SPRINGER REFERENCE

Wei Zhang
Editor

Handbook of Cognitive Radio

Springer

Handbook of Cognitive Radio

Wei Zhang
Editor

Handbook of Cognitive Radio

With 657 Figures and 136 Tables

Springer

Editor
Wei Zhang
School of Electrical Engineering and Telecommunications
The University of New South Wales
Sydney, NSW, Australia

ISBN 978-981-10-1393-5 ISBN 978-981-10-1394-2 (eBook)
ISBN 978-981-10-1395-9 (print and electronic bundle)
https://doi.org/10.1007/978-981-10-1394-2

Library of Congress Control Number: 2018964907

This Springer imprint is published by the registered company Springer Nature Singapore Pte Ltd.
The registered company address is: 152 Beach Road, #21-01/04 Gateway East, Singapore 189721, Singapore

Contents

Volume 1

Volume 2

About the Editor

Wei Zhang
School of Electrical Engineering and Telecommunications
The University of New South Wales
Sydney, NSW, Australia

Wei Zhang is a Professor at the University of New South Wales, Sydney, Australia. His current research interests include UAV communications, millimeter-wave communications, space information networks, and massive MIMO. He is the Editor-in-Chief of *IEEE Wireless Communications Letters* and Editor-in-Chief of *Journal of Communications and Information Networks* (JCIN). He is a TPC Co-Chair of IEEE/CIC ICCC 2019, Changchun, China. He also serves as Chair for IEEE Wireless Communications Technical Committee and Vice Director of IEEE Communications Society Asia Pacific Board. He is a member of Board of Governors of IEEE Communications Society. He is an IEEE fellow.

Editorial Board

Cognitive Radio Communications

Wei Zhang School of Electrical Engineering and Telecommunications, The University of New South Wales, Sydney, NSW, Australia

Dynamic Spectrum Access and Sharing

Dusit Niyato School of Computer Science and Engineering (SCSE), Nanyang Technological University, Singapore, Singapore

Ping Wang School of Computer Science and Engineering (SCSE), Nanyang Technological University, Singapore, Singapore

Cognitive Radio Resource Management

Jianwei Huang Department of Information Engineering, The Chinese University of Hong Kong, Shatin, New Territory, Hong Kong, China

Xu Chen School of Data and Computer Science, Sun Yat-Sen University, Guangzhou, China

Cognitive Cellular Networks

Lingyang Song School of Electronics Engineering and Computer Science, Peking University, Beijing, China

Spectrum Policy and Cognitive Radio Standards

Oliver Holland Centre for Telecommunications Research, King's College London, London, UK

Cognitive Radio Applications and Practices

Yue Gao School of Electronic Engineering and Computer Science (EECS), Queen Mary University of London, London, UK

Contributors

Ahmed Abdelhadi ICTAS/ECE, Virginia Tech, Blacksburg, VA, USA

Satyam Agarwal Indian Institute of Technology Guwahati, Guwahati, India

Peter Anker Ministry of Economic Affairs, Delft University of Technology, Haarlem, The Netherlands

Alagan Anpalagan Electrical and Computer Engineering, Ryerson University, Toronto, ON, Canada

G. Araniti DIIES Department, University Mediterranea of Reggio Calabria, Reggio Calabria, RC, Italy

Huseyin Arslan Department of Electrical and Electronics Engineering, Istanbul Medipol University, Istanbul, Turkey

Department of Electrical Engineering, University of South Florida, Tampa, FL, USA

Luca Bedogni Department of Computer Science and Engineering, University of Bologna, Bologna, Italy

Maria-Gabriella Di Benedetto Department of Information Engineering, Electronics and Telecommunications (DIET), Sapienza University of Rome, Rome, Italy

Kostas Berberidis Department of Computer Engineering and Informatics, University of Patras, Patras, Greece

CTI "Diophantus", Patras, Greece

Jim Beveridge Faileas Limited, Buckinghamshire, UK

Kaigui Bian School of EECS, Peking University, Beijing, China

Luciano Bononi Department of Computer Science and Engineering, University of Bologna, Bologna, Italy

Joseph M. Bruno ECE Department, George Mason University, Fairfax, VA, USA

Danijela Cabric Electrical Engineering, University of California, Los Angeles (UCLA), Los Angeles, CA, USA

Haofan Cai Southern University of Science and Technology, Shenzhen, China

Giuseppe Caso Department of Information Engineering, Electronics and Telecommunications (DIET), Sapienza University of Rome, Rome, Italy

Gianni Cerro Department of Electrical and Information Engineering, University of Cassino and Southern Lazio, Cassino, Italy

Symeon Chatzinotas SnT – securityandtrust, University of Luxembourg, Luxembourg City, Luxembourg

Xu Chen School of Data and Computer Science, Sun Yat-Sen University, Guangzhou, China

Yanjiao Chen Wuhan University, Wuhan, China

Julian Cheng School of Engineering, The University of British Columbia, Kelowna, BC, Canada

Man Hon Cheung Department of Information Engineering, The Chinese University of Hong Kong, Hong Kong, China

Charles Clancy ICTAS/ECE, Virginia Tech, Arlington, VA, USA

Deborah Cohen Electrical Engineering, Technion – Israel Institute of Technology, Haifa, Israel

Shuguang Cui University of California, Davis, CA, USA

Department of Electrical and Computer Engineering, University of California, Davis, CA, USA

Zhiyu Dai D&B Cloud Innovation Center, Vancouver, BC, Canada

Swades De Indian Institute of Technology Delhi, New Delhi, India

Marco Di Felice Department of Computer Science and Engineering, University of Bologna, Bologna, Italy

Haichuan Ding Department of Electrical and Computer Engineering, University of Florida, Gainesville, FL, USA

Zhi Ding University of California, Davis, CA, USA

L. S. Dooley School of Computing and Communications, The Open University, Milton Keynes, UK

Dongliang Duan Department of Electrical and Computer Engineering, University of Wyoming, Laramie, WY, USA

Yonina C. Eldar Electrical Engineering, Technion – Israel Institute of Technology, Haifa, Israel

Mohamed Elkourdi Department of Electrical Engineering, University of South Florida, Tampa, FL, USA

Hesham M. Elmaghraby University of California, Davis, CA, USA

Ahmed R. Elsherif University of California, Davis, CA, USA

Yariv Ephraim ECE Department, George Mason University, Fairfax, VA, USA

Yuguang Fang Department of Electrical and Computer Engineering, University of Florida, Gainesville, FL, USA

Zhiyong Feng Key Laboratory of Universal Wireless Communications, Ministry of Education, Beijing University of Posts and Telecommunications, Beijing, China

Liqun Fu Department of Communication Engineering, Xiamen University, Xiamen, China

Takeo Fujii Advanced Wireless and Communication Research Center, The University of Electro-Communications, Tokyo, Japan

Cunhao Gao Virginia Polytechnic Institute and State University, Blacksburg, VA, USA

Lin Gao School of Electronic and Information Engineering, Harbin Institute of Technology, Shenzhen, China

Yue Gao School of Electronic Engineering and Computer Science (EECS), Queen Mary University of London, London, UK

Savo Glisic Department of Communication Engineering, University of Oulu, Oulu, Finland

Shengjie Guo Louisiana State University, Baton Rouge, LA, USA

Zhu Han Electrical and Computer Engineering Department, University of Houston, Houston, TX, USA

Xiaolei Hao Department of Electrical and Computer Engineering, The University of British Columbia, Vancouver, BC, Canada

Hiroshi Harada Department of Communications and Computer Engineering, Kyoto University, Kyoto, Japan

Ghaith Hattab Electrical Engineering, University of California, Los Angeles (UCLA), Los Angeles, CA, USA

Biao He Department of Electronic and Computer Engineering, The Hong Kong University of Science and Technology, Hong Kong, Hong Kong

Dinh Thai Hoang School of Computer Science and Engineering, Nanyang Technological University, Singapore, Singapore

Oliver Holland Centre for Telecommunications Research, King's College London, London, UK

Y. Thomas Hou Virginia Polytechnic Institute and State University, Blacksburg, VA, USA

Xiaoxia Huang Shenzhen Institutes of Advanced Technology, China Academy of Sciences, Shenzhen, Guangdong, China

Jianwei Huang Department of Information Engineering, The Chinese University of Hong Kong, Shatin, New Territory, Hong Kong, China

A. Iera DIIES Department, University Mediterranea of Reggio Calabria, Reggio Calabria, RC, Italy

Kei Inage Electrical and Electronics Engineering Course, Tokyo Metropolitan College of Industrial Technology, Tokyo, Japan

Kentaro Ishizu National Institute of Information and Communications Technology, Yokosuka, Japan

Muhammad Nazmul Islam Qualcomm Corporate R&D, Bridgewater, NJ, USA

Linshan Jiang Southern University of Science and Technology, Shenzhen, China

Friedrich K. Jondral Communications Engineering Lab, Karlsruhe Institute of Technology, Karlsruhe, Germany

Jung-Min Jerry Park Department of Electrical and Computer Engineering, Virginia Tech, Blacksburg, VA, USA

Xin Kang National Key Laboratory of Science and Technology on Communications, University of Electronic Science and Technology of China, Chengdu, China

Ankit Kaushik Communications Engineering Lab, Karlsruhe Institute of Technology, Karlsruhe, Germany

Lamiaa Khalid Electrical and Computer Engineering, Ryerson University, Toronto, ON, Canada

Muhammad R. A. Khandaker Electronic and Electrical Engineering, University College London, London, UK

Sastry Kompella Information Technology Division, Naval Research Laboratory, Washington, DC, USA

U.S. Naval Research Laboratory, Washington, DC, USA

Lifeng Lai University of California, Davis, CA, USA

Zhou Lan Broadcom Ltd., Irvine, CA, USA

Vincent K. N. Lau Department of Electronic and Computer Engineering, The Hong Kong University of Science and Technology, Hong Kong, Hong Kong

Mai T. Phuong Le Department of Information Engineering, Electronics and Telecommunications (DIET), Sapienza University of Rome, Rome, Italy

Olga León Telematics Department, Universitat Politècnica de Catalunya, Castelldefels, Barcelona, Spain

Victor C. M. Leung Department of Electrical and Computer Engineering, The University of British Columbia, Vancouver, BC, Canada

Husheng Li Department of Electrical Engineering and Computer Science, The University of Tennessee, Knoxville, TN, USA

Pan Li Department of Electrical Engineering and Computer Science, Case Western Reserve University, Cleveland, OH, USA

Xuanheng Li School of Information and Communication Engineering, Dalian University of Technology, Dalian, Liaoning, China

Yun Liao School of Electrical Engineering and Computer Science, Peking University, Beijing, China

Mingyan Liu EECS, University of Michigan, Ann Arbor, MI, USA

Yang Liu SEAS, Harvard University, Cambridge, MA, USA

Miguel López-Benítez Department of Electrical Engineering and Electronics, University of Liverpool, Liverpool, UK

Wenjing Lou Virginia Polytechnic Institute and State University, Blacksburg, VA, USA

Yuan Ma School of Electronic Engineering and Computer Science (EECS), Queen Mary University of London, London, UK

S. Eman Mahmoodi Electrical and Computer Engineering, Stevens Institute of Technology, Hoboken, NJ, USA

Narayan B. Mandayam WINLAB, Department of ECE, Rutgers University, North Brunswick, NJ, USA

Lucio Marcenaro Department of Electrical, Electronic, Telecommunications Engineering and Naval Architecture (DITEN), University of Genoa, Genoa, Italy

Brian L. Mark ECE Department, George Mason University, Fairfax, VA, USA

J. H. Martin IP/Optical Networks (ION), Nokia, Bristol, UK

School of Computing and Communications, The Open University, Milton Keynes, UK

Marja Matinmikko Centre for Wireless Communications (CWC), University of Oulu, Oulu, Finland

Takeshi Matsumura Department of Communications and Computer Engineering, Kyoto University, Kyoto, Japan

Morteza Mehrnoush University of Washington, Seattle, WA, USA

Scott F. Midkiff Virginia Polytechnic Institute and State University, Blacksburg, VA, USA

Gianfranco Miele Department of Electrical and Information Engineering, University of Cassino and Southern Lazio, Cassino, Italy

L. Militano DIIES Department, University Mediterranea of Reggio Calabria, Reggio Calabria, RC, Italy

Keiichi Mizutani Department of Communications and Computer Engineering, Kyoto University, Kyoto, Japan

Apurva Mody WhiteSpace Alliance®, Chelmsford, MA, USA

Markus Mueck Next Generation and Standards, INTEL Deutschland GmbH, Neubiberg, Germany

Miia Mustonen VTT Technical Research Centre of Finland Ltd., Oulu, Finland

Luca De Nardis Department of Information Engineering, Electronics and Telecommunications (DIET), Sapienza University of Rome, Rome, Italy

Maziar Nekovee Department of Engineering and Design, School of Engineering and Informatics, University of Sussex, Brighton, UK

Dusit Niyato School of Computer Science and Engineering, Nanyang Technological University, Singapore, Singapore

A. Orsino ELS Department, Tampere University of Technology, Tampere, Finland

Björn Ottersten SnT – securityandtrust, University of Luxembourg, Luxembourg City, Luxembourg

Jarkko Paavola Turku University of Applied Sciences, Turku, Finland

Miao Pan Department of Electrical and Computer Engineering, University of Houston, Houston, TX, USA

Lee Pucker The Wireless Innovation Forum, Reston, VA, USA

A. Raschellà Department of Computer Science, Liverpool John Moores University, Liverpool, MSY, UK

Jeffrey H. Reed Virginia Polytechnic Institute and State University, Blacksburg, VA, USA

Ivan Reede AmeriSys, Oviedo, FL, USA

Carlo Regazzoni Department of Electrical, Electronic, Telecommunications Engineering and Naval Architecture (DITEN), University of Genoa, Genoa, Italy

Jie Ren Electronic and Information Engineering, Beijing Jiaotong University, Beijing, China

Sumit Roy University of Washington, Seattle, WA, USA

Anindya Saha Saankhya Labs Pvt Ltd, Bangalore, India

Koya Sato Department of Electrical Engineering, Tokyo University of Science, Tokyo, Japan

Ivan Seskar WINLAB, Rutgers University, North Brunswick, NJ, USA

Shree Krishna Sharma Department of Electrical and Computer Engineering, Western University, London, Ontario, Canada

SnT – securityandtrust, University of Luxembourg, Luxembourg City, Luxembourg

Yi Shi Intelligent Automation Inc., Rockville, MD, USA

Lingyang Song School of Electrical Engineering and Computer Science, Peking University, Beijing, China

Liwei Song School of Electrical Engineering and Computer Science, Peking University, Beijing, China

Andrew Stirling Larkhill Consultancy Limited, Surrey, UK

K. P. Subbalakshmi Electrical and Computer Engineering, Stevens Institute of Technology, Hoboken, NJ, USA

Sumei Sun Institute for Infocomm Research, South Tower, Singapore

Yi Sun School of Information and Communication Engineering, Dalian University of Technology, Dalian, Liaoning, China

Chintha Tellambura Electrical and Computer Engineering, University of Alberta, Edmonton, AB, Canada

Feng Tian Nanjing University of Posts and Telecommunications, Nanjing, China

Zhi Tian ECE Department, George Mason University, Fairfax, VA, USA

Andrea Toma Department of Electrical, Electronic, Telecommunications Engineering and Naval Architecture (DITEN), University of Genoa, Genoa, Italy

School of Electronic Engineering and Computer Science (EECS), Queen Mary University of London, London, UK

Wade Trappe Rutgers University, New Brunswick, NJ, USA

Theodoros A. Tsiftsis School of Engineering, Nazarbayev University, Astana, Akmola, Kazakhstan

Christos G. Tsinos Interdisciplinary Centre for Security, Reliability and Trust (SnT), University of Luxembourg, Luxembourg City, Luxembourg

Shahar Tsiper Electrical Engineering, Technion – Israel Institute of Technology, Haifa, Israel

Jitendra K. Tugnait Department of Electrical and Computer Engineering, Auburn University, Auburn, AL, USA

R. N. Uma Mathematics and Physics, North Carolina Central University, Durham, NC, USA

Mihaela van der Schaar Oxford – Man Institute of Quantitative Finance (OMI), Oxford, UK

Department of Engineering Science, University of Oxford, Oxford, UK

Jingqing Wang Networking and Information Systems Laboratory, Department of Electrical and Computer Engineering, Texas A&M University, College Station, TX, USA

Xinbing Wang EE and CS Department in School of Electronic Information and Electrical Engineering, Shanghai Jiao Tong University, Shanghai, China

Zehua Wang Department of Electrical and Computer Engineering, The University of British Columbia, Vancouver, BC, Canada

Zhiqing Wei Key Laboratory of Universal Wireless Communications, Ministry of Education, Beijing University of Posts and Telecommunications, Beijing, China

K. C. P. Wong School of Computing and Communications, The Open University, Milton Keynes, UK

Kai-Kit Wong Electronic and Electrical Engineering, University College London, London, UK

Vincent W. S. Wong Department of Electrical and Computer Engineering, The University of British Columbia, Vancouver, BC, Canada

Liang Wu Department of Electronic Engineering and Information Science, University of Science and Technology of China, Hefei, China

Huawei Technologies, Shanghai, China

Yuanzhang Xiao Department of Electrical Engineering and Computer Science, Northwestern University, Evanston, IL, USA

Yan Xin Futurewei Technologies Inc., Bridgewater, NJ, USA

Xiaoming Xu College of Communications Engineering, PLA University of Science and Technology, Nanjing, Jiangsu, China

Youyun Xu National Engineering Research Center for Communications and Networking, Nanjing University of Posts and Telecommunications, Nanjing, China

Liuqing Yang Department of Electrical and Computer Engineering, Colorado State University, Fort Collins, CO, USA

Weiwei Yang College of Communications Engineering, PLA University of Science and Technology, Nanjing, Jiangsu, China

Ahmet Yazar Department of Electrical and Electronics Engineering, Istanbul Medipol University, Istanbul, Turkey

Toby Youell Spectrum Group, Ofcom (writing in a personal capacity), London, UK

Xu Yuan Virginia Polytechnic Institute and State University, Blacksburg, VA, USA

Chiya Zhang School of Electrical Engineering and Telecommunications, The University of New South Wales, Sydney, NSW, Australia

Haijun Zhang Beijing Engineering and Technology Research Center for Convergence Networks and Ubiquitous Services, University of Science and Technology Beijing, Beijing, China

Hongliang Zhang School of Electronics Engineering and Computer Science, Peking University, Beijing, China

Huaqing Zhang Electrical and Computer Engineering Department, University of Houston, Houston, TX, USA

Jin Zhang Southern University of Science and Technology, Shenzhen, China

Qinyu Zhang School of Electronic and Information Engineering, Harbin Institute of Technology, Shenzhen, China

Wei Zhang School of Electrical Engineering and Telecommunications, The University of New South Wales, Sydney, NSW, Australia

Wenyi Zhang Key Laboratory of Wireless-Optical Communications, Chinese Academy of Sciences, Hefei, China

Department of Electronic Engineering and Information Science, University of Science and Technology of China, Hefei, China

Xi Zhang Networking and Information Systems Laboratory, Department of Electrical and Computer Engineering, Texas A&M University, College Station, TX, USA

Yong Zhou Department of Electrical and Computer Engineering, The University of British Columbia, Vancouver, BC, Canada

Xiangwei Zhou Louisiana State University, Baton Rouge, LA, USA

Part I
Cognitive Radio Communications

Multiple Antenna Spectrum Sensing in Colored Noise

1

Jitendra K. Tugnait

Contents

Abstract

The problem of multiple antenna spectrum sensing is addressed where the receiver noise is allowed to be temporally colored with unknown power spectral density, but must be spatially uncorrelated. The signal is received over a possibly frequency-selective, unknown channel. A comprehensive overview of spectrum sensing approaches under colored noise is presented. Both time-domain and frequency-domain approaches exploiting stationarity are presented. Cyclostationarity-based spectrum sensing methods are also reviewed.

J. K. Tugnait (✉)
Department of Electrical and Computer Engineering, Auburn University, Auburn, AL, USA
e-mail: tugnajk@auburn.edu

W. Zhang (ed.), *Handbook of Cognitive Radio*,
https://doi.org/10.1007/978-981-10-1394-2_1

Introduction

Cognitive radio (CR) allows for usage of licensed frequency bands (rights held by primary users) by unlicensed users (secondary or cognitive users) when the licensed spectrum bands are unoccupied (a function of time and location). Therefore, one of the first steps to be accomplished by a cognitive user is *spectrum sensing*: analysis of the received electromagnetic transmissions to search for unoccupied spectrum bands (*spectrum holes*). Based on the received signal $x(t)$, the cognitive user's spectrum sensing problem is to decide if the primary user (PU) is present or not. This may be formulated as a binary hypothesis testing problem:

$$x(t) = \begin{cases} n(t) & : \mathscr{H}_0 \\ s(t) + n(t) & : \mathscr{H}_1 \end{cases} \tag{1}$$

where $\mathscr{H}_0$ is the null hypothesis that cognitive user is receiving just noise $n(t)$ and $\mathscr{H}_1$ is the alternative that PU signal $s(t)$ is also present. A popular approach is that of energy detection; see [8, 15] and references therein. One designs a CFAR (constant false alarm rate) test requiring prior knowledge of some of the signal statistics under $\mathscr{H}_0$. For instance, $n(t)$ is taken to be thermal noise with known variance.

Quite often, as a result of receive filters at the cognitive user's receiver, the filtered thermal noise will not be white. Most existing approaches assume white noise sequences at the receiver. The goal of this chapter is to present a comprehensive overview of spectrum sensing approaches when noise is colored. Emphasis is on multiple antenna receivers which rely on the fact that noise is spatially (across antennas) independent and PU signals are spatially dependent while temporal properties of signal and noise become "irrelevant."

Notation: Notations $|\mathbf{D}|$ and $\text{tr}(\mathbf{D})$ stand for the determinant and trace of square matrix $\mathbf{D}$, respectively, $\text{etr}(\mathbf{D}) = \exp(\text{tr}(\mathbf{D}))$, $\mathbf{D}_{ij}$ is the ijth element of $\mathbf{D}$, $\mathbf{I}$ is the identity matrix and superscripts $*$ and H denote the complex conjugate and the conjugate transpose (Hermitian) operations, respectively. The notation $y = \mathscr{O}(g(x))$ means that there exists some finite real number $b > 0$ such that $\lim_{x\to\infty} |y/g(x)| \leq b$. Given a column vector $\mathbf{y}$, $\text{diag}\{\mathbf{y}\}$ denotes a square matrix with elements of $\mathbf{y}$ along its main diagonal and zeros everywhere else. Covariance $\text{cov}(\mathbf{x}, \mathbf{y}^*) := E\{\mathbf{x}\mathbf{y}^H\} - E\{\mathbf{x}\}E\{\mathbf{y}^H\}$ where E denotes expectation, and let $\text{cum}_4(x_1, x_2, x_3, x_4)$ denote the joint fourth cumulant of random variables x_i ($i = 1, 2, 3, 4$). Note that $\text{cum}_4(x_1, x_2, x_3, x_4) = E\{x_1x_2x_3x_4\} - E\{x_1x_2\}E\{x_3x_4\} - E\{x_1x_3\}E\{x_2x_4\} - E\{x_1x_4\}E\{x_2x_3\}$ when all x_i's are zero mean. The function $\delta_{i,j}$ denotes the Kronecker delta function, i.e., $\delta_{i,j} = 1$ if $i = j$, 0 otherwise. The abbreviations i.i.d. and w.r.t. stand for "independent and identically distributed" and "with respect to," respectively.

Colored Noise

An irreducible source of noise at the receiver is thermal noise which is zero-mean white Gaussian and whose baseband-equivalent model is that of a zero-mean, white, circularly symmetric complex Gaussian random process $v(t)$. Before processing the (continuous-time) received noisy signal, at the receiver front-end, the noisy (baseband-equivalent) signal is passed through a receive filter $g_r(t)$. Let $\tilde{v}(t)$ denote the filtered noise:

$$\tilde{v}(t) = v(t) \circledast g_r(t) = \int v(t-\lambda) g_r(\lambda)\, d\lambda$$

where $\circledast$ denotes convolution. The autocorrelation function of $\tilde{v}(t)$ is

$$R_{\tilde{v}\tilde{v}}(\tau) = E\{\tilde{v}(t)\tilde{v}^*(t-\tau)\} = \frac{N_0}{2} \int g_r(t) g_r^*(t-\tau)\, dt$$

where $R_{vv}(\tau) = \frac{N_0}{2}\delta(\tau)$. If $g_r(t)$ is a square-root raised cosine filter with bandwidth $(1+\alpha)/(2T_s)$, $0 \le \alpha \le 1$, where T_s is the symbol interval, then $R_{\tilde{v}\tilde{v}}(nT_s) = 0$ for $n = \pm 1, \pm 2, \cdots$. That is, $\{\tilde{v}(t)\big|_{t=nT_s}\}_n$ is white Gaussian sample sequence when $\tilde{v}(t)$ is sampled at the symbol rate. But if one oversamples (more than one sample in T_s sec, called fractional sampling), then $\{\tilde{v}(t)\big|_{t=nT}\}_n$, $T < T_s$, is colored.

Thus, if the filters are not necessarily the ones that yield white noise at symbol rate sampling, or the sampling rate exceeds the symbol rate, the sampled filtered thermal noise will be a colored random sequence. For CR applications, active RC filters with tunable cutoff frequencies have been proposed in the literature [23, 32]. Sampling of the filtered thermal noise using such RC filters will invariably result in colored noise. The effect of noise correlation on spectrum sensing performance for a class of spectrum sensing algorithms has been analyzed in [22].

Spectral Sensing Models

Assume that there are p antennas at the cognitive user. Then the hypothesis testing problem (1) is reformulated as

$$\mathbf{x}(t) = \begin{cases} \mathbf{n}(t) & : \mathscr{H}_0 \\ \underbrace{\sum_{l=0}^{L} \mathbf{h}(l) s_{pu}(t-l)}_{=\mathbf{s}(t)} + \mathbf{n}(t) & : \mathscr{H}_1 \end{cases} \tag{2}$$

where under $\mathscr{H}_0$, cognitive user is receiving just noise $\mathbf{n}(t)$ (assumed to be zero-mean, complex-valued, possibly colored, Gaussian, and spatially uncorrelated),

and under $\mathscr{H}_1$, (scalar) PU signal $s_{pu}(t)$ is also present where p-column $\mathbf{h}(l)$ is the complex channel impulse response and $s_{pu}(t)$ is the scalar (non-Gaussian) complex-valued proper i.i.d. information sequence with zero mean and variance $E\{|s_{pu}(t)|^2\} = \sigma_s^2$.

Spectrum sensing methods considered here include time-domain approaches that exploit either stationarity or cyclostationarity properties of the received noisy signals and also include frequency-domain approaches based on multivariate spectral analysis that exploit stationarity properties of the received noisy signals. To this end, first some of these properties are briefly reviewed.

Large Sample Statistics of Sample Correlation

In (2), $\mathbf{n}(t)$ is complex (proper) possibly colored Gaussian with

$$E\{\mathbf{n}(t)\mathbf{n}^H(t+\tau)\} = \text{diag}\left\{R_{11,n}(\tau),\ R_{22,n}(\tau),\ \cdots,\ R_{pp,n}(\tau)\right\}. \tag{3}$$

Given an observation length of N samples of $\mathbf{x}(t)$ in (2), estimate the correlation function $\mathbf{R}_{xx}(\tau) = E\{\mathbf{x}(t)\mathbf{x}^H(t-\tau)\}$ as

$$\hat{\mathbf{R}}_{xx}(\tau) = \frac{1}{N}\sum_{t=1}^{N}\mathbf{x}(t)\mathbf{x}^H(t-\tau). \tag{4}$$

It is easy to see that $E\{\hat{\mathbf{R}}_{xx}(\tau)\} = \mathbf{R}_{xx}(\tau)$. With $R_{ij,xx}(\tau)$ denoting the ijth element of matrix $\mathbf{R}_{xx}(\tau)$, one has

$$\begin{aligned}
&E\{x_i(t_1)x_j^*(t_1-\tau_1)x_k^*(t_2)x_l(t_2-\tau_2)\}\\
&\quad= \text{cum}_4\left(x_i(t_1), x_j^*(t_1-\tau_1), x_k^*(t_2), x_l(t_2-\tau_2)\right) + R_{ij,xx}(\tau_1)R_{kl,xx}^*(\tau_2)\\
&\qquad+R_{ik,xx}(t_1-t_2)R_{lj,xx}(t_2-t_1-\tau_2+\tau_1).
\end{aligned} \tag{5}$$

Hence,

$$\begin{aligned}
&\text{cov}\left(\hat{R}_{ij,xx}(\tau_1), \hat{R}_{kl,xx}^*(\tau_2)\right)\\
&\quad= \frac{1}{N^2}\sum_{t_1=1}^{N}\sum_{t_2=1}^{N}\left[R_{ik,xx}(t_1-t_2)R_{lj,xx}^*(t_1-t_2+\tau_2-\tau_1) + A_2\right]
\end{aligned} \tag{6}$$

where

$$A_2 := \text{cum}_4\left(x_i(t_1), x_j^*(t_1-\tau_1), x_k^*(t_2), x_l(t_2-\tau_2)\right). \tag{7}$$

Denote the first double summation term in (6) by B_1 and set $t_1 - t_2 = m$ therein to obtain

$$B_1 = \frac{1}{N^2} \sum_{t_1=1,\, t_1-t_2=m}^{N} \sum_{t_2=1}^{N} R_{ik,xx}(m) R^*_{lj,xx}(m + \tau_2 - \tau_1)$$

$$= \frac{1}{N^2} \sum_{m=-(N-1)}^{N-1} (N - |m|) R_{ik,xx}(m) R^*_{lj,xx}(m + \tau_2 - \tau_1), \tag{8}$$

leading to

$$\lim_{N\to\infty} NB_1 = \sum_{m=-\infty}^{\infty} R_{ik,xx}(m) R^*_{lj,xx}(m + \tau_2 - \tau_1). \tag{9}$$

It then follows that ($\gamma_{4s} := \mathrm{cum}_4(s(t), s^*(t), s(t), s^*(t))$)

$$A_2 = \gamma_{4s} \sum_{m=-\infty}^{\infty} h_i(m+\tau_1) h^*_j(m) h^*_k(t_2 - t_1 + m + \tau_1) h_l(t_2 - t_1 + m + \tau_1 - \tau_2). \tag{10}$$

Using $R^{(s)}_{ij,ss}(\tau) = E\{[x_i(t) - n_i(t)][x_i(t-\tau) - n_i(t-\tau)]^*\} = \sigma_s^2 \sum_{l=-\infty}^{\infty} h_i(l) h^*_j(l - \tau)$ and mimicking (8) and (9), one obtains

$$\lim_{N\to\infty} \frac{1}{N} \sum_{t_1=1}^{N} \sum_{t_2=1}^{N} A_2 = \frac{\gamma_{4s}}{\sigma_s^4} R_{ij,ss}(\tau_1) R^*_{kl,ss}(\tau_2). \tag{11}$$

From (6), (9), and (11), one has

$$\lim_{N\to\infty} N \mathrm{cov}\left(\hat{R}_{ij,xx}(\tau_1), \hat{R}^*_{kl,xx}(\tau_2)\right)$$

$$= \frac{\gamma_{4s}}{\sigma_s^4} R_{ij,ss}(\tau_1) R^{(*}_{kl,ss}(\tau_2) + \sum_{m=-\infty}^{\infty} R_{ik,xx}(m) R^*_{lj,xx}(m + \tau_2 - \tau_1). \tag{12}$$

Spatially Uncorrelated, Temporally Colored Noise

If $\mathbf{x}(t)$ is Gaussian, then

$$\lim_{N\to\infty} N \mathrm{cov}\left(\hat{R}_{ij,xx}(\tau_1), \hat{R}^*_{kl,xx}(\tau_2)\right) = \sum_{m=-\infty}^{\infty} R_{ik,xx}(m) R^*_{lj,xx}(m + \tau_2 - \tau_1). \tag{13}$$

If $\mathbf{x}(t) = \mathbf{n}(t)$, then

$$\lim_{N\to\infty} N \mathrm{cov}\left(\hat{R}_{ij,nn}(\tau_1), \hat{R}^*_{kl,nn}(\tau_2)\right) = \delta_{i,k}\delta_{j,l} \sum_{m=-\infty}^{\infty} R_{ii,nn}(m) R^*_{jj,nn}(m + \tau_2 - \tau_1). \tag{14}$$

In particular, with $\tau_1 = \tau_2 = 0$, one obtains

$$\lim_{N\to\infty} N\mathrm{cov}\left(\hat{R}_{ij,nn}(0), \hat{R}^*_{kl,nn}(0)\right) = \delta_{i,k}\delta_{j,l} \sum_{m=-\infty}^{\infty} R_{ii,nn}(m) R^*_{jj,nn}(m) \tag{15}$$

and

$$\begin{aligned}\lim_{N\to\infty} N\mathrm{cov}\left(\hat{R}_{ij,nn}(0), \hat{R}_{kl,nn}(0)\right) &= \lim_{N\to\infty} N\mathrm{cov}\left(\hat{R}_{ij,nn}(0), \hat{R}^*_{lk,nn}(0)\right) \\ &= \delta_{i,l}\delta_{j,k} \sum_{m=-\infty}^{\infty} R_{ii,nn}(m) R^*_{jj,nn}(m)\end{aligned} \tag{16}$$

It is assumed that $R_{ij,nn}(\tau) = 0$ for $|\tau| > L_n$ for some L_n (finite memory). Invoking the central limit theorem, it is seen that for $i \neq j$,

$$\lim_{N\to\infty} \sqrt{N}\,\hat{R}_{ij,nn}(0) \sim \mathcal{N}_c\left(0, \sum_{m=-\infty}^{\infty} R_{ii,nn}(m) R^*_{jj,nn}(m)\right) \tag{17}$$

where $\mathcal{N}_c(\boldsymbol{\mu}, \Sigma)$ denotes a complex (proper) Gaussian (vector) distribution with mean $\boldsymbol{\mu}$ and covariance matrix Σ. Furthermore, by the central limit theorem and (14), (15), and (16), the upper (lower) triangular off-diagonal elements of $\hat{\mathbf{R}}_{nn}(0)$ are asymptotically independent of the other upper (lower) triangular off-diagonal elements.

Spectral Analysis Background

Suppose that $\mathbf{x}(t)$, $t = 0, 1, \cdots, N-1$, has zero mean and $p \times p$ power spectral density (PSD) matrix $\mathbf{S}(f)$. Numerous approaches are available [3, 19] to estimate $\mathbf{S}(f)$ on a grid $f_n := n/N$, $n = 0, 1, \cdots, N-1$. Consider the Daniell method (unweighted frequency-domain averaging) to estimate PSD. Given $p \times 1$ time series $\mathbf{x}(t)$, $t = 0, 1, \cdots, N-1$, first the periodogram estimator of the $\mathbf{S}(f)$ is calculated as

$$\hat{\mathbf{S}}_p(f) = N^{-1}\mathbf{I}(f)\mathbf{I}^H(f), \quad \mathbf{I}(f) := \sum_{t=0}^{N-1} \mathbf{x}(t) e^{-j2\pi ft}. \tag{18}$$

In the Daniell method, the periodogram is averaged over $K = 2m_t + 1$ nonoverlapping frequency bins:

$$\hat{\mathbf{S}}(f_n) = \frac{1}{K} \sum_{l=-m_t}^{m_t} \hat{\mathbf{S}}_p(f_{n+l}) \tag{19}$$

where $f_n := n/N, n = 0, 1, \cdots, N-1$ and there are N data observation samples. A key fact is that at any frequency f (on the appropriate FFT grid in the interval $(0, 2\pi) \equiv (0, 1.0)$), the PSD estimator $\hat{\mathbf{S}}(f)$ of the true $p \times p$ PSD matrix $\mathbf{S}(f)$ has the (asymptotic: N "large") distribution

$$\hat{\mathbf{S}}(f) \sim (1/K) W_C(p, K, \mathbf{S}(f)) \tag{20}$$

where $W_C(p, K, \mathbf{S}(f))$ denotes the complex Wishart distribution of dimension p and degrees of freedom K. These results follow from [3] (and others). It has been shown in [19, Sec. 6.19] that for circularly symmetric complex-valued time series, the spectral estimators are (asymptotically) statistically independent on an appropriate discrete grid on $(0, 2\pi)$, in contrast to the case of real-valued time series where this property holds true on just $(0, \pi)$.

If $\mathbf{X} \sim W_C(p, K, \mathbf{S}(f))$, then by [3, Sec. 4.2], $E\{\mathbf{X}\} = K\mathbf{S}(f)$, $\text{cov}\{\mathbf{X}_{jk}, \mathbf{X}_{lm}\} = K\mathbf{S}_{jl}(f)\mathbf{S}^*_{km}(f)$, and the probability density function (pdf) of $\mathbf{X}$ is given by

$$f_{\mathbf{X}}(\mathbf{X}) = \frac{1}{\Gamma_p(K)} \frac{1}{|\mathbf{S}(f)|^K} |\mathbf{X}|^{K-p} \,\text{etr}\{-\mathbf{S}^{-1}(f)\mathbf{X}\} \tag{21}$$

where (21) is defined for positive-definite Hermitian $\mathbf{X}$ and is otherwise zero, and

$$\Gamma_p(K) := \pi^{p(p-1)/2} \prod_{j=1}^{p} \Gamma(K - j + 1)$$

where $\Gamma(n)$ denotes the (complete) gamma function $\Gamma(z) := \int_0^\infty t^{z-1} e^{-t}\, dt$. Applying [16, Thm. 3.2.5] to complex-valued random vectors, if $\mathbf{X} \sim W_C(p, K, \mathbf{S}(f))$, then $\mathbf{AXA}^H \sim W_C\left(m, K, \mathbf{AS}(f)\mathbf{A}^H\right)$ for any $m \times p$ matrix $\mathbf{A}$ of rank m. It then follows that $\mathbf{Y} = \hat{\mathbf{S}}(f_k) = (1/K)\mathbf{X}$ and the pdf of $\mathbf{Y}$ is given by

$$f_{\mathbf{Y}}(\mathbf{Y}) = \frac{1}{\Gamma_p(K)} \frac{K^{pK}}{|\mathbf{S}(f_k)|^K} |\mathbf{Y}|^{K-p} \,\text{etr}\{-K(\mathbf{S}(f_k))^{-1}\mathbf{Y}\}. \tag{22}$$

Cyclostationarity Background

First consider scalar signals to fix notation and concepts.

Scalar Processes

A discrete-time, zero-mean, scalar complex-valued cyclostationary signal $x(t)$ is characterized by a time-varying autocorrelation function $R_{xx}(t, t+\tau) := E\{x(t)x^*(t+\tau)\}$ which has a Fourier series representation [4, 17]

$$R_{xx}(t, t+\tau) = \sum_{\alpha \in \mathscr{A}} R_{xx}(\alpha; \tau) e^{j2\pi\alpha t} \tag{23}$$

where given $x(t)$ for $t = 1, 2, \cdots, M$, the *cyclic autocorrelation function* (CAF) $R_{xx}(\alpha;\tau)$ at cycle frequency $\alpha \in \mathscr{A}$ is given by

$$R_{xx}(\alpha;\tau) = \lim_{M\to\infty} \frac{1}{M} \sum_{t=1}^{M} R_{xx}(t, t+\tau) e^{-j2\pi\alpha t} \tag{24}$$

and $\mathscr{A}$ is the set of cycle frequencies [4]

$$\mathscr{A} := \{\alpha \,|\, 0 \le \alpha < 1,\ R_{xx}(\alpha;\tau) \not\equiv 0\}\,. \tag{25}$$

A conjugate CAF is defined as

$$R_{xx(*)}(\alpha;\tau) = \lim_{M\to\infty} \frac{1}{M} \sum_{t=1}^{M} R_{xx^*}(t, t+\tau) e^{-j2\pi\alpha t} \tag{26}$$

where $R_{xx^*}(t, t+\tau) := E\{x(t)x(t+\tau)\}$. Reference [4] considers conjugate CAFs whereas [14, 17] consider both types of CAFs. For wide-sense stationary (WSS) signals, $R_{xx}(\alpha;\tau) = 0$ as well as $R_{xx(*)}(\alpha;\tau) = 0$ for any $\alpha \neq 0$.

OFDM Signals

As shown in [17] and [18], an OFDM signal exhibits nonconjugate cyclostationarity with cycle frequencies $\alpha = kF_s$, $k = \pm1, \pm2, \cdots$ and lags $\tau = \pm T_u$ where the OFDM symbol duration is $T_s = T_u + T_c = (1/F_s)$, T_c is the duration of the cyclic prefix, and T_u is the useful symbol duration. Consider a (continuous-time) baseband OFDM signal with N_c subcarriers given by

$$s(t) = \sum_{n=-\infty}^{\infty} \sum_{i=0}^{N_c-1} d_{n,i}\, g(t - nT_s) e^{-j2\pi(i-\frac{N_c-1}{2})(t-nT_s)/T_u} \tag{27}$$

where $d_{n,i}$ is the complex nth information symbol modulating the ith subcarrier, T_u^{-1} is the subcarrier separation, and $g(t)$ is the rectangular pulse of duration T_s centered at 0. If $E\{d_{n,i}d_{m,k}\} = 0$ (as for M-PSK ($M \neq 2$) or QAM modulation), then the OFDM signal does not exhibit conjugate cyclostationarity. The continuous-time nonconjugate CAF of (27) is given by [18]

$$R_{ss}(\alpha;\tau) = \begin{cases} \sigma_d^2 \frac{\sin(\pi N_c \tau/T_u)\sin(\pi k F_s(T_s - |\tau|))}{\pi k \sin(\pi\tau/T_u)}, & \alpha = kF_s,\ \ k = \pm1, \pm2, \cdots,\ \ |\tau| < T_s \\ 0, & \text{otherwise}\,, \end{cases} \tag{28}$$

where $\sigma_d^2 = E\{|d_{n,i}|^2\}$. As noted in [17, 18], the CAF (28) exhibits discrete cyclic autocorrelation surfaces for $\alpha = kF_s$ ($k = \pm1, \pm2, \cdots$), which peak at $\tau = \pm T_u$. If one samples $s(t)$ in (27) with $N = N_c + N_{cp}$ samples every T_s sec with N_c samples in useful symbol duration T_u and N_{cp} samples in cyclic prefix duration T_c, then,

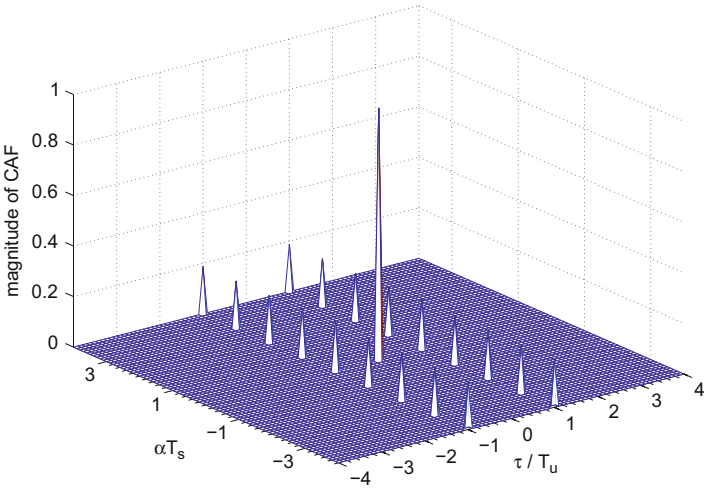

Fig. 1 CAF magnitude for an OFDM signal with $N_c = 32$, $N_{cp} = 8$

in terms of normalized frequency and sampled signal, the discrete-time sampled OFDM signal has normalized cyclic frequencies $\alpha = k/N$ ($k = \pm 1, \pm 2, \cdots$), and the nonconjugate CAF peaks at $\tau = \pm N_c$. Thus the set $\mathscr{A}$ in (25) for sampled OFDM signals is $\mathscr{A} = \{\frac{k}{N},\ k = 0, 1, 2, \cdots, N-1\}$.

Figure 1 shows the magnitude of $R_{ss}(\alpha; \tau)$ when $N_c = 32$, $N_{cp} = 8$, and $\sigma_d^2 = 1$.

GMSK signals

Using a linearization approximation, it has been shown in [17] and [18] that a GMSK (Gaussian Minimum Shift Keying) signal with symbol rate F_s exhibits conjugate cyclostationarity with cycle frequencies of $\alpha = \pm k F_s/2$, k odd, and the conjugate CAF for $k = 1$ peaks at $\tau = 0$. It is also shown in [18] that for GMSK-based GSM signals, nonconjugate cyclostationarity can be quite weak. For further details, one is referred to [17] and [18]. If there are N (even) samples per GMSK symbols, then in terms of normalized frequency, $\mathscr{A} = \{\frac{k}{2N},\ k = 1, 3, \cdots, 2N-1\}$.

Multivariate Processes

One has a vector random process arising due to a multiple antenna receiver with $p \geq 1$ antennas. Therefore, consider a $p \times 1$ discrete-time zero-mean complex-valued cyclostationary signal $\mathbf{x}(t)$ with time-varying autocorrelation function $\mathbf{R}_{xx}(t, t+\tau) := E\{\mathbf{x}(t)\mathbf{x}^H(t+\tau)\}$ which has a Fourier series representation [4, 17]

$$\mathbf{R}_{xx}(t, t+\tau) = \sum_{\alpha \in \mathscr{A}} \mathbf{R}_{xx}(\alpha; \tau) e^{j 2\pi \alpha t} \tag{29}$$

where the nonconjugate *cyclic autocorrelation function* (CAF) $\mathbf{R}_{xx}(\alpha;\tau)$ at cycle frequency $\alpha \in \mathscr{A}$ is given by

$$\mathbf{R}_{xx}(\alpha;\tau) = \lim_{M\to\infty} \frac{1}{M} \sum_{t=1}^{M} \mathbf{R}_{xx}(t, t+\tau) e^{-j2\pi\alpha t}. \tag{30}$$

Similar comments apply to conjugate CAFs.

Tests Using Stationarity

The spectrum sensing tests considered here assume that the noisy signal is stationary during the time interval over which the measurements are collected and processed at the cognitive receiver.

Correlation-Based Approaches

Consider the binary hypothesis testing problem (2). The PU channel impulse response and the noise correlation are unknown. It is known that noise is zero-mean complex (proper) Gaussian, spatially uncorrelated and temporally possibly colored. Assume further that correlation function of noise is "effectively" zero for lags $> L_n$ where L_n is known, i.e.,

$$\mathbf{R}_{nn}(\tau) = 0 \text{ for } |\tau| > L_n. \tag{31}$$

The binary hypothesis testing problem in this case is formulated as

$$\begin{aligned} &\mathscr{H}_0 : \mathbf{R}_{ij,xx}(0) = 0 \ \text{ for } i \neq j, \ \ i,j = 1,2,\cdots,p \\ &\mathscr{H}_1 : \mathbf{R}_{ij,xx}(0) \not\equiv 0 \ \text{ for some } i \neq j, \ \ i,j = 1,2,\cdots,p \end{aligned} \tag{32}$$

In view of the earlier results of section "Large Sample Statistics of Sample Correlation", consider the following ad hoc test statistic

$$\mathscr{T} := 2N \sum_{i=1}^{p-1} \sum_{j=i+1}^{p} \frac{|\hat{R}_{ij,xx}(0)|^2}{\sum_{m=-M}^{M} \hat{R}_{ii,xx}(m)\hat{R}^*_{jj,xx}(m)} \tag{33}$$

where $M \ll N$ is an upperbound on "effective" memory of the colored noise sequence. Under $\mathscr{H}_0$, $\hat{R}_{ij,xx}(0)$ has zero mean for every $i \neq j$, and under $\mathscr{H}_1$, it has nonzero mean for some $i \neq j$. This motivates the (ad hoc) CFAR (constant false alarm rate) test

$$\mathscr{T} \underset{\mathscr{H}_0}{\overset{\mathscr{H}_1}{\gtrless}} \eta \tag{34}$$

where the threshold η is picked to achieve a specified probability of false alarm $P_{fa} = P\{\mathscr{T} \geq \eta \,|\, \mathscr{H}_0\}$. By the results of section "Large Sample Statistics of Sample Correlation", asymptotic distribution of $\mathscr{T}$ under $\mathscr{H}_0$ can be found to enable design of a CFAR test. Such CFAR tests are not optimal in any sense but do yield a constant false alarm rate, a desirable property, under model parameter uncertainties. CFAR tests have been used in radar and other problems under parameter uncertainty [9, Sec. 8.1].

The threshold η is calculated based on asymptotic considerations as follows. It follows from (17) that asymptotically (as $N \to \infty$),

$$2N \frac{|\hat{R}_{ij,xx}(0)|^2}{\sum_{m=-M}^{M} R_{ii,xx}(m) R^*_{jj,xx}(m)} \overset{\mathscr{H}_0}{\sim} \chi^2_2 \tag{35}$$

where χ^2_n denotes the central chi-square distribution with n degrees of freedom (dof). Equation (13) applied to finite-memory sequences also implies that as $N \to \infty$, $\hat{R}_{ii,xx}(0)$ converges in the mean-square sense, hence in probability (i.p.), to $R_{ii,xx}(0)$. Together with (35) this result implies that asymptotically

$$2N \frac{|\hat{R}_{ij,xx}(0)|^2}{\sum_{m=-M}^{M} \hat{R}_{ii,xx}(m) \hat{R}^*_{jj,xx}(m)} \overset{\mathscr{H}_0}{\sim} \chi^2_2. \tag{36}$$

As noted earlier, the upper (lower) triangular off-diagonal elements of $\hat{\mathbf{R}}_{nn}(0)$ are asymptotically independent of the other upper (lower) triangular off-diagonal elements; therefore, for distinct ij pairs with $i \neq j$, the left side of (35) results in mutually independent random variables for distinct ij pairs. Therefore, since there are $p(p-1)/2$ such terms in $\mathscr{T}$, asymptotically

$$\mathscr{T} \overset{\mathscr{H}_0}{\sim} \chi^2_{p(p-1)}. \tag{37}$$

This allows one to pick the test threshold for a given P_{fa}.

PSD Based Approaches

Here the generalized likelihood ratio test (GLRT) proposed in [27] is summarized. Denote the spectral estimator at the k-th frequency bin f_k as $\mathbf{X}_k$ with its true value denoted as $\mathbf{S}(f_k)$. Thus, $\mathbf{X}_k \sim (1/K) W_C(p, K, \mathbf{S}(f_k))$. Attention is confined to the frequency points over which the spectral estimators are independent. If one uses the Daniell method, then the frequencies over which the estimators are (asymptotically) independent, given by $f_k = (kK + \lceil (K/2) \rceil)/N$, $k \in [0, \lfloor$

$(N-(K/2)-1)/K\rfloor]$. After reindexing the frequency subscripts to run from 1 through M, let $\mathscr{M} := \{f_k : 1 \le k \le M\}$ denote the set of M frequency bins under consideration.

The binary hypothesis testing problem under consideration is

$$\begin{aligned} &\mathscr{H}_0 : \mathbf{S}(f_k) = \text{diag}\left\{\mathbf{S}_{11}(f_k), \cdots, \mathbf{S}_{pp}(f_k)\right\} \ \forall f_k \in \mathscr{M} \\ &\mathscr{H}_1 : \mathscr{H}_0^c, \text{ i.e., } \mathbf{S}_{lm}(f_k) \not\equiv 0 \text{ for some } l \ne m \end{aligned} \tag{38}$$

given the "data" $\mathbf{X}_k$. Under $\mathscr{H}_0$ noise is spatially uncorrelated, while under $\mathscr{H}_1$, spatially correlated signal may also be present; no assumptions are made regarding temporal correlations. Under $\mathscr{H}_0$, the joint pdf of $\mathbf{X}_k$ for $k \in \mathscr{M}$ is maximized w.r.t. $\mathbf{S}_{ii}(f_k)$ for $\widehat{\mathbf{S}}_{ii}(f_k) = (\mathbf{X}_k)_{ii}$, $i = 1, 2, \cdots, p$. Under $\mathscr{H}_1$, the joint pdf of $\mathbf{X}_k$ for $k \in \mathscr{M}$ is maximized w.r.t. the Hermitian matrix $\mathbf{S}(f_k)$ for $\hat{\mathbf{S}}(f_k) = \mathbf{X}_k$. Then one gets the GLRT

$$\begin{aligned} \mathscr{L} &:= \frac{f\left(\mathbf{X}_k,\ 1 \le k \le M | \mathscr{H}_1, \hat{\mathbf{S}}(f_k),\right)}{f\left(\mathbf{X}_k,\ 1 \le k \le M | \mathscr{H}_0, \widehat{\mathbf{S}}_{ii}(f_k), i = 1, 2, \cdots, p,\ \ 1 \le k \le M\right)} \\ &= \prod_{k=1}^{M} \frac{\prod_{i=1}^{p} \left[(\mathbf{X}_k)_{ii}\right]^K}{|\mathbf{X}_k|^K} \underset{\mathscr{H}_0}{\overset{\mathscr{H}_1}{\gtrless}} \tau \end{aligned} \tag{39}$$

where the threshold τ is picked to achieve a prespecified probability of false alarm $P_{fa} = P\{\mathscr{L} \ge \tau \,|\, \mathscr{H}_0\}$. This requires pdf of $\mathscr{L}$ under $\mathscr{H}_0$. This problem is addressed in [27] which is reviewed next after introducing some notation.

Let $B_r(n)$ denote the Bernoulli polynomial of degree r and order unity. The first five Bernoulli polynomials are $(B_0(n) = 1)$ [1]:

$$\begin{aligned} &B_1(n) = n - \frac{1}{2},\ B_2(n) = n^2 - n + \frac{1}{6}, \\ &B_3(n) = n^3 - \frac{3}{2}n^2 + \frac{1}{2}n,\ B_4(n) = n^4 - 2n^3 + n^2 - \frac{1}{30}, \\ &B_5(n) = n^5 - \frac{5}{2}n^4 + \frac{5}{3}n^3 - \frac{1}{6}n. \end{aligned}$$

Let

$$\nu = Mp^2 - Mp,\ \ \rho = 1 - \frac{1}{\nu}\left[\frac{Mp(p^2-1)}{3K}\right], \tag{40}$$

and for $r = 1, 2, \cdots$

$$\omega_r = \frac{(-1)^{r+1}M}{r(r+1)(\rho K)^r}\left[\left\{\sum_{l=1}^{p} B_{r+1}((1-\rho)K+1-l)\right\} - pB_{r+1}((1-\rho)K)\right]. \tag{41}$$

Theorem 1 ([27]). *The GLRT for the binary hypothesis testing problem (38) is given by*

$$2\rho\ \ln(\mathscr{L}) \underset{\mathscr{H}_0}{\overset{\mathscr{H}_1}{\gtrless}} \tau \tag{42}$$

where ρ is given by (40) and

$$\ln(\mathscr{L}) = K\left\{\sum_{k=1}^{M}\left(\left[\sum_{i=1}^{p}\ln\left(\mathbf{X}_k\right)_{ii}\right] - \ln(|\mathbf{X}_k|)\right)\right\}. \tag{43}$$

The threshold τ is picked to achieve a specified probability of false alarm $P_{fa} = P\{2\rho\ \ln(\mathscr{L}) > \tau \,|\, \mathscr{H}_0\} = 1 - P\{2\rho\ \ln(\mathscr{L}) \leq \tau \,|\, \mathscr{H}_0\}$. The probability $P\{2\rho\ \ln(\mathscr{L}) \leq \tau \,|\, \mathscr{H}_0\}$ is given by

$$\begin{aligned} P\{2\rho\ \ln(\mathscr{L}) \leq \tau \,|\, \mathscr{H}_0\} = {} & P\{\chi_\nu^2 \leq \tau\} + \omega_2\big[P\{\chi_{\nu+4}^2 \leq \tau\} \\ & - P\{\chi_\nu^2 \leq \tau\}\big] + \omega_3\big[P\{\chi_{\nu+6}^2 \leq \tau\} - P\{\chi_\nu^2 \leq \tau\}\big] \\ & + \Big\{\omega_4\big[P\{\chi_{\nu+8}^2 \leq \tau\} - P\{\chi_\nu^2 \leq \tau\}\big] \\ & + \frac{1}{2}\omega_2^2\big[P\{\chi_{\nu+8}^2 \leq \tau\} - 2P\{\chi_{\nu+4}^2 \leq \tau\} + P\{\chi_\nu^2 \leq \tau\}\big]\Big\} \\ & + \mathscr{O}(K^{-5}) \end{aligned} \tag{44}$$

where χ_n^2 denotes a random variable with central chi-square distribution with n degrees of freedom (as well as the distribution itself), and ω_r's are given by (41).

Remark 1. Under some very general conditions, the following results hold ([7] and [6, Chapter 22]) asymptotically (as $N \to \infty$ with $K \to \infty$, $M \to \infty$ and $M/K \to 0$) for the problem under consideration

$$2\ \ln(\mathscr{L}) \sim \begin{cases} \chi^2_{M(p^2-p)} & : \mathscr{H}_0 \\ \chi^2_{M(p^2-p)}(\lambda) & : \mathscr{H}_1 \end{cases} \tag{45}$$

for some $\lambda > 0$ where $\chi_n^2(\lambda)$ denotes the noncentral chi-square distribution with n degrees of freedom and non-centrality parameter λ. As pointed out in [1, 2, 16],

under $\mathscr{H}_0$, the distribution $\chi^2_{M(p^2-p)}$ is often not accurate unless N is quite large, hence the extra terms and the Bartlett scale factor ρ in Theorem 1. As $N \to \infty$, $\rho \to 1$ and $\omega_r \to 0$ for $r = 2, 3, \cdots$. □

Performance: Probability of Detection

Under "local" alternatives, using [7] and [6, Chapter 22] (see also Remark 1), it follows that asymptotically, under $\mathscr{H}_1$, $2\ln(\mathscr{L}) \sim \chi^2_{M(p^2-p)}(\lambda)$. Typically (see, for instance, [7], [6, Chapter 22] and [33]) one calculates first- and second-order derivatives of the log-likelihood ratio and then takes their expectation (essentially one needs the Fisher information matrix [33]) in order to compute λ. Alternatively, an indirect approach to compute λ can be used. Under $\mathscr{H}_1$, one must have $E\{2\ln(\mathscr{L})\} = M(p^2-p) + \lambda$. In [29] an asymptotic expression ("large" K) for the non-centrality parameter λ via $E\{2\ln(\mathscr{L})\}$ has been derived as

$$\lambda = 2K \sum_{k=1}^{M} \left[\sum_{i=1}^{p} \ln(\mathbf{S}(f_k))_{ii} - \ln|\mathbf{S}(f_k)| \right]. \tag{46}$$

Remark 2. As noted in Remark 1, under $\mathscr{H}_0$, the distribution $\chi^2_{M(p^2-p)}$ is often not accurate unless N is "quite large," hence the extra terms and the Bartlett scale factor ρ in Theorem 1. Just as Theorem 1 accounts for "smaller" data sizes and modifies the distribution $\chi^2_{M(p^2-p)}$ under $\mathscr{H}_0$, one may follow (45) to modify the distribution $\chi^2_{M(p^2-p)}(\lambda)$ under $\mathscr{H}_1$ exploiting Theorem 1. That is, [29] proposes to use the distributions

$$\begin{aligned}
&P\{2\rho\ln(\mathscr{L}) \le \tau \mid \mathscr{H}_0\} \text{ is given by (44)},\\
&P\{2\rho\ln(\mathscr{L}) \le \tau \mid \mathscr{H}_1\} = P\{\chi^2_\nu(\lambda) \le \tau\}\\
&\qquad + \omega_2\big[P\{\chi^2_{\nu+4}(\lambda) \le \tau\} - P\{\chi^2_\nu(\lambda) \le \tau\}\big]\\
&\qquad + \omega_3\big[P\{\chi^2_{\nu+6}(\lambda) \le \tau\} - P\{\chi^2_\nu(\lambda) \le \tau\}\big]\\
&\qquad + \Big\{\omega_4\big[P\{\chi^2_{\nu+8}(\lambda) \le \tau\} - P\{\chi^2_\nu(\lambda) \le \tau\}\big]\\
&\qquad + \frac{1}{2}\omega_2^2\big[P\{\chi^2_{\nu+8}(\lambda) \le \tau\} - 2P\{\chi^2_{\nu+4}(\lambda) \le \tau\}\\
&\qquad + P\{\chi^2_\nu(\lambda) \le \tau\}\big]\Big\} + \mathscr{O}(K^{-5})
\end{aligned} \tag{47}$$

where $f = M(p^2-p)$ and λ is given by (46). Under $\mathscr{H}_0$, $\lambda = 0$ and under $\mathscr{H}_1$, as signal gets weaker, $\lambda \to 0$; under both these cases, (44) and (47) become the same. Also, as $N \to \infty$, we have $\rho \to 1$ and $\omega_r \to 0$ for $r = 2, 3, \cdots$, and we get (45). Thus use of (47) is well justified. □

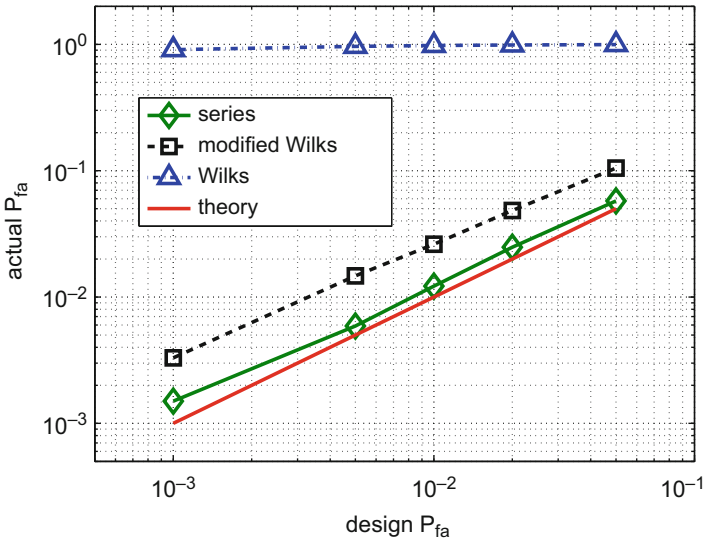

Fig. 2 Actual P_{fa} versus design P_{fa} based on 10,000 runs, $p = 4$, N=256, $K = 7$, $M = 36$.

Analytical Threshold Calculation Verification Example

This example is taken from [27] where efficacy of Theorem 1 in analytically computing the GLRT threshold for a given P_{fa} is investigated. There are four antennas (p=4) with independent complex Gaussian noise. First generate i.i.d. noise sequences at the antennas with variances σ_n^2, $2\sigma_n^2$, $0.75\sigma_n^2$, and $0.25\sigma_n^2$ with $\sigma_n^2 = 0.01$, and then filter each of them through the same linear filter with impulse response $\{0.3, 1.0, 0.3\}$. For $N = 256$, $m_t = 3$ was picked in (19) for spectral estimation, leading to $K = 7$ and $M = 36$. In Fig. 2 actual P_{fa} and design P_{fa} based on 10,000 runs are compared for N=256. It is seen that calculation of the test threshold via Theorem 1 is effective. In Fig. 2, "Wilks" refers to the test (42) with $\rho = 1$ and $2\ln(\mathscr{L}) \sim \chi^2_\nu$ under $\mathscr{H}_0$, and "modified Wilks" (more generally known as Bartlett's correction [2]) refers to the test (42) with $2\rho\ln(\mathscr{L}) \sim \chi^2_\nu$. It is seen that both Wilks approximation and Bartlett's correction for threshold calculation are ineffective.

Performance Analysis Verification Example

Here comparison of theoretical performance as predicted by the results of section "Performance: Probability of Detection" (in particular Remark 2) with the simulations-based performance for the proposed detector is presented when $N = 256$. Detection simulation results based on 5000 runs are shown. The noise sequences are as in the previous example. The signal is scalar QPSK filtered through impulse response $\{0.227, -0.460, 0.688, -0.460, 0.227\}$ and then passed through a flat-fading channel with random gain $\mathbf{h}$ (4×1) having mutually independent components, zero-mean proper complex-Gaussian with unit variance. The information

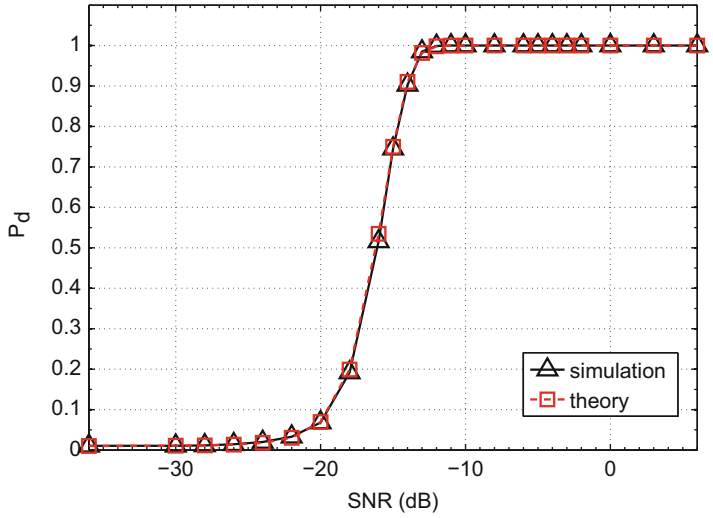

Fig. 3 Verification of theoretical performance analysis: N=256, $p = 4$, $P_{fa} = 0.01$

sequence variance σ_s^2 is scaled to achieve the desired SNR across antennas, defined as ratio of the sum of signal powers at the antennas to the sum of noise powers. Figure 3 shows the probability of detection ($P_d = P\{2\rho \ln(\mathscr{L}) > \tau \,|\, \mathscr{H}_1\}$ computed using (47)) versus average SNR results based on 5000 runs for $P_{fa} = 0.01$ and $p = 4$ for a randomly generated PU channel response which was then kept fixed for all Monte Carlo runs, only the noise sequence realization varied from run to run. It is seen from Fig. 3 that the theoretical- and simulation-based results are in excellent agreement.

Other Approaches

Several time-domain approaches relying on the generalized likelihood ratio test (GLRT) paradigm have been proposed for multiple antenna spectrum sensing in cognitive radios [24, 33, 35]. These approaches are suitable for flat-fading signals in white noise. They can obviate the need for the precise knowledge of the noise variance, but they do assume that noise variance is the same at all antennas. In sections "Correlation-Based Approaches" and "PSD Based Approaches", noise is allowed to be colored, and its variances can be different at different antennas without requiring knowledge of their spectra. In [13] various approaches are discussed to handle unequal noise variances across sensors. However, [13] (also [12]) assumes that noise is white and the primary user's signal is temporally white Gaussian, whereas in sections "Correlation-Based Approaches" and "PSD Based Approaches", one only requires it to be ergodic (it can be non-Gaussian). In [11] a spectral covariance sensing approach has been discussed where one

first computes the spectrogram of downconverted baseband signal. For analysis [11] also assumes both signal and noise samples to be temporally independent and identically distributed, and only a single antenna has been considered. In [26] an autocorrelation-based multiantenna spectrum sensing approach in white Gaussian noise is presented, and an extension of this approach to colored Gaussian noise is in [28]. There exist other non-GLRT approaches to the problem under consideration; see, for instance, [34] and references therein. In [34] two sample covariance-based test statistics have been proposed and analyzed for multi-antenna real-valued colored signals in real-valued white noise. Colored (complex) signals have been considered within the GLRT paradigm in [21] assuming multiple records (snapshots) and Gaussian PU signals; the results of sections "Correlation-Based Approaches" and "PSD Based Approaches" are based on a single observation record (snapshot).

A PSD-based GLRT approach was recently proposed in [27]. Except for [27] (and [28]), the PU signal is always assumed to be Gaussian in existing approaches, and most often noise is assumed to be white, and when handling colored noise/signal, both [20] and [21] (others consider white signal in white noise) require multiple independent data realizations (measurements) whereas only one data realization is needed in [27]. In [20] the test threshold is selected via simulations whereas [27] provides an analytical formulation. In [20] a frequency-domain test statistic (see (2) therein) similar to [27, Eqn. (6)] is derived via a time-domain formulation under the Gaussian assumption and some asymptotic considerations.

Tests Using Cyclostationarity

The problem under consideration is as in (2) except that now $s_{pu}(t)$ is a scalar cyclostationary signal (emitted by a primary user) with at least one known cycle frequency α and at least one known lag τ such that $R_{s_{pu}s_{pu}}(\alpha;\tau) \neq 0$. The approach taken here is similar to section "Correlation-Based Approaches" except that one uses estimated CAFs. To this end, first the large sample statistics of sample CAF are discussed.

Large Sample Statistics of Sample CAF

We are interested only in nonzero cycle frequencies.

Nonconjugate CAF

These results are appropriate for OFDM signals.

Spatially White and Temporally Correlated Gaussian Noise

Consider a $p \times 1$ WSS proper (circularly symmetric) complex-valued zero-mean colored Gaussian sequence $\mathbf{x}(t) = \mathbf{n}(t)$ with correlation function $\mathbf{R}_{xx}(t, t+\tau) =$

$\mathbf{R}_{nn}(t, t+\tau) = \mathbf{R}_{nn}(\tau) = \text{diag}\{R_{ii,n}(\tau),\ 1 \le i \le p\}$. Also, $E\{\mathbf{n}(t)\mathbf{n}^T(t+\tau)\} \equiv 0$ since $\mathbf{n}(t)$ is proper. Given an observation length of M samples, one can estimate the (nonconjugate) CAF $\mathbf{R}_{xx}(\alpha;\tau)$ as

$$\hat{\mathbf{R}}_{xx}(\alpha;\tau) = \frac{1}{M}\sum_{t=1}^{M} \mathbf{x}(t)\mathbf{x}^H(t+\tau)e^{-j2\pi\alpha t}. \tag{48}$$

It is easy to see that $\lim_{M\to\infty} E\{\hat{\mathbf{R}}_{xx}(\alpha;\tau)\} = \mathbf{R}_{xx}(\alpha;\tau)$. Let ($x_i$ is the i-th component of $\mathbf{x}$)

$$\hat{R}_{ik,x}(\alpha;\tau) := \frac{1}{M}\sum_{t=1}^{M} x_i(t)x_k^*(t+\tau)e^{-j2\pi\alpha t}. \tag{49}$$

Then

$$E\{\hat{R}_{ik,x}(\alpha;\tau)\} = R_{ik,x}(\tau)\left[\frac{1}{M}\sum_{t=1}^{M} e^{-j2\pi\alpha t}\right] \tag{50}$$

where $R_{ik,x}(\tau) := E\{x_i(t)x_k^*(t+\tau)\}$. It follows that

$$\begin{aligned} &E\{x_i(t_1)x_j^*(t_1+\tau_1)e^{-j2\pi\alpha t_1}x_k^*(t_2)x_l(t_2+\tau_2)e^{j2\pi\beta t_2}\} \\ &\quad= \text{cum}_4\left(x_i(t_1), x_j^*(t_1+\tau_1), x_k^*(t_2), x_l(t_2+\tau_2)\right)e^{-j2\pi(\alpha t_1-\beta t_2)} \\ &\qquad+R_{ij,x}(\tau_1)R_{kl,x}^*(\tau_2)e^{-j2\pi(\alpha t_1-\beta t_2)} \\ &\qquad+R_{ik,x}(t_2-t_1)R_{lj,x}(t_1-t_2-\tau_2+\tau_1)e^{-j2\pi(\alpha t_1-\beta t_2)}. \end{aligned} \tag{51}$$

For Gaussian sequences, the fourth cumulants are identically zero. Hence,

$$\begin{aligned} &\text{cov}\left(\hat{R}_{ij,x}(\alpha;\tau_1), \hat{R}_{kl,x}^*(\beta;\tau_2)\right) \\ &\quad= E\left\{\hat{R}_{ij,x}(\alpha;\tau_1)\hat{R}_{kl,x}^*(\beta;\tau_2)\right\} - E\left\{\hat{R}_{ij,x}(\alpha;\tau_1)\right\}E\left\{\hat{R}_{kl,x}^*(\beta;\tau_2)\right\} \\ &\quad= \frac{1}{M^2}\sum_{t_1=1}^{M}\sum_{t_2=1}^{M}\left[R_{ik,x}(t_2-t_1)R_{lj,x}(t_1-t_2-\tau_2+\tau_1)e^{-j2\pi(\alpha t_1-\beta t_2)}\right] =: A. \end{aligned} \tag{52}$$

Setting $t_1 - t_2 = m$ in (52) and with $\mathbf{x}(t) = \mathbf{n}(t)$, one obtains

$$A = \frac{1}{M^2}\sum_{m=-(M-1)}^{M-1} e^{-j2\pi\beta m}R_{ik,n}(-m)R_{lj,n}(m+\tau_1-\tau_2)\left[\sum_{t_1=|m|+1}^{M} e^{-j2\pi(\alpha-\beta)t_1}\right]. \tag{53}$$

It follows that

$$\frac{1}{M}\sum_{t=1}^{M} e^{-j2\pi(\alpha-\beta)t} = \begin{cases} 1 & \text{for } \alpha = \beta \in \mathscr{A} \\ \frac{e^{-j\pi(\alpha-\beta)(M+1)}}{M}\frac{\sin(\pi(\alpha-\beta)M)}{\sin(\pi(\alpha-\beta))} & \text{for } \alpha \neq \beta,\ \alpha,\beta \in \mathscr{A}. \end{cases} \tag{54}$$

It then follows that for any fixed m,

$$\begin{aligned} \lim_{M\to\infty}\frac{1}{M}\sum_{t=|m|+1}^{M} e^{-j2\pi(\alpha-\beta)t} &= \lim_{M\to\infty}\frac{1}{M}\left[\sum_{t=1}^{M} e^{-j2\pi(\alpha-\beta)t} - \sum_{t=1}^{|m|} e^{-j2\pi(\alpha-\beta)t}\right] \\ &= \delta_{\alpha,\beta}. \end{aligned} \tag{55}$$

Using (52), (53), and (55) and the fact that $\mathbf{n}(t)$ is spatially uncorrelated, one has

$$\lim_{M\to\infty} M\,\mathrm{cov}\left(\hat{R}_{ij,n}(\alpha;\tau_1), \hat{R}^*_{kl,n}(\beta;\tau_2)\right) = \tilde{\gamma}_{ij,n}(\alpha;\tau_1-\tau_2)\delta_{i,k}\delta_{j,l}\delta_{\alpha,\beta} \tag{56}$$

where

$$\tilde{\gamma}_{ij,n}(\alpha;\tau_1-\tau_2) := \sum_{m=-\infty}^{\infty} R_{ii,n}(-m)R_{jj,n}(m+\tau_1-\tau_2)e^{-j2\pi\alpha m}. \tag{57}$$

Using (49) it follows that

$$\hat{R}^*_{ik,x}(\alpha;\tau) = \hat{R}_{ki,x}(-\alpha;-\tau) = \hat{R}_{ki,x}(1-\alpha;-\tau). \tag{58}$$

Therefore, from (56) and (58), one obtains

$$\begin{aligned} &\lim_{M\to\infty} M\,\mathrm{cov}\left(\hat{R}_{ij,n}(\alpha;\tau_1), \hat{R}_{kl,n}(\beta;\tau_2)\right) \\ &\quad= \lim_{M\to\infty} M\,\mathrm{cov}\left(\hat{R}_{ij,n}(\alpha;\tau_1), \hat{R}^*_{lk,n}(-\beta;-\tau_2)\right) \\ &\quad= \tilde{\gamma}_{ij,n}(\alpha;\tau_1+\tau_2)\delta_{i,l}\delta_{j,k}\delta_{\alpha,-\beta}. \end{aligned} \tag{59}$$

Finite-Memory Colored Gaussian Noise

It is analytically convenient to make a further assumption that correlation function of noise is "effectively" zero for lags $> L_n$ where L_n is known, i.e.,

$$\mathbf{R}_{nn}(\tau) = 0 \text{ for } |\tau| > L_n. \tag{60}$$

By (56), (59), and (60), for $\alpha, \beta \in \mathscr{A}$, we have

$$\begin{aligned} &\lim_{M\to\infty} M\,\mathrm{cov}\big(\hat{R}_{ij,n}(\alpha;\tau_1), \hat{R}^*_{kl,n}(\beta;\tau_2)\big) \\ &\quad= \tilde{\gamma}_{ij,n}(\alpha;0)\delta_{i,k}\delta_{j,l}\delta_{\tau_1,\tau_2}\delta_{\alpha,\beta} \text{ for } |\tau_1-\tau_2| > L_n, \end{aligned} \tag{61}$$

$$\lim_{M\to\infty} M \operatorname{cov}\left(\hat{R}_{ij,n}(\alpha;\tau_1), \hat{R}_{kl,n}(\beta;\tau_2)\right) = 0. \tag{62}$$

Also, by [4, 14, 17], asymptotically (as $M \to \infty$), $\hat{R}_{ik,x}(\alpha;\tau)$ is a Gaussian random variable (complex-valued but not necessarily circularly symmetric), and "vectorized" matrix $\hat{\mathbf{R}}_{xx}(\alpha;\tau)$ is a Gaussian random vector for any α and τ, for $\mathbf{x}(t)$ under either $\mathscr{H}_0$ or $\mathscr{H}_1$ and whether $\mathbf{x}(t)$ is finite memory or not. Invoking asymptotic Gaussianity, it then follows that

$$\lim_{M\to\infty} \sqrt{M}\,\hat{R}_{ij,n}(\alpha;\tau) \sim \mathscr{N}_c\left(0, \tilde{\gamma}_{ij,n}(\alpha;0)\right) \quad \forall i, j \tag{63}$$

where $\mathscr{N}_c(\mathbf{m}, \Sigma)$ denotes a circularly symmetric (proper) complex Gaussian (vector) distribution with mean $\mathbf{m}$ and covariance matrix Σ. Furthermore, $\hat{R}_{ij,x}(\alpha;\tau)$ is asymptotically independent of $\hat{R}_{kl,x}(\alpha;\tau)$ if $i \neq k$ or $j \neq l$. Moreover, $\hat{R}_{ij,x}(\alpha;\tau_1)$ is asymptotically independent of $\hat{R}_{kl,x}(\beta;\tau_2)$ if $\alpha \neq \beta$ ($\alpha, \beta \in \mathscr{A}$) or $\tau_1 \neq \tau_2$, for any i, j, k, l.

As discussed in section "OFDM Signals", for OFDM signals, the nonconjugate CAF peaks at $\tau = \pm N_c$ (N_c = number of subcarriers). If $\tau_1 = N_c$ and $\tau_2 = -N_c$, then one must have $L_n < 2N_c$ for (61) to hold true.

Conjugate CAF

These results are appropriate for GMSK signals. Given an observation length of M samples, one can estimate the conjugate CAF

$$\mathbf{R}_{xx(*)}(\alpha;\tau) := \lim_{M\to\infty} \frac{1}{M} \sum_{t=1}^{M} E\{\mathbf{x}(t)\mathbf{x}^T(t+\tau)\} e^{-j2\pi\alpha t} \tag{64}$$

as

$$\hat{\mathbf{R}}_{xx(*)}(\alpha;\tau) = \frac{1}{M} \sum_{t=1}^{M} \mathbf{x}(t)\mathbf{x}^T(t+\tau) e^{-j2\pi\alpha t}. \tag{65}$$

Spatially White and Temporally Correlated Gaussian Noise

When $\mathbf{n}(t)$ is proper and $\mathbf{x}(t) = \mathbf{n}(t)$, it follows easily that $E\{\hat{\mathbf{R}}_{nn(*)}(\alpha;\tau)\} = 0$ and

$$\operatorname{cov}\left(\hat{R}_{(*)ij,n}(\alpha;\tau_1), \hat{R}_{(*)kl,n}(\beta;\tau_2)\right) = E\{\hat{R}_{(*)ij,n}(\alpha;\tau_1)\hat{R}_{(*)kl,n}(\beta;\tau_2)\} = 0 \tag{66}$$

where $R_{(*)ik,x}(\tau) := E\{x_i(t)x_k(t+\tau)\}$. Mimicking section "Spatially White and Temporally Correlated Gaussian Noise" one has

$$\operatorname{cov}\left(\hat{R}_{(*)ij,n}(\alpha;\tau_1), \hat{R}^*_{(*)kl,n}(\beta;\tau_2)\right) = E\{\hat{R}_{(*)ij,n}(\alpha;\tau_1)\hat{R}^*_{(*)kl,n}(\beta;\tau_2)\}$$

$$= \frac{1}{M^2}\sum_{t_1=1}^{M}\sum_{t_2=1}^{M}\Big[R_{ik,n}(t_2-t_1)R_{jl,n}(t_2-t_1+\tau_2-\tau_1)$$
$$+R_{il,n}(t_2-t_1+\tau_2)R_{jk,n}(t_2-t_1-\tau_1)\Big]e^{-j2\pi(\alpha t_1-\beta t_2)}$$
$$= \frac{1}{M^2}\sum_{m=-(M-1)}^{M-1} e^{j2\pi\alpha m}\Big[R_{ik,n}(m)R_{jl,n}(m+\tau_2-\tau_1)$$
$$+R_{il,n}(m+\tau_2)R_{jk,n}(m-\tau_1)\Big]\left[\sum_{t_2=|m|+1}^{M} e^{-j2\pi(\alpha-\beta)t_2}\right]. \tag{67}$$

It then follows that

$$\lim_{M\to\infty} M\,\mathrm{cov}\left(\hat{R}_{(*)ij,n}(\alpha;\tau_1),\hat{R}^*_{(*)kl,n}(\beta;\tau_2)\right)$$
$$= \sum_{m=-\infty}^{\infty}\left[R_{ik,n}(m)R_{jl,n}(m+\tau_2-\tau_1)+R_{il,n}(m+\tau_2)R_{jk,n}(m-\tau_1)\right]e^{j2\pi\alpha m}\delta_{\alpha,\beta}. \tag{68}$$

For GMSK signals, the nonconjugate CAF peaks at $\tau = 0$. Confining one's attention to $\tau_1 = \tau_2 = 0$, for finite-memory, spatially uncorrelated, colored Gaussian noise, one obtains

$$\lim_{M\to\infty} M\,\mathrm{cov}\left(\hat{R}_{(*)ij,n}(\alpha;0),\hat{R}^*_{(*)kl,n}(\beta;0)\right)$$
$$= \begin{cases} 2\sum_{m=-L_n}^{L_n} R^2_{ii}(n)e^{j2\pi\alpha m}\delta_{\alpha,\beta} & \text{if } i=k=l=j \\ \sum_{m=-L_n}^{L_n} R_{ii,n}(m)R_{jj,n}(m)e^{j2\pi\alpha m}\delta_{\alpha,\beta} & \text{if } (i,j)=(k,l) \text{ but } i\neq j, \\ & \quad \text{or } (i,j)=(l,k) \\ 0 & \text{otherwise.} \end{cases} \tag{69}$$

Specializing (68) to white, spatially uncorrelated, Gaussian noise with $\tau_1 = \tau_2 = \tau$, it follows that

$$\lim_{M\to\infty} M\,\mathrm{cov}\left(\hat{R}_{(*)ij,n}(\alpha;\tau),\hat{R}^*_{(*)kl,n}(\beta;\tau)\right)$$
$$= \begin{cases} 2R_{ii,n}(0)R_{jj,n}(0)\delta_{\alpha,\beta} & \text{if } i=k=l=j \text{ and } \tau=0 \\ R_{ii,n}(0)R_{jj,n}(0)\delta_{\alpha,\beta} & \text{if } (i,j)=(k,l) \text{ but } i\neq j, \text{ or } (i,j)=(l,k) \text{ and } \tau=0 \\ 0 & \text{otherwise.} \end{cases} \tag{70}$$

Invoking asymptotic Gaussianity, it then follows that for finite-memory colored Gaussian noise

$$\lim_{M\to\infty} \sqrt{M}\,\hat{R}_{(*)ij,n}(\alpha;0) \sim \mathcal{N}_c\left(0,\ \sum_{m=-L_n}^{L_n} (1+\delta_{i,j})R_{ii,n}(m)R_{jj,n}(m)e^{j2\pi\alpha m}\right) \quad \forall i,j. \tag{71}$$

Similarly for white Gaussian noise, one has

$$\lim_{M\to\infty} \sqrt{M}\,\hat{R}_{(*)ij,n}(\alpha;0) \sim \mathcal{N}_c\left(0,(1+\delta_{\tau,0}\delta_{i,j})R_{ii,n}(0)R_{jj,n}(0)\right) \quad \forall i,j. \tag{72}$$

Noting that since $\lim_{M\to\infty} \hat{R}_{(*)ij,x}(\alpha;\tau) = \lim_{M\to\infty} \hat{R}_{(*)ji,x}(\alpha;\tau)$ and $\hat{R}_{(*)ij,x}(\alpha;0) = \hat{R}_{(*)ji,x}(\alpha;0)$, unlike nonconjugate CAFs, in case of conjugate CAFs, $\hat{R}_{(*)ij,x}(\alpha;\tau)$ is asymptotically independent of $\hat{R}_{(*)kl,x}(\alpha;\tau)$ for $i \neq k$ or $j \neq l$ if $i \geq j$ and $k \geq l$ (or if $i \leq j$ and $k \leq l$).

Test Statistics

Based on the large sample statistics of CAFs of colored Gaussian noise discussed in section "Large Sample Statistics of Sample CAF", one can devise ad hoc CFAR (constant false alarm rate) detectors for detection of nonzero nonconjugate as well as conjugate CAFs. They are ad hoc as they do not follow any optimality criterion. Since no knowledge is assumed about the structure of the colored noise (its variance or correlation function) or the underlying channel (flat or frequency selective), an optimal detector based on the likelihood ratio or generalized likelihood ratio test does not appear to be possible. It is assumed that the finite-memory assumption (60) holds true. The desired PU signals are assumed to have nonzero CAF at certain known nonzero cycle frequencies and lags, whereas CAF of colored noise is zero at all lags and nonzero cycle frequencies. The considered tests exploit the large sample statistics of the estimated CAF to yield CFAR detectors.

Nonconjugate CAF: OFDM Signals

Consider the binary hypothesis testing problem (2). The PU channel impulse response and the noise correlation function are unknown. Also, $s_{pu}(t)$ is a scalar cyclostationary signal (emitted by PUs) with $K \geq 1$ known cycle frequency and lag pairs (α_k, τ_k), $k = 1, 2, \cdots, K$, such that $R_{s_{pu}s_{pu}}(\alpha_k;\tau_k) \neq 0$ and $|\tau_1 - \tau_2| > L_n$ so that (61) holds true. The binary hypothesis testing problem in this case can be formulated as

$$\begin{aligned} \mathcal{H}_0 &: R_{ij,x}(\alpha_k;\tau_k) = 0 \ \ \forall\, i,j,k \\ \mathcal{H}_1 &: R_{ij,x}(\alpha_k;\tau_k) \not\equiv 0 \ \ \text{for some } i,j,k. \end{aligned} \tag{73}$$

Under both hypotheses, $\lim_{M\to\infty} E\{\hat{\mathbf{R}}(\alpha;\tau)\} = \mathbf{R}(\alpha;\tau)$. Under $\mathcal{H}_0$, by the results of section "Spatially Uncorrelated, Temporally Colored Noise", $\hat{R}_{ij}(\alpha_k;\tau_k)$ has zero-mean $\forall\, i,j,k$, and under $\mathcal{H}_1$, it has nonzero mean for some i,j,k; therefore, $|R_{ij}(\alpha_k;\tau_k)| > 0$ for some i,j,k. Define (see also (57))

$$\bar{\gamma}_{ij,n}(\alpha_k) := \sum_{m=-L_n}^{L_n} R_{ii,n}(-m) R_{jj,n}(m) e^{-j2\pi\alpha_k m} \tag{74}$$

and let $\tilde{\mathbf{r}}$ denote the $Kp^2 \times 1$ vector composed of elements $\hat{R}_{ij,x}(\alpha_k;\tau_k)/\sqrt{\bar{\gamma}_{ij,x}(\alpha_k)}$ for all distinct triplets (i,j,k). Then by (63), one has $\lim_{M\to\infty} \sqrt{M}\tilde{\mathbf{r}} \overset{\mathscr{H}_0}{\sim} \mathcal{N}_c(0,\mathbf{I})$ leading to $2M\tilde{\mathbf{r}}^H\tilde{\mathbf{r}} \overset{\mathscr{H}_0}{\sim} \chi^2_{2Kp^2}$ where χ^2_n denotes the central chi-square distribution with n degrees of freedom (dof). Since $|R_{ij}(\alpha_k;\tau_k)| > 0$ for some i,j,k, it follows that $E\{\tilde{\mathbf{r}}^H\tilde{\mathbf{r}} \,|\, \mathscr{H}_1\} > E\{\tilde{\mathbf{r}}^H\tilde{\mathbf{r}} \,|\, \mathscr{H}_0\}$. Furthermore, since the true values $\bar{\gamma}_{ij,n}(\alpha_k)$, $(k = 1,2,\cdots,K)$, are not available, they are replaced with estimates $\hat{\gamma}_{ij,x}(\alpha_k)$, and consider the following ad hoc test motivated by $2M\tilde{\mathbf{r}}^H\tilde{\mathbf{r}}$ and $E\{\tilde{\mathbf{r}}^H\tilde{\mathbf{r}} \,|\, \mathscr{H}_1\} > E\{\tilde{\mathbf{r}}^H\tilde{\mathbf{r}} \,|\, \mathscr{H}_0\}$:

$$\mathscr{T} := 2M \sum_{k=1}^{K} \sum_{i=1}^{p} \sum_{j=1}^{p} \frac{|\hat{R}_{ij,x}(\alpha_k;\tau_k)|^2}{\hat{\gamma}_{ij,x}(\alpha_k)} \underset{\mathscr{H}_0}{\overset{\mathscr{H}_1}{\gtrless}} \eta \tag{75}$$

where

$$\hat{\gamma}_{ij,x}(\alpha_k) := \sum_{m=-L_n}^{L_n} \hat{R}_{ii,x}(-m) \hat{R}_{jj,x}(m) e^{-j2\pi\alpha_k m}, \tag{76}$$

$$\hat{R}_{ii,x}(m) := \frac{1}{M-m} \sum_{k=1}^{M-m} x_i(k) x_i^*(k+m), \quad m \geq 0, \tag{77}$$

$\hat{R}_{ii,x}(-m) = \hat{R}^*_{ii,x}(m)$, and the threshold η is picked to achieve a specified probability of false alarm $P_{fa} = P\{\mathscr{T} \geq \eta \,|\, \mathscr{H}_0\}$. By the results of section "Spatially Uncorrelated, Temporally Colored Noise", one can find asymptotic distribution of $\mathscr{T}$ under $\mathscr{H}_0$ and design a CFAR test. Such CFAR tests are not optimal in any sense but do yield a constant false alarm rate, a desirable property, under model parameter uncertainties.

How does one calculate η? It follows from (63) that asymptotically (as $M \to \infty$),

$$2M \frac{|\hat{R}_{ij,x}(\alpha_k;\tau_k)|^2}{\bar{\gamma}_{ij,x}(\alpha_k)} \overset{\mathscr{H}_0}{\sim} \chi^2_2. \tag{78}$$

Equation (61) applied to finite-memory colored Gaussian noise also implies that as $M \to \infty$, under $\mathscr{H}_0$, $\hat{R}_{ii,x}(m)$ converges in the mean-square sense, hence in probability (i.p.), to $R_{ii,x}(m)$. Together with (78) this result implies that asymptotically

$$2M \frac{|\hat{R}_{ij,x}(\alpha;\tau)|^2}{\hat{\gamma}_{ij,x}(\alpha_k)} \overset{\mathscr{H}_0}{\sim} \chi^2_2. \tag{79}$$

As noted in section "Spatially Uncorrelated, Temporally Colored Noise", any element of $\hat{\mathbf{R}}_{xx}(\alpha_k;\tau_k)$ is asymptotically independent of all other elements, and the same holds true for distinct cycle frequencies; therefore, in (75) one has (asymptotically) mutually independent random variables for distinct (i,j,k) triples. Since there are Kp^2 such terms in $\mathscr{T}$, asymptotically

$$\mathscr{T} \overset{\mathscr{H}_0}{\sim} \chi^2_{2Kp^2}. \tag{80}$$

Conjugate CAF: GMSK Signals

In this case too, the binary hypothesis testing problem is formulated as (73) except that one uses $R_{(*)ij,x}(\alpha_k;\tau_k)$ instead of $R_{ij,x}(\alpha_k;\tau_k)$, and one should take $\tau_k = 0\ \forall k$ since that is where the GMSK CAF is the strongest [18]. Following sections "Conjugate CAF" and "Nonconjugate CAF: OFDM Signals", consider the test statistic

$$\mathscr{T}_{conj} := 2M \sum_{k=1}^{K} \sum_{i=1}^{p} \sum_{j=i}^{p} \frac{|\hat{R}_{(*)ij,x}(\alpha_k;0)|^2}{\sum_{m=-L_n}^{L_n}(1+\delta_{i,j})\hat{R}_{ii,x}(m)\hat{R}_{jj,x}(m)e^{j2\pi\alpha_k m}} \underset{\mathscr{H}_0}{\overset{\mathscr{H}_1}{\gtrless}} \eta_{conj}. \tag{81}$$

Using the results of section "Conjugate CAF" and noting that there are $K(p^2+p)/2$ terms in the double summation in (81), it follows that

$$\mathscr{T}_{conj} \overset{\mathscr{H}_0}{\sim} \chi^2_{K(p^2+p)} \tag{82}$$

which allows for calculation of the test threshold η_{conj} corresponding to a specified P_{fa}.

Single Antenna Case: Nonconjugate CAF

Here some existing tests for $p = 1$ are briefly discussed and compared.

Test of [10]

For $p = 1$ (single antenna), the considered nonconjugate CAF test reduces to

$$2M \sum_{k=1}^{K} \frac{|\hat{R}_{11,x}(\alpha_k;\tau_k)|^2}{\sum_{m=-L_n}^{L_n}|\hat{R}_{11,x}(m)|^2 e^{-j2\pi\alpha_k m}} \underset{\mathscr{H}_0}{\overset{\mathscr{H}_1}{\gtrless}} \eta. \tag{83}$$

Dandawate-Giannakis and Related Tests [4, 14, 17]

It is interesting to compare the above test with the corresponding tests in [4, 14]. Define

$$\hat{\mathbf{c}}(\alpha;\tau) := \begin{bmatrix} \mathrm{Re}\left\{\hat{R}_{11,x}(\alpha;\tau)\right\} \\ \mathrm{Im}\left\{\hat{R}_{11,x}(\alpha;\tau)\right\} \end{bmatrix},$$

$$F(f) := \sum_{t=1}^{M} x(t)x^*(t+\tau)e^{-j2\pi ft}, \tag{84}$$

$$\hat{S} := \frac{1}{ML_w} \sum_{s=-(L_w-1)/2}^{s=(L_w-1)/2} W(s)F(\alpha - \frac{s}{M})F(\alpha + \frac{s}{M}), \tag{85}$$

$$\hat{S}^{(*)} := \frac{1}{ML_w} \sum_{s=-(L_w-1)/2}^{s=(L_w-1)/2} W(s)F^*(\alpha + \frac{s}{M})F(\alpha + \frac{s}{M}), \tag{86}$$

$$\hat{\Gamma}(\alpha;\tau) := \begin{bmatrix} \text{Re}\left\{\frac{\hat{S}+\hat{S}^{(*)}}{2}\right\} & \text{Im}\left\{\frac{\hat{S}-\hat{S}^{(*)}}{2}\right\} \\ \text{Im}\left\{\frac{\hat{S}+\hat{S}^{(*)}}{2}\right\} & \text{Re}\left\{\frac{\hat{S}^{(*)}-\hat{S}}{2}\right\} \end{bmatrix} \tag{87}$$

where $W(s)$ is a spectral smoothing window of odd length L_w. The test of [4] is given by

$$\mathscr{T}_{2c}(\alpha;\tau) := M\hat{\mathbf{c}}^T(\alpha;\tau)\hat{\Gamma}^{-1}(\alpha;\tau)\hat{\mathbf{c}}(\alpha;\tau) \underset{\mathscr{H}_0}{\overset{\mathscr{H}_1}{\gtrless}} \gamma \tag{88}$$

where $\mathscr{T}_{2c}(\alpha;\tau) \overset{\mathscr{H}_0}{\sim} \chi^2_2$. A multi-antenna version of this test for conjugate CAFs may be found in [36]. A Kaiser window function has been used for $W(s)$ in [4, 14, 17, 18, 36]. It is given by

$$W(s) = \begin{cases} I_0\left(\beta\sqrt{1-(\frac{s}{L_w/2})^2}\right), -\frac{L_w-1}{2} \le s \le \frac{L_w+1}{2} \\ 0 \text{ elsewhere} \end{cases} \tag{89}$$

where I_0 is zero-order modified Bessel function of the first kind and β and L_w are parameters to be selected. In [14] a multifrequency-multilag version has been proposed as

$$\sum_{k=1}^{K} \mathscr{T}_{2c}(\alpha_k;\tau_k) \underset{\mathscr{H}_0}{\overset{\mathscr{H}_1}{\gtrless}} \gamma_K \text{ where } \sum_{k=1}^{K} \mathscr{T}_{2c}(\alpha_k;\tau_k) \overset{\mathscr{H}_0}{\sim} \chi^2_{2K}. \tag{90}$$

Computational requirements for these tests are discussed in [10]. In (85) and (86), $\hat{S}$ and $\hat{S}^{(*)}$ are estimates of nonconjugate and conjugate cyclic spectra of $f(t,\tau) = x(t)x(t+\tau)$, respectively [4, 14, 17]. Thus, while in [4, 14, 17] cyclic spectra of $x(t)x(t+\tau)$ are used in the test statistic; in [10], one only needs the autocorrelation (equivalently power spectral density) of $x(t)$.

It should be pointed out that the tests of [4, 14, 17, 18, 36] are not generalized likelihood ratio tests (GLRTs), contrary to the claims made therein. It is more appropriate to view $\mathscr{T}_{2c}$ in (88) as an ad hoc test statistic resulting in a CFAR test; same remark applies to [14, 17, 18, 36] (all based on [4]).

Tani-Fantacci Test [25]
This test applies to OFDM signals only. Given an OFDM signal as discussed in section "OFDM Signals", the test statistic of [25, Sec. IV.A] is given by

$$T_\alpha := \left| \frac{\hat{R}^{\alpha}_{11}(N_c)}{\hat{R}^{\alpha+S}_{11}(N_c)} \right| \underset{\mathscr{H}_0}{\overset{\mathscr{H}_1}{\gtrless}} \eta_T, \tag{91}$$

where

$$\alpha = \frac{1}{N_c + N_{cp}} = \frac{1}{N}, \tag{92}$$

$$\hat{R}^{\alpha}_{11}(\tau) := \frac{1}{M} \sum_{n=1}^{M} \left(\frac{1}{L} \sum_{k=n}^{n+L-1} x(k) x^*(k+\tau) \right) e^{-j2\pi\alpha n} \tag{93}$$

and L is picked to be shorter than the OFDM symbol duration. One picks the (fundamental) cycle frequency $\alpha = \alpha_0 = \frac{1}{N}$ (for sampled OFDM signal), and S is an arbitrary integer value that does not belong to the set of cycle frequencies $\{\frac{k}{T_s},\ k = 1, 2, \cdots\}$ for continuous-time OFDM signal. For sampled signals, [25] suggests choosing $S = S_{bin}/M$ where S_{bin} is the "frequency bin number." It is established in [25] that under $\mathscr{H}_0$, asymptotically T_α follows a Cauchy distribution.

Two-Window Approaches

Suppose the model (1) is changed to the following

$$x(t) = \begin{cases} i(t) + n(t) & : \mathscr{H}_0 \\ s(t) + i(t) + n(t) & : \mathscr{H}_1 \end{cases} \tag{94}$$

where now one includes interference $i(t)$. In all of the approaches discussed thus far, under $\mathscr{H}_0$, $i(t)$ is assumed to be absent and $n(t)$ represents thermal noise or filtered thermal noise. One designs a CFAR test requiring prior knowledge of some of the signal statistics under $\mathscr{H}_0$. For instance, for spectrum sensing one needs to know the PSD under $\mathscr{H}_0$ to design the CFAR test. Typically, $i(t)$ is ignored and $n(t)$ is taken to be thermal noise with known white PSD. An interesting approach not requiring any prior knowledge of the PSD under $\mathscr{H}_0$ was proposed in [5]. Reference [5] assumes that a PU-free data record is available in an *assessment window* of observations which allows one to acquire signal statistics of interest under $\mathscr{H}_0$. Then the PSD of the current observations segment (*evaluation window*) is estimated and compared with the PSD of the assessment window "bin by bin" on the frequency grid to test for the presence/absence of the PU. Reference [5] uses a single antenna receiver. The approaches of [30, 31] proposed in the context of wireless user authentication and comparison of random processes can be exploited for spectrum sensing based on two windows.

Reference [30] analyzes a single antenna receiver whereas [31] discusses multiple antenna receivers. Following [5] two nonoverlapping time windows, each of N samples, are considered, where the first window (occurring earlier in time) is called the *assessment window* and the second window is called the *evaluation window*. As in [5], a key assumption is that the time location of *assessment window* is such that the measurements made during this window consist of just noise and interference (i.e., it is free of the primary user signal). The PSD estimated from the *assessment window* serves a reference against which the PSD obtained from the *evaluation window* is compared. If there is a statistically significant deviation between the two estimated PSDs, one declares presence of PU over a particular frequency bin or over a particular frequency band. Thus, prior knowledge of noise and interference spectrum is not needed. On the other hand, a PU-free set of measurements must be available. Note that the time interval within which the two windows reside must be less than the channel coherence time for the procedure to work.

Summary

Quite often, as a result of receive filters at the cognitive user's receiver, the filtered thermal noise will not be white. Most existing approaches assume white noise sequences at the receiver. The goal of this chapter was to present a comprehensive overview of spectrum sensing approaches when noise is colored. Emphasis was on multiple antenna receivers which rely on the fact that noise is spatially (across antennas) independent, and PU signals are spatially dependent, while temporal properties of signal and noise become irrelevant to design of the PU signal detector. Both time-domain and frequency-domain approaches exploiting stationarity were presented. Cyclostationarity-based spectrum sensing methods were also reviewed. Enough details were presented to allow the reader to understand the underlying model assumptions and their consequences. There is no single best approach, and the detection results will depend upon the prior knowledge about the sensing environment.

Acknowledgements This work was supported by NSF Grant CCF-1617610.

References

1. Anderson TW (2003) An introduction to multivariate statistical analysis, 3rd edn. John Wiley, Hoboken
2. Box GEP (1949) A general distribution theory for a class of likelihood criteria. Biometrika 36:317–246
3. Brillinger DR (1981) Time series: data analysis and theory, expanded edn. McGraw Hill, New York
4. Dandawate AV, Giannakis, GB (1994) Statistical tests for presence of cyclostationarity. IEEE Trans Signal Process 42:2255–2369

5. Fantacci R, Tani A (2009) Performance evaluation of a spectrum-sensing technique for cognitive radio applications in B-VHF communication systems. IEEE Trans Veh Technol 58:1722–1730
6. Ferguson TS (1996) A course in large sample theory. Chapman & Hall, London
7. Hayakawa T (1975) The likelihood ratio criterion for a composite hypothesis under a local alternative. Biometrika 62:451–460
8. Haykin S, Thomson DJ, Reed JH (2009) Spectrum sensing for cognitive radio. Proc IEEE 97:849–877
9. Helstrom CW (1995) Elements of signal detection and estimation. Prentice Hall, Englewood Cliffs
10. Huang G, Tugnait JK (2013) On cyclic autocorrelation based spectrum sensing under uncertain Gaussian noise. IEEE Trans Signal Process 61:2042–2054
11. Kim J, Andrews JG (2010) Sensitive white space detection with spectral covariance sensing. IEEE Trans Wirel Commun 9:2945–2955
12. Leshem A. van der Veen AJ (2001) Multichannel detection of Gaussian signals with uncalibrated receivers. IEEE Signal Process Lett 8:120–122
13. Lopez-Valcarce R,Vazquez-Vilar G, Sala J (2010) Multiantenna spectrum sensing for cognitive radio: overcoming noise uncertainty. In: Proceedings of the 2010 2nd International Workshop Cognitive Information Processing, Elba Island, pp 310–315
14. Lunden J, Koivunen V, Huttunen A, Poor HV (2009) Collaborative cyclostationary spectrum sensing for cognitive radio systems. IEEE Trans Signal Process 57:4182–4195
15. Ma J, Li GY, Juang BH (2009) Signal processing in cognitive radio. Proc IEEE 97:805–823
16. Muirhead RJ (1982) Aspects of multivariate statistical theory. John Wiley, New York
17. Oner M, Jondral, F (2004) Cyclostationarity based air interface recognition for software radio systems. In: Proceedings of the 2004 Radio Wireless Conference, pp 263–266
18. Oner M, Jondral, F (2007) On the extraction of the channel allocation information in spectrum pooling systems. IEEE J Sel Areas Commun 25:558–565
19. Percival DB, Walden AT (1993) Spectral analysis for physical applications. Cambridge University Press, Cambridge
20. Ramirez D, Via J, Santamaria I, Scharf LL (2010) Detection of spatially correlated Gaussian time series. IEEE Trans Signal Process 58:5006–5015
21. Ramirez D, Vazquez-Vilar G, Lopez-Valcarce R, Via J, Santamaria I (2011) Multiantenna detection of rank-P signals in cognitive radio networks. IEEE Trans Signal Process 59: 3764–3774
22. Sharma SK, Chatzinotas S, Ottersten B (2013) The effect of noise correlation on fractional sampling based spectrum sensing. In: Proceedings of the 2013 IEEE International Conference Communications, Budapest, pp 1183–1187
23. Shin H, Kim Y (2010) A CMOS active RC low-pass filter with simultaneously tunable high and low cutoff frequencies for IEEE 802.22 applications. IEEE Trans Circuits Syst Express Briefs 57:85–89
24. Taherpour A, Nasiri-Kenari M, Gazor S (2010) Multiple antenna spectrum sensing in cognitive radios. IEEE Trans Wirel Commun 9:814–823
25. Tani A, Fantacci R (2010) Low-complexity cyclostationary-based spectrum sensing for UWB and WiMAX coexistence with noise uncertainty. IEEE Trans Veh Technol 59:2940–2950
26. Tugnait JK (2011) On autocorrelation-based multiantenna spectrum sensing for cognitive radios in unknown noise. In: Proceedings of the 2011 IEEE International Conference Acoustics, Speech & Signal Processing, Prague
27. Tugnait JK (2011) Multichannel spectrum sensing via multivariate power spectrum analysis. In: Proceedings of the 12th IEEE International Workshop on Signal Processing Advances in Wireless Communication, San Francisco, pp 106–110
28. Tugnait JK (2011) Autocorrelation-based multi-antenna spectrum sensing in colored noise. In: Proceedings of the 45th Asilomar Conference Signals, Systems, Computers, Pacific Grove, pp 1737–1741

29. Tugnait JK (2013) Further results on multiantenna spectrum sensing in colored noise. In: Proceedings of the IEEE 2013 Digital Signal Processing & Signal Processing Education Workshop, Napa, pp 30–35
30. Tugnait JK (2013) Wireless user authentication via comparison of power spectral densities. IEEE J Sel Areas Commun 31:1791–1802
31. Tugnait JK (2016) Comparing multivariate complex random signals: algorithm, performance analysis and application. IEEE Trans Signal Process 64:934–947
32. Vasilopoulos A, Vitzilaios G, Theodoratos G, Papananos Y (2006) A low-power wideband reconfigurable integrated active RC filter with 73 dB SFDR. IEEE J Solid-State Circuits 41:1997–2008
33. Wang P, Fang J, Han N, Li H (2010) Multiantenna-assisted spectrum sensing for cognitive radio. IEEE Trans Veh Technol 59:1791–1800
34. Zeng Y, Liang YC (2009) Spectrum-sensing algorithms for cognitive radio based on statistical covariances. IEEE Trans Veh Technol 58:1804–1815
35. Zhang R, Lim TJ, Liang YC, Zeng Y (2010) Multi-antenna based spectrum sensing for cognitive radios: a GLRT approach. IEEE Trans Commun 58:84–88
36. Zhong G, Guo J, Zhao Z, Qu D (2010) Cyclostationarity based multi-antenna spectrum sensing in cognitive radio networks. In: Proceedings of the IEEE 2010 Vehicular Technology Conference, pp 1–5

Spectrum Sensing Using Markovian Models

2

Joseph M. Bruno, Yariv Ephraim, Brian L. Mark, and Zhi Tian

Contents

J. M. Bruno (✉) · Y. Ephraim · B. L. Mark · Z. Tian
ECE Department, George Mason University, Fairfax, VA, USA
e-mail: jbruno2@gmu.edu; yephraim@gmu.edu; bmark@gmu.edu; ztian1@gmu.edu

W. Zhang (ed.), *Handbook of Cognitive Radio*,
https://doi.org/10.1007/978-981-10-1394-2_2

Abstract

Markovian models, as well as other statistical models, have been applied in the context of cognitive radio communications to characterize user activity in a given spectrum band and to develop algorithms for temporal spectrum sensing. In this chapter, we discuss spectrum sensing based on Markovian models. We provide an overview of the related literature and then discuss the application of discrete-time Markov chain models to spectrum sensing, in particular the hidden bivariate Markov chain. We focus on the modeling of cognitive radio channels using Markov chains, spectrum detection, and parameter estimation. We then discuss various spectrum sensing scenarios in which the Markovian models are used. Finally, we discuss open problems and topics for further research related to spectrum sensing using Markovian models.

Introduction

The conventional approach to spectrum management is to partition the spectrum into bands and issue licenses for spectrum usage in those bands. Studies of spectrum usage have shown that this spectrum allocation paradigm often results in severe underutilization of the spectrum; see, e.g., [22, 45]. In opportunistic or dynamic spectrum access, a band of licensed spectrum can be used by unlicensed users whenever it is not being used by licensed users. The licensed user is often referred to as the primary user, whereas the unlicensed user is called the secondary user. To take advantage of the portions of the spectrum unused by the primary users, also known as spectrum holes, the secondary users must be capable of dynamically switching their transmissions among different frequency bands, i.e., they must be frequency agile. In addition, the secondary users must be capable of sensing the radio environment to determine the spectrum hole opportunities for dynamic spectrum access. Such capabilities are realized in cognitive radio technologies [26]. A group of communicating secondary users equipped with cognitive radios forms a cognitive radio network. In the context of dynamic spectrum access, the goal of the cognitive radio network is to maximize spectrum utilization while avoiding harmful interference to the primary users.

Dynamic spectrum access can be seen as a "fix" to the problem over spectrum underutilization caused by static allocation of spectrum to licensed users. The primary users maintain strict priority over the secondary users with respect to access to the licensed spectrum. The onus is on the secondary users to identify spectrum holes and transmit in such a way as to avoid harmful interference to the primary users. In a more general dynamic spectrum *sharing* framework, a given spectrum band may be shared among different groups of users rather than being licensed to a certain group of primary users. The spectrum may be shared according to some criterion of fairness, and the different groups of users may collaborate with each other to maximize overall spectrum efficiency while achieving their own individual communication goals. As in dynamic spectrum access, the users in a dynamic

spectrum sharing network must be capable of sensing the radio environment to determine spectrum holes and be frequency agile.

In this chapter, we focus on the problem of spectrum sensing, specifically the temporal aspect of identifying when spectrum holes occur in time. Our treatment of temporal spectrum sensing is based on Markovian models of user activity. To simplify the discussion, we will use the terminology of primary users and secondary users associated with the dynamic spectrum access paradigm, but the same principles of spectrum sensing will be applicable in a more general dynamic spectrum sharing setting. We will mainly look at applying Markovian models to characterize spectrum usage, detection of spectrum activity, and parameter estimation. For a given user, there is an important trade-off between devoting resources toward spectrum sensing vs. actually using spectrum for transmission. In the terminology of multiarmed bandit problems, this is the trade-off between "exploration" and "exploitation." To limit the scope of this chapter, we shall focus almost exclusively on the exploration aspect and consider only discrete-time models in detail. The spectrum sensing techniques discussed here could be applied in a dedicated spectrum monitoring infrastructure independently from the users. In this setting, the users would consult the spectrum monitoring system to determine spectrum availability, rather than perform the spectrum sensing themselves. Nevertheless, we will touch upon some of the related work in the literature that deals with both the exploration and exploitation aspects of spectrum sensing.

The remainder of this book chapter is organized as follows. In section "Background and Overview of Related Work," we provide an overview of the literature related to spectrum sensing using Markovian models. In section "Markovian Models," we introduce some terminology and notation for Markovian models as they are applied to temporal spectrum sensing. We focus on the hidden bivariate Markov chain and discuss the associated problems of spectrum detection and parameter estimation. In section "Spectrum Sensing Scenarios," we discuss various spectrum sensing scenarios in which the Markovian models can be applied. In section "Research Challenges and Open Problems," we consider some future challenges and areas of further research involving spectrum sensing via Markovian models. A brief summary and concluding remarks are given in section "Conclusion."

Background and Overview of Related Work

In this section, we provide background on applications of Markovian models to spectrum sensing and an overview of the related work in the literature. Some of the material discussed at a high level in this section is treated in greater detail in subsequent sections.

Applications of Markovian Models

Markovian models have been applied in many different areas, including network traffic modeling [23], speech processing [17], and ion channel current modeling [4], just to name a few. In such applications, some aspect of the system or signal of interest is represented by a Markov process either in discrete time or continuous time. Depending on the application, a discrete-time or a continuous-time model may be preferred for various reasons such as model fidelity, mathematical tractability, or computational complexity. Typically, the number of states of the Markov process is assumed to be finite. In general, Markovian models are attractive because of their mathematical tractability relative to other statistical models and their wide applicability. The fidelity of the Markovian model representation can sometimes be improved by increasing the number of states of the Markov process, but often at the expense of higher computational complexity and the need for a larger training set for parameter estimation.

In some applications, the purpose of the Markovian model is to represent the system or signal as closely as possible in a statistical sense. In other applications, the Markovian model may be only a means to an end, and accuracy of the model itself is of less importance than that of the final result, though the two are obviously closely related. In queueing applications, for instance, the arrival process may not need to be modeled with high accuracy if only the mean queue length is desired. For such a situation, a Poisson arrival process may be sufficient. If the queue length distribution is desired, a more sophisticated model such as the Markov-modulated Poisson process (MMPP) may be necessary. In teletraffic applications, the Poisson process has been found to be sufficiently accurate for modeling call arrivals, but does not provide a good model for bursty packet traffic. The MMPP model can represent the burstiness in packet arrivals [27], but may not be sufficiently rich to represent other phenomena such as long-range dependence or self-similarity, which have been observed in empirical studies of packetized traffic. Modeling of such phenomena takes us outside the realm of Markovian models, so some authors have devised approaches to approximate, in a local sense, characteristics such as long-range dependence using Markovian models.

Markovian Models in Cognitive Radio Systems

In a cognitive radio system, where the secondary user must vacate a channel before a primary user accesses it, statistical prediction of the future primary user state can reduce the probability of interference. Therefore, a Markovian model of the primary user can be used for state prediction, which in turn can prevent unintended collisions. Several cognitive radio media access control methods have been developed which model the primary user as a Markovian process. In [58], the primary user is modeled as a discrete-time partially observable Markov decision process (POMDP), where only part of the state of the system is observed. The

system consists of a set of independent channels, each occupied by a primary user that is modeled as a two-state discrete-time Markov chain. At a given time slot, the states of only a small subset of the total set of channels can be observed. Based on the partially observed state, the secondary user makes a decision on which channel or channels to sense or access in the next time slot. The Markov chain parameters for the primary users on the channels are assumed to be known. The basic POMDP model is augmented to account for errors in observing the partial system state.

Markovian models have been used to model primary users in optimization of exploration/exploitation of channels in cognitive radio systems. In [39, 59], a restless multiarmed bandit model is used to model dynamic spectrum access in the presence of multiple primary users on different channels. Solutions are presented to determine how much time should be spent sensing each channel with the objective of maximizing system throughput. In these works, the primary users are modeled by two-state discrete-time Markov chains, but estimation of the Markov chain parameters is not performed explicitly. In [39], estimation of the stationary distribution in the formulation of the reward function is performed.

Hidden Markov Models

In cognitive radio applications, the state of the primary user must be inferred by observing the signal through a noisy channel. When the primary user is modeled as a Markov chain, and the process is observed through a memoryless channel, the resulting model is a hidden Markov process. The bivariate process which comprises the Markovian primary user chain and the observations from the channel observations is a Markov process. The observable process alone is not Markov. The hidden Markov process is a natural model, which allows for inference of the underlying state, while still allowing for prediction of future states. A hidden Markov model consists of the underlying or hidden state process, together with an observable process that is conditionally dependent on the underlying state. The joint bivariate process retains the Markov property, so HMMs fall under the purview of Markovian models. As an additional benefit, HMMs allow for smoothing of decisions by performing maximum likelihood sequence estimation with the Viterbi algorithm, which can reduce the probability of detection error [20]. The HMM has been applied in many different fields including speech and image processing. A comprehensive review of HMMs is given in [20].

HMMs were first introduced as a model for spectrum sensing in cognitive radio networks independently in [1] and [40]. Although an HMM may use any conditional distribution to model signal impairments, the conditional normal distribution is of particular interest for its ability to model additive white Gaussian noise, Rayleigh fading [7], and lognormal shadowing [38].

Parameter Estimation for Markovian Models

Much of the research regarding cognitive radio media access using Markovian models relies on knowledge of the Markov chain parameters, either the state transition rates for continuous-time Markov chains or the state transition probabilities for discrete-time Markov chains. In practice, these parameters are unlikely to be known a priori, so a secondary user would have to perform parameter estimation as part of its spectrum sensing process. In [50], multichannel Markov parameter estimation for cognitive radio is considered. Multiple channels, each containing a single primary user, are observed by the secondary user. The primary user is modeled as a continuous-time Markov chain, and each channel is sensed sequentially using a maximum likelihood estimator [2]. Per-channel sensing times are allocated such that the total variance across all channels is minimized.

For HMMs, additional parameters of the conditional distributions must be estimated with the Markov chain parameter. The Baum algorithm (Also known as the Baum-Welch algorithm.), described in detail in [20], is used to estimate the Markov chain transition matrix and the conditional distribution. The Baum algorithm is a specific realization of the expectation-maximization algorithm [15]. An initial parameter is specified, and the algorithm alternates between computing the state probability distribution for each data point and reestimating the parameters.

The Baum algorithm is considered an *offline* parameter estimation algorithm because it requires a relatively large record of sample data. Reestimation of parameters if new data is received would require iterating again over the entire data set. In [44] and [46], recursive HMM parameter estimators were proposed. Recursive parameter estimation allows for *online* processing of data, where single samples or small blocks of samples may be used to update the HMM parameter estimates, rather than a large block of sample data.

Multivariate Markovian Models

As discussed above, the HMM is an example of a bivariate Markovian model. The underlying Markov chain of an HMM has geometrically distributed so journ times in each state. In many applications, including spectrum sensing, the state sojourn times may have non-geometric distributions such that the HMM is not a suitable model. A more general model that has been proposed is the hidden semi-Markov model [55], in which the sojourn time distributions are explicitly represented in the parameter of the model. The hidden semi-Markov model, however, is not Markovian. Consequently, parameter estimation for the hidden semi-Markov model has significantly higher computational complexity.

As an alternative to the semi-Markov model, a bivariate Markov chain can be used to model the underlying state. The bivariate Markov chain consists of two processes: one represents the observed state and the other represents phases during which the first process remains in a given state. This gives rise to discrete phase-type

state sojourn time distributions. By observing a bivariate Markov chain through a channel, we obtain a hidden bivariate Markov chain, which generalizes the HMM, but remains within the realm of Markovian models, i.e., the hidden bivariate Markov chain is a trivariate Markov process. A review of bivariate and multivariate Markov processes is given in [18].

The hidden bivariate Markov chain enjoys many of the same properties of an HMM. For example, the Baum algorithm can be used to perform parameter estimation for the hidden bivariate Markov chain. The hidden bivariate Markov chain may be considered a special case of a hidden semi-Markov model, in which the sojourn time distributions are of discrete-phase type. Unlike the hidden semi-Markov model, however, the sojourn time distribution is implicit in the model, rather than specified as a separate component of the model parameter. With a single underlying state, the bivariate Markov chain is equivalent to a standard univariate Markov chain. Increasing the number of phases or order of the bivariate Markov chain allows for modeling the state sojourn time distributions with more general phase-type distributions. On the other hand, the parameter estimation becomes more computationally complex, and more observation data is required to avoid overfitting the model.

In [38], hidden bivariate Markov chains were applied to spectrum sensing, and it was shown that when predicting many steps in the future, the bivariate Markov process was substantially more accurate. In [48], the work in [38] was extended using a recursive parameter estimation algorithm to perform online spectrum sensing. The algorithm from [44] was extended to perform parameter estimation of hidden bivariate Markov processes.

Markovian Models

Markov Chains

A Markov chain is a discrete-time random process with finite or countably infinite alphabet. Each letter of the alphabet is commonly referred to as a *state*, and the collection of states, i.e., the alphabet, is commonly referred to as the *state space*. The Markov chain may start from one of the states and subsequently visits any state that is reachable from the present state. A state is reachable if the probability of jumping to that state in one or more steps is positive. Self-transitions are allowed. In a Markov chain, future states are conditionally independent of past states given the current state. Thus, a Markov chain is characterized by the initial distribution which represents the probability of the chain to start from any given state and by the transition matrix which contains all conditional probabilities of the chain to visit any state given any current state. Each such conditional probability is referred to as the *transition probability*.

A discrete-time memoryless random process with finite alphabet is a particular Markov chain. Markov chains enable dependence of the process at various times and thus are more suitable for many applications. Furthermore, since their mathematical

structure is relatively simple, they are amenable to mathematical analysis, and they are well understood.

We denote the Markov chain by $X = \{X_0, X_1, \ldots, X_t, \ldots\}$ where $X_t \in \mathbb{X}$ and $\mathbb{X} = \{0, 1, \ldots, d\}$ denotes the state space for some finite integer d. In cognitive radio applications, the process X represents the status of the primary user at any given moment. Thus, $X_t = 0$ when the primary user is idle at time t and $X_t = 1$ when the primary user is active. Clearly, in that case $d = 1$. It is possible to choose $d > 1$ to refine the description of the status of the primary user. For example, various states may represent different levels of transmission power by the primary user. We assume that the Markov chain is homogeneous and irreducible. Homogeneity means that transition probabilities are independent of time. Irreducibility means that each state may be reached from any other state, that is, $\mathbf{P}(X_{t+k} = j \,|\, X_t = i) > 0$ for any $i, j \in \mathbb{X}$, any $t \geq 0$, and some $k > 0$. We use the row vector $\pi = \text{row}(\pi_0, \pi_1, \ldots, \pi_d)$ to denote the initial distribution of the process X and $A = \{a_{ij}, i, j = 0, 1, \ldots, d\}$ to denote the *transition matrix* of X. For given (i, j), π_i is the probability of $X_0 = i$, and a_{ij} represents the conditional probability of $X_t = j$ given $X_{t-1} = i$ for any $t \geq 1$. From the Chapman-Kolmogorov theorem, A^k represents the k-step transition matrix. That is, $A^k(i, j) = \mathbf{P}(X_{t+k} = j \mid X_t = i)$ for any positive integer k and any $t \geq 0$. The Markov chain is a stationary process if and only if its initial distribution π satisfies $\pi = \pi A$. In that case, π is called the stationary distribution of X, and $\pi_i = \mathbf{P}(X_t = i)$ for any $t \geq 0$. By the Perron-Frobenius theorem [29, p. 536], a sufficient condition for a finite state Markov chain to have a unique stationary distribution is that the chain be irreducible. A well-known result for an irreducible aperiodic finite state Markov chain is

$$\lim_{k \to \infty} A^k = \Pi \tag{1}$$

where Π is a matrix with identical rows each equal to the stationary distribution π. A Markov chain is *aperiodic* if the greatest common divisor of its returning epochs to a given state is one. This result shows that for sufficiently large t, $\mathbf{P}(X_t = j \mid X_{t-1} = i) = \pi_j$, $j = 1, \ldots, d$, regardless of i, where π is the stationary distribution of the chain.

There are many excellent books on Markov chains. The book by [5] contains an elementary chapter on finite-state Markov chains. The book by Kemeny and Snell [28] is very accessible, and there is the classic and more advanced book by Çinlar [11].

Hidden Markov Models

Normally, the process X cannot be observed directly. When the channel is sensed, noise is inevitably present at the cognitive radio receiver. A Markov chain observed through noisy memoryless channel is commonly referred to as a hidden Markov

model (HMM). An HMM is not a Markov chain, and its analysis is far more complex. HMMs, however, have numerous applications, and their statistical theory is very well understood. A review of HMMs may be found in [20]. Let $Y = \{Y_0, Y_1, \ldots, Y_t, \ldots\}$ denote the received signal by the cognitive radio receiver. The HMM is characterized by (π, A) as well as by the transition density of the channel. This is the conditional density of Y_t given X_t. We denote this conditional density by $b(y_t \mid x_t)$. The density $b(y_t \mid x_t)$ could be normal, exponential, Poisson, Gamma, etc. Let $B = \{b(y_t \mid x_t), x_t = 0, 1, \ldots, d\}$ denote the collection of all possible densities associated with the various states. In cognitive radio applications, when $x_t = 0$, $b(y_t \mid x_t)$ represents the density of the received signal when the primary user is idle, and when $x_t = 1$, $b(y_t \mid x_t)$ represents the density of the received signal when the primary user is active. Motivated by a central limit theorem, the density $b(y_t \mid x_t)$ is usually assumed normal with mean and variance dependent on the value of x_t. If we denote the mean and variance by μ_{x_t} and $\sigma^2_{x_t}$, respectively, then the parameter of the HMM is given by $\phi = \left(\pi, A, \{(\mu_i, \sigma_i^2), i = 0, \ldots, d\}\right)$. Hidden Markov models in the forms of a Markov chain observed through a channel with memory are also possible.

Let y^n denote a realization of the observation sequence $Y^n = \{Y_0, Y_1, \ldots, Y_n\}$ at the input of the cognitive radio receiver. The density of y^n is then given by

$$p(y^n; \phi) = \sum_{x_0, \ldots, x_n} \pi_{x_0} \prod_{t=1}^{n} a_{x_{t-1} x_t} b(y_t \mid x_t) \tag{2}$$

The parameter ϕ of the HMM may be estimated in an unsupervised offline manner from some training data. This is usually done by the Baum algorithm which is the earliest form of the expectation-maximization (EM) algorithm. The Baum algorithm is an iterative approach for generating a sequence of parameter estimates with increasing likelihood values unless a fixed point in the parameter space is reached. In the latter case, the algorithm is terminated, and the fixed point is a stationary point of the likelihood function. The algorithm is not guaranteed to reach a fixed point and hence is practically terminated when the relative likelihood values in two consecutive iterations fall below a preset threshold. Conditions for convergence of the sequence of estimates generated by the EM algorithm were given by Wu [54].

Given a value ϕ_κ of the true parameter of the HMM at the conclusion of the κth iteration, a new estimate is obtained as

$$\begin{aligned} \phi_{\kappa+1} &= \arg\max_\phi E\{\log p(x^n, y^n; \phi) \mid y^n; \phi_\kappa\} \\ &= \arg\max_\phi \sum_{x^n} p(x^n \mid y^n; \phi_\kappa) \log p(x^n, y^n; \phi). \end{aligned} \tag{3}$$

The density $p(x^n, y^n; \phi)$ is given by the summand of (2). Implementation of the Baum algorithm requires the density $p(x_t \mid y^n; \phi_\kappa)$, $t = 1, 2, \ldots, n$, which is

efficiently calculated using the so-called forward-backward algorithm. The forward density is given by $p(x_t, y^t; \phi_\kappa)$, $t = 0, 1, \ldots, n$, and the backward density is given by $p(y_{t+1}^n \mid x_t; \phi_\kappa)$, $t = n, n-1, \ldots, 0$, where $p(y_{n+1}^n) = 1$ and $y_{t+1}^n = \{y_{t+1}, \ldots, y_n\}$. Both densities are calculated recursively in forward and backward modes, respectively. Progressive scaling is required for better numerical stability. Scaling of the forward density, for example, results in recursive evaluation of $p(x_t \mid y^t; \phi_\kappa)$. We demonstrate the recursive calculation of the forward-backward formulas and the scaling procedure in section "Forward-Backward Matrix Recursions." The Baum algorithm is well known for its slow convergence which cannot be controlled by a choice of a step size as in Newton's methods for maximizing a function.

In cognitive radio applications, a fading channel with thermal additive noise is assumed. The measurements $\{Y_t\}$ constitute the logarithm of the power of the signal in a given narrowband portion of the available spectrum. When the state of the primary user is $X_t = a$, then Y_t is assumed normal with mean μ_a and variance σ_a^2. The samples $\{Y_t\}$ are assumed statistically independent. This model is motivated by a central limit theorem developed in [21]. The relation between $\{\mu_a, \sigma_a^2\}$ and the parameters of the fading additive noise channel is nontrivial. In [21, Corollary 5.6.3], the statistics of the logarithm of the smoothed periodogram of a stationary process with small dependence span were studied. The power of each narrowband signal may be seen as a value of the smoothed periodogram of a broadband process measured at a particular frequency. It was shown in [21] that the log-smoothed periodogram at a given frequency is asymptotically normal with mean that depends on the underlying power spectral density and a constant variance that is independent of the underlying power spectral density. In the proposed model, we allow both the mean and variance of each Y_t to depend on the state of the primary user, and hence on the underlying power of the received signal, in order to accommodate possible deviations from the model of [21]. If the variance of Y_t is somewhat independent of the underlying hypothesis, then that should be reflected in its estimated values.

When the active/idle process of the primary user in cognitive radio is represented by a Markov chain as described in this article, the sojourn time of the primary user in each of the two states has a geometric distribution with parameter that depends on the present state. The geometric distribution presents an unrealistic restriction since it does not conform with the typical sojourn time distributions of the primary user. That well-known fact in cognitive radio applications, as well as in other applications such as speech recognition, has led to the use of semi-Markov models [10,11,55]. In these models, which are not Markov processes, a desired sojourn time distribution is imposed. A semi-Markov process may be seen as a pair of processes comprising a Markov jump process for the states and a sequence of conditionally independent sojourn times given the sequence of states. Estimation of the parameter of a semi-Markov process is far more complicated than that of an HMM. This difficulty may be circumvented by substituting the Markov chain of the HMM by a bivariate Markov chain.

Bivariate Markov Chains

A bivariate Markov chain is a pair of discrete-time finite state random processes that are jointly Markov. Each of the individual processes is not necessarily Markov. When a bivariate Markov chain is used in cognitive radio sensing, one of the two processes represents the state process of the primary user while the other is an auxiliary process which endows the primary process with some desired statistical properties. A particularly useful property is a new distribution of the sojourn time of the primary process in each of its state. This distribution is phase type and is far more general than the geometric sojourn time distribution of the univariate Markov chain. The set of discrete phase-type distributions is dense in the set of distributions on $0, 1, 2, \ldots$. This means that every distribution in that family is either a phase type or it can be approximated arbitrarily well by a phase-type distribution. The family of phase-type distributions includes mixtures of convolutions of geometric distributions. Intuitively, either a jump of the two processes comprising the bivariate Markov chain or a joint jump of the two processes constitutes a jump of the bivariate Markov chain. The sojourn time in each pair of states of the bivariate Markov chain has geometric distribution like in any other Markov chain. Consecutive jumps of the primary process may occur while the secondary process has undergone several jumps along some path in the state space. Thus, the sojourn time of the primary process in each of its states is the sum of multiple independent geometric random variables. Considering different paths, we see that the sojourn time in each state of the primary process could have a mixture of convolutions of geometric distributions. A review of bivariate Markov chains may be found in [18].

Let $Z = \{Z_t = (X_t, S_t), t = 0, 1, \ldots\}$ denote a bivariate Markov chain where $X = \{X_t, t = 0, 1, \ldots\}$ represents the primary process and $S = \{S_t, t = 0, 1, \ldots\}$ represents the auxiliary process. We assume that X takes values in the state space $\mathbb{X} = \{0, 1, \ldots, d\}$, S takes values in the state space $\mathbb{S} = \{0, 1, \ldots, r\}$, and Z takes values in the state space $\mathbb{Z} = \mathbb{X} \times \mathbb{S}$. The state pairs $\{(a, i) \in \mathbb{Z}\}$ are assumed to be ordered lexicographically, and the transition probability of Z is given by

$$h_{ab}(ij) = P_\phi(Z_{t+1} = (b, j) \mid Z_t = (a, i)) \tag{4}$$

where ϕ is the parameter of the process, that is, ϕ comprises the set of independent entries of initial distribution and transition matrix of the bivariate Markov chain. The transition matrix $H = \{h_{ab}(ij)\}$ is written as a block matrix $H = \{H_{ab}; a, b \in \mathbb{X}\}$, where $H_{ab} = \{h_{ab}(ij); i, j \in \mathbb{S}\}$ is an $r \times r$ matrix. The underlying chain S is Markov with transition matrix Q if and only if the equation $\sum_{b \in \mathbb{X}} H_{ab} = Q$ holds independently of a. A similar condition can be given for the observable chain X to be Markov. When H is irreducible, it has a unique stationary distribution $\pi = \text{row}\{\pi_{ai}, a \in \mathbb{X}, i \in \mathbb{S}\}$ satisfying $\pi = \pi H$. The process $\{Z_t\}$ is stationary if and only if $P_\phi(Z_0 = (a, i)) = \pi_{a,i}$ for all $(a, i) \in \mathbb{Z}$.

The probability mass function of the sojourn time of the primary process in each state in $\mathbb{X}$ is given by [38]

$$p_\phi(l \mid a) = \bar{\nu}_a(\phi) H_{aa}^{l-1}(I - H_{aa})\mathbf{1} \tag{5}$$

for $l = 1, 2, \ldots$, where $\mathbf{1}$ is a column vector of all ones of suitable dimension, and $\bar{\nu}_a$ is defined as follows. Let $\nu_{a,i}(\phi) = P_\phi(Z_0 = (a, i))$ denote the initial probability of the bivariate Markov chain to be in state (a, i) at time $t = 0$, and let

$$\nu_a(\phi) = (\nu_{a,1}(\phi), \nu_{a,2}(\phi), \ldots, \nu_{a,r}(\phi)). \tag{6}$$

Then, $\bar{\nu}_a(\phi) = \nu_a(\phi)/(\nu_a(\phi)\mathbf{1})$ is a normalized version of $\nu_a(\phi)$. Equation (5) provides the *discrete-time phase-type* probability mass function with parameter $(\bar{\nu}_a(\phi), H_{aa})$ [37, p. 46]. This probability mass function is derived under the assumptions that the matrices H and $\{H_{aa}, a \in \mathbb{X}\}$ are irreducible and that the diagonal elements of H are positive.

Consider now substitution of the univariate Markov chain of an HMM with the bivariate Markov chain described above. The bivariate Markov chain is now observed through a memoryless channel with output denoted by $Y = \{Y_0, Y_1, \ldots, Y_t, \ldots\}$ as before. The resulting process (Y, X, S) is an HMM with a bivariate Markov chain $Z = (X, S)$ rather than the univariate Markov chain X. The sojourn time in each pair of states of the bivariate Markov chain is geometrically distributed. Assume now that the triplet process (Y, X, S) possesses a Markov property such that the processes Y and S are conditionally independent given the process X. With this assumption, the observable process Y inherits its sojourn time from the non-Markovian process X, rather than from the Markovian process Z, and hence, the sojourn time distribution of Y in each state of X is discrete phase-type rather than geometric [38], [18, Eq. 8.7]. The process (Y, X, S) with the Markovian property provides a realistic model for the received signal in a cognitive radio receiver [38]. We refer to the model that incorporates the above Markovian property as a *hidden bivariate Markov chain*.

Likelihood of Observable Process

Proceeding with the Markovian assumption, for each time instant t, Y_t is independent of S_t given X_t. That is, $b(y_t \mid z_t) = b(y_t \mid x_t)$. We next develop expressions for the likelihood function of the observable process and for the forward-backward formulas for both the HMM and the hidden bivariate Markov chain.

Define the conditional distribution

$$F_{ij}^{ab}(y) := P_\phi(Y_t \le y_t, Z_t = (b, j) \mid Z_{t-1} = (a, i)) \tag{7}$$

and the corresponding transition density

$$f_{ij}^{ab}(y_t) = \frac{\partial}{\partial y_t} F_{ij}^{ab}(y_t) = p_\phi(y_t, z_t = (b, j) \mid z_{t-1} = (a, i)). \tag{8}$$

Recall that the states (X, S) are ordered lexicographically. Define the $dr \times dr$ *transition density matrix* by

$$f(y_t) = \left\{ f_{ij}^{ab}(y_t); (a,i),(b,j) \in \mathbb{Z} \right\}. \tag{9}$$

The transition density matrix for the HMM where Y_t depends on Z_t is given in terms of the transition matrix H from (4) and the density which corresponds to $P_\phi(Y_t \leq y_t \mid Z_t = (b,j))$. We denote that density by $g_{\theta_{bj}}(y_t)$ where θ_{bj} is its parameter. This density is determined by the channel. For memoryless Gaussian channel as is assumed here, the parameter $\theta_{bj} = (\mu_{bj}, \sigma_{bj}^2)$, where μ_{bj} denotes the mean and σ_{bj}^2 denotes the variance. For the hidden bivariate Markov chain where Y_t given X_t is independent of S_t, the density $g_{\theta_{bj}}(y_t)$ is independent of j and is given by $g_{\theta_b}(y_t)$. In either case,

$$f(y_t) = HG(y_t) \tag{10}$$

where for the HMM,

$$G(y_t) = \text{diag}(g_{\theta_{bj}}(y_t), (b,j) \in \mathbb{Z}), \tag{11}$$

and for the hidden bivariate Markov chain,

$$G(y_t) = \text{diag}(g_{\theta_b}(y_t) I, b = 1, \ldots, d) \tag{12}$$

where I is an $r \times r$ identity matrix. Define the $1 \times dr$ row vector $\zeta_{y_0} = \left\{ p_\phi(y_0, z_0); z_0 \in \mathbb{Z} \right\}$ representing the initial density of (Y_0, Z_0). Then, the likelihood function of the hidden bivariate Markov chain is given by

$$p_\phi(y_0^n) = \zeta_{y_0} \prod_{t=1}^{n} f(y_t) \mathbf{1}. \tag{13}$$

The likelihood function of the HMM is given by a similar expression. The parameter ϕ of the HMM comprises the independent components of the initial distribution π and of the transition matrix H and $\{\theta_{bj}, (b,j) \in \mathbb{Z}\}$. For the hidden bivariate Markov chain, the relevant entries of π and H are the same as for the HMM, but the parameter of the channel densities is given by $\{\theta_b, b \in \mathbb{X}\}$. The difference is due to the Markovian assumption making Y and S conditionally independent given X.

Forward-Backward Matrix Recursions

Evaluation of the likelihood function of the hidden bivariate Markov chain, as well as iterative estimation of its parameter using the EM algorithm, is facilitated by the use of the forward-backward recursions. We present here a slightly more general

form of the standard recursions for HMMs due to Stiller and Radons [46]. This version is useful in recursive estimation of the parameter of the model [19]. Define

$$R(k,m) := \prod_{t=k}^{m} f(y_t) \tag{14}$$

where $1 \leq k \leq m \leq n$. For fixed k, we have the forward recursion (in m) on the backward density as follows:

$$\begin{aligned} R(m,m-1) &:= I \\ R(k,m) &= R(k,m-1)\, f(y_m) \end{aligned} \tag{15}$$

where I is an identity matrix. For fixed $m = n$, the backward recursion (in k) on the backward density is given as follows:

$$\begin{aligned} R(n+1,n) &:= I \\ R(k,n) &= R(k+1,n)\, f(y_k) \end{aligned} \tag{16}$$

for $k = n, n-1, \ldots, 0$. The forward recursion for the forward density is given by

$$L(m) = L(m-1)\, f(y_m) \tag{17}$$

where $m = 1, 2, \ldots, n$ and $L(m) = \nu_{y_0} R(1,m)$, and let $L(0) = \nu_{y_0}$. Note that for a given parameter ϕ and observation sequence $Y_0^n = y_0^n$, the $((a,i),(b,j))$ element of $R(k,m)$ is given by

$$R_{ai,bj}(k,m) = p_\phi(y_k^m, z_m = (b,j) \mid z_{k-1} = (a,i)), \tag{18}$$

and the (b,j) element of $L(m)$ is given by

$$L_{bj}(m) = p_\phi(y_0^m, z_m = (b,j)). \tag{19}$$

Numerical stability of the recursions in (15) and (17) is improved when scaling is introduced in each iteration. It is instructive to start with the description of the scaled version of $L(m)$, which we denote by $\tilde{L}(m)$. Let $c_0 = \nu_{y_0}\mathbf{1}$, and let $\tilde{L}(0) = \nu_{y_0}/c_0$. The scaled version of (17) is given by

$$\tilde{L}(m) = \frac{1}{c_m} \tilde{L}(m-1)\, f(y_m) \tag{20}$$

where

$$c_m = \tilde{L}(m-1)\, f(y_m)\mathbf{1}. \tag{21}$$

It follows that

$$\tilde{L}(m) = \frac{1}{\prod_{t=0}^{m} c_t} L(m), \tag{22}$$

$p_\phi(y_0^m) = \prod_{t=0}^{m} c_t$, $c_t = p_\phi(y_t \mid y_0^{t-1})$ for $t \geq 1$, and the (b, j) component of $\tilde{L}(m)$ is given by $\tilde{L}_{bj}(m) = P_\phi(Z_m = (b, j) \mid y_0^m)$. The scaled version of forward recursion on $R(k, m)$ is given by

$$\begin{aligned} \tilde{R}(k, m) &= \frac{1}{\prod_{t=k}^{m} c_t} R(k, m) \\ &= \tilde{R}(k, m-1) \frac{f(y_m)}{c_m}. \end{aligned} \tag{23}$$

where c_m is given in (21). The recursion $\tilde{R}(k, m)$ does not enjoy an appealing probabilistic interpretation as $\tilde{L}(m)$. A similar scaled backward recursion on $R(k, n)$ can be written.

The parameter of the hidden bivariate Markov chain may essentially be estimated as the parameter of an HMM using the Baum or the EM algorithm as is demonstrated in the next section "Estimation of the Bivariate Markov Chain Parameter." Batch estimation of the parameter from a given training sequence was detailed in [19, 38]. Sequential estimation of the parameter using an EM iterate was described in [19].

Estimation of the Bivariate Markov Chain Parameter

In this section we demonstrate how the parameter of the hidden bivariate Markov chain can be estimated from a sequence of observations y_0^n using the batch EM algorithm. Our presentation follows that in [19]. A sequential estimation approach which is based on the EM iteration may also be found in [19]. It turns out that the estimation procedure can be described simultaneously for an HMM as well as for a hidden bivariate Markov chain. We shall thus start with estimation of the HMM parameter and then infer about estimation of the hidden bivariate Markov chain.

Assume that ϕ_κ is the parameter estimate at the end of the κth iteration. At the conclusion of the $(\kappa + 1)$th iteration, the new estimate of the initial distribution π_{bj} is given by

$$\hat{\pi}_{bj}(n) = P_{\phi_\kappa}(Z_0 = (b, j) \mid y_0^n), \tag{24}$$

and the new estimate of $h_{ab}(ij)$ is given by

$$\hat{h}_{ab}(ij) = \frac{\hat{M}_{ij}^{ab}(n)}{\sum_{(\beta,l)} \hat{M}_{il}^{a\beta}(n)} \tag{25}$$

where $\hat{M}_{ij}^{ab}(n)$ denotes the conditional mean estimate given y_0^n of the number of transitions of Z from (a, i) to (b, j) in $[0, n]$. This number includes self-transitions.

Using the indicator function

$$\varphi_{bj}(t) = \begin{cases} 1, & Z_t = (b, j) \\ 0, & \text{otherwise,} \end{cases} \tag{26}$$

the number of transitions is given by

$$M_{ij}^{ab}(n) = \sum_{t=1}^{n} \varphi_{ai}(t-1)\varphi_{bj}(t), \tag{27}$$

and

$$\begin{aligned} \hat{M}_{ij}^{ab}(n) &= E_{\phi_\kappa}\left\{ M_{ij}^{ab}(n) \mid y_0^n \right\} \\ &= \sum_{t=1}^{n} P_{\phi_\kappa}\left(Z_{t-1} = (a, i), Z_t = (b, j) \mid y_0^n \right). \end{aligned} \tag{28}$$

For an HMM with normal densities, $\{b_{\phi_\kappa}(y_t \mid z_t), z_t \in \mathbb{Z}\}$, with mean μ_{bj} and variance σ_{bj}^2 when $z_t = (b, j)$, define

$$N_j^b(n; \lambda) = \sum_{t=0}^{n} y_t^\lambda \varphi_{bj}(t) \tag{29}$$

for $\lambda \in \{0, 1, 2\}$. Note, for example, that if the observations $\{y_t\}$ are clustered into the various states of the HMM, then $N_j^b(n; 1)$ is the sum of the observations associated with state (b, j). Let

$$\begin{aligned} \hat{N}_j^b(n; \lambda) &= E_{\phi_\kappa}\left\{ N_j^b(n; \lambda) \mid y_0^n \right\} \\ &= \sum_{t=0}^{n} y_t^\lambda P_{\phi_\kappa}(Z_t = (b, j) \mid y_0^n). \end{aligned} \tag{30}$$

The new estimates of the mean and variance at the conclusion of the $(\kappa + 1)$th iteration are, respectively, given by

$$\hat{\mu}_{bj}(n) = \frac{\hat{N}_j^b(n; 1)}{\hat{N}_j^b(n; 0)}, \tag{31}$$

$$\widehat{\sigma_{bj}^2}(n) = \frac{\hat{N}_j^b(n; 2)}{\hat{N}_j^b(n; 0)} - \hat{\mu}_{bj}^2(n). \tag{32}$$

For a hidden bivariate Markov chain, μ_{bj} and σ_{bj}^2 are reduced to μ_b and σ_b^2, respectively. Thus, $P_{\phi_\kappa}(Z_t = (b, j) \mid y_0^n)$ in (31) and (32) should be substituted

by $P_{\phi_\kappa}(X_t = b \mid y_0^n)$. It is well known that the conditional probability in (28), and hence in (24) and (30), may be efficiently implemented using forward-backward recursions.

Spectrum Sensing Scenarios

In this section, we shall discuss the application of spectrum sensing techniques based on Markovian models to a variety of scenarios. Temporal spectrum sensing scenarios can be organized into three basic categories [47]:

1. *Narrowband:* The secondary user senses a single channel that is clearly defined in terms of center frequency and bandwidth.
2. *Multiband:* The secondary user senses multiple independent narrowband channels.
3. *Wideband:* The secondary user senses a spectrum band with no prior knowledge of channel boundaries or channel occupancy.

In the descriptions of the above categories, we "the secondary user" may refer to a group of several secondary users collaboratively sensing the given spectrum band. Spectrum sensing performance can be significantly enhanced by employing collaborative sensing among a group of several secondary users [30]. Multiband temporal sensing techniques are useful for applications such as TV whitespace where multiple independent primary users operate on clearly defined channels. To simplify our discussion, we shall assume that only a single primary user occupies a given narrowband channel. The wideband temporal sensing problem can be transformed into a multiband sensing problem by first identifying the channel boundaries [6].

Narrowband Sensing

Well-known signal detection algorithms for a narrowband channel include energy detection, cyclostationary feature detection, and matched filter detection [56]. The energy detector is the simplest of the narrowband detectors and requires no a priori knowledge of the channel, but performs poorly in low signal-to-noise ratio (SNR) conditions. The matched filter detector can detect primary user activity at very low SNR, but requires a priori knowledge of the primary user waveform. Cyclostationary feature detection lies between the matched filter and energy detector with respect to performance at low SNR, but requires significant computation times and long integration windows. The performance of all three signal detection methods can be degraded by low primary user duty cycle. By characterizing the primary user signal using a Markovian model, the temporal dynamics of primary user activity on the channel can be taken into account in detecting the signal. Spectrum sensing

based on a Markovian model can lead to better detection performance in lower SNR scenarios, since the past history of primary user activity is incorporated into the detection process. Moreover, use of a Markovian model can provide predictive information that can be applied to achieve more effective dynamic spectrum access.

In [38], the hidden bivariate Markov chain model discussed in section "Bivariate Markov Chains" was proposed as a model for the received primary user signal in a narrowband channel. Consider a system consisting of one primary user transmitting on the narrowband channel. The primary user alternates between an active state, in which a signal of fixed power is transmitted over the narrowband channel, and an idle state, in which no signal is transmitted. We denote the idle state of the primary user at time $t\Delta$ by $X_t = 0$ and the active state by $X_t = 1$, where Δ is a sampling period. The process $X = \{X_t\}$, taking values in the set $\mathbb{X} \in \{0, 1\}$, models the directly observed state of the primary user.

The wireless propagation environment is assumed to be governed by a standard path loss with lognormal shadowing model [35, pp. 40–41]. We ignore fast fading since it can be reduced effectively by an averaging filter (cf. [34]). Let $u(t)$ denote the complex baseband demodulated primary user signal. For a particular secondary user, let $c(t)$ denote a random process representing the fading, and let $w(t)$ denote the additive thermal noise of the channel. The signal received by the secondary user is given by $y(t) = c(t)u(t) + w(t)$. The received baseband signal may be envisioned as a phasor perturbed by the additive noise. The received signal is sampled every Δ seconds, and each sample is represented by the logarithm of its power.

Let Y_t denote the logarithm of the power of the tth sample of the received signal of the secondary user. Given the state $X_t = a$ of the primary user, the samples $\{Y_t\}$ are assumed statistically independent, and each Y_t is assumed normally distributed with some mean μ_a and variance σ_a^2. The process $Y = \{Y_t\}$ represents the received primary user signal, which can be interpreted as the primary user state observed through the narrowband channel. Further motivation and discussion of this model for the cognitive radio channel is given in section "Hidden Markov Models."

If the primary user state process X is modeled as a Markov chain, the joint process (Y, X) is an HMM. In this case, the primary user sojourn times in the active and idle states are given by geometric distributions. We now introduce an underlying process S, taking values in $\mathbb{S} = \{0, 1, \ldots, r\}$, such that $Z = (X, S)$ is a bivariate Markov chain. In this case, the sojourn time of the process X in each state $a \in \{0, 1\}$ takes on a discrete-time phase-type distribution with r phases [38]. The trivariate process (Y, X, S) is then a hidden bivariate Markov chain. In the nomenclature of section "Bivariate Markov Chains," the conditional density of Y given $X = a$ is denoted by $g_{\theta_a}(y) = \mathcal{N}(\mu_a, \sigma_a^2)$, where $\mathcal{N}(\mu, \sigma^2)$ is the normal density with mean μ and variance σ^2. The parameter ϕ of the hidden bivariate Markov chain consists of the initial distribution of Z, denoted by $\boldsymbol{\pi}$, and the independent components of the generator of Z, denoted by H and $\{\theta_a; a \in \mathbb{X}\}$.

Assume that the parameter ϕ of the hidden bivariate Markov chain is given. The conditional probability of the bivariate state at time $t + \tau$ given the observations up

to and including time t can then be computed as follows (cf. [38, Eq. (22)]):

$$p_\phi(z_{t+\tau} \mid y^t) = \sum_{z_t \in \mathbb{Z}} p_\phi(z_k \mid y^t)\; p_\phi(z_{t+\tau} \mid z_t)$$
$$= \sum_{z_t \in \mathbb{Z}} \tilde{L}_{z_t}(t)\, [H^\tau]_{z_t, z_{t+\tau}}\,, \tag{33}$$

where $[H^\tau]_{ai,bj}$ denotes the $((a,i);(b,j))$ entry of the generator matrix given by H^τ. A detection scheme for the state of the primary user at time $t+\tau$ given the received signal power y^t is specified by (cf. [38, Eq. (23)]):

$$\hat{X}_{t+\tau|t} = \begin{cases} 0, \sum_s p_\phi(z_{t+\tau} = (0,s) \mid y^t) \geq \eta, \\ 1, \text{ otherwise}, \end{cases} \tag{34}$$

for $t = 0, 1, \ldots$, where η is a decision threshold, $0 < \eta < 1$. The detection scheme is a maximum a posteriori detector when $\eta = 0.5$. When $\tau = 0$, $\hat{X}_{t+\tau|t} = \hat{X}_{t|t}$ is an estimate of the current state X_t. When $\tau = 1, 2, \ldots$, $\hat{X}_{t+\tau|t}$ is the τ-step predicted estimate of the state $X_{t+\tau}$. The current and predicted state estimates $\hat{X}_{t+\tau|t}$ can be directly applied to make dynamic spectrum access decisions.

The parameter ϕ of the hidden bivariate Markov chain can be estimated offline from training data using the EM algorithm described in section "Estimation of the Bivariate Markov Chain Parameter"; see also [38]. A major advantage of online parameter estimation is that it can adapt to changes in the behavior of the primary user or the channel. An online approach to estimating the parameter, based on Rydén's recursive algorithm HMM parameter estimation, is developed in [48]. An alternative approach to online parameter estimation, based on the EM iteration discussed in section "Estimation of the Bivariate Markov Chain Parameter," is discussed in [19].

Collaborative Sensing

In radio environments with severe shadowing and fading effects, spectrum sensing by a single secondary user can lead to hidden terminal effects and other errors which can result in harmful interference to the primary users. Collaborative spectrum sensing techniques leverage multiuser diversity to improve sensing performance, particularly in severely shadowed environments with hidden terminals. Collaborative sensing involves multiple secondary users in a joint decision-making process to determine when a given channel is idle or active [30, 57]. Collaborative sensing schemes can be categorized into two main types: hard fusion and soft fusion. In this discussion, we review hard and soft fusion collaborative sensing and summarize the collaborative sensing schemes based on hidden bivariate Markov chain modeling developed in [49].

Hard Fusion

In a hard fusion scheme, at each time t, each secondary user q makes an independent decision, $X_{t|t}^{(q)}$, on the primary user state based on the observations $Y_1^{(q)}, \ldots, Y_t^{(q)}$. The 1-bit secondary user hard decisions are transmitted to the fusion center, which computes a final decision, denoted by $\hat{X}_{t|t}$, according to a hard fusion rule. For example, the "OR" rule decides that the primary user is active, i.e., state 1, if at least one of the secondary user hard decisions has the value 1. The "majority voting" rule decides that the primary user is active if more than half of the Q secondary user hard decisions have value 1. The OR rule and majority voting rule are special cases of the q-out-of-Q rule, where $1 \leq q \leq Q$ is an integer constant. Here, the primary user state is determined to be active if q or more of the individual hard decisions are "active"; otherwise, the primary user state is determined to be idle. The OR and majority voting rules are equivalent to the q-out-of-Q rule when $q = 1$ and $q = \lfloor Q/2 \rfloor$, respectively. The q-out-of-Q fusion rule is in turn a special case of linear hard fusion (cf. [41]). Under linear combining, the decision variable is computed as $V_t = \sum_{q=1}^{Q} w_q \hat{X}_{t|t}^{(q)}$, where the w_q are predetermined weights. The decision variable V_t is then compared to a threshold ψ to obtain the final decision $\hat{X}_{t|t}$. The q-out-of-Q fusion rule is a special case of linear hard fusion.

In conventional hard fusion schemes, each secondary user employs an energy detector to obtain a hard decision at each time t. Typically, a majority voting rule is applied at the fusion center. In the hard fusion scheme proposed in [49], each secondary user independently estimates the parameter of a hidden bivariate Markov chain to characterize the observed primary user signal on the channel. An estimator of the form (34) is employed to obtain a hard decision at the secondary user. The hard decisions are combined at the fusion center using a linear fusion rule proposed in [42] based on maximizing a so-called modified deflection coefficient.

Soft Fusion

In soft fusion, at each time t, the secondary users transmit quantized versions of their received signals $Y_t^{(1)}, \ldots, Y_t^{(q)}$, to the fusion center, where they are collectively used to predict the state of the primary user at time $t + \tau$ for some nonnegative integer τ. The state estimator is denoted by $\hat{X}_{t+\tau|t}$. For conventional fusion schemes that do not have predictive capability, $\tau = 0$. In a *linear* soft fusion scheme, a weighted sum, $V_t = \sum_{q=1}^{Q} w_q Y_t^{(q)}$, of the observations at time k is computed and compared to a threshold ψ as follows [33,41,42]:

$$\hat{X}_{t|t} = \begin{cases} 0, & V_t < \psi, \\ 1, & V_t \geq \psi, \end{cases} \tag{35}$$

where $w_1, \ldots, w_Q$ are the weights. Typically, the threshold and weights for soft fusion are computed offline [33,42].

In [48], at each time t, the observation sample $Y_t^{(q)}$ from each secondary user q is transmitted directly to the fusion center, which forms the vector observation sample $\boldsymbol{Y}_t = (Y_t^{(1)}, \ldots, Y_t^{(Q)})$. The soft fusion scheme is based on hidden bivariate Markov chain modeling of the *vector* observation sequence $\boldsymbol{Y} = \{\boldsymbol{Y}_t; t = 0, 1, \ldots\}$ generated by the Q secondary users. Here, the conditional output density parameter is given by $\boldsymbol{\theta} = (\boldsymbol{\theta}_a : a \in \mathbb{X})$, where $\boldsymbol{\theta}_a = (\theta_a^{(1)}, \ldots, \theta_a^{(Q)})$, and $\theta_a^{(q)}$ is the conditional output density parameter of each secondary user q when the primary user is in state a. With this definition of $\boldsymbol{\theta}$, the parameter ϕ of the hidden bivariate Markov chain is given by the independent elements of $(\pi, \boldsymbol{\theta}, H)$, where π is the initial state probability distribution and H is the generator of the underlying bivariate Markov chain.

Parameter estimation of the hidden bivariate Markov chain with vector observation input $\boldsymbol{Y}$ can be carried out at the fusion center using the EM approach discussed in section "Estimation of the Bivariate Markov Chain Parameter" by replacing the scalar sequence y^t with the vector sequence $\boldsymbol{y}^t$ and interpreting the parameter ϕ as discussed above. Similarly, state estimation can be performed via (34). The online parameter estimation approach in [48] can be extended to handle vector observation input, as described in [49].

Performance Comparison

Receiver operating characteristic (ROC) curves presented in [49] show a significant improvement in detection performance of collaborative sensing schemes based on the hidden bivariate Markov chain compared to conventional hard and soft fusion schemes based on energy detectors. In particular, the Markovian model-based soft fusion scheme performs markedly better than the linear soft fusion-based scheme proposed in [42]. Linear soft fusion performs better than the hard fusion scheme based on hidden bivariate Markov chain modeling, which in turn performs substantially better than conventional hard fusion based on energy detection. A disadvantage of soft fusion schemes is that they incur substantially higher communication overhead than the hard fusion schemes. This overhead can be reduced by quantizing the received signal strength values using a smaller number of bits at the expense of poorer detection accuracy, as proposed in [49]. Using a simple uniform quantization scheme, soft fusion based on the hidden bivariate Markov chain with 4-bit observation samples was shown to outperform linear soft fusion with 8-bit samples.

Multiband Sensing

In multiband spectrum sensing, the secondary user tracks the states of primary users operating on a given set of channels to determine spectrum access opportunities. The center frequency and bandwidth of each channel are assumed known. In a given sensing interval, the secondary user must allocate time for sensing each of

the channels. A Markovian model for multiband sensing was proposed by [50], in which each primary user on a given channel is modeled as a two-state homogeneous continuous-time Markov chain. Hence, the state of the primary user on each channel is assumed to be observable directly, or at least the signal-to-noise ratio is sufficiently high that sensing errors are negligible. The Markov chains corresponding to different primary users are assumed statistically independent. One of the basic issues in multiband sensing involves how much time should be allocated to sensing each channel.

To discuss this model further, let us assume there are M independent channels, each having the same bandwidth, but the primary user model parameters for the channels may be different. The parameter of each Markov chain is not known in advance and hence is estimated from observations of the state processes. In a given sensing interval of length T seconds, the secondary user senses each channel i for T_i seconds, where $\sum_{i=1}^{M} T_i = T$. In [50], the sensing times $\{T_i\}$ are determined by minimizing the Cramer-Rao lower bound on the minimum mean squared error in estimating the parameters of *all* M channels. An approximation for the inverse Fisher information matrix, asymptotic in the sensing interval length T, is used to obtain closed-form formulas for the MMSE sensing time allocations.

Since not all M channels may provide equally *good* secondary user spectrum access opportunities, allocating channel sensing times with the objective of minimizing the overall estimation error may not be optimal for dynamic spectrum access. In [8], a preprocessing step to determine the *best* $N < M$ channels, with respect to a criterion related to the spectrum opportunity on the channel, is performed first. The criterion used in [8] was based on the mean idle time on the channel. Then the approach of [50] is applied to the remaining N channels from the first step. The preprocessing step in [8] is based on the optimal computing budget allocation (OCBA) methodology [12] from the field of simulation optimization. The OCBA approach was originally developed to test multiple designs through simulation by allocating simulation time to the designs with the objective of maximizing the probability that the best design is selected according to a given cost function under a Gaussian model [13]. The technique was subsequently extended to determine the best $N > 1$ designs among a given set of M designs [14]. In the context of multichannel parameter estimation, sensing times are allocated rather than simulation times, and the multiple designs correspond to the multiple channels in multiband sensing.

A number of articles on multiband spectrum sensing have approached the problem as a type of multiarmed bandit problem [3,39,53,59] or the related partially observable Markov decision process (POMDP) [58]. Several assume knowledge of the parameters of the underlying Markov chains, but do not address the important issue of parameter estimation [3, 53, 58]. The multichannel parameter estimation algorithm proposed in [8] obtains estimates of this parameter and thus could, in principle, be used in conjunction with these approaches. Knowledge of the model parameter can be used to improve spectrum detection performance and allows the prediction of future primary user state, which provides clear advantages for spectrum sensing [38, 53].

Wideband Sensing

In the wideband spectrum sensing scenario, a secondary user must sense an entire band and determine channel boundaries. The bandwidth that must be sensed can vary from the order of 1 MHz to 1 GHz. This is required if the secondary user cannot leverage any external information about channel allocation. A secondary user need only perform wideband sensing during initialization and may then revert to multiband or narrowband sensing during normal operation. In general, primary user signals may be heterogeneous in frequency, bandwidth, and power, so robust wideband sensing algorithms must be developed to detect all primary user activity within the spectrum band.

State-of-the-art techniques for wideband sensing include wideband energy detection [9] and frequency-domain edge detection [51]. The wideband energy detector is a very simple wideband sensing technique in which the secondary user estimates the power spectral density over the entire band and applies an energy threshold to determine primary user activity [9,25]. Many power spectral density frames may be averaged to increase reliability. This simple algorithm has several limitations. Like all energy detectors in additive white Gaussian noise (AWGN), this technique has limited sensitivity, and performance is severely degraded at low SNR. Furthermore, this technique operates on a snapshot in time, and dynamic behavior of the primary user will degrade performance, since both the on and off cycles will be averaged into the power spectral density estimate.

Edge detectors can offer an improvement over energy detection in terms of SNR threshold, but they can also perform relatively poorly on signals with gradual roll-offs in their band edges. An alternative wideband spectrum sensing technique that has been studied in the literature employs frequency-domain edge detection to determine channel boundaries. A popular edge detection technique uses the continuous wavelet transform to decompose the edge detector into multiple resolutions and multiplies the resolutions together, which has a beneficial effect of reducing the noise [51]. While the edge detectors do offer an improvement over energy detectors in terms of SNR threshold, they come with several limitations. Most importantly, the edge detectors require that primary user signals have sharp transitions in the frequency domain. This allows them to work well with the rectangular spectra of OFDM and quadrature amplitude modulation (QAM) with low excess bandwidth, but edge detectors tend to fail on signals with gradual roll-offs on their band edges, such as QAM with large excess bandwidth and GMSK.

Neither energy detection nor edge detection alone takes into account the temporal dynamics of primary user signals and consequently can perform rather poorly when primary user signals have low duty cycles. In [6], a framework for wideband temporal spectrum sensing is proposed in which a given spectrum band is divided into smaller channels and modeled as a balanced binary tree. In [6], a sensing framework for reliable wideband detection of primary users with low duty cycle was developed. The approach, referred to as wideband temporal sensing, involves partitioning the given spectrum band into smaller subchannels. The energy in each subchannel is measured and an HMM-based spectrum sensing approach is applied

to each subchannel. A recursive tree search is performed to aggregate correlated subchannels into a set of independent narrowband channels, which effectively reduces the sensing task to the multiband case. The wideband temporal sensing approach developed in [6] allows primary user signals with low duty cycle to be detected accurately at high to moderate SNR. This approach was demonstrated to outperform both wideband energy and edge detection techniques particularly in the presence of dynamic primary user signals. In principle, the recursive tree search could be based on a hidden bivariate Markov chain in lieu of the HMM to provide more accurate modeling of the state sojourn times.

In [7], the wideband temporal sensing approach of [6] is extended to incorporate edge detection. In particular, the wavelet-based edge detection algorithm in [51] is incorporated into the wideband temporal sensing framework of [6]. The use of edge detection avoids the need for the recursive tree search used in the wideband temporal energy detector, resulting in a computationally more efficient spectrum sensing scheme. Moreover, the wideband temporal edge detector was shown to perform better in low SNR scenarios in the presence of primary user signals with sharp band edges, i.e., OFDM signals.

Research Challenges and Open Problems

In this section, we discuss future challenges and open research problems related to spectrum sensing using Markovian models.

Signal Feature vs. Energy Detection

In the Markovian model-based spectrum sensing techniques discussed in section "Spectrum Sensing Scenarios," the front end for spectrum sensing was assumed to be similar to that of an energy detector. The energy of the received signal samples was measured and used to perform parameter estimation of a hidden bivariate Markov chain, as well as detection and prediction of primary user spectrum usage. The energy-based front end could, in principle, be replaced by a front end that extracts certain features of the received signal. This could potentially improve the performance of Markovian-based spectrum sensing in low SNR scenarios.

Cyclic feature detection, for example, is based on computing the cyclic or cyclostationary spectrum of the received signal. Modulated signals are often readily identifiable based on their cyclic spectra. Therefore, cyclic feature detection has been proposed as an approach to spectrum sensing that has the potential to perform much better than energy detection or edge detection in low SNR scenarios [16, 31, 32]. A drawback of cyclic feature detection is the usual requirement to sample above the Nyquist rate to recover the cyclic spectrum. Furthermore, long sensing periods are typically required to obtain a statistically reliable estimate of the cyclic spectrum [24]. A cyclic feature detector also has much higher computational complexity compared to an energy detector. Nevertheless, practical implementation

of cyclic feature detection for spectrum sensing is the subject of ongoing research. Aside from the cyclic spectrum, other features of the received signal could be used to perform spectrum sensing based on Markovian models. For example, the cepstrum has been used successfully in speech recognition in conjunction with HMMs [21,43].

Multiband Sensing with Channel Impairments

Multiband sensing was discussed in section "Multiband Sensing" mainly in the context of determining appropriate sensing intervals for each channel, based on the framework of [50]. In [8,50], the primary user activity on each channel is modeled by a two-state continuous-time Markov chain in which the primary user state was assumed to be observed directly. In practice, the primary user state is observed only through the received signal, which is subject to channel impairments such as fading, shadowing, and additive white Gaussian noise. Therefore, it would be of interest to extend the approach to incorporate channel impairments. Some form of noise could be incorporated into the continuous-time Markov primary user state model. Alternatively, a multiband sensing approach based on the HMM or hidden bivariate Markov model in discrete time could be developed.

Multiuser Channels

In the temporal spectrum sensing scenarios discussed in section "Spectrum Sensing Scenarios," a single primary user was assumed to occupy a given narrowband channel. More generally, multiple primary users could share a given channel in a dynamic spectrum sensing scenario. In this case, the two-state Markov model discussed previously would not be sufficient to characterize the channel. One approach is to increase the number of states in the model. For example, if there were N distinct primary users sharing a channel, with different received signal characteristics, an $(N+1)$-state Markov channel could be used to model the channel. An alternative approach is to introduce a Gaussian mixture model for the primary user state. In this case, the Markov model would still consist of two states, i.e., an active and an idle state, but the conditional distribution in the active state would be governed by a mixture of N Gaussian random variables.

Wideband Sensing

The wideband temporal spectrum sensing approach discussed in section "Wideband Sensing" has limitations with respect to the spectrum bandwidth that can be sensed in a practical implementation. This approach could be extended to cover larger spectrum bands by partitioning the spectrum into smaller chunks and then employing high-performance hardware to implement wideband temporal sensing in

parallel over the spectrum chunks. However, for very wide spectrum bands, e.g., on the order of tens or hundreds of GHz, the required hardware may be too expensive in terms of actual cost and/or power consumption.

Detection of temporal spectrum hole opportunities over a wide spectrum band remains an open problem. In general, spectrum sensing over very wide spectrum bands requires prohibitively high sampling rates for current analog to digital converters. A drawback of cyclic feature detection is the usual requirement to sample above the Nyquist rate to recover the cyclic spectrum. Compressive sensing has been proposed as a technique to exploit the sparsity of primary user signal occupancy within a wide spectrum band. In [52], the inherent sparsity in the two-dimensional cyclic spectrum of communication signals is leveraged, and compressive sensing and sparse signal techniques are developed to recover the desired cyclic statistics with sub-Nyquist samples in a robust manner. Related work along these lines is reported in [36].

Wideband spectrum sensing techniques based on compressive sensing do not take into account the bursting nature of primary user signals, which may result in false detection of spectrum holes in the spectrum band. Moreover, compressive sensing techniques provide only a snapshot of primary user activity over the given spectrum and do not provide a mean of exploiting temporal spectrum hole opportunities. In principle, the primary user activity over the spectrum band during a given time slot could be characterized by a state, and the temporal dynamics could then be modeled using a Markov chain. Unfortunately, the number of states required for such a Markovian model would be infeasible for practical implementation.

A possible solution may involve a two-stage approach in which wideband sensing techniques such as those based on compressive sensing may be applied in the first stage to provide a rough picture of the spectrum occupancy at a given epoch. Portions of the spectrum may then be characterized as being idle, fully occupied, or partially occupied. In the second stage, the Markovian-based wideband temporal sensing approach may be applied to the portions of the spectrum deemed partially occupied based on the results of the first stage. A partially occupied spectrum band may be classified as such because of bursting primary user signal activity, or simply because of a weak primary user signal. In the former case, temporal spectrum hole opportunities may exist, whereas in the latter case, a spatial spectrum hole opportunity may exist. Clearly, these cases must be treated differently in a dynamic spectrum access or dynamic spectrum sharing systems.

Resource Allocation

In this chapter, we have focused on Markovian-based spectrum sensing methods to detect and predict spectrum hole opportunities in the settings of a narrowband channel, a multiband scenario, and a wideband scenario. Emphasis has been placed on estimating the parameter of a Markovian model to characterize primary user occupancy in a given spectrum band. Given an estimate of the model parameter, detection and prediction of the primary user state for spectrum sensing follows

from the Markovian model. On the other hand, we have not discussed the important issue of how to allocate harvested spectrum resources to the secondary users. In the language of multiarmed bandit problems, our focus has been on *exploration* rather than *exploitation* of the spectrum.

The spectrum sensing techniques we have discussed may be employed by a spectrum monitoring service. In this scenario, the secondary users may contribute observation data to the spectrum monitoring service, but they do not make the spectrum sensing decisions per se. The secondary users access the spectrum holes by making requests to the spectrum monitoring service. In this way, exploration of the spectrum is decoupled from its exploitation by secondary users. In this setting, the spectrum monitoring service is responsible both for making spectrum sensing decisions and spectrum allocation decisions to the secondary users. An interesting problem requiring further research is how the Markovian characterization of primary user spectrum occupancy can be leveraged to perform spectrum allocation to secondary users in an efficient manner. In the multiband scenario, for example, when multiple channels are detected to be idle, a secondary user requesting a channel for dynamic spectrum access may be assigned the best channel with respect to some criterion such as the expected sojourn time in the idle state. Such resource allocation could also depend on further information provided by the secondary user, for example, the expected length of time that the channel would be needed. Furthermore, the transmission requirements of secondary users may play a role in which portions of the spectrum are sensed by the spectrum monitoring service.

The presence of a spectrum monitoring service effectively decouples the exploration task from the exploitation task in dynamic spectrum access or sharing. When the secondary users are responsible for both tasks, an important trade-off between exploration and exploitation arises. As discussed in section "Background and Overview of Related Work," several works in the literature have addressed this issue by modeling the dynamic spectrum access problem as POMDP or multiarmed bandit problem. These problems are formulated in a multiband setting in which the the underlying model of primary user activity for a given channel is assumed to be Markovian. A given secondary user must decide, in a given time slot, whether to perform sensing, i.e., explore, or to access a channel, i.e., exploit. If it decides to explore, the secondary user must further decide which channel or channels to sense. Similarly, if it decides to exploit, the secondary user must decide which channel or channels to exploit. In the POMDP formulations, the parameter of the underlying Markov process is assumed to be known either a prior or via parameter estimation. In the multiarmed bandit formulations, usually full knowledge of the parameter is not needed.

In the OCBA-based approach to multiband sensing proposed in [8], the N *best* channels out of a total M channels is selected, based on a parameter estimation process. In the context of a secondary user implementing a POMDP or multiarmed bandit approach to joint sensing and resource allocation, this approach is particularly beneficial when $N \ll M$. Reducing the number of channels under consideration from N to M can have a significant impact on the computational burden. Moreover, the parameter estimates for the M channels can be used in both the POMDP and

multiarmed bandit approaches. It would be of interest to investigate further the role that parameter estimation could play with respect to the exploration/exploitation trade-off in the multiband setting.

Conclusion

In this chapter, we have discussed the application of Markovian models to spectrum sensing in cognitive radio networks. The focus of the chapter has been on the formulation of the Markovian models, parameter estimation, and detection/prediction of primary user activity in a given spectrum band based on knowledge of the model parameter. We provided an overview of background material and related work on spectrum sensing using Markovian models. We reviewed relevant Markovian models for spectrum sensing, primarily in discrete time, including Markov chains, hidden Markov models, and multivariate Markov chains. We also reviewed parameter estimation techniques for these models, particularly the Baum algorithm. We then discussed the application of Markovian-based spectrum sensing in the three progressively more difficult settings of narrowband, multiband, and wideband sensing. Finally, we discussed some interesting issues and open problems for further research on spectrum sensing using Markovian models.

Acknowledgements This work was supported in part by the US National Science Foundation under Grants CNS-1421869 and AST-1547329.

References

1. Akbar IA, Tranter WH (2007) Dynamic spectrum allocation in cognitive radio using hidden Markov models: poisson distributed case. In: Proceedings 2007 IEEE SoutheastCon, pp 196–201
2. Albert A (1962) Estimating the infinitesimal generator of a continuous time, finite state Markov process. Ann Math Stat 23(2):727–753
3. Bagheri S, Scaglione A (2015) The restless multi-armed bandit formulation of the cognitive compressive sensing problem. IEEE Trans Signal Process 63(5):1183–1198
4. Ball FG, Rice JA (1992) Stochastic models for ion channels: introduction and bibliography. Math Biosci 112:189–206
5. Bertsekas DP, Tsitsiklis JN (2008) Introduction to probability, 2nd edn. Athena Scientific, Belmont
6. Bruno JM, Mark BL (2015) A recursive algorithm for joint time-frequency wideband spectrum sensing. In: 2015 IEEE Wireless Communications and Networking Conference Workshops (WCNCW), pp 235–240
7. Bruno JM, Mark BL, Tian Z (2016) An edge detection approach to wideband temporal spectrum sensing. In: IEEE Global Communications Conference (GLOBECOM), pp 1–6
8. Bruno JM, Mark BL, Ephraim Y, Chen C-H (2017) An edge detection approach to wideband temporal spectrum sensing. In: IEEE Wireless Communications and Networking Conference (WCNC), pp 1–6
9. Cabric D, Mishra S, Brodersen R (2004) Implementation issues in spectrum sensing for cognitive radios. In: Conference Record of the Thirty-Eighth Asilomar Conference on Signals, Systems and Computers, vol 1, pp 772–776

10. Çinlar E (1975) Markov renewal theory: a survey. Manage Sci 21(7):727–752
11. Çinlar E (2013) Introduction to stochastic processes. Dover Publications, Mineola/New York. Reprint of 1975 edition published by Prentice-Hall
12. Chen CH, Lee LH (2010) Stochastic simulation optimization: an optimal computing budget allocation. World Scientific Publishing Co., Singapore
13. Chen C-H, Lin J, Yücesan E, Chick SE (2000) Simulation budget allocation for further enhancing the efficiency of ordinal optimization. Discret Event Dyn Syst 10(3):251–270
14. Chen C-H, He D, Fu M, Lee LH (2008) Efficient simulation budget allocation for selecting an optimal subset. INFORMS J Comput 20(4):579–595
15. Dempster AP, Laird NM, Rubin DB (1977) Maximum likelihood from incomplete data via the EM algorithm. J R Stat Soci Ser B 39(1):1–38
16. Dobre OA, Rajan S, Inkol R (2009) Joint signal detection and classification based on first-order cyclostationarity for cognitive radios. EURASIP J Adv Signal Process (7). Special issue on dynamic spectrum access for wireless networking. http://dl.acm.org/citation.cfm?id=1661353
17. Ephraim Y (1992) Statistical model based speech enhancement systems. Proc IEEE 80: 1526–1555
18. Ephraim Y, Mark BL (2013) Bivariate Markov processes and their estimation. Found Trends Signal Process 6(1):1–95
19. Ephraim Y, Mark BL (2015) Causal recursive parameter estimation for discrete-time hidden bivariate Markov chains. IEEE Trans Signal Process 63:2108–2117
20. Ephraim Y, Merhav N (2002) Hidden Markov processes. IEEE Trans Inf Theory 48(6): 1518–1569
21. Ephraim Y, Rahim M (1999) On second order statistics and linear estimation of cepstral coefficients. IEEE Trans Acoust Speech Signal Process 7:162–176
22. FCC (2002) Spectrum policy task force. Technical report 02-135, Rep. ET Docket, Federal Communications Commission
23. Frost VS, Melamed B (1994) Traffic modeling for telecommunications networks. IEEE Commun Mag 32(3):70–81
24. Gardner W (1991) Exploitation of spectral redundancy in cyclostationary signals. IEEE Signal Process Mag 8(2):14–36
25. Hayes MH (1996) Statistical digital signal processing and modeling, 1st edn. Wiley, New York
26. Haykin S (2005) Cognitive radio: brain-empowered wireless communications. IEEE J Sel Areas Commun 23(2):201–220
27. Heffes H, Lucantoni D (1986) A Markov modulated characterization of packetized voice and data traffic and related statistical multiplexer performance. IEEE J Sel Areas Commun 4(6):856–868
28. Kemeny JG, Snell JL (1983) Finite Markov chains, 3rd edn. Springer, New York
29. Lancaster P, Tismenetsky M (1985) The theory of matrices, 2nd edn. Academic Press, Orlando
30. Leu AE, McHenry M, Mark BL (2006) Modeling and analysis of interference in listen-before-talk spectrum access schemes. Int J Netw Manage 16(2):131–147
31. Lunden J, Koivunen V, Huttunen A, Poor HV (2009) Collaborative cyclostationary spectrum sensing for cognitive radio systems. IEEE Trans Signal Process 57(11):4182–4195
32. Lunden J, Kassam SA, Koivunen V (2010) Robust nonparametric cyclic correlation-based spectrum sensing for cognitive radio. IEEE Trans Signal Process 58(1):38–52
33. Ma J, Zhao G, Li Y (2008) Soft combination and detection for cooperative spectrum sensing in cognitive radio networks. IEEE Trans on Wirel Commun 7(11):4502–4507
34. Mark BL, Leu AE (2007) Local averaging for fast handoffs in cellular networks. IEEE Trans Wirel Commun 6(3):866–874
35. Mark JW, Zhuang W (2003) Wireless communications and networking. Pearson Education, Inc., Piscataway
36. Mishali M, Eldar YC (2011) Wideband spectrum sensing at sub-Nyquist rates. IEEE Signal Process Mag 28(4):102–135
37. Neuts MF (1981) Matrix-geometric solutions in stochastic models. Johns Hopkins University Press, Baltimore

38. Nguyen T, Mark BL, Ephraim Y (2013) Spectrum sensing using a hidden bivariate Markov model. IEEE Trans Wirel Commun 12(9):4582–4591
39. Oksanen J, Koivunen V, Poor HV (2012) A sensing policy based on confidence bounds and a restless multi-armed bandit model. In: 2012 Conference Record of the Forty Sixth Asilomar Conference on Signals, Systems and Computers (ASILOMAR), pp 318–323
40. Park CH, Kim SW, Lim SM, Song MS (2007) HMM based channel status predictor for cognitive radio. In: 2007 Asia-Pacific Microwave Conference, pp 1–4
41. Peh E, Liang Y-C, Guan YL, Zeng Y (2010) Cooperative spectrum sensing in cognitive radio networks with weighted decision fusion schemes. IEEE Trans Wirel Commun 9(12): 3838–3847
42. Quan Z, Ma W-K, Cui S (2008) Optimal linear cooperation for spectrum sensing in cognitive radio networks. IEEE J Sel Top Signal Process 2(1):28–40
43. Rabiner LR (1989) A tutorial on hidden Markov models and selected applications in speech recognition. Proc IEEE 77:257–286
44. Rydén T (1997) On recursive estimation for hidden Markov models. Stoch Process Appl 66(1):79–96
45. Shared Spectrum Company (2010) General survey of radio frequency bands: 30 MHz to 3 GHz. Technical report
46. Stiller JC, Radons G (1999) Online estimation of hidden Markov models. IEEE Signal Process Lett 6(8):213–215
47. Sun Y, Mark BL (2013) Interference model for spectrum sensing with power control. In: Proceeding of Conference on Information Science and Systems (CISS), Baltimore, pp 1–6
48. Sun Y, Mark BL, Ephraim Y (2015) Online parameter estimation for temporal spectrum sensing. IEEE Trans Wirel Commun 14(8):4105–4114
49. Sun Y, Mark BL, Ephraim Y (2016) Collaborative spectrum sensing via online estimation of hidden bivariate Markov models. IEEE Trans Wirel Commun 15(8):5430–5439
50. Tehrani P, Tong L, Zhao Q (2012) Asymptotically efficient multi-channel estimation for opportunistic spectrum access. IEEE Trans Signal Process 60(10):5347–5360
51. Tian Z, Giannakis GB (2006) A wavelet approach to wideband spectrum sensing for cognitive radios. In: Proceedings of 1st International Conference on Cognitive Radio Oriented Wireless Networks and Communications (CROWNCOM), pp 1–5
52. Tian Z, Tafesse Y, Sadler BM (2012) Cyclic feature detection from sub-Nyquist samples for wideband spectrum sensing. IEEE J Sel Top Signal Process 6(1):58–69. Special Issue on Robust Measures and Tests Using Sparse Data for Detection and Estimation
53. Wang K, Chen L, Liu Q, Wang W, Li F (2015) One step beyond myopic probing policy: a heuristic lookahead policy for multi-channel opportunistic access. IEEE Trans Wirel Commun 14(2):759–769
54. Wu FCJ (1983) On the convergence properties of the EM algorithm. Ann Stat 11(1):95–103
55. Yu S-Z (2010) Hidden semi-Markov models. Artif Intell 174(2):215–243
56. Yucek T, Arslan H (2009) A survey of spectrum sensing algorithms for cognitive radio applications. IEEE Commun Surv Tuts 11(1):116–130
57. Zhang W, Mallik RK, Letaief KB (2009) Optimization of cooperative spectrum sensing with enrgy detection in cognitive radio networks. IEEE Trans Wirel Commun 8(12):5761–5766
58. Zhao Q, Tong L, Swami A, Chen Y (2007) Decentralized cognitive MAC for opportunistic spectrum access in ad hoc networks: a POMDP framework. IEEE J Sel Areas Commun 25(3):589–600
59. Zhao Q, Krishnamachari B, Liu K (2008) On myopic sensing for multi-channel opportunistic access: structure, optimality, and performance. IEEE Trans Wirel Commun 7(12):5431–5440

Waveform Designs for Cognitive Radio and Dynamic Spectrum Access Applications

3

Ahmet Yazar, Mohamed Elkourdi, and Huseyin Arslan

Contents

Abstract

Cognitive radio and dynamic spectrum access systems are effective ways of using radio spectrum which is a scarce source. Cognitive radio applications changed the

A. Yazar (✉)
Department of Electrical and Electronics Engineering, Istanbul Medipol University, Istanbul, Turkey
e-mail: ayazar@medipol.edu.tr

H. Arslan
Department of Electrical and Electronics Engineering, Istanbul Medipol University, Istanbul, Turkey

Department of Electrical Engineering, University of South Florida, Tampa, FL, USA
e-mail: arslan@usf.edu; huseyinarslan@medipol.edu.tr

M. Elkourdi
Department of Electrical Engineering, University of South Florida, Tampa, FL, USA
e-mail: elkourdi@mail.usf.edu

W. Zhang (ed.), *Handbook of Cognitive Radio*,
https://doi.org/10.1007/978-981-10-1394-2_3

paradigm for the wireless communications systems in the past decades. Besides that, different communications systems and wireless communications channels require different waveform designs and radio access technologies. In this study, a general design and evaluation procedure for the new waveform techniques are presented based on cognitive radio and dynamic spectrum access requirements. Radio access technology researches for the future-generation cellular systems and cognitive radio systems intersect to each other. Therefore, some of the future waveform designs and related modifications are analyzed under the cognitive radio perspective. Several waveforms which have various trade-off situations are discussed from a general perspective and an adaptivity/flexibility perspective.

Introduction

Cellular communications systems have seen a huge growth of data usage in the past decades. In parallel, cognitive radio (CR) and dynamic spectrum access (DSA) systems are developed to create alternative ways of using radio spectrum efficiently for the wireless communications systems. CR and DSA systems provide spectrally efficient solutions by exploiting the unused but licensed radio spectrum, while primary users (licensed users, LUs) are not using the same frequency bands because the radio spectrum is generally underutilized [1]. By this way, frequency spectrum can be utilized efficiently. CR and DSA applications changed the paradigm in the wireless communications system development.

The performance of a wireless communications system depends on the radio access technology (RAT). Different parameters such as the compactness of symbols (localization) which are in time-frequency plane and the robustness issues against channel impairments are determined by the RAT. Also, it has to overcome the new challenges and problems which come with the new-generation systems including decreasing the out-of-band (OOB) emission, increasing spectral efficiency, enabling asynchronous communications, decreasing latency, and decreasing complexity. Different communications systems and wireless channels require different waveform designs and different RATs [2, 3].

Orthogonal Frequency Division Multiplexing (OFDM) has been popularly used in broadband wireless and wired communications systems, but it suffers from several limitations such as high spectral leakage, large peak-to-average power ratio (PAPR), and strict synchronization requirements and is not considered a strong waveform candidate to be used in future communications systems [2, 4]. Generally, existing new waveform designs aim to decrease OOB leakage and increase spectral efficiency compared to OFDM technique which is taken as a reference waveform in most of the waveform studies. However, computational complexity is an important problem for most of the new waveforms. Because of that, modified OFDM methods are also very important in new waveform researches because their complexities are generally low. Today, RAT researches for the future-generation cellular systems and CR systems can intersect to each other. Hence, the future waveform designs need to be analyzed also for CR and DSA systems.

The main goal of this chapter is to provide a general design and evaluation procedure that allows the reader to tailor new waveform techniques based on CR and DSA requirements.

This book chapter is organized as follows: Requirements for CR and DSA systems are given in section "Requirements for Cognitive Radio and Dynamic Spectrum Access". Advantages and disadvantages of OFDM for the CR and DSA applications are presented in section "OFDM for Cognitive Radio". New waveforms beyond OFDM from the general and adaptivity perspectives are explained in sections "Beyond OFDM from Dynamic Spectrum Access Perspectives" and "Beyond OFDM for Adaptation and Flexible Utilization of Various Resources". Finally, in section "Conclusion and Future Directions", future work and concluding remarks are given.

Requirements for Cognitive Radio and Dynamic Spectrum Access

CR and DSA systems need flexible and adaptable physical layer design to provide spectrally efficient solutions. By this perspective, requirements for the opportunistic usage of the underutilized spectrum by CR and DSA applications are given in this section to understand the relationship between the relevant requirements and waveform design parameters better.

As a fundamental requirement, CR systems need to have the ability to utilize scattered and narrow spectrum opportunities. Available signal bandwidth which is a very broadband is divided into smaller bands to exploit the narrow spectrum opportunities for the multiband signaling approach, and it enables better spectrum allocation. On the contrary, the single broadband signaling approach is not preferred for the CR and DSA systems because it is not a spectrally efficient solution. If single broadband signaling approach is employed, fractional frequency usage cannot be maintained and many subcarriers might be deactivated. Hence, single-carrier waveform designs do not fulfill the fundamental requirement of CR and DSA systems. When the multiband signaling approach is considered, the portion of the time and spectrum resources need to be dynamically turned on and off. Multicarrier waveform signals can be shaped adaptively in time and frequency by deactivating a set of subcarriers where primary users exist. To activate/deactivate the subcarriers dynamically, suitable algorithms need to be employed like FFT/IFFT to provide a flexible waveform design.

Spectrum powers of subcarriers leak to adjacent nulled subcarriers especially while activating/deactivating the subcarriers dynamically. This type of situations causes mutual interference to LUs, and it is desired to provide minimal OOB leakage to prevent the interference. There are many techniques to minimize OOB emission in the literature given in the next sections of this chapter. Additionally, orthogonality between subcarriers and user synchronization to the receiver are also important concepts for the CR waveform design.

As another requirement, parameters of the waveform need to be changed on the fly in real time. Waveform parameters such as center frequency, signal bandwidth,

power levels of subcarriers, FFT size, subcarrier spacing, cyclic prefix (CP) size, modulation type and order, coding, etc. should be adaptable and controllable for different wireless channel environments and user requirements. Therefore, CR and DSA systems need highly flexible waveform designs. They need to sense the opportunity in frequency domain while utilizing the spectrum. Actually, CR must sense and exploit the spectrum holes very fast and efficiently. Because of that, awareness of the radio channel characteristics is a critical issue. Besides, the computational complexity of the sensing algorithms should be reduced to provide this awareness. Computationally efficient FFT/IFFT operations are very helpful for the spectrum sensing algorithms in the frequency domain. Simple one-tap frequency domain equalizers are more suitable for the CR and DSA applications in respect to computational complexity requirements. Additionally, minimal latency is another requirement for the CR waveform designs because transmission parameters need to be changed very fast.

In section "OFDM for Cognitive Radio", all requirements given in this section are analyzed considering the OFDM technique as a CR and DSA waveform.

OFDM for Cognitive Radio

OFDM can be thought of as a candidate for the physical layer transmission technology in CR because of its flexibility and adaptivity aspects [1]. OFDM has its wide range of pros and some cons that should be taken into account. In this section, a brief summary of the pros and cons when using OFDM as a physical layer technology for CR systems is provided. The pros of using OFDM as the physical layer technology in CR can be described as follows:

- The process of sensing the spectrum can be done quickly and efficiently using OFDM as the physical layer for CR. OFDM inherently uses the IFFT block to perform the conversion from the frequency domain to the time domain. Therefore, the process of scanning the time-frequency grids, looking for untapped resources, can be done by just reusing the IFFT block at the transmitter, without the need of any supplementary hardware or computation.
- CR shares the system bandwidth with LUs of narrowband. The LUs can operate on a predefined bands or operate at any location of the bands that CR could be operating on causing an interference from and to the LUs. OFDM can avoid this problem by enabling the fractional bandwidth (FBW) mode, where it can deactivate some of the subcarrier by transmitting zeros at that portion of the IFFT block.
- OFDM can adaptively shape its spectrum to fit within the required spectrum mask by simply turning off some of the subcarrier from the IFFT block.
- OFDM provides a high degree of flexibility through the wide range of parameters it has, which can be adjusted accordingly to adapt its waveform to different situations [5]. It can adaptively change the modulation order, the power transmitted for each subcarrier, and the coding according to the channel quality and the user's

need [6]. This adaptation can be performed to serve different design targets, such as lowering the bit error rate (BER), enhancing the system's throughput, controlling the interference, extending the user's battery life or increasing the coverage. OFDM systems also have the flexibility to adaptively change the subcarrier spacing to maintain it less than the coherence bandwidth; thus, the equalization process at the receiver can be done by simple one-tap equalizer. Furthermore, the subcarrier spacing can be adaptively adjusted to reduce the inter-carrier interference (ICI) caused by Doppler spread [7]. Also, OFDM systems deal elegantly with the inter-symbol interference (ISI) caused by the multipath channel effect by appending a CP to each OFDM symbol, the CP duration needs to be larger than maximum channel delay spread to eliminate any ISI that could happen. In OFDM, the CP duration can also be adaptively adjusted according to each user's channel to cope with the amount of ISI observed by each user's channel and maximize the total system throughput.

- In multiuser CR radio scenario, the resources need to be shared and accessed by different users. There are many access technologies that can perform this task in different ways. OFDM supports many access technologies such as Frequency Division Multiple Access (FDMA), Time Division Multiple Access (TDMA) and Carrier Sense Multiple Access (CSMA). Also, OFDM can be combined with Code Division Multiple Access (CDMA) technology, where this transmission is called Multicarrier Code Division Multiple Access (MC-CDMA) or multicarrier Direct Spread Code Division Multiple Access (DS-CDMA). OFDMA, which is an extension of FDM for the multiuser case, is also considered as flexible access technique that can be used for CR. In Orthogonal Frequency Division Multiple Access (OFDMA), the subcarrier of each user (unlicensed user or renter) can either be grouped into a cluster of adjacent subcarriers or to be interleaved among other user's subcarrier according to the availability of free spectrum.
- Since OFDM has been implemented in many of the standards such as WLAN (IEEE 208.11), WMAN (IEEE 802.16), WRAN (IEEE 802.22), and WPAN (IEEE 802.15.3a). This brings another key advantage which is referred to as the interoperability.

On the other hand, OFDM has some limitation when it is considered as the physical layer for CR. OFDM cons can be described as follows:

- The OFDM modulated subcarriers have the sinc shape that is considered to have large sidelobes in both sides. The presence of the large sidelobes of the OFDM signal results in an interference in the adjacent subcarrier. Many techniques have been proposed to lower the power leakage to enable the coexistence of CR-OFDM systems with the primary users.
- In single band CR-OFDM systems, after searching for an available free portion of the spectrum, one OFDM signal can be transmitted over the available free parts of the spectrum. Then by shaping the OFDM spectrum, CR can avoid interfering with the LUs operating on the same band because OFDM is a multiband approach. Although using single broadband transmission approach facilities the

system design, it requires high-speed analog to digital converter (ADC) to be able to sample the wide band signal. On the other hand, the implementation of wideband multiband OFDM system includes the need for a wide range of frequency synthesizer, broadband TX/RX switch at the antenna and fast band hopping to avoid interference to the occupied bands.

- Synchronization is one of the fatal issues that should be taken care of when designing any OFDM system. In CR, a narrow band interference (NBI) can interfere with the preamble sequence causing a synchronization problem [8]. Also, pilots could fall into the place of the unused subcarriers which can also cause a synchronization problem. Therefore, to keep the orthogonality between subcarrier and to avoid the ICI, all users should be synchronized to the receiver. Adding longer preambles to CR-OFDM compared to conventional systems is proposed as a solution [8].

Beyond OFDM from Dynamic Spectrum Access Perspectives

In the previous sections, it is mentioned about that the future-generation cellular system and CR requirements can intersect to each other. Existing new waveform designs generally aim to decrease OOB leakage and increase spectral efficiency compared to OFDM technique which is taken as a reference waveform in most of the studies. However, computational complexity is an important problem for most of the new waveforms. Because of that, modified OFDM methods are also very important in fifth-generation (5G) waveform researches as analyzed in section "Sidelobe Suppression Techniques". And, new multicarrier waveforms beyond OFDM are discussed from a general perspective under two main groups: Orthogonal waveforms in section "New Waveforms" and non-orthogonal waveforms section "Non-orthogonal Waveforms".

Sidelobe Suppression Techniques

Based on the advantages and disadvantages of OFDM, which are given in section "OFDM for Cognitive Radio", there are various modification methods to overcome some drawbacks of OFDM. The most important and widely used modifications are related to the sidelobe suppression techniques. OFDM can be employed in a better way especially for CR applications by using these sidelobe suppression methods. In this subsection, various sidelobe suppression techniques are presented under a common umbrella.

There are too many different sidelobe suppression approaches in the literature. Their performances change according to the various trade-off situations which are generally originated from the amount of spectral leakage, computational complexity performance, and BER performance. Among these performance metrics, if the spectral leakage is not handled, the high spectral sidelobes can create severe adjacent

channel interference (ACI) problems. Superiorities and drawbacks of these sidelobe suppression techniques differ.

Time windowing techniques are known as the computationally efficient way for the sidelobe suppression [9–11]. They modify the shape of OFDM symbols to suppress sidelobes. Generally, the guard interval is increased while windowing the time domain OFDM symbols and spectral efficiency is decreased because of these guard intervals. In one similar time domain approach called as adaptive symbol transition (AST) [12], the OFDM symbols are extended in time like in the windowing technique, but the transition signal is optimized adaptively to minimize ACI. By this way, spectral efficiency can be increased in exchange for the computational complexity. Rather than windowing techniques, there are also some filtering methods in the literature; however, they usually increase the computational complexity and cause long delays while employing filtering operations [12].

For the frequency domain approaches, active interference cancellation (AIC) [13] and cancellation carriers (CC) [14] are two techniques which smooth the sharp transitions between OFDM symbols. They reduce interference to white spaces and provide high spectral efficiency. However, these methods are known as computationally complex techniques. For example, calculation of cancellation carrier values increases the complexity. Subcarrier weighting (SW) [15], constellation adjustment (CA) [16], and constellation expansion [17] are other schemes which include an extension for the OFDM symbols in time. SW technique multiplies all subcarriers in specific weights to reduce the sidelobe powers.

A precoder for shaping the spectrum of OFDM is given under mask compliant precoder (MCP) technique [18] which aims to control the OOB emission levels without impacting the BER performance. There are also different precoder methods like N-continuous precoder (NCP) [19], least square notch precoder (LSNP) [20], and orthogonal precoder (OP) [21]. For NCP technique, OFDM signals are constructed by precoder that renders the phase and amplitude of the emitted signal and this method leaves the effective length of the CP unchanged. BER performance of the NCP method is low compared to conventional OFDM. Generalization of the N-continuous method with using more degrees of freedom is achieved by enabling disturbance-free data subcarriers at the receiver [22]. LNSP scheme is introduced as a spectrum-sculpting and linear precoder that suppresses the power in predefined parts of the related spectrum flexibly. The computational complexity of this method is low because of the notching process. In OP technique, N-continuous OFDM signals are realized as an orthogonal multiplex to increase BER performance compared to other precoder methods.

One of the low-complexity techniques is sidelobe suppression with orthogonal projection (SSOP) which is based on orthogonal projection matrix and uses one reserved subcarrier for recovering the distorted signal in the receiver [23]. In this method, ISI between the symbols can be removed in the absence of noise by using the reserved subcarriers. Another sidelobe suppression method is multiple choice sequences (MCS), and it is based on the idea that transforming the original transmit sequence into a set of sequences [24]. After that, the sequence with the lowest sidelobe power is chosen.

There are also various joint PAPR and OOBE reduction methods in the literature [25, 26]. And, instead of the sidelobe suppression techniques, there are also new waveform designs which can be considered as waveform candidates of 5G and beyond cellular systems. In sections "New Waveforms" and "Non-orthogonal Waveforms", some of these approaches are analyzed from a general perspective.

New Waveforms

Current waveforms all have various positive and negative properties which push the research for new waveforms [27]. Optimization of any parameter results in losses in other parameters. This game of trade-offs has not converged to a fully optimal solution yet [2]. The proposed waveforms are usually benchmarked against OFDM.

As mentioned in section "OFDM for Cognitive Radio", OFDM has the following advantages: It has low computational complexity due to the FFT algorithms, adjustable bandwidth, simple equalization, and good coupling with multi-input multi-output (MIMO) systems. The disadvantages of OFDM are high PAPR, synchronization requirement between users, sensitivity against time and frequency shifts, and high level of OOBE.

The high OOBE problem limits the OFDM in the framework of new cognitive radio systems. Most of the new waveforms are generally better than OFDM with respect to their OOB leakage amounts. However, they generally have some computational complexity problems compared to OFDM or modified OFDM methods.

Some of the new waveforms proposed to address challenges associated with 5G and beyond include filtered OFDM (f-OFDM) [28], universal filtered multicarrier (UFMC) (aka universal filtered OFDM, UF-OFDM) [29], and unique word OFDM (UW-OFDM) [30]. These waveform designs are backward compatible because the main structure of the OFDM frame is maintained. However, some other waveform designs do not have the same frame structure such as FBMC [31,32] and generalized frequency division multiplexing (GFDM) [33]. FBMC and GFDM are analyzed under non-orthogonal waveforms in section "Non-orthogonal Waveforms". Additionally, some waveform techniques are analyzed from an adaptivity perspective in section "Beyond OFDM for Adaptation and Flexible Utilization of Various Resources".

As mentioned previously, filtering and windowing methods can be used to suppress the sidelobes after pulse shaping. At the transmitter, the OOB emission levels are suppressed when the windowing technique is applied. Suppressing the OOB emission levels reduces the interference among adjacent channels and provides better adjacent channel leakage power ratio. Alternatively, different-length filters can be applied either to a group of subcarriers or to all the subcarriers for one OFDM frame in f-OFDM and UF-OFDM techniques. Besides, the windowing technique helps to reduce the interference between the users within one band by lowering the in-band emissions at the receiver.

In f-OFDM, a different number of subcarriers are grouped into subbands for different users and applications. Based on these subbands, the appropriate IFFT, different length CP addition and filtering operations are performed [28]. Filters are designed to reduce OOBE. However, these operations destroy the orthogonality between the subbands and may cause inter-user interference. Some other details related with the adaptivity of f-OFDM are presented in section "Filtered OFDM with an Adaptivity Perspective".

In UFMC, subcarriers are grouped in subbands, and these subbands are filtered with either the same filter or different filter functions. IFFT is performed to each subband separately and zero guard (ZG) is added afterward in place of CP [29]. UFMC has less OOBE and higher spectral efficiency when compared to CP-OFDM due to the filtering performed.

Conventional pulse shaping and filtering may not be sufficient to meet the needs of a wide range of transmitted and received signals. Additional processing on top of grid design, filtering, and pulse shaping can be used to modify the signal and its structure to optimize the waveform design. For example, unique word (UW) [30] and zero tail (ZT) [34] have been proposed for future-generation wireless communications systems which can be considered as pre/post processes. These techniques aim to deal with disadvantages of the hard-coded CP.

The pre- and post-processing techniques may have purposes such as easing the equalization [34,35], reducing spectral leakage emission [18], reducing PAPR [36], improving physical layer security [37], and even joint goals [38]. Structural or adaptive processing techniques are used to improve different aspects of the wireless communications system that cannot be solved only by filtering and lattice design. They can be gathered under the pre- and post-processing at transmitter and receiver, respectively.

In CP-OFDM, CP is used to prevent ISI between consecutive symbols and eases the frequency domain equalization by transforming the linear convolution of transmitted OFDM symbols to a circular convolution. In UW-OFDM, the UW process improves the aforementioned gains by placing the same known sequence between all consecutive symbols [30]. Since the sequence is known, it can be used for the synchronization, and channel estimation can be done at the receiver. Also, it eliminates the need for dedicated pilot subcarriers used in CP-OFDM. Compared to CP-OFDM, UW-OFDM trades off a gain in OOBE with increased computational complexity.

The inflexibility of the duration of hard-coded CP is another disadvantage of CP-OFDM. If CP length is longer than required duration, resources are not used efficiently. Otherwise, it causes an insufficient mitigation against ISI. In zero-tail DFT-spread OFDM (ZT DFT-s OFDM), the ZT procedure generates low power samples, which are called as tails, inside the FFT duration, and they are adjusted according to different channel delay spreads to increase spectral efficiency [34]. This conserves the same total symbol duration even with different guard durations. For 5G heterogeneous networks operating over different frame structures and different symbol lengths, the usage of flexible guard time becomes a promising

feature, making ZT DFT-s OFDM a candidate. The drawback is the uncontrollable ISI in the case of unusually long delay spreads.

By the way, from the CR design perspectives, multicarrier waveform methods need to be discussed rather than single-carrier methods. There are various single-carrier waveform methods especially for the 5G uplink systems. However, they are not suitable for the CR applications because it is a need for more carriers to switch on and switch off between these carriers. At this point, DFT-s techniques can be thought as mixed waveform types of multicarrier and single-carrier methods according to the number of subcarrier groups. If there are fewer subcarrier groups, DFT-s method behaves like a single-carrier method. On the contrary, DFT-s method can be analyzed like a multicarrier waveform technique. DFT-s OFDM techniques and their variations introduce flexible physical layer for the future-generation cellular systems and CR applications.

There are also some other DFT-s OFDM-based waveform suggestions in various publications. These suggestions include some modifications to the new waveforms which are given in this subsection. UW DFT-s OFDM method modifies ZT DFT-s OFDM and UW-OFDM techniques by removing the impact of symbols on the tail of the transmitted signal [39]. In another study of the same authors, UW DFT-s Windowed OFDM is proposed which uses a frequency domain windowing technique as in GFDM to suppress the leakage to the tail of the DFT-s OFDM symbols [40]. Guard interval (GI) DFT-s OFDM scheme uses an adaptive GI of variable size to decrease PAPR while providing similar OOBE compared to DFT-s OFDM and CP-OFDM techniques [41]. Another paper introduces generalized DFT-s OFDM which replaces the CP with a sequence having a tunable length to provide more flexibility [42]. Some other details related with the adaptivity of DFT-s OFDM methods are presented in section "New Adaptive Waveforms".

A generic block diagram of the transmitter and receiver designs for major waveforms developed for 5G can be seen in Tables 1 and 2, respectively. Some basic differences between these waveform designs are given in these tables. For ZT DFT-s OFDM method, M is less than N.

Non-orthogonal Waveforms

There are also new non-orthogonal waveforms which ignore the assumption of strict synchronization and orthogonality in the wireless network systems. For example, different non-orthogonal waveform designs were studied in some EU projects like PHYDYAS (Physical Layer for Dynamic Access and Cognitive Radio) and 5GNOW (5th Generation Non-Orthogonal Waveforms for Asynchronous Signalling). FBMC and GFDM are two techniques analyzed in these EU projects. Generally, these methods may need interference suppression techniques on the receiver side of the transceiver systems.

In FBMC, a different filter is used for each subcarrier and these filters are not orthogonal in the complex plane. Polyphase network (PPN) approaches are taken for better performance [43]. To achieve better filtering performance, symbols are

Table 1 Generic block diagram of the transmitter designs for major waveforms developed for 5G

	ZT	DFT	OFDM synthesis	CP/ZG/UW	Filtering
CP-OFDM			IFFT	CP	
f-OFDM			IFFT with different lengths for each subband	Different-length CPs for each subband	Subband filtering using filters with different lengths
UFMC			Separate N-point IFFT for each subband	ZG between subbands	Subband filtering
UW-OFDM			IFFT	UW	
ZT DFT-s OFDM	ZT	M-point DFT	N-point IFFT		
FBMC			IFFT		Subcarrier filtering
GFDM			GFDM modulator	CP	

Table 2 Generic block diagram of the receiver designs for major waveforms developed for 5G

	Filtering	Removing CP	FFT	IDFT	Other processes
CP-OFDM		Yes	FFT		
f-OFDM	Yes	Yes	FFT		
UFMC			2N-point FFT		
UW-OFDM			FFT		Removing UW
ZT DFT-s OFDM			N-point FFT	M-point IFFT	Removing zeros
FBMC	Yes		FFT		
GFDM		Yes			GFDM demodulator

modulated using offset QAM (OQAM) [32]. FBMC has extremely low OOBE due to the utilization of very long filters. However, these long filters increase the computational complexity and decrease the spectral efficiency with their tails. FBMC is not well suitable for MIMO since the filters span a few symbols [44].

Comparing UFMC to FBMC, the shorter filters utilized in UFMC decrease the access delays introduced by the waveform. The same reason makes UFMC less computationally complex compared to FBMC, but UFMC is still more computationally complex than CP-OFDM.

In GFDM, time blocks are divided into shorter duration symbols, which results in wider band subcarriers compared to CP-OFDM [33]. The cyclic filters used for each subsymbol adds CP before GFDM blocks. Filtering is performed per subcarrier as in FBMC. Different than FBMC, the subcarriers are upsampled before filtering is performed, resulting in shorter access delays. ICI introduced by the non-orthogonality requires utilization of cyclostationarity-based interference suppression techniques at the receiver, which greatly increases receiver complexity. Some other details related with the adaptivity of GFDM are presented in section "Generalized Frequency Division Multiplexing with an Adaptivity Perspective".

For the beyond of 5G, more adaptive, flexible, and hybrid systems with mixed numerology structures are needed. In section "Beyond OFDM for Adaptation and Flexible Utilization of Various Resources", this type of systems is explained in more details, and new waveforms beyond OFDM are discussed from an adaptivity perspective.

Beyond OFDM for Adaptation and Flexible Utilization of Various Resources

From the adaptivitiy perspective, OFDM is a multicarrier modulation scheme that has the potentials that makes it suitable for CR. OFDM provides a high degree of adaptation in many aspects which are described in section "OFDM from the Adaptivity Perspective". There are also other new adaptive waveforms like DFT-s methods which are explained in section "New Adaptive Waveforms".

OFDM from the Adaptivity Perspective

Adaptive CP

In a multipath environment, the transmitted symbol reaches the receiver from different propagation paths with different time delays. Therefore, the duration of the received symbol is stretched causing some overlapping with the previously received symbols. This overlapping caused by the multipath propagation is usually referred to as ISI. Also, there is another kind of interference called ICI that arises with the ISI when there is no guard time between the consecutive OFDM symbols or when the guard time is insufficient. The integer number of cycles for each subcarrier within the FFT interval is no longer maintained due to the phase transition introduced by the previous symbol. A zero guard time that has a length greater than or equal to the maximum excess delay can be used to accommodate the spreading of the previous symbol and eliminate the ISI. At the receiver, the guard time including the interfering parts is discarded before the FFT operation. Although the guard time can be sufficient to cope with the ISI between the adjacent received OFDM symbols, OFDM symbol still suffers from a self-interference caused by the delayed replicas arriving from different propagation paths as shown in Fig. 1. The orthogonality of subcarriers is lost due to the multipath propagations. The reason is that there is no longer an integer number of cycle's difference between the subcarrier within the FFT interval. Alternatively, CP that is a guard time inserted between consecutive OFDM symbols, can restore the orthogonality by converting the linear convolution channel into a circular convolution channel. It is done by copying enough number of time samples from the end of the OFDM symbol and appending them into the front.

In order to handle with this distortion, a one-tap channel equalizer can be used for each subcarrier. In the receiver, the output samples of the FFT is multiplied by the corresponding channel equalizer coefficient. On the other hand, using CP

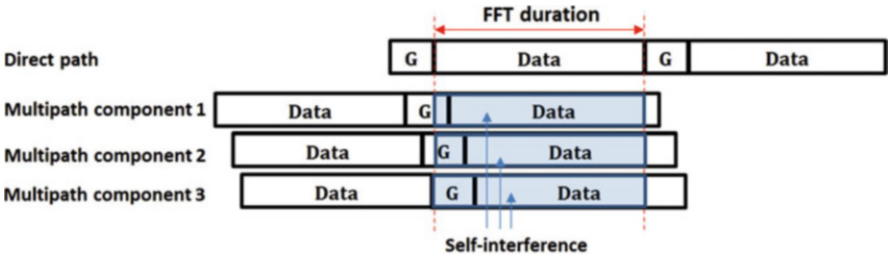

Fig. 1 Guard interval solves ISI, but does not solve the self-interference due to multipath propagation

results in energy waste by transmitting redundant OFDM samples that are used to mitigate ICI and ISI. Also, ICI occurs in the time-varying multipath channels, where the Doppler shifts cause frequency offset on the subcarriers, then ICI and a loss of orthogonality. For large Doppler frequency, f_d, values, the channel varies faster relatively to the OFDM symbol duration resulting in ICI and a degradation in the BER performance. While, for small Doppler frequency values, the channel varies slowly relative to OFDM symbol duration yielding to performance that is close to the flat fading channel.

As not having a sufficient CP length can cause interference problems and degradation on the quality of communication, also having unnecessary long CP causes a waste of resources and degradation in the throughput. CP contains a redundant data that is not being processed and discarded at the receiver prior to demodulation. Therefore, CR needs to adaptively change CP duration after estimating the channel in order to maintain ISI and ICI-free signal while achieving the maximum throughput possible. As discussed previously, the amount of effect that ISI causes can be reduced by increasing the OFDM symbol duration. And the symbol duration is proportional to the number of subcarriers for a given bandwidth. Therefore, it shows that a small number of subcarriers is better than a large number of subcarriers for ISI. Long OFDM symbols are more immune to frequency-selective fading channels. However, they are more sensitive to time-selective fading channels. Time selectivity causes the loss of orthogonality. Therefore, in doubly dispersive channels an optimum combination of CP and number of subcarriers should be selected depending on the required BER performance, available bandwidth, and the available transmitted power.

Adaptive Modulation and Subcarrier Allocation

Adaptive modulation is one of the techniques used to enhance the performance of an OFDM system. Assuming all subcarriers transmit at the same power level. If the transmitter knows the instantaneous channel transfer function, then the subcarriers with large channel gains can transmit more bits per OFDM symbol using higher order modulations, while the subcarrier that suffers from low channel gains "deep fading" can carry less number of bits or no bits per OFDM symbol to enhance the

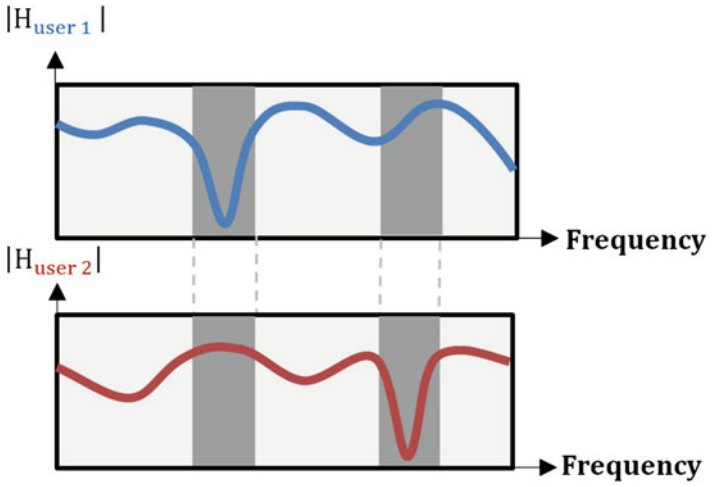

Fig. 2 Low channel gains at the locations of the subcarriers of the first user corresponds to high channel gains for the same group of subcarrier of the second user

BER performance. Since different subcarriers suffer from different channel gains and transmit at different rates "bits per OFDM symbol," then the transmit power level of each subcarrier should be changed accordingly. In frequency-selective channels, some subcarriers suffer from deep fades, as a result, a large number of subcarriers could be left without being utilized causing waste of resources. In a multiuser scenario, the deep fading affecting portion of the subcarriers of one user might not also be affecting the same portion of subcarriers of other users, as illustrated in Fig. 2. In static resource allocation such as TDMA and FDMA, users are allocated to predetermined time slots or frequency bands, the unused subcarriers in the time slots or frequency bands of one user cannot be used by the other users. Figure 3 shows the differences between the three static resource allocation schemes. In OFDM-TDMA, the subcarriers are not shared with other user(s) during a predetermined TDMA time slot. Each user is assigned in a predetermined time slot to use the subcarriers in that time slot separately. While in OFDM-FDMA, each user is assigned a predetermined group of subcarriers to be used at all times by single users. Another version of OFDM-FDMA is referred to as OFDM-interleaved-FDMA, which is similar to OFDM-FDMA, except that the subcarriers assigned to each user are not consecutive, the subcarriers of one user are merged within the other user's subcarriers. Therefore, multiuser adaptive subcarrier allocation, depending on the instantaneous channel response of the users, allows better utilization of the resources since there is a benefit of the subcarriers that suffers from deep fade at one user by other users.

One of the objectives in an adaptive multiuser subcarrier, bit, and power allocation system is to minimize the overall transmit power [45]. At the transmitter, the total number of bits that need to be transmitted from K users are fed to subcarrier and bit allocation block that allocates the bits from different users to

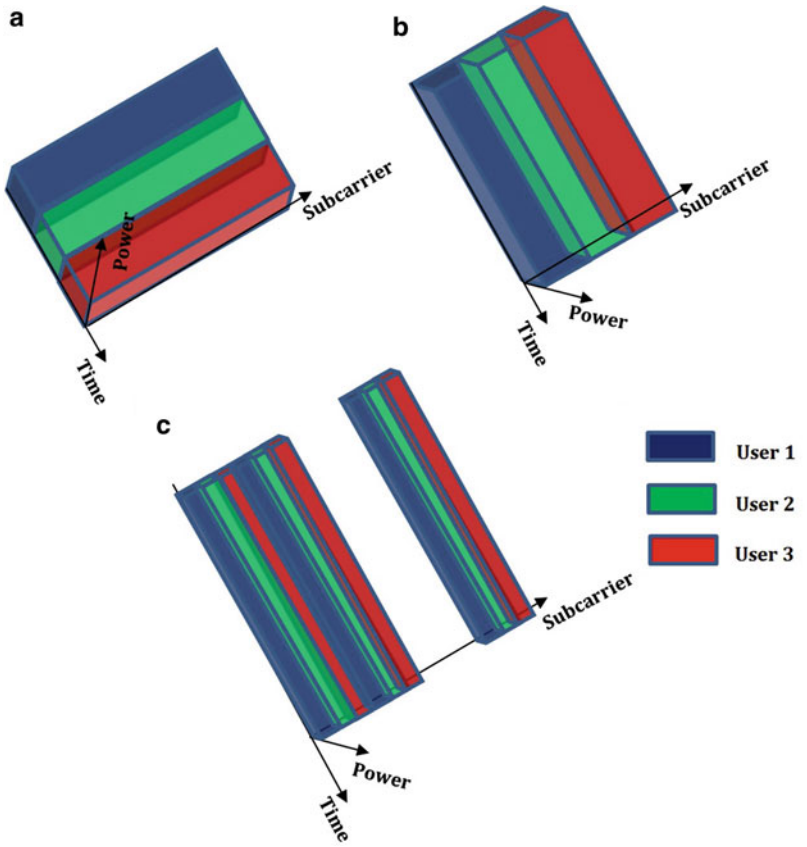

Fig. 3 (**a**) OFDM-TDMA, (**b**) OFDM-FDMA, (**c**) OFDM-interleaved-FDMA

different subcarriers. The transmitter is aware of the instantaneous channel gains from the K users on all the subcarriers. The transmitter exploits the extracted channel information by applying them to a subcarrier, bit, and power allocation algorithm which assigns different subcarriers to different users. And, the adaptive modulator chooses a modulation scheme and the transmit power level depending on the number of bits assigned on each subcarrier.

Adaptive OFDMA Frame Structure: "Adaptive Lattice"

The frame consists of multiple OFDMA symbols that have a structure in time and frequency referred to as lattice. The structure of all the OFDMA symbols within the frame defines the structure of the whole frame. The structure of OFDMA symbols in time and frequency domains is determined by different parameters, but the fundamental parameters are mainly the subcarrier spacing (Δ_f) and the cyclic prefix duration (T_{cp}). In conventional OFDMA systems, the frame structure is fixed, meaning that the design parameters chosen (T_{cp} and Δ_f) for all the OFDM symbols within the frame are set to a fixed value that is chosen considering the worst

case communication channel to guarantee to maintain the orthogonality between the subcarriers within one OFDM frame. The interference is composed of ISI in doubly dispersive channels. It is caused by the time dispersion due to the multipath propagation and ICI. The motion of the transmitter, the receiver, or the objects in between causes a frequency spreading which is also the reason of ICI. Depending on the channel characteristics of the users, the time and frequency dimensions might be exposed to different time and frequency responses at the same. Although the conventional approach in designing the frame structure provides an immunity to different channel conditions, it ignores the fact that not all the users within the frame undergoes to the worst channel condition in time and frequency at all times. For example, the conventional approach does not consider the user with a less maximum excess delay than the worst maximum excess delay spread as the users close to the base station; also it doesn't consider stationary users with narrower subcarrier spacing. Other approaches follow different strategies by treating the user's communication channels fairly rather than equally when designing the frame structure. The new approach in [46] aims to improve the spectral efficiency while maintaining the frequency spread immunity by classifying the OFDMA symbols within the frame into different cases according to the user's channel response in doubly dispersive channel as shown in Fig. 4. Having multiple users with different doubly dispersive channels is exploited by adapting the time-frequency structure of OFDMA scheme. Having large subcarrier spacing provides immunity to ICI, but on the other hand, smaller subcarrier spacing improves the spectral efficiency. Also, the subcarrier spacing is related to delay spread characteristics of the channel by the relation that connects the subcarrier spacing and the symbol duration T_s by:

$$T_s = \frac{1}{\Delta_f} \tag{1}$$

Additionally, the subcarrier spacing indirectly impacts T_{cp}, which depends on the delay spread characteristics of the channel. Longer T_{cp} is desirable to avoid ISI between OFDMA symbols, while shorter T_{cp} increases the spectral efficiency. This approach is based on prior knowledge of the channel statistic that the frame structure is designed base upon it. Prior knowledge of channel statistics is used to reduce feedback requirements.

New Adaptive Waveforms

Zero-Tail DFT-s OFDM with an Adaptivity Perspective

As being mentioned previously, in OFDM and DFT-spread-OFDM, the problem of ISI that is caused by the multipath channel effect is being taken care of by copying the last part of the time domain signal and appending it at the beginning before the transmission which is referred to as CP. Then at the receiver, the effect of ISI is being removed by discarding the CP part and applying single tap equalizer after the IFFT process to get rid of the ICI caused by the multipath effect [47].

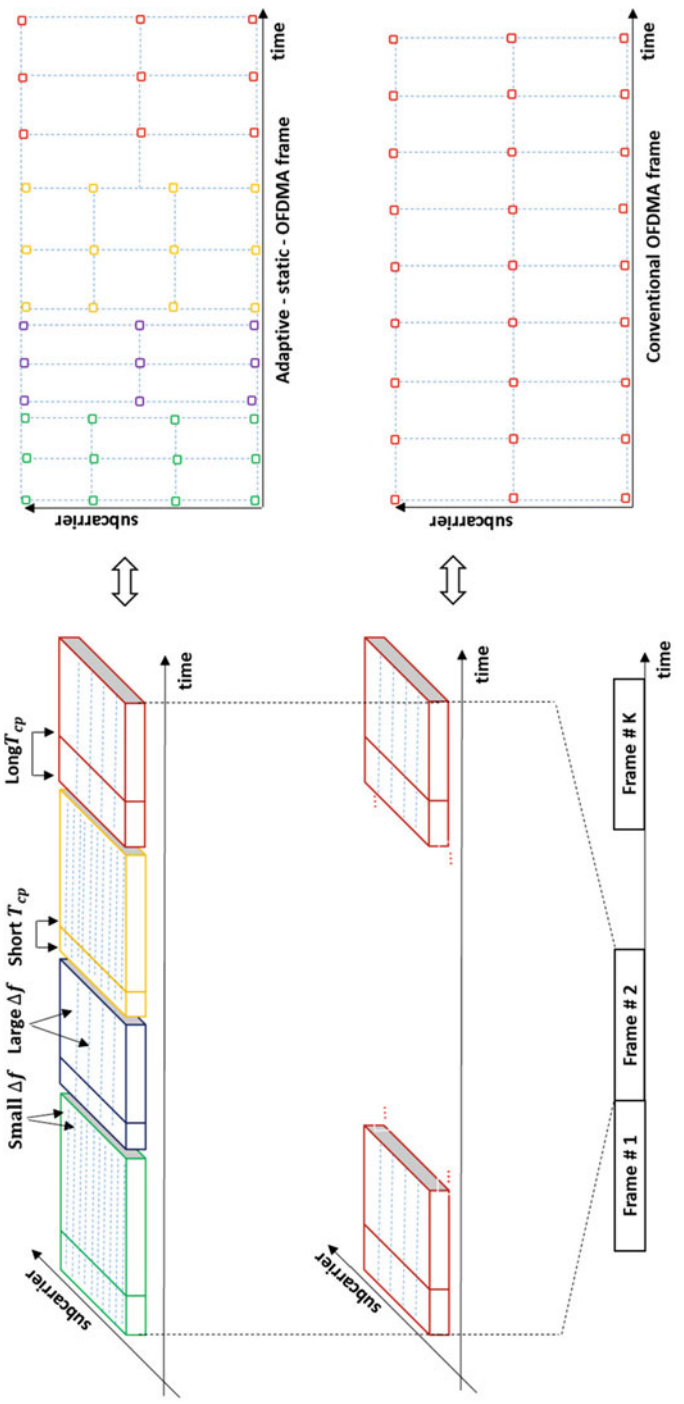

Fig. 4 Adaptive OFDMA frame structure [46]

Although CP approach has a great role in protecting the signal against the multipath channel effect, it still suffers from some limitation in terms of its flexibility. Since, CP duration is agreed on in prior according to the channel characteristics, e.g., maximum channel delay spread, it becomes not feasible to change the CP duration while maintaining their fit in one millisecond subframe duration. Also, since the CP is pre-agreed on prior to channel delay spread then this either results in and excessive CP duration for the users who observe less channel delay spread, or it can result in insufficient CP duration for user who observe high channel delay spread, allowing some leakage from the previous symbols which result in degradation in the system performance. While ZT DFT-s OFDM is a new approach which generates an internal GI between the consecutive symbols by adding zero tail at the beginning of the DFT process after the data symbols [34]. Thus, even if the guard interval changes, the complete symbol duration remains the same. Also, it is worth mentioning that this GI that appears after the IFFT process; it does not have a zero power; however, it has a low-power samples at the tail due to the spreading that happens after the DFT and IDFT processes. Furthermore, adding some zero before the data symbols (at the header of the data symbols) to the input of DFT block enhances the OOB emission by making the smooth transition between the consecutive symbols. The basic structure for the ZT DFT-s OFDM is shown in Fig. 5.

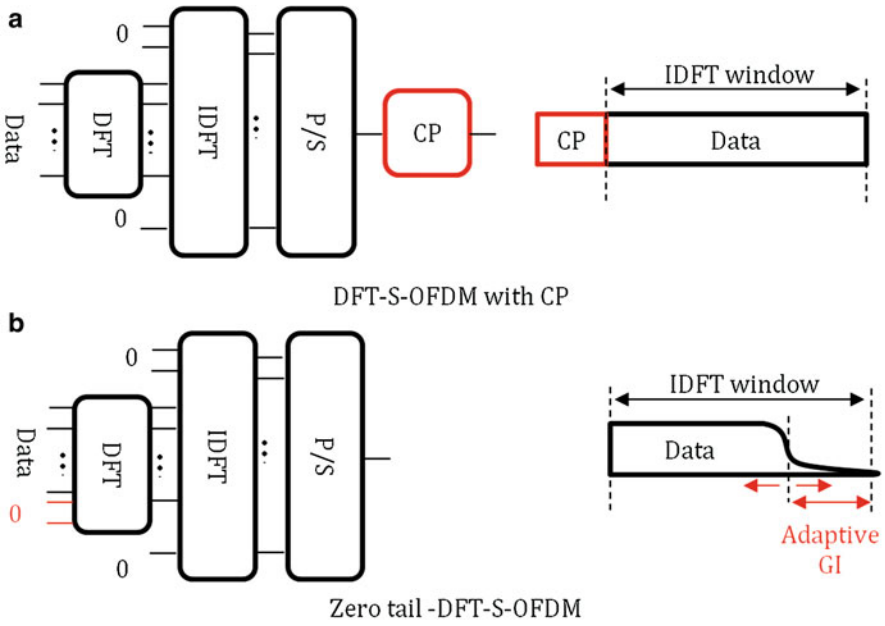

Fig. 5 ZT DFT-s OFDM structure

Unique Word DFT-s OFDM

UW DFT-s OFDM can be seen as a general case which ZT DFT-s OFDM have flowed from it. Instead of generating a zero (or low-power) time domain samples at the beginning and at the end of the DFT-s OFDM symbol, UW DFT-s OFDM generates a non-zero fixed samples at the end and the beginning of the DFT-s OFDM symbol. This non-zero-sample can be generated by adding a signal which is referred to as UW. This UW signal can either be added in time domain with two steps, or in the frequency domain in one step [30]. The two-step approach is done be firstly generating a ZT DFT-s OFDM symbol by inserting zeros at the head and tail of the data symbols before the DFT process. Then add the UW signal in time domain after the IDFT process. This two-step approach is used, then the UW should be generated within the transmission bandwidth. Additionally, any interference that could occur due to the addition of the UW signal should be handled at the receiver. Alternatively, the second approach which is a one-step approach maintains the orthogonally between the UW signal and the DFT-s OFDM signal by replacing the zeros added at the beginning of DFT block by a unique fixed sequence to generate the unique word at the output of the IDFT block. Thus, the UW signal and the DFT-s OFDM signal are orthogonal since they use different input signals at the DFT block. Additionally, it worth to mention that the since the UW is generated by a fixed sequence, it can be used in the estimation of noise variance and tracking [48] and also in phase tracking algorithms [49]. General solutions and challenges for the flexible DFT-s OFDM techniques are analyzed in [40]. The basic structure for the UW DFT-s OFDM is given in Fig. 6.

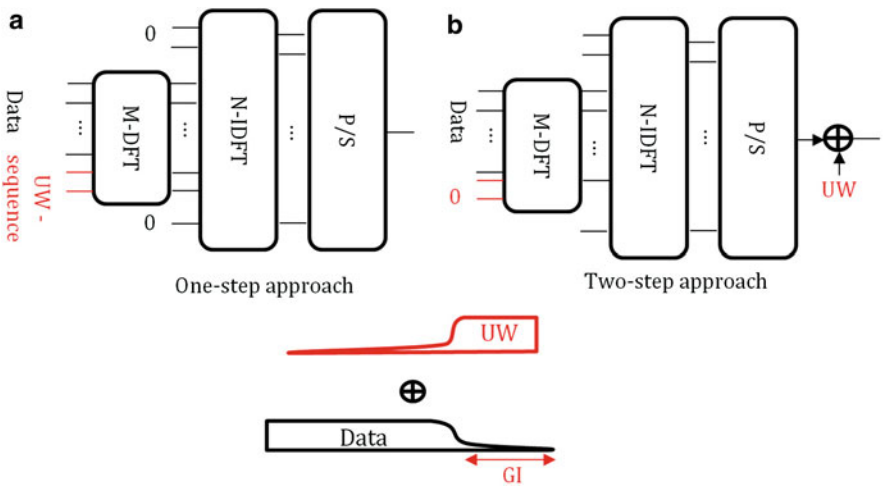

Fig. 6 UW DFT-s OFDM structure

Filtered OFDM with an Adaptivity Perspective

OFDM signal is not well localized in frequency due to the presence of the large sidelobes. Therefore, at least 10% guard band is required to meet the OOB leakage rejection requirements. Also, OFDM is not a flexible waveform with fixed subcarrier spacing and have limited options in CP. Also, OFDM is not suitable for asynchronous transmission across different subbands do to the high OOB emission. And most importantly, conventional OFDM does not allow using different configurations (e.g., subcarrier spacing, CP duration, etc.) across different subbands. f-OFDM enables the use of different waveforms with different configurations. While the conventional OFDM makes the whole frequency band as one block with the same subcarrier spacing and the same CP. While in f-OFDM the whole frequency band is divided into smaller subbands with different bandwidths and different subcarrier spacing and each subband can have different CP duration, this provides the flexibility in both frequency (subcarrier spacing and subband bandwidth) and in time (symbol duration, CP duration). Then after each subband has its own filter that is applied to it. f-OFDM allows the support of asynchronous transmission across the subbands and the support of mixed numerologies due to better OOBE at the expense of a lower number of guard tones between neighboring subbands.

The filters considered in f-OFDM is designed by multiplying a sinc function in time domain, which has an ideal response in the frequency domain, by a time domain window function (e.g., Hanning, root-raised cosine (RRC)), which is well localized in time, to produce a filter which has better localization in time and frequency domains for better ICI and ISI. Frequency domain filtering is preferred for simple implementation via an overlap-save algorithm [50]. The basic structure of f-OFDM is given in Fig. 7.

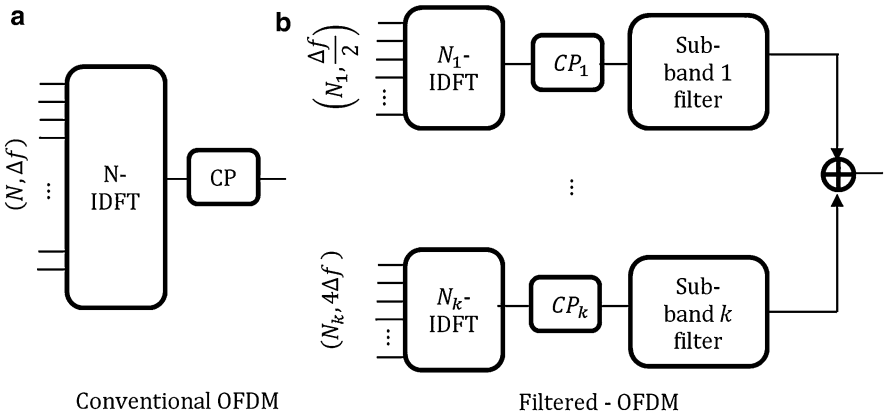

Fig. 7 f-OFDM structure

Generalized Frequency Division Multiplexing with an Adaptivity Perspective

In the literature, GFDM is presented as a flexible waveform that can be customized to correspond to either OFDM or DFT-s OFDM as two extreme cases of GFDM. Also, GFDM can be customized by adjusting some of its parameters to be able to adapt to different requirements and channel conditions. Moreover, GFDM has shown enhancement in lowering the OOB radiation when it is compared with OFDM. However, even a lower OOB can be achieved by applying windowing to GFDM as an additional process at the expense of increasing the complexity.

These features of flexibility and lowering the OOB are achieved by changing the building unit of the system which is the pulse shape. Unlike OFDM which uses a rectangular pulse shape in time domain that extends to only one OFDM symbol, GFDM uses a pulse shape that spreads to multiple subsymbols. In GFDM, the pulse shapes are overlapped in time domain by circularly shifting the pulse shape across all the subsymbols within one GFDM symbol. GFDM, like some other waveforms, works on enhancing the OOB emission by filtering each subcarrier, leading to better immunity against ICI and relaxing synchronization requirements. As illustrated in Fig. 8, GFDM can be converted to DFT-s OFDM by setting $K = 1$; thus, the number of subsymbols increases $M = N$. On the other hand, GFDM can correspond

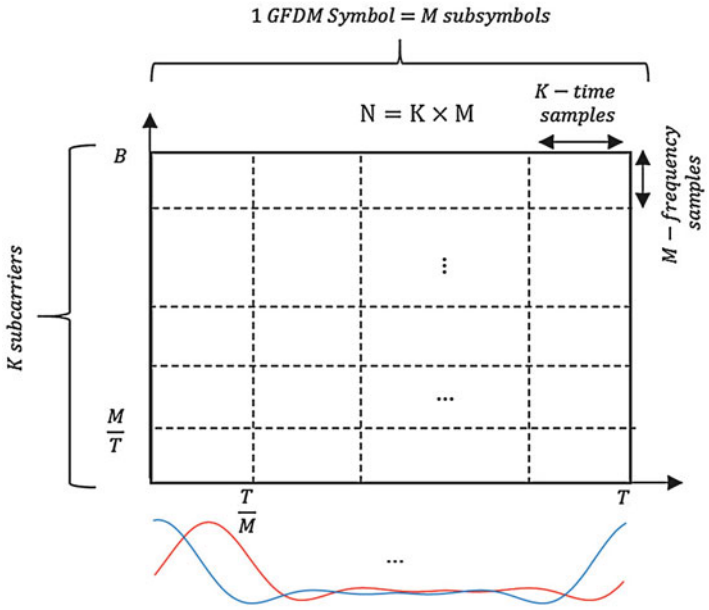

Fig. 8 GFDM structure

to OFDM waveform by elegantly setting $M = 1$ and increasing the number of subcarriers to $K = N$.

Conclusion and Future Directions

As it is discussed, OFDM is seen as a promising physical layer candidate for CR. It has high level of flexibility and high level of adaptation to the open opportunities in the spectrum and to different conditions. However, OFDM still suffers from limitation such as high OOBE, requiring strict synchronization, and some other drawbacks. Some of those problems have been solved with some additional processing done on the OFDM signal. On the other hand, other waveforms that have better characteristics than OFDM can be thought of as a good alternative for CR physical layer. Those waveforms have a wide range of adjustable parameters that grants them a high level of flexibility and adaptivity which are important aspects of the CR physical layer. Moreover, adaptive waveform designs can be multiplexed in a hybrid structure to provide more flexible and adaptive solutions. In hybrid structures, different waveforms may be employed under the same cell. Thus, hybrid structure designs can let the future communications systems benefit from different techniques and choices for different times and conditions.

References

1. Mahmoud HA, Yucek T, Arslan H (2009) OFDM for cognitive radio: merits and challenges. IEEE Wirel Commun 16(2):6–15
2. Yazar A, Onat FA, Arslan H (2016) New generation waveform approaches for 5G and beyond. In: IEEE Signal Processing and Communications Applications Conference (SIU), pp 961–964
3. I C-L, Han S, Xu Z, Wang S, Sun Q, Chen Y (2016) New paradigm of 5G wireless internet. IEEE J Sel Areas Commun 34(3):474–482
4. Elkourdi M, Pekoz B, Guvenkaya E, Arslan H (2016) Waveform design principles for 5G and beyond. In: IEEE Wireless and Microwave Technology Conference (WAMICON), pp 1–6
5. Arslan H, Yucek T (2006) Adaptation of wireless mobile multi-carrier systems. In: Li W, Xiao Y (eds) Adaptation techniques in wireless multimedia networks, 1st edn. Nova Science Publishers, New York, pp 215–240
6. Keller T, Hanzo L (2000) Adaptive modulation techniques for duplex OFDM transmission. IEEE Trans Veh Technol 49(5):1893–1906
7. Harvatin DT, Ziemer RE (1997) Orthogonal frequency division multiplexing performance in delay and doppler spread channels. In: IEEE Vehicular Technology Conference (VTC), vol 3, pp 1644–1647
8. Weiss T, Krohn A, Capar F, Martoyo I, Jondral FK (2003) Synchronization algorithms and preamble concepts for spectrum pooling systems. In: IST Mobile & Wireless Telecommunications Summit, pp 788–792
9. Sahin A, Arslan H (2011) Edge windowing for OFDM based systems. IEEE Commun Lett 15(11):1208–1211
10. Bala E, Li J, Yang R (2013) Shaping specktral leakage: a novel low-complexity transceiver architecture for cognitive radio. IEEE Veh Technol Mag 8(3):38–46

11. Guvenkaya E, Sahin A, Bala E, Yang R, Arslan H (2015) A windowing technique for optimal time-frequency concentration and ACI rejection in OFDM-based systems. IEEE Trans Commun 63(12):4977–4989
12. Mahmoud HA, Arslan H (2008) Sidelobe Suppression in OFDM-based spectrum sharing systems using adaptive symbol transition. IEEE Commun Lett 12(2):133–135
13. Yamaguchi H (2004) Active interference cancellation technique for MB-OFDM cognitive radio. In: IEEE European Microwave Conference, pp 1105–1108
14. Brandes S, Cosovic I, Schnell M (2006) Reduction of out-of-band radiation in OFDM systems by insertion of cancellation carriers. IEEE Commun Lett 10(6):420–422
15. Cosovic I, Brandes S, Schnell M (2006) Subcarrier weighting: a method for sidelobe suppression in OFDM systems. IEEE Commun Lett 10(6):444–446
16. Li D, Dai X, Zhang H (2009) Sidelobe suppression in NC-OFDM systems using constellation adjustment. IEEE Commun Lett 13(5):327–329
17. Joshi DR, Popescu DC, Dobre OA, Baddour KE (2011) Spectral shaping for adjacent band interference suppression in cognitive radio systems. In: IEEE Global Telecommunications Conference (GLOBECOM), pp 1–5
18. Tom A, Sahin A, Arslan H (2013) Mask compliant precoder for OFDM spectrum shaping. IEEE Commun Lett 17(3):447–450
19. Beek J, Berggren F (2009) N-continuous OFDM. IEEE Commun Lett 13(1):1–3
20. Beek J (2009) Sculpting the multicarrier spectrum: a novel projection precoder. IEEE Commun Lett 13(12):881–883
21. Beek J (2010) Orthogonal multiplexing in a subspace of frequency well-localized signals. IEEE Commun Lett 14(10):882–884
22. Guvenkaya E, Sahin E, Arslan H (2015) N-coninuous OFDM with CP alignment. In: IEEE Military Communications Conference (MILCOM), pp 587–592
23. Zhang JA, Huang X, Cantoni A, Guo YJ (2012) Sidelobe suppression with orthogonal projection for multicarrier systems. IEEE Trans Commun 60(2):589–599
24. Cosovic I, Mazzon T (2006) Suppression of sidelobes in OFDM systems by multiple-choice sequence. Eur Trans Telecommun 17:623–630
25. Tom A, Sahin A, Arslan H (2016) Suppressing alignment: joint PAPR and out-of-band power leakage reduction for OFDM-based systems. IEEE Trans Commun 64(3):1100–1109
26. Ni C, Jiang T, Peng W (2015) Joint PAPR reduction and sidelobe suppression using signal cancellation in NC-OFDM-based cognitive radio systems. IEEE Trans Veh Technol 64(3):964–972
27. Sahin A, Guvenc I, Arslan H (2014) A survey on multicarrier communications: prototype filters, lattice structures, and implementation aspects. IEEE Commun Surv Tutorials 16(3):1312–1338
28. Zhang X, Jia M, Chen L, Ma J, Qiu J (2015) Filtered-OFDM – enabler for flexible waveform in the 5th generation cellular networks. In: IEEE Global Telecommunications Conference (GLOBECOM), pp 1–6
29. Vakilian V, Wild T, Schaich F, Brink ST, Frigon JF (2013) Universal-filtered multi-carrier technique for wireless systems beyond LTE. In: IEEE Global Telecommunications Conference (GLOBECOM), pp 223–228
30. Huemer M, Hofbauer C, Huber JB (2012) Non-systematic complex number RS coded OFDM by unique word prefix. IEEE Trans Signal Process 60(1):285–299
31. Bellanger M (2010) FBMC physical layer: a primer. In: Physical Layer for Dynamic Spectrum Access and Cognitive Radio (PHYDYAS)
32. Farhang-Boroujeny B (2011) OFDM versus filter bank multicarrier. IEEE Signal Process Mag 28(3):92–112
33. Fettweis G, Krondorf M, Bittner S (2009) GFDM – generalized frequency division multiplexing. In: IEEE VTC-Spring, pp 1–4
34. Berardinelli G, Tavares FML, Sorensen TB, Mogensen P, Pajukoski K (2013) Zero-tail DFT-spread-OFDM signals. In: IEEE Global Telecommunications Conference (GLOBECOM), pp 229–234

35. Benvenuto N, Tomasin S, Tomba L (2002) Equalization methods in OFDM and FMT systems for broadband wireless communications. IEEE Trans Commun 50(9):1413–1418
36. Berardinelli G, Temino LR, Frattasi S, Rahman M, Mogensen P (2008) OFDMA vs. SC-FDMA: performance comparison in local area IMT-A scenarios. IEEE Wirel Commun 15(5):64–72
37. Ankarali Z, Karabacak M, Arslan H (2014) Cyclic feature concealing CP selection for physical layer security. In: IEEE Military Communications Conference (MILCOM), pp 485–489
38. Guvenkaya E, Tom A, Arslan H (2013) Joint sidelobe suppression and PAPR reduction in OFDM using partial transmit sequences. In: IEEE Military Communications Conference (MILCOM), pp 95–100
39. Sahin A, Yang R, Ghosh M, Olesen RL (2015) An improved unique word DFT-spread OFDM scheme for 5G systems. In: IEEE Global Telecommunications Conference (GLOBECOM), pp 1–6
40. Sahin A, Yang R, Bala E, Beluri CM, Olesen RL (2016) Flexible DFT-S-OFDM: solutions and challenges. IEEE Commun Mag 54(11):106–112
41. Kumar U, Ibars C, Bhorkar A, Jung H (2015) A waveform for 5G: guard interval DFT-s OFDM. In: IEEE Global Telecommunications Conference (GLOBECOM), pp 1–6
42. Berardinelli G, Pederson KI, Sorensen TB, Mogensen P (2016) Generalized DFT-spread-OFDM as 5G waveform. IEEE Commun Mag 54(11):99–105
43. Devi B, Lalleima N, Singh S (2014) Comparative analysis of FBMC and OFDM multicarrier techniques for wireless communication networks. Int J Comput Appl 100(19):27–31
44. Farhang A, Marchetti N, Figueiredo F, Miranda J (2014) Massive MIMO and waveform design for 5th generation wireless communication systems. In: International Conference on 5G for Ubiquitous Connectivity (5GU), pp 70–75
45. Wong CY, Cheng RS, Lataief KB, Murch RD (1999) Multiuser OFDM with adaptive subcarrier, bit, and power allocation. IEEE J Sel Areas Commun 17(10):1747–1758
46. Sahin A, Arslan H (2012) Multi-user aware frame structure for OFDMA based system. In: IEEE Vehicular Technology Conference (VTC Fall), pp 1–5
47. Falconer D, Ariyavisitakul SL, Benyamin-Seeyar A, Eidson B (2002) Frequency domain equalization for single-carrier broadband wireless systems. IEEE Commun Mag 40(4):58–66
48. Coon J, Sandell M, Beach M, McGeehan J (2006) Channel and noise variance estimation and tracking algorithms for unique-word based single-carrier systems. IEEE Trans Wirel Commun 5(6):1488–1496
49. Huemer M, Witschnig H, Hausner J (2003) Unique word based phase tracking algorithms for SC/FDE-systems. In: IEEE Global Telecommunications Conference (GLOBECOM), pp 70–74
50. Daher A, Baghious EH, Burel G, Radoi E (2010) Overlap-save and overlap-add filters: optimal design and comparison. IEEE Trans Signal Process 58(6):3066–3075

4 Modeling and Performance Analysis of Cognitive Radio Systems from a Deployment Perspective

Ankit Kaushik, Shree Krishna Sharma, Symeon Chatzinotas, Björn Ottersten, and Friedrich K. Jondral

Contents

A. Kaushik (✉) · F. K. Jondral
Communications Engineering Lab, Karlsruhe Institute of Technology, Karlsruhe, Germany
e-mail: Ankit.Kaushik@kit.edu; Friedrich.Jondral@kit.edu

S. K. Sharma
Department of Electrical and Computer Engineering, Western University, London, Ontario, Canada

SnT – securityandtrust, University of Luxembourg, Luxembourg City, Luxembourg
e-mail: sshar323@uwo.ca

S. Chatzinotas · B. Ottersten
SnT – securityandtrust, University of Luxembourg, Luxembourg City, Luxembourg
e-mail: symeon.chatzinotas@uni.lu; bjorn.ottersten@uni.lu

W. Zhang (ed.), *Handbook of Cognitive Radio*,
https://doi.org/10.1007/978-981-10-1394-2_4

Abstract

A cognitive radio (CR) system aims at an efficient utilization of the spectrum below 6 GHz – suitable for mobile communications – by enabling a secondary access to the licensed spectrum while ensuring a sufficient protection to the licensed users. Despite the fact that an extensive amount of literature has been dedicated to the field of CR, its performance analysis has been dealt inadequately from a deployment perspective, therefore making it difficult to understand the extent of vulnerability caused to the primary system. Following a deployment perspective, it has been identified that the involved channels' knowledge is pivotal for the realization of CR techniques. However, the aspect of channel knowledge in context of CR systems, particularly its detrimental effect on the performance, has not been clearly understood. With the purpose of curtailing this gap, this chapter proposes a successful integration of this knowledge by carrying out estimation of the involved channels within a CR system. More specifically, this chapter outlines the following two aspects: first, this chapter establishes an analytical framework to characterize the degradation in the performance due to effects such as time allocation and variation, arising due to imperfect channel knowledge. Second, this chapter features performance tradeoffs that determine the maximum achievable throughput of the CR systems while satisfying the interference constraint.

Introduction

Since the invention of smart devices, the mobile traffic has been increasing tremendously over the last decade. According to the recent surveys on mobile traffic by prominent market leaders (Cisco [15] and Ericsson [20]), the existing mobile traffic is expected to increase 11-fold by 2021. The wireless community including the standardization bodies (3GPP) believe that the state-of-the-art standards (fourth-generation (4G) – LTE, WiMAX) are not capable of sustaining these ever-increasing demands in the upcoming decade. With this situation in hand, the standardization bodies are currently in the phase of conceptualizing the requirements of the fifth generation (5G) of mobile wireless systems. Some of these major requirements are (i) areal capacity in bits/sec/m^2 must increase by a factor of 1000 compared to 4G, (ii) low latency of approximately 1 ms, and (iii) energy- and cost-efficient deployment [3].

The feasibility of these requirements can be envisaged through the application of promising approaches such as maximization of the spatial degrees of freedom (using techniques like massive MIMO [50] and 3D-beamforming [33]), in-band full duplex communications [64], small cell densification [2, 24], alternatives to the already allocated spectrum – such as millimeter-wave technology (mmW) [62], visible light communications [76], and cognitive radio (CR) communications – and waveform design [65]. A classification of these approaches is described in Fig. 1. In order to narrow down the perspective, in this chapter, a deployment scenario that lays

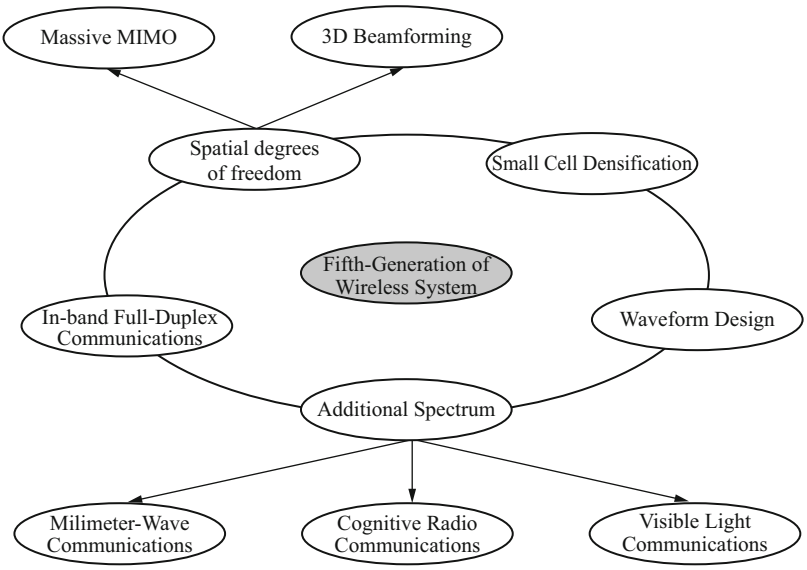

Fig. 1 An illustration of the potential approaches considered under the 5G framework

emphasis on the small cell densification and the implementation of CR is proposed. Before proceeding further, it is essential to briefly discuss some of the prerequisites that render small cell densification and CR communication approaches, particularly their combination, a suitable candidate for a 5G network.

Small Cell Densification

In the recent past, small cells (SCs) have emerged as a potential solution for coverage and capacity enhancements inside a wireless network. An SC represents a low-power station that ranges from 10 to 100 m. The reduced transmit distance accomplished with the deployment of SCs enhances the link quality and aids spatial reuse [13]. As a result, small cell densification can leverage the areal capacity of a 5G network [3]. Because the capacity increases linearly with the number of SCs, it is infeasible to procure the factor of 1000 in the areal capacity with densification alone. In addition, the operation and the integration of these substantial number of SCs to the backhaul network are cost- and energy-intensive for the mobile operator. Therefore, the degree to which the densification can be achieved by a wireless network is rather limited.

Additional Spectrum

Complementing the SCs, an additional spectrum is envisioned as a power source that is capable of sustaining the desired areal capacity for 5G. In consideration to the present allocation of the spectrum below 6 Hz to different wireless services, it is difficult to procure an extension to the already available spectrum to the mobile

communication. Before investigating the potential candidates for the spectrum extension, it is necessary to consider the following classification of the spectrum: (i) $>$ 6 GHz; (ii) $\leq$ 6 GHz. This sort of classification allows us to focus on the feasibility characteristics and the issues thereof.

The spectrum beyond 6 GHz largely entails the mmW, which is well known for point-to-point communications. Recently, it is envisaged as a powerful source of spectrum for 5G wireless systems. However, the mmW technology is still in its initial stage, and along with complex regulatory requirements in this regime, it has to address several challenges like propagation loss, low efficiency of radio-frequency components such as power amplifiers, small size of the antenna, and link acquisition [62]. Therefore, in order to capture a deeper insight of its feasibility in 5G, it is essential to overcome the aforementioned challenges in the near future.

In contrast to the spectrum beyond 6 GHz, an efficient utilization of the spectrum below 6 GHz presents an alternative solution. The use of the spectrum in this regime (below 6 GHz) is fragmented and statically allocated [56, 57], leading to inefficiencies and the shortage in the availability of the spectrum for new services. A glimpse of the measurement campaign demonstrating the underutilized spectrum is presented in Fig. 2. The measurements, acquired during the peak hours, illustrate the spectrum occupancy for the GSM 1800 MHz downlink sub-channels. The low spectrum occupancy for most of the sub-channels clearly signifies the fact that the demand for the additional spectrum can be fulfilled only by managing the utilization of the available spectrum efficiently.

In this perspective, CR is foreseen as one of the potential contenders that addresses the spectrum scarcity problem. Since its origin by Mitola et al. in 1999 [58], this notion has evolved at a significant pace and consequently has acquired certain maturity. Despite the existence of the theoretical analysis, from a deployment perspective, this technology is still in its preliminary phase [60]. In order to curtail the gap between the theoretical models and the practical implementations, recently, the wireless community has started to show an inclination toward models and/or techniques as indicated by the increased promotion of hardware implementation/demonstration or the events such as spectrum challenge [44] in conferences like IEEE DySPAN. Hence, facilitating a hardware implementation of this concept in a way encourages the disposition of CR systems in the upcoming 5G wireless systems. Motivated by this fact, this chapter focuses on the performance analysis of CR systems from a deployment perspective.

In contrast to the radio-frequency (RF) spectrum, visible light communication (VLC) has started to gain extensive attention for 5G wireless communication and hence deserves consideration in context to spectrum extension. Despite the fact that VLC offers some attractive characteristics like spatial, spectrum reuse, high-energy efficiency, and security, it has to overcome certain challenges such as mobility and adverse effect of atmospheric conditions while operating outdoor [76].

In order to enhance the readability, this chapter is organized as follows: section "Cognitive Radio Systems " features different CR systems. Next, to illustrate a successful incorporation of the CR in a 5G network, a specific use-case (deployment

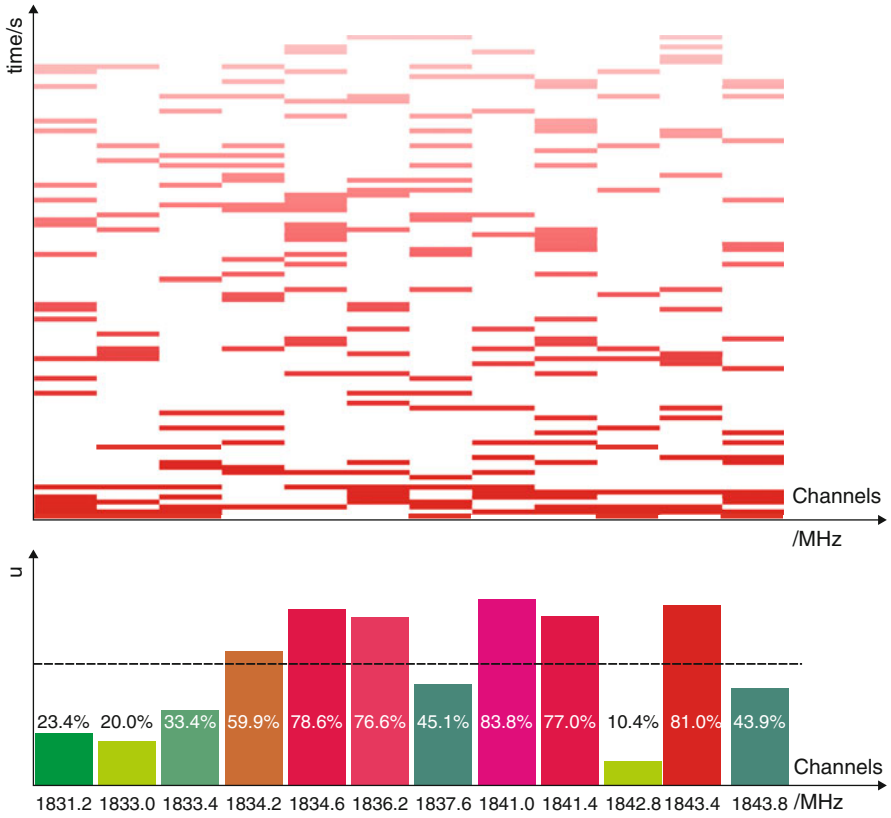

Fig. 2 A snapshot of a hardware demonstrator that measures the spectral occupancy in GSM 1800 MHz downlink channels, whereby the red slices represent the spectrum occupancy (1 or 0) corresponding to a single measurement at a given time instant. The bar plots illustrate the spectrum occupancy (u) for each channel with a history of 500 measurements [40]

scenario) is presented subsequently in section "Cognitive Small Cell: A Prominent Use-Case". Section "Performance Analysis of CR Systems: A Challenging Task" brings out the key aspects that are pivotal to performance analysis of a CR system. Subsection "Imperfect Channel Knowledge" underlines the significance channel knowledge with regard to the realization of CR techniques on a hardware platform. It also describes the harmful effects arising due to the imperfect channel knowledge, leading to performance degradation. In order to justify this argument, section "Interweave System: A Case Study" presents a case study that incorporates channel estimation to characterize the performance of CR as interweave system. Thus, the indoor deployment scenario is transformed into an interweave scenario, whereby a spectrum sensing mechanism is employed at the CR, enabling a secondary access to the licensed spectrum. In addition, this section establishes an analytical framework to capture the effect of imperfect channel knowledge on the

Table 1 Definitions of acronyms and notations used

Acronyms and notations	Definitions
AC, OC	Average Constraint, Outage Constraint
CR	Cognitive Radio
CSC, CSC-BS, MC-BS, MS	Cognitive Small Cell, Cognitive Small Cell-Base Station, Macro Cell-Base Station, Mobile Station
IM, EM	Ideal Model, Estimation Model
IS	Interweave System
PU – PT, PR	Primary User – Primary Transmitter, Primary Receiver
SU – ST, SR	Secondary User – Secondary Transmitter, Secondary Receiver
$\mathscr{H}_1, \mathscr{H}_0$	Signal plus noise hypothesis, noise only hypothesis
f_s	Sampling frequency
τ_{est}, τ_{sen}	Estimation time, sensing time interval
T	Frame duration
P_d, P_{fa}	Detection probability, false alarm probability
$\bar{P}_d$	Target detection probability
ρ_d	Outage constraint over detection probability
$h_{p,1}, h_{p,2}, h_s$	Channel coefficient for the link PT-ST, PT-SR, ST-SR
$\gamma_{p,1}, \gamma_s$	Signal to noise ratio for the link PT-ST, ST-SR
$\gamma_{p,2}$	Interference (from PT) to noise ratio for the link PT-SR
R_s	Throughput at SR
C_0, C_1	Date rate at SR without and with interference from PT
μ	Threshold for the energy detector
$F_{(\cdot)}$	Cumulative distribution function of random variable $(\cdot)$
$f_{(\cdot)}$	Probability density function of random variable $(\cdot)$
$\widehat{(\cdot)}$	Estimated value of $(\cdot)$
$\widetilde{(\cdot)}$	Suitable value of the parameter $(\cdot)$ that achieves maximum performance
$\mathbb{E}_{(\cdot)}$	Expectation with respect to $(\cdot)$
$\mathbb{P}$	Probability measure
$\mathbf{T}(\cdot)$	Test statistics
σ_s^2, σ_w^2	Signal variance at PT, noise variance at ST and SR

performance. Section "Research Directions" presents some possible direction for further research. Finally, section "Conclusion" concludes this chapter. Table 1 lists the definitions of acronyms and important mathematical notations used throughout this chapter.

Cognitive Radio Systems

In order to proceed further, it is essential to understand the classification of different CR systems described in the literature. An access to the licensed spectrum is an outcome of the paradigm employed by a secondary user (SU). In this context, all CR

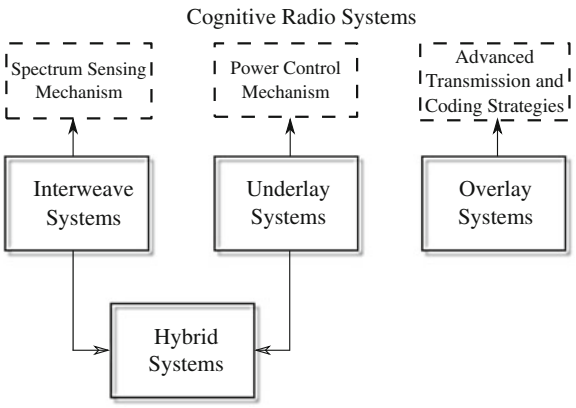

Fig. 3 A classification of different CR systems and some specific CR techniques that allow shared access to the licensed spectrum

systems that provide shared access (used interchangeably with secondary access) to the spectrum mainly fall under the following categories [30]; please consider Fig. 3 for a graphical illustration of different CR systems, including some specific CR techniques:

- According to interweave system (IS) , the SUs render an interference-free access to the licensed spectrum by exploiting spectral holes in different domains such as time, frequency, space, and polarization.
- An underlay system (US) enables an interference-tolerant access, according to which the SUs are allowed to use the licensed spectrum (e.g., ultra-wide band (UWB)) as long as they respect the interference constraints of the primary receivers (PRs).
- A hybrid system (HS) combines the benefits of the IS (agility to detect spectrum holes in different domains) and the US (interference-tolerant capability) so that the spectrum available for performing secondary access can be used efficiently.
- An overlay system considers advanced transmission and coding strategies, which include the participation of higher layers for enabling the spectral coexistence between two or more wireless networks.

The IS, the US, and the HS are closely associated with the physical layer; hence, these systems are mostly considered not only for the theoretical analysis but for practical implementations as well [6, 9, 10, 40, 41, 44, 47, 63]. Underlying this fact, this chapter establishes a deployment-centric viewpoint toward these CR systems. In order to illustrate a successful incorporation of the CR in a 5G network, a specific use-case (deployment scenario) is presented subsequently.

Cognitive Small Cell: A Prominent Use-Case

It is evident from the previous discussion in section "Introduction" that the spectrum extension via CR systems and SC densification is significant to the 5G system.

Based on this, a preliminary concept of cognitive small cell (CSC), a promising application that combines the benefits from the SC deployment and the efficient usage of the spectrum below 6 GHz, by realizing CR, is presented. A typical scenario where the CSC finds its application would be the coexistence of Wi-Fi or unlicensed small cell and wireless cellular systems [7]. The notion of CSC has been previously investigated by Elsawy et al. [19], where the authors primarily emphasized on the modeling techniques that depict the positioning of several CSCs inside the network. The modeling is based on stochastic geometry, which allows a spatial averaging over multiple network geometries [32]. Due to this, the performance analysis of the CSC has been limited mainly to network abstraction. In contrast, this chapter examines the fundamental aspects encountered while deploying a CSC, which otherwise could forbid its realization of this concept over the hardware. A comprehensive incorporation of CSC in a preliminary 5G architecture is illustrated in Fig. 4. In order to enhance the viability of the proposed network architecture, it is reasonable to highlight some of the essential ingredients pertaining to the deployment of the CSC.

Network Elements

In order to propose a successful integration of CSC in a 5G network, the following key elements are essential: a CSC-base station (CSC-BS), a macro-cell-base station (MC-BS), and mobile stations (MSs), cf. Fig. 4. MSs are the devices either served

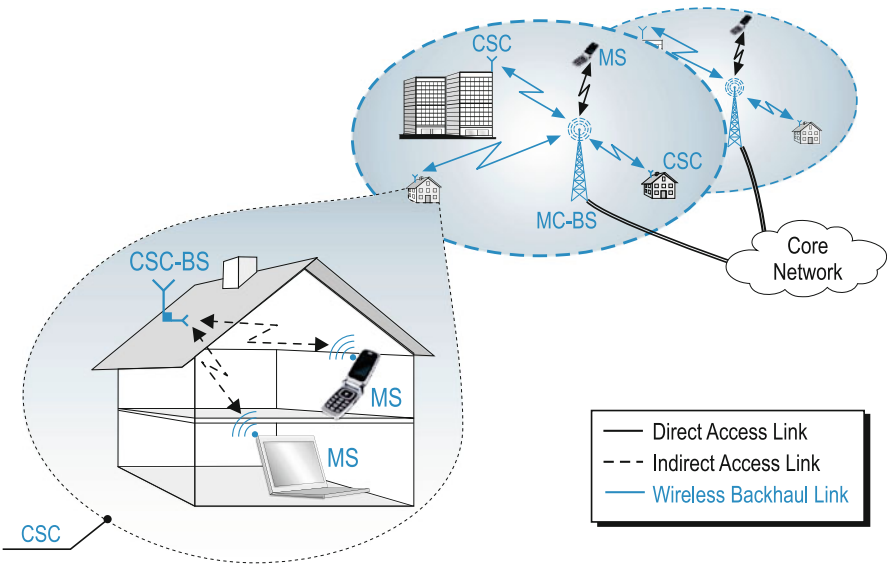

Fig. 4 An illustration of the CSC deployment in a 5G network

by the MC-BS over a *direct access* link or the CSC-BS over an *indirect access* link. The direct access and the indirect access are the nomenclature used to distinguish a state-of-the-art (spectrum) access between the MC-BS and the MS from an access between the CSC-BS and the MS representing a CR communication, respectively. Furthermore, the MC-BS is connected to several CSC-BSs over a *wireless backhaul* link. Although the MC-BS and the MS already exist in the conventional cellular architecture, to incorporate the opportunistic access inside the CSC, it is necessary to consider a functionality upgrade.

Spectrum Access

In the proposed network architecture, the access to the spectrum is realized over the wireless backhaul, the direct access, and the indirect access links, cf. Fig. 4.

1. A wireless backhaul is a point-to-point wireless link between the CSC-BS and the MC-BS that relays the traffic generated from the CSC to the core network. With regard to the densification of the CSC in 5G network, the wireless backhaul link, in contrast to the optical fiber link, presents a cost-effective and energy-efficient alternative to the mobile operator. With limited infrastructure required for the deployment, wireless backhauling accelerates the installation process and promotes scalability of the network. For the wireless backhaul link, considering that it is utilized for a longer time duration, an exclusive spectrum represents a viable option. In this context, it is sensible to nominate a mmW band; alternatively, an exclusive band below 6 GHz can be acquired using the principles of licensed shared access (LSA) [21].
2. A direct access link represents a direct access of the MS at the MC-BS over the allocated spectrum. Consequently, the spectrum access for this link is analogous to the one existing in the state-of-the-art wireless standards.
3. The CSC elements (the CSC-BS and the MS) are responsible for executing the secondary access to the licensed spectrum. The additional spectrum, acquired through the realization of CR techniques, including spectrum sensing and power control, at the CSC-BS, is used for the communication between the CSC-BS and the MS over the indirect access link.

Hardware Feasibility

Along with other ingredients, it is essential to outline certain aspects that pertain to the hardware realizability of the CSC. For the CSC-BS, an antenna mount system consisting of an indoor and an outdoor antenna is proposed. The indoor antenna exploits the walls of the building to physically separate the indoor transmissions over the indirect access link. In this way, the CSC is able to mitigate the interference to the primary system and to the neighboring CSCs and vice versa. However, the outdoor antenna secures a narrow beam transmission to enhance the link quality for the wireless backhaul link. Besides this, it is a well-known fact that software-

defined radio (SDR) has played an important role in the genesis of the CR [37]. This means that the SDR can serve as a suitable platform for executing CR techniques, accomplishing rapid prototyping for the CR systems. Taking this into account, the SDR platform is utilized for realizing (or demonstrating) the CR functionality pursued by the CSC-BS over a hardware.

Indoor Deployment

From a market survey, it has been depicted that 70% of the mobile traffic is originated from indoor locations [13]. Another survey of the leading WiMAX operators revealed that 80% of their subscribers will be connected indoors [59]. In addition, a new range of wireless services, categorized as Internet of things (IoT), will operate indoors. Following these facts, it is clear that the performance gains in terms of spectrum reuse will be far more consequential if we manage to consolidate these sources of traffic by means of SCs deployment. In order to capture the indoor-originated traffic, it is sensible to consider the residential and enterprise as the main deployment scenarios for the CSC, cf. Fig. 4. Except for a different coverage regime, the operating principles of these scenarios are analogous. Besides, in context with the CR, where the interference mitigation between the primary and the secondary systems is a significant aspect, a CR communication within walls (which attributes to an indoor deployment) provides a spatial separation between the two systems. This, however, does not indicate that CR communication is limited to indoor scenarios. As the matter of fact, the indoor deployment is opted to:

- Exploit the behavioral dimension of the traffic source (traffic management) and
- Mitigate the interference between the two systems

so that coexistence with the licensed users is encouraged. In this regard, an indoor scenario is considered for the deployment of the CSC, cf. Fig. 4. Besides employing such interference mitigation approach, an effective control over the interference is essential for a successful operation of the CR systems. Therefore, the next section extensively discusses the performance of the CR systems.

Performance Analysis of CR Systems: A Challenging Task

Since the evolution of wireless systems, understanding the performance of novel algorithms/techniques related to the wireless systems has always been a challenging task. With regard to this, for a CR system, because of the involvement of two different systems, namely, primary and secondary systems, this task is even more difficult. On one end, it has been engaging a large number of researchers that are eager to find solutions for the new set of problems that are emerging from an interplay between these two systems, leading them to develop theoretical models (system models). As a result, these models allow us to determine the performance

limits of the CR system. However, to sustain analytical tractability, they tend to consider assumptions that in most situations are unrealistic for a hardware deployment.

On the other end, due to the coexistence of the two systems sharing the same spectrum, the performance of a CR system is critical to the regulatory bodies and the mobile operators, responsible for managing the spectrum. These operators are the ones who are willing to share their license (as primary system) or the ones who are willing to access the licensed spectrum (as secondary system). In this regard, despite the numerous theoretical models that exist in the literature, when it comes to judging the performance of a CR system, the regulatory bodies give more preference to the hardware implementations.

These different mindsets and the lack of proper guidelines ultimately slow down the evolution of the CR in realistic scenarios. Under this situation, it is advisable to merge these mindsets and establish a deployment-centric viewpoint toward the CR systems, according to which the upcoming models and/or techniques not only associate themselves to the performance characterization but also eligible for practical implementations.

The coexistence between the primary and the secondary systems can be accomplished only through a detailed analysis of the performance of these systems. To address this issue, the researchers have made an intensive effort to develop system models [38, 39, 52] that characterize the performance of the CR systems. The performed analysis boils down to the fact that the CR systems are allowed to successfully coexist with the primary system only if they respect the interference power (or interference) at the primary system caused due to an access to the licensed spectrum. In other words, imposing an interference constraint ensures a sufficient protection to the primary systems and enables the CR system to perform secondary access.

With regard to the aforementioned constraint, the CR system also intends to deliver a certain quality of service/quality of experience (QoS/QoE) in the form of throughput to its corresponding secondary receiver (SR), defined as *secondary throughput*. Such a QoS/QoE provisioning helps us to determine the potential applications or prominent use-cases for the CR system. For instance, the secondary throughput's knowledge over the access link enables the CR to execute a band allocation policy, based on which the CR can relinquish those channels that ineffectively contribute to the secondary throughput, and/or are responsible for causing interference at the primary system. As a result, the performance of a CR system can be jointly characterized in terms of the harmful interference received at the primary system and the throughput achieved by the secondary system.

The fact is that the derived expressions depicting the performance of the CR systems are rarely examined over the hardware, mainly because of the complicated deployment scenario or the computational complexity of the employed CR techniques, leaving the validity of the existing theoretical analysis questionable. Because of this, we tend to overlook certain imperfections (or uncertainties) inherent to the CR systems, including noise uncertainty, channel imperfections, signal uncertainty, noise/channel correlation, hardware imperfections, and modeling imperfections

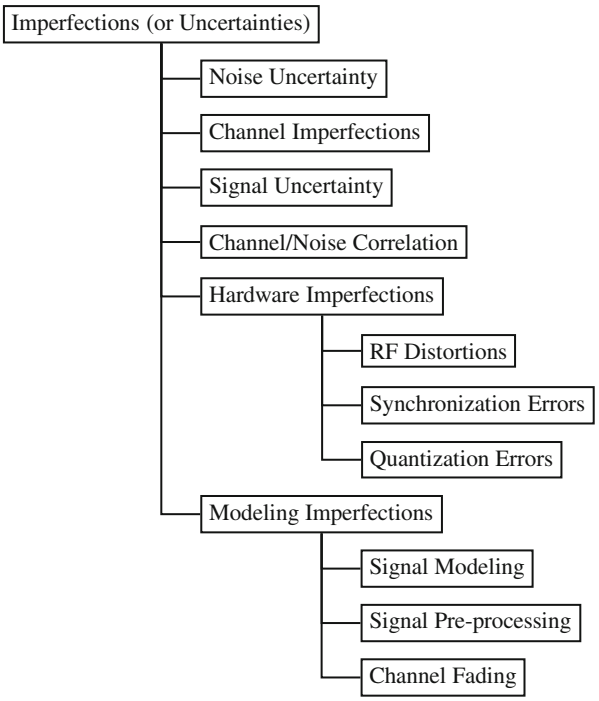

Fig. 5 An illustration of major imperfections (or uncertainties) in CR systems [68]

[68], which may be responsible for degrading the performance of CR systems; refer to Fig. 5. In other words, by neglecting these imperfections in the system model, the performance of a CR system is overestimated. To narrow down the perspective, this chapter considers the effect on performance of CR systems due to imperfect channel while putting emphasis on the fact that the performed analysis can be easily validated through a hardware implementation.

Imperfect Channel Knowledge

In a nutshell, *a CR is an agile system that possesses the ability to adapt to the changes in the environment*. From a physical layer perspective, this corresponds to the response to the changes incurred within the system or from the outside environment, which in a way leads to a performance enhancement. Inherent to the wireless systems, these changes may arise due to the variations in the signal caused by the presence of the thermal noise at the receiver and the fading in the channel. It is well known from the textbooks, related to wireless communications [29, 74], that the channel fading, in particular, is critical for wireless systems. As a matter of fact, channel knowledge – in the form of channel state information at the transmitter (CSIT) available through a feedback from the receiver – has rendered a substantial

improvement in the performance in terms of data rate, for instance, multiplexing gains for a MIMO system [55].

In context with a CR system, the channel knowledge, unlike the conventional or state-of-the-art wireless systems, is not confined to a single transmitter-receiver link. It rather includes all the related channels that exist within as well as across the primary and the secondary systems. Therefore, at this stage, it is worth understanding the fact that channel knowledge is paramount for the hardware implementation of the CR systems. This knowledge allows them to exercise CR techniques and to respect the desired interference constraints, which are necessary for their coexistence with the primary systems. Besides, from a theoretical perspective, the channel knowledge is required for the performance characterization. The absence of this knowledge, especially of those channels that are related to the interference at the primary systems, renders the performance characterization of a CR system inadequate for the practical implementations.

Despite the existence of multitude of analytical models in the literature [25, 52, 67] that consider with the performance analysis of a CR system, its performance with regard to the channel estimation, due to the complexity of the underlying problem, has never been completely understood. In order to curtail this gap, this chapter capitalizes on the estimation of the involved channels in a CR system. In this sense, the accessibility of the channel knowledge at the CSC-BS facilitates the implementation of the CR techniques at the CSC-BS, establishing a CR communication link with the MS over the acquired spectrum. More importantly, this knowledge allows us to regulate the interference at the PR below a desired level.

Certainly, an access to the channel knowledge comes at a certain cost. Firstly, the inclusion of channel estimation demands an allocation of a certain time interval by the CSC-BS. In consideration to the time allocation, a certain degradation in the performance in terms of the throughput is obvious. Secondly, the variations introduced due to the estimation process, also treated as imperfect channel knowledge, lead to an uncertainty in the interference, defined as *uncertain interference*, to the primary systems. The uncertain here specifically symbolizes the variations in the interference power received at the PR that exists because of the imperfect channel knowledge. If not considered, this uncertain interference may severely degrade the performance of the CR systems. In order to approach a successful integration of channel estimation into the CR system, it is essential to consider the performance degradation arising due to the time allocation and the uncertain interference in the system model. These effects concerning the performance degradation have been completely left aside in the existing models that consider the perfect channel knowledge. Section "Interweave System: A Case Study" takes these effects into account to establish analytical frameworks that allow us to understand the behavior of the CR systems as interweave systems under those situations that are close to realistic scenarios.

Shifting the focus back to the deployment, it is worthy to understand that the channel estimation, facilitating shared access to the licensed spectrum, is viable only if the CR system is equipped with the knowledge about the primary system. This implies that in order to perform channel estimation based on conventional

techniques – such as training-based [70], pilot-based [27, 28], and signal to noise ratio-based [14, 66] channel estimation, which already exist in the literature – a preliminary processing in the form of synchronization and demodulation of the baseband signal received from the primary system is necessary. The existence of multiple wireless standards and their complexity preclude us from deploying a dedicated circuitry corresponding to each primary system [26]. The fact is, these conventional channel estimation techniques are well known for delivering accurate channel estimates, which is employed in state-of-the-art wireless standards. However, in context of the CR systems, these techniques

- Increase the complexity related to the channel estimation, evaluated in terms of the mathematical operations,
- Demand the demodulation of the primary user (PU) signal.

Under these circumstances, it is advisable to consider only those solutions that offer low complexity and show versatility toward different PU signals. Generally speaking, such solutions will not only ease the deployment process but also have a large acceptance among the CR community. For instance, energy-based detection (or energy detection) has been a popular choice compared to its counterparts such as matched filtering-based and cyclostationary-based detection for detecting a PU signal, required for performing spectrum sensing for the interweave systems (discussed later in section "Interweave System: A Case Study"). A direct comparison of these techniques by simply counting their implementations for hardware demonstration has been done in [60].

On similar grounds as energy detection, in order to approach the channel estimation for the CR system, particularly for the channels that involve the primary systems, a *received power-based* channel estimation technique is proposed as a part of the analytical framework. It is worthy to understand that the received power refers to the signal power measured after analog to digital conversion; hence, it consists of the signal and the noise power. Traditionally, received signal strength is a metric used for measuring signal quality to perform tasks such as cell association and handover [8]. This channel estimation technique is introduced to substitute the conventional techniques because, like energy detection, employing received power-based estimation assures the low complexity and the versatility toward unknown PU signal requirements of the CR system, and consequently facilitates its deployment. Besides, the channel within the secondary framework, treated as a conventional transmitter-receiver link, does not fall in the aforementioned category. Therefore, its knowledge is procured by employing a pilot-based channel estimation technique.

Modeling Imperfections

Besides imperfect channel knowledge, this section briefly discusses some key issues that are necessary from a deployment perspective but left aside while establishing the system model.

Signal Modeling

The Gaussian and the constant power signals are generally used for modeling the PU signals, which correspond to orthogonal frequency-division multiplexing (OFDM) and phase-shift keying (PSK) modulated signals, respectively. In practice, this modeling can be employed only if the sampling point is selected appropriately, hence resulting in i.i.d. samples. In other situations, the samples are correlated. This correlation is not considered while modeling the system, hence leading to deviation of the performance parameters (false alarm probability and detection probability) obtained theoretically from the ones obtained by performing the measurements. In order to resolve this issue, the OFDM and PSK-modulated signals can be replaced with their mathematical counterparts for signal transmission; these include a Gaussian and a sinusoidal signal, respectively. By doing this, we are able to avoid the correlation between the samples that are used for computing the energy.

Signal Preprocessing

Generally, ST is emulated using an SDR platform (for instance, Universal Software Radio Peripheral (USRP) B210, an SDR from Ettus Research [22]). Such low-cost hardwares are associated with a direct downconversion of the bandpass to the baseband signal – a homodyne receiver. Spurious effects such as DC offset, flicker noise $(1/f)$, and I/Q imbalance arising from the analog front-end can affect the accuracy of the analytical expressions. These spurious effects, particularly the DC offset and the flicker noise, become significant at low signal to noise ratio. In order to retrieve the complex samples close to the one obtained while characterizing the system model that do not take such spurious effects into account, the following signal processing (referred as preprocessing) is proposed; please consider Fig. 6:

- The received PU signal (a complex sinusoid) is oversampled with sampling frequency of 200 kHz. In order to filter out the spurious effects, the local oscillator is tuned at a certain offset frequency defined as $f_{\text{LO-Offset}} = 50\,\text{kHz}$, refer to Fig. 6a.
- Subsequently, a bandpass filter with bandwidth = 50 kHz, corresponding to an oversampling factor = 4, is employed to obtain the desired bandpass signal at the $f_{\text{LO-Offset}}$. This filters out the DC offset and the flicker noise present at low frequencies, cf. Fig. 6b.
- In order to obtain the lowpass equivalent of the desired signal, a digital down-conversion (i.e., multiplying with a complex sinusoid with frequency $f_{\text{LO-Offset}} = 50\,\text{kHz}$) of the bandpass filtered signal is performed, cf. Fig. 6c.
- Lastly, a decimation filter (with decimation factor = 4) over the downconverted signal is applied, cf. Fig. 6d, to reduce the correlation between the samples, arising due to oversampling.

Channel Fading

Channel fading is essential to establish a macroscopic view toward the performance of a CR system. With regard to this, Rayleigh block fading is mostly preferred for modeling channel fading. However, block fading considers uncorrelated over the

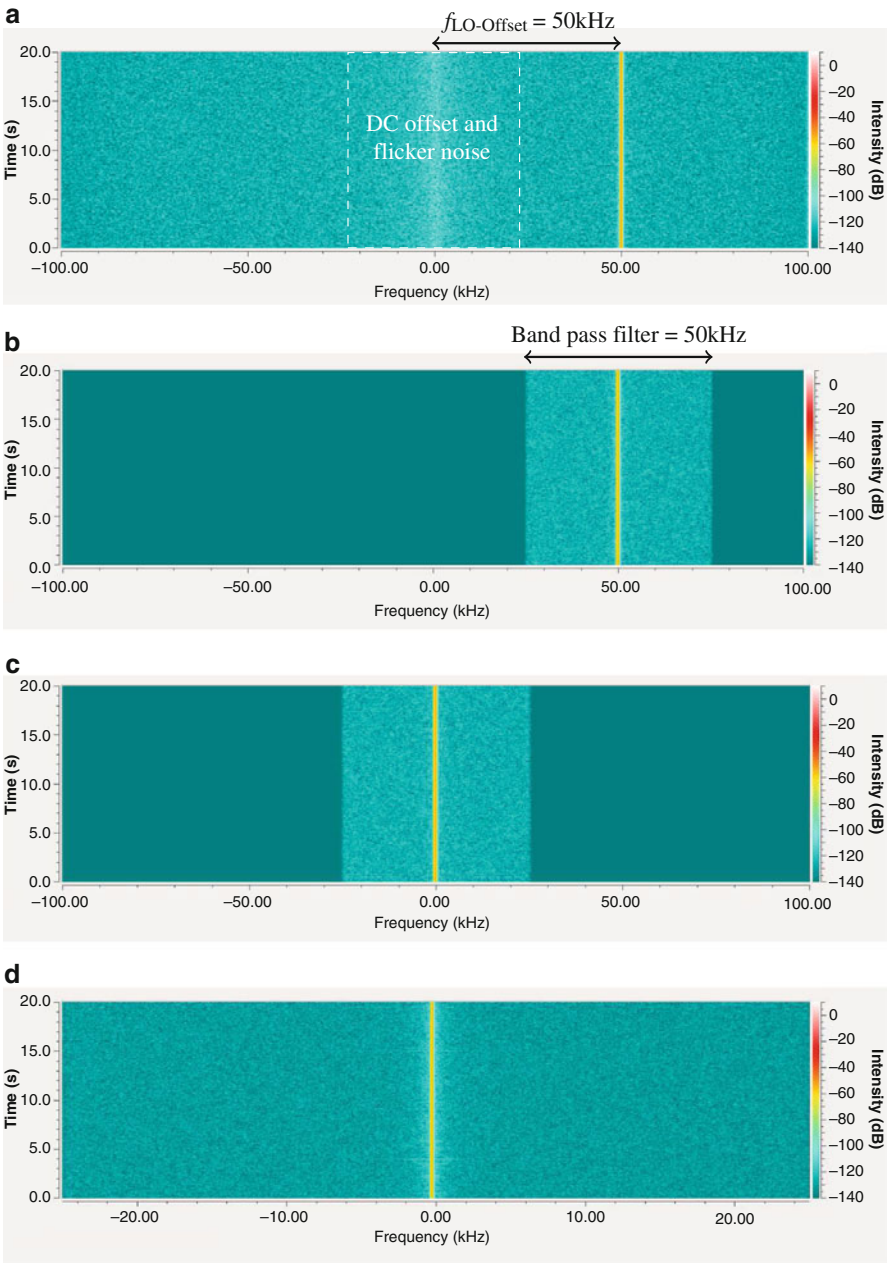

Fig. 6 An illustration of the signal processing steps carried out at the host computer to preclude the spurious effects such as the DC offset and the flicker noise on the signal received at the ST. (**a**) Signal with oversampling, where the local oscillator is tuned at $f_{\text{LO-Offset}} = 50\,\text{kHz}$. (**b**) Signal after bandpass filtering, filter bandwidth $= 50\,\text{kHz}$. (**c**) Signal after digital downconversion. (**d**) Signal after decimation

different energy measurements. However, in practice, either uncorrelated fading is not encountered or the measurements may converge to a different fading model such as Nakagami-*m* fading model [41]. Due to this issue, hardware validation of the analytical expressions that incorporates channel fading models is rarely considered.

One possible way of resolving this issue is to emulate fading at the ST, according to which the transmit signal is modulated with channel gains at the PT using software [63]. This allows us to establish a close relation between the analytical model and the acquired energy measurements, which consequently enhances the validation of a CR system that incorporates channel fading for the performance analysis. However, to proceed with the hardware validation pertaining to scenarios that involve channel fading, in the future, it is essential to incorporate correlated fading model into the system and estimate the related parameters [41].

Interweave System: A Case Study

At this stage, it is well-understood that the knowledge of the related channels is crucial for the application of CR techniques in the practical scenarios. This section capitalizes on the successful integration of this knowledge on interweave system. In this context, the indoor deployment scenario is transformed into an interweave scenario, whereby a spectrum sensing mechanism is employed at the CSC-BS enabling a secondary access to the licensed spectrum. Section "Theoretical Analysis" derives the theoretical expressions to capture the effect of imperfect channel knowledge on the performance of an IS. Further, section "Numerical Results" establishes an estimation-sensing-throughput tradeoff that depicts the suitable estimation and the suitable sensing time intervals at which the maximum secondary throughput is achieved by an IS. Please note that this section contains material from the following publication [45].

For detecting a PU signal, several techniques such as energy-based detection (or energy detection), matched filtering-based, cyclostationary-based, and feature-based detection exist [5]. Because of its versatility toward unknown PU signals and its low computational complexity, energy detection has been extensively investigated in the literature [34,75]. In this technique, the decision is accomplished by comparing the power received at the ST to a decision threshold. In reality, the ST encounters variations in the received power due to the existence of thermal noise at the receiver and fading in the channel. Subsequently, these variations lead to sensing errors described as misdetection and false alarm, which limit the performance of the IS. In order to determine the performance of a detector, it is essential to obtain the expressions of detection probability and false alarm probability.

In particular, detection probability is critical for IS because it protects the PR from the interference induced by the ST. As a result, the IS has to ensure that they operate above a target detection probability [61]. Therefore, the characterization of the detection probability becomes absolutely necessary for the performance analysis of the IS. In this context, Urkowitz [75] introduced a probabilistic framework for characterizing the sensing errors; however, the characterization accounts only for the noise in the system.

To encounter the variation caused by channel fading, a frame structure has been introduced in [52], assuming that the channel remains constant over the frame duration (corresponds to a quasi-static block fading). Upon exceeding the frame duration, the system may observe a different realization of the channel. Based on this frame structure, the performance of the IS has been investigated in terms of a deterministic (corresponding to a nonrandom behavior) channel [52, 67] and a random channel [16, 34]. These deterministic and random behaviors of the channel illustrate a microscopic and a macroscopic view toward the performance characterization, respectively, of a CR system. In this chapter, the former approach is considered; hence, the performance is analyzed for a specific frame, i.e., for a certain (unknown) realization of the channel.

Besides the detection probability, false alarm probability has a large influence on the throughput achieved by the secondary system. Recently, the performance characterization of CR systems in terms of a sensing-throughput tradeoff has received significant attention [12, 52]. According to Liang et al. [52], the ST assures a reliable detection of a PU signal by retaining the detection probability above a desired level with an objective of maximizing the throughput at the SR. In this way, the sensing-throughput tradeoff depicts a suitable sensing time interval that achieves a maximum secondary throughput. To characterize the detection probability and the secondary throughput, the system requires the knowledge of interacting channels, namely, a *sensing* channel, an *access* channel, and an *interference* channel; refer to Fig. 7. Since the interference to the PR is controlled by a regulatory constraint over the detection probability, in this view, the interaction with the PR is excluded in the considered scenario [52]. The baseline models, investigated in the literature, assume the knowledge of these channels to be available at the ST. However, in practice, this knowledge is not available; thus, it needs to be estimated by the secondary system. As a result, the existing solutions for the IS are considered inadequate from a practical viewpoint.

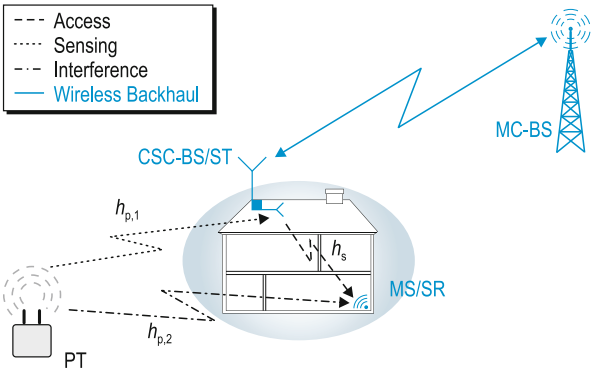

Fig. 7 A cognitive small cell scenario demonstrating: (i) the interweave paradigm, (ii) the associated network elements, which constitute cognitive small cell-base station/secondary transmitter (CSC-BS/ST), mobile station/secondary receiver (MS/SR), macro cell-base station (MC-BS) and primary transmitter (PT), (iii) the interacting channels: sensing ($h_{p,1}$), access (h_s) and interference ($h_{p,2}$)

As a matter of fact, the sensing and the interference channels related to the CR system (refer to Fig. 7) represent the channels between two different (primary and secondary) systems. In this context, it becomes challenging to select the estimation methods in such a way that low complexity and versatility (towards different PU signals) requirements are satisfied. These issues, discussed later in section "Proposed Approach", render the existing estimation techniques [14, 27, 28, 66, 70] unsuitable for hardware implementations. To tackle the issue related to the channel estimation, as discussed previously in section "Imperfect Channel Knowledge", a received power-based estimation at the ST and at the SR for the sensing and the interference channels is employed, respectively. Considering the fact that the access channel corresponds to the link between the ST and the SR, conventional channel estimation techniques such as pilot-based channel estimation at the ST is employed.

Inherent to the estimation process, the variations due to the channel estimation translate to the variations in the performance parameters, namely, detection probability and secondary throughput. In particular, the variations induced in the detection probability cause uncertain interference at the PR, which may severely degrade the performance of a CR system. The detrimental effect due to the time allocation for the channel estimation and the uncertain interference due to imperfect channel knowledge have not been considered in [12, 52] or studied partially in [11, 14]. In this context, the performance characterization of an IS with imperfect channel knowledge remains an open problem. Motivated by this fact, this section focuses on the performance characterization of the IS in terms of sensing-throughput tradeoff taking these aforementioned aspects into account.

System Model

Interweave Scenario

To consider the applicability of IS, the CSC, a CR application illustrated previously in Fig. 4 is transformed into an interweave scenario. Considering the fact that the IS is employed at the CSC-BS, the CSC-BS and the MS represent the ST and the SR, respectively. A hardware prototype of the CSC-BS operating as IS was presented in [40]. For simplification, a PU constraint based on false alarm probability (Neyman-Pearson criterion) was considered in [40]. With the purpose of improving system's reliability, the analysis is extended to employ a PU constraint on the detection probability.

Signal Model

Subject to the underlying hypothesis that illustrates the presence ($\mathscr{H}_1$) or the absence ($\mathscr{H}_0$) of a PU signal, the discrete and complex signal received at the ST is given by

$$y_{\mathrm{ST}}[n] = \begin{cases} h_{\mathrm{p},1} \cdot x_{\mathrm{PT}}[n] + w_{\mathrm{ST}}[n] & : \mathscr{H}_1 \\ w_{\mathrm{ST}}[n] & : \mathscr{H}_0 \end{cases}, \tag{1}$$

The signal $x_{\mathrm{PT}}[n]$ transmitted by the PUs can be modeled as (i) a PSK modulated signal or (ii) a Gaussian signal. The signals that are prone to high inter-symbol interference or entail precoding, for instance, OFDM signal with linear precoding, can be modeled as Gaussian signals [52]. In this chapter, the analysis is focused on the latter case, i.e., the primary and the secondary systems employ OFDM to carry out their transmission. As a result, the mean and the variance for the signal and the noise are determined as $\mathbb{E}\left[x_{\mathrm{PT}}[n]\right] = 0$, $\mathbb{E}\left[w_{\mathrm{ST}}[n]\right] = 0$, $\mathbb{E}\left[|x_{\mathrm{PT}}[n]|^2\right] = \sigma_{\mathrm{s}}^2$ ($= P_{\mathrm{Tx,PT}}$) and $\mathbb{E}\left[|w_{\mathrm{ST}}[n]|^2\right] = \sigma_{\mathrm{w}}^2$. The channel $h_{\mathrm{p},1}$ is considered to be independent of $x_{\mathrm{PT}}[n]$ and $w_{\mathrm{ST}}[n]$. Thus, $y_{\mathrm{ST}}[n]$ is also an independent and identically distributed (i.i.d.) random process.

Similar to (1), during data transmission, the discrete and complex received signal at the SR conditioned on the detection probability ($\mathrm{P_d}$) and the false alarm probability ($\mathrm{P_{fa}}$) is given by

$$y_{\mathrm{SR}}[n] = \begin{cases} h_{\mathrm{s}} \cdot x_{\mathrm{ST}}[n] + h_{\mathrm{p},2} \cdot x_{\mathrm{PT}}[n] + w_{\mathrm{SR}}[n] & : 1 - \mathrm{P_d} \\ h_{\mathrm{s}} \cdot x_{\mathrm{ST}}[n] + w_{\mathrm{SR}}[n] & : 1 - \mathrm{P_{fa}} \end{cases}, \tag{2}$$

where $x_{\mathrm{ST}}[n]$ corresponds to discrete and complex sample transmitted by the ST and $w_{\mathrm{SR}}[n]$ is the AWGN at the SR with $\mathscr{CN}(0, \sigma_{\mathrm{w}}^2)$. In practice, the noise power at different network nodes (the ST, the SR, and the PR) has different values. The fact is, only the signal to noise ratios received at these nodes are affected due to these different values, which are already included in the performance analysis. For the brevity of the exposition, the noise powers at these nodes are expressed using a single notation (σ_{w}^2). Further, $|h_{\mathrm{s}}|^2$ and $|h_{\mathrm{p},2}|^2$ represent the power gains for the access and the interference channels, refer to Fig. 7.

Problem Description

In accordance with the conventional frame structure, the ST performs sensing for a duration of τ_{sen}. The test statistics at the ST is evaluated as

$$\mathrm{T}(\mathbf{y}) = \frac{1}{\tau_{\mathrm{sen}} f_{\mathrm{s}}} \sum_{n=1}^{\tau_{\mathrm{sen}} f_{\mathrm{s}}} |y_{\mathrm{ST}}[n]|^2 \underset{\mathscr{H}_0}{\overset{\mathscr{H}_1}{\gtrless}} \mu, \tag{3}$$

where μ is the decision threshold, f_{s} represents the sampling frequency, and $\mathbf{y}$ is a vector with $\tau_{\mathrm{sen}} f_{\mathrm{s}}$ samples. $\mathrm{T}(\mathbf{y})$ represents a random variable, whereby the characterization of the cdf depends on the underlying hypothesis. With regard to the Gaussian signal model, which corresponds to the OFDM signal transmitted by the PU, $\mathrm{T}(\mathbf{y})$ follows a central chi-squared ($\mathscr{X}^2$) distribution for both hypotheses $\mathscr{H}_0$ and $\mathscr{H}_1$ [46]. It is worthy to mention here that the Gaussian approximation that exists due to application of central limit theorem – confining the applicability of the considered analysis to large samples only – is avoided. in this context, an effort has been made to derive the theoretical expressions so that the performance analysis is valid for all sample sizes.

As a result, the detection probability ($\mathrm{P_d}$) and the false alarm probability ($\mathrm{P_{fa}}$) corresponding to (3) are determined as [73]

$$\mathrm{P_d} = \Gamma\left(\frac{\tau_{\mathrm{sen}} f_{\mathrm{s}}}{2}, \frac{\tau_{\mathrm{sen}} f_{\mathrm{s}} \mu}{2 P_{\mathrm{Rx,ST},h_{\mathrm{p,1}}}}\right), \tag{4}$$

$$\mathrm{P_{fa}} = \Gamma\left(\frac{\tau_{\mathrm{sen}} f_{\mathrm{s}}}{2}, \frac{\tau_{\mathrm{sen}} f_{\mathrm{s}} \mu}{2\sigma_{\mathrm{w}}^2}\right), \tag{5}$$

where $P_{\mathrm{Rx,ST},h_{\mathrm{p,1}}}$ is the power received over the sensing channel and $\Gamma(\cdot,\cdot)$ represents a regularized upper-incomplete Gamma function [31].

Following the characterization of $\mathrm{P_{fa}}$ and $\mathrm{P_d}$, Liang et al. [52] established a tradeoff between the sensing time and the secondary throughput (R_{s}) subject to a target detection probability ($\bar{\mathrm{P}}_{\mathrm{d}}$). This tradeoff is represented as

$$\begin{aligned} R_{\mathrm{s}}(\tilde{\tau}_{\mathrm{sen}}) &= \max_{\tau_{\mathrm{sen}}} R_{\mathrm{s}}(\tau_{\mathrm{sen}}) \\ &= \frac{T - \tau_{\mathrm{sen}}}{T}\Big[\mathrm{C_0}(1-\mathrm{P_{fa}})\mathbb{P}(\mathscr{H}_0) + \mathrm{C_1}(1-\mathrm{P_d})\mathbb{P}(\mathscr{H}_1)\Big], \end{aligned} \tag{6}$$

$$\text{s.t. } \mathrm{P_d} \geq \bar{\mathrm{P}}_{\mathrm{d}}, \tag{7}$$

$$\text{where } \mathrm{C_0} = \log_2\left(1 + |h_{\mathrm{s}}|^2 \frac{P_{\mathrm{Tx,ST}}}{\sigma_{\mathrm{w}}^2}\right) = \log_2\left(1+\gamma_{\mathrm{s}}\right), \tag{8}$$

$$\begin{aligned} \mathrm{C_1} &= \log_2\left(1 + \frac{|h_{\mathrm{s}}|^2 P_{\mathrm{Tx,ST}}}{|h_{\mathrm{p,2}}|^2 P_{\mathrm{Tx,PT}} + \sigma_{\mathrm{w}}^2}\right) \\ &= \log_2\left(1 + \frac{|h_{\mathrm{s}}|^2 P_{\mathrm{Tx,ST}}}{P_{\mathrm{Rx,SR}}}\right) = \log_2\left(1 + \frac{\gamma_{\mathrm{s}}}{\gamma_{\mathrm{p,2}}+1}\right), \end{aligned} \tag{9}$$

where $\mathbb{P}(\mathscr{H}_0)$ and $\mathbb{P}(\mathscr{H}_1)$ are the occurrence probabilities for the respective hypothesis, whereas $\gamma_{\mathrm{p,1}}$ and γ_{s} represent the signal to noise ratios for the links PT-ST and ST-SR, respectively, and $\gamma_{\mathrm{p,2}}$ corresponds to interference (from the PT) to noise ratio for the link PT-SR. Moreover, $P_{\mathrm{Tx,PT}}$ and $P_{\mathrm{Tx,ST}}$ represent the transmit power at the PT and the ST, whereas $P_{\mathrm{Rx,SR}}$ corresponds to the received power (which includes the interference power from the PT and the noise power) at the SR. In addition, $\mathrm{C_0}$ and $\mathrm{C_1}$ represent the data rate without and with the interference from the PT. Please note that the following terms the data rate $\mathrm{C_0}$, $\mathrm{C_1}$ and the throughput R_{s} have been introduced to make a clear distinction between the instantaneous data rate and its average value over the frame duration. Also, the use of the term "capacity" is avoided for representing $\mathrm{C_0}$ and $\mathrm{C_1}$, since it implies the optimization of the mutual information over the cognitive channel.

In other words, using (6), the ST determines a suitable sensing time $\tau_{\text{sen}} = \tilde{\tau}_{\text{sen}}$, such that the secondary throughput is maximized subject to a target detection probability; refer to (7). From the deployment perspective, the tradeoff depicted above has the following fundamental issues:

- Without the knowledge of the received power $P_{\text{Rx,ST},h_{\text{p,I}}}$ over the sensing channel, it is not feasible to characterize P_d, refer to (4). This renders the characterization of the secondary throughput (6) impossible and the constraint defined in (7) inappropriate.
- Moreover, the knowledge of the interference and the access channels is required at the ST; refer to (8) and (9) for characterizing the throughput in terms of C_0 and C_1 at the SR.

Proposed Approach

In order to overcome the difficulties discussed in section "Problem Description", the following strategy is proposed:

1. As a first step, the estimation of the involved channels is considered. In order to characterize the detection probability, a received power-based estimation at the ST for the sensing channel is employed. This is done to ensure that the detection probability remains above a desired level. Further, a pilot-based estimation and a received power-based estimation for the access channel and the interference channel are employed at the ST and the SR, respectively, to characterize the secondary throughput.
2. Next, the variations due to channel estimation in the estimated parameters, namely, received power (for the sensing and the interference channels) and the power gain (for the access channel) are characterized in terms of their cdfs.
3. In order to investigate the performance of the IS subject to the channel estimation, these variations in the performance parameters, which include the detection probability and the secondary throughput, are characterized in terms of their cdfs.
4. Finally, the derived cdfs are utilized to obtain the expressions of sensing-throughput tradeoff. Hence, based on these expressions, the impact of imperfect channel knowledge on the performance of the ISs is qualified, and subsequently the achievable secondary throughput at a suitable sensing time is determined.

Considering the channel estimation, it is well known that systems with transmitter information (which includes the filter parameters, pilot symbols, modulation type, and time-frequency synchronization) at the receiver acquire the channel knowledge by listening to the pilot data sent by the ST [4, 23, 27, 28]. Other systems, where the receiver possesses either no access to this information or is limited by hardware complexity, procure channel knowledge indirectly by estimating a different parameter that entails the channel knowledge, for instance, received signal power [43] or received signal to noise ratio [14,66]. Recently, estimation techniques such as pilot-based estimation [48, 71] and received power-based estimation [42] have been applied to obtain channel knowledge for the CR systems. However, the

performance analysis has been limited to the underlay systems, where the emphasis has been given on modeling the interference at the PR.

Since the pilot-based estimation requires the knowledge of the PU signal at the secondary system, the versatility (in terms of PU signals) of the secondary system is compromised. On the other side, for the estimation of the received signal to noise ratio, Eigenvalue (which involves matrix operations)-based approach [66] or iterative approaches such as expectation-maximization have been proposed [14]. Due to the complicated mathematical operations or the complexity of the iterative algorithms, such approaches tend to increase the hardware complexity of the ISs. In order to resolve these issues, a received power-based estimation for the sensing and the interference channels and a pilot-based estimation for the access channel are employed. Similar to the energy-based detection, since the received power-based estimation involves simple operations on the obtained samples such as magnitude squared followed by summation, the proposed estimation provides a reasonable tradeoff between complexity and versatility.

Frame Structure

In order to include channel estimation, a frame structure that constitutes estimation τ_{est}, sensing τ_{sen} and data transmission $T - \tau_{\text{sen}}$ is proposed, where τ_{est} and τ_{sen} correspond to time intervals and $0 < \tau_{\text{est}} \leq \tau_{\text{sen}} < T$; refer to Fig. 8. Since the estimated values of the interacting channels are required for determining the suitable sensing time (the duration of the sensing phase), the sequence depicted in Fig. 8 is reasonable for the hardware deployment, whereby estimation is followed by sensing. Particularly for the sensing channel, it is worthy to note that the samples used for estimation can be combined with the samples acquired for sensing

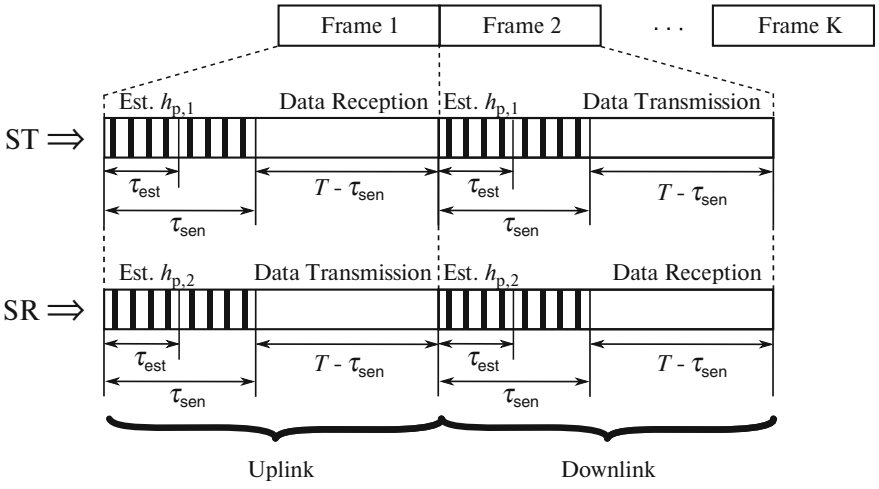

Fig. 8 Frame structure of the IS illustrating the time allocation of the channel estimation, sensing, and data transmission from the perspective of the ST and the SR

(therefore, the sensing phase incorporates the estimation phase, see Fig. 8) such that the time resources within the frame duration can be utilized efficiently, as shown in the frame structure in Fig. 8. Considering the fact that the number of pilot symbols is relatively small in comparison to the samples used for performing received power-based channel estimation, the time allocation of the pilot symbols does not affect the overall performance of the ISs. Hence, no time resources are allocated for the estimation of the access channel in the frame structure. In the following paragraphs, the estimation of the involved channels is considered.

Estimation of Sensing Channel ($h_{\mathrm{p},1}$)

Following the previous discussions, the ST acquires the knowledge of $|h_{\mathrm{p},1}|^2$ (included in $P_{\mathrm{Rx,ST},h_{\mathrm{p},1}}$, cf. (4)) to characterize $\mathrm{P_d}$ and to further evaluate the detector's performance. This knowledge is acquired by estimating the power received at the ST over the sensing channel.

Under $\mathscr{H}_1$, the received power-based estimated during the estimation phase at the ST is given as [75]

$$\widehat{P}_{\mathrm{Rx,ST},h_{\mathrm{p},1}} = \frac{1}{\tau_{\mathrm{est}} f_{\mathrm{s}}} \sum_{n=1}^{\tau_{\mathrm{est}} f_{\mathrm{s}}} |y_{\mathrm{ST}}[n]|^2. \tag{10}$$

$\widehat{P}_{\mathrm{Rx,ST},h_{\mathrm{p},1}}$ determined in (10) using $\tau_{\mathrm{est}} f_{\mathrm{s}}$ samples follows a central chi-squared distribution $\mathscr{X}^2$ [46]. f_{s} and τ_{est} are such that the number of samples $\tau_{\mathrm{est}} f_{\mathrm{s}}$ is an integer. The cdf of $\widehat{P}_{\mathrm{Rx,ST},h_{\mathrm{p},1}}$ is given by

$$F_{\widehat{P}_{\mathrm{Rx,ST},h_{\mathrm{p},1}}}(x) = 1 - \Gamma\left(\frac{\tau_{\mathrm{est}} f_{\mathrm{s}}}{2}, \frac{\tau_{\mathrm{est}} f_{\mathrm{s}} x}{2 P_{\mathrm{Rx,ST},h_{\mathrm{p},1}}}\right). \tag{11}$$

Estimation of Access Channel (h_{s})

The signal received from the SR undergoes matched filtering and demodulation at the ST; hence, it is reasonable to employ pilot-based estimation for h_{s}. Unlike received power-based estimation, pilot-based estimation renders a direct estimation of the channel. Now, to accomplish pilot-based estimation, the ST aligns itself to the pilot symbols transmitted by the SR.

Under $\mathscr{H}_0$, the discrete and complex pilot symbol at the output of the demodulator is given by [28]

$$p[n] = \sqrt{E_{\mathrm{s}}} h_{\mathrm{s}} + w_{\mathrm{ST}}[n], \tag{12}$$

where E_{s} denotes the pilot energy. Without loss of generality, the pilot symbols are considered to be +1. The maximum likelihood estimate, representing a sample average of N_{s} pilot symbols, is given by [27]

$$\widehat{h}_{\mathrm{s}} = h_{\mathrm{s}} + \underbrace{\frac{\sum_{n=1}^{N_{\mathrm{s}}} w_{\mathrm{ST}}[n]}{N_{\mathrm{s}}}}_{\epsilon}, \tag{13}$$

where ϵ denotes the estimation error. The estimate $\widehat{h}_{\mathrm{s}}$ is unbiased, is efficient, and achieves a Cramér-Rao bound with equality, with variance $\mathbb{E}\left[|h_{\mathrm{s}} - \widehat{h}_{\mathrm{s}}|^2\right] = \sigma_{\mathrm{w}}^2/N_{\mathrm{s}}$ [28].

Consequently, $\widehat{h}_{\mathrm{s}}$ conditioned on h_{s} follows a circularly symmetric Gaussian distribution:

$$\widehat{h}_{\mathrm{s}}|h_{\mathrm{s}} \sim \mathscr{CN}\left(h_{\mathrm{s}}, \frac{\sigma_{\mathrm{w}}^2}{N_{\mathrm{s}}}\right). \tag{14}$$

As a result, the power gain $|\widehat{h}_{\mathrm{s}}|^2$ follows a noncentral chi-squared $\left(\mathscr{X}'^2\right)$ distribution with two degrees of freedom and noncentrality parameter $\lambda_{\mathrm{s}} = \frac{N_{\mathrm{s}}|h_{\mathrm{s}}|^2}{\sigma_{\mathrm{w}}^2}$.

Estimation of Interference Channel ($h_{\mathrm{p,2}}$)

The knowledge of $|h_{\mathrm{p,2}}|^2$ is required to characterize the interference from the PT. Analog to the sensing channel, the SR performs received power-based estimation by listening to the signal transmitted by the PT.

Under $\mathscr{H}_1$, in the estimation phase (which implies ST is not transmitting, please consider Fig. 8), the discrete and complex signal received at the SR is given as

$$y_{\mathrm{SR}}[n] = h_{\mathrm{p,2}} \cdot x_{\mathrm{PT}}[n] + w_{\mathrm{SR}}[n]. \tag{15}$$

As a result, the estimated power at the SR, from the signal transmitted by the PT, is given by

$$\widehat{P}_{\mathrm{Rx,SR}} = \frac{1}{\tau_{\mathrm{est}} f_{\mathrm{s}}} \sum_{n=1}^{\tau_{\mathrm{est}} f_{\mathrm{s}}} |y_{\mathrm{SR}}[n]|^2, \tag{16}$$

where $\widehat{P}_{\mathrm{Rx,SR}}$ follows a $\mathscr{X}^2$ distribution.

Validation

At this stage, it is clear that the estimates $\widehat{P}_{\mathrm{Rx,ST},h_{\mathrm{p,1}}}$, $|\widehat{h}_{\mathrm{s}}|^2$ and $\widehat{P}_{\mathrm{Rx,SR}}$ exhibit the knowledge corresponding to the involved channels; however, it is essential to validate them, mainly $\widehat{P}_{\mathrm{Rx,ST},h_{\mathrm{p,1}}}$ and $\widehat{P}_{\mathrm{Rx,SR}}$. In this context, it is necessary to ensure the presence of the PU signal ($\mathscr{H}_1$) for that particular frame. In this direction, Chavali et al. [14] recently proposed a detection followed by the estimation of the signal to noise ratio, while [11] implemented a blind technique for estimating the signal power of noncoherent PU signals.

Here, a different methodology is proposed, according to which a coarse detection on the estimates $\left(\widehat{P}_{\mathrm{Rx,ST},h_{\mathrm{p,l}}}, \widehat{P}_{\mathrm{Rx,SR}}\right)$ at the end of the estimation phase τ_{est} is applied. For the coarse detection, an energy detection is employed whose threshold can be determined by means of Neyman-Pearson criterion. Through an appropriate selection of the time interval τ_{est} (for instance, $\tau_{\mathrm{est}} \in [1, 10]$ms) during the system design, the reliability of the coarse detection can be ensured. With the existence of a separate control channel such as cognitive pilot channel, the reliability of the coarse detection can be further enhanced by exchanging the detection results between the ST and the SR.

The estimation and the coarse detection processes in the proposed method are equivalent in terms of their mathematical operations, consisting of magnitude squared and summation. In this regard, the validity of the channel estimates with certain reliability and without comprising the complexity of the estimators, employed by the secondary system, is considered. Moreover, by performing a joint estimation and (coarse) detection, an efficient way of utilizing the time resources within the frame duration is proposed. The ST considers these estimates to determine a suitable sensing time based on the sensing-throughput tradeoff such that the desired detector's performance is ensured. At the end of the detection phase, a fine detection of the PU signals is carried out, thereby improving the performance of the detector. In accordance with the proposed frame structure in Fig. 8, fine detection represents the main detection, which also includes the samples acquired during the estimation phase.

Assumptions and Approximation

To simplify the analysis and sustain analytical tractability for the proposed approach, several assumptions, considered in this section, are summarized as follows:

- All transmitted signals are subjected to distance-dependent path loss and small-scale fading gain. With no loss of generality, it is considered that the channel gains include distance-dependent path loss and small-scale gain. Moreover, the coherence time for the channel gain is considered to be greater than the frame duration. In scenarios, where the coherence time exceeds the frame duration, the proposed characterization depicts a lower performance bound.
- Perfect knowledge of the noise power is assumed in the system; however, the uncertainty in noise power can be captured as a bounded interval [73]. Inserting this interval in the derived expressions, refer to subsection "Theoretical Analysis", the performance of the IS can be expressed in terms of the upper and the lower bounds.

For analytical tractability, the following approximation is considered.

Approximation 1. *For all degrees of freedom, $\mathscr{X}'^2$ distribution can be approximated by a gamma distribution [1]. The parameters of the gamma distribution are obtained by matching the first two central moments to those of $\mathscr{X}'^2$.*

Theoretical Analysis

At this stage, it is evident that the variation due to the imperfect channel knowledge translates to the variations in the performance parameters:

$$\widehat{\mathrm{P}}_{\mathrm{d}} = \Gamma\left(\frac{\tau_{\mathrm{sen}} f_{\mathrm{s}}}{2}, \frac{\tau_{\mathrm{sen}} f_{\mathrm{s}} \mu}{2\widehat{P}_{\mathrm{Rx,ST},h_{\mathrm{p},1}}}\right), \tag{17}$$

$$\widehat{\mathrm{C}}_0 = \log_2\left(1 + |\widehat{h}_{\mathrm{s}}|^2 \frac{P_{\mathrm{Tx,ST}}}{\sigma_{\mathrm{w}}^2}\right), \tag{18}$$

and

$$\widehat{\mathrm{C}}_1 = \log_2\left(1 + \frac{|\widehat{h}_{\mathrm{s}}|^2 P_{\mathrm{Tx,ST}}}{\widehat{P}_{\mathrm{Rx,SR}}}\right), \tag{19}$$

which are fundamental to sensing-throughput tradeoff. It is worth noticing the fact (17), (18) and (19) are determined using the estimated parameters, which include $\widehat{P}_{\mathrm{Rx,ST},h_{\mathrm{p},1}}$, $|\widehat{h}_{\mathrm{s}}|^2$ and $\widehat{P}_{\mathrm{Rx,SR}}$, determined in previous section. Below, the variations in these performance parameters are characterized in terms of their cdfs: $F_{\widehat{\mathrm{P}}_{\mathrm{d}}}(\cdot)$, $F_{\widehat{\mathrm{C}}_0}(\cdot)$ and $F_{\widehat{\mathrm{C}}_1}(\cdot)$.

Lemma 1. The cdf of $\widehat{\mathrm{P}}_{\mathrm{d}}$ is characterized as

$$F_{\widehat{\mathrm{P}}_{\mathrm{d}}}(x) = 1 - \Gamma\left(\frac{\tau_{\mathrm{est}} f_{\mathrm{s}}}{2}, \frac{\tau_{\mathrm{est}} \tau_{\mathrm{sen}} f_{\mathrm{s}}^2 \mu}{4P_{\mathrm{Rx,ST},h_{\mathrm{p},1}} \Gamma^{-1}(x, \frac{\tau_{\mathrm{sen}} f_{\mathrm{s}}}{2})}\right), \tag{20}$$

where $\Gamma^{-1}(\cdot,\cdot)$ is the inverse of the regularized upper-incomplete gamma function [31].

Solution 1. The cdf of $\widehat{\mathrm{P}}_{\mathrm{d}}$ is defined as

$$F_{\widehat{\mathrm{P}}_{\mathrm{d}}}(x) = \mathbb{P}(\widehat{\mathrm{P}}_{\mathrm{d}} \leq x). \tag{21}$$

Using (17)

$$= \mathbb{P}\left(\Gamma\left(\frac{\tau_{\mathrm{sen}} f_{\mathrm{s}}}{2}, \frac{\tau_{\mathrm{sen}} f_{\mathrm{s}} \mu}{2\widehat{P}_{\mathrm{Rx,ST},h_{\mathrm{p},1}}}\right) \leq x\right), \tag{22}$$

$$= 1 - \mathbb{P}\left(\widehat{P}_{\mathrm{Rx,ST},h_{\mathrm{p},1}} \geq \frac{\mu \tau_{\mathrm{sen}} f_{\mathrm{s}}}{2\Gamma^{-1}\left(x, \frac{\tau_{\mathrm{sen}} f_{\mathrm{s}}}{2}\right)}\right). \tag{23}$$

Replacing the cdf of $\widehat{P}_{\mathrm{Rx,ST},h_{\mathrm{p},1}}$ in (23), an expression of $F_{\widehat{\mathrm{P}}_{\mathrm{d}}}(\cdot)$ is obtained.

Lemma 2. *The cdf of $\widehat{C}_0$ is defined as*

$$F_{\widehat{C}_0}(x) = \int_0^x f_{\widehat{C}_0}(t)dt, \tag{24}$$

where

$$f_{\widehat{C}_0}(x) = 2^x \ln 2 \frac{(2^x-1)^{a_s-1}}{\Gamma(a_s)b_s^{a_s}} \exp\left(-\frac{2^x-1}{b_s}\right), \tag{25}$$

and

$$a_s = \frac{(2+\lambda_s)^2}{(4+4\lambda_s)} \text{ and } b_s = \sigma_w^2 \frac{(4+4\lambda_s)}{(2+\lambda_s)}. \tag{26}$$

Solution 2. See [45, Section IV, Lemma 2].

Lemma 3. *The cdf of $\widehat{C}_1$ is given by*

$$F_{\widehat{C}_1}(x) = \int_0^x f_{\widehat{C}_1}(t)dt, \tag{27}$$

where

$$f_{\widehat{C}_1}(x) = 2^x \ln 2 \frac{(2^x-1)^{a_s-1}\Gamma(a_s+a_p)}{\Gamma(a_s)\Gamma(a_p)b_s^{a_s}b_p^{a_p}} \left(\frac{1}{b_p} + \frac{2^x-1}{b_s}\right)^{(a_s+a_p)}, \tag{28}$$

and

$$a_p = \frac{\tau_{\text{sen}} f_s}{2} \text{ and } b_p = \frac{2P_{Rx,SR}}{\sigma_w^2 \tau_{\text{sen}} f_s}. \tag{29}$$

where a_s and b_s are defined in (26).

Solution 3. See [45, Appendix A].

Next, a sensing-throughput tradeoff for the estimation model is established that includes the estimation time and incorporates the variations in the performance parameter. Most importantly, to restrain the harmful effect of the uncertain interference at the PR due to the variations in the detection probability, two new PU constraints at the PR, namely, an average constraint (AC) and an outage constraint (OC) on the detection probability are proposed. Based on these constraints, the sensing-throughput tradeoff for the IS is characterized.

Problem 1. The achievable expected secondary throughput subject to an average constraint on $\widehat{\mathrm{P}}_{\mathrm{d}}$ that employs channel estimation corresponding to the deterministic behavior of the interacting channels is given by

$$\begin{aligned} R_{\mathrm{s}}(\tilde{\tau}_{\mathrm{est}}, \tilde{\tau}_{\mathrm{sen}}) &= \max_{\tau_{\mathrm{est}}, \tau_{\mathrm{sen}}} \mathbb{E}_{\widehat{\mathrm{P}}_{\mathrm{d}}, \widehat{\mathrm{C}}_0, \widehat{\mathrm{C}}_1} \left[R_{\mathrm{s}}(\tau_{\mathrm{est}}, \tau_{\mathrm{sen}}) \right] \\ &= \frac{T - \tau_{\mathrm{sen}}}{T} \Bigg[\mathbb{E}_{\widehat{\mathrm{C}}_0} \left[\widehat{\mathrm{C}}_0 \right] (1 - \mathrm{P}_{\mathrm{fa}}) \mathbb{P}(\mathscr{H}_0) + \\ &\quad \mathbb{E}_{\widehat{\mathrm{C}}_1} \left[\widehat{\mathrm{C}}_1 \right] \left(1 - \mathbb{E}_{\widehat{\mathrm{P}}_{\mathrm{d}}} \left[\widehat{\mathrm{P}}_{\mathrm{d}} \right] \right) \mathbb{P}(\mathscr{H}_1) \Bigg], \qquad (30) \\ &\text{s.t. } \mathbb{E}_{\widehat{\mathrm{P}}_{\mathrm{d}}} \left[\widehat{\mathrm{P}}_{\mathrm{d}} \right] \geq \bar{\mathrm{P}}_{\mathrm{d}}, \qquad (31) \\ &\text{s.t. } 0 < \tau_{\mathrm{est}} \leq \tau_{\mathrm{sen}} \leq T, \end{aligned}$$

where $\mathbb{E}_{\widehat{\mathrm{P}}_{\mathrm{d}}} [\cdot]$ represents the expectation with respect to $\widehat{\mathrm{P}}_{\mathrm{d}}$, $\mathbb{E}_{\widehat{\mathrm{P}}_{\mathrm{d}}, \widehat{\mathrm{C}}_0, \widehat{\mathrm{C}}_1} [\cdot]$ denotes the expectation with respect to $\widehat{\mathrm{P}}_{\mathrm{d}}$, $\widehat{\mathrm{C}}_0$ and $\widehat{\mathrm{C}}_1$. Unlike (7), $\bar{\mathrm{P}}_{\mathrm{d}}$ in (30) represents the constraint on expected detection probability.

Solution 4. See [45, Appendix B].

Problem 2. The achievable expected secondary throughput subject to an outage constraint on $\widehat{\mathrm{P}}_{\mathrm{d}}$ that employs channel estimation corresponding to the deterministic behavior of the interacting channels is given by

$$\begin{aligned} R_{\mathrm{s}}(\tilde{\tau}_{\mathrm{est}}, \tilde{\tau}_{\mathrm{sen}}) &= \max_{\tau_{\mathrm{est}}, \tau_{\mathrm{sen}}} \mathbb{E}_{\widehat{\mathrm{P}}_{\mathrm{d}}, \widehat{\mathrm{C}}_0, \widehat{\mathrm{C}}_1} \left[R_{\mathrm{s}}(\tau_{\mathrm{est}}, \tau_{\mathrm{sen}}) \right] \\ &= \frac{T - \tau_{\mathrm{sen}}}{T} \Bigg[\mathbb{E}_{\widehat{\mathrm{C}}_0} \left[\widehat{\mathrm{C}}_0 \right] (1 - \mathrm{P}_{\mathrm{fa}}) \mathbb{P}(\mathscr{H}_0) + \\ &\quad \mathbb{E}_{\widehat{\mathrm{C}}_1} \left[\widehat{\mathrm{C}}_1 \right] \left(1 - \mathbb{E}_{\widehat{\mathrm{P}}_{\mathrm{d}}} \left[\widehat{\mathrm{P}}_{\mathrm{d}} \right] \right) \mathbb{P}(\mathscr{H}_1) \Bigg], \qquad (32) \\ &\text{s.t. } \mathbb{P}(\widehat{\mathrm{P}}_{\mathrm{d}} \leq \bar{\mathrm{P}}_{\mathrm{d}}) \leq \rho_{\mathrm{d}}, \qquad (33) \\ &\text{s.t. } 0 < \tau_{\mathrm{est}} \leq \tau_{\mathrm{sen}} \leq T, \end{aligned}$$

where ρ_{d} represents the outage constraint.

Solution 5. See [45, Appendix B].
In contrast to the ideal model, the sensing-throughput tradeoff investigated by the estimation model (refer to Problems 1 and 2) incorporates the imperfect channel knowledge. In this context, the performance characterization considered by the proposed framework is closer to the realistic situations. Herein, based on the

estimation model, a fundamental relation between estimation time (which regulates the variation in the detection probability according to the PU constraint), sensing time (which represents the detector performance) and achievable throughput is established. This relationship is characterized as estimation-sensing-throughput tradeoff. Based on this tradeoff, a suitable estimation time $\tau_{\text{est}} = \tilde{\tau}_{\text{est}}$ and a suitable sensing time $\tau_{\text{sen}} = \tilde{\tau}_{\text{sen}}$ that attains a maximum achievable throughput $R_{\text{s}}(\tilde{\tau}_{\text{est}}, \tilde{\tau}_{\text{sen}})$ for the IS are determined.

Corollary 1. *Problems 1 and 2 consider the optimization of the expected secondary throughput to incorporate the effect of variations due to the channel estimation and subsequently determine the suitable sensing and the suitable estimation time. Here, an alternative approach to the optimization problem that captures the effect of imperfect channel knowledge is investigated. According to which, the suitable sensing time for a certain value of estimation time, subject to the average constraint, is determined as*

$$\begin{aligned}
\tilde{\tau}_{\text{sen}} &= \underset{\tau_{\text{sen}}}{\text{argmax}}\ R_s(\tau_{\text{est}}, \tau_{\text{sen}}) \\
&= \frac{T - \tau_{\text{sen}}}{T}\left[\widehat{C}_0(1 - P_{fa})\mathbb{P}(\mathscr{H}_0) + \widehat{C}_1(1 - \widehat{P}_d)\mathbb{P}(\mathscr{H}_1)\right], \\
&\text{s.t. } \mathbb{E}_{\widehat{P}_d}\left[\widehat{P}_d\right] \geq \bar{P}_d, \\
&\text{s.t. } 0 < \tau_{\text{est}} \leq \tau_{\text{sen}} \leq T.
\end{aligned} \tag{34}$$

Similarly, the suitable sensing time for a certain value of estimation time, subject to the outage constraint, is determined as

$$\begin{aligned}
\tilde{\tau}_{\text{sen}} &= \underset{\tau_{\text{sen}}}{\text{argmax}}\ R_s(\tau_{\text{est}}, \tau_{\text{sen}}) \\
&= \frac{T - \tau_{\text{sen}}}{T}\left[\widehat{C}_0(1 - P_{fa})\mathbb{P}(\mathscr{H}_0) + \widehat{C}_1(1 - \widehat{P}_d)\mathbb{P}(\mathscr{H}_1)\right], \\
&\text{s.t. } \mathbb{P}(\widehat{P}_d \leq \bar{P}_d) \leq \rho_d, \\
&\text{s.t. } 0 < \tau_{\text{est}} \leq \tau_{\text{sen}} \leq T.
\end{aligned} \tag{35}$$

In contrast to (30) and (32), the suitable sensing time evaluated in (34) and (35) entails the variations due to the channel estimation from the performance parameters $(\widehat{P}_d, \widehat{C}_0, \widehat{C}_1)$. Hence, the expected secondary throughput subject to the average and the outage constraints that captures the variations in the suitable sensing time and the performance parameters is determined as

$$\mathbb{E}_{\widehat{P}_d, \widehat{C}_0, \widehat{C}_1, \tilde{\tau}_{\text{sen}}}\left[R_s(\tau_{\text{est}}, \tilde{\tau}_{\text{sen}})\right], \tag{36}$$

where $\mathbb{E}_{\widehat{P}_d, \widehat{C}_0, \widehat{C}_1, \tilde{\tau}_{\text{sen}}}[\cdot]$ corresponds to an expectation over $\widehat{P}_d, \widehat{C}_0, \widehat{C}_1, \tilde{\tau}_{\text{sen}}$.

In accordance with the Problems 1 and 2, the expected secondary throughput, defined in (36), is further optimized over the estimation time to yield the achievable expected secondary throughput:

$$R_s(\tilde{\tau}_{\text{est}}, \tilde{\tau}_{\text{sen}}) = \max_{\tau_{\text{est}}} \mathbb{E}_{\widehat{P}_d, \widehat{C}_0, \widehat{C}_1, \tilde{\tau}_{\text{sen}}} \left[R_s(\tau_{\text{est}}, \tilde{\tau}_{\text{sen}}) \right]. \tag{37}$$

In this way, an estimation-sensing-throughput tradeoff for the alternative approach is established that determines the suitable estimation and the suitable sensing time intervals.

Remark 1. Complementing the analysis in [52], it is complicated to obtain a closed-form expression of $\tilde{\tau}_{\text{sen}}$, thereby rendering the analytical tractability of its cdf difficult. In this view, the performance of the alternative approach is captured by means of simulations.

Numerical Results

Here, the performance of the IS based on the proposed approach is investigated. In this regard, (i) the simulations are performed to validate the expressions obtained, and (ii) the performance degradation incurred due to the channel estimation is analyzed. In this regard, the ideal model is considered to benchmark and to evaluate the performance loss; (iii) the mathematical justification to the considered approximations is established. Although the derived expressions, depicting the performance analysis, are general and applicable to all CR systems, the parameters are selected in such a way that they closely relate to the deployment scenario described in Fig. 7. Unless stated explicitly, the choice of the parameters given in Table 2 is considered for the analysis.

At first, the performance of the IS in terms of sensing-throughput tradeoff corresponding to the ideal model (IM) and estimation model (EM) for a fixed $\tau_{\text{est}} = 5$ ms is analyzed; refer to Fig. 9. In contrast to constraint on P_d for the ideal model, the average constraint (EM-AC) and the outage constraint (EM-OC) for the proposed estimation model are employed. With the inclusion of received power-based estimation in the frame structure, the ST achieves no throughput at the SR for the interval τ_{est}. For the given cases, namely, IM, EM-AC, and EM-OC, a suitable sensing time that results in a maximum secondary throughput $R_\text{s}(\tau_{\text{est}} = 5\,\text{ms}, \tilde{\tau}_{\text{sen}})$ is determined. Apart from that, a performance degradation is depicted in terms of the achievable throughput; refer to Fig. 9. For $\rho_\text{d} = 0.05$, it is observed that the outage constraint is more sensitive to the performance loss in comparison to the average constraint. It is clear that the analysis, illustrated in Fig. 9, is obtained for a certain choice of system parameters, particularly $\gamma_{\text{p},1} = -10\,\text{dB}$, $\tau_{\text{est}} = 5\,\text{ms}$, and $\rho_\text{d} = 0.05$. To acquire more insights, the effect of these variations on the performance parameters is considered, subsequently.

Table 2 Parameters for numerical analysis

Parameter	Value
f_s	1 MHz
$\lvert h_{p,1}\rvert^2$	-100 dB
$\lvert h_{p,2}\rvert^2$	-100 dB
$\lvert h_s\rvert^2$	-80 dB
T	100 ms
$\bar{P}_d$	0.9
ρ_d	0.05
σ_w^2	-100 dBm
$\gamma_{p,1}$	-10 dB
$\gamma_{p,2}$	-10 dB
γ_s	10 dB
$\sigma_s^2 = P_{Tx,PT}$	-10 dBm
$P_{Tx,ST}$	-10 dBm
$\mathbb{P}(\mathscr{H}_1) = 1 - \mathbb{P}(\mathscr{H}_0)$	0.2
τ_{est}	5 ms
N_s	10

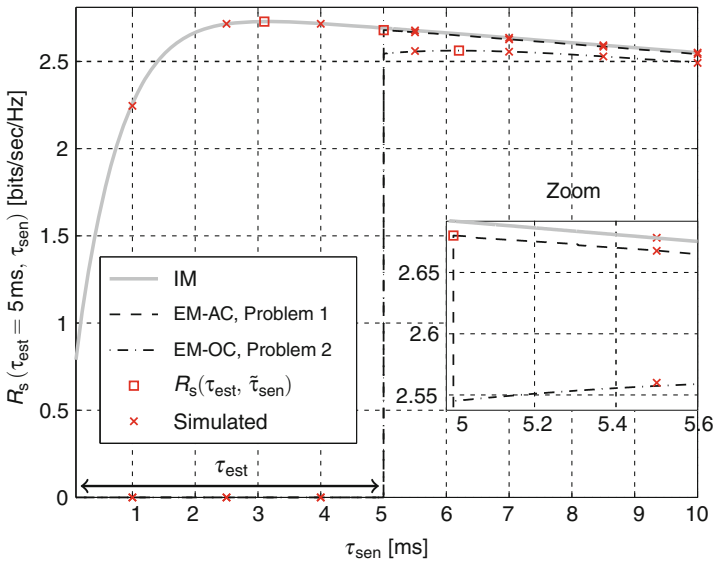

Fig. 9 Sensing-throughput tradeoff for the ideal model (IM) and estimation model (EM), $\gamma_{p,1} = -10$ dB, $\tau_{est} = 5$ ms and $\rho_d = 0.05$

Hereafter, the theoretical expressions are considered for the analysis; in addition, the IS is operated at the suitable sensing time. Next, the variation in the achievable throughput $R_s(\tau_{est}, \tilde{\tau}_{sen})$ against the received signal to noise ratio $\gamma_{p,1}$ at the ST with $\tau_{est} = 5$ ms is considered; refer to Fig. 10. For $\gamma_{p,1} < -10$ dB, the estimation model incurs a significant performance loss. This clearly reveals that the ideal

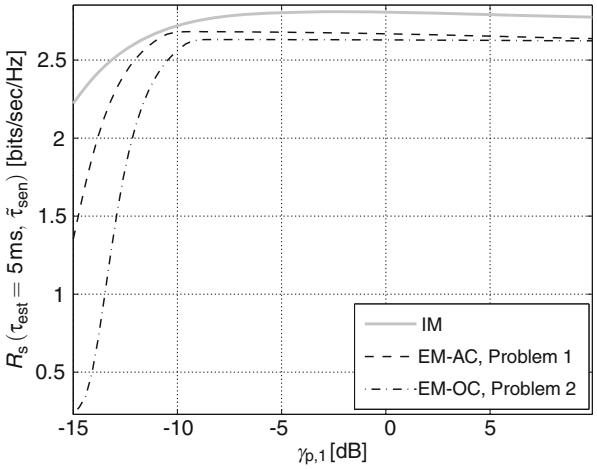

Fig. 10 Secondary throughput versus $\gamma_{p,1}$ with $\tau_{est} = 5$ ms for the deterministic channel

model overestimates the performance of the IS. From the previous discussion, it is concluded that the inclusion of the average and the outage constraints (depicted by the proposed framework) precisely tackles the uncertainty in the interference at the PR, arising due to channel estimation, without considerably degrading the performance of the IS.

Upon maximizing the secondary throughput, it is interesting to analyze the variation of the secondary throughput with the estimation time. Corresponding to the estimation model, Fig. 11 illustrates a tradeoff among the estimation time, the sensing time, and the secondary throughput. From Fig. 11, it can be noticed that the function $R_s(\tau_{est}, \tau_{sen})$ is well behaved in the region $0 < \tau_{est} \leq \tau_{sen} \leq T$ and consists of a global maximum, yielding the achievable secondary throughput.

This tradeoff depicted by the proposed framework can be explained from the fact that low values of the estimation time result in large variations in $\widehat{P}_d$. To counteract and satisfy the average and the outage constraints, the corresponding thresholds shift to a lower value. This causes an increase in P_{fa}, thereby increasing the sensing-throughput curvature. As a result, the suitable sensing time is obtained at a higher value. However, beyond a certain value ($\tilde{\tau}_{est}$), a further increase in the estimation time slightly contributes to the performance improvement and largely consumes the time resources. As a consequence to the estimation-sensing-throughput tradeoff, the suitable estimation time that yields an achievable throughput $R_s(\tilde{\tau}_{est}, \tilde{\tau}_{sen})$ is determined.

To procure further insights, the variations of expected $\widehat{P}_d$ and P_{fa} with the estimation time are studied. From Fig. 12, it is observed that the expected $\widehat{P}_d$ corresponding to the outage constraint is strictly above the desired level $\bar{P}_d$ for all values of the estimation time. However, for lower values of the estimation time, this margin reduces. This is based on the fact that lower estimation time shifts the probability mass of P_d to a lower value.

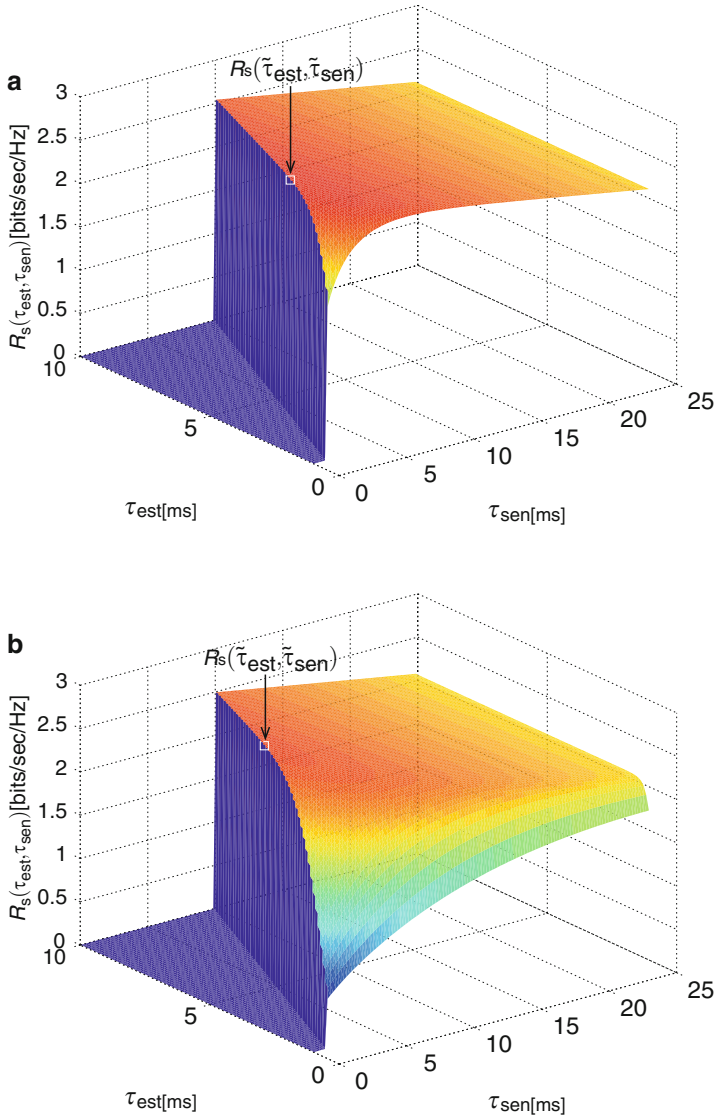

Fig. 11 Estimation-sensing-throughput tradeoff for the estimation model for (**a**) average constraint and (**b**) outage constraint with $\rho_d = 0.05$

According to Fig. 13, the system notices a considerable improvement in P_{fa} at small values of τ_{est}, which saturates for a certain period and falls drastically beyond a certain value. To understand this, it is important to study the dynamics between the estimation and the sensing time. Low τ_{est} increases the variations in the detection probability, these variations are compensated by an increase in the suitable sensing time, and vice versa. The performance improves until a maximum ($\tilde{\tau}_{est}$, $\tilde{\tau}_{sen}$) is

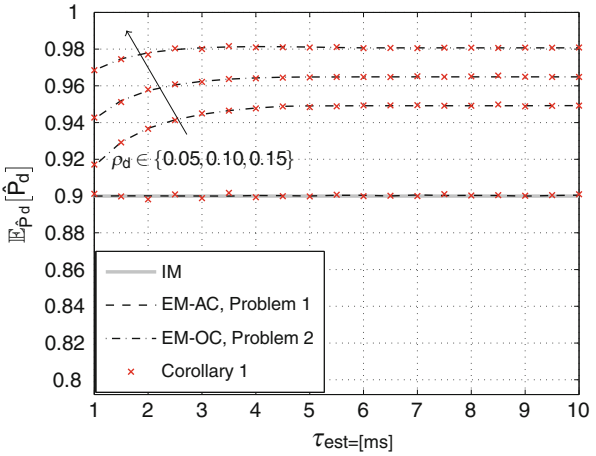

Fig. 12 Variation of $\mathbb{E}_{\widehat{P_d}}\left[\widehat{P}_d\right]$ versus the τ_{est}, where the secondary throughput is maximized over the sensing time, $R_s(\tau_{est}, \tilde{\tau}_{sen})$

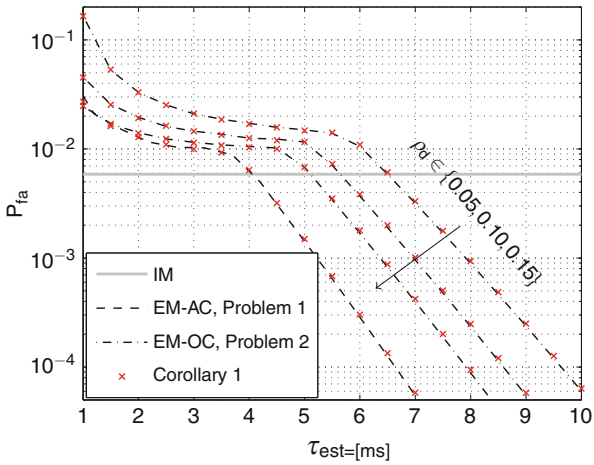

Fig. 13 Variation of P_{fa} versus the τ_{est}, where the secondary throughput is maximized over the sensing time, $R_s(\tau_{est}, \tilde{\tau}_{sen})$

reached, beyond this, the time resources (allocated in terms of the sensing and the estimation time) contribute more in improving the detector's performance (in terms of P_{fa} as P_d is already constrained) and less in reducing the variations due to the channel estimation.

Summary

This section investigated the performance of cognitive radio as an interweave system from a deployment perspective. It has been argued that the knowledge of the

interacting channels is a key aspect that enables the performance characterization of the interweave system. In this regard, a novel framework that facilitates channel estimation and captures the effect of channel estimation in the system model has been proposed. As a major outcome of the analysis, it has been justified that the existing model, illustrating an ideal scenario, disregards the effects such as time allocation and imperfect channel knowledge encountered by the IS due to the inclusion of channel estimation. In this context, the existing model overestimates the performance of the interweave system and, hence, is less suitable for deployment.

Moreover, it has been clearly identified that the variations induced in the system, specially in the detection probability, cause uncertain interference. Unless controlled, this uncertain interference may severely degrade the performance of the primary system. To overcome this situation, average and outage constraints as primary user constraints have been employed. As a consequence, for the proposed estimation model, novel expressions for the sensing-throughput tradeoff based on the mentioned constraints have been established. More importantly, by analyzing the estimation-sensing-throughput tradeoff, the suitable estimation time and the suitable sensing time that maximize the secondary throughput have been determined.

Research Directions

With regard to the performance analysis and the deployment-centric viewpoint toward CR systems emphasized in this chapter, the following extensions or considerations to the proposed framework could be of great interest for future investigations.

In-Band Full-Duplex

For instance, this chapter focused only on a half duplex CR communication, i.e., the CR techniques (which include spectrum sensing and power control) are time-interlaced with the data transmission. Recently, there has been significant advancement concerning the feasibility of in-band full duplex communication; for a detailed discussion over in-band full duplex communication, please consider [54, 64] and the references therein. In this context, the CR communication can be transformed into the in-band full duplex, whereby the CR techniques and the data transmission occur simultaneously in time and over the same frequency channel. The design challenges and the corresponding performance tradeoffs related to the in-band full duplex CR communication are precisely dealt within [49, 53].

Multiple Antennas at ST

In addition, the performed analysis considers that the ST and the SR are installed with single antenna. As a matter of fact, state-of-the-art standards are mostly equipped with multiple antennas. With an intention of establishing a preliminary analysis involving channel estimation in context of the CR systems, the performance enhancement procured by upgrading the existing spectrum sensing (detector performance) due to the deployment of multiple antennas [17, 72], has been completely neglected in the chapter. Based on a hardware deployment, the authors in [63]

argued that the hardware complexity in context with the CR system escalates with the deployment of multiple antennas, prohibiting the usage of well-known combining techniques such as equal-gain combining and maximum-ratio combining [16]. In this regard, nonconventional techniques, such as square-law selector and square-law combiner (following the principle of energy detection) are able to reduce complexity, thereby promoting the feasibility of multiple antennas.

Asynchronous Access

Given the complexity of the underlying problem, impairments due to the asynchronous (in time domain) access by the secondary system to the licensed spectrum is left aside throughout the chapter. The asynchronous access is due to the unknown (which can be random also) behavior of PU traffic. In these circumstances, the assumption concerning the synchronous access (i.e., perfect alignment to the primary system's medium access) becomes invalid. As a consequence, this asynchronous access certainly has an impact on the performance of the CR systems. A careful integration of the asynchronous access to the proposed analysis presents a promising research direction. To tackle this problem, the reader is encouraged to consult the references [35, 36].

Network-Wide Perspective

Finally, the performance analysis in this chapter has been confined to a single of PT, PR, ST, and SR, a classical way of illustrating a node-wide perspective of a CR system. The effect of the presence of other PTs and other STs in the network on the performance – evaluated using parameters such as spatial interference at the PR and spatial throughput at the SR, illustrating a network-wide perspective – has not been treated in the chapter. The concept of stochastic geometry, widely accepted for modeling the wireless networks, has been recently applied to the perform analysis for the cognitive radio networks. In order to establish an in-depth understanding of this concept, it is advisable to consult the references [18, 51, 69].

Conclusion

Despite its huge popularity and in-depth knowledge acquired on this topic, an autonomous as well as exhaustive implementation of such a concept is underdeveloped. One main reason behind this is the fact that the existing models (developed for the performance characterization) have focused more on theoretical analysis and less on the hardware deployment. In this regard, due to the complexity of the underlying problem, these models tend to overlook certain aspects such as noise uncertainty, channel knowledge, signal uncertainty, and hardware and model imperfections that are fundamental to a hardware implementation. The lack of such imperfections in the system model renders the performance analysis of the CR system incomplete.

The knowledge of the involved channels residing within a CR system is one of such aspects dealt in this chapter. From a physical layer perspective, it has been

identified that the channel knowledge is extremely necessary for the realization of the CR techniques on a hardware, thus allowing a CR system to control the interference accumulated by the primary system. In this chapter, this notion has been extensively justified and resolved through adequate analysis while considering a hardware deployment.

Above all, the inclusion of the channel estimation requires a proper allocation of time resources in the frame structure and appropriate measures to counter variations due to the estimation error induced in the system. Surely, these factors have a detrimental effect on the performance of a CR system, leading to the performance degradation. These channel estimation-related issues have been carefully identified and characterized, which ultimately allows us to depict the performance of the CR systems in a fairly realistic scenario. Besides, following the deployment perspective, a received power-based channel estimation technique is proposed for the estimation, particularly, for the channels that exist between the two systems.

Briefly, the analysis performed in this chapter does not only provide answers to specific questions related to imperfect channel knowledge, including:

1. How to counter the uncertain interference induced in different CR systems?
2. How to evaluate the performance degradation?
3. How to determine the suitable estimation time and suitable sensing time that yields the maximum throughput achieved?

but also promotes techniques such as:

1. implementation of the channel estimation at the secondary system
2. energy-based detection and
3. received power-based channel estimation

that ultimately encourage hardware feasibility of CR systems.

As a closing remark, spectrum is a precious component that can enable wireless connectivity to the billions of devices residing inside a 5G network. To meet this escalating demand of more spectrum, cognitive radio, competing with technologies such as the millimeter-wave technology and the visible light communication, represents a viable option. Having said that, there exist certain scenarios, including the one considered in this chapter (refer to section "Cognitive Small Cell: A Prominent Use-Case") that facilitate the coexistence of these technologies within a 5G system.

References

1. Abramowitz M, Stegun IA (1964) Handbook of mathematical functions with formulas, graphs, and mathematical tables, ninth dover printing, tenth GPO printing edition. Dover, New York
2. Andrews JG, Claussen H, Dohler M, Rangan S, Reed MC (2012) Femtocells: past, present, and future. IEEE J Sel Areas Commun 30(3):497–508. https://doi.org/10.1109/JSAC.2012.120401

3. Andrews JG, Buzzi S, Choi W, Hanly SV, Lozano A, Soong ACK, Zhang JC (2014) What will 5G be? IEEE J Sel Areas Commun 32(6):1065–1082. https://doi.org/10.1109/JSAC.2014.2328098
4. Annavajjala R, Milstein LB (2005) Performance analysis of linear diversity-combining schemes on Rayleigh fading channels with binary signaling and Gaussian weighting errors. IEEE Trans Wirel Commun 4(5):2267–2278. https://doi.org/10.1109/TWC.2005.853834
5. Axell E, Leus G, Larsson EG, Poor HV (2012) Spectrum sensing for cognitive radio: state-of-the-art and recent advances. IEEE Sign Process Mag 29(3):101–116. https://doi.org/10.1109/MSP.2012.2183771
6. Becker H, Kaushik A, Sharma SK, Chatzinotas S, Jondral FK (2016) Experimental study of an underlay cognitive radio system: model validation and demonstration. In: 11th International Conference on Cognitive Radio Oriented Wireless Networks and Communications (CROWNCOM), pp 511–523
7. Bennis M, Simsek M, Czylwik A, Saad W, Valentin S, Debbah M (2013) When cellular meets WiFi in wireless small cell networks. IEEE Commun Mag 51(6):44–50. https://doi.org/10.1109/MCOM.2013.6525594
8. Bogale TE, Le LB (2016) Massive MIMO and mmWave for 5G wireless HetNet: potential benefits and challenges. IEEE Veh Technol Mag 11(1):64–75. https://doi.org/10.1109/MVT.2015.2496240
9. Cabric D, Mishra SM, Brodersen RW (2004) Implementation issues in spectrum sensing for cognitive radios. In: Conference Record of the Thirty-Eighth Asilomar Conference on Signals, Systems and Computers, vol 1, pp 772–776. https://doi.org/10.1109/ACSSC.2004.1399240
10. Cabric D, Tkachenko A, Brodersen RW (2006) Experimental study of spectrum sensing based on energy detection and network cooperation. In: Proceedings of the First International Workshop on Technology and Policy for Accessing Spectrum. ACM. http://doi.acm.org/10.1145/1234388.1234400
11. Cao N, Mao M, Chen Y, Long M (2014) Analysis of collaborative spectrum sensing with binary phase shift keying signal power estimation errors. IET Sci Meas Technol 8(6):350–358. https://doi.org/10.1049/iet-smt.2013.0218
12. Cardenas-Juarez M, Ghogho M (2011) Spectrum sensing and throughput trade-off in cognitive radio under outage constraints over Nakagami fading. IEEE Commun Lett 15(10):1110–1113. https://doi.org/10.1109/LCOMM.2011.080811.111127
13. Chandrasekhar V, Andrews JG, Gatherer A (2008) Femtocell networks: a survey. IEEE Commun Mag 46(9):59–67. https://doi.org/10.1109/MCOM.2008.4623708
14. Chavali VG, da Silva CRCM (2011) Collaborative spectrum sensing based on a new SNR estimation and energy combining method. IEEE Trans Veh Technol 60(8):4024–4029. https://doi.org/10.1109/TVT.2011.2166284
15. Cisco (2014) Cisco visual networking index: global mobile data traffic forecast update, 2013–2018. White Paper
16. Digham FF, Alouini MS, Simon MK (2003) On the energy detection of unknown signals over fading channels. In: IEEE International Conference on Communications (ICC), vol 5, pp 3575–3579. https://doi.org/10.1109/ICC.2003.1204119
17. Digham FF, Alouini MS, Simon MK (2007) On the energy detection of unknown signals over fading channels. IEEE Trans Commun 55(1):21–24. https://doi.org/10.1109/TCOMM.2006.887483
18. ElSawy H, Hossain E, Haenggi M (2013) Stochastic geometry for modeling, analysis, and design of multi-tier and cognitive cellular wireless networks: a survey. IEEE Commun Surv Tutorials 15(3):996–1019. https://doi.org/10.1109/SURV.2013.052213.00000
19. ElSawy H, Hossain E, Kim DI (2013) HetNets with cognitive small cells: user offloading and distributed channel access techniques. IEEE Commun Mag 51(6):28–36. https://doi.org/10.1109/MCOM.2013.6525592
20. Ericsson (2015) Ericsson mobility report. Technical report. http://www.ericsson.com/res/docs/2015/mobility-report/ericsson-mobility-report-nov-2015.pdf

21. ETSI TS 103 113 (2013) Electromagnetic compatibility and radio spectrum matters (ERM); system reference document (SRdoc); mobile broadband services in the 2300–2400 MHz frequency band under licensed shared acces regime
22. Ettus Research (2015) http://www.ettus.com/. [Online; Accessed 2 Dec 2015]
23. Gans M (1971) The effect of Gaussian error in maximal ratio combiners. IEEE Trans Commun Technol 19(4):492–500. https://doi.org/10.1109/TCOM.1971.1090666
24. Gelabert X, Legg P, Qvarfordt C (2013) Small cell densification requirements in high capacity future cellular networks. In: IEEE International Conference on Communications (ICC) Workshops, pp 1112–1116. https://doi.org/10.1109/ICCW.2013.6649403
25. Ghasemi A, Sousa ES (2007) Fundamental limits of spectrum-sharing in fading environments. IEEE Trans Wirel Commun 6(2):649–658. https://doi.org/10.1109/TWC.2007.05447
26. Ghasemi A, Sousa ES (2008) Spectrum sensing in cognitive radio networks: requirements, challenges and design trade-offs. IEEE Commun Mag 46(4):32–39. https://doi.org/10.1109/MCOM.2008.4481338
27. Gifford WM, Win MZ, Chiani M (2005) Diversity with practical channel estimation. IEEE Trans Wirel Commun 4(4):1935–1947. https://doi.org/10.1109/TWC.2005.852127
28. Gifford WM, Win MZ, Chiani M (2008) Antenna subset diversity with non-ideal channel estimation. IEEE Trans Wirel Commun 7(5):1527–1539. https://doi.org/10.1109/TWC.2008.05744
29. Goldsmith A (2005) Wireless communications. Cambridge University Press, New York
30. Goldsmith A, Jafar SA, Maric I, Srinivasa S (2009) Breaking spectrum gridlock with cognitive radios: an information theoretic perspective. Proc IEEE 97(5):894–914. https://doi.org/10.1109/JPROC.2009.2015717
31. Gradshteyn IS, Ryzhik IM (2000) Table of integrals, series, and products, 6th edn. Academic Press, San Diego
32. Haenggi M (2013) Stochastic geometry for wireless networks. Cambridge University Press, Cambridge
33. Halbauer H, Saur S, Koppenborg J, Hoek C (2013) 3D beamforming: performance improvement for cellular networks. Bell Labs Tech J 18(2):37–56. https://doi.org/10.1002/bltj.21604
34. Herath SP, Rajatheva N, Tellambura C (2009) Unified approach for energy detection of unknown deterministic signal in cognitive radio over fading channels. In: IEEE International Conference on Communications (ICC) Workshops, pp 1–5. https://doi.org/10.1109/ICCW.2009.5208031
35. Jiang C, Beaulieu NC, Jiang C (2013) A novel asynchronous cooperative spectrum sensing scheme. In: IEEE International Conference on Communications (ICC), pp 2606–2611. https://doi.org/10.1109/ICC.2013.6654928
36. Jiang C, Beaulieu NC, Zhang L, Ren Y, Peng M, Chen HH (2015) Cognitive radio networks with asynchronous spectrum sensing and access. IEEE Netw 29(3):88–95. https://doi.org/10.1109/MNET.2015.7113231
37. Jondral FK (2005) Software-defined radio-basic and evolution to cognitive radio. EURASIP J Wirel Commun Netw 2005(3):275–283
38. Kang X, Liang YC, Garg HK, Zhang L (2009) Sensing-based spectrum sharing in cognitive radio networks. IEEE Trans Veh Technol 58(8):4649–4654. https://doi.org/10.1109/TVT.2009.2018258
39. Kang X, Liang YC, Nallanathan A, Garg HK, Zhang R (2009) Optimal power allocation for fading channels in cognitive radio networks: ergodic capacity and outage capacity. IEEE Trans Wirel Commun 8(2):940–950. https://doi.org/10.1109/TWC.2009.071448
40. Kaushik A, Mueller M, Jondral FK (2013) Cognitive relay: detecting spectrum holes in a dynamic scenario. In: Tenth International Symposium on Wireless Communication Systems (ISWCS), pp 1–2
41. Kaushik A, Raza MR, Jondral FK (2014) On the deployment of cognitive relay as underlay systems. In: 9th International Conference on Cognitive Radio Oriented Wireless Networks and Communications (CROWNCOM), pp 329–334

42. Kaushik A, Sharma SK, Chatzinotas S, Ottersten B, Jondral FK (2015) Estimation-throughput tradeoff for underlay cognitive radio systems. In: IEEE International Conference on Communications (ICC), pp 7701–7706
43. Kaushik A, Sharma SK, Chatzinotas S, Ottersten B, Jondral FK (2015) Sensing-throughput tradeoff for cognitive radio systems with unknown received power. In: 10th International Conference on Cognitive Radio Oriented Wireless Networks and Communications (CROWNCOM), pp 308–320
44. Kaushik A, Wunsch F, Sagainov A, Cuervo N, Demel J, Koslowski S, Jäkel H, Jondral F (2015) Spectrum sharing for 5G wireless systems (Spectrum sharing challenge). In: IEEE International Symposium on Dynamic Spectrum Access Networks (DySPAN), pp 1–2. https://doi.org/10.1109/DySPAN.2015.7343841
45. Kaushik A, Sharma SK, Chatzinotas S, Ottersten B, Jondral FK (2016) Sensing-throughput tradeoff for interweave cognitive radio system: a deployment-centric viewpoint. IEEE Trans Wirel Commun 15(5):3690–3702. https://doi.org/10.1109/TWC.2016.2525986
46. Kay S (1998) Fundamentals of statistical signal processing: detection theory. Prentice hall signal processing series. Prentice-Hall PTR, Upper Saddle River
47. Kim K, Xin Y, Rangarajan S (2010) Energy detection based spectrum sensing for cognitive radio: an experimental study. In: IEEE Global Telecommunications Conference (GLOBECOM), pp 1–5. https://doi.org/10.1109/GLOCOM.2010.5683560
48. Kim H, Wang H, Lim S, Hong D (2012) On the impact of outdated channel information on the capacity of secondary user in spectrum sharing environments. IEEE Trans Wirel Commun 11(1):284–295. https://doi.org/10.1109/TWC.2011.112311.110307
49. Kim D, Lee H, Hong D (2015) A survey of in-band full-duplex transmission: from the perspective of PHY and MAC layers. IEEE Commun Surv Tutorials 17(4):2017–2046. https://doi.org/10.1109/COMST.2015.2403614
50. Larsson EG, Edfors O, Tufvesson F, Marzetta TL (2014) Massive MIMO for next generation wireless systems. IEEE Commun Mag 52(2):186–195. https://doi.org/10.1109/MCOM.2014.6736761
51. Lee C, Haenggi M (2012) Interference and outage in poisson cognitive networks. IEEE Trans Wirel Commun 11(4):1392–1401. https://doi.org/10.1109/TWC.2012.021512.110131
52. Liang YC, Zeng Y, Peh ECY, Hoang AT (2008) Sensing-throughput tradeoff for cognitive radio networks. IEEE Trans Wirel Commun 7(4):1326–1337. https://doi.org/10.1109/TWC.2008.060869
53. Liao Y, Song L, Han Z, Li Y (2015) Full duplex cognitive radio: a new design paradigm for enhancing spectrum usage. IEEE Commun Mag 53(5):138–145. https://doi.org/10.1109/MCOM.2015.7105652
54. Liu G, Yu FR, Ji H, Leung VCM, Li X (2015) In-band full-duplex relaying: a survey, research issues and challenges. IEEE Commun Surv Tutorials 17(2):500–524. https://doi.org/10.1109/COMST.2015.2394324
55. Maddah-Ali MA, Tse D (2012) Completely stale transmitter channel state information is still very useful. IEEE Trans Inf Theory 58(7):4418–4431. https://doi.org/10.1109/TIT.2012.2193116
56. McHenry MA (2005) NSF spectrum occupancy measurements project summary. Shared Spectrum Company Report
57. McHenry M, Livsics E, Nguyen T, Majumdar N (2007) XG dynamic spectrum access field test results. IEEE Commun Mag 45(6):51–57. https://doi.org/10.1109/MCOM.2007.374432
58. Mitola J, Maguire GQ Jr (1999) Cognitive radio: making software radios more personal. IEEE Pers Commun Mag 6(4):13–18. https://doi.org/10.1109/98.788210
59. Paolini M (2007) Meeting the challenges of high-capacity indoor and outdoor coverage. Senza Fili Consulting. Available at http://www.senzafiliconsulting.com/downloads/SenzaFili_IndoorCoverageSurvey.pdf
60. Pawelczak P, Nolan K, Doyle L, Oh SW, Cabric D (2011) Cognitive radio: ten years of experimentation and development. IEEE Commun Mag 49(3):90–100. https://doi.org/10.1109/MCOM.2011.5723805

61. Peh E, Liang YC (2007) Optimization for cooperative sensing in cognitive radio networks. In: IEEE Wireless Communications and Networking Conference (WCNC), pp 27–32. https://doi.org/10.1109/WCNC.2007.11
62. Rappaport TS, Sun S, Mayzus R, Zhao H, Azar Y, Wang K, Wong GN, Schulz JK, Samimi M, Gutierrez F (2013) Millimeter wave mobile communications for 5G cellular: it will work!. IEEE Access 1:335–349. https://doi.org/10.1109/ACCESS.2013.2260813
63. Rodes L, Kaushik A, Sharma SK, Chatzinotas S, Jondral FK (2016, to appear) Square-law selector and square-law combiner for cognitive radio systems: an experimental study. In: IEEE 84th Vehicular Technology Conference (VTC)
64. Sabharwal A, Schniter P, Guo D, Bliss DW, Rangarajan S, Wichman R (2014) In-band full-duplex wireless: challenges and opportunities. IEEE J Sel Areas Commun 32(9):1637–1652. https://doi.org/10.1109/JSAC.2014.2330193
65. Schaich F, Wild T (2014) Waveform contenders for 5G – OFDM vs. FBMC vs. UFMC. In: 6th International Symposium on Communications, Control and Signal Processing (ISCCSP), pp 457–460. https://doi.org/10.1109/ISCCSP.2014.6877912
66. Sharma SK, Chatzinotas S, Ottersten B (2013) SNR estimation for multi-dimensional cognitive receiver under correlated channel/noise. IEEE Trans Wirel Commun 12(12):6392–6405. https://doi.org/10.1109/TWC.2013.103113.130523
67. Sharma S, Chatzinotas S, Ottersten B (2014) A hybrid cognitive transceiver architecture: sensing-throughput tradeoff. In: 9th International Conference on Cognitive Radio Oriented Wireless Networks and Communications (CROWNCOM), pp 143–149
68. Sharma S, Bogale T, Chatzinotas S, Ottersten B, Le L, Wang X (2015) Cognitive radio techniques under practical imperfections: a survey. IEEE Commun Surv Tutorials 17(4):1858–1884. https://doi.org/10.1109/COMST.2015.2452414
69. Song X, Yin C, Liu D, Zhang R (2014) Spatial throughput characterization in cognitive radio networks with threshold-based opportunistic spectrum access. IEEE J Sel Areas Commun 32(11):2190–2204. https://doi.org/10.1109/JSAC.2014.1411RP05
70. Stoica P, Besson O (2003) Training sequence design for frequency offset and frequency-selective channel estimation. IEEE Trans Commun 51(11):1910–1917. https://doi.org/10.1109/TCOMM.2003.819199
71. Suraweera HA, Smith PJ, Shafi M (2010) Capacity limits and performance analysis of cognitive radio with imperfect channel knowledge. IEEE Trans Veh Technol 59(4):1811–1822. https://doi.org/10.1109/TVT.2010.2043454
72. Taherpour A, Nasiri-Kenari M, Gazor S (2010) Multiple antenna spectrum sensing in cognitive radios. IEEE Trans Wirel Commun 9(2):814–823. https://doi.org/10.1109/TWC.2009.02.090385
73. Tandra R, Sahai A (2008) SNR walls for signal detection. IEEE J Sel Top Signal Proces 2(1):4–17. https://doi.org/10.1109/JSTSP.2007.914879
74. Tse D, Viswanath P (2005) Fundamentals of wireless communication. Cambridge University Press, Cambridge
75. Urkowitz H (1967) Energy detection of unknown deterministic signals. Proc IEEE 55(4):523–531. https://doi.org/10.1109/PROC.1967.5573
76. Wu S, Wang H, Youn CH (2014) Visible light communications for 5G wireless networking systems: from fixed to mobile communications. IEEE Netw 28(6):41–45. https://doi.org/10.1109/MNET.2014.6963803

Spectrum Sensing, Measurement, and Modeling

5

Ghaith Hattab and Danijela Cabric

Contents

Abstract

Modeling spectrum sensing is a critical step that paves the way to (i) identify the key impairments that affect the detection performance and (ii) help develop algorithms and receiver architectures that mitigate these impairments. In this chapter, realistic and practical sensing models are presented beyond those

G. Hattab (✉) · D. Cabric
Electrical Engineering, University of California, Los Angeles (UCLA), Los Angeles, CA, USA
e-mail: ghattab@ucla.edu; danijela@ee.ucla.edu

W. Zhang (ed.), *Handbook of Cognitive Radio*,
https://doi.org/10.1007/978-981-10-1394-2_5

developed for classical detection theory. These models capture the impact of different sensing receiver impairments on several detectors such as the energy, the pilot, and the cyclostationarity detectors. Several receiver nonidealities are investigated, including noise uncertainty, imperfect synchronization, and cyclic frequency offsets. In addition, challenges and impairments pertaining to wideband sensing are analyzed, including the presence of strong adjacent interferers as well as the nonlinearities of the receiver RF front-end. From these models, several mitigation techniques are developed to compensate for the presence of the different sensing receiver impairments. Measurements and simulation results are presented throughout the chapter to show the negative impact of such impairments and validate that the developed mitigation techniques provide tangible performance gains.

Introduction

A standard cognitive radio (CR) system seeks to identify channels that are not occupied by primary systems so it can access them. Such cognitive and dynamic approach promises to enhance spectrum utilization. For this reason, the CR receiver must be equipped with a spectrum sensor that helps scan a single (in case of narrowband) or multiple (in case of wideband) spectrum bands. The objective of the spectrum sensing receiver is to employ detection algorithms to quickly and reliably detect primary systems and identify available spectral resources.

Among the most popular spectrum sensing techniques proposed in the literature are the energy, pilot, and cyclostationarity detectors. The theoretical detection performance of these detectors has been thoroughly investigated in the literature, yet the derived expressions are assumed to hold under ideal assumptions irrespective of the signal-to-noise ratio (SNR) at the sensing receiver front-end, as will be discussed in section "Spectrum Sensing Techniques". Indeed, measurements have verified that in negative SNR regimes, many of these assumptions do not hold. In this chapter, more accurate spectrum sensing models are presented, where several receiver impairments are included to better capture the performance attained via experimental studies. Specifically, the energy detector requires noise power estimation, which is commonly assumed to be perfect. Such assumption is dropped, and the detection performance is analyzed in the presence of noise uncertainty. Similarly, pilot and cyclostationarity detectors require tight synchronization to reap the coherent gains achieved via signal feature exploitation. This synchronization is difficult to attain in practice, where frequency, cyclic frequency, and sampling clock offsets are inevitable. Modeling these impairments and studying their impact on energy detection, pilot detection, and cyclostationarity detection will be discussed in details in sections "Energy Detection Under Noise Uncertainty," "Pilot Detection Under Frequency Offsets," and "Cyclostationarity Detection Under Imperfect Synchronization", respectively. Several mitigation algorithms are also presented in their corresponding sections.

While narrowband sensing is fundamental, wideband sensing is a highly desirable feature since it enables the CR receiver to explore more spectral resources and switch between different channels in case some of them become occupied by primary systems. To this end, modeling the wideband sensing problem has been reduced to modeling several narrowband sensing problems by dividing the wideband into many narrowbands. Such approach typically assumes an ideal channelization process, which is infeasible in practice. Indeed, two major bottlenecks arise in wideband sensing. First, a band that is adjacent to other bands with strong signals can suffer from high interference due to the nonideal filter mask in practice, which is commonly assumed to be a brick wall in theory. In addition, strong signals can saturate the RF front-end components such as the low-power amplifier (LNA). This pushes the LNA to operate in a nonlinear region, introducing spurious terms that can affect the detection performance. These two challenges and the mitigation techniques to overcome them will be presented in section "Wideband Sensing: Challenges and Solutions".

The different sensing impairments require revisiting the sensing models for two reasons. First, it is important to understand how the presence of these impairments affects the performance. Second, by identifying the key parameters that affect the performance, it becomes feasible to develop compensation algorithms and architectures to mitigate these impairments. The design procedure, which will be followed throughout this chapter, is summarized below:

1. Include the impairment in the sensing model. Such impairment may be identified through measurements or more practical modeling.
2. For a given detection algorithm, derive the detection performance in the presence of the impairment. The theoretical derivations help identify the key parameters that affect the detection performance.
3. Develop a compensation algorithm that mitigates the issues introduced by the impairment.

Spectrum Sensing Techniques

The CR receiver must have sensing capabilities to decide whether a channel is occupied by other users or not. Generally, physical layer sensing relies on estimating parameters that convey information about the channel such as the signal energy in that channel or the presence of signal features or pilots. In essence, the spectrum sensing problem can be viewed as a classical binary hypothesis test, where H_0 stands for the absence of primary user signals, i.e., noise-only samples, and H_1 stands for the presence of users, i.e., both noise and signal samples are present. This is a digital implementation, where a test statistic, Λ, is used to process N samples and estimate a desired parameter. Then, the statistic is compared to a predetermined decision threshold. Mathematically, this is expressed as

$$\Lambda \underset{H_0}{\overset{H_1}{\gtrless}} \lambda, \tag{1}$$

where λ is a threshold that can be optimized to attain a certain objective, e.g., meet a false alarm constraint.

There are a plethora of spectrum sensing techniques [2, 11, 23, 28], but the most prominent candidates for practical implementation are the energy detector, the pilot detector, and the cyclostationarity detector, which will be reviewed next.

Energy Detection

This is one of the simplest forms of detection because the CR receiver does not require any knowledge about the received samples beforehand. Specifically, the objective is to process the received samples to compute the energy level in the channel. Let $r(n)$ denote the n-th sample of the received signal; then the energy detector is expressed as

$$\Lambda_E = \frac{1}{N} \sum_{n=0}^{N-1} |r(n)|^2. \tag{2}$$

The detection performance of this test statistic is well-investigated in the literature for different signal and noise models. For instance, it can be shown that under the additive white Gaussian noise (AWGN) channel, the receiver operating characteristic (ROC) performance is expressed as [24]

$$P_d = Q\left(\frac{1}{1+\text{SNR}}\left[Q^{-1}(P_f) - \sqrt{N}\,\text{SNR}\right]\right), \tag{3}$$

where P_d is the probability of detection, P_f is the probability of false alarm, $Q(\cdot)$ is the Q-function, and $Q^{-1}(\cdot)$ is the inverse Q-function. It can be observed that the performance improves for higher SNR or longer sensing times, i.e., larger N. Note that this expression is assumed to be valid for any SNR value.

Pilot Detection

While the energy detector is a *universal* detector, since it does not need any specific signal structure, some practical communication systems deliberately embed signal features to either perform synchronization and acquisition or help improve signal decoding. For instance, in some broadcast communication systems, e.g., digital television, sinewave pilot tones are transmitted for data frame synchronization. Mathematically, the transmitted primary signal can be expressed as [10, 24]

$$x(n) = \sqrt{\varepsilon} x_p(n) + \sqrt{1-\varepsilon} x_d(n), \tag{4}$$

where $x_p(n)$ is a known pilot tone, $x_d(n)$ is the data-carrying signal, and ε is the pilot power factor, i.e., the fraction of the total power allocated to the pilot tone. For example, pilots in digital TV signals are 11 dB weaker than the average signal power, i.e., $\varepsilon \approx 0.1$ [1].

Pilot detection infers the occupancy of a channel by utilizing prior knowledge about pilots embedded in transmitted signals. One common approach for pilot detection is the following test statistic [5, 24]

$$\Lambda_P = \frac{1}{N} \sum_{n=0}^{N-1} \hat{x}_p^*(n) r(n), \tag{5}$$

where $\hat{\mathbf{x}}_p = [\hat{x}_p(1), \hat{x}_p(2), \cdots, \hat{x}_p(N)]^T$ is a unit vector in the direction of the pilot tone. The ROC performance of this statistic in an AWGN channel can be shown to be [10]

$$P_d = Q\left(Q^{-1}(P_f) - \sqrt{N\varepsilon\,\mathrm{SNR}}\right). \tag{6}$$

It can be observed that the performance depends on the power allocated to the pilot tone.

Cyclostationarity Detection

In the absence of deterministic pilot tones, the CR receiver can instead utilize the inherit features of modulated signals, which exhibit periodic statistical properties [7, 8]. Specifically, many of the modulated signals are second-order *cyclostationary*, i.e., their means and autocorrelation functions are periodic, where the period depends on the symbol period and the carrier frequency of the signal [21].

Cyclostationarity properties can be observed via the spectral correlation function, a two-dimensional complex transform [8]. This transform is actually a generalization of the power spectral density function, and it maintains several key advantages. First, it preserves phase and frequency information related to certain parameters in modulated signals. Second, features that overlap in the power spectrum are nonoverlapping features in the spectral correlation domain, making it easier to detect them. Third, different modulation schemes, e.g., BPSK and QPSK, have identical power spectral density functions, yet they can have highly distinct spectral correlation functions [4]. Last, noise samples are typically uncorrelated, and hence noise does not exhibit any cyclic features, making the detection in low SNR regime robust. Indeed, the measured spectral correlation of a receiver sensing noise-only samples is illustrated in Fig. 1, which confirms that noise does not have any peaks in the spectral correlation function except at zero cyclic frequencies.

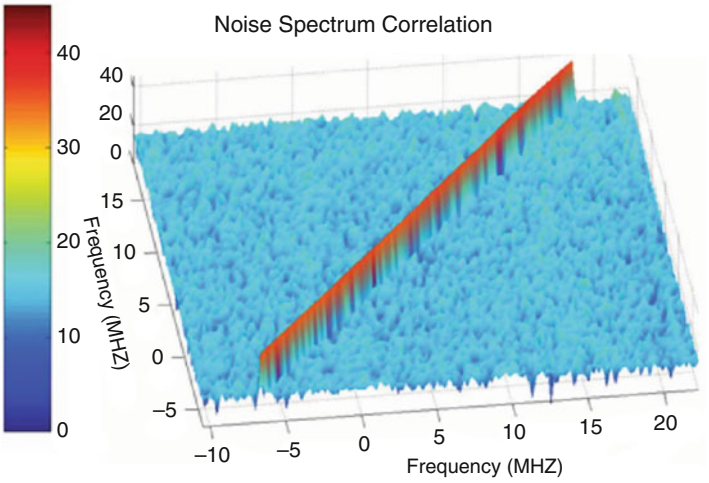

Fig. 1 Measured spectral correlation function of the noise at the 2.4 GHz receiver

The detection of cyclic features in the received signal is typically done by computing the *cyclic autocorrelation function* (CAF), where the received signal is correlated with a frequency-shifted version of itself [7]. More formally, the CAF can be estimated using N samples as follows [14, 21]

$$R_r^{\alpha}(\tau) = \frac{1}{N} \sum_{n=0}^{N-1} r(n) r^*(n-\tau) e^{-j2\pi\alpha n T_s}, \tag{7}$$

where α is the cyclic frequency and T_s is the sampling period. Once the CAF is computed at the CR receiver, the following test statistic can be performed:

$$\Lambda_{\alpha} = |R_r^{\alpha}(\tau)|. \tag{8}$$

As stated, different modulation schemes have peaks at different cyclic frequencies, and hence by varying α, it can be possible to not only detect signals but also classify them [9, 22].

Beyond Classical Detection Theory

Modeling the binary hypothesis testing problem in classical detection theory generally includes many ideal assumptions. For instance, it is commonly assumed that noise samples are generated from a white Gaussian wide-stationary process with a noise variance that is precisely known. This means that the threshold used for the energy detector can be accurately optimized to achieve any desired detection performance. Similarly, for pilot detection, tight synchronization is assumed between

the transmitter and the sensing receiver to properly correlate the received signal with a replica of the pilot tone, whereas frequency and clock offsets are neglected in the analysis of cyclostationarity detection.

Such ideal assumptions can be warranted if detection is done in good SNR conditions, where noise estimation and receiver synchronization are more reliable. However, primary user systems require protection even in the worst-case scenarios when the received signal at a CR receiver could be far below noise floor. For example, for a cognitive radio operation in licensed TV bands, IEEE 802.22 working group defined required SNR sensitivities for primary user signals to be -22 dB for DTV signals and -10 dB for wireless microphones [6]. Hence, spectrum sensing must be reliable in negative SNR regimes.

In addition to the reliable operation under stringent SNR requirements, the CR receiver must seek spectral opportunities over a wide swath of the spectrum, elevating the need for wideband spectrum sensing. The problem of wideband sensing has been typically approached by breaking the spectrum into many narrowband channels, and hence the problem is converted into several binary hypotheses tests, one per channel [11, 12, 16–18]. Such simplification, however, neglects many design challenges inherited with wideband sensing, including the impact of strong interferers in some channels [26, 27], spectral leakage due to nonideal filters [26], or the presence of spurious harmonics generated from nonlinearities in the receiver front-end [19].

The aforementioned design challenges require revisiting the sensing models for two reasons. First, it is important to accurately understand the impact of operating in negative SNR regions with nonideal wideband receiver front-ends on the detection performance. Second, by identifying the key parameters that affect the detection performance, the sensing algorithms can be enhanced to compensate for the different impairments that affect the detection reliability.

Energy Detection Under Noise Uncertainty

In an unoccupied channel, the CR receiver collects noise-only samples. From these samples, the noise variance can be estimated using the energy detector to optimize the detection threshold λ in order to achieve *any* desired probability of detection. Indeed, it can be observed from the ROC performance of the energy detector in (3) that controlling the sensing time N can help meet any specified (P_d, P_f) pair. Specifically, the following relation holds

$$N = \frac{\left[Q^{-1}(P_f) - Q^{-1}(P_d)(1 + \text{SNR})\right]^2}{\text{SNR}^2}. \tag{9}$$

In other words, the theoretical analysis shows that the number of samples asymptotically scales as $1/\text{SNR}^2$, which follows using the approximation $1 + \text{SNR} \approx 1$ in negative SNR regimes. To verify this scaling law, an experimental study is

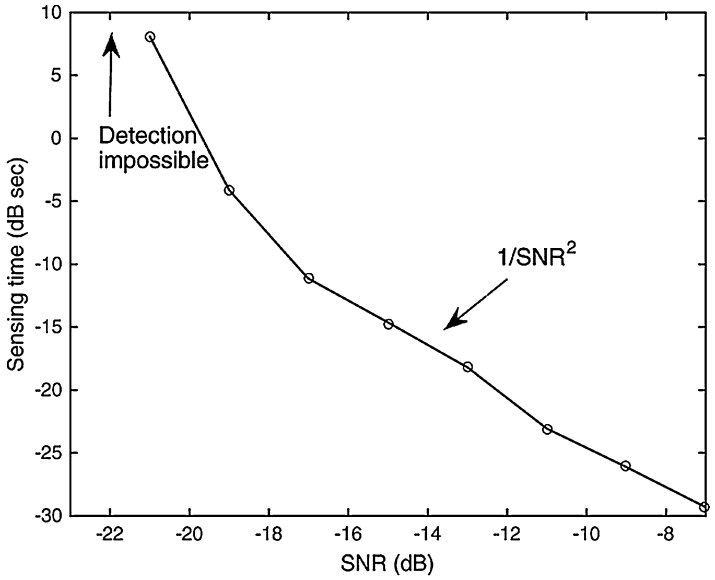

Fig. 2 Measured sensing time versus SNR for energy detector

performed using a real CR test bed [3]. In this study, the objective is to detect a QPSK signal under different SNR values. For each value, two different sets of energy values are collected: one in the absence of the signal and one in its presence. When the signal is absent, the noise-only samples are used to estimate the detection threshold λ that achieves a false alarm of $P_f = 0.05$. The threshold is then applied to compute P_d. From these measurements, the sensing time for a given SNR is derived to achieve a detection performance of $P_d = 0.9$ as shown in Fig. 2. It can be observed that the theoretical scaling law holds for SNR values above -20 dB. However, as the signal becomes weaker, detection becomes progressively harder, and when the signal is below -23 dB, the detector cannot sense the signal irrespective of the sensing time, leading to a phenomenon known as the *SNR wall* [24]. Such deviation illustrates that the energy detector lacks robustness in negative SNR regimes. In addition, the measurements show that the existing sensing model must be revisited to accurately capture the SNR wall phenomenon.

To understand the deviation of the measured sensing time curve from the predicted one, it is imperative to address the assumptions used in the existing sensing model. Specifically, there are two strong assumptions used here. First, noise is assumed to be an additive white Gaussian wide-sense stationary process with zero-mean and known variance. However, noise is an aggregation of various sources including not only thermal noise at the receiver and underlined circuits but also interference due to nearby unintended emissions, weak signals from transmitters very far away, etc. Second, by assuming that the noise variance is perfectly known, the detection threshold can be optimized with infinite precision. However, in the

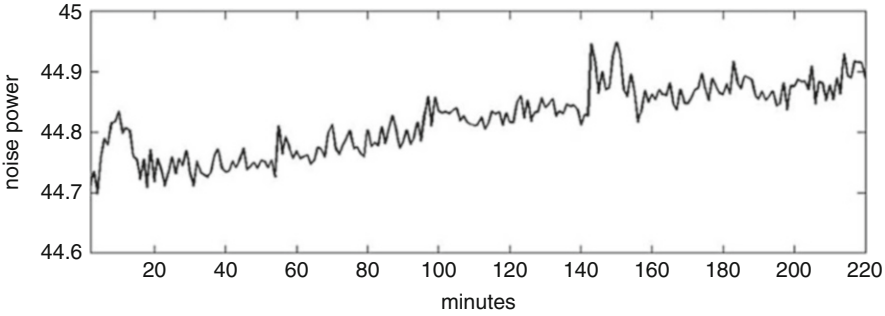

Fig. 3 Measured noise power at the CR receiver

actual implementation, this is practically impossible as noise could vary over time due to temperature change, ambient interference, filtering, etc. Indeed, Fig. 3 shows that the measured noise power level in the receiver used for testing of energy detection varies over time. The impact of the time-varying nature of the noise process on detection becomes tangible when the signal strength is below the estimation error of the noise variance. Hence, these temporal changes must be captured in the sensing model, particularly when the receiver operates in negative SNR regimes.

Modeling Noise Uncertainty

In a standard sensing model, it is common to model the noise-only samples as $w(n) \sim \mathcal{N}(0, \sigma_w^2)$, i.e., a Gaussian random variable with zero-mean and perfectly known variance σ_w^2. However, it is more accurate to assume that such noise samples are instead generated from $\tilde{w}(n) \sim \mathcal{N}(0, \tilde{\sigma}_w^2)$ such that

$$\tilde{\sigma}_w^2 \in \left[\frac{1}{\rho}\sigma_w^2, \rho\sigma_w^2\right], \tag{10}$$

where $\rho \geq 1$ is a parameter that quantifies the noise uncertainty. Note that $\rho = 1$ implies perfect knowledge of the noise variance. In other words, the CR receiver estimates that the noise variance is σ_w^2, whereas the *actual* variance is $\tilde{\sigma}_w^2$.

To understand how such noise uncertainty leads to an SNR wall, consider the worst-case scenario. Specifically, the highest false alarm probability occurs when the actual noise variance is $\tilde{\sigma}_w^2 = \rho\sigma_w^2$ since in this case σ_w^2 becomes an underestimate of the true variance, forcing the CR receiver to more frequently decide that the channel is occupied. Similarly, the lowest probability of detection occurs when the actual noise variance is $\tilde{\sigma}_w^2 = (1/\rho)\sigma_w^2$. In this case, the CR receiver overestimates the true variance, leading to increasing the frequency of declaring a channel to be empty. Under such worst-case scenario, it can be shown that the ROC of the energy detector becomes [24]

$$P_d = Q\left(\frac{\rho Q^{-1}(P_f) - \sqrt{N}(\text{SNR} + 1/\rho - \rho)}{\text{SNR} + 1/\rho}\right). \tag{11}$$

Clearly, for $\rho = 1$, (11) simplifies to (3). From this expression, the sensing time can be derived to be

$$N = \frac{\left[\rho Q^{-1}(P_f) - Q^{-1}(P_d)(1/\rho + \text{SNR})\right]^2}{(\text{SNR} + 1/\rho - \rho)^2}. \tag{12}$$

It is evident that $N \to \infty$ when $\text{SNR} + 1/\rho - \rho = 0$, i.e., there exists an SNR wall where detection below that SNR value becomes impossible. More formally, for $\rho > 1$, the SNR wall occurs at

$$\text{SNR}_{\text{wall}} = \frac{\rho^2 - 1}{\rho}. \tag{13}$$

Figure 4 illustrates the theoretical sensing time in the presence and absence of noise uncertainty where $\rho_{dB} = 10\log_{10}(\rho)$. It is evident that even small uncertainty makes the energy detector poor in highly negative SNR regions. It is also observed that the modified sensing model captures the behavior observed in the experimental study illustrated in Fig. 2.

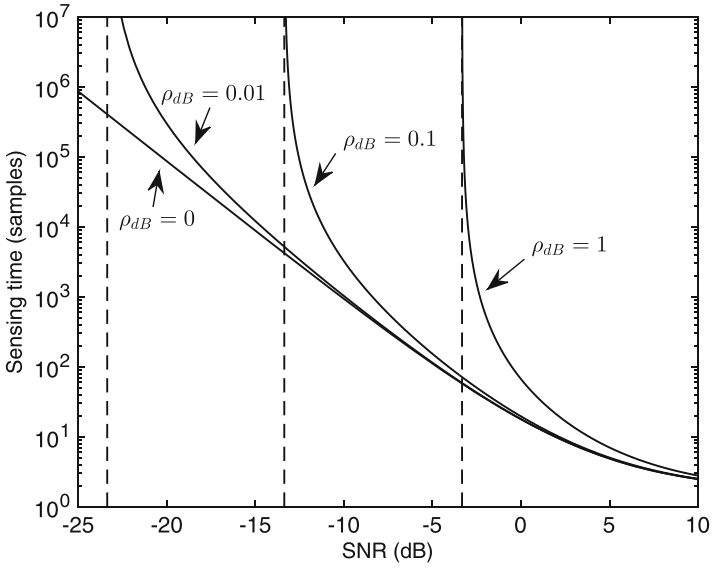

Fig. 4 Sensing time in the presence of noise uncertainty

Compensating Noise Uncertainty

Frequent noise power estimation becomes imperative, particularly in low SNR regimes. To this end, the CR receiver must collect noise-only samples. These samples, denoted as $w(n)$, can be used to estimate the noise variance using the following maximum likelihood (ML) estimator [13]

$$\hat{\sigma}_w^2 = \frac{1}{M} \sum_{m=0}^{M-1} |w(m)|^2. \tag{14}$$

The key issue here is the availability of such samples or inferring that the collected samples are actually noise-only samples instead of samples of a weak signal. One solution to this issue is to infrequently trigger a fine-sensing stage, where a feature detector is used [15]. Specifically, during the fine-sensing stage, if the decision is H_0, then the collected samples can, with high accuracy, be declared as noise-only samples, and hence they can be used to update $\hat{\sigma}_w^2$ for subsequent energy detection. Such approach can be implemented using the following detector:

$$\begin{aligned} \Lambda'_E &= \frac{\Lambda_E}{\hat{\sigma}_w^2} \\ &= \frac{M}{N} \frac{\sum_{n=0}^{N-1} |r(n)|^2}{\sum_{m=0}^{M-1} |w(m)|^2}. \end{aligned} \tag{15}$$

Figure 5 illustrates the enhanced energy detector. It consists of two stages: fine sensing of duration M, that is triggered infrequently, and energy sensing for duration N, which is triggered frequently. The former is motivated to reliably update the noise variance estimate, which will be used for subsequent fast energy detection.

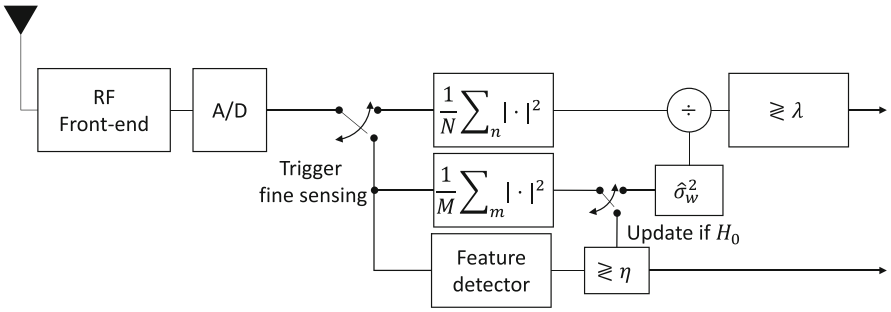

Fig. 5 The enhanced energy detector utilizes the noise variance estimate, which is periodically updated

The detection performance of this detector can be approximated as [15]

$$P_d = Q\left(\frac{1}{1+\text{SNR}}\left[Q^{-1}(P_f) - \sqrt{\frac{N \cdot M}{N+M}}\,\text{SNR}\right]\right). \tag{16}$$

From this expression, the sensing time of the energy detector is derived as follows:

$$\sqrt{\frac{N \cdot M}{N+M}} = \frac{Q^{-1}(P_f) - Q^{-1}(P_d)(1+\text{SNR})}{\text{SNR}}. \tag{17}$$

For instance, if $M = N$, the sensing time needed to achieve a specific (P_d, P_f) pair is

$$N = \frac{2\left[Q^{-1}(P_f) - Q^{-1}(P_d)(1+\text{SNR})\right]^2}{\text{SNR}^2}. \tag{18}$$

That is, there is an SNR penalty of $10\log_{10}(\sqrt{2}) \approx 1.5\,\text{dB}$ in comparison with the ideal energy detector. Note, however, that if $M = N^2$, then $\sqrt{\frac{N \cdot M}{N+M}} \approx \sqrt{N}$, i.e., the performance of Λ'_E reaches the ideal performance of Λ_E in the negative SNR regime.

Alternatively, the minimum SNR for which the detection is possible can be derived as [15]

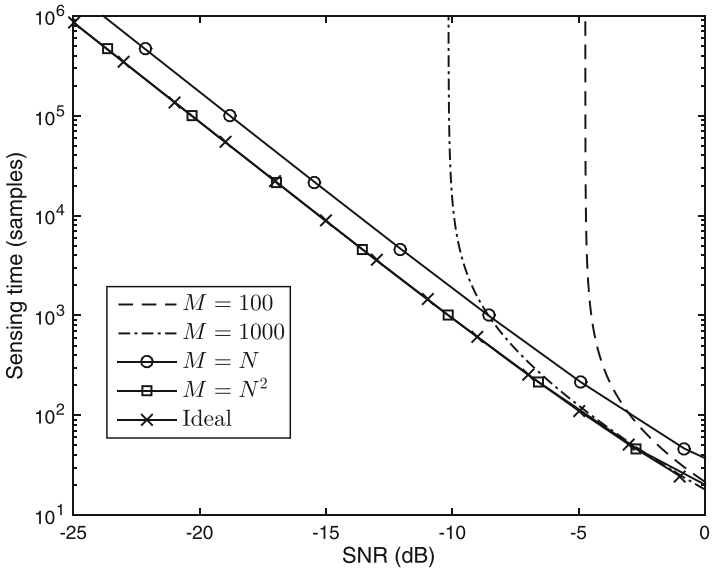

Fig. 6 Performance of the enhanced energy detector

$$\mathrm{SNR}_{\min} = \frac{1 + \sqrt{\frac{M+N}{N \cdot M}} Q^{-1}(P_f)}{1 + \sqrt{\frac{M+N}{N \cdot M}} Q^{-1}(P_d)} - 1. \tag{19}$$

It is clear that if $M = N$ or $M = N^2$, then $\mathrm{SNR}_{\min} \to 0$ as $N \to \infty$, i.e., there is no SNR wall. However, if M is a constant, e.g., $M = 100$, then $\mathrm{SNR}_{\min} > 0$ as $N \to \infty$.

Figure 6 illustrates the sensing time needed to achieve $P_f = 0.05$ and $P_d = 0.9$ when Λ'_E is used. As expected, having longer sensing periods to estimate the noise variance, i.e., larger M, improves the performance of the energy detector. However, to mitigate the SNR wall, the noise power estimation period should scale with the duration of the energy detector, e.g., $M = N$ and $M = N^2$.

Pilot Detection Under Frequency Offsets

The simplicity of the energy detector comes at the expense of a poor performance in negative SNR regimes. To circumvent this, pilot detection exploits certain signal features to robustify the detection performance, and particularly it relies on pilot tones that are sent alongside data-carrying signals. Indeed, the processing of the received samples via correlation provides *coherent* gains that make detection of very weak signals possible. However, this coherent processing requires the CR receiver to be in perfect synchronization with the pilot in the received signal.

Consider the ROC performance of the pilot detector in (6); then the sensing time needed to achieve any desired (P_d, P_f) pair can be shown to be

$$N = \frac{\left[Q^{-1}(P_f) - Q^{-1}(P_d)\right]^2}{\varepsilon\,\mathrm{SNR}}. \tag{20}$$

Thus, the theoretical scaling law of the sensing time is $N \sim 1/\mathrm{SNR}$. Comparing this scaling law with the one achieved using the energy detector, then it can be observed that the sensing time under pilot detection is a lower bound on that achieved using energy detection as long as $\varepsilon > \mathrm{SNR}$.

To verify the scaling law of the pilot detector, an experimental study is performed on a sinewave pilot, with signal levels varying from -110 to -136 dB. The measured sensing time is shown in Fig. 7 in the presence of different frequency offsets. It is observed that for strong pilot tones, the measured sensing time follows the theoretical scaling law. However, as the pilot power decreases, the sensing time deviates from the theoretical curve, leading to the SNR wall phenomenon.

The deviation of the experimental result from the theoretical curve is explained as follows. Practical receivers have imperfect thus inaccurate oscillators and circuitry, deeming perfect synchronization near impossible, particularly in negative SNR regimes. Typically, synchronization loops can estimate and reliably correct frequency offsets when the SNR at the receiver is positive. However, in negative

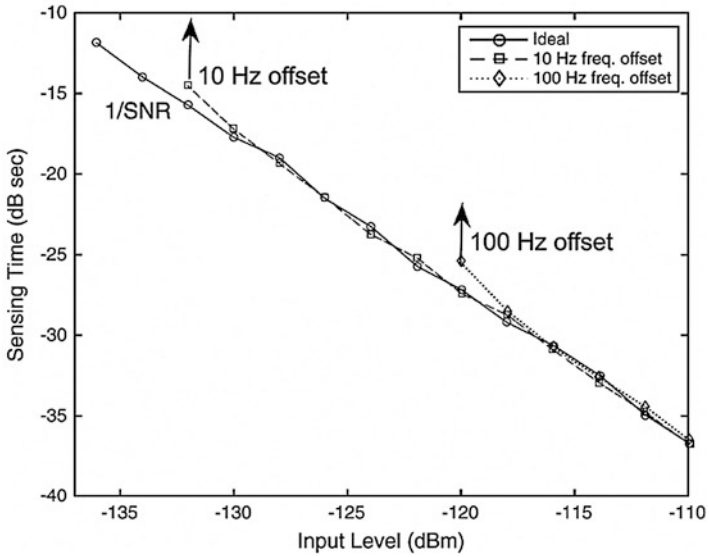

Fig. 7 Measured sensing time with variations of the sine wave signal power under different frequency offsets

SNRs these loops are driven by noise and cannot perform robust synchronization. The imperfect synchronization can severely affect the coherent processing gains achieved by correlating the received signal with the pilot tone.

Modeling Frequency Offsets

Consider the sinewave pilot tone $x_p(n) = \exp(j(\omega_o n + \theta))$, where ω_0 is the carrier frequency. Suppose there exists a frequency offset, ψ, between the primary transmitter and the CR receiver. This can be modeled by assuming that the pilot tone replica used at the receiver is equal to $\hat{x}_p(n) = x_p(n)\exp(j\psi n)$. Using the pilot detector, it can be shown that under H_1

$$\begin{aligned} \Lambda_P &= \frac{1}{N}\sum_{n=0}^{N-1} \hat{x}_p(n)^* r(n) \\ &\approx \frac{\sqrt{\varepsilon}}{N}\sum_{n=0}^{N-1} \exp(-j\psi n). \end{aligned} \tag{21}$$

If the sensing time N becomes comparable or larger than the period of the frequency offset, then the pilot detector loses its coherent processing gain. In other words, in

the presence of frequency offsets, the pilot detector can suffer from the SNR wall, explaining the measured curve in Fig. 7.

Compensating Frequency Offsets

As discussed in the previous section, the presence of frequency offsets can be detrimental if the sensing time is in the order of frequency offset time period. Thus, it is intuitive to break down the sensing time into shorter time periods to help achieve partial coherent processing gains. This motivates the following enhanced pilot detector [5]:

$$\Lambda'_P = \frac{1}{K}\sum_{k=0}^{K-1}\frac{1}{M}\left[\sum_{m=0}^{M-1}\hat{x}_p^*(kM+m)r(kM+m)\right]^2. \tag{22}$$

This detector can be interpreted as a two-stage pilot detector. Specifically, in the first stage, the CR receiver correlates the received signal with a replica of the pilot tone, but this time it is done over a short period, i.e., $M \ll N$. This process is repeated K times, and hence in the second stage, the CR receiver noncoherently averages over these collected K blocks, making the total sensing time $N = K \cdot M$. The receiver architecture of the two-stage pilot detector is shown in Fig. 8.

It can be shown that the performance of the enhanced pilot detector is

$$P_d = Q\left(\frac{1}{\sqrt{1+2M\varepsilon\,\mathrm{SNR}}}\left[Q^{-1}(P_f) - \sqrt{\frac{K}{2}}M\varepsilon\,\mathrm{SNR}\right]\right). \tag{23}$$

There are several key observations here. First, if $\varepsilon\,\mathrm{SNR} \ll 1$, then the performance can be approximated as

$$P_d \approx Q\left(Q^{-1}(P_f) - \sqrt{\frac{K}{2}}M\varepsilon\,\mathrm{SNR}\right). \tag{24}$$

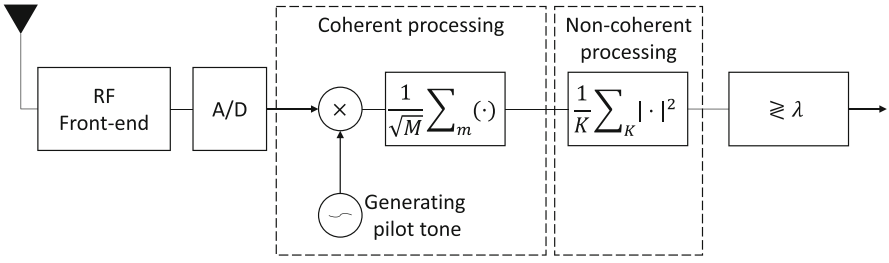

Fig. 8 The two-stage pilot detector complements coherent processing with noncoherent processing

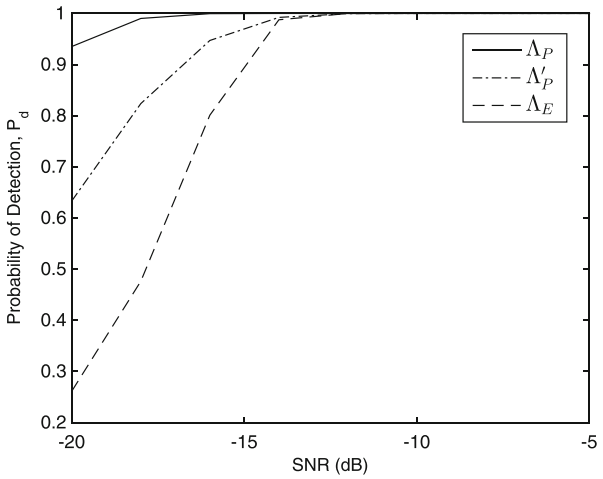

Fig. 9 The detection performance of the enhanced pilot detector

In this case, increasing K improves the performance with a similar scaling to the energy detector (cf. (3)). Yet, the coherent processing effectively improves the SNR by $10\log_{10}(M)$dB. In other words, comparing (24) with (3), it can be observed that under noise uncertainty, which affects nocoherent processing, the enhanced pilot detector moves the SNR wall by $10\log_{10}(M)$dB.

Second, if $\varepsilon\,\mathrm{SNR} \gg 1$, then the performance can be approximated as

$$P_d \approx Q\left(\frac{Q^{-1}(P_f)}{\sqrt{2M\varepsilon\,\mathrm{SNR}}} - \sqrt{\frac{KM\varepsilon\,\mathrm{SNR}}{4}}\right). \tag{25}$$

In this case, the performance of the enhanced pilot detector is similar to the performance of the ideal pilot detector (cf. (6)).

Figure 9 shows the detection performance of the enhanced pilot detector in negative SNR regimes. The enhanced detector is compared with the ideal energy and pilot detectors in (2) and (5), respectively. It is assumed that $P_f = 0.05$, $\varepsilon = 0.1$, and $N = 10{,}000$, where $K = 10$ and $M = 1000$. It is clear that the enhanced pilot detector benefits from the coherent processing gains in very negative SNRs, and since $M \ll N$, the robustness against frequency offsets improves.

Cyclostationarity Detection Under Imperfect Synchronization

Similar to pilot detection, where prior knowledge about pilot tones is needed, cyclostationarity detection requires knowledge about the cyclic frequency of the modulated signal. Such feature exploitation helps robustify detection in negative SNR regimes. However, it is critical to analyze the detection performance when such knowledge is not perfectly known.

Consider the zero-lag CAF, i.e., $\tau = 0$, which is expressed as

$$R_r^{\alpha}(0) = \frac{1}{N} \sum_{n=0}^{N-1} r(n) r^*(n) e^{-j2\pi\alpha n T_s}. \tag{26}$$

Clearly, for $\alpha = 0$, the cyclostationarity detector simplifies to the energy detector in (2). From this, one can interpret this detector for $\alpha \neq 0$ as computing the energy of the received signal at a cyclic frequency α. In the presence of noise-only samples, it can be shown that as $N \to \infty$ then $R_r^{\alpha}(0) \to 0$ for $\alpha \neq 0$ at all SNRs. That is, the detector can *theoretically* suppress noise at the negative SNR regime by increasing the sensing time N due to averaging a stationary noise process.

The robustness of the cyclostationarity detector in negative SNR regimes is attained when α is perfectly known, yet this is difficult to achieve in practice. Specifically, the presence of Doppler shifts, imperfect estimation of carrier frequencies, and the frequency mismatch due to local oscillators all introduce *cyclic frequency offsets* (CFOs) that can degrade the performance. Such performance degradation is verified experimentally [20]. In particular, a BPSK signal with a symbol period $T = 10\mu s$ is generated. At the receiver end, the detector in (26) is implemented at $\alpha = 1/T = 100\,\text{KHz}$ with a sampling frequency $1/T_s = 2\,\text{MHz}$. The cyclic feature of the BPSK signal is analyzed in the presence of different frequency offsets Δ_α given in units per million (ppm). Figure 10 shows the impact of increasing the sensing time N on the cyclic feature. Interestingly, as the sensing time increases, it

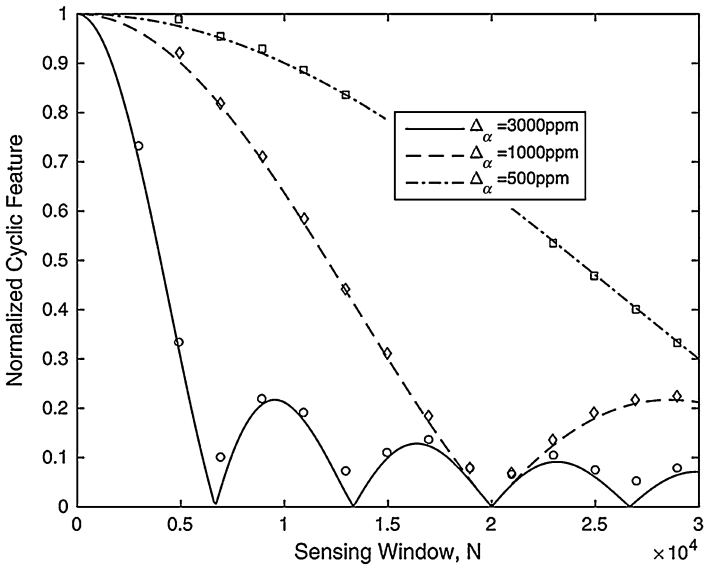

Fig. 10 Normalized cylic feature in the presence of CFOs. *Markers* denote the experimental results and *curves* denote the theoretical expression in (29)

becomes harder to detect the cyclic feature. Thus, although increasing N averages the noise process in negative SNR regimes, the cyclic feature becomes harder to detect, leading to an SNR wall phenomenon. The decay in the cyclic feature is theoretically investigated in the next section.

Modeling Cyclic Frequency Offsets

To model the CFO, it can be assumed that the test statistic is computed at a cyclic frequency that is deviated from the correct one by Δ_α, i.e., the cyclic frequency used is

$$\hat{\alpha} = \alpha(1 + \Delta_\alpha). \tag{27}$$

Note that the CFO will not affect the noise process since it is stationary. Hence, noiseless signals are considered in the subsequent analysis.

For illustration purposes, consider a single-carrier signal $r(n) = \sum_m a(mT_b)\, p(nT_s - mT) \exp(-2\pi f_0 nT_s)$, where $a(mT_b)$ are data symbols with period T_b, e.g., for BPSK $a(mT_b) \in \{+1, -1\}$, $p(\cdot)$ is a pulse shaping filter, and f_0 is the carrier frequency. Then,

$$\begin{aligned} R_r^{\hat{\alpha}}(0) &= \frac{1}{N}\sum_{n=0}^{N-1} r(n) r^*(n) e^{-j2\pi\hat{\alpha}nT_s} \\ &= \frac{1}{N}\sum_{n=0}^{N-1} \left|\sum_m a(mT_b)\, p(nT_s - mT)\right|^2 e^{-j2\pi\alpha nT_s} e^{-j2\pi\alpha\Delta_\alpha nT_s} \\ &\approx \frac{R_r^\alpha(0)}{N} \frac{e^{-j2\pi\alpha\Delta_\alpha NT_s} - 1}{e^{-j2\pi\alpha\Delta_\alpha T_s} - 1} \\ &= R_r^\alpha(0) e^{-j2\pi\alpha\Delta_\alpha(N-1)T_s} \frac{\sin(\pi\alpha\Delta_\alpha NT_s)}{N\sin(\pi\alpha\Delta_\alpha T_s)}. \end{aligned} \tag{28}$$

Note that $R_r^{\hat{\alpha}}(0) \to R_r^\alpha(0)$ as $\Delta_\alpha \to 0$. The test statistic to detect the cyclic feature is shown to be [20, 29]

$$|R_r^{\hat{\alpha}}(0)| = |R_r^\alpha(0)| \left|\frac{\sin(\pi\alpha\Delta_\alpha NT_s)}{N\sin(\pi\alpha\Delta_\alpha T_s)}\right|. \tag{29}$$

It can be observed that for $\Delta_\alpha \neq 0$, the cyclic feature decays as N increases. This makes $|R_r^{\hat{\alpha}}(0)|$ under H_1 to be similar to $|R_r^{\hat{\alpha}}(0)|$ under H_0, making detection very difficult. Figure 10 shows the theoretical curves of the normalized cyclic feature in the presence of CFOs, which match the results obtained via the experimental study.

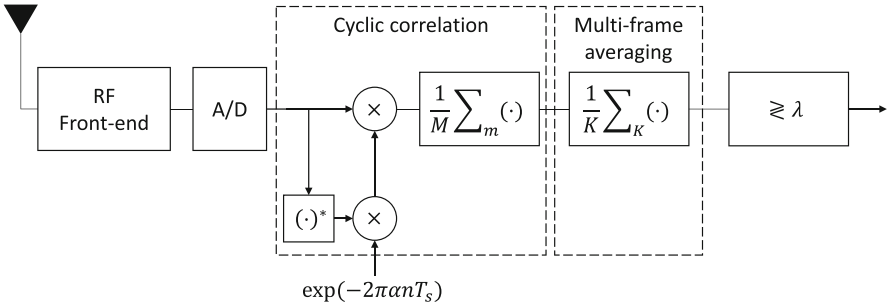

Fig. 11 The enhanced cyclostationarity detector

Compensating Frequency Offsets

It is shown that long sensing windows severely impact the cyclostationarity detector in the presence of CFOs. However, long sensing windows are necessary to average noise, particularly in negative SNR regimes. This suggests a two-stage sensing detector similar to the approach used in improving the pilot detector. Specifically, the N samples are broken into K blocks, where each one is of length M. In each block of samples, cyclostationarity detection is done, yet $M < N$, and hence the impact of the CFO is reduced. At the same time, $K > 1$ in order to average noise. Mathematically, the two-stage detector is given as [21]

$$R_r^{\alpha}(0)' = \frac{1}{K \cdot M} \sum_{k=0}^{K-1} \sum_{m=0}^{M-1} r(kM + m) r^*(kM + m) e^{-j2\pi\alpha m T_s}. \tag{30}$$

The enhanced cyclostationarity detector is shown in Fig. 11. Similar to the analysis given for $R_r^{\hat{\alpha}}(0)$, it can be shown that the impact of the CFO on $R_r^{\alpha}(0)'$ is given by

$$|R_r^{\hat{\alpha}}(0)'| = |R_r^{\alpha}(0)'| \left| \frac{\sin(\pi\alpha\Delta_{\alpha} M T_s)}{M \sin(\pi\alpha\Delta_{\alpha} T_s)} \cdot \frac{\sin(\pi\alpha K M T_s)}{K \sin(\pi\alpha M T_s)} \right|. \tag{31}$$

Figure 12a shows the normalized cyclic frequency under the enhanced detector for different number of frames. It is evident that breaking the N samples into several frames can significantly reduce the rate at which the cyclic feature decays, making it more reliable to detect in negative SNR regimes. Figure 12b illustrates the cyclic feature with variations of the CFO, where $N = 20{,}000$. It can be observed that increasing K does not always provide the highest gains. For instance, the cyclic feature is weak for $K = 5$ when the CFO is small. This emphasizes that the number of samples and how these samples are divided into blocks both affect the performance. This suggests an optimization framework that maximizes the cyclic feature by optimizing K and M [20].

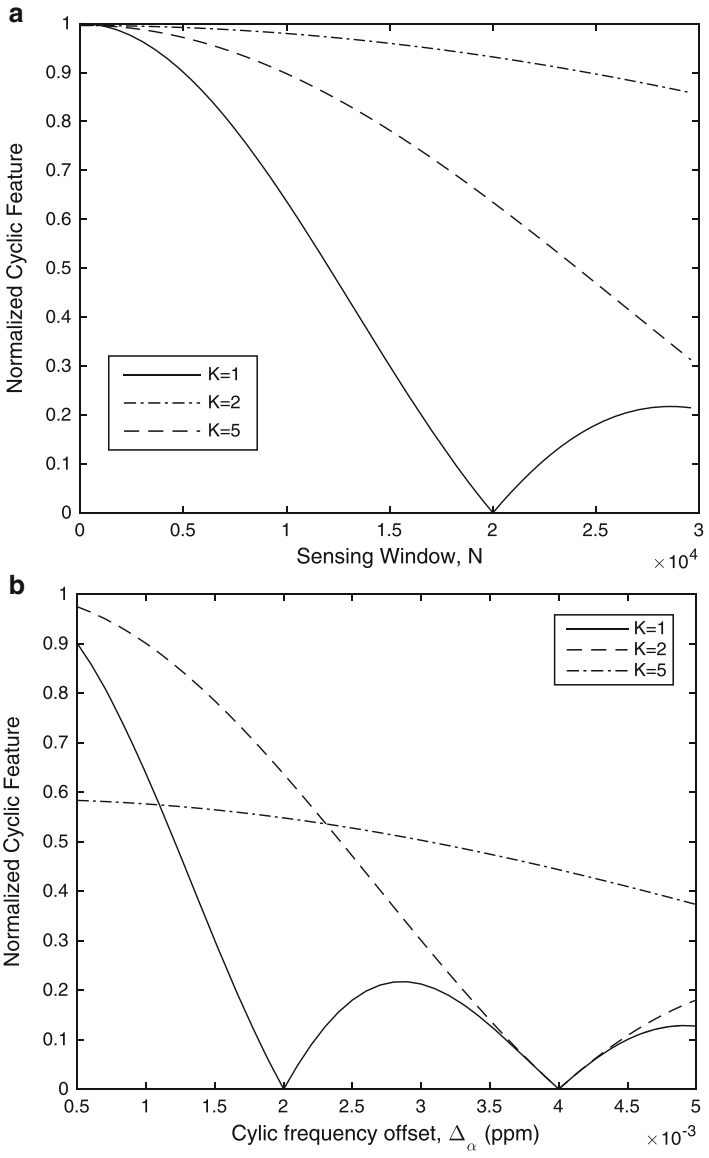

Fig. 12 Normalized cyclic frequency under the enhanced cyclostationarity detector

So far, it is assumed that there are no phase offsets between the different blocks, which occur when $M \alpha T_s$ is an integer, i.e., the estimation of the CAF is done over an integer number of periods of the cyclic frequency. However, *sampling clock offsets* (SCOs) resulted in the analog-to-digital conversion stage may prevent coherent integration of the different blocks.

One way to model the SCO is to rewrite the sampling period as

$$\hat{T}_s = T_s(1+\delta). \tag{32}$$

Here, it is assumed that $\Delta_\alpha = 0$ to explicitly understand how the SCO affects the performance of the enhanced cyclostationarity detector. Hence, and similar to the analysis done for the CFO, it can be shown that

$$|\hat{R}_r^\alpha(0)'| = |R_r^\alpha(0)'| \left| \frac{\sin(\pi\alpha K M T_s(1+\delta))}{K \sin(\pi\alpha M T_s(1+\delta))} \right|, \tag{33}$$

where $\hat{R}_r^\alpha(0)'$ denotes the enhanced detector in the presence of the SCO.

The impact of the SCO on the enhanced detector is studied for $K = 5$. Figure 13a shows the normalized cyclic frequency with variations of the number of samples, whereas Fig. 13b shows the impact of δ, where $N = 10{,}000$. It is assumed that $\alpha = 1/T = 100\,\text{KHz}$ and $1/T_s = 2\,\text{MHz}$. It is clear that sampling offsets have detrimental effects on the performance.

The enhanced detector, in general, requires optimizing K and M to limit the performance loss due to CFOs and SCOs [21]. An optimization framework can be formulated when these two impairments are modeled as random variables. Figure 14 illustrates the detection performance of the enhanced detector, where both impairments are modeled as zero-mean Gaussian random variables with variances $\sigma_{cfo}^2 = 2 \times 10^{-4}$ and $\sigma_{sco}^2 = 1 \times 10^{-5}$. The signal to be detected is assumed to be BPSK with $\alpha = 5\,\text{MHz}$, and $1/T_s = 10\,\text{MHz}$. Figure 14a shows the simulated ROC performance for different number of frames, where SNR $= -5\,\text{dB}$. The total sensing window is fixed at $N = K \cdot M = 5000$ samples. It can be observed that the way by which the samples are split is critical to the detector's performance. Figure 14b shows the detection performance for $K = 12$ under different SNR regimes. Overall, the detector provides robust performance in negative SNR regimes if K and M are optimized.

Wideband Sensing: Challenges and Solutions

To realize a full-scale uptake of cognitive radio systems, it is imperative to explore a wide swath of the spectrum in order to identify as many spectral opportunities as possible. Hence, it is critical to equip CR receivers with wideband sensing capabilities, i.e., scanners that can scan many channels in parallel. Not only this provides more bandwidth, and hence more throughput, but also enables the receiver to move from one channel to another when a primary system reappears.

Typically in wideband sensing, the received wideband signal is fed into a filter bank to channelize it into nonoverlapping subbands. In this case, the wideband sensing model becomes a collection of narrowband sensing models. Hence, the

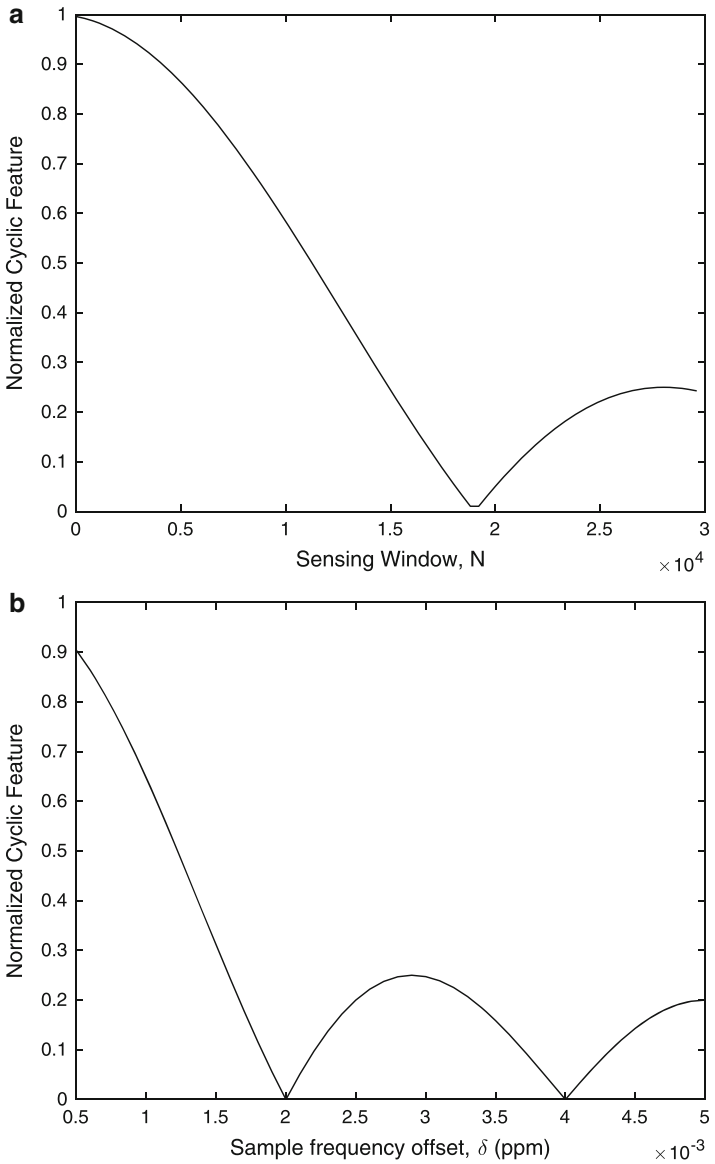

Fig. 13 Normalized cyclic frequency in the presence of SCOs

impairments discussed in the previous sections can still occur for each subband, e.g., noise uncertainty, imperfect synchronization, frequency offsets, etc.

Besides the aforementioned impairments, there are other impairments and design challenges inherited in wideband sensing. For instance, consider the general wideband sensing architecture shown in Fig. 15. Observe that the digital signal

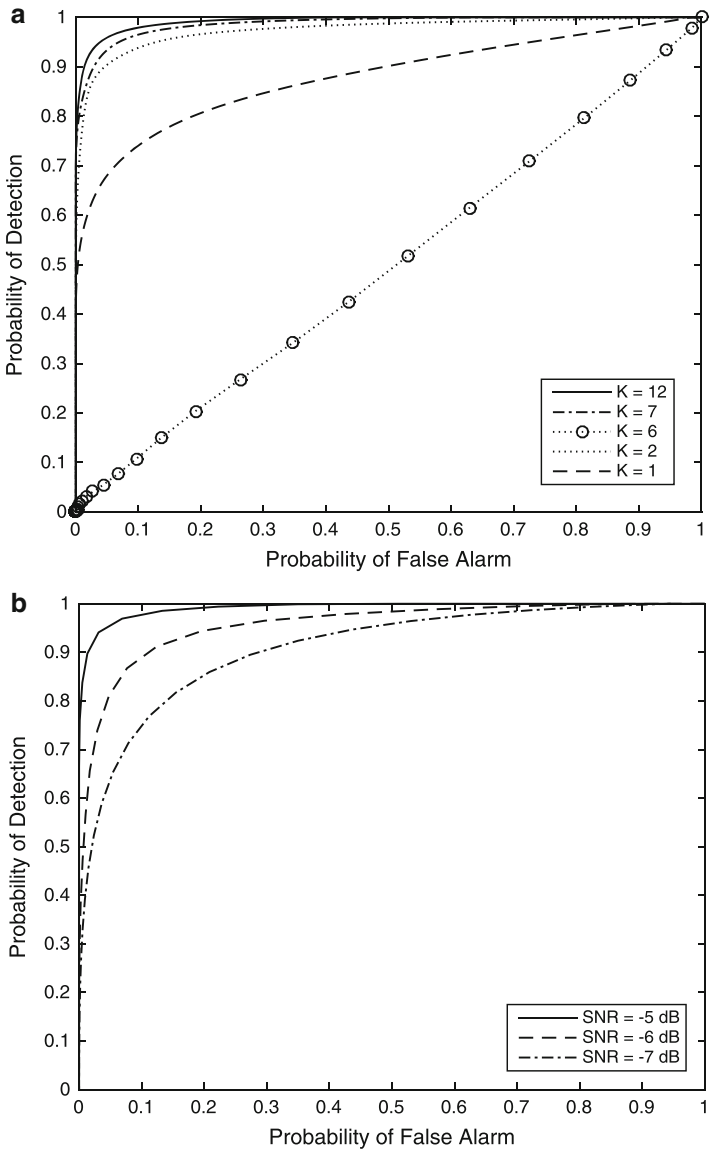

Fig. 14 Detection performance of the enhanced detector in the presence of CFOs and SCOs

processor (DSP) has the additional block *channelization* (or filtering) to convert the wideband signal into several narrowbands. Such filtering procedure is nonideal, causing leakage and interference in the channel of interest. In addition, due to the high bandwidth of the signal, the low-power amplifier (LNA) in the RF front-end may be pushed to operate in a nonlinear region, causing the wideband signal to be distorted. These two impairments will be the focus of this section.

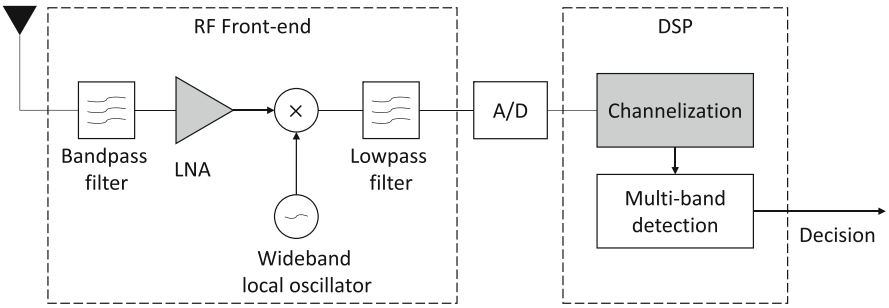

Fig. 15 A typical wideband sensing architecture

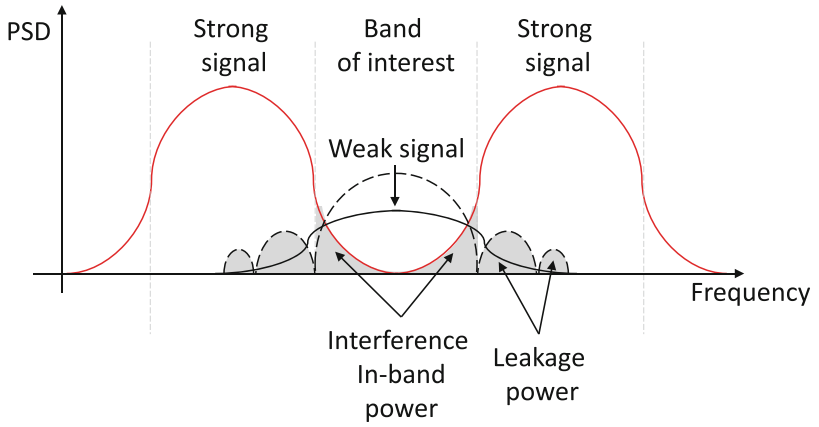

Fig. 16 Nonideal channelization and filtering result in adjacent interfering power

Adjacent Band Interfering Power

Consider a wideband signal that is composed of several nonoverlapping narrowband primary users, where for simplicity all bands are assumed to be of equal bandwidth and modulation scheme. Figure 16 illustrates an example of the power spectral density (PSD) of three nonoverlapping signals. Consider detecting the weak primary signal, which is adjacent to two strong primary signals. In an ideal architecture, each signal can be processed and detected independently of the other signals. However, in a practical receiver, there are two issues that arise. First, the filters in frequency domain are not perfectly rectangular, with sharp edges. Hence, the tail of a strong adjacent signal may introduce interference to the band of interest. In other words, even if the band of interest is unoccupied, the interference present in that channel may increase false alarms. Second, the channelization of the time-domain samples can introduce spectral leakage to other channels. These two issues will be collectively referred as *adjacent band interfering power* [26].

Modeling Adjacent Interference Power

The discrete-time domain received wideband signal $r(n)$ is a superposition of primary signals corrupted with noise. In other words, let $w(n) \sim \mathcal{N}(0, \sigma_w^2)$ be the noise samples; then $r(n) = \sum_{l=1}^{L} x_l(n) + w(n)$, where $x_l(n)$ is the transmitted primary signal over the l-th channel. The received signal can be decoupled into narrowband signals using the frequency domain representation of $r(n)$, which is computed by the normalized fast Fourier transform (FFT) as follows

$$R_k[m] = \frac{1}{N_F} \sum_{n=0}^{N_F-1} r(n + kN_F) e^{-2\pi nm/N_F}, \tag{34}$$

where k is the FFT block index, m is the frequency bin, and N_F is the FFT size. Each channel is represented by M bins. Using Parseval's theorem, the signal power in the l-th channel can be computed in frequency domain as

$$\Lambda_{E,l} = \frac{1}{KM} \sum_{k=0}^{K-1} \sum_{m} |R_k[m]|^2, \tag{35}$$

where the second sum term is over the l-th channel bins. The issue here is that $R_{k,l} = \sum_m |R_k[m]|^2$ is not the power of noise-only samples in case of H_0 (or noise-plus-signal samples in case of H_1) since now these samples are corrupted by the adjacent interference. In this case, the variance of the samples under H_0 is higher than σ_w^2, increasing false alarms if the threshold is not corrected. As a result, it is critical to not only reduce the interference but also to estimate it in order to correct the decision threshold.

Mitigating Adjacent Interference Power

The high-level overview of the procedure that mitigates the adjacent interference power is shown in Fig. 17. In the first step, the RF antennas are switched off to calibrate the noise power. In the second step, a coarse estimation of the PSD is performed, where each channel is sensed using an energy detector with the same number of samples. By measuring the power in each adjacent channel to the band of interest, the interfering power is estimated in the third step.

Once the interference power, $\sigma_{I,l}^2$, is estimated for each channel, the sensing time needed for each channel to perform a fine PSD estimation is optimized. The PSD estimation can be robustified against power leakages using a windowed FFT instead of using (34). In the windowed FFT, the received samples $r(n)$ are weighted first by a normalized window coefficient $\omega(n)$ before computing the FFT. This weighting, however, comes at the expense of reducing the spectral resolution. To maintain a high spectral resolution, a multitap-windowed FFT can be used instead. Mathematically, the multitap-windowed FFT is implemented as [26]

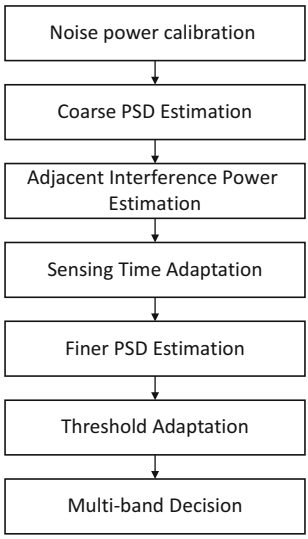

Fig. 17 A high-level procedure to mitigate adjacent interference power

$$\hat{R}_k[m] = \frac{1}{N_F} \sum_{n=0}^{N_F-1} \left(\sum_{p=0}^{P-1} \omega(n + pN_F) r(n + pN_F + kN_F) \right) e^{-2\pi nm/N_F}, \quad (36)$$

where p is the tap index and P is the total number of taps. In this case, the multitap-windowed energy detector is expressed as

$$\Lambda_{ME,l} = \frac{1}{N_l} \sum_{k=0}^{N_l-1} \sum_{m} |\hat{R}_k[m]|^2, \quad (37)$$

where N_l is the channel-specific sensing time. The sensing time differs across channels depending on the interfering powers in each channel. For a desired (P_f, P_d) pair and SNR sensitivity, N_l can be computed as follows:

$$N_l = \mu \left[\left(1 + \frac{\sigma_{I,l}^2}{\sigma_w^2} \right) \frac{Q^{-1}(P_f) - Q^{-1}(P_d)}{\text{SNR}} - Q^{-1}(P_d) \right]^2, \quad (38)$$

where μ is a fitting factor that can be calculated beforehand. This expression can be derived from the detection performance of the multitap-windowed energy detector, which is shown to be [25]

$$P_d = Q \left(\frac{1}{1 + \text{SNR} + \sigma_{I,l}^2/\sigma_w^2} \left[Q^{-1}(P_f)(1 + \sigma_{I,l}^2/\sigma_w^2) - \sqrt{\frac{N_l}{\mu}}\, \text{SNR} \right] \right). \quad (39)$$

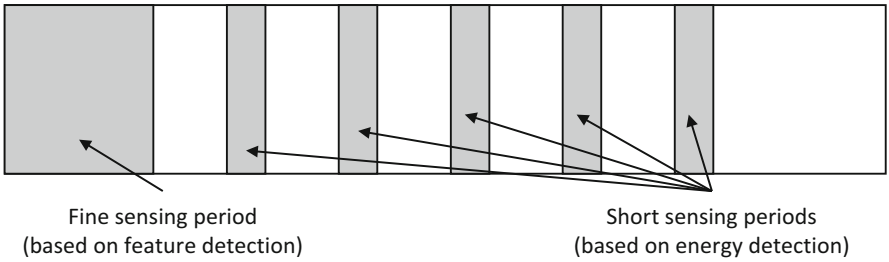

Fig. 18 The multitap-windowed energy detector

Once the PSD is finely estimated for each channel, the threshold is corrected before the multiband detection. Specifically, it is computed as

$$\lambda_l = \left(\sigma_w^2 + \sigma_{I,l}^2\right)\left(\sqrt{\mu/N_l}\,Q^{-1}(P_f) + 1\right). \tag{40}$$

Figure 18 illustrates the DSP used for the multitap-windowed energy detector.

Figure 19a shows the number of samples needed for $(P_f, P_d) = (0.1, 0.9)$ with variations on the interfere-to-noise-power ratio (INR), i.e., $\sigma_{I,l}^2/\sigma_w^2$. Three detectors are shown: the multitap-windowed detector; the windowed detector, i.e., $P = 1$; and the conventional one, i.e., no windowing is used. It is assumed that SNR $= -5$ dB, and the adjacent interferes are one bin away from the band of interest. It is evident that the multitap-windowed detector provides a significant reduction in the sensing time. Figure 19b shows the false alarm probability with variations of the INR. It is clear that adapting the threshold maintains the false alarm to 0.1 as desired.

RF Front-End Nonlinearity

In wideband sensing, the received signal may contain multiple primary user signals. Even if all primary signals are transmitted with the same power, at the CR receiver, these signals can have various power levels, depending on the distance of these users to the CR receiver and channel fading. In the presence of strong signals, the receiver's LNA may operate in a nonlinear region. Such nonlinearity introduces harmonics and intermodulation (IM) terms.

Figure 20 shows a receiver sensing a wideband spectrum that contains two strong signals, henceforth denoted as *blockers*, located at f_{b1} and f_{b2}. The signal of interest is located at $f_0 = 2f_{b2} - f_{b1}$. At the output of the LNA, the blockers introduce IM terms in the same band as the desired signal. These spurious terms remain after downconverting the wideband spectrum into baseband. Hence, the received samples, resulted from digitizing the baseband, are corrupted with the IM terms.

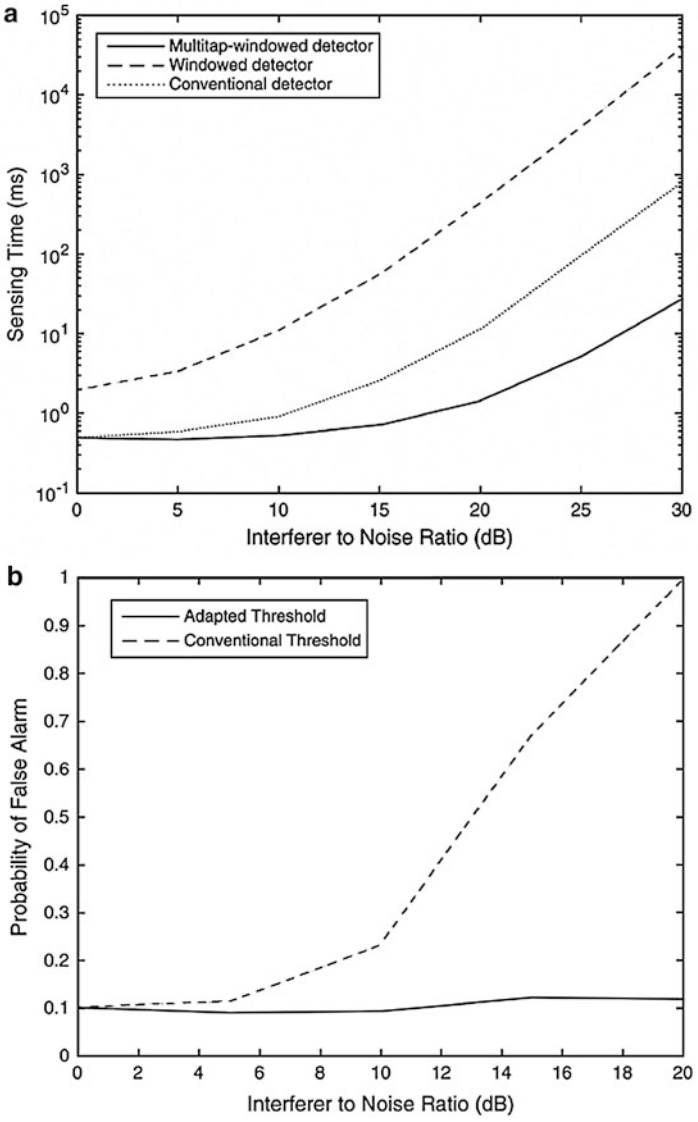

Fig. 19 Performance of different energy-based detectors in the presence of adjacent interference

Modeling LNA Nonlinearities

Different IM terms are generated due to the nonlinearity of the LNA. However, not all these terms affect the received samples. For instance, even-order IM terms lie outside the frequency support of the signal of interest, and hence they can be filtered efficiently. Similarly, odd-order nonlinearities are typically dominated by third-order nonlinearities, making the impact of high odd-order terms, e.g., 5th order

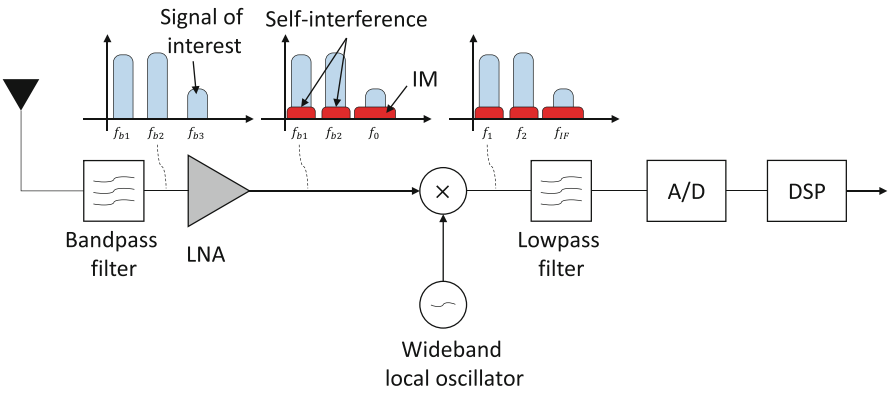

Fig. 20 LNA nonlinearity introduces IM terms

and higher, negligible. Hence, only third-order nonlinearities are considered in the subsequent analysis.

In the presence of nonlinearities, the received samples can be modeled as [19,30]

$$r(n) = \beta_1 x(n) + \beta_3 x(n)|x(n)|^2 + w(n), \tag{41}$$

where $x(n)$ is the wideband signal and $w(n)$ is an additive white Gaussian noise. Here, β_1 and β_3 are constants that are characteristics of the receiver front-end. Note that $\beta_1 x(n)$ is the linear term, whereas $\beta_3 x(n)|x(n)|^2$ is the third-order nonlinear term.

In the example of a single pair of blockers, it can be shown that the signal in the channel of interest is given by [30]

$$r_d(n) \approx \left(\beta_1 x_d(n) + \frac{3}{2}\beta_3 x_{b1}^*(n) x_{b2}^2(n)\right) e^{2\pi f_{if} n T_s} + w(n), \tag{42}$$

where $x_d(n)$ is the signal of interest, $x_{b1}(n)$ and $x_{b2}(n)$ are the two blockers, and $f_{if} = 2f_2 - f_1$ is the intermediate frequency, where the signal of interest resides. Note that $x_d(n)$ is present in H_1 and absent in H_0, and the CR receiver must determine which hypothesis is true. The challenge here is that in the presence of strong blockers, the IM terms can be stronger than the signal of interest, making the detection difficult.

Mitigating LNA Nonlinearities

By viewing the IM terms as interference, one may follow the same approach used in Fig. 17, where the sensing time and the decision threshold are adapted. This requires estimating the blocker power [19]. The challenge here is that estimating the blocker, say in f_{b1}, cannot be directly done by measuring the energy in that channel since it

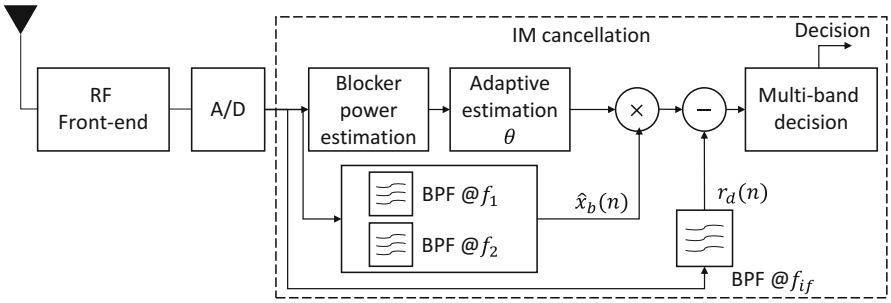

Fig. 21 An architecture that cancels the IM terms

does not only contain the blocker signal but also the self-interference as shown in Fig. 20. Indeed, recall the received signal:

$$r(n) = \underbrace{\left(\beta_1 x_d(n) + \frac{3}{2} x_{b1}^*(n) x_{b2}^2(n)\right) e^{2\pi f_{if} n T_s}}_{\text{signal at } f_{if}} + \underbrace{\bar{x}_{b1}(n) e^{2\pi f_1 n T_s}}_{\text{signal at } f_1} + \underbrace{\bar{x}_{b2}(n) e^{2\pi f_2 n T_s}}_{\text{signal at } f_2}$$

$$+ w(n), \tag{43}$$

where $\bar{x}_{bi}(n)$ is a function of the i-th blocker signal $x_{bi}(n)$, and it can be shown that [19]

$$\bar{x}_{b1}(n) = \beta_1 x_{b1}(n) + \frac{3}{2}\beta_3 x_{b1}(n)|x_{b1}(n)|^2 + 3\beta_3 x_{b1}(n)|x_{b2}(n)|^2. \tag{44}$$

The self-interference is hence defined as $\phi_i(n) = \bar{x}_{bi}(n) - \beta_1 x_{bi}(n)$. It is observed that estimating the blocker power cannot be implemented using a time average of $\bar{x}_{bi}(n)$ due to the presence of self-interference. Hence, a more advanced estimation is needed. Once estimated, the sensing time and the decision threshold can be adapted.

An alternative approach is to cancel the IM terms instead of estimating them since the latter approach typically requires increasing the sensing time to mitigate the presence of interference. Indeed, it is shown in (38) that $N_l \propto \sigma_{I,l}^2/\sigma_w^2$, which shows that higher interference power requires longer sensing duration in order to mitigate it.

The cancellation scheme is as follows. An additional band-pass filtering stage is applied to the received samples to estimate the IM terms that fall in the channel of interest, i.e.,

$$\hat{x}_b(n) = \frac{1}{\beta_1^3} \bar{x}_{b1}(n) \bar{x}_{b2}^2(n). \tag{45}$$

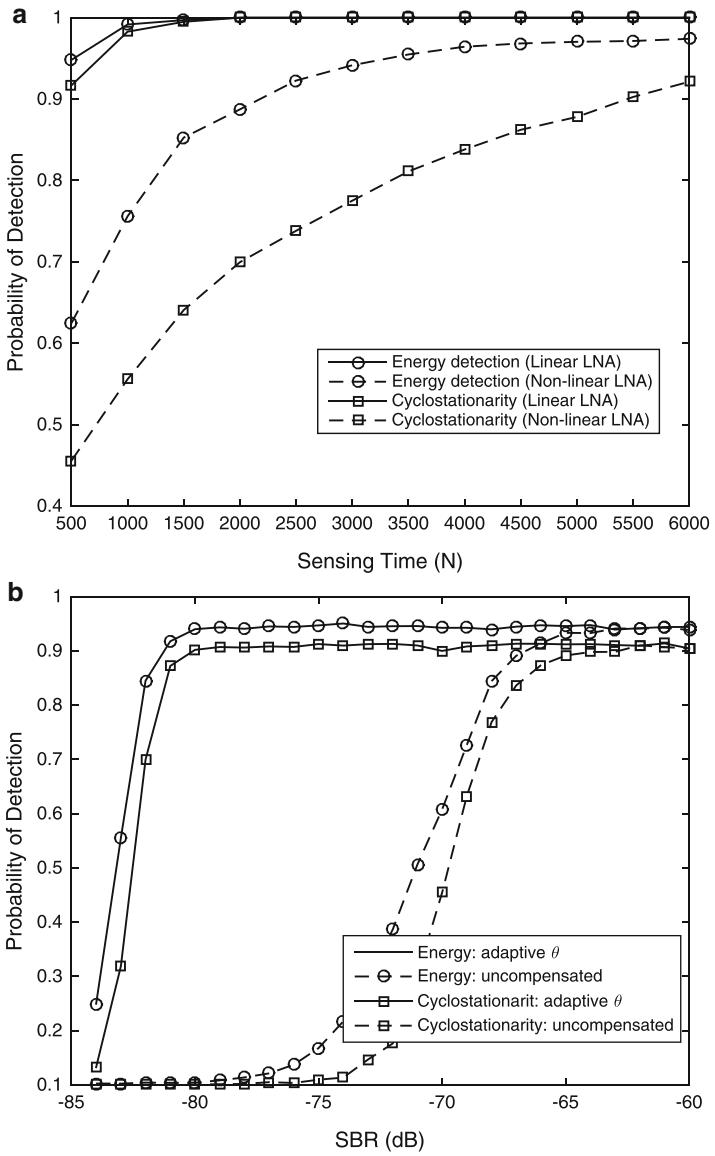

Fig. 22 Effect of nonlinearities on detection performance in the presence and absence of the compensation algorithm

Then, this estimate is subtracted from the received signal in the band of interest, i.e.,

$$\hat{r}_d(n) = r_d(n) - \frac{3}{2}\theta \hat{x}_b(n), \tag{46}$$

where θ is a parameter that can be optimized using an adaptive filter to minimize the IM term. The receiver architecture of this method is shown in Fig. 21.

Figure 22a shows the detection performance of the energy and cyclostationarity detectors in the presence and absence of LNA nonlinearities. It is assumed that the signal-to-blocker ratio (SBR) is set to -70 dB, SNR $= 3$ dB, and the thresholds are optimized to achieve $P_f = 0.1$. It is observed that the detection performance is degraded when the LNA operates in the nonlinear regime, making it critical to compensate for this impairment. Figure 22b shows the probability of detection with variations of the SBR, where the compensation algorithm presented in Fig. 21 is used with adaptive θ [19]. It is assumed that $N = 500$ and SNR $= 3$ dB. Using the cancellation algorithm, the performance significantly improves particularly when the blocker power is strong relative to the signal power.

Summary

Spectrum sensing is an integral component of the cognitive radio system. To this end, modeling the different sensing techniques is critical to ensure reliable detection. While spectrum sensing has been largely studied using the classical detection modeling tools, there are key differences that are inherited to cognitive radio. In particular, spectrum sensing should be robust in negative SNR regimes, where measurements have shown that the detection performance may deviate from that predicted by the theoretical expressions. Indeed, in negative SNRs, noise power estimation becomes difficult and synchronization leads to frequency offsets. In addition, it is shown that converting the wideband sensing problem into several narrowband sensing problems requires additional care due to the adjacent interfering power resulted from the presence of strong signals and the IM terms resulted from the RF front-end nonlinearities.

References

1. ATSC Digital Television Standard (2007) ATSC Std. A/53. http://www.atsc.org/standards.html
2. Axell E, Leus G, Larsson EG, Poor HV (2012) Spectrum sensing for cognitive radio: state-of-the-art and recent advances. IEEE Signal Proc Mag 29(3):101–116. https://doi.org/10.1109/MSP.2012.2183771
3. Cabric D (2008) Addressing feasibility of cognitive radios. IEEE Signal Proc Mag 25(6):85–93. https://doi.org/10.1109/MSP.2008.929367
4. Cabric D, Mishra S, Brodersen R (2004) Implementation issues in spectrum sensing for cognitive radios. In: Proceedings of the 38th Asilomar Conference on Signals, System and Computers (ASILOMAR'04), vol 1, pp 772–776

5. Cabric D, Tkachenko A, Brodersen R (2006) Spectrum sensing measurements of pilot, energy, and collaborative detection. In: Proceedings of the IEEE Military Communications Conference (MILCOM'06), pp 1–7
6. Chuinard G, Cabric D, Ghosh M (2006) Sensing thresholds. Technical report, EEE 802.22-06/005/r3
7. Dandawate AV, Giannakis GB (1994) Statistical tests for presence of cyclostationarity. IEEE Trans Signal Process 42(9):2355–2369. https://doi.org/10.1109/78.317857
8. Gardner W (1991) Exploitation of spectral redundancy in cyclostationary signals 8(2): 14–36
9. Harjani R, Cabric D, Markovic D, Sadler BM, Palani RK, Saha A, Shin H, Rebeiz E, Basir-Kazeruni S, Yuan FL (2015) Wideband blind signal classification on a battery budget. IEEE Commun Mag 53(10):173–181. https://doi.org/10.1109/MCOM.2015.7295481
10. Hattab G, Ibnkahla M (2014) Enhanced pilot-based spectrum sensing algorithm. In: Proceedings of the IEEE Biennial Symposium on Communication (QBSC'14), pp 57–60. https://doi.org/10.1109/QBSC.2014.6841184
11. Hattab G, Ibnkahla M (2014) Multiband spectrum access: great promises for future cognitive radio networks. Proc IEEE 102(3):282–306. https://doi.org/10.1109/JPROC.2014.2303977
12. Hossain K, Champagne B (2011) Wideband spectrum sensing for cognitive radios with correlated subband occupancy. IEEE Signal Proc Lett 18(1):35–38. https://doi.org/10.1109/LSP.2010.2091405
13. Kay S (1993) Fundamentals of statistical signal processing, vol I – estimation theory. Prentice Hall
14. Lunden J, Koivunen V, Huttunen A, Poor HV (2009) Collaborative cyclostationary spectrum sensing for cognitive radio systems. IEEE Trans Signal Process 57(11):4182–4195. https://doi.org/10.1109/TSP.2009.2025152
15. Mariani A, Giorgetti A, Chiani M (2011) Effects of noise power estimation on energy detection for cognitive radio applications. IEEE Trans Commun 59(12):3410–3420. https://doi.org/10.1109/TCOMM.2011.102011.100708
16. Paysarvi-Hoseini P, Beaulieu NC (2011) Optimal wideband spectrum sensing framework for cognitive radio systems. IEEE Trans Signal Process 59(3):1170–1182. https://doi.org/10.1109/TSP.2010.2096220
17. Pei Y, Liang YC, Teh KC, Li KH (2009) How much time is needed for wideband spectrum sensing? IEEE Trans Wirel Commun 8(11):5466–5471. https://doi.org/10.1109/TWC.2009.090350
18. Quan Z, Cui S, Sayed A, Poor H (2009) Optimal multiband joint detection for spectrum sensing in cognitive radio networks. IEEE Trans Signal Process 57(3):1128–1140. https://doi.org/10.1109/TSP.2008.2008540
19. Rebeiz E, Ghadam ASH, Valkama M, Cabric D (2015) Spectrum sensing under RF non-linearities: performance analysis and DSP-enhanced receivers. IEEE Trans Signal Process 63(8):1950–1964. https://doi.org/10.1109/TSP.2015.2401532
20. Rebeiz E, Urriza P, Cabric D (2012) Experimental analysis of cyclostationary detectors under cyclic frequency offsets. In: Conference on Signals, Systems and Computers (ASILOMAR'12), pp 1031–1035
21. Rebeiz E, Urriza P, Cabric D (2013) Optimizing wideband cyclostationary spectrum sensing under receiver impairments. IEEE Trans Signal Process 61(15):3931–3943. https://doi.org/10.1109/TSP.2013.2262680
22. Rebeiz E, Yuan FL, Urriza P, Markovi D, Cabric D (2014) Energy-efficient processor for blind signal classification in cognitive radio networks. IEEE Trans Circuits Syst I Regul Pap 61(2):587–599. https://doi.org/10.1109/TCSI.2013.2278392
23. Sun H, Nallanathan A, Wang CX, Chen Y (2013) Wideband spectrum sensing for cognitive radio networks: a survey. IEEE Wirel Commun 20(2):74–81. https://doi.org/10.1109/MWC.2013.6507397
24. Tandra R, Sahai A (2008) SNR walls for signal detection. IEEE J Sel Top Signal Process 2(1):4–17. https://doi.org/10.1109/JSTSP.2007.914879

25. Yu TH, Rodriguez-Parera S, Markovic D, Cabric D (2010) Cognitive radio wideband spectrum sensing using multitap windowing and power detection with threshold adaptation. In: 2010 IEEE International Conference on Communications, pp 1–6. https://doi.org/10.1109/ICC.2010.5502024
26. Yu TH, Sekkat O, Rodriguez-Parera S, Markovic D, Cabric D (2011) A wideband spectrum-sensing processor with adaptive detection threshold and sensing time. IEEE Trans Circuits Syst I Regul Pap 58(11):2765–2775. https://doi.org/10.1109/TCSI.2011.2143010
27. Yu TH, Yang CH, Cabric D, Markovic D (2012) A 7.4-mW 200-MS/s wideband spectrum sensing digital baseband processor for cognitive radios. IEEE J Solid-State Circuits 47(9):2235–2245. https://doi.org/10.1109/JSSC.2012.2195933
28. Yucek T, Arslan H (2009) A survey of spectrum sensing algorithms for cognitive radio applications. Commun Surveys Tutor 11(1):116–130. https://doi.org/10.1109/SURV.2009.090109
29. Zeng Y, Liang YC (2010) Robustness of the cyclostationary detection to cyclic frequency mismatch. In: 21st Annual IEEE International Symposium on Personal, Indoor and Mobile Radio Communications, pp 2704–2709. https://doi.org/10.1109/PIMRC.2010.5671799
30. Zou Q, Mikhemar M, Sayed AH (2009) Digital compensation of cross-modulation distortion in software-defined radios. IEEE J Sel Top Signal Process 3(3):348–361. https://doi.org/10.1109/JSTSP.2009.2020266

Spectrum Sensing Methods and Their Performance

6

Chintha Tellambura

Contents

C. Tellambura (✉)
Electrical and Computer Engineering, University of Alberta, Edmonton, AB, Canada
e-mail: ct4@ualberta.ca

W. Zhang (ed.), *Handbook of Cognitive Radio*,
https://doi.org/10.1007/978-981-10-1394-2_6

Abstract

Spectrum sensing is the process of determining if a spectrum slot is occupied or not by a primary signal. This tutorial emphasizes energy detection based spectrum sensing and provides a broad overview of the tools necessary for performance analysis of several spectrum sensing algorithms. A detailed description of the spectrum sensing problem is provided as a binary hypothesis test. The main parameters of interest – decision statistic, detection, and false-alarm probabilities and the decision threshold – are discussed. These parameters of the energy detector, which computes the energy of the received signal, are described. The use of the central limit theorem (CLT) to achieve energy detection with prescribed performance level is discussed. The receiver operating characteristic (ROC) curve and area under the curve (AUC) are described. Fading, a fundamental wireless channel impairment, can be mitigated with multiple antenna techniques, which provide spatial diversity gains. The performance of the energy detector with two low-complexity diversity techniques is described. The performance is analyzed for Rayleigh fading, for spatial correlation, and in the high signal-to-noise ratio (SNR) regime. General analytical techniques are highlighted. Double-threshold energy detector, P-norm detector, and energy detection for full-duplex nodes are described. Alternative to energy detection includes cyclostationary detection, matched filter-based detection, and waveform-based detection. These methods are briefly discussed. Spectrum sensing is an essential part of smart grid, Internet of things, and cognitive radio. An overview is provided.

Introduction

The growth of global mobile wireless networks is exponential and robust. It is driven by the use of smartphones, tablets, laptops, and other wireless devices that allow subscribers to browse the Web, use email, and download videos, multimedia, and applications. For example, by 2021, the monthly mobile data traffic will exceed 49 exabytes, mobile devices per capita will be 1.5, the wireless connection rate will increase to 20 Mbps, over 50% of mobile connections will be from smartphones, and mobile-to-mobile connections will be the majority [1].

Consequently, increasing demands for wireless mobile broadband are likely to outstrip the available radio spectrum. For example, while the 0.1–5 GHz band is perhaps the most advantageous for communications, much of it has already been allocated to about 40 different radio services such as fixed, mobile, satellite, amateur, radio navigation and radio astronomy. In fact, International Telecommunication Union (ITU) divides spectrum in to bands and assigns them to these services in order to avoid radio interference [30]. Moreover, although frequencies above 5 GHz offer the potential vast bandwidths, high attenuation, blockage, and other impairments pose significant difficulties. Therefore, spectrum congestion may hem the rapid growth of next-generation (e.g., 5G) wireless networks and users.

One potential solution is to note that much of the current licensed/assigned spectrum remains unused at different times and/or locations. Those temporary spectrum slots (aka spectrum holes or white spaces) [19, 39] can be as high as 15–85% of the licensed spectrum [29]. Radio nodes that can identify and utilize such spectrum holes while minimizing potential interference on licensed users (aka primary users) are called cognitive radios (aka secondary users). They clearly improve overall spectrum usage, alleviating the need for new spectrum. The process of identification of spectrum holes is called spectrum sensing.

Depending on when a secondary user accesses a primary spectrum slot regardless if it is occupied or not, there are three different cognitive radio paradigms [30]:

1. Interweave – secondary user transmits only in an unused spectrum hole currently unoccupied by a primary user. To do so, secondary user must know if primary signals are present or absent in the frequency band. Thus, this paradigm clearly needs spectrum sensing.
2. Underlay – secondary user is allowed to transmit in both unused and used spectrum slots. In the latter, secondary user must adjust its transmission power such that interference on primary network is below a certain threshold. Again, the secondary requires spectrum sensing, for instance, to determine its transmit power levels.
3. Overlay – the secondary access mechanism is similar to that of underlay mode. However, secondary user earns the right to spectrum access by helping to enhance primary communication capability and by taking suitable measures to limit interference on the primary network. To achieve these two goals, secondary user needs to know some characteristics of primary signals (e.g., modulation formats, frequency, and more) in advance. This information is then used to improve communication quality of both the primary and secondary users. For example, secondary user may take proactive signal coding solutions to cancel interference on primary network. To enhance primary rates, secondary user can relay primary data. Thus, in this paradigm, secondary user must acquire much more primary information than is the case with overlay and underlay modes. Nevertheless, a critical part of the overall acquisition process is spectrum sensing.

Overall, since spectrum is essential to all the three paradigms, solid understanding of the performance of sensing algorithms in different propagation environments and in network configurations is necessary. The reliability and performance can be quantified with rigorous analytical techniques. Before discussing the basics of the performance analysis, it should be mentioned that standards with spectrum sensing include IEEE 802.22 WRAN (wireless regional area network) and its amendments, IEEE 802.11af for wireless LANs, IEEE 1900.x series, and licensed shared access (LSA) for LTE mobile operators [17]. In particular, WRAN is cognitive radio designed to operate in empty TV bands, which provides additional spectrum for wireless mobile networks on a non-interfering basis.

This tutorial aims to provide a broad overview of the tools necessary for performance analysis of spectrum sensing algorithms, with particular emphasis on energy detection. The tutorial is organized as follows:

1. The spectrum sensing problem is formulated as a binary hypothesis test. The decision statistic, detection, false-alarm probabilities, and decision threshold are discussed. The energy detector, one of the most common sensing algorithms, is described in terms of its basic performance parameters. The use of CLT to estimate the number of samples needed for the energy detection with prescribed performance level is discussed. The ROC curve and AUC are described.
2. Fading is mitigated by the use of multiple antenna techniques, which provide spatial diversity gains. The performance of the energy detector with selection and combining diversity techniques is described. Moreover, the performance is analyzed for Rayleigh fading, for spatial correlation, and in the high-SNR regime. General analytical techniques based on probability density function (PDF) and moment generating function (MGF) are highlighted.
3. Double-threshold energy detector, P-norm detector, and energy detection for full-duplex nodes are described. Alternative to energy detection includes cyclostationary detection, matched filter-based detection, and waveform-based detection. These methods are briefly discussed.
4. An overview of spectrum sensing for smart grid, Internet of things, and cognitive radio is provided.

Spectrum Sensing Problem Formulation

Clearly, accurate, reliable, and low-complexity spectrum sensing is essential for opportunistic spectrum access. To this end, secondary nodes must detect the presence/absence of a primary signal in a given frequency band $[f_0, f_1]$ for a particular time slot. This process is commonly called spectrum sensing. It can be readily formulated as a binary hypothesis test. For example, the complex signal observed at time t by the secondary user in the desired band $[f_0, f_1]$ may be modeled as [47]

$$y(t) = \begin{cases} n(t) & : H_0 \\ h(t)s(t) + n(t) & : H_1 \end{cases} \tag{1}$$

where $n(t)$ is an additive complex white Gaussian noise process, $h(t)$ represents a fading process (e.g., nonfading means $h(t) = 1$), and $s(t)$ is a signal transmitted by the primary node [47]. The sensing decisions are made using $N \gg 1$ samples of $y(t)$. The choice of N will be discussed later. Starting with this observational model, it is possible to formulate a wide array of spectrum sensing techniques based on signal energy, matched filtering, cyclostationary features, covariances, and others. These will be discussed subsequently.

Let $y(k)$ be the k-th ($k = 1, 2, \ldots, N$) sample of $y(t)$. All the samples are placed in to the vector $\mathbf{y} = [y(1), \ldots, y(n)]'$. These samples are used to compute a decision statistic $T(\mathbf{y})$. The hypothesis test for spectrum sensing is then given by

$$\text{if} \begin{cases} T(\mathbf{y}) < \lambda & \text{accept} \ : H_0 \\ T(\mathbf{y}) > \lambda & \text{accept} \ : H_1 \end{cases} \tag{2}$$

where $0 < \lambda < \infty$ is called the decision threshold. The reliability associated with the decision the rule (2) can be characterized by probability of detection P_d and probability of false alarm P_f. The former is the probability of detecting the primary signal when it is actually present in the frequency band, $[f_0, f_1]$. Consequently, large detection probability is highly desirable. Mathematically, it is a conditional probability given by

$$P_d = \Pr(T(\mathbf{y}) > \lambda | H_1).$$

Equivalently, the complement of this probability $P_{md} = 1 - P_d$ is also widely used for illustration and design purposes.

On the other hand, the test might incorrectly decide that $s(t)$ is present in $[f_0, f_1]$ when it actually is not, and this false-alarm probability may be written as

$$P_f = \Pr\left(T(\mathbf{y}) > \lambda | H_0\right).$$

The exact values of P_d and P_f depend on how $T(\mathbf{y})$ is constructed using received samples, channel estimates, propagation characteristics, the choice of the threshold, and other information. The false alarms will clearly reduce spectrum access opportunities for secondary users, and hence the expected improvements in spectral efficiency are not materialized. This problem may be alleviated by choosing the decision threshold λ for an optimum balance between P_d and P_f. However, this requires knowledge of noise and detected signal powers. Estimation of both noise power and signal power can be challenging as they are depend on evolving transmission standards and the locations of primary and secondary nodes. In practice, with the knowledge of noise variance, the threshold is chosen to obtain a certain false-alarm rate (section "Threshold Optimization Techniques").

Notations

$\mathbb{P}(\cdot)$, $\mathbb{E}(\cdot)$, $\mathrm{Var}(\cdot)$ denote the probability measure, expectation, and variance. $\Gamma(z) = \int_0^\infty t^{z-1}e^{-t}dt$, $\Gamma(z, x) = \int_x^\infty t^{z-1}e^{-t}dt$, ${}_2F_1(a, b; c; z) = \sum_{k=0}^\infty \frac{(a)_k (b)_k (z)^k}{(c)_k k!}$ is the Gauss hypergeometric function, with $(x)_y$ denoting the Pochhammer symbol. If $X_1, \ldots, X_k$ are independent Gaussian $N(0, \mu_k)$ random variables, then $Y = \sum_{i=1}^k X_i^2$, is noncentral chi-square, $\chi_k^2(\delta)$, with k degrees of freedom and $\delta = \sum \mu_k^2$. If all $\mu_k = 0$, Y is central chi-square, χ_k^2. The generalized

Marcum-Q function is $Q_l(a,b) = \int_b^\infty \frac{x^l}{a^{l-1}} e^{-(x^2+a^2)/2} I_{l-1}(ax)dx$, where $I_l(x)$ is the l-th order modified Bessel function. The Gaussian-Q function is $Q(x) = \int_x^\infty \frac{e^{-t^2/2}}{\sqrt{2\pi}} dt$.

Classical Energy Detector

As mentioned before, although the exponential growth of mobile data traffic is likely to outstrip the available spectrum, licensed users may not be active at a given spectrum slot (e.g., 54–806 MHz TV band), a time, and a location. To access those spectral holes, secondary user may first sense them via the most popular spectrum sensing algorithm: energy detector, which has thus attracted massive wireless research interest due to its simple structure and low hardware complexity [7].

This detector computes a proxy for the energy of received signal over the spectrum slot that is being tested. The basic concept is that the computed energy must be sufficiently high if the slot contains primary signals; otherwise, the slot contains noise only. Thus, this detection problem can be formulated as a special case of the hypothesis test (2) with the decision statistic given by

$$T(\mathbf{y}) = \sum_{i=1}^{N} |y_i|^2 \tag{3}$$

where y_i is the i-th ($i = 1, 2, \ldots, N$) sample of $y(t)$ and N is the number of samples. It can be readily shown that $T(\mathbf{y})$ conditional on H_0 and H_1 are distributed as central chi-square χ^2_{2N} and noncentral chi-square $\chi^2_{2N}(2\gamma)$, respectively, both with $2N$ degrees of freedom. The noncentrality parameter is 2γ where γ is the SNR. For a static channel scenario, false-alarm and detection probabilities may be expressed as

$$P_f = \Gamma(N, \lambda/2)/\Gamma(N) \tag{4}$$

$$P_d = Q_N(\sqrt{2\gamma}, \sqrt{\lambda}), \tag{5}$$

where $\Gamma(a,b)$ and $Q_N(a,b)$ are incomplete Gamma function and the Marcum-Q function, respectively. The choice of a suitable value for N has critical ramifications on both performance and complexity. The method of choosing N will be discussed in Sect. "Use of the CLT." The SNR γ is a fixed quantity if the channel is static (e.g., $h(t) = 1$); otherwise, it will be modeled as a random variable (this case will be treated subsequently).

The Eqs. (4) and (5) connect false-alarm and missed-detection probabilities with the SNR, the decision threshold, and the number of samples. Thus, many design choices and requirements can be made depending on specific requirements. For example, very low SNR is -20 dB with a signal power of -116 dBm and a noise

floor of −96 dBm [7]. For this reason, IEEE 802.22 prescribes both P_d and P_f be less than 0.1. While energy detection performs well at moderate and high SNRs, low-SNR operation typically requires large N, which impacts the sensing and processing time. For example, IEEE 802.22 limits the maximal detection latency to 2 s which may include sensing time and subsequent processing time. This maximal time limit is critical at low-SNR spectrum sensing.

In the literature, the detection probability P_d has also been analyzed extensively, treating propagation characteristics, multiple antennas, cooperative diversity, and other factors [3, 5, 16, 20, 42]. However, exact analysis tends to be complicated (special functions, infinite series, and so on). Moreover, since closed-form P_d for more complicated versions of energy detection appears intractable, several computational methods have been developed [40]. To detect potential spectrum opportunities rapidly, sensing algorithms must operate with the fewest possible number of samples and offer high reliability. Therefore, selection of a suitable number of samples, N, is considered next.

Use of the CLT

When the number of samples N is sufficiently large, CLT can be used instead of the exact equations (4) and (5) [7]. Thus, false-alarm and detection probabilities may be approximated as

$$P_{f,CLT} \approx Q\left(\frac{\lambda - 2N}{2\sqrt{N}}\right) \tag{6}$$

$$P_{d,CLT} \approx Q\left(\frac{\lambda - 2N(1+\gamma)}{2(1+\gamma)\sqrt{N}}\right) \tag{7}$$

where primary signal $s(t)$ is assumed to be zero-mean, complex Gaussian and $Q(x)$ is the standard Gaussian upper tail probability function. Although it is possible to consider different models for $s(t)$, the details are omitted for brevity. This approximation has been utilized to investigate sensing-throughput tradeoff [28], multiple-band spectrum sensing [35], low-SNR spectrum sensing [6, 31], and numerous others. However, it may not be accurate enough for small sample sizes [37].

Next the above is used to determine the suitable sample size N. Suppose the prescribed performance point is (P_f, Pd). By using (6) and (7), and solving for N, it turns out that

$$N \approx \left[\gamma^{-1}Q^{-1}(P_f) - (1+\gamma^{-1})Q^{-1}(P_d)\right]^2.$$

Based on the CLT, this estimate may be accurate only when N is sufficiently high but not when P_f is low and P_d is high [37]. To get around these challenges, [37]

has developed an estimate of N using the cube-of-Gaussian approximation (CGA), and further results have been reported in [9, 38].

Threshold Optimization Techniques

In (2), the key parameter is the decision threshold, λ. This threshold must be optimized for each detection technique to improve its performance. The threshold may be chosen by considering P_f and P_d. A common practice is to set the threshold is based on a constant false-alarm probability, say, P_f. For example, then based on the normalized threshold is

$$\lambda^* = 2\sqrt{N}\left(Q^{-1}(P_f) + \sqrt{N}\right)$$

which must adjusted based on the variance of the additive noise. Note that P_d and P_f are functions of λ. In general, it is chosen to make P_d large and P_f small as possible (e.g., in IEEE 802.22 WRAN needs $P_f \leq 0.1$ and $P_d \geq 0.9$). More generally, the threshold may be optimized by considering noise level, total error rate, and other factors [7].

ROC Curves

Although detection (or missed detection) and false-alarm probabilities are key measures, detection capability is typically illustrated with a so-called ROC curve – a plot of the detection probability versus the false-alarm probability when the threshold varies from 0 to ∞. Thus, the ROC curve is defined parametrically as pair (x, y) with

$$x = P_f(\lambda) \quad y = P_d(\lambda), \quad 0 \leq \lambda < \infty. \tag{8}$$

A set of ROC curves for the basic energy detector ($N = 10$) in a static channel is depicted in Fig. 1. Each ROC curve corresponds to a particular SNR, γ. The upper left corner or coordinate (0,1) of the ROC space, representing 0% false alarms and 100% detection, depicts the best possible detector. The diagonal line ($P_d = P_f$) from the left bottom to the top right corners depicts a random detector such as detection by flipping coins (heads or tails). The further away is the ROC curve from the diagonal, the better is the detector performance. The ROC figures have been widely used to illustrate the energy detector performance for small-scale and large-scale fading, diversity reception techniques, and cooperative spectrum sensing [7].

However, a single summarizer of detection capability is also desirable. This is called area under the ROC curve (AUC) [2]. The AUC is a number between 0 and 1, and a perfect detector has an AUC of 1. Moreover, an AUC of 0.5 represents a random detector (e.g., coin flip). In fact, the more far AUC is from 0.5, the better

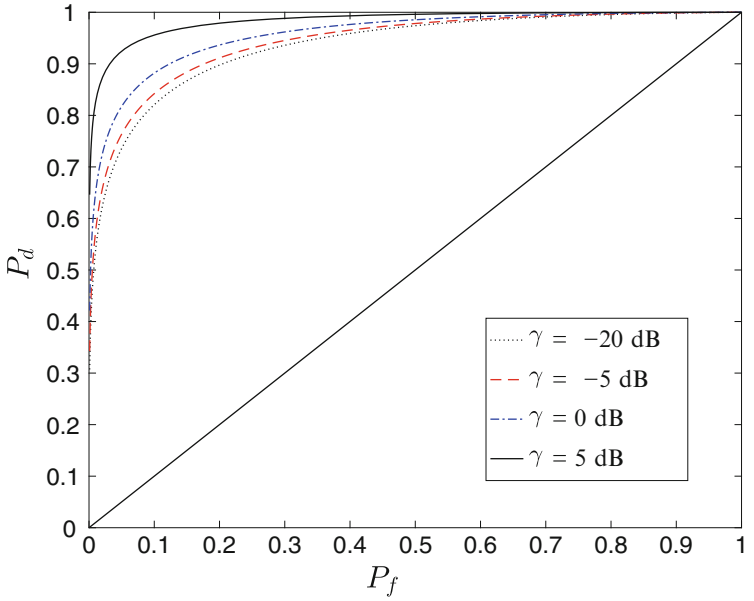

Fig. 1 ROC for energy detection

is performance. If AUC is below 0.5, the detector output must be inverted. For example, if AUC is zero, the inverted detector output yields a perfect decision. The AUC may be evaluated as

$$\mathscr{A} = \int_0^1 P_d \, dP_f. \tag{9}$$

By substituting the values of P_d and P_f from (5) and (4), the AUC of classical energy detector can be obtained as [2]

$$\mathscr{A}(\gamma) = 1 - \sum_{k=0}^{u-1} \frac{1}{2^k k!} \gamma^k e^{\frac{-\gamma}{2}} + \sum_{k=1-u}^{u-1} \frac{\Gamma(u+k)}{2^{u+k}\Gamma(u)} e^{-\gamma} \, {}_1F_1\left(u+k; 1+k; \frac{\gamma}{2}\right) \tag{10}$$

where ${}_1F_1(a, b, c)$ is the regularized confluent hypergeometric function. The expression (10) shows that as SNR tends to infinity, the AUC approaches one, which is desirable.

AUC and complementary AUC (CAUC) (e.g., $1 - \mathscr{A}$) have been derived for an energy detector with no diversity reception, with several popular diversity schemes, with channel estimation errors, with fading correlations, and with relay signaling [2] and [4]. However, the analysis of [2,4] may not work for cooperative spectrum sensing. Moreover, special functions (e.g., Marcum-Q and confluent and regularized confluent hypergeometric functions) in P_d make closed-form evaluation

of the AUC rather intractable. To circumvent these drawbacks, AUC can be related to the MGF of the received SNR. The resulting calculations are simple, avoid special functions, and are readily available in modern mathematical platforms (e.g., Mathematica and MAPLE). This approach will be developed in Sect. "MGF-Based Approach."

Performance in Fading Channels

Wireless channel impairments include small-scale fading, shadowing, and path loss [18,32]. Modeling these impairments is critical to characterize and analyze spectrum sensing algorithms. Small-scale fading is characterized by various models such as Rayleigh, Nakagami-m, and Rician [32]. A detailed sensing performance analysis for these channels is beyond the scope of this tutorial. Moreover, although fading does not impact P_f (4), P_d (5) must be averaged over the distribution. For instance, the performance under Rayleigh fading (i.e., $f_\gamma(x) = \frac{1}{\bar{\gamma}} e^{-x/\bar{\gamma}}, 0 \le x < \infty$) is given as [16,21]

$$\overline{P}_d = e^{-\frac{\lambda}{2}} \sum_{i=0}^{N-2} \frac{\left(\frac{\lambda}{2}\right)^i}{i!} + \left(\frac{1+\bar{\gamma}}{\bar{\gamma}}\right)^{N-1} \times \left[e^{-\frac{\lambda}{2(1+\bar{\gamma})}} - e^{-\frac{\lambda}{2}} \sum_{i=0}^{N-2} \frac{\left(\frac{\lambda\bar{\gamma}}{2(1+\bar{\gamma})}\right)^i}{i!} \right]. \quad (11)$$

A set of ROC curves for the basic energy detector ($N = 10$) in a Rayleigh fading channel is depicted in Fig. 2. Each ROC curve corresponds to a particular SNR, $\bar{\gamma}$. The diagonal line ($\bar{P}_d = P_f$) from the left bottom to the top right corners depicts a random detector such as detection by flipping coins (heads or tails). The further away is the ROC curve from the diagonal, the better is the detector performance. Thus, note that as $\bar{\gamma}$ increases, the ROC moves away from the diagonal and toward the (0,1) point, which is the ideal performance.

Spatial Diversity for Spectrum Sensing

Spatial diversity (e.g., multiple antennas) can be exploited to mitigate fading. In the literature, a large body of research has investigated the use of $L > 1$ antennas to enhance the performance of spectrum sensing (see [7] and references therein). With multiple antenna systems, channel states of individual antenna branches and spatial correlations must be considered. These factor will complicate the analysis and operation of common energy detector. Nevertheless, two diversity schemes are briefly described next. In square-law combiner (SLC), the individual energy measurements of different antennas are added together to form the total. The decision statistics is thus $T(\mathbf{y}) = \sum_{i=}^{L} Y_i$ where Y_i is the decision statistic for the i-th antenna branch ($i = 1, \ldots, L$). The equivalent SNR is thus given by $\gamma_{SLC} = \sum_{i=1}^{L} \gamma_i$ where γ_i is the SNR associated with the i-th antenna branch

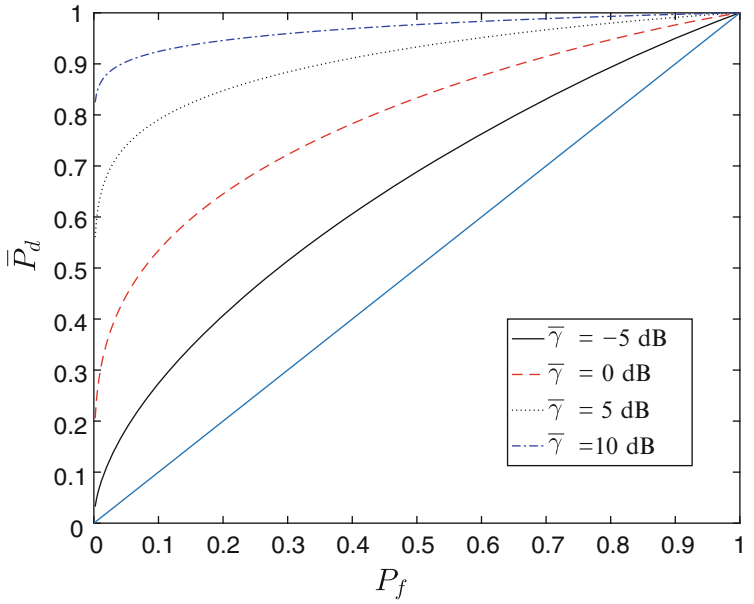

Fig. 2 ROC for energy detection in a Rayleigh channel

($i = 1, \ldots, L$). The final decision is made after comparing $T(\mathbf{y})$ against the threshold. The false-alarm and the detection probabilities are thus obtained as [16]

$$P_{f,SLC} = \frac{\Gamma(LN, \frac{\lambda}{2})}{\Gamma(LN)},$$

$$P_{d,SLC} = Q_{LN}\left(\sqrt{2\gamma_{SLC}}, \sqrt{\lambda}\right).$$

In square-law selection (SLS), only the branch with the largest energy is selected. The decision statistics is thus $T(\mathbf{y}) = \max(Y_1, \ldots, Y_L)$ where Y_i is the decision statistic for the i-th antenna branch ($i = 1, \ldots, L$). Thus, false-alarm and detection probabilities can be obtained as [16]

$$P_{f,SLS} = 1 - \left[1 - \frac{\Gamma\left(N, \frac{\lambda}{2}\right)}{\Gamma(N)}\right]^L$$

$$P_{d,SLS} = 1 - \prod_{i=1}^{L}\left[1 - Q_N\left(\sqrt{2\gamma_i}, \sqrt{\lambda}\right)\right].$$

A set of ROC curves for the basic energy detector ($N = 10$) with SLC in Rayleigh fading is depicted in Fig. 3. Each ROC curve corresponds to a particular

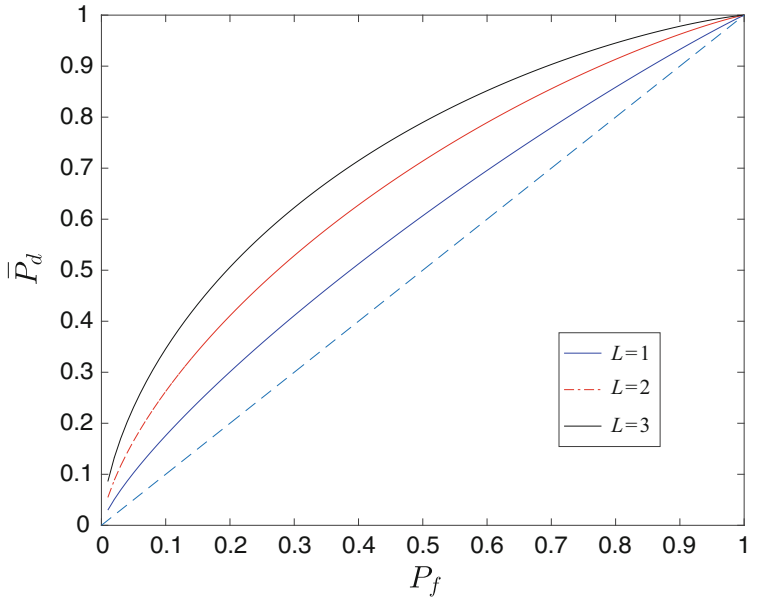

Fig. 3 ROC for energy detection and SLC for different numbers of antennas

number of antennas, L. The diagonal line ($\bar{P}_d = P_f$) from the left bottom to the top right corners depicts a random detector such as detection by flipping coins (heads or tails). The further away is the ROC curve from the diagonal, the better is the detector performance. Thus, note that as L increases, the ROC moves away from the diagonal and toward the (0,1) point, which is the ideal performance. This suggests that the spatial diversity of SLC improves the energy detector performance.

Thus far, it has been seen that the average of P_d in fading channels requires the PDF of γ. In many wireless problems, this PDF can be a highly complex expression or even intractable.

MGF-Based Approach

To avoid such difficulties, the MGF of γ can be utilized for analysis [43–45]. The reason of this wide applicability is that MGF of a sum of independent random variables is equal to the product of individual MGFs [25, 26].

Using the alternative representation of the Marcum-Q function [44], the average of P_d (5) in a multiple antenna system can be expressed as

$$\overline{P}_d = \frac{e^{-\frac{\lambda}{2}}}{2\pi j} \oint_{\Delta} M\left(1 - \frac{1}{z}\right) \frac{e^{\frac{\lambda}{2} z}}{z^q (1-z)} dz \tag{12}$$

where MGF $M(s) = \mathbb{E}(e^{-s\gamma})$, $j = \sqrt{-1}$, $\triangle$ is a circular contour of radius $0 < r < 1$ that encloses origin, and q is a positive integer which depends on N, the number of antennas and diversity combining method. For example, with SLC described earlier, $q = LN$. The integral expression (12) can thus be customized for many diversity systems where the MGF is readily available.

This equation (12) can also be used to derive average AUC under different fading channels. Since $\bar{\mathscr{A}} = \int_0^1 \bar{P}_d dP_f$, average AUC is obtained as

$$\bar{\mathscr{A}} = \frac{1}{j2\pi} \oint_{\triangle} M\left(1 - \frac{1}{z}\right) \frac{1}{z^q (1-z)(z-2)^N} dz. \tag{13}$$

Both (12) and (13) are versatile and provide a powerful basis for analysis of energy detector with various diversity schemes (see [7] for further examples).

Antenna Correlation

Standards like the Long-Term Evolution (LTE) Advanced, WiMax, and International Mobile Telecommunications (IMT) Advanced have promised high data rate services; they motivate the use of multiple antenna terminals. With such secondary nodes, the antenna correlation is an important factor that affects the overall performance of energy detection. To illustrate the impact of antenna correlation, energy detection with SLC can be analyzed. The branch SNR's γ_i $(i = 1, \ldots, L)$ are related by a correlation matrix. The PDF of SNR may be written as

$$f_{\gamma_{SLC}}(x) = \frac{1}{\bar{\gamma}} \sum_{k=1}^{L} \frac{\pi_k}{\mu_k} e^{-x/(\bar{\gamma}\mu_k)}, \quad 0 \le x < \infty \tag{14}$$

where μ_k is the k-th eigenvalue of the correlation matrix and $\pi_k = \prod_{i \neq k} \frac{\mu_k}{\mu_k - \mu_i}$. The correlation matrix is called exponential if the ij-th entry $\rho_{ij} = \rho^{|i-j|}$. However, this model is not universal. For example, the correlation depends the placement, spacing and height of antenna elements, signal incident angles, and so on. Another common model is the Toeplitz structure where $\rho_{ij} = [\rho_{|i-j|}]$ with $\rho_0 = 1$.

For illustration purposes, consider two correlated (ρ) antennas. The two eigenvalues can be shown to be

$$\mu_1, \mu_2 = (1 \pm \rho). \tag{15}$$

The ROC curves for this system are shown in Fig. 4. It is clear that the correlation penalizes the performance. That is, as ρ increases, the ROC curves move toward the diagonal line. The impact of correlation is not high because this is

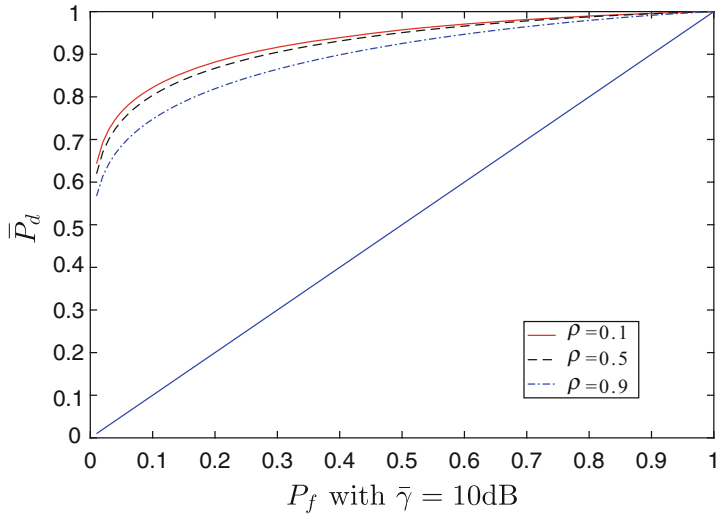

Fig. 4 ROC for SLC energy detection with antenna correlation

a system with two branches only. A higher impact can be expected for systems with more antennas.

Asymptotic Performance Measures

As mentioned before, the SNR γ in a fading environment is a random variable, and hence average of P_d over the distribution of γ, denoted by $\overline{P}_d$, is often computed. The details of the averaging process are as follows. First, $P_d(\gamma)$ for a fixed channel realization is given in (5). It is convenient to express SNR as the product $\gamma = \overline{\gamma}\beta$, where $\overline{\gamma}$ is the average SNR (in static channels $\beta = 1$ and $\gamma = \overline{\gamma}$), and β is a nonnegative random variable, which accounts for system conditions including channel propagation conditions, antenna diversity, interference, and others. Thus, β is characterized by PDF $f(\beta)$. In the second step, $P_d(\gamma)$ is integrated over $f(\beta)$.

The average probability detection can thus be expressed as

$$\overline{P}_d = \int_0^\infty Q_N(\sqrt{2\overline{\gamma}\beta}, \sqrt{\lambda}) f(\beta) d\beta. \tag{16}$$

Thus, the main challenge in (16) is the lack of closed-form solutions for integrals involving the Marcum-Q function or tedious analytical expressions involving complicated special functions and/or infinite series [33]. One solution is to use the MGF approach (12).

An alternative solution is to simplify $f(\beta)$ in order to facilitate the evaluation of (16) in simple yet accurate form. To this end, an idea of Wang and Giannakis [49] may be utilized. The basic concept is that in the high-SNR regime (e.g., $\bar{\gamma} \to \infty$),

the integral (16) can be tightly approximated by simply using just the first term of the Taylor series expansion of $f(\beta)$ at $\beta = 0$. Thus, let exact PDF $f(\beta)$ have the monomial expansion as $\beta \to 0^+$ [49]

$$f^{\text{wg}}(\beta) = a\beta^t + O(\beta^{t+1}), \tag{17}$$

where the parameters a and t define the first term of the PDF expansion, which in turn depend on the operating conditions. These two can be obtained by utilizing the exact PDF or MGF of the diversity structure. Moreover, (17) holds for many practical fading models like Rayleigh, Nakagami-q, Nakagami-n, and Nakagami-m [49]. Further developments on (17) can be found in [14, 15].

By utilizing $f^{\text{wg}}(\beta)$, [48] has derived the asymptotic

$$\overline{P}_{md} \approx \frac{A}{\bar{\gamma}^{t+1}}, \quad \bar{\gamma} \to \infty \tag{18}$$

where A is a constant independent of $\bar{\gamma}$. This shows that for large SNRs ($\overline{\gamma} \gg 1$), missed-detection probability decreases at rate of $t + 1$ on a log-log scale. This observation leads to the notion of sensing gain, which is equal to $t + 1$. However, this approximation is accurate only in the high-SNR regime (say, $\overline{\gamma} \geq 20\,\text{dB}$). This means something other than $f^{\text{wg}}(\beta)$ is needed to approximate $\overline{P}_{md}$ which is accurate over a wider range of SNRs (say, $0 \leq \overline{\gamma} < \infty$). New approximations with such properties can be developed [14, 15, 41].

P-Norm Detection

This idea generalizes classical energy detection (19). Instead of simply squaring, the magnitudes of the signal samples are raised to power $p > 0$ [12, 31, 40]. Thus, the decision variable becomes

$$T(\mathbf{y}) = \sum_{i=1}^{N} |y_i|^p \tag{19}$$

where y_i is the i-th sample and N is the number of samples. Note that $p = 2$ reverts to the classical energy detector (Sect. "Classical Energy Detector"). Several approximations for conditional decision variables $T|H_0, T|H_1$ and probabilities P_f and P_d are analyzed in [8]. One idea is to approximate $T(\mathbf{y})$ a three-parameter gamma distribution. The approximate detection probability is given as [8]

$$P_d^{tg} = \frac{1}{\Gamma(\alpha)} \Gamma\left(\alpha, \frac{\lambda - \delta}{\beta}\right). \tag{20}$$

where δ, α, and β are calculated by cumulant matching. Using this, AUC or area under the ROC curve can be derived. This single figure of merit for P-norm detection [7] has been elusive for arbitrary sample sizes. As well, exact computational methods for P_d and P_f exploiting Talbot's method of numerical integration and Laguerre-polynomials can be found in [40].

Double Threshold Energy Detection

Although the classical energy detector has the benefits of low complexity and blind operation (e.g., without needing primary signal information), the optimum threshold value to achieve target probabilities of false alarm and detection is prone to estimation errors, e.g., noise estimation error. Moreover, these two probabilities cannot be independently adjusted to desirable levels using a single decision threshold. These drawbacks can be alleviated with a double threshold energy detection [22], which allows independent setting of arbitrarily low P_f and P_{md} at the cost of an increased uncertainty region. For this detector, the hypothesis test is thus defined as

$$\text{if} \begin{cases} T(\mathbf{y}) < \lambda_0 & \text{accept} \ : H_0 \\ \lambda_0 \leq T(\mathbf{y}) < \lambda_1 & \text{No decision} \\ T(\mathbf{y}) \geq \lambda_1 & \text{accept} \ : H_1 \end{cases} \tag{21}$$

Thus, false-alarm and detection probabilities (4) and (5) depend on λ_0 and λ_1. However, for double threshold energy detection, a new parameter of probability of uncertainty is incorporated and expressed as a function of λ_0 and λ_1. Probability of uncertainty is given by [22]

$$P_c = \frac{\Gamma(N, \lambda_0/2) - \Gamma(N, \lambda_1/2)}{\Gamma(N)} + Q_N\left(\sqrt{2\gamma}, \sqrt{\lambda_0}\right) - Q_N\left(\sqrt{2\gamma}, \sqrt{\lambda_1}\right). \tag{22}$$

If $\lambda_0 = \lambda_1$, this rule reverts to the classical (2).

Energy Detection with Full Duplex Nodes

Radio nodes typically operate in half-duplex (HD) mode, e.g., transmission and reception functions require distinct, separate time or frequency slots. However, if both functions occur simultaneously on the same frequency band, spectral efficiency potentially doubles at the cost of self-interference. Since this self-interference poses a fundamental limit, cancellation methods have been developed with recent advances in antenna design and analog/digital signal processing techniques [10]. Nevertheless, residual self-interference will limit the system performance.

This residual interference will affect the ability of a radio node to sense spectrum holes. Thus, the complex signal observed at time t by the secondary full-duplex user in the desired band $[f_0, f_1]$ may be modeled as [36]

$$y(t) = \begin{cases} d(t) + n(t) & : H_0 \\ h(t)s(t) + d(t)n(t) & : H_1 \end{cases} \tag{23}$$

where $d(t)$ is the residual self-interference signal. According to this model, the effective SNR can be expressed as [36]

$$\gamma_{FD} = \frac{\gamma_t}{\gamma_i + 1}, \tag{24}$$

where γ_t and γ_i denote SNR at transmitter and the ratio between self-interference power and thermal noise, respectively. Assuming self-interference $d(t)$ to follow complex Gaussian with mean 0 and variance σ_i^2 [36], false-alarm and detection probabilities may be expressed as

$$P_f = \Gamma\left(N, \lambda/2\left(1+\sigma_i^2\right)\right)/\Gamma(N) \tag{25}$$

$$P_d = Q_N\left(\sqrt{2\gamma_{FD}}, \sqrt{\lambda}/\left(1+\sigma_i^2\right)\right). \tag{26}$$

The ROC curves can be plotted by using these equations. Thus, it is possible to evaluate the performance of full-duplex energy detection.

Alternatives

As mentioned before, energy detection offers not only a low-complexity and low-cost solution for spectrum sensing but also avoids a prior information about primary signals. However, it sometimes performs poorly. For example, when a primary signal and multiple interfering signals are present in a band, the energy detector may not readily differentiate among these, and hence spectrum access decisions can be overly conservative. In the following, three alternatives are briefly described.

Cyclostationary Based Detection

Cyclostationarity signals are signals that exhibit periodic probability structures (e.g., periodic mean and autocorrelation). These periodicities are in turn caused by special features such as modulation formats and cyclic components of primary signals or may even be introduced deliberately in order to assist spectrum sensing. Such detection algorithms can readily differentiate H_0 from H_1 because simply additive noise does not exhibit any correlation structures. Furthermore, they may

even distinguish among different types of transmissions and primary users. Their performance has been surveyed in [11, 50].

Matched Filter Based Detection

The received signal is correlated with a copy of the primary signal [7, 27]. If the primary signal and channel response are known, this detector is thus optimal (Neyman-Pearson sense) and maximizes the SNR. It can also take advantage of matched-filter implementations ion existing networks. For example, a matched filter is used by IEEE 802.11 (WiFi) nodes to detect incoming packets, and the same filter may also be leveraged to help with spectrum sensing. This detector also requires perfect timing and synchronization and thus incur computational complexity. Its performance decreases dramatically when channel response changes rapidly or when there are multiple primary user signals over the same band. However, a matched filter can be customized for each primary signal, but the overall complexity will be high. The performance of a matched filter (noise level of one) is given in [11].

Waveform-Based Detection

Current wireless networks periodically transmit special signal patterns for synchronization or for other purposes. They include prefixes for frame delineation, pilot patterns, spreading sequences, and others [50]. Thus, such a preamble can be correlated with the received signal. Such waveform-based (WF) sensing or coherent sensing can outperform energy detector in terms of reliability and convergence time. The performance advantage increases as the length of the known signal pattern increases. WF sensing performs well even with very low SNRs.

Applications

Smart Grids

A smart electrical grid includes a variety of operational and energy measures including smart meters, smart appliances, renewable energy resources, and energy-efficient resources. The communication goals of smart grid can be served by the use of spectrum sensing. For example, [13] studied the energy detector-based spectrum sensing in smart grids and its impact on the performance of demand response management. Matched filter-based spectrum sensing may also be used. A feature detection-based spectrum sensing for smart grid has been examined in [34]. However, sophisticated spectrum sensing algorithms may require significantly high power requirements. On the other hand, cooperative energy-efficient sensing schemes are suitable for dense smart grid environments [24]. Several practical spectral sensing approaches for CR in smart grids have been surveyed in [24].

Internet of Things (IoT)

Cognitive radio is expected to have a variety of IoT applications where very large numbers of sensors will coexist in a small physical space. Thus, spectrum sensing technologies are highly important for WSAN (wireless sensor and actuator networks) based IoT and the requirements and issues related to adaptive systems and architectures [23]. WSANs generally utilize the industrial, scientific, and medical (ISM) radio bands. However, overcrowded ISM bands negatively affect WSAN performance. Thus, improved spectrum sensing and spectrum data processing must be developed [46].

Spectrum Sensing in Standards

Spectrum sensing has been considered in IEEE 802.22 (for TV white spaces) and ECMA 392 [30]. However, specific techniques are not prescribed. Thus, anyone which satisfies the false-alarm and missed-detection requirements of the standard can be chosen. Coexistence among different standards is also important. For example, in heterogeneous network settings, coexistence between IEEE 802.22 WRAN and IEEE 802.11af Super Wi-Fi in the TV white spaces may be required. However, maximum transmit power of an 802.22 node is 1 W while that for an 802.11af is 100 mW. Thus, such power disparities will affect the ability of the spectrum sensing algorithm to differentiate between presence/absence of primary signals. Moreover, its performance may also be affected by interference from random numbers of nodes located randomly.

Summary

This tutorial provides a broad overview of the tools necessary for performance analysis of spectrum sensing algorithms, with particular emphasize on energy detection. The following contributions are made.

1. The spectrum sensing problem is provided as a binary hypothesis test. The decision statistic, detection, and false-alarm probabilities and the decision threshold are discussed. The basic parameters of the energy detector are described. The use of CLT to estimate the number of samples and prescribed performance levels is discussed. The ROC and AUC are described.
2. Fading is mitigated with multiple antenna techniques, which provide spatial diversity gains. The performance is analyzed for Rayleigh fading, diversity combining, and spatial correlation and in the high-SNR regime. General analytical techniques are highlighted.
3. Double-threshold energy detector, P-norm detector, and energy detection for full-duplex nodes are described. Alternative to energy detection includes cyclo-

stationary detection, matched filter-based detection, and waveform-based detection. These methods are briefly discussed. Spectrum sensing is an essential part of smart grid, Internet of things, and cognitive radio. An overview is provided.

References

1. Cisco visual networking index (2017) Global mobile data traffic forecast update, 2016–2021. http://www.cisco.com/c/en/us/solutions/collateral/service-provider/visual-networking-index-vni/mobile-white-paper-c11-520862.pdf
2. Atapattu S, Tellambura C, Jiang H (2010) Analysis of area under the ROC curve of energy detection. IEEE Trans Wirel Commun 9(3):1216–1225
3. Atapattu S, Tellambura C, Jiang H (2010) Performance of an energy detector over channels with both multipath fading and shadowing. IEEE Trans Wirel Commun 9(12):3662–3670
4. Atapattu S, Tellambura C, Jiang H (2010) Performance of energy detection: a complementary AUC approach. In: IEEE Global Telecommunications Conference (GLOBECOM)
5. Atapattu S, Tellambura C, Jiang H (2011) Energy detection based cooperative spectrum sensing in cognitive radio networks. IEEE Trans Wirel Commun 10(4):1232–1241
6. Atapattu S, Tellambura C, Jiang H (2011) Spectrum sensing via energy detector in low SNR. In: Proceedings of the IEEE International Conference on Communications (ICC)
7. Atapattu S, Tellambura C, Jiang H (2014) Energy detection for spectrum sensing in cognitive radio. Springer, New York
8. Banjade VRS, Tellambura C, Jiang H (2014) Performance of p-norm detector in AWGN, fading, and diversity reception. IEEE Trans Veh Technol 63(7):3209–3222. https://doi.org/10.1109/TVT.2014.2298395
9. Banjade VRS, Tellambura C, Jiang H (2015) Approximations for performance of energy detector and p-norm detector. IEEE Commun Lett 19(10):1678–1681
10. Bharadia D, Katti S (2014) Full-duplex MIMO radios. In: Proceedings of the 11th USENIX Symposium on Networked System, Design and Implementation (NSDI'14), Seattle, pp 359–372
11. Bhargavi D, Murthy CR (2010) Performance comparison of energy, matched-filter and cyclostationarity-based spectrum sensing. In: 2010 IEEE 11th International Workshop on Signal Processing Advances in Wireless Communications (SPAWC), pp 1–5. https://doi.org/10.1109/SPAWC.2010.5670882
12. Chen Y (2010) Improved energy detector for random signals in Gaussian noise. IEEE Trans Wirel Commun 9(2):558–563
13. Deng R, Chen J, Cao X, Zhang Y, Maharjan S, Gjessing S (2013) Sensing-performance tradeoff in cognitive radio enabled smart grid. IEEE Trans Smart Grid 4(1):302–310. https://doi.org/10.1109/TSG.2012.2210058
14. Dhungana Y, Tellambura C (2012) New simple approximations for error probability and outage in fading. IEEE Commun Lett 16(11):1760–1763
15. Dhungana Y, Tellambura C (2013) Uniform approximations for wireless performance in fading channels. IEEE Trans Commun 61(11):4768–4779
16. Digham F, Alouini MS, Simon MK (2007) On the energy detection of unknown signals over fading channels. IEEE Trans Commun 55(1):21–24
17. Gavrilovska L, Denkovski D, Rakovic V, Angjelichinoski M (2014) Medium access control protocols in cognitive radio networks: overview and general classification. IEEE Commun Surveys Tutor 16(4):2092–2124
18. Goldsmith A (2005) Wireless communications. Cambridge University Press
19. Haykin S (2005) Cognitive radio: brain-empowered wireless communications. IEEE J Sel Areas Commun 23(2):201–220. https://doi.org/10.1109/JSAC.2004.839380

20. Herath S, Rajatheva N, Tellambura C (2009) On the energy detection of unknown deterministic signal over Nakagami channels with selection combining. In: Proceedings of the IEEE Canadian Conference on Electrical and Computer Engineering
21. Herath SP, Rajatheva N, Tellambura C (2011) Energy detection of unknown signals in fading and diversity reception. IEEE Trans Commun 59(9):2443–2453
22. Horgan D, Murphy CC (2010) Voting rule optimisation for double threshold energy detector-based cognitive radio networks. In: 2010 4th International Conference on Signal Processing and Communication Systems, pp 1–8. https://doi.org/10.1109/ICSPCS.2010.5709679
23. Khan AA, Rehmani MH, Rachedi A (2016) When cognitive radio meets the internet of things? In: 2016 International Wireless Communications and Mobile Computing Conference (IWCMC), pp 469–474. https://doi.org/10.1109/IWCMC.2016.7577103
24. Khan AA, Rehmani MH, Reisslein M (2016) Cognitive radio for smart grids: survey of architectures, spectrum sensing mechanisms, and networking protocols. IEEE Commun Surveys Tutor 18(1):860–898. https://doi.org/10.1109/COMST.2015.2481722
25. Kusaladharma S, Tellambura C (2012) Aggregate interference analysis for underlay cognitive radio networks. IEEE Wirel Commun Lett 1(6):641–644. https://doi.org/10.1109/WCL.2012.091312.120600
26. Kusaladharma S, Tellambura C (2013) On approximating the cognitive radio aggregate interference. IEEE Wirel Commun Lett 2(1):58–61. https://doi.org/10.1109/WCL.2012.101812.120671
27. Lee WY, Akyildiz IF (2008) Optimal spectrum sensing framework for cognitive radio networks. IEEE Trans Wirel Commun 7(10):3845–3857. https://doi.org/10.1109/T-WC.2008.070391
28. Liang YC, Zeng Y, Peh E, Hoang AT (2008) Sensing-throughput tradeoff for cognitive radio networks. IEEE Trans Wirel Commun 7(4):1326–1337
29. Masonta MT, Mzyece M, Ntlatlapa N (2013) Spectrum decision in cognitive radio networks: a survey. IEEE Commun Surveys Tutor 15(3):1088–1107
30. Medeisis A, Holland O (2014) Cognitive radio policy and regulation. Springer
31. Moghimi F, Nasri A, Schober R (2011) Adaptive L_p-norm spectrum sensing for cognitive radio networks. IEEE Trans Commun 59(7):1934–1945
32. Molisch A (2011) Wireless communications. Wiley-IEEE Press
33. Nuttall AH (1972) Some integrals involving the Q function. Naval Underwater Systems Center (NUSC), Technical report
34. Qiu RC, Chen Z, Guo N, Song Y, Zhang P, Li H, Lai L (2010) Towards a real-time cognitive radio network testbed: architecture, hardware platform, and application to smart grid. In: 2010 Fifth IEEE Workshop on Networking Technologies for Software Defined Radio Networks (SDR), pp 1–6. https://doi.org/10.1109/SDR.2010.5507920
35. Quan Z, Cui S, Sayed A, Poor H (2009) Optimal multiband joint detection for spectrum sensing in cognitive radio networks. IEEE Trans Signal Process 57(3):1128–1140
36. Riihonen T, Wichman R (2014) Energy detection in full-duplex cognitive radios under residual self-interference. In: 2014 9th International Conference on Cognitive Radio Oriented Wireless Networks and Communications (CROWNCOM), pp 57–60. https://doi.org/10.4108/icst.crowncom.2014.255395
37. Rugini L, Banelli P, Leus G (2013) Small sample size performance of the energy detector. IEEE Commun Lett 17(9):1814–1817
38. Rugini L, Banelli P, Leus G (2016) Spectrum sensing using energy detectors with performance computation capabilities. In: 2016 24th European Signal Processing Conference (EUSIPCO), pp 1608–1612
39. Shahraki HS (2015) Opportunistic usage of television white space with respect to the long term evolution-advanced parameters. IET Commun 9(9):1240–1247
40. Sharma Banjade V, Tellambura C, Jiang H (2014) Performance of p-norm detector in AWGN, fading and diversity reception. IEEE Trans Veh Technol 63(7):3209–3222
41. Sharma Banjade VR, Tellambura C, Jiang H (2015) Asymptotic performance of energy detector in fading and diversity reception. IEEE Trans Commun 63(6):2031–2043

42. Sofotasios P, Rebeiz E, Zhang L, Tsiftsis T, Cabric D, Freear S (2013) Energy detection based spectrum sensing over κ-μ and κ-μ extreme fading channels. IEEE Trans Veh Technol 62(3):1031–1040
43. Tellambura C (1996) Evaluation of the exact union bound for trellis-coded modulations over fading channels. IEEE Trans Commun 44(12):1693–1699. https://doi.org/10.1109/26.545899
44. Tellambura C, Annamalai A, Bhargava VK (2003) Closed form and infinite series solutions for the MGF of a dual-diversity selection combiner output in bivariate Nakagami fading. IEEE Trans Commun 51(4):539–542. https://doi.org/10.1109/TCOMM.2003.810870
45. Tellambura C, Mueller AJ, Bhargawa VK (1997) Analysis of M-ary phase-shift keying with diversity reception for land-mobile satellite channels. IEEE Trans Veh Technol 46(4):910–922. https://doi.org/10.1109/25.653065
46. Tervonen J, Mikhaylov K, Piesk S, Jms J, Heikkil M (2014) Cognitive internet-of-things solutions enabled by wireless sensor and actuator networks. In: 2014 5th IEEE Conference on Cognitive Infocommunications (CogInfoCom), pp 97–102. https://doi.org/10.1109/CogInfoCom.2014.7020426
47. Urkowitz H (1967) Energy detection of unknown deterministic signals. Proc IEEE 55(4): 523–531
48. Wang Q, Yue DW (2009) A general parameterization quantifying performance in energy detection. IEEE Signal Process Lett 16(8):699–702
49. Wang Z, Giannakis G (2003) A simple and general parameterization quantifying performance in fading channels. IEEE Trans Commun 51(8):1389–1398
50. Yucek T, Arslan H (2009) A survey of spectrum sensing algorithms for cognitive radio applications. IEEE Commun Surveys Tutor 11(1):116–130. https://doi.org/10.1109/SURV.2009.090109

Non-cooperative and Cooperative Spectrum Sensing in 5G Cognitive Networks

7

Giuseppe Caso, Mai T. Phuong Le, Luca De Nardis, and Maria-Gabriella Di Benedetto

Contents

Abstract

5G is the expected next step of the mobile cellular network evolution, and it is considered as the answer to the ongoing huge increase of cellular users and services. The architecture envisioned for 5G includes a large number of different network entities and systems that share a common spectrum resource via a dynamic spectrum access (DSA) approach. This solution is expected to significantly increase the overall spectrum efficiency but also introduces the challenge of optimizing the coexistence between the entities forming the overall

G. Caso (✉) · M. T. P. Le · L. De Nardis · M.-G. Di Benedetto
Department of Information Engineering, Electronics and Telecommunications (DIET), Sapienza University of Rome, Rome, Italy
e-mail: giuseppe.caso@uniroma1.it; caso@diet.uniroma1.it; mai.le.it@ieee.org; luca.denardis@uniroma1.it; mariagabriella.dibenedetto@uniroma1.it

W. Zhang (ed.), *Handbook of Cognitive Radio*,
https://doi.org/10.1007/978-981-10-1394-2_7

network, by limiting their mutual interference. Within this context, the cognitive radio (CR) paradigm, mainly focusing on its peculiar function, that is, spectrum sensing (SS), is being currently proposed as one of the main enablers for efficient DSA with limited interference. The goal of this chapter is to provide a comparative analysis on CR-inspired spectrum resource management (CR-SRM) mechanisms recently proposed for the 5G architecture, which mainly exploit SS, in order to characterize up-to-date research trends on the topic and highlight still-open challenges and possible future work directions.

Introduction

The rapid increase of cellular devices and services calls for the development of a new generation of the mobile cellular system, and considering the previous generations, the 5G acronym is currently widely adopted for indicating both envisioned requirements and possible solutions. On one hand, three main pillars synthesize the 5G requirements: (a) ubiquitous connectivity, (b) extreme low latency, and (c) very high data rate [1]; on the other hand, three categories identify the possible solutions: (a) massive and heterogeneous network densification, (b) increased bandwidth and spectrum efficiency, and (c) improved energy efficiency [2]. All together, the 5G architecture will include a huge number of different network entities mostly sharing a common spectrum resource, formed by licensed and unlicensed frequency bands, via a *dynamic spectrum access* (DSA) approach rather than traditional, and less efficient, static band assignment; while this solution is expected to significantly increase the overall spectrum efficiency, it also introduces the challenge of optimizing the coexistence between different devices, systems, and technologies.

Within this context, the *cognitive radio* (CR) paradigm and technology, as envisioned in [3], is being currently proposed as one of the main enablers for efficient and dynamic spectrum sharing between 5G network entities. For this reason, in recent years, several *CR*-inspired *spectrum resource management* (CR-SRM) mechanisms have been proposed, at different levels of the 5G architecture, for efficient DSA with limited interference. The key idea of these mechanisms is to exploit the CR capability of obtaining information on the occupation of a spectrum resource and subsequently apply an appropriate action strategy. The function of gathering information on the spectrum resource is usually referred to as *spectrum sensing* (SS); results of spectrum sensing are then used for optimizing the spectrum sharing among network entities.

The goal of this chapter is to provide a comparative analysis on CR-SRM mechanisms recently proposed for the 5G architecture, which mainly exploit SS, in order to characterize up-to-date research trends on the topic and also highlight still-open challenges and possible future work directions.

The rest of the work is organized as follows: section "Towards the 5G Era: Requirements, Enabling Technologies, and the Interference Challenge" introduces 5G basic concepts, first reporting a brief history of the mobile cellular system evolution and then highlighting requirements, most investigated solutions, and one of the

main challenges of the incoming generation, that is, the interference management. Section "The Cognitive Radio Paradigm for 5G" frames the topic of this work, providing a brief introduction to DSA and CR paradigms, while also considering the 5G scenarios in which they are envisioned to be applied. Section "CR-Inspired Spectrum Resource Management" is focused on the comparative analysis of recent CR-SRM mechanisms proposed for 5G. Finally, section "Conclusions and Future Work" concludes the chapter and describes open challenges and possible future work.

Towards the 5G Era: Requirements, Enabling Technologies, and the Interference Challenge

Evolution of the Mobile Cellular System

The 5G technology is the next step of the mobile cellular network evolution, and it is globally considered as the answer to the enormous increase of cellular users and cellular-based services. Research communities and industries hypothesize that 5G standards might be introduced in early 2020s. This prediction might confirm the chronological rule of thumb on the development of a new cellular system generation each ten years approximately: the introduction of 1G systems are in fact dated 1982, while the 2G ones were commercially distributed in 1992. 3G systems were then deployed in early 2000s, while 4G systems are being fully exploited since 2010s. Considering the huge amount of users, devices, and systems, the 5G network is expected to have capabilities that significantly overcome the previous system generations, particularly in terms of system capacity, data rate, latency, network reliability and availability, and energy costs and consumption. Many recent reports and projects summarize numerical requirements for the above categories [4–9], and the comparison with the previous generations, in particular with the 4G one, highlights the huge scale of the forecast (see section "5G Requirements" for details). Several proposals are being currently analyzed in terms of solutions and enabling technologies. On one hand, the improved use of existing 3G/4G architectures and systems is considered a good practice, in order to allow interoperability and compatibility; on the other hand, new technological solutions are needed in order to achieve the 5G requirements (see section "5G Enabling Technologies" for details).

5G Requirements

This section highlights the most important 5G requirements, which range from expected data rates to latency indicators, reporting either their absolute values or, when possible, comparative indicators with the 4G assessed performance. References for the reported data are in particular industry reports such as [4–9], among the others.

Massive capacity. In order to deal with the exponential growth of traffic volume, 5G technologies target to increase the overall network capacity, compared with the existing architectures. In particular, when compared to LTE-A, a 100-fold or higher increase of area capacity in Mbit/s per unit area is being targeted.

High connectivity. Compared to LTE-A, a $\geq$ tenfold increase in the number of connected users is expected.

High data rate everywhere. 5G data rate will also significantly increase. In particular, the target of network operators is a $\geq$ tenfold increase in user-experienced throughput (Mbits/s) compared to 4G, aiming at a maximum of 1 Gbps experienced user throughput everywhere, including sparsely populated rural areas. For indoor and dense outdoor environments, a peak data rate exceeding 10 Gbps is expected.

Ultralow latency. Real-time applications, such as tactile Internet, augmented reality, traffic safety, and control of critical infrastructures and industry processes, require much lower latency compared to the 4G performance. 5G is expected to provide an end-to-end latency of about 1 ms or less and almost "zero latency" in case of cloud-based applications.

Improved energy efficiency. This factor is considered extremely important in the 5G context, because it can help in reducing costs and allow energy harvesting, making the network more sustainable. A 100-fold increase of network energy efficiency in bits/Joule is being targeted, together with a ten times prolonged battery life of devices.

Ultrahigh reliability and availability. Besides the above requirements, 5G network should provide connectivity with ultrahigh reliability and availability. In particular, high availability has to be ensured in new mission-critical control services, such as control of critical infrastructures and traffic safety. An availability of 99.999% can be sought in many industrial applications, e.g., energy/smart grid or medical services, to guarantee successful packet delivery within 1 ms. For autonomous vehicles and industrial automation, ultrahigh reliability is expected to be provided with extremely low loss rate.

Table 1 reports a numerical comparison of the main performance indicators between 4G, in particular the LTE-A technology, and 5G, also highlighting the expected order of increase.

Table 1 Comparison of 4G performance and 5G requirements

Performance indicator	4G	5G	Order of increase
Area capacity [Mbits/s/m^2]	0.1	10–100	100–1000
Connection density [devices/km^2]	10^5	10^6–10^7	10–100
User data rate [Mbits/s]	10	100–1000	10–100
Latency [ms]	10	$\leq$1	$\geq$10
Energy efficiency (bits/Joule)	–	–	100

5G Enabling Technologies

This section highlights the most investigated enabling technologies for the 5G vision. References for the reported solutions are in particular survey papers on 5G such as [1, 2, 10] and [11], among the others.

Network heterogeneous densification. The 5G architecture will be an ultra-dense mixture of network tiers of different sizes and transmit powers, front/backhaul connections, device-to-device (D2D) links, and different radio access technologies (RATs) [12]. Focusing on the cellular network, the coexistence of several classes of base stations (BSs), including macrocells (MBSs) and femto-, pico-, and microcells, generically indicated as small cells (SBSs), will provide improved coverage and spectrum efficiency, if robust mechanisms for interference avoidance are provided. This aspect is analyzed in detail in the following chapter, together with a discussion on cognitive radio-based mechanisms for interference mitigation.

Massive multiple-input multiple-output technology. Massive MIMO, also referred to as large-scale antenna systems, very large MIMO, hyper-MIMO, and full-dimension MIMO and ARGOS, has been recently added to the 5G vision. A massive MIMO system is formed by a BS equipped with a very large number (hundreds to thousands) of colocated or distributed antennas that coherently serves many users within the same time-frequency resource. On one hand, the large number of simultaneously operating antennas can improve significantly the performance in terms of data rate, link reliability, and energy efficiency due to multiplexing and array gains [13, 14]; on the other hand, it increases the hardware complexity while stressing out the need of efficient cooperation between many low-cost low-precision components.

Millimeter-wave communications. The 5G system is expected to work at new, high-frequency bands that are nowadays unused. Among the others, the use of the millimeter-wave (mm-wave) frequency spectrum is of great interest, considering that it exists a vast amount of idle spectrum in the range from 30 to 300 GHz, and preliminary measurements showed that 28 and 38 GHz frequency bands can be used with steerable directional antennas [15]. Issues of using the mm-wave spectrum derive from strong pathloss and atmospheric absorption, low diffraction and penetration around/through obstacles, strong phase noise, and high equipment costs.

Full-duplex communications. Thanks to recent advances in interference cancelation techniques and digital baseband technologies, a full-duplex (FD) transceiver is nowadays capable of transmitting and receiving signals on the same frequency at the same time, thus solving the old days issue of simultaneous Tx/Rx due to high self-interference [16]. FD systems are envisioned to be applied to 5G, thus furtherly increasing the spectrum efficiency. However, several complex types of interference are also introduced, for example, in a multiuser channel sharing system, besides intra-cell interference (among the users in a

Table 2 5G requirements and enabling technologies

Requirement	Main enabling technologies
Massive capacity and connectivity	Network heterogeneous densification, massive MIMO, mm-wave, C-RAN
High data rate everywhere	Network heterogeneous densification, massive MIMO, mm-wave, full-duplex
Ultralow latency	Full-duplex, C-RAN, D2D
Improved energy efficiency	Energy harvesting, D2D
Ultrahigh reliability and availability	Network heterogeneous densification, C-RAN, WNV

cell), intercell downlink-to-uplink interference, and intercell inter-user uplink-to-downlink interference also appear.

Energy harvesting. Energy harvesting has been recently proposed as a potential enabler for solving the energy efficiency requirement. Among the others, several environmental energy sources (e.g., solar and wind energy) and ambient radio signals (e.g., RF energy harvesting) are being analyzed as possible harvesting solutions [17].

Cloud-based access and wireless network virtualization. Cooperation and network virtualization are promising methodologies to be applied in the 5G system; cloud-based radio access network (C-RAN) and wireless network virtualization (WNV), as examples, make possible (a) a distributed architecture for a single BS and (b) simplified resource sharing among many operators, respectively [11]. Several advantages and challenges are being investigated in C-RAN and WNV, as summarized in [18] and [19], respectively.

Table 2 summarizes the above technologies, matching them with the 5G requirements.

The 5G Interference Challenge

In order to highlight the challenge regarding the interference among the heterogeneous 5G network entities, this section introduces in detail the architecture envisioned for the 5G system, first focusing on the cellular network (section "The 5G Cellular Network") and then moving on the more general view of 5G as network of networks (section "5G as Network of Networks"). Definitions of interference at various levels of the 5G architecture are consequently provided and discussed.

The 5G Cellular Network

As briefly introduced in section "5G Enabling Technologies", the cellular part of the overall 5G network will continue the process of *heterogeneous densification* started with the 4G systems. The cellular heterogeneous networks, referred in the following to as *HetNets* or multitier networks, will be the core of the overall 5G architecture:

traditional outdoor MBSs will be massively overlaid with power-limited SBSs, e.g., femtocells, picocells, and microcells (in order to provide a general analysis, this work discusses the interference challenge with the wide concept of small cells. For this reason, the difference between femto-/pico-/microcells is not furtherly highlighted), in space and, possibly, spectrum domains, thus providing an improved network capacity, thanks to (a) a cost-efficient network expansion, in particular for indoor areas [2, 20], and (b) an intelligent traffic balance at each tier via offloading techniques and cell association schemes [21, 22]. Moreover, in a more general view of the network, entities such as relays, operating in a decode-and-forward (DF) mode, and repeaters, working in an amplify-and-forward (AF) mode, will be also developed to increase the coverage area and decrease the power consumption of the network entities [23,24]. It is being proposed that either SBSs or their corresponding users (SUEs) could act as relays for either MBSs or MUEs when needed, thus defining *cooperative* HetNets, in contrast with *noncooperative* ones [25]. While it is clear that MBSs and SBSs will spatially overlay, three main solutions are being proposed for the spectrum domain [26]:

1. **Dedicated-channel**, in which the overall HetNets bandwidth is statically divided in two portions, one dedicated to MBSs/MUEs and the other to SBSs/SUEs.
2. **Partial-channel-sharing**, in which the SBSs/SUEs bandwidth portion is shared with MBSs/MUEs.
3. **Co-channel**, in which the HetNets bandwidth is globally shared between macro- and small cell tiers.

Regarding the HetNets bandwidth, it is assumed that, due to limited availability of the licensed cellular spectrum, it will be formed by both licensed and unlicensed bands, with the latter being free to be used by different systems (e.g., the ISM band). Partial-channel-sharing and co-channel solutions are applicative scenarios of the DSA approach, as will be descripted in section "Dynamic Spectrum Access and Cognitive Radio": in both cases, macro- and small cell tier coexistence is challenging, and the interference arising among them is traditionally referred to as *cross-tier interference* (Cr-TI). Moreover, in all previous spectrum solutions, efficient coexistence between entities within small cell tiers is also a challenge, mainly due to the extremely dense deployment at random locations of SBSs; the interference in this case is referred to as *co-tier interference* (Co-TI). Cr/Co-TI can be seen as particular cases of *intra-network interference* (Intra-NI). In detail, this kind of interference can appear under different forms: the up-/downlink scheduling of macro- and small cell tiers will be in fact asynchronous, and for this reason, if difference between SBSs and SUEs is negligible due to similar locations and transmission powers, intra-NI appears a) from SBSs/SUEs to MBSs, b) from SBSs/SUEs to MUEs, c) from MBSs to SBSs/SUEs, d) from MUEs to SBSs/SUEs, and e) from SBSs/SUEs to SBSs/SUEs [23]. Figure 1 shows the intra-NI scenario in case of downlink transmissions (from MBSs/SBSs to corresponding MUEs/SUEs): intra-NI is indicated as generically affecting the Tx/Rx data link, thus causing interference to both involved transmitter and receiver.

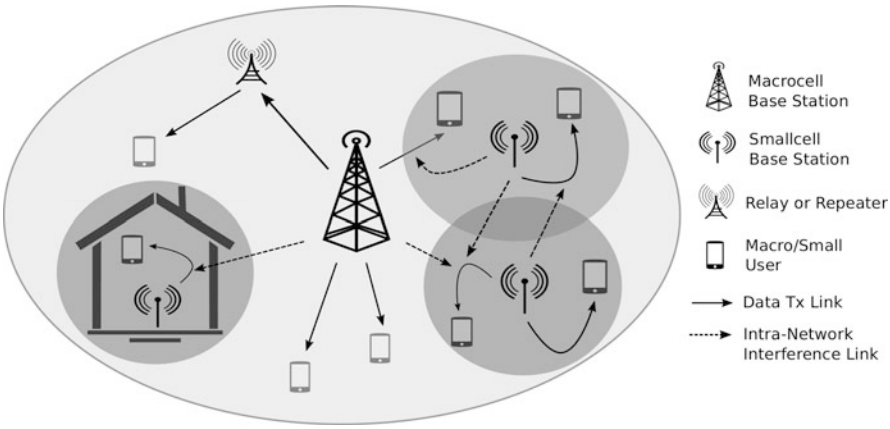

Fig. 1 Representation of HetNets intra-NI scenario in case of downlink transmissions (*straight lines* indicate data links; *dashed lines* indicate intra-NI links)

5G as Network of Networks

As mentioned in section "5G Enabling Technologies", besides the cellular network, the overall 5G architecture will be a mixture of several *radio access technologies* (RATs), allowing the generic 5G user to dynamically connect to different RATs, in order to preserve its required quality of service/experience and the overall network capacity. Among the others, 5G devices will support new 5G standards but also numerous releases of 3G/4G systems, several types of Wi-Fi, and device-to-device (D2D) direct links, all across many spectrum resources [2]. The 5G network will be thus a combination of *multi-RAT HetNets*, and the definition of optimized RAT selection and automatic offloading schemes will be of paramount importance [27].

Within this vision, the use of unlicensed bands opens new opportunities and challenges: some of the RATs will overlay in the spectrum domain (e.g., different releases of Wi-Fi and the small cell tiers, at ISM band and higher frequencies), and these scenarios will require efficient resource management in order to limit the arising *inter-network interference* (inter-NI) [28]. Figure 2 shows the inter-NI scenario in case of downlink transmissions for both cellular network and Wi-Fi and in the presence of D2D communication links: inter-NI is indicated as generically affecting the Tx/Rx data link, thus causing interference to both involved transmitter and receiver.

The Cognitive Radio Paradigm for 5G

In this section, a brief introduction to DSA and CR is provided, in order to highlight general definitions and contributions within this research area, and a focus on SS approaches and techniques is also reported; the application of DSA and CR to the 5G architecture is then discussed.

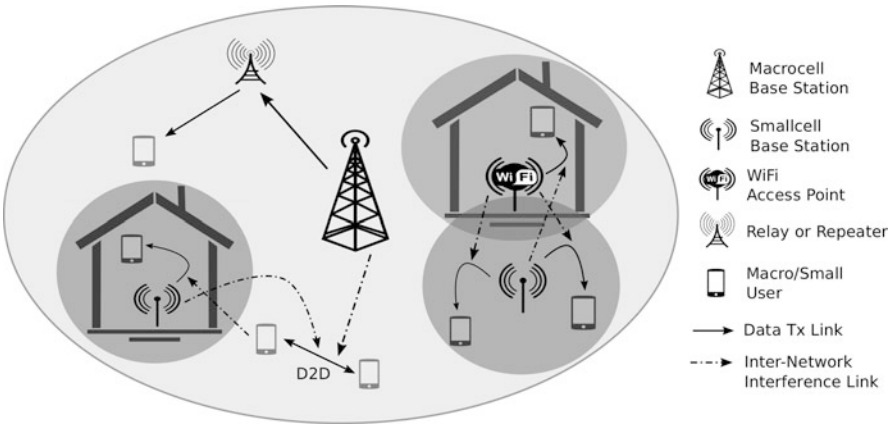

Fig. 2 Representation of multi-RAT HetNets inter-NI scenario in case of downlink transmissions and D2D direct links (*straight lines* indicate data links; *slash-dotted lines* indicate inter-NI links)

Dynamic Spectrum Access and Cognitive Radio

The optimal use of the spectrum resource is an important challenge given the ongoing increase of wireless technologies, systems, and applications. The inefficient spectrum used is largely due to the static assignment of frequency bands to different systems rather than physical shortage, given that, as suggested by several measurements campaigns, many portions of the licensed spectrum are not used either for significant periods of time or in specific geographical areas by the incumbent systems [29, 30]. The need of reforming the spectrum usage has stimulated several activities in the engineering, economics, and regulation communities, having the common goal of optimizing the use of spectrum resources, allowing their use to new services and systems, without damaging the existing ones.

The term dynamic spectrum access is generally used to encompass various approaches to the spectrum reform. According to taxonomy and definitions in [31], DSA approaches can be roughly divided in three main categories:

1. **Dynamic exclusive use model**, in which the static and licensed spectrum assignment is saved but flexibility is introduced in the form of different solutions such as spectrum trading, leasing, and short-time agreement between licensed and unlicensed systems [32].
2. **Hierarchical access model**, mostly applied in case of a licensed band to be shared between licensed primary users (PUs) and unlicensed secondary users (SUs), with the goal of letting the SUs access to the band by exploiting its possible underutilization, while limiting the interference to the PUs [33]. The modalities of the SU spectrum access furtherly identify three sharing scenarios within this model: (a) *underlay* spectrum access, in which the interference between PUs and SUs is controlled by limiting the SUs transmission power;

(b) *overlay* spectrum access, also known as *opportunistic* access, in which the SUs are allowed to transmit full power if they are able to discover, within the licensed band, portions temporarily PU-free; and (c) *hybrid* spectrum access, which combines overlay and underlay access in order to increase the sharing efficiency [34].

3. **Open sharing model**, in which, inspired by the huge success of wireless services operating at unlicensed bands (e.g., the ISM band), different systems openly share the spectrum resource by adopting efficient, either centralized or distributed spectrum sharing mechanisms, with the latter including solutions with roots in game, graphs, and optimization theories [35].

Software-defined radio (SDR) and CR paradigms find a basic application scenario within the DSA context, particularly for hierarchical access and open sharing models. While SDR has been defined as a software-reconfigurable, multi-band device supporting multiple interfaces and protocols, CR, built upon SDR, has been introduced as a context-aware intelligent radio, capable of autonomous reconfiguration by learning from and adapting to the communication environment [3]. The theoretical CR exploits the spectrum resource, by adapting its behavior to the environment, while also considering the requirements of the specific user. Moreover, it is able to learn from past situations in order to always provide the best possible configuration. CR actions are typically scheduled in the so-called cognitive cycle: (a) observe the surrounding environment, (b) plan possible action strategies, (c) decide the optimal operative strategy, (d) learn from experience and derive new action strategies, and (e) act by applying the selected strategy.

While theoretical CR could process an extremely wide range of contextual information, including audiovisual and spatial inputs, CR-related research has been traditionally focused on analyzing and deriving information on the spectrum resource, limiting the contextual information to the one obtained by observing the spectrum domain. In this case, as introduced above, the main function of CRs is spectrum sensing and the cognitive cycle can be simplified in four steps [34], reported in Table 3.

Table 3 The cognitive cycle

Phase	Description
Spectrum sensing	The CRs observe the targeted spectrum resource, thus detecting the traffic activities of noncognitive users and highlighting possible transmission opportunities
Spectrum decision	Depending on the SS results, the CRs plan and decide the action strategy in terms of several functions, e.g., the selection of the best spectrum opportunity, modulation type, and transmission power
Spectrum sharing	The strategy for accessing the spectrum opportunity is applied among all CRs requiring to transmit
Spectrum mobility	The CRs modify their action strategies if a noncognitive user changes its behavior within the spectrum opportunities

The design of a CR network results of paramount importance in all DSA scenarios where different entities and/or networks share the same spectrum resource and therefore could mutually interfere [36]. From the perspective of a hierarchical access model, for example, the SUs should undoubtedly synthesize a CR network while the PUs might be traditional devices: on one hand, in the underlay mode, the SUs can sense the PU activities, estimate the current interference from/to the PUs, and adapt, if necessary, their transmission features, in order to minimize the interference; on the other hand, in the overlay mode, the SUs try to discover via SS, on the overall band, spectrum opportunities free from PUs, and opportunistically use them, until one or more PUs reappear.

The Spectrum Sensing Function

Spectrum sensing plays a fundamental role toward the success of the CR paradigm in terms of spectrum efficiency and coexistence capability, and its definition closely follows the definition of spectrum opportunity. For example, by defining the spectrum opportunity as a band of frequencies that are not being used by the licensed PU at a particular time and/or in a particular geographical area, it immediately arises that SS at least involves frequency, time, and space domains. There are several other dimensions that are possible to explore in order to define and find a spectrum opportunity, e.g., the code and signal propagation direction. On one hand, it is important to define an SS acting across many domains; on the other hand, this requires increased computational complexity and costs for developing and managing the SS function [37].

When focusing on traditional frequency/time/space SS, several definitions can be provided, each one related to a particular highlighted feature [37, 38]. Considering the size of the spectrum resource of interest, SS can be classified into *wideband* and *narrowband* SS: in the first case, the goal is the detection of spectrum opportunities as portions of the overall resource, while, in the second case, the SS is focused on a single portion. Wideband and narrowband SS are usually operated jointly, assuming an intermediate phase in which the sensing device decides a single opportunity where narrowband SS should be applied, among several opportunities previously discovered with wideband SS. In terms of device architecture, SS can be performed in *single radio* and *dual radio*: in the single radio case, specific time allocation for SS is assumed, thus leading to performance of detection and spectrum efficiency depending on the sensing time duration; in the dual radio case, one Tx/Rx chain is dedicated to data transmission/reception, while another chain is dedicated to SS. In this case, SS is also referred to as spectrum monitoring, and performance is improved at the cost of increased hardware complexity and power consumption. The previous definitions assume that the sensing devices are also the ones asking for data transmission such as the SUs in a hierarchical access model. This approach is referred to as *internal* SS, in contrast with *external* SS, where the presence of external network agents, dedicated to SS and able to broadcast the results to the communication devices, is assumed. External SS can solve some problems related to internal SS, such as spectrum and power efficiency, but it introduces new challenges because of the need of exchanging the sensing results on a dedicated

control channel. This challenge arises in general when cooperation between sensing devices, in both internal and external SS configurations, is introduced. In fact, in contrast to *local* SS (LSS), in which each device takes independent decisions on the spectrum status, a *cooperative* SS (CSS) approach can be defined, in which the devices share their decisions in order to improve the overall accuracy of SS. Decisions can be shared either with a central unit, also named fusion center, thus defining *centralized* CSS, or among all neighboring devices, referred to as *distributed* CSS. Cooperation leads in general to SS performance improvement, but this depends on the control channel reliability, the type and the fusion rules of shared information, and the number of involved devices; the trade-off between SS accuracy improvement, on one hand, and architecture complexity and overhead due to control message exchange, on the other, have to be considered while designing CSS algorithms [39].

Besides the above definitions, a plethora of SS techniques, approaches, and methodologies, together with challenges and issues, can be highlighted. Providing a survey on SS is out of the scope of this chapter and the interested reader can refer to [37,38,40], among the others, for detailed and complete reviews. However, observing that CR devices do not in general interact with noncognitive users to verify their presence, indirect detection sensing techniques for (a) *transmitter*, (b) *receiver*, and (c) *interference temperature* detection have been introduced in recent years. The first case is the most investigated one, and the corresponding techniques, ranging from traditional energy and feature detectors to recent wavelet transform-based, statistical and sub-Nyquist approaches, differ each other depending on the a priori knowledge on the device to be detected and the accuracy/complexity trade-off. Complexity and adaptability of the SS technique to different environments play a fundamental role in the 5G context, considering the high number of possible scenarios of interference, and the level of heterogeneity expected for and required by the 5G architecture, as already reported in section "5G Enabling Technologies".

CR-Inspired Spectrum Resource Management

In this section, the state of the art of CR-SRM mechanisms proposed for the 5G architecture is reported and analyzed, first focusing on the HetNets case and then moving on the more general multi-RAT HetNets one.

Focus on HetNets

Focusing on the HetNets forming the cellular network, the application of CR capabilities depends on the possible HetNets usage scenarios. On one hand, with reference to noncooperative HetNets, the scenario in which cognitive small cell tiers provide support to the macrocell tiers while acting on the same spectrum resource is particularly analyzed in recent literature, and it is also actively pursued by the industry; on the other hand, in case of cooperative HetNets, the scenario suggesting

the presence of cognitive relays/repeaters, capable of autonomously selecting the optimal relying/amplifying strategy for further cellular coverage enhancement, is of particular interest. Since centralized control for both spectrum access and intra-NI mitigation is hard to implement, because of scalability of control message exchange among and within tiers [41], CR-SRM mechanisms in the form of cognitive DSA are highly desirable, also considering that the DSA hierarchical access model perfectly matches the HetNets scenarios of partial-channel sharing and co-channel deployment, with macrocells and small cell tiers having the role of PUs and cognitive SUs, respectively.

Solutions Based on Local Spectrum Sensing

Within this context, SS is mainly adopted for a direct analysis of the spectrum resource, in order to estimate and mitigate the intra-NI. Focusing on Cr-TI, several approaches might be used for making possible an efficient spectrum access to low-priority small cell tiers: on one hand, considering an overlay access scenario, interference from/to MBSs/MUEs might be avoided through direct SS by SBSs/SUEs [21]; on the other hand, considering an underlay access scenario, SS-based mechanisms might be used to estimate the interference from/to MBSs/MUEs within the targeted spectrum resource. More complex hybrid access might be also considered: in [23], for example, when considering SBSs/SUEs and MBSs/MUEs spatially overlapped, overlay access is proposed on the spectrum opportunities, while underlay access is carried out on spectrum portions being used by MBSs/MUEs covering different geographical areas, after estimating, through SS-based mechanisms, the possible interference caused to them.

Focusing on Co-TI, several different approaches can be highlighted. On one hand, SBSs/SUEs access might be regulated via SS-based access schemes, as proposed in [21], where Aloha-like access vs. SS-based CSMA have been comparatively evaluated; on the other hand, the recent trend seems to prefer solutions based on game theory [42] and optimization methods [43, 44], with a particular emphasis on maximizing the small cell throughput.

Cr-TI and Co-TI are mostly analyzed in conjunction and, also in this case, SS mechanisms are used in particular for Cr-TI mitigation, while game and optimization theories are preferred for Co-TI [26, 28]. Furthermore, it can be highlighted that the reuse of existing 4G functionalities is being widely analyzed for 5G SS mechanisms: in [26], each SBS mitigates Cr-TI by comparing the gathered information on macrocell scheduled transmission activities, broadcasted by the MBSs in a common dedicated signaling channel, with the SS measurements of the received interference power, which is an indicator already adopted as a sensing quantity in LTE-A tiers. Besides the received interference power, reference signal received quality and number of neighboring cells are the others 4G indicators to be possibly used in 5G interference scenarios, as analyzed in [28]; Cr-TI mitigation is here achieved by also introducing a first step of cooperation within the small cell tier: while the SBS measures the received interference power, thus obtaining a global tier interference indicator, the SUEs measure their own reference signal received quality, thus obtaining a local interference indicator. The SUE measurements are

then reported to the SBS, which decides on the spectrum resource occupancy, by applying a compressed sensing approach for overcoming the possible huge amount of received data.

Solutions Based on Cooperative Spectrum Sensing

While in [28] a centralized CSS scheme has been suggested for Cr-TI mitigation only, both centralized and distributed CSS approaches are being proposed for global intra-NI interference mitigation. Within this context, one of the main challenges is the energy efficiency, to be achieved by minimizing SS efforts and control message exchange. For this reason, when considering centralized CSS, a sequential SS algorithm with hibernation state for the sensing devices has been proposed in [45], while external CSS architecture with dedicated network entities referred to as spectrum agents (SAs) has been recently discussed in [46]. Even in this case, mechanisms for energy efficiency are highlighted: the SAs are in fact supposed to be activated through an explicit sensing request either by the SBS/SUE needed to transmit or by a central unit that is also in charge of the final decision on the resource occupancy. Figures 3 and 4 graphically clarify some of the concepts being discussed; on one hand, Fig. 3 reports a representation of three different internal SS mechanisms that are local SS, centralized CSS, and distributed CSS: considering the downlink scenario, it is assumed that, in all cases, the SBS activates the SS function in order to transmit data to the SUEs, and in case of centralized CSS, it also acts as central unit. On the other hand, Fig. 4 reports two simplified scenarios of external and centralized CSS: in this case, considering again the downlink scenario, it is assumed that, the SBS needed to transmit activates the SAs, they apply SS and report the results either to the SBS or to a dedicated central unit. It is worth noting that the cases reported in both Figs. 3 and 4 consider the execution of SS within an isolated small cell tier: approaches considering possible cooperation between near/overlapping small cell tiers can be also taken into account.

Considering that the reliability of the common control channel is another factor significantly affecting the CSS performance, an MAC protocol with dynamic common control channel selection has been recently proposed in [47], referred to as DCCC-MAC, and formed by four phases: (a) CSS by the SUEs on the channels forming the spectrum resource, (b) selection by the SBS of a common control channel among the channels sensed as free from macrocell activities, (c) contention-free allocation and data transmission of the cooperative SUEs on the other channels detected as free, and (d) beaconing for synchronization purposes within the cell.

In the context of distributed CSS, joint optimization of sensing parameters, transmission powers, and spectrum resource allocation has been discussed in [48], where an optimal trade-off between the power spent for transmission and the power spent for sensing is also derived. CSS has been also proposed in the hypothesis of mobile PUs, which mainly matches the HetNets uplink scenario (MUE/SUE transmitting to corresponding MBS/SBS), for joint estimation of spectrum occupancy and spatial localization of MUEs [49].

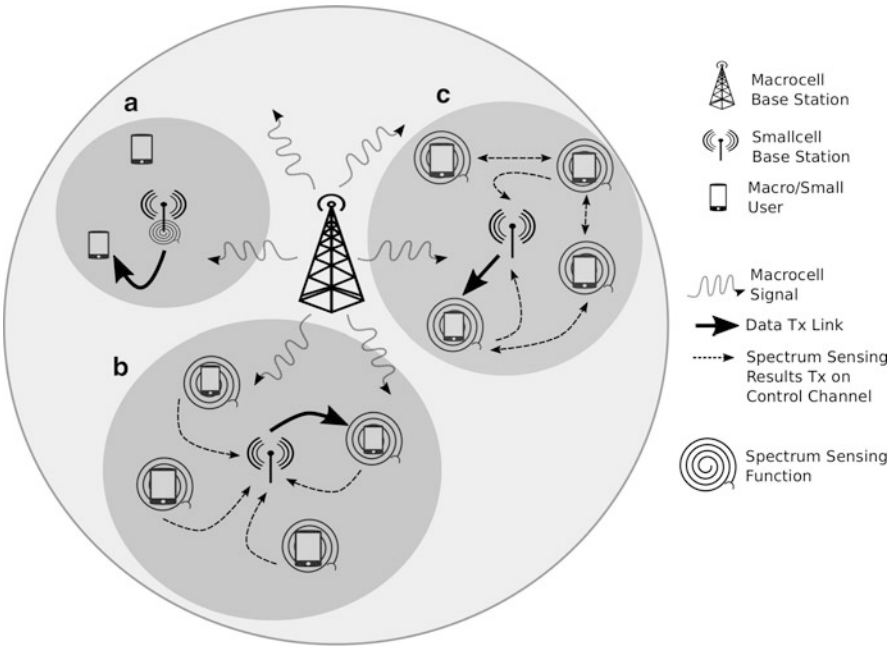

Fig. 3 Representation of three internal SS scenarios, in case of downlink transmissions: (**a**) local SS by the SBS; (**b**) centralized CSS, the SUEs, activated by the SBS, apply SS and report their results to the SBS that also acts as central unit; (**c**) distributed CSS, the SUEs, activated by the SBS, apply SS and forward their results to the nearest neighbors

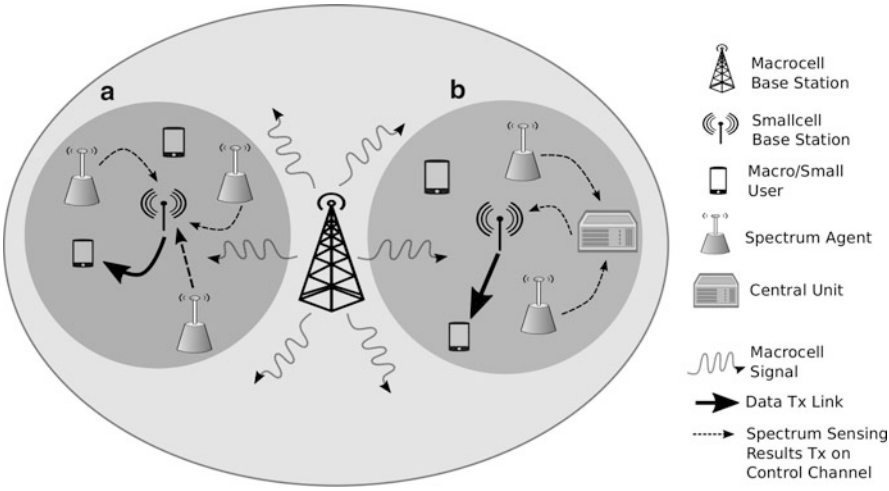

Fig. 4 Representation of two external SS scenarios, in case of downlink transmissions: (**a**) centralized SS mode 1, the SBS activates the SAs and acts as control unit; (**b**) centralized SS mode 2, the SBS activates the SAs and receives the final SS decision from a dedicated central unit

Imperfect Spectrum Sensing

The imperfection of SS due to possible miss-detections and false alarms is a nontrivial problem that significantly affects the expected network performance. It recently started to be explicitly considered in the HetNets design and spectrum allocation schemes: on one hand, the spectrum allocation framework proposed in [50, 51] for OFDMA small cells considers both constraints deriving from intra-NI and SS errors on the channels forming the spectrum resource; on the other hand, the problem deriving from possible SS low reliability can be mitigated by limiting its use within a more sophisticated sharing mechanism, as suggested in [52], where a centralized spectrum sharing has been proposed: distributed SS is executed by SUEs, and results are reported to the nearest SBS. However, the SS results are only used by MBSs/SBSs as side information, and the final spectrum sharing decisions are mainly based on the policies defined by a centralized controller.

Energy Efficiency

Spectrum efficiency and interference mitigation issues are mostly analyzed in conjunction with many other challenges deriving from 5G requirements. As already observed in section "Solutions Based on Cooperative Spectrum Sensing", one of the most investigated combinations is with energy efficiency and harvesting, considering their paramount importance for the creation of 5G devices and infrastructures [25]. When considering CR-SRM mechanisms, energy efficiency of spectrum sensing and sharing assumes primary importance: it has been demonstrated that the energy consumption of energy detector SS with off-the-shelf components is nearly twice the one of a normal transmission state, and for this reason, the constraint on the power consumption has to be considered in the SS time duration optimization [53]. Moreover, in the context of HetNets, energy-efficient SBS/SUE spectrum sharing is being investigated: once a spectrum opportunity has been discovered, the optimization of the SBS/SUE transmission power can be achieved by considering that the highest its value, the highest the possible intra-NI and power consumption [53].

Energy harvesting is also highlighted in the 5G HetNets scenarios: different network entities can be empowered by different energy harvesting solutions, and CSS mechanisms for discovering spectrum opportunities should take this aspect into account in order to adaptively selecting the optimal number of cooperative neighbors and the energy that can be consumed by each one in the SS phase. In [54] an MAC protocol synthesizing these aspects, divided into contention, sensing, and transmission phases, has been proposed and analyzed.

Focus on Multi-RAT HetNets

As discussed in section "The 5G Cellular Network", the HetNets architecture is interference-affected, given that macro- and small cell tiers share the licensed spectrum. Even if the CR-SRM mechanisms discussed in section "Focus on

HetNets" could mitigate this interference, the large-scale deployment of small cells is posing an increasing challenge. For this reason, research communities and industries are discussing on the utilization of other spectrum resources for small cells, including unlicensed spectrum bands, such as the 2.4 and 5 GHz bands that Wi-Fi systems operate in [55].

Within the 4G context, tentatives of exploring the unlicensed spectrum currently used by Wi-Fi systems for LTE/LTE-A systems are mainly known as LTE-unlicensed (LTE-U) or licensed-assisted access using LTE (LAA-LTE) and clearly pose an initial inter-NI issue to be managed between the cellular network and the Wi-Fi systems; when considering 5G networks, the coexistence of HetNets and Wi-Fi becomes even more challenging and requires in-depth research, considering the increasing number of overall network scenarios and entities. As an example, the same systems are also possibly interfering at the 60 GHz mm-wave bands, where the new IEEE 802.11ad standard, also known as WiGig, is about to work, and on parallel, 5G small cell SBSs/core network backhaul links are being envisioned, given that wired and in-band wireless links may not perform well because of the dense deployment of small cells [56].

Nowadays, considering their huge proliferation, Wi-Fi systems are mainly playing an important role in offloading traffic from the heavily loaded cellular network, especially in indoor traffic hotspots and in poor cellular coverage areas, and the huge amount of recent work on the topic proves that efficient offloading schemes and intelligent RAT selection are fundamental tools in achieving satisfactory network performance, if inter-NI mitigation is provided [57].

HetNets vs. Wi-Fi: Inter-NI Mitigation

HetNets and Wi-Fi coexistence can be envisioned to be cooperative or otherwise; considering that the first case implies modification of existing protocols due to the need of control message exchange, most of the work has been nowadays focused on noncooperative RATs, thus proposing CR-based solutions.

Resource partitioning between HetNets and Wi-Fi are being discussed: while unlicensed spectrum partitioning guarantees fairness between small cells and Wi-Fi but suboptimal spectrum efficiency [58], time-domain dynamic resource sharing, based on the almost blank subframe (ABSs) mechanism, is expected to be a more efficient solution. In the context of LTE/Wi-Fi coexistence, the ABSs, which are subframes with reduced power and data, are randomly transmitted by the LTE network, without coordination with the Wi-Fi system; the Wi-Fi access points can detect the ABSs (via CSMA/CA or SS) and use them for their own transmissions. It has been shown that this mechanism sets a reasonable trade-off between the Wi-Fi and the LTE throughput performance [59,60]. Moreover, interference avoidance can be obtained, as previously discussed in section "Solutions Based on Local Spectrum Sensing", by adopting 4G SS indicators [28] and estimating the density of nearby Wi-Fi transmissions [60]. Coexistence at the 60 GHz mm-wave has been recently investigated in [61], where wavelet transform-based SS and filter bank multicarrier modulation techniques have been proposed to increase the small cell tier throughput.

Conclusions and Future Work

This chapter has presented a comparative analysis of recent CR-SRM mechanisms proposed in literature for the incoming 5G network and exploiting, in particular, the SS function. After reporting a summary on 5G envisioned requirements and possible enabling technologies, the interference challenge at different levels of the 5G architecture has been discussed, and the application of the CR paradigm, with a particular focus on SS and CSS, has been descripted in light of recent literature. The analysis suggests that CR is being extensively analyzed in the context of 4G/5G multi-RAT HetNets: in particular, when considering the cellular part of the 5G network, SS-based approaches seem to be extremely suitable for Cr-TI mitigation scenarios, where a particular emphasis is being given to cooperative approaches, energy efficiency, and an overall optimal sensing/transmission network organization through specific MAC protocols; when considering the multi-RAT scenarios, SS-based approaches are being proposed for improving the coexistence of different RATs on a common unlicensed spectrum resource, with a particular focus on the optimization of HetNets and Wi-Fi coexistence, given the importance of Wi-Fi, as supporting technology for offloading, in the general 5G vision.

Nowadays, the presented topic is still extremely open and challenging and calls for further research in a broad range of scenarios. For example, most of the work either does not indicate the SS technique to be used or assumes simple energy detector SS schemes. However, the SS technique might be selected with reference to the applicative scenarios: for example, in case of Cr-TI mitigation within the cellular licensed spectrum, it can be assumed that small cell tiers are focused on discovering macrocell activities and thus, knowing their transmission features, more complex and performing SS techniques might be used. In general, specificity of SS should be considered for more detailed performance analysis. Another aspect that might be addressed more in detail is the possible users' mobility, considering that majority of 5G users is assumed to be mobile in the area of interest; this is extremely relevant also for D2D communications and cooperative architectures with relays and repeaters. Finally, full-duplex and massive MIMO might be taken into account in all the above scenarios, given that they are considered as fundamental technologies for a complete success of the 5G era.

References

1. Panwar N, Sharma S, Kumar Singh A (2016) A survey on 5G: the next generation of mobile communication. Elsevier Phys Commun 18(2):64–84
2. Andrews JG et al (2014) What will 5G be? IEEE J Sel Areas Commun 32(6):1065–1082
3. Mitola J, Maguire GQ (1999) Cognitive radio: making software radios more personal. IEEE Pers Commun 6(4):13–18
4. Ericsson (2016) 5G radio access – capabilities and technologies. White paper Uen 284:23–3204. Rev C
5. NTT DoCoMo Inc (2014) 5G radio access: requirements, concept and technologies. White paper

6. 5GPPP (2015) The next generation of communication networks and services, the 5G infrastructure public private partnership (5GPPP), European Commission
7. GSMA Intelligence (2014) Understanding 5G: perspectives on future technological advancements in mobile. White paper
8. METIS Project (2013) Scenarios, requirements and KPIs for 5G mobile and wireless system, Doc. ID:ICT-317669-METIS/D1.1
9. Qualcomm Technologies Inc (2016) Leading the world to 5G. White paper
10. Demestichas P et al (2013) 5G on the horizon: key challenges for the radio-access network. IEEE Veh Technol Mag 8(3):47–53
11. Hossain E, Hasan M (2015) 5G cellular: key enabling technologies and research challenges. IEEE Instrum Meas Mag 18(3):11–21
12. Bhushan N et al (2014) Network densification: the dominant theme for wireless evolution into 5G. IEEE Commun Mag 52(2):82–89
13. Larsson EG, Edfors O, Tufvesson F, Marzetta TL (2014) Massive MIMO for next generation wireless systems. IEEE Commun Mag 52(2):186–195
14. Ngo HQ (2015) Massive MIMO: fundamentals and system designs. PhD thesis, Linkoping University Electronic Press
15. Rappaport TS et al (2013) Millimiter wave mobile communications for 5G cellular: it will work! IEEE Access 1:335–349
16. Hong S et al (2014) Applications of self-interference cancellation in 5G and beyond. IEEE Commun Mag 52(2):114–121
17. Xiao L, Wang P, Niyato D, Kim D, Han Z (2014) Wireless networks with RF energy harvesting: a contemporary survey. IEEE Commun Surv Tutorials 17(2):757–789
18. Checko A et al (2015) Cloud RAN for mobile networks – a technology overview. IEEE Commun Surv Tutorials 17(1):405–426
19. Liang C, Yu F (2015) Wireless network virtualization: a survey, some research issues and challenges. IEEE Commun Surv Tutorials 17(1):358–380
20. Andrews JG, Claussen H, Dohler M, Rangan S, Reed MC (2012) Femtocells: past, present, and future. IEEE J Sel Areas Commun 30(3):497–508
21. ElSawy H, Hossain E, Kim DI (2013) HetNets with cognitive small cells: user offloading and distributed channel access techniques. IEEE Commun Mag 51(6):28–36
22. Hossain E, Rasti M, Tabassum H, Abdelnasser A (2014) Evolution toward 5G multi-tier cellular wireless networks: an interference management perspective. IEEE Wirel Commun 21(3):118–127
23. Wang W, Yu G, Huang A (2013) Cognitive radio enhanced interference coordination for femtocell networks. IEEE Commun Mag 51(6):37–43
24. Sharma SK, Patwary M, Chatzinotas S, Ottersten B, Abdel-Maguid M (2015) Repeater for 5G wireless: a complementary contender for spectrum sensing intelligence. In: Proceedings of the IEEE International Conference on Communications. IEEE Press, pp 1416–1421
25. Hong X, Wang J, Wang CX, Shi J (2014) Cognitive radio in 5G: a perspective on energy-spectral efficiency trade-off. IEEE Commun Mag 52(7):46–53
26. Huang L, Zhu G, Du X (2013) Cognitive femtocell networks: an opportunistic spectrum access for future indoor wireless coverage. IEEE Wirel Commun 20(2):44–51
27. Galinina O et al (2014) Capturing spatial randomness of heterogeneous cellular/WLAN deployments with dynamic traffic. IEEE J Sel Areas Commun 32(6):1083–1099
28. Lien S-Y, Chen K-C, Liang Y-C, Lin Y (2014) Cognitive radio resource management for future cellular networks. IEEE Wirel Commun 21(1):70–79
29. FCC Spectrum Policy Task Force (2002) Report of the spectrum efficiency working group. Technical report 02–155
30. Staple G, Werbach K (2004) The end of spectrum scarcity. IEEE Spectr 41(3):48–52
31. Zhao Q, Swami A (2007) A survey of dynamic spectrum access: signal processing and networking perspectives. In: Proceedings of the IEEE International Conference on Acoustics, Speech and Signal Processing. IEEE Press, pp IV-1349–IV-1352

32. Hatfield DN, Weiser PJ (2005) Property rights in spectrum: taking the next step. In: Proceedings of the IEEE Symposium on New Frontiers in Dynamic Spectrum Access Networks. IEEE Press, pp 43–55
33. Akyildiz IF, Altunbasak Y, Fekri F, Sivakumar R (2004) AdaptNet: adaptive protocol suite for next generation wireless internet. IEEE Commun Mag 42(3):128–138
34. Akyildiz IF, Lee W-Y, Vuran MC, Mohanty S (2006) Next generation/dynamic spectrum access/cognitive radio wireless networks: a survey. Elsevier Comput Netw 50:2127–2159
35. Etkin R, Parekh A, Tse D (2007) Spectrum sharing for unlicensed bands. IEEE J Sel Areas Commun 25(3):517–528
36. Di Benedetto M-G, Cattoni AF, Fiorina J, Bader F, De Nardis L (eds) (2015) Cognitive radio and networking for heterogeneous wireless networks. Springer, Cham
37. Yucek T, Arslan H (2009) A survey of spectrum sensing algorithms for cognitive radio applications. IEEE Commun Surv Tutorials 11(1):116–130
38. Ali A, Hamouda W (2016) Advances on spectrum sensing for cognitive radio networks: theory and applications. IEEE Commun Surv Tutorials PP(99):1
39. Caso G, De Nardis L, Thobaben R, Di Benedetto M-G (2015) Cooperative sensing of spectrum opportunities. In: Holland O, Bogucka H, Medeisis A (eds) Opportunistic spectrum sharing and white space access: the practical reality. John Wiley & Sons, Hoboken, New Jersey, pp 143–165
40. Axell A, Leus G, Larsson E, Poor HV (2012) Spectrum sensing for cognitive radio: state-of-the-art and recent advances. IEEE Signal Process Mag 29(3):101–116
41. ElSawy H, Hossain E (2013) Channel assignment and opportunistic spectrum access in two-tier cellular networks with cognitive small cells. In: Proceedings of the IEEE Global Communications Conference. IEEE Press, pp 4477–4482
42. Pantisano F, Bennis M, Saad W, Debbah M, Latva-Aho M (2013) interference alignment for cooperative femtocell networks: a game-theoretic approach. IEEE Trans Mob Comput 12(11):2233–2246
43. Zhuang B, Guo D, Honig ML (2015) Traffic-driven spectrum allocation in heterogeneous networks. IEEE J Sel Areas Commun 33(10):2027–2038
44. Qiu J et al (2016) Hierarchical resource allocation framework for hyper-dense small cell networks. IEEE Access 4:8657–8669
45. Qiao X, Xie W, Yang F (2015) Cooperative sequential sensing of radio transmissions in 5G with improved cost-delay tradeoff. Hindawi Int J Distrib Sens Netw 2015:1–12. ID:456074
46. Zhang Z, Zhang W, Zeadally S, Wang Y, Liu Y (2015) Cognitive radio spectrum sensing framework based on multi-agent architecture for 5G networks. IEEE Wirel Commun 22(6): 34–39
47. Thilina KGM, Hossain E, Kim DI (2016) DCCC-MAC: a dynamic common-control-channel-based MAC protocol for cellular cognitive radio networks. IEEE Trans Veh Technol 65(5):3597–3613
48. Sardellitti S, Barbarossa S (2013) Joint optimization of collaborative sensing and radio resource allocation in small-cell networks. IEEE Trans Signal Process 61(18):4506–4520
49. Li B, Li S, Nallanathan A, Zhao C (2015) Deep sensing for future spectrum and location awareness 5G communications. IEEE J Sel Areas Commun 33(7):1331–1344
50. Zhang H, Jiang C, Mao X, Chen HH (2016) Interference-limited resource optimization in cognitive femtocells with fairness and imperfect spectrum sensing. IEEE Trans Veh Technol 65(3):1761–1771
51. Zhang H, Nie Y, Cheng J, Leung VCM, Arumugam N (2016) Sensing time optimization and power control for energy efficient cognitive small cell with imperfect hybrid spectrum sensing. IEEE Trans Wirel Commun PP(99):1
52. Akhtar AM, Wang X, Hanzo L (2016) Synergistic spectrum sharing in 5G HetNets: a harmonized SDN-enabled approach. IEEE Commun Mag 54(1):40–47
53. Jiang C, Zhang H, Ren Y, Chen HH (2014) Energy-efficient non-cooperative cognitive radio networks: micro, meso, and macro views. IEEE Commun Mag 52(7):14–20
54. Liu Y, Zhang Y, Yu R, Xie S (2015) Integrated energy and spectrum harvesting for 5G wireless communications. IEEE Netw 29(3):75–81

55. Huawei et al (2013) Discussion paper on unlicensed spectrum integration to IMT systems, 3GPP RAN 62 RP-131723
56. Hur S et al (2013) Millimeter wave beamforming for wireless backhaul and access in small cell networks. IEEE Trans Commun 61(10):4391–4403
57. Bennis M et al (2013) When cellular meets WiFi in wireless small cell networks. IEEE Commun Mag 51(6):44–50
58. Hajmohammad S, Elbiaze H (2013) Unlicensed spectrum splitting between femtocell and WiFi. In: Proceedings of the IEEE International Conference on Communications. IEEE Press, pp 1883–1888
59. Almeida E et al (2013) Enabling LTE/WiFi coexistence by LTE blank subframe allocation. In: Proceedings of the IEEE International Conference on Communications. IEEE Press, pp 5083–5088
60. Zhang H, Chu X, Guo W, Wang S (2015) Coexistence of WiFi and heterogeneous small cell networks sharing unlicensed spectrum. IEEE Commun Mag 53(3):158–164
61. Hosseini H, Anpalagan A, Raahemifar K, Erkucuk S, Habib S (2016) Joint wavelet-based spectrum sensing and FBMC modulation for cognitive mmWave small cell networks. IET Commun 10(14):1803–1809

Spectrum Sensing, Database, and Its Hybrid

8

Yue Gao and Yuan Ma

Contents

Abstract

The rising popularity of wireless services resulting in spectrum shortage has motivated dynamic spectrum sharing to facilitate efficient usage of the under-utilized spectrum. Cognitive radio has emerged as one of the most promising candidate solutions to improve spectrum utilization, by allowing secondary users (SUs) to opportunistically access the temporarily unused spectrum, without introducing harmful interference to primary users (PUs). A crucial requirement in cognitive radio networks (CRNs) is wideband spectrum sensing, in which SUs

Y. Gao (✉) · Y. Ma
School of Electronic Engineering and Computer Science (EECS), Queen Mary University of London, London, UK
e-mail: yue.gao@qmul.ac.uk; y.ma@qmul.ac.uk

W. Zhang (ed.), *Handbook of Cognitive Radio*,
https://doi.org/10.1007/978-981-10-1394-2_8

should detect spectral opportunities across a wide frequency range. However, wideband spectrum sensing could lead to unaffordable high sampling rates at energy-constrained SUs. Sub-Nyquist sampling was developed to overcome this issue by exploiting the sparse property of the wideband signals. Additionally, to relax the sensing requirements, hybrid framework that combines the advantages of both geo-location database and spectrum sensing is explored. The experimental results show that the hybrid schemes can achieve improved detection performance with reduced hardware and computation complexity in comparison with the sensing and database only approach.

Introduction

With the explosive proliferation of wireless devices and rapid growth of wireless services, spectrum scarcity has become a major bottleneck for wireless industry. The threat of spectrum shortage has encouraged the governments to take critical steps toward releasing multiple bands for dynamic spectrum sharing, motivated by the fact that the actual spectrum is underutilized in practice [13, 22]. In particular, TV white space (TVWS) is one of the most promising section for dynamic spectrum sharing, which is composed of the channels that are not used by digital terrestrial televisions (DTT) or program making and special events (PMSE) users, and those freed up by the switchover from analog to digital TV broadcasting [11,22]. The UK communications regulator, Office of Communications (Ofcom), has announced the license exempt regulations for TVWS in December 2015 [24]. Compact and low-power white space devices for rural broadband/WiFi-like accesses and machine-to-machine (M2M) communications could therefore operate on these vacant channels without causing interferences to the primary transmissions [9].

To make the SUs aware of the spectrum occupancy, one way is geo-location database, which is a centralized database to store the maximum allowed equivalent isotropic radiated power (EIRP) for each vacant TVWS channel at a specific location [13]. However, the real-time changes of the propagation environment pose significant challenges to the database approach [23]. Spectrum sensing over the wide bandwidth is thus desirable to detect spectral opportunities over a wide frequency range. However, for the wideband sensing at high frequency, it requires a high-rate analog-to-digital converter (ADC) for the signal sampling, which is quite expensive and high-power consuming. Sub-Nyquist sampling techniques were thus introduced to implement wideband sensing using sampling rate lower than the Nyquist rate to reduce the requirements of high-speed signal processing. In [39], Tian and Giannaki first applied compressed sensing to implement wideband sensing by exploiting the sparseness of the wideband signal in the frequency domain. In [30], each SU implements wideband channel division to sense K out of L channels, and then matrix completion is performed at a fusion center to reconstruct the original spectrum for decision making. To further relax the sensing requirements, an efficient blind sub-Nyquist cooperative wideband spectrum sensing scheme is proposed in [17] that reduce energy consumption in wideband signal acquisition, processing and transmission, with reliable performance guarantee.

Spectrum sensing provides instant channel occupancy information but may cause interference to some reserved channels as they would be determined as vacant by sensing and hence utilized by SUs for unlicensed transmission. To reduce the risk of interference caused by the unregistered PMSE and improve the spectrum efficiency, Wang et al. proposed a hybrid framework incorporating the advantages of both geo-location database and spectrum sensing, in which different spectrum sensing modules are performed after the spectrum occupancies were initially determined by geo-location database in [47]. Due to the energy constraint in compact SUs, efficient and reliable real-time wideband spectrum sensing emerges as a crucial challenge for dynamic spectrum sharing in CRNs. To further relax the sensing requirements, the data provided by the geo-location database calculation algorithm can be utilized to improve the detection performance.

Spectrum Sensing

Spectrum sensing is a critical functionality to enable the implementation of dynamic spectrum access in cognitive radio systems [20]. Its goal is to allow SUs to identify the spectrum occupancy states before opportunistically exploiting the temporarily vacant frequency channels while protecting PUs from harmful interferences caused by secondary transmissions.

Many narrowband spectrum sensing algorithms have been studied in the literature [35], including matched filtering [7], energy detection [15], and cyclostationary feature detection [37]. While present narrowband spectrum sensing algorithms focus on exploiting spectral opportunities over a narrow frequency range, cognitive radio networks will eventually be required to exploit spectral opportunities over a wide frequency range for achieving higher opportunistic throughput. If a PU reappears over a certain band, the availability of several other possible vacant channels facilitates the seamless handoff from one spectrum channel to another, which reduces secondary data transmission interruptions. However, for conventional wideband spectrum sensing, a stringent requirement arises from the Nyquist signal acquisition, which is quite expensive, power-consuming, and computation intensive. Efficient real-time wideband spectrum sensing emerges as a crucial challenge for dynamic spectrum sharing.

Narrowband Spectrum Sensing

As the core component of cognitive radio, spectrum sensing aims to obtain awareness about the spectrum usage and the existence of PU in a certain geographical area at a particular duration of time. The spectrum sensing problem can be formulated as follows.

Assume that the received signal is sampled at sampling frequency f_s. To detect the primary signal, SU poses a binary hypothesis testing problem as

$$\begin{aligned} H_0 &: r(t) = w(t), \\ H_1 &: r(t) = h(t) * s(t) + w(t), \end{aligned} \tag{1}$$

where $s(t) \in C^{N\times 1}$ is the transmitted signal, $h(t)$ is the channel gain between the transmitter and receiver, $w(t) \sim \mathscr{CN}(0, \sigma_\omega^2 \mathbf{I}_N)$ refers to additive white Gaussian noise (AWGN) distributed independently and identically with zero mean and variance σ_ω^2, $\mathbf{I}_N$ is the identity matrix, and N is the product of the sensing duration T_s and the sampling frequency f_s.

Traditional narrowband sensing can be mainly divided into three types, matched filtering [7], energy detection [15], and cyclostationary feature detection [37].

Among there three methods, energy detection is a non-coherent detection method that avoids the need for prior knowledge of the PUs. It is easy to implement and the computational complexity is relatively low but with a drawback of poor detection resolution under low SNR scenarios. Once the signal is received by SUs, the energy detector is used to calculate the energy of the received signal over the sensing interval and compare it with a predefined threshold to decide whether the frequency band is occupied or not.

Based on the central limit theorem, the test statistic T approximately follows the Gaussian Distribution [36]:

$$\begin{aligned} T &\sim \mathscr{N}(\sigma_\omega^2, 2\sigma_\omega^4/N), && H_0 \\ T &\sim \mathscr{N}((1+\gamma)\sigma_\omega^2, 2(1+\gamma)^2\sigma_\omega^4/N), && H_1, \end{aligned} \tag{2}$$

where N is the signal size and γ is the received SNR at the SU.

The performance of the detection scheme can be evaluated by two metrics: probability of detection P_d and probability of false-alarm P_f. P_d is the probability of correctly detecting the existence of PU on the sensing sub-channel when it is truly present and thus can be formulated as

$$P_d = P(T > \lambda | H_1) = Q\left(\frac{\lambda - \sigma_\omega^2(\gamma+1)}{\sigma_\omega^2(\gamma+1)\sqrt{\frac{2}{N}}}\right). \tag{3}$$

P_f is the probability of falsely testing that the considered channel is occupied by PU when it is actually not and can be computed as

$$P_f = P(T > \lambda | H_0) = Q\left(\frac{\lambda - \sigma_\omega^2}{\sigma_\omega^2\sqrt{\frac{2}{N}}}\right), \tag{4}$$

where $Q(x)$ is the standard Gaussian complementary distribution function (CDF).

To achieve the predefined false-alarm probability P_f, the threshold λ in each channel is set as

$$\lambda = \left[\sqrt{\frac{2}{N}}Q^{-1}(P_f) + 1\right] \cdot \sigma_\omega^2, \tag{5}$$

where $Q^{-1}(\cdot)$ denotes the inverse complementary distribution function of the standard normal distribution.

In order to maximize the benefit for both PUs and SUs, an adaptive threshold setting algorithm is developed in [48] to achieve the best trade-off between detection probability P_d and false alarm probability P_f, which can be formulated to an equivalent form of minimizing the error decision probability P_e as

$$\lambda^* = \arg\min_{\lambda} P_e(\lambda) = \arg\min_{\lambda}\{(1-\Omega)P_f + \Omega(1-P_d)\}, \tag{6}$$

where Ω ($0 \leq \Omega \leq 1$) is the PU's spectrum utilization ratio, $(1-\Omega)$ stands for the probability that the channel being vacant and full of noise, and $(1-P_d)$ represents the missed detection probability that indicates PUs are absent while actually present. After mathematical derivation, the adaptive threshold λ^* that can minimize the error decision probability is

$$\lambda^* = \sigma_n^2 \cdot \frac{1 + \sqrt{1 + \frac{4}{N} \cdot \left(1 + \frac{2}{SNR}\right) \cdot \ln\left(\frac{(1-\Omega)}{\Omega} \cdot (1+SNR)\right)}}{(2+SNR)/(1+SNR)}, \tag{7}$$

and it can be further simplified when the sample points N is approaching to positive infinite:

$$\lambda^* \approx \frac{2\sigma_n^2 \cdot (1+SNR)}{(2+SNR)} (N \to +\infty). \tag{8}$$

Wideband Spectrum Sensing

Against narrowband techniques aforementioned, wideband spectrum sensing techniques aim to sense a frequency bandwidth that exceeds the coherence bandwidth of the channel. For example, for exploiting spectral opportunities in the whole ultrahigh frequency (UHF) TV band (between 300 MHz and 3 GHz), wideband spectrum sensing techniques should be employed. Narrowband sensing techniques cannot be directly used for performing wideband spectrum sensing, because they make a single binary decision for the whole spectrum and thus cannot identify individual spectral opportunities that lie within the wideband spectrum [3].

Wideband spectrum sensing can be broadly divided into two types: Nyquist wideband sensing and sub-Nyquist wideband sensing. Nyquist wideband sensing processes the received signals at or above the Nyquist rate, which can lead to unaffordable high sampling rate or implementation complexity. Sub-Nyquist sampling technique therefore attracts more and more attention to achieve a more flexible and faster wideband spectrum sensing, such as compressive sensing (CS) [39, 52, 53], multicoset sampling [8, 46], etc.

Nyquist Wideband Sensing

A direct approach of wideband spectrum sensing is to directly acquire the wideband signal using a standard ADC and then use the digital signal processing techniques to detect spectral opportunities. In [31], a multiband joint detection algorithm is proposed. As shown in Fig. 1, the wideband signal is directly sensed by a wideband ADC, and then it is processed by a serial-to-parallel conversion circuit to divide the sampled data into parallel data streams. Fast Fourier transform (FFT) is implemented to covert the wideband signals into frequency domain. Then the wideband spectrum is divided into series of narrowband spectrum. Finally, spectrum occupancy of each narrow band is determined by using an optimized threshold. It achieved a better detection performance than the aforementioned narrowband spectrum sensing.

In addition, a wavelet-based spectrum sensing algorithm was proposed in [38]. In this algorithm, the power spectral density (PSD) of the wideband spectrum was modeled as a train of consecutive frequency subbands, where the PSD is smooth within each subband but exhibits discontinuities and irregularities on the border of two neighboring subbands. The wavelet transform was then used to locate the singularities of the wideband PSD, and the wideband spectrum sensing was formulated as a spectral edge detection problem.

However, in the wideband regime, a major challenge arises from the stringent requirements on the high sampling rate at the ADCs to transform the received signals into digital signals by sampling at the Nyquist rate, which presents significant challenges in the high-speed sampling hardware and signal processing algorithms.

A simple approach to relax the high sampling rate requirement for wideband spectrum sensing is to use a tunable narrowband bandpass filter (BPF) at the radio-frequency (RF) front-end to scan through all of the narrow channels one by one to detect the existence or nonexistence of licensed primary transmissions [26,50]. The tuning range of each BPF needs to be preselected. The occupancy of each channel can be determined by measuring the energy of the signal at the output of each filter. However, the sequential nature of such scheme could introduce a long sensing period. Such delay in the sensing process will also cause missed opportunities or interferences to PUs.

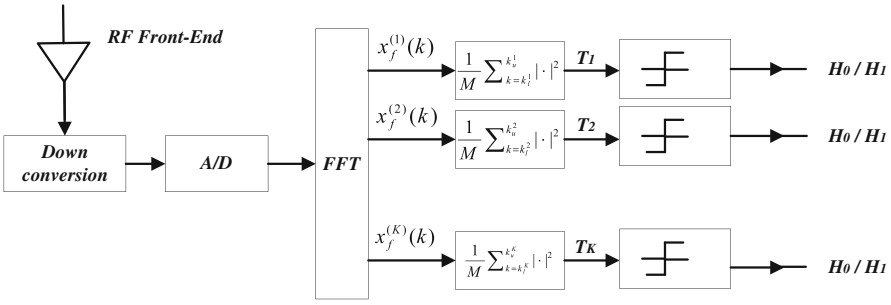

Fig. 1 Schematic illustration of multiband joint detection

Sub-Nyquist Wideband Sensing

Due to the drawbacks of high sampling rate or high implementation complexity in Nyquist systems, sub-Nyquist approaches are drawing more and more attention. Sub-Nyquist wideband spectrum sensing refers to the procedure of acquiring wideband signals using a sampling rate lower than the Nyquist rate and detecting spectral opportunities using these partial measurements. Two important types of sub-Nyquist wideband sensing are CS-based wideband sensing and multichannel sub-Nyquist wideband sensing. In the subsequent section, we give some discussions and comparisons regarding these sub-Nyquist algorithms and their applications to the wideband spectrum sensing.

Sub-Nyquist Wideband Spectrum Sensing

The well-known Nyquist sampling theory requires that sampling rate should be at least twice of the signal bandwidth. Therefore, the sampling rate is very challenging for wideband spectrum sensing. The high-speed ADC for wideband signals is difficult or expensive to implement at SUs, especially for power-limited devices. To guarantee the stable reconstruction of multiband signals, Landau [14] demonstrated that the sampling rate should be no less than the measure of the occupied part of the spectrum, which is below the corresponding Nyquist sampling rate. As the wideband spectrum of interest is normally underutilized in reality [22], the spectrum exhibits a sparse property in the frequency domain, which makes sub-Nyquist sampling possible for spectrum sensing.

Compressed Sensing

Compressed sensing (CS) is a technique that can efficiently acquire a signal using relatively few measurements, by which unique representation of the signal can be found based on the signal's sparseness in some domain. As the wideband spectrum is sparse due to its low spectrum utilization, CS becomes a promising candidate to realize wideband spectrum sensing by using sub-Nyquist sampling rates. The process of CS can be summarized as follows:

1. *Sparse representation of received signals.*
   It is assumed that bandwidth of the whole spectrum is B Hz. The received signal at an SU is given by:

$$r(t) = h(t) * s(t) + w(t), \tag{9}$$

   where $s(t) \in C^{N\times 1}$ is the transmitted signal, $h(t)$ is the channel gain between the transmitter and receiver, and $w(t) \sim \mathscr{CN}(0, \sigma_\omega^2 \mathbf{I}_N)$ refers to AWGN where σ_ω^2 refers to the noise variance and $\mathbf{I}_N$ is the identity matrix.

The received signals $r(t)$ is assumed to be sparse in the frequency domain. It can be expressed as $r_f = s_f + w_f$, where r_f, s_f, and w_f are the discrete Fourier transform (DFT) of $r(t)$, $s(t)$, and $w(t)$. As aforementioned, s_f is sparse since the spectrum is normally underutilized. This sparse property makes it possible to reduce sampling rates by implementing CS at the SU.

2. *Compressed measurement collection.*

The received compressed measurements at the SU can be expressed by:

$$x = \Phi \mathscr{F}^{-1} r_f = \Theta r_f = \Theta \left(s_f + w_f \right), \tag{10}$$

where $\Phi \in C^{P \times N}$ $(P \leq N)$ is a measurement matrix to collect the compressed measurements $x \in C^{P \times 1}$, where $P/N \leq 1$ refers to the compression ratio.

There are three conditions that should be fulfilled by the measurement matrix: (i) each column of it is normalized, (ii) each row of it has approximately equal norm, and (iii) the rows of it are orthogonal [42]. In practical settings, structured random matrices are often employed for improved implementation affordability, such as the analog-to-information converter (AIC sampler) [41]. The AIC sampler mainly contains three components: a high-rate pseudonoise sequence, a low-pass anti-aliasing filter, and a low-speed ADC. This structure alleviates the burden on the ADCs, at the expense of slightly degraded recovery performance compared with those fully random Gaussian samplers.

3. *Signal recovery.*

In order to make accurate decisions about spectrum occupancy, the signal recovery should be performed by solving the following l_1 norm minimization as:

$$\widehat{s}_f = \arg \ \min \ \left\| \widehat{s}_f \right\|_1, \ s.t. \ \left\| \theta \cdot \widehat{s}_f - x \right\|_2^2 \leq \varepsilon \tag{11}$$

where ε is an upper bound on the size of the noisy contribution.

4. *Decision making.* When the estimated signal $\hat{s}_f$ is obtained, energy detection is performed to determine the spectrum occupancy. Specifically, the energy density of each channel in the recovered signal is compared with a predefined threshold to make a decision. In practice, the noise power (σ_w^2) can be calibrated in a given channel which is known to be idle, such as channel 21 in TVWS that is supposed to be vacant currently in the UK.

If the energy of the reconstructed signal is higher than the threshold, the corresponding channel is determined as occupied, and SUs are forbidden to access it. Otherwise, the corresponding channel is determined as vacant, and SUs can access it for transmission.

In order to reduce the complexity in signal recovery and enhance the robustness to imperfect channel environments, a two-phase spectrum sensing algorithm is proposed in [30]. In the first phase, a channel division scheme is applied to reduce the computation complexity for signal recovery. In the second phase, a denoising algorithm is proposed to improve the sensing robustness against heavy channel noise.

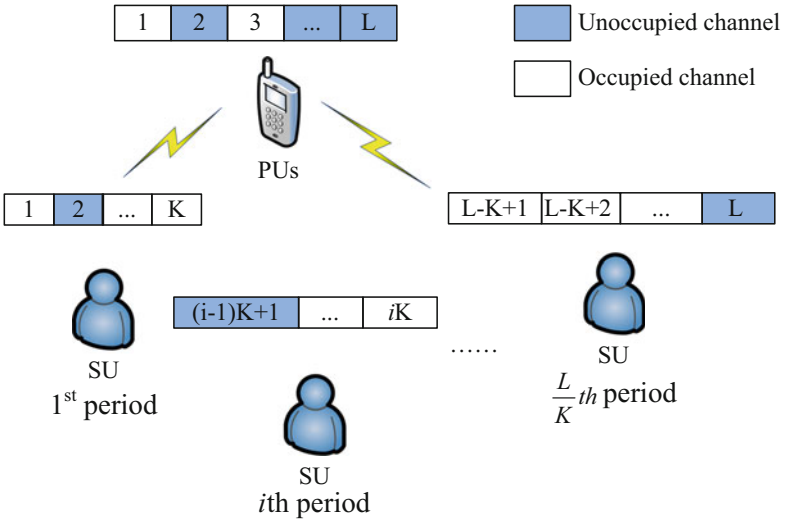

Fig. 2 Channel division scheme

1. *The efficient channel division scheme*

   In the l_1 minimization recovery process, the computational complexity is dependent on the number of samples to be recovered. Assuming that there are L channels in the spectrum of interest, a channel division scheme is proposed in which only K ($K < L$) channels are expected to be sensed in each sensing period to reduce the number of samples to be recovered. As shown in Fig. 2, each K-channel group is indexed by i $\left(i = 1, 2, \cdots, \frac{L}{K}\right)$. If any vacant channel is detected, the SU would stop sensing and start data transmission. Otherwise, it senses the next channel group in the following sensing period. As a result, the required sampling rates for exact recovery are reduced at the SU.

   Once signal for a K channel group $s_{fi} \in C^{n\times 1}$ ($n = \frac{KN}{L}$) arrives, compressed samples x_i are collected at the SU, and its original spectrum can be recovered by l_1 norm minimization as:

$$\hat{s}_{fi} = \arg \min \left\|\hat{s}_{fi}\right\|_1, \text{ s.t. } \left\|\Theta_i \cdot \hat{s}_{fi} - x_i\right\|_2^2 \leq \varepsilon_i, \tag{12}$$

   where $\Theta_i \in C^{p\times n}$, $p = \frac{KP}{L}$ and ε_i is the error tolerance in the reconstruction process.

2. *The denoised spectrum sensing algorithm*

   The recovery performance of the l_1 norm minimization is degraded by heavy channel noise and reduced number of compressed samples. Furthermore, it is noticed that the amplitudes of recovered signal $\hat{s}_{fi}$ may be negative with high absolute values. As the power spectrum s_{fi} is nonnegative, if those negative values are used to calculate the energy density, it would become higher than

its real energy value. Therefore, it will result in a higher P_f, so that the vacant channels might be determined as occupied. In order to improve the detection performance, a denoising algorithm is proposed to implement at each SU.

In the denoising algorithm, the amplitude of each frequency bin in the recovered signal $\hat{s}_{fi}$ is compared with the noise level. If the amplitude of is higher than the noise level, the compressed measurement collected $r_{fi}(b)$ is kept for the recovered signal. Otherwise, the corresponding value will be set to zero to reduce the recovery error. The denoised signal $\hat{s}_{fi\_d}$ can be expressed as:

$$\hat{s}_{fi\_d}(b) = \begin{cases} r_{fi}(b) & \text{if } \hat{s}_{fi}(b) \geq \sigma(b) \\ 0 & \text{otherwise,} \end{cases} \tag{13}$$

where b is the index of each frequency bin.

After the denoising algorithm, the energy density in the denoised signal is compared with the corresponding threshold to determine the spectrum occupancy of each considered K channel group. If any channel group is determined as vacant, it can be used by SUs to transmit the unlicensed signals. Otherwise, the SU should continue sensing the next channel group until any vacant channel is found out or the final $\frac{L}{K}$ sensing periods are run out. As there is a high probability that the spectrum vacant in last loop remains free in the current sensing loop, the SU should sense the channel group determined as free in the last sensing loop at the beginning of the new sensing loop. The whole process of the two-phase spectrum sensing algorithm based on CS is summarized as Algorithm 1.

Algorithm 1 Two-phase CS-based single node spectrum sensing scheme

Initialization:

Set threshold λ as (5);

$i = 1$.

1: **while** $i \leq \frac{L}{K}$ or $E\left(\hat{s}_{fi\_d}\right) < \lambda$ **do**

2: The SU takes measurements at sub-Nyquist rate for the i-th K-channel group to collect r_i in the i-th sensing period.

3: Perform signal recovery by l_1 algorithm as (12) to get the recovered signal $\hat{s}_{fi}$.

4: Perform denoising to $\hat{s}_{fi}$ to get $\hat{s}_{fi\_d}$.

5: Increase i by 1.

6: **end while**

Decision:

If $E\left(\hat{s}_{fi\_d}\right) < \lambda$, SU can access the i-th K-channel group. If $i = \frac{L}{K}$, a new sensing loop begins. The SU senses from the K-channel group which is vacant in last sensing loop or from the first K-channel group in the new sensing loop.

Figure 3 shows P_d for the traditional l_1 norm minimization based spectrum sensing (labeled as traditional CS-based SS) and the two-phase CS-based spectrum sensing (labeled as denoised CS-based SS) under a different number of collected measurements. The detection performance is also compared with that of spectrum

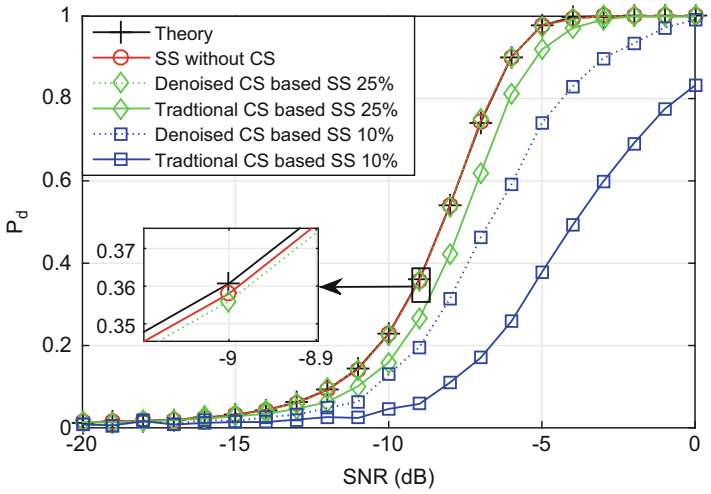

Fig. 3 Probability of detection P_d comparison with different compression ratios under different SNR values

sensing without CS implementation (labeled as SS without CS), as well as the theoretical values derived from (3). In the simulation, primary signals are orthogonal frequency-division multiplexing (OFDM) generated, which is used in Digital Video Broadcasting-Terrestrial (DVB-T) over the TVWS from 470 MHz to 790 MHz in the UK [22]. There are $L = 40$ channels in total with 8MHz for each channel. The number of channels sensed by the SU in each sensing period is set to be $K = 8$. Therefore, at most $\frac{L}{K} = 5$ sensing periods are needed for the whole spectrum of interest. The P_f is set to be 0.01. The SNR is defined as the ratio of signal power and noise power of the K channel group. The number of occupied channels is 1 among 8. Therefore, the sparsity level is set to be 12.5%.

As Fig. 3 shows, performance of the two-phase spectrum sensing based on CS is better than that of the CS-based spectrum sensing without denoising when the compression ratio is 25% and 10%. This gain benefits from the denoising algorithm to improve the signal recovery accuracy. As the recovery accuracy becomes higher with higher compression ratio, detection performance of the two-phase spectrum sensing algorithm gets closer to the theoretical curves. The simulation result shows that the two-phase spectrum sensing algorithm can reduce the sampling rates by 75% without degrading detection performance.

Multichannel Sub-Nyquist Sampling

Although the energy consumption at the CS-based wideband signal sampling part is reduced, compressive sensing requires random sub-Nyquist projections [3]. Therefore, custom ADCs with complex hardware that can perform analog mixing or

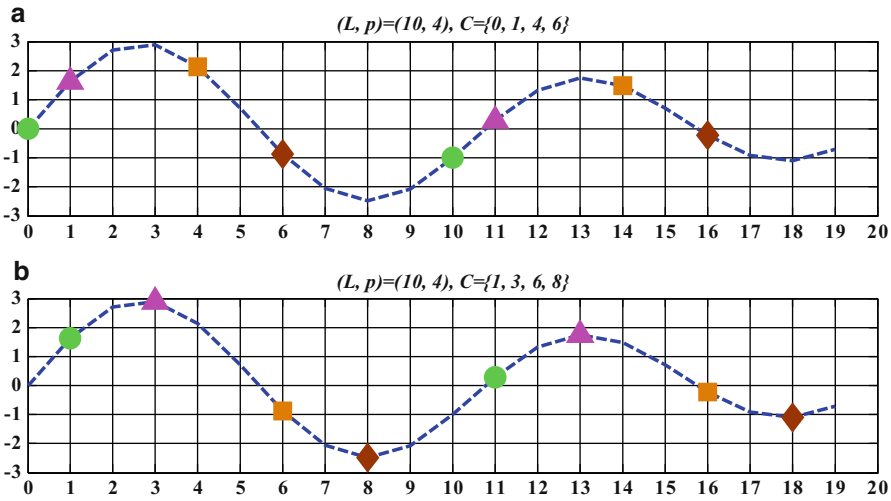

Fig. 4 Examples of two sampling patterns for $(L, p) = (10, 4)$. (**a**) $C = \{0, 1, 4, 6\}$; (**b**) $C = \{1, 3, 6, 8\}$

analog matrix multiplication at high frequency are needed in compressive wideband spectrum sensing schemes, which do not work well with low-power commodity hardware [10, 19, 41].

In [8], a wideband spectrum sensing scheme based on multicoset sampling was proposed, which is a nonuniform sub-Nyquist sampling technique and can be realized using an efficient multichannel architecture. Given the prior information on the number of channels L, multicoset sampling is first executed at each SU by taking nonuniform samples at the time instants $t = (mL + c_i)T$, where $i = 1, \ldots, p$, $p \leq L$, $m \in \mathbb{Z}$, and $1/T = f_s$ is the Nyquist sampling rate. The set $C = \{c_i\}_{i=1}^{p}$, which comprises of p distinct integers chosen from $\{0, 1, \ldots, L-1\}$, is referred as a (L, p) sampling pattern. Figure 4 presents two multicoset sampling patterns for $(L, p) = (10, 4)$.

To implement the periodic nonuniform sampling, a multicoset sampler can be realized by p parallel cosets, each of which takes uniform samples at time instants $\{mLT + c_i T\}$, $m \in \mathbb{Z}$, via a decimated sampling rate $\frac{1}{LT} = f_s/L$ with a sampling time offset of $\{c_i T\}$, $i = 1, \ldots, p$, as shown in Fig. 5.

From the practical standpoint, the nonuniform sub-Nyquist sampling can be realized by a time-interleaved ADC, in which only a subset of channels are used. In [16, 28], efficient fabrications of time-interleaved ADC implemented as a single integrated circuit are proposed. As multicoset sampler only needs fewer channels than the time-interleaved ADC ($p \leq L$), the hardware implementation would be simpler and less power-consuming. In addition, the time offsets can be realized by connecting the antenna to different ADCs using different delay lines.

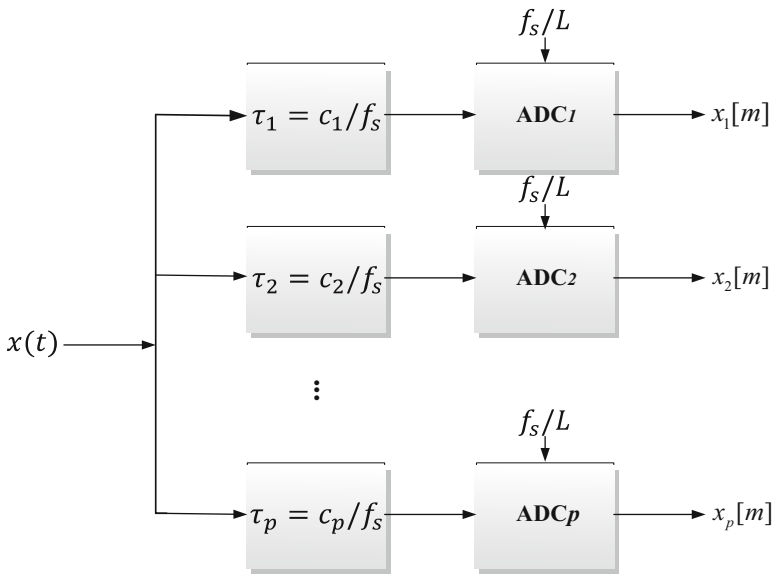

Fig. 5 The parallel implementation of the nonuniform sub-Nyquist sampling

The measurement sequence of the i-th coset is defined as

$$x_{c_i}[n] = \begin{cases} x(nT), & n = mL + c_i, m \in \mathbb{Z} \\ 0, & \text{otherwise} \end{cases} \tag{14}$$

In practice, the ADCs of the parallel cosets provide p sample sequences, given by

$$x_i[m] = x[(mL + c_i)T], \ m \in \mathbb{Z}, \ i = 1, 2, \ldots, p. \tag{15}$$

In (14), each sequence $x_{c_i}[n], \ i = 1, \ldots, p$, contains $L - 1$ zeros in between the downsampled signals. To get $x_{c_i}[n]$, each $x_i[m]$ is upsampled by a factor of L:

$$x_{u_i}[n] = \begin{cases} x_i\left[\frac{n}{L}\right], & n = mL, \ m \in \mathbb{Z} \\ 0, & \text{otherwise}, \end{cases} \tag{16}$$

and then filtered to get $x_{h_i}[n] = x_{u_i}[n] * h[n]$, where $h[n]$ is an interpolation filter with the frequency response:

$$H(f) = \begin{cases} 1, & f \in [0, B] \\ 0, & \text{otherwise}. \end{cases} \tag{17}$$

The filtered sequence is then delayed with c_i samples to obtain $x_{c_i}[n]$ as

$$x_{c_i}[n] = x_{h_i}[n - c_i]. \tag{18}$$

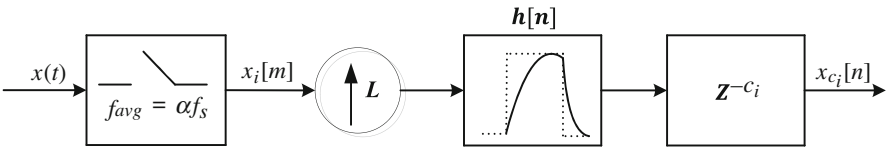

Fig. 6 Flow chart to get the multicoset sampling measurements

The whole process to obtain the compressed measurements in multicoset sampling can be implemented as shown in Fig. 6 [8].

The average sampling rate of each (L, p) multicoset sampling pattern is

$$\frac{1}{T_{\text{avg}}} = \frac{p}{LT}, \tag{19}$$

where $\alpha = p/L$ is termed as the sub-Nyquist sampling ratio. According to the Landau's theorem [14], α is lower-bounded by the maximum possible spectrum occupancy ratio. However, an average sampling rate above the Landau's rate, which equals the total bandwidth of the occupied spectrum, may not be sufficient for individual blind spectrum recovery, and the number of cosets $p \geq 2\kappa$ is needed when the band locations are unknown [18], where κ is the number of active channels occupied by PUs during the sensing period.

Applying Fourier transform to $x_{c_i}[n]$ gives the link between its spectrum $X_{c_i}(e^{j2\pi fT})$ and the unknown Fourier Transform of $x(t)$ [8]:

$$\begin{aligned} X_{c_i}(e^{j2\pi fT}) &= \textstyle\sum_{n=-\infty}^{+\infty} x_{c_i}[n] e^{-j2\pi fnT} \\ &= \tfrac{1}{LT} \textstyle\sum_{l=0}^{L-1} \underbrace{X\left(f + \dfrac{l}{LT}\right)}_{X_l(f)} e^{j\frac{2\pi}{L}c_i l} \\ &= \tfrac{1}{LT} \textstyle\sum_{l=0}^{L-1} X_l(f) e^{j\frac{2\pi}{L}c_i l} \quad \forall f \in [0, B], \end{aligned} \tag{20}$$

for every $1 \leq i \leq p$, where $X_l(f)$, $l = 0, \ldots, L-1$, corresponds to the pieces of the original spectrum $X(f)$ in the channel l, which is shifted to the left by $\frac{l}{LT}$ units such that all L channels are folded into the first narrowband $[0, B]$.

Assume that the observed signal is given by $x(t) = s(t) + n(t)$, where $s(t)$ is the primary signal and $n(t)$ is the additive white Gaussian noise with zero mean and variance σ_n^2. The corresponding Fourier transform is given by $X(f) = S(f) + N(f)$. Define $S_l(f) = S(f + \frac{l}{LT})$, $l = 0, \ldots, L-1$, and $\mathbf{S}(f) = [S_0(f), S_1(f), \ldots, S_{L-1}(f)]^T$. Similarly we define $N_l(f)$ and $\mathbf{N}(f)$. We can rewrite (20) into the matrix form as

$$\underbrace{\begin{bmatrix} X_{c_1}(e^{j2\pi fT}) \\ X_{c_2}(e^{j2\pi fT}) \\ \vdots \\ X_{c_p}(e^{j2\pi fT}) \end{bmatrix}}_{\mathbf{Y}(f)} = \underbrace{\frac{1}{LT}\begin{bmatrix} e^{\frac{j2\pi c_1 0}{L}} & e^{\frac{j2\pi c_1 1}{L}} & \cdots & e^{\frac{j2\pi c_1 (L-1)}{L}} \\ e^{\frac{j2\pi c_2 0}{L}} & e^{\frac{j2\pi c_2 1}{L}} & \cdots & e^{\frac{j2\pi c_2 (L-1)}{L}} \\ \vdots & \vdots & \vdots & \vdots \\ e^{\frac{j2\pi c_p 0}{L}} & e^{\frac{j2\pi c_2 1}{L}} & \cdots & e^{\frac{j2\pi c_p (L-1)}{L}} \end{bmatrix}}_{\mathbf{A}} \times \underbrace{\begin{bmatrix} X_0(f) \\ X_1(f) \\ \vdots \\ X_{L-1}(f) \end{bmatrix}}_{\mathbf{X}(f)} = \mathbf{A}[\mathbf{S}(f) + \mathbf{N}(f)], \quad \forall f \in [0, B], \tag{21}$$

where $\mathbf{Y}(f)$ is a matrix whose i-th row is $X_{c_i}(e^{j2\pi fT})$, $\mathbf{X}(f) = [X_0(f), X_1(f), \ldots, X_{L-1}(f)]^T$ is the unknown spectrum vectors of $x(t)$ in the L channels, and $\mathbf{A} \in \mathbb{C}^{p \times L}$ is a matrix with (i, j)-th element given by

$$\mathbf{A}_{i,j} = \frac{1}{LT} e^{j\frac{2\pi}{L}c_i(j-1)}. \tag{22}$$

As the parameter L in the adopted multicoset sampler is set according to the number of channels in the original spectrum, the support of the original spectrum $supp(\mathbf{S}(f))$ in (21) is equivalent to the active channel index set S. Thus, signal reconstruction is unnecessary and only the support of the spectrum is of interest in this wideband spectrum sensing scheme.

With multicoset samplers, each SU gets p sample sequences in a matrix from $\mathbf{Y}(f) \in \mathbb{C}^{p \times N}$, where N is the number of samples in each coset. The correlation matrix of the sampled sequence $\mathbf{Y}(f)$ is defined as

$$\mathbf{R} \triangleq \mathbb{E}[\mathbf{Y}(f)\mathbf{Y}^H(f)], \tag{23}$$

where the superscript $()^H$ denotes the Hermitian transpose. Since there is no correlation between the signal and the noise, it follows that

$$\mathbf{R} = \mathbf{A}[\mathbf{R}_s + \sigma_n^2 \mathbf{I}]\mathbf{A}^H, \tag{24}$$

where $\mathbf{R}_s \triangleq \mathbb{E}[\mathbf{S}(f)\mathbf{S}^H(f)]$ is the primary signal correlation matrix. Note that $\mathbf{A}$ is a sub-matrix of the complex conjugate of the $L \times L$ discrete Fourier transform

matrix (consisting of p rows indexed by the sampling pattern C) multiplied by a factor of $\frac{1}{LT}$. It is shown that for a larger L, the randomly selected sampling pattern C enables the matrix $\mathbf{A}$ to have almost orthogonal columns, i.e., $<a_i, a_j> = 0$ for $i \neq j$ and $<a_i, a_j> = \frac{1}{LT^2}$ for $i = j$ with a high probability [2,3]. Therefore, $\mathbf{R}$ can be derived as:

$$\mathbf{R} = \mathbf{A}\mathbf{R}_s\mathbf{A}^H + \frac{\sigma_n^2}{LT^2}\mathbf{I}. \tag{25}$$

From Parseval's identity [1, 51], the correlation matrix $\hat{\mathbf{R}}$ can be computed directly from the sampled sequence $x_{c_i}[n]$ in the time domain, where $\hat{\mathbf{R}}_{ij} = \frac{1}{N}\sum_{n=1}^{N} x_{c_i}[n]x_{c_j}^H[n]$. It is shown in [21,45] that when the number of measurement samples N is much larger than the observation dimension p, $\hat{\mathbf{R}}$ is an accurate estimator of the true correlation matrix.

As there are up to κ active channels occupied during the sensing period, i.e., $\mathbf{R}_s$ has a rank of κ and $\mathbf{A}$ is of full rank, it follows that the rank of $\mathbf{A}\mathbf{R}_s\mathbf{A}^H$ equals κ. Denoting $\lambda_1 \geq \lambda_2 \geq \ldots \geq \lambda_p$ and $\mu_1, \mu_2, \ldots, \mu_p$ as the eigenvalues and corresponding eigenvectors of $\mathbf{R}$, respectively, i.e.,

$$\mathbf{R}\mu_i = \lambda_i\mu_i,\ i = 1, \ldots, p. \tag{26}$$

We then have

$$[\mathbf{A}\mathbf{R}_s\mathbf{A}^H + \frac{\sigma_n^2}{LT^2}\mathbf{I}][\mu_1, \ldots, \mu_p] = [\mu_1, \ldots, \mu_p]\begin{bmatrix}\lambda_1 & & & 0\\ & \lambda_2 & & \\ & & \ddots & \\ 0 & & & \lambda_p,\end{bmatrix}, \tag{27}$$

i.e.,

$$\begin{aligned}&[\mathbf{A}\mathbf{R}_s\mathbf{A}^H][\mu_1, \ldots, \mu_p]\\ &\quad = [\mu_1, \ldots, \mu_p]\begin{bmatrix}\lambda_1 - \frac{\sigma_n^2}{LT^2} & & & 0\\ & \lambda_2 - \frac{\sigma_n^2}{LT^2} & & \\ & & \ddots & \\ 0 & & & \lambda_p - \frac{\sigma_n^2}{LT^2},\end{bmatrix}.\end{aligned} \tag{28}$$

Since $\mathbf{A}\mathbf{R}_s\mathbf{A}^H$ has a rank of κ, there must be $p - \kappa\lambda_i$'s equal to $\frac{\sigma_n^2}{LT^2}$. As $\mathbf{A}\mathbf{R}_s\mathbf{A}^H$ is positive semidefinite, the λ_i's with values equal to $\frac{\sigma_n^2}{LT^2}$ must be the smallest ones of λ_i's. Therefore, we have

$$\lambda_{\kappa+1} = \lambda_{\kappa+2} = \ldots = \lambda_p = \frac{\sigma_n^2}{LT^2}. \tag{29}$$

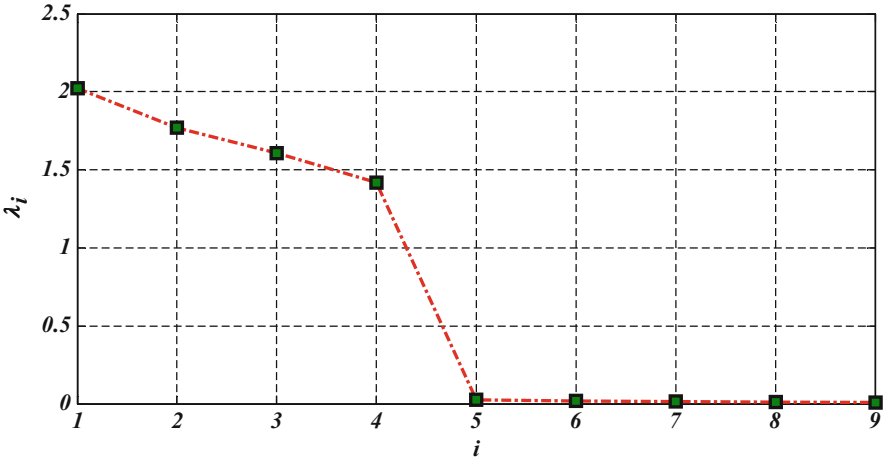

Fig. 7 Eigenvalues of the sample correlation matrix ordered in decreasing order with $p = 9$, $\kappa = 4$

As $N \to \infty$, it follows that except for the κ largest, the eigenvalues of $\mathbf{R}$ are related to the noise variance σ_n^2, as shown in Fig. 7.

Thus $\mathbf{R}$ can be decomposed via the rank-revealing eigenvalue decomposition (RREVD) as

$$\mathbf{R} = \mathbf{U}\boldsymbol{\Lambda}\mathbf{U}^H = \mathbf{U}_s\boldsymbol{\Lambda}_s\mathbf{U}_s^H + \frac{\sigma_n^2}{LT^2}\mathbf{U}_n\mathbf{U}_n^H, \tag{30}$$

where $\mathbf{U} = [\mathbf{U}_s, \mathbf{U}_n]$, $\boldsymbol{\Lambda}_s = \text{diag}\{\lambda_1, \ldots, \lambda_\kappa\}$ contains the κ non-increasing principal eigenvalues and $\mathbf{U}_s$ contains the corresponding eigenvectors, while $\mathbf{U}_n$ contains the corresponding eigenvectors associated with the smallest $p - \kappa$ eigenvalues $\frac{\sigma_n^2}{LT^2}$. As the noise term only perturbs the eigenvalues, the range of $\mathbf{R}$, spanned by $\mathbf{U}_s$, coincides with the signal subspace spanned by $\mathbf{AS}(f)$, and its orthogonal complement spanned by $\mathbf{U}_n$ is the noise subspace. Therefore, we choose the κ largest eigenvalues $\boldsymbol{\Lambda}_s$ and the corresponding eigenvectors $\mathbf{U}_s$ to construct the measurement matrix as $\boldsymbol{\chi}_s = \mathbf{U}_s\sqrt{\boldsymbol{\Lambda}_s}$; so we can define the following linear system

$$\boldsymbol{\chi}_s = \mathbf{A}\boldsymbol{v}_s, \tag{31}$$

where the support of the sparest solution to (31) converges to the original primary signal, i.e., $supp(\boldsymbol{v}_s) = supp(\mathbf{S}(f))$. Moreover, using $\boldsymbol{\chi}_s \in \mathbb{C}^{p\times\kappa}$ for support recovery instead of $\mathbf{Y}(f) \in \mathbb{C}^{p\times N}$ reduces the transmission overhead and enhances the computational efficiency.

The separation between the signal and noise eigenvalues needs a threshold. Depending on the noise variance and the number of samples, the threshold could vary. To avoid the tricky threshold setting, some information theoretic criteria for

Algorithm 2 Joint sparse recovery in SA-SOMP

Initialization: $\mathbf{R} \in \mathbb{C}^{p\times p}$, $\hat{\kappa}$, $\mathbf{A} = [\mathbf{a}_1, \ldots, \mathbf{a}_L] \in \mathbb{C}^{p\times L}$
Decision: S
1: $[\mathbf{U}_s, \boldsymbol{\Lambda}_s] \leftarrow \text{RREVD}(\mathbf{R}, \hat{\kappa})$, $\boldsymbol{\chi}_s = \mathbf{U}_s\sqrt{\boldsymbol{\Lambda}_s}$
2: $t = 0$, $\mathbf{R}_0 = \boldsymbol{\chi}_s$, $\boldsymbol{\nu}_0 = \varnothing$, $S = \varnothing$
3: **while** $t \le \hat{\kappa}$ **do**
4: $t \leftarrow t + 1$
5: $l_t = \arg\max_l \parallel \mathbf{a}_l^{\mathbf{H}}\mathbf{R}_{t-1} \parallel_2, l \in 1, \ldots, L$
6: $S \leftarrow S \cup l_t$, $\boldsymbol{\nu}_t = \mathbf{A}_S^{\dagger}\boldsymbol{\chi}_s$
7: $\mathbf{R}_t \leftarrow \boldsymbol{\chi}_s - \mathbf{A}_S\boldsymbol{\nu}_t$
8: **end while**
9: **return** S=S-1

the model order selection, such as exponential fitting test (EFT), can be applied for the estimation of the signal support dimension $\hat{\kappa}$ [32].

As only κ active channels are assumed to be occupied by primary transmissions, $\boldsymbol{\nu}_s$ can be approximated to be jointly κ-sparse as it contains no more than κ significant rows. Reconstruction of the unknown matrix $\boldsymbol{\nu}_s$ with jointly sparse columns in (31) is referred to as the joint sparse problem, which aims to estimate the support of $\boldsymbol{\nu}_s$ from the measurement matrix $\boldsymbol{\chi}_s$. Some existing greedy algorithms for the sparse recovery problem could be extended to this joint sparse problem, such as SOMP [40]. To improve the detection robustness against noise interference and reduce the computation complexity, SOMP is applied to the constructed low-dimensional measurement matrix $\boldsymbol{\chi}_s$, denoted as subspace-augmented SOMP (SA-SOMP). The detailed procedure of the joint sparse recovery in the individual wideband spectrum sensing is summarized in Algorithm 2.

As sub-Nyquist measurements are quite vulnerable to channel degradations, cooperation among multiple SUs is necessary in sub-Nyquist wideband sensing. Assume that there are J coexisting SUs within the local region that cooperatively sense the wideband to locate the active channel set S. The received signals at the SUs are from the same primary transmissions but affected differently by fading and shadowing from the common PU transmitter to each SU. Thus all SUs share a common sparse support with different amplitudes.

The cooperative spectrum sensing based on the multicoset sampling scheme can be formulated into a three-step framework:

1. Each SU implements a multicoset sampler that independently samples the signal with a different sampling pattern $C^{(j)}$ from the others, e.g., randomly chosen to allow for more sampling diversity.
2. Measurement matrix $\boldsymbol{\chi}_s^{(j)}$ is constructed at each SU from its sub-Nyquist samples based on subspace decomposition. Then the local matrix $\boldsymbol{\chi}_s^{(j)}$ with the sampling pattern $C^{(j)}$ is transmitted to the fusion center.
3. The fusion center locates the active channels by jointly fusing measurements shared among the SUs to reach a global sensing decision with enhanced accuracy.

Based on the measurement matrix $\boldsymbol{\chi}_s^{(j)}$ and the sampling pattern $C^{(j)}$ sent from each SU, the fusion center computes the corresponding reconstruction matrix $\mathbf{A}^{(j)}$ and then locates the active channels by exploiting the common signal support shared by $\boldsymbol{v}_s^{(j)}$, $j = 1, \cdots, J$, across all SUs. At each SU, the following relationship holds:

$$\boldsymbol{\chi}_s^{(j)} = \mathbf{A}^{(j)} \boldsymbol{v}_s^{(j)}, \ 1 \leq j \leq J. \tag{32}$$

Exploiting the common sparse support shared by the J SUs, the fusion center fuses measurements sent from all SUs to locate the original active channels. Grouping the rows of $\boldsymbol{v}_s^{(j)}$, $j = 1, \ldots, J$, with the same indices, forms the matrix $\boldsymbol{\zeta}_s$ as

$$\boldsymbol{\zeta}_s = \left[\underbrace{\boldsymbol{v}_s^{(1)}[1]^T \cdots \boldsymbol{v}_s^{(J)}[1]^T}_{\boldsymbol{v}_s[1]^T} \cdots \underbrace{\boldsymbol{v}_s^{(1)}[L]^T \cdots \boldsymbol{v}_s^{(J)}[L]^T}_{\boldsymbol{v}_s[L]^T} \right]^T, \tag{33}$$

where $\boldsymbol{v}_s^{(j)}[i]$ denotes the i-th row of $\boldsymbol{v}_s^{(j)}$ at the j-th SU. Furthermore, $\boldsymbol{\zeta}_s$ can be partitioned as a concatenation of blocks $\boldsymbol{v}_s[l]^T$, $l = 1, \ldots, L$, and the block size is equal to the number of SUs J. As there are at most κ channels occupied, $\boldsymbol{\zeta}_s$ can be modeled as a block κ-sparse matrix. Thus, in each iteration, the block index that accounts for the largest residual norm among all SUs is selected, i.e.,

$$l_t = \arg\max_{l} \sum_{j=1}^{J} \parallel \mathbf{a}_l^{(j)\mathbf{H}} \mathbf{R}_{t-1}^{(j)} \parallel_2, \ l \in 1, \ldots, L, \tag{34}$$

where $\mathbf{R}_{t-1}^{(j)}$ is the residue at the $(t-1)$-th iteration at the j-th SU, $\mathbf{a}_l^{(j)}$ is the l-th column in $\mathbf{A}^{(j)}$, and l_t is the selected index. The detailed algorithm for the joint support recovery at the fusion center is described in Algorithm 3, where each SU implements EFT to estimate the signal sparsity $\hat{\kappa}^{(j)}$, and then the fusion center takes the average $\hat{\kappa}$, i.e.,

$$\hat{\kappa} = \frac{1}{J} \sum_{j=1}^{J} \hat{\kappa}^{(j)}, \tag{35}$$

for the number of iterations at the joint support recovery in Algorithm 3.

Based on the measurements shared among the SUs, the detection performance is improved in low SNR regimes. Moreover, thanks to the measurement diversity across multiple SUs given the different sampling patterns, the fusion center could obtain an accurate estimate of the occupied channel locations at the sampling rate approaching the Landau's rate as the number of SUs increases [17]. This is due to the fact that the sub-coherence within the block,

$$\mu = \max_{1 \leq l \leq L} \ (\max_{1 \leq i \neq j \leq J} ||a_l^{(i)H} a_l^{(j)}||), \tag{36}$$

Algorithm 3 Measurement fusion in the proposed centralized cooperative spectrum sensing scheme

Initialization: $\boldsymbol{\chi}_s^{(j)} \in \mathbb{C}^{p\times\hat{\kappa}^{(j)}}, \hat{\kappa}^{(j)}, \mathbf{A}^{(j)} = [\mathbf{a}_1^{(j)}, \ldots, \mathbf{a}_L^{(j)}] \in \mathbb{C}^{p\times L}$
Decision: S
1: $\hat{\kappa} = \frac{1}{J}\sum_{j=1}^{J}\hat{\kappa}^{(j)}$
2: $t = 0, \mathbf{R}_0^{(j)} = \boldsymbol{\chi}_s^{(j)}, \boldsymbol{\nu}_0^{(j)} = \varnothing, S = \varnothing$
3: **while** $t \leq \hat{\kappa}$ **do**
4: $t \leftarrow t + 1$
5: $l_t = \arg\max_{l} \sum_{j=1}^{J} \parallel \mathbf{a}_l^{(j)\mathbf{H}}\mathbf{R}_{t-1}^{(j)} \parallel_2,\ l \in 1, \ldots, L$
6: $S \leftarrow S \cup l_t, \boldsymbol{\nu}_t^{(j)} = \mathbf{A}_S^{(j)\dagger}\boldsymbol{\chi}_s^{(j)}$
7: $\mathbf{R}_t^{(j)} \leftarrow \boldsymbol{\chi}_s^{(j)} - \mathbf{A}_S^{(j)}\boldsymbol{\nu}_t^{(j)}$
8: **end while**
9: **return** $S = S - 1$

is substantially smaller than the conventional coherence in the equivalent reconstruction matrix $\mathbf{A}$ [5]. Reconstruction of the block sparse signal in the cooperative sensing scheme therefore can be guaranteed with an eased requirement comparing to the reconstruction in the individual scheme. Therefore, a small number of cosets p proportional to the signal sparsity κ is sufficient for cooperative spectrum sensing. The computation complexity of support recovery at the fusion center could be expressed as $O(\kappa^3 LJ)$.

Geo-Location and Its Hybrid

As reported by the Federal Communications Commission (FCC) and the Ofcom in the UK, a large percentage of spectrum resources are underutilized [22]. It is noticed that spectrum used to be allocated to analog TV signals has been cleaned and opened to access due to the digital-switchover. To implement cognitive radio in TVWS successfully, there are mainly two goals to be achieved: (1) to protect incumbent licensed users from harmful interference and (2) to utilize the available spectrum efficiently [20].

In order to avoid any harmful interference to primary services, SUs, also named as white space devices (WSDs), should have the knowledge of spectrum occupancy. Two approaches have been proposed to make SUs aware of the spectrum occupancy. One is geo-location database which is a centralized database to store the maximum allowable EIRP for each vacant TVWS channel. So far, several geo-location database providers such as Google, Nominet, Spectrum Bridge, etc. have been approved by Ofcom in UK [24]. The geo-location database calculates the interference generated in wireless communication systems through theoretical propagation models rather than actual measurements, which may result in inaccurate results for spectrum occupancy [25]. Furthermore, the real-time events and dynamic changes of the propagation environment pose significant challenges to the database approach, as it can only protect the registered users. Some PMSE users, such as the

wireless microphone, operate mostly on an unlicensed basis, without any record in the database [23]. The other is spectrum sensing, which provides instant channel occupancy information but may cause interference to some reserved channels as they would be determined as vacant by sensing alone and hence utilized by SUs for unlicensed transmission. To relax the sensing requirements on the WSDs, hybrid framework that combines the advantages of both geo-location database and spectrum sensing is explored.

Geo-Location Database Model

For geo-location databases, a power control model is used to calculate the maximum permitted EIRP [49]. It makes use of a two-ray path loss model to measure the power attenuation. However, there are two main problems for this model. Firstly, the DTT receivers cannot be located precisely which leads that the path loss cannot be calculated by the exact distance between SUs and DTT receivers. All known information is the number of households located within a 100×100 m pixel [43]. Secondly, different environmental scenarios, which would lead to different tolerance levels for DTT receivers, are not considered in the power control model. For example, the power attenuation in urban areas is much higher than that of open areas. As a result, the maximum allowable EIRP of a specific SU in open areas is higher than that in urban areas.

To solve these problems, the concept of location uncertainty is introduced in the location probability model, which classifies the location relationship between SUs and DTT receivers into four different scenarios. In addition, transmission environment can be classified as open, suburban, and urban areas. Power attenuation is measured by coupling gain that depends both on location relationship and transmission environment. Figure 8 shows the location probability model for the geo-location database. It is assumed that a DTT reception is located on the edge

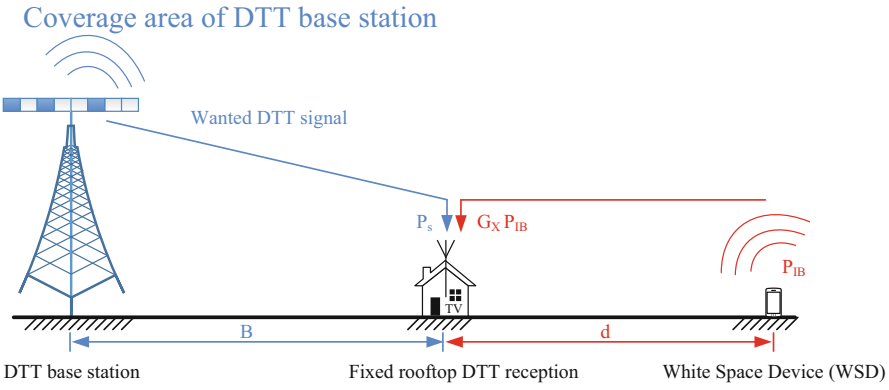

Fig. 8 DTT location probability model

area of a DTT base station, which receives the lowest wanted power from the DTT base station. The average received power of wanted DTT signal is labeled as P_s, and R is the coverage radius of the DTT base station and d is distance between the DTT receiver and the mobile WSD, which can be obtained from the DTT transmitter's database available at [44]. A mobile WSD radiates an inbound EIRP P_{IB} with a power attenuation factor coupling gain (G), which is dependent on the different areas.

DTT location probability is defined as the probability with which a DTT receiver could operate accurately at a specific location, i.e., the probability with which the average received wanted signal level is appropriately greater than a minimum required value. DTT location probability is used to limit the maximum allowable EIRP and it can be expressed in linear domain as follows [43]:

$$q_1 = \Pr\left\{ P_s \geq P_{s,\min} + \sum\nolimits_{k=1}^{K} r_{U,k} P_{U,k} \right\}, \tag{37}$$

$$q_2 = \Pr\left\{ P_s \geq P_{s,\min} + \sum\nolimits_{k=1}^{K} r_{U,k} P_{U,k} + r\left(\Delta f, m_s\right) G P_{IB} \right\}, \tag{38}$$

where $P_{s(dBm)}$ is modeled as a Gaussian random variable with median m_s and standard deviation σ_s, and $P_{s,\min}$ is DTT receiver's reference sensitivity level. The parameter $P_{U,k}$ refers to received power of the k-th unwanted DTT signals, and $r_{U,k}$ is the protection ratio of the received wanted DTT power and received k-th unwanted DTT power at the point where DTT receiver fails. $\Delta f = f_{\mathrm{WSD}} - f_{\mathrm{DTT}}$, where f_{WSD} is the frequency in which a WSD device operates and f_{DTT} is the DTT carrier frequency. The mean value of received power of wanted DTT signal P_s is labeled as m_s. The DTT receiver's location probability in the absence of interference from WSDs is labeled as q_1, and q_2 is the DTT receiver's location probability when considering the additional WSDs' interference. When the interference from WSDs is considered, it results in a reduction in location probability $\Delta q = q_1 - q_2$. To identify the maximum allowable EIRP P_{IB} in (38), Δq is maximized by assigning a maximal allowed value Δq_T to Δq.

We can express (37) in decibel domain as follows [34]:

$$\begin{aligned} q_1 &= \Pr\left\{ P_s \geq P_{s,\min} + \sum\nolimits_{k=1}^{K} r_{U,k} P_{U,k} \right\} \\ &= \Pr\left\{ P_s \geq P_{s,\min} + V \right\} \\ &= \Pr\left\{ 1 \geq \frac{P_{s,\min}}{P_s} + \frac{V}{P_s} \right\} \\ &= \Pr\left\{ 1 \geq A + B \right\} \\ &= \Pr\left\{ 1 \geq X \right\} \end{aligned}, \tag{39}$$

where $V_{(dBm)}$ is modeled as a Gaussian random variable with median m_V and standard deviation σ_V. Furthermore, $A_{(dB)}$ and $B_{(dB)}$ can be modeled as Gaussian random variables. In addition, $X_{(dB)}$ can be modeled as a Gaussian random

variable with median m_X and standard deviation σ_X. As a result, (39) can be given by:

$$q_1 = \Pr\left\{0 \geq X_{(dB)}\right\} = \frac{1}{2}\text{erfc}\left(\frac{m_X}{\sqrt{2}\sigma_X}\right). \tag{40}$$

Similarly, q_2 can be expressed in decibel domain as follows:

$$\begin{aligned} q_2 &= \Pr\left\{P_s \geq P_{s,\min} + \sum_{k=1}^{K} r_{U,k} P_{U,k} + r\left(\Delta f, m_s\right) G P_{IB}\right\} \\ &= \Pr\left\{P_s \geq P_{s,\min} + V + r\left(\Delta f, m_s\right) G P_{IB}\right\} \\ &= \Pr\left\{1 \geq \frac{P_{s,\min}}{P_s} + \frac{V + r(\Delta f, m_s) G P_{IB}}{P_s}\right\} \\ &= \Pr\left\{1 \geq A + \frac{V+C}{P_s}\right\} \\ &= \Pr\left\{1 \geq A + \frac{D}{P_s}\right\} \\ &= \Pr\{1 \geq A + E\} \\ &= \Pr\{1 \geq Y\} \end{aligned}, \tag{41}$$

where $C_{(dBm)}$ is a Gaussian random variable. V and C are two uncorrelated log-normal random variables, $D_{(dBm)}$ can be modeled as a Gaussian random variable with median m_D and standard deviation σ_D. Furthermore, as D and P_S are both log-normal random variables, $E_{(dB)}$ is also Gaussian variable with $m_E = m_D - m_S$ and $\sigma_E = \sqrt{\sigma_D^2 + \sigma_S^2}$. Eventually, as A and E are both log-normal random variables, $Y_{(dB)}$ can be modeled as a Gaussian random variable with mean m_Y and standard deviation σ_Y.Furthermore, (41) can be expressed as:

$$q_2 = \Pr\left\{0 \geq Y_{(dB)}\right\} = \frac{1}{2}\text{erfc}\left(\frac{m_Y}{\sqrt{2}\sigma_Y}\right). \tag{42}$$

Once q_2 is obtained, the corresponding P_{IB} can be calculated for each channel to indicate the maximum allowable EIRP as the output of the geo-location database.

Hybrid Framework with Spectrum Sensing and Geo-Location Database

Geo-location database can only protect registered channel users, while some of the PUs may not be registered, which may pose significant challenges to a geo-location database. For example, PMSE devices operate mostly on an unlicensed basis, without any record in TVWS [33]. Therefore, the approach to protect unregistered applications such as wireless microphone is through spectrum sensing. Spectrum sensing requires SUs to have the capability to detect spectrum holes that are not occupied by PUs. However, it may cause interference to some reserved channels as they would be determined as vacant by sensing alone.

As the geo-location database will not be updated instantly when the PUs temporally stop or begin the data transmission, conventional geo-location database cannot make a full utilization of vacant channels and prevent interference to the incumbent users concurrently. To reduce the risk of interference caused by the unregistered PMSE and improve the spectrum efficiency, Wang et al. proposed a hybrid framework incorporating the advantages of both geo-location database and spectrum sensing, where different spectrum sensing modules will be performed when the channel state is initially determined by the geo-location database [47], as illustrated in Fig. 9. WSDs classifies the vacant and occupied channels by referring to the geo-location database which contains the information of registered licensed users. If the channel is vacant on the geo-location database, PMSE sensing module will be applied such that if unregistered PMSE users appear on the vacant channel, instant sensing will provide a good protection to these users. While if geo-location database presents that the channel is occupied, the assistance of the DTT sensing module shown in the left dotted square circle of Fig. 9 helps the SUs to use the bands in which PUs temporally pause the data transmission.

Considering the appearance of unregistered PMSE users with probability 0.1, Fig. 10 shows the spectral efficiency of SUs against different SNRs for the geo-location database alone, hybrid database-augmented sensing with fixed (5) or adaptive threshold (7), and sensing only algorithm. Both fixed and adaptive database-augmented sensing algorithms' spectral efficiency outperform that of the

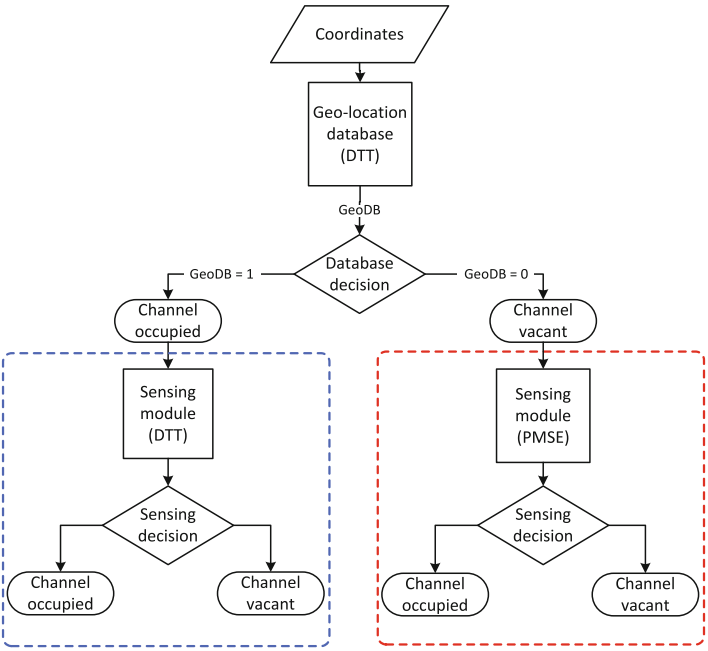

Fig. 9 The framework of the database-augmented spectrum sensing algorithm in [47]

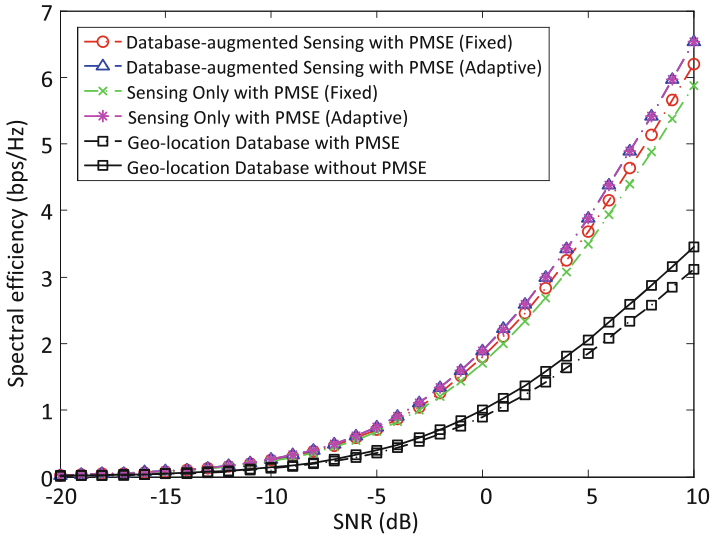

Fig. 10 Spectral efficiency for geo-location database, the database-augmented sensing with fixed and adaptive threshold

geo-location database alone approach about 1.83 bps/Hz at SNR $= 5$ dB. This is because of the increased number of paused transmission bands. The database-augmented sensing algorithm incorporated with the adaptive sensing algorithm has a better spectral efficiency than that of the fixed threshold, especially with the increasing SNRs. This is due to the lower P_f obtained by the adaptive sensing approach compared to that of the fixed one. Generally, it seems the sensing only algorithm could have almost the same spectral efficiency with that of the database-augmented sensing one. However, due to the reduced number of sensing bands, the database-augmented sensing algorithm relaxes the computation complexity required for the secondary device.

However, the hybrid framework requires the WSDs to set up a direct link to the remote geo-location database, which will require an initial wired or wireless link available at the WSD in order to report its location to the central database and retrieve the related channel state information from database. Moreover, the sensing module is based on the sequential manner to scan through the multiple channels one by one, which could introduce a long sensing period and thus cause missed opportunities or interferences to PUs.

In order to reduce the necessary sampling rate, the network load, and the inevitable transmission errors between geo-location database and SUs, a hybrid framework combining geo-location database and compressive spectrum sensing is proposed in [29], called as data-assisted non-iterative reweighted least square (DNRLS)-based compressive wideband sensing, where the maximum permitted EIRP P_{IB} of each channel obtained from geo-location database is utilized as the prior information for compressive spectrum sensing. In addition, in order to further

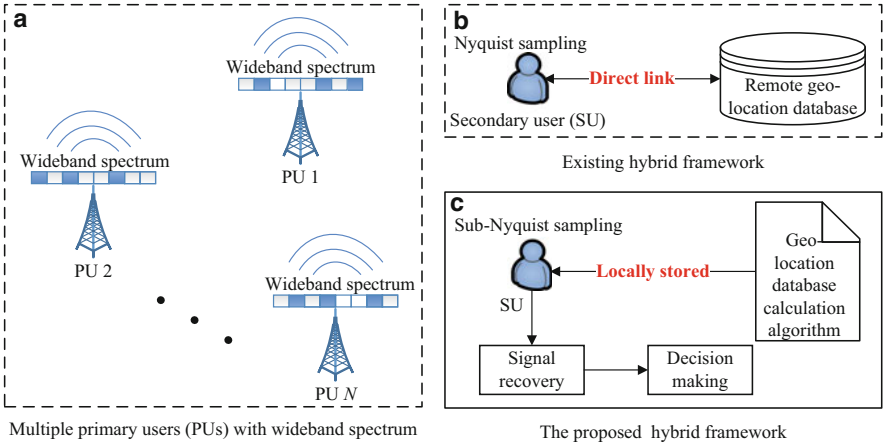

Fig. 11 (**a**) Scenario of wideband spectrum sensing with multiple primary users; (**b**) the existing hybrid framework with a direct link to remote database and conventional spectrum sensing at Nyquist rate; and (**c**) the hybrid framework with the locally stored geo-location database calculation algorithm and the data-assisted non-iterative reweighted least square (DNRLS)-based compressive spectrum sensing at sub-Nyquist rate [29]

relax the SU, a Wilkinson's method [6]-based DTT location probability is proposed to calculate the maximum permitted EIRP P_{IB} of each channel locally at the SU. The whole procedure of the proposed standalone hybrid framework is shown in Fig. 11c.

In order to rectify a key difference between l_0 and l_1 minimization and balance the penalty on large coefficients and smaller coefficients of the sparse signal, Candes et al. [19] proposed an iteratively reweighted l_1 minimization algorithm by introducing weight for each bin of the signal to be recovered. Another approach to recover a sparse signal with fewer measurements is to replace the l_1 norm with l_P norm. In order to solve the l_p norm problem, an iteratively reweighted least squares (IRLS) algorithm was proposed to perform sparse signal reconstruction [22–24,47–49]. The optimization problem can be formulated in Lagrangian form as follows:

$$\min \quad \left\| \Theta \cdot h_f \hat{s}_f - x \right\|_2^2 + \lambda W \cdot \hat{s}_f^2, \tag{43}$$

where W is a diagonal matrix $W = diag\{w_1, \ldots, w_n, \ldots, w_N\}$, which is updated in each iteration. In the l-th $(l = 0, 1, \ldots, L)$ iteration of IRLS algorithm, the weights are calculated with the recovered signal $\hat{s}_{f\_n}^{(l-1)}$ in the $(l-1)$-th iteration as:

$$w_n^{(l)} = \left(\left(\hat{s}_{f\_n}^{(l-1)} \right)^2 + \varepsilon^{(l)} \right)^{1-\frac{p}{2}}, \tag{44}$$

where $\varepsilon^{(l)}$ is updated in each iteration, and it is a positive value to make sure that a zero-valued component in $\bar{s}_f$ does not strictly prohibit a nonzero estimate in the next iteration of weights update. In addition, the solution of (43) at the l-th iteration can be expressed as:

$$\begin{aligned}\hat{s}_{f\_n}^{(l)} &= \arg\ \min\ \left\|\Theta \cdot h_f \hat{s}_f - x\right\|_2^2 + \lambda W^{(l)} \cdot \hat{s}_f^2 \\ &= W^{(l)}\Theta^{\mathrm{T}}\left(h_f \Theta W^{(l)}\Theta^{\mathrm{T}} + \lambda \mathbf{I}_P\right)^{-1} x,\end{aligned} \tag{45}$$

where the initial value for the weights w_n in W is 1, and then $W^{(0)} = \mathbf{I}_N$. As a result, $\hat{s}_{f\_n}^{(0)} = \Theta^{\mathrm{T}}\left(h_f + \lambda \mathbf{I}_P\right)^{-1} x$. It is noticed that (43) is a nonconvex optimization problem when $p < 1$. As a result, the solution to (43) is a local minima. It is proved in [4] that the computed local minimizers of (43) are actually global minimizer when solved by IRLS.

In the traditional IRLS-based compressive spectrum sensing, it is noticed that the key challenge is to find the optimal set of weights W in an iterative process for a better estimate of the original signal. The iteration process generates more computational complexities during signal recovery process. When part of the allowable maximum EIRPs is available in advance, the iterative process can be removed without degrading the recovery performance. The geo-location database calculation algorithm is implemented at SUs locally to provide data for weights calculation in a non-iterative method so that SUs would not need any additional link to a centralized geo-location database. The weights are calculated as:

$$w_n = \frac{1}{|\overline{\gamma_n}| + \varepsilon}, \tag{46}$$

where $\bar{\gamma}_n$ is constructed by the channel history information which would be introduced in details in the following part.

In the $(t+1)$-th sensing period, the geo-location database calculates the maximum allowable EIRP $P_{IB}(t+1)$ for current period before performing spectrum sensing by the Wilkinson's method-based DTT location probability model. It is mapped to $\gamma(t+1)$. Furthermore, the averaged $\bar{\gamma}(t+1)$ is calculated as:

$$\bar{\gamma}(t+1) = (\bar{\gamma}(t) + \gamma(t+1))/2, \tag{47}$$

where $\bar{\gamma}(t)$ is the average values to construct the weights at the t-th sensing period, $t = \{0, 1, \ldots, T\}$, and T is the window size for SUs to fuse the current allowable maximum P_{IB} with the history data. At an SU, only the $\bar{\gamma}(t)$ is stored locally after the t-th sensing period. If there is any new unregistered user showing up in the spectrum of interest in t-th period, the DTT transmitter database, which is used to calculate P_{IB}, is updated locally. This rule makes the weights calculation robust to the new unregistered users. Meanwhile, the DTT transmitter database at other SUs would not be influenced. In the $(t+1)$-th period, the $\gamma(t+1)$ provided

by the local geo-location database would be updated accordingly by considering the unregistered users. After $\bar{\gamma}(t+1)$ for the current sensing period obtained to calculate the weights, a better spectrum estimation can be obtained by solving the following non-iterative problem:

$$\begin{aligned}\hat{s}_f &= \arg \min \left\|\Theta \cdot h_f \hat{s}_f - x\right\|_2^2 + \lambda \tilde{W} \cdot \hat{s}_f^2 \\ &= \tilde{W}\Theta^{\mathrm{T}}\left(h_f \hat{s}_f \tilde{W}\Theta^{\mathrm{T}} + \lambda \mathrm{I}_P\right)^{-1} x,\end{aligned} \tag{48}$$

where $\tilde{W} = diag(w_1, \ldots, w_n, \ldots, w_N)$ is a diagonal matrix in which w_n is calculated by (46) to replace the iterative update of (44). In the DNRLS-based compressive spectrum sensing algorithm, the accuracy of $\bar{\gamma}$ would influence the recovery performance.

If there is no unregistered user in the spectrum of interest, which means the values of γ used to construct the weights are accurate, the recovery performance of DNRLS is very good. When unregistered users show up in the spectrum of interest at the first period, the $\bar{\gamma}(1)$ is not accurate on all the bins of the signal to be recovered as $\gamma(1)$ is not accurate. As a result, the detection performance would be degraded correspondingly. In the $(t+1)$-th period after the unregistered user shows up in the spectrum of interest, $\gamma(t+1)$ provided by the local geo-location database is updated corresponding to the decision in t-th period. The accuracy of weights would depend on the window size T for the weights fusion at SUs. The weights fusion process is shown as follows when unregistered users show up in the spectrum of interest:

$$\begin{aligned}\bar{\gamma}(1) &= \frac{\bar{\gamma}(0)+\gamma(1)}{2}, \text{(1st period)} \\ \bar{\gamma}(2) &= \frac{\bar{\gamma}(1)+\gamma(2)}{2}, \text{(2nd period)} \\ &\vdots \\ \bar{\gamma}(t) &= \frac{\bar{\gamma}(T-1)+\gamma(t)}{2}, \text{(Tth period)}\end{aligned} \tag{49}$$

where $\bar{\gamma}(0)$ is the history average value for weights construction before unregistered user showing up, and $\gamma(1)$ is the data obtained from the geo-location database in current period. As $\gamma(2) = \cdots = \gamma(t) = \gamma$, which is the data from local geo-location database after the unregistered users show up, $\bar{\gamma}(t)$ can be expressed as:

$$\begin{aligned}\bar{\gamma}(t) &= \frac{\bar{\gamma}(0)}{2^T} + \frac{\gamma(1)}{2^T} + \frac{\frac{1}{2} \times \left(1 - \left(\frac{1}{2}\right)^{T-1}\right) \times \gamma}{1 - \frac{1}{2}} \\ &= \frac{\bar{\gamma}(0)}{2^T} + \frac{\gamma(1)}{2^T} + \left(1 - \left(\frac{1}{2}\right)^{T-1}\right) \times \gamma.\end{aligned} \tag{50}$$

Algorithm 4 Data-assisted non-iterative reweighted least square-based compressive spectrum sensing

1: Input: $p, \lambda, \Theta, x, \varepsilon, \bar{\gamma}(t)$.
2: Calculate $P_{IB}(t+1)$ by the Wilkinson's method.
3: Map $P_{IB}(t+1)$ to $\gamma(t+1)$.
4: Calculate $\bar{\gamma}(t+1)$ by (47).
5: Perform signal recovery by (48) to get $\hat{s}_f$.
6: Make decision on spectrum occupancy by compare $\hat{s}_f$ with the threshold λ defined in (5).

It is noticed that $\bar{\gamma}(t)$ would converge fast to γ after unregistered users show up in the spectrum of interest. In addition, part of channels are fixed and utilized by DTV signals in TVWS and some channels are reserved for other purposes. Therefore, at least the weights for those fixed channels in $\bar{\gamma}(0)$ and $\gamma(1)$ are accurate. This would make sure the recovery performance would not be degraded heavily when unregistered users show up in the spectrum of interest. With increasing window size T, the influence of inaccurate parts in $\bar{\gamma}(0)$ and $\gamma(1)$ degrades.

The computational complexity reduction of the DNRLS-based compressive spectrum sensing comes from two parts. In the traditional IRLS algorithm, the inverse of $\left(h_f \Theta W^{(l)} \Theta^T + \lambda \mathrm{I}_P\right)$ takes $\mathrm{O}\left(P^3\right)$ and it is required in each iteration. In large-size compressive sensing problem, solving a problem with complexity $\mathrm{O}\left(P^3\right)$ L times is time consuming. By implementing the DNRLS-based compressive spectrum sensing to update the weights at SUs as summarized in Algorithm 4, the signal recovery step in the algorithm is performed in a non-iterative approach. Therefore, the computational complexity is $\frac{1}{L}$ of the traditional IRLS-based compressive spectrum sensing in which L iterations are required to get a good estimation of the spectrum. Another reason of complexity reduction is that the DNRLS algorithm can achieve exact recovery with fewer measurements. In the DNRLS algorithm, the minimal number of measurements P for exact recovery can be reduced to $\tilde{P}\left(\tilde{P} < P\right)$ which leads to a big complexity reduction as the complexity of solving the inverse of $\left(h_f \Theta W^{(l)} \Theta^T + \lambda \mathrm{I}_P\right)$ is $\mathrm{O}\left(\tilde{P}^3\right)$. The additional complexity of the DNRLS-based compressive spectrum sensing comes from the calculation of P_{IB} for each channel in TVWS. To minimize the necessary computational complexity at SU, the Wilkilson's method is proposed to calculate P_{IB} with lower complexity.

At an SU, the calculation of maximum permitted EIRP P_{IB} of each channel in TVWS should be efficient and accurate. Monte Carlo method and Schwartz-Yeh's method are the two algorithms approved by Ofcom to calculate the maximum allowable EIRP P_{IB}. Schwartz-Yeh's method is an approximate algorithm in which infinite loops are used to calculate the mean and standard deviation values of log-normal distribution variables like variables A, B, and E in (39) and (41) [27]. As a result, the large computational complexity and low efficiency are difficult to overcome at power-limited SUs. Therefore, Wilkinson's method is proposed to calculate the median and standard deviation values of log-normal distribution variables for the calculation of q_1, q_2 and P_{IB} in a more efficient way.

Assuming variable I_k $(k = 1, 2, \ldots, K)$ is a log-normal random variable, $M_k = 10\log_{10} I_k$ can be modeled as a Gaussian random variable and $M = 10\log_{10}\left(\sum_{k=1}^{K} 10^{\frac{M_k}{10}}\right)$. It is assumed that $e^{\Lambda_1} + e^{\Lambda_2} + \cdots + e^{\Lambda_K} = e^Z = 10^M$ and $Z = \rho M$, $\rho = \frac{1}{10}\ln 10 = 0.2302$, the mean and standard deviation of parameter M could be calculated by bringing in two parameters μ_1 and μ_2 as follows:

$$\mu_1 = \mathrm{E}\left(m_Z + \frac{1}{2}\sigma_Z^2\right) = \sum\nolimits_{i=1}^{K} \mathrm{E}\left(m_{\Lambda_i} + \frac{1}{2}\sigma_{\Lambda_i}^2\right), \tag{51}$$

$$\begin{aligned}\mu_2 = \mathrm{E}\left(2m_Z + 2\sigma_Z^2\right) &= \sum\nolimits_{i=1}^{K} \mathrm{E}\left(2m_{\Lambda_i} + 2\sigma_{\Lambda_i}^2\right) \\ &+ 2\sum\nolimits_{i=1}^{K-1}\sum\nolimits_{j=i+1}^{K} \mathrm{E}\left(m_{\Lambda_i} + m_{\Lambda_j}\right) \\ &\times \mathrm{E}\left[\frac{1}{2}\left(\sigma_{\Lambda_i}^2 + \sigma_{\Lambda_j}^2 + 2r_{ij}\sigma_{\Lambda_i}\sigma_{\Lambda_j}\right)\right],\end{aligned} \tag{52}$$

where m_{Λ_i} and σ_{Λ_i} are the median and standard deviation of Λ_i, and r_{ij} are the correlation coefficients of Λ_i and Λ_j. Consequently, the median and standard deviation of M can be calculated as:

$$\sigma_M = \frac{1}{\rho}(2\ln\mu_1 - \frac{1}{2}\ln\mu_2), \tag{53}$$

$$\sigma_M = \frac{1}{\rho}(\ln\mu_2 - 2\ln\mu_1)^{\frac{1}{2}}. \tag{54}$$

Based on the Wilkinson's method explained above, q_1 and q_2 can be calculated. Taking the calculation of q_1 as an example, as shown in (39), $\frac{P_{s,\min}}{P_s} + \frac{V}{P_s} = A + B \leq 1$. $10\log_{10}(A + B) \leq 0$, which is equivalent to $X_{(dB)} = 10\log_{10}\left(10^{\frac{A_{dB}}{10}} + 10^{\frac{B_{dB}}{10}}\right) \leq 0$. It can be fitted into the precondition of Wilkinson's method to get $10^{\frac{A_{dB}}{10}} + 10^{\frac{B_{dB}}{10}} = 10^{X_{dB}} = e^{\Lambda_1} + e^{\Lambda_2}$. Therefore, $\Lambda_1 = \rho \times A_{(dB)}$ and $\Lambda_2 = \rho \times B_{(dB)}$. The relevant correlation coefficient of A and B can be given as:

$$r_{A,B} = \frac{\mathrm{cov}\left(A_{(dB)},\ B_{(dB)}\right)}{\sqrt{\mathrm{var}\left(A_{(dB)}\right)\mathrm{var}\left(B_{(dB)}\right)}} = \frac{\sigma_S}{\sqrt{\sigma_S^2 + \sigma_V^2}}, \tag{55}$$

where σ_S and σ_V can be calculated based on the DTT transmitter database available at [44]. According to (51) and (52), μ_1 and μ_2 can be obtained. Consequently, m_X and σ_X can be calculated according to (53) and (54).

Similarly, q_2 can be calculated by Wilkinson's method by the following procedure:

1. Input m_S, σ_S, m_V, σ_V, m_C, and σ_C as shown in (41), which can be calculated based on the DTT transmitter database available at [44];
2. Calculate m_D and σ_D by Wilkinson's method based on m_V, σ_V, m_C, and σ_C;
3. Calculate m_A, σ_A, m_E, and σ_E by Wilkinson's method based on m_S, σ_S, m_D, and σ_D;
4. Calculate m_Y and σ_Y by Wilkinson's method based on m_A, σ_A, m_E, and σ_E;
5. Calculate q_2 by (42) based on m_A, σ_A, m_E, and σ_E.

In summary, the procedure of calculating P_{IB} with the Wilkinson's method is shown in Fig. 12. Firstly, input the median and standard derivation of the received power of wanted DTT signal, i.e., P_s and the minimum required power of wanted DTT signal, i.e., V which can be obtained from the DTT transmitter database from [44]. Secondly, the predefined maximum permitted value is assigned to P_{IB}. As defined in IEEE 802.22 standard, the maximum permitted EIRP that can be utilized in TV frequency band is 4 watts [12]. In addition, q_1 and q_2 are calculated by the Wilkinson's method as aforementioned. Consequently, the corresponding P_{IB} is updated until $q_2 \leq q_1 - \Delta q_T$.

By taking the values calculated by Monte Carlo simulation as a benchmark, the accuracy of the Schwartz-Yeh's method and Wilkinson's method can be measured by error rate $\Delta Q(\cdot)/Q_{(\text{Monte Carlo})}(\cdot)$, where $Q_{(\text{Monte Carlo})}(\cdot)$ refers to values calculated by Monte Carlo simulation and $\Delta Q(\cdot)$ refers to the absolute difference of parameters' values calculated by the Schwartz-Yeh's method and Wilkinson's method and that calculated by Monte Carlo simulation. More specifically, $\Delta Q(q_1) = \left|q_1^{S,W} - q_1^M\right|$, $\Delta Q(q_2) = \left|q_2^{S,W} - q_2^M\right|$, and $\Delta Q(P_{IB}) =$

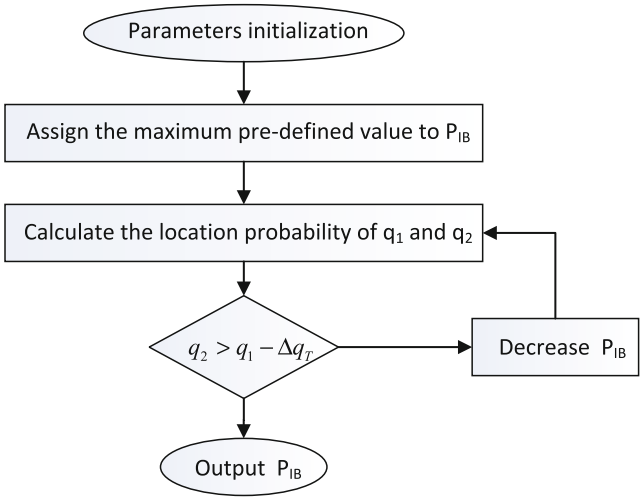

Fig. 12 The procedure of calculating maximum allowable P_{IB} by the Wilkinson's method

Table 1 Error rates comparison

	q_1	q_2	P_{IB}
Schwartz-Yeh's method	31.25%	4.76%	7.87%
Wilkinson's method	9.36%	1.31%	1.54%

Table 2 Running time comparison

	q_1	q_2	P_{IB}
Schwartz-Yeh's method	15966.04%	153278.65%	75462.57%
Wilkinson's method	99.06%	98.89%	99.47%

$\left|P_{IB}^{S,W} - P_{IB}^{M}\right|$, where $q_1^{S,W}$, $q_2^{S,W}$, and $P_{IB}^{S,W}$ refer to the corresponding values calculated by the Schwartz-Yeh's method and Wilkinson's method, respectively, and q_1^M, q_2^M, and P_{IB}^M refer to the corresponding values calculated by Monte Carlo simulation. The error rates of q_1, q_2, and P_{IB} calculated by the Schwartz-Yeh's method and Wilkinson's method are shown in Table 1. It shows that the Wilkinson's method-based DTT location probability calculation outperforms that of the Schwartz-Yeh's method.

Similarly as the error rate calculation, running time of Monte Carlo simulation with 10,000 points is chosen as a benchmark when measuring the running time for q_1, q_2, and q_{IB} calculation. Table 2 shows the running time comparison of the Schwartz-Yeh's and Wilkinson's methods for the calculation of q_1, q_2, and P_{IB}. We can see that the Wilkinson's method can reduce the running time significantly in comparison with the Schwartz-Yeh's method. Therefore, the Wilkinson's method is more suitable for SUs with limited power to obtain the q_1, q_2, and P_{IB} efficiently.

With the validation of the accuracy and efficiency of the Wilkinson's method, a national grid reference (NGR)-based geo-location database is built with the Wilkinson's method. By using the data from the DTT transmitter database available at [44], P_{IB} can be calculated by the Wilkinson's method-based DTT location probability model for a specific location. To show the performance, an NGR number of SP515065 in Oxford is chosen as a test location. The average allowed EIRP calculated by the power control and the proposed location probability model are shown in Table 3.

As shown in Table 3, there are 11 available channels at SP515065 in total. In the Wilkinson's location probability model, the transmission environment is classified into three situations: open, suburban, and urban. Coupling gain in different situations is treated differently, leading to different interference toleration levels of DTT receivers. It is obvious that the power attenuation in open areas is much lower than suburban and urban areas. As a result, the actual maximum allowable EIRP P_{IB} in open areas is lower than the other two situations at a certain NGR location. Taking channel 51 as an example, the P_{IB} is 0.0002 watts in power control model, while the power could be utilized more effectively if the environment is classified into

Table 3 Comparison of actual maximum allowable EIRP P_{IB} in Oxford

	Actual maximum allowable EIRP P_{IB} (Watt)			
	The latest release of Ofcom TV white space model by Wilkinson's method			
Available Channel	Open	Suburban	Urban	Power control model
22	0	4.0000	4.0000	4.0000
25	0	4.0000	4.0000	4.0000
28	0	4.0000	4.0000	4.0000
29	0.0025	4.0000	4.0000	4.0000
40	0	4.0000	4.0000	4.0000
43	0	4.0000	4.0000	4.0000
46	0	4.0000	4.0000	4.0000
49	0.0013	4.0000	4.0000	4.0000
51	0.3981	1.2589	4.0000	0.0002
54	0.0013	4.0000	4.0000	4.0000
58	0.0013	4.0000	4.0000	4.0000

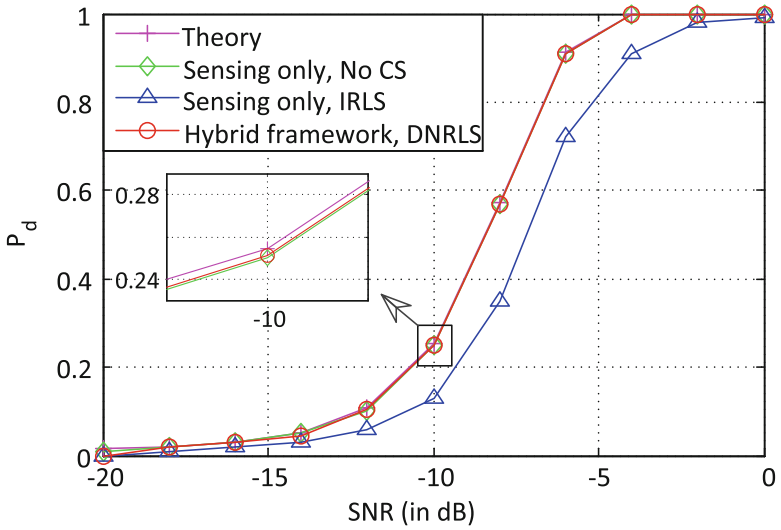

Fig. 13 Detection performance on the simulated signals and data under different SNR values, $p = 0.1$, compression ratio = 20%

different scenarios in location probability model. It is 0.3981 watts in open areas, 1.2589 watts in suburban areas, and 4.0000 watts in urban areas.

Based on the maximum allowable EIRP P_{IB} from the local geo-location database, the weights for the DNRLS-based compressive spectrum sensing can be constructed by fusing with the historical data. Figure 13 shows detection performance of the sensing only approach with IRLS and the hybrid framework with DNRLS algorithms implemented at SUs, where p is set to be 0.1. It is observed

that the detection performance of spectrum sensing only approach without CS implemented at an SU is matched with the theoretical curve, which is presented as a benchmark.

Figure 13 shows that detection performance of the sensing only approach with IRLS used for signal recovery is lower than the theoretic curve due to the signal recovery errors caused by the sub-Nyquist sampling (20%). However, it is noticed that the sensing only approach with IRLS requires an iterative process to update the weights. When the hybrid framework with DNRLS is performed, detection probability increases greatly which can almost match with the theoretic curve. The reason for the large performance improvement is that the data used to constructed the weights is the exact representation of the spectrum of interest if there is no unregistered user. As a result, the DNRLS-based compressive spectrum sensing can achieve better detection performance with $\frac{L-1}{L}$ of computational complexity reduced in comparison with the sensing only approach with IRLS.

Conclusion

Cognitive radio has emerged as one of the most crucial candidate solutions to improve spectrum utilization in next-generation cellular networks. An important requirement for future cognitive radio networks is wideband spectrum sensing, where SUs can detect spectral opportunities across a wide frequency range. However, special attention should be paid to the high signal sampling rate. Therefore, sensing wideband spectrum presents a significant challenge in building sampling hardware that operates at a sufficiently high rate and designing high-speed signal processing algorithms. Sub-Nyquist approaches are drawing more and more attention in wideband spectrum sensing, which refers to the procedure of acquiring wideband signals using sampling rates lower than the Nyquist rate and detecting spectral opportunities using these partial measurements. To fully explore the advantages of both geo-location database and spectrum sensing, hybrid frameworks are explored to maximize the benefits for both PUs and SUs based on the initial information from geo-location database. The partially information from geo-location database can be utilized to further reduce the number of sampling measurements and computation complexity and improve the detection performance for dynamic spectrum sensing.

References

1. Arfken GB, Weber HJ, Harris FE (2001) Mathematical methods for physicists, 7th edn. Academic Press, San Diego
2. Candes EJ, Tao T (2005) Decoding by linear programming. IEEE Trans Inf Theory 51(12):4203–4215
3. Candes EJ, Romberg J, Tao T (2006) Robust uncertainty principles: exact signal reconstruction from highly incomplete frequency information. IEEE Trans Inf Theory 52(2):489–509

4. Chartrand R (2007) Exact reconstruction of sparse signals via nonconvex minimization. IEEE Signal Process Lett 14(10):707–710
5. Eldar YC, Kuppinger P, Bolcskei H (2010) Block-Sparse signals: uncertainty relations and efficient recovery. IEEE Trans Signal Process 58(6):3042–3054
6. Fenton L (1960) The sum of log-normal probability distributions in scatter transmission systems. IRE Trans Commun Syst 8(1):57–67
7. Forney G (1972) Maximum-likelihood sequence estimation of digital sequences in the presence of intersymbol interference. IEEE Trans Inf Theory 18(3):363–378
8. Feng P, Bresler Y (1996) Spectrum-blind minimum-rate sampling and reconstruction of multiband signals. In: Proceedings of IEEE International Conference on Acoustics, Speech and Signal Process (ICASSP), Atlanta, vol 3, pp 1688–1691
9. Gao Y, Qin Z, Feng Z, Zhang Q, Holland O, Dohler M (2016) Scalable and reliable IoT Enabled By Dynamic Spectrum Management for M2M in LTE-A. IEEE Internet Things J 3(6): 1135–1145
10. Hassanieh H, Shi L, Abari O, Hamed E, Katabi D (2014) GHz-wide sensing and decoding using the sparse Fourier transform. In: Proceedings of IEEE International Conference on Computer Communication (INFOCOM), Toronto, pp 2256–2264
11. Holland O, Ping S, Gao Y, Qin Z, Aijaz A, Chareau J, Chawdhry P, Kokkinen H (2015) To white space or not to white space: that is the trial within the ofcom TV white spaces pilot. In: Proceedings of IEEE International Conference on Dynamic Spectrum Access Network (DYSPAN), Stockholm, pp 11–22
12. IEEE Standard for Wireless Regional Area Networks (2011) Part 22: Cognitive Wireless RAN MAC & PHY Specifications: Policies and Procedures for Operation in the TV Bands. IEEE Std. 802.22–2011
13. Kolodzy P, Avoidance I (2002) Spectrum policy task force. Federal Communications Commission, Washington, DC, Report of ET Docket, no. 02–135
14. Landau HJ (1967) Necessary density conditions for sampling and interpolation of certain entire functions. Acta Math 117(1):37–52
15. Liang Y-C, Zeng Y, Peh EC, Hoang AT (2008) Sensing-Throughput tradeoff for cognitive radio networks. IEEE Trans Wirel Commun 7(4):1326–1337
16. Louwsma SM, van Tuijl AJM, Vertregt M, Nauta B (2008) A 1.35 GS/s, 10 b, 175 mW Time-interleaved AD converter in 0.13 m CMOS. J Solid-State Circuits 43(4): 778–786
17. Ma Y, Gao Y, Liang Y-C, Cui S (2016) Reliable and efficient sub-Nyquist wideband spectrum sensing in cooperative cognitive radio networks. IEEE J Sel Areas Commun 34(10): 2750–2762
18. Mishali M, Eldar YC (2009) Blind multiband signal reconstruction: compressed sensing for analog signals. IEEE Trans Signal Process 57(3):993–1009
19. Mishali M, Eldar YC (2010) From theory to practice: sub-Nyquist sampling of sparse wideband analog signals. IEEE J Sel Signal Process 4(2):375–391
20. Mitola J, Maguire G JR (1999) Cognitive radio: making software radios more personal. IEEE Pers Commun 6(4):13–18
21. Nielson B, Cox DR (1989) Asymptotic techniques for use in statistics, 1st edn. Chapman and Hall/CRC, London/New York
22. Office of Communications (2009) Digital dividend: cognitive access. [Online]. Available: http://stakeholders.ofcom.org.uk/binaries/consultations/cognitive/statement/statement.pdf
23. Office of Communications (2010) Implementing Geolocation. [Online]. Available: https://www.ofcom.org.uk/data/assets/pdffile/0035/46889/statement.pdf
24. Office of Communications (2015) Implementing TV White Spaces. [Online]. Available: http://stakeholders.ofcom.org.uk/binaries/consultations/white-space-coexistence/statement/tvws-statement.pdf
25. Paisana F, Marchetti N, DaSilva L (2014) Radar, TV and cellular bands: which spectrum access techniques for which bands? IEEE Commun Surv Tutorials 16(3):1193–1220. Third Quarter

26. Pei Y, Liang Y-C, Teh KC, Li KH (2011) Energy-efficient design of sequential channel sensing in cognitive radio networks: optimal sensing strategy, power allocation, and sensing order. IEEE J Sel Areas Commun 29(8):1648–1659
27. Petrini V, Karimi H (2012) TV white space databases: algorithms for the calculation of maximum permitted radiated power levels. In: IEEE international symposium on dynamic spectrum access networks (DYSPAN), Bellevue, pp 552–560
28. Poulton K, Neff R, Setterberg B, Wuppermann B, Kopley T, Jewett R, Pernillo J, Tan C, Montijo A (2003) A 20 GS/s 8 b ADC with a 1 MB memory in 0.18 m CMOS. In: Proceedings of IEEE International Solid-State Circuits Conference, Digest of Technical Papers, vol 1, pp 318–496
29. Qin Z, Gao Y, Parini CG (2016) Data-assisted low complexity compressive spectrum sensing on real-time signals under sub-nyquist rate. IEEE Trans Wireless Commun 15(2):1174–1185
30. Qin Z, Gao Y, Plumbley M, Parini C (2016) Wideband spectrum sensing on real-time signals at sub-nyquist sampling rates in single and cooperative multiple nodes. IEEE Trans Signal Process 64(12):3106–3117
31. Quan Z, Cui S, Sayed AH, Poor HV (2009) Optimal multiband joint detection for spectrum sensing in cognitive radio networks. IEEE Trans Signal Process 57(3):1128–1140
32. Quinlan A, Barbot J-P, Larzabal P, Haardt M (2006) Model order selection for short data: an exponential fitting test (EFT). EURASIP J Adv Signal Process 2007:Art. ID 71953
33. Ribeiro J, Ribeiro J, Rodriguez J, Dionisio R, Esteves H, Duarte P, Marques P (2012) Testbed for combination of local sensing with geolocation database in real environments. IEEE Wirel Commun 19(4):59–66
34. Schwartz SC, Yeh Y-S (1982) On the distribution function and moments of power sums with log-normal components. Bell Syst Tech J 61(7):1441–1462
35. Sun H, Nallanathan A, Wang C-X, Chen Y (2013) Wideband spectrum sensing for cognitive radio network: a survey. IEEE Trans Wireless Commun 20(2):74–81
36. Tandra R, Sahai A (2008) SNR walls for signal detection. IEEE J Sel Top Sign Proces 2(1): 4–17
37. Tani A, Fantacci R (2010) A low-complexity cyclostationary-based spectrum sensing for UWB and WiMAX coexistence With noise uncertainty. IEEE Trans Veh Technol 59(6):2940–2950
38. Tian Z, Giannakis GB (2006) A wavelet approach to wideband spectrum sensing for cognitive radios. In: Proceedings of International Conference on Cognitive Radio Oriented Wireless Network and Commun (CROWNCOM), Mykonos Island, pp 1–5
39. Tian Z, Giannakis GB (2007) Compressed sensing for wideband cognitive radios. In: Proceedings of IEEE International Conference on Acoustics, Speech and Signal Process (ICASSP), Honolulu, vol 4, pp 1357–1360
40. Tropp JA, Gilbert AC, Strauss MJ (2005) Simultaneous sparse approximation via greedy pursuit. In: Proceedings of IEEE International Conference on Acoustics, Speech and Signal Process (ICASSP), Philadelphia, vol 5, pp. v/721–v/724
41. Tropp JA, Laska JN, Duarte MF, Romberg JK, Baraniuk RG (2010) Beyond Nyquist: efficient sampling of sparse bandlimited signals. IEEE Trans Inf Theory 56(1):520–544
42. Treichler J, Davenport M, Baraniuk R (2009) Application of compressive sensing to the design of wideband signal acquisition receivers. In: US/Australia Joint Work. Defense Apps. of Signal Processing (DASP), Lihue, vol 5
43. UK Office of Communications (Ofcom) (2013) TV white spaces-approach to coexistence, p 26 [Online]. Available: http://stakeholders.ofcom.org.uk/consultations/white-space-coexistence/
44. UK Television Stations (UHF Digital System). [Online]. Available: http://www.wolfbane.com/ukdtt.htm
45. Vallet P, Mestre X, Loubaton P (2015) Performance analysis of an improved MUSIC DoA estimator. IEEE Trans Signal Process 63(23):6407–6422
46. Venkataramani R, Bresler Y (2001) Optimal sub-Nyquist nonuniform sampling and reconstruction for multiband signals. IEEE Trans Signal Process 49(10):2301–2313
47. Wang N, Gao Y, Evans B (2015) Database-augmented spectrum sensing algorithm for cognitive radio. In: Proceedings of IEEE International Conference on Communication (ICC), London

48. Wang N, Gao Y, Zhang X (2013) Adaptive spectrum sensing algorithm under different primary user utilizations. IEEE Commun Lett 17(9):1838–1841
49. Wang N, Gao Y, Chen Y, Bodanese E, Cuthbert L (2011) A power control algorithm for TV white space cognitive radio system. In: IET international conference on communication technology and application (ICCTA), London, pp 546–550
50. Yu R, Zhang Y, Yi L, Xie S, Song L, Guizani M (2012) Secondary users cooperation in cognitive radio networks: balancing sensing accuracy and efficiency. IEEE Wireless Commun 19(2):30–37
51. Zeng Y, Liang Y-C (2009) Eigenvalue-based spectrum sensing algorithms for cognitive radio. IEEE Trans Commun 57(6):1784–1793
52. Zhang Z, Han Z, Li H, Yang D, Pei C (2011) Belief propagation based cooperative compressed spectrum sensing in wideband cognitive radio networks. IEEE Trans Wireless Commun 10(9):3020–3031
53. Zhang X, Ma Y, Gao Y (2016, to appear) Adaptively regularized compressive spectrum sensing from real-time signals to real-time processing. In: Proceedings of IEEE Global Communication Conference (GLOBECOM), Washington, DC

Further Reading

1. Digham F, Alouini M-S, Simon MK (2003) On the energy detection of unknown signals over fading channels. In: IEEE International Conference on Communications (ICC), Anchorage, pp 3575–3579
2. Ye Z, Memik G, Grosspietsch J (2008) Energy detection using estimated noise variance for spectrum sensing in cognitive radio networks. In: IEEE Wireless Communications and Networking Conference (WCNC), Las Vegas, pp 711–716

Sequential Methods for Spectrum Sensing

9

Yan Xin and Lifeng Lai

Contents

Abstract

Spectrum sensing is widely regarded as a key enabling technology to support dynamic spectrum access (DSA) for cognitive radio (CR). Though in principle spectrum sensing can be viewed as a traditional signal detection problem, the design of spectrum sensing algorithms needs to take into account certain stringent

Y. Xin (✉)
Futurewei Technologies Inc., Bridgewater, NJ, USA
e-mail: yan03xin@gmail.com

L. Lai
University of California, Davis, CA, USA
e-mail: lflai@ucdavis.edu

W. Zhang (ed.), *Handbook of Cognitive Radio*,
https://doi.org/10.1007/978-981-10-1394-2_9

requirements due to the nature of CR systems. Firstly, it is important for spectrum sensing algorithms to be robust to signal models as it is often difficult in practice for secondary users (SUs) to acquire complete or even partial knowledge about primary signals. Secondly, a small detection delay is essential for the spectrum sensing even under a fairly low detection signal-to-noise ratio (SNR) level with low detection error probabilities. This chapter focuses on a particular type of spectrum sensing algorithms, called *sequential* spectrum sensing algorithms for CR systems. Compared with block-based sensing algorithms, sequential sensing algorithms enable us to make detection decision with minimum delay while still providing certain performance guarantee. We will first illustrate the benefits of sequential detection for a single-band system. We will then discuss how to design quickest sequential scanning algorithms for multiband systems to quickly identify free channels.

Keywords
Detection delay · Sequential detection · Sequential probability ratio testing · Spectrum scanning

Introduction

Spectrum sensing is widely regarded as a key enabling technology to support dynamic spectrum access (DSA) for cognitive radio (CR) systems[1–20]. Though in principle spectrum sensing can be viewed as a traditional signal detection problem, the design of spectrum sensing algorithms needs to take into account certain stringent requirements due to the nature of CR systems. Firstly, it is important for spectrum sensing algorithms to be robust to signal models as it is often difficult in practice for secondary users (SUs) to acquire complete or even partial knowledge about primary signals. Secondly, a small detection delay is essential for the spectrum sensing even under a fairly low detection signal-to-noise ratio (SNR) level with low detection error probabilities. To this end, a number of spectrum sensing algorithms have been proposed and studied [21–26]. Roughly speaking, spectrum sensing can be classified into two categories: single-band sensing and multiband sensing. As far as spectrum sensing is concerned, the major difference between single-band sensing and multiband sensing is that in a multiband system, sensing needs to be performed over spectrum bands that support different primary user (PU) activities. In this chapter, we treat each single band as an entity in the sense that a single band no matter whether it is a single-carrier or multi-carrier single band only has two possible states: unoccupied or occupied.

This chapter focuses on a particular type of spectrum sensing algorithms, called *sequential* spectrum sensing algorithms for CR systems. Compared with block-based sensing algorithms, sequential sensing algorithms enable us to make important detection decision with minimum delay while still providing certain performance guarantee. The goal of this chapter is to introduce the sequential sensing method and the performance benefits it brings under various scenarios.

In particular, we will first illustrate the benefits of sequential sensing for single-band systems in section "Sequential Detection for Single Channel." We will then present sequential algorithms that enable us to quickly locate all available channels for multiband systems in section "Quickest Spectrum Scanning."

Single-Band Sensing

Typical examples of single-band spectrum sensing algorithms include energy detection [27], generalized likelihood ratio test [7], covariance sensing [21–23], and feature detection [24]. From a practical point of view, energy detection is very attractive, primarily because it has a low implementation complexity and requires no deterministic knowledge of PU signals. However, to achieve a high sensing accuracy, energy detection entails a large amount of sensing time especially when the detection SNR is low [28].

To reduce sensing time, several sequential probability ratio test (SPRT)-based sensing algorithms have been proposed under various CR settings [26, 29, 30]. The main motivation of using SPRT as a sensing algorithm is that SPRT requires the shortest average sensing time for any given false-alarm and misdetection probabilities in the simple hypothesis testing case [31, 32]. However, the detection delay of SPRT is highly variable. Although the average detection delay of SPRT is less than that of the fixed-sample-size detection algorithm under the same error probabilities requirements, the detection delay of SPRT in a particular realization might be significantly larger than the average value. In CR systems, on the other hand, the decision must be made within a short period of sensing time [37]. In other words, sequential sensing algorithms used in practice are essentially truncated algorithms. There are two major drawbacks in the existing (truncated) SPRT-based sensing algorithms [26, 29]. First, the complexity of SPRT under practical signal models is high. In particular, the test statistic of SPRT is updated and is compared to lower and upper thresholds after taking each sample. Thus, the computational complexity of the test statistic determines the feasibility of SPRT. While in the simple hypothesis testing case, evaluating the test statistic of SPRT is simple, but it requires the perfect knowledge of primary signals. However, acquiring such knowledge in practice is difficult in general. In the absence of such knowledge, the evaluation of the test statistics at each time slot involves significant computation. Second, the performance of SPRT is fairly sensitive to the choices of upper and lower thresholds. In [31], Wald proposed an elegant method for selecting upper and lower thresholds for the non-truncated SPRT. Existing SPRT-based algorithms simply apply Wald's method to select thresholds. Such selection does not work well for truncated sensing algorithms since it leads to an increase in detection error probabilities.

In this chapter, we introduce a low-complexity truncated sequential spectrum sensing algorithm, called the sequential shifted chi-square test (SSCT). SSCT possesses several attractive features: (1) similar to energy detection, SSCT requires only the knowledge on the noise power and does not require any deterministic knowledge

of primary signals; (2) compared to fixed-sample-size detection algorithms such as energy detection, SSCT is capable of achieving a comparable detection performance with much reduced average sensing time; (3) in comparison with existing SPRT-based sensing algorithms [29], SSCT has a much simpler test statistic and a lower implementation complexity; and (4) SSCT offers desirable flexibility to strike a trade-off between detection performance and sensing delay when the operating SNR is higher than the minimum detection SNR. Furthermore, to evaluate the detection performance of SSCT and hence guide the proper choice of parameters, which is typically a challenging task, we derive the exact false-alarm probability and provide numerical integration algorithms to compute the misdetection probability and the average sample number (ASN) in a recursive manner.

Multiband Sensing

Besides single-band sensing, multiband (multichannel) spectrum sensing has recently gained considerable research attention. More specifically, in [25] and [26], multiple narrow-band sensors (detectors), each for a spectrum band, are used to simultaneously observe multiple spectrum bands. Multiband joint energy detection [25] and sequential detection [26] were developed to maximize overall throughput performance. When the number of candidate bands is large, these spectrum sensing schemes require a large number of sensors and joint simultaneous operation of these sensors and thus are of prohibitively large implementation complexity. In [33] and [34], a detector based on a wide-band receiver is used to collect signal samples from all multiple candidate bands. SPRT and fixed-sample-size (FSS) sensing algorithms are developed to minimize multiband sensing delay. However, a wide-band detector typically requires a high-speed analog-to-digital converter (ADC) and extra signal processing elements, thus incurring additional cost/complexity.

This chapter considers the problem of how to determine the availability of each spectrum band in a multiband primary system with small delay and small error probabilities using a single or few sensors. With one or a small number of sensors, SUs are able to observe one band or a small subset of candidate bands at a time. Two scenarios of practical interests are investigated. In the first scenario, there is a strict delay constraint on the spectrum scanning. That is, the spectrum scanning needs to be complete within a certain time period. In the second scenario, there is no strict time constraint for the scanning. That is, the spectrum scanning continues until the completion of the entire detection process. In both scenarios, our goal is to design spectrum scanning schemes that minimize a cost function that strikes a balance between error probabilities and detection delay.

We first consider a single sensor case, in which only one spectrum band is observed at a time. To minimize the scanning cost, the detector needs to design (1) *selection rules* that decide which band to collect signal samples at each time; (2) *termination rules* that decide when to terminate the entire scanning process; and (3) *terminal decision rules* that decide the availability of each band after the scanning process is complete. We first show that the problem at hand can be converted

into a Markovian optimal stopping time problem [35]. Using mathematical tools from the optimal stopping theory, we derive the optimal algorithms for both scenarios with and without a delay constraint. We show that in the scenario without a delay constraint, the optimal scanning algorithm is a concatenated sequential probability ratio test (C-SPRT). More specifically, we perform a SPRT test for the first band. Once the SPRT test is complete for this band, we switch to another band and carry out another SPRT on the newly switched band. The scanning process completes once all the bands have been detected by using SPRT. Hence, the scanning algorithm can be efficiently implemented. On the other hand, the implementation of the optimal algorithm for the scenario with a strict delay constraint requires large lookup tables and frequent updating of posterior probabilities, thus incurring a prohibitively high computational complexity. To reduce the complexity for the delay-constrained scenario, we also propose several truncated C-SPRT algorithms that have very low implementation complexity yet are asymptotically optimal.

We next generalize the study to the multiple sensor case, in which multiple spectrum bands can be simultaneously observed. The detector again needs to design band selection rules (in this case, select a subset of bands), termination rules, and terminal decision rules to minimize the cost function. The problem can also be converted into a Markovian optimal stopping time problem, and optimal rules can be derived using the tools from the optimal stopping theory. To reduce the complexity, we also design several low-complexity algorithms. Extensive numerical results are presented to show the effectiveness of the proposed algorithms.

Notation: Boldface upper and lower case letters are used to denote matrices and vectors, respectively; $\boldsymbol{I}_k$ denotes a $k \times k$ identity matrix; $E[\cdot]$ denotes the expectation operator. $(\cdot)^T$ denotes the transpose operation; $\mathbf{1}_k$ denotes a $k \times 1$ vector whose entries are all ones; $\aleph_p^q$ denotes a set of consecutive integers from p to q, i.e., $\aleph_p^q := \{p, \ldots, q\}$, where p is a non-negative integer and q is a positive integer greater than p or $+\infty$; $(\cdot)^c$ denotes a complement of a set; $\mathbb{I}_{\{x \geq t\}}$ denotes an indicator function defined as $\mathbb{I}_{\{x \geq t\}} = 1$ if $x \geq t$ and $\mathbb{I}_{\{x \geq t\}} = 0$ if $x < t$, where x is a variable and t is a constant.

Sequential Detection for Single Channel

In this section, we start by presenting a statistical formulation of the spectrum sensing problem for a single SU CR system. We next give a brief overview on two sensing algorithms that are closely related to SSCT: energy detection and a SPRT-based sensing algorithm.

Problem Formulation

In this section, we assume that there is a single SU in the CR system, which is allowed to access the licensed spectrum of PU in an opportunistic manner. Upon receiving signal samples, denoted by r_i, SU is required to detect whether there are primary signals or not before using the licensed spectrum. We use s_i, $i = 1, 2, \ldots$ to

denote the primary signal samples. Such a signal detection problem can be written as the following classic binary hypothesis testing problem:

$$H_0: \ r_i = w_i, \ i = 1, 2, \ldots, \tag{1}$$

$$H_1: \ r_i = hs_i + w_i, \ i = 1, 2, \ldots, \tag{2}$$

where w_i denotes additive white Gaussian noise (AWGN) with zero mean and variance $\sigma_w^2/2$ per dimension, i.e., $w_i \sim \mathscr{CN}(0, \sigma_w^2)$, and h is the channel coefficient between PU and SU. We further assume that the channel coefficient h is a constant during the sensing process, and the primary signal samples s_i are independent and identically distributed (i.i.d.).

Preliminaries

Energy detection is a fixed-sample-size sensing algorithm in the sense that the decision is made after collecting a fixed number of samples, say, M. Let $\boldsymbol{r}$ be the $1 \times M$ received signal vector defined as $\boldsymbol{r} := [r_1, r_2, \ldots, r_M]$. In energy detection, we compute the energy of $\boldsymbol{r}$ and compare it with a predetermined value. Mathematically, the testing procedure is described as: accept H_1, if $T(\boldsymbol{r}) := \sum_{i=1}^{M} |r_i|^2 \geq \gamma_{\text{ed}}$; Accept H_0, if $T(\boldsymbol{r}) < \gamma_{\text{ed}}$, where γ_{ed} denotes a threshold for energy detection.

Since w_i is a zero mean complex Gaussian random variable (RV) with variance $\sigma_w^2/2$ per dimension, $2T(\boldsymbol{r})/\sigma_w^2$ is a central chi-square RV with $2M$ degrees of freedom under H_0 and is a noncentral chi-square RV with $2M$ degrees of freedom and noncentrality parameter $2|h|^2 \sum_{i=1}^{M} |s_i|^2/\sigma_w^2$ under H_1 conditioning on $|s_i|^2, i = 1, \ldots, M$. As M increases, $2|h|^2 \sum_{i=1}^{M} |s_i|^2/\sigma_w^2$ approaches $2M|h|^2\sigma_s^2/\sigma_w^2$, where σ_s^2 denotes the average symbol energy. Define $\texttt{SNR}_m$ as the minimum detection SNR, at which the requirements on the target false-alarm and misdetection probabilities are satisfied. The minimum detection SNR is a design parameter, which depends on implementation scenarios but is not directly related to a particular channel realization. In practice, it is highly likely that $\texttt{SNR}_m$ is different from the exact operating SNR, which is defined as $|h|^2\sigma_s^2/\sigma_w^2$. The exact operating SNR depends on the channel gain h between PU and SU, which is difficult to acquire in practice. To distinguish these two different SNRs, we denote by $\texttt{SNR}_o$ the exact operating SNR.

It follows directly from the central limit theorem (CLT) that as M approaches infinity, the distribution of $2T(\boldsymbol{r})/\sigma_w^2$ converges to a normal distribution as follows [36]: $2T(\boldsymbol{r})/\sigma_w^2 \sim \mathscr{N}(2M, 4M)$ under H_0 while $2T(\boldsymbol{r})/\sigma_w^2 \sim \mathscr{N}\big(2M(1 + \texttt{SNR}_m), 4M(1 + 2\texttt{SNR}_m)\big)$ under H_1. Let $\bar{\alpha}_{\text{ed}}$ and $\bar{\beta}_{\text{ed}}$ be the target false-alarm and misdetection probabilities, respectively. Generally speaking, the number of required signal samples M is determined by $\bar{\alpha}_{\text{ed}}$ and $\bar{\beta}_{\text{ed}}$. We use $M_{\text{ed}}^{\min}$ to denote the minimum number of sensing samples required to meet the target $\bar{\alpha}_{\text{ed}}$ and $\bar{\beta}_{\text{ed}}$ requirements when the detection SNR is $\texttt{SNR}_m$. As shown in [37], we have

$$M_{\text{ed}}^{\min} = \left\lceil \ \texttt{SNR}_m^{-2}\left[\mu - \nu \cdot \sqrt{2\texttt{SNR}_m + 1}\right]^2 \right\rceil \tag{3}$$

where $\mu := Q^{-1}(\bar{\alpha}_{\text{ed}})$, $\nu := Q^{-1}(1-\bar{\beta}_{\text{ed}})$, and $\lceil x \rceil$ denotes the smallest integer greater than or equal to x, $Q(\cdot)$ denotes the complementary cumulative distribution function of the standard normal RV, i.e., $Q(x) := (2\pi)^{-1/2}\int_x^\infty e^{-t^2/2}dt$, and $Q^{-1}(\cdot)$ denotes its inverse function. It is evident from (3) that for energy detection, the minimum number of samples is proportional to $\texttt{SNR}_m^{-2}$ for a sufficiently small $\texttt{SNR}_m$ [28].

It is clear from the description above that energy detection has a simple test statistic and a low implementation complexity [27]. In addition, known as a form of non-coherent detection, energy detection requires only the knowledge of noise power and does not rely on any deterministic knowledge about the primary signal s_i. However, one major drawback of the energy detection is that, at a low SNR, it requires a large amount of sensing time to achieve low detection error probabilities.

In comparison with a fixed-sample-size detection such as energy detection, SPRT is capable of achieving the same detection performance with a much reduced ASN [32]. We next investigate a SPRT-based sensing algorithm that relies on the amplitude squares of the received signal samples [26, 29].

To simplify the description, we review a case in which the amplitude squares of primary signals, $|s_i|^2$, $i = 1, 2, \ldots$, are perfectly known at SU. In this case, the spectrum sensing problem formulated in (1) becomes a simple hypothesis testing problem, which is the original setup considered by Wald [31]. Normalize $|r_i|^2$ as $v_i := 2|r_i|^2/\sigma_w^2$ for the convenience of derivation. Note that under H_0, v_i is an exponential RV with rate parameter $1/2$, and under H_1, v_i is a noncentral chi-square RV (conditional on $|s_i|^2$) with two degrees of freedom and noncentrality parameter λ_i that can be readily obtained as $\lambda_i = 2|h|^2|s_i|^2/\sigma_w^2$. Hence, the probability density function (PDF) of v_i under H_0 is

$$q_0(v_i) = \frac{1}{2}e^{-v_i/2} \tag{4}$$

whereas under H_1, the PDF of v_i (conditional on λ_i) is

$$q_1(v_i|\lambda_i) = \frac{1}{2}e^{-(v_i+\lambda_i)/2} I_0(\sqrt{\lambda_i v_i}) \tag{5}$$

where $I_0(\cdot)$ is the zeroth-order modified Bessel function of the first kind. After collecting N samples, we can express the accumulative log-likelihood ratio as

$$L_N(\boldsymbol{v}_N|\boldsymbol{\lambda}_N) = \log\frac{q_{\boldsymbol{v}|H_1}(\boldsymbol{v}_N|\boldsymbol{\lambda}_N)}{q_{\boldsymbol{v}|H_0}(\boldsymbol{v}_N)} = \sum_{i=1}^N z_i = -\sum_{i=1}^N \lambda_i/2 + \sum_{i=1}^N \log I_0(\sqrt{\lambda_i v_i}) \tag{6}$$

where $\boldsymbol{v}_N := (v_1, v_2, \ldots, v_N)$, $z_i = \log\big(q_1(v_i|\lambda_i)/q_0(v_i)\big)$, and $\boldsymbol{\lambda}_N := (\lambda_1, \lambda_2, \ldots, \lambda_N)$. The test procedure is given as follows: accept H_1, if $L_N(\boldsymbol{v}_N|\boldsymbol{\lambda}_N) \geq b_L$; accept H_0, if $L_N(\boldsymbol{v}_N|\boldsymbol{\lambda}_N) \leq a_L$; and continue sensing, if $a_L < L_N(\boldsymbol{v}_N|\boldsymbol{\lambda}_N) < b_L$. In [31], Wald specified a particular choice of

thresholds a_L and b_L for the *non-truncated* SPRT as follows: $a_L = \log \bar{\beta}_{\text{sprt}}/(1 - \bar{\alpha}_{\text{sprt}})$, and $b_L = \log(1 - \bar{\beta}_{\text{sprt}})/\bar{\alpha}_{\text{sprt}}$ where $\bar{\alpha}_{\text{sprt}}$ and $\bar{\beta}_{\text{sprt}}$ denote the target false-alarm and misdetection probabilities, respectively. For a non-truncated SPRT, the Wald's choice on a_L and b_L yields true false-alarm and misdetection probabilities that are fairly close to the target ones.

Let z be a RV having the same PDF as z_i. It has been pointed out in [39] that, in SPRT, if hypotheses H_0 and H_1 are distinct, then $E_{H_0}(z) < 0 < E_{H_1}(z)$, where $E_{H_i}(\cdot)$ denotes the expectation under H_i, $i = 1, 2$. As evident from (6), one shortcoming of this SPRT-based sensing algorithm is that the test statistic contains a modified Bessel function, which may result in a high implementation complexity. When the perfect knowledge of the instantaneous amplitude squares of the primary signals is not available, PDF under H_1 is not completely known, i.e., the alternative hypothesis is composite. Generally speaking, two approaches, the Bayesian approach and the generalized likelihood ratio test, can be used to deal with such a case. In the Bayesian approach, *a prior* PDF of the amplitude squares of the primary signals is required and multiple summations over all possible amplitudes of the primary signals need to be performed, whereas in the generalized likelihood ratio test, a maximum likelihood estimation (MLE) of the amplitude squares of the primary signals is needed [7]. Either of these two approaches, however, leads to a considerable increase in the implementation complexity.

A Low-Complexity Sequential Spectrum Sensing Algorithm

We now propose a low-complexity sequential spectrum sensing algorithm depicted as follows:

$$\Lambda_N = \sum_{i=1}^{N} \left(|r_i|^2 - \Delta \right), \tag{7}$$

in which Δ is a fixed and predetermined parameter. Suppose that the detector has a decision deadline M. That is, the detector needs to make a decision within M samples. We propose the following test procedure:

$$\texttt{Accept } H_1 :$$

$$\text{if } \Lambda_N \geq b \text{ for } 0 < N \leq M - 1, \text{ or if } \Lambda_M \geq \gamma; \tag{8}$$

$$\texttt{Accept } H_0 :$$

$$\text{if } \Lambda_N \leq a \text{ for } 0 < N \leq M - 1, \text{ or if } \Lambda_M < \gamma; \tag{9}$$

$$\texttt{Continue Sensing} :$$

$$\text{if } \Lambda_N \in (a, b) \text{ for } 0 < N \leq M - 1 \tag{10}$$

where a, b, and γ denote three predetermined and fixed constants satisfying the following conditions: $a < 0$, $b > 0$, and $\gamma \in (a, b)$. In statistical term, the test

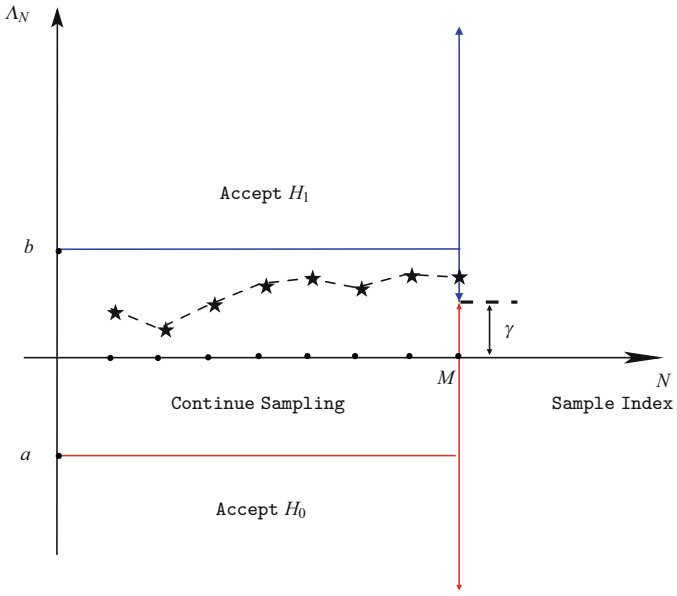

Fig. 1 The test region of SSCT

procedure given in (8), (9), and (10) is nothing but a *truncated* sequential test. As depicted in Fig. 1, the stopping boundaries of the test region consist of horizontal lines b and a, which we call the upper and lower boundary, respectively. Notice that each term $|r_i|^2 - \Delta$ in Λ_N is nothing but a shifted chi-square RV. Hence, we simply name this sensing algorithm described in (8), (9), and (10) *sequential shifted chi-square test* (SSCT). As can be seen from (7), SSCT has a simple test statistic that contains only the amplitude squares of the received signals and the parameter Δ.

Let r be a RV with the same PDF as $|r_i|^2 - \Delta$, which is the ith incremental term in the test statistic (7). Similar to the SPRT case, we choose $\sigma_w^2 < \Delta < \sigma_w^2(1 + \mathrm{SNR}_m)$ to ensure $E_{H_0}(r) < 0 < E_{H_1}(r)$. In SSCT, we have $E_{H_0}(r) = \sigma_w^2 - \Delta$ and $E_{H_1}(r) = \sigma_w^2(1 + \mathrm{SNR}_o) - \Delta$. Using $\mathrm{SNR}_m \le \mathrm{SNR}_o$ and $\sigma_w^2 < \Delta < \sigma_w^2(1 + \mathrm{SNR}_m)$, we always have $E_{H_0}(r) < 0 \le \mathrm{SNR}_o - \mathrm{SNR}_m < E_{H_1}(r)$. Note that with this choice, the constant Δ depends on the minimum detection SNR instead of the exact operating SNR. Normalize the test statistic Λ_N by $\sigma_w^2/2$ and define $\bar{\Lambda}_N := 2\Lambda_N/\sigma_w^2$. We rewrite (7) as

$$\bar{\Lambda}_N = \sum_{i=1}^{N} (v_i - 2\Delta/\sigma_w^2) \tag{11}$$

where $v_i := 2|r_i|^2/\sigma_w^2$. Let ξ_N denote the sum of v_i for $i = 1, \ldots, N$, i.e., $\xi_N = \sum_{i=1}^{N} v_i$ and let $\bar{\Delta}$ denote $2\Delta/\sigma_w^2$. Applying this notation, we rewrite $\bar{\Lambda}_N$ as $\bar{\Lambda}_N = \xi_N - N\bar{\Delta}$. We let $\bar{\Lambda}_0$ and ξ_0 be 0 for notational simplicity. We further define a_i and

b_i as: $a_i = 0$ for $\aleph_0^P$, $a_i = \bar{a} + i\bar{\Delta}$ for $i \in \aleph_{P+1}^{\infty}$, and $b_i = \bar{b} + i\bar{\Delta}$ for $b \in \aleph_0^{\infty}$, where $\bar{a} := 2a/\sigma_w^2$, $\bar{b} := 2b/\sigma_w^2$, and P denotes the largest integer not greater than $-a/\Delta$, i.e., $P := \texttt{floor}(-a/\Delta)$. Applying the notation $\xi_N = \sum_{i=1}^{N} v_i$, we express the test procedure (8), (9), and (10) as

$$\texttt{Accept } H_1 : \tag{12}$$
$$\texttt{if } \xi_N \geq b_N \text{ for } 0 < N \leq M-1, \texttt{ or if } \xi_M \geq \bar{\gamma}_M;$$
$$\texttt{Accept } H_0 : \tag{13}$$
$$\texttt{if } \xi_N \leq a_N \text{ for } 0 < N \leq M-1, \texttt{ or if } \xi_M < \bar{\gamma}_M;$$
$$\texttt{Continue Sensing} : \tag{14}$$
$$\texttt{if } \xi_N \in (a_N, b_N) \text{ for } 0 < N \leq M-1$$

where $\bar{\gamma}_M = \bar{\gamma} + M\bar{\Delta}$ with $\bar{\gamma} := 2\gamma/\sigma_w^2$. The corresponding test region is depicted in Fig. 2, where the stopping boundaries comprise two slant line segments.

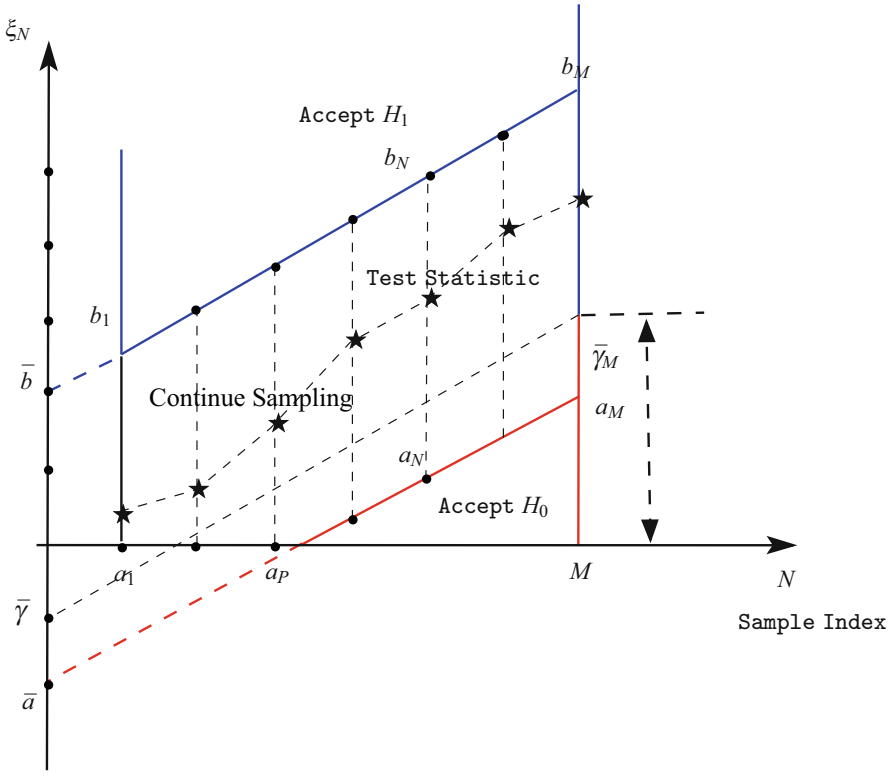

Fig. 2 The test region of the transformed test procedure

Define α_{ssct} and β_{ssct} as the false-alarm and misdetection probabilities of SSCT, respectively.

The issue of how to select thresholds a, b, and γ is critical to the performance of SSCT. In [31], Wald proposed a method to select appropriate thresholds for the non-truncated SPRT. Since the proposed test procedure in (8), (9), and (10) is a truncated sequential test and is not necessarily a SPRT, the thresholds selected by the Wald's method cannot meet target detection performance requirements in general.

As a result, an alternative approach to select thresholds is needed. Typically, the thresholds a, b, γ, the parameter Δ, and the truncated size M are selected *beforehand and off-line*, either purposefully or randomly, and the corresponding α_{ssct} and β_{ssct} are then computed. If the resulted α_{ssct} and β_{ssct} do not meet the requirement, the thresholds and truncated size are subsequently adjusted. This process continues until a desirable error probability performance is obtained. In the above process, the key and challenging step is to accurately and efficiently evaluate α_{ssct} and β_{ssct} as well as ASN for any prescribed thresholds a, b, γ, the parameter Δ, and the truncated size M. In the following section, we will show how to evaluate these quantities for SSCT.

Evaluations of False-Alarm and Misdetection Probabilities

In this section, we present the exact false-alarm probability result and a numerical integration algorithm that obtains the misdetection probability in a recursive manner [38] for any given thresholds.

Preparatory Tools

We introduce the first integral as follows:

$$f_{\boldsymbol{\chi}_k}^{(k)}(\xi) = \int_{\chi_k}^{\xi} d\xi_k \int_{\chi_{k-1}}^{\xi_k} d\xi_{k-1} \cdots \int_{\chi_1}^{\xi_2} d\xi_1, \ k \geq 1$$

and $f_{\boldsymbol{\chi}_k}^{(k)}(\xi) = 1$ for $k = 0$, where $\boldsymbol{\chi}_0 = \emptyset$ and $\boldsymbol{\chi}_k := [\chi_1, \ldots, \chi_{k-1}, \chi_k]$ with $0 \leq \chi_1 \leq \ldots \leq \chi_k$. The superscript k and the subscript $\boldsymbol{\chi}_k$ are used to indicate that $f_{\boldsymbol{\chi}_k}^{(k)}(\xi)$ is a k-fold multiple integral with ordered lower limits specified by $\boldsymbol{\chi}_k$. Evidently, the integral $f_{\boldsymbol{\chi}_k}^{(k)}(\xi)$ is a polynomial in ξ of degree k. Lemma 1 shows that the exact value of $f_{\boldsymbol{\chi}_k}^{(k)}(\xi)$ can be computed recursively.

Lemma 1. *The integral $f_{\boldsymbol{\chi}_k}^{(k)}(\xi)$ is given by*

$$f_{\boldsymbol{\chi}_k}^{(k)}(\xi) = \sum_{i=0}^{k-1} \frac{f_i^{(k)}(\xi - \chi_{i+1})^{k-i}}{(k-i)!} + f_k^{(k)} \tag{15}$$

where $f_i^{(k)}$, $i = 0, \ldots, k$, *for* $k \geq 1$ *can be obtained recursively as follows:* $f_i^{(k)} = f_i^{(k-1)}$, $i \in \aleph_0^{k-1}$ *and*

$$f_k^{(k)} = -\sum_{i=0}^{k-1} \frac{f_i^{(k-1)}}{(k-i)!}(\chi_k - \chi_{i+1})^{k-i}$$

with $f_0^{(0)} = 1$. *For the case where* $\chi_1 = \chi_2 = \ldots = \chi_k = \chi$, *the coefficients* $f_{\boldsymbol{\chi}_k}^{(k)}$ *is given by*

$$f_{\boldsymbol{\chi}_k}^{(k)} = \frac{1}{k!}(\xi - \chi)^k.$$

Additionally, the integral $f_{\boldsymbol{\chi}_k}^{(k)}(\xi)$ *has the following useful properties: 1) Differential Property:* $df_{\boldsymbol{\chi}_k}^{(k)}(\xi)/d\xi = f_{\boldsymbol{\chi}_{k-1}}^{(k-1)}(\xi)$ *with* $\boldsymbol{\chi}_{k-1} = [\chi_1, \ldots, \chi_{k-1}]$ *and* $k \geq 2$*; 2) Scaling Property:* $f_{t\boldsymbol{\chi}_k}^{(k)}(t\xi) = t^k f_{\boldsymbol{\chi}_k}^{(k)}(\xi)$ *for* $t > 0$*; 3) Shift Property:* $f_{\boldsymbol{\chi}_k - \delta \mathbf{1}_k}^{(k)}(\xi - \delta) = f_{\boldsymbol{\chi}_k}^{(k)}(\xi)$.

It is noteworthy to mention that formula (15) together with scaling and shift properties are particularly useful in reducing round-off errors when evaluating $f_{\boldsymbol{\chi}_k}^{(k)}(\xi)$. These two properties will be used to ensure the numerical stability of the false-alarm probability computation method presented later in this section. The second integral that will be useful is

$$I^{(0)} := 1, \text{ and } I^{(n)} := \int_{\Omega^{(n)}} \cdots \int d\boldsymbol{\xi}_n, \; n \geq 1 \tag{16}$$

where $\boldsymbol{\xi}_n := [\xi_1, \xi_2, \ldots, \xi_n]$ with $0 \leq \xi_1 \leq \xi_2 \cdots \leq \xi_n$, and $\Omega^{(n)} = \{(\xi_1, \xi_2, \ldots, \xi_n) : 0 \leq \xi_1 \leq \cdots \leq \xi_n; a_i < \xi_i < b_i, i \in \aleph_1^n\}$. For $n = 1$, we have $I^{(1)} = \int_{a_1}^{b_1} d\xi_1 = b_1 - a_1$. We define c and d as two parameters satisfying $0 \leq c < d$, $a_{N-1} \leq c \leq b_N$ and $a_N \leq d$. For $N \geq 2$, we define the following vector

$$\boldsymbol{\psi}_{n,c}^N = \begin{cases} [\underbrace{b_{n+1}, \ldots, b_{n+1}}_{Q}, \underbrace{a_{Q+n+1}, \ldots, a_{N-1}, c}_{N-Q-n}], n \in \aleph_0^{N-Q-2} \\ [\underbrace{b_{n+1}, \ldots, b_{n+1}, c}_{N-n}], n \in \aleph_{N-Q-1}^{s-1} \\ b_{n+1}\mathbf{1}_{N-n}, n \in \aleph_s^{N-2} \end{cases}$$

where s and Q denote the integers satisfying $b_s < c \leq b_{s+1}$ and $a_Q \leq b_1 < a_{Q+1}$ respectively. Let us define $\boldsymbol{A}_i$ as an $(N-n) \times (N-n-i)$ matrix $\boldsymbol{A}_i = [\boldsymbol{I}_{N-i-n} | \mathbf{0}_{(N-i-n)\times i}]^T$ with $i \in \aleph_1^{N-n}$. In addition, we define the following vectors $\boldsymbol{\psi}_{n,c}^{N-i} = \boldsymbol{\psi}_{n,c}^N \cdot \boldsymbol{A}_i$, $i \in \aleph_1^{N-n} \boldsymbol{a}_{n_1}^{n_2} = [a_{n_1+1}, \ldots, a_{n_2}]$, $n_2 \geq n_1 \geq 0$, where $\boldsymbol{\psi}_{n,c}^{N-i}$

is an $(N-i-n)\times 1$ vector and $\boldsymbol{a}_{n_1}^{n_2}$ is an $(n_1-n_2)\times 1$ vector. If $n_1=n_2$, we define $a_{n_1}^{n_2}$ as $\emptyset$. In what follows, we show that we can compute the exact value of $I^{(N)}$ in (16) recursively.

Lemma 2. *The exact value of the integral $I^{(N)}$ is given by*

$$I^{(N)}=f_{\boldsymbol{a}_0^N}^{(N)}(b_N)-\begin{cases}\mathbb{I}_{\{N\geq 2\}}\sum_{n=0}^{N-2}\dfrac{(b_N-b_{n+1})^{N-n}I^{(n)}}{(N-n)!}, & N\in\aleph_1^Q\\ \sum_{n=0}^{N-2}f_{\boldsymbol{\psi}_{n,a_N}^N}^{(N-n)}(b_N)I^{(n)}, & N\in\aleph_{Q+1}^{\infty}\end{cases}$$

with $I^{(0)}=1$.

The third integral is given by

$$J_{c,d}^{(N)}(\theta):=\underset{\Upsilon_{c,d}^{(N)}}{\int\cdots\int}e^{-\theta\xi_N}d\boldsymbol{\xi}_N$$

where $\theta>0$, $N\geq 1$, and $\Upsilon_{c,d}^{(N)}:=\{(\xi_1,\ldots,\xi_N):0\leq\xi_1\leq\ldots\leq\xi_N;a_i<\xi_i<b_i,i\in\aleph_1^{N-1};c<\xi_N<d\}$. Recall that c and d are two non-negative numbers satisfying $a_{N-1}\leq c\leq b_N$ and $0\leq c<d$ and $d\geq a_N$. We define the following function

$$g_{c,d}^{(n)}(\theta)=\begin{cases}I^{(n)}\Big[\theta^{n-N}e^{-\theta b_{n+1}}-\sum_{i=1}^{N-n}\theta^{-i}\times f_{b_{n+1}\mathbf{1}_{N-n-i}}^{(N-n-i)}(d)e^{-\theta d}\Big], & c\leq b_1,n\in\aleph_0^{N-2}\\ I^{(n)}\sum_{i=1}^{N-n}\theta^{-i}\Big[f_{\boldsymbol{\psi}_{n,c}^{N-i}}^{(N-n-i)}(c)e^{-\theta c}-f_{\boldsymbol{\psi}_{n,c}^{N-i}}^{(N-n-i)}(d)e^{-\theta d}\Big], & c>b_1,n\in\aleph_0^{s-1}\\ I^{(n)}\Big[\theta^{n-N}e^{-\theta b_{n+1}}-\sum_{i=1}^{N-n}\theta^{-i}\times f_{b_{n+1}\mathbf{1}_{N-n-i}}^{(N-n-i)}(d)e^{-\theta d}\Big], & c>b_1,n\in\aleph_s^{N-2}.\end{cases}$$

In the cases of $(c,d)=(\bar{\gamma}_N,\infty)$ and $(c,d)=(a_N,b_N)$, the exact values of the integral $J_{c,d}^{(N)}(\theta)$ in (17) can be obtained from the following lemma.

Lemma 3. *For any $\bar{\gamma}_N$ satisfying $a_N\leq\bar{\gamma}_N<b_N$, the exact values of the integrals $J_{\bar{\gamma}_N,\infty}^{(N)}(\theta)$ and $J_{a_N,b_N}^{(N)}(\theta)$ are given by*

$$J_{\bar{\gamma}_N,\infty}^{(N)}(\theta)=\sum_{i=1}^{N}\theta^{-i}f_{\boldsymbol{a}_0^{N-i}}^{(N-i)}(\bar{\gamma}_N)e^{-\theta\bar{\gamma}_N}-\mathbb{I}_{\{N\geq 2\}}\sum_{n=0}^{N-2}g_{\bar{\gamma}_N,\infty}^{(n)}(\theta)$$

$$J_{a_N,b_N}^{(N)}(\theta)=\sum_{i=1}^{N}\theta^{-i}\Big[f_{\boldsymbol{a}_0^{N-i}}^{(N-i)}(a_N)e^{-\theta a_N}-f_{\boldsymbol{a}_0^{N-i}}^{(N-i)}(b_N)e^{-\theta b_N}\Big]-\mathbb{I}_{\{N\geq 2\}}\sum_{n=0}^{N-2}g_{a_N,b_N}^{(n)}(\theta).$$

We next show how to apply these preparatory results to evaluate the exact false-alarm probability.

False-Alarm Probability

Define $E_N := \{\Lambda_N \geq b \text{ and } a < \Lambda_n < b \text{ for } n \in \aleph_1^{N-1} \text{ with } N \in \aleph_1^{M-1}\}$ and $E_M := \{\Lambda_M \geq \gamma \text{ and } a < \Lambda_n < b \text{ for } n \in \aleph_1^{M-1}\}$ and let $P_{H_0}(E_N)$ be the probability of event E_N occurring under H_0. Since the test procedure described in (8), (9), and (10) is the same as that described in (12) (13), and (14), we have

$$P_{H_0}(E_N) = \begin{cases} P_{H_0}(a_i < \xi_i < b_i, i \in \aleph_1^{N-1}; \xi_N \geq b_N), \text{for } N \in \aleph_1^{M-1}; \\ P_{H_0}(a_i < \xi_i < b_i, i \in \aleph_1^{M-1}; \xi_M \geq \bar{\gamma}_M), \text{for } N = M. \end{cases} \tag{17}$$

Clearly, the false-alarm probability α_{ssct} can be written $\alpha_{\text{ssct}} = \sum_{N=1}^{M} P_{H_0}(E_N)$. The following proposition gives the exact false-alarm probability α_{ssct}.

Proposition 1. *The false-alarm probability, α_{ssct}, is given by $\alpha_{ssct} = \sum_{N=1}^{M} P_{H_0}(E_N)$, where $P_{H_0}(E_N)$ is given by*

$$P_{H_0}(E_N) = \begin{cases} A_N \dfrac{b_1 b_N^{N-2}}{(N-1)!}, \ N \in \aleph_1^{P+1}; \\ A_N \Big[f_{\boldsymbol{a}_0^{N-1}}^{(N-1)}(b_{N-1}) - \mathbb{I}_{\{N \geq 3\}} \displaystyle\sum_{n=0}^{N-3} e^{\frac{b_{n+1}}{2}} \frac{P_{H_0}(E_{n+1})(b_{N-1} - b_{n+1})^{N-n-1} 2^n}{(N-n-1)!} \Big], \\ \qquad\qquad\qquad\qquad\qquad\qquad\qquad\qquad N \in \aleph_{P+2}^{Q+1}; \\ A_N \Big[f_{\boldsymbol{a}_0^{N-1}}^{(N-1)}(b_{N-1}) - \displaystyle\sum_{n=0}^{N-3} f_{\boldsymbol{\psi}_{n,a_{N-1}}^{N-1}}^{(N-1-n)}(b_{N-1}) 2^n e^{\frac{b_{n+1}}{2}} P_{H_0}(E_{n+1}) \Big], \ N \in \aleph_{Q+2}^{M-1}; \\ 2^{-M} J_{\bar{\gamma}_M, \infty}^{(M)}(1/2), \ N = M, \end{cases} \tag{18}$$

where $A_N := 2^{-(N-1)} e^{-b_N/2}$.

Misdetection Probability

We now show how to evaluate the misdetection probability β_{ssct} for SSCT. Evaluating β_{ssct} is more difficult than evaluating α_{ssct}. The main reason is that to compute β_{ssct}, one needs to know $q_1(v_i)$. However, computing $q_1(v_i)$ is intractable except when primary signal samples have the constant-modulus property, i.e., $|s_i|^2 = \sigma_s^2$. We next show that at a relatively low detection SNR level, the misdetection probability obtained by using constant-modulus primary signals can be used to well approximate the actual β_{ssct}. Our arguments are primarily based on the following two properties of SSCT.

The first property shows that as N approaches infinity, the distribution of the test statistic ξ_N in SSCT converges to a normal distribution that is independent of a specific choice of $\lambda_1, \lambda_2, \ldots, \lambda_N$.

Property 1. *The statistical distribution of ξ_N converges to a normal distribution given by*

$$\xi_N \sim \begin{cases} \mathcal{N}(2N, 4N), & \text{under } H_0, \\ \mathcal{N}\big(2N(1+\mathtt{SNR}_m), 4N(1+2\mathtt{SNR}_m)\big), & \text{under } H_1, \end{cases}$$

as N approaches infinity.

The property can be readily proved by using CLT [39]. However, unlike energy detection, this property alone is not sufficient to explain that the constant-modulus assumption is valid in approximating β_{ssct}. This is because each ξ_N for $N = 1, \ldots, M$, including small values of N, may potentially affect the value of β_{ssct}. To complete our argument, we first present the following definitions. Let $\tilde{\xi}_i$ denote the test statistic using the constant-modulus assumption, i.e., $|s_i|^2 = \sigma_s^2$. Define $\rho_N := b_N$ for $N \in \aleph_1^{M-1}$ and $\rho_M := \bar{\gamma}_M$ for $N = M$. Let F_N and $\tilde{F}_N$ denote the events that $\xi_N \geq \rho_N$, and $a_i < \xi_i < b_i$ for $i \in \aleph_1^M$, and $\tilde{\xi}_N \geq \rho_N$ and $a_i < \tilde{\xi}_i < b_i$ for $i \in \aleph_1^M$, respectively. Let $P_{H_1}(F_N)$ and $P_{H_1}(\tilde{F}_N)$ denote the probabilities of the events F_N and $\tilde{F}_N$ under H_1. Let $\tilde{\beta}_{\text{ssct}}$ denote the misdetection probability obtained by assuming constant-modulus signals with average symbol energy σ_s^2, i.e., $|s_i|^2 = \sigma_s^2$. As clear from their definitions, we have $\beta_{\text{ssct}} = \sum_{N=1}^{M} P_{H_1}(F_N)$ and $\tilde{\beta}_{\text{ssct}} = \sum_{N=1}^{M} P_{H_1}(\tilde{F}_N)$.

Let $\mathscr{A}_N^{l_N}$ denote the event that $a_i < \xi_i < b_i$, $i \in \aleph_1^{l_N}$ for some integer $l_N \in \aleph_1^N$, and let $\tilde{\mathscr{A}}_N^{l_N}$ denote its counterpart for the constant-modulus case. Let $\mathscr{B}_N^{l_N}$ denote the event that $\xi_N \geq \rho_N$ and $a_i < \xi_i < b_i$, $i \in \aleph_{l_N+1}^N$ and let $\tilde{\mathscr{B}}_N^{l_N}$ denote its counterpart in the constant-modulus case. We now present the second property.

Property 2. *For any $\varepsilon > 0$, if for each N, there exists a positive integer $l_N \in \aleph_1^N$ such that $P_{H_1}(\mathscr{A}_N^{l_N}) \geq 1 - \varepsilon/(3M)$, $P_{H_1}(\tilde{\mathscr{A}}_N^{l_N}) \geq 1 - \varepsilon/(3M)$, and $|P_{H_1}(\mathscr{B}_N^{l_N}) - P_{H_1}(\tilde{\mathscr{B}}_N^{l_N})| < \varepsilon/(3M)$, then $|\beta_{ssct} - \tilde{\beta}_{ssct}| \leq \varepsilon$.*

Relying on these two properties, we provide an outline of our arguments. To achieve a high detection accuracy at a low SNR level, ASN and M are typically quite large. When the sample index N is relatively small, it is highly unlikely that the test statistics ξ_N and $\tilde{\xi}_N$ cross either of the two boundaries. In such a situation, there exists some integer l_N such that $P_{H_1}(\mathscr{A}_N^{l_N})$ and $P_{H_1}(\tilde{\mathscr{A}}_N^{l_N})$ are fairly close to 1, whereas $P_{H_1}(\mathscr{B}_N^{l_N})$ and $P_{H_1}(\tilde{\mathscr{B}}_N^{l_N})$ are fairly close to 0. Hence, the conditions in Property 2 can be easily satisfied. On the other hand, when N is relatively large, one can find a sufficiently large l_N such that $P_{H_1}(\mathscr{A}_N^{l_N})$ and $P_{H_1}(\tilde{\mathscr{A}}_N^{l_N})$ are fairly close to one, while $|P_{H_1}(\mathscr{B}_N^{l_N}) - P_{H_1}(\tilde{\mathscr{B}}_N^{l_N})|$ is sufficiently small due to Property 1 guaranteed by the CLT. Collectively, at a low detection SNR level, $\tilde{\beta}_{\text{ssct}}$ evaluated under the constant-modulus assumption is a close approximation of

β_{ssct}. Therefore, we will focus on the case in which all λ_i's are equal to a constant $\lambda := 2|h|^2\sigma_s^2/\sigma_w^2 = 2\text{SNR}_m$.

Recall that under H_1, v_i is a noncentral chi-square random variable, whose PDF involves the zeroth-order modified Bessel function of the first kind as given in (5). Hence, it is mathematically intractable to evaluate $\tilde{\beta}_{\text{ssct}}$ by applying the computational approach used in section "False-Alarm Probability." To obtain $\tilde{\beta}_{\text{ssct}}$, we apply a numerical integration algorithm proposed in [38].

Defining $u_i = v_i - \bar{\Delta}$, we express $\bar{\Lambda}_N$ in (11) as $\bar{\Lambda}_N = \sum_{i=1}^{N} u_i$. Clearly, the PDF of u_i under hypothesis H_1 can be rewritten as

$$q_1(u_i) = \frac{1}{2} e^{-(u_i+\bar{\Delta}+\lambda)} I_0\Big(\sqrt{\lambda(u_i+\bar{\Delta})}\Big), u_i > -\bar{\Delta}.$$

Note that SSCT observes at most M samples before making a decision. Let t_k denote $\bar{\Lambda}_{M-k}$. We also use $G_k(t_k)$ to denote the conditional misdetection probability conditioning on the follow event: the first $(M-k)$ samples have been collected, the present observation value is $t_k = \bar{\Lambda}_{M-k}$, and the test statistic of the previous $(M-k-1)$ samples has not crossed either the upper or lower boundary. When $\bar{a} < t_k < \bar{b}$ for $k = 1, \ldots, M$, SSCT needs to collect an additional sample (the $(M-k+1)$th sample). For notation simplicity, we use u to denote the next observed value of u_i. We can write the conditional probability $G_k(t_k|u)$ as

$$G_k(t_k|u) = \begin{cases} 0 & \text{if } u > \bar{b} - t_k \\ 1 & \text{if } u < \bar{a} - t_k \\ G_{k-1}(t_k + u) & \text{if } \bar{a} - t_k \le u \le \bar{b} - t_k. \end{cases} \tag{19}$$

Using (19), we can compute $G_k(t_k)$ as

$$G_k(t_k) = \int_{-\infty}^{\bar{a}-t_k} q_1(u)du + \int_{\bar{a}-t_k}^{\bar{b}-t_k} G_{k-1}(t_k+u)q_1(u)du \tag{20}$$

for $k = 1, \cdots, M$ with the following initial condition: $G_0(t_0) = 0$ if $t_0 \ge \bar{\gamma}$ and $G_0(t_0) = 1$, otherwise. Note that $G_M(0)$ is indeed the misdetection probability $\tilde{\beta}_{\text{ssct}}$. By applying the backward recursion algorithm described above, the value of $G_M(0)$ is obtained.

Evaluation of the Average Sample Number

In this section, we discuss how to evaluate ASN of the proposed algorithm. Let N_s denote the number of samples required to yield a decision. Clearly, N_s is a RV in SSCT, and its mean value is ASN, which can be written as

$$E(N_s) = E_{H_0}(N_s)\pi_0 + E_{H_1}(N_s)\pi_1 \tag{21}$$

where $E_{H_i}(N_s)$ denotes ASN under H_i, and π_i denotes the priori probability of hypothesis H_i, for $i = 0, 1$.

According to (8), (9), and (10), we have $1 \leq N_s \leq M$. Hence, we can express $E_{H_i}(N_s)$ as

$$E_{H_i}(N_s) = \sum_{N=1}^{M} N P_{H_i}(N_s = N),\ i = 0, 1 \tag{22}$$

where $P_{H_i}(N_s = N)$ is the probability that the detector makes a decision at the Nth sample under H_i. We now need to determine $P_{H_i}(N_s = N)$. Let $\mathscr{C}_N$ denote the event that the test statistics $(\xi_1, \xi_2, \ldots, \xi_N)$ do not cross either the upper or lower boundary before or at the Nth sample, i.e., $\mathscr{C}_N = \{(\xi_1, \xi_2, \ldots, \xi_N) \in \Upsilon^{(N)}_{a_N, b_N}\}$ for $N \in \aleph_1^M$. For notional convenience, let us define $\mathscr{C}_0$ as a universe set. Hence, we have $P(\mathscr{C}_0) = 1$. The test procedure described in (12) (13), and (14) implies that $P_{H_i}(N_s = N),\ i = 0, 1$ can be obtained as

$$P_{H_i}(N_s = N) \overset{(a)}{=} P_{H_i}\left(\mathscr{C}_{N-1}\right) - P_{H_i}\left(\mathscr{C}_N\right),\ N \in \aleph_1^{M-1} \tag{23}$$

$$P_{H_i}(N_s = M) \overset{(b)}{=} P_{H_i}\left(\mathscr{C}_{M-1}\right), \qquad N = M \tag{24}$$

where $P_{H_i}(\mathscr{C}_{N-1})$ and $P_{H_i}(\mathscr{C}_N)$ in (a) denote the respective probabilities of the following events: under H_i, the test statistic does not cross either the upper or lower boundary before or at the $(N-1)$th sample and the Nth sample for $N \in \aleph_1^{M-1}$; and $P_{H_i}(\mathscr{C}_{M-1})$ in (b) denotes the probability of the following event: under H_i, the test statistic does not cross either upper or lower boundary before or at the $(M-1)$th sample. Clearly, using (23) and (24), we can express (22) as

$$E_{H_i}(N_s) = \sum_{N=1}^{M-1} N\left(P_{H_i}(\mathscr{C}_{N-1}) - P_{H_i}(\mathscr{C}_N)\right) + M P_{H_i}(\mathscr{C}_{M-1}) = 1 + \sum_{N=1}^{M-1} P_{H_i}(\mathscr{C}_N). \tag{25}$$

Applying (23), and (24), we obtain $P_{H_0}\left(\mathscr{C}_N\right) = 2^{-N} J^{(N)}_{a_N, b_N}(1/2),\ N \in \aleph_1^{M-1}$. Hence, according to (25), we have

$$E_{H_0}(N_s) = 1 + \sum_{N=1}^{M-1} 2^{-N} J^{(N)}_{a_N, b_N}(1/2). \tag{26}$$

We next show how to obtain $P_{H_1}(\mathscr{C}_N)$ or equivalently how to obtain $P_{H_1}(\mathscr{C}_N^c)$. To compute $P_{H_1}(\mathscr{C}_N^c)$, we apply a similar computation method to the one used in computing the misdetection probability. It should be noted that $\mathscr{C}_N^c$ indicates the following event: under H_1, the test procedure given in (12) (13), and (14) stops before or at the Nth sample, i.e., the test statistic crosses either the upper or lower

boundary before or at the Nth sample. With a slight abuse of notation, we rewrite $G_k(t_k)$ as $G_k(t_k, \bar{\gamma})$. We use V_N to denote the following event: the test statistic crosses the lower boundary before or at the Nth sample under H_1, and we use U_N to denote the following event: the test statistic *does not* cross the upper boundary before or at the Nth sample under H_1. By the definitions of V_N, U_N, and G_N, we have $P_{H_1}(V_N) = G_N(0, \bar{a})$ and $P_{H_1}(U_N) = G_N(0, \bar{b})$. Clearly, we can write $P_{H_1}(\mathscr{C}_N^c)$ as

$$P_{H_1}\left(\mathscr{C}_N^c\right) = G_N(0, \bar{a}) + 1 - G_N(0, \bar{b}) \tag{27}$$

where $G_N(t, \bar{a})$ and $G_N(t, \bar{b})$ can be obtained by applying (20) recursively. From (27), we have $P_{H_1}(\mathscr{C}_N) = G_N(0, \bar{b}) - G_N(0, \bar{a})$. According to (25), we have

$$E_{H_1}(N_s) = 1 + \sum_{N=1}^{M-1} (G_N(0, \bar{b}) - G_N(0, \bar{a})). \tag{28}$$

In the following proposition, we present the ASN of SSCT.

Proposition 2. *The ASN of SSCT can be obtained as*

$$E(N_s) = \pi_0 \left(1 + \sum_{N=1}^{M-1} 2^{-N} J_{a_N, b_N}^{(N)}(1/2)\right) + \pi_1 \left(1 + \sum_{N=1}^{M-1} (G_N(0, \bar{b}) - G_N(0, \bar{a}))\right).$$

Numerical Examples

In this section, we present several numerical examples to test the SSCT algorithm and validate the results obtained in sections "Evaluations of False-Alarm and Misdetection Probabilities" and "Evaluation of the Average Sample Number." In these examples, the parameter $\bar{\Delta}$ is selected to be $2 + \mathtt{SNR}_m$. With this choice of $\bar{\Delta}$, we have $E_{H_0}(|r_i|^2 - \Delta) = E_{H_1}(|r_i|^2 - \Delta) = -\sigma_s^2/2$ and thus $E_{H_0}(\Lambda_N) = -E_{H_1}(\Lambda_N)$ for every $N \geq 0$. It implies that statically, the test statistic Λ_N moves the same distance on average upward or downward at each step. Roughly speaking, such choice of the parameter Δ will lead to an approximately same average sample number under H_0 or H_1. In the first three test examples, we select the parameter M to be the minimum required sample number $M_{\text{ed}}^{\min}$ for energy detection to achieve the target false-alarm and misdetection probabilities, and we choose $\bar{a}$ to be $-\bar{b}$. In all test examples, the channel gains $|h|$ are equal to one, and primary signals are constant-modulus quadrature phase shift-keying (QPSK) signals except for Test Example 2, in which the modulation formats of the primary signals are explicitly stated. Following conventional terminology in the sequential detection, we define the efficiency of SSCT as $\mathscr{E}_{\text{SSCT}} = 1 - \text{ASN}_{\text{SSCT}}/M_{\min}^{ed}$.

Table 1 SCCT versus energy detection

$\mathtt{SNR}_m$ (dB)	0	−5	−10	−15
$\bar{\gamma}$	−8.5	−5.69	−4	−1.897
$\bar{b}$	27	35.32	69.30	158.47
$\bar{\Delta}$	3	2.316	2.100	2.032
α_{ssct} (Monte Carlo)	0.011	0.055	0.103	0.153
α_{ssct} (Numerical)	0.011	0.055	0.103	0.153
α_{ed} (Energy detect.)	0.011	0.055	0.101	0.150
β_{ssct} (Monte Carlo)	0.008	0.046	0.099	0.154
β_{ssct} (Numerical)	0.008	0.047	0.100	0.156
β_{ed} (Energy detect.)	0.008	0.046	0.096	0.149
ASN (Monte Carlo)	26	95	509	3154
ASN (Numerical)	26	96	515	3185
M (Energy detect.)	40	140	730	4450
Efficiency η	35%	32%	30%	29%

Test Example 1: Table 1 lists false-alarm and misdetection probabilities and ASN for different $\mathtt{SNR}_m$ for both SSCT and energy detection. For $\mathtt{SNR}_m = 0, -5, -10$, and -15 dB, we select the corresponding truncation sizes to be the minimum sample sizes required by energy detection to achieve $(\bar{\alpha}_{\text{ed}}, \bar{\beta}_{\text{ed}}) = (0.01, 0.01), (0.05, 0.05)$, $(0.1, 0.1)$, and $(0.15, 0.15)$, respectively. The parameters $\bar{b}$, $\bar{\Delta}$, and $\bar{\gamma}$ are given in the table. Table 1 shows that while maintaining a comparable detection performance, SSCT is capable of achieving about $29\% \sim 35\%$ savings in terms of the average sensing time as compared with energy detection. We use an abbreviation, numerical, in the parenthesis, to indicate the results obtained by either the exact formula (18) for false-alarm probabilities or by the numerical integration algorithm for misdetection probabilities. As can be seen from the table, the results obtained by the numerical approach and those obtained by the Monte Carlo simulation are fairly close.

Test Example 2: In this example, we assume that primary signals are square 64-quadrature amplitude modulation (QAM) signals with $\sigma_s^2 = 10^{\mathtt{SNR}_m/10}\sigma_w^2$. Table 2 lists misdetection probabilities and ASN for SSCT and energy detection when $\mathtt{SNR}_m = 0, -5, -10$, and -15 dB. To demonstrate the fact that SSCT does not rely on the knowledge of the modulation format of primary signals, we determine the parameters $\bar{a}$, $\bar{b}$, $\bar{\gamma}$, $\bar{\Delta}$, and M in SSCT, by applying QPSK signals with average symbol energy $\sigma_s^2 = 10^{\mathtt{SNR}_m/10}\sigma_w^2$ while we apply these design parameters determined by QPSK primary signals to detect the i.i.d. 64-QAM signal samples, which are drawn from 64-QAM constellation points with equal probability. It is evident from the table that the misdetection probabilities obtained in the 64-QAM case and the QPSK case match well except for the case of $\mathtt{SNR}_m = 0$ dB (correspondingly, $M = 40$). This is because M is not large enough to neglect errors caused by using the CLT approximation. However, the energy detection and SSCT sensing algorithms have a similar amount of approximation error in terms of the misdetection probability.

Table 2 Detection performance without knowing modulation types of the primary signals

$\mathtt{SNR}_m$ (dB)	0	−5	−10	−15
β_{ssct} (QPSK,Monte Carlo)	0.008	0.046	0.099	0.154
β_{ssct} (QPSK,Numerical)	0.008	0.047	0.100	0.156
β_{ed} (QPSK,Energy detect.)	0.008	0.046	0.096	0.149
β_{ssct} (64-QAM,Monte Carlo)	0.012	0.048	0.099	0.154
β_{ssct} (64-QAM,Numerical)	0.012	0.050	0.103	0.157
β_{ed} (64-QAM,Energy detect.)	0.012	0.047	0.096	0.149
ASN (QPSK,Monte Carlo)	26	95	509	3154
ASN (QPSK,Numerical)	26	96	515	3185
ASN (64-QAM,Monte Carlo)	26	95	509	3154
ASN (64-QAM,Numerical)	26	96	514	3190

Table 3 Mismatch between $\mathtt{SNR}_m$ and $\mathtt{SNR}_o$ ($\mathtt{SNR}_m = -15$ dB)

$\mathtt{SNR}_o$ (dB)	−12	−13	−14	−15
β_{ssct} (Monte Carlo)	0.0018	0.0153	0.0629	0.154
β_{ssct} (Numerical)	0.0017	0.0151	0.0628	0.156
β_{ed} (Energy detect.)	0.0012	0.0131	0.0584	0.149
ASN (Monte Carlo)	2425	2686	2948	3154
ASN (Numerical)	2499	2769	3035	3185
M (Energy detect.)	4450	4450	4450	4450
$\mathscr{E}_{ssct}$	46%	40%	34%	29%

Test Example 3: In this example, we study the detection performance of SSCT and the energy detection when there is a mismatch between $\mathtt{SNR}_o$ and $\mathtt{SNR}_m$. For $\mathtt{SNR}_o = -12, -13, -14$ dB, and $\mathtt{SNR}_m = -15$ dB, the false-alarm and misdetection probabilities and ASN are listed in Table 3. We choose the parameters for SSCT and energy detection such that target false-alarm and misdetection probabilities are around $(0.15, 0.15)$ at $\mathtt{SNR}_m = -15$ dB. As can be seen from the table, for both SSCT and energy detection, the misdetection probabilities decrease as $\mathtt{SNR}_o$ increases, while the false-alarm probabilities keep the same. It is clear from the table that the false-alarm and misdetection $(\alpha_{\text{ssct}}, \beta_{\text{ssct}})$ satisfy the target detection error probability requirements. As the mismatch between $\mathtt{SNR}_o$ and $\mathtt{SNR}_m$ increases, the efficiency of SSCT increases from 29% to 46%. This implies that compared with the energy detection, SSCT offers an additional flexibility in striking a desirable sensing time and detection performance trade-off in the SNR mismatch case.

Quickest Spectrum Scanning

In this section, we consider the problem of how to determine the availability of each spectrum band in a multiband primary system with small delay and small error probabilities using a single or few sensors. With one or a small number of

sensors, secondary users (SUs) are able to observe one band or a small subset of candidate bands at a time. Two scenarios of practical interests are investigated. In the first scenario, there is a strict delay constraint on the spectrum scanning. That is, the spectrum scanning needs to be complete within a certain time period. In the second scenario, there is no strict time constraint for the scanning. That is, the spectrum scanning continues until the completion of the entire detection process. In both scenarios, our goal is to design spectrum scanning schemes that minimize a cost function that strikes a balance between error probabilities and detection delay.

System Model and Problem Formulation

In the system considered, the SU can make simultaneous observations on a subset of M spectrum bands from the set $\mathscr{K}$, which consists of all K candidate spectrum bands. Let $r_i^{(k)}$ denote the signal sample received by the SU, at time i from band k. Compared with section "Sequential Detection for Single Channel," we have multiple channels in this section, and hence we additionally use (k) to denote the channel index. If there is no primary transmission over band k at time i, then the received signal sample $r_i^{(k)}$ can be written as $r_i^{(k)} = w_i^{(k)}$, in which $w_i^{(k)}$ is the background noise, whereas, if there is a primary transmission over band k at time i, then $r_i^{(k)}$ can be written as $r_i^{(k)} = h^{(k)} s_i^{(k)} + w_i^{(k)}$, in which $h^{(k)} s_i^{(k)}$ is the primary signal sample. Mathematically, the detection of the primary signals at the kth band can be formulated as a binary hypothesis testing problem as follows:

$$\begin{aligned} H_0^{(k)} &: r_i^{(k)} = w_i^{(k)}, \quad i = 1, 2, \cdots, \\ H_1^{(k)} &: r_i^{(k)} = h^{(k)} s_i^{(k)} + w_i^{(k)}, \quad i = 1, 2, \cdots \end{aligned} \tag{29}$$

where $H_0^{(k)}$ refers to the hypothesis that channel k is free and $H_1^{(k)}$ refers to the hypothesis that channel k is occupied. We use $q_0^{(k)}(\cdot)$ to denote the density function of the signal received at the k^{th} band when there is only noise and use $q_1^{(k)}(\cdot)$ to denote the density function of the signal received at the k^{th} band when there is primary signal. The algorithms developed in this chapter work for any form of density functions $q_0^{(k)}(\cdot)$ and $q_1^{(k)}(\cdot)$. Furthermore, for generality, we allow the density functions to be different for different k.

Let $\pi_0^{(k)}$ denote the a priori probability that band k is occupied by the primary user (PU). Generally speaking, the values of $\pi_0^{(k)}$ can be different for different bands. We further assume that the status (occupied/unoccupied) of each band is independent of the status of other bands and the channel status remains unchanged during the scanning process. Our goal is to design an algorithm to decide the presence/absence of the PU on each band in a way that minimizes an appropriate measure, which takes into account detection error probabilities and the sampling

cost. We consider a sequential testing setup in which the SU needs to detect the status of all K candidate spectrum bands. At each time i, the SU tunes to a subset of bands $\mathscr{M}$ from the set $\mathscr{K}$ to make an observation, the set $\mathscr{M}$ has a size of M that represents the number of simultaneous observations. After taking one observation each from these M bands, the detector needs to decide whether to terminate the scanning or to continue. Let τ denote the *termination rule* that SU uses to decide whether or not to terminate the scanning. If SU terminates the scanning at time i, then it determines the occupancy of all bands using a *terminal decision rule* $\boldsymbol{\delta}_i = (\delta_i^{(1)}, \cdots, \delta_i^{(K)})$, in which $\delta_i^{(k)}$ takes values in $\{0, 1\}$ with 0 indicating that band k is free and 1 indicating that band k is occupied. Let $\boldsymbol{\delta} = \{\boldsymbol{\delta}_i,\ i = 1, 2, \cdots\}$ denote the sequence of decision rules used at the SU. If SU chooses to continue scanning, then it uses the *band selection function* ϕ_i to select M bands from the set $\mathscr{K}$ and makes another observation from the selected band. We use $\boldsymbol{\phi} = \{\phi_i,\ i = 1, 2, \ldots, \}$ to denote the sequence of band selection functions. At the end of the scanning process, there are two types of error probabilities for band k. The first one is the false-alarm probability $P_{FA}^{(k)}$ that is the probability of declaring hypothesis $H_1^{(k)}$ is true, while hypothesis $H_0^{(k)}$ is true, and the second one is the misdetection probability $P_{MD}^{(k)}$ that is the probability of declaring hypothesis $H_0^{(k)}$ to be true while hypothesis $H_1^{(k)}$ is true.

Intuitively speaking, the lower $P_{FA}^{(k)}$ is, the higher number of spectrum bands are successfully identified as free and hence more secondary transmission opportunities can be exploited. Whereas the lower $P_{MD}^{(k)}$ is, the lower the probability that the SU interferes with primary transmissions. Both types of error probabilities can be made arbitrarily small by letting the number of samples go to infinity. However, this will incur significant delay to reach a decision. Therefore, an appropriate cost function needs to strike a desirable trade-off between the decision delay and the detection error probabilities. In this chapter, we aim to determine the *termination rule* τ, the *terminal decision rules* $\boldsymbol{\delta}$ and the *band selection rules* $\boldsymbol{\phi}$ that minimize the cost

$$\inf_{\tau, \boldsymbol{\delta}, \boldsymbol{\phi}} \left[c\mathbb{E}\{\tau\} + \sum_{k=1}^{K} \left(c_0^{(k)} (1 - \pi_0^{(k)}) P_{FA}^{(k)} + c_1^{(k)} \pi_0^{(k)} P_{MD}^{(k)} \right) \right], \tag{30}$$

where $\mathbb{E}$ is expectation under the probability measure $\boldsymbol{q}_\pi = [q^{(1)}, q^{(2)}, \ldots, q^{(K)}]$ with $q^{(k)} := (1 - \pi_0^{(k)}) q_0^{(k)} + \pi_0^{(k)} q_1^{(k)}$. The parameter c denotes the cost of unit delay, and hence the term $c\mathbb{E}\{\tau\}$ in the cost function represents the average cost of scanning delay. Similarly, $c_0^{(k)}$ denotes the cost of a false-alarm event happening over band k, and $c_1^{(k)}$ denotes the cost of a misdetection event happening over band k. For generality, we allow $c_0^{(k)}$ and $c_1^{(k)}$ to be different for different bands. Clearly, the term $(1 - \pi_0^{(k)}) c_0^{(k)} P_{FA}^{(k)} + \pi_0^{(k)} c_1^{(k)} P_{MD}^{(k)}$ is the average cost of detection errors over band k. Hence, the cost function specified in (30) takes into consideration detection error probabilities and sampling cost, which are two key parameters closely related to the throughput of the SU systems.

Two different scenarios will be considered. In the first scenario, the SU needs to stop the scanning by time T. That is, the stopping time τ is restricted to a finite interval $[0, T]$, called the delay-constrained scenario. This models the situation in which there is a strict delay constraint. In the second scenario, there is no delay constraint on the scanning time, called the non-delay-constrained scenario. Relying on results from optimal stopping theory, we obtain optimal solutions for both scenarios.

The Single Observation Case

In this section, we develop scanning algorithms that solve (30) for both delay-constrained and non-delay-constrained scenarios when $M = 1$, i.e., the single observation case. Hence, at time i, the detector will use the band selection rule ϕ_i to select which band to perform sensing. The results for this special case provide insights for the solution of the general case.

Let $\pi_i^{(k)}$ denote the posterior probability that band k is occupied after collecting observations up to time i. We define $\boldsymbol{\pi}_i := (\pi_i^{(1)}, \cdots, \pi_i^{(K)})$. If $\phi_i = k$, then the SU selects band k to sense at time i. Via Bayesian rule, we can update the posterior probability of band k being occupied after collecting an observation $r_i^{(k)}$ using the following equation

$$\pi_i^{(k)} = \frac{\pi_{i-1}^{(k)} q_1^{(k)}(r_i^{(k)})}{\pi_{i-1}^{(k)} q_1^{(k)}(r_i^{(k)}) + (1 - \pi_{i-1}^{(k)}) q_0^{(k)}(r_i^{(k)})}, \tag{31}$$

where the sequence $\pi_i^{(k)}$ is evaluated recursively as in [35]. For band k that is not selected at time i, the posterior probability $\pi_i^{(k)}$ is not updated, i.e., $\pi_i^{(k)} = \pi_{i-1}^{(k)}$.

At this point, it is not clear whether or not $\boldsymbol{\pi}_i$ is a sufficient statistic for the optimization problem (30). If $\boldsymbol{\pi}_i$ is a sufficient statistic, then at time i, we can make our termination rule τ, terminal decision rule $\boldsymbol{\delta}$ and band selection rule $\boldsymbol{\phi}$ solely based on $\boldsymbol{\pi}_i$. This will greatly simplify our problem. We will show below that $\boldsymbol{\pi}_i$ is indeed a sufficient statistic for the problem under study.

We first study the optimal terminal decision rule $\boldsymbol{\delta}$. For any given termination rule τ and band selection rules $\boldsymbol{\phi}$, following a standard argument in [40], it is easy to show that the following simple terminal decision rule is optimal:

$$\delta_\tau^{(k)} = \begin{cases} 1, & \text{if } \ c_1^{(k)} \pi_\tau^{(k)} \geq c_0^{(k)} (1 - \pi_\tau^{(k)}), \\ 0, & \text{if } \ c_1^{(k)} \pi_\tau^{(k)} < c_0^{(k)} (1 - \pi_\tau^{(k)}), \end{cases} \tag{32}$$

for any $k \in \{1, \ldots, K\}$. The interpretation of this decision rule is clear. More specifically, $c_1^{(k)} \pi_\tau^{(k)}$ is the average cost of making a misdetection error. That is, we declare band k to be free while band k is busy. Similarly $c_0^{(k)}(1 - \pi_\tau^{(k)})$ is the average cost of making a false-alarm error, that is we declare band k to be busy while

band k is free. Thus, we declare that band k is occupied if the cost of a misdetection event is larger than that of a false-alarm event and vice visa. This result suggests that the terminal decisions can be made only based on $\boldsymbol{\pi}_i$. With these terminal decision rules, the objective function in (30) is then converted into

$$\inf_{\tau,\boldsymbol{\phi}} \mathbb{E}\left[c\tau + \sum_{k=1}^{K} \min\left\{ c_0^{(k)}(1-\pi_\tau^{(k)}), c_1^{(k)}\pi_\tau^{(k)} \right\} \right]. \tag{33}$$

We will use results from optimal stopping theory [35] to solve this problem.

The Delay-Constrained Scenario

We first consider the scenario in which we have strict delay constraint T, i.e., we need to finish the scanning by time T. At each time instant i, the SU needs to decide whether or not to terminate the scanning based on the observations that have been collected so far. Let $\mathscr{F}_i$ denote the set of observations till time i, and let $\tilde{J}_{i,T}(\mathscr{F}_i)$ denote the minimal expected cost-to-go function at time i. This is the minimal value of the expected additional cost that will incur by any strategy between time i and T. Note that $\tilde{J}_{i,T}(\mathscr{F}_i)$ is a function of $\mathscr{F}_i$, i and T. At this stage, it is not clear what the optimal strategy between time i and T is, and it is also not clear what the form of the function $\tilde{J}_{i,T}(\mathscr{F}_i)$ is. In the following, we will obtain the form of this function recursively using dynamic programming and then obtain the optimal solution based on this function.

At first, it is clear that $\tilde{J}_{T,T} = \sum_{k=1}^{K} \min\left\{ c_0^{(k)}(1-\pi_T^{(k)}), c_1^{(k)}\pi_T^{(k)} \right\}$, since we have to stop at time T. Given $\tilde{J}_{i+1,T}(\mathscr{F}_{i+1})$, we have the following equation:

$$\tilde{J}_{i,T}(\mathscr{F}_i) = \min\left\{ \sum_{k=1}^{K} \min\left\{ c_0^{(k)}(1-\pi_i^{(k)}), c_1^{(k)}\pi_i^{(k)} \right\}, c + \inf_{\phi_i} \mathbb{E}\left\{ \tilde{J}_{i+1,T}(\mathscr{F}_{i+1}) | \mathscr{F}_i, \phi_i \right\} \right\}.$$

In this equation, the term $\sum_{k=1}^{K} \min\left\{ c_0^{(k)}(1-\pi_i^{(k)}), c_1^{(k)}\pi_i^{(k)} \right\}$ is the additional cost that will incur if the SU decides to stop scanning at time i. The term

$$c + \inf_{\phi_i} \mathbb{E}\left\{ \tilde{J}_{i+1,T}(\mathscr{F}_{i+1}) | \mathscr{F}_i, \phi_i \right\}$$

is the minimal expected additional cost that will incur if the SU does not stop at time i. Note that the term $\mathbb{E}\left\{ \tilde{J}_{i+1,T}(\mathscr{F}_{i+1}) | \mathscr{F}_i, \phi_i \right\}$ depends on $\mathscr{F}_i$, the observation up to time i and ϕ_i, the band selection rule. Hence, $\tilde{J}_{i,T}(\mathscr{F}_i)$ also depends on the entire observation up to time i, namely, $\mathscr{F}_i$. The following lemma shows that one can greatly simplify the form of these functions.

Lemma 4. *For each i, the minimal expected cost-to-go function $\tilde{J}_{i,T}(\mathscr{F}_i)$ can be written as a function of $\boldsymbol{\pi}_i$, say, $J_{i,T}(\boldsymbol{\pi}_i)$ and the optimal band selection function ϕ_i depends only on $\boldsymbol{\pi}_i$.*

Proof. We will prove the lemma by induction. Clearly,

$$\tilde{J}_{T,T}(\mathscr{F}_T) = \sum_{k=1}^{K} \min\left\{c_0^{(k)}(1-\pi_T^{(k)}), c_1^{(k)}\pi_T^{(k)}\right\} \tag{34}$$

is a function of $\boldsymbol{\pi}_T$ only. Let $J_{T,T}(\boldsymbol{\pi}_T)$ denote this function.

Suppose that $\tilde{J}_{i+1,T}(\mathscr{F}_{i+1})$ depends on $\boldsymbol{\pi}_{i+1}$ only. Let us use $J_{i+1,T}(\boldsymbol{\pi}_{i+1})$ to denote it. We now show that $\tilde{J}_{i,T}(\mathscr{F}_i)$ depends on $\boldsymbol{\pi}_i$ only. First, we have

$$\begin{aligned}\tilde{J}_{i,T}(\mathscr{F}_i) &= \min\left\{\sum_{k=1}^{K} \min\left\{c_0^{(k)}(1-\pi_i^{(k)}), c_1^{(k)}\pi_i^{(k)}\right\}, c + \inf_{\phi_i} \mathbb{E}\left\{\tilde{J}_{i+1,T}(\mathscr{F}_{i+1})|\mathscr{F}_i, \phi_i\right\}\right\} \\ &= \min\left\{\sum_{k=1}^{K} \min\left\{c_0^{(k)}(1-\pi_i^{(k)}), c_1^{(k)}\pi_i^{(k)}\right\}, c + \inf_{\phi_i} \mathbb{E}\left\{J_{i+1,T}(\boldsymbol{\pi}_{i+1})|\mathscr{F}_i, \phi_i\right\}\right\}.\end{aligned}$$

Since ϕ_i admits only K possible values, the term $c + \inf_{\phi_i} \mathbb{E}\left\{J_{i+1,T}(\boldsymbol{\pi}_{i+1})|\mathscr{F}_i, \phi_i\right\}$ can be written as $c + \min_{\phi_i} \mathbb{E}\left\{J_{i+1,T}(\boldsymbol{\pi}_{i+1})|\mathscr{F}_i, \phi_i\right\}$. If $\phi_i = k$, then

$$\begin{aligned}&\mathbb{E}\left\{J_{i+1,T}(\boldsymbol{\pi}_{i+1})|\mathscr{F}_i, \phi_i = k\right\} \\ &\quad= \int J_{i+1,T}\left(\pi_i^{(1)}, \cdots, \frac{\pi_i^{(k)} q_1^{(k)}(y_{i+1}^{(k)})}{\pi_i^{(k)} q_1^{(k)}(y_{i+1}^{(k)}) + (1-\pi_i^{(k)}) q_0^{(k)}(y_{i+1}^{(k)})}, \cdots, \pi_i^{(k)}\right) \\ &\qquad\left[\pi_i^{(k)} q_1^{(k)}(y_{i+1}^{(k)}) + (1-\pi_i^{(k)}) q_0^{(k)}(y_{i+1}^{(k)})\right] dy_{i+1}^{(k)} := A_{i,T}^{(k)}(\boldsymbol{\pi}_i),\end{aligned} \tag{35}$$

since if we select band k, only the posterior probability of band k will be updated. Clearly, this is a function of $\boldsymbol{\pi}_i$, and we will use $A_{i,T}^{(k)}(\boldsymbol{\pi}_i)$ to denote this function.

As a result, we have

$$\begin{aligned}\tilde{J}_{i,T}(\mathscr{F}_i) &= \min\left\{\sum_{k=1}^{K} \min\left\{c_0^{(k)}(1-\pi_i^{(k)}), c_1^{(k)}\pi_i^{(k)}\right\}, c + \inf_{\phi_i} \mathbb{E}\left\{\tilde{J}_{i+1}^{T}(\mathscr{F}_{i+1})|\mathscr{F}_i, \phi_i\right\}\right\} \\ &= \min\left\{\sum_{k=1}^{K} \min\left\{c_0^{(k)}(1-\pi_i^{(k)}), c_1^{(k)}\pi_i^{(k)}\right\}, c + \min_{k}\left\{A_{i,T}^{(k)}(\boldsymbol{\pi}_i)\right\}\right\},\end{aligned} \tag{36}$$

is a function of $\boldsymbol{\pi}_i$ only, and we will use $J_{i,T}(\boldsymbol{\pi}_i)$ to denote this function.

Now, the optimal band selection function is given by

$$\phi_i = \arg\left\{A_{i,T}^{(k)}(\boldsymbol{\pi}_i)\right\}, \tag{37}$$

which depends on $\boldsymbol{\pi}_i$.

From this result, we know that $\boldsymbol{\pi}_i$ is a sufficient statistic for this problem. Without loss of optimality, we can make our decisions solely based on $\boldsymbol{\pi}_i$. Furthermore, since ϕ_i depends on $\boldsymbol{\pi}_i$ only, we have that $\{\boldsymbol{\pi}_i : i = 0, 1, \cdots\}$ forms a Markov process.

Regarding the functions $J_{i,T}(\boldsymbol{\pi}_i)$ and $A_{i,T}^{(k)}(\boldsymbol{\pi}_i)$, we have the following result. Let $\mathbf{0}$ denote a vector whose entries are all zeros and $\mathbf{1}$ denote a vector whose entries are all ones.

Lemma 5. *The functions $J_{i,T}(\boldsymbol{\pi}_i)$ and $A_{i,T}^{(k)}(\boldsymbol{\pi}_i)$ are non-negative concave functions of $\boldsymbol{\pi}_i$. And $J_{i,T}(\mathbf{0}) = J_{i,T}(\mathbf{1}) = A_{i,T}^{(k)}(\mathbf{0}) = A_{i,T}^{(k)}(\mathbf{1}) = 0$.*

These supporting lemmas show that the finite-horizon version of the optimization problem (33) can be converted to a Markov optimal stopping time problem [35]. Using the results from optimal stopping theory, we know that the optimal termination rule τ has the following form

$$\tau_{\text{opt}} = \inf\left\{ i : \sum_{k=1}^{K} \min\left\{ c_0^{(k)}(1-\pi_i^{(k)}), c_1^{(k)}\pi_i^{(k)} \right\} = c + \min_k \left\{ A_{i,T}^{(k)}(\boldsymbol{\pi}_i) \right\} \right\}. \quad (38)$$

That is, the optimal time to terminate the scanning is the time when the cost that will incur if SU decides to stop scanning is equal to the minimal expected cost that will incur if SU does not stop.

In summary, the optimal scanning algorithm with a deadline T is described as follows:

1. Initialization: Given the maximum sensing time T, density functions $q_0^{(k)}$ and $q_1^{(k)}$, the cost of errors $c_0^{(k)}$ and $c_1^{(k)}$, we use (34), (35), and (36) to recursively compute the functions $J_{i,T}(\boldsymbol{\pi})$ and $A_{i,T}^{(k)}(\boldsymbol{\pi})$.
2. After collecting a sample, we use (31) to update the posterior probability that a selected band is being occupied.
3. Use (37) to select which band to sense if we decide to continuing sensing.
4. Use (38) to decide whether we should terminate scanning or not. If we decide to continue scanning, go back to (2). If we decide to terminate scanning, then we use decision rule (32) to decide the availability of each band.

Remark 1. In the delay-constrained scenario, the optimal algorithm involves recursive computation of $J_{i,T}(\boldsymbol{\pi})$ and $A_{i,T}^{(k)}(\boldsymbol{\pi})$ and frequent updating of the posterior probability $\pi_j^{(k)}$. These steps incur high computational complexity and thus are the major hurdles in the implementation. We will develop several low-complexity algorithms in section "Truncated C-SPRT Schemes" based on insights gained from the non-delay-constrained scenario discussed in section "The Non-delay-Constrained Scenario."

The Non-delay-Constrained Scenario

In this section, we consider the non-delay-constrained scenario. We can obtain the optimal solution for this problem via two approaches. The first one is to let the delay constraint T defined in section "The Delay-Constrained Scenario" go to ∞. For each T, we obtain the optimal solution as outlined in section "The Delay-Constrained Scenario." As T increases, the solution will converge to the optimal solution for the case with no deadline constraint. The convergence is guaranteed by Theorem 3.7 of [35].

Another approach is to exploit the **decoupled** structure of the optimization problem (33). In the following, we will adopt this approach. For any stopping time τ, let $\tau^{(k)}$ be the amount of time we spend on detecting band k. We can express (33) as

$$c\mathbb{E}\left\{\sum_{k=1}^{K}\tau^{(k)}\right\}+\sum_{k=1}^{K}\min\left\{c_0^{(k)}(1-\pi_\tau^{(k)}),c_1^{(k)}\pi_\tau^{(k)}\right\}$$

$$=\sum_{k=1}^{K}\left\{c\mathbb{E}\{\tau^{(k)}\}+\min\left\{c_0^{(k)}(1-\pi_\tau^{(k)}),c_1^{(k)}\pi_\tau^{(k)}\right\}\right\}. \quad (39)$$

As a result, the quantity to be minimized is related to only the total amount of detection time. Particularly, the quantity is irrespective of sensing ordering $\boldsymbol{\phi}$ (band selection rules). Once $\mathbb{E}\{\tau^{(k)}\}+\min\left\{c_0^{(k)}(1-\pi_\tau^{(k)}),c_1^{(k)}\pi_\tau^{(k)}\right\}$ is minimized for each band, the summation is also minimized. One key observation is that these K optimization problems are **independent** of each other. We can minimize each term independently. Note that this is not the case for the scenario considered in section "The Delay-Constrained Scenario." In section "The Delay-Constrained Scenario", we need to stop before time T, and hence we have an additional constraint $\sum_{k=1}^{K}\tau^{(k)}\le T$, which couples these K optimization problems.

For each k, the solution that minimizes $\mathbb{E}\{\tau^{(k)}\}+\min\left\{c_0^{(k)}(1-\pi_\tau^{(k)}),c_1^{(k)}\pi_\tau^{(k)}\right\}$ is the well-known SPRT algorithm [35]. More specifically, for any c, $c_0^{(k)}$, $c_1^{(k)}$, $q_0^{(k)}$ and $q_1^{(k)}$, the solution is parameterized by two parameters $U^{(k)}$ and $L^{(k)}$. The stopping rule of the sequential test at the kth band is

$$\psi_\tau^{(k)}=\begin{cases}0, & \text{if } L^{(k)}<\pi_i^{(k)}<U^{(k)},\\ 1, & \text{otherwise,}\end{cases} \quad (40)$$

and the terminal decision rule in (32) becomes

$$\delta_\tau^{(k)}=\begin{cases}1, & \text{if } \pi_i^{(k)}\ge U^{(k)},\\ 0, & \text{if } \pi_i^{(k)}\le L^{(k)}.\end{cases} \quad (41)$$

The stopping rule in (40) requires the sequential test to continue if the posterior probability lies within the boundaries $U^{(k)}$ and $L^{(k)}$ and to stop sensing otherwise. Once the sequential test is stopped, a decision should be made based on the terminal

decision rule of (41). That is, claiming hypothesis $H_0^{(k)}$ if $\pi_i^{(k)} \leq L^{(k)}$ or claiming hypothesis $H_1^{(k)}$ if $\pi_i^{(k)} \geq U^{(k)}$. In the original Wald's SPRT [41], there is no upper limit on the number of observations required to reach a decision. This may lead to an increase in number of samples in case of ambiguous observations. However, this problem will be treated in section "Truncated C-SPRT Schemes" by truncation as we propose different truncation schemes as an alternative to the optimal multiband delay-constrained scenario.

The optimization problem does not depend on $\boldsymbol{\phi}$, and no delay constraint is imposed on the scanning process. Hence, with no loss of optimality, we can start scanning from band 1; once we finish scanning band 1, we switch to band 2. The entire scanning process is terminated, once we finish scanning band K. In summary, we have the following solution:

1. Initialization: Given density functions $q_0^{(k)}$ and $q_1^{(k)}$, the costs of errors $c_0^{(k)}$ and $c_1^{(k)}$, compute parameters $L^{(k)}$ and $U^{(k)}$.
2. Starting from band 1, after taking each sample from band k, use (31) to update the posterior probability. If $\pi^{(k)} \in (L^{(k)}, U^{(k)})$, stay on band k to collect more samples. If $\pi_k \geq U^{(k)}$, claim that band k is busy, and switch to band $k+1$ to sense. If $\pi^{(k)} \leq L^{(k)}$, claim that band k is free, and switch to band $k+1$ to sense.
3. The scanning is finished, once we finish scanning band K.

Remark 2. It is clear that the optimal algorithm is a concatenation of SPRTs (C-SPRT), which is much simpler as compared with the solution for the delay-constrained scenario.

This algorithm can be further simplified for specific density functions. Here, we give an example for Gaussian random variables. In this example, we assume

$$q_0(r_i^{(k)}) = \frac{1}{\pi[\sigma^{(k)}]^2} \exp\Big(-\frac{|r_i^{(k)}|^2}{[\sigma^{(k)}]^2}\Big), \tag{42}$$

$$\text{and} \quad q_1(r_i^{(k)}) = \frac{1}{\pi(P^{(k)} + [\sigma^{(k)}]^2)} \exp\Big(-\frac{|r_i^{(k)}|^2}{P^{(k)} + [\sigma^{(k)}]^2}\Big). \tag{43}$$

Here, $[\sigma^{(k)}]^2$ is the variance of the Gaussian noise over band k and $P^{(k)}$ is the power of the signal over band k. Let $\mathscr{S}^{(k)}$ denote the set of time slot in which we select band k to sense up to time j. Using Bayes' rule and the fact that the observations are assumed to be independent and identically distributed (i.i.d.) [40], the posterior probability can be written as

$$\pi_i^{(k)} = \frac{\pi_0^{(k)} \prod\limits_{i \in \mathscr{S}^{(k)}} q_1^{(k)}(Y_i^{(k)})}{\pi_0^{(k)} \prod\limits_{i \in \mathscr{S}^{(k)}} q_1^{(k)}(Y_i^{(k)}) + (1-\pi_0^{(k)}) \prod\limits_{i \in \mathscr{S}^{(k)}} q_0^{(k)}(Y_i^{(k)})},$$

hence $\pi_i^{(k)} > U^{(k)}$ and $\pi_i^{(k)} < L^{(k)}$ imply that

$$\frac{\prod_{l\in\mathscr{S}^{(k)}} q_1^{(k)}(Y_l^{(k)})}{\prod_{l\in\mathscr{S}^{(k)}} q_0^{(k)}(Y_l^{(k)})} > \frac{U^{(k)}(1-\pi_0^{(k)})}{\pi_0^{(k)}(1-U^{(k)})} := B_U^{(k)}, \tag{44}$$

$$\text{and} \quad \frac{\prod_{l\in\mathscr{S}^{(k)}} q_1^{(k)}(Y_l^{(k)})}{\prod_{l\in\mathscr{S}^{(k)}} q_0^{(k)}(Y_l^{(k)})} < \frac{L^{(k)}(1-\pi_0^{(k)})}{\pi_0^{(k)}(1-L^{(k)})} := B_L^{(k)},$$

respectively. Let $SNR^{(k)} = P^{(k)}/[\sigma^{(k)}]^2$ denote the signal-to-noise ratio (SNR) at band k. Since $Q_0 \sim \mathscr{CN}(0, [\sigma^{(k)}]^2)$ and $Q_1 \sim \mathscr{CN}(0, P^{(k)} + [\sigma^{(k)}]^2)$, these two equations can be further simplified as

$$\sum_{l\in\mathscr{S}^{(k)}} [Y_l^{(k)}]^2 > d^{(k)} \left(|\mathscr{S}^{(k)}| \log\left(1 + SNR^{(k)}\right) + \log B_U^{(k)} \right), \tag{45}$$

$$\sum_{l\in\mathscr{S}^{(k)}} [Y_l^{(k)}]^2 < d^{(k)} \left(|\mathscr{S}^{(k)}| \log\left(1 + SNR^{(k)}\right) + \log B_L^{(k)} \right), \tag{46}$$

in which $d^{(k)} = [\sigma^{(k)}]^2(SNR^{(k)}+1)/SNR^{(k)}$ and $|\mathscr{S}^{(k)}|$ is the size of the set $\mathscr{S}^{(k)}$.

In general, it is difficult to obtain a closed form expressions for the boundary values $B_U^{(k)}$ and $B_L^{(k)}$ [41]. Since the optimal solution is the concatenated SPRT, we can use the approximation techniques for the SPRT to simplify the computation of $B_L^{(k)}$ and $B_U^{(k)}$. In practice, we will first specify the target error probabilities. That is, $\bar{P}_{FA}^{(k)}$ and $\bar{P}_{MD}^{(k)}$ are given. Then, using Wald's approximation [35,41], we have

$$B_U^{(k)} = (1 - \bar{P}_{MD}^{(k)})/\bar{P}_{FA}^{(k)}, \quad B_L^{(k)} = \bar{P}_{MD}^{(k)}/(1 - \bar{P}_{FA}^{(k)}). \tag{47}$$

The actual false-alarm and misdetection probabilities of SPRT using upper- and lower bounds in (47) are upper bounded by the target $\bar{P}_{FA}^{(k)}$ and $\bar{P}_{MD}^{(k)}$, respectively, and more importantly the actual error probabilities become quite close to the target counterparts when $\bar{P}_{FA}^{(k)}$ and $\bar{P}_{MD}^{(k)}$ are small. In SPRT, the number of observations required to reach a decision is a random number. The average (expected) sample number (ASN) is thus considered as a useful benchmark for SPRT.

We next evaluate ASN of C-SPRT. Let us first consider the kth band. Let $\tau_l^{(k)}$ be the sample number required to reach a decision for the kth band under H_l for $l = 0, 1$. Let us define $Z_i^{(k)} := \log\left[q_1^{(k)}(Y_i^{(k)})/q_0^{(k)}(Y_i^{(k)})\right]$ and $r^{(k)} = 1/(SNR^{(k)}+1)$. We can readily compute $Z_i^{(k)}$ as

$$Z_i^{(k)} = \log r^{(k)} + |Y_i^{(k)}|^2/d^{(k)},$$

By some straightforward computation, we have

$$\mu_0^{(k)} := E[Z_i^{(k)}|H_0] = \log r^{(k)} + 1 - r^{(k)}, \text{ and } \mu_1^{(k)} := E[Z_i^{(k)}|H_1] = \log r^{(k)} + [r^{(k)}]^{-1} - 1.$$

Following from [35], we have

$$E\left[\tau_l^{(k)}|H_l\right] \approx \frac{1}{\mu_l^{(k)}} \frac{B_L^{(k)}[\exp(t_l B_U^{(k)}) - 1] + B_U^{(k)}[1 - \exp(t_l B_L^{(k)})]}{\exp(t_l B_U^{(k)}) - \exp(t_l B_L^{(k)})}, \ l = 0, 1$$

where t_l is a nonzero constant satisfying $E[\exp(t_l Z_i^{(k)})|H_l] = 1$. It can be readily determined that t_0 is equal to 1 while t_1 is equal to -1. Clearly, the overall ASN can be expressed as

$$E(\tau) = \sum_{k=1}^{K} E\left[\tau_l^{(k)}|H_0\right](1 - \pi_0^{(k)}) + E\left[\tau_l^{(k)}|H_1\right]\pi_0^{(k)}. \tag{48}$$

To compare the ASN of C-SPRT with the fixed sample size (FSS) of the energy detector, we compute the minimum FSS required to achieve target $\bar{P}_{FA}^{(k)}$ and $\bar{P}_{MD}^{(k)}$ in the multiband setup for the same density functions above. The test statistic in this case is the energy of the received signal compared to a threshold [42]. By simple manipulations, the FSS can be expressed as

$$FSS = \sum_{k=1}^{K} \left(\frac{1}{SNR^{(k)}} \left[Q^{-1}(\bar{P}_{FA}^{(k)}) - (SNR^{(k)} + 1) Q^{-1}(1 - \bar{P}_{MD}^{(k)}) \right] \right)^2. \tag{49}$$

In summary, we have the following simplified scanning scheme:

1. Given target error probabilities $\bar{P}_{MD}^{(k)}$ and $\bar{P}_{FA}^{(k)}$, we use (47) to compute $B_L^{(k)}$ and $B_U^{(k)}$.
2. After taking a sample $Y_i^{(k)}$ from band k, we use (45) and (46) to decide whether we should skip to the next band or not. If (45) is satisfied, claim that band k is busy and skip to the next band. If (46) is satisfied, then we declare that band k is free and skip to the next band. If neither of these two is satisfied, stay on band k to observe more samples.

Truncated C-SPRT Schemes

As mentioned above, the complexity of the optimal solution for the delay-constrained scenario is very high. Inspired by the solution for the scenario with no delay constraint, we propose several truncated C-SPRT that can be used for the delay-constrained scenario. In the truncated C-SPRT, SPRT will be run on

each band. However, a deadline will be imposed on each band. If SPRT does not finish before the deadline is reached, then it will be forced to finish, and a decision will be made using the information gathered at that time. In the following, we consider several truncation methods, namely, uniform truncation, tail truncation, uniformly added truncation, and sequentially added truncation. All these truncated algorithms are asymptotically optimal as the delay constraint is relaxed. In these truncation schemes, we adopt a simple scanning order (from channel 1 to channel K), which is not necessarily optimal. One can find the optimal scanning order following the steps in [43]. However, the complexity of the algorithm for finding the optimal scanning order is very high. Since our goal is to find a low complexity but asymptotically optimal schemes, we opt to use this simple scanning order.

Uniform Truncation

In the uniform truncation, we need to finish detecting each band within a period of time T/K as illustrated in Fig. 3. That is, the maximal detection time is equal for all bands. In particular, the saved time for detecting a band will not be reallocated for detecting other bands. As it can be seen from the above description, the advantage of uniform truncation is that it can always guarantee no random decision will take place in the detection process, but the disadvantage of the method is that it does not utilize the saved time from the bands that can be quickly detected.

Tail Truncation

In the tail truncation, we need to finish the detection process within a period of time T. It implies that detection time is distributed unevenly among K bands. To be specific, the maximum detection time for the kth band is $T - \sum_{l=1}^{k-1} \tau^{(l)}$ as shown in Fig. 4. Intuitively, if T is sufficiently large, then C-SPRT with tail truncation will be able to scan all the bands, thus being able to achieve a probability similar to one achieved by the non-truncated C-SPRT. If T is quite small, then it is highly likely that C-SPRT with tail truncation will not have time to finish detecting

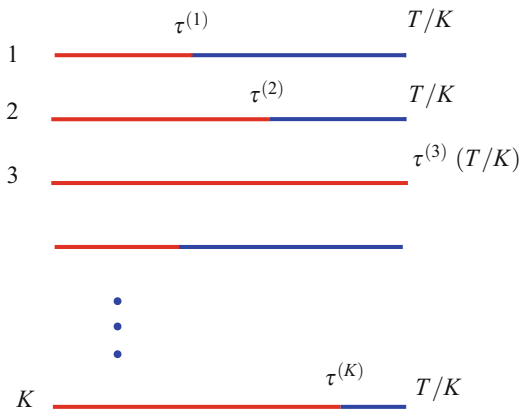

Fig. 3 An illustration of C-SPRT with the uniform truncation

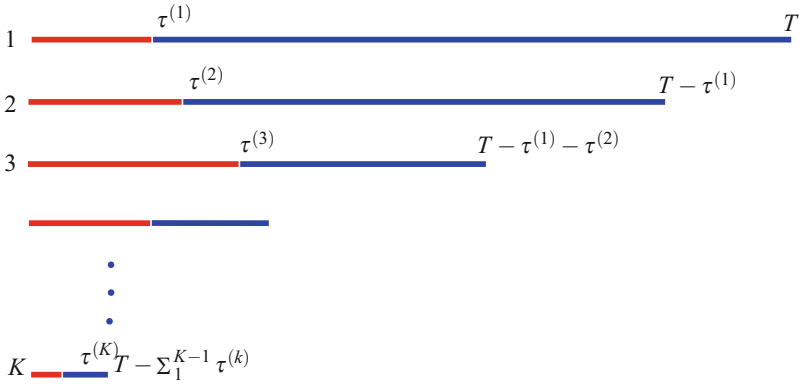

Fig. 4 An illustration of C-SPRT with the tail truncation

all K bands. In such a case, we assume that a random decision (like tossing a coin) will be made for undetected bands, thus incurring high detection errors. This is the major disadvantage of C-SPRT with tail truncation.

Uniformly Added Truncation

To overcome potential drawbacks of the uniform truncation and the tail truncation, we next present the uniformly added truncation. As shown in Fig. 5, we initially set the maximal detection time to be T. During the detection process, we will use the detection time saved in any detection stage to extend the maximal detection time for a later detection stage in a uniform manner. That is, the saved detection time will be added to the maximum detection time of the undetected bands equally. The maximum detection time for the kth band is $T/K + \Delta^{(k-1)}$, where $\Delta^{(k)}$ can be recursively computed as

$$\Delta^{(0)} = 0, \text{ and } \Delta^{(k)} = \Delta^{(k-1)} + \left\lceil \frac{T/K + \Delta^{(k-1)} - \tau^{(k)}}{K-k} \right\rceil^{+}, \ k = 1, \ldots, K-1,$$

where $\lceil x \rceil^{+}$ denotes $\max\{0, x\}$. As an example, if $K = 16$, $T = 1600$ and $\tau^{(1)} = 10$, then after detecting the first band, we save 90 sample periods and will use it to equally extend the maximum detection time for the rest 15 bands. Thus, the maximum detection time for the rest bands now is 106 sample periods. By doing so, uniformly added truncation can guarantee that no random detection will take place and the detector can fully utilize available detection time.

Sequentially Added Truncation

In the uniformly added truncation, the saved detection time will be added to the maximum detection time of the undetected bands in a uniform manner. Apparently,

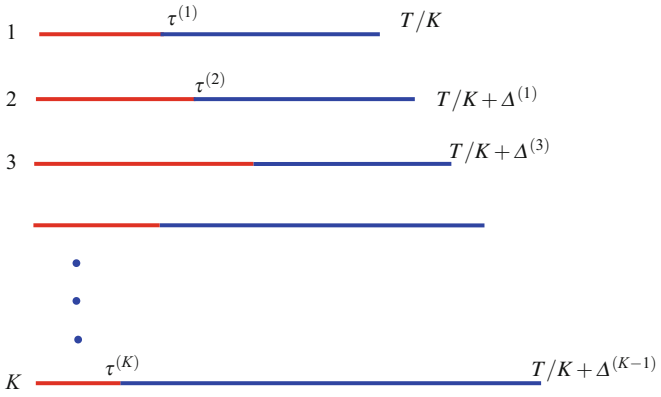

Fig. 5 An illustration of C-SPRT with the uniformly added truncation

when T is small, it may lead to too much truncation in an early detection stage. To amend this deficiency, we next propose an alternative truncation method, called the sequential added truncation. The method is the same as the uniformly add truncation except that the saved time on detecting the current band will be used to extend only the maximum detection time of the next band. The maximum detection time of the kth band can be written as $T/K + \delta^{(k-1)}$, where $\delta^{(0)} = 0$ and $\delta^{(k)} = \delta^{(k-1)} + \lceil T/K - \tau^{(k)} \rceil^+$.

Numerical Examples

In this section, we provide several numerical examples to illustrate the effectiveness of the algorithms developed in this chapter. In all the examples, we assume that $\pi_0^{(k)}$ for $k = 1, \ldots, K$ is equal to $1/2$ unless indicated otherwise, and the results are obtained by using Monte Carlo simulations. Furthermore, we assume that both noise and signal are complex Gaussian.

Table 4 compares C-SPRT in terms of false-alarm and misdetection probabilities and ASN for different SNR for $K = 4, 16, 64$ for the single observation case. In this table, we use P_{FA} and P_{MD} to denote average false-alarm and misdetection probabilities. That is, $P_{FA} = \sum_{k=1}^{K} P_{FA}^{(k)}/K$ and $P_{MD} = \sum_{k=1}^{K} P_{MD}^{(k)}/K$. As can be observed from the table, ASN increases linearly as K increases. ASN obtained by Monte Carlo simulation is quite close to one obtained by using an approximation in (48). Table 4 also compares C-SPRT and energy detection in terms of the number of samples required to achieve the same false-alarm and misdetection probabilities. As can be seen from the table, C-SPRT requires much less ASN than energy detection in the cases of $(P_{FA}, P_{MD}) = (0.1, 0.1)$ and $(P_{FA}, P_{MD}) = (0.01, 0.01)$. Furthermore, it can be observed from the table that as compared to energy detection, the lower the target error probabilities are, the higher the ASN savings can be achieved for C-SPRT.

Table 4 Detection performance of C-SPRT for $K = 4, 16, 64$

SNR (dB)	0	−5	−10
P_{FA} ($K = 4$, Monte Carlo)	0.005	0.04	0.09
P_{FA} ($K = 16$, Monte Carlo)	0.005	0.04	0.09
P_{FA} ($K = 64$, Monte Carlo)	0.005	0.04	0.09
P_{MD} ($K = 4$, Monte Carlo)	0.008	0.05	0.1
P_{MD} ($K = 16$, Monte Carlo)	0.008	0.05	0.1
P_{MD} ($K = 64$, Monte Carlo)	0.008	0.05	0.1
ASN ($K = 4$, Monte Carlo)	85	305	1615
ASN ($K = 16$, Monte Carlo)	342	1222	6468
ASN ($K = 64$, Monte Carlo)	1368	4888	25,875
ASN ($K = 4$, Numerical)	76	281	1548
ASN ($K = 16$, Numerical)	304	1126	6194
ASN ($K = 64$, Numerical)	1216	4502	24,775
ASN ($K = 16$, $P_{FA} = P_{MD} = 0.1$)	161	844	6468
FSS ($K = 16$, $P_{FA} = P_{MD} = 0.1$)	240	1424	11,600
ASN ($K = 16$, $P_{FA} = P_{MD} = 0.01$)	342	1990	16,138
FSS ($K = 16$, $P_{FA} = P_{MD} = 0.01$)	784	4656	38,192

In this example, we compare four truncation methods in terms of the false-alarm probability, the misdetection probability for different cases of SNR, the number of bands, and truncation time for the single observation case. The results of the error probabilities for three different parameter configuration cases are shown in Table 5.

Figure 6 shows ASN versus SNR for the first case. Comparing the results of P_{FA} and P_{MD} in this case (i.e., $K = 16$, $T = 3560$) and ASN in Fig. 6 yields to a conclusion that when the delay constraint is strict, all truncations suffers from large error when SNR is small while the non-truncated C-SPRT suffers from large ASN to scan all the available bands when SNR is small. The tail truncation approach suffers a large number of random decision errors and requires the largest ASN among these truncation methods to achieve similar detection performance. The overall performance shows that among the four truncation methods, the sequentially added truncation method yields the most desirable trade-off between the detection performance and the detection delay. This is because the sequentially added truncation method avoids random detection and fully utilizes available detection time. In the second case, both the number of bands K and the allowed time T are increased by a factor of 4. From Table 5, it is clear that the performance is very similar to the first case. The results in the third case shows that the average number of errors decreases considerably when the allowable delay T is increased while K is fixed. The truncated schemes perform similarly to non-truncated C-SPRT when SNR increases.

Table 5 Detection performance of C-SPRT for different values of SNR

		SNR = −15 dB		SNR = −10 dB		SNR = −5 dB	
Case 1: $K = 16, T = 3560$	Methods	P_{FA}	P_{MD}	P_{FA}	P_{MD}	P_{FA}	P_{MD}
	No truncation	0.1014	0.1051	0.0917	0.0933	0.0773	0.0875
	Uniform truncation	0.4052	0.4262	0.2357	0.2528	0.0793	0.0913
	Uniformly added truncation	0.4032	0.4147	0.2145	0.2341	0.0791	0.0922
	Tail truncation	0.4720	0.4670	0.2767	0.2747	0.0799	0.0933
	Sequentially added truncation	0.3958	0.4183	0.2139	0.2239	0.0730	0.0951
Case 2: $K = 64$, $T = 14240$	No Truncation	0.0960	0.0983	0.0902	0.0973	0.0747	0.0933
	Uniform truncation	0.3986	0.4181	0.2339	0.2446	0.0745	0.0959
	Uniformly added truncation	0.3988	0.4168	0.2201	0.2292	0.0773	0.0919
	Tail truncation	0.4693	0.4765	0.2750	0.2797	0.07916	0.0921
	Sequentially added truncation	0.3969	0.4159	0.2184	0.2278	0.0768	0.0936
Case 3: $K = 64$, $T = 113920$	No truncation	0.0962	0.0982	0.0910	0.0972	0.0751	0.0929
	Uniform truncation	0.2534	0.2624	0.0957	0.0997	0.0780	0.0961
	Uniformly added truncation	0.2460	0.2535	0.0925	0.0973	0.0737	0.0931
	Tail truncation	0.3027	0.2991	0.0916	0.0980	0.0762	0.0922
	Sequentially added truncation	0.2427	0.2454	0.0923	0.0945	0.0739	0.0913

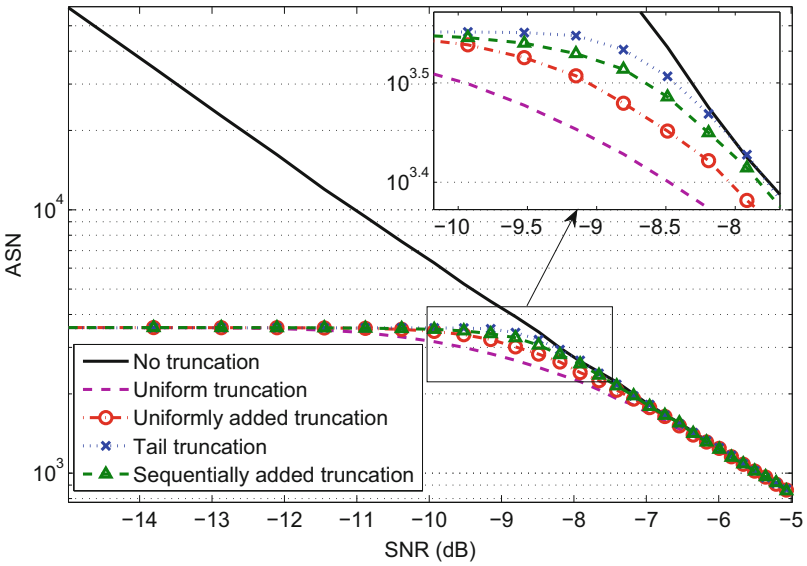

Fig. 6 ASN versus SNR of the truncation C-SPRT with $K = 16$, $T = 3560$

Conclusion

In this chapter, we have reviewed sequential spectrum sensing algorithms for CR systems. Compared with block-based sensing algorithms, sequential sensing algorithms enable us to make detection decision with minimum delay while still providing certain performance guarantee. We have illustrated the benefits of sequential detection for a single-band system. We have also discussed how to design quickest sequential scanning algoithms for multiband systems to quickly identify free channels. These algorithms enable us to deal with scenarios where SUs do not have complete or even partial knowledge about primary signals. They also enable us to achieve a small detection delay even under a fairly low detection SNR level with low detection error probabilities.

Acknowledgements The work of L. Lai was supported by National Science Foundation under grant CNS-1660128.

References

1. Zhang W, Letaief KB (2008) Cooperative spectrum sensing with transmit and relay diversity in cognitive radio networks. IEEE Trans Wirel Commun 7(12):4761–4766
2. Zhang W, Mallik RK, Letaief KB (2009) Optimization of cooperative spectrum sensing with energy detection in cognitive radio networks. IEEE Trans Wirel Commun 8(12):5761–5766
3. Duan D, Yang L, Principe JC (2010) Cooperative diversity of spectrum sensing for cognitive radio systems. IEEE Trans Signal Process 58(6):3218–3227
4. Quan Z, Cui S, Sayed AH (2007) An optimal strategy for cooperative spectrum sensing in cognitive radio networks. In: Proceedings of the IEEE Global Telecommunications Conference, Washington, DC, pp 2947–2951
5. Quan Z, Cui S, Sayed AH (2008) Optimal linear cooperation for spectrum sensing in cognitive radio networks. IEEE J Spec Top Signal Process 2(1):28–40
6. Zeng Y, Liang Y (2007) Maximum-minimum eigenvalue detection for cognitive radio. In: Proceedings of the IEEE 18th International Symposium on Personal, Indoor, and Mobile Radio Communication (PIMRC), Athens, pp 1–5
7. Lim TH, Zhang R, Liang Y-C, Zeng H (2008) GLRT-based spectrum sensing for cognitive radio. In: Proceedings of the IEEE Global Telecommunications Conference (GLOBECOM), New Orleans, pp 1–5
8. Cabric D, Mishra SM, Brodersen RW (2004) Implementation issues in spectrum sensing for cognitive radios. In: Proceedings of the Asilomar Conference on Signals, Systems and Computers, Pacific Grove, pp 772–776
9. Tang H (2005) Some physical layer issues of wide-band cognitive radio systems. In: Proceedings of the IEEE International Symposium on New Frontiers in Dynamic Spectrum Access Networks, Baltimore, pp 151–159
10. Shankar S, Cordeiro C, Challapali K (2005) Spectrum agile radios: utilization and sensing architectures. In: Proceedings of the IEEE International Symposium on New Frontiers in Dynamic Spectrum Access Networks, Baltimore, pp 160–169
11. Lunden J, Huttunen A, Koivunen V, Poor HV (2007) Multiple sensing in cognitive radios based on multiple cyclic frequencies. In: Proceedings of the International Conference on Cognitive Radio Oriented Wireless Networks and Communications, Orlando, pp 1583–1590
12. Sutton PD, Nolan KE, Doyle LE (2008) Cyclostationary signatures in practical cognitive radio applications. IEEE J Sel Areas Commun 2(1):13–24

13. Tian Z, Giannakis GB (2006) A wavelet approach to wideband spectrum sensing for cognitive radios. In: Proceedings of the International Conference on Cognitive Radio Oriented Wireless Networks and Communications, Mykonos Island, pp 1–5
14. Ghasemi A, Sousa ES (2005) Collaborative spectrum sensing in cognitive radio networks. In: Proceedings of the IEEE International Symposium on New Frontiers in Dynamic Spectrum Access Networks, Baltimore, pp 131–136
15. Ganesan G, Li YG (2007) Cooperative spectrum sensing in cognitive radio, part I: two user networks. IEEE Trans Wirel Commun 6(6):2204–2213
16. Ganesan G, Li YG (2007) Cooperative spectrum sensing in cognitive radio, part II: multiuser networks. IEEE Trans Wirel Commun 6(6):2214–2222
17. Ganesan G, Li YG, Bing B, Li S (2008) Spatiotemporal sensing in cognitive radio networks. IEEE J Sel Areas Commun 28(1):5–12
18. Mishra SM, Sahai A, Brodersen RW (2006) Cooperative sensing among cognitive radios. In: Proceedings of the IEEE International Conference on Communication, vol 4, Istanbul, pp 1658–1663
19. Vistotsky E, Kuffner S, Peterson R (2005) On collaborative detection of TV transmissions in support of dynamic spectrum sharing. In: Proceedings of the IEEE International Symposium on New Frontiers in Dynamic Spectrum Access Networks, Baltimore, pp 338–345
20. Unnikrishnan J, Veeravalli VV (2008) Cooperative sensing for primary detection in cognitive radio. IEEE J Spec Top Signal Process 2(1):18–27
21. Kim J, Andrews JG (2010) Sensitive white space detection with spectral covariance sensing. IEEE Trans Wirel Commun 9:2945–2955
22. Kim J, Chae C-B, Andrews JG (2011) Cooperative spectral covariance sensing under correlated shadowing. IEEE Trans Wirel Commun 10:3589–3593
23. Zeng Y, Liang Y (2007) Covariance based signal detections for cognitive radio. In: Proceedings of the IEEE International Symposium on New Frontiers in Dynamic Spectrum Access Networks (DySPAN), Dublin, pp 202–207
24. Lundén J, Koivunen V, Huttunen A, Poor HV (2007) Spectrum sensing in cognitive radios based on multiple cyclic frequencies. In: Proceedings of the IEEE Cognitive Radio Oriented Wireless Networks and Communications (CrownCom), Orlando, pp 37–43
25. Quan Z, Cui S, Sayed AH, Poor HV (2008) Wideband spectrum sensing in cognitive radio networks. In: Proceedings of the International Conference on Communications, Beijing, pp 901–906
26. Kim SJ, Giannakis GB (2009) Rate-optimal and reduced-complexity sequential sensing algorithms for cognitive OFDM radios. In: Proceedings of the Conference on Information Science and System. Johns Hopkins University, Baltimore, pp 141–146
27. Urkowitz H (1967) Energy detection of unknown deterministic signals. Proc IEEE 55(4): 523–531
28. Tandra R, Sahai A (2008) SNR walls for signal detection. IEEE J Sel Top Signal Process 2(1):4–17
29. Kundargi N, Tewfik A (2007) Hierarchical sequential detection in the context of dynamic spectrum access for cognitive radios. In: Proceedings of the IEEE 14th International Conference on Electronics, Circuits and Systems, Marrakech, pp 514–517
30. Chen B, Park J, Bian K (2006) Robust distributed spectrum sensing in cognitive radio networks. Technical report TR-ECE-06–07, Department of Electrical and Computer Engineering, Virginia Tech
31. Wald A (1945) Sequential tests of statistical hypothesis. Ann Math Stat 17:117–186
32. Wald A, Wolfowitz J (1948) Optimum character of the sequential probability ratio test. Ann Math Stat 19:326–329
33. Kim SJ, Li G, Giannakis GB (2010) Minimum-delay spectrum sensing for multi-band cognitive radios. In: Proceedings of the IEEE GLOBECOM Conference, Miami, pp 1–5
34. Kim SJ, Giannakis GB (2010) Sequential and cooperative sensing for multichannel cognitive radios. IEEE Trans Signal Process 58(8):4239–4253
35. Poor HV, Hadjiliadis O (2008) Quickest detection. Cambridge University Press, Cambridge

36. Quan Z, Cui S, Sayed A (2008) Optimal linear cooperation for spectrum sensing in cognitive radio networks. IEEE J Sel Top Signal Process 2(1):28–40
37. Liang Y-C, Zeng Y, Peh E, Hoang A (2008) Sensing-throughput tradeoff for cognitive radio networks. IEEE Trans Wirel Commun 7(4):1326–1337
38. Pollock SM, Golhar D (1985) Efficient recursions for truncation of the SPRT. Technical report No. 85–24, Department of Industrial and Operations Engineering, University of Michigan
39. Johnson NL (1961) Sequential analysis: a survey. J R Stat Soc Ser A (Gen) 3:372–411
40. Poor HV (1994) An introduction to signal detection and estimation. Springer, New York
41. Wald A (1947) Sequential analysis. Prentice Hall, Englewood Cliffs
42. Kay SM (1998) Fundamentals of statistical signal processing. Volume 2: Detection theory. Prentice Hall, Upper Saddle River
43. Jiang H, Lai L, Fan R, Poor HV (2009) Optimal selection of channel sensing order in cognitive radios. IEEE Trans Wirel Commun 8(1):297–307

Recommended Reading

1. Hassibi B, Hochwald B (2003) How much training is needed in multiple-antenna wireless links? IEEE Trans Inf Theory 49(4):951–963
2. Kay SM (1993) Fundamentals of statistical processing. Volume I: Estimation theory. Prentice Hall, Englewood Cliffs

Cooperative Spectrum Sensing: From Fundamental Limits to Practical Designs

10

Dongliang Duan, Liuqing Yang, and Shuguang Cui

Contents

D. Duan (✉)
Department of Electrical and Computer Engineering, University of Wyoming, Laramie, WY, USA
e-mail: dduan@uwyo.edu

L. Yang
Department of Electrical and Computer Engineering, Colorado State University, Fort Collins, CO, USA
e-mail: lqyang@engr.colostate.edu

S. Cui
University of California, Davis, CA, USA

Department of Electrical and Computer Engineering, University of California, Davis, CA, USA
e-mail: sgcui@ucdavis.edu

W. Zhang (ed.), *Handbook of Cognitive Radio*,
https://doi.org/10.1007/978-981-10-1394-2_10

Abstract

The first and foremost function in cognitive radio is spectrum sensing. To overcome the performance bottleneck created by fading and shadowing effects of the wireless channel, cooperation among sensing users is proposed as a promising solution. However, most designs of cooperative sensing strategies are developed in a rather ad hoc manner due to the lack of the fundamental knowledge on the cooperation gain. Hence, in this chapter, the cooperation gain in the context of cooperative spectrum sensing is rigorously quantified via diversity and error exponent analyses. The fundamental limits of the diversity and error exponent are derived as functions of key system parameters. After that, a couple of case studies are presented to illustrate how the concepts of diversity and error exponent can guide practical designs of cooperative spectrum sensing.

Introduction

In cognitive radio systems, the unlicensed wireless users (a.k.a. secondary users) take chances to access the spectrum (temporarily or spatially) released by the licensed users (a.k.a. primary users) so that the spectrum access is dynamic and somewhat opportunistic [27]. To realize this, the first step is to find such opportunities in the primary users' spectrum usage; this is spectrum sensing.

Among existing work on spectrum sensing, some focus on algorithms to improve a single-user's sensing performance by utilizing some side information (see, e.g., [2, 13]). Nonetheless, single-user spectrum sensing is still the system performance bottleneck due to fading and shadowing effects of the wireless channel, as well as the noise uncertainty of the device [22]. To this end, cooperative spectrum sensing by multiple secondary users can significantly improve the sensing performance. Hence, this has become the focus of most ongoing research (see, e.g., [10, 12, 13, 20, 26]).

At the center of all these research reside the rules by which the cooperating sensing users and the fusion center act and interact. These rules determine how each sensing user processes the local sensing data, what information the sensing users will forward to the fusion center, and how the fusion center makes a decision on the spectrum sensing. However, most existing designs of such rules are developed in a rather ad hoc manner due to the lack of the fundamental knowledge on the cooperation gain. In fact, though the benefit of cooperative sensing as

opposed to an individual user sensing has been recognized in various scenarios, the fundamental cooperation gain has never been rigorously defined, proved, or quantified.

Hence, the rigorous quantification of the cooperation gain in the context of cooperative spectrum sensing has both scientific and practical promises: in addition to furthering the fundamental understanding of this very problem, it can also provide the necessary knowledge to guide systematic design of the rules governing the sensing user interactions. In this chapter, we discuss the fundamental limits and practical designs of cooperative spectrum sensing in the following two aspects: (i) cooperative spectrum sensing performance scaling with signal parameters: we will quantify the cooperation gain using the notion of "diversity," which characterizes how the cooperative spectrum sensing performance scales with the signal parameter when the number of cooperative sensing users is fixed (section "Performance Scaling with SNR: Cooperative Diversity"); (ii) cooperative spectrum sensing performance scaling with the number of cooperative sensing users: we will extract this scaling factor in the form of the error exponent based on large deviation analysis. We will first determine the exact scaling factor. Due to the interweaved nature of this scaling factor and the optimum local and fusion rules, we show that the local rules that are globally optimum can be obtained (section "Performance Scaling with the Number of Sensing Users: Error Exponent"). Based on the discussions on the fundamental limits in these two aspects, a couple of practical design issues will be investigated in section "Practical Designs: Case Studies". Specifically, in section "Sensing with Ternary Local Decisions: A Design from the Diversity Perspective", diversity is used as a guideline to design a simple but effective fusion rule for sensing fusion with local ternary decisions, and in section "Sensing with Joint Diversity and Error Exponent Considerations", a joint analysis of diversity and error exponent is used to derive a closed-form local threshold for cooperative spectrum sensing to achieve both the maximum diversity and error exponent.

Notation: Subscripts "f," "md," "d," and 'e' refer to false alarm, missed detection, detection, and average error, respectively. $x \sim \mathcal{CN}(\mu, \sigma^2)$ denotes a proper complex Gaussian random variable x with mean μ and variance σ^2; $b \sim \text{Ber}(p_0)$ denotes a Bernoulli random variable b with $p_0 = Pr[b = 0]$; $X \sim \text{Bin}(N, p)$ denotes a binomial random variable; $u \sim \mathcal{U}(a, b)$ denotes a real random variable u uniformly distributed over interval $[a, b]$. $f(\gamma) \sim g(\gamma)$ denotes two functions of γ with $\lim_{\gamma\to+\infty} \frac{f(\gamma)}{g(\gamma)} = k$, where k is a nonzero constant; $g(\gamma) \approx f(\gamma)$ means $\lim_{\gamma\to+\infty} \frac{g(\gamma)}{f(\gamma)} = 1$. Throughout this chapter, $D_{\text{KL}}(p||q)$ denotes the Kullback-Leibler distance between Bernouilli distributions, $\text{Ber}(p)$ and $\text{Ber}(q)$. That is,

$$D_{\text{KL}}(p||q) = E_p \log\left(\frac{\text{Ber}(p)}{\text{Ber}(q)}\right) = p \log\left(\frac{p}{q}\right) + (1-p)\log\left(\frac{1-p}{1-q}\right).$$

Performance Scaling with SNR: Cooperative Diversity

While *diversity* has been well acknowledged as the intuitive benefit of cooperative sensing, its rigorous meaning in this setup has remained largely unexplored. In this section, we will determine quantitatively the diversity order in various cooperative spectrum sensing schemes.

Diversity has been widely adopted as a fundamental performance indicator in communication systems, where it is defined and quantified in terms of the signal-to-noise ratio (SNR)-dependent behavior of the bit error rate (BER) for symbol detection [23, Chapter 3] or the probability distribution of the mutual information [23, Chapter 5]. This concept was also extended to the context of cooperative estimation in wireless sensor networks [5]. Therein, diversity refers to the SNR-dependent behavior of the outage probability that the estimation variance exceeds a predefined value. In [18], the missed detection probability is adopted for the determination of diversity in a cooperative detection scenario while keeping the false alarm probability fixed (SNR independent). In [26], the opposite is considered by emphasizing the false alarm probability while fixing the missed detection probability. However, in the spectrum sensing problem, none of these measures can sufficiently and appropriately quantify diversity.

Unlike traditional detection problems where focusing on either the false alarm or missed detection probabilities while fixing the other is a rather common exercise, doing so in a spectrum sensing problem will risk unbalanced treatment between the system *efficiency* and *reliability*. On the one hand, false alarm probability is of critical importance because the whole purpose of cognitive radio is to maximally utilize the spectrum vacancies, while false alarms lead to undetected spectrum holes and can significantly reduce the efficiency of such usage. On the other hand, missed detections lead to deteriorated "cognition" level and give rise to unexpected interference from the secondary users to the primary ones. In short, false alarm and missed detection probabilities, respectively, capture the *efficiency* and *reliability* of the overall cognitive system. Hence, a diversity measure of cooperative sensing performance should fairly account for both probabilities. In this work, we consider the false alarm and missed detection probabilities both individually and jointly in terms of the average error probability, which balances system efficiency and reliability.

The technical contributions of this section are summarized as follows: (i) We derive the optimum detection thresholds by minimizing the average error probability in both noncooperative single-user and cooperative multiuser sensing scenarios. The diversity orders of all three probabilities are then quantified under the optimum thresholds. We also prove that such thresholds lead to the maximum diversity order in both sensing scenarios. (ii) We consider two cooperative strategies, namely, multiuser sensing with soft information fusion and hard/binary information fusion. The former provides a theoretical bound on the diversity orders and error probability performance in an ideal cooperative sensing setup, whereas the latter leads to practical fusion and decision rules together with their respective quantified diversity orders. (iii) We investigate the trade-off between the system efficiency (via false

alarm probability) and reliability (via missed detection probability) and present analytical results to guide practical system designs with differing preferences. (iv) Depending on whether the secondary users have knowledge of the number of cooperative users, we find that the optimal hard fusion rules are, respectively, the majority-fusion rule and the OR-fusion rule. (v) We verify the benefit of cooperative sensing and compare the performances of majority-fusion and OR-fusion rules at low SNR.

Sensing Strategies and Performance Metrics

In the spectrum sensing process, the sensing users observe signals under the following two hypotheses:

H_0 : absence of primary user in the spectrum band of interest,

H_1 : presence of primary user in the spectrum band of interest.

We adopt the signal model in [13], where the channels between the primary and the sensing users are Rayleigh fading with additive white Gaussian noise (AWGN). Then the received signal at the sensing user is given by [13]:

$$\begin{aligned} r|H_0 &= n \sim \mathscr{CN}(0, \sigma_n^2), \\ r|H_1 &= hx + n \sim \mathscr{CN}(0, E_x\sigma_h^2 + \sigma_n^2), \end{aligned}$$

where n is AWGN with variance σ_n^2, h is the channel coefficient with variance σ_h^2, and x is the signal from the primary user with energy E_x. Suppose that the sensing users know the noise variance, hence, without loss of generality, we normalize the noise variance to 1. Accordingly, the signal at the sensing users becomes:

$$\begin{aligned} r|H_0 &= n \sim \mathscr{CN}(0, 1), \\ r|H_1 &= hx + n \sim \mathscr{CN}(0, \gamma + 1), \end{aligned} \tag{1}$$

where $\gamma \triangleq E_x\sigma_h^2/\sigma_n^2$ is the average signal-to-noise ratio (SNR) at the sensing users.

With geographically distributed sensing users, it is reasonable to assume that they experience independent fading channels. Thus, the received signals for different sensing users r_is are conditionally identically independently distributed (i.i.d.) under each hypothesis.

Cooperative spectrum sensing requires cooperation among multiple sensing users. In our analysis, a fusion center collects information from all secondary users and facilitates their cooperation. Ideally, the cooperation benefit is maximized if all sensing information from all secondary users reaches the fusion center without any loss. This condition, however, cannot always be satisfied due to the limited spectrum resource available to the secondary user system. Hence, we will next

consider two types of sensing strategies, namely, cooperative multiuser sensing with soft information fusion and cooperative multiuser sensing with hard/binary information fusion.

Cooperative Sensing with Soft Information Fusion

In this case, the fusion center can obtain information from the distributed secondary users perfectly. This provides a best case scenario for cooperative sensing among multiple secondary users. Although this may not be practically achievable, it does provide a useful bound on the multiuser sensing performance. Moreover, this is also a good model for the case where multiple independent faded copies of the primary user's signal are collected at a single secondary user. For example, multiple receive antennas with appropriate antenna spacing can provide independent faded copies of the signal, or in the case of a fast fading scenario, the signals from different time slots are independently distributed. In these cases, the single secondary user can be regarded as the fusion center and the different sources of independent faded signals can be regarded as the multiple spectrum sensing nodes with lossless transmission to the fusion center, leading to soft information fusion.

Cooperative Sensing with Hard/Binary Information Fusion

In a more practical multiuser setup, each distributed secondary user senses the spectrum usage and then only transmits the one-bit sensing decision, "0" for absence of primary users or "1" for presence of primary users, to the fusion center.

Performance Metric and Diversity Order

In traditional signal detection problems, the receiver operating characteristic (ROC) curves (false alarm probability P_f vs. missed detection probability P_{md}) are generally used to graphically illustrate the detection performance [19]. Every ROC curve is plotted for a certain combination of the system parameters such as SNR, number of cooperative users, and so on. As a result, they do not provide an explicit quantitative relationship between the system parameters and the system metrics (false alarm, missed detection, and average detection error probabilities) [10]. Hence, to better illustrate the effects of the system parameters on the performance, in this chapter, we analyze each single system metric as a function of the system parameter variables.

As aforementioned, the performance of spectrum sensing is indicated by the false alarm probability P_f, the missed detection probability P_{md}, and the average error probability P_e. P_f is the probability of deciding on H_1 when H_0 is true (type I error); P_{md} is the probability of deciding on H_0 when H_1 is true (type II error); P_e is the average probability of making a wrong decision. Physically, P_f determines the capability of detecting the available spectrum resource, and thus the *efficiency* of the system; and P_{md} indicates the level of interference that the secondary user system introduces to the primary user system and thus the *reliability* of the system. As a result, P_e combines the efficiency and reliability considerations. We denote the probability of the absence of the primary user (H_0) as π_0 and thus that of the

presence of the primary user (H_1) as $(1-\pi_0)$, and then the average error probability is $P_e = \pi_0 P_f + (1-\pi_0) P_{md}$.

The concept of diversity was introduced in wireless communications to quantify the effects of independent fading in space, time, frequency, or code space on the improvement of the system performance [23]. Quantitatively, the diversity order is defined as:

$$d = -\lim_{\text{SNR}\to+\infty} \frac{\log P}{\log \text{SNR}}$$

where P can be the bit error rate or the outage probability of the communication system and SNR is the average signal-to-noise ratio. In cooperative sensing, the fusion center also receives multiple copies of the original signal under independent fading. Hence, the sensing performance is expected to exhibit a similar behavior. Here we define the diversity order in sensing scenarios as:

$$d_* = -\lim_{\gamma\to+\infty} \frac{\log P_*}{\log \gamma}$$

where $*$ can be f (false alarm), md (missed detection), or e (average error). Accordingly, there will be false alarm diversity d_f, missed detection diversity d_{md} and average error diversity d_e. Obviously, $d_e = \min\{d_f, d_{md}\}$ when $d_f \neq d_{md}$. In the following, we will quantify the diversity order of spectrum sensing according to the definitions above for three cases: single-user sensing, multiuser cooperative sensing with soft information fusion, and multiuser cooperative sensing with hard/binary information fusion. In addition, we will show that, though the diversity order is defined in the limit when $\gamma \to +\infty$, it actually shows up quite early at low SNR.

Diversity Analysis for Single-User Sensing

To achieve uniformly most powerful detection performance, we use the Neyman-Pearson (NP) detector [19]. With our signal model, the NP test is the likelihood ratio test:

$$\lambda = |r|^2 \underset{H_0}{\overset{H_1}{\gtrless}} \theta \tag{2}$$

where θ is the threshold of the test. According to (1), the distribution of the decision statistic is:

$$\begin{aligned} f(\lambda|H_0) &= e^{-\lambda} \quad (\lambda > 0) \\ f(\lambda|H_1) &= \frac{1}{\gamma+1} e^{-\frac{\lambda}{\gamma+1}} \quad (\lambda > 0). \end{aligned} \tag{3}$$

Hence, the probabilities of false alarm and missed detection are, respectively:

$$P_f = \int_{\theta}^{+\infty} f(\lambda|H_0)d\lambda = \int_{\theta}^{+\infty} e^{-\lambda}d\lambda = e^{-\theta} \tag{4}$$

and

$$P_{md} = \int_{0}^{\theta} f(\lambda|H_1)d\lambda = \int_{0}^{\theta} \frac{1}{\gamma+1} e^{-\frac{\lambda}{\gamma+1}} d\lambda = 1 - e^{-\frac{\theta}{\gamma+1}}. \tag{5}$$

Diversity Order When Minimizing P_e

As shown in (4) and (5), the performance metrics P_f, P_{md}, and P_e all rely on the choice of the decision threshold θ. Clearly, one may choose different thresholds when optimizing different performance metrics. Recall that P_f captures the cognitive system's *efficiency* while P_{md} captures its *reliability*. To balance the system efficiency and reliability, we will optimize the threshold θ by minimizing the average error probability $P_e = \pi_0 P_f + (1-\pi_0)P_{md}$. Setting $dP_e/d\theta = 0$ and solving for θ, we obtain the optimum threshold as:

$$\theta^o = \left(1 + \frac{1}{\gamma}\right) \log\left[\frac{\pi_0}{1-\pi_0}(\gamma+1)\right], \tag{6}$$

where log is base-e throughout this chapter unless otherwise specified. Using this threshold, as $\gamma \to +\infty$, we have:

$$\begin{aligned} P_f = e^{-\theta} &= e^{-(1+\frac{1}{\gamma})\log\left[\frac{\pi_0}{1-\pi_0}(\gamma+1)\right]} \\ &= (\gamma+1)^{-(1+\frac{1}{\gamma})} \left(\frac{\pi_0}{1-\pi_0}\right)^{-\left(1+\frac{1}{\gamma}\right)} \sim (1+\gamma)^{-1} \end{aligned} \tag{7}$$

and

$$\begin{aligned} P_{md} = 1 - e^{-\frac{\theta}{\gamma+1}} &= 1 - e^{-\frac{1}{\gamma}\log\left[\frac{\pi_0}{1-\pi_0}(\gamma+1)\right]} \\ &\sim \gamma^{-1} \log\left[\frac{\pi_0}{1-\pi_0}(\gamma+1)\right]. \end{aligned} \tag{8}$$

Thus, their respective diversity orders can be obtained as:

$$\begin{aligned} d_f &= -\lim_{\gamma\to+\infty} \frac{\log P_f}{\log \gamma} = 1 \\ d_{md} &= -\lim_{\gamma\to+\infty} \frac{\log P_{md}}{\log \gamma} = 1 \\ d_e &= \min(d_f, d_{md}) = 1. \end{aligned} \tag{9}$$

Accordingly, we establish the following result:

Theorem 1. *For single-user spectrum sensing, when the threshold θ is chosen to minimize the average error probability P_e as in (6), the diversity order of the NP detector is $d_e = d_f = d_{md} = 1$.*

This theorem is quite intuitive since any single sensing user only has one copy of the original signal going through the fading channel, and it is well known that the probability of deep fading in this case is proportional to γ^{-1} (see, e.g., [23]).

From the analysis above, we see that the prior probabilities of the hypotheses π_0 and $(1-\pi_0)$ do not affect the diversity orders of the performance. Without loss of generality, to simplify the following analyses on the diversity orders, we choose $\pi_0 = \frac{1}{2}$ for the rest of this chapter.

False Alarm Diversity Versus Missed Detection SNR Gain

In Theorem 1, we choose θ^o to minimize the average detection error probability P_e, which is the average of efficiency and reliability. However, in some systems, the two features may have different levels of importance. Thus, we will next analyze P_f and P_{md} separately. Our analysis will reveal an interesting trade-off between the system efficiency and reliability. This trade-off can be exploited to achieve the desirable P_f and P_{md} performance and accordingly the preferable spectrum usage efficiency and interference level.

From (4) and (6), we notice that, if one changes the threshold to $\theta' = d_0\theta^o$, then the false alarm diversity order changes from 1 in (9) to:

$$d'_f = -\lim_{\gamma\to+\infty}\frac{\log P'_f}{\log\gamma} = -\lim_{\gamma\to+\infty}\frac{-d_0(1+\frac{1}{\gamma})\log(\gamma+1)}{\log\gamma} = d_0. \tag{10}$$

On the other hand, with this new threshold θ', as $\gamma\to+\infty$, we have:

$$P'_{md} = 1 - e^{-\frac{\theta'}{\gamma+1}} = 1 - e^{-\frac{d_0}{\gamma}\log(\gamma+1)} \sim d_0\gamma^{-1}\log(\gamma+1). \tag{11}$$

This implies that $d'_{md} = 1$, which is identical to d_{md} in (9) with threshold θ^o. In other words, the missed detection diversity order remains unaltered. However, the scalar difference between (8) and (11) suggests that, to ensure $P'_{md} \approx P_{md}$ as $\gamma\to+\infty$, ones needs $\gamma' = d_0\gamma$. This implies that the missed detection probability P_{md} exhibits a $-10\log_{10}d_0$ dB SNR gain (or equivalently $10\log_{10}d_0$ dB SNR loss) when the threshold is chosen as $\theta = d_0\theta^o$. This interesting phenomenon may result from the fact that the false alarm probability is the right tail of the Rayleigh distribution which decays very rapidly, whereas the missed detection is the left tail of the Rayleigh distribution which decays quite slowly.

We summarize the trade-off between the false alarm diversity and the missed detection SNR gain in the following corollary:

Corollary 1. *For single-user spectrum sensing, when the threshold is set to* $d_0\theta^o$ *with* θ^o *given in* (6)*, the false alarm diversity order becomes* $d_f = d_0$*, while the missed detection diversity order remains* $d_{md} = 1$ *but the* P_{md} *curve exhibits* $a - \log_{10} d_0$ *dB SNR gain.*

The trade-off between the false alarm diversity and the missed detection SNR gain presented above provides system designers with a flexible tool to achieve the desirable trade-off between the spectrum usage efficiency of the secondary users and the reliability of the primary users. For example, if the primary users in the cognitive system are capable of interference suppression and the spectrum usage efficiency is of major concern for the system designer, then, by the properties above, the secondary users can set the threshold as $d_0\theta^o$ with $d_0 > 1$. This means, the false alarm diversity is increased to $d_0(> 1)$ by sacrificing a $10\log_{10} d_0$ dB SNR loss for the missed detection probability. On the other hand, if the primary users are vulnerable to interference and the performance of primary users in the cognitive system is of the major concern, then the secondary users can set the threshold at $d_0\theta^o$ with $0 < d_0 < 1$. As a result, there will be a $-10\log_{10} d_0$ dB SNR gain for the missed detection probability by reducing the false alarm diversity to $d_0(< 1)$.

As shown later in section "Hard/Binary Information Fusion", this flexibility of the false alarm diversity can also be utilized to maximize the diversity order of the multiuser sensing with hard/binary information fusion.

Diversity Analysis for Multiuser Sensing

Soft Information Fusion

With a soft information fusion strategy, the fusion center receives $r_1, r_2, \ldots, r_N$ from the distributed sensing users, where N is the total number of cooperative sensing users and r_is are conditionally independent identically distributed (i.i.d.) under both H_0 and H_1. Similar to section "Diversity Analysis for Single-User Sensing", the NP test is

$$\lambda_s = \sum_{i=1}^{N} |r_i|^2 \underset{H_0}{\overset{H_1}{\gtrless}} \theta_s, \tag{12}$$

where the subscript "s" refers to soft information fusion.

Since r_is are conditionally independent, and according to (1), we have:

$$\begin{aligned} f(\lambda_s|H_0) &= \lambda_s^{N-1} \frac{e^{-\lambda_s}}{(N-1)!} \quad (\lambda_s > 0) \\ f(\lambda_s|H_1) &= \lambda_s^{N-1} \frac{e^{-\frac{\lambda_s}{\gamma+1}}}{(N-1)!(\gamma+1)^N} \quad (\lambda_s > 0). \end{aligned} \tag{13}$$

Hence, the probabilities of false alarm and missed detection are, respectively:

$$P_{f,s} = \int_{\theta_s}^{+\infty} f(\lambda_s|H_0)d\lambda_s = \left(\sum_{i=0}^{N-1} \frac{\theta_s^i}{i!}\right) e^{-\theta_s} \tag{14}$$

and

$$P_{md,s} = \int_{0}^{\theta_s} f(\lambda_s|H_1)d\lambda_s = \left(\sum_{i=N}^{+\infty} \frac{\theta_s^i}{i!(\gamma+1)^i}\right) e^{-\frac{\theta_s}{\gamma+1}}. \tag{15}$$

Accordingly, the average error probability is $P_{e,s} = \frac{1}{2}P_{f,s} + \frac{1}{2}P_{md,s}$. Similar to section "Diversity Analysis for Single-User Sensing", minimizing $P_{e,s}$ by taking $dP_{e,s}/d\theta_s = 0$, we obtain the optimum threshold as:

$$\theta_s^o = N\left(1 + \frac{1}{\gamma}\right)\log(\gamma+1). \tag{16}$$

Using this threshold, we establish the following theorem:

Theorem 2. *For multiuser sensing with soft information fusion, when the threshold θ_s is chosen as in (16) to minimize the average error probability $P_{e,s}$, the diversity order of the NP detector is $d_{e,s} = d_{f,s} = d_{md,s} = N$, where N is the number of cooperative users.*

Proof. See section "Appendix 1: Proof of Theorem 2".

This theorem is also intuitive in that the fusion center has copies of the original received signals from N independently fading channels. Similar to section "False Alarm Diversity Versus Missed Detection SNR Gain", we can also choose the threshold as $\theta_s' = d_0\theta_s^o$, where d_0 can be any positive number and is not necessarily an integer, to increase the false alarm diversity to d_0N while keeping the missed detection diversity unaltered at N. In this case, there is also a trade-off between the missed detection SNR gain and the false alarm diversity. For the false alarm diversity to be d_0N, the missed detection probability will exhibit a $-10\log_{10} d_0$ dB SNR gain (or equivalently $10\log_{10} d_0$ dB SNR loss).

Hard/Binary Information Fusion

With the hard/binary information fusion strategy, each sensing user makes its own local hard decision and then sends the binary decision b_i to the fusion center. For simplicity, we assume that all distributed sensing users employ the same threshold θ_l for their local decisions where subscript "l" stands for local. The corresponding local false alarm and missed detection probabilities are denoted as $P_{f,l}$ and $P_{md,l}$, respectively. Clearly, b_i follows conditionally i.i.d. Bernoulli distribution with $(1 - P_{f,l})$ and $P_{md,l}$ as the probabilities of value 0 under H_0 and H_1, respectively; that is:

$$\begin{aligned} b_i|H_0 &\sim \text{Ber}(1-P_{f,l}) \\ b_i|H_1 &\sim \text{Ber}(P_{md,l}). \end{aligned} \tag{17}$$

In this case, the NP test becomes:

$$\lambda_h = \sum_{i=1}^{N} b_i \underset{H_0}{\overset{H_1}{\gtrless}} \theta_h, \quad \theta_h = 1, 2, \ldots, N, \tag{18}$$

where subscript "h" refers to hard information fusion. Accordingly, the distribution of λ_h is:

$$\begin{aligned} f(\lambda_h|H_0) &= \binom{N}{\lambda_h} P_{f,l}^{\lambda_h}(1-P_{f,l})^{N-\lambda_h}, \ \lambda_h = 0, 1, \ldots, N; \\ f(\lambda_h|H_1) &= \binom{N}{\lambda_h}(1-P_{md,l})^{\lambda_h} P_{md,l}^{N-\lambda_h}, \ \lambda_h = 0, 1, \ldots, N. \end{aligned} \tag{19}$$

In hard information fusion, there are two levels of decision making, each level having its own decision performance. For the local decision, there are diversity orders for the local false alarm probabilities ($d_{f,l}$) and local missed detection probabilities ($d_{md,l}$). At the fusion center, there are also corresponding diversity orders for the overall hard decision false alarm probability ($d_{f,h}$), missed detection probability ($d_{md,h}$), and average error probability ($d_{e,h}$). Here we establish the relationship between the local decision diversity orders with the overall diversity orders at the fusion center in the following theorem:

Theorem 3. *For multiuser sensing with* 1*-bit hard information fusion, and with the fusion center threshold* θ_h *(*$\theta_h = 1, 2, \ldots, N$*), the diversity orders of the NP detector are* $d_{f,h} = \theta_h d_{f,l}$, $d_{md,h} = (N-\theta_h+1)d_{md,l}$, *and* $d_{e,h} = \min\{\theta_h d_{f,l}, (N-\theta_h+1)d_{md,l}\}$, *where* N *is the number of cooperative users.*

Proof. See section "Appendix 2: Proof of Theorem 3".

Similar to the single-user sensing and cooperative sensing with soft information fusion, cooperative sensing with hard information fusion also provides the system designer with the flexibility of balancing between the spectrum efficiency of the secondary users (via $d_{f,h}$) and the reliability of the primary users (via $d_{md,h}$) by the choice of the threshold θ_h. A larger θ_h will improve the false alarm performance, leading to higher spectrum usage efficiency of the secondary users, while a smaller θ_h will improve the missed detection performance, leading to enhanced reliability of the primary users. However, it is worth noting that the trade-off and flexibility here are very different from what we have discussed in Corollary 1 for the single-user sensing and the multiuser soft-fusion cases. In previous cases, the trade-off was between the false alarm *diversity* and the missed detection *SNR gain*, while here in

the case of multiuser hard fusion, the trade-off is between the false alarm *diversity* and the missed detection *diversity*.

Note that, though the local threshold θ_l does not appear explicitly in Theorem 3, it affects the overall system implicitly via $d_{f,l}$ and $d_{md,l}$. Hence, if one opts to minimize $P_{e,h} = \frac{1}{2}P_{f,h} + \frac{1}{2}P_{md,h}$, one needs to jointly choose both the optimum local threshold θ_l at the individual sensing users and the optimum hard decision threshold θ_h at the fusion center. However, under this fusion rule, θ_l has a very complicated form in $P_{e,h}$ through parameters $P_{f,l}$ and $P_{md,l}$, rendering optimization intractable. Even with numerical techniques, the optimization over θ_l still requires knowledge of the total number of distributed sensors in the network N, which is not always available to the secondary users in real applications. However, with Theorem 3, one can optimize the overall hard decision fusion performance from the diversity perspective with different strategies as detailed in the following two scenarios.

(B.1) Number of Cooperative Users *N* Unknown

In this case, the sensing users can only perform their optimum detection locally. From Theorem 1, the local threshold is $\theta_l = \theta^o$ and the local diversities are $d_{f,l} = d_{md,l} = 1$. According to Theorem 3, the diversity orders at the fusion center are $d_{f,h} = \theta_h$, $d_{md,h} = N-\theta_h+1$ and $d_{e,h} = \min\{\theta_h, N-\theta_h+1\}$. With equal emphasis on false alarm and missed detection performance, by maximizing $\min\{\theta_h, N - \theta_h + 1\}$, we obtain the optimum threshold θ_h^o at the fusion center that maximizes the detection error diversity:

Corollary 2. *For multiuser sensing with* 1*-bit hard information fusion, and with each sensing user using the locally optimum threshold* $\theta_l = \theta^o$*, the optimum threshold at the fusion center in the sense of maximizing the detection error diversity is* $\theta_h^o = \lfloor \frac{N+1}{2} \rfloor$ *or* $\theta_h^o = \lceil \frac{N+1}{2} \rceil$ *with* $d_{e,h} = \lfloor \frac{N+1}{2} \rfloor$*, where* N *is the number of cooperative users.*

In this case, the strategy is the so-termed majority-fusion rule. Notice that under this rule, about half of the diversity is lost compared with the soft information fusion. This indicates that a hard decision at each local sensing user leads to considerable information loss of the received signal.

(B.2) Number of Cooperative Users *N* Known

From Corollary 1, we have seen that the false alarm diversity at each local sensing user is flexible. It is shown in the following corollary that this property can be utilized to maximize the average error diversity.

Corollary 3. *For multiuser sensing with* 1*-bit hard information fusion, if each distributed sensing user knows the number of cooperative users* N*, the average error diversity order at the fusion center can be maximized by choosing local decision threshold* $\theta_l = N\theta^o$ *with* θ^o *given in* (6) *and the fusion decision threshold* $\theta_h = 1$.

Proof. See section "Appendix 3: Proof of Corollary 3".
Notice that the decision strategy turns out to be the so-termed OR-fusion rule. From this corollary, we see that with the number of sensors known at each local sensor, the diversity of the average detection error probability of hard information fusion equals that of soft information fusion ($d_{e,h} = d_{e,s} = N$). In other words, knowledge of N completely compensates for the loss of information by local hard decisions, in terms of the detection error diversity. However, we should also notice that though the diversity performance of the two cases are identical, their average error probability performances are still different. As detailed in section "False Alarm Diversity Versus Missed Detection SNR Gain", there is a $10 \log N$ SNR loss for the missed detection probability $P_{md,l}$ by setting $\theta_l = N\theta^o$ (such that $d_{f,l} = N$).

Remark 1. As stated in section "Sensing Strategies and Performance Metrics", our results on multiuser sensing with soft information fusion can be readily applied to the case of combining signals from different multiple time slots at a single user, as long as the combined received signals experience independent fading. In this case, if the system also uses cooperative multiuser sensing with hard/binary information fusion among these multiple time slot sensors, our analysis in this section can be readily extended by combining the results in Theorems 2 and 3. In addition, for the correlated fading case, intuitively, we expect that the diversity orders equal the rank of the correlation matrix of the received signals, which will be justified in the following section.

Simulations

Single-User Sensing

For single-user sensing, we use the test given by (2) and the threshold of (6) to obtain the average error probability, false alarm probability, and the missed detection probability. These probabilities are shown as the solid curves in Fig. 1. All three curves exhibit the same slope, indicating diversity orders $d_f = d_{md} = d_e = 1$.

To illustrate the trade-off between the false alarm diversity and missed detection SNR gain (loss) discussed in section "False Alarm Diversity Versus Missed Detection SNR Gain", we change the threshold to $\theta' = 2\theta^o$ and obtain the dashed curves in Fig. 1. From the figure, we see that $d'_f = 2$ and $d'_{md} = d_{md} = 1$, as predicted by Corollary 1. In addition, by comparing the solid curve with the dashed one for P_{md}, one can easily verify that at high SNR, there is an approximately $10 \log_{10} d_0 = 3$ dB SNR loss. This is the price paid for the increase of the diversity for the false alarm probability.

Multiuser Sensing with Soft Information Fusion

Here, we simulate the multiuser sensing with soft information fusion strategy. The total number of cooperative users is $N = 5$. From the analysis in section "Soft Information Fusion", we expect the relative performance of $P_{e,s}$, $P_{f,s}$ and $P_{md,s}$ to

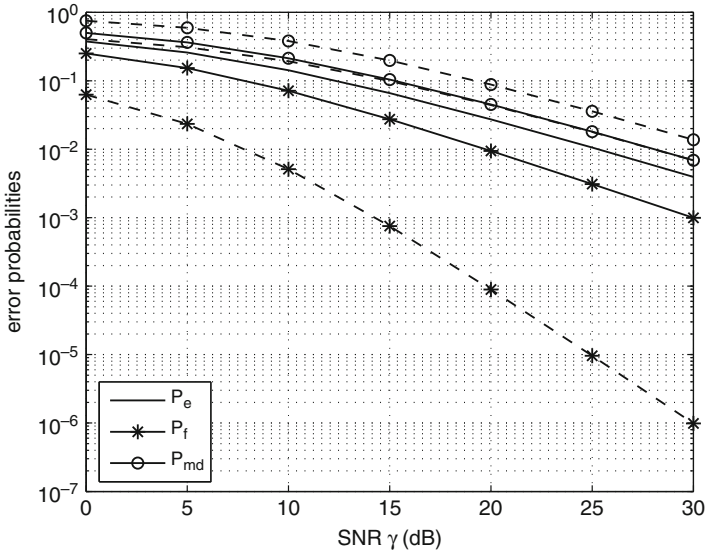

Fig. 1 Single-user sensing. *Solid curves*: threshold $\theta = \theta^o$; *dashed curves*: threshold $\theta = 2\theta^o$

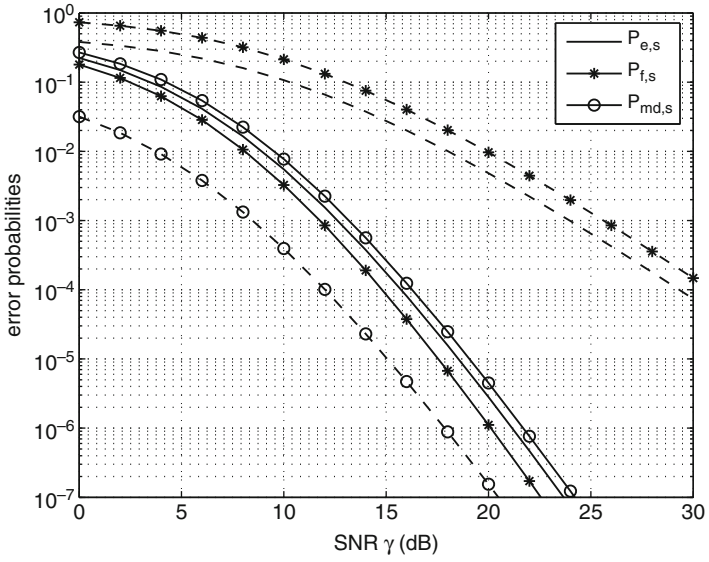

Fig. 2 $N = 5$ multiuser sensing with soft decision fusion *Solid curves*: threshold $\theta = \theta_s^o$; *dashed curves*: threshold $\theta = 0.5\theta_s^o$

be similar to the single-user sensing case, except for the diversity order of 5. This is verified in Fig. 2. The solid curves show that with the threshold minimizing the average error probability, the diversity orders are $d_{e,s} = d_{f,s} = d_{md,s} = N = 5$. In multiuser sensing with soft information fusion, we can also set the threshold

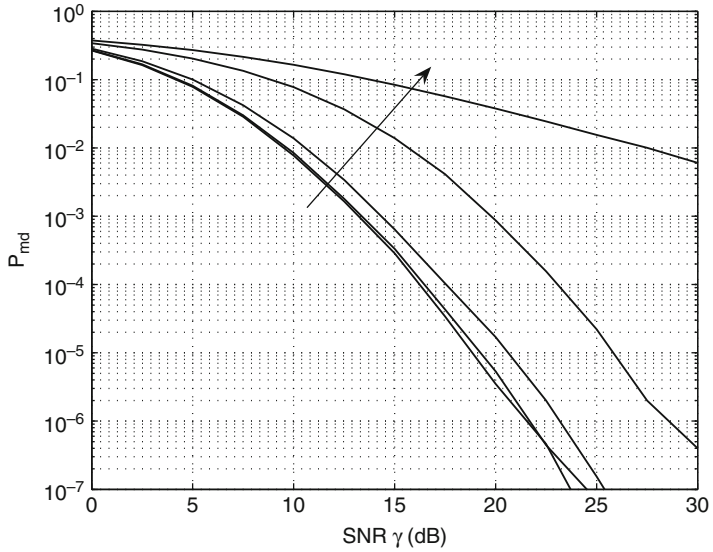

Fig. 3 $N = 5$ multiuser sensing with soft decision fusion on correlated signals with correlation $\mathbb{E}[h_i^* h_j] = r^{|i-j|}$. In the direction of *arrow*: $r = 0, r = 0.2, r = 0.5, r = 0.9, r = 1$, respectively

to $\theta_s' = d_0\theta_s^o$ to make $d_{f,s} = d_0 N$. The dashed curves in Fig. 2 show $P_{f,s}$ and $P_{md,s}$ with $d_0 = 0.5$. Similar to the single-user sensing case, comparing the solid curve with the dashed one for $P_{md,s}$, we verify that at high SNR, there is approximately $-10\log_{10} d_0 = 3$ dB SNR gain for the decrease of the false alarm diversity (from 5 to 2.5).

In the simulations above, the fading coefficients at each user are assumed to be independent. However, for multi-time-slot sensing which can be modeled as multiuser sensing with soft information fusion, the fading coefficients can be correlated. To investigate the diversities in this case, we plot the simulation results of the detector under the threshold η_s^o in Fig. 3. Notice that in this case, the signals under hypothesis H_0 remains unaltered; thus, it suffices to give the missed detection performances only. In this simulation, the number of time slots $N = 5$ and the correlations of the fading coefficients are assumed to be $\mathbb{E}[h_i^* h_j] = r^{|i-j|}$ where i and j are indices for the time slot. Under this assumption, the correlation matrix is

$$\Lambda_{\mathbf{h}} = \mathbb{E}[\mathbf{h}^H \mathbf{h}] = \begin{bmatrix} 1 & r & r^2 & r^3 & r^4 \\ r & 1 & r & r^2 & r^3 \\ r^2 & r & 1 & r & r^2 \\ r^3 & r^2 & r & 1 & r \\ r^4 & r^3 & r^2 & r & 1 \end{bmatrix}$$

In Fig. 3, we see that when the correlation (r) among the fading coefficients increases, the performance degrades. However, as long as the correlation matrix $\Lambda_{\mathbf{h}}$ is full rank, the diversity results obtained under the independent fading scenario still hold. When the matrix loses rank to rank 1 at $r = 1$, the diversity order reduces to 1.

Multiuser Sensing with Hard/Binary Information Fusion

For the multiuser sensing with hard/binary information fusion in section "Hard/Binary Information Fusion", we first consider the case where the number of cooperative users N is not available to the individual sensing users. Then, each distributed sensing user makes the locally optimum hard decision, i.e., $\theta_l = \theta^o$ as defined in (6). In this case, as Theorem 3 dictates, the false alarm diversity, the missed detection diversity, and the average error diversity are all heavily dependent on the threshold θ_h at the fusion center. Figure 4 shows the behavior of $P_{f,h}$, $P_{md,h}$, and $P_{e,h}$ of the hard information fusion strategy with $\theta_h = 1$ (solid curves) and $\theta_h = 2$ (dashed curves) when the number of cooperative users is $N = 5$. When $\theta_h = 1$, the solid curves show that $d_{f,h} = 1$, $d_{md,h} = 5$, and $d_{e,h} = 1$; when $\theta_h = 2$, the dashed curves show that $d_{f,h} = 2$, $d_{md,h} = 4$, and $d_{e,h} = 2$. These results are consistent with Theorem 3 and illustrate the trade-off between the false alarm diversity and the missed detection diversity.

With locally optimum hard decision ($\theta_l = \theta^o$) at distributed sensing users, the threshold maximizing the average error diversity should be chosen as $\lfloor \frac{N+1}{2} \rfloor$ or $\lceil \frac{N+1}{2} \rceil$ according to Corollary 2. This result is shown in Fig. 5 when $N = 5$.

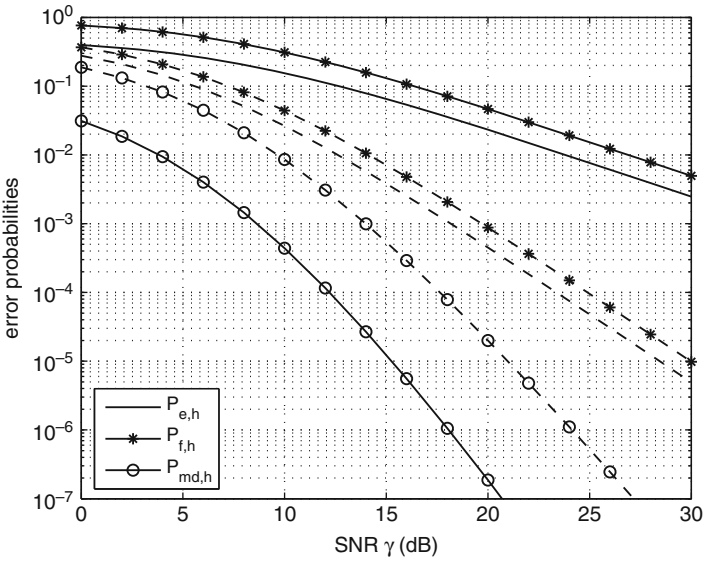

Fig. 4 $N = 5$ multiuser sensing with hard decision fusion. *Solid curves*: threshold $\theta_l = \theta^o$, $\theta_h = 1$; *dashed curves*: threshold $\theta_l = \theta^o$, $\theta_h = 2$

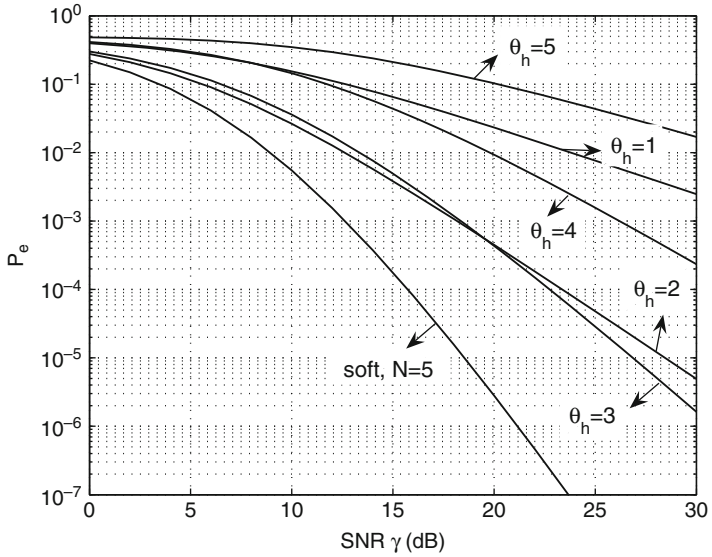

Fig. 5 $N = 5$ multiuser sensing with soft information fusion and hard information fusion with $\theta_l = \theta^o$ and various θ_hs

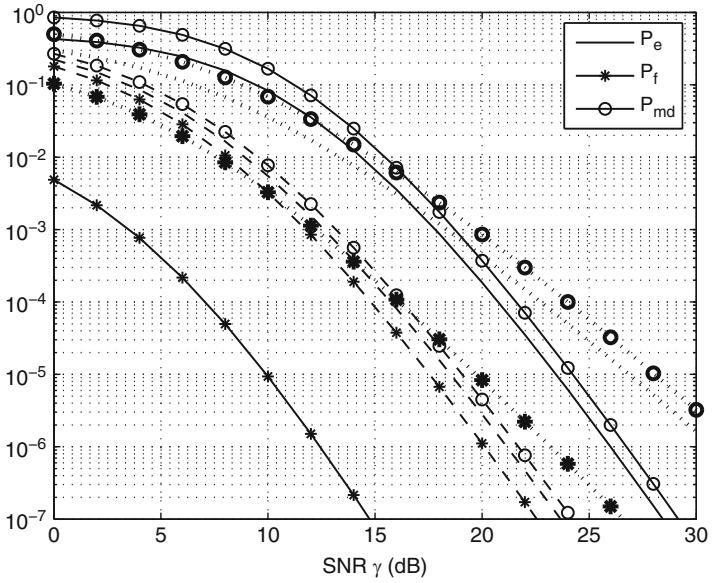

Fig. 6 $N = 5$ multiuser sensing with OR-fusion rule with $\theta_l = N\theta^o$ (*solid curves*), majority-fusion rule with $\theta_l = \theta^o$ (*dotted curves*), and soft information fusion (*dashed curves*)

From this figure, we see that $\theta_h = 3$ gives the maximum average error diversity. Compared with the error performance under soft information fusion, we see here that this locally optimum hard decision strategy suffers from a large loss of diversity.

When the distributed sensing users know the number of cooperative users in the network, then the flexibility of the false alarm diversity in Corollary 1 can be utilized to maximize the diversities of the hard information fusion. In this case, the local decision threshold is $\theta_l = N\theta^o$ where θ^o is defined in (6). Figure 6 shows the performance with this strategy and compares this with that of the soft information fusion strategy. From this figure, we see that in terms of diversity order d_e, the hard information fusion with adjusted local threshold equals the soft information fusion. However, the soft information fusion has a huge SNR advantage over the hard information fusion on the missed detection and average error probabilities. This is due to the fact that in the local decisions, a $10\log_{10} 5 = 7$ dB SNR loss of missed detection probability is introduced to increase the false alarm diversity from $d_{f,l} = 1$ to $d_{f,l} = 5$ by setting $\theta_l = 5\theta^o$. This also explains why the false alarm performance in this hard information fusion strategy with knowledge of the number of cooperative users is better than that in the soft information fusion strategy. In addition, compared with the dotted curves, we see that this strategy recovers the diversity loss introduced by the locally optimum hard decision.

Discussions

In this section, we analyzed various cooperative spectrum sensing strategies under different scenarios. By considering both false alarm and missed detection probabilities individually and jointly via the average error probability, we found several trade-offs between the system efficiency and reliability under three different spectrum sensing strategies. For single-user sensing and multiuser sensing with soft information fusion, the trade-off is between the false alarm diversity gain and the missed detection SNR loss by altering the detection threshold. For multiuser sensing with hard/binary information fusion without information of cooperative user number, there is a trade-off between the diversities of false alarm and missed detection. In addition, under hard information fusion, with the knowledge of cooperative user number, the soft decision diversity can be achieved at a given missed detection SNR loss. With these diversity and trade-off results, we derived the optimum threshold in each cooperative strategy to guide practical system design. Simulations have also been presented to further illustrate the analytical results and compare the various cooperative strategies.

Performance Scaling with the Number of Sensing Users: Error Exponent

In our previous discussions, we have characterized the cooperative sensing performance scaling with the signal parameter (i.e., SNR) for *fixed number of cooperative users* by diversity. In this section, we will see how the cooperative sensing

performance scales with the number of cooperative users for *fixed signal model*. Since now we are not aiming at writing the sensing performance as a function of any signal parameter, we start with a general sensing problem without any particular signal model and then apply the results to our spectrum sensing problem with the signal model given in section "Performance Scaling with SNR: Cooperative Diversity".

For a general detection fusion problem, we begin by assuming the prior probability of an event is known, and the number of functioning sensors is known. Each of these assumptions may be called into question. When they are, then various strategies may be considered, which we review and analyze in this section. Interestingly enough, when the asymptotically optimum detector is derived, it is found to be an equalizer rule that is invariant to the prior probability of an event, and therefore it is a minimax rule. Moreover the threshold setting at the fusion center scales with the number of reported sensor decisions, so that the number of cooperative sensors is not required to be known a priori.

The crux of the problem is this. At the global fusion center, the decision rule to minimize the global error probability is known. It depends on the number of sensors in the network, the prior probabilities of the underlying state, and the operating point on the ROC curve of each individual sensor. So the only problem is to determine the operating point on the local ROC curve for each individual sensor that minimizes the global error probability. This problem is intractable [24], so approximations are sought. Some designs for the operating point simply ignore the global error probability and use an operating point at the local sensors that achieves an objective like maximum entropy (ME), minimum error probability (MEP), or maximum mutual information (MMI). None of these designs has any claim to optimality. Other designs use an asymptotic theory to exponentially bound global error probability and seek an operating point that maximizes the error exponent. The result of this section uses the method of large deviations (LD) to do it.

Joint Optimization of Local and Fusion Decisions

In our analysis of the error exponent, we assume that the system is applying the cooperative sensing scheme with hard/binary information fusion. As discussed at the beginning of this section, we start with the sensing with any general signal models. That is, with probability π_0, each sensor (sensing user) measures a random variable distributed as F_0, and with probability π_1 each sensor measures a random variable distributed as F_1. Each local detector will make its own local decision $D_i \in \{0, 1\}$ based on its observed signal (i.e., information fusion with hard/binary information fusion). Then, a fusion center will collect all D_i's and make a fused binary decision $\phi(D_1, D_2, \ldots, D_N) = 0$ or $\phi(D_1, D_2, \ldots, D_N) = 1$.

Tsitsiklis [24] has shown that in the case of dependent signals at the local detectors, the solution for optimal detection fusion is non-deterministic polynomial-time hard [25]. Therefore, in our analysis, we assume that the signals at different detectors are independent, which is the case in many applications, including our

cooperative spectrum sensing problem discussed so far. Under this assumption, Tsitsiklis [24] proved that, asymptotically in the number of sensors, all local detectors use the same decision rule. For a finite number of local detectors, it is suboptimal. Under this setup, the D_is are conditionally i.i.d. binary random variables.

To describe the distribution of the local decision D_i, we denote $P_{f,l} = P(D_i = 1|H_0)$ as the local false alarm probability and $P_{d,l} = P(D_i = 1|H_1)$ as the local detection probability. Then, the local decisions $\{D_i\}$ are conditionally i.i.d. Bernoulli distributed with probabilities $P_{f,l}$ and $P_{d,l}$ under H_0 and H_1, respectively. Note that $(P_{f,l}, P_{d,l}) \in [0, 1] \times [0, 1]$ is constrained to lie on ROC curve for the local sensors, governed by the measurement model. At the fusion center that collects all N detectors' local decisions, $D_i \in \{0, 1\}$, the joint distribution of $(D_1, D_2, \ldots, D_N)$ is

$$P(D_1, D_2, \ldots, D_N|H_0) = P_{f,l}^{\sum_{i=1}^N D_i} \left(1 - P_{f,l}\right)^{N-\sum_{i=1}^N D_i},$$
$$P(D_1, D_2, \ldots, D_N|H_1) = P_{d,l}^{\sum_{i=1}^N D_i} \left(1 - P_{d,l}\right)^{N-\sum_{i=1}^N D_i}.$$

Accordingly, $V = \sum_{i=1}^{N} D_i$ is the sufficient statistic and it follows a binomial distribution under each hypothesis; that is,

$$\begin{aligned} V|H_0 &\sim \text{Bin}(N, P_{f,l}), \\ V|H_1 &\sim \text{Bin}(N, P_{d,l}). \end{aligned} \tag{20}$$

A global binary decision strategy will involve both a detection rule for mapping measurements into decision D_i at local detectors and a detection rule ϕ at the fusion center. We adopt the global average error probability $P_{e,h} = \pi_0 P(\phi(V) = 1|H_0) + \pi_1 P(\phi(V) = 0|H_1)$ as the performance metric. To obtain the optimum performance, one needs to find a local threshold and a corresponding fusion rule that jointly minimize $P_{e,h}$.

At the fusion center, if the local detector performance $(P_{f,l}, P_{d,l})$ is known, then the maximum *a posteriori* (MAP) detector will minimize the global error probability, $P_{e,h}$, via the likelihood ratio test:

$$\frac{\pi_1 P_{d,l}^v (1 - P_{d,l})^{N-v}}{\pi_0 P_{f,l}^v (1 - P_{f,l})^{N-v}} \underset{H_0}{\overset{H_1}{\gtrless}} 1. \tag{21}$$

The result is a threshold test,

$$v \underset{H_0}{\overset{H_1}{\gtrless}} v^{\text{MAP}} \tag{22}$$

where

$$v^{\mathrm{MAP}} = \frac{\left(\log \frac{1-P_{f,l}}{1-P_{d,l}}\right) N + \log\left(\frac{\pi_0}{\pi_1}\right)}{\log \frac{P_{d,l}}{P_{f,l}} + \log \frac{1-P_{f,l}}{1-P_{d,l}}}. \tag{23}$$

Importantly, this threshold may be written, asymptotically in N, as

$$v^{\mathrm{MAP}} = N\theta^{\mathrm{LD}};\ \theta^{\mathrm{LD}} = \frac{\left(\log \frac{1-P_{f,l}}{1-P_{d,l}}\right)}{\log \frac{P_{d,l}}{P_{f,l}} + \log \frac{1-P_{f,l}}{1-P_{d,l}}}. \tag{24}$$

The θ^{LD} is the LD solution to be found in section "A Large Deviation (LD) Solution of the Local Threshold". It is also the finite-N solution when $\pi_0 = \pi_1$.

This solution scales with N, the number of decisions reported to the global fusion center, and it is independent of the prior probabilities, π_0 and π_1. It will be shown that the threshold $N\theta^{\mathrm{LD}}$ is in fact the asymptotically optimum solution returned from a large deviations error bound. So already the asymptotic solution for the fusion threshold is known. The problem is to determine the asymptotic expression for the global error probability,

$$P_{e,h} = \pi_0 \sum_{v \geq v^{\mathrm{MAP}}} \binom{N}{v} P_{f,l}^{v} (1 - P_{f,l})^{N-v} + \pi_1 \sum_{v < v^{\mathrm{MAP}}} \binom{N}{v} P_{d,l}^{V} (1 - P_{d,l})^{N-v}. \tag{25}$$

The theory of LD will allow us to tightly bound this error probability for large N and solve for the operating point that minimizes it.

From (23) and (25), it can be readily verified that for any given local false alarm probability $P_{f,l}$, the larger the local detection probability $P_{d,l}$ is, the smaller the global average error probability $P_{e,h}$ will be. Therefore, at the local detectors, the NP detection rule maximizes the detection probability $P_{d,l}$ for any given false alarm probability P_f. However, the NP detector only determines an ROC curve $(P_{f,l}, P_{d,l})$ for the individual detectors. What remains to be determined is how to select the operating point $(P_{f,l}, P_{d,l})$ on the ROC curve for the local NP detector that minimizes the global error probability, $P_{e,h}$. From (23) and (25), we see that the minimization of $P_{e,h}$ depends on the prior probabilities, the number of sensors reporting, and the local error probabilities. This optimization problem is non-convex. However, asymptotically, the operating point $(P_{f,l}, P_{d,l})$ may be determined independently of these parameters.

In summary,

- It is asymptotically optimal to select the same decision strategy for all local sensors [24];
- The minimization of the average global error probability forces the local sensors to use an NP detector;

- Given the local operating point on a local ROC curve, the optimum fusion rule is the threshold test of (21),
- The fundamental design problem is to determine the operating point $(P_{f,l}, P_{d,l})$ on the ROC curve for the local NP detector.

Detectors Based Only on a Local Optimality Criterion

None of the local detectors described in this section has any claim to global optimality. But each has been proposed as a candidate for sensor fusion when the prior probability of an event, π_0, is known, but the number of functioning sensors in the network is unknown.

Maximum Entropy (ME)

The local maximum entropy detector maximizes the entropy of the local decision by equalizing $P(D_i = 0)$ and $P(D_i = 1)$ (see, e.g., [3]). Under this condition, the local operating point $(P_{f,l}, P_{d,l}) \in$ local ROC is determined as

$$\text{choose}_{(P_{f,l},P_{d,l})\in \text{ local ROC}} \text{ such that } .\pi_1 P_{d,l} - \pi_0 P_{f,l} = 0 \tag{26}$$

This operating point treats each sensor as a source encoder, which "encodes" the sensor measurement into the reported decision. However, this decision rule has nothing to do with how the binary decision variable D carries the information about the binary state variable H, so it is expected to perform poorly.

Local MEP

The local MEP detector selects the operating point on the local ROC that minimizes the local average error probability:

$$\min_{(P_{f,l},P_{d,l})\in \text{ local ROC}} \left(\pi_0 P_{f,l} + \pi_1(1 - P_{d,l})\right). \tag{27}$$

This detection rule minimizes local error probability, but it does not minimize global error probability.

Maximum Mutual Information (MMI)

Maximizing the mutual information between the local decision D and the hypothesis H maximizes the rate at which D carries information about the hypothesis H, and it minimizes equivocation. Similar performance metrics were introduced in [11] where the aim was to optimize over dependent operating points rather than common points.

The mutual information $I(H, D)$ between the binary decision variable $D \in \{0, 1\}$ and the binary hypothesized state $H \in \{H_0, H_1\}$ is defined to be $E_{H,D}\left[\log\left(\frac{P(H,D)}{P(H)P(D)}\right)\right]$. Then, with prior probabilities $P(H_0) = \pi_0$, $P(H_1) = \pi_1$;

and conditional probabilities $P(D = 1|H_0) = P_{f,l}$, $P(D = 1|H_1) = P_{d,l}$, a few lines of algebra shows mutual information to be

$$I(D, H) = \pi_0 D_{\mathrm{KL}}\left(P_{f,l}||\left(\pi_0 P_{f,l} + \pi_1 P_{d,l}\right)\right) + \pi_1 D_{\mathrm{KL}}\left(P_{d,l}||\left(\pi_0 P_{f,l} + \pi_1 P_{d,l}\right)\right). \tag{28}$$

So the local operating point that maximizes mutual information is determined as,

$$\max_{(P_{f,l}, P_{d,l}) \in \text{ local ROC}} I(D, H) \tag{29}$$

It will be shown in due course that the local MMI operating point is superior to the MEP operating point, which is superior to the ME operating point.

A Large Deviation (LD) Solution of the Local Threshold

In this section the operating point on the local ROC that minimizes global error probability, asymptotically when the number of sensors approaches infinity, is designed using LD.

Asymptotically Optimum Local Decision Rule

The sufficient statistics at the fusion center $V = \sum_{i=1}^{N} D_i$ is binomial distributed as in (20). With $\theta \in (0, 1)$ such that $P_{f,l} < \theta < P_{d,l}$, and by large deviation analysis, the global error probabilities are asymptotically exponential decaying functions of N [1]:

$$\begin{aligned} P_{f,h} &= P(V \geq \theta N|H_0) \quad \sim e^{-N D_{\mathrm{KL}}(\theta||P_{f,l})}, \\ P_{md,h} &= P(V < \theta N|H_1) \quad \sim e^{-N D_{\mathrm{KL}}(\theta||P_{d,l})}. \end{aligned} \tag{30}$$

Accordingly, the global average error probability is asymptotically

$$\begin{aligned} P_{e,h} &= \pi_0 P_{f,h} + \pi_1 P_{md,h} \\ &\sim \pi_0 e^{-N D_{\mathrm{KL}}(\theta||P_{f,l})} + \pi_1 e^{-N D_{\mathrm{KL}}(\theta||P_{d,l})} \sim e^{-N \min\left(D_{\mathrm{KL}}(\theta||P_{f,l}), D_{\mathrm{KL}}(\theta||P_{d,l})\right)}. \end{aligned} \tag{31}$$

This error probability is maximized, globally, by maximizing the error exponent, $\min(D_{\mathrm{KL}}(\theta||P_{f,l}),\ D_{\mathrm{KL}}(\theta||P_{d,l}))$. Hence, the operating point $(P_{f,l},\ P_{d,l})$ is determined as

$$\max_{(P_{f,l}, P_{d,l}) \in \text{ local ROC}} \min_{\theta} \left(D_{\mathrm{KL}}(\theta||P_{f,l}), D_{\mathrm{KL}}(\theta||P_{d,l})\right). \tag{32}$$

For $P_{f,l} < \theta < P_{d,l}$, $D_{\mathrm{KL}}(\theta||P_{f,l})$ is an increasing function of θ and $D_{\mathrm{KL}}(\theta||P_{d,l})$ is a decreasing function of θ. As a result, the maximum is achieved when $D_{\mathrm{KL}}(\theta||P_{f,l}) = D_{\mathrm{KL}}(\theta||P_{d,l})$. Accordingly, the equalizing value of θ is

$$\theta^{\mathrm{LD}} = \frac{\log \frac{1-P_{d,l}}{1-P_{f,l}}}{\log \frac{P_{f,l}}{P_{d,l}} + \log \frac{1-P_{d,l}}{1-P_{f,l}}}, \tag{33}$$

and the corresponding value of the error exponent is

$$D_{\mathrm{KL}}(\theta^{\mathrm{LD}}||P_{f,l}) = D_{\mathrm{KL}}\left(\frac{\log \frac{1-P_{d,l}}{1-P_{f,l}}}{\log \frac{P_{f,l}}{P_{d,l}} + \log \frac{1-P_{d,l}}{1-P_{f,l}}}||P_{f,l}\right). \tag{34}$$

Notice that the operating point $(P_{f,l}, P_{d,l})$ and resulting error exponent are independent of the prior probabilities π_0 and π_1. Thus the LD solution is asymptotically an equalizer rule and therefore minimax.

In summary, the asymptotically optimum local decision rule is determined as

$$\max_{(P_{f,l},P_{d,l})\in \text{ local ROC}} D_{\mathrm{KL}}(\theta^{\mathrm{LD}}||P_{f,l}). \tag{35}$$

This large deviation (LD) solution for the local threshold has a number of important properties:

- *Semi-parametric*. The asymptotically optimal local decision strategy is *independent* of the total number of sensors N and the prior probabilities π_0 and π_1 but only dependent on the measurement model at the local sensors.
- *Asymptotically Minimax*. As shown in (32), the LD solution maximizes the minimum of the false alarm and missed detection error exponents. Therefore, asymptotically, the LD solution is an equalizer rule and consequently minimax [21, Chapter 5.3]. In other words, the LD solution has constant error exponents under any prior probabilities of the local hypotheses.
- *One-Dimensional Search*. In (35), we see that though $(P_{f,l}, P_{d,l})$ is two-dimensional, it actually only has one degree of freedom, as $(P_{f,l}, P_{d,l})$ is constrained by the ROC of the local detectors. This renders the optimization a one-dimensional search. In fact, under many signal models, the NP local detectors are in the form of a scalar compared against a single threshold, and in this case $P_{f,l}$ and $P_{d,l}$ can be computed as a function of this threshold, analytically in closed form. The objective function $D_{\mathrm{KL}}(\theta^{\mathrm{LD}}||P_{f,l})$ is convex and hence can be easily optimized by line search techniques such as those in [4, Chapter 7].
- *Universality*. The $(P_{f,l}, P_{d,l})$ pair in (35) has to reside within the $[0, 1] \times [0, 1]$ region of the local ROC curve. In Fig. 7, we plot the contours of the error exponent $D_{\mathrm{KL}}(\theta^{\mathrm{LD}}||P_{f,l})$ vs. the pair $(P_{f,l}, P_{d,l})$. This function is symmetrical

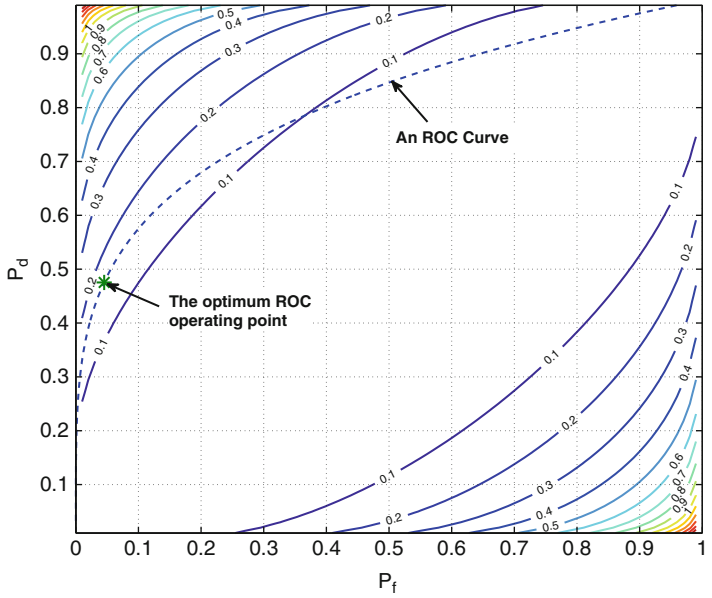

Fig. 7 Contours of error exponent in ROC region

about the line $P_{f,l} = P_{d,l}$ which agrees with the fact that the fusion center can always treat the hypotheses H_0 and H_1 symmetrically. These contours are convex and universal, in the sense that they depend only on the binomial distribution at the fusion center and are independent of the local measurement model. The local measurement model determines where the local ROC intersects the universal set of error exponents.

Simulations

The LD result obtained is applicable to general detection fusion problems with any signal models. Here, we apply the result to our cooperative spectrum sensing problems with the signal model given in section "Sensing Strategies and Performance Metrics".

Performance Surface and Local Threshold Convergence

In Fig. 8 the global error probability ($P_{e,h}$) for the energy sensing problem is plotted versus the local and fusion thresholds according to (25). In this figure, the number of local detectors is $N = 20$. Evidently, there are four local minima. This verifies our discussion of non-convexity in section "Joint Optimization of Local and Fusion Decisions".

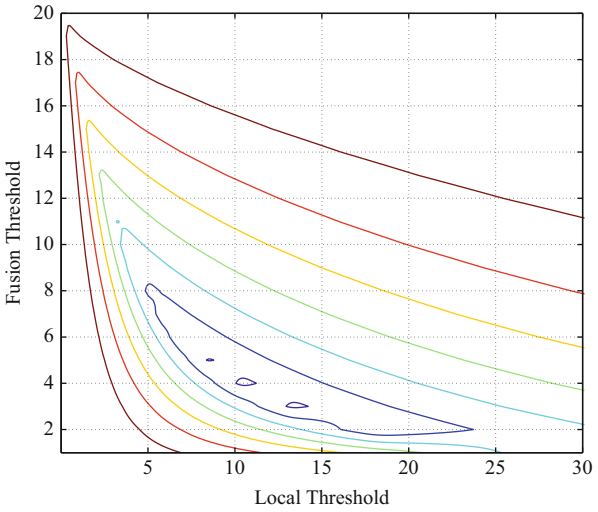

Fig. 8 The performance surface under local and fusion thresholds with $N = 20$

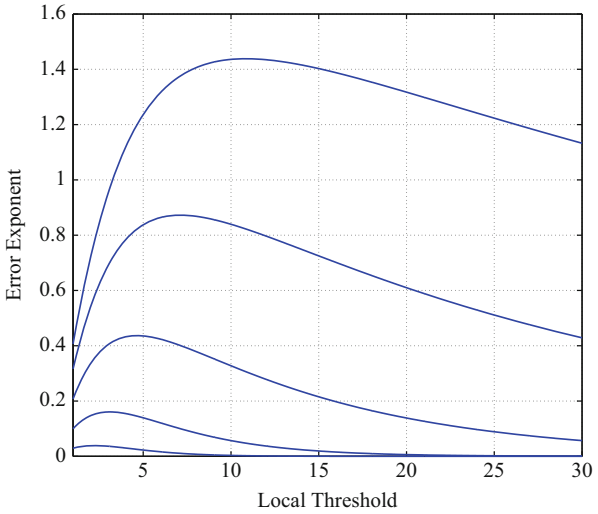

Fig. 9 Error exponent under different local thresholds. From bottom to top, the SNR is $\gamma = 0, 5, 10, 15, 20$ dB

The LD error exponent is plotted versus the local decision threshold in Fig. 9. In this figure, it can be observed that the error exponent is a unimodal function of the local threshold. Therefore, the optimal local threshold can be found using a one-dimensional line search algorithm.

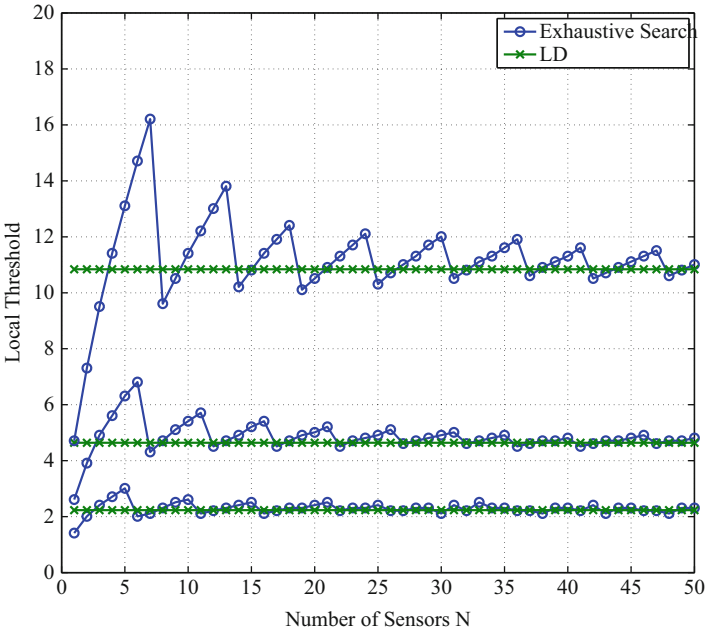

Fig. 10 Local decision thresholds under joint optimization by exhaustive search and large deviation analysis. From bottom to top, the per sensor SNR is $\gamma = 0, 10, 20$ dB

In Fig. 10, the optimum local thresholds, obtained by exhaustive search, are plotted versus N and compared with the thresholds determined by LD. There are three curves, for three values of SNR γ. These curves illustrate the approximation of the optimum thresholds, which depend on N, by the LD thresholds.

The behavior of the corresponding global fusion threshold is also interesting. In Fig. 11, we see that, instead of converging to the LD solution from one side of the ROC curve, the trace of the optimum operating points starts from the right side (larger P_f and P_d) of the LD solution, and then as the number of sensors increases, it passes through the LD solution and then reaches the leftmost point (smaller P_d and P_f). Then, the optimum operating point will return to the other side of, but at a closer distance to, the LD. This pattern repeats. This phenomenon comes from the fact that the value of the global fusion statistics can only take integer values. Within a certain range of N, the number of terms in the first summation in (25) will remain at a constant, so the increase of N within this range is accounted for by an increasing local threshold moving from right to left on the ROC curve in Fig. 11. As N increases beyond this range, the number of terms in the first summation in (25) will be increased by 1, bringing the local threshold down to the right side again.

To see this more clearly, consider a given number of sensors N, and the corresponding optimal local ROC operating point $(P_{f,l}(N), P_{d,l}(N))$ and fusion threshold $v^{\mathrm{MAP}}(N)$. It then follows that

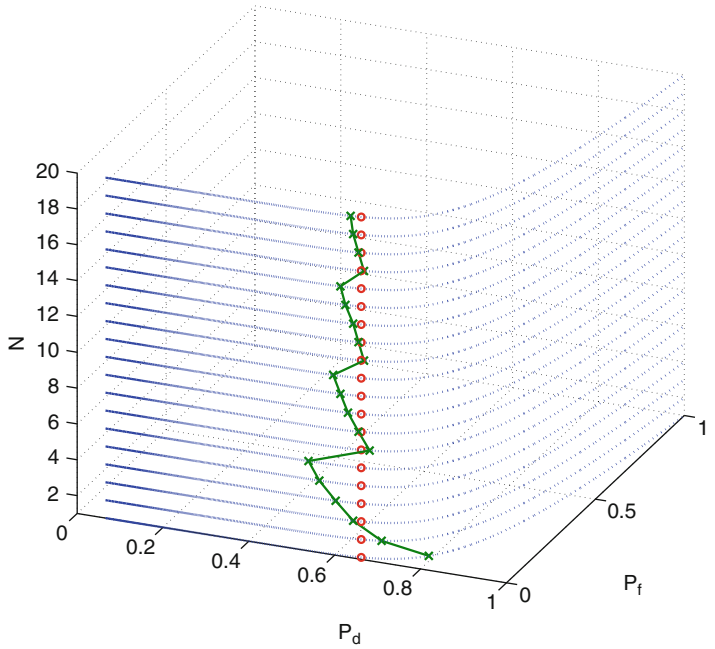

Fig. 11 The convergence of the optimal ROC operating points. SNR = 0 dB

$$
\begin{aligned}
P_{f,h}(N) &= \pi_0 \sum_{v=\lceil v^{\mathrm{MAP}}(N)\rceil}^{N} \binom{N}{v} \left(P_{f,l}(N)\right)^{v} \left(1-P_{f,l}(N)\right)^{N-v}, \\
P_{md,h}(N) &= \pi_1 \sum_{v=0}^{\lceil v^{\mathrm{MAP}}(N)\rceil-1} \binom{N}{v} \left(P_{d,l}(N)\right)^{v} \left(1-P_{d,l}(N)\right)^{N-v}.
\end{aligned}
\tag{36}
$$

When the number of sensors increases to $(N+1)$, we have

$$
\begin{aligned}
P_{f,h}(N+1) &= \pi_0 \sum_{v=\lceil v^{\mathrm{MAP}}(N+1)\rceil}^{N+1} \binom{N+1}{v} \left(P_{f,l}(N+1)\right)^{v} \left(1-P_{f,l}(N+1)\right)^{N+1-v}, \\
P_{md,h}(N+1) &= \pi_1 \sum_{v=0}^{\lceil v^{\mathrm{MAP}}(N+1)\rceil-1} \binom{N+1}{v} \left(P_{d,l}(N)\right)^{v} \left(1-P_{d,l}(N)\right)^{N+1-v}.
\end{aligned}
\tag{37}
$$

If $\lceil v^{\mathrm{MAP}}(N+1)\rceil = \lceil v^{\mathrm{MAP}}(N)\rceil$, $P_{f,h}(N+1)$ has one additional term compared with $P_{f,h}(N)$, whereas $P_{md,h}(N+1)$ has the same number of terms as $P_{md,h}(N)$. To minimize $(\pi_0 P_{f,h}(N+1) + \pi_1 P_{md,h}(N+1))$, one has to reduce $P_{f,l}(N)$ to

compensate for the extra term in $P_{f,h}(N+1)$. This leads to a higher local threshold and results in the leftward movement of the optimal ROC point in Fig. 11. On the other hand, if $\lceil v^{\text{MAP}}(N+1)\rceil = \lceil v^{\text{MAP}}(N)\rceil + 1$, there will be one additional term in $P_{md,h}(N+1)$, which by a similar argument will require a larger $P_{d,l}(N)$ and hence a lower local threshold. As a result, we have the abrupt changes of the ROC operating point when N increases from 6 to 7, from 11 to 12 and from 16 to 17 in Fig. 11.

Performance Comparisons

In this section, we compare the performance of the LD solution with previously proposed local detectors. In Fig. 12, we show the traces of their respective local detectors on the ROC curve as the SNR varies. Three of the ROC curves are illustrated, but operating points are computed for 20 different SNRs. We see that the LD solution has a lower operating point than other alternatives, and it remains very close to the exhaustive search solution for any SNR value. Among local detectors, the MMI detector is far superior to the others and nearly globally optimum for this example.

In Fig. 13, we plot the global average error probability at SNR $\gamma = 15$ dB as a function of the number of local sensors N, using various local decision rules. It can be observed that the average error probability decays exponentially with N as the large deviation analysis indicates. In addition, LD closely approximates the performance optimized by exhaustive search and actually does not require N to be very large to approach the optimal performance. Interestingly, from Figs. 10 and 13,

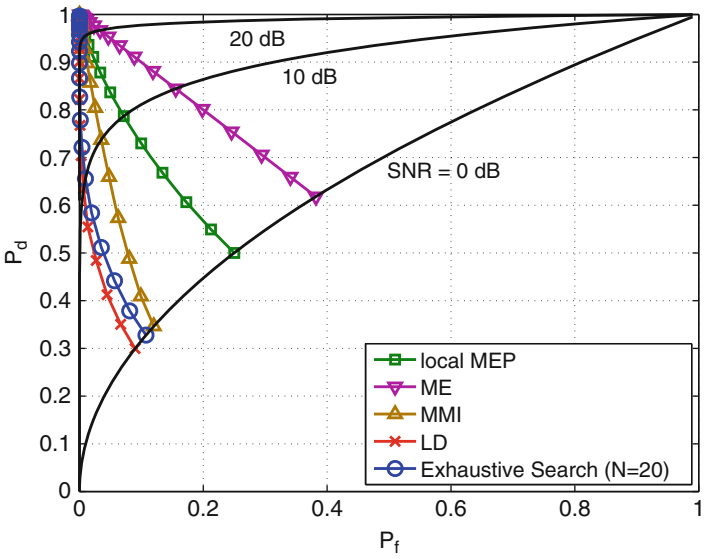

Fig. 12 The operating ROC trace under different local thresholds

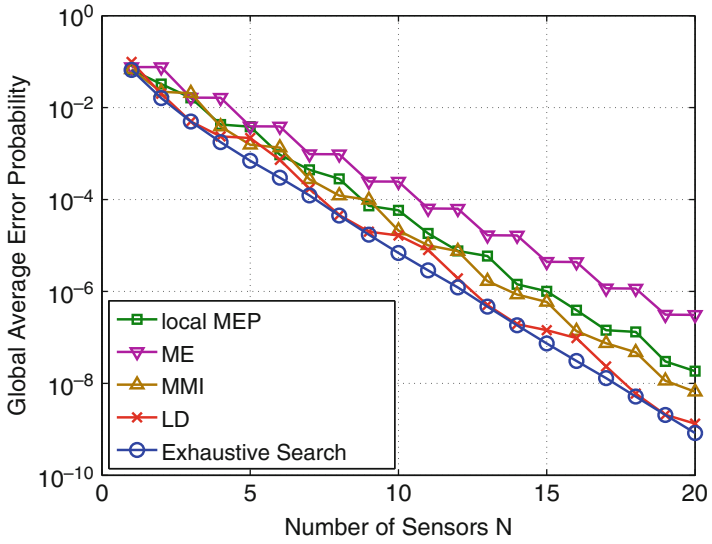

Fig. 13 Global average error probability under different local decision criteria at SNR $\gamma = 15$ dB as a function of the number of local sensing users N

we see that the exhaustive search solution with a fluctuating threshold results in a smooth performance curve, while LD with a constant threshold leads to a fluctuating performance curve, as our analysis in the preceding subsection implies.

Discussions

In this section, the method of LD is used to derive the operating point on local ROCs that minimizes the global error probability in cooperative sensing, asymptotically as the number of sensors grows large. The LD solution also establishes an important connection with Kullback-Leibler divergence and with a solution that maximizes mutual information at the local sensors. The LD solution is independent of the prior probabilities of the hypotheses and the total number of sensors, can be found by a simple line search, and is asymptotically minimax. It is also worth noting that the LD solution is applicable so long as a local (theoretical or empirical) ROC curve is known, regardless of whether or not it is the ROC curve for an NP detector.

Practical Designs: Case Studies

In this section, we will use two case studies to show how the fundamental limits in terms of diversity and error exponent we derived can guide practical designs in various system setups.

Sensing with Ternary Local Decisions: A Design from the Diversity Perspective

In section "Performance Scaling with SNR: Cooperative Diversity", the gain of cooperation is quantified in terms of the *cooperative diversities* for missed detection, false alarm, and average error probabilities. Using diversity as the performance metric, we optimally designed the sensing threshold strategies for cooperative sensing with both soft information fusion (SCoS) and hard information fusion or equivalently binary information fusion (BCoS). We found that while SCoS can achieve the maximum diversity, BCoS either loses half of the diversity or achieves the full diversity at the price of some signal-to-noise ratio (SNR) loss.

While the performance of SCoS is desirable, it is impractical since it requires infinite bandwidth for the communications between the sensing users and the fusion center. Intuitively, the performance gap between SCoS and BCoS results from the loss of information with the single-bit local decisions in BCoS. It should be possible to improve the performance by allowing the sensing users to provide more information. In this section, we investigate a cooperative sensing scheme with local ternary decisions. While developing the optimum strategies is complicated and mathematically intractable, our focus is to show that with local ternary decisions, it is possible to gain in terms of both diversity and SNR. This is in sharp contrary with the inevitable diversity-SNR trade-off when binary local decisions are used.

Compared with existing work on cooperative spectrum sensing with multi-threshold local decisions such as [3, 14–16] and [17], our design provides simple and closed-form expressions for both the local thresholds and fusion rule based on the metric of cooperative diversity. Moreover, we also obtain an explicit analytical expression for the performance gain, which has only been illustrated by simulations in the literature.

Binary Local Decision vs. Ternary Local Decision

Binary Local Decision (BD) and BCoS-k_0

For BCoS introduced in section "Performance Scaling with SNR: Cooperative Diversity", the secondary users make local binary decisions $D_i \in \{0, 1\}$ and a fusion center will collect all decisions and make a global decision. The local decisions are:

$$D_i = \begin{cases} 0 & \text{if } 0 \le \|r_i\|^2 < \theta_{l,B} \\ 1 & \text{if } \|r_i\|^2 > \theta_{l,B}. \end{cases} \tag{38}$$

If the local decision threshold is $\theta_{l,B} = k_0\theta^o$, where $\theta^o = (1 + \frac{1}{\gamma})\log(1 + \gamma)$ is the local optimum threshold. Then, as $\gamma \to +\infty$, $P_{f,l} = e^{-\theta_{l,B}} \approx \gamma^{-k_0}$, and $P_{md,l} = e^{\frac{\theta_{l,B}}{\gamma+1}} \approx k_0\gamma^{-1}$. With the NP detector $\sum_{i=1}^{N} D_i \underset{<H_0}{\overset{\ge H_1}{}} \theta_{f,B}$, the diversities are $d_{f,B} = k_0\theta_{f,B}$ and $d_{md,B} = N - \theta_{f,B} - 1$, where N is the total number of secondary users. To jointly optimize both diversities, the fusion threshold can

be selected as (It should be noticed that at the fusion center, $\sum D_i$'s can only take integer values. However, to simplify the notation, the integer restrictions are neglected without affecting the analysis.): $\arg\max_{\theta_{f,B}}(\min(k_0\theta_{f,B}, N-\theta_{f,B}-1)) = \frac{N+1}{k_0+1}$. The optimized diversities can be determined accordingly as $d_e = d_f = d_{md} = \frac{k_0}{k_0+1}(N+1)$.

This indicates that with larger k_0, BCoS-k_0 can achieve higher diversities by setting larger local threshold. However, in this case, the local decisions have missed detection probabilities $P_{md,B} \approx k_0\gamma^{-1}$ with $-10\log_{10}k_0$ SNR loss and smaller false alarm probabilities $P_{f,B} \approx \gamma^{-k_0}$. The larger missed detection probability P_{md} will dominate the overall average error probabilities performance P_e. Furthermore, instead of the diversity gain, the SNR losses for the missed detection probabilities will dominate the overall average error probability P_e at low-to-medium SNR.

Ternary Local Decision (TD)

The local decisions for TD are:

$$D_i = \begin{cases} 0 & \text{if } 0 \le \|r_i\|^2 < \theta_{l,1} \\ \spadesuit & \text{if } \theta_{l,1} \le \|r_i\|^2 \le \theta_{l,2} \\ 1 & \text{if } \|r_i\|^2 > \theta_{l,2}, \end{cases} \tag{39}$$

where $\theta_{l,2} > \theta_{l,1}$ are two local decision thresholds and $\spadesuit$ means "not sure." Then, the "0" or "1" decisions (Note that the sensor will remain silent when the local decision is $\spadesuit$.) are sent to the fusion center for the global decision $D \in \{0, 1\}$.

Under this local decisions, the conditional probabilities under each hypothesis are:

$$\begin{aligned} P(D_i = 0|H_0) &= \alpha_1 = 1 - e^{-\theta_{l,1}}, \\ P(D_i = \spadesuit|H_0) &= \alpha_2 = e^{-\theta_{l,1}} - e^{-\theta_{l,2}}, \\ P(D_i = 1|H_0) &= \alpha_3 = e^{-\theta_{l,2}}, \\ P(D_i = 0|H_1) &= \beta_1 = 1 - e^{-\frac{\theta_{l,1}}{\gamma+1}}, \\ P(D_i = \spadesuit|H_1) &= \beta_2 = e^{-\frac{\theta_{l,1}}{\gamma+1}} - e^{-\frac{\theta_{l,2}}{\gamma+1}}, \\ P(D_i = 1|H_1) &= \beta_3 = e^{-\frac{\theta_{l,2}}{\gamma+1}}. \end{aligned} \tag{40}$$

At the fusion center, D_is follow the trinomial distribution as:

$$\begin{aligned} P(D_1, D_2, \ldots, D_N|H_0) &= \alpha_1^{n_0}\alpha_2^{N-n_0-n_1}\alpha_3^{n_1}, \\ P(D_1, D_2, \ldots, D_N|H_1) &= \beta_1^{n_0}\beta_2^{N-n_0-n_1}\beta_3^{n_1}, \end{aligned} \tag{41}$$

where $n_0 = \{\text{the number of } D_i = 0\}$, $n_1 = \{\text{the number of } D_i = 1\}$, and N is the total number of cooperating local detectors. Accordingly, the sufficient statistics is (n_0, n_1). Denoting $\mathscr{R}_1$ as the set of (n_0, n_1) to make global decision $D = 1$ and $\mathscr{R}_0$ vice versa, we have:

$$\begin{aligned} P_f &= \sum_{(n_0,n_1)\in\mathscr{R}_1} P(n_0, n_1|H_0), \\ P_{md} &= \sum_{(n_0,n_1)\in\mathscr{R}_0} P(n_0, n_1|H_1). \end{aligned} \tag{42}$$

Based on Eqs. (40), (41), and (42), the optimum fusion rule can be obtained by jointly optimizing $P_e = \frac{1}{2}(P_f + P_{md})$ over $\theta_{l,1}$, $\theta_{l,2}$, and $\mathscr{R}_1$. However, not only that this is mathematically intractable, the solution also does not provide any clear insights on the diversity-SNR trade-off. As an alternative, we will first find the relationship between fusions with TD and BD and then develop the fusion rule for cooperative sensing with ternary local decisions (TCoS).

TCoS Fusion Rule

It is worth noting that at the fusion center, BD has a one-dimensional sufficient statistics set with $n_0 + n_1 = N$, while TD has a two-dimensional set with $n_0 + n_1 \leq N$. We find that when the fusion center with TD makes a global decision based on only one of n_0 and n_1, it is equivalent to the fusion with BD as the following:

Theorem 4. *For cooperative sensing based on local ternary decisions with thresholds $\theta_{l,1}$ and $\theta_{l,2}$:*

1. *If $\mathscr{R}_1 = \{(n_0, n_1) : n_1 \geq \theta_t\}$, this TD fusion is equivalent to BD fusion with local threshold $\theta_{l,B} = \theta_{l,2}$ and fusion threshold $\theta_{f,B} = \theta_t$;*
2. *If $\mathscr{R}_0 = \{(n_0, n_1) : n_0 \geq N - \theta_t + 1\}$, this TD fusion is equivalent to BD fusion with local threshold $\theta_{l,B} = \theta_{l,1}$ and fusion threshold $\theta_{f,B} = \theta_t$;*

Proof. See section "Appendix 4: Proof of Theorem 4".

With the relationship between BD and TD established in Theorem 4, we will next develop the fusion rule for TCoS. In particular, with local sensing thresholds $\theta_{l,1} = k_1\theta^o$ and $\theta_{l,2} = k_2\theta^o$ and $k_1 < k_2$, the corresponding sensing strategy is termed as TCoS-k_1-k_2.

Recall that from section "Binary Local Decision vs. Ternary Local Decision", BCoS-k_1 has a smaller diversity order. On the other hand, BCoS-k_2 achieves larger diversity but suffers from the SNR loss with the missed detection probability. Therefore, here we try to improve BCoS-k_2 missed detection performance by moving part of the decision region $\mathscr{R}_0$ to $\mathscr{R}_1$ while maintaining its larger false alarm and hence the overall diversity.

With TCoS-k_1-k_2, the probabilities for local decisions are $\alpha_1 \approx 1 - \gamma^{-k_1}, \alpha_2 \approx \gamma^{-k_1}, \alpha_3 \approx \gamma^{-k_2}$ and $\beta_1 \approx k_1\gamma^{-1}, \beta_2 \approx (k_2 - k_1)\gamma^{-1}, \beta_3 \approx 1 - k_2\gamma^{-1}$. Accordingly,

$$P(n_0, n_1|H_0) \approx \alpha_2^{N-n_0-n_1}\alpha_3^{n_1} \sim \gamma^{-(k_1N-k_1n_0+(k_2-k_1)n_1)}, \tag{43}$$

$$P(n_0, n_1|H_1) \approx \beta_1^{n_0}\beta_2^{N-n_0-n_1} \sim \gamma^{-(N-k_1)}. \tag{44}$$

The false alarm probability can be then calculated as:

$$\begin{aligned} P_f &= \sum_{(n_0,n_1)\in\mathscr{R}_1} P(n_0, n_1|H_0) \\ &\sim \sum_{(n_0,n_1)\in\mathscr{R}_1} \gamma^{-(k_1N-k_1n_0+(k_2-k_1)n_1)}. \end{aligned} \tag{45}$$

By Theorem 4, the decision region corresponding to BCoS-k_2 is $\mathscr{R}_1 = \{(n_0, n_1) : n_1 \geq \frac{N+1}{k_2+1}\}$, $\mathscr{R}_0 = \{(n_0, n_1) : n_1 < \frac{N+1}{k_2+1}\}$, and $d_{f,\text{BCoS}-k_2} = \frac{k_2}{k_2+1}(N+1)$. In order to reduce the missed detection probability which dominates the average error performance, we want to increase the decision region of $\mathscr{R}_1$ or equivalently decrease $\mathscr{R}_0$. At the same time, however, the false alarm diversity should be preserved. From Eq. (43), if $k_1N - k_1n_0 + (k_2 - k_1)n_1 \geq \frac{k_2}{k_2+1}(N+1)$, or equivalently $n_0 \leq (k_2 - k_1)n_1 + \frac{k_1(k_2+1)N-k_2(N+1)}{k_2+1}$, $P(n_0, n_1|H_0)$ will have a larger exponent of γ^{-1} than $d_{f,\text{BCoS}-k_2}$. Therefore, all points in $\mathscr{R}_0$ satisfying $n_0 \leq (k_2 - k_1)n_1 + \frac{k_1(k_2+1)N-k_2(N+1)}{k_2+1}$ can be moved into $\mathscr{R}_1$ without affecting the false alarm diversity according to (45). As a result, the boundary between $\mathscr{R}_1$ and $\mathscr{R}_0$ of the resultant fusion rule is the line $n_0 = (\frac{k_2}{k_1} - 1)n_1 + \frac{k_1(k_2+1)N-k_2(N+1)}{k_1(k_2+1)}$, which starts from $(n_0, n_1) = \left(\frac{k_1(k_2+1)N-k_2(N+1)}{k_1(k_2+1)}, 0\right)$ and ends at $(n_0, n_1) = \left(\frac{k_2N-1}{k_2+1}, \frac{N+1}{k_2+1}\right)$ where $\frac{k_2N-1}{k_2+1} + \frac{N+1}{k_2+1} = N$.

The decision region for TCoS-k_1-k_2 is illustrated in Fig. 14. The bold line is the boundary between $\mathscr{R}_0$ and $\mathscr{R}_1$ for TCoS-k_1-k_2, while the dashed line is the boundary corresponding to BCoS-k_2.

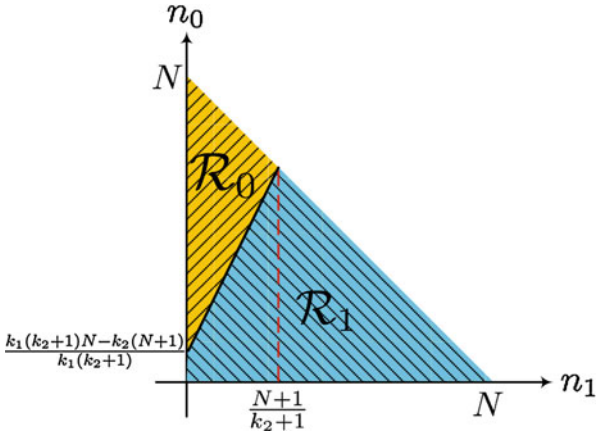

Fig. 14 The decision region for TCoS-k_1-k_2 with the points at the boundary belonging to $\mathscr{R}_1$

Compared with BCoS-k_2, TCoS-k_1-k_2 will provide the same overall diversities with $d_e = d_{md} = d_f = \frac{N+1}{k_2+1}$. Denoting

$$\Delta\mathscr{R} = \left\{(n_0, n_1) : 0 \le n_1 < \frac{N+1}{k_2+1}, 0 \le n_0 \le (k_2 - k_1)n_1 + \frac{k_1(k_2+1)N - k_2(N+1)}{k_2+1}\right\},$$

the difference between the missed detection probabilities of TCoS-k_1-k_2 and BCoS-k_2 is

$$\Delta P_{md} = P_{md,\text{TCoS}-k_1-k_2} - P_{md,\text{BCoS}-k_2} = -\sum_{\Delta\mathscr{R}} \beta_1^{n_0} \beta_2^{N-n_0-n_1} \beta_3^{n_1}, \tag{46}$$

and the difference between the false alarm probabilities of TCoS-k_1-k_2 and BCoS-k_2 is

$$\Delta P_f = P_{f,\text{TCoS}-k_1-k_2} - P_{f,\text{BCoS}-k_2} = \sum_{\Delta\mathscr{R}} \alpha_1^{n_0} \alpha_2^{N-n_0-n_1} \alpha_3^{n_1}. \tag{47}$$

It should be noticed that $\Delta P_e = P_{e,\text{TCoS}-k_1-k_2} - P_{e,\text{BCoS}-k_2} = \frac{1}{2}(\Delta P_{md} + \Delta P_f) < 0$. Therefore, we obtain overall performance gain over BCoS-k_2. This once again confirms that TCoS not only keeps the diversity gain that captures high SNR performance but also improves the SNR gain that characterizes the low to medium.

Simulations

Although it is possible to optimize k_1 for any given k_2 to obtain the maximum performance gain of TCoS by the analytical expressions given in section "TCoS Fusion Rule", the complexity is high. Therefore, we opt to verify and demonstrate the performance gain of TCoS over BCoS using some simple k_1 and k_2 values.

To illustrate the performance gain of TCoS-k_1-k_2 over both BCoS-k_1 and BCoS-k_2, we simulate TCoS-1-2 with 5 cooperating users and compare its performance with BCoS-1 and BCoS-2 in Fig. 15. We see that BCoS-2 exhibit a higher diversity than BCoS-1, but a worse performance at low SNR. Our proposed TCoS-1-2 not only retains the higher diversity of BCoS-2 but also has better performance at low SNR.

In Fig. 16, the performance of our proposed TCoS-1-2 is compared with the optimal TCoS with exhaustive search. It can be seen that our TCoS-1-2 only sacrifices a little performance ($\approx$1.5 dB) in exchange for the low-complexity closed-form local and global decision rules.

In addition, we know that BCoS-N achieves the maximum diversity but suffers from considerable SNR loss. Here, we compare the performance of TCoS-2.5-5

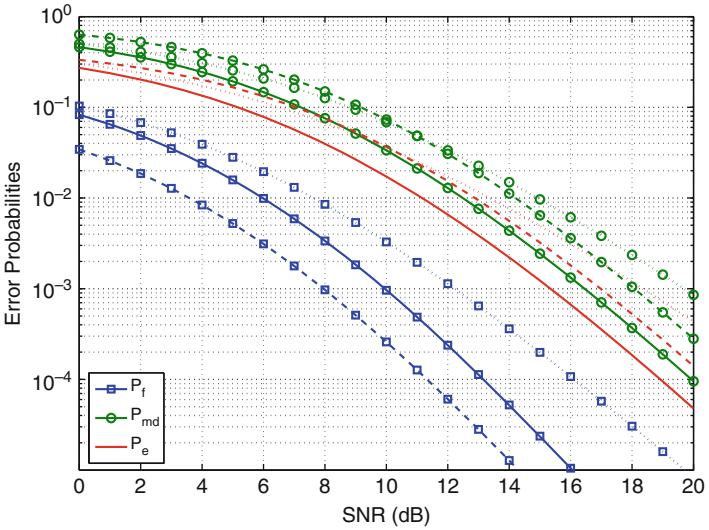

Fig. 15 TCoS-1-2 (*solid*) vs. BCoS-1 (*dotted*) and BCoS-2 (*dashed*) with $N = 5$

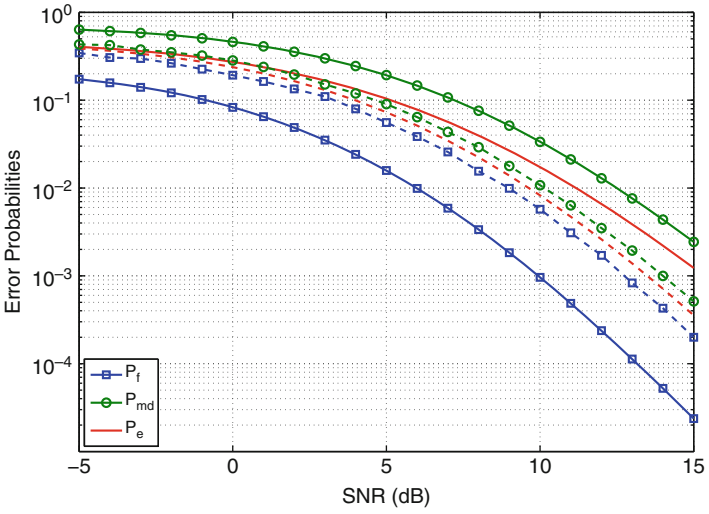

Fig. 16 TCoS-1-2 (*solid*) vs. optimal TCoS by exhaustive search (*dashed*) with $N = 5$

and BCoS-5 in Fig. 17. It can be observed that TCoS-2.5-5 also achieves the same full diversity ($d_e = 5$), but has about 2dB SNR gain. Together with Fig. 15, it is confirmed that the overall SNR gain is obtained without losing any false alarm diversity.

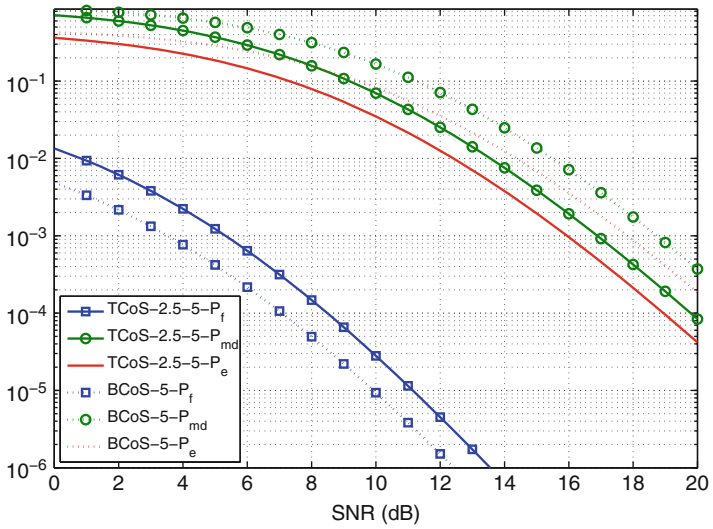

Fig. 17 TCoS-2.5-5 vs. BCoS-5 with $N = 5$

Discussions

In this case study, we introduced cooperative sensing with ternary local decisions (TCoS) to improve upon binary hard decisions (BCoS) by gaining SNR while maintaining the same diversity. The link between the fusion with BD and TD has been established and further used to determine the fusion rule for TCoS. The algorithm developed in this section provides simple and closed-form expressions for both the local decision thresholds and the fusion rule. The performance gain was also derived analytically. Furthermore, simulations confirmed that, as the middle ground between BCoS and SCoS, TCoS provides a practical yet effective solution for the inevitable diversity-SNR trade-off encountered by BCoS.

Sensing with Joint Diversity and Error Exponent Considerations

As discussed in section "Performance Scaling with SNR: Cooperative Diversity", for cooperative spectrum sensing, when the number of cooperative sensing users N is fixed, the error probability decreases with SNR γ at a certain rate. Generally speaking, when the number of cooperating sensing users N increases, the decreasing rate of error probabilities in λ will increase, thanks to more extensive sensing cooperation. To quantify the gain of multiple sensors, the diversity order is defined as

$$d(N) = -\lim_{\gamma \to +\infty} \frac{\log P_{e,h}(N, \gamma)}{\log \gamma}, \tag{48}$$

where $P_{e,h}$ is the global average error probability for the hard/binary information fusion. By definition, the diversity notion comes from the asymptotic performance in terms of the signal model parameter γ. It is shown in section "Performance Scaling with SNR: Cooperative Diversity" that the maximum diversity order for fusion with N sensors is N. It is interesting to see whether the large deviation solution proposed in section "Performance Scaling with the Number of Sensing Users: Error Exponent" also achieves the maximum diversity.

Diversity Analysis of the LD Solution for Spectrum Sensing

To evaluate the diversity of the LD solution which is the asymptotic performance in terms of the average SNR γ, we take $\gamma \to +\infty$. In this case, the local probabilities will have $P_{f,l} \to 0$ and $P_{d,l} \to 1$. Then, the first term within the KL divergence in (34) is

$$\frac{\log \frac{1-P_{d,l}}{1-P_{f,l}}}{\log \frac{P_{f,l}}{P_{d,l}} + \log \frac{1-P_{d,l}}{1-P_{f,l}}} \approx \frac{\log(1-P_{d,l})}{\log P_{f,l} + \log(1-P_{d,l})} \triangleq \theta^{\mathrm{LD}}. \tag{49}$$

As such, the objective function in (35) can be expanded as

$$\begin{aligned} D_{\mathrm{KL}}(\theta^{\mathrm{LD}} || P_{f,l}) &= \theta^{\mathrm{LD}} \log \frac{\theta^{\mathrm{LD}}}{P_{f,l}} + (1-\theta^{\mathrm{LD}}) \log \frac{1-\theta^{\mathrm{LD}}}{1-P_{f,l}} \\ &= \theta^{\mathrm{LD}} \log \theta^{\mathrm{LD}} + (1-\theta^{\mathrm{LD}}) \log(1-\theta^{\mathrm{LD}}) \theta^{\mathrm{LD}} \log P_{f,l} - (1-\theta^{\mathrm{LD}}) \log(1-P_{f,l}). \end{aligned}$$

In the four terms of the resulting expansion, when $P_{f,l} \to 0$, we have

$$\begin{aligned} &0 \le \theta^{\mathrm{LD}} \log \theta^{\mathrm{LD}} + (1-\theta^{\mathrm{LD}}) \log(1-\theta^{\mathrm{LD}}) \le 1 \ll E(\gamma), \\ &(1-\theta^{\mathrm{LD}}) \log(1-P_{f,l}) \approx 0. \end{aligned} \tag{50}$$

As a result, the error exponent

$$E(P_{f,l}, P_{d,l}) \approx \max_{(P_{f,l}, P_{d,l})} (-\theta^{\mathrm{LD}} \log P_{f,l}) = \max_{(P_{f,l}, P_{d,l})} \frac{-\log P_{f,l} \log(1-P_{d,l})}{\log P_{f,l} + \log(1-P_{d,l})}, \tag{51}$$

where $P_{f,l}$ and $P_{d,l}$ are

$$\begin{aligned} P_{f,l} &= e^{-\theta_l}, \\ P_{d,l} &= e^{-\frac{\theta_l}{\gamma+1}}, \end{aligned} \tag{52}$$

according to the signal model given in (1) and θ_l is the local decision threshold in (2).

When $\gamma \to +\infty$, $P_{d,l} = e^{-\frac{\theta_l}{\gamma+1}} \approx 1 - \frac{\theta_l}{\gamma+1}$, then

$$E(P_{f,l}, P_{d,l}) \approx \frac{-\log P_{f,l} \log(1 - P_{d,l})}{\log P_{f,l} + \log(1 - P_{d,l})} = \frac{-(-\theta_l) \log \frac{\theta_l}{\gamma+1}}{(-\theta_l) + \log \frac{\theta_l}{\gamma+1}}. \tag{53}$$

Setting $\frac{dE(P_{f,l}, P_{d,l})}{d\theta_l} = 0$, we can see that the large deviation local threshold satisfies

$$\log \theta_l + \theta_l^{\frac{1}{2}} = \log(\gamma + 1). \tag{54}$$

When $\gamma \to +\infty$, we have $\theta_l \to +\infty$, and therefore $\log \theta_l \ll \theta_l^{\frac{1}{2}}$. Ignoring the term $\log \theta_l$ in (54), we have an approximated optimal threshold in closed form:

$$\tilde{\theta}_l^{\mathrm{LD}} \approx (\log(\gamma + 1))^2 . \tag{55}$$

With this large deviation solution $\tilde{\theta}_l^{\mathrm{LD}}$ and by (53), the error exponent becomes

$$\tilde{E}^{\mathrm{LD}}(\gamma) \approx \log(\gamma + 1). \tag{56}$$

An illustration of the resultant error exponents under the threshold achieved by (35), (54) and (55) is given in Fig. 18. It could be observed that the closed-form expression

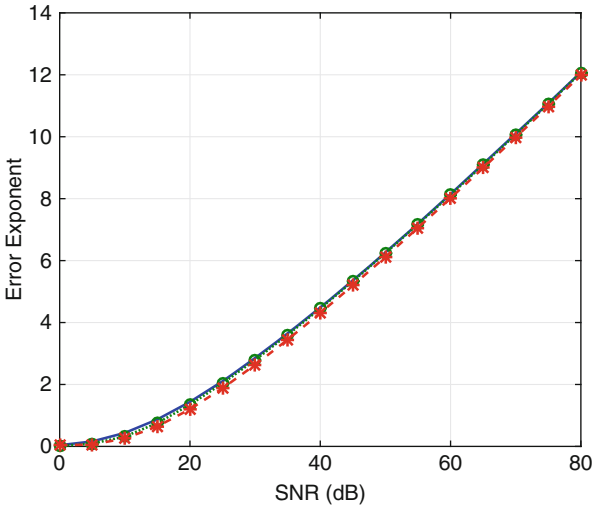

Fig. 18 The error exponent $E(\gamma)$ for cooperative spectrum sensing using different thresholds: (1) *solid curve*, by solving (35); (2) *dotted curve* with *circles*, by solving (54); and (3) *dashed curve* with *stars*: by using the closed-form expression (55)

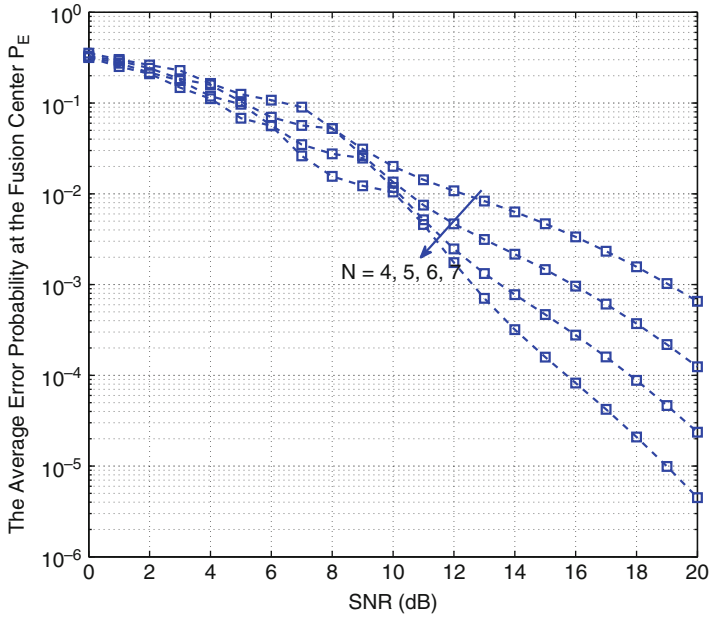

Fig. 19 The LD solution achieves full diversity

can achieve the error exponent of the optimum large deviation solution given in (35) very well.

To obtain the diversity of the resultant cooperative sensing strategy, by the definition of the error exponent, as $N \to +\infty$,

$$\begin{aligned} d(N) &= -\lim_{\lambda \to +\infty} \frac{\log P_{e,h}(N,\gamma)}{\log \gamma} = -\lim_{\gamma \to +\infty} \frac{\log(e^{-NE(\gamma)})}{\log \gamma} \\ &= -\lim_{\gamma \to +\infty} \frac{-N \log(\gamma+1)}{\log \gamma} = N. \end{aligned} \tag{57}$$

That is, the proposed large deviation solution can achieve the maximum diversity gain. An illustration of the average error probability vs. N is shown in Fig. 19.

Discussions

From our analysis, we see that although in general the LD solution requires a one-dimensional search, at high SNR we find a closed-form analytical solution for large N, for the cooperative spectrum sensing problem. It should be noticed that this closed-form solution will only be expected to achieve the optimal performance when both the SNR γ and the number of cooperative users N approaches infinity. For cooperative spectrum sensing with fixed finite number of users, the strategies provides in section "Performance Scaling with SNR: Cooperative Diversity" might

still be better alternatives. However, another unique advantage of the closed-form strategy given by joint considerations of diversity and error exponent is that the resultant solution is entirely local and independent of the total number of sensing users in cooperations. Therefore, it can be readily applied in the cases where the number of sensing users is unknown and/or changing over time.

Summary

In this chapter, we have quantified the fundamental limits of cooperative spectrum sensing performance (i) by diversity when the signal parameter SNR approaches infinity and (ii) by error exponent when the number of cooperative users approaches infinity. These fundamental limits can effectively guide practical designs under different system setups. In particular, with the notion of diversity, we have seen how cooperative spectrum sensing with ternary local decisions can be designed to approach the performance with soft information fusion. On the other hand, combining the LD solution with the notion of diversity in our spectrum sensing problem, we have obtained a closed-form expression for the optimal local threshold when both the SNR and the number of cooperative users approaches infinity.

Appendices

Appendix 1: Proof of Theorem 2

With $\theta_s = N(1+\frac{1}{\gamma})\log(\gamma+1)$, as $\gamma \to +\infty$, $e^{-\theta_s} = (1+\gamma)^{-N(1+\frac{1}{\gamma})} \sim (\gamma+1)^{-N}$ and $\sum_{i=0}^{N-1} \theta_s^i/i! = \sum_{i=0}^{N-1} N^i(1+\frac{1}{\gamma})^i(\log(\gamma+1))^i/i! \sim N^{N-1}(\log(\gamma+1))^{N-1}/(N-1)!$. Thus, according to (14), $P_{f,s} \sim \frac{N^{N-1}}{(N-1)!}(\log(\gamma+1))^{N-1}(\gamma+1)^{-N}$ and

$$d_{f,s} = -\lim_{\gamma\to+\infty} \frac{\log P_{f,s}}{\log \gamma} = N.$$

Also, with θ_s defined above, as $\gamma \to +\infty$, $e^{-\theta_s/(\gamma+1)} = e^{-\frac{N}{\gamma}\log(\gamma+1)} \to 1$ and $\sum_{i=N}^{+\infty} \theta_s^i/(i!(\gamma+1)^i) = \sum_{i=N}^{+\infty} N^i(1+\frac{1}{\gamma})^i(\log(\gamma+1))^i/(i!(\gamma+1)^i) \sim N^N(\log(\gamma+1))^N(\gamma+1)^{-N}/N!$. Thus, according to (15), $P_{md,s} \sim \frac{N^N}{N!}(\log(\gamma+1))^N(\gamma+1)^{-N}$ and

$$d_{md,s} = -\lim_{\gamma\to+\infty} \frac{\log P_{md,s}}{\log \gamma} = N.$$

Accordingly, $d_{e,s} = \min(d_{f,s}, d_{md,s}) = N$.

Appendix 2: Proof of Theorem 3

From (18) and (19),

$$P_{f,h} = P(\lambda_h \geq \theta_h | H_0) = \sum_{i=\theta_h}^{N} \binom{N}{i} P_{f,l}^{i} (1 - P_{f,l})^{N-i}.$$

The false alarm diversity at the local sensing decision is $d_{f,l}$, so as $\gamma \to +\infty$, $P_{f,l} \sim (\gamma+1)^{-d_{f,l}}$, $1 - P_{f,l} \to 1$; thus $P_{f,l}^{i}(1 - P_{f,l})^{N-i} \sim (\gamma+1)^{-i d_{f,l}}$. In the summation of $P_{f,h}$, as $\gamma \to +\infty$, the term with lowest power order of $(\gamma+1)^{-1}$ will dominate; thus $P_{f,h} \sim \binom{N}{\theta_h}(\gamma+1)^{-\theta_h d_{f,l}}$, and the false alarm diversity order is

$$d_{f,h} = -\lim_{\gamma \to +\infty} \frac{\log P_{f,h}}{\log \gamma} = \theta_h d_{f,l}, \quad \theta_h = 1, 2, \ldots, N.$$

From (18) and (19),

$$P_{md,h} = P(\lambda_h < \theta_h | H_1) = \sum_{i=0}^{\theta_h - 1} \binom{N}{i} (1 - P_{md,l})^{i} P_{md,l}^{N-i}.$$

From the same argument, the missed detection diversity order is

$$d_{md,h} = -\lim_{\gamma \to +\infty} \frac{\log P_{md,h}}{\log \gamma} = (N - \theta_h + 1) d_{md,l}, \ \theta_h = 1, 2, \ldots, N.$$

Appendix 3: Proof of Corollary 3

From Corollary 1, we know that the local threshold can be chosen as $\theta_l = d_0 \theta^o$ ($d_0 > 0$). In this case, $d_{f,l} = d_0$ and $d_{md,l} = 1$. By Theorem 3, if the hard decision threshold is θ_h ($\theta_h \in \{1, 2, \ldots, N\}$), the average error diversity is $d_{e,h} = \min(\theta_h d_0, N - \theta_h + 1)$. To maximize $d_{e,h}$, we need to maximize both $\theta_h d_0$ and $(N - \theta_h + 1)$ simultaneously. By maximizing the latter, we obtain $\theta_h = 1$. Then $d_{e,h} = \min(d_0, N)$. Thus, as long as $d_0 \geq N$, we obtain the maximum diversity $d_{e,h} = N$. However, as stated in Corollary 1, higher d_0 will cause higher SNR loss for the missed detection performance. Thus, we choose $d_0 = N$ to minimize the SNR loss for the missed detection performance while achieving the maximum average error diversity.

Appendix 4: Proof of Theorem 4

If $\mathscr{R}_1 = \{(n_0, n_1) : n_1 \geq \theta_t\}$, then:

$$P_{f,t} = \sum_{n_1=\theta_t}^{N} \sum_{n_0=0}^{N-n_1} \frac{N!}{n_0!(N-n_0-n_1)!n_1!} \alpha_1^{n_0} \alpha_2^{N-n_0-n_1} \alpha_3^{n_1}$$
$$= \sum_{n_1=\theta_t}^{N} \frac{N}{n_1!(N-n_1)!} (1-\alpha_3)^{N-n_1} \alpha_3^{n_1},$$

and

$$P_{md,t} = \sum_{n_1=0}^{\theta_t-1} \sum_{n_0=0}^{N-n_1} \frac{N!}{n_0!(N-n_0-n_1)!n_1!} \beta_1^{n_0} \beta_2^{N-n_0-n_1} \beta_3^{n_1}$$
$$= \sum_{n_1=0}^{\theta_t-1} \frac{N}{n_1!(N-n_1)!} (1-\beta_3)^{N-n_1} \beta_3^{n_1}.$$

This is equivalent to BT with $\theta_{l,B} = \theta_{l,2}$ and $\theta_{f,B} = \theta_t$.

If $\mathscr{R}_0 = \{(n_0, n_1) : n_0 \geq N + 1 - \theta_t\}$, then:

$$P_{f,t} = \sum_{n_0=0}^{N-\theta_t+1} \sum_{n_1=0}^{N-n_0} \frac{N!}{n_0!(N-n_0-n_1)!n_1!} \alpha_1^{n_0} \alpha_2^{N-n_0-n_1} \alpha_3^{n_1}$$
$$= \sum_{n_0=0}^{N-\theta_t+1} \frac{N}{n_0!(N-n_0)!} \alpha_1^{n_0} (1-\alpha_1)^{N-n_0},$$

and

$$P_{md,t} = \sum_{n_0=N-\theta_t+1}^{N} \sum_{n_1=0}^{N-n_1} \frac{N!}{n_0!(N-n_0-n_1)!n_1!} \beta_1^{n_0} \beta_2^{N-n_0-n_1} \beta_3^{n_1}$$
$$= \sum_{n_0=N-\theta_t+1}^{N} \frac{N}{n_0!(N-n_0)!} \beta_1^{n_0} (1-\beta_1)^{N-n_0}.$$

This is equivalent to BT with $\theta_{l,B} = \theta_{l,1}$ and $\theta_{f,B} = \theta_t$.

References

1. Arratia R, Gordon L (1989) Tutorial on large deviations for the binomial distribution. Bull Math Biol 51(1):125–131
2. Cabric D, Tkachenko A, Brodersen RW (2006) Experimental study of spectrum sensing based on energy detection and network cooperation. In: Proceedings of ACM 1st International

Workshop on Technology and Policy for Accessing Spectrum (TAPAS), Boston, Aug 2006, pp 1–8
3. Chaudhari S, Lunden J, Koivunen V, Poor HV (2010) Cooperative sensing with imperfect reporting channels: hard decisions or soft decisions? IEEE Trans Signal Process 60(1):18–28
4. Chong EK, Zak SH (2013) An introduction to optimization, 3rd edn. Wiley, Hoboken
5. Cui S, Xiao J, Goldsmith AJ, Luo Z, Poor HV (2007) Estimation diversity and energy efficiency in distributed sensing. IEEE Trans Signal Process 55(9):4683–4695
6. Duan D, Yang L, Principe JC (2010) Cooperative diversity of spectrum sensing for cognitive radio systems. IEEE Trans Sig Process 58(6):3218–3227
7. Duan D, Yang L (2012) Cooperative spectrum sensing with ternary local decisions. IEEE Commun Lett 16(9):1512–1515
8. Duan D, Yang L, Scharf LL, Cui S (2013) Large deviation solution for cooperative spectrum sensing with diversity analysis. In: Proceedings of IEEE Global Communications Conference (GLOBECOM), Atlanta, 9–13 Dec 2013
9. Duan D, Scharf L, Yang L (2017) LD approach to asymptotically optimum sensor fusion. IET Commun 11(5):680–686
10. Ghasemi A, Sousa ES (2005) Collaborative spectrum sensing for opportunistic access in fading environments. In: Proceedings of the First IEEE International Symposium on New Frontiers in Dynamic Spectrum Access Networks (DySPAN), Baltimore, 8–11 Nov 2005, pp 131–136
11. Han YI, Kim T (2001) Mutual and conditional mutual informations for optimizing distributed Bayes detectors. IEEE Trans Aerosp Electron Syst 37(1):147–157
12. Haykin S (2005) Cognitive radio: brain-empowered wireless communications. IEEE J Select Areas Commun 23(2):201–220
13. Hong S, Vu MH, Tarokh V (2008) Cognitive sensing based on side information. In: IEEE Sarnoff Symposium, Princeton, 28–30 Apr 2008, pp 1–6
14. Kaewprapha P, Li J, Yu Y (2010) Cooperative spectrum sensing with tri-state probabilistic inference. In: Proceedings of Military Communications Conference, San Jose, 31 Oct–3 Nov 2010, pp 318–323
15. Ma J, Zhao G, Li Y (2008) Soft combination and detection for cooperative spectrum sensing in cognitive radio networks. IEEE Trans Wirel Commun 7(11):4502–4507
16. Mishra SM, Tandra R, Sahai A (2007) The case for multiband sensing. In: Proceedings of the Forty-Fifth Annual Allerton Conference on Communication, Control, and Computing, The Allerton House, University of Illinois, Sept 2007.
17. Mustonen M, Matinmikko M, Mämmalä A (2009) Cooperative spectrum sensing using quantized soft decision combining. In: Proceedings of the Fourth International Conference on Cognitive Radio Oriented Wireless Networks and Communications, Hannover, 22–24 June 2009, pp 1–5
18. Pezeshki A, Calderbank R, Howard SD (2007) Diversity order for detection with distributed sensors. IEEE Trans Signal Process Submitted November 2007
19. Poor HV (1994) An introduction to signal detection and estimation, 2nd edn. Springer, New York
20. Quan Z, Cui S, Sayed AH (2008) Optimal linear cooperation for spectrum sensing in cognitive radio networks. IEEE J Sel Top Singal Process 2(1):28–40
21. Scharf L (1991) Statistical signal processing-detection, estimation and time series analysis. Addison-Wesley, Reading
22. Tandra R, Sahai A (2008) SNR walls for signal detection. IEEE J Sel Top Signal Process 2:4–17
23. Tse DNC, Viswanath P (2005) Fundamentals of wireless communications. Cambridge University Press, Cambridge
24. Tsitsiklis JN (1988) Decentralized detection by a large number of sensors. Math Control Signals Syst 1(2):167–182

25. Tsitsiklis J, Athans M (1985) On the complexity of decentralized decision making and detection problems. IEEE Trans Autom Control 30(5):440–446
26. Unnikrishnan J, Veeravalli VV (2008) Cooperative sensing for primary detection in cognitive radio. IEEE J Sel Top Singal Process 2(1):18–27
27. Zhao Q, Sadler BM (2007) A survey of dynamic spectrum access. IEEE Signal Process Mag 24(3):79–89

Analog to Digital Cognitive Radio

11

Deborah Cohen, Shahar Tsiper, and Yonina C. Eldar

Contents

D. Cohen (✉) · S. Tsiper · Y. C. Eldar
Electrical Engineering, Technion – Israel Institute of Technology, Haifa, Israel
e-mail: debby@technion.ac.il; tsiper@technion.ac.il; yonina@ee.technion.ac.il

W. Zhang (ed.), *Handbook of Cognitive Radio*,
https://doi.org/10.1007/978-981-10-1394-2_11

Abstract

Enabling cognitive radio (CR) requires revisiting the traditional task of spectrum sensing with specific and demanding requirements in terms of detection performance, real-time processing, and robustness to noise. Unfortunately, conventional spectrum sensing methods do not satisfy these demands. In particular, the Nyquist rate of signals typically sensed by a CR is prohibitively high so that sampling at this rate necessitates sophisticated and expensive analog to digital converters, which lead to a torrent of samples. Over the past few years, several sampling methods have been proposed that exploit signals' a priori known structure to sample them below Nyquist. In this chapter, we review some of these techniques and tie them to the task of spectrum sensing for CRs. We then show how other spectrum sensing challenges can be tackled in the sub-Nyquist regime. First, to cope with low signal-to-noise ratios, spectrum sensing may be based on second-order statistics recovered from the low rate samples. In particular, cyclostationary detection allows to differentiate between communication signals and stationary noise. Next, CR networks, that perform collaborative low rate spectrum sensing, have been proposed to overcome fading and shadowing channel effects. Last, to enhance CR efficiency, we present joint spectrum sensing and direction of arrival estimation methods from sub-Nyquist samples. These allow to map the temporarily vacant bands both in terms of frequency and space. Throughout this chapter, we highlight the relation between theoretical algorithms and results and their practical implementation. We show hardware simulations performed on a prototype built with off-the-shelf devices, demonstrating the feasibility of sub-Nyquist spectrum sensing in the context of CR.

Introduction

In order to increase the chance of finding an unoccupied spectral band, cognitive radios (CRs) have to sense a wide band of spectrum. Nyquist rates of wideband signals are high and can even exceed today's best analog to digital converters (ADCs) front-end bandwidths. In addition, such high sampling rates generate a large number of samples to process, affecting speed and power consumption. To overcome the rate bottleneck, several sampling methods have been proposed that leverage the a priori known received signal's structure, enabling sampling rate reduction [1,2]. These include the random demodulator [3], multi-rate sampling [4], multicoset sampling, and the modulated wideband converter (MWC) [5–8].

The CR then performs spectrum sensing on the acquired samples to detect the presence of primary users' (PUs) transmissions. The simplest and most common spectrum sensing approach is energy detection [9], which does not require any a priori knowledge on the input signal. Unfortunately, energy detection is very sensitive to noise and performs poorly in low signal-to-noise ratio (SNR) regimes. This becomes even more critical in sub-Nyquist regimes since the sensitivity of energy detection is amplified due to aliasing of the noise [10]. Therefore, this

scheme fails to meet CR performance requirements in low SNRs. In contrast, matched filter (MF) detection [11, 12], which correlates a known waveform with the input signal to detect the presence of a transmission, is the optimal linear filter for maximizing SNR in the presence of additive stochastic noise. However, this technique requires perfect knowledge of the potential received transmission. When no a priori knowledge is assumed on the received signals' waveform, MF is difficult to implement. A compromise between both methods is cyclostationary detection [13, 14]. This strategy is more robust to noise than energy detection but at the same time only assumes that the signal of interest exhibits cyclostationarity, which is a typical characteristic of communication signals. Consequently, cyclostationary detection is a natural candidate for spectrum sensing from sub-Nyquist samples in low SNRs.

Besides noise, the task of spectrum sensing for CRs is further complicated due to path loss, fading, and shadowing [15]. These phenomena are due to the signal's propagation that can be affected by obstacles and multipath and result in the attenuation of the signal's power. To overcome these practical issues, collaborative CR networks have been considered, where different users share their sensing results and cooperatively decide on the licensed spectrum occupancy [15–17]. Cooperative spectrum sensing can be classified into three categories based on the way the data is shared by the CRs in the network: centralized, distributed, and relay-assisted. In each of these settings, two options of data fusion arise: decision fusion, or hard decision, where the CRs only report their binary local decisions, and measurement fusion, or soft decision, where they share their samples [15]. Cooperation has been shown to improve detection performance and relax sensitivity requirements by exploiting spatial diversity.

Finally, CRs may require, or at least benefit from, joint spectrum sensing and direction of arrival (DOA) estimation. DOA recovery can enhance CR performance by allowing exploitation of vacant bands in space in addition to the frequency domain. For example, a spectral band occupied by a PU situated in a certain direction with respect to the CR may be used by the latter for transmission to the opposite direction, where receivers do not sense the PU's signal. In order to estimate jointly the carrier frequencies and DOAs of the received transmissions, arrays of sensors have been considered. DOA recovery techniques, such as MUSIC [18, 19], ESPRIT [20], or compressed sensing (CS) [21] techniques, may then be adapted to the joint carrier and DOA estimation problem both in Nyquist and sub-Nyquist regimes.

This chapter focuses on the spectrum sensing challenges for CR outlined above. We first review sub-Nyquist sampling methods for multiband signals and then consider different aspects of spectrum sensing performed on low rate samples, including cyclostationary detection, collaborative spectrum sensing, and joint carrier frequency and DOA estimation. Our emphasis is on practical low rate acquisition schemes and tailored recovery that can be implemented in real CR settings. The approach adopted here focuses on the analog to digital interface of CRs. In particular, we are concerned with compressive spectrum sensing, including the application of CS to analog signals. Modeling the analog to digital conversion

allows demonstrating the realization of the theoretical concepts on hardware prototypes. We focus on the implementation of one sampling scheme reviewed here, the MWC, and show how the same low rate samples can be used in the different extensions of spectrum sensing described above.

Sub-Nyquist Sampling for CR

CR receivers sense signals composed of several transmissions with unknown support, spread over a wide spectrum. Such sparse wideband signals belong to the so-called multiband model [6, 7]. An example of a multiband signal $x(t)$ with K bands is illustrated in Fig. 1. The bandwidth of each band is no greater than B and is centered around unknown carrier frequencies $|f_i| \leq f_{\text{Nyq}}/2$, where f_{Nyq} denotes the signals' Nyquist rate and i indexes the transmissions. Note that, for real-valued signals, K is an even integer due to spectral conjugate symmetry and the number of transmissions is $N_{\text{sig}} = K/2$.

When the frequency support of $x(t)$ is known, classic sampling methods such as demodulation, undersampling ADCs, and interleaved ADCs (see [1, 2] and references therein) may be used to reduce the sampling rate below Nyquist. Here, since the frequency location of the transmissions are unknown, classic processing first samples $x(t)$ at its Nyquist rate f_{Nyq}, which may be prohibitively high. To overcome the sampling rate bottleneck, several blind sub-Nyquist sampling and recovery schemes have been proposed that exploit the signal's structure and in particular its sparsity in the frequency domain, but do not require knowledge of the carrier frequencies. It has been shown in [6] that the minimal sampling rate for perfect blind recovery in multiband settings is twice the Landau rate [22], that is twice the occupied bandwidth. This rate can be orders of magnitude lower than Nyquist. In the remainder of this section, we survey several sub-Nyquist methods that theoretically achieve this minimal sampling rate.

Multitone Model and the Random Demodulator

Tropp et al. [3] consider a discrete multitone model for multiband signals and suggest sampling using the random demodulator, depicted in Fig. 2. Multitone functions are composed of K active tones spread over a bandwidth W, such that

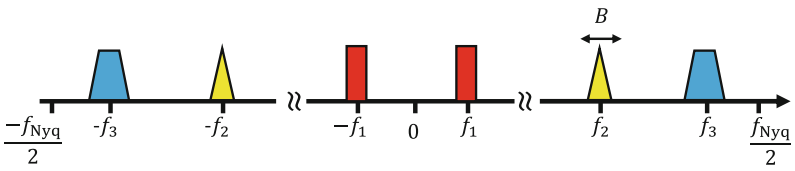

Fig. 1 Multiband model with $K = 6$ bands. Each band does not exceed the bandwidth B and is modulated by an unknown carrier frequency $|f_i| \leq f_{\text{Nyq}}/2$, for $i = 1, 2, 3$

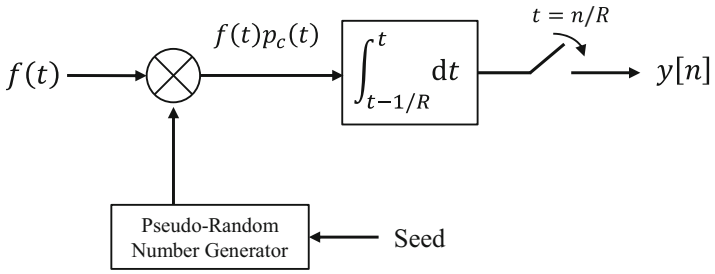

Fig. 2 Block diagram for the random demodulator, including a random number generator, a mixer, an accumulator, and a sampler [3]

$$f(t) = \sum_{\omega \in \Omega} b_\omega \mathrm{e}^{-2\pi i \omega t}, \quad t \in [0, 1). \tag{1}$$

Here, Ω is a set of K normalized frequencies, or tones, that satisfies

$$\Omega \subset \{0, \pm 1, \pm 2, \ldots, \pm(W/2 - 1), \pm W/2\}, \tag{2}$$

and b_ω, for $\omega \in \Omega$, are a set of complex-valued amplitudes. The number of active tones K is assumed to be much smaller than the bandwidth W. The goal is to recover both the tones ω and the corresponding amplitudes b_ω.

To sample the signal $f(t)$, it is first modulated by a high rate sequence $p_c(t)$ created by a pseudorandom number generator. It is then integrated and sampled at a low rate, as shown in Fig. 2. The random sequence used for modulation is a square wave, which alternates between the levels ± 1 with equal probability. The K tones present in $f(t)$ are thus aliased by the pseudorandom sequence. The resulting modulated signal $y(t) = f(t)p_c(t)$ is integrated over a period $1/R$ and sampled at the low rate R. This integrate-and-dump approach results in the following samples

$$y_m = R \int_{m/R}^{(m+1)/R} y(t)\mathrm{d}t, \quad m = 0, 1, \ldots, R - 1. \tag{3}$$

The samples y_m acquired by the random demodulator can be written as a linear combination of the $W \times 1$ sparse amplitude vector $\mathbf{b}$ that contains the coefficients b_ω at the corresponding locations ω [3]. In matrix form, we write

$$\mathbf{y} = \mathbf{A}\mathbf{b}, \tag{4}$$

where $\mathbf{y}$ is the vector of size R that contains the samples y_m and $\mathbf{A}$ is the known sampling matrix that describes the overall action of the system on the vector of amplitudes $\mathbf{b}$, namely, modulation and filtering (see [3] for more details). Capitalizing on the sparsity of the vector $\mathbf{b}$, the amplitudes b_ω and their respective locations ω can be recovered from the low rate samples $\mathbf{y}$ using CS [21] techniques,

in turn allowing for the recovery of $f(t)$. CS provides a framework for simultaneous sensing and compression of finite-dimensional vectors, which relies on linear dimensionality reduction. It provides both recovery conditions and algorithms to reconstruct sparse vectors from low-dimensional measurement vectors, represented as linear combinations of the former. Here, the minimal required number of samples R for perfect recovery of $f(t)$ in noiseless settings is $2K$ [21].

The random demodulator is one of the pioneer attempts to extend the inherently discrete and finite CS theory to analog signals. However, truly analog signals, as those we consider here, require a prohibitively large number of harmonics to approximate them well within the discrete model. When attempting to approximate signals such as those from the multiband model, the number of tones W is on the order of the Nyquist rate, and the number of samples R is a multiple of KB. This in turn renders the reconstruction computationally prohibitive and very sensitive to the grid choice (see [1] for a detailed analysis). Furthermore, the time domain approach precludes processing at a low rate, even for multitone inputs since interpolation to the Nyquist rate is an essential ingredient of signal reconstruction. In terms of hardware and practical implementation, the random demodulator requires accurate modulation by a periodic square mixing sequence and accurate integration, which may be challenging when using analog signal generators, mixers, and filters.

In contrast to the random demodulator, which adopts a discrete multitone model, the rest of the approaches we focus on treat the analog multiband model, illustrated in Fig. 1, which is of interest to us in the context of CR.

Multi-rate Sampling

An alternative sampling approach is based on the synchronous multi-rate sampling (SMRS) [4] scheme, which has been proposed in the context of electro-optical systems to undersample multiband signals. The SMRS samples the input signal at P different sampling rates F_i, each of which is an integer multiple of a basic sampling rate Δf. This procedure aliases the signal with different aliasing intervals, as illustrated in Fig. 3. The Fourier transform of the undersampled signals is then related to the original signal through an underdetermined system of linear equations,

$$\mathbf{z}(f) = \mathbf{Q}\mathbf{x}(f). \tag{5}$$

Here, $\mathbf{x}(f)$ contains frequency slices of size Δf of the original signal $x(t)$ and $\mathbf{z}(f)$ is composed of the Fourier transform of the sampled signal. Each channel contributes $M_i = F_i/\Delta f$ equations to the system (5), which concatenates the observation vector of all the channels. The measurement matrix $\mathbf{Q}$ has exactly P nonzero elements in every column that correspond to the locations of the spectral replica in each channel baseband $[0, F_i]$.

This approach assumes that either the signal or the sampling time window is finite. The continuous variable f is then discretized to a frequency resolution of Δf. Since $x(t)$ is sparse in the frequency domain, the vector $\mathbf{x}(f)$ is sparse and

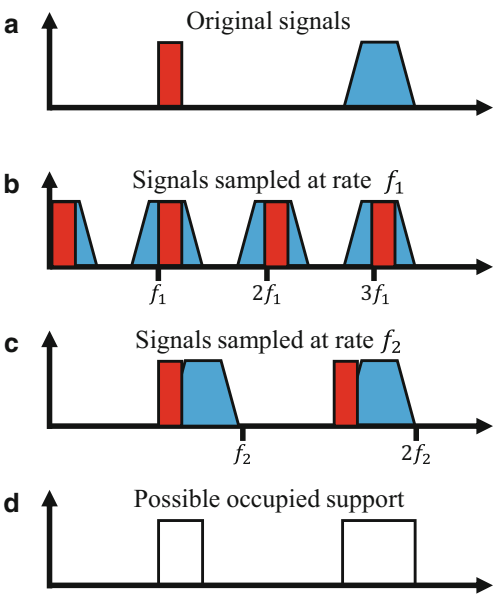

Fig. 3 Action of the SMRS on a multiband signal: (**a**) the input signal with $K = 2$ bands, (**b**) signals sampled at rate F_1 in channel 1, (**c**) signals sampled at rate F_2 in channel 2, and (**d**) possible support which is the intersection of the supports in channel 1 and 2 [4]

can be recovered from (5) using CS techniques, for each discrete frequency f. An alternative recovery method, referred to as the reduction procedure, consists of detecting baseband frequencies in which there is no signal, by observing the samples. These frequencies are assumed to account for the absence of signals of interest in all the frequencies that are down-converted to that baseband frequency. This allows to reduce the number of sampling channels. This assumption does not hold in the case where two or more frequency components cancel each other due to aliasing, which happens with probability zero. The procedure is illustrated in Fig. 3. Once the corresponding components are eliminated from (5), the reduced system can be inverted using the Moore-Penrose pseudo-inverse to recover $\mathbf{x}(f)$.

There are several drawbacks to the SMRS that limit its performance and potential implementation. First, the discretization process affects the SNR since some of the samples are thrown out. Furthermore, spectral components down-converted to off the grid frequencies are missed. In addition, the first recovery approach requires a large number of sampling channels, proportional to the number of active bands K, whereas the reduction procedure does not ensure a unique solution and the inversion problem is ill-posed in many cases. Finally, in practice, synchronization between channels sampling at different rates is challenging. Moreover, this scheme samples wideband signals using low rate samplers. Practical ADCs introduce an inherent bandwidth limitation, modeled by an anti-aliasing low-pass filter (LPF) with cutoff frequency determined by the sampling rate, which distorts the samples. To avoid this issue, the multi-rate strategy would require low rate samplers with large analog bandwidth.

Multicoset Sampling

A popular sampling scheme for sampling wideband signals at the Nyquist rate is multicoset or interleaved ADCs [1, 6, 23] in which several channels are used, each operating at a lower rate. We now discuss how such systems can be used in the sub-Nyquist regime.

Multicoset sampling may be described as the selection of certain samples from the uniform Nyquist grid, as shown in Fig. 4, where $T_{\text{Nyq}} = 1/f_{\text{Nyq}}$ denotes the Nyquist period. More precisely, the uniform grid is divided into blocks of N consecutive samples, from which only $M < N$ are kept. Mathematically, the ith sampling sequence is defined as

$$x_{c_i}[n] = \begin{cases} x(nT_{\text{Nyq}}), & n = mN + c_i, m \in \mathbb{Z} \\ 0, & \text{otherwise}, \end{cases} \tag{6}$$

where the cosets c_i are ordered integers so that $0 \le c_1 < c_2 < \cdots < c_M < N$. A possible implementation of the sampling sequences (6) is depicted in Fig. 5. The building blocks are M uniform samplers at rate $1/NT_{\text{Nyq}}$, where the ith sampler is shifted by $c_i T_{\text{Nyq}}$ from the origin. When sampling at the Nyquist rate, $M = N$ and $c_i = (i-1)$.

The samples in the Fourier domain can be written as linear combinations of spectrum slices of $x(t)$, such that [6]

$$\mathbf{z}(f) = \mathbf{A}\mathbf{x}(f), \qquad f \in \mathscr{F}_s. \tag{7}$$

Here, $\mathscr{F}_s = [-f_s/2, f_s/2]$ with $f_s = \frac{1}{NT_{\text{Nyq}}} \ge B$ the sampling rate of each channel. The mth row of $\mathbf{z}(f)$ contains the discrete time Fourier transform of the samples $z_m[n]$. The $N \times 1$ vector $\mathbf{x}(f)$ denotes the spectrum slices of $x(t)$, where the ith row of $\mathbf{x}(f)$ is $\mathbf{x}_i(f) = X(f + (i - \lfloor (N+2)/2 \rfloor) f_p)$, and $X(f)$ is the Fourier transform of $x(t)$. Since $x(t)$ is assumed to be sparse, $\mathbf{x}(f)$ is sparse as well, and its support, that is the set that contains the indices corresponding to its nonzero rows, is determined by the frequency locations of the transmissions of $x(t)$. The $M \times N$

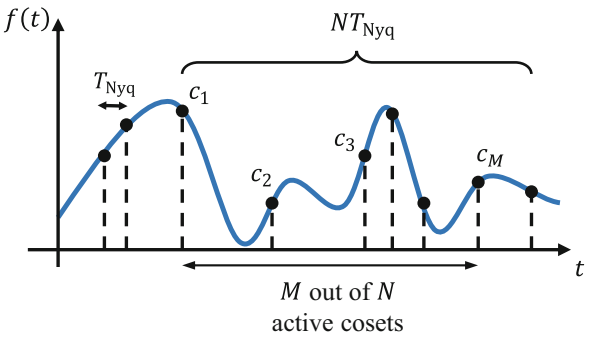

Fig. 4 Illustration of multicoset sampling

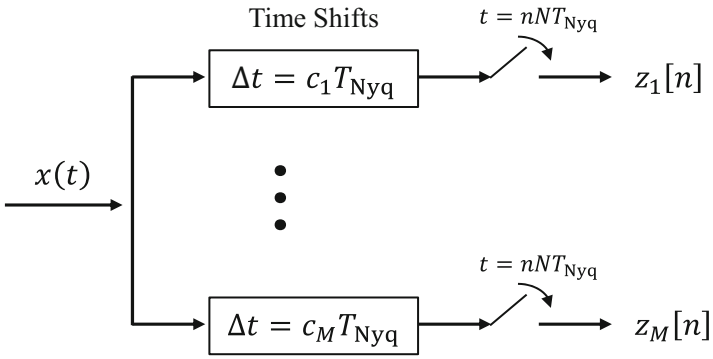

Fig. 5 Schematic implementation of multicoset sampling. The input signal $x(t)$ is inserted into the multicoset sampler that splits the signal into M branches and delays each one by a fixed coefficient $c_i T_{\text{Nyq}}$. Every branch is sampled at the low rate $1/(NT_{\text{Nyq}})$ and then digitally processed to perform spectrum sensing and signal reconstruction

sampling matrix $\mathbf{A}$ is a Vandermonde matrix with factors determined by the selected delays or cosets c_i. This relation is illustrated in Fig. 6. In the Nyquist regime, when $M = N$, $\mathbf{A}$ is the Fourier matrix. The recovery processing described below is performed in the time domain, where we have

$$\mathbf{z}[n] = \mathbf{A}\mathbf{x}[n], \qquad n \in \mathbb{Z}. \tag{8}$$

The vector $\mathbf{z}[n]$ collects the measurements at $t = n/f_s$ and $\mathbf{x}[n]$ contains the sample sequences corresponding to the spectrum slices of $x(t)$. Obviously, the sparsity pattern of $\mathbf{x}[n]$ is identical to that of $\mathbf{x}(f)$, and it follows that $\mathbf{x}[n]$ are jointly sparse over time.

Our goal is to recover $\mathbf{x}[n]$ from the samples $\mathbf{z}[n]$. The system (8) is underdetermined due to the sub-Nyquist setup and known as infinite measurement vector (IMV) in the CS literature [2, 21]. The digital reconstruction algorithm consists of the following three stages [6] that we explain in more detail below:

1. The continuous-to-finite (CTF) block constructs a finite frame (or basis) from the samples.
2. The support recovery formulates an optimization problem whose solution's support is identical to the support S of $\mathbf{x}[n]$, that is the active slices.
3. The signal is then digitally recovered by reducing (8) to the support of $\mathbf{x}[n]$.

The recovery of $\mathbf{x}[n]$ for every n independently is inefficient and not robust to noise. Instead, the CTF method, developed in [6], exploits the fact that the bands occupy continuous spectral intervals so that $\mathbf{x}[n]$ are jointly sparse, that is they have the same spectral support S over time. The CTF then produces a finite system of equations, called multiple measurement vectors (MMV) [2, 21] from the infinite number of linear systems described by (8). The samples are first summed as

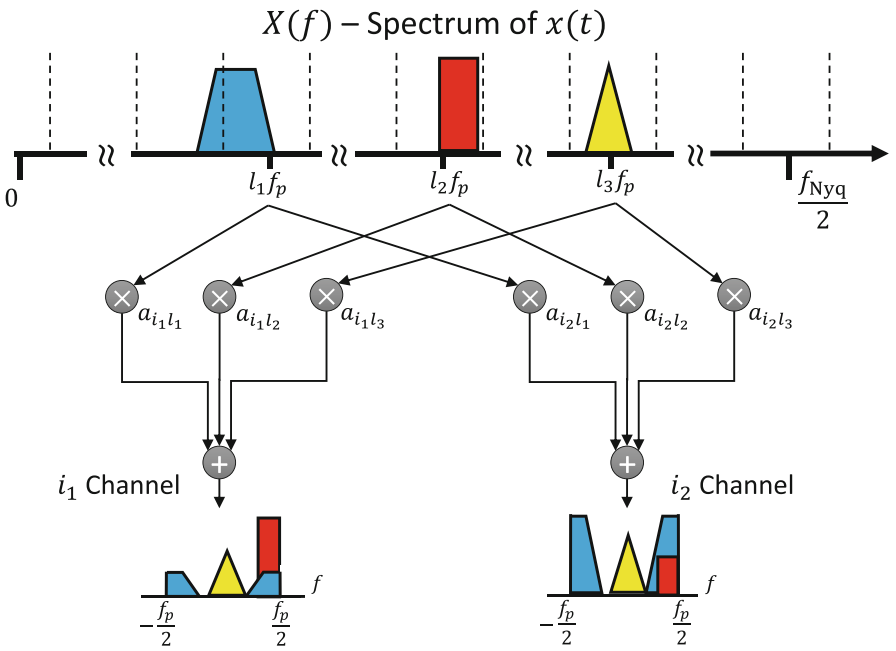

Fig. 6 The spectrum slices of the input signal $\mathbf{x}(f)$ are shown here to be multiplied by the coefficients a_{il} of the sensing matrix $\mathbf{A}$, resulting in the measurements z_i for the ith channel. Note that in multicoset sampling, only the slices' complex phase is modified by the coefficients a_{il}. In the MWC sampling described below, both the phases and amplitudes are affected

$$\mathbf{Q} = \sum_n \mathbf{z}[n]\mathbf{z}^H[n], \tag{9}$$

and then decomposed to a frame $\mathbf{V}$ such that $\mathbf{Q} = \mathbf{V}\mathbf{V}^H$. Clearly, there are many possible ways to select $\mathbf{V}$. One option is to construct it by performing an eigendecomposition of $\mathbf{Q}$ and choosing $\mathbf{V}$ as the matrix of eigenvectors corresponding to the nonzero (or large enough) eigenvalues. The finite-dimensional MMV system

$$\mathbf{V} = \mathbf{A}\mathbf{U} \tag{10}$$

is then solved for the sparsest matrix $\mathbf{U}$ with minimal number of nonidentically zero rows using CS techniques [2, 21]. The key observation of this recovery strategy is that the indices of the nonzero rows of $\mathbf{U}$ coincide with the active spectrum slices of $\mathbf{z}[n]$ [6]. These indices are referred to as the support of $\mathbf{z}[n]$ and are denoted by S.

Once the support S is known, $\mathbf{x}[n]$ is recovered by reducing the system of equations (8) to S. The resulting matrix $\mathbf{A}_S$, that contains the columns of $\mathbf{A}$ corresponding to S, is then inverted

$$\mathbf{x}_S[n] = \mathbf{A}_S^{\dagger}\mathbf{z}[n]. \tag{11}$$

Here, $\mathbf{x}_S[n]$ denotes the vector $\mathbf{x}[n]$ reduced to its support. The remaining entries of $\mathbf{x}[n]$ are equal to zero.

The overall sampling rate of the multicoset system is

$$f_{\text{Total}} = Mf_s = \frac{M}{N} f_{\text{Nyq}}. \tag{12}$$

The minimal number of channels is dictated by CS results [21] which imply that $M \geq 2K$ with $f_s \geq B$ per channel. The sampling rate can thus be as low as $2KB$, which is twice the Landau rate [22].

Although this sampling scheme seems relatively simple and straightforward, it suffers from several practical drawbacks [1]. First, as in the multi-rate approach, multicoset sampling requires low rate ADCs with large analog bandwidth. Another issue arises from the time shift elements, since maintaining accurate time delays between the ADCs on the order of the Nyquist interval T_{Nyq} is difficult. Last, the number of channels M required for recovery of the active bands can be prohibitively high. The MWC, presented in the next section, uses similar recovery techniques while overcoming these practical sampling issues.

MWC Sampling

The MWC [7] exploits the blind recovery ideas developed in [6] and combines them with the advantages of analog RF demodulation. To circumvent the analog bandwidth issue in the ADCs, an RF front-end mixes the input signal $x(t)$ with periodic waveforms. This operation imitates the effect of delayed undersampling used in the multicoset scheme and results in folding the spectrum to baseband with different weights for each frequency interval. The MWC achieves aliasing by mixing the signal, which is filtered prior to sampling. The ADC's input is thus a narrowband signal in contrast with multicoset which samples a wideband signal at a low rate to create aliasing. This characteristic of the MWC enables practical hardware implementation, which will be described in section "MWC Hardware".

More specifically, the MWC is composed of M parallel channels. In each channel, $x(t)$ is multiplied by a periodic mixing function $p_i(t)$ with period $T_p = 1/f_p$ and Fourier expansion

$$p_i(t) = \sum_{l=-\infty}^{\infty} a_{il} \mathrm{e}^{j\frac{2\pi}{T_p}lt}. \tag{13}$$

The mixing process aliases the spectrum, such that each band appears in baseband. The signal then goes through a LPF with cutoff frequency $f_s/2$ and is sampled at rate $f_s \geq f_p$. The analog mixture boils down to the same mathematical relation between the samples and the $N = f_{\text{Nyq}}/f_s$ frequency slices of $x(t)$ as in multicoset sampling, namely, (7) in frequency and (8) in time, as shown in Fig. 6. Here, the

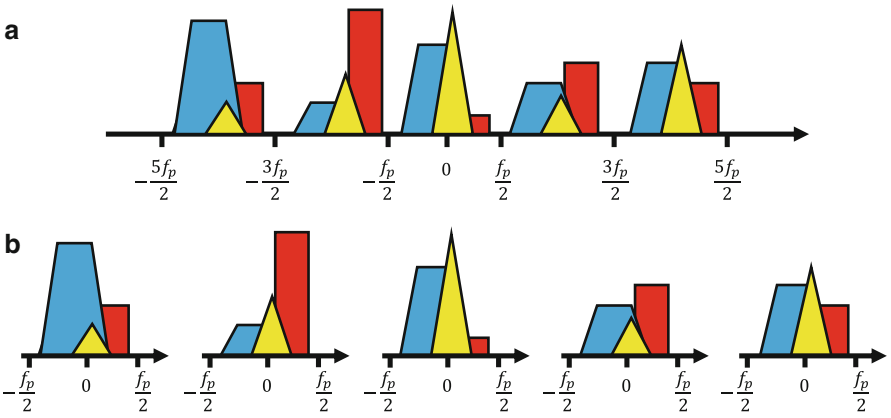

Fig. 7 Illustration of the expander configuration for $q = 5$. (**a**) Spectrum of the output $\tilde{z}_i[n]$ of the physical ith channel, (**b**) spectrum of the samples $z_{i,j}[n]$ of the $q = 5$ equivalent virtual channels, for $j = 1, \ldots, 5$, after digital expansion

$M \times N$ sampling matrix $\mathbf{A}$ contains the Fourier coefficients a_{il} of the periodic mixing functions. The recovery conditions and algorithm are identical to those described for multicoset sampling.

Choosing the channels' sampling rate f_s to be equal to the mixing rate f_p results in a similar configuration as the multicoset scheme in terms of the number of channels. In this case, the minimal number of channels required for the recovery of K bands is $2K$. The number of branches dictates the total number of hardware devices and thus governs the level of complexity of the practical implementation. Reducing the number of channels is a crucial challenge for practical implementation of a CR receiver. The MWC architecture presents an interesting flexibility property that permits trading channels for sampling rate, allowing to drastically reduce the number of channels, even down to a single channel.

Consider a configuration where $f_s = qf_p$, with odd q. In this case, the ith physical channel provides q equations over $\mathscr{F}_p = [-f_p/2, f_p/2]$, as illustrated in Fig. 7. Conceptually, M physical channels sampled at rate $f_s = qf_p$ are equivalent to Mq channels sampled at $f_s = f_p$. The number of channels is thus reduced at the expense of higher sampling rate f_s in each channel and additional digital processing. The output of each of the M physical channels is digitally demodulated and filtered to produce samples that would result from Mq equivalent virtual branches. This happens in the so-called expander module, directly after the sampling stage and before the digital processing described above, in the context of multicoset sampling. At its brink, this strategy allows to collapse a system with M channels to a single branch with sampling rate $f_s = Mf_p$ (further details can be found in [7, 24, 25]).

The MWC sampling and recovery processes are illustrated in Fig. 8. This approach results in a hardware-efficient sub-Nyquist sampling method that does not suffer from the practical limitations described in previous sections, in particular,

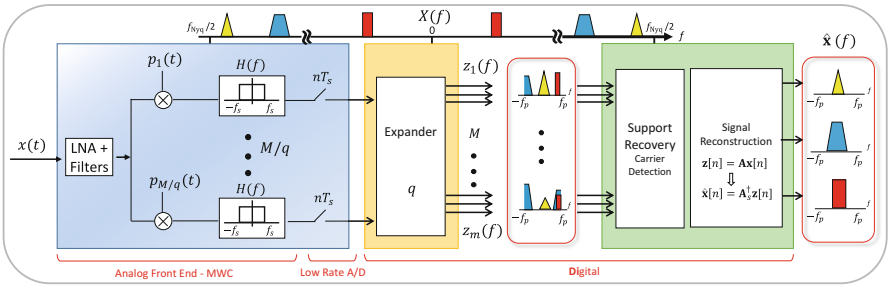

Fig. 8 Schematic implementation of the MWC analog sampling front-end and digital signal recovery from low rate samples

the analog bandwidth limitation of low rate ADCs. In addition, the number of MWC channels can be drastically reduced below $2K$ to as few as one, using a higher sampling rate f_s in each channel and additional digital processing. This tremendously reduces the burden on hardware implementation. However, the choice of appropriate periodic functions $p_i(t)$ to ensure correct recovery is challenging. Some guidelines are provided in [2, 26, 27].

Uniform Linear Array-Based MWC

An alternative sensing configuration, composed of a uniform linear array (ULA) and relying on the sampling paradigm of the MWC, is presented in [28]. The sensing system consists of a ULA composed of M sensors, with two adjacent sensors separated by a distance d, such that $d < c/(|\cos(\theta)| f_{\text{Nyq}})$, where c is the speed of light and θ is the angle representing the DOA of the signal $x(t)$. This system, illustrated in Fig. 9, capitalizes on the different accumulated phases of the input signal between sensors, given by $e^{j2\pi f_i \tau_m}$, where

$$\tau_m = \frac{d\,m}{c}\cos(\theta) \tag{14}$$

is the delay at the mth sensor with respect to the first one. Each sensor implements one channel of the MWC, that is the input signal is mixed with a periodic function, low-pass filtered and then sampled at a low rate.

This configuration has three main advantages over the standard MWC. First, it allows for a simpler design of the mixing functions which can be identical in all sensors. The only requirement on $p(t)$, besides being periodic with period $T_p \leq 1/B$, is that none of its Fourier series coefficients within the signal's Nyquist bandwidth is zero. Second, the ULA-based system outperforms the MWC in terms of recovery performance in low SNR regimes. Since all the MWC channels belong to the same sensor, they are all affected by the same additive sensor noise. In the ULA architecture, each channel belongs to a different sensor with uncorrelated

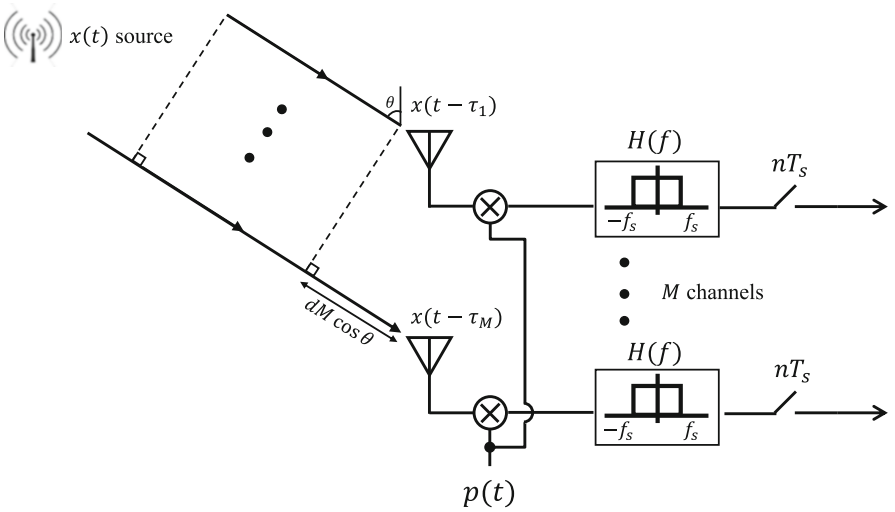

Fig. 9 ULA configuration with M sensors, with distance d between two adjacent sensors. Each sensor includes an analog front-end composed of a mixer with the same periodic function $p(t)$, a LPF and a sampler, at rate f_s

sensor noise between channels. The alternative approach benefits from the same flexibility as the standard MWC in terms of collapsing the channels, which translates into reducing the antennas in the alternative configuration. This lead to a trade-off exists between hardware complexity, governed by the number of antennas, and SNR. Finally, as will be shown in section "The CaSCADE System", the modified system can be easily extended to enable joint spectrum sensing and DOA estimation.

Similarly to the previous sampling schemes, the samples $\mathbf{z}(f)$ can be expressed as a linear transformation of the unknown vector of slices $\mathbf{x}(f)$, such that

$$\mathbf{z}(f) = \mathbf{A}\mathbf{x}(f), \qquad f \in \mathscr{F}_s. \tag{15}$$

Here, $\mathbf{x}(f)$ is a non-sparse vector that contains cyclic shifted, scaled, and sampled versions of the active bands, as shown in Fig. 10. In contrast to the previous methods, in this configuration, the matrix $\mathbf{A}$, defined by

$$\mathbf{A} = \begin{pmatrix} \mathrm{e}^{j2\pi f_1 \tau_1} & \cdots & \mathrm{e}^{j2\pi f_N \tau_1} \\ \vdots & & \vdots \\ \mathrm{e}^{j2\pi f_1 \tau_M} & \cdots & \mathrm{e}^{j2\pi f_N \tau_M} \end{pmatrix}, \tag{16}$$

depends on the unknown carrier frequencies. As before, in the time domain

$$\mathbf{z}[n] = \mathbf{A}\mathbf{x}[n], \quad n \in \mathbb{Z}. \tag{17}$$

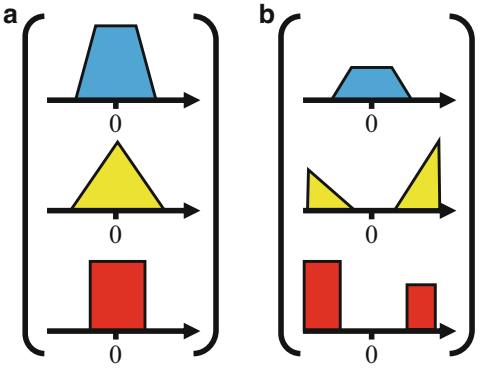

Fig. 10 (**a**) Original source signals at baseband (before modulation), (**b**) output signals at baseband $\mathbf{x}(f)$ after modulation, mixing, filtering, and sampling

Two approaches are presented in [28] to recover the carrier frequencies of the transmissions composing the input signal. The first is based on CS algorithms and assumes that the carriers lie on a predefined grid. In this case, the resulting sensing matrix, which extends $\mathbf{A}$ with respect to the grid, is known and the expanded vector $\mathbf{x}(f)$ is sparse. This leads to a similar system as (7) or (8) which can be solved using the recovery paradigm from [6], described in the context of multicoset sampling.

In the second technique, the grid assumption is dropped, and ESPRIT [20] is used to estimate the carrier frequencies. This approach first computes the sample covariance of the measurements

$$\mathbf{R} = \sum_n \mathbf{z}[n]\mathbf{z}^H[n] \tag{18}$$

and performs a singular value decomposition (SVD). The nonzero singular values correspond to the signal's subspace, and the carrier frequencies are then estimated from these. Once the carriers are recovered, the signal itself is reconstructed by inverting the sampling matrix $\mathbf{A}$ in (17).

The minimal number of sensors required by both reconstruction methods in noiseless settings is $M = 2K$, with each sensor sampling at the minimal rate of $f_s = B$ to allow for perfect signal recovery [28]. The proposed system thus achieves the minimal sampling rate $2KB$ derived in [6]. We note that the expander strategy proposed in the context of the MWC can be applied in this configuration as well.

MWC Hardware

MWC Prototype

One of the main aspects that distinguish the sub-Nyquist MWC from other sampling schemes is its practical implementation [24], proving the feasibility of sub-Nyquist sampling even under distorting effects of analog components and

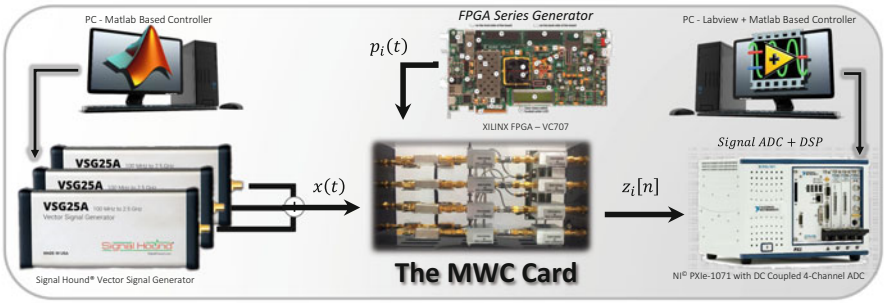

Fig. 11 Hardware implementation of the MWC prototype, including the RF signal generators, analog front-end board, FPGA series generator, ADC, and DSP

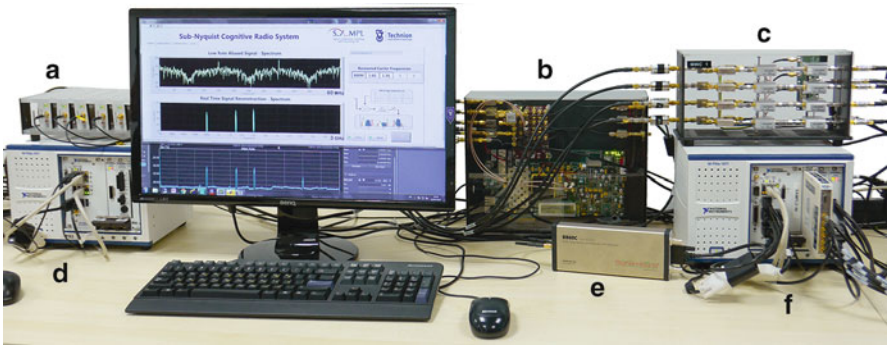

Fig. 12 MWC CR system prototype: (**a**) vector signal generator (VSG), (**b**) FPGA mixing sequences generator, (**c**) MWC analog front-end board, (**d**) RF combiner, (**e**) spectrum analyzer, (**f**) ADC, and DSP

physical phenomena. A hardware prototype, shown in Fig. 11, was developed and built according to the block diagram in Fig. 8. The main hardware components that were used in the prototype can be seen in Fig. 11. In particular, the system receives an input signal with Nyquist rate of 6 GHz and spectral occupancy of up to 200 MHz and samples at an effective rate of 480 MHz, that is only 8% of the Nyquist rate and 2.4 times the Landau rate. This rate constitutes a relatively small oversampling factor of 20% with respect to the theoretical lower sampling bound. This section describes the different components of the hardware prototype, shown in Fig. 12, explaining the various considerations that were taken into account when implementing the theoretical concepts on actual analog components.

At the heart of the system lies the proprietary MWC board [24] that implements the sub-Nyquist analog front-end. The card uses a high-speed 1-to-4 analog splitter that duplicates the wideband signal to $M = 4$ channels, with an expansion factor of $q = 5$, yielding $Mq = 20$ virtual channels after digital expansion. Then, an analog preprocessing step, composed of preliminary equalization, impedance

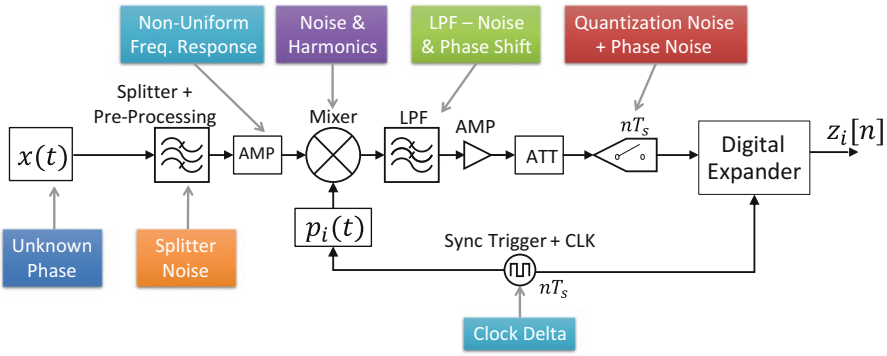

Fig. 13 Hardware RF chain detailed schematics, including amplifiers, attenuators, filters, mixers, samplers, and synchronization signals required for precise and accurate operation. The distortions induced by each component are indicated as well

corrections, and gain adjustments, aims at maintaining the dynamic range and fidelity of the input in each channel. Indeed, the signal and mixing sequences must be amplified to specific levels before entering the analog mixers to ensure proper behavior emulating mathematical multiplication with the mixing sequences. The entire analog path of the multiband input signal is described in Fig. 13.

The modulated signal next passes through an analog anti-aliasing LPF. The anti-aliasing filter must be characterized by both an almost linear phase response in the pass band, between 0 to 50 MHz, and an attenuation of more than 20 dB at $f_s/2 = 60$ MHz. A Chebyshev LPF of 7th order with cutoff frequency (-3 dB) of 50 MHz was chosen for the implementation. After impedance and gain corrections, the signal now has a spectral content limited to 50 MHz that contains a linear combination of the occupied bands with different amplitudes and phases, as seen in Fig. 6. Finally the low rate analog signal is sampled by a National Instruments© ADC operating at 120 MHz, leading to a total sampling rate of 480 MHz.

The mixing sequences that modulate the signal play an essential part in signal recovery. They must have low cross-correlations with each other, while spanning a large bandwidth determined by the Nyquist rate of the input signal, and yet be easy enough to generate with relatively cheap, off-the-shelf hardware. The sequences $p_i(t)$, for $i = 1, \ldots, 4$, are chosen as truncated versions of Gold Codes [29], which are commonly used in telecommunication (CDMA) and satellite navigation (GPS). Mixing sequences based on Gold codes were found to give good results in the MWC system [26], primarily due to small bounded cross-correlations within a set.

Since Gold codes are binary, the mixing sequences are restricted to alternating ± 1 values. This fact allows to digitally generate the sequences on a dedicated FPGA. Alternatively, they can be implemented on a small chip with very low power and complexity. The added benefit of producing the mixing sequences on such a platform is that the entire sampling scheme can be synchronized and triggered using the same FPGA with minimally added phase noise and jitter, keeping a closed

synchronization loop with the samplers and mixers. A XiLinX VC707 FPGA acts as the central timing unit of the entire sub-Nyquist CR setup by generating the mixing sequences and the synchronization signals required for successful operation. It is crucial that both the mixing period $T_p = 1/f_p$ and the low rate samplers operating at $(q+1)f_p$ (due to intended oversampling) are fully synchronized, in order to ensure correct modeling of the entire system and consequently guarantee accurate support detection and signal reconstruction.

The digital back-end is implemented using a National Instruments© PXIe-1065 computer with DC-coupled ADC. Since the digital processing is performed at the low rate f_s, very low computational load is required in order to achieve real-time recovery. MATLAB®and LabVIEW® environments are used for implementing the various digital operations and provide an easy and flexible research platform for further experimentations, as discussed in the next sections. The sampling matrix $\mathbf{A}$ is computed once off-line, using the calibration process outlined in [25].

Support Recovery

The prototype is fed with RF signals composed of up to 5 carrier transmissions with an unknown total bandwidth occupancy of up to 200 MHz and Nyquist rate of 6 GHz. An RF input $x(t)$ is generated using vector signal generators (VSG), each producing one modulated data channel with individual bandwidth of up to 20 MHz. The input transmissions then go through an RF combiner, resulting in a dynamic multiband input signal. This allows to test the system's ability to rapidly sense the input spectrum and adapt to changes, as required by modern CR standards (e.g., IEEE 802.22). In addition, the described setup is able to simulate more complex scenarios, including collaborative spectrum sensing [30,31], joint DOA estimation [28], cyclostationary-based detection [32], and various modulation schemes such as PSK, OFDM, and more, for verifying sub-Nyquist data reconstruction capabilities.

Support recovery is digitally performed on the low rate samples, as presented above in the context of multicoset sampling. The prototype successfully recovers the support of the transmitted bands transmitted, when SNR levels are above 15 dB, as demonstrated in Fig. 14. Additional simulations presenting different input scenarios can be found in [2]. More sophisticated detection schemes, such as cyclostationary detection, allow to achieve perfect support recovery from the same sub-Nyquist samples in lower SNR regimes of $0-10$ dB, as seen in Figs. 23 and 24, and will be further discussed in section "Cyclostationary Detection".

The main advantage of the MWC is that sensing is performed in real time for the entire spectral range, even though the operation is performed solely on sub-Nyquist samples, which results in substantial savings in both computational and memory complexity. In additional tests, it is shown that the bandwidth occupied in each band can also be very low without impeding the performance, as seen in Fig. 15, where the support of signals with very low bandwidth (just 10% occupancy within the 20 MHz band) is correctly detected.

Fig. 14 Screenshot from the MWC recovery software: low rate samples acquired from one MWC channel at rate 120 MHz (*top*), digital reconstruction of the entire spectrum, performed from sub-Nyquist samples (*middle*), true input signal $x(t)$ showed using a fast spectrum analyzer (*bottom*)

Signal Reconstruction

Once the support is recovered, the data is reconstructed from the sub-Nyquist samples. Reconstruction is performed by inverting the reduced sampling matrix $\mathbf{A}_S$ in the recovered support, applying (11). This step is performed in real time, reconstructing the signal bands $\mathbf{z}[n]$ one sample at a time, with low complexity due to the small dimensions of the matrix-vector multiplication. We note that reconstruction does not require interpolation to the Nyquist grid. The active transmissions are recovered at the low rate of 20 MHz, corresponding to the bandwidth of the slices $\mathbf{z}(f)$.

The prototype's digital recovery stage is further expanded to support decoding of common communication modulations, including BPSK, QPSK, QAM, and OFDM. An example for the decoding of three QPSK modulated bands is given in Fig. 16, where the I/Q constellations are shown after reconstructing the original transmitted signals $\mathbf{x}_S$ (11), from their low rate and aliased sampled signals $\mathbf{z}_n$ (8). The I/Q constellations of the baseband signals is displayed, each individually decoded using a general QPSK decoder. In this example, the user broadcasts text strings that are then deciphered and displayed on screen.

Fig. 15 The setup is identical to Fig. 14. In this case, the individual transmissions have low bandwidth, highlighting the structure of the signal when folding to baseband

There are no restrictions regarding the modulation type, bandwidth, or other parameters, since the baseband information is exactly reconstructed regardless of its respective content. Therefore, any digital modulation method, as well as analog broadcasts, can be transmitted and deciphered without loss of information, by applying any desirable decoding scheme directly on the sub-Nyquist samples.

By combining both spectrum sensing and signal reconstruction, the MWC prototype serves as two separate communication devices. The first is a state-of-the-art CR that can perform real-time spectrum sensing at sub-Nyquist rates, and the second is a unique receiver able to decode multiple data transmissions simultaneously, regardless of their carrier frequencies while adapting to temporal spectral changes in real time. In cases where the support of the potential active transmissions is a priori known (e.g., potential cellular carriers), the MWC may be used as an RF demodulator that efficiently acquires several frequency bands simultaneously. Other schemes would require a dedicated demodulation channel for each potentially active band. In this case, the mixing sequences should be designed so that their Fourier coefficients are nonzero only in the bands of interest, increasing SNR, and the support recovery stage is not needed [33].

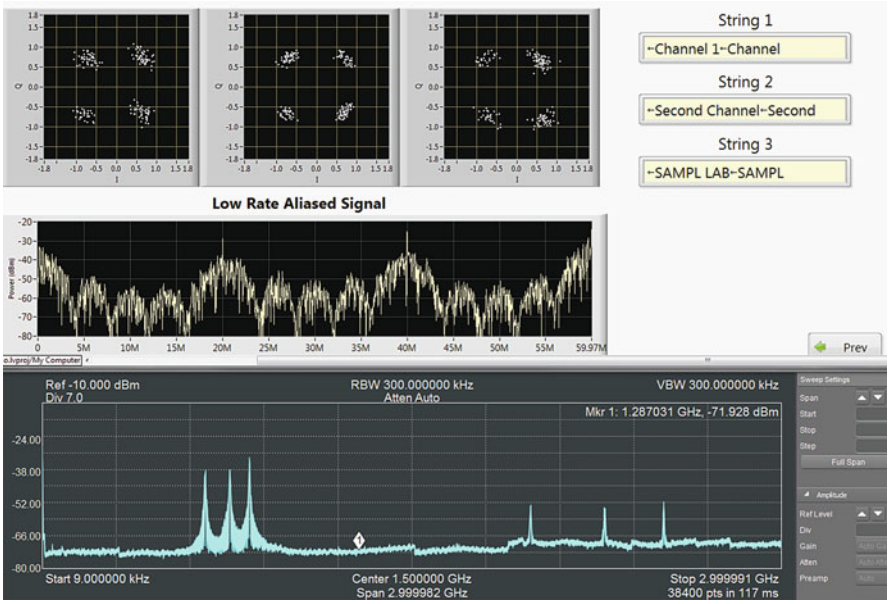

Fig. 16 Demodulation, reconstruction, and detection of $N_{\text{sig}} = 3$ inputs from sub-Nyquist samples using the MWC CR prototype. At the *bottom*, the signal is sampled by an external spectrum analyzer showing the entire bandwidth of 3 GHz. Sub-Nyquist samples from an MWC channel $z_i[n]$ in the Fourier domain are displayed in the *middle*. The I/Q phase diagrams, showing the modulation pattern of the transmitted bands after reconstruction from the low rate samples, are presented at the *top left*. In the *upper right corner*, we see the information that was sent on each carrier, proving successful reconstruction

Statistics Detection

In the previous sections, we reviewed recent sub-Nyquist sampling methods that reconstruct a multiband signal, such as a CR signal, from low rate samples. However, the final goal of CRs often only requires detection of the presence or absence of the PUs' transmissions and not necessarily their perfect reconstruction. In this case, several works have proposed performing detection on second-order signal statistics, which share the same frequency support as the original signal. In particular, power and cyclic spectra have been considered for stationary and cyclostationary [13] signals, respectively. Instead of recovering the signal from the low rate samples, its statistics are reconstructed and the support is estimated [32, 34–40].

Recovering second-order statistics rather than the signal itself benefits from two main advantages. First, it allows to further reduce the sampling rate, as we will discuss in the remainder of this section. Intuitively, statistics have fewer degrees of freedom than the signal itself, requiring less samples for their reconstruction. This follows from the assumption that the signal of interest is either stationary or

cyclostationary. Going one step further, the sparsity constraint can even be removed in this case, and the power/cyclic spectrum of non-sparse signals is recoverable from samples obtained below the Nyquist rate [32, 34, 37, 38, 40]. This is useful for CRs operating in less sparse environments, in which the lower bound of twice the Landau rate may exceed the Nyquist rate. Second, the robustness to noise is increased due to the averaging performed to estimate statistics. This is drastically improved in the case of cyclostationary signals in the presence of stationary noise. Indeed, exploiting cyclostationarity properties exhibited by communication signals allows to separate them from stationary noise, leading to better detection in low SNR regimes [41]. In this section, we first review power spectrum detection techniques in stationary settings and then extend these to cyclic spectrum detection of cyclostationary signals.

Power Spectrum-Based Detection

In the statistical setting, the signal $x(t)$ is modeled as the sum of uncorrelated wide-sense stationary transmissions. The stationarity assumption is key to further reducing the sampling rate. In frequency, stationarity is expressed by the absence of correlation between distinct frequency components. Specifically, as shown in [42], the Fourier transform of a wide-sense stationary signal is a nonstationary white process, such that

$$\mathbb{E}[X(f_1)X^*(f_2)] = S_x(f_1)\delta(f_1 - f_2). \tag{19}$$

Here, the power spectrum $S_x(f)$ of $x(t)$ is the Fourier transform of its autocorrelation $r_x(\tau)$. Thus, obviously, the support of $S_x(f)$ is identical to that of $X(f)$. In addition, due to (19), the autocorrelation matrix of the N spectrum frequency slices of $x(t)$ comprising $\mathbf{x}(f)$ is diagonal, containing only N degrees of freedom, which allows sampling rate reduction.

Another intuitive interpretation to the reduced number of degrees of freedom in statistics recovery is given in the time domain. There, the autocorrelation of stationary signals $r_x(\tau) = \mathbb{E}[x(t)x(t-\tau)]$ is only a function of the time lags τ. The cardinality of the difference set, namely, the set that contains the time lags, may be greater than that of its associated original set, up to the order of its square, for an appropriate choice of sampling times [35, 43]. When the sampling scheme is not tailored to power spectrum recovery, the sampling rate can be as low as the Landau rate [38], which constitutes a worst-case scenario in terms of sampling rate. With appropriate design, the autocorrelation or power spectrum may be estimated from samples with arbitrarily low average sampling rate [34, 35, 43–45] at the expense of increased latency.

We first review power spectrum recovery techniques that do not exploit any specific design. We then present methods that further reduce the sampling rate by adapting the sampling scheme to the purpose of autocorrelation or power spectrum estimation. Finally, we extend these results to the cyclostationary model.

Power Spectrum Recovery

In this section, we first focus on sampling with generic MWC or multicoset schemes without specific design of the mixing sequences or cosets, respectively.

To recover $S_x(f)$ from the low rates samples $\mathbf{z}(f)$, consider the correlation matrix of the latter $\mathbf{R_z}(f) = \mathbb{E}[\mathbf{z}(f)\mathbf{z}^H(f)]$ [38]. Using (7), $\mathbf{R_z}(f)$ can be related to correlations between the slices $\mathbf{x}(f)$, that is $\mathbf{R_x}(f) = \mathbb{E}[\mathbf{x}(f)\mathbf{x}^H(f)]$ as follows

$$\mathbf{R_z}(f) = \mathbf{A}\mathbf{R_x}(f)\mathbf{A}^H, \qquad f \in \mathscr{F}_s. \tag{20}$$

From (19), the correlation matrix $\mathbf{R_x}(f)$ is diagonal and contains the power spectrum $S_x(f)$ at the corresponding frequencies, as

$$\mathbf{R}_{\mathbf{x}_{(i,i)}}(f) = S_x(f + if_s - \frac{f_{\text{Nyq}}}{2}), \qquad f \in \mathscr{F}_s. \tag{21}$$

Recovering the power spectrum $S_x(f)$ is thus equivalent to recovering the matrix $\mathbf{R_x}(f)$. Exploiting the fact that $\mathbf{R_x}(f)$ is diagonal and denoting by $\mathbf{r_x}(f)$ its diagonal, (20) can be reduced to

$$\mathbf{r_z}(f) = (\bar{\mathbf{A}} \odot \mathbf{A})\mathbf{r_x}(f), \tag{22}$$

where $\mathbf{r_z}(f) = \text{vec}(\mathbf{R_z}(f))$ concatenates the columns of $\mathbf{R_z}(f)$. The matrix $\bar{\mathbf{A}}$ is the conjugate of $\mathbf{A}$ and $\odot$ denotes the Khatri-Rao product [46].

Generic choices of the sampling parameters, either mixing sequences or cosets, which are only required to ensure that $\mathbf{A}$ is full spark, are investigated in [38]. Then, the Khatri-Rao product $(\bar{\mathbf{A}} \odot \mathbf{A})$ is full spark as well if $M > N/2$, that is the number of rows of $\mathbf{A}$ is at least half the number of slices N. The minimal sampling rate to recover $\mathbf{r_x}(f)$, and consequently $S_x(f)$, from $\mathbf{r_z}(f)$ in (22) is thus equal to the Landau rate KB, namely, half the rate required for signal recovery [38]. The recovery of $\mathbf{r_x}(f)$ is performed using the procedure presented in the context of signal recovery on (22), that is CTF, support recovery, and power spectrum reconstruction (rather than signal reconstruction).

The same result for the minimal sampling rate is valid for non-sparse signals, for which KB is in the order of f_{Nyq} [38]. The power spectrum of such signals may be recovered at half their Nyquist rate. This means that even without any sparsity constraints on the signal in crowded environments, a CR can retrieve the power spectrum of the received signal by exploiting the stationarity property of the latter. In this case, the system (22) is overdetermined, and $\mathbf{r_x}(f)$ is obtained by a simple pseudo-inverse operation.

Obviously, in practice, we do not have access to $\mathbf{R_z}(f)$, which thus needs to be estimated. The overall sensing time is divided into N_f frames of length N_s samples. In [38], different choices of N_f and N_s are examined for a fixed sensing time. In order to estimate the autocorrelation matrix $\mathbf{R_z}(f)$ in the frequency domain, we first compute the estimates of $\mathbf{z}_i(f), 1 \leq i \leq M$, denoted by $\hat{\mathbf{z}}_i(f)$, using the fast

Fourier transform (FFT) on the samples $z_i[n]$ over a finite time window. We then estimate the elements of $\mathbf{R}_\mathbf{z}(f)$ as

$$\hat{\mathbf{R}}_\mathbf{z}(i,j,f) = \frac{1}{N_f}\sum_{\ell=1}^{N_f} \hat{\mathbf{z}}^\ell(i,f)\hat{\mathbf{z}}^\ell(j,f), \quad f \in \mathscr{F}_s, \tag{23}$$

where $\hat{\mathbf{z}}^\ell(i,f)$ is the value of the FFT of the samples $\mathbf{z}_i[n]$ from the ℓth frame, at frequency f. In practice, the number of samples dictates the number of FFT coefficients in the frequency domain and therefore the resolution of the reconstructed power spectrum.

Once $\hat{\mathbf{r}}_\mathbf{x}(f)$ is reconstructed, the following test statistic,

$$\Gamma_i = \sum_{f\in\mathscr{F}_s} |\hat{\mathbf{r}}_{\mathbf{x}_i}(f)|^2, \qquad 1 \le i \le N, \tag{24}$$

may be adopted in order to detect the occupied support. Here, $\hat{\mathbf{r}}_{\mathbf{x}_i}(f)$ is the ith entry of $\hat{\mathbf{r}}_\mathbf{x}(f)$, and the sum is performed over the frequency band of interest to detect the presence of a PU. Alternatively, other detection statistics can be used on the reconstructed power spectrum, such as eigenvalue-based test statistics [47].

Power Spectrum Sensing: Tailored Design

Sampling approaches specifically designed for estimating the autocorrelation of stationary signals at much finer lags than the sample spacings have been studied recently in detail [35,43,44,48]. The key observation here is that the autocorrelation is a function of the lags only, namely, the differences between pairs of sample times. Thus, it is estimated at all-time lags contained in the difference co-array, composed of all the differences between pairs of elements from the original sampling array. Since the size of the difference co-array may be greater than that of the sampling set, it is possible to sample below the Nyquist rate and estimate the correlation at all lags on the Nyquist grid, from the low rate samples. Therefore, the sampling times should be carefully chosen so as to maximize the cardinality of the difference co-array.

The first approach we present adopts multicoset sampling previously reviewed while specifically designing the cosets to obtain a maximal number of differences. In the previous section, the results were derived for any coset selection. Here, we show that the sampling rate may be lower if the cosets are carefully chosen. When using multicoset sampling, the sampling matrix $\mathbf{A}$ in (20) or (22) is a partial Fourier matrix with (i,k)th element $e^{j\frac{2\pi}{N}c_i k}$. A typical element of $(\bar{\mathbf{A}} \odot \mathbf{A})$ is then $e^{j\frac{2\pi}{N}(c_i - c_j)k}$. If all cosets are distinct, then the size of the difference set over one period is greater than or equal to $2M-1$. This bound corresponds to a worst-case scenario, as discussed in the previous section, and leads to a sampling rate of at least half Nyquist in the non-sparse setting and at least Landau for a sparse signal with unknown support. This happens, for example, if we select the first or last M cosets or if we keep only the even or odd cosets.

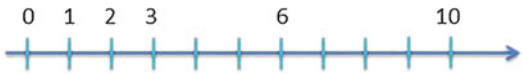

Fig. 17 Minimal sparse ruler of order $M = 6$ and length $N = 10$

To maximize the size of the difference set and increase the rank of $(\bar{\mathbf{A}} \odot \mathbf{A})$, the cosets can be chosen [35,48] using minimal linear and circular sparse rulers [49]. A linear sparse ruler is a set of integers from the interval $[0, N]$, such that the associated difference sets contain all integers in $[0, N]$. Intuitively, it can be seen as a ruler with some marks erased but still able to measure all integer distances between 0 and its length. For example, consider the minimal sparse ruler of length $N = 10$. This ruler requires $M = 6$ marks, as shown in Fig. 17. Obviously, all the lags $0 \leq \tau \leq 10$ on the integer grid are identifiable. There is no closed form expression for the maximum compression ratio M/N that is achievable using a sparse ruler; however, the following bounds hold

$$\frac{\sqrt{\tau(N-1)}}{N} \leq \frac{M}{N} \leq \frac{\sqrt{3(N-1)}}{N}, \tag{25}$$

where $\tau \approx 2.4345$ [48]. A circular or modular sparse ruler extends this idea to include periodicity. Such designs that seek minimal sparse rulers, that is rulers with minimal number of marks M, allow to achieve compression ratios M/N on the order of $\sqrt{N}$. As N increases, the compression ratio may be arbitrarily low.

Two additional sampling techniques specifically designed for autocorrelation recovery are nested arrays [43] and co-prime sampling [44], presented in the context of autocorrelation estimation as well as beamforming and DOA estimation applications. In nested and co-prime structures, similarly to multicoset, the corresponding co-arrays have more degrees of freedom than those of the original arrays, leading to a finer grid for the time lags with respect to the sampling times. We now briefly review both sampling structures and their corresponding difference co-arrays and show how the autocorrelation of an arbitrary stationary signal can be recovered on the Nyquist grid from these low rate samples.

In its simplest form, the nested array [43] structure has two levels of sampling density. The first-level samples are at the N_1 locations $\{\ell T_{\text{Nyq}}\}_{1 \leq \ell \leq N_1}$, and the second-level samples are at the N_2 locations $\{(N_1+1)kT_{\text{Nyq}}\}_{1 \leq k \leq N_2}$. This nonuniform sampling is then repeated with period $(N_1+1)N_2T_{\text{Nyq}}$. Since there are N_1+N_2 samples in intervals of length $(N_1+1)N_2T_{\text{Nyq}}$, the average sampling rate of a nested array sampling set is given by

$$f_s = \frac{N_1+N_2}{(N_1+1)N_2T_{\text{Nyq}}} \equiv \frac{1}{N_1T_{\text{Nyq}}} + \frac{1}{N_2T_{\text{Nyq}}}, \tag{26}$$

which can be arbitrarily low since N_1 and N_2 may be as large as we choose, at the expense of latency.

Now, consider the difference co-array which has contribution from the cross-differences and the self-differences. The non-negative cross-differences, normalized by T_{Nyq} for clarity, are given by

$$n = (N_1 + 1)k - \ell, \quad 1 \le k \le N_2, 1 \le \ell \le N_1. \tag{27}$$

All differences in the range $1 \le n \le (N_1 + 1)N_2 - 1$ are covered, except for the multiples of $N_1 + 1$. These are precisely the self-differences among the second array. As a result, the difference co-array is a filled array represented by the set of all integers $-[(N_1 + 1)N_2 - 1] \le n \le [(N_1 + 1)N_2 - 1]$. Going back to our autocorrelation or power spectrum estimation problem, this result shows that by proper averaging, we can estimate $R(\tau)$ at any lag τ on the Nyquist grid for any stationary signal from the nested array samples, with arbitrarily low sampling rate.

Co-prime sampling involves two uniform sampling sets with spacing $N_1 T_{\text{Nyq}}$ and $N_2 T_{\text{Nyq}}$, respectively, where N_1 and N_2 are co-prime integers. Therefore, the average sampling rate of such a sampling set, given by

$$f_s = \frac{1}{N_1 T_{\text{Nyq}}} + \frac{1}{N_2 T_{\text{Nyq}}}, \tag{28}$$

can be made arbitrarily small compared to the Nyquist rate $1/T_{\text{Nyq}}$.

The associated difference set normalized by T_{Nyq} is composed of elements of the form $n = N_1 k - N_2 \ell$. Since N_1 and N_2 are co-prime, there exist integers k and ℓ such that the above difference achieves any integer value n. Therefore, the autocorrelation can be estimated by proper averaging, as

$$\hat{R}[n] = \frac{1}{Q} \sum_{q=0}^{Q-1} x(N_1(k + N_2 q)) x^*(N_2(\ell + N_1 q)), \tag{29}$$

where Q is the number of snapshots used for averaging. Again, the autocorrelation of any stationary signal may be estimated over the Nyquist grid from samples with arbitrarily low rate, and without any sparsity constraint.

The main drawback of both techniques, besides the practical issue of analog bandwidth and channel synchronization similarly to multicoset sampling, is the added latency required for sufficient averaging. In addition, nested array sampling still requires one sampler operating at the Nyquist rate. Thus, there is no saving in terms of hardware but only in memory and computation.

Cyclostationary Detection

Communication signals typically exhibit statistical periodicity, due to modulation schemes such as carrier modulation or periodic keying [50]. Therefore, such signals are better modeled as cyclostationary rather than stationary processes. A characteristic function of such processes, the cyclic spectrum $S_x^{\alpha}(f)$, extends the traditional power spectrum to a two dimensional map, with respect to two frequency variables, angular and cyclic. The cyclic spectrum exhibits spectral peaks at certain frequency

locations, the cyclic frequencies, which are determined by the signal's parameters, particularly the carrier frequency and symbol rate [41]. This constitutes the main advantage of cyclostationary detection. Stationary noise and interference exhibit no spectral correlation [41], as shown in (19), rendering such detectors highly robust to noise. Compressive power spectrum recovery techniques have been extended to reconstruction of the cyclic spectrum from the same compressive measurements. In this section, we first provide some general background on cyclostationarity and then review sub-Nyquist cyclostationary detection approaches.

Cyclostationarity

A process $x(t)$ is said to be wide-sense cyclostationary with period T_0 if its mean $\mu_x(t) = \mathbb{E}[x(t)]$ and autocorrelation $R_s(t,\tau) = \mathbb{E}[x(t)x(t+\tau)]$ are both periodic with period T_0 [13], that is

$$\mu_x(t+T_0) = \mu_x(t), \qquad R_x(t+T_0,\tau) = R_x(t,\tau), \tag{30}$$

for all $t \in \mathbb{R}$. Given a wide-sense cyclostationary random process, its autocorrelation $R_x(t,\tau)$ can be expanded in a Fourier series

$$R_x(t,\tau) = \sum_{\alpha} R_x^{\alpha}(\tau) \mathrm{e}^{j2\pi\alpha t}, \tag{31}$$

where the sum is over integer multiples of the fundamental frequency $1/T_0$ and the Fourier coefficients, referred to as cyclic autocorrelation functions, are given by

$$R_x^{\alpha}(\tau) = \frac{1}{T_0} \int_{-T_0/2}^{T_0/2} R_x(t,\tau) \mathrm{e}^{-j2\pi\alpha t} \mathrm{d}t. \tag{32}$$

The cyclic spectrum is the Fourier transform of (32) with respect to τ, namely,

$$S_x^{\alpha}(f) = \int_{-\infty}^{\infty} R_x^{\alpha}(\tau) \mathrm{e}^{-j2\pi f\tau} \mathrm{d}\tau, \tag{33}$$

where α is referred to as the cyclic frequency and f is the angular frequency [13]. If there is more than one fundamental frequency $1/T_0$, then the process $x(t)$ is said to be poly-cyclostationary in the wide sense. In this case, the cyclic spectrum contains harmonics (integer multiples) of each of the fundamental cyclic frequencies [41]. These cyclic frequencies are governed by the transmissions' carrier frequencies and symbol rates as well as modulation types.

An alternative and more intuitive interpretation of the cyclic spectrum expresses it as the cross-spectral density $S_x^{\alpha}(f) = S_{uv}(f)$ of two frequency-shifted versions of $x(t)$, $u(t)$ and $v(t)$, such that

$$u(t) \triangleq x(t)\mathrm{e}^{-j\pi\alpha t}, \quad v(t) \triangleq x(t)\mathrm{e}^{+j\pi\alpha t}. \tag{34}$$

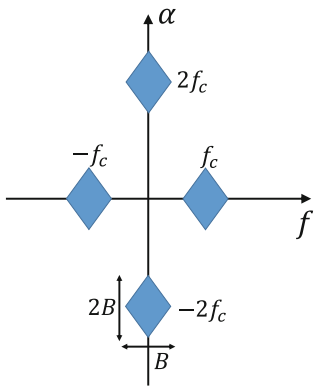

Fig. 18 Support region of the cyclic spectrum of a bandpass cyclostationary signal with carrier frequency f_c and bandwidth B

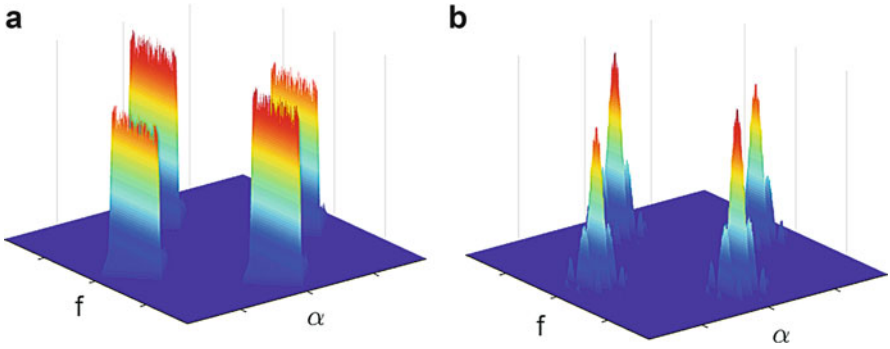

Fig. 19 Cyclic spectrum magnitude of signals with (**a**) AM and (**b**) BPSK modulations

Then, from [42], it holds that

$$S_x^{\alpha}(f) = S_{uv}(f) = \mathbb{E}\left[X\left(f + \frac{\alpha}{2}\right)X^*\left(f - \frac{\alpha}{2}\right)\right]. \tag{35}$$

Thus, the cyclic spectrum $S_x^{\alpha}(f)$ measures correlations between different spectral components of $x(t)$. Stationary signals, which do not exhibit spectral correlation between distinct frequency components, appear only at $\alpha = 0$. This property is the key to robust detection of cyclostationary signals in the presence of stationary noise, in low SNR regimes.

The support region in the (f, α) plane of the cyclic spectrum of a bandpass cyclostationary signal is composed of four diamonds, as shown in Fig. 18. Therefore, the cyclic spectrum $S_x^{\alpha}(f)$ of a multiband signal with K uncorrelated transmissions is supported over $4K$ diamond-shaped areas. Figure 19 illustrates the cyclic spectrum of two modulation types, AM and BPSK.

Cyclic Spectrum Recovery

In the previous section, we showed how the power spectrum $S_x(f)$ can be reconstructed from correlations $\mathbf{R_z}(f)$ between the samples obtained using the

MWC or multicoset sampling. To that end, we first related $S_x(f)$ to the slices' correlation matrix $\mathbf{R}_\mathbf{x}(f)$ and then recovered the latter from $\mathbf{R}_\mathbf{z}(f)$. Here, this approach is extended to the cyclic spectrum $S_x^\alpha(f)$. We first show how it is related to shifted correlations between the slices, namely, $\mathbf{R}_\mathbf{x}^a(\tilde{f}) = \mathbb{E}\left[\mathbf{x}(\tilde{f})\mathbf{x}^H(\tilde{f}+a)\right]$, for $a \in [0, f_s]$ and $\tilde{f} \in [0, f_s - a]$. Next, similarly to power spectrum recovery, $\mathbf{R}_\mathbf{x}^a(\tilde{f})$ is reconstructed from shifted correlations of the samples $\mathbf{R}_\mathbf{z}^a(\tilde{f}) = \mathbb{E}\left[\mathbf{z}(\tilde{f})\mathbf{z}^H(\tilde{f}+a)\right]$. Once the cyclic spectrum $S_x^\alpha(f)$ is recovered, we estimate the transmissions' carriers and bandwidth by locating its peaks. Since the cyclic spectrum of stationary noise $n(t)$ is zero for $\alpha \neq 0$, cyclostationary detection is more robust to noise than stationary detection.

The alternative definition of the cyclic spectrum (35) implies that the elements in the matrix $\mathbf{R}_\mathbf{x}^a(\tilde{f})$ are equal to $S_x^\alpha(f)$ at the corresponding α and f. Indeed, it is easily shown [32] that

$$\mathbf{R}_\mathbf{x}^a(\tilde{f})_{(i,j)} = S_x^\alpha(f), \tag{36}$$

for

$$\begin{aligned} \alpha &= (j-i)f_s + a \\ f &= -\frac{f_{\text{Nyq}}}{2} + \tilde{f} - \frac{f_s}{2} + \frac{(j+i)f_s}{2} + \frac{a}{2}. \end{aligned} \tag{37}$$

Here $\mathbf{R}_\mathbf{x}^a(\tilde{f})_{(i,j)}$ denotes the (i,j)th element of $\mathbf{R}_\mathbf{x}^a(\tilde{f})$. This means that each entry of the cyclic spectrum $S_x^\alpha(f)$ can be mapped to an element from one of the correlation matrices $\mathbf{R}_\mathbf{x}^a(\tilde{f})$ and vice versa. Using (7) and similarly to (20) in the context of power spectrum recovery, we relate the shifted correlations matrices of $\mathbf{x}(f)$ and $\mathbf{z}(f)$ as

$$\mathbf{R}_\mathbf{z}^a(\tilde{f}) = \mathbf{A}\mathbf{R}_\mathbf{x}^a(\tilde{f})\mathbf{A}^H, \quad \tilde{f} \in [0, f_s - a], \tag{38}$$

for all $a \in [0, f_s]$.

Recall that, in the context of stationary signals, $\mathbf{R}_\mathbf{x}(f)$ is diagonal. Here, understanding the structure of $\mathbf{R}_\mathbf{x}^a(\tilde{f})$ is more involved. It was shown [32] that $\mathbf{R}_\mathbf{x}^a(\tilde{f})$ contains nonzero elements on its 0, 1, and -1 diagonals and anti-diagonals. Besides the nonzero entries being contained only in the three main and anti-diagonals, additional structure is exhibited, limiting to two the number of nonzero elements per row and column of the matrix $\mathbf{R}_\mathbf{x}^a(\tilde{f})$. The above pattern follows from two main considerations. First, each frequency component, namely, each entry of $\mathbf{x}(f)$, is correlated to at most two frequencies from the shifted vector of slices $\mathbf{x}(\tilde{f}+a)$, one from the same frequency band and one from the symmetric band. Second, the correlated component can be either in the same/symmetric slice or in one of the adjacent slices.

Figures 21 and 22 illustrate these correlations for $a = 0$ and $a = f_s/2$, respectively. First, in Fig. 20, an illustration of the spectrum of $x(t)$, namely, $X(f)$,

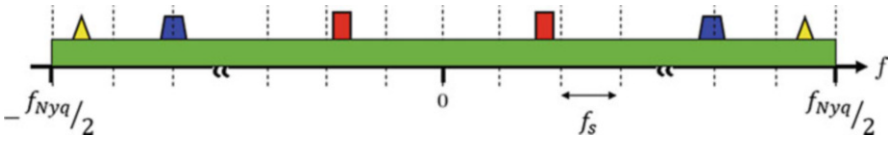

Fig. 20 Original spectrum $X(f)$. The cyclostationary transmissions are shown as a *triangle-*, *trapezoid-*, and *rectangle-shaped* spectral components, buried in a flat stationary noise

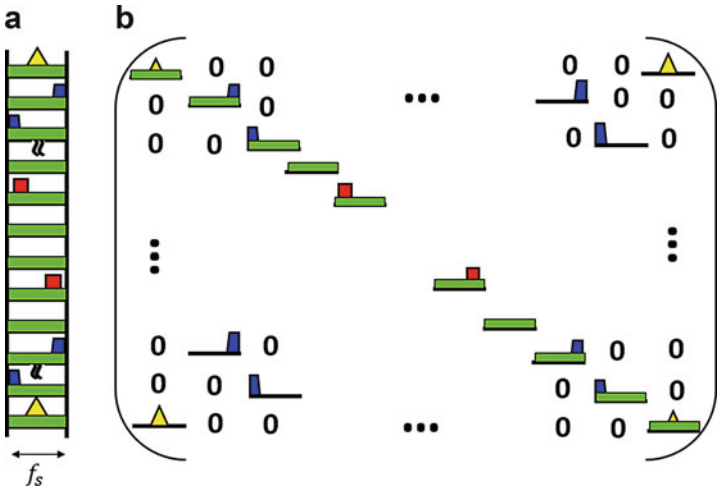

Fig. 21 (**a**) Spectrum slices vector $\mathbf{x}(\tilde{f})$, (**b**) correlated slices of $\mathbf{x}(\tilde{f})$ in the matrix $\mathbf{R}_{\mathbf{x}}^{0}(\tilde{f})$

is presented for the case of a sparse signal buried in stationary noise. It can be seen that frequency bands of $X(f)$ either appear in one f_p-slice or are split between two slices at most since $f_p \geq B$. The resulting vector of spectrum slices $\mathbf{x}(f)$ and the correlations between these slices without any shift, namely, $\mathbf{R}_{\mathbf{x}}^{0}(\tilde{f})$, are shown in Fig. 21a, b, respectively. In Fig. 21b, we observe that self-correlations appear only on the main diagonal since every frequency component is correlated with itself. In particular, the main diagonal contains the noise's power spectrum (in green). Cross-correlations between the yellow symmetric triangles appear in the 0-anti-diagonal, whereas those of the blue trapezes are contained in the -1 and $+1$ anti-diagonals. The red rectangles do not contribute any cross-correlations for $a = 0$.

Figure 22a, b show the vector $x(\tilde{f})$ and its shifted version $x(\tilde{f}+a)$ for $a = f_s/2$, respectively. The resulting correlation matrix $\mathbf{R}_{\mathbf{x}}^{a}(\tilde{f})$ appears in Fig. 22c. Here, the self-correlations of the triangle-shaped frequency component appear in the main diagonal and that of the trapezoid-shaped component in the -1 diagonal. The cross-correlations all appear in the anti-diagonal for the shift $a = f_s/2$. Note that since the noise is assumed to be wide-sense stationary, from (19), a noise frequency component is correlated only with itself. Thus, $n(t)$ contributes nonzero elements only on the diagonal of $\mathbf{R}_{\mathbf{x}}^{0}(\tilde{f})$.

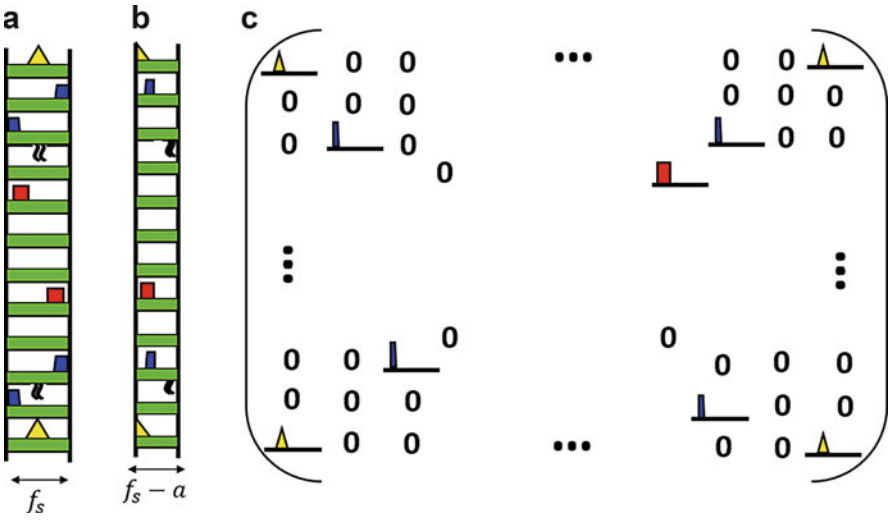

Fig. 22 (**a**) Spectrum slices vector $\mathbf{x}(\tilde{f})$, (**b**) spectrum slices shifted vector $\mathbf{x}(\tilde{f}+a)$, for $a = f_s/2$, (**c**) correlated slices of $\mathbf{x}(\tilde{f})$ and $\mathbf{x}(\tilde{f}+a)$ in the matrix $\mathbf{R}^a_{\mathbf{x}}(\tilde{f})$, with $a = f_s/2$

To recover $\mathbf{R}^a_{\mathbf{x}}(\tilde{f})$ from $\mathbf{R}^a_{\mathbf{z}}(\tilde{f})$, structured CS techniques are used in [32] that aim at reconstructing a sparse matrix while taking into account its specific structure, as described above. Once the cyclic spectrum is reconstructed, the number of transmissions and their respective carrier frequencies and bandwidths are estimated, as discussed in the next section. The detection performed on the cyclic spectrum is more robust to stationary noise than power spectrum-based detection, at the expense of a slightly higher sampling rate, as shown in [32]. More precisely, in the presence of stationary noise, the cyclic spectrum may be reconstructed from samples obtained at $4/5$ of the Nyquist rate, without any sparsity assumption on the signal. If the signal of interest is sparse, then the minimal sampling rate is further reduced to $8/5$ of the Landau rate [32].

Carrier Frequency and Bandwidth Estimation

Many detection and classification algorithms based on cyclostationarity have been proposed (see reviews [13, 14]). To assess the presence or absence of a signal, a first group of techniques requires a priori knowledge of its parameters and particularly of the carrier frequency, which is the information that CRs should uncover in the first place. A second strategy focuses on a single transmission, which does not fit the multiband model. Alternative approaches apply machine learning tools to the modulation classification of a single signal with unknown carrier frequency and symbol rate. Besides being only suitable for a single transmission, these methods require a training phase, which would be a main drawback for CR purposes. In particular, these techniques can only cope with PUs whose modulation type and parameters were part of the training set.

For CR purposes, we need a detector designed to comply with certain requirements: (1) carrier frequency and bandwidth estimation rather than simple detection of the presence or absence of a signal; (2) blind detection, namely, without knowledge of the carrier frequencies, bandwidths, and symbol rates of the transmissions; (3) simultaneous detection of several transmissions; (4) non-learning approach, i.e., with no training phase. The parameter estimation algorithm, presented in [51], is a simple parameter extraction method from the cyclic spectrum of multiband signals that answers these requirements. It allows the estimation of several carriers and several bandwidths simultaneously, as well as the number of transmissions, namely, half the number of occupied bands $K/2$ for real-valued signals. The proposed parameter estimation algorithm can be decomposed into the following four main steps: preprocessing, thresholding, clustering, and parameter estimation.

The preprocessing simply aims at compensating for the presence of stationary noise in the cyclic spectrum at the cyclic frequency $\alpha = 0$, by attenuating the energy of the cyclic spectrum at this frequency. Thresholding is then applied to the resulting cyclic spectrum in order to find its peaks. The locations and values of the selected peaks are then clustered using k-means to find the corresponding cyclic feature, after estimating the number of clusters by applying the elbow method [52]. It follows that, apart from the cluster present in DC, the number of real signals, namely, $N_{\text{sig}} = K/2$, is equal to half the number of clusters. Next, the carrier frequency f_i, which corresponds to the highest peak [41], is estimated for each transmission. The bandwidth B_i is found by locating the edge of the support of the angular frequencies at the corresponding cyclic frequency $\alpha_i = 2f_i$.

Results presented in [32] demonstrate that cyclostationary-based detection, as described in this section, outperforms energy detection carried on the signal's spectrum or power spectrum, at the expense of increased complexity. We now show similar results obtained from hardware simulations, performed using the prototype from Fig. 12.

Hardware Simulations: Robustness to Noise

Cyclostationary detection has been implemented in the MWC CR prototype. The analog front-end is identical to that of the original prototype, and only the digital recovery part is modified since the cyclic spectrum is recovered directly from the MWC low rate samples. Preliminary testing suggests that sensing success is achievable at SNRs lower by 10 dB than those allowed by energy detection performed on the recovered spectrum or power spectrum. Representative results shown in Figs. 23 and 24 demonstrate the advantage of cyclostationary detection over energy detection in the presence of noise. The figures show the reconstructed cyclic spectrum from samples of the MWC prototype as well as cross-sections at $f = 0$ and $\alpha = 0$, which corresponds to the power spectrum. This increased robustness to noise comes at the expense of more complex digital processing on the low rate samples, stemming from the higher dimensionality involved, since we reconstruct the 2-dimensional cyclic spectrum rather than the 1-dimensional (power) spectrum.

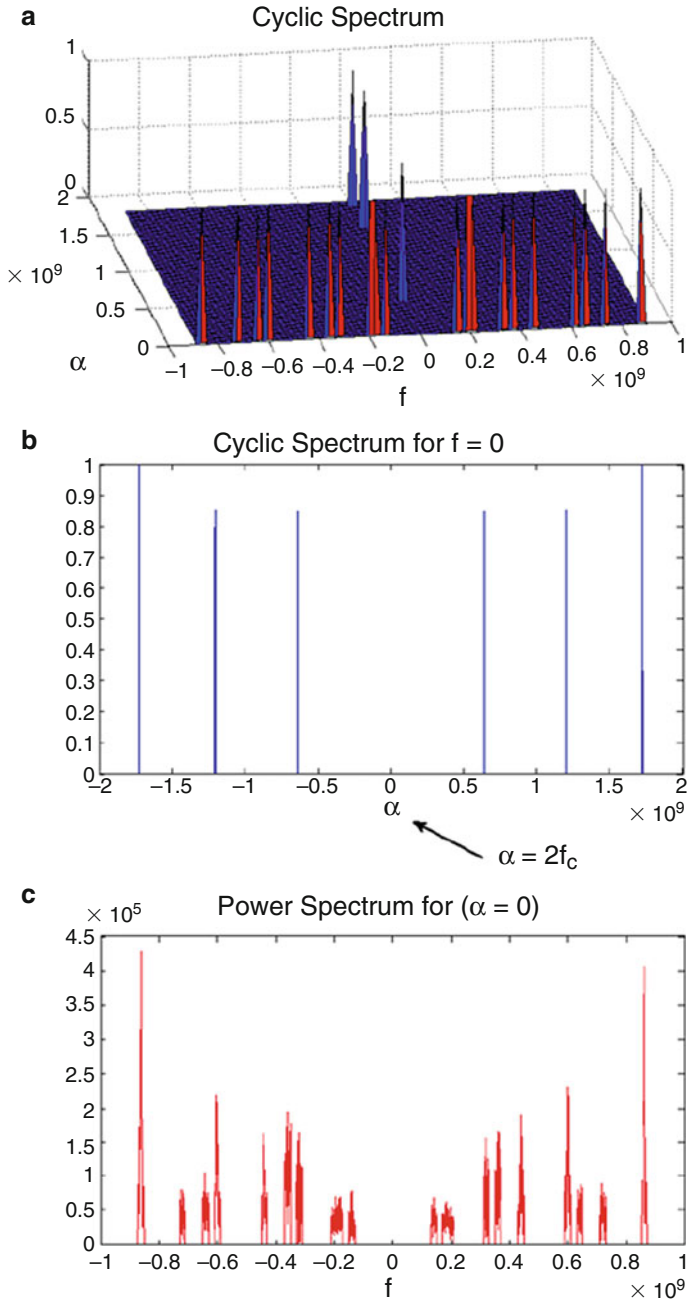

Fig. 23 Screenshot from the MWC with cyclostationary detection. The input signal is composed of $N_{\text{sig}} = 3$ transmissions (or $K = 6$ bands) with carriers $f_1 = 320\,\text{MHz}$, $f_2 = 600\,\text{MHz}$ and $f_3 = 860\,\text{MHz}$. (**a**) The recovered cyclic spectrum from low rate samples. (**b**) The cyclic spectrum profile at the angular frequency $f = 0$; the cyclic peaks are clearly visible at twice the carrier frequencies. (**c**) The power spectrum recovery is displayed and shown to fail in the presence of noise

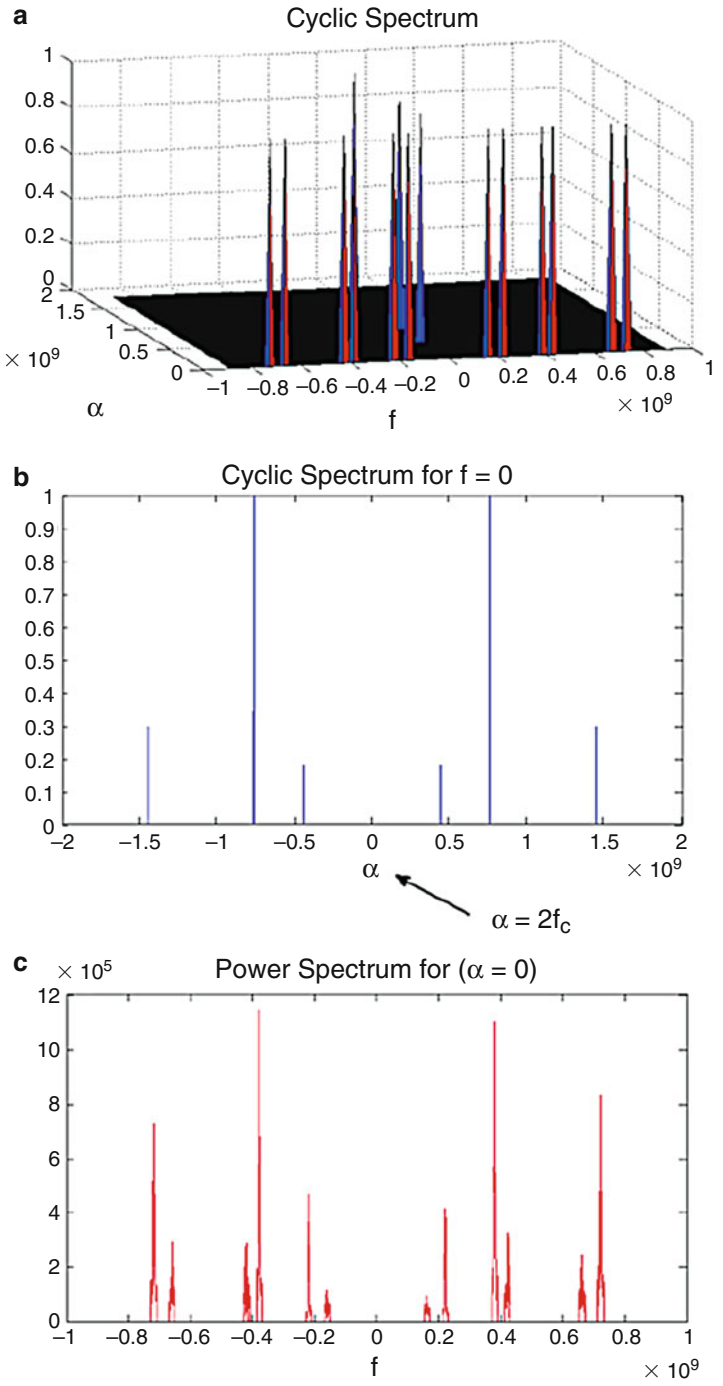

Fig. 24 The setup is identical to Fig. 23, with carrier frequencies $f_1 = 220\,\text{MHz}$, $f_2 = 380\,\text{MHz}$ and $f_3 = 720\,\text{MHz}$

Collaborative Spectrum Sensing

Collaborative Model

Until now, we assumed direct observation of the spectrum. In practice, the task of spectrum sensing for CR is further complicated due to physical channel effects such as path loss, fading, and shadowing [15]. To overcome these practical issues, collaborative CR networks have been considered, where different users share their sensing results and cooperatively decide on the licensed spectrum occupancy.

The different collaborative approaches can be distinguished according to several criteria [15]. First, cooperation can be either centralized or distributed. In centralized settings, the data is sent to a fusion center which combines the shared data to jointly estimate the spectrum or determine its occupancy. In the distributed approach, the CRs communicate among themselves and iteratively converge to a common estimate or decision. While centralized cooperation does not require iterations and can reach the optimal estimate based on the shared data, convergence to this estimate is not always guaranteed in its distributed counterpart. On the other hand, the latter is less power hungry and more robust to node and link failure, increasing the network survivability. An additional criterion concerns the shared data type; the CRs may share local binary decisions on the spectrum occupation (hard decision) or a portion of their samples (soft decision).

We consider the following collaborative model. A network of N_{rec} CRs receives the N_{sig} transmissions, such that the received signal at the jth CR is given by

$$x^{(j)}(t) = \sum_{i=1}^{N_{\text{sig}}} r_{ij}(t) = \sum_{i=1}^{N_{\text{sig}}} s_i(t) * h_{ij}(t). \tag{39}$$

The channel response $h_{ij}(t)$ is determined by fading and shadowing effects. Typical models are Rayleigh fading, or small-scale fading, and log-normal shadowing, or large-scale fading [16, 53, 54]. In the frequency domain, the Fourier transform of the jth received signal is given by

$$X^{(j)}(f) = \sum_{i=1}^{N_{\text{sig}}} S_i(f) H_{ij}(f). \tag{40}$$

Therefore, the support of $x^{(j)}(t)$ is included in the support of the original signal $x(t)$. Since the transmissions are affected differently by fading and shadowing from each transmitter to each CR, we can assume that the union of their respective supports is equivalent to the frequency support of $x(t)$. The goal here is therefore to assess the support of the transmitted signal $x(t)$ from sub-Nyquist samples of the received $x^{(j)}(t), 1 \leq j \leq N_{\text{rec}}$, by exploiting their joint frequency sparsity.

A simple and naive approach is to perform support recovery at each CR from its low rate samples and combine the local binary decisions, either in a fusion center for centralized collaboration or in a distributed manner. In this hard decision

strategy, the combination can be performed using several fusion rules such as AND, OR, or majority rule. Although this method is attractive due to its simplicity and low communication overhead, it typically achieves lower performance than its soft decision counterpart. To mitigate the communication overhead, soft decision-based methods can rely on sharing observations based on the low rate samples with smaller dimensions, rather than the samples themselves. In the next section, we review such techniques both in centralized and distributed contexts.

Centralized Collaborative Support Recovery

One approach [55, 56] to centralized spectrum sensing considers a digital model based upon a linear relation between the M sub-Nyquist samples $\mathbf{z}^{(j)}$ at CR j and N Nyquist samples $\mathbf{x}^{(j)}$ obtained for a given sensing time frame, namely,

$$\mathbf{z}^{(j)} = \mathbf{A}\mathbf{x}^{(j)}, \tag{41}$$

where $\mathbf{A}$ is the sampling matrix. In particular, the authors consider multicoset sampling where $\mathbf{z}$ selects certain samples from the Nyquist grid $\mathbf{x}$ and $\mathbf{A}$ is the corresponding selection matrix. The goal is to recover the power spectrum of the true signal $\mathbf{x}$, assumed to be stationary. To that end, the covariance matrices of sub-Nyquist and Nyquist samples are related by the following quadratic equation

$$\mathbf{R_z}^{(j)} = \mathbf{A}\mathbf{R_x}^{(j)}\mathbf{A}^H, \tag{42}$$

where $\mathbf{R_x}^{(j)}$ is diagonal. Each CR sends its autocorrelation matrix $\mathbf{R_z}^{(j)}$ to the fusion center. The common sparsity of the diagonal of $\mathbf{R_x}^{(j)}$ is then exploited in the frequency domain across all CRs to jointly reconstruct them at the fusion center, using a modified simultaneous orthogonal matching pursuit (SOMP) [21] algorithm.

In [55] only the autocorrelation $\mathbf{R_z}^{(j)}$ between the samples of each CR j is considered. This approach is extended in [56] to include cross-correlations between measurements from different CRs,

$$\mathbf{R}_{\mathbf{z}^{(j)}\mathbf{z}^{(k)}} = \mathbb{E}[\mathbf{z}^{(j)}(\mathbf{z}^{(k)})^H], \tag{43}$$

where j and k are the indices of two CRs. Here, each CR sends its measurement vector $\mathbf{z}^{(j)}$ to the fusion center and the cross-correlations are then computed. The cross-correlations are related to the common power spectrum $\mathbf{s_x} = \mathbf{F}\mathbf{r_x}$ by

$$\mathbf{R}_{\mathbf{z}^{(j)}\mathbf{z}^{(j)}} = \mathbf{C}^{(j)}\mathbf{S_x}(\mathbf{C}^{(j)})^H, \tag{44}$$

where $\mathbf{S_x}$ is the diagonal matrix that contains the power spectrum vector $\mathbf{s_x}$ and $\mathbf{C}^{(j)} = \mathbf{A}^{(j)}\mathbf{F}^H\mathbf{H}^{(j)}$. The sampling matrix $\mathbf{A}^{(j)}$ can be different for each CR j, $\mathbf{F}$ is the $N \times N$ Fourier matrix, and $\mathbf{H}^{(j)}$ is a diagonal matrix that contains the frequency channel state information (CSI). After vectorization, similarly to (42), the N^2 auto- and cross-correlation measurements are concatenated and the goal is to

recover $\mathbf{s_x}$, that is the diagonal of $\mathbf{S_x}$ from these. It is shown that if the total number of samples $N_{\text{rec}}M$ is greater than N and these are suitably chosen to account for enough measurement diversity, then the power spectrum $\mathbf{s_x}$ of a non-sparse signal can be recovered from compressed samples from a sufficient number of CRs. This shows that the minimal rate per CR is lower by a factor of N_{rec} with respect to that required for an individual CR and the number of receivers may be traded for the number of samples per CR. However, increasing the number of samples per CR does not increase spatial diversity, as does increasing the number of receivers. A drawback of this technique is that CSI is traditionally unknown by the CRs and should be estimated prior to detection.

An alternative approach [31] relies on the analog model from (7) and does not assume any a priori knowledge on the CSI. This method considers collaborative spectrum sensing from samples acquired via multicoset sampling or the MWC at each CR. In this approach, the j th CR shares its observation matrix $\mathbf{V}^{(j)}$, as defined in (10), rather than the sub-Nyquist samples themselves, and its measurement matrix $\mathbf{A}^{(j)}$, with a fusion center. The sampling matrices are considered to be different from one another in order to allow for more measurement diversity. However, the same known matrix may be used to reduce the communication overhead. The underlying matrices $\mathbf{U}^{(j)}$ are jointly sparse since fading and shadowing do not affect the original signal's support. Capitalizing on the joint support of $\mathbf{U}^{(j)}$, the support of the transmitted signal $x(t)$ can be recovered at the fusion center by solving

$$\begin{aligned} \arg\min_{\mathbf{U}^{(j)}} \quad & \bigcup_{i=1}^{N_{\text{rec}}} ||\mathbf{U}^{(j)}||_0 \\ \text{s.t.} \quad & \mathbf{V}^{(j)} = \mathbf{A}^{(j)}\mathbf{U}^{(j)}, \text{ for all } 1 \leq j \leq N_{\text{rec}}. \end{aligned} \tag{45}$$

To recover the joint support of $\mathbf{U}^{(j)}$ from the observation matrices $\mathbf{V}^{(j)}$, both the orthogonal matching pursuit (OMP) and iterative hard thresholding (IHT) algorithms, two popular CS techniques, are extended to the collaborative setting [31]. Previously we considered support recovery from an individual CR, which boils down to an MMV system of equations (10). CS algorithms have been extended to this case, such as SOMP from [57] and simultaneous IHT (SIHT) presented in [58]. These now need to account for the joint sparsity across the CRs.

The distributed CS-SOMP (DCS-SOMP) algorithm [59], which extends the original SOMP to allow for different sampling matrices $\mathbf{A}^{(j)}$ for each receiver, is adapted to the CR collaborative setting [31]. The main modification appears in the computation of the index that accounts for the greatest amount of residual energy. Here, the selected index is the one that maximizes the sum of residual projections over all the receivers. Once the shared support is updated, the residual matrices can be computed for each CR separately. The resulting modified algorithm is referred to as block sparse OMP (BSOMP) [31]. The sparse IHT algorithm can also be extended to this setting by selecting the indices of the common support though averaging over all the estimated $\mathbf{U}^{(j)}$ in each iteration. Once the support is selected, the update calculations are performed separately for each receiver [31]. Both methods are suitable for centralized cooperation, in the presence of a fusion

center. As in the previous approach, if the CSI is known, then the sampling rate per CR can be reduced by a factor of N_{rec} with respect to the rate required from an individual CR.

Distributed Collaborative Support Recovery

In the distributed approach, there is no fusion center, and the CRs are restricted to communicate only with their neighbors. Both the digital and analog centralized approaches have been extended to the distributed settings. First, in [60, 61], the digital model (41) is used, and the low rate samples $\mathbf{z}^{(j)}$ of the jth CR are expressed with respect to the spectrum $\mathbf{w}^{(j)} = \mathbf{F}\mathbf{x}^{(j)}$, such that

$$\mathbf{z}^{(j)} = \mathbf{A}^{(j)}\mathbf{F}^H\mathbf{H}^{(j)}\mathbf{w}^{(j)}. \tag{46}$$

Both unknown and known CSI cases are considered. In the first case, each CR computes its local binary decision $\mathbf{c}^{(j)}$ for each spectral band by recovering the sparse spectrum using CS techniques and comparing the local spectrum estimate $\mathbf{w}^{(j)}$ to a chosen threshold. Then, an average consensus approach is adopted, with respect to the shared hard decision. Specifically, each node j broadcasts its current decision $\mathbf{c}^{(j)}(t)$ to its neighbors $\mathcal{N}^{(j)}$ and updates itself by adding a weighted sum of the local discrepancies, that is

$$\mathbf{c}^{(j)}(t+1) = \mathbf{c}^{(j)}(t) + \sum_{k\in\mathcal{N}^{(j)}} \alpha_{jk}(\mathbf{c}^{(k)}(t) - \mathbf{c}^{(j)}(t)), \tag{47}$$

where α_{jk} is a weight associated with the edge (j,k). If the CSI is known, then the joint spectrum itself and not only its support can be collaboratively recovered. Each CR iteratively solves an ℓ_1 optimization problem for the sparse spectrum $\mathbf{w}^{(j)}$ constrained to consent with one-hop neighbors. In [60], the proposed algorithm iterates through the following steps: local spectrum reconstruction given the support and consensus averaging on the spectrum estimate. In [61], a distributed augmented Lagrangian algorithm is adopted.

Another approach extends the method presented in [31], based on the analog model (7), to comply with distributed settings [30]. The ith CR contacts a random neighbor j, chosen with some probability P_{ij}, according to the Metropolis-Hastings scheme for random transition probabilities,

$$P_{ij} = \begin{cases} \min\{\frac{1}{d_i}, \frac{1}{d_j}\} & (i,j) \in E, \\ \sum_{(i,k)\in E} \max\{0, \frac{1}{d_i} - \frac{1}{d_k}\} & i = j, \\ 0 & \text{otherwise.} \end{cases} \tag{48}$$

Here d_i denotes the cardinality of the neighbor set of the ith CR, and E is the set of communication links between CRs in the network.

A single vector, computed from the low rate samples (and that will be defined below for each recovery algorithm), is passed between the CR nodes in the network, rather than the samples themselves, effectively reducing communication overhead. When a CR receives this vector, it performs local computation to update both the shared vector and its own estimate of the signal support accordingly. Finally, the vector is sent to a neighbor CR, chosen according to the random walk with probability (48). Two distributed algorithms are presented in [30]. The first, distributed one-step greedy algorithm (DOSGA), extends the OSGA from [59] to distributed settings. The second method, referred to as randomized distributed IHT (RDSIHT), adapts the centralized BSIHT [31] to the distributed case.

To describe the DOSGA algorithm, we first present its centralized counterpart OSGA. Each CR computes the ℓ_2-norm of the projections of the observation matrix $\mathbf{V}^{(j)}$ onto the columns of the measurement matrix $\mathbf{A}^{(j)}$, stored in the vector $\mathbf{w}^{(j)}$ of size N. The fusion center then averages over all receivers' vectors, such that

$$\hat{\mathbf{w}} = \frac{1}{N_{\text{rec}}} \sum_{j=1}^{N_{\text{rec}}} \mathbf{w}^{(j)}, \tag{49}$$

and retains the highest values of $\hat{\mathbf{w}}$ whose indices constitute the support of interest. In the absence of a fusion center, finding this average is a standard distributed average consensus problem, also referred to as distributed averaging or distributed consensus. DOSGA [30] then uses a randomized gossip algorithm [62] for this purpose, where the vectors $\mathbf{w}^{(j)}$ are exchanged, with the Metropolis-Hastings transition probabilities.

Next, we turn to the RDSIHT algorithm, which adapts the centralized BSIHT [31] to the distributed scenario. The distributed approach from [30] was inspired by the randomized incremental subgradient method proposed in [63] and recent work on a stochastic version of IHT [64]. A vector $\mathbf{w}$ of size N, that sums the ℓ_2-norms of the rows of the estimates of $\mathbf{U}^{(j)}$ before thresholding, is shared in the network through a random walk. The indices of its k largest values correspond to the current estimated support. When the ith CR receives $\mathbf{w}$, it locally updates it by performing a gradient step using its own objective function that is then added to $\mathbf{w}$. Next, it selects a neighbor j to send the vector to with probability P_{ij} (48). The joint sparsity across the CRs is exploited by sharing one common vector $\mathbf{w}$ by the network. It is shown numerically in [30] that both DOSGA and RDSIHT converge to their centralized counterparts.

Hardware Simulations: Collaborative vs. Individual Spectrum Sensing

Here, we would like to confirm that the collaborative algorithms for spectrum sensing perform better than their individual counterparts. We demonstrate a collaborative setting simulated on the MWC CR prototype, as can be seen in Fig. 25.

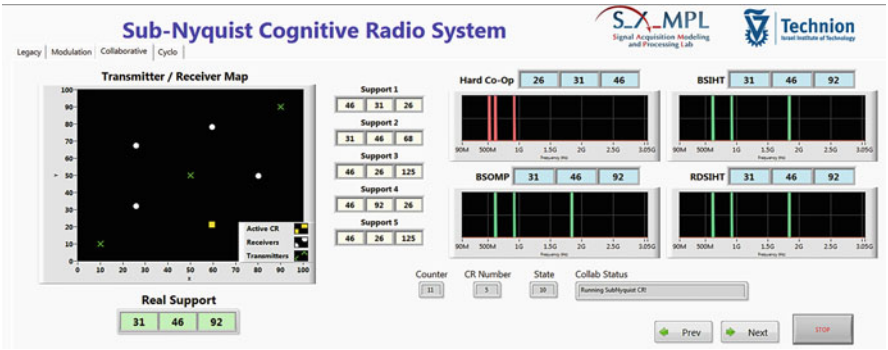

Fig. 25 Screenshot from the MWC CR collaborative hardware prototype. On the upper left side, we see the spatial map of the receivers in *white* and transmitters in *green*. On the bottom left, the occupied band indices of the real spectral support are shown, while to the right of the transmitter/receiver map, the estimated indices by each CR individually are presented. On the right, we see the spectrum sensing results of 4 different algorithms: Hard Co-Op (hard decision collaboration that selects the most popular frequency band indices), BSIHT, BSOMP, and RDSIHT. These results show both the superiority of collaborative spectrum sensing methods over individual detection and that of soft decision methods compared to the plain union of all the CR results

During the simulations conducted, $N_{\text{rec}} = 5$ CR receivers, spread across different locations, are emulated, denoted by white circles on the transmitter/receiver map. The transmitters are also positioned in various locations depicted by green x-marks. The transmitter positions and broadcasts are mimicking the effects of physical channel phenomena, i.e., fading and shadowing. The frequency support recovered by each of the CRs is false, since they individually receive only a partial spectral image of their surroundings, as expected in a real-world scenario.

In all simulated scenarios, collaborative spectrum sensing outperforms detection realized by individual CRs. This result is expected, since the soft collaborative methods take advantage of the spatial deployment of the receivers to reproduce the exact spectral map of the environment. Moreover, the centralized and distributed algorithms BSOMP, BSIHT and RDSIHT, based on soft decisions, showed superior results in comparison with a hard decision method. The same result can be seen in Fig. 25, where the hard decision support algorithm (Hard Co-Op) fails to recover the entire active frequency support (depicted by red bins).

Joint Carrier Frequency and Direction Estimation

The final extension we consider is joint spectrum sensing and DOA estimation. In order for CRs to map vacant bands more efficiently, spatial information about the PUs' locations can be of great interest. Consider the network of CRs presented in Fig. 26 and focus on CR1. Now, picture a scenario where PU2, with DOA θ_2 with respect to CR1, is transmitting in a certain frequency band with carrier f_2.

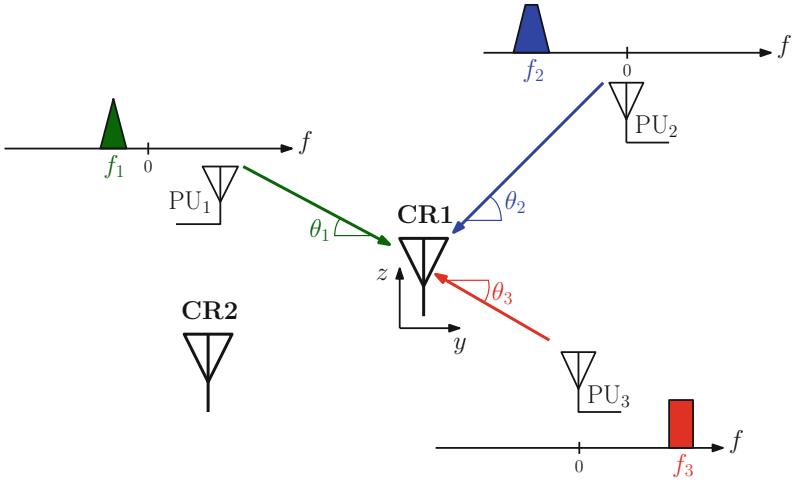

Fig. 26 Illustration of $N_{\text{sig}} = 3$ source signals in the yz plane. Each transmission is associated with a carrier frequency f_i and DOA θ_i

Assuming that CR2 does not receive PU2's transmission, CR1 may transmit in the same frequency band in the opposite direction of PU2 toward CR2. DOA estimation can thus enhance CR performance by allowing exploitation of vacant bands in space in addition to the frequency domain.

Model and System Description

To formulate the joint spectrum sensing and DOA estimation problem mathematically, assume that the input signal $x(t)$ is composed of N_{sig} source signals $s_i(t)$ with both unknown and different carrier frequencies f_i and DOAs θ_i. The main difference between this scenario and the one that has been discussed in the previous sections is the additional unknown DOAs θ_i. Figure 26 illustrates this signal model. To recover the unknown DOAs, an array of sensors is required. A similar problem thoroughly treated in the literature is the 2D-DOA recovery problem, where two angles are traditionally recovered and paired. In our case, the second variable is the signal's carrier frequency instead of an additional angle.

Multicoset Approach

A few works have recently considered joint DOA and spectrum sensing of multiband signals from sub-Nyquist samples. In [65] and [66], the low rate samples are obtained using multicoset sampling. In [65], which considers the digital model (41), both time and spatial compression are applied by selecting samples from the Nyquist grid and receivers from a uniform linear array (ULA), such that

$$\mathbf{Z}[n] = \mathbf{C}_s \mathbf{X}[n] \mathbf{C}_t. \tag{50}$$

Here, $\mathbf{X}[n]$ is the matrix of Nyquist samples from all receivers in the ULA, the selection matrices $\mathbf{C}_s$ and $\mathbf{C}_t$ operate on the spatial and time domain, respectively, to form the matrix of compressed samples $\mathbf{Z}[n]$. The 2D power spectrum matrix of the underlying signal is then reconstructed from the samples, where every row gives the power spectrum in the frequency domain for a given DOA and every column provides the power spectrum information in the angular domain for a given frequency.

In [66], an L-shaped array with two interleaved, or multicoset, channels, with a fixed delay between the two, τT_{Nyq} with $\tau \in [0, 1]$, samples the signal below the Nyquist rate. The delayed path signal received at the mth sensor is approximated by

$$x_m^d(t) = \sum_{i=1}^{K} s_i(t) \mathrm{e}^{j 2\pi f_i \left(t - \tau T_{\text{Nyq}} + \tau_m(\theta_i)\right)}, \tag{51}$$

using the narrowband assumption on the envelope $s_i(t)$. Here, K denotes the number of transmissions, f_i and θ_i are the carrier and DOAs of transmission i and $\tau_m(\theta_i)$ is the time difference between the mth element to the reference point for a plane wave arriving from the source i in direction θ_i. The samples of both paths is then written in frequency as

$$\mathbf{Z} = \mathbf{A}\mathbf{X}, \quad \mathbf{Z}^d = \mathbf{A}\mathbf{D}\mathbf{X}, \tag{52}$$

where $\mathbf{Z}$ and $\mathbf{Z}^d$ concatenate all samples for each sensor of the direct and delayed path, respectively. Here, $\mathbf{A}$ is the unknown steering matrix that depends on f_i and θ_i, $\mathbf{X}$ is the unknown matrix that contains frequency slices of the signal, and

$$\mathbf{D} \triangleq \operatorname{diag}\left[\mathrm{e}^{j 2\pi f_1 \tau T_{\text{Nyq}}} \cdots \mathrm{e}^{j 2\pi f_K \tau T_{\text{Nyq}}}\right]. \tag{53}$$

Exploiting correlations between samples from the direct path and its delayed version, the frequencies and their corresponding DOAs are estimated using MUSIC [18, 19]. However, the pairing issue between the two, that is matching each frequency with its corresponding angle, is not discussed.

In the next section, we describe the compressed carrier and DOA estimation (CaSCADE) system, presented in [28], that utilizes the sampling principles of the MWC. This technique addresses the pairing problem and avoids the hardware issues involved in multicoset sampling.

The CaSCADE System

The CaSCADE system implements the modified, or ULA based, MWC over an L-shaped array with $2M - 1$ sensors (M sensors along the y axis and M sensors

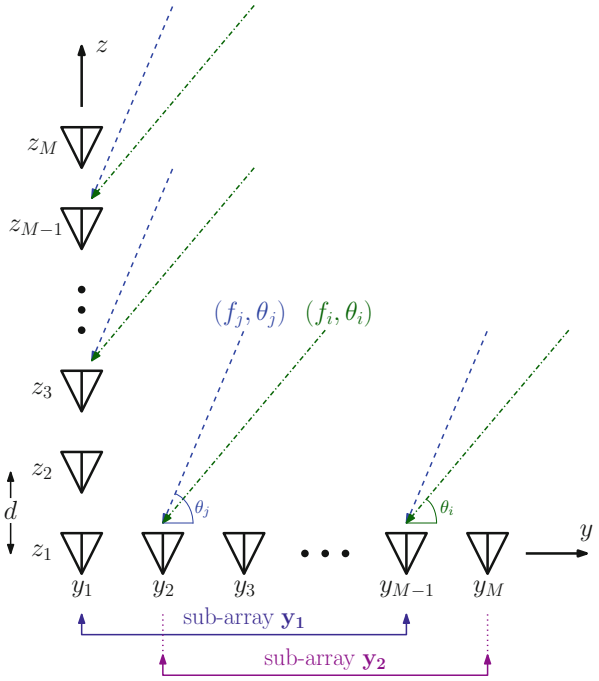

Fig. 27 CaSCADE system: L-shaped array with M sensors along the y axis and M sensors along the z axis including a common sensor at the origin. The sub-arrays $\mathbf{y}_1$ and $\mathbf{y}_2$ (and similarly $\mathbf{z}_1$ and $\mathbf{z}_2$) are defined in the derivation of the 2D-ESPRIT algorithm

along the z axis including a common sensor at the origin) in the yz plane. Each transmission $s_i(t)$ impinges on the array with its corresponding DOA θ_i, as shown in Fig. 27. The array sensors have the same sampling pattern as the alternative MWC. Each sensor is composed of an analog mixing front-end, implementing one physical branch of the MWC, that includes a mixer, a LPF, and a sampler.

By treating the L-shaped array as two orthogonal ULAs, one along the y axis and the other along the z axis, two systems of equations similar to (15) can be derived. For the ULA along the y axis, we obtain

$$\mathbf{y}(f) = \mathbf{A}_y \mathbf{x}(f), \quad f \in \mathscr{F}_s, \tag{54}$$

where

$$\mathbf{A}_y = \begin{bmatrix} e^{j2\pi f_1 \tau_1^y(\theta_1)} & \cdots & e^{j2\pi f_K \tau_1^y(\theta_K)} \\ \vdots & & \vdots \\ e^{j2\pi f_1 \tau_M^y(\theta_1)} & \cdots & e^{j2\pi f_K \tau_M^y(\theta_K)} \end{bmatrix}. \tag{55}$$

Similarly, along the z axis, we get

$$\mathbf{z}(f) = \mathbf{A}_z \mathbf{x}(f), \quad f \in \mathscr{F}_s, \tag{56}$$

where $\mathbf{A}_z$ is defined accordingly. Here,

$$\tau_m^y(\theta) = \frac{d\,m}{c}\cos(\theta), \quad \tau_m^z(\theta) = \frac{d\,m}{c}\sin(\theta) \tag{57}$$

denote the delays at the mth sensors in the y and z axis, respectively, with respect to the first sensor. The matrices $\mathbf{A}_y$ and $\mathbf{A}_z$ thus depend on both the unknown carrier frequencies and DOAs. In the time domain,

$$\mathbf{y}[n] = \mathbf{A}_y\mathbf{x}[n], \quad n \in \mathbb{Z} \tag{58}$$

$$\mathbf{z}[n] = \mathbf{A}_z\mathbf{x}[n], \quad n \in \mathbb{Z}. \tag{59}$$

Two joint recovery approaches for the carrier frequencies and DOAs of the transmissions are proposed in [28]. Note that once the carriers and DOAs are estimated, the signals can be reconstructed, as shown for the alternative MWC. For the sake of simplicity, a statistical model where $x(t)$ is wide-sense stationary is considered. The first recovery approach is based on CS techniques and allows recovery of both parameters assuming the electronic angles $f_i\cos\theta_i$ and $f_i\sin\theta_i$ lie on a predefined grid. The CS problem is formulated in such a way that no pairing issue arises between the carrier frequencies and their corresponding DOAs. To that end, the samples from both ULAs are concatenated into one vector $\mathbf{v}[n] = \left[\mathbf{y}^T[n]\,\mathbf{z}^T[n]\right]^T$, whose correlation matrix,

$$\mathbf{R} = \mathbb{E}\left[\mathbf{v}[n]\mathbf{v}^H[n]\right] = \mathbf{A}\mathbf{R}_x\mathbf{A}^H, \tag{60}$$

is computed. Here, $\mathbf{A} = [\mathbf{A}_y^T\,\mathbf{A}_z^T]^T$ and the autocorrelation matrix $\mathbf{R}_x = \mathbb{E}\left[\mathbf{x}[k]\mathbf{x}^H[k]\right]$ is sparse and diagonal, from the stationarity of $x(t)$. From the grid assumption, (60) may be discretized with respect to the possible values taken by the electronic angles. The resulting sparse matrix derived from $\mathbf{R}_x$ is diagonal as well, and its sparse diagonal is recovered using traditional CS techniques, similarly to (22).

The second recovery approach, inspired by [67], extends the ESPRIT algorithm to the joint estimation of carriers and DOAs while overcoming the pairing issue. The 2D-ESPRIT algorithm presented in [28] is directly applied to the sub-Nyquist samples, by considering cross-correlation matrices between the sub-arrays of both axis. Dropping the time variable n for clarity, the samples from the sub-arrays can be written as

$$\begin{aligned} \mathbf{y}_1 &= \mathbf{A}_{y_1}\mathbf{x}, \quad & \mathbf{y}_2 &= \mathbf{A}_{y_2}\mathbf{x} \\ \mathbf{z}_1 &= \mathbf{A}_{z_1}\mathbf{x}, \quad & \mathbf{z}_2 &= \mathbf{A}_{z_2}\mathbf{x}, \end{aligned} \tag{61}$$

where $\mathbf{y}_1, \mathbf{y}_2, \mathbf{z}_1, \mathbf{z}_2$ are samples from the sub-arrays shown in Fig. 27. The matrices $\mathbf{A}_{y_1}$ and $\mathbf{A}_{y_2}$ are the first and last $M-1$ rows of $\mathbf{A}_y$, respectively, and $\mathbf{A}_{z_1}$ and $\mathbf{A}_{z_2}$

are similarly defined. Each couple of sub-array matrices along the same axis are related by

$$\begin{aligned} \mathbf{A}_{y_2} &= \mathbf{A}_{y_1}\mathbf{D}_{\phi} \\ \mathbf{A}_{z_2} &= \mathbf{A}_{z_1}\mathbf{D}_{\psi}, \end{aligned} \tag{62}$$

where

$$\begin{aligned} \mathbf{D}_{\phi} &\triangleq \text{diag}\left[\mathrm{e}^{j2\pi f_1 \tau_1^y(\theta_1)} \cdots \mathrm{e}^{j2\pi f_K \tau_1^y(\theta_K)}\right] \\ \mathbf{D}_{\psi} &\triangleq \text{diag}\left[\mathrm{e}^{j2\pi f_1 \tau_1^z(\theta_1)} \cdots \mathrm{e}^{j2\pi f_K \tau_1^z(\theta_K)}\right]. \end{aligned} \tag{63}$$

We can see from (63) that the carrier frequencies f_i and DOAs θ_i are embedded in the diagonal matrices $\mathbf{D}_{\phi}$ and $\mathbf{D}_{\psi}$. Applying the ESPRIT framework on cross-correlations matrices between the subarrays of both axis allows to jointly recover $\mathbf{D}_{\phi}$ and $\mathbf{D}_{\psi}$ [28]. This leads to proper pairing of the corresponding elements $f_i\tau_1^y(\theta_i)$ and $f_i\tau_1^z(\theta_i)$. The DOAs θ_i and carrier frequencies f_i are then given by

$$\theta_i = \tan^{-1}\left(\frac{\angle(D_{\psi})_{ii}}{\angle(D_{\phi})_{ii}}\right) \quad f_i = \frac{\angle(D_{\phi})_{ii}}{2\pi\frac{d}{c}\cos(\theta_i)}. \tag{64}$$

It is proven in [28] that the minimal number of sensors required for perfect recovery is $2K+1$. This leads to a minimal sampling rate of $(2K+1)B$, which is slightly higher than the minimal rate $2KB$ required for spectrum sensing in the absence of DOA recovery. These ideas can also be extended to jointly recover the transmissions' carrier frequencies, azimuth, and elevation angles in a 3D framework.

Summary

In this chapter, we reviewed several challenges imposed on the traditional task of spectrum sensing by the new application of CR. We first investigated sub-Nyquist sampling schemes, enabling sampling, and processing of wideband signals at low rate, by exploiting their a priori known structure. A possible extension of these works is to include adaptive updating of the detected support, triggered by a change in a PU's activity, either starting a transmission in a previously vacant band or withdrawing from an active band. To increase efficiency, this should be performed by taking the current detected support as a prior and updating it with respect to the newly acquired samples, without going through the entire support recovery process from scratch. Additional preliminary assumptions on the structure or statistical behavior of the potentially active signals, such as statistics on channel occupancy, can be exploited as well.

We then considered detection challenges in the presence of noise, where second-order statistics recovery, and in particular cyclostationary detection, is shown to

perform better than simple energy detection. Next, fading and shadowing channel effects were overcome by collaborative CR networks. We then addressed the joint spectrum sensing and DOA estimation problem, allowing for better exploitation of frequency vacant bands by exploiting spatial sparsity as well. All these methods should next be combined in order to map the occupied spectrum, in frequency, time, and space, thus maximizing the CR network's throughput. This would require an adequate spectrum access protocol as well that translates the data acquired by spectrum sensing into transmission opportunities for the CRs.

An essential part of the approach adopted in this survey is the relation between the theoretical algorithms and practical implementation, demonstrating real-time spectrum sensing from low rate samples using off-the-shelf hardware components. Indeed, we believe that prototype development is an important component to enabling sub-Nyquist sampling as a solution to the task of spectrum sensing in CR platforms.

References

1. Mishali M, Eldar YC (2011) Sub-Nyquist sampling: bridging theory and practice. IEEE Signal Process Mag 28(6):98–124
2. Eldar YC (2015) Sampling theory: beyond bandlimited systems. Cambridge University Press, Cambridge
3. Tropp JA, Laska JN, Duarte MF, Romberg JK, Baraniuk RG (2010) Beyond Nyquist: efficient sampling of sparse bandlimited signals. IEEE Trans Inf Theory 56:520–544
4. Fleyer M, Linden A, Horowitz M, Rosenthal A (2010) Multirate synchronous sampling of sparse multiband signals. IEEE Trans Signal Process 58:1144–1156
5. Mishali M, Eldar YC (2011) Wideband spectrum sensing at sub-Nyquist rates. IEEE Signal Process Mag 28:102–135
6. Mishali M, Eldar YC (2009) Blind multi-band signal reconstruction: compressed sensing for analog signals. IEEE Trans Signal Process 57(3):993–1009
7. Mishali M, Eldar YC (2010) From theory to practice: sub-Nyquist sampling of sparse wideband analog signals. IEEE J Sel Top Signal Process 4(2):375–391
8. Mishali M, Eldar YC, Elron AJ (2011) Xampling: signal acquisition and processing in union of subspaces. IEEE Trans Signal Process 59:4719–4734
9. Urkowitz H (1967) Energy detection of unknown deterministic signals. Proc IEEE 55:523–531
10. Arias-Castro E, Eldar YC (2011) Noise folding in compressed sensing. IEEE Signal Process Lett 18(8):478–481
11. North DO (1963) An analysis of the factors which determine signal/noise discrimination in pulsed carrier systems. Proc IEEE 51:1016–1027
12. Turin GL (1960) An introduction to matched filters. IRE Trans Inf Theory 6:311–329
13. Gardner WA, Napolitano A, Paura L (2006) Cyclostationarity: half a century of research. Signal Process 86:639–697
14. Napolitano A (2016) Cyclostationarity: new trends and applications. Signal Process 120: 385–408
15. Akyildiz IF, Lo BF, Balakrishnan R (2011) Cooperative spectrum sensing in cognitive radio networks: a survey. Phys Commun 4:40–62
16. Mishra SM, Sahai A, Brodersen RW (2006) Cooperative sensing among cognitive radios. IEEE Int Conf Commun 1658–1663
17. Letaief KB, Zhang W (2009) Cooperative communications for cognitive radio networks. Proc IEEE 97(5):878–893

18. Pisarenko VF (1973) The retrieval of harmonics from a covariance function. Geophys J R Astron Soc 33:347–366
19. Schmidt RO (1986) Multiple emitter location and signal parameter estimation. IEEE Trans Antennas Propag 34:276–280
20. Roy R, Kailath T (1989) ESPRIT-estimation of signal parameters via rotational invariance techniques. IEEE Trans Signal Process 37:984–995
21. Eldar YC, Kutyniok G (2012) Compressed sensing: theory and applications. Cambridge University Press, Cambridge
22. Landau H (1967) Necessary density conditions for sampling and interpolation of certain entire functions. Acta Math 117:37–52
23. Venkataramani R, Bresler Y (2000) Perfect reconstruction formulas and bounds on aliasing error in sub-Nyquist nonuniform sampling of multiband signals. IEEE Trans Inf Theory 46:2173–2183
24. Mishali M, Eldar YC, Dounaevsky O, Shoshan E (2011) Xampling: analog to digital at sub-Nyquist rates. IET Circuits Devices Syst 5:8–20
25. Israeli E, Tsiper S, Cohen D, Reysenson A, Hilgendorf R, Shoshan E, Eldar YC (2014) Hardware calibration of the modulated wideband converter. In: IEEE Global Communications Conference, Austin, pp 948–953
26. Mishali M, Eldar YC (2009) Expected RIP: conditioning of the modulated wideband converter. In: IEEE Information Theory Workshop, Volos, pp 343–347
27. Gan HWL, Wang H (2013) Deterministic binary sequences for modulated wideband converter. In: International Conference Sampling Theory and Applications, Bremen
28. Stein S, Yair O, Cohen D, Eldar YC (2016) CaSCADE: compressed carrier and DOA estimation. Arxiv:1604.02723 [cs.IT]
29. Gold R (1967) Optimal binary sequences for spread spectrum multiplexing (corresp.). IEEE Trans Inf Theory 13(4):619–621
30. Cohen D, Akiva A, Avraham B, Eldar YC (2015) Distributed cooperative spectrum sensing from sub-Nyquist samples for cognitive radios. In: IEEE Workshop Signal Proceedings of Advances Wireless Communications, Stockholm, pp 336–340
31. Cohen D, Akiva A, Avraham B, Eldar YC (2015) Centralized cooperative spectrum sensing from sub-Nyquist samples for cognitive radios. In: IEEE International Conference on Communications, London, pp 7487–7491
32. Cohen D, Eldar YC (2016) Sub-Nyquist cyclostationary detection for cognitive radio. Arxiv:1604.02659 [cs.IT]
33. Adams D, Eldar Y, Murmann B (2016) A mixer frontend for a four-channel modulated wideband converter with 62 db blocker rejection. In: 2016 IEEE Radio Frequency Integrated Circuits Symposium (RFIC), May 2016, San Francisco, pp 286–289
34. Lexa MA, Davies ME, Thompson JS (2011) Compressive and noncompressive power spectral density estimation from periodic nonuniform samples. CoRR, vol. abs/1110.2722
35. Arianandа DD, Leus G (2012) Compressive wideband power spectrum estimation. IEEE Trans Signal Process 60:4775–4789
36. Romero D, Leus G (2013) Compressive covariance sampling. In: Proceedings Information Theory and Applications Workshop, San Diego, pp 1–8
37. Yen CP, Tsai Y, Wang X (2013) Wideband spectrum sensing based on sub-Nyquist sampling. IEEE Trans Signal Process 61:3028–3040
38. Cohen D, Eldar YC (2014) Sub-Nyquist sampling for power spectrum sensing in cognitive radios: a unified approach. IEEE Trans Signal Process 62:3897–3910
39. Tian Z, Tafesse Y, Sadler BM (2012) Cyclic feature detection with sub-nyquist sampling for wideband spectrum sensing. IEEE J Select Top Signal Process 6(1):58–69
40. Leus G, Tian Z (2011) Recovering second-order statistics from compressive measurements. In: IEEE International Workshop on Computational Advances in Multi-sensor Adaptive Processing, San Juan, pp 337–340
41. Gardner W (1988) Statistical spectral analysis: a non probabilistic theory. Prentice Hall, Englewood Cliffs, NJ, USA

42. Papoulis A (1991) Probability, random variables, and stochastic processes. McGraw Hill, Boston
43. Pal P, Vaidyanathan PP (2010) Nested array: a novel approach to array processing with enhanced degrees of freedom. IEEE Trans Signal Process 58:4167–4181
44. Vaidyanathan PP, Pal P (2011) Sparse sensing with co-prime samplers and arrays. IEEE Trans Signal Process 59:573–586
45. Qu D, Tarczynski A (2007) A novel spectral estimation method by using periodic nonuniform sampling. In: Asilomar Conference on Signals, Systems and Computers, Pacific Grove, pp 1134–1138
46. Khatri CG, Rao CR (1968) Solutions to some functional equations and their applications to characterization of probability distributions. Sankhyā: Indian J Stat Ser A 30:167–180
47. Arts M, Bollig A, Mathar R (2015) Analytical test statistic distributions of the mmme eigenvalue-based detector for spectrum sensing. In: 2015 International Symposium on Wireless Communication Systems (ISWCS). IEEE, Brussels, pp 496–500
48. Romero D, López-Valcarce R, Leus G (2015) Compression limits for random vectors with linearly parameterized second-order statistics. IEEE Trans Inf Theory 61(3):1410–1425
49. Leech J (1956) On the representation of 1, 2, 3,...n by differences. J Lond Math Soc 1(2): 160–169
50. Gardner WA (1986) The spectral correlation theory of cyclostationary time-series. Signal Process 11:13–36
51. Cohen D, Pollak L, Eldar YC (2016) Carrier frequency and bandwidth estimation of cyclostationary multiband signals. IEEE ICASSP, Shanghai
52. Thorndike RL (1953) Who belong in the family? Psychometrika 18:267–276
53. Ghasemi A, Sousa ES (2005) Collaborative spectrum sensing for opportunistic access in fading environments. In: IEEE International Symposium on New Frontiers in Dynamic Spectrum Access Networks, pp 131–136
54. Sklar B (1997) Rayleigh fading channels in mobile digital communication systems part I: characterization. IEEE Commun Mag 35:90–100
55. Wang Y, Pandharipande A, Polo YL, Leus G (2009) Distributed compressive wideband spectrum sensing. In: IEEE Information Theory and Applications Workshop, Volos, pp 178–183
56. Ariananda DD, Leus G (2012) A study on cooperative compressive wideband power spectrum sensing. In: Joint WIC/IEEE Symposium on Information Theory and Signal Process, pp 102–109
57. Tropp J, Gilbert AC, Strauss MJ (2005) Simultaneous sparse approximation via greedy pursuit. In: IEEE International Conference on Acoustics, Speech and Signal Process, Philadelphia, vol 5, pp 721–724
58. Makhzani A, Valaee S (2012) Reconstruction of jointly sparse signals using iterative hard thresholding. In: IEEE International Conference on Communications, Beijing, pp 3564–3568
59. Duarte MF, Sarvotham S, Baron D, Wakin MB, Baraniuk RG (2005) Distributed compressed sensing of jointly sparse signals. In: IEEE Asilomar Conference on Signals, Systems and Computers, pp 1537–1541
60. Tian Z (2008) Compressed wideband sensing in cooperative cognitive radio networks. In: IEEE Global Communications Conference, New Orleans, pp 1–5
61. Zeng F, Li C, Tian Z (2011) Distributed compressive spectrum sensing in cooperative multihop cognitive networks. J Select Topics Signal Process 5:37–48
62. Boyd S, Ghosh A, Prabhakar B, Shah D (2006) Randomized gossip algorithms. IEEE Trans Inf Theory 52:2508–2530
63. Rabi BJM, Johansson M (2009) A randomized incremental subgradient method for distributed optimization in networked systems. SIAM J Optim 20(3):1157–1170
64. Nguyen N, Needell D, Woolf T (2014) Linear convergence of stochastic iterative greedy algorithms with sparse constraints. CoRR abs/1407.0088, [Online]. Available: http://arxiv.org/abs/1407.0088

65. Arianandа DD, Leus G (2013) Compressive joint angular-frequency power spectrum estimation. In: Proceedings of European Signal Processing Conference, Piscataway, pp 1–5
66. Kumar AA, Razul SG, See CS (2014) An efficient sub-Nyquist receiver architecture for spectrum blind reconstruction and direction of arrival estimation. In: IEEE International Conference on Acoustics, Speech and Signal Processing, Florence, pp 6781–6785
67. Gu J-F, Zhu W-P, Swamy MNS (2015) Joint 2-D DOA estimation via sparse L-shaped array. IEEE Trans Signal Process 63:1171–1182

Part II
Dynamic Spectrum Access and Sharing

Principles and Challenges of Cooperative Spectrum Sensing in Cognitive Radio Networks

12

Lamiaa Khalid and Alagan Anpalagan

Contents

Abstract

Cognitive radio (CR) technology is a promising solution to the inevitable problem of spectrum scarcity and underutilization. Cognitive radios can perform spectrum sensing, dynamically identify unused spectrum, and opportunistically utilize those spectrum holes for their own transmission. Cognitive radio

L. Khalid (✉) · A. Anpalagan
Electrical and Computer Engineering, Ryerson University, Toronto, ON, Canada
e-mail: lkhalid@ryerson.ca; alagan@ieee.org

W. Zhang (ed.), *Handbook of Cognitive Radio*,
https://doi.org/10.1007/978-981-10-1394-2_12

technology is also a key concept suggested to be part of the fifth generation of cellular wireless standards (5G). Efficient spectrum sensing is crucial to the effective deployment of CR networks. Cooperative spectrum sensing (CSS) schemes can significantly improve the sensing accuracy of CR networks by exploiting multiuser spatial diversity. However, the cooperative gain can be impacted by factors such as the detection performance of each secondary user (SU) and the fusion techniques used to combine the secondary users' decisions. Moreover, CSS incurs cooperation overhead that may deteriorate its overall performance. In this chapter, we provide a comprehensive survey on the different factors that contribute to the efficient design of CSS schemes for cognitive radio networks. We specifically focus on the elements of cooperative sensing that can leverage the achievable cooperative gain, limit the cooperation overhead, or provide trade-off between the gain and overhead such as the number of channels sensed in each sensing period, the selection of secondary users, the selection of the fusion scheme, and the correlation between the cooperating secondary users. We also highlight key open research challenges in cooperative spectrum sensing.

Introduction

Driven by the proliferation of new wireless services and applications, as well as the steadily increasing number of wireless users, the demand for radio spectrum has increased dramatically. The government regulatory agencies employ inflexible spectrum management approaches by granting each operator an exclusive license to operate in a certain frequency band. With most of the prime radio frequency spectrum already exclusively assigned, it is becoming exceedingly hard to find vacant bands to either deploy new services or enhance existing ones. However, this spectrum scarcity is mainly due to inefficient fixed frequency allocations rather than a physical shortage in the spectrum. This inefficiency in the spectrum usage necessitates a new communication paradigm to exploit the existing wireless spectrum opportunistically. Dynamic spectrum access (DSA) has been proposed as an alternative policy to allow the radio spectrum to be more efficiently utilized [1]. Using DSA, a portion of the spectrum can be licensed to one or more users, which are called primary users (PUs); however, the use of that spectrum is not exclusively granted to these licensed users, although they have higher priority in using it. The unlicensed users, which are referred to as secondary users, are allowed to opportunistically utilize the unused licensed bands, commonly referred to as "white spaces" or "spectrum holes," as long as the primary users' transmissions can be adequately protected. By doing so, the radio spectrum can be reused in an opportunistic manner or shared all the time which can significantly improve the spectrum utilization efficiency [2]. The key enabling technology of DSA is the cognitive radio (CR) technology.

A cognitive radio system is a radio system which is aware of its operational and geographical environment, established policies, and its internal state. Moreover, it is able to dynamically and autonomously adapt its operational parameters and

protocols and to learn from its previous experience [3]. Cognitive radios are enabled by the rapid and significant advancements in radio technologies (e.g., software-defined radios, frequency agility, power control, etc.) and can be characterized by the utilization of disruptive techniques such as wideband spectrum sensing, real-time spectrum allocation and acquisition, and real-time measurement dissemination [4]. To reliably identify the vacant licensed bands, some methods that the secondary users can employ are geolocation combined with access to database, beacons, spectrum sensing, or a combination of any of those methods [5,6]. In the geolocation method, primary users register the relevant data such as their location and transmit power as well as expected duration of usage at a centralized database. Secondary users then have to access this database to determine the availability of vacant licensed bands at their location. Geolocation database is based on field strength estimates for the primary users obtained using terrain-based radio propagation models. However, the limited geographical information restricts the achievable accuracy of the field strength estimates. Therefore, radio environment mapping (REM) has been introduced as an alternative or complementary procedure to radio propagation models [7–9].

In the beacon method, secondary users only transmit if they receive a control signal (beacon) identifying vacant channels within their service areas. Without reception of this control signal, no transmissions are permitted by the secondary users. In [10], beacon-assisted channel access was assumed in which a codeword from the codebook of the primary users is reserved as a beacon, and each time a primary user releases a channel, it broadcasts this beacon message. The authors assumed that the codebook of the primary users as well as the beacon codeword was a priori known to the secondary users. The proposed protocol showed performance gain in terms of more reliable detection of spectrum holes as well as achieving higher secondary channel capacity. In [11], novel detection schemes employed at the fusion center, namely, the robust estimator-correlator detector and the robust generalized likelihood detector, were proposed for multiple beacon signaling-based cooperative spectrum sensing in multiple-input multiple-output wireless cognitive radio networks with channel state information (CSI) uncertainty. Simulation results demonstrated that the proposed detection techniques yield a significant improvement in the detection performance compared to the conventional CSI uncertainty matched filter detector.

With the aforementioned methods, secondary devices will need additional connectivity in a different band in order to be able to access the database [5] or a dedicated standardized channel will be needed to broadcast the beacons [6]. In the spectrum sensing method, secondary users autonomously detect the presence of the primary signals and only use the channels that are not used by the primary users. All the abovementioned methods have their advantages and disadvantages. It is up to the regulator to decide on the best approach with the considerations from all the stakeholders. However, it is expected that in the future, both database and spectrum sensing techniques will be used together in order to have flexibility and achieve maximum efficiency for secondary users [12]. In this chapter, we focus on spectrum sensing performed by cognitive radios because of its relatively lower

infrastructure cost and its compatibility with licensed primary systems which allows for broader application areas.

Spectrum sensing enables the capability of a cognitive radio to measure, learn, and be aware of the radio's operating environment, such as the spectrum availability and interference status. Availability of radio spectrum varies depending on time, frequency, and location resulting in spectrum access opportunities. Secondary users can use the available idle spectrum in an opportunistic manner by identifying the available spectrum reliably and rapidly. It also helps in quickly determining if the primary users have become active in the bands used by secondary users so that those bands can be vacated immediately. This is important for ensuring that the interference caused to the primary users' transmissions remains below a permitted level. Moreover, detection of other secondary users may be necessary as well for coexistence with other secondary networks. However, due to the effects of multipath fading and shadowing, the signal-to-noise ratio (SNR) of the received primary signal can be extremely low, and a secondary user may not be able to distinguish between a deeply faded band and an idle one. Since receiver sensitivity indicates the capability of detecting weak signals, the sensitivity requirement of the secondary user's receiver may end up being too stringent. In order to mitigate these effects, secondary users often cooperate for spectrum sensing.

The main idea of cooperative spectrum sensing (CSS) is to enhance the sensing performance by exploiting the spatial diversity in the observations of spatially located secondary users [13–17]. Having multiple cooperating secondary users increases diversity by providing multiple measurements of the signal and, therefore, guarantees a better detection performance. Consequently, the diversity gain achieved through cooperative spectrum sensing improves the overall detection sensitivity without imposing higher sensitivity requirements on individual secondary users [18]. A less stringent sensitivity requirement is particularly appealing from the implementation point of view due to the reduced hardware cost and complexity. The performance improvement due to spatial diversity is called cooperative gain. However, cooperative gain is not limited to the improved detection performance and relaxed sensitivity requirement. For instance, since it is difficult, using a single radio, to transmit on a licensed band and sense it simultaneously, sensing has to be interleaved with data transmission [13, 19]. Therefore, if the sensing time can be reduced due to cooperation, secondary users will have more time for data transmission so as to improve their opportunistic throughput which is also considered a part of the cooperative gain. From the above discussion, it is apparent that well-designed techniques for cooperative spectrum sensing can significantly contribute to improving the achievable cooperative gain. However, CSS can incur cooperation overhead and the achievable cooperative gain can be impacted by many factors. The goal of this chapter is to point out several aspects of cooperative spectrum sensing. These aspects are discussed in the rest of this chapter.

In section "Fundamental Concepts of Spectrum Sensing," we present the fundamental concepts of spectrum sensing. In section "Sensing Techniques," we review the most common spectrum sensing techniques for cognitive radio networks and detail their advantages and disadvantages. In section "Cooperative Spectrum

Sensing (CSS)," we present the different elements of cooperative spectrum sensing. In section "Performance of Cooperative Spectrum Sensing," we discuss the different factors impacting the performance of cooperative spectrum sensing. We present some research challenges which offer directions for future work in section "Research Challenges." Section "Conclusions" concludes this chapter.

Fundamental Concepts of Spectrum Sensing

The spectrum sensing problem is traditionally formulated as a binary hypothesis testing problem as described below. To identify the idle spectrum and protect the primary users' transmissions, different local spectrum sensing techniques have been proposed for individual secondary users based on hypothesis testing. Some of the most common spectrum sensing techniques for the detection of primary users' transmissions for cognitive radio networks are discussed in section Sensing Techniques.

Hypothesis Testing

A key task in spectrum sensing is to decide whether the spectrum is idle or busy. The spectrum sensing problem is traditionally formulated as a binary hypothesis test [20]. The null hypothesis denoted by H_0 corresponds to the absence of the primary user's transmission, i.e., the received signal being only noise. On the other hand, the alternative hypothesis denoted by H_1 indicates that the primary user's transmission is present, i.e., the received signal contains the primary signal along with noise. In case the hypotheses have no unknown parameters, the hypotheses are called simple. If there are unknown or unspecified parameters, then the hypotheses are called composite. As an example, a binary hypothesis test for detecting the primary user's transmission in an additive white Gaussian noise (AWGN) channel is given by

$$x(n) = \begin{cases} v(n), & H_0 \\ h(n)s(n) + v(n), & H_1 \end{cases} \tag{1}$$

where $x(n)$ denotes the sampled received signal with sampling rate f_s (Hz) and an observation time T. The channel gain and primary user's transmitted signal are denoted by $h(n)$ and $s(n)$, respectively, and $v(n)$ is the AWGN noise.

In most practical cases, a test statistic Y is computed from the observation vector $\mathbf{x} = [x(1), x(2), .., x(N)]$ containing N observation samples, where $N \triangleq f_s T$ is assumed to be an integer. The detection is based on comparing the test statistic Y to the threshold γ. If the test statistic is greater than the threshold, i.e., $Y > \gamma$, then H_1 is declared true. Otherwise, H_0 is declared true. Two main performance metrics that are crucial in the design of spectrum sensing techniques are the probability

of miss-detection, P_m, and the probability of false alarm, P_f. The probability of miss-detection is defined as the probability that the detector declares the absence of a primary user (PU) transmission (decide H_0), when PU transmission is actually present (H_1 is true). The probability of false alarm is defined as the probability that the detector declares the presence of PU transmission (decide H_1), when PU transmission is actually absent (H_0 is true). Therefore, we represent the probabilities of miss-detection and false alarm, respectively, as [21]

$$P_m = P(H_0|H_1) = P(Y \leq \gamma|H_1), \tag{2}$$

and

$$P_f = P(H_1|H_0) = P(Y > \gamma|H_0). \tag{3}$$

It is clear that we need the probability of detection to be high as it indicates the level of protection of the primary users' transmissions from the interfering secondary users' transmissions. On the other hand, low probabilities of false alarm are necessary in order to maintain high opportunistic secondary throughput, since a false alarm would prevent the unused bands from being accessed by secondary users leading to inefficient spectrum usage.

Primary Transmitter Detection

The transmitter detection model is based on the detection of weak signals from a primary transmitter through the local observations of secondary users. This model has a wider applicability due to its compatibility with the licensed systems. The main drawback of the primary transmitter sensing model is its reliance on the detection of primary transmitters to infer the availability of white spaces while the interference happens at the primary receivers. As such, a detection margin has to be included in order to protect primary receivers [6].

When the primary system employs bursty transmission, the secondary user can detect the empty time slots and multiplex its signal over them without causing any performance degradation at the primary receivers. On the other hand, when the primary system employs continuous transmission, the secondary user has to estimate the interference it generates at the primary receivers by using signal level measurements. If the transmitter of the secondary user is far from the primary receiver, depending on the signal-to-interference ratio (SIR) limit at the receiver of the primary user supplied by the regulatory bodies, both the primary user and the secondary user could transmit data simultaneously [6, 22]. In this case, the interference range is defined as the minimum distance that a secondary transmitter should be away from the primary receiver such that it does not cause harmful interference at this receiver. Figure 1 shows the primary receiver located at a

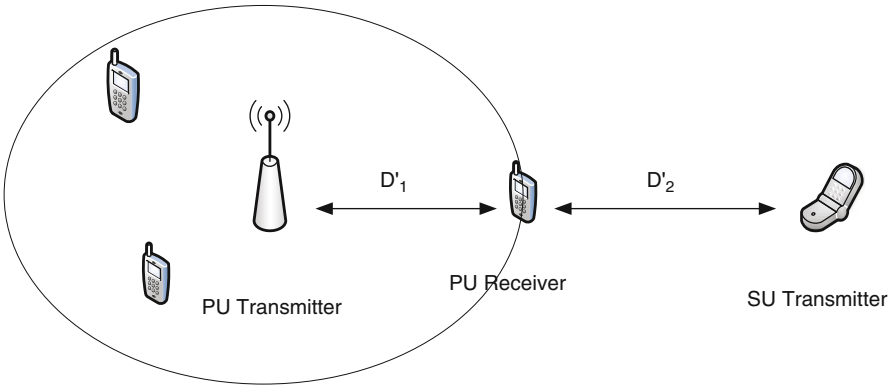

Fig. 1 Interference range of a cognitive radio

distance D_1' from the primary transmitter and D_2' is the interference range. The interference range will depend on the SU-transmitted power and the primary receiver's interference tolerance and can be obtained from [23]

$$\text{SIR} = \frac{P_u' h(D_1')}{P_s' h(D_2') + P_b'}, \tag{4}$$

where P_u' and P_s' are the transmit power of the primary and secondary users, respectively, $h(D')$ is the channel gain at distance D' from the transmitter, and P_b' is the background interference power at the primary receiver.

To avoid causing harmful interference to the primary receiver, the secondary user must be able to detect a signal from the primary transmitter within the range of $D_1' + D_2'$ which can translate to a certain sensitivity requirement for the secondary detector. Although the cases where an active primary transmitter is present but it is far away from the secondary user fall under hypothesis H_1, the interference to the primary receiver would not be harmful, and as such these cases should be treated as white space by definition. In particular, since the detection of the primary transmitter is dependent on the SNR at the secondary user as seen in (1), it would be unlikely for low-SNR primary signals to trigger the secondary user's detector resulting in unusable white spaces [24].

Sensing Techniques

In this section, we will discuss some of the most common spectrum sensing techniques for the detection of the primary transmitter in the cognitive radio literature. From the perspective of signal detection, sensing techniques can be classified into two broad categories: coherent and noncoherent detection. In coherent detection,

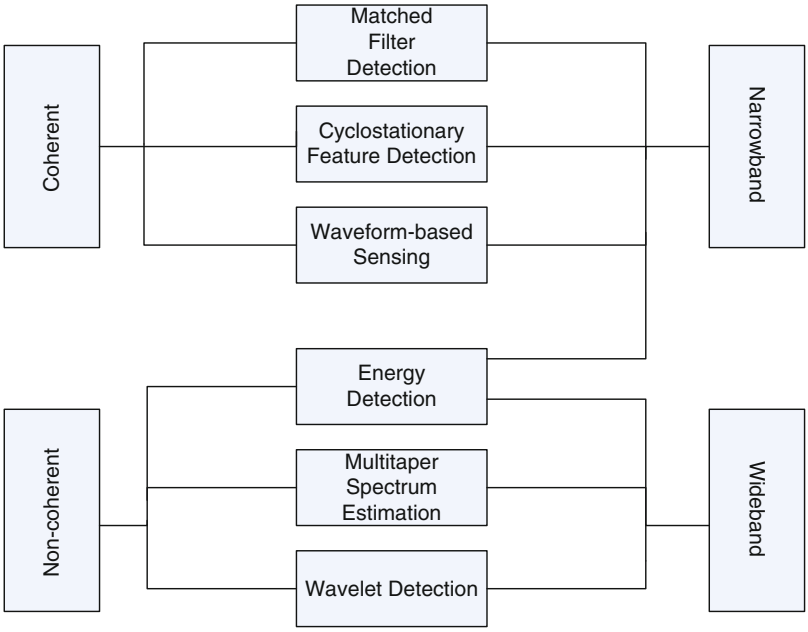

Fig. 2 Classification of spectrum sensing techniques

the primary signal can be coherently detected by comparing the received signal or the extracted signal characteristics with prior knowledge of primary signals. In noncoherent detection, no prior knowledge of the primary signal is required for detection. Another way to classify sensing techniques is based on the bandwidth of the spectrum of interest, that is, narrowband and wideband. The classification of sensing techniques is shown in Fig. 2. Next, we introduce matched filter detection, energy detection, and cyclostationary detection and briefly discuss some other spectrum sensing techniques. A more complete review on various spectrum sensing techniques and design challenges can be found in [25, 26].

Matched Filter Detection

Matched filtering is known as the optimum method for the detection of the primary signal when the transmitted signal is known, since it maximizes the received signal-to-noise ratio (SNR). The main advantage of matched filtering is the short time it requires to achieve a certain detection performance, such as low probabilities of miss-detection and false alarm [27], since a matched filter needs less received signal samples. However, matched filtering requires the secondary users to demodulate the received signals. Therefore, it requires perfect knowledge of the primary users' signaling features such as bandwidth, operating frequency, modulation type and

order, and pulse shaping as well as accurate synchronization at the secondary user [25, 28, 29]. However, in cognitive radio networks, such knowledge is not readily available to secondary users, and the implementation cost and complexity of this detector are high. Another significant drawback of matched filter detection is that a secondary user would need a dedicated receiver for every primary user class [30].

Energy Detection

Energy detection [21, 31] is a noncoherent detection method that is most commonly used if the receiver cannot gather sufficient information about the primary user's signal. This simple scheme accumulates the energy of the received signal during the sensing interval and declares the primary band to be occupied if the energy surpasses a certain threshold which depends on the noise floor [21]. Due to its simplicity and the fact that it does not require prior knowledge of the primary users' signals, energy detection is the most popular sensing technique among others for spectrum sensing [6, 15, 32–34]. However, some of the challenges with energy detection include selection of the threshold for detecting primary users, inability to differentiate interference from primary users' transmission and noise, and poor performance under low signal-to-noise ratio [29]. Moreover, energy detection does not work efficiently for detecting spread spectrum signals for which more sophisticated signal processing algorithms need to be devised [35].

In addition to narrowband sensing, energy detection has been used for multiband joint detection in wideband sensing by employing an array of energy detectors, each of which detects one frequency band [36]. The multiband joint detection framework enables secondary users to simultaneously detect primary users' signals across multiple frequency bands for efficient management of the wideband spectrum resource at the cost of detection hardware.

Cyclostationary Feature Detection

Another detection method that can be applied for spectrum sensing is the cyclostationary feature detection. Modulated signals are in general coupled with sinusoidal wave carriers, pulse trains, repeated spreading or hopping sequences, or cyclic prefixes, which result in built-in periodicity. Cyclostationary features are caused by the periodicity in the signal or in its statistics such as mean and autocorrelation [29]. Cyclostationary feature detection is a method for detecting primary user transmissions by exploiting the cyclostationary features of the received signals. Instead of power spectral density (PSD), cyclic correlation function is used for detecting signals present in a given spectrum. The cyclostationary-based detection algorithms can differentiate noise from primary users' signals. This is a result of the fact that noise is wide-sense stationary with no correlation, while modulated signals are cyclostationary with spectral correlation due to the redundancy of signal periodicity. Therefore, a cyclostationary feature detector can perform better than

the energy detector in discriminating against noise due to its robustness to the uncertainty in noise power [28, 37]. However, it is computationally complex and requires significantly long observation time. Moreover, it requires the knowledge of the cyclic frequencies of the primary users, which may not be available to the secondary users.

Other Sensing Techniques

Alternative spectrum sensing methods include waveform-based sensing, multitaper spectral estimation, and wavelet detection. Waveform-based sensing is usually based on correlation with known signal patterns. Known patterns are usually utilized in wireless systems to assist synchronization or for other purposes. Such patterns include preambles, regularly transmitted pilot patterns, and spreading sequences. In [35], it was shown that waveform-based sensing outperforms energy detector-based sensing in reliability and convergence time. Furthermore, it was shown that the performance of the sensing algorithm increases as the length of the known signal pattern increases. Waveform-based sensing, however, is only possible when the target primary user's signal contains known signal patterns.

In [38], the authors proposed a spectrum sensing method based on the auto-correlation of the received samples. The proposed method was evaluated by means of experiments wherein the probabilities of detection and false alarm at different signal-to-noise ratios (SNRs) were observed. A metric called the Euclidean distance was derived to analyze the autocorrelation of the received samples in order to decide whether only noise was present or signal plus noise. Simulation results showed that the proposed method is more efficient than using autocorrelation function at first lag method in terms of probability of detection and false alarm and more efficient than the energy detection method in terms of probability of false alarm.

Multitaper spectrum estimation was proposed in [39]. The proposed algorithm was shown to be an approximation to the maximum likelihood power spectral density estimator, and for wideband signals, it is nearly optimal. Most importantly, unlike the maximum likelihood spectral estimator, the multitaper spectral estimator is computationally feasible. In [40], wavelets are used for detecting edges in the power spectral density of a wideband channel. Once the edges, which correspond to transitions from an occupied band to an empty band or vice versa, are detected, the power within the bands between two edges is estimated. Using this information and the edges' positions, the power spectral density can be characterized as occupied or empty in a binary fashion. The assumptions made in [40], however, need to be relaxed for building a practical sensing algorithm. The method proposed in [40] was extended in [41] by using sub-Nyquist sampling (compressed sensing). Assuming that the signal spectrum is sparse, sub-Nyquist sampling is used to obtain a coarse spectrum knowledge in an efficient way. Table 1 presents a brief comparison of the above spectrum sensing techniques.

Table 1 Comparison of spectrum sensing techniques

Spectrum sensing technique	Advantages	Disadvantages
Matched filter detection	- Optimal performance - Low computational cost	Requires prior knowledge of the primary user's signal
Energy detection	- Low complexity - No primary knowledge required	- Poor performance for low SNR - Cannot differentiate signal and noise
Cyclostationary detection	- Robust in low SNR region - Robust against interference	- Requires partial prior information - High computational cost
Waveform-based detection	- Robust in low SNR region - Short measuring time	- Requires prior knowledge of the primary user's signal - Susceptible to synchronization errors
Multitaper spectrum estimation	- Near-optimal performance for wideband signals - No primary knowledge required	High implementation complexity
Wavelet detection	Effective for wideband signal detection	- Requires high sampling rate analog-to-digital converter - High computational cost

Cooperative Spectrum Sensing (CSS)

In cooperative spectrum sensing, information from multiple secondary users are incorporated for the detection of the primary signal. In the literature, cooperative sensing is discussed as a solution to problems that arise in spectrum sensing due to noise uncertainty, fading, and shadowing since the uncertainty in a single user's detection can be minimized [32]. The main idea of cooperative sensing is to enhance the sensing performance by exploiting the spatial diversity in the observations of spatially located secondary users. By cooperation, secondary users can share their sensing information for making a combined decision more accurate than the individual decisions [17]. The performance improvement due to spatial diversity is called cooperative gain. While cooperative gain such as improved detection performance and relaxed sensitivity requirement can be obtained, cooperative sensing can incur cooperation overhead. Cooperation overhead refers to any extra sensing time, delay, energy, and operations devoted to cooperative sensing and any performance degradation caused by cooperative sensing.

Cooperation Architecture

Depending on how the secondary users share their sensing data, several cooperative spectrum sensing architectures for CR networks have been proposed in the literature [15, 42–44]. The most commonly proposed architecture is the parallel fusion

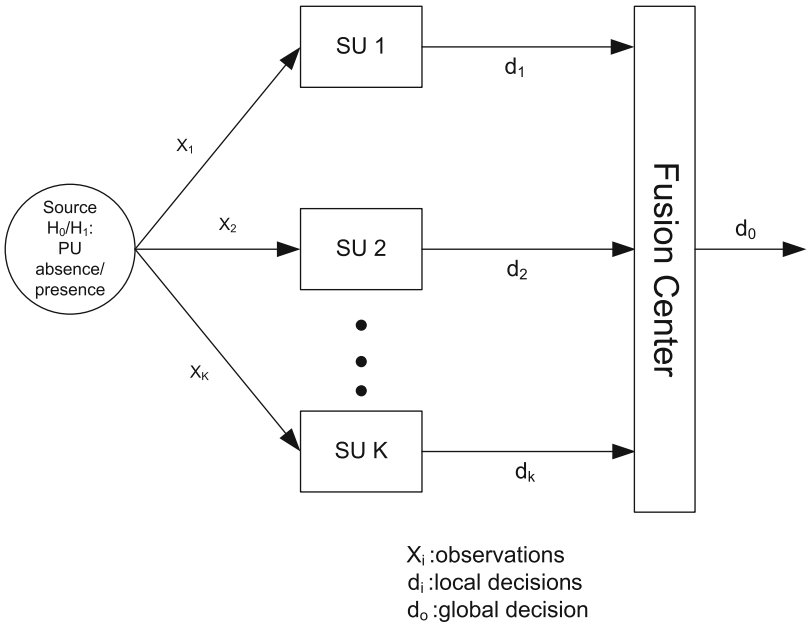

Fig. 3 Parallel fusion architecture

architecture, in which all the sensing secondary users send their sensing information directly to a centralized controller called a fusion center. This fusion center then makes a final decision regarding the presence or absence of the primary signal and broadcasts this information to other secondary users or directly controls the cognitive radio network traffic [15, 32, 42]. The parallel fusion architecture is illustrated in Fig. 3.

Another possible sensing architecture is the decentralized sensing architecture which does not rely on a fusion center for making the cooperative decision [16, 35, 44]. In this case, secondary users exchange the sensing observations and converge to a unified decision on the presence or absence of primary user's transmissions by iterations. Based on a distributed algorithm, each secondary user sends its own sensing data to other users, combines its data with the received sensing data, and decides whether or not the primary user's transmission is present by using a local criterion. If the criterion is not satisfied, secondary users send their combined results to other users again and repeat this process until the algorithm is converged and a decision is reached. The decentralized sensing architecture is illustrated in Fig. 4.

Fusion Schemes

In cooperative sensing, a fusion scheme refers to the process of combining locally sensed data of individual secondary users. Depending on which type of sensing data

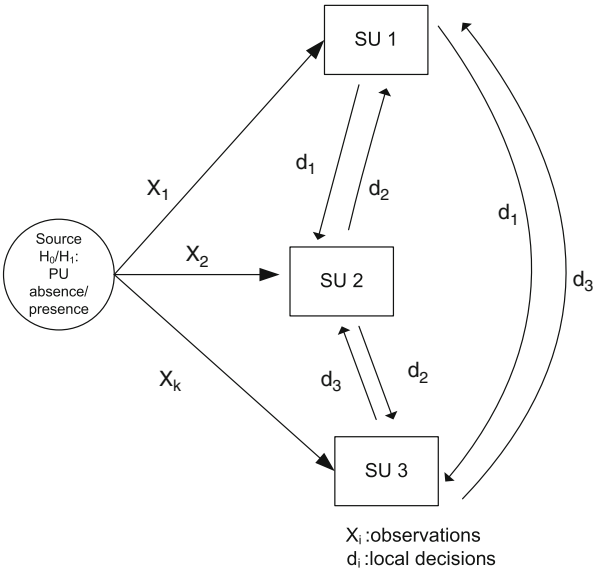

Fig. 4 Decentralized fusion architecture

is transmitted to the fusion center or shared with neighboring users, CSS can employ data or decision fusion schemes. In soft-decision schemes (data fusion), secondary users exchange their test statistics calculated from their local observations. On the other hand, in the hard decision schemes (decision fusion), secondary users only exchange their individual binary decisions.

Soft Combining and Data Fusion

Existing receiver diversity techniques such as equal gain combining (EGC) and maximal ratio combining (MRC) can be utilized for soft combining of local observations or test statistics. If the channel state information (CSI) between the primary users and the secondary users are perfectly known, the optimal combining strategy, which is MRC, can be used for achieving the highest output SNR. In MRC, the local observations of secondary users are weighted proportionately to their channel gain and then summed up [45]. In EGC, the local observations of secondary users are weighted equally [46]. The EGC scheme has a performance close to that of MRC but with simpler implementation.

It was shown in [47] that the soft combining scheme yields better gain than the hard combining scheme. However, there is a significant difference in the cooperation overhead between the hard- and soft-decision-based detectors, which requires a wideband control channel for the soft-decision cooperative approach. The soft information-based signal detection method for the single-carrier case and multi-carrier case was investigated in [48]. In [33], a linear cooperation strategy was developed which is based on the optimal combination of the local statistics from

spatially distributed secondary users. In [49], an optimal soft combination scheme based on Neyman-Pearson criterion was proposed to combine the weighted local observations. The proposed scheme reduces to EGC at high SNR and reduces to MRC at low SNR. Since such a soft combining scheme results in large overhead, a softened two-bit combining scheme was also proposed for energy detection. In this method, there are three decision thresholds dividing the whole range of test statistics into four regions. Each secondary user reports the quantized two-bit information of its local test statistics. The performance of this method is comparable to the performance of the EGC scheme with less complexity and overhead.

In [50], the authors proposed a cooperation strategy in which the local decisions are combined with weighting factors that reflect the local sensing reliability of each secondary user based on partial channel side information to make a final decision with the correspondingly optimized threshold level. In [51], the authors proposed a weighted cooperative spectrum sensing scheme for which the optimal weights are derived under the constraint of equal probabilities of false alarm and miss-detection. They also incorporated reference matrix into the weight setting procedure to store the most recent sensing data in either noise matrix or signal energy matrix according to their corresponding sensing decisions in order to acquire the primary user signal energies from the sensing data of the cooperating sensing nodes. In [52], the authors proposed a cooperative spectrum sensing technique which considers the spatial variation of secondary users, and each user's contribution is weighted by a factor that depends on the received power and path loss. The proposed scheme provides better probability of detection and spectrum utilization when compared to EGC scheme.

In [53], the authors proposed a weighted cooperative sensing scheme that assigns weights to secondary users based on the local detection accuracy of each SU, instead of SNR. In this scheme, the authors used the total error probability, which combines the false-alarm probability and miss-detection probability, to measure the detection accuracy. At the fusion center, each cooperating user is assigned a weight corresponding to its probability of error, i.e., an SU with higher probability of error is assigned lower weight. The optimal detection threshold, as well as the number of SUs required to participate in cooperative sensing, was derived, subject to a given total error probability. Simulation results showed that the proposed scheme provides performance improvement, in terms of the probability of error, when compared to the equal weighted and SNR-based weighted schemes. The authors in [54] proposed a penalty-based weight adjustment mechanism for cooperative spectrum sensing (CSS) to enhance the adaptability of secondary users in time-varying environments. Similar to [53], each secondary user is characterized by its probability of error but the weight factor is adjusted using a penalty mechanism based on the current local decision made by the secondary user. The final result is then computed by fusion of weighted soft decisions made by each cooperating secondary user.

In [55], an adaptive weighting scheme with double threshold energy detection based on the water-filling principle was proposed for cooperative spectrum sensing. For this scheme, each secondary user was allocated a weighting factor based on the relation between the instantaneous SNR of the sensing channel and the water

level. The authors showed that the proposed weighting scheme can achieve better detection performance and lower average number of sensing bits when compared to the equal weighted and SNR weighted schemes. A cooperative spectrum sensing scheme based on ROCQ reputation management model for cognitive radio networks was proposed in [56]. The ROCQ scheme is a reputation-based trust management system that computes the trustworthiness of peers on the basis of transaction-based feedback. The ROCQ model combines four parameters: (i) reputation, (ii) a peer's global trust rating or opinion formed by a peer's firsthand interactions, (iii) credibility of a reporting peer, and (iv) the quality or the confidence a reporting peer puts on the feedback it provides. In this scheme, each secondary user has a reputation degree used to calculate its coefficient in the linear fusion process, and the reputation degree is initialized and adjusted by the fusion center according to each secondary user's sensing result, sensing correctness, and report consistency. Simulation results showed that the detection performance of the proposed scheme in [56] is approximately the same as that of the optimal linear fusion scheme while it requires no instantaneous SNR.

Hard Combining and Decision Fusion

In the hard combining scheme, the final decision is reached by taking into consideration the individual local decisions reported by each secondary user. When binary local decisions are reported to the fusion center, it is convenient to apply linear fusion rules to obtain the cooperative decision. The main advantage of the hard combining scheme is the reduction of communication overhead. Hard decision combining for CSS has been considered in several works [47,49,57]. The commonly used fusion rules are AND, OR, and majority voting rules which are special cases of the general K-out-of-M rule. Those decision fusion rules can be summarized as below [58]:

- **K-out-of-M rule**: In this fusion rule, the fusion center decides on the presence of the primary user's transmission if, and only if, K or more than K secondary users out of the total M cooperating secondary users report the detection of the primary user's signal, where $K \in [1, M]$. Therefore, in the K-out-of-M rule, if K users or more decide in favor of H_1, then the cooperative decision declares that H_1 is true. If the decisions from all the secondary users are independent, the network probabilities of detection and false alarm are, respectively, given by [59]

$$P_D = \sum_{k=0}^{M-K} \binom{M}{K+k} (1 - P_{d,k})^{M-K-k} (P_{d,k})^{K+k}, \tag{5}$$

and

$$P_F = \sum_{k=0}^{M-K} \binom{M}{K+k} (1 - P_{f,k})^{M-K-k} (P_{f,k})^{K+k}, \tag{6}$$

where $P_{d,k}$ and $P_{f,k}$ are, respectively, the probabilities of detection and false alarm of the kth secondary user and $\binom{M}{K+k} = \frac{M!}{(K+k)!(M-K-k)!}$.

- **Majority voting (MV) rule**: In the MV fusion rule, also known as half-voting rule, if half, or more than half, of the local detectors decide that there is a primary user's transmission, then the final decision at the fusion center declares that there is a primary user's transmission [58]. Therefore, for the MV rule, the cooperative decision declares H_1 only if half or more than half of the secondary users decide on H_1, i.e., $K = \lceil \frac{M}{2} \rceil$ in (5) and (6), where $\lceil \frac{M}{2} \rceil$ denotes the smallest integer not less than $\frac{M}{2}$. If the decisions from all the secondary users are independent, the network probabilities of detection and false alarm are, respectively, given by

$$P_D = \sum_{k=0}^{M-\lceil \frac{M}{2} \rceil} \binom{M}{\lceil \frac{M}{2} \rceil + k} (1 - P_{d,k})^{M-\lceil \frac{M}{2} \rceil - k} (P_{d,k})^{\lceil \frac{M}{2} \rceil + k}, \tag{7}$$

and

$$P_F = \sum_{k=0}^{M-\lceil \frac{M}{2} \rceil} \binom{M}{\lceil \frac{M}{2} \rceil + k} (1 - P_{f,k})^{M-\lceil \frac{M}{2} \rceil - k} (P_{f,k})^{\lceil \frac{M}{2} \rceil + k}. \tag{8}$$

- **Logical OR rule**: In this fusion rule, the fusion decides on the presence of primary user's transmission if any of the secondary users reports the detection of the primary user's transmission. Therefore, for the OR rule, the cooperative decision declares H_1 if any of the secondary users decides on H_1, i.e., setting $K = 1$ in (5) and (6). Since an SU occupying a licensed frequency band may cause interference to the primary users, the risk of SUs causing interference to the primary users is minimized using the logical OR rule. If the decisions from all the secondary users are independent, the network probabilities of detection and false alarm are, respectively, given by

$$P_D = 1 - \prod_{k=1}^{M} (1 - P_{d,k}), \tag{9}$$

and

$$P_F = 1 - \prod_{k=1}^{M} (1 - P_{f,k}). \tag{10}$$

- **Logical AND rule**: In the AND fusion rule, if all local detectors decide that there is a primary user's transmission, then the final decision at the fusion center declares that there is a primary user's transmission [58]. Therefore, for the AND rule, the cooperative decision declares H_1 only if all of the secondary users decide on H_1, i.e., setting $K = M$ in (5) and (6). Using this fusion rule, the

probability of false alarm is minimized, but the risk of causing interference to primary users will increase. If the decisions from all the secondary users are independent, the network probabilities of detection and false alarm are, respectively, given by

$$P_D = \prod_{k=1}^{M} P_{d,k}, \tag{11}$$

and

$$P_F = \prod_{k=1}^{M} P_{f,k}. \tag{12}$$

In [60], the authors proposed a decision fusion rule for the sensing-throughput trade-off design that considers the differences in the signal-to-noise ratios of the secondary users. These differences were reflected in the weighing of the decisions based on the likelihood ratio test at the fusion center. A decision fusion scheme was proposed in [61] that combines all secondary users decisions, taking into account the credibility of each decision via Dempster-Shafer (D-S) theory of evidence. This scheme can give a significant improvement in detection probability as well as reduction in false-alarm rate and is best suited for a fast-changing radio frequency environment. In [62], an enhanced scheme was proposed that assigns a reliability value to each detector based on its SNR. This value reflects the relative relationship between detectors and is used to adjust the credibility of each decision to a more accurate value before combining the decisions via D-S theory. In [63], the authors proposed a trust weighted cooperative spectrum sensing scheme to identify malicious secondary users and mitigate their harmful effect on sensing performance. To make an accurate final decision, the trust weight factor of each SU is calculated by their trust values. The fusion center initializes the trust values of SUs by the number of true sensing that agrees with the primary user's actual behavior and the number of total sensing. The trust value for each secondary user is then increased or decreased according to whether it provides true or false sensing information. Simulation results showed a performance improvement in the probability of detection as compared to the conventional cooperative spectrum sensing scheme without trust weighted factors for OR, AND, and majority fusion rules. In [64], a centralized trust management scheme for secondary user base station was proposed. The authors introduced the notion of self-confidence and trust. Self-confidence is a rate supplied by a sensing secondary user of its own confidence on the accuracy of its sensing results. Trust is a measure of reputation and represents the historical accuracy of secondary user's sensing reports. The authors incorporated the trustworthiness evaluation from a modified beta reputation model into the K-out-of-M decision fusion rule to give greater weight to the opinions of more trustworthy secondary users.

Performance of Cooperative Spectrum Sensing

In this section, we discuss some of the factors affecting the performance of CSS, in terms of cooperation gain or incurred overhead, such as the number of channels sensed in each sensing period, the selection of secondary users, the selection of the fusion scheme, and the correlation between the cooperating secondary users. We also discuss the performance of cooperative wideband spectrum sensing.

Cooperative User Selection

The selection of secondary users for cooperative sensing plays a key role in determining the performance of CSS because it can be utilized to improve the trade-off between cooperative gain and cooperation overhead. In [57], for the case of independent secondary users' observations with energy detection-based cooperation, it was shown that cooperating with all users in the network does not necessarily achieve the optimum performance. It was observed that including secondary users experiencing bad channels, in terms of the SNR received at a secondary user, for cooperation may degrade the performance. In order to relax the requirement on prior knowledge of the received SNR at each secondary user, the authors in [65] proposed to select the sensing secondary users that have the best detection probabilities with respect to a given false-alarm probability. Specifically, the false-alarm probability is set to be identical at each secondary user. Therefore, the SU that reports the largest number of 1's is first chosen to participate in cooperative sensing. In [66], the optimal number of secondary users, K, that minimizes the total error probability for secondary users with independent local decisions for the general K-out-of-M fusion rule was found to be approximately half of the total number of secondary users M. A user selection strategy based on a modified deflection coefficient with low complexity was proposed in [67]. The optimal number of secondary users and the user set were obtained in order to provide sufficient protection to the primary users and improve the total throughput of the cognitive radio network. CSS using counting rule was studied in [68], and the sensing errors were minimized by choosing the optimal probability of false alarm to satisfy a given constraint and the optimal number of cooperating secondary users for both matched filtering and energy detection.

When the cooperating secondary users experience correlated shadowing, it was shown in [18] that selecting independent secondary users for cooperation can improve the robustness of sensing results. In [69], a correlation-aware user selection algorithm was developed to address the dynamic changes in the spatial correlation experienced by mobile secondary users. To accurately derive the spatial correlation coefficient, a correlation model between mobile secondary users was first developed. Based on this correlation model, a distributed user selection algorithm that adaptively selects uncorrelated secondary users through the spatial correlation coefficient was designed. In [70], a joint spatial-temporal sensing scheme for CR

networks was proposed, where secondary users collaboratively estimate the location and transmit power of the primary transmitter. Based on those estimates, secondary users determine their maximum allowable transmission power and use the location information to decide which users should participate in cooperative sensing in order to minimize the correlation among the secondary users' observations. CSS with correlated secondary users' local decisions was studied in [71]. The probability of sensing error was minimized by choosing the optimal assignments for the number of cooperating secondary users, K, in the K-out-of-M fusion rule and the local threshold for a certain correlation index.

Moreover, removing malicious users from cooperation ensures the security and the reliability of the network. A robust secondary user selection algorithm for CSS considering the presence of malicious users was proposed in [72]. The users were selected based on the consistency check with known trusted users, and simulation results showed that the proposed algorithm is effective in identifying and excluding malicious secondary users. The authors in [73] presented a soft-decision reporting scheme that is robust against malicious users. They proposed a heuristic approach to iteratively identify malicious users, where the fusion center computes the secondary user's suspicious level, i.e., the posterior probability that this SU is an attacker, based on the honest SU and malicious SU report probabilities. These probabilities are estimated assuming that the fusion center knows the position of the users' and the attackers' policy. When the suspicious level of the secondary user goes beyond a threshold, it is discarded from the final decision process and moved into a malicious user set. This process is repeated until no more malicious users can be found, and only the reports from honest users are fused to make the final decision.

Most of the existing cooperative sensing schemes assume all the secondary users are willing to cooperate. In reality, some selfish secondary users may refuse to provide the sensing results to save energy or transmission time, while benefiting from sensing results of other users which may disrupt CSS. To enhance the cooperation, several researchers investigate this incentive problem from the perspective of game theory.

In [74], the authors modeled the cooperative spectrum sensing as an N-player horizontal infinite game and then studied various strategies with it. They examined the classical grim trigger strategy and proved it can sustain cooperation easily but will result in poor performance under uncertainty of wireless channel. They then proposed a strategy based on the carrot-and- stick strategy which can recover cooperation from deviation. The authors proved that the proposed strategy can achieve mutual cooperation as well as recover from failures. Performance evaluation showed that the proposed strategy can achieve good network performance and reduce interference to primary users.

In [75], the author proposed an evolutionary game-theoretic framework to develop the best cooperation strategy for cooperative sensing with selfish users. Using replicator dynamics, users can try different strategies (behavior dynamics) and learn a better strategy through strategic interactions (evolutionarily stable strategy). The authors also proposed a distributed learning algorithm that aids the secondary users approach the evolutionarily stable strategy only with their own

payoff history. Simulation results showed that the proposed game has a better performance, in terms of total throughput, than having all secondary users sense at every time slot.

In [76], the authors proposed a game in which every user can choose to collaborate or not in each time slot depending on whether the benefit of the cooperation is worth the cost. From this perspective, the cooperative spectrum sensing game was modeled as the stag hunt game. The authors then proposed cooperative communication incentive scheme (CCIS) to enhance the cooperative sensing. The basic idea is to introduce a periodically available trusted authority to compensate the secondary users (e.g., using the relay to help transmit their data during transmission time) who suffer losses in the cooperative sensing.

Cooperation Overhead

The exploitation of spatial diversity in cooperative sensing results in a significant improvement in detection performance. However, cooperation among secondary users may also introduce a variety of overheads that limit or even compromise this improved detection performance. The overhead associated with all elements of cooperative sensing is called cooperation overhead. Cooperation overhead can refer to any transmission cost, extra sensing time, delay, energy, and operations devoted to cooperative sensing and any performance degradation caused by cooperative sensing.

Since the sensing time is proportional to the number of samples taken by each individual secondary user, the longer the sensing time is, the better the detection performance will be. However, when each secondary user is equipped with a single radio transceiver, it will be difficult for the secondary users to simultaneously perform sensing and transmission. Therefore, the more time is devoted to sensing, the less time is available for transmissions which reduces the secondary users' throughput, also known as opportunistic throughput. In addition, the cooperation overhead due to the extra sensing time will generally increase with the number of cooperating users due to the increased volume of data that needs to be reported to and be processed by the fusion center. This is known as the sensing efficiency problem [77] or the sensing-throughput trade-off [59] in spectrum sensing.

The cooperation overhead, in terms of the extra sensing time or reduced opportunistic throughput, will also increase as the delay in finding an available channel increases [78]. In [79], a sensing-period optimization mechanism and an optimal channel-sequencing algorithm were developed to maximize the discovery of spectrum access opportunities and minimize the delay in discovering an available channel when all secondary users participate in sensing an identical channel in each sensing period. In [80], two different channel sensing policies, the random sensing policy and the negotiation-based sensing policy, were proposed to discover the available channels. In both policies, different users are allowed to sense different channels that are selected either randomly or through negotiation, which enables SUs to identify and utilize the maximum number of vacant channels. The authors

assumed that each secondary user is equipped with two transceivers. One transceiver is tuned to the dedicated control channel, and another transceiver is used to periodically sense and dynamically use the identified unused channels. Parallel cooperative sensing was proposed in [81,82] where the cooperative secondary users are divided into multiple groups, and each group senses one channel such that more than one channel are sensed in each sensing period. Since multiple channels are detected in one sensing period, the cooperation overhead associated with the delay in finding an available channel is significantly reduced.

Since each sensing phase is usually separated into several subslots used for signal detection and decision reporting, reporting delay will also affect the performance of cooperative spectrum sensing. In [83], the authors proposed cooperative spectrum sensing where the secondary network optimizes the decision thresholds at the sensors and the division between time samples used for sensing the primary users and time slots used for reporting the sensing results. Simulation results showed that joint optimization of thresholds and sensing/reporting time slots achieve good sensing performance in terms of the network probabilities of false alarm and miss-detection.

In [84], the authors proposed two distributed reporting SU selection methods to reduce the overall sensing overhead and to mitigate the interference to PUs in CR networks. The authors also considered the reporting channel errors and the interference impact on PUs induced by decision reporting. Simulation results showed that the proposed strategies achieve better detection performance and lower sensing overhead than the traditional case.

In cooperative sensing, secondary users involve in activities such as local sensing and data reporting that consume additional energy. The energy consumption overhead can be significant if the number of cooperating secondary users or the amount of sensing results to be reported is large. One approach to address this issue is to use censoring to limit the amount of reported sensing data according to certain criteria or constraints. Since the censoring criteria are chosen to refrain cooperating secondary users from transmitting unnecessary or uninformative data, the energy efficiency can be improved in cooperative sensing. In [85], a simple censoring method was proposed to decrease the average number of sensing bits reported to the fusion center. In this method, the energy detector output of each secondary user is compared to two thresholds, and the decision is sent to the fusion center if the energy detector output is between those two thresholds. Otherwise, no decision is made and this sensing output is censored from reporting. The simulation results showed that even though the network probability of false alarm may degrade due to the possibility that the sensing outputs of all secondary users are censored, the amount of reported local decisions can be dramatically reduced. Therefore, the energy efficiency can be traded off with the network probability of false alarm.

Another approach to reduce the cooperation overhead in terms of energy consumption is to minimize the energy consumption with detection performance constraints. In [86], the energy efficiency problem was addressed by energy minimization under detection performance constraints. This method investigates the trade-off between the two aspects of sensing time. On one hand, longer sensing

time consumes more energy at each secondary user. On the other hand, longer sensing time can improve detection performance at each secondary user and reduce the number of cooperating users and the associated energy consumption overhead. Therefore, this method finds the optimal sensing time and the optimal number of cooperating users to balance the energy consumption in local sensing and the energy overhead due to cooperation for a required detection performance.

An energy-efficient CSS scheme was proposed in [87] to maximize the energy efficiency. The authors proposed a method in which sensing time, sensing threshold, and the number of cooperating SUs are jointly optimized. In [88], the authors proposed an efficient algorithm to solve the general problem of spectrum efficiency and energy efficiency trade-off in cognitive radio with cooperative sensing. The authors then considered the trade-off between spectrum efficiency and energy efficiency such that the energy efficiency (spectrum efficiency) is maximized via joint optimization of sensing duration and final decision threshold under the constraint that the spectrum efficiency (energy efficiency) requirement is satisfied. Simulation results showed that different spectrum efficiency (energy efficiency) requirements need different optimal values of sensing duration and final decision threshold, and there exists a trade-off between the spectrum efficiency and energy efficiency.

To alleviate the energy deficiency, radio frequency (RF) harvesting techniques have become alternative methods through which green energy can be used to power the next generation wireless networks [89]. Recently, energy harvesting communication has been considered for cognitive radio networks in order to improve both energy and spectral efficiency in wireless and mobile networks. In [90], the transmitters in a CR network either opportunistically harvest RF energy from transmissions by nearby devices in a primary network or transmit data if the devices are not in the interference range of any other primary network. The optimal transmit power and density of the secondary transmitters that maximize the throughput of the CR network were derived under an outage probability constraint. The authors in [91] investigated the optimal detection threshold for opportunistic spectrum access in an energy harvesting CR network to maximize the expected total throughput under both the energy causality constraint and the collision constraint. In [92], the authors extended the work in [91] to investigate the optimal sensing duration and sensing threshold that jointly maximize the average throughput for a given amount of harvested energy.

Multiband Spectrum Sensing

Wideband spectrum sensing, which we also refer to in this chapter as multiband sensing, faces technical challenges, and there is limited work on it in the literature. To sense multiple frequency bands simultaneously, secondary users may need to scan the spectrum or use multiple radio frequency (RF) front ends for sensing multiple bands. However, using these approaches for wideband sensing either causes long sensing delay or incurs high computational complexity and hardware

cost. Recent advances in compressed sensing [41, 93] enable the sampling of the wideband signals at sub-Nyquist rate to relax the analog-to-digital converter (ADC) requirements. The techniques of compressed sensing provide promising solutions to promptly recover wideband signals and facilitate wideband sensing at a reasonable computational complexity. Compressed sensing can be achieved by various sensing matrix techniques such as random matrices. However, due to the sub-Nyquist rate sampling and insufficient number of samples, a weak primary user's signal with a nearby strong signal may not be properly reconstructed for detection in a wideband spectrum [17]. In addition, a new ADC architecture with nonuniform timing and a pseudorandom clock generator is needed [94]. In [95], the authors proposed two algorithms for wideband spectrum sensing at sub-Nyquist sampling rates for the single node and cooperative multiple nodes, respectively. In single node spectrum sensing, a two-phase spectrum sensing algorithm based on compressive sensing is proposed to reduce the computational complexity and improve the robustness at secondary users. In the cooperative multiple node case, the signals received at SUs exhibit a sparsity property that yields a low-rank matrix of compressed measurements at the fusion center. This leads to a two-phase cooperative spectrum sensing algorithm for cooperative multiple SUs based on low-rank matrix completion. The numerical results showed that the proposed algorithms are robust to channel noise with low computational complexity.

In multiband cooperative sensing, secondary users cooperate to sense multiple narrowbands instead of focusing on one band at a time. In [36], a multiband joint detection scheme was proposed for combining the statistics of sensing multiple bands from spatially distributed secondary users. The fusion center calculates the test statistic and makes a cooperative decision in each band. The weight coefficients and detection thresholds of all bands were obtained by jointly maximizing the aggregate opportunistic throughput in each band subject to constraints on the miss-detection and false-alarm probabilities. To enable the multiband sensing at each secondary user, an energy detector is required for each band of interest. As a result, the method may incur high hardware cost when the number of bands for cooperative sensing is large. In [96], the authors proposed a multiband adaptive joint detection framework for wideband spectrum sensing that collectively searches the secondary transmission opportunities over multiple frequency bands. In this framework, both the sensing slot duration and detection thresholds for each narrowband detector were jointly optimized to maximize the achievable opportunistic throughput of the secondary network subject to a limit on the interference introduced to primary users.

In [81], a parallel cooperative sensing scheme was proposed to enable the multichannel sensing by optimally selected cooperating secondary users. Different from the multiband sensing scheme in [36, 96], each cooperating secondary user senses a different channel. In [82], the authors proposed a group-based CSS scheme in which the cooperative secondary users are divided into several groups, and each group senses a different channel during a sensing period, while the secondary users in the same group perform joint detection on the targeted channel. In [97], the authors proposed an adaptive user-group assignment algorithm for group-based CSS that considers cooperating secondary users with heterogeneous sensing ability in

terms of the sensing accuracy. By the methods in [81,82,97], multiple channels can be cooperatively sensed in each sensing period. The objective is to maximize the secondary opportunistic throughput while minimizing the sensing overhead such as the sensing time and the number of secondary users required for cooperation.

Implementation of Sensing Techniques on Testbeds

Testbeds are essential to advance the development of cognitive radio networks by verification of proposed sensing techniques in a practical system and evaluation of key performance metrics. Some of the existing CR testbed researches are focusing on the algorithms of spectrum sensing and signal processing. In [98], the authors proposed an experimental setup based on the Berkeley Emulation Engine 2 (BEE2) platform, which is a multi-FPGA emulation platform, to experiment with various sensing techniques and develop a set of metrics and test cases to allow them to measure the sensing performance of these techniques. The authors in [99] proposed KNOWS, which has a reconfigurable transceiver based on a modified Wi-Fi hardware. The hardware consists of a development board with a scanner/receiver radio and a reconfigurable transceiver. KNOWS spectrum allocation engine maintains up-to-date information about the spectrum usage by all its neighbors and stores it in a resource allocation matrix (RAM). The authors studied the bandwidth allocation problem and designed a spectrum-aware medium access control (MAC) protocol. The MAC protocol uses the RAM to dynamically decide on the portion of the spectrum to use for a given communication. Simulations results showed that KNOWS significantly increases the capacity when compared to IEEE 802.11-based systems.

In [100], the authors presented a real-time testbed, based on programmable system-on-chip processors, for the evaluation of cognitive radio MAC algorithms. The proposed testbed is much easier to configure and control than the traditional FPGA-based testbed. The authors introduced the testbed implementation details of the spectrum sensing of PHY layer, the channel selection strategy, and the access control strategy of MAC layer.

In [101], the author studied the performance of normal collaborative spectrum sensing (NCSS) based on coalitional games and implemented NCSS in wireless open-access research platform. Wireless open-access research platform is a scalable and extensible programmable wireless platform, developed by Rice University [102], to prototype advanced wireless networks. Based on testbed implementation, the authors showed that under poor reporting channel conditions, the coalition splits and the weaker SUs exhibit inefficient sensing performance. The authors then proposed relay-based collaborative spectrum sensing that uses neighboring SU with low error-prone relay path to share sensing results between affected SUs and channel. Testbed results revealed that relay-based collaborative spectrum sensing performs better than all other collections of coalitions, and it improves sum-utility by 20%, as compared to NCSS at the cost of minimal 2.3% loss in energy efficiency.

Research Challenges

Many operations in cooperative spectrum sensing, such as sharing data, broadcasting spectrum-aware routing information, and coordinating spectrum access, rely on control message exchange on a common control channel. The implementation of a common control channel is one of the most challenging issues in cognitive radio networks, since a fully reliable control channel cannot be created without reserving bandwidth specifically for this purpose. However, if a dedicated channel is used, the bandwidth available for traffic communications reduces. In addition, since the common control channel may be subject to primary user's activity, secondary users have to negotiate a new control channel when the original one is occupied by primary users. In [103], the authors investigate a promising solution that exploits the ultrawideband (UWB) technology to allow the secondary users to discover each other and exchange control information for establishing a communication link. Other works assume that secondary users use an out-of-band common control channel to report the local sensing results to the fusion center to avoid interfering with the primary user [104, 105]. Setting up and maintaining common control channel is still an open issue for CR networks.

In cooperative spectrum sensing, it is usually assumed that all cooperating CR users are perfectly synchronized, and their sensing results are also assumed to be available instantly at the fusion center. In reality, this is not always valid, and therefore, the CSS scheme should consider the case of asynchronous observations and reporting delay which result in time offsets between local sensing observations and the final decision at the fusion center. In [106], a probability-based combination scheme was proposed to combine asynchronous reports at the fusion center. The proposed combining scheme considers both detection errors and time offsets between local sensing observations and the final decision. Based on the knowledge of the primary user channel usage model and the Bayesian decision rule, the conditional probabilities of the local sensing decisions received at different times, conditioned on each hypothesis, and their combined likelihood ratio were calculated to make the final decision at the fusion center.

Most of the studies on CSS analyze its performance based on the assumption of perfect knowledge of the average received SNR at the secondary user. However, in practice, this is not always the case. The effect of average SNR estimation errors on the performance of CSS was examined in [107]. In the noiseless sample-based case, it was found that the probability of false alarm decreases as the average SNR estimation error decreases for both independent and correlated shadowing. In the noise sample-based case, it was found that there exists a threshold for the noise level. Below this threshold, the probability of false alarm increases as the noise level increases, while above the threshold, the probability of false alarm decreases as the noise level increases.

Spectrum mobility, in which SU has to move from one spectrum hole to another to avoid interference in case of the reappearance of PU, is another challenging problem in CR networks. CR networks need to perform mobility management

adaptively depending on the heterogeneous spectrum availability that is dependent on the primary traffic.

Some new research directions focus on the design of architectures for the integration of cognition network and cooperative communications in wireless heterogeneous networks (HetNet) for better utilization of radio resources and guaranteeing quality of service. The authors in [108] have focused their research on the coexistence of wireless fidelity (Wi-Fi)and 4G cellular networks sharing the unlicensed spectrum. They have introduced the network architecture for long-term evolution (LTE)/LTE-advanced small cells to exploit unlicensed spectrum used by Wi-Fi systems. They showed that the proposed architecture along with interference avoidance schemes increases the capacity of 4G cellular networks by maintaining the quality of service (QoS)of Wi-Fi systems. Cognitive radio networks are also highly promising for providing timely smart grid wireless communications by utilizing all available spectrum resources [109].

Conclusions

Cognitive radio technology allows a wireless network to expand its spectrum on demand at a relatively low cost, thereby offering a natural solution to cope with random and diverse mobile data traffic which makes it a promising candidate for 5G communication networks. In this chapter, the most common spectrum sensing techniques for cognitive radio networks were surveyed and classified to provide an overview of the research direction in the area of cognitive radio networks. To address the limitations of the spectrum sensing techniques by a single secondary user, cooperative spectrum sensing and its main elements have been discussed. Different cooperation architectures and fusion schemes for fusion the decisions of cooperating secondary users were presented, and their advantages and disadvantages were highlighted.

We further identified some of the main factors that contribute to the efficient design of cooperative spectrum sensing schemes for cognitive radio networks. Different criteria for selecting the cooperating secondary users were discussed, and the performance improvement achieved by the different selection criteria was highlighted. The performance degradation due to cooperation overhead in terms of transmission cost, extra sensing time, delay, energy, and operations devoted to cooperative sensing was investigated which provided an insight on some of the key challenges facing cooperative spectrum sensing in cognitive radio networks.

References

1. Mitola I, Maguire J (1999) Cognitive radio: making software radios more personal. IEEE Pers Commun Mag 6:13–18
2. Liang Y, Chen K, Li GY, Mhnen P (2011) Cognitive radio networking and communications: an overview. IEEE Trans Veh Technol 60:3386–3407

3. Federal Communications Commission (2002) Spectrum policy task force report. ET Docket no. 02-135
4. Stevenson CR, Chouinard G, Lei Z, Hu W, Shellhammer SJ, Caldwell W (2009) IEEE 802.22: the first cognitive radio wireless regional area network standard. IEEE Commun Mag 47: 130–138
5. Nekovee M (2010) Cognitive radio access to TV white spaces: spectrum opportunities, commercial applications and remaining technology challenges. In: IEEE International Symposium on New Frontiers in Dynamic Spectrum Access Networks, Singapore, Apr 2010, pp 1–10
6. Ghasemi A, Sousa ES (2008) Spectrum sensing in cognitive radio networks: requirements, challenges and design trade-offs. IEEE Commun Mag 46:32–39
7. Gavrilovska L, Atanasovski VM (2013) Dynamic REM towards flexible spectrum management. In: International Conference on Telecommunication in Modern Satellite, Cable and Broadcasting Services, Oct 2013, pp 287–296
8. Li S, Zhao Y, Sun C, Guo X (2014) Development of an advanced geolocation engine-based cognitive radio testbed. In: IEEE/CIC ICCC 2014 Symposium on Wireless Communications Systems, Oct 2014, pp 528–533
9. Yilmaz HB, Chae C-B, Tugcub T (2014) Sensor placement algorithm for radio environment map construction in cognitive radio networks. In: IEEE Wireless Communications and Networking Conference, Apr 2014, pp 2096–2101
10. Tajer A, Wang X (2009) Beacon-assisted spectrum access with cooperative cognitive transmitter and receiver. In: IEEE International Conference on Acoustics, Speech and Signal Processing, Apr 2009, pp 2341–2344
11. Patel A, Biswas S, Jagannatham AK (2013) Multiple beacon based robust cooperative spectrum sensing in MIMO cognitive radio networks. In: IEEE Vehicular Technology Conference, Sept 2013, pp 1–5
12. Fitch M, Nekovee M, Kawade S, Briggs K, MacKenzie R (2011) Wireless services provision in TV white space with cognitive radio technology: a telecom operator's perspective and experience. IEEE Commun Mag 49:64–73
13. Ghasemi A, Sousa E (2007) Optimization of spectrum sensing for opportunistic spectrum access in cognitive radio networks. In: IEEE Consumer Communications and Networking Conference, Las Vegas, Jan 2007, pp 1022–1026
14. Unnikrishnan J, Veeravalli V (2007) Cooperative spectrum sensing and detection for cognitive radio. In: IEEE Global Telecommunications Conference, Washington, DC, Nov 2007, pp 2972–2976
15. Unnikrishnan J, Veeravalli VV (2008) Cooperative sensing for primary detection in cognitive radio. IEEE J Sel Top Signal Proces 2:18–27
16. Ganesan G, Li Y (2005) Cooperative spectrum sensing in cognitive radio networks. In: IEEE International Symposium on New Frontiers in Dynamic Spectrum Access Networks, Baltimore, Nov 2005, pp 137–143
17. Akyildiz IF, Lo BF, Balakrishnan R (2011) Cooperative spectrum sensing in cognitive radio networks: a survey. Phys Commun (Elsevier) J 4:40–62
18. Mishra S, Sahai A, Brodersen R (2006) Cooperative sensing among cognitive radios. In: IEEE International Conference on Communications, Istanbul, June 2006, vol 4, pp 1658–1663
19. Huang S, Liu X, Ding Z (2009) Optimal sensing-transmission structure for dynamic spectrum access. In: IEEE Conference on Computer Communications, Rio de Janeiro, Apr 2009, pp 2295–2303
20. Sahai A, Hoven N, Tandra R (2004) Some fundamental limits on cognitive radio. In: Allerton Conference on Communication, Control and Computing, Monticello, Oct 2004
21. Digham F, Alouini M, Simon M (2003) On the energy detection of unknown signals over fading channels. In: IEEE International Conference on Communications, Anchorage, May 2003, vol 5, pp 3575–3579
22. Koufos K (2013) Spectrum access in white spaces using spectrum sensing and geolocation databases. PhD thesis, Aalto University

23. Hossain E, Niyato D, Han Z (2009) Dynamic spectrum access and management in cognitive radio networks. Cambridge University Press, Amsterdam
24. Varnamkhasti AG (2008) Spectrum sensing in cognitive wireless networks: requirements, challenges annd design trade-offs. PhD thesis, University of Toronto
25. Zeng Y, Liang Y, Hoang AT, Zhang R (2010) A review on spectrum sensing techniques for cognitive radio: challenges and solutions. EURASIP J Adv Signal Process 2010:1–15
26. Haykin S, Thomson D, Reed J (2010) Spectrum sensing for cognitive radio. Proc IEEE 97:849–877
27. Tandra R, Sahai A (2005) Some fundamental limits on detection in low SNR under noise uncertainty. In: IEEE International Conference on Wireless Networks, Communications and Mobile Computing, Wuhan, June 2005, vol 1, pp 464–469
28. Yucek T, Arslan H (2009) A survey of spectrum sensing algorithms for cognitive radio applications. IEEE Commun Surv Tutorials 11:116–130
29. Cabric D, Mishra S, Brodersen R (2004) Implementation issues in spectrum sensing for cognitive radio. In: Asilomar Conference on Signals, Systems and Computers, Pacific Grove, Nov 2004, vol 1, pp 772–776
30. Arslan H (2007) Cognitive radio, software defined radio, and adaptive wireless systems. Springer, Dordrecht
31. Urkowitz H (1967) Energy detection of unknown deterministic signal. Proc IEEE 55:523–531
32. Ghasemi A, Sousa E (2005) Collaborative spectrum sensing for opportunistic access in fading environment. In: IEEE International Symposium on New Frontiers in Dynamic Spectrum Access Networks, Baltimore, Nov 2005, pp 131–136
33. Quan Z, Cui S, Sayed A (2008) Optimal linear cooperation for spectrum sensing in cognitive radio networks. IEEE J Sel Top Signal Proces 2:28–40
34. Quan Z, Cui S, Sayed A, Poor H (2008) Wideband spectrum sensing in cognitive radio networks. In: IEEE International Conference on Communications, Beijing, May 2008, pp 901–906
35. Tang H (2005) Some physical layer issues of wide-band cognitive radio systems. In: IEEE International Symposium on New Frontiers in Dynamic Spectrum Access Networks, Baltimore, Nov 2005, pp 151–159
36. Quan Z, Cui S, Sayed A, Poor H (2009) Optimal multiband joint detection for spectrum sensing in cognitive radio networks. IEEE Trans Signal Process 57:1128–1140
37. Cabric D, Brodersen R (2005) Physical layer design issues unique to cognitive radio systems. In: IEEE Personal Indoor and Mobile Radio Communications, Berlin, Sept 2005, vol 2, pp 759–763
38. Reyes H, Subramaniam S, Kaabouch N, Hu W (2016) A spectrum sensing technique based on autocorrelation and euclidean distance and its comparison with energy detection for cognitive radio networks. Elsevier Comput Electr Eng J 52:319–327
39. Haykin S (2005) Cognitive radio: brain-empowered wireless communications. IEEE J Sel Areas Commun 23:201–220
40. Tian Z, Giannakis GB (2006) A wavelet approach to wideband spectrum sensing for cognitive radios. In: IEEE International Conference on Cognitive Radio Oriented Wireless Networks and Communications, Mykonos Island, June 2006, pp 151–159
41. Tian Z, Giannakis G (2007) Compressed sensing for wideband cognitive radios. In: IEEE International Conference on Acoustics, Speech, and Signal Processing, Honolulu, Apr 2007, pp 1357–1360
42. Ganesan G, Li Y (2007) Cooperative spectrum sensing in cognitive radio: part I: two user networks. IEEE Trans Wirel Commun 6:2204–2213
43. Shankar NS, Cordeiro C, Challapali K (2005) Spectrum agile radios: utilization and sensing architectures. In: IEEE International Symposium on New Frontiers in Dynamic Spectrum Access Networks, Baltimore, Nov 2005, pp 160–169
44. Ganesan G, Li Y (2007) Cooperative spectrum sensing in cognitive radio: part II: multiuser networks. IEEE Trans Wirel Commun 6:2214–2222

45. Ahn KS, Jr Heath RW (2009) Performance analysis of maximum ratio combining with imperfect channel estimation in the presence of cochannel interferences. IEEE Trans Wirel Commun 8:1080–1085
46. Song Y, Blostein SD, Cheng J (2003) Exact outage probability for equal gain combining with cochannel interference in Rayleigh Fading. IEEE Trans Wirel Commun 2:865–870
47. Vistotsky E, Kuffner S, Peterson R (2005) On collaborative detection of TV transmissions in support of dynamic spectrum sharing. In: IEEE International Symposium on New Frontiers in Dynamic Spectrum Access Networks, Baltimore, Nov 2005, pp 338–345
48. Uchiyama H, Umebayashi K, Fujii T, Ono F, Sakaguchi K, Kamiya Y, and Suzuki Y (2008) Study on soft decision based cooperative sensing for cognitive radio networks. IEICE Trans Commun E91-B:95–101
49. Ma J, Zhao G, Li Y (2008) Soft combination and detection for cooperative spectrum sensing in cognitive radio networks. IEEE Trans Wirel Commun 7:4502–4507
50. Oh DC, Lee HC, Lee YH (2010) Linear hard decision combining for cooperative spectrum sensing in cognitive radio systems. In: IEEE Vehicular Technology Conference, Ottawa, Sept 2010, pp 1–5
51. Shen B, Huang L, Zhao C, Kwak K, Zhou Z (2008) Weighted cooperative spectrum sensing in cognitive radio networks. In: International Conference on Convergence and Hybrid Information Technology, Busan, Nov 2008, vol 1, pp 1074–1079
52. Shahid MB, Kamruzzaman J (2008) Weighted soft decision for cooperative sensing in cognitive radio networks. In: IEEE International Conference on Networks, New Delhi, Dec 2008, pp 1–6
53. Zhao Y, Song M, Xin C (2011) A weighted cooperative spectrum sensing framework for infrastructure-based cognitive radio networks. Comput Commun 34:1510–1517
54. Hasan N, Ejaz W, Kim HS (2012) PWAM: penalty-based weighted adjustment mechanism for cooperative spectrum sensing in centralized cognitive radios networks. Int J Innov Comput Inf Cont 8:1510–1517
55. Chuan L-qing, Zhi-ming W (2011) Adaptive weighted algorithm Of cooperative spectrum sensing in cognitive radio networks. In: IET International Communication Conference on Wireless Mobile and Computing, Shanghi, Nov 2011, pp 121–126
56. Zhou M, Chen H, Xie L, Wang K (2012) A reliable collaborative spectrum sensing scheme based on the ROCQ reputation model for cognitive radio networks, In: IEEE Vehicular Technology Conference, Quebec, May 2012, pp 1–5
57. Peh E, Liang Y (2007) Optimization for cooperative sensing in cognitive radio networks. In: IEEE Wireless Communications and Networking Conference, Hong Kong, Mar 2007, pp 27–32
58. Hossain E, Bhargava V (2007) Cognitive wireless communication networks. Springer, New York
59. Liang Y, Zeng Y, Peh EC, Hoang AT (2008) Sensing-throughput tradeoff for cognitive radio networks. IEEE Trans Wirel Commun 7:1326–1337
60. Peh EC, Liang Y, Guan YL, Zeng Y (2010) Cooperative spectrum sensing in cognitive radio networks with weighted decision fusion schemes. IEEE Trans Wirel Commun 9:3838–3847
61. Qihang P, Kun Z, Jun W, Shaoqian L (2006) A distributed spectrum sensing scheme based on credibility and evidence theory in cognitive radio context. In: IEEE International Symposium on Personal, Indoor and Mobile Radio Communications, Helsinki, Sept 2006, pp 1–5
62. Nguyen-Thanh N, Koo I (2009) An enhanced cooperative spectrum sensing scheme based on evidence theory and reliability source evaluation in cognitive radio context. IEEE Commun Lett 13:492–494
63. Feng J, Lu G, Bao Z (2012) Weighted-cooperative spectrum sensing scheme using trust in cognitive radio networks. In: IEEE International Conference on Signal Processing, Beijing, Oct 2012, pp 1693–1696
64. Qin T, Yu H, Leung C, Shen Z, Miao C (2009) Towards a trust aware cognitive radio architecture. ACM SIGMOBILE Mob Comput Commun Rev 13:86–95

65. Khan Z, Lehtomaki J, Umebayashi K, Vartiainen J (2010) On the selection of the best detection performance sensors for cognitive radio networks. IEEE Signal Process Lett 17:359–362
66. Zhang W, Mallik RK, Letaief KB (2008) Cooperative spectrum sensing optimization in cognitive radio networks. In: IEEE International Conference on Communications, Beijing, May 2008, pp 3411–3415
67. Li X, Li W, Hei Y (2012) Joint spectrum sensing and user selection strategy for cognitive radio networks. In: IEEE International Conference on Wireless Communications and Signal Processing, Huangshan, Oct 2012, pp 1–6
68. Jiang T, Qu D (2008) On minimum sensing error with spectrum sensing using counting rule in cognitive radio networks. In: International ICST Conference on Wireless Internet, Maui, Nov 2008, pp 1–9
69. Cacciapuoti AS, Akyildiz IF, Paura L (2012) Correlation-aware user selection for cooperative spectrum sensing in cognitive radio ad hoc networks. IEEE J Sel Areas Commun 30:297–306
70. Do T, Mark BL (2009) Joint spatial-temporal spectrum sensing for cognitive radio networks. In: Conference on Information Sciences and Systems, Baltimore, Mar 2009, pp 124–129
71. Khalid L, Anpalagan A (2012) Cooperative sensing with correlated local decisions in cognitive radio networks. IEEE Trans Veh Technol 61:843–849
72. Zeng K, Wang J, Li S, Cabric D (2011) Robust node selection for cooperative spectrum sensing with malicious users. In: IEEE Military Communications Conference, Baltimore, Nov 2011, pp 79–84
73. Wang W, Li H, Sun Y, Han Z (2010) Securing collaborative spectrum sensing against untrustworthy secondary users in cognitive radio networks. EURASIP J Adv Signal Process 2010:106–117
74. Song C, Zhang Q (2009) Achieving cooperative spectrum sensing in wireless cognitive radio networks. ACM SIGMOBILE Mob Comput Commun Spec Issue Cognit Radio Technol Syst 13:14–25
75. Wang B, Liu K, Clancy T (2010) Evolutionary cooperative spectrum sensing game:how to collaborate? IEEE Trans Commun 58:890–900
76. Li S, Zhu H, Yang B, Chen C, Guan X, Lin X (2012) Towards a game theoretical modeling of rational collaborative spectrum sensing in cognitive radio networks. In: IEEE Conference on Communications June 2012, pp 88–92
77. Lee WY, Akyildiz IF (2008) Optimal spectrum sensing framework for cognitive radio networks. IEEE Trans Wirel Commun 7:3845–3857
78. Yu R, Zhang Y, Yi L, Xie S, Song L, and Guizani M (2012) Secondary users cooperation in cognitive radio networks: balancing sensing accuracy and efficiency. IEEE Wirel Commun 19:30–37
79. Kim H, Shin KG (2008) Efficient discovery of spectrum opportunities with MAC-layer sensing in cognitive radio networks. IEEE Trans Mob Comput 7:533–545
80. Su H, Zhang X (2008) Cross-layer based opportunistic MAC protocols for QoS provisionings over cognitive radio wireless networks. IEEE J Sel Areas Commun 26:118–129
81. Xie S, Liu Y, Zhang Y, Yu R (2010) A parallel cooperative spectrum sensing in cognitive radio networks. IEEE Trans Veh Technol 59:4079–4092
82. Liu Y, Yu R, Zhang Y, Yuen C (2013) An efficient MAC protocol with selective grouping and cooperative sensing in cognitive radio networks. IEEE Trans Veh Technol 62:3928–3941
83. Noel A, Schober R (2012) Convex sensing-reporting optimization for cooperative spectrum sensing. IEEE Trans Wire Commun 11:1900–1910
84. Dai Z, Liu J, Long K (2015) Selective-reporting-based cooperative spectrum sensing strategies for cognitive radio networks. IEEE Trans Veh Technol 64:3043–3055
85. Sun C, Zhang W, Letaief K (2007) Cooperative spectrum sensing for cognitive radios under bandwidth constraints. In: IEEE Wireless Communications and Networking Conference, Hong Kong, Mar 2007, pp 1–5
86. Pham H, Zhang Y, Engelstad P, Skeie T, Eliassen F (2010) Energy minimization approach for optimal cooperative spectrum sensing in sensor-aided cognitive radio networks. In: International ICST Conference on Wireless Internet, Singapore, Mar 2010, pp 1–9

87. Gao Y, Xu W, Yang K, Niu K, Lin J (2013) Energy-efficient transmission with cooperative spectrum sensing in cognitive radio networks. In: IEEE Wireless Communications and Networking Conference, Apr 2013, pp 7–12
88. Hu H, Zhang H, Liang Y-C (2016) On the spectrum- and energy-efficiency tradeoff in cognitive radio networks. IEEE Trans Commun 64(2):490–501
89. Huang K (2013) Spatial throughput of mobile ad hoc networks powered by energy harvesting. IEEE Trans Inf Theory 59:7597–7612
90. Lee S, Zhang R, Huang K (2013) Opportunistic wireless energy harvesting in cognitive radio networks. IEEE Trans Wirel Commun 12:4788–4799
91. Park S, Kim H, Hong D (2013) Cognitive radio networks with energy harvesting. IEEE Trans Wirel Commun 12:1386–1397
92. Chung W, Park S, Lim S, Hong D (2014) Spectrum sensing optimization for energy-harvesting cognitive radio systems. IEEE Trans Wirel Commun 13:2601–2613
93. Donoho D (2006) Compressed sensing. IEEE Trans Inf Theory 52:1289–1306
94. Ragheb T, Kirolos S, Laska J, Gilbert A, Strauss M, Baraniuk R, Massoud Y (2007) Implementation models for analog-to-information conversion via random sampling. In: Midwest Symposium on Circuits and Systems, Montreal, Aug 2007, pp 325–328
95. Qin Z, Gao Y, Plumbley MD, Parini CG (2015) Wideband spectrum sensing on real time signals at sub-nyquist sampling rates in single and cooperative multiple nodes. IEEE Trans Signal Process 64(12):3106–3117
96. Paysarvi-Hoseini P, Beaulieu NC (2011) Optimal wideband spectrum sensing framework for cognitive radio systems. IEEE Trans Signal Process 59:1170–1182
97. Khalid L, Anpalagan A (2014) Adaptive grouping scheme for cooperative spectrum sensing in cognitive radio networks. In: IEEE Vehicular Technology Conference, May 2014, pp 1–5
98. Mishra S, Cabric D, Chang C, Willkomm D, van Schewick B, Wolisz A, Brodersen R (2005) A real time cognitive radio testbed for physical and link layer experiments. In: IEEE Symposium on New Frontiers in Dynamic Spectrum Access Networks, Nov 2005, pp 8–11
99. Yuan Y, Bahl P, Chandra R, Chou P, Ferrell J, Moscibroda T, Narlanka S, Wu Y (2007) KNOWS: kognitiv networking over white spaces. In: IEEE Symposium on New Frontiers in Dynamic Spectrum Access Networks, Apr 2007, pp 416–427
100. Gu S, Xu P, Wang X, Gan X, Yu H (2010) A real time testbed for the evaluation of cognitive radio MAC. In: IEEE Global Telecommunications Conference, Dec 2010, pp 1–5
101. Manna T, Misra IS (2013) Implementation of relay based collaborative spectrum sensing using coalitional games in wireless cognitive radio networks. Elsevier Comput Electr Eng J 45:77–99
102. Rice University, "warp.rice.edu." WARP homepage, 2013
103. Masri A, Chiasserini C-F, Casetti C, Perotti A (2012) Common control channel allocation in cognitive radio networks through UWB communication. J Commun Netw 14:710–718
104. Chowdhury K, Akyildiz I (2011) OFDM based common control channel design for cognitive radio ad hoc networks. IEEE Trans Mob Comput 10:228–238
105. Jia J, Zhang Q, Shen X (2008) HC-MAC: a hardware constrained cognitive MAC for efficient spectrum management. IEEE J Sel Areas Commun 26:106–117
106. Zhou X, Ma J, Li GY, Kwon YH, Soong AC (2010) Probability-based combination for cooperative spectrum sensing. IEEE Trans Commun 58:463–466
107. Chen Y, Beaulieu N (2009) Performance of collaborative spectrum sensing for cognitive radio in the presence of gaussian channel estimation errors. IEEE Trans Commun 57:1944–1947
108. Zhang R, Wang M, Caiy LX, Zheng Z, Shen X, Xie L-L (2015) LTE-unlicensed: the future of spectrum aggregation for cellular networks. IEEE Wirel Commun 22:150–159
109. Khan AA, Rehmani MH, Reisslein M (2015) Cognitive radio for smart grids: survey of architectures, spectrum sensing mechanisms, and networking protocols. IEEE Commun Surv Tutorials 18:860–898

Application-Aware Spectrum Sharing

13

Ahmed Abdelhadi and Charles Clancy

Contents

The content in this chapter is reproduced with permission after modifications (License numbers 3975601299718, 3975601157846, 3975600417474). For the original articles please refer to [1–3].

A. Abdelhadi (✉)
ICTAS/ECE, Virginia Tech, Blacksburg, VA, USA
e-mail: aabdelhadi@vt.edu

C. Clancy
ICTAS/ECE, Virginia Tech, Arlington, VA, USA
e-mail: tcc@vt.edu

W. Zhang (ed.), *Handbook of Cognitive Radio*,
https://doi.org/10.1007/978-981-10-1394-2_13

Abstract

In this chapter, an application-aware spectrum sharing and allocation problem for cellular systems with multiple frequency bands is presented. Mobile users are categorized based on applications running on their devices. They could be either delay-tolerant or real-time applications which are approximated by logarithmic utility functions and sigmoidal-like utility functions, respectively. The objective is to share spectrum resources from multiple base stations with different frequency bands according to a utility proportional fairness policy. This policy guarantees no user is dropped, i.e., allocated zero resource. Additionally, it ensures that mobile users with real-time applications are given priority in resource allocation to achieve higher overall user satisfaction with the available shared resources. Hence, this problem is casted as a convex optimization problem to ensure optimality and the existence of a tractable global optimal solution. Using optimization techniques, e.g., duality and Lagrange multipliers, a distributed spectrum sharing and allocation algorithm is constructed. This algorithm is tested for convergence in different traffic conditions. Based on the convergence analysis, a robust resource allocation and sharing algorithm is developed to allocate the optimal resources for high-traffic situations where conventional resource allocation algorithms fail to converge. Additionally, this algorithm provides the option of traffic-dependent pricing for network providers. This pricing approach can be used to flatten the network traffic and decrease cost per bandwidth for mobile users. The simulation results of the performance of this robust optimal algorithm are explored for a single-carrier and two-carrier scenarios.

Keywords

Inelastic traffic · Convex optimization · Robust algorithm · Traffic-dependent pricing · Optimal resource allocation · Joint carrier aggregation · Application-aware · Sigmoidal-like utility

Introduction

Nowadays, mobile phones are becoming smarter with a wide variety of advanced applications that are hungry for bandwidth resources. Mobile phone industry is witnessing a rapid growth in both number of subscribers and traffic consumption per subscriber. Mobile subscribers are currently running multiple applications, simultaneously, on their smart phones. Network providers are moving from single service (e.g., Internet access) to multiple service offering (e.g., multimedia telephony, mobile-TV, etc.) [16]. In order to meet this strong demand for wireless resources by mobile users, more spectrum resources are needed [40]. However, due to the scarcity of the dedicated cellular spectrum, it is difficult to have a single frequency band fulfilling this demand. Therefore, the dedicated cellular frequency bands are not sufficient to satisfy demands of this industry, and sharing other frequency bands is necessary for pushing further advances in the mobile phone industry.

The National Broadband Plan (NBP) and the findings of the President's Council of Advisors on Science and Technology (PCAST) spectrum study have recommended that underutilized federal spectrum be made available for secondary use [19,36]. Furthermore, National Telecommunications and Information Administration (NTIA) findings revealed that not efficiently sharing radar band can result in large exclusion zones that reach up to tens of kilometers from the west and east coasts [34]. Hence, this excludes millions of mobile users living within tens of kilometers from the west and east coasts from aggregating additional secondary band to their existing primary spectrum. Additionally, the Federal Communications Commission (FCC) recommended the use of small cells, i.e., low-power wireless base stations, to operate in the 3.5 GHz radar band efficiently [21]. Hence, radar band can be shared by cellular networks similar to previous sharing examples, e.g., Wi-Fi, Bluetooth, wireless local area network (WLAN), etc. [20].

Making more spectrum available will certainly provide opportunities for mobile broadband capacity gains, but only if those resources can be aggregated efficiently with the existing commercial mobile system [35,49,50]. The efficient sharing and aggregation of federal spectrum with the existing cellular network is a challenging task. The challenges are both in hardware implementation and sharing and allocation of spectrum resource from multiple carriers with different bands. Hardware implementation challenges are in the need for multiple oscillators, multiple RF chains, more powerful signal processing, and longer battery life [5]. For sharing of spectrum resources from multiple base stations, e.g., macro cells and small cells, with multiple bands, e.g., dedicated cellular bands and secondary radar bands, a distributed resource allocation and aggregation algorithm is needed to optimally allocate these spectrum resources from different carriers operating using different frequency bands. Hence, the problem boils down to optimally allocating resources from different carriers with different frequency bands. In other words, it is a resource allocation optimization problem with carrier aggregation. This problem holds for sharing federal or commercial spectrum from various network providers as well [39].

The area of resource allocation optimization has received significant interest since the seminal network utility maximization problem presented in [28]. The network utility maximization problem allocates the resources among users based on bandwidth proportional fairness and using Lagrange multiplier methods of optimization theory. An iterative algorithm based on the dual problem has been proposed to solve the resource allocation optimization problem in [32]. The utility functions used in early research work, as in [28] and [32], are logarithmic utility functions that are good approximations of elastic Internet traffic for wired communication networks. Therefore, all utility functions are strictly concave functions, and hence the optimization problem is convex and converges to the global optimal solution.

Nowadays, there has been an increasing demand for wireless adaptive real-time applications. The utility functions that approximate real-time applications are non-concave functions. Applications with utility functions that are not strictly concave are presented in [41]. For example, voice-over-IP (VoIP) can be approximated as a step function where the utility percentage is zero below a certain rate threshold

and is 100% above that threshold, while rate-adaptive applications, e.g., video streaming, have utility functions that can be approximated as a sigmoidal-like function according to [41]. The sigmoidal-like function is a convex function for rates below the curve inflection point and is a concave function for rates above that inflection point. Hence, there is an urgent need to provide an optimal sharing and allocation algorithm that is aware of different applications running on mobile devices. The developed algorithm has to allocate shared spectrum resources based on the characteristics of the applications running on users' devices and the impact of that on users' experience. In other words, an application-aware spectrum sharing solution is needed.

In this chapter, a single carrier resource allocation optimization problem that includes users with non-concave utility functions (i.e., sigmoidal-like functions) and users with strictly concave utility functions (i.e., logarithmic utility functions) is discussed first. The optimization problem is formulated to ensure application awareness and fairness when allocating available evolved Node B (eNodeB) resources to all users. A resource allocation algorithm is developed to give priority to real-time application users who have non-concave utility functions approximated by sigmoidal-like functions with different parameters for different real-time applications. The algorithm and corresponding optimization problem inherently guarantee by construction that all users are assigned a fraction of the resources. This satisfies the objective of cellular system to provide a minimum quality of service (QoS) for all the users subscribing for the mobile service.

This developed rate allocation algorithm converges to the optimal rate only when the maximum available rate by the eNodeB exceeds the mid-utilization point for all the real-time application users as shown in section "Convergence Analysis". So, this algorithm does not converge for eNodeB with scarce bandwidth resources with respect to the number of users. This situation is a realistic situation during peak network traffic hours. Therefore, a modified algorithm to solve this problem is presented in section "A More Robust Algorithm". The modified algorithm provides a more robust algorithm that converges for both scarce and abundant bandwidth resources. Additionally, this robust algorithm provides traffic-dependent pricing. This pricing approach can be utilized by network providers to incentivize users to use the mobile service during less congested times [25].

By extending the single carrier optimization problem, an application-aware spectrum sharing optimization problem is formulated. In this problem multiple spectrum bands are shared by solving for resource allocation of multiple carriers. This resource allocation optimization problem with joint carrier aggregation is casted into a convex optimization framework. Application awareness is augmented by usage of logarithmic and sigmoidal-like utility functions to represent delay-tolerant and real-time applications, respectively. This model supports both contiguous and noncontiguous carrier aggregation from one or more frequency bands. The corresponding distributed algorithm allocates resources from one or more carriers to provide the lowest resource prices for mobile users. In addition, this algorithm uses utility proportional fairness policy to be aware of the priority of real-time applications over delay-tolerant applications when allocating resources.

Related Work

A distributed power allocation algorithm for mobile cellular system is presented in [30]. The authors used non-concave sigmoidal-like utility functions. The proposed algorithm approximates the global optimal solution but could drop users to maximize the overall system utilities; therefore, it does not guarantee minimum QoS for all users. In [7,46,47], the authors presented novel algorithms for different scenarios of power allocation in cellular systems that are optimal based on the optimality proof in [24].

A weighted aggregation of elastic and inelastic utility functions in each user equipment (UE) is presented in [29]. These aggregated utility functions are then approximated to the nearest concave utility function from a set of functions using minimum mean-square error. That approximate utility function is used to solve the rate allocation problem using a modified version of distributed rate allocation algorithm presented in [28]. In [24], the authors showed that sigmoidal-like and logarithmic utility functions are suitable for representing real-time and delay-tolerant applications, respectively.

In [43] and [44], the authors presented a non-convex optimization formulation for the maximization of utility functions in wireless networks. They used both elastic and sigmoidal-like utility functions and proposed a distributed algorithm to solve it when the duality gap is zero. But the algorithm does not converge to the optimal solution for a positive duality gap. A fair allocation heuristic is included to ensure network stability which resulted in a high aggregated utility.

In [26], the authors proposed a utility max-min fairness resource allocation for users with elastic and real-time traffic sharing a single path in the network. In [45], the authors proposed a utility proportional fair optimization formulation for high-SINR wireless networks using a utility max-min architecture. They compared their algorithm to the traditional bandwidth proportional fair algorithms [33] and presented a closed form solution that prevents oscillations in the network.

In [25], the authors conducted a pilot trial with 50 iPhone or iPad 3G data users, who were charged according to time-dependent pricing algorithms. Their results show that time-dependent pricing benefits both operators and customers. The algorithms flatten demand fluctuations over time. It also allows users to choose the time and volume of their usage and hence save money. However, this method lacks application awareness which is essential in advancing mobile service industry.

A Round Robin packet scheduling method which distributes the load among multiple component carriers across the network is proposed in [48]. A collaborative scheme, where users covered by multiple base stations are allocated resources from the base station with the best channel, is presented in [15]. The problem of spectrum sharing of resources using carrier aggregation for LTE Advanced is addressed in [42]. The authors consider modulation and coding scheme (MCS) selection and mobile users' MIMO capabilities. These proposed methods in [15, 42, 48] are not application-aware and hence are less efficient in maximizing user's satisfaction and quality of experience. In this chapter, we address quality of experience by including application-awareness into spectrum sharing problem.

Our Contributions

Our contributions in this chapter are summarized as:

- An application-aware utility proportional fairness optimization problem that solves for utility functions that are both strictly concave and non-concave (i.e., sigmoidal-like [24]) is formulated. In addition, the optimization problem inherently gives priority to real-time application users (i.e., with sigmoidal-like utility functions) while allocating resources.
- The proposed application-aware optimization problem is convex, and therefore the global optimal solution is tractable. A distributed rate allocation algorithm is presented.
- The convergence of the distributed rate allocation algorithm is analyzed. A modified distributed rate allocation algorithm that converges to the optimal rates for high-traffic and low-traffic periods is identified.
- A pricing policy is proposed for service providers to charge to service subscribers that can flatten traffic load on the network.
- Extension of the application-aware optimization problem to include spectrum sharing with carrier aggregation between multiple different frequency bands is formulated.
- Simulation results for one- and two-carrier scenarios are explored.

The chapter is organized as follows. Section "Single-Carrier Scenario" presents the single-carrier problem formulation. Section "Optimality" shows that the single-carrier optimization problem is convex, and section "UE and eNodeB Subproblems" provides the corresponding distributed subproblems. Section "Distributed Algorithm for Single-Carrier Scenario" presents a single-carrier algorithm. Section "Simulation Example: One Carrier" explores the simulation results for a single-carrier scenario setup. Section "Convergence Analysis" analyzes the algorithm convergence. Section "A More Robust Algorithm" constructs a more robust single-carrier algorithm, and the corresponding simulation results are shown in section "Simulation Example: One Carrier (Cont.)". The multiple-carrier optimization problem is formulated in section "Multiple-Carrier Scenario", its optimality shown in section "Optimality and Subproblems", corresponding algorithm developed in section "Distributed Algorithm for Multiple-Carrier Scenario", and its simulation results provided in section "Simulation Example: Two Carriers". Section "Conclusion and Future Direction" concludes the chapter with future direction.

Single-Carrier Scenario

A single-cell system consisting of a single eNodeB and M UEs is considered as our system model. The bandwidth allocated by the eNodeB to ith UE is given by r_i. Each UE has its own utility function $U_i(r_i)$ that corresponds to the type of traffic

being handled by it. Our objective is to determine the bandwidth the eNodeB should allocate to the UEs. We assume the utility functions $U_i(r_i)$ to be strictly concave or a sigmoidal-like functions. The utility functions have the following properties:

- $U_i(0) = 0$, and $U_i(r_i)$ is an increasing function of r_i.
- $U_i(r_i)$ is twice continuously differentiable in r_i.

In our model, we use the normalized sigmoidal-like utility function, as in [24, 30], that can be expressed as

$$U_i(r_i) = c_i\left(\frac{1}{1+e^{-a_i(r_i-b_i)}} - d_i\right) \tag{1}$$

where $c_i = \frac{1+e^{a_i b_i}}{e^{a_i b_i}}$ and $d_i = \frac{1}{1+e^{a_i b_i}}$. So, it satisfies $U(0) = 0$ and $U(\infty) = 1$. In Fig. 1, the normalized sigmoidal-like utility function with $a = 5$ and $b = 10$ is a good approximation for a step function (e.g., VoIP), and $a = 0.5$ and $b = 20$ is a good approximation to an adaptive real-time application (e.g., video streaming). In addition, we use the normalized logarithmic utility function, as in [18, 45], that can be expressed as

$$U_i(r_i) = \frac{\log(1+k_i r_i)}{\log(1+k_i r_{\max})} \tag{2}$$

where $r_{\max}$ is the required rate for the user to achieve 100% utility percentage and k_i is the rate of increase of utility percentage with the allocated rate r_i. So, it satisfies $U(0) = 0$ and $U(r_{\max}) = 1$. The logarithmic utility functions with $k = 15$ and

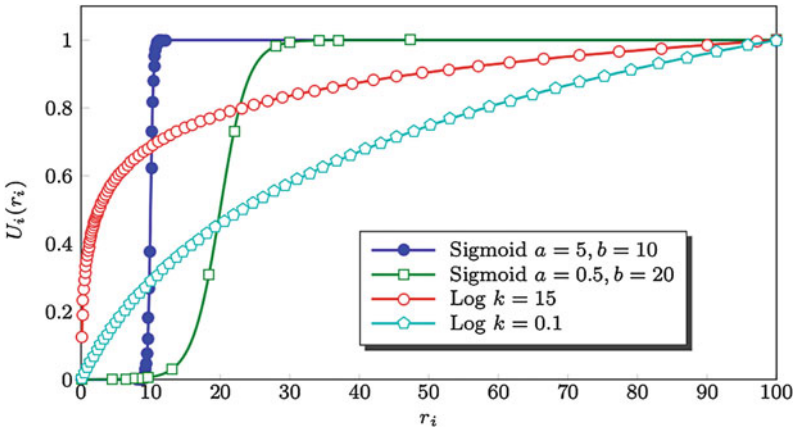

Fig. 1 The sigmoidal-like utility functions (representing real-time traffic) and logarithmic utility functions (representing delay-tolerant traffic) $U_i(r_i)$

$k = 0.1$ are shown in Fig. 1. We consider the utility proportional fairness objective function given by

$$\max_{\mathbf{r}} \prod_{i=1}^{M} U_i(r_i) \tag{3}$$

where $\mathbf{r} = \{r_1, r_2, \ldots, r_M\}$ and M is the number of UEs in the coverage area of the eNodeB. The goal of this resource allocation objective function is to allocate the resources for each UE that maximize the total mobile system objective (i.e., the product of the utilities of all the UEs) while ensuring proportional fairness between individual utilities. This resource allocation objective function ensures nonzero resource allocation for all users. Therefore, the corresponding resource allocation optimization problem guarantees minimum QoS for all users. In addition, this approach allocates more resources to users with real-time applications providing improvement to the QoS of cellular system.

The basic formulation of the utility proportional fairness resource allocation problem is given by the following optimization problem:

$$\begin{aligned} \max_{\mathbf{r}} \quad & \prod_{i=1}^{M} U_i(r_i) \\ \text{subject to} \quad & \sum_{i=1}^{M} r_i \leq R \\ & r_i \geq 0, \quad i = 1, 2, \ldots, M. \end{aligned} \tag{4}$$

where R is the total rate of the eNodeB covering the M UEs, and $\mathbf{r} = \{r_1, r_2, \ldots, r_M\}$.

We prove in section "Optimality" that there exists a tractable global optimal solution to the optimization problem (4).

Optimality

In the optimization problem (4), since the objective function $\arg\max_{\mathbf{r}} \prod_{i=1}^{M} U_i(r_i)$ is equivalent to $\arg\max_{\mathbf{r}} \sum_{i=1}^{M} \log(U_i(r_i))$, then optimization problem (4) can be written as:

$$\begin{aligned} \max_{\mathbf{r}} \quad & \sum_{i=1}^{M} \log(U_i(r_i)) \\ \text{subject to} \quad & \sum_{i=1}^{M} r_i \leq R \\ & r_i \geq 0, \quad i = 1, 2, \ldots, M. \end{aligned} \tag{5}$$

In section "Single-Carrier Scenario", we assume that all the utility functions of the UEs are strictly concave or sigmoidal-like functions. In the strictly concave utility function case, recall the utility function properties in section "Single-Carrier Scenario"; the utility function is positive $U_i(r_i) > 0$, increasing, and twice differentiable with respect to r_i. Then, it follows that $U_i'(r_i) = \frac{dU_i(r_i)}{dr_i} > 0$ and $U_i''(r_i) = \frac{d^2U_i(r_i)}{dr_i^2} < 0$. It follows that, the utility function $\log(U_i(r_i))$ in the optimization problem (5) has $\frac{d\log(U_i(r_i))}{dr_i} = \frac{U_i'(r_i)}{U_i(r_i)} > 0$ and $\frac{d^2\log(U_i(r_i))}{dr_i^2} = \frac{U_i''(r_i)U_i(r_i) - U_i'^2(r_i)}{U_i^2(r_i)} < 0$. Therefore, the strictly concave utility function $U_i(r_i)$ natural logarithm $\log(U_i(r_i))$ is also strictly concave. It follows that the natural logarithm of the logarithmic utility function in equation (2) is strictly concave.

In the sigmoidal-like utility function case, the utility function of the normalized sigmoidal-like function is given by equation (1) as $U_i(r_i) = c\left(\frac{1}{1+e^{-a_i(r_i-b_i)}} - d\right)$. For $0 < r_i < R$, we have $0 < 1 - d_i(1 + e^{-a_i(r_i-b_i)}) < \frac{1}{1+c_i d_i}$. It follows that for $0 < r_i < R$, we have the first and second derivative as

$$\frac{d}{dr_i}\log U_i(r_i) > 0 \text{ and } \frac{d^2}{dr_i^2}\log U_i(r_i) < 0.$$

Therefore, the sigmoidal-like utility function $U_i(r_i)$ natural logarithm $\log(U_i(r_i))$ is strictly a concave function.

All the utility functions in the optimization problem presented in equation (5) have strictly concave natural logarithms. For visualization, an example of four users is shown in Fig. 1 where two users run applications with sigmoidal-like utility functions and the other two users run application with logarithmic utility functions. The sigmoidal-like utility functions parameters are $a = \{5, 0.5\}$ and $b = \{10, 20\}$, respectively. The logarithmic utility functions parameters are $k = \{15, 0.1\}$ and $r_{\max} = 100$. The natural logarithms of the utility functions of Fig. 1 are shown in Fig. 2, and the derivatives of natural logarithms of the utility functions are shown in Fig. 3. It follows that for all UEs, utility functions are strictly concave. Therefore, the

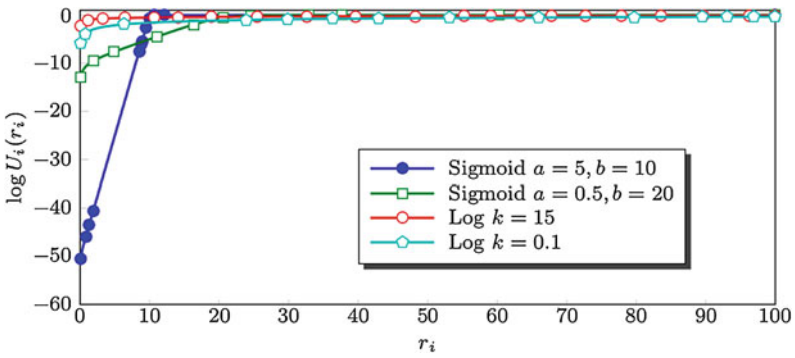

Fig. 2 The natural logarithm of sigmoidal-like and logarithmic utility functions $\log U_i(r_i)$

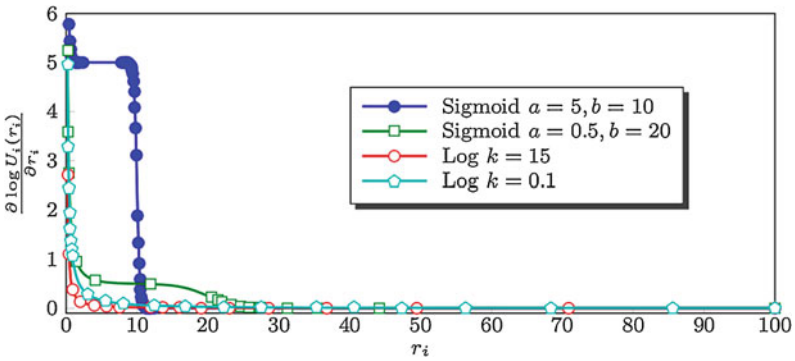

Fig. 3 The first derivative of the natural logarithm of sigmoidal-like and logarithmic utility functions $\frac{\partial \log U_i(r_i)}{\partial r_i}$

optimization problem (5) is a convex optimization problem [10]. The optimization problem (5) is equivalent to optimization problem (4); therefore it is also a convex optimization problem. For a convex optimization problem, there exists a unique tractable global optimal solution [8].

UE and eNodeB Subproblems

The key to UE and eNodeB subproblems from the primal problem in (5) is to convert to the dual problem, similar to [28] and [32]. The optimization problem (5) can be divided into two simpler problems by using the dual problem. We define the Lagrangian

$$L(\mathbf{r}, p) = \sum_{i=1}^{M} \log(U_i(r_i)) - p\left(\sum_{i=1}^{M} r_i + z - R\right) \tag{6}$$

where $z \geq 0$ is the slack variable and p is Lagrange multiplier or the shadow price (i.e., the total price per unit bandwidth for all the M channels). Therefore, the ith UE bid for bandwidth can be given by $w_i = pr_i$, and we have $\sum_{i=1}^{M} w_i = p\sum_{i=1}^{M} r_i$. The first term in equation (6) is separable in r_i. Hence, the dual problem objective function can be written as

$$D(p) = \sum_{i=1}^{M} \max_{r_i}\Big(\log(U_i(r_i)) - pr_i\Big) + p(R - z) \tag{7}$$

The dual problem is given by

$$\begin{aligned} \min_{p} \quad & D(p) \\ \text{subject to} \quad & p \geq 0. \end{aligned} \tag{8}$$

Hence,

$$\frac{\partial D(p)}{\partial p} = R - \sum_{i=1}^{M} r_i - z = 0 \tag{9}$$

substituting by $\sum_{i=1}^{M} w_i = p \sum_{i=1}^{M} r_i$ we have

$$p = \frac{\sum_{i=1}^{M} w_i}{R - z} \tag{10}$$

Now, divide the primal problem (5) into two simpler optimization problems in the UEs and the eNodeB. The ith UE optimization problem is given by:

$$\begin{aligned} \max_{r_i} \quad & \log U_i(r_i) - p r_i \\ \text{subject to} \quad & p \geq 0 \\ & r_i \geq 0, \quad i = 1, 2, \ldots, M. \end{aligned} \tag{11}$$

The eNodeB optimization problem is given by:

$$\begin{aligned} \min_{p} \quad & D(p) \\ \text{subject to} \quad & p \geq 0. \end{aligned} \tag{12}$$

The minimization of shadow price p is achieved by the minimization of the slack variable $z \geq 0$ from equation (10). Therefore, the maximum utility percentage for the available eNodeB bandwidth is achieved by setting the slack variable $z = 0$. In this case, we replace the inequality in primal problem (5) constraint by equality constraint, and so we have $\sum_{i=1}^{M} w_i = pR$. Therefore, we have $p = \frac{\sum_{i=1}^{M} w_i}{R}$ where $w_i = p r_i$ is transmitted by the ith UE to the eNodeB. The utility proportional fairness in the objective function of the optimization problem (4) is guaranteed in the solution of the optimization problems (11) and (12).

Distributed Algorithm for Single-Carrier Scenario

The distributed application-aware resource allocation algorithm for optimization problems (11) and (12) is an iterative algorithm for allocating the network resources with awareness of applications running on UEs. For the Algorithm in (1) and (2), each UE starts with an initial bid $w_i(1)$ which is transmitted to the eNodeB. The eNodeB calculates the difference between the received bid $w_i(n)$ and the previously received bid $w_i(n-1)$ and exits if it is less than a prespecified threshold δ. Note that $w_i(0) = 0$. If the value is greater than the threshold δ, eNodeB calculates the shadow price $p(n) = \frac{\sum_{i=1}^{M} w_i(n)}{R}$ and sends that value to all the UEs. Each UE receives the

Algorithm 1 UE algorithm for a single-carrier scenario

Send initial bid $w_i(1)$ to eNodeB
loop
  Receive shadow price $p(n)$ from eNodeB
  if STOP from eNodeB **then**
    Calculate allocated rate $r_i^{\text{opt}} = \frac{w_i(n)}{p(n)}$
    STOP
  else
    Solve $r_i(n) = \arg\max_{r_i} \left(\log U_i(r_i) - p(n) r_i \right)$
    Send new bid $w_i(n) = p(n) r_i(n)$ to eNodeB
  end if
end loop

Algorithm 2 eNodeB algorithm for a single-carrier scenario

loop
  Receive bids $w_i(n)$ from UEs {Let $w_i(0) = 0 \ \forall i$}
  if $|w_i(n) - w_i(n-1)| < \delta \ \forall i$ **then**
    Allocate rates, $r_i^{\text{opt}} = \frac{w_i(n)}{p(n)}$ to user i
    STOP
  else
    Calculate $p(n) = \frac{\sum_{i=1}^{M} w_i(n)}{R}$
    Send new shadow price $p(n)$ to all UEs
  end if
end loop

shadow price to solve for the rate r_i that maximizes $\log U_i(r_i) - p(n) r_i$. That rate is used to calculate the new bid $w_i(n) = p(n) r_i(n)$. Each UE sends the value of its new bid $w_i(n)$ to the eNodeB. This process is repeated until $|w_i(n) - w_i(n-1)|$ is less than the prespecified threshold δ.

Simulation Example: One Carrier

In this section, the Algorithm in (1) and (2) is applied to the cell in Fig. 4 with six utility functions corresponding to six UEs shown in Fig. 5. We use real-time applications represented by equation (1) with different parameters, $a = 5, b = 10$, which is an approximation to VoIP application at rate $r = 10$, $a = 3, b = 20$ which is an approximation of a standard definition video streaming application with inflection point at rate $r = 20$, and $a = 1, b = 30$ which is also an approximation of a high definition video streaming application with inflection point at rate $r = 30$. We use three logarithmic functions that are expressed by equation (2) with $r_{\max}$ =100 and different k_i parameters which are approximations for delay-tolerant applications (e.g., browsing, FTP, emails). We use $k = \{15, 3, 0.5\}$, and eNodeB has $R = 100$ [23].

In Fig. 6, the allocated rates for each users per iteration are shown. The real-time applications have priority over delay-tolerant applications. In Fig. 7, the

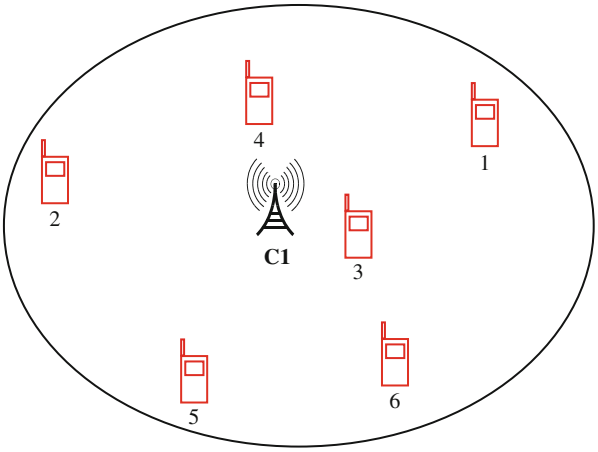

Fig. 4 System model with one carrier and six users

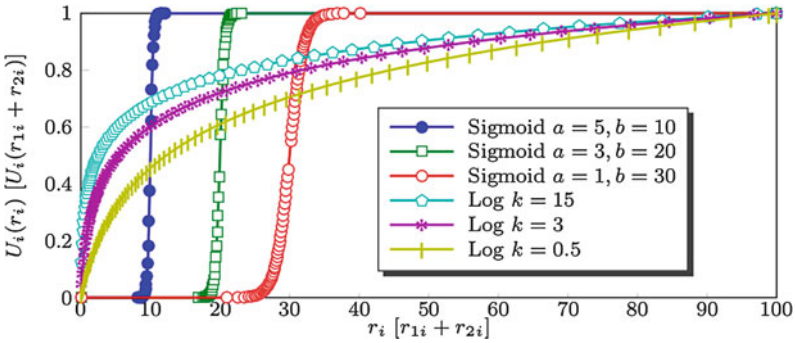

Fig. 5 The users utility functions $U_i(r_i)$ [or $U_i(r_{1i} + r_{2i})$ for section "Simulation Example: Two Carriers"] used in the simulation (three sigmoidal-like functions and three logarithmic functions)

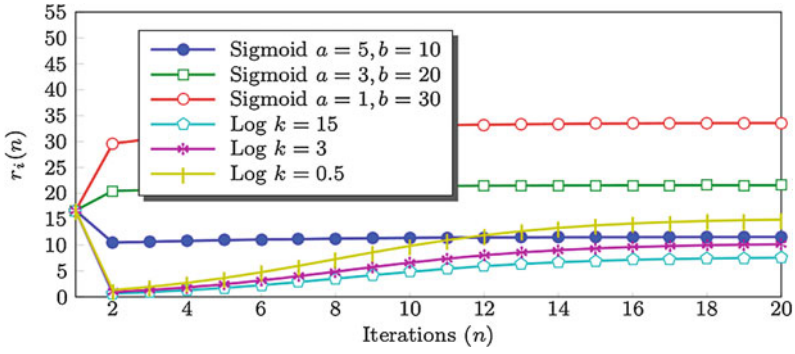

Fig. 6 The users allocated rate convergence $r_i(n)$ with number of iterations n for eNodeB rate $R = 100$

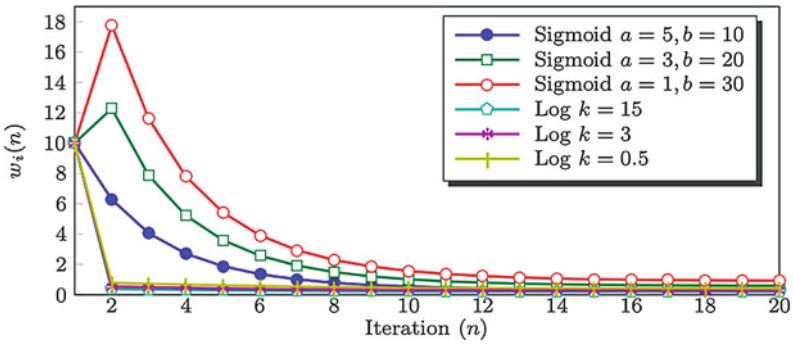

Fig. 7 The users bid convergence $w_i(n)$ with number of iterations n for eNodeB rate $R = 100$

corresponding bids per iteration are shown. Note that the distributed algorithm avoids the situation of allocating zero rate to any user (i.e., no user is dropped).

Convergence Analysis

In this section, the convergence analysis of Algorithms (1) and (2) for different values of R is explored.

For the sigmoidal-like function $U_i(r_i) = c_i(\frac{1}{1+e^{-a_i(r_i-b_i)}} - d_i)$, let $S_i(r_i) = \frac{\partial \log U_i(r_i)}{\partial r_i}$ be the slope curvature function. Then,

$$\frac{\partial S_i}{\partial r_i} = \frac{-a_i^2 d_i e^{-a_i(r_i-b_i)}}{c_i\left(1 - d_i(1+e^{-a_i(r_i-b_i)})\right)^2} - \frac{a_i^2 e^{-a_i(r_i-b_i)}}{\left(1+e^{-a_i(r_i-b_i)}\right)^2}$$

and

$$\frac{\partial^2 S_i}{\partial r_i^2} = \frac{a_i^3 d_i e^{-a_i(r_i-b_i)}\left(1 - d_i(1-e^{-a_i(r_i-b_i)})\right)}{c_i\left(1 - d_i\left(1+e^{-a_i(r_i-b_i)}\right)\right)^3} + \frac{a_i^3 e^{-a_i(r_i-b_i)}(1-e^{-a_i(r_i-b_i)})}{\left(1+e^{-a_i(r_i-b_i)}\right)^3}. \tag{13}$$

By inspection, $\frac{\partial S_i}{\partial r_i} < 0 \quad \forall\, r_i$. The first term S_i^1 of $\frac{\partial^2 S_i}{\partial r_i^2}$ in equation (13) can be written as

$$S_i^1 = \frac{a_i^3 e^{a_i b_i}(e^{a_i b_i} + e^{-a_i(r_i-b_i)})}{(e^{a_i b_i} - e^{-a_i(r_i-b_i)})^3} \tag{14}$$

and hence

$$\lim_{r_i \to 0} S_i^1 = \infty, \text{ and } \lim_{r_i \to b_i} S_i^1 = 0 \text{ for } b_i \gg \frac{1}{a_i}. \tag{15}$$

For second term S_i^2 of $\frac{\partial^2 S_i}{\partial r_i^2}$ in equation (13), the following properties are satisfied

$$S_i^2(b_i) = 0, \ S_i^2(r_i > b_i) > 0, \text{ and } S_i^2(r_i < b_i) < 0. \tag{16}$$

From equations (15) and (16), S_i has an inflection point at $r_i = r_i^s \approx b_i$. In addition, the curvature of S_i changes from a convex function close to origin to a concave function before the inflection point $r_i = r_i^s$ then to a convex function after the inflection point. **Therefore, the first remark is that for sigmoidal-like utility functions $U_i(r_i)$, the slope curvature function $\frac{\partial \log U_i(r_i)}{\partial r_i}$ has an inflection point at $r_i = r_i^s \approx b_i$ and is convex for $r_i > r_i^s$.**

For the sigmoidal-like function $U_i(r_i) = c_i(\frac{1}{1+e^{-a_i(r_i - b_i)}} - d_i)$, the optimal solution is achieved by solving the optimization problem (5). In Algorithms (1), an important step to reach to the optimal solution is to solve the optimization problem $r_i(n) = \arg\max_{r_i}(\log U_i(r_i) - p(n) r_i)$ for every UE. The solution of this problem can be written using Lagrange multipliers method in the form

$$\frac{\partial \log U_i(r_i)}{\partial r_i} - p = S_i(r_i) - p = 0. \tag{17}$$

From equation (15) and (16), the curvature of $S_i(r_i)$ is convex for $r_i > r_i^s \approx b_i$. The Algorithm in (1) and (2) is guaranteed to converge to the global optimal solution when the slope $S_i(r_i)$ of all the utility functions natural logarithm $\log U_i(r_i)$ is in a convex domain, similar to the analysis of logarithmic functions in [27] and [12]. Therefore, the natural logarithm of sigmoidal-like functions $\log U_i(r_i)$ converges to the global optimal solution for $r_i > r_i^{\approx} b_i$. The inflection point of sigmoidal-like function $U_i(r_i)$ is at $r_i^{\inf} = b_i$. For $\sum_{i=1}^{M} r_i^{\inf} \ll R$, Algorithms (1) and (2) allocate rates $r_i > b_i$ for all users. Since $S_i(r_i)$ is convex for $r_i > r_i^s \approx b_i$, then the optimal solution can be achieved by Algorithm (1) and (2). We have from equation (17), and $S_i(r_i)$ is convex for $r_i > r_i^s \approx b_i$, that $p_{ss} < S_i(r_i = \max b_i)$ where $S_i(r_i = \max b_i) = \frac{a_{i_{\max}} d_{i_{\max}}}{1 - d_{i_{\max}}} + \frac{a_{i_{\max}}}{2}$ and $i_{\max} = \arg\max_i b_i$. **Therefore, the second remark is that if $\sum_{i=1}^{M} r_i^{\inf} \ll R$ then Algorithms (1) and (2) converge to the global optimal rates which corresponds to the steady state shadow price $p_{ss} < \frac{a_{i_{\max}} d_{i_{\max}}}{1 - d_{i_{\max}}} + \frac{a_{i_{\max}}}{2}$ where $i_{\max} = \arg\max_i b_i$.**

For $\sum_{i=1}^{M} r_i^{\inf} > R$ there exists i such that the allocated rates $r_i^{\text{opt}} < b_i$. Therefore, if $p_{ss} \approx \frac{a_i d_i e^{\frac{a_i b_i}{2}}}{1 - d_i(1 + e^{\frac{a_i b_i}{2}})} + \frac{a_i e^{\frac{a_i b_i}{2}}}{(1 + e^{\frac{a_i b_i}{2}})}$ is the optimal shadow price for optimization problem (5), then a small change in the shadow price $p(n)$ in the nth iteration can lead to rate $r_i(n)$ (root of $S_i(r_i) - p(n) = 0$) to fluctuate

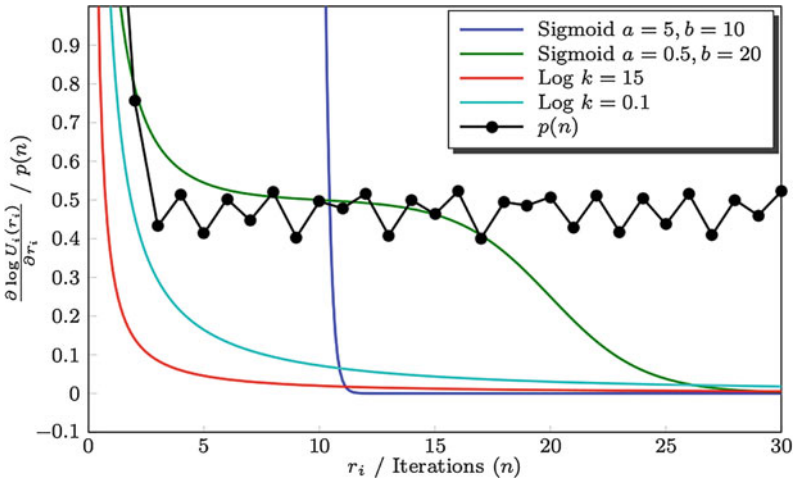

Fig. 8 The $\frac{\partial \log U_i(r_i)}{\partial r_i}$ diff log of sigmoidal-like utility function and shadow price $p(n)$ in algorithm (1) and (2) for $R = 25$

between the concave and convex curvature of slope curvature $S_i(r_i)$ for the ith user. Hence, this causes fluctuation in the bid $w_i(n)$ sent to eNodeB and fluctuation in the shadow price $p(n)$ set by eNodeB. Then, the iterative solution of Algorithms (1) and (2) fluctuates about the global optimal rates r_i^{opt}. **Therefore, the third remark is that for $\sum_{i=1}^{M} r_i^{\text{inf}} > R$ and the global optimal shadow price $p_{ss} \approx \frac{a_i d_i e^{\frac{a_i b_i}{2}}}{1-d_i(1+e^{\frac{a_i b_i}{2}})} + \frac{a_i e^{\frac{a_i b_i}{2}}}{(1+e^{\frac{a_i b_i}{2}})}$, then Algorithms (1) and (2) fluctuate about the global optimal solution.**

From the first, second, and third remarks, the Algorithm in (1) and (2) does not converge to the global optimal solution for all values of R.

Oscillation example: An example of four users with the utilities shown in Fig. 1 and the assumption that eNodeB maximum rate is $R = 25$, i.e., $\sum_{i=1}^{4} r_i^{\text{inf}} = 30 > R = 25$. Therefore, we cannot guarantee convergence with Algorithms (1) and (2), as stated in section "Convergence Analysis". In Fig. 8, the shadow price $p(n)$ oscillates between a concave and convex curvature of the $\frac{\partial \log U_i(r_i)}{\partial r_i}$ curve. The oscillation in the shadow price $p(n)$ causes an oscillation in the allocated rates and hinders the convergence to the optimal rates, and therefore the optimal rate allocation is not achievable by Algorithm in (1) and (2).

A More Robust Algorithm

In this section, a robust algorithm is developed to ensure the proposed rate allocation algorithm converges for all values of the eNodeB rate R. For $\sum r_i^{\text{inf}} > R$, the

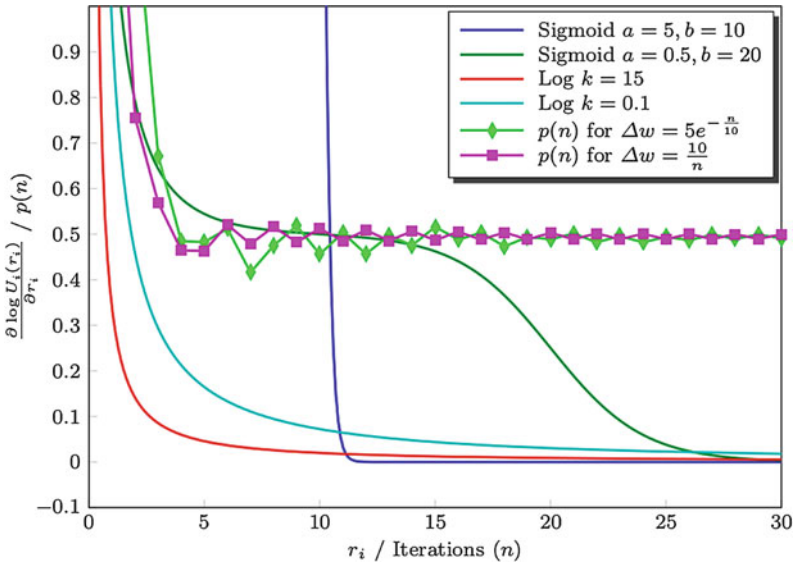

Fig. 9 The $\frac{\partial \log U_i(r_i)}{\partial r_i}$ diff log of sigmoidal-like utility function and $p(n)$ for Algorithm in (3) and (4) with $\Delta w = 5e^{-\frac{n}{10}}$ and $\Delta w = \frac{10}{n}$ and $R = 25$

algorithm must avoid fluctuations in the non-convergent region discussed in section "Convergence Analysis". This is achievable by adding a convergence measure $\Delta w(n)$ that senses the fluctuations in the bids w_is. In case of fluctuations, this robust algorithm decreases the step size between current and previous bid $w_i(n) - w_i(n-1)$ for each user i using fluctuations decay function. The fluctuations decay function could be in the following forms:

- *Exponential function*: It takes the form $\Delta w(n) = l_1 e^{-\frac{n}{l_2}}$.
- *Rational function*: It takes the form $\Delta w(n) = \frac{l_3}{n}$.

where l_1, l_2, l_3 can be adjusted to change the rate of decay of the bids w_is. The fluctuations decay function can be included in Algorithm (3) of the UE or Algorithm (4) of the eNodeB. In this model, the decay part is added to Algorithm (3) of the UE. The example of four users with the utilities shown in Fig. 1 and $R = 25$ is executed with fluctuation decay functions as shown in Fig. 9.

Simulation Example: One Carrier (Cont.)

In this section, simulation setup and parameters are similar to section "Simulation Example: One Carrier" with the exception of $R = 45$ for a comparison between Algorithm in (1) and (2) and Algorithm in (3) and (4). Here, we choose the

Algorithm 3 Modified UE algorithm for a single-carrier scenario

Send initial bid $w_i(1)$ to eNodeB
Set $r_i^{\min} = 0$
loop
  Receive shadow price $p(n)$ from eNodeB
  if STOP from eNodeB **then**
    Calculate allocated rate $r_i^{\text{opt}} = \frac{w_i(n)}{p(n)}$
  else
    Calculate new bid $w_i(n) = p(n) r_i(n)$
    if $|w_i(n) - w_i(n-1)| > \Delta w(n)$ **then**
      $w_i(n) = w_i(n-1) + \text{sign}(w_i(n) - w_i(n-1))\Delta w(n)$ $\{\Delta w = l_1 e^{-\frac{n}{l_2}}$ or $\Delta w = \frac{l_3}{n}\}$
    end if
    Send new bid $w_i(n)$ to eNodeB
  end if
end loop

Algorithm 4 Modified eNodeB algorithm for a single-carrier scenario

Receive r_i^{inf} from UEs
loop
  Receive bids $w_i(n)$ from UEs {Let $w_i(0) = 0 \ \forall i$}
  if $|w_i(n) - w_i(n-1)| < \delta \ \forall i$ **then**
    STOP and calculate rates $r_i^{\text{opt}} = \frac{w_i(n)}{p(n)}$
  else
    Calculate $p(n) = \frac{\sum_{i=1}^{M} w_i(n)}{R}$
    Send new shadow price $p(n)$ to all UEs
  end if
end loop

eNodeB rate R to be less than the sum of real-time application user inflection points $\sum b_i$. As expected Algorithm in (1) and (2) does not converge in this region as shown in Fig. 10 for rates and in Fig. 11 for bids. On the other hand, Algorithm in (3) and (4) behavior is more robust due to the fluctuation decay function. It damps the fluctuations with every iteration for rates as shown in Fig. 12 and for bids as shown in Fig. 13. Figure 14 shows the oscillatory shadow price $p(n)$ of Algorithm in (1) and (2) and the damping shadow price $p(n)$ of Algorithm in (3) and (4).

For $\delta = 10^{-3}$ and R changing between 5 and 100 with step of 5, the final rates and the corresponding final bids of different users with different eNodeB rate R are shown in Figs. 15 and 16, respectively. Note that the eNodeB allocates the majority of its resources to the UEs running adaptive real-time application until they reach their inflection rates $r_i = b_i$. When the total rate R exceeds the sum of the inflection rates $\sum b_i$ of all the adaptive real-time applications, eNodeB allocates more resources to the UEs with delay-tolerant application. Additionally, real-time application users bid higher when the resources are scare, and their bids decrease as R increases. Therefore, the pricing which is proportional to the bids is traffic-dependent. This gives the service providers the option to increase the service price

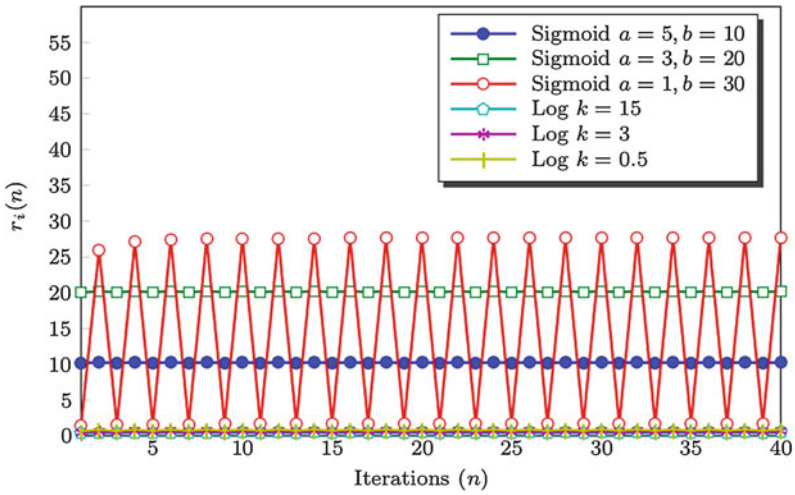

Fig. 10 The rate convergence $r_i(n)$ of Algorithm in (1) and (2) with number of iterations n for different users and $R = 45$

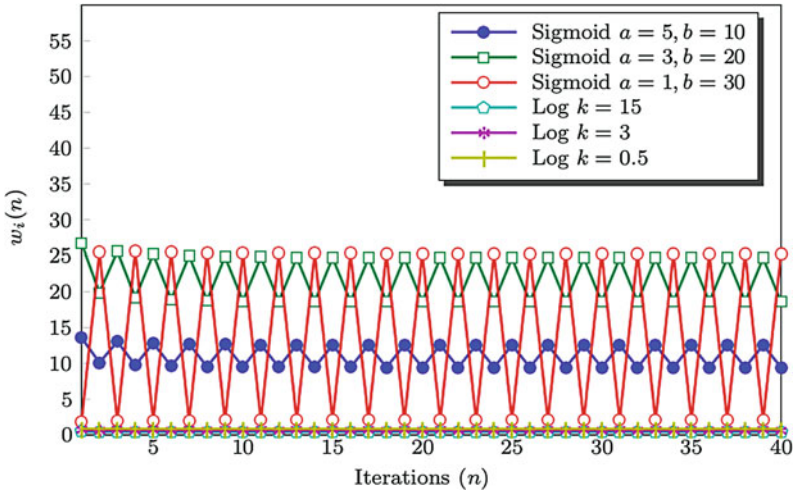

Fig. 11 The bid convergence $w_i(n)$ of Algorithm in (1) and (2) with number of iterations n for different users and $R = 45$

for subscribers when the traffic load on the cellular system is high. In other words, service providers can motivate subscribers to use the network when the traffic is lower as they pay less for the same QoS. Figure 17 shows the shadow price $p(n)$ with eNodeB rate R. The price is high for high-traffic case (i.e., fixed number of users but less resources, R is small) which decreases for low traffic (i.e., same number of users but more resources, R is large).

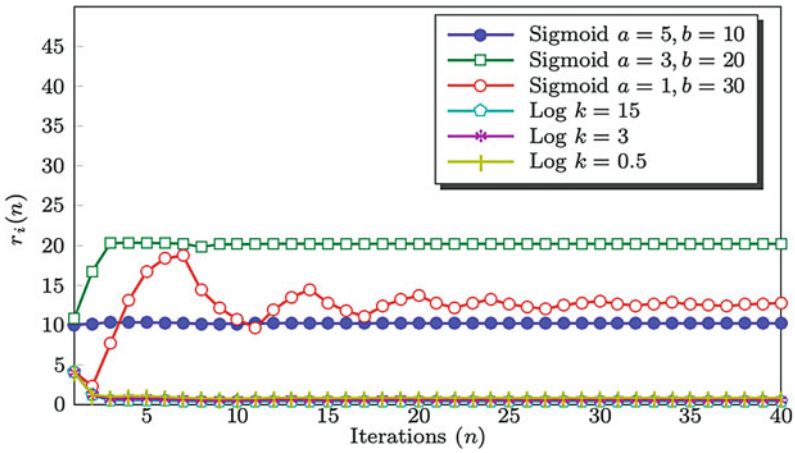

Fig. 12 The rate convergence $r_i(n)$ of Algorithm in (3) and (4) with number of iterations n for different users and $R = 45$

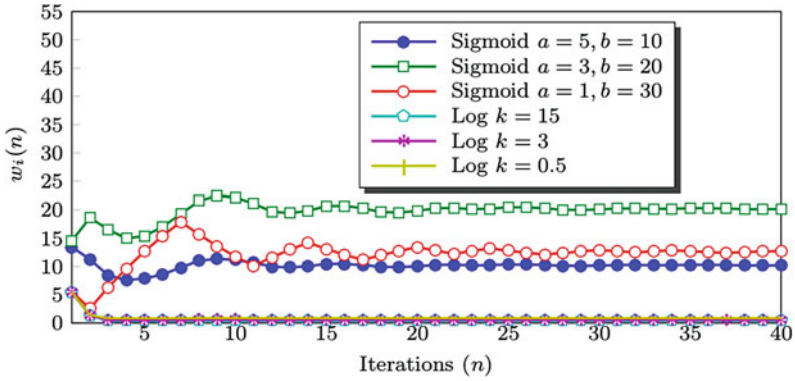

Fig. 13 The bid convergence $w_i(n)$ of Algorithm in (3) and (4) with number of iterations n for different users and $R = 45$

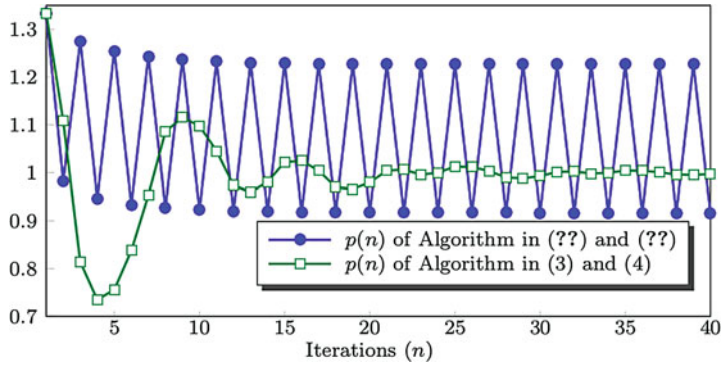

Fig. 14 The shadow price $p(n)$ convergence with the number of iterations n

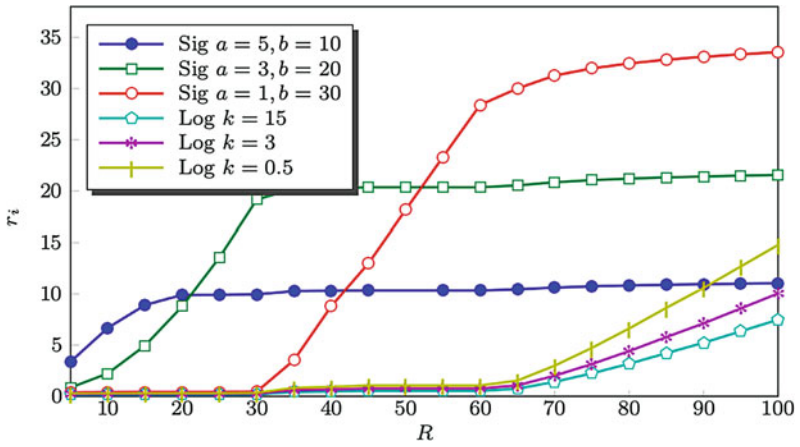

Fig. 15 The allocated rates r_i for different values of R and $\delta = 10^{-3}$ for Algorithm in (3) and (4)

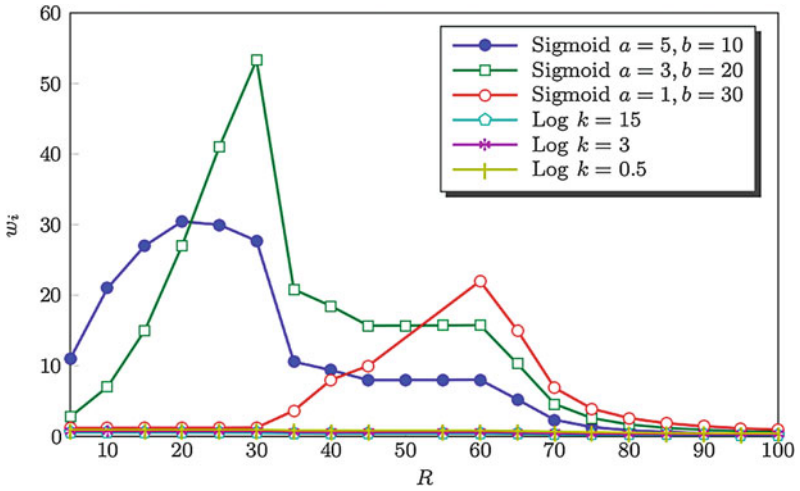

Fig. 16 The final bids w_i for different values of R and $\delta = 10^{-3}$ for Algorithm in (3) and (4)

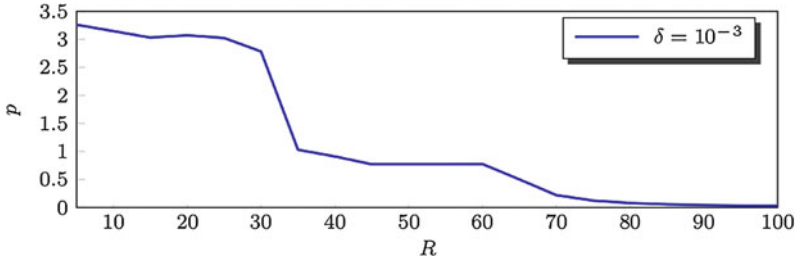

Fig. 17 The final shadow price p for different values of R and $\delta = 10^{-3}$ for Algorithm in (3) and (4)

Multiple-Carrier Scenario

In this scenario, UEs share the spectrum of K carriers eNodeBs. These carriers could be forming macro or small cells, i.e., K cells, with M UEs distributed in these cells. The rate allocated by the lth carrier eNodeB to ith UE is given by r_{li} where $l = \{1, 2, \ldots, K\}$ and $i = \{1, 2, \ldots, M\}$. Each UE has its own utility function $U_i(r_{1i} + r_{2i} + \ldots + r_{Ki})$ that corresponds to the type of traffic being handled by the ith UE. The objective is similar to section "Single-Carrier Scenario" which is to determine the optimal rates that the lth carrier eNodeB should allocate to UEs under its coverage. The utility functions $U_i(r_{1i} + r_{2i} + \ldots + r_{Ki})$ are assumed to be a strictly concave or a sigmoidal-like functions. Hence, the utility functions satisfy the following properties:

- $U_i(0) = 0$ and $U_i(r_{1i} + r_{2i} + \ldots + r_{Ki})$ is an increasing function of r_{li} for all l.
- $U_i(r_{1i} + r_{2i} + \ldots + r_{Ki})$ is twice continuously differentiable in r_{li} for all l.

In our model, we use the normalized sigmoidal-like utility function, as in [37], that can be expressed as

$$U_i(r_{1i} + r_{2i} + \ldots + r_{Ki}) = c_i\left(\frac{1}{1 + e^{-a_i(\sum_{l=1}^{K} r_{li} - b_i)}} - d_i\right) \tag{18}$$

where $c_i = \frac{1+e^{a_i b_i}}{e^{a_i b_i}}$ and $d_i = \frac{1}{1+e^{a_i b_i}}$. So, it satisfies $U_i(0) = 0$ and $U_i(\infty) = 1$. We use the normalized logarithmic utility function, as in [38], that can be expressed as

$$U_i(r_{1i} + r_{2i} + \ldots + r_{Ki}) = \frac{\log(1 + k_i \sum_{l=1}^{K} r_{li})}{\log(1 + k_i r_{\max})} \tag{19}$$

where $r_{\max}$ is the required rate for the user to achieve 100% utilization and k_i is the rate of increase of utilization with allocated rates. So, it satisfies $U_i(0) = 0$ and $U_i(r_{\max}) = 1$. We consider the utility proportional fairness objective function given by

$$\max_{\mathbf{r}} \prod_{i=1}^{M} U_i(r_{1i} + r_{2i} + \ldots + r_{Ki}) \tag{20}$$

where $\mathbf{r} = \{\mathbf{r}_1, \mathbf{r}_2, \ldots, \mathbf{r}_M\}$ and $\mathbf{r}_i = \{r_{1i}, r_{2i}, \ldots, r_{Ki}\}$. This resource allocation objective function has a similar goal which is to allocate the resources that maximizes the total system utility while ensuring proportional fairness between utilities (i.e., the product of the utilities of all UEs). This construction of resource allocation objective function ensures nonzero resource allocation for all users. Therefore, the corresponding resource allocation optimization problem provides minimum QoS for all users. In addition, this approach allocates more resources to users with real-time applications which improves QoS for cellular system.

Hence, the formulation of application-aware resource allocation with spectrum sharing is given by the following optimization problem:

$$\begin{aligned} \max_{\mathbf{r}} \quad & \prod_{i=1}^{M} U_i(r_{1i} + r_{2i} + \ldots + r_{Ki}) \\ \text{subject to} \quad & \sum_{i=1}^{M} r_{1i} \le R_1, \sum_{i=1}^{M} r_{2i} \le R_2, \ldots \\ & \ldots \ , \ \sum_{i=1}^{M} r_{Ki} \le R_K, \\ & r_{li} \ge 0, \quad l = 1, 2, \ldots, K, i = 1, 2, \ldots, M. \end{aligned} \tag{21}$$

where R_l is the total available rate at the lth carrier eNodeB.

Optimality and Subproblems

Similar to the analysis in section "Optimality", the optimization problem (21) can be written as:

$$\begin{aligned} \max_{\mathbf{r}} \quad & \sum_{i=1}^{M} \log\left(U_i(r_{1i} + r_{2i} + \ldots + r_{Ki})\right) \\ \text{subject to} \quad & \sum_{i=1}^{M} r_{1i} \le R_1, \sum_{i=1}^{M} r_{2i} \le R_2, \ldots \\ & \ldots \ , \ \sum_{i=1}^{M} r_{Ki} \le R_K, \\ & r_{li} \ge 0, \quad l = 1, 2, \ldots, K, i = 1, 2, \ldots, M. \end{aligned} \tag{22}$$

For strictly concave utility function in section "Multiple-Carrier Scenario", the utility function is positive $U_i(r_{1i} + \ldots + r_{Ki}) > 0$, increasing, and twice differentiable with respect to r_{li}. Then, it follows that $\frac{\partial U_i(r_{1i}+\ldots+r_{Ki})}{\partial r_{li}} > 0$ and $\frac{\partial^2 U_i(r_{1i}+\ldots+r_{Ki})}{\partial r_{li}^2} < 0$. It follows that the utility function $\log(U_i(r_{1i}+r_{2i}+\ldots+r_{Ki}))$ in the optimization problem (22) has $\frac{\partial \log(U_i(r_{1i}+\ldots+r_{Ki}))}{\partial r_{li}} > 0$ and $\frac{\partial^2 \log(U_i(r_{1i}+\ldots+r_{Ki}))}{\partial r_{li}^2} < 0$. Hence, the strictly concave utility function $U_i(r_{1i}+r_{2i}+\ldots+r_{Ki})$ natural logarithm $\log(U_i(r_{1i} + r_{2i} + \ldots + r_{Ki}))$ is also strictly concave. It follows that the natural logarithm of the logarithmic utility function in equation (19) is strictly concave.

In the sigmoidal-like utility function case, the utility function of the normalized sigmoidal-like function is given by equation (18) as $U_i(r_{1i} + r_{2i} + \ldots + r_{Ki}) = c_i\left(\frac{1}{1+e^{-a_i(\sum_{l=1}^{K} r_{li} - b_i)}} - d_i\right)$. For $0 < \sum_{l=1}^{K} r_{li} < \sum_{l=1}^{K} R_l$, we have

$$0 < 1 - d_i\left(1 + e^{-a_i(\sum_{l=1}^{K} r_{li} - b_i)}\right) < \frac{1}{1 + c_i d_i}.$$

It follows that for $0 < \sum_{l=1}^{K} r_{li} < \sum_{l=1}^{K} R_l$, we have the first and second derivative as $\frac{\partial}{\partial r_{li}} \log U_i(r_{1i} + \ldots + r_{Ki}) > 0$ and $\frac{\partial^2}{\partial r_{li}^2} \log U_i(r_{1i} + \ldots + r_{Ki}) < 0$. Hence, the sigmoidal-like utility function $U_i(r_{1i} + \ldots + r_{Ki})$ natural logarithm $\log(U_i(r_{1i} + \ldots + r_{Ki}))$ is strictly concave function. Then, all the utility functions in our model have strictly concave natural logarithm. Therefore, the optimization problem (22) is a convex optimization problem [10]. The optimization problem (22) is equivalent to optimization problem (21); therefore it is a convex optimization problem. For a convex optimization problem, there exists a unique tractable global optimal solution [9].

Similar to section "UE and eNodeB Subproblems", the optimization problem (22) can be divided into simpler subproblems by using the dual problem. We define the Lagrangian

$$\begin{aligned} L(\mathbf{r}, \mathbf{p}) = &\sum_{i=1}^{M} \log\left(U_i\left(r_{1i} + r_{2i} + \ldots + r_{Ki}\right)\right) \\ &- p_1\left(\sum_{i=1}^{M} r_{1i} + z_1 - R_1\right) - \ldots \\ &- p_K\left(\sum_{i=1}^{M} r_{Ki} + z_K - R_K\right) \end{aligned} \tag{23}$$

where $z_l \geq 0$ is the lth slack variable and p_l is Lagrange multiplier or the shadow price of the lth carrier eNodeB and $\mathbf{p} = \{p_1, p_2, \ldots, p_K\}$. Therefore, the ith UE bid for rate from the lth carrier eNodeB can be written as $w_{li} = p_l r_{li}$, and we have $\sum_{i=1}^{M} w_{li} = p_l \sum_{i=1}^{M} r_{li}$. The first term in equation (23) is separable in $\mathbf{r}_i$. Hence, the dual problem objective function can be written as

$$D(\mathbf{p}) = \sum_{i=1}^{M} \max_{\mathbf{r}_i}\left(L_i\left(\mathbf{r}_i, \mathbf{p}\right)\right) + \sum_{l=1}^{K} p_l(R_l - z_l) \tag{24}$$

and the corresponding dual problem is given by

$$\begin{aligned} \min_{\mathbf{p}} \quad & D(\mathbf{p}) \\ \text{subject to} \quad & p_l \geq 0, \quad l = 1, 2, \ldots, K. \end{aligned} \tag{25}$$

By differentiating $\frac{\partial D(\mathbf{p})}{\partial p_l}$ and substituting by $\sum_{i=1}^{M} w_{li} = p_l \sum_{i=1}^{M} r_{li}$, we have

$$p_l = \frac{\sum_{i=1}^{M} w_{li}}{R_l - z_l}. \tag{26}$$

Now, divide the primal problem (22) into simpler optimization problems in the UEs and the eNodeBs. The ith UE optimization problem is given by:

$$\begin{aligned} \max_{r_i} \quad & \log(U_i(r_{1i} + r_{2i} + \ldots + r_{Ki})) - \sum_{l=1}^{K} p_l r_{li} \\ \text{subject to} \quad & p_l \geq 0 \\ & r_{li} \geq 0, \quad i = 1, 2, \ldots, M, l = 1, 2, \ldots, K. \end{aligned} \tag{27}$$

The second problem is the lth eNodeB optimization problem for rate proportional fairness that is given by:

$$\begin{aligned} \min_{p_l} \quad & D(\mathbf{p}) \\ \text{subject to} \quad & p_l \geq 0. \end{aligned} \tag{28}$$

The minimization of shadow price p_l is achieved by the minimization of the slack variable $z_l \geq 0$ from equation (26). Therefore, the maximum utilization of the lth eNodeB rate R_l is achieved by setting the slack variable $z_l = 0$. In this case, replace the inequality in primal problem (22) constraints by equality constraints and so $\sum_{i=1}^{M} w_{li} = p_l R_l$. Accordingly, $p_l = \frac{\sum_{i=1}^{M} w_{li}}{R_l}$ where $w_{li} = p_l r_{li}$ is transmitted by the ith UE to lth eNodeB. The utility proportional fairness in the objective function of the optimization problem (21) is guaranteed in the solution of the optimization problems (27) and (28).

Distributed Algorithm for Multiple-Carrier Scenario

In this section, a distributed algorithm for multiple-carrier scenario using optimization problems (27) and (28) is presented. The algorithm provides a share spectrum mechanism from multiple carriers simultaneously with an application awareness policy. The algorithm is divided into the ith UE algorithm shown in Algorithm (5) and the lth eNodeB carrier algorithm shown in Algorithm (6). In Algorithms

(5) and (6), the ith UE starts with an initial bid $w_{li}(1)$ which is transmitted to the lth carrier eNodeB. The lth eNodeB calculates the difference between the received bid $w_{li}(n)$ and the previously received bid $w_{li}(n-1)$ and exits if it is less than a prespecified threshold δ. We set $w_{li}(0) = 0$. If the value is greater than the threshold, the lth eNodeB calculates the shadow price $p_l(n) = \frac{\sum_{i=1}^{M} w_{li}(n)}{R_l}$ and sends that value to all the UEs in its coverage area. The ith UE receives the shadow prices p_l from the in-range carrier eNodeBs and compares them to find the first minimum shadow price $p^1_{\min}(n)$ and the corresponding carrier index $l_1 \in L$ where $L \in \{1, 2, \ldots, K\}$. The ith UE solves for the l_1 carrier rate $r_{l_1 i}(n)$ that maximizes $\log U_i(r_{1i} + \ldots + r_{Ki}) - \sum_{l=1}^{K} p_l(n) r_{li}$ with respect to $r_{l_1 i}$. The rate $r^1_i(n) = r_{l_1 i}(n)$ is used to calculate the new bid $w_{l_1 i}(n) = p^1_{\min}(n) r^1_i(n)$. The ith UE sends the value of its new bid $w_{l_1 i}(n)$ to the l_1 carrier eNodeB. Then, the ith selects the second minimum shadow price $p^2_{\min}(n)$ and the corresponding carrier index $l_2 \in L$. The ith UE solves for the l_2 carrier rate $r_{l_2 i}(n)$ that maximizes $\log U_i(r_{1i} + \ldots + r_{Ki}) - \sum_{l=1}^{K} p_l(n) r_{li}$ with respect to $r_{l_2 i}$. The rate $r_{l_2 i}(n)$ subtracted by the rate from l_1 carrier $r^2_i(n) = r_{l_2 i}(n) - r^1_i(n)$ is used to calculate the new bid $w_{l_2 i}(n) = p^2_{\min}(n) r^2_i(n)$ which is sent to l_2 carrier eNodeB. In general, the ith UE selects the mth minimum shadow price $p^m_{\min}(n)$ with carrier index $l_m \in L$ and solves for the l_m carrier rate $r_{l_m i}(n)$ that maximizes $\log U_i(r_{1i} + \ldots + r_{Ki}) - \sum_{l=1}^{K} p_l(n) r_{li}$ with respect to $r_{l_m i}$. The rate $r_{l_m i}(n)$ subtracted by $l_1, l_2, \ldots, l_{m-1}$ carrier rates $r^m_i(n) = r_{l_m i}(n) - (r^1_i(n) + r^2_i(n) + \ldots + r^{m-1}_i(n))$ is used to calculate the new bid $w_{l_m i}(n) = p^m_{\min}(n) r^m_i(n)$ which is sent to l_m carrier eNodeB. This process is repeated until $|w_{li}(n) - w_{li}(n-1)|$ is less than the threshold δ.

This application-aware spectrum sharing algorithm ensures no user is dropped. Additionally, the UE chooses from the nearby carrier eNodeBs the one with the lowest shadow price and request spectrum resources from that carrier eNodeB. If the allocated rate is not enough or the price of the resources increases due to high demand on that carrier eNodeB resources from other UEs, the UE switches to allocate the rest of the required resources from another nearby eNodeB carrier with a lower resource price. This is done iteratively until an equilibrium between demand and supply of resources is achieved and the optimal rates are allocated in the mobile network.

Simulation Example: Two Carriers

In this section, Algorithm in (5) and (6) is used to simulate spectrum sharing of frequency bands of two carriers and 18 UEs shown in Fig. 18. The UEs are divided into three groups. The 1st group is connected to 1st carrier eNodeB only (index $i = 1, 2, 3, 4, 5, 6$), the 2nd group is connected to 2nd carrier eNodeB only (index $i = 7, 8, 9, 10, 11, 12$), and the 3rd group is connected to both 1st and 2nd carrier eNodeBs (index $i = 13, 14, 15, 16, 17, 18$). Hence, the 3rd group of users experiences spectrum sharing from 1st and 2nd carrier eNodeBs. Similar utility functions as in section "Simulation Example: One Carrier", shown in Fig. 5,

Algorithm 5 The ith UE algorithm for multiple-carrier scenario

Send initial bid $w_{li}(1)$ to lth carrier eNodeB (where $l \in L = \{1, 2, \ldots, K\}$)
loop
  Receive shadow prices $p_{l \in L}(n)$ from all in range carriers eNodeBs
  if STOP from all in range carriers eNodeBs **then**
    Calculate allocated rates $r_{li}^{\text{opt}} = \frac{w_{li}(n)}{p_l(n)}$
    STOP
  else
    Set $p_{\min}^0 = \{\}$ and $r_i^0 = 0$
    for $m = 1 \rightarrow K$ **do**
      $p_{\min}^m(n) = \min(\mathbf{p} \setminus \{p_{\min}^0, p_{\min}^1, \ldots, p_{\min}^{m-1}\})$
      $l_m = \{l \in L : p_l = \min(\mathbf{p} \setminus \{p_{\min}^0, p_{\min}^1, \ldots, p_{\min}^{m-1}\})\}$ {l_m is the index of the corresponding carrier}
      Solve $r_{l_m i}(n) = \arg\max_{r_{l_m i}} \left(\log U_i(r_{1i} + \ldots + r_{Ki}) - \sum_{l=1}^{K} p_l(n) r_{li} \right)$ for the l_m carrier eNodeB
      $r_i^m(n) = r_{l_m i}(n) - \sum_{j=0}^{m-1} r_i^j(n)$
      if $r_i^m(n) < 0$ **then**
        Set $r_i^m(n) = 0$
      end if
      Calculate new bid $w_{l_m i}(n) = p_{\min}^m(n) r_i^m(n)$
      if $|w_{l_m i}(n) - w_{l_m i}(n-1)| > \Delta w(n)$ **then**
        $w_{l_m i}(n) = w_i(n-1) + \text{sign}(w_{l_m i}(n) - w_{l_m i}(n-1)) \Delta w(n)$ {$\Delta w = h_1 e^{-\frac{n}{h_2}}$ or $\Delta w = \frac{h_3}{n}$}
      end if
    end for
  end if
end loop

Algorithm 6 The lth eNodeB algorithm for multiple-carrier scenario

loop
  Receive bids $w_{li}(n)$ from UEs {Let $w_{li}(0) = 0 \ \forall i$}
  if $|w_{li}(n) - w_{li}(n-1)| < \delta \ \forall i$ **then**
    Allocate rates, $r_{li}^{\text{opt}} = \frac{w_{li}(n)}{p_l(n)}$ to ith UE
    STOP
  else
    Calculate $p_l(n) = \frac{\sum_{i=1}^{M} w_{li}(n)}{R_l}$
    Send new shadow price $p_l(n)$ to all UEs
  end if
end loop

are used. UEs with indexes $i = \{1, 7, 13\}$ have utility parameters $a = 5$ and $b = 10$, indexes $i = \{2, 8, 14\}$ have utility parameters $a = 3$ and $b = 20$, and indexes $i = \{3, 9, 15\}$ have utility parameters $a = 1$ and $b = 30$, while UEs with indexes $i = \{4, 10, 16\}$ have utility parameters $k = 15$ and $r_{\max} = 100$, indexes $i = \{5, 11, 17\}$ have utility parameters $k = 3$ and $r_{\max} = 100$, and indexes $i = \{6, 12, 18\}$ have utility parameters $k = 0.5$ and $r_{\max} = 100$.

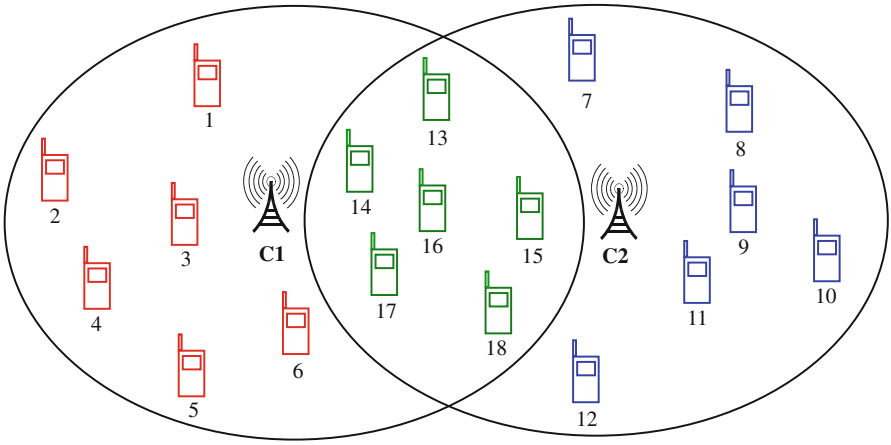

Fig. 18 System model with three groups of users and two carriers. The 1st group with UE indexes $i = \{1, 2, 3, 4, 5, 6\}$ (*red*), 2nd group with UE indexes $i = \{7, 8, 9, 10, 11, 12\}$ (*blue*), and 3rd group with UE indexes $i = \{13, 14, 15, 16, 17, 18\}$ (*green*)

The simulation setup is $\delta = 10^{-3}$, the 1st carrier eNodeB rate R_1 takes values between 20 and 300 with step of 10, and the 2nd carrier eNodeB rate is fixed at $R_2 = 100$. In Fig. 19, the final rates of different users with different 1st carrier eNodeB total rates R_1 are shown. In Fig. 19a, c, the increase in the rate allocated to the users of 1st and 3rd groups is due to the increase in R_1 (i.e., in range carrier). In Fig. 19b, the increase in the rate allocated to the users of 2nd groups is associated with the increase in R_1 (i.e., out of range carrier). This is due to the decrease in the number of users requesting resources from the 2nd carrier eNodeB (the users of the 3rd group allocate most of their rates from the resources of 1st carrier eNodeB and so decrease the load/demand on the 2nd carrier eNodeB). In spite of fixed 2nd carrier eNodeB rate at $R_2 = 100$, an increase in the allocated rates in the 2nd group is observed with the increase in R_1. This is more clear when monitoring the change in the rates allocated to the 3rd group of users from the 1st carrier eNodeB in Fig. 20a and from the 2nd carrier eNodeB in Fig. 20b. In Fig. 20a, b, when the resources available at the 2nd carrier is more than that at 1st carrier, most of the 3rd group rates are allocated by the 2nd carrier. With the increase in R_1, a gradual increase in the 3rd group rates allocated from the 1st carrier is observed as well as a gradual decrease from the 2nd carrier eNodeB resources. This shift in the resource allocation increases the available resources to be allocated to 2nd group of users by 2nd carrier eNodeB.

The final bids of different users with different values of R_1 are shown in Fig. 21. It is observed that the users bid high when the resources are scarce and their bids decrease as R_1 increases. Hence, pricing in this model is traffic-dependent

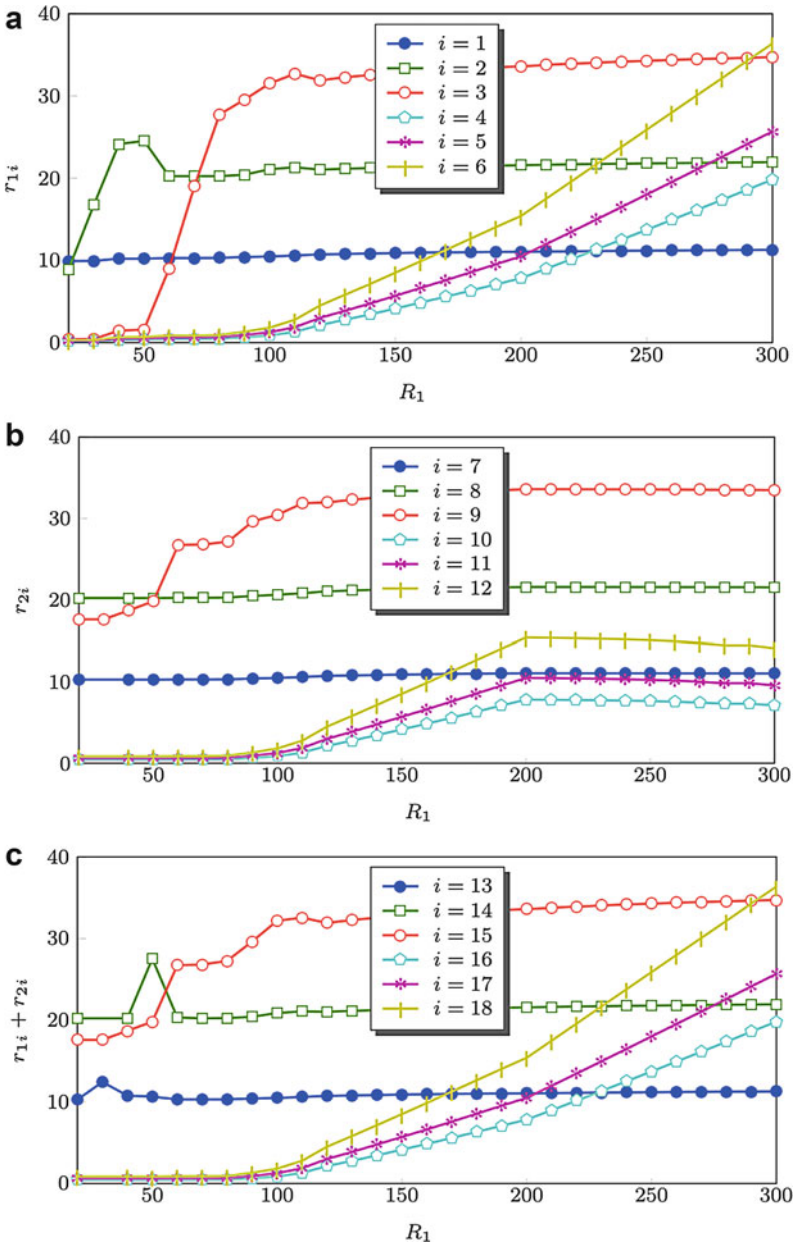

Fig. 19 The rates r_{li} of the 3rd group of users verses 1st carrier rate $20 < R_1 < 300$ with 2nd carrier rate fixed at $R_2 = 100$. (**a**) The rates allocated r_{1i} from the 1st carrier eNodeB to users of the 1st group (i.e., $i = 1, 2, 3, 4, 5, 6$). (**b**) The rates allocated r_{2i} from 2nd carrier eNodeB to users of the 2nd group (i.e., $i = 7, 8, 9, 10, 11, 12$). (**c**) The rates allocated $r_{1i} + r_{2i}$ from 1st and 2nd carriers eNodeBs to users of the 3rd group (i.e., $i = 13, 14, 15, 16, 17, 18$)

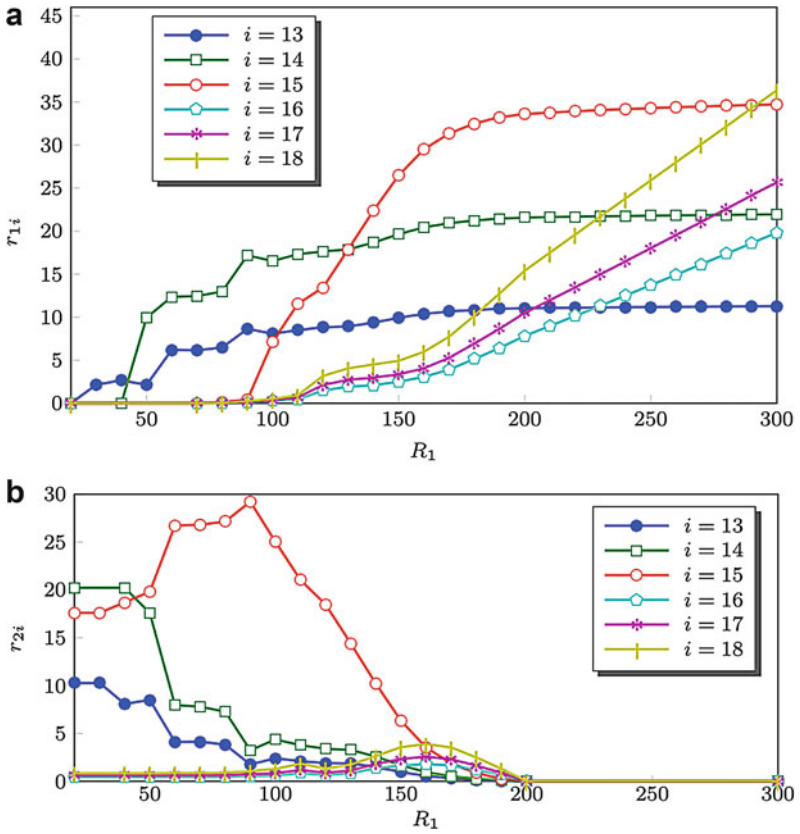

Fig. 20 The allocated rates r_{li} from the lth carrier eNodeB to the 3rd group of users with 1st carrier eNodeB rate $20 < R_1 < 300$ and 2nd carrier eNodeB rate fixed at $R_2 = 100$. (**a**) The allocated rates r_{1i} from the 1st carrier eNodeB to the 3rd group of users. (**b**) The allocated rates r_{2i} from the 2nd carrier eNodeB to the 3rd group of users

(i.e., demand by users increase the price increase and vice versa). In Fig. 21a, c, the decrease in the 1st and 3rd group users' bids with the increase in R_1 is noticeable. The supply increases, and the demand is still the same. In Fig. 21b, the decrease in the 2nd group users' bids with the increase in R_1 (which is an out-of-range carrier) is observable. This is due to the decrease in the demand on 2nd carrier eNodeB resources with fixed supply from 2nd carrier. In Fig. 22, the shadow price of the 1st carrier eNodeB is higher than that of 2nd carrier eNodeB for $R_1 \leq 50$, approximately equal for $60 < R_1 \leq 200$, and lower for $R_1 > 200$. This shows how it is very efficient to have joint carrier aggregation on the pricing of the user. In addition, provided this traffic-dependent pricing, the network providers can flatten the traffic specially during peak hours by setting traffic-dependent bandwidth resource price, which gives an incentive for users to use the network during less-congested hours.

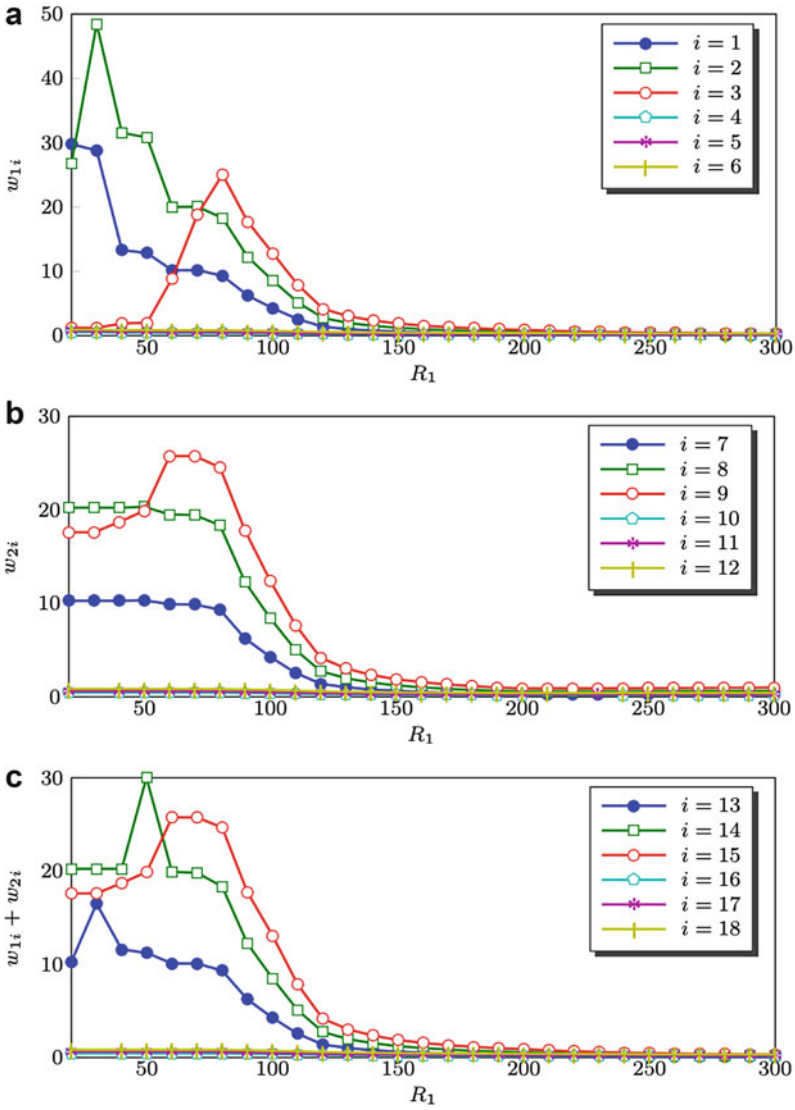

Fig. 21 The users final bids w_{1i} (i.e., network provider pricing) for the three group of users vs 1st carrier eNodeB available rate $20 < R_1 < 300$ with 2nd carrier rate fixed at $R_2 = 100$. (**a**) The bids w_{1i} of users of the 1st group (i.e., $i = 1, 2, 3, 4, 5, 6$). (**b**) The bids w_{2i} of users of the 2nd group (i.e., $i = 7, 8, 9, 10, 11, 12$). (**c**) The bids $w_{1i} + w_{2i}$ of users of the 3rd group (i.e., $i = 13, 14, 15, 16, 17, 18$)

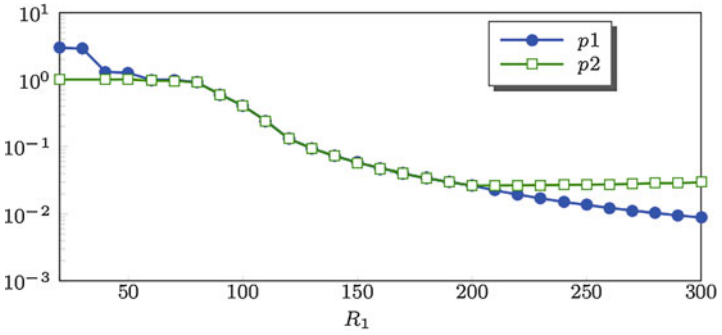

Fig. 22 The 1st carrier shadow price p_1 and 2nd carrier shadow price p_2 with the 1st carrier eNodeB rate $20 < R_1 < 300$ and the 2nd carrier eNodeB rate $R_2 = 100$

Conclusion and Future Direction

In this chapter, an application-aware optimization problem for UEs with delay-tolerant and real-time applications in cellular networks is presented. Two scenarios are discussed, i.e., one-carrier scenario and multiple-carrier scenario. Starting with one-carrier scenario, the global optimal solution exists and is tractable for the resource allocation optimization problem for UEs with logarithmic (delay-tolerant applications) and sigmoidal-like (real-time application) utility functions. A distributed algorithm for allocating the eNodeB resources optimally to the UEs is presented. Additionally, convergence analysis is discussed. A solution for ensuring convergence for different network traffic conditions is discussed. Hence, this modified robust algorithm converges for high and low traffic loads. The algorithm is aware of different applications and ensures fairness in the utility percentage achieved by the allocated resources for all the users. Therefore, the algorithm gives priority to the users with real-time applications over delay-tolerant applications. In addition, a minimum resource allocation for users with elastic or inelastic traffic is guaranteed to satisfy a minimum QoS for all service subscribers. Simulations provide that the robust algorithm converges to the optimal rates and allocates the eNodeB resources with priority to users running real-time applications. For multiple-carrier scenario, spectrum sharing through carrier aggregation is presented. The assumptions of applications running on smart phones are similar to one-carrier scenario. But in this case, users share multiple bands in an application-aware scheme. Optimality is shown for this scenario as well, and robustness of convergence is considered in the resource allocation algorithm design. Simulations provided for the two-carrier scenario for a proof of concept. The algorithm guarantees allocating resources from the carrier with the lowest resource price for the user. Hence, the algorithm converges to the optimal rate allocation with the lowest possible resource price.

The algorithms discussed in this chapter can be extended to include cellular system features such as frequency reuse [6]. Additionally, resource block allocation

problems for an application-aware spectrum sharing can be included in the mathematical model presented in this chapter. Some preliminary examples are shown in [17, 23]. The algorithm, presented in this chapter, provides a pricing approach for network providers to flatten network traffic over time. Hence, it provides a traffic-dependent pricing approach. This could be utilized to give the subscribers the incentive to decrease the cost of using the network by choosing to access the network at low-cost low-traffic load time. Additionally, the provided algorithm in this chapter can be extended to a centralized method rather than distributed to minimize overheads; more details are in [24].

The presented techniques could be used for allocating resources for smart grids and power system as well, for example, the extension of the research work in [31] to include sigmoidal-like utilities. Additionally, the pricing incentive used in the presented model could be extended to improve smart grid current models, e.g., [11]. Finally, this work can provide a platform for sharing radar spectrum with communication systems. For instance, carrier aggregation between radar and communication bands can improve the overall user QoS as shown in [22], radar transmitters can be utilized as auxiliary network base stations as shown in [4], and cooperative radar and communications signaling schemes can be considered as shown in [13, 14].

References

1. Abdelhadi A, Clancy T (2013) A robust optimal rate allocation algorithm and pricing policy for hybrid traffic in 4G-LTE. In: IEEE International Symposium on Personal, Indoor, and Mobile Radio Communications (PIMRC)
2. Abdelhadi A, Clancy T (2014) A utility proportional fairness approach for resource allocation in 4G-LTE. In: IEEE International Conference on Computing, Networking, and Communications (ICNC), CNC Workshop
3. Abdelhadi A, Clancy C (2015) An optimal resource allocation with joint carrier aggregation in 4G-LTE. In: 2015 International Conference on Computing, Networking and Communications (ICNC), pp 138–142
4. Abdelhadi A, Clancy TC (2016) Network MIMO with partial cooperation between radar and cellular systems. In: 2016 International Conference on Computing, Networking and Communications (ICNC), pp 1–5. https://doi.org/10.1109/ICCNC.2016.7440576
5. Abdelhadi A, Clancy TC (2016) Optimal context-aware resource allocation in cellular networks. In: 2016 International Conference on Computing, Networking and Communications (ICNC), pp 1–5
6. Abdelhadi A, Clancy TC (2016) An optimal resource allocation with frequency reuse in cellular networks. In: 2016 International Conference on Computing, Networking and Communications (ICNC), pp 1–5. https://doi.org/10.1109/ICCNC.2016.7440718
7. Abdelhadi A, Khawar A, Clancy TC (2015) Optimal downlink power allocation in cellular networks. Phys Commun 17:1–14
8. Bertsekas D (2009) Convex optimization theory. Athena scientific optimization and computation series. Athena Scientific. https://books.google.com/books?id=0H1iQwAACAAJ
9. Bertsekas DP (2015) Convex optimization algorithms. Athena Scientific, Nashua. http://opac.inria.fr/record=b1135903
10. Boyd S, Vandenberghe L (2004) Convex optimization. Cambridge University Press, New York

11. Chen L, Li N, Low SH, Doyle JC (2010) Two market models for demand response in power networks. IEEE Smart Grid Commun 10:397–402
12. Chiang M, Low SH, Calderbank AR, Doyle JC (2007) Layering as optimization decomposition: a mathematical theory of network architectures. Proc IEEE 95(1):255–312
13. Chiriyath AR, Bliss DW (2015) Joint radar-communications performance bounds: data versus estimation information rates. In: MILCOM 2015–2015 IEEE Military Communications Conference, pp 1491–1496. https://doi.org/10.1109/MILCOM.2015.7357655
14. Chiriyath AR, Paul B, Jacyna GM, Bliss DW (2016) Inner bounds on performance of radar and communications co-existence. IEEE Trans Signal Process 64(2):464–474. https://doi.org/10.1109/TSP.2015.2483485
15. Dianati M, Shen X, Naik K (2007) Cooperative fair scheduling for the downlink of CDMA cellular networks. IEEE Trans Veh Technol 56(4):1749–1760. https://doi.org/10.1109/TVT.2007.897209
16. Ekstrom H (2009) QoS control in the 3GPP evolved packet system. IEEE Commun Mag 47(2):76 –83. https://doi.org/10.1109/MCOM.2009.4785383
17. Erpek T, Abdelhadi A, Clancy C (2015) An optimal application-aware resource block scheduling in LTE. In: IEEE International Conference on Computing, Networking and Communications (ICNC) Worshop (CCS)
18. Erpek T, Abdelhadi A, Clancy TC (2016) Application-aware resource block and power allocation for LTE. In: 2016 Annual IEEE Systems Conference (SysCon), pp 1–5. https://doi.org/10.1109/SYSCON.2016.7490591
19. FCC (2010) Connecting America: the national broadband plan. http://download.broadband.gov/plan/national-broadband-plan.pdf, http://download.broadband.gov/plan/national-broadband-plan.pdf
20. Federal Communications Commission (FCC) (2006) In the matter of revision of parts 2 and 15 of the commission's rules to permit unlicensed national information infrastructure (U-NII) devices in the 5 GHz band. MO&O, ET Docket No. 03-122
21. Federal Communications Commission (FCC) (2012) FCC proposes innovative small cell use in 3.5 GHz band. Online: http://www.fcc.gov/document/fcc-proposes-innovative-small-cell-use-35-ghz-band, http://www.fcc.gov/document/fcc-proposes-innovative-small-cell-use-35-ghz-band
22. Ghorbanzadeh M, Abdelhadi A, Clancy C (2014) A utility proportional fairness resource allocation in spectrally radar-coexistent cellular networks. In: Military Communications Conference (MILCOM)
23. Ghorbanzadeh M, Abdelhadi A, Clancy T (2015) A utility proportional fairness approach for resource block allocation in cellular networks. In: IEEE International Conference on Computing, Networking and Communications (ICNC)
24. Ghorbonzadeh M, Abdelhadi A, Clancy TC (2017) Cellular communications systems in congested environments: resource allocation and end-to-end quality of service solutions with MATLAB. Springer International Publishing, Switzerland
25. Ha S, Sen S, Joe-Wong C, Im Y, Chiang M (2012) Tube: time-dependent pricing for mobile data. In: Proceedings of the ACM SIGCOMM 2012 Conference on Applications, Technologies, Architectures, and Protocols for Computer Communication, SIGCOMM '12. ACM, New York, pp 247–258. https://doi.org/10.1145/2342356.2342402. http://doi.acm.org/10.1145/2342356.2342402
26. Harks T (2005) Utility proportional fair bandwidth allocation: an optimization oriented approach. In: QoS-IP, pp 61–74
27. Kelly F (1997) Charging and rate control for elastic traffic. Eur Trans Telecommun 8(1):33–37
28. Kelly F, Maulloo A, Tan D (1998) Rate control in communication networks: shadow prices, proportional fairness and stability. J Oper Res Soc 49. citeseer.ist.psu.edu/kelly98rate.html
29. Kurrle RL (2012) Resource allocation for smart phones in 4G LTE advanced carrier aggregation. MS Thesis, Virginia Tech

30. Lee JW, Mazumdar RR, Shroff NB (2005) Downlink power allocation for multi-class wireless systems. IEEE/ACM Trans Netw 13(4):854–867. https://doi.org/10.1109/TNET.2005.852888. http://doi.org/10.1109/TNET.2005.852888
31. Li N, Chen L, Low SH (2011) Optimal demand response based on utility maximization in power networks. In: 2011 IEEE Power and Energy Society General Meeting, pp 1–8. https://doi.org/10.1109/PES.2011.6039082
32. Low SH, Lapsley DE (1999) Optimization flow control, I: basic algorithm and convergence. IEEE/ACM Trans Netw 7(6):861–874
33. Nandagopal T, Kim TE, Gao X, Bharghavan V (2000) Achieving MAC layer fairness in wireless packet networks. In: Proceedings of the 6th Annual International Conference on Mobile Computing and Networking, MobiCom'00. ACM, New York, pp 87–98. https://doi.org/10.1145/345910.345925. http://doi.acm.org/10.1145/345910.345925
34. National Telecommunications and Information Administration (NTIA) (2012) Analysis and resolution of RF interference to radars operating in the band 2700–2900 MHz from broadband communication transmitters. Online, NTIA Report 13-490. https://www.its.bldrdoc.gov/publications/download/13-490.pdf
35. Parkvall S, Furuskar A, Dahlman E (2011) Evolution of LTE toward IMT-advanced. IEEE Commun Mag 49(2):84–91. https://doi.org/10.1109/MCOM.2011.5706315
36. PCAST (2012) Final PCAST Spectrum Report
37. Shajaiah H, Abdelhadi A, Clancy T (2013) Utility proportional fairness resource allocation with carrier aggregation in 4G-LTE. In: IEEE Military Communications Conference (MILCOM)
38. Shajaiah H, Abdelhadi A, Clancy T (2014) Multi-application resource allocation with users discrimination in cellular networks. In: IEEE International Symposium on Personal, Indoor and Mobile Radio Communications (PIMRC)
39. Shajaiah H, Abdelhadi A, Clancy T (2014) Spectrum sharing between public safety and commercial users in 4G-LTE. In: IEEE International Conference on Computing, Networking and Communications (ICNC)
40. Shajaiah H, Abdelhadi A, Clancy C (2015) A price selective centralized algorithm for resource allocation with carrier aggregation in LTE cellular networks. In: 2015 IEEE Wireless Communications and Networking Conference (WCNC), pp 813–818. https://doi.org/10.1109/WCNC.2015.7127574
41. Shenker S (1995) Fundamental design issues for the future internet. IEEE J Sel Areas Commun 13:1176–1188
42. Tsai PL, Lin KJ, Chen WT (2014) Downlink radio resource allocation with carrier aggregation in MIMO LTE-advanced systems. In: 2014 IEEE International Conference on Communications (ICC), pp 2332–2337. https://doi.org/10.1109/ICC.2014.6883671
43. Tychogiorgos G, Gkelias A, Leung KK (2011) A new distributed optimization framework for hybrid ad-hoc networks. In: GLOBECOM Workshops, pp 293–297
44. Tychogiorgos G, Gkelias A, Leung KK (2011) Towards a fair non-convex resource allocation in wireless networks. In: PIMRC, pp 36–40
45. Tychogiorgos G, Gkelias A, Leung KK (2012) Utility-proportional fairness in wireless networks. In: PIMRC, IEEE, pp 839–844
46. Wang Y, Abdelhadi A (2016) A QoS-based power allocation for cellular users with different modulations. In: 2016 International Conference on Computing, Networking and Communications (ICNC), pp 1–5. https://doi.org/10.1109/ICCNC.2016.7440595
47. Wang Y, Abdelhadi A, Clancy TC (2016) Optimal power allocation for LTE users with different modulations. In: 2016 Annual IEEE Systems Conference (SysCon), pp 1–5. https://doi.org/10.1109/SYSCON.2016.7490537
48. Wang Y, Pedersen K, Mogensen P, Sorensen T (2009) Resource allocation considerations for multi-carrier LTE-advanced systems operating in backward compatible mode. In: 2009 IEEE 20th International Symposium on Personal, Indoor and Mobile Radio Communications, pp 370–374. https://doi.org/10.1109/PIMRC.2009.5450150

49. Wang Y, Pedersen K, Sorensen T, Mogensen P (2011) Utility maximization in LTE-advanced systems with carrier aggregation. In: 2011 IEEE 73rd Vehicular Technology Conference (VTC Spring), pp 1–5. https://doi.org/10.1109/VETECS.2011.5956494
50. Yuan G, Zhang X, Wang W, Yang Y (2010) Carrier aggregation for LTE-advanced mobile communication systems. In: IEEE Commun Mag 48:88–93

Autonomous Spectrum Sharing by Well-Designed Games

14

Jie Ren, Kai-Kit Wong, and Muhammad R. A. Khandaker

Contents

J. Ren (✉)
Electronic and Information Engineering, Beijing Jiaotong University, Beijing, China
e-mail: renjie@bjtu.edu.cn

K.-K. Wong · M. R. A. Khandaker
Electronic and Electrical Engineering, University College London, London, UK
e-mail: kai-kit.wong@ucl.ac.uk; m.khandaker@ucl.ac.uk

W. Zhang (ed.), *Handbook of Cognitive Radio*,
https://doi.org/10.1007/978-981-10-1394-2_14

Abstract

From static spectrum allocation to nowadays more liberated policies such as spectrum refarming or even opportunistically exploiting the so-called spectrum holes or "white spaces," we have witnessed many changes all over the world regarding how spectrum is being allocated. The message is clear, and that spectrum allocation needs to be more dynamic and adaptive to the environment and applications. However, dynamic spectrum sharing and access is complicated in many ways. Firstly, it requires global knowledge of channel states for all communication links in the entire network and, secondly, the required large-scale optimization would be computationally prohibitive to achieve, not to mention that channel states vary over time as well. Importantly, there is a strong desire that such dynamic spectrum sharing be realized by a large number of uncoordinated mobile radios in a distributed and autonomous fashion. This is the focus of this chapter which discusses game-theoretic methods for self-optimization of cognitive mobile radios in spectrum sharing. The chapter will begin by reviewing the not-so-flexible spectrum management in cellular networks and then covering the topics of using forward-looking games in spectrum allocation. A major result is that autonomous spectrum sharing leading to spectral-efficient solutions is shown possible by well-designed games requiring only local channel knowledge at individual mobile radios and such interactive self-optimization can also be employed under the hierarchical spectrum sharing model in which primary spectrum owners are present and need to be protected.

Introduction

Wireless is an open medium that has not only given us the convenience for boundaryless communications, but its openness is unfortunately exposed to unwanted interference. For wireless communications to be useful, simultaneous communications have to be managed in a way that mutual interference is either eliminated or controlled to an acceptable level. In the past, this was usually achieved by separating coexisting communication links onto disjoint radio resource units (e.g., time, frequency, code, etc.), and occupying the same radio channel was deemed destructive and therefore prohibitive. On the policy level, this approach implies an exclusive use spectrum allocation model which grants exclusive use to licensees who pay multibillion dollars for several MHz of spectrum. This static spectrum management policy has, nevertheless, fueled the misbelief that the spectrum was precious.

The fundamental problem of today's wireless communications provision is spectrum scarcity because the usable spectrum is inevitably limited, while the demand is kept on increasing at an alarming rate. The wasteful static allocations

from tight regulations on the spectrum use and lack of network coordination have made the problem even worse [1]. Historically, spectrum regulation is more about "command and control" with primary considerations on economics and politics. Since mid-1980s, a market-based approach by various forms of auction has been adopted to assign new spectrum. A well-known example was the multibillion dollars price for a 20 MHz frequency band at the European 3G spectrum auction [2].

In the command-and-control management approach, the allocation decisions are often static in both temporal and spatial dimensions, which are valid for extended periods of time (usually 10s of years) and for large geographical regions (countrywide). The usage for each spectrum band is often set to be exclusive to a single provider (licensee), hence maintaining interference-free communication. However, this approach is unable to encourage the development and use of some spectrum-efficient technologies because it may not provide the freedom needed for these technologies to operate across existing spectrum designations.

The issue is further clarified by the regulatory bodies such as FCC in the USA and Ofcom in the UK, reporting that most of the radio spectrum was inefficiently utilized and that spectrum usage depends strongly on both time and place. For example, amateur radio and paging frequencies are very lightly loaded most of the time. Spectrum will become abundant if these spectrum holes, a.k.a. "white spaces," can be released for use by other users in need. In an attempt to unlock those available spectrum spaces, we have witnessed some radical changes on spectrum allocation in recent years worldwide. For instance, FCC has reclaimed approximately 85 MHz of UHF broadcast spectrum and authorized the reuse of 500 MHz of spectrum for a novel tower-based video and data service that shares spectrum with existing satellite television. Germany also switched off analogue broadcasting in Berlin and reclaimed the spectrum for other uses. In the UK, Ofcom also granted permission to the UK's mobile operators to redeploy their existing 2G and 3G radio spectrum for 4G services in 2013. The decision was Ofcom's one of many attempts to liberalize mobile spectrum for use with all currently available technologies for improved spectrum utilization. It is also anticipated that there will be relaxation of the commercial limitations on existing spectrum licenses by, for example, granting existing mobile radio licensees the right to lease or resell their spectrum to third parties that value it most. An example of this was the May 2003 order by FCC in the USA, permitting cellular licensees to lease some or their entire spectrum, reshaping the market, and leading to a new business model for service providers.

Recognizing the fact that the low spectral efficiency is all down to the rigid and inflexible use of spectrum, there have been restless efforts attempting to make spectrum utilization more intelligent, from reusing the frequency bands of the macrocells for small cells in a heterogeneous network (HetNet) to a conventional cellular network permitting the use of frequency channels in adjacent cells and to the dynamic frequency allocation autonomously achieved by a self-organizing group of cognitive radios in an open spectrum access environment, just to name a few.

The focus of this chapter is on *autonomous dynamic spectrum access technologies* that allow mobile radios to compete and share the same spectrum in a healthy and self-organizing fashion without coordination. This setup is motivated by the new

understanding of spectrum scarcity together with the increasing capability of mobile handsets, leading to reconfigurable software-defined radios, a.k.a. *cognitive radios*, which are expected to possess the ability to sense, observe the radio environment, and adapt their operating parameters for optimized performance on the fly.

Before we describe autonomous technologies for dynamic spectrum access, this chapter will first review the spectrum management in cellular networks in section "Spectrum Management in Cellular Networks" and the well-known models for dynamic spectrum access in section "Models for Dynamic Spectrum Access Strategies." In section "Dynamic Spectrum Access as a Global Resource Allocation Optimization Problem," we describe the orthogonal frequency-division multiple-access (OFDMA) interference channel model and use it as the model to discuss how to achieve the optimal frequency allocation to users, if a centralized spectrum manager exists. Section "The OFDMA Forward-Looking Game" then views the OFDMA interference channel as a resource competition game with radio users modeled as players so that self-optimization of the radio users can be investigated and analyzed. In particular, section "The OFDMA Forward-Looking Game" will introduce the forward-looking game, a specific type of games that is especially useful for designing efficient games. This chapter will be concluded by considering the cognitive radio scenarios where the frequency allocation of the secondary users (SUs) is optimized autonomously and at the same time avoiding the channels occupied by the primary users (PUs) by using well-designed games. Concluding remarks will be provided in section "Conclusions."

Spectrum Management in Cellular Networks

Radio spectrum is a precious natural resource, and mobile service providers need to pay billions and billions of dollars to operate on those designated frequency bands. Notwithstanding this, providing radio coverage is far more challenging than simply assigning a band to a service user. First, in order to generate revenues, there is a strong desire to cope with as many users as possible for the given bandwidth, with the aim to maximizing the spectral efficiency (sometimes measured in bps/Hz/km^2). In addition, coverage is an important criterion for reflecting the quality of service (QoS) of a mobile service operator. Nevertheless, a radio base station can provide radio coverage over only a limited area because the power of a radio wave attenuates as it propagates, regardless of whether it is in indoor or outdoor. It is thus important not to drain the power of the base station while not compromising the coverage. Meeting these mutually conflicting objectives requires the cellular radio approach.

In a cellular radio system, a large area is divided into many small areas (usually called *cells*), each of which is served by a base station located at the center of the cell. When joined together, these cells provide radio coverage over a wide geographic area. This enables a large number of portable transceivers (e.g., mobile phones, etc.) to communicate with each other anywhere in the network, via base stations.

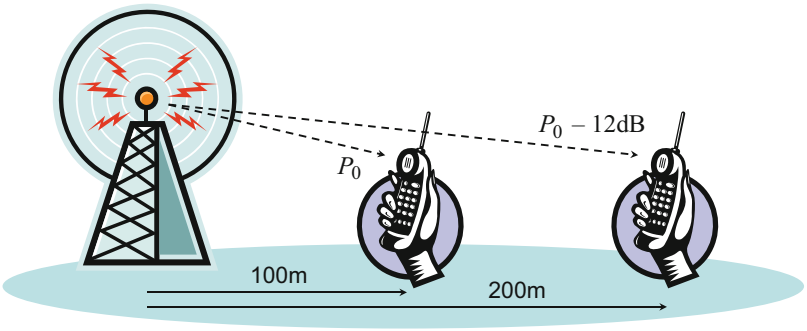

Fig. 1 The range-and-power relationship if $\alpha = 4$

Moving from a single large cell to many small cells has many advantages. First of all, radiation power attenuates severely as it propagates (i.e., $\propto d^{-\alpha}$ with distance d and the pathloss exponent α typically ranging from 3 to 6). Thus, just to extend the range only slightly would require a substantial effort in raising the transmit power of the base station in the downlink (or mobile terminal in the uplink). For instance, as shown in Fig. 1, if we like to extend the range from 100 to 200 m, then one will need to increase its transmit power by 16 times or 12 dB for the same quality to be achieved if $\alpha = 4$. Secondly, in general, the actual coverage of a cell can be very irregular due to different propagation environments in different directions. This will either cause coverage holes (or dead spots) in certain directions or excessive transmit power will have to be used in some directions leading to excessive interference in these directions. This problem will be greatly alleviated if the cell is smaller, hence motivating the small cell architecture in recent years. These properties can be easily converted to increased capacity, larger coverage area, and reduced interference.

The requirement of a cellular radio system is that more base stations need to be placed to provide coverage and they are required to be connected to the mobile switching centers (MSCs) to handle mobility managements and handover from one cell to another. The MSCs are also connected to the wider public switched telephone network (PSTN), a worldwide net of telephone lines, fiber-optic and undersea telephone cables, microwave transmission links, cellular networks, and satellites.

Frequency Reuse

To design a cellular radio system and characterize its network performance, it is required to consider the geometrical tessellation of the overall coverage region. With idealized propagation (i.e., same pathloss properties in all directions, no shadowing and fading), the most natural choice is to fill the region by circular coverage areas; see Fig. 2b. However, circles overlap (or leave gaps) which confuses the responsibility of the base stations. Hexagonal cells are therefore a much better

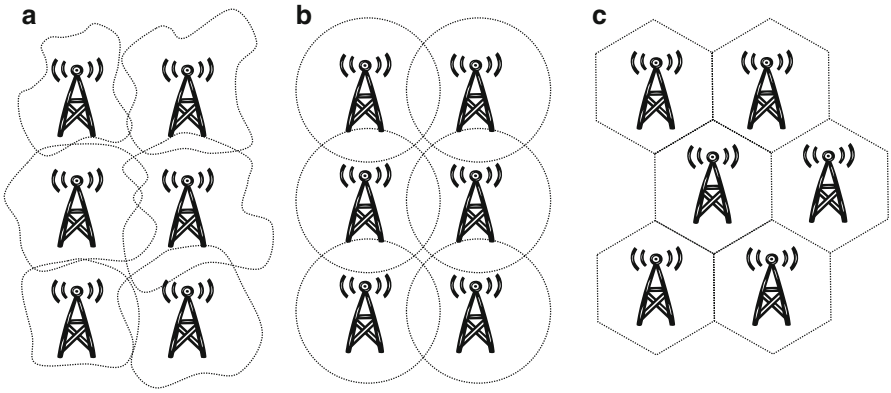

Fig. 2 Illustration of cell tessellation. (**a**) Actual coverage areas. (**b**) Circular coverage areas. (**c**) Hexagonal coverage areas

choice which can partly reflect the circular propagation pattern and fill the area without gaps or overlapping areas, as shown in Fig. 2c.

In conventional designs, the base station of each cell is only responsible for providing coverage of its own cell, and its transmit power should be assigned to just do that. As such, it is possible to reuse the same set of frequency channels at a different cell (referred to as a co-channel cell) or location if it is sufficiently far away so that the interference has traveled long enough to die down to an acceptable level. Frequency reuse is an important concept for cellular networks which allows us to increase the network capacity per unit area. Much of the work for cellular radio system planning is to do with choosing an appropriate *frequency reuse factor* to yield a desirable system performance. Before we discuss this, let us introduce the mathematical tools to describe the frequency reuse system and define the parameters.

For two-dimensional systems, only certain channel reuse patterns are allowable, with a few examples given in Fig. 3. To see this, we define shift parameters, k and l, that range over the positive integers. For hexagonal cells, the procedure for determining co-channel cells is as follows (see Fig. 4a):

- Pick a starting cell with the frequency channel set, say A.
- Move k cells along any one of the six directions perpendicular to the sides of the hexagons.
- Then, turn clockwise 120° and move l cells. The resulting cell is a cell that reuses the same channel set A as the starting cell and is by definition a co-channel cell.
- Repeat the same procedure for each of the other 5 sides of the starting hexagonal cell identifies all the 6 closest co-channel cells. Repeat for each of the co-channel cells will identify all co-channel cells on the entire coverage region.

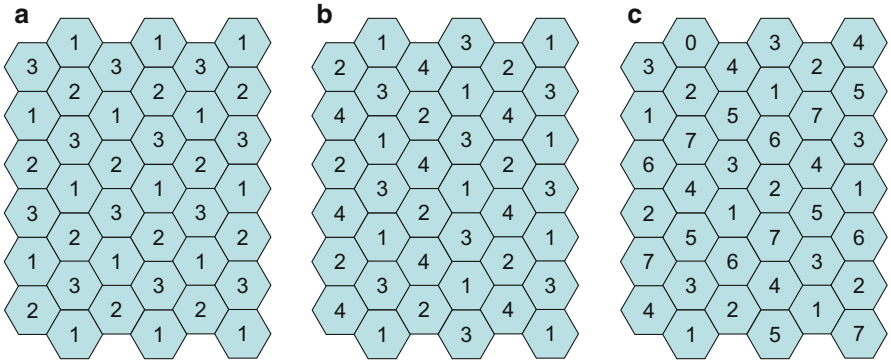

Fig. 3 Examples of cellular systems with different reuse patterns. (**a**) Reuse factor = 3. (**b**) Reuse factor = 4. (**c**) Reuse factor = 7

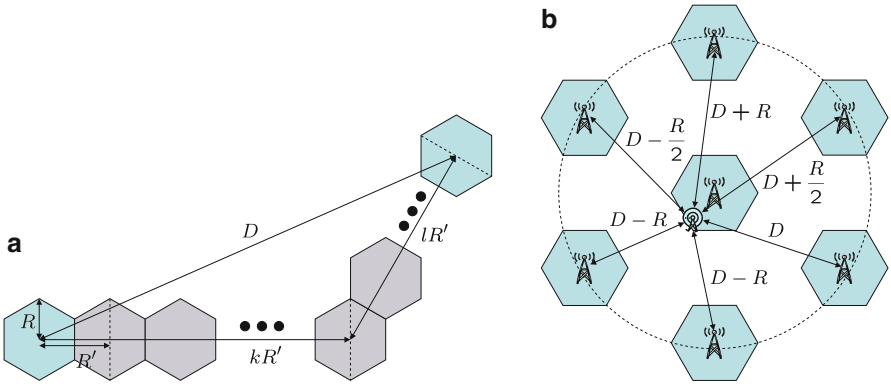

Fig. 4 Identifying the co-channel cell through the shift parameters, k and l. (**a**) Geometry of locating a co-channel cell. (**b**) Worst-case first-tier co-channel interference (CCI) in the downlink

The number of channel sets in the reuse pattern, defined as the *frequency reuse factor*, N, depends on k and l. To obtain N, let R be the radius of each cell, R' be the center-to-cell distance of two neighboring cells, and D be the center-to-center distance of two co-channel cells, as shown in Fig. 4a. As such,

$$N = \frac{\text{Area of the group}}{\text{Area of the cell}} \equiv \frac{A}{a}. \tag{1}$$

The area of the cell, a, can be easily found as

$$a = 6\left(\frac{1}{2}R^2 \sin 60^\circ\right) = \frac{3\sqrt{3}R^2}{2}, \tag{2}$$

while the area of the group, A, can be evaluated similarly by imagining a group radius $\frac{\left(\frac{D}{2}\right)}{\cos 30^\circ} = \frac{D}{\sqrt{3}}$ so that

$$A = 6\left(\frac{1}{2}\left(\frac{D}{\sqrt{3}}\right)^2 \sin 60^\circ\right) = \frac{\sqrt{3}D^2}{2}. \tag{3}$$

As a consequence, we have

$$N = \frac{D^2}{3R^2} \text{ or } Q \triangleq \frac{D}{R} = \sqrt{3N}, \tag{4}$$

where Q is regarded as the co-channel reuse ratio. On the other hand, from the basic geometry, we can express D in terms of R' (or $R' = \sqrt{3}R$) by

$$D^2 = \left(kR' + \frac{lR'}{2}\right)^2 + \left(\frac{lR'\sqrt{3}}{2}\right)^2 = \left(k^2 + kl + l^2\right) R'^2 = 3\left(k^2 + kl + l^2\right) R^2. \tag{5}$$

As a result, it can be derived by substituting (5) into (4) that

$$N = k^2 + kl + l^2. \tag{6}$$

The allowable reuse pattern therefore ranges over $1, 3, 4, 7, 9, 12, 13, \ldots$.

SIR Versus Cell Capacity

Frequency reuse greatly enhances the network capacity. This can be exemplified by considering a 50 MHz band, half of which is dedicated for the forward link or downlink (the communication path from a base station transmitter to its mobile user receivers) and another half for the reverse link or uplink (the communication path from the mobile user transmitters to a base station receiver). Assume that the band is divided into 200-kHz-wide frequency channels, each of which can support 8 users by, say, time-division multiple-access (TDMA) technologies. Then without cellular structure and frequency reuse, at any given time, at most $\frac{25\text{M}}{200\text{k}} \times 8 = 1000$ full-duplex users can be accommodated. In contrast, if each frequency channel is reused M times, then $1000M$ full-duplex users will be supported.

Network or cell capacity is increased with M. Increasing M implies a smaller co-channel reuse ratio Q and a smaller reuse factor N. For instance, when $N = 1$, the same channel set will be reused at every cell. However, the capacity performance for each cell will be limited by the interference or CCI, as users in co-channel cells interfere with each other. Signal-to-interference ratio (SIR) is therefore an important performance measure to the optimization of N for acceptable cell performance. In particular, the worst-case SIR in the downlink can be directly expressed as

$$\text{SIR} = \frac{S}{\sum_\ell I_\ell} = \frac{P_0 R^{-\alpha}}{\sum_\ell P_0 D_\ell^{-\alpha}}, \tag{7}$$

where P_0 is the transmit power of the base station. Taking into account only the first-tier CCI, i.e., the nearest adjacent co-channel cells, and assuming equal distance D from the 6 interfering cells, then we have

$$\text{SIR} = \frac{\left(\sqrt{3N}\right)^\alpha}{6}. \tag{8}$$

As such, N cannot be too small; otherwise, the SIR may be too low to have any acceptable performance. There is hence a trade-off between SIR and cell capacity. Advanced coding and decoding methods will be able to help the terminals to operate at low SIRs for decent performance. Other alternative approaches may avoid as much as possible the co-channel cells to operate at the same time by scheduling.

An accurate estimate of the SIR can be obtained by an observation in Fig. 4b so that

$$\begin{aligned}
\text{SIR} &= \frac{R^{-\alpha}}{\sum_\ell D_\ell^{-\alpha}} \\
&= \frac{R^{-\alpha}}{(D+R)^{-\alpha} + \left(D+\frac{R}{2}\right)^{-\alpha} + D^{-\alpha} + 2(D-R)^{-\alpha} + \left(D-\frac{R}{2}\right)^{-\alpha}} \qquad (9) \\
&= \frac{1}{\frac{2(Q+1)^\alpha + (Q-1)^\alpha}{(Q^2-1)^\alpha} + \frac{(Q+0.5)^\alpha + (Q-0.5)^\alpha}{(Q^2-0.25)^\alpha} + \frac{1}{Q^\alpha}}. \qquad (10)
\end{aligned}$$

For $\alpha = 4$, to achieve SIR ≥ 10 dB, we need to have $Q \geq 3.325$ and $N \geq 3.7$. Thus, the minimum reuse factor is $N = 4$. Similarly, if SIR ≥ 20 dB is required, $N \geq 9.58$, and the reuse factor will be 12. Note that the contributions from higher-tier co-channel base stations are much weaker (especially when $\alpha > 3$ as is typical in real environments) than those from the first tier and hence neglected in the evaluation.

Evaluation of SIR in the case of downlink above is relatively straightforward. In the uplink, however, the interference situation is highly variable depending upon the locations of co-channel mobile users at other base stations. For this reason, even if the uplink and downlink propagation is reciprocal, the uplink and downlink CCI will not be reciprocal. Uplink CCI is a more complex function of mobile user positions, and in real systems the mobile user positions tend to be random. Though it may still be possible to estimate the worst case, such result may be overly conservative.

Fixed and Dynamic Frequency Assignment

Following the above, in a cellular radio system, the same set of frequency channels is assigned to co-channel cells, with properly chosen N to control the CCI. Different

channels are assigned such that channels adjacent in the frequency domain are not in the same cells as well as neighboring cells so that adjacent channel interference is minimized. Because of that, each cell has only a fraction of the total channels and call may be blocked if all the channels assigned to a cell are all occupied, even though channels in other cells are unused. To improve trunking efficiency, possible solutions include channel borrowing (see section "Channel Borrowing in Cellular Networks") and more generally dynamic frequency assignment (DFA) (see section "Dynamic Spectrum Access as a Global Resource Allocation Optimization Problem"). In DFA, MSC holds all the frequency channels and allocates a channel to a user based on demand and performance considerations in order that some or more of the followings are achieved:

- Interference (CCI, adjacent channel) is managed in meeting the minimum SIR;
- The likelihood of future blocking using current traffic information is minimized or controlled to an acceptable level with the aid of queueing analysis;
- The likelihood of future drop call during unsuccessful handoff from one cell to another is minimized or controlled to an acceptable level.

The network-centric approach by DFA has the ability to design for actual interference, as opposed to the worst case in the fixed frequency assignment and can therefore reduce the probability of blocking and drop call considerably as well as increase the network capacity. More discussion and practical algorithms on DFA in the context of dynamic spectrum access will be presented in sections "Dynamic Spectrum Access as a Global Resource Allocation Optimization Problem," "The OFDMA Forward-Looking Game," and "Cognitive OFDMA."

The disadvantages of DFA are mainly the increased processing complexities and loading on MSC which are required to keep track of channel allocation, received signal strength indicator (RSSI) measurement for all the links, the user traffic and usage, etc. Estimating the SIR accurately for all the communication links at all available channels itself is challenging, and even with today's technologies, it is not feasible. In addition, the global optimization of the entire network is utterly complex and to achieve this in real-time where users are mobile, some at high speeds, is inconceivable, if not impossible. In section "The OFDMA Forward-Looking Game," we will discuss autonomous schemes that could achieve DFA in a self-optimizing manner while possessing only local channel information. This will make DFA much more attractive and practical.

Channel Borrowing in Cellular Networks

In this section, we will consider the basic cellular network where frequency channels are assigned to individual cells but can be borrowed from one to another, in order to enhance the spectral efficiency of the network. This method relaxes the rigidity of the original static frequency allocation among the cells. Adding flexibility to the static fixed frequency allocation can be very simple, and the simplest scheme is the

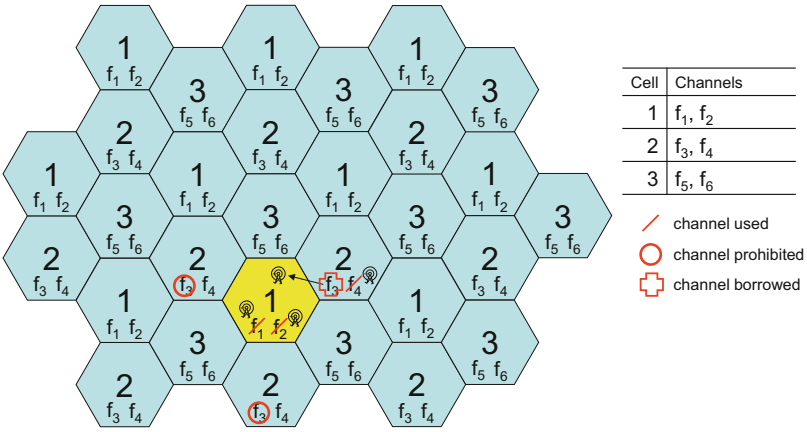

Fig. 5 Channel borrowing in a cellular radio system with frequency reuse factor of 3

channel borrowing scheme in [3, 4], where a channel in a cell (the donor cells) can be borrowed by another cell (the acceptor cell) if needed and if the borrowed channel does not interfere with existing calls. When a channel is borrowed, several other cells are prohibited from using it, due to CCI. Hence, the reduction in call blocking probability of the acceptor cell is achieved at the expense of the increase in call blocking probability of not only the donor cell but also many other cells.

The idea can be clearly explained by the diagram in Fig. 5 in which it can be seen that in the light-colored cell 1, all channels have been used and it needs an extra channel to serve the new arrival user. Therefore, channel f_3 from the donor cell 2 is borrowed and used to serve this new user by the acceptor cell 1. In this case, f_3 will be locked in the other two neighboring cells to avoid CCI.

Once the call dealt with by the borrowed channel is completed, the borrowed channel is returned to the original donor cell. It has been illustrated that channel borrowing can greatly decrease the call blocking probability under light and moderate traffic. Nonetheless, in heavy traffic conditions, such *channel locking* will worsen the overall blocking probability. On the other hand, it is quite possible that when channel borrowing is needed, there may be more than one candidate channels for borrowing. In this case, channel selection can be done with an aim to minimize the future call blocking probability in the cell that is most affected by the channel borrowing. A variety of ad hoc channel borrowing schemes with various objectives have been developed, some with sectoring, to achieve different trade-offs.

Models for Dynamic Spectrum Access Strategies

At present, spectrum is exclusively used by the licensee, and due to the problem of interference, for cellular radio systems, as discussed in the previous section, frequency allocation is carefully, but rigidly, planned for the worst-case scenarios in

terms of the SIR for every cell. One can choose an appropriate frequency reuse factor to yield an acceptable SIR performance. In practice, an SIR guard margin will be added as a precaution to deal with the possible channel fading effects. Overall, this static approach will be overly conservative, sacrificing the trunking efficiency for each cell, and has been the culprit for the poor spectrum utilization. There is clearly a need for spectrum reform so that more flexible use of spectrum will be permitted. Depending on the approaches to spectrum reform, such *dynamic spectrum access* will appear in different forms. Here, we review three main models [2].

Dynamic Exclusive Use Model

The first model is the dynamic exclusive use model which is by and large the traditional exclusive use model, with the major difference that the licensees are now allowed to sell and trade spectrum and to freely choose technology. This approach is also widely referred to as the spectrum property rights model [5] in which the licensees will be incentivized to achieve the most profitable use of spectrum which in return should lead to an increase in the spectrum utilization. However, in this approach, economy and market will play a more important role than any physical performance metrics, which may not necessarily improve spectrum utilization.

In the exclusive use model, dynamic spectrum access will still be possible if all channels are placed in a pool and there exists a *centralized and global* spectrum manager who assigns channels from the pool to new calls as needed, while monitoring to make sure that every user's SIR performance is acceptable. To optimize the performance of dynamic channel allocation, adaptive power control is usually employed to have better control on the CCI. The joint optimization of power control and dynamic channel allocation will be discussed in section "Dynamic Spectrum Access as a Global Resource Allocation Optimization Problem." It should be noted however that even a fully dynamic approach will not eliminate spectrum holes because nonsubscribers of the spectrum licensees will not be allowed to access the spectrum even if it is idle. This motivates the next two models.

Open Sharing Model

In open sharing model, the spectrum is open to everyone who wants to access it. The most well-known successful example of such is the unlicensed industrial, scientific, and medical (ISM) band. In this case, the spectrum usage will be maximized; however, it does not always translate to high spectrum utilization in terms of bits per second per Hz because users are inherently selfish, and if they do not control their signals properly, every user will suffer excessive CCI and the entire network may collapse. A great deal of researches have made progress toward dynamic spectrum access in this highly competitive wireless environment by a centralized spectrum server or manager [6] or distributed schemes, e.g., [7–9]. When a centralized spectrum server exists, the dynamic spectrum access technique will operate in the

same way as those for the exclusive use model. By contrast, if dynamic spectrum access were to achieve in a distributed and self-organized fashion, a whole new approach such as game-theoretic techniques, which allow users to negotiate the spectrum among themselves, will be required. This will be discussed in section "The OFDMA Forward-Looking Game."

Hierarchical Access Model

It is possible to have a hierarchical access model in which users are classified into primary and secondary, with the PUs (primary users) being the licensees who have the primary right to use the spectrum and SUs (secondary users) being the cognitive users who may share the spectrum with the PUs if their signals are properly controlled so that the interference perceived by the PUs is tolerable.

Under this hierarchical access model, coexistence of PUs and SUs may be achieved by one of the following three approaches:

- Underlay – If the SUs can control their signal power to be below the noise floor of the PU receivers, then the SU's communications in the same channel will not harm or affect the PU's communications, allowing them to coexist to increase the spectrum efficiency. This approach is the most natural and nonintrusive way to boost the spectrum utilization. However, the main drawback is that it might not always be possible to obtain useful rates for the SUs if their power is too low.
- Overlay – Advanced signal processing techniques such as dirty-paper coding [10] permit simultaneous transmission of PU and SU signals with zero interference at the PU receivers. In addition, the SUs can also act as relays to enhance the achievable rates of the PU links. The challenge of realizing this, however, is that the SUs need to have knowledge of the PUs' messages, which may not always be realistic. Also, the tremendous increase in processing complexity at the SUs may be an issue, as SUs are sometimes expected to be simple devices.
- Interweave – The interweave paradigm adopts the *opportunistic spectrum access* approach in which spectrum holes will be filled by SUs if they are identified [11, 12]. If those filled spectrum holes are reclaimed by any of the PUs, then the SUs will cease their transmissions immediately and return the spectrum back to the PUs who have the access priority over SUs. The main issue for the interweave approach is erroneous detection of spectrum holes caused by the hidden-terminal problem. The problem of automatically identifying and filling spectrum holes left out from the PUs by the SUs will be discussed in section "Cognitive OFDMA."

Self-Optimizing Cognitive Mobile Radios

There is a huge scope for dynamic spectrum access or DFA as discussed in the previous sections. The more challenging scenario is, though, when those DFA algorithms need to be achieved in a distributed fashion without any centralized

spectrum manager. This is greatly motivated by recent advances in digital signal processing (DSP), and general-purpose microprocessing technologies have brought *software-defined radio* to become reality. In particular, the term "software-defined radio" is often used to refer to the new digital radio technology which operates by software modules running on field programmable gate arrays (FPGAs), DSPs, and general-purpose processors (GPPs) and can change its operation characteristics by simply loading a new software. A software-defined radio can be reconfigured to switch functions and operations, but it generally does not imply capability of reconfiguring itself into the most effective form. The self-reconfigurable radio, now widely known as *cognitive radio*, was first envisioned by Mitola and Maguire in 1999 [13].

In addition to being programmable, a cognitive mobile radio is trainable, capable of being aware of its radio environments, and has the ability to learn and adaptively change its operating parameters in real time with the objective of providing reliable and spectral-efficient communications anywhere anytime [14]. An important application for cognitive radio is therefore dynamic spectrum access, due to its environmental awareness and the intelligence of rapidly reconfiguring itself for interference avoidance to other users sharing the same spectrum.

A cognitive radio network finds applications in the open sharing model in section "Open Sharing Model" and the hierarchical sharing model in section "Hierarchical Access Model," in the latter of which it operates in a spectrum originally allocated to a primary network consisting of one or more PUs. The fundamental principle of cognitive radio is to identify PUs that use the spectral resource and then design a transmission strategy that minimizes interference to and from those PUs in a nonintrusive manner [14–16]. When the PUs are idle and not occupying the spectrum, which is referred to as spectrum holes or white spaces, spectrum certainly can be reused by SUs. A great deal of efforts to achieve such opportunistic spectrum access are to sense and predict the PUs' activities and then take advantages of any vacant channels accurately.

Next, we will briefly review some basics of cognitive radios before providing a mathematical treatment in the dynamic spectrum access of cognitive radio using a game-theoretic framework later in sections "The OFDMA Forward-Looking Game" and "Cognitive OFDMA."

Spectrum Sensing

A cognitive radio needs to understand the status of the spectrum to take judicious decisions, and a continuous monitoring of the spectrum of interest is usually needed to preserve and maximize its adaptive capability. For instance, in the hierarchical model, a white space (i.e., an empty spectrum space) which is taken by a cognitive SU may be reclaimed by the PU at a later time. The detection of PU activities which relies on accurate spectrum sensing will be crucial. Sensing process could be performed in a centralized or distributed fashion and should be as accurate as possible because the QoS requirements for the PUs are rigorous.

Spectrum Analysis and Decision

Based on the spectrum availability and possibly the internal and external policies, a cognitive SU has to decide which channels it will occupy. Making a spectrum decision is complex, and it has to minimize the impact on the PUs while providing sufficient spectrum resources for this SU to achieve its QoS. For instance, the decision may be obtained by solving some resource allocation problems, through a centralized manager. Once spectrum decision is made, the cognitive SU will select and adjust its operating parameters to adapt to the decision for transmission.

Spectrum Sharing

Since there may be many SUs trying to access the same spectrum, cognitive spectrum access should be coordinated, and there should be a negotiation process for the SUs to come to a desirable operating point. This operation is required to ensure compliance of the secondary system with license issues and also take care of issues regarding collision, transmission, synchronization, and other relevant parameters.

Spectrum Mobility

SUs are regarded as visitors to the spectrum where the PUs are the owners. Therefore, if a PU reclaims certain part of the spectrum, where an SU is active, then the latter will have to cease its transmission or continue operating in another band, to avoid disturbance of the licensed system under certain QoS requirements.

Dynamic Spectrum Access as a Global Resource Allocation Optimization Problem

Section "Channel Borrowing in Cellular Networks" has given a taste of what is possible for more flexible frequency allocation as an attempt to unlock the spectrum in cellular networks. In the extreme case, however, one would anticipate that if all the frequency channels are available for all cells, the spectral efficiency will then be fully maximized, realizing the true dynamic spectrum access [2, 17]. In this section, we will characterize the mobile communications network as an OFDMA interference channel where multiple users share the same number of narrow frequency bands, but interfere with each other when more than one users occupy the same bands. We will first review some simple strategies to dynamically allocate channels to users. Then a global perspective which looks at dynamic channel allocation as a global optimization problem is studied.

Dynamic spectrum access is all about to assign the best channel to each user so that the interference to other co-channel users is properly controlled to an acceptable level, while maintaining the flexibility of using any channel in the central pool to take new calls (i.e., no more channel locking) (see section "Channel Borrowing in Cellular Networks"). Since the amount of CCI received by a user depends on the transmit power of the users causing the CCI, the performance of dynamic channel allocation is closely related to how well the users' transmit power is controlled. In fact, the overall dynamic spectrum access problem can be viewed as

a resource allocation optimization problem that deals with jointly the power control and channel allocation. It is fair to say that Wong et al. [18] were arguably the first work that illustrated the importance of multiuser diversity in the DFA problem for OFDM communications. In [18], the transmit power minimization problem in the downlink was addressed, with joint subcarrier and bit allocation to all users. This is regarded as a margin adaptive optimization.

The OFDMA Interference Channel

The dynamic power and channel allocation problem can be viewed as finding the optimal strategy for an OFDMA interference channel. Consider a K-user OFDMA system, as shown in Fig. 6, in which each user is free to occupy any of the N orthogonal frequency channels (or subcarriers) for communications to its designated destination receiver. The users operate in a noncooperative manner (i.e., no signal and information exchange between the base stations and between the mobile users is permitted), forming a multi-carrier interference channel where they inherently compete with and cause interference to each other, if they communicate on the same subcarriers. For user k, typically, the total transmitted power is constrained by

$$\sum_{n=1}^{N} p_k[n] \leq P_k, \ \forall k \in \{1, 2, \ldots, K\}, \tag{11}$$

where $p_k[n] \geq 0$ denotes the power allocated for the nth subcarrier (or subchannel) by user k and P_k represents the total power budget for user k. We also define the power allocation vector

$$\mathsf{p}_k \triangleq \{p_k[1], p_k[2], \ldots, p_k[N]\} \tag{12}$$

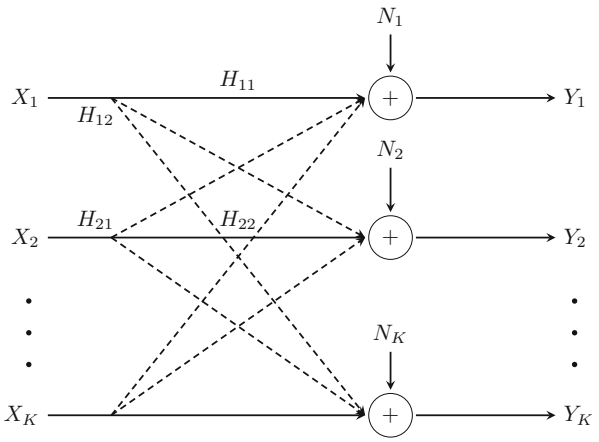

Fig. 6 A multiuser interference channel model

as the power allocation pattern of user k, which is drawn from some power allocation strategy $\mathscr{P}_k$, or it can be written as $\mathsf{p}_k \in \mathscr{P}_k$.

Let $H_{ij}[n]$ be the channel coefficient from transmitter i to receiver j (which is subject to channel flat fading and regarded as static under which the rate is evaluated) and $N_k[n]$ be the noise power density for the complex additive white Gaussian noise (AWGN) at receiver k on the nth subchannel. The flat fading assumption would be valid as long as the each subcarrier is sufficiently narrow compared to the coherence bandwidth of the channel. The achievable rate for user k can be written as

$$R_k = \sum_{n=1}^{N} R_k[n] = \sum_{n=1}^{N} \log_2 \left(1 + \frac{p_k[n]\,|H_{kk}[n]|^2}{N_k[n] + \sum_{\substack{i=1 \\ i \neq k}}^{K} p_i[n]\,|H_{ik}[n]|^2} \right), \tag{13}$$

which can be further reexpressed as

$$\begin{aligned} R_k &= \sum_{n=1}^{N} \log_2 \left(1 + \frac{p_k[n]}{\frac{N_k[n]}{|H_{kk}[n]|^2} + \sum_{\substack{i=1 \\ i \neq k}}^{K} p_i[n] \frac{|H_{ik}[n]|^2}{|H_{kk}[n]|^2}} \right) \\ &= \sum_{n=1}^{N} \log_2 \left(1 + \frac{p_k[n]}{\sigma_k[n] + \sum_{\substack{i=1 \\ i \neq k}}^{K} p_i[n]\theta_{ik}[n]} \right) \qquad (14) \\ &= \sum_{n=1}^{N} \log_2 \left(1 + \frac{p_k[n]}{\sigma_k[n] + I_k[n]} \right) \equiv \sum_{n=1}^{N} \log_2 \left(1 + \frac{p_k[n]}{c_k[n]} \right), \qquad (15) \end{aligned}$$

where in (14), $\sigma_k[n] \triangleq \frac{N_k[n]}{|H_{kk}[n]|^2}$ is the normalized noise power on subchannel n, $\theta_{ik}[n] \triangleq \frac{|H_{ik}[n]|^2}{|H_{kk}[n]|^2}$ denotes the normalized (by user k) channel power gain from transmitter (or interference) i to receiver k, and $I_k[n] = \sum_{\substack{i=1 \\ i \neq k}}^{K} p_i[n] \frac{|H_{ik}[n]|^2}{|H_{kk}[n]|^2}$ is the total interference power on subchannel n for user k and, in (15), $c_k[n] \triangleq \sigma_k[n] + I_k[n]$ corresponds to the overall "noise" on subchannel n for user k.

Under this interference model, users compete on their individual achievable rates. In particular, a user may choose to allocate more power on its own good subchannels to boost its rate but will interfere other users more on these subchannels. Channel allocation will be automatically done through the power allocation. If $p_k[n] = 0$ for some n, then it means that the nth subchannel is not assigned to user k.

Optimal Spectrum Balancing

Typically, the problem of interest is to maximize the network capacity under the power constraints of the transmitters (base stations in the downlink and

mobile users in the uplink). This is called a rate-adaptive optimization problem. That is,

$$\max_{\{p_k[n]\geq 0,\forall k,n\}} \sum_{k=1}^{K} R_k \quad \text{s.t.} \quad \sum_{n=1}^{N} p_k[n] \leq P_k \ \forall k. \tag{16}$$

When a global optimizer or centralized spectrum manager who knows the channel state information (CSI) of all the user links exists, it is possible to find the optimal solution of (16). The problem (16), however, is not convex and a multidimensional global optimization problem involving a large number of variables (KN unknowns).

In [19], (16) is optimally solved by considering the dual domain and forming the Lagrangian dual

$$\mathscr{L}(\{p_k[n]\},\{\lambda_k\}) = \sum_{k=1}^{K} R_k + \sum_{k=1}^{K} \lambda_k \left(P_k - \sum_{n=1}^{N} p_k[n] \right), \tag{17}$$

where $\{\lambda_k\}$ are the Lagrange multipliers. The dual objective function $g(\{\lambda\})$ can be defined as the maximization of an unconstrained maximization of the Lagrangian

$$g(\{\lambda_k\}) = \max_{\{p_k[n]\geq 0,\forall k,n\}} \mathscr{L}(\{p_k[n]\},\{\lambda_k\}). \tag{18}$$

The dual optimization problem is $\min_{\{\lambda_k\geq 0,\forall k\}} g(\{\lambda_k\})$.

The optimal solution may be found by a nested bisection search in the λ-space. It can be shown that the optimal spectrum balancing (OSB) algorithm has a computational complexity that is linear in the number of frequency carriers N.

However, the computational complexity of the OSB algorithm, although linear in N, is exponential in the number of users K. For a cellular radio system where the number of users, K, is in the order of thousands or more and it has hundreds of channels, it would be too demanding to solve hundreds of thousands unknowns in real-time resource allocation. The required complexity is prohibitive.

Iterative Spectrum Balancing

To solve (16) at much lower complexity, [20] established a general theory of dual optimization for OFDMA systems and showed that the duality gap for multiuser spectrum optimization always tends to zero as the number of frequency subcarriers goes to infinity, regardless of whether the optimization problem is convex. This observation has led to efficient search methods that optimize the dual objective function (17) directly. In particular, evaluating (17) can be realized by decoupling into N independent problems as

$$g(\{\lambda_k\}) = \sum_{n=1}^{N} \left\{ \max_{\{p_k[n] \geq 0, \forall k\}} \left[\sum_{k=1}^{K} \log_2 \left(1 + \frac{p_k[n]}{c_k[n]} \right) - \sum_{k=1}^{K} \lambda_k \, p_k[n] \right] \right\} + \sum_{k=1}^{K} \lambda_k \, P_k, \tag{19}$$

which, even though may still involve an exhaustive search, is unconstrained and much more manageable. Sub-gradient and ellipsoidal searches were also possible to improve the efficiency of the search over the λ-space.

The OFDMA Forward-Looking Game

In section "A Belief-Directed Game of Forward-Looking Players," we have revealed that the dynamic power and channel allocation can be obtained by solving the problem (16) which can be solved optimally by the OSB algorithm in [19] and near optimally by the ISB algorithm in [20]. Such optimization is able to reconcile the users' interest to maximize the achievable network sum-rate by a central spectrum manager. The major drawback of this approach is unfortunately that in a cellular radio network where there are a large number of users, such centralized optimization would be too complex to perform. For open spectrum access such as the white space, such centralized manager is also unlikely to exist. An alternative approach is to view the competition between users as a game, and negotiation on the resource allocation between users may be achieved by *playing* in which mobile users (considered as players) negotiate with each other by varying their actions intelligently and interactively according to the network response.

Consider the OFDMA interference channel described in section "A Subsystem Model for the OFDMA Game" (see also Fig. 6). Let $\mathscr{P} = \{\mathscr{P}_1, \mathscr{P}_2, \ldots, \mathscr{P}_K\}$ denote the set of collection for all users' power allocation strategies, with $\mathsf{p}_k \in \mathscr{P}_k \ \forall k$, and define $\mathsf{p}_{-k} \triangleq \{\mathsf{p}_1, \ldots, \mathsf{p}_{k-1}, \mathsf{p}_{k+1}, \ldots, \mathsf{p}_K\}$. We also let $\mathsf{BP}_k \in \mathscr{P}_k$ be user k's best power allocation strategy in response to the interference pattern seen by that user $\mathsf{I}_k \triangleq \{I_k[1], I_k[2], \ldots, I_k[N]\}$. Then, mathematically, BP_k is given by

$$\mathsf{BP}_k = \arg \max_{\mathsf{p}_k \in \mathscr{P}_k} \sum_{n=1}^{N} \log_2 \left(1 + \frac{p_k[n]}{\sigma_k[n] + I_k[n]} \right) \ \text{s.t.} \ \sum_{n=1}^{N} p_k[n] \leq P_k. \tag{20}$$

Figure 7 shows a power game subsystem which illustrates how users interact with each other in a competitive way. Given the interference pattern seen by user k, it optimizes its power allocation to give $\mathsf{p}_k = \mathsf{BP}(\mathsf{I}_k)$ which in return changes the interference patterns of other users $\{\mathsf{I}_l\}_{l \neq k}$ giving rise to their new power allocation strategies $\{\mathsf{BP}(\mathsf{I}_l)\}_{l \neq k}$. The power $\{\mathsf{BP}(\mathsf{I}_l)\}_{l \neq k}$ will become the cause of the changes in the interference pattern for user k, I_k. That is,

$$\mathsf{I}_k = \mathsf{I}_k \left(\{\mathsf{BP}(\mathsf{I}_l(\mathsf{p}_k))\}_{l \neq k} \right). \tag{21}$$

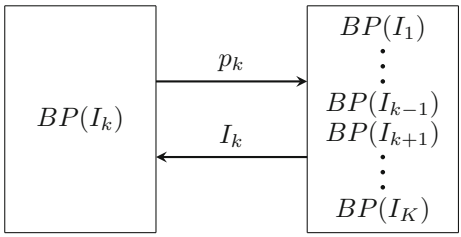

Fig. 7 The power game subsystem

For convenience, we abuse our notation slightly and define

$$\mathsf{BP}_{-k}(\mathsf{p}_k) \triangleq \{\mathsf{BP}(\mathsf{I}_1), \ldots, \mathsf{BP}(\mathsf{I}_{k-1}), \mathsf{BP}(\mathsf{I}_{k+1}), \ldots, \mathsf{BP}(\mathsf{I}_K)\}. \tag{22}$$

Clearly, the interference pattern for user k, $\mathsf{I}_k(\mathsf{BP}_{-k}(\mathsf{p}_k))$, is recognized to be a function of its own power allocation strategy p_k. Depending on how users react to the change of the environments and how the power game runs, if the system converges, then it will converge to some equilibrium.

Throughout, we shall use the superscript $*$ to denote the parameters at the equilibrium so that at the equilibrium, the power allocation strategy is $\mathbf{P}^* = \{\mathsf{p}_k^*, \mathsf{p}_{-k}^*\}$.

A Subsystem Model for the OFDMA Game

In this setup, users are all uncoordinated individuals, and each allocates its power over the subcarriers to maximize its own rate based on its observation of the environment, $\{c_k[n]\}$ for all n (which is referred to as the local CSI possessed by user k), and its belief on how the environment would react to its action. The environment user k observations can change because other users may alter their strategies to respond to user k's action. It is a dynamic process where users all interact and may compromise to an equilibrium, if their interactions converge over time.

To model this interaction, from user k's viewpoint, we can regard other users as a subsystem (or the environment seen by user k), as shown in Fig. 7, which takes its action at time t as inputs (i.e., $\mathsf{p}_k^t = \{p_k^t[n]\}$) and produces a new interference pattern at time $t+1$ as outputs (i.e., $\mathsf{c}_k^{t+1} = \{c_k^{t+1}[n]\}$). The subsystem reacts by an overall response from the actions of all other users, $\mathsf{p}_{-k}^t \triangleq \{\mathsf{p}_1^t, \ldots, \mathsf{p}_{k-1}^t, \mathsf{p}_{k+1}^t, \ldots, \mathsf{p}_K^t\}$.

Based on the rate (15), the distributed optimization problem for the OFDMA channel can be written as

$$\max_{\mathsf{p}_k \in \mathscr{S}_k} R_k, \ \forall k, \tag{23}$$

where $\mathscr{S}_k \triangleq \{\mathsf{p}_k : \sum_{n=1}^{N} p_k[n] \leq P_k\}$. The challenge to the above optimization is that R_k is a time-varying function (via c_k) which changes, according to the action or reaction of the remaining users. One way of characterizing the interactive process is to use the framework of the Nash game with forward-looking players in [21].

A Belief-Directed Game of Forward-Looking Players

Definitions

A player is said to be forward-looking if it uses some belief function to quantify the future reaction of the environment according to its action at present. Before presenting the definition of a Nash game with forward-looking players, the following functions are introduced:

- *Environmental function* – In a competition process, the reward for player k depends not only on its own strategy x_k but also others' strategies $\boldsymbol{x}_{-k}$ at any given time instant t. We use the environmental function $r_k(\boldsymbol{x}^t_{-k})$ to quantify the influence of other players' strategies onto player k's reward.
- *Belief function* – A player's understanding on its environmental function reflects its cognition about the competition in the game. In a belief-directed game, it is considered that player k possesses the knowledge of a belief function, which is denoted as $r^{\mathsf{B}}_k(x_k, \boldsymbol{x}^t_{-k})$, where $\boldsymbol{x}^t_{-k}$ denotes the strategies from all the players at time instant t except player k, and, clearly, $r^{\mathsf{B}}_k(x^t_k, \boldsymbol{x}^t_{-k}) = r_k(\boldsymbol{x}^t_{-k})$. The belief function may be constructed using some form of Taylor series expansion, e.g.,

$$r^{\mathsf{B}}_k(x_k, \boldsymbol{x}^t_{-k}) = r_k(\boldsymbol{x}^t_{-k}) + \varphi^t_k(x_k - x^t_k), \tag{24}$$

  where $\varphi^t_k \triangleq \frac{\partial r^{\mathsf{B}}_k(x_k, \boldsymbol{x}^t_{-k})}{\partial x_k}$ is regarded as the *interference derivative* that predicts the amount of future reaction from the environment due to present change in strategy. The selection of the interference derivative φ^t_k by the player permits engineering of the equilibrium of the game. Moreover, the belief function $r^{\mathsf{B}}_k(\cdots)$ can be understood as player k's cognition on what the environment function $r_k(\cdots)$ would be, given a strategy x_k and the present state $\boldsymbol{x}^t_{-k}$. Note that φ^t_k is only a belief for player k and whether the derivative $\frac{\partial r_k}{\partial x_k}$ actually exists or not is irrelevant.
- *Predicted reward* – The predicted reward function, $f_k(x_k, r^{\mathsf{B}}_k(x_k, \boldsymbol{x}^t_{-k}))$, gives the amount of reward player k believes to achieve by the strategy, x_k, given other players' strategies at time t, $\boldsymbol{x}^t_{-k}$, and the belief function $r^{\mathsf{B}}_k(\cdots)$ that player k uses to predict the future impact in the environment.

Based on the above definitions, we now can present the Nash equilibrium with forward-looking players (i.e., with some cognition in the form of belief functions). Mathematically, it is written as

$$f_k(x_k^*, r_k^{\mathsf{B}}(x_k^*, \boldsymbol{x}_{-k}^*) \geq f_k(x_k, r_k^{\mathsf{B}}(x_k, \boldsymbol{x}_{-k}^*)), \ \forall k, \tag{25}$$

where $r_k^{\mathsf{B}}(\cdot)$ is the belief function reflecting player k's cognition ability and $f_k(\cdot)$ is the predicted reward function for player k. Note that (25) can be rewritten as

$$f_k(x_k^*, \boldsymbol{x}_{-k}^*) \geq f_k(x_k, r_k^{\mathsf{B}}(x_k, \boldsymbol{x}_{-k}^*)), \ \forall k. \tag{26}$$

This can be explained by recognizing the fact that according to (24), $r_k^{\mathsf{B}}(x_k^*, \boldsymbol{x}_{-k}^*) = r_k(\boldsymbol{x}_{-k}^*)$ and as such at the equilibrium, we have

$$f_k(x_k^*, r_k^{\mathsf{B}}(x_k^*, \boldsymbol{x}_{-k}^*) = f_k(x_k^*, r_k(\boldsymbol{x}_{-k}^*)) = f_k(x_k^*, \boldsymbol{x}_{-k}^*). \tag{27}$$

In this model, the belief function $r_k^{\mathsf{B}}(\cdot)$ can be chosen arbitrarily, and it only serves to indicate player k's understanding about the competition environment. In fact, (26) embraces the conventional Nash equilibrium in which players have the belief function $r_k^{\mathsf{B}}(x_k, \boldsymbol{x}_{-k}^t) = r_k(\boldsymbol{x}_{-k}^t)$ which effectively treats the environment player k observations at any present time instant t as fixed and constant and ignores the subsequent changes in other players' strategies provoked by player k's new strategy.

The equilibrium of a Nash game with belief functions is referred to as a belief-directed Nash equilibrium (BNE).

The OFDMA BNE

For the OFDMA system, the reward function is the achievable rate R_k in (15), and the strategy for player k (or user k) is the power allocation strategy p_k. Also, the environmental function is the overall interference resulting from other users' strategies $\mathsf{c}_k(\mathsf{p}_{-k}^t)$. As a result, under BNE, we can form the belief function to enable player k's cognition using a general form inspired by the Taylor series

$$c_k^{\mathsf{B}}[n] \triangleq c_k^t[n] + \sum_{\ell=1}^{\infty} \varphi_k^{t\,(\ell)}[n](p_k[n] - p_k^t[n])^{\ell}, \tag{28}$$

where $\varphi_k^{t\,(\ell)}[n]$ denotes the ℓth order derivative of the belief function with respect to (w.r.t.) the strategy $p_k[n]$ at time t. The derivatives $\{\varphi_k^{t\,(\ell)}[n]\}$ can be chosen freely to give a different belief function for the player (which will result in a different BNE) and hence play the role of the engineering parameters for the BNE. Also, we write $\mathsf{c}_k^{\mathsf{B}}(\mathsf{p}_k, \mathsf{p}_{-k}^t) = \{c_k^{\mathsf{B}}[1], c_k^{\mathsf{B}}[2], \ldots, c_k^{\mathsf{B}}[N]\}$, which may be viewed as a prediction to $\mathsf{c}_k(\mathsf{p}_{-k})$. Based on the belief function $\mathsf{c}_k^{\mathsf{B}}$, user k has the predicted reward function (or predicted rate) given by

$$f_k(\mathsf{p}_k, \mathsf{c}_k^{\mathsf{B}}(\mathsf{p}_k, \mathsf{p}_{-k}^t)) \triangleq \sum_{n=1}^{N} \log_2\left(1 + \frac{p_k[n]}{c_k^{\mathsf{B}}[n]}\right), \tag{29}$$

which is the achievable rate in (15) after replacing $c_k[n]$ by $c_k^{\mathsf{B}}[n]$. Note that $f_k(\cdots)$ provides a predictive rate given the strategy p_k and the present state p_{-k}^t at time instant t. Mathematically, at the BNE, we have

$$f_k(\mathsf{p}_k^*, \mathsf{c}_k^{\mathsf{B}}(\mathsf{p}_k^*, \mathsf{p}_{-k}^*)) \geq f_k(\mathsf{p}_k, \mathsf{c}_k^{\mathsf{B}}(\mathsf{p}_k, \mathsf{p}_{-k}^*)), \ \forall \mathsf{p}_k \in \mathscr{S}_k \text{ and } \forall k. \tag{30}$$

Nash equilibrium is a special case of BNE, and this can be seen when $\varphi_k^{(\ell)*}[n] = 0 \ \forall \ell \geq 1$ and $\forall n, k$. In this case, $\mathsf{c}_k^{\mathsf{B}} = \mathsf{c}_k^t$ and the BNE is therefore degenerated to

$$f_k(\mathsf{p}_k^*, \mathsf{c}_k(\mathsf{p}_{-k}^*)) \geq f_k(\mathsf{p}_k, \mathsf{c}_k(\mathsf{p}_{-k}^*)), \ \forall \mathsf{p}_k \in \mathscr{S}_k \text{ and } \forall k. \tag{31}$$

The above basically states that at the equilibrium, the rewards for all the players are maximized, giving no incentive for players to deviate from it. In other words, the mobile users all settle on their power allocation strategies $\{\mathsf{p}_k^*\}$.

It is worth emphasizing that the predicted rate does not need to be accurate for the game to work, though the general sense is that an accurate prediction should help the users find better strategies. Note that Nash equilibrium is a result from an unrealistic prediction (based on the assumption of a static environment).

Forward-Looking Water-Filling Optimization

It is well known that for the power allocation of the OFDM type problem, the solution usually has an interpretation of water filling over the subchannels. It is no different in the OFDMA scenario even if the mobile users are forward-looking.

In the OFDMA BNE game, at time t, user k aims to find the strategy for time $t+1$ by solving

$$\mathsf{p}_k^{t+1} = \arg \max_{\mathsf{p}_k \in \mathscr{S}_k} f_k(\mathsf{p}_k, \mathsf{c}_k^{\mathsf{B}}(\mathsf{p}_k, \mathsf{p}_{-k}^t)). \tag{32}$$

In order to make (32) solvable, it is advisable to choose $\{\varphi_k^{t\,(\ell)}[n]\}$ such that

$$c_k^{\mathsf{B}}[n] > 0, \tag{33a}$$

$$\frac{\partial f_k(\mathsf{p}_k, \mathsf{c}_k^{\mathsf{B}})}{\partial p_k[n]} > 0, \tag{33b}$$

$$\frac{\partial^2 f_k(\mathsf{p}_k, \mathsf{c}_k^{\mathsf{B}})}{\partial (p_k[n])^2} < 0, \tag{33c}$$

so that (32) is a convex optimization problem. Note that (28) is a very general form to define the belief function, and how to best utilize it to design the most spectral efficient OFDMA BNE game is unknown. In this chapter, for mathematical tractability, we propose to choose $\{\varphi_k^{t\,(1)}[n]\}$ appropriately to optimize the BNE while setting $\varphi_k^{t\,(\ell)}[n] = 0$ for $\ell \geq 3$ and $\forall t, n$. Also, we can set

$$\varphi_k^{t\,(2)}[n] > -\frac{c_k^t[n] + \varphi_k^t[n](p_k[n] - p_k^t[n])}{(p_k[n] - p_k^t[n])^2} \tag{34}$$

to ensure that $c_k^{\mathsf{B}}[n] > 0$ is satisfied, where $\varphi_k^t[n] = \varphi_k^{t\,(1)}[n]$ for notational brevity.

Based on the definition of BNE (30), at time instant t, forward-looking user k aims to solve

$$\mathsf{p}_k^{t+1} = \arg\max_{\mathsf{p}_k \in \mathscr{S}_k} \sum_{n=1}^{N} \log_2\left(1 + \frac{p_k[n]}{c_k^{\mathsf{B}}(\mathsf{p}_k, \mathsf{p}_{-k}^t)[n]}\right). \tag{35}$$

The following theorem gives the optimal strategy update for p_k^{t+1}.

Theorem 1. *Assuming that any (infinitesimal) change in user k's strategy on subcarrier n only affects the interference on subcarrier n but not others $m \neq n$, the optimal strategy update for user k is given by*

$$p_k^{t+1}[n] = \left(\frac{w_k^t x_k^t[n] - (x_k^t[n])^2}{w_k^t y_k^t[n] + x_k^t[n]}\right)^+, \tag{36}$$

where $(a)^+ = \max\{0, a\}$, $x_k^t[n] \triangleq c_k^{\mathsf{B}}(\mathsf{p}_k^{t+1}, \mathsf{p}_{-k}^t)[n]$, $y_k^t[n] \triangleq \left.\frac{\partial c_k^{\mathsf{B}}[n]}{\partial p_k[n]}\right|_{p_k[n]=p_k^{t+1}[n]}$ *and* $w_k^t (> 0)$ *is regarded as the water level that ensures the equality of the power constraint (11) for the maximization.*

Proof. The problem (35) can be solved by introducing the Lagrange multiplier λ, using a Lagrangian multiplier formulation

$$\mathscr{L} = \sum_{n=1}^{N} \ln\left(1 + \frac{p_k[n]}{c_k^{\mathsf{B}}(\mathsf{p}_k, \mathsf{p}_{-k}^t)[n]}\right) - \lambda\left(\sum_{n=1}^{N} p_k[n] - P_k\right). \tag{37}$$

To proceed, we first obtain

$$\frac{\partial \mathscr{L}}{\partial p_k[n]} = \frac{1}{1 + \frac{p_k[n]}{c_k^{\mathsf{B}}(\mathsf{p}_k, \mathsf{p}_{-k}^t)[n]}}\left(\frac{c_k^{\mathsf{B}}(\mathsf{p}_k, \mathsf{p}_{-k}^t)[n] - p_k[n]\frac{\partial c_k^{\mathsf{B}}(\mathsf{p}_k, \mathsf{p}_{-k}^t)[n]}{\partial p_k[n]}}{(c_k^{\mathsf{B}}(\mathsf{p}_k, \mathsf{p}_{-k}^t)[n])^2}\right) - \lambda. \tag{38}$$

Then by setting $\left.\frac{\partial \mathscr{L}}{\partial p_k[n]}\right|_{p_k[n]=p_k^{t+1}[n]} = 0$ (which is the necessary condition for the maximization), and using the definitions

$$\begin{cases} x_k^t[n] \triangleq c_k^{\mathsf{B}}(\mathsf{p}_k^{t+1}, \mathsf{p}_{-k}^t)[n], \\ y_k^t[n] \triangleq \left.\dfrac{\partial c_k^{\mathsf{B}}[n]}{\partial p_k[n]}\right|_{p_k[n]=p_k^{t+1}[n]}, \end{cases} \tag{39}$$

we get

$$p_k^{t+1}[n] = \left(\frac{\frac{1}{\lambda}x_k^t[n] - (x_k^t[n])^2}{\frac{1}{\lambda}y_k^t[n] + x_k^t[n]}\right)^+, \tag{40}$$

where $(\cdot)^+$ ensures the positiveness of the power. Finally, renaming $\frac{1}{\lambda}$ as w_k^t yields the desired result, which completes the proof. □

The power allocation solution (36) is based on the maximization of a forward-looking achievable rate (via the belief function $\mathsf{c}_k^{\mathsf{B}}$). Note that its water-filling interpretation follows exactly the same way as the conventional water-filling power allocation for a single-user OFDM system with water-level w_k^t. As $t \to \infty$, if all users' strategies converge to a stable state, then from (28), we have

$$\begin{cases} x_k^*[n] = \left. c_k^{\mathsf{B}*}[n]\right|_{p_k[n]=p_k^*[n]} = c_k^*[n], \\ y_k^*[n] = \left.\dfrac{\partial c_k^{\mathsf{B}*}[n]}{\partial p_k[n]}\right|_{p_k[n]=p_k^*[n]} = \varphi_k^*[n], \end{cases} \tag{41}$$

and as a consequence, at the equilibrium, we obtain the users' strategies

$$p_k^*[n] = \left(\frac{w_k^* c_k^*[n] - (c_k^*[n])^2}{w_k^* \varphi_k^*[n] + c_k^*[n]}\right)^+, \quad \forall k, n. \tag{42}$$

The intuition is that although there can be many parameters $\{\varphi_k^{t\,(m)}[n]\}_{\forall m,n}$ that can be adjusted in a player's belief, the power allocation strategy at the equilibrium depends only on $\varphi_k^*[n]$ (i.e., the first derivative but not the higher-order ones), or the choice of $\{\varphi_k^{t\,(m)}[n]\}_{\forall m \geq 2}$ plays no role in defining the BNE. This justifies the earlier assumption of setting the higher-order derivatives in the belief function to zeros.

A common structure in the OFDMA power allocation game, regardless of the equilibrium, is to solve (20), which can be tackled by the Lagrangian multiplier method. In particular, this is done by defining

$$\mathscr{L} = \sum_{n=1}^{N} \log_2\left(1 + \frac{p_k[n]}{\sigma_k[n] + I_k[n]}\right) - \lambda \sum_{n=1}^{N} p_k[n], \tag{43}$$

where λ denotes the Lagrange multiplier, and finding p_k that maximizes $\mathscr{L}$. The Karush-Kuhn-Tucker (KKT) conditions for optimality can be derived as

$$\frac{\partial \mathscr{L}}{\partial p_k[n]} \begin{cases} = 0 \text{ for } p_k[n] > 0, \\ \leq 0 \text{ for } p_k[n] = 0. \end{cases} \tag{44}$$

Moreover, with

$$\frac{\partial \mathscr{L}}{\partial p_k[n]} = \frac{1}{\sigma_k[n] + I_k[n] + p_k[n]} \left(\frac{\sigma_k[n] + I_k[n] - p_k[n] \frac{\partial I_k[n]}{\partial p_k[n]}}{\sigma_k[n] + I_k[n]} \right) - \lambda \tag{45}$$

and defining $\varphi_k[n] \triangleq \frac{\partial I_k[n]}{\partial p_k[n]}$, it can be simplified as

$$\frac{\partial \mathscr{L}}{\partial p_k[n]} = \frac{1}{\frac{c_k^2[n] + \varphi_k[n] p_k^2[n]}{c_k[n] - \varphi_k[n] p_k[n]} + p_k[n]} - \lambda \equiv \frac{1}{\eta_k[n] + p_k[n]} - \lambda. \tag{46}$$

As a consequence, the optimal power allocation (or best power) for user k has the well-known water-filling interpretation and is given by

$$p_k[n] = (w_k - \eta_k[n])^+, \tag{47}$$

where $(a)^+ = \max(0, a)$ and

$$w_k = \frac{(\sigma_k[n] + I_k[n])^2 + \varphi_k[n] p_k^2[n]}{\sigma_k[n] + I_k[n] - \varphi_k[n] p_k[n]} + p_k[n], \tag{48}$$

which is chosen to satisfy the user's power constraint $\sum_n p_k[n] \leq P_k$ and is interpreted as the "water level" of the solution. Though this version of water-filling solution may appear complicated (as both w_k and $\eta_k[n]$ are functions of $\{p_k[n]\}$), this is much more general and facilitates the design of algorithms converging to different equilibria by obtaining an appropriate (belief) function $\varphi_k[n]$ to model various level of cognition ability of the user. The introduction of the interference derivative $\varphi_k[n]$ is significant because this provides the parameter that, if properly chosen, can guide the negotiation process between the users to reach a desired equilibrium.

For Nash equilibrium as an example, $\varphi_k[n] = 0$ is applied (because the user believes that $c_k^{\mathsf{B}}[n]$ is fixed and does not depend on the strategy $p_k[n]$ or $\varphi_k[n] = \frac{\partial c_k^{\mathsf{B}}[n]}{p_k[n]} = 0$) and (47) can therefore be greatly simplified as

$$p_k[n] = (w_k - \sigma_k[n] - I_k[n])^+. \tag{49}$$

Various Equilibria

Nash Equilibrium

At Nash equilibrium, $\mathsf{p}_k^* = \mathsf{BP}(\mathsf{I}_k^*)$ and $\mathsf{p}_{-k}^* = \mathsf{BP}_{-k}(\mathsf{p}_k^*)$, so the strategy profile can be written as

$$\mathbf{P}^* = \{\mathsf{BP}(\mathsf{I}_k^*), \mathsf{BP}_{-k}(\mathsf{p}_k^*)\}. \tag{50}$$

Additionally, Nash equilibrium can be formulated formally as

$$R_k(\mathsf{p}_k^*, \mathsf{BP}_{-k}(\mathsf{p}_k^*)) \geq R_k(\mathsf{p}_k, \mathsf{BP}_{-k}(\mathsf{p}_k^*)),\ \forall \mathsf{p}_k \in \mathscr{P}_k \text{ and } \forall k \in \{1, 2, \ldots, K\}. \tag{51}$$

User k's data rate, R_k^*, is therefore given by

$$\begin{aligned} R_k^* &= \max_{\mathsf{p}_k \in \mathscr{P}_k} \sum_n \log_2\left(1 + \frac{p_k[n]}{\sigma_k[n] + I_k^*[n]}\right) \\ &= \max_{\mathsf{p}_k \in \mathscr{P}_k} \sum_n \log_2\left(1 + \frac{p_k[n]}{\sigma_k[n] + I_k(\mathsf{BP}_{-k}(\mathsf{p}_k^*))[n]}\right). \end{aligned} \tag{52}$$

Note that the above maximization is done under a fixed interference pattern I_k^*. As mentioned before, achieving Nash equilibrium will have $\varphi_k[n] = \frac{\partial I_k^*[n]}{\partial p_k[n]} = 0$ and

$$\mathsf{p}_k^* = \mathsf{BP}(\mathsf{I}_k(\mathsf{BP}_{-k}(\mathsf{p}_k^*)))\ \forall k. \tag{53}$$

This can be achieved by the iterative (multiuser) water-filling algorithm as follows:

$$p_k^t + \sigma_k + I_k(\mathsf{BP}_{-k}(\mathsf{p}_k^{t-1})) = w_k^t \tag{54a}$$

$$p_k^{t+1} + \sigma_k + I_k(\mathsf{BP}_{-k}(\mathsf{p}_k^t)) = w_k^{t+1} \tag{54b}$$

$$\vdots$$

$$p_k^* + \sigma_k + I_k(\mathsf{BP}_{-k}(\mathsf{p}_k^*)) = w_k^* \tag{54c}$$

where the superscript t denotes the iteration time index and becomes $*$ at the equilibrium, and in the above the subchannel index $[n]$ has been omitted for convenience. The iterations (54) follow largely from the single-user water-filling solution in (49), but the only difference is that the interference pattern seen by user k changes due to a new response from other users before reaching to the steady state.

Every user in the equilibrium is deemed self-optimal giving the highest possible rate, with respect to other users' steady-state power allocation. Thus, a user does not gain by not agreeing to the equilibrium. However, the Nash system can be overly competitive leading to a very suboptimal power game equilibrium.

Stackelberg Equilibrium

It is possible to reach a different equilibrium that to some user allows better reconciliation between users to outperform Nash equilibrium. One such equilibrium is the Stackelberg equilibrium where one user is regarded as the Stackelberg leader, say user κ, who can maximize its own rate, R_κ, by finding its optimal strategy knowing that other users (regarded as followers) will know its action and respond by their (Nash-like) best power allocation. Mathematically, we have, for user κ,

$$R_\kappa(\mathsf{p}_\kappa^*, \mathsf{BP}_{-\kappa}(\mathsf{p}_\kappa^*)) \geq R_\kappa(\mathsf{p}_\kappa, \mathsf{BP}_{-\kappa}(\mathsf{p}_\kappa)),\ \forall \mathsf{p}_\kappa \in \mathscr{P}_\kappa. \tag{55}$$

As a result, user κ's data rate, R_κ^*, can be formulated as

$$\begin{aligned} R_\kappa^* &= \sum_n \log_2\left(1 + \frac{p_\kappa^*[n]}{\sigma_\kappa[n] + I_\kappa^*[n]}\right) \\ &= \max_{\mathsf{p}_\kappa \in \mathscr{P}_\kappa} \sum_n \log_2\left(1 + \frac{BP(\mathsf{I}_\kappa(\mathsf{BP}_{-\kappa}(\mathsf{p}_\kappa)))[n]}{\sigma_\kappa[n] + I_\kappa(\mathsf{BP}_{-\kappa}(\mathsf{p}_\kappa))[n]}\right). \end{aligned} \tag{56}$$

To reach the leader-followers Stackelberg equilibrium, the leader (i.e., user κ) can play the generalized water-filling power allocation (47) with appropriately chosen $\{\varphi_\kappa[n]\}$ while the followers (i.e., the remaining users) respond by the traditional water-filling power allocation (49) with $\varphi_k[n] = 0$. As such, the following iterative water-filling algorithm can take the users to the Stackelberg equilibrium:

$$\text{Leader } \kappa \begin{cases} p_\kappa^t + \eta_\kappa^t(\mathsf{p}_\kappa^{t-1}) = w_\kappa^t \\ p_\kappa^{t+1} + \eta_\kappa^t(\mathsf{p}_\kappa^t) = w_\kappa^{t+1} \\ \qquad\qquad \vdots \\ p_\kappa^* + \eta_\kappa^* = w_\kappa^* \end{cases} \tag{57}$$

and

$$\text{for all Followers } k \neq \kappa \begin{cases} p_k^t + \sigma_k + I_k(\mathsf{BP}_{-k}(\mathsf{p}_k^{t-1})) = w_k^t, \\ p_k^{t+1} + \sigma_k + I_k(\mathsf{BP}_{-k}(\mathsf{p}_k^t)) = w_k^{t+1}, \\ \qquad\qquad\qquad\qquad \vdots \\ p_k^* + \sigma_k + I_k(\mathsf{BP}_{-k}(\mathsf{p}_k^*)) = w_k^*. \end{cases} \tag{58}$$

Note that $\eta_\kappa^t[n] \triangleq \frac{(c_\kappa^t[n])^2 + \varphi_\kappa^t[n](p_\kappa^t[n])^2}{c_\kappa^t[n] - \varphi_\kappa^t[n]p_\kappa^t[n]}$ (which was defined in (46) earlier).

In the literature, when solving (56), a brute-force optimization is usually needed, which is not only prohibitively complex but also that no known method exists to play the leader to reach the Stackelberg equilibrium. However, using the BNE game as

a tool, one could choose $\varphi_\kappa[n]$ appropriately to reach the Stackelberg equilibrium. Note that there are likely many choices of $\varphi_\kappa[n]$ that can all permit the users to converge to the Stackelberg equilibrium. Here, nevertheless, we provide a choice without proof by setting

$$\varphi_\kappa[n] = -\frac{c_\kappa[n]}{2c_\kappa[n] + p_\kappa[n]} \ \forall n. \tag{59}$$

There are a few observations we can make to understand why this choice is good. First, to derive a judicious belief on $\varphi_\kappa^*[n]$, the interference derivative should be negative, or $\varphi_\kappa^*[n] \leq 0$ because it then has a strong tendency to invest power on a good subcarrier. In contrast, if $\varphi_\kappa^*[n] > 0$, this will imply that the more the power it allocates for a subcarrier, the more the interference it gets, thus ending up occupying a poor subcarrier at the equilibrium. On the other hand, it can be shown that as long as $-\frac{c_\kappa^*[n]}{2c_\kappa^*[n]+p_\kappa^*[n]} \leq \varphi_\kappa^*[n] \leq 0$ is true, the equilibrium is unique, and therefore, any value in this interval could be a sensible choice for the interference derivative $\varphi_\kappa^t[n]$. However, it should also be noted that the magnitude of $\varphi_\kappa^*[n]$ reflects the forward-looking capability, or if $\varphi_\kappa^*[n] = 0$, the user is myopic and not forward-looking. As a result, (59) is a proper choice that is anticipated to optimize user κ's rate.

In Fig. 8, we provide a simulation example for the power allocation of a 3-user 9-subcarrier interference channel (e.g., cellular system with game-theoretic dynamic spectrum access) under different game-theoretic equilibria. In the simulations, every subcarrier channel is modeled by an equal-power four-independent-ray Rayleigh fading channel (see Fig. 9) [22], i.e., $|H_{ij}[n]|^2 = |h_{ij}^{(1)}[n]|^2 + |h_{ij}^{(2)}[n]|^2 + |h_{ij}^{(3)}[n]|^2 + |h_{ij}^{(4)}[n]|^2, \ \forall i, j$, with $\mathrm{E}[|H_{ij}[n]|^2] = x$ and $\mathrm{E}[|h_{ij}^{(\ell)}[n]|^2] = 0.25x \ \forall \ell$, for $i \neq j$, where x measures the relative severeness of the interference channel. For $i = j$, it is set that $\mathrm{E}[|H_{kk}[n]|^2] = 1$ and $\mathrm{E}[|h_{kk}^{(\ell)}[n]|^2] = 0.25 \ \forall \ell$. We also assumed that $P_k = 100 \ \forall k$, $N_k[n] = 0.01 \ \forall k, n$ and $x = 0.4$ (a typical interference channel).

Several observations can be made from the results in Fig. 8. First of all, for Nash equilibrium, all three users are Nash users, and they operate using the conventional water-filling power allocation. Therefore, we can see that the water level for each user, which is shown in this example, is very close to each other because their power constraints as well as the channel statistics are set to be the same. Also, users 2 and 3 in one-leader Stackelberg equilibrium are Nash users, and the same is observed in their power allocation strategies. By contrast, user 1 in OSE is the Stackelberg leader, and its water level depends upon η_k (not c_k) and cannot be directly visualized. In addition, the results illustrate that the power allocation strategies for users 2 and 3 in both equilibria are very similar, while the Stackelberg leader, user 1 in OSE, and the Nash user 1 in NE have profoundly different strategies. Specifically, the Stackelberg leader recognizes the fact that subcarriers 2, 5, and 6 are weak and very noisy, so decides not to occupy these subcarriers and concentrates on the good subcarriers 3, 4, and 8 leading to a substantial increase in its sum-rate from 14.8 to 19.3 (bps/Hz), whereas the sum-rates for users 2 and 3 in both equilibria are very similar and they are not compromised.

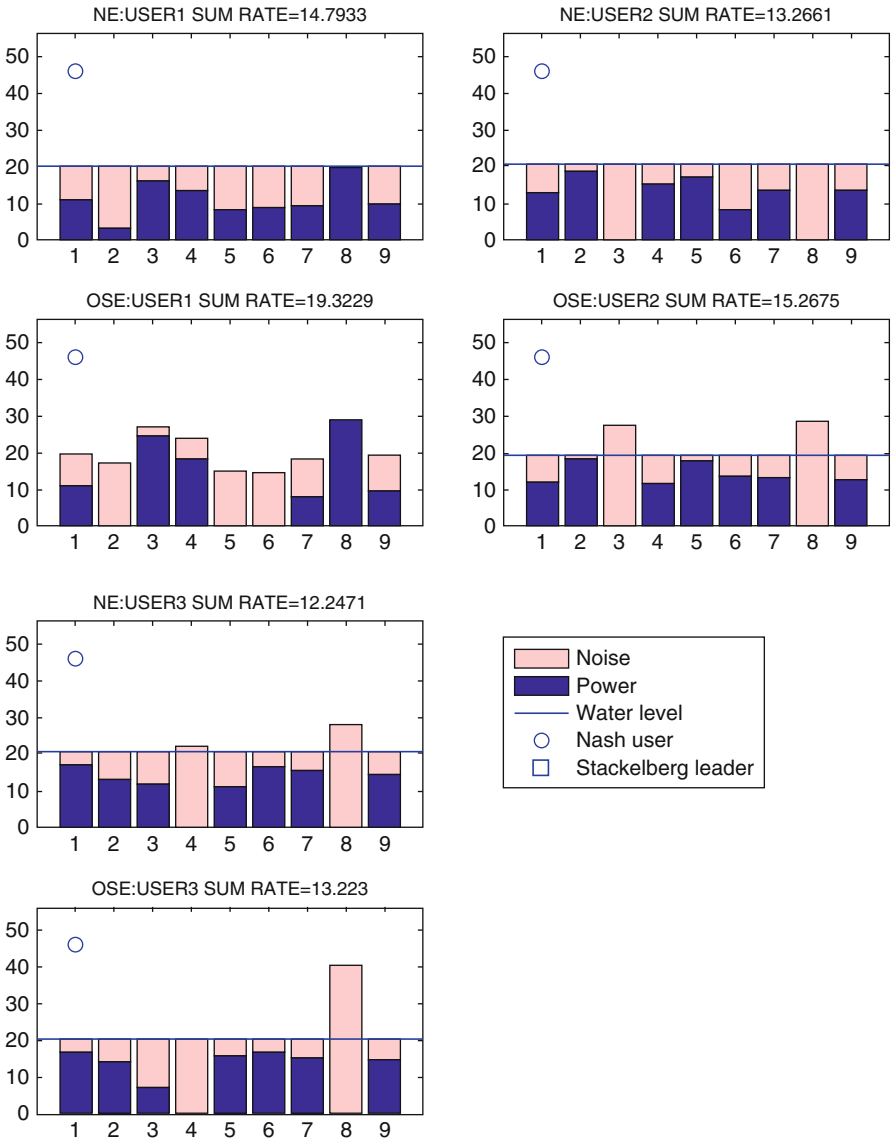

Fig. 8 An example showing the power allocation for each user over a 3-user 9-subcarrier interference channel under Nash and one-leader Stackelberg equilibria (NE and OSE)

Equilibrium Resulting from All Forward-Looking Players

Both Nash and Stackelberg equilibria can be achieved autonomously as each individual user simply needs to perform its water-filling power allocation, and their simultaneous interactions, once converged, will lead to the results. Therefore, spectrum sharing is done in a self-organizing and autonomous way. However, so

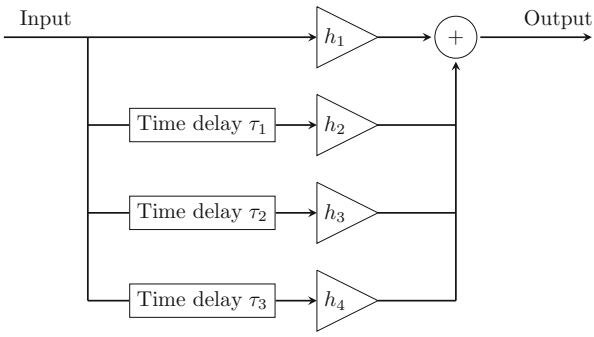

Fig. 9 A four-ray Rayleigh fading channel model

Table 1 Average users' sum-rates for the 3-user 9-subcarrier interference channel

Sum-rate	User 1	User 2	User 3
NE	13.9944	13.8966	13.8021
OSE	16.5275	15.5493	15.4743
AFE	32.6641	32.8518	33.0399

far, only the Stackelberg leader is forward-looking, while the Nash users are all myopic. In order to let all users become forward-looking, all $\{\varphi_k[n]\}$ need to be set to nonzero. It is in fact possible to use (59) for all the users, but further analysis, which is omitted here, can show that by setting

$$\varphi_k[n] = -\sqrt{\frac{c_k[n]}{2c_k[n] + p_k[n]}} \ \forall k, n, \tag{60}$$

the results are even better. The idea is to harmonize their competition, avoid destructive competition, and facilitate autonomous negotiation.

In Table 1, results are provided for the average users' sum-rates for a 3-user 9-subcarrier interference channel, with $P_k = 100 \ \forall k$, $N_k[n] = 0.01 \ \forall k, n$, and $x = 0.4$. Results show that there is a considerable gain in the sum-rates using AFE (the equilibrium achieved by having all forward-looking users using (60)) over NE and OSE. Furthermore, we compare the rate performance between AFE and ISB [20] in Fig. 10 for $x = 0.5$ and various signal-to-noise ratio (SNR) which is defined as $\frac{P_0}{NN_0}$ where $P_k = P_0 \ \forall k$, $N_k[n] = N_0 \ \forall k, n$. Results show that AFE achieves nearly the same average sum-rate as ISB and significantly outperforms OSE and NE in terms of rates for the entire range of SNR. Note that ISB is the centralized approach that has been known to achieve nearly the optimal performance.

OFDMA with MIMO Antennas

Multiple-input multiple-output (MIMO) antennas promise to deliver extraordinary gains in energy and spectral efficiencies and have been adopted in the current-

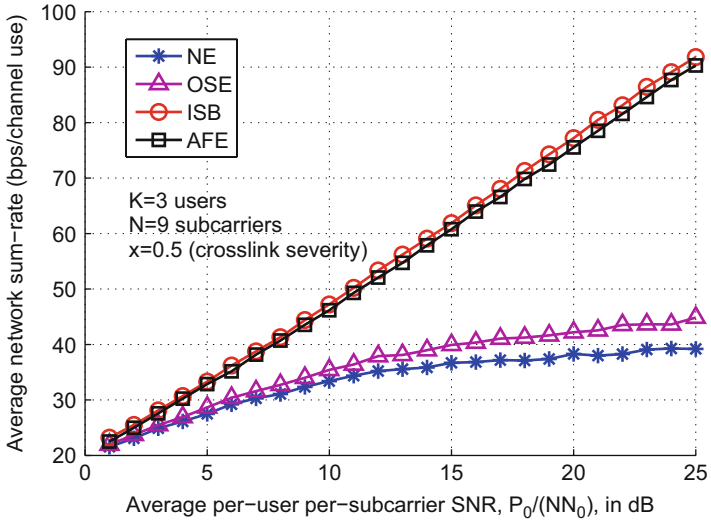

Fig. 10 The average sum-rate comparison against the SNR

as well as future-generation mobile communications networks. The autonomous spectrum sharing approaches discussed earlier, if adopted, will need to be integrated with MIMO antenna technologies. The extension is nevertheless not trivial as the spatial subchannels brought by MIMO compete within and among users.

Consider the OFDMA system with MIMO user terminals. We assume that every transmitter has N_t antennas and every receiver has N_r antennas. (Different numbers of antennas at the terminals can be easily incorporated.) In this case, assuming full-rank MIMO channels, a user, say k, has $N_t \times N$ subchannels (N_t spatial subchannels on each subcarrier) to transmit with power $p_k[\ell, n]$, on spatial subchannel ℓ and subcarrier n. For user k, the total transmit power is constrained by

$$\sum_{n=1}^{N} \sum_{\ell=1}^{N_t} p_k[\ell, n] \leq P_k, \ \forall k \in \{1, 2, \ldots, K\}. \tag{61}$$

With MIMO links, we denote the channel matrix between transmitter i and receiver j on subcarrier n by $\mathbf{H}_{ij}[n]$, and $N_k[n]$ is still the noise power spectral density at receiver k, but at every receive antenna. Assuming that user k has perfect CSI knowledge of $\{\mathbf{H}_{kk}[n]\}_{\forall n}$, the capacity-achieving scheme (from user k's viewpoint and ignoring the interference) is to use singular-value decomposition to diagonalize the channel using the right singular matrix $\mathbf{V}_k[n]$ as the precoding matrix and the left singular matrix $\mathbf{U}_k^{\dagger}[n]$ as the decoding matrix (where $\dagger$ denotes the hermitian operation) so that the received spatial subchannel signals at receiver k is

$$\mathbf{y}_k[n] = \Lambda_k[n]\mathbf{x}_k[n] + \mathbf{U}_k^{\dagger}[n]\left(\sum_{\substack{j=1\\ j\neq k}}^{K}\mathbf{H}_{jk}[n]\mathbf{V}_j[n]\mathbf{x}_j[n] + \boldsymbol{\mu}_k[n]\right), \tag{62}$$

in which $\Lambda_k[n]$ is the diagonal matrix containing the singular values of $\mathbf{H}_{kk}[n]$, $\mathbf{x}_j[n]$ denotes the information vector transmitted from user j on subcarrier n, and $\boldsymbol{\mu}_k[n]$ is the complex AWGN vector at user k. Now, define $\tilde{\boldsymbol{\mu}}_k[n] \triangleq \mathbf{U}_k^{\dagger}[n]\boldsymbol{\mu}_k[n]$ and $\tilde{\mathbf{H}}_{jk}[n] \triangleq \mathbf{U}_k^{\dagger}[n]\mathbf{H}_{jk}[n]\mathbf{V}_j[n]$. Then we have

$$\mathbf{y}_k[n] = \Lambda_k[n]\mathbf{x}_k[n] + \sum_{\substack{j=1\\ j\neq k}}^{K}\tilde{\mathbf{H}}_{jk}[n]\mathbf{x}_j[n] + \tilde{\boldsymbol{\mu}}_k[n]. \tag{63}$$

As a result, the achievable rate for user k is given by

$$\begin{aligned} R_k &\equiv \sum_{n=1}^{N}\sum_{\ell=1}^{M} R_k[\ell,n] \\ &= \sum_{n=1}^{N}\sum_{\ell=1}^{M}\log_2\left(1 + \frac{|(\Lambda_k[n])_{\ell,\ell}|^2 p_k[\ell,n]}{\sum_{\substack{j=1\\ j\neq k}}^{K}\sum_{\ell=1}^{M}|(\tilde{\mathbf{H}}_{jk}[n])_{\ell,j}|^2 p_j[\ell,n] + N_k[n]}\right), \end{aligned} \tag{64}$$

where $M = \min(N_t, N_r)$ and $(\cdot)_{\ell,j}$ returns the (ℓ, j)th entry of the input matrix. Now, introducing

$$c_k[\ell,n] \triangleq \sum_{\substack{j=1\\ j\neq k}}^{K}\sum_{\ell=1}^{M}\frac{|(\tilde{\mathbf{H}}_{jk}[n])_{\ell,j}|^2 p_j[\ell,n]}{|(\Lambda_k[n])_{\ell,\ell}|^2} + \frac{N_k[n]}{|(\Lambda_k[n])_{\ell,\ell}|^2}, \tag{65}$$

which is the overall noise (interference plus noise) on spatial subchannel ℓ and subcarrier n for user k, (64) is then written as

$$R_k = \sum_{n=1}^{N}\sum_{\ell=1}^{M}\log_2\left(1 + \frac{p_k[\ell,n]}{c_k[\ell,n]}\right), \tag{66}$$

which has a similar form as (15) in the single-antenna case.

The Nash-Stackelberg Game

For OFDMA without MIMO antennas, it is possible to use the BNE analysis or the belief function to regulate user competition. However, the MIMO channels make it difficult to extend the analysis, and how users can be regulated to approach a desirable equilibrium is unknown. To get round this, we regard the resource

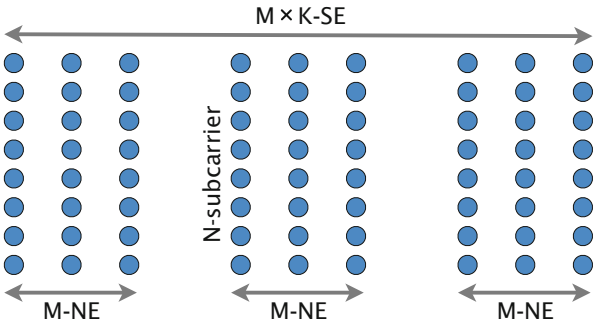

Fig. 11 The Nash-Stackelberg game: M OFDMA AFE games competing in a Nash manner

negotiation game as M mutually interfering single-antenna OFDMA AFE games; see Fig. 11.

To proceed, we let

$$r_k[\ell] = \sum_{n=1}^{N} \log_2 \left(1 + \frac{p_k[\ell, n]}{c_k[\ell, n]}\right), \tag{67}$$

which corresponds to the sum-rate of all the subcarriers over spatial subchannel ℓ achieved by user k. Hence,

$$R_k = \sum_{\ell=1}^{M} r_k[\ell]. \tag{68}$$

For each spatial OFDMA game, say spatial subchannel ℓ, we have the constraints

$$\sum_{n=1}^{N} p_k[\ell, n] \leq P_k[\ell], \text{ for some } P_k[\ell], \tag{69a}$$

$$\sum_{\ell=1}^{M} P_k[\ell] \leq P_k. \tag{69b}$$

For a given spatial subchannel ℓ and if $P_k[\ell]$ is known, (67) can be maximized to approach the AFE of the single-antenna OFDMA network by the generalized water-filling method (47). Thus, the power allocation on subcarrier n by user k is

$$p_k[\ell, n] = (w_k[\ell] - \eta_k[\ell, n])^+, \ \forall n, \tag{70}$$

where the water level, $w_k[\ell]$, is chosen to satisfy (69a) and

$$\begin{cases} \eta_k[\ell,n] = \dfrac{c_k^2[\ell,n] + \varphi_k[\ell,n]p_k^2[\ell,n]}{c_k[\ell,n] - \varphi_k[\ell,n]p_k[\ell,n]}, \\ \varphi_k[\ell,n] = -\sqrt{\dfrac{c_k[\ell,n]}{2c_k[\ell,n] + p_k[\ell,n]}}. \end{cases} \tag{71}$$

For user k, the M chunks of OFDMA subcarriers compete with each other as well in terms of the power resources. With the simplified view that at a good steady state, the M-chunk AFE games should have the same achievable sum-rate, i.e., $r_k[\ell]$ is the same for all ℓ, the total sum-rate for user k (68) can be maximized by reinforcing a Nash equilibrium. To do so, we set

$$w_k[\ell] = \frac{1}{M}\sum_{l=1}^{M} w_k[\ell] \equiv w_k^{\mathsf{NE}} \text{ for } \ell = 1, 2, \ldots, M. \tag{72}$$

This results in changes of the power constraints in the spatial domain $\{P_k[\ell]\}_{\forall \ell}$.

Figure 11 shows a Nash-Stackelberg game which can be formulated as

$$R_k(\tilde{\mathsf{p}}_k^{NE}, \boldsymbol{\eta}_k^{AFE}(\tilde{\mathsf{p}}_k^{NE})) \geq R_k(\tilde{\mathsf{p}}_k, \boldsymbol{\eta}_k^{AFE}(\tilde{\mathsf{p}}_k^{NE})),\ \forall \tilde{\mathsf{p}}_k \in \tilde{\mathscr{P}}_k \text{ and } \forall k, \tag{73}$$

and all users' rates can be enhanced and formulated as

$$R_k^{N-S} = \max_{\tilde{\mathsf{p}}_k \in \tilde{\mathscr{P}}_k} \sum_{\ell} R_{k(\ell)}^{AFE}\ \forall k. \tag{74}$$

For approaching the Nash-Stackelberg equilibrium (N-SE), (70) and (71) are used, and the iterative water-filling algorithm runs for all users as follows:

$$p_k^t + \eta_k^t(\mathsf{p}_k^{t-1}) \xrightarrow{t \text{ increasing}} \cdots\cdots \rightarrow p_k^* + \eta_k^* = w_k^*. \tag{75}$$

In the simulations, we model each subcarrier by a Rayleigh fading channel with $\mathrm{E}[|\mathbf{H}_{jk}[n]|^2] = 0.4$, which is the severeness indicator for the interference channel. There are $K = 3$ users and $N = 14$ subcarriers with $N_k[n] = N_0$, $P_k = P_0$, and $\mathrm{E}[|\mathbf{H}_{kk}[n]|^2] = 1$ for those subcarriers. The SNR for all users is defined as $\frac{P_0}{NN_0}$.

Figure 12 compares the N-SE and Nash equilibrium (NE in the figure) for various SNR assuming $N_0 = 0.01$. Results illustrate that NE game fails to reconcile users' competition and has pretty *flat* user rates as a function of SNR but the N-SE game can achieve an order of magnitude gain in user rates which also grow with the SNR.

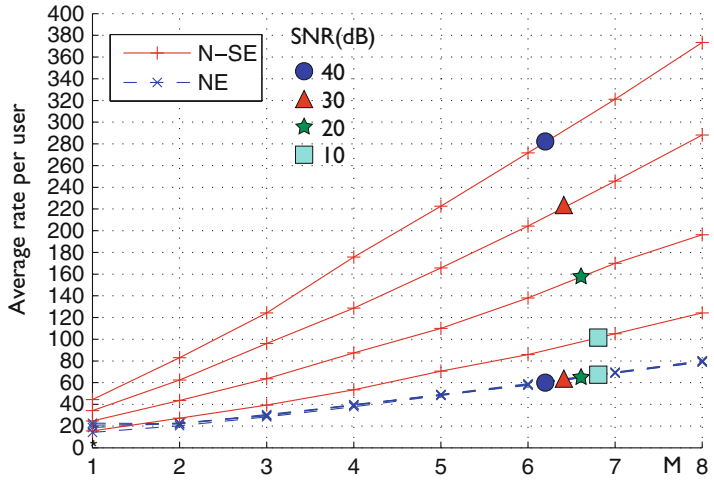

Fig. 12 The sum-rate results against M

Self-Optimization by Virtual Channel Construction

The Nash competition among the AFE games appears to degrade the performance of the resulting equilibrium. This can be improved using the virtual channel construction approach, which is discussed in this section.

Before we present this, let us extend the system model by writing

$$\mathsf{P}_k \triangleq \{p_k[1,1], p_k[2,1], \ldots, p_k[M,1], p_k[1,2], p_k[2,2], \ldots, p_k[M,2], \cdots, p_k[1,N], p_k[2,N] \ldots, p_k[M,N]\} \tag{76}$$

as the spatial-frequency power allocation profile for the kth user, which is drawn from some strategy $\mathscr{P}_k$, or $\mathsf{P}_k \in \mathscr{P}_k$. For convenience, we also define the non-k user's power profile:

$$\mathsf{P}_{-k} \triangleq \{\mathsf{P}_1, \ldots, \mathsf{P}_{k-1}, \mathsf{P}_{k+1}, \ldots, \mathsf{P}_K\}. \tag{77}$$

We let $\mathsf{BP}_k \in \mathscr{P}_k$ be user k's best power allocation strategy in response to the overall noise pattern experienced by that user $\mathsf{C}_k \triangleq \{c_k[\ell,n]\}_{\forall \ell,n}$. Then BP_k is given by

$$\mathsf{BP}_k = \arg \max_{\mathsf{P}_k \in \mathscr{P}_k} \sum_{n=1}^{N} \sum_{\ell=1}^{M} \log_2 \left(1 + \frac{p_k[\ell,n]}{c_k[\ell,n]}\right) \text{ s.t. (61).} \tag{78}$$

Given the overall noise pattern seen by user k, i.e., local CSI C_k, it optimizes its power allocation by $\mathsf{P}_k = \mathsf{BP}_k(\mathsf{C}_k)$ which changes the noise patterns of other users

$\{\mathsf{C}_l\}_{l\neq k}$ resulting in their new power allocation profiles $\{\mathsf{BP}_l(\mathsf{C}_l)\}_{l\neq k}$ which will become the cause of the changes in C_k. That is,

$$\mathsf{C}_k = \mathsf{C}_k\left(\{\mathsf{BP}_l(\mathsf{C}_l(\mathsf{P}_k))\}_{l\neq k}\right). \tag{79}$$

For convenience, we abuse our notation slightly and define

$$\mathsf{BP}_{-k}(\mathsf{P}_k) \triangleq \{\mathsf{BP}_1(\mathsf{C}_1),\ldots,\mathsf{BP}_{k-1}(\mathsf{C}_{k-1}),\mathsf{BP}_{k+1}(\mathsf{C}_{k+1}),\ldots,\mathsf{BP}_K(\mathsf{C}_K)\}. \tag{80}$$

Clearly, the noise pattern observed by user k, $\mathsf{C}_k(\mathsf{BP}_{-k}(\mathsf{P}_k))$, is a function of its own strategy P_k. At the equilibrium, the strategy is denoted by $\mathsf{P}^* = \{\mathsf{P}_k^*, \mathsf{P}_{-k}^*\}$.

Depending on how users react to the environmental changes, the system may converge to an equilibrium. For autonomous sharing in OFDMA, we need algorithms that can take users to equilibriums that benefit all by exploiting users' local CSI. Without MIMO antennas, this was shown possible using AFE (based on BNE).

Formally, under the MIMO-OFDMA model, we have, for all k,

$$R_k(\mathsf{P}_k^*, \mathsf{BP}_{-k}(\mathsf{P}_k^*)) \geq R_k(\mathsf{P}_k, \mathsf{BP}_{-k}(\mathsf{P}_k)),\ \forall \mathsf{P}_k \in \mathscr{P}_k. \tag{81}$$

Hence, all users' rates can be enhanced and formulated as

$$R_k^* = \max_{\mathsf{P}_k\in\mathscr{P}_k} \sum_{n,\ell} \log_2\left(1+\frac{p_k[\ell,n]}{c_k(\mathsf{BP}_{-k}(\mathsf{P}_k))[\ell,n]}\right)\ \forall k. \tag{82}$$

The challenge of a MIMO-OFDMA power allocation game is the competition in both spatial and frequency domains and that the interference derivative analysis for the single-antenna OFDMA in section "The OFDMA BNE" does not seem to be generalizable. To get round this, section "The Nash-Stackelberg Game" uses an N-SE game, but the Nash subgame unnecessarily restricts the optimization and competes harmfully in the spatial domain.

Here, based on the MIMO-OFDMA system, we provide an alternative approach by constructing a virtual *single-antenna* OFDMA game in which we have

$$\check{R}_k \equiv \sum_{n=1}^{N} \check{R}_k[n] = \sum_{n=1}^{N} \log_2\left(1+\frac{\check{p}_k[n]}{\check{c}_k[n]}\right), \tag{83}$$

where $\check{c}_k[n] \triangleq \sum_{\ell=1}^{M} c_k[\ell,n]$ denotes the overall noise power over the virtual subcarrier n seen by user k and $\check{p}_k[n]$ is the power allocated for the nth virtual subcarrier.

To achieve AFE of the virtual OFDMA network in (81), it has been shown that the optimal power allocation for user k is given by

$$\check{p}_k[n] = (\check{w}_k - \eta_k[n])^+, \tag{84}$$

where for those n such that $\check{p}_k[n] \geq 0$, we have

$$\check{w}_k = \underbrace{\frac{(\check{c}_k[n])^2 + \varphi_k[n]\check{p}_k^2[n]}{\check{c}_k[n] - \varphi_k[n]\check{p}_k[n]}}_{\eta_k[n]} + \check{p}_k[n], \tag{85}$$

which is the "water level" satisfying the total power constraint P_k, and as discussed before, $\varphi_k[n]$ is the *interference derivative* that helps regulate user competition to converge to a desired equilibrium, chosen as

$$\varphi_k[n] = -\sqrt{\frac{\check{c}_k[n]}{2\check{c}_k[n] + \check{p}_k[n]}}, \ \forall k, n. \tag{86}$$

The power allocation on the nth virtual subcarrier, $\check{p}_k[n]$, provides a useful estimate on the overall power budget for the spatial subchannels of subcarrier n, i.e., $\sum_{\ell=1}^{M} p_k[\ell, n] = \check{p}_k[n]$. Thus, to obtain the actual power allocation, user k can suballocate $\check{p}_k[n]$ into the spatial subchannels by a water-filling procedure according to the noise pattern $\{c_k[\ell, n]\}_{\forall \ell}$. As such, we get

$$p_k[\ell, n] = (w_k[n] - c_k[\ell, n])^+, \ \forall \ell, \tag{87}$$

where $w_k[n]$ is the water level on subcarrier n for user k and chosen to satisfy the power constraint $\check{p}_k[n]$.

The proposed interactive game, which does the autonomous spectrum sharing in MIMO-OFDMA systems, therefore runs for all users from the tth iteration until convergence, i.e.,

$$\begin{cases} \check{p}_k^t[n] + \eta_k^t(\check{\mathbf{p}}_k^{t-1}, \check{\mathbf{c}}_k^t)[n] = \check{w}_k^t \ \forall n \text{ (virtual)} \\ \quad p_k^t[\ell, n] + c_k^t[\ell, n] = w_k^t[n] \ \forall n, \ell \text{ (actual)} \\ \quad \xrightarrow{t \text{ increasing}} \cdots\cdots \rightarrow \begin{cases} \check{p}_k^*[n] + \eta_k^*[n] = \check{w}_k^* \ \forall n \text{ (virtual)} \\ p_k^*[\ell, n] + c_k^*[\ell, n] = w_k^*[n] \ \forall n, \ell \text{ (actual).} \end{cases} \end{cases} \tag{88}$$

In the simulations, we assume $\mathrm{E}[|\mathbf{H}_{jk}[n]|^2] = 1$, $N_k[n] = N_0 \ \forall k, n$, and $P_k = P_0 \ \forall k$ and define the system SNR as $\frac{P_0}{N_0}$ (slightly different from before). Results for the proposed virtual AFE (labeled "VAFE" in the figure), the N-S game ("N-SE") in the previous section, NE, and a single-user MIMO-OFDMA ("Single") performance bound are provided and compared. For "single," the optimal sum-rate per subcarrier with the same total network sum-power KP_0, which is the one with zero interference by default, is provided for comparison and also an important benchmark.

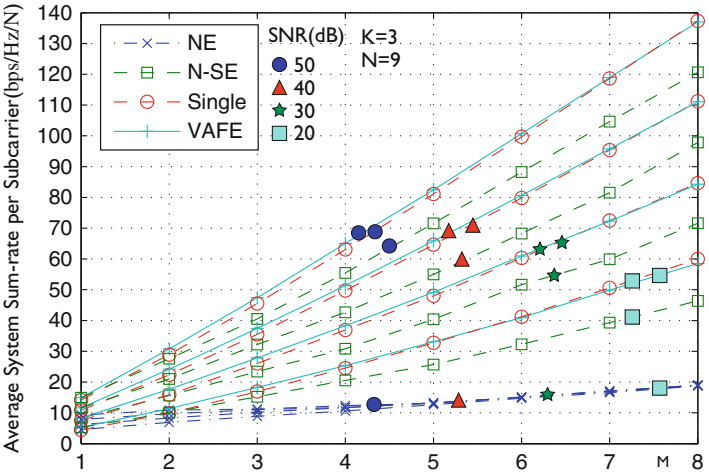

Fig. 13 The network sum-rate per subcarrier against M

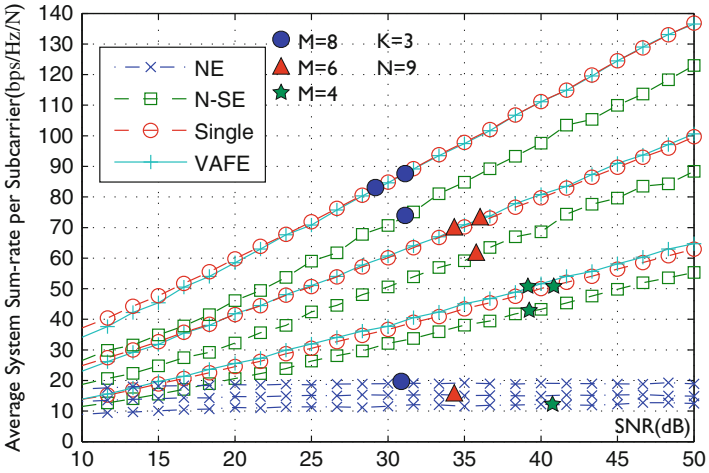

Fig. 14 The network sum-rate per subcarrier against the SNR

Figures 13 and 14 show the average sum-rate results for various SNR and sizes of MIMO when there are 9 subcarriers and 3 users. As can be seen, the sum-rates of NE increase only very slowly with M and are even flat with the SNR indicating that inter-user interference is not managed. In contrast, this is not true for VAFE, N-SE, and the single-user case. Results also illustrate that VAFE outperforms significantly N-SE and achieves the sum-rates very close to the single-user case.

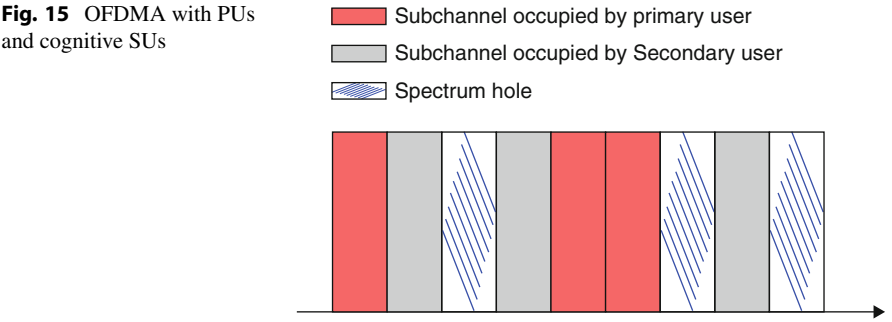

Fig. 15 OFDMA with PUs and cognitive SUs

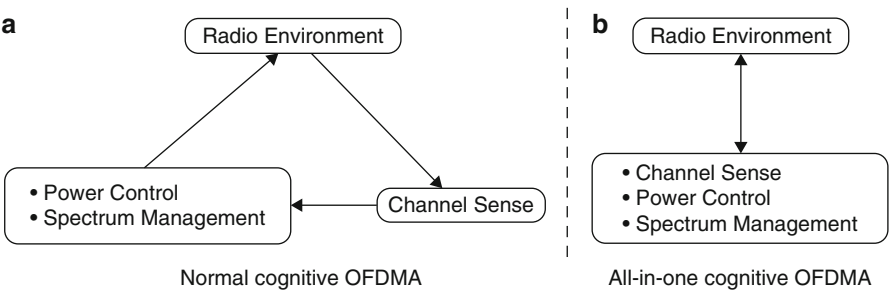

Fig. 16 The cognition cycle

Cognitive OFDMA

Game-theoretic approaches such as described above provide a promising method for uncoordinated users to negotiate and share spectrum resources among themselves in a distributed and autonomous manner. Remarkably, it has been demonstrated that playing strategies can be devised to take users to a desired equilibrium yielding the network sum-rate close to what previously only achievable by a centralized ISB optimization approach in [20]. This makes it a perfect solution for cognitive SUs to maximize their achievable rates among themselves *by playing* when they see white space opportunities, where the PUs are idle in the hierarchical model.

A typical scenario in cognitive radio networks is that there will be a number of PU transmitter-and-receiver pairs with ongoing communications and a number of SUs are observing the radio environment to identify any white spaces for their disposal. For instance, if the PUs have occupied the first, fifth, and sixth channels, as shown in Fig. 15, then ideally, the SUs should optimize their channel allocation and power control over the remaining channels (i.e., white spaces) by either a centralized spectrum manager or the game-theoretic techniques. If a centralized manager is present, then the channels used by the PUs will be obviously quarantined for the OSB (or ISB) optimization for the SUs. However, in playing the game without a centralized manager, how do the SUs know about the quarantined channels?

This is a very challenging problem because a seemingly occupied channel does not necessarily mean that it is being used by a PU and quarantined, as it might be occupied by another SU who is yet to negotiate with any other SU for the channel use. Cognitive transmission is normally done in the following way. First, the SUs will sense the channels and then gather the information about the channel occupancy for spectrum management and power control through a centralized spectrum manager or by some exchange of information. As a final step, the centralized optimal (or suboptimal) solution will be performed that affects the radio environment. By contrast, the cognition cycle in game-theoretic approaches is lumped into a single iteration process of playing the game, which may be designed to arrive at a desired equilibrium, as discussed previously. Figure 16 compares the cognition cycles between standard approaches and the game-theoretic approaches. Nevertheless, it is not at all clear how game-theoretic techniques can coexist with the PUs while being operated for optimizing the access capacity of the SUs. Clearly, the SUs are required to have the *cognition* capability to avoid those channels used by PUs and also compete among themselves for rate maximization. We will defer such discussion by first introducing the use of the transmit interference temperature limit (ITL).

In fact, regulators are skeptical about the effectiveness of ITL model in cognitive radio. FCC defined the model in 2003 intending to control cognitive SUs' interference to the spectrum PUs but abandoned it in 2007 [23] because having an ITL to constrain the transmit power of SUs not only fails to guarantee the PUs' performance but greatly compromises the SUs' achievable performance [24].

Limiting interference to the PUs is the primary concern for cognitive radios [25, 26]. Yet, using an ITL as a precautionary measure has been ineffective as the actual interference experienced by the PUs depends not only upon the transmit power of SUs but the channels between the SUs and the PUs. A too low ITL would provide no protection to the PUs, but if the ITL is set too high, meaningful communications of SUs would be impossible. This is an unresolved challenge of the model, and there has not been a solution to make it sustainable. Another weakness of the model is that even if the channel is genuinely idle, the SUs can never be certain and will not operate at full power to avoid any potential harmful interference to PUs.

Despite the problems it faces, the ITL model's beauty is its simplicity. In this section, we will show that there are ways to make this model useful. In particular, an ITL can work if used as a threshold for the SUs to decide whether or not to transmit rather than to impose a limit on the transmit power. The ITL can also be set very low for extra protection to the PUs and other coexisting users.

Transmit ITL

Consider the OFDMA model without MIMO antennas in section "A Subsystem Model for the OFDMA Game." Now, we introduce an ITL, S_k, for user k, serving

as a threshold for the channel activity to decide whether user k should transmit on a subcarrier. In particular, user k should only occupy subcarrier n if $I_k[n] < S_k$, or it satisfies

$$p_k[n](S_k - I_k[n]) \geq 0. \tag{89}$$

The value of S_k reflects the level of protection to the PUs. In the extreme cases, if $S_k = 0$, the SUs will never be admitted, while if $S_k = \infty$, there will be no protection to the PUs. There is clearly a trade-off between SUs' capacity and protection for PUs. Later, we will propose to use a *transient* ITL, $\tilde{S}_k$, for SU power allocation so that the SUs could violate S_k to gain useful spectrum information for optimizing their strategies but should satisfy the ITL S_k after the adaptation process. Such violation in S_k is undesirable but necessary for distributed learning and self-optimization.

LCP Formulation with ITL

This section presents a linear complementarity problem (LCP) formulation for the OFDMA model given a fixed interference pattern $\{I_k[n]\}$ and a fixed ITL $\tilde{S}_k$. The LCP permits the optimal power allocation strategy $\mathsf{p}_k \triangleq (p_k[1], p_k[2], \ldots, p_k[N])$ to be solved by the well-known Lemke's method [27] and can be viewed as an extension of [28] to cope with the transmit ITL for PU protection.

From user k's point of view, the optimal power allocation strategy in response to the interference pattern experienced by that user can be found by solving the following problem:

$$\max_{\mathsf{p}_k} \sum_{n=1}^{N} \log_2 \left(1 + \frac{p_k[n]}{c_k[n]}\right) \quad \text{s.t. (11) \& } \tilde{S}_k \text{ in (89).} \tag{90}$$

The solution to this is the water-filling power allocation:

$$\begin{cases} p_k[n] = (w_k - c_k[n])^+, & \text{if } I_k[n] < \tilde{S}_k, \\ p_k[n] = 0, & \text{if } I_k[n] \geq \tilde{S}_k, \end{cases} \tag{91}$$

in which w_k is the water level satisfying the power constraint (11). (Note that (91) is of the form of the well-known water-filling solution, which can be optimally realized by a one-dimensional search of w_k satisfying the power constraint. However, motivated by the increased analytical capability, an LCP formulation is preferred here [28].)

The problem (91) can be converted into an LCP of the form:

$$\begin{cases} \mathbf{z}_k \geq \mathbf{0}, \\ \mathbf{M_k z}_k + \mathbf{q}_k \geq \mathbf{0}, \\ \mathbf{z}_k^T (\mathbf{M}_k \mathbf{z}_k + \mathbf{q}_k) = 0, \end{cases} \tag{92}$$

which aims to find a vector $\mathbf{z}_k$ for some vector $\mathbf{q}_k$ and matrix $\mathbf{M}_k$. In (92), the superscript T denotes the transposition and $\mathbf{0}$ is an all-zero column vector. The LCP in (92) can be efficiently and optimally solved by the Lemke's method [27].

To convert (90) into an LCP, we see that when $I_k[n] < \tilde{S}_k$, we have

$$\begin{cases} p_k[n] \geq 0, \\ p_k[n] + c_k[n] - w_k \geq 0, \\ p_k[n](p_k[n] + c_k[n] - w_k) = 0. \end{cases} \tag{93}$$

On the other hand, when $I_k[n] \geq \tilde{S}_k$, we only need to replace $c_k[n] - w_k$ in (93) by 0. For $\sum_{n=1}^{N} p_k[n] = P_k$, we have

$$\begin{cases} \sum_{n=1}^{N} p_k[n] \geq 0, \\ P_k - \sum_{n=1}^{N} p_k[n] \geq 0, \\ \sum_{n=1}^{N} p_k[n] \left(P_k - \sum_{n=1}^{N} p_k[n] \right) = 0. \end{cases} \tag{94}$$

The unknowns are the power allocation p_k and its water-level w_k. From (93) and (94), we can form an LCP by setting

$$\mathbf{z}_k = (p_k[1], p_k[2], \ldots, p_k[N], w_k)^T, \tag{95}$$

$\mathbf{q}_k = (q_k[1], q_k[2], \ldots, q_k[N])^T$ where

$$q_k[n] = \begin{cases} c_k[n] & \text{if } I_k[n] < \tilde{S}_k, \\ 0 & \text{if } I_k[n] \geq \tilde{S}_k, \\ P_k & \text{if } n = N + 1, \end{cases} \tag{96}$$

and

$$\mathbf{M}_k = \begin{pmatrix} 1 & 0 & \cdots & 0 & m_k[1] \\ 0 & 1 & \ddots & \vdots & m_k[2] \\ \vdots & \ddots & \ddots & 0 & \vdots \\ 0 & \cdots & 0 & 1 & m_k[N] \\ -1 & -1 & \cdots & -1 & 0 \end{pmatrix}, \tag{97}$$

where $m_k[n] = -\mathsf{sgn}(\tilde{S}_k - I_k[n])$, in which $\mathsf{sgn}(x)$ returns one if $x > 0$ and zero otherwise. With the above formulation, (92) and (95), (96), and (97), the optimal power allocation strategy for a user for a given interference pattern can be obtained.

The next section will address the interaction between users (both PUs and SUs) using game theory and a proper adaptation in $\tilde{S}_k$ for trading off between SU admission and interference avoidance (i.e., the more we allow users to coexist, the more likely an SU is admitted but a higher level of interference).

A Cognitive Nash Game with Transmit ITL

NE for Rate Competition

From the SUs' perspective and viewing the PU signals as *fixed* background noise, (We assume that the PUs do not change their strategies during which the SUs adapt their strategies, since the PUs are the primary owner and should not be altered regardless of what the SUs do.) we here focus on how the SUs self-optimize their strategies through interaction under the game-theoretic framework. In particular, in the ITL-aided OFDMA model, one can use simultaneous water-filling procedures (similar to the one in [29]) for the SUs to learn each other's action and compromise to an agreed operating point, also known as the NE (or BNE if users are considered forward-looking based on some belief functions). Here, we consider NE as an example. Mathematically, the steady-state solution at the NE, denoted by $(\cdot)^*$, is defined as the strategy which satisfies

$$R_k(\mathsf{p}_k^*, \mathsf{p}_{-k}^*) \geq R_k(\mathsf{p}_k, \mathsf{p}_{-k}^*), \ \forall \mathsf{p}_k \text{ s.t. (11) and } \forall k. \tag{98}$$

Note that while (98) appears to be identical to the simultaneous water-filling process in [29], the key difference is the introduction of $\tilde{S}_k$ into the solution for each SU; see (91). It is however true that without properly designing $\tilde{S}_k$, such NE rate competition could give rise to a highly inefficient operating point causing severe interference to both the SUs and the PUs. It is worth pointing out that in the ITL approach, $\tilde{S}_k$ plays the key role to harmonize the competition among users, analogous to the roles of the belief functions in BNE. Thus, with the transmit ITL integrated with the water-filling competition, a pure NE is sufficient to deliver good results.

The Algorithm, ITL Violation, and Settlement

The main idea of the game-theoretic water-filling interaction is to give opportunity to the SUs to learn the spectrum environment and decide on their resource allocation strategies. Nevertheless, the drawback is that during this interaction and before the SUs identify the subcarriers occupied by the PUs, there will be interference spikes to the PUs. As a result, it is necessary that the water-filling iteration converges rapidly to minimize the impact to the PUs and that at the equilibrium, for all the subcarriers chosen by the SUs, they should satisfy $I_k^*[n] < S_k$.

In particular, a good transient ITL can be chosen as

$$\tilde{S}_k = \max\left(S_k, \frac{\sum_{n=1}^{N} I_k[n]\mathsf{sgn}(p_k[n])}{\sum_{n=1}^{N} \mathsf{sgn}(p_k[n])}\right). \tag{99}$$

For each iteration, SU k uses $\tilde{S}_k$ as a criterion to eliminate the subcarriers and performs the water-filling power allocation based on the LCP described in section "LCP Formulation with ITL." The iterative water-filling procedure can be viewed as a process of sequentially eliminating highly probable "poor" subcarriers and is described as follows:

Step (1) For any SU k, it evaluates $\tilde{S}_k$ by (99);
Step (2) Obtain $\{p_k[n]\}$ by solving the LCP in (92);
Step (3) Repeat Steps 1 and 2 until convergence.

Assuming convergence, the following two propositions analyze the properties of the algorithm at the equilibrium (i.e., NE) and give justification of $\tilde{S}_k$ in (99).

Proposition 1. *At the NE, the transient ITL is given by*

$$\tilde{S}_k^* = \max\left(S_k, \min_n I_k^*[n]\right). \tag{100}$$

Proof. From (99), it is seen that the iterative water-filling process subsequently eliminates weaker subcarriers, and less subcarriers will be remained toward convergence. If

$$\min_n I_k^*[n] > S_k, \tag{101}$$

then only one subcarrier will be hired by SU k and

$$\tilde{S}_k^* = \min_n I_k^*[n]. \tag{102}$$

In this case, however, the converged $\tilde{S}_k^*$ will exceed the preset ITL S_k, which is undesirable and should be avoided. On the other hand, $\tilde{S}_k^* = S_k$, which means that the transient ITL will converge to the preset ITL. As a result, (100) is obtained. □

Note that if $\min_n I_k^*[n] > S_k$, this means that there should not be any subcarrier available for use by SU k. This algorithm manages to learn this by water-filling interaction at the cost of interference spikes during the interaction. The proposition below presents a property of the algorithm if $\tilde{S}_k^* = S_k$.

Proposition 2. *At the NE, if* $\sum_{n=1}^{N} \mathsf{sgn}\left(p_k^*[n]\right) \geq 2$, *then*

$$\tilde{S}_k^* = S_k, \tag{103}$$

or if there are more than one subcarriers selected by SU k after convergence, then they will all satisfy the ITL S_k.

Proof. Obtained immediately by definition. □

Propositions 1 and 2 together assert that using this algorithm the possible outcome for each SU is either that the SU cannot be admitted if the ITL condition $I_k^*[n] < S_k$ cannot be satisfied or the SU has (self-)optimized its power allocation to maximize its rate after negotiation with other SUs while satisfying the ITL $I_k^*[n] < S_k$ (i.e., meeting the requirement for avoiding the PUs).

Analysis

The ITL-regulated Nash game has always at least one NE. The proof follows immediately from [30, Theorem 1]. However, whether the NE is unique is not understood. For large S_k, the algorithm is reduced to the traditional iterative water-filling algorithm, and the convergence condition has been studied in [29,31]. For small S_k, users will have strong tendency to avoid each other and should converge.

The choice of S_k governs the admission of SUs based on an artificial projection of interference to the PUs, with the thought that a small S_k would provide strong protection to the PUs. It is therefore important to see if it is possible to have a small S_k for the game to be carried out effectively for self-optimization of the SUs. This will be answered by the numerical results in the next section.

Results

In this section, simulation results are provided to evaluate the performance of the proposed ITL-aided simultaneous water-filling solution, which is referred to as a cognitive NE ("CNE" in the figures). The benchmark to be compared to is the traditional simultaneous water-filling solution, or simply "NE," where no control is imposed onto the SUs and the SUs can freely compete with the PUs for transmission. In the simulations, it is assumed that there are totally 20 subcarriers or $N = 20$, randomly selected four of which are occupied by the PUs. For SU k, we have

$$I_k[n] = \sum_{\substack{j=1 \\ j \neq k}} p_j[n] \frac{|H_{jk}[n]|^2}{|H_{kk}[n]|^2} + \tilde{p}[n] \frac{|\tilde{h}_k[n]|^2}{|H_{kk}[n]|^2} + \frac{N_k[n]}{|H_{kk}[n]|^2}, \tag{104}$$

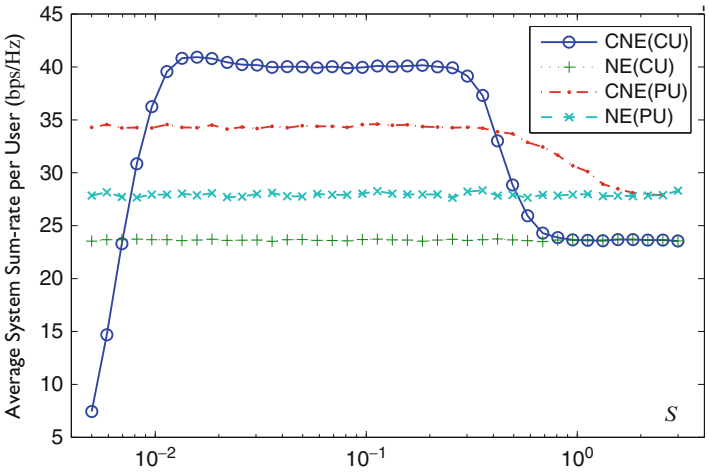

Fig. 17 Sum-rate against the ITL S with $H_0 = 0.4$ and SNR $= 16.5$ dB

where $\tilde{p}[n]$ denotes the transmit power of the PU on subcarrier n, $\tilde{h}_k[n]$ is the channel between the PU and SU k on the nth subcarrier, and $N_k[n]$ is the noise power at user k on the nth subcarrier. It is also assumed that $N_k[n] = N_0 \ \forall k, n$ and $\frac{\tilde{p}[n]}{N_0} = 27$ dB for all those subcarriers used by the PU. We model each cross talk link for every subcarrier by an equal-power four-ray Rayleigh fading channel with $\mathrm{E}[|H_{jk}[n]|^2] = \mathrm{E}[|\tilde{h}_k[n]|^2] = H_0$, and H_0 indicates the severeness for the interference. For the desired link, $\mathrm{E}[|H_{kk}[n]|^2] = 1 \ \forall k, n$. Three SUs are assumed, i.e., $K = 3$ and $S_k = S \ \forall k$. Also, $P_k = P_0 \ \forall k$ and the SNR for an SU is defined as $\frac{P_0}{NN_0}$. In the figures, the sum-rate per PU or SU averaged over independent channel realizations is provided.

First, we investigate how the sum-rate performance of the ITL-aided Nash game varies with the choice of the transmit ITL S. In Fig. 17, it is observed that CNE (i.e., the ITL-based scheme) significantly outperforms the conventional NE in that the SUs can achieve a much higher rate and at the same time the PUs suffer the least, if the ITL is chosen to be $0.01 \leq S \leq 0.3$. For NE, they are independent of S.

Setting the ITL $S = 0.1$ (a good choice as suggested by the results in Fig. 17), Fig. 18 shows the sum-rate results against the SNR of the SU. Results illustrate that as expected the sum-rates of the SUs increase with the SNR for both the ITL-based CNE and NE. However, for NE, the PUs suffer a huge rate loss due to interference from the SUs. In contrast, in the ITL-based CNE, the PU sum-rate is unaffected meaning that the SUs can avoid the subcarriers used by the PUs.

Figure 19 shows the rate performance against the number of interactions between the users. In the simulations, we assume that the SUs interact in a sequential order. Results reveal that both CNE and NE converge very quickly in a few interactions. Also, we see that there is only a slight dip in the PU rate for CNE during which the

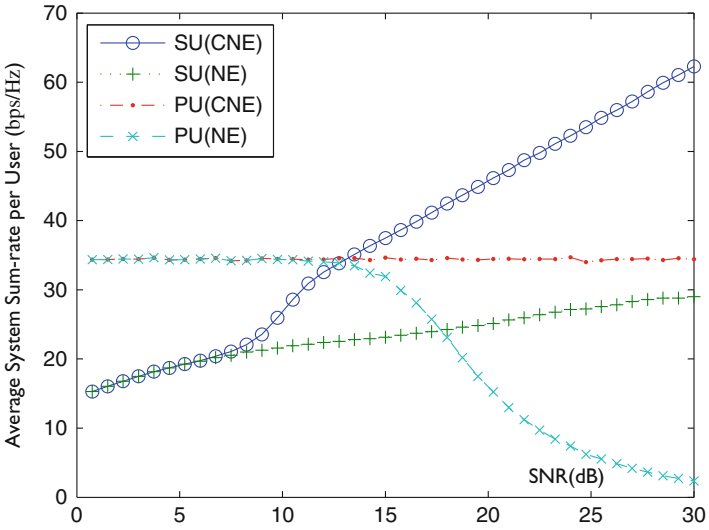

Fig. 18 Sum-rate against the SNR with $H_0 = 0.4$ and $S = 0.1$

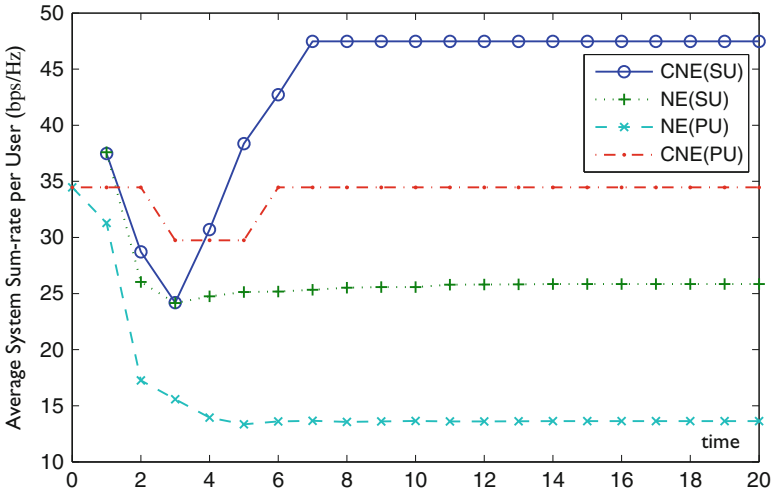

Fig. 19 Sum-rate against the number of interactions for the cognitive Nash game between users with $H_0 = 0.4$, $S = 0.1$, and SNR= 20 dB

SUs learn the spectrum environment to maximize their rates. At convergence, the PUs can regain their rate since the SUs then avoid their subcarriers completely.

As a major result, it has been shown possible to design a game-theoretic strategy for cognitive SUs to optimize their access to the shared spectrum, while completely avoiding the PUs without prior knowledge of the channels occupied by the PUs.

Conclusions

In this chapter, well-designed games utilizing the concepts of forward-looking players and the transmit ITL have been investigated to achieve spectrally efficient autonomous spectrum sharing. The mathematical framework of a belief-directed game has been shown suitable to characterize the cognition ability of mobile radios via a belief function, which can then be designed to facilitate negotiation among competing radios to reach a rate-maximization equilibrium. The use of a transmit ITL on the other hand has been demonstrated as a simple way to effectively protect the PUs while the SUs negotiate among themselves to optimize their access. The extraordinary network performance of these approaches appears to come from the users' forward-lookingness empowering their acceptance and willingness to trade strategies for negotiating toward a desirable equilibrium. This chapter, however, has only touched upon a tip of an iceberg and more have to be done. For example:

- How chaotic a wireless environment would be and any harmful impact, if such game-theoretic methods are adopted? Note that there could be new joining users every now and then inviting negotiation. Do these methods really work?
- An assumption that is implicit in the game-theoretic approaches is that every user has instant knowledge of its own predicted reward function. In the OFDMA rate-maximization problem, it means that each user knows its instantaneous achievable rate. Although it can be easily measured and fed back to its transmitter, the feedback could be too much, if the game takes many cycles to converge.
- Would it be possible for adversarial users to manipulate the game for better self-returns? In the ITL-aided method, for example, the reason why the PUs can be avoided even if the SUs do not know a priori which channels they are using is that the PUs are not responding to the SUs' actions and thus the SUs end up trading among themselves leaving the PUs' channels unaffected. If an adversary plays stubbornness to own certain channels, it will win. How to avoid that?

Obviously, many directions still need to be conquered in the future, but it is hoped that this chapter has shed sufficient light on the possible performance that could be resulted from well-designed games, and more researches will follow suit.

References

1. Staple G, Werbach K (2004) The end of spectrum scarcity. IEEE Spectr 41(3):48–52
2. Zhao Q, Sadler BM (2007) A survey of dynamic spectrum access. IEEE Signal Process Mag 24(3):79–89
3. Anderson T (1973) A simulation study of some dynamic channel assignment algorithms in high capacity mobile telecommunications system. IEEE Trans Veh Technol 22:210
4. Zhang M (1989) Comparisons of channel assignment strategies in cellular mobile telephone systems. IEEE Trans Veh Technol 38:211–215
5. Hatfield D, Weiser P (2005) Property rights in spectrum: taking the next step. In: Proceedings of the 1st IEEE Symposium on New Frontiers Dynamic Spectrum Access Networks, pp 43–55

6. Ileri O, Samardzija D, Mandayam N (2005) Demand responsive pricing and competitive spectrum allocation via a spectrum server. In: Proceedings of the 1st IEEE Symposium on New Frontiers Dynamic Spectrum Access Networks, pp 194–202
7. Chung S, Kim S, Lee J, Cioffi J (2003) A game-theoretic approach to power allocation in frequency-selective Gaussian interference channels. In: Proceedings of the IEEE International Symposium Information Theory, p 316
8. Etkin R, Parekh A, Tse D (2005) Spectrum sharing for unlicensed bands. In: Proceedings of the 1st IEEE Symposium on New Frontiers Dynamic Spectrum Access Networks, pp 251–258
9. Huang J, Berry R, Honig M (2005) Spectrum sharing with distributed interference compensation. In: Proceedings of the 1st IEEE Symposium on New Frontiers Dynamic Spectrum Access Networks, pp 88–93
10. Costa M (1983) Writing on dirty paper. IEEE Trans Inf Theory 29:439–441
11. Simeone O, Bar-Ness Y, Spagnolini U (2007) Stable throughput of cognitive radios with and without relaying capabilities. IEEE Trans Commun 55(12):2351–2360
12. Sadek AK, Liu KJR, Ephremides A (2007) Cognitive multiple access via cooperation: protocol design and performance analysis. IEEE Trans Inf Theory 53(10):3677–3696
13. Mitola J III, Maguire GQ Jr (1999) Cognitive radio: making software radios more personal. IEEE Commun Mag 6(4):13–18
14. Haykin S (2005) Cognitive radio: brain-empowered wireless communications. IEEE J Select Areas Commun 23(2):201–220
15. Commission FC (2002) Spectrum Policy Task Force: ET Docket no. 02-135
16. Molisch AF, Greenstein LJ, Shafi M (2009) Propagation issues for cognitive radio. Proc IEEE 97(5):787–804
17. Akyildiz IF, Lee W-Y, Vuran MC, Mohanty S (2006) NeXt generation/dynamic spectrum access/cognitive radio wireless networks: a survey. Comput Netw 50(13):2127–2159
18. Wong CY, Cheng RS, Letaief KB, Murch RD (1999) Multiuser OFDM with adaptive subcarrier, bit, and power allocation. IEEE J Select Areas Commun 17(10):1747–1758
19. Cendrillon R, Yu W, Moonen M, Verlinden J, Bostoen T (2006) Optimal multiuser spectrum balancing for digital subscriber lines. IEEE Trans Commun 54(5):922–933
20. Yu W, Lui R (2006) Dual methods for nonconvex spectrum optimization of multicarrier systems. IEEE Trans Commun 54(7):1310–1322
21. Ren J, Wong KK, Hou J (2013) A forward-looking Nash game and its application to achieving Pareto-efficient optimization. Appl Math 4(12):1609–1615
22. Rappaport TS (1996) Wireless communications: principles and practice. Prentice-Hall, Englewood Cliffs
23. FCC (2007) Interference temperature operation. ET docket no. 03-237, FCC 07-78
24. Clancy TC (2007) Achievable capacity under the interference temperature model. In: IEEE International Conference on Computer Communications, Anchorage, 6–12 May 2007, pp 794–802
25. Mitola J, Maguire GQ (1999) Cognitive radio: making software radios more personal. IEEE Per Commun 6(6):13–18
26. Haykin S (2005) Cognitive radio: brain-empowered wireless communications. IEEE J Select Areas Commun 23(2):201–220
27. Cottle RW, Pang J-S, Stone RE (1992) The linear complementarity problem. Academic Press, Boston
28. Luo ZQ, Pang JS (2006) Analysis of iterative waterfilling algorithm for multiuser power control in digital subscriber lines. EURASIP J Appl Signal Proc 2006:Article ID 24012, 10 pages
29. Popescu O, Rose C, Popescu DC (2007) Simultaneous water-filling in mutually interfering systems. IEEE Trans Wireless Commun 6(3):1102–1113
30. Rosen JB (1965) Existence and uniqueness of equilibrium points for concave n-person games. Econometrica 33(3):520–534
31. Yu W, Ginis G, Cioffi J (2002) Distributed multiuser power control for digital subscriber lines. IEEE J Select Areas Commun 20(5):1105–1115

Further Reading

1. Debreu DA (1952) Social equilibrium existence. Proc Natl Acad Sci 38:886–893
2. Ren J, Hou J, Wong KK (2011) Self-optimized MIMO-OFDMA: a nash-stackelberg game-theoretic approach. In: Proceedings of the Asilomar Conference on Signals, Systems and Computers, Pacific Grove, 6–9 Nov 2011

Spectrum Sensing in Multi-antenna Cognitive Radio Systems via Distributed Subspace Tracking Techniques

15

Christos G. Tsinos and Kostas Berberidis

Contents

C. G. Tsinos (✉)
Interdisciplinary Centre for Security, Reliability and Trust (SnT), University of Luxembourg, Luxembourg City, Luxembourg
e-mail: christos.tsinos@uni.lu

K. Berberidis
Department of Computer Engineering and Informatics, University of Patras, Patras, Greece

CTI "Diophantus", Patras, Greece
e-mail: berberid@ceid.upatras.gr

W. Zhang (ed.), *Handbook of Cognitive Radio*,
https://doi.org/10.1007/978-981-10-1394-2_15

Abstract

Among the many different techniques that have been suggested for spectrum sensing, the eigenvalue-based spectrum sensing (EBSS) techniques exhibit some important advantages. Specifically, they can operate in a totally blind manner while they offer remarkably improved performance for specific types of signals, especially when compared to energy-based methods. Until recently, most of the cooperative EBSS techniques that could be found in the literature were batch and centralized ones, thus suffering from limitations that render them impractical in several cases. Practical cooperative adaptive versions of typical EBSS techniques, which could be applied in a completely distributed manner, have been proposed very recently. The aim of this chapter is (a) to briefly review existing cooperative EBSS techniques of the batch and centralized type and (b) to present in more detail adaptive and distributed versions of typical EBSS techniques. Focusing on the latter case, at first, we present adaptive EBSS techniques for the maximum eigenvalue detector (MED), the maximum-minimum eigenvalue detector (MMED), and the generalized likelihood ratio test (GLRT) scheme, respectively, for a single-user (noncooperative) case. Then, a distributed subspace tracking method is presented which enables the cooperating nodes to track the joint subspace of their received signals. Based on this method, cooperative distributed versions of the adaptive EBSS techniques have been developed that overcome the limitations of the previous batch centralized approaches. Numerical results show that the distributed techniques exhibit good performance, even though they require reduced computational complexity compared to their batch and centralized counterparts.

Introduction

The exponentially increasing demands for higher data rate mobile communication services [6] require new methods for efficient managing the available spectrum resources. Current wireless services are "squeezed" in a spectrum area of a few GHz, and several studies conducted worldwide [4,5,7,41,48] have shown that many of the frequency bands licensed to wireless systems are significantly underutilized. This motivated the development of techniques within the context of cognitive radio (CR) [17]. The concept of CR was introduced via the seminal works [32–34], and its core idea is to allow non-licensed users (Secondary Users – SUs) to transmit their data in a spectrum area that is licensed to the so-called primary users (PUs) of the system.

A large part of the related literature is mainly addressing the co-existence problem between the PUs-SUs by proposing efficient techniques for different examined system models. According to the spectrum access policy, the CR techniques can be categorized into three different categories [13]. In the underlay techniques, the SUs are allowed to transmit simultaneously with the PUs as long as the generated interference is below a predefined threshold. In the overlay CR techniques, cooperation is allowed between the SUs and PUs nodes so as to jointly

optimize their transmissions. Finally, the interweave, techniques which are based on the so-called opportunistic communications concept, rely on the idea that the SUs can operate via spectrum areas that are not used temporally by the PUs. The latter unused spectrum areas are commonly referred to as "spectral holes," and they provide transmission opportunities to the SU without degrading the performance of the PU. A desired characteristic of the interweave approach is that the SUs can employ transmission techniques that require very little or no interaction with the corresponding PUs.

Key role in the interweave/opportunistic approaches play the spectrum sensing techniques which are employed by the SUs in order to detect the spectrum holes. Due to the fact that the performance of both the PUs and SUs depends highly on the successful detection of the corresponding spectrum holes, a major part of the recent CR literature has focused on the design of efficient spectrum sensing techniques.

Spectrum sensing may be implemented either by a single-radio architecture or by a dual-radio one [40,61,69]. In the single-radio case, which is the most common one, a fixed portion of each time slot is dedicated to spectrum sensing, and the remaining part is employed for data transmission. As a consequence, the accuracy of the spectrum sensing results is limited. Furthermore, single-radio architectures are less spectrally efficient, since a portion of the available time slot is allocated to spectrum sensing, instead of data transmission [40, 62]. On the contrary, it is obvious that a single-radio architecture is simple to implement and of low cost. In the dual-radio architecture, one radio-frequency (RF) chain is dedicated to data transmission and reception, while a second RF chain is dedicated to continuous spectrum monitoring [19, 73]. In general, the dual-radio approach provides higher spectrum efficiency and better sensing accuracy; however it should employ very low-complexity spectrum sensing techniques due to its "continuous" nature.

Several spectrum sensing schemes have been proposed over the last few years. The most common approach is via energy-based detectors (EBD) [8, 11, 24] which are usually simple to implement; however, they require knowledge of the involved noise variance. The test statistic of the energy detector is the average energy of the observed samples. The decision is taken by comparing that test statistic with a threshold, usually related to the underlying statistics of the noise that corrupts the received samples. In case, the noise variance is not known, it is estimated via standard methods, though this results in significant performance degradation of the EBD techniques [21, 46, 50]. If information related to the PU signal is available at the SU, the optimal detection method is the matched filter approach [18, 30]. In these techniques, the known primary signal is correlated with the received secondary signal to detect the PU existence in the latter and thus maximize the signal-to-noise ratio. The matched filter detection achieves satisfactory performance, even for very small number of samples, though as already mentioned, it requires the strong assumption that the PU signal is known at the SU. The estimation of the required information at the SU side may be very difficult or even impossible, and thus the matched filter approach, in many cases, cannot be applied. The cyclostationary-based spectrum sensing techniques [12, 47] belong to the feature detector's category and exploit the cyclostationary feature of the

signals in order to detect the PU's presence. It is based on the analysis of the cyclic autocorrelation function of the received signal or its Fourier series expansion. The Fourier series expansion exhibits peaks when cyclostationary signals are present on the received one. Thus, if the PU is not present, no peaks are observed, since the noise is considered as a non-cyclostationary signal, in general. A cyclostationary-based detector achieves satisfactory performance on detecting weak signals even for low SNR values. A category that has gained significant interest over the past years is that of the eigenvalue-based spectrum sensing techniques (EBSS) [23, 35, 36, 49, 63, 71, 72]. The EBSS methods (particularly, the MMED and GLRT) may operate without the knowledge of the noise variance, and, moreover, they may offer remarkably improved performance for specific signal categories. However, this is done at the expense of high complexity since they require the EigenValue Decomposition (EVD) of the received signal's sample covariance matrix. Moreover, the computation of the involved decision thresholds is generally based on the asymptotic (limiting) distributions of the corresponding test statistics and requires a large number of samples in order to attain a satisfactory performance. Recently, close approximations for the distribution functions of the test statistics have been proposed in the literature [23, 36] though they have quite a complex form. Thus, the computation of the decision thresholds is actually performed by numerical methods which increase even further the computational complexity.

The high complexity required for implementing the batch EBSS techniques makes them impractical for cases where continuous monitoring of a specific spectrum band is required (dual-radio approach). In such cases, the aim is to detect as soon as possible an abrupt change (i.e., the PU starts or stops its transmission at a random time). To this end, a number of different solutions have been proposed in literature so far based on the quickest detection of change as well as sequential detection approaches [3, 15, 22, 65, 68, 70, 74]. According to the aforementioned approaches, the SU updates sequentially its corresponding tests statistics upon the reception of a new data sample and decides if a change has occurred in the spectrum area of interest. The decision is based on thresholds which are computed in order to optimize a metric, i.e., a mean detection delay which is usually defined as the mean time required by the SU to detect a change subject to the targeted probability of false alarms.

There are two standard formulations in the area of change detection: Bayesian and min-max. The Bayesian formulation was developed by Shiryaev [43–45]. In this approach the change point is assumed to be a random variable with a certain (known) prior distribution, and the objective is to minimize the mean detection delay subject to an upper bound on the false alarm probability. In the min-max approach, introduced by Lorden [28], the change point is assumed to be an unknown deterministic parameter, and the objective is to minimize the worst-case conditional detection delay subject to an inequality constraint on the average run false alarm length. Each one of the approaches is suited for different regimes, and both of them have been applied in the cognitive radio literature during the past years [3, 15, 22, 65, 68, 70, 74]. Note that these approaches are mainly based on the energy detector whereas, to the best of our knowledge, none of them was of the EBSS type.

An approach based on the batch EBSS techniques would require high computational complexity if small mean detection delay was sought since periodic computation of the EVD of the SU's sample covariance matrix would be required for updating the corresponding test statistics so as to detect as quickly as possible an abrupt change in the PU's behavior.

Thus, in this chapter which is an updated and extended version of [56,58], at first, online implementations of the EBSS techniques based on low-complexity subspace tracking (ST) techniques [9–67] (and references therein) are presented. The aim of a ST technique is to update in an adaptive manner the estimation of the subspace of an input signal provided that a new data sample of the signal is available at each time index. In other words the EVD of the sample covariance matrix is updated each time a new data sample is received. The main advantage of a ST technique is that the EVD update can be done with complexity of $O(R_x L)$ operations, where L is the rank of the desired subspace. Contrariwise, recall that in the batch approach, the subspace of the signal is updated by computing the EVD of the sample covariance matrix at each time index which exhibits a prohibited computational complexity of $O(R_x^3)$ operations.

The previously mentioned spectrum sensing techniques are suitable for single-user systems. The performance of a single-user spectrum sensing technique deteriorates significantly in environments where the fading and shadowing effects of the wireless channels degrade the quality of the received signals. Cooperation among multiple secondary users has been proposed in literature in order to improve the sensing performance. It is noteworthy, however, that the existing approaches (see [1, 2, 10, 25, 27, 31, 37, 60, 75] and references therein) are cooperative variations of the generic energy detector. To the best of our knowledge, cooperative techniques of the EBSS type have not been considered in literature so far, apart from the case where a fusion center collects the sensed data and applies the EBSS in a centralized batch manner [23]. A centralized approach comes with a number of limitations concerning the high-power costs in transmitting local information to the fusion center and conveying global decisions back to the SUs. Furthermore, a centralized SU network is quite sensitive to node and link failures. On the contrary, a decentralized approach exhibits low communication overhead, and it is robust to node and link failures. Each SU node communicates only with its adjacent SU nodes via one-hop transmissions resulting in transmissions with reduced power consumption during the sensing period. The SU nodes exchange information for several rounds so as to reach global convergence. Upon convergence, each node can reach the same decision concerning the PU existence without the need of a fusion center node.

Thus, in the second part of this chapter, cooperative adaptive EBSS techniques [58] are presented that function in a completely decentralized manner so as to overcome the limitations of the centralized batch approaches. It is noteworthy to mention that a constituent part of the these cooperative EBSS techniques is a distributed ST algorithm which is also presented here. In literature so far, little work concerning the problem of distributed ST has been published. The authors in [26] develop a consensus-based technique of the so-called OJA rule in which

several ST methods are based. In [39] a distributed version of the well-known PAST technique is presented. The previous methods are more suitable for ad hoc wireless sensor networks with a large number of nodes since they are based on consensus strategies. In the scenario studied in this chapter, the number of nodes that are involved in the network topology is relatively small, and thus, distributed strategies that minimize the required communication overhead are more suitable. Moreover, the approaches of [26] and [39] provide estimations for the eigenvectors only and not for the corresponding eigenvalues. Furthermore, they converge rather slowly since they are gradient flow-based approaches [9], and finally they do not guarantee the orthogonality of the estimated eigenvectors resulting in severe performance degradation.

More specifically, the techniques that are presented in this chapter are the following ones. At first, single SU (noncooperative) adaptive EBSS techniques are discussed based on well-known ST methods. Then, the distributions of the adaptive test statistics are derived in order to compute the required decisions thresholds. It turns out that accurate approximations of the test statistics correspond to well-known tabulated functions improving further the practicality of the presented adaptive schemes over the batch ones. Next, a cooperative adaptive EBSS method is proposed by first developing a distributed adaptive ST algorithm. The adaptive EBSS and cooperative adaptive EBSS methods that are presented in this chapter are compared to the corresponding batch EBSS approaches, in terms of performance for single (fixed spectrum sensing time)- and dual (continuous spectrum monitoring)-radio architectures.

The rest of this chapter is organized as follows. In section "System Description," the system description is provided. In section "Centralized Batch Cooperative Eigenvalue-Based Spectrum Sensing," a brief description is given for the EBSS techniques considered here. In section "Adaptive Eigenvalue-Based Spectrum Sensing for the Single SU Case," adaptive versions of the EBSS (AD-EBSS) techniques are derived. In section "Test Statistics Distributions and Decision Thresholds," the test statistics' distribution functions of the proposed AD-EBSS techniques, and the corresponding decision thresholds are derived. In section "Cooperative Decentralized Adaptive Eigenvalue-Based Spectrum Sensing," the cooperative EBSS schemes are presented. Section "Numerical Results" presents the numerical results, and section "Conclusion" concludes the chapter.

System Description

Let us assume that a single-antenna PU node and K SU nodes of R_x antennas each one are operating in the same frequency band in a typical interweave CR scheme (Fig. 1) [13]. The system description is given for the single-radio approach, though it can be easily modified for the dual-radio one. Thus, the time axis is assumed to be divided into transmit time intervals (time slots). The time slot is considered as the basic unit of time scheduling. At the beginning of each SU time slot, the SUs sense the frequency band so as to determine if it is occupied by a PU transmission.

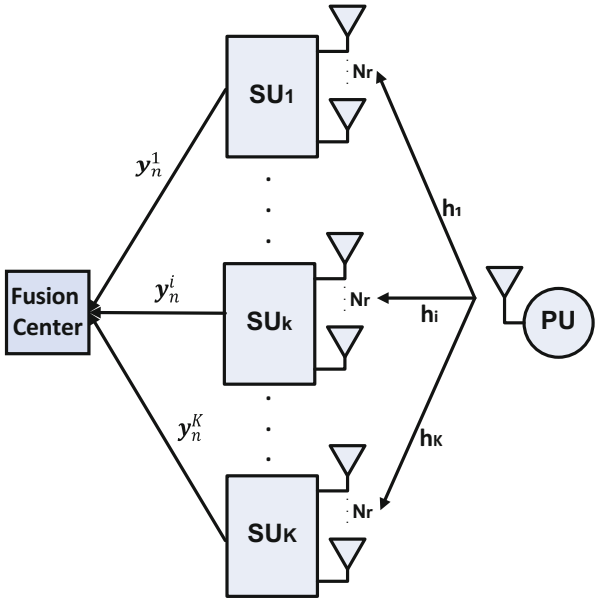

Fig. 1 Fusion based centralized EBSS technique

Let us also assume that during each sensing period, each one of the K SUs collects N sample vectors $\mathbf{y}_n^i$, $1 \leq n \leq N$ and $1 \leq i \leq K$, of dimensions $1 \times R_x$. In a centralized approach, a node that plays the role of the fusion center (Fig. 1) receives from the SUs the collected vector samples. Then, the fusion center node processes the samples jointly, decides if active PU transmissions exist in the environment, and notifies accordingly the SUs. More specifically, in the related cooperative spectrum sensing problem, the following hypothesis test is considered at the fusion center,

$$\mathscr{H}_0 : \mathbf{y}_n = \mathbf{z}_n \tag{1}$$

$$\mathscr{H}_1 : \mathbf{y}_n = \mathbf{h}x_n + \mathbf{z}_n, \tag{2}$$

where $\mathbf{y}_n = \left[\mathbf{y}_n^1, \ldots, \mathbf{y}_n^K\right]^T$, $\mathbf{z}_n$ is an $KR_x \times 1$ additive noise random variable modeled as $\mathscr{CN}\left(0, \sigma_z^2\right)$, $\mathbf{h} = [\mathbf{h}_1, \ldots, \mathbf{h}_K]^T$ is a $KR_x \times 1$ vector that contains all complex flat channel gains that correspond to the links between the PU and the antennas of all SUs, and x_n is the transmitted PU symbol. That is, under the hypothesis $\mathscr{H}_0$, the PU is idle and the received signals $\mathbf{y}_n^i$ at the SUs contain only noise. On the other hand, under the hypothesis $\mathscr{H}_1$, the PU transmits data, and the received SUs' signals are a superposition of these data (scaled by the channel gains) and noise. An EBSS technique decides between the two hypotheses by employing test statistics that are functions of the eigenvalues of the received signals' sample covariance matrix. In the following section, a brief description of the existing EBSS techniques is given.

Centralized Batch Cooperative Eigenvalue-Based Spectrum Sensing

In literature so far, only batch EBSS techniques have been considered, in the sense that the derivation of the test statistics is based on the EVD of the sample covariance matrix formed by a number of N collected vectors. Moreover, only centralized cooperative extensions of the EBSS techniques have been proposed so far. As long as a fusion center exists to collect the SU vector samples $\mathbf{y}_n^i$ in the cooperative case, the application of a batch EBSS technique is almost identical for both the noncooperative (single) SU and the cooperative cases.

In the rest of this section, we provide a brief description of the existing approaches for the cooperative case, though they are directly applicable to the noncooperative case by setting the number of SU nodes equal to $K = 1$. We consider that the fusion center receives the SUs' sample vectors $\mathbf{y}_n^i$ through noise-free communication links and forms the aggregate vector $\mathbf{y}_n = \left[\mathbf{y}_n^1, \ldots, \mathbf{y}_n^K\right]^T$ as discussed in the previous section. The covariance matrix $\mathbf{R}$ of the received signal $\mathbf{y}_n$, under the two hypotheses, is given by

$$\mathbf{R} = \mathbb{E}\{\mathbf{y}_n \mathbf{y}_n^H\} = \begin{cases} \sigma_z^2 \mathbf{I}_{KR_x} & \mathscr{H}_0 \\ \sigma_x^2 \mathbf{h}\mathbf{h}^H + \sigma_z^2 \mathbf{I}_{KR_x} & \mathscr{H}_1 \end{cases}, \tag{3}$$

where $\mathbb{E}\{\cdot\}$ denotes the expectation operator, σ_x^2 is the PU's transmitted signal's variance, and $(\cdot)^H$ denotes the Hermitian of a matrix. In practice, the fusion center (or a single SU) computes the sample covariance matrix of the received signals, which is given by

$$\hat{\mathbf{R}} = \frac{1}{N} \sum_{i=1}^{N} \mathbf{y}_n \mathbf{y}_n^H. \tag{4}$$

Let us denote with $\lambda_1 \geq \cdots \geq \lambda_{R_x}$ the ordered eigenvalues of matrix $\hat{\mathbf{R}}$. As it is known from the relevant literature, the eigenvalues of the sample covariance matrix can be used to form a sufficient test statistics for the spectrum sensing problem. In the following equations, three different test statistics are defined:

$$T^{MED}(\lambda_1) = \frac{\lambda_1}{\sigma_z^2}, \tag{5}$$

$$T^{GLRT}(\lambda_1, \ldots, \lambda_{R_x}) = \frac{\lambda_1}{\frac{1}{N-1} \sum_{m=2}^{R_x} \lambda_m}, \tag{6}$$

$$T^{MMED}(\lambda_1, \lambda_{R_x}) = \frac{\lambda_1}{\lambda_{R_x}}. \tag{7}$$

The noise eigenvalues of the sample covariance matrix are random variables due to the finite number of samples that are used for its computation. The distribution of these noise eigenvalues is used to compute the decision threshold

in a Neyman-Pearson sense for a predefined probability of false alarm. Detailed information on how to compute the decision thresholds is given in [49, 71, 72].

We may now proceed with the development of the cooperative adaptive EBSS methods. For clarity purposes, we first deal with the noncooperative case in which only a single SU is involved. Then, the extension of the proposed adaptive approaches to the cooperative case is derived.

Adaptive Eigenvalue-Based Spectrum Sensing for the Single SU Case

In this section the adaptive eigenvalue-based spectrum sensing techniques are presented for the single-user (noncooperative) case. First, the single-radio-fixed spectrum sensing time case will be considered. Then, the double-radio-continuous spectrum monitoring scenario will be developed. The complexity analysis for both the adaptive approaches is also analyzed and compared to the one of the corresponding batch counterparts.

Single-Radio Approach

Let us now proceed to the description of the adaptive EBSS technique for the single-radio approach. In this paper the complex version of the Fast Data Projection Method (FDPM) is employed [9]. The FDPM steps are summarized in the following equations:

$$\mathbf{r}_n = \mathbf{U}_{n-1}^H \mathbf{y}_n \tag{8}$$

$$\mathbf{U}_n = \mathbf{U}_{n-1} \pm \mu \mathbf{y}_n \mathbf{r}_n^H \tag{9}$$

$$\mathbf{U}_n = orth\{\mathbf{U}_n\} \tag{10}$$

$$\boldsymbol{\lambda}_n = \alpha \boldsymbol{\lambda}_{n-1} + (1-\alpha)|\mathbf{r}_n|^2, \tag{11}$$

where $\mathbf{U}_n$ and $\boldsymbol{\lambda}_n$ are the $R_x \times L$ matrix and $L \times 1$ vector that contain the L principal (minor) eigenvectors and eigenvalues, respectively; $|\mathbf{r}_n|^2$ is the vector of the squared absolute values of the elements of vector $\mathbf{r}_n$; and α, μ are step-size parameters. Note that in (9) the sign is a $(+)$ or $(-)$ depending on whether the signal or the noise subspace, respectively, is updated. Equation (11) tracks the corresponding eigenvalues. An orthonormalization procedure is applied in (10) based on a low-complexity Householder transformation [9] given by the following equations:

$$\mathbf{a}_n = \mathbf{r}_n - \|\mathbf{r}_n\| e^{j(angle(\mathbf{e}_1^H \mathbf{y}_n))} \mathbf{e}_1 \tag{12}$$

$$\mathbf{U}_n = \mathbf{U}_n - \frac{2}{\|\mathbf{a}_n\|^2} (\mathbf{U}_n \mathbf{a}_n) \mathbf{a}_n^H \tag{13}$$

$$\mathbf{U}_n = norm\{\mathbf{U}_n\} \tag{14}$$

In (12) $\mathbf{e}_1 = [1, 0 \dots 0, 0]$ and in (13), $norm\{\cdot\}$ denotes the operator that normalizes the columns of a matrix. For the MED test statistic, only the first (maximum) eigenvalue is required, so $\mathbf{U}_n$ is a $R_x \times 1$ matrix and $\boldsymbol{\lambda}_n$ is a scalar that contains the current estimate of the maximum eigenvalue. The orthonormalization step is also reduced to a simple normalization one, i.e., $\mathbf{U}_n = \mathbf{U}_n / \|\mathbf{U}_n\|$. In a similar way, the MMED test statistic is estimated. At first, the signal subspace version of the FDPM is employed (with $(+)$ in (9)) to track the maximum eigenvalue, and then the noise subspace version follows (with $(-)$ in (9)) to track the minimum one. For the GLRT test statistic, the complete FDPM (8), (9), (10), and (11) is used since all the R_x eigenvalues of $\hat{\mathbf{R}}_n$ are required in (6).

It is evident that, by employing the FDPM method, the SU is capable of tracking, with low complexity, the value of any of the test statistics under consideration at every time index within the sensing period. Therefore, once a new signal vector is received, the SU updates the employed test statistic and decides if a change in the state has been occurred (from $\mathscr{H}_0$ to $\mathscr{H}_1$ and vice versa). Thus, the adaptive EBSS techniques can be applied in both the single- and in the dual-radio approach. In the single-radio approach, the adaptive techniques can be applied in fixed sensing periods in a similar way to the batch ones. That is for each time slot within the sensing period, the corresponding test statistics are updated and at the end of the sensing period a decision is taken according to a threshold whose computation is given in section "Test Statistics Distributions and Decision Thresholds".

Complexity Analysis for the Single-Radio Approach

Let us now derive the complexity of the adaptive and the batch EBSS techniques for the single-radio case. The complexity is given in terms of the total required complex mathematical operations (additions/subtractions, multiplications/divisions, and square roots) at a sensing period of N timeslots. According to [9], the FDPM algorithm requires at each timeslot $12R_xL+5L+2$ operations, to update L principal components of the covariance matrix $\mathbf{R}$ at the SU receiver, provided that a new $R_x \times 1$ sample $\mathbf{y}_n$ is available (see [9] for a detailed analysis). In the aforementioned complexity, we must add $3L$ operations since (11) is not included in the original version of the FDPM presented in [9]. Note that (11) requires only $3L$ operations since the entries of the vector $|\mathbf{r}_n|$ are already computed in (8) and in (12). Thus, the overall complexity is $12R_xL + 8L + 2$ per update/timeslot. Since the sensing period is associated with N signals, a total of $N(12R_xL + 8L + 2)$ operations are required. Now the complexity of each one of the adaptive EBSS techniques can be derived by properly setting the value of the parameter L and then adding the number of operations that are required for the computation of the specific test statistic according to (5), (6), an(7). That is, for the MED test statistic $L = 1$ and the complexity is $N(12R_x + 10) + 1$ operations. In a similar way, the MMED test statistic requires two applications of the FDPM with $L = 1$ (section "Single-Radio Approach") resulting in complexity of $2N(12R_x + 10) + 1$ operations. Finally,

$L = R_x$ for the GLRT test statistic and the complexity is $N(12R_x^2 + 8R_x + 2) + R_x$ operations.

Let us now derive the complexity of the batch approaches. In this case matrix $\hat{\mathbf{R}}$ is updated at each timeslot. The latter requires $2NR_x^2$ complex operations. Then, the SVD of the $\mathbf{R}$ is computed requiring approximately $13R_x^3$ operations according to [51]. Thus, the overall computational cost of each one of the batch EBSS techniques is equal to $13R_x^3 + 2NR_x^2$. Now, in order to derive the explicit complexity of each one of the test statistics, we should count for the operations of (5), (6), and (7), similarly to the adaptive case. Therefore, the MED and MMED test statistics require $13R_x^3 + 2NR_x^2 + 1$ operations, and the GLRT one requires $13R_x^3 + 2NR_x^2 + R_x$ operations. It is evident that the adaptive methods exhibit significantly reduced complexity compared to the batch ones. As it is shown in the following section, the complexity savings can be more significant for the case of the dual-radio approach.

Dual-Radio Approach

We now present the adaptive EBSS techniques for the dual-radio architecture. Let us assume that the SU employs the FDPM method so as to track continuously the test statistics during consecutive periods of N samples. We follow the approach of [74] where it is assumed that the PU changes its behavior at a random sample number within the sensing period. The change point T_0 is assumed to follow a known geometric distribution parametrized by p, that is,

$$P\{T_0 = n\} = p(1-p)^{n-1}(1-\lambda_0),\ 0 < n \leq N, \tag{15}$$

where $\lambda_0 = P\{T_0 = 0\}$ denotes the probability that a change occurs before the sensing period. According to the Bayesian formulation, the problem of quickest detection of change is to design a detection rule that gives the stopping time T_d so that the mean detection delay $E\{(T_d - T_0)^+\}$ is minimized subject to a constraint on the probability of false alarm, that is $P\{T_d < T_0\} \leq \zeta$. Note that the definition of the probability of false alarm here differs from the single-radio approach, since now is denoted as the probability that a change is detected prior the actual time of change ($T_d < T_0$). The solution to that problem requires the knowledge of the exact distribution of the samples under both hypotheses which is not possible to be derived for the case of the EBSS techniques. Moreover a closed form is in general intractable even in case of the simple energy detector. Thus, in order to develop an efficient and simple technique, the following approach is adopted which is summed up in Algorithm 1. The SU for each block of N samples updates sequentially the EBSS test statistics under consideration. At each time index n of the sensing block, the updated test statistic is compared to a global threshold. The global threshold is computed so as the probability of false alarm is set to a specific value

Algorithm 1 : Adaptive EBSS for the single SU case

Initialization:
The SU detects the present state ($\mathscr{H}_0$ or $\mathscr{H}_1$) by applying the adaptive EBSS technique for a sufficient number of received signals, until an initial decision is taken. For each block of N symbols
for $n = 1 \rightarrow N$ **do**
  Update the employed Test-Statistic T via the FDPM (8), (9), (10), and (11)
  if $T \geq \eta_d$ under $\mathscr{H}_0$ || $T < \eta_d$ under $\mathscr{H}_1$ **then**
    Raise an alarm, change in the state has been detected;
  end if
end for

$P\{T_d < T_0\} = \zeta$. The threshold computation in this approach is more complex than the simple radio one, and it is described in section "Test Statistics Distributions and Decision Thresholds".

Remark 1. One may argue that the batch EBSS approaches can be extended easily to the dual-radio case. Indeed, let us assume that within the sensing period of N symbols, the EVD of the sample covariance matrix is periodically computed every $N_s < N$ samples so as to update the values of the test statistics. This could increase significantly the complexity due to a number of $\lfloor \frac{N}{Ns} \rfloor$ SVD that are required. Clearly a small number of N_s reduces the detection delay though it results in high complexity and vice versa. A detailed analysis of the complexity is given in the following subsection.

Complexity Analysis for the Dual-Radio Approach

Let us assume that a dual-radio sensing approach is applied for a period of N symbols. For the subspace update given in section "Single-Radio Approach", the adaptive techniques require the same complexity with the single-radio case. The difference in the dual-radio case is that the computation of the test statistics is done at every timeslot $n \in [1, N]$, and thus, the operations of (5), (6), and (7) must be added N times to the overall complexity. Thus, it is easy to see that in the dual-radio approach, the complexity for the MED technique is $N(12R_x + 10) + N$; for the MMED one, it is $2N(12R_x + 10) + N$; and for the GLRT one, it is $N(12R_x^2 + 8R_x + 2) + NR_x$ operations, respectively.

According to Remark 1, the dual-radio version of the batch approaches requires the computation of $\lfloor \frac{N}{Ns} \rfloor$ SVDs for a sensing period of N symbols. According to section "Complexity Analysis for the Single-Radio Approach," the latter costs $13\lfloor \frac{N}{Ns} \rfloor R_x^3$ operations. In order to derive the overall complexity, one should also add $\lfloor \frac{N}{Ns} \rfloor$ times the operations of (5), (6), and (7) similarly to the adaptive case. Therefore, the MED and MMED test techniques require $13\lfloor \frac{N}{Ns} \rfloor R_x^3 + \left(2N + \lfloor \frac{N}{Ns} \rfloor - 1\right) R_x^2 + \lfloor \frac{N}{Ns} \rfloor$ operations, and the GLRT one requires

$13\lfloor\frac{N}{Ns}\rfloor R_x^3 + \left(2N + \lfloor\frac{N}{Ns}\rfloor - 1\right) R_x^2 + \lfloor\frac{N}{Ns}\rfloor R_x$ operations. Clearly, the complexity gains for employing the adaptive EBSS techniques are even greater in the dual-radio sensing approach especially for small values of the parameter N_s. In Fig. 10 of section "Numerical Results," the complexity of the adaptive EBSS techniques is compared to the one of the batch techniques for different values of the involved parameters.

Test Statistics Distributions and Decision Thresholds

In this section, the cumulative distribution functions (CDF) of the three test statistics of (5), (6), and (7) are derived for the adaptive case, under the hypothesis $\mathscr{H}_0$, i.e., when no information signal is present in the signal received by the SU. Based on (11) of the FDPM, the distribution functions of the involved test statistics can be tracked at every time index n. The following lemma provides expressions for the distribution functions of the corresponding test statistics.

Lemma 1. *The distribution functions of the adaptive test statistics updated by (11) for a SU of R_x antennas under the hypothesis $\mathscr{H}_0$ can be approximated by the functions*

$$F_{T^{MED}}(x;\xi,\rho) \approx \frac{\gamma(\xi x,\rho)}{\Gamma(\rho)}, \tag{16}$$

$$F_{T^{GLRT}}(x;\rho,R_x) \approx \mathscr{I}_{\frac{(R_x-1)x}{x+1}}(\rho,(R_x-1)\rho), \tag{17}$$

$$F_{T^{MMED}}(x;\rho) \approx \mathscr{I}_{\frac{x}{x+1}}(\rho,\rho), \tag{18}$$

respectively, where $\xi = \frac{(1-\alpha^n)(1+\alpha)}{((1-\alpha)(1-\alpha^{2n}))}$, $\rho = \frac{(1-\alpha^n)^2(1+\alpha)}{((1-\alpha)(1-\alpha^{2n}))}$, $\gamma(x,\rho) = \int_0^x t^{\rho-1}e^{-t}dt$ is the lower incomplete gamma function, $\Gamma(\rho) = \int_0^\infty t^{\rho-1}e^{-t}dt$ denotes the ordinary gamma function, and $\mathscr{I}_x(\rho_1,\rho_2) = \int_0^x t^{\rho_1-1}(1-t)^{\rho_2-1}dt$ is the incomplete beta function.

Proof. Observe that, under hypothesis $\mathscr{H}_0$, the signal vector $\mathbf{y}_n$ received by the SU consists of i.i.d. complex Gaussian noise samples $\mathscr{CN}(0,\sigma_z^2)$. Since matrix $\mathbf{U}_{n-1}$ is orthonormal, the entries $\mathbf{r}_n^{(i)}$ of vector $\mathbf{r}_n = \mathbf{U}_{n-1}^H\mathbf{y}_n$ are also i.i.d. $\mathscr{CN}(0,\sigma_z^2)$. From (11), the l-th eigenvalue of the covariance matrix is estimated as

$$\lambda_l(n) = \sum_{i=0}^{n} \alpha^i(1-\alpha)|\mathbf{r}_n^{(i)}|^2. \tag{19}$$

According to the previous equation, the MED test statistic can be expressed as a weighted sum of chi-squared variables with each one derived by squaring the absolute value of a random variable $\phi_i \sim \mathscr{CN}(0,1)$. A close approximation to the

previous distribution can be derived by properly applying the results of [64] to our case. Let us consider the following RV:

$$T \triangleq \sum_{i=1}^{m} w_i \zeta_i^2, \tag{20}$$

where $\zeta_i \sim \mathcal{N}(0,1)$ and $w_i \in \mathbb{R}$. Welch, in a 1938 paper [64], proposed an approximation of the distribution of variable T by a scaled chi-squared distribution of ρ degrees of freedom. That is, $T \sim \frac{1}{\xi}\chi^2_\rho$, where $\xi = \frac{\sum_{i=1}^m w_i}{\sum_{i=1}^m w_i^2}$, $\rho = \frac{(\sum_{i=1}^m w_i)^2}{\sum_{i=1}^m w_i^2}$, and the corresponding CDF is given by

$$F_T(x;\xi,\rho) = \frac{\gamma(\xi/2x, \rho/2)}{\Gamma(\rho/2)}. \tag{21}$$

Now, by defining $w_i = \alpha^i(1-\alpha)/2$ and using (21) in the case of complex normal variables ϕ_i, we can apply the previous results to the MED test statistic (5). Moreover, observe that the weights w_i are actually terms of a geometric sequence enabling as to compute closed forms for the parameters ρ and ξ. Thus, it can be verified that $\xi = \frac{2(1-\alpha^n)(1+\alpha)}{((1-\alpha)(1-\alpha^{2n}))}$ and $\rho = \frac{2(1-\alpha^n)^2(1+\alpha)}{((1-\alpha)(1-\alpha^{2n}))}$. Finally, by combining these expressions with (21), the proof for MED is completed.

In the case of the MMED test statistic, we seek for the distribution of the ratio of two eigenvalues of matrix $\hat{\mathbf{R}}_n$ that are estimated via (11). The required distribution is equivalent to the distribution of the ratio $\frac{T^{MED}(\lambda_1)}{T^{MED}(\lambda_{R_x})}$. Therefore, the corresponding CDF is equal to the one of the ratio of two independent T^{MED} random variables. It turns out that the distribution of the MMED statistic can be approximated by the beta prime distribution with the corresponding CDF given by (18). The detailed proof is given at Appendix.

Finally, the CDF of the GLRT test statistic can be computed by firstly observing that the random variable $\sum_{m=2}^{R_x}\lambda_m \sim \frac{1}{\xi}\chi^2_{(R_x-1)\rho}$, where the parameters ξ and ρ are defined similar to the case of the MED distribution. Then, the CDF of the ratio of the two independent random variables $\frac{\lambda_1}{\sum_{m=2}^{R_x}\lambda_m}$ is computed in a similar way to the MMED case. As long as the CDF of the ratio under consideration is computed, it is easy then to compute the CDF of the scaled random variable $T^{GLRT} = \frac{\lambda_1}{\frac{1}{R_x-1}\sum_{m=2}^{R_x}\lambda_m}$, given by (17). □

Threshold Computation for the Single-Radio Approach

From Lemma 1, the CDFs of the adaptive test statistics involve the computation of well-known tabulated functions, and the same comment is true for their corresponding inverse functions. The latter observation enables the SU to easily compute the

decision thresholds in a Neyman-Pearson sense, for a predefined probability of false alarm $\mathscr{P}_f$, as opposed to the case of the batch test statistics where usually numerical methods are required. To proceed further, first, the decision threshold η^{MED} for the MED test statistic is computed. We equivalently have

$$P_f = P\left\{T^{MED} > \eta^{MED} | \mathscr{H}_0\right\} = 1 - F_{T^{MED}}(x; \xi, \rho) \Rightarrow$$

$$\eta^{MED} = F^{-1}_{T^{MED}}\left(1 - P_f; \xi, \rho\right). \tag{22}$$

The decision thresholds for the adaptive MMED and GLRT test statistics can be computed in a similar way, and they are given by the following equations:

$$\eta^{MMED} = \frac{\mathscr{I}^{-1}\left(1 - P_f; \rho, \rho\right)}{1 - \mathscr{I}^{-1}\left(1 - P_f; \rho, \rho\right)}, \tag{23}$$

$$\eta^{GLRT} = \frac{\mathscr{I}^{-1}\left(1 - P_f; \rho, (R_x - 1)\rho\right)}{(R_x - 1) - \mathscr{I}^{-1}\left(1 - P_f; \rho, (R_x - 1)\rho\right)}. \tag{24}$$

Threshold Computation for the Dual-Radio Approach

According to section "Complexity Analysis for the Single-Radio Approach" in the dual-radio approach, the threshold is computed so as to set the probability of false alarm $P\{T_d < T_0\}$ to a specific value ζ. In order to compute the previous probability, we require the probability that a PU is detected at least one time before the time index of change T_0 under $\mathscr{H}_0$. Given the fact that the test statistics are updated by adding each time index a new positive random variable and that the parameter α is set to values close to 1, the latter probability can be approximated by the probability the test statistic is greater than the threshold at time index $T_0 - 1$, that is $P\{T_{T_0-1} > \eta_d | \mathscr{H}_0\} = 1 - F_{T_{T_0-1}}(\eta_d)$, where $F_{T_{T_0-1}}(\eta_d)$ denotes the CDF of the corresponding test statistic given by (16), (17), and (18) for each one of the cases considered here. Now, by assuming that the time of change is independent to the values of the test statistics and taking the summation over all the $0 < n \leq N$, it can be seen that the required false alarm probability can be approximated by the following equation:

$$P\{T_d < T_0\} \approx \sum_{n=0}^{N} (1 - F_{T_{n-1}}(\eta_d)) p (1-p)^{n-1} (1 - \lambda_0). \tag{25}$$

Finally, by setting $P\{T_d < T_0\} = \zeta$ and solving numerically (25), the desired threshold is computed.

Cooperative Decentralized Adaptive Eigenvalue-Based Spectrum Sensing

In this section, the previously derived adaptive EBSS techniques are extended to the cooperative case, in which multiple SUs sense the spectrum in a collaborative manner. The distributed technique is designed so as (a) to improve the sensing performance by forming a virtual multiple antenna system that performs a joint EBSS technique, (b) to distribute the computation overhead among the SU nodes, and (c) to enable each user to track the joint test statistics at each time index within the sensing period so as to reach a common decision in a decentralized manner. Apart from the benefits of a decentralized approach discussed in the Introduction, the latter feature is crucial in scenarios where the multiple nodes employ a cooperative transmission scheme [16,52–55,57,59], and thus all the involved nodes should reach a common decision concerning the PU existence. Clearly, the proposed decentralized adaptive EBSS methods require the development of a distributed adaptive subspace tracking method in order to track the corresponding test statistics of (5), (6), and (7). Therefore, a novel distributed subspace tracking scheme is first developed by extending the FDPM of [9]. The present section is divided into two subsections. In section "Distributed Data Projection Method (DDPM)," the proposed distributed subspace tracking method is described. Then, in section "Cooperative EBSS Techniques," the cooperative EBSS methods are described.

Distributed Data Projection Method (DDPM)

Let us assume that K SU nodes form a network where the i-th node is connected via direct links only to the $(i-1)$-th and the $(i+1)$-th nodes. The communication links are assumed to be established via ideal (noise-free) channels. Note that the latter assumption is typical in both the distributed adaptive signal processing [42] and cooperative spectrum sensing literature [10, 31, 37, 60, 75]. For simplicity, we assume that each SU node has the same number of R_x antennas, though the results are directly applicable in cases where the nodes may have different numbers of antennas. At each time index of the sensing period, the i-th SU obtains a $R_x \times 1$ vector of samples $\mathbf{y}_n^i$. Let us now assume that we are interested in tracking the L first principal (or minor) components of the correlation matrix $\mathbf{R}$ of the aggregate vector $\left[\mathbf{y}_n^1, \ldots, \mathbf{y}_n^K\right]^T$. The task of tracking each one of the L eigenvectors is properly distributed to the SU nodes in a way that the i-th node tracks the elements of the sub-matrix $\mathbf{U}_n\left((i-1)R_x+1 : iR_x, 1 : L\right)$ of the aggregate eigenvectors matrix $\mathbf{U}_n$. For simplicity, the later sub-matrix will be denoted by $\mathbf{U}_n^i$. Thus, each node needs to update only a specific part of the subspace. Moreover, each node is capable of tracking the corresponding L principal (minor) eigenvalues of the aggregate system, denoted by $\boldsymbol{\lambda}_n^i$. As explained below, at each time index n, the DDPM requires three spatial iterations in order to update the eigenvectors and eigenvalues matrices. By observing (9), the subspace update can be done in a local computation step at node i given by

$$\mathbf{U}_n^i = \mathbf{U}_{n-1}^i \pm \mu \mathbf{y}_n^i \mathbf{r}_n^H \tag{26}$$

Now, in order to execute the local update step of (26), each node must know the value of $\mathbf{r}_n$. Observe that the computation of $\mathbf{r}_n$ requires a spatial iteration in which the i-th node performs the local computation of (27) and sends the quantity $\mathbf{r}_{loc}^i$ to the $(i+1)$-th node. That is,

$$\mathbf{r}_{\text{loc}}^i = \mathbf{r}_{\text{loc}}^{i-1} + \mathbf{U}_{n-1}^{*^i} \mathbf{y}_n^i \tag{27}$$

Thus, starting from the first node, the variable $\mathbf{r}_{\text{loc}}^i$ is updated in an incremental manner, and at the end of this first spatial iteration, the K-th node has the exact value of $\mathbf{r}_n$ given by

$$\mathbf{r}_n = \sum_{i=1}^{K} \mathbf{r}_{\text{loc}}^i \tag{28}$$

The second spatial iteration starts from the last node K of the network. As it was mentioned, the K-th node has already the exact value of $\mathbf{r}_n$ in (28), and therefore it is able to update the corresponding sub-matrix of eigenvectors as determined by (26), then update the eigenvalues by using (11) locally, and apply the orthogonalization transformation to the updated eigenvectors sub-matrix, that is

$$\mathbf{U}_n^i = \mathbf{U}_n^i - \frac{2}{\|\mathbf{a}_n\|^2} \left(\mathbf{U}_n^i \mathbf{a}_n\right) \mathbf{a}_n^H, \tag{29}$$

where the quantity $\mathbf{a}_n$ is computed by applying (12) locally. Clearly, in order to complete the eigenvectors update, the normalization step of (13) is required. Therefore, the last local computation of the $i-th$ node at the second spatial iteration is given by

$$\mathbf{T}_{\text{loc}}^i = \mathbf{T}_{\text{loc}}^{i-1} + \sum_{l=1}^{L} |\mathbf{U}_n^j(:, l)|^2 \tag{30}$$

Now observe that by incrementally applying (30) at the end of the second spatial iteration, the first node has the vector $\mathbf{T}_n = \left[\|\mathbf{U}_n(:, l)\|^2, \ldots, \|\mathbf{U}_n(:, L)\|^2\right]$ whose i-th element is the squared normed of the i-th eigenvector. Note that as already mentioned, the incremental strategy requires the transmission of the quantities $\mathbf{r}_n$ and $\mathbf{T}_{\text{loc}}^i$ from the i-th node to the $(i+1)$-th one.

The aim of the third iteration is to normalize the updated eigenvalues matrix $\mathbf{U}_n$. It is easy to see that the latter can be done by performing sequentially the following steps at the i-th node

$$\mathbf{U}_n^i = diag\left(\mathbf{T}_n\right)^{1/2} \mathbf{U}_n^i \tag{31}$$

Algorithm 2 : The DDPM algorithm

1: **Initialization:** $\mathbf{U}_0 \leftarrow \mathbf{I}_{R_x \times L}$ & $\boldsymbol{\lambda}_0 \leftarrow \mathbf{0}_{L\times 1}$
2: **Previous Instant Data:** Node i has $\mathbf{U}^i_{n-1}$ and $\boldsymbol{\lambda}^i_{n-1}$
3: **New Data:** Node i has a new vector sample $\mathbf{y}^i_n$
4: **Apply:**
5: **1st Spatial Iteration:**
6: $\mathbf{r}^0_{\text{loc}} \leftarrow \mathbf{0}_{L\times 1}$ $\mathbf{T}^{K+1}_{\text{loc}} \leftarrow \mathbf{0}_{L\times 1}$
7: **for** $i = 1 \rightarrow K$ **do**
8: $\quad \mathbf{r}^i_{\text{loc}} \leftarrow \mathbf{r}^{i-1}_{\text{loc}} + \mathbf{U}^{i*}_{n-1}\mathbf{y}_n(i)$ % Incremental Computation of $\mathbf{r}_n$
9: **end for**
10: **2nd Spatial Iteration:**
11: **for** $i = K \rightarrow 1$ **do**
12: $\quad \boldsymbol{\lambda}^i_n = \alpha\boldsymbol{\lambda}^i_{n-1} + (1-\alpha)|\mathbf{r}_n|^2$, % Update of $\boldsymbol{\lambda}^i_n$
13: $\quad \mathbf{U}^i_n \leftarrow \mathbf{U}^i_{n-1} \pm \mu \mathbf{y}^i_n \mathbf{r}^H_n$ % Update of $\mathbf{U}^i_n$
14: $\quad \mathbf{a}_n \leftarrow \mathbf{r}_n - \|\mathbf{r}_n\|\mathbf{e}_1$ % Distributed Orthogonalization of $\mathbf{U}_n$
15: $\quad \mathbf{U}^i_n \leftarrow \mathbf{U}^i_n - \frac{2}{\|\mathbf{a}_n\|^2}\left(\mathbf{U}^i_n\mathbf{a}_n\right)\mathbf{a}^H_n$
16: $\quad \mathbf{T}^i_{\text{loc}} \leftarrow \mathbf{T}^{i-1}_{\text{loc}} + \sum_{l=1}^{L}|\mathbf{U}^j_n(:,l)|^2$ % Incremental Computation of $\mathbf{T}_n$
17: **end for**
18: **3rd Spatial Iteration:**
19: **for** $i = 1 \rightarrow K$ **do**
20: $\quad \mathbf{U}^i_n \leftarrow diag\left(\mathbf{T}_n\right)^{1/2}\mathbf{U}^i_n$ % Distributed Normalization of $\mathbf{U}_n$
21: **end for**

where $diag\,(\cdot)$ denotes the operator that transforms the vector operand to a diagonal matrix. The complete DDPM is summarized in Algorithm 2.

Cooperative EBSS Techniques

In this subsection the extension of the adaptive EBSS technique to the case of multiple SUs is described. Let us consider that the nodes of SUs network apply the DDPM of Algorithm 2 so as to jointly track the subspace of the received data covariance matrix of the aggregate virtual multi-antenna SU system (Fig. 2). As it is evident from line 13 of Algorithm 2, each node, at each time index, updates the local estimates of the eigenvalues of the sample covariance matrix. Therefore, each node is also able to compute the test statistics of (5), (6), and (7) of the aggregate system and can perform the detection tests independently. Moreover, the test statistics distributions, under the hypothesis $\mathscr{H}_0$, are again given by Lemma 1, by replacing R_x with KR_x. Observe also that in a dual-radio approach, each SU node can employ independently Algorithm 1 so as to reach a common decision concerning a detection of a change in the PU activity.

Let us now comment on the specificities of each one of the cooperative EBSS techniques. If the MED method is employed, then it suffices to track only the maximum eigenvalue, and thus, in the DDPM algorithm the cooperating SUs may set $L = 1$. Moreover, the distributed orthogonalization steps (lines 15–16 on

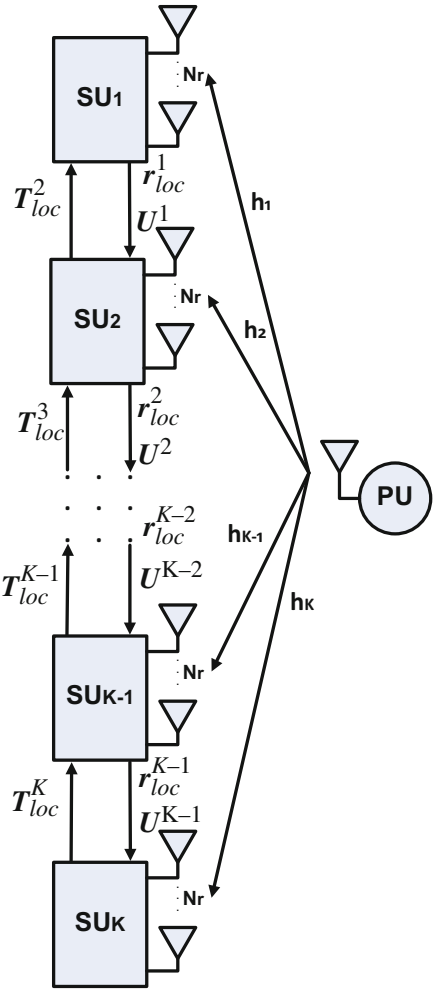

Fig. 2 Distributed EBSS technique

Algorithm 2) are not performed at all, in a way similar to the single SU case. In the case of the MMED method, again in a similar way to the single SU one, each of the SUs tracks the maximum and the minimum eigenvalues of the covariance matrix by employing twice the DDPM for $L = 1$. Specifically, first the signal subspace version (with $(+)$ in (9)) is employed so as to track the maximum eigenvalue, and then the noise subspace version follows (with $(-)$ in (9)) in order to track the minimum one. Recall that this approach has been adopted in order to avoid the complexity of tracking the complete subspace of the covariance matrix. Of course the steps of each one of the two versions of the DDPM can be applied simultaneously at each time index. Finally, for the adaptive GLRT EBSS method, the SU nodes should apply the complete DDPM algorithm with $L = KR_x$.

Computational and Network Complexity of the Decentralized Adaptive EBSS Techniques

Let us first examine the computational complexity. From the description of the DDPM technique, it is evident that its computational complexity equals to the one of a centralized FDPM for a system of $K \times R_x$ receiver antennas, though (11) is executed K times, that is one time for each one of the participating SUs. Therefore according to [9] and the discussion of section "Complexity Analysis for the Single-Radio Approach," the complexity for subspace estimation for a sensing period of N timeslots is $N(12KR_xL + 5L + 3KL + 2)$ operations. Now, by noting that each one of the SUs employs (22) and (23), and following the same procedure with the single SU case, the complexity at both the single- and the dual-radio case can be derived easily. Thus, we have for the single-radio case $N(12KR_x+3K+7)+K$ operations for the MED test statistic, $2N(12KR_x+3K+7)+K$ operations for the MMED, one and $N(12K^2R_x^2+11KR_x+2)+KR_x$ for the GLRT one, respectively. Accordingly we have for the dual-radio case $N(12KR_x+3K+7)+NK$ operations for the MED test statistic, $2N(12KR_x + 3K + 7) + KN$ operations for the MMED one and $N(12K^2R_x^2 + 11KR_x + 2) + NKR_x$ operations for the GLRT one, respectively.

Note that in a similar way, one may also derive the complexity of the batch EBSS techniques by simply replacing R_x with KR_x in the expressions derived in sections "Complexity Analysis for the Single-Radio Approach" and "Complexity Analysis for the Dual-Radio Approach" (omitted here to avoid repetition).

The network complexity is derived in terms of the complex scalar quantities that must be transmitted during a sensing period of N data samples. From the description of the DDPM technique (Algorithm 2), the MED test statistic requires $3NK$ scalar quantities to be transmitted, and the MMED and the GLRT require $6NK$ and $3NKR_x$, respectively. A centralized approach requires NKR_x scalar transmissions in order for the SUs to transmit the data samples to the fusion center and K transmissions to notify the users for its decision. Clearly, for SUs with number of antennas greater than 3, the decentralized MED test statistic exhibits lower complexity than the corresponding centralized approach. In a similar way, the MMED test statistic exhibits less communication burden when the number of antennas of each node is greater than 6. Finally, the GLRT exhibit always greater communication complexity than the centralized. The network complexity is depicted also in Fig. 11 in the simulations section.

Numerical Results

In this section, numerical results are presented in order to evaluate the performance of the adaptive EBSS methods. We assume that the PU transmits a binary phase-shift keying (BPSK) modulated signal. The step of the FDPM algorithm is set to $\mu = 0.8/\|\mathbf{y}_n\|^2$. First, the methods for the single SU case are tested.

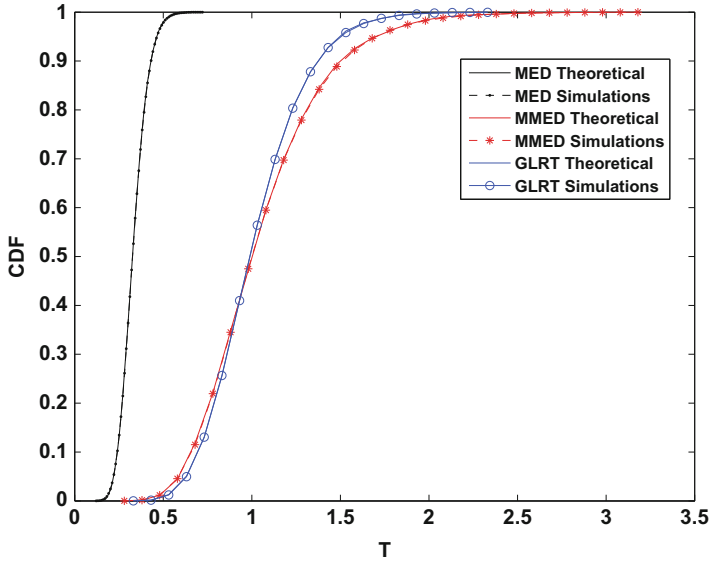

Fig. 3 CDFs of the test statistics under $\mathscr{H}_0$ (16), (17), and (18)

In Fig. 3, the theoretical CDFs of the MED, MMED, and GLRT adaptive test statistics under the $\mathscr{H}_0$ (Lemma 1) are compared to the empirical ones when a block of $N = 20$ received signal vectors at the SU is used to estimate them. The results of 10000 simulations are averaged so as to compute the empirical CDFs for a SU receiver with $R_x = 4$. As it is shown, the derived theoretical CDFs are very close to the empirical ones even for this small number of received signals.

In Fig. 4, the performance of the AD-EBSS techniques is compared to the one of the batch techniques in terms of the achieved probability of detection $\mathscr{P}_d$ under different SNR values for probability of false alarm $\mathscr{P}_f = 0.1$ for the single-radio case.

The parameter a of the FDPM algorithm in (11) is set to $a = 0.98$. The performance is examined considering constant channels within each timeslot of duration $N = 100$ symbols. The taps of all the involved channels are derived as $\mathscr{CN}(0, 1)$, and the results of 10000 realizations are averaged. Note that, even in single-radio approach, the AD-EBSS techniques exhibit reduced complexity compared to the batch ones, as they do not require the computation of the sample covariance matrix given by (4).

As it is shown, the adaptive versions of the test statistics achieve, in general, performance close to the batch ones (or even better, in some cases). This is due to the fact that the CDFs of the adaptive test statistics (16) (17), and (18) are close approximations to the exact ones, whereas for the batch case asymptotic expressions are used. This can be also verified by the results depicted in Fig. 5 where the simulations of Fig. 4 were repeated, but now the decision thresholds

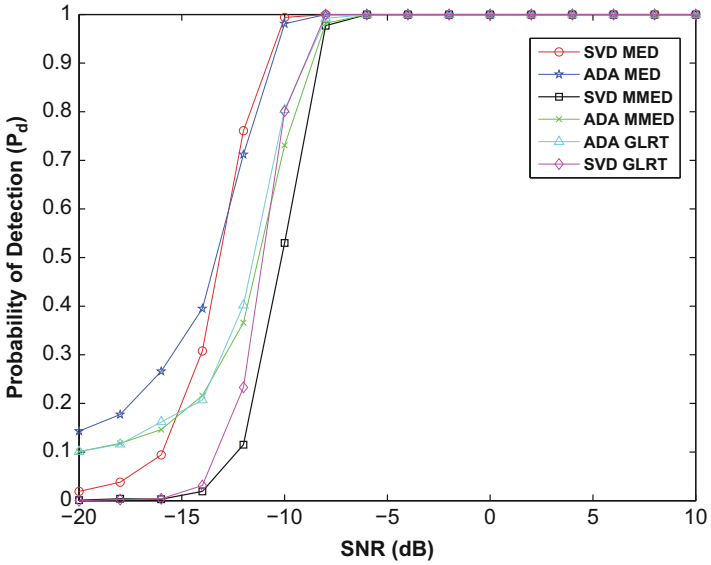

Fig. 4 $\mathscr{P}_d$ for i.i.d. noise samples and uncorrelated fading

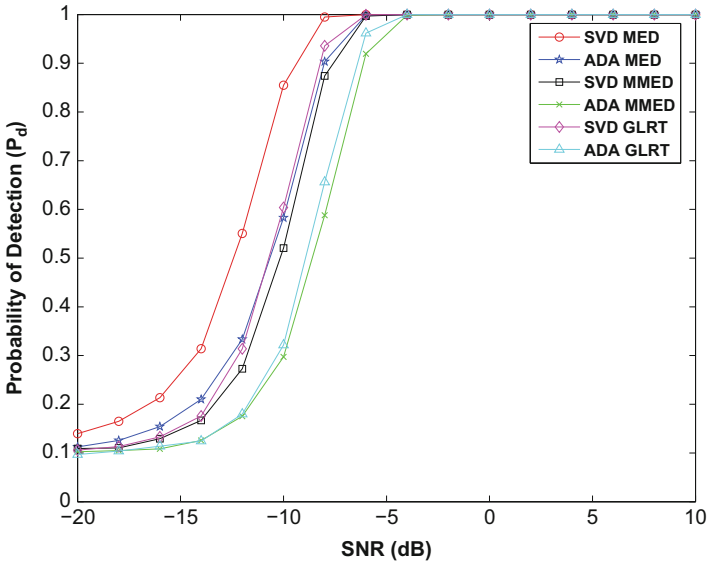

Fig. 5 Experimental setup of Fig. 4 for numerical thresholds

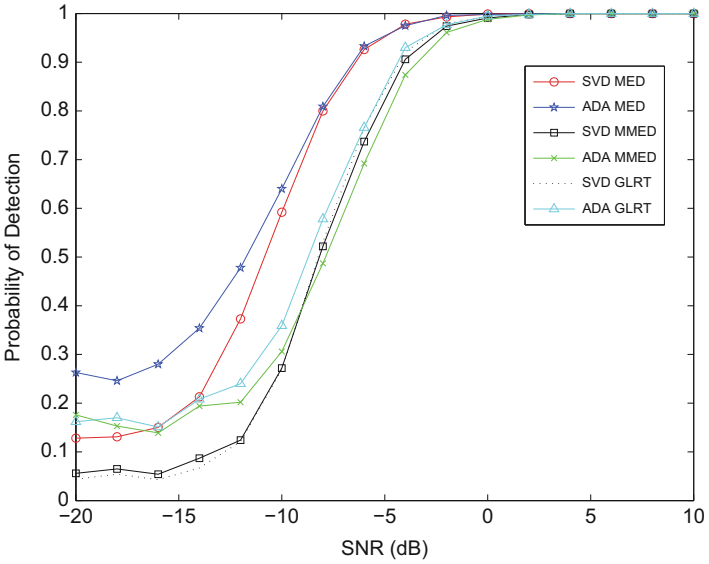

Fig. 6 $\mathscr{P}_d$ for non i.i.d. noise samples and uncorrelated fading

were computed numerically. The batch techniques exhibit improved performance due to accurate values of the employed thresholds. In Fig. 6, the same experiment of Fig. 4 is repeated, though now, we consider that the noise samples are no longer i.i.d. due to calibration errors at the SU. According to the relevant literature [14, 38], the correlation matrix of the noise samples can be considered diagonal. In the simulations of the present figure, the noise covariance matrix is given by $\mathbf{R}_z = diag\{1.1, 0.9, 0.8, 1.2\}$. As it was expected, both the adaptive and the batch techniques exhibit worse performance compared to the i.i.d. case. Nevertheless, for high SNR regimes, the EBSS techniques achieve high detection rates. Similar conclusions can be derived in the case of correlated fading coefficients at the SU antennas. The results are depicted in Fig. 7, where the fading coefficients are correlated such that each entry of their covariance matrix is given by $c_{m,n} = \rho_c^{|m-n|}$ [29], where $\rho_c \in \mathbb{R}$ is the correlation coefficient that satisfies $|\rho_c| \leq 1$.

Note that the noise samples are assumed to be i.i.d. in order to evaluate the effect of correlated fading to the EBSS techniques' performance. Again, for low SNR regimes, performance degradation is observed for both the adaptive and the batch EBSS methods.

In Fig. 8, the mean detection delay of an abrupt change is compared for each one of the batch and the adaptive EBSS techniques for different SNR values in order to evaluate the performance of the method in the dual-radio case. We consider timeslots of N = 1000 symbols in which an abrupt change in the channel state occurred at a random symbol time. The time at which a change occurs is assumed to follow the geometric distribution of (15) with parameters $p = 0.1$, $\lambda_0 = 0.01$ and a targeted

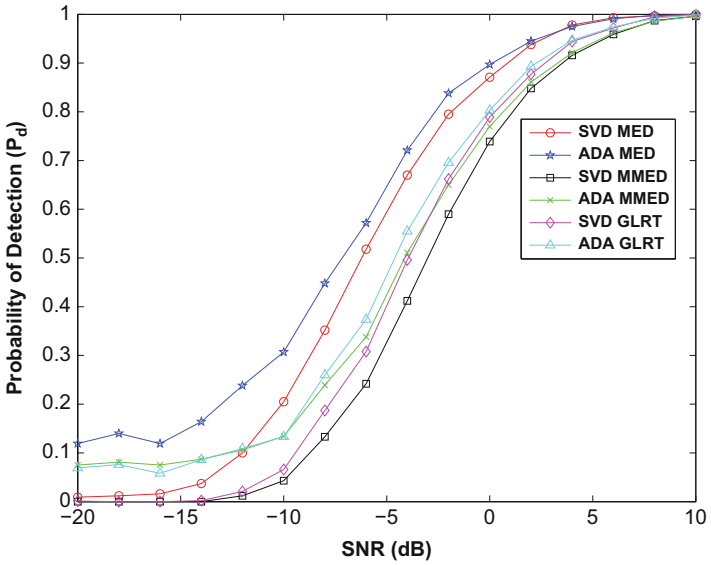

Fig. 7 $\mathscr{P}_d$ for i.i.d. noise samples and correlated fading

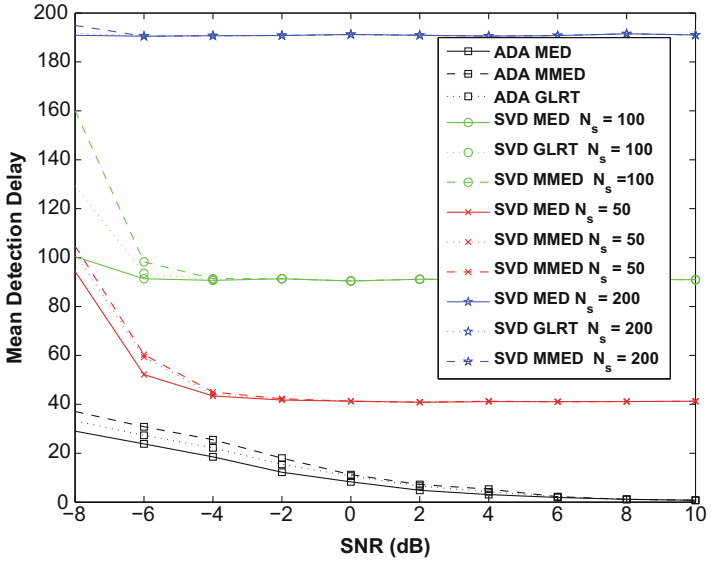

Fig. 8 Mean detection delay of an abrupt change

probability of false alarm $P_f = 0.01$. The decision threshold of the adaptive methods is computed by (25), as it is described in section "Threshold Computation for the Dual-Radio Approach." The threshold of the batch EBSS techniques is computed by simulations since a similar expression of the probability of false alarm was not possible to be found for this case. The adaptive EBSS techniques employ Algorithm 1. The batch EBSS techniques are employed periodically at every block of $N_s = \{50, 100, 200\}$ symbols, as it is described in Remark 1. It is evident that the adaptive EBSS techniques detect very fast the change even for low SNR regimes, since the detection test is applied at every sample time. The batch techniques' detection delay is related to the number N_s that dictates the frequency of their application.

Let us now study the multiple SUs case. In Fig. 9, the experiments of Fig. 4 are repeated, though now 7 SUs of 4 antennas each one are cooperating. The performance of the cooperative adaptive EBSS methods that employ the DDPM of Algorithm 2 is compared to the one of the single-user adaptive EBSS methods. The performance improvement offered by the cooperative methods is evident, and it is due to the fact that they process jointly the samples of the aggregate system of the KR_x receive antennas. In the same figure, the performance of a fusion-based method, that collects the samples for all the users and performs the batch EBSS techniques, is shown for comparison purposes. As it is shown, the cooperative adaptive EBSS schemes, apart from their benefits due to their completely decentralized nature and their low complexity, exhibit also satisfactory performance compared to the centralized batch ones, as it was also shown in the single SU case. Finally in Figs. 10 and 11, the computational and network

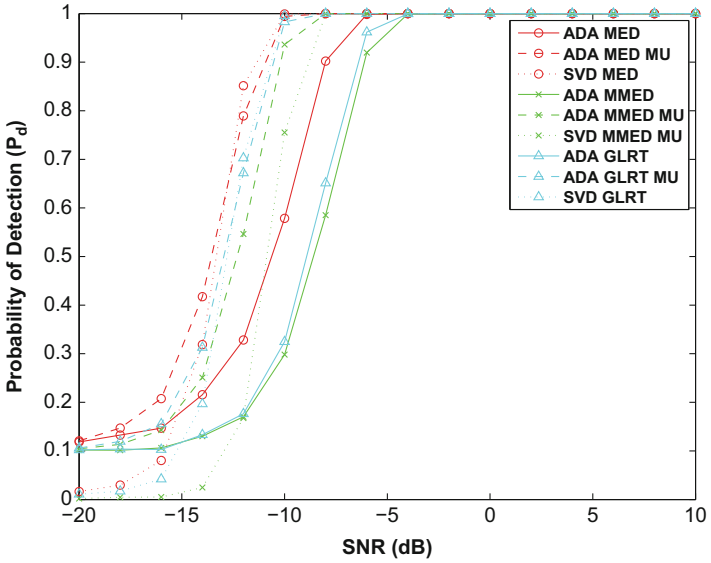

Fig. 9 Probability of detection ($\mathscr{P}_d$) for $K = 7$ SUs

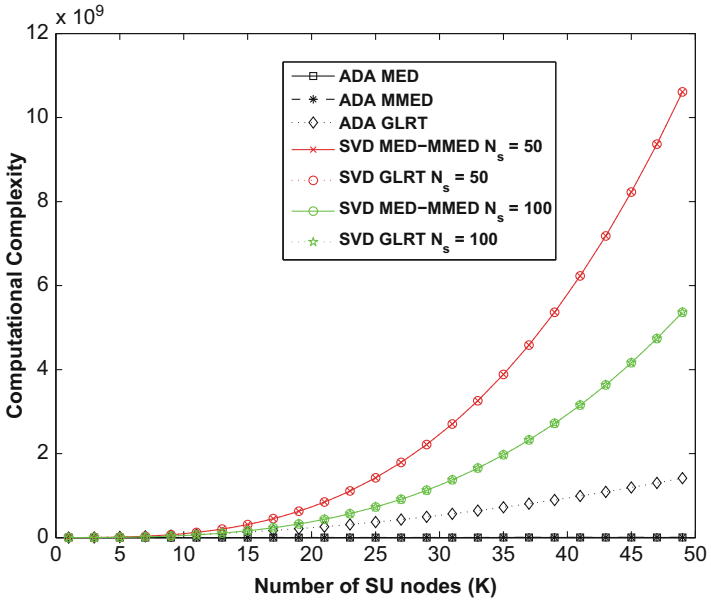

Fig. 10 Computational complexity vs. number of SUs

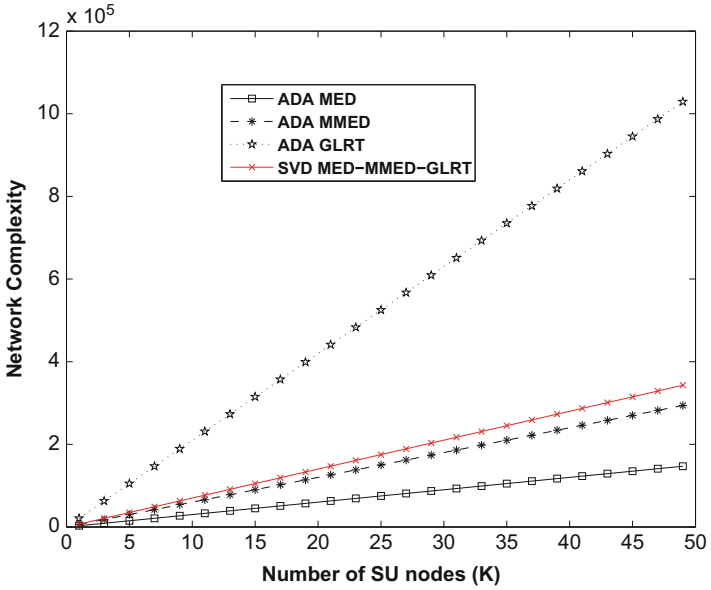

Fig. 11 Network complexity vs. number of SUs

complexity of the decentralized dual-radio approach is examined for a different number K of SUs. Each one of the SUs is considered to have $R_x = 7$ antennas. In the same figures, we present also the corresponding complexities for the batch centralized EBSS techniques. As it is evident, the adaptive EBSS techniques can provide significant reduction in the required complexities, especially for large network sizes.

Conclusion

In this chapter, cooperative decentralized adaptive versions of the well-known EBSS techniques were presented for multi-antenna cognitive receivers. The proposed techniques offer low complexity and improved performance especially in cases when continuous spectrum monitoring is applied. Moreover due to their decentralized nature, they exhibit reduced power consumption at the transmissions during the sensing period and provide robustness against node and link failures. In order to compute the decision thresholds for each one of the adaptive test statistics, the derivation of close approximations for the associated distribution functions was shown. A novel distributed subspace tracking method was also presented as a constituent part of the proposed decentralized EBSS techniques. The distributed ST method enables the SUs to track jointly the subspace of their received signals in a completely decentralized manner. The performance of the presented EBSS techniques was verified via indicative simulations and compared to those of the corresponding batch centralized approaches.

Appendix: Derivation of the Distribution of the MMED Test Statistic Under the $\mathscr{H}_0$ Hypothesis

Let us assume that two RVs T_1 and T_2 follow the same distribution with that of the MED test statistic. The CDF of the later distribution is given by (16). The corresponding probability density function (PDF) is computed by taking the derivative of (16). That is,

$$f_{T_i}(\tau_i) = \frac{\xi^\rho}{\Gamma(\rho)} \tau_i^{\rho-1} e^{-\rho\tau_i}. \tag{32}$$

We are interested in the distribution of the random variable $Y_1 = T_1/T_2$. Let us also define the auxiliary random variable $Y_2 = T_2$. Thus we have,

$$\begin{aligned} f_1(t_1, t_2) &= \frac{t_1}{t_2} \\ f_2(t_1, t_2) &= t_2, \end{aligned} \tag{33}$$

where $t_i \in \mathbb{R}^+$. The inverse functions of the ones of (33) are given by

$$f_1^{-1}(t_1, t_2) = t_1 t_2$$
$$f_2^{-1}(t_1, t_2) = t_2, \tag{34}$$

The joint PDF of variables Y_1 and Y_2 is given by

$$f_{Y_1,Y_2}(y_1, y_2) = f_{T_1,T_2}\big(f_1^{-1}(y_1, y_2), f_2^{-1}(y_1, y_2)\big)|J(y_1, y_2)|, \tag{35}$$

where $J(y_1, y_2) = \frac{\partial(t_1,t_2)}{\partial(y_1,y_2)}$ is the Jacobian matrix of the transformation and $|J(y_1, y_2)| = y_2$ is its determinant.

Observe now that, since the eigenvalues are estimated via (11), there are statistically independent. That is, the joint PDF of the variables under consideration T_1 and T_2 can be computed as the product of the corresponding marginal ones (16). Therefore, from (35) the joint PDF of Y_1 and Y_2 is given by

$$\begin{aligned} f_{Y_1,Y_2}(y_1, y_2) &= f_{T_1}(y_1 y_2) f_{T_2}(y_2) y_2 \\ &= \frac{\xi^{2\rho}}{\Gamma^2(\rho)} y_1^{\rho-1} y_2^{2\rho-1} e^{-\xi y_2(y_1+1)} \end{aligned} \tag{36}$$

In order to compute the marginal PDF of RV Y_1, we integrate the joint one of (36) with respect to y_2. That is

$$\begin{aligned} f_{Y_1}(y_1) &= \frac{y_1^{\rho-1}}{\xi^{2\rho}\Gamma^2(\rho)} \int_0^{+\infty} y_2^{2\rho-1} e^{-\xi y_2(y_1+1)} dy_2 \\ &= \frac{y_1^{\rho-1}\xi^{2\rho}\Gamma(2\rho)}{(1+y_1)^{2\rho}\xi^{2\rho}\Gamma^2(\rho)} = \frac{y_1^{\rho-1}}{B(\rho,\rho)(1+y_1)^{2\rho}}, \end{aligned} \tag{37}$$

where the following property of the beta function [20] was used

$$B(\rho_1, \rho_2) = \int_0^1 x^{\rho_1}(1-x)^{\rho_2-1} dx = \frac{\Gamma(\rho_1+\rho_2)}{\Gamma(\rho_1)\Gamma(\rho_2)}. \tag{38}$$

By integrating (37) we derive the corresponding CDF of the beta prime distribution given by (18) of Lemma 1, and the proof is completed. □

References

1. Bazerque JA, Giannakis GB (2010) Distributed spectrum sensing for cognitive radio networks by exploiting sparsity. IEEE Trans Signal Process 58(3):1847–1862

2. Cardoso LS, Debbah M, Bianchi P, Najim J (2008) Cooperative spectrum sensing using random matrix theory. In: 3rd International Symposium on Wireless Pervasive Computing – ISWPC 2008, pp 334–338
3. Chaudhari S, Koivunen V, Poor HV (2009) Autocorrelation-based decentralized sequential detection of OFDM signals in cognitive radios. IEEE Trans Signal Process 57(7): 2690–2700
4. Chen Y, Oh HS (2016) A survey of measurement-based spectrum occupancy modeling for cognitive radios. IEEE Commun Surv Tutorials 18(1):848–859. Firstquarter
5. Cicho K, Kliks A, Bogucka H (2016) Energy-efficient cooperative spectrum sensing: a survey. IEEE Commun Surv Tutorials 18(3):1861–1886. Thirdquarter
6. Cisco Visual Networking Index Cisco (2014) Global mobile data traffic forecast update, pp 2013–2018. White paper
7. de Lima MV, Mello LdS (2013) Cognitive radio simulation based on spectrum occupancy measurements at one site in Brazil. In: Microwave Optoelectronics Conference (IMOC), 2013 SBMO/IEEE MTT-S International, pp 1–5
8. Digham FF, Alouini M-S, Simon MK (2003) On the energy detection of unknown signals over fading channels. In: IEEE International Conference on Communications – ICC 2003, vol 5, pp 3575–3579
9. Doukopoulos XG, Moustakides GV (2008) Fast and stable subspace tracking. IEEE Trans Signal Process 56(4):1452–1465
10. Duan D, Yang L, Principe JC (2010) Cooperative diversity of spectrum sensing for cognitive radio systems. IEEE Trans Signal Process 58(6):3218–3227
11. Ghasemi A, Sousa ES (2005) Collaborative spectrum sensing for opportunistic access in fading environments. In: First IEEE International Symposium on New Frontiers in Dynamic Spectrum Access Networks, DySPAN 2005, Baltimore, pp 131–136
12. Ghozzi M, Marx F, Dohler M, Palicot J (2006) Cyclostatilonarilty-based test for detection of vacant frequency bands. In: First International Conference on Cognitive Radio Oriented Wireless Networks and Communications, CROWNCOM 2006, Mykonos Island, pp 1–5
13. Goldsmith A, Jafar SA, Maric I, Srinivasa S (2009) Breaking spectrum gridlock with cognitive radios: an information theoretic perspective. Proc IEEE 97(5):894–914
14. Hack DE, Rossler CW, Patton LK (2014) Multichannel detection of an unknown rank-n signal using uncalibrated receivers. IEEE Signal Process Lett 21(8):998–1002
15. Hanafi E, Martin PA, Smith PJ, Coulson AJ (2013) Extension of quickest spectrum sensing to multiple antennas and rayleigh channels. IEEE Commun Lett 17(4):625–628
16. Havary-Nassab V, ShahbazPanahi S, Grami A, Luo Z-Q (2008) Distributed beamforming for relay networks based on second-order statistics of the channel state information. IEEE Trans Signal Process 56(9):4306–4316
17. Haykin S (2005) Cognitive radio: brain-empowered wireless communications. IEEE J Sel Areas Commun 23(2):201–220
18. Haykin S, Thomson DJ, Reed JH (2009) Spectrum sensing for cognitive radio. Proc IEEE 97(5):849–877
19. Hur Y, Park J, Woo W, Lim K, Lee CH, Kim SH, Laskar J (2006) A wideband analog multi-resolution spectrum sensing (MRSS) technique for cognitive radio (CR) systems. In: 2006 IEEE International Symposium on Circuits and Systems, p 4
20. Johnson NL, Kotz S, Balakrishnan N (1994) Continuous univariate distributions. Wiley Series in Probability and Statistics, vol 1, 2nd edn. Wiley-Interscience, New York
21. Jouini W (2011) Energy detection limits under log-normal approximated noise uncertainty. IEEE Signal Process Lett 18(7):423–426
22. Kim S-J, Giannakis GB (2010) Sequential and cooperative sensing for multi-channel cognitive radios. IEEE Trans Signal Process 58(8):4239–4253
23. Kortun A, Ratnarajah T, Sellathurai M, Zhong C, Papadias CB (2011) On the performance of eigenvalue-based cooperative spectrum sensing for cognitive radio. IEEE J Sel Top Signal Process 5(1):49–55

24. Kostylev VI (2002) Energy detection of a signal with random amplitude. In: IEEE International Conference on Communications – ICC 2002, vol 3, pp 1606–1610
25. Li Z, Yu FR, Huang M (2010) A distributed consensus-based cooperative spectrum-sensing scheme in cognitive radios. IEEE Trans Veh Technol 59(1):383–393
26. Li L, Scaglione A, Manton JH (2011) Distributed principal subspace estimation in wireless sensor networks. IEEE J Sel Top Signal Process 5(4):725–738
27. Long C, Wang H, Li B (2010) Collaborative spectrum sensing based on signal correlation in cognitive radio networks. In: IEEE Global Telecommunications Conference – GLOBECOM 2010, pp 1–5
28. Lorden G (1971) Procedures for reacting to a change in distribution. Ann Math Stat 42:18971908
29. Loyka SL (2001) Channel capacity of MIMO architecture using the exponential correlation matrix. IEEE Commun Lett 5(9):369–371
30. Ma J, Li GY, Juang B-H (2009) Signal processing in cognitive radio. Proc IEEE 97(5):805–823
31. Matsui M, Shiba H, Akabane K, Uehara K (2007) A novel cooperative sensing technique for cognitive radio. In: IEEE 18th International Symposium on Personal, Indoor and Mobile Radio Communications, PIMRC 2007, Athens, pp 1–5
32. Mitola J (1999) Cognitive radio for flexible mobile multimedia communications. In: 1999 IEEE International Workshop on Mobile Multimedia Communications (MoMuC'99), pp 3–10
33. Mitola J (2000) Cognitive radio – an integrated agent architecture for software defined radio. DTech thesis, Royal Institute of Technology (KTH), Kista
34. Mitola J, Maguire GQ (1999) Cognitive radio: making software radios more personal. IEEE Pers Commun 6(4):13–18
35. Nadler B, Penna F, Garello R (2011) Performance of eigenvalue-based signal detectors with known and unknown noise level. In: Proceedings of the 2011 IEEE International Conference on Communications – ICC 2011, Kyoto, pp 1–5
36. Penna F, Garello R, Figlioli D, Spirito MA (2009) Exact non-asymptotic threshold for eigenvalue-based spectrum sensing. In: Proceedings of the Fourth International Conference on Cognitive Radio Oriented Wireless Networks and Communications – CROWNCOM 2009, Hannover, pp 1–5
37. Quan Z, Cui S, Sayed AH (2008) Optimal linear cooperation for spectrum sensing in cognitive radio networks. IEEE J Sel Top Signal Process 2(1):28–40
38. Ramirez D, Vazquez-Vilar G, Lopez-Valcarce R, Via J, Santamaria I (2011) Detection of rank-p signals in cognitive radio networks with uncalibrated multiple antennas. IEEE Trans Signal Processing 59(8):3764–3774
39. Reyes C, Hilaire T, Mecklenbrauker CF (2009) Distributed projection approximation subspace tracking based on consensus propagation. In: 3rd IEEE International Workshop on Computational Advances in Multi-Sensor Adaptive Processing – CAMSAP 2009, Dutch Antilles, pp 340–343
40. Sai Shankar N, Cordeiro C, Challapali K (2005) Spectrum agile radios: utilization and sensing architectures. In: First IEEE International Symposium on New Frontiers in Dynamic Spectrum Access Networks – DySPAN 2005, pp 160–169
41. Sanders FH (1998) Broadband spectrum surveys in Denver, CO, San Diego, CA, and Los Angeles, CA: methodology, analysis, and comparative results. In: 1998 IEEE International Symposium on Electromagnetic Compatibility, vol 2, pp 988–993
42. Sayed AH, Lopes CG (2007) Distributed processing over adaptive networks. In: 9th International Symposium on Signal Processing and Its Applications – ISSPA 2007, Sharjah, pp 1–3
43. Shiryaev AN (1961) The problem of quickest detection of a violation of stationary behavior. Dokl Akad Nauk SSSR 138:10391042
44. Shiryaev AN (1961) The problem of the most rapid detection of a disturbance in a stationary process. Sov Math Dokl 2:795799

45. Shiryaev AN (1963) On optimum methods in quickest detection problems, theory. Theory Prob Appl 8:2246
46. Sonnenschein A, Fishman PM (1992) Radiometric detection of spread-spectrum signals in noise of uncertain power. IEEE Trans Aerosp Electron Syst 28(3):654–660
47. Sutton PD, Nolan KE, Doyle LE (2008) Cyclostationary signatures in practical cognitive radio applications. IEEE J Sel Areas Commun 26(1):13–24
48. Taher TM, Bacchus RB, Zdunek KJ, Roberson DA (2011) Long-term spectral occupancy findings in Chicago. In: 2011 IEEE Symposium on New Frontiers in Dynamic Spectrum Access Networks (DySPAN), pp 100–107
49. Taherpour A, Nasiri-Kenari M, Gazor S (2010) Multiple antenna spectrum sensing in cognitive radios. IEEE Trans Wirel Commun 9(2):814–823
50. Tandra R, Sahai A (2008) SNR walls for signal detection. IEEE J Sel Top Signal Process 2(1):4–17
51. Trefethen LN, Bau D (1997) Numerical linear algebra, 1st edn. SIAM, Philadelphia
52. Tsinos CG, Berberidis K (2009) An adaptive beamforming scheme for cooperative wireless networks. In: 16th International Conference on Digital Signal Processing, pp 1–6
53. Tsinos CG, Berberidis K (2009) A new cooperative technique for wireless communications with improved diversity-multiplexing tradeoff. In: 17th European Signal Processing Conference, pp 135–139
54. Tsinos CG, Berberidis K (2010) A cooperative uplink transmission technique for the single- and multi-user case. In: IEEE International Conference on Communications, pp 1–5
55. Tsinos CG, Berberidis K (2012) Multi-antenna cooperative systems with improved diversity multiplexing tradeoff. In: IEEE Wireless Communications and Networking Conference (WCNC), pp 1093–1097
56. Tsinos CG, Berberidis K (2013) Adaptive eigenvalue-based spectrum sensing for multi-antenna cognitive radio systems. In: IEEE International Conference on Acoustics, Speech and Signal Processing, pp 4454–4458
57. Tsinos CG, Berberidis K (2015) A cooperative uplink transmission technique with improved diversity-multiplexing tradeoff. IEEE Trans Veh Technol 64(7):2883–2896
58. Tsinos CG, Berberidis K (2015) Decentralized adaptive eigenvalue-based spectrum sensing for multiantenna cognitive radio systems. IEEE Trans Wirel Commun 14(3):1703–1715
59. Tsinos CG, Vlachos E, Berberidis K (2013) Distributed blind adaptive computation of beamforming weights for relay networks. In: 24th IEEE Annual International Symposium on Personal, Indoor, and Mobile Radio Communications (PIMRC), pp 570–574
60. Unnikrishnan J, Veeravalli VV (2008) Cooperative sensing for primary detection in cognitive radio. IEEE J Sel Top Signal Process 2(1):18–27
61. Vardoulias G, Faroughi-Esfahani J, Clemo G, Haines R (2001) Blind radio access technology discovery and monitoring for software defined radio communication systems: problems and techniques. In: Second International Conference on 3G Mobile Communication Technologies (Conference Publication No. 477), pp 306–310
62. Wang P, Xiao L, Zhou S, Wang J (2007) Optimization of detection time for channel efficiency in cognitive radio systems. In: 2007 IEEE Wireless Communications and Networking Conference, pp 111–115
63. Wang P, Fang J, Han N, Li H (2010) Multiantenna-assisted spectrum sensing for cognitive radio. IEEE Trans Veh Technol 59(4):1791–1800
64. Welch BL (1938) The significance of the difference between two means when the population variances are unequal. Biometrika 29(3/4):350–362
65. Xin Y, Zhang H, Lai L (2014) A low-complexity sequential spectrum sensing algorithm for cognitive radio. IEEE J Sel Areas Commun 32(3):387–399
66. Yang B (1995) Projection approximation subspace tracking. IEEE Trans Signal Process 43(1):95–107
67. Yang J-F, Kaveh M (1988) Adaptive eigensubspace algorithms for direction or frequency estimation and tracking. IEEE Trans Acoust Speech Signal Process 36(2):241–251

68. Yilmaz Y, Moustakides GV, Wang X (2012) Cooperative sequential spectrum sensing based on level-triggered sampling. IEEE Trans Signal Process 60(9):4509–4524
69. Yucek T, Arslan H (2009) A survey of spectrum sensing algorithms for cognitive radio applications. IEEE Commun Surv Tutorials 11(1):116–130
70. Zarrin S, Lim TJ (2009) Cooperative quickest spectrum sensing in cognitive radios with unknown parameters. In: IEEE Global Telecommunications Conference – GLOBECOM 2009, pp 1–6
71. Zeng Y, Koh CL, Liang Y-C (2008) Maximum eigenvalue detection: theory and application. In: Proceedings of the 2008 IEEE International Conference on Communications – ICC 2008, Beijing, pp 4160–4164
72. Zeng Y, Liang Y-C (2009) Eigenvalue-based spectrum sensing algorithms for cognitive radio. IEEE Trans Commun 57(6):1784–1793
73. Zhao Q, Geirhofer S, Tong L, Sadler BM (2007) Optimal dynamic spectrum access via periodic channel sensing. In: 2007 IEEE Wireless Communications and Networking Conference, pp 33–37
74. Zhao Q, Ye J (2010) Quickest detection in multiple on-off processes. IEEE Trans Signal Process 58(12):5994–6006
75. Zou Q, Zheng S, Sayed AH (2010) Cooperative sensing via sequential detection. IEEE Trans Signal Process 58(12):6266–6283

Further Reading

1. Badeau R, David B, Richard G (2005) Fast approximated power iteration subspace tracking. IEEE Trans Signal Process 53(8):2931–2941

Cognitive Management Strategies for Dynamic Spectrum Access

16

A. Raschellà, L. Militano, G. Araniti, A. Orsino, and A. Iera

Contents

A. Raschellà (✉)
Department of Computer Science, Liverpool John Moores University, Liverpool, MSY, UK
e-mail: a.raschella@ljmu.ac.uk

L. Militano · G. Araniti · A. Iera
DIIES Department, University Mediterranea of Reggio Calabria, Reggio Calabria, RC, Italy
e-mail: leonardo.militano@unirc.it; araniti@unirc.it; antonio.iera@unirc.it

A. Orsino
ELS Department, Tampere University of Technology, Tampere, Finland
e-mail: antonino.orsino@tut.fi

W. Zhang (ed.), *Handbook of Cognitive Radio*,
https://doi.org/10.1007/978-981-10-1394-2_16

Abstract

The Cognitive Radio (CR) paradigm represents an innovative solution to mitigate the spectrum scarcity problem. Enabling a Dynamic Spectrum Access (DSA), it conciliates the existing conflict between the ever-increasing spectrum demand and the currently inefficient spectrum utilization. The basic idea of DSA is to provide proper solutions that allow sharing radio spectrum among several radio communication systems and optimize the overall spectrum utilization. The first part of this chapter gives a general overview of the CR concept to enable DSA, whereas the second part of the chapter addresses the problem of modeling a cognitive management framework with innovative strategies for spectrum management in different scenarios. The presented framework is able to characterize the environment dynamicity through long-term predictions based on the so-called belief vector. This demonstrates that a reliable characterization of the radio environment that combines awareness of its surrounding with a statistical evaluation of the system dynamics in terms of traffic generation patterns is able to guarantee an efficient utilization of the available spectrum resources. From a methodological point of view, the development and assessment of the proposed cognitive management framework involves an analytical study and a real-time platform implementation.

Introduction

The licensed static spectrum allocation policy, in use since the early days of radio communications, was proved to effectively control interference among the radio communication systems. However, the overwhelming proliferation of new operators, innovative services, and wireless technologies during the last years resulted, under the static regulatory regime, in the exhaustion of spectrum bands with commercially attractive radio propagation characteristics. The vast majority of spectrum considered as usable has already been assigned hindering commercial rollout of new emerging services. This situation produced a common belief of a depletion the usable radio frequencies. This was certainly strengthened by the overly crowded frequency allocation charts of many countries worldwide. Notwithstanding, some preliminary field measurements of spectrum usage revealed that most of the allocated spectrum was vastly underutilized [1], with temporal and geographical variations in the use of the assigned spectrum ranging from 15 to 85% [2].

More recent spectrum measurement campaigns carried out all over the world have confirmed the underutilization of the spectrum. This indicated also that the spectrum scarcity problem actually results from the static and inflexible spectrum management policies rather than the physical depletion of usable radio frequencies. For instance, in [3], the authors illustrate a spectral occupancy measurement campaign conducted in the frequency range between 806 and 2750 MHz in Auckland, New Zealand. In [4], a detailed analysis from 20 MHz to 3 GHz spectrum band in

different locations in Guangdong (province of China) is presented. Several spectrum measurement campaigns covering wide frequency ranges have been carried out in different locations and scenarios also in the USA [5–9] to determine the usage degree of allocated spectrum bands in real wireless communication systems. In [10], the authors provide an extensive measurement campaign conducted in Germany, comparing indoor and outdoor measurement results in the band from 20 MHz to 3 GHz. All these studies have confirmed that the static spectrum allocation policy which was appropriate in the recent past is becoming an outdated scheme that has become obsolete. Therefore, new spectrum management paradigms are required for a more efficient exploitation of the scarce radio resources. This has motivated the emergence of flexible spectrum access policies to overcome the shortcomings of the inefficient static allocation policies.

In this context, the so-called Cognitive Radio (CR) represents an innovative way to detect and use the wireless spectrum resources. CR was originally defined as a context-aware intelligent radio, capable of autonomous reconfiguration by learning from and adapting to the surrounding. In particular, it interacts with the environment following the cognition cycle as defined in [11], which allows CRs to continually observe their Radio Frequency (RF) environment, orienting themselves, creating a plan, deciding, and then acting. In addition, learning may be pursued in the background. Enabling Dynamic Spectrum Access (DSA), the CR paradigm is considered as a key solution to mitigate the spectrum scarcity problem [12].

DSA is the opposite of the static spectrum management policy and covers any innovative solution to share spectrum among several radio systems and increase the overall spectrum utilization. The basic idea of the DSA is to allow the so-called secondary users to access in an opportunistic and noninterfering way some licensed bands temporarily unoccupied by the licensed (or primary) users. Secondary terminals monitor the spectrum in order to identify time and unused frequency gaps, perform transmissions, and vacate the channel as soon as primary users return active. Secondary transmissions are allowed as long as they do not result in harmful interference to primary users. The temporarily unused portions of spectrum in time, frequency, and space domains are called spectrum White Spaces (WSs).

The basic concept of the CR paradigm introduced in [11] has been reconsidered in the literature in several papers which aimed at redefining it for specific scenarios. In the DSA context, the tasks of the CR cycle (see section "Cognitive Radio Paradigm" for more details) should be characterized to enable the following capabilities [12]:

- *Radio-scene analysis*: which consists in estimating interference conditions of the radio environment and identifying the set of available spectrum holes or WSs.
- *Channel identification*: which consists in estimating the Channel State Information (CSI) and predicting the channel capacity.
- *Transmit-power control and spectrum management*: which adjusts transmission parameters based on a received feedback.

With the advent of the CR, high interest has been devoted to Cognitive Radio Networks (CRNs) which allow a wireless communication system based on the cognitive cycle to observe the environment, act, and learn in order to optimize its performance. For instance, in [13], a CRN is defined as a wireless network with the capabilities of radio environment awareness, autonomous decision-making, adaptive reconfiguration of its infrastructure, and intelligent learning from experience of a continuously changing environment to solve the challenges of efficient spectrum management and high-quality end-to-end performance. Hence, a CRN foresees the ability to be aware of certain information, such as the available spectrum, the operation mode of the wireless network, the transmitted waveform, the network protocol, the geographical information, the type of services, the user needs, and the security policy. Furthermore, a CRN must analyze the achieved information and make the decision to optimize the end-to-end performance of the wireless network. Based on the optimized decision, a CRN must finally reconfigure its network parameters when necessary. Moreover, CRNs deal with challenges in terms of coexistence with primary users and different Quality of Service (QoS) requirements associated with the various cognitive communications. According to [14], in a network that guarantees the cognitive capabilities, the following issues have to be considered:

- *Interference avoidance*: to operate while controlling the amount of interference perceived by primary networks.
- *QoS awareness*: to enable QoS-aware communications in dynamic and heterogeneous spectrum environments.
- *Seamless communication*: to provide seamless communications regardless of the activity of primary users.

Several contributions in the literature have illustrated the expected benefits of developing cognitive management functional architectures, which support CRNs to exploit the mentioned cognitive radio capabilities for efficient spectrum management and high-quality end-to-end performance [13, 15, 16]. These studies have motivated the development of advanced cognitive management tools in many specific scenarios. For instance, in [16], a cognitive management framework is illustrated to carry out an autonomous optimization of resource usage in next-generation home networks. The proposed framework is able to autonomously improve the performance of network nodes in a dynamic environment according to the objectives, the restrictions, and the policy regulations formulated by network stakeholders. Although the benefits of CR and DSA supported by cognitive management architectures have been discussed in several studies (e.g., [17–20]), many aspects are still under investigation. Spectrum sensing strategies to identify spectrum opportunities, coordination of opportunistic spectrum access among different users, or spectrum selection are some examples for this.

The main objective of this chapter is to propose a cognitive management framework that provides innovative strategies for spectrum management exploiting the CR capabilities. The proposed framework is developed in order to combine the

observations carried out during the CR cycle with a statistical characterization of the system dynamic. The spectrum management strategies illustrated in this chapter rely on the so-called belief vector concept as a means to characterize and predict the environmental dynamics. The belief vector assesses the probability that the radio environment is under specific conditions (e.g., interference levels) at a certain instant of time based on past measurements. As long as the belief vector predicts the existing conditions with sufficient accuracy when the decision is made, proper decisions can be made with minimum requirements in terms of observations. The proposed framework aims at demonstrating that a reliable characterization of the radio environment in terms of traffic generation pattern that combines awareness of its surrounding with a statistical evaluation of the system dynamics can guarantee an efficient utilization of the available spectrum resources in CRNs. The proposed framework is experimentally evaluated making use of a real-time platform.

The rest of this chapter is organized as follows. The introduction of CR and a detailed description of the CR cycle are provided in section "Cognitive Radio Paradigm". Section "Dynamic Spectrum Access to Exploit Cognitive Radio Paradigm" presents the basic concepts of the DSA and how it is enabled by the CR. A typical example of CRNs with the corresponding functionalities, which enables DSA, is also provided. Section "Proposed Framework for Spectrum Management" presents the proposed framework, which implements the spectrum management strategies. Section "Real-Time Testbed Design and Implementation" illustrates the implementation of the real-time testbed used to assess the performance of the proposed framework, while a detailed analysis in different scenarios is presented in section "Performance Evaluation". Concluding remarks are given in section "Conclusions and Future Directions".

Cognitive Radio Paradigm

The CR concept was introduced by J. Mitola III as a smart, context-sensitive radio that can be programmed and configured dynamically under varying environmental conditions [11]. The operations of the CR systems are typically assumed to follow the cognitive cycle illustrated in Fig. 1 in order to interact with the environment. Any CR system following this cycle gathers observations from the outside world through different types of sensors, orients itself, creates a plan of possible courses of actions, decides, and then acts. During this cycle, the CR system also learns from the outcomes of its decisions and sensory inputs from the outside world. Clearly this original definition of CR is very general, applicable to a vast number of scenarios; in details, in the original study of J. Mitola III, the observations were focused on the following inputs: (i) radio spectrum, (ii) images from cameras, (iii) speech recognition, and (iv) geo-location. Hence, a general CR paradigm is an adaptive, self-organizing architecture for holistic resource management in wireless networks, capable of adjusting its own behavior through learning.

A CR system can observe a number of different aspects of its environment. The most commonly mentioned example is the radio environmental information

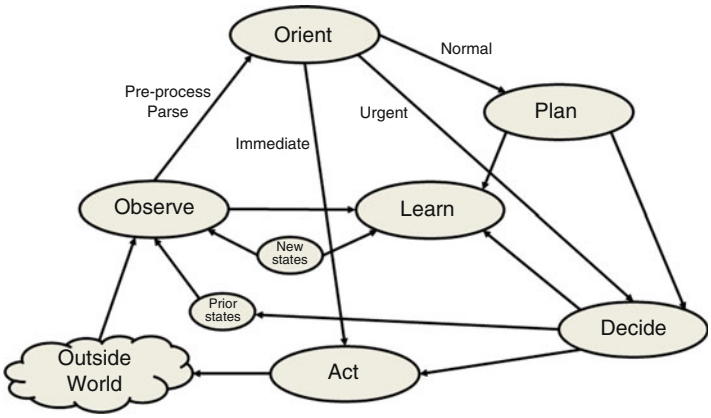

Fig. 1 Cognitive cycle

achieved by a spectrum sensor. Usually, a spectrum sensor would measure features such as either the sensed power in a range of frequencies or the presence of signals transmitted through particular technologies or digital modulation schemes. This spectrum sensor could also be implemented either on an individual CR system by a hardware component, or it could be based on cooperation between several CR systems in the neighborhood. The observations could also be done through explicit communication among different radios such as transmitters that send control information on the used frequencies.

The orientation stage involves the processing of the information achieved from the different sensors and the integration with any prior knowledge for updating the estimated state of the system and its environment. Depending on the diversity of the sensing information and available prior knowledge, numerous different state estimation and learning mechanisms can be used in the orientation state. For instance, further processing of information achieved by spectrum sensors can be gathered with location information to make logical conclusions whether certain transmitters are active or not. Depending on the change in state, the CR shifts either to the planning state or, in case urgent reaction is needed, to the decision state. After reaching the decision-making state, the CR should potentially act according to the decisions made. Actions here would usually relate to change in any of the tuneable parameters across the entire protocol stack, including selection of protocols to be used, and actual links or end-to-end connections established to other nodes. During the learning state, the CR updates the different models that have been constructed on the environment, on the properties of other radios, and on the dynamics of its own state.

The CR paradigm relies often, but not necessarily, on the use of the Software-Defined Radio (SDR) technology, which is a multiband radio supporting multiple air interfaces and protocols. It is reconfigurable through software running on a Digital Signal Processor (DSP), Field-Programmable Gate Array (FPGA), or general purpose microprocessor [21]. Hence, CR systems, usually built upon a SDR

platform, are context-aware intelligent radio capable of autonomous reconfiguration by learning from and adapting to the surrounding communication environment [22]. They are capable of sensing their Radio Frequency (RF) environment, learning about their radio resources and user and application requirements, and adapting their behavior accordingly. The idea behind SDR is to define all radio functionalities in software rather than in dedicated hardware, in order to reuse a single platform for many different radio standards.

Through SDR the following main characteristics of the CR defined in [12, 15] can be exploited: cognitive capability, i.e., the ability to capture information from the radio environment, and reconfigurability, which enables the transmitter parameters to be dynamically programmed and modified according to the radio environment. In fact, SDR is capable of sensing spectrum occupancy and opportunistically adapting transmission parameters to utilize empty frequency bands without causing harmful interference to primary networks. Moreover, through SDR, a CR system is able to reconfigure several parameters such as the operating frequency (to take profit of spectrum holes detected on different frequency bands), modulation and/or channel coding (to adapt to the application requirements and the instantaneous channel quality conditions), transmission power (to control interference), and communication technology (to adapt to specific communication needs). Based on the characteristics of the detected spectrum holes, these parameters can be reconfigured so that the CR is switched to a different spectrum band, transmitter and receiver parameters are reconfigured, and the appropriate communication protocols and modulation schemes are used.

Dynamic Spectrum Access to Exploit Cognitive Radio Paradigm

Spectrum underutilization has motivated different activities and initiatives in the regulatory, economic, and research communities, to look for better spectrum management policies [23]. DSA solutions have been proposed to provide procedures or schemes to achieve flexible spectrum access approaches aimed at overcoming the disadvantages and shortcoming of the currently inefficient static allocation policies. The key enabler of the DSA concept is the CR that provides functionalities such as the possibility to use the spectrum in an opportunistic way observing the outside world.

Dynamic Spectrum Access Models

Several DSA models have been defined to optimize the spectrum usage depending on the particular radio environment as shown in Fig. 2. The following classification can be defined:

- **Dynamic exclusive use model.** It basically keeps the structure of the static spectrum allocation policy. Spectrum bands are licensed to operators, technologies,

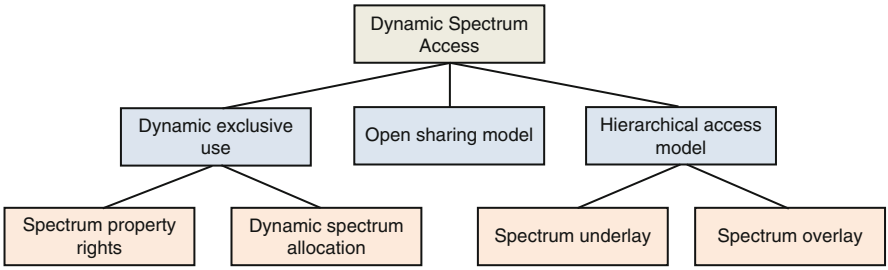

Fig. 2 Classification of the dynamic spectrum access models

and/or services for exclusive use, but some flexibility is introduced to optimize the spectrum efficiency. Two different approaches can be distinguished in this model:

- *Spectrum property rights* [24]. It enables licensed users to sell and lease some portions of its licensed spectrum and to select the technology to be employed as well as the service to be given in that band. Hence, in this context, economy and market would play a more important role in driving the most profitable use of spectrum under this scheme. It is worth highlighting that even though licensed users can sell or lease the spectrum for economic profit, this spectrum sharing is not mandated by the regulatory organism.
- *Dynamic spectrum allocation* [25]. It aims at managing the spectrum used by a converged radio system and sharing it between participating Radio Access Networks (RANs) over space and time to optimize overall spectrum efficiency. A bandwidth reservation will result in unused spectrum for long periods of time and along large geographical areas. Hence, spectrum efficiency can be improved by exploiting the spatial and temporal traffic variations of different services. The underlying idea of DSA methods is to enable two or more networks of a converged radio system to share an overall block of spectrum such that spectrum allocations can adapt to either temporal or spatial variations. However, these strategies allocate, at a given time and region, a portion of the spectrum to a RAN for its exclusive use. Furthermore, the allocation varies at a much faster scale than the current policy (e.g., traffic demands usually exhibit a periodic daily pattern).

- **Open sharing model** [26]. Also defined as spectrum commons, it considers open sharing among peer users as the basis for managing a spectral region in a similar way as wireless services operating in the unlicensed Industrial, Scientific, and Medical (ISM) band. Spectrum commons proponents declare that wireless transmissions can be regulated by baseline rules enabling users to coordinate their utilization, avoiding interference-producing collisions, and preventing congestion.
- **Hierarchical access model.** This is a hybrid model of the dynamic exclusive use model and the open sharing model. It is built upon a hierarchical access structure that distinguishes between primary or licensed users and secondary or

license-exempt users. The basic idea is to open licensed spectrum to secondary users limiting the interference perceived by primary ones. Two approaches to spectrum sharing between primary and secondary users have been considered:

- *Spectrum underlay*. It enables to overlap transmissions from secondary users but imposes severe constraints on their transmission power so that they operate below the noise floor of primary users. Therefore, secondary transmissions have to spread over a wide frequency band, which can be achieved by means of technologies such as Code Division Multiple Access (CDMA) or Ultra Wide Band (UWB). This approach enables secondary users to potentially obtain short-range high data rates with extremely low transmission power. Another advantage is that the activity of primary users does not need to be tracked by secondary ones. The most important problem in this approach is that the low transmission power still limits the applicability of spectrum underlay to short-range applications [27].
- *Spectrum overlay.* It is not necessarily characterized by severe restrictions on the transmission power of secondary users but rather on when and where they may transmit. The basic idea of this approach is to define spatial and temporal spectrum gaps not occupied by primary users, referred to as spectrum holes or white spaces, and place secondary transmissions within these spaces. Hence, the purpose of this scheme is to define and exploit local and instantaneous spectrum availability in a nonintrusive and opportunistic way. This approach is also defined as Opportunistic Spectrum Access (OSA) [28].

Cognitive Radio as an Enabler of Dynamic Spectrum Access

The CR technology in the context of DSA enables the users to (1) determine which portion of the spectrum is available and detect the presence of licensed users when a user operates in a licensed band (spectrum sensing), (2) select the best available channel (spectrum decision), (3) coordinate access to this channel with other users (spectrum sharing), and (4) free the channel when a licensed user is detected (spectrum mobility). Focusing on these functions, the result is the simplified version of the full cognitive cycle and is shown in Fig. 3 [29]. The states defined in the cycle can be characterized as:

1. *Spectrum sensing*. A CR user can only allocate an unused portion of the spectrum. Therefore, the CR user should monitor the available spectrum bands, capture their information, and then detect the spectrum holes.
2. *Spectrum decision.* Based on the spectrum availability, CR users can allocate a channel. This allocation not only depends on spectrum availability, but it is also determined based on internal (and possibly external) policies.
3. *Spectrum sharing.* Since there may be multiple CR users trying to access the spectrum, CR network access should be coordinated in order to prevent multiple users colliding in overlapping portions of the spectrum.

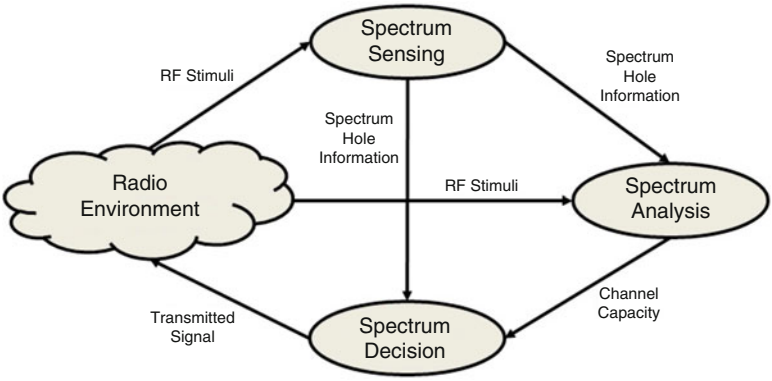

Fig. 3 Specialization of the cognitive cycle to the DSA case

4. *Spectrum mobility.* If the specific portion of the spectrum in use is required by a primary user, or if the Quality of Service (QoS) of the spectrum worsens, the communication needs to be continued in another vacant portion of the spectrum.

However, compared to the full cognitive cycle, the loop missed a few important components. For instance, one is the learning module, which prevents mistakes from previous iterations from being made on future ones. Several schemes have been proposed to classify the functions required in the context of the described CR and the DSA cycle. For instance, according to [1], the main functions are categorized into:

1. *Spectrum opportunity identification.* It is responsible for accurately identifying and intelligently tracking idle frequency bands that are dynamic in both time and space. Hence, this function is equivalent to the spectrum sensing function previously described.
2. *Spectrum opportunity exploitation.* It takes input from the spectrum opportunity identification function, and it decides whether and how a transmission should be carried out. This function comprises the aforementioned spectrum decision and spectrum sharing ones.
3. *Regulatory policy.* It defines the basic etiquette for secondary users, dictated by a regulatory body, to guarantee compatibility with legacy systems. An example of this DSA policy is Dynamic Frequency Selection (DFS) [2]. DFS allows unlicensed 802.11 communications devices in the 5 GHz band to coexist with legacy radar systems. The policy specifies the sensor detection threshold as well as the timeline for radar sensing, usage, abandoning the channel, and a non-occupancy time after detection. This policy allows limited but minimal harm to legacy radar systems by accounting for the specific form of sensor for detection and prescribing the timeline for channel use and release.

The spectrum mobility function is not explicitly considered in the classification criterion proposed in [1], but it could be included within the spectrum opportunity exploitation function.

DSA/CR Networks Architecture

Once a radio supports the capability to select the best available channel, the next challenge is to make the network protocols adaptive to the available spectrum. Therefore, new functionalities are required in a DSA/CRN (CRN for simplicity from here on) to support this adaptively and to achieve spectrum-aware communication protocols. A typical CRN architecture is illustrated in Fig. 4 according to the open sharing and hierarchical DSA models described in section "Dynamic Spectrum Access Models" [29]. For each of these models, the interconnection architecture may be built without a central network entity, such as a Base Station (BS) or an access point (CR ad hoc Access), or rely on some additional network nodes (CR Network Access). Moreover, the figure illustrates how the network allows the access to both unlicensed band and licensed bands according to the open sharing and hierarchical access models, respectively. In case of hierarchical access model, when licensed bands are considered, the components of the network can be classified in two groups: the primary network and the CR network or secondary network. The primary network is the legacy network having an exclusive right to a certain spectrum band such as the common cellular and TV broadcast networks, while the CR network does not have a license to operate in the desired band.

The spectrum access is allowed only in an opportunistic manner. The basic components of primary networks are:

- *Primary user.* It is authorized to use always a particular spectrum band. This use is controlled only by the primary BS, and it should not be affected by the operations of other unlicensed users. Primary users do not need any modification or additional functions for coexistence with BSs and CR users.
- *Primary BS.* It is a fixed infrastructure network component which has a spectrum license such as BS Transceiver system (BST) in a cellular system. In principle, the primary BS does not have any CR capability for sharing spectrum with CR users. However, the primary BS may be requested to have both legacy and CR protocols for the primary network access of CR users.

The basic elements of the CR network are defined as follows:

- *CR user.* It does not hold a spectrum license, and it uses detected spectrum holes in an opportunistic way which requires additional functionalities to share the licensed spectrum band.
- *CR BS.* It is a fixed infrastructure component with CR capabilities. The CR BS provides single hop connection to CR users without spectrum access license. Through this connection, a CR user can access other networks.

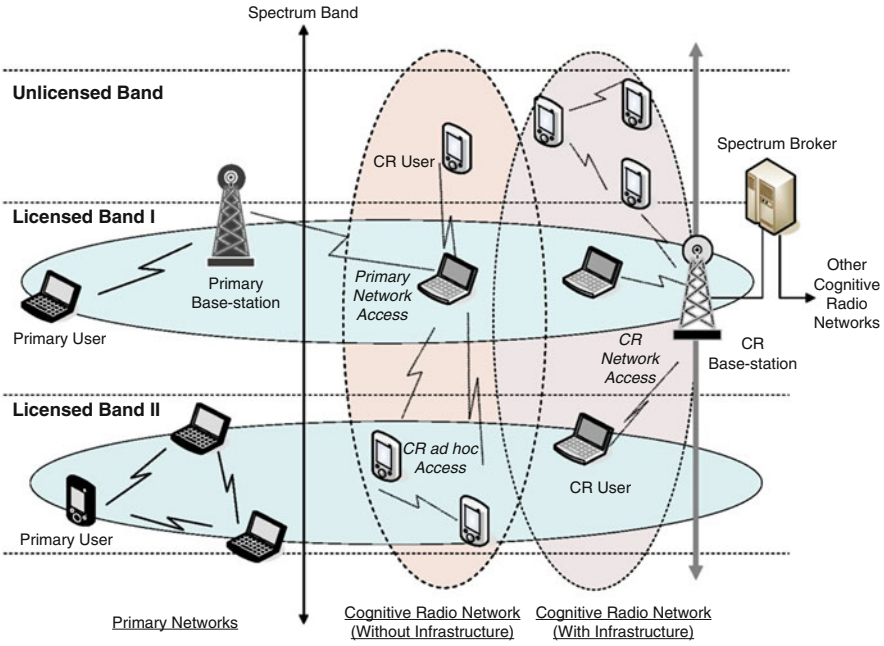

Fig. 4 CRN architecture for DSA applications [29]

- *CR spectrum broker.* It is a central network entity that controls the spectrum sharing among different CRNs. The spectrum broker can be connected to each network and can serve as a spectrum information manager to enable coexistence of multiple CRNs.

Since CRNs can operate in both licensed and unlicensed bands, the required functionalities that the cognitive management tools should provide vary according to the characteristic of the spectrum. The following CRNs operations can be distinguished [29]:

- **CRN on licensed band.** In this case, there are temporarily unused spectrum holes. Therefore, CRNs can be deployed to use these spectrum holes through cognitive communication techniques. This architecture is illustrated in Fig. 5. It can be observed that the CRN coexists with the primary network at the same location and on the same spectrum band. There exist various challenges for CRNs on licensed band due to the existence of the primary users. Although the main objective of the CRN is to find the best available spectrum, the interference avoidance with primary users is the most important issue in this architecture. In fact, when primary users appear in the spectrum band occupied by CR users, this must release the current spectrum band and select a new available spectrum.

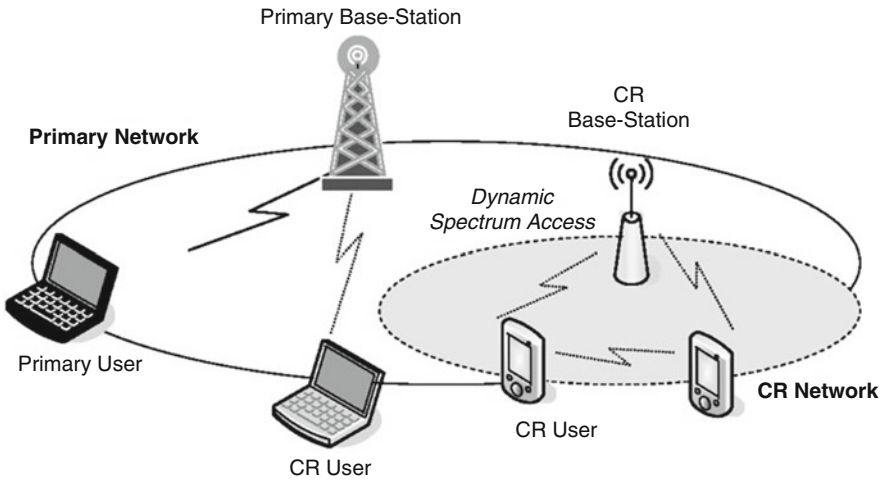

Fig. 5 CRN on licensed band [29]

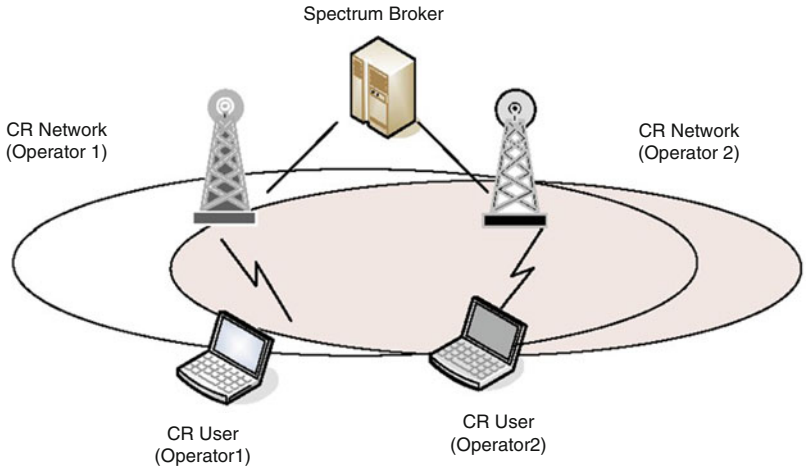

Fig. 6 CRN on unlicensed band [29]

- **CRN on unlicensed band.** The open spectrum policy that began in the ISM band has provoked a wide variety of innovative technologies. Notwithstanding, due to the interference among multiple heterogeneous networks, the spectrum efficiency of the ISM band is worsening. CRNs can be designed for operation on unlicensed bands such that the efficiency is improved in this portion of the spectrum. The CRN on unlicensed band architecture is shown in Fig. 6. As there are no license holders, all the entities of the network have the same right to access the spectrum bands. Multiple CRNs can coexist in the same area and share the same portion of the spectrum. Therefore, intelligent spectrum sharing algorithms are needed

to improve the efficiency of spectrum usage. In this architecture, CR users focus on detecting the transmissions of other CR users; hence, sophisticated spectrum sharing methods among CR users are required. If multiple CRN operators reside in the same unlicensed band, a fair spectrum sharing among these networks is also required.

Proposed Framework for Spectrum Management

Motivations

The cognitive management framework proposed in this chapter is designed to provide a powerful tool to assess efficient spectrum management solutions in different scenarios and use cases. Specifically, the framework is based on the DSA/CR cycle paradigm presented in section "Cognitive Radio as an Enabler of Dynamic Spectrum Access". This includes observation, analysis, decision, and action in order to perform efficient decision-making strategies for spectrum selection in CRNs. Moreover, it is implemented for the open sharing model and spectrum overlay hierarchical DSA model introduced in section "Dynamic Spectrum Access Models".

The observation of the radio environment and the analysis of such observations will allow to acquire knowledge about the state of the potential spectrum blocks that can be selected (e.g., the amount of measured interference, their occupation, etc.) as well as their dynamic behavior (e.g., how the interference changes with time). Observations of the radio environment involve making measurements at several nodes of a CRN. Then, these measurements need to be reported to the node in charge of the decision-making. This is usually done through signaling procedures supported by cognitive control channels [30]. As a result, the observation stage can be very costly in terms of practical requirements such as signaling overhead, battery consumption, etc. Consequently, decision-making strategies able to efficiently operate with the minimum amount of measurements would be of high interest. The proposed spectrum management framework is based on the so-called belief vector to predict the environment dynamics, which allows avoiding measurements when possible.

In detail, the belief vector assesses the probability that the radio environment is under specific conditions at a certain time, based on past measurements (observations). Moreover, the proposed framework can be particularized to different observation strategies to determine the instants when measurements of the radio environment need to be performed, assessing the trade-off existing between performance and observation requirements of the cognitive cycle. Some illustrative use cases representing DSA-based scenarios where this framework can be applicable are (1) a Digital Home (DH) environment in which different devices need to communicate, (2) a set of cognitive small cells deployed in a cellular network that make use of an additional spectrum to increase the network capacity, and (3) an opportunistic Device-to-Device (D2D) radio link created to extend the coverage

of certain cellular terminals that are outside the coverage area of the cellular infrastructure.

The authors in [31] have introduced the spectrum management approach based on the belief vector concept, which can be particularized for different observation strategies relying only on simulation analysis. In particular, the achieved results have assessed the impact of the environment dynamics in terms of the traffic generation patterns in the observation strategies supporting the decision-making solution in Matlab-based simulated scenarios. The spectrum management framework has also been assessed experimentally in [32] through a real-time testbed, evaluating an actual scenario where the best trade-off between performance and measurements requirements has been achieved through an appropriate combination between periodical measurements of the radio environment and statistical characterization of the interference variations. Finally, in [33], the authors have compared the belief-based spectrum management approach against other state-of-the-art solutions to demonstrate the effectiveness of this spectrum selection strategy through Matlab-based simulations. Hence, the functionalities of this framework have already achieved satisfactory results [31–33]. Notwithstanding, these publications either provide only simulation analysis [31] and [33] or address a particular use case in a real-time scenario [32]. The use of simulations is typical within the research and industrial communities and can be convenient for achieving preliminary performance results. However, to carry out appropriate and relevant studies and to properly evaluate the performance of innovative solutions before progressing to a prototype or full-scale deployment, assessment on realistic platforms is a crucial step. In this context, real-time platforms enable the emulation of realistic scenarios to test algorithms, applications, protocols, and policies under realistic conditions and represent a powerful tool for assessing the Quality of Experience (QoE) of end-users that could not be obtained through off-line simulations, as well as the QoS. Guided by these motivations, this chapter extends (i) the results achieved in [31] and [33] in a realistic environment provided by a real-time platform and (ii) the preliminary experimental results obtained in [32] providing new functionalities that enhance the proposed framework.

System Model and Problem Formulation

The considered system model assumes a set of $j = 1, \cdots, L$ radio links, each intended to support data transmission between either a pair of terminals or between a terminal and an infrastructure node. The j-th radio link will support a certain data service characterized by a required bit rate $R_{\text{req},j}$ and will generate data transmission sessions of a certain duration D_j. The focus will be to take the *decision* based on observations, which determines the spectrum to be assigned to each radio link. For this purpose, it is assumed that the L radio links are controlled by a centralized cognitive management entity in charge of spectrum selection decisions.

The spectrum is organized in a set of $i = 1, \cdots, M$ spectrum blocks, each characterized by a central frequency and bandwidth. The considered candidate

spectrum blocks can belong to different bands allowing different degrees of spectrum sharing with other systems in accordance with the DSA models considered in our implementation (e.g., non-licensed ISM bands, licensed bands allowing primary/secondary spectrum sharing such as TV White Spaces bands, licensed bands with exclusive use such as those belonging to the mobile network operator in charge of the CRN, etc.).

The considered strategies consist in performing an efficient allocation of the j-th spectrum block to the j-th radio link by properly matching the bit rate requirements with the achievable bit rate in each spectrum block. This will be conducted by the execution of the spectrum selection decision-making, which will take a so-called *action*, corresponding to the allocation of a spectrum block to a radio link, anytime that a data transmission session is initiated on this radio link. The action made for the j-th link at time t is denoted as $a_i(t) \in \{1, \cdots, M\}$ and corresponds to the selected spectrum block among those currently available.

For the interference model, we denote as $I_{i,j} = I_{\max,j,i} \cdot \sigma_i(t)$ the interference spectral density measured by the receiver of the j-th in the i-th spectrum block at a given time due to other external transmitters (i.e., outside the control of the decision-making entity). In order to capture that interfering sources may exhibit time-varying characteristics, we consider the term $\sigma_i(t)$ which is a spectrum block-specific term between 0 and 1 (i.e., $\sigma_i(t) = 0$ when no interference exists and $\sigma_i(t) = 1$ when interference reaches its maximum value $I_{\max,j,i}$). For modeling purposes, the set of possible values of $\sigma_i(t)$ is translated into a discrete set of interference states $S^{(i)}(t) \in \{0, 1, \cdots, K\}$ where state $S^{(i)}(t) = k$ corresponds to $\sigma_{k-1} < \sigma_i(t) < \sigma_k$ for $k > 0$ and to $\sigma_i(t) = \sigma_0 = 0$ for $K = 0$; note also that $\sigma_K = 1$. The system state at time t is given by the M-column vector $S(t) = [S^{(i)}(t)]$. Moreover, assuming that the state of each spectrum block remains the same for a time step of duration Δt, the interference evolution for the i-th block is modeled as a discrete-time Markov process with the state transition probability from state k to k' given by:

$$P^{(i)_{k,k'}} = P_r[S^{(i)}(t + \Delta t) = k' | S^{(i)}(t) = k] \tag{1}$$

Then, the state transition probability matrix for the i-th spectrum block is defined as:

$$\mathbf{P^{(i)}} = \begin{Bmatrix} p^{(i)}_{0,0} & \cdots & p^{(i)}_{0,K} \\ \vdots & \ddots & \vdots \\ p^{(i)}_{K,0} & \cdots & p^{(i)}_{K,K} \end{Bmatrix} \tag{2}$$

It is assumed that the state of the i-th spectrum block $S^{(i)}(t)$ evolves independently from the other blocks and that the state evolution is independent from the assignments made by the spectrum selection strategy. Moreover, let us define $\phi^{(i)} = [\phi^{(i)}_0 \phi^{(i)}_1 \cdots \phi^{(i)}_k]^T$, where superscript T denotes the transpose operation, as

the steady-state probability vector. $\phi_k^{(i)}$ is the probability that the i-th spectrum block is in the k-th interference state. Each radio link with a data session in progress (referred to as an active link) will obtain a reward that measures the obtained performance depending on the interference state of the allocated spectrum block at each time. The reward vector of the j-th link in the different interference states of the i-th SB is $r^{(i)} = [r_0^{(i)} r_1^{(i)} \cdots r_k^{(i)}]^T$. Supposing the use of the j-th link, the element $r_{j,k}^{(i)}$ denotes the reward that this link receives when using its allocated spectrum block i and the interference state is $S^{(i)}(t)$. The reward is a metric between 0 and 1 capturing how suitable the i-th spectrum block is for the j-th radio link, depending on the bit rate that can be achieved in this spectrum block with respect to the bit rate required by the application. Several possible definitions of the reward metric as a function of the bit rate may exist such as sigmoid functions, linear functions, or fittingness factor [34, 35]. The average reward experienced by the j-th link in the i-th spectrum block along a session starting to transmit data at time $t+1$ and ending after a certain duration of D_j time steps is given by:

$$r_{\text{Session},j}^{(i)} = \frac{1}{D_j} \sum_{n=1}^{D_j} r_{j,S^{(i)}(t+n)}^{(i)} \tag{3}$$

The spectrum selection policy illustrated in this chapter is executed at time t for the j-th radio link and targets the maximization of the expected reward that the session will experience along its duration:

$$a_i(t) = \arg\max_i \frac{1}{\overline{D_j}} \sum_{n=1}^{\overline{D_j}} r_{j,S^{(i)}(t+n)}^{(i)} \tag{4}$$

The selection is made among the available spectrum blocks, i.e., those that are not allocated to any other radio link at the decision-making time t. The analysis of the future evolution of the reward in each of the spectrum blocks until the session ends exploits the measurements of the interference state of the different spectrum blocks carried out at specific time instants in the past, together with the statistical characterization of the interference dynamics in each spectrum block. In details, the statistical characterization of the interference dynamics in the i-th spectrum block is given by the belief vector $\mathbf{b^{(i)}}(t)$. The computation of the belief vector of the i-th spectrum block at a certain time instant t is performed recursively, starting from the last observation of the actual interference state that was taken in the i-th spectrum block at time step $t - m^{(i)}$. In particular, the belief vector at a time instant $t > t - m^{(i)}$ can be obtained from the belief vector at the previous $m^{(i)}$ time steps using the state transition probabilities of the interference states recursively.

The envisaged framework to implement the spectrum selection strategies consists of the main entities illustrated in Fig. 7 and is described in the following.

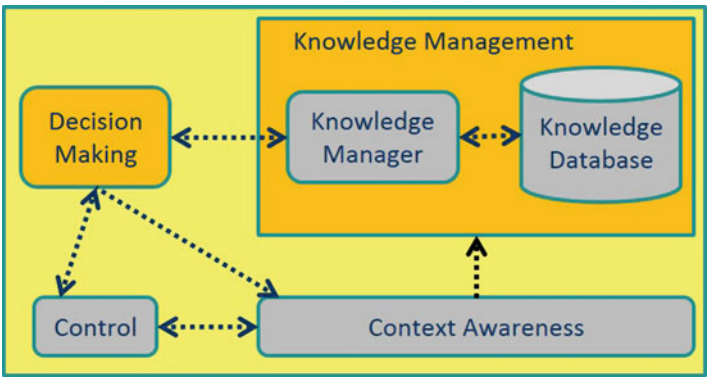

Fig. 7 Proposed framework for spectrum management

The Knowledge Management block is in charge of storing and managing the relevant knowledge obtained from the radio environment that will be used by the decision-making entity. In details, it includes the Knowledge Database (KD) that stores different statistic information about the radio environment and the Knowledge Manager (KM), which is in charge of computing and updating this information. The Knowledge Management relies on an *initial acquisition functionality* implemented in the KM to perform an estimation of the parameters stored in the KD based on real-time observations of the interference states in the different spectrum blocks. The estimation is done by averaging a sufficient number of samples for each parameter. To ensure that the estimated value has properly converged to the real value, the γ confidence interval is used. More specifically, let us consider the estimation of a transition probability of link i from state k to state k' as $P_{k,k'}^{(i)}$, called P from now on for simplicity reasons. Let us define $\overline{P}$ as the mean of this parameter after averaging a total of N samples. The Υ confidence interval can be defined as the interval $[\overline{P_{\min}(N)}, \overline{P_{\max}(N)}]$ such that the real value of P falls within this interval with probability Υ:

$$P_r\left[P \in [\overline{P_{\min}(N)}, \overline{P_{\max}(N)}]\right] = \Upsilon \tag{5}$$

Assuming large-sample conditions, the values of the Υ confidence interval after averaging N samples are given by:

$$\overline{P_{\min}(N)} = \overline{P(N)} - z_{(1-\Upsilon)/2}\frac{\overline{\sigma_P(N)}}{\sqrt{N}}\Upsilon \tag{6}$$

$$\overline{P_{\max}(N)} = \overline{P(N)} + z_{(1-\Upsilon)/2}\frac{\overline{\sigma_P(N)}}{\sqrt{N}}\Upsilon \tag{7}$$

where $z_{(1-\Upsilon)/2}$ is defined as follows:

$$z_{(1-\Upsilon)/2} = \Phi^{-1}(1 - \frac{1-\Upsilon}{2}) \tag{8}$$

Function $\Phi(\cdot)$ denotes the inverse of the normal cumulative distribution function, and $\overline{\sigma_P(N)}$ in (6) and (7) is the standard deviation with N samples. Note that as the number of samples N increases, the Υ confidence interval gets narrower, meaning that the estimation given by the sample mean $P_{\min}(N)$ tends to converge to the real value. Then, the required number of samples N that provides a sufficiently accurate estimate of parameter P by its sample mean $\overline{P(N)}$ is the first value of N that fulfills the following convergence condition:

$$\overline{P_{\max}(N)} - \overline{P_{\min}(N)} < \eta \overline{P(N)} \tag{9}$$

where $0 < \eta < 1$ is a parameter to be set; here it is assumed to have $\Upsilon = 95\%$, so that the term $z_{(1-\Upsilon)/2}$ in (6) and (7) equals 1.96.

The KM is also in charge of computing the analysis of the belief vector based on the information stored in the KD. In detail, the belief vector $\mathrm{b}^{(\mathrm{i})}$ at time $t - m^{(i)}$ (i.e., when the last observation of the actual interference state was taken in the i-th spectrum block) is given by:

$$\mathbf{b^{(i)}}(t - m^{(i)}) = \mathbf{x}(S^{(i)}(t - m^{(i)})) \tag{10}$$

where $\mathbf{x}(k)$ is defined as a column vector of $K + 1$ components numbered from 0 to K that has all of them equal to 0 except the k-th component, which is equal to 1. Then, the belief vector at a time instant $t - m^{(i)}$ can be obtained at the previous time step $t - 1$ using the state transition probability matrix $\mathbf{P^{(i)}}$ stored in the KD as follows:

$$\mathbf{b^{(i)}}(t) = \mathbf{b^{(i)}}(t-1)[\mathbf{P^{(i)}}] \tag{11}$$

By recursively applying (11) for the last $m^{(i)}$ time steps and making use of (10), the belief vector at time t as a function of the last observation is given by:

$$\mathbf{b^{(i)}}(t) = \mathbf{b^{(i)}}(t - m^{(i)})[\mathbf{P^{(i)}}]^{m^{(i)}} \tag{12}$$

This functionality executes the selection of the most appropriate radio spectrum block whenever requested by a radio link in accordance with the statistic information stored in the knowledge management. It also triggers the execution of the measurements of the radio environment made by the Context Awareness (CA). In particular, the proposed spectrum selection strategy based on the belief vector implements the decision provided by the decision-making functionality, which maximizes the expected reward and that can be particularized for the following observation strategies:

- *Instantaneous Measurements (IM) strategy*: It consists of performing instantaneous measurements of the interference states in all the spectrum blocks at the time t when a new session has to be established, i.e., at the time when the spectrum selection decision-making is executed. In this case, the belief vector always is computed with $m^{(i)} = 0$ to capture the exact interference state at time t.
- *Periodic Measurements (PM) strategy*: It consists of performing periodic measurements of the i-th spectrum block with observation period $T_{\text{obs}}^{((i))}$. In this manner, the elapsed time $m^{(i)}$ between the last observation of the i-th spectrum block and the decision-making time t will always be upper-bounded by $m^{(i)} < T_{\text{obs}}^{((i))}$.
- *Steady-state (StS) strategy:* It is the case when no actual observations are performed. In this case, it can be easily proved making use of the properties of the ergodic discrete-time Markov processes that the values of the belief vector will be equal to the steady-state probabilities [36].

In the decision-making entity, the following functionalities are implemented: (i) the *observation strategy decision-making* in charge of selecting one of the observation strategies among the IM, the PM, and the StS to be applied in the i-th spectrum block depending on the traffic generation patterns and the interference behavior and (ii) the *spectrum selection decision-making* in charge of selecting a spectrum block each time that a new session is established in the j-th radio link particularized for one of selected observation strategies. Moreover, it targets the maximization of the expected reward that the session will experience along its duration D_j at future time instants $t + n$ relying on the belief vector, which can be achieved recursively through (11), leading to:

$$\mathbf{b^{(i)}}(t+n) = \mathbf{b^{(i)}}(t)[\mathbf{P^{(i)}}]^n \tag{13}$$

Then, the *action* implemented in the spectrum selection decision-making policy introduced by (4) is reformulated as:

$$a_i(t) = \arg\max_i \frac{1}{\overline{D_j}} \sum_{n=1}^{\overline{D_j}} \mathbf{b^{(i)}}(t+n)\mathbf{r_j^{(i)}} \tag{14}$$

where $\mathbf{r_j^{(i)}}$ represents the reward vector of the j-th link in the different interference states of the i-th spectrum block and $\mathbf{b^{(i)}}(t+n)$ is achieved by (13). Notice that $\mathrm{b^{(i)}}(t)$ in (13), which is computed through (12) by the KM, provides at the decision-making time t the future evolution of the reward in each of the spectrum blocks until the session end, exploiting past measurements of the interference state together with the statistical characterization of the interference dynamics. Finally, given that the session duration D_j is typically unknown at the decision-making time t, it is assumed to be characterized statistically in terms of its average value.

The CA entity is responsible for acquiring the required measurements to support the operation of the Knowledge Management entity. Specifically, it will provide the different observations that will be used by the KM and stored in the KD. Measurements will be triggered either by the decision-making functionality in accordance with the observation strategy or by the *initial acquisition functionality* implemented in the KM.

The control entity will provide the signaling means to support the communication between the cognitive management entity and the different nodes of the network. In the context of the spectrum selection processes considered in this chapter, two main functions are envisaged for this control entity:

- Whenever a new session has to be established in a given radio link, the control entity will trigger the decision-making requesting the allocation of a spectrum block and will inform the involved nodes about the result of this allocation.
- Whenever the CA needs to collect a measurement at a certain node of the network, the control entity will exchange the necessary signaling messages with this node to request and retrieve the measurement.

The signaling exchange relies on a cognitive control channel that allows for the transmission of different information elements and the realization of diverse operations within a cognitive radio system. Details on the specific implementation and signaling exchange are outside the scope of this chapter.

Real-Time Testbed Design and Implementation

This section presents the real-time testbed developed to implement and evaluate the spectrum management solutions illustrated in section "Proposed Framework for Spectrum Management". In detail, section "Individual Node" presents the implementation of the individual node with details about hardware and software components, while section "Testbed Architecture" illustrates the architecture of the platform for the implementation of the framework for spectrum management based on the belief vector, in which an individual node can implement both the centralized framework and a user node.

Individual Node

Each individual node is implemented through Universal Software Radio Peripheral (USRP) version 1 integrated boards [37] controlled by a Personal Computer (PC) running Linux Operating System (OS) where GNU radio [38], a software for properly configuring the transmission and reception parameters of the USRP modules, is implemented. The Linux OS was selected for the implementation of the testbed for its capability to guarantee appropriate levels of real-time management while guaranteeing a high degree of flexibility and for its interprocess communication

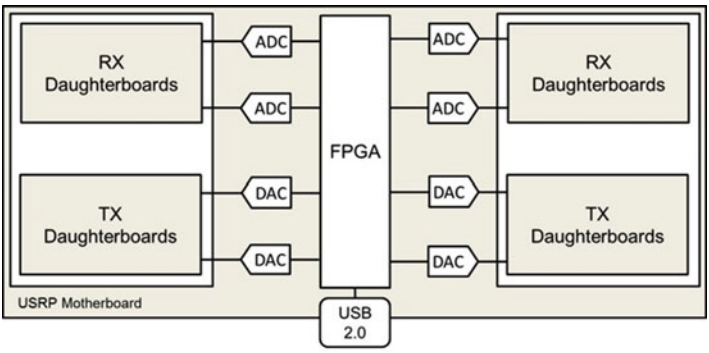

Fig. 8 USRP motherboard

methods considered in order to exploit the auto reconfigurability functionality of the hardware.

USRP incorporates Analog to Digital and Digital to Analog Converters (ADC/DAC), a Radio Frequency (RF) front end, a Field-Programmable Gate Array (FPGA), and a USB 2.0 interface to connect to the PC. A typical setup of the USRP board is illustrated in Fig. 8, and it consists of one motherboard that supports up to four daughterboards, where up to two receivers and up to two transmitters can be plugged in. The RF front ends are implemented on the daughterboards.

In details, the motherboard contains 4 high-speed 12-bit ADCs and 4 high-speed 14-bit DACs. All the ADCs and DACs are connected to the FPGA that performs high bandwidth math procedures such as filtering, interpolation, and decimation. The DACs clock frequency is 128 Msample/s, while ADCs work at 64 Msample/s to digitize the received signal. The USB 2.0 controller sends the digital signal samples to the PC in 16-bit I and 16-bit Q complex data format (4 bytes per complex sample); since the maximum USB data rate is 32 MB/s, 8 Msample/s is the maximum sample rate manageable by the USB controller. Consequently, the FPGA has to perform filtering and digital down-conversion (decimation) to adapt the incoming data rate to the USB 2.0 and PC computing capabilities. The maximum RF bandwidth that can be handled is thus 8 MHz. There exist different kinds of daughterboards that allow a very high USRP reconfigurability. A complete list of daughterboards that can be used with the USRP motherboard can be found in [37], while, in the testbed proposed in this chapter, Transceivers *XCVR2450* working in the frequency ranges 2.4–2.5 GHz and 4.9–5.9 GHz have been used.

Notice that the first range includes specifically the 13 sub-bands around the 2.4 ISM band (2.412–2.472 GHz in 5 MHz steps), used by Wi-Fi applications (i.e., IEEE 802.11b, 802.11g, and 802.11n standards). The bands from 5.170 to 5.320 GHz and from 5.500 to 5.825 GHz are also used by Wi-Fi applications (i.e., IEEE 802.11a standard). The bandwidth of each Wi-Fi channel is 20 MHz, and the mentioned ranges are illustrated in Fig. 9.

GNU radio software is a free and open-source toolkit that provides a library of signal processing blocks like modulators, demodulators, lters, etc., for building

Channel Number	Channel GHz	Channel Number	Channel GHz	104	5.520
1	2.412	34	5.170	108	5.540
2	2.417	36	5.180	112	5.560
3	2.422	38	5.190	116	5.580
4	2.427	40	5.200	120	5.600
5	2.432	42	5.210	124	5.620
6	2.437	44	5.220	128	5.640
7	2.442	46	5.230	132	5.660
8	2.447	48	5.240	136	5.680
9	2.452	52	5.260	140	5.700
10	2.457	56	5.280	149	5.745
11	2.462	60	5.300	153	5.765
12	2.467	64	5.320	157	5.785
13	2.472	100	5.500	161	5.805
				165	5.825

2.4GHz – has 3 non-overlapping channels separated by 20MHz.

5GHz – has 24 non-overlapping channels separated by 20MHz.

Fig. 9 ISM channels

SDRs. It is an empowering tool that enables to explore new ways of using the electromagnetic spectrum growing into a widely used cross-platform package that supports SDRs. In GNU radio, the programmer builds a SDR by creating a graph where the vertices are signal processing blocks and the edges represent the data flow between them. All the signal processing blocks are written in C++; these blocks process streams of data from their input port to their output one. The input and output ports of a signal process block are variable; hence, a block can have multiple outputs and multiple inputs. Python programming language is used to create a network or graphs and glue the signal processing blocks together.

The Simplified Wrapper and Interface Generator (SWIG) is an open-source package used by GNU radio as a glue such that the C++ classes can be used from Python. SWIG has the ability to convert the C++ classes into Python-compatible ones. As a result, the whole GNU radio framework is capable of putting together and exploiting the benefits of both C++ and Python. The input and output ports of a signal process block are variable; hence, a block can have multiple outputs and multiple inputs. GNU radio has been used to implement all the processes carried out at the different entities of the proposed cognitive management framework described section "Proposed Framework for Spectrum Management". Moreover, GNU radio has been considered to enable the data and control communication between USRP transceivers. There is also a graphical environment available to create a custom radio called GNU Radio Companion (GRC) [38], which allows connecting graphically the signal processing blocks. Figure 10 illustrates an example of screenshot of the GRC.

Figure 11 illustrates a general scheme of two USRP nodes acting as transmitter and receiver, respectively, reflecting the transmission and reception processes and

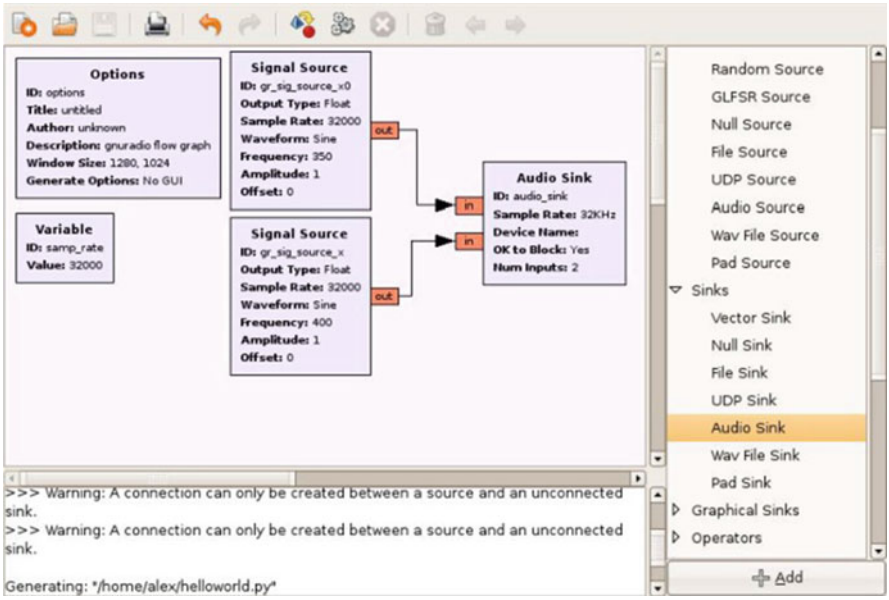

Fig. 10 GNU Radio Companion screenshot

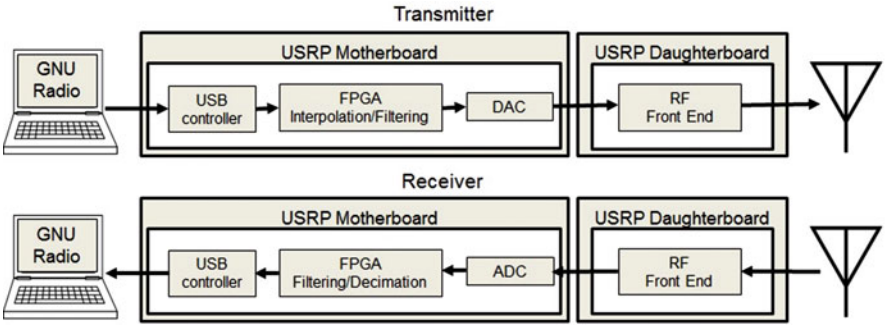

Fig. 11 Transmitter/receiver nodes implemented through USRP and GNU radio

the connection of the PCs running GNU radio software to the hardware platforms. Each individual node can act as either transmitter or receiver in the testbed, and it provides spectrum sensing and data transmission functionalities. Regarding the spectrum sensing functionality, it is exploited by the CA implemented in the node that represents the cognitive management entity in order to provide the observations in the belief-based spectrum selection solution proposed in section "Proposed Framework for Spectrum Management". Moreover, this functionality is exploited by the KM during the *initial acquisition functionality* implemented to estimate the transition probabilities stored in the KD. The spectrum sensing implemented in the nodes is based on measurements performed by means of the energy detection

functionality implemented in the USRPs. Energy detection for each spectrum block is performed during a sensing time Δt_m. Then, based on the detected energy, the CA identifies the interference states of each spectrum block. The energy threshold to decide if a spectrum block is free of interference is set based on [39].

The script "*usrp_spectrum_sense.py*" has been considered for the design of the spectrum sensing functionality implemented in the individual node of the testbed; it can be found in the toolkit provided by GNU radio software. This script has been used as a basic code for implementing a wideband spectrum analyzer. In details, the script has been extended in order to properly sense the spectrum bands considered in the strategies explained in the next sections. The USRP cannot examine more than 8 MHz of RF spectrum due to the USB 2.0 limitations. Notwithstanding, USRP RF front end can be tuned in suitable steps in order to scan across a RF spectrum wider than 8 MHz.

The script receives several input parameters from the user such as the lowest frequency of the band to be sensed $f_{\min}$, the highest frequency of the band to be sensed $f_{\max}$, how long the spectrum sensing functionality is executed in the entire frequency range whose bandwidth is $f_{\max} - f_{\min}$, the decimation factor that adapts the incoming data rate to the USB 2.0 and PC computing capabilities, and the Fast Fourier Transform (FFT) size parameter that is the number of samples considered to perform the magnitude analysis of the sensed signal. In particular, the selection of this parameter allows dividing the entire frequency range to be sensed into smaller spectrum blocks. The output of this script provides the signal energy detected in each sample during the execution of the spectrum sensing functionality.

Regarding the data transmission functionality, it allows sending either signaling messages among nodes or user data between a pair of terminals. The data transmission functionality has been implemented through the GNU radio "*benchmark_tx.py*" and "*benchmark_rx.py*" scripts. In details, the file "*benchmark_tx.py*" is the transmitter code that generates packets whose size is specified by the user, while the file "*benchmark_rx.py*" is the receiver code, which listens for incoming packets and checks for errors in each received one through the Cyclic Redundancy Check (CRC) error-detecting code. These scripts take the following input parameters from the users: a modulation scheme between the Gaussian Minimum Shift Keying (GMSK) and the Differential Binary Phase Shift Keying (DBPSK), the data transmission bit rate, the packet size, and the central frequency of the spectrum block for the data transmission.

The main problem found in these scripts is that the implementation uses only one way data flow; therefore, the transmitter cannot receive ACK (positive acknowledge) or NACK (negative acknowledge) messages useful to allow retransmissions of either lost or erroneous packets. Hence, these scripts have been modified by adding a stop and wait error-control method that uses acknowledgement messages in order to monitor the performance of the data transmission. Stop and wait is the simplest kind of Automatic Repeat reQuest (ARQ) method.

In an ARQ scheme, a number of parity-check bits are generated for each block of information and then transmitted together with the information. At the receiver side, the parity checking is performed on the received data. If the parity checking

is successful, the received block is assumed to be error-free, delivered to higher layers, and the receiver notifies that the block has been successfully received sending an ACK. If there is a parity failure, errors are detected in the received data, and the transmitter is requested sending a NACK in order to retransmit the same block of information. The stop and wait scheme implemented in the testbed enables the following procedures illustrated in time line order:

- "*benchmark_rx.py*" takes the input parameter and then it listens to the selected spectrum block waiting for data reception;
- "*benchmark_tx.py*" takes the input parameter and then it sends the i-th packet to "*benchmark_rx.py*";
- "*benchmark_rx.py*" checks for a possible error in the received packet through the CRC, and it sends the corresponding acknowledgement message to "*benchmark_tx.py*";
- "*benchmark_tx.py*" waits for the i-th ACK or NACK message from "*benchmark_rx.py*" during a certain time (defined as timeout);
- if the i-th ACK is received before the timeout is expired, then "*benchmark_tx.py*" sends the next packet to "*benchmark_rx.py*";
- if the i-th NACK is received or the i-th ACK is not received before the timeout is expired, "*benchmark_tx.py*" retransmits the i-th packet to "*benchmark_rx.py*".

Testbed Architecture

The testbed consists of six reconfigurable individual nodes to implement two terminals communicating through the radio link, the central node where the cognitive management processes are executed, and three nodes representing interference sources; see Fig. 12. Node#1 in the figure is the centralized entity where the framework of Fig. 7 has been implemented. Node#2 and Node#3 are the terminals that need to establish a radio link for supporting a data communication under the control of Node#1 that will decide the spectrum block to be used by this radio link. The control messages are sent among the nodes through Ethernet cables. Nodes#4, #5, and #6 are external interference sources transmitting in certain spectrum blocks.

Node#1 includes the decision-making, the knowledge management, and the CA functionalities. Specifically, the CA entity performs measurements by means of the spectrum sensing functionality implemented in the USRPs for each spectrum block during a sensing time Δt_m. Then, based on the detected energy, the CA identifies the interference states of each spectrum block. These measurements are triggered either by the KM during the *initial acquisition functionality* in order to fill the KD with transition probabilities of the spectrum blocks or by the decision-making in accordance to an observation strategy selected among the IM, PM, and StS by the *observation strategy decision-making*.

By properly processing the measurements of the interference states, the KM derives samples of the durations of each state. From these durations, the KM estimates the values of state transition probabilities and steady-state probabilities

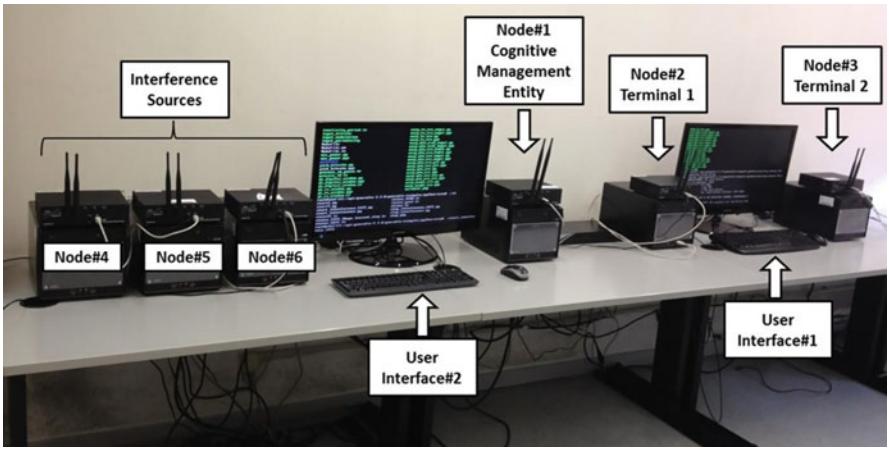

Fig. 12 Testbed architecture for the belief-based spectrum selection

to be stored in the KD through the *initial acquisition functionality*. The estimation of each parameter will be done as the average of a sufficient number of sample that ensures convergence under some reasonable limits, as explained in section "Proposed Framework for Spectrum Management". In particular, the considered convergence condition in this chapter is that the size of the 95% confidence interval of every measured parameter is below a fraction of the measured average value. The convergence criterion defined in section "Proposed Framework for Spectrum Management" is used with $\eta = 0.2\%$.

The KM is in charge of providing the *observation strategy decision-making* implemented in the decision-making with the dynamism information of the radio environment in terms of traffic generation patterns. Moreover, each time that a new session is established in a radio link, the KM provides the data function parameters to the *spectrum selection decision-making* that selects the most appropriate spectrum block following (12) particularized for the observation strategy decided in the *observation strategy decision-making* entity.

Node#2 is programmed to compute periodically the system session reward in order to measure the achieved performance depending on the experienced bit rate in the allocated spectrum block. Moreover, the USRP-based interference sources implemented in Nodes #4, #5, and #6 are transmitting in specific spectrum blocks following random patterns whose statistics can be controlled at the testbed configuration. As seen in Fig. 12, two screens connected to two switches are the user interfaces that allow running and controlling the testbed operation. Specifically, the User Interface#1 allows configuring the parameters of the cognitive management entity and the communicating terminals, while the User Interface#2 allows the configuration of the interference sources. In each emulation run, the testbed produces a number of performance statistics that are stored in files so that they can be post-processed later on. In particular, statistics related to the performance obtained in the

communication through the radio link between Terminal 1 and Terminal 2 are stored in Node#2, while the statistics related to the cognitive management entity are stored in Node#1.

Performance Evaluation

Configuration

The emulation assumptions and scenario parameters that have been considered are described in the following. A set of $M = 3$ spectrum blocks are taken into account. The bandwidth is 200 kHz for all the spectrum blocks, and the central frequencies are 5472, 5490, and 5508 MHz. Two different interference states are considered for the spectrum blocks: $S^{(i)} = 0$ when no interference exists and $S^{(i)} = 1$ when the interference corresponds to its maximum value. The average durations of the interferences states for each spectrum block are presented in Table 1, considering that the testbed operates in time steps of 10 s.

$L = 1$ radio link is considered to transfer the data flow between Node#2 and Node#3 of the testbed (see Fig. 12) with bit rate requirement $R_{\text{req}} = 512$ kbps. During the data transmission sessions, Node#2 computes the system session reward value in the selected i-th spectrum block. Different values of the average link session duration $\overline{D_j} = \overline{D}$ and average session rate ρ are considered as indicated in Table 2. Specifically, three different scenarios are considered with different values of session duration and session generation rate. This allows demonstrating the effect of the observation and decision-making strategies under different situations in terms of traffic patterns. For the PM strategy, the observation period $T_{\text{obs}}^{(i)}$ is set to 2 time steps.

In order to assess the performance of the proposed observation strategies, appropriate KPIs are also defined for the belief-based policy for the performance study in the real-time environment provided by the testbed. In particular:

Table 1 Characterization of the interference states

Spectrum block	State $S^{(i)} = 0$ (time steps)	State $S^{(i)} = 1$ (time steps)
#1	480	120
#2	60	480
#3	480	160

Table 2 Characterization of the scenarios

Scenario	$\overline{D_j} = \overline{D}$ (time steps)	ρ (sessions/time step)
1	15	0.013
2	15	0.063
3	500	1.810-3

- *Average system session reward:* it is the reward experienced by each data transmission session depending on the interference state of the allocated spectrum block averaged along the total emulation time.
- *Average throughput:* it is the bit rate in kb/s achieved in the radio link averaged along the total emulation time.
- *Observation rate:* it is the average number of observations per time step that are performed to determine the interference state of the different spectrum blocks during the system operation. This KPI is only applicable to IM and PM policies, while StS strategy does not require observations.

Performance Results

This section compares the performance obtained in a real-time environment by each of the observation strategies and associated spectrum selection decision-making criteria considered in section "Proposed Framework for Spectrum Management", namely, IM, PM, and StS, respectively. For this purpose, the different scenarios considered in Table 2 are evaluated during a total emulation time $T_{em} = 3600$ steps (i.e., 10 h) starting from the time when the KD statistics have been acquired under the considered convergence criterion enabled through the *initial acquisition functionality* and implemented in the KD.

Figures 13, 14, and 15 present the time evolution of the average system reward for the different strategies in all the scenarios. As a baseline reference, the random strategy in which the spectrum block is randomly selected among the available ones at the time that each session is established is also included in the comparison. Table 3 summarizes the average reward, throughput, and observation rate for the different strategies along the whole emulation time. Moreover, the last column of Table 3 indicates the strategy that will be selected by the proposed *observation strategy decision-making* entity in each of the considered scenarios.

It can be observed from the figures and Table 3 that the proposed strategies in all the scenarios allow achieving a clear improvement in terms of both reward and throughput with respect to the random selection of the spectrum block. Focusing on scenario 1, the session duration is much shorter than the interference dynamics, and the session generation rate is low. Results in Fig. 13 and Table 3 show that IM outperforms PM and StS in terms of reward and throughput. Moreover, it allows achieving the highest reward and throughput with reduced requirements in terms of observation rate. On the contrary, scenario 2 is characterized by a higher session generation rate. In this case, it can be noticed that IM suffers an increase in the observation rate that is almost five times higher than with scenario 1. PM strategy becomes a better option since it allows achieving a similar reward and throughput as IM but with much less observation requirements, as seen in Table 3 and Fig. 14. Moreover, it achieves an important improvement in terms of reward and throughput in around 15% with respect to StS.

Scenario 3 is characterized by a session duration that is much longer compared to the session generation rate. In this case, results in Table 3 and Fig. 15 reveal

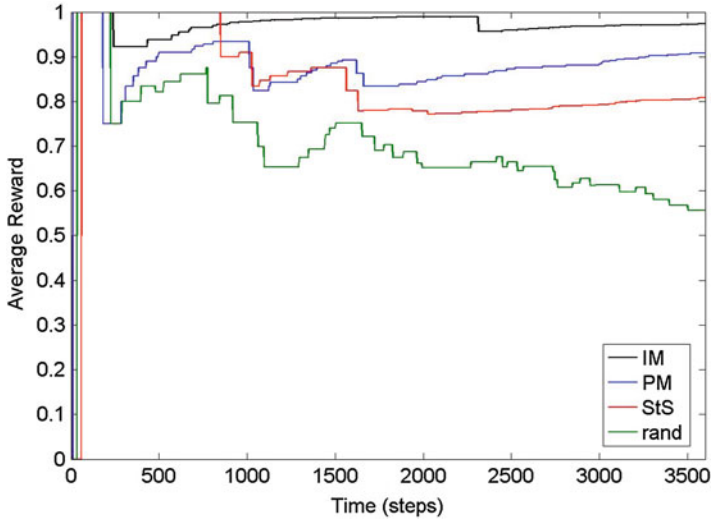

Fig. 13 Avg. system reward scenario 1 emulated by the testbed

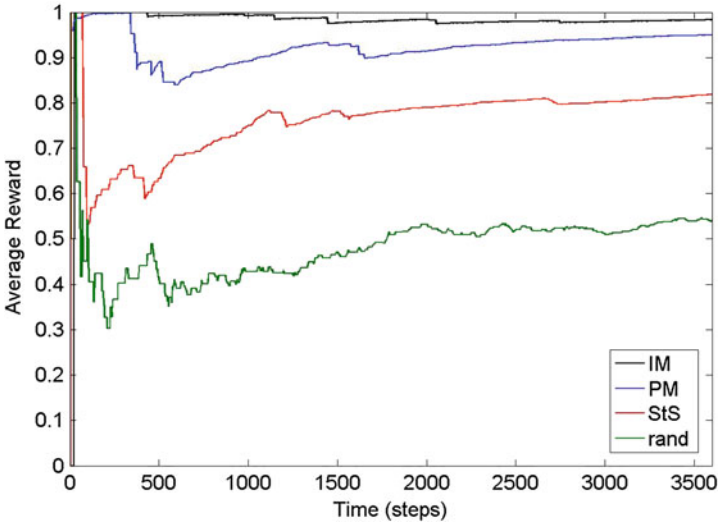

Fig. 14 Avg. system reward scenario 2 emulated by the testbed

that IM, PM, and StS techniques tend to converge to similar values of the reward and the throughput. The reason is that, when a spectrum block is allocated to a link for a long time, the link will tend to experience the steady-state conditions in this spectrum block. Therefore, the reward estimation based on the steady-state probabilities made by the StS at the decision-making time becomes a good estimate

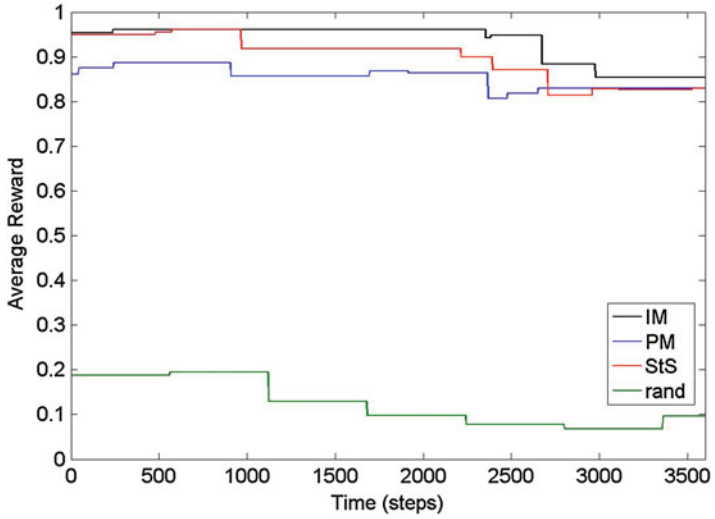

Fig. 15 Avg. system reward scenario 3 emulated by the testbed

of the actual performance that will be achieved. Correspondingly, for long session durations, StS becomes the most adequate strategy because it is capable of properly estimating the performance without requiring any observations.

Based on the obtained results, it can be concluded that the traffic generation pattern plays a key role when deciding the most adequate observation strategy in a belief-based decision-making approach. For long session durations (see scenario 3 with D_j equal to 500 time steps), the best approach is the decision-making based on steady-state conditions because it allows properly estimating the performance without requiring dynamic observations of the environment. On the contrary, for shorter session durations, the choice between IM and PM is related to the session arrival rate ρ that reflects the rate at which the spectrum selection functionality is triggered. In particular, a belief-based decision-making with periodic observations becomes a good approach for large session generation rates ρ, because it allows achieving good performance in terms of reward while significantly reducing the observation rate requirements, while for lower session generation rates, it is more convenient the IM approach.

The presented results focused on the performance achieved after the proper convergence of the KD statistics in the *initial acquisition functionality*. In order to complement the analysis, the operation of this functionality is studied next. Specifically, Fig. 16 depicts the initial acquisition process for one of the parameters stored in the KD, namely, the state transition probability $p^{(1)}_{(0,0)}$ for spectrum block #1. To compute it, the CA entity performs on spectrum block #1 a measurement once per time step during a sensing time $\Delta t_m = 2$s. Then, based on the detected energy, it sends the interference state to the KD acquisition entity where the different samples

Table 3 Average performance in terms of reward, throughput (kb/s), and observation rate (observations/time step)

Scenario	KPI	IM	PM	StS	Random	Best observation strategy
1	Reward	0.97	0.91	0.79	0.55	IM
	Throughput	491	465	406	274	
	Observation rate	0.04	0.06	0.0	0.0	
2	Reward	0.98	0.95	0.82	0.54	PM
	Throughput	502	486	413	305	
	Observation rate	0.19	0.06	0.0	0.0	
3	Reward	0.85	0.83	0.83	0.09	StS
	Throughput	441	388	409	47	
	Observation rate	0.01	0.07	0.0	0.0	

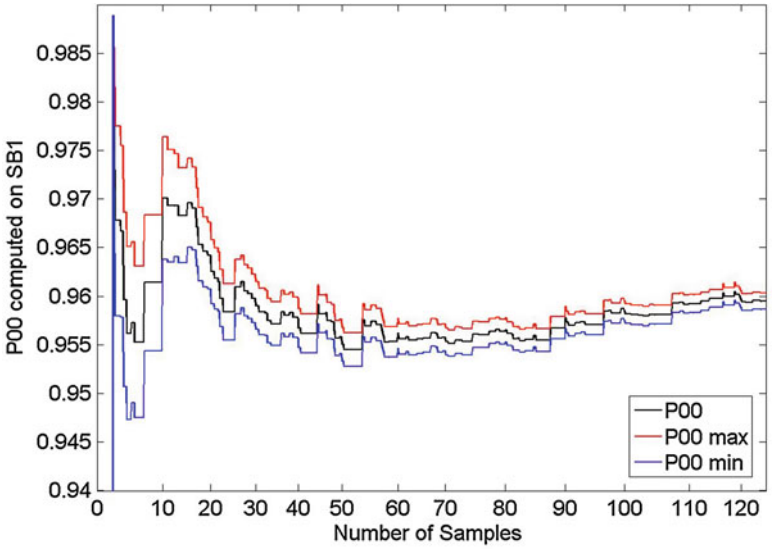

Fig. 16 Evolution of the initial acquisition process for parameter $p^{(1)}_{(0,0)}$

of $p^{(1)}_{(0,0)}$ are computed. Figure 16 presents the evolution of the sample average $\overline{p^{(1)}_{(0,0)}}$ and the 95% confidence interval bounds $p^{(1)}_{(0,0,\text{min})}$ and $p^{(1)}_{(0,0,\text{max})}$ as a function of the number of samples N. It can be observed in the figure how the confidence interval gets narrower when increasing the number of samples. Then, considering the convergence condition with parameter $\eta = 0.2\%$, it is shown in the figure that the convergence is achieved after $N = 100$ samples. The sample average $\overline{p^{(1)}_{(0,0)}}$ existing at this point of time is the one stored in the KD.

Conclusions and Future Directions

In this chapter, an overview of the Cognitive Radio paradigm has been presented as an innovative solution to mitigate the spectrum scarcity problem by enabling Dynamic Spectrum Access. It provided a general description of the CR paradigm including the so-called cognitive cycle and then the basic DSA concepts with particular emphasis on the different existing models and the exploitation of the CR cycle. The modeling of cognitive strategies for spectrum management suitable for different scenarios and use cases in the context of DSA/CR networks is also presented. A belief-based framework for decision-making in CR networks has been introduced, focusing on the spectrum selection problem where a number of radio links with different requirements have to be established. This exploits the belief vector concept to predict the environment dynamics at the decision-making time and in later instants based on past measurements. In this context, the chapter has analyzed the trade-off existing between performance and observation requirements of the cognitive cycle. For that purpose, a general formulation of the belief-based decision-making has been presented and has been particularized for different observation strategies. These have been evaluated to assess the impact of the environment dynamics in terms of the traffic generation patterns.

Results have demonstrated that for long session durations, a steady-state-based strategy that does not require dynamic observations becomes the best approach. Instead, for short session durations, the use of periodic measurements achieves a good trade-off between reward and observation rate for large session generation rates, while for low session generation rates, the use of instantaneous measurements made at the decision-making time becomes adequate.

The cognitive management frameworks presented in this chapter provide new research possibilities in the practical development of other aspects in the context of LTE that currently is the most advanced International Mobile Telecommunications (IMT) technology. Although LTE operating in licensed spectrum is characterized by a prominent deployment across the world, the integration of unlicensed carrier has been proposed as an innovative and promising way to further expand its capacity and to meet the growing traffic demands. This integration, which is carried out by adapting LTE air interface to operate in the unlicensed spectrum, leads to the so-called Unlicensed LTE (U-LTE) technology. Regarding the spectrum regulation in the context of U-LTE, the 5 GHz band is considered as the main candidate in terms of large amounts of unlicensed available spectrum, as well as relatively good channel propagation performance. One of the challenging topics in the context of U-LTE is the definition of spectrum management policies [40, 41] such as mechanisms of Dynamic Frequency Selection (DFS) based on spectrum sensing strategies, which allow avoiding interference among IMT devices and to non-IMT systems working at the same band (e.g., radar systems). For instance, Listen-Before-Talk (LBT) techniques are designed and enforced by EU regulations, in order to impose a flexible and fair coexistence among IMT systems by enabling channel sensing before the use of the spectrum resource and dynamic channel occupancy.

References

1. Federal Communications Commission (FCC) (2002) Spectrum Policy Task Force. Report of the spectrum efficiency working group
2. Federal Communications Commission (FCC) (2003) ET Docket no. 03-287: Notice of proposed rule making and order
3. Chiang RIC, Rowe GB, Sowerby KW (2007) A quantitative analysis of spectral occupancy measurements for cognitive radio. In: 63rd Vehicular Technology Conference (VTC Spring 2007), Dublin, pp 22–25
4. Yin S, Chen D, Zhang Q, Liu M, Li S (2012) Mining spectrum usage data: a large-scale spectrum measurement study. IEEE Trans Mob Comput 11(6):1033–1046
5. Sanders FH, Lawrence VS (1995) Broadband spectrum survey at Denver, Colorado. National Telecommunications and Information Administration (NTIA), Techncal report, pp 95–321
6. Sanders FH, Ramsey BJ, Lawrence VS (1996) Broadband spectrum survey at San Diego, California. National Telecommunications and Information Administration (NTIA), Technical report, pp 97–334
7. McHenry MA, Steadman K (2005) Spectrum occupancy measurements, location 1 of 6: Riverbend Park, Great Falls, 7 Apr 2004. Shared Spectrum Company, Technical report, available at: http://www.sharedspectrum.com
8. McHenry MA, McCloskey D, Lane-Roberts G (2005) Spectrum occupancy measurements, location 4 of 6: Republican National Convention, New York City, 30 Aug 2004–3 Sept 2004, revision 2, Shared Spectrum Company, Technical report, available at: http://www.sharedspectrum.com
9. McHenry MA, Tenhula PA, McCloskey D, Roberson DA, Hood CS (2006) Chicago spectrum occupancy measurements & analysis and a long-term studies proposal. In: 1st International Workshop on Technology and Policy for Accessing Spectrum (TAPAS 2006), Boston
10. Wellens M, Wu J, Mahonen P (2007) Evaluation of spectrum occupancy in indoor and outdoor scenario in the context of cognitive radio. In: 2nd International Conference on Cognitive Radio Oriented Wireless Networks (CROWNCOM 2007), Orlando
11. Mitola J III (2000) Cognitive radio: an integrated agent architecture for software defined radio. Ph.D. dissertation, KTH Royal Institute of Technology
12. Shin KG, Kim H, Min AW, Kumar A (2010) Cognitive radios for dynamic spectrum access: from concept to reality. IEEE Wirel Commun 17(6):64–74
13. Demestichas P, Dimitrakopoulos G, Strassner J, Bourse D (2006) Introducing reconfigurability and cognitive networks concepts in the wireless world. IEEE Veh Technol Mag 1(2):32–39
14. Akyildiz I, Lee W-Y, Vuran MC, Mohanty S (2008) A survey on spectrum management in cognitive radio networks. IEEE Commun Mag 46(4):40–48
15. Thomas RW, Friend DH, Dasilva LA, Mackenzie AB (2006) Cognitive networks: adaptation and learning to achieve end-to-end performance objectives. IEEE Commun Mag 44(12):51–57
16. Kephart J, Chess D (2003) The vision of autonomic computing. Computer 36(1):41–50
17. ETSI Technical Committee (TC) on Reconfigurable Radio Systems (RRS). Online Available: http://www.etsi.org/WebSite/technologies/RRS.aspx
18. Seidel S, Breinig R (2005) Autonomous dynamic spectrum access system behaviour and performance. In: 1st IEEE International Symposium on New Frontiers in Dynamic Spectrum Access Networks (DySPAN 2005), Baltimore
19. DeGroot RJ, Gurney DP, Hutchinson K, Johnson ML, Kuffner S, Schooler A, Silk SD, Visotsky E (2005) A cognitive-enabled experimental system. In: 1st IEEE International Symposium on New Frontiers in Dynamic Spectrum Access Networks (DySPAN 2005), Baltimore
20. Yuan Y, Bahl P, Chandra R, Chou PA, Ferrell JI, Moscibroda T, Narlanka S, Wu Y (2007) KNOWS: cognitive radio networks over white spaces. In: 2nd IEEE International Symposium on New Frontiers in Dynamic Spectrum Access Networks (DySPAN 2007), Dublin
21. Mitola J III (2000) Software radio architecture. Wiley-Interscience, New York
22. Mitola J III (2006) Cognitive radio architecture. Wiley-Interscience, Hoboken

23. Jackson C (2005) Dynamic sharing of radio spectrum: a brief history. In: 1st IEEE International Symposium on New Frontiers in Dynamic Spectrum Access Networks (DySPAN 2005), Baltimore
24. Zhao Q, Swami A (2007) A survey of dynamic spectrum access: signal processing and networking perspectives. In: IEEE International Conference on Acoustics, Speech and Signal Processing (ICASSP 2007), Honolulu
25. Hatfield DN, Weiser PJ (2005) Property rights in spectrum: taking the next step. In: 1st IEEE International Symposium on New Frontiers in Dynamic Spectrum Access Networks (DySPAN 2005), Baltimore
26. Leaves P, Moessner K, Tafazolli R, Grandblaise D, Bourse D, Tönjes R, Breveglieri M (2004) Dynamic spectrum allocation in composite reconfigurable wireless networks. IEEE Commun Mag 42(5):72–81
27. Lehr W, Crowcroft J (2005) Managing shared access to a spectrum commons. In: 1st IEEE International Symposium on New Frontiers in Dynamic Spectrum Access Networks (DySPAN 2005), Baltimore
28. Santivanez C, Ramanathan R, Partridge C, Krishnan R, Condell M, Polit S (2006) Opportunistic spectrum access: challenges, architecture, protocols. In: 2nd Annual International Workshop on Wireless Internet (WICON 2006), Boston
29. Akyildiz IF, Lee W-Y, Vuran MC, Mohanty S (2006) NeXt generation/dynamic spectrum access/cognitive radio wireless networks: a survey. Comput Netw 50(13):2127–2159
30. ETSI, TC RRS (2009) Reconfigurable radio systems (RRS); functional architecture (FA) for the management and the control of reconfigurable radio systems, Technical report 102 682 V1.1.1
31. Pérez-Romero J, Raschellà A, Sallent O, Umbert A (2014) Enhanced cognitive radio operation through belief-based decision making. In: 20th European Wireless Conference, Barcelona
32. Raschellà A, Pérez-Romero J, Sallent O, Umbert A (2014) Evaluation of a belief-based decision making in a real-time platform for cognitive radio networks. In: 9th International Conference on Cognitive Radio Oriented Wireless Networks (CROWNCOM), Oulu
33. Pérez-Romero J, Raschellà A, Sallent O, Umbert A (2015) A belief-based decision making framework for spectrum selection in cognitive radio networks. IEEE Trans Veh Technol 65(10):8283–8296
34. Raschellà A, Pérez-Romero J, Sallent O, Umbert A (2013) On the use of POMDP for spectrum selection in cognitive radio networks. In: CROWNCOM 2013, Washington DC
35. Raschellà A, Umbert A (2016) Implementation of cognitive radio networks to evaluate spectrum management strategies in real-time. Elsevier Comput Commun 79:37–52
36. Kleinrock L (1975) Queueing systems. Volume I: theory. Wiley, New York
37. Ettus Research TM Distribution. http://www.ettus.com. Accessed Mar 2010
38. Free and Open Software Distribution. http://www.gnuradio.org. Accessed Apr 2010
39. López-Benítez M, Casadevall F (2010) Methodological aspects of spectrum occupancy evaluation in the context of cognitive radio. In: European Transactions on Telecommunications (Wiley), Special Issue on European Wireless 2009 Conference, vol 1, no 8, pp 680–693
40. Federal Communications Commission (FCC) White Paper (2013) The mobile broadband spectrum challenge: International comparisons
41. ITU Radio Regulations Articles Tech. Rep. (2016) International Telecommunication Union

Full-Duplex WiFi Networks

17

Liwei Song, Yun Liao, and Lingyang Song

Contents

Abstract

The device in conventional half-duplex WiFi networks cannot perform carrier sensing while in data transmission; thus it suffers from long collision duration. To mitigate this problem, this chapter introduces full-duplex (FD) technology into WiFi networks. A novel CSMA/CD protocol design is first presented for single-channel FD-WiFi, which facilitates continuous carrier sensing and transmission suspension. The network throughput performance is comprehensively analyzed by considering possible sensing errors (i.e., false alarm and miss detection) due to self-interference, and simulation results verify the performance analysis and the effectiveness of CSMA/CD protocol. Then the protocol for multi-channel FD-

L. Song · Y. Liao · L. Song
School of Electrical Engineering and Computer Science, Peking University, Beijing, China
e-mail: songliwei@pku.edu.cn; yun.liao@pku.edu.cn; lingyang.song@pku.edu.cn

W. Zhang (ed.), *Handbook of Cognitive Radio*,
https://doi.org/10.1007/978-981-10-1394-2_17

WiFi is provided, where the CSMA/CD protocol for accessing a certain channel is modified by adopting a contention window adjustment rule, and a distributed channel selection strategy is proposed based on the best-response algorithm. Simulation results indicate the performance improvement of multi-channel FD-WiFi protocol design.

WiFi Network Basics

WiFi technologies have received a rapid proliferation over the past few decades [1]. As a part of the 802 standard family, IEEE 802.11 provides an international standard for the conventional WiFi networks. Detailed medium access control (MAC) and physical layer (PHY) specifications for the 802.11 protocol are summarized in [2].

The fundamental access mechanism for 802.11 protocol is the distributed coordination function (DCF), which is a random access scheme and based on carrier sense multiple access with collision avoidance (CSMA/CA) [3, 4]. In DCF, users are required to listen to the channel before access. If the channel is sensed busy, users need to wait until channel becomes idle; then they enter into a random backoff procedure. This prevents multiple users from accessing the medium immediately after completion of the preceding transmission and leading to collisions.

Specifically, in the CSMA/CA protocol, every active node which has a new packet for transmission monitors the channel activity first. The node persists to carrier sense until the channel is measured idle for a period of time equal to a distributed interframe space (DIFS). At this point, the node generates a random backoff time by setting an internal timer to an integer number of slot times, which can be expressed as the following:

$$\text{Backoff Time} = \text{Rand(CW)} \times \text{Slot Time}, \tag{1}$$

where CW is called the contention window. The backoff time decreases in any slot as long as the channel is sensed to be idle, "freezes" when the channel is judged busy, and "reactivates" decrement when the channel is sensed idle again for a DIFS. The active node transmits the data packet when its backoff timer counts down to zero.

However, the collision is still possible due to concurrent transmission between different users. The exponential backoff scheme is thus adopted in the CSMA/CA protocol to further reduce collision. At the first transmission attempt, the user's backoff stage is zero and CW is set equal to $\text{CW}_{\min}$, called the minimum contention window. After each successful transmission, the backoff stage increases and CW is doubled, up to the maximum contention window $\text{CW}_{\max} = 2^{W_{\max}}\text{CW}_{\min}$, in which $W_{\max}$ is called the maximum backoff stage.

Upon packet reception, the acknowledgment (ACK) is required, i.e., the receiver transmits an ACK signal back after the interval of one short interframe space (SIFS)

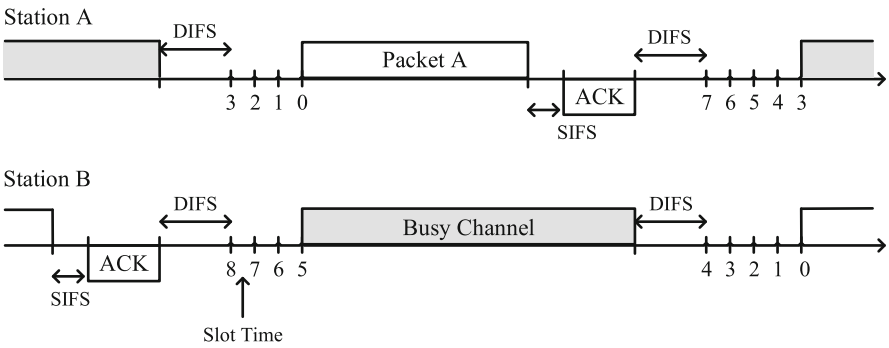

Fig. 1 Example of CSMA/CA protocol in conventional WiFi networks

when transmission is finished. The SIFS is shorter than the DIFS so that the other contending users cannot start to decrease their backoff time, which means that the ACK has higher priority than other regular transmissions. The transmission is unsuccessful if the transmitter fails to receive the ACK signal.

Figure 1 illustrates an example of the CSMA/CA protocol. Two stations A and B share the same wireless channel for data transmission. At the end of previous data transmission, they wait for a DIFS and randomly choose backoff time. Station A chooses 3 while station B chooses 8. Thus, after three slots, the backoff time of station A counts down to zero, and station A starts to transmit its data packet, during which station B has its backoff time frozen. After station A finishes transmission and the channel is sensed idle again for a DIFS, station B decrements its backoff time, and station A again chooses backoff time and contends the channel.

Although carrier sense is performed in the CSMA/CA protocol, the transmitter's sensing result may wrongly indicate the channel condition at the receiver due to different network topology, which leads to two problems called hidden terminal and exposed terminal [5]. A hidden terminal lies in the transmission range of a receiving station, but it is out of the range of the transmitting station. Therefore, the hidden terminal is oblivious of the ongoing transmission and can initiate a new transmission that will cause a collision at the receiver. The occurrence of these collisions reduces the overall performance of the network. On the other hand, an exposed terminal lies in the transmission range of the transmitter but out of the transmission range of the receiver. Therefore, a transmission initiated by this terminal would not cause a collision at the receiver. However, it remains silent due to the busy channel detection. This effect reduces the overall throughput by stopping some stations from transmitting despite the fact that they would not cause a collision.

To resolve the two problems, the RTS/CTS (request to send/clear to send) scheme is adopted by IEEE 802.11 as an optional mechanism [6]. In this scheme, an active node which wants to transmit a packet, waits until the channel is sensed idle for a DIFS, follows the backoff procedure explained above, and then, instead of the packet, preliminarily transmits a special RTS frame. When the receiving node

detects an RTS frame, it responds, after a SIFS, with a CTS frame. The transmitting node is allowed to transmit data packet only if the CTS frame is correctly received. By listening to RTS/CTS frame, the neighboring nodes of transmitter and receiver can get the transmission range information; thus hidden terminal and exposed terminal problems can be resolved. The main drawback of RTS/CTS scheme is long overhead caused by two frames.

Although the CSMA/CA protocol has been shown effective in the WiFi networks, it suffers from the problem of long collision duration. The main reason is that conventional WiFi networks are based on the half-duplex (HD) technology, due to the limitation of which, unlike the CSMA/CD (collision detection) protocol in Ethernet, the WiFi users cannot perform carrier sense and collision detection once transmitting. Thus if collision happens between some transmitting users, they cannot detect it and still transmit left collided data packets.

The full-duplex (FD) communication technology [7], by which the users can simultaneously transmit and receive data on the same band, has the potential to resolve the problem in conventional HD-WiFi networks. Recent years witness the revival of FD research due to the development of self-interference suppression (SIS) techniques in propagation, analog circuit, and digital domains, which significantly reduce the self-interference to a limited level [8, 9]. Apart from the development of the SIS techniques in PHY layer, some FD-MAC protocols have also been proposed recently [10–13]. In [10], a centralized FD-MAC protocol is proposed with shared random backoff, header snooping, and virtual backoffs. In [11], the authors design a decentralized FD-MAC protocol by adding FD acknowledgment bits. Both protocols in [10] and [11] discuss dual-link transmissions between two and three nodes. While [12] and [13] enable simultaneous spectrum sensing and data transmission for wireless users, the former is for cognitive radio networks and the latter is for ad hoc networks.

To mitigate the long collision duration problem in conventional HD-WiFi networks, similar to [12] and [13], this chapter introduces the FD technology into WiFi networks to realize simultaneous carrier sensing and data transmission. In the rest of this chapter, we first present the proposed CSMA/CD protocol for single-channel FD-WiFi networks [14]; then we extend this FD protocol to the multi-channel WiFi scenario [15].

Full-Duplex CSMA/CD Protocol

In this section, we elaborate the CSMA/CD protocol for single-channel FD-WiFi networks to resolve the long collision duration problem in conventional HD-WiFi networks. By taking advantage of FD techniques, each user can sense the spectrum and determine whether other users are occupying it while transmitting its own data simultaneously. We start with the system model, followed by the FD-WiFi protocol description. Performance analysis and simulation results are provided to show the protocol's effectiveness.

System Model

As shown in Fig. 2, we consider a FD-WiFi network consisting of one access point (AP) and N users $(U_1, \ldots, U_N)$, where the users are independently and randomly distributed in the coverage area of the AP. Each user is equipped with two antennas to realize FD communications. We focus on the uplink traffic, in which data packets are transmitted from the users to the AP, and each user is assumed to always have a packet to transmit with the same transmission power.

The channel can serve at most one user at a time; otherwise the collision happens. Therefore, as shown in the upper part of Fig. 2, each user performs carrier sensing to detect the channel state and contends for the idle channel against each other by the proposed protocol. When a certain user, say U_n $(n \in \{1, 2, \ldots, N\})$, accesses the channel, it uses one antenna for carrier sensing and the other antenna for data transmission simultaneously. However, the residual self-interference (RSI) between those two antennas leads to imperfect sensing, as shown in the lower part of Fig. 2. False alarm happens when the user mistakenly judges the channel to be occupied by other users when it is not, while miss detection means that the user fails to detect the channel occupation of other transmitting users. Both of the sensing errors degrade the network performance and, thus, should be taken into consideration for performance analysis. We now further discuss the carrier sensing in FD-WiFi networks as follows.

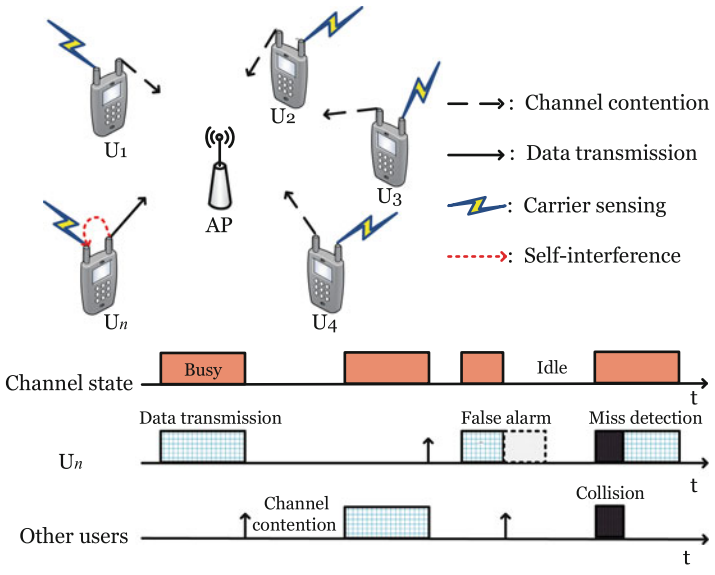

Fig. 2 The CSMA/CD protocol for the uplink traffic of FD-WiFi and two types of sensing errors (false alarm and miss detection) due to self-interference

Full-Duplex Carrier Sensing

Since noise is negligible compared to collision signal and self-interference, it is omitted in this chapter. Thus, a silent user has a perfect sensing, and we only need to analyze the sensing errors for transmitting users. Furthermore, the probability for the case with more than two collided users is negligible compared to the probability that only two users collide, and even when the case happens, the sensing performance is also better due to the accumulated collision signal. Thus perfect sensing is also assumed for the case that three or more users collide, and the sensing errors only exist in the following two cases: (1) $\mathscr{H}_0$, the transmitting user singly occupies the channel and (2) $\mathscr{H}_1$, the transmitting user has a collision with another user.

The received signal for sensing at the transmitting user can be given by

$$y = \begin{cases} h_r s_t, & \mathscr{H}_0, \\ h_r s_t + h_c s_c, & \mathscr{H}_1, \end{cases} \tag{2}$$

where s_t denotes the transmitting user's signal and s_c is the collided user's signal, h_c represents the collision channel, and h_r denotes the equivalent RSI channel indicating the SIS degree, which depends on the adopted SIS techniques and network environment. We adopt a typical path loss Rayleigh fading channel; thus, $h_c s_c$ is zero-mean complex Gaussian distributed with average power $\overline{P}_r(\frac{\overline{d}}{d})^{\alpha}$, where α is the path loss exponent, $\overline{P}_r$ is the reference received signal power at the reference distance $\overline{d}$, and d is the distance between two users. Moreover, according to [16], $h_r s_t$ is also a complex Gaussian variable with zero mean and average power $\beta^2 \overline{P}_r$, where β^2 denotes the SIS factor.

As for the sensing strategy, energy detection is adopted, and we assume the process is time slotted. Thus the sensing test statistics can be given by

$$M = \sum_{m=1}^{N_s} |y(m)|^2, \tag{3}$$

where $y(m)$ denotes the mth sample of received sensing signal and N_s is the sampling number in one slot.

The transmitting user compares M with the sensing threshold to decide whether a collision happens or not. Two types of sensing errors exist, i.e., false alarm and miss detection. As shown in the lower part of Fig. 2, false alarm wastes available channel slots, while miss detection causes collisions. We need to balance the two types of sensing errors to ensure network performance.

CSMA/CD Protocol Design

Based on the FD technology and conventional CSMA/CA concepts, we now propose the CSMA/CD protocol for FD-WiFi networks. Figure 3 shows the proposed protocol, which consists of the following several parts.

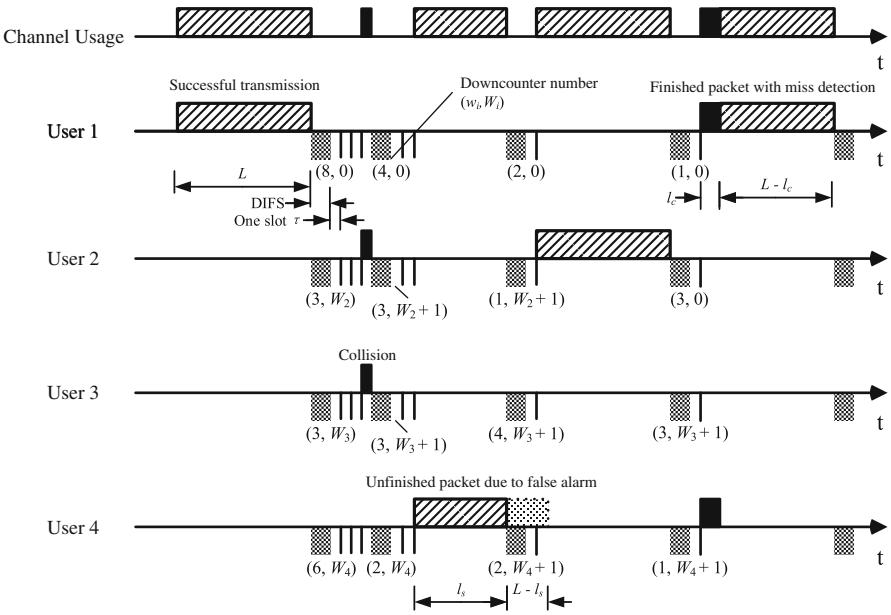

Fig. 3 The proposed CSMA/CD protocol for FD-WiFi networks, in which (w_i, W_i) denotes the residual backoff time and the backoff stage of U_i

Sensing: All users keep sensing the channel continuously regardless of its own activity and make decisions of the channel usage at the end of each slot with duration τ, which is the required time to reliably detect the transmission of any other user.

Backoff mechanism: Once the channel is judged idle without interruption for a certain period of time as long as a distributed interframe space (DIFS) (shown as the dotted area below each line), users check their own backoff timers and generate a random backoff time for additional deferral if their timers have counted down to zero. The additional backoff time after a DIFS is also slotted by τ, i.e., the backoff time is expressed as

$$\text{Backoff Time} = w \times \tau = \text{Random}\,(\text{CW}) \times \tau, \tag{4}$$

where $\text{CW} = 2^W \cdot \text{CW}_{\min}$ is the contention window length and $w = \text{Random}\,(\text{CW})$ is a random integer drawn from the uniform distribution over the interval $[0, \text{CW})$, where $W \in [0, W_{\max}]$ is the backoff stage depending on the number of unsuccessful transmissions for a packet. The countdown starts right after the DIFS and suspends when the channel is detected occupied by others.

Channel access and transmission suspension: A user accesses the channel and begins transmission when its timer reaches zero. During the transmission, if it

detects the signal from other users, it stops its transmission and switches to the backoff procedure immediately. If the packet is finished, the user resets the backoff stage $W = 0$. Otherwise, it sets $W = \min\{W + 1, W_{\max}\}$.

Performance Analysis

In this part, we study the analytical performance of the proposed FD-WiFi CSMA/CD protocol and derive its saturation throughput. We first analyze the carrier sensing performance and derive expressions for sensing error probabilities; then we derive the throughput performance of the CSMA/CD protocol by taking the sensing errors into consideration. Note that when only one user is transmitting, all other users can detect its transmission perfectly, which means that once a collision-free transmission begins, it either completes the packet or suspends it because of false alarm. This process is independent with other users' sensing and contending, and thus, contention and transmission can be considered separately.

Carrier Sensing Performance

We mainly derive the expressions of false alarm probability (p_f) and miss detection probability (p_m). With Rayleigh fading channels, the sampling signal power ($|y(m)|^2$) is Chi-square distributed. Furthermore, M is the sum of sampling signal power in one slot; thus according to [17], M is gamma distributed, the probability density function of which can be expressed as

$$f_M(x) = \frac{x^{N_s-1}e^{-\frac{x}{\phi}}}{\phi^{N_s}\Gamma(N_s)}, \tag{5}$$

where $\phi = \beta^2\overline{P}_r$ and $\phi = \left(\beta^2 + \left(\frac{\overline{d}}{d}\right)^{\alpha}\right)\overline{P}_r$ for $\mathscr{H}_0$ and $\mathscr{H}_1$, respectively.

With a certain sensing threshold ϵ, we can obtain the expressions of p_f and p_m

$$p_f = \mathrm{P_r}(M > \epsilon \mid \mathscr{H}_0) = 1 - \Gamma\left(N_s, \frac{\epsilon}{\beta^2\overline{P}_r}\right), \tag{6}$$

$$p_m(d) = \mathrm{P_r}(M < \epsilon \mid \mathscr{H}_1) = \Gamma\left(N_s, \frac{\epsilon}{\left(\beta^2 + \left(\frac{\overline{d}}{d}\right)^{\alpha}\right)\overline{P}_r}\right), \tag{7}$$

where $\Gamma(m, x) = \frac{1}{\Gamma(m)}\int_0^x t^{m-1}e^{-t}dt$ is the incomplete gamma function. By deriving the expression of ϵ in terms of p_f from (6) and substituting that into (7), the following equations are presented:

$$\epsilon(p_f) = a\beta^2\overline{P}_r, \tag{8}$$

$$p_m(d) = \Gamma\left(N_s, a - \frac{b}{d^\alpha + c}\right), \tag{9}$$

where $a = \Gamma^{-1}\left(N_s, 1 - p_f\right)$, $b = a\frac{\overline{d}^\alpha}{\beta^2}$, and $c = \frac{\overline{d}^\alpha}{\beta^2}$, in which $\Gamma^{-1}(m, x)$ is the inverse incomplete gamma function.

Furthermore, users are independently and randomly distributed in AP's coverage area, the radius of which is denoted by R. Then we can derive the average miss detection probability:

$$p_m = \frac{2}{\pi R^4}\int_0^R \int_0^R \int_0^{2\pi} \Gamma\left(N_s, a - \frac{b}{d^\alpha + c}\right) r_0 r_1 d\theta dr_0 dr_1, \tag{10}$$

where r_0, r_1 are the distances of transmitting user and collided user away from the AP, θ is their included angle, and $d = \sqrt{r_0^2 + r_1^2 - 2r_0 r_1 \cos\theta}$ is the distance between them. We can find that the expression of p_m is related to the path loss exponent. Particularly, when free-space channel is considered, i.e., $\alpha = 2$, we can derive an approximation of p_m:

$$\begin{aligned} p_m &= \frac{2}{\pi R^4}\int_0^R \int_0^R \int_0^{2\pi} \Gamma\left(N_s, a - \frac{b}{d^2 + c}\right) r_0 r_1 d\theta dr_0 dr_1 \\ &\approx \frac{1}{R^4}\left(\int_0^{R^2} x\Gamma\left(N_s, a - \frac{b}{x + c}\right) dx + \int_{R^2}^{2R^2} \left(2R^2 - x\right)\Gamma\left(N_s, a - \frac{b}{x + c}\right) dx\right) \\ &\approx \frac{2}{3}\Gamma\left(N_s, a - \frac{b}{R^2 + c}\right) + \frac{1}{6}\Gamma\left(N_s, a - \frac{b}{2R^2 + c}\right). \end{aligned} \tag{11}$$

According to (6), (7), (8), (9), (10), and (11), p_f is negatively related to ϵ, while p_m is positively related. Therefore, the sensing threshold should be well designed to balance false alarm probability and miss detection probability.

Transmission Probability

To obtain the network throughput, we need to calculate users' transmission probability first. We follow the assumption in [4] that each packet gets collided with the same probability independent of the value of CW_i. Let $\{w_n, W_n\}$ denote the state of the nth contending user. For each user, the state change can be modeled as a discrete-time Markov chain illustrated in Fig. 4. The nonzero transition probabilities are given as

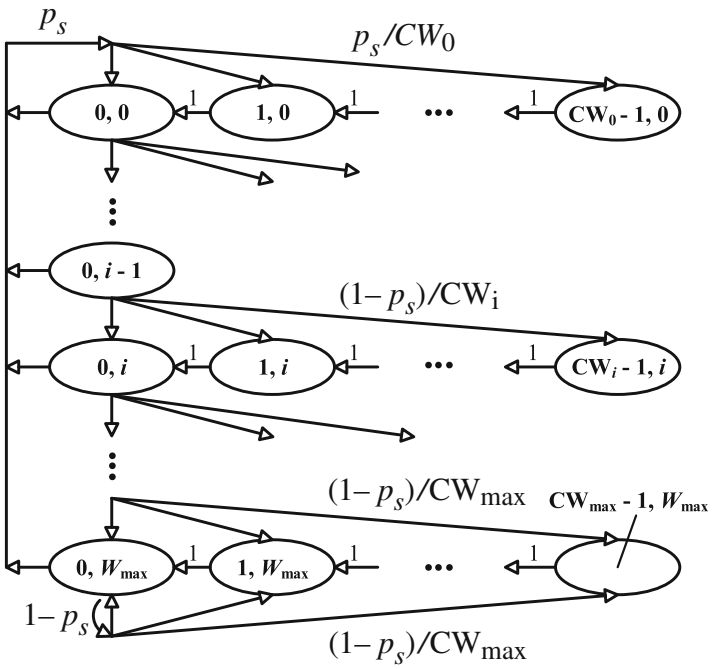

Fig. 4 Discrete-time Markov chain of the backoff window size

$$\begin{cases} P\left(w_n - 1, W_n | w_n, W_n\right) = 1, & w_n \in (0, \mathrm{CW}_i), W_n \in [0, W_{\max}], \\ P\left(w_n, 0 | 0, W_n\right) = \dfrac{p_s}{\mathrm{CW}_{\min}}, & w_n \in [0, \mathrm{CW}_{\min}), W_n \in [0, W_{\max}], \\ P\left(w_n, W_n + 1 | 0, W_n\right) = \dfrac{1 - p_s}{\mathrm{CW}_{i+1}}, & w_n \in [0, \mathrm{CW}_{i+1}), W_n \in [0, W_{\max}), \\ P\left(w_n, W_{\max} | 0, W_{\max}\right) = \dfrac{1 - p_s}{\mathrm{CW}_{\max}}, & w_n \in [0, \mathrm{CW}_{\max}), \end{cases} \tag{12}$$

where p_s denotes the probability that the considered user successfully finishes its transmission without awareness of collision. Note that p_s does not equal to the non-collision probability due to imperfect sensing. Specifically, if two users collide, it is possible that only one user stops and the other user still transmits due to miss detection, and even when one single user is transmitting without collision, it may cease the transmission due to false alarm.

Considering the steady-state distribution of the discrete-time Markov chain, the probability that one user stays in each state can be calculated. Let $p_{w,W}$ denote the probability that one user is in the state of $\{w, \mathrm{W}\}$, and the probability that a certain user begins transmission in the next slot is

$$p = \sum_{W=0}^{W_{\max}} p_{0,W} = \frac{2\left(2p_s - 1\right)}{\left(2p_s - 1\right)\left(\mathrm{CW}_{\min} + 1\right) + \left(1 - p_s\right)\mathrm{CW}_{\min}\left(1 - \left(2 - 2p_s\right)^{W_{\max}}\right)}. \tag{13}$$

Then, we consider the relation between p_s and p. For simplicity, we assume the packet length L is fixed. The calculation of p_s has two prerequisites:

1. The probability that the transmitting user begins collision-free transmission after colliding for l slots, which can be expressed as

$$p_a\left(l\right) = \begin{cases} \left(1-p\right)^{N-1}, & l = 0, \\ \left(N-1\right)p\left(1-p\right)^{N-2} p_m^{2l-1}\left(1-p_m\right), & 1 \le l \le L-1, \\ \left(N-1\right)p\left(1-p\right)^{N-2} p_m^{2L-1}, & l = L. \end{cases} \tag{14}$$

2. The probability that the transmitting user successfully transmits l collision-free slots, which can be denoted as

$$p_b\left(l\right) = \left(1-p_f\right)^l, 0 \le l \le L. \tag{15}$$

Successful transmission requires at least one user transmits the entire packet without the awareness of collision. Thus, p_s can be calculated as

$$\begin{aligned} p_s =& \sum_{l=0}^{L} p_a(l) p_b(L-l), \\ =& (1-p)^{N-1}(1-p_f)^L + (N-1)p(1-p)^{N-2} p_m \frac{(1-p_f)^L - p_m^{2L}}{1-p_f-p_m^2}. \end{aligned} \tag{16}$$

Combining (13) and (16), the values of p and p_s can be solved numerically.

Throughput Performance

We use the time fraction that the channel is occupied for successful transmission as the normalized throughput, i.e., the throughput is defined as

$$\begin{aligned} C =& \frac{\mathbb{E}\left[\text{Successful transmission length}\right]}{\mathbb{E}\left[\text{Consumed time for a successful transmission}\right]} \\ =& \frac{P_s L_s}{P_e + P_s\left(L_s + \mathrm{DIFS}\right) + P_c\left(L_c + \mathrm{DIFS}\right)}, \end{aligned} \tag{17}$$

where $P_s = Np\left(1-p\right)^{N-1}$ denotes the probability that a successful transmission occurs, $P_e = \left(1-p\right)^N$ is the probability that the channel is empty, $P_c = 1 - P_e - P_s$ represents the collision probability, and L_s, L_e, and L_c denote the average length of

successful transmission, empty state, and collision, respectively. The average length of successful transmission and collision can be calculated as, respectively,

$$\begin{aligned} L_s &= \sum_{l=1}^{L-1} l\left(1-p_f\right)^{l-1} p_f + L\left(1-p_f\right)^{L-1} \\ &= \frac{1-(1-p_f)^{L-1}}{p_f} + (1-p_f)^{L-1}, \end{aligned} \tag{18}$$

$$\begin{aligned} L_c &= \frac{P_c + \binom{N}{2} p^2 (1-p)^{N-2} \sum_{l=1}^{L-1} p_m^{2l}\left(1-p_m^2\right) l}{P_c} \\ &= 1 + \binom{N}{2} p^2 (1-p)^{N-2} \frac{p_m^2\left(1-p_m^{2L-2}\right)}{P_c\left(1-p_m^2\right)}. \end{aligned} \tag{19}$$

The throughput is readily obtained by substituting (18) and (19) into (17). We can find that L_s is negatively related to p_f, while L_c is positively proportional to p_m. Thus, the network with a larger sensing threshold can obtain a longer average successful transmission length; however, it also suffers from a longer average collision length. Therefore, the sensing threshold should be properly designed to achieve the maximum throughput, which can be obtained through numerical.

Comparison with the Basic CSMA/CA Mechanism

We make a comparison between the proposed protocol for FD-WiFi with the conventional CSMA/CA for HD-WiFi in this part. For fairness, we consider the same system with N users and omit the noise term. The analytical performance of the CSMA/CA protocol is elaborated in [4], which are omitted here due to the space limitation. Some main differences between the two protocols are listed as follows.

- **Collision length.** In conventional CSMA/CA, the "blindness" in transmission results in long collision, which is typically a packet length. FD allows users to detect collision while transmitting. Thus, the average collision length L_c, as is derived in (19), is slightly more than one slot, which is sharply reduced compared with CSMA/CA.
- **Successful transmission length.** In CSMA/CA, once a collision-free transmission begins, it can always be finished successfully without interruption. However, in the FD-WiFi network, the transmission may get ceased due to false alarm, especially for long packets. According to (18), if L is sufficiently large, L_s goes to $\frac{1}{p_f}$. Also, false alarm leads to unnecessary backoff and increase of contention window, which may further degrade the performance of FD-WiFi. Thus, in FD-WiFi networks, the sensing threshold should be well designed to balance the probabilities of two sensing errors.

Simulation Results

In this subsection, simulation results are presented to show the performance of the proposed FD-WiFi CSMA/CD protocol. We consider 20 users and AP's radius R is set as 10 m. We set $\alpha = 2$ and $\overline{P}_r = 10\,\text{mW}$ with $\overline{d} = 1$ unit. The slot sampling number N_s is set as 100. Furthermore, the packet length is fixed to be 100 slots and DIFS is 2 slots. We run for 10^3 transmission attempts to fully develop the WiFi network and proceed with another 10^6 packet transmissions to obtain the simulated results by MATLAB. For comparison, we provide the throughput performance of conventional HD-WiFi and bidirectional FD transmission, which is similar to [10] and [11] and named by "dual-link FD-WiFi." Specifically, for the dual-link simulation, once a certain user transmits data to the AP, AP also transmits data packets back to this user. Moreover, due to RSI, the rate of dual link at one end is less than that of single link. For simplicity, the single-link sum rate is normalized as 1, and the dual-link sum rate is denoted as the relevant ratio.

In Fig. 5, we show the throughput of the proposed FD-WiFi protocol versus false alarm probability, which consists of two cases with the SIS factor $\beta^2 = 0.15$ and $\beta^2 = 0.3$, respectively. Note that the normalized throughput is denoted as the time ratio that the channel is occupied for successful transmissions, as shown in (17); thus it has no dimension. Figure 5 shows that there exists an optimal value of p_f

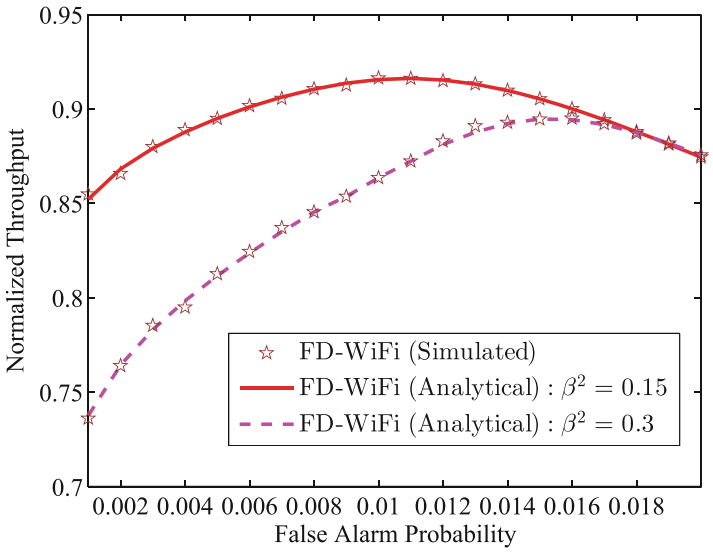

Fig. 5 Normalized throughput C versus false alarm probability p_f, where the number of users $N = 20$, the minimum contention window size $\text{CW}_{\text{min}} = 2^3$, and the maximum contention window size $\text{CW}_{\text{max}} = 2^8$

for FD-WiFi to achieve the maximum throughput. Since p_f is determined by ϵ, as shown in (6), the sensing threshold should be well designed to achieve the maximum throughput. We can also find that the optimal value of p_f for the case with $\beta^2 = 0.3$ is higher than that with $\beta^2 = 0.15$, which can be explained as follows. Higher SIS factor leads to worse sensing performance. Setting p_f the optimal value for the case with $\beta^2 = 0.15$, the collision is more frequent due to higher p_m when β^2 increases to 0.3. Thus, to obtain the maximum throughput, p_m should be decreased by increasing p_f.

In Fig. 6, by considering two cases with the packet length $L = 50$ and $L = 200$, we present the relationship between network throughput and the maximum backoff stage, with the throughput of convention HD-WiFi and dual-link FD-WiFi for comparison. According to Fig. 6, we can find that with proper parameters, the proposed FD-WiFi protocol has a better throughput performance than HD-WiFi and dual-link FD-WiFi. For the HD-WiFi and dual-link FD-WiFi, with higher $W_{\max}$, collision is less likely to happen, so the throughput increases monotonously. However, the throughput of proposed FD-WiFi protocol may drop with large $W_{\max}$, which can be found in the dashed line. The reason is that the asymptotic value of L_s is 100 with $p_f = 0.01$, and for $L > 100$ slots, false alarm is quite likely to happen during transmission, and the users are likely to enlarge their contention windows up to $\mathrm{CW}_{\max}$ due to the unsuccessful transmissions. Thus, more time is spent in the backoff procedure and the throughput gets smaller.

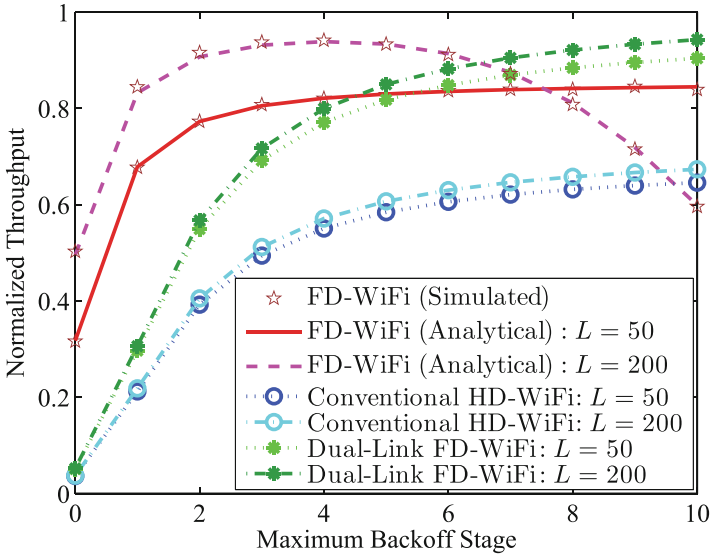

Fig. 6 Normalized throughput C of different protocols versus the maximum backoff stage $W_{\max}$, where $\mathrm{CW}_{\min} = 2^3$, SIS factor $\beta^2 = 0.15$, and the false alarm probability in FD-WiFi CSMA/CD protocol $p_f = 0.01$

Multi-channel Full-Duplex WiFi

In this section, we extend the proposed single-channel CSMA/CD protocol to the scenario with multiple available wireless channels in the FD-WiFi networks. For the multi-channel scenario, the WiFi users need to resolve the following two problems: (1) channel selection, users choose certain channels for access according to their channel state information (CSI), and (2) channel access, the contending users, which select the same channel, need to perform a contention-based access mechanism to alleviate collisions (Fig. 7).

For the channel access problem, we propose a random access strategy based on the CSMA/CD protocol described in section "Full-Duplex CSMA/CD Protocol." With the existence of multiple channels, the number of contending users on a certain channel change with time, and a fixed setting of contention parameters may lead to severe collision or over much waiting time in some cases. Therefore, different from the single-channel scenario, an adjustment of contention window is added in the channel access strategy.

As for the channel selection problem, some previous papers present their protocol designs for HD multi-channel systems. In [18], the authors propose a multiple spanning tree-based load-balancing routing algorithm for wireless mesh network. In [19], the authors design a multi-channel MAC protocol for ad hoc networks by channel preference negotiation between the transmitter and the receiver. In [20], the authors derive game theoretic results for multi-channel cognitive radio networks. In this section, we take advantage of game theory to propose a distributed channel selection scheme for multi-channel FD-WiFi networks. Our goal is to improve network performance, so user's channel selection strategy is based on comparison of

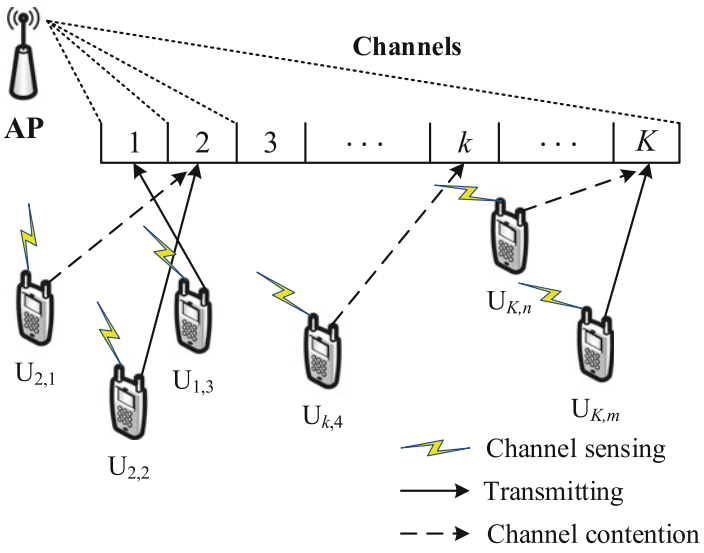

Fig. 7 Multi-channel full-duplex WiFi networks with one AP, N users and K orthogonal channels

expected throughput on different channels, which can be evaluated from the channel access strategy.

The rest of this section is organized as follows. We first discuss the system model for multi-channel FD-WiFi networks; then the channel access strategy and channel selection strategy are presented, respectively. Comparison with CSMA/CA and HD protocols and simulation results are provided finally.

System Model

We consider a network consisting of one AP and N FD users. There are K orthogonal channels, denoted by $\mathcal{K} = \{1, 2, \ldots, K\}$, each of which can serve at most one user at a time; otherwise the collision happens. The FD users, whose set is denoted by $\mathcal{N} = \{1, 2, \ldots, N\}$, have the same self-interference cancelation capability and the same transmission power P. Each user $n \in \mathcal{N}$ is assumed to have the knowledge of perfect CSI of any channel $k \in \mathcal{K}$ between the AP and itself, denoted by $\{h_{nk}\}_{k=1}^{K}$.

Similar to section "Full-Duplex CSMA/CD Protocol," we mainly focus on the uplink transmissions, where data are sent by users to the AP. Moreover, the WiFi network is considered to be distributed, which means that the AP has no way to allocate the users or schedule their traffic. We also assume that each user is capable of detecting the occupancy of all channels and transmitting on at most one channel at a time. Let τ be the minimum required time for each user to make a reliable channel sensing decision. We assume a time-slotted system in which users can transmit the data during each slot. The users can change their channels and activity only at the beginning of a slot.

By taking advantage of FD techniques, simultaneous carrier sensing and data transmission become possible [21,22]. In particular, one antenna is for transmission, while the other can be used as a receiver to sense the channel information. However, when a user is transmitting, the RSI due to the imperfect self-interference cancelation degrades the reliability of sensing on its own current operating channel [23]. Let P_f be the false alarm probability that one user falsely detects others' presence on the channel, and P_m denote the miss detection probability that one user fails to detect the collision while it is transmitting on the channel. Since the RSI exists only when a user is transmitting, we can simply assume perfect sensing for silent users.

The transmission procedure contains the following two steps:

1. According to the expected utilities of different channels, each user n selects a certain channel c_n to contend.
2. User n preforms a CSMA-/CD-based channel access strategy to avoid collision. After each successful or suspended transmission attempt, user n adjusts the contention window and the expected utility of channel c_n.

Since the expected channel utility is derived according to the specific channel access strategy, in the remaining section, we first present the CSMA-/CD-based

channel access mechanism and then propose the channel selection algorithm by taking advantage of game theory.

Channel Access Strategy

In this part, based on the CSMA/CD protocol in section "Full-Duplex CSMA/CD Protocol," we present a random access strategy adopted by the FD users when they are contending for the same channel. Here, the number of contending users is unknown to users, and it may change with time. By using FD technology, users can sense the channel while transmitting and stop transmission immediately when a collision is detected. Thus, collided transmissions can be significantly shorter than successful transmissions, which can be observed by all contending users, who can adjust the contention window size accordingly.

Protocol Description

As shown in Fig. 8, the proposed random access protocol for FD users on a single channel includes the following four phases:

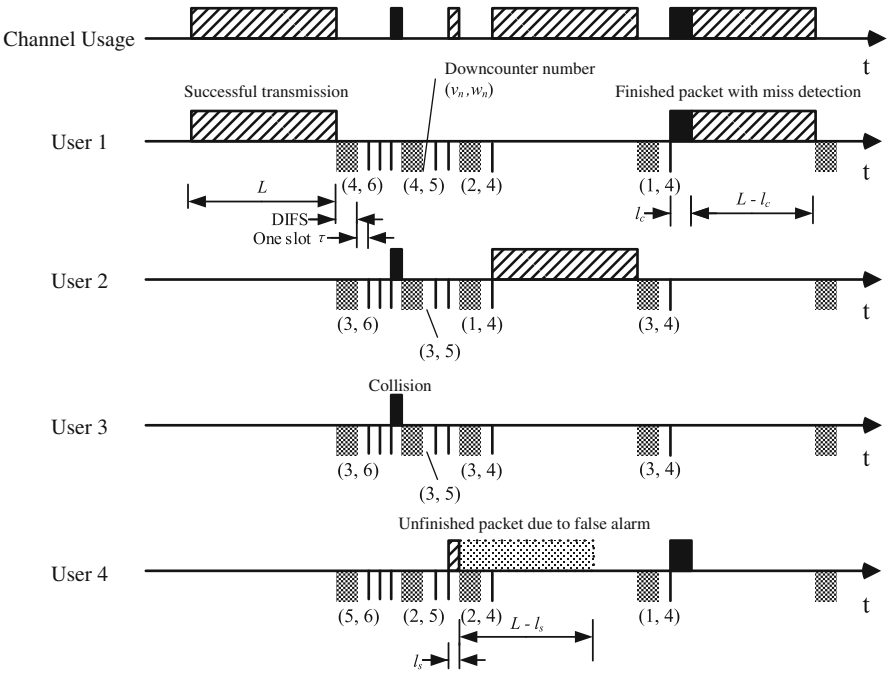

Fig. 8 Channel access protocol in decentralized FD networks, in which (v_n, w_n) denotes the residual backoff time and the contention window of user n

Sensing: All users keep sensing the channel continuously regardless of its own activity and make decisions of the channel usage at the end of each slot.

Backoff mechanism: Once the channel is sensed idle without interruption for a certain period of time equal to DIFS, users generate a random backoff time for an additional deferral, which can be expressed as follows:

$$\text{Backoff Time} = v \times \tau = \text{Random}\,(w) \times \tau, \tag{20}$$

where w is the length of contention window and $v = \text{Random}\,(w)$ is a random integer drawn from the uniform distribution over the interval $[0, w)$. The backoff timer starts countdown immediately after the DIFS and suspends when the channel is detected occupied by others.

Channel access and transmission suspension: A user accesses the channel and begins transmission when its backoff timer reaches zero before other transmissions are detected. During the first slot of the transmission, if it detects the signal from other users, a user stops its transmission and switches to the backoff procedure immediately. Otherwise, it keeps transmitting the packet until finished.

Adjustment of the contention window: When a transmission on the channel is detected finished, all users adjust the contention window size by the following contention window adjustment rule and begin the contention procedure for the next round.

Adjustment Rule of the Contention Window Size

When there are m users contending for a single channel, the optimum contention window size can be proved to be m. However, in a fully distributed system, the number of users, m, is unknown, and it may change dynamically. Thus, users cannot directly use m as the contention window. In this scenario, the conventional CSMA/CA mechanism cannot perform well, when m is smaller than the minimum contention window size or larger than the maximum size. Note that the lengths of collisions and successful transmissions can be different. All users are aware of whether the previous transmission is successful or not, as well as the average interval between two transmission attempts, based on which they can estimate the number of contending users and adjust the contention window accordingly.

When there are m users contending for a single channel with the contention window size w, the access probability for a certain user can be calculated as $p_{a,w} = \frac{2}{w+1}$ [4], and the probability that none of these users accesses the channel in the next coming slot can be expressed as the following:

$$p_i = (1 - p_{a,w})^m . \tag{21}$$

Moreover, the waiting time between two transmission attempts has the geometric distribution with parameter p_i and mean $L_w = \frac{p_i}{1-p_i}$. Thus, with the observed average waiting time, the number of contending users can be estimated as follows:

$$\hat{m} = \frac{\ln\left(\frac{L_w}{L_w+1}\right)}{\ln\left(1-p_{a,w}\right)} = \frac{\ln\left(\frac{L_w}{L_w+1}\right)}{\ln\left(\frac{w-1}{w+1}\right)}. \tag{22}$$

Remark 1. Notice that there exists a special case in (22) when the contention window $w = 0$. In this case, users access the channel with probability one, and average waiting time is 0. Collisions occur once there are more than one user on the channel. Thus, it is only possible to tell whether there are multiple users on the channel by observing the length of transmissions.

Remark 2. If users can sense the channel for a long time without changing the contention window, $\hat{m}$ can be a precise estimation of m, and the users can change their contention window to m to achieve the optimal throughput. However, it is inefficient and may be ineffective if the value of m varies during the longtime estimation. Thus, we propose the adjustment rule in a dynamic learning way as shown in Algorithm 1.

In Algorithm 1, T is the number of transmissions for calculating the average waiting time, and β is the step length in the adjustment rule. These two parameters directly influence the convergence time and stability of the algorithm. Generally, when β is large, the contention window size approaches the number of contending users more quickly, but meanwhile, the contention window size is more vulnerable to the fluctuation of the estimation of L_w, which may lead to the instability of the network. On the other hand, small β guarantees the stability, but the contention

Algorithm 1 Contention window size adjustment rule

INPUT:

Current contention window w;
Average waiting time L_w among the previous T transmissions;
Whether the previous transmission is successful;

OUTPUT:

New contention window w';

---

if $w = 1$ **then**
  if Previous transmission is successful **then**
    $w' \leftarrow 1$;
  else
    $w' \leftarrow 2$;
  end if
else
  Estimate number of users $\hat{m}$ according to (22);
  $w' \leftarrow \lceil w + \beta(\hat{m} - w) \rceil$, where $\beta \in (0, 1)$;
end if

window size may be unable to keep pace with the change of the number of contention users. Thus, a mediate value of β requires careful design. Similar analysis can be applied for T: shorter T introduces instability to the network, while longer T leads to low sensitivity to the change of number of users.

Expected Throughput

Since our goal is to improve the network throughput performance, the expected throughput on certain channel is considerably important for the channel selection strategy, which is derived as follows. For any user n attempting to transmit on the channel, the expected throughput can be written as follows:

$$u_n = \frac{p_s L_s \cdot r_n}{p_s L_s + p_c L_c + L_w + \text{DIFS}}, \tag{23}$$

where p_s is the probability that the user successfully accesses the channel without collision, $p_c = 1 - p_s$ is the collision probability, L_s is the average successful transmission length, L_c is the average collision length, L_w is the average waiting time for channel contention, and $r_n = \log_2(1 + \lambda |h_n|^2)$ is the achievable rate of user n, in which λ is proportional to each user's transmit power.

The probability that the user n successfully accesses the channel k without collision can be estimated as follows:

$$p_s = \begin{cases} \left(\frac{w-1}{w+1}\right)^{\hat{m}-1} & n \text{ is on the channel,} \\ \left(\frac{w-1}{w+1}\right)^{\hat{m}} & n \text{ is not on the channel,} \end{cases} \tag{24}$$

and the collision probability is $p_c = 1 - p_s$.

Then, we consider the average successful transmission and the collision length. We assume a fixed packet length L for all users. Taking the false alarm probability into account, the average successful transmission length can be written as follows:

$$L_s = \left(1 - P_f\right) L + P_f. \tag{25}$$

Similarly, the average collision length is given by considering the miss detection probability:

$$L_c = (1 - P_m) + P_m L. \tag{26}$$

It can be seen from Algorithm 1 and (24) that all users can adjust the contention window size to the same value and estimate the expected throughput on the channel in a fully distributed manner.

Channel Selection Strategy

In this part, we tackle with the channel selection problem and formulate it as a distributed multi-channel random access game, in which each user uses the local information and observation of all channels to determine its channel selection strategy. Since our goal is to improve the network throughput, the expected throughput on each channel is adopted as the utility.

More specifically, in the multi-channel FD-WiFi network, each user needs to choose one channel to contend. After selecting the channel, the user performs access or backoff using the strategy described in section "Channel Access Strategy." According to our assumption, all users can monitor the occupancy of all channels. Thus, a user can estimate its expected throughput on each channel by using the method in section"Expected Throughput," and we can assume that when a user switches to a new channel, it can automatically adopt the same contention window size as the ongoing users on the same channel.

By extending (24) to multi-channel scenario, we can derive the utility for any user n attempting to transmit on channel k_n as the following:

$$u_n\left(k_n, \boldsymbol{k}_{-n}\right) = \frac{p_{s,k_n} L_s \cdot r_{nk_n}}{p_{s,k_n} L_s + p_{c,k_n} L_c + L_{w,k_n} + \mathrm{DIFS}}, \tag{27}$$

where $k_n \in \mathscr{S}_n$ is the strategy of user n, $\boldsymbol{k}_{-n} = (k_1, k_2, \ldots, k_{n-1}, k_{n+1}, \ldots, k_N)$ is the strategy vector of all users except user n, p_{s,k_n} is the probability that user n successfully accesses channel k_n, p_{c,k_n} is the collision probability, L_{w,k_n} is the average waiting time for channel contention on channel k, and $r_{nk} = \log_2(1 + \lambda|h_{nk}|^2)$ is the achievable rate of user n on channel k.

In this distributed network, each user tries to maximize its own expected throughput by adjusting its channel selection strategy, which can be formally written as follows:

$$k_n^* = \arg \max_{k_n \in \mathscr{S}_n} u_n\left(k_n, \boldsymbol{k}_{-n}\right), \ \forall n \in \mathscr{N}. \tag{28}$$

Note that the expected throughput of any user n on any channel k is largely dependent on the choices of other users. Thus, we formulate the channel selection process as a game defined as follows.

Definition 1. A channel selection game $\mathscr{G}$ is defined as $\mathscr{G} := < \mathscr{N}, (\mathscr{S}_n)_{n\in\mathscr{N}}, (u_n)_{n\in\mathscr{N}} >$, where $\mathscr{N} = \{1, 2, \ldots, N\}$ is the set of users, $\mathscr{S}_n := \{k_n = 1, 2, \ldots, K\}$ is the set of all possible choices of user n, and $u_n\left(k_n, \boldsymbol{k}_{-n}\right)$ is the utility function of user n when all users choose $\boldsymbol{k}_{-n}$.

We are interested in the Nash equilibrium of the channel selection game, which provides the strategy stability of each user's selection strategy.

Definition 2 (Nash Equilibrium). A strategy profile $\boldsymbol{k}^*$ is a pure strategy Nash equilibrium if and only if no user can improve its utility by deviating unilaterally, i.e.,

$$u_n\left(k_n^*, \boldsymbol{k}_{-n}^*\right) \geq u_n\left(k_n, \boldsymbol{k}_{-n}^*\right), \ \forall n \in \mathcal{N}, \ k_n \in \mathcal{S}_n. \tag{29}$$

Theorem 1. *The channel selection game $\mathcal{G}$ has at least one pure strategy Nash equilibrium.*

Proof. The utility function $u_n\left(k_n, \boldsymbol{k}_{-n}\right)$ defined in (27) is quasiconcave continuous in k. The feasible set is also compact and convex. Consequently, according to [24], there exists at least a pure Nash equilibrium. Similar proof for Aloha game can be also found in [25].

To achieve the Nash equilibrium, we present a best-response-based channel selection mechanism. In this algorithm, each user chooses the channel with the largest expected throughput to contend on and then performs random channel access strategy in section "Channel Access Strategy." Meanwhile, each user monitors the states of all channels continuously and adjusts the contention window size according to the channels' occupancy. Once the user fails to contend for a channel or finishes a transmission, it estimates the expected throughput of all channels and chooses the channel with the largest expected throughput to update its selection strategy. This channel selection mechanism is formally described in Algorithm 2.

Performance Analysis and Comparison

In this subsection, we provide theoretical comparison of the proposed FD protocol with CSMA/CA and HD protocols.

Comparison with CSMA/CA Protocols

We make a comparison between the proposed FD-WiFi channel access protocol on a single channel with the conventional CSMA/CA mechanism in this part. For fairness, we consider the single-channel network with m users and omit the noise term.

In CSMA/CA, there exists the minimum contention window length $\mathrm{CW}_{\min}$ and the maximum backoff stage $w_{\max}$. After each failed transmission attempt, the transmitted user doubles its contention window until to the maximum contention window length $\mathrm{CW}_{\max} = 2^{w_{\max}}\mathrm{CW}_{\min}$. After each successful transmission, the user resets the contention window as $\mathrm{CW}_{\min}$. According to the analysis in [4], the average access probability can be written as follows:

$$p = \frac{2\left(2p_s - 1\right)}{\left(2p_s - 1\right)\left(\mathrm{CW}_{\min} + 1\right) + \left(1 - p_s\right)\mathrm{CW}_{\min}\left(1 - \left(2 - 2p_s\right)^{w_{\max}}\right)}, \tag{30}$$

where p_s is the successful transmission probability, given by

Algorithm 2 Channel selection mechanism

Step 1: Initialization

1: $\forall n \in \mathcal{N}$, estimate the value of h_{nk}, for all $k = 1, 2, \ldots, K$;
2: Initialize contention window $w_k = 1, \forall k \in \mathcal{K}$;
3: Initialize backoff time $v_{nk} = 0, \forall n \in \mathcal{N},\ k \in \mathcal{K}$;
4: Set $c_n = \arg \max_k \{|h_{nk}|^2\}$;

Step 2: Channel selection and random access

1: **while** in each time slot **do**
2: **for** $k = 1 : K$ **do**
3: **if** Channel is currently occupied **then**
4: Transmitting users keep transmitting and detecting whether their current transmissions collide with other transmissions. If collision is detected, stop transmission;
5: **else**
6: All users on channel k keep downcounting v_{nk}, a user n accesses channel k when v_{nk} reaches 0;
7: **end if**
8: **end for**
9: All users sense and judge the occupancy of all channels during the whole slot;
10: **for** all channel k whose occupancy has just changed **do**
11: All users that fail to contend for channel k or users that just finish a transmission collect $L_{w,k'}$ ($k' = 1, 2, \ldots, K$), and update the utilities $u_{nk'}$ of all channels according to (27). We denote the set of these users as $\mathcal{N}_{\text{tochange}}$;
12: $\forall n \in \mathcal{N}_{\text{tochange}}$, update channel selection strategy as $c_n = \arg \max_k \{u_{nk}\}$;
13: Update contention window w_k according to Algorithm 1;
14: **end for**
15: **if** there exists a set of channels $\mathcal{K}_i$ whose waiting time exceeds the contention window **then**
16: Judge all the channels $k \in \mathcal{K}_i$ as unoccupied by any users, and set contention windows $w_k = 1$;
17: **end if**
18: **end while**

$$p_s = 1 - (1 - p)^{m-1}. \tag{31}$$

It can be verified that the access probability is less than $\frac{2}{m+1}$, which is the asymptotic value of access probability under the proposed contention adjustment rule.

Comparison with Half-Duplex Protocols

Compared with the HD protocols, the most significant difference is that users can sense the channels while transmitting, i.e., users are no longer "blind" in transmission. Once a collision is detected, users can stop transmission immediately. This feature can significantly reduce the average length of collision. Additionally, contending users can obtain additional information of whether the previous transmission is successful by simply detecting the length of the transmission.

- **Collision length.** In HD protocols, the "blindness" in transmission results in long collision, which is typically a packet length. FD allows users to detect

collision while transmitting. As derived in (26), the average collision length $L_c = 1 + P_m (L - 1)$, as is derived in (26), is slightly more than one slot, which is substantially reduced from a packet length L.

- **Successful transmission length.** In HD protocols, once a collision-free transmission begins, it can always be finished successfully without interruption. However, in the proposed FD protocol, the transmission may be ceased due to false alarm. According to (25), it can be seen that $L_s = L - (L - 1) P_f$ is reduced because of false alarm. Furthermore, false alarm may lead to unnecessary increase of contention window and decrease of expected throughput of the channel, which may further degrade the performance of the proposed protocol.

Simulation Results

In this part, simulation results are presented to evaluate the performance of the proposed protocol for multi-channel FD-WiFi network. We consider $K = 4$ channels with up to $N = 15$ users. The packet length L is fixed on 50 slots, and DIFS time is 2 slots. The number of transmissions taken into account for contention window adjustment is $T = 10$. The channel sensing error probabilities, i.e., P_m and P_f, are set as 0.01.

In Fig. 9, we first verify the effectiveness of the proposed FD protocol. We consider the channel selection process of ten users. It can be seen from Fig. 9 that the channel selection mechanism converges to the Nash equilibrium quickly, and all users do not change their strategies afterward.

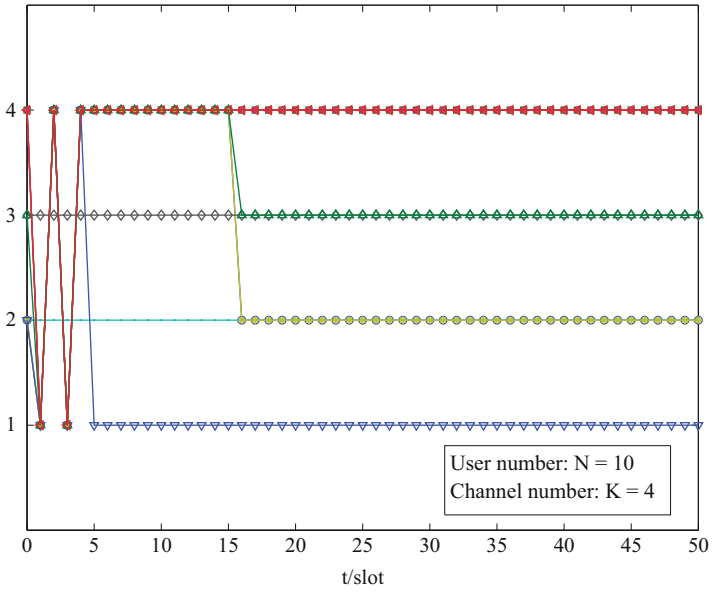

Fig. 9 Channel selection process under the proposed mechanism

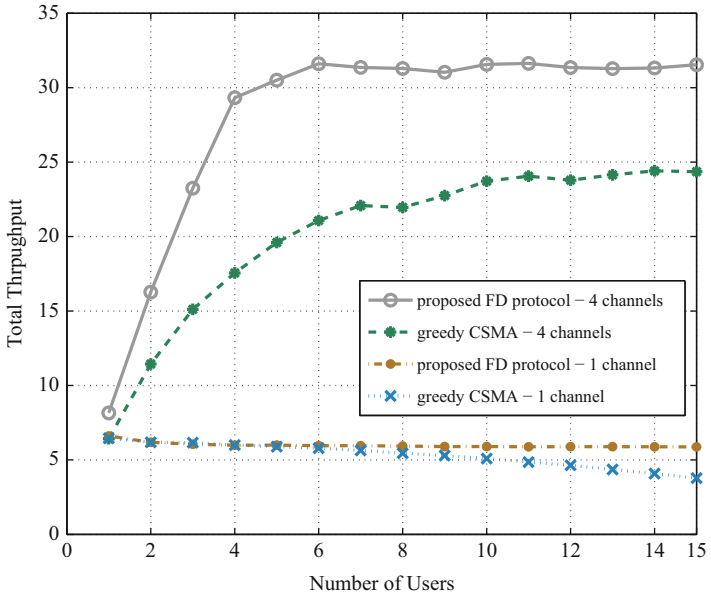

Fig. 10 Channel selection process under the proposed mechanism

In Fig. 10, we consider the total throughput of the multichannel network, which is the throughput of all the N users on all K channels. We present comparison between the proposed FD protocol and a greedy CSMA-based FD protocol in which each user accesses the channel with maximum achievable rate and performs contention based on CSMA mechanism with minimum contention window $\mathrm{CW}_{\min} = 1$ and maximum backoff stage $w_{\max} = 4$. Note that we do not adopt the original window size $\mathrm{CW}_{\min} = 8$ and $w_{\max} = 5$ in CSMA in the simulation since the number of users is small, and the adoption of large contention window size leads to worse performance. Firstly, it is shown in the dash-dotted and dotted lines in Fig. 10 that the proposed protocol can achieve higher throughput in single-channel case, especially when the number of users is large. This is because the contention window adjustment rule guarantees a more proper window size for all users to maximize their access and successful transmission probability. Also, Fig. 10 shows in the solid and dashed lines that the proposed protocol can achieve higher total throughput than that of the greedy CSMA, especially when the number of users is close to the number of channels. This is because in the proposed protocol, users can automatically avoid to choose crowded channels to increase their access and successful transmission probability. Additionally, it can be seen that when $N \leq K$ ($N \leq 4$ in Fig. 10), the throughput increases almost proportionally with the number of users, and the slope is close to $\mathbb{E}[\log_2(1 + \lambda|h|^2)]$. This indicates that all users intend to occupy a channel exclusively without sharing with other users. However, when the number of users increases, the greedy mechanism may gradually approach the proposed protocol. This is because when many users contending for

limited channels, it is likely that all channels are crowded at a similar level, and the users do not have the much motivation to deviate from the channel with the largest rate. This makes the channel selection profile almost the same as the greedy mechanism.

Summary

This chapter has first discussed the CSMA/CA protocol in conventional HD-WiFi networks and pointed out its long collision duration problem due to the failure of carrier sensing during transmission. To mitigate this problem, the CSMA/CD protocol has been proposed for single-channel WiFi networks by taking advantage of the FD technology. Compared with CSMA/CA protocol, the new CSMA/CD protocol has two adaptations: (1) continuous carrier sensing by enabling simultaneous sensing and transmission and (2) transmission suspension procedure, by which users stop transmitting immediately once detecting a collision. To obtain a comprehensive network performance analysis, this chapter has calculated two types of sensing error probabilities due to residual self-interference, namely, false alarm and miss detection. The normalized throughput has also been derived as the average channel utilization for successful data transmission. Both performance analysis and simulation results have shown that the full-duplex CSMA/CD protocol improves WiFi throughput performance.

Then this chapter has extended the CSMA/CD protocol to the multi-channel FD-WiFi network and divided this scenario into two parts: (1) channel selection, each user selects which channel for access, and (2) channel access, all contending users, which select same channel, perform a contention-based channel access scheme. For the channel access problem, a random access strategy has been proposed based on the described CSMA/CD protocol for single-channel scenario, except not adopting the exponential backoff scheme. Instead, by learning from historical waiting time, the proposed channel access strategy provides an adjustment rule of contention window size to accommodate the number change of contending users. For the channel selection problem, a distributed selection protocol has also been provided based on the best-response algorithm, by which the WiFi user always selects the channel with the highest expected throughput. Simulation results have also been provided to verify the effectiveness of multi-channel FD-WiFi protocol.

References

1. Afanasyev M, Chen T, Voelker GM, Snoeren AC (2010) Usage patterns in an urban WiFi network. IEEE Trans Netw 18(5):1359–1372
2. IEEE Standard for Wireless LAN Medium Access Control (MAC) and Physical Layer (PHY) Specifications, Jan 2016, IEEE P802.11
3. Crow BP, Widjaja I, Kim JG, Sakai PT (1997) IEEE 802.11 wireless local area networks. IEEE Commun Mag 35(9):116–126

4. Bianchi G (2000) Performance analysis of the IEEE 802.11 distributed coordination function. IEEE J Sel Areas Commun 18(3):535–547
5. Jayasuriya A, Perreau S, Dadej A, Gordon S (2004) Hidden vs. exposed terminal problem in ad hoc networks. In: Australian Telecommunication Networks and Applications Conference, Sydney
6. Ray S, Carruthers JB, Starobinski D (2003) RTS/CTS-induced congestion in Ad Hoc wireless LANs. In: Wireless Communications and Networking Conference (WCNC), New Orleans, pp 1516–1521
7. Song L, Wichman R, Li Y, Han Z (2017) Full-duplex communications and network. Cambridge University Press, UK
8. Jain M, Choi JI, Kim T, Bharadia D, Seth S, Srinivasan K, Levis P, Katti S, Sinha P (2011) Practical, real-time, full duplex wireless. In: ACM MobiCom, New York
9. Sabharwal A, Schniter P, Guo D, Bliss DW, Rangarajan S, Wichman R (2014) In-band full-duplex wirelss: challenges and opportunities. IEEE J Sel Areas Commun 32(9):1637–1652
10. Sahai A, Patel G, Sabharwal A (2011) Pushing the limits of full-duplex: design and real-time implementation. Rice University, Houston. Rep. TREE1104, http://arxiv.org/pdf/1107.0607.pdf
11. Goyal S, Liu P, Gurbuz O, Erkip E, Panwar S (2013) A distributed MAC protocol for full duplex radio. In: Asilomar Conference on Signals, Systems and Computers, Pacfic Grove, pp 788–792
12. Liao Y, Song L, Han Z, Li Y (2015) Full-duplex cognitive radio: a new design paradigm for enhancing spectrum usage. IEEE Commun Mag 53(5):138–145
13. Liao Y, Bian K, Song L, Han Z (2015) Full-duplex MAC protocol design and analysis. IEEE Commun Lett 19(7):1185–1188
14. Song L, Liao Y, Bian K, Song L, Han Z (2016) Cross-layer protocol design for CSMA/CD in full-duplex WiFi networks. IEEE Commun Lett 20(4):792–795
15. Liao Y, Di B, Bian K, Song L, Niyato D, Han Z (2015) Cross-layer protocol design for distributed full-duplex network. In: IEEE Global Communications Conference (GLOBECOM), San Diego
16. Afifi W, Krunz M (2013) Exploiting self-interference suppression for improved spectrum awareness/efficiency in cognitive radio systems. In: IEEE INFOCOM, Turin, pp 1258–1266
17. Poor HV (1994) An introduction to signal detection and estimation, 2nd edn. Springer, New York
18. Raniwala A, Chiueh T (2005) Architecture and algorithms for an IEEE 802.11-based multi-channel wireless mesh network. In: IEEE INFORCOM'05, Miami, vol 3
19. So J, Vaidya N (2004) Multi-channl MAC for Ad Hoc networks: handling multi-channel hidden terminals using a single transceiver. In: ACM MobiHoc'04, Roppongi
20. Cohen K, Leshem A, Zehavi E (2013) Game theoretic aspects of the multi-channel ALOHA protocol in cognitive radio networks. IEEE J Sel Areas Commun 31(11):2276–2288
21. Liao Y, Wang T, Song L, Han Z (2014) Listen-and-talk: full-duplex cognitive radio. In: IEEE Globecom'2014, Austin
22. Song L, Liao Y, Song L (2015) Flexible full-duplex cognitive radio networks by antenna reconfiguration. In: IEEE/CIC International Conference on Communications in China (ICCC), Shenzhen, pp 1–5
23. Singh N, Gunawardena D, Proutiere A, Radunovic B, Balan HV, Key P (2011) Efficient and fair MAC for wireless networks with self-interference cancellation. In: International Symposium on Modeling and Optimization in Mobile, Ad Hoc and Wireless Networks (WiOpt), Princeton, pp 94–101
24. Han Z, Niyato D, Saad W, Başar T, Hjørungnes A (2011) Game theory in wireless and communication networks: theory, models, and applications. Cambridge University Press, North Miami Beach
25. MacKenzie AB, Wicker SB (2003) Stability of multipacket slotted aloha with selfish users and perfect information. In: IEEE INFOCOM'03, San Franciso, vol 3, pp 1583–1590

Mobile Data Offloading Through Third-Party Wi-Fis: Association Rules and Incentive Mechanisms

18

Xin Kang and Sumei Sun

Contents

X. Kang (✉)
National Key Laboratory of Science and Technology on Communications, University of Electronic Science and Technology of China, Chengdu, China
e-mail: kangxin83@gmail.com

S. Sun
Institute for Infocomm Research, South Tower, Singapore
e-mail: sunsm@i2r.a-star.edu.sg

W. Zhang (ed.), *Handbook of Cognitive Radio*,
https://doi.org/10.1007/978-981-10-1394-2_18

Abstract

WiFi offloading is regarded as one of the most promising techniques to deal with the explosive increasing data usage over the existing 4G cellular network due to its high quality of service, high data transmission rate, and low requirement on devices. In this chapter, we investigate two key issues, i.e., association rules and incentive mechanisms, for data offloading through third-party WiFi access points (APs) in a cellular mobile system. Firstly, by assuming the data offloaded through the third-party WiFi AP is charged based on usage, we formulate the user association problem as an utility maximization problem from the cellular operator's perspective. By considering whether the successive interference cancelation (SIC) decoders are available at the BS and/or the WiFi AP, different utility functions are considered. Then, the optimal user association rules are derived for each case when the number of users is large. Secondly, incentive mechanisms to motivate WiFi APs to provide data offloading services are studied. In particular, a salary plus bonus-based incentive mechanism is proposed. Under the proposed incentive scheme, WiFi APs are rewarded not only based on the amount of offloaded data but also based on the quality of the offloading service. The interactions between the WiFi APs and the mobile network operator are investigated using Stackelberg game.

Introduction

Background and Motivation

Due to the rapid development in mobile phones and wireless communications in the recent years, the popularity of using smartphones to access the Internet and the social networking services, which generates a lot of data usage over the cellular network, is increasing [1]. Due to the unprecedented explosion of mobile data traffic, the cellular operators around the world are facing the glut of mobile data on their networks because of the capacity constraints of these networks. Most cellular networks are of high probability to be overloaded in the near future. In fact, most 4G networks are already overloaded, especially in crowded areas and during peak hours. Mobile users in overloaded areas are forced to use the degraded cellular services, such as low transmission rate, missed calls, and unreliable coverage.

To tackle with these problems and enhance users' network experience, cellular operators are forced to increase their network capacity. A straightforward way to is to add more base stations with smaller cell size such as femtocells [2, 3]. However, these options require large investment in the network equipment and are not cost-effective. A more promising approach is to offload portion of the mobile data usage through the existing WiFi networks. WiFi offloading is a strong candidate for mobile data offloading due to the following reasons: (1) No equipment upgrading is required at the user side. This is due to the fact that the bulk of the demand for high-speed data services is created by smartphones, which have already integrated WiFi modules.

(2) No licensed spectrum band is required. WiFi devices operate in unlicensed ISM 2.4 and 5 GHz bands. (3) High quality of service and high data rates. WiFi is the only wireless technology that can deliver data rates as high as 600 Mbps, which is much faster than the current 4G technology.

Though WiFi offloading is a promising technology and has many advantages, without economic incentives, WiFi APs may be reluctant to provide data offloading service for the mobile network operator (MNO). This is because providing offloading service for the MNO will inevitably incur additional operation cost, such as energy cost and data-usage cost. Besides, when providing data service for guest users from the cellular network, WiFi APs may have to sacrifice its own users' benefit, such as bandwidth, transmission rate, and quality of service. Thus, a WiFi AP has no reason to providing offloading service for the MNO unless it is purely altruistic. Therefore, there is a compelling need to design effective incentive mechanisms to motivate WiFi APs to participate in WiFi offloading. Using monetary reward as an incentive to motivate the WiFi APs will inevitably decrease the profit of the MNO. Thus, when and how the users should be offloaded to the WiFi APs is another important issue for data offloading. Therefore, we also investigate the user association problem in this chapter.

Related Work

Due to various advantages and its promising future, WiFi offloading becomes a hot research topic and has attracted the attention of many researchers all over the world. In [4], the authors investigated the feasibility of augmenting 3G using WiFi. The key ideas is to leverage WiFi's delay tolerance property and its fast switching mechanism. They have shown that WiFi can greatly reduce the burden on the cellular network. In [5], the authors conducted a quantitative study on the performance of 3G mobile data offloading through WiFi networks. Their trace-driven simulation showed that WiFi can offload about 65% of the total mobile data traffic and saves 55% of battery power without using any delayed transmission for 97 iPhone users from metropolitan areas. In [6], the authors quantitatively evaluated the gains of citywide WiFi offloading using real traces and gave out the numbers of APs needed for different requirements of quality of service for data delivery in large metropolitan area. In [7], the authors proposed to opportunistically offload traffic from the cellular network to WiFi with the aid of social participation. The authors showed that through identifying the social groups of the users and delivering specific contents to a particular social group, a large fraction of data can be offloaded from the cellular network. In [8], the author gives a tutorial on the basics and key concepts of data offloading techniques from the network layer perspective. In [9], based on Lyapunov optimization, a dynamic offloading algorithm is proposed to save energy for mobile computing. In [10], the authors investigate the outage probability and ergodic rate for a heterogeneous network when flexible cell association scheme is adopted. In [11], the authors investigate the downlink user association problem for

loading balancing in a heterogeneous cellular networks. In [12], the authors develop a general and tractable model for data offloading in heterogeneous networks with different tiers of APs.

Some recent works, such as [13–15], investigate the network economics of the mobile data offloading through WiFi APs using the game theory [16]. In [13], the authors proposed the so-called market-based data offloading where the MNO pays WiFi APs for offloading traffic. An offloading game between the MNO and WiFi APs was formulated to study the pricing strategy of the MNO and the offloading strategies of WiFi APs. However, in [13], the MNO pays WiFi APs only based on the amount of data offloaded, while the quality of the data offloading service was not taken into consideration in designing the incentive mechanism. In [14], the authors focused on the interactions between the MNO and the mobile users. The MNO pays the mobile users if they direct their delay-tolerant data service to WiFi APs. The economic benefits brought to the MNO and the users due to the delayed WiFi offloading were then studied. In [15], the authors investigated the tradeoff between the amount of traffic being offloaded and the users' satisfaction. An incentive framework to motivate users to leverage their delay tolerance for cellular traffic offloading was proposed. However, the proposed incentive mechanisms in [14, 15] are aimed at providing incentives for mobile users rather than WiFi APs.

Main Contribution

Different from the aforementioned research works, in this chapter, we investigate the user association rules and incentive mechanisms for data offloading through a third-party WiFi AP in a cellular mobile system. The main contribution and results of this chapter can be summarized as follow.

Association rules: In this chapter, by assuming the data offloaded through the third-party WiFi AP is charged based on usage, we formulate mobile data offloading problem as an utility maximization problem from the cellular operators perspective. By considering whether the successive interference cancelation (SIC) decoders are available at the BS and/or the WiFi AP, three different cases are considered. Then, the optimal data offloading scheme is derived for each case when the number of users is large. It is shown that the optimal data offloading schemes for different cases are not alike and have their own characteristics. When *SIC decoders are not available at both the BS and the WiFi AP*, it is shown that one-one association is optimal, i.e., one user with the best channel connects to the BS and the other user with the best channel to the AP connects to the WiFi AP. When *the SIC decoder is available only at the BS*, the optimal solution is at most one user connecting to the WiFi AP, and all the other users connect to the BS. When *SIC decoders are available at both the BS and the WiFi AP*, a centralized association algorithm is obtained by solving the relaxation problem. We have rigorously proved that SIC decoders are beneficial for the cellular operator in terms of maximizing its utility.

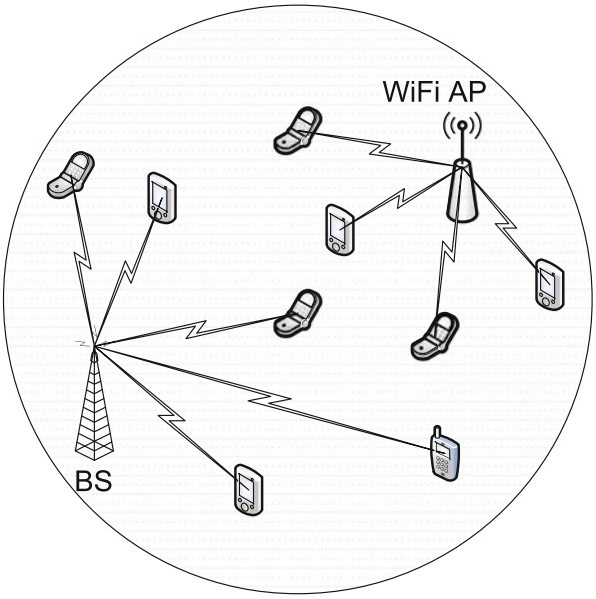

Fig. 1 System model

Incentive mechanisms: For providing strong incentives for WiFi APs to participate in data offloading, we further investigate the incentive mechanisms and propose a *salary plus bonus* reward scheme. Particularly, the proposed incentive mechanism rewards WiFi APs not only based on the amount of data offloaded but also based on the quality of the offloading service. Under the proposed incentive mechanism, we investigate the interactions between the MNO and WiFi APs using Stackelberg game. We derive the best response functions for WiFi APs which lead to the Nash equilibrium (NE). From the economic point of view, we investigate the optimal bonus and salary rate that the MNO should set in order to maximize its utility. Closed-form solutions are obtained when all WiFi AP cases are of the same type. For the heterogeneous WiFi AP case, we start with the two-AP case and then extend the results to the multi-AP case. It is shown that the MNO should adopt a low-salary high-bonus strategy or a high-salary low-bonus strategy to achieve a higher utility (Fig. 1).

System Model

In this chapter, to study the association rule, we first consider a cellular network with N users served by a base station (BS). We assume that there is a third-party WiFi access point (AP) within the coverage area of the BS. We assume that the WiFi AP and the BS use orthogonal frequencies. Thus, there is no inter-network interference between WiFi and cellular network. To maximize its network

throughput and improve the overall network performance, the cellular operator is able to direct its users to transmit through the WiFi AP rather than its BS. Since the WiFi AP is operating by a third-party operator, the cellular operator has to pay the third-party AP operator for the data usage. This monetary reward serves as an incentive for the third-party operator to operate its WiFi AP in an open access model for the users served by the cellular operator.

We assume that all the users adopt fixed power transmission, i.e., P_i for user i. For the convenience of analysis, we assume that $P_i = P, \forall i$. We assume the users are uniformly distributed in the coverage area. The channel power gain between user i and the BS is denoted by $g_{i,B}$, and the channel power gain between user i and the WiFi AP is denoted by $g_{i,A}$. We assume that $g_{i,B}$s and $g_{i,A}$s are mutually independent and have continuous probability distribution function (pdf). Besides, we assume that the power of the additive Gaussian noises at the BS and the AP is σ_B^2 and σ_A^2, respectively. Without specific declaration, we assume that all the channel state information and users' transmit power are known at the BS. We only consider the uplink scenario. Now, we define $x_i \in \{0, 1\}$ and $y_i \in \{0, 1\}$ as two indicator functions to indicate user i's connection to BS or AP, respectively. If user i connects to BS, $x_i = 1$; otherwise, $x_i = 0$. Similarly, if user i connects to AP, $y_i = 1$; otherwise, $y_i = 0$. Besides, at any time, user i is only allowed to connect to either BS or AP, but not allowed to connect to both of them simultaneously, i.e., $x_i + y_i \leq 1, \forall i$.

We assume that the cellular operator charges its users at λ per nat of data sent for data usage, and it pays the third-party operator at μ per nat of data sent through its WiFi AP. Thus, its utility can be defined as

$$U(\boldsymbol{x}, \boldsymbol{y}) = \lambda R_B(\boldsymbol{x}) + (\lambda - \mu) R_A(\boldsymbol{y}), \tag{1}$$

where $R_B(\boldsymbol{x})$ is the sum rate at the BS and $R_A(\boldsymbol{y})$ is the sum rate at the WiFi AP. Then, according to [17], if the successive interference cancelation (SIC) decoder is available at the BS, the sum-rate at the BS can be written as $R_B^w(\boldsymbol{x}) = \ln(1 + \sum_{i=1}^N \frac{g_{i,B} P_i}{\sigma_B^2} x_i)$; on the other hand, if the SIC decoder is not available at the BS, $R_B^o(\boldsymbol{x}) = \sum_{i=1}^N \ln\big(1 + \frac{x_i g_{i,B} P}{\sum_{j=1, j\neq i}^N x_j g_{j,B} P + \sigma_B^2}\big)$. Similarly, at the WiFi AP side, with SIC decoder, we have $R_A^w(\boldsymbol{x}) = \ln\big(1 + \sum_{i=1}^N \frac{g_{i,A} P_i}{\sigma_A^2} y_i\big)$; without SIC decoder, we have $R_A^o(\boldsymbol{x}) = \sum_{i=1}^N \ln\big(1 + \frac{y_i g_{i,A} P}{\sum_{j=1, j\neq i}^N y_j g_{j,A} P + \sigma_A^2}\big)$.

Then, based on the fact that whether SIC decoder is available at BS/AP, we have the following four possible utility functions:

$$U^{ww}(\boldsymbol{x}, \boldsymbol{y}) = \lambda R_B^w(\boldsymbol{x}) + (\lambda - \mu) R_A^w(\boldsymbol{y}), \tag{2}$$

$$U^{oo}(\boldsymbol{x}, \boldsymbol{y}) = \lambda R_B^o(\boldsymbol{x}) + (\lambda - \mu) R_A^o(\boldsymbol{y}), \tag{3}$$

$$U^{wo}(\boldsymbol{x}, \boldsymbol{y}) = \lambda R_B^w(\boldsymbol{x}) + (\lambda - \mu) R_A^o(\boldsymbol{y}), \tag{4}$$

$$U^{ow}(\boldsymbol{x}, \boldsymbol{y}) = \lambda R_B^o(\boldsymbol{x}) + (\lambda - \mu) R_A^w(\boldsymbol{y}). \tag{5}$$

Association Rules

With SIC Decoder at Both Sides

In this subsection, we investigate the case that both the BS and the WiFi AP are equipped with a SIC decoder. Thus, the utility maximization problem of the cellular operator can be formulated as

Problem 1.

$$\max_{\{x_i,y_i,\forall i\}} \ \lambda \ln\left(1+\sum_{i=1}^{N} S_{i,B}x_i\right)+(\lambda-\mu)\ln\left(1+\sum_{i=1}^{N} S_{i,A}y_i\right), \tag{6}$$

$$\text{s.t. } x_i \in \{0,1\}, \ \forall i, \tag{7}$$

$$y_i \in \{0,1\}, \ \forall i, \tag{8}$$

$$x_i + y_i \leq 1, \ \forall i, \tag{9}$$

where $S_{i,B} \triangleq \frac{g_{i,B}P_i}{\sigma_B^2}$ and $S_{i,A} \triangleq \frac{g_{i,A}P_i}{\sigma_A^2}$.

It is observed from this problem formulation that the third-party operator's pricing strategy μ has a great influence on the optimal solution of the above problem. When μ is larger than λ, the cellular operator will not assign any user to the AP, which is rigorously proved by the following proposition.

Proposition 1. *When $\lambda \leq \mu$, the optimal solution of Problem 1 is $\boldsymbol{x}^* = \mathbf{1}_N, \boldsymbol{y}^* = \mathbf{0}_N$, where $\mathbf{1}_N$ and $\mathbf{0}_N$ denote the N-dimension all-one vector and all-zero vector, respectively.*

Proof. To prove $\boldsymbol{x}^* = \mathbf{1}_N$ and $\boldsymbol{y}^* = \mathbf{0}_N$ is the optimal solution of Problem 3.1, we have to show that $f(\boldsymbol{x}^*, \boldsymbol{y}^*)$ is larger than $f(\boldsymbol{x}, \boldsymbol{y})$, where $f(\boldsymbol{x}, \boldsymbol{y})$ denotes the objective function of Problem 1 and $(\boldsymbol{x}, \boldsymbol{y})$ is any feasible solution of Problem 1. Suppose $(\tilde{\boldsymbol{x}}, \tilde{\boldsymbol{y}})$ is a feasible solution of Problem 1, then it follows that

$$\begin{aligned} f(\tilde{\boldsymbol{x}}, \tilde{\boldsymbol{y}}) &= \lambda f_B(\tilde{\boldsymbol{x}}) + (\lambda-\mu) f_A(\tilde{\boldsymbol{y}}) \\ &\overset{a}{\leq} \lambda f_B(\tilde{\boldsymbol{x}}) + (\lambda-\mu) f_A(\mathbf{0}_N) \\ &\overset{b}{\leq} \lambda f_B(\mathbf{1}_N) + (\lambda-\mu) f_A(\mathbf{0}_N), \end{aligned} \tag{10}$$

where the inequality "a" results from the fact that $\lambda - \mu \leq 0$ and $f_A(\boldsymbol{y})$ is always nonnegative. The inequality "b" results from the fact that $f_B(\boldsymbol{x})$ is an increasing function with respect to $\boldsymbol{x}$, and thus the equality holds only when $\boldsymbol{x}^* = \mathbf{1}_N$.

The above proposition indicates that the cellular operator will not offload any mobile data through the WiFi AP if the third-party operator charges at a price higher than its revenue, i.e., $\mu \geq \lambda$. On the other hand, from the third-party operator's

perspective, if the cellular operator does not offload mobile data through its WiFi AP, it will earn nothing, which is a lose-lose situation. Thus, a reasonable third-party operator will charge a price lower than λ, which is the scenario we consider in the following studies, i.e., $\mu < \lambda$.

Proposition 2. *The optimal solution of Problem 1 is obtained when (9) holds with equality for arbitrary i.*

Proof. This can be proved by contradiction. Suppose $(\boldsymbol{x}^*, \boldsymbol{y}^*)$ is the optimal solution of Problem 1, and it has an element (x_k^*, y_k^*) satisfying $x_k^* + y_k^* < 1$. Then, from (7) and (8), it follows that $x_k^* = 0, y_k^* = 0$. Now, we show that we can always find a feasible solution $(\tilde{\boldsymbol{x}}, \tilde{\boldsymbol{y}})$ with its elements satisfying $x_i^* + y_i^* = 1, \forall i$, which will result in a higher value of (6). We let $\tilde{\boldsymbol{x}}_{-k} = \boldsymbol{x}_{-k}^*, \tilde{\boldsymbol{y}}_{-k} = \boldsymbol{y}_{-k}^*$. Then, since the logarithm function is an increasing function, it is clear that if we set $\tilde{x}_k^* = 1, \tilde{y}_k^* = 0$ or $\tilde{x}_k^* = 0, \tilde{y}_k^* = 1$ will result in a higher value of (6) than that resulted by $x_k^* = 0, y_k^* = 0$. This contradicts with our presumption. Proposition 2 is thus proved.

With the results given in Proposition 2, we can reduce the complexity of Problem 1 by setting $y_i = 1 - x_i$. Problem 1 can be converted to the following problem.

Problem 2.

$$\max_{x_i, \forall i} \ \lambda \ln\left(1+\sum_{i=1}^{N} S_{i,B} x_i\right) + (\lambda-\mu) \ln\left(1+\sum_{i=1}^{N} S_{i,A}(1-x_i)\right), \tag{11}$$

$$\text{s.t. } x_i \in \{0, 1\}, \ \forall i. \tag{12}$$

This problem is a nonlinear integer programming problem. When the number of users is small, it can be solved by exhaustive search. However, when the number of users is large, exhaustive search is not applicable due to the high complexity. Thus, we solve Problem 2 by solving its relaxation problem and rigorously prove that the gap between the relaxation problem and Problem 2 is negligible when the number of the users is large.

The **relaxation problem** of Problem 2 is given as follows:

Problem 3.

$$\max_{x_i, \forall i} \ \lambda \ln\left(1+\sum_{i=1}^{N} S_{i,B} x_i\right) + (\lambda-\mu) \ln\left(1+\sum_{i=1}^{N} S_{i,A}(1-x_i)\right), \tag{13}$$

$$\text{s.t. } 0 \le x_i \le 1, \ \forall i. \tag{14}$$

This problem is easy to solve as it is a convex optimization problem. To show its convexity, we only need to show that the objective function is convex or concave

since all the constraints are linear. Denote the objective function of the relaxation problem as f_r, then f_r is convex/concave if its Hessian is positive/negative semidefinite. Denote the Hessian of f_r as $\boldsymbol{H}$, we show that $\boldsymbol{H}$ is negative semidefinite by the following proposition.

Proposition 3. *The Hessian $\boldsymbol{H}$ is negative semidefinite.*

Proof. The Hessian of f can be written as

$$\boldsymbol{H} = \begin{pmatrix} \frac{\partial^2 f}{\partial x_1^2} & \cdots & \frac{\partial^2 f}{\partial x_1 \partial x_N} \\ \vdots & \ddots & \vdots \\ \frac{\partial^2 f}{\partial x_N \partial x_1} & \cdots & \frac{\partial^2 f}{\partial x_N^2} \end{pmatrix}, \tag{15}$$

where the diagonal elements and off-diagonal elements can be obtained as $\frac{\partial^2 f}{\partial x_k^2} = -\frac{\lambda S_{k,B}^2}{\left(1+\sum_{i=1}^N S_{i,B} x_i\right)^2} - \frac{(\lambda-\mu) S_{k,A}^2}{\left(1+\sum_{i=1}^N S_{i,A}(1-x_i)\right)^2}$, and $\frac{\partial^2 f}{\partial x_k \partial x_j} = -\frac{\lambda S_{k,B} S_{j,B}}{\left(1+\sum_{i=1}^N S_{i,B} x_i\right)^2} - \frac{(\lambda-\mu) S_{k,A} S_{j,A}}{\left(1+\sum_{i=1}^N S_{i,A}(1-x_i)\right)^2}$.

It is observed that $\boldsymbol{H}$ can be rewritten as

$$\boldsymbol{H} = -\frac{\lambda}{\left(1+\sum_{i=1}^N S_{i,B} x_i\right)^2} \boldsymbol{B} - \frac{(\lambda-\mu)}{\left(1+\sum_{i=1}^N S_{i,A}(1-x_i)\right)^2} \boldsymbol{A}, \tag{16}$$

where the matrices $\boldsymbol{B}$ and $\boldsymbol{A}$ have the same structure as the following matrix $\boldsymbol{X}$

$$\boldsymbol{X} = \begin{pmatrix} S_{1,X}^2 & \cdots & S_{1,X} S_{N,X} \\ \vdots & \ddots & \vdots \\ S_{N,X} S_{1,X} & \cdots & S_{N,X}^2 \end{pmatrix}, \tag{17}$$

where $X = B$ for matrix $\boldsymbol{B}$ and $X = A$ for matrix $\boldsymbol{A}$.

It can be shown that for any vector $\boldsymbol{c} = [c_1 \ \cdots \ c_N]^T$, $\boldsymbol{c}^T \boldsymbol{X} \boldsymbol{c}$ can be obtained as

$$\boldsymbol{c}^T \boldsymbol{X} \boldsymbol{c} = (c_1 S_{1,X} + \cdots + c_N S_{N,X})^2 \geq 0. \tag{18}$$

Thus, it is clear that both $\boldsymbol{B}$ and $\boldsymbol{A}$ are positive semidefinite. Then, since both λ and $\lambda - \mu$ are nonnegative, it is easy to see that $\boldsymbol{H}$ is negative semidefinite. Therefore, the objective function is strictly concave.

Since Problem 3 is a convex optimization problem, the duality gap between it and its dual problem is zero. Thus, solving its dual problem is equivalent to solving the original problem. Now, we consider its dual problem.

The Lagrangian of the relaxation problem can be written as

$$L(\boldsymbol{x},\boldsymbol{\alpha},\boldsymbol{\beta}) = (\lambda-\mu)\ln\left(1+\sum_{i=1}^{N} S_{i,A}(1-x_i)\right)$$
$$+\lambda\ln\left(1+\sum_{i=1}^{N} S_{i,B}x_i\right) - \sum_{i=1}^{N}\alpha_i(x_i-1) + \sum_{i=1}^{N}\beta_i x_i, \tag{19}$$

where $\boldsymbol{\alpha} = [\alpha_1 \ \cdots \ \alpha_N]^T$ and $\boldsymbol{\beta} = [\beta_1 \ \cdots \ \beta_N]^T$ are the nonnegative dual variables associated with the constraints.

The dual function is $q(\boldsymbol{\alpha},\boldsymbol{\beta}) = \max_{\boldsymbol{x}} L(\boldsymbol{x},\boldsymbol{\alpha},\boldsymbol{\beta})$. The Lagrange dual problem is then given by $\min_{\boldsymbol{\alpha}\succcurlyeq 0,\boldsymbol{\beta}\succcurlyeq 0} q(\boldsymbol{\alpha},\boldsymbol{\beta})$. Therefore, the optimal solutions need to satisfy the following Karush-Kuhn-Tucker (KKT) conditions [18]:

$$\alpha_k(x_k^*-1) = 0, \tag{20}$$
$$\beta_k x_k^* = 0, \tag{21}$$
$$0 \le x_k^* \le 1, \tag{22}$$
$$\alpha_k^* \ge 0, \ \beta_k^* \ge 0, \tag{23}$$
$$\frac{\partial L(\boldsymbol{x},\boldsymbol{\alpha},\boldsymbol{\beta})}{\partial x_k^*} = -\frac{(\lambda-\mu)S_{k,A}}{1+\sum_{i=1}^{N} S_{i,A}(1-x_i^*)} + \frac{\lambda S_{k,B}}{1+\sum_{i=1}^{N} S_{i,B}x_i^*} - \alpha_k + \beta_k = 0, \tag{24}$$

Due to the complexity of the problem, solving the above KKT conditions will not render us a closed-form solution. However, from these KKT conditions, we are able to gain some significant features of the optimal solution.

Theorem 1. *The optimal solution of the relaxation problem has at most one user indexed by k ($k \in \{1,2,\cdots,N\}$), with a fractional x_k satisfying $0 < x_k < 1$.*

Proof. This theorem can be proved by contradiction. Suppose that there are two arbitrary users denoted by m and n having fractional x_m and x_n, respectively, i.e., $0 < x_m < 1$ and $0 < x_n < 1$. From (20) and (21), it follows that $\alpha_m = 0$, $\alpha_n = 0$, $\beta_m = 0$, and $\beta_n = 0$. Then, applying these facts to (24), it follows that

$$\frac{\lambda S_{m,B}}{1+\sum_{i=1}^{N} S_{i,B}x_i^*} - \frac{(\lambda-\mu)S_{m,A}}{1+\sum_{i=1}^{N} S_{i,A}(1-x_i^*)} = 0, \tag{25}$$
$$\frac{\lambda S_{n,B}}{1+\sum_{i=1}^{N} S_{i,B}x_i^*} - \frac{(\lambda-\mu)S_{n,A}}{1+\sum_{i=1}^{N} S_{i,A}(1-x_i^*)} = 0. \tag{26}$$

Then, for these two users, the following equality must hold

$$\frac{S_{m,B}}{S_{m,A}} = \frac{S_{n,B}}{S_{n,A}} = \frac{(\lambda-\mu)}{\lambda}\frac{1+\sum_{i=1}^{N} S_{i,B}x_i^*}{1+\sum_{i=1}^{N} S_{i,A}(1-x_i^*)}. \tag{27}$$

Table 1 Proposed centralized data offloading scheme

Proposed centralized data offloading scheme
(1) Solve Problem 3 by standard convex optimization algorithms, such as interior-point method [19], or existing solvers such as CVX [20]
(2) Convert the obtained solution into a feasible solution of Problem 2 by rounding the fractional indicator function to its nearest integer (0 or 1)

It is easy to observe that $\frac{S_{m,B}}{S_{m,A}} = \frac{S_{n,B}}{S_{n,A}}$ is equivalent to $\frac{g_{m,B}}{g_{m,A}} = \frac{g_{n,B}}{g_{n,A}}$, However, it can be verified that the equality $\frac{g_{m,B}}{g_{m,A}} = \frac{g_{n,B}}{g_{n,A}}$ is satisfied with a zero probability since the channel power gains are mutually independent and have continuous pdf. This result contradicts with our presumption. Thus, it is concluded that there is at most one user with a fractional x_k, i.e., $0 < x_k < 1$. Theorem 1 is thus proved.

From Theorem 1, it is observed that there is at most one user with a fractional indicator for the optimal solution of the relaxation problem. This indicates that the optimal solution of Problem 3 is either equal to or just one-user away from that of Problem 2. Thus, the following scheme is proposed to find the optimal solution of Problem 2.

In general, the above algorithm provides a suboptimal solution to Problem 2. However, due to the special feature presented in Theorem 1, we are able to prove that the proposed solution given in the Table 1 is near optimal when the number of users is large, which is given below.

Theorem 2. *The gap between the optimal solution of the Problem 2 and the proposed solution given in Table 1 is negligible when the number of users is large.*

Proof. For the convenience of exposition, we denote the maximum values of Problem 2 attained at the optimal solution and at the proposed solution given in Table 1 as f_o^* and f_s^*, respectively. Since the solution given in Table 1 is also a feasible solution of Problem 2. Thus, it follows that

$$f_s^* \leq f_o^*. \tag{28}$$

On the other hand, it is clear that the maximum value of Problem 2 is upper bounded by its relaxation problem. Thus, if we denote the maximum values of the relaxation problem attained at the optimal solution as f_r^*, it follows that

$$f_o^* \leq f_r^*. \tag{29}$$

Combining the above facts together, we have

$$f_s^* \leq f_o^* \leq f_r^*. \tag{30}$$

Thus, if we are able to show that the gap between f_s^* and f_r^* is negligible when the number of users is large, it is clear that the gap between f_s^* and f_o^* will also be negligible when the number of users is large.

Now, we show that the gap between f_s^* and f_r^* is negligible when the number of users is large. Suppose $\boldsymbol{x}^*$ is the optimal solution of the relaxation problem and user k is the user who has a fractional indicator function x_k^*. Then, the value of f_r^* is $\lambda \ln\left(1+\sum_{i=1}^{N} S_{i,B} x_i^*\right)+ (\lambda - \mu) \ln\left(1+\sum_{i=1}^{N} S_{i,A}(1 - x_i^*)\right)$. While the value of f_s^* is obtained by either setting $x_k = 0$ when $x_k < 0.5$ or setting $x_k = 1$ when $x_k \geq 0.5$. Obviously, it follows that $f_s^* > \tilde{f}_s{}^*$, where $\tilde{f}_s{}^* \triangleq \lambda \ln\left(1 + \sum_{i=1,i\neq k}^{N} S_{i,B} x_i^*\right) + (\lambda - \mu) \ln\left(1 + \sum_{i=1,i\neq k}^{N} S_{i,A}(1 - x_i^*)\right)$, which corresponds to the scenario where user k connects to neither the BS nor the AP.

Then, the gap Δ between f_s^* and f_r^* satisfies

$$\begin{aligned}\Delta < f_r^* - \tilde{f}_s{}^* &= \lambda \ln\left(1 + \frac{S_{k,B} x_k^*}{1+\sum_{i=1,i\neq k}^{N} S_{i,B} x_i^*}\right) \\ &+ (\lambda - \mu) \ln\left(1 + \frac{S_{k,A}(1-x_k^*)}{1+\sum_{i=1,i\neq k}^{N} S_{i,A}(1 - x_i^*)}\right). \end{aligned} \tag{31}$$

Since the users are uniformly distributed in the area, thus when the number of users is large, it is inferred that the denominators of the above equation will be very large. Consequently, the value of Δ is close to zero. Theorem 2 is thus proved.

Without SIC Decoder at Both Sides

In this subsection, we consider the scenario that both the BS and the WiFi AP are not equipped with SIC decoder. Then, the utility maximization problem of the cellular operator for this case can be formulated as

Problem 4.

$$\begin{aligned}\max_{\{x_i, y_i\}} \ & \lambda \sum_{i=1}^{N} \ln\left(1 + \frac{x_i g_{i,B} P}{\sum_{j=1,j\neq i}^{N} x_j g_{j,B} P + \sigma_B^2}\right) \\ & + (\lambda - \mu) \sum_{i=1}^{N} \ln\left(1 + \frac{y_i g_{i,A} P}{\sum_{j=1,j\neq i}^{N} y_j g_{j,A} P + \sigma_A^2}\right), \end{aligned} \tag{32}$$

$$\text{s.t.} \quad x_i \in \{0, 1\}, \ \forall i, \tag{33}$$

$$y_i \in \{0, 1\}, \ \forall i, \tag{34}$$

$$x_i + y_i \leq 1, \ \forall i. \tag{35}$$

Problem 4 is a nonlinear integer programming problem which is difficult to solve directly due to its high complexity. Besides, it is not difficult to verify that the relaxation problem of Problem 4 is non-convex. Thus, we are able not to solve this problem in the same way as Problem 1. Therefore, to solve Problem 4, we first consider the following two subproblems.

Subproblem 4a.

$$\max_{\{x_i,\forall i\}} \quad \lambda \sum_{i=1}^{N} \ln\left(1+\frac{x_i g_{i,B} P}{\sum_{j=1,j\neq i}^{N} x_j g_{j,B} P + \sigma_B^2}\right), \tag{36}$$

$$\text{s.t.} \quad x_i \in \{0,1\},\ \forall i. \tag{37}$$

Subproblem 4b.

$$\max_{\{y_i,\forall i\}} \quad (\lambda-\mu) \sum_{i=1}^{N} \ln\left(1+\frac{y_i g_{i,A} P}{\sum_{j=1,j\neq i}^{N} y_j g_{j,A} P + \sigma_A^2}\right), \tag{38}$$

$$\text{s.t.} \quad y_i \in \{0,1\},\ \forall i. \tag{39}$$

Denote the optimal solution of Subproblem 4a as $x_i^*,\ \forall i \in \{1,2,\cdots,N\}$ and that of Subproblem 4b as $y_i^*,\ \forall i \in \{1,2,\cdots,N\}$. Then, it is clear that if x_i^* and y_i^* satisfy the constraints (35) for all $i \in \{1,2,\cdots,N\}$, x_i^* and y_i^* will be the optimal solution for Problem 4. In the following, we will show that when the number of users is large, Problem 4 can be solved by individually solving Subproblems 4a and 4b. It is seen that Subproblems 4a and 4b have the same structure. As a result, the optimal solutions of these two subproblems should also have the same structure. Thus, we only need to solve one of them. In the following, using Subproblem 4b as an example, we present the optimal solution of subproblems.

Lemma 1. *If we sort the users according to their channel power gains in the following order:* $g_{1,A} \geq g_{2,A} \geq \cdots \geq g_{N,A}$, *then only the first* k^* *users are allowed to transmit at the optimal solution, where* k^* *is given by* $k^* = argmax_k \sum_{i=1}^{k} \ln\left(1+\frac{h_i P}{\sum_{j=1,j\neq i}^{k} h_j P+\sigma_A^2}\right)$ *and* $k \in \{1,2,\cdots,N\}$. *Especially, if* $g_{1,A} \geq \frac{(e-1)\sigma_A^2}{P}$ *is satisfied,* $k^* = 1$, *i.e., only the user with the largest channel power gain is allowed to transmit at the optimal solution.*

Proof. To solve Subproblem 4b, we first consider its relaxation problem, which is given as below.

Problem 5.

$$\max_{\{y_i,\forall i\}} \quad \sum_{i=1}^{N} \ln\left(1+\frac{y_i g_{i,A} P}{\sum_{j=1,j\neq i}^{N} y_j g_{j,A} P + \sigma_A^2}\right), \tag{40}$$

$$\text{s.t.} \quad 0 \leq y_i \leq 1,\ \forall i. \tag{41}$$

Let $P_i \triangleq y_i P, \forall i$; it is not difficult to observe that Problem 5 can be converted to the following problem,

Problem 6.

$$\max_{\{P_i, \forall i\}} \sum_{i=1}^{N} \ln\left(1 + \frac{g_{i,A} P_i}{\sum_{j=1, j\neq i}^{N} g_{j,A} P_j + \sigma_A^2}\right), \tag{42}$$

$$\text{s.t.} \quad 0 \leq P_i \leq P, \ \forall i. \tag{43}$$

This problem is shown to be Schur convex in [21]. By using the Schur convex properties, they showed that the optimal power allocation is binary power allocation, i.e., either 0 or P for all i. This indicates that the optimal solution for Problem 5 is either 0 or 1 for all i. Thus, it can be observed that Problem 5 is actually equivalent to Subproblem 4b. Then, the results obtained for Problem 6 can be directly applied to Subproblem 4b. Based on the results obtained in [21] (Theorems 1 and 4), it is not difficult to obtain the results presented in this lemma. Details are omitted here for brevity.

With the results given in Lemma 1, we are now ready for the following theorem.

Theorem 3. *When the number of users N is sufficiently large, the optimal solution for Problem 4 is as below.*

- *Only two users are left in the network: one connects to the BS, and the other one connects to the WiFi AP.*
- *Denote the index of the users connecting to the BS and the WiFi AP as m and n, respectively. Then, user m has the best channel between it and the BS, i.e., $m = argmax_i \ g_{i,B}$, and user n has the best channel between it and the WiFi AP, i.e., $n = argmax_i \ g_{i,A}$.*

Proof. This proof consists of two steps.

Step 1. Denote the probability that there exists at least one user satisfying $g_{i,A} \geq \frac{(e-1)\sigma_A^2}{P}$ as $\mathscr{P}_A$, and denote the probability that there exists at least one user satisfying $g_{i,B} \geq \frac{(e-1)\sigma_B^2}{P}$ as $\mathscr{P}_B$. Now, we show that when the number of users is large, both $\mathscr{P}_A$ and $\mathscr{P}_B$ are large.

$$\mathscr{P}_A = 1 - \text{Prob}\left\{g_{i,A} < \frac{(e-1)\sigma_A^2}{P}, \forall i\right\} \tag{44}$$

$$\stackrel{a}{=} 1 - \left(\text{Prob}\left\{g_A < \frac{(e-1)\sigma_A^2}{P}\right\}\right)^N \tag{45}$$

$$= 1 - \left(\int_0^{(e-1)\sigma_A^2/P} dF(g_A) \right)^N, \tag{46}$$

where the equality "a" results from the fact that the channel power gains are i.i.d. and $F(g_A)$ denotes the CDF of the channel power gain. Since $\int_0^{(e-1)\sigma_A^2/P} dF(g_A)$ is less than 1, it is clear that $\mathscr{P}_A$ goes to 1 as N goes to $+\infty$. Then, based on Lemma 4.1, as long as there exists a user satisfying $g_{i,A} \geq \frac{(e-1)\sigma_A^2}{P}$, the optimal solution for the Subproblem 4.1b should be $k^* = 1$, and the user should have the largest channel power gain among all the users, i.e., $n = \text{argmax}_i \; g_{i,A}$.

Using the same approach, we can show that when N is large, the optimal solution for the Subproblem 4a is that only the user with the largest channel power gain of the channel between it and the BS is allowed to transmit, i.e., $m = \text{argmax}_i \; g_{i,m}$. Details are omitted here for brevity.

Step 2. Denote the probability that there exists one user having the best channel between it and the BS and simultaneously having the best channel between it and the WiFi AP as $\mathscr{P}_C$. Now, we show that $\mathscr{P}_C$ is zero when the number of users is large.

$$\mathscr{P}_C = \binom{1}{N} \text{Prob}\{j = \text{argmax}_i \; g_{i,A} \text{ and } j = \text{argmax}_i \; g_{i,B}\} \tag{47}$$

$$\overset{a}{=} N \text{Prob}\{j = \text{argmax}_i \; g_{i,A}\} \text{Prob}\{j = \text{argmax}_i \; g_{i,B}\} \tag{48}$$

$$= \frac{1}{N} \tag{49}$$

where the equality "a" results from the fact that the channel power gains are i.i.d. Then, it is observed that $\mathscr{P}_C$ is a decreasing function with respect to N. Thus, it is clear that $\mathscr{P}_C$ goes to 0 as N goes to $+\infty$.

Theorem 3 is thus proved.

With SIC Decoder at One Side

In this subsection, we consider the scenario that the SIC decoder is only available at one side. Particularly, we only study the case that the SIC decoder is only available at the BS. This is due to the fact that the case that the SIC decoder is only available at the WiFi AP is a symmetric case of the case studied here and thus can be solved in the same way.

Problem 7.

$$\max_{\{x_i, y_i, \forall i\}} \; \lambda \ln\left(1 + \sum_{i=1}^N \frac{x_i g_{i,B} P}{\sigma_B^2}\right) + (\lambda - \mu) \sum_{i=1}^N \ln\left(1 + \frac{y_i g_{i,A} P}{\sum_{j=1, j\neq i}^N y_j g_{j,A} P + \sigma_A^2}\right), \tag{50}$$

$$\text{s.t.} \quad x_i \in \{0,1\},\ \forall i, \tag{51}$$

$$y_i \in \{0,1\},\ \forall i, \tag{52}$$

$$x_i + y_i \leq 1,\ \forall i. \tag{53}$$

Similar as Problem 4, we are not able to solve this problem directly or by solving its relaxation problem. Thus, to solve Problem 7, we first consider the following two subproblems.

Subproblem 7a.

$$\max_{\{x_i,\forall i\}} \ \lambda \ln\left(1+\sum_{i=1}^{N} \frac{x_i g_{i,B} P}{\sigma_B^2}\right), \tag{54}$$

$$\text{s.t.} \quad x_i \in \{0,1\},\ \forall i. \tag{55}$$

Subproblem 7b.

$$\max_{\{y_i,\forall i\}} \ (\lambda-\mu)\sum_{i=1}^{N} \ln\left(1+\frac{y_i g_{i,A} P}{\sum_{j=1,j\neq i}^{N} y_j g_{j,A} P + \sigma_A^2}\right), \tag{56}$$

$$\text{s.t.} \quad y_i \in \{0,1\},\ \forall i. \tag{57}$$

Denote the optimal solution of Subproblem 7a as $x_i^*,\ \forall i \in \{1,2,\cdots,N\}$ and that of Subproblem 7b as $y_i^*,\ \forall i \in \{1,2,\cdots,N\}$. Subproblem 7a is easy to solve, and the optimal solution is $x_i^* = 1, \forall i$. Subproblem 7b is exactly the same as Subproblem 4b, and thus the optimal solution of Subproblem 7b can be obtained from Lemma 1. It is obvious that x_i^* and y_i^* cannot satisfy the constraints (53) for all $i \in \{1,2,\cdots,N\}$. Thus, Problem 7 cannot be solved by directly solving Subproblems 7a and 7b. This makes Problem 7 more challenging than Problem 4.

To solve Problem 7, we need the following lemma.

Lemma 2. *The optimal solution of Problem 7 is obtained when* (53) *holds with equality for all* i.

Proof. This can be proved by contradiction. Suppose $(\boldsymbol{x}^*, \boldsymbol{y}^*)$ is the optimal solution of Problem 7 and it has an element (x_k^*, y_k^*) satisfying $x_k^* + y_k^* < 1$. Then, from (51) and (52), it follows that $x_k^* = 0, y_k^* = 0$. Now, we show that we can always find a feasible solution $(\tilde{\boldsymbol{x}}, \tilde{\boldsymbol{y}})$ with its elements satisfying $x_i^* + y_i^* = 1, \forall i$, which will result in a higher value of (50). We let $\tilde{\boldsymbol{x}}_{-k} = \boldsymbol{x}_{-k}^*, \tilde{\boldsymbol{y}}_{-k} = \boldsymbol{y}_{-k}^*$. Clearly, if we set $\tilde{x}_k^* = 1, \tilde{y}_k^* = 0$ will result in a higher value of (50) than that resulted by $x_k^* = 0, y_k^* = 0$ since the logarithm function is an increasing function. This contradicts with our presumption. Lemma 2 is thus proved.

Based on Lemma 2 and the optimal solutions of Subproblems 7a and 7b, we are able to obtain the following theorem.

Theorem 4. *When the number of users N is sufficiently large, the optimal solution for Problem 7 is: At most one user connects to the AP, and all the other users connect to the BS.*

Proof. Using the same approach as the proof of Theorem 3, we can easily show that the optimal solution of subproblems 7b is one-user dominant transmission (i.e. $k^* = 1$, only the user with the best channel is allowed to transmit.) when the number of users N is large. Based on this result, we prove Theorem 4 by contradictory as follows.

Let $\mathscr{S}^*$ be the optimal set of users connecting to the WiFi AP. Suppose $|\mathscr{S}^*| = 2$, where $|\cdot|$ denotes the cardinality of a set. Given this assumption, we have two possible cases: (1) There is a dominant user is in the set $\mathscr{S}^*$. (2) There is no dominant user in the set $\mathscr{S}^*$. In the following, we investigate these two cases, respectively.

- Case 1: *With a dominant user in* $\mathscr{S}^*$. In this case, if we assign the nondominant user to the BS, the utility at the BS side $\lambda R_B^w(\boldsymbol{x})$ will increase. On the other hand, based on Lemma 1, we know that the utility at the AP side is maximized if only the dominant user connects to the AP. Thus, by assigning the nondominant user to the BS, we can also increase the utility at the AP side $(\lambda - \mu) R_B^o(\boldsymbol{y})$. Then, it is clear that the total utility of the operator increases if we assign the nondominant user to the BS. This contradicts with our presumption.
- Case 2: *Without a dominant user in* $\mathscr{S}^*$. In this case, we assume that the dominant user is not in $\mathscr{S}^*$. We denote the channel power gain of the channel between the dominant user and the BS as $h_{1,B}$. Besides, we denote the channel power gains of the channels between the two nondominant users and the BS as $h_{m,B}$ and $h_{n,B}$, respectively. Based on the relationship between $h_{1,B}$ and $h_{m,B}$, $h_{n,B}$. It can be observed that if we switch the two nondominant users to the BS side and switch the dominant user to the WiFi AP side, we have four possible scenarios, which are listed in the following Table 2.

  It is observed that for the first three cases, the total utility of the cellular operator increases if we switch the connections of the nondominant users with that of the dominant user. However, for the last case, though the utility at the AP side increases, whether the utility at the BS side increase or not is uncertain. It is not difficult to observe that the utility at the BS side will increase if the following condition is satisfied.

Table 2 Four possible scenarios

	Conditions	Utility at BS	Utility at AP	Total utility
1	$h_{1,B} < h_{m,B},\ h_{1,B} < h_{n,B}$	Increase	Increase	Increase
2	$h_{1,B} < h_{m,B},\ h_{1,B} > h_{n,B}$	Increase	Increase	Increase
3	$h_{1,B} > h_{m,B},\ h_{1,B} < h_{n,B}$	Increase	Increase	Increase
4	$h_{1,B} > h_{m,B},\ h_{1,B} > h_{n,B}$	Uncertain	Increase	Uncertain

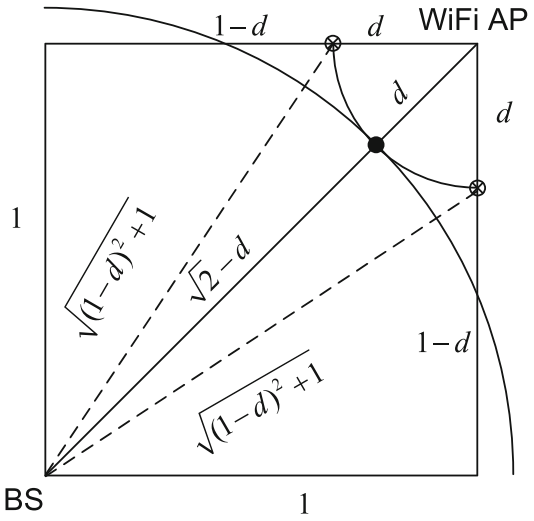

Fig. 2 Path loss model. ⊗ denotes the nondominant user, and • denotes the dominant user

$$h_{m,B}P + h_{n,B}P \geq h_{1,B}P. \tag{58}$$

In the following, we show that (58) always holds when the number of users is large. For the convenience of illustration, the proof given out here is based on the geometry of the network given in Fig. 2. However, it is worthy pointing out that the same result obtained here can be extended to any other geometries with minor revisions. In Fig. 2, we consider a 1 by 1 square area with the BS at coordinate $(0, 0)$ and the WiFi AP at $(1, 1)$. The number of users is denoted by N, and we assume these N users are uniformly scattered in the square area. The channel power gains are modeled by path loss model, i.e., $g = d^{-\gamma}$, where γ is the path loss exponent. For the convenience of analysis, we assume that $\gamma = 2$.

Based on the geometry given in Fig. 2, we consider the worst-case scenario. Thus, the utility of the BS will increase if $\frac{2P}{(1-d)^2+1} \geq \frac{P}{(\sqrt{2}-d)^2}$ holds, which is equivalent to $d < 0.67$. When there are N users in the network, the probability that this condition holds is given by $\mathscr{P}_{\text{in}} = 1 - (\text{Prob}\{d > C\})^N$. It can be observed that $\mathscr{P}_{\text{in}}$ goes to 1 when N goes to $+\infty$. This indicates that when the number of users is very large, the utility at the BS side will increase with almost probability one. Based on the results given above, it is concluded that when the number of users is large, switching the two nondominant users with the dominant user will always result in the increase of the total utility. This contradicts with our presumption.

Combining the results obtained in Cases 1 and 2, it is observed that $|\mathscr{S}^*|$ should not be equal to 2. Using the same approach, we can show that $|\mathscr{S}^*|$ cannot be equal to any number in the set $\{3, 4, \cdots, N\}$. Therefore, it is concluded that there is at most one user connecting to the WiFi AP at the optimal solution of Problem 7.

Table 3 Proposed data offloading scheme for Problem 7

Proposed data offloading scheme for Problem 7
1. **For** $k = 1 : N$;
initialize $\boldsymbol{x} = [1, 1, \cdots, 1]^T$; $\boldsymbol{y} = [0, 0, \cdots, 0]^T$;
set $\boldsymbol{x}(k) = 0$; $\boldsymbol{y}(k) = 1$;
compute $\boldsymbol{F}(k) = U(\boldsymbol{x}, \boldsymbol{y})$;
end
2. Find the optimal allocation and the maximum value of $\boldsymbol{F}$, $[F_{\max}, \text{index}] = \max \boldsymbol{F}$;
3. Compare $F_{\max}$ with the utility without offloading $U(\mathbf{1}_N, \mathbf{0}_N)$

Theorem 4 is thus proved.

Based on the result given in Theorem 4, the optimal solution of Problem 7 can be easily found by the following algorithm (Table 3).

Benefit of SIC Decoder

In this subsection, we investigate the role of the SIC decoder plays in the utility maximization of the cellular operator. We rigorously prove that the SIC decoder is beneficial for the cellular operator in terms of maximizing its utility.

Theorem 5. *Let* $(\boldsymbol{x}^*, \boldsymbol{y}^*)$, $(\hat{\boldsymbol{x}}^*, \hat{\boldsymbol{y}}^*)$, *and* $(\tilde{\boldsymbol{x}}^*, \tilde{\boldsymbol{y}}^*)$ *be the optimal solutions of Problems 1, 4, and 7, respectively. In general, the following inequality always holds*

$$U^{ww}(\boldsymbol{x}^*, \boldsymbol{y}^*) \geq U^{wo}(\tilde{\boldsymbol{x}}^*, \tilde{\boldsymbol{y}}^*) \geq U^{oo}(\hat{\boldsymbol{x}}^*, \hat{\boldsymbol{y}}^*). \tag{59}$$

Proof. To prove Theorem 5, we first show that $U^{ww}(\boldsymbol{x}^*, \boldsymbol{y}^*) \geq U^{wo}(\tilde{\boldsymbol{x}}^*, \tilde{\boldsymbol{y}}^*)$. It can be observed that $U^{ww}(\boldsymbol{x}^*, \boldsymbol{y}^*) \geq U^{ww}(\tilde{\boldsymbol{x}}^*, \tilde{\boldsymbol{y}}^*)$. This is due to the fact that $(\tilde{\boldsymbol{x}}^*, \tilde{\boldsymbol{y}}^*)$ is a feasible solution of Problem 1, while $(\boldsymbol{x}^*, \boldsymbol{y}^*)$ is the optimal solution of Problem 1. Thus, if we can show that $U^{ww}(\tilde{\boldsymbol{x}}^*, \tilde{\boldsymbol{y}}^*) \geq U^{wo}(\tilde{\boldsymbol{x}}^*, \tilde{\boldsymbol{y}}^*)$ holds, $U^{ww}(\boldsymbol{x}^*, \boldsymbol{y}^*) \geq U^{wo}(\tilde{\boldsymbol{x}}^*, \tilde{\boldsymbol{y}}^*)$ will hold. In the following, we show that $U^{ww}(\tilde{\boldsymbol{x}}^*, \tilde{\boldsymbol{y}}^*) \geq U^{wo}(\tilde{\boldsymbol{x}}^*, \tilde{\boldsymbol{y}}^*)$ always holds. Since $U^{ww}(\tilde{\boldsymbol{x}}^*, \tilde{\boldsymbol{y}}^*) = \lambda R_B^w(\tilde{\boldsymbol{x}}^*) + (\lambda - \mu) R_A^w(\tilde{\boldsymbol{y}}^*)$ and $U^{wo}(\tilde{\boldsymbol{x}}^*, \tilde{\boldsymbol{y}}^*) = \lambda R_B^w(\tilde{\boldsymbol{x}}^*) + (\lambda - \mu) R_A^o(\tilde{\boldsymbol{y}}^*)$, we only need to show that $R_A^w(\tilde{\boldsymbol{y}}^*) \geq R_A^o(\tilde{\boldsymbol{y}}^*)$ always holds, which is presented as below.

Assume that K elements of $\tilde{\boldsymbol{y}}^*$ are equal to 1, where $K \in \{1, 2, \cdots, N\}$. Then, it follows that

$$\begin{aligned} R_A^w(\tilde{\boldsymbol{y}}^*) &= \ln\left(1 + \sum_{i=1}^{K} \frac{g_{i,A} P}{\sigma_A^2}\right) \\ &= \ln\left(\frac{\sigma_A^2 + \sum_{i=1}^{K} g_{i,A} P}{\sigma_A^2}\right) \end{aligned}$$

$$
\begin{aligned}
&= \ln\left[\left(\frac{\sigma_A^2+\sum_{i=1}^{K} g_{i,A}P}{\sigma_A^2+\sum_{i=2}^{K} g_{i,A}P}\right)\left(\frac{\sigma_A^2+\sum_{i=2}^{K} g_{i,A}P}{\sigma_A^2+\sum_{i=3}^{K} g_{i,A}P}\right)\cdots\left(\frac{\sigma_A^2+\sum_{i=K}^{K} g_{i,A}P}{\sigma_A^2}\right)\right] \\
&\overset{a}{=} \sum_{j=1}^{K} \ln\left(\frac{\sigma_A^2+\sum_{i=j}^{K} g_{i,A}P}{\sigma_A^2+\sum_{i=j+1}^{K} g_{i,A}P}\right) \\
&= \sum_{j=1}^{K} \ln\left(1+\frac{g_{j,A}P}{\sigma_A^2+\sum_{i=j+1}^{K} g_{i,A}P}\right) \\
&\overset{b}{\geq} \sum_{j=1}^{K} \ln\left(1+\frac{g_{j,A}P}{\sigma_A^2+\sum_{i=1,i\neq j}^{K} g_{i,A}P}\right) = R_A^o(\tilde{\boldsymbol{y}}^*),
\end{aligned} \tag{60}
$$

where we introduce a dumb item $\sum_{i=K+1}^{K} g_{i,A}P = 0$ in the equality "a" for notation convenience. The inequality "b" follows from the fact that $\sum_{i=1,i\neq j}^{K} g_{i,A}P \geq \sum_{i=j+1}^{K} g_{i,A}P$ for each j.

Then, it is clear that $U^{ww}(\boldsymbol{x}^*, \boldsymbol{y}^*) \geq U^{wo}(\tilde{\boldsymbol{x}}^*, \tilde{\boldsymbol{y}}^*)$ always holds. Using the same approach, we can easily show that $U^{wo}(\tilde{\boldsymbol{x}}^*, \tilde{\boldsymbol{y}}^*) \geq U^{oo}(\hat{\boldsymbol{x}}^*, \hat{\boldsymbol{y}}^*)$ always holds. Theorem 5 is thus proved.

From Theorem 5, it is observed that SIC decoder plays an important role in the utility maximization of the cellular operator. In the long run, it is always beneficial for the operator to equip the BS and/or AP with SIC decoders in terms of maximizing its utility.

Incentive Mechanisms

In the previous section, we use a very simple incentive mechanism when studying the association rules. In this section, we investigate the incentive mechanisms and show its impact on the system performance. Stackelberg game is adopted to design and analyze the proposed incentive mechanism.

Game Formulation

A Stackelberg game [3] is a strategic game that consists of a leader and several followers competing with each other on certain resources. The leader moves first and the followers move subsequently. We consider a heterogeneous network with a MNO and multiple WiFi APs. The set of WiFi APs is denoted by $\mathcal{N}$. All the WiFi APs can provide data offloading service for the MNO. In particular, we consider the case that each WiFi AP may have its home users (HUs), and thus it should reserve certain bandwidth for its HUs. Like the existing work [13–15], we design incentive mechanism purely from the data level. Thus, the related physical layer and MAC layer issues to implement the data offloading schemes are out of concern.

We formulate the MNO as the leader and the WiFi APs as the followers. The MNO (leader) announces a salary and a bonus to the WiFi APs. Then, each WiFi AP (follower) determines its optimal amount of data (that it intends to offload) to maximize its utility based on the salary and the bonus. Thus, the Stackelberg game consists of two parts, the game at the WiFi APs and the game at the MNO, which are introduced as follows.

Game at the WiFi APs

Let p denote the pay rate, i.e., cash paid to a WiFi AP on per unit of data offloaded. Let B denote the total amount of bonus paid to all WiFi APs for data offloading. Then, the utility function of an arbitrary WiFi AP can be modeled as

$$\mathscr{U}_i^F(\boldsymbol{d}, p, B) = \mathscr{S}_i(p, d_i) + \mathscr{B}_i(B, \boldsymbol{w}, \boldsymbol{d}) - \mathscr{C}_i(d_i), \tag{61}$$

where $\boldsymbol{d} \triangleq [d_1, \cdots, d_N]^T$ with entry d_i denoting the amount of data that AP_i offloads for the MNO and $\boldsymbol{w} \triangleq [w_1, \cdots, w_N]^T$ with entry w_i denoting the quality of offloading service provided by AP_i.

It is observed from (61) that each AP's utility function consists of three parts: $\mathscr{S}_i(p, d_i)$, $\mathscr{B}_i(B, \boldsymbol{w}, \boldsymbol{d})$, and $\mathscr{C}_i(d_i)$. In the following, we present how to model them under the proposed incentive mechanism.

Salary: $\mathscr{S}_i(p, d_i)$ denotes the salary of AP_i, i.e., the payment received for providing data offloading service for the MNO. $\mathscr{S}_i(p, d_i)$ is a function of d_i and p. Intuitively, the more work you have done, the more payment you should receive. Thus, $\mathscr{S}_i(p, d_i)$ should be an increasing function of d_i. Besides, $\mathscr{S}_i(p, d_i)$ also should be an increasing function of p, since the higher the pay rate is, the more payment you will receive. In this paper, for simplicity, we use a linear function to model the salary, which is given as

$$\mathscr{S}_i(p, d_i) = p d_i. \tag{62}$$

Bonus: $\mathscr{B}_i(B, \boldsymbol{w}, \boldsymbol{d})$ denotes the bonus paid to AP_i by the MNO. In game theory literature, there are many bonus distribution models, such as equal share, Shapley value [16], and marginal contribution. In this work, to better stimulate WiFi APs to participate in data offloading, we use the weighted proportional share model, which is

$$\mathscr{B}_i(B, \boldsymbol{w}, \boldsymbol{d}) = \frac{w_i d_i}{\sum_{j \in \mathscr{N}} w_j d_j} B. \tag{63}$$

It is observed from (61) that AP_i's bonus $\mathscr{B}_i$ not only depends on its own performance (quality of offloading service w_i and amount of data offloaded d_i) but also depends on other APs' performance ($\boldsymbol{w}_{-i}$ and $\boldsymbol{d}_{-i}$). This is analogous to the bonus system in human's society, where a staff's bonus not only depends on his/her own performance but also depends on other staffs' performance.

Cost: $\mathscr{C}_i(d_i)$ denotes the cost incurred when AP_i provides data offloading service for the MNO. Usually, when a WiFi AP provides data service for more users, it will incur more cost, such as electricity cost, data usage cost, etc. In general, the cost increases with the increasing of the amount of data offloaded. Thus, in this work, we model the cost as

$$\mathscr{C}_i(d_i) = c_i d_i, \tag{64}$$

where c_i is a positive constant that relates the amount of data offloaded to the cost of AP_i.

Under the Stackelberg game formulation, the amount of data that AP_i intends to offload depends on the pay rate p and the bonus B. In general, if the MNO sets a high p and a high B, AP_i is willing to offload more data and vice versa. Thus, each WiFi AP has to determine its optimal d_i^* given p, B and other APs' offloading amount. Mathematically, the problem can be written as

Problem 8.

$$\max_{d_i \geq 0} \quad p d_i + \frac{w_i d_i}{\sum_{j \in \mathscr{N}} w_j d_j} B - c_i d_i, \tag{65}$$

$$\text{s.t.} \quad d_i \leq T_i, \tag{66}$$

where $T_i \triangleq T_i^C - T_i^H$. T_i^C is the maximum amount of data that can be admitted within the AP_i's capacity and T_i^H is the data quota reserved for its HUs. Thus, the constraint (66) represents the maximum amount of data that a WiFi AP can offload.

Game at the MNO

We define the MNO's utility and present the game at the MNO. Without loss of generality, in this paper, we define the MNO's utility function as

$$\mathscr{U}^L(p, B, \boldsymbol{d}) \triangleq \mathscr{R}^L(p, B, \boldsymbol{d}) - \mathscr{C}^L(p, B, \boldsymbol{d}), \tag{67}$$

where $\mathscr{R}^L(p, B, \boldsymbol{d})$ is the payoff/benefit gained from offloading data and $\mathscr{C}^L(p, B, \boldsymbol{d})$ is the cost incurred due to data offloading.

Note that the MNO's utility function consists of two parts: payoff and cost. Both of them are functions of p, B, and $\boldsymbol{d}$. In the following, we present how to model them under the proposed incentive mechanism.

Payoff: The MNO's payoff is the benefit or reward gained from offloading data. In this paper, we model the MNO's payoff as

$$\mathscr{R}^L(p, B, \boldsymbol{d}) = \lambda f(\boldsymbol{d}), \tag{68}$$

where $f(\boldsymbol{d})$ is the *offloading beneficial factor* (OBF) for the MNO and λ is a positive constant converting the offloading benefit into monetary reward. In this paper, we use a log function to model the OBF, i.e.,

$$f(\boldsymbol{d}) \triangleq \log_2\left(1+\sum_{i\in\mathcal{N}} d_i\right). \tag{69}$$

Though other functions (such as linear functions or exponential functions) can also be used to model OBE, log functions are shown in literatures to be more suitable to representing the relationship between the network performance and a large class of elastic data traffics [22]. It is observed from (69) that when the amount of data offloaded is zero ($\sum_{i\in\mathcal{N}} d_i = 0$), the OBE f is zero. Besides, the OBE increases with the increasing of the amount of data offloaded. These indicate that (69) is able to capture the relationship between the MNO's benefit and the data offloaded.

Cost: The MNO's cost includes two parts: the salary and the bonus. With a unified pay rate p, the total salary paid to WiFi APs is $p\sum_{i\in\mathcal{N}} d_i$. We assume that the bonus that the MNO intends to hand out is B. Thus, the cost function of the MNO can be modelled as

$$\mathscr{C}^L(p, B, \boldsymbol{d}) = p\sum_{i\in\mathcal{N}} d_i + B. \tag{70}$$

As pointed out in the previous subsection, the amount of data that each AP intends to offload depends on the pay rate p and the bonus B. Thus, the MNO can easily control the total amount of data offloaded to WiFi APs by controlling p and B. However, the benefit of the MNO received from data offloading also depends on p and B. Setting high pay rate and high bonus can help the MNO offload more data; however, this also increases the operating cost of the MNO. Therefore, the MNO needs to find the optimal p^* and B^* in order to maximize its utility. Mathematically, the problem can be written as

Problem 9.

$$\max_{p,\ B}\ \lambda \ln\left(1+\sum_{i\in\mathcal{N}} d_i(p,B)\right) - p\sum_{i\in\mathcal{N}} d_i(p,B) - B, \tag{71}$$

$$\text{s.t.}\quad p \geq 0,\ B \geq 0. \tag{72}$$

Optimal Solutions and Equilibrium Analysis

Problems 8 and 9 together form a Stackelberg game. The objective of this game is to find the Stackelberg equilibrium (SE) point(s) from which neither the MNO (leader) nor the WiFi APs (followers) have incentives to deviate. For the proposed Stackelberg game, the SE is defined as follows.

Definition 1. Let d_i^* be the solution for Problem 8 and (p^*, B^*) be the solution for Problem 9. Then, the point $(\boldsymbol{d}^*, p^*, B^*)$ is a SE for the proposed Stackelberg game if, for any $(\boldsymbol{d}, p, B)$, the following conditions are satisfied:

$$\mathscr{U}^L(p^*, B^*, \boldsymbol{d}^*) \geq \mathscr{U}^L(p, B, \boldsymbol{d}^*), \tag{73}$$

$$\mathscr{U}_i^F(d_i^*, p^*, B^*) \geq \mathscr{U}_i^F(d_i, p^*, B^*), \forall i. \tag{74}$$

where $\mathscr{U}^L$ and $\mathscr{U}_i^F$ are the utilities of the MNO and the WiFi AP$_i$, respectively.

To find the SE, the optimal strategies for the followers (WiFi APs) must be obtained first, and then the leader (MNO) derives its optimal strategy on those of the followers. This is also known as *backward induction* in game-theoretic studies. For the proposed game, the optimal strategies are derived in the following two subsections, respectively.

Optimal Strategies of WiFi APs

To find the optimal strategies of WiFi APs, we first look at the best response of each WiFi AP given p, B, and other APs' strategies, which is given in the following theorem.

Theorem 6. *The best response function of AP$_i$ is*

$$d_i^* = \begin{cases} 0, & \text{if } a_i > 0 \text{ and } B \leq a_i \frac{z_i}{w_i}, \\ T_i, & \text{if } a_i \leq 0 \text{ or } B \geq a_i \frac{z_i}{w_i}(1 + \frac{w_i T_i}{z_i})^2, \\ \sqrt{\frac{B z_i}{a_i w_i}} - \frac{z_i}{w_i}, & \text{otherwise.} \end{cases} \tag{75}$$

where

$$z_i \triangleq \sum_{j \in \mathscr{N}/\{i\}} w_j d_j \text{ and } a_i \triangleq c_i - p. \tag{76}$$

Proof. Take the derivative of $\mathscr{U}_i^F$ with respect to d_i, we have

$$\frac{\partial \mathscr{U}_i^F}{\partial d_i} = p + \frac{B w_i \sum_{j \in \mathscr{N}/\{i\}} w_j d_j}{\left(\sum_{j \in \mathscr{N}} w_j d_j\right)^2} - c_i, \tag{77}$$

- Case 1: $p - c_i \geq 0$. When $p - c_i \geq 0$, $\frac{\partial \mathscr{U}_i^F}{\partial d_i}$ is always positive, which indicates $\mathscr{U}_i^F$ is monotonically increasing with d_i. Thus, $\mathscr{U}_i^F$ attains its maximum when $d_i^* = T_i$.
- Case 2: $p - c_i < 0$. When $p - c_i < 0$, let $\frac{\partial \mathscr{U}_i^F}{\partial d_i}\big|_{d_i = d_i^\circ} = 0$, we have

$$d_i^\circ = \sqrt{\frac{B \sum_{j \in \mathscr{N}/\{i\}} w_j d_j}{w_i (c_i - p)}} - \frac{\sum_{j \in \mathscr{N}/\{i\}} w_j d_j}{w_i}. \tag{78}$$

Since $\frac{\partial^2 \mathscr{U}_i^F}{\partial d_i^2} = -\frac{2Bw_i^2 \sum_{j\in\mathscr{N}/\{i\}} w_j d_j}{\left(\sum_{j\in\mathscr{N}} w_j d_j\right)^3} < 0$, $\mathscr{U}_i^F$ is concave in d_i, and it follows that

$$d_i^* = \begin{cases} 0, & \text{if } d_i^\circ \le 0, \\ d_i^\circ, & \text{if } 0 < d_i^\circ < T_i, \\ T_i, & \text{if } d_i^\circ \ge T_i. \end{cases} \tag{79}$$

Then, let $z_i \triangleq \sum_{j\in\mathscr{N}/\{i\}} w_j d_j$ and $a_i \triangleq c_i - p$. Theorem 6 follows by combining the results obtained in Cases 1 and 2.

Now, we investigate the Nash equilibrium (NE) of this subgame. First, we show the existence of NE.

Existence of NE: It is observed from Problem 8 that APs' strategy set is compact and convex. The utility of AP_i is continuous and concave in d_i and continuous in $\boldsymbol{d}_{-i}$. Thus, according to the **Debreu-Glicksberg-Fan** theorem [16], a pure strategy NE exists.

Next, we show how to find the NE. To find the multiuser NE is very difficult and may be mathematically intractable. Thus, to get close-form solutions and obtain useful insights, we assume all the WiFi APs are of the same type, i.e., $w_i = w$, $c_i = c$, $T_i = T$, $\forall i$. For this case, the NE is computed as follows.

- When $a \le 0$, the NE is

$$d_i^{ne} = T, \ \forall i. \tag{80}$$

- When $a > 0$, the NE is

$$d_i^{ne} = \begin{cases} \frac{B(|\mathscr{N}|-1)}{a|\mathscr{N}|^2}, & \text{if } \frac{B}{a} < \frac{|\mathscr{N}|^2 T}{|\mathscr{N}|-1}, \\ T, & \text{if } \frac{B}{a} \ge \frac{|\mathscr{N}|^2 T}{|\mathscr{N}|-1}, \end{cases} \tag{81}$$

where $|\cdot|$ denotes the cardinality of a set.

It is observed that (i) different values of p and B will result in different NE; (ii) for given p and B, the NE is unique; and (iii) all the WiFi APs have the same strategy at the NE.

Optimal Strategy of the MNO

Given the AP's strategy, we now study the best strategy of the MNO. To find the optimal strategy of the MNO, we need to substitute the subgame NE given in (81) into Problem 9.

First, we look at the case that $a \le 0$, i.e., $p \ge c$. For this case, the subgame NE is given by (80). Substitute (80) into Problem 9, the MNO's utility maximization problem becomes

$$\max_{p,B} \ \lambda \ln(1+|\mathcal{N}|T) - p|\mathcal{N}|T - B, \tag{82}$$

$$\text{s.t.} \quad p \geq 0, \ B \geq 0. \tag{83}$$

The optimal solution of this problem is

$$p^* = c, \ B^* = 0. \tag{84}$$

This result indicates that p is bounded by c and the MNO will never set a p^* larger than c.

Now, we look at the case that $a > 0$, i.e., $p < c$. For this case, we first present the following theorem.

Theorem 7. *For any given p with $0 \leq p < c$, the best strategy of the MNO is*

$$B^* = \begin{cases} \frac{\lambda}{1+p\frac{|\mathcal{N}|-1}{a|\mathcal{N}|}} - \frac{1}{\frac{|\mathcal{N}|-1}{a|\mathcal{N}|}}, & \text{if } \tilde{\mathscr{U}}^{\mathrm{L}} < \hat{\mathscr{U}}^{\mathrm{L}}, \\ \frac{a|\mathcal{N}|^2 T}{|\mathcal{N}|-1}, & \text{if } \tilde{\mathscr{U}}^{\mathrm{L}} \geq \hat{\mathscr{U}}^{\mathrm{L}}. \end{cases} \tag{85}$$

where $\tilde{\mathscr{U}}^{L} \triangleq \lambda \ln(1+|\mathcal{N}|T) - p|\mathcal{N}|T - \frac{a|\mathcal{N}|^2 T}{|\mathcal{N}|-1}$ *and* $\hat{\mathscr{U}}^{L} \triangleq \ln\left(\frac{\lambda}{p+\frac{a|\mathcal{N}|}{|\mathcal{N}|-1}}\right) + \frac{a|\mathcal{N}|}{|\mathcal{N}|-1} + p - \lambda$.

Proof. (i) When $B < \frac{a|\mathcal{N}|^2 T}{|\mathcal{N}|-1}$, the MNO's utility can be written as

$$\max_{B \geq 0} \ \lambda \ln\left(1 + \frac{B(|\mathcal{N}|-1)}{a|\mathcal{N}|}\right) - p\frac{B(|\mathcal{N}|-1)}{a|\mathcal{N}|} - B, \tag{86}$$

It is easy to verify (86) is concave in B by looking at its second-order derivative. Then, the optimal $\hat{B}^*$ can be obtained by setting the first-order derivative of (86) to zero, which is

$$\lambda \frac{\frac{(|\mathcal{N}|-1)}{a|\mathcal{N}|}}{\frac{(|\mathcal{N}|-1)}{a|\mathcal{N}|}\hat{B}^* + 1} - p\frac{(|\mathcal{N}|-1)}{a|\mathcal{N}|} - 1 = 0, \tag{87}$$

Then, it follows that

$$\hat{B}^* = \frac{\lambda}{1+p\frac{|\mathcal{N}|-1}{a|\mathcal{N}|}} - \frac{1}{\frac{|\mathcal{N}|-1}{a|\mathcal{N}|}}. \tag{88}$$

and the resultant utility is

$$\hat{\mathscr{U}}^L = \ln\left(\frac{\lambda}{p + \frac{a|\mathscr{N}|}{|\mathscr{N}|-1}}\right) + \frac{a|\mathscr{N}|}{|\mathscr{N}|-1} + p - \lambda. \tag{89}$$

(ii) When $B \geq \frac{a|\mathscr{N}|^2 T}{|\mathscr{N}|-1}$, it is easy to observe that

$$\tilde{B}^* = \frac{a|\mathscr{N}|^2 T}{|\mathscr{N}|-1}, \tag{90}$$

and the resultant utility is

$$\tilde{\mathscr{U}}^L = \lambda \ln(1 + |\mathscr{N}|T) - p|\mathscr{N}|T - \frac{a|\mathscr{N}|^2 T}{|\mathscr{N}|-1}. \tag{91}$$

Combining (i) and (ii), (85) follows.
It is observed from Theorem 7 that for any given p satisfying $0 \leq p < c$, the optimal B^* is unique. Besides, as pointed out in (84), p^* is bounded by c. Thus, the optimal p^* can be obtained by searching over the region $[0, c]$. Therefore, the Stackelberg game is solved, and the SE always exists since there exists a unique subgame NE for any given p and B.

Heterogeneous WiFi APs

In the previous subsection, to obtain closed-form solutions and get useful insights, we assume all the WiFi APs are homogeneous, i.e., having the same type. In this subsection, we consider the case that different WiFi APs have different parameters. To facilitate the analysis, we start with the two-AP case and then extend the results to multi-AP case.

Optimal Strategies of WiFi APs

We first derive the optimal strategies of WiFi APs. For given p and B, the best response functions of WiFi APs are given by (75). Based on (75), the subgame NE is obtained in the following theorem.

Theorem 8. *Assume $c_2 > c_1$, the subgame NE denoted by (d_1^{ne}, d_2^{ne}) is given as*

(i) When $p \geq c_2 > c_1$, the NE is

$$(d_1^{ne}, d_2^{ne}) = (T_1, T_2). \tag{92}$$

(ii) When $c_2 > p \geq c_1$, the NE is

$$(d_1^{ne}, d_2^{ne}) = \begin{cases} (T_1, 0), & \text{if } 0 \leq B < \frac{a_2}{w_2} w_1 T_1, \\ \left(T_1, \sqrt{\frac{B w_1 T_1}{w_2 a_2}} - \frac{w_1 T_1}{w_2}\right), & \text{if } \frac{a_2 w_1 T_1}{w_2} \leq B < \frac{a_2}{T_1} \frac{(w_1 T_1 + w_2 T_2)^2}{w_1 w_2}, \\ (T_1, T_2), & \text{if } \frac{a_2}{T_1} \frac{(w_1 T_1 + w_2 T_2)^2}{w_1 w_2} \leq B. \end{cases} \tag{93}$$

(iii) When $c_2 > c_1 > p \geq 0$ and $a_1 T_1 < a_2 T_2$, the NE is

$$(d_1^{ne}, d_2^{ne}) = \begin{cases} \left(\frac{B w_1 w_2 a_2}{(w_1 a_2 + w_2 a_1)^2}, \frac{B w_1 w_2 a_1}{(w_1 a_2 + w_2 a_1)^2}\right) & \text{if } B \in \mathscr{A}_1, \\ \left(T_1, \sqrt{\frac{B w_1 T_1}{w_2 a_2}} - \frac{w_1 T_1}{w_2}\right), & \text{if } B \in \mathscr{A}_2, \\ (T_1, T_2), & \text{if } B \in \mathscr{A}_3. \end{cases} \tag{94}$$

where the regions are defined as: $\mathscr{A}_1 \triangleq \left(0, \frac{(w_1 a_2 + w_2 a_1)^2}{w_1 w_2} \frac{T_1}{a_2}\right)$, $\mathscr{A}_2 \triangleq \left[\frac{(w_1 a_2 + w_2 a_1)^2}{w_1 w_2} \frac{T_1}{a_2}, \frac{a_2}{T_1} \frac{(w_1 T_1 + w_2 T_2)^2}{w_1 w_2}\right)$, *and* $\mathscr{A}_3 \triangleq \left[\frac{a_2}{T_1} \frac{(w_1 T_1 + w_2 T_2)^2}{w_1 w_2}, \infty\right)$.

(iv) When $c_2 > c_1 > p \geq 0$ and $a_1 T_1 > a_2 T_2$, the NE is

$$(d_1^{ne}, d_2^{ne}) = \begin{cases} \left(\frac{B w_1 w_2 a_2}{(w_1 a_2 + w_2 a_1)^2}, \frac{B w_1 w_2 a_1}{(w_1 a_2 + w_2 a_1)^2}\right) & \text{if } B \in \tilde{\mathscr{A}_1}, \\ \left(\sqrt{\frac{B w_2 T_2}{w_1 a_1}} - \frac{w_2 T_2}{w_1}, T_2\right), & \text{if } B \in \tilde{\mathscr{A}_2}, \\ (T_1, T_2), & \text{if } B \in \tilde{\mathscr{A}_3}. \end{cases} \tag{95}$$

where the regions are defined as: $\tilde{\mathscr{A}_1} \triangleq \left(0, \frac{(w_1 a_2 + w_2 a_1)^2}{w_1 w_2} \frac{T_2}{a_1}\right)$, $\tilde{\mathscr{A}_2} \triangleq \left[\frac{(w_1 a_2 + w_2 a_1)^2}{w_1 w_2} \frac{T_2}{a_1}, \frac{a_1}{T_2} \frac{(w_1 T_1 + w_2 T_2)^2}{w_1 w_2}\right)$, *and* $\tilde{\mathscr{A}_3} \triangleq \left[\frac{a_1}{T_2} \frac{(w_1 T_1 + w_2 T_2)^2}{w_1 w_2}, \infty\right)$.

From Theorem 8, we can observe that:

- For any given p and B, the NE is unique.
- The order of $a_i T_i$s has an impact on the NE. The WiFi AP with lower $a_i T_i$ is more likely to reach its capacity limit T_i first.

Optimal Strategy of the MNO

Now, given WiFi AP's strategy, we derive the optimal strategies of the MNO. Problem 9 becomes a non-convex optimization problem given WiFi AP's strategy. Thus, convex optimization techniques or existing convex optimizers cannot be applied here. However, we can show that (i) the optimal p^* is bounded by c_2 and

(ii) for a given p, Problem 9 is concave in B for each separate region of B (such as $\mathscr{A}_1$, $\mathscr{A}_2$, and $\mathscr{A}_3$). Thus, the optimal B for each separate region can be easily obtained using the convex optimization techniques. Then, the optimal B^* can be obtained by comparing the maximum utility function of each separate region. Based on these facts, the optimal strategy of the MNO can be obtained in the following two steps: (i) For a given p, compute the optimal B^*. (ii) Search for the optimal p^* over the region $[0, c_2]$.

Multi-AP Case

For given p and B, the best response for each AP is given by (75). However, the subgame NE cannot be obtained in closed-form due to the high complexity. Numerically, the subgame NE can be computed by the simplicial method [23]. The basic idea is to solve the nonlinear equilibrium problem by solving a piecewise linear approximation of the problem. Details are omitted here for brevity. Interested readers can refer to [23] for details. For the MNO's side, the optimal strategy cannot be obtained in closed form since there is no explicit expression of the WiFi AP's strategy. Numerically, we can solve the MNO's optimal strategy in the following way. Similar as the two-AP case, we can show that p^* is bounded by $\text{argmax}_i c_i$. We can further show that B^* is bounded by $\text{argmax}_i \frac{a_i}{w_i z_i} \left(\sum_{i \in \mathscr{N}} w_i T_i\right)^2$. Since both p^* and B^* are bounded, the MNO's optimal strategy can be obtained by performing a two-dimensional grid search over p and B.

Numerical Results

In this section, numerical results are provided to evaluate the performance of the proposed studies.

Simulation Parameters

The simulation setup is as follows. We consider a 1 by 1 square area with the base station at coordinate $(0, 0)$ and the WiFi AP at $(1, 1)$. The number of users is denoted by N, and we assume these N users are uniformly scattered in the square area. For simplicity, without specific declaration, we assume that the transmit power of each user is the same and given by 1. For the convenience of exposition, the path loss model is adopted to model the channel power gain. Let $(\text{posx}_i, \text{posy}_i)$ denotes the position of user i; then the channel power gain between it and the BS can be modeled as $g_{i,B} = \left(\sqrt{\text{posx}_i^2 + \text{posy}_i^2}\right)^{-\gamma}$, where γ is the path loss coefficient. Similarly, the channel power gain between the user i and the AP can be modeled as $g_{i,A} = \left(\sqrt{(1 - \text{posx}_i)^2 + (1 - \text{posy}_i)^2}\right)^{-\gamma}$. In this paper, we adopt the free space path loss model where $\gamma = 2$. The power of the additive Gaussian noises at the BS

and the AP is set to 1, i.e., $\sigma_B^2 = 1$ and $\sigma_A^2 = 1$. The revenue coefficient λ of the BS is set to 1, and the cost coefficient μ is set to 0.5.

Association Rules

With SIC Decoder at Both Sides

In Fig. 3, we investigate the gap between the proposed centralized data offloading scheme given in Table 1 and the optimal solution. For the purpose of illustration, the gap is normalized by the value of the utility attained at the optimal solution. The result presented in Fig. 3 is averaged over 100 channel realizations for each N. It is observed from Fig. 3 that the normalized utility gap decreases with the increase of the number of users. When there are only two users in the network, the normalized utility gap is as large as 0.85%. When the number of users goes up to 16, the normalized utility gap is almost zero.

In Fig. 4, we study the performance of the proposed centralized data offloading scheme. In this case, we also generate 1000 channel realizations for each N. We count the number of realizations, in which the normalized utility gap exceeds the given values. The given values actually indicate the accuracy of the proposed data offloading scheme. It is observed from Fig. 4 that the number of realizations decreases with the increasing number of users for all the four given values as expected. It is also observed from Fig. 4 that, when there are only two users in the

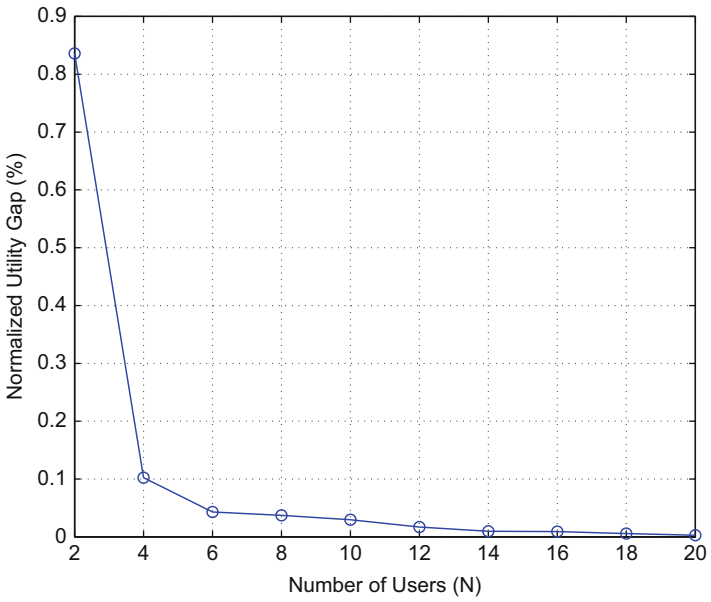

Fig. 3 Normalized utility gap vs. the number of users

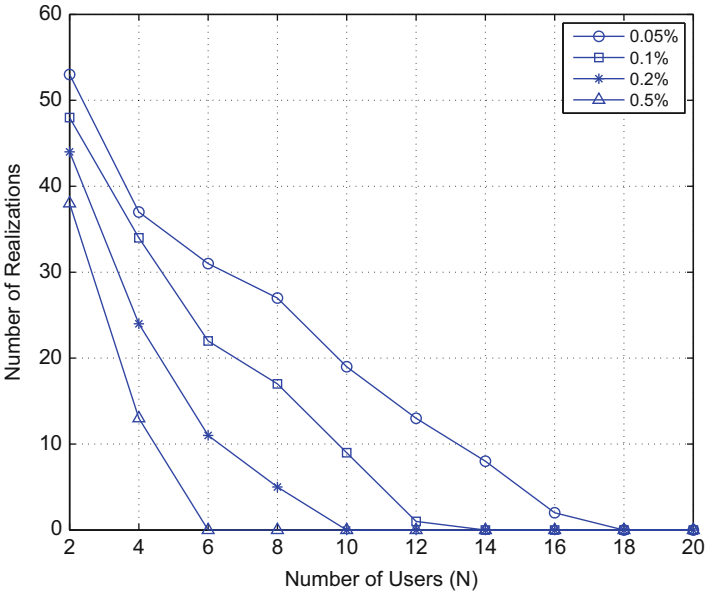

Fig. 4 Performance of the centralized data offloading scheme

network, almost 40 realizations will result in the utility gap that is larger than 0.5%. However, when the number of users increases to 6, the number of realizations that results in a utility gap larger than 0.5% is zero. This indicates that when the system requirement is not too high, the proposed data offloading scheme will perform well even when the number of users is not large. It is also observed from Fig. 4 that, even when the system requirement is very high, such as 0.05%, the proposed data offloading scheme can produce a satisfactory performance when there are more than 16 users in the network.

Without SIC Decoder at Both Sides

In Figs. 5 and 6, we investigate the performance of the proposed data offloading scheme for the case that SIC decoders are not available at both BS and the AP side. In Fig. 5, we generate 1000 channel realizations for each N. We count the number of realizations, in which the proposed data offloading scheme is optimal. First, it is observed that for all the curves, the number of realizations that the proposed data offloading scheme is optimal increases with the increasing of the number of users. This is in accordance with our theoretic analysis. Secondly, it is observed that the transmit power of the users also plays an important role in the performance of the proposed data offloading scheme. For the same number of users, when the transmit power of the users is large, the number of realizations that the proposed data offloading scheme is optimal is large. This is due to the fact that when P is large, the value of $\frac{(e-1)\sigma_A^2}{P}$ is small, and thus the probability that $g_{1,A} \geq \frac{(e-1)\sigma_A^2}{P}$ is

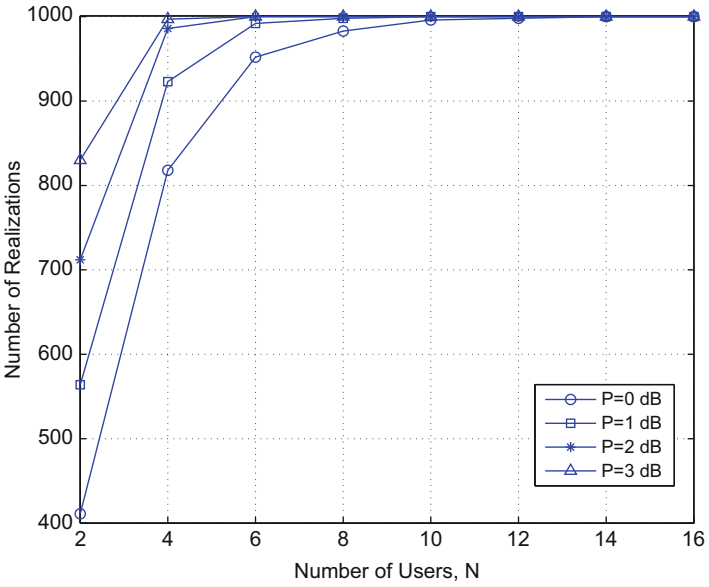

Fig. 5 Performance of the data offloading scheme: without SIC decoder at both sides

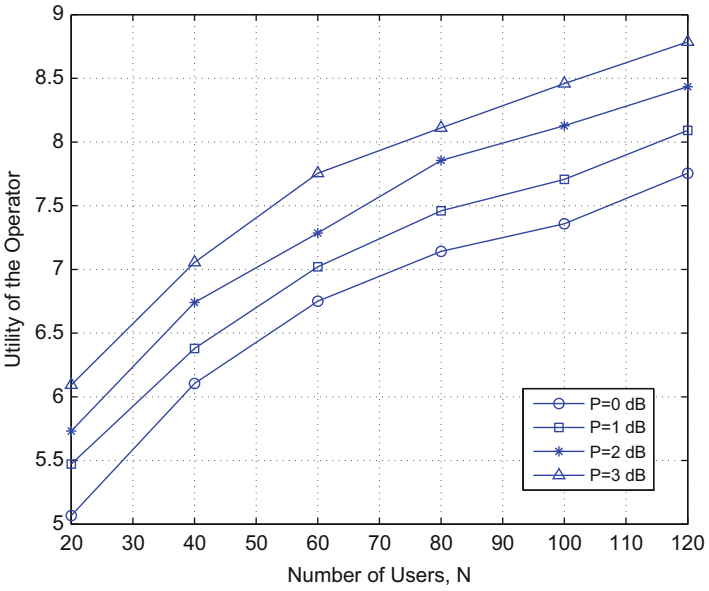

Fig. 6 Performance of the data offloading scheme: without SIC decoder at both sides

large for the same number of users. Thirdly, it is observed that when the number of users is larger than 10, the proposed data offloading scheme is always optimal for all the cases. This indicates that the proposed data offloading scheme can achieve a satisfactory performance even when the number of users is not very large.

With SIC Decoder at One Side

In Figs. 7 and 8, we investigate the performance of the proposed data offloading scheme for the case that SIC decoders are only available at the BS side. In Fig. 7, we generate 1000 channel realizations for each N. We count the number of realizations, in which the proposed data offloading scheme is optimal. It is observed that for all the curves, the number of realizations that the proposed data offloading scheme is optimal increases with the increasing of the number of users. This is in accordance with our theoretic analysis. Secondly, it is observed that the transmit power of the users almost does not affect the performance of the proposed data offloading scheme. This is quite different from the results obtained in Fig. 5. This is due to the fact that for this case, the proposed data offloading scheme is optimal only when both $g_{1,A} \geq \frac{(e-1)\sigma_A^2}{P}$ and $d < 0.67$ are satisfied simultaneously. For the case considered here, the condition that $d < 0.67$ always dominates. Since this condition is irrelevant with the transmit power, the performance of the proposed date offloading scheme is not affected by the transmit power of the users. Finally, it is observed that when the number of users is larger than 12, the proposed data offloading scheme is always optimal. This indicates that the proposed data

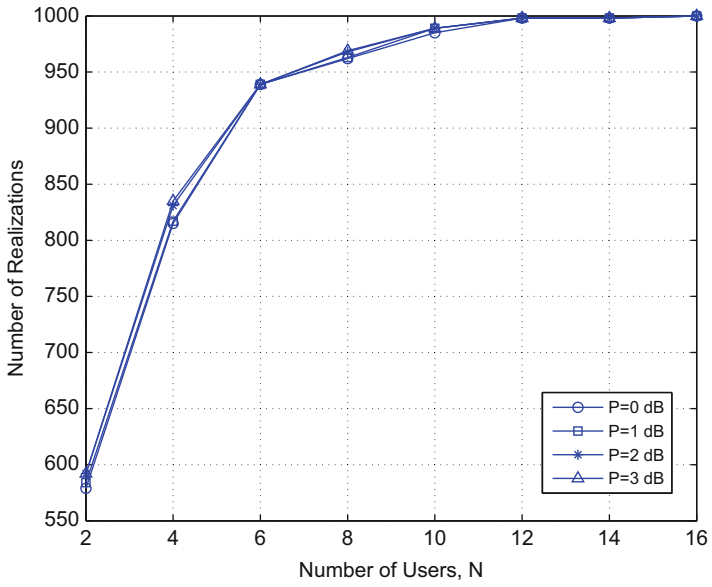

Fig. 7 Performance of the data offloading scheme: with SIC decoder at one side

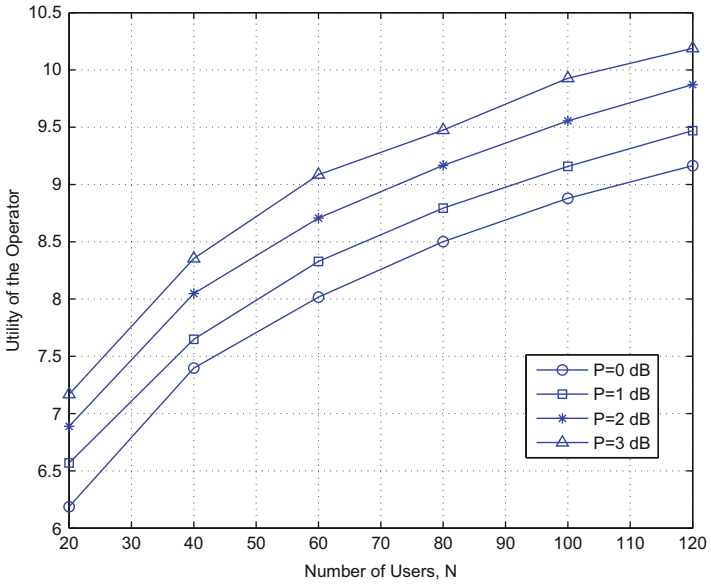

Fig. 8 Performance of the data offloading scheme: with SIC decoder at one side

offloading scheme can achieve a good performance even when the number of users is not large.

Incentive Mechanisms

In this subsection, two numerical examples are given to investigate the proposed incentive mechanisms.

Example 1: The Utility of the MNO

In this example, we assume that there are two heterogeneous APs existing in the HetNet. The simulation parameters are given as $c_1 = 2$, $c_2 = 3$, $T_1 = T_2 = 5$, $w_1 = 0.2$, $w_2 = 0.3$, and $\lambda = 50$. It is observed from Fig. 9 that the utility function of the MNO is neither convex nor concave in p and B. It is also observed that when both p and B are large or small, the utility of the MNO is low, while the MNO's utility is high when one of them (either p or B) is large and the other one of them is small. This indicates that the MNO should in general adopt either the low-salary high-bonus strategy or the high-salary low-bonus strategy to achieve high utilities.

Example 2: Subgame NE Analysis

In this example, we assume that there are three heterogeneous APs existing in the HetNet. The simulation parameters are chosen as follows: $c_1 = 2$, $c_2 = 3$, $c_3 = 4$, $T_1 = T_2 = T_3 = 5$, $w_1 = 0.2$, $w_2 = 0.3$, and $w_3 = 0.5$. In this example, we

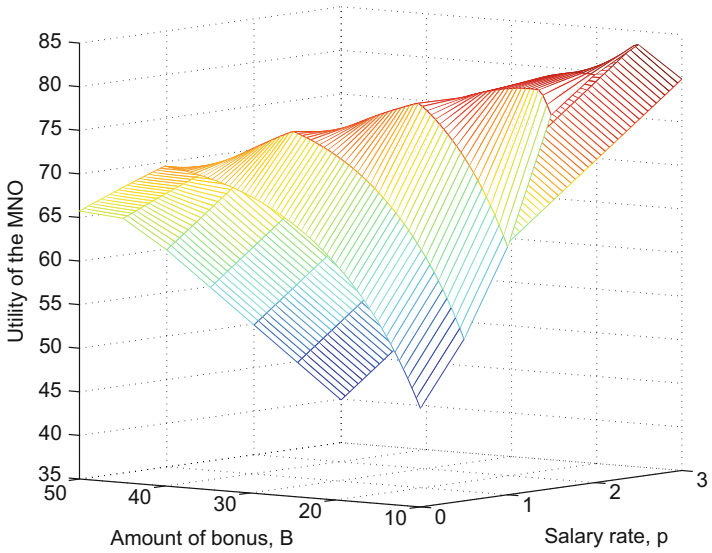

Fig. 9 Utility of the MNO under the Stackelberg game formulation

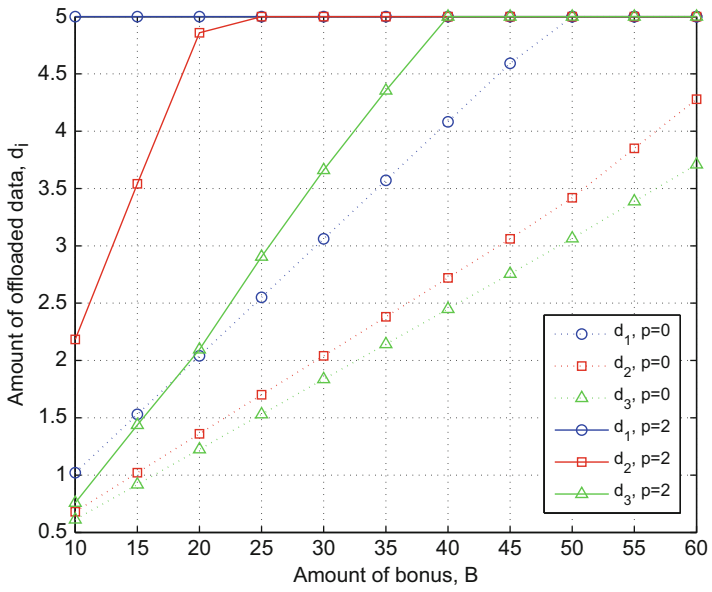

Fig. 10 Subgame nash equilibrium of three heterogeneous WiFi APs under different bonus B and different salary rate p

investigate the subgame equilibrium behavior of WiFi APs for given p and B. It is observed that for the same p and B, the AP with lower cost is willing to offload more data. Increasing the salary rate p is more effective in boosting up the amount of data offloaded. The AP with lower w_i is more sensitive to the bonus changes. When the bonus increases, the amount of offloaded data increases faster for the AP with lower w_i. This is because that the bonus distribution not only depends on d_i but also depends on w_i in the proposed incentive mechanism. Thus, in order to get the same partition of the bonus, the AP with lower w_i must offload more data than the AP with higher w_i. This also indicates that the proposed bonus scheme is bias toward to the AP with good quality of service w_i and thus provides an incentive for APs to improve their service quality (Fig. 10).

Conclusions

In this chapter, we have investigated the association rules and incentive mechanisms for mobile data offloading problem through a third-party WiFi AP in a cellular mobile system. Firstly, using a simple incentive mechanism, we have formulated the user association problem as an utility maximization problem. By considering whether the successive interference cancelation (SIC) decoders are available at the BS and/or the WiFi AP, different utility functions are considered. When the SIC decoders are available at both the BS and the WiFi AP, the utility maximization problem can be solved by considering its relaxation problem. It is strictly proved that the proposed user association scheme is near optimal when the number of users is large. When the SIC decoders are not available at both the BS and the WiFi AP, we have rigorously proved that the optimal solution is one-one association, i.e., one user connects to the BS, and the other user connects to the WiFi AP. When the SIC decoder is only available at the BS, we have shown that there is at most one user connecting to the WiFi AP and all the other users connect to the BS. We have rigorously proved that SIC decoders are beneficial for the cellular operator in terms of maximizing its utility. Secondly, to provide strong incentives for WiFi APs to provide data offloading service, we proposed an incentive mechanism using both salary and bonus. We investigated the interactions between the MNO and the WiFi APs using the Stackelberg game model. Under the Stackelberg game formulation, we derived the optimal amount of data that each WiFi AP was willing to offload and investigated the optimal bonus and salary rate that the MNO should set in order to maximize its utility. It has been shown that the MNO should adopt a low-salary high-bonus strategy or a high-salary low-bonus strategy to achieve a higher utility.

References

1. Cisco Systems Inc. (2012) Cisco visual networking index: global mobile data traffic forecast update, 2011–2016

2. Chandrasekhar V, Andrews JG, Gatherer A (2008) Femtocell networks: a survey. IEEE Commun Mag 46(9):59–67
3. Kang X, Zhang R, Motani M (2012) Price-based resource allocation for spectrum-sharing femtocell networks: a stackelberg game approach. IEEE J Sel Areas Commun 30(3):538–549
4. Balasubramanian A, Mahajan R, Venkataramani A (2010) Augmenting mobile 3G using WiFi. In: Proceedings of ACM MobiSys, pp 209–222
5. Lee K, Lee J, Yi Y, Rhee I, Chong S (2010) Mobile data offloading: how much can WiFi deliver? In: Proceedings of ACM Sigcomm, pp 425–426
6. Dimatteocy S, Huiy P, Hanyz B, Lix V (2011) Cellular traffic offloading through WiFi networks. In: Proceedings of IEEE MASS, pp 192–201
7. Han B, Hui P, Kumar V, Marathe M, Shao J, Srinivasan A (2012) Mobile data offloading through opportunistic communications and social participation. IEEE Trans Mobile Comput 11(5):821–834
8. Sankaran CB (2012) Data offloading techniques in 3GPP Rel-10 networks: a tutorial. IEEE Commun Mag 50(6):46–53
9. Dong H, Wang P, Niyato D (2012) A dynamic offloading algorithm for mobile computing. IEEE Trans Wirel Commun 11(6):1991–1995
10. Jo H, Sang Y, Xia P, Andrews JG (2012) Heterogeneous cellular networks with flexible cell association: a comprehensive downlink SINR analysis IEEE Trans Wirel Commun 11(10):3484–3495
11. Ye Q, Rong B, Chen Y, Al-Shalash M, Caramanis C, Andrews JG, User association for load balancing in heterogeneous cellular networks. Avaiable at http://arxiv.org/pdf/1205.2833.pdf
12. Singh S, Dhillon HS, Andrews JG, Offloading in heterogeneous networks: modeling, analysis, and design insights. Avaiable at http://arxiv.org/pdf/1208.1977.pdf
13. Gao L, Iosifidisy G, Huang J, Tassiulasy L (2013) Economics of mobile data offloading. In: Proceedings of Infocom Workshop on SDP
14. Lee J, Yi Y, Chong S, Jin Y (2013) Economics of WiFi offloading: trading delay for cellular capacity. In: Proceedings of Infocom Workshop on SDP
15. Zhuo X, Gao W, Cao G, Hua S (2014) An incentive framework for cellular traffic offloading. IEEE Trans Mobile Comput 13(3):541–555
16. Fudenberg D, Tirole J (1993) Game theory. MIT Press
17. Cover T, Thomas J (1991) Elements of information theory. Wiley, Hoboken
18. Kang X, Liang Y-C, Nallanathan A, Garg HK, Zhang R (2009) Optimal power allocation for fading channels in cognitive radio networks: ergodic capacity and outage capacity. IEEE Trans Wirel Commun 8(2):940–950
19. Boyd S, Vandenberghe L (2004) Convex optimization. Cambridge University Press
20. CVX Research, Inc. CVX: Matlab software for disciplined convex programming, version 2.0 beta. http://cvxr.com/cvx. Sept 2012
21. Inaltekin H, Hanly SV (2012) Optimality of binary power control for the single cell uplink. IEEE Trans Inform Theory 58(10):6484–6498
22. Kelly FP, Maulloo A, Tan D (1998) Rate control for communication netowrks: shadow prices, proportional fairness and stability. J Oper Res Soci 29(3):237–252
23. Herings PJ-J, van den Elzen A (2002) Computation of the nash equilbirum selected by the tracing procedure in n-person games. Games Econo Behav 38(1):89–117

Resource Allocation in Spectrum-Sharing Cognitive Heterogeneous Networks

19

Haijun Zhang, Theodoros A. Tsiftsis, Julian Cheng, and Victor C. M. Leung

Contents

H. Zhang (✉)
Beijing Engineering and Technology Research Center for Convergence Networks and Ubiquitous Services, University of Science and Technology Beijing, Beijing, China
e-mail: haijunzhang@ieee.org

T. A. Tsiftsis
School of Engineering, Nazarbayev University, Astana, Akmola, Kazakhstan
e-mail: theodoros.tsiftsis@nu.edu.kz

J. Cheng
School of Engineering, The University of British Columbia, Kelowna, BC, Canada
e-mail: julian.cheng@ubc.ca

V. C. M. Leung
Department of Electrical and Computer Engineering, The University of British Columbia, Vancouver, BC, Canada
e-mail: vleung@ece.ubc.ca

W. Zhang (ed.), *Handbook of Cognitive Radio*,
https://doi.org/10.1007/978-981-10-1394-2_19

Abstract

Cognitive radio-enabled heterogeneous networks are an emerging technology to address the exponential increase of mobile traffic demand in the next-generation mobile communications. Recently, many technological issues such as resource allocation and interference mitigation pertaining to cognitive heterogeneous networks have been studied, but most studies focus on maximizing spectral efficiency. This chapter introduces the resource allocation problem in cognitive heterogeneous networks, where the cross-tier interference mitigation, imperfect spectrum sensing, and energy efficiency are considered. The optimization of power allocation is formulated as a non-convex optimization problem, which is then transformed to a convex optimization problem. An iterative power control algorithm is developed by considering imperfect spectrum sensing, cross-tier interference mitigation, and energy efficiency.

Keywords

Cognitive heterogeneous networks · Fairness · Imperfect spectrum sensing · Orthogonal frequency division multiple access (OFDMA) · Power control · Resource allocation Sensing time optimization

Introduction

Demand for mobile data traffic is increasing exponentially due to the wide usage of smart mobile devices and data-centric applications in mobile Internet. As a promising technology in the fifth-generation (5G) mobile communications, small cell can offload heavy traffics from primary macrocells by shortening the distance between basestation and users. Since small cell can effectively improve the coverage and spatial reuse of spectrum by deploying low-power access points, it is not surprising that small cell has attracted much research interests in both industry and academia. However, the benefits of small cell deployments come with a number of fundamental challenges, which include spectrum access, resource allocation, and interference mitigation [1–7].

Cognitive radio is also an emerging technology to improve the efficiency of spectrum access in the 5G networks [8]. The cognitive capabilities can improve the spectrum efficiency, radio resource utilization, and interference mitigation by efficient spectrum sensing, interference sensing, and adaptive transmission. Therefore, a cognitive radio-enabled small cell network can further improve the system performance by coexisting with a macrocell network [9]. There are three ways for a cognitive small cell to access the spectrum potentially used by a primary macrocell: (1) spectrum sharing, where the cognitive small cell can share the

spectrum with the primary macrocell; (2) opportunistic spectrum access, where the cognitive small cell can opportunistically access the spectrum that is detected to be idle; and (3) hybrid spectrum sensing, where the cognitive small cell senses the channel status and optimizes the power allocation based on the spectrum sensing result.

Orthogonal frequency division multiple access (OFDMA) working jointly with cognitive small cell can improve spectrum efficiency and energy efficiency via resource allocation and interference mitigation [10]. In [11], the authors investigated the resource allocation problems based on multistage stochastic programming for stringent quality of service (QoS) requirements of real-time streaming scalable videos in cognitive small cell networks. The issues on spectrum sensing and interference mitigation were studied in [12], where an interference coordination approach was adopted. Opportunistic cooperation between cognitive small cell users and primary macrocell users was provided for cognitive small cell networks based on a generalized Lyapunov optimization technique [13]. In [14], a spectrum-sharing scheme between primary macrocell and secondary small cell was investigated, and bounds on maximum intensity of simultaneously transmitting cognitive small cell that satisfies a given per-tier outage constraint in these schemes were theoretically derived using a stochastic geometry model. In [15], interferences due to different interfering sources were analyzed within cognitive-empowered small cell networks, and a stochastic dual control approach was introduced for dynamic sensing coordination and interference mitigation without involving global and centralized control efforts. Moreover, energy-efficient resource allocation has also been investigated for cognitive radio and small cell. In [16], the energy efficiency aspect of spectrum sharing and power allocation was studied using a Stackelberg game in heterogeneous cognitive radio networks with femtocells. While in [17], Nash equilibrium of a power adaptation game was derived to reduce energy consumption. Moreover, interference temperature limits, originated from the cognitive radio, were used in [18] to mitigate cross-tier interferences between macrocell and small cell.

This chapter includes two parts. In the first part, the power control and sensing time optimization problem in a cognitive small cell network are discussed. The resource allocation problem is solved by two new algorithms. In the second part, an iterative subchannel and power allocation algorithm is applied to the cognitive femtocells. The effectiveness of the provided algorithm in terms of capacity and fairness when compared to the other existing algorithms is verified by simulation.

Sensing Time Optimization and Power Control for Energy-Efficient Cognitive Small Cell with Imperfect Hybrid Spectrum Sensing

In this part, we study the optimization of sensing time and power control in an OFDMA-based cognitive small cell by considering energy efficiency, QoS requirement, cross-tier interference limitation, and imperfect hybrid spectrum sensing.

System Model and Problem Formulation

System Model

We consider an OFDMA cognitive small cell network where a co-channel cognitive small cell is overlaid on a primary macrocell and focus on resource allocation in the downlink of the cognitive small cell. The OFDMA system has a bandwidth of B, which is divided into N subchannels. The channel fading of each subcarrier is assumed to be the same within a subchannel, but may vary across different subchannels. The channel model for each subchannel includes path loss and frequency-nonselective Rayleigh fading. Before the small cell accesses the spectrum licensed to the primary macrocell, cognitive small basestation (CSBS) performs spectrum sensing to determine the occupation status of the subchannels. In each time frame, the cognitive small cell can sense N subchannels by energy detection-based spectrum sensing. The CSBS adapts the transmit power based on the spectrum sensing result [19]. The H_n^o is the hypothesis that the nth subchannel is occupied by the primary macrocell. The $\tilde{\mathscr{H}}_n^o$ represents the spectrum sensing result that the nth subchannel is occupied by the primary macrocell. The H_n^v is the hypothesis that the nth subchannel is not occupied by the primary macrocell. The $\tilde{\mathscr{H}}_n^v$ represents the spectrum sensing result that the nth subchannel is not occupied by the primary macrocell. The probabilities of false alarm and mis-detection on subchannel n are q_n^f and q_n^m, respectively. The user signal of the primary macrocell is a complex-valued phase shift keying (PSK) signal, and the noise at CSBS is circularly symmetric complex Gaussian (CSCG) with mean zero and variance σ^2 [19]. According to [20], the probability of mis-detection q_n^m can be approximated by

$$q_n^m(\varepsilon_n, \tau) = 1 - Q\left(\left(\frac{\varepsilon_n}{\sigma^2} - \gamma_n - 1\right)\sqrt{\frac{\tau f}{2\gamma_n + 1}}\right) \tag{1}$$

where ε_n is a chosen threshold of energy detector on subchannel n, τ is the spectrum sensing time, γ_n is the received signal-to-noise ratio (SNR) of the primary macrocell user measured at the CSBS on subchannel n, f is the sampling frequency, and the standard Gaussian Q-function is defined as

$$Q(x) = \frac{1}{\sqrt{2\pi}}\int_x^\infty \exp(-t^2/2)dt. \tag{2}$$

The probability of false alarm q_n^f can be approximated by [20]

$$\begin{aligned} q_n^f(\varepsilon_n, \tau) &= Q\left(\left(\tfrac{\varepsilon_n}{\sigma^2} - 1\right)\sqrt{\tau f}\right) \\ &= Q\left(\sqrt{2\gamma_n + 1}\left(Q^{-1}\left(\hat{q}_n^d\right)\right) + \sqrt{\tau f}\gamma_n\right) \end{aligned} \tag{3}$$

where $\hat{q}_n^d$ is the target probability of detection.

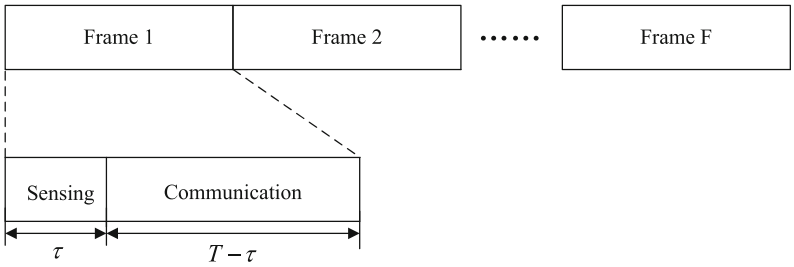

Fig. 1 The frame structure of cognitive small cell networks

The frame structure of the considered cognitive small cell network is shown in Fig. 1 [20]. As can be seen from Fig. 1, a spectrum sensing duration/time τ is inserted in the beginning of each frame. The CSBS adapts its transmit power based on the spectrum sensing decision made in the beginning of each frame. If the subchannel n is detected to be idle ($\tilde{\mathscr{H}}_n^v$), the cognitive small cell can transmit high-power $P_{s,n}^v$; if the subchannel n is detected to be occupied ($\tilde{\mathscr{H}}_n^o$), the cognitive small cell can transmit low-power $P_{s,n}^o$ in order to mitigate the interference caused to the primary macrocell. This approach is called hybrid spectrum sensing, and it is different from the opportunistic spectrum access and the spectrum-sharing approach. Based on the Shannon's capacity formula, when the spectrum sensing result is idle, the achievable capacity on subchannel n in the small cell is given by [19]

$$R_{v,n} = \log_2\left(1 + \frac{g_{ss,n} \cdot P_{s,n}^v}{\sigma^2}\right) \tag{4}$$

where $g_{ss,n}$ is the channel gain of subchannel n between the small cell user and CSBS. If the spectrum sensing result is active/occupied, the achievable capacity on subchannel n in the small cell is given by [19]

$$R_{o,n} = \log_2\left(1 + \frac{g_{ss,n} \cdot P_{s,n}^o}{g_{ms,n} \cdot P_{m,n}^o + \sigma^2}\right) \tag{5}$$

where $g_{ms,n}$ is the channel gain of subchannel n between the macrocell basestation (MBS) and CSBS and $P_{m,n}^o$ is the transmit power of MBS on subchannel n.

In a cognitive heterogeneous network, which typically consists of a cognitive small cell and a primary macrocell, imperfect spectrum sensing of CSBS can cause severe co-channel interference to the primary macrocell and thus degrade the performance of the heterogeneous cognitive small cell networks [19]. Since it is the CSBS that determines whether a subchannel is occupied by the primary

macrocell or not, according to [19], four different cases are to be considered as follows.

- Case 1: subchannel n is vacant in primary macrocell, and the spectrum sensing decision made by CSBS is vacant;
- Case 2: subchannel n is vacant in primary macrocell, but the spectrum sensing decision made by CSBS is occupied;
- Case 3: subchannel n is occupied in primary macrocell, but the spectrum sensing decision made by CSBS is vacant;
- Case 4: subchannel n is occupied in primary macrocell, and the spectrum sensing decision made by CSBS is occupied.

For the first and fourth cases, the CSBS makes the correct decisions. On the other hand, the second case is false alarm, and the third case is mis-detection. Therefore, the achievable capacities on subchannel n in small cell can be calculated for the four different cases as [19]

$$R_{1,n} = \log_2\left(1 + \frac{g_{ss,n} \cdot P_{s,n}^{v}}{\sigma^2}\right), \tag{6}$$

$$R_{2,n} = \log_2\left(1 + \frac{g_{ss,n} \cdot P_{s,n}^{o}}{\sigma^2}\right), \tag{7}$$

$$R_{3,n} = \log_2\left(1 + \frac{g_{ss,n} \cdot P_{s,n}^{v}}{g_{ms,n} \cdot P_{m,n} + \sigma^2}\right), \tag{8}$$

$$R_{4,n} = \log_2\left(1 + \frac{g_{ss,n} \cdot P_{s,n}^{o}}{g_{ms,n} \cdot P_{m,n} + \sigma^2}\right). \tag{9}$$

Our objective is to maximize energy efficiency of cognitive small cell networks by optimizing sensing time and power allocation. The energy efficiencies of those four cases [19] are defined as follows:

$$\eta_{1,n} = \frac{R_{1,n}}{P_{s,n}^{v} + P_c}, \tag{10}$$

$$\eta_{2,n} = \frac{R_{2,n}}{P_{s,n}^{o} + P_c}, \tag{11}$$

$$\eta_{3,n} = \frac{R_{3,n}}{P_{s,n}^{v} + P_c}, \tag{12}$$

$$\eta_{4,n} = \frac{R_{4,n}}{P_{s,n}^{o} + P_c} \tag{13}$$

where P_c is the constant circuit power consumption which includes lowpass filter, mixer for modulation, frequency synthesizer, and digital-to-analog converter [21] and P_c is assumed to be independent of the transmitted power [22].

The average energy efficiency of subchannel n in the hybrid spectrum sensing scheme is [19]

$$\begin{aligned}\eta_n = & P\left(\mathscr{H}_n^v\right)\left(1-q_n^f\left(\varepsilon_n,\tau\right)\right)\eta_{1,n} \\ & +P\left(\mathscr{H}_n^v\right)q_n^f\left(\varepsilon_n,\tau\right)\eta_{2,n} \\ & +P\left(\mathscr{H}_n^o\right)q_n^m\left(\varepsilon_n,\tau\right)\eta_{3,n} \\ & +P\left(\mathscr{H}_n^o\right)\left(1-q_n^m\left(\varepsilon_n,\tau\right)\right)\eta_{4,n}\end{aligned} \tag{14}$$

where $P\left(\mathscr{H}_n^v\right)$ and $P\left(\mathscr{H}_n^o\right)$ are the probabilities of vacant status and occupied status of subchannel n, respectively.

Since the resource allocation is performed in CSBS, the transmit power of CSBS on subchannel n is constrained by [19]

$$\sum_{n=1}^{N}\left[\begin{array}{l}P\left(\mathscr{H}_n^v\right)\left(1-q_n^f\left(\varepsilon_n,\tau\right)\right)P_{s,n}^v \\ +P\left(\mathscr{H}_n^v\right)q_n^f\left(\varepsilon_n,\tau\right)P_{s,n}^o \\ +P\left(\mathscr{H}_n^o\right)q_n^m\left(\varepsilon_n,\tau\right)P_{s,n}^v \\ +P\left(\mathscr{H}_n^o\right)\left(1-q_n^m\left(\varepsilon_n,\tau\right)\right)P_{s,n}^o\end{array}\right]\frac{T-\tau}{T}\le P_{\max} \tag{15}$$

where $P_{\max}$ is the maximum average transmit power of CSBS.

Since primary macrocells play a fundamental role in providing cellular coverage, macrocell users' QoS should not be affected by cognitive small cell's deployment. Therefore, to implement cross-tier interference protection, an average interference power limit is imposed to constrain the cross-tier interference suffered by macrocell [19]. Let I_n^{th} denote the maximum tolerable interference level on subchannel n for the macrocell user. We have

$$P\left(\mathscr{H}_n^o\right)\cdot g_{sm,n}\left[\begin{array}{l}q_n^m\left(\varepsilon_n,\tau\right)P_{s,n}^v+ \\ \left(1-q_n^m\left(\varepsilon_n,\tau\right)\right)P_{s,n}^o\end{array}\right]\frac{T-\tau}{T}\le I_n^{th},\forall n \tag{16}$$

where $g_{sm,n}$ is the channel power gain from the small cell to the macrocell user on subchannel n.

In order to guarantee the QoS for the small cell, a minimum transmit data rate constraint is introduced as [19]

$$\begin{aligned}& P\left(\mathscr{H}_n^v\right)\left(1-q_n^f\left(\varepsilon_n,\tau\right)\right)R_{1,n}+P\left(\mathscr{H}_n^v\right)q_n^f\left(\varepsilon_n,\tau\right)R_{2,n} \\ & +P\left(\mathscr{H}_n^o\right)q_n^m\left(\varepsilon_n,\tau\right)R_{3,n}+P\left(\mathscr{H}_n^o\right)\left(1-q_n^m\left(\varepsilon_n,\tau\right)\right)R_{4,n}\ge R_{\min}\end{aligned} \tag{17}$$

where $R_{\min}$ is the minimum transmit data rate requirement of each subchannel.

For a target detection probability of $\widehat{q}_n^d$ on subchannel n, substituting $\widehat{q}_n^d$ into (1), we obtain

$$\left(\frac{\varepsilon_n}{\sigma^2} - \gamma_n - 1\right)\sqrt{\frac{\tau f}{2\gamma_n + 1}} = Q^{-1}\left(\widehat{q}_n^d\right). \tag{18}$$

Therefore, for a given sensing time $\widehat{\tau}$, the detection threshold ε_n can be determined as

$$\varepsilon_n = \left(\sqrt{\frac{2\gamma_n + 1}{\widehat{\tau} f}} Q^{-1}\left(\widehat{q}_n^d\right) + \gamma_n + 1\right)\sigma^2, \forall n. \tag{19}$$

Problem Formulation

In this part, the aim is to maximize the cognitive small cell's energy efficiency while protecting QoS of the primary macrocell users. The cross-tier interference power limit is sent by a primary MBS periodically. This process requires little overhead in the primary macrocell. In this case, the sensing time optimization and power control in primary macrocell are not part of optimization [19]. Thus, the corresponding sensing time optimization and power allocation problem for the downlink CSBS can be mathematically formulated as [19]

$$\max_{\{\tau, \mathbf{P}_s^v, \mathbf{P}_s^o\}} \sum_{n=1}^{N} \frac{T-\tau}{T} \eta_n\left(\tau, P_{s,n}^v, P_{s,n}^o\right) \tag{20}$$

s.t.

$$\begin{aligned}
&C1: \sum_{n=1}^{N} \left[\begin{array}{l} P(\mathscr{H}_n^v)(1 - q_n^f(\varepsilon_n, \tau))P_{s,n}^v + P(\mathscr{H}_n^v)q_n^f(\varepsilon_n, \tau)P_{s,n}^o \\ + P(\mathscr{H}_n^o)q_n^m(\varepsilon_n, \tau)P_{s,n}^v + P(\mathscr{H}_n^o)(1 - q_n^m(\varepsilon_n, \tau))P_{s,n}^o \end{array}\right]\frac{T-\tau}{T} \le P_{\max} \\
&C2: P(\mathscr{H}_n^o) \cdot g_{sm,n}\left[q_n^m(\varepsilon_n, \tau)P_{s,n}^v + (1 - q_n^m(\varepsilon_n, \tau))P_{s,n}^o\right]\frac{T-\tau}{T} \le I_n^{th}, \forall n \\
&C3: \begin{array}{l} P(\mathscr{H}_n^v)(1 - q_n^f(\varepsilon_n, \tau))R_{1,n} + P(\mathscr{H}_n^v)q_n^f(\varepsilon_n, \tau)R_{2,n} \\ + P(\mathscr{H}_n^o)q_n^m(\varepsilon_n, \tau)R_{3,n} + P(\mathscr{H}_n^o)(1 - q_n^m(\varepsilon_n, \tau))R_{4,n} \ge R_{\min}, \forall n \end{array} \\
&C4: P_{s,n}^v \ge 0, P_{s,n}^o \ge 0, \forall n \\
&C5: 0 \le \tau \le T
\end{aligned} \tag{21}$$

where $\mathbf{P}_s^v = [p_{s,n}^v]_{1\times N}$ and $\mathbf{P}_s^o = [p_{s,n}^o]_{1\times N}$ are the power allocation vectors of the N subchannels in the cognitive small cell. In (21), $C1$ limits the maximum transmit power of each CSBS to $P_{\max}$; $C2$ sets the tolerable interference power level on each subchannel of the macrocell user on subchannel n; $C3$ represents minimum QoS requirement of each subchannel; $C4$ represents the nonnegative power constraint of the transmit power on each subchannel; $C5$ expresses the constraint of sensing time in each frame.

Note that the optimization problem in (20) under the constraints of (21) is nonconvex with respect to $\{\tau, \mathbf{P}_s^v, \mathbf{P}_s^o\}$ [19]. Therefore, the problem of energy-efficient power control is investigated given the sensing time $\widehat{\tau}$.

Energy-Efficient Resource Optimization in One Cognitive Small Cell

Transformation of the Optimization Problem

Given the sensing time $\widehat{\tau}$, the power control problem in (20) under the constraints of (21) can be classified as a nonlinear fractional programming problem. Since the joint optimization problem of $\mathbf{P}_s^v$ and $\mathbf{P}_s^o$ in (20) can be decoupled into two separate subproblems, namely, one for $\mathbf{P}_s^v$ and the other for $\mathbf{P}_s^o$ [19]. The subproblem related to $\mathbf{P}_s^v$ is first solved. Since subchannels in (20) are independent, a nonnegative variable $\eta_{13,n}^*$ is defined for the sum of average energy efficiencies on subchannel n in Case 1 and Case 3 as [19]

$$\eta_{13,n}^* = \frac{\left\{\begin{array}{l} P(\mathscr{H}_n^v)(1-q_n^f(\varepsilon_n,\hat{\tau}))R_{1,n}(\hat{\tau},\tilde{P}_{s,n}^v) \\ +P(\mathscr{H}_n^o)q_n^m(\varepsilon_n,\hat{\tau})R_{3,n}(\hat{\tau},\tilde{P}_{s,n}^v) \end{array}\right\}}{\tilde{P}_{s,n}^v + P_c} \tag{22}$$

where $\widetilde{P}_{s,n}^v$ is the optimal solution to the problem of (20) under the constraints of (21).

Theorem 1. *$\eta_{13,n}^*$ is achieved if and only if (80) where the $P_{s,n}^v$ in (80) is one of the feasible solutions to (20) under the constraints of (21).*

The proof is provided in Appendix.

According to the Theorem 1, the objective function with respect to $\mathbf{P}_s^o$ in fractional form can also be transformed to a subtractive form by introducing a nonnegative variable $\eta_{24,n}^*$.

Iterative Energy Efficiency Maximization Algorithm

To solve the transformed optimization problem in the subtractive form under the constraints of (20), Algorithm 1 [19] is provided.

Algorithm 1 Energy-efficient power control algorithm

Initialize the maximum number of iterations $L_{\max}$ and convergence tolerance ε_η;
Set $\eta_{13,n}(1)=0$, $\eta_{24,n}(1)=0$, $l=0$;
Initialize power allocation with an equal power distribution and begin the outer loop;
for $n=1$ to N **do**
  repeat
    a) The inner loop power control problem is solved with outer loop results $\eta^*_{13,n}(l)$, $\eta^*_{24,n}(l)$, the Lagrangian method and (28), (31);
    b) Then, the power control solution $\underline{P}^v_{s,n}(l)$ and $\underline{P}^o_{s,n}(l)$ can be obtained;
    if $(P(\mathscr{H}^v_n)(1-q^f_n(\varepsilon_n,\widehat{\tau}))R_{1,n}(\widehat{\tau},\underline{P}^v_{s,n}(l)) + P(\mathscr{H}^o_n)q^m_n(\varepsilon_n,\widehat{\tau})R_{3,n}(\widehat{\tau},\underline{P}^v_{s,n}(l)) - \eta_{13,n}(l)(\underline{P}^v_{s,n}(l)+P_c)) < \varepsilon_\eta$ **then**
      Convergence= **true**; $\widetilde{P}^v_{s,n}=\underline{P}^v_{s,n}(l)$
      $\eta^*_{13,n}=\dfrac{P(H^v_n)(1-q^f_n(\varepsilon_n,\hat{\tau}))R_{1,n}(\hat{\tau},\tilde{P}^v_{s,n})+P(H^o_n)q^m_n(\varepsilon_n,\hat{\tau})R_{3,n}(\hat{\tau},\tilde{P}^v_{s,n})}{\tilde{P}^v_{s,n}+P_c}$
    else
      $\eta_{13,n}(l+1)=\dfrac{P(H^v_n)(1-q^f_n(\varepsilon_n,\hat{\tau}))R_{1,n}(\hat{\tau},\underline{P}^v_{s,n}(l))+P(H^o_n)q^m_n(\varepsilon_n,\hat{\tau})R_{3,n}(\hat{\tau},\underline{P}^v_{s,n}(l))}{\underline{P}^v_{s,n}(l)+P_c}$
      Convergence= **false**, $l=l+1$;
    end if
    if $(P(\mathscr{H}^v_n)q^f_n(\varepsilon_n,\widehat{\tau})R_{2,n}(\widehat{\tau},\underline{P}^o_{s,n}(l)) + P(\mathscr{H}^o_n)(1-q^m_n(\varepsilon_n,\widehat{\tau}))R_{4,n}(\widehat{\tau},\underline{P}^o_{s,n}(l)) - \eta_{24,n}(l)(\underline{P}^o_{s,n}(l)+P_c)) < \varepsilon_\eta$ **then**
      Convergence= **true**; $\widetilde{P}^o_{s,n}=\underline{P}^o_{s,n}(l)$
      $\eta^*_{24,n}=\dfrac{P(H^v_n)q^f_n(\varepsilon_n,\hat{\tau})R_{2,n}(\hat{\tau},\tilde{P}^o_{s,n})+P(H^o_n)(1-q^m_n(\varepsilon_n,\hat{\tau}))R_{4,n}(\hat{\tau},\tilde{P}^o_{s,n})}{\tilde{P}^o_{s,n}+P_c}$
    else
      $\eta_{24,n}(l+1)=\dfrac{P(H^v_n)q^f_n(\varepsilon_n,\hat{\tau})R_{2,n}(\hat{\tau},\underline{P}^o_{s,n}(l))+P(H^o_n)(1-q^m_n(\varepsilon_n,\hat{\tau}))R_{4,n}(\hat{\tau},\underline{P}^o_{s,n}(l))}{\underline{P}^o_{s,n}(l)+P_c}$
      Convergence= **false**, $l=l+1$;
    end if
  until Convergence= **true** or $l=L_{\max}$
end for

As shown in Algorithm 1, in each iteration of the outer loop, the lth inner loop power control problem is given as

$$\max_{\{\mathbf{P}^v_s,\mathbf{P}^o_s\}}\sum_{n=1}^{N}\frac{T-\hat{\tau}}{T}\left\{\begin{array}{l}P(\mathscr{H}^v_n)(1-q^f_n(\varepsilon_n,\hat{\tau}))R_{1,n}(\hat{\tau},P^v_{s,n})\\+P(\mathscr{H}^o_n)q^m_n(\varepsilon_n,\hat{\tau})R_{3,n}(\hat{\tau},P^v_{s,n})\\+P(\mathscr{H}^v_n)q^f_n(\varepsilon_n,\hat{\tau})R_{2,n}(\hat{\tau},P^o_{s,n})\\+P(\mathscr{H}^o_n)(1-q^m_n(\varepsilon_n,\hat{\tau}))R_{4,n}(\hat{\tau},P^o_{s,n})\\-\eta_{13,n}(l)(P^v_{s,n}+P_c)\\-\eta_{24,n}(l)(P^o_{s,n}+P_c)\end{array}\right\} \tag{23}$$

$$\text{s.t. } C1-C4. \tag{24}$$

Since the optimization problem of (23) under the constraints of (24) is convex with respect to $\mathbf{P}_s^v$ and $\mathbf{P}_s^o$. The Lagrangian function is given by (25)

$$
\begin{aligned}
&L(\mathbf{P}_s^v, \mathbf{P}_s^o, \lambda, \boldsymbol{\mu}, \boldsymbol{\nu}) = \\
&\left\{ \sum_{n=1}^{N} \frac{T-\hat{\tau}}{T} \left[\begin{array}{l} (P(\mathscr{H}_n^v)(1-q_n^f(\varepsilon_n,\hat{\tau}))R_{1,n}(\hat{\tau}, P_{s,n}^v) \\ \quad + P(\mathscr{H}_n^o)q_n^m(\varepsilon_n,\hat{\tau})R_{3,n}(\hat{\tau}, P_{s,n}^v) - \eta_{13,n}(l)P_{s,n}^v \\ \quad + P(\mathscr{H}_n^v)q_n^f(\varepsilon_n,\hat{\tau})R_{2,n}(\hat{\tau}, P_{s,n}^o) \\ \quad + P(\mathscr{H}_n^o)(1-q_n^m(\varepsilon_n,\hat{\tau}))R_{4,n}(\hat{\tau}, P_{s,n}^o) - \eta_{24,n}(l)P_{s,n}^o \end{array} \right] \right\} \\
&-\lambda \left\{ \sum_{n=1}^{N} \left[\begin{array}{l} P(\mathscr{H}_n^v)(1-q_n^f(\varepsilon_n,\hat{\tau}))P_{s,n}^v + P(\mathscr{H}_n^v)q_n^f(\varepsilon_n,\hat{\tau})P_{s,n}^o + \\ P(\mathscr{H}_n^o)q_n^m(\varepsilon_n,\hat{\tau})P_{s,n}^v + P(\mathscr{H}_n^o)(1-q_n^m(\varepsilon_n,\hat{\tau}))P_{s,n}^o \end{array} \right] \frac{T-\hat{\tau}}{T} - P_{\max} \right\} \\
&- \sum_{n=1}^{N} \mu_n \left\{ \left[\sum_{n=1}^{N} P(\mathscr{H}_n^o) g_{sm,n} (q_n^m(\varepsilon_n,\hat{\tau})P_{s,n}^v + (1-q_n^m(\varepsilon_n,\hat{\tau}))P_{s,n}^o) \right] \frac{T-\hat{\tau}}{T} - I_n^{th} \right\} \\
&+ \sum_{n=1}^{N} \nu_n \left\{ \left[\begin{array}{l} P(\mathscr{H}_n^v)(1-q_n^f(\varepsilon_n,\tau))R_{1,n} + P(\mathscr{H}_n^v)q_n^f(\varepsilon_n,\tau)R_{2,n} \\ + P(\mathscr{H}_n^o)q_n^m(\varepsilon_n,\tau)R_{3,n} + P(\mathscr{H}_n^o)(1-q_n^m(\varepsilon_n,\tau))R_{4,n} \end{array} \right] - R_{\min} \right\}
\end{aligned}
\tag{25}
$$

where λ, $\boldsymbol{\mu_n}$, and $\boldsymbol{\nu_n}$ are the Lagrangian multipliers (also called dual variables) vectors for the constraints C1, C2, and C3 in (21), respectively. Thus, the Lagrangian dual function is [19] defined as

$$
g(\lambda, \boldsymbol{\mu}, \boldsymbol{\nu}) = \max_{\mathbf{P}_s^v, \mathbf{P}_s^o} \; L(\mathbf{P}_s^v, \mathbf{P}_s^o, \lambda, \boldsymbol{\mu}, \boldsymbol{\nu}). \tag{26}
$$

The dual problem can be expressed as [19]

$$
\min_{\lambda, \boldsymbol{\mu}, \boldsymbol{\nu} \geq 0} \; g(\lambda, \boldsymbol{\mu}, \boldsymbol{\nu}). \tag{27}
$$

Using Lagrangian function and the Karush-Kuhn-Tucker (KKT) conditions, the near optimal solution of $\widetilde{P}_{s,n}^v$ on subchannel n can be obtained as

$$
\tilde{P}_{s,n}^v = \left[\frac{A_{v,n} + \sqrt{B_{v,n}}}{2} \right]^+ \tag{28}
$$

where $[x]^+ = \max\{x, 0\}$, and $A_{v,n}$ and $B_{v,n}$ are given by (29) and (30), respectively.

$$
\begin{aligned}
A_{v,n} = &\frac{(1+\nu_n)(P(\mathscr{H}_n^v)(1-q_n^f(\varepsilon_n,\widehat{\tau})) + P(\mathscr{H}_n^o)q_n^m(\varepsilon_n,\widehat{\tau}))}{\ln 2(\eta_{13,n}(l) + \lambda(P(\mathscr{H}_n^v)(1-q_n^f(\varepsilon_n,\hat{\tau})) + P(\mathscr{H}_n^o)q_n^m(\varepsilon_n,\widehat{\tau})) \\
&\qquad + \mu_n g_{sm,n} P(\mathscr{H}_n^o)q_n^m(\varepsilon_n,\widehat{\tau}))} \\
&- \frac{2\sigma^2 + g_{ms,n} P_{m,n}^o}{g_{ss,n}}
\end{aligned}
\tag{29}
$$

$$B_{v,n} = A_{v,n}^2 - \frac{4}{g_{ss,n}} \cdot \left\{ \frac{\sigma^4 + \sigma^2 g_{ms,n} P_{m,n}^o}{g_{ss,n}} - \frac{\begin{array}{c}(1+\nu_n)[P(\mathscr{H}_n^v)(1-q_n^f(\varepsilon_n,\widehat{\tau})(\sigma^2+g_{ms,n}P_{m,n}^o)) \\ +P(\mathscr{H}_n^o)q_n^m(\varepsilon_n,\widehat{\tau})\sigma^2]\end{array}}{\begin{array}{c}\ln 2(\eta_{13,n}(l)+\lambda(P(\mathscr{H}_n^v)(1-q_n^f(\varepsilon_n,\widehat{\tau})+P(\mathscr{H}_n^o)q_n^m(\varepsilon_n,\widehat{\tau})) \\ +\mu_n g_{sm,n} P(\mathscr{H}_n^o) q_n^m(\varepsilon_n,\widehat{\tau})))\end{array}} \right\}. \tag{30}$$

Similar to $\widetilde{P}_{s,n}^v$, the near optimal solution of $\widetilde{P}_{s,n}^o$ on subchannel n can be obtained as

$$\tilde{P}_{s,n}^o = \left[\frac{A_{o,n} + \sqrt{B_{o,n}}}{2} \right]^+ \tag{31}$$

$$A_{o,n} = \frac{(1+\nu_n)(P(\mathscr{H}_n^v)q_n^f(\varepsilon_n,\widehat{\tau}) + P(\mathscr{H}_n^o)(1-q_n^m(\varepsilon_n,\widehat{\tau})))}{\begin{array}{c}\ln 2(\eta_{24,n}(l)+\lambda(P(\mathscr{H}_n^v)q_n^f(\varepsilon_n,\widehat{\tau})+P(\mathscr{H}_n^o)(1-q_n^m(\varepsilon_n,\widehat{\tau}))) \\ +\mu_n g_{sm,n} P(\mathscr{H}_n^o)(1-q_n^m(\varepsilon_n,\widehat{\tau})))\end{array}} - \frac{2\sigma^2 + g_{ms,n}P_{m,n}^o}{g_{ss,n}} \tag{32}$$

$$B_{o,n} = A_{o,n}^2 - \frac{4}{g_{ss,n}} \cdot \left\{ \frac{\sigma^4 + \sigma^2 g_{ms,n} P_{m,n}^o}{g_{ss,n}} - \frac{\begin{array}{c}(1+\nu_n)[P(\mathscr{H}_n^v)q_n^f(\varepsilon_n,\hat{\tau})(\sigma^2+g_{ms,n}P_{m,n}^o) \\ +P(\mathscr{H}_n^o)(1-q_n^m(\varepsilon_n,\hat{\tau}))\sigma^2]\end{array}}{\begin{array}{c}\ln 2(\eta_{13,n}(l)+\lambda(P(\mathscr{H}_n^v)q_n^f(\varepsilon_n,\hat{\tau})+P(\mathscr{H}_n^o)(1-q_n^m(\varepsilon_n,\hat{\tau})) \\ +\mu_n g_{sm,n} P(\mathscr{H}_n^o)(1-q_n^m(\varepsilon_n,\hat{\tau})))\end{array}} \right\}. \tag{33}$$

where $A_{o,n}$ and $B_{o,n}$ are given by (32) and (33), respectively.

Either the ellipsoid or the subgradient method can be adopted in updating the dual variables [23]. Here, the subgradient method is chosen to update the dual variables, and the update formulas are (34), (35), and (36)

$$\lambda^{l+1} = \lambda^l - \vartheta_1^l \left(P_{\max} - \sum_{n=1}^{N} \left[\begin{array}{l} P(\mathscr{H}_n^v)(1-q_n^f(\varepsilon_n,\tau))P_{s,n}^v + P(\mathscr{H}_n^v)q_n^f(\varepsilon_n,\tau)P_{s,n}^o + \\ P(\mathscr{H}_n^o)q_n^m(\varepsilon_n,\tau)P_{s,n}^v + P(\mathscr{H}_n^o)(1-q_n^m(\varepsilon_n,\tau))P_{s,n}^o \end{array} \right] \frac{T-\tau}{T} \right) \tag{34}$$

$$\mu_n^{l+1} = \mu_n^l - \vartheta_2^l \left(I_n^{th} - P(\mathscr{H}_n^o) \cdot g_{sm,n} \left[q_n^m(\varepsilon_n,\tau)P_{s,n}^v + (1-q_n^m(\varepsilon_n,\tau))P_{s,n}^o \right] \frac{T-\tau}{T} \right), \forall n \tag{35}$$

$$\nu_n^{l+1} = \nu_n^l - \vartheta_3^l \left(\left\{ \begin{array}{l} P(\mathscr{H}_n^v)(1-q_n^f(\varepsilon_n,\tau))R_{1,n} + P(\mathscr{H}_n^v)q_n^f(\varepsilon_n,\tau)R_{2,n} + \\ P(\mathscr{H}_n^o)q_n^m(\varepsilon_n,\tau)R_{3,n} + P(\mathscr{H}_n^o)(1-q_n^m(\varepsilon_n,\tau)R_{4,n} \end{array} \right\} \frac{T-\tau}{T} - R_{\min} \right), \forall n \tag{36}$$

where ϑ_1^l, ϑ_2^l, and ϑ_3^l denote the step size of iteration l ($l \in \{1, 2, \ldots, L_{\max}\}$)for λ, $\boldsymbol{\mu}$, and $\boldsymbol{\nu}$, respectively, and $L_{\max}$ is the maximum number of iterations. Meanwhile, the step size must meet the following conditions

$$\sum_{l=1}^{\infty} \vartheta_i^l = \infty, \lim_{l \to \infty} \vartheta_i^l = 0, \ \forall i \in \{1, 2, 3\}. \tag{37}$$

Algorithm 1 is provided to optimize the power $P_{s,n}^v$ and $P_{s,n}^o$ of (20) given the sensing time $\hat{\tau}$ [19]. In Algorithm 1, the process of power control is decomposed to inner loop problem and outer loop problem. In each iteration, both $\eta_{13,n}^*(l)$ and $\eta_{24,n}^*(l)$ can be found through outer loop, the inner loop control problem is solved by the outer loop results $\eta_{13,n}^*(l)$ and $\eta_{24,n}^*(l)$, the Lagrangian method and (28), (31).

The near optimal sensing time scheme can be found in Algorithm 2 [19] based on a one-dimensional exhaustive search.

Algorithm 2 is provided to optimize the sensing time in (20) when the optimal power through Algorithm 1 has been obtained. Therefore, running Algorithm 1 with $\widehat{\tau}(l)$ to obtain the optimal power $\widetilde{P}_{s,n}^v$ and $\widetilde{P}_{s,n}^o$ has to be firstly done in Algorithm 2. Then the optimal sensing time is found based on a one-dimensional exhaustive search.

Complexity Analysis

The computational complexity of the provided algorithms is analyzed in this subsection. Suppose the subgradient method used in Algorithm 1 reguires Δ_1 iterations to converge; the updates of λ need $O(1)$ operations; $\boldsymbol{\mu}$ and $\boldsymbol{\nu}$ need $O(N)$ operations each. The method used in Algorithm 1 to calculate $\eta_{13,n}^*$ and $\eta_{24,n}^*$ on each subchannel in a small cell needs Δ_2 iterations to converge. The total complexity of Algorithm 1 is thus $O(N^2 \Delta_1 \Delta_2)$. The parameters Δ_1 and Δ_2 can be small enough if the initial values of λ, $\boldsymbol{\mu}$ and $\boldsymbol{\nu}$ are well chosen, together with suitable

Algorithm 2 Near optimal energy-efficient sensing time scheme

1: Initialize the maximum number of iterations $L_{\max}$ and convergence tolerance ε_τ
2: Set $l = 0$; Initialize $\widehat{\tau}(l)$;
3: **repeat**
4: Run Algorithm 1 with $\widehat{\tau}(l)$ to obtain the optimal power $\widetilde{P}_{s,n}^v$ and $\widetilde{P}_{s,n}^o$;
5: $P_{s,n}^v(l) = \widetilde{P}_{s,n}^v$, $P_{s,n}^o(l) = \widetilde{P}_{s,n}^o$;
6: $\widehat{\tau}(l) = \max_{\tau} \sum_{n=1}^{N} \frac{T-\tau}{T} \eta_n \left(\tau, P_{s,n}^v(l), P_{s,n}^o(l)\right)$;
7: **if** $\left|\widehat{\tau}(l) - \widehat{\tau}(l-1)\right| \le \varepsilon_\tau$ **then**
8: Convergence= **true**, $\widetilde{\tau} = \widehat{\tau}(l)$;
9: **else**
10: Convergence= **false**, $l = l + 1$;
11: **end if**
12: **until** Convergence= **true** or $l = L_{\max}$

values of iteration step sizes. In Algorithm 2, finding the optimal sensing time for each subchannel requires $O(L)$ operations. Therefore, the total computational complexity of Algorithm 2 is $O(NL)$ for the network with N subchannels [19].

Energy-Efficient Resource Optimization in Multiple Cognitive Small Cells

Multiple Cognitive Small Cells Scenario

In this subsection, the energy-efficient resource optimization is investigated in multiple cognitive small cells. The aforementioned method is applied to optimize the energy efficiency in multiple cognitive small cells network, where the interference between small cells will be considered. In multiple cognitive small cells, to maximize the total energy efficiency with the consideration of co-tier interference mitigation, the problem in (20) under the constraints of (21) can be formulated as [19]

$$\max_{\{\boldsymbol{\tau},\mathbf{P}^{\mathbf{v}}_{\mathbf{ms}},\mathbf{P}^{\mathbf{o}}_{\mathbf{ms}}\}} \sum_{k=1}^{K}\sum_{n=1}^{N} \frac{T-\tau_k}{T}\eta_{k,n}\left(\tau_k, P^v_{s,k,n}, P^o_{s,k,n}\right) \tag{38}$$

$$\begin{aligned}
\text{s.t.}\quad & C1: \sum_{n=1}^{N}\left[\begin{array}{l} P(\mathscr{H}^v_{k,n})(1-q^f_{k,n}(\varepsilon_{k,n},\tau_k))P^v_{s,k,n} + P(\mathscr{H}^v_{k,n})q^f_{k,n}(\varepsilon_{k,n},\tau_k)P^o_{s,k,n} \\ +P(\mathscr{H}^o_{k,n})q^m_{k,n}(\varepsilon_{k,n},\tau_k)P^v_{s,k,n} + P(\mathscr{H}^o_{k,n})(1-q^m_{k,n}(\varepsilon_{k,n},\tau_k))P^o_{s,k,n}\end{array}\right] \\
& \times \frac{T-\tau_k}{T} \le P_{\max} \\
& C2: P(H^o_{k,n})\cdot g^{sm}_{k,n}\left[q^m_{k,n}(\varepsilon_{k,n},\tau_k)P^v_{s,k,n} + (1-q^m_{k,n}(\varepsilon_{k,n},\tau_k))P^o_{s,k,n}\right]\frac{T-\tau_k}{T} \\
& \le I^{th}_{k,n}, \forall k,n \\
& C3: \begin{array}{l} P(\mathscr{H}^v_{k,n})(1-q^f_{k,n}(\varepsilon_{k,n},\tau_k))R^1_{k,n} + P(\mathscr{H}^v_{k,n})q^f_{k,n}(\varepsilon_{k,n},\tau_k)R^2_{k,n} \\ +P(\mathscr{H}^o_{k,n})q^m_{k,n}(\varepsilon_{k,n},\tau_k)R^3_{k,n} + P(\mathscr{H}^o_{k,n})(1-q^m_{k,n}(\varepsilon_{k,n},\tau_k))R^4_{k,n} \ge R_{\min}\end{array} \\
& C4: \sum_{j=1,j\neq k}^{K}\frac{T-\tau_k}{T}g_{k,j,n} \\
& \left\{\begin{array}{l} P(\mathscr{H}^o_{j,n})\left[q^m_{j,n}(\varepsilon_{j,n},\tau_j)P^v_{s,j,n} + (1-q^m_{j,n}(\varepsilon_{j,n},\tau_j))P^o_{s,j,n}\right] + \\ P(\mathscr{H}^v_{j,n})\left[q^f_{j,n}(\varepsilon_{j,n},\tau_j)P^o_{s,j,n} + (1-q^f_{n,j}(\varepsilon_{j,n},\tau_j))P^v_{s,j,n}\right]\end{array}\right\} \\
& \le \gamma^{th}_{k,n}, \forall n,k \\
& C5: P^v_{s,k,n} \ge 0, P^o_{s,k,n} \ge 0, \forall n,k \\
& C6: 0 \le \tau_k \le T, \forall k
\end{aligned} \tag{39}$$

where $\boldsymbol{\tau} = [\tau]_{1\times K}$ is the sensing time vector of K cognitive small cells, N is the number of subchannels in each small cell, and $\mathbf{P^v_{ms}} = \left[P^v_{s,k,n}\right]_{K\times N}$ and $\mathbf{P^o_{ms}} = \left[P^o_{s,k,n}\right]_{K\times N}$ are the power allocation vectors of the N subchannels in K cognitive small cells. Constraint $C1$ limits the maximum transmit power of each CSBS to $P_{\max}$; $C2$ sets the tolerable interference power level for each small cell on each subchannel of the macrocell user on subchannel n; $C3$ represents minimum QoS requirement of each subchannel; $C4$ represents the tolerable interference power level from other small cells, where $\gamma^{th}_{k,n}$ denotes the co-tier interference limits on the nth subchannel in the kth small cell; $C5$ represents the nonnegative power constraint of the transmit power on each subchannel; $C6$ expresses the constraint of sensing time in each frame.

First of all, similar to the problem in (20), the problem of power control in (38) under the constraints of (39) can be decoupled into two separate subproblems respect to $\mathbf{P^v_{ms}}$ and $\mathbf{P^o_{ms}}$, respectively, when the sensing time $\hat{\tau}_k$ is given. The subproblem respect to $\mathbf{P^v_{ms}}$ is dealt with [19]. The variable $\eta^{13^*}_{k,n}$ is defined as

$$\eta^{13^*}_{k,n} = \frac{P(\mathscr{H}^v_{k,n})(1-q^f_{k,n}(\varepsilon_{k,n},\hat{\tau}_k))R^1_{k,n}(\hat{\tau}_k,\tilde{P}^v_{s,k,n}) + P(\mathscr{H}^o_{k,n})q^m_{k,n}(\varepsilon_{k,n},\hat{\tau}_k)R^3_{k,n}(\hat{\tau}_k,\tilde{P}^v_{s,k,n})}{\tilde{P}^v_{s,k,n}+P_c} \tag{40}$$

where $\eta^{13^*}_{k,n}$ represents the sum of average energy efficiencies on the nth subchannel of the kth small cell in Case 1 and Case 3. $\tilde{P}^v_{s,k,n}$ is the optimal solution to the problem of (38) under the constraints of (39).

Therefore, the optimization problem of (38) is transformed as optimization problem of (40) under the constraints of (39) [19]. Subsequently, Algorithm 1 is used to solve the transformed problem [19], and the near optimal solution can be obtained [19]

$$\tilde{P}^v_{s,k,n} = \left[\frac{A_{v,k,n}+\sqrt{B_{v,k,n}}}{2}\right]^+ \tag{41}$$

where $A_{v,k,n}$ and $B_{v,k,n}$ are given by

$$A_{v,k,n} = \frac{(1+\nu_{k,n})(P(\mathscr{H}^v_{k,n})(1-q^f_{k,n}(\varepsilon_{k,n},\hat{\tau}_k)) + P(\mathscr{H}^o_{k,n})q^m_{k,n}(\varepsilon_{k,n},\hat{\tau}_k))}{\left\{\begin{array}{l}\ln 2\left(\eta^{13}_{k,n}(l)+\lambda_{k,n}\left(P(\mathscr{H}^v_{k,n})\left(1-q^f_{k,n}(\varepsilon_{k,n},\hat{\tau}_k)\right)\right.\right.\\ \left.+P\left(\mathscr{H}^o_{k,n}\right)q^m_{k,n}(\varepsilon_{k,n},\hat{\tau}_k)\right)+\mu_{k,n}g^{sm}_{k,n}P(\mathscr{H}^o_{k,n})q^m_{k,n}(\varepsilon_{k,n},\hat{\tau}_k)\\ -\xi_{k,n}\sum\limits_{j=1,j\neq k}^{K}g_{j,k,n}\left[\begin{array}{l}P\left(\mathscr{H}^v_{j,n}\right)\left(1-q^f_{j,n}\left(\varepsilon_{j,n},\hat{\tau}_j\right)\right)\\ +P(\mathscr{H}^o_{j,n})q^m_{j,n}\left(\varepsilon_{j,n},\hat{\tau}_j\right)\end{array}\right]\end{array}\right\}}\\ -\frac{2\sigma^2+g^{ms}_{k,n}P^o_{m,n}}{g^{ss}_{k,n}} \tag{42}$$

$$B_{v,k,n} = A_{v,k,n}^2 \left\{ -\frac{4}{g_{k,n}^{ss}} \cdot \left\{ \frac{\sigma^4 + \sigma^2 g_{k,n}^{ms} P_{m,k,n}^o}{g_{k,n}^{ss}} - \frac{(1+\nu_{k,n})[P(\mathscr{H}_{k,n}^v)(1-q_{k,n}^f(\varepsilon_{k,n},\hat{\tau}_k))(\sigma^2 + g_{k,n}^{ms} P_{m,k,n}^o) + P(\mathscr{H}_{k,n}^o) q_{k,n}^m(\varepsilon_{k,n},\hat{\tau}_k)\sigma^2]}{\left\{ \begin{array}{l} \ln 2(\eta_{k,n}^{13}(l) + \lambda_k(P(\mathscr{H}_{k,n}^v)(1-q_{k,n}^f(\varepsilon_{k,n},\hat{\tau}_k)) + P(\mathscr{H}_{k,n}^o) q_{k,n}^m(\varepsilon_{k,n},\hat{\tau}_k) \\ +\mu_{k,n} g_{k,n}^{ms} P(\mathscr{H}_{k,n}^o) q_{k,n}^m(\varepsilon_{k,n},\hat{\tau}_k) \\ -\xi_{k,n} \sum\limits_{j=1,j\neq k}^{K} g_{j,k,n} \left[P(\mathscr{H}_{j,n}^v)(1-q_{j,n}^f(\varepsilon_{j,n},\hat{\tau}_j)) + P(\mathscr{H}_{j,n}^o) q_{j,n}^m(\varepsilon_{j,n},\hat{\tau}_j) \right] \end{array} \right\} \right\} \tag{43}$$

Similar to $\tilde{P}_{s,k,n}^v$, the near optimal solution can be obtained

$$\tilde{P}_{s,k,n}^o = \left[\frac{A_{o,k,n} + \sqrt{B_{o,k,n}}}{2} \right]^+ \tag{44}$$

where $A_{o,k,n}$ and $B_{o,k,n}$ are given by (45) and (46), respectively.

$$A_{o,k,n} = \frac{(1+\nu_{k,n}) P(\mathscr{H}_{k,n}^v) q_{k,n}^f(\varepsilon_{k,n},\hat{\tau}_k) + P(\mathscr{H}_{k,n}^o)(1-q_{k,n}^m(\varepsilon_{k,n},\hat{\tau}_k))}{\left\{ \begin{array}{l} \ln 2(\eta_{k,n}^{24}(l) + \lambda_{k,n} P(\mathscr{H}_{k,n}^v) q_{k,n}^f(\varepsilon_{k,n},\hat{\tau}_k) \\ +P(\mathscr{H}_{k,n}^o)(1-q_{k,n}^m(\varepsilon_{k,n},\hat{\tau}_k)) + \mu_{k,n} g_{k,n}^{sm} P(\mathscr{H}_{k,n}^o)(1-q_{k,n}^m(\varepsilon_{k,n},\hat{\tau}_k)) \\ -\xi_{k,n} \sum\limits_{j=1,j\neq k}^{K} g_{j,k,n} \left[\begin{array}{l} P(\mathscr{H}_{j,n}^v) q_{j,n}^f(\varepsilon_{j,n},\hat{\tau}_j) \\ +P(\mathscr{H}_{j,n}^o)(1-q_{j,n}^m(\varepsilon_{j,n},\hat{\tau}_j)) \end{array} \right] \end{array} \right\}} - \frac{2\sigma^2 + g_{k,n}^{ms} P_{m,n}^o}{g_{k,n}^{ss}} \tag{45}$$

$$B_{o,k,n} = A_{o,k,n}^2 \left\{ -\frac{4}{g_{k,n}^{ss}} \cdot \left\{ \frac{\sigma^4 + \sigma^2 g_{k,n}^{ms} P_{m,k,n}^o}{g_{k,n}^{ss}} \right. \right. \left. \left. - \frac{(1+\nu_{k,n})[P(\mathscr{H}_{k,n}^v) q_{k,n}^f(\varepsilon_{k,n}, \hat{\tau}_k)(\sigma^2 + g_{k,n}^{ms} P_{m,k,n}^o) + P(\mathscr{H}_{k,n}^o)(1 - q_{k,n}^m(\varepsilon_{k,n}, \hat{\tau}_k))\sigma^2]}{\left\{ \begin{array}{l} \ln 2(\eta_{k,n}^{13}(l) + \lambda_k(P(\mathscr{H}_{k,n}^v) q_{k,n}^f(\varepsilon_{k,n}, \hat{\tau}_k) + P(\mathscr{H}_{k,n}^o)(1 - q_{k,n}^m(\varepsilon_{k,n}, \hat{\tau}_k)) \\ +\mu_{k,n} g_{k,n}^{ms} P(\mathscr{H}_{k,n}^o)(1 - q_{k,n}^m(\varepsilon_{k,n}, \hat{\tau}_k)) \\ -\xi_{k,n} \sum\limits_{j=1, j\neq k}^{K} g_{j,k,n} \left[P(\mathscr{H}_{j,n}^v) q_{j,n}^f(\varepsilon_{j,n}, \hat{\tau}_j) + P(\mathscr{H}_{j,n}^o)(1 - q_{j,n}^m(\varepsilon_{j,n}, \hat{\tau}_j)) \right] \end{array} \right\} } \right\} \tag{46}$$

Finally, the near optimal sensing time for each small cell can be found in Algorithm 2 based on a one-dimensional exhaustive search [19].

Complexity Analysis

In this part, the computational complexity of the provided algorithms in multiple small cells network is analyzed. Similar to the single small cell case, suppose the subgradient method used in Algorithm 1 needs Δ_1 iterations to converge; the updates of $\boldsymbol{\lambda}$ need $O(N)$ operations; $\boldsymbol{\mu}$ and $\boldsymbol{\nu}$ need $O(KN)$ operations each. The method used in Algorithm 1 to calculate $\eta_{13,n}^*$ and $\eta_{24,n}^*$ on each subchannel in a small cell needs Δ_2 iterations to converge. The total complexity of Algorithm 1 is thus $O(N^2K^2\Delta_1\Delta_2)$. The parameters Δ_1 and Δ_2 can be small enough if the values of iteration step sizes and initial values of $\boldsymbol{\lambda}$, $\boldsymbol{\mu}$, and $\boldsymbol{\nu}$ are well chosen. In Algorithm 2, finding the optimal sensing time for each subchannel requires $O(L)$ operations. Therefore, the total computational complexity of Algorithm 2 is $O(KNL)$.

Simulation Results and Discussion

In this part, simulation results are presented to evaluate the performance of the provided algorithms. The sampling frequency f is 6 MHz, $T = 0.1$ s, $N = 50$, and $\sigma^2 = 1 \times 10^{-4}$. The channel gains are modeled as block faded and exponentially

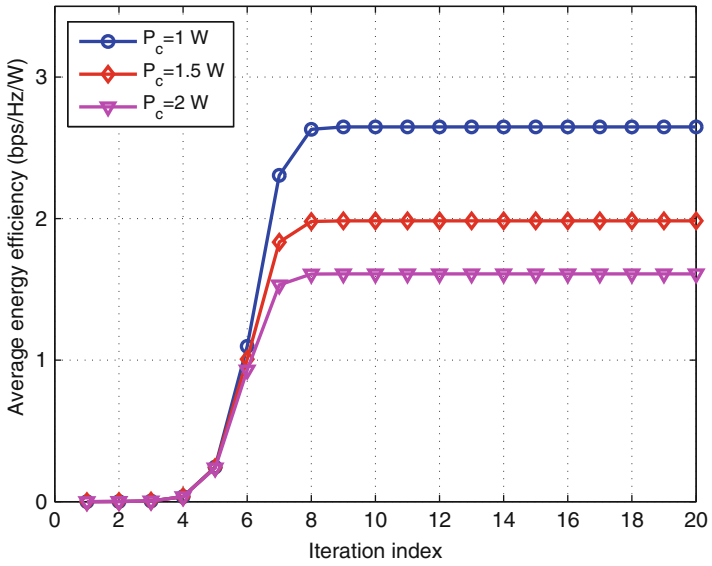

Fig. 2 Convergence in terms of average energy efficiency of small cell on each subchannel versus the number of iterations

distributed with mean of 0.1. The transmit power on each subchannel of primary macrocell is set at 25 mW. The QoS requirement of minimum data rate requirement is set as 0.3 bps/Hz. The target detection probability $\widehat{q}_n^d$ is set as 90% unless otherwise specified [19].

In Fig. 2, the convergence of Algorithm 1 is evaluated with the $P_{\max} = 15\,\text{dBm}$, the cross-tier interference limit $I_n^{th} = -10\,\text{dBm}$. As can be seen from Fig. 2, the average energy efficiency of small cell on each subchannel converges after nine iterations. This result, together with the previous analysis, indicates that the provided Algorithm 1 is practical in cognitive small cell [19].

Figure 3 displays the average energy efficiency of each subchannel in cognitive small cell network when the sensing time increases from 0.0005 to 0.015 s with $P_{\max} = 5, 10, 13, 15\,\text{dBm}$, the cross-tier interference limit $I_n^{th} = -10\,\text{dBm}$. The relation between sensing time and the average energy efficiency of each subchannel is exhibited [19]. As shown in Fig. 3, the average energy efficiency of each subchannel in cognitive small cell first increases and then drops when the sensing time is increased from 0.0005 to 0.015 s. It is estimated that the near optimal sensing time is between 0.002 and 0.004 s. Larger value of $P_{\max}$ results in higher average energy efficiency because a larger value of $P_{\max}$ enlarges the feasible region of the variables in the original optimization problem in (20)–(21).

Figure 4 shows the trend of average energy efficiency of each subchannel in cognitive small cell when $P_{\max}$ increases from 5 to 25 dBm [19]. The target detection probabilities $\widehat{q}_n^d = 0.8, 0.9$ and cross-tier interference limit $I_n^{th} = -10\,\text{dBm}$ in Fig. 4. As shown in Fig. 4, the average energy efficiency of each subchannel of

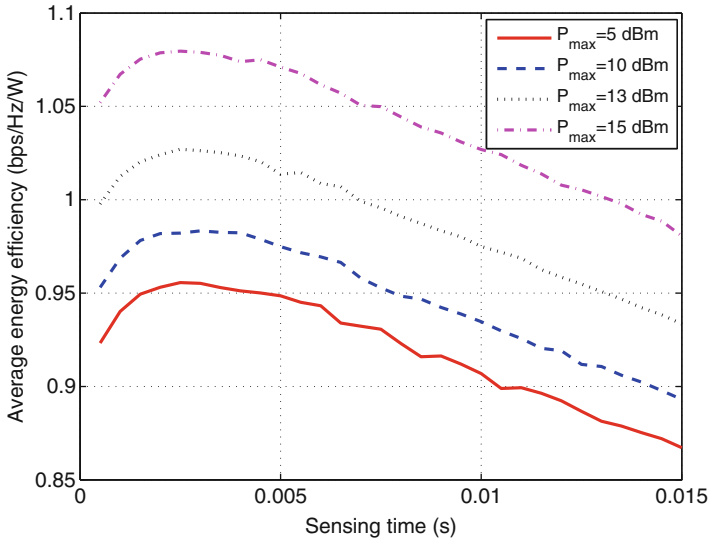

Fig. 3 Average energy efficiency versus sensing time with different $P_{\max}$ values

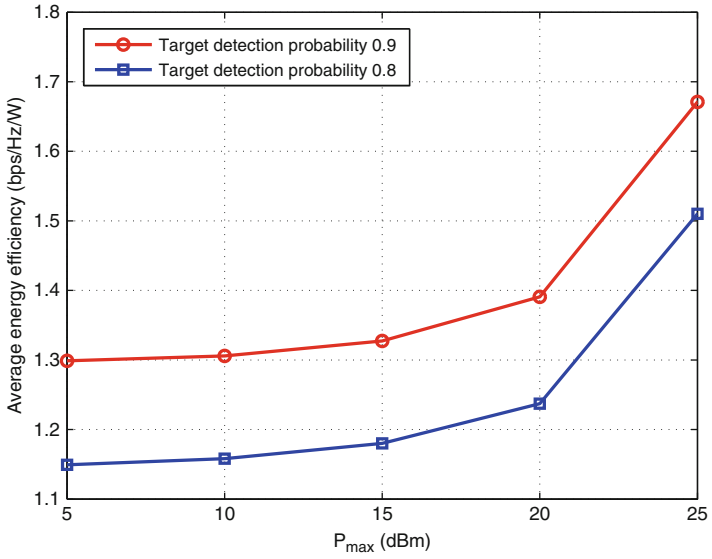

Fig. 4 Average energy efficiency versus $P_{\max}$ with different target detection probabilities

cognitive small cell increases when $P_{\max}$ is increased from 5 to 25 dBm, because a larger value of $P_{\max}$ results in a larger optimal power in (20)–(21). A larger target detection probability which results in better performance of the optimal average energy efficiency from Fig. 4 can be seen. The reason is that a larger target detection probability makes it more accurate in detection of spectrum sensing [19].

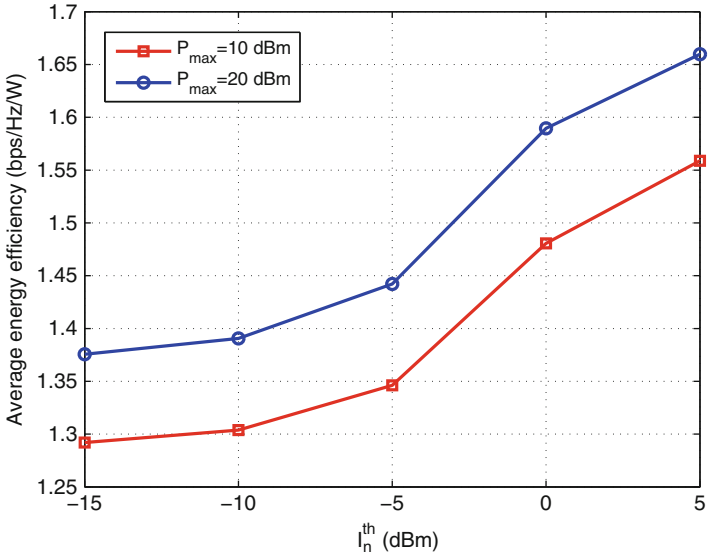

Fig. 5 Average energy efficiency versus the cross-tier interference limit with different $P_{\max}$ values

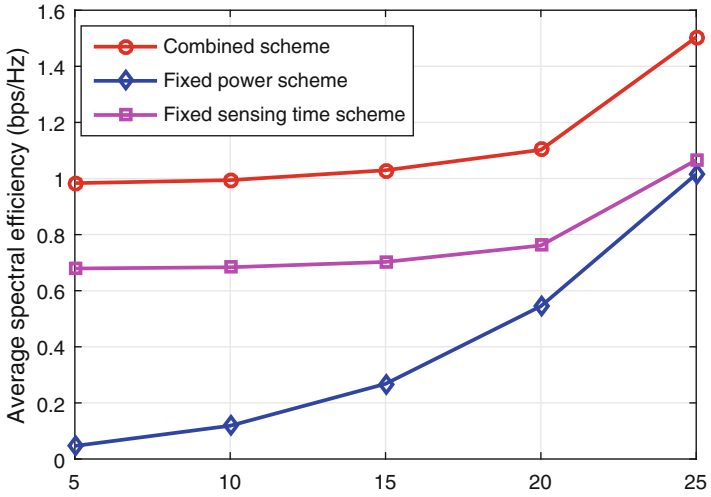

Fig. 6 Performance comparison of different schemes in terms of average spectral efficiency of small cell on each subchannel

Figure 5 shows the relation between cross-tier interference limit and the average energy efficiency of each subchannel with a different target detection probability. As shown in Fig. 5, the average energy efficiency of each subchannel in cognitive small cell increases when I_n^{th} is changed from −15 to 5 dBm. Similar to Fig. 3, this is because that a larger value of I_n^{th} can enlarge the feasible region of the optimizing variable of power in (20)–(21).

Figure 6 shows the performance comparison of average spectral efficiency with different schemes. The combined scheme is the combination of the provided Algorithm 1 and the provided near optimal sensing time scheme. Fixed sensing time scheme is the combination of the provided Algorithm 1 and a random selected sensing time scheme. Fixed power scheme is the combination of equal power allocation and the provided optimal sensing time scheme [19]. As shown in Fig. 6, the average spectral efficiency of each subchannel in the cognitive small cell with $P_{\max}$ increases from 5 to 25 mW. However, the combined scheme outperforms the fixed sensing time scheme and the fixed power scheme obviously.

Figure 7 provides the energy efficiency performance comparison between combined scheme and the other methods. In Fig. 7, the average energy efficiency of each subchannel in the cognitive small cell is shown when $P_{\max}$ increases from 8 to 18 mW, where the target detection probability $\widehat{q}_n^d = 0.9$ and cross-tier interference limit $I_n^{th} = -10$ dBm. As shown in Fig. 7, the combined scheme can achieve 15% higher energy efficiency than the fixed sensing time scheme. Fixed power scheme has the lowest curve, because of equal power allocation [19].

Figure 8 shows the relation between cross-tier interference limit and the optimal sensing time. As shown in Fig. 8, the near optimal sensing time decreases with an increase of I_n^{th}. Because when using KKT conditions related to $C2$, larger I_n^{th} results in larger optimized sensing time. Moreover, a larger value of $P_{\max}$ results in smaller optimized sensing time.

Figure 9 shows the relation between the sensing time and average energy efficiency of each subchannel in cognitive small cell network with a different cross-tier interference limit. As shown in Fig. 9, similar to Fig. 3, the average energy efficiency of each subchannel in cognitive small cell first increases and then drops as the sensing time is increased from 0.0005 to 0.015 s. It is because that the near

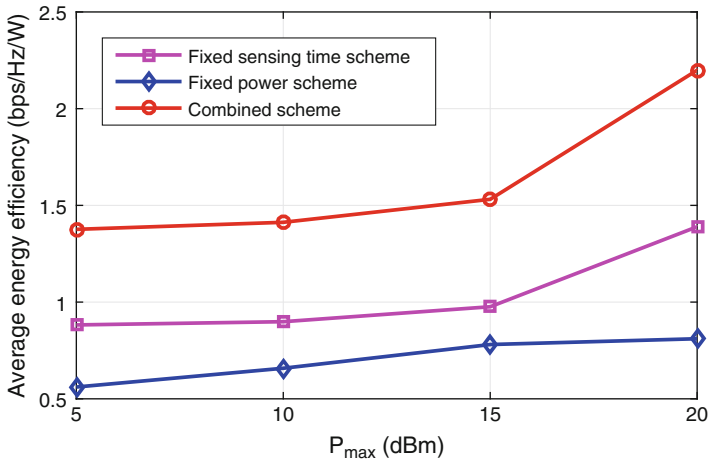

Fig. 7 Performance comparison of different schemes in terms of average energy efficiency of small cell on each subchannel

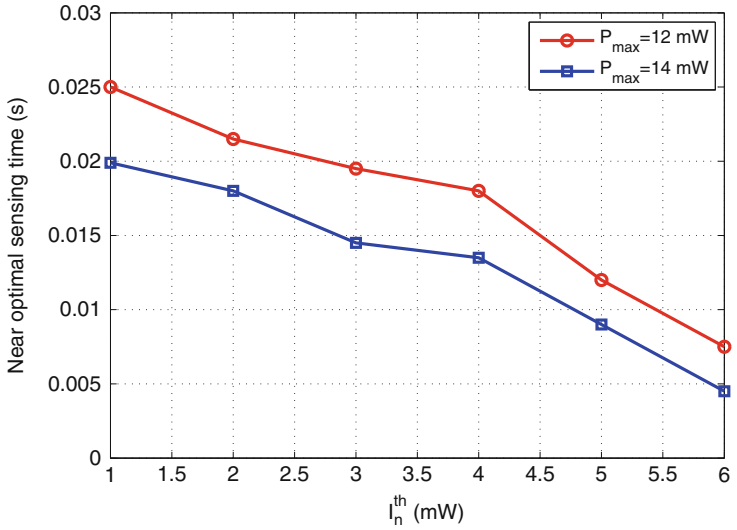

Fig. 8 Near optimal sensing time versus the cross-tier interference limit with different $P_{\max}$ values

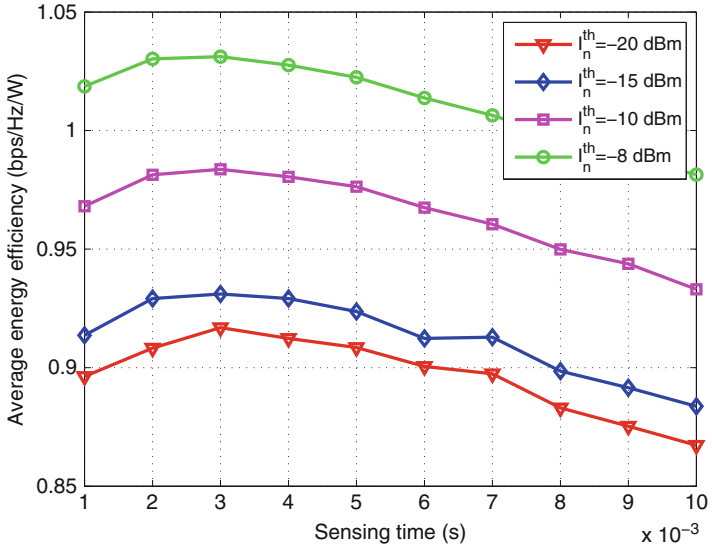

Fig. 9 Average energy efficiency versus sensing time with different cross-tier interference limits

optimal sensing time is between 0.002 and 0.004 s. Larger I_n^{th} value results in higher average energy efficiency since a larger of value of I_n^{th} leads to a larger optimization variable region in (20)–(21) [19].

Figure 10 displays the trend of average energy efficiency of each subchannel in cognitive small cell when $P_{\max}$ increases from 5 to 25 dBm with cross-tier

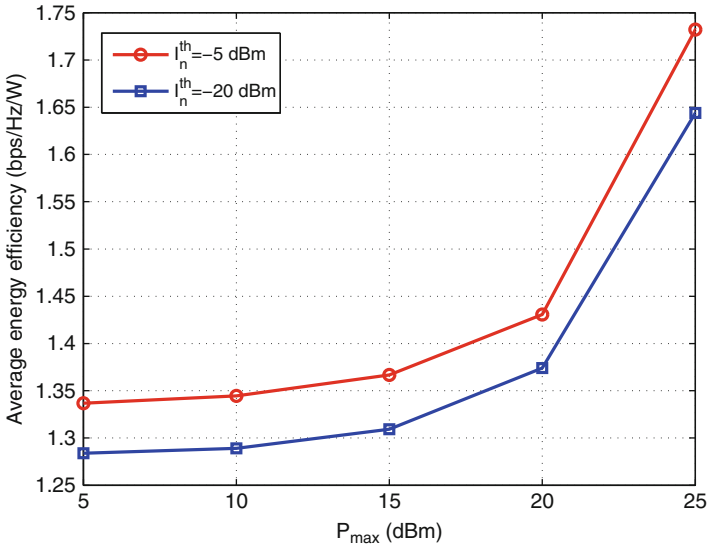

Fig. 10 Average energy efficiency versus $P_{\max}$ with different cross-tier interference limits

interference limit $I_n^{th} = -20, -5\,\text{dBm}$ and target detection probability $\widehat{q}_n^d = 0.9$ [19]. Similar to Fig. 4, Fig. 10 shows that the average energy efficiency of each subchannel in cognitive small cell increases when $P_{\max}$ is increased from 5 to 25 dBm. Besides, the larger cross-tier interference limit can result in improved performance in average energy efficiency.

Figure 11 shows the convergence performance of Algorithm 1 in the network consists of multiple cognitive small cells under the different circuit power P_c. As shown in Fig. 11, the total average energy efficiency on each subchannel of all small cells converges after 12 iterations. The practical applicability of Algorithm 1 in the multiple cognitive small cells is demonstrated through this figure.

Figure 12 shows that the total average energy efficiency on each subchannel of all small cells versus the number of small cells in network with the co-tier interference limits $\gamma^{th} = -10, -20\,\text{dBm}$, and $P_{\max} = 15\,\text{dBm}$. As shown in Fig. 12, the total average energy efficiency on each subchannel of all small cells increase gradually with the number of small cells. However, the rate of increase is diminishing, and it is caused by the co-tier interference among small cells [19]. A larger co-tier interference limit which results in better performance of the optimal total average energy efficiency can be seen. It implies that the provided method not only can optimize the energy efficiency but also can mitigate the co-tier interference in multiple cognitive small cells.

Figure 13 shows the total average energy efficiency on each subchannel of all the small cells versus the number of small cells in network with the cross-tier interference limits $I_n^{th} = -10, -13\,\text{dBm}$, and $P_{\max} = 15\,\text{dBm}$. The total average energy efficiency on each subchannel increases and then drops when the number of

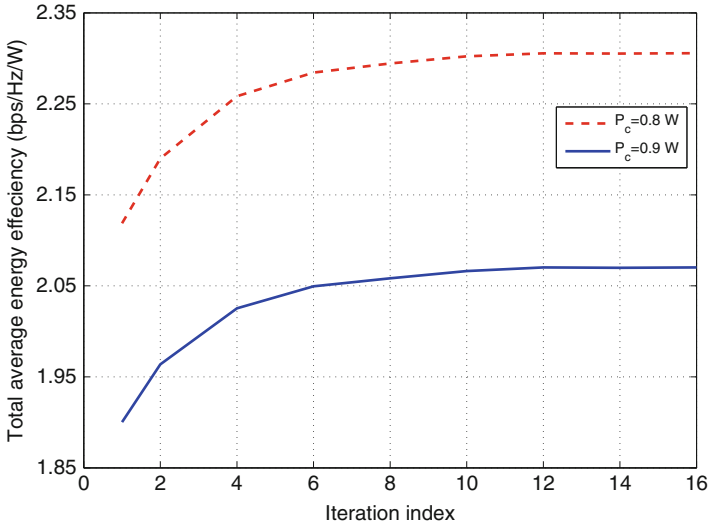

Fig. 11 Convergence in terms of sum of the average energy efficiency of small cells versus the number of iterations

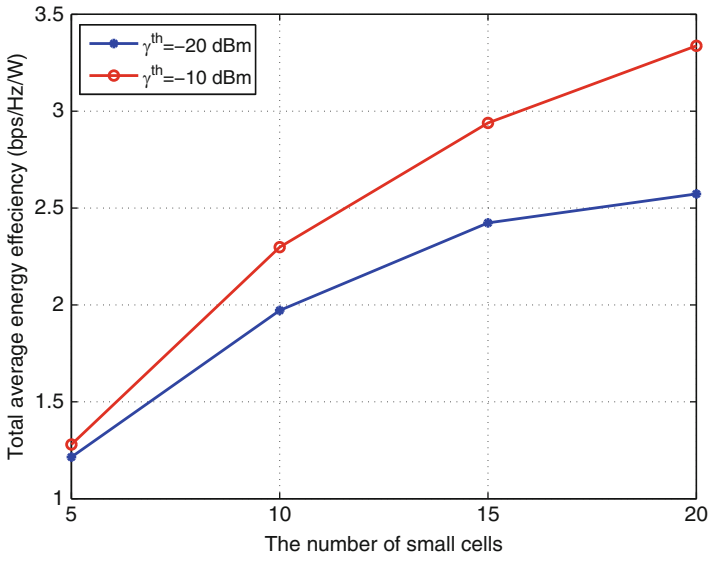

Fig. 12 Sum of the average energy efficiency versus the number of small cells with different co-tier interference limits

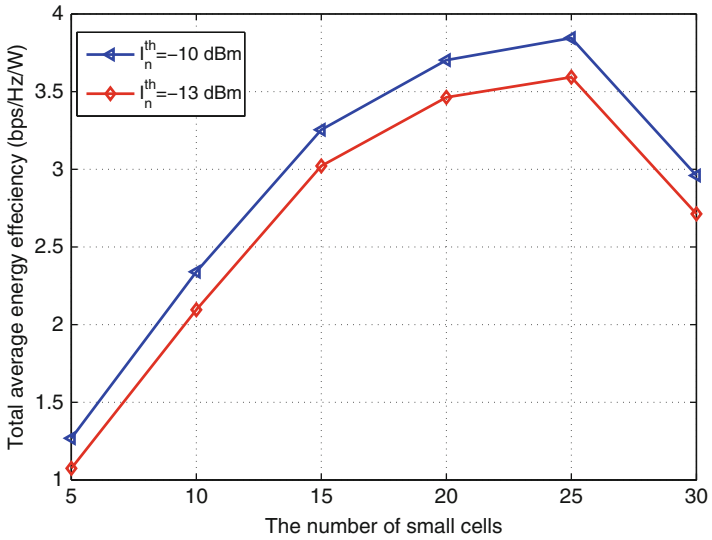

Fig. 13 Sum of the average energy efficiency versus the number of small cells with different cross-tier interference limits

small cells is increased from 5 to 30. The slope of lines is diminishing. Therefore, the provided scheme can mitigate the cross-tier interference when optimizing the energy efficiency.

Interference-Limited Resource Optimization in Cognitive Femtocells with Fairness and Imperfect Spectrum Sensing

This part studies joint subchannel and power allocation in OFDMA-based cognitive femtocells under femtocell user (FU) fairness constraints, QoS requirement, and co-/cross-tier interference temperature limits with imperfect spectrum sensing.

System Model

In the system model [18], we consider an OFDMA uplink of a network with one primary macrocell and K co-channel cognitive femtocells which are deployed randomly in the coverage area of a macrocell. Let M and F denote the numbers of active macro users (MUs) inside the primary macrocell and FUs in each cognitive femtocell, respectively. The OFDMA system has a bandwidth of B_w, which is divided into N_{total} subchannels. The channel model for each subchannel includes path loss and frequency-nonselective Rayleigh fading [18]. We focus on a resource allocation problem in the uplink of cognitive femtocells. The FUs opportunistically access the spectrum licensed to the primary macrocells via cognitive FBS, as illustrated in Fig. 14 [18]. In each time slot, the secondary network can sense N_{total}

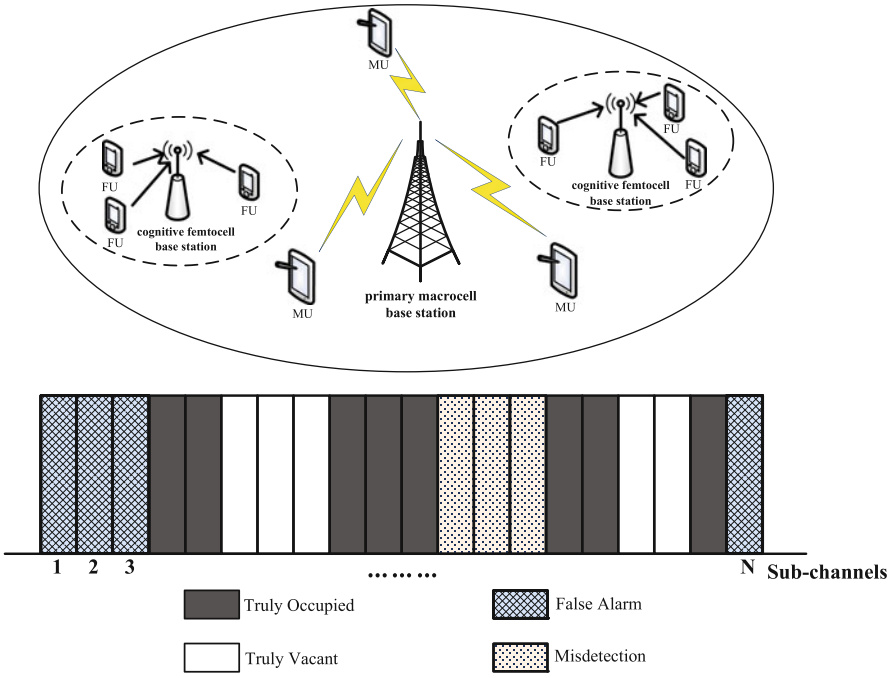

Fig. 14 A cognitive heterogeneous macro/femto network model

subchannels and opportunistically access idle channels by energy detection-based spectrum sensing. In a spectrum sensing period, the cognitive femtocell network senses N_{total} subchannels licensed to the primary macrocell network and determines available vacant/idle subchannels, which are denoted as $\mathcal{N} = 1, 2, \ldots, N$. Throughout this part, a cognitive femto base station is assumed to have perfect channel state information (CSI) between FBS and cognitive FUs/primary MUs. Therefore, the total capacity of the cognitive femtocell networks using resource scheduling schemes [18] will serve as an upper bound of the achievable capacity with channel estimation errors in practical scenarios.

The received signal-to-interference-plus-noise ratio (SINR) $\ell^{\text{F}}_{k,i,n}$ at the kth ($k \in \{1, \ldots, K\}$) cognitive FBS from its FU i ($i \in \{1, \ldots, F\}$) in the nth ($n \in \{1, \ldots, N\}$) subchannel is given as [18]

$$\ell^{\text{F}}_{k,i,n} = \frac{p^{\text{F}}_{k,i,n} \hbar^{\text{FF}}_{k,k,i,n}}{\sum\limits_{j=1, j\neq k}^{K} \sum\limits_{v=1}^{F} p^{\text{F}}_{j,v,n} \hbar^{\text{FF}}_{k,j,v,n} + p^{\text{M}}_{w,n} \hbar^{\text{FM}}_{k,w,n} + \sigma^2} \tag{47}$$

where $p^{\text{F}}_{k,i,n}$ is FU i's transmit power on subchannel n in cognitive femtocell k; $\hbar^{\text{FF}}_{k,j,v,n}$ and $\hbar^{\text{FM}}_{k,w,n}$ are the channel gains on subchannel n from FU v in cognitive femtocell j and from MU w to FBS k, respectively; w is a specific MU using

subchannel n; $p^{\mathrm{M}}_{w,n}$ is MU w's transmit power in subchannel n; and σ^2 is the additive white Gaussian noise (AWGN) power [18]. In such a case, based on the Shannon's capacity formula, the uplink capacity on subchannel n of FU i in cognitive femtocell k can be calculated by [18]

$$R^{\mathrm{F}}_{k,i,n} = \log_2\left(1 + \ell^{\mathrm{F}}_{k,i,n}\right). \tag{48}$$

Optimization Framework with Imperfect Spectrum Sensing

Imperfect Spectrum Sensing

Spectrum sensing has been extensively investigated in the previous works [24, 25]. Here, a cooperative spectrum sensing scheme [26] is presented, in which each cognitive FU senses subchannels and sends the sensing results to a cognitive FBS. Then, the cognitive FBS makes decision to determine whether or not the subchannels are vacant.

The interference from cognitive femtocell networks to primary macrocell networks occurs due to the following two reasons. One is the out-of-band emissions and the other is the spectrum sensing errors. The out-of-band emissions are due to power leakage in the sidelobes of OFDM signals [27]. The amount of out-of-band interference power of subchannel n introduced to subchannel j occupied by a primary macrocell (with unit transmit power) can be expressed as [18]

$$I^{s}_{k,i,n} = \int_{f^c_s - \frac{B_w}{2N_{\mathrm{total}}} + f^c_n}^{f^c_s + \frac{B_w}{2N_{\mathrm{total}}} + f^c_n} \varphi(f)\hbar^{FM}_{k,i,n,s}\,df \tag{49}$$

where f^c_n and f^c_s are the center frequencies of subchannel n and s, respectively, and $\hbar^{FM}_{k,i,n,s}$ is the channel gain from cognitive FU to primary MBS in subchannel s. In (47), power spectrum density (PSD) of OFDM signal $\varphi(f)$ is given as [18]

$$\varphi(f) = \frac{1}{T}\left(\frac{\sin(\pi(f - f^c_n)T)}{\pi(f - f^c_n)}\right)^2 \tag{50}$$

where T is the duration of an OFDM symbol.

Based on the analysis of the last part, there are four different cases in the cognitive femtocells network. Similarly, the probabilities for Cases 1, 2, 3, and 4 [18] for subchannel s are defined $\rho_{1,s}$, $\rho_{2,s}$, $\rho_{3,s}$, and $\rho_{1,s}$, respectively.

Based on the above analysis, the uplink cross-tier interference from cognitive femtocell to primary MBS, caused by out-of-band emission and co-channel interference, can be formulated as [18]

$$I^{MF}_{k,i,n} = p^{F}_{k,i,n} \underbrace{\left(\sum_{s\in\mathcal{N}_0} \rho_{3,s} I^{s}_{k,i,n} + \sum_{s\in\mathcal{N}_0} \rho_{4,s} I^{s}_{k,i,n}\right)}_{\tilde{G}^{MF}_{k,i,n}} \tag{51}$$

where $\mathcal{N}_v$ and $\mathcal{N}_o$ are the sets of vacant and occupied subchannels, respectively, and they are determined by the cognitive FBS. The amount of out-of-band interference power of subchannel n introduced to a primary macrocell-occupied subchannel j, with unit transmit power, can be expressed as $I^s_{k,i,n}$. In other words, since $I^s_{k,i,n}$ is calculated by unit transmit power, $I^s_{k,i,n}$ is the unit interference power here, which can be seen as channel gain. Moreover, both $\rho_{3,s}$ and $\rho_{4,s}$ are the probabilities, and therefore $\tilde{G}^{MF}_{k,i,n}$ can be interpreted as the channel gain on subchannel n from user i in cognitive femtocell k to the primary MBS [18].

General Optimization Framework

First, for resource allocation in cognitive femtocell networks, the total transmit power of cognitive FU is constrained by

$$\sum_{n=1}^{N} \tau_{k,i,n} p^{\mathrm{F}}_{k,i,n} \leq P_{\max}, \quad \forall k,\ i \tag{52}$$

where $\tau_{k,i,n} \in \{0, 1\}$ is the subchannel allocation indicator, and $\tau_{k,i,n} = 1$ indicates that subchannel n is occupied by user i in cognitive femtocell k; otherwise $\tau_{k,i,n} = 0$. $P_{\max}$ is the maximum transmit power of each cognitive FU [18].

Second, to maintain communication quality of cognitive FUs, a QoS requirement in terms of SINR is introduced for each FU. Thus, the QoS requirement can be written as [18]

$$\sum_{n=1}^{N} \tau_{k,i,n} R^{\mathrm{F}}_{k,i,n} \geq R^0_{k,i}, \quad \forall k, i \tag{53}$$

where $R^0_{k,i}$ is the QoS requirement for user i in cognitive femtocell k.

Third, a subchannel should be assigned to no more than one user at a time in a cognitive femtocell. Therefore, the subchannel assignment can be performed based on [18]

$$\sum_{i=1}^{F} \tau_{k,i,n} \leq 1, \quad \forall k, n. \tag{54}$$

Fourth, to obtain the fairness on FUs' level, the upper and lower bounds of the number of subchannels assigned to user i in cognitive femtocell k are set as [18]

$$\Gamma_{L,k,i} \leq \sum_{n=1}^{N} \tau_{k,i,n} \leq \Gamma_{U,k,i}, \quad \forall k, i \tag{55}$$

where $\Gamma_{U,k,i}$ and $\Gamma_{L,k,i}$ are the upper and lower bounds of the number of subchannels assigned to user i in cognitive femtocell k, respectively. Finally, to protect the primary macrocell's transmission, an interference temperature limit is introduced to constrain cross-tier interference from cognitive femtocell to primary macrocell [18], i.e.,

$$\sum_{k=1}^{K}\sum_{i=1}^{F}\tau_{k,i,n}p_{k,i,n}^{F}\tilde{G}_{k,i,n}^{MF} \le I_{th,n}^{\mathrm{MF}}, \quad \forall n \tag{56}$$

where $I_{th,n}^{\mathrm{MF}}$ is the maximum tolerable cross-tier interference temperature in subchannel n in the primary macrocell.

Our resource allocation problem aims to maximize the total uplink capacity of K cognitive femtocells under a cross-tier interference constraint and FUs' QoS constraints, i.e. [18],

$$\max_{\{\tau_{k,i,n}\},\{p_{k,i,n}^{\mathrm{F}}\}} \sum_{k=1}^{K}\sum_{1=1}^{F}\sum_{n=1}^{N}\tau_{k,i,n}R_{k,i,n}^{\mathrm{F}} \tag{57}$$

$$\begin{aligned}
\text{s.t.} \quad & C_1 : \sum_{n=1}^{N}\tau_{k,i,n}p_{k,i,n}^{\mathrm{F}} \le P_{\max}, \quad \forall k,i, \\
& C_2 : p_{k,i,n}^{\mathrm{F}} \ge 0, \quad \forall k,i,n, \\
& C_3 : \sum_{n=1}^{N}\tau_{k,i,n}R_{k,i,n}^{\mathrm{F}} \ge R_{k,i}^{0}, \quad \forall k,i, \\
& C_4 : \tau_{k,i,n} \in \{0,1\}, \quad \forall k,i,n, \\
& C_5 : \sum_{i=1}^{F}\tau_{k,i,n} \le 1, \quad \forall k,n, \\
& C_6 : \Gamma_{L,k,i} \le \sum_{n=1}^{N}\tau_{k,i,n} \le \Gamma_{U,k,i}, \quad \forall k,i, \\
& C_7 : \sum_{k=1}^{K}\sum_{i=1}^{F}\tau_{k,i,n}p_{k,i,n}^{F}\tilde{G}_{k,i,n}^{MF} \le I_{th,n}^{\mathrm{MF}}, \quad \forall n
\end{aligned}$$

where C_1 limits the transmit power of each FU below the maximum power $P_{\max}$; C_2 indicates that the transmit power is nonnegative; C_3 sets the QoS requirement $R_{k,i}^{0}$ for user i in cognitive femtocell k; C_4 and C_5 guarantee that each subchannel can be assigned to no more than one user in each femtocell; C_6 ensures a fairness among users by setting $\Gamma_{U,k,i}$ and $\Gamma_{L,k,i}$ as the upper and lower bounds of the number of subchannels assigned to user i in cognitive femtocell k, respectively. The priority of the user can be adjusted by setting appropriate values of $\Gamma_{U,k,i}$ and $\Gamma_{L,k,i}$. The constraint C_7 imposes the maximum tolerable cross-tier interference temperature $I_{th,n}^{\mathrm{MF}}$ in subchannel n for the primary macrocell [18].

Joint Resource Optimization with Fairness and Imperfect Sensing

Transformation of the Optimization Problem

The problem in (57) is a non-convex mixed integer programming problem. It can be solved using a brute-force method, which however incurs a high computational complexity. To make the problem tractable, an additional co-tier interference temperature constraint C_8 is introduced as [18]

$$C_8: \sum_{j=1, j\neq k}^{K} \sum_{v=1}^{F} \tau_{j,v,n} p^{\mathrm{F}}_{j,v,n} \hbar^{\mathrm{FF}}_{k,j,v,n} \leq I^{\mathrm{FF}}_{th,n}, \quad \forall k, n \tag{58}$$

where $I^{\mathrm{FF}}_{th,n}$ is the co-tier interference limit in subchannel n for a cognitive femtocell. Each femtocell will potentially interfere each other when two neighbor femtocells use the same subchannel. Therefore, from physical/engineering point view in the real-world applications, $I^{\mathrm{FF}}_{th,n}$ is a co-tier interference limit for neighbor femtocell to mitigate co-tier interference. The value of $I^{\mathrm{FF}}_{th,n}$ can be broadcasted by each femtocell or set by each femtocell.

Moreover, inspired by [28], the $\tau_{k,i,n}$ in C_4 is relaxed to be a real variable in the range of [0,1], in which case $\tau_{k,i,n}$ can be interpreted as the fraction of time that subchannel n is assigned to user i in cognitive femtocell k during one transmission frame. Denote $\widehat{p}_{k,i,n} = \tau_{k,i,n} p^{\mathrm{F}}_{k,i,n}$ as the actual power allocated to user i in cognitive femtocell k on subchannel n. Denote $I_{k,i,n} = p^{\mathrm{M}}_{w,n} \hbar^{\mathrm{FM}}_{k,w,n} + I^{\mathrm{FF}}_{th,n} + \sigma^2$ and $\hat{R}^{\mathrm{F}}_{k,i,n} = \log_2\left(1 + \frac{\hat{p}_{k,i,n} \hbar^{\mathrm{FF}}_{k,k,i,n}}{\tau_{k,i,n} I_{k,i,n}}\right)$ as the upper bound of the total received interference power and lower bound of the capacity of user i on subchannel n in cognitive femtocell k, respectively. In such a case, the optimization problem in (57) can be rewritten as [18]

$$\max_{\{\tau_{k,i,n}\}, \{\widehat{p}_{k,i,n}\}} \sum_{k=1}^{K} \sum_{i=1}^{F} \sum_{n=1}^{N} \tau_{k,i,n} \widehat{R}^{\mathrm{F}}_{k,i,n} \tag{59}$$

$$\text{s.t. } C_1: \sum_{n=1}^{N} \widehat{p}_{k,i,n} \leq P_{\max}, \quad \forall k, i,$$

$$C_2: \widehat{p}_{k,i,n} \geq 0, \quad \forall k, i, n,$$

$$C_3: \sum_{n=1}^{N} \tau_{k,i,n} \widehat{R}^{\mathrm{F}}_{k,i,n} \geq R^0_{k,i}, \quad \forall k, i,$$

$$C_4: 0 \leq \tau_{k,i,n} \leq 1, \quad \forall k, i, n,$$

$$C_5: \sum_{i=1}^{F} \tau_{k,i,n} \leq 1, \quad \forall k, n,$$

$$C_6 : \Gamma_{L,k,i} \leq \sum_{n=1}^{N} \tau_{k,i,n} \leq \Gamma_{U,k,i}, \quad \forall k, i,$$

$$C_7 : \sum_{k=1}^{K} \sum_{i=1}^{F} \widehat{p}_{k,i,n} \tilde{G}^{\mathrm{MF}}_{k,i,n} \leq I^{\mathrm{MF}}_{th,n}, \quad \forall n,$$

$$C_8 : \sum_{j=1, j\neq k}^{K} \sum_{v=1}^{F} \tau_{j,v,n} \hbar^{\mathrm{FF}}_{k,j,v,n} \leq I^{\mathrm{FF}}_{th,n}, \quad \forall k, n.$$

Theorem 2. *The objective function in (59) is concave, and the corresponding optimization problem under the constraints C_1 to C_8 is a convex problem.*

The proof is provided in Appendix.

According to Theorem 2, the objective function in (59) is concave, and the corresponding optimization problem under the constraints C_1 to C_8 is a convex problem.

Joint Subchannel and Power Allocation with Imperfect Spectrum Sensing

The joint subchannel and power allocation problem in (59) can be solved using the Lagrangian dual decomposition method, which has been widely used in solving resource allocation problems. The Lagrangian function is given by [18]

$$\begin{aligned}
\mathscr{L}(\{\tau_{k,i,n}\}, \{\widehat{p}_{k,i,n}\}, \boldsymbol{\lambda}, \boldsymbol{\nu}, \boldsymbol{\delta}, \boldsymbol{\mu}, \boldsymbol{\eta}) = & \sum_{k=1}^{K} \sum_{u=1}^{F} \sum_{n=1}^{N} \tau_{k,i,n} \widehat{R}^{\mathrm{F}}_{k,i,n} \\
& + \sum_{k=1}^{K} \sum_{i=1}^{F} \lambda_{k,i} \left(P_{\max} - \sum_{n=1}^{N} \widehat{p}_{k,i,n} \right) + \sum_{n=1}^{N} \delta_n \left(I^{\mathrm{MF}}_{th,n} - \sum_{k=1}^{K} \sum_{i=1}^{F} \widehat{p}_{k,i,n} \tilde{G}^{\mathrm{MF}}_{k,i,n} \right) \\
& + \sum_{k=1}^{K} \sum_{n=1}^{N} \mu_{k,n} \left(I^{\mathrm{FF}}_{th,n} - \sum_{j=1, j\neq k}^{K} \sum_{v=1}^{F} \widehat{p}_{j,v,n} \hbar^{\mathrm{FF}}_{k,j,v,n} \right) + \sum_{k=1}^{K} \sum_{n=1}^{N} \eta_{k,n} \left(1 - \sum_{i=1}^{F} \tau_{k,i,n} \right) \\
& + \sum_{k=1}^{K} \sum_{i=1}^{F} \nu_{k,i} \left(\sum_{n=1}^{N} \tau_{k,i,n} \widehat{R}^{\mathrm{F}}_{k,i,n} - R^{0}_{k,i} \right)
\end{aligned} \tag{60}$$

where $\boldsymbol{\lambda}$, $\boldsymbol{\nu}$, $\boldsymbol{\delta}$, $\boldsymbol{\mu}$, and $\boldsymbol{\eta}$ are the Lagrange multiplier vectors for C_1, C_3, C_7, C_8, and C_5 in (59), respectively. The boundary constraints C_2, C_4, and C_6 in (59) are absorbed in the KKT conditions [23], which will be shown later. The dual function is defined as

$$g(\boldsymbol{\lambda}, \boldsymbol{\nu}, \boldsymbol{\delta}, \boldsymbol{\mu}, \boldsymbol{\eta}) = \max_{\{\tau_{k,i,n}\}, \{\widehat{p}_{k,i,n}\}} \mathscr{L}\Big(\{\tau_{k,i,n}\}, \{\widehat{p}_{k,i,n}\}, \boldsymbol{\lambda}, \boldsymbol{\nu}, \boldsymbol{\delta}, \boldsymbol{\mu}, \boldsymbol{\eta} \Big) \tag{61}$$

and the dual problem can be expressed by

$$\min_{\boldsymbol{\lambda},\boldsymbol{\nu},\boldsymbol{\delta},\boldsymbol{\mu},\boldsymbol{\eta}\geq 0} g\Big(\boldsymbol{\lambda},\boldsymbol{\nu},\boldsymbol{\delta},\boldsymbol{\mu},\boldsymbol{\eta}\Big). \tag{62}$$

Decomposing the Lagrangian dual problem into a master problem and $K \times N$ subproblems that can be solved iteratively [18]. Here the MBS solves the master problem, and each FBS solves N subproblems based on local information in each iteration. Accordingly, Eq. (60) is rewritten as [18]

$$\mathscr{L}(\{\tau_{k,i,n}\},\{\widehat{p}_{k,i,n}\},\boldsymbol{\lambda},\boldsymbol{\nu},\boldsymbol{\delta},\boldsymbol{\mu},\boldsymbol{\eta}) = \sum_{k=1}^{K}\sum_{n=1}^{N} L_{k,n}(\{\tau_{k,i,n}\},\{\widehat{p}_{k,i,n}\},\boldsymbol{\lambda},\boldsymbol{\nu},\boldsymbol{\delta},\boldsymbol{\mu},\boldsymbol{\eta})$$
$$+\sum_{k=1}^{K}\sum_{i=1}^{F}\lambda_{k,i}P_{\max}-\sum_{k=1}^{K}\sum_{i=1}^{F}\nu_{k,i}R_{k,i}^{0}+\sum_{n=1}^{N}\delta_n I_{th,n}^{\mathrm{MF}}+\sum_{k=1}^{K}\sum_{n=1}^{N}\mu_{k,n}I_{th,n}^{\mathrm{FF}}+\sum_{k=1}^{K}\sum_{n=1}^{N}\eta_{k,n} \tag{63}$$

where

$$\mathscr{L}_{k,n}(\{\tau_{k,i,n}\},\{\widehat{p}_{k,i,n}\},\boldsymbol{\lambda},\boldsymbol{\nu},\boldsymbol{\delta},\boldsymbol{\mu},\boldsymbol{\eta}) = \sum_{i=1}^{F}\tau_{k,i,n}\widehat{R}_{k,i,n}^{\mathrm{F}}-\sum_{i=1}^{F}\lambda_{k,i}\widehat{p}_{k,i,n}-\sum_{i=1}^{F}\eta_{k,n}\tau_{k,i,n}$$
$$+\sum_{i=1}^{F}\nu_{k,i}\tau_{k,i,n}\widehat{R}_{k,i,n}^{\mathrm{F}}-\mu_{k,n}\sum_{j=1,j\neq k}^{K}\sum_{l\in U_j}\widehat{p}_{j,l,n}\hbar_{k,j,l,n}^{\mathrm{FF}}-\sum_{g\neq k}^{K}\sum_{u\in U_k}\mu_{g,n}\widehat{p}_{k,i,n}\hbar_{g,k,i,n}^{\mathrm{FF}}$$
$$-\sum_{i=1}^{F}\delta_n\widehat{p}_{k,i,n}\tilde{G}_{k,i,n}^{\mathrm{MF}}. \tag{64}$$

The calculation of the derivatives with respect to $\hat{p}_{k,i,n}$ and $\tau_{k,i,n}$, respectively, gives the KKT condition as

$$\frac{\partial L_{k,n}(\ldots)}{\partial \hat{p}_{k,i,n}} = \Lambda_{k,i,n}-\lambda_{k,i}\leq 0 \tag{65}$$

where

$$\Lambda_{k,i,n} = \frac{(1+\nu_{k,i})\tau_{k,i,n}\hbar_{k,k,i,n}^{FF}}{\ln 2(\tau_{k,i,n}I_{k,i,n}+\hat{p}_{k,i,n}\hbar_{k,k,i,n}^{FF})}-\sum_{g=1,g\neq k}^{K}\mu_{g,n}\hbar_{g,k,i,n}^{\mathrm{FF}}-\delta_n\tilde{G}_{k,i,n}^{\mathrm{MF}}, \tag{66}$$

$$\hat{p}_{k,i,n}\left(\Lambda_{k,i,n}-\lambda_{k,i}\right)=0, \tag{67}$$

$$\lambda_{k,i}\left(P_{\max}-\sum_{n=1}^{N}\hat{p}_{k,i,n}\right)=0. \tag{68}$$

According to (65), (66), (67), and (68), the optimal power allocated to user i in cognitive femtocell k in subchannel n for (59) is [18]

$$p_{k,i,n}^{*\mathrm{F}} = \frac{\hat{p}_{k,i,n}}{\tau_{k,i,n}} = \left[\frac{(1+\nu_{k,i})}{\ln 2 \left(\lambda_{k,i} + \sum\limits_{g=1,g\neq k}^{K} \mu_{g,n} \hbar_{g,k,i,n}^{\mathrm{FF}} + \delta_n \tilde{G}_{k,i,n}^{\mathrm{MF}} \right)} - \frac{I_{k,i,n}}{\hbar_{k,k,i,n}^{\mathrm{FF}}} \right]^+, \forall k,i \tag{69}$$

where $[x]^+ = \max\{0, x\}$. Moreover, there is

$$\frac{\partial L_{k,n}(\ldots)}{\partial \tau_{k,i,n}} = \Xi_{k,i,n} - \eta_{k,n} \leq 0 \tag{70}$$

where

$$\Xi_{k,i,n} = (1+\nu_{k,i}) \left[\log_2 \left(1 + \frac{p_{k,i,n}^{*\mathrm{F}} \hbar_{k,k,i,n}^{\mathrm{FF}}}{I_{k,i,n}} \right) - \frac{1}{\ln 2} \left(\frac{p_{k,i,n}^{*\mathrm{F}} \hbar_{k,k,i,n}^{\mathrm{FF}}}{p_{k,i,n}^{*\mathrm{F}} \hbar_{k,k,i,n}^{\mathrm{FF}} + I_{k,i,n}} \right) \right], \tag{71}$$

$$\tau_{k,i,n} \left(\Xi_{k,i,n} - \eta_{k,n} \right) = 0, \tag{72}$$

$$\eta_{k,n} \left(1 - \sum_{i=1}^{F} \tau_{k,i,n} \right) = 0. \tag{73}$$

Based on (70), (71), (72), and (73), subchannel n is assigned to the user with the largest $\Xi_{k,i,n}$ in femtocell k, i.e.,

$$\widehat{\tau}_{k,i^*,n} = 1 \Big|_{i^* = \max\limits_{i} \Xi_{k,i,n}}, \quad \forall k,n. \tag{74}$$

Since the dual function is differentiable, the subgradient method can be used to solve the master dual minimization problem in (62). Based on the subgradient method, the master dual problem in (62) can be solved as [18]

$$\lambda_{k,i}^{(l+1)} = \left[\lambda_{k,i}^{(l)} - \varepsilon_1^{(l)} \left(P_{\max} - \sum_{n=1}^{N} \widehat{p}_{k,i,n} \right) \right]^+, \quad \forall k,i, \tag{75}$$

$$\nu_{k,i}^{(l+1)} = \left[\nu_{k,i}^{(l)} - \varepsilon_2^{(l)} \left(\sum_{n=1}^{N} \widehat{R}_{k,i,n}^{\mathrm{F}} - R_{k,i}^{0} \right) \right]^+, \quad \forall k,i, \tag{76}$$

$$\mu_{k,n}^{(l+1)} = \left[\mu_{k,n}^{(l)} - \varepsilon_3^{(l)} \left(I_{th,n}^{\mathrm{FF}} - \sum_{j \neq k}^{K} \sum_{l \in U_j} s_{j,l,n} \hbar_{k,j,l,n}^{\mathrm{FF}} \right) \right]^+, \quad \forall k, n, \tag{77}$$

$$\delta_n^{(l+1)} = \left[\delta_n^{(l)} - \varepsilon_4^{(l)} \left(I_{th,n}^{\mathrm{MF}} - \sum_{k=1}^{K} \sum_{i=1}^{F} \widehat{p}_{k,i,n} \tilde{G}_{k,i,n}^{\mathrm{MF}} \right) \right]^+, \quad \forall n \tag{78}$$

where $\varepsilon_1^{(l)}$, $\varepsilon_2^{(l)}$, $\varepsilon_3^{(l)}$, and $\varepsilon_4^{(l)}$ are step sizes of iteration i, $l \in \{1, 2, \ldots, L_{\max}\}$, $L_{\max}$ is the maximal number of iterations. The step sizes should satisfy $\sum_{l=1}^{\infty} \varepsilon_t^{(l)} = \infty$, $\lim_{l \to \infty} \varepsilon_t^{(l)} = 0$, $\forall t \in 1, \ldots, 4$. λ, ν, and μ are updated by the cognitive femtocells in a distributed manner, and $\delta_n^{(l+1)}$ is updated by the primary MBS. Figure 15 shows the three-layer architecture of the decomposed dual problem.

Iterative Resource Optimization Algorithm with Fairness

Although in the solution in (69), (74), (75), (76), (77), and (78) give a complete algorithm for the original problem, the fairness in subchannel occupation was not considered. Therefore, Algorithm 3 is provided as an implementation of the joint subchannel and power allocation scheme, as shown in the pseudo codes below.

In this part, the fairness is taken into consideration in terms of subchannel allocation. Specifically, to ensure the fairness on FUs' level, the upper and lower bounds of the number of subchannels are assigned to the users in a cognitive femtocell as shown in (55). In the problem formulation, C_6 ensures fairness among users by setting $\Gamma_{U,k,i}$ and $\Gamma_{L,k,i}$ as the upper and lower bounds of the number of

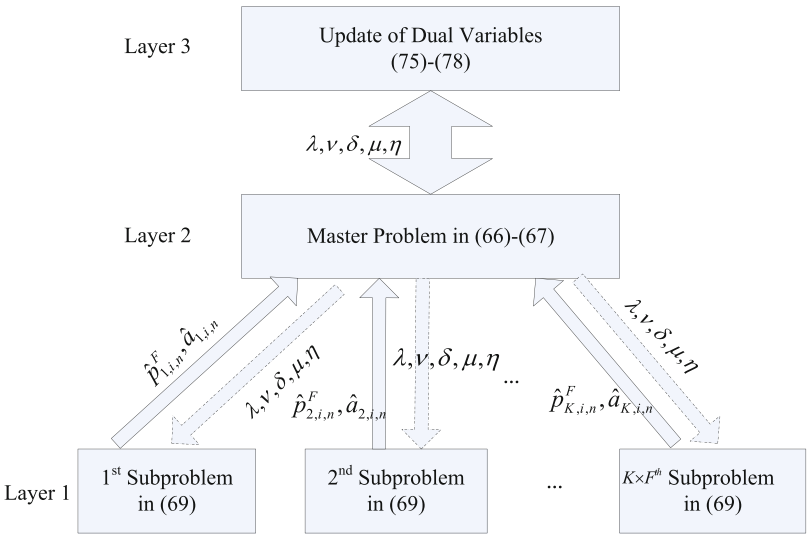

Fig. 15 Three-layer architecture of the decomposed dual problem

Algorithm 3 Iterative resource allocation algorithm

Cognitive FBS set: $\mathcal{K} = \{1, 2, \ldots K\}$; Cognitive FU set per femtocell: $\mathcal{U} = \{1, 2, \ldots F\}$.
Initialize $I_{\max}$ and Lagrangian variables vectors $\boldsymbol{\lambda}, \boldsymbol{\nu}, \boldsymbol{\mu}$, and set $i = 0$.
Allocate the same power to each subchannel, set $\tau_{k,i,n} = 0$, $\forall k, i, n$.
repeat
  Cognitive FBS k measures $\hbar^{\mathrm{FF}}_{k,k,i,n}$ and $I_{k,i,n}$, $\forall k, i, n$;
  for each FBS **do**
    subchannel set: $\mathcal{N} = \{1, 2, \ldots, N\}$;
    Set $N_i = 0$, $\forall i \in \mathcal{U}$
    subchannel allocation for user fairness
    while $N_i < \Gamma_{L,k,i}$, $\forall i \in \mathcal{U}$ **do**
      a) find $n^* = \arg\max_{n \in \mathcal{N}} \Xi_{k,i,n}$ according to (71);
      b) $\tau_{k,i,n^*} = 1$, $\mathcal{N} = \mathcal{N} - \{n^*\}$, $N_i = N_i + 1$;
      if $N_i = N_{U,k,i}$ **then**
        $\mathcal{U} = \mathcal{U} - \{i\}$;
      end if
    end while
    subchannel allocation for capacity enhancement
    while $\mathcal{N} \neq \phi$ **do**
      a) find $(i^*, n^*) = \arg\max_{i \in \mathcal{U}, n \in \mathcal{N}} \Xi_{k,i,n}$;
      b) $\tau_{k,i^*,n^*} = 1$, $\mathcal{N} = \mathcal{N} - \{n^*\}$;
      if $N_{i^*} = N_{U,k,i^*}$ **then**
        $\mathcal{U} = \mathcal{U} - \{i^*\}$;
      end if
    end while
    Every FBS j ($j \neq k$) measures $\mu_{j,n} \hbar^{\mathrm{FF}}_{j,k,i,n}$ and feeds it back to FBS k
    Power Allocation
    for $n = 1$ to N **do**
      a) FUs update $p^{*\mathrm{F}}_{k,i,n}$ according to (69);
      b) Cognitive FBS k updates $\boldsymbol{\lambda}, \boldsymbol{\nu}, \boldsymbol{\mu}$ according to (75), (76) and (77), respectively;
      c) Cognitive FBS k updates $\Xi_{k,i,n}$ according to (71).
    end for
  end for
  Primary MBS updates $\boldsymbol{\delta}$ according to (78), and broadcasts the updated value to all FBSs via backhaul, $l = l + 1$.
until convergence or $l = L_{\max}$

subchannels assigned to user i in cognitive femtocell k, respectively, and the priority of the user can be adjusted by setting values of $\Gamma_{U,k,i}$ and $\Gamma_{L,k,i}$ appropriately. After the transformation, the optimization problem is solved by Algorithm 3 [18].

In Algorithm 3, there are two procedures to ensure users' fairness in subchannel allocation. First, subchannels are allocated for the users whose subchannel occupation is below $\Gamma_{L,k,i}$, and this procedure is named as "subchannel allocation for user fairness" in Algorithm 3, to guarantee user's lowest requirement. In the second procedure, which is called "subchannel allocation for capacity enhancement," the algorithm tries to enhance the user's capacity while keeping users' subchannel occupation below the upper bound of $\Gamma_{U,k,i}$. With the help of the two procedures, Algorithm 3 can ensure that the subchannels assigned to user i in femtocell k is

between $\Gamma_{U,k,i}$ and $\Gamma_{L,k,i}$. Moreover, from lines 9–16 of Algorithm 3, subchannels will be assigned to cognitive femto users, and the used subchannels will be removed from subchannel set $\mathcal{N}$ based on line 12 of Algorithm 3. Algorithm 3 will check that whether any unused subchannels are left in line 18; if true, lines 19–20 will be executed until the subchannel set is empty. Therefore, lines 9–24 can ensure a full utilization of all vacant subchannels [18].

In practical scenarios, users' subchannel requirements are different, and traditional capacity-maximum subchannel algorithms tend to allocate the subchannels to the users with better channel conditions according to users' subchannel requirements. Therefore, the subchannel requirements of the other users with relatively poor channel conditions may not be satisfied. This is unfair for the users with poor subchannel conditions. In Algorithm 3, Procedure 1 can guarantee the lowest requirements of subchannels for users with poor channel conditions, and Procedure 2 can maximize the users' capacity while keeping the number of user's subchannel occupation below the upper bound.

Note that $\hbar^{\mathrm{FF}}_{g,k,i,n}$ required in (69), (71), and (77) can be known by a cognitive FBS from a FBS gateway or through available interfaces between FBSs, and $\tilde{G}^{\mathrm{MF}}_{k,i,n}$ required in (69) and (78) can be estimated by user i in femtocell k by measuring downlink channel gain of subchannel n from the MBS, assuming a symmetry between uplink and downlink channels. Furthermore, it is assumed that there are wired connections between FBSs and MBS [29,30], so that $\tilde{G}^{\mathrm{MF}}_{k,i,n}$ can be exchanged between the MBS and FBS's.

The following is the complexity analysis of the provided algorithm. Suppose that the subgradient method used in Algorithm 3 needs Δ iterations to converge. Since the updates of each $\boldsymbol{\lambda}$ and $\boldsymbol{\nu}$ need $O(F)$ operations [23], the computation of $\boldsymbol{\mu}$ and $\boldsymbol{\delta}$ requires $O(N)$ operations each, and Δ is a polynomial function of FN. Therefore, the asymptotic complexity of Algorithm 3 is $O(KFN(\log_2 N + \log_2 F)\Delta)$. Compared to the brute-force method, which has a complexity of $O(KF^N)$, the provided Algorithm 3 has a lower complexity, especially for a large N.

Simulation Results and Discussions

In the simulations, the primary macrocell's radius is set to 500 m, and the radius of each cognitive femtocell is set to 10 m. Cognitive femtocells and MUs are distributed randomly in the macrocell coverage area. The carrier frequency is 2 GHz. $B_w = 10\,\mathrm{MHz}$, $N_0 = -174\,\mathrm{dBm/Hz}$, $N = 50$, and $M = 20$ were used in the simulations, respectively [18]. The block-fading channel gains are modeled as independent identically distributed exponential random variables with unit mean. MUs' maximum transmit power is 23 dBm. The standard deviation of lognormal shadowing between MBS and users is 8 dB, while between an FBS and users is 10 dB. The probability of false alarm q_s^f, mis-detection q_s^m, and primary MU's occupation q_s^p are uniformly distributed over [0.05,0.1], [0.01,0.05], and [0,1], respectively. Assuming that $\mathcal{N}_o = \{1, 3, 5, \ldots, 49\}$ and $\mathcal{N}_v = \{2, 4, 6, \ldots, 50\}$,

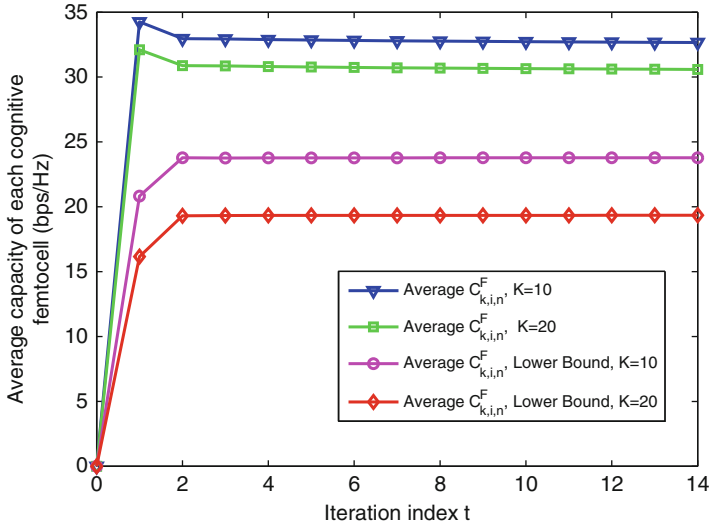

Fig. 16 Convergence in terms of average capacity of each femtocell versus the number of iterations

while the upper bounds [7, 7, 14, 14] and the lower bounds [3, 3, 7, 7] of subchannel assignment for FUs $i = \{1, 2, 3, 4\}$ per femtocell are assumed. For comparison purpose, the simulation included the scheduling scheme in [31] in conjunction with the power allocation scheme in Algorithm 3 and refered to it as the "existing scheme" hereafter. The indoor and outdoor pathloss models are based on [32].

Figure 16 shows the convergence of the Algorithm 3 in terms of the average capacity per femtocell versus the number of iterations i, where $K = 10, 20$, $R_{k,i}^0 = 9$ bps/Hz for all FUs, $P_{\max} = 23$ dBm, and $I_{th,n}^{\mathrm{FF}} = I_{th,n}^{\mathrm{MF}} = -100$ dBm. The provided algorithm in [18] takes only four iterations to converge, indicating that it is suitable for real-time implementation. The average capacity per femtocell for $K = 10$ is higher than that for $K = 20$, because co-tier interference increases with K. The lower bound of cognitive femtocell capacity used in (59) is also plotted and is shown to be in reasonably close agreement with the simulation results.

Figure 17 shows the total capacity of K cognitive femtocells versus the number of femtocells in term of different co-/cross-tier interference limits. The Algorithm 3 [18] with higher co-/cross-tier interference limits, $I_{th,n}^{\mathrm{FF}}$ and $I_{th,n}^{\mathrm{MF}}$, provides a higher total capacity of K cognitive femtocells, because of the higher transmit power used by users under the slacker constraint of co-/cross-tier interference. The effect on how additional constraint of C_8 affects the overall performance of the Algorithm 3 is investigated in the simulations, as showed in Fig. 17. The brute-force method without constraint of co-tier interference limit C_8 has a better performance in terms of total capacity of K cognitive femtocells than the provided algorithm with C_8, because of the slacker constraint of co-/cross-tier interference in the optimization problem [18].

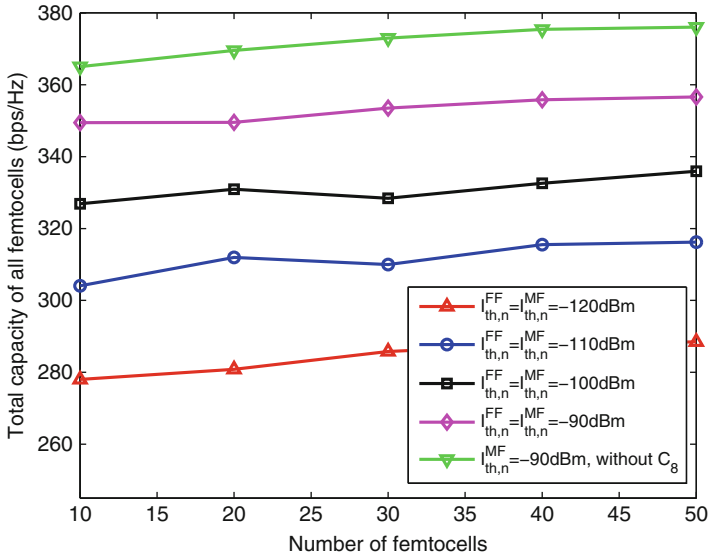

Fig. 17 Total capacity of femtocells versus number of femtocells

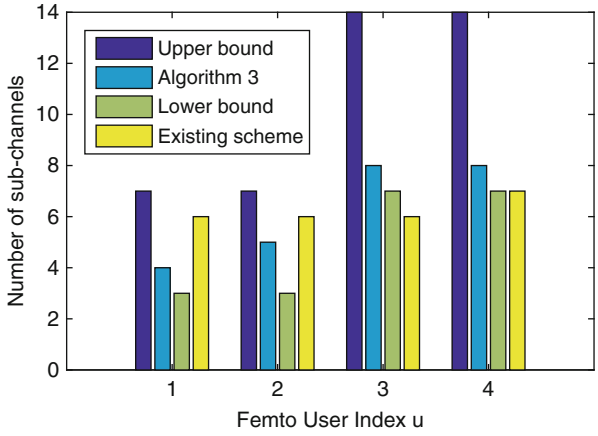

Fig. 18 Number of subchannels occupied by each FU

Figure 18 shows the average number of subchannels allocated by the provided Algorithm 3 [18] to each FU as compared with the "existing algorithm." It can be seen that subchannel assignments of the provided algorithm meet the requirements of different users given in C_6, while the "existing algorithm" does not always satisfy C_6, e.g., the number of assigned subchannels may fall below the lower bound. The provided algorithm tends to allocate a number of subchannels, which

is only slightly larger than the lower bound to each FU, leading to an efficient reuse of subchannels. The procedure of "subchannel allocation for user fairness" guarantees the lower bound for users' subchannel requirement, while the procedure of "subchannel allocation for capacity enhancement" guarantees that it does not exceed the upper bound.

Figure 19a shows the average cross-tier interference suffered in each subchannel of primary macrocell when the maximum transmit power $P_{\max}$ increases from 20 to 30 dBm, for the number of users per femtocell $F = 4$ and the number of femtocells $K = 10$. The other simulation parameters are set as $R_{k,i}^0 = 9$ bps/Hz for all k, and $I_{th,n}^{MF} = I_{th,n}^{FF} = -100$ dBm for all n. The total cross-tier interference increases as the increase of $P_{\max}$. This is because that the cross-tier interference is caused by transmit power per subchannel and the cross-tier channel gain, and a large value of $P_{\max}$ enlarges the feasible domain of the optimizing variable [18]. It also can be seen from the figure that the perfect spectrum sensing scheme has a higher cross-tier interference than the imperfect spectrum sensing scheme. The reason of this phenomenon is that mis-detection and false alarm in imperfect spectrum sensing overestimate the cross-tier interference. Moreover, the average interference from cognitive femtocell to primary macrocell in each su-channel in imperfect spectrum sensing is below the cross-tier interference threshold. Figure 19b shows the average co-tier interference suffered in each subchannel of neighboring femtocells when maximum transmit power $P_{\max}$ increases from 20 to 30 dBm. Note that perfect spectrum sensing of cross-tier channel gain at cognitive FBS side results in a higher co-tier interference than the imperfect spectrum sensing scheme [18], because mis-detection and false alarm in imperfect spectrum sensing overestimate the cross-tier interference.

Figure 20 shows the total capacity of all cognitive femtocells when maximum transmit power $P_{\max}$ increases from 20 to 30 dBm, for the number of users per femtocell $F = 4$ and the number of femtocells $K = 10$. The other simulation parameters are set as $R_{k,i}^0 = 9$ bps/Hz for all k, and $I_{th,n}^{MF} = I_{th,n}^{FF} = -100$ dBm for all n. The total capacity of all femtocells increases with $P_{\max}$. This is because a large value of $P_{\max}$ enlarges the feasible domain of the optimizing variable [18]. It also can be seen from the figure that perfect spectrum sensing scheme has a higher capacity of all cognitive femtocells than the imperfect spectrum sensing scheme, because mis-detection and false alarm in imperfect spectrum sensing overestimate the cross-tier interference, which shrinks the feasible domain of the optimizing variable.

Figure 21 shows the total capacity of all cognitive femtocells when minimum transmit rate requirement $R_{k,i}$ increases from 2 to 10 bps/Hz for the number of users per femtocell $F = 2, 3, 4$ and the number of femtocells $K = 10$. The other simulation parameters are set as $I_{th,n}^{MF} = I_{th,n}^{FF} = -100$ dBm for all n. The total capacity of all femtocells decreases as the decrease of $R_{k,i}^0$. This is because a large value of $R_{k,i}^0$ narrows the feasible domain of the optimizing variable. It can also be seen from the figure that a larger number of FUs per femtocell results in a higher capacity, because of the multiuser diversity in the resource allocation [18].

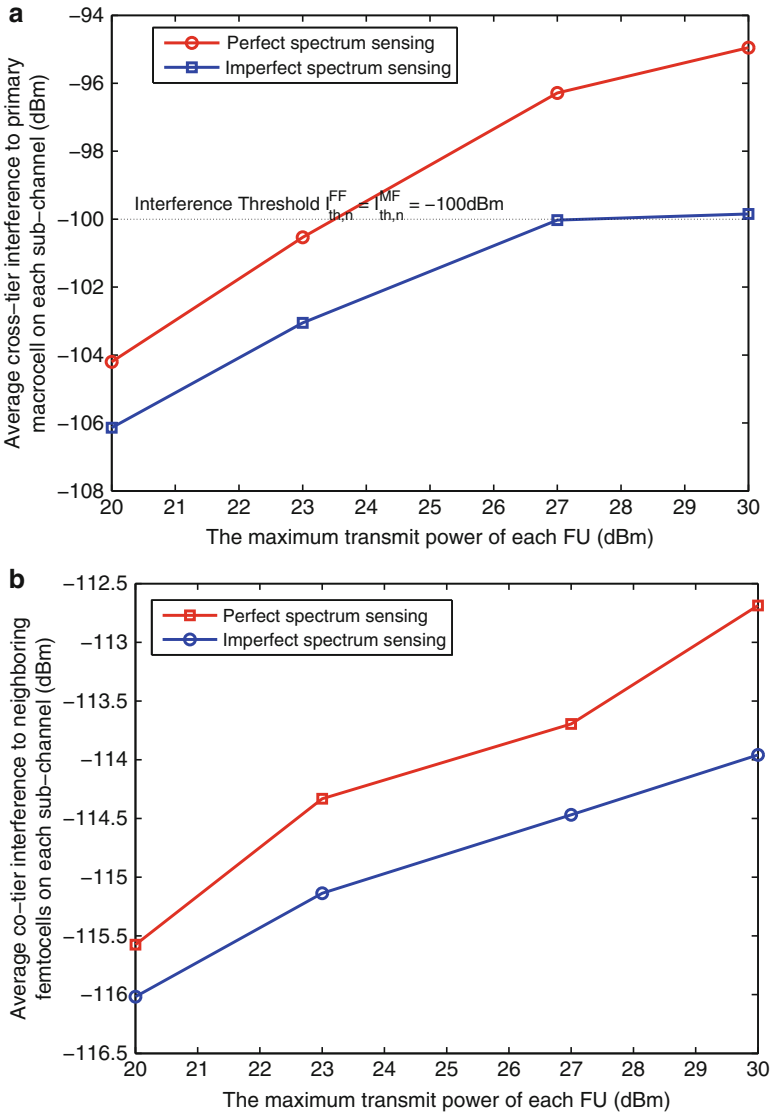

Fig. 19 Average cross-tier interference to primary macrocell and average co-tier interference to neighboring femtocells in each subchannel versus the maximum transmit power of each FU. (**a**) Average cross-tier interference to primary macrocell in each subchannel. (**b**) Average co-tier interference to neighboring femtocells in each subchannel

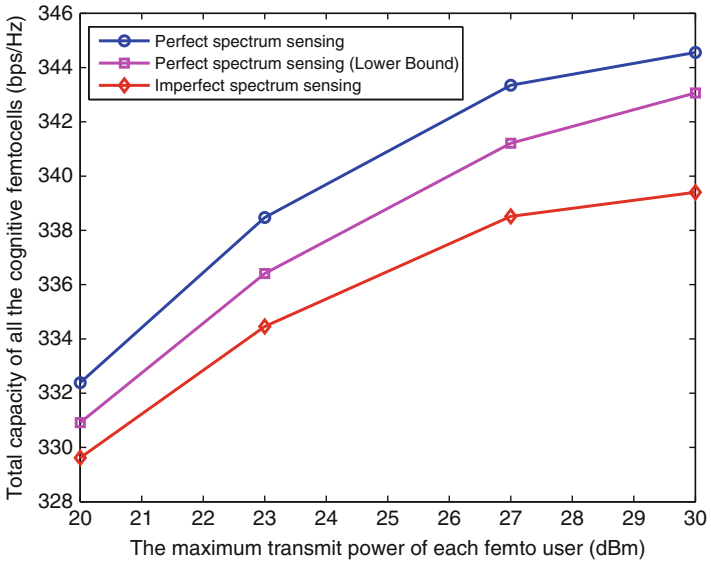

Fig. 20 Total capacity of all cognitive femtocells versus the maximum transmit power of each FU

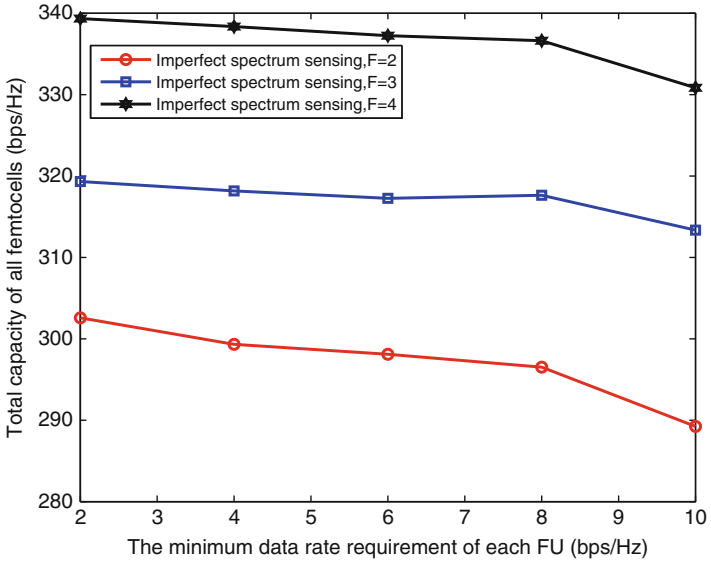

Fig. 21 Total capacity of all cognitive femtocells versus the minimum QoS requirement of each FU

Conclusion

This chapter introduced the resource allocation problem in cognitive heterogeneous networks, where the cross-tier interference mitigation, imperfect spectrum sensing, and energy efficiency are considered. Through provided three algorithms for cognitive heterogeneous networks, the resource allocation problems were solved. Furthermore, the simulation results showed that the provided algorithms achieve improved performance.

Appendix

The proof of Theorem 1.

Proof. (1) Suppose that $\eta^*_{13,n}$ is the optimal solution of (22), the inequality can be obtained

$$\begin{aligned}\eta^*_{13,n} &= \frac{P(\mathscr{H}_n^v)(1-q_n^f(\varepsilon_n,\hat{\tau}))R_{1,n}(\hat{\tau},\tilde{P}^v_{s,n}) + P(\mathscr{H}_n^o)q_n^m(\varepsilon_n,\hat{\tau})R_{3,n}(\hat{\tau},\tilde{P}^v_{s,n})}{\tilde{P}^v_{s,n}+P_c} \\ &\geq \frac{P(\mathscr{H}_n^v)(1-q_n^f(\varepsilon_n,\hat{\tau}))R_{1,n}(\hat{\tau},P^v_{s,n}) + P(\mathscr{H}_n^o)q_n^m(\varepsilon_n,\hat{\tau})R_{3,n}(\hat{\tau},P^v_{s,n})}{P^v_{s,n}+P_c}\end{aligned} \tag{79}$$

$$\begin{aligned}&\max_{P^v_{s,n}}\left\{P(\mathscr{H}_n^v)(1-q_n^f(\varepsilon_n,\hat{\tau}))R_{1,n}(\hat{\tau},P^v_{s,n}) + P(\mathscr{H}_n^o)q_n^m(\varepsilon_n,\hat{\tau})R_{3,n}(\hat{\tau},P^v_{s,n}) - \eta^*_{13,n}(P^v_{s,n}+P_c)\right\} \\ &= P(\mathscr{H}_n^v)(1-q_n^f(\varepsilon_n,\hat{\tau}))R_{1,n}(\hat{\tau},P^v_{s,n}) + P(\mathscr{H}_n^o)q_n^m(\varepsilon_n,\hat{\tau})R_{3,n}(\hat{\tau},P^v_{s,n}) - \eta^*_{13,n}(P^v_{s,n}+P_c) = 0.\end{aligned} \tag{80}$$

Hence, we have (81)

$$\begin{cases} P(\mathscr{H}_n^v)(1-q_n^f(\varepsilon_n,\hat{\tau}))R_{1,n}(\hat{\tau},\tilde{P}^v_{s,n}) + P(\mathscr{H}_n^o)q_n^m(\varepsilon_n,\hat{\tau})R_{3,n}(\hat{\tau},\tilde{P}^v_{s,n}) - \eta^*_{13,n}\left(\tilde{P}^v_{s,n}+P_c\right) = 0 \\ P(\mathscr{H}_n^v)(1-q_n^f(\varepsilon_n,\hat{\tau}))R_{1,n}(\hat{\tau},P^v_{s,n}) + P(\mathscr{H}_n^o)q_n^m(\varepsilon_n,\hat{\tau})R_{3,n}(\hat{\tau},P^v_{s,n}) - \eta^*_{13,n}\left(P^v_{s,n}+P_c\right) \leq 0. \end{cases} \tag{81}$$

Therefore, $\max\limits_{P^v_{s,n}} \left\{ \begin{array}{l} P(\mathscr{H}_n^v)(1-q_n^f(\varepsilon_n,\hat{\tau}))R_{1,n}(\hat{\tau},P^v_{s,n}) \\ + P(\mathscr{H}_n^o)q_n^m(\varepsilon_n,\hat{\tau})R_{3,n}(\hat{\tau},P^v_{s,n}) \\ - \eta^*_{13,n}(P^v_{s,n}+P_c) \end{array} \right\} = 0$ can be concluded.
That is, eq. (80) is achieved.

(2) Suppose that $\widetilde{P}^v_{s,n}$ is a solution to the problem of (80). The definition of (80) implies that (82)

$$
\begin{aligned}
&P(\mathscr{H}_n^v)(1-q_n^f(\varepsilon_n,\hat{\tau}))R_{1,n}(\hat{\tau},P_{s,n}^v)+P(\mathscr{H}_n^o)q_n^m(\varepsilon_n,\hat{\tau})R_{3,n}(\hat{\tau},P_{s,n}^v)\\
&-\eta_{13,n}^*\left(P_{s,n}^v+P_c\right)\le P(\mathscr{H}_n^v)(1-q_n^f(\varepsilon_n,\hat{\tau}))R_{1,n}(\hat{\tau},\tilde{P}_{s,n}^v)\\
&+P(\mathscr{H}_n^o)q_n^m(\varepsilon_n,\hat{\tau})R_{3,n}(\hat{\tau},\tilde{P}_{s,n}^v)-\eta_{13,n}^*\left(\tilde{P}_{s,n}^v+P_c\right)=0\\
&or\\
&\begin{cases}
P(\mathscr{H}_n^v)(1-q_n^f(\varepsilon_n,\hat{\tau}))R_{1,n}(\hat{\tau},P_{s,n}^v)+P(\mathscr{H}_n^o)q_n^m(\varepsilon_n,\hat{\tau})R_{3,n}(\hat{\tau},P_{s,n}^v)\\
-\eta_{13,n}^*\left(P_{s,n}^v+P_c\right)\le 0\\
P(\mathscr{H}_n^v)(1-q_n^f(\varepsilon_n,\hat{\tau}))R_{1,n}(\hat{\tau},\tilde{P}_{s,n}^v)+P(\mathscr{H}_n^o)q_n^m(\varepsilon_n,\hat{\tau})R_{3,n}(\hat{\tau},\tilde{P}_{s,n}^v)\\
-\eta_{13,n}^*\left(\tilde{P}_{s,n}^v+P_c\right)=0.
\end{cases}
\end{aligned}
\tag{82}
$$

Therefore, we obtain

$$
\frac{\left\{\begin{array}{l}P(\mathscr{H}_n^v)(1-q_n^f(\varepsilon_n,\hat{\tau}))R_{1,n}(\hat{\tau},\tilde{P}_{s,n}^v)\\+P(\mathscr{H}_n^o)q_n^m(\varepsilon_n,\hat{\tau})R_{3,n}(\hat{\tau},\tilde{P}_{s,n}^v)\end{array}\right\}}{\tilde{P}_{s,n}^v+P_c}=\eta_{13,n}^* \tag{83}
$$

and

$$
\frac{\left\{\begin{array}{l}P(\mathscr{H}_n^v)(1-q_n^f(\varepsilon_n,\hat{\tau}))R_{1,n}(\hat{\tau},P_{s,n}^v)\\+P(\mathscr{H}_n^o)q_n^m(\varepsilon_n,\hat{\tau})R_{3,n}(\hat{\tau},P_{s,n}^v)\end{array}\right\}}{P_{s,n}^v+P_c}\le\eta_{13,n}^*. \tag{84}
$$

□

Lemma 1. *Let $\boldsymbol{A}$ be an $N\times N$ symmetric matrix, $\boldsymbol{A}$ is negative semidefinite if and only if all the kth order principal minors of $\boldsymbol{A}$ are no larger than zero if k is odd, and not less than zero if k is even, where $1\le k\le N$.*

The proof of Theorem 2.

Proof. First, define the element $\tau_{k,i,n}\widehat{R}_{k,i,n}^{\mathrm{F}}$ in (59) as $f(\tau_{k,i,n},\widehat{p}_{k,i,n})=\tau_{k,i,n}\widehat{R}_{k,i,n}^{\mathrm{F}}$. The objective function in (59) is the sum of $f(\tau_{k,i,n},\widehat{p}_{k,i,n})$ over all possible values of k, i, and n. Substituting $\widehat{R}_{k,i,n}^{\mathrm{F}}=\log_2\left(1+\frac{\widehat{p}_{k,i,n}\hbar_{k,k,i,n}^{\mathrm{FF}}}{\tau_{k,i,n}I_{k,i,n}}\right)$ into $f(\tau_{k,i,n},\widehat{p}_{k,i,n})$, so we have

$$
f(\tau_{k,i,n},\widehat{p}_{k,i,n})=\tau_{k,i,n}\log_2\left(1+\frac{\widehat{p}_{k,i,n}\hbar_{k,k,i,n}^{\mathrm{FF}}}{\tau_{k,i,n}I_{k,i,n}}\right). \tag{85}
$$

Based on (85), one obtains

$$
\frac{\partial^2 f}{\partial{\tau_{k,i,n}}^2}=-\frac{1}{\ln 2}\frac{\left(\widehat{p}_{k,i,n}\hbar_{k,k,i,n}^{\mathrm{FF}}\right)^2}{\tau_{k,i,n}\left(\tau_{k,i,n}I_{k,i,n}+\widehat{p}_{k,i,n}\hbar_{k,k,i,n}^{\mathrm{FF}}\right)^2}, \tag{86}
$$

$$\frac{\partial^2 f}{\partial \tau_{k,i,n} \partial \widehat{p}_{k,i,n}} = \frac{\partial^2 f}{\partial \widehat{p}_{k,i,n} \partial \tau_{k,i,n}} = \frac{1}{\ln 2} \frac{\widehat{p}_{k,i,n} \left(\hbar^{\mathrm{FF}}_{k,k,i,n}\right)^2}{\left(\tau_{k,i,n} I_{k,i,n} + \widehat{p}_{k,i,n} \hbar^{\mathrm{FF}}_{k,k,i,n}\right)^2}, \tag{87}$$

$$\frac{\partial^2 f}{\partial \widehat{p}_{k,i,n}{}^2} = -\frac{1}{\ln 2} \frac{\tau_{k,i,n} \left(\hbar^{\mathrm{FF}}_{k,k,i,n}\right)^2}{\left(\tau_{k,i,n} I_{k,i,n} + \widehat{p}_{k,i,n} \hbar^{\mathrm{FF}}_{k,k,i,n}\right)^2}. \tag{88}$$

Consequently, the Hessian matrix of $f(\tau_{k,i,n}, \widehat{p}_{k,i,n})$ can be written as

$$\boldsymbol{H} = \begin{bmatrix} \frac{\partial^2 f}{\partial \tau_{k,i,n}{}^2} & \frac{\partial^2 f}{\partial \tau_{k,i,n} \partial \widehat{p}_{k,i,n}} \\ \frac{\partial^2 f}{\partial \widehat{p}_{k,i,n} \partial \tau_{k,i,n}} & \frac{\partial^2 f}{\partial \widehat{p}_{k,i,n}{}^2} \end{bmatrix}. \tag{89}$$

Substituting (86), (87), (88) to (89), we can show that the first-order principal minors of $\boldsymbol{H}$ are negative, and the second-order principal minor of $\boldsymbol{H}$ is zero. Therefore, $\boldsymbol{H}$ is negative semidefinite according to Lemma 1, and $f(\tau_{k,i,n}, \widehat{p}_{k,i,n})$ is concave. The objective function of (59) is concave because any positive linear combination of concave functions is concave [23,33]. As the inequality constraints in (59) are convex, the feasible set of the objective function in (59) is convex, and the corresponding optimization problem is a convex problem. This completes the proof. □

References

1. Zhang H, Chu X, Guo W, Wang S (2015) Coexistence of Wi-Fi and heterogeneous small cell networks sharing unlicensed spectrum. IEEE Commun Mag 22(3):92–99
2. Samarakoon S, Bennis M, Saad W, Debbah M, Latva-aho M (2016) Ultra dense small cell networks: turning density into energy efficiency. IEEE J Sel Areas Commun 34(5): 1267–1280
3. Zhang H, Dong Y, Cheng J, Hossain Md J, Leung VCM (2016) Fronthauling for 5G LTE-U ultra dense cloud small cell networks. IEEE Wirel Commun 23(6):48–53
4. Bennis M, Simsek M, Czylwik A, Saad W, Valentin S, Debbah M (2013) When cellular meets WiFi in wireless small cell networks. IEEE Commun Mag 51(6):44–50
5. Zhang H, Jiang C, Beaulieu NC, Chu X, Wen X, Tao M (2014) Resource allocation in spectrum-sharing OFDMA femtocells with heterogeneous services. IEEE Trans Commun 62(7):2366–2377
6. Bennis M, Perlaza SM, Blasco P, Han Z, Poor HV (2013) Self-organization in small cell networks: a reinforcement learning approach. IEEE Trans Commun 12(7): 3202–3212
7. Zhang H, Jiang C, Beaulieu NC, Chu X, Wang X, Quek T (2015) Resource allocation for cognitive small cell networks: a cooperative bargaining game theoretic approach. IEEE Trans Wirel Commun 14(6):3481–3493
8. Hong X, Wang J, Wang C, Shi J (2014) Cognitive radio in 5G: a perspective on energy-spectral efficiency trade-off. IEEE Commun Mag 52(7):46–53

9. Huang L, Zhu G, Du X (2013) Cognitive femtocell networks: an opportunistic spectrum access for future indoor wireless coverage. IEEE Wirel Commun 20(2):44–51
10. Chen X, Zhao Z, Zhang H (2013) Stochastic power adaptation with multiagent reinforcement learning for cognitive wireless mesh networks. IEEE Trans Mob Comput 12(11): 2155–2166
11. Wang W, Yu G, Huang A (2013) Cognitive radio enhanced interference coordination for femtocell networks. IEEE Commun Mag 51(6):37–43
12. Hu D, Mao S (2012) On medium grain scalable video streaming over femtocell cognitive radio networks. IEEE J Sel Areas Commun 30(3):641–651
13. Urgaonkar R, Neely MJ (2012) Opportunistic cooperation in cognitive femtocell networks. IEEE J Sel Areas Commun 30(3):607–616
14. Cheng S, Ao W, Tseng F, Chen K (2012) Design and analysis of downlink spectrum sharing in two-tier cognitive femto networks. IEEE Trans Veh Technol 61(5):2194–2207
15. Wang X, Ho P, Chen K (2012) Interference analysis and mitigation for cognitive-empowered femtocells through stochastic dual control. IEEE Trans Wirel Commun 11(6): 2065–2075
16. Xie R, Yu FR, Ji H, Li Y (2012) Energy-efficient resource allocation for heterogeneous cognitive radio networks with femtocells. IEEE Trans Wirel Commun 11(11): 3910–3920
17. Le L, Niyato D, Hossain E, Kim DI, Hoang DT (2013) QoS-aware and energy-efficient resource management in OFDMA femtocells. IEEE Trans Wirel Commun 12(1): 180–194
18. Zhang H, Jiang C, Mao X, Chen H (2016) Interference-limit resource allocation in cognitive femtocells with fairness and imperfect spectrum sensing, accepted. IEEE Trans Veh Technol 65(3):1761–1771
19. Zhang H, Nie Y, Cheng J, Leung VCM, Nallanathan A (2017) Sensing time optimization and power control for energy efficient cognitive small cell with imperfect hybrid spectrum sensing. IEEE Trans Wirel Commun 16(2):730–743
20. Liang Y, Zeng Y, Peh ECY, Hoang A (2008) Sensing-throughput tradeoff for cognitive radio networks. IEEE Trans Wirel Commun 7(4):1326–1337
21. Ng DWK, Lo ES, Schober R (2012) Energy-efficient resource allocation in multi-cell OFDMA systems with limited backhaul capacity. IEEE Trans Wirel Commun 11(10):3618–3631
22. Xiong C, Li GY, Liu Y, Chen Y, Xu S (2013) Energy-efficient design for downlink OFDMA with delay-sensitive traffic. IEEE Trans Wirel Commun 12(6):3085–3095
23. Boyd S, Vandenberghe L (2004) Convex optimization. Cambridge University Press, Cambridge
24. Chen Y, Zhao Q, Swami A (2008) Joint design and separation principle for opportunistic spectrum access in the presence of sensing errors. IEEE Trans Inf Theory 54(5): 2053–2071
25. Jiang C, Chen Y, Gao Y, Liu KJR (2013) Joint spectrum sensing and access evolutionary game in cognitive radio networks. IEEE Trans Wirel Commun 12(5):2470–2483
26. Xie R, Yu FR, Ji H (2012) Dynamic resource allocation for heterogeneous services in cognitive radio networks with imperfect channel sensing. IEEE Trans Veh Technol 61(2):770–780
27. Almalfouh SM, Stuber GL (2011) Interference-aware radio resource allocation in OFDMA-based cognitive radio networks. IEEE Trans Veh Technol 60(4):1699–1713
28. Wong CY, Cheng R, Lataief K, Murch R (1999) Multiuser OFDM with adaptive subcarrier, bit, and power allocation. IEEE J Sel Areas Commun 17(10):1747–1758
29. Kang X, Zhang R, Motani M (2012) Price-based resource allocation for spectrum-sharing femtocell networks: a stackelberg game approach. IEEE J Sel Areas Commun 30(3): 538–549
30. Son K, Lee S, Yi Y, Chong S (2011) Refim: a practical interference management in heterogeneous wireless access networks. IEEE J Sel Areas Commun 29(6):1260–1272
31. Shen Z, Andrews JG, Evans BL (2005) Adaptive resource allocation in multiuser OFDM systems with proportional rate constraints. IEEE Trans Wirel Commun 4(6):2726–2737

32. Further advancements for E-UTRA, physical layer aspects, 3GPP Std. TR 36.814 v9.0.0, 2010
33. Tao M, Liang Y-C, Zhang F (2008) Resource allocation for delay differentiated traffic in multiuser OFDM systems. IEEE Trans Wirel Commun 7(6):2190–2201

Further Reading

1. Hsiung CY, Mao GY (1998) Linear algebra. Allied Publishers

Dynamic Spectrum Sharing in Secure Cognitive Radio Networks

20

Biao He, Xiaoming Xu, Vincent K. N. Lau, and Weiwei Yang

Contents

Abstract

In this chapter, the physical layer security in cognitive radio networks with dynamic spectrum sharing is discussed. A brief overview on the security threats

B. He (✉) · V. K. N. Lau
Department of Electronic and Computer Engineering, The Hong Kong University of Science and Technology, Hong Kong, Hong Kong
e-mail: eebiaohe@ust.hk; eeknlau@ee.ust.hk

X. Xu · W. Yang
College of Communications Engineering, PLA University of Science and Technology, Nanjing, Jiangsu, China
e-mail: xiaomingxu.plaust@gmail.com; wwyang1981@163.com

W. Zhang (ed.), *Handbook of Cognitive Radio*,
https://doi.org/10.1007/978-981-10-1394-2_20

in cognitive ratio networks is given. Focusing on the eavesdropping attack, a secrecy problem of the communication between a secondary transmitter-receiver pair in the presence of randomly distributed eavesdroppers is specifically investigated. The dynamic transmit power control is adopted at the secondary-user transmitter to ensure that the spectrum sharing does not harm the primary network. Depending on the knowledge of the channel and the eavesdropper locations, four secure transmission schemes with dynamic spectrum sharing are introduced. A comprehensive performance analysis of each scheme is given. Moreover, the optimal design of the transmission scheme that maximizes the secrecy throughput subject to the secrecy constraint and the reliability constraint is derived. Numerical illustrations on the performance comparison between different schemes are also presented.

Keywords
Physical layer security · Cognitive radio network · Dynamic transmit power · On-off transmission · Secrecy guard zone

Security Issues in Cognitive Radio Networks

With the rapid adoption of wireless devices, there is an unprecedented growth in the demand for radio spectrum. To address the conflict between spectrum scarcity and spectrum underutilization, dynamic spectrum sharing has been regarded as a promising technology to solve the problem of inefficient spectrum usage. Spectrum sharing allows the primary and secondary users transmit concurrently while ensuring that the secondary network do not harm the primary network.

The adoption of spectrum sharing is not without drawbacks. The coexistence of licensed and unlicensed users in the same network makes the data transmissions vulnerable to security attacks [23]. The key security threats in cognitive radio networks include but not limited to the primary user emulation, the spectrum sensing data falsification, the jamming attack, and the eavesdropping.

When launching a primary user emulation attack, the attacker pretends to be a primary user and sends signals in the licensed band. As a result, second users may regard the attacker as a primary user, and the precious unused spectrum would be wasted. For the spectrum sensing data falsification, attackers intentionally send incorrect spectrum sensing signals to fusion centers or secondary users, which may lead to legitimate users' wrong decisions on the spectrum access and sharing. In a jamming attack, the attacker continuously or randomly broadcast interference signals to jam legitimate channels, so that the legitimate users may not be able to send or receive messages reliably. By eavesdropping attacks, malicious users attempt to listen to the transmission between legitimate users, which can result in the leakage of sensitive and confidential information of legitimated users. The detailed introduction on the security threats in cognitive radio networks and the conventional countermeasures can be found in [21] and [23].

Eavesdropping Threat

In the following, the eavesdropping threat in the cognitive network and the related studies are specifically discussed. Secure communication against eavesdropping attacks has drawn considerable attention from wireless researchers and engineers in recent years [2, 29], due to the unprecedented amount of private and sensitive data transmitted over wireless channels as a result of the ubiquitous adoption of wireless technology.

In cognitive radio networks, both primary and secondary networks are subject to the threat of eavesdropping, and protecting the transmission is not easy. For example, a transmitter in the secondary network wishes to send confidential information to a receiver the secondary network by dynamically sharing the spectrum with preliminary users. They have to make sure that the transmission is reliable to the receiver, unharmful to primary users, and not interceptable by eavesdroppers.

From an information-theoretic perspective, the performance of PLS in cognitive radio networks was studied in, e.g., [1, 16, 17, 26, 31]. The ergodic secrecy capacity for the cognitive radio network was evaluated in [16, 17] with the consideration of fast fading channels where the encoded messages are assumed to span sufficient channel realizations to capture the ergodic features of the fading channel. Considering the slow fading channels, the secrecy performance of the cognitive radio network was evaluated in [31] by the outage-based formulation. The secrecy throughput scaling laws were investigated in [1, 26]. More recently, various signal processing techniques and system design protocols were proposed to improve the secrecy performance of cognitive radio networks. For the multi-antenna cognitive radio network, beamforming designs and cooperative jamming techniques were studied in [5, 8, 22]. For the cognitive radio network with multiple SUs, the user scheduling scheme for improving the security level of cognitive transmissions was proposed in [30]. Furthermore, the cognitive radio network with decode and forward relays was studied in [19] where the optimal relay selection scheme to minimize the secrecy outage probability was proposed.

Randomly Distributed Eavesdroppers

Although considerable efforts have been paid to the PLS in cognitive radio networks, the practical situation where a large number of malicious users inside the cognitive radio network at random and possibly changing locations has been rarely studied. In practice, the number of malicious users in the network can be large, and the passive eavesdroppers would not reveal their location information to legitimate users. In addition, the eavesdroppers may frequently change their location to avoid being detected. Since the PLS relies on the characteristics of wireless channels, the lack of information on eavesdroppers' channels and locations makes it challenging to protect cognitive radio networks in such a situation.

Without the consideration of fading effects, the secrecy issue of cognitive radio networks with distributed eavesdroppers has been studied in [20, 21], in which a simplified channel model consisting of the pass loss effect only is assumed. It is worth mentioning that the performance of secure communication is very different between a fading and a non-fading scenario, and the presence of fading can be smartly utilized to achieve a better secrecy performance. Thus, it is important to take the fading effects into account when analyzing the physical layer security of cognitive radio networks with randomly distributed eavesdroppers [25].

Dynamic Spectrum Sharing in the Presence of Poisson Distributed Eavesdroppers

Consider a situation where a secondary transmitter (SU-Tx) wants to sends confidential messages to a secondary receiver (SU-Rx) in the presence of randomly distributed eavesdroppers. The secondary users dynamically share the spectrum with the primary users and guarantee that the transmission does not affect primary users. The eavesdroppers are assume to movable, and their locations change at each snapshot of time.

Problem Formulation

An illustration of the network model is shown in Fig. 1. The SU-Tx sends confidential messages to the SU-Rx in the presence of multiple movable eavesdroppers. The secondary network dynamically shares the spectrum of the primary network by an underlay method. That is, secondary users are allowed to utilize the licensed

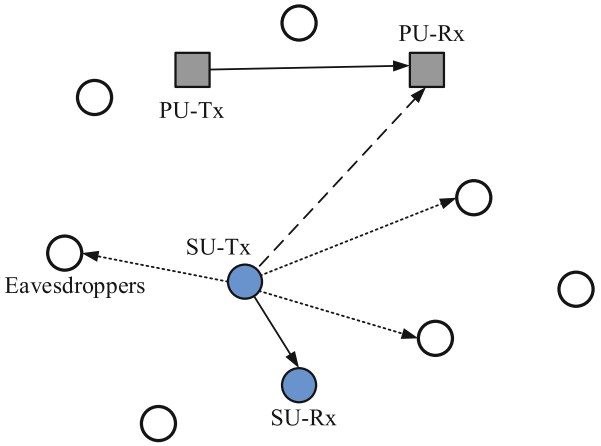

Fig. 1 Illustration of a cognitive radio network with randomly distributed eavesdroppers

spectrum while guaranteeing the interference at primary users not beyond an acceptable threshold.

The path-loss plus quasi-static Rayleigh fading channel model is considered and each communication node is assumed to have a single antenna. The received signal-to-noise ratios (SNRs) at the SU-Rx or the j-th eavesdropper is given by

$$\gamma_i = \frac{P}{\sigma_i^2} |h_i|^2 d_i^{-\alpha}, \quad i = s \text{ or } j \tag{1}$$

respectively, where the subscripts s and j denote the SU-Rx and the j-th eavesdropper, respectively, P denotes the transmitter power at SU-Tx, $\alpha \geq 2$ denotes the path-loss exponent, d_i denotes the distance from SU-Tx to the receiver, σ_i^2 denotes the variance of additive white Gaussian noise (AWGN) at the receiver, and $h_i \sim \mathcal{CN}(0, 1)$ denotes the normalized fading channel coefficient. It is assumed that $\sigma_s^2 = \sigma_j^2 = \sigma^2$ and the interferences from PU-Tx to the SU-Rx and the eavesdroppers are neglectable. It is assume that the receivers have the perfect estimation of their own channel, i.e., h_i. A low-complexity feedback scheme is possibly available from the SU-Rx to the SU-Tx, in which one-bit information about the instantaneous channel condition can be fed back to the SU-Tx. The eavesdroppers are totally passive and do not real their channel state information (CSI) to legitimate users.

Dynamic Transmit Power Control

The PU-Rx informs the SU-Tx of the instantaneous channel gain between them to enable the SU-Tx to dynamically control the transmit power so that its transmission does not harm the primary network. A spectrum-band manager may be required to mediate between the licensed and unlicensed users [15]. The instantaneous interference power at the PU-Rx from the SU-Tx is required to be lower than a threshold, denoted by I_0. Then, the SU-Tx adjusts its transmit power as

$$P = \frac{I_0}{\left|h_p\right|^2 d_p^{-\alpha}} \mathbf{1}_{(\text{condition})}, \tag{2}$$

where $h_p \sim \mathcal{CN}(0, 1)$ and d_p denote the fading channel coefficient and the distance between the SU-Tx and the PU-Rx, respectively. The $\mathbf{1}_{(\text{condition})}$ in (2) denotes an indicator function for whether the transmission is "on" or "off," which is given by

$$\mathbf{1}_{(\text{condition})} = \begin{cases} 1, & \text{if the condition holds} \\ 0, & \text{otherwise,} \end{cases} \tag{3}$$

where the condition depends on the specifical transmission scheme and will be detailed later.

Poisson Model of Eavesdropper Locations

The scenario where a large number of eavesdroppers are randomly distributed in the network is consider. The network with a large number of randomly distributed eavesdroppers is often investigated by adopting the tool from stochastic geometry [10]. Stochastic geometry is proved to be a good mathematic tool in analyzing wireless networks with a larger number of nodes [10]. The location set of the eavesdroppers, denoted by Φ_e, is modeled by a homogeneous Poisson point process (PPP) with density λ_e. The homogeneous PPP well models the set of communication nodes contained in large-scale wireless networks [9], which not only provides tractable closed-form results but also describes the randomness of eavesdropper locations in practical scenarios [4]. Thus, the homogeneous PPP model of eavesdropper locations has been widely adopted in the literature, e.g., [4,6,13,14,18,27].

The worst-case scenario is considered for a robust approach to analyzing the system. Specifically, all eavesdroppers are assumed to be able to collude and exchange the received information. The multiple eavesdroppers is then regarded as a single eavesdropper with multiple distributed antennas, and the equivalent received SNR at the colluding eavesdroppers is given by

$$\gamma_e = \frac{P}{\sigma^2} \sum\nolimits_{j \in \Phi_e} \left| h_j \right|^2 d_j^{-\alpha} = \frac{P}{\sigma^2} Z_{\Phi_e} \tag{4}$$

where $Z_{\Phi_e} = \sum_{j \in \Phi_e} |h_j|^2 d_j^{-\alpha}$.

Secure Encoding

The wiretap code [24] is adopted at the SU-Tx to encode the confidential messages. Denote the set of all possible Wyner codes as $\mathbb{C}(R_t, R_s)$, where R_t is the rate of transmitted codewords and R_s is the rate of confidential messages with $R_t > R_s$. The rate difference $R_t - R_s$ reflects the rate cost to secure the message against eavesdropping. The encoding rates are assumed to have been already designed, so that R_t and R_s are fixed during the transmission. In practice, applications like video streaming in multimedia applications often require fixed-rate transmission.

Performance Metrics

The metrics to comprehensively evaluate the performance are introduced as follows.

Transmission Probability

Depending on the transmission scheme, SU-Tx may not always transmit to avoid eavesdropping. Then, there exists a probability of transmission. A small probability of transmission will cause the delay of the information delivery. Thus, the

transmission probability is adopted to measure the performance of transmission delay given by

$$p_{\text{tx}} = \mathbb{P}\left(\mathbf{1}_{(\text{condition})} = 1\right), \tag{5}$$

where $\mathbb{P}(\cdot)$ denotes the probability measure.

Connection Outage Probability

A connection outage event happens when the message cannot be decoded at the intended receiver without error. The reliability performance is then measured by the connection outage probability given by

$$p_{\text{co}} = \mathbb{P}\left(C_s < R_t \,|\, \mathbf{1}_{(\text{condition})} = 1\right), \tag{6}$$

where $C_s = \log\left(1 + \gamma_s\right)$ denotes the channel capacity of the SU-Rx.

Secrecy Outage Probability

A secrecy outage event happens when the perfect secrecy of the message cannot be guaranteed. The secrecy performance is then measure by the secrecy outage probability, which is given by [28]

$$p_{\text{so}} = \mathbb{P}\left(C_e > R_t - R_s \mid \mathbf{1}_{(\text{condition})} = 1\right), \tag{7}$$

where $C_e = \log\left(1 + \gamma_e\right)$ denotes the channel capacity of the colluding eavesdroppers.

Secrecy Throughput

The overall performance of the system is measured by the secrecy throughput taking into account the transmission delay, the security performance and the reliability performance together. The secrecy throughput quantizes the average rate at which the messages are securely and reliably transmitted to the SU-Rx, which is given by

$$\eta = p_{\text{tx}} p_{\text{no}} R_s, \tag{8}$$

where p_{no} denotes the non-outage probability. The non-outage probability in (8) characterizes the probability that neither the secrecy outage event nor the connection outage event happens, which is given by

$$p_{\text{no}} = \mathbb{P}\left(C_s \geq R_t \;\&\; C_e \leq R_t - R_s \mid \mathbf{1}_{(\text{condition})} = 1\right). \tag{9}$$

Note that p_{no} cannot be simply given as a function of p_{co} and p_{so}, since p_{co} in (6) and p_{so} in (7) are correlated due to the correlation between γ_s and γ_e.

Secure Transmission Schemes with Dynamic Spectrum Sharing

There are mainly four secure transmission schemes with the dynamic spectrum sharing as introduced in [25]. These four schemes are suitable in different situations depending on the SU-Tx's knowledge about the channel and the eavesdropper locations. Specifically, the situations of interest are given as follows:

1. SU-Tx does not know any information about the channel condition to the SU-Rx and the eavesdropper locations;
2. SU-Tx does not know any information about the channel condition to the SU-Rx but can detect the existence of eavesdroppers in its vicinity;
3. SU-Rx has the one-bit feedback about the channel condition to the SU-Rx but does not know any information about the eavesdropper locations;
4. SU-Rx has the one-bit feedback about the channel condition to the SU-Rx and can detect the existence of eavesdroppers in its vicinity.

Full-Active Scheme

The full activity scheme is adopted in the situation where the SU-Tx can neither obtain the one-bit feedback from the SU-Rx nor detect the existence of eavesdroppers in its vicinity. In such a situation, the SU-Tx transmits all the time with the dynamic power control, and the indicator function in (3) is always equal to one.

The SNRs at the SU-Rx and the colluding eavesdroppers are given by

$$\gamma_s = \frac{I_0 |h_s|^2 d_s^{-\alpha}}{\sigma^2 |h_p|^2 d_p^{-\alpha}} \tag{10}$$

and

$$\gamma_e = \frac{I_0}{\sigma^2 |h_p|^2 d_p^{-\alpha}} Z_{\Phi_e}, \tag{11}$$

respectively. The transmission probability is given by

$$p_{\text{tx}} = \mathbb{P}\left(\mathbf{1}_{(\text{condition})} = 1\right) = 1, \tag{12}$$

which indicates that there is no transmission delay. The connection outage probability can be obtained by substituting (10) into (6), which is given by

$$
\begin{aligned}
p_{\text{co}} &= \mathbb{P}\left(C_s < R_t \,|\, \mathbf{1}_{(\text{condition})} = 1\right) \\
&= \mathbb{P}\left(|h_s|^2 < \frac{\left(2^{R_t}-1\right)\sigma^2 d_s^{\alpha}}{I_0 d_p^{\alpha}} \left|h_p\right|^2\right) \\
&= \frac{\left(2^{R_t}-1\right)\sigma^2 d_s^{\alpha}}{\left(2^{R_t}-1\right)\sigma^2 d_s^{\alpha} + I_0 d_p^{\alpha}}.
\end{aligned} \tag{13}
$$

The secrecy outage probability can be obtained by substituting (11) into (7), which is given by

$$
\begin{aligned}
p_{\text{so}} &= \mathbb{P}\left(C_e > R_t - R_s \mid \mathbf{1}_{(\text{condition})} = 1\right) \\
&= \mathbb{P}\left(\log_2\left(1 + \frac{I_0}{\sigma^2 \left|h_p\right|^2 d_p^{-\alpha}} Z_{\Phi_e}\right) > R_t - R_s\right) \\
&= \mathbb{E}_{\Phi_e}\left\{1 - \exp\left(-\frac{I_0 Z_{\Phi_e} d_p^{\alpha}}{\left(2^{R_t-R_s}-1\right)\sigma^2}\right)\right\} \\
&= 1 - L_{Z_{\Phi_e}}\left(\frac{I_0 d_p^{\alpha}}{\left(2^{R_t-R_s}-1\right)\sigma^2}\right),
\end{aligned} \tag{14}
$$

where $\mathbb{E}_{\Phi_E}\{\cdot\}$ denotes the expectation operator over Φ_e and $L_{Z_{\Phi_e}}(\cdot)$ denotes the Laplace transform of Z_{Φ_e}. From [3], $L_{Z_{\Phi_e}}(\cdot)$ is given by

$$
L_{Z_{\Phi_e}}(x) = \exp\left(-\frac{2\pi}{\alpha}\Gamma\left(\frac{2}{\alpha}\right)\Gamma\left(1-\frac{2}{\alpha}\right)\lambda_e x^{\frac{2}{\alpha}}\right) \tag{15}
$$

where $\Gamma(\cdot)$ denotes the gamma function. The non-outage probability can be obtained by substituting (10) and (11) into (9), which is given by

$$
\begin{aligned}
p_{\text{no}} &= \mathbb{P}\left(C_s \geq R_t \;\&\; C_e \leq R_t - R_s \mid \mathbf{1}_{(\text{condition})} = 1\right) \\
&= \mathbb{E}_{\Phi_e}\left\{\int_{\frac{I_0 d_p^{\alpha} Z_{\Phi_e}}{\left(2^{R_t-R_s}-1\right)\sigma^2}}^{\infty} \exp\left(-\left(\frac{\left(2^{R_B}-1\right)\sigma^2 d_s^{\alpha}}{I_0 d_p^{\alpha}} + 1\right)x\right)\mathrm{d}x\right\} \\
&= \frac{I_0 d_p^{\alpha}}{\left(2^{R_t}-1\right)\sigma^2 d_s^{\alpha} + I_0 d_p^{\alpha}} L_{Z_{\Phi_e}}\left(\frac{\left(2^{R_t}-1\right)\sigma^2 d_s^{\alpha} + I_0 d_p^{\alpha}}{\left(2^{R_t-R_s}-1\right)\sigma^2}\right).
\end{aligned} \tag{16}
$$

Based on (8), (12), and (16), the secrecy throughput is given by

$$\begin{aligned}\eta &= p_{\text{tx}} p_{\text{no}} R_s \\ &= \frac{I_0 d_p^{\alpha} R_s}{\left(2^{R_t}-1\right)\sigma^2 d_s^{\alpha} + I_0 d_p^{\alpha}} L_{Z_{\Phi_e}}\left(\frac{\left(2^{R_t}-1\right)\sigma^2 d_s^{\alpha} + I_0 d_p^{\alpha}}{\left(2^{R_t-R_s}-1\right)\sigma^2}\right).\end{aligned} \tag{17}$$

Secrecy Guard Zone Scheme

The secrecy guard scheme is adopted in the situation where the SU-Tx is able to detect the existence of eavesdroppers within a finite range. As per the mechanism of secrecy guard zone [11,27], the finite range near the SU-Tx is modeled as a secrecy guard circle. Denote the location of the SU-Tx as the origin o. The secrecy guard circle around the SU-Tx with radius r is then denoted by $\mathcal{B}(o,r)$. With the secrecy guard zone scheme, the SU-Tx transmits only when no eavesdropper is detected inside $\mathcal{B}(o,r)$.

The SNRs at the SU-Rx and the colluding eavesdroppers are given by

$$\gamma_s = \frac{I_0 |h_s|^2 d_s^{-\alpha}}{\sigma^2 \left|h_p\right|^2 d_p^{-\alpha}} \mathbf{1}_{(C_1)} \tag{18}$$

and

$$\gamma_e = \frac{I_0}{\sigma^2 \left|h_p\right|^2 d_p^{-\alpha}} Z_{\Phi_e} \mathbf{1}_{(C_1)}, \tag{19}$$

respectively, where C_1 denotes the event that all eavesdroppers are outside of the secrecy guard zone, i.e., $\left\{C_1 : \forall j \in \Phi_e, d_j > r\right\}$. Denote the number of eavesdroppers inside $\mathcal{B}(o,r)$ as $\pi r^2 \lambda_e$. Note that N is a Poisson random variable with mean $\pi r^2 \lambda_e$, and its probability mass function (PMF) is given by

$$\mathbb{P}(N=n) = \exp\left(-\pi r^2 \lambda_e\right) \frac{\left(\pi r^2 \lambda_e\right)^n}{n!}. \tag{20}$$

The transmission probability is then derived as

$$\begin{aligned} p_{\text{tx}} &= \mathbb{P}\left(\mathbf{1}_{(\text{condition})} = 1\right) \\ &= \mathbb{P}\left(C_1 : \forall j \in \Phi_e, d_j > r\right) \\ &= \mathbb{P}(N=0) \\ &= \exp\left(-\pi \lambda_e r^2\right). \end{aligned} \tag{21}$$

The connection outage probability can be obtained by substituting (18) into (6), which is identical to (13) and omitted here.

Denote $\widetilde{\Phi}_e$ as the new location set of the colluding eavesdroppers for the scenario where no eavesdropper is inside the secrecy guard zone. Following the steps of obtaining (14), the secrecy outage probability is given by

$$\begin{aligned} p_{\text{so}} &= \mathbb{P}\left(C_e > R_t - R_s \mid \mathbf{1}_{(\text{condition})} = 1\right) \\ &= 1 - L_{Z_{\widetilde{\Phi}_E}}\left(\frac{I_0 d_{SP}^{\alpha}}{\left(2^{R_B - R_S} - 1\right)\sigma^2}\right). \end{aligned} \tag{22}$$

where $Z_{\widetilde{\Phi}_E} = \sum_{E_j \in \widetilde{\Phi}_E} \left|h_{SE_j}\right|^2 d_{SE_j}^{-\alpha}$. The Laplace transform of $Z_{\widetilde{\Phi}_E}$, i.e., $L_{Z_{\widetilde{\Phi}_E}}$, is given by

$$\begin{aligned} L_{Z_{\widetilde{\Phi}_e}}(x) &= \mathbb{E}_{\widetilde{\Phi}_e, \left|h_{SE_j}\right|^2}\left\{\exp\left(-x \sum_{j \in \widetilde{\Phi}_e} \left|h_j\right|^2 d_j^{-\alpha}\right)\right\} \\ &\overset{(a)}{=} \mathbb{E}_{\widetilde{\Phi}_e}\left\{\prod_{j \in \widetilde{\Phi}_e} \mathbb{E}_{\left|h_j\right|^2}\left\{\exp\left(-x\left|h_j\right|^2 d_j^{-\alpha}\right)\right\}\right\} \\ &\overset{(b)}{=} \mathbb{E}_{\widetilde{\Phi}_e}\left\{\prod_{j \in \widetilde{\Phi}_e} \frac{1}{1 + x d_j^{-\alpha}}\right\} \\ &\overset{(c)}{=} \exp\left(-\lambda_e \int_{\mathbb{R}^2 \setminus \mathcal{B}(o,r)} \left(1 - \frac{1}{1 + x s^{-\alpha}}\right) ds\right) \\ &= \exp\left(-\frac{2\pi}{\alpha} \lambda_e x^{\frac{2}{\alpha}} \mathrm{B}_{\left(r^{\alpha} x^{-1} + 1\right)^{-1}}\left(1 - \frac{2}{\alpha}, \frac{2}{\alpha}\right)\right), \end{aligned} \tag{23}$$

where $\mathrm{B}_a(p, q) = \int_0^a t^{p-1}(1-t)^{q-1}\,\mathrm{d}t$ is the incomplete Beta function [7], (a) follows from the independence between the channel gain $\left|h_j\right|^2$ and the location of eavesdroppers, (b) follows from the exponential distribution of $\left|h_j\right|^2$, and (c) follows from the generating function of the homogeneous PPP $\widetilde{\Phi}_E$.

Based on (18), (19), and (9), the non-outage probability is given by

$$\begin{aligned} p_{\text{no}} &= \mathbb{P}\left(C_s \geq R_t \;\&\; C_e \leq R_t - R_s \mid \mathbf{1}_{(\text{condition})} = 1\right) \\ &= \frac{I_0 d_p^{\alpha}}{\left(2^{R_t} - 1\right)\sigma^2 d_s^{\alpha} + I_0 d_p^{\alpha}} L_{Z_{\widetilde{\Phi}_e}}\left(\frac{\left(2^{R_t} - 1\right)\sigma^2 d_s^{\alpha} + I_0 d_p^{\alpha}}{\left(2^{R_t - R_s} - 1\right)\sigma^2}\right). \end{aligned} \tag{24}$$

With (8), (21), and (24), the secrecy throughput is derived as

$$\begin{aligned}\eta &= p_{\text{tx}} p_{\text{no}} R_s \\ &= \frac{I_0 d_p^{\alpha} R_s \exp\left(-\pi \lambda_e r^2\right)}{\left(2^{R_t}-1\right)\sigma^2 d_s^{\alpha} + I_0 d_p^{\alpha}} L_{\widetilde{Z}_{\Phi_e}}\left(\frac{\left(2^{R_t}-1\right)\sigma^2 d_s^{\alpha} + I_0 d_p^{\alpha}}{\left(2^{R_t-R_s}-1\right)\sigma^2}\right).\end{aligned} \tag{25}$$

From (21), one can find that p_{tx} decreases as r increases, which implies that a large secrecy guard zone worsens the delay performance of the system. From (22), one can also find that p_{so} decreases as r increases, which implies that a large secrecy guard zone improves the secrecy performance of the network. Hence, the size of secrecy guard zone incurs a trade-off between the delay performance and the secrecy performance of the system.

Threshold-Based Scheme

The threshold-based scheme is adopted in the situation where the SU-Tx can obtain a one-bit feedback from the SU-Rx to enable a threshold-based on-off transmission. With the secrecy guard zone scheme, the SU-Tx transmits only when the received SNR at SU-Rx is larger than a predetermined threshold μ. To this end, the SU-Rx sends an instantaneous one-bit feedback to the SU-Tx for indicating whether its received SNR is larger the threshold μ.

The SNRs at the SU-Rx and the colluding eavesdroppers are given by

$$\gamma_s = \frac{I_0 |h_s|^2 d_s^{-\alpha}}{\sigma^2 |h_p|^2 d_p^{-\alpha}} \mathbf{1}_{(C_2)} \tag{26}$$

and

$$\gamma_e = \frac{I_0}{\sigma^2 |h_p|^2 d_p^{-\alpha}} Z_{\Phi_e} \mathbf{1}_{(C_2)} \tag{27}$$

respectively, where C_2 denotes the event that the received SNR at the SU-Rx is larger than μ, i.e., $\left\{C_2 : \frac{I_0 |h_s|^2 d_s^{-\alpha}}{\sigma^2 |h_p|^2 d_p^{-\alpha}} > \mu\right\}$. The transmission probability is given by

$$\begin{aligned} p_{\text{tx}} &= \mathbb{P}\left(\mathbf{1}_{(\text{condition})} = 1\right) \\ &= \mathbb{P}\left(C_2 : \frac{I_0 |h_s|^2 d_s^{-\alpha}}{\sigma^2 |h_p|^2 d_p^{-\alpha}} > \mu\right) \\ &= \frac{I_0 d_p^{\alpha}}{\mu \sigma^2 d_s^{\alpha} + I_0 d_p^{\alpha}}. \end{aligned} \tag{28}$$

The connection outage probability can be obtained by substituting (26) into (6), which is given by

$$\begin{aligned} p_{\text{co}} &= \mathbb{P}\left(C_s < R_t \,|\, \mathbf{1}_{(\text{condition})} = 1\right) \\ &= \begin{cases} 1 - \frac{\mu\sigma^2 d_s^\alpha + I_0 d_p^\alpha}{\left(2^{R_t}-1\right)\sigma^2 d_s^\alpha + I_0 d_p^\alpha}, & 0 \le \mu < 2^{R_t} - 1, \\ 0, & 2^{R_t} - 1 \le \mu. \end{cases} \end{aligned} \tag{29}$$

The secrecy outage probability can be obtained by substituting (27) into (7), which is given by

$$\begin{aligned} p_{\text{so}} &= \mathbb{P}\left(C_e > R_t - R_s \mid \mathbf{1}_{(\text{condition})} = 1\right) \\ &= \frac{\mu\sigma^2 d_s^\alpha + I_0 d_p^\alpha}{I_0 d_p^\alpha} \mathbb{E}_{\Phi_e} \left\{ \int_0^{\frac{I_0 d_p^\alpha Z_{\Phi_e}}{\left(2^{R_t - R_s}-1\right)N_0}} \exp\left(-\left(\frac{\mu\sigma^2 d_s^\alpha}{I_0 d_p^\alpha} + 1 \right) x \right) \mathrm{d}x \right\} \\ &= 1 - L_{Z_{\Phi_e}} \left(\frac{\mu\sigma^2 d_s^\alpha + I_0 d_p^\alpha}{\left(2^{R_t - R_s} - 1\right)\sigma^2} \right). \end{aligned} \tag{30}$$

The non-outage probability can be obtained by substituting (26) and (27) into (9), which is given by

$$\begin{aligned} p_{\text{no}} &= \mathbb{P}\left(C_s \ge R_t \;\&\; C_e \le R_t - R_s \mid \mathbf{1}_{(\text{condition})} = 1\right) \\ &= \frac{1}{p_{\text{tx}}} \mathbb{E}_{\Phi_e} \left\{ \int_{\frac{I_0 d_p^\alpha}{\left(2^{R_t - R_s}-1\right)\sigma^2} Z_{\Phi_e}}^{\infty} \exp\left(-\left(\frac{\max\left\{\mu, 2^{R_t} - 1\right\}\sigma^2 d_s^\alpha}{I_0 d_p^\alpha} + 1 \right) x \right) \mathrm{d}x \right\} \\ &= \begin{cases} \frac{\mu\sigma^2 d_s^\alpha + I_0 d_p^\alpha}{\left(2^{R_t}-1\right)\sigma^2 d_s^\alpha + I_0 d_p^\alpha} L_{Z_{\Phi_e}} \left(\frac{\left(2^{R_t}-1\right)\sigma^2 d_s^\alpha + I_0 d_p^\alpha}{\left(2^{R_t - R_s}-1\right)\sigma^2} \right), & 0 \le \mu < 2^{R_t} - 1, \\ L_{Z_{\Phi_e}} \left(\frac{\mu\sigma^2 d_s^\alpha + I_0 d_p^\alpha}{\left(2^{R_t - R_s}-1\right)\sigma^2} \right), & 2^{R_t} - 1 \le \mu. \end{cases} \end{aligned} \tag{31}$$

Based on (8), (28), and (31), the secrecy throughput is given by

$$\begin{aligned} \eta &= p_{\text{tx}} p_{\text{no}} R_s \\ &= \begin{cases} \frac{I_0 d_p^\alpha R_s}{\left(2^{R_t}-1\right)\sigma^2 d_s^\alpha + I_0 d_p^\alpha} L_{Z_{\Phi_e}} \left(\frac{\left(2^{R_t}-1\right)\sigma^2 d_s^\alpha + I_0 d_p^\alpha}{\left(2^{R_t - R_s}-1\right)\sigma^2} \right), & 0 \le \mu < 2^{R_t} - 1, \\ \frac{I_0 d_p^\alpha R_s}{\mu\sigma^2 d_s^\alpha + I_0 d_p^\alpha} L_{Z_{\Phi_e}} \left(\frac{\mu\sigma^2 d_s^\alpha + I_0 d_p^\alpha}{\left(2^{R_t - R_s}-1\right)\sigma^2} \right), & 2^{R_t} - 1 \le \mu. \end{cases} \end{aligned} \tag{32}$$

From (29) and (30), one can note that p_{co} decreases as μ increases, while p_{so} increases as μ increases. This is due to the dynamic transmit power control at the SU-Tx to satisfy the requirement of spectrum sharing with the primary network.

Under the dynamic transmit power control, the received SNR at the eavesdropper is probably large when the received SNR at the SU-Rx is large. Thus, the value of SNR threshold arises a trade-off between the reliability performance and the secrecy performance of the system. In addition, one can find from (28) that p_{tx} decreases as μ increases, which implies that there is also a trade-off between the delay performance and the reliability performance incurred by the value of SNR threshold.

Hybrid Scheme

The hybrid scheme is adopted in the situation where the SU-Tx can obtain the one-bit feedback from the SU-Rx and detect the existence of eavesdroppers in its vicinity. In such a situation, the SU-Tx adopts a joint secrecy guard zone and SNR threshold-based transmission strategy. The SU-Tx transmits only when no eavesdropper is detected in the secrecy guard zone and the received SNR at SU-Rx is larger than the SNR threshold.

The SNRs at the SU-Rx and the colluding eavesdroppers are given by

$$\gamma_s = \frac{I_0 |h_s|^2 d_s^{-\alpha}}{\sigma^2 \left|h_p\right|^2 d_p^{-\alpha}} \mathbf{1}_{(C_1 \& C_2)} \tag{33}$$

and

$$\gamma_e = \frac{I_0}{\sigma^2 \left|h_p\right|^2 d_p^{-\alpha}} Z_{\Phi_e} \mathbf{1}_{(C_1 \& C_2)}, \tag{34}$$

respectively, where $\{C_1 \& C_2 : \forall j \in \Phi_e, d_j > r \text{ and } \frac{I_0 |h_s|^2 d_s^{-\alpha}}{\sigma^2 \left|h_p\right|^2 d_p^{-\alpha}} > \mu\}$. The transmission probability is given by

$$\begin{aligned} p_{\text{tx}} &= \mathbb{P}\left(\mathbf{1}_{(\text{condition})} = 1\right) \\ &= \mathbb{P}\left(C_1 \& C_2 : \forall j \in \Phi_e, d_j > r \text{ and } \frac{I_0 |h_s|^2 d_s^{-\alpha}}{\sigma^2 \left|h_p\right|^2 d_p^{-\alpha}} > \mu\right) \\ &= \frac{I_0 d_p^{\alpha} \exp\left(-\pi \lambda_e r^2\right)}{\mu \sigma^2 d_s^{\alpha} + I_0 d_p^{\alpha}}. \end{aligned} \tag{35}$$

The expression for the connection outage probability is identical to (29) in the threshold-based scheme. The secrecy outage probability is derived as

$$\begin{aligned} p_{\text{so}} &= \mathbb{P}\left(C_e > R_t - R_s \mid \mathbf{1}_{(\text{condition})} = 1\right) \\ &= 1 - L_{Z_{\Phi_e}}\left(\frac{\mu \sigma^2 d_s^{\alpha} + I_0 d_p^{\alpha}}{\left(2^{R_t - R_s} - 1\right) \sigma^2}\right). \end{aligned} \tag{36}$$

The non-outage probability can be obtained by substituting (33) and (34) into (9), which is given by

$$p_{\text{no}} = \mathbb{P}\left(C_s \geq R_t \;\&\; C_e \leq R_t - R_s \mid \mathbf{1}_{(\text{condition})} = 1\right) = \begin{cases} \frac{\mu\sigma^2 d_s^\alpha + I_0 d_p^\alpha}{(2^{R_t}-1)\sigma^2 d_s^\alpha + I_0 d_p^\alpha} L_{\widetilde{Z}_{\Phi_e}}\left(\frac{(2^{R_t}-1)\sigma^2 d_s^\alpha + I_0 d_p^\alpha}{(2^{R_t-R_s}-1)\sigma^2}\right), & 0 < \mu < 2^{R_t} - 1, \\ L_{\widetilde{Z}_{\Phi_e}}\left(\frac{\mu\sigma^2 d_s^\alpha + I_0 d_p^\alpha}{(2^{R_t-R_s}-1)\sigma^2}\right), & 2^{R_t} - 1 \leq \mu. \end{cases} \tag{37}$$

Based on (8), (35), and (37), the secrecy throughput is derived as

$$\eta = p_{\text{tx}} p_{\text{no}} R_s = \begin{cases} \frac{I_0 d_p^\alpha \exp(-\pi\lambda_e r^2) R_s}{(2^{R_t}-1)\sigma^2 d_s^\alpha + I_0 d_p^\alpha} L_{\widetilde{Z}_{\Phi_e}}\left(\frac{(2^{R_t}-1)\sigma^2 d_s^\alpha + I_0 d_p^\alpha}{(2^{R_t-R_s}-1)\sigma^2}\right), & 0 < \mu < 2^{R_t} - 1, \\ \frac{I_0 d_p^\alpha \exp(-\pi\lambda_e r^2) R_s}{\mu\sigma^2 d_s^\alpha + I_0 d_p^\alpha} L_{\widetilde{Z}_{\Phi_e}}\left(\frac{\mu\sigma^2 d_s^\alpha + I_0 d_p^\alpha}{(2^{R_t-R_s}-1)\sigma^2}\right), & 2^{R_t} - 1 \leq \mu. \end{cases} \tag{38}$$

Illustration of Performance of Transmission Schemes

In the following, we present and discuss the figure results that illustrate the performance of different transmission schemes.

Figure 2 shows the secrecy outage probability, p_{so}, and the connection outage probability, p_{co}, of different transmission schemes versus the density of eavesdroppers, λ_e. As depicted in the figure, p_{so} increases as λ_e increases, while p_{co} remains constant as λ_e increases. This is because the increase of eavesdropper density worsens the secrecy performance of the network but does not affect the reliability performance. Consider the full-active scheme as a baseline scheme for comparison. One can find that the secrecy guard zone scheme improves the secrecy performance without affecting the reliability performance. In contrast, the threshold-based scheme improves the reliability performance but at a cost of worsening the secrecy performance. Note that the finding of the impact of the threshold-based scheme is different from the results for the networks without dynamic spectrum sharing; see, e.g., [12, 28], in which the threshold-based scheme does not worsen the secrecy performance. As previously explained in section "Threshold-Based Scheme", the increase of p_{so} in the threshold-based scheme is because of the dynamic transmit power control at the SU-Tx for the spectrum sharing requirement. Moreover, taking the advantages of both the secrecy guard zone scheme and the threshold-based scheme, the hybrid scheme improves both the secrecy and reliability performance.

Figure 3 presents the impact of the radius of the secrecy guard zone, r; on the transmission probability, p_{tx}; the connection outage probability, p_{co}; and the secrecy outage probability, p_{so}. As shown in the figure, both p_{so} and p_{tx} decrease as r

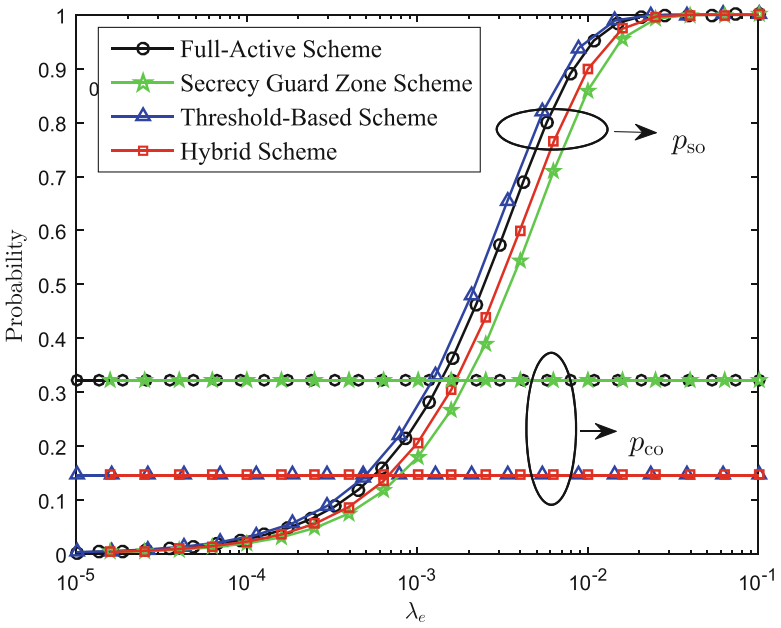

Fig. 2 The connection outage probability and the secrecy outage probability versus the eavesdropper density. The system parameters are $\alpha = 4$, $I_0/\sigma^2 = 10\,\mathrm{dB}$, $R_t = 1.5$, $R_s = 0.5$, $d_s = 5.4$, $d_p = 4.2$, $\mu = 1$, and $r = 5.4$

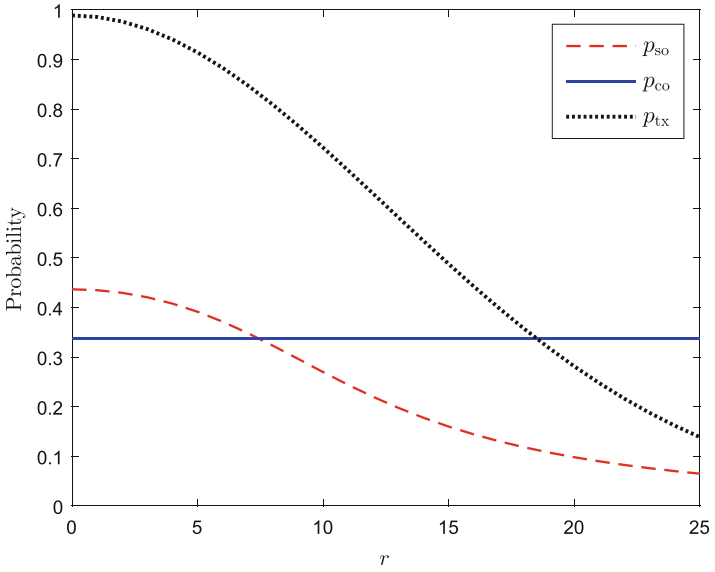

Fig. 3 The transmission probability, the connection outage probability, and the secrecy outage probability versus the radius of the secrecy guard zone. The system parameters are $\alpha = 4$, $I_0/\sigma^2 = 10\,\mathrm{dB}$, $R_t = 3$, $R_s = 1$, $d_s = 8.5$, $d_p = 7$, $\lambda_e = 10^{-3}$, and $\mu = 3$

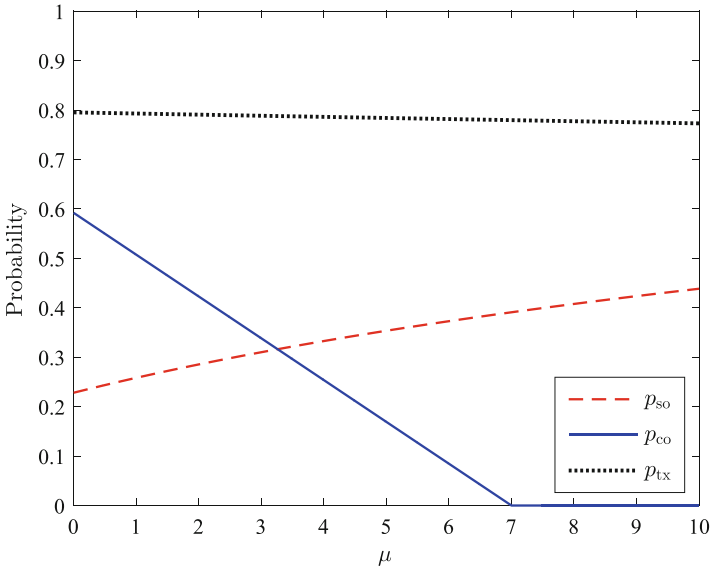

Fig. 4 The transmission probability, the connection outage probability, and the secrecy outage probability versus the SNR threshold. The system parameters are $\alpha = 4$, $I_0/\sigma^2 = 10$ dB, $R_t = 3$, $R_s = 1$, $d_s = 8.5$, $d_p = 7$, $\lambda_e = 10^{-3}$, and $r = 8.5$

increases, which implies that the radius of the secrecy guard zone incurs a trade-off between the secrecy performance and the performance of transmission delay. In addition, one can note that p_{co} does not change as r increases, which confirms that the reliability performance is not related to design of secrecy guard zone. Figure 4 demonstrates the impact of the SNR threshold, μ; on the transmission probability, p_{tx}; the connection outage probability, p_{co}; and the secrecy outage probability, p_{so}. As the figure shows, p_{co} decreases as μ increases, and it reaches zero when $\mu \geq 2^{R_t} - 1$, which indicates that the system can be perfectly reliable by having a sufficiently large SNR threshold. Besides, p_{so} increases as μ increases and p_{tx} decreases as μ increases. These observations confirms that a larger SNR threshold benefits the reliability performance but harms the secrecy performance and the performance of transmission delay.

Transmission Scheme Design

As previously discussed, the radius of the secrecy guard zone r and the SNR threshold μ play important roles in the performance of the system. Specifically, r incurs a trade-off between the delay performance and the secrecy performance. μ incurs trade-offs not only between the reliability performance and the secrecy performance, but also between the reliability performance and the delay performance.

In this section, the optimal design of r and/or μ that maximizes the secrecy throughput subject to secrecy outage and connection outage constraints is studied. The optimization problem is formulated as

$$\max_{r \text{ and/or } \mu} \quad \eta = p_{\text{tx}} p_{\text{no}} R_s \tag{39a}$$

$$\text{s.t.} \quad p_{\text{co}} \leq \delta, p_{\text{so}} \leq \varepsilon, r \geq 0, \mu \geq 0, \tag{39b}$$

where δ and ε denote the maximum acceptable connection outage probability and the maximum acceptable secrecy outage probability, respectively. For the secrecy guard zone scheme, the parameter to optimize is r. For the threshold-based scheme, the parameter to optimize is μ. For the hybrid scheme, the parameters to optimize are μ and r.

Feasibility of Constraints

Not all constraints on the connection outage probability and the connection outage probability, i.e., δ and ε, are feasible. Under infeasible constraints, the positive secrecy throughput is not achievable. The feasible constraint regions for the full-active scheme, the secrecy guard zone scheme, the threshold-based scheme, and the hybrid scheme, denoted by $F(1)$, $F(2)$, $F(3)$ and $F(4)$, respectively, are detailed as follows.

For the full-active scheme, the connection outage probability and the secrecy outage probability are uncontrollable, and hence the reliability and secrecy constraints are either always achievable or always not achievable. The feasible constraint region for the full-active scheme is given by

$$F(1) = \{(\delta, \varepsilon) : \delta_1 \leq \delta \leq 1, \varepsilon_1 \leq \varepsilon \leq 1\}, \tag{40}$$

where δ_1 and ε_1 denote the COP in (13) and the SOP in (14), respectively.

For the secrecy guard zone scheme, the secrecy outage probability is a decreasing function of r and $\lim_{r\to\infty} p_{\text{so}} = 0$, while the connection outage probability is still uncontrollable. The feasible constraint region for the secrecy guard zone scheme is given by

$$F(2) = \{(\delta, \varepsilon) : 0 < \varepsilon \leq 1, \delta_1 \leq \delta \leq 1\}. \tag{41}$$

For the threshold-based scheme, the connection outage probability is a decreasing function of μ, while the secrecy outage probability is an increasing function of μ. When $\delta \geq \delta_1$, the minimum achievable p_{so} is ε_1 by setting $\mu = 0$; when $\delta < \delta_1$, the minimum achievable p_{so} is given by

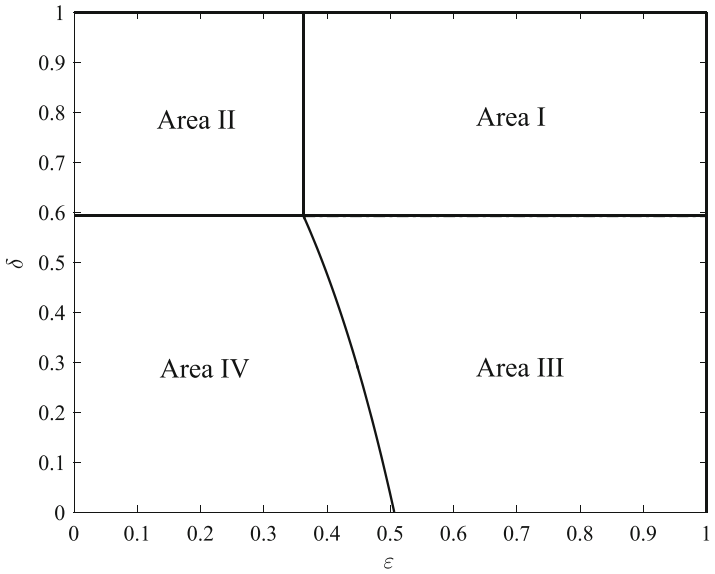

Fig. 5 An illustration of the feasible constraint region for the network with $\alpha = 4$, $I_0/\sigma^2 = 10\,\text{dB}$, $R_t = 3$, $R_s = 1$, $d_s = 8.5$, $d_p = 7$, and $\lambda_e = 10^{-3}$. $F(1)$ = Area I, $F(2)$ = Area I ∪ Area II, $F(3)$ = Area I ∪ Area III, and $F(4)$ = Area I ∪ Area II ∪ Area III ∪ Area IV

$$\varepsilon_2 = 1 - L_{Z_{\Phi_e}}\left(\frac{(1-\delta)\left(2^{R_t-1}\right)\sigma^2 d_s^{\alpha} + I_0 d_p^{\alpha}}{\left(2^{R_t-R_s}-1\right)\sigma^2}\right). \tag{42}$$

Thus, the constraint region for the threshold-based scheme is given by

$$F\,(3) = \{(\delta,\varepsilon) : 0 \le \delta \le 1, \max(\varepsilon_1,\varepsilon_2) \le \varepsilon \le 1\}. \tag{43}$$

$F\,(4)$: For the hybrid scheme, any required connection outage probability and secrecy outage probability are achievable by adjusting r and μ. Thus, the feasible constraint region for the hybrid scheme is given by

$$F\,(4) = \{(\delta,\varepsilon) : 0 \le \delta \le 1, 0 < \varepsilon \le 1\}. \tag{44}$$

An illustration of the feasible reliability and secrecy constraints for a different scheme is given in Fig. 5. As shown in the figure, the feasible constraint region for the full-active scheme is represented by Area I. The feasible constraint region for the secrecy guard zone scheme is depicted by Area I and Area II. The feasible constraint region of the threshold-based scheme is given by Area I and Area III. The feasible constraint region of the hybrid scheme is demonstrated by Area I, Area II, Area III, and Area IV. Compared with the full-active scheme, the secrecy guard zone scheme extends the feasible range of the secrecy constraint, and the threshold-based scheme

extends the feasible range of the reliability constraint. The feasible constraint region of the hybrid scheme becomes the whole $\varepsilon - \delta$ plane field.

Optimal Design

Note that the design of the hybrid scheme mathematically includes all of the other three transmission schemes as special cases. The hybrid protocol reduces to the full activity protocol when $r = 0$ and $\mu = 0$. The hybrid scheme reduces to the secrecy guard zone zone when $\mu = 0$. The hybrid scheme reduces to the threshold-based protocol when $r = 0$. Therefore, the optimal design of the hybrid protocol is presented only, and the designs of other schemes can be easily obtained accordingly.

Proposition 1. *The optimal design parameters* (r^*, μ^*) *of the hybrid scheme are given by*

$$\left(r^*, \mu^*\right) = \begin{cases} \left(0, [0, \mu_u]\right), & \text{if } \varepsilon \geq \varepsilon_1 \text{ and } \delta \geq \delta_1, \\ \left(g\left(0\right), 0\right), & \text{if } 0 < \varepsilon < \varepsilon_1 \text{ and } \delta \geq \delta_1, \\ \left(0, [\mu_l, \mu_u]\right), & \text{if } \varepsilon \geq \varepsilon_2 \text{ and } 0 \leq \delta < \delta_1, \\ \left(g\left(\mu_l\right), \mu_l\right), & \text{if } 0 < \varepsilon < \varepsilon_2 \text{ and } 0 \leq \delta < \delta_1, \end{cases} \tag{45}$$

where

$$g\left(x\right) = \left(\frac{x\sigma^2 d_s^{\alpha} + I_0 d_p^{\alpha}}{\left(2^{R_t} - R_s - 1\right)\sigma^2} \left(\left(B^{-1}_{\frac{-\alpha \ln(1-\varepsilon)}{2\pi\lambda_e \left(\phi(x)\right)^{1/\alpha}}} \left(1 - \frac{2}{\alpha}, \frac{2}{\alpha}\right) \right)^{-1} - 1 \right) \right)^{\frac{1}{\alpha}}, \tag{46}$$

$$\mu_l = \left(1 - \delta\right)\left(2^{R_t} - 1\right) - \frac{I_0 d_p^{\alpha}}{\sigma^2 d_s^{\alpha}}\delta, \tag{47}$$

$$\mu_u = \min\left\{ 2^{R_t} - 1, \left(\frac{-\alpha \ln\left(1 - \varepsilon\right)}{2\pi\lambda_e \Gamma\left(1 - \frac{2}{\alpha}\right)\Gamma\left(\frac{2}{\alpha}\right)} \right)^{\frac{\alpha}{2}} \frac{2^{R_t - R_s} - 1}{d_s^{\alpha}} - \frac{I_0 d_p^{\alpha}}{\sigma^2 d_s^{\alpha}} \right\} \tag{48}$$

Proof. Substituting (35) and (37) into (8), the secrecy throughput η is given by

$$\eta = \frac{I_0 d_p^{\alpha} \exp\left(-\pi\lambda_e r^2\right) R_s}{\max\left\{2^{R_t} - 1, \mu\right\}\sigma^2 d_s^{\alpha} + I_0 d_s^{\alpha}} L_{\widetilde{Z}_{\Phi_e}}\left(\frac{\max\left\{2^{R_t} - 1, \mu\right\}\sigma^2 d_s^{\alpha} + I_0 d_p^{\alpha}}{\left(2^{R_t - R_s} - 1\right)\sigma^2} \right). \tag{49}$$

Taking first-order derivative of η with respect to r yields

$$\frac{\partial \eta\left(r, \mu\right)}{\partial r} = -2\pi\lambda_e r \left(1 - \left(r^{\alpha}\omega^{-1} + 1\right)^{-1}\right)\eta < 0, \tag{50}$$

where $\omega = \left(\max\left\{\mu, 2^{R_B}-1\right\}\sigma^2 d_{SD}^{\alpha} + I_0 d_{SP}^{\alpha}\right) / \left(\sigma^2\left(2^{R_B-R_S}-1\right)\right)$. This implies that the secrecy throughput decreases as r increases. From (49), one can also find that η decreases as μ increases when $\mu > 2^{R_t}-1$, while η remains constant when $\mu \leq 2^{R_t}-1$. Thus, it is wise to have $\mu \leq 2^{R_t}-1$. The optimal r and μ subject to different reliability and secrecy constraints are discussed as follows:

Case 1: $\delta \geq \delta_1$ and $\varepsilon \geq \varepsilon_1$. Since the secrecy constraint is very loose and η decreases as r increases, it is optimal to set $r = 0$. The lower bound of μ is equal to zero due to the loose reliability constraint. While to satisfy the secrecy constraint, there is an upper bound of μ. By solving $p_{\text{so}} = \varepsilon$ for μ with the consideration of $\mu \leq 2^{R_B}-1$, the upper bound of μ is given as (48). Thus, the optimal r and μ for this case are given by $(r^*, \mu^*) = (0, [0, \mu_u])$.

Case 2: $\delta \geq \delta_1$ and $0 < \varepsilon < \varepsilon_1$. To satisfy the secrecy constraint, there is a lower bound of r. By solving $p_{\text{so}} = \varepsilon$ for r, the lower bound of r is given as (46). From (46), one can find that $g(\mu)$ increases as μ increases. Since $\delta \geq \delta_1$, it is optimal have $\mu = 0$. Hence, the optimal r and μ for this case are given by $(r^*, \mu^*) = (g(0), 0)$.

Case 3: $0 \leq \delta < \delta_1$ and $\varepsilon \geq \varepsilon_2$. To satisfy the reliability constraint, there is a lower bound of μ. By solving $p_{\text{co}} = \delta$ for μ, we derive the lower bound of μ as (47). Also, there is also an upper bound of μ given by (48) to satisfy the secrecy constraint. Thus, the optimal r and μ for this case are given by $(r^*, \mu^*) = (0, [\mu_l, \mu_u])$.

Case 4: $0 < \varepsilon < \varepsilon_2$ and $0 \leq \delta < \delta_1$. To satisfy the reliability constraint, there is a lower bound of μ given by (47). There is also a lower bound of r given by (46). Since $g(\mu)$ increases as μ increases, it is optimal to set $\mu = \mu_{\text{LB}}$. Hence, the optimal r and μ are given by $(r^*, \mu^*) = (g(\mu_l), \mu_l)$.

Summarizing the optimal r and μ for the four cases completes the proof. ■

From Proposition 1, one can note that the optimal r and μ are influenced by the reliability and secrecy constraints. In general, a stringent reliability constraint leads to a large μ^*, and a stringent secrecy constraint leads to a large r^*. One can also note that as the eavesdropper density increases, r^* increases and μ_u decreases, which will result in a decrease of the achievable secrecy throughput.

Figure 6 plots the secrecy throughput, η, against the SNR threshold, μ, and the radius of the secrecy guard zone, r. The reliability constraint and the secrecy constraint are set as $\delta = 0.4 < \delta_1$ and and $\varepsilon = 0.4 < \max(\varepsilon_1, \varepsilon_2)$, respectively. As shown in the figure, the positive secrecy throughput is achievable in the network with the appropriate design of μ and r. However, the unwise design of μ and r may result in the zero secrecy throughput. These observations emphasize the importance of the design of the SNR threshold and the radius of secrecy guard zone on overall performance of the network, i.e., the secrecy throughput. In addition, there is an optimal pair of (r, μ) which maximizes the secrecy throughput. From Proposition 1, one can obtain that the optimal pair of (r, μ) for the given network is $(r^*, \mu^*) = (2.7, 5.0)$, which is consistent with the results shown in the figure.

Figure 7 compares the achievable secrecy throughput for different transmission schemes versus the reliability constraint, δ, and the secrecy constraint, ε. Still con-

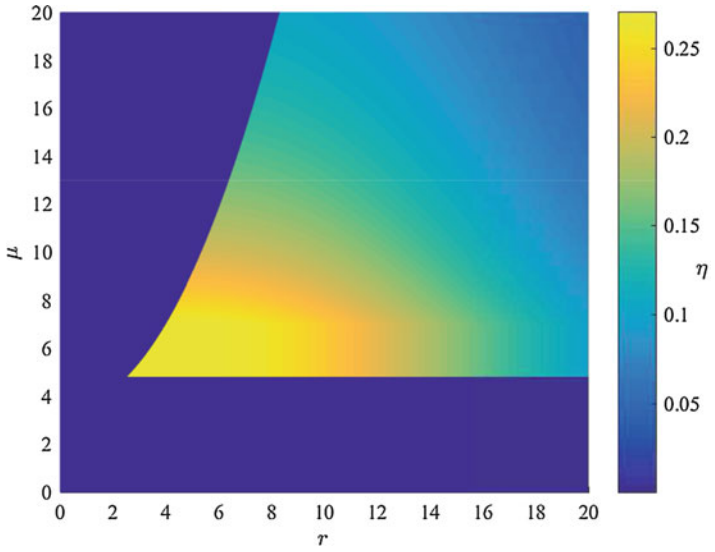

Fig. 6 The secrecy throughput versus the secrecy guard radius and the SNR threshold. The system parameters are $\alpha = 4$, $I_0/\sigma^2 = 10\,\text{dB}$, $R_t = 3$, $R_s = 1$, $d_s = 5.4$, $d_p = 4.2$, $\varepsilon = 0.2$, $\delta = 0.2$, and $\lambda_e = 10^{-3}$

sider the full-active scheme as the baseline scheme for comparison. As presented in the figure, the secrecy guard zone scheme enhances the achievability of the positive secrecy throughput subject to the stringent security constraint. The threshold-based scheme enhances the achievability of the positive secrecy throughput subject to the stringent reliability constraint. It is worth noting from the threshold-based scheme that the secrecy performance has to be compromised to obtain the positive secrecy throughput as the reliability constraint becomes stringent. Besides, the hybrid scheme can achieve the positive secrecy throughput under the most stringent secrecy and reliability constraints, compared with all three other three schemes. Based on these findings, one can summarize how to wisely choose the transmission scheme according to the condition/requirement of the system. When the secrecy constraint and the reliability constraint are loose, one can adopt the full-active scheme with its simple mechanism. When the secrecy constraint is stringent while the reliability constraint is loose, it is wise to use the secrecy guard zone scheme. When the reliability constraint is stringent while the security constraint is loose, it is preferable to adopt the threshold-based protocol. When both the secrecy constraint and the reliability constraint are stringent, one has to adopt the hybrid protocol. Of course, the adoption of different transmission schemes with the dynamic spectrum sharing is still mainly determined by the practical situations, i.e., the SU-Tx's knowledge about the channel and the eavesdropper locations.

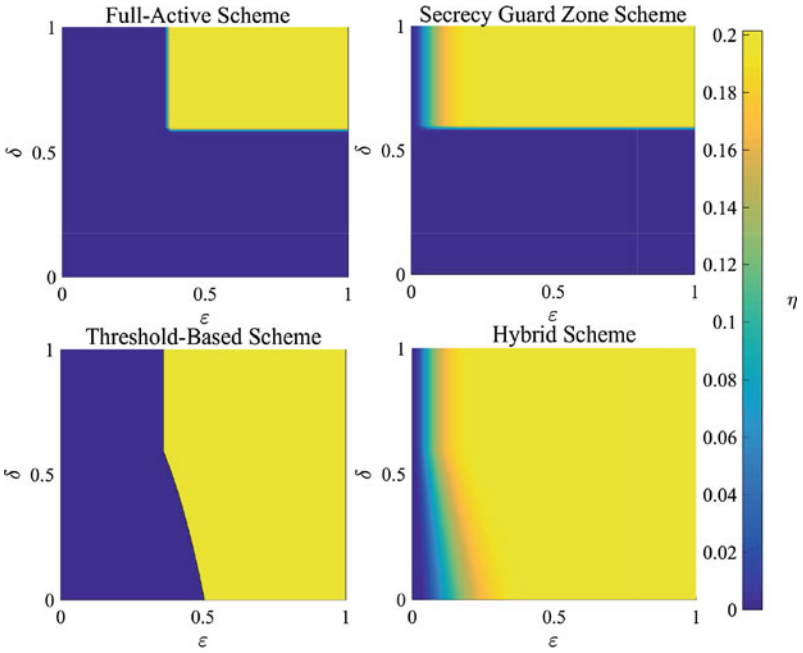

Fig. 7 The maximum achievable secrecy throughput versus the reliability constraint and the secrecy constraint. The system parameters are $\alpha = 4$, $I_0/\sigma^2 = 10\,\text{dB}$, $R_t = 3$, $R_s = 1$, $d_s = 8.5$, $d_p = 7$, $\lambda_e = 10^{-3}$

Conclusion and Future Directions

In this chapter, the security threats in cognitive radio networks have been briefly discussed. The secure transmission schemes with dynamic spectrum sharing in the presence of randomly distributed eavesdroppers have been introduced. Specifically, the secure communication in an underlay cognitive radio networks in the presence of multiple movable eavesdroppers has been studied. The location set of the eavesdroppers is modeled by a homogeneous PPP. The SU-Tx sends confidential messages to the SU-Rx with a dynamic transmit power in order not to interfere with the primary user. To combat eavesdropping in such a cognitive radio network, four transmission schemes have been introduced and investigated. The transmission delay performance, the secrecy performance, the reliability performance, and the overall secrecy throughout performance of different schemes have been comprehensively analyzed and compared. The optimal design parameters that maximize the secrecy throughput subject to the secrecy and reliability constraints have been further derived. It is shown that the secrecy guard zone

scheme improves the secrecy performance, the threshold-based scheme improves the reliability performance, and the hybrid protocol achieves the best overall performance.

In the considered transmission schemes, the encoding rates are assumed to be fixed and predesigned. An interesting future direction is to give more degrees of freedom for the transmission design by considering the encoding rates as designable parameters as well. Another interesting future direction is to investigate the physical layer security techniques to solve other security threats, while most existing studies on the physical layer security have focused on the eavesdropping threat only. As mentioned in section "Security Issues in Cognitive Radio Networks", there are many other security threats in cognitive radio network including but not limited to the primary user emulation, the spectrum sensing data falsification, and the jamming attack. Therefore, how to solve different security threats by physical layer security techniques is an important future direction.

References

1. Attar A, Tang H, Vasilakos AV, Yu FR, Leung VCM (2012) A survey of security challenges in cognitive radio networks: solutions and future research directions. Proc IEEE 100(12): 3172–3186
2. Bloch M, Barros J (2011) Physical layer security: from information theory to security engineering. Cambridge University Press, New York
3. Cai C, Cai Y, Zhou X, Yang W, Yang W (2014) When does relay transmission give a more secure connection in wireless ad hoc networks? IEEE Trans Inf Forensics Secur 9(4):624–632
4. Capar C, Goeckel D, Liu B, Towsley D (2012) Secret communication in large wireless networks without eavesdropper location information. In: Proceedings of IEEE International Conference on Computer Communications (INFOCOM), Orlando, pp 1152–1160
5. Gabry F, Zappone A, Thobaben R, Jorswieck E, Skoglund M (2015) Energy efficiency analysis of cooperative jamming in cognitive radio networks with secrecy constraints. IEEE Wirel Commun Lett 4(4):437–440
6. Goel S, Aggarwal V, Yener A, Calderbank AR (2010) Modeling location uncertainty for eavesdroppers: a secrecy graph approach. In: Proceedings of IEEE International Symposium on Information Theory (ISIT), Austin, pp 2627–2631
7. Gradshteyn IS, Ryzhik IM (2007) Tables of integrals, series, and products, 7th edn. Academic, Amsterdam/Boston
8. Guan X, Cai Y, Yang W (2011) Increasing secrecy capacity via joint design of cooperative beamforming and jamming. In: Proceedings of IEEE International Symposium on Personal, Indoor and Mobile Radio Communications (PIMRC), Toronto, pp 1274–1278
9. Haenggi M, Ganti RK (2009) Interference in large wireless networks, 1st edn. Now Publishers Inc., Hanover
10. Haenggi M, Andrews J, Baccelli F, Dousse O, Franceschetti M (2012) Stochastic geometry and random graphs for the analysis and design of wireless networks. IEEE J Sel Areas Commun 27(7):1029–1046
11. Hasan A, Andrews JG (2013) The guard zone in wireless ad hoc networks. IEEE Trans Wirel Commun 6(3):897–906
12. He B, Zhou X (2013) Secure on-off transmission design with channel estimation errors. IEEE Trans Inf Forensics Secur 8(12):1923–1936
13. Koyluoglu OO, Koksal CE, Gamal HE (2012) On secrecy capacity scaling in wireless networks. IEEE Trans Inform Theory 58(5):3000–3015

14. Liang Y, Poor H, Ying L (2009) Secrecy throughput of MANETs with malicious nodes. In: Proceedings of IEEE International Symposium on Information Theory (ISIT), Seoul, pp 1189–1193
15. Musavian L, Aïssa S, Lambotharan S (2010) Effective capacity for interference and delay constrained cognitive-radio relay channels. IEEE Trans Wirel Commun 9(5):1698–1707
16. Pei Y, Liang YC, Teh KC, Li KH (2009) Achieving cognitive and secure transmissions using multiple antennas. In: Proceedings of IEEE International Symposium on Personal, Indoor and Mobile Radio Communications (PIMRC), Singapore, pp 1–5
17. Pei Y, Liang YC, Teh KC, Li KH (2010) Secure communication over MISO cognitive radio channels. IEEE Trans Wirel Commun 9(4):1494–1502
18. Pinto PC, Barros J, Win MZ (2012) Secure communication in stochastic wireless networks – Part I: connectivity. IEEE Trans Inf Forensics Secur 7(1):125–138
19. Sakran H, Shokair M, Nasr O, EI-Rabaie S, EI-Azm AA (2012) Proposed relay selection scheme for physical layer security in cognitive radio networks. IET Commun 6(16):2676–2687
20. Shu Z, Yang Y, Qian Y, Hu RQ (2011) Impact of interference on secrecy capacity in a cognitive radio network. In: Proceedings of IEEE Global Telecommunications Conference (GLOBECOM), Houston, pp 1–6
21. Shu Z, Qian Y, Ci S (2013) On physical layer security for cognitive radio networks. IEEE Netw 27(3):28–33
22. Wang C, Wang H (2014) On the secrecy throughput maximization for MISO cognitive radio network in slow fading channels. IEEE Trans Inf Forensics Secur 9(11):1814–1827
23. Wen H, Zhu X, Zhou L (2013) A framework of the PHY-layer approach to defense against security threats in cognitive radio networks. IEEE Netw 27(3):34–39
24. Wyner A (1975) The wire-tap channel. Bell Syst Tech J 54(8):1355–1387
25. Xu X, He B, Yang W, Zhou X, Cai Y (2016) secure transmission design for cognitive radio networks with Poisson distributed eavesdroppers. IEEE Trans Inf Forensics Secur 11(2):373–387
26. Youssef M, Ibrahim M, Abdelatif M, Chen L, Vasilakos AV (2014) Routing metrics of cognitive radio networks: a survey. IEEE Commun Surv Tuts 16(1):92–109
27. Zhou X, Ganti RK, Andrews JG, Hjørungnes A (2011) On the throughput cost of physical layer security in decentralized wireless networks. IEEE Trans Wirel Commun 10(8):2764–2775
28. Zhou X, McKay MR, Maham B, Hjørungnes A (2011) Rethinking the secrecy outage formulation: a secure transmission design perspective. IEEE Commun Lett 15(3):302–304
29. Zhou X, Song L, Zhang Y (2013) Physical layer security in wireless communications. CRC Press, US
30. Zou Y, Wang X, Shen W (2013) Physical-layer security with multiuser scheduling in cognitive radio networks. IEEE Trans Commun 61(12):5103–5113
31. Zou Y, Li X, Liang YC (2014) Secrecy outage and diversity analysis of cognitive radio systems. IEEE J Sel Areas Commun 32(11):2222–2236

Heterogeneous Statistical QoS Provisioning Over Cognitive-Radio Based 5G Mobile Wireless Networks

21

Xi Zhang and Jingqing Wang

Contents

Abstract

As one of the critical techniques to support the multimedia services over mobile wireless networks, the statistical quality of service (QoS) technique has been proved to be effective in statistically guaranteeing delay-bounded video transmissions over the time-varying wireless channels. In the meantime,

X. Zhang (✉) · J. Wang
Networking and Information Systems Laboratory, Department of Electrical and Computer Engineering, Texas A&M University, College Station, TX, USA
e-mail: xizhang@ece.tamu.edu; wang12078@tamu.edu

W. Zhang (ed.), *Handbook of Cognitive Radio*,
https://doi.org/10.1007/978-981-10-1394-2_21

the full-duplex spectrum sensing (FD-SS) has been widely recognized as the promising candidate technique for maximizing the spectrum efficiency while provisioning the heterogeneous statistical QoS guarantees over cognitive radio-based 5G mobile wireless networks. However, due to the heterogeneity caused by different scenarios and applications of the multimedia traffics over CRNs, supporting diverse delay-bounded QoS guarantees for cognitive radio networks imposes many new challenges not encountered before. To effectively overcome the aforementioned problems, in this book chapter, we propose the heterogeneous statistical QoS provisioning schemes by applying the multiple-input-multiple-output generalized frequency division multiplexing (MIMO-GFDM) techniques to implement the FD-SS-based multimedia services in CRNs. In particular, under the Nakagami-*m* wireless channels, we derive the MIMO-GFDM-based physical (PHY)-layer model and the self-interference cancelation model. We develop the MIMO-GFDM-based FD-SS schemes and derive the miss-detection and false-alarm probabilities. Under the heterogeneous statistical QoS constraints, we develop the Markov chain model to characterize the aggregate effective capacity under the optimal power allocation policies using our proposed MIMO-GFDM architecture over FD-SS CRNs. Also conducted is a set of simulations which validate our proposed schemes, evaluate their performances, and show that our proposed schemes can outperform the other existing solutions under the heterogeneous statistical delay-bounded QoS constraints over cognitive radio-based 5G mobile wireless networks.

Keywords

Heterogeneous statistical quality of service (QoS) · Cognitive radio networks (CRNs) · Full-duplex spectrum sensing (FD-SS) · Self-interference cancelation · Multiple-input-multiple-output generalized frequency division multiplexing (MIMO-GFDM)

Introduction

With the explosive advances and emerging applications of wireless communications and networks, most available spectrum has already been allocated. However, there exists a large amount of white space in time and frequency. Most traditional fixed frequency allocation policies experience low spectrum utilization. As a result, researchers have made a great deal of efforts in investigating promising techniques to support the increasing demand of high-speed data rate and bandwidth for multimedia services over 5G mobile wireless networks [1, 2]. One of the most effective ways to solve the low spectrum utilization problem is the cognitive radio scheme, which is proposed to alleviate the severe scarcity of the spectrum with spectrum sensing technique.

In order to support the demands of multimedia applications, delay-bounded quality of service (QoS) [3, 4] guarantees are critically important for time-sensitive traffics over CRNs. One of the key design issues for multimedia wireless services –

the major traffic in 5G mobile wireless networks is how to efficiently guarantee the timely multimedia data transmissions within specified delay bounds. Due to the highly varying wireless channels, the deterministic delay-bounded QoS requirements are usually hard to guarantee. As a result, the statistical delay-bounded QoS guarantees [5–7], in terms of effective capacity and queue-length-bound/delay-bound violation probabilities, have been proposed and demonstrated as the powerful technique to characterize delay-bounded QoS requirements for wireless traffics.

However, the existing homogeneous statistical QoS guarantee techniques typically assume that the QoS provisioning for each link can be individually processed. Since all different links in wireless transmissions have joint power constraints, the statistical delay-bound QoS provisioning needs to be jointly considered for all links simultaneously. Under this circumstance, the users in the wireless mobile networks need to satisfy different delay-bound QoS requirements under the joint power constraint, simultaneously. The time sensitivities of different sets of services vary from 1 ms to a few seconds across different wireless links for different mobile users. As a result, the delay-bounded QoS guarantees for the different types of services in 5G mobile wireless networks demand the new heterogeneous statistical delay-bounded QoS provisioning architectures [8], schemes, algorithms, and 5G candidate framework, which can be implemented by integrating several 5G candidates, including massive MIMO and relay-based 5G promising techniques. Until now, how to guarantee heterogeneous statistical delay-bounded QoS requirements over relay-based cognitive radio networks (CRNs) is one of the main challenges for next generation wireless network services.

On the other hand, in traditional CRNs, secondary users (SUs) typically access the spectrum of primary users (SUs) by a two-stage listen-before-talk (LBT) protocol with the help of the wireless half-duplex (HD) energy detection spectrum sensing (HDSS) scheme, in which SUs sense the target channel before transmission. While the LBT protocol requires little infrastructure support, it suffers from sacrifice of transmitting time and discontinuity of transmission even if the white space of the spectrum is continuous. In order to fully utilize the channel spectrum, researchers have proposed an efficient listen-and-talk (LAT) protocol [8, 9] with the help of the wireless full-duplex (FD) spectrum sensing (FD-SS) technique [10, 11] that enables SUs to sense and access the vacant spectrum simultaneously. However, the self-interference introduced by the FD-SS transmission mode imposes many new challenges in decoding process.

In addition, to support the next-generation wideband wireless networks, various advanced wireless techniques, such as multiple-input multiple-output (MIMO) and orthogonal frequency division multiple (OFDM) [12, 13] techniques, have received widely attention in the past few years. MIMO technology utilizes the spatial multiplexing gain to achieve the higher spectral efficiency. Compared with the MIMO technology, OFDM scheme has been identified as a promising interface solution for wideband wireless networks for its excellence performance over frequency-selective channels. As multiple transmit antennas can be applied to OFDM-based cognitive radio systems, researchers have designed and proposed the very promising

candidate, called MIMO-OFDM [14, 15], which can compensate for shortage of capacity while increasing the spectral efficiency.

However, the complicated application scenarios associated with CRNs present new challenges making the OFDM technique less efficient in various advanced wireless networks. Therefore, the novel generalized frequency division multiplexing (GFDM) [16, 17] technique has been designed and implemented in order to overcome the aforementioned challenges. GFDM is well suitable for cognitive radio as the choice of pulse shaping filters makes the out-of-band leakage extremely small. Compared to OFDM, which has rectangular pulse shaping, GFDM with a choice of transmit pulse shaping causes less interference to the adjacent incumbent frequency bands, which leads to better peak-to-average ratio. However, how to efficiently integrate the wireless FD-SS-based system with the underlying MIMO-GFDM framework on supporting statistical QoS constraints over CRNs still remains as an open and challenging problem.

To effectively overcome the abovementioned challenges, in this chapter, we propose the heterogeneous statistical QoS provisioning schemes by extending MIMO-GFDM system to implement the FD-SS-based multimedia services in cognitive radio networks. In particular, under the Nakagami-*m* wireless channels, we establish MIMO-GFDM-based PHY-layer model, the non-time-slotted CRN model, and the self-interference cancelation model. We develop the FD-SS-based MIMO scheme to fully utilize the channel spectrum and derive the probabilities of miss-detection and false alarm for the proposed FD-SS-based MIMO model over CRNs. Under the heterogeneous statistical QoS constraints, we develop the Markov chain model to characterize the correctness of detections in channel sensing and then derive and analyze the aggregate effective capacity under our proposed optimal power allocation policies using the proposed GFDM architecture over FD CRNs. Also conducted is a set of simulations which evaluate the system performances and show that our proposed power allocation policies can outperform the other existing schemes under the heterogeneous statistical delay-bounded QoS constraints over cognitive radio-based 5G mobile wireless networks.

The rest of this chapter is organized as follows: section "Cognitive Radio-Based 5G Wireless Networks" establishes the spectrum sensing model under Nakagami-*m* wireless channels and also develops the MIMO-GFDM-based PHY-layer model, the non-time-slotted CRN model, and the self-interference cancelation model. Section "MIMO-GFDM-Based FD-SS Relaying Scheme" develops and analyzes the FD-SS-based MIMO-GFDM scheme to fully utilize the channel spectrum and derive the probabilities of miss-detection and false alarm for the proposed FD-SS-based MIMO-GFDM model over cognitive radio networks. Under the heterogeneous statistical QoS constraints, section "Heterogeneous Statistical Delay-Bounded QoS Guarantees Through Effective Capacity Over CRNs" develops the Markov chain model to characterize the correctness of detections in channel sensing and then derives and analyzes the aggregate effective capacity under our proposed optimal power allocation policies using the proposed MIMO-GFDM architecture over FD cognitive radio networks. Section "Simulation Evaluations" evaluates the system performances and shows

that our proposed scheme outperforms the other existing schemes in terms of aggregate effective capacity to efficiently implement the heterogeneous statistical QoS over MIMO-GFDM-based full-duplex CRNs. The chapter concludes with section "Conclusions".

Cognitive Radio-Based 5G Wireless Networks

Cognitive radio networks, where the secondary users (SUs) dynamically utilize the idle licensed channels of primary users (PUs), have been designed to effectively achieve high spectrum utilization and improve the quality of wireless applications. In CRNs, the SUs can sense the occupancy of the licensed channels and use the licensed channels when they are not occupied by the PUs based on the sensing results. The PUs and the SUs form the primary wireless network and the secondary wireless network, respectively. Although the basic idea of cognitive radio networks is simple, the efficient design imposes many new challenges that are not presented in the conventional wireless networks.

Spectrum Sensing Model Over CRNs

For the spectrum sensing model over CRNs, the MIMO-GFDM technique [15] is applied on the relay station. Consider K secondary source nodes ($S_1, S_2, \ldots, S_K$), K secondary destination nodes ($D_1, D_2, \ldots, D_K$), and one MIMO-GFDM-based full-duplex relay station in coexistence with primary users (PUs) for the CRNs, as illustrated in Fig. 1. Assume each source node and destination node is equipped with one transmit antenna and one receive antenna, while the relay station consists of M_t transmit antennas and M_r receive antennas. In order to achieve the wideband spectrum sensing, the entire system band is partitioned into several subbands with relatively small bandwidth. Suppose a licensed wideband spectrum having bandwidth B with Q nonoverlapping narrowband subchannels are licensed to a primary wireless network, where the channels are implemented by the same frequency spectra and time slots. PUs have the high priority to access the licensed channels over secondary users (SUs), which have low priority in using the licensed spectrum band. SUs with the low-priority queue seek idle spectrum opportunities in the licensed spectrum band. Using LAT protocol [9, 11], the secondary relay station needs to employ the wireless FD mode for transmitting data and sensing licensed spectrum simultaneously.

Assume that the cognitive relay station is within the transmission range of one PU node. Suppose that when one PU is in operation, it may occupy the whole or part of the wideband, and more than one relay node can share the radio spectrum within one PU operating range when the PU is inactive. This is the case for the current GFDM-based communication infrastructure where some of the GFDM subchannels are allocated to different users.

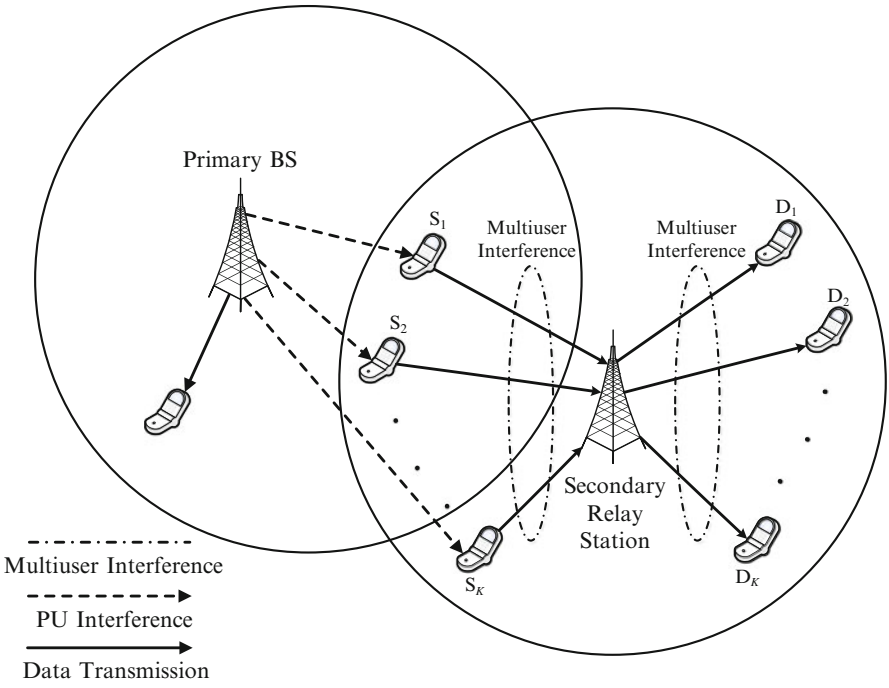

Fig. 1 MIMO-GFDM-based full-duplex cognitive radio network architecture with K secondary-user source-destination pairs

Assume that the PUs operate independently over a wideband spectrum; it is most likely that some portions of the spectrum may not be utilized by the primary systems over some time. In order to realize this seamless transmission within the cognitive relay network and share the radio spectrum when PU is inactive, cognitive relays first get the spectrum map of their local channel environment by spectrum sensing. Define the *spectrum indicator*, denoted by $\boldsymbol{b}_k$, of the kth user, where the entries of $\boldsymbol{b}_k \in \{\mathscr{H}_0, \mathscr{H}_1\}$ $(k = 1, 2, \ldots, K)$ denote the availability for the subchannel, where $\mathscr{H}_1$ implies that PU is active and $\mathscr{H}_0$ implies that PU is inactive while the kth secondary source node S_k is transmitting signals to the destination node, and $\mathscr{H}_0, \mathscr{H}_1 \in \{0, 1\}$. Clearly, the spectrum environment of the whole cognitive relay network can be characterized as follows:

$$\boldsymbol{B} = [\boldsymbol{b}_1, \boldsymbol{b}_2, \ldots, \boldsymbol{b}_K]^T, \tag{1}$$

where the matrix $\boldsymbol{B}$ is a binary matrix in which each entry is either zero or one. The total number of ones in $\boldsymbol{B}$ indicates the amount of spectrum opportunities and represents a degree of freedom in the cognitive relay network. When $\boldsymbol{B}$ is an all-one matrix, it is a special case for the conventional relay network, such as the

GFDM-based relay network where every relay has the same number of available subchannels.

MIMO-GFDM-Based PHY-Layer Model

The MIMO-GFDM-based system applies and analyzes for energy-efficient and low-complex communications over Nakagami-m wireless channels. The block diagram of MIMO-based GFDM system between the transmitter and the receiver under statistical QoS guarantees over MIMO wireless networks is shown in Fig. 2. The channel state information (CSI) is estimated at the receiver and fed back to the transmitter for advanced modulation techniques and MIMO diversity deployments. Based on the statistical QoS constraint θ (to be detailed soon in section "Heterogeneous Statistical Delay-Bounded QoS Guarantees Through Effective Capacity Over CRNs") required by the service, the transmitter needs to determine the optimal transmit power to jointly optimize the effective spectrum and power efficiencies. We concentrate on discrete time channel, indexed by $l = 1, 2, \ldots$.

In order to achieve the novel GFDM scheme [16], the initial binary data is modulated and divided into sequences of $Q \times P$ complex-valued data symbols, where each such sequence is spread across Q subcarriers and P time slots for transmission. The data sequence is denoted by means of block structure as follows:

$$\boldsymbol{D} = \begin{bmatrix} \boldsymbol{d}_0 \\ \boldsymbol{d}_1 \\ \vdots \\ \boldsymbol{d}_{(Q-1)} \end{bmatrix} = \begin{bmatrix} d_{0,0} & \cdots & d_{0,(P-1)} \\ \vdots & \ddots & \vdots \\ d_{(Q-1),0} & \cdots & d_{(Q-1),(P-1)} \end{bmatrix} \tag{2}$$

where $d_{q,p}$, with $p \in \{0, 1, \ldots, (P-1)\}$ and $q \in \{0, 1, \ldots, (Q-1)\}$, is the data sequence on the qth subchannel and in the pth time slot. Clearly, OFDM is a special case of GFDM, where $P = 1$, i.e., the data is spread only across frequencies and not in time.

After pulse shaping filter and carrier up-conversion, the resulting subchannel transmit signal, denoted by $x(n)$, can be derived as follows:

$$x(n) = \sum_{q=0}^{Q-1} \sum_{p=0}^{P-1} g_{q,p}(n) d_{q,p} \tag{3}$$

where $d_{q,p}$ is the data sequence specified by Eq. (2), and $g_{q,p}$(n) is the circular pulse shaping filter defined as follows:

$$q_{q,p}(n) = g[(n - pQ) \bmod N] e^{-\widetilde{j}\pi qn/N} \tag{4}$$

where $N \geq Q$ is the number of samples per time slot and $\widetilde{j} = \sqrt{-1}$.

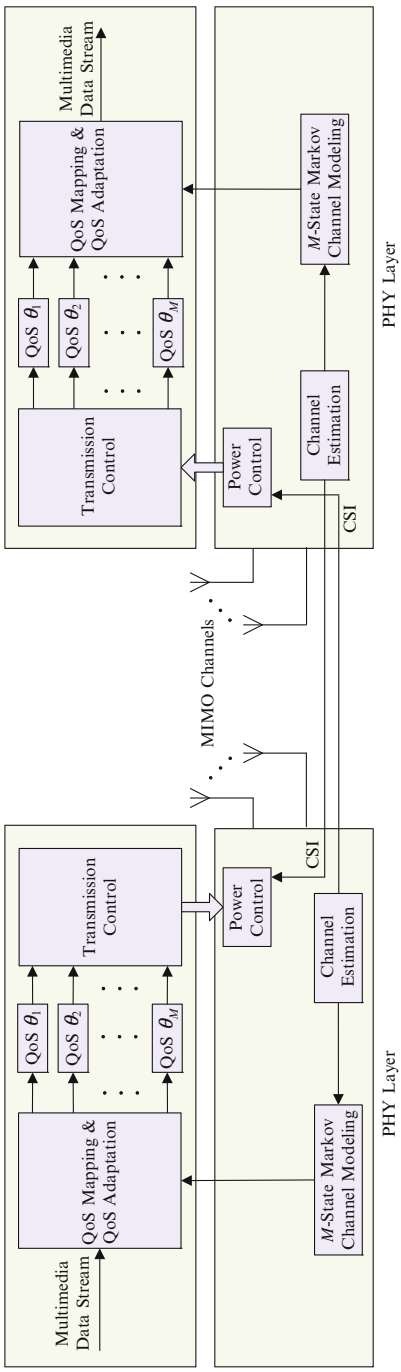

Fig. 2 The block diagram of MIMO-GFDM transceiver system model under cross-layer QoS mapping architecture with M_t transmit antennas and M_r receive antennas over CRNs, where the wireless channels experiencing the Nakagami-m fading

According to Eq. (3), a linear mapping from data symbols to transmit signal is applied as follows [16]:

$$\boldsymbol{x} = \boldsymbol{A}\boldsymbol{d} \tag{5}$$

where $\boldsymbol{d}$ represents the data symbols given by

$$\boldsymbol{d} = [d_{0,0}, d_{1,0}, \ldots, d_{(Q-1),0}, d_{0,1}, \ldots, d_{(Q-1),(P-1)}]^T \tag{6}$$

and $\boldsymbol{A}$ is a $(Q \times P) \times (Q \times P)$ modulation matrix given by

$$\boldsymbol{A} = [g_{0,0}(n), \ldots, g_{(Q-1),0}(n), g_{0,1}(n), \ldots, g_{(Q-1),(P-1)}(n)] \tag{7}$$

with all possible pulse shaping filter functions $g_{q,p}(n)$, where $p \in \{0, 1, \ldots, (P-1)\}$ and $q \in \{0, 1, \ldots, (Q-1)\}$.

In order to compare and analyze the performance of GFDM and OFDM systems, the peak-to-average ratio (PAPR), denoted by $f_r(\boldsymbol{x})$, can be expressed as follows:

$$f_r(\boldsymbol{x}) = 10 \log_{10} \frac{\max\limits_{0 \le n < N} |x(n)|^2}{\mathbb{E}_x[|x(n)|^2]} \tag{8}$$

Then, the complementary cumulative distribution function (CCDF), denoted by $F_c(\boldsymbol{x})$, which is one of the key performance measures for PAPR representing the probability that the PAPR of an GFDM symbol exceeds the given threshold, denoted by $f_{r_0}(\boldsymbol{x})$, can be determined as follows:

$$F_c(\boldsymbol{x}) = \Pr\{f_r(\boldsymbol{x}) > f_{r_0}(\boldsymbol{x})\} \tag{9}$$

Assume that the discrete-time channel is block fading. And the path gains are assumed to be invariant within a frame duration T_f, but vary independently from one frame to another. In the following discussions, the discrete-time index l when representing the channel's impulse response can be omitted. The multiple parallel spatial channel's impulse response, denoted by $\boldsymbol{H}$, can be derived as follows:

$$\boldsymbol{H} = \begin{bmatrix} H^{(0,0)} & \cdots & H^{(0,(M_t-1))} \\ \vdots & \ddots & \vdots \\ H^{((M_r-1),0)} & \cdots & H^{((M_r-1),(M_t-1))} \end{bmatrix} \tag{10}$$

where $H^{(i,j)}$ with $i \in \{0, 1, \ldots, (M_r - 1)\}$ and $j \in \{0, 1, \ldots, (M_t - 1)\}$ is a $(Q \times P) \times (Q \times P)$ matrix given by

$$H^{(i,j)} = \begin{bmatrix} \begin{matrix} h_{0,0}^{(i,j)} & h_{1,0}^{(i,j)} & \cdots & h_{0,(P-1)}^{(i,j)} \\ h_{0,1}^{(i,j)} & h_{1,1}^{(i,j)} & \cdots & h_{1,(P-1)}^{(i,j)} \\ \vdots & \vdots & \ddots & \vdots \\ h_{(Q-1),0}^{(i,j)} & h_{(Q-1),1}^{(i,j)} & \cdots & h_{(Q-1),(P-1)}^{(i,j)} \end{matrix} & & \mathbf{0} \\ & \ddots & \\ \mathbf{0} & & \begin{matrix} h_{0,0}^{(i,j)} & h_{1,0}^{(i,j)} & \cdots & h_{0,(P-1)}^{(i,j)} \\ h_{0,1}^{(i,j)} & h_{1,1}^{(i,j)} & \cdots & h_{1,(P-1)}^{(i,j)} \\ \vdots & \vdots & \ddots & \vdots \\ h_{(Q-1),0}^{(i,j)} & h_{(Q-1),1,}^{(i,j)} & \cdots & h_{(Q-1),(P-1)}^{(i,j)} \end{matrix} \end{bmatrix} \tag{11}$$

where $h_{q,p}^{(i,j)}$ with $p \in \{0, 1, \ldots, (P-1)\}$ and $q \in \{0, 1, \ldots, (Q-1)\}$ is the channel's impulse response over the Nakagami-m fading channels, where m is the shape factor of the Nakagami-m model, in our proposed system. In the special case, $m = 1$ represents Rayleigh fading, and $m = \infty$ corresponds to the Gaussian channel. The Nakagami-m channel impulse response function, denoted by $h_{q,p}^{(i,j)}(l)$, over qth subchannel between ith transmit antenna and jth receive antenna at time l over qth subchannel can be expressed as

$$h_{q,p}^{(i,j)}(l) = \alpha_{q,p}^{(i,j)} \delta\left(l - \tau_{q,p}^{(i,j)}\right) \exp\left(-\widetilde{j}\phi_{q,p}^{(i,j)}\right) \tag{12}$$

where $\widetilde{j} = \sqrt{-1}$; $q \in \{0, 1, \ldots, (Q-1)\}$; $\left\{\tau_{q,p}^{(i,j)}\right\}$ is the path delay; $\left\{\alpha_{q,p}^{(i,j)}\right\}$ is the path envelope; and $\left\{\phi_{q,p}^{(i,j)}\right\}$ is the phase shift. Assume that $\left\{\phi_{q,p}^{(i,j)}\right\}$ is independent and identically distributed (i.i.d) random variable uniformly distributed between $[0, 2\pi)$, and $\left\{\alpha_{q,p}^{(i,j)}\right\}$ is i.i.d. random variable following Nakagami-m distribution, which is specified by

$$f_\alpha(\alpha) = 2\left(\frac{m}{\Omega}\right)^m \frac{\alpha^{2m-1}}{\Gamma(m)} \exp\left(-m\frac{\alpha^2}{\Omega}\right) \tag{13}$$

where $\Omega = \mathbb{E}_\alpha\{[\alpha]^2\}$ is the average path gain and $\Gamma(\cdot)$ denotes the Gamma function.

The Non-time-Slotted Cognitive Radio Network Protocol

In this chapter, we focus on the non-time-slotted cognitive radio networks, which impose more challenges as compared with the time-slotted cognitive radio networks. The non-time-slotted cognitive radio network is defined as the wireless cognitive radio network where the PUs and the SUs are asynchronous. In particular, consider a scenario where a spectrum licensed to the PUs consists of Q subchannels,

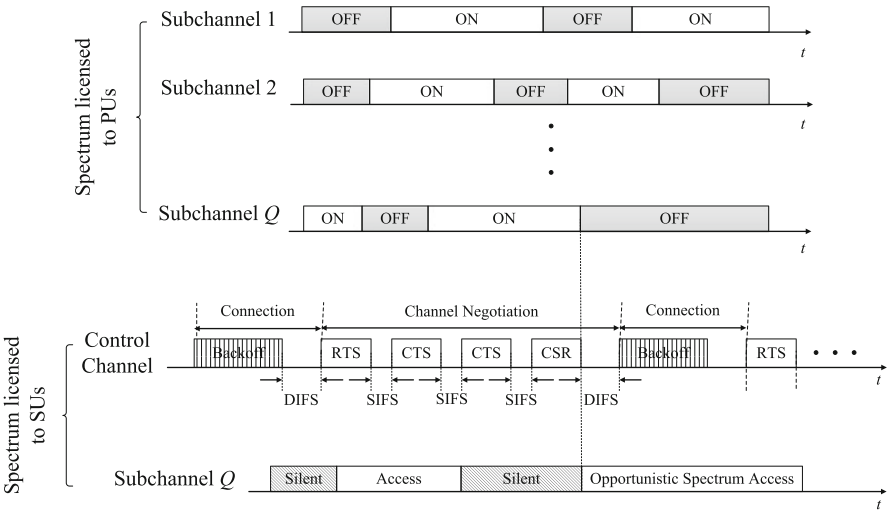

Fig. 3 The non-time-slotted cognitive radio network model, where SIFS is the duration of the short inter-frame space, and DIFS is the duration of DCF inter-frame space

as illustrated in Fig. 3, in which the PUs operating at different subchannels are unsynchronized. Figure 3 shows the timing control sequences of PUs and SUs in non-time-slotted CRNs, where the PUs randomly access and leave the licensed channels. Assume that for each subchannel, the subchannel usage pattern of the PUs follows independent and identically distributed (i.i.d.) ON/OFF renewal process. An ON state represents that the channel is occupied by the PUs. An OFF state represents that the PU is idle and thus the channel can be opportunistically used by the SUs. Note that the average ON and OFF periods depend on the channel usage pattern of the PUs.

On the other hand, as for SUs, the channel is alternating between ON (busy) and OFF (idle) states. Let random variables $T_{q,1}$ and $T_{q,0}$ represent the idle and busy duration, respectively, for the qth licensed subchannel. Without loss of generality, assume that $T_{q,1}$ is independent of $T_{q,0}$. Denote $f_{q,1}(n)$ and $f_{q,0}(n)$ as the probability density functions (pdf) for the durations of the ON state and OFF state for the qth licensed subchannel, respectively. Then, the probability, denoted by $p_{q,0}$, that the channel is in its ON state at an arbitrary time instance can be derived as follows:

$$p_{q,0} = \frac{\int_0^\infty n f_{q,1}(n) dn}{\int_0^\infty n f_{q,1}(n) dn + \int_0^\infty n f_{q,0}(n) dn} = \frac{\overline{T}_{q,1}}{\overline{T}_{q,1} + \overline{T}_{q,0}} \tag{14}$$

where $\overline{T}_{q,1}$ and $\overline{T}_{q,0}$ denote the mean duration of ON and OFF states, respectively, for qth subchannel. Assume that the PUs' subchannel utilization pattern is homogeneous.

The non-time-slotted cognitive radio protocol employs a common control channel as the rendezvous where SUs exchange control packets for multichannel resource reservation [18]. Under the non-time-slotted cognitive radio protocol, the interference from SU's transmission must be constrained in a modest level which the PUs can tolerate; we limit each channel access time of SUs to be not more than the maximum tolerable interference period. The key of the non-time-slotted cognitive radio protocol is to employ four types (two pairs) of control packets, namely, ready-to-send/clear-to-send (RTS/CTS) packets and channel-state-transmitter/channel-state-receiver (CST/CSR) packets, to implement the channel negotiation. All of the above four types of control packets are exchanged over the control channel. The goal of the RTS/CTS control packets is to prevent the collisions among the SUs, while the object of the CST/CSR control packets is to avoid the collisions between the SUs and the PUs. In particular, when a SU sender wants to communicate with a SU receiver over the cognitive radio networks, the SU sender contends for the data channels via the control channel, as shown in Fig. 3. After successful backoff stage, the SU sender conducts the channel negotiation with the SU receiver by exchanging RTS/CTS/CST/CSR control packets over the control channel. As shown in Fig. 3, the common idle licensed channels for the SU sender and SU receiver are subchannel Q; after the successful channel negotiation, the SU sender utilizes subchannel Q to send the data to the SU receiver.

Self-Interference Cancelation-Based Full-Duplex System Model

In this section, consider the full-duplex MIMO-GFDM-based wireless communication at the relay station, as illustrated in Fig. 4. To suppress the self-interference caused by FD communication, the combined analog-domain and digital-domain interference cancelation (ADIC) [19, 20] technique is employed at the receiver of the relay node to cancel the residual self-interference after the propagation-domain interference suppression (PDIS) schemes.

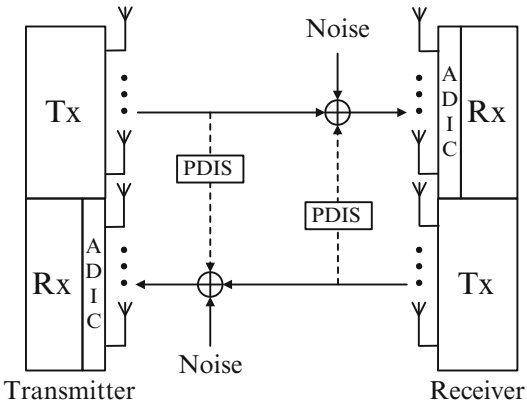

Fig. 4 Full-duplex communications across the secondary source users and the relay station

Let $M = M_r = M_t$. The full-duplex transceiver receives not only the signal of interest $\widehat{\boldsymbol{y}}_a^{(k)}(l) \in \mathbb{C}^{M\times 1}$ but also a self-interference signal $\widetilde{\boldsymbol{y}}_a^{(k)}(l) \in \mathbb{C}^{M\times 1}$ due to bidirectional transmissions. As illustrated in Fig. 4, we can denote the MIMO channel's impulse response for wireless channels from the source node S_k to the relay station in a considered kth source-destination pair as $\boldsymbol{H}_S^{(k)}(l) \in \mathbb{C}^{M\times M}$, which is specified in Eq. (10). Denote the channel's impulse response for wireless channels from the relay station to the destination node D_k as $\boldsymbol{H}_R^{(k)}(l) \in \mathbb{C}^{M\times M}$. The self-interference experiences the channel's impulse responses, denoted by $\boldsymbol{\Phi}^{(k)}(n) \in \mathbb{C}^{M\times M}$, with $n = 1, 2, \ldots$ being the delay index from local transmitter to local receiver at the relay station. Consequently, the received analog composite signal can be determined as follows:

$$\overline{\boldsymbol{y}}_a^{(k)}(l) = \widehat{\boldsymbol{y}}_a^{(k)}(l) + \widetilde{\boldsymbol{y}}_a^{(k)}(l) \tag{15}$$

for which the self-interference signal at the relay node yields

$$\widetilde{\boldsymbol{y}}_a^{(k)}(l) = \sum_{n=0}^{\infty} \boldsymbol{\Phi}^{(k)}(n)\boldsymbol{x}^{(k)}(l-n) \tag{16}$$

The principle of ADIC scheme can be briefly described in the following two aspects:

1. **Analog Cancelation**: Analog cancelation technique uses knowledge of the transmission to cancel self-interference in the RF signal, before it is digitized. The principle of analog self-interference cancelation is to process the known transmitted signal with a frequency-selective filter to generate a negative signal that, when added to the composite signal, reverts the effect of the self-interference propagating through $\boldsymbol{\Phi}^{(k)}(n)$. Denoting the channel's impulse response of the cancelation filter by $\boldsymbol{C}_a^{(k)}(n) \in \mathbb{C}^{M\times M}$, then, the signal, denoted by $\boldsymbol{y}_a^{(k)}(l)$, after analog cancelation can be determined as follows:

$$\boldsymbol{y}_a^{(k)}(l) = \overline{\boldsymbol{y}}_a^{(k)}(l) \sum_{n=0}^{\infty} \boldsymbol{C}_a^{(k)}(n)\boldsymbol{x}^{(k)}(l-n) \tag{17}$$

The self-interference could be ideally removed already in analog domain by choosing $\boldsymbol{C}_a^{(k)}(n) = -\boldsymbol{\Phi}^{(k)}(n)$ for all n. However, in reality, $\boldsymbol{C}_a^{(k)}(n)$ is an analog filter which is difficult and expensive to implement. For example, a practical implementation may include only an $M \times M$ matrix of amplification and phase shift operations which can cancel at its best the strongest multipath component of each MIMO branch as follows [21]:

$$\left\{\boldsymbol{C}_a^{(k)}(n)\right\}_{i,j} = \begin{cases} \left\{\boldsymbol{\Phi}^{(k)}(n)\right\}_{i,j}, & \text{if } n = n_{i,j}^* \\ 0, & \text{otherwise} \end{cases} \tag{18}$$

where $n_{i,j}^* = \arg\max_n \left|\left\{\boldsymbol{\Phi}^{(k)}(n)\right\}_{i,j}\right|^2$.

2. **Digital Cancelation**: Denoting the impulse response of the cancelation filter by $\boldsymbol{C}_d^{(k)}(n) \in \boldsymbol{C}^{M\times M}$, then, we can derive the signal, denoted by $\boldsymbol{y}_d^{(k)}(l)$, after digital cancelation as follows:

$$\boldsymbol{y}_d^{(k)}(l) = \overline{\boldsymbol{y}}_d^{(k)}(l) \sum_{n=0}^{\infty} \boldsymbol{C}_d^{(k)}(n)\boldsymbol{x}^{(k)}(l-n) \tag{19}$$

where $\overline{\boldsymbol{y}}_d^{(k)}(l)$ represents the received digital composite signal. The self-interference could be removed now by choosing

$$\boldsymbol{C}_d^{(k)}(n) = -\boldsymbol{A}\left(\boldsymbol{\Phi}^{(k)}(n) + \boldsymbol{C}_a^{(k)}(n)\right) \tag{20}$$

where $\boldsymbol{A}$ is a real diagonal matrix, and we can obtain that $\widehat{\boldsymbol{y}}_d^{(k)}(l) = \boldsymbol{A}\widehat{\boldsymbol{y}}_a^{(k)}(l)$ and $\widetilde{\boldsymbol{y}}_d^{(k)}(l) = \boldsymbol{A}\widetilde{\boldsymbol{y}}_a^{(k)}(l)$.

MIMO-GFDM-Based FD-SS Relaying Scheme

FD-SS Scheme with Imperfect CSI

To detect the random access and departure of the PUs, the SUs need to sense the licensed channel not only in the sensing period but also in the transmission period. To enable the SU sensing during the transmission period, the SUs need to use the wireless FD mode with transmitting and sensing simultaneously. Consequently, we apply the wireless FD-SS scheme [9] over CRNs.

Since we assume that the source node and the destination node are far enough from each other, there is no direct channel link between them due to shadowing conditions and the transmit power limitation, thus the information needs to be forwarded through the MIMO-based relay node in the networks. The relaying process consists of two phases. In the first phase, the source nodes transmit signals to the relay station after detecting the spectral white space.

Under the wireless FD-SS-based MIMO-GFDM model, the kth secondary source node S_k detects the PU's presence while it is transmitting signals to the relay station. Consequently, the self-interference is introduced to S_k because of S_k's FD transmission with PU. When S_k is transmitting signals to the destination node, the spectrum detection problem as a hypothesis testing problem presents with the

following two hypotheses:

$$\boldsymbol{y}_S^{(k)} = \begin{cases} \sqrt{P_P}\boldsymbol{H}_P^{(k)}\boldsymbol{x}^{(p)} + \sum\limits_{n\neq k}^{K}\sqrt{P_S^{(n)}}\boldsymbol{H}_S^{(n)}\boldsymbol{x}_S^{(n)} + \boldsymbol{n}_S^{(k)}, & \text{if } \mathscr{H}_1; \\ \sqrt{\kappa P_S^{(k)}}\boldsymbol{H}_S^{(k)}\boldsymbol{x}_S^{(k)} + \sum\limits_{n\neq k}^{K}\sqrt{P_S^{(n)}}\boldsymbol{H}_S^{(n)}\boldsymbol{x}_S^{(n)} + \boldsymbol{n}_S^{(k)}, & \text{if } \mathscr{H}_0; \end{cases} \tag{21}$$

where $\mathscr{H}_1$ implies that PU is active and $\mathscr{H}_0$ implies that PU is inactive while the secondary source node S_k is transmitting signals to the destination node; κ with $0 \leq \kappa \leq 1$ is the self-interference suppression coefficient defined as the impact of self-interference mitigation on the wireless FD communication [22]; $P_S^{(k)}$ and $P_S^{(n)}$ are the transmit power of the kth source node and nth source node, respectively; P_P represents the transmit power of the PU base station (BS). $\boldsymbol{x}_S^{(k)}$ and $\boldsymbol{x}_S^{(n)}$ denote the signals sent from the kth secondary-user source node and nth secondary-user source node, respectively; $\boldsymbol{x}^{(p)}$ denotes the signals sent from the PU BS. $\boldsymbol{H}_S^{(k)}$ and $\boldsymbol{H}_S^{(n)}$ denote the channel's impulse response from the transmitter of kth source node and nth source node to the receiver of the relay node, specified by Eq. (10), respectively; $\boldsymbol{H}_P^{(k)}$ denotes the channel's impulse response from the PU base station to the receiver of the relay node; and $\boldsymbol{n}_S^{(k)}$ represents the additive white Gaussian noise (AWGN) with zero mean and unit variance matrix.

In practice, the relay station usually does not have perfect knowledge of CSI. With imperfect CSI, the minimum mean-square error (MMSE) channel estimation for $\boldsymbol{H}_S^{(k)}$ and $\boldsymbol{H}_R^{(k)}$ can be derived as follows:

$$\begin{cases} \widehat{\boldsymbol{H}}_S^{(k)} = \boldsymbol{H}_S^{(k)} - \boldsymbol{\varepsilon}_S^{(k)}; \\ \widehat{\boldsymbol{H}}_R^{(k)} = \boldsymbol{H}_R^{(k)} - \boldsymbol{\varepsilon}_R^{(k)}, \end{cases} \tag{22}$$

where $\boldsymbol{\varepsilon}_S^{(k)}$ and $\boldsymbol{\varepsilon}_R^{(k)}$ represent the estimation error matrices for $\boldsymbol{H}_S^{(k)}$ and $\boldsymbol{H}_R^{(k)}$, respectively. According to [23], rows of $\widehat{\boldsymbol{H}}_S^{(k)}$, $\boldsymbol{\varepsilon}_S^{(k)}$, $\widehat{\boldsymbol{H}}_R^{(k)}$, and $\boldsymbol{\varepsilon}_R^{(k)}$ are mutually independent and distributed as $\mathscr{CN}\left(\boldsymbol{0}, \widehat{\boldsymbol{D}}_S^{(k)}\right)$, $\mathscr{CN}\left(\boldsymbol{0}, \boldsymbol{D}_S^{(k)} - \widehat{\boldsymbol{D}}_S^{(k)}\right)$, $\mathscr{CN}\left(\boldsymbol{0}, \widehat{\boldsymbol{D}}_R^{(k)}\right)$, and $\mathscr{CN}\left(\boldsymbol{0}, \boldsymbol{D}_R^{(k)} - \widehat{\boldsymbol{D}}_R^{(k)}\right)$, respectively, where $\widehat{\boldsymbol{D}}_S^{(k)}$ and $\widehat{\boldsymbol{D}}_R^{(k)}$ are the diagonal matrices and $\boldsymbol{x} \sim \mathscr{CN}(\boldsymbol{0}, \boldsymbol{\Sigma})$ denotes a complex Gaussian vector $\boldsymbol{x}$ with zero mean and covariance matrix $\boldsymbol{\Sigma}$. Define $\mathbf{W}_S^{(k)} \triangleq \widehat{\boldsymbol{H}}_S^{(k)}\left(\widehat{\boldsymbol{H}}_S^{(k)}\right)^H$, as a random nonnegative definite matrix, which has real, nonnegative eigenvalues, denoted by $\lambda_S^{(k)}$. Also, define $\mathbf{W}_R^{(k)} \triangleq \widehat{\boldsymbol{H}}_R^{(k)}\left(\widehat{\boldsymbol{H}}_R^{(k)}\right)^H$, as a random nonnegative definite matrix with eigenvalues, denoted by $\lambda_R^{(k)}$. Assuming that each eigenvalues is i.i.d..

By applying the MMSE channel estimation technique, the channel's impulse response is estimated at the receiver of the relay station as $\widehat{\boldsymbol{H}}_P^{(k)}$ and $\widehat{\boldsymbol{H}}_S^{(k)}$. Because

$\boldsymbol{x}_S^{(k)}$ is known to the receiver of the relay station, in conjunction with the channel estimation results specified by Eq. (21), the received signal after combined ADIC at the relay station, denoted by $\boldsymbol{z}_S^{(k)}$, takes the following form:

$$\boldsymbol{z}_S^{(k)} = \begin{cases} \sqrt{P_P}\widehat{\boldsymbol{H}}_P^{(k)}\boldsymbol{x}^{(p)} + \boldsymbol{I}_{S,1}^{(k)}, & \text{if } \mathscr{H}_1; \\ \sqrt{\kappa P_S^{(k)}}\widehat{\boldsymbol{H}}_S^{(k)}\boldsymbol{x}_S^{(k)} + \boldsymbol{I}_{S,0}^{(k)}, & \text{if } \mathscr{H}_0, \end{cases} \tag{23}$$

where $\boldsymbol{I}_{S,1}^{(k)}$ and $\boldsymbol{I}_{S,0}^{(k)}$ are the residual self-interference-plus-noise items after combined ADIC at the relay station given by

$$\begin{cases} \boldsymbol{I}_{S,1}^{(k)} = \sqrt{P_P}\boldsymbol{\varepsilon}_P^{(k)}\boldsymbol{x}^{(p)} + \sum\limits_{n\neq k}^{K}\sqrt{P_S^{(n)}}\left(\widehat{\boldsymbol{H}}_S^{(n)} + \boldsymbol{\varepsilon}_S^{(n)}\right)\boldsymbol{x}_S^{(n)} + \boldsymbol{n}_S^{(k)}, & \text{if } \mathscr{H}_1; \\ \boldsymbol{I}_{S,0}^{(k)} = \sqrt{\kappa P_S^{(k)}}\boldsymbol{\varepsilon}_S^{(k)}\boldsymbol{x}_S^{(k)} + \sum\limits_{n\neq k}^{K}\sqrt{P_S^{(n)}}\left(\widehat{\boldsymbol{H}}_S^{(n)} + \boldsymbol{\varepsilon}_S^{(n)}\right)\boldsymbol{x}_S^{(n)} + \boldsymbol{n}_S^{(k)}, & \text{if } \mathscr{H}_0, \end{cases} \tag{24}$$

where $\boldsymbol{\varepsilon}_P^{(k)}$ represents the channel estimation error coefficients for the PU communication link. Then, the power of $\boldsymbol{I}_{S,1}^{(k)}$ and $\boldsymbol{I}_{S,0}^{(k)}$, denoted by $\Theta_{S,1}^{(k)}$ and $\Theta_{S,0}^{(k)}$, respectively, can be derived as follows:

$$\begin{cases} \Theta_{S,1}^{(k)} = \boldsymbol{I} + P_p\left\|\boldsymbol{\varepsilon}_P^{(k)}\right\|^2 + \sum\limits_{n\neq k}^{K}P_S^{(n)}\left\|\widehat{\boldsymbol{H}}_S^{(n)}\right\|^2 + \sum\limits_{n\neq k}^{K}P_S^{(n)}\left\|\boldsymbol{\varepsilon}_S^{(n)}\right\|^2, & \text{if } \mathscr{H}_1; \\ \Theta_{S,0}^{(k)} = \boldsymbol{I} + \kappa P_S^{(k)}\left\|\boldsymbol{\varepsilon}_S^{(k)}\right\|^2 + \sum\limits_{n\neq k}^{K}P_S^{(n)}\left\|\widehat{\boldsymbol{H}}_S^{(n)}\right\|^2 + \sum\limits_{n\neq k}^{K}P_S^{(n)}\left\|\boldsymbol{\varepsilon}_S^{(n)}\right\|^2, & \text{if } \mathscr{H}_0; \end{cases} \tag{25}$$

where $\boldsymbol{I}$ is the identity matrix. According to Eqs. (23) and (25), the received signal-to-noise-plus interference ratio (SINR), denoted by $\gamma_{S,1}^{(k)}$ and $\gamma_{S,0}^{(k)}$, at the relay station when the channels are idle or not can be expressed as follows:

$$\begin{cases} \gamma_{S,1}^{(k)} = \dfrac{P_p\left\|\boldsymbol{H}^{(p)}\right\|^2}{\Theta_{S,1}^{(k)}}, & \text{if } \mathscr{H}_1; \\ \gamma_{S,0}^{(k)} = \dfrac{\kappa P_S^{(k)}\left\|\boldsymbol{H}_S^{(k)}\right\|^2}{\Theta_{S,0}^{(k)}}, & \text{if } \mathscr{H}_0. \end{cases} \tag{26}$$

In the second phase, considering the MIMO-based FD relay networks, to keep the system complexity low, linear processing schemes are proven to be close to optimal [23]. Among all the linear processing techniques, we adopt the zero-forcing (ZF) processing technique. Define the vector for the received signal at the relay station as $\boldsymbol{Z}_S \triangleq \left[\boldsymbol{z}_S^{(1)}, \boldsymbol{z}_S^{(2)}, \ldots, \boldsymbol{z}_S^{(K)}\right]$, where $\boldsymbol{z}_S^{(k)}$ $(k = 1, 2, \ldots, K)$ is specified by Eq. (23). Then, after receiving the signal from the source node, the relay station applies the ZF receiver to detect the received signal. Thus, we have

$$\boldsymbol{s}_R^{(k)} = \left(\boldsymbol{W}^{(k)}\right)^H \boldsymbol{z}_S^{(k)}, \tag{27}$$

where $(\cdot)^H$ denotes the Hermitian transpose and $\boldsymbol{W} = \left[\boldsymbol{w}^{(1)}, \boldsymbol{w}^{(2)}, \ldots, \boldsymbol{w}^{(K)}\right]$ is the $M \times M$ beamforming matrix given by [24, 25]

$$\boldsymbol{W}^H \triangleq \left(\widehat{\boldsymbol{H}}_R^H \widehat{\boldsymbol{H}}_R\right)^{-1} \widehat{\boldsymbol{H}}_R^H. \tag{28}$$

The estimated received signal is then amplified and forwarded to the destination node using the beamforming matrix $\boldsymbol{A} = \left[\boldsymbol{A}^{(1)}, \boldsymbol{A}^{(2)}, \ldots, \boldsymbol{A}^{(K)}\right]$. Consequently, after linear processing, the transmit signal at the relay station can be expressed as $\boldsymbol{x}_R^{(k)} = \left(\boldsymbol{A}^{(k)}\right)^H \boldsymbol{s}_R^{(k)}$ where

$$\boldsymbol{A}^{(k)} = a_{ZF} \widehat{\boldsymbol{H}}_R^{(k)} \left(\left(\widehat{\boldsymbol{H}}_R^{(k)}\right)^H \widehat{\boldsymbol{H}}_R^{(k)}\right)^{-1}, \tag{29}$$

where a_{ZF} denotes the normalization constant, chosen to satisfy a long-term total meet the power constraint at the relay node, we have [25]

$$a_{ZF} = \sqrt{\frac{M-K}{\sum_{k=1}^{K} \left(\lambda_R^{(k)}\right)^{-2}}}. \tag{30}$$

Consequently, with imperfect knowledge of desired channels, the received signal, denoted by $\boldsymbol{y}_R^{(k)}$, at the kth destination node can be derived as follows:

$$\begin{cases} \boldsymbol{y}_R^{(k)} = \sqrt{P_P} \left(\widehat{\boldsymbol{H}}_P^{(k)}\right)^H \boldsymbol{A}^{(k)} \boldsymbol{x}_P^{(k)} + \sum_{n \neq k}^{K} \sqrt{P_R^{(n)}} \left(\widehat{\boldsymbol{H}}_R^{(k)}\right)^H \boldsymbol{A}^{(n)} \boldsymbol{x}_R^{(n)} \\ \qquad + \sum_{n=1}^{K} \sqrt{P_R^{(n)}} \left(\boldsymbol{\varepsilon}_R^{(k)}\right)^H \boldsymbol{A}^{(n)} \boldsymbol{x}_R^{(n)} + \boldsymbol{n}_D^{(k)}, & \text{if } \mathscr{H}_1; \\ \boldsymbol{y}_R^{(k)} = \sqrt{\kappa P_R^{(k)}} \left(\widehat{\boldsymbol{H}}_R^{(k)}\right)^H \boldsymbol{A}^{(k)} \boldsymbol{x}_R^{(k)} + \sum_{n \neq k}^{K} \sqrt{P_R^{(n)}} \left(\widehat{\boldsymbol{H}}_R^{(k)}\right)^H \boldsymbol{A}^{(n)} \boldsymbol{x}_R^{(n)} \\ \qquad + \sum_{n=1}^{K} \sqrt{P_R^{(n)}} \left(\boldsymbol{\varepsilon}_R^{(k)}\right)^H \boldsymbol{A}^{(n)} \boldsymbol{x}_R^{(n)} + \boldsymbol{n}_D^{(k)}, & \text{if } \mathscr{H}_0, \end{cases} \tag{31}$$

where $\widehat{\boldsymbol{H}}_R^{(k)}$ denotes the estimated channel's impulse response from the relay node to kth secondary destination node; $\boldsymbol{\varepsilon}_R^{(k)}$ represents the estimation error for $\boldsymbol{H}_R^{(k)}$; $P_R^{(k)}$ is the transmit power at the relay node; and $\boldsymbol{n}_R^{(k)}$ represents the additive white Gaussian noise (AWGN) with zero mean and unit variance matrix.

Define the power of the interference-plus-noise item for the received signal at the kth secondary destination node when PU is active or not as follows:

$$\boldsymbol{\Theta}_{R,1}^{(k)} = \boldsymbol{\Theta}_{R,0}^{(k)} = \sum_{n\neq k}^{K} P_R^{(n)} \left\| \left(\widehat{\boldsymbol{H}}_R^{(k)}\right)^H \boldsymbol{A}^{(n)} \right\|^2 + \sum_{n=1}^{K} P_R^{(n)} \left\| \left(\boldsymbol{\varepsilon}_R^{(n)}\right)^H \boldsymbol{A}^{(n)} \right\|^2. \tag{32}$$

Consequently, the SNR, denoted by $\gamma_{R,1}^{(k)}$ and $\gamma_{R,0}^{(k)}$, from the relay station to the kth secondary destination node can be derived as follows:

$$\begin{cases} \gamma_{R,1}^{(k)} = \dfrac{P_P \left| \left(\widehat{\boldsymbol{H}}_P^{(k)}\right)^H \boldsymbol{A}^{(k)} \right|^2}{\boldsymbol{\Theta}_{R,1}^{(k)}}, & \text{if } \mathscr{H}_1; \\ \gamma_{R,0}^{(k)} = \dfrac{\kappa P_R^{(k)} \left| \left(\widehat{\boldsymbol{H}}_R^{(k)}\right)^H \boldsymbol{A}^{(k)} \right|^2}{\boldsymbol{\Theta}_{R,1}^{(k)}}, & \text{if } \mathscr{H}_0. \end{cases} \tag{33}$$

Probability of Miss-Detection and False Alarm

We assume the detection threshold is ε. We can rewrite the test statistics of wireless FD energy detection for the channel from the secondary source node to the secondary destination node, denoted by $Y_k(n)$, as follows:

$$Y_k(n) = \frac{1}{N_s} \left(\sum_{n=0}^{N_s} \left| y_R^{(k)}(n) \right|^2 \right) \tag{34}$$

where N_s is the number of samples for the entire sensing period. Note that $y_R^{(k)}(n)$ in each sample is i.i.d. and we assume N_s is large enough. According to the central limit theorem (CLT), the probability density function (pdf) of $Y_k(n)$ can be approximated by a Gaussian distribution.

Lemma 1. *The false-alarm probability, denoted by p_f, and the miss-detection probability, denoted by p_m, for our proposed MIMO-GFDM-based full-duplex cognitive radio networks are determined, respectively, as follows:*

$$\begin{cases} p_f = \Pr\{Y_k(n) > \varepsilon | \mathscr{H}_0\} = Q\left(\left(\frac{\varepsilon}{(1+\gamma_0)} - 1 \right) \sqrt{N_s} \right); \\ p_m = \Pr\{Y_k(n) < \varepsilon | \mathscr{H}_1\} = 1 - Q\left(\left(\frac{\varepsilon}{(1+\gamma_1+\gamma_0)} - 1 \right) \sqrt{N_s} \right), \end{cases} \tag{35}$$

where $Q(\cdot)$ represents the Q function, ε is the detection threshold and N_s denotes the number of samples for the entire sensing period; the end-to-end SINR, denoted by γ_1 and γ_0 when PU is present or not, is given as follows:

$$\begin{cases} \gamma_1 = \sum_{k=1}^{K} \frac{\gamma_{S,1}^{(k)} \gamma_{R,1}^{(k)}}{1+\gamma_{S,1}^{(k)}+\gamma_{R,1}^{(k)}}; \\ \gamma_0 = \sum_{k=1}^{K} \frac{\gamma_{S,0}^{(k)} \gamma_{R,0}^{(k)}}{1+\gamma_{S,0}^{(k)}+\gamma_{R,0}^{(k)}}. \end{cases} \tag{36}$$

Proof. The expression for SINR received at the destination node due to the kth secondary-user source-destination link is given by [26]

$$\gamma_0^{(k)} = \frac{\gamma_{S,0}^{(k)} \gamma_{R,0}^{(k)}}{1 + \gamma_{S,0}^{(k)} + \gamma_{R,0}^{(k)}}. \tag{37}$$

Consequently, using the maximum ratio combining (MRC) at the secondary destination node, the total end-to-end SINR due to the full-duplex-based relay network is given as

$$\gamma_0 = \sum_{k=1}^{K} \gamma_0^{(k)}. \tag{38}$$

Because the pdf of $Y_k(n)$ under hypothesis $\mathscr{H}_0$ can be approximated by a Gaussian distribution with mean, denoted by μ_0, as follows:

$$\mu_0^{(k)} = 1 + \gamma_0, \tag{39}$$

where γ_0 is the end-to-end SINR at the secondary destination node when the channels are idle. Then, we can derive the variance, denoted by σ_0 as follows:

$$\sigma_0^2 = \frac{(1 + \gamma_0)^2}{N_s} \tag{40}$$

Thus, we can derive the probability of false alarm as follows:

$$\begin{aligned} p_f &= \Pr\{Y_k(n) > \varepsilon | \mathscr{H}_0\} = \int_{\varepsilon}^{\infty} \frac{1}{\sqrt{2\pi}\sigma_0} \exp\left(-\frac{(x-\mu_0)^2}{2\sigma_0^2}\right) dx \\ &= \frac{1}{\sqrt{2\pi}} \int_{\varepsilon}^{\infty} \frac{\sqrt{N_s}}{(1+\gamma_0)} \exp\left(-\frac{(x-(1+\gamma_0))^2}{2\frac{(1+\gamma_0)^2}{N_s}}\right) dx \end{aligned} \tag{41}$$

Defining new function $z_0(x)$ as follows:

$$z_0(x) \triangleq \frac{x - (1 + \gamma_0)}{1 + \gamma_0} \sqrt{N_s} \tag{42}$$

and plugging Eq. (42) into Eq. (41), we can obtain

$$p_f = Q\left(\left(\frac{\varepsilon}{(1+\gamma_0)} - 1\right)\sqrt{N_s}\right) \tag{43}$$

which is Eq. (35). In the similar way, we can derive the miss-detection probability p_m specified in Eq. (35). Thus, Lemma 1 follows. □

Heterogeneous Statistical Delay-Bounded QoS Guarantees Through Effective Capacity Over CRNs

In this section, we apply the heterogeneous statistical QoS-driven power allocation scheme to maximize the aggregate effective capacity of the FD-based MIMO-GFDM system with heterogeneous statistical delay-bound QoS requirements.

Preliminary for Effective Capacity for Homogeneous Statistical QoS

The statistical QoS guarantees [27, 28] have been extensively studied for analyzing the queueing behavior for time-varying arrival and service processes. Based on large deviation principle (LDP), under sufficient conditions, the queue length process $Q(l)$ converges in distribution to a random variable $Q(\infty)$ such that

$$-\lim_{Q_{th}\to\infty} \frac{\log\left(\Pr\{Q(\infty) > Q_{th}\}\right)}{Q_{th}} = \theta \tag{44}$$

To be more specific, Eq. (44) states that the probability of the queue length exceeding a certain threshold Q_{th} decays exponentially fast as the threshold Q_{th} increases. The parameter θ is called QoS exponent and plays a critically important role for statistical QoS guarantees. The larger θ corresponds to the more stringent QoS requirement, while the smaller θ leads to the looser delay constraint, which implies the system can only provide a looser QoS guarantee. For a certain $\theta > 0$, Q_{th} denotes the queue length bound.

Definition 1. The *effective capacity* [29] is defined as the maximum constant arrival rate that a given service process can support in order to guarantee a QoS requirement specified by θ. Given a service process $R(l)$, the effective capacity of the service process, denoted by $E_c(\theta)$, where $\theta > 0$, is defined as follows [29]:

$$E_c(\theta) = -\frac{1}{\theta}\log\left(\mathbb{E}\left[e^{-\theta R(l)}\right]\right) = -\frac{1}{\theta}\log\left(\mathbb{E}\left[e^{-\theta R(1)}\right]\right) \tag{45}$$

where $\mathbb{E}(\cdot)$ is the expectation operation.

Furthermore, define the resource allocation policy, denoted by $\boldsymbol{\mu} \triangleq \boldsymbol{\mu}(\theta, \gamma)$, as a function of not only the SNR γ but also of the QoS exponent θ [4]. Applying the resource allocation policy, the instantaneous transmit power becomes $P(\boldsymbol{\mu}) = \boldsymbol{\mu}\overline{P}$. Assume that the channel is block fading. In addition, assume that all secondary users are heterogeneous, that is, they have different power allocation schemes but they all subject to the same unit mean power constraint. Let the mean transmit power be upper-bounded by $\overline{P}$. Therefore, the power control law needs to satisfy the mean power constraint:

$$\int_0^\infty P(\boldsymbol{\mu}) p_\gamma(\gamma) d\gamma \leq 1, \qquad \text{for all } \theta > 0 \tag{46}$$

where $p_\gamma(\gamma)$ denotes the pdf of the SINR over Nakagami-m fading channel given by

$$p_\gamma(\gamma) = \frac{\gamma^{m-1}}{\Gamma(m)} \left(\frac{m}{\overline{\gamma}}\right)^m \exp\left(-\frac{m\gamma}{\overline{\gamma}}\right) \tag{47}$$

where $\overline{\gamma}$ denotes the average SINR.

Markov Chain Model for QoS-Driven CRN

Each channel is modeled as an ON/OFF source alternating between state ON (busy) and state OFF (idle) [30]. Suppose that each channel changes its state independently, and the state transition probabilities do not depend on the original state. To characterize the correctness of detections in channel sensing, there are three possible scenarios, as illustrated in Fig. 5, as shown in the following:

Scenario 1: When channel is busy and detected as busy, or when channel is idle but detected as busy, implying that channel is in ON state. As a result, the probability of staying in ON state can be derived as follows [31]:

$$p_{11} = p_{21} = p_{31} = \left[p_0(1 - p_m) + (1 - p_0)p_f\right]^M \tag{48}$$

where p_0 denotes the prior probability of channel being busy; p_f is the false-alarm probability, specified by Eq. (13);

Scenario 2: When channel is idle and detected as idle, implying that channel is in OFF state, that is, the probability of staying in OFF state is determined as follows:

$$p_{12} = p_{22} = p_{32} = \widetilde{c}(1 - p_0)(1 - p_f) \tag{49}$$

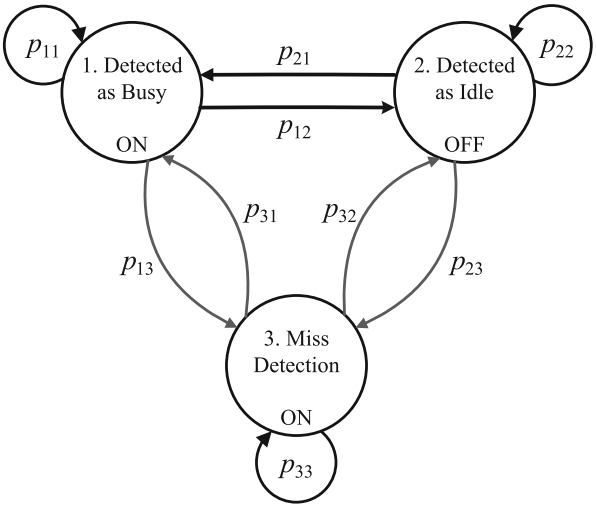

Fig. 5 Markov chain modeling for cognitive radio channel state transitions

where

$$\widetilde{c} = \sum_{i=0}^{M-1} (1 - p_{11})^{M-1-i} (p_{11})^{i} \frac{M!}{(M-i)!i!} = \frac{1 - (p_{11})^{M}}{p_{11}} \tag{50}$$

where let $M = M_t = M_r$.

Scenario 3: When channel is busy but detected as idle, implying that there is no reliable transmitted data. The probability of staying in this scenario is denoted as follows:

$$p_{13} = p_{23} = p_{33} = \widetilde{c} p_0 p_m \tag{51}$$

where p_m denotes the miss-detection probability, specified by Eq. (13).

Then, the 3×3 state transition probability matrix can be derived as follows:

$$\mathbf{S} = \begin{bmatrix} p_{11} & p_{12} & p_{13} \\ p_{21} & p_{22} & p_{23} \\ p_{31} & p_{32} & p_{33} \end{bmatrix} = \begin{bmatrix} p_1 & p_2 & p_3 \\ p_1 & p_2 & p_3 \\ p_1 & p_2 & p_3 \end{bmatrix} \tag{52}$$

Note that in each frame duration, data is transmitted and received at rate R_1 and R_2 bits in the **Scenario 1** and **Scenario 2**, respectively, while the transmitted number of bits is assumed to be zero in **Scenario 3**.

Assume that if the channel is detected as busy, SUs are considered in the listen-and-talk mode, that is, SUs simultaneously transmit data and sense the target spectrum band with transmitting power $P_S^{(k)}$ and $P_R^{(k)}$. Otherwise, SUs are considered in the half-duplex (HD) sensing mode, that is, SUs just sense the target spectrum band.

Optimizing Effective Capacity with Heterogeneous Statistical QoS Requirements Over CRNs

Considering the Markov-based relaying model, for the different K-link transmissions at the relay station, it is unrealistic to still assume that all the links have the homogeneous statistical QoS requirements. Thus, the diverse delay-bound QoS provisionings for different links at the same time, which represents the new heterogeneous statistical QoS provisioning framework and imposes many new challenges, need to be considered. Let θ_k ($k \in [1, K]$) denote the QoS exponents for different link transmissions at the relay station. Define the power allocation vector $\mathbf{P}_S(\boldsymbol{\mu}) = [P_S^{(1)}(\boldsymbol{\mu}), P_S^{(2)}(\boldsymbol{\mu}), \cdots, P_S^{(K)}(\boldsymbol{\mu})]$ and $\mathbf{P}_R(\boldsymbol{\mu}) = [P_R^{(1)}(\boldsymbol{\mu}), P_R^{(2)}(\boldsymbol{\mu}), \cdots, P_R^{(K)}(\boldsymbol{\mu})]$.

Different relay protocols have been investigated in the last decades [4, 8]. In this section, we mainly focus on the simple relay protocols proposed, that is, amplify-and-forward (AF) and decode-and-forward (DF) protocols as follows:

1. AF Protocol: In AF mode, the relay station simply amplifies and then forwards what it receives to the destination node. This strategy is also called non-regenerative relay or analog relay protocol. Then, with the assumption that there is no direct channel link between the source node and the destination node, the achievable rate of AF protocol, denoted by R_{AF}, can be derived as follows [32]:

$$R_{AF} = T_f B \log_2 \left(1 + \frac{4P_S^{(k)}(\boldsymbol{\mu})P_R^{(k)}(\boldsymbol{\mu})\gamma_S^{(k)}\gamma_R^{(k)}}{1 + 2P_S^{(k)}(\boldsymbol{\mu})\gamma_S^{(k)} + 2P_R^{(k)}(\boldsymbol{\mu})\gamma_R^{(k)}}\right), \tag{53}$$

   where $\gamma_S^{(k)}$ and $\gamma_R^{(k)}$ denote the SINR from the secondary source node k to the relay station and from the relay station to the secondary destination node k, respectively.
2. DF Protocol: With DF protocol, the relay station can decode its received message and forward it to the destination node. The achievable rate of DF protocol, denoted by R_{DF}, can be expressed as follows:

$$R_{DF} = T_f B \log_2 \min\left\{\left(1 + \kappa\gamma_S^{(k)}P_S^{(k)}\right), \left(1 + \gamma_R^{(k)}P_R^{(k)}\right)\right\}. \tag{54}$$

Scenario 1: According to the Markov state transition model, for the first scenario (channel is in ON state, $\mathscr{H}_0$), the transmission rate as a function of $\boldsymbol{\mu}$ is derived as follows:

$$\begin{cases} R_{S,0}^{(k)}(\boldsymbol{\mu}) = T_f B \left\{ \log_2 \left(1 + \gamma_{S,0}^{(k)} \right) \right\}; \\ R_{R,0}^{(k)}(\boldsymbol{\mu}) = T_f B \left\{ \log_2 \left(1 + \gamma_{R,0}^{(k)} \right) \right\}. \end{cases} \tag{55}$$

Based on AF protocol in Eq. (53), the achievable rate, denoted by $R_{AF,0}^{(k)}(\boldsymbol{\mu})$, of the MIMO-GFDM-based relaying scheme can be expressed as follows:

$$R_{AF,0}^{(k)}(\boldsymbol{\mu}) = T_f B \left\{ \log_2 \left(1 + \frac{4 P_S^{(k)}(\boldsymbol{\mu}) P_R^{(k)}(\boldsymbol{\mu}) \gamma_{S,0}^{(k)} \gamma_{R,0}^{(k)}}{1 + 2 P_S^{(k)}(\boldsymbol{\mu}) \gamma_{S,0}^{(k)} + 2 P_R^{(k)}(\boldsymbol{\mu}) \gamma_{R,0}^{(k)}} \right) \right\} \tag{56}$$

Suppose a set $\mathscr{S}_k$ of subchannels allocated to the kth secondary source-destination pair. Since in the MIMO-GFDM structure each subchannel is only allocated to one secondary pair, $\mathscr{S}_k \bigcap \mathscr{S}_n = \emptyset$ where $k \neq n$ and $\bigcup_{k=1}^{K} \mathscr{S}_k = \{1, 2, \ldots, K\}$. With regard to the abovementioned assumptions and long-term power constraint, our maximization problem $\mathbf{P_1}$ with heterogeneous statistical delay-bound QoS requirements under $\mathscr{H}_0$ hypnosis can be formulated as follows:

$$\mathbf{P_1} : = \arg \max_{P_S^{(k)}(\boldsymbol{\mu}), P_R^{(k)}(\boldsymbol{\mu})} C_{AF,0}^{\text{opt}}(\theta_1, \theta_2, \ldots, \theta_K) \tag{57}$$

$$\begin{aligned} \text{s.t.}: \quad & (1)\ \mathscr{S}_k \bigcap \mathscr{S}_n = \emptyset \quad \text{if } k \neq n; \\ & (2)\ P_S^{(k)}(\boldsymbol{\mu}) > 0 \quad \text{and} \quad P_R^{(k)}(\boldsymbol{\mu}) > 0; \\ & (3)\ \mathbb{E}\left[\sum_{k=1}^{K} P_S^{(k)}(\boldsymbol{\mu}) \right] \leq \overline{P}_S, \quad \mathbb{E}\left[\sum_{k=1}^{K} P_R^{(k)}(\boldsymbol{\mu}) \right] \leq \overline{P}_R. \end{aligned} \tag{58}$$

Theorem 1. *For optimizing the aggregate effective capacity for problem* $\mathbf{P_1}$*, there exists the unique optimal QoS exponent* θ_o ($\theta_{\min} \leq \theta_o \leq \theta_{\max}$ *where* $\theta_{\min} = \min\{\theta_1, \theta_2, \ldots, \theta_K\}, \theta_{\max} = \max\{\theta_1, \theta_2, \ldots, \theta_K\}$) *such that the equivalent aggregate effective capacity, denoted by* $\widetilde{C}_{AF,0}(\theta_1, \theta_2, \ldots, \theta_K)$*, for different links in the relay-based cognitive radio networks is given as follows [8]:*

$$\widetilde{C}_{AF,0}(\theta_1,\theta_2,\ldots,\theta_K) \triangleq -\frac{1}{\theta_o}\log\left\{\mathbb{E}_\gamma\left[\exp\left\{-\sum_{k=1}^{K}\theta_k T_f B \cdot \left\{\log_2\left(1+\frac{4P_S^{(k)}(\boldsymbol{\mu})P_R^{(k)}(\boldsymbol{\mu})\gamma_{S,0}^{(k)}\gamma_{R,0}^{(k)}}{1+2P_S^{(k)}(\boldsymbol{\mu})\gamma_{S,0}^{(k)}+2P_R^{(k)}(\boldsymbol{\mu})\gamma_{R,0}^{(k)}}\right)\right\}\right\}\right]\right\} \tag{59}$$

and the approximation for the optimal value of θ_o in the high-end SINR region is determined as follows:

$$\theta_o \approx \begin{cases} \dfrac{\prod_{k=1}^{K}\theta_k \sum_{n=1}^{K}\log\left\{\mathbb{E}_\gamma\left[\exp\left[-\theta_k T_f B\log_2\left(1+\frac{2\overline{P}_S^{(n)}(\boldsymbol{\mu})\overline{P}_R^{(n)}(\boldsymbol{\mu})\gamma_{S,0}^{(n)}\gamma_{R,0}^{(n)}}{\overline{P}_S^{(n)}(\boldsymbol{\mu})\gamma_{S,0}^{(n)}+\overline{P}_R^{(n)}(\boldsymbol{\mu})\gamma_{R,0}^{(n)}}\right)\right]\right]\right\}}{\sum_{k=1}^{K}\left(\prod_{n\neq k}^{K}\theta_n\right)\log\left\{\mathbb{E}_\gamma\left[\exp\left[-\theta_k T_f B\log_2\left(1+\frac{2\overline{P}_S^{(k)}(\boldsymbol{\mu})\overline{P}_R^{(k)}(\boldsymbol{\mu})\gamma_{S,0}^{(k)}\gamma_{R,0}^{(k)}}{\overline{P}_S^{(k)}(\boldsymbol{\mu})\gamma_{S,0}^{(k)}+\overline{P}_R^{(k)}(\boldsymbol{\mu})\gamma_{R,0}^{(k)}}\right)\right]\right]\right\}}, \\ \qquad\qquad \text{if } m\le 1 \text{ or } m>1 \text{ and } \theta_{\max}\le 10^{-2}; \\ \frac{1}{K}\sum_{k=1}^{K}\theta_k, \qquad\qquad \text{if } m>1 \text{ and } \theta_{\min}>10^{-2}; \\ \dfrac{\prod_{k=1}^{N}\theta_k \sum_{n=1}^{N}\log\left\{\mathbb{E}_\gamma\left[\exp\left[-\theta_k T_f B\log_2\left(1+\frac{2\overline{P}_S^{(n)}(\boldsymbol{\mu})\overline{P}_R^{(n)}(\boldsymbol{\mu})\gamma_{S,0}^{(n)}\gamma_{R,0}^{(n)}}{\overline{P}_S^{(n)}(\boldsymbol{\mu})\gamma_{S,0}^{(n)}+\overline{P}_R^{(n)}(\boldsymbol{\mu})\gamma_{R,0}^{(n)}}\right)\right]\right]\right\}}{\sum_{k=1}^{N}\left(\prod_{n\neq k}^{N}\theta_n\right)\log\left\{\mathbb{E}_\gamma\left[\exp\left[-\theta_k T_f B\log_2\left(1+\frac{2\overline{P}_S^{(k)}(\boldsymbol{\mu})\overline{P}_R^{(k)}(\boldsymbol{\mu})\gamma_{S,0}^{(k)}\gamma_{R,0}^{(k)}}{\overline{P}_S^{(k)}(\boldsymbol{\mu})\gamma_{S,0}^{(k)}+\overline{P}_R^{(k)}(\boldsymbol{\mu})\gamma_{R,0}^{(k)}}\right)\right]\right]\right\}}, \\ \qquad\qquad \text{if } m>1, \theta_{\min}\le 10^{-2}, \text{ and } \theta_{\max}>10^{-2}, \end{cases} \tag{60}$$

where N $(1 \le N \le K)$ is the number of QoS exponents which are less than or equal to 10^{-2} and $\overline{P}_S^{(k)}(\boldsymbol{\mu})$ and $\overline{P}_R^{(k)}(\boldsymbol{\mu})$ are the average transmit power.

Proof. The proof is provided in section "Appendix A: Proof of Theorem 1". □

According to Theorem 1, in the high-end SINR region, the above non-convex optimization problem $\mathbf{P_1}$ can be converted into a convex problem $\mathbf{P_2}$ as follows:

$$\begin{aligned}\mathbf{P_2}: &\arg\min_{P_S^{(k)}(\boldsymbol{\mu}),P_R^{(k)}(\boldsymbol{\mu})} \mathbb{E}_\gamma\left[\exp\left\{-\sum_{k=1}^{K}\theta_k T_f B\left\{\log_2\left(1+\frac{2P_S^{(k)}(\boldsymbol{\mu})P_R^{(k)}(\boldsymbol{\mu})\gamma_{S,0}^{(k)}\gamma_{R,0}^{(k)}}{P_S^{(k)}(\boldsymbol{\mu})\gamma_{S,0}^{(k)}+P_R^{(k)}(\boldsymbol{\mu})\gamma_{R,0}^{(k)}}\right)\right\}\right\}\right] \\ &= \arg\min_{P_S^{(k)}(\boldsymbol{\mu}),P_R^{(k)}(\boldsymbol{\mu})} \mathbb{E}_\gamma\left[\prod_{k=1}^{K}\left(1+\frac{2P_S^{(k)}(\boldsymbol{\mu})P_R^{(k)}(\boldsymbol{\mu})\gamma_{S,0}^{(k)}\gamma_{R,0}^{(k)}}{P_S^{(k)}(\boldsymbol{\mu})\gamma_{S,0}^{(k)}+P_R^{(k)}(\boldsymbol{\mu})\gamma_{R,0}^{(k)}}\right)^{-\beta_k}\right]\end{aligned} \tag{61}$$

subject to the same constraints given in Eq. (58). Define $\beta_k \triangleq \theta_k T_f B/(2\log 2)$ as the normalized QoS exponent corresponding to θ_k.

To obtain the global optimal solution for $\mathbf{P_2}$, first the Lagrangian function is applied for problem $\mathbf{P_2}$ as follows:

$$J = \mathbb{E}_{\gamma}\left[\prod_{k=1}^{K}\left(1+\frac{2P_S^{(k)}(\boldsymbol{\mu})P_R^{(k)}(\boldsymbol{\mu})\gamma_{S,0}^{(k)}\gamma_{R,0}^{(k)}}{P_S^{(k)}(\boldsymbol{\mu})\gamma_{S,0}^{(k)}+P_R^{(k)}(\boldsymbol{\mu})\gamma_{R,0}^{(k)}}\right)^{-\beta_k}\right]+\widetilde{\lambda}_S\mathbb{E}\left[P_S^{(k)}(\boldsymbol{\mu})-\overline{P}_S\right] + \widetilde{\lambda}_R\mathbb{E}\left[P_R^{(k)}(\boldsymbol{\mu})-\overline{P}_R\right], \tag{62}$$

where $\widetilde{\lambda}_S$ and $\widetilde{\lambda}_R$ are the Lagrange multipliers. Then, applying the Karush-Kuhn-Tucker (KKT) condition, we can take the derivative of J with respect to $P_S^{(k)}(\boldsymbol{\mu})$ and $P_R^{(k)}(\boldsymbol{\mu})$ and set the results to zero as follows:

$$\begin{cases} \frac{\partial J}{\partial P_S^{(k)}(\boldsymbol{\mu})} = -\beta_k\frac{2\gamma_{S,0}^{(k)}\left(\gamma_{R,0}^{(k)}\right)^2\left(P_R^{(k)}(\boldsymbol{\mu})\right)^2}{\left(P_S^{(k)}(\boldsymbol{\mu})\gamma_{S,0}^{(k)}+P_R^{(k)}(\boldsymbol{\mu})\gamma_{R,0}^{(k)}\right)^2}\prod_{k=1}^{K}\left(1+\frac{2P_S^{(k)}(\boldsymbol{\mu})P_R^{(k)}(\boldsymbol{\mu})\gamma_{S,0}^{(k)}\gamma_{R,0}^{(k)}}{P_S^{(k)}(\boldsymbol{\mu})\gamma_{S,0}^{(k)}+P_R^{(k)}(\boldsymbol{\mu})\gamma_{R,0}^{(k)}}\right)^{-\beta_k-1} \\ \qquad \cdot p_\gamma(\gamma)+\widetilde{\lambda}_S p_\gamma(\gamma)=0; \\ \frac{\partial J}{\partial P_S^{(k)}(\boldsymbol{\mu})} = -\beta_k\frac{2\left(\gamma_{S,0}^{(k)}\right)^2\gamma_{R,0}^{(k)}\left(P_S^{(k)}(\boldsymbol{\mu})\right)^2}{\left(P_S^{(k)}(\boldsymbol{\mu})\gamma_{S,0}^{(k)}+P_R^{(k)}(\boldsymbol{\mu})\gamma_{R,0}^{(k)}\right)^2}\prod_{k=1}^{K}\left(1+\frac{2P_S^{(k)}(\boldsymbol{\mu})P_R^{(k)}(\boldsymbol{\mu})\gamma_{S,0}^{(k)}\gamma_{R,0}^{(k)}}{P_S^{(k)}(\boldsymbol{\mu})\gamma_{S,0}^{(k)}+P_R^{(k)}(\boldsymbol{\mu})\gamma_{R,0}^{(k)}}\right)^{-\beta_k-1} \\ \qquad \cdot p_\gamma(\gamma)+\widetilde{\lambda}_R p_\gamma(\gamma)=0. \end{cases} \tag{63}$$

Thus,

$$\widetilde{\lambda}_S\gamma_{S,0}^{(k)}\left(\gamma_{R,0}^{(k)}\right)^2\left(P_R^{(k)}(\boldsymbol{\mu})\right)^2=\widetilde{\lambda}_R\left(\gamma_{S,0}^{(k)}\right)^2\gamma_{R,0}^{(k)}\left(P_S^{(k)}(\boldsymbol{\mu})\right)^2 \tag{64}$$

Plugging Eq. (64) back into Eq. (63), we can observe that although the generic optimal heterogeneous statistical QoS-driven recourse allocation for the MIMO-GFDM-based cognitive radio networks can only be obtained through numerical methods, the closed-form for the special case with $K=1$ which can maximize the effective capacity given in Eq. (57) under **Scenario 1** can be derived as follows:

$$\begin{cases} P_S^{(k)}(\boldsymbol{\mu})=\frac{\gamma_{S,0}^{(k)}+\nu^{(k)}\gamma_{R,0}^{(k)}}{2\nu^{(k)}\gamma_{S,0}^{(k)}\gamma_{R,0}^{(k)}}\left[\left(\frac{\widetilde{\lambda}_S^{\text{opt}}\left(\gamma_{S,0}^{(k)}+\nu^{(k)}\gamma_{R,0}^{(k)}\right)^2}{2\beta_k\gamma_{S,0}^{(k)}\left(\nu^{(k)}\gamma_{R,0}^{(k)}\right)^2}\right)^{-\frac{1}{\beta_k+1}}-1\right]; \\ P_R^{(k)}(\boldsymbol{\mu})=\nu^{(k)}P_S^{(k)}(\boldsymbol{\mu}), \end{cases} \tag{65}$$

where $\nu^{(k)}\triangleq\sqrt{\widetilde{\lambda}_S^{\text{opt}}\gamma_{S,0}^{(k)}/\left(\widetilde{\lambda}_R^{\text{opt}}\gamma_{R,0}^{(k)}\right)}$ and $\widetilde{\lambda}_S^{\text{opt}}$ and $\widetilde{\lambda}_R^{\text{opt}}$ are the optimal Lagrangian multipliers and can be numerically obtained by substituting Eq. (65) into Eq. (58). Then, the rest of the cases where $K=2,3,\ldots$ can be determined. Consequently, the maximum aggregate effective capacity using the optimal resource allocation policy is obtained.

Scenario 2: Similar with **Scenario 1**, using $\gamma_{S,1}^{(k)}$ and $\gamma_{R,1}^{(k)}$, we can obtain the optimal power allocation policy for our proposed MIMO-GFDM-based full-duplex cognitive radio networks when channel is in OFF state ($\mathscr{H}_1$). Therefore, the maximum effective capacity, denoted by $C_{AF,1}^{\text{opt}}(\theta_1, \theta_2, \ldots, \theta_K)$, can be derived.

Scenario 3: In this scenario, since the transmitted number of bits is assumed to be zero, the value of the QoS exponent θ does not affect the value of effective capacity. Consequently, the effective capacity in **Scenario 3** can be omitted.

Based on the abovementioned three scenarios, the maximum aggregate effective capacity, denoted by $E_c^{\text{opt}}(\theta_1, \theta_2, \ldots, \theta_K)$, can be derived as follows:

$$C_{AF,0}^{\text{opt}}(\theta_1, \theta_2, \ldots, \theta_K) = p_1 C_{AF,0}^{\text{opt}}(\theta_1, \theta_2, \ldots, \theta_K) + p_2 C_{AF,1}^{\text{opt}}(\theta_1, \theta_2, \ldots, \theta_K). \tag{66}$$

Dynamic Power Allocations for DF Relay-Based Massive MIMO Cognitive Radio Networks

In the FD relaying network, interference may degrade system performance severely, and MIMO is proposed for interference suppression with the help of its extra spatial dimensions. In order to mitigate the self-interference introduced by FD scheme, during the last decades, massive MIMO systems [33, 34] that use large antenna arrays with a few hundred antennas for multiuser operation have been an emerging technology that delivers all the attractive benefits compared with the traditional MIMO system, but at a much larger scale. Such massive MIMO system substantially reduces the effects of noise, fast fading, and interference and provide increased capacity. Researchers have been studying the massive MIMO system and identify the key result is that, with very large antenna arrays at each base station, both the intracell and intercell interferences can be substantially reduced with simple linear beamforming (BF) processing techniques.

Scenario 1: For the massive MIMO system, according to DF protocol in Eq. (54), the achievable rate, denoted by $R_{DF,0}^{(k)}(\boldsymbol{\mu})$, of the MIMO-GFDM-based relaying scheme can be expressed as follows:

$$R_{DF,0}^{(k)}(\boldsymbol{\mu}) = T_f B \log_2 \min\left\{\left(1 + \kappa \gamma_{S,0}^{(k)} P_S^{(k)}\right), \left(1 + \gamma_{R,0}^{(k)} P_R^{(k)}\right)\right\}. \tag{67}$$

Similar with the AF protocol, we can derive a function for the maximization problem under DF protocol as follows:

$$\widetilde{C}_{DF,0}^{(k)}(\theta_1, \theta_2) = -\frac{1}{\theta_i} \log\left\{\mathbb{E}\left[\exp\left\{-\theta_i T_f B \min\left\{\left(1 + \kappa \gamma_{S,0}^{(k)} P_S^{(k)}\right), \left(1 + \gamma_{R,0}^{(k)} P_R^{(k)}\right)\right\}\right\}\right]\right\}, \tag{68}$$

the QoS exponent θ_i $(i = \{1, 2\})$ with $i = 1$ if $R_{S,0}^{(k)} < R_{R,0}^{(k)}$ and $i = 2$ if $R_{S,0}^{(k)} > R_{S,0}^{(k)}$. Then, the maximization problem $\mathbf{P_3}$ with heterogeneous statistical delay-bound QoS requirements under $\mathscr{H}_0$ hypnosis can be formulated as follows:

$$\mathbf{P_3}: \arg \min_{P_S, P_R} \{\mathbb{E}[\max\{\mathscr{F}_1(\boldsymbol{\nu}), \mathscr{F}_2(\boldsymbol{\nu})\}]\} \geq \arg \min_{P_S, P_R} \{\max\{\mathbb{E}[\mathscr{F}_1(\boldsymbol{\nu})], \mathbb{E}[\mathscr{F}_2(\boldsymbol{\nu})]\}\} \tag{69}$$

subject to the same constraints given in Eq. (58) where

$$\begin{cases} \mathscr{F}_1(\boldsymbol{\nu}) = \left(1 + \kappa \gamma_{S,0}^{(k)} P_S^{(k)}\right)^{-\beta_1}; \\ \mathscr{F}_2(\boldsymbol{\nu}) = \left(1 + \gamma_{R,0}^{(k)} P_R^{(k)}\right)^{-\beta_2}, \end{cases} \tag{70}$$

where $\beta_1 \triangleq \theta_1 T_f B / \log 2$ and $\beta_2 \triangleq \theta_2 T_f B / \log 2$ are defined as the normalized QoS exponents.

With ZF linear processing techniques at the relay station, the closed-form expression for $\mathbb{E}[\{\mathscr{F}_1(\boldsymbol{\nu})\}]$ and $\mathbb{E}[\{\mathscr{F}_2(\boldsymbol{\nu})\}]$ of the FD relaying system in the high-end SNR region with a finite number of transmit and receive antennas can be, respectively, approximated as follows [35]:

$$\begin{cases} \mathbb{E}[\{\mathscr{F}_1(\boldsymbol{\nu})\}] \approx \left(\dfrac{P_S(M-K)\left(\lambda_S^{(k)}\right)^2}{\sum\limits_{n=1}^{K} P_S\left(\alpha_S^{(k)} - \left(\lambda_S^{(n)}\right)^2\right) + \frac{K(M-K)}{M}\kappa^2 P_R + 1} \right)^{-\beta_1}; \\ \mathbb{E}[\{\mathscr{F}_2(\boldsymbol{\nu})\}] \approx \left(\dfrac{P_R(M-K)\left(\lambda_R^{(k)}\right)^2}{KP_R\left(1 - \frac{K}{M}\alpha_R^{(k)} - \left(\lambda_R^{(k)}\right)^2\right) + 1} \right)^{-\beta_2}. \end{cases} \tag{71}$$

where $\alpha_R^{(k)}$ is the path envelop of the Nakagami-m fading channels.

To obtain the global optimal solution for $\mathbf{P_3}$, we need to convert the non-convex optimization problem $\mathbf{P_3}$ to an equivalent convex optimization problem. Because $\mathbb{E}[\mathscr{F}_1(\boldsymbol{\nu})]$ and $\mathbb{E}[\mathscr{F}_2(\boldsymbol{\nu})]$ are both convex functions, their point-wise maximum function $\max\{\mathbb{E}[\mathscr{F}_1(\boldsymbol{\nu})], \mathbb{E}[\mathscr{F}_2(\boldsymbol{\nu})]\}$ is also a convex function [28]. Therefore, problem $\mathbf{P_3}$ is a strictly convex problem. To fine the optimal power adaptation, we have

$$\mathbb{E}[\mathscr{F}_1(\boldsymbol{\nu})] = \mathbb{E}[\mathscr{F}_2(\boldsymbol{\nu})] \tag{72}$$

Thus, we can derive an equivalent problem $\mathbf{P_4}$ as follows:

$$\mathbf{P_4}: \arg \min_{P_R} \{\mathbb{E}[\mathscr{F}_2(\boldsymbol{\nu})]\} \tag{73}$$

subject to the same constraints given in Eq. (58). For the FD-based massive MIMO system, as $M \gg K$, we can rewrite the approximate expression for $\mathbb{E}\left[\{\mathscr{F}_1(\boldsymbol{\nu})\}\right]$ and $\mathbb{E}\left[\{\mathscr{F}_2(\boldsymbol{\nu})\}\right]$ as follows:

$$\begin{cases} \mathbb{E}\left[\{\mathscr{F}_1(\boldsymbol{\nu})\}\right] \approx \left(\dfrac{MP_S\left(\lambda_S^{(k)}\right)^2}{\sum\limits_{n=1}^{K} P_S\left(\alpha_S^{(n)} - \left(\lambda_S^{(n)}\right)^2\right) + K\kappa^2 P_R + 1} \right)^{-\beta_1}; \\ \mathbb{E}\left[\{\mathscr{F}_2(\boldsymbol{\nu})\}\right] \approx \left(\dfrac{MP_R\left(\lambda_R^{(k)}\right)^2}{KP_R\left(1 - \left(\lambda_R^{(k)}\right)^2\right) + 1} \right)^{-\beta_2}. \end{cases} \tag{74}$$

Consequently, for massive MIMO system, we can formulate an equivalent problem $\mathbf{P_4}$ as follows:

$$\mathbf{P_4} : \arg\min_{P_R} \left\{ \left(\frac{MP_R\left(\lambda_R^{(k)}\right)^2}{KP_R\left(1 - \lambda_{R,k}^2\right) + 1} \right)^{-\beta_2} \right\} \tag{75}$$

subject to the same constraints given in Eq. (58).

Theorem 2. *For our proposed massive MIMO system, the optimal resource adaptation policy which maximizes the effective capacity at the relay station given in Eq. (26) is derived as follows:*

$$P_R^{\text{opt}} = \left(\frac{\mu^{\text{opt}}\left(M\left(\lambda_R^{(k)}\right)^2\right)^{\beta_2}}{\beta_2\left(K\left(1 - \left(\lambda_R^{(k)}\right)^2\right)\right)^{\beta_2 - 1}} \right)^{\frac{1-\beta_2}{1+\beta_2}}, \tag{76}$$

where μ^{opt} can be obtained by substituting Eq. (76) into Eq. (58).

Proof. The proof is provided in section "Appendix B: Proof of Theorem 2". □

Substituting Eq. (76) into Eqs. (72) and (74), the optimal power adaptation policy, denoted by P_S^{opt}, for the source node can be determined as follows:

$$P_S^{\text{opt}} = \frac{\left(\dfrac{M\left(\lambda_R^{(k)}\right)^2 P_R^{\text{opt}}}{K\left(1 - \left(\lambda_R^{(k)}\right)^2\right) P_R^{\text{opt}} + 1} \right)^{\frac{\beta_2}{\beta_1}} \left(K\kappa^2 P_R^{\text{opt}} + 1\right)}{M\left(\lambda_S^{(k)}\right)^2 - \sum\limits_{n=1}^{K} \left(\alpha_S^{(n)}\left(\lambda_S^{(n)}\right)^2\right) \left(\dfrac{M\left(\lambda_R^{(k)}\right)^2 P_R^{\text{opt}}}{K\left(1 - \left(\lambda_R^{(k)}\right)^2\right) P_R^{\text{opt}} + 1} \right)^{\frac{\beta_2}{\beta_1}}}. \tag{77}$$

Scenario 2: Similar with **Scenario 1**, using $\gamma_{S,1}^{(k)}$ and $\gamma_{R,1}^{(k)}$, we can obtain the optimal power allocation policy for our proposed MIMO-GFDM-based full-duplex cognitive radio networks when channel is in OFF state ($\mathscr{H}_1$).

Scenario 3: In this scenario, the effective capacity in **Scenario 3** can be omitted.

Simulation Evaluations

MATLAB simulation is used to validate and evaluate the QoS-aware MIMO-GFDM-based CRNs. Throughout our simulations, set the bandwidth $B = 100$ KHz, the time frame length $T_f = 2$ ms, the average transmit power for the source nodes and the relay station $\overline{P}_S = 0.5$ W, and $\overline{P}_R = 1$ W. Without loss of generality, we set the self-interference mitigation factors for secondary users as $\kappa = 0.95$.

For analyzing and comparing the system performance of both a 2×2 MIMO channel and an FD channel, we consider the simplest case of two SUs trying to constantly send data to each other. Both SUs have two antennas that can be used for transmitting or receiving. We compare the case when the SUs use the two antennas

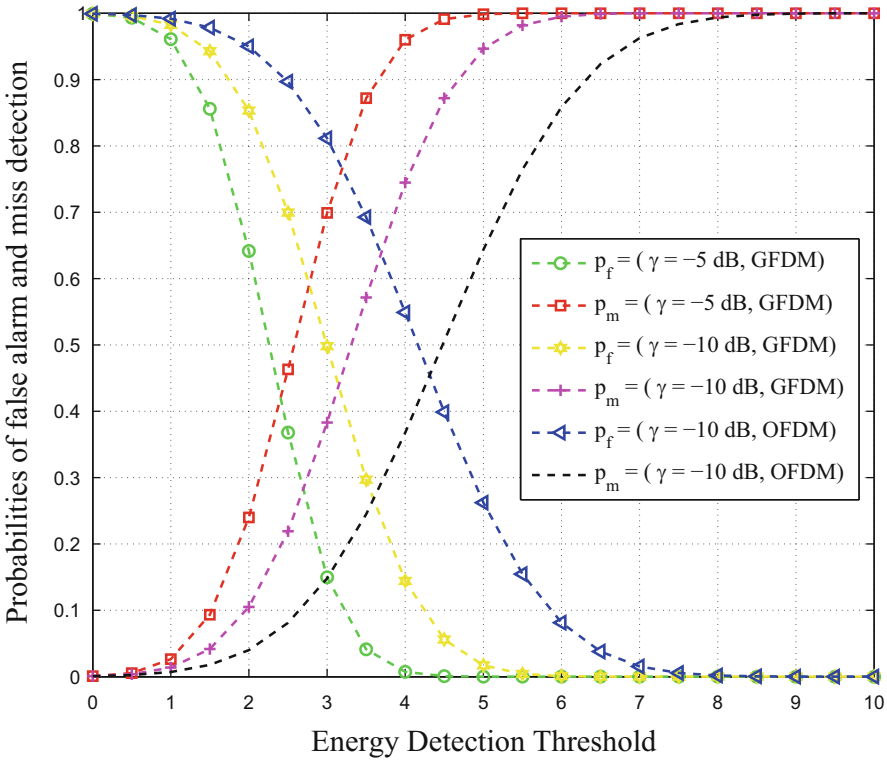

Fig. 6 The probabilities of false alarm and miss-detection with varying SNR over FD CRNs

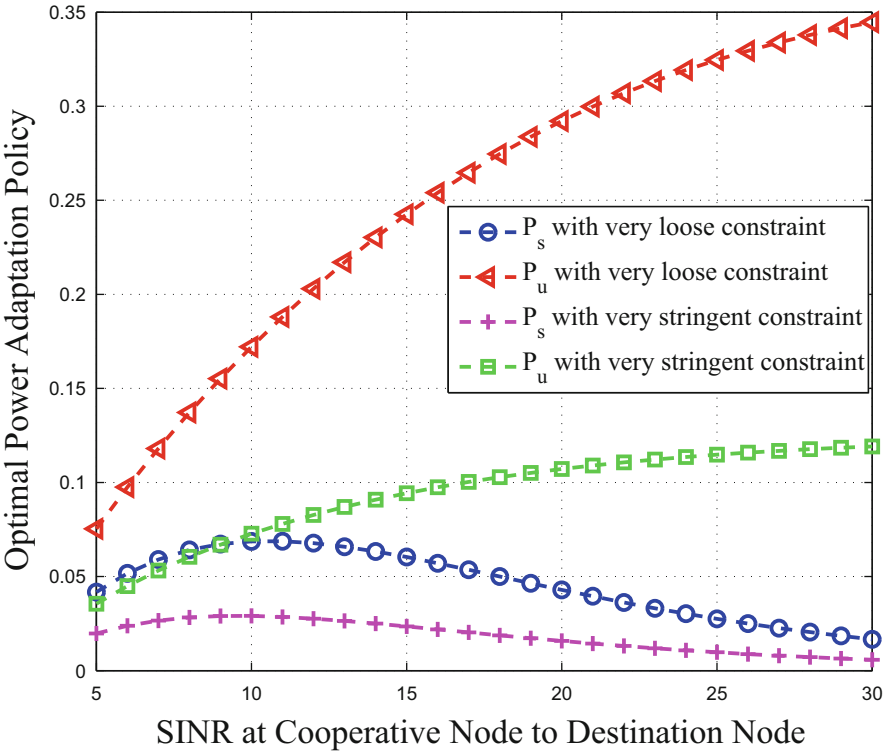

Fig. 7 The comparison of QoS-driven optimal resource allocation policy with different QoS constraints

to implement a 2×2 MIMO system v.s. implement a FD system. We can make two assumptions in this comparison [36]:

- SUs have the same power constraint during the transmission regardless of its duplex mode. This means that an HD SU cannot double its transmit power even though it remains silent half of the time (compared to the FD SU which always transmits). Under this assumption, a 2×2 MIMO system is able to use the maximum power of only a single SU at a given time, since only one of two communicating SUs can transmit at a given time. On the other hand, with FD scheme, the system uses the maximum power of both communicating SUs at the same time, thus allowing the use of more total power in the system.
- The transmitter knows the state of the wireless channel from itself to the receiver perfectly. For a MIMO system, this increases the transmission rate by allowing an additional transmitter processing technique, called MIMO precoding. In case of FD scheme, if both the SUs know the channels between all the antenna pairs, they can agree on the best transmit-receive antenna pair to maximize the transmission rate in both directions.

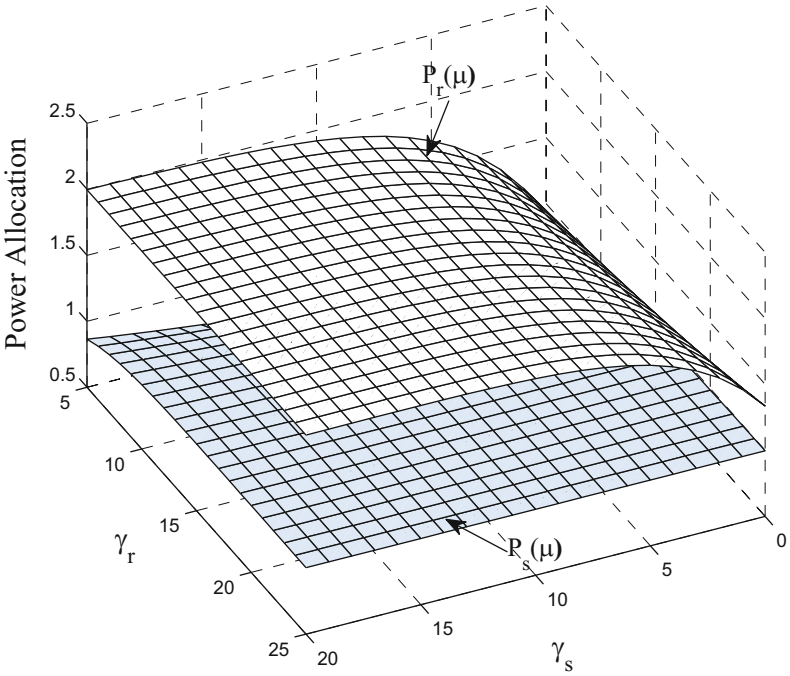

Fig. 8 The optimal power allocation policy for our proposed MIMO-GFDM-based cognitive radio networks

We consider GFDM system and OFDM system with 1024 subcarriers ($P = 1024$) and $Q = 256$. Using Eq. (35), Fig. 6 plots and evaluates the probability of false alarm and the probability of miss-detecting the channel with varying SNR corresponding to GFDM system, compared with the OFDM system. As illustrated in Fig. 6, our proposed GFDM system outperforms OFDM system in terms of the false-alarm probability and miss-detection probability. Figure 6 also shows that the probability of false alarm decreases as the energy detection threshold ε decreases. We can observe from Fig. 6 that the probability of false alarm and the probability of miss-detection both increase as the value of SNR decreases, while the gap between each curve is decreasing as SNR increases. This implies that the energy detection performance of one cognitive node gets worse when the SNR decreases, which is the case when the cognitive node experiences heavy shadowing or fading.

According to the statistical QoS scheme, when $\theta \to \infty$, this implies that the system cannot tolerate any delay, which corresponds to the very stringent statistical delay-bound QoS constraint. On the other hand, when $\theta \to 0$, the system can tolerate an arbitrarily long delay, which corresponds to the very loose statistical delay-bound QoS constraint. Figure 7 depicts the QoS-driven optimal power allocation policy with different QoS constraints, where we plot and compare four curves with very loose constraint ($\theta_1 = \theta_2 = 1 \times 10^{-4}$) and very stringent

constraint ($\theta_1 = \theta_2 = 0.6$). Figure 7 shows that the loose and stringent QoS constraints set the upper bound and lower bound for the power allocation policy, respectively. As illustrated in Fig. 7, we can also observe that for a given SNR, the optimal resource allocation scheme allocates more power for $P_u^{(k)}$ than $P_s^{(k)}$, which implies that the SU consumes more power for LAT mode than HD sensing mode.

Let $\theta_1 = \theta_2 = \cdots = \theta_K = 0.5$, $K = 2$, and $M = 2$. According to Eq. (65), to evaluate the performance of the MIMO-GFDM-based system, Fig. 8 depicts the optimal power allocation policy for our relay-based cognitive radio networks. As illustrated in Fig. 8, the relay station is allocated more power compared with the power allocation policy at the source nodes $P_S^{(k)}$. It makes sense since the average transmit power at the secondary relay station is set larger than the power at the secondary source nodes.

Figure 9 depicts the aggregate effective capacity for the MIMO-GFDM-based cognitive radio networks corresponding to the heterogeneous statistical QoS-driven power allocation scheme compared with the homogeneous QoS-driven power allocation scheme with $K = 2$ and $M = 2$. As shown in Fig. 9, the aggregate effective capacity converges to zero as the statistical QoS constraint becomes more stringent.

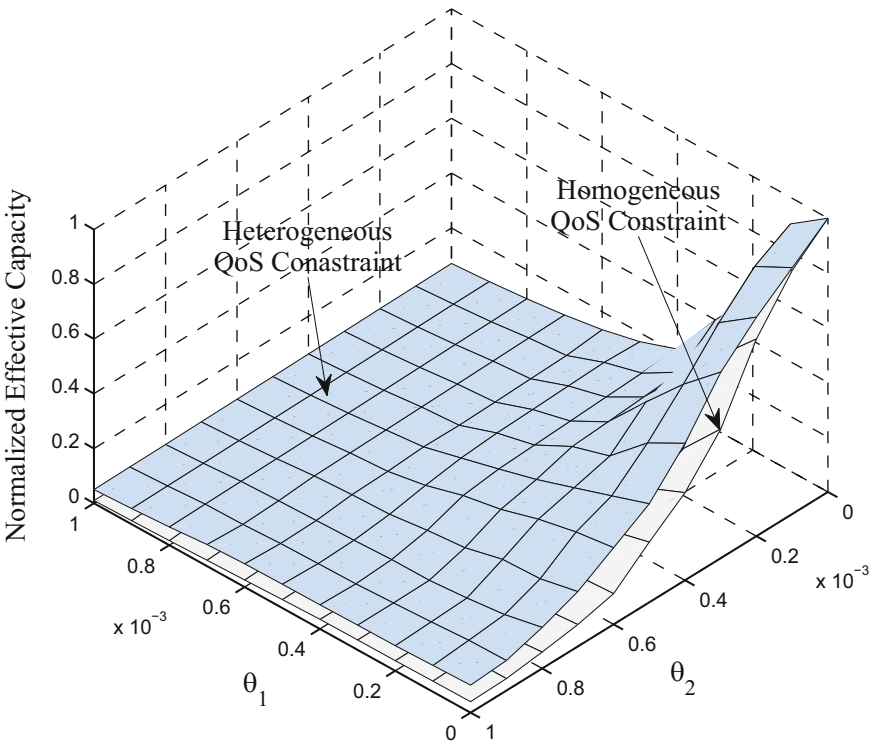

Fig. 9 The heterogeneous statistical QoS-driven power allocation policy v.s. homogeneous QoS-driven power allocation policy

When $\theta_1 = \theta_2$, the aggregate effective capacity for heterogeneous statistical QoS scheme is the same as the homogeneous statistical QoS scheme, which implies that the homogeneous statistical QoS provisioning is a special case of the heterogeneous statistical QoS provisioning. When $\theta_1 \neq \theta_2$, the effective capacity corresponding to the heterogeneous statistical QoS scheme is larger than the effective capacity corresponding to the homogeneous statistical QoS provisioning, implying that the heterogeneous statistical QoS scheme outperforms the existing homogeneous statistical QoS scheme in terms of the aggregate effective capacity for the MIMO-GFDM-based cognitive radio networks.

Set $K = 2$, $\gamma_{S,0}^{(1)} = 10\,\text{dB}$, and $\gamma_{S,0}^{(2)} = 5\,\text{dB}$. Figure 10 plots the aggregate effective capacity for the MIMO-GFDM-based cognitive radio system under different QoS constraints. As shown in Fig. 10, with looser QoS constraint ($\theta = 10^{-2}$), the system can achieve higher aggregate effective capacity, which implies that loose QoS constraint ($\theta = 10^{-3}$) and stringent QoS constraint ($\theta = 10^{-2}$) can set the upper bound and lower bound for the aggregate effective capacity, respectively.

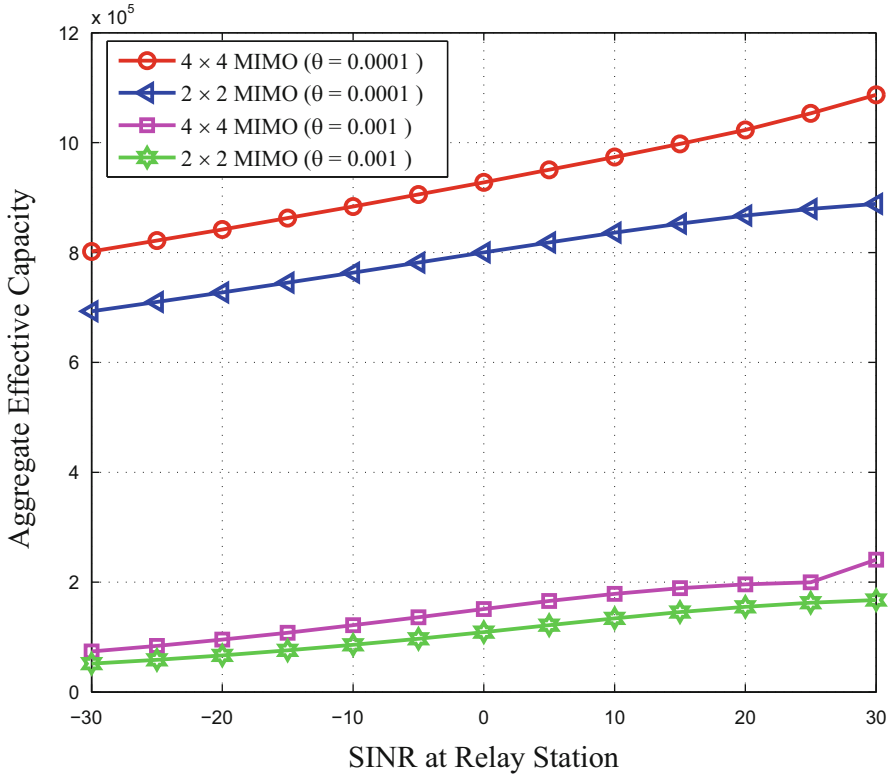

Fig. 10 The aggregate effective capacity under different QoS constraints for our proposed MIMO-GFDM-based cognitive radio networks

Using Eq. (57), Fig. 11 depicts the aggregate effective capacity for the MIMO-GFDM-based cognitive radio system with different number of transmit and receive antennas M compared with single-input single-output (SISO) scheme. As shown in Fig. 11, as the QoS exponent θ becomes larger, the effective capacity decreases. As illustrated in Fig. 11, as the number of transmit and receive antennas increases, the MIMO-based relaying system achieves better aggregate effective capacity over the cognitive radio networks, implying that larger antenna arrays at the relay station can achieve better performance, that is, the MIMO-GFDM-based relaying system can outperform the traditional SISO system in terms of the aggregate effective capacity. From Fig. 11, it is obvious that the gap between the plots becomes smaller as M increases, which implies that the aggregate effective capacity cannot always increase as $M \to \infty$; instead, the transmission rate finally converges to a certain value.

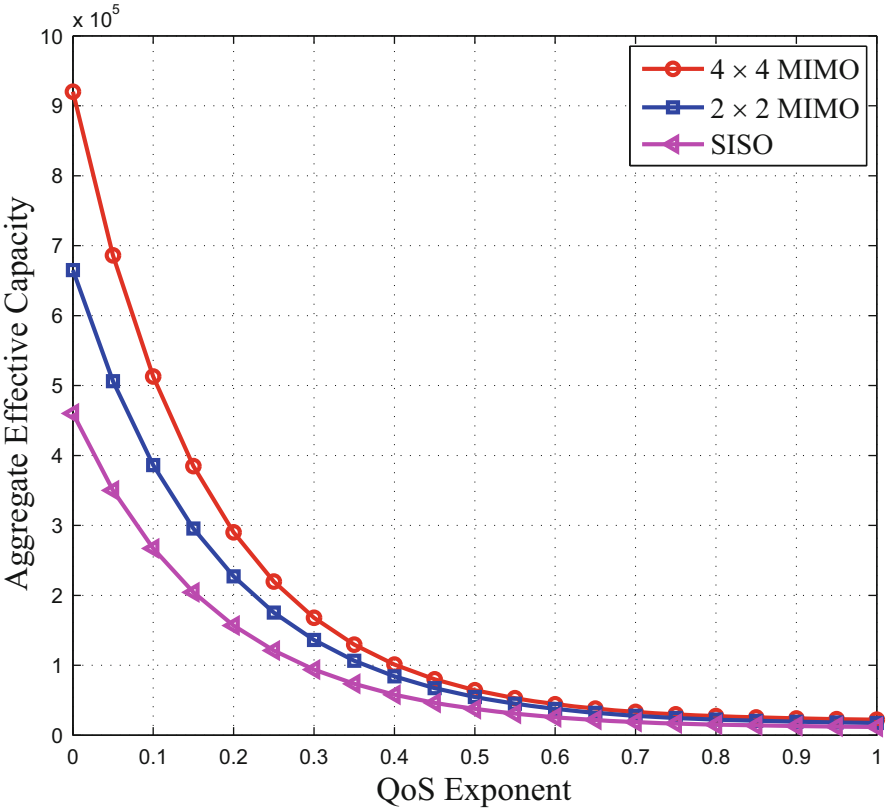

Fig. 11 The aggregate effective capacity with different number of antennas for our proposed MIMO-GFDM-based cognitive radio networks

Conclusions

We proposed the heterogeneous statistical QoS provisioning schemes by applying MIMO-GFDM technique to implement FD-SS-based multimedia services in CRNs. In particular, under the Nakagami-m wireless channels, we established the spectrum sensing model, the MIMO-GFDM-based PHY-layer model, the non-time-slotted CRN model, and the self-interference cancelation model. We developed and analyzed the FD-SS-based MIMO-GFDM scheme to fully utilize the channel spectrum and derived the probabilities of miss-detection and false alarm for the proposed FD-SS-based MIMO-GFDM model over cognitive radio networks. Under the heterogeneous statistical QoS constraints, we developed the Markov chain model to characterize the correctness of detections in channel sensing and then derived and analyzed the aggregate effective capacity under our proposed optimal power allocation policies using the proposed MIMO-GFDM architecture over FD cognitive radio networks. Also conducted was a set of simulations which showed that our proposed scheme outperformed the other existing schemes in terms of aggregate effective capacity to efficiently implement the heterogeneous statistical QoS over cognitive radio-based 5G mobile wireless networks.

Acknowledgements This work was supported in part by the U.S. National Science Foundation under Grants ECCS-1408601 and CNS-1205726, and the U.S. Air Force under Grant FA9453-15-C-0423.

Appendix A: Proof of Theorem 1

Proof. The aggregate effective capacity, denoted by $\widetilde{C}_{AF,0}(\theta_1, \theta_2, \ldots, \theta_K)$, for different links in the relay-based cognitive radio networks can be derived as follows:

$$\widetilde{C}_{AF,0}(\theta_1, \theta_2, \ldots, \theta_K) \triangleq -\frac{1}{\theta_o} \log \left\{ \mathbb{E}_\gamma \left[\exp \left\{ -\sum_{k=1}^{K} \theta_k T_f B \right. \right. \right.$$
$$\left. \left. \left. \cdot \log_2 \left(1 + \frac{4 P_S^{(k)}(\boldsymbol{\mu}) P_R^{(k)}(\boldsymbol{\mu}) \gamma_{S,0}^{(k)} \gamma_{R,0}^{(k)}}{1 + 2 P_S^{(k)}(\boldsymbol{\mu}) \gamma_{S,0}^{(k)} + 2 P_R^{(k)}(\boldsymbol{\mu}) \gamma_{R,0}^{(k)}} \right) \right\} \right] \right\}. \tag{78}$$

Then, the value of θ_o needs to be derived before solving the optimization problem. The optimal θ_o needs to satisfy the following equation:

$$\sum_{k=1}^{K} -\frac{1}{\theta_k} \log \left\{ \mathbb{E}_\gamma \left[\exp \left\{ -\theta_k T_f B \log_2 \left(1 + \frac{4P_S^{(k)}(\boldsymbol{\mu}) P_R^{(k)}(\boldsymbol{\mu}) \gamma_{S,0}^{(k)} \gamma_{R,0}^{(k)}}{1 + 2P_S^{(k)}(\boldsymbol{\mu}) \gamma_{S,0}^{(k)} + 2P_R^{(k)}(\boldsymbol{\mu}) \gamma_{R,0}^{(k)}} \right) \right\} \right] \right\}$$

$$= -\frac{1}{\theta_o} \sum_{k=1}^{K} \log \left\{ \mathbb{E}_\gamma \left[\exp \left\{ -\theta_k T_f B \cdot \log_2 \left(1 + \frac{4P_S^{(k)}(\boldsymbol{\mu}) P_R^{(k)}(\boldsymbol{\mu}) \gamma_{S,0}^{(k)} \gamma_{R,0}^{(k)}}{1 + 2P_S^{(k)}(\boldsymbol{\mu}) \gamma_{S,0}^{(k)} + 2P_R^{(k)}(\boldsymbol{\mu}) \gamma_{R,0}^{(k)}} \right) \right\} \right] \right\} \tag{79}$$

Considering that the effective capacity for one link can be increased when using the QoS-driven power allocation as compared with the effective capacity using the average transmit power control, we have

$$-\frac{1}{\theta_k} \log \left\{ \mathbb{E}_\gamma \left[\exp \left\{ -\theta_k T_f B \log_2 \left(1 + \frac{4P_S^{(k)}(\boldsymbol{\mu}) P_R^{(k)}(\boldsymbol{\mu}) \gamma_{S,0}^{(k)} \gamma_{R,0}^{(k)}}{1 + 2P_S^{(k)}(\boldsymbol{\mu}) \gamma_{S,0}^{(k)} + 2P_R^{(k)}(\boldsymbol{\mu}) \gamma_{R,0}^{(k)}} \right) \right\} \right] \right\}$$

$$= -\frac{1}{\theta_k} \log \left\{ \mathbb{E}_\gamma \left[\exp \left\{ -\theta_k T_f B \cdot \log_2 \left(1 + \frac{4P_S^{(k)}(\boldsymbol{\mu}) P_R^{(k)}(\boldsymbol{\mu}) \gamma_{S,0}^{(k)} \gamma_{R,0}^{(k)}}{1 + 2P_S^{(k)}(\boldsymbol{\mu}) \gamma_{S,0}^{(k)} + 2P_R^{(k)}(\boldsymbol{\mu}) \gamma_{R,0}^{(k)}} \right) \right\} \right] \right\} + I_k, \tag{80}$$

for $1 \leq k \leq K$ where I_k represents the increased aggregate effective capacity when using the heterogeneous-statistical-QoS-driven power allocation scheme for the kth downlink. Then, substituting Eq. (80) back into Eq. (79), we can obtain the expression for θ_o in Eq. (81) as follows:

$$\theta_o = \frac{\prod_{n=1}^{K} \theta_n \left[\sum_{k=1}^{K} \log \left\{ \mathbb{E}_\gamma \left[\exp \left\{ -\theta_k T_f B \log_2 \left(1 + \frac{4\overline{P}_S^{(k)}(\boldsymbol{\mu}) \overline{P}_R^{(k)}(\boldsymbol{\mu}) \gamma_{S,0}^{(k)} \gamma_{R,0}^{(k)}}{1 + 2\overline{P}_S^{(k)}(\boldsymbol{\mu}) \gamma_{S,0}^{(k)} + 2\overline{P}_R^{(k)}(\boldsymbol{\mu}) \gamma_{R,0}^{(k)}} \right) \right\} \right] \right\} \right] - \Lambda_1}{\sum_{k=1}^{K} \left[\left(\prod_{n \neq k}^{K} \theta_n \right) \log \left\{ \mathbb{E}_\gamma \left[\exp \left\{ -\theta_k T_f B \log_2 \left(1 + \frac{4\overline{P}_S^{(k)}(\boldsymbol{\mu}) \overline{P}_R^{(k)}(\boldsymbol{\mu}) \gamma_{S,0}^{(k)} \gamma_{R,0}^{(k)}}{1 + 2\overline{P}_S^{(k)}(\boldsymbol{\mu}) \gamma_{S,0}^{(k)} + 2\overline{P}_R^{(k)}(\boldsymbol{\mu}) \gamma_{R,0}^{(k)}} \right) \right\} \right] \right\} \right] - \Lambda_2}, \tag{81}$$

where

$$\begin{cases} \Lambda_1 \triangleq \sum\limits_{k=1}^{K} \theta_k I_k \left(\prod\limits_{n=1}^{K} \theta_n \right); \\ \Lambda_2 \triangleq \prod\limits_{k=1}^{K} \theta_k \left(\sum\limits_{n=1}^{K} I_n \right). \end{cases} \tag{82}$$

According to [7], the approximation of θ_o can be classified into the following four cases based on the values of Nakagami-m channel parameter m:

Case 1: $m \leq 1$. For this case, because the average transmit power is the determining factor for the effective capacity, we have

$$-\frac{1}{\theta_k} \log \left\{ \mathbb{E}_\gamma \left[\exp \left\{ -\theta_k T_f B \cdot \log_2 \left(1 + \frac{4\overline{P}_S^{(k)}(\boldsymbol{\mu}) \overline{P}_R^{(k)}(\boldsymbol{\mu}) \gamma_{S,0}^{(k)} \gamma_{R,0}^{(k)}}{1 + 2\overline{P}_S^{(k)}(\boldsymbol{\mu}) \gamma_{S,0}^{(k)} + 2\overline{P}_R^{(k)}(\boldsymbol{\mu}) \gamma_{R,0}^{(k)}} \right) \right\} \right] \right\} \gg I_k \tag{83}$$

for $1 \leq k \leq K$. Thus, we can omit the terms containing I_k in Eq. (81).

Case 2: $m > 1$ and $\theta_{\max}$ is small ($\theta_{\max} \leq 10^{-2}$). We consider θ is large if $\theta > 10^{-2}$ and if $\theta \leq 10^{-2}$, we claim that θ is small [7]. For small θ, the optimal power-adaptation law allocates more power to worse channel. In contrast, for large θ, the power control assigns less power to the better channel, but more power to the worse channel. Because the average transmit power is the determining factor for the effective capacity, it is the same as **Case 1**.

Case 3: $m > 1$ and $\theta_{\min}$ is large ($\theta_{\min} > 10^{-2}$). For this case, because the QoS-driven power control is the determining factor for the effective capacity, we only need to consider each term containing I_k in Eq. (81), we have

$$-\frac{1}{\theta_k} \log \left\{ \mathbb{E}_\gamma \left[\exp \left\{ -\theta_k T_f B \cdot \log_2 \left(1 + \frac{4\overline{P}_S^{(k)}(\boldsymbol{\mu}) \overline{P}_R^{(k)}(\boldsymbol{\mu}) \gamma_{S,0}^{(k)} \gamma_{R,0}^{(k)}}{1 + 2\overline{P}_S^{(k)}(\boldsymbol{\mu}) \gamma_{S,0}^{(k)} + 2\overline{P}_R^{(k)}(\boldsymbol{\mu}) \gamma_{R,0}^{(k)}} \right) \right\} \right] \right\} \ll I_k \tag{84}$$

for $1 \leq k \leq K$. Thus, we can obtain

$$\theta_o \approx \frac{\sum_{k=1}^{K} \theta_k I_k}{\sum_{k=1}^{K} I_k} \approx \frac{\sum_{k=1}^{K} \theta_k}{K}. \tag{85}$$

Case 4: $m > 1$, $\theta_{\min}$ is small and $\theta_{\max}$ is large. For this case, because we have

$$-\frac{1}{\theta_k} \log \left\{ \mathbb{E}_\gamma \left[\exp \left\{ -\theta_k T_f B \cdot \log_2 \left(1 + \frac{4\overline{P}_S^{(k)}(\boldsymbol{\mu})\overline{P}_R^{(k)}(\boldsymbol{\mu})\gamma_{S,0}^{(k)}\gamma_{R,0}^{(k)}}{1 + 2\overline{P}_S^{(k)}(\boldsymbol{\mu})\gamma_{S,0}^{(k)} + 2\overline{P}_R^{(k)}(\boldsymbol{\mu})\gamma_{R,0}^{(k)}} \right) \right\} \right] \right\} \gg I_k \quad \text{and} \quad I_n \tag{86}$$

and

$$-\frac{1}{\theta_k} \log \left\{ \mathbb{E}_\gamma \left[\exp \left\{ -\theta_k T_f B \log_2 \left(1 + \frac{4\overline{P}_S^{(k)}(\boldsymbol{\mu})\overline{P}_R^{(k)}(\boldsymbol{\mu})\gamma_{S,0}^{(k)}\gamma_{R,0}^{(k)}}{1 + 2\overline{P}_S^{(k)}(\boldsymbol{\mu})\gamma_{S,0}^{(k)} + 2\overline{P}_R^{(k)}(\boldsymbol{\mu})\gamma_{R,0}^{(k)}} \right) \right\} \right] \right\}$$
$$\gg -\frac{1}{\theta_n} \log \left\{ \mathbb{E}_\gamma \left[\exp \left\{ -\theta_n T_f B \cdot \log_2 \left(1 + \frac{4\overline{P}_S^{(n)}(\boldsymbol{\mu})\overline{P}_R^{(n)}(\boldsymbol{\mu})\gamma_{S,0}^{(n)}\gamma_{R,0}^{(n)}}{1 + 2\overline{P}_S^{(n)}(\boldsymbol{\mu})\gamma_{S,0}^{(n)} + 2\overline{P}_R^{(n)}(\boldsymbol{\mu})\gamma_{R,0}^{(n)}} \right) \right\} \right] \right\} \tag{87}$$

where θ_k $(1 \leq k \leq N \leq K)$ is small $(\theta_k \leq 10^{-2})$ and θ_n $((N+1) \leq n \leq K)$ is large $(\theta_n > 10^{-2})$. Then, we can derive Eq. (60).

In order to derive the value of θ_o, we also need to obtain the optimal values of $\overline{P}_S^{(k)}$ and $\overline{P}_R^{(k)}$ $(1 \leq k \leq K)$, which can be obtained by solving the optimization problem $\mathbf{P_2}$. Therefore, the proof for Theorem 1 follows. □

Appendix B: Proof of Theorem 2

Proof. Since $\mathbf{P_4}$ is a strictly convex optimization problem, and thus it has the unique optimal solution. We construct the Lagrangian function for $\mathbf{P_4}$, denoted by J, as follows:

$$J = \left(\frac{MP_R \left(\lambda_R^{(k)}\right)^2}{KP_R(\boldsymbol{\nu}) \left(1 - \left(\lambda_R^{(k)}\right)^2\right) + 1} \right)^{-\beta_2} + \mu \left(\mathbb{E}\left[P_R\right] - \overline{P}_R \right) \tag{88}$$

where μ is the Lagrangian multiplier associated with the constraint specified by Eq. (58). Thus, the optimal solutions for the recourse adaptation law, and the optimal Lagrangian multiplier μ^{opt} of the problem $\mathbf{P_4}$ need to satisfy the following Karush-Kuhn-Tucker (KKT) conditions:

$$\begin{cases} \left.\frac{\partial J}{\partial P_R}\right|_{P_R=P_R^{\text{opt}}} = 0; \\ \mu^{\text{opt}}\left(\mathbb{E}\left[P_R\right] - \overline{P}_R\right) = 0; \\ \mu^{\text{opt}} \geq 0; \\ P_R > 0. \end{cases} \tag{89}$$

Taking derivative of J with respect to P_R, we can obtain

$$\frac{\partial J}{\partial P_R} = \frac{-\beta_2 \left(P_R\right)^{-\beta_2-1}\left(M\left(\lambda_R^{(k)}\right)^2\right)^{-\beta_2}}{\left(KP_R\left(1-\left(\lambda_R^{(k)}\right)^2\right)+1\right)^{-\beta_2+1}} + \mu. \tag{90}$$

Then, for our proposed massive MIMO system ($M \to \infty$), associated with Eq. (89), we can derive the optimal solutions expressed by Eq. (76). Therefore, the proof for Theorem 2 follows. □

References

1. Zhang X, Wang J (2017) Statistical QoS-driven power adaptation in Q-OFDMA-Based full-duplex D2D 5G mobile wireless networks. In: IEEE WCNC 2017, San Francisco
2. Wang J, Zhang X (2017) Statistical QoS-Driven cooperative power allocation game over wireless cognitive radio networks. In: IEEE WCNC 2017, San Francisco
3. Tang J, Zhang X (2007) Quality-of-service driven power and rate adaptation over wireless links. IEEE Trans Wirel Commun 6(8):3058–3068
4. Tang J, Zhang X (2007) Cross-layer resource allocation over wireless relay networks for quality of service provisioning. IEEE J Sel Areas Commun 25(4):645–656
5. Wang J, Zhang X (2015) Adaptive power control for maximizing channel capacity over full-duplex D2D Q-OFDMA ad hoc networks. In: IEEE GLOBECOM 2015, San Francisco
6. Wang J, Zhang X (2016) Statistical QoS-driven resource allocation over FD-SS cooperative cognitive radios networks. In: IEEE GLOBECOM 2016, Washington DC
7. Cheng W, Zhang X, Zhang H (2014) Heterogeneous statistical QoS provisioning for downlink transmissions over mobile wireless cellular networks. In: IEEE GLOBECOM 2014, pp 4757–4763
8. Wang J, Zhang X (2016) Heterogeneous QoS-driven resource adaptation over full-duplex relay networks. In: IEEE GLOBECOM 2016, Washington DC
9. Cheng W, Zhang X, Zhang H (2014) Full-duplex spectrum-sensing and MAC-protocol for multichannel non-time-slotted cognitive radio networks. IEEE J Sel Areas Commun 33(5):820–831
10. Liao Y, Wang T, Song L, Han Z (2014) Listen-and-talk: full-duplex cognitive radio networks. In: IEEE GLOBECOM 2014, pp 3068–3073

11. Cheng W, Zhang X, Zhang H (2011) Full duplex spectrum sensing in non-time-slotted cognitive radio networks. In: IEEE MILCOM 2011, Baltimore, pp 1029–1034
12. Luo L, Zhang JA, Davis LM (2012) Space-time block code and spatial multiplexing design for quadrature-OFDMA systems. IEEE Trans Commun 60(10):3133–3142
13. Zhang X, Wang J (2017) Heterogeneous statistical QoS-driven resource allocation over MIMO-OFDMA based 5G cognitive radio networks. In: IEEE WCNC 2017, San Francisco
14. Shahrakia HS, Mohamed-pourb K, Vangelista L (2014) Sum capacity maximization for MIMO-OFDMA based cognitive radio networks. Phys Commun 10(12):106–115
15. Li S, Li B, Xing C (2013) Joint resource allocation for learning-based cognitive radio networks with MIMO-OFDMA relay-aided transmissions. In: 2013 IEEE Wireless Communications and Networking Conference (WCNC): PHY, pp 3271–3276
16. Michailow N, Matthe M, Gaspar IS, Mendes ANCLL, Festag A, Fettweis G (2014) Generalized frequency division multiplexing for 5th generation cellular networks. IEEE Trans Commun 62(9):3045–3061
17. Datta R, Michailow N, Lentmaier M, Fettweis G (2012) GFDM interference cancellation for flexible cognitive radio PHY design. In: IEEE Vehicular Technology Conference (VTC Fall), Quebec City, pp 1–5
18. Zhang X, Su H (2011) CREAM-MAC: cognitive radio-enabled multi-channel MAC protocol over dynamic spectrum access networks. IEEE J Sel Top Signal Process 5(1): 110–123
19. Wang C, Au EKS, Murch RD, Mow WH, Cheng RS, Lau V (2007) On the performance of the MIMO zero-forcing receiver in the presence of channel estimation error. IEEE Trans Wirel Commun 6(3):805–810
20. Senaratne D, Tellambura C (2011) Beamforming for space division duplexing. In: IEEE ICC 2011, Kyoto, pp 1–5
21. Riihonen T, Wichman R (2012) Analog and digital self-interference cancellation in full-duplex MIMO-OFDM transceivers with limited resolution in A/D conversion. In: 2012 Conference Record of the Forty Sixth Asilomar Conference on Signals, Systems and Computers (ASILOMAR), Pacific Grove, pp 45–49
22. Cheng W, Zhang X, Zhang H (2013) Optimal dynamic power control for full-duplex bidirectional-channel based wireless networks. In: IEEE INFOCOM 2013, pp 3120–3128
23. Ngo HQ, Suraweera HA, Matthaiou M, Larsson EG (May 2014) Multipair full-duplex relaying with massive arrays and linear processing. IEEE Trans Veh Technol 32(9):1721–1737
24. Zheng G (2015) Joint beamforming optimization and power control for full-duplex MIMO two-way relay channel. IEEE Trans Signal Process 63(3):555–566
25. Yang H, Marzetta TL (2013) Performance of conjugate and zero-forcing beamforming in large-scale antenna systems. IEEE J Sel Areas Commun 31(2):172–179
26. Chen M, Liu TC-K, Dong X (2012) Opportunistic multiple relay selection with outdated channel state information. IEEE Trans Veh Technol 61(3):1333–1345
27. Chang C-S (1994) Stability, queue length, and delay of deterministic and stochastic queueing networks. IEEE Trans Auto Control 39(5):913–931
28. Cheng W, Zhang X, Zhang H (2012) Full/half duplex based resource allocations for statistical quality of service provisioning in wireless relay networks. In: 2012 Proceedings IEEE INFOCOM, Orlando, pp 864–872
29. Tang J, Zhang X (2007) Cross-layer resource allocation over wireless relay networks for quality of service provisioning. IEEE J Sel Areas Commun 25(4):645–656
30. Su H, Zhang X (2008) Cross-layer based opportunistic MAC protocols for QoS provisionings over cognitive radio wireless networks. IEEE J Sel Areas Commun 26(1):118–129
31. Akin S, Gursoy MC (2010) Effective capacity analysis of cognitive radio channels for quality of service provisioning. IEEE Trans Wirel Commun 9(11):3354–3364
32. Laneman JN, Tse DNC, Wornell GW (2004) Cooperative diversity in wireless networks: efficient protocols and outage behavior. IEEE Trans Inf Theory 50(12):3062–3080

33. Xia X, Zhang D, Xu K, Ma W, Xu Y (2015) Hardware impairments aware transceiver for full-duplex massive MIMO relaying. IEEE Trans Signal Process 63(24):6565–6580
34. Xu K, Gao Y, Xie W, Xia X, Xu Y (2015) Achievable rate of full-duplex massive MIMO relaying with hardware impairments. In: 2015 IEEE Pacific Rim Conference on Communications, Computers and Signal Processing (PACRIM), Victoria, pp 84–89
35. Li Y, Fan P, Leukhin A, Liu L (2016) On the spectral and energy efficiency of full-duplex small cell wireless systems with massive MIMO. IEEE Trans Veh Technol PP(99):1–15
36. Jainy M, Choiy JI, Kim TM, Bharadia D, Seth KSS, Levis P, Katti S, Sinha P (2011) Practical, real-time, full duplex wireless. In: The 17th Annual International Conference on Mobile Computing and Networking (MobiCom), Las Vegas

Spectrum-Aware Mobile Computing Using Cognitive Networks

22

S. Eman Mahmoodi, K. P. Subbalakshmi, and R. N. Uma

Contents

Abstract

With the advent of mobile cloud computing, the expectation of the mobile users for anywhere, anytime, content-rich experience will see a significant increase. The users' expectation on quality of experience for content-rich applications can only be met through offloading computationally intensive application tasks to a remote cloud since mobile devices are still constrained by their battery power. This, however, leads to an increase in mobile web traffic. The success of computation offloading techniques, therefore, depends on being able to effectively trade-off resource usage at the mobile device against efficiently managing the spectrum for mobile computing. Hence it is essential for cloud offloading techniques to take advantage of recent advances in cognitive network-

S. E. Mahmoodi (✉) · K. P. Subbalakshmi
Electrical and Computer Engineering, Stevens Institute of Technology, Hoboken, NJ, USA
e-mail: smahmood@stevens.edu; ksubbala@stevens.edu

R. N. Uma
Mathematics and Physics, North Carolina Central University, Durham, NC, USA
e-mail: ruma@nccu.edu

W. Zhang (ed.), *Handbook of Cognitive Radio*,
https://doi.org/10.1007/978-981-10-1394-2_22

ing and spectrum-aware scheduling of application components. The convergence of cognitive networking and spectrum-aware mobile computing is propelling research in this area. The current state-of-the-art includes techniques that offload application data using all viable multiple radio interfaces (e.g., WiFi, LTE, etc.) in multi-RAT-enabled devices, while being adaptive to the conditions of the mobile network. This chapter presents a survey of the existing spectrum-aware mobile computing techniques and proposes a vision for the future for a 5G-enabled, cognitive mobile computing platform. Implementation setups using real data measurements from an HTC phone running multicomponent applications and using different cloud servers such as Amazon EC2 and NSFCloud over LTE and WiFi are also discussed.

Keywords
Spectrum-aware computing · Mobile cloud computing · Cognitive networking · Computation offloading · Scheduling · Optimization

Introduction

The advent of cognitive radio technology, proposed almost two decades ago, has enabled dynamic spectrum access and sharing. Additionally, since 2013, many modern phones have been designed to support multiple radio access technologies (RATs) such as bluetooth, WiFi, and 3G/4G/LTE. The coexistence of these two technologies has spawned a fertile research area in spectrum-aware mobile computing. Furthermore, current and future mobile devices are expected to deliver a lot more than handling basic applications like phone calls, emails, texting, and video sharing. They are expected to run data-intensive and compute-intensive applications such as face recognition software. Users' desired quality of service and experience and resource limitations at the end device will warrant computation offloading to the cloud.

Cloud offloading can be interpreted as (i) data flow offloading in networking applications [8] or (ii) offloading computationally intensive tasks to the cloud [33] or mobile edge devices [67], a self-managing data center in the layer of network infrastructure [53]. The focus of this chapter is on computation offloading to the cloud. State-of-the-art techniques in spectrum-aware mobile computing in this context are presented.

Mobile computation offloading techniques can be classified along four axes as shown in Fig. 1 based on (i) radio access technology (RAT), (ii) time adaptability, (iii) scheduling order of application components, and (iv) extent of offloading. RAT strategies for wireless-aware computation offloading are presented for single-RAT devices (section "Spectrum-Aware Offloading Using Single-RAT Devices") and multi-RAT devices (on/off networking is addressed in section "Spectrum-Aware Cloud Offloading Using On/Off Multi-RAT Networking", and cognitive networking is addressed in section "Spectrum-Aware Cloud Offloading Using Cognitive Networking"). The second classification is based on flexibility of mobile computing

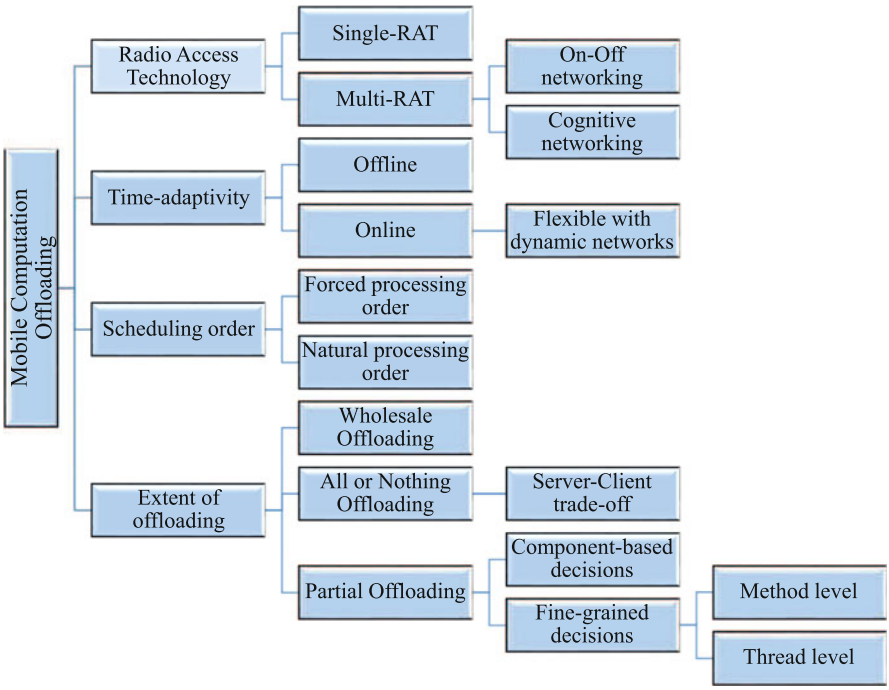

Fig. 1 Classification of mobile computation offloading

techniques with either static variations of wireless network parameters (offline strategies) (sections "Offline Approach", "Offline Approach", "Offline Approach") or dynamic variations of wireless network parameters (online strategies) (sections "Online Approach", "Online Approach", "Online Approach"). The third classification is based on the schedule order of component tasks for spectrum-aware computation offloading – trivial order or nontrivial order. In trivial ordering, the application components are scheduled in a sequential order computed either arbitrarily or based on the compiler-generated call graph. In nontrivial ordering, a sophisticated schedule is computed that allows for simultaneous processing of components on the mobile and the cloud while maintaining the integrity of the application (section "The Effect of Spectrum-Aware Scheduling in Mobile Computing"). Finally, the extent of offloading can be either complete offloading, all-or-nothing offloading, or partial offloading. This chapter focuses only on partial offloading. Hence the different extents of offloading are briefly discussed below.

Extent of offloading: Mobile computation offloading can be classified into three types: (1) complete offloading, where everything is offloaded for remote execution [31, 56]; (2) all-or-nothing offloading, where the required computations for the mobile app are totally offloaded to a cloud server, or everything is

processed in the mobile device [62]; and (3) partial offloading, where the app is partitioned into smaller component tasks, and piecewise decisions are made for individual tasks to be executed either in the mobile device or in the cloud [4, 11, 26, 27, 35, 55].

Partitioning the mobile apps for partial offloading strategies can be divided into two groups: (1) coarse-level partitioning of the applications where the code is pre-partitioned into components [4, 20, 35, 60]; (2) fine-grained offloading using method-level partitioning like MAUI [11] and ThinkAir [26]. ThinkAir focuses on scalability issues and parallel processing of offloaded tasks using multiple virtual machines (VMs). Mobile Augmentation Cloud Service (MACS) [27], which provides an Android service-based mobile computing middleware, allows for seamless offloading of the application component tasks to the cloud. COSMOS [55] is also a new offload platform where fine-grained partial mobile computing of sequential tasks is performed as a service.

Partial offloading can provide more efficient spectrum-aware mobile cloud offloading strategies because decision, for each component task, on whether to offload or execute on the mobile is dynamic with the wireless network parameters such as delay, offloading energy consumption, and queue backlog [4, 11, 26, 27, 35, 55, 65]. The decision for either offloading a component task or executing it on the mobile device can be considered based on the following objectives: minimizing the battery consumption by the mobile device, providing shorter runtimes for the execution of sophisticated mobile apps, and efficiently using the limited spectrum for offloading. Although partial offloading reduces computational burden on the mobile device, it adds to the communication cost on the networks. Therefore, in order to fully harness the power of partial cloud offloading, the resource constraints on the mobile device should be addressed jointly with the recent trends in wireless networking.

For the above reasons, only partial offloading is considered in this chapter. Hence the current research literature in spectrum-aware mobile cloud offloading can be schematically presented along only three axes as shown in Fig. 2.

The existing work can be represented along three axes, namely, the radio access technology (R-axis), time adaptability (T-axis), and scheduling order (S-axis). All the research contributions indicated in this schematic figure are discussed in the following sections. Most of the prior existing work only concerns the radio technology and time adaptability with a predetermined scheduling order (on the R-T plane). The work in [34] was the first to introduce work along the S-axis and the R-T-S-space (addressed in section "Joint Scheduling and Computation Offloading in Time-Adaptive Cognitive Networks").

The rest of this chapter is organized as follows. Section "Spectrum-Aware Cloud Offloading Using Cognitive Radios (Offline/Online Scenarios)" presents the work in the R-T plane. Section "The Effect of Spectrum-Aware Scheduling in Mobile Computing" presents the work along the S-axis. Section "Joint Scheduling and Computation Offloading in Time-Adaptive Cognitive Networks" discusses the work in the R-T-S-space. Finally, section "Summary and Future Directions of Spectrum-Aware Mobile Computing" concludes with future directions.

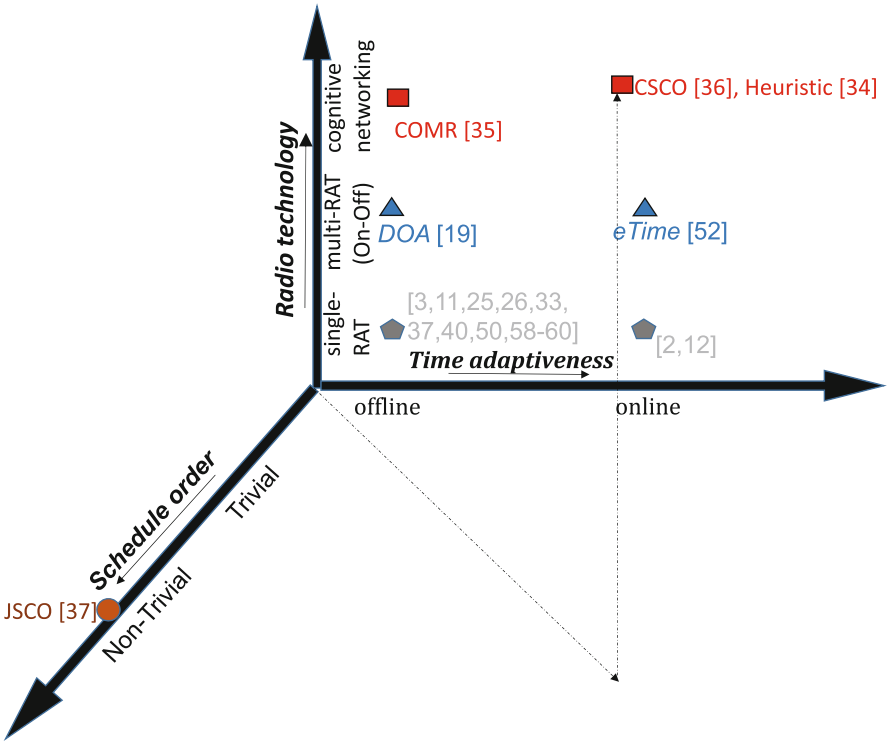

Fig. 2 Schematic of the spectrum-aware mobile computing schemes in context of the state of arts

Spectrum-Aware Cloud Offloading Using Cognitive Radios (Offline/Online Scenarios)

Multiple radio access technology (multi-RAT) is increasingly being supported by mobile devices of today. For example, current iPhones use multipath TCP to create backup connections for iOS [38], and Samsung phones combine WiFi and LTE to provide Gigabit mobile services [45]. Also, exploiting multiple radio interfaces in mobile heterogeneous networks (HetNets) and next-generation cellular networks is necessary to utilize maximum achievable network capacity [24]. Several approaches can be used for multi-RAT networking such as carrier aggregation (CA) and channel bonding (CB) [23, 24, 49]; multipath TCP (MPTCP) protocols that simultaneously access multiple networks [30]; using proper strategies for network selection, which is to select the best network for various communications at any time anywhere [59]; dynamic switching with heterogeneous channels [14]; and concurrent transmission of multi-array antennas [3].

Nowadays, different techniques for aggregation of wireless radio interfaces have been introduced. However, multiple overlapping exists as a main problem in primary

channels (say WiFi) and also uncoordinated frequency bands (e.g., 802.15.4 that uses 2 MHz). Dynamic carrier aggregation between licensed and unlicensed carriers is a technique for multi-RAT networking that has been addressed in [24]. Carrier aggregation is also addressed in [49] where the reference signal design for uplink transmission is based on selections of best combination of distinct sequences and cyclic shifts in each carrier. In [59] the utility function for *network selection* is based on multiple attributes, including bandwidth [21,40], cell radius [28], security [7], battery [51], SNR/ SIR [57], price [40], hand-off failure probability [19,25], data traffic [29], power consumption [1,21], BER [57], delay [28,47], and packet loss and jitter [5]. Another solution for muti-RAT networking is opportunistic channel switching that allows a link to dynamically search for a channel. This technique maximizes the real-time system performance among heterogeneous channels [14].

The emerging technology of cognitive networking is the appropriate solution in the cloud offloading scenario where there is a need for offloading computationally intensive parts of the applications to a resource-rich cloud. Cognitive cloud offloading is a new concept (introduced in [34]) where the computational cloud offloader decides which radio interfaces must be used in the associated data transfers and what percentage of the data should be communicated through each interface, as well as which components of a sophisticated multicomponent application should be offloaded and which should run locally. Cognitive networking and using all the viable networks simultaneously for cloud offloading lead to a higher throughput of the network.

An example of a complex multicomponent mobile application, that is computed through offloading, is shown in Fig. 3. This application consists of ten components, and the dependencies between the components are indicated. A cloud server, such as NSFCloud or Amazon Elastic Compute Cloud (Amazon EC2), is used for cloud computing, scheduling the tasks, and aggregating of the data related to the computations from all the networks. A mobile device with K radio interfaces (networks) is used. In the uplink scenario, at time slot t, $\alpha_k(t)\%$ of the required data for offloading is sent by the mobile device through radio interface k. Similarly in the downlink scenario, $\beta_k(t)\%$ of the data is sent by the cloud to the mobile device using radio interface k $\forall k$. The goal is to find an online scheduling-offloading policy for all components as well as the optimal wireless resource allocation between the multi-RAT networks for two-way data transfers between mobile and cloud.

This section elaborates on research in the R-T plane in the schematic presented in Fig. 2. The R-axis indicates wireless-aware cloud offloading using single radio interface, multiple radio interfaces, and cognitive networking. The cloud offloading algorithms are developed either for single radio access technology (single-RAT) or multiple radio access technology (multi-RAT) devices. Multi-RAT-enabled mobile devices increase the capacity for offloading [30]. In multi-RAT networking, there are two options: the wireless interfaces are used in either an on/off mode or a hybrid mode. In the on/off mode, only one network is offloading at a time, whereas in the hybrid mode *cognitive networking* is applied for cloud offloading.

Recall that offloading with single network can be done using single channel or multiple channels. The multi*channel* single-RAT scenario is totally different from

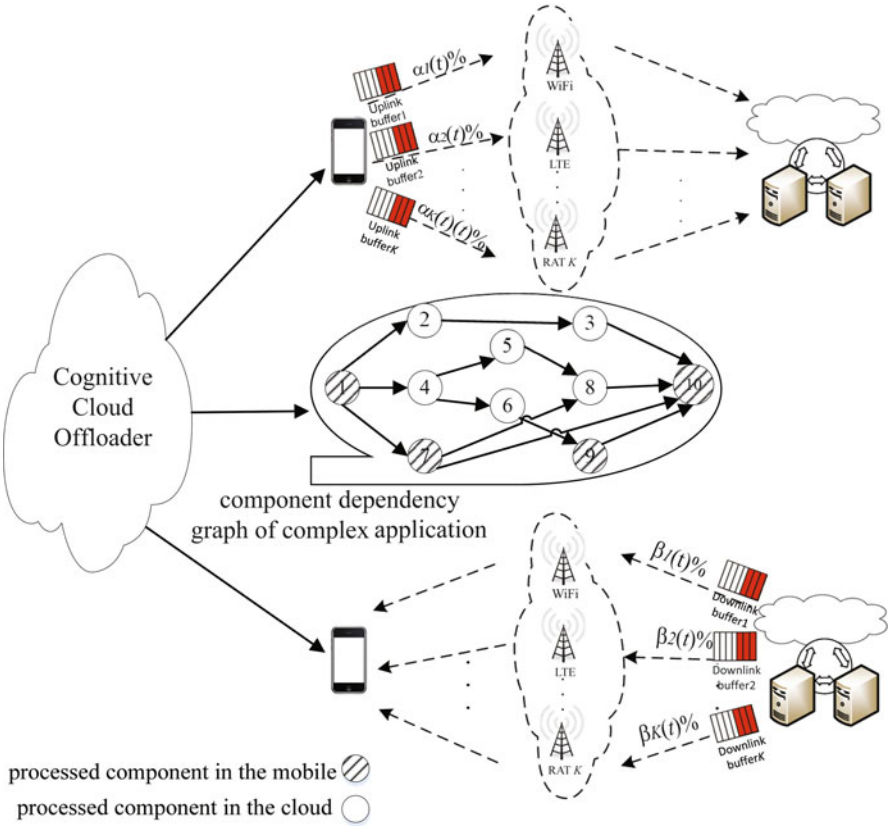

Fig. 3 Cognitive offloading for multi-RAT-enabled wireless devices

the multi-*RAT* scenario. The parameters of *channels* (path characteristics such as rate and delay) in the same radio network vary widely in comparison with radio interfaces such as WiFi and LTE supported by multi-RAT-enabled devices [48]. On the one hand, a multi-RAT system is transparent to underlying wireless network and technology. On the other hand, it makes coarse decision on offloading computation of components from one radio to another unlike multichannel approach which does provide fine grain decisions between different channels. A multi*channel* partial offline offloading solution was proposed in [4] for queue stability. The extension of [4] to joint allocation of transmit power in single and multichannel scenarios in single-RAT devices was studied in [13].

Partial cloud offloading for mobile applications with predetermined compiler-generated call graphs is expressed jointly with allocation of transmit power level, and the constellation size of OFDM subcarriers used for offloading in [13] such that the constraints of latency, packet loss, and execution time are satisfied. The authors of [13] then extended the wireless communication environment of their work to MIMO multiple system where multiple mobile devices demand cloud

offloading [52]. However, decision making is on the CPU cycles/second assigned for the computations on each mobile device by the cloud rather than offloading strategy.

The time (adaptiveness) axis (T-axis) in spectrum-aware cloud offloading indicates that the existing offloading techniques are classified based on offline or online techniques. In the offline approach, the offloading decisions are static and done at the start of processing. In the online approach, the offloading decisions are dynamic and are made on the fly [18].

The research represented in the $R-T$-plane is divided into six categories: (1) offline offloading strategies using single-RAT for networking; (2) online offloading strategies using single-RAT for networking; (3) offline offloading strategies using on/off multi-RAT for networking; (4) online offloading strategies using on/off multi-RAT for networking; (5) offline offloading strategies using cognitive networking; and (6) online offloading strategies using cognitive networking. These 6 classes are discussed below.

Spectrum-Aware Offloading Using Single-RAT Devices

Offline Approach

The offline (static) offloading strategies using single radio includes classic computation offloading approaches such as MAUI [11]. MAUI presented an offline fine-grained partial offloading strategy using WiFi network for communication. This energy-efficient strategy provides minimum burden on the programming support for implementation. It specifies which methods must be offloaded to the cloud using WiFi RAT under the mobile's wireless connectivity constraints at runtime and which methods must be processed in the mobile device. This fine-grained partial offloading scheme maximizes the energy savings. MAUI achieves these advantages using some properties of current code environments for mobile apps as follows:

1. Code portability is used to provide two versions of a mobile app in the infrastructure, one for mobile execution and another one for cloud execution; this flexible code provides adaptability in the instruction set architecture between the mobile app and the cloud servers.
2. Programming reflection is combined with safety to enable the offload scheduler to automatically identify the offloadable methods (tasks) and extract only the program state needed by those methods.
3. Each method of the mobile app is profiled, and *serialization* is used for method processing.

In this work, resources are managed based on the wireless connectivity (bandwidth and latency) using a linear programming formulation of the computation offloading problem. The authors have tested their strategy using several apps including a computationally intensive face recognition mobile application for the specific purpose of energy minimization and a delay-sensitive arcade game application. Other related work on offline single-RAT computation offloading include [2, 26, 27, 33, 36, 41, 55, 62, 63, 66].

In [41], an offline offloading policy is proposed to minimize the energy consumption of the mobile device with overall application deadline constraints. A more precise algorithm for individual deadline constraints on application tasks is also mentioned in [2]. A partial offline computation offloading scheme is used in [54] where a predictive algorithm is used for wireless connectivity. Here, a risk control strategy is used to make the prediction analysis more reliable.

Online Approach

Online (dynamic) computation offloading is fundamentally influenced by instantaneous changes of the data rates, latency, communication power, and buffer queuing at the radio interface. A partial dynamic offloading for frame-based tasks with response time guarantees from the cloud servers is studied in [58]. The server estimates the response time for remote execution of each task based on total bandwidth server model. Also a fault-tolerant strategy for online partial cloud offloading of the mobile applications with sequential component dependency is proposed in [12] such that the trajectory of mobility of users is modeled by random waypoint (RWP). In this fault-tolerant strategy, there is a trade-off to balance waiting for reconnections and restarting failed services from beginning.

Spectrum-Aware Cloud Offloading Using On/Off Multi-RAT Networking

Computation offloading strategies using multi-RAT networking [20, 35, 56] have recently gained interest because of the new features and capabilities in cognitive radio networking [68] and wireless HetNets in the 5G evolution. In the classic multi-RAT offloading [20,56], only one of the radio interfaces, which has the best wireless characteristics, will be selected for offloading. Thus, these schemes use an *on/off* selection model for the networks.

Offline Approach

A classic energy-efficient partial computation offloading algorithm using on/off multi-RAT networking was proposed in [20]. The main objective of this work is to reduce the communication costs (energy and delay) between the mobile device and the cloud server while guaranteeing the given application runtime. Note that although this algorithm works in offline mode, it assumes that the viable wireless networks change over time depending on the current location of the mobile device. However, during the runtime of the application, the parameters of available wireless networks are assumed to not change. Huang et al. [20] considers that cellular network is accessible everywhere while WiFi network is available only in special places. When two networks are available, the controller in the mobile device selects the best RAT based on the higher data rate before making decision on offloading. The offloading decision is obtained based on minimization of the energy consumption by the mobile device (the energy consumed for mobile execution of local tasks of the app plus the energy consumption in the idle mode due to offloading

plus the energy consumed for offloading). The constraints of this optimization problem are designed such that the maximum number of computation requests would not violate a given threshold, and the system stability will also be guaranteed. Lyapunov optimization is applied to solve this problem.

Online Approach

A wholesale offloading strategy is addressed in eTime [56] based on energy and delay trade-off. Although the authors assume a multi-RAT device, only the *best single* wireless interface is used for offloading. This work proposes a strategy for **E**nergy-efficient data **T**ransm**I**ssion from the cloud to **M**obile d**E**vices (eTime) such that online decisions are made for time-adaptive scheduling of the data communication based on wireless connectivity between the two entities. eTime strategy uses the online information of data traffic to specify the amount of data to be transmitted at the current time such that jointly the energy consumed by the mobile device for communication is minimized and the queue of ambient data traffic is stabilized. Therefore, an energy-delay trade-off algorithm was designed to solve the problem using Lyapunov optimization technique. To test the proposed strategy, the authors considered ten applications running in the cloud with specific data-arrival distributions, and the corresponding data of applications were transmitted to the mobile devices based on the current online connectivity through WiFi and cellular networks. The implementation results show that using the eTime strategy, 20–35% less energy was consumed by the mobile device in comparison to a random strategy, where the user may run applications on the mobile device and request data in a random time slot, and the data are offloaded instantly from the cloud to the mobile user without wireless connectivity prediction.

Spectrum-Aware Cloud Offloading Using Cognitive Networking

Offline Approach

Cognitive cloud offloading was first considered in [35] for multi-RAT devices, where all viable networks are simultaneously used to offload. An optimal one shot solution (in offline mode) is used to obtain the percentage of data over each wireless interface. In previous multiple radio-aware computation offloading strategies, including [20], the best of the available wireless interfaces was selected (only one of the wireless interfaces) for computation offloading, rather than a strategy that addresses using all viable radio interfaces simultaneously. In [35], the associated data transfer was optimized over all viable networks at the mobile device transmitter in uplink (not at the cloud transmitter end in downlink scenario). This work assumes one best radio interface for downlink data transfer. The optimization of radio resource allocation for cognitive networking in downlink was addressed in a later work [34]. They also assume that the application components are processed in a predetermined manner like [11, 20].

A comprehensive model is proposed in [35] for energy consumption by the mobile device to run the application component task i, given as $E_i = E_i^{(\mathrm{m})} + E_i^{(\mathrm{c})} + E_i^{(\mathrm{com})}$, where $E_i^{(\mathrm{m})}$ ($E_i^{(\mathrm{c})}$) is defined as the energy consumed by the mobile device to run component i in the mobile (cloud), and $E_i^{(\mathrm{com})}$ is defined as the energy consumed by the mobile for data transfer of component i between cloud and mobile. The energy consumption for mobile execution of component i is expressed as $E_i^{(\mathrm{m})} = (1-I_i)P_{\mathrm{ac}}^{(\mathrm{m})}(i)q_i^{\mathrm{m}}$. I_i is the execution place indicator, assigned 1 if component i is offloaded to the cloud and assigned 0 if processed on the mobile device, $P_{\mathrm{ac}}^{(\mathrm{m})}(i)$ is the power consumed by the mobile device when it is actively processing component i, and q_i^{m} represents the time to process component i in the mobile device. If the component should be offloaded, then the mobile device will spend the idle power for the duration of this execution. The energy consumption by the mobile device when component i is being remotely processed is $E_i^{(\mathrm{c})} = I_i P_{\mathrm{id}} q_i^{\mathrm{c}}$. P_{id} shows the power consumed by the mobile in the idle mode, and q_i^{c} presents the time to process component i in the cloud. $E_i^{(\mathrm{com})}$ comes into play when either the component immediately preceding the component i or immediately succeeding component i is executed in the other entity. $E_i^{(\mathrm{com})}$ is the energy consumed by the mobile device for associated data transfer between the cloud and mobile. $E_i^{(\mathrm{com})}$ represents (1) the energy consumed in transmitting or receiving the relevant data and (2) the idle energy consumption when the relevant computations are being transferred to the cloud (different from $E_i^{(\mathrm{c})}$, which shows the idle energy consumption by the mobile device while component i is running in the cloud). The time to transfer data in the downlink and uplink scenarios are respectively given by $\tau_{ij,k}^{(\mathrm{cm})} = \frac{d_{ij}}{R_k^{(\mathrm{d})}}$ and $\tau_{ij,k}^{(\mathrm{mc})} = \frac{d_{ji}}{R_k^{(\mathrm{u})}}$, where $R_k^{(\mathrm{d})}$ and $R_k^{(\mathrm{u})}$ are the downlink and uplink rates on radio interface k. d_{ij} is the data size that must be transferred from component i to j.

The optimization problem is formulated to minimize the overall energy consumption by the mobile device in processing a sophisticated, multicomponent application under three constraints.

$$\min_{\boldsymbol{\nu},\boldsymbol{I}} E \triangleq \sum_{i=1}^{M} E_i, \tag{1}$$

where M shows the number of components in the application, $\boldsymbol{I} = [I_1 I_2 \ldots I_M]$, $\boldsymbol{\nu}$ is a matrix with entries $\nu_{i,k}$, $\forall i,k$, and $\nu_{i,k}$ is the percentage of data upload using radio interface k, for execution of component i in the cloud. The constraints are given as follows: (1) deadline on the runtime of the application; (2) flow rate control on each network used for cloud offloading; and (3) the overall value of data percentage allocated to the network interface for each offloaded component.

The constraint on the runtime of application is given as

$$\sum_{i=1}^{M} T_i \leq T_{\text{req}}, \tag{2}$$

where T_{req} is the deadline of the application, $T_i = T_i^{(\text{m})} + T_i^{(\text{c})} + T_i^{(\text{com})}, \forall i.\ T_i^{(\text{m})}$, $T_i^{(\text{c})}$ represent the time taken for component i to execute in the mobile device and cloud, respectively, and $T_i^{(\text{com})}$ is the time taken to complete the necessary data transfer for execution of component i. The detailed formulation of these variables is presented in [35]. A solution to the optimization problem indicates where each component should be processed, in the mobile device or in the cloud, and what percentage of data must be allocated to each radio link for necessary uplink data transfer.

In order for the cognitive network model to be stable, the transmit data rate on the radio interfaces must be less than the service rate of each radio interface. Moreover, the overall data allocations to the radio interfaces for each component must sum up to the total data that needs to be transferred. Since this optimization problem is nonlinear and hence computationally intractable, an iterative algorithm that converges to a local optimum is also proposed. Simulations show that the proposed iterative algorithm performs very close to the optimal solution for a significant reduction in complexity.

Online Approach

While [35] was an offline offloading strategy, an online dynamic strategy for cognitive offloading was presented later in [34]. The online strategy addressed both uplink and downlink scenarios and also considered a joint scheduling-offloading policy for applications with arbitrary dependency constraints between components of an application. Moreover, an optimal solution is proposed in [37] for online joint cognitive scheduling and cloud offloading discussed in section "Joint Scheduling and Computation Offloading in Time-Adaptive Cognitive Networks".

The Effect of Spectrum-Aware Scheduling in Mobile Computing

Scheduling of application tasks is studied in [2] and *eTime* [56] where a predetermined compiler-generated order of execution for the application components is used, and all the component tasks are offloaded for cloud execution. *eTime* explores an energy-delay trade-off in scheduling the required data transmissions for wholesale offloading such that offloading is done when the wireless connectivity is sufficiently good. Efficient computing for mobile applications requires spectrum-aware scheduling of the tasks particularly for apps with general arbitrary dependency constraints between components rather than sequential schedule order or predetermined compiler-generated schedule order. Since computation offloading

strategy relies on the task scheduling decisions for the application components, this spectrum-aware scheduling must be considered jointly with the offloading policies.

A joint optimal scheduling and partial offloading solution for sophisticated apps in single-RAT-enabled mobile devices was proposed in [36] where a net utility function was maximized to provide a trade-off between the battery energy saved in the mobile device and the communication costs involved in the offloading. The constraints of the formulation accounted for the precedence ordering for task execution of the application components, the overall execution runtime of the application, and parallel execution of an application between the mobile device and the cloud server. Note that *the accommodation of parallel processing reduces the time to complete the application significantly*. Therefore, efficient task scheduling of the application components in addition to partial cloud offloading decisions provides a more comprehensive solution in comparison with the partial offloading strategies using a predetermined compiler-generated schedule order for processing the individual application components.

Most of the related work on partial computation offloading address mobile applications with forced sequential component dependencies or a scheduling order which is predetermined by a compiler. However in real-life scenarios, applications may have arbitrary dependency constraints between their components. Therefore, efficient strategies for *joint scheduling-offloading* policies must address wireless network aware scheduling order of the components based on the topology of component dependency graphs (CDGs) between the components of the mobile applications.

Component dependency graphs (CDGs) of mobile applications considered in [36] are assumed to have the following properties:

1. All the components, except the first component, must have an in-degree of at least 1.
2. Each component, except the last component which corresponds to the output, must have an out-degree of at least 1.
3. Every component must have at least 1 path from the first component, directly or indirectly. This shows that all the components are dependent on the starting point of the application.
4. Each component must have at least 1 path to the last component. This shows that all the components collaborate in processing the app.
5. There is no self-dependency in the CDG, that is no component must depend on itself. The component dependencies can be represented using an adjacency matrix where entry (i, j) is 1 if component j depends on component i and 0 otherwise.

Since self-dependencies are not allowed, the diagonal entries of the adjacency matrix are all 0.

The sequential and parallel dependency graphs present the two extreme level of dependencies between components. These two CDGs can, therefore, be used

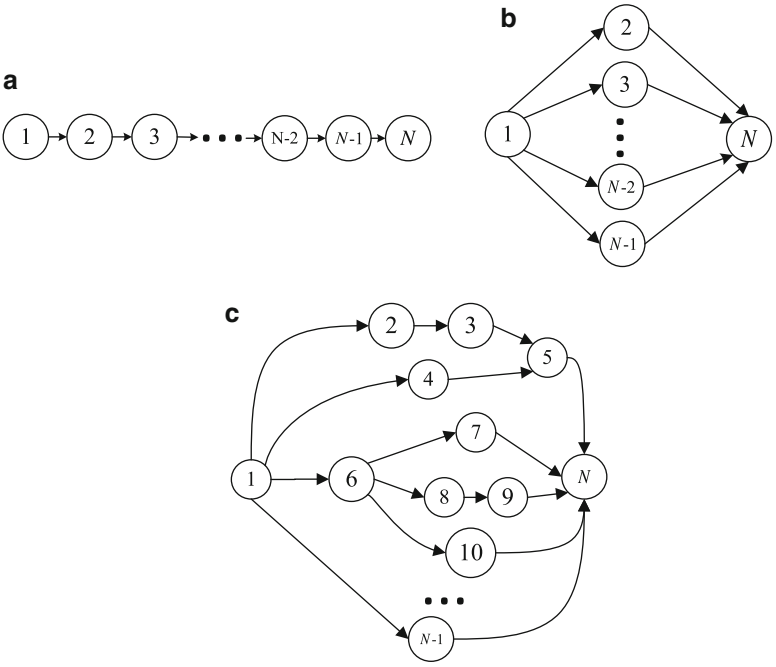

Fig. 4 Examples of various topologies for CDGs of the mobile applications with N components. (**a**) Sequential CDG. (**b**) Parallel CDG. (**c**) Arbitrary CDG

to achieve the upper and lower bounds for the cost of offloading applications. Figure 4 shows different types of CDGs for an N-component application (N=10): (i) sequential dependency graphs where all the components are sequentially dependent (Fig. 4a); (ii) parallel dependency graph where component 1 must be executed before all the other components, and component N must be executed after all the other components (Fig. 4b); and (iii) arbitrary dependency graph, a special class of precedence constraints, where there is a combination of sequential and parallel dependencies between components.

A scheduling scheme for partial cloud offloading is discussed in [66] for a sequence of fine-grained tasks with serial CDG (Fig. 4a) that guarantees the application runtime. A partial mobile offloading strategy based on probabilistic estimations of the offloading effectiveness is proposed in [15] for a variety of mobile applications with serial CDGs. To determine the offloading effectiveness, a semi-Markov framework is used where runtime heterogeneity of application execution characteristics is taken into account. Existing component-based partial cloud offloading strategies use a predetermined compiler-generated serial order that does not lend itself to parallel computation of components in the mobile device and cloud (DOA [20] and MACS [27]). In [4], sequential scheduling of the components is studied in both single-channel and multichannel radio links. The objective is minimization of the energy consumption in the mobile device

while meeting the delay constraints of the application. Another scheduling strategy, designed for energy minimization in a multiuser network, is presented in [41], where a centralized broker partially offloads tasks to the cloud in a serial order. In their work, a centralized strategy is investigated to offload the tasks in two hops where the broker is an intermediary between the mobile user and the cloud. However, the scheme in [36] determines the scheduling decision as well and therefore affords parallel computation of components.

In comparison with the state of the art, joint scheduling and cloud offloading strategies such as [36] have several benefits. These strategies combine computation offloading and task scheduling in the presence of arbitrary component dependencies (precedence constraints between app components) such that parallel execution of components will be possible between the mobile device and the cloud. To achieve this multi-term objective, a holistic optimization problem is solved in [36] for real mobile applications that guarantees deadline for application runtime, ordering of task execution for individual components, and saving of battery energy in the mobile device. The authors of [36] introduced the first energy-efficient joint scheduling and cloud offloading scheme for mobile users running applications with arbitrary component dependency graphs. Earlier state-of-the-art techniques consider either trivial serial ordering of the components or a predetermined compiler-generated ordering, leading to less adaptability with wireless conditions. In [36], real data was measured from an HTC smartphone using real and randomly generated mobile applications, WiFi network was used for partial offloading, and Amazon Elastic Compute Cloud (EC2) was used for remote processing of the application components. The optimal solution is obtained under these real data measurements using IBM CPLEX optimizer [10]. This strategy is analyzed and tested by varying several parameters: the number of application components (up to 150 components), topology of application component dependency graphs (CDGs), application runtime, and wireless parameters such as rates, latencies, and data sizes. The results show that the proposed JSCO reduces energy consumption by 54, 37, 16, 30, and 11% compared to local execution, remote execution, DOA [20], HELVM [43], and RHJS [32], respectively.

Joint Scheduling and Computation Offloading in Time-Adaptive Cognitive Networks

Online cognitive cloud offloading strategies make it possible to realize a more realistic spectrum-aware mobile computing that accommodates (1) arbitrary dependencies between the component tasks of the applications (as opposed to the predetermined schedule order) and (2) online strategies that adapt to the dynamic changes in the mobile networks over time.

The first work in this area of cognitive cloud offloading, [35], proposed an offline optimal solution for applications with predetermined schedule order considering multiple wireless network parameters. Then, a joint scheduling and computation offloading (JSCO) solution was proposed that allows for more degrees of freedom in

the solution by moving away from a predetermined compiler-generated scheduling order for the components toward a more component dependency aware scheduling order [36]. However, this work uses a single-RAT offloader and applies fixed wireless parameters for making decision on offloading and scheduling in the offline mode.

In [34,37], authors move to a more realistic and comprehensive extension of the problem, where an optimal *online* solution (adaptive to changing wireless network parameters) is obtained for applications with *arbitrary component dependencies* over *multi-RAT*-enabled mobile devices. This is indicated schematically, in the context of the existing works in this area, in Fig. 2.

In [34], heuristic strategies are proposed to jointly schedule the application's component tasks for processing and simultaneously optimizing the percentage of the associated data for transferring by the mobile device in uplink and the cloud in downlink via each mobile network. A holistic multi-term net utility function is defined that trades-off costs of resources (energy, memory, and CPU) of the mobile device with the communication costs of offloading including the communication energy and the data queue length at the multiple radio interfaces. Moreover, the offloading strategies for transmission, at the mobile and cloud, use past mobile network data history, queue status, and the current data flow to update the current queue status.

Mahmoodi and Subbalakshmi [34] is implemented in two ways: (i) a fast algorithm with two stages where some of the components are eliminated as unsuitable for offloading at the outset and maximizing the instantaneous utility values in the offline mode (first stage). In the second stage, the selected components for online offloading will be verified for scheduling constraints. (ii) a single stage algorithm (with more complexity but closer to the optimal solution in performance) where all the components are verified for offloading in the online mode. The notations used for the parameters in this work are defined in Table 1.

Consider a scenario as in Fig. 3 where there are K radio interfaces in a wireless network, and a multicomponent app is running on a mobile device with N number of task components. The objective of the algorithm in [34] is to provide an online cognitive offloading and scheduling strategy and an allocation of wireless resource among the multi-RAT interfaces for data transfers of both the uplink and downlink scenarios. Figure 3 shows that at time t, $\alpha_k(t)\%$ of the data for computation offloading is uploaded by the mobile user through network link k. Similarly, $\beta_k(t)\%$ of the data is downloaded from the cloud through network link k. The authors of [34] assume that the battery power and the time required to transfer data between components that are processed in the same place (cloud or mobile device) are negligible in comparison to when the data must be transferred between the mobile device and the cloud. Also, another assumption is that the cloud and the mobile clocks are synchronized (as thoroughly discussed in [9]). Here, the cognitive cloud offloading approach makes a balance in the benefits of cloud execution such as energy and time savings on the mobile device with the costs of cloud offloading including the energy and delay values involved in the associated data transfer. Based on this determination of balance, simultaneous decisions are made on the optimal

Table 1 Parameter definitions

Parameters	Definitions
$A_k^{\mathrm{mc}}(t)(A_k^{\mathrm{cm}}(t))$	Data rate transmitted from the mobile (cloud) to the cloud (mobile) through radio interface k at time slot t
$B_i^{\mathrm{mc}}(t)$ $(B_i^{\mathrm{cm}}(t))$	Arrival data rate at the mobile (cloud), including the ambient traffic as well as the data generated by offloaded component i (arrival data in time slot t)
$c_i(t)$	Indicator function that takes on a value of 1, if the component i has started execution in the cloud at any time between 1 and t
code_i	Code size to launch component i
$E_{\mathrm{com}}^{\mathrm{Tx}}(t)$	Energy consumed for the mobile transmission due to cloud offloading
$I_i(t)$	Offloading indicator: 1 if the mobile starts to offload component i at time slot t
K	Number of wireless radio interfaces
$l_{ji}(t)$	The time slots to process the preceding component j and transfer the output data from component j to i by t
M_i	RAM memory consumed by the mobile device to launch component i
$m_i(t)$	Indicator function that takes on a value of 1, if the component i has started local execution at any time slot between 1 and t
N	Number of components in the application
P_i^{m}	Power consumed by the mobile device when it is actively processing component i
$P_k^{\mathrm{Tx}}(t)$	Transmit power consumed by the mobile device through radio interface k at time slot t
$Q_k(t)$	The transmission queue of data from the mobile (cloud) side for wireless interface k at time slot t
q_i^{m} (q_i^{c})	Number of time slots to process component i in the mobile (cloud)
T	Number of time slots to complete processing the application
$T_{\mathrm{th}}^{\mathrm{Tx}}$	Threshold number of time slots for transmission from mobile to cloud
$U(t)$	Net utility function at time t
V_{mc}	Control parameter in mobile (cloud) transmission for Lyapunov optimization
w_x	Weight factor of function x
$X_i(t)$	Local execution indicator: 1 if the mobile starts to execute component i locally at time slot t
$\alpha_k(t)$	Percentage of allocated uplink (mobile to cloud) rate using radio interface k for communication at t
$\beta_k(t)$	Percentage of allocated downlink (cloud to mobile) rate using radio interface k for communication at t
ε	Mapping factor to relate code size and the CPU instructions [44]
γ	Weight factor (to adjust the wait time for offloading)
μ_{ij}	Dependency indicator: 1 if component i must be processed before j and 0 otherwise
$\Omega_{\mathrm{mc}}(t)$	The objective function for mobile transmission strategy at time t
$\tau_{i,k}^{\mathrm{mc}}(t)$	Delay (in number of time slots) to transmit the output data from component i in the mobile to the cloud at interface k starting by t

percentage of the data to be uploaded and downloaded via each network link. Note that this heuristic cognitive cloud offloading strategy is managed in the cloud, and the feedback decision for offloading will be sent to the mobile user. The mobile user also sends the required information of wireless parameters (delay, rate, queue size, and communication power) to the cloud through control signaling before cognitive cloud offloading. The latency of sending data related to the wireless parameters is negligible in comparison with the computation offloading costs which may require transferring megabytes of data.

An appropriate net utility function is defined based on saving the computational resources of the mobile user and the costs of cloud offloading. To determine the heuristic decision for component task i, two variable parameters must be obtained (at each time slot t) as follows: $I_i(t) = 1$, if component task i starts offloading at t, and otherwise it is assigned 0; $X_i(t) = 1$, if component task i starts processing in the mobile device at t, and otherwise it is assigned 0. This net utility function is defined as a weighted sum of the energy, memory, and CPU cycles saved at the mobile device by cognitive offloading minus the communication costs arising from running some components locally and some remotely. This is given as $U(t) = w_{\text{saved}} E_{\text{saved}}(t) + w_{\text{memory}} M_{\text{saved}}(t) + w_{\text{CPU}} CPU_{\text{saved}}(t) - w_{\text{com}} C_{\text{com}}(t)$. The weight factors for the benefits and costs are chosen such that $w_{\text{saved}} = 1 - w_{\text{com}}$, and $w_{\text{CPU}} = 1 - w_{\text{memory}}$. The weight factors show the relative importance of the utility functions, namely, memory saved, CPU saved, the communication costs, and battery power. The solution can be pre-biased toward different goals by setting weights appropriately. If w_{saved} is assigned a higher value than w_{com}, then it means that saving battery power at the mobile device is preferred; if w_{com} is assigned a higher value, it shows that minimizing the communication costs for cloud offloading is more important. Note that monetary costs of using cloud services could be significant; in which case, this financial cost can be incorporated into the weight factors so that offloading to the cloud is favored a little less.

The overall energy saved by executing the component tasks in the cloud at time t is computed as the energy cost for running it in the mobile device ($P_i^{\text{m}} q_i^{\text{m}}$), and is given by $E_{\text{saved}}(t) = \sum_{i=1}^{N} c_i(t) P_i^{\text{m}} q_i^{\text{m}}$, where $c_i(t) = \sum_{s=1}^{t} I_i(s)$, that is, $c_i(t) = 1$ if component i is processed in the cloud during some time slot s for $s \in \{1, \ldots, t\}$. Similarly, $m_i(t) = \sum_{s=1}^{t} X_i(s)$.

The memory saved in the mobile device by offloading the components to the cloud is illustrated as $M_{\text{saved}}(t) = \sum_{i=1}^{N} c_i(t) M_i$, where M_i is the memory consumed by the mobile device to launch component i. The number of CPU cycles saved is given by $CPU_{\text{saved}}(t) = \sum_{i=1}^{N} c_i(t)(\varepsilon(\text{code}_i))$, where code_i is the code size for instructions that is used for executing component i and ε is the mapping between code size and the CPU instructions. The communication cost at time slot t ($C_{\text{com}}(t)$) will be discussed later.

Besides specifying the components that are selected for computation offloading, the objective of this heuristic strategy is to decide on the time that each component should be scheduled for local or remote processing, and the network link allocation for offloading at each time slot for both uplink and downlink transmission. Accordingly, decision variables are (i) offloading indicator ($I_i(t)$), (ii) local execution

indicator ($X_i(t)$) for component i at time slot t, and, (iii) the percentage of allocated uplink ($\alpha_k(t)$) and downlink ($\beta_k(t)$) rates through network link k at time t.

In the heuristic algorithm, the following two scheduling constraints must be checked to see if a component is eligible for processing at the current time t: First, each component task should be executed only once, either in the mobile device or in the cloud server. This constraint is mathematically written as $m_i(t-1) + c_i(t-1) < 1$, $\forall i$. indicating component i has not started execution by time slot t. Second constraint is to ensure the precedence ordering of component tasks of the application is respected. For running component i at t, it is required that all the components j on which component i depends ($j \prec i$) should have completed processing before starting the offload process for component i or execution of component i (either in the mobile device or in the cloud). If these two constraints are guaranteed, then component i is safe to be executed.

Uplink Transmission Strategy: After the offloading component has been identified and the component is scheduled for execution, the radio allocation for the transmission from the mobile device to the cloud must be calculated. Since the proposed cognitive cloud offloader [34] works with multiple networks at the same time, the queue stability of the uplink data transmission buffers must be monitored to guarantee no buffer overflows. This is stated as follows: $\overline{Q} = \lim_{T\to\infty} \sup \frac{1}{T} \sum_{t=1}^{T} \sum_{k=1}^{K} \mathbb{E}\{|Q_k(t)|\} < \infty$, where $Q_k(t)$ is the transmission queue of radio k at time t in uplink scenario. This problem is cast as a Lyapunov optimization [39] problem. The Lyapunov function is given as $L(Q(t)) = \frac{1}{2} \sum_{k=1}^{K} Q_k^2(t)$ where $Q(t)=[Q_1(t)\ Q_2(t) \ldots\ Q_K(t)]$. When the queue of mobile transmission is updated with time, the Lyapunov drift is given as $\Delta_{\text{mc}}(Q(t)) \triangleq \mathbb{E}\{L(Q(t+1)) - L(Q(t))|Q(t)\}$. The Lyapunov drift is minimized when the cost of the energy consumed for mobile transmission is taken into account: $\Delta_{\text{mc}}(Q(t)) + V_{\text{mc}}\mathbb{E}\{E_{\text{com}}^{\text{Tx}}(t)|Q(t)\}$ [16], where V_{mc} is the control parameter for the queuing of the mobile transmission, considering the balance between the Lyapunov drift and the cost of energy consumed for transmission ($E_{\text{com}}^{\text{Tx}}(t)$), where $E_{\text{com}}^{\text{Tx}}(t) = \sum_{k=1}^{K} P_k^{\text{Tx}}(t) \sum_{i=1}^{N} I_i(t)\alpha_k(t)\tau_{i,k}^{\text{mc}}(t)$,

Following the Lyapunov optimization framework, the upper bound of the objective function must be minimized as:

$$\text{OP1}: \min_{\boldsymbol{\alpha}} \Omega_{\text{mc}}(t) = V_{\text{mc}} E_{\text{com}}^{\text{Tx}} - \sum_{k=1}^{K} \left(Q_k(t) A_k^{\text{mc}}(t)\right), \tag{3}$$

s.t.

$$\sum_{k=1}^{K} \alpha_k(t) \sum_{i=1}^{N} I_i(t)\tau_{i,k}^{\text{mc}}(t) \le T_{\text{th}}^{\text{Tx}}, \tag{4}$$

$$\sum_{k=1}^{K} \alpha_k(t) = 1, \alpha_k(t) \ge 0, \forall k, \tag{5}$$

where $\boldsymbol{\alpha} = [\alpha_1(t)\ \alpha_2(t)\ \ldots \alpha_K(t)]$. Here, V_{mc} is a control-knob parameter that trades-off wireless communication costs with decreasing the uplink communication energy ($E_{\text{com}}^{\text{Tx}}$) and satisfying the queue stability constraint for all the radios. The RHS of the objective function of the optimization problem shows the averaged aggregated queue length ($\overline{Q}$). Reducing V_{mc} emphasizes on reducing the aggregated queue length, while increasing it enforces possible minimization of the uplink transmission energy. Constraint (4) requires that the transmission time lies below a given threshold, $T_{\text{th}}^{\text{Tx}}$. Constraint (5) ensures that the amount of data offloaded at time t does not exceed the transmission capacity of all the multi-RAT interfaces taken together.

The heuristic cognitive offloading strategy (for uplink scenario) in the online stage is as follows. For every qualified component i for processing that meets the scheduling constraints, if there is a feasible solution for OP1 with variable parameter set $\boldsymbol{\alpha}$, then i is offloaded starting at time t ($I_i(t) = 1$) through K radio interfaces at the optimal percentage values $\alpha_k^*(t)\ \forall k$. If there is no feasible solution for optimization problem, OP1, then there are two options: (1) wait for the next time slot; (2) run the component in the mobile device. The difference between the current time slot t and the time slot requested for execution of component i (t_i^{req}) must be much lower than the processing time in the mobile device. This is written as $|t - t_i^{\text{req}}| < \gamma q_i^{\text{m}}$, where γ is the weight factor. If the wait time does not exceed the processing time in the mobile device for component i (q_i^{m}), then $I_i(t)$ gets 0 and the component i is left to await its turn for execution. However, if $|t - t_i^{\text{req}}| \geq \gamma q_i^{\text{m}}$, the component is sent for mobile execution in the next time slot and will not be considered for offloading again.

The transmission queue for the next time slot at radio interface k will be updated as follows: $Q_k(t+1) = \max[Q_k(t) - A_k^{\text{mc}}(t), 0] + \alpha_k(t) \sum_{i=1}^{N} B_i^{\text{mc}}(t)$, where $\max[Q_k(t) - A_k^{\text{mc}}(t), 0]$ shows the data remaining in the queue for interface k, and $\alpha_k(t) \sum_{i=1}^{N} B_i^{\text{mc}}(t)$ represents the data arrival at radio interface k in time slot t. Note that the queue is a function of percentage of allocated uplink. Also, if component i, that is originally scheduled for remote execution, is not offloaded at time t due to not finding a feasible solution for OP1, then the delay values for transmission of the output data from component i in the mobile to the cloud via wireless interface k will be updated to $\tau_{i,k}^{\text{mc}}(t+1) + 1$. Hence, after each time slot, if the scheduled component for cloud execution is not offloaded, the delay cost will be updated by the delay value at the next time slot plus one.

An optimal cognitive scheduling and cloud offloading solution is proposed in [37] that decides on the following features jointly: (1) which application components must be scheduled for offloading and which must be executed locally, (2) which radio interfaces (networks) should be used in the associated data transfers, and (3) what percentage of the associated data must be offloaded through each radio interface (Fig. 3). This work also achieves the optimal solution for online cognitive scheduling and cloud offloading strategies. While the heuristic algorithm in [34] can be implemented in the mobile device, the optimal solution in [37] is managed in the cloud, and the decision on offloading is sent to the mobile device. The mobile device sends the corresponding parameters via control signaling to inform

the cloud. A holistic optimization problem with several constraints is formulated in [37] as a time-indexed mixed-integer linear program (MILP) and is relaxed to a corresponding linear programming problem. The multi-term net utility in [37] is a combination of the cost of mobile resources saved due to cognitive cloud offloading including the energy, memory, and CPU minus the penalty for offloading. This penalty includes the energy consumed for transmission and reception, latencies due to offloading, and the data queue backlog for buffers of uplink and downlink scenarios, using all multi-RAT interfaces. The constraints of this optimization problem take into account: (1) the total deadline of the application; (2) the schedule order of the application components; (3) the percentages of data transferred with each network in uplink and downlink at each time slot; (4) the serial computation of the components for local execution where parallel processing is not feasible; and (5) the completion deadline of application components. This optimal cognitive scheduling and cloud offloading scheme is compared experimentally to the state-of-the-art techniques using real data that includes values for active power, transmission and reception powers of radio interfaces, time to process components in the mobile and cloud, uplink and downlink delays, and queue buffer lengths for wireless interfaces. The real data was obtained from an HTC vivid smartphone and two wireless networks: WiFi and LTE. NSFCloud [42] was used as the cloud server for these comparisons and measurements were taken for both indoor and outdoor environments.

This work [37] proposes a holistic approach for optimal cognitive mobile cloud offloading and scheduling in multi-RAT-enabled mobile devices where the component dependencies are kept intact for partial offloading decisions either on the mobile or on the cloud. Simultaneously, the strategy remains adaptive to the instantaneous changes of wireless network parameters under the presence of several system constraints. The implementation results illustrated that the energy consumed by the mobile device using this approach is 51, 23, 68, and 42% lower in comparison to the best-interface protocol, offline schemes, mobile-only, and cloud-only executions, respectively.

Summary and Future Directions of Spectrum-Aware Mobile Computing

Cognitive radio networking, a relatively newer paradigm in wireless networking, offers among other things a strong feature to opportunistically share spectrum. Using this technology, recent commercial wireless platforms offer bandwidth aggregation services such that the mobile user can use several wireless networks (e.g., WiFi and Cellular) simultaneously to distribute their load and achieve an aggregate throughput. SpiderRadio, a cognitive radio prototype router, developed at Stevens Institute of Technology, offers cloud controlled dynamic spectrum access and management [50]. Among other things, this router can aggregate bandwidth from multiple wireless networks in the licensed as well as unlicensed bands.

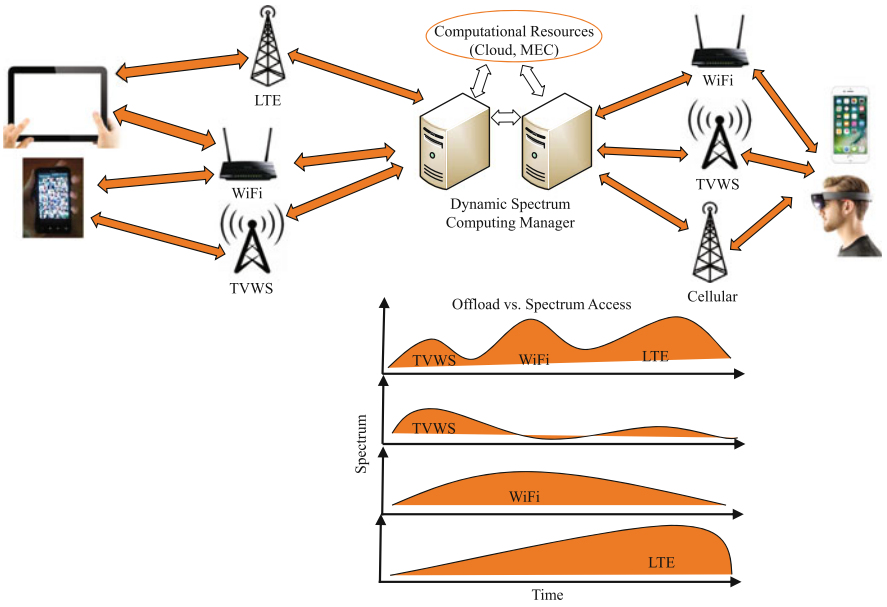

Fig. 5 Cognitive cloud offloader-spectrum manager. The future of mobile computing can apply cognitive radio networking technologies to efficiently use spectrum opportunities when offloading components to the cloud while also being able to aggregate bandwidths from appropriate wireless networks

Given these developments, the future of cloud offloading lies in a holistic approach that will be cognizant of spectrum diversity and opportunity and will be able to access more than one network at a time for offloading needs. We envisage a future as depicted in Fig. 5. The framework will be an integrated cognitive cloud offloader-spectrum manager that is categorized into two parts of dynamic computation offloader that schedules energy and radio spectrum-aware offloaders for application components and the dynamic spectrum manager that will determine spectrum management decisions adaptive with the online network parameters. Therefore, dynamic spectrum management and offloading strategies will be obtained jointly.

As detailed in sections "Spectrum-Aware Offloading Using Single-RAT Devices" and "Spectrum-Aware Cloud Offloading Using On/Off Multi-RAT Networking", there is a good body of work that considers wireless-aware mobile computing. These works have used only *single-RAT* wireless networks at a time or *multichannel* wireless (as opposed to multi-RAT network). In cases where multiple wireless networks have been used [20], the offload scheduler typically only chooses *one* of the available networks for offloading. The first *cognitive computation offloading* strategy for multi-RAT devices, where all viable wireless interfaces are simultaneously used to offload using the optimal distribution of offload data over wireless interfaces, was proposed in [35]. While this strategy was a one-shot (offline) offloading strategy, online (time-adaptive) strategies for cognitive offloading were studied in [34, 37]

where dynamic parameters for wireless environment are considered. These works also remove the assumption of a serial dependency graph and allows for an organic execution order to be determined by the spectrum-aware scheduler. This parallel processing scheme also allows for more degrees of freedom in the solution by moving away from a predetermined compiler-generated scheduling order for the components toward a more wireless-aware scheduling order. A spectrum-aware optimization problem was developed in [37] to determine the best cognitive computation offloading-scheduling policy for multi-radio-enabled mobile devices. The constraints of this offloading-scheduling scheme include overall runtime of the application, precedence of application components, percentages of associated data transfer via each radio, and completion deadline of components. Since the optimization problem is NP-hard and the system complexity will be high, an online heuristic algorithm that converges to a local optimum was studied in [34].

The preliminary results in [34, 37] are encouraging and make a case for the joint design of offloading and spectrum management. Clearly, components of applications can have more complex relationships, which might mean that parts of the program can be parallelized. Taking care of these complex relationships and parallelizing where possible in the joint scheduling-bandwidth management solutions can be expected to pay much better dividends in terms of energy costs as well as better and more informed utilization of the available wireless networks. Looking further into the future, it is possible to imagine that the spectrum-aware cloud offload manager will become spectrum-opportunistic, in the sense that the cognitive cloud offload manager will not only respond to known available wireless networks but will also actively seek spectrum opportunities at runtime to distribute the load more effectively.

Mobility models also can be incorporated to further enhance the understanding of spectrum-aware mobile computing in a mobile multi-network environment. This concept offers new research topics that guarantee promise of 5G technologies such that more resource-aware schemes and faster application runtimes will be provided. The impact of mobility in cloud offloading have been addressed recently in [4, 12, 13, 15, 22, 31, 52, 61, 66]. Some works have addressed this problem for the scenarios where centralized cloud resources are used [4, 12, 13, 52, 66], and the others considered the scenario where computations are offloaded to nearby mobile resource-rich devices (i.e., mobile edge computing (MEC) devices) [6, 22, 61]. There are open problems to be solved in considering the mobile heterogeneous networks such as achieving the capacity of mobile HetNets [24], hand-off [25, 28], impact of geographical and spectral mobility of the users [28, 46], quality of service (QoS)/quality of experience (QoE) [64], and interference between wireless radio interfaces [1].

In heterogeneous delay-tolerant networks (DTNs) (including broadcasting and unicasting routing and distributed systems), a probabilistic epidemic spreading scheme regarding the mobility of the users' neighbors is considered for data offloading [47]. In epidemic spreading, delay is analyzed under a large class of node mobility patterns in a set of fully heterogeneous Poisson processes. A mobile HetNet topology challenges the classic cellular system framework in (i) using uniform

hexagonal grid to model the base station locations (ii) using the concept that a mobile user should generally connect to the one base station providing the strongest signal, which in a HetNet is quite often not the one providing the best rate or network performance [17].

Another approach to monitor the mobility model of the users in HetNets is hierarchical interference management based on clustering and resource allocation for dense cells (especially Femtocells) [1]. In this approach, correlation clustering is used for Femtocell grouping and within each cluster, one Femto access point is elected as a cluster head that is responsible for power and subchannel allocation among the Femtocells in that cluster. Also, joint reduction of mobile data traffic and delay is investigated in [29] where different operation modes are defined depending on the popularity of the data object (e.g., those that are frequently updated such as stock information), and only popular data objects are proactively pushed to the access point to minimize the delay while mitigating the traffic load over the wireless link. A network mobility management framework is introduced in [28] to mitigate heterogeneous spectrum availability such that a target cell and spectrum band for cognitive radio users are dynamically relied on time-varying spectrum opportunities. Also a proper hand-off mechanism to minimize the switching latency at the cell boundary is discussed by considering spatially heterogeneous spectrum availability. Mobility-aware call admission control with hand-off queuing is analyzed in [25] for two vehicular scenarios: (i) when vehicle is static – a hand-off priority scheme with guard channels is studied to protect vehicular hand-off users; (ii) when vehicle is moving: no guard channels for hand-off users are allocated to maximize the channel utilization.

Offloading computations to the nearby mobile resource-rich devices such as MECs [22, 61] and fog services [6] is another research area for mobile computing that has recently been significantly developed. There are two limitations in the approach of using these cloudlets: intermittent connectivity to cloudlet and cloudlet capacity. An optimal partial offloading algorithm, considering the users' mobility patterns and cloudlets' admission control, is proposed in [61]. This algorithm is obtained by deriving the probability of successful offloading actions.

Fog computing is also a framework that uses some end-user clients or near-user edge devices for storage and offloading (rather than routed over the Internet backbone). Using the mobility characteristics, such as edge location, location awareness, and latency, Internet of things (IoT) services will be applicable in this framework [6].

References

1. Abdelnasser A, Hossain E, Dong IK (2014) Clustering and resource allocation for dense femtocells in a two-tier cellular OFDMA network. IEEE Trans Wirel Commun 13:3:1628–1644
2. Balakrishnan P, Tham C-K (2013) Energy-efficient mapping and scheduling of task interaction graphs for code offloading in mobile cloud computing. In: IEEE/ACM 6th International Conference on Utility and Cloud Computing (UCC), pp 34–41

3. Barak O, Touboul A (2009) Point to point link and communication method. US Patent 7,593,729: https://www.google.com/patents/US7593729
4. Barbarossa S, Sardellitti S, Di Lorenzo P (2013) Computation offloading for mobile cloud computing based on wide cross-layer optimization. In: Future Network and Mobile Summit (FutureNetworkSummit), pp 1–10
5. Bari F, Leung VCM (2007) Automated network selection in a heterogeneous wireless network environment. IEEE Netw 21:1:34–40
6. Bonomi F, Milito R, Zhu J, Addepalli S (2012) Fog computing and its role in the Internet of things. In: Proceedings of the First Edition of the MCC Workshop on Mobile Cloud Computing. ACM, pp 13–16
7. Cai X, Chen L, Sofia R, Wu Y (2007) Dynamic and user-centric network selection in heterogeneous networks. In: IEEE International Performance, Computing, and Communications Conference (IPCCC), pp 538–544
8. Chen X, Wu J, Cai Y, Zhang H, Chen T (2015) Energy-efficiency oriented traffic offloading in wireless networks: a brief survey and a learning approach for heterogeneous cellular networks. IEEE J Sel Areas Commun 33:4:627–640
9. Chun B-G, Maniatis P (2009) Augmented smartphone applications through clone cloud execution. In: Proceedings of the 12th Conference on Hot Topics in Operating Systems, Monte Verit, pp 8–8
10. CPLEX, IBM (2017). http://www-01.ibm.com/software/commerce/optimization/cplex-optimizer/
11. Cuervo E, Balasubramanian A, Cho D-k, Wolman A, Saroiu S, Chandra R, Bahl P (2010) MAUI: making smartphones last longer with code offload. In: International Conference on Mobile Systems, Applications, and Services, pp 49–62
12. Deng S, Huang L, Taheri J, Zomaya AY (2015) Computation offloading for service workflow in mobile cloud computing. In: IEEE Transactions on Parallel and Distributed Systems (early access)
13. Di Lorenzo P, Barbarossa S, Sardellitti S (2015) Joint optimization of radio resources and code partitioning in mobile cloud computing. IEEE Trans Mob Comput. Under second round of review, arXiv preprint arXiv:1307.383
14. Galvez JJ, Vaidya N (2014) Dynamic switching with heterogeneous channels in multichannel 802.11 WLANs. University of Illinois. http://www.crhc.illinois.edu/wireless/papers/galvez-ocs.pdf
15. Gao W, Li Y, Lu H, Wang T, Liu C (2014) On exploiting dynamic execution patterns for workload offloading in mobile cloud applications. In: IEEE 22nd International Conference on Network Protocols (ICNP), pp 1–12
16. Georgiadis L, Neely MJ, Tassiulas L (2006) Resource allocation and cross-layer control in wireless networks. Foundations and trends in networking. Now Publishers Inc., Hanover, pp 1:1:1–144
17. Ghosh A, Mangalvedhe N, Ratasuk R, Mondal B, Cudak M, Visotsky E, Thomas TA, Andrews JG, Xia P, Jo HS, Dhillon HS, Novlan TD (2012) Heterogeneous cellular networks: from theory to practice. IEEE Commun Mag 50:6:54–64
18. Hall LA, Schulz AS, Shmoys DB, Wein J (1996) Scheduling to minimize average completion time: off-line and on-line approximation algorithms. Universität Berlin. Fachbereich 3 - Mathematik, Berlin
19. Hou J, O'brien D (2006) Vertical handover-decision-making algorithm using fuzzy logic for the integrated radio-and-OW system. IEEE Trans Wirel Commun 5:1:176–185
20. Huang D, Wang P, Niyato D (2012) A dynamic offloading algorithm for mobile computing. IEEE Trans Wirel Commun 11:6:1991–1995
21. Ismail M, Gamage AT, Weihua Z, Xuemin S, Serpedin E, Qaraqe K (2015) Uplink decentralized joint bandwidth and power allocation for energy-efficient operation in a heterogeneous wireless medium. IEEE Trans Commun 63:4:1483–1495
22. Jin A, Song W, Wang P, Niyato D, Ju P (2015) Auction mechanisms toward efficient resource sharing for cloudlets in mobile cloud computing. IEEE Trans Serv Comput 99:1–1

23. Johansson K, Bergman J, Gerstenberger D, Blomgren M, Wallén A (2009) Multi-carrier HSPA evolution. In: IEEE Vehicular Technology Conference, pp 1–5
24. Khan Z, Ahmadi H, Hossain E, Coupechoux M, DaSilva L, Lehtomaki J (2014) Carrier aggregation/channel bonding in next generation cellular networks: methods and challenges. IEEE Netw 28:6:34–40
25. Kim Y, Ko H, Pack S, Lee W, Shen X (2013) Mobility-aware call admission control algorithm with handoff queue in mobile hotspots. IEEE Trans Veh Technol 62:8:3903–3912
26. Kosta S, Aucinas A, Hui P, Mortier R, Zhang X (2012) ThinkAir: dynamic resource allocation and parallel execution in the cloud for mobile code offloading. In: IEEE Proceedings of INFOCOM, pp 945–953
27. Kovachev D, Yu T, Klamma R (2012) Adaptive computation offloading from mobile devices into the cloud. In: IEEE International Symposium on Parallel and Distributed Processing with Applications (ISPA), pp 784–791
28. Lee W-Y, Akyildiz IF (2012) Spectrum-aware mobility management in cognitive radio cellular networks. IEEE Trans Mob Comput 11:4:529–542
29. Lee G, Jang I, Pack S, Shen X (2014) FW-DAS: fast wireless data access scheme in mobile networks. IEEE Trans Wirel Commun 13:8:4260:4272
30. Lim Y-s, Chen Y-C, Nahum EM, Towsley D, Gibbens RJ (2014) Improving energy efficiency of MPTCP for mobile devices. arXiv preprint arXiv:1406.4463
31. Lin Y, Chu ET, Lai Y, Huang T (2013) Time-and-energy-aware computation offloading in handheld devices to coprocessors and clouds. IEEE Syst J 9:2:393–405
32. Lin X, Wang Y, Xie Q, Pedram M (2015) Task scheduling with dynamic voltage and frequency scaling for energy minimization in the mobile cloud computing environment. IEEE Trans Serv Comput 8:2:175–186
33. Ma X, Zhao Y, Zhang L, Wang H, Peng L (2013) When mobile terminals meet the cloud: computation offloading as the bridge. IEEE Netw 27:5:28–33
34. Mahmoodi SE, Subbalakshmi KP (2016) A time-adaptive heuristic for cognitive cloud offloading in multi-RAT enabled wireless devices. IEEE Trans Cogn Commun Netw 2:2:194–207
35. Mahmoodi SE, Subbalakshmi KP, Sagar V (2015) Cloud offloading for multi-radio enabled mobile devices. In: IEEE International Communication Conference (ICC), pp 1–6
36. Mahmoodi SE, Uma RN, Subbalakshmi KP (2016) Optimal joint scheduling and cloud offloading for mobile applications. IEEE Trans Cloud Comput PP(99):1. doi:10.1109/TCC.2016.2560808
37. Mahmoodi SE, Subbalakshmi KP, Uma RN (2017) Optimal cognitive scheduling and cloud offloading for mobile applications in multi-radio enabled devices. IEEE Trans Mob Comput. Under 2nd round of review, pp 1–11
38. MPTCP in iOS (2017). https://support.apple.com/en-us/HT201373
39. Neely MJ (2010) Stochastic network optimization with application to communication and queuing systems. Morgan and Claypool Publishers. ISBN:160845455X, 9781608454556
40. Nguyen-Vuong Q-T, Ghamri-Doudane Y, Agoulmine N (2008) On utility models for access network selection in wireless heterogeneous networks. In: IEEE Network Operations and Management Symposium, pp 144–151
41. Nir M, Matrawy A, St-Hilaire M (2014) An energy optimizing scheduler for mobile cloud computing environments. In: IEEE Conference on Computer Communications Workshops (INFOCOM), pp 404–409
42. NSFCloud (2017). https://www.chameleoncloud.org/nsf-cloud-workshop/
43. Ou S, Yang K, Zhang J (2007) An effective offloading middleware for pervasive services on mobile devices. Pervasive Mob Comput 3:4:362–385
44. Ousterhout JK (1998) Scripting: higher level programming for the 21st century. Computer 31(3):23–30
45. PC World (2017). http://www.pcworld.com/article/2936872/wifi-and-lte-join-up-for-gigabit-mobile-service-in-korea.html
46. Peng M, Li Y, Jiang J, Li J, Wang C (2014) Heterogeneous cloud radio access networks: a new perspective for enhancing spectral and energy efficiencies. IEEE Wirel Commun 21:6:126–135

47. Picu A, Spyropoulos T, Hossmann T (2012) An analysis of the information spreading delay in heterogeneous mobility DTNs. In: IEEE International Symposium on a World of Wireless, Mobile and Multimedia Networks (WoWMoM), pp 1–10
48. Ramachandran KN, Belding EM, Almeroth KC, Buddhikot MM (2006) Interference-aware channel assignment in multi-radio wireless mesh networks. In: IEEE Conference on Computer Communications (INFOCOM), pp 1–12
49. Rui Y, Cheng P, Li M, Zhang QT, Guizani M (2013) Carrier aggregation for LTE-advanced: uplink multiple access and transmission enhancement features. IEEE Wirel Commun 20:4:101–108
50. Sagar V (2016) Software defined access: cognition in multi-radio networks. PhD dissertation at Stevens Institute of Technology, Hoboken
51. Saquib N, Hossain E, Dong IK (2013) Fractional frequency reuse for interference management in LTE-advanced hetnets. IEEE Wirel Commun 20:2:113–122
52. Sardellitti S, Scutari G, Barbarossa S (2014) Joint optimization of radio and computational resources for multicell mobile cloud computing. In: IEEE 15th International Workshop on Signal Processing Advances in Wireless Communications (SPAWC), pp 354–358
53. Satyanarayanan M, Bahl P, Caceres R, Davies N (2009) The case for VM-based cloudlets in mobile computing. IEEE Pervasive Comput 8:4:14–23
54. Shi C, Pandurangan P, Ni K, Yang J, Ammar M, Naik M, Zegura E (2013) IC-cloud: computation offloading to an intermittently-connected cloud. In: SCS Technical Report in Georgia Institute of Technology. http://hdl.handle.net/1853/45985
55. Shi C, Habak K, Pandurangan P, Ammar M, Naik M, Zegura E (2014) COSMOS: computation offloading as a service for mobile devices. In: Proceedings of the ACM International Symposium on Mobile Ad Hoc Networking and Computing (MobiHoc), pp 287–296
56. Shu P, Liu F, Jin H, Chen M, Wen F, Qu Y (2013) eTime: energy-efficient transmission between cloud and mobile devices. In: IEEE Proceedings of INFOCOM, pp 195–199
57. Stevens-Navarro E, Wong VWS (2006) Comparison between vertical handoff decision algorithms for heterogeneous wireless networks. IEEE Veh Technol Conf (VTC) 2: 947–951
58. Toma ASM, Chen J-J (2014) Computation offloading for frame-based real-time tasks under given server response time guarantees. Leibniz Trans Embed Syst 1:2:1–21
59. Wang L, Kuo G-SGS (2013) Mathematical modeling for network selection in heterogeneous wireless networks; a tutorial. IEEE Commun Surv Tutorials 15:1:271–292
60. Wu H, Wang Q, Wolter K (2013) Tradeoff between performance improvement and energy saving in mobile cloud offloading systems. In: IEEE International Conference on Communications Workshops (ICC), pp 728–732
61. Zhang Y, Niyato D, Wang P (2015) Offloading in mobile cloudlet systems with intermittent connectivity. IEEE Trans Mob Comput 14(12):2516–2529
62. Zhang W, Wen Y, Guan K, Kilper D, Luo H, Wu DO (2013) Energy-optimal mobile cloud computing under stochastic wireless channel. IEEE Trans Wirel Commun 12:9:4569–4581
63. Zhang W, Wen Y, Wu DO (2013) Energy-efficient scheduling policy for collaborative execution in mobile cloud computing. In: IEEE Proceedings of INFOCOM, pp 190–194
64. Zhang X, Zhang Y, Yu R, Wang W, Guizani M (2014) Enhancing spectral-energy efficiency for LTE-advanced heterogeneous networks: a users social pattern perspective. IEEE Wirel Commun 21:2:10–17
65. Zhang Y, Niyato D, Wang P (2015) Offloading in mobile cloudlet systems with intermittent connectivity. IEEE Trans Mob Comput 14:12:2516:25291–10
66. Zhang W, Wen Y, Wu DO (2015) Collaborative task execution in mobile cloud computing under a stochastic wireless channel. IEEE Trans Wirel Commun 14:1:81–93
67. Zhou B, Dastjerdi AV, Calheiros RN, Srirama SN, Buyya R (2015) A context sensitive offloading scheme for mobile cloud computing service. In: IEEE International Conference on Cloud Computing (CLOUD), pp 869–876
68. Zorzi M, Zanella A, Testolin A, De Filippo De Grazia M, Zorzi M (2015) Cognition-based networks: a new perspective on network optimization using learning and distributed intelligence. IEEE Access 3:1512–1530

Cognitive Radio Network Security

23

Olga León and K. P. Subbalakshmi

Contents

Abstract

Cognitive radio networks (CRNs) emerge as a possible solution to increase spectrum efficiency by allowing cognitive radios (CRs) to access spectrum in an opportunistic manner. Although security in CRNs has received less attention than other areas of CR technology, the need for addressing security issues is evidenced by two facts. First, as for any other type of wireless network, an open

O. León (✉)
Telematics department, Universitat Politècnica de Catalunya, Castelldefels, Barcelona, Spain
e-mail: olga@entel.upc.edu

K. P. Subbalakshmi
Electrical and Computer Engineering, Stevens Institute of Technology, Hoboken, NJ, USA
e-mail: ksubbala@stevens.edu

W. Zhang (ed.), *Handbook of Cognitive Radio*,
https://doi.org/10.1007/978-981-10-1394-2_23

channel is used for communications that can easily be accessed by attackers. On the other hand, the particular attributes of CRNs raise new opportunities to malicious users, which can disrupt network operation. In this chapter, we provide an overview of those threats that are specific to CRNs. We classify them according to the layer in which the attacks are performed, give an insight of their impact on the network performance, and describe potential countermeasures that can be used to prevent them or mitigate their effect.

Introduction

The proliferation of wireless applications during the last years has led to spectrum shortage. Most of the frequency bands have been assigned by regulator bodies, such as the Federal Communications Commission (FCC) in the USA, to specific services that operate under license. License-free bands, such as the Industrial, Medical and Scientific (ISM) band, rapidly became overcrowded with the explosion of new technologies. However, recent studies show that many licensed spectrum bands are being infra-utilized by their legitimate users, which gives rise to usage of this spectrum in an opportunistic manner.

Cognitive radio networks (CRNs) [4] can improve spectrum utilization by allowing non-licensed users to act as secondary users (SUs) of those portions of the spectrum left unused by the licensed services or primary users (PUs), provided that no interferences are caused to the latter. With the emergence of software-defined radios (SDRs) [15], cognitive radio (CR) systems can become a reality. An SDR can be defined as a radio where transmission frequency, modulation type, and other radio frequency (RF) parameters can be configured and reconfigured by software. As a consequence, they can provide a wide range of services with variable quality of service (QoS) in order to adapt to different network technologies and to the dynamics of radio propagation. The addition of cognition capability to an SDR led to the idea of a CR, an intelligent radio capable of tuning itself based on its own perception of the spectrum availability and the environment conditions, and learn from past experiences.

Consider the network model shown in Fig. 1; a primary network is an existing network infrastructure operating with license in a given spectrum band, such as current cellular or TV broadcast networks and offering its services to incumbents or PUs. In this context, a CRN is allowed to operate in both licensed and unlicensed bands. When using the licensed band, the CRN may coexist with existing primary networks, and thus it is seen as a secondary network, where secondary users are allowed to use the spectrum in an opportunistic manner. Therefore, a CRN must perform spectrum sensing in order to identify the portions of spectrum left unused by primary networks and, among those available, select the channel with best conditions. During its operation in a given channel, a CRN must keep on performing spectrum sensing, and, whenever a primary transmission is detected in the current band of operation, it must immediately vacate the channel and switch to another one, a process known as spectrum handoff. Note that many CRN may overlap

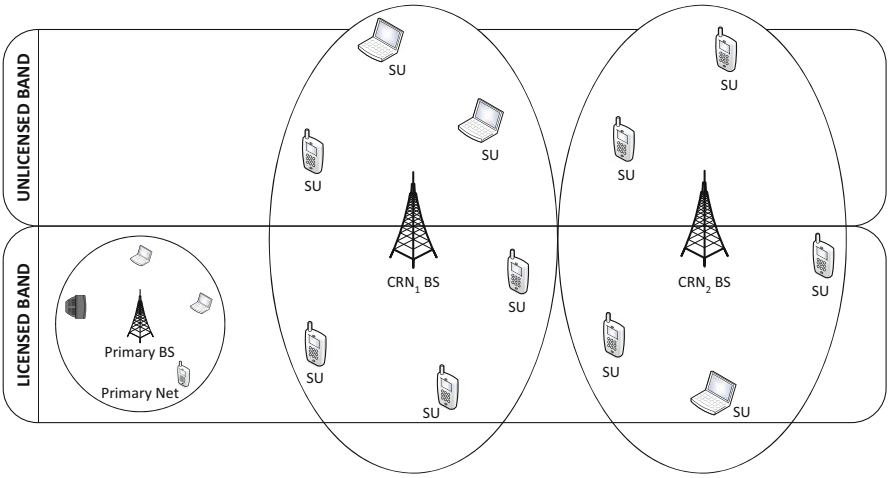

Fig. 1 CRN model

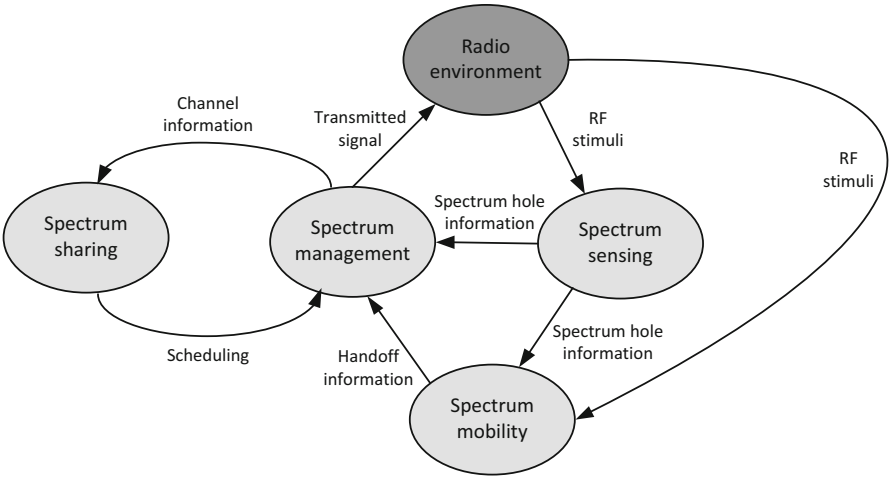

Fig. 2 Cognitive radio cycle

trying to make use of the spectrum left by a primary network, also referred as self-coexistence. As a consequence, there is also a need for mechanisms to enable coexistence among overlapping CRNs. CRs must perform several functions in order to adapt to the environment, known as the cognitive cycle (see Fig. 2):

- Spectrum sensing: it is needed to sense the medium in order to detect unused spectrum and avoid causing harmful interference to legitimate users of the spectrum.

- Spectrum management: a CRN must select the best available channel to meet user communication requirements.
- Spectrum mobility: a channel must be vacated when a licensed user is detected while maintaining seamless communication requirements during the transition to better spectrum.
- Spectrum sharing: a fair spectrum scheduling method among coexisting secondary users must be provided.

Spectrum Sensing in CRNs

Spectrum sensing mechanisms are thus indispensable to prevent harmful interferences to PUs. An SU can use several detection mechanisms in order to detect the existence of PUs [39]:

- Matched filter detection. A matched filter is obtained by correlating the unknown signal with a known signal or a template. When there is prior knowledge of the primary signal, it is the optimal detection method.
- Energy detection. In this approach the received signal strength is measured and compared to a threshold to determine if the channel is idle or not. Its performance is poor under low signal-to-noise ratios (SNRs) and cannot discriminate between signals, i.e., cannot distinguish between a primary signal and interference signals coming from other secondary users. However, it is considered the optimal detection method when there is no a priori knowledge of the primary signal.
- Radio identification-based detection. This category covers a set of techniques which are based on extracting several features from the signal such as frequency, transmission range, modulation technique, etc. One of these techniques is cyclostationary detection, which exploits the periodic properties of the received signal that cannot be found in random noise or interferences signals.

Matched filter detection and radio identification-based detection are more robust to noise uncertainties than energy detection but they are rather complex and require a significantly long observation time. Because of its simplicity and less overhead, energy detection is the most widely used technique in CRNs.

Typically, local sensing for primary signal detection can be formulated as a binary hypothesis problem as in 1.

$$x(t) = \begin{cases} n(t) & H_0 \\ h(t) \cdot s(t) + n(t) & H_1 \end{cases} \tag{1}$$

where $x(t)$ is the received signal at the SU, $s(t)$ is the PU signal, $h(t)$ is the channel gain, $n(t)$ is the zero-mean additive white Gaussian noise (AWGN), and $H0$ and

$H1$ denote the test hypothesis denoting the absence and presence, respectively, of the PU signal. Detection mechanisms are evaluated by means of two parameters: the probabilities of detection P_d and false alarm P_f are defined as in (2) and (3).

$$p_d = \Pr(\text{decision} = H_1|H_1) = \Pr(Y > \lambda|H_1) \tag{2}$$

$$p_{fa} = \Pr(\text{decision} = H_1|H_0) = \Pr(Y > \lambda|H_0) \tag{3}$$

where Y is the decision statistic and λ is the decision threshold. The value of λ is set depending on the requirements of detection performance. Based on an AWGN channel, these values can be computed as in (4) and (5).

$$p_d = Q_m(\sqrt{2\gamma}, \sqrt{\lambda}) \tag{4}$$

$$p_{fa} = \frac{\Gamma(m, \frac{\lambda}{2})}{\Gamma(m)} \tag{5}$$

where $m = TW$, which is the time-bandwidth product of the energy detector, $Q_m(a, b)$ is the generalized Marcum Q-function, $\Gamma(.)$ the complete gamma function and $\Gamma(.,.)$ the upper incomplete gamma function.

Low values for p_d result in missing the presence of a primary user with high probability and can lead to interferences to primary transmissions. On the other hand, a high p_d results in low spectrum utilization, since secondary users miss spectrum opportunities. The probability of misdetection can then be computed as $p_{md} = 1 - p_d$. Typical values are $p_d = 0.1$, $p_{md} = 0.9$, and $p_{fa} = 01$.

A single CR may fail to detect the presence of a primary signal due to fading or shadowing. However, it is unlikely that all secondary users within a CRN experience fading or shadowing concurrently. Therefore, cooperative spectrum sensing (CSS) [5] can help to improve the probability of detection by taking into account sensing reports from several CRs. Cooperation provides with space diversity and overcomes the limitations introduced by bad environment conditions in a particular area of the network.

In CSS, each secondary user takes a measurement and shares its report in order to take a global decision. The combination of all reports, a.k.a. data fusion, can be centralized or distributed; when it is centralized, all CRs sent the reports to a single fusion center (FC), e.g., the BS, which is responsible for taking a global decision and report back the results to the members of the CRN. If it distributed, every CR can act as an FC receiving sensing information from the neighboring nodes and taking a decision locally. Then, individual decisions can be shared among CRs and converge by iterations to a unified decision. On the other hand, sensing reports may contain the observed data by a particular receiver, an approach known as **soft fusion**, or its individual decision about the existence of a primary, known as **hard**

fusion. Soft fusion generally provides better results in terms of primary detection but requires the transmission of a high volume of data. Hard fusion reduces the amount of transmitted data because each node only needs to send one bit of information.

Fusion Data Mechanisms

Hypothesis testing is usually used in soft-fusion mechanisms, which relies on statistical tests used to determine whether there is enough evidence in a sample of data to infer that a certain condition is true for the entire population. In the cooperative spectrum sensing mechanism of CRNs, the sample of data is composed of the set of reports sent by SUs.

The test examines two opposing hypotheses: H_0 or the absence of PU and H_1 or the presence of PU. One of the basic hypothesis testing methods is the Neyman-Pearson (NP) test. The NP test aims at maximizing the detection probability p_d given the constraint $p_{fa} \leq \alpha$, being α is the maximum false alarm probability.

According to the individual signal detection in (1), the NP test is equivalent to the following test:

$$\Lambda(\mathbf{y}) = \frac{f(\mathbf{y}|H_1)}{f(\mathbf{y}|H_0)} = \prod_{k=1}^{N} \frac{f(\mathbf{y}_k|H_1)}{f(\mathbf{y}_k|H_0)} \underset{<H_1}{\geq H_0} \lambda \tag{6}$$

where $\Lambda(\mathbf{y})$ is the likelihood ratio, $f(\mathbf{y}|H_1)$ is the distribution of observations $\mathbf{y}$ under hypothesis H_j, $j \in (0, 1)$, λ is the detection threshold, and N is the number of samples. The likelihood ratio indicates how many times more likely the set of measurements are under one model than the other.

The second equality in (6) holds only if the observations $\mathbf{y}_k$ are independent and identically distributed (i.i.d.) under H_j. As a result, it is the optimal test if the conditional independence is assumed. Another disadvantage of this method is that it requires a fixed number of measurements, which can lead to a large sensing time.

An alternative to reduce the sensing time is the sequential probability ratio test (SPRT). In SPRT, samples are taken sequentially, and the test statistics are compared with two thresholds λ_0 and λ_1, with $\lambda_0 < \lambda_1$, which are determined by detection requirements. If the likelihood ratio is greater than λ_1, the detector outputs $H1$, and H_0 if it is smaller than λ_0. Otherwise, it waits for the next measurement, as more samples are needed in order to take a decision. The main advantage of the SPRT is that it requires fewer samples on the average than those fixed-sample testing methods to achieve the same detection performance, but it also requires a priori knowledge of the distribution probability of measurements and assumes identical probability distributions for all users.

Regarding hard-fusion mechanisms, the OR, AND, and the "k out of N" rules can be used. Q_d and Q_{fa} are then defined, respectively, as the probability of detection and false alarm of the fusion mechanism given the reports of a set of N SUs.

- **OR rule**. The final decision is H_1 if at least one of N SUs reports "1." The probabilities of false detection and false alarm are then given by (7).
- **AND rule**. The final decision is H_1 if all SUs report "1." The probabilities of false detection and false alarm are then given by (8).
- **k out of N rule**. The final decision is H_1 if at least k out of the N SUs report "1." The probabilities of false detection and false alarm are then given by (9).

$$Q_d = \prod_{i=1}^{N}(1 - p_{d,i}) \quad Q_{fa} = \prod_{i=1}^{N}(1 - p_{fa,i}) \tag{7}$$

$$Q_d = \prod_{i=1}^{N} p_{d,i} \quad Q_{fa} = \prod_{i=1}^{N} p_{fa,i} \tag{8}$$

$$Q_d = \sum_{i=k}^{N} \binom{N}{i} p_{d,i}^{i}(1 - p_{d,i})^{N-i} \quad Q_{fa} = \sum_{i=k}^{N} \binom{N}{i} p_{fa,i}^{i}(1 - p_{fa,i})^{N-i} \tag{9}$$

where $p_{d,i}$ and $p_{fa,i}$ are the individual probabilities of detection and false alarm of user i.

The OR rule works best, i.e., maximizes the detection probability and minimizes the false alarm probability, for a large number of cooperative users, while the AND rule presents its best performance for a small number of users. The majority rule can be obtained by means of the k out of N rule, under the condition $k \geq N/2$. In such case, it is important to obtain the value of k for which the detection errors are minimized. It can be shown [5] that this value depends on the individual detection threshold λ (see Eqs. 2 and 3).

Classification of CRNs

CRNs can be classified into **centralized** or **distributed** according to their architecture. In centralized networks there is a single top-level entity in charge of network management, typically a base station (BS). In this type of networks, CSS is performed in a centralized way, and the BS takes decisions about spectrum access.

In a distributed network, management is shared by several entities, and communications takes place in an ad hoc manner. Because of this, distributed CRNs are also known as cognitive radio ad hoc networks (CRAHNs) [3]. When these entities are a subset of SUs, we refer to these networks as partially distributed. SUs are grouped into clusters according to some parameters, such as distance, and a cluster head is selected to be in charge of the cluster management. The CSS in partially distributed CRNs is performed in a centralized way, so members of a given cluster report their measurements to the cluster head, who takes decisions about spectrum availability. Note that the cluster head selection mechanism adds a significant overhead and can pose serious security problems if the cluster head node

is compromised. When the management is shared among all SUs and there is no central entity, then we talk about fully distributed networks. The CSS mechanism is distributed, and SUs exchange their reports among their neighbors in order to reach a joint spectrum decision. Due to the lack of a trusted central entity, management is much more complex, and the design of efficient security policies is hard to achieve. On the other hand, by distributing spectrum decisions among several SUs, the risk of denial of service (DoS) attacks against a single point of failure (i.e., the central entity) is eliminated.

CRNs can also be classified according to what extent they make use of the spectrum:

- **Spectrum interweave networks**. SUs use the spectrum without interfering PUs transmission either by accessing the spectrum in a TDMA (time division multiple access) or FDMA (frequency division multiple access). The goal is to find the spatial, temporal, or spectral gaps and use them for SUs transmission.
- **Spectrum underlay networks**. SUs transmit over the same spectrum as PUs but keeping interferences below a given level by means of spread spectrum techniques. This option requires, however, knowledge of the channel between the CRN transmitters and the PU receivers.
- **Spectrum overlay networks**. This sharing mechanism is similar to spectrum underlay, but in addition it requires the CRN to know about the PU operation. As an example, the CRN should know about the PU's codebooks allowing SUs to decode PU's transmissions.

The type of network plays an important role with regard to security issues. Generally speaking, distributed networks are more likely to be attacked since, due to the lack of a central entity, attack detection and prevention mechanisms are harder to implement. With regard to the use of the spectrum, underlay and overlay networks will require a more precise CSS mechanism in order to prevent harmful interferences to PUs. Thus, attacks to the CSS mechanism in such networks may be easier to implement and have a stronger impact on network performance.

Security in CRNs

Due to the openness of the wireless transmission channel, CRNs are exposed to well- known threats [35] but in addition, their particular features make them vulnerable to new attacks. Security attacks can be implemented against CRN functionalities by altering the radio environment or disrupting CSS mechanisms. CSS is built on the basis that nodes are honest and altruistic, making CRNs vulnerable to security threats such as selfish or malicious behaviors.

As in any other type of wireless network, the following security requirements should be fulfilled:

- Confidentiality, to ensure that data is not accessed by unauthorized users.
- Authentication, in order to verify the identity of the parties involved in a communication, ensure that data comes from a trusted source and prevent unauthorized injection of data.
- Integrity, to prevent an unauthorized user from altering data.
- Availability, to ensure that legitimate users can access network services.

The first three security services can be achieved by means of traditional cryptographic mechanisms, i.e., encryption, message authentication codes, and digital signatures. In fact, the IEEE 802.22 WRAN (wireless rural area networks) standard [1], the first wireless air interface standard based on CR technology, defines a MAC (medium access layer) security sublayer which provides basic security services by applying cryptographic transformations. This security sublayer has two main components: an encapsulation protocol and a PKM (Public Key Management) protocol. The encapsulation protocol defines a set of supported cryptographic suites and the rules for applying these algorithms to data. Confidentiality and integrity is achieved by means of AES-GCM, and network entry authorization is obtained by means of RSA and ECC-based X.509 certificates. On the other hand, the PKM protocol ensures the secure distribution of keying material among the members of the network.

Despite the abovementioned security mechanisms can be efficient to prevent some basic attacks, additional countermeasures are needed to deal with those that are specific to CRNs. As it will be shown in the following sections, most threats to CRNs are targeted to the spectrum sensing process used for detecting portions of free spectrum and selection of channels. These threats may lead to a DoS, thus preventing SUs from accessing network services.

In this chapter we provide an overview of the potential threats to CRNs and focus on those specific to CRNs. We classify them according to the layer in which they are performed, give an insight of their impact on the network performance, and describe potential countermeasures that can be used to prevent them or mitigate their effect.

Physical Layer Security

Eavesdropping

Wireless networks use an open transmission medium, and therefore they are susceptible to eavesdropping, meaning that an unauthorized user can access the

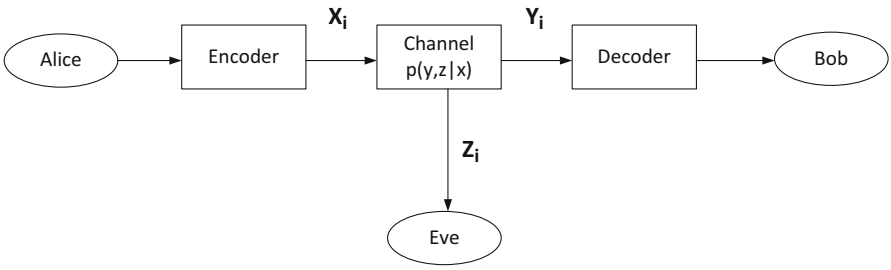

Fig. 3 Wiretap channel model

information transmitted by SUs. Traditionally, this attack has been addressed by means of cryptography implemented at the application level. However, in some scenarios, such as in ad hoc networks, it may be hard to distribute the cryptographic material, i.e., algorithms, keys, etc.

As a consequence, physical-layer security emerges as an effective mean to secure the wireless communications by exploiting the physical-layer characteristics of wireless channels. Wyner proposed the well-known wiretap channel model, a secrecy system consisting of a legitimate transmitter (Alice), a legitimate receiver (Bob), and an eavesdropper (Eve). Wyner showed that Alice can send confidential information to Bob while keeping it secret from Eve if the transmission rate is kept below a given threshold, which is known as **secrecy rate** or **secrecy capacity**. Figure 3 depicts the wiretap channel model. It has been shown that the secrecy capacity is the difference in capacities between the main channel (i.e., the channel from the transmitter to the legitimate receiver) and the eavesdropper channel (i.e., the channel from the transmitter to the eavesdropper) for a degraded discrete memoryless channel (DMC), as in (10).

$$C_s = \max_{p(x)} I(X;Y|Z) = \max_{p(x)}(I(X;Y) - I(X;Z)) \tag{10}$$

where the mutual information $I(X;Y)$ measures how much information the variables X and Y share.

Communication over a discrete memoryless channel, such as an AWGN channel, takes place in a discrete number of channel uses, indexed by a number $i \in N$. Alice sends a message to Bob by transmitting codewords which span n. Bob decodes the received signal, which is often corrupted by noise according to the statistical channel model and recovers the message. A discrete channel has finite input alphabets and output alphabets X_i and Y_i, respectively, which are related through a collection of conditional probability mass functions (pmfs) $p(y|x)$. In its turn, the wiretap channel is modeled by a set of pmfs $p(z|x)$.

Besides secrecy capacity, there are also some other parameters that depict the security of wireless networks. One is the leakage probability, which is the probability that the eavesdropper decodes its received codeword with an error

probability less than its target bit error rate. Another one is the security gap, which is the ratio of two SNRs, the SNR at which a very low-target bit error rate (BER) is achieved at the intended receiver and that at which a high BER is achieved at the eavesdropper. The smaller the security gap, the more likely that the transmitter can transmit over a time-varying wireless channel successfully.

Countermeasures

In order to prevent eavesdropping, it is needed to maximize the secrecy capacity of the main channel (Alice to Bob), while minimizing the capacity of the wiretap channel (Alice to Eve). This can be achieved by means of several techniques [44].

- **Security-oriented beamforming** consists in transmitting a signal in a given direction so that the signal received by the eavesdropper experiences destructive interference and becomes weaker, while the signal received by the legitimate receiver experiences constructive interference. In this way, the capacity of the main channel is higher than the capacity of the wiretap channel.
- **Relay-based techniques**. Relays are cooperative nodes that help the source to relay signals to the destination. The relay selection can also be employed to enhance the physical layer security in the presence of an eavesdropper. In a scenario where multiple relays are available, the relay node with the highest secrecy rate may be invoked if the channel state information (CSI) of both the main channel and the eavesdropper is known. If this information is not available, then the relay with the highest capacity will be chosen. When a relay assists nodes message transmission from a source to a destination, it forwards the signal to the destination by means of a given protocol: amplify and forward (AF) or decode and forward (DF) [23]. With the AF protocol, the relay node just simply retransmits a scaled version of its received noisy signal to the destination. By contrast, the DF protocol enables the relay first to decode its received signal and then forward its decode result to the destination. The AF protocol is simpler, but as a drawback, with this protocol the relay may also amplify and forward the received noise. This may result in a performance degradation at the destination in decoding the signal.
- **Artificial noise aided**. This approach enables the source to generate an interfering signal (referred to as artificial noise) in a such a way that it only interferes the eavesdropper. As a consequence, the capacity of the wiretap channel is decreased, and thus the secrecy capacity is increased. The main drawback of this proposal is that it requires more power consumption to generate the artificial noise and knowledge about the attacker. This strategy is also known as cooperative jamming, and it is usually performed by means of some relays that, instead of forwarding the legitimate signal, jam or generate interferences to prevent an attacker from eavesdropping the legitimate signal.
- **Multi-antenna-Based Techniques**. Multiple-input multiple-out (MIMO) is a method for increasing the capacity of a radio link by taking advantage of the extra degrees of freedom provided by multiple antennas. This technique increases the

capacity of the main channel by using multiple antennas to transmit and receive to exploit multipath propagation.

Jamming

Jamming in wireless networks is defined as the intentional disruption of existing communications by decreasing the signal-to-noise ratio at the receiver through the transmission of interfering wireless signals. In CRNs, a jammer may have two objectives: disrupting all the communications of primary and secondary users or preventing only secondary users from accessing the free spectrum bands. The former goal is a general problem of standard wireless communications, the latter one is specific to CRNs. Note that by disrupting the secondary users communications an attacker increases its chances to use the free spectrum.

Jamming can be achieved by spreading a flat spectrum power in the bandwidth of interest, i.e., band jamming, or by generating a sinusoidal waveform whose power is concentrated on the target carrier frequency, known as tone jamming. The latter might be more expensive and require more specific hardware, but in turn it is more effective and disruptive.

Depending on how a jammer selects the channels to perform the jamming attack, it can be classified into:

- **Sweeping attack**. A malicious node attacks a channel regardless of whether there is activity or not in that channel. In this attack, the jammer may waste resources by transmitting signals on a free channel that do not cause any interference to secondary users.
- **Fixed-strategy jamming**. The jammer senses the spectrum in order to identify the channel being used by the transmitter and the receiver and transmits an interfering signal on that channel. It is thus more efficient than a sweeping attack, since it only generates interfering signals on those channels that are being used by the network. However, because CRNs perform spectrum sensing and may switch to a better channel, such an attack would be inefficient once the CRN has moved to a different channel.
- **Cognitive jamming**. A cognitive jammer is defined in [16] as an adversary equipped with cognitive radio technology, which adapts to the CRN strategy with regard to channel selection in order to maximize the efficiency of the attack.

The impact of the attack will depend on the number of available channels, the number and location of jammers and their capabilities regarding power transmission and channel selection, but in any case it will degrade the overall network performance [36] and can lead to a DoS for some users.

Countermeasures

Traditional jamming countermeasures include the use of directional antennas instead of omnidirectional antennas, or spread spectrum (SS) techniques [18].

Directional antennas are used to improve energy efficiency by only radiating in the sector where the receiver is located, thus reducing the network interference level. In its turn, spread spectrum can be direct sequence (DSSS) or frequency hopping (FHSS) based. The former uses a wider bandwidth for signal transmission, allowing for greater resistance to unintentional and intentional interference. DSSS can be achieved by using the signal to be transmitted to modulate a bit sequence, known as a pseudo noise (PN) code that is much shorter in duration than the original signal. In FHSS, each available frequency band is divided into sub-frequencies, and the signal rapidly changes or hops among them in a predetermined order. In this way, interference at a specific frequency will only affect the signal during a short interval. A major disadvantage of this approach is that the channel switching algorithm, i.e., the sequence of channels that will be followed by the network, must be shared in advance between the sender and receiver. Also, this technique will be only effective provided that such algorithm is kept secret from the attacker.

Channel/frequency hopping has also been proposed as a countermeasure [43] in the context of CRNs. Channel hopping can be performed in a reactive or proactive way, depending on whether the CRN switches to another channel upon detection of the attack or according to a predetermined sequence or algorithm, which is shared in advance among the members of the network. In both cases, the hopping information must be exchanged through a shared control channel. This scheme is time-consuming due to the required frequency synchronization, channel estimation, handshaking for information exchange, and network setup. This approach will be more efficient in preventing jamming attacks, since generally speaking it may be difficult for an attacker to guess the hopping sequence. A major drawback, however, is that in a CRN, the available channels may be time-varying due to PUs activity, and using a fixed channel sequence may greatly reduce the throughput of the CRN.

Some recent works [37] propose to optimize channel selection based on network conditions but also on jammer patterns. The interaction between the CRN and the jammers is modeled as a stochastic game where the CRN goal is to maximize secondary users' throughput. At each stage of the game, secondary users observe the spectrum availability, the channel quality, and the attacker's strategy from the status of jammed channels. According to this observation, they will decide how many channels they should reserve for transmitting control and data messages and how to switch between the different channels. Because these techniques rely on observations of jammers behavior, they are more robust to cognitive jammers than the previous ones. Some works present similar countermeasures but targeted to mitigate the PUE attack (see section "PUE Attack"), which could also be applied to mitigate the effect of jamming.

Finding the location of a jammer is of paramount importance in order to prevent further interferences by, once the jammer is located, taking the appropiate security actions [30]. A CRN can take advantage of its cooperative nature to estimate the position of the attacker by making use of measurements provided by secondary users. This is also one of the countermeasures proposed for the PUE attack and will be discussed in detail in the next section.

Finally, the techniques presented in section "Countermeasures" to prevent eavesdropping can also be applied in order to enhance the throughput of jammed links.

PUE Attack

The primary user emulation (PUE) attack, first presented in [12], can be considered a sophisticated version of a jamming attack. Although both of them can degrade the performance of the network and reduce the throughput, they differ in that:

- While a jammer transmits an interfering signal, a PUE attacker transmits a signal emulating a PU transmission.
- The main goal of a jammer is to disrupt communications, while a PUE attack aims at preventing the CRN from using a free channel due to the (false) detected presence of a PU.

Generally speaking, a PUE attack is less resource-consuming since the transmission power required for a successful attack is lower than in a jamming attack. In particular, it is required that the received power at the secondary users is above the threshold set by the CRN for PU detection. However, it can be more complex depending on the selected detection mechanism (see section "Spectrum Sensing in CRNs"). Mechanisms such as cyclostationary detection will not consider the signal a legitimate PU transmission unless the PUE signal has the same characteristics as a real one in terms of power, modulation, etc. On the other hand, if energy detection is used, an attacker can succeed by transmitting any type of signal with the required transmission power. The ability of the attacker of mimicking a PU transmission is key to the success of a PUE attack. Parameters such as the characteristics of the transmitted signal, transmission power, and location of the attacker will determine the efficiency of the attack.

A PUE attacker can be malicious, if its only purpose is to interrupt the activity of the CRN, or selfish, if it aims at making use of the available bandwidth left by the CRN because of the attack. The PUE attack can be performed against a free channel during sensing period of the CRN or against the channel in use, forcing the CRN to vacate the channel and leading to the interruption of all communications until a new channel is available. In the worst scenario, the attack can lead to a DoS if the CRN fails to get an available channel. This may happen whenever the number of channels left unused by PUs is small or if the attacker resources are enough to perform PUE attacks over several channels simultaneously.

The activity of PUs and channel occupancy is often modeled as a Markov process with arrival rate λ_p and permanence time μ_p, in which every state represents the number of available channels for the CRN. Based on this model and on the attacker model, it is possible to get an estimate of the impact of a PUE attack on the network performance and the probability of a DoS. In [6], a model for the probability of a successful PUE attack is derived, as a function of the distance of the attacker from

the SUs and the energy threshold used during the PU detection. The authors state that under suitable power control and with more than an attacker, it is possible to obtain a probability equal to 1.

Countermeasures

The countermeasures for PUE attacks can be classified into:

- **Channel hopping**. As previously mentioned, channel hopping represents an effective countermeasure to avoid PUE [19] and jamming attacks, provided that the channel sequence cannot be predicted by an attacker. However, it leads the CRN to continuously perform frequency handoffs, implying the interruption of all communications until the CRN is completely operating at a new frequency. CRNs have been designed to deal with mild disruption due to the presence of PUs, and thus they can tolerate PUE attacks that have a similar impact. However, this measure will not be effective when a PUE attack is performed by an intelligent attacker that can guess the next channel to be selected by the CRN, or if the number of available channels is low.
- **Radio fingerprinting** is a process that identifies the device from which a radio transmission originated by looking at the properties of its transmission, including specific radio frequencies. Each signal originator has its own specific "fingerprint" based on the location and configuration of its transmitted signals. Even transmitters of the same type will show different characteristics during a transient period of time due to factors such as age or tolerance levels, which allow to uniquely identify every single transmitter. As a disadvantage, this method requires physical proximity to the PU in order to verify the fingerprints and the use of dedicated nodes to this end, a fact that considerably increases the cost of the method.
- **Cryptographic approaches**. Solutions based on cryptography can be integrated to prevent PUE attacks, such as including cryptographic signatures in PU signals or using integrity and authentication mechanisms for communications between primary and secondary CR users. The main problem with these approaches is that they do not meet the requirement of the FCC, which states that the utilization of available spectrum by SUs should be possible without requiring any modification to the incumbent users and their signals. Therefore, PU authentication is a challenging issue, and existing proposals are subject to practical limitations [24].
- **Location based**. If the location of the true PUs is known in advance, a PUE attacker can be detected by estimating the position of the transmission source and comparing it with the known locations. As an example, in IEEE 802.22 networks, the location of TV broadcast towers (PUs) can be obtained through access to geo-location databases.

The position of an emitter is usually estimated based on measures of certain distance-dependent parameters, such as the received signal strength (RSS), the time it takes to the signal to travel from the emitter to the receiver or time of arrival (ToA), or the angle of arrival (AoA) of the signal. These measurements are performed at

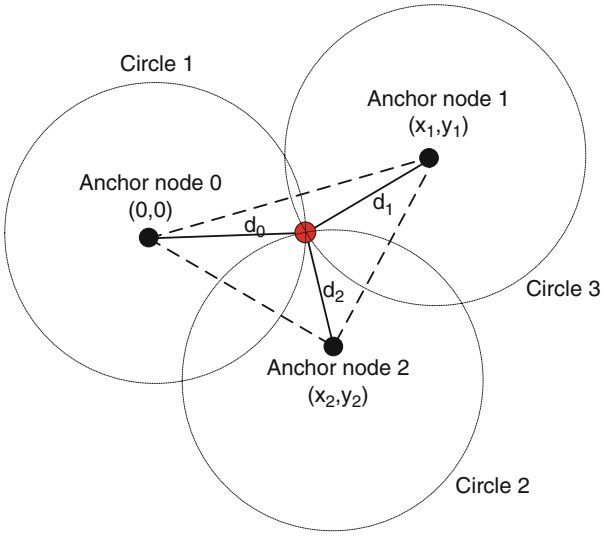

Fig. 4 Trilateration based on RSS/ToA measures

a set of reference nodes whose position is known, which we will refer to as anchor nodes. Distance or angle information is then used to estimate the position of the node, typically by applying a method such as lateration or angulation. Whenever the number of observations is reduced to three, then the process is referred to as trilateration for distance measurements, or triangulation for angles measurements.

Lateration consists in measuring distances between the node to be located and three or more anchor nodes with known positions. When distance measures are obtained by means of ToA or RSS, the position is estimated via the intersection of three circles, as depicted in Fig. 4. Let (x, y) be the 2-D position of the emitter to be located, which is in the range of 3 anchor nodes whose positions (x_i, y_i) are known. Let d_i be the distance from anchor node i to the emitter, which has been derived from a ToA or RSS measurement. Then, the equation of a circle (11) can be derived for each one.

$$d_i = \sqrt{(x - x_i)^2 + (y - y_i)^2} \tag{11}$$

If the transmission time or the transmission power at the sender is not known, the difference in RSS or ToA measurements between pairs of anchor nodes can still be computed. This is known as hyperbolic positioning, as the equation of a hyperbola is derived from each pair of difference measurement. The location of the emitter is then defined by the intersection of three hyperbolas. Regarding angulation, three or more AoA measures (triangulation or multiangulation) are used to obtain a 2-D location estimation, which is given by the intersection of the lines of bearing. For more details on these techniques, we refer the reader to [29].

In practice, measurements are subjected to errors, and the geometrical approaches previously presented lead to position estimation ambiguities. The effect of noisy measures, from the geometric point of view, is that the set of circles defined by equations in (11) rarely intersect. Then, the position estimate is usually approximated by using as many anchor nodes as possible (and therefore more measurements) and applying heuristic approaches which try to minimize the error performed in the estimation.

RSS-based techniques are relatively inexpensive and simple to implement in hardware, but they are susceptible of high errors due to the dynamics of indoor/outdoor environments, mainly due to multipath signals and shadowing. The effect of shadowing is usually modeled as log-normal with standard deviation σ_{dB}. This parameter is relatively constant with distance and typically takes values between 4 and 12 dB depending on the environment considered. This model leads to RSS estimates with variance proportional to their range, i.e., to the distance between the emitter and the node performing the RSS measurement. With regard to time-based techniques, measures may be affected mainly by multipath effect. Because of this, the accuracy of the method strongly depends on the ability to estimate the line-of-sight (LoS) signal. In its turn, angle-based approaches require the use of several antennas, thus increasing the cost and size of nodes.

A number of other methods exist to estimate the position of a node, such location fingerprinting. It consists in storing at a database a set of location signatures, which are built based on the signal characteristics obtained from a set of locations. Then, the position of a given emitter is estimated by comparing its received signal characteristics with those signatures previously stored in a database. This proposal requires being aware of the position of all PUs in advance and also, it may pose scalability problems in large networks.

Attacks to the Learning Engine

One of the key features of CRs is their capability of adapting to changing conditions in order to enhance network performance, based on current observations of the environment and past experiences. Learning from the past requires the introduction of a learning engine that makes use of **machine learning** or **artificial intelligence** (AI) algorithms. The term machine learning refers to the automated detection of meaningful patterns in data, while AI is defined as intelligence exhibited by machines. An intelligent machine perceives its environment and takes decisions that maximize its chance of achieving some goal. Typical algorithms for a learning engine include support vector machines (SVM), reinforcement learning (RL), and neural networks or genetic algorithms.

In the context of CRNs, learning techniques can be a valuable tool to get knowledge about environment conditions and its variability over time, and more specifically about spectrum availability [2]. As an example, knowledge about typical PU activity can reduce the burden of CSS mechanisms and speed up the channel selection process. A CRN may decide not to use a given channel that is available

at some specific time, because it has learned that it is frequently used by PUs that intermittently occupies and vacates the channel. This will prevent the CRN from spending unnecessary time on sensing that channel but also from performing spectrum handoffs whenever that is the channel in use, and it detects the presence of a PU. Recall that spectrum handoffs cause interruption of all communications until a new channel is available, and therefore avoiding spectrum handoffs leads to a higher efficiency in terms of network throughput. Learning machine may also be an aid for other CR functionalities, such as spectrum allocation or even detection of attacks, such as jamming or the PUE attack.

Learning algorithms can be classified into supervised or unsupervised. In supervised learning the algorithm is fed with the input and the desired results during the training phase, while in unsupervised learning it is not provided with the correct results. Usually, this technique is used for classification. When supervised learning is used, input data has already been classified, so that we know how the output of the algorithm should be, and we can modify its internal parameters if the output is not the expected one. In unsupervised learning, the input data has no label yet, and it must be classified according to their statistical properties.

The benefit of applying supervised learning to a CRN is that the algorithm is fed in a controlled environment during the training phase. However, given the dynamics of wireless environments which frequently change due to phenomena such as noise, multipath, etc., it can lead to wrong decisions due to the huge difference between training data and the data acquired during the performance phase. In this sense, unsupervised learning may have a better performance, but it is susceptible to attacks during the training phase. A learning engine attacker could alter the wireless medium by transmitting jamming signals, replaying PU transmissions, or generating interferences to prevent the system from detecting true PU transmissions. This would lead the learning algorithm to a bad classification of environment conditions and thus to take wrong decisions about spectrum availability.

Despite being an important feature of CRs, learning engine issues have received less attention than other areas of CRNs, and, therefore, how to protect the learning phase of such engines still remains an open issue.

Link Layer Security

Byzantine Attack

The need for spectrum sensing mechanisms to protect PU transmissions gives rise to specific threats to CRNs that have been widely studied by the research community [8], such as the Byzantine attack, in which adversaries gain control of one or more authenticated devices with the aim of degrading network performance. In the context of CRNs, this attack is also referred to as spectrum sensing data falsification (SSDF) [11], and it relies on the transmission of false spectrum sensing data by malicious SUs that aim at disrupting the cooperative sensing mechanism of the network.

Recall that in CSS mechanisms, each SU performs energy measurements, and report them to a central entity or FC, or exchange this measurements among its neighboring nodes, depending on whether the network is centralized or distributed.

According to the model of attacker, the Byzantine attack can be classified into [38]:

- Always Yes, if the SU always declares that the primary user is active.
- Always NO, if the SU always reports an absence of primary signal.
- Always FALSE, if the SU always reports the contrary result to its observation.

In addition, when there is more than one compromised or malicious node, attacks can be classified into [32]:

- Independent attack, each attacker forges its sensing result with a given probability regardless of what other attackers do.
- Dependent attack, if the attacker know the sensing reports of other attackers and forges its own reports according to these information in order to minimize the probability of being detected.
- Collaborative attack, if the attackers exchange their sensing information and decide their response in a collaborative way.

The two last attacks might be harder to implement, since they require the set of attackers to exchange their reports in advance, and thus they are more costly. Besides, such an exchange should be done very quickly in order to be able to send the reports to the FC during the sensing period of the CRN. As in other attacks to CRNs, a Byzantine attacker can be malicious or selfish, depending on whether its main goal is to disrupt network performance or make use of the bandwidth left unused by the CRN because of the attack.

Figures 5 and 6 depict the effect of the Byzantine attack, in terms of Q_{md} and Q_{fa}, on the decision of the FC when the fusion mechanism used is the k out of N rule, in a CRN with $N = 100$ SUs and $k = 30$ and $k = 50$, respectively. The number of Byzantine attackers M ranges from 10 to 60, and they forge their report with probability $p_l \in (0, 1)$ in an independent way. Note that for $p_l = 0$, no Byzantine attacker forges its report, and therefore it is equivalent to have a CRN with N honest SUs. As it can be seen, a low threshold ($k = 30$) leads to good performance in terms of misdetections Q_{md}, but also to high values of Q_{fa} for any value of $M > 10$. As a consequence, Byzantine attackers can easily lead the CRN to a wrong decision when there is no PU and take the available bandwidth. In Fig. 6 it can be seen that there is a tradeoff between both metrics Q_{fa} and Q_{md}, so if the threshold k is raised, Q_{fa} decreases but Q_{md} increases.

In [42], a formula is derived for the optimal value of k_{opt} that minimizes $Q_{md} + Q_{fa}$ as a function of the number of users N and the individual probabilities p_{md} and p_{fa}.

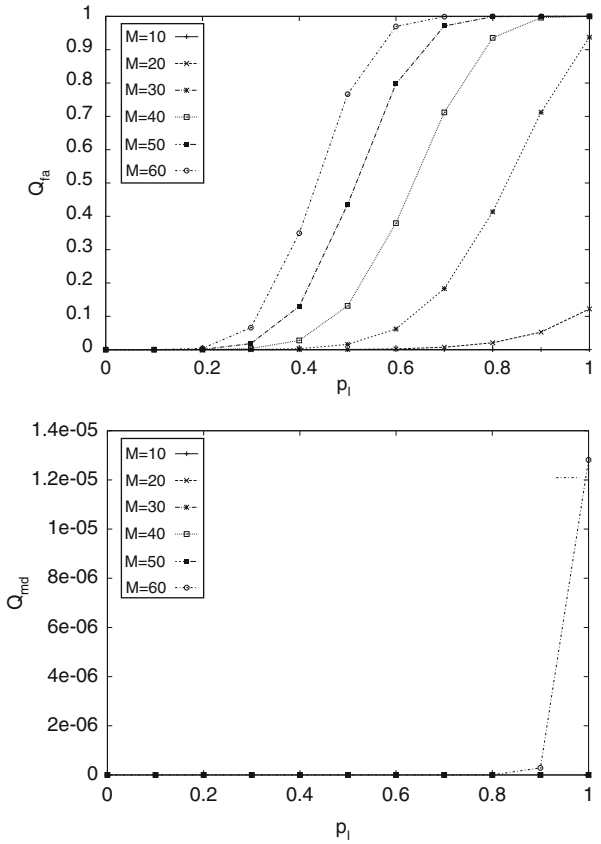

Fig. 5 P_{md} and P_{fa} with $N_{th} = 30$

$$k_{\text{opt}} = \min(N, \lceil \frac{N}{1+\alpha} \rceil) \tag{12}$$

with

$$\alpha = \frac{\log\left(\frac{p_{fa}}{1-p_{md}}\right)}{\log\left(\frac{p_{md}}{1-p_{fa}}\right)} \tag{13}$$

For typical values $p_{fa} = 0.1$ and $p_{md} = 0.1$ and $N = 100$, the optimal value is given by expression (12) is $k_{opt} = 50$.

Countermeasures

Byzantine defense is targeted to detect anomalies in the reported sensing data and discriminate between malicious and honest users. As a consequence, these schemes

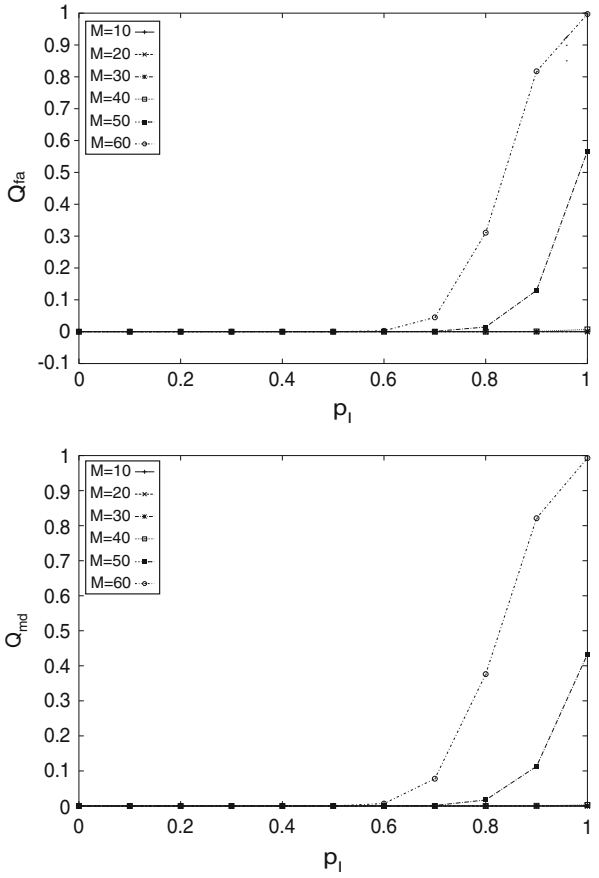

Fig. 6 P_{md} and P_{fa} with $N_{th} = 50$

require references representing normal behavior. In practice, it is hard to get a true reference, since a CRN does not know in advance which of the reports are honest. Besides, the fact that sensing mechanisms are extremely sensitive to the varying channel conditions and even honest users may report incorrect values, makes the task of identifying malicious users more challenging.

The general approach to counteract Byzantine attacks is to identify suspicious reports from potential malicious users and discard or give them a lower weight in the fusion data mechanism [10,31,32]. With that purpose, reputation mechanisms, a.k.a. as trust mechanisms, are typically used. Trust mechanisms have been extensively studied in the context of sensor networks and ad hoc networks [14]. The concept of *trust* has its origin in social sciences and is defined as the degree of subjective belief about the behavior of an entity [22]. Trust in CSS mechanisms is essential in order to ensure the correct detection of PU signals and identify holes in the spectrum.

The rationale behind it is to assign a low trust value to those SUs that deviate from the expected behavior. When an SU joins the network, it is assigned an initial trust value, and it will be updated in each sensing round according to it. Generally, the sensing decision procedure is performed as follows:

- Prefiltering. SUs with low reputation may be excluded from the fusion process.
- Data fusion. A data fusion rule is applied to the remaining reports, which are weighted according to the SU reputation.
- Reputation update. Trust values are updated for the next sensing round.

The way in which trust values are computed can be:

- Global decision based. Trust for a given SU is increased whenever the SUs report matches the final decision and decreased otherwise.
- Outliers detection based. These methods rely on different parameters such as the mean, the standard deviation, or the median, in order to identify those reports which clearly deviated from the data set.
- Correlation based. Relies on the correlation among measurements from neighboring nodes in order to detect abnormal values.

In global decision-based methods, trust is computed by comparing SU reports with the final decision. If a hard-fusion method is used, both SU reports and the final decision are binary variables, and to decide whether there is a match or not is straightforward. When soft fusion is used, however, it is needed to use a threshold. As an example, in [10], trust for a node k, r_k is initially set to zero, and it is incremented or decremented by one whenever the local sensing report is consistent with the final decision or not, respectively. The trust value is mapped to a weight w_k that is used by a SPRT fusion data mechanism (see section "Spectrum Sensing in CRNs") to reach a decision as in (14). This approach is known as weighted SPRT (WPSRT). The mapping between r_k and w_k is done in such a way that $w_i \in (0, 1)$ and ensures that an SU with a slightly negative reputation will have some contribution on the final decision.

$$W_N = \prod_{k=0}^{N} \left(\frac{f(y_k|H_1)}{f(y_k|H_0)} \right)^{w_k} \underset{<H_1}{\geq H_0} \lambda \tag{14}$$

Trust values depend on the report provided by the SU during a sensing round, but also on its past behavior. It is possible, though, to give higher weights to recent behaviors and gradually decrease the influence of older ones by means of a forgetting factor, as in [31]. In this way, an honest SU that reported several erroneous reports in the past due to channel degradation can recover faster.

Outliers detection is a technique that can be used to identify abnormal reports. In statistics, an outlier is an observation that is numerically distant from the rest of the data. When applied to cooperative spectrum sensing, identification of outliers allows

discarding those energy measures which are highly improbable and take a more reliable final decision about the existence of a PU. To this end, different statistical parameters can be used.

The simplest outlier detection technique makes use of the mean and the standard deviation of the set of reported energy values. In [20], an outlier factor is assigned to SU n at the ith sensing round as in (15), where $\sigma_n[i]$ is the outlier factor, $e_n[i]$ represents the reported energy value of a given secondary user, and $\mu[i]$ and $\sigma[i]$ are the sample mean and the sample standard deviation, respectively.

$$\sigma_n[i] = \frac{e_n[i] - \mu[i]}{\sigma[i]} \tag{15}$$

However, as the authors pointed out in [21], this technique does not perform well when the distribution of the energy values is highly skewed. In such case, valid values lying on the heavy-tailed side of the distribution will be assigned a high outlier factor, meaning that they will have a very low impact on the final decision. Other statistical parameters such as the median absolute deviation (MAD) or the bi-weight scale (BWS) are known to be more robust than the mean and the standard deviation. The MAD measures the median of the absolute distances of the data points from the sample median as in (16).

$$\sigma_n[i] = \text{median}_n \left\{ |e_n[i] - \mu[i]| \right\} \tag{16}$$

In its turn, the BWS can be computed as in (17). It has been shown that it is more sensitive to data samples that are at a moderate distance from the estimate and only ignores extremely data points [21]. Given the spatial diversity in CRNs, it makes sense to take into account those measures that slightly differ from the expected and only discard those that extremely deviate.

$$\sigma_n[i] = \sqrt{\left(\frac{N \sum\limits_{u_n^2<1} (e_n[i] - \mu[i])^2 \left(1 - u_n^2\right)^4}{s\,(-1+s)}\right)} \tag{17}$$

where

$$s = \sum_{u_n^2<1} \left(1 - u_n^2\right)\left(1 - 5u_n^2\right) \tag{18}$$

and

$$u_n = \frac{e_n[i] - \mu[i]}{\text{median}_n \left\{ |e_n[i] - \mu[i]| \right\}} \tag{19}$$

with c_2 a tuning constant which can be used to determine the impact of extreme points on BWS estimates.

Correlation between reports can also be applied to detect abnormal reports, under specific circumstances. This method relies on the fact that shadowing correlation decays exponentially with distance, and thus neighboring SUs should report similar values. This approach was followed in [27], where WSPRT is used as data fusion scheme, and the weights assigned to each node are computed according to a shadowing correlation model applied to a two-dimensional area. The authors define the shadowing random field of a given point (x, y) as the shadowing gain at unit grid area, i.e., δm $\times$ δm, centered at the coordinate (x, y). Then, the covariance of the shadowing random field between two different points (x_i, y_i) and (x_j, y_j) is modeled as in (20), with d_{ij} the Euclidean distance between the two nodes, σ the standard deviation of shadow fading. D_{corr} is the decorrelation distance which determines the distance above which the correlation falls to e^{-1} and depends on the environment (urban, suburban...). In suburban areas, it typically takes values between 120 and 200 m.

$$R_p(d_{ij}) = \sigma^2 \cdot e^{-d_{ij}/D_{\text{corr}}} \tag{20}$$

Abnormal reports are then detected by analyzing their similarity (or difference) with reports from neighboring nodes. Note that such an approach can only be applied in small CRNs where all SUs are close to each other, e.g., sensor networks, or in CRNs in rural areas where households tend to be clustered [33]. In the latter case, reports from SUs belonging to the same cluster should be highly correlated. To this end, the set of CR is divided into clusters according to their proximity so that nodes belonging to the same cluster should be highly correlated.

Regardless of the approach followed by the CRN to detect abnormal reports and exclude them from the CSS process, a major concern is to identify Byzantine attackers. Based on outliers detection, global decision-based methods, or correlation, the CRN can compute a trust value and establish a threshold to determine whether a given node is an attacker or a honest node reporting erroneous values due to bad channel conditions. It would be reasonable to penalize those users that are regarded as attackers by denying them access to the network. However, because every detection mechanism exhibits a certain rate of false positives, this would lead to expel some honest users of the CRN.

Utility-based methods circumvent this problem by, rather than identifying malicious users, incentivizing them to behave in an honest way [40]. The utility of a user is an economic term introduced by Daniel Bernoulli referring to the total satisfaction received from consuming a good or a service. When applied to CRNs, the utility may refer, for example, to the bandwidth that a given user is assigned. The key idea is to design the appropriate fusion and resource allocation mechanisms such that the utility of a Byzantine attacker gradually decreases if it keeps forging reports. Note that such approaches can only counteract the Byzantine attack based on selfish profiles, since malicious users do not care about bandwidth, and its only purpose is to disrupt network performance.

The malicious user utility $\hat{U}$ consists of two elements: the utility U acquired by the user as a member of the CRN and the utility achieved by forging reports

(e.g., available bandwidth when the CRN erroneously decides that no PU exists in a channel). The goal is to ensure $\hat{U} < U$ to incentivize SUs to behave honestly and report accurate sensing reports. Utility-based approaches rely on game theory, and some examples of its application to CRNs can be found in [13].

Note that in a centralized CRN, the FC is responsible for computing the trust value for each SU, according to the matches between the reports sent by the SU and the final decisions of the FC regarding the existence of a PU. In a fully distributed network, each SU must compute the trust values for its one-hop neighbors and reach a final decision. This fact increases node complexity due to the computations needed to run the sensing decision procedure and the exchange of reports among neighbors. Besides, it is prone to exhibit a higher error rate due to the lack of a trusted central entity and because the amount of reports combined by fusion data mechanisms is limited to the number of neighbors, and thus lower than in infrastructure-based networks..

Selfish Behavior

In a cooperative framework, selfish behavior refers to a set of actions performed by a node in order to increase its benefit while decreasing the average benefit for the rest of participants. Because CSS is known to improve the performance of PU detection, selfish behaviors may increase the probability of wrong decisions regarding spectrum opportunities. Selfish SUs may not cooperate in the sensing process in order to save energy while still making use of the network resources.

Due to the negative impact of selfish nodes on the CSS mechanisms of a CRN, appropriate strategies are needed in order to enforce cooperation. In wireless networks, this is a hard problem to deal with, since lack of feedback may be either due to selfishness or information loss. The community research has put a big effort on this topic in the context of ad hoc networks [26], mostly regarding routing mechanisms. Although these approaches cannot be directly applied to CRN, they can be used as a basis to develop efficient methods to detect selfish behaviors and to incentivize CR to cooperate. In addition, these methods should be also tailored to the type of CRN: ad hoc or infrastructure based. In ad hoc networks, selfish detection must be performed locally by neighboring nodes, and cooperative enforcement may be achieved by traditional mechanisms that penalize selfish nodes by, for example, not forwarding packets coming from them. On the other hand, in infrastructure-based networks, the FC is responsible for gathering the sensing reports from all CRs and therefore can easily verify which SUs do not report sensing measurement.

Cooperation enforcement can be achieved by means of utility-based methods. As an example, in [34] the CSS process is modeled as an N-player noncooperative, non-zero-sum repeated game. Two different strategies based on game theory are analyzed in order to incentive cooperation: grim trigger and carrot and stick. In grim trigger, cooperation from each node is measured, and all nodes stop cooperation whenever deviation from any node is detected. This technique can effectively motivate nodes to cooperate, but results in poor performance when channel errors

are not negligible. On the other hand, carrot and stick is an iterative approach where, at each step, a given node only cooperates if all nodes cooperated or deviated in the previous step. This approach recovers cooperation when all nodes deviate at the risk of leaving the CRN with no information about spectrum availability.

A more elaborated proposal is presented in [41], where reputation is used as a pricing factor in the spectrum allocation process to incentivize cooperative sensing in distributed CRNs. The reputation values are computed according to the sensing accuracy of the reports and the participation of SUs in the CSS process. SUs with low reputation are allocated bandwidth at the expenses of paying a higher price for it, thus forcing selfish nodes to cooperate if they want to maximize its utility.

Application Layer Security

As previously mentioned, SDRs are key for the deployment of CRNs, as they can provide the flexibility and reconfiguration capability needed by CRs. An SDR must be capable of downloading new software or updates that, once they are activated, may change the radio transmission parameters or implement new learning or decision algorithms. The reconfigurability property gives rise, however, to a number of software-related attacks [17].

The software is downloaded over the air, and therefore an unauthorized user could obtain a copy of the software, modify it, or inject malicious code. On the one hand, knowledge about a CR operation, in terms of channel selection, can be very valuable information to perform a different type of attack, such as a PUE attack. On the other hand, malicious code can lead a CR to behave in an unexpected way and even propagate the attack to other CRs, as it occurs with worms. Overall, the likelihood of causing network disruption because of software attacks is very high.

As a consequence, it is essential to provide confidentiality, authentication, access control and integrity in all communications used to distribute SDR software:

- Confidentiality will prevent unauthorized users to obtain a copy of the software.
- Authentication ensures that the downloaded software comes from a trusted source. Only authorized software should be activated in an SDR.
- Integrity guarantees that the downloaded software has not been altered.

A straightforward solution to provide confidentiality is symmetric encryption, by means of a shared secret key between the network administrator and the device. The key should be unique to each terminal and should be stored in **tamper-proof** hardware on the device [25]. Tamper-resistant devices may be designed to reset to zero, a.k.a. zeroise, sensitive data, such as cryptographic keys, if they detect penetration of their security encapsulation or out-of-specification environmental parameters.

Authentication and integrity can be achieved by means of digital signatures, which are sent together with the software to be downloaded. The main disadvantage of this approach is that it is computationally expensive, and some limited devices

Table 1 Main threats to SDRs

Threat	Security requirement
Insertion of malicious software	Integrity
Alteration or destruction of data	Integrity
Alteration or destruction of software	Integrity
Extraction of data	Confidentiality

may not support them. A lightweight mechanism, such as the one presented in [9], may be more suitable for constraint devices.

A method to ensure a secure execution of downloaded software is the implementation of trusted computing (TC) [28]. TC is a technology aiming at guaranteeing that a device will consistently behave in an expected way, and those behaviors will be enforced by computer hardware and software. This is achieved by loading the hardware with a unique private key that is not accessible to the rest of the system.

In [7] a complete list of threats to SDRs is given. Table 1 show the most relevant ones along with their security requirements.

Conclusions

CR paradigm is considered a key solution to mitigate the spectrum scarcity problem by enabling spectrum access in an opportunistic manner. CRNs are allowed to act as secondary users of the licensed spectrum on a non-interference basis, thus requiring the use of spectrum sensing mechanisms to identify free portions of the spectrum. Detection performance improves by means of spatial diversity and therefore all the members of the network are expected to cooperate by sharing their sensing reports.

The successful deployment of these networks relies on the proper design of mechanisms for cooperative sensing, adapt to changing environment conditions, and manage the available spectrum. However, CRNs use an open transmission medium that open doors to a myriad of attacks that can severely degrade network performance. On the one hand, CRNs are susceptible to well-known attacks that apply to any conventional wireless network. On the other hand, new threats that are based on the specific features or mechanisms of CRNs have been identified.

In this chapter we have provided an overview of the main threats to CRNs, with special emphasis on those inherent to CR functionalities. These threats and their possible countermeasures are summarized in Table 2. Most of the attacks are targeted to disrupt the CSS process of the network, either by altering the medium or by forging sensing reports. The consequences of these attacks are twofold. First, they may cause interference to the legitimate users of the spectrum, thus violating one of the basic principles of CRNs, and, second, they may prevent CRNs from accessing available spectrum, which degrades the quality of the communications. In some extreme situations, these attacks can cause a DoS, meaning that legitimate users will be denied access to network resources.

Table 2 Threats to CRNs and countermeasures

Threat	Layer	Countermeasures
Eavesdropping	Physical	Beamforming/relays/MIMO/artificial noise
Jamming	Physical	Channel hopping/location of attacker
PUE	Physical	Fingerprinting/cryptography/location of attacker
Learning	Physical	Training in a secure environment
Byzantine	Link layer	Trust schemes/utility-based schemes (game theory)
Selfish	Link layer	Utility-based schemes (game theory)
Threats to SDRs	Application	Secure software download and execution

Throughout this chapter we have discussed several countermeasures for each attack and evaluated their pros and cons. Some of them, being effective in mitigating the attack, may not be practical from a deployment point of view. Limitations regarding cost, size of devices, and deployment of additional infrastructure or FCC rules could restrain their realization. Two key aspects make hard the design of efficient countermeasures: first, the lack of real scenarios to evaluate the impact of the attacks with more accuracy and the feasibility of deploying specific countermeasures, and, second, the heterogeneity in CRN architectures and mechanisms to implement all functionalities. Despite the research community has put a big effort in developing the IEEE 802.22 standard, its application is limited to a few scenarios, since it was conceived to be used in large rural areas. As a result, the mechanisms and features defined in IEEE 802.22 may not apply to other CRNs. Therefore, further work in this direction is needed in order to deploy secure CRNs.

References

1. 802.22 WG (2015) IEEE Standard for Information Technology – Telecommunications and Information Exchange Between Systems Wireless Regional Area Networks (WRAN) – Specific Requirements Part 22: Cognitive Wireless RAN Medium Access Control (MAC) and Physical Layer (PHY) Specifications: Policies and Procedures for Operation in the TV Bands. http://ieeexplore.ieee.org. Cited 15 Nov 2016
2. Abbas N, Nasser Y, El Ahmad K (2015) EURASIP J Wirel Commun Netw 174:1–20. https://doi.org/10.1186/s13638-015-0381-7
3. Akyildiz IF, Lee W-Y, Chowdhury KR (2009) CRAHNs: cognitive radio ad hoc networks. Ad Hoc Netw 7(5):810–836
4. Akyildiz IF, Lee W-Y, Vuran MC, Mohanty S (2006) NeXt generation/dynamic spectrum access/cognitive radio wireless networks: a survey. Comput Netw 50(13):2127–2159
5. Akyildiz IF, Lo BF, Balakrishnan R (2011) Cooperative spectrum sensing in cognitive radio networks: a survey. Phys Commun 4(1):40–62. https://doi.org/10.1016/j.phycom.2010.12.003
6. Anand S, Jin Z, Subbalakshmi KP (2008) An analytical model for primary user emulation attacks in cognitive radio networks. Paper Presented at the 3rd IEEE Symposium on New Frontiers in Dynamic Spectrum Access Networks, Chicago, 14–17 Oct 2008
7. Baldini G, Sturman T, Biswas AR, Leschhorn R, Godor G, Street M (2012) Security aspects in software defined radio and cognitive radio networks: a survey and a way ahead. IEEE Commun Surv Tutorials 14(2):355–379

8. Bhattacharjee S, Sengupta S, Chatterjee M (2013) Vulnerabilities in cognitive radio networks: a survey. Comput Commun 36(13):1387–1398
9. Brawerman A, Blough D, Bing B (2004) Securing the download of radio configuration files for software defined radio devices. In: Proceedings of the Second International Workshop on Mobility Management & Wireless Access Protocols, Philadelphia, 1 Oct 2004
10. Chen R, Park JM, Bian K (2008) Robust distributed spectrum sensing in cognitive radio networks. In: Proceedings of the IEEE 27th Conference on Computer Communications (INFOCOM 2008), Phoenix, 16–17 Apr 2008
11. Chen R, Park J-M, Hou YT, Reed JH (2008) Toward secure distributed spectrum sensing in cognitive radio networks. IEEE Commun Mag 46(4):50–55
12. Chen R, Park J-M, Reed JH (2008) Defense against primary user emulation attacks in cognitive radio networks. IEEE J Sel Areas Commun 26(1):25–37
13. Chen H, Zhou M, Xie L, Wang K, Li J (2016) Joint spectrum sensing and resource allocation scheme in cognitive radio networks with spectrum sensing data falsification attack. IEEE Trans Veh Technol 65(11):9181–9191
14. Cho J-H, Swami A, Chen R (2011) A survey on trust management for mobile ad hoc networks. IEEE Commun Surv Tutorials 13(4):562–583
15. Dillinger M, Madani K, Alonistioti N (2005) Software defined radio: architectures, systems and functions. Wiley, Hoboken
16. Di Pietro R, Oligeri G (2013) Jamming mitigation in cognitive radio networks. IEEE Netw 27(3):10–15
17. Fragkiadakis AG, Tragos EZ, Askoxylakis IG (2013) A survey on security threats and detection techniques in cognitive radio networks. IEEE Commun Surv Tutorials 15(1):428–445
18. Grover K, Lim A, Yang Q (2014) Jamming and anti–jamming techniques in wireless networks: a survey. N Engl J Med 17(4):197–215
19. Husheng L, Zhu H (2010) Catch me if you can: an abnormality detection approach for collaborative spectrum sensing in cognitive radio networks. IEEE Trans Wirel Commun 9(11):3554–3565; 2(5-6):399–413. https://doi.org/10.1504/IJSNET.2007.014364
20. Kaligineedi P, Khabbazian M, Bhargava VK (2008) Secure cooperative sensing techniques for cognitive radio systems. Paper Presented at the IEEE International Conference on Communications (ICC'08), Beijing, 19–23 May 2008
21. Kaligineedi P, Khabbazian M, Bhargava VK (2010) Malicious user detection in a cognitive radio cooperative sensing system. IEEE Trans Wirel Commun 9(8):2488–2497
22. Kramer RM, Cook KS (2004) Trust and distrust in organizations: dilemmas and approaches. The future of modern genomics. Russell Sage Foundation, New York
23. Lee J-H (2015) Cooperative relaying protocol for improving physical layer security in wireless decode-and-forward relaying networks. Wirel Pers Commun 83(4):3033–3044
24. Marinho J, Granjal J, Monteiro E (2015) A survey on security attacks and countermeasures with primary user detection in cognitive radio networks. EURASIP J Inf Secur 2015(1):1–14
25. Michael LB, Mihaljevic MJ, Haruyama S, Kohno R (2002) A framework for secure download for software-defined radio. IEEE Commun Mag 40(7):88–96
26. Michiardi P, Molva R (2003) Secure cooperative sensing techniques for cognitive radio systems. In: Proceedings of WiOpt 2003, INRIA, Sophia-Antipolis, 3–5 May 2003
27. Min AW, Shin KG, Hu X (2010) Secure cooperative sensing in IEEE 802.22 WRANs using shadow fading correlation. IEEE Trans Mob Comput 10(10):1434–1447
28. Mitchell C (2005) Trusted computing. Iet, London
29. Patwari N, Ash JN, Kyperountas S, Hero AO III, Moses RL, Correal NS (2005) Locating the nodes: cooperative localization in wireless sensor networks. Signal Process Mag 22(4):54–69
30. Pelechrinis K, Koutsopoulos I, Broustis I, Krishnamurthy SV (2009) Lightweight jammer localization in wireless networks: system design and implementation. In: Proceedings of the Global Telecommunications Conference (GLOBECOM 2009), Hawai, 30 Nov–4 Dec 2009
31. Qin T, Yu H, Leung C, Shen Z, Miao C (2009) Towards a trust aware cognitive radio architecture. SIGMOBILE Mob Comput Commun Rev 13(2):86–95. https://doi.org/10.1145/1621076.1621085

32. Rawat AS, Anand P, Hao C, Varshney PK (2011) Collaborative spectrum sensing in the presence of Byzantine attacks in cognitive radio networks. IEEE Trans Signal Process 59(2):774–786
33. Sawada M, Cossette D, Wellar B, Kurt T (2006) Analysis of the urban/rural broadband divide in Canada: using GIS in planning terrestrial wireless deployment. Gov Inf Q 23(3):454–479
34. Song C, Zhang Q (2009) Achieving cooperative spectrum sensing in wireless cognitive radio networks. ACM SIGMOBILE Mob Comput Commun Rev 13(2):14–25
35. Walters JP, Liang Z, Shi W, Chaudhary V (2007) Wireless sensor network security: a survey. Secur Distrib Grid Mob Pervasive Comput 1:367
36. Wang W, Bhattacharjee S, Chatterjee M, Kwiat K (2013) Collaborative jamming and collaborative defense in cognitive radio networks. Pervasive Mob Comput 9(4):572–587
37. Wang B, Wu Y, Liu KJR, Clancy TC (2011) An anti-jamming stochastic game for cognitive radio networks. IEEE J Sel Areas Commun 29(4):877–889
38. Yifeng C, Yijun M, Ota K, Changqing L, Mianxiong D, Yang L (2014) Optimal data fusion of collaborative spectrum sensing under attack in cognitive radio networks. IEEE Netw 28(1):17–23
39. Zeng Y, Liang Y-C, Hoang AT, Zhang R (2010) A review on spectrum sensing for cognitive radio: challenges and solutions. EURASIP J Adv Signal Process 78(2):74 2010. https://doi.org/10.1155/2010/381465
40. Zhang L, Ding G, Wu Q, Zou Y, Han Z, Wang J (2015) Byzantine attack and defense in cognitive radio networks: a survey. IEEE Commun Surv Tutorials 17(3):1342–1363
41. Zhang T, Li Z, Safavi-Naini R (2014) Incentivize cooperative sensing in distributed cognitive radio networks with reputation-based pricing. In: Proceedings of IEEE Conference on Computer Communications (INFOCOM 2014), Toronto, 27 Apr–2 May 2014
42. Zhang W, Mallik RK, Letaief K (2008) Cooperative spectrum sensing optimization in cognitive radio networks. In: Proceedings of the IEEE International Conference on Communications (ICC 2008), Beijing, 19–23 May 2008
43. Zhang K, Mao Y, Leng S, Fang S (2013) Efficient anti-jamming strategies in multi-channel wireless networks. In: Proceedings of the 2013 International Conference on Computational Problem-solving (ICCP), Jiuzhai, 22–23 Oct 2013
44. Zou Y, Zhu J (2016) Physical-layer security for cooperative relay networks. Springer, Berlin

Physical Layer Coexistence: WLAN/Radar Case Study

24

Morteza Mehrnoush and Sumit Roy

Contents

Abstract

Spectrum sharing of 802.11 wireless local area network (WLAN) and radars operating in co-/adjacent channel scenarios (notably 5 GHz) is a problem of considerable importance that requires new innovations. The spectrum sharing explored in this chapter is based on unilateral action by Wi-Fi networks to prevent

This work was supported in part by AFRL CERFER Under Contract FA8650-14-D-1722

M. Mehrnoush (✉) · S. Roy
University of Washington, Seattle, WA, USA
e-mail: mortezam@uw.edu; sroy@u.washington.edu; sroy@uw.edu

W. Zhang (ed.), *Handbook of Cognitive Radio*,
https://doi.org/10.1007/978-981-10-1394-2_44

unacceptable interference to incumbent radar and also mitigating the interference from radar to Wi-Fi. Specifically, the ability of a single Wi-Fi network inside the exclusion region is to *speedily detect* radar operation and to subsequently switch to a clear channel as a means of protecting them. The approach is relied on the opportunistic use of naturally occurring *random* quiet/idle periods in a Wi-Fi network employing distributed coordination function (DCF) to detect the presence of a radar using energy detection. Moreover, the Wi-Fi systems outside the exclusion region are modified to mitigate the interference from a pulsed search radar such that the WLAN continues to operate with no noticeable performance degradation. The radar pulse detection is required to mitigate the radar interference.

Keywords
WLAN · Radar system · Network coexistence · Radar pulse detection · Interference mitigation

Introduction

The fundamental challenge facing mobile network operators is the scarcity of spectrum allocated for civilian use. The demand (and hence the price) for spectrum has skyrocketed as cellular data, and WLAN services have become ubiquitous in response to ever-richer multimedia and interactive applications running on higher-end consumer devices. Acknowledging this recent exponential growth in data traffic on cellular networks, regulatory authorities have aimed at various strategies for systematically increasing the spectral efficiency of wireless networks, as means for alleviating the spectrum crunch.

Looking ahead, the need for coexistence among dissimilar technologies will be a fundamental feature of wireless networks as a broad principle. For example, a significant chunk of Wi-Fi channels in the 5 GHz bands (declared U-NII, i.e., unlicensed, for North America) are utilized by various radar systems worldwide [14,28], in fact, only 36% of 5 GHz channels are unencumbered by radar protection requirements. Hence, 802.11 WLAN networks in the 5 GHz band was the first significant instance of coexistence/spectrum sharing. To that end, dynamic frequency selection (DFS) by Wi-Fi (based on channel sensing and radar avoidance) was the solution proposed to protect radars from WLAN systems [19]. An examination of the 225 MHz–3.7 GHz band assignments shows that 1700 MHz in this range has been set aside for radar and radiolocation operation in the United States [25] making it a virtual certainty that issues of coexistence of radars with civilian systems will recur. In fact, the US Department of Commerce has already recommended that 150 MHz of spectrum between 3550 and 3700 MHz be made available for wireless broadband applications [2,6] which has led to further coexistence studies.

The foundation of protecting radar operation is based on the notion of an *exclusion or protection region* as shown in Fig. 1 – this defines a spatial region centered around the radar location where no co-channel use by WLAN is permitted

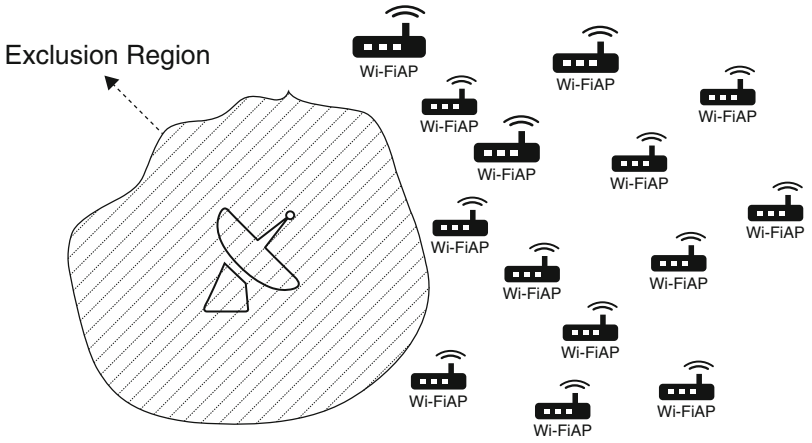

Fig. 1 Wi-Fi access points outside the radar exclusion region that benefit from proposed idea

(and by implication, reuse of the channel is permitted only outside this region). This topic was explored in [18] for a search pulsed radar rotating with a constant angular rotation (speed) and employing a known transmit main beam-pattern in azimuth (For simplicity, the formulation in [18] assumes a 2D model, whereby the radar and Wi-Fi networks operate in the same plane.). Thus the exclusion region is time varying, consist with the current location of the radar beam-pointing angle. Clearly, minimizing the area of the protection region (equivalently, expanding the co-channel reuse opportunities for the secondary Wi-Fi networks) is an appropriate design goal, and a method for achieving this is shown in [18] as a function of the WLAN deployment geometry.

In Fig. 2, the exclusion regions are determined by regulatory organizations (such as the NTIA) under the assumption that secondary networks (e.g., Wi-Fi) do not take any measures to mitigate interference to the radar systems [22]. In such scenarios, these no-go exclusion regions can extend for hundreds of kilometers radially from radar location, which given the proximity of radars to population centers (precisely the places where there is demand for such secondary networks) makes deployment of secondary systems unattractive as a business proposition.

Enabling mitigation between two dissimilar radio networks (such as radar and Wi-Fi) can be accomplished (at a conceptual level) in several ways. The most obvious is for one system to retrofit so as to become more resilient in operation to the presence of the other. This is the methodology which is adopted in this work, i.e., explore enhancements to Wi-Fi system that enable it to (a) rapidly detect the presence of (pulsed) radars and avoid (via evacuating the channel) when it is

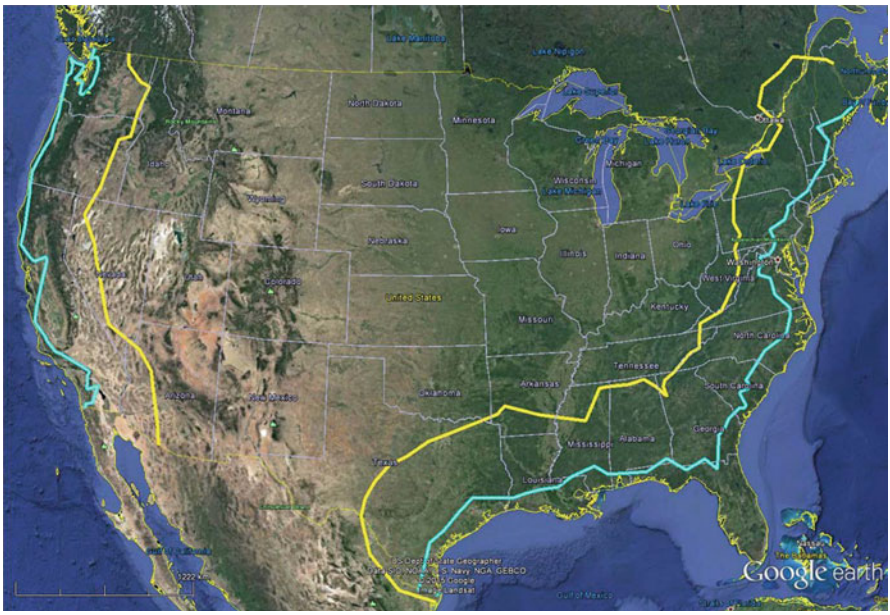

Fig. 2 The original exclusion regions computed by the NTIA (*yellow contours*) were revised recently in [8] (*blue contours*). Even the revised region encompasses many of the major population centers such as Los Angeles and New York City

inside the exclusion region and/or (b) detect and perform interference mitigation during WLAN packet transmission when it is outside the exclusion region. The first conforms to regulatory requirements so as to protect the incumbent radar from undue interference, whereas for WLAN nodes at a distance from the radar (i.e., outside the exclusion region), radar pulses that impact WLAN packets in flight contribute low interference that make (WLAN) packet decoding feasible with suitable interference mitigation.

Inside the exclusion region, it is crucial that communication systems detect active radars *accurately and speedily* in order to limit interference to incumbents. The FCC's current plans for spectrum sharing in the 3.5 GHz band forgo sensing and instead rely solely on a Spectrum Access System to govern usage of the shared spectrum [6]. However, a full coexistence solution will likely employ detect and switch via run-time channel sensing in conjunction with spectrum sharing database assistance. The latter contains all available system information regarding incumbent operation [8] that can assist secondary a priori for interference avoidance; however, in case of any updates to primary operation, such database information may possibly be out of date, and thus run-time sensing will likely be needed.

A traditional approach for a WLAN (inside the protection region) attempting to detect a radar pulse is based on requiring all in-network transmissions to cease (via scheduling) so as to create quiet/idle periods wherein radar pulses that happen to arrive can be accurately detected. In [9], the authors propose periodically

scheduling idle intervals for the purposes of channel sensing. The scheme incurs some complication in implementation due to the increase in packet fragmentation and consequent loss in throughput. In [16], extending (some of) naturally occurring idle periods in the Wi-Fi DCF MAC for the purposes of channel sensing is considered which did not suffer from the complications of [9] and was shown to detect transient out-of-network interference reliably. However, subsequently the requirement for any scheduled quiet period was dropped, and radar detection was based solely on *inherent natural periods of network operation whereby* ***all*** *nodes are backing off*, leading to randomly occurring quiet periods of random duration [24]. However, such naturally occurring idle periods typically comprise only a small portion of channel time on average (This fraction decreases with Wi-Fi node density or traffic load increase, i.e., factors that are beyond direct control.); hence, the chances of detecting the short-duration and low-duty cycle radar pulses within such random quiet intervals reliably is a largely open question. On the other hand, if the number or duration of such quiet intervals is increased (via means to be described later) to improve radar detection probability, it will result in a commensurate loss in communication network throughput, leading to an inherent trade-off that is explored and characterized.

Finally, *outside the exclusion region*, it is possible that a Wi-Fi node is able to detect radar pulses reliably *even during transmission of WLAN packets*, due to the lower interference power at the Wi-Fi receiver. Thus in contrast to the method in [24] that waited for the (probabilistic) event that a pulse falls within a quiet duration, it is proposed to investigate how WLAN may detect the presence of an interfering (narrow) radar pulse while there is a payload on the channel. Accordingly, two modifications to generic Wi-Fi transmitter/receiver chain are suggested toward achieving the goal of radar pulse detection cum interference mitigation.

DFS Requirement in 5 GHz

DFS comprises of a radar detection and avoidance scheme by the secondary (Wi-Fi) network. The detection algorithm has two primary components:

1. **Out-of-service monitoring:** This refers to the period at the start when each access point (AP) must scan the channels to determine if radar is present. The requirement is to detect radar signals above −62 dBm with detection rate of 99.99% within a scan duration of 60 s.
2. **In-service monitoring:** This refers to the ability of an active Wi-Fi network to detect a radar that begins operation after initial setup. DFS requires that during the regular operation, WLANs must detect a radar with a success rate of 60% for radar signals above −62 dBm in 60 s.

The detection rate is determined by the probability that a radar pulse is detected by a Wi-Fi network in each detection phase. Compliance with the radar protection requirements is based primarily on verifying these detection rates under the test scenarios, and example radars are defined in [14]. These DFS rules were aimed specifically at the 5 GHz band (Hence they may be insufficient for protecting radars in other bands.) and will be used as a performance benchmark for the novel schemes. [29] analyzed the radar detection delay in a simple time division duplex (TDD) system.

Radar Pulse Detection Using Quiet Periods in Wi-Fi

Model of Wi-Fi Network

In this work, an isolated Wi-Fi "cell," i.e., a single access point with n connected clients, is considered. In the following sections, the following two cases are studied:

1. Downlink-only traffic from the access point (AP) to the associated stations;
2. Full buffer at *all* nodes in the network.

The second setup corresponds to the model analyzed in [10]. Slot durations and frame spacings conform to the 802.11 standards [4] as indicated in Table 1. Network time is *slotted* with a resolution of $t_{\text{slot}} = 1\,\mu\text{s}$ as baseline. Typical parameters for radars operating in 3.5 and 5 GHz are included in Table 2 based on [1, 14, 17]. The radars transmit a series of equally spaced pulses called a pulse *burst* with low-duty cycles (often less than 1%) in a given direction (Directionality could be achieved through a phased array in place of mechanical rotation.), with peak transmit powers that can exceed 90 dBm. Accordingly, a simple link-budget analysis using an irregular terrain path-loss model (e.g., Fig. 5 in [15]) indicates that

Table 1 Wi-Fi timing parameters

Parameter	Description	Duration
t_{slot}	Timing slot	$1\,\mu\text{s}$
t_{bo}	Backoff	$9 \times t_{\text{slot}}$
t_{difs}	DIFS	$34 \times t_{\text{slot}}$ (5 GHz)
t_{sifs}	SIFS	$16 \times t_{\text{slot}}$ (5 GHz)
t_{ack}	ACK	$48 \times t_{\text{slot}}$
t_{payload}	Payload	up to $\approx 3000 \times t_{\text{slot}}$
$t_{\text{slot}} = 1$ slot $= 1\,\mu\text{s}$		

Table 2 Example radar parameters

Parameter	Values
Pulse repitition interval (t_{pri})	100 μs–5 ms
Pulse duration	0.8–50 μs
Pulses per burst	10–25
Peak power	up to 90 dBm
Antenna main beam gain	up to 40 dBi

radar interference power at a Wi-Fi AP can exceed −62 dBm at distances of tens of kilometers from the radar. As a result, energy detection schemes can be effective in the exclusion region for meeting the 5 GHz DFS latency requirements. It noteworthy that radar detection is conducted typically by the AP and any information (such as DFS triggering) disseminated via broadcast to all clients.

Challenges in Radar Pulse Detection

Performance of radar pulse detector by the secondary user (Wi-Fi) in order to limit interference (by either controlling its own in-band transmission or switching to a different unoccupied channel) is measured by the obvious metric:

- **Detection delay:** The interval from the instant the incumbent (radar) becomes active until its successful detection by the secondary network (Wi-Fi).

which is impacted by (a) radar pulse duration and (b) pulse repetition interval (PRI).

Typically, in other applications of the shared spectrum paradigm (e.g., wireless microphones), the incumbents transmit high-duty cycle signals; any Wi-Fi idle period will thus overlap with multiple incumbent transmissions with high probability allowing for effective detection. In contrast, radars with low-duty cycles pose a significant challenge. In this work, the detection delay of radar by Wi-Fi systems for various Wi-Fi/radar system parameters is presented to establish the conditions under which such a system can adequately protect radar and if the associated cost (loss of WLAN throughput) is acceptable.

Wi-Fi Basics

The Wi-Fi standard employs a CSMA/CA-based approach [4] within a distributed slotted medium access scheme.

A brief summary of the core algorithm follows: each node attempting transmission must first ensure that the medium has been idle for a duration labeled the DCF interframe spacing period (DIFS) which is typically in the range of 28–50 μs. Once the medium has remained idle for a DIFS period, the node selects a backoff counter uniformly at random in the range of $[0, 2^m W - 1]$ (Typical W values are 16, 32.)

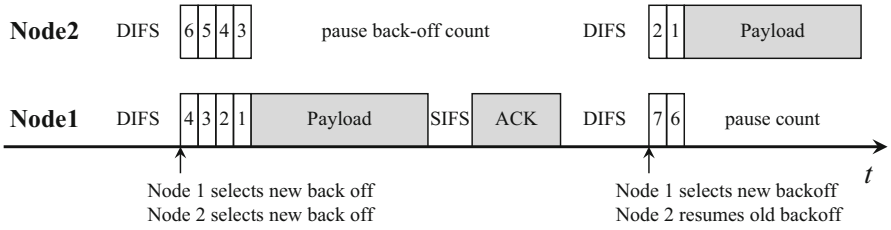

Fig. 3 This parallel timeline for two nodes contending for access to the same channel shows the role of the random backoff in reducing collisions

where the value of m is initialized to 0. The node then counts down from the selected backoff value in a slotted fashion (i.e., the node decrements the counter every t_{BO} microseconds corresponding to a backoff slot) as long as no other transmissions are detected. If during the countdown a transmission is detected, the counting is paused, and nodes continue to monitor the busy channel until it goes idle; thereafter the medium must remain idle for a further DIFS period before the backoff down-counting is resumed. Once the counter hits zero, the node transmits its payload (illustrated in Fig. 3). Any node that did not complete its countdown to zero in the previous transmission round resumes the countdown at the next opportunity without selecting a new backoff value.

A collision event occurs if and only if two nodes select the same backoff counter value at the end of a DIFS period. In case of a collision, the value of m (the backoff stage) is incremented by one (binary exponential backoff) such that the backoff counter is doubled for the next attempt, thereby reducing the probability that any two nodes select the same backoff counter repeatedly. Once a transmission has been completed successfully, the value of m is reset to 0. The value of m cannot exceed a maximum value $m_{\max}$ (typically values are 3–5).

Analytical Evaluation of Radar Detection in Wi-Fi Quiet Periods

Since no synchronization between the radar pulses and the Wi-Fi network is assumed, once the radar becomes active, the first pulse it transmits will arrive at random in relation to the Wi-Fi network state. From the alternating renewal theorem, it can be shown that if a pulse arrives at a random time instant, the Wi-Fi network will be in an idle state with probability P_{idle} (Fig. 4a, b) and in a busy state with probability P_{busy} (Fig. 4c) computed as below:

$$P_{\text{busy}} = \frac{\mathbb{E}[B_k]}{\mathbb{E}[B_k] + \mathbb{E}[I_k]} \tag{1}$$

$$P_{\text{idle}} = 1 - P_{\text{busy}} \tag{2}$$

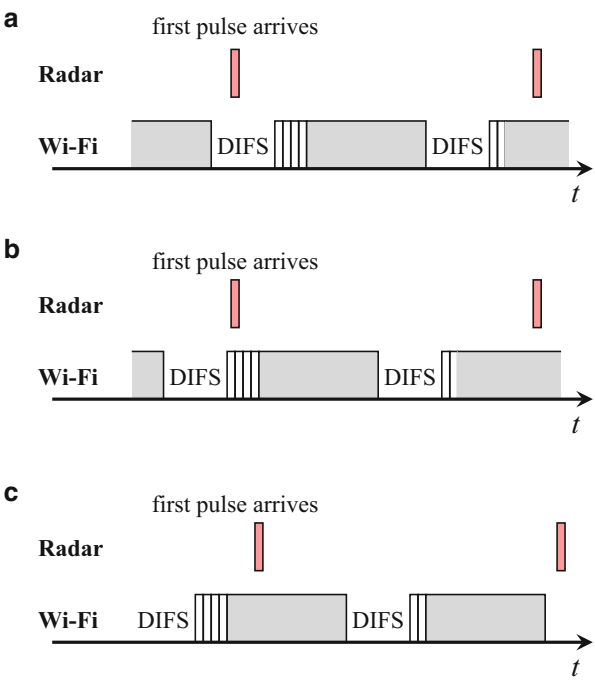

Fig. 4 (**a**) In this case, the first pulse arrives during a DIFS portion of the idle period. (**b**) In this case, the first pulse arrives during the backoff portion of the idle period. (**c**) In this case, the first pulse arrives during the busy period

where,

B_k The *random* duration of the busy period in the kth renewal cycle. Randomness is due to the success or failure of transmission.

I_k The *random* duration of the idle period in the kth renewal cycle. The randomness in the idle duration is due to the random backoff

Q_k The *random* number of backoff slots during idle period I_k. $Q_k \sim \text{Geo}(P_{\text{tr}})$ (P_{tr} is the probability that at least one node attempts transmission in a backoff slot)

It is assumed that for any radar pulse arriving during an idle period is detected perfectly (i.e., with probability 1, an approximation which is good for Wi-Fi nodes within the exclusion region for reasons stated earlier) and the (additional) processing delay for detection (post arrival) is negligible. Thus the detection delay is the interval measured from the first (reference) pulse, till the first time a pulse arrives during a Wi-Fi idle period, as shown in Fig. 5. Hence, if the first pulse arrives during an idle period, the detection delay is zero.

For the remainder of the analysis, the random variable B_k is replaced by a constant t_{busy} equal to expected duration of $E[B]$. This is reasonable for all *fixed packet length* scenarios since the ACK/SIFS durations are typically negligible compared to the payload duration (in the downlink-only case, this approximation is exact). Thus

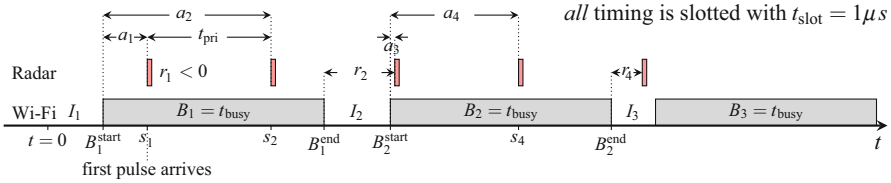

Fig. 5 Example timeline for a detection delay of 5 ($D = 5$) for $t_{pri} < t_{busy}$. The fifth pulse is the first that arrives during an idle period. Busy periods are of fixed duration t_{busy}, while idle periods are of a random duration

$$t_{busy} \triangleq \mathbb{E}[B] = t_{PAYLOAD} + P_s(t_{SIFS} + t_{ACK})$$

where P_s is the probability of successful packet transmission. Next, let us define:

S_i The *random* arrival time of the ith radar pulse. Since all timing is *slotted*, $S_i \in \mathbb{N}$ and clearly $S_i = S_{i-1} + t_{pri}$

N_i The index of the renewal period in which pulse i arrives (e.g., in Fig. 5, $N_1 = N_2 = 1$ since pulses 1 and 2 arrive during busy period 1, and $N_3 = N_4 = 2$)

A_i The *random offset* of the ith pulse inside the associated busy period. $A_i \in \{1, 2, \cdots, t_{busy}\}$. $A_i \triangleq S_i - B_{N_i}^{start}$

r_i The remaining time from the end of the busy period till the arrival of pulse $i+1$ as calculated in (4). A negative value for r_i signifies that a pair of pulses arrives in the same busy period (e.g., pulses 1 and 2 in Fig. 5)

D The random variable describing the detection delay in number of pulses where $D = 1$ signifies detection of the first arriving pulse. $D \in \{1, 2, \ldots\}$

d_{burst} The number of pulses in a radar pulse burst

For the radar to be detected with the first arriving pulse ($D = 1$), the network must be idle at arrival time which occurs with probability P_{idle} according to (2). For $D > 1$, the approach is to compute the detection delay distribution recursively; therefore, the derivation focuses on obtaining an expression for the following conditional probability:

$$\mathbf{P}(A_{i+1} = a_{i+1} | A_i = a_i) \tag{3}$$

which denotes the probability that pulse $i + 1$ arrives at offset a_{i+1} in an upcoming busy period given that pulse i arrived at offset a_i in a busy period.

One key observation is that (3) *does not* depend on arrival values prior to i (e.g., A_{i-1}), a fact that is used to help simplify the analysis. Even so, two separate classes should be considered in the upcoming subsections:

1. $t_{pri} < t_{busy}$ (Fig. 5)
2. $t_{pri} \geq t_{busy}$ (Fig. 6)

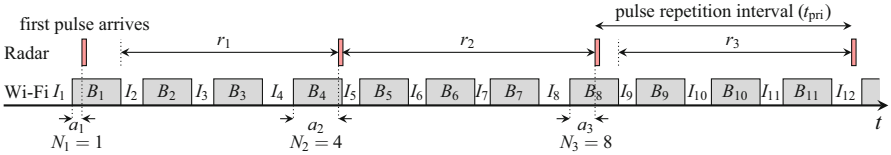

Fig. 6 Sample timeline for a detection delay of four pulses (i.e., $D = 4$) for $t_{\text{pri}} > t_{\text{busy}}$. Note that $N_i = n_i$ signifies that pulse i arrives during busy period B_{n_i}

Before doing so, let's define:

$$r_i \triangleq a_i + t_{\text{pri}} - t_{\text{busy}} \tag{4}$$

$t_{\text{Pri}} < t_{\text{Busy}}$

When $t_{\text{pri}} < t_{\text{busy}}$, multiple radar pulses can arrive within a single busy period (Fig. 5). An example of this coexistence class is when a radar with short PRI (e.g., 200 μs) is sharing spectrum with an 802.11 WLAN employing 3 ms aggregated frames.

Case 1: $r_i < 0$

This condition is satisfied if and only if both pulses fall within the same busy period. An example of this case can be observed with pulses 1 and 2 in Fig. 5. As shown, a_1 and a_2 differ by exactly t_{pri}. In this case, the trivial (deterministic) result is as

$$\mathbf{P}(A_{i+1} = a_{i+1} | A_i = a_i) = \begin{cases} 1 & \text{when } a_{i+1} = a_i + t_{\text{pri}} \\ 0 & \text{otherwise} \end{cases} \tag{5}$$

Case 2: $r_i \geq 0$

If pulse $i + 1$ falls within the next renewal cycle, it can be shown that

$$\mathbf{P}(A_{i+1} = a_{i+1} | A_i = a_i) = \mathbf{P}(I_{N_i+1} = r_i - a_{i+1}) \tag{6}$$

Moreover,

$$I_{N_i+1} = Q_{N_i+1} \cdot t_{\text{bo}} + t_{\text{difs}};\ Q_{N_i+1} \in \mathbb{N}, \tag{7}$$

therefore, it can be written:

$$\mathbf{P}(I_{N_i+1} = r_i - a_{i+1}) = \mathbf{P}\left(Q_{N_i+1} = q_{N_i+1}\right), \tag{8}$$

where

$$q_{N_i+1} = \frac{r_i - a_{i+1} - t_{\text{difs}}}{t_{\text{bo}}}. \tag{9}$$

Hence,

$$\mathbf{P}(A_{i+1} = a_{i+1} | A_i = a_i) = \begin{cases} \mathbf{P}(Q_{N_i+1} = q_{N_i+1}) & r_i \geq 0 \\ 1 & r_i < 0 \text{ and } a_{i+1} = a_i + t_{\text{pri}} \\ 0 & \text{otherwise} \end{cases}, \tag{10}$$

where $\mathbf{P}(Q_{N_i+1} = q_{N_i+1})$ for the uplink/downlink configuration is calculated as

$$\mathbf{P}(Q_{N_i+1} = q_{N_i+1}) = P_{tr}.(1 - P_{tr})^{q_{N_i+1}} \; q_{N_i+1} = 0, 1, \ldots \tag{11}$$

and for the downlink only there will be no collisions and therefore the success probability of any transmission equals 1. So,

$$\mathbf{P}(Q_{N_i+1} = q_{N_i+1}) = \frac{1}{W}, \; 0 \leq q_{N_i+1} < W. \tag{12}$$

$t_{\text{Pri}} \geq t_{\text{Busy}}$

For this class, it is possible for multiple busy periods to occur in a single PRI as would be the case for a long PRI radar coexisting with a WLAN not using frame aggregation. An example is shown in Fig. 6. It is straightforward to see that given some remainder time r_i, the next pulse cannot occur any later than busy period $N_i + K$, where

$$K = \left\lceil \frac{r_i}{t_{\text{busy}} + t_{\text{difs}}} \right\rceil, \tag{13}$$

therefore:

$$N_i < N_{i+1} \leq N_i + K. \tag{14}$$

Provided the value of r_i as calculated in (4), so

$$\mathbf{P}(A_{i+1} = a_{i+1} | A_i = a_i) = 0 \;\text{ if } r_i - t_{\text{difs}} < 0, \tag{15}$$

Otherwise, if $r_i \geq 0$, for each $k = 1, \ldots, K$, it can be shown that

$$\mathbf{P}\left(\sum_{j=1}^{k} I_{N_i+j} = r_i - a_{i+1} - t_{\text{busy}}(k-1) \right) = \mathbf{P}\left(\sum_{j=1}^{k} Q_{N_i+j} = \hat{q} \right),$$

$$\text{where } \hat{q} = \frac{r_i - a_{i+1} - t_{\text{busy}}(k-1) - t_{\text{difs}} k}{t_{\text{bo}}}$$

$$r_i - t_{\text{difs}} \geq 0 \text{ and } \hat{q} = 0, 1, \ldots$$

The intuition behind this formulation is that for pulse $i+1$ to fall within busy period $N_i + k$, $k-1$ busy periods and k idle periods must have elapsed prior to B_{N_i+k}. Meanwhile, the quantity $\hat{q}$ is nothing, but the sum of all backoff slots that must be remained idle for this event to occur.

Now, depending on the network configuration of interest (uplink/downlink or downlink only), the distribution of Q_k will differ as will the distribution of the sum. When considering an uplink/downlink network, Q_k is distributed geometrically; hence, the sum can be computed using a negative binomial:

$$\mathbf{P}\left(\sum_{j=1}^{k} Q_{N_i+j} = \hat{q}\right) = \binom{k-1+\hat{q}}{k-1} P_{\text{tr}}^{k}(1-P_{\text{tr}})^{\hat{q}} \tag{16}$$

In contrast, in the downlink-only case, Q is discrete uniform and the sum distribution can be calculated as [24]

$$\mathbf{P}\left(\sum_{j=1}^{k} Q_{N_i+j} = \hat{q}\right) = \frac{k}{(W+1)^k} \times \sum_{u=0}^{\lfloor \hat{q}/W \rfloor} \frac{\Gamma(k+\hat{q}-u\cdot W)(-1)^u}{\Gamma(u+1)\Gamma(k-u+1)\Gamma(\hat{q}-u\cdot W+1)} \tag{17}$$

where $\Gamma(.)$ is the gamma function for integer arguments. As a final step, the sum over all possible values of k is as

$$\mathbf{P}(A_{i+1} = a_{i+1} | A_i = a_i) = \sum_{k=1}^{K} \mathbf{P}\left(\sum_{j=1}^{k} Q_{N_i+j} = \hat{q}\right), \tag{18}$$

$$\text{where } \hat{q} = \frac{r_i - a_{i+1} - t_{\text{busy}}(k-1) - t_{\text{difs}}k}{t_{\text{bo}}}$$

$$r_i - t_{\text{difs}} \geq 0 \text{ and } \hat{q} = 0, 1, \ldots$$

Detection Delay

We gather and summarize the result for $\mathbf{P}(A_{i+1} = a_{i+1} | A_i = a_i)$ as follows:

$t_{\text{pri}} < t_{\text{busy}}$ and	uplink/downlink: Eq. 10, 11
$t_{\text{pri}} < t_{\text{busy}}$ and	downlink only: Eq. 10, 12
$t_{\text{pri}} \geq t_{\text{busy}}$ and	uplink/downlink: Eq. 16
$t_{\text{pri}} \geq t_{\text{busy}}$ and	downlink only: Eq. 18

With expressions in hand for the various network configurations and coexistence classes, the detection delay can be computed recursively. If the first pulse arrives at $a_1 = \alpha$, so

$$\mathbf{P}(D = 2|\alpha) = 1 - \sum_{\alpha'=1}^{t_{\text{busy}}} \mathbf{P}(A_{i+1} = \alpha' | A_i = \alpha), \tag{19}$$

then for $d > 2$,

$$\mathbf{P}(D = d|\alpha) = \sum_{\alpha'=1}^{t_{\text{busy}}} \mathbf{P}(A_{i+1} = \alpha' | A_i = \alpha)\mathbf{P}(D = d - 1|\alpha'), \tag{20}$$

and the full expression for the detection delay can be written as

$$\mathbf{P}(D = d) = \begin{cases} 1 - P_{\text{busy}} & \text{when } d = 1 \\ \frac{P_{\text{busy}}}{t_{\text{busy}}} \sum_{a_1=1}^{t_{\text{busy}}} \mathbf{P}(D = d|A_1 = a_1) & \text{otherwise} \end{cases}, \tag{21}$$

where

$$A_1 \sim \text{Unif}(1, t_{\text{busy}}). \tag{22}$$

Finally, the detection rate for a radar burst of d_{burst} pulses is as

$$P_d(d_{\text{burst}}) = \mathbf{P}(D < d_{\text{burst}}). \tag{23}$$

Simulation Results and Discussion

In this section, the results for several radar parameter sets are presented to gain some insight into suitability of the proposed sensing/detection as a coexistence mechanism. Later, using the analysis developed is considered as a guideline for selecting Wi-Fi parameters that allows to achieve some desired detection requirements.

The Impact of Wi-Fi and Radar Parameters

Figure 7 shows the dramatic affect of payload size on the detection delay when comparing corresponding results for the different payloads; increases in the payload duration negatively impact detection delay (by comparing a with b). In the worst case, it can take hundreds of pulses for detection when the secondary network's channel utilization is high. Thus increased payloads both reduce the frequency with which idle periods occur as well as the overall average idle time duration, making it less likely for the low-duty cycle radar signal to be detected.

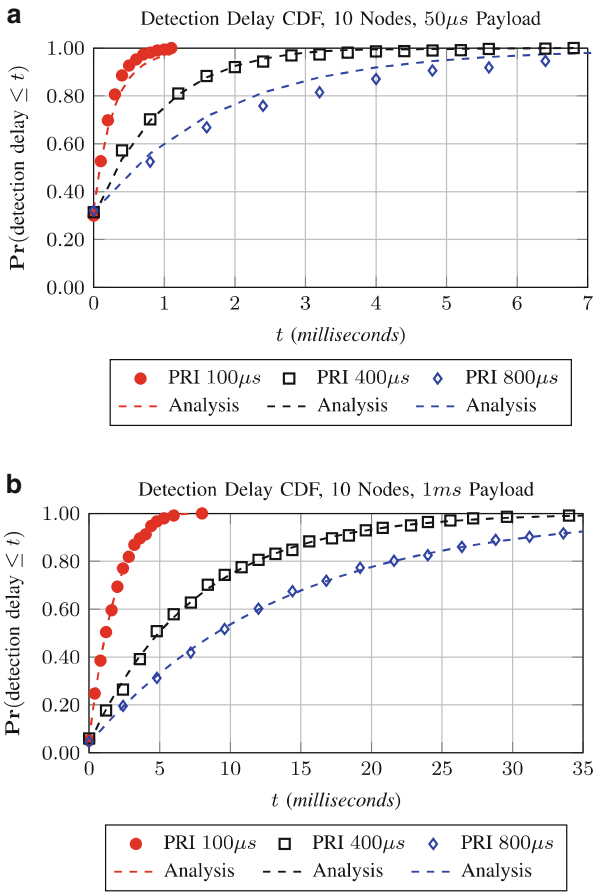

Fig. 7 Detection delay (in seconds) as a function of radar PRI for two fixed payloads. Aside from the PRI, all parameters match those in Table 3. (**a**) shows a ten-node saturated network with a fixed payload size of 50 μs. Wi-Fi throughput at this setting is 0.299. (**b**) shows the detection delay for a similar network but with a longer payload duration of 1 ms. Wi-Fi throughput at this setting is 0.725

The Detection Versus Throughput Trade-Off

The framework developed is now applied to achieving good WLAN throughput subject to the detection requirements, i.e., explore the detection-throughput trade-off. To do so, the length of the payload (busy period) and the DIFS (idle period) is tuned to achieve two goals:

1. Modifying the proportion of network idle time,
2. Adjusting the frequency with which idle periods occur.

From a secondary network throughput perspective, these constitute necessary overheads while they reduce detection delay. Note that any desired detection delay $D_{\text{des}} > 1$ can be trivially guaranteed by imposing the following conditions:

$$I^{\min} \geq t_{\text{pri}} \implies t_{\text{difs}} \geq t_{\text{pri}} \tag{24}$$

which ensures that every idle period is of sufficient duration to contain at least a single pulse arrival. The second condition ensures that at least one such idle period occurs by the desired detection delay (D_{des})

$$D_{\text{des}} t_{\text{pri}} \geq I^{\min} + B^{\max} \tag{25}$$

While feasible, this guarantee comes at a (potentially) heavy cost. In essence, by lengthening the inter-frame spacing which reduces throughput while simultaneously, the duration of the payload is decreased which compounds the effect. Such overheads impose a heavy penalty that would significantly degrade Wi-Fi throughput. However, by forgoing strict requirements and adopt statistical guarantees instead, one will be able to achieve far better network performance while maintaining acceptable protection for radars. Currently, the specific detection requirements available in the public literature are those applying to the 5 GHz band [14]. Hence, these numbers simply is considered as a benchmark.

The derivations in the previous section show that the distribution of detection delay is a function of the distributions of I and B. However, they cannot be considered as independent "knobs" used for tuning. Modifying either one affects both throughput and detection; in fact, adjusting the payload seems to be clearly sufficient.

Based on the calculations, WLAN parameters can be selected to achieve a particular in-service detection probability given particular radar characteristics. As an example, a radar with a PRI of 200 μs in line with [14] is considered. Table 3 shows the parameter sets that yield a 60% detection rate for a PRI of 200 μs. When the payload size is 3 ms (which is close to the maximum allowable by Wi-Fi), the throughput is maximized; however, $d_{\text{burst}} > 40$ pulses is needed before it can be detected with desired reliability. Reducing the payload size to 1 ms deceases the number of pulses required for detection by more than one half. Evidently, this improvement results in only a minimal loss of throughput (less than 10%) though additional improvements through further reductions of the payload size come at a much greater cost. It can be concluded that high throughput (by using 1 ms Wi-Fi payloads) and a 60% detection rate for bursts longer than 16 pulses can be obtained

Table 3 Simulation verification scenarios

Scenario:	1	2	3	4	5
t_{payload}	50 μs	150 μs	250 μs	1 ms	3 ms
Clients			10		
Radar pulse			4 μs		
Radar PRI			200 μs		
Energy detection			Ideal		
d_{burst} for $P_d = 0.6$	4	6	6	16	44
Throughput (Analysis)	0.299	0.571	0.599	0.718	0.7553
Throughput (Sim.)	0.3	0.58	0.61	0.725	0.75

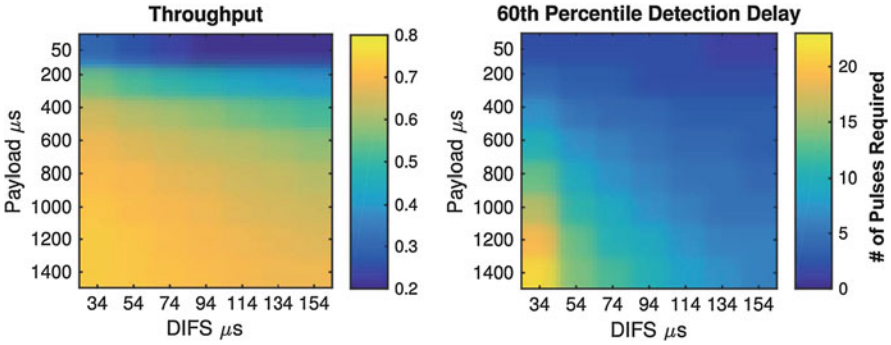

Fig. 8 For $t_{\text{pri}} = 200\,\mu\text{s}$, these figures illustrate the detection delay vs. throughput trade-off for various t_{difs} and t_{payload}

Table 4 DFS scenarios

PRI	250 μs	1429 μs	5000 μs
Pulse duration	1 μs	1 μs	5 μs
d_{burst}	25	18	10
Target burst P_d		0.6	
Clients		10	
Max throughput	0.7363	0.715	0.6470
Payload duration	1.5 ms	930 μs	400 μs

simultaneously; this is an indication that through careful selection of the appropriate parameters, a Wi-Fi network can achieve acceptable throughput while adequately protecting a radar.

Figure 8 shows a complete picture of the detection vs. throughput trade-off for a radar with a PRI of 200 μs as a function of payload and DIFS duration. As alluded to earlier, it is evident that for almost any desired pulse burst, the best throughput can be attained by simply adjusting the payload. To conclude, the results for a selection of other radar parameters indicated in [14] is presented, namely, those listed in Table 4. Evidently, radars that transmit less frequently (i.e., longer PRIs as well as fewer pulses per burst) are more difficult to detect reliably. Nevertheless, the key insight from this exercise points to the feasibility of achieving desired detection rates with latency budgets for specific radar parameter sets, while preserving a good throughput for the Wi-Fi network.

WLAN Modifications for Radar Interference Mitigation

In this section, the Wi-Fi networks outside the exclusion region is considered that have an opportunity to detect pulse interference during a packet transmission and subsequently mitigate it to preserve WLAN throughput. This section begins with

the description of a standard Wi-Fi transceiver chain and indicates the sort of modifications necessary for this purpose [21].

WLAN Generic System Architecture

A generic Wi-Fi link is illustrated in Fig. 9, where the blocks without red circles constitute the generic receiver and transmitter chain. The system has one transmit and two receive antennas and uses maximal ratio combining (MRC) in the receiver. There are two error correction coding options available in the 802.11 standard [3,5]: binary convolutional code (BCC) and low-density parity check (LDPC). The LDPC code with 1944 coded bits is chosen because of its superior performance in burst error circumstances. The LDPC decoder uses a sum-product algorithm-based soft-input decoder. The traditional symbol interleaver interleaves among a sequence of encoded data corresponding to each OFDM symbol. The constellation mapper takes a group of bits (depending on the modulation index and scheme) and maps them to a constellation point. After OFDM modulation of the payload, the framing block in Fig. 9a constructs a frame with preamble and payload (Fig. 11). Automatic gain control (AGC) block regulates the received signal power at the input prior to analog to digital conversion (ADC). The frame synchronization block achieves frame (timing) synch and pilot common phase error (CPE) estimator uses transmitted pilots to estimate the oscillator phase noise which causes rotation of all subcarriers and causes intercarrier interference (ICI). The standard soft demodulator passes an

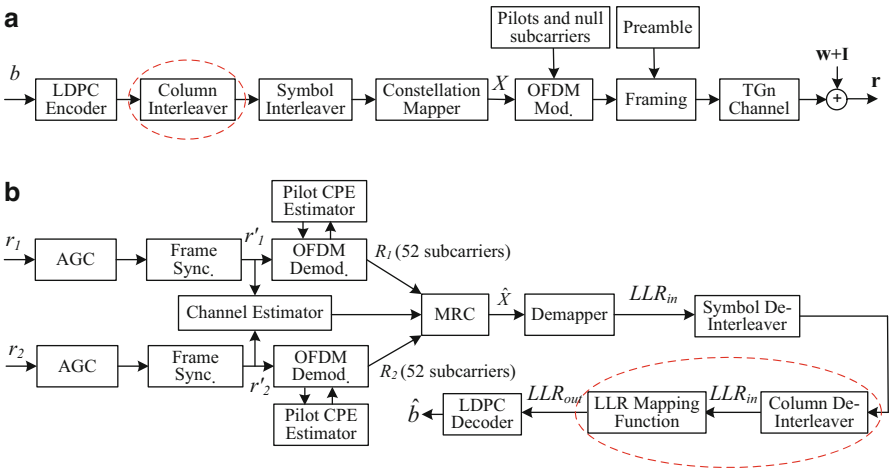

Fig. 9 The transmitter and receiver block diagrams of the Wi-Fi system. The blocks without *red circles* shows the generic Wi-Fi system receiver and transmitter chain. The blocks with *red circles* are the new components added to the genetic system that is the modified Wi-Fi system receiver and transmitter chain. (**a**) The transmitter block diagram of the Wi-Fi system, (**b**) The receiver block diagram of the Wi-Fi system

Table 5 Wi-Fi system parameters

BW	Pilots	Number of data subcarriers	Cyclic prefix	OFDM symbol duration
20 MHz	11, 25, 40, 54	52	16 Samples (0.8 μs)	80 Samples (4 μs)

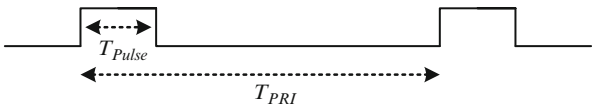

Fig. 10 The radar pulse repetition interval and pulse duration

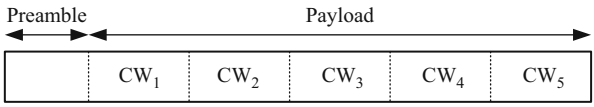

Fig. 11 The structure of a WLAN frame consisting of preamble data and several CWs

LLR value for each encoded bit to the LDPC soft input decoder. Finally, the blocks with red circles represent the new components to be added to the generic Wi-Fi system receiver and transmitter chain, and their role is explained in section "Wi-Fi System Modifications for Interference Mitigation".

Table 5 lists the Wi-Fi system parameters used in this work, consistent with 802.11ac WLAN: a 64 subcarrier OFDM with spacing of 312.5 KHz. The 20 MHz channel has 4(3) guard subcarriers at the left (right) band edge, and the DC (center) subcarrier that are unused. The remaining subcarriers as listed in Table 5 are pilot and data subcarriers. For simulations, the MATLAB 2015 WLAN toolbox [7] is used that implements the IEEE 802.11ac PHY layer, adapted for radar/Wi-Fi coexistence by (a) adding the new elements of the modified Wi-Fi system as described and (b) injecting a suitably modeled pulsed radar signal as additive interference at the Wi-Fi receiver input.

We consider linear frequency modulation (LFM) radar pulse as shown in Fig. 10 with $T_{PRI} = 200\,\mu s$ and pulse duration (T_p) of 4 μs. The LFM radar waveform has sweep frequency of $f_s = 4$ MHz and relative carrier frequency offset of $\Delta f_r = [-4, 4]$ MHz relative to the center of the Wi-Fi channel.

The baseband LFM radar waveform is given by

$$I(t) = Ae^{j(\pi \frac{f_s}{T_p} t + 2\pi \Delta f_r)t} \quad 0 \le t \le T_p. \tag{26}$$

The radar pulse arriving are assumed to hit the payload randomly (we ignore the small probability that it hits the preamble, which is much smaller than the payload as indicated in Fig. 11). The received OFDM symbol at the Wi-Fi receiver under the two hypothesis (radar pulse present or absent) can be written as

$$\begin{aligned} \mathscr{H}_0 &: \text{(W/O Interference) } \mathbf{r}(n) = x_s(n) * h(n) + \mathbf{w}(n) \\ \mathscr{H}_1 &: \text{(W/ Interference) } \mathbf{r}(n) = x_s(n) * h(n) + \mathbf{w}(n) + \mathbf{I}(n), \end{aligned} \tag{27}$$

where **r** is the received data vector at the Wi-Fi receiver input as indicated in Fig. 9b, h is the WLAN channel, **w** is the additive white Gaussian noise vector, **I** is the radar interference vector, x_s is the OFDM modulated signal and $*$ denotes convolution. The modulated signal and noise is assumed to the following the complex normal distribution, i.e.,

$$w \sim CN(0, \sigma_w^2), \qquad x_s \sim CN(0, \sigma_s^2). \tag{28}$$

Hence, the signal to noise ratio (SNR) at the receiver input is calculated as

$$\text{SNR} = 10 \log_{10} \left(\frac{\sigma_s^2}{\sigma_w^2} \right), \tag{29}$$

since the frequency selective channel $h(n)$ is assumed normalized (i.e. $\sum_n |h(n)|^2 = 1$), σ_s^2 is equal to the power of $x_s(n) * h(n)$ at the receiver. The interference to noise ratio (INR) seen at Wi-Fi receiver is thus

$$\text{INR} = 10 \log_{10} \left(\frac{A^2}{\sigma_w^2} \right), \tag{30}$$

where A is the radar signal magnitude.

Exclusion Region Calculation

The numerical results in [18] shows that for a single co-channel Wi-Fi network impacted by continuous wave pulse radar, the effective interference from radar to the Wi-Fi receiver can be calculated as

$$\text{INR}_{eff} = 10 \log_{10} \left(\frac{PWf_R P_T G_w G_{max} l(d)}{N_0 BW} \right), \tag{31}$$

$l(d) = k_0 d^{-\alpha}$ is the path loss model between radar and Wi-Fi receiver [18] and BW is the Wi-Fi channel bandwidth. The other parameters are defined in Table 6. Based on (31), the maximum INR_{eff} from radar to the Wi-Fi receiver at the border of exclusion region (the exclusion region range is 20 Km in the main lobe direction) is computed to be 43.8 dB.

Wi-Fi System Modifications for Interference Mitigation

Pulsed radar interference causes – in general – burst or consecutive error events at the Wi-Fi receiver. As explained in section "WLAN Generic System Architecture", the symbol interleaver just interleaves among the sequence of data corresponding to one OFDM symbol. If the radar pulse impacts the OFDM symbols, it is

Table 6 Wi-Fi and radar parameters for maximum interference calculation

Parameters	Descriptions	Values
PW	Radar pulse width	1.03 (μs)
f_R	Pulse repetition frequency	1115.5
P_T	Radar Tx power	1.32 (MW)
G_w	Wi-Fi antenna gain	2.15 (dBi)
$G_{\max}$	Radar maximum antenna gain	33.5 (dBi)
NF	Noise figure	8 (dB)
k_0	Path loss constant	259
α	Path loss constant	3.97

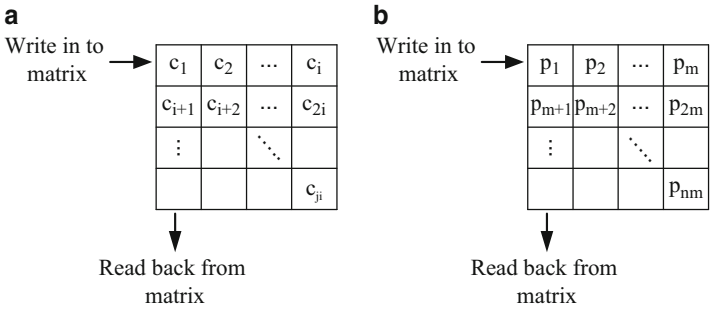

Fig. 12 (**a**) Column CW interleaver. (**b**) Column frame interleaver

typically lost, i.e., results in decoding failure. So a longer interleaver is needed (that interleaves among several OFDM symbols) to distribute the error burst through the frame and potentially mitigate the burst error event. To deal with this problem, a column interleaver/de-interleaver is added to the Wi-Fi transmitter/receiver as illustrated in Fig. 9.

Two types of column interleaving – (i) codeword (CW) interleaving and (ii) frame interleaving are proposed that both interleave over several OFDM symbols, as shown in Fig. 12. In CW interleaver, an LDPC CW is interleaved denoted by the sequence of $C = (c_1, c_2, \ldots, c_{ji})$ and length of $N_{cw} = j \times i$ as follows – it is written row by row into a matrix (N_{cw} = 1944, corresponding to $j = 9$ and $i = 216$) and read back column by column from the matrix as shown in Fig. 12a. To de-interleave, the identical process is conducted at the receiver.

In the frame interleaver, a frame of data is interleaved which consists of several CWs. For example, in the case of modulation and coding scheme (MCS) 4, a frame consists of 5 CWs with the length of 1944 followed by a small set of data to construct a standard size frame. A frame sequence of $P = (p_1, p_2, \ldots, p_{nm})$ and length of $N_p = n \times m$ is written row by row into a matrix (N_p in this case is 9776, n is 52 and m is 188) and read back column by column from the matrix as shown in Fig. 12b. To de-interleave, the same process is performed at the receiver. In CW interleaving, the objective is to distribute the symbols with interfered LLR among a CW so to remove the burst error effect (for MCS4, each CWs consists of almost nine payload

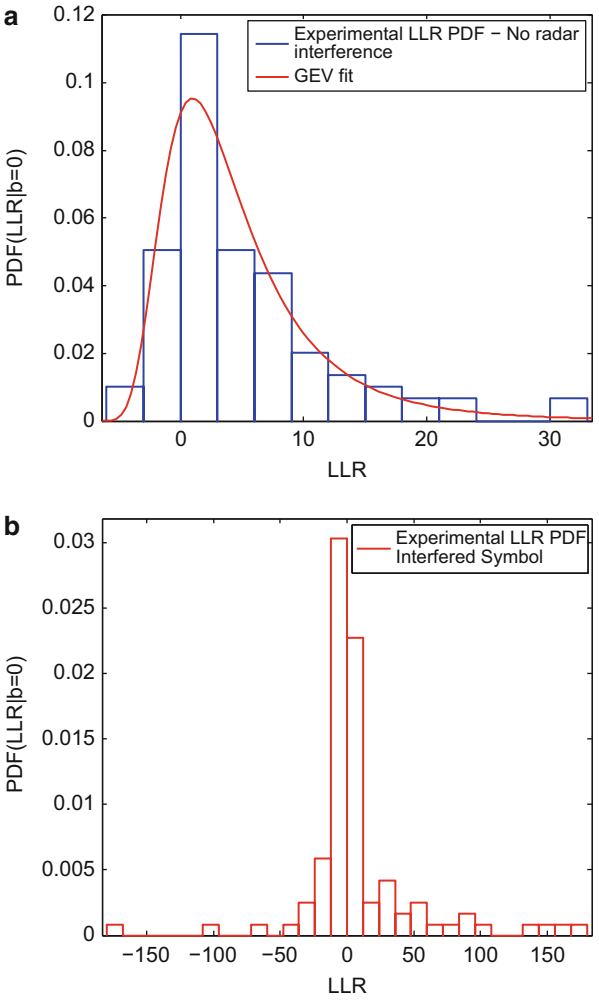

Fig. 13 Conditional LLR PDF of an OFDM symbol interfered by the radar pulse. For (a) the label is "No Radar interference" and for (b) the label is "Radar interference"

OFDM symbols). A frame consists of several CWs (Fig. 11), so frame interleaving distributes the symbols with interfered LLRs over the multiple CWs, and hence the decoder needs to correct for fewer interfered symbols per CW.

Figure 13 compares the conditional distribution of LLR_{in} at the output of demapper in Fig. 9b) for the cases of with and without radar pulse interference, at SNR=15 dB, INR=30 dB and MCS4. In the demapper implementation of MATLAB 2015 WLAN toolbox, the generic LLR calculation for BPSK modulation is done via

$$LLR_d = \log\left(\frac{P(b=0|\hat{X})}{P(b=1|\hat{X})}\right), \tag{32}$$

LLR_d is then multiplied by the channel gain inside the demapper to yield [27],

$$LLR_{in}(l) = |H_{k,l}|^2 LLR_d(l) \tag{33}$$

where $H_{k,l}$ is the (estimated) frequency-domain channel coefficient for kth OFDM symbol in a frame and lth subcarrier ($H_{k,l}$ is assumed constant for all OFDM symbols in a frame, i.e., for different k), $LLR_{in}(l)$ is the LLR for the lth subcarrier after weighting. The distribution of LLR_{in} corresponds to the multiplication of the channel gain represented by a Rayleigh-distributed random variable and LLR_d, represented by a Gaussian distribution. By fitting the experimental LLR_{in} histogram (as illustrated in Fig. 13a), it is observed that the generalized extreme value (GEV) distribution [13] achieves a good fit as can be seen in Fig. 13a. The GEV distribution is given by

$$f(x|k_v, \mu_v, \sigma_v) = \frac{1}{\sigma_v} \exp\left(-\left(1 + k_v \frac{(x-\mu_v)}{\sigma_v}\right)^{-\frac{1}{k_v}}\right)\left(1 + k_v \frac{(x-\mu_v)}{\sigma_v}\right)^{-1-\frac{1}{k_v}}, \tag{34}$$

where the GEV parameters in Fig. 13a are the following: $k_v = 0.2$, $\mu_v = 3.93$, and $\sigma_v = 1.69$.

Figure 13b shows the LLR_{in} for interference due to the radar pulse; most noticeably, it shows significantly larger LLR magnitudes compared with the no interference case. Hence, for a transmitted symbol that is interfered by the radar pulse, the constellation symbol value is superimposed with additive, random interference component with large magnitude. As a result, the LLR calculated in the demapper has a large value either to the left or right of the median in Fig. 13b. Since large LLR values (even if due to an external interference) imply high confidence about the correctness of the bit, the LDPC soft-in decoder cannot recover the transmitted CW as is.

To help the LDPC decoder to recover CW in the presence of large interference, a new LLR mapping function is proposed as shown in Fig. 14, given by

$$LLR_{out} = \begin{cases} Th_{out} \times sign(Th_{in}) & \text{if } |LLR_{in}| >= Th_{in} \\ \frac{Th_{out}}{Th_{in}} \times LLR_{in} & \text{if } |LLR_{in}| < Th_{in} \end{cases} \tag{35}$$

representing a thresholded linear function where Th_{in} – the input threshold – is determined by the *maximum LLR value in the noninterfered OFDM symbols*, i.e., $Th_{in} = th_1 \times \max(LLR)$, and $\max(LLR)$ is calculated based on the noninterfered OFDM symbol. Input LLRs with magnitude larger than Th_{in} map to Th_{out} where $Th_{out} = th_2 \times \max(LLR)$. The slope or gain of the linear region equals $\frac{th_2}{th_1}$, where th_1 and th_2 are selected by searching over a discretized set of values during training phase. Via the thresholding, the LLR to the LDPC decoder is desensitized to large LLR values and can detect instances where large LLRs result due to interference. Thus, smaller LLRs represent either noninterfered symbols or ones

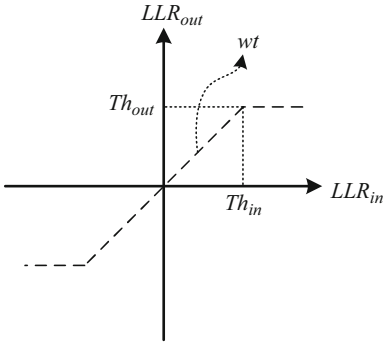

Fig. 14 The LLR mapping function

Table 7 LLR mapping function parameters for the frame interleaving cases

MCS	SNR	th_1, th_2, INR	th_1, th_2, INR
0	4	0.1, 0.001, [−5, 40]	–
0	8	0.05, 0.01, [−5, 40]	–
4	15	0.1, 0.05, [−5, 20]	0.1, 0.01, (20, 40]
4	20	0.01, 0.001, [−5, 40]	–
8	25	0.1, 0.01, [−5, 25]	0.05, 0.001, (25, 40]
8	30	0.01, 0.001, [−5, 40]	–

with small interference; by appropriately weighting them, the mapping function aids the decoding.

Simulation Results for Interference Mitigation

We simulate the modified Wi-Fi system under different MCSs. MCS0 uses BPSK modulation, whereas MCS4 uses 16QAM modulation and MCS8 uses 256QAM modulation. The LDPC code rate for MCS0 is $\frac{1}{2}$ and for the two other MCSs is $\frac{3}{4}$. The maximum number of LDPC decoder iteration is 50. The LDPC iteration is terminated when either the CW is detected or the maximum number of iteration is reached. For each frame error rate (FER) point in the figures, 2500 frames were used in simulation. The parameter values selected for the LLR mapping function (contained in Table 7) are chosen to yield low FER in the different scenarios; in general, the choice of (th_1, th_2) are seen to depend (mildly) on both the SNR and INR in some cases.

Figure 15 illustrates the performance of the Wi-Fi system interfered with the co-channel radar interference in comparison with the modified Wi-Fi system for MCS0. When the interference mitigation is not performed, the FER increases very rapidly as the INR increases even at high SNR case (e.g., SNR=8 dB). The modified Wi-Fi system shows a better FER performance compared with the no-mitigation system. In this figure, the FER performances of the system with CW interleaver and frame interleaver are almost the same and follow a flat curve under the no-mitigation

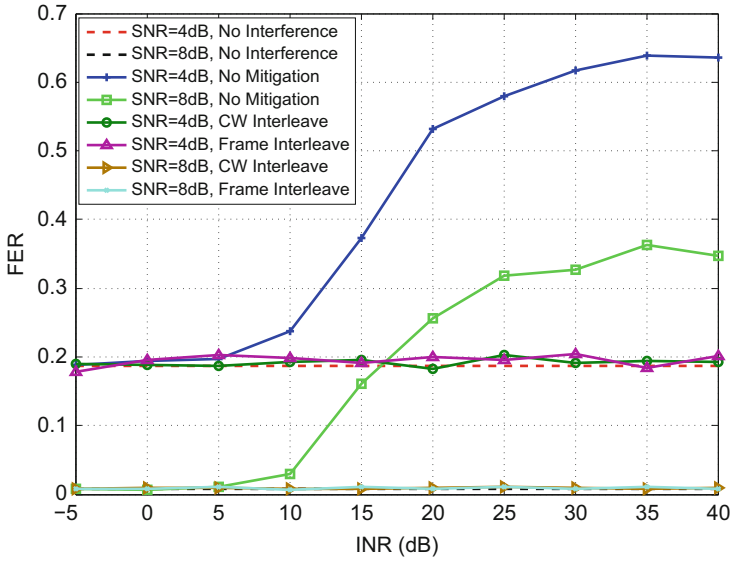

Fig. 15 FER comparison of the Wi-Fi system without interference mitigation and a modified Wi-Fi system for two different cases of CW interleave and frame interleave at MCS0

Wi-Fi system curve. In MCS0 the number of interfered coded bits is relatively small compared with the CW length because of the fewer number of bits in one OFDM symbol, so smaller column interleaver like CW interleaver is enough for mitigating the radar interference burst effect.

Figure 16 compares the performance of the Wi-Fi systems at MCS4. When the interference mitigation is not performed, the FER increases much faster in MCS4 compared with the MCS0. It implies that the radar interference has a greater (deteriorating) effect at higher MCSs. The modified receiver shows a very good FER performance compared with the no-mitigation system. When the total frame is interleaved, the FER curves remain below the no-mitigation curves for all of the INR values. In the CW interleave case, the FER is higher than the no-mitigation case for small INR values (especially at 15 dB SNR curve). Also, there is an (expected) FER gap between the CW interleave and frame interleave cases; by interleaving a frame, the incorrect interfered LLRs are distributed among multiple CWs, so the decoder needs to deal with fewer corrupted LLRs. At higher SNR, the gap between the CW interleave and frame interleave curves is smaller because fewer error happens anyway, so each LDPC CW has fewer corrupted LLRs for correction. The performance of the modified system compared with the system without interference mitigation for MCS8 is also illustrated in Fig. 17 as a benchmark. The FER curve for the modified system is flat (insensitive to INR) and very close to the "no-interference" curve, suggesting that the modified Wi-Fi receiver can completely mitigate the radar interference.

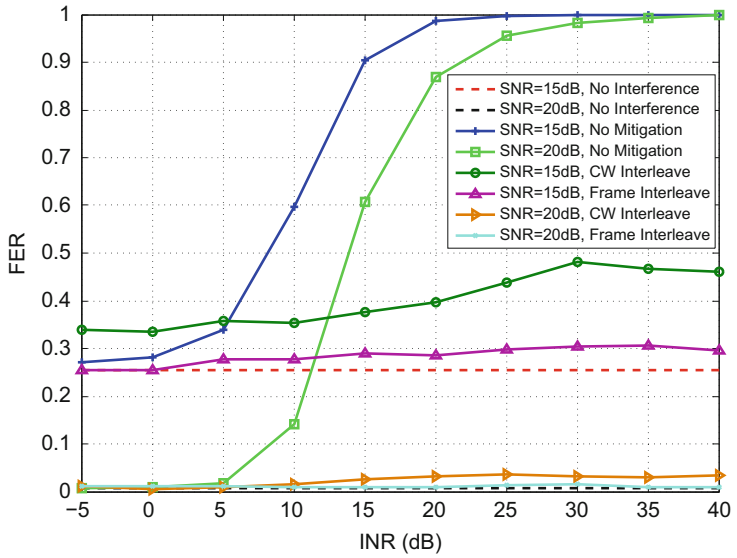

Fig. 16 FER comparison of the Wi-Fi system without interference mitigation and a modified Wi-Fi system for two different cases of CW interleave and frame interleave at MCS4

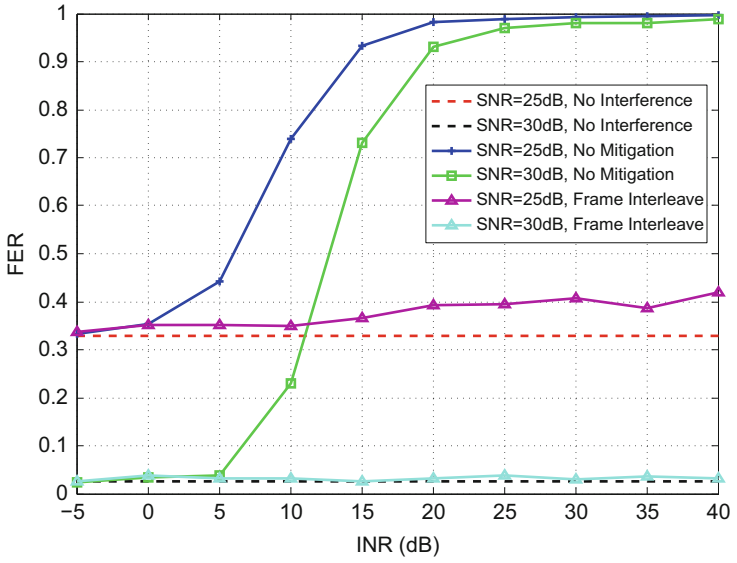

Fig. 17 FER comparison of the Wi-Fi system without interference mitigation and a modified Wi-Fi system at MCS8

Radar Pulse Detection During Wi-Fi Transmission

Interference mitigation requires accurate radar pulse detection first. Generic approaches proposed in the literature include energy-based detection (that does not require any knowledge of the radar pulse shape) or some feature-based detection schemes such as cyclostationary and autocorrelation-based sensing [11, 20, 23]. Specifically for OFDM transmission, signal detectors using embedded pilots were proposed in [12]. In [11], cyclic prefix (CP)-based autocorrelation detection is considered, and cyclostationary-based detection proposed in [26]. Following the above, two detection approaches are proposed: (a) CP-based autocorrelation detector and (b) frequency domain data subcarrier detector.

(a) CP is inherent in 802.11 WLAN modulation in an OFDM symbol (by repeating the trailing samples as prefix data) to combat ISI for a frequency selective channel. Thus at the receiver, there is a high correlation between prefix data samples and those at the end of OFDM symbol. When a symbol is interfered by a radar pulse, it decreases the correlation between these two pieces of an OFDM symbol, which can be used as a criterion to detect the presence of radar interference.
(b) Spectral shape of the radar pulse in frequency domain may also be used for OFDM subcarrier based detector. The interference in the frequency domain is spectrally limited to subset of the OFDM subcarriers; thus, the energy concentrated in a portion of the impacted subcarriers compared to the rest provides another heuristic for improved radar pulse detection.

Conclusion and Future Directions

In this chapter, the statistical properties of randomly occurring quiet periods in Wi-Fi networks for the purposes of radar detection using DFS in a Wi-Fi/radar coexistence scenario was first studied. In many circumstances, these random quiet periods occur with sufficient frequency to provide some statistical guarantees for in-service radar detection, especially in the regions close to the radar that are designated as exclusion or no-transmit zones. An intelligent method to adjust Wi-Fi parameters is proposed in order to achieve the desired protection for the radar while attaining acceptable throughput. Lastly, it is shown that modifying the payload duration is the most effective adjustment for Wi-Fi to speedily detect radars and provide adequate in-service protection.

Next, the Wi-Fi transmitter/receiver chains were modified to enable the coexistence of WLAN and radar by mitigating the radar interference. The impact of radar interference on the generic Wi-Fi system and the modified Wi-Fi system was studied in terms of FER. The simulation results show that by a relatively small modification to the Wi-Fi system, the FER performance is significantly improved; the modified Wi-Fi system can perform at very high INR.

As a final step, it is clear that in order to mitigate radar interference, accurate radar (pulse) detector is required. This suggests a path for future extension of this work. Radar pulse detection has focused thus far on detecting a single pulse; however, in almost all cases, radar sources emit a pulse burst, which provides significant potential for further improvement if this property were to be suitably exploited.

References

1. (2000–2003) Characteristics of radiolocation radars, and characteristics and protection criteria for sharing studies for aeronautical radionavigation and meteorological radars in the radiodetermination service operating in the frequency band 2700–2900 MHz. In: International Telecommunication Union, Technical Report
2. (2010) An assessment of the near-term viability of accommodating wireless broadband systems in the 1675–1710 MHz, 1755–1780 MHz, 3500–3650 MHz and 4200–4220 MHz, 4380–4400 MHz bands. US Department of Commerce, Technical Report
3. (2012) Wireless LAN Medium Access Control (MAC) and Physical Layer (PHY) specifications. IEEE Std 80211
4. (2013) Part 11: Wireless LAN Medium Access Control (MAC) and Physical Layer (PHY) specification. IEEE Std 80211n
5. (2013) Wireless LAN Medium Access Control (MAC) and Physical Layer (PHY) specifications. IEEE Std 80211ac
6. (2015) Amendment of the commissions rules with regard to commercial operations in the 3550–3650 MHz band. In: FCC Report and Order 15-47A1
7. (2015) The MathWorks Inc., Using MATLAB Version 8.6
8. (2015) NTIA letter to FCC on commercial operations in the 3550–3650 MHz band
9. Adamis AV, Constantinou P (2009) Intermittent DCF: a MAC protocol for cognitive radios in overlay access networks. In: Wang W (ed) Cognitive radio systems. InTech. https://www.intechopen.com/books/howtoreference/cognitive-radio-systems/intermittent-dcf-a-mac-protocol-for-cognitive-radios-in-overlay-access-networks
10. Bianchi G (2000) Performance analysis of the IEEE 802.11 distributed coordination function. IEEE J Sel Areas Commun 18(3):535–547
11. Chaudhari S, Koivunen V, Poor HV (2009) Autocorrelation-based decentralized sequential detection of OFDM signals in cognitive radios. IEEE Trans Signal Process 57(7):2690–2700
12. Chen HS, Gao W, Daut DG (2009) Spectrum sensing for OFDM systems employing pilot tones. IEEE Trans Wirel Commun 8(12):5862–5870
13. Coles S (2001) An introduction to statistical modeling of extreme values. Springer, London
14. ETSI (2012) Broadband radio access networks (BRAN); 5 GHz high performance RLAN; harmonized EN covering the essential requirements of article 3.2 of the R&TTE directive. EN 301 893
15. Ghorbanzadeh M, Visotsky E, Moorut P, Yang W, Clancy C (2015) Radar inband and out-of-band interference into LTE macro and small cell uplinks in the 3.5 GHz band. In: IEEE Wireless Communications and Networking Conference (WCNC), pp 1829–1834
16. Ghosh C, Safavi-Naeini HA, Roy S, Doppler K, Stahl J (2012) QP-CSMA-CA: a modified CSMA-CA-based cognitive channel access mechanism with testbed implementation. In: IEEE International Symposium on Dynamic Spectrum Access Networks, pp 501–509
17. Griffiths H, Cohen L, Watts S, Mokole E, Baker C, Wicks M, Blunt S (2015) Radar spectrum engineering and management: technical and regulatory issues. Proc IEEE 103(1):85–102
18. Hessar F, Roy S (2016) Spectrum sharing between a surveillance radar and secondary Wi-Fi networks. IEEE Trans Aerosp Electron Syst 52(3):1434–1448

19. Kruys J, Vangeel E, Kraemer B, Auluck V, Kennedy R, Raab J, Kubik R (2007) Spectrum sharing in the 5 GHz band – DFS best practices. Wi-Fi Alliance, Technical Report
20. Lunden J, Koivunen V, Huttunen A, Poor HV (2007) Spectrum sensing in cognitive radios based on multiple cyclic frequencies. In: 2nd International Conference on Cognitive Radio Oriented Wireless Networks and Communications, pp 37–43
21. Mehrnoush M, Roy S (2017) Interference mitigation in coexistence of WLAN network with radar. In: IEEE Radar Conference, pp 1–6
22. Drocella E, Richards J, Sole R, Najmy F, Lundy A, McKenna P (2015) 3.5 GHz exclusion zone analyses and methodology. NTIA technical report TR-15-517
23. Peh E, Liang YC (2007) Optimization for cooperative sensing in cognitive radio networks. In: IEEE Wireless Communications and Networking Conference, pp 27–32
24. Safavi-Naeini HA, Roy S, Ashrafi S (2015) Spectrum sharing of radar and Wi-Fi networks: the sensing/throughput tradeoff. IEEE Trans Cogn Commun Netw 1(4):372–382
25. Sanders FH, Carroll JE, Sanders GA, Sole RL (2013) Effects of radar interference on LTE base station receiver performance. NTIA, Technical Report TR-14-499
26. Sutton PD, Nolan KE, Doyle LE (2008) Cyclostationary signatures in practical cognitive radio applications. IEEE J Sel Areas Commun 26(1):13–24
27. Tosato F, Bisaglia P (2002) Simplified soft-output demapper for binary interleaved COFDM with application to HIPERLAN/2. In: IEEE International Conference on Communications (ICC), vol 2, pp 664–668
28. US Department of Commerce (2013) Fast track evaluation of the 5350–5470 MHz and 5850–5925 MHz bands pursuant to section 6406(b) of the middle class tax relief and job creation act of 2012. Technical Report
29. Zarikoff BW, Weldon D (2011) Detection of pulsed radar in a time division duplexed system. In: IEEE 73rd Vehicular Technology Conference (VTC Spring), pp 1–5

Part III
Cognitive Radio Resource Management

System Power Minimization in Non-contiguous Spectrum Access

25

Muhammad Nazmul Islam, Narayan B. Mandayam, Ivan Seskar, and Sastry Kompella

Contents

M. N. Islam (✉)
Qualcomm Corporate R&D, Bridgewater, NJ, USA
e-mail: mislam@qti.qualcomm.com

N. B. Mandayam
WINLAB, Department of ECE, Rutgers University, North Brunswick, NJ, USA
e-mail: narayan@winlab.rutgers.edu

I. Seskar
WINLAB, Rutgers University, North Brunswick, NJ, USA
e-mail: seskar@winlab.rutgers.edu

S. Kompella
Information Technology Division, Naval Research Laboratory, Washington, DC, USA

U.S. Naval Research Laboratory, Washington, DC, USA
e-mail: sastry.kompella@nrl.navy.mil

W. Zhang (ed.), *Handbook of Cognitive Radio*,
https://doi.org/10.1007/978-981-10-1394-2_24

Abstract

Wireless transmission using non-contiguous chunks of spectrum is becoming increasingly important due to a variety of scenarios such as secondary users avoiding incumbent users in TV white space, anticipated spectrum sharing between commercial and military systems, and spectrum sharing among uncoordinated interferers in unlicensed bands. multichannel multi-radio (MC-MR) platforms and non-contiguous orthogonal frequency division multiple access (NC-OFDMA) technology are the two commercially viable transmission choices to access these non-contiguous spectrum chunks. Fixed MC-MRs do not scale with increasing number of non-contiguous spectrum chunks due to their fixed set of supporting radio front ends. NC-OFDMA allows nodes to access these non-contiguous spectrum chunks and put null subcarriers in the remaining chunks. However, nulling subcarriers increases the sampling rate (spectrum span) which, in turn, increases the power consumption of radio front ends. Our work characterizes this trade-off from a cross-layer perspective, specifically by showing how the slope of ADC/DAC's power consumption versus sampling rate curve influences scheduling decisions in a multi-hop network. Specifically, we provide a branch and bound algorithm-based mixed integer linear programming solution that performs joint power control, spectrum span selection, scheduling, and routing in order to minimize the system power of multi-hop NC-OFDMA networks. We also provide a low-complexity ($O(E^2M^2)$) greedy algorithm where M and E denote the number of channels and links, respectively. Numerical simulations suggest that our approach reduces system power by 30% over classical transmit power minimization based cross-layer algorithms.

Keywords

Cognitive radio networks · Software defined radio · NC-OFDMA · TV white space · Circuit power

Introduction

Demand for wireless services is becoming much greater than the currently available spectrum [22]. FCC has already opened up 300 MHz in TV bands [6] and plans to open up an additional 500 MHz by 2020 [14] to meet this demand. Any radio can use these channels if it abides by FCC specifications [14]. If uncoordinated networks (e.g., different broadband wireless service providers) use these channels, they will adjust spectrum usage according to their individual traffic demands. Available spectrum will become partitioned into a set of non-contiguous segments. For some bands, like white space [6], available spectrum itself is non-contiguous.

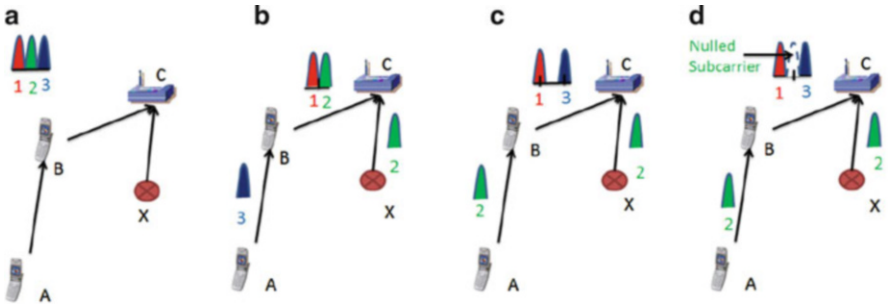

Fig. 1 Motivation of non-contiguous spectrum access. (**a**) Three node network. (**b**) Contiguous OFDMA implementation. (**c**) MC-MR implementation. (**d**) NC-OFDMA implementation

Multichannel multi-radio (MC-MR) technology allows nodes to simultaneously access multiple fragmented spectrum chunks [24, 25]. However, the number of non-contiguous spectrum chunks that fixed MC-MR can access is limited by the number of available radio front ends, which is often constrained due to the size and power limitations of the transmission device [16]. Software defined radio-based non-contiguous orthogonal frequency division multiple access (NC-OFDMA) technology allows nodes to transmit in these non-contiguous spectrum chunks with a single radio front end. Nodes can null interference-limited subcarriers and select better channels in NC-OFDMA-enabled networks. Hence, NC-OFDMA has grabbed a lot of attention in resource allocation [34–36], cooperative forwarding [21,38], and experimental research [39, 40]. However, nulling unwanted channels increases the spectrum span and the sampling rate of nodes.

Figure 1 illustrates the benefits and inherent challenges of NC-OFDMA using the example of a two-hop network. Figure 1a shows a two-hop network where node A transmits to node C via node B; node B relays node A's data and also transmits its own data to node C. Channel 1, 2, and 3 are available channels, and let us assume, without loss of generality, that transmission on any of these channels results in identical signal quality. Node X, an external and uncontrollable interferer, transmits in channel 2. If we want to minimize the maximum rate between node A and B and allocate channels accordingly, node B will require two channels and node A will require one channel. There are three possible techniques/configurations to allocate the three available channels as shown in Fig. 1b–d. Figure 1b shows contiguous OFDMA that suffers from interference in link BC at channel 2. Figure 1c shows MC-MR that requires two radio front ends to capture channels 1 and 3 in link BC. Figure 1d shows NC-OFDMA that uses only one radio front end, transmits at channels 1, and 3 and nulls channel 2. However, due to the nulling of channel 2, NC-OFDMA spans three channels, instead of two.

It is well known that the circuit power consumption of ADC and DAC increases linearly and exponentially with sampling rate and the number of quantization bits, respectively [3, 9]. As software defined radios continue to improve their higher quantization resolution, the ADC and DAC that are used in the radio circuits will

dominate the amount of power consumption. A comparison between Tables 1 and 2 shows that the power consumption of some commercial ADCs is more than 10 dB higher than the maximum allowed transmission power for portable devices in the 802.22 standard. On the one side, NC-OFDMA reduces transmission power by selecting channels with better link gains, while on the other side, this increased spectrum span increases circuit power consumption of the transceiver. In this chapter, we investigate this trade-off between transmission power reduction and circuit power increase in the context of cross-layer optimization of NC-OFDMA-based wireless networks.

Specifically, we ask the following question in this work: *How can single front-end radio-based nodes of a multi-hop network access non-contiguous spectrum chunks?* We investigate this question from a system power perspective and find that *scheduling a small subset of channels may outperform traditional transmit power minimization based approaches – which allocate power across all "good" channels – since it consumes less circuit power.* Our algorithm selects scheduling variables based on the slope of ADC and DAC power consumption versus sampling rate curves. Figure 2a, b the power consumption versus sampling rate curves of some commercial DACs and ADCs, respectively. These figures show that the slope of the

Table 1 Maximum sampling rates and power dissipation of different ADC/DAC

Device name	Device type	Max. sampling rate (MS/s)	Power dissipation (mW)
AD 9777 [2]	DAC	150	1056
ADS62P4 [11]	ADC	125	908
ADC 9467B [1]	ADC	250	1333

Table 2 Maximum allowed power and operating frequencies in IEEE 802.22 [17]

Device type	Allowed power (mW)	Operating frequency (MHz)
Fixed	4000	54–698
Portable	100	512–698

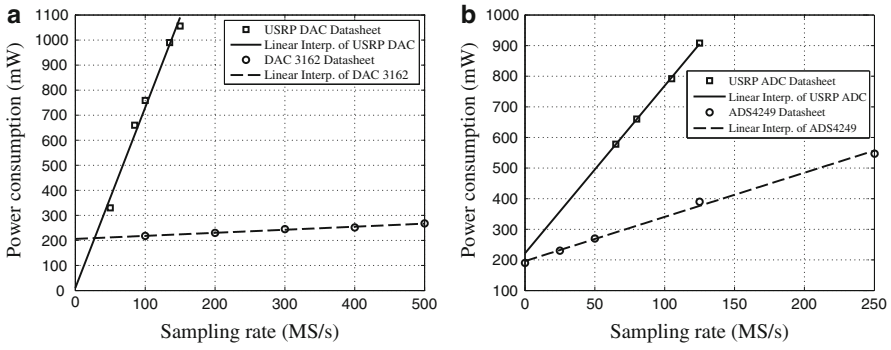

Fig. 2 (**a**) Power consumption of AD 9777 [2] (DAC of USRP radio) and DAC 3162 [12]. (**b**) Power consumption of ADS 62P4 [11] (ADC of USRP radio) and ADS 4249 [13]

power consumption curve varies from device to device. We show two special subcases of our finding based on the slope of the curves. We find that if the curves are almost flat, our algorithm converges to the transmission power minimization-based scheduling algorithms. If the curves are very steep, our algorithm selects the channel with the highest link gain. For commercial ADC & DACs, whose slopes lie between these two extreme cases, our algorithm selects channels to minimize the summation of transmit and circuit powers of the network.

In general, we provide a branch and bound algorithm-based mixed integer linear programming solution that performs joint power control, spectrum span selection, scheduling, and routing and minimizes system power of multi-hop NC-OFDMA networks. We also provide a greedy algorithm that runs in $O(E^2M^2)$ time where E and M denote the number of links and channels, respectively. *To the best of our knowledge, ours is the first work that shows how the slope of ADC/DAC's power consumption curve influences the scheduling decisions of a multi-hop network*. Numerical simulations suggest that our approach reduces system power by 30% over classical transmission power minimization-based cross-layer algorithms.

Related Work

The authors of [24, 25] characterized the capacity region of an MC-MR-based multi-hop network. The authors of [34,36] focused on software-defined radio-based multi-hop networks and performed cross-layer optimization using a protocol and signal-to-interference-plus-noise-ratio model, respectively. Shi and Hou extended the work of [34] and provided a distributed algorithm in [35]. None of these works considered circuit power and addressed how non-contiguous spectrum access influences cross-layer decisions.

Consideration of system power has been gaining attention in energy-efficient wireless communication literature [27]. Cui et. al. focused on system energy constrained modulation optimization in [9]. Sahai et. al. investigated system power consumption – especially decoder power consumption – in [18]. Isheden and Fettweis assumed circuit power to be a linear function of the data rate [20]. All these works focused on single transceiver pair. Our approach differs from these works in the following way: in NC-OFDMA technology, ADC and DAC consume power not only for used channels (i.e., transmitted data) but also for nulled channels. Our work considers the power consumption related to spectrum span and investigates the performance of NC-OFDMA-based multi-hop networks.

The impact of hardware constraints on the performance of NC-OFDMA networks was previously raised in [5, 23]. The authors of [23] performed cross-layer resource allocation when each node's maximum spectrum span is limited by its ADC/DAC. The authors of [5] investigated how the size of the guard band, required to reduce cross-band interference, affects the performance of NC-OFDMA-based distributed transceiver pairs. Our work uses system power to investigate the performance of NC-OFDMA-based multi-hop networks.

Periodic nonuniform sampling (PNS) can recover a sparsely located non-contiguous signal with sub-Nyquist sampling rate [28] and potentially reduce the power consumption of the ADC circuits. However, PNS requires Nyquist rate circuitry at track-and-hold stages. PNS also needs compensation for imperfect production of the time delay elements. As a result, PNS is not widely used by industry to access non-contiguous spectrum [30]. Our work focuses on the system power minimization of an NC-OFDMA network that uses commercial ADCs and DACs with Nyquist sampling rate to access non-contiguous spectrum.

Time and frequency mismatch affect an NC-OFDMA network more severely due to its use of a large number of nulled subcarriers. Several researchers have implemented different techniques to reduce interference between unsynchronized NC-OFDMA nodes. The authors of [39] have used adaptive multibank stop-band filters to reduce interference of unwanted channels. The authors of [40] have used wider guard bands to reduce leakage power into neighboring channels. We do not focus on synchronization techniques and test bed implementation of NC-OFDMA nodes in our work. Interested readers are suggested to go through [19, 39–41] to understand the implementation and synchronization details of NC-OFDMA.

The remainder of the chapter is organized as follows: section "System Model" presents system power and multi-hop network model. Section "Branch-and-Bound Based Solution Overview" provides a branch and bound-based solution of the optimization problem. We present theoretical insights of our algorithm in section "Low-Complexity Algorithm Design" and a low-complexity algorithm in section "Polynomial Time Algorithm for a Multi-hop Networks." After showing numerical results in section "Simulation Results," we conclude in section "Conclusion."

System Model

System Power Model

We assume that baseband signal processing techniques like multiuser detection and iterative decoding are not employed in the system. In this context, power consumption in the baseband is negligible compared with that in the radio frequency (RF) circuitry [29]. Each radio node has two front ends: one for transmission and the other for reception. Nodes are half-duplex, i.e., they can simultaneously transmit and receive using these two front ends but not in the same channel.

Figure 3 shows signal level blocks in the transmitter and receiver. At the transmitter, the baseband digital signal goes through DAC, filters, mixer (where it gets multiplied by the local oscillator (LO)), and programmable amplifier (PA) before reaching transmitter antenna. The received signal at the antenna goes through low-noise amplifiers (LNA), filters, mixer, intermediate-frequency amplifier (IFA), and ADC to reach the baseband circuit [9].

Typically, transceiver circuits work on a multimode basis. When there is a signal to transmit, all RF circuits work in active mode; when there is no signal to transmit,

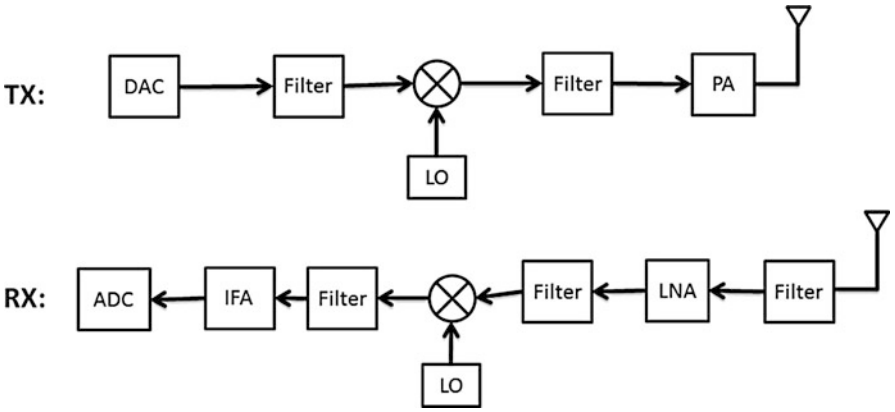

Fig. 3 Radio front-end circuit blocks (Reproduced from [9])

all RF circuits remain in sleep mode; circuits switch from sleep to active mode through transient mode [9]. Here, we focus on system power minimization of all RF circuits in the active mode. Let p_t, p_r and p denote active mode power consumption of transmitter and receiver and transmitter's emitted power at radio frequency, respectively. Now,

$$p_t = \frac{PAPR}{\eta} p + p_{tc}, \quad p_r = p_{rc}. \tag{1}$$

where $PAPR$ and η denote the peak-to-average-power ratio (PAPR) and drain efficiency of the programmable amplifier. $\frac{PAPR}{\eta} p$ denote the total power consumption of programmable amplifier [9]. Also, p_{tc} and p_{rc} are the circuit power consumption of transmitter (excluding programmable amplifier's power consumption) and receiver, respectively.

The power consumption at almost all blocks of the radio front end, except ADC and DAC, does not depend on sampling rate [9, 26]. The power consumption of ADC and DAC is affine functions of the sampling rate [3,9]. Denoting $k_{pa} = \frac{PAPR}{\eta}$, system power consumption in the transmitter and receiver front end become

$$p_t = \alpha_1 + \alpha_2 f_{st} + k_{pa} p. \tag{2}$$

$$p_r = \beta_1 + \beta_2 f_{sr}. \tag{3}$$

In the above, f_{st} and f_{sr} are the sampling rates of the transmitter and receiver path. α_1, α_2, β_1 and β_2 are constants that depend on the power consumption of different blocks. Appendix Power Consumption of Different Blocks in Transmitter and Receiver describes the power consumption of each block in details. Table 3 shows the list of notations that we have used throughout the chapter.

Table 3 List of notations

Notation	Description
$\mathscr{N}$	Set of nodes
N	Total number of nodes
$\mathscr{E}$	Set of edges
E	Total number of edges
$\mathscr{L}$	Set of sessions
L	Total number of sessions
$(s(l), d(l))$	Source and destination of session l
$r(l)$	Rate requirements of session l
W	Bandwidth of each channel
N_0	Noise spectral density
$f_{ij}^m(l)$	Flow on link ij in channel m for session l
c_{ij}^m	Capacity on link ij in channel m
s_{ij}^m	Signal-to-noise ratio on link ij in channel m
M	Total number of channels
$\mathscr{M}$	Set of all available channels across all nodes
$\mathscr{M}_i$	Set of available channels in node i
P_I	Interference threshold
$\mathscr{M}_{ij}$	Set of available channels between node i and j
M	Total number of available channels
g_{ij}^m	Link gain of ij in channel m
$p_{ij,m}$	Allocated power between i and j in channel m
x_{ij}^m	If link ij uses channel m
$x_i^{t,m}$	If node i uses channel m for transmission
$x_i^{r,m}$	If node i uses channel m for reception
$q_{t,i}$	Spectrum span of the transmitter path of node i
$q_{r,i}$	Spectrum span of the receiver path of node i
$f_{st,i}$	Sampling rate of node i's transmitter path
$f_{sr,i}$	Sampling rate of node i's receiver path
$f_{s,\max}$	Maximum allowed sampling rate of the nodes
$P_{s,\max}$	Maximum allowed system power consumption
A	An arbitrary large number

Multi-hop Cross-Layer Model

We consider a multi-hop network with a set of $\mathscr{N}$ cognitive radio nodes. Let $\mathscr{M}$ denote the set of all available channels. Bandwidth of each channel is W.

Power Control and Scheduling Constraints

The number of available channels may vary in different (spatial) parts of the network due to interference and other spectrum constraints such as primary users and systems. Hence, we focus on frequency scheduling. Denote the binary scheduling decision x_{ij}^m as follows:

$$x_{ij}^m = \begin{cases} 1, & \text{if node } i \text{ transmits to node } j \text{ using channel } m. \\ 0, & \text{otherwise.} \end{cases} \tag{4}$$

Due to self-interference, node i can use channel m only for receiving from node k or transmitting to node j. In other words:

$$\sum_{j \in \mathcal{N}, j \neq i} x_{ij}^m + \sum_{k \in \mathcal{N}, k \neq i} x_{ki}^m \leq 1 \quad \forall\, i \in \mathcal{N}\,,\ \forall\, m \in \mathcal{M}_i\,. \tag{5}$$

We use protocol interference model. Assume that node i transmits to node j in channel m, i.e., $x_{ij}^m = 1$. Let p_{ij}^m and g_{ij}^m denote the transmission power and channel gain in channel m of link ij. Let P_I denote the interference threshold. P_I should be chosen in such a way so that it is negligible compared to the noise power $N_0 W$ where N_0 is the noise spectral density. Another node k can transmit to node h in channel m if p_{kh}^m causes negligible interference in node j. Hence,

$$p_{kh}^m \leq \frac{P_I}{g_{kj}^m} x_{ij}^m \ \forall (k,h) \in \mathcal{N},\ k \neq i,\ h \neq j. \tag{6}$$

Also, a node can allocate power in a link only if it is scheduled, i.e.,

$$p_{ij}^m \leq A x_{ij}^m \ \forall\, (i\,,\, j\ \in \mathcal{N})\,,\ m \in \mathcal{M}\,. \tag{7}$$

Here, A is a big number that couples power control and scheduling variables.

Routing and Link Capacity Constraints

Let $\mathcal{L}$ be the set of active sessions and $|\mathcal{L}| = L$. Let $s(l)$, $d(l)$, and $r(l)$ denote the source node, destination node, and minimum rate requirements of session l. Let $f_{ij}^m(l)$ denote the flow from node i to node j in channel m for session l. If i is the source (destination) node of session l, the total outgoing (incoming) flow from (to) node i should exceed the minimum rate requirements of session l, i.e.,

$$\sum_{j \in \mathcal{N}} \sum_{m \in \mathcal{M}_{ij}} f_{ij}^m(l) \geq r(l) \quad (l \in \mathcal{L}\,,\ i = s(l)). \tag{8}$$

$$\sum_{k \in \mathcal{N}} \sum_{m \in \mathcal{M}_{ki}} f_{ki}^m(l) \geq r(l) \quad (l \in \mathcal{L}\,,\ i = d(l)). \tag{9}$$

The incoming flow of session l should match the outgoing flow in an intermediate node i:

$$\sum_{j \in \mathcal{N}}^{j \neq s(l)} \sum_{m \in \mathcal{M}_{ij}} f_{ij}^m(l) = \sum_{k \in \mathcal{N}}^{k \neq d(l)} \sum_{m \in \mathcal{M}_{ki}} f_{ki}^m(l) \ \forall\, (l \in \mathcal{L},\ i \in \mathcal{N},\ i \neq s(l), d(l)). \tag{10}$$

Additionally, the aggregated flows of all sessions in a particular link should not exceed the capacity of the link. Therefore,

$$\sum_{l\in\mathscr{L}}^{s(l)\neq j\,,\,d(l)\neq i} f_{ij}^{m}(l) \leq c_{ij}^{m}\ (i\,,\,j\ \in\mathscr{N}\,,\,i\neq j\,,\,\forall\, m\ \in\mathscr{M}_{ij}\,,\,\mathscr{M}_{ij}\neq\emptyset). \tag{11}$$

where

$$c_{ij}^{m} \leq W\log(1+s_{ij}^{m})\ \ (i\,,\,j\ \in\mathscr{N}\,,\,i\neq j), \tag{12}$$

$$s_{ij}^{m} = \frac{g_{ij}^{m}\,p_{ij}^{m}}{N_0 W},\ \ (i\,,\,j\ \in\mathscr{N}\,,\,i\neq j). \tag{13}$$

In the above, c_{ij}^{m} and s_{ij}^{m} denote the capacity and signal-to-noise ratio in link ij of channel m. The denominator of s_{ij}^{m} only contains $N_0 W$ because (6) ensures that the interference from other nodes is negligible compared to the noise power.

The constraints described above resemble previous works that focus on *transmission power* based cross-layer optimization (i.e., power control, scheduling and routing). The novelty of the work here is in relating the hardware constraints imposed by the radio front end to the above cross-layer optimization as we describe next.

System Power Constraints

Let $p_{t,i}$ and $p_{r,i}$ denote the system power consumption in the transmitter and receiver path of node i. The total system power consumption, P_{tot}, is:

$$P_{\text{tot}} = \sum_{i\in\mathscr{N}}\left(p_{t,i}+p_{r,i}\right). \tag{14}$$

Equations (2) and (3) show a radio node also contains a fixed amount of power (independent of sampling rate) if it transmits or receives in a channel. Denoting α_{1_i} and β_{1_i} as this fixed power consumption of node i's transmit and receive path respectively, we find,

$$\alpha_{1_i} \geq \alpha_1 x_{ij}^{m}\ \ \forall m\in\mathscr{M}_{ij},\ j\in\mathscr{N},\ i\in\mathscr{N}, \tag{15}$$

$$\beta_{1_i} \geq \beta_1 x_{ki}^{m}\ \ \forall m\in\mathscr{M}_{ij},\ k\in\mathscr{N}\ i\in\mathscr{N}. \tag{16}$$

Using (2), (3), (14), (15) and (16),

$$\sum_{i\in\mathscr{N}}\left(\alpha_{1_i}+\alpha_2 f_{st,i}+\sum_{j\in\mathscr{N}}\sum_{m\in\mathscr{M}_{ij}} k_{pa}\,p_{ij}^{m}+\beta_{1_i}+\beta_2 f_{sr,i}\right) = P_{\text{tot}}, \tag{17}$$

where $f_{st,i}$ and $f_{sr,i}$ denote the sampling rates in the transmitter and receiver of node i.

The constraints introduced so far involve channel scheduling decisions and sampling rate of different nodes. We now show how channel scheduling decisions influence the sampling rate of the nodes, which in turn influences the total system power.

Relation Between Channel Scheduling and System Power

The sampling rate of a transceiver depends on its spectrum span, which in turn is determined by the choice of channels selected for its intended transmission.

Let $x_i^{t,m}$ and $x_i^{r,m}$ denote the following:

$$x_i^{t,m} = \begin{cases} 1, & \text{if } i \text{ transmits to any node } j \in \mathcal{N} \text{ in channel } m. \\ 0, & \text{otherwise.} \end{cases}$$

$$x_i^{r,m} = \begin{cases} 1, & \text{if } i \text{ receives from any node } j \in \mathcal{N} \text{ in channel } m. \\ 0, & \text{otherwise.} \end{cases}$$

In other words,

$$\begin{aligned} x_i^{t,m} &\geq x_{ij}^m \ \forall\, j \in \mathcal{N}, \\ x_i^{r,m} &\geq x_{ki}^m \ \forall\, k \in \mathcal{N}, \end{aligned} \tag{18}$$

Using this notation, analog power equations of (15) and (16) are redefined as

$$\alpha_{1_i} \geq \alpha_1 x_i^{t,m}, \quad \beta_{1_i} \geq \beta_1 x_i^{r,m}, \ \forall m \in \mathcal{M}_i, \ \forall i \in \mathcal{N}. \tag{19}$$

We define spectrum span as the gap between the furthest edges of the used channels. Node i's uppermost used channel index in the transmitter path is

$$\max_{m \in \mathcal{M}_i} m \cdot x_i^{t,m}. \tag{20}$$

Node i's lowermost used channel index in the transmitter path is

$$\min_{m \in \mathcal{M}_i} \left(m \cdot x_i^{t,m} + |M| \cdot (1 - x_i^{t,m}) \right). \tag{21}$$

The second term of (21) ensures that we do not consider the index i's for which $x_i^{t,m} = 0$. Let $q_{t,i}$ and $q_{r,i}$ denote the spectrum spans of the transmitter and receiver path of node i. Now,

$$q_{t,i} = W \cdot \max\left(\left(\max_{m \in \mathcal{M}_i} \left(m \cdot x_i^{t,m} \right) - \min_{m \in \mathcal{M}_i} \left(m \cdot x_i^{t,m} + |M| \cdot (1 - x_i^{t,m}) \right) + 1 \right), 0 \right). \tag{22}$$

$$q_{r,i} = W \cdot \max\left(\left(\max_{m \in \mathcal{M}_i} \left(m \cdot x_i^{r,m} \right) - \min_{m \in \mathcal{M}_i} \left(m \cdot x_i^{r,m} + |M| \cdot (1 - x_i^{r,m}) \right) + 1 \right), 0 \right). \tag{23}$$

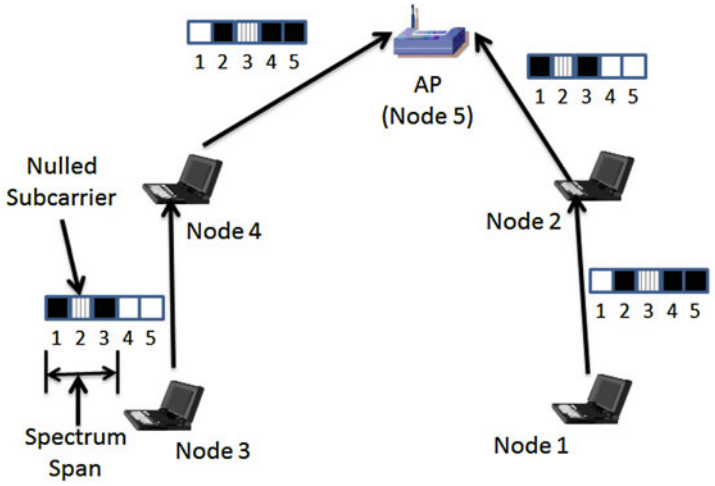

Fig. 4 Spectrum span, occupied, and nulled subcarrier in an NC-OFDMA-based multi-hop network. *Black solid, lined ash,* and *white boxes* denote occupied, nulled, and un-spanned subcarriers, respectively. Spectrum span is the summation of occupied and nulled subcarriers

Figure 4 illustrates the concept of spectrum span in a five node multi-hop network. We now verify (20), (21), (22) and (23) by focusing on the spectrum span of node 3 of Fig. 4. There are 5 available channels. Node 3 transmits in channels 1 and 3 and nulls channel 2. Node 3 does not receive in any channel from other nodes. Hence,

$$\mathscr{M} = \{1, 2, 3, 4, 5\}\,,\; x_3^{r,m} = 0\;\forall\, m \in \mathscr{M},$$

$$x_3^{t,m} = 1\;\forall m \in \{1, 3\}\,,\; x_3^{t,m} = 0\;\forall m \in \{2, 4, 5\}.$$

Using the values of $\mathscr{M}$, $x_3^{r,m}$ and $x_3^{t,m}$ in (22) and (23), $q_{r,3} = 0$ and $q_{t,3} = 3W$. Figure 4 shows that node 3 does not receive from any node and spans three channels while transmitting to node 4.

Now, using (19), (22) and (23), along with the fact that sampling rate of a transceiver should be at least twice its spectrum span, we convert (17) to the following:

$$\sum_{i\in\mathscr{N}}\left(\alpha_{1_i} + 2\alpha_2 q_{t,i} + \sum_{j\in\mathscr{N}}\sum_{m\in\mathscr{M}_{ij}} p_{ij}^m + \beta_{1_i} + 2\beta_2 q_{r,i}\right) = P_{\text{tot}}. \tag{24}$$

Equations (19), (22), (23), and (24) relate total system power to the scheduling variables.

In this work, our objective is to minimize the total system power subject to rate requirements. Using the above equations, we formulate our optimization problem and show it in (25).

$$\min \quad P_{\text{tot}} \tag{25a}$$

$$s.t. \sum_{j\in\mathcal{N}} \sum_{m\in\mathcal{M}_{ij}} f_{ij}^{m}(l) \geq r(l) \quad (l \in \mathcal{L}\,,\, i = s(l)) \,,\, \sum_{k\in\mathcal{N}} \sum_{m\in\mathcal{M}_{ki}} f_{ki}^{m}(l) \geq r(l)$$

$$(l \in \mathcal{L}\,,\, i = d(l)). \tag{25b}$$

$$\sum_{j\in\mathcal{N}}^{j\neq s(l)} \sum_{m\in\mathcal{M}_{ij}} f_{ij}^{m}(l) = \sum_{k\in\mathcal{N}}^{k\neq d(l)} \sum_{m\in\mathcal{M}_{ki}} f_{ki}^{m}(l) \;\; (l \in \mathcal{L},\, i \in \mathcal{N},\, i \neq s(l), d(l)). \tag{25c}$$

$$\sum_{l\in\mathcal{L}}^{s(l)\neq j\,,\, d(l)\neq i} f_{ij}^{m}(l) \leq c_{ij}^{m} \;\; (i\,,\, j \;\in \mathcal{N}\,,\, i \neq j\,,\, \mathcal{M}_{ij} \neq \emptyset). \tag{25d}$$

$$c_{ij}^{m} \leq W \log(1 + s_{ij}^{m}) \;\; (i\,,\, j \;\in \mathcal{N}\,,\, i \neq j) \,,\; s_{ij}^{m} = \frac{g_{ij}^{m} p_{ij}^{m}}{N_0 W},\; (i\,,\, j \;\in \mathcal{N}\,,\, i \neq j). \tag{25e}$$

$$p_{kh}^{m} \leq \frac{P_I}{g_{kj}} x_{ij}^{m} \;\forall\, k \in \mathcal{N},\, h \in \mathcal{N},\, k \neq h \;,\; p_{ij}^{m} \leq A x_{ij}^{m} \;\forall\, (i\,,\, j \;\in \mathcal{N})\,,\, m \in \mathcal{M}. \tag{25f}$$

$$q_{t,i} \geq W \cdot \Big(\max_{m\in\mathcal{M}_i} \big(m \cdot x_i^{t,m}\big) - \min_{m\in\mathcal{M}_i} \big(m \cdot x_i^{t,m} + |M| \cdot (1 - x_i^{t,m})\big) + 1\Big). \tag{25g}$$

$$q_{r,i} \geq W \cdot \Big(\max_{m\in\mathcal{M}_i} \big(m \cdot x_i^{r,m}\big) - \min_{m\in\mathcal{M}_i} \big(m \cdot x_i^{r,m} + |M| \cdot (1 - x_i^{r,m})\big) + 1\Big). \tag{25h}$$

$$\alpha_{1_i} \geq \alpha_1 x_i^{t,m} \,,\quad \beta_{1_i} \geq \beta_1 x_i^{r,m} \;\; \forall m \in \mathcal{M}_i \;\forall i \in \mathcal{N}. \tag{25i}$$

$$\sum_{j\in\mathcal{N}\,,j\neq i} x_{ij}^{m} + \sum_{k\in\mathcal{N}\,,k\neq i} x_{ki}^{m} \leq 1 \quad \forall\, i \in \mathcal{N}\,,\, \forall\, m \in \mathcal{M}_i. \tag{25j}$$

$$\sum_{i\in\mathcal{N}} \Big(\alpha_{1_i} + 2\alpha_2 q_{t,i} + \sum_{j\in\mathcal{N}} \sum_{m\in\mathcal{M}_{ij}} p_{ij}^{m} + \beta_{1_i} + 2\beta_2 q_{r,i}\Big) \leq P_{\text{tot}}. \tag{25k}$$

$$x_{ij}^{m} \in \{0, 1\}\,,\, s_{ij}^{m} \geq 0 \;\; (i, j \in \mathcal{N},\, i \neq j,\, m \in \mathcal{M}_{ij})\,,\; q_{t,i} \geq 0,\, q_{r,i} \geq 0 \;\forall i \in \mathcal{N}. \tag{25l}$$

$$P_{\text{tot}}\,,\, f_{ij}^{m}(l)$$

$$\geq 0 \,\big(l \in \mathcal{L}, m \in \mathcal{M}_{ij},\, i, j \in \mathcal{N},\, i \neq j,\, i \neq d(l),\; j \neq s(l),\, \mathcal{M}_{ij} \neq \emptyset\big). \tag{25m}$$

Next two sections provide solution methodologies of (25).

Branch-and-Bound Based Solution Overview

Linearization of the Optimization Problem

The optimization problem of (25) is a mixed integer nonlinear program (MINLP). The nonlinearity of (25) comes from the logarithm function of (25e) and max-min functions of (25g) and (25h).

The logarithmic function of the capacity term in (25e) can be linearized by reformulation linearization technique (RLT) [33]. RLT uses a number of tangential supports at different points of the logarithmic curve and generates a convex hull linear relaxation of the logarithmic function. We ask interested readers to go through [33] for the details of RLT.

The max-min equations of (22) and (23) can be rewritten in following linear forms:

$$\begin{aligned} & q_{t,i} + W\left(m_2 \cdot x_i^{t,m_2} + |M| \cdot (1 - x_i^{t,m_2})\right) \\ & \geq W\left(m_1 \cdot x_i^{t,m_1} + 1\right) \ \forall (m_1, m_2) \in \mathscr{M}_i \,, \ \forall i \in \mathscr{N}. \end{aligned} \tag{26}$$

$$\begin{aligned} & q_{r,i} + W\left(m_2 \cdot x_i^{r,m_2} + |M| \cdot (1 - x_i^{r,m_2})\right) \\ & \geq W\left(m_1 \cdot x_i^{r,m_1} + 1\right) \ \ \forall (m_1, m_2) \in \mathscr{M}_i \,, \ \forall i \in \mathscr{N}. \end{aligned} \tag{27}$$

$$q_{t,i} \geq 0 \,, \ q_{r,i} \geq 0 \ \ \forall i \in \mathscr{N}. \tag{28}$$

The optimization problem of (25) with the reformulated linear equations can be directly solved in CVX [10] (with MOSEK [31]) software. This problem is a MILP. CVX uses branch-and-bound algorithm [33] to solve this problem.

Feasible Solution

CVX outputs flow variables $f_{ij}^m(l)$, scheduling decisions x_{ij}^m and power variables $p_{ij}^m\big(l \in \mathscr{L}, m \in \mathscr{M}_{ij}, i, j \in \mathscr{N}, i \neq j,\big)$. Since we relaxed flow capacity equations to get this output, the resultant flow rates may exceed the capacity of the links. We keep flow variables and scheduling decisions unperturbed and increase power variables to get feasible solutions. We use the following set of equations for flows and powers:

$$\begin{aligned} & \sum_{i \in \mathscr{L}} f_{ij}^m(l) = W \log\left(1 + \frac{p_{ij}^m g_{ij}^m}{N_0 W}\right), \\ & p_{ij}^m = \frac{N_0 W}{g_{ij}^m}\left[\exp\left\{\frac{\sum_{i \in \mathscr{L}} f_{ij}^m(l)}{W}\right\} - 1\right] \ \ \forall m \in \mathscr{M}_{ij}, \, i, j \in \mathscr{N}, \, i \neq j. \end{aligned} \tag{29}$$

These power variables along with flow and scheduling decisions of the CVX output form a feasible solution. We refer to this solution as "BnBSysPowerMin." The resulting algorithm however suffers from exponential complexity in the worst-case scenario. Next section develops low-complexity algorithms to minimize system power in a multi-hop network, i.e., to solve the original optimization problem of (25).

Low-Complexity Algorithm Design

We first focus on the system power minimization of a point-to-point link. Thereafter, we use the insights obtained from this scenario to develop a low-complexity algorithm to minimize system power in a multi-hop network.

Theoretical Insights from Point-to-Point Link Case

In a point-to-point link, the optimization problem of (25) takes the following form:

$$\min \quad \sum_{m \in \mathscr{M}} p^m + \alpha_1 + 2\alpha_2 q + \beta + 2\beta_2 q, \tag{30a}$$

$$s.t. \;\; q \geq W \left(\max_{m \in \mathscr{M}} (m \cdot x^m) - \min_{m \in \mathscr{M}} (m \cdot x^m + |M|(1 - x^m)) + 1 \right),$$

$$x^m \in \{0, 1\}, \; \forall m \in \mathscr{M}, \; q \geq 0, \tag{30b}$$

$$\sum_{m \in \mathscr{M}} W \log_2 \left(1 + \frac{p^m g^m}{N_0 W} \right) \geq r \;, \;\; p^m \geq 0, \;\; \forall m \in \mathscr{M}, \tag{30c}$$

$$p^m \leq A x^m \;\; \forall m \in \mathscr{M}. \tag{30d}$$

In above equations, p^m and g^m denote the allotted power and link gain in channel m, respectively. Rate requirement and spectrum span are denoted by r and q, respectively. In the objective function, $\sum_{m \mathscr{M}} p^m$ denotes transmit power, and $\alpha_1 + 2\alpha_2 q + \beta + 2\beta_2 q$ denotes circuit power consumption.

The optimization problem of (30) is the combination of two separate optimization problems. The objective is to minimize the summation of transmit and circuit power. Equation (30b) denotes the constraints associated with circuit power minimization problem, and it only involves spectrum span and scheduling variables. Equation (30c) denotes the constraints associated with transmit power minimization problem, and it only involves power variables. Equation (30d) relates the power and scheduling variables and couples these two optimization problems.

The optimization problem of (30) has two sub-cases. These sub-cases depend on the values of α_2 and β_2, i.e., the slope of ADC and DAC's power consumption versus sampling rate curves

Case I: Transmit Power Minimization

When α_2 and β_2 are very small, i.e., ADC and DAC's power consumption versus sampling rate curves are very flat, the impact of spectrum span on system power becomes negligible. Scheduling decisions do not influence system power that much, and we can concentrate on minimizing transmit power. Then the optimization problem gets reduced to

$$\min \sum_{m \in \mathscr{M}} p^m, \tag{31a}$$

$$s.t. \sum_{m \in \mathscr{M}} W \log_2 \left(1 + \frac{p^m g^m}{N_0 W}\right) \geq r \ , \ p^m \leq A x^m \ , \ p^m \geq 0, \ x^m \in \{0, 1\} \ \forall m \in \mathscr{M}. \tag{31b}$$

Since x^m's are not present in the objective function, we can just solve the problem with p^m variables and then enforce $x^m = 1$ for every positive p^m.

The optimization problem of (31) is similar to the classical waterfilling [8] problem, which maximizes rate subject to a total power constraint. In the remainder of the chapter, we refer to the above problem "TxPowerMin." The solution to this problem selects the "good" channels in the network and spreads power across the whole spectrum [8].

Case II: Circuit Power Minimization

When α_2 and β_2 are very large, i.e., ADC and DAC's power consumption are very steep, circuit power consumption dominates system power. Transmit power variables do not influence circuit power that much, and we can just concentrate on minimizing circuit power. The optimization problem reduces to

$$\min \quad \alpha_1 + 2\alpha_2 q + \beta + 2\beta_2 q, \tag{32a}$$

$$s.t. \ \ q \geq W \left(\max_{m \in \mathscr{M}} (m \cdot x^m) - \min_{m \in \mathscr{M}} (m \cdot x^m + |M|(1 - x^m)) + 1 \right),$$

$$x^m \in \{0, 1\}, \ \forall m \in \mathscr{M}, \ q \geq 0, \tag{32b}$$

$$\sum_{m \in \mathscr{M}} W \log_2 \left(1 + \frac{p^m g^m}{N_0 W}\right) \geq r \ , \ p^m \geq 0, \ \forall m \in \mathscr{M} \ , \ p^m \leq A x^m \ \forall m \in \mathscr{M}. \tag{32c}$$

The objective of the optimization problem of (32) increases with spectrum span q. Minimum circuit power occurs if we schedule only one channel and allocate enough power in that channel so that it can meet rate requirement. Scheduling any single channel leads to same circuit power in the above optimization problem. Since the original system power minimization problem contains both transmit and

circuit powers, it is prudent to select the channel with the best link gain. This greedy selection requires less transmit power to meet rate requirement.

Trade-Off Between Transmit and Circuit Power Minimization

If ADC and DAC's power consumption versus sampling rate curves are very flat, our algorithm selects all good channels in the network. If ADC and DAC's power consumption vs. sampling rate curves are very steep, our algorithm selects the channel with the best link gain. In a practical setting with commercial ADCs and DAC, our algorithm trades off between transmit and circuit power.

Polynomial Time Algorithm for a Multi-hop Networks

The analysis from the point-to-point link case provides us insights to develop a low-complexity greedy algorithm to solve the optimization problem of (25). The algorithm minimizes the circuit power by using only one channel at the first step and then tries to minimize the system power, i.e., the combination of transmit and circuit power, by greedily selecting more and more channels in the subsequent steps. Our greedy algorithm can be explained simply as follows:

- Find the initial route between each sender and receiver using the shortest path algorithm [7].
- Assign the best channel to each link unless the current assignment interferes with previously assigned channels.
- For each active link, check if any other channel assignment reduces system power.
- Once channels are scheduled, determine power allocation and routing through a convex optimization program.

Our greedy system power minimization algorithm consists of the central program of Algorithm 1 and the subroutines of Algorithms 2 and 3. Next three subsections describe the central program and the subroutines. We analyze the complexity of our algorithm in section "Computational Complexity."

Central Program

Algorithm 1 shows the pseudocode of our greedy polynomial time algorithm. Operation 1 finds large-scale gains of all links by averaging small-scale fading in time or frequency domain. Operation 2 assigns weight to each link. Operation 3 finds the shortest path between each sender and forwarder based on the assigned weights of operation 2. Operation 5 finds the active links and operation 7 calculates the flow requirement among these links. Operation 8 initiates total power (P_{tot}), power allocation (p_{ij}^m), and scheduling (x_{ij}^m) variables to zero for the greedy channel scheduling algorithm. We initiate an outer loop in operation 9. Operations 11, 12, and 13 calls the subroutine of Algorithm 2 and checks if any link should be assigned a channel. The outer loop breaks if none of the active links becomes suitable to

Algorithm 1 Polynomial time algorithm to minimize system power in a multi-hop network

Input : $\mathscr{M}, s(l), d(l), r(l)\ \forall l \in \mathscr{L}, W, N_0, g_m\ \forall m \in \mathscr{M}$
. **Output**: $x_m,\ p_m \forall m \in \mathscr{M}$, P_{tot} , $f_{ij}^m(l)\ \forall m \in \mathscr{M},\ \forall l \in \mathscr{L},\ \forall (i,j)\ \in \mathscr{E}$
.

1: Denote g_{ij} as the average gain (e.g., path loss plus shadowing) of link ij.
2: Assign weight w_{ij} to each link, $w_{ij} = \frac{1}{g_{ij}}$.
3: Find shortest path between between source $(s(l))$ and destination $(d(l))$ of every session $l \in \mathscr{L}$ based on the link weight w.
4: $b_{ij}(l) = 1$ if link ij falls in the routing path of any session $l \in \mathscr{L}$.
5: A link is active if it falls in the routing path of any session, i.e., $x_{ij} = 1$ if $\exists l \in \mathscr{L}$ s.t. $b_{ij}(l) = 1$.
6: Define $\mathscr{A}$ to be set of active links.
7: Flow in each link, $f_{ij} = \sum_{l \in \mathscr{L}} b_{ij}(l) r(l)$.
8: $P_{\text{tot}} = \infty$, $x_{ij}^m = p_{ij}^m = 0\ \forall (i,j) \in \mathscr{E}$, $\forall m \in \mathscr{M}$, $x_i^{t,m} = x_i^{r,m} = 0$, $\alpha_{1_i} = \beta_{1_i} = 0, \forall i \in \mathscr{N}, \forall m \in \mathscr{M}$.
9: **while** True **do**
10: $flag = 0$.
11: **for** $(a,b) \in \mathscr{A}$ **do**
12: $\big(flag, x_{ij}^m, p_{ij}^m\ \forall m \in \mathscr{M}, (i,j) \in \mathscr{E}\big) =$ GreedyAlgo$\big(\mathscr{M}, (a,b), f_{ab}, r, W, N_0, flag, P_{\text{tot}}, \alpha_{1_i}, \beta_{1_i}, x_i^{t,m}, x_i^{r,m}, x_{ij}^m, p_{ij}^m, g_{ij}^m$ $\forall m \in \mathscr{M}, i \in \mathscr{N}, (i,j) \in \mathscr{E}\big)$.
13: **end for**
14: **if** $flag = |A|$ **then**
15: Break.
16: **end if**
17: **end while**
18: Solve the optimization problem of (25) where scheduling variables $(x_{ij}^m\ \forall m \in \mathscr{M}, \forall (i,j) \in \mathscr{E})$ are constants, not variables. Find power allocation, scheduling and routing variables, and total power, P_{tot}.

be assigned a channel. This outer loop determines the channel scheduling (x_{ij}^m) variables.

We obtain power allocation (p_{ij}^m) and routing path $(f_{ij}(l))$ variables from the optimization problem of (25) where scheduling variables (x_{ij}^m) are constants. Since we fix the integer variables of (25), the total power minimization problem becomes a convex optimization program and can be solved in polynomial time [4].

We assume one path (shortest path), i.e., no flow splitting, per session during the initial routing topology design of operations 1, 2, and 3. This allows us to easily calculate the flow requirement of each link which we later use in the greedy scheduling algorithm. We consider optimal flow splitting, based on the selected scheduling variables, in the final optimization of operation 18 of Algorithm 1.

Greedy Scheduling Algorithm

The greedy scheduling algorithm of Algorithm 2 is a subroutine that's called from operation 12 of the central program of Algorithm 1. The subroutine receives previously assigned scheduling and power allocation variables from the central

Algorithm 2 Greedy scheduling algorithm

Input : $\mathscr{M}$, Link (a,b), f_{ab}, r, W, N_0, $flag$, α_{1_i}, β_{1_i}, $x_i^{t,m}$, $x_i^{r,m}$, x_{ij}^m, p_{ij}^m, g_{ij}^m $\forall\,(i,j) \in \mathscr{E}$, $\forall\, i \in \mathscr{N}$, $\forall m \in \mathscr{M}$

. **Output**: $flag$, x_{ij}^m, $\forall\,(i,j) \in \mathscr{E}$, $\forall m \in \mathscr{M}$

.

1: $x_{\text{new},ij}^m = x_{ij}^m$, $p_{\text{new},ij}^m = p_{ij}^m$, $\forall\,(i,j) \in \mathscr{E}$, $\forall m \in \mathscr{M}$.

2: $f_{\text{new},ab}^m = \frac{f_{ab}}{\sum_{m\in\mathscr{M}} x_{\text{new},ab}^m + 1} \cdot x_{\text{new},ab}^m$, $p_{\text{new},ab}^m = \frac{N_0 W}{g_{ab}^m} \cdot \left(2^{\frac{f_{\text{new},ab}^m}{W}} - 1\right) x_{\text{new},ab}^m$ $\forall\, m \in \mathscr{M}$.

3: **for** $m \in \mathscr{M}$ where $x_{ab}^m \neq 1$. **do**

4: $x_{\text{new},ab}^m = 1$. $x_a^{t,m} = 1$. $x_b^{r,m} = 1$. $\alpha_{1_a} = \alpha_1$. $\beta_{1_b} = \beta_1$.

5: $q_{t,i} = W \cdot \left(\max_{m\in\mathscr{M}} \left(m \cdot x_i^{t,m}\right) - \min_{m\in\mathscr{M}} \left(m \cdot x_i^{t,m} + |M| \cdot (1 - x_i^{t,m})\right) + 1\right)$ $\forall\, i \in \mathscr{N}$.

6: $q_{r,i} = W \cdot \left(\max_{m\in\mathscr{M}_i} \left(m \cdot x_i^{r,m}\right) - \min_{m\in\mathscr{M}_i} \left(m \cdot x_i^{r,m} + |M| \cdot (1 - x_i^{r,m})\right) + 1\right)$ $\forall\, i \in \mathscr{N}$.

7: $f_{\text{new},ab}^m = \frac{f_{ab}}{\sum_{m\in\mathscr{M}} x_{\text{new},ab}^m} \cdot x_{\text{new},ab}^m$, $p_{\text{new},ab}^m = \frac{N_0 W}{g_{ab}^m} \cdot \left(2^{\frac{f_{\text{new},ab}^m}{W}} - 1\right) x_{\text{new},ab}^m$.

8: $IntFlag = \text{IntCheck}\left(x_{\text{new},ab}^m, p_{\text{new},ab}^m, \mathscr{M}, \mathscr{A}, W, N_0, x_{ij}^m, p_{ij}^m\ \forall\,(i,j) \in \mathscr{E}\right)$.

9: **if** IntCheck(·) = 1 **then**

10: $P_{\text{new,tot}}^m = \infty$.

11: **else**

12: $P_{\text{new,tot}}^m = \sum_{i\in\mathscr{N}} \left(\alpha_{1_i} + 2\alpha_2 q_{t,i} + \sum_{j\in\mathscr{N}} \sum_{m\in\mathscr{M}_{ij}} p_{\text{new},ij}^m + \beta_{1_i} + 2\beta_2 q_{r,i}\right)$.

13: **end if**

14: $x_a^{t,m} = 0$, $x_b^{r,m} = 0$.

15: **end for**

16: $P_{\text{tot,new}} = \min_{m\in\mathscr{M}} P_{\text{tot,new}}^m$. ind $= \arg\min_{m\in\mathscr{M}} P_{\text{tot,new}}^m$.

17: **if** $P_{\text{tot,new}} < P_{\text{tot}}$ **then**

18: $x_{ab}^{\text{ind}} = 1$.

19: $x_a^{t,\text{ind}} = 1$. $x_b^{r,\text{ind}} = 1$. $\alpha_{1_a} = \alpha_1$. $\beta_{1_b} = \beta_1$.

20: $f_{ab}^m = \frac{f_{ab}}{\sum_{m\in\mathscr{M}} x_{ab}^m} \cdot x_{ab}^m$, $p_{ab}^m = \frac{N_0 W}{g_{ab}^m} \cdot \left(2^{\frac{f}{W}} - 1\right) x_{ab}^m$ $\forall\, m \in \mathscr{M}$.

21: **else**

22: $flag = flag + 1$.

23: **end if**

24: **return**

program. The central controller also asks the subroutine to focus on a particular link (a,b). The subroutine iterates through all available channels and finds the best available channel for (a,b).

Operation 1 stores the global scheduling (x_{ij}^m) and power allocation (p_{ij}^m) variables in local dummy variables $x_{\text{new},ij}^m$ and $p_{\text{new},ij}^m$, respectively. Operation 3 of Algorithm 2 starts the iteration for all channels. Operation 4 assigns the current channel to the focus link (a,b). Operation 5 and 6 calculate the transmit span $(q_{t,i})$ and receiver span $(q_{r,i})$ for all nodes $i \in \mathscr{N}$. Operation 7 assumes equal flow allocation among the selected channels and finds the power allocation in link (a,b) to meet rate requirement. Operation 8 calls the subroutine of Algorithm 3 and checks if current channel assignment causes interference to other links. Operation 12 calculates total system power of the current iteration. Operation 15 comes out of the loop. Operation 16 finds the minimum system power $(P_{\text{tot,new}})$ among all possible channel allocations. Operations 17, 18, 19, 20, 21, 22, and 23 compare the achievable minimum system power $(P_{\text{tot,new}})$ with the stored global system power (P_{tot}) and update scheduling and power variables accordingly.

Algorithm 3 Primary and secondary interference checking algorithm

Input : $x^m_{\text{new},ab}$, $p^m_{\text{new},ab}$, $\mathscr{M}$, $\mathscr{A}$, W, N_0, x^m_{ij}, p^m_{ij} $\forall(i,j) \in \mathscr{A}$
Output: $Intflag$
1: $count = 0$. $Intflag = 0$.
2: **for** $(i,j) \in \mathscr{A}$, $i \neq a$, $j \neq b$ **do**
3: **if** $\left((p^m_{\text{new},ab} g^m_{aj} \geq 0.1 N_0 W x^m_{ij}) || (p^m_{ij} g^m_{ib} \geq 0.1 N_0 W x^m_{\text{new},ab})\right)$ **then**
4: $count = count + 1$.
5: **end if**
6: **if** $\left(x^m_{ia} + x^m_{ab} + x^m_{bj} > 0\right)$ **then**
7: $count = count + 1$.
8: **end if**
9: **end for**
10: **if** $count > 0$ **then**
11: $Intflag = 1$.
12: **end if**
13: **return**

We assume equal flow per channel in each link in operation 7 and 20 of Algorithm 2. This simplifies the calculation of transmission power per channel and avoids the computation of a convex optimization program in each loop. However, we consider optimal flow and power allocation in our final optimization problem of operation 18 of Algorithm 1.

Interference Checking Algorithm

The subroutine of Algorithm 3 gets called from operation 8 of the greedy scheduling algorithm of Algorithm 2. This subroutine checks if the scheduling and power allocation of link ab in channel m, calculated in Algorithm 2, interferes with other links. Operation 3 of Algorithm 3 checks if transmitted power in link ab causes interference to any nonadjacent link that uses channel m. Operation 6 checks if link ab maintains half-duplex relationships with its adjacent links. Operation 11 updates the interference flag and returns this value to the greedy scheduling subroutine of Algorithm 2.

Computational Complexity

Global system power minimization algorithm of Algorithm 1 contains three major parts: (1) Initial routing path selection (operations 1, 2, and 3) of Algorithm 1, (2) channel scheduling (operations 9, 10, 11, 12, 13, 14, 15, 16, and 17) of Algorithm 1 along with Algorithm 2 and Algorithm 3 , and (3) optimal power control and routing path design (operation 18 of Algorithm 1).

Initial routing path selection involves computing link weights ($O(E)$) and shortest path ($O(E + N \log N)$) for L sessions. Therefore, the overall complexity for this part is $O\big(L(E + N \log N)\big)$.

The greedy scheduling algorithm starts with a while loop. The while loop iterates through all active links ($O(E)$). Each link calls the subroutine of Algorithm 2, iterates through M channels. Inside each channel, the code calls the subroutine of Algorithm 3. Algorithm 3 checks if the current channel assignment interferes with

Table 4 Summary of algorithms

Algorithm index	Objective	Complexity
1	Minimize system power of the multi-hop network	$O(E^2M^2)$
2	Schedule channel for a given link of the multi-hop network	$O(EM)$
3	Check if current schedule interferes with other links of the multi-hop network	$O(E)$

other links ($O(E)$). The global while loop of Algorithm 1 can iterate at most $O(M)$ times since each iteration will either select a channel for a link or the loop will break. Therefore, the greedy scheduling algorithm runs in $O(E^2M^2)$ time.

The optimal power allocation and routing path selection problem of operation 18 of Algorithm 1 is a convex optimization program. Barrier method [4] can solve this in $O(R\log(R))$ steps where R is the number of inequality constraints. From (25), we find the complexity to be $O(EM\log(EM))$.

The greedy scheduling part dominates the overall complexity ($O(E^2M^2)$) of Algorithm 1. We term this algorithm "GreedySysPowerMin." We compare the performance of both "GreedySysPowerMin" and "BnBSysPowerMin" with that of "TxPowerMin" in section "Simulation Results."

Table 4 summarizes the objective and computational complexity of the three algorithms presented in the paper. As mentioned before, Algorithms 2 and 3 are subroutines of Algorithm 1, which is the greedy algorithm that solves the optimization problem of (25) with polynomial complexity. This greedy algorithm does not provide any optimality guarantee.

The number of channel M does not denote the number of subcarriers in a multi-hop network. It represents the number of wideband channels, e.g., 6 MHz TV channels in white space and 20 MHz channels in 5.8 GHz, in the network. This ensures that our overall complexity ($O(E^2M^2)$) remains reasonable for a moderately sized network.

Simulation Results

System Power Minimization in a Single Point-to-Point Link

We focus on an NC-OFDMA-based single transceiver pair. There is only one session in the network and minimum data rate requirement is 18 Mbps. There are 20 channels available for transmission. Each channel is 3 MHz wide. The left subplot of Fig. 5 shows the link gains across these channels. We designed the link gains so that every other channel has better link gain than its adjacent neighbors.

The second subplot (from the left) of Fig. 5 shows the power allocation and scheduling variables of TxPowerMin approach. This approach minimizes transmit power subject to the rate constraint. Similar to the concept of "waterfilling" algorithm [8], this approach spreads power across all ten "good" channels of the network.

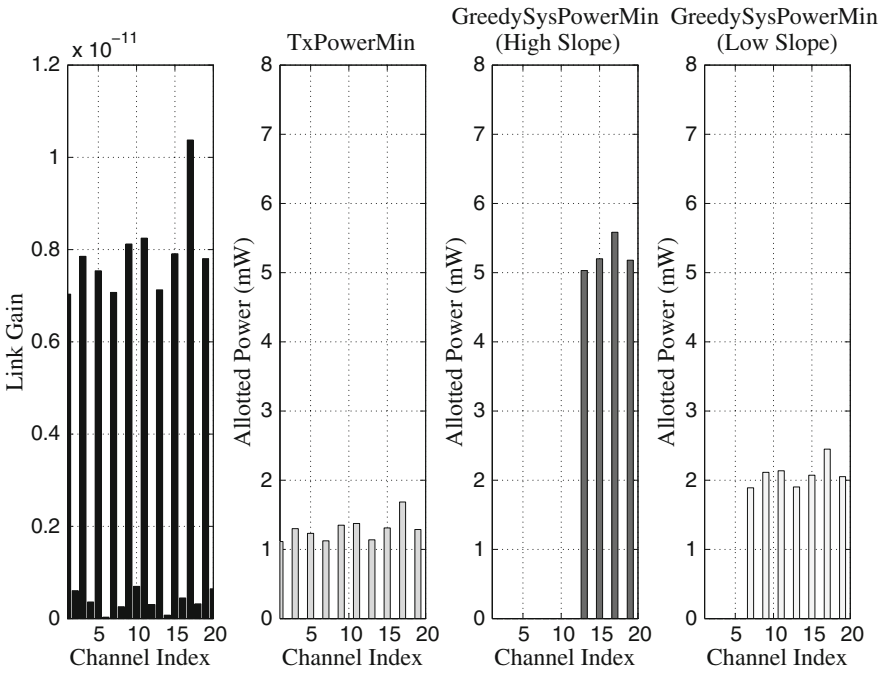

Fig. 5 Comparison of 'TxPowerMin' and our approach in power allocation and scheduling

The third and fourth subplot (from the left) of Fig. 5 shows the scheduling and power variables of our greedy algorithm (GreedySysMin). We use two different types of ADC and DAC models to investigate the influence of ADC/DAC slopes on our algorithm. We use the high-slope ADC and DAC models – ADC 9777 and ADS 62P4 (see Fig. 2a, b) – in the third subplot of Fig. 5 and the low-slope ADC and DAC model, DAC 3162 and ADS 4249 (see Fig. 2a, b), in the fourth subplot (the rightmost one) of Fig. 5. With high-slope ADC and DAC, our algorithm focuses more on minimizing circuit power and selects only four channels. With low-slope ADC and DAC, our approach finds a trade-off between transmit and circuit power and selects seven channels.

Figure 6 compares the performance of our algorithm with that of TxPowerMin approach in high ADC/DAC slope setting. "TxPowerMin" approach minimizes transmit power by spreading data across all "good" channels of the network. Both of our algorithms consume more transmit power than the "TxPowerMin" approach since selecting a subset of available good channels is a suboptimal policy in terms of transmit power. Our algorithms consume less circuit power due to the reduced spectrum span. Overall, our algorithms reduce system power – summation of transmit and circuit power – consumption by almost 30%.

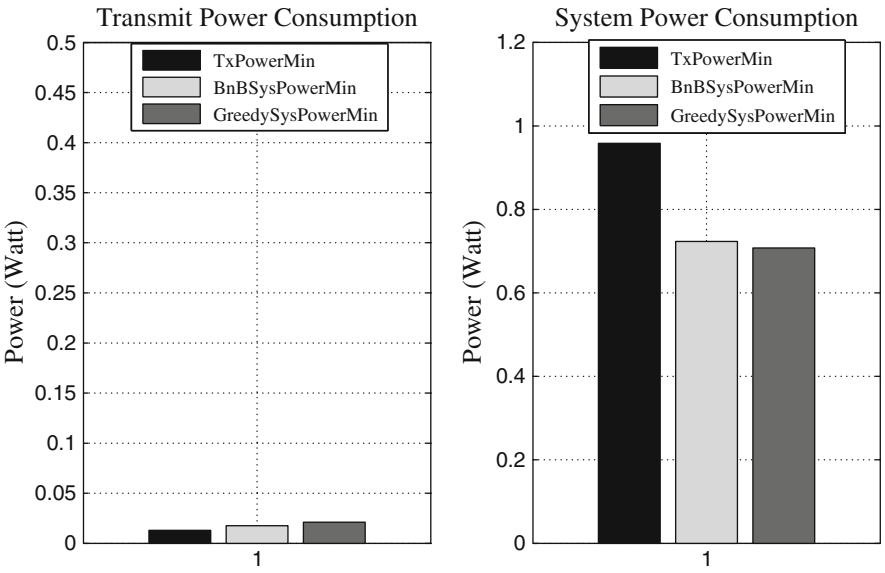

Fig. 6 Comparison of our algorithms with the "TxPowerMin" approach using the high-slope ADC/DAC's of Fig. 2a, b

Note that the lower bound of the system power consumption (obtained from the mixed integer linear programming relaxation) was 0.63 W in this scenario. Hence, both of our algorithms gave feasible results with roughly 15% optimality gap.

Figure 7 compares the performance of our algorithm with that of "TxPowerMin" approach in low ADC/DAC slope setting. We use the same link gain, bandwidth, and traffic demands of Fig. 6, but we use the low power consumption ADC and DAC's to generate these new figures. Our algorithm performs almost similar to the "TxPowerMin" approach here because the power consumption of these low power ADC & DAC is negligible compared to the transmit power requirement.

System Power Minimization in a Multi-hop Network

To illustrate the influence of system power minimization in a practical setting of non-contiguous spectrum access, we consider an exemplary scenario of multi-hop networking among fixed devices in the TV white space channels of Wichita, Kansas, USA. We use standard spectrum databases [37] to find the available TV channels in Wichita, Kansas. Figure 8 shows the locations of nodes. Nodes 1, 2, and 3 transmit to nodes 12, 11, and 10, respectively. Each session requires 10 Mbps data rate. Table 5 shows the available channel indexes. Each channel is 6 MHz wide. We consider both large-scale fading (with path loss exponent 3) and small-scale fading (with

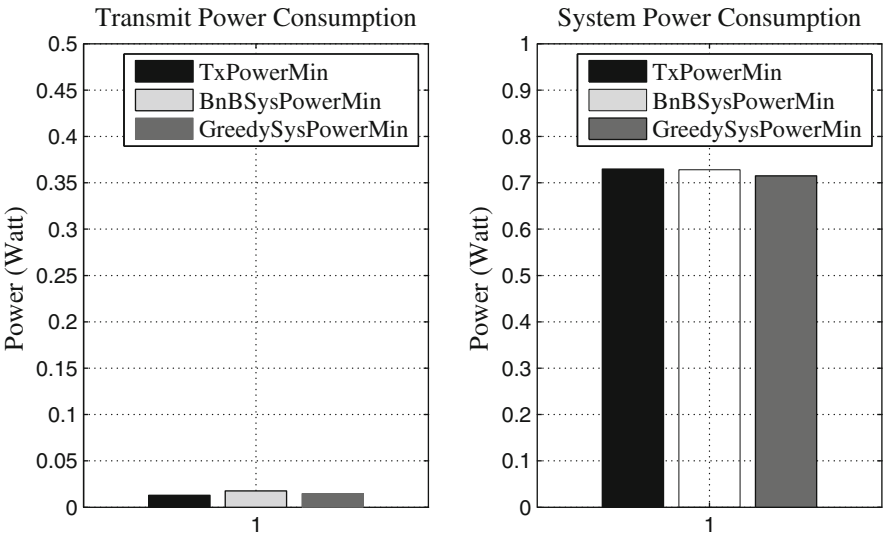

Fig. 7 Comparison of our algorithms with the "TxPowerMin" approach using the low-slope ADC/DAC's of Fig. 2a, b

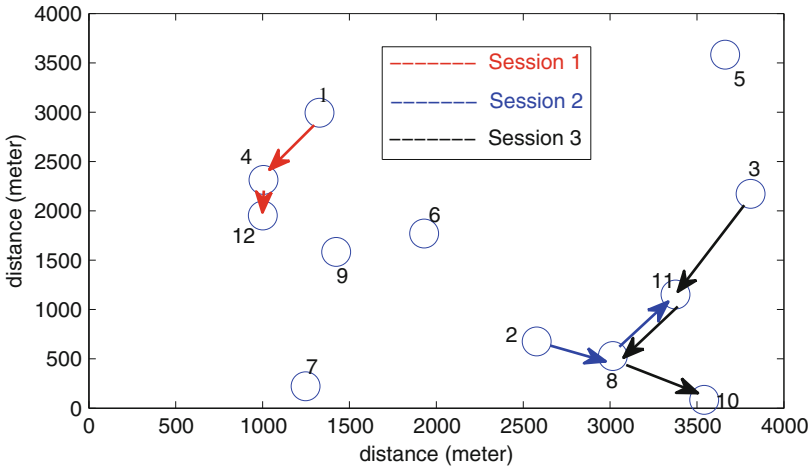

Fig. 8 Twelve-node three-session multi-hop network

12 dB random fluctuation) in each channel. Maximum allowed transmission power is 4 W [17].

Channel Indexing Notations in Optimization Formulation

The difference between channel's carrier frequencies in TV bands are not always proportional to the index differences. Channel 17's center frequency is $((23-17)*6)$

Table 5 Available TV channels for fixed devices in Wichita, Kansas

Channel index	2	5	6	17	23	24	47
Center freq. (MHz)	57	79	85	491	527	533	671

Table 6 Comparison between the spectrum span of "TxPowerMin" and our "BnBSysPowerMin" algorithm in the network of Fig. 8

Node	Mode	TxPowerMin		BnBSysPowerMin	
		Channel index	Spectrum span (MHz)	Channel index	Spectrum span (MHz)
1	Tx	{23, 47}	150	{17, 23}	42
	Rx	{Ø}	0	{Ø}	0
2	Tx	{17}	6	{23}	6
	Rx	{Ø}	0	{Ø}	0
3	Tx	{6, 47}	592	{5, 6}	12
	Rx	{Ø}	0	{Ø}	0
4	Tx	{17}	6	{6}	6
	Rx	{23, 47}	150	{17, 23}	42
8	Tx	{2, 23}	476	{2, 47}	620
	Rx	{5, 24}	460	{17, 23, 24}	48
10	Tx	{Ø}	0	{Ø}	0
	Rx	{23}	6	{47}	6
11	Tx	{5, 24}	460	{17, 24}	48
	Rx	{2, 6, 47}	620	{2, 5, 6}	34
12	Tx	{Ø}	0	{Ø}	0
	Rx	{17}	6	{6}	6

36 MHz far from that of channel 23 but not $((17 - 6) * 6)$ 66 MHz far from that of channel 6. The spectrum span calculation of our optimization formulations depends heavily on the coherence of channel indexing differences. Therefore, we use an index set of $\{9, 13, 14, 81, 87, 88, 111\}$ to denote the channel list of $\{2, 5, 6, 17, 23, 24, 47\}$ in the optimization formulations. We use the original channel list to show the numerical results.

Comparison of "Waterfilling" Algorithm and Our Approach

Here, we use the low-slope ADC and DAC models of Fig. 2b, a. We also use Hou and Shi's algorithm [34] to illustrate the scheduling and power control decisions of "TxPowerMin" approach.

Table 6 compares the channel scheduling decisions and spectrum spans of "TxPowerMin" approach and our algorithm. Although "TxPowerMin" minimizes transmit power by selecting channels with better quality, it increases radio front-end power by selecting channels that are too far apart. Our approach spans narrow spectrum and reduces circuit power consumption. Figure 9 shows that our algorithm reduces system power by 30%.

The 30% system power saving achieved here was obtained with the low-slope ADC and DAC models of Fig. 2b, a – termed as "ultralow-power ADC" and

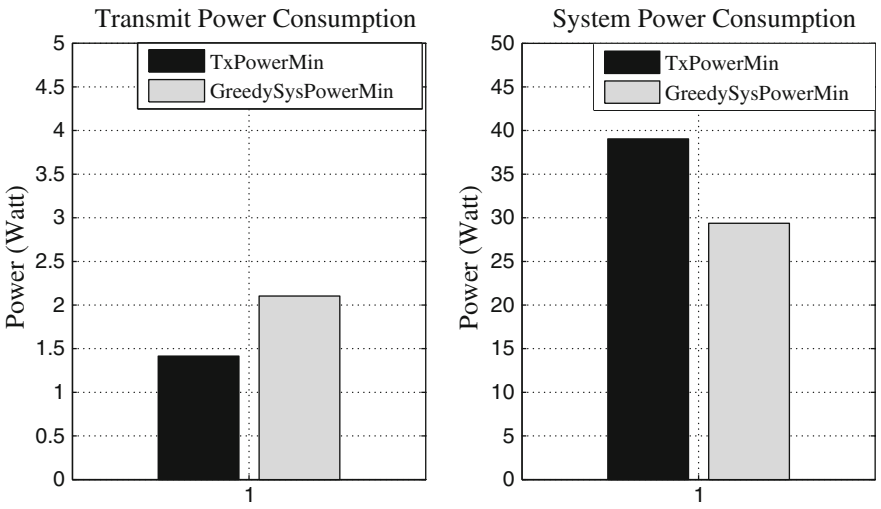

Fig. 9 Performance comparison of "TxPowerMin" approach and our algorithm in the network of Fig. 8, based on the low-slope ADC and DAC models of Fig. 2b, a

"low-power DAC" by their maker, Texas Instruments. Had we used the high-slope ADC and DAC models of Fig. 2b, a, our algorithm would have saved system power by a much higher amount in this simulation. In the future, even if the power consumption curves of ADC and DAC become flatter, our algorithm will reduce the system power considerably as long as the number of available channels is sparsely located – which is often the case in a cognitive radio network.

The lower bound of system power consumption is 24 W in this scenario. Our algorithm provides a feasible solution (29 W) with 20% optimality gap.

Conclusion

Wireless transmission using non-contiguous chunks of spectrum is becoming increasingly essential. MC-MR and NC-OFDMA are the two commercially viable choices to access these non-contiguous spectrum chunks. Fixed MC-MRs do not scale with increasing number of non-contiguous spectrum chunks. NC-OFDMA accesses non-contiguous spectrum chunks with a single front-end radio but increases circuit power consumption by spanning wider spectrum. Our approach characterized this trade-off and performed joint power control, channel scheduling, spectrum span selection, and routing to minimize system power consumption in an NC-OFDMA-based multi-hop network. Our algorithm showed how the slopes of ADC and DAC's power consumption versus sampling rate curves influence the scheduling decisions of a multi-hop network. Numerical results suggested that our algorithm can save 30% system power over classical

transmission power-based cross-layer algorithms in single front-end radios. We developed a branch-and-bound-based mixed integer linear programming model to optimize the cross-layer decisions of a general multi-hop network. Furthermore, we also provided a low-complexity ($O(E^2M^2)$) greedy algorithm.

The optimal fragmentation results presented here have only accounted for the radio front-end power and transmitters' emitted power. Future work will incorporate baseband power in the optimization formulation.

We focused on system power consumption of single front-end radio in this work. A multifront-end programmable radio can dynamically switch its multiple set of center frequencies and access several spectrum chunks in each radio front end with less spectrum span by using NC-OFDMA technology [15]. In the future, we will focus on optimal system power consumption of multifront-end radios.

Acknowledgements This work is supported in part by a grant from the US Office of Naval Research (ONR) under grant number N000014-15-1-2168. The work of S. Kompella is supported directly by the Office of Naval Research.

Power Consumption of Different Blocks in Transmitter and Receiver

Based on Fig. 3, power consumption of transmitter and receiver are:

$$p_{tc} = p_{dac} + p_{tfilt} + p_{mix} + p_{pa}. \tag{33}$$

$$p_{rc} = p_{adc} + p_{rfilt} + p_{mix} + p_{ifa} + p_{lna}. \tag{34}$$

In the above, p_{dac}, p_{mix}, p_{pa}, p_{adc}, p_{ifa} and p_{lna} denote the circuit power consumption in the DAC, mixer, PA, ADC, IFA and LNA respectively. p_{tfilt} and p_{rfilt} represent the summation of circuit powers in the filters of transmitter and receiver respectively.

The power consumption in the mixer, LNA and IFA are constants with respect to the sampling rate [26]. Baseband filter power depends on sampling rate but we assume it to be constant due to its low power consumption [9]. Let us assume,

$$p_{tfilt} + p_{mix} = k_t\,,\ \ p_{rfilt} + p_{mix} + p_{ifa} + p_{lna} = k_r. \tag{35}$$

DAC and ADC power consumptions are affine functions of sampling rate [9]. Hence,

$$p_{dac} = k_1 + k_2 fs\,,\ \ p_{adc} = k_3 + k_4 fs. \tag{36}$$

Now, using(36) and (35) in (33) and (34).

$$p_{tc} = k_1 + k_2 fs + k_t = \alpha_1 + \alpha_2 fs\,,\ \ p_{rc} = k_3 + k_4 fs + k_r = \beta_1 + \beta_2 f. \tag{37}$$

In the above equation, $\alpha_1 = k_1 + k_t$, $\beta_1 = k_3 + k_r$, $\alpha_2 = k_2$ and $\beta_2 = k_4$.

We assume low power consumption at these blocks and use the following values [9]: $p_{tfilt} = 5\,\text{mW}$, $p_{mix} = 30.3\,\text{mW}$, $p_{rfilt} = 7.5\,\text{mW}$, $p_{ifa} = 3\,\text{mW}$, $p_{lna} = 20\,\text{mW}$.

Due to its dependence on transmit power, we do not include programmable amplifier's circuit power consumption term p_{pa} in the overall circuit power consumption equations of (33) and (34). Instead, we couple it with the transmit power consumption p and include it in the total power equations of (2) and (3).

Power Consumption of Programmable Amplifier

Power consumption of programmable amplifier is, $p_{pa} = \frac{PAPR}{\eta} p$. We assume a class-B or a higher class (C, D or E) amplifier with $\eta = 0.75$ [9].

We consider OFDM to be our modulation scheme. The authors of [32] have related the PAPR with the number of subcarriers in OFDM systems as:

$$\text{Prob}\{\text{PAPR} > \gamma\} \approx 1 - \exp\left\{-Ne^{-\gamma}\sqrt{\frac{\pi}{3}\gamma}\right\}, \tag{38}$$

where N is the number of subcarriers.

In the presence of large number of subcarriers, the statistical distribution of the PAPR does not remain sensitive to the increase of the number of subcarriers [32]. During the simulations, we consider the worst case PAPR by assuming maximum possible spectrum span and highest number of subcarriers. We plug the value of maximum number of possible subcarriers of TV white space in (38), and assume $\gamma = 0.005$ and a 3–4 dB reduction in PAPR. Based on these calculations, we find PAPR to be around 9 dB.

Power Consumption of ADC and DAC

Figure 2a plots the power consumption vs. sampling rate curve of AD 9777 [2] (DAC of USRP radio) and DAC 3162 [12]. Figure 2b plots the power consumption vs. sampling rate curve of ADS62P4 [11] (ADC of USRP radio) and ADS4249 [13]. We obtain specific values of k_1, k_2, k_3 and k_4 from these plots.

References

1. AD9467: 16 bit, 200 MSPS/250 MSPS, analog-to-digital converter. http://www.analog.com/media/en/technical-documentation/data-sheets/AD9467.pdf. Accessed Jan 2016
2. AD9777: 16-Bit interpolating dual DAC converter. http://www.analog.com/media/en/technical-documentation/data-sheets/AD9777.pdf. Accessed Jan 2016
3. ADC performance evolution; Walden figure-out-merit (FOM). http://converterpassion.wordpress.com/2012/08/21/. Accessed Jan 2016

4. Boyd S, Vandenberghe L (1999) Convex optimization. Cambridge University Press, Cambridge
5. Cao L, Yang L, Zheng H (2010) The impact of frequency-agility on dynamic spectrum sharing. In: IEEE DySPAN 2010, pp 1–12. https://doi.org/10.1109/DYSPAN.2010.5457889
6. Cordeiro C, Challapali, Birru D et al (2005) IEEE 802.22: the first worldwide wireless standard based on cognitive radios. In: IEEE DySPAN 2005 Nov, pp 328–337. https://doi.org/10.1109/DYSPAN.2005.1542649
7. Cormen TH, Leiserson CE, Rivest RL et al (2009) Introduction to algorithms. The MIT Press, Cambridge
8. Cover TM, Thomas JA (2005) Elements of information theory. Wiley, Hoboken
9. Cui S, Goldsmith A, Bahai A (2005) Energy-constrained modulation optimization. In: IEEE TWC 2005 Sep:2349–2360. https://doi.org/10.1109/TWC.2005.853882
10. CVX: Matlab software for disciplined convex programming. http://cvxr.com/cvx/. Accessed Jan 2016
11. Dual channel, 14 bit, 125/105/80/65 MSPS ADC with DDR LVDS/CMOS outputs. http://www.ti.com/lit/ds/symlink/ads62p42.pdf. Accessed Jan 2016
12. Dual-channel 10/12 bit 500 MSPS digital-to-analog converters. http://www.ti.com/lit/ds/symlink/dac3162.pdf. Accessed Jan 2016
13. Dual-channel 14 bit 250 MSPS ultralow-power ADC. http://www.ti.com/lit/ds/symlink/ads4249.pdf. Accessed Jan 2016
14. Enabling innovative small cell use in 3.5 GHz band NPRM and order. Available via FCC. http://www.fcc.gov/document/enabling-innovative-small-cell-use-35-ghz-band-nprm-order. Accessed Jan 2016
15. Fettwis G, Krondorf M, Bittner S (2009) GFDM – generalized frequency division multiplexing. In: IEEE VTC 2009 June, pp 1–4. https://doi.org/10.1109/VETECS.2009.5073571
16. Fredriksson K, Guhl M (2011) Multi-channel, multi-radio in wireless mesh networks. Available via Chalmers institute of technology, Goteborg. http://publications.lib.chalmers.se/records/fulltext/138138.pdf. Accessed Nov 2016
17. Gerami C, Mandayam NB, Greenstein LJ (2010) Backhauling in TV white space. In: IEEE Globecom 2010, pp 1–6. https://doi.org/10.1109/GLOCOM.2010.5684131
18. Grover P, Woyach KA, Sahai A (2011) Towards a communication theoretic understanding of system level power consumption. In: IEEE JSAC 2011, vol 29, pp 1744–1755. https://doi.org/10.1109/JSAC.2011.110922
19. Hou W, Yang L, Zhang L et al (2009) Understanding the impact of cross-band interference. In: ACM CoRoNet 2009, pp 19–24. https://doi.org/10.1145/1614235.1614241
20. Isheden C, Fettweis GP (2010) Energy efficient multi-carrier link adaptation with sum rate-dependent circuit power. In: IEEE GLOBECOMM 2010, pp 1–6. https://doi.org/10.1109/GLOCOM.2010.5683700
21. Islam MN, Mandayam NB, Kompella S (2012) Optimal resource allocation and relay selection in bandwidth exchange based cooperative forwarding. In: IEEE WiOpt 2012, pp 192–199. http://ieeexplore.ieee.org/document/6260454/. Accessed Nov 2016
22. Islam MN, Sampath A, Maharshi A et al (2014) Wireless backhaul node placement for small cell networks. In: IEEE CISS 2014, pp 1–6. https://doi.org/10.1109/CISS.2014.6814156
23. Jia J, Zhuang W (2011) Capacity of multi-hop wireless network with frequency agile software defined radio. In: IEEE INFOCOM WKSHPs 2011 Apr, pp 41–46. https://doi.org/10.1109/INFCOMW.2011.5928850
24. Kodialam M, Nandagopal T (2005) Characterizing the capacity region in multi-radio multi-channel wireless mesh networks. In: ACM MOBICOM 2005 Aug, pp 73–87. https://doi.org/10.1145/1080829.1080837
25. Kyasanur P, Vaidya NH (2005) Capacity of multi-channel wireless networks: impact of number of channels and interfaces. In: ACM MOBICOM 2005 Aug, pp 43–57. https://doi.org/10.1145/1080829.1080835
26. Li Y, Bakkaloglu B, Chakrabarti C (2007) A system level energy model and energy quality evaluation for integrated transceiver front-ends. In: Proceedings of IEEE Transactions on VLSI 2007, vol 15, no 1, pp 90–103. https://doi.org/10.1109/TVLSI.2007.891095

27. Li G, Xu Z, Xiong C et al (2011) Energy efficient wireless communications: tutorial, survey, and open issues. In: IEEE TWC 2011, vol 18, no 6, pp 28–35. https://doi.org/10.1109/MWC.2011.6108331
28. Lin YP, Vaidyanathan PP (1998) Periodically nonuniform sampling of bandpass signals. In: IEEE TCS II 1998, vol 43, no 3, pp 340–351. https://doi.org/10.1109/82.664240
29. Liu HC, Min JS, Samueli H (1996) A low power baseband receiver IC for frequency-hopped spread spectrum communications. In: Proceedings of IEEE Journal of SSC 1996, vol 31, no 3, pp 384–394. https://doi.org/10.1109/4.494200
30. Mishali M, Eldar YC (2011) From theory to practice: sub-Nyquist sampling of sparse wideband analog signals. In: IEEE JSTSP 2010, vol 4, no 2, pp 375–391. https://doi.org/10.1109/JSTSP.2010.2042414
31. Mosek optimization. http://www.mosek.com/. Accessed Jan 2016
32. Ochiai H, Imai H (2001) On the distribution of peak-to-average power ratio in OFDM signals. In: IEEE Transactions on COM 2001, vol 49, no 2, pp 282–289. https://doi.org/10.1109/26.905885
33. Sherali HD, Adams WP (1999) A reformulation linearization technique for solving discrete and continuous nonconvex problems. Kluwer Academic Publishers, Dordrecht/Boston/London
34. Shi Y, Hou YT (2007) Optimal power control for multi-hop software defined radio networks. In: IEEE INFOCOM 2007, pp 1694–1702. https://doi.org/10.1109/INFCOM.2007.198
35. Shi Y, Hou T et al (2008) A distributed optimization algorithm for multi-hop cognitive radio networks. In: IEEE INFOCOM 2008, pp 1292–1300. https://doi.org/10.1109/INFOCOM.2008.186
36. Shi Y, Hou T, Komeplla S et al (2011) Maximizing capacity in multihop cognitive radio networks under the SINR model. In: IEEE TMC 2011, vol 10, no 7, pp 954–967. https://doi.org/10.1109/TMC.2010.204
37. Show my white space. http://whitespaces.spectrumbridge.com/whitespaces. Accessed Jan 2016
38. Xu H, Li B (2010) Efficient resource allocation with flexible channel cooperation in OFDMA cognitive radio networks. In: IEEE INFOCOM 2010, pp 1–9. https://doi.org/10.1109/INFCOM.2010.5462169
39. Yang L, Hou W, Cao L et al (2010) Supporting demanding wireless applications with frequency agile radios. In: USENIX Symposium on NSDI 2010, pp 1–5
40. Yang L, Zhao BY, Zheng H (2010) The spaces between us: setting and maintaining boundaries in wireless spectrum access. In: ACM MOBICOM 2010, pp 37–48. https://doi.org/10.1145/1859995.1860001
41. Yang L, Zhang Z, Hou W et al (2011) Papyrus: a software platform for distributed dynamic spectrum sharing using SDRs. In: ACM SIGCOMM 2011, vol 41, no 1, pp 31–37. https://doi.org/10.1145/1925861.1925866

Sequential Learning and Decision-Making in Dynamic Channel Access and Transmission Scheduling

26

Yang Liu and Mingyan Liu

Contents

Y. Liu (✉)
SEAS, Harvard University, Cambridge, MA, USA
e-mail: yangl@seas.harvard.edu

M. Liu
EECS, University of Michigan, Ann Arbor, MI, USA
e-mail: mingyan@eecs.umich.edu

W. Zhang (ed.), *Handbook of Cognitive Radio*,
https://doi.org/10.1007/978-981-10-1394-2_25

Abstract

Making judicious channel access and transmission scheduling decisions is essential for improving performance (delay, throughput, etc.) as well as energy and spectral efficiency in multichannel wireless systems. This problem has been a subject of extensive study in the past decade, and the resulting dynamic and opportunistic channel access schemes can bring potentially significant improvement over traditional schemes. In this chapter, a couple of classical settings and problems for this decision-making question in cognitive radio networks, namely, multiuser, single-channel model and single-user, multichannel model, as well as their solutions, will be surveyed first. Toward making such studies more practical, we point to a common and severe limitation of these dynamic schemes in that they almost always require some form of a priori knowledge of the channel statistics. On the other hand, what is often available to the decision-maker is a rather rich stream of network data that can jointly describe channel conditions.

Then a natural remedy is to consider a learning framework, which has also been extensively studied in the same context, but a typical learning algorithm in this literature seeks only the best static policy (i.e., to stay in the best channel), with performance measured by *weak regret*, rather than learning a good dynamic channel access policy. There is thus a clear disconnect between what an optimal channel access policy can achieve with known channel statistics that actively exploits temporal, spatial, and spectral diversity and what a typical existing learning algorithm aims for, which is the static use of a single-channel devoid of diversity gain.

In this chapter, this gap is bridged by designing learning algorithms that track known optimal or suboptimal dynamic channel access and transmission scheduling policies via using collected observations following the made decisions, thereby yielding performance measured by a form of *strong regret*, the accumulated difference between the reward returned by an optimal solution when a priori information is available and that by our online algorithm. We do so in the context of two specific algorithms that appeared in [1] and [2], respectively, the former for a multiuser single-channel setting and the latter for a single-user multichannel setting. In both cases we show that our algorithms achieve sublinear regret uniform in time and outperform the standard weak-regret learning algorithms.

Keywords

Sequential learning · Decision-making · Dynamic access · Transmission scheduling · Multiuser · Multichannel

Introduction

Making judicious channel access and transmission scheduling decisions is essential for improving performance (delay, throughput, etc.) as well as energy and spectral efficiency in wireless systems, especially those consisting of multiple users and multiple channels. Such decisions are often nontrivial because of the time-varying nature of the wireless channel condition, which further varies across different users and different spectrum bands. Such variations bring in diversities that can provide opportunities for a radio transceiver to exploit for performance gain, and the past decade has seen many research advances in this area. For instance, a transmitter can seek the best channel through channel sensing before transmission, see, e.g., [3–5] for such dynamic multichannel MAC schemes that allow transmitters to opportunistically switch between channels in search of good instantaneous channel conditions; if a transmitter consistently selects a channel with better instantaneous condition (e.g., higher instantaneous received SNR) from a set of channels, then over time it sees (potentially much) higher average rate [6–8]. Similarly, a transmitter can postpone transmission if the sensed instantaneous condition is poor in hopes of better condition later, see e.g., [1] for stopping rule-based sequential channel sensing policies, in the single-user multichannel and single-channel multiuser scenarios, respectively. Variations on the same theme include [9] where a distributed opportunistic scheduling problem under delay constraints is investigated and [2] where a generalized stopping rule is developed for the single-user multichannel setting.

These dynamic channel access schemes (both optimal and suboptimal) improve upon traditional schemes such as channel splitting [10, 11], multichannel CSMA [12], and multi-rate systems [13]. In this chapter, we first go through two representative models, namely, single-user, multichannel model and multiuser, single-channel model, and we revisit their solutions.

In these solutions, formally there are three types of diversity gains being commonly explored. The first is *temporal diversity*, where the natural temporal variation in the wireless channel causes a user to experience or perceive different transmission conditions over time even when it stays on the same channel, and the idea is to have the user access to the channel for data transmission when the condition is good, which may require and warrant a certain amount of waiting. Studies like [14] investigate the trade-off involved in waiting for a better condition and when is the best time to stop.

The second is *spectral diversity*, where different channels experience different temporal variations, so for a given user at any given time, a set of channels present different transmission conditions. The idea is then to have the user select a channel with the best condition at any given time for data transmission, which typically involves probing multiple channels to find out their conditions. Protocols like [15] does exactly this, and studies like [16, 17] further seek to identify the best sequential probing policies using a decision framework.

The third is *user diversity* or *spatial diversity*, where the same frequency band at the same time can offer different transmission qualities to different users due to their differences in transceiver design, geographic location, etc. The idea is to have the user with the best condition on a channel use it. This diversity gain can be obtained to some degree by using techniques like stopping rules whereby a user essentially judges for himself whether the condition is sufficiently good before transmitting, which comes as a by-product of utilizing temporal diversity.

Harnessing the above forms of diversities is studied in different scenarios. For instance, temporal diversity is studied in a multiuser setting but with a single channel in [1, 18]; spectral diversity is analyzed for a single user in [4], among others. More specifically, [1] developed optimal stopping policies for single-channel multiuser access. [18] considered a distributed opportunistic scheduling problem for ad hoc communications under delay constraints. In [4], authors exploited spectral diversity in OSA for a single user with sensing errors, where the multi-channel overhead is captured by a generic penalty on each channel switching. This becomes insufficient in a multiuser setting as such overhead will obviously depend on the level of congestion in the system that results in different amount of collision and the time it takes to regain access to a channel. In [15], an opportunistic auto rate multichannel MAC protocol MOAR is presented to exploit spectral diversity for a multichannel multi-rate IEEE 802.11-enabled wireless ad hoc network. However, this scheme does not allow parallel use of multiple channels by different users due to its reservation mechanism. Other works that study multichannel access by a single user include [14, 17, 19–22].

Toward making such studies more practical, we note a common and severe limitation of these dynamic schemes in that they almost always require some form of a priori knowledge of the channel statistics. For instance, a typical assumption is that the channel conditions evolve as an IID process and that its distribution for each channel is known to the transmitter/user, see, e.g., [1, 2, 5]. While in some limited setting, such information may be acquired with high accuracy and low latency, this assumption does not generally hold. Furthermore, the channel statistics may be time-varying, in which case such an assumption can only be justified if there exists a separate channel sampling process which keeps the assumed channel statistics information updated.

To relax such an assumption, it is therefore natural to cast the dynamic channel sensing and transmission scheduling problem in a learning context, where the user is not required to possess a priori channel statistics but will try to learn as actions are taken and observations are made. Within this context, the type of *online* learning or *regret* learning, also often referred to as the Multi-Armed Bandit (MAB) [23–25] framework, is particularly attractive, as it allows a user to optimize its performance throughout its learning process. For this reason, this learning framework has also been extensively studied within the context of multichannel dynamic spectrum access, see, e.g., [26] for single-user and [27, 28] for multiuser settings. However, in most of this literature, the purpose of the learning algorithm is for a transmitter to find the best channel in terms of its average condition and then use this channel for transmission most of the time. It follows that the performance of such learning

algorithms is measured by *weak regret*, the difference between a learning algorithm and the best single-action policy which in this context is to always use the channel with the best average condition. Accordingly, the key ingredient in these algorithms is to form accurate estimates on the average condition for each channel.

We therefore see a clear disconnect between what an optimal channel access policy can achieve with known channel statistics (e.g., by employing a stopping rule-based algorithm) that actively exploits temporal, spatial, and spectral diversity and what a typical existing learning algorithm aims for, i.e., essentially the static use of a single channel, which unfortunately completely eliminates the utilization of diversity gain. Note that some multiuser learning algorithms attempt to separate users into different channels, so to exploit to some degree the multiuser diversity gain, see, e.g., [29]. Further in practice, when such an algorithm is deployed for users to shoot for the single best channel, a load balancing issue will arise.

Our goal is to bridge this gap and seek to design learning algorithms that, instead of trying to track the best average-condition channel, attempt to track a known optimal or suboptimal channel access and transmission scheduling algorithm, thereby yielding performance measured by a form of *strong regret*. Our presentation and analysis strongly suggest that such learning algorithms may be constructed in a much broader context, i.e., they can be made to track any prescribed policy and not just those cited earlier or even limited to the dynamic spectrum access context. However, to make our discussion concrete, we shall present our results in the context of specific channel sensing and access algorithms.

Specifically, we present the general framework of such a learning algorithm, followed by the detailed instances designed to track the stopping rule policies given in [1] and [2], respectively. The choice of these two algorithms is not an arbitrary one. Our intention is to use two representatives to capture a fairly wide array of similar algorithms of this kind. The stopping rule algorithm in [1] is a relatively simple one, designed for multiple users competing for access to a single channel; it exploits temporal and spatial (multiuser) diversity, the idea being for a user to defer transmission if it perceives poor channel quality thereby giving the opportunity to another user with better condition. The stopping rule algorithm in [2], on the other hand, is much more complex in construction; it is designed for a single user with access to multiple channels by exploiting spectral and temporal diversity, with the idea being to find the channel with the best instantaneous condition. Both algorithms assume that channel qualities evolve in an IID fashion with known probability distributions, though different channels may have different statistics [2]; both are provably optimal (or near-optimal) under mild technical conditions. For other stopping rule-based policies, see also [3–5]. We show that in both cases our algorithms achieve a sublinear cumulative strong regret (against their respective reference algorithms from [1] and [2]), thus achieving zero-regret averaged over time (Table 1).

The rest of the chapter is organized as follows. Problem formulation is presented in section "Preliminaries" and the two reference optimal offline algorithms in section "Offline Solutions Revisited". We present the setting of our online learning algorithms in section "Goal of Online Learning" and their details in section "Design

Table 1 Our contribution. Weak regret is often used as the performance measure when targeting a single best option on average over time. On the other hand, strong regret is defined as the performance loss w.r.t. selecting the best option at any time step. So far results on strong regret have largely focused on the case when channel statistics are known (decision-maker's perspective)

Measure \ channel stat.	Available	Not available
Weak regret	Trivial	[25–28]: best average option; easier to achieve
Strong regret	[1–5]: harness temporal/spatial diversity at any time; harder to achieve	Our work: minimize strong regret w/o channel information

of Online Algorithms." We brief over their performance analysis in section "Regret Analysis". Numerical results are given in section "Simulation", and possible extensions to this work are discussed in section "Discussion". Section "Conclusion" concludes the chapter.

Preliminaries

In this section, we present two system models and their corresponding transmission scheduling problems. These two models are generally regarded as the most fundamental ones that are analytically tractable, yet powerful, in characterizing key properties of these decision-making settings. Also this lays the foundation for us to introduce the two offline optimal stopping rule policies from [1] and [2], respectively, in section "Offline Solutions Revisited"; these are the policies our learning algorithm presented in section "Design of Online Algorithms" aims to track.

Model I: Multiuser, Single-Channel

Under the first model (studied in [1]), there is a finite number of users/transmitters, indexed by the set $\mathscr{M} = \{1, 2, \ldots, M\}$, $M \geq 1$, and a single channel. The system works in discrete time slots indexed by $n = 1, 2, \cdots$. Denote the channel quality by $X(n)$, $n = 1, 2, \cdots$. This quantity measures how good a channel is; for example, $X(n)$ could model the Signal-Noise-Ratio (SNR) for the channel at time n. At time n, if no one is transmitting on the channel, a user $i \in \mathscr{M}$ attempts to access with probability $0 \leq p_i \leq 1$ by sending a carrier sensing packet. A carrier sensing period takes a constant amount of time denoted by ζ (slots). The contention resolution is done by random access, i.e., an access attempt is successful with probability $p_s = \sum_{i \in \mathscr{M}} p_i \cdot \prod_{j \neq i}(1 - p_i)$, when there is only one user attempting access. Denote the random contention time between two successful accesses by η; it follows that $E[\eta] = \zeta / p_s$ (slots). We assume the process $\{X(n_k)\}_{k=1,2,\ldots,}$ forms an IID process, where n_k is the time the k-th contention succeeds. That is, we assume the

samples collected at successful accesses are generated in an IID fashion (as assumed and argued in [1]). Upon a collision, the current slot will be abandoned, and users recompete in the next time slot. On the other hand, users keep silent if there is an active transmission on the channel. For simplicity, it is assumed that $X(n)$ stays unchanged during each transmission, which may be justified if transmission times are kept on a smaller time scale than channel coherence times [30]. Once a user gains access right (and sees the channel quality $X(n)$), it has two options:

- Access the channel right away for K time slots (*stop*)
- Give up the access opportunity and release the channel for all users to recompete (*continue*)

This can be more formally stated as an optimal stopping rule (OSR) problem: users decide at which time to stop the decision process and use the channel. There are a number of variations of this problem with slightly different model, see, e.g., [4]. The idea is when the channel quality is poor, a user would give up the transmission opportunity so that it is more likely that a user with better perceived channel quality will get to use it. Denote the stopping time by τ, then the objective is to design a stopping rule for all users so as to maximize the rate of return, which is the effective data rate for each successful access ([1])

$$J_I^* = \max_{\tau \in \Pi} J_I^\tau = \max_{\tau \in \Pi} E\left[\frac{X(\sum_{k=1}^{\tau} \eta_k) \cdot K}{K_\tau}\right] \underbrace{\longrightarrow}_{\text{Renewal theory}} \max_{\tau \in \Pi} \frac{E[X(\sum_{k=1}^{\tau} \eta_k) \cdot K]}{E[K_\tau]}, \tag{1}$$

where Π is the strategy space and η_k is the k-th contention time and $K_\tau = \sum_{k=1}^{\tau} \eta_k + K$ is the total amount of time spent for each successful transmission.

Model II: Single-User, Multichannel

Under the second model (studied in [2]), there is a finite number of channels, denoted and indexed by $\mathcal{O} = \{1, 2, \ldots, N\}$, each of which yields a non-negative reward when selected for transmission (e.g., throughput, delay, etc.). For any subset $S \subseteq \mathcal{O}$ we will use $\mathcal{O} - S$ to denote the set $\{j : j \in \mathcal{O} \ \& \ j \notin S\}$. There is one decision-maker (user/transmitter) within the system. The system again works in discrete time slots $n = 1, 2, \ldots, \tau \leq N$; these however are much smaller time units than those under Model I because they are used only for channel sensing and not transmission. The user sequentially chooses a set of channels to probe for their condition, stops at a stopping time τ using certain stopping rule, and selects a channel for transmission (over a period of time larger than a slot). The decision process thus consists of determining in which sequence to sense the channels, when to stop, and which channel to use for transmission when stopping.

For consistency we reuse the terminology *meta stage* to describe the above decision process between $n = 1$ and τ; this will be referred to as one *meta stage*. Each time a new meta stage starts, the clock is reset to $n = 1$. The meta stages are indexed by $t = 1, 2, \ldots, T$. There is a period of transmission between two successive meta stages. It is assumed that the channel condition remains constant within a single meta stage and forms an IID process over successive meta stages. This is modeled by a reward X_i (to generate $\{X_i(t)\}_t$) for the i-th channel given by a pdf $f_{X_i}(\cdot)$ and cdf $F_{X_i}(\cdot)$, respectively. Channels are independent of each other, i.e., a specific channel i's realization $X_i(t;\omega)$ does not reveal any information for channels in $\mathcal{O} - \{i\}$.

The transmitter is able to sense one channel (to observe X_i) at each decision step n with a finite and constant sensing cost $c_i \geq 0$ for each channel i. The system works in the following way at each n of meta stage t: The transmitter makes a decision between the following choices:

- Continues sensing. If this is the case, then furthermore decides which channel to probe next (*sense*).
- Stops sensing and proceeds to transmit (*access*). Under this case, there are two more options to choose from:
  - Access the channel with the best observed instantaneous condition (*access with recall*)
  - Access the best channel (with highest expected reward) from the unprobed set without sensing (*access with guess*)

For the offline problem, due to the IID assumption on the channel condition, the decision strategy at each meta stage t is the same. We thus suppress the time index t; the transmitter's objective is to choose the strategy that maximizes the collected reward minus the sum of probing costs:

$$J_{II}^* = \max_{\pi \in \Pi} J_{II}^{\pi} = \max_{\pi \in \Pi} E\left[X_{\pi(\tau)} - \sum_{n=1}^{\tau-1} c_{\pi(n)} \right], \tag{2}$$

where π denotes a probing strategy and τ the stopping time. From [2], it can be shown that for time slots $n = 1, 2, \ldots, \tau$ at any meta stage t, a sufficient information state is given by the pair $(x(n), S_n)$ where S_n is the unprobed channel set and $x(n)$ is the highest observed reward among the set of probed channels $\mathcal{O} - S_n$. Let $V(x, S)$ denote the value function, the maximum expected remaining reward given the system state is (x, S); the problem/decision process at the n-th decision step is equivalent to the following dynamic programming (DP) formulation

$$\begin{aligned} &V(x(n), S_n) \\ &= \max \left\{ \max_{j \in S_n} \{-c_j + E[V(\max\{x(n), X_j\}, S_n - j)]\}, x(n), \max_{j \in S_n} E[X_j] \right\}, \end{aligned}$$

where the three terms on the RHS correspond to the decision options sense, access with recall, and access with guess, respectively.

Offline Solutions Revisited

To be self-contained as well as to provide certain intuition for the design of the online algorithms, below we present the optimal offline solutions to the scheduling problems in Model I and Model II, respectively.

Algorithm Description: Model I

The solution for the scheduling problem in Model I is surprisingly clean and elegant and can be easily described as follows. Within each meta stage l, the optimal stopping rule is given by a threshold policy [1]:

$$\tau^* = \min\{n \geq 1 : X(n) \geq x^*\}\,, \tag{3}$$

where x^* is given by the solution for u in the following equation:

$$E[X(n) - u]^+ = \frac{u \cdot \zeta}{p_s \cdot K}\,. \tag{4}$$

Intuitively the LHS captures the potential room for gain, compared with the "reserve price" μ (if gave up the chance for access). While RHS captures the loss in the rate of return, if user is up to "continue" the decision-making procedure. The stopping time occurs exactly when the above two terms equal to each other.

The above equation is guaranteed to have a unique solution. This can be intuitively explained by observing that the LHS is decreasing in u, while the RHS is increasing w.r.t. it; thus the two sides intersect exactly once, which corresponds to the solution. Then the corresponding algorithm is straightforward – at each n when a user needs to make a decision:

- If $X(n) \geq x^*$, a user will transmit.
- Otherwise he will release the channel.

Intuitively this says that when the channel quality is sufficiently good (as compared to x^* which separates the decision regions for stop and continue), a user should transmit. This algorithm will be referred to as (Offline_MU) (MultiUser) in our subsequent discussion.

Such a stopping rule-based solution framework can be extended to slightly more complicated settings, such as when there are delay constraints for the access procedures.

Algorithm Description: Model II

The solution for Model II is much more involved; this is primarily due to it allowing *access with guess* as an option, which is very different from classical stopping time problems. In this sense this model presents a generalization. Particularly the optimal policy is shown to have three major steps in [2]: parameter calculation, sorting, and decision-making, as detailed below.

STEP 1: Parameter calculation for channels

Compute the following two parameters $\forall j \in \mathscr{O}$:

$$a_j = \min\{u : u \geq E[X_j], c_j \geq E[\max(X_j - u, 0)]\},$$
$$b_j = \max\{u : u \leq E[X_j], c_j \geq E[\max(u - X_j, 0)]\}.$$

STEP 1 is based on a threshold property for the optimal policy proved in [2]. The first term on the RHS is the maximum reward by continuing sensing. The second term corresponds to stop and access best sensed option while the last term corresponds to the action selecting the best option (highest expected reward) from the unsensed set w/o sensing to access. It could be easily established that $a_j \geq E[X_j] \geq b_j$ and $a_j = b_j$ if and only if we have $a_j = b_j = E[X_j], \forall j$. Intuitively speaking, a, b separates the decision region as follows. A state larger than a_j means further probing is not profitable, whereas a state below b_j suggests gain from continued sensing (Fig. 1).

First we prove the following proposition for a_j, b_j [31].

Proposition 1. $a_j, b_j > 0, \forall j \in \mathscr{O}$.

For STEP 2, we refer to each of its sub-steps **m** as STEP 2.**m** (we will reuse this numbering style in later discussions). The sorting process is straightforward: we start with the full set $\mathscr{O}$, and at each step, we first calculate $\mathscr{R}$, the set of channels

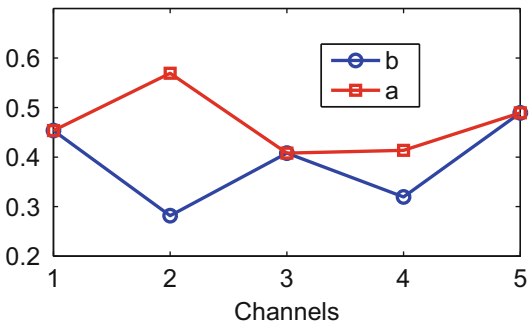

Fig. 1 Illustration of a, b

STEP 2: Channel sorting

1: Initialize $k = 1,\ S = \mathscr{O}$.

2: First compute $\mathscr{R} := \left\{ j \in S, a_j = \max_{i \in S} a_i \right\}$, and then j^*:

$$j^* = \text{argmax}_{j \in \mathscr{R}} \left\{ I_{b_j = a_j} \cdot E[X_j] + I_{a_j > b_j} \cdot \left[E[X_j | X_j \geq a_j] - \frac{c_j}{P(X_j \geq a_j)} \right] \right\}.$$

3: Let $o_k = j^*$ (randomly select one if multiple j^* exists) and set $k := k + 1$. $S = S - \{j^*\}$.

4: If $|S| \geq 1$, repeat **2**; o.w. return the sorted set $\{o_1, \ldots, o_N\}$.

5: Relabel the sorted set as $\{1, 2, \ldots, N\}$.

with the highest a_j. Then within $\mathscr{R}$, we further order the channels based on the one-step reward of probing channel j when $x(n) = a_j$ with j being the only remaining channel. The ordering repeats until all channels are in order.

The above two steps serve as processing steps toward the optimal decision-making. However as noted in [2], it is not easy to calculate the optimal solution in the last decision-making step which involves solving dynamic programming equations with exponentially growing (in N) state space. Instead of seeking the optimal solution, [2] gives out a suboptimal solution which has been shown (analytically and simulation-wise) to be performing well. The idea is, instead of iterating value functions over all remaining unprobed channels, we only consider the 1st & 2nd channels on the remaining options set S_n (ordered).

Given the current information state is $(x(n), S_n)$ at decision epoch n and denoting by d_s the solution to the following equation (solution is guaranteed to exist [2]):

$$V(0, S_n) = -c_1 + E[V(\max\{d_s, X_1\}, S_n - \{1\})],$$

where in above equation 1 denotes the first channel in the remaining channel set S_n (ordered). The decision-making process in STEP 3 can be intuitively explained as follows. First if the current observed maximum reward is larger than the remaining maximum a_j, we stop and access with recall. Otherwise if the current maximum reward $x(n)$ is below a_j but higher than d_s, we proceed to probe the 1st channel in S_n. When $x(n)$ is less than d_s, we further need to differentiate the decisions based on three conditions. Define

$$g_i(x) = -c_i + E[V(\max(X_i, x), -i + 3)],\ i = 1, 2,$$

then $g_1(x)$ is the expected reward of probing channel 1 facing information state $(x, \{1, 2\})$, while $g_2(x)$ is the reward for probing channel 2. $f_1(x)$ is the expected reward of probing 1 facing information state $(x, \{1, 2\})$, while $f_2(x)$ is the one for probing channel 2.

STEP 3: Decision-making step

1: If $x(n) \geq \max_{i \in S_n} a_i$, stop and access the best sensed channel.
2: Otherwise if $x(n) > d_s$, probe the first channel in S_n.
3: If $x(n) \leq d_s$ consider the following sub-cases
(1) : If $b_1 \geq a_2$, then access/guess 1st channel (in S_n, w/o sensing).
(2) : If $b_2 \geq b_1$ or $g_1(0) \geq \max\{E[X_1], g_2(0)\}$, probe 1 in S_n.
(3) : There exists a unique b_0, where $b_1 > b_0 > b_2$ and $g_1(b_0) = \max\{E[X_1], g_2(0)\}$:
– If $x(n) \geq b_0$: probe 1st channel.
– $x(n) < b_0$: guess channel 1 if $E[X_1] \geq g_2(0)$; probe channel 2 o.w.

We denote the algorithm consisting of (**STEP 1, STEP 2, STEP 3**) as (Offline_MC) (MultiChannel) and it serves as the offline benchmark solution for the multichannel scheduling problem.

Goal of Online Learning

Model I: Multiuser, Single-Channel

As can be readily seen from Eq. (4) and the whole procedures documented in (Offline_MC), in order to compute the optimal threshold access strategy x^*, users need to be fully aware of the distribution of channels' transmission qualities, i.e., the distribution of $X(n)$. In practice, such knowledge can only be collected gradually along with users' accesses.

In this model, we regard the decision process between two consecutive successful transmissions (note that no successful transmission occurs if a user who wins access forgoes the transmission opportunity) as one *meta stage*. Suppose there are all together H meta stages (thus H successful transmissions). We define the following *strong regret* performance measure,

$$R_I(H) = \sup_{\boldsymbol{\tau} \in \Pi^H} E^{\boldsymbol{\tau}}\left[\sum_{l=1}^{H} \frac{X(\sum_{k=1}^{\tau_l} \eta_k) \cdot K}{K_{\tau_l}}\right] - E^{\boldsymbol{\alpha}}\left[\sum_{l=1}^{H} \frac{X(\sum_{k=1}^{\alpha_l} \eta_k) \cdot K}{K_{\alpha_l}} | \mathscr{F}_{l-1}, \ldots, \mathscr{F}_0\right].$$

In the above formulation, since channel conditions are IID over time, for each meta stage we restart the clock, i.e., we always set the first time slot for each meta stage as $n = 1$. α_l is the stopping time for the l-th meta stage and $X(\sum_{k=1}^{\alpha_l} \eta_k)$ is the corresponding reward. Here we denote by the $\mathscr{F}_l := \cup_{j \in \mathscr{M}} \mathscr{F}_l^j$ the set of observations of channel qualities at meta stage l (with $\mathscr{F}_l^j$ for each user j).

Model II: Single-User, Multichannel

For this model, our goal is to design an online algorithm $\alpha_t, t = 1, 2, \ldots, T$ based on past observed history $\mathscr{F}_{t-1}, \ldots, \mathscr{F}_1$, so as to minimize the expected reward loss from the one-stage decision-making process. Or in other words, to minimize the following strong regret measure,

$$R_{II}(T) = \sup_{\boldsymbol{\pi} \in \Pi^T} E^{\boldsymbol{\pi}}\left[\sum_{t=1}^{T}(X_{\pi_t(\tau)}(t) - \sum_{n=1}^{\tau-1} c_{\pi_t(n)})\right] - E^{\boldsymbol{\alpha}}\left[\sum_{t=1}^{T}(X_{\alpha_t(\tau)}(t) - \sum_{n=1}^{\tau-1} c_{\alpha_t(n)})|\mathscr{F}_{t-1}, \ldots, \mathscr{F}_0\right], \tag{5}$$

where π_t is the optimal decision at meta stage t when the information on $\{X_i\}_{i\in\mathscr{O}}$ is known and τ the stopping time; $\pi_t(n), n = 1, 2, \ldots, \tau$ are the channels selected at decision step n of each meta stage t. α_t is the decision actually made at t by the user based on past observations when channel statistics is unknown.

For both problems, if an algorithm can achieve regret $\frac{R_I(H)}{H}$ (respectively, $\frac{R_{II}(T)}{T}$) $\to 0$ then it is called sublinear in total regret and zero-regret in time average.

Weak Regret

As mentioned earlier in the introduction, when the statistics for decision-making processes are missing, there is a large body of literature on online decision-making. Among all the solutions, Multi-Armed Bandit stands out as one of the most widely adopted solution, due to both its simple, elegant solution structure, as well as its very minor restriction on prior knowledge of models' statistics. However the distinct feature that sets our goal different from the existing one lies in that such policies try to minimize the notion of weak regret, a more commonly used objective as mentioned earlier. This is in contrast to *strong regret* that we are aiming to study.

Weak regret generally refers to the difference between an algorithm and the best single-action policy that always uses the option with the best average. For instance, under Model II, the weak regret is given by

$$R^{\text{weak}}(T) = T \cdot \max_i E[X_i] - E[\sum_{t=1}^{T} X_{\alpha_t}]\,. \tag{6}$$

This can be similarity defined for Model I, where $\max_i E[X_i]$ corresponds to always letting the "best user" (with the highest average access rate) use the channel.

The above weak regret minimization problem can be readily solved within the context of Multi-Armed Bandit, Existing online algorithms developed under this

category of studies can often help achieve a sublinearly growing $R^{\text{weak}}(T)$, that is, $R^{\text{weak}}(T) = o(T)$. For example, the celebrated UCB1 [25] algorithm:

Upper Confidence Bound 1 (UCB1) Auer et al. [25]

1: Initialization: for $t \leq N$, play arm/choice t, $t = t + 1$.
2: While $t > N$:

- For each choice k, calculate its sample mean:

$$\bar{X}_k(t) = \frac{X_k(1) + X_k(2) + \ldots + X_k(n_k(t))}{n_k(t)}$$

- Its index:

$$I_{k,t,n_k(t)} = X_k(t) + \sqrt{\frac{L \log t}{n_k(t)}}, \quad \forall k$$

- Play the arm with the highest index; $t = t + 1$

The algorithm executes the notion of exploration and exploitation implicitly. To be more specific, the sample mean term controls how often the learner exploits by favoring the arms that turned to be good empirically. The confidence terms regulate how often a user should *explore* by sampling less confident options.

The regret of running UCB1 is bounded at the order of $\log T$. Specifically, suppose $E[X_1] > E[X_2] > \ldots > E[X_N]$. Denote by $\Delta_k := E[X_1] - E[X_k]$

Theorem 1 ([25]). *$R^{\text{weak}}(T)$ when running UCB1 is bounded as follows:*

$$R^{\text{weak}}(T) \leq \sum_{k>1} \lceil \frac{8 \log T}{\Delta_i} \rceil + \text{const.} \tag{7}$$

Design of Online Algorithms

We detail our online learning algorithm in this section. To generalize the discussion we shall refer to the users in Model I and the channels in Model II as *units*. Then for a unifying framework of the online learning process, there are two main phases, *exploration* and *exploitation*, described as follows.

- Exploration: sample the units with sampling times less than $D_1(t) = L \cdot t^z \cdot \log t$ up to meta stage t, with $L > 0$, $0 < z < 1$ being constant parameters. Here L is a sufficiently large (we shall specify its bounds later alongside the analysis) *exploration* parameter. When the unit represents a channel, the sampling process

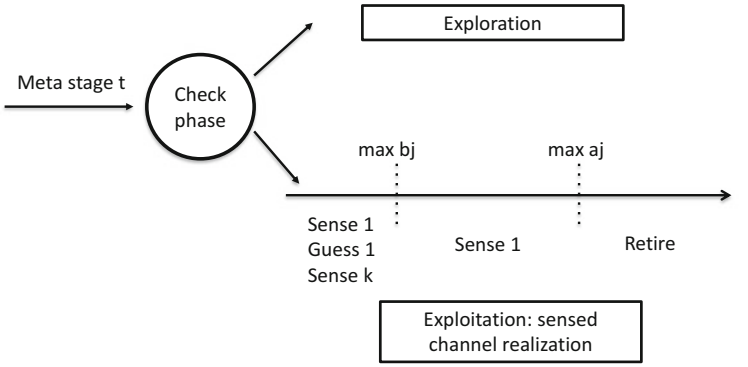

Fig. 2 Illustration of our online algorithm for Model II

is to probe the channel quality; when such a unit represents a user, the process corresponds to letting the user gain access to the channel to gather samples.

- Exploitation: execute the optimal scheduling policy using collected statistics as detailed in the offline solution, but with built-in tolerance for estimation errors as detailed below. The sensing results (possibly multiple) from exploitation phases will also be collected and utilized for training purpose.

The above steps are rather standard within the regret learning literature: when a unit has not been explored/sensed sufficiently (e.g., a user has not accessed a channel for a sufficient number of times in Model I or a channel has not been sampled sufficiently in Model II), the algorithm enters the exploration phase. Otherwise the algorithm mimics the procedures of calculating the optimal strategies as detailed in the offline solutions but with empirically estimated channel statistics. One notable difference here is that since the offline dynamic policies involve channel sensing as part of the decision process, effectively additional samples are collected during exploitation phases and used toward estimation. The general framework of this online approach is summarized as follows. We also illustrate above procedure with Model II in Fig. 2.

Online Solution: A unifying framework

1: *Initialization*: Initialize $L, z, t = 1$ and sample each unit at least once. Update the collection of sample as $\mathscr{F}_0$ and the number of samples for each unit j as $n_j(t)$.
2: *Exploration*: At stage t, if $\mathscr{E}(t) := \{j : n_j(t) < D_1(t)\} \neq \emptyset$, sense the set $\mathscr{E}(t)$ of units.
3: *Exploitation*: If $\mathscr{E}(t) = \emptyset$, calculate the optimal strategy according to steps in the corresponding offline algorithm (with relaxation) based on collected statistics $\{\mathscr{F}_{\hat{t}}\}_{\hat{t}=1}^{t-1}$.
4: *Update*: $t := t + 1$; update sample set and for sampled unit j update $n_j(t) := n_j(t) + 1$.

The exploitation phase is intended for the algorithm to compute and execute the optimal offline strategy using statistics collected during the exploration phase.

However, due to the estimation error, the executed version has to be error tolerant, e.g., by relaxing the conditions for the steps involving strict equalities. We show how this relaxation is done for the problem in Model II below.

(Online_MU) and (Online_MC)

We now detail the online counterparts for (Offline_MU) and (Offline_MC) by filling the details in above general framework. As a notational convention, we will denote by $\tilde{y}$ the estimated version of y, $t_j(k)$ the meta stage when the k-th sample is collected for channel j and $E[\tilde{X}]$ the sample mean of X.

Online_MU: Algorithm details

1: *Initialization*: Initialize $L, z, l = 1$ and let each user access the channel once. Denote the collected sample for user j at stage l as $\mathscr{F}_l^j$. Update $n_j(0) = 1$ and $\mathscr{F}_0^j$.
2: *Exploration*: At stage l, let

$$\mathscr{E}(l) := \{j : n_j(l) < D_1(l)\}.$$

At any decision epoch, if $\mathscr{E}(l) \neq \emptyset$ and let user $j \in \mathscr{E}(l)$ transmit right away. If multiple such j exist, a user is selected randomly from $\mathscr{E}(l)$.
3: *Exploitation*: Otherwise if $\mathscr{E}(l) = \emptyset$, calculate the optimal threshold $\tilde{x}^*$ according to Eq. (4) using collected statistics $\{\mathscr{F}_{\hat{l}}^j\}_{\hat{l}=0}^{l-1}$ for each user j and following the scheduling strategy detailed in (Offline_MU).
4: *Update*: $l := l + 1$; for user j who accessed the channel update $n_j(l) := n_j(l) + 1$ and its sample set $\{\mathscr{F}_{\hat{l}}^j\}_{\hat{l}=0}^{l}$.

In (Online_MC), besides the clear separation between exploration and exploitation phases, several relaxations are invoked and the relaxation term $\frac{1}{t^{z/2}}$ could be viewed as the tolerance/confidence region. This tolerance region decreases in time t and approaches 0 asymptotically as the estimation errors decrease as well. There is an inherent trade-off between exploration and the tolerance region. With more exploration steps (a larger z), a finer degree of tolerance region could be achieved. We shall further discuss the roles of z in the analysis.

Regret Analysis

In this section, we analyze performance of the online algorithm. We present the main results for both (Online_MU) and (Online_MC). Since (Online_MC) is a much more complex algorithm and its analysis can be easily adapted for (Online_MU), as well as for brevity, we will only provide details for (Online_MC).

Before formalizing the regret analysis for (Online_MC), we outline the key steps. The regret consists of two parts: that incurred during exploration phases and that during exploitation phases. For exploration regret, we will try to bound the

number of exploration steps that are needed. For the exploitation phase, the regret is determined by how accurate decisions are made using estimated values. Specifically, *Online.STEP 1* does not have a decision-making step as it is simply a calculation, though we will show later in the proof that the calculation of $\{a_j, b_j\}_{j\in\mathscr{O}}$ does play an important role in the sorting and decision-making process. In *Online.STEP 2*, if the sorting is done incorrectly, then this could lead to errors in *Online.STEP 3*, as all decision-making and sensing orders are based upon the ordering of the channels. *Online.STEP 3* has the following error: (1) error in computing a_j, b_js, (2) error in calculating d_s, and (3) error in calculating a set of value functions for sub-step 3.3.

Assumptions

We state a few mild technical assumptions. We will assume nontrivial channels, i.e., $E[X_j] > 0, \forall j \in \mathscr{O}$, so that they all have positive average rates. We will also assume all channel realizations are bounded, i.e., finite support over all channel condition, $0 \leq \sup_{j\in\mathscr{O},\omega} X_j(t;\omega) < \infty$, $\forall t$, with ω being an arbitrary channel realization. This is not a restrictive assumption since in reality the transmission rate is almost always nontrivial and bounded. Moreover denote

$$\Delta^* = \max_{t,i\neq j,\omega_i,\,\omega_j} |X_j(t;\omega_j) - X_i(t;\omega_i)| + \sum_{i\in\mathscr{O}} c_i \ .$$

Δ^* can be viewed as an upper bound for a one step loss when a suboptimal decision is made and $\Delta^* < +\infty$ (note c_is are finite). Finally, we assume the cdf of each channel i's condition satisfies the Lipschitz condition, i.e., there exists $\mathscr{L}$(note different from L), $\alpha > 0$ such that

$$|F_{X_i}(x+\delta) - F_{X_i}(x)| \leq \mathscr{L}\cdot|\delta|^\alpha, \forall i, x, \delta \ . \tag{8}$$

The Lipschitz condition has been observed to hold for various distributions, for example, the exponential distribution and uniform distribution [32].

Main Results for (Online_MC)

Full details can be found in [31]. We first separate the regret for different phases. We have the following simple upper bound on the regret $R_{II}(T)$,

$$R_{II}(T) = R_e(T) + R_s(T) \leq R_e(T) + \Big(R_2(T) + R_3(T)\Big) \ .$$

The first term $R_e(T)$ is the regret from exploration phases. $R_s(T)$ is the regret from exploitation which could be further upper bounded by the two terms from *Online.STEP 2&3* of (Online_MC), respectively: $R_2(T)$ comes from the sorting

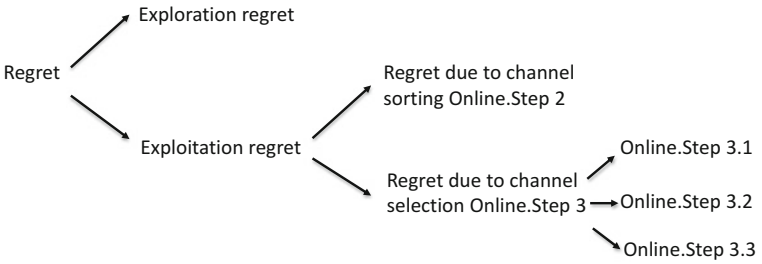

Fig. 3 Illustration of our regret analysis for (Online_MC)

procedure and $R_3(T)$ comes from the last step of decision-making. Notice for *Online.STEP 1* there is no direct regret incurred from parameter calculation: the errors in the calculation are reflected in *Online.STEP 2&3* later. The idea of upper bounding the regret by a union bound will be repeatedly utilized in the following analysis. For example, we can show that the regret in each step above can again be upper bounded by the sum of regrets of each of its sub-steps. This is illustrated in Fig. 3. Therefore we will not restate the details of the bounding for the rest of the proof. Denote the sum $s_p(T) := \sum_{t=1}^{T} \frac{1}{t^p}$. We have our main result for the regret analysis summarized as follows.

Theorem 2. *There exists a constant L s.t. the regret for (Online_MC) is bounded by*

$$R_{II}(T) \leq \Delta^* \left\{ NLT^z \log T + C_1 \cdot s_{\alpha \cdot z/2}(T) + C_2 \cdot s_2(T) \right\},$$

time uniformly, where $C_1, C_2 > 0$ are constants.

Here L is larger than a certain positive constant which we detail later. It is easy to notice since $T^z \log T$ and $s_{\alpha \cdot z/2}$ are both sublinear terms ($s_{\alpha \cdot z/2}$ is on the order of $1 - \frac{\alpha \cdot z}{2}$, while $s_2(\cdot)$ is bounded by a constant since $s_p(T) < \infty, \forall\, p > 1, T.$), $R_{II}(T)$ is also sublinear and asymptotically we achieve zero-regret on average ($\lim_{T \to \infty} R_{II}(T)/T = 0$). The first term $T^z \log T$ is due to the exploration while the term $s_{\alpha \cdot z/2}$ comes from exploitation. Clearly we see with a larger z (more exploration invoked), we will have a larger regret term from exploration phases; however the regret for exploitation will decrease. The balanced setting is achieved at $z = 1 - \frac{\alpha \cdot z}{2} \Rightarrow z = \frac{2}{2+\alpha}$.

Interesting to note when $\alpha \to \infty$, $z \to 0$, that is, similar to the weak regret results of MAB literature, our strong regret reduces from a sublinear order to the logarithmic one. What $\alpha \to \infty$ implies is that the Lipschitz condition becomes

$$|F_{X_i}(x + \delta) - F_{X_i}(x)| \leq \mathscr{L} \cdot |\delta|^{\alpha} = 0,$$

i.e., $F_{X_i}(x+\delta) - F_{X_i}(x) = 0$ when δ is small enough. This further implies when the channel quality state X_i is discrete, we are able to achieve a $O(\log T)$ strong regret, compared to a $O(T^z \log T)$ one.

Bounding the Exploration Regret

We start with bounding the exploration regret $R_e(T)$.

Lemma 1. *The exploration regret $R_e(T)$ is bounded as*

$$R_e(T) \leq D_1(T) \cdot N\Delta^*. \tag{9}$$

Proof. Note that since the exploration phase requires $D_1(T)$ samples for each channel up to time T, we know there are at most $N \cdot D_1(T)$ exploration phases being triggered. For each exploration phase, the regret is bounded by Δ^*, completing the proof. □

Bounding the Exploitation Regret

We next consider regret incurred during exploitation phases, that associated with the sorting (*Online.STEP 2*) and that associated with decision-making (*Online.STEP 3*), respectively. Main steps and sketches of the proofs are given below, while the details can be found in [31].

To bound the regret associated with the sorting step, we have the following result.

Lemma 2. *Regret $R_2(T)$ is bounded as follows, $R_2(T) \leq \Delta^* \cdot 2 \cdot N \sum_{t=1}^{T} \frac{2}{t^2}$.*

Proof. First of all, we could easily show the calculation of $E[X_j], a_j, b_j$ will fall into certain confidence region when the number of exploration steps are large enough (L). Moreover the estimation errors of a_j, b_j are proportional to the one for $E[X_j]$. Intuitively this is due to the calculation of a_j, b_j which relates to the calculation of $E[X_j]$ in a piece-wise linear way.

Lemma 3. *With sufficiently large $L(\geq \frac{1}{\varepsilon^2})$, $\forall j$ we have,*

$$P(|E[\tilde{X}_j] - E[X_j]| > \varepsilon) \leq \frac{2}{t^2}\ , \ \textit{and}$$

$$P(|\tilde{a}_j - a_j| > c_{1,j} \cdot \varepsilon) \leq \frac{2}{t^2},\ P(|\tilde{b}_j - b_j| > c_{2,j} \cdot \varepsilon) \leq \frac{2}{t^2}\ ,$$

where $\varepsilon, c_{1,j}, c_{2,j}$ are positive constants.

Accurate estimations of the parameters lead us to a small probability event of miscomputing $\mathscr{R}$:

Lemma 4. *At time t with sufficiently large L, and any iteration steps of the sorting procedure of Online.STEP 2, we have* $P(\mathscr{R} \neq \tilde{\mathscr{R}}) \leq N \cdot \frac{2}{t^2}$.

The above lemma helps us prove the following results for sorting S:

Lemma 5. *At t with sufficiently large L, the error for sorting set S is bounded as,*

$$P(\tilde{S} \neq S) \leq N \cdot \frac{2}{t^2} .$$

Putting up all terms and multiple by Δ^*, we have results claimed in Lemma 2. □

To bound the regret associated with decision-making (STEP 3), we have the following result.

Lemma 6. *Regret $R_3(T)$ is bounded as follows,*

$$R_3(T) \leq \Delta^* \cdot \left(C_1 \cdot s_{\alpha \cdot z/2}(T) + C_2^* \cdot s_2(T) \right),$$

where C_1, C_2^* are positive constants.

Proof. We sketch the key steps toward getting the claim.

Online.STEP 3.1

At first step of deciding whether $x(n) \geq a_1$ of *Online.STEP 3*, there will be no error when $x \leq \min\{\tilde{a}_1, a_1\}$ or $x \geq \max\{\tilde{a}_1, a_1\}$. Consider x falling in the middle. Make ε being small enough, $\varepsilon = \frac{1}{t^{z/2}}$. As we already proved $P(|\tilde{a}_1 - a_1| > c_{1,1} \cdot \varepsilon) < \frac{2}{t^2}$, and also due to the relaxation of $\mathscr{R}$, the difference between $\tilde{a}_1$ and the true a_1 is bounded away by at most $c_{1,1} \cdot \varepsilon + \varepsilon$. For $|\tilde{a}_1 - a_1| \leq (c_{1,1} + 1) \cdot \varepsilon$, the probability that x falls within the middle is bounded as

$$\begin{aligned} & P(\exists i \text{ s.t. } X_i(t) \in [\min\{\tilde{a}_1, a_1\}, \max\{\tilde{a}_1, a_1\}]) \\ & \leq \sum_i P(X_i(t) \in [\min\{\tilde{a}_1, a_1\}, \max\{\tilde{a}_1, a_1\}]) \\ & \leq N \cdot |F_{X_i}(\tilde{a}_1) - F_{X_i}(a_1)| \leq \frac{N \mathscr{L} \cdot (c_{1,1} + 1)^\alpha}{t^{\alpha \cdot z/2}} , \end{aligned}$$

by Lipschitz condition. Add up for all t we have a sublinear term.

Online.STEP 3.2

We first prove the following results:

Lemma 7. *With sufficiently large L, $\forall$ information state (x, S), we have at time t $\forall \varepsilon > 0$* $P(|\tilde{V}(x, \tilde{S}) - V(x, S)| > |S| \cdot \varepsilon) \leq \frac{2}{t^2}$.

This lemma bounds the difference in estimating the value function with enough samples. The proof is done by induction over the size S and relies heavily on the dynamic equations for $V(\cdot,\cdot)$. Based on above results, we prove that the estimation of d_s can be bounded by a confidence region, which we detail as follows:

Lemma 8. *With sufficiently large L and channel set S*

$$P(|\tilde{d}_s - d_s| > \frac{2|S|+3}{C_{d_s}} \cdot \varepsilon) \leq \frac{4}{t^2} ,$$

at time step t, $\forall \varepsilon > 0$, *where* $C_{d_s} = P(X_1 \leq d_s)$.
The proof is primarily done via analyzing the estimation errors from both sides of the equation

$$V(0, S_n) = -c_1 + E[V(\max\{d_s, X_1\}, S_n - \{1\})] ,$$

which decides d_s. For bounding the value functions, we repeatedly use Lemma 7. Taking $L \geq 4$ and $\varepsilon = \frac{1}{t^{z/2}}$ will lead to our bounds.

Remark 1. The above result invokes a constant $C_{d_s} = P(X_1 \leq d_s)$. If $P(X_1 \leq d_s) = 0$, i.e., $X_1(\omega) > d_s, \forall \omega$ our bound is not well defined. In fact under this case, what really matters is the overlapping between $[0, \tilde{d}_s]$ and $[\underline{X}_j, \overline{X}_j]$ (support of X_j). So long as the overlapping is bounded small enough, the decision error is again bounded.

Online.STEP 3.3

When $x(n) < d_s$, the optimal decision comes from one of three cases. For the first two cases, we have the following lemmas characterizing the regrets: for sub-steps *Online.STEP 3.3.1 and 3.3.2*, there are possibly three decisions to make and we have their error bounded as follows

Lemma 9. *With sufficiently large L, we have the following concentration results: (1). if* $b_1 \geq a_2$, $P(\tilde{b}_1 < \tilde{a}_2 - \frac{1}{t^{z/2}}) \leq \frac{2}{t^2}$. *(2). If* $b_2 \geq b_1$, $P(\tilde{b}_2 < \tilde{b}_1 - \frac{1}{t^{z/2}}) \leq \frac{2}{t^2}$. *(3). If* $g_1(0) \geq \max\{E[X_1], g_2(0)\}$, $P(\tilde{g}_1(0) < \max\{E[\tilde{X}_1], \tilde{g}_2(0)\} - \frac{2}{t^{z/2}}) \leq \frac{2}{t^2}$.

For error in b_1 in *Online.STEP 3.3.2*, the analysis is the same as for a_1 as in *Online.STEP 3.1* since we already established its estimation error bounds.

For the last case in *Online.STEP 3.3.3*, first notice if $E[X_1] = g_2(0)$, there is no error associated with the last step since guessing (access w/o sensing) the first channel and probing the second essentially return the same expected reward. Therefore we show the error analysis when $E[X_1] \neq g_2(0)$. We then bound the error of estimating b_0 (this is similar with proving the bound for d_s and we omit the details for proof): with C_{b_0} being certain constant, $P(|\tilde{b}_0 - b_0| > \frac{2\varepsilon}{C_{b_0}}) \leq \frac{2}{t^2}$. Moreover we have the following results: At time t

$$P(\mathbf{sign}(E[\tilde{X}_1] - \tilde{g}_2(0)) \neq \mathbf{sign}(E[X_1] - g_2(0))) \leq \frac{2}{t^2}.$$

These cover all parameters needed for the decision-making queries.

Putting up all terms we have results claimed in Lemma 6. □
Combining $R_e(T), R_2(T), and R_3(T)$ gives us the main result.

Discussion on Parameter *L*

In most of our proved results, we assumed L to be significantly large. We summarize the actual conditions on L below:

$$\textbf{(Condition 1):}\ L \geq \max\{4, 1/(\frac{\min_{a_{k_1} \neq a_{k_2}} |a_{k_1} - a_{k_2}|}{2 \max_j c_{1,j}})^2\}\ ,$$

$$\textbf{(Condition 2):}\ L \geq 1/\varepsilon_o^2\ ,$$

where $\{c_{1,j}\}_{j \in \mathscr{O}}$ is a set of positive constants and ε_o is a solution of ε for

$$C \cdot (\varepsilon + \mathscr{L} \cdot (c_{1,j} + 1)^\alpha \varepsilon^\alpha) \leq \frac{\min\{\varepsilon_3, \varepsilon_4\}}{2}\ ,$$

where C is a positive constant and

$$\varepsilon_3 = \min_{j \neq k} |E[X_j] - E[X_k]|,\ \varepsilon_4 = \min_{j \neq k} |\frac{E[X_j] - c_j}{P(X \geq a_j)} - \frac{E[X_k] - c_k}{P(X \geq a_k)}|$$

and for simplicity we assume $\varepsilon_3, \varepsilon_4 > 0$, that is, channels have different values in above two parameters.

From **(Condition 1)** we know when $\{a_i\}$s are closer to each other, L should be chosen to be larger. Also from **(Condition 2)** we know when channels' expected reward $E[X_j]$ and $\frac{E[X_j] - c_j}{P(X \geq a_j)}$ (can be viewed as potential term when sensed) are closer to each other, again L should be chosen to be larger. The intuition here is that in such cases a larger L can help achieve higher accuracy for the estimations to differentiate two channels that are similar.

The selection of L depends on a set of εs, which further depends on statistical information of X_js (though weaker as we only need to know a lower bound on them), but this is assumed unknown. Following a common technique [33], this assumption can be relaxed but with potentially larger regret. In particular, one can show that at any time t with L being a positive constant, the estimation error ε_t for any terms (e.g., a, b or $E[X_j]$) satisfies the following: $P(\varepsilon_t > \frac{1}{t^\theta}) \leq \frac{1}{t^\nu}$, with $\theta, \nu > 1$. Therefore with the error region ε_t being small enough, there would be no error associated with differentiating the channels of the algorithm. Thus there exists a constant T_0 such that $\varepsilon_t < \min \varepsilon, \forall t > T_0$. Consider the case $\varepsilon_t \leq \frac{1}{t^\theta}$. Since when the error happens under this case, two estimated terms (the suboptimal and optimal

one) are separated by at most $2\varepsilon_t$. The probability of the corresponding term falls into this region is bounded as $|F_{X_i}(x+\varepsilon_t) - F_{X_i}(x-\varepsilon_t)| \leq \mathscr{L} \cdot 2^{\alpha} \cdot \frac{1}{t^{\alpha \cdot \theta}}$ by the Lipschitz condition. Therefore we have the extra error bounded by $\sum_{t=1}^{T_0} \mathscr{L} \cdot 2^{\alpha} \cdot \frac{1}{t^{\alpha \cdot \theta}}$, which is a constant growing sublinearly up to time T_0.

Main Results for (Online_MU)

For (Online_MU) we can similarly prove the following result

Theorem 3. *There exists a constant L s.t. the regret for (Online_MU) is bounded by*

$$R_I(H) \leq \Delta^* \left\{ MLH^z \log H + \hat{C}_1 \cdot s_{\alpha \cdot z/2}(H) + \hat{C}_2 \cdot s_2(H) \right\},$$

time uniformly, where $\hat{C}_1, \hat{C}_2 > 0$ are constants.
Notice that though $R_I(H)$ looks similar to $R_{II}(T)$, they may have very different parameters for each term, i.e., $\hat{C}_1, \hat{C}_2$ may be quite different from C_1, C_2, as well as different constraints for L due to the different statistical structure of the two problems. Again the first term is coming from exploration phases, the second term is due to inaccurate calculations of x^*, and last term bounds the event that $\tilde{x}^*$ is too different from x^*.

Simulation

In this section we show a few examples of the performance of the proposed online algorithm via simulation. We measure the average *regret* rate $R_I(l)/l(R_{II}(t)/t)$ and compare our performance to the optimal offline algorithm, a static best single-channel policy, as well as that of a weak-regret algorithm.

For simplicity of demonstration, we assume channel qualities follow *exponential distribution* but with different parameters (We have similar observations for other distributions. The details are omitted for brevity.). The corresponding distributions' parameters are generated uniformly and randomly between $[0, 0.5]$. Users' attempt rates p_is are uniformly generated in the interval $[0, 0.5]$ (in Model I). The costs for sensing the channels (in Model II) are also randomly generated according to uniform distribution between $[0, 0.1]$. In the following simulation for Model I, we have $M = 5$ users, while for Model II, we have $N = 5$ channels. Simulation cycle is set to be $H = T = 4,000$. In the set of results for performance comparison with offline solutions, we set the exploration parameters as $L = 10, z = 1/5$. Later on we show the performance comparison w.r.t. different selection of L and z.

Comparison with Offline Solution

We first take the difference between the oracle ((Offline_MU)) and (Online_MU) at each step t and divide it by t (i.e., we plot $R_I(t)/t$). This regret rate is plotted in Fig. 4, and clearly we see a sublinear convergence rate. We repeat the experiment for (Online_MC), and the regret convergence is shown in Fig. 5, which validate our analytical results. To make the comparison more convincing, we compare the accumulated reward between (Online_MC), (Offline_MC), and the best single-channel (action) policy, which always selects the best channel in terms of its average rate (channel statistics is assumed to be known a priori) in Fig. 6. In particular, we see the accumulated rewards of (Online_MC) (red square) are close to the performance of the oracle (blue circle) who has all channel statistical information and follows the optimal decision process as we previously depicted in (Offline_MC). We observe that the dynamic policies clearly outperform the best single-channel policy.

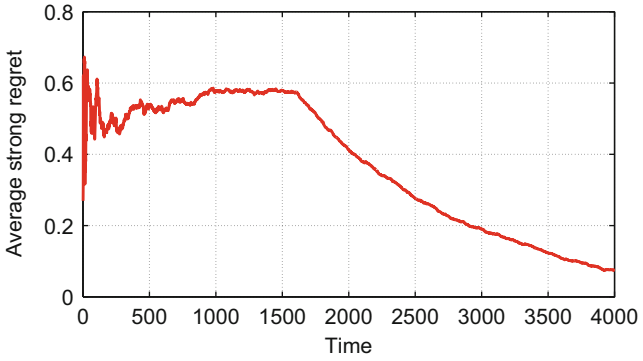

Fig. 4 Convergence of average regret: (Online_MU)

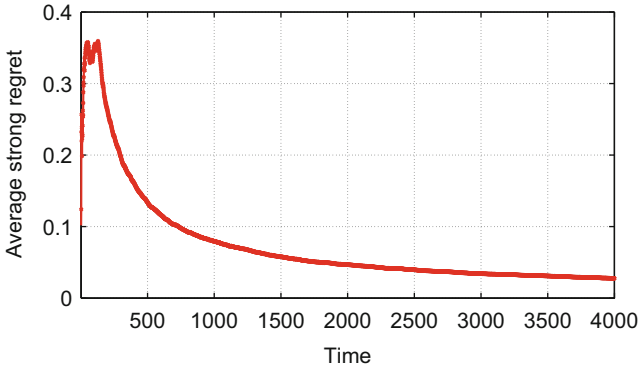

Fig. 5 Convergence of average regret: (Online_MC)

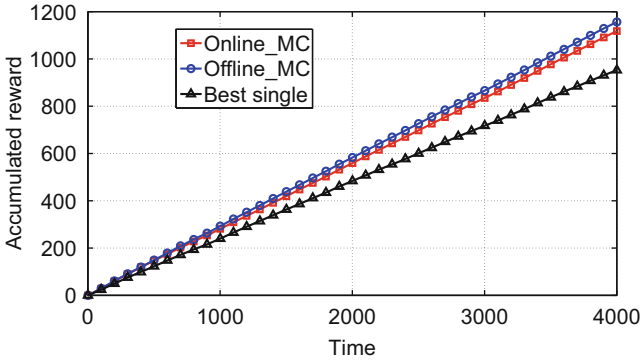

Fig. 6 (Online_MC) v.s. (Offline_MC) v.s. Best single

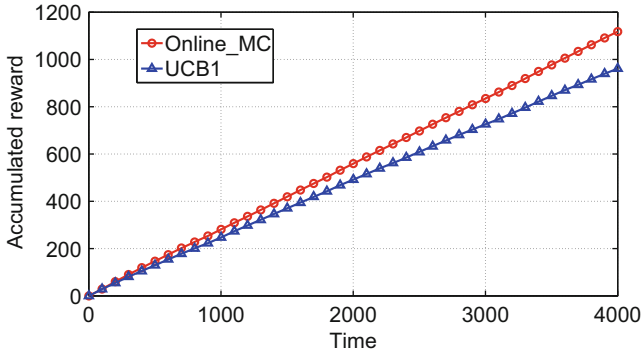

Fig. 7 (Online_MC) v.s. UCB1

Comparison with UCB1

We next demonstrate the advantages of our algorithm (Online_MC) by comparing it with UCB1, a classical online learning algorithm that achieves logarithmic weak regret for IID bandits [25]. The performance gain is quite clearly seen in Fig. 7. It is worth pointing out that there also exists extensive literature in reinforcement learning (RL), which is generally targeted at a broader set of learning problems in Markov Decision Processes (MDPs) [34]. Bandit problems constitute a special class of MDPs, for which the regret learning framework (using index policies) is generally viewed as more effective both in terms of convergence and computational complexity.

Effects of Parameter Selection

We next take a closer look at the effects of parameter selection, primarily with L and z. We demonstrate with (Online_MC). We repeat the above sets of experiment

Table 2 Average collected reward under different L (Avg. = 0.27 with random channel selection)

$L(z = 1/5)$	5	10	20	30	40
Average reward	0.3391	**0.3522**	0.3353	0.3183	0.3166

Table 3 Average collected reward under different z (Avg. = 0.27 with random channel selection)

$z(L = 10)$	1/6	1/5	1/4	1/3	1/2
Average reward	0.3411	0.3522	**0.3557**	0.3017	0.1949

w/ different L, z combinations and tabulate the average reward per time step. From Table 2, we observe the selection of L is not monotonic: a smaller L incurs less exploration steps, but more errors will be invoked at exploitation steps due to its less confidence in calculating the optimal strategy. On the other hand, a large L inevitably imposes higher burden on sampling and thus becomes less and less favorable with its increase. Similar observations hold for z since z controls the length of exploration phases jointly with L but with different scale. However it is indeed interesting to observe that when z grows large enough (e.g., $z = \frac{1}{2}$), the performance drops drastically: this is due to the fact in such a case more than enough efforts have been spent in sensing steps (Table 3).

Discussion

We discuss several possible extensions of existing results, concerning the relaxation of assumptions on channel properties. Note that our basic idea and method of tracking an offline optimal (or near-optimal) algorithm by estimating key parameters remain unchanged regardless of the assumptions on the channel model. However, two factors will be at play with more challenging models: (1) Different channel models may lead to only suboptimal offline solutions or approximations which may or may not have a performance guarantee; tracking such algorithms would lead to a "weakened" strong regret measure. (2) If the computation of an offline algorithm is complex either in terms of computation or in the amount of information it requires, then this could also affect the effectiveness of our learning procedure.

For instance, throughout the paper, we have assumed that the channel quality over time evolves as an IID process, though with unknown distributions. An immediate extension is to consider Markovian channel evolution, which leads to a restless bandit problem which does not have a known structured solution in general. In some special cases, optimal solutions can be derived and may take on a simple form, see, e.g., the greedy policy under the two-state channel model considered in [35, 36], or the LP relaxation approximation developed in [37]. Tracking these algorithms

requires the estimation of a set of two-state transition probability matrices and conceptually can be done and likely will not change the order of the regret bound; however, none of these algorithms are generally optimal so in some cases we could be tracking a target with poor performance. On the other hand, computing the optimal offline algorithm even with full-channel statistics is computationally intensive (restless bandit problems are known to be PSPACE complete [38], so tracking it becomes nontrivial).

Similarly, throughout this study, we have not considered interferences from multiple users; the channel quality perceived by a user is assumed to be entirely the result of factors like fading and shadowing but not interference. It would be an interesting extension to consider multiuser interference and investigate the effectiveness of our learning approach in tracking a certain offline multiuser algorithm. A natural way to design the learning procedure in this case is to combine stochastic bandit learning (for channel availability) with adversarial learning (for user interference). Possible candidates of target offline algorithms include, e.g., [39], which studied a capacity maximization problem in distributed wireless network under SINR interference model and showed a constant factor approximation bound compared to the global optimum is achievable, by using an adversarial model to capture the effects of interference, and [40] that proposed scheduling algorithms for a similar problem but under Rayleigh-fading interference models and showed a logarithmic order approximation.

Last but not least, the assumption that the channel statistics stay unchanged is needed only in deriving the bound under the current technique. It is however not needed for the learning algorithm to work as the exploration aspect of the algorithm is in principle designed to detect and adapt to changes in the underlying statistics. The challenge is in how to quantify the learning/adaptation performance when such changes are present. Some recent results may prove very helpful, see, e.g., [41] on a sharp bound (sublinear) for certain cases when such non-stationary statistical properties satisfy bounded variation [41].

Conclusion

In this chapter, we discuss several decision-making issues in channel switching and transmission scheduling in cognitive networks. We present a couple of classical results for single-user, multichannel model and multiuser, single channel model. We point out to a common limitation in all existing solutions in such decision-making solutions that often channel statistics are unknown a priori. Without knowing such information, we propose an online learning algorithm which helps collect samples of channel realization while making optimal scheduling decisions. We show our proposed learning algorithm (for both a multiuser and multichannel model) achieves sublinear regret uniform in time, which further gives us a zero-regret algorithm on average.

References

1. Zheng D, Ge W, Zhang J (2009) Distributed opportunistic scheduling for ad hoc networks with random access: an optimal stopping approach. IEEE Trans Inf Theory 55(1):205–222
2. Chang NB, Liu M (2009) Optimal channel probing and transmission scheduling for opportunistic spectrum access. IEEE/ACM Trans Netw 17(6):1805–1818
3. Kanodia V, Sabharwal A, Knightly E (2004) MOAR: a multi-channel opportunistic auto-rate media access protocol for ad hoc networks. In: International Conference on Broadband Networks, pp 600–610
4. Shu T, Krunz M (2009) Throughput-efficient sequential channel sensing and probing in cognitive radio networks under sensing errors. In: Proceedings of the 15th Annual International Conference on Mobile Computing and Networking (MobiCom'09). ACM, New York, pp 37–48
5. Sabharwal A, Khoshnevis A, Knightly E (2006) Opportunistic spectral usage: bounds and a multi-band CSMA/CA protocol. IEEE/ACM Trans Netw 2006:533545
6. Liu Y, Knightly E (2003) Opportunistic fair scheduling over multiple wireless channels. In: Twenty-Second Annual Joint Conference of the IEEE Computer and Communications Societies (INFOCOM 2003), vol 2. IEEE, pp 1106–1115
7. Andrews M, Kumaran K, Ramanan K, Stolyar A, Whiting P, Vijayakumar R (2001) Providing quality of service over a shared wireless link. IEEE Commun Mag 39(2):150–154
8. Borst S, Whiting P (2001) Dynamic rate control algorithms for HDR throughput optimization. In: Proceedings of the Twentieth Annual Joint Conference of the IEEE Computer and Communications Societies (INFOCOM 2001), vol 2, pp 976–985
9. Tan S-S, Zheng D, Zhang J, Zeidler B (2010) Distributed opportunistic scheduling for ad-hoc communications under delay constraints. In: INFOCOM, 2010 Proceedings IEEE, IEEE
10. Muqattash A, Krunz M (2003) Power controlled dual channel (PCDC) medium access protocol for wireless ad hoc networks. In: Twenty-Second Annual Joint Conference of the IEEE Computer and Communications Societies (INFOCOM 2003), vol 1. IEEE, pp 470–480
11. Yang X, Vaidya NH (2003) Explicit and implicit pipelining for wireless medium access control. In: 2003 IEEE 58th Vehicular Technology Conference (VTC 2003-Fall), vol 3, pp 1427–1431
12. Marsan MA, Neri F (1991) A simulation study of delay in multichannel CSMA/CD protocols. IEEE Trans Commun 39(11):1590–1603
13. Kamerman A, Monteban L (1997) WaveLAN-II: a high-performance wireless LAN for the unlicensed band. Bell Labs Tech J 2(3):118–133
14. Chang NB, Liu M (2009) Optimal channel probing and transmission scheduling for opportunistic spectrum access. IEEE/ACM Trans Netw 17(6):1805–1818
15. Kanodia V, Sabharwal A, Knightly E (2004) MOAR: a multi-channel opportunistic auto-rate media access protocol for ad hoc networks. In: Proceedings of the First International Conference on Broadband Networks (BROADNETS'04). IEEE Computer Society, Washington DC, pp 600–610
16. Zhao Q, Tong L, Swami A, Chen Y (2007) Decentralized cognitive MAC for opportunistic spectrum access in ad hoc networks: a POMDP framework. IEEE J Sel Areas Commun 25(3):589–600
17. Ahmad SHA, Liu M, Javidi T, Zhao Q, Krishnamachari B (2009) Optimality of myopic sensing in multichannel opportunistic access. IEEE Trans Inf Theory 55(9):4040–4050
18. Tan S-S, Zheng D, Zhang J, Zeidler J (2010) Distributed opportunistic scheduling for ad-hoc communications under delay constraints. In: Proceedings of the 29th Conference on Information communications (INFOCOM'10). IEEE Press, Piscataway, pp 2874–2882
19. Zhao Q, Krishnamachari B, Liu K (2008) On myopic sensing for multi-channel opportunistic access: structure, optimality, and performance. IEEE Trans Wirel Commun 7(12):5431–5440
20. Liu K, Zhao Q (2010) Indexability of restless bandit problems and optimality of whittle index for dynamic multichannel access. IEEE Trans Inf Theory 56(11):5547–5567

21. Liang YC, Zeng Y, Peh ECY, Hoang AT (2008) Sensing-throughput tradeoff for cognitive radio networks. IEEE Trans Wirel Commun 7(4):1326–1337
22. Chang NB, Liu M (2008) Optimal competitive algorithms for opportunistic spectrum access. IEEE J Sel Areas Commun 26(7):1183–1192
23. Lai TL, Robbins H (1985) Asymptotically efficient adaptive allocation rules. Adv Appl Math 6:4–22
24. Anantharam V, Varaiya P, Walrand J (1986) Asymptotically efficient allocation rules for the multiarmed bandit problem with multiple plays part I: I.I.D. rewards, part II: Markovian rewards. Technical report UCB/ERL M86/62. EECS Department, University of California, Berkeley
25. Auer P, Cesa-Bianchi N, Fischer P (2002) Finite-time analysis of the multiarmed bandit problem. Mach Learn 47:235–256
26. Tekin C, Liu M (2011) Online learning in opportunistic spectrum access: a restless bandit approach. In: 2011 Proceedings IEEE INFOCOM. IEEE, pp 2462–2470
27. Tekin C, Liu M (2012) Online learning in decentralized multi-user spectrum access with synchronized explorations. In: Military Communications Conference (MILCOM 2012), pp 1–6
28. Liu H, Liu K, Zhao Q (2011) Learning and sharing in a changing world: non-bayesian restless bandit with multiple players. In: Information Theory and Applications Workshop (ITA 2011). IEEE, pp 1–7
29. Tekin C, Liu M (2012) Performance and convergence of multi-user online learning. In: Game theory for networks. Springer, pp 321–336
30. Zheng L, Tse D, Médard M (2007) Channel coherence in the low-SNR regime. IEEE Trans Inf Theory 53(3):976–997
31. Liu Y, Liu M (2015) An online approach to dynamic channel access and transmission scheduling. Preliminary version published at MobiHoc'15. arXiv:1504.01050
32. Heinonen J (2005) Lectures on Lipschitz analysis. University of Jyväskylä, Jyväskylä https://books.google.com/books/about/Lectures_on_Lipschitz_Analysis.html?id=mCIsAAAACAAJ
33. Agrawal R (1995) The continuum-armed bandit problem. SIAM J Control Optim 33(6):1926–1951
34. Barto AG (1998) Reinforcement learning: an introduction. MIT Press, Cambridge
35. Ahmad SHA, Liu M, Javidi T, Zhao Q, Krishnamachari B (2009) Optimality of myopic sensing in multichannel opportunistic access. IEEE Trans Inf Theory 55(9):4040–4050
36. Liu Y, Liu M, Ahmed SHA (2014) Sufficient conditions on the optimality of myopic sensing in opportunistic channel access: a unifying framework. IEEE Trans Inf Theory 60(8):4922–4940
37. Le Ny JL, Dahleh M, Feron E (2006) Multi-agent task assignment in the bandit framework. In: 2006 45th IEEE Conference on Decision and Control. IEEE, pp 5281–5286
38. Bertsimas D, Niño-Mora J (2000) Restless bandits, linear programming relaxations, and a primal-dual index heuristic. Oper Res 48(1):80–90
39. Asgeirsson EI, Mitra P (2011) On a game theoretic approach to capacity maximization in wireless networks. In: 2011 Proceedings IEEE INFOCOM. IEEE, pp 3029–3037
40. Dams J, Hoefer M, Kesselheim T (2014) Scheduling in wireless networks with rayleigh-fading interference. IEEE Trans Mob Comput PP(99):1–1
41. Besbes O, Gur Y, Zeevi A (2014) Optimal exploration-exploitation in a multi-armed-bandit problem with non-stationary rewards. Available at SSRN:2436629

Energy-Efficient Design in Cognitive MIMO Systems

27

Liqun Fu

Contents

Abstract

The energy-efficient design for TDMA (time-division multiple access) MIMO (multiple-input multiple-output) cognitive radio (CR) networks can be treated as the joint optimization over both the time resource and the transmit precoding

L. Fu (✉)
Department of Communication Engineering, Xiamen University, Xiamen, China
e-mail: liqun@xmu.edu.cn

W. Zhang (ed.), *Handbook of Cognitive Radio*,
https://doi.org/10.1007/978-981-10-1394-2_26

matrices to minimize the overall energy consumption. Compared with the traditional MIMO networks, the challenge here is that the secondary users (SUs) may not be able to obtain the channel state information (CSI) to the primary receivers. The corresponding mathematical formulation turns out to be non-convex and thus of high complexity to solve in general. This chapter covers both the transmission choices for each SU: single-data-stream transmission and multiple-data-stream transmission. Fortunately, by applying a proper optimization decomposition, it can be shown that the optimal solution can be found in polynomial time in both cases. In practical wireless system, the time is usually allocated in the unit of slot. Moreover, by exploring the special structure of this particular problem, it can be shown that the optimal time slots allocation can be obtained in polynomial time with a simple greedy algorithm. Simulation results show that the energy-optimal transmission scheme adapts to the traffic load of the secondary system to create a win-win situation where the SUs are able to decrease the energy consumption and the PUs experience less interference from the secondary system. The effect is particularly pronounced when the secondary system is underutilized.

Keywords
Cognitive radio networks · MIMO · Energy efficiency · Scheduling · Beamforming

Introduction

Background

Cognitive radio (CR), which allows secondary users (SUs) to opportunistically access the spectrum that is underutilized by the primary licensed users, is a promising approach to improve the spectrum efficiency [11, 17]. With the aid of multiple-input multiple-output (MIMO) techniques [9], the cognitive spectrum may efficiently work in the underlay mode, where the SUs transmit concurrently with the primary users (PUs) as long as the interferences from the SUs to the PUs are below a tolerable threshold [17]. Future wireless systems are evolving to support the exponentially increasing traffic demands, which, in most cases, are achieved at the expense of a higher energy consumption and a considerable impact on the environment. Energy-efficient transmission is of critical importance to reduce the carbon footprint and to prolong the battery lifetime of wireless devices [6–8, 12, 15, 16, 20, 27]. Performing energy-efficient transmissions among the SUs could also alleviate the interference to the primary system.

The key idea that enables the underlay mode in a CR network is that with multiple antennae, the SU can carefully design its precoding matrix so as to suppress the interference at the primary receivers. Such a technique normally requires channel state information (CSI), which can be assumed to be available in the traditional MIMO network setup. However, in a CR network, the PUs are usually not aware of the existence of the SUs. This has two effects: (1) the primary receivers may not

feed back the CSI to the SUs; (2) the primary receiver will not perform interference cancellation at the receiver side. In other words, the SUs are only able to do pre-interference suppression and may have to do this with only access to statistical CSI. This is the main challenge when designing energy-efficient transmission strategies for MIMO CR networks.

Related Works

Studies of energy-efficient transmissions of MIMO networks fall into two main classes: traditional MIMO networks [6, 8, 15, 16, 24, 27] and MIMO CR networks [12, 20]. For example, in the former class, [6] investigated the energy consumption of a single MIMO/SISO link by considering both the transmission energy and the circuit energy consumption. In [24], the authors considered the transmit power minimization through downlink transmit beamforming. In [8], the authors considered power minimization through downlink transmit beamforming and solved it with semidefinite programming (SDP) approach. In [15], the authors studied the energy efficiency of a MIMO-based TDMA cellular system. In particular, the authors proposed a cross-layer approach of joint rate selection and mode switching to save the system energy consumption. As discussed above, perfect CSI is typically assumed in traditional MIMO networks.

In the latter class, some recent papers, [12, 20, 34], considered the energy/power minimization problem in MIMO CR networks. When perfect CSI is not available to the secondary system, the deterministic interference constraints at the primary receivers cannot be satisfied and thus are not proper. A robust optimization framework is proposed in [12, 34], which requires the constraints to hold for every possible realization of the channel. Such an approach guarantees the worst-case performance and is thus overly conservative. In practice, many wireless applications can tolerate occasional outages without affecting users' QoS. Therefore, it is sufficient to consider a more realistic interference constraint which is to satisfy the interference constraints with high probability [28]. In [20], the authors considered the multicast precoding where a secondary transmitter communicates with multiple secondary receivers under statistical CSI. The problem was shown to be non-convex [24], and an SDP relaxation was proposed. Since there is only one secondary transmitter, it is sufficient to optimize the SU's precoding matrix only at the physical layer. This chapter focuses on the uplink transmission scenario involving multiple secondary transmitters. In this case, the scheduling and beamforming need to be jointly optimized in order to minimize the total energy consumption of all the SUs.

A closely related problem to energy minimization is rate maximization. Rate maximization in MIMO CR networks has been considered in [29–34]. In [31], Zhang et al. showed that rate maximization for a single secondary link under perfect CSI and no interference from the primary system to the secondary system is a convex optimization problem. Practical algorithms based on the singular-value decomposition of the SU's MIMO channel matrix were proposed. In [29], weighted sum-rate maximization of the multiple access channel in a MIMO CR network was

investigated and a capped multilevel water-filling algorithm was proposed. In [33], the authors considered maximizing the rate of a single secondary link under different levels of CSI availability of the channels from the SUs to the primary receivers. A unified homogeneous QCQP formulation was proposed, and an SDP relaxation was shown to produce the optimal solution in some special cases.

Summary

The joint design of physical and MAC layer techniques can further reduce the overall energy consumption of the secondary network with multiple SUs. With the aid of MIMO techniques, it is possible that multiple SUs send uplink traffic to the secondary base station (BS) simultaneously with spatial multiplexing. However, in a CR network, the interference power at each secondary receiver does not only come from the primary users but also from other SUs. The MIMO interference channel is well known to result in NP-hard problems [22]. Therefore, in order to avoid excessive interference among the SUs, the SUs send their traffic via TDMA. There is no interference among the SUs. However, the SUs share the same spectrum with some PUs, and thus the concurrent transmissions of SUs and PUs will cause interference to each other. Shannon's capacity formula implies that we can reduce the energy consumption for delivering a certain amount of traffic by increasing the transmission time [26]. However, in a TDMA network, the total transmission time is shared by multiple SUs. Increasing transmission time for one SU leads to the reduction of transmission time for others. Therefore, the energy consumptions of SUs trade off against each other. Meanwhile, each SU has a QoS requirement, measured as a target rate, to be satisfied. Therefore, the secondary BS needs to allocate the time resource and configure the beamforming patterns for the SUs in a way that could achieve the desirable balance between the SUs' target rates and the interference at the primary receivers.

The problem formulation involves jointly optimizing the time allocation and precoding for the SUs, with statistical CSI. As will be elaborated in section "Problem Formulations", the problem formulations are non-convex and thus can be expected to be hard to solve in general. This chapter covers a comprehensive investigation on this problem, under two different transmission choices for SUs: single-data-stream transmission and multiple-data-stream transmission. Quite surprisingly, it is possible to develop efficient algorithms that are guaranteed to find the optimal solutions in both cases. To tackle the non-convexity, the decomposition method that subdivides the overall problem into two separate problems is applied so that the problem can be solved efficiently. In particular, the optimal time allocation can be found by solving a convex optimization problem for each case. When each SU only transmits one data stream on all its transmit antennae, the transmit precoding matrix then reduces to a beamforming vector. This choice is more preferable in an interference-limited network to avoid excessive interference to other links [4, 18].Given the optimal time allocation, the optimal beamforming vector for each SU can be obtained efficiently through a simple matrix eigenvalue-eigenvector

computation. When each SU transmits multiple data streams, the SU further utilizes the multiplexing gain of MIMO systems. In this case, the number of data streams is also a system design variable, which is discrete by nature. In this case, given the optimal time allocation, the optimal precoding matrix can be found by "water-filling."

Furthermore, in practical wireless systems, a slot is the smallest unit during time allocation, which implies that there is additional integer constraint on the time variable. The overall problem formulation then becomes a mixed-integer non-convex optimization problem, which is typically even more complicated. By exploring the special structure of the time optimization problem, it can be shown that the optimal integer time allocation can be found in polynomial time with a simple greedy algorithm.

The remainder of this paper is organized as follows. Section "System Model" introduces the system model. Section "Problem Formulations" lays out the problem formulations in both the single-data-stream transmission case and the multiple-data-stream transmission case for each SU. Section "Single-Data-Stream Transmission: Problem Decomposition and Optimal Solution" is devoted to the optimization decomposition and the solution method when each SU transmits only one data stream on all its transmit antennae. Section "Multiple-Data-Stream Transmission: Problem Decomposition and Optimal Solution" covers the solution methods under the multiple-data-stream transmission case for each SU. Section "Simulation Results" is the simulation results. Section "Conclusion" concludes this chapter.

System Model

In a CR network with K SUs and J PUs, the primary links could potentially always be active and thus need to be protected at all times. The primary network is composed of J pairs of transmitters and receivers. The secondary system is a single-cell network, where the SUs send uplink traffic to the same secondary BS via TDMA. The uplink transmissions are synchronized by the secondary BS so that they are allocated different time slots for their transmissions and thus do not cause interference to each other.

Let S_k denote the kth SU. Let M_{S_k} denote the number of transmit antennas of S_k and N_{BS} denote the number of receive antennas at the secondary BS. Let $\mathbf{H}_{BS,S_k} \in \mathbb{C}^{N_{BS} \times M_{S_k}}$ denote the channel matrix from S_k to the secondary BS. There are J links in the primary network. Let P_j denote the jth primary transmitter-receiver pair. Let M_{P_j} and N_{P_j} denote the number of transmit antennas and the number of receive antennas of P_j, respectively. Let $\mathbf{H}_{P_i,P_j}$ denote the $N_{P_i} \times M_{P_j}$ channel matrix from the jth primary transmitter to the ith primary receiver. Since the SUs coexist with the PUs, their signals may interfere with each other. Let $\mathbf{H}_{P_j,S_k} \in \mathbb{C}^{N_{P_j} \times M_{S_k}}$ and $\mathbf{H}_{BS,P_j} \in \mathbb{C}^{N_{BS} \times M_{P_j}}$ denote the channel matrix from S_k to the receiver of P_j and the channel matrix from the transmitter of P_j to the secondary BS, respectively. The channel is assumed to be a frequency flat fading channel so that it is the same for the considered bandwidth. Furthermore,

the channel is assumed to be block fading channel, so that the channel matrices do not change during a TDMA frame, and the channel realizations in different frames are uncorrelated. This assumption is valid if the mobile user does not move very fast. In this case, the coherence time is long enough to cover the whole TDMA frame. In particular, it is assumed that the channel is Rayleigh fading channel in a rich scattering environment, so that the entries of the channel matrices are independently and identically distributed (i.i.d.) complex Gaussian random variables with a zero mean [21]. The variance of the complex Gaussian variables is half of the path loss from the corresponding transmitter to the corresponding receiver. Since the secondary system is centralized, the secondary BS can estimate $\mathbf{H}_{BS,S_k}$ and feed back it to each S_k with a separate control channel. Thus, it is reasonable to assume that $\mathbf{H}_{BS,S_k}$ is known to both S_k and the secondary BS.

Single-Data-Stream Transmission for Each SU

When each SU transmits the same data stream on all its transmit antennae, the transmit and receive beamforming can be defined on vector. Let $\mathbf{u}_{S_k} \in \mathbb{C}^{M_{S_k}\times 1}$ and $\mathbf{v}_{BS_k} \in \mathbb{C}^{N}_{BS} \times 1$ denote the transmit beamforming vector of S_k and the receive beamforming vector of the secondary BS when S_k is active, respectively. Let $\mathbf{u}_{P_j} \in \mathbb{C}^{M_{P_j}\times 1}$ and $\mathbf{v}_{P_j} \in \mathbb{C}^{N_{P_j}\times 1}$ denote the transmit beamforming vector and the receive beamforming vector of the primary link P_j, respectively. Without loss of generality, the receive beamforming vectors are normalized such that $\|\mathbf{v}_{BS_k}\|_2^2 = 1$ and $\|\mathbf{v}_{P_j}\|_2^2 = 1$. Let scalars x_{S_k} and x_{P_j} denote the transmit signals of S_k and P_j, respectively. Without loss of generality, it can be assumed that $\mathbb{E}[|x_{S_k}|^2] = 1$ and $\mathbb{E}[|x_{P_j}|^2] = 1$. The received signal of S_k after receive beamforming at the secondary BS is

$$y_{BS_k} = \mathbf{v}_{BS_k}{}^H \mathbf{H}_{BS,S_k}\mathbf{u}_{S_k}x_{S_k} + \sum_{j=1}^{J} \mathbf{v}_{BS_k}{}^H \mathbf{H}_{BS,P_j}\mathbf{u}_{P_j}x_{P_j} + \mathbf{v}_{BS_k}^H \mathbf{n}_{BS}, \quad k=1,\cdots,K.$$

The vector $\mathbf{n}_{BS} \in \mathbb{C}^{N_{BS}\times 1}$ is a circular complex additive Gaussian noise vector with a noise power of $N_0 w$ at the secondary BS, where $N_0/2$ is the noise power spectral density and w is the bandwidth used in the secondary system. The received signal-to-interference-plus-noise ratio (SINR) of S_k then becomes

$$\begin{aligned}\gamma_{BS_k} &= \frac{\mathbb{E}\left[\left|\mathbf{v}_{BS_k}{}^H \mathbf{H}_{BS,S_k}\mathbf{u}_{S_k}x_{S_k}\right|^2\right]}{\mathbb{E}\left[\sum_{j=1}^{J}\left|\mathbf{v}_{BS_k}{}^H \mathbf{H}_{BS,P_j}\mathbf{u}_{P_j}x_{P_j}\right|^2 + \left|\mathbf{v}_{BS_k}^H \mathbf{n}_{BS}\right|^2\right]} \\ &= \frac{\left|\mathbf{v}_{BS_k}{}^H \mathbf{H}_{BS,S_k}\mathbf{u}_{S_k}\right|^2}{\sum_{j=1}^{J}\left|\mathbf{v}_{BS_k}{}^H \mathbf{H}_{BS,P_j}\mathbf{u}_{P_j}\right|^2 + N_0 w}, \quad k=1,\cdots,K. \end{aligned} \tag{1}$$

According to the Shannon's capacity formula, the achievable transmission rate of S_k is

$$r_{S_k} = w \log\left(1 + \gamma_{BS_k}\right) = w \log\left(1 + \frac{\left|\mathbf{v}_{BS_k}{}^H \mathbf{H}_{BS,S_k} \mathbf{u}_{S_k}\right|^2}{\sum_{j=1}^{J} \left|\mathbf{v}_{BS_k}{}^H \mathbf{H}_{BS,P_j} \mathbf{u}_{P_j}\right|^2 + N_0 w}\right).$$

The transmit power of S_k is $p_{S_k} = \|\mathbf{u}_{S_k}\|_2^2$, and S_k causes an interference to the jth primary receiver at the level of

$$q_{P_j S_k} = \left|\mathbf{v}_{P_j}^H \mathbf{H}_{P_j,S_k} \mathbf{u}_{S_k}\right|^2, \quad k = 1, \cdots, K, \quad j = 1, \cdots, J.$$

Multiple-Data-Stream Transmission for Each SU

To further explore the multiplexing gain of MIMO system, both the primary and secondary users can transmit multiple data streams. Let D_{S_k} and D_{P_j} denote the number of data streams of S_k and P_j, respectively. Let $\mathbf{x}_{S_k} \in \mathbb{C}^{M_{S_k} \times 1}$ and $\mathbf{x}_{P_j} \in \mathbb{C}^{M_{P_j} \times 1}$ denote the actual transmitted vectors of S_k and P_j, respectively. The covariance matrices of $\mathbf{x}_{S_k}$ and $\mathbf{x}_{P_j}$ are denoted by $\mathbf{Q}_{S_k}$ and $\mathbf{Q}_{P_j}$, which are Hermitian positive semidefinite matrices.

The received vector of S_k at the secondary BS is

$$\mathbf{y}_{BS_k} = \mathbf{H}_{BS,S_k} \mathbf{x}_{S_k} + \sum_{j=1}^{J} \mathbf{H}_{BS,P_j} \mathbf{x}_{P_j} + \mathbf{n}_{BS}, \; k = 1, \cdots, K.$$

The secondary BS treats the interference from the primary transmitters as noise, and there is no successive interference cancellation at the secondary BS. The interference-plus-noise covariance matrix at the secondary BS when S_k transmits is then

$$\mathbf{C}_{S_k} = \sum_{j=1}^{J} \mathbf{H}_{BS,P_j} \mathbf{Q}_{P_j} \mathbf{H}_{BS,P_j}^H + N_0 w \mathbf{I}_{N_{BS}},$$

which is an $N_{BS} \times N_{BS}$ Hermitian positive semidefinite matrix.

According to Shannon's capacity formula for a MIMO link [9,25], the achievable transmission rate of S_k is

$$r_{S_k} = w \log\left[\det\left(\mathbf{I} + \mathbf{H}_{BS,S_k} \mathbf{Q}_{S_k} \mathbf{H}_{BS,S_k}^H \mathbf{C}_{S_k}^{-1}\right)\right], k = 1, \cdots, K.$$

Here r_{S_k} is the instantaneous transmission rate (in nats/second) when S_k is active. The total transmit power of S_k on all its transmit antennas is $p_{S_k} = \mathrm{tr}\left(\mathbf{Q}_{S_k}\right)$, and S_k causes a total interference power to the jth primary receiver at the level of

$$q_{P_j,S_k} = \mathrm{tr}\left(\mathbf{H}_{P_j,S_k}\mathbf{Q}_{S_k}\mathbf{H}_{P_j,S_k}^H\right),\ k = 1,\cdots,K, j = 1,\cdots,J.$$

Problem Formulations

The system target is to choose the proper time allocation and the transmit precoding design for each SU to minimize the total energy consumption of all the SUs while protecting the PUs and ensuring a minimum QoS for each SU. Specifically, the interference from each SU to each of the PUs needs to be below a certain threshold, and each SU has a rate requirement R_{S_k} to be satisfied. Here R_{S_k} (with the unit of nats/frame) is the number of nats that S_k needs to transmit in each time frame. Without loss of generality, the TDMA frame length of the secondary system is normalized to be 1. Each S_k is allocated a time fraction t_{S_k} $(0 \le t_{S_k} \le 1)$ to transmit its data. The instantaneous transmit power of S_k is limited by a maximum power of $p_{S_k,\max}$.

Problem Formulation for Single-Data-Stream Transmission

This problem can be mathematically formulated as follows:

$$\min_{t_{S_k},\mathbf{u}_{S_k},\mathbf{v}_{BS_k}} \quad \sum_{k=1}^{K} t_{S_k}\|\mathbf{u}_{S_k}\|_2^2$$

$$\text{s.t.} \quad t_{S_k} w \log\left(1 + \frac{\left|\mathbf{v}_{BS_k}{}^H\mathbf{H}_{BS,S_k}\mathbf{u}_{S_k}\right|^2}{\sum_{j=1}^{J}\left|\mathbf{v}_{BS_k}{}^H\mathbf{H}_{BS,P_j}\mathbf{u}_{P_j}\right|^2 + N_0 w}\right) \ge R_{S_k}, \quad \forall k, \tag{2a}$$

$$\sum_{k=1}^{K} t_{S_k} \le 1, \tag{2b}$$

$$\left|\mathbf{v}_{P_j}^H\mathbf{H}_{P_j,S_k}\mathbf{u}_{S_k}\right|^2 \le \phi_{P_j}, \quad \forall k, \quad \forall j, \tag{2c}$$

$$\|\mathbf{u}_{S_k}\|_2^2 \le p_{S_k,\max}, \quad \forall k, \tag{2d}$$

$$t_{S_k} \ge 0, \quad \forall k.$$

The objective function in (2) is the total energy consumption of all the SUs. Constraint (2a) guarantees each SU's rate requirement. Constraint (2b) states that the total time allocated to all the SUs is no larger than the TDMA frame length. Constraint (2c) ensures that the interference from each secondary transmitter to each primary receiver is no larger than a tolerable threshold ϕ_{P_j}. Constraint (2d) states that the SUs have limited transmission power. The variables in (2) are the time fraction variables t_{S_k}, the transmit beamforming vectors $\mathbf{u}_{S_k}$, and the receive beamforming vectors $\mathbf{v}_{BS_k}$ of the SUs.

Since the secondary system is a centralized TDMA network, it is reasonable to assume that $\mathbf{H}_{BS,S_k}$ is known to both S_k and the secondary BS. As, in a CR network, the secondary system is usually aware of the existence of the primary system, it is also reasonable to assume that the secondary BS can overhear the transmissions on the primary links. At the secondary BS, the overheard signal of P_j is $\mathbf{H}_{BS,P_j}\mathbf{u}_{P_j}$. Therefore, the secondary BS is able to estimate $\mathbf{H}_{BS,P_j}\mathbf{u}_{P_j}$ for all PUs. However, in a CR network, the secondary system is usually transparent to the primary system. The primary system would not deliberately provide the CSI to the secondary system. Therefore, the secondary system may only know the statistics of coefficient vectors $\mathbf{v}_{P_j}^H\mathbf{H}_{P_j,S_k}$ in constraint (2c) (e.g., the type of distribution and $\mathbb{E}[\mathbf{v}_{P_j}^H\mathbf{H}_{P_j,S_k}\mathbf{H}_{P_j,S_k}^H\mathbf{v}_{P_j}]$). However, it does not know the precise realization of $\mathbf{v}_{P_j}^H\mathbf{H}_{P_j,S_k}$.

Notice that in formulation (2), the receive beamforming variables $\mathbf{v}_{BS_k}$ only appear in constraint (2a). These variables can be eliminated by exploring the optimal receive beamforming, which are the minimum-mean-square-error (MMSE) receivers [14]:

$$\mathbf{v}_{BS_k}^* = \theta_{S_k}\mathbf{B}_{S_k}^{-1}\mathbf{H}_{BS,S_k}\mathbf{u}_{S_k}, \quad k = 1, \cdots, K, \tag{3}$$

where $\mathbf{B}_{S_k} = \sum_{j=1}^{J}\mathbf{H}_{BS,P_j}\mathbf{u}_{P_j}\mathbf{u}_{P_j}^H\mathbf{H}_{BS,P_j}^H + N_0 w\mathbf{I}$, and θ_{S_k} is the normalized factor given by $\theta_{S_k} = \frac{1}{\|\mathbf{B}_{S_k}^{-1}\mathbf{H}_{BS,S_k}\mathbf{u}_{S_k}\|_2}$, which ensures $\|\mathbf{v}_{BS_k}^*\|_2^2 = 1$. The maximum received SINR is then given by

$$\gamma_{BS_k} = \mathbf{u}_{S_k}^H\mathbf{A}_{S_k}\mathbf{u}_{S_k}, \quad k = 1, \cdots, K, \tag{4}$$

where $\mathbf{A}_{S_k} = \mathbf{H}_{BS,S_k}^H\mathbf{B}_{S_k}^{-1}\mathbf{H}_{BS,S_k}$, which is an $M_{S_k} \times M_{S_k}$ Hermitian matrix.

Substituting (4) into constraint (2a), formulation (2) can be simplified to

$$\min_{t_{S_k},\mathbf{u}_{S_k}} \quad \sum_{k=1}^{K} t_{S_k}\|\mathbf{u}_{S_k}\|_2^2$$

$$\text{s.t.} \quad t_{S_k} w \log\left(1 + \mathbf{u}_{S_k}^H\mathbf{A}_{S_k}\mathbf{u}_{S_k}\right) \geq R_{S_k}, \quad \forall k, \tag{5a}$$

$$\sum_{k=1}^{K} t_{S_k} \leq 1, \tag{5b}$$

$$\left|\mathbf{v}_{P_j}^H \mathbf{H}_{P_j,S_k} \mathbf{u}_{S_k}\right|^2 \leq \phi_{P_j}, \quad \forall k, \quad \forall j, \tag{5c}$$

$$\|\mathbf{u}_{S_k}\|_2^2 \leq p_{S_k,\max}, \quad \forall k, \tag{5d}$$

$$t_{S_k} \geq 0, \quad \forall k,$$

The receive beamforming vectors $\mathbf{v}_{BS_k}$ are removed, and the variables in formulation (5) are the time fraction variables t_{S_k} and the transmit beamforming vectors $\mathbf{u}_{S_k}$ of the SUs.

Since the secondary system does not know the precise realization of $\mathbf{v}_{P_j}^H \mathbf{H}_{P_j,S_k}$, the left-hand side of constraint (5c) is random for any given $\mathbf{u}_{S_k}$. The requirement of satisfying constraint (5c) would easily lead to suboptimal or infeasible solutions. Interestingly, many wireless applications (such as video streaming, voice over IP) can tolerate occasional outages without affecting users' QoS. Thus, in a more realistic requirement, it is sufficient to satisfy the interference constraints with a high probability. In other words, the CR network allows the interference from the secondary transmitters to the primary receivers to exceed the power threshold ϕ_{P_j} with a small outage probability δ_{P_j}. Constraint (5c) is then replaced by

$$\Pr_{\mathbf{H}_{P_j,S_k},\mathbf{v}_{P_j}} \left\{ \left|\mathbf{v}_{P_j}^H \mathbf{H}_{P_j,S_k} \mathbf{u}_{S_k}\right|^2 \leq \phi_{P_j} \right\} \geq 1 - \delta_{P_j}, \quad \forall k, \forall j, \tag{6}$$

where the probability is taken over both $\mathbf{H}_{P_j,S_k}$ and $\mathbf{v}_{P_j}$.

Under Rayleigh fading channel assumption, the entries of the channel matrix $\mathbf{H}_{P_j,S_k}$ are i.i.d. complex Gaussian random variables with a zero mean and a variance of $\frac{\beta_{P_j,S_k}}{2}$, where β_{P_j,S_k} denotes the path loss from S_k to the jth primary receiver. Furthermore, because $\mathbf{H}_{P_j,S_k}$ and $\mathbf{v}_{P_j}$ are independent of each other, $\left|\mathbf{v}_{P_j}^H \mathbf{H}_{P_j,S_k} \mathbf{u}_{S_k}\right|^2$ follows an exponential distribution with the parameter $\frac{1}{\beta_{P_j,S_k}\|\mathbf{u}_{S_k}\|_2^2}$ [33]. So we have

$$\Pr_{\mathbf{H}_{P_j,S_k},\mathbf{v}_{P_j}} \left\{ \left|\mathbf{v}_{P_j}^H \mathbf{H}_{P_j,S_k} \mathbf{u}_{S_k}\right|^2 \leq \phi_{P_j} \right\} = 1 - \exp\left(-\frac{\phi_{P_j}}{\beta_{P_j,S_k}\|\mathbf{u}_{S_k}\|_2^2} \right).$$

Therefore, the outage probability constraint (6) is equivalent to

$$\|\mathbf{u}_{S_k}\|_2^2 \leq \frac{-\phi_{P_j}}{\beta_{P_j,S_k} \log \delta_{P_j}}, \quad \forall k, \quad \forall j. \tag{7}$$

Furthermore, after converting the outage probability constraint to (7), it can be shown that (7) can be combined with the maximum transmission power

constraint (5d). Let $\rho_{S_k} = \min\left\{\frac{-\phi_{P_1}}{\beta_{P_1,S_k}\log\delta_{P_1}},\cdots,\frac{-\phi_{P_J}}{\beta_{P_J,S_k}\log\delta_{P_J}},p_{S_k,\max}\right\}$. Constraints (7) and (5d) are equivalent to

$$\|\mathbf{u}_{S_k}\|_2^2 \le \rho_{S_k}, \quad \forall k = 1,\cdots,K.$$

Therefore, problem (5) can be recast as follows:

$$\begin{aligned}
\min_{t_{S_k},\mathbf{u}_{S_k}} \quad & \sum_{k=1}^{K} t_{S_k}\|\mathbf{u}_{S_k}\|_2^2 \\
\text{s.t.} \quad & t_{S_k} w \log\left(1+\mathbf{u}_{S_k}^H \mathbf{A}_{S_k}\mathbf{u}_{S_k}\right) \ge R_{S_k}, \forall k, && \text{(8a)}\\
& \sum_{k=1}^{K} t_{S_k} \le 1, && \text{(8b)}\\
& \|\mathbf{u}_{S_k}\|_2^2 \le \rho_{S_k}, \quad \forall k, && \text{(8c)}\\
& t_{S_k} \ge 0, \quad \forall k.
\end{aligned}$$

Problem Formulation for Multiple-Data-Stream Transmission

When each SU transmits multiple data streams, the joint design of time allocation and the transmit precoding matrix to minimize the energy consumption of all the SUs can be mathematically formulated as follows:

$$\begin{aligned}
\min_{t_{S_k},\mathbf{Q}_{S_k}} \quad & \sum_{k=1}^{K} t_{S_k}\,\mathrm{tr}\left(\mathbf{Q}_{S_k}\right) \\
\text{s.t.} \quad & t_{S_k} w \log\left[\det\left(\mathbf{I}+\mathbf{H}_{BS,S_k}\mathbf{Q}_{S_k}\mathbf{H}_{BS,S_k}^H\mathbf{C}_{S_k}^{-1}\right)\right] \ge R_{S_k}, \quad \forall k, && \text{(9a)}\\
& \sum_{k=1}^{K} t_{S_k} \le 1, && \text{(9b)}\\
& \mathrm{tr}\left(\mathbf{H}_{P_j,S_k}\mathbf{Q}_{S_k}\mathbf{H}_{P_j,S_k}^H\right) \le \phi_{P_j}, \quad \forall k, \quad \forall j, && \text{(9c)}\\
& \mathrm{tr}\left(\mathbf{Q}_{S_k}\right) \le p_{S_k,\max}, \quad \forall k, && \text{(9d)}\\
& t_{S_k} \ge 0, \quad \forall k,\\
& \mathbf{Q}_{S_k} \succeq \mathbf{0}, \quad \forall k.
\end{aligned}$$

Problem (9) is non-convex due to both the objective function and Constraint (9a) and is thus in general difficult to solve. It can be shown that the rank of the optimal covariance matrix to Problem (9) is never higher than the corresponding channel, i.e., $\text{rank}(\mathbf{Q}_{S_k}^*) \leq \text{rank}(\mathbf{H}_{BS,S_k}^H \mathbf{C}_{S_k}^{-1} \mathbf{H}_{BS,S_k}) \leq \text{rank}(\mathbf{H}_{BS,S_k})$. Suppose there is one optimal $\mathbf{Q}_{S_k}^*$ with a higher rank than $\text{rank}(\mathbf{H}_{BS,S_k})$. It is easy to obtain a new solution of the transmit covariance matrix by projecting $\mathbf{Q}_{S_k}^*$ to the row space of $\mathbf{H}_{BS,S_k}^H \mathbf{C}_{S_k}^{-1} \mathbf{H}_{BS,S_k}$. The new solution obtained by the projection satisfies Constraints (9a) and (9c). Further, it reduces the LHS of Constraint (9d) and the objective function. This contradicts with that $\mathbf{Q}_{S_k}^*$ with a higher rank than $\text{rank}(\mathbf{H}_{BS,S_k})$ is the optimal solution. Therefore, we do not need to impose rank constraint on $\mathbf{Q}_{S_k}$ in Problem (9).

The secondary system only knows the statistics of $\mathbf{H}_{P_j,S_k}$ (e.g., the type of distribution and $\mathbb{E}[\mathbf{H}_{P_j,S_k} \mathbf{H}_{P_j,S_k}^H]$). It does not know the precise realization of $\mathbf{H}_{P_j,S_k}$. Similarly, under the probabilistic interference constraints, the CR network allows the interference from each secondary transmitter to each primary receiver to exceed the power threshold ϕ_{P_j} with a small outage probability δ_{P_j}. Constraint (9c) is then replaced by

$$\Pr_{\mathbf{H}_{P_j,S_k}} \left\{ \text{tr}\left(\mathbf{H}_{P_j,S_k} \mathbf{Q}_{S_k} \mathbf{H}_{P_j,S_k}^H \right) \leq \phi_{P_j} \right\} \geq 1 - \delta_{P_j}, \ \forall k, \ \forall j, \tag{10}$$

where the probability is taken over $\mathbf{H}_{P_j,S_k}$.

Given the Rayleigh distribution of the channels, $\text{tr}\left(\mathbf{H}_{P_j,S_k} \mathbf{Q}_{S_k} \mathbf{H}_{P_j,S_k}^H \right)$ follows an exponential distribution with the parameter $\frac{1}{\beta_{P_j,S_k} \text{tr}(\mathbf{Q}_{S_k})}$ [33]:

$$\Pr_{\mathbf{H}_{P_j,S_k}} \left\{ \text{tr}\left(\mathbf{H}_{P_j,S_k} \mathbf{Q}_{S_k} \mathbf{H}_{P_j,S_k}^H \right) \leq \phi_{P_j} \right\} = 1 - \exp\left(-\frac{\phi_{P_j}}{\beta_{P_j,S_k} \text{tr}\left(\mathbf{Q}_{S_k}\right)} \right).$$

Thus, the outage probability constraint (10) is equivalent to

$$\text{tr}\left(\mathbf{Q}_{S_k}\right) \leq \frac{-\phi_{P_j}}{\beta_{P_j,S_k} \log \delta_{P_j}}, \quad \forall k, \ \forall j. \tag{11}$$

Furthermore, (11) can be combined with Constraint (9d), which can be expressed by

$$\text{tr}\left(\mathbf{Q}_{S_k}\right) \leq \rho_{S_k}, \quad \forall k.$$

Therefore, the problem formulation can be recast as follows:

$$
\begin{aligned}
\min_{t_{S_k},\mathbf{Q}_{S_k}} \quad & \sum_{k=1}^{K} t_{S_k} \operatorname{tr}\left(\mathbf{Q}_{S_k}\right) \\
\text{s.t.} \quad & t_{S_k} w \log\left[\det\left(\mathbf{I}+\mathbf{H}_{BS,S_k}\mathbf{Q}_{S_k}\mathbf{H}_{BS,S_k}^{H}\mathbf{C}_{S_k}^{-1}\right)\right] \geq R_{S_k}, \quad \forall k, && \text{(12a)} \\
& \sum_{k=1}^{K} t_{S_k} \leq 1, && \text{(12b)} \\
& \operatorname{tr}\left(\mathbf{Q}_{S_k}\right) \leq \rho_{S_k}, \quad \forall k, && \text{(12c)} \\
& t_{S_k} \geq 0, \quad \forall k, \\
& \mathbf{Q}_{S_k} \succeq \mathbf{0}, \quad \forall k.
\end{aligned}
$$

Note that similar to Problem (9), it does not need to add rank constraint on $\mathbf{Q}_{S_k}$ in Problem (12). Furthermore, Problem (12) is also a non-convex optimization problem. It is challenging to solve the non-convex Problems (8) and (12) directly. As can be seen in the subsequent sections, we will tackle this difficulty by finding a closed-form solution for $\mathbf{u}_{S_k}$ and $\mathbf{Q}_{S_k}$, respectively. Therefore, (8) and (12) can be further reduced to convex optimization problems in t_{S_k} only. As a result, the optimal solutions to both Problem (8) and Problem (12) can be found efficiently.

Feasibility

The feasible set in Problem (8) (or (12)) may not always be nonempty. For each S_k, its maximum feasible instantaneous transmission rate $r_{S_k,\max}$, with the unit of nats/second, depends on its maximum transmit power and the interference constraints at the primary receivers. In the single-data-stream transmission case, the maximum link rate for S_k can be computed by solving the following problem:

$$
\begin{aligned}
\max_{\mathbf{u}_{S_k}} \quad & w \log\left(1+\mathbf{u}_{S_k}^{H}\mathbf{A}_{S_k}\mathbf{u}_{S_k}\right) \\
\text{s.t.} \quad & \|\mathbf{u}_{S_k}\|_2^2 \leq \rho_{S_k}.
\end{aligned}
\tag{13}
$$

In the multiple-data-stream transmission case, the maximum link rate for S_k can be obtained by solving

$$
\begin{aligned}
\max_{\mathbf{Q}_{S_k}} \quad & w \log\left[\det\left(\mathbf{I}+\mathbf{H}_{BS,S_k}\mathbf{Q}_{S_k}\mathbf{H}_{BS,S_k}^{H}\mathbf{C}_{S_k}^{-1}\right)\right] \\
\text{s.t.} \quad & \operatorname{tr}\left(\mathbf{Q}_{S_k}\right) \leq \rho_{S_k}, \\
& \mathbf{Q}_{S_k} \succeq \mathbf{0}.
\end{aligned}
\tag{14}
$$

Problem (14) can be solved with standard "water-filling" [9, 25].

The minimum time resource $t_{S_k,\min}$ that each S_k needs to satisfy its rate requirement is

$$t_{S_k,\min} = \frac{R_{S_k}}{r_{S_k,\max}}.$$

Problem (8) (or (12)) is feasible when the traffic load in the secondary system does not exceed its capacity, i.e.,

$$\sum_{k=1}^{K} t_{S_k,\min} \leq 1. \tag{15}$$

In section "Single-Data-Stream Transmission: Problem Decomposition and Optimal Solution", it can be shown that there is a closed-form feasibility condition in the single-data-stream transmission case. In the multiple-data-stream transmission case, first it is required to solve Problem (14) to obtain $r_{S_k,\max}$. Then the feasibility of Problem (12) can be guaranteed if Condition (15) is satisfied.

Single-Data-Stream Transmission: Problem Decomposition and Optimal Solution

It can be shown that there is a closed-form feasibility condition in the single-data-stream transmission case. Furthermore, the optimal time fractions and transmit beamforming vectors can be obtained efficiently through a proper decomposition. Therefore, the time fractions t_{S_k} and the transmit beamforming vectors $\mathbf{u}_{S_k}$ can be separately optimized without affecting the overall optimality.

Given any time fraction allocation $(t_{S_1}, \cdots, t_{S_K})$, Problem (8) reduces to K separate optimization problems among the SUs. For each S_k, the optimization problem is given by

$$\begin{aligned} \min_{\mathbf{u}_{S_k}} \quad & \|\mathbf{u}_{S_k}\|_2^2 \\ \text{s.t.} \quad & w \log\left(1 + \mathbf{u}_{S_k}^H \mathbf{A}_{S_k} \mathbf{u}_{S_k}\right) \geq \frac{R_{S_k}}{t_{S_k}}, && \text{(16a)} \\ & \|\mathbf{u}_{S_k}\|_2^2 \leq \rho_{S_k}. && \text{(16b)} \end{aligned}$$

It can be shown that the optimization problem (16) has a closed-form solution by a simple eigenvalue-eigenvector computation. Let $\pi_{S_k,1}, \pi_{S_k,2}, \cdots, \pi_{S_k,M_{S_k}}$ denote all the eigenvalues of matrix $\mathbf{A}_{S_k}$. Let $\mathbf{z}_{S_k,i}$ $(\|\mathbf{z}_{S_k,i}\|_2^2 = 1)$ denote the normalized eigenvector of $\mathbf{A}_{S_k}$ associated with eigenvalue $\pi_{S_k,i}, (1 \leq i \leq M_{S_k})$. Let $\pi_{S_k,\max}$ denote the largest eigenvalue of $\mathbf{A}_{S_k}$ and $\mathbf{z}_{S_k,\max}$ denote the normalized eigenvector

of $\mathbf{A}_{S_k}$ associated with $\pi_{S_k,\max}$. The closed-form solution to (16) is given in the following lemma.

Lemma 1. *The necessary and sufficient condition for optimization problem* (16) *to be feasible is*

$$t_{S_k} \geq \frac{R_{S_k}}{w \log\left(\rho_{S_k} \pi_{S_k,\max} + 1\right)}, \quad k = 1, \cdots, K. \tag{17}$$

When condition (17) *is satisfied, the optimal solution to* (16) *is*

$$\mathbf{u}_{S_k}^* = \sqrt{\frac{\exp\left(\frac{R_{S_k}}{wt_{S_k}}\right) - 1}{\pi_{S_k,\max}}} \mathbf{z}_{S_k,\max}, \quad k = 1, \cdots, K. \tag{18}$$

Proof. Matrix $\mathbf{A}_{S_k}$ is a Hermitian matrix. Therefore $\mathbf{A}_{S_k}$ can be unitarily diagonalized as $\mathbf{A}_{S_k} = \mathbf{P}_{S_k} \mathbf{\Pi}_{S_k} \mathbf{P}_{S_k}^H$, where $\mathbf{P}_{S_k}$ is a unitary matrix and $\mathbf{\Pi}_{S_k}$ is a diagonal matrix containing all the eigenvalues of $\mathbf{A}_{S_k}$. So we have

$$\mathbf{u}_{S_k}^H \mathbf{A}_{S_k} \mathbf{u}_{S_k} = \mathbf{u}_{S_k}^H \mathbf{P}_{S_k} \mathbf{\Pi}_{S_k} \mathbf{P}_{S_k}^H \mathbf{u}_{S_k} = \left(\mathbf{P}_{S_k}^H \mathbf{u}_{S_k}\right)^H \mathbf{\Pi}_{S_k} \left(\mathbf{P}_{S_k}^H \mathbf{u}_{S_k}\right) \leq \pi_{S_k,\max} \|\mathbf{P}_{S_k}^H \mathbf{u}_{S_k}\|_2^2.$$

Since matrix $\mathbf{P}_{S_k}$ is unitary, we further know that $\|\mathbf{P}_{S_k}^H \mathbf{u}_{S_k}\|_2^2 = \|\mathbf{u}_{S_k}\|_2^2$. So we have

$$\mathbf{u}_{S_k}^H \mathbf{A}_{S_k} \mathbf{u}_{S_k} \leq \pi_{S_k,\max} \|\mathbf{u}_{S_k}\|_2^2, \tag{19}$$

where the equality is achieved when $\mathbf{u}_{S_k}$ is an eigenvector of $\mathbf{A}_{S_k}$ corresponding to $\pi_{S_k,\max}$.

On the other hand, constraint (16a) is equivalent to

$$\mathbf{u}_{S_k}^H \mathbf{A}_{S_k} \mathbf{u}_{S_k} \geq \exp\left(\frac{R_{S_k}}{wt_{S_k}}\right) - 1. \tag{20}$$

According to (19) and (20), we know that if we only consider constraint (16a) in optimizing Problem (16), the minimum value of the objective function in (16) is $\|\mathbf{u}_{S_k}^*\|_2^2 = \frac{\exp\left(\frac{R_{S_k}}{wt_{S_k}}\right)-1}{\rho_{S_k,\max}}$, and the optimal solution is $\mathbf{u}_{S_k}^* = \sqrt{\frac{\exp\left(\frac{R_{S_k}}{wt_{S_k}}\right)-1}{\pi_{S_k,\max}}} \mathbf{z}_{S_k,\max}$. Since constraint (16b) only states that $\|\mathbf{u}_{S_k}\|_2^2$ should be no greater than ρ_{S_k}, therefore (16) is feasible if and only if the minimum value of $\|\mathbf{u}_{S_k}\|_2^2$ satisfies constraint (16b). That is,

$$\frac{\exp\left(\frac{R_{S_k}}{wt_{S_k}}\right) - 1}{\pi_{S_k,\max}} \leq \rho_{S_k} \Rightarrow t_{S_k} \geq \frac{R_{S_k}}{w \log\left(\rho_{S_k} \pi_{S_k,\max} + 1\right)}. \quad \square$$

According to Lemma 1, the optimal transmit beamforming vectors are explicit functions of the time fraction allocation $(t_{S_1}, \cdots, t_{S_K})$. This enables us to solve optimization problem (8) through a proper decomposition.

Theorem 1. *In the single-data-stream transmission case, the necessary and sufficient condition for optimization problem* (8) *to be feasible is*

$$\sum_{k=1}^{K} \frac{R_{S_k}}{w \log\left(\rho_{S_k} \pi_{S_k,\max} + 1\right)} \leq 1. \tag{21}$$

Furthermore, problem (8) *can be solved in polynomial time. In particular, the optimal time fractions are the optimal solutions to the convex optimization*

$$\begin{aligned} \min_{t_{S_k}} \quad & \sum_{k=1}^{K} t_{S_k} \frac{\exp\left(\frac{R_{S_k}}{w t_{S_k}}\right) - 1}{\pi_{S_k,\max}} \\ \text{s. t.} \quad & \sum_{k=1}^{K} t_{S_k} \leq 1, \\ & t_{S_k} \geq \frac{R_{S_k}}{w \log\left(\rho_{S_k} \pi_{S_k,\max} + 1\right)}, \quad \forall k. \end{aligned} \tag{22}$$

The optimal transmit beamforming vectors are then given by the closed-form solution in (18).

Proof. Substituting (18) into Problem (8), then (8) becomes (22). The condition for the constraint set of (22) to be nonempty is $\sum_{k=1}^{K} \frac{R_{S_k}}{w \log\left(\rho_{S_k} \pi_{S_k,\max}+1\right)} \leq 1$.

Problem (22) is an optimization problem with the time fraction variables t_{S_k} only. The second order derivative of the objective function in (22) with respect to variable t_{S_k} is

$$\frac{R_{S_k}^2}{w^2 \pi_{S_k,\max} t_{S_k}^3} \exp\left(\frac{R_{S_k}}{w t_{S_k}}\right),$$

which is always positive for any nonnegative t_{S_k}. Thus, the objective function in (22) is a convex function. Furthermore, the constraints in (22) are linear. Therefore, (22) is a convex optimization problem, which can be solved in polynomial time with the standard interior-point method [5]. □

Two remarks are in order for Theorem 1:

1. In the single-data-stream transmission case, it is energy-optimal for each SU to scale its transmit beamforming vector with the eigenvector corresponding to the largest eigenvalue of its $\mathbf{A}_{S_k}$. The scaling factor depends on the time resource

for each SU. Furthermore, the energy-optimal time allocation can be found by solving convex optimization problem (22).

2. Finding the optimal solutions in the single-data-stream transmission case is straightforward. When a new SU sends transmission request to the secondary BS, the secondary BS first checks whether Condition (21) is satisfied. If yes, the secondary BS solves the convex optimization Problem (22) to obtain the optimal time fractions. Furthermore, the optimal transmit beamforming vectors are then computed by (18). After obtaining the optimal transmit beamforming vectors, the optimal receive beamforming vectors can be computed by (3). If Condition (21) is not satisfied, the rate requirements of all the SUs cannot be satisfied. In this case, the secondary BS performs call admission control to block the new SU.

Multiple-Data-Stream Transmission: Problem Decomposition and Optimal Solution

In the multiple-data-stream transmission case, the optimal solutions to the non-convex Problem (12) can be found in polynomial time by first optimizing the time fractions t_{S_k} and then the transmit covariance matrices $\mathbf{Q}_{S_k}$. Furthermore, it can be shown that the optimal time slot allocation (discrete time allocation) can be obtained with a polynomial-time algorithm.

Optimal Solution for Continuous Time Allocation

Given any feasible time allocation $(t_{S_1}, \cdots, t_{S_K})$, Problem (12) reduces to K separate transmit covariance matrix optimization problems, one for each S_k:

$$\min_{\mathbf{Q}_{S_k}} \quad \mathrm{tr}\left(\mathbf{Q}_{S_k}\right)$$

$$\text{s.t.} \quad w \log\left[\det\left(\mathbf{I} + \mathbf{H}_{BS,S_k}\mathbf{Q}_{S_k}\mathbf{H}_{BS,S_k}^H\mathbf{C}_{S_k}^{-1}\right)\right] \geq \frac{R_{S_k}}{t_{S_k}}, \tag{23a}$$

$$\mathrm{tr}\left(\mathbf{Q}_{S_k}\right) \leq \rho_{S_k}, \tag{23b}$$

$$\mathbf{Q}_{S_k} \succeq \mathbf{0}.$$

The optimal solution to Problem (23) can be computed by standard "water-filling" [9, 25]. Let $\mathbf{F}_{S_k}$ denote $\mathbf{H}_{BS,S_k}^H\mathbf{C}_{S_k}^{-1}\mathbf{H}_{BS,S_k}$, which is an $M_{S_k} \times M_{S_k}$ Hermitian positive semidefinite matrix. Let $W_{S_k} = \mathrm{rank}\left(\mathbf{F}_{S_k}\right)$ and $\lambda_{S_k,1} \geq \lambda_{S_k,2} \geq \cdots \geq \lambda_{S_k,W_{S_k}}$ denote all the nonnegative eigenvalues of matrix $\mathbf{F}_{S_k}$. Let $\mathbf{g}_{S_k,i}$ ($\|\mathbf{g}_{S_k,i}\|_2^2 = 1$) denote the normalized eigenvector of $\mathbf{F}_{S_k}$ associated with eigenvalue $\lambda_{S_k,i}$, $(1 \leq i \leq W_{S_k})$ and $\mathbf{G}_{S_k}$ be a matrix whose ith column is $\mathbf{g}_{S_k,i}$. The optimal solution to Problem (23) is given in the following lemma.

Lemma 2. *The necessary and sufficient condition for Problem (23) to be feasible is*

$$t_{S_k} \geq t_{S_k,\min}. \tag{24}$$

Furthmore, let $\tilde{\mathbf{Q}}^*_{S_k}$ *be a diagonal matrix with entries*

$$\tilde{Q}^*_{S_k,ii} = \left(\mu_{S_k} - \frac{1}{\lambda_{S_k,i}}\right)^+, \tag{25}$$

where $(x)^+ = \max\{x, 0\}$*, and the value of* μ_{S_k} *is chosen to sastisfy*

$$\prod_{i=1}^{W_{S_k}} \left(\lambda_{S_k,i}\mu_{S_k}\right)^+ = \exp\left(\frac{R_{S_k}}{wt_{S_k}}\right). \tag{26}$$

Then, when Condition (24) is satisfied, the optimal solution to Problem (23) is

$$\mathbf{Q}^*_{S_k} = \mathbf{G}_{S_k}\tilde{\mathbf{Q}}^*_{S_k}\mathbf{G}^H_{S_k}. \tag{27}$$

Proof. If we do not consider Constraint (23b) when solving Problem (23), the optimal solution is given by standard "water-filling." Constraint (23b) only states that the minimum objective value should be no greater than ρ_{S_k}. Since the MIMO link rate obtained from the water-filling is an increasing function in $\mathrm{tr}\left(\mathbf{Q}_{S_k}\right)$ [25], we can find that Constraint (23b) is satisfied if t_{S_k} satisfies Condition (24). □

The optimal transmit covariance matrices are functions of the time allocation $(t_{S_1}, \cdots, t_{S_K})$. Thus, the optimal number of data streams and the optimal energy consumption of each S_k are dependent on its time resource allocation. To simplify the notation, let

$$\tau_{S_k}\left(m_{S_k}\right) = \frac{R_{S_k}}{w\left(\left(\sum_{i=1}^{m_{S_k}} \log\lambda_{S_k,i}\right) - m_{S_k}\log\lambda_{S_k,(m_{S_k}+1)}\right)},$$

where $m_{S_k} \in \left\{1, \cdots, \left(W_{S_k} - 1\right)\right\}$. Observe that τ_{S_k} is a decreasing function of m_{S_k}. The optimal number of data streams $D^*_{S_k}$ is a stepwise function of t_{S_k}, given by

$$D^*_{S_k}\left(t_{S_k}\right) = \begin{cases} W_{S_k}, & 0 < t_{S_k} < \tau_{S_k}\left(W_{S_k} - 1\right), \\ m_{S_k}, & \tau_{S_k}\left(m_{S_k}\right) \leq t_{S_k} < \tau_{S_k}\left(m_{S_k} - 1\right), \\ 1, & t_{S_k} \geq \tau_{S_k}\left(1\right). \end{cases} \tag{28}$$

Furthermore, the optimal "water level" $\mu^*_{S_k}$ is a function of t_{S_k}, given by

$$\mu_{S_k}^* \left(t_{S_k}\right) = \left(\frac{\exp\left(\frac{R_{S_k}}{wt_{S_k}}\right)}{\prod_{i=1}^{D_{S_k}^*\left(t_{S_k}\right)} \lambda_{S_k,i}} \right)^{\frac{1}{D_{S_k}^*\left(t_{S_k}\right)}}.$$

Therefore, the optimal energy consumption of S_k is a function of t_{S_k}, which can be computed according to

$$E_{S_k}\left(t_{S_k}\right) = t_{S_k} \left(D_{S_k}^*\left(t_{S_k}\right) \left(\frac{\exp\left(\frac{R_{S_k}}{wt_{S_k}}\right)}{\prod_{i=1}^{D_{S_k}^*\left(t_{S_k}\right)} \lambda_{S_k,i}} \right)^{\frac{1}{D_{S_k}^*\left(t_{S_k}\right)}} - \sum_{i=1}^{D_{S_k}^*\left(t_{S_k}\right)} \frac{1}{\lambda_{S_k,i}} \right), \tag{29}$$

Note that because the optimal number of data streams $D_{S_k}^*\left(t_{S_k}\right)$ is a stepwise function of t_{S_k}, $E_{S_k}\left(t_{S_k}\right)$ is a piecewise defined function of t_{S_k}. Here the piecewise defined function means that $E_{S_k}\left(t_{S_k}\right)$ takes on different forms for different intervals of t_{S_k}. As shown in Proposition 1, $E_{S_k}\left(t_{S_k}\right)$ is a continuous function in t_{S_k}. The following proposition establishes some key properties of the optimal energy consumption $E_{S_k}\left(t_{S_k}\right)$, which will be useful later when solving the time allocation problem among the SUs.

Proposition 1. *The optimal energy consumption $E_{S_k}\left(t_{S_k}\right)$ is a strictly convex, continuous, first-order differentiable, and monotonically decreasing function in t_{S_k}.*

Proof. The proof is in the Appendix. □

Substituting (24), (27), and (29) into Problem (12), it then becomes an optimization problem in the time fraction variables t_{S_k} only. Furthermore, as shown in Proposition 1, the energy consumption (29) is a monotonically decreasing function in t_{S_k}. Thus, the optimal solution could be achieved only when Constraint (12b) is satisfied with equality. Therefore, the time resource optimization problem among the SUs is given by

$$\begin{aligned} \min_{t_{S_k}} \quad & \sum_{k=1}^{K} E_{S_k}\left(t_{S_k}\right) \\ \text{s.t.} \quad & \sum_{k=1}^{K} t_{S_k} = 1, \\ & t_{S_k} \geq t_{S_k,\min}, \quad \forall k. \end{aligned} \tag{30}$$

The objective function $E_{S_k}\left(t_{S_k}\right)$ is convex as shown in Proposition 1, and the constraints in (30) are linear. Therefore, Problem (30) is a convex optimization problem. Problem (12) can be solved efficiently through the decomposition method.

Theorem 2. *In the multiple-data-stream transmission case, the optimal time allocation and the optimal transmit covariance matrices can be found separately. In particular, the optimal time allocation is the optimal solution to the convex optimization problem* (30)*. After obtaining the optimal* $t^*_{S_k}$*, the optimal transmit covariance matrix of each SU can then be computed by "water-filling," given in* (27)*.*

Proof. From Lemma 2, it can be shown that given any feasible time allocation, the optimal transmit covariance matrix is computed by "water-filling." Proposition 1 further shows that the energy consumption, based on the optimal covariance matrix, is a strictly convex function of t_{S_k}. Thus, the optimal solution to Problem (30) is the global optimal time allocation. Given this optimal $t^*_{S_k}$, the optimal transmit covariance matrix is then computed by "water-filling." □

Note that although the objective function in (30) is a piecewise defined function in t_{S_k}, it is continuous, and its first-order derivative is also continuous. However, it is not second-order differentiable. Thus, only first-order methods for convex optimization problems (such as the gradient methods) can be applied to solve Problem (30) [2, 5]. Here the spectral projected gradient (SPG) method [3], which is a variation of the projected gradient method, is a time-efficient algorithm for Problem (30). The SPG method makes two modifications. First, it incorporates the non-monotone line search scheme proposed in [10]. Second, the step size is chosen to be the one introduced in [1]. With these two modifications, the number of iterations can be significantly reduced. Thus, the SPG method has been shown to converge to the global optimal solution with a competitive convergence rate for convex optimization problems [3, 23].

The time complexity for the SPG method to solve Problem (30) is $O\left(K^2\right)$ in terms of iterations [3]. In each iteration, the gradient can be easily updated from an explicit function. The time complexity for each SU to obtain the optimal transmit covariance matrix by "water-filling" is $O\left(W^3_{S_k}\right)$, where $W_{S_k} = \min\{M_{S_k}, N_{BS}\}$ [19]. Therefore, the overall time complexity to obtain the optimal solution in multiple-data-stream transmission case is $O\left(K^2\right) + O\left(K W^3_{S_k}\right)$.

Optimal Solution for Discrete Time Allocation

In many wireless systems, the time frame is divided into a number of time slots. A slot is the smallest unit in the time allocation process. The time resource allocated to each S_k should be an integer indicating the number of time slots instead of a real number. With the additional integer constraint on the variable t_{S_k} in Problem (12), it then becomes a mixed-integer non-convex optimization problem, which is generally very difficult to solve. Fortunately, by exploring the special structure of Problem (12), optimal solutions can be obtained within polynomial time.

Without loss of generality, suppose each normalized frame has a total number of T time slots, the time resource optimization problem among the SUs is given by

$$\begin{aligned} \min_{t_{S_k}} \quad & \sum_{k=1}^{K} E_{S_k}\left(t_{S_k}\right) \\ \text{s. t.} \quad & \sum_{k=1}^{K} t_{S_k} = T, \\ & t_{S_k} \in \left\{t_{S_k,\min}^{(I)}, \left(t_{S_k,\min}^{(I)}+1\right), \cdots, T\right\}, \quad \forall k, \end{aligned} \tag{31}$$

where $t_{S_k,\min}^{(I)} = \lceil t_{S_k,\min} T \rceil$ is the minimum number of time slots that each S_k needs.

Problem (31) is an integer optimization problem, which is feasible if and only if

$$\sum_{k=1}^{K} t_{S_k,\min}^{(I)} \leq T.$$

The objective function of (31) is a separable sum of convex functions. With this special property, it is not difficult to find the optimal solution to (31) with a greedy algorithm [13]. Let $\Delta_k(t_{S_k})$ denote the change in the energy consumption when the number of time slots allocated to S_k is increased from $t_{S_k}-1$ to t_{S_k},

$$\Delta_k(t_{S_k}) = E_{S_k}\left(t_{S_k}\right) - E_{S_k}\left(t_{S_k}-1\right), \quad t_{S_k} \in \left\{\left(t_{S_k,\min}^{(I)}+1\right), \cdots, T\right\}.$$

The value of $\Delta_k(t_{S_k,\min}^{(I)})$ can be defined as $-\infty$.

As shown in Proposition 1, the energy consumption $E_{S_k}\left(t_{S_k}\right)$ is strictly convex and monotonically decreasing in t_{S_k}. We then have

$$\Delta_k(t_{S_k,\min}^{(I)}) \leq \Delta_k(t_{S_k,\min}^{(I)}+1) \leq, \cdots, \leq \Delta_k(T), \quad \forall k.$$

In the greedy algorithm, starting from the minimum slot allocation $\mathbf{t}_{\min}^{(I)} = \left(t_{S_1,\min}^{(I)}, \cdots, t_{S_K,\min}^{(I)}\right)$, one time slot is allocated at a time. A time slot is added to the S_k which has the minimum $\Delta_k(t_{S_k})$ among all the SUs. The algorithm stops when all the T time slots are allocated. The optimal solution to Problem (31) can be characterized by

$$\begin{cases} \Delta_k(t_{S_k}^*) \leq \varphi^*, & \forall k, \\ \Delta_k(t_{S_k}^*+1) \geq \varphi^*, & \forall k, \\ \sum_{k=1}^{K} t_{S_k}^* = T, & \\ t_{S_k}^* \in \left\{t_{S_k,\min}^{(I)}, \left(t_{S_k,\min}^{(I)}+1\right), \cdots, T\right\}, & \forall k. \end{cases}$$

In the allocation of one slot, the energy consumption can be easily computed from an explicit function. The time complexity for finding the minimum $\Delta_k(t_{S_k})$ among all the SUs is $O(K)$. Therefore, the overall time complexity to obtain the optimal discrete time allocation with the greedy algorithm is $O(KT)$.

Simulation Results

The performance of the proposed algorithms is evaluated in terms of energy consumption, interference to primary system, convergence, and optimality. In the simulation setup, there are two primary links with 10 m distance between the transmitter and corresponding receiver. The SUs are uniformly distributed in a square area of 200 m×200 m, with a minimum separation of 35 m from the primary receivers. An example CR network with 35 SUs is shown in Fig. 1. Each node in the network has 4 antennae. For each network setting, 1000 independent simulation runs are performed.

The frame length of the secondary system is 20 ms, and each SU has a rate requirement of 32 kbps. The carrier frequency is 1 GHz and the network bandwidth is 20 MHz. The wireless channel is assumed to be the i.i.d. Rayleigh fading channel with path loss exponent equal to 4. The PUs transmit at the maximum power of 20 dBm, while the maximum transmit power for each SU is 27.5 dBm. The noise power density is −174 dBm/Hz. The interference power threshold ϕ_{P_j} is set such that $\frac{\phi_{P_j}}{N_0 w}$ is 25 dB. The outage probability δ_{P_j} in the statistical CSI scenario is 1%.

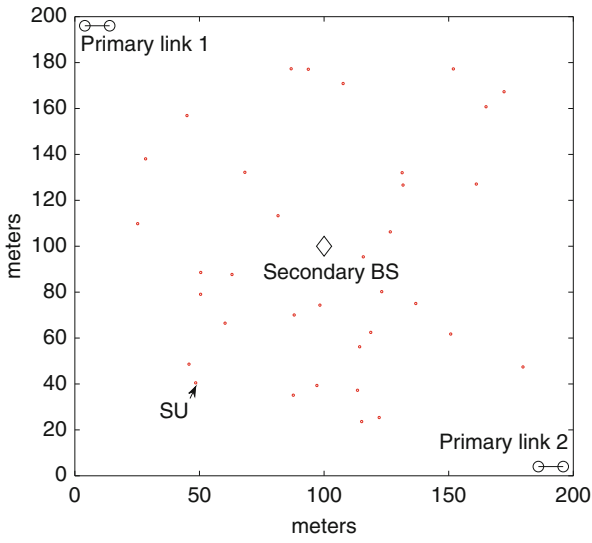

Fig. 1 A sample random CR network with 2 primary links and 35 secondary users

Energy Consumption

The energy consumptions per bit of the SUs, for both the single-data-stream transmission case and the multiple-data-stream transmission case, named "optimal time & single stream" and "optimal time & multiple streams," are shown in Fig. 2. For comparison, the energy consumption of the "max-rate" transmission schemes is shown. In the "max-rate" scheme, each SU uses the minimum time resource and the transmit covariance matrix of the solution to Problem (14).

Compared with the "max-rate" scheme, the energy consumption of both the "optimal time & single stream" and "optimal time & multiple streams" is reduced significantly. The energy consumption per bit roughly remains constant in the "max-rate" scheme. In the "optimal time & single stream" and "optimal time & multiple streams" schemes, there is a trade-off between the energy consumption and the system traffic load (i.e., the number of SUs). Taking the "max-rate" scheme as the baseline, the energy reduction of "optimal time & multiple streams" is up to 78% when the secondary system is underutilized. During simulations, it can be observed that when the secondary system is underutilized or when it experiences a strong interference from the primary system, the optimal way for each SU to perform transmit precoding is to do the single-data-stream transmission. This can be seen in Fig. 2: when the secondary system has less than 8 SUs, both the "optimal time & single stream" and "optimal time & multiple streams" produce the same result. As the traffic load further increases, the optimal number of data streams will increase to

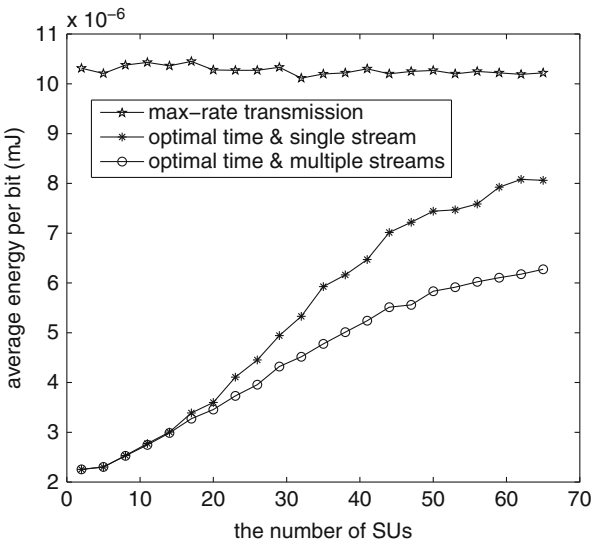

Fig. 2 Average energy consumption per bit of the secondary system

exploit the multiplexing gain and further reduce the energy consumption. Compared with the "optimal time & single stream" scheme, the energy consumption of the "optimal time & multiple streams" scheme is reduced by 23% when the secondary system has 65 users.

Interference to the Primary Receivers

Figure 3 shows the average interference power from the SUs to the primary receivers in the statistical CSI scenario, which is measured by the interference-to-noise ratio (in dB).

In the "max-rate" scheme, the average interference-to-noise ratio is smaller than the required 25 dB. This is because the secondary transmitter needs to satisfy the interference constraint at both primary receivers in each simulated network. Therefore, the interference-to-noise ratio at each primary receiver is smaller than 25 dB in many simulation runs. The interference to the primary system is also alleviated in the "optimal time & single stream" and "optimal time & multiple streams" schemes. The interference power to the primary system adapts to the traffic load of the secondary system. Moreover, it can be observed that in the "optimal time & multiple streams" scheme, the interference power increases slower compared with the "optimal time & single stream" scheme.

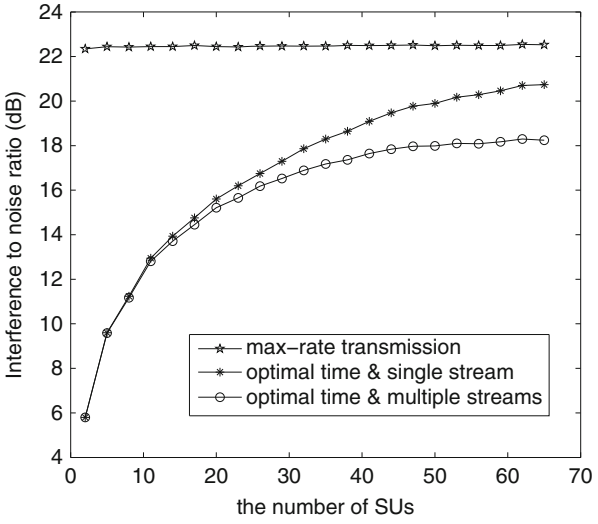

Fig. 3 Average interference power at primary receiver vs. the number of SUs

Convergence

As shown in section "Optimal Solution for Continuous Time Allocation", the SPG method is guaranteed to converge to the optimal time allocation in multiple-data-stream transmission case. Figure 4 shows the convergence performance for the sample random secondary network with 35 users, as shown in Fig. 1. It can be found that the objective function is reduced significantly during the first 10 iterations. Another observation is that the objective function in the SPG method may not monotonically decrease in every iteration, which has also been discussed in [23].

Figure 5 shows the convergence performance, plotted in terms of the average number of iterations. The stopping criterion is $\|\mathbf{t}^{(n+1)} - \mathbf{t}^{(n)}\|_\infty < 10^{-5}$. The number of iterations first increases and then decreases with the number of SUs and always stays below 85 iterations. This indicates that the SPG method has a good convergence rate even in a secondary system with many users. Note that in the perfect CSI scenario, the SPG method is also guaranteed to converge to the optimal solution with similar convergence performance when the secondary system is underutilized.

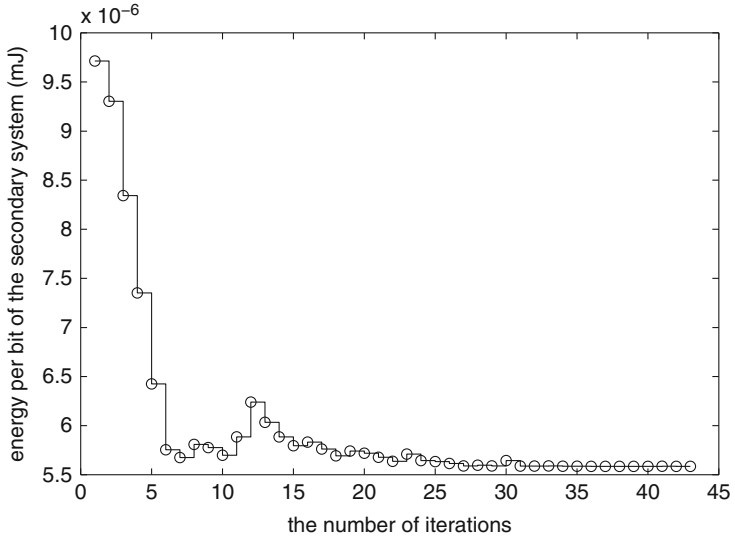

Fig. 4 The energy consumption of the secondary network as a function of the number of iterations in the multiple-data-stream transmission case. The secondary network has 35 users with the topology shown in Fig. 1

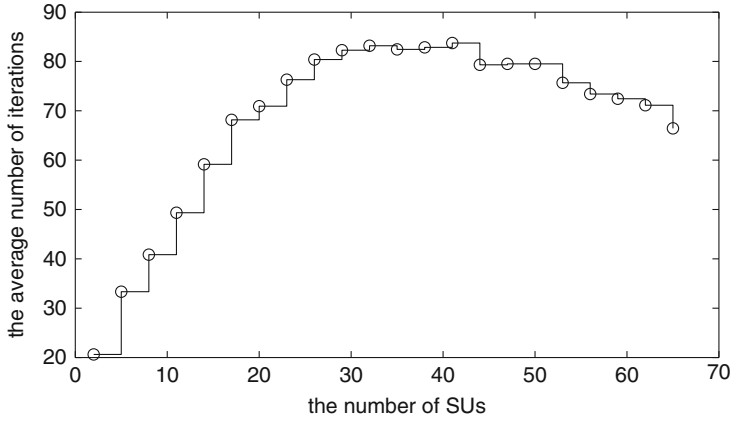

Fig. 5 Average number of iterations needed to converge to the optimal solution in the multiple-data-stream transmission case

Conclusion

This chapter discusses the jointly energy-optimal time allocation and precoding design in MIMO CR networks. In particular, it covers two transmission choices for each SU: single-data-stream transmission and multiple-data-stream transmission. The problem formulations turn out to be non-convex optimization problems. The non-convexity can be conquered by applying an optimization decomposition technique. As a result, in the single-data-stream transmission case, the global optimal time allocation can be found by solving a convex optimization problem. Furthermore, the optimal beamforming vector can be found by simple matrix eigenvalue-eigenvector computation.

In the multiple-data-stream transmission case, since the number of data streams in the transmit covariance matrix is discrete by nature, the energy consumption is a piecewise defined function in the time variable. In this case, the optimal energy consumption is shown to be continuous, first-order differentiable, strictly convex, and monotonically decreasing in the time variable. Thus the SPG algorithm can be applied to quickly find the optimal time allocation. In a slotted system, where time is a discrete variable, the optimal number of time slots can be found with a greedy algorithm. Given the optimal time allocation, the optimal transmit covariance matrix is obtained by water-filling.

Note that spectrum efficiency can be further improved if the SUs send simultaneous uplink transmissions with spatial multiplexing. However, in this case, the SUs will interfere with each other. Finding the optimal transmit covariance matrices for the SUs is more challenging. Considering the trade-off between the diversity gain and the spatial multiplexing gain for energy-efficient MIMO CR networks is an interesting yet challenging topic for future investigation.

Appendix

Proof of Proposition 1:

We first show that $E_{S_k}\left(t_{S_k}\right)$ is a continuous function in t_{S_k} by showing $\lim_{t_{S_k}\to\tau_{S_k}^{-}(m_{S_k})} E_{S_k}\left(t_{S_k}\right) = \lim_{t_{S_k}\to\tau_{S_k}^{+}(m_{S_k})} E_{S_k}\left(t_{S_k}\right)$:

$$\lim_{t_{S_k}\to\tau_{S_k}^{-}(m_{S_k})} E_{S_k}\left(t_{S_k}\right) = \tau_{S_k}\left(m_{S_k}\right)\left(\left(m_{S_k}+1\right)\left(\frac{\exp\left(\frac{R_{S_k}}{w\tau_{S_k}\left(m_{S_k}\right)}\right)}{\prod_{i=1}^{m_{S_k}+1}\lambda_{S_k,i}}\right)^{\frac{1}{m_{S_k}+1}} - \sum_{i=1}^{m_{S_k}+1}\frac{1}{\lambda_{S_k,i}}\right)$$

$$= \tau_{S_k}\left(m_{S_k}\right)\left(\left(m_{S_k}+1\right)\left(\frac{\exp\left(\left(\sum_{i=1}^{m_{S_k}}\log\lambda_{S_k,i}\right) - m_{S_k}\log\lambda_{S_k,\left(m_{S_k}+1\right)}\right)}{\prod_{i=1}^{m_{S_k}+1}\lambda_{S_k,i}}\right)^{\frac{1}{m_{S_k}+1}} - \sum_{i=1}^{m_{S_k}+1}\frac{1}{\lambda_{S_k,i}}\right)$$

$$= \tau_{S_k}\left(m_{S_k}\right)\left(\left(m_{S_k}+1\right)\left(\frac{\prod_{i=1}^{m_{S_k}}\lambda_{S_k,i}}{\lambda_{S_k,\left(m_{S_k}+1\right)}^{m_{S_k}}\prod_{i=1}^{m_{S_k}+1}\lambda_{S_k,i}}\right)^{\frac{1}{m_{S_k}+1}} - \sum_{i=1}^{m_{S_k}+1}\frac{1}{\lambda_{S_k,i}}\right)$$

$$= \tau_{S_k}\left(m_{S_k}\right)\left(\frac{m_{S_k}}{\lambda_{S_k,\left(m_{S_k}+1\right)}} - \sum_{i=1}^{m_{S_k}}\frac{1}{\lambda_{S_k,i}}\right),$$

and

$$\lim_{t_{S_k}\to\tau_{S_k}^{+}(m_{S_k})} E_{S_k}\left(t_{S_k}\right) = \tau_{S_k}\left(m_{S_k}\right)\left(m_{S_k}\left(\frac{\exp\left(\frac{R_{S_k}}{w\tau_{S_k}\left(m_{S_k}\right)}\right)}{\prod_{i=1}^{m_{S_k}}\lambda_{S_k,i}}\right)^{\frac{1}{m_{S_k}}} - \sum_{i=1}^{m_{S_k}}\frac{1}{\lambda_{S_k,i}}\right)$$

$$= \tau_{S_k}\left(m_{S_k}\right)\left(m_{S_k}\left(\frac{\exp\left(\left(\sum_{i=1}^{m_{S_k}}\log\lambda_{S_k,i}\right) - m_{S_k}\log\lambda_{S_k,\left(m_{S_k}+1\right)}\right)}{\prod_{i=1}^{m_{S_k}}\lambda_{S_k,i}}\right)^{\frac{1}{m_{S_k}}} - \sum_{i=1}^{m_{S_k}}\frac{1}{\lambda_{S_k,i}}\right)$$

$$= \tau_{S_k}\left(m_{S_k}\right)\left(\frac{m_{S_k}}{\lambda_{S_k,\left(m_{S_k}+1\right)}} - \sum_{i=1}^{m_{S_k}}\frac{1}{\lambda_{S_k,i}}\right).$$

Thus we have

$$\lim_{t_{S_k}\to\tau_{S_k}^{-}(m_{S_k})} E_{S_k}\left(t_{S_k}\right) = \lim_{t_{S_k}\to\tau_{S_k}^{+}(m_{S_k})} E_{S_k}\left(t_{S_k}\right).$$

Therefore, $E_{S_k}\left(t_{S_k}\right)$ is a continuous function in t_{S_k}.

Next, we show that $\frac{dE_{S_k}}{dt_{S_k}}$ is a continuous function in t_{S_k} by showing $\lim_{t_{S_k}\to\tau_{S_k}^{-}(m_{S_k})}\frac{dE_{S_k}}{dt_{S_k}} = \lim_{t_{S_k}\to\tau_{S_k}^{+}(m_{S_k})}\frac{dE_{S_k}}{dt_{S_k}}$. The first-order derivative of $E_{S_k}\left(t_{S_k}\right)$ with respect to t_{S_k} is

$$\frac{dE_{S_k}}{dt_{S_k}} = \left(D_{S_k}^{*}\left(t_{S_k}\right) - \frac{R_{S_k}}{wt_{S_k}}\right)\left(\frac{\exp\left(\frac{R_{S_k}}{wt_{S_k}}\right)}{\prod_{i=1}^{D_{S_k}^{*}\left(t_{S_k}\right)}\lambda_{S_k,i}}\right)^{\frac{1}{D_{S_k}^{*}\left(t_{S_k}\right)}} - \sum_{i=1}^{D_{S_k}^{*}\left(t_{S_k}\right)}\frac{1}{\lambda_{S_k,i}}.$$

It can be shown that

$$\lim_{t_{S_k}\to\tau_{S_k}^{-}(m_{S_k})}\frac{dE_{S_k}}{dt_{S_k}} = \left(\left(m_{S_k}+1\right) - \frac{R_{S_k}}{w\tau_{S_k}\left(m_{S_k}\right)}\right)\left(\frac{\exp\left(\frac{R_{S_k}}{w\tau_{S_k}\left(m_{S_k}\right)}\right)}{\prod_{i=1}^{m_{S_k}+1}\lambda_{S_k,i}}\right)^{\frac{1}{m_{S_k}+1}} - \sum_{i=1}^{m_{S_k}+1}\frac{1}{\lambda_{S_k,i}}$$

$$= \left(\left(m_{S_k}+1\right) - \frac{R_{S_k}}{w\tau_{S_k}\left(m_{S_k}\right)}\right)\left(\frac{\exp\left(\left(\sum_{i=1}^{m_{S_k}}\log\lambda_{S_k,i}\right) - m_{S_k}\log\lambda_{S_k,(m_{S_k}+1)}\right)}{\prod_{i=1}^{m_{S_k}+1}\lambda_{S_k,i}}\right)^{\frac{1}{m_{S_k}+1}}$$

$$- \sum_{i=1}^{m_{S_k}+1}\frac{1}{\lambda_{S_k,i}}$$

$$= \left(\left(m_{S_k}+1\right) - \frac{R_{S_k}}{w\tau_{S_k}\left(m_{S_k}\right)}\right)\frac{1}{\lambda_{S_k,(m_{S_k}+1)}} - \sum_{i=1}^{m_{S_k}+1}\frac{1}{\lambda_{S_k,i}}$$

$$= \left(m_{S_k} - \frac{R_{S_k}}{w\tau_{S_k}\left(m_{S_k}\right)}\right)\frac{1}{\lambda_{S_k,(m_{S_k}+1)}} - \sum_{i=1}^{m_{S_k}}\frac{1}{\lambda_{S_k,i}},$$

and

$$\lim_{t_{S_k}\to\tau_{S_k}^{+}(m_{S_k})}\frac{dE_{S_k}}{dt_{S_k}} = \left(m_{S_k} - \frac{R_{S_k}}{w\tau_{S_k}\left(m_{S_k}\right)}\right)\left(\frac{\exp\left(\frac{R_{S_k}}{w\tau_{S_k}\left(m_{S_k}\right)}\right)}{\prod_{i=1}^{m_{S_k}}\lambda_{S_k,i}}\right)^{\frac{1}{m_{S_k}}} - \sum_{i=1}^{m_{S_k}}\frac{1}{\lambda_{S_k,i}}$$

$$= \left(m_{S_k} - \frac{R_{S_k}}{w\tau_{S_k}\left(m_{S_k}\right)}\right)\left(\frac{\exp\left(\left(\sum_{i=1}^{m_{S_k}}\log\lambda_{S_k,i}\right) - m_{S_k}\log\lambda_{S_k,(m_{S_k}+1)}\right)}{\prod_{i=1}^{m_{S_k}}\lambda_{S_k,i}}\right)^{\frac{1}{m_{S_k}}} - \sum_{i=1}^{m_{S_k}}\frac{1}{\lambda_{S_k,i}}$$

$$= \left(m_{S_k} - \frac{R_{S_k}}{w\tau_{S_k}\left(m_{S_k}\right)}\right)\frac{1}{\lambda_{S_k,(m_{S_k}+1)}} - \sum_{i=1}^{m_{S_k}}\frac{1}{\lambda_{S_k,i}}.$$

Thus, we have

$$\lim_{t_{S_k}\to\tau_{S_k}^{-}(m_{S_k})}\frac{dE_{S_k}}{dt_{S_k}}=\lim_{t_{S_k}\to\tau_{S_k}^{+}(m_{S_k})}\frac{dE_{S_k}}{dt_{S_k}}.$$

Therefore, $\frac{dE_{S_k}}{dt_{S_k}}$ is a continuous function in t_{S_k}.

The second-order derivative of $E_{S_k}\left(t_{S_k}\right)$ with respect to t_{S_k} is

$$\frac{d^2E_{S_k}}{dt_{S_k}^2}=\frac{R_{S_k}^2}{w^2t_{S_k}^3D_{S_k}^*\left(t_{S_k}\right)}\left(\frac{\exp\left(\frac{R_{S_k}}{wt_{S_k}}\right)}{\prod_{i=1}^{D_{S_k}^*\left(t_{S_k}\right)}\lambda_{S_k,i}}\right)^{\frac{1}{D_{S_k}^*\left(t_{S_k}\right)}},$$

which is always positive for any positive t_{S_k}. However, it is not continuous in t_{S_k}, with the noncontinuous points at $t_{S_k}=\tau_{S_k}\left(m_{S_k}\right)$, $(m_{S_k}=\left\{1,\cdots,\left(W_{S_k}-1\right)\right\})$.

Next we show that $\frac{dE_{S_k}}{dt_{S_k}}$ is always negative for any positive t_{S_k}. Since $\frac{d^2E_{S_k}}{dt_{S_k}^2}$ is always positive, this means that $\frac{dE_{S_k}}{dt_{S_k}}$ is an increasing function in t_{S_k}. Thus, we have

$$\begin{aligned}\frac{dE_{S_k}}{dt_{S_k}}&<\lim_{t_{S_k}\to\infty}\left(\left(D_{S_k}^*\left(t_{S_k}\right)-\frac{R_{S_k}}{wt_{S_k}}\right)\left(\frac{\exp\left(\frac{R_{S_k}}{wt_{S_k}}\right)}{\prod_{i=1}^{D_{S_k}^*\left(t_{S_k}\right)}\lambda_{S_k,i}}\right)^{\frac{1}{D_{S_k}^*\left(t_{S_k}\right)}}-\sum_{i=1}^{D_{S_k}^*\left(t_{S_k}\right)}\frac{1}{\lambda_{S_k,i}}\right)\\&=\left(D_{S_k}^*\left(t_{S_k}\right)\left(\frac{1}{\prod_{i=1}^{D_{S_k}^*\left(t_{S_k}\right)}\lambda_{S_k,i}}\right)^{\frac{1}{D_{S_k}^*\left(t_{S_k}\right)}}-\sum_{i=1}^{D_{S_k}^*\left(t_{S_k}\right)}\frac{1}{\lambda_{S_k,i}}\right)\Bigg|_{D_{S_k}^*\left(t_{S_k}\right)=1}=\frac{1}{\lambda_{S_k,1}}-\frac{1}{\lambda_{S_k,1}}=0.\end{aligned}\tag{32}$$

The second line of (32) follows from (28), which states that when t_{S_k} approaches infinity, the optimal number of data streams equals 1. Therefore, we can find that the optimal energy consumption $E_{S_k}\left(t_{S_k}\right)$ is a strictly convex, continuous, first-order differentiable, and monotonically decreasing function in t_{S_k}. □

References

1. Barzilai J, Borwein J (1988) Two-point step size gradient methods. IMA J Numer Anal 8(1):141–148
2. Bertsekas DP (1999) Nonlinear programming, 2nd edn. Athena Scientific, Belmont
3. Birgin E, Martínez J, Raydan M (2000) Nonmonotone spectral projected gradient methods on convex sets. SIAM J Optim 10(4):1196–1211

4. Blum RS (2003) MIMO capacity with interference. IEEE J Sel Areas Commun 21(5):793–801
5. Boyd S, Vandenberghe L (2004) Convex optimization. Cambridge University Press, Cambridge
6. Cui S, Goldsmith AJ, Bahai A (2004) Energy-efficiency of MIMO and cooperative MIMO techniques in sensor networks. IEEE J Sel Areas Commun 22(6):1089–1098
7. Fu L, Kim H, Huang J, Liew SC, Chiang M (2011) Energy conservation and interference mitigation: from decoupling property to win-win strategy. IEEE Trans Wirel Commun 10(11):3943–3955
8. Gershman AB, Sidiropoulos ND, Shahbazpanahi S, Bengtsson M, Ottersten B (2010) Convex optimization-based beamforming: from receive to transmit and network designs. IEEE Signal Process Mag 27(3):62–75
9. Gesbert D, Shafi M, shan Shiu D, Smith PJ, Naguib A (2003) From theory to practice: an overview of MIMO space-time coded wireless systems. IEEE J Sel Areas Commun 21(3):281–302
10. Grippo L, Lampariello F, Lucidi S (1986) A nonmonotone line search technique for Newton's method. SIAM J Numer Anal 23(4):707–716
11. Haykin S (2005) Cognitive radio: brain-empowered wireless communications. IEEE J Sel Areas Commun 23(2):201–220
12. Huang Y, Li Q, Ma WK, Zhang S (2012) Robust multicast beamforming for spectrum sharing-based cognitive radios. IEEE Trans Signal Process 60(1):527–533
13. Ibaraki T, Katoh N (1988) Resource allocation problems: algorithmic approaches. MIT Press, Cambridge
14. Johnson DH, Dudgeon DE (1993) Array signal processing: concepts and techniques. Prentice Hall signal processing series. P T R Prentice-Hall Inc., Englewood Cliffs
15. Kim H, Chae CB, de Veciana G, Heath RW Jr (2009) A cross-layer approach to energy efficiency for adaptive MIMO systems exploiting spare capacity. IEEE Trans Wirel Commun 8(8):4264–4275
16. Kobayashi M, Caire G (2007) Joint beamforming and scheduling for a multi-antenna downlink with imperfect transmitter channel knowledge. IEEE J Sel Areas Commun 25(7):1468–1477
17. Liang YC, Chen KC, Li GY, Mähönen P (2011) Cognitive radio networking and communications: an overview. IEEE Trans Veh Technol 60(7):3386–3407
18. Ma J, Zhang YJ, Su X, Yao Y (2008) On capacity of wireless ad hoc networks with MIMO MMSE receivers. IEEE Trans Wirel Commun 7(12):5493–5503
19. Palomar DP, Fonollosa JR (2005) Practical algorithms for a family of waterfilling solutions. IEEE Trans Signal Process 53(2):686–695
20. Phan KT, Vorobyov SA, Sidiropoulos ND, Tellambura C (2009) Spectrum sharing in wireless networks via QoS-aware secondary multicast beamforming. IEEE Trans Signal Process 57(6):2323–2335
21. Rappaport TS (2002) Wireless communications: principles and practice, 2nd edn. Prentice Hall PTR, Upper Saddle River
22. Razaviyayn M, Sanjabi M, Luo ZQ (2012) Linear transceiver design for interference alignment: complexity and computation. IEEE Trans Inf Theory 58(5):2896–2910
23. Schmidt M (2010) Graphical model structure learning with l_1-regularization. Ph.D. thesis, University of British Columbia
24. Sidiropoulos ND, Davidson TN, Luo ZQ (2006) Transmit beamforming for physical-layer multicasting. IEEE Trans Signal Process 54(6):2239–2251
25. Telatar E (1995) Capacity of multi-antenna gaussian channels. AT&T Bell Laboratories, Tech. Memo
26. Uysal-Biyikoglu E, Prabhakar B, Gamal AE (2002) Energy-efficient packet transmission over a wireless link. IEEE ACM Trans Netw 10(4):487–499
27. Yu W, Lan T (2007) Transmitter optimization for the multi-antenna downlink with per-antenna power constraints. IEEE Trans Signal Process 55(6):2646–2660
28. Zhang G, Ma S, Wong KK, Ng TS (2010) Robust beamforming in cognitive radio. IEEE Trans Wirel Commun 9(2):570–576

29. Zhang L, Liang YC, Xin Y (2008) Joint beamforming and power allocation for multiple access channels in cognitive radio networks. IEEE J Sel Areas Commun 26(1):38–51
30. Zhang L, Xin Y, Liang YC (2009) Weighted sum rate optimization for cognitive radio MIMO broadcast channels. IEEE Trans Wirel Commun 8(6):2950–2959
31. Zhang R, Liang YC (2008) Exploiting multi-antennas for opportunistic spectrum sharing in cognitive radio networks. IEEE J Sel Topics Signal Process 2(1):88–102
32. Zhang R, Liang YC, Cui S (2010) Dynamic resource allocation in cognitive radio networks: a convex optimization perspective. IEEE Signal Process Mag 27(3):102–114
33. Zhang YJ, So AMC (2011) Optimal spectrum sharing in MIMO cognitive radio networks via semidefinite programming. IEEE J Sel Areas Commun 29(2):362–373
34. Zheng G, Wong KK, Ottersten B (2009) Robust cognitive beamforming with bounded channel uncertainties. IEEE Trans Signal Process 57(12):4871–4881

Collaborative Spectrum Trading and Sharing for Cognitive Radio Networks

28

Xuanheng Li, Haichuan Ding, Yuguang Fang, Miao Pan, Pan Li, Xiaoxia Huang, Yi Sun, and Savo Glisic

Contents

X. Li (✉) · Y. Sun
School of Information and Communication Engineering, Dalian University of Technology, Dalian, Liaoning, China
e-mail: lixuanheng@mail.dlut.edu.cn; lslwf@dlut.edu.cn

H. Ding · Y. Fang
Department of Electrical and Computer Engineering, University of Florida, Gainesville, FL, USA
e-mail: dhcbit@gmail.com; fang@ece.ufl.edu

M. Pan
Department of Electrical and Computer Engineering, University of Houston, Houston, TX, USA
e-mail: mpan2@uh.edu

P. Li
Department of Electrical Engineering and Computer Science, Case Western Reserve University, Cleveland, OH, USA
e-mail: lipan@case.edu

X. Huang
Shenzhen Institutes of Advanced Technology, China Academy of Sciences, Shenzhen, Guangdong, China
e-mail: xx.huang@siat.ac.cn

S. Glisic
Department of Communication Engineering, University of Oulu, Oulu, Finland
e-mail: savo.glisic@ee.oulu.fi

W. Zhang (ed.), *Handbook of Cognitive Radio*,
https://doi.org/10.1007/978-981-10-1394-2_27

Abstract

Spectrum trading is one of the most promising approaches to enabling dynamic spectrum access (DSA) in cognitive radio networks (CRNs). With this approach, unlicensed users (a.k.a. secondary users) offer licensed users (a.k.a. primary users) with monetary rewards or improved quality of services (QoSs) in exchange for spectrum access rights. In this chapter, we present a comprehensive introduction to spectrum trading. First, we provide a brief introduction to DSA and CRNs as the background and motivation for the spectrum trading. Then, we present various state-of-the-art spectrum trading mechanisms for spectrum sharing. Finally, by analyzing various design issues in these mechanisms, we introduce the concept of service-oriented spectrum trading and offer a novel collaborative network architecture, called a cognitive mesh assisted network, to effectively utilize unused licensed/unlicensed spectrums with high spectral efficiency. We expect that this chapter provides readers with basic understanding on spectrum trading technology and foster future research initiatives.

Keywords

Dynamic spectrum access · Cognitive radio networks · Spectrum trading · Cognitive mesh assisted networks · Game theory · Auction theory

Introduction

In recent years, the popularity of smart devices, such as smartphones and tablets, and wireless services, such as mobile health (mHealth), online social networking, and mobile gaming, has led to the exponential growth in data traffic. According to the Cisco Visual Networking Index, mobile traffic has raised up to almost 400-million-fold over the past 15 years through the end of 2015 and will continue to grow by about eightfold between 2015 and 2020 [1]. This surge of data traffic will ultimately cause congestion over existing telecommunication systems, which calls for more spectrum resource. Nevertheless, current spectrum allocation adopted by Federal Communications Commission (FCC) is static and inefficient because spectrums are licensed to authorized users (a.k.a. licensed users) for long-term (often for 10 or more years with possible renewal) prespecified service provisioning

across a relatively large geographical region. Licensees cannot change the type of use or transfer the right to others, and thus the current spectrum allocation policy is commonly referred to as the static spectrum access (SSA) [2]. Obviously, the SSA scheme is inflexible and leads to low spectrum utilization because the right to access certain spectrum bands is only limited to license owners even if the band is temporally or spatially unoccupied. Experimental tests in academia and measurements conducted in industries both show that even in some big cities with dense populations, many licensed spectrum bands have surprisingly low utilization (e.g., less than 20% on average in Chicago city across all bands [3]). The conflicts between high demands for spectrum resources and inflexibility in SSA have spurred government to open the discussions on intelligently sharing licensed spectrums. As reported by the President's Council of Advisors on Science and Technology (PCAST) in July 2012, exclusive licensing is not the way to stepping forward, and advanced spectrum sharing should become the new paradigm, which has the potential to transform spectrum scarcity into abundancy [4]. In July 2016, US National Science Foundation (NSF) declared an investment of over $400 million to foster advanced wireless research, and dynamic spectrum sharing, also known as dynamic spectrum access (DSA), is regarded as a promising research direction [5].

Dynamic Spectrum Access

As defined in [6], DSA can be treated as the near-real-time adjustment of spectrum usage toward varying environments, operating states (e.g., operational modes, battery life, location, etc.), and external constraints (e.g., propagation characteristics, operational policies, etc.). In general, DSA schemes can be categorized into the following three models [7].

Spectrum Commons Model

In this model, also referred to as the open sharing model, spectrum resources are openly shared among different users. All users have equal rights to access a spectrum band once they obey certain operational rules. For example, unlicensed industrial, scientific, and medical (ISM) radio bands (e.g., WiFi) are used under this open sharing model. The phenomenal success of WiFi networks has motivated mobile operators to take advantage of the spectrum commons model for traffic offloading purpose. To be specific, instead of using their cellular networks, cellular operators can offload some broadband services to WiFi networks and save precious cellular bands for more QoS stringent services. In such a way, WiFi-offloading technique could help relieve high demands on cellular bands and mitigate congestion in cellular networks. However, it mainly targets at delay-tolerant services and the quality of service (QoS) cannot be guaranteed. Having in mind that cellular networks and WiFi networks adopt different spectrum access schemes, how to effectively manage interference among accessing users in such a heterogeneous network is one of the most important issues to address for this model. Otherwise,

packet collisions and retransmissions will seriously degrade the performance of these networks, particularly the WiFi networks, which will lead to low network throughput.

Hierarchical Access Model

In this model, users are classified into two types. One is the license owners, a.k.a. primary users (PUs), and the other is the unlicensed users, a.k.a. secondary users (SUs). Hierarchical access-based spectrum sharing allows SUs to access the PUs' spectrum with limited interference imposed on them, which is thus also referred to as the shared use model (note that, unlike the open sharing model, the users in this model have different priorities). Two approaches, i.e., the *underlay* and the *overlay* approaches, can be adopted by SUs when they access the PUs' spectrums [8].

In the underlay approach, SUs and PUs can transmit over the same spectrum simultaneously, but SUs should comply with restrictions on their transmit power so that the interference imposed on primary receivers does not exceed certain level (also known as interference temperature) [9]. Generally speaking, the optimal underlay spectrum sharing can be formulated as an optimization problem with a suitable objective function reflecting the performance of secondary network and a set of constraints with different considerations, such as fairness, quality of service (QoS), interference management, etc., which can be mathematically expressed as

$$\begin{aligned} &\text{Max} \quad f\left(R_1, \cdots, R_n\right) \\ &\text{s.t.} \quad R_i \geq R_{\text{th}}^i, \ \forall i \in \{1, \cdots, n\}; \quad \sum_{i=1}^{n} h_{ij} \cdot p_i \leq I_{\text{th}}^j, \ \forall j \in \{1, \cdots, m\}. \end{aligned} \tag{1}$$

Here, R_i, R_{th}^i, and p_i denote the achievable rate, the minimal guaranteed rate, and the transmit power of the i-th SU, respectively, h_{ij} is the channel gain from the i-th secondary transmitter to the j-th primary receiver, and I_{th}^j signifies the maximum tolerable interference level (threshold) on the j-th primary receiver. To satisfy the stringent limits on interferences for PUs, some sophisticated power control schemes for secondary transmitters can be adopted. Furthermore, if the constraints are too strict and/or the network load is too high, admission control mechanisms can be embedded as well to limit the number of admitted SUs. Moreover, beamforming techniques can also be jointly considered with power control to improve the performance of the secondary network. In addition to power control, SUs can also use spread-spectrum techniques (i.e., spread transmitted signals over a wide frequency band) to achieve short-range high-rate transmissions with extremely low power to avoid interference to the narrowband transmissions of the PUs.

In the overlay approach, there is no strict limits on SUs' transmission powers. Instead, SUs exploit spectrum white spaces (spectrum holes), i.e., spatially and/or temporally unoccupied parts of the spectrum, and access them opportunistically. Therefore, different from the interference control approach (underlay), to adopt the interference avoidance approach (overlay), SUs need to have the knowledge about spectrum holes so that they can ensure no interference caused to PUs. To gather the timely and accurate information about the usage of PUs' spectrum,

either noncooperative or cooperative way can be employed. In the former case, SUs must have the ability to perceive and analyze the surrounding radios by using various spectrum sensing methods. This could accomplish the noninterfering communications between PUs and SUs. In the latter case, the exclusive spectrum usage information is provided by PUs. Since PUs cannot get any benefit from sharing spectrum with SUs and thus usually have no motivation to participate in the spectrum sharing process, this approach mainly applies to the government-issued cases or the spectrum trading market where PUs lease/sell their unused spectrum resources to SUs in order to create additional revenue. A typical example of overlay spectrum sharing is the approval by FCC in November 2008 of the unlicensed use of the TV white spaces (TVWS) (54–72, 76–88, 174–216, and 470–806 MHz bands, which have superior radio propagation characteristics) based on spectrum sensing as well as consultation with an FCC-mandated database. In September 2010, FCC released new rules for the use of white space for unlicensed wireless devices, which removed the mandatory sensing requirements and facilitated the use of the spectrum with geolocation-based channel allocation. In the TVWS, the TV broadcasting stations and low-power wireless microphones are PUs, and the secondary systems such as the IEEE 802.22-based WRANs, the WiFi hot-spots, and home networks can coexist in an overlay sharing manner.

Dynamic Exclusive Use Model

This model is the closest to the current spectrum regulation policy (spectrum licenses are granted for exclusive use by the corresponding licensees) but in a more flexible way and at smaller time scale, which improves spectrum efficiency. Two approaches, namely, *spectrum property rights transfer* and *dynamic spectrum allocation*, have been proposed under this model. The former approach makes the spectrum property rights transferable from one licensee to another. In order to explore the most profitable use of the spectrum resource, economic market is adopted as an important method, which leads to spectrum trading. To be specific, in general, three factors, i.e., time, geographic area, and spectrum frequency, can be used to specify the spectrum property rights. Based on this approach, the spectrum licensees are allowed to flexibly sell or lease portions of their spectrums, such as the unused bands, to SUs and authorize them to use in certain geographic areas during certain time periods, which in turn creates revenue return for themselves. Note that spectrum trading is not limited to this model. For example, the shared-use-based spectrum trading model also exists, which is very practical because in some cases it is difficult for licensees to give up their precious spectrum rights considering the unpredictable demands in the future. Such a shared-use-based spectrum trading model has been implemented by FCC on 3.5 G band [2], which will be introduced in detail in section "The State-of-the-Art of Spectrum Trading". The latter approach is introduced by the European DRiVE project [10]. Such an approach aims to improve spectrum efficiency through dynamic spectrum assignment according to the spatial and temporal traffic statistics of different services. Similar to the current static spectrum licensing policy, this approach allocates spectrums to services for exclusive use, but the spectrum relocation occurs at a much smaller scale.

Cognitive Radios

With regard to the aforementioned DSA models, hierarchical access-based spectrum sharing has attracted increasing attention and been treated as a promising solution to the low spectrum utilization problem in the traditional SSA scheme. It allows unlicensed users to access a licensed spectrum under certain restrictions, which makes spectrum access more flexible. In such a way, spectrum efficiency can be improved significantly without losing the benefits associated with the traditional SSA scheme. However, legacy wireless devices were usually designed for a dedicated frequency band and incapable of spectrum sensing to identify spectrum holes, which makes them hardly utilize the improved flexibility provided by this sharing scheme. Cognitive radios (CRs), as smart radios, provide the adaptability and technologies for wireless transmissions and enable the spectrum sharing. Specifically, it can be regarded as a sophisticated radio device that mimics the human brain, perceives and learns the radio environment, and adjusts the transmission parameters accordingly (e.g., frequency band, modulation mode, transmission power, etc.) [8]. CR devices usually work collaboratively to form a network, a.k.a. the cognitive radio network (CRN). To achieve self-adaptive transmissions in a CRN, each CR device senses its local radio environment (distributed sensing), or a centralized sensing controller senses the whole network (centralized sensing). Then, the sensing results are processed either centrally or distributedly, which guide CR devices to control their transmission patterns, including modulation, transmission power, error control methods, etc., and establish communications accordingly.

Consequently, three main functionalities are associated with a CR device, namely, *spectrum sensing*, *spectrum management*, and *spectrum mobility* [8]. These three mechanisms can facilitate SUs to access the PUs' spectrum under the hierarchical access-based spectrum sharing. To be more specific, *spectrum sensing* can be employed to determine the status of PUs' spectrum bands. By periodically sensing PUs' activities on target spectrum bands, spectrum holes in temporal and/or spatial domain can be detected and thus leveraged by SUs (with CR devices) without causing too much interference. Then, based on the *spectrum management*, SUs can conduct their spectrum access and optimize their transmission parameters. By analyzing the sensed information, SUs can learn about spectrum access related information, such as interference estimation, available duration, collision probability, etc., and make spectrum access decisions, including frequency band, transmit power, time duration, etc., by optimizing their performance (e.g., achievable rate) under certain constraints (e.g., limited interference). When the PU returns or shifts to services with high QoS requirements, *spectrum mobility*, which is also called spectrum hand-off, plays an important role in making the SU switch to another idle spectrum band. Such a spectrum hand-off process must ensure that the parameters at different protocol layers can be adjusted to match the new frequency band so that the data transmissions of this SU can be continued.

In summary, the emergence of CR technologies makes the hierarchical access-based spectrum sharing possible. If the SU has CR ability, it can obtain and utilize the information on PUs' spectrums through spectrum sensing function, make

optimal decisions on spectrum access through spectrum management function, and change the operating frequency bands in order to continue data transmissions even in the context of the unpredictable return of PUs through spectrum mobility function.

Trading-Based Spectrum Sharing Mechanism

Although the emerging CR technology could provide a strong technical support for DSA and eliminate PUs' concerns on interference imposed by SUs if they open up their licensed bands, one key issue is why PUs are willing to share their preciously owned spectrums with others. To guarantee their QoSs, if there is no incentive, PUs might even prefer to transmit bogus data to keep spectrums occupied and deter SUs from using it. Therefore, it is essential to design proper mechanisms to provide incentives for PUs to share out their spectrum bands. From the economic aspect, spectrum trading, referring to the process of selling and buying spectrum resources, has been widely advocated as a promising mechanism for DSA and attracted a lot of attention. In spectrum trading, the spectrum owners (PUs) can sell their unused spectrum resources in certain geographic areas during certain time periods to unlicensed users (SUs) for monetary gains or performance improvements, and unlicensed users can purchase them to fulfill their desired communication goals at the monetary cost or resources (e.g., serving as relays for PUs). As a result, such a secondary spectrum market can realize the DSA with a win-win situation while generating high economic profits. In what follows, along with different directions, we will discuss various spectrum trading mechanisms proposed in the current literature.

Exclusive-Use Mode vs. Shared-Use Mode

As aforementioned, DSA can be implemented in an exclusive-use mode or a shared-use mode, which corresponds to two different spectrum trading operations. These two types of trading have different characteristics with different relevant problems, which, however, are ambiguous in many existing research works. To be specific, in the former case (exclusive-use), the spectrum access rights (including specific frequency bands, available regions, and time durations) are traded for exclusive use by SUs. In other words, within the leasing duration, the SUs who have purchased the access right turn to be the PUs and can exclusively use the purchased bands at the corresponding geographic areas. In turn, the original PUs cannot use them until the end of the leasing period. As for this mode, spectrum sensing and interference management are not critical issues anymore because the spectrum is exclusively used by either PUs or SUs. One key challenge here is on the seller side (PUs), namely, how to design an optimal selling/leasing strategy. Since the spectrum owners have to guarantee the QoS for their subscribed users, they have to reserve enough resource, and it is not an easy task to determine the access right for selling due to the unpredictable traffic in the future.

In the latter case (shared-use), if SUs want to use the purchased spectrum access right, they have to obey certain rules, rather than exclusively use it as PUs. In other words, the sold spectrum access right is utilized based on spectrum sharing among both PUs and SUs where PUs have higher priority. Generally speaking, overlay-based sharing has been widely adopted, where SUs have to monitor the PUs' activities and vacate the spectrum if PUs return even though they have purchased the access right. Actually, this mode can be treated as a hybrid mode with both exclusive-use and shared-use. Between PUs and SUs, it is based on shared-use to ensure PUs' QoS; and among SUs, it is based on exclusive-use that only the SUs who have purchased the access right can opportunistically access the spectrum. In fact, in comparison with the former mode, the shared-use mode is more practical because the rational spectrum owners are usually unwilling to totally give up their access right considering their unpredictable traffic demands. In the shared-use mode, one key challenge is on the buyer side (SUs), i.e., how to valuate the reward under the uncertain risk of purchasing certain access right. Due to the hierarchical sharing mode, it is important for SUs to capture the statistical features of the sold spectrums (e.g., by taking spectrum measurements) and determine an optimal buying strategy [11].

Monetary Reward vs. Resource Exchange

It is known that the radio spectrum resource is very valuable. In 2008, the auction of 700 MHz frequency band in the United States raised $19.59 billion for the US government. Therefore, as the traditional trading market in economics, currency, also referred to as money, is widely used as the payment in the spectrum trading market as well, i.e., in the so-called money-exchange trading model. Generally speaking, this model is most effective if PUs have redundant spectrum resource to sell because in this case, SUs are transparent to PUs and high monetary revenue can be gained, which is most interesting to PUs. However, if PUs' own traffic load is heavy or the primary channels' qualities are poor (e.g., due to the severe channel fading), there might be no extra spectrum resource left for sale. In this scenario, resource-exchange spectrum trading becomes an attractive option, where PUs could share spectrum with SUs in exchange for the performance improvement, such as increasing data rate or reducing probability of outage [12]. Under the barter-like trading rule, SUs provide communication resources for PUs in exchange for the access right to PUs' certain spectrum (also known as cooperative spectrum sharing).

Serving as relays is one typical way for SUs to obtain the spectrum access right in the resource-exchange trading model [13, 14]. To be specific, direct transmission of a primary session may be at a low data rate due to poor channel condition or long transmission distance. Thus, suitable SUs could be utilized as the cooperative relays for the PU's traffic to achieve a higher data rate accordingly. If the selected SUs join the cooperation and the primary session's data rate can be increased, the time occupied by this primary session on the licensed band can be decreased.

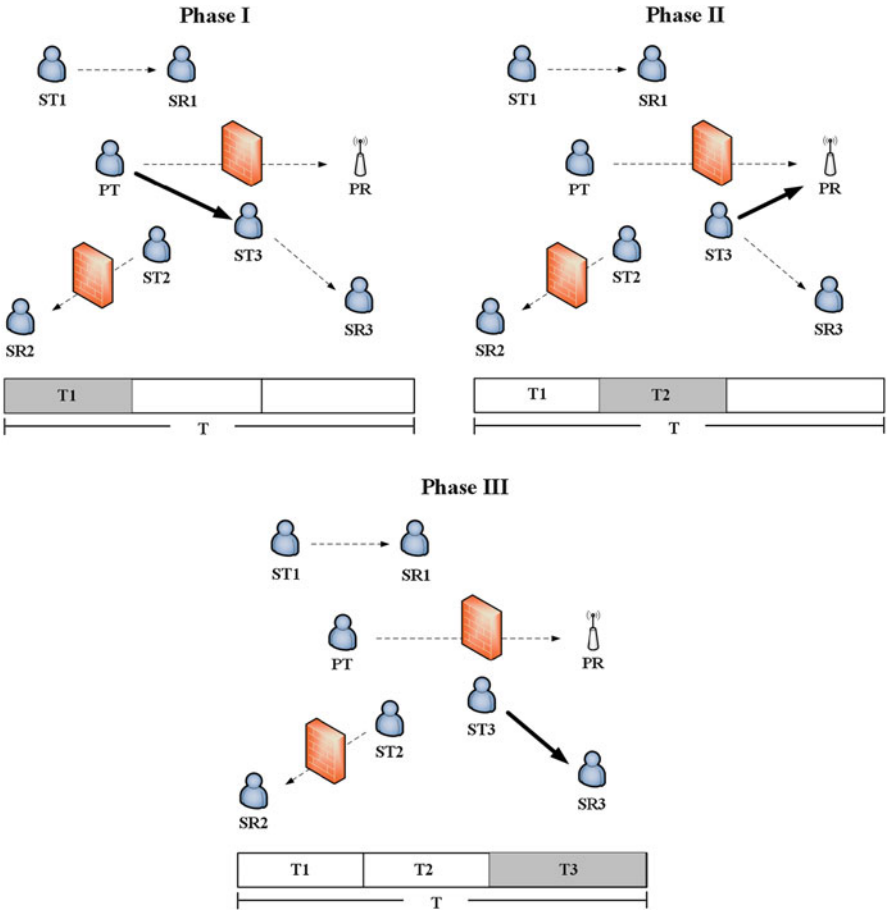

Fig. 1 A toy example of the relay-based resource-exchange spectrum trading

In return, the involved SUs could gain the access right for the remaining session period. Therefore, by exploiting relay-based cooperation between PUs and SUs as a resource-exchange trading mechanism, both sides can increase their own interests. Here, a toy example is presented as Fig. 1, where one primary transmission pair (PU) and three secondary transmission pairs (SU) coexist.

The PU has the exclusive access right to the licensed band with certain transmission task, but experiences a poor channel condition from its transmitter PT to its receiver PR, and the SUs have no right to use the spectrum for their transmissions unless explicitly permitted by the PU. Based on the resource-exchange trading, the PU employs some SUs to relay its traffic and allows involved SUs to use the spectrum after the primary session is completed. Suppose that the primary session is scheduled as T. In phase I, the primary transmitter PT broadcasts its data to the involved SUs who are willing to join the cooperation, by using T_1. In this

example, ST1 rejects the invitation because it is quite far away from PR, and ST2 rejects as well because of its poor channel condition between ST2 and SR2. The trading agreement can be reached by bargaining between the PU and SUs or adopting a contract-based approach in which the PU can claim different reward-effort combinations and design contracts for different SUs. In phase II, the involved SUs (ST3) relay the primary traffic to PR in either amplify-and-forward or decode-and-forward manner by using T_2. In phase III, the PU rewards the involved SUs (ST3) to use the spectrum within the remaining time period, i.e., $T - T_1 - T_2$ (if multiple SUs participate in the cooperation, they can share the spectrum by using TDMA with a dedicated time allocation managed by the PU).

Auction Market vs. Open Market

Auction Market

An auction is a process of procurement via competitive bidding. It is a traditional but efficient way to distribute commodities and especially suitable for the spectrum trading market because the price of a radio spectrum is difficult to be determined precisely in advance.

First, some basic terminologies in auction theory are introduced as follows [15]. (a) *Seller and bidder*: In auctions, a seller and a bidder (buyer) are the one who owns and wants to sell commodities and the one who wants to buy them, respectively. In the secondary spectrum market, the seller is usually the spectrum owner, and the bidder is usually a secondary user or a secondary service provider who wants to obtain the spectrum access right. (b) *Auctioneer*: An auctioneer works as an intermediate agent who receives bids/asks from both bidders and sellers and hosts and directs the auction process. In general, the auctioneer could be employed by the seller or certain third-party institution such as government agencies. (c) *Valuation:* In an auction, for each commodity, a bidder/seller has a reserved valuation in his mind, i.e., the monetary estimated value of it. Different players may value commodities with different valuations depending on their preferences. (d) *Clearing price*: According to the bids from bidders and asks from the seller, auctioneer will determine winners, charge them by certain price (so-called clearing price) and clear the market. Note that, for each winner, the charging price may not be equal to his bid. Generally, it is not higher/lower than the valuation of the bidder/seller on this commodity.

After introducing some basic definitions, we next present some typical auction types, which could be embedded in the spectrum trading market. (a) *Open-cry and sealed-bid auction*: In an open-cry auction, each buyer calls out his bid, i.e., the bidding strategy of each buyer is public. This type of auction is usually held in several rounds, and each buyer could adjust his bidding strategy according to others' calls which could reach a high revenue for the seller. However, generally, it is time-consuming and needs to make all bidders stay in one room. On the contrary, in a sealed-bid auction, buyers privately submit bids to the auctioneer without knowing others' bidding strategies, which is more suitable for the dynamic spectrum

trading. Specifically, first-price and second-price sealed-bid auctions are the two most important sealed-bid auctions. In both auctions, the winner is the buyer who submits the highest bid, but the charging prices are different. As for the first-price mechanism, the charging price is just his highest bid, but as for the second-price mechanism (also known as Vickrey auction), the charging price is equal to the second highest bid among all bidders. As a generalized Vickrey auction, Vickrey-Clarke-Groves (VCG) auction has attracted great attention because it can achieve the maximal social welfare due to its truthfulness property (introduced later), and many VCG-styled auction mechanisms have been proposed for the auction-based spectrum trading market. For an overview see section "The State-of-the-Art of Spectrum Trading". (b) *Single-sided and double-sided auction*: In the single-sided auction [16–19], the competition only happens on either seller side or buyer side, corresponding to the following two cases, one is that multiple sellers compete with each other to sell commodities to one buyer. In this case, Dutch auction (descending-bid auction) is usually adopted where each seller decreases the price from the initial setting ceiling price over time until the deal is completed. The other case is that multiple buyers compete for the commodity from one seller. Then English auction (ascending-bid auction) can be employed, in which the bids submitted by buyers increase monotonically until no higher bid comes out, and the buyer who offers the highest bid wins the auction. In practice, generally, multiple sellers and buyers coexist in the market, and thus double auction emerges to handle this scenario [20–23]. In a double auction, the auctioneer matches the asks from multiple sellers and bids from multiple buyers by allocating commodities from sellers to buyers and payments from buyers to sellers accordingly. (c) *Offline and online auction*: In an offline auction, the auctioneer will keep listening to asks from sellers and bids from buyers and determine the auction result at certain specified time points, i.e., the auction is based on a wait-and-clear procedure. Nevertheless, in an online auction [18, 22, 23], whenever the asks and the bids arrive, the market is cleared immediately, i.e., the auction is based on a real-time procedure. The online auction is more complicated than its offline counterpart but could reach a more flexible spectrum trading market, where the auction requests could be generated randomly and handled as soon as possible. (d) *Single-unit, multiunit, and combinatorial auction*: In single-unit auctions, each buyer bids for one commodity unit, while in multiunit auctions, each buyer bids for multiple commodities. The requested commodities may be partly or fully allocated to the buyers, and buyers can accept the case if only some of the requested commodities are received. However, in some cases, buyers may need a complete set of commodities. In other words, buyers bid for certain commodity bundles in an all-or-none mode, i.e., each bid for the whole bundle is either fully accepted or rejected. Such a scenario is common in spectrum trading market because a SU may need to use a set of bands within a large area to provide end-to-end services. To deal with such bidding requests, combinatorial auctions [24–26] can be applied. Since each buyer bids for certain bundles, the conflict relationships among different bidders will be more complicated and thus makes the optimal commodity allocation more difficult.

In general, an auction mechanism design mainly contains two components (no matter what type the auction is), namely, the winner determination and the pricing mechanism. There are many key issues to be considered.

(a) Winner determination: As for the winner determination process, social welfare maximum is usually adopted as the decision metric, which is defined as the sum of all auction participants' utilities, indicating the total profits produced in the market. By maximizing the social welfare, an auction could allocate each commodity to the buyer who values it the most, which is called allocation efficient or Pareto efficient. To be specific, for a buyer, if he wins the commodity, his utility is equal to the difference between his valuation and his payment (clearing price). For a seller who sells the commodity, his utility is the gap between the charging price and his valuation (reserved price). Then, for the auctioned commodity, the achieved social welfare is equal to the sum of all winners' valuations minus the reserved price of the sold commodity, and the optimal decision can be obtained by solving certain optimization problems. In addition to efficiency, fairness issue is also considered in some research works to ensure that different participants can benefit fairly in the auction, which could encourage buyers to join the auction. Different fairness levels can be developed, such as the basic level ensuring the equal chance for buyers to participate in an auction and the max-min fairness level to make each buyer at least receive a basic portion of commodities [27]. Generally speaking, in an auction market, efficiency and fairness cannot be achieved at the same time, and there should be trade-offs between these two metrics. Furthermore, different from the conventional auction, for the commodity which is not reusable, i.e., an auction in which commodity claimed by one buyer cannot be allocated again to others, in the spectrum auction, the radio resource can be allocated to many buyers simultaneously as long as they will not interfere with each other (e.g., sufficiently apart from each other). Such a special feature makes the winner determination process more complicated, and conflict graph model has been regarded as an effective way to handle the interference issue. Furthermore, the reusability also leads to some other interesting research works, such as the group-based auction [28] where multiple buyers targeting at the same radio resource group together as a virtual bidder and the corresponding profit sharing problem, i.e., how to share the profit among individual buyers in the same virtual bidder group [29].

(b) Pricing mechanism: With regard to the pricing mechanism design, the following three important economic properties are usually taken into account, namely, individual rationality (IR), budget balanced (BB), and incentive compatibility (IC, also known as truthfulness or strategy proof) [30, 37]. To be specific, IR property means that the charging price to certain winner cannot be higher than his bid. BB property indicates that the generated revenue of the trader should be nonnegative. These two properties are relatively easy to achieve. However, satisfying IC property, as an extremely important property to realize the maximal social welfare, is usually challenging for an auction design. In general, buyers in the market are selfish and may deceive others by submitting false information about their private valuations to gain more profit. In such a way, although some lying buyers may earn more profit, the social welfare may be impaired seriously. From this point of view, a

truthful auction design with IC feature can guarantee that each buyer will achieve the optimal utility only when he submits the truthful bid, reflecting his real valuation on the requested commodity. In other words, when IC property is satisfied, each buyer's dominant strategy (social choice) is to submit the true valuation no matter what other buyers' bidding strategies are. In such a way, the auctioneer can make the socially optimal winner determination just according to buyers' bids, which reflect their real valuations, and also prevent market manipulations. A simpler approach to achieve IC is referring to the existing auction mechanisms that have been proved to be IC, such as the typical VCG auction.

Open Market

Unlike the auction-based spectrum trading, instead of being controlled by an auctioneer, in an open market, PUs and SUs are allowed to sell and buy radio resources freely. Due to the flexibility in the open market, some new issues emerge accordingly, which lead to several interesting research directions. In the following, three popular marketing mechanisms are introduced, namely, pricing based, contract based, and bargaining based.

(a) Pricing-based mechanism: Different from the auction market, where the final price of the commodity is derived from buyers' bidding strategies (e.g., first-price or second-price mechanism), in the open market, the price of the commodity is designed by its corresponding seller. As the most important role in the open market, the pricing strategy of a seller will not only determine his revenue but also influence the decision of buyers, which usually stand on two opposite sides, e.g., a high price will increase the seller's revenue while reducing the satisfaction of the buyer. Due to the complicated relationships among different market participants, several factors will impact the price setting, such as the demand/supply of buyers/sellers, the competition among buyers/sellers, etc. Considering a typical scenario where multiple sellers and multiple buyers coexist, generally, three pricing models are involved, i.e., market-equilibrium model, competitive model, and cooperative model, corresponding to different levels of competition and cooperation among different sellers [31]. In the market-equilibrium pricing model, each seller is not aware of others, and the prices of commodities of each seller are natively set by himself according to the demand in the market. Specifically, since the price of commodities will influence the demand of buyers, the market-equilibrium price represents the price that makes the demand just equal to the supply in the market. Such a pricing strategy could ensure that there is no excess supply in the market and maximize both seller's profit and buyer's satisfaction. In general, demand function and supply function are considered in this model to derive the market-equilibrium-based solution. In the latter two models, sellers are aware of each other, and the prices are set in either a competitive or a cooperative manner. To be specific, in the competitive pricing model, each seller has its own interest to maximize his individual profit. Therefore, competition occurs in terms of pricing, and game theory can be used to deal with this situation. In general, a game formulation consists of three main components, i.e., players, actions, and corresponding payoffs. As for this situation, multiple sellers (i.e., players) offer prices (i.e., actions) to

sell commodities to buyers trying to maximize their profits (i.e., payoffs), and thus a noncooperative game can be adopted to model such a situation. The Nash equilibrium is usually considered as the solution to such a game model, where no seller can improve his payoff by deviating from the equilibrium, and the Nash equilibrium can be obtained by analyzing the best response function, i.e., the best strategy adopted by one player given others' strategies. Although more buyers could be attracted in the market through the competition among sellers, it may result in a low revenue for each seller. Therefore, instead of competing with each other, sellers may be willing to cooperate together to choose higher prices so that they can earn a higher profit than that in case of competition, i.e., the so-called cooperative pricing model. In addition to game theory (i.e., cooperative game), optimi zation approach could be employed as well in the cooperative pricing model, e.g., to achieve the highest total profit for all sellers.

(b) Contract-based mechanism: In some cases, precisely pricing commodities is inflexible or even hardly achievable for sellers (e.g., due to the limited knowledge about buyers' valuations). As a result, contract mechanism has been regarded as an effective approach in the open market [32–35]. To be specific, the seller can design a contract by offering different supply-price options to different buyers, such as different effort-reward combinations in resource-exchange market or different quality-price combinations in money-exchange market. Each buyer can choose to sign one of the contract items or reject. A typical example is the labor market, in which an employer offers a contract with several different items specifying different combinations of effort level and salary level. Each potential employee can select one of the contract items or refuse it to maximize his payoff according to his own capability and valuation. By means of the contract, buyers will gain enhanced satisfactions, and meanwhile sellers can optimally allocate their commodities to maximize own revenue or the social efficiency. Consequently, how to optimally specify the class of contracts so that both sellers and buyers are able to maximize their individual utilities is the most important issue for contract mechanism design.

(c) Bargaining-based mechanism: In the former two market mechanisms, the trading process is based on a monopoly market, in which the seller acts as a monopolist who sets prices or contracts for the sold commodities. Different from that, in the bargaining mechanism, the buyer and the seller can negotiate on the price and the requested commodities repeatedly until an acceptable solution for both sides is achieved (i.e., for certain commodity, the seller and the buyer take turns to offer and counteroffer until reaching an agreement). Such a bargaining mode is especially suitable for the multiplayer scenario, where each player prefers to reach an agreement rather than not, however, with conflicting interests. As a mathematical basis for modeling and analyzing interactive decision-making problems, game theory is commonly used for bargaining scheme design. For example, the Stackelberg game as a strategic game has attracted intensive attention, which contains two types of players, i.e., leader and followers. In the Stackelberg game, the leader moves first, and then the followers move subsequently. For the bargaining market, the seller acts as the leader, and the buyers acts as the followers, and the Nash equilibrium solution can be solved through backward induction, i.e., the leader makes the best decision

by predicting what the possible best response of the followers is and the follower moves according to the adopted strategy of the leader. In addition to the Stackelberg game, Bayesian game can also be used in the bargaining market when considering a common scenario that sellers and buyers do not have complete information about each other, in which probabilistic analysis plays an important role.

Summary

The aforementioned various classifications of spectrum trading along with different directions have been summarized as Fig. 2, including their categories, descriptions, features, and possible application scenarios.

The State-of-the-Art of Spectrum Trading

In this section, we present the state-of-the art of spectrum trading, including both practical initiatives implemented by the government and theoretical research works developed in the academic research community.

Auction-Based Spectrum Sharing Initiatives by Government

Although the dynamic spectrum trading market, where spectrum owners and unlicensed users can trade spectrum access right freely, is still in the draft, in practice, such an economic-based spectrum sharing mechanism has been implemented by the government to provide more spectrum for commercial use due to the booming growth on wireless services. In the United States, the radio spectrum is managed by two governmental agencies, namely, the Federal Communications Commission (FCC) and the National Telecommunications and Information Administration (NTIA). The former is responsible for managing the non-Federal use (e.g., commercial, private internal business, and personal use) and the latter for Federal use (e.g., used by the Army, the FAA, and the FBI) of the spectrum. In order to enable various wireless broadband technologies, the Presidential Memorandum in June 2010, "Unleashing the Wireless Broadband Revolution," called for the NTIA and the FCC to make 500 MHz of spectrum available for the wireless broadband use within 10 years [36]. Generally, the traditional way to make additional frequency bands available for commercial use is based on a clear-and-relocate process, i.e., clear the target spectrum (original users are moved to other bands) and relocate the cleared spectrum to new commercial users (e.g., by an auction). For example, in 2002, the NTIA and the FCC jointly reallocated the 1710–1755 MHz band from Federal use to non-Federal Advanced Wireless Service (AWS) use, also referred to as AWS-1. The spectrum relocation, although additional spectrum could be made available for commercial use as well, is extremely expensive and time-consuming. Take the case AWS-1 as an example, 12 Federal agencies representing 173 separate

	Categories		Descriptions	Features	Application Scenarios
Sharing Scheme	Exclusive-use		SUs can exclusively use the purchased spectrum access rights	Guaranteed QoS for SUs (higher selling price); No access by PUs; Selling strategies on spectrum owner side	Spectrum holes are determinant in both spatial and temporal domains, i.e., PUs have regular activities, e.g., TVWS
	Shared-use		SUs can use the purchased spectrum access rights only when PUs are inactive	Non-guaranteed QoS for SUs; Sharing mechanisms (PU protection); Buying strategies on SU-side (spectrum uncertainty)	Spectrum holes are unpredictable, e.g., 3.5GHz
Payment Mode	Monetary Reward		SUs pay money to spectrum owners for spectrum access rights	High monetary revenue gained by spectrum owners; Transparency of SUs for PUs	Spectrum holes exist
	Resource Exchange		SUs improve the QoS of PUs by using their own resources, e.g., as relays, to gain spectrum access rights in return	Improved QoS gained by PUs; Cooperation between SUs and PUs	No spectrum hole exists because of the heavy traffic of PUs or the primary channels' conditions are poor
Market Mechanism	Auction Market	Open-cry/Sealed-bid	SUs buy spectrum access rights through competitive bidding in an auction managed by an auctioneer	buyer-driven prices; Time-consuming (bidding decision-making, multi-round auction process, etc.); Two main steps: Winner Determination (social welfare maximum)+Pricing Mechanism (economic-robustness)	Difficult to pre-determine the selling price; Time scale is relatively large; A trusted auctioneer can be found to manage the auction process
		Single-sided/Double-sided			
		Offline/Online			
		Single-unit/Multi-unit/ Combinatorial			
	Open Market	Pricing-based Mechanism	SUs buy spectrum access rights directly from sellers based on their selling mechanisms	Specific price determined by the seller based on Market-equilibrium/Competive/Cooperation model	Sellers are willing to pre-determine the selling price; Time scale can be small because the trading process is flexible and simple without auctioneer as a controller
		Contract-based Mechanism		Multiple supply-price options offered by the seller	
		Bargaining-based Mechanism		Negotiation between buyers and sellers; Game theory	

Fig. 2 Summary of various spectrum trading classifications

systems with thousands of radio equipments in hundreds of locations have to move away from the 1710–1755 MHz band. Facing the serious drawback of the clear-and-relocate process, the NTIA and the FCC have been cooperating to develop advanced spectrum sharing schemes to fulfill the 500 MHz goal. Due to the high economic revenue of the spectrum resource, auction has been considered as an effective way to grant new licenses. As a result, many auction-based spectrum sharing actions on different frequency bands have been executed recently. Next, two concrete examples are presented, namely, AWS-3 and Citizens Broadband Radio Service (CBRS) at 3.5 GHz [2].

AWS-3

In March 2014, the Report and Order makes 65 MHz available for commercial use via auction (including 1695–1710, 1755–1780, and 2155–2180 MHz) and specifies some rules for sharing with incumbent Federal users (40 MHz to be shared). The incumbent Federal users will either relocate to other bands or share with the incoming commercial systems based on the establishment of certain geographic protection zones. In January 2015, the AWS-3 auction was conducted, which raised $41.3 billion in total with 31 winning bidders granted 1611 licenses. The new AWS-3 licensees must agree on the transmission rule where the incumbent Federal users within protection zones have higher priority for operation. In other words, the sharing is based on the underlay mode where the AWS-3 licensees within protect zones need to control their transmission power in order to avoid harmful interference imposed on incumbent Federal users. By using such an auction-based underlay spectrum sharing mechanism, high economic revenue has been generated, more spectrum has been made available to carriers, and meanwhile disruptions to Federal missions can be prevented.

CBRS at 3.5 GHz

In July 2012, the President's Council of Advisors on Science and Technology (PCAST) released its report "Realizing the Full Potential of Government-Held Spectrum to Spur Economic Growth," which claims that exclusive licensing is not the way to stepping forward and the advanced spectrum sharing should become the new paradigm [4]. The report proposes a new spectrum management mode by dividing the spectrum into large blocks, called spectrum superhighways, and allowing users with compatible services to dynamically share them on a priority basis. To be specific, users are classified into three tiers with different priorities, and all users are required to register in a database, called Spectrum Access System (SAS) database, which acts as the controller to manage the dynamic spectrum access. (a) The incumbent users, also called primary access users, are at the top tier with the highest access right. They would register their actual deployments in the SAS database and obtain the guaranteed protection against harmful interference in their deployment areas. (b) Secondary access users, also called priority access licensees, are at the secondary tier, who are issued short-term operating rights in certain specified geographic areas and would be protected from interference caused by the third tier users. However, they are required to vacate the spectrum when a

primary access user registers a conflicting deployment in the database. (c) General authorized access (GAA) users are at the third tier, who would be allowed to access the unoccupied spectrum opportunistically if there is no conflicting primary and secondary access users registering in the database. Particularly, the secondary access users and GAA users are required to query the SAS database to gain the permission to access certain spectrum. The implementation of CBRS at 3.5 GHz is just based on this three-tier sharing model proposed in the PCAST Spectrum Report, which enables incumbent Federal users, operating at the first tier, and CBRS users, operating at the second and third tier, to share spectrum via a dynamic spectrum access system, and the priority access licenses (PALs) at the secondary tier are allocated by an auction. Obviously, different from the AWS-3 case, the spectrum sharing for CBRS at 3.5 GHz is in an overlay sharing mode, and the auction for the PALs belongs to the shared-use trading model.

Spectrum Auction

The aforementioned spectrum auction, as a well-known economic-effective allocation mechanism, has been widely adopted for spectrum trading. Different auction models with different features have been embedded in the spectrum auction design.

VCG Auction

Vickrey-Clarke-Groves (VCG) auction is a type of truthful sealed-bid auction for multiple commodities. Such an auction allocates commodities in a socially optimal way (i.e., to maximize the total valuation of winners) based on the bidders' bids (equal to their true valuations) and charges each winner the harm he causes to other bidders. Suppose that there are $\mathscr{M} = \{c_1, \cdots, c_m\}$ commodities and $\mathscr{N} = \{k_1, \cdots, k_n\}$ bidders in the auction. For the bidder k_i, his bid for the commodity c_j is expressed as $b_i\left(c_j\right)$, which is equal to his valuation due to the guarantee of truthfulness in VCG auctions. Then, based on the VCG mechanism, the socially optimal allocation can be formulated as the following optimization problem

$$\begin{aligned} &\text{Max} \quad \sum_{j=1}^{m} \sum_{i=1}^{n} b_i\left(c_j\right) \cdot x_{ij} \\ &\text{s.t.} \quad \sum_{i=1}^{n} x_{ij} \leq 1, \ \forall j \in \mathscr{M}, \quad x_{ij} \in \{0,1\}, \end{aligned} \tag{2}$$

in which the integer x_{ij} indicates whether or not k_i wins c_j. In some cases, each bidder only allows to win one item, then, the constraint $\sum_{j=1}^{m} x_{ij} \leq 1, \forall i \in \mathscr{N}$ can be included as well. Denote the achievable social value of this VCG auction as $V_{\mathscr{N}}^{\mathscr{M}}$, i.e., $V_{\mathscr{N}}^{\mathscr{M}} = \sum_{j=1}^{m} \sum_{i=1}^{n} b_i\left(c_j\right) \cdot x_{ij}$, and use $\mathscr{A} \backslash \mathscr{B}$ to represent the set of elements of $\mathscr{A}$

which do not belong to $\mathscr{B}$. Assume that k_i wins c_j, i.e., $x_{ij} = 1$, then, the charging price to k_i for c_j can be calculated as $V^{\mathscr{M}}_{\mathscr{N}\setminus\{k_i\}} - V^{\mathscr{M}\setminus\{c_j\}}_{\mathscr{N}\setminus\{k_i\}}$. The first term represents the total valuation of others if the bidder i does not participate into the auction, and in the second term, the commodity c_j is excluded from the available commodity set due to the participation of the bidder i. Therefore, such a gap indicates the harm that the bidder i causes to others. A simple example is presented here for a better understanding. Assume that there are two bidders with bidding values $b_1(c_1) = 10$, $b_1(c_2) = 6$, $b_2(c_1) = 7$, $b_2(c_2) = 5$ for two commodities and each bidder is allowed to get only one commodity. Obviously, the socially optimal allocation is to let k_1 get c_1 and k_2 get c_2, achieving the maximal social value 15. According to the aforementioned pricing mechanism, the charging price to k_1 for c_1 should be $7 - 5 = 2$ and that to k_2 for c_2 should be $10 - 10 = 0$.

The VCG auction guarantees the most important truthfulness property, i.e., forces buyers to bid truthfully in the sense that bidding lower than the true valuation does not gain anything advantage, and thus achieves the maximal social welfare. Therefore, it has attracted great attention and inspired many truthful VCG-styled spectrum auction development. Due to the specific feature of radio resource, i.e., spectrum reusability in different regions, the truthful design on spectrum auction is different from (and much more difficult than) that in conventional auctions. Zhou et al. developed the first truthful and computationally efficient spectrum auction scheme, called VERITAS, in [16], which consists of a greedy spectrum allocation algorithm for winner determination and a VCG-styled pricing mechanism to charge winners. Take the scenario (conflict graph) in Fig. 3 as an example. Each vertex represents a bidder, i.e., there are totally five bidders in this auction. The edge between two vertices indicates that they conflict with each other, i.e., a spectrum band cannot be allocated to these two bidders at the same time. Suppose that there are two bands auctioned in this market denoted as f_1 and f_2 and each bidder bids for one (for each bidder, either f_1 or f_2 is acceptable). The bidding values of the five bidders are shown in Fig. 3 as $b_1 = 6, b_2 = 5, b_3 = 4, b_4 = 3$, and $b_5 = 1$. First, the greedy algorithm is adopted to allocate the two bands. Specifically, it sequentially allocates spectrums to bidders from the one with the highest bid to the one with the lowest bid, considering their conflicting relationships. For each bidder, the algorithm first checks whether or not there is an available band for him. If so, it assigns him one band with the lowest available index. Consequently, the allocation process can

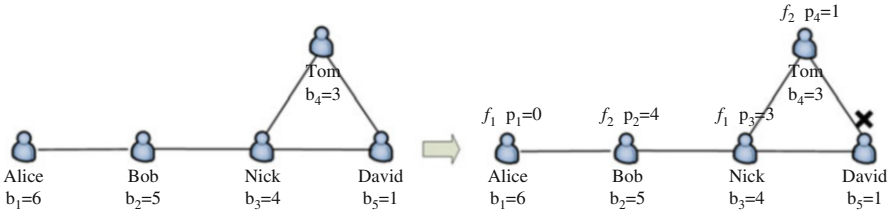

Fig. 3 An example of VERITAS scheme

be described as follows: (Alice gets f_1) → (Bob gets f_2) → (Nick gets f_1) → (Tom gets f_2) → (David gets nothing). After the greedy allocation, a VCG-styled pricing mechanism is applied on the winners to calculate their payments. To be specific, the charging price of each winner i is the bidding value of his critical neighbor (i.e., the one of the i's conflicting neighbors where if i bids lower than his, i will lose, and if i bids higher than his, i will win). Take Alice and Nick as an example. Alice does not have a critical neighbor because even if she bids lower than her neighbor Bob, e.g., 4.5, she can also win the auction with f_2, i.e., (Bob gets f_1) → (Alice gets f_2) → (Nick gets f_2) → (Tom gets f_1) → (David gets nothing). Therefore, the charging price to Alice is 0. Nick has three conflicting neighbors, i.e., Bob, Tom and David, and Tom is his critical neighbor because if he bids lower than Tom's bid 3, Tom will get f_1 based on the greedy algorithm and Nick will lose the auction. Therefore, the charging price to Nick is 3. Similarly, the charging price to Bob and Tom is 4 and 1, respectively. It is noteworthy that comparing with the aforementioned VCG pricing mechanism, the charging price to winner i in VERITAS can be denoted as $V^{\mathscr{M}}_{\mathscr{N}\setminus\{k_i\}} - \left(V^{\mathscr{M}}_{\mathscr{N}} - b_i\right)$, which can be treated as a special VCG mechanism due to the reusability of the auctioned commodity. Such an auction mechanism can be proved to be truthful, and detailed proof can be found in [16].

According to the VERITAS design, a key rule for truthful spectrum auction design is summarized here by satisfying the following two crucial factors: (a) The resource allocation process (winner determination) is monotonic, i.e., if a bidder could win/lose by certain bid, he could also win/lose if he bids higher/lower. (b) The charging price for a winner is the critical value (boundary value) of him, i.e., if he bids higher than that, he would win, otherwise, he would lose. Under different scenarios, the monotonic allocation and the critical value could be different, and readers could refer to such a design rule to develop different truthful spectrum auction schemes. For example, in [17], Li et al. considered the multi-hop scenario by modeling unlicensed users as secondary networks (SNs) with end-to-end routing service requests. A truthful heuristic auction scheme with the consideration of inter-SN interference and a truthful randomized auction framework based on primal-dual linear optimization were proposed. Also targeting at the multi-hop communication scenario, in [37], Li et al. proposed a novel economic-robust transmission opportunity auction scheme (TOA). Different from the case in [17], in [37], the bidders are the individual SUs with certain multi-hop data transmission tasks, rather than SNs, which are deployed by a secondary service provider working as a network operator. To support the multi-hop data traffic, instead of using spectrum bands as the auctioned commodities, in the TOA scheme, each SU bids for transmission opportunities (TOs), i.e., the permit of data transmission on a specific link using a certain band (link-band pair). Based on the sophisticated design on TO allocation, TO scheduling, and TO pricing, the developed TOA scheme can satisfy all the IC, IR, and BB properties. Similarly, to support the end-to-end service in multi-hop networks, Pan et al. developed a session-based spectrum trading system in [38] and [39] and further designed an economic-robust session-based auction scheme in [40] by following the aforementioned design rule. In [18], considering the dynamic CRN environment, Sodagari et al. developed a truthful online auction

for expiring spectrum sharing, where the SUs are allowed to arrive and participate in the auction with expiring spectrum bands at any time. The SUs are required to submit their valuations and arrival-departure time instances, which can be enforced to be truthful. In order to enable bidders' flexible strategies in terms of demands and valuations, in [19], Feng et al. designed a novel truthful auction mechanism called Flexauc, in which each bidder can bid for any amount of demands with different valuations and will be satisfied with any possible result.

Double Auction

Double auction is also a common auction model when multiple sellers are involved, in which buyers bid for resources and sellers compete for demands. As an extension of the single-sided truthful auction design in [16], in [20], Zhou et al. proposed a framework for truthful double auctions called TRUST. To be specific, based on the conflicting relationships, buyers are formed into many groups. Then, by comparing the sellers' asks with the buyer groups' bids, several matching seller/buyer-group pairs are selected as the auction winners, and payments are made from the winning buyers to the winning sellers. In [21], Chen et al. developed a truthful double auction mechanism with the consideration of the heterogeneity of spectrum, called TAMES, in which each buyer is allowed to submit a bidding profile to express his diversified valuations for different spectrum bands. Similarly, buyer grouping, matching allocation, and VCG-styled pricing are adopted by the TAMES. In [22], Wang et al. designed a truthful online double auction (TODA) scheme because the selling/buying requests from PUs/SUs often come in an online fashion. In the TODA, once the auctioneer receives spectrum requests, it will decide and match winning SUs and PUs immediately and also determine how much SUs should pay and PUs should get. By incorporating the buyers' location information into the auction mechanism design, a location-aware online truthful double auction scheme called LOTUS was proposed in [23], which has considered the sporadic nature of spectrum requests and the geographic feature of buyers.

Combinatorial Auction

Combinatorial auction has been regarded as a widely used model for spectrum auction as well because in general, to satisfy the end-to-end QoS, the SU may need to bid for a whole bundle of frequency bands covering certain regions during an extended time period in an all-or-none mode. In [24], Zheng et al. modeled the heterogeneous spectrum allocation as a combinatorial auction, named AEGIS, with the consideration of five features, i.e., strategic behaviors of unknown users, channel heterogeneity, preference diversity, channel spatial reusability, and social welfare maximization. Specifically, two mechanisms are developed, i.e., a direct revelation combinatorial spectrum auction mechanism for unknown single-minded users (AEGIS-SG) and an iterative ascending one for unknown multiple-minded users (AEGIS-MP). In [25], Dong et al. modeled the spectrum opportunity in a time-frequency division mode and proposed a truthful combinatorial auction with the consideration of time-frequency flexibility. It consists of a polynomial-time and near-optimal winner determination algorithm and a novel payment mechanism that

guarantees the truthfulness. Many-to-many matching theory was adopted in [26] to realize the combinatorial auction, in which buyers can freely express their preferences for different combinations of spectrum bands. Instead of achieving the maximal social welfare, the stable status is the main goal of the interference-free spectrum matching where both sellers and buyers are satisfied with the result.

In addition to the investigation of various auction models, there are also many other hot research directions for spectrum auction in the literature, such as the allocation objective design, the bidding strategy adaption, the multitier architecture development, etc. (a) With regard to the optimization objective for resource allocation (winner determination), in [41], Huang et al. proposed a flexible one that can be set to maximize either the overall social efficiency (social welfare) or the expected revenue. In order to prevent some bidders from starvation in the long run, in [27], Gopinathan et al. brought the fairness criterion into the objective to increase the diversity of the winners. In general, such an optimization problem involving interference-free scheduling is essentially an NP-hard graph coloring problem [15], which, therefore, attracts many research works to develop approximation algorithms. For example, in [41], a series of near-optimal mechanisms were proposed based on many approximation techniques, namely, linear programming (LP) relaxation, randomized and de-randomized rounding, monotone de-randomization, and Lavi-Swamy method. In [16] and [17], heuristic algorithms were employed to achieve the truthful auction based on the rule that combines the monotonic allocation and critical value-based pricing. In [25], a polynomial-time approximation algorithm that could reach the upper bound of the worst-case approximation ratio was developed. (b) Furthermore, as for the bidding strategy adaption, many interesting updating techniques have been proposed, which are usually based on the auction results in the past and other auction participants' statistical information. For example, in [42], Fu et al. proposed a best-response learning algorithm for bidders to improve their bidding policies based on the historical information on bidding and allocation, the current auction participants' statuses, and the estimated future auction results. In [43], Han et al. considered a repeated auction game and developed a Bayesian nonparametric belief update scheme based on the Dirichlet process. According to the proposed bidding learning algorithm, buyers can alter their bidding strategies optimally. (c) Moreover, to enable a more flexible auction market, the multitier auction framework has been studied as well. For example, in [44], Tang and Jain presented a hierarchical auction model where multiple auction markets are cascaded as multiple tiers to iteratively trade the spectrum resource. In [45], Lin et al. developed a three-stage auction framework, including an outer auction between secondary access point (SAP) and SUs and an inner auction between spectrum holder and SAPs.

Spectrum Trading in Open Market

Different from the auction market where the trading process is hosted by an auctioneer, the open market is more flexible where sellers and buyers could freely conclude the transactions with each other by reaching certain agreement, which

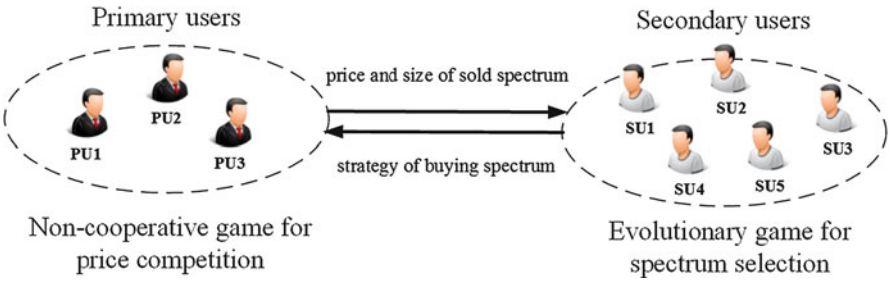

Fig. 4 A game-theoretic framework for spectrum trading in an open market

makes the relationship among the market participants more complicated. A typical open market with multiple PUs selling spectrum opportunities to multiple SUs was considered in [46], and the interactions among PUs and SUs were modeled by a game-theoretic framework. As shown in Fig. 4, in general, there are two levels of competition in such an open market. The first one happens among different PUs in terms of the size and the price on their sold spectrum bands. Denote the total bandwidth owned by PU i as B_i, the size for sale as b_i, and the number of SUs demanding that spectrum as n_i. Assume that all spectrum demanding SUs are allocated with the same size of the spectrum, i.e., b_i/n_i, and charged with the same price p_i. Then, the payoff, also called *net utility*, of PU i can be defined as

$$\gamma_i\left(\mathbf{b},\mathbf{p}\right)=\mathscr{U}\left(B_i-b_i\right)+p_i\cdot n_i\left(\mathbf{b},\mathbf{p}\right), \tag{3}$$

in which $\mathscr{U}(b)$ represents the utility function of a user when using the spectrum with bandwidth b, and it is usually defined as a logarithmic function, e.g., $\mathscr{U}(b)=u_1\log\left(u_2\cdot b\right)$ (u_1 and u_2 are constants that depend on the application type). $\mathbf{b}$ and $\mathbf{p}$ indicate the size and the price vectors, respectively, corresponding to all PUs, which will influence the demanded spectrum from SUs. In order to maximize its own payoff, each PU should set the size and the price carefully. If the size is small and/or the price is high, SUs may buy from other PUs. Conversely, if the size is large and/or the price is low, although many SUs may be attracted, the payoff may be low because of the low price and the poor utility of their usage. Such a competitive spectrum selling can be modeled as a noncooperative game, and the Nash equilibrium may provide an optimal solution. In this case, the Nash equilibrium can be obtained by using the best response function, i.e., the best strategy of one player given others' strategies, which can be described as

$$\{b_i^*,p_i^*\}=\arg\max_{b_i,p_i}\gamma_i\left(b_i,p_i,\mathbf{b}_{-i},\mathbf{p}_{-i}\right). \tag{4}$$

The other level of competition occurs among the SUs. The payoff of one SU, if he buys spectrum from PU i, can be expressed as

$$\phi_i=\mathscr{U}\left(b_i/n_i\right)-p_i. \tag{5}$$

Obviously, if many SUs choose to buy spectrum from the same PU, the spectrum may become overutilized, or the price may be increased, resulting in poor performance and low payoff for each SU. Consequently, the rational SUs will buy spectrum bands with low price while achieving reasonable performance, which can be modeled as an evolutionary game. Note that the evolutionary equilibrium, i.e., the final buying strategy of each SU, will in turn influence the selling strategies of PUs, which has been considered in the best response function to achieve the Nash equilibrium.

As for the spectrum trading in an open market, the pricing strategy of PUs is usually treated as the most important design issue because it influences the benefit of each trading participant. In [31], Niyato et al. investigated three typical pricing models for spectrum trading, namely, market-equilibrium, competitive, and cooperative pricing models, which aims at satisfying spectrum demands from SUs, maximizing individual profit, and maximizing total profit, respectively. In [47], Xing et al. explored the price dynamics in the market with multiple competitive sellers. A myopically optimal strategy was developed when full information is available to the sellers, and a stochastic learning-based strategy was studied when the information is limited. In [48], by considering different states of the primary channel (e.g., good or bad), Bajaj et al. investigated the optimal pricing that maximizes the PU's payoff under three scenarios, i.e., overlay-based spectrum sharing, relaying-based spectrum sharing, and underlay-based spectrum sharing.

In addition to the pricing mechanism, contract mechanism has also been regarded as an effective mechanism for spectrum trading, in which the seller could design several options with different supplies and prices as a contract or the items in one contract for different buyers by considering their different characteristics, and each buyer could choose one to sign or reject. For example, in [32], Gao et al. designed a monopolist-dominated quality-price contract, which is offered by the PU with a set of quality-price combinations corresponding to different consumer types, and further derived the optimal contract, which maximizes PU's utility. In [33], Gao et al. investigated a hybrid spectrum market, consisting of both future market with guaranteed contracts (including the price, the guaranteed supply, and the penalty if PU violates the contract) and spot market with spot transactions (where SUs buy spectrum in a real-time and on-demand mode). They focused on the PU's expected profit maximization and addressed the problem on how to optimally allocate the idle spectrum among contract users and spot market users. Similarly, a two-stage spectrum trading market, including a long-term market and a short-term market, was studied in [34]. In the long-term market, the PU designs a set of contracts for different types of SUs, and the optimal contract is developed. In the short-term market, SUs can buy some amount of spectrum in a real-time manner, and the interaction between the PU and SUs is modeled as a Stackelberg game. In [35], Jin et al. proposed a novel insurance mechanism for spectrum trading, in which the PUs serve as spectrum sellers as well as insurers. With the insurance contracts, SUs simply purchase the spectrum or sign an insurance contract with the PU to obtain insurance for the potential accident, i.e., transmission failure incurred by the excessively poor channel quality. Such a market game was modeled as a four-stage

Bayesian game characterized by the second-best Pareto optimal allocations and the perfect Bayesian equilibrium.

Instead of the preceding monopolistic market, in which sellers as monopolists to determine prices or contracts, in some cases, buyers are allowed to negotiate with sellers, which is called the bargaining-based market. Such a market mechanism could provide more incentives for buyers to participate because they could express their intentions in the market and thus more transactions could be achieved. In [49], a two-tier market was proposed for decentralized dynamic spectrum access. To be specific, in the tier-1 market, spectrum is traded from a PU to several SUs in a relatively large time scale, which is modeled by a Nash bargain game, and the equilibrium prices are derived. The tier-2 market is set up by SUs to redistribute channels among themselves in a small time scale, which is modeled by a strategic bargain game that SUs can exchange channels with low overhead through random matching, bilateral bargain, and the predetermined market equilibrium price. Actually, such a bargaining mode is especially suitable for the resource-exchange-based spectrum trading, also referred to as cooperative spectrum sharing/trading. For example, in [13], Yan et al. studied a cooperative spectrum sharing scenario with one PU and one SU where the SU was allowed to opportunistically use the licensed band if he relays the PU's traffic. By considering the incomplete information obtained by the PU, the dynamic bargaining process was modeled as a dynamic Bayesian game, and the equilibria was investigated under both single-slot and multi-slot bargaining models. In [14], Simeone et al. considered the cooperative spectrum sharing scenario with multiple SUs. The PU leases the spectrum for a fraction of time to a subset of SUs in exchange for the cooperation, i.e., relaying. On the one hand, the PU attempts to maximize his QoS in terms of either rate or probability of outage. On the other hand, the SUs compete with each other for transmission within the leased time period based on a distributed power control mechanism.

After reviewing the state-of-art of spectrum trading, in the next section, we will discuss some related practical issues and then present a novel flexible network architecture, called *cognitive mesh assisted network*, accordingly. Furthermore, we will demonstrate how to leverage the new network architecture to design an efficient service-oriented spectrum trading scheme.

Service-Oriented Spectrum Trading

Given all these spectrum trading schemes, natural questions to ask are how much cost do they have to pay to implement such schemes and how much end-users can benefit. To address these questions, we may have to revisit our prior research on cognitive radio networks [38, 39, 50–53], particularly on practical implementation consideration. In this section, we first discuss some of the practical issues, then present our flexible network architecture developed previously, followed by our recently proposed service-oriented spectrum trading (SOST) scheme to facilitate end-users to benefit from the spectrum trading [55].

Design Issues and Concerns for CRNs

In this subsection, we first discuss several issues when end-users are directly involved in spectrum trading processes.

Decision-Making for End-Users: End-users might lack necessary expertise and intelligence to join the spectrum trading processes. Similar to its counterpart in economics, spectrum trading requires buyers to specify desired commodities (i.e., spectrum bands) with certain valuations. In contrast, what end-users exactly know is just the service they want to acquire, such as downloading an HQ-video with 1.5 Gbits from Dropbox within 10 min. To join the spectrum trading processes, end-users must convert their service requests to desired bands and the corresponding valuations. Specifically, end-users should decide how much spectrum is needed to meet the QoS, which set of bands is the best choice, how to evaluate different bands, and so on. Clearly, it is not an easy task to make these decisions without specialized knowledge in telecommunications. Even with necessary knowledge, end-users might still not be able to specify their desired bands because of difficulties in gathering intelligence. How much each end-user can gain from purchased spectrum bands depends on PUs' activities, network topology, and the decisions of other end-users, particularly when destinations cannot be reached within one hop. When end-users look for extra spectrum resources for service delivery, they have already suffered from the lack of spectrum resources and might not have enough spectrum bands to collect necessary information for decision-making.

Implementation of Spectrum Markets: Considering the large number of end-users, it will cast a heavy burden on spectrum markets if these users directly join spectrum markets. On the one hand, spectrum markets should be able to interact with substantial number of end-users. To facilitate spectrum trading, spectrum markets need to exchange various kinds of information with end-users, including spectrum band availability, reserve price for each band, and end-users' desired bands and the corresponding valuations. This implies that some exclusive reliable bands/channels must be reserved for fast information exchange, but where do they come from? On the other hand, the extremely large number of end-users will impose considerable computational complexity on spectrum markets, which may become the bottleneck, even for some heuristic algorithms to achieve an approximate maximum of social welfare. For example, unlike traditional trading in economics, since one band can be shared among many nonconflicting users in spectrum trading, spectrum markets need to figure out the conflict relationships among different users' transmissions, which is a very daunting task.

Uncertain Spectrum Availability: Other than above issues, spectrum uncertainty is also an important factor for spectrum trading, which makes it challenging for end-users to directly participate in the spectrum trading processes. The basic premise of CRNs is to protect PUs from being interfered by SUs. In other words, despite end-users' payments for spectrum access, what they obtained is actually

the right to *opportunistically access* these licensed bands, rather than accessing them freely and unconditionally as PUs. End-users still need to obey the FCC ruling and immediately evacuate from the licensed band if the PU returns. This observation has two implications. First, end-users should consider potential risks (service interruptions due to the return of the PU) when purchasing a band. However, due to limited information, it is difficult for end-users to make the appropriate judgement on the potential risk. Second, end-users need to execute spectrum sensing to monitor PUs' activities when accessing licensed bands. These spectrum sensing may consume too power, imposing unbearable burdens on SUs' lightweight mobile devices in terms of energy consumptions.

Capabilities of End-Users' Devices: Even if the aforementioned issues could be well addressed and end-users could get what they need from the spectrum market, they might still not be interested in joining spectrum markets due to limitations of their communication devices. To trade and access licensed spectrum bands, end-users must have frequency-agile communication devices to search for unused licensed bands, reconfigure the RF front end, switch among a wide range of spectrum bands (e.g., from MHz bands such as TV bands to GHz bands such as 5 GHz unlicensed bands), and send and receive packets over potentially noncontiguous spectrum bands. According to [1], by 2020, nearly 50% of global devices and connections will be handheld smartphones which will account for more than four-fifths of mobile data traffic. Due to limited size, it is extremely difficult to embed cognitive radio capability into these lightweight handheld devices. Although some of the desired features could be implemented in these devices in the future, significant amount of time and efforts must be devoted to design more capable hardware devices as well as more efficient signal processing algorithms. Besides, even if it is possible to have lightweight handheld communication devices with CR capability, the prohibitively high price of these new fancy devices might discourage end-users, especially the economically disadvantaged ones, from joining the spectrum trading processes.

In view of above concerns, it would be ideal if there is a network to assist end-users to join spectrum markets, which is the theme of the next subsection.

Cognitive Mesh Assisted Network Architecture

In this subsection, we elaborate our formerly proposed flexible network architecture, called *cognitive mesh assisted network (CMAN)* or *cognitive capacity harvesting network (CCHN)*, as shown in Fig. 5, where an SSP is introduced to manage the services for end-users [38–40, 50, 53, 54]. Our CMAN consists of an SSP, a group of SUs, a set of base stations (BSs) and cognitive radio routers (CR routers), and a collection of licensed spectrum bands, i.e., *basic bands*. The SSP can be either an existing wireless service provider or an independent wireless service provider which is willing to provide better or new kinds of services to their customers. BSs are deployed by the SSP via, for example, leasing infrastructure (towers and cables)

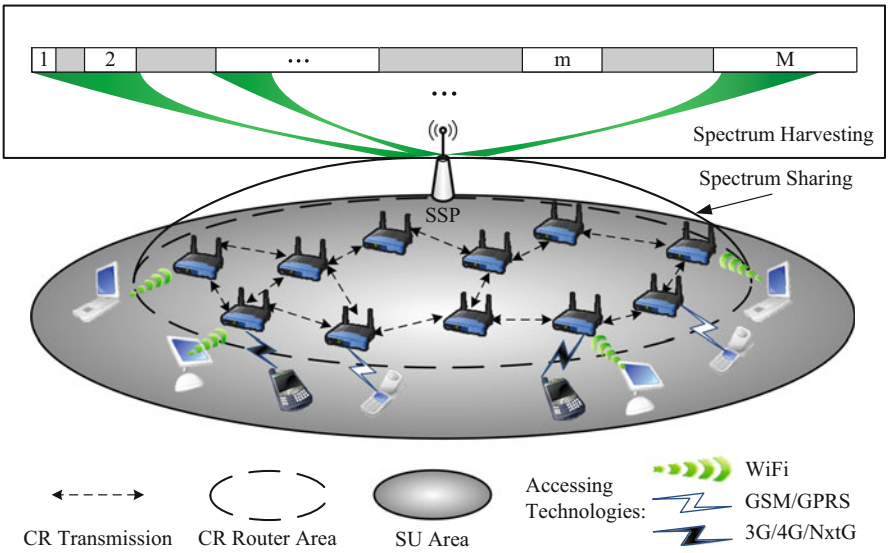

Fig. 5 The cognitive capacity harvesting network architecture for spectrum trading

from an existing cellular operator but with its own transceivers and spectrum bands to reduce initial deployment costs. BSs are interconnected via data networks and allow the SSP to gain access to data networks. The SSP employs BSs as an agent to exchange control signaling with CR routers and SUs as well as to provide basic coverage services. CR routers are deployed by the SSP to assist BSs in service provisioning. Specifically, under the supervision of the SSP, CR routers collectively form a cognitive radio mesh network (CMN) as a backhaul network between SUs and BSs for data transportation. It should be noted that BSs and CR routers are equipped with cognitive radios and communication interfaces, including the basic band interface. The basic band is mainly used for control message exchange between BSs and CR routers, user access related control signaling, and, if possible, data delivery in both the access network and the CMN. The cognitive radio interface is mainly used for data delivery in the CMN. Depending on SUs' locations, mobility, and service requests, they connect to either BSs or CR routers for services. If SUs have cognitive capability (i.e., equipped with cognitive radios), BSs and CR routers can deliver data services to these SUs via cognitive radio interfaces. If SUs do not have cognitive radio interfaces, BSs and CR routers can tune to the interfaces which SUs normally use for service delivery. CR routers collect SUs' traffic requests via basic bands and submit the aggregated traffic requests to the SSP. After receiving these data requests, the SSP make centralized network optimization by jointly considering link scheduling, flow routing, and resource allocation and sends the coordination decisions back to CR routers via BSs. According to these decisions, CR routers in the CMN collectively deliver data services to SUs. Since this may potentially reduce the transmission range for the last-hop communications

to the end SUs, the frequency reuse for the bands used for network access can be significantly increased with proper frequency planning, resulting in high spectral efficiency.

The CMAN architecture can help end-users interact with spectrum markets without knowing what the spectrum market is, which spectrum bands are needed, and how to complete their data transmissions. End-users only need to know their expected services and affordable monetary costs. They submit their service requests and their valuations of these services to the SSP, i.e., end-users bid for services from the SSP instead of spectrum resources from the spectrum markets. Once end-users' data requests are received, the SSP will search for appropriate spectrum resources in spectrum markets according to end-users' service requests and spatial distributions, prices of different bands and how these bands will be utilized, etc. As an operator, the SSP always attempts to maximize its own profits, and thus how much spectrum the SSP should purchase from spectrum markets is closely related to end-users' bids, which implies that end-users interact with spectrum markets via the CMAN. Such a spectrum trading scheme is referred to as the SOST scheme to emphasize the fact that end-users purchase services instead of directly purchasing spectrum bands in most existing research works.

Compared with end-user-based spectrum trading, the SOST scheme has many attractive features. First, in the SOST scheme, each end-user only needs to submit its service request and bidding allowance to the SSP, and the SSP will act as an agent to bid for bands that can support the requested services. This shifts the complexity from SUs' side to the operator which is more trustworthy and has more bargaining power and credibility. Second, as a network operator, the SSP can collect necessary network intelligence and make centralized optimization accordingly to determine which bands to purchase. Third, the number of SSPs will be much fewer than that of end-users, which not only reduces the complexity but also improves the efficiency of spectrum markets. Fourth, since services in the CMAN are carried over the CMN, end-users are not aware of the specific spectrum allocation across the whole session (i.e., from the source to the destination). Even if an SU overhears the bids of other SUs, it is not helpful since the SU is not sure who are his competitors for spectrum usage, which simplify the spectrum trading mechanism design. Finally, this SOST scheme does not pose any additional requirements on end-users' communication devices. Even for end-users without cognitive radio devices, they can still benefit from spectrum trading, which allows the SSP to extend its services and enhance the prosperity of spectrum markets.

CMAN-Based Two-Tier Service-Oriented Spectrum Auction

In this subsection, we introduce the basic operation process of the SOST scheme by taking the auction market as a concrete example. For illustration, we consider a secondary spectrum market with one primary service provider (PSP) and N infrastructure-based secondary service providers (SSPs). The PSP can share its licensed bands for economic profits, and SSPs can bid for them to support their own

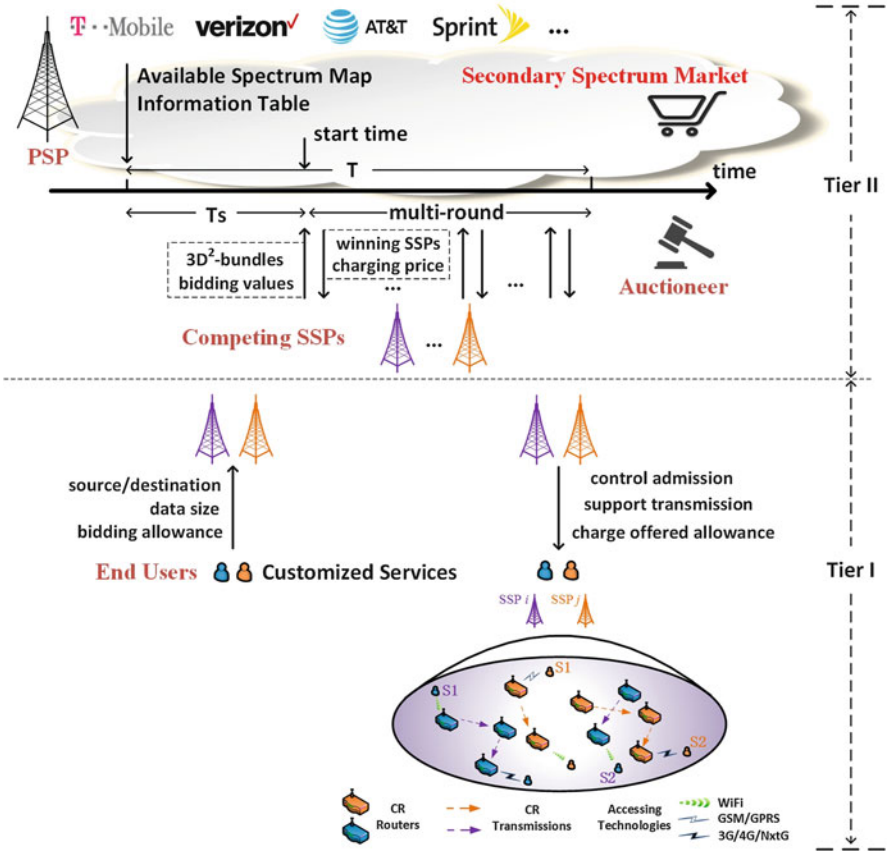

Fig. 6 Two-Tier framework for multi-round service-oriented combinatorial spectrum auction

wireless services. To be specific, a multi-round auction is held periodically in the market. At each period, the PSP constructs a fine-grained available spectrum map (ASM) and an information table (IT) to show which bands are idle within which regions in the next time period. Each SSP bids for needed bands within certain regions in an all-or-none mode, i.e., either fully obtained or rejected, according to users' service requests. Different from the traditional spectrum market, where end-users directly bid for specific bands, in this market, although the initiators are still the end-users, they only need to submit their service requests, and the buyers who truly participate in the auction are the SSPs. To be specific, such a market has a two-tier framework as shown in Fig. 6.

Mesh Network of an SSP in Tier I

Tier I is between SSPs and their end-users. End-users do not need to know what the spectrum market is, which spectrum bands are needed, and how to complete their

data transmissions, other than their expected services and affordable monetary costs. Each SSP acts as an admission controller, a bidding agent, and a service provider for end-users. Specifically, as shown in Fig. 6, each SSP deploys BSs and CR routers to deliver data services to end-users. Each BS serves as a central controller in its coverage area with some basic bands to provide reliable common control signaling to manage the network resources (both basic bands and harvested bands). The BS also manages a group of CR routers deployed in its coverage area, which have CR capability to operate over the purchased PSP's bands. These CR routers form a mesh network to relay data traffic between the BS and end-users. If possible, end-users can access CR routers through the SSP's basic bands using any available interfaces, e.g., Wi-Fi, GSM/GPRS, 3G/4G/NxtG, etc., without making any changes on their devices.

Two main functions are provided by the CR mesh network. One is aggregating information from its end-users. Assume that each end-user generates a specific service request, which will be submitted to the SSP through the closest CR router. Each service request includes its source/destination, data size, and bidding allowance, and each SSP aggregates end-users' service information through CR routers via basic bands. According to the aggregated information from end-users and available bands in the market, each SSP bids for needed bands during the auction. According to the results, each SSP broadcasts its admission decisions and charges each admitted end-user its bidding allowance via basic bands and, then, provides requested services to end-users with CR routers and purchased PSP's bands according to predetermined routing and scheduling decisions.

Auction-Based Spectrum Market in Tier II

In Tier II, a series of multi-round auctions are held by a third-party auctioneer every time period T for access rights to the opened bands in the next time period, where T is a controllable time parameter. As shown in Fig. 6, at the starting time of each auction period, the seller, the PSP, provides a fine-grained ASM and an IT to reveal available bands and regions in the next period T. An example of the fine-grained ASM is shown as Fig. 7. It has several overlapped zones, and each one represents an available region for an unoccupied band, which is further divided into many blocks with corresponding specific location coordinates. The bands in separated zones can be either different or the same. In the considered spectrum market, for certain band m, if certain SSP wants to bid for it, he has to specify which blocks he wants to get, i.e., he has to bid for a set corresponding to all needed blocks for this band. Therefore, while bidding for the band m, the SSP needs to specify both the band's index and the block's coordinates which form a spectrum bundle as $\{m, (x, y)\}$. All the requested spectrum bundles of an SSP is called a three-dimensional desired bundle ($3D^2$-bundle). Note that the $3D^2$-bundle is purchased in an all-or-none mode, i.e., only part of it is unacceptable.

IT is provided as the supplement to the ASM including multidimensional information of the sold bands. First, it contains the specific spectrum range with the bandwidth and the available blocks' coordinates. Second, for each band within certain available block, a reserved price required by the PSP is also included in

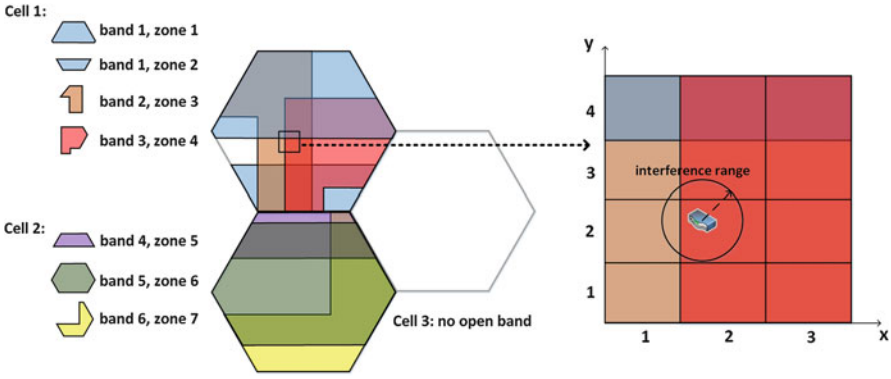

Fig. 7 An example of the fine-grained available spectrum map

the IT. Furthermore, it is noteworthy that PUs' activities are diverse in different areas during different time periods. Therefore, to capture the spatial variation in spectrum availability, the actual available bandwidth of certain band within certain available zone can be treated as a random variable. In order to help SSPs take such an uncertainty into consideration, in the IT, as a reference, historical usage data for each band is also provided (e.g., the average available bandwidth during the same time period everyday in previous several days collected via spectrum measurements).

The competing SSPs should submit their $3D^2$-bundles to the auctioneer before the auction starts, i.e., within the first T_s, in each period. Considering certain CR router, if its SSP wants to obtain certain band for its data transmissions, he has to claim an exclusive area, i.e., specify certain needed blocks. On the one hand, no other SSPs can use this band within this area if it has been claimed already. On the other hand, the CR router can transmit data using this band only within this area and will not cause interference to other areas. For certain transmit power, the exclusive area can be described as a circle, with the CR router as the center and the interference range as the radius, and the desired set of blocks corresponds to the minimal set of blocks covering this circle. A band is called an available band to certain CR router only if its SSP can find available blocks to cover the corresponding exclusive area.

Summary

After aggregating end-users' service requests, according to the available bands of each router, each SSP optimally schedules its network transmissions to obtain its needed $3D^2$-bundle which is submitted to the auctioneer along with certain bidding value. When the auction begins, the auctioneer determines winners and their charging prices. After that, the sold blocks of bands will be deleted from the ASM, and each losing SSP can reschedule its network transmissions according to the updated ASM and bids for desired spectrum bands during the next auction round. The auction continues multiple rounds until no available bands on ASM or no participating SSPs, or this auction period is over. In such a way, more transactions

are achievable in this market and thus generate higher revenue for both PSP and SSPs. It should be noted that many other mechanisms, such as other auction models or game-based open market, can also be adapted in the CCHN based SOST scheme to fulfill different design goals.

Case Study

Next, we present a one-shot experiment as a case study to illustrate the whole process of the SOST scheme. We consider a $1000 \times 600\,\mathrm{m}^2$ grid network with 3 SSPs owning 9 CR routers, respectively, as shown in Fig. 8.

SSP_1 has two end-users with request as ($7 \to 5$, $r_1^1 = 6\,\mathrm{Mbps}$, $p_1^1 = 20$) and ($1 \to 3$, $r_2^1 = 1.3\,\mathrm{Mbps}$, $p_2^1 = 10$), respectively. SSP_2 has three end-users with request as ($5 \to 1$, $r_1^2 = 6\,\mathrm{Mbps}$, $p_1^2 = 19$), ($5 \to 1$, $r_2^2 = 4\,\mathrm{Mbps}$, $p_2^2 = 7$), and ($5 \to 7$, $r_3^2 = 5\,\mathrm{Mbps}$, $p_3^2 = 17$), respectively. SSP_3 has one end-user with request as ($6 \to 4$, $r_1^3 = 7\,\mathrm{Mbps}$, $p_1^3 = 25$). Assume that four bands are opened by PSP and each one is available to all CR routers in all 15 blocks. The four numbers in each block in Fig. 8 represent the reserve price of the four unoccupied bands within this block, respectively, and some other information including bandwidth and 13 historical data is shown as Table 1. According to the bands' information and its own end-users' service requests, each SSP makes an optimal scheduling to determine a $3D^2$-bundle (the needed blocks outside this map are not considered). For the 3 SSPs, suppose that they have the same path loss factor $\beta = 4$, the antenna related parameter $\lambda = 4$, and the noise density power at each CR router $\eta = 10^{-16}\,\mathrm{W/Hz}$. The transmission power at each CR router on each band of each

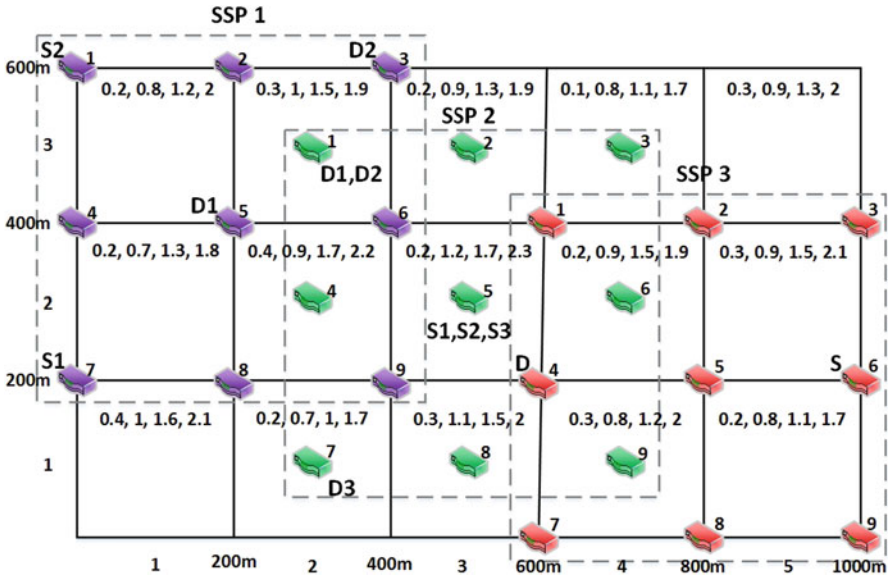

Fig. 8 Topology of the grid network for the case study

Table 1 Information of the four unoccupied bands

Band	Bandwidth (MHz)	Historical data (MHz)												
1	0.4	0.34	0.37	0.13	0.37	0.28	0.12	0.18	0.26	0.38	0.38	0.14	0.39	0.38
2	1.8	1.54	1.19	1.45	0.97	1.50	0.83	1.07	0.84	0.89	1.62	1.49	1.11	1.75
3	4.0	2.06	2.87	2.76	3.53	3.59	2.37	2.97	2.89	3.29	3.41	3.50	2.55	3.35
4	5.5	4.21	5.00	3.35	4.05	5.28	4.98	5.39	4.63	3.08	5.12	5.33	4.69	4.89

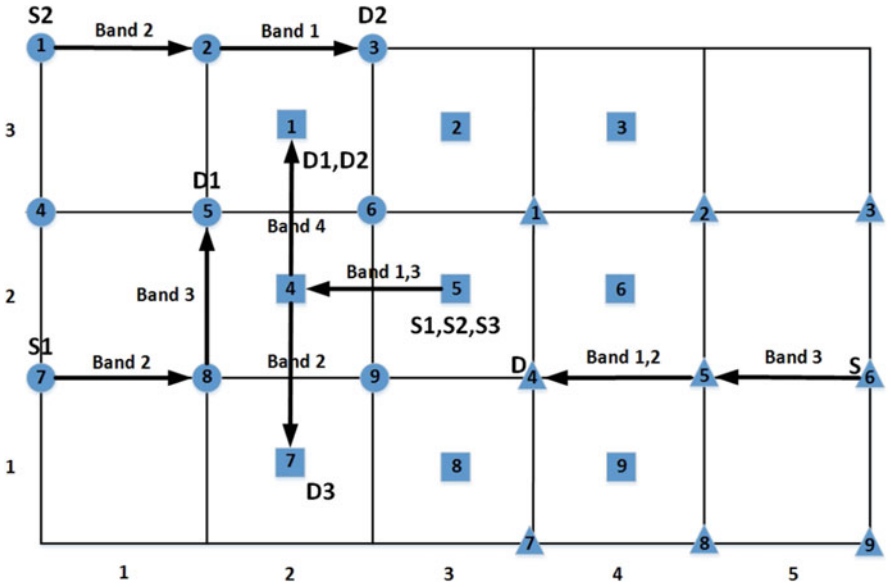

Fig. 9 The optimal transmission schedule of each SSP

SSP is assumed to be equal as 5 W with a transmission/interference range as 210 and 350 m, respectively, and the confidence level for probabilistic link capacity $\alpha = 0.8$. Then, through the optimal network scheduling, the transmission schedule of each SSP is shown as Fig. 9 (readers can refer to [55] for the details of the optimal network scheduling).

According to the optimal schedule, at the first round of the auction, SSP_1 has a $3D^2$-bundle as $\hat{\mathscr{B}}_1^1 = \{\{m, (x_m, y_m)\}\}$, $m = 1, 2, 3$, $x_1, y_2, x_3, y_3 = 1, 2, 3$, $y_1 = 2, 3$, $x_2 = 1, 2$, with a total reserve price as 18.4 and its bidding value $b_1^1 = v_1^1 = 30$, and SSP_2 has a $3D^2$-bundle as $\hat{\mathscr{B}}_1^2 = \{\{m, (x_m, y_m)\}\}$, $m = 1, 2, 3, 4$, $x_1, x_3 = 2, 3, 4$, $y_1, y_3, x_2, x_4, y_2, y_4 = 1, 2, 3$, with a total reserve price as 40.9 and its bidding value $b_1^2 = v_1^2 = 43$, and SSP_3 has a $3D^2$-bundle as $\hat{\mathscr{B}}_1^2 = \{\{m, (x_m, y_m)\}\}, m = 1, 2, 3, x_1, x_2 = 3, 4, 5, x_3 = 4, 5, y_1, y_2, y_3 = 1, 2, 3$, with a total reserve price as 18.2 and its bidding value $b_1^3 = v_1^3 = 25$. Obviously, three SSPs conflict with each other. By taking the social welfare maximum as the

metric to determine winners, since the bid of SSP_2 is the maximum, it becomes the winner. To guarantee the truthfulness property, the corresponding clearing price is set as its critical value, i.e., $\max(40.9, 30) = 40.9$. The auction only has one round because all bands within the middle region have been sold to SSP_2, and SSP_1 and SSP_3 cannot find any bundled remaining bands to support any service. More detailed mechanism design and performance evaluation can be found in [55].

Conclusion and Future Directions

Facing the dramatic increase of wireless data traffic, making more spectrum available is imperative. Consequently, dynamic spectrum sharing via spectrum trading, as one promising technique with the potential to transforming spectrum scarcity into abundancy, has attracted great attentions. In order to provide incentives for spectrum owners to open up their licensed spectrum, economic perspective has been embedded to burst the spectrum trading. In the spectrum trading market, the spectrum owners could sell/lease their radio resources for monetary revenue or performance improvement, and unlicensed users could buy/rent the spectrum access opportunities for their own services. Based on different characteristics, the spectrum trading market could be categorized into many different types, such as exclusive-use based and shared-use based, money exchange and resource exchange, and auction market and open market, which have been elaborated in this chapter. By referring to the overview of the state of the art, readers could acquire a broad view of the spectrum trading on both governmental issued mechanisms and those designed by the academic research community. Furthermore, some practical issues have been summarized, and a novel service-oriented spectrum trading scheme based on a newly developed network architecture has been presented as a promising solution. As the future research direction, spectrum trading market will become more and more flexible in spatial, temporal, and frequency dimensions, which still needs lots of research efforts, including the sophisticated market frameworks to enable such an extremely dynamic trading, the superior bidding languages with low overhead, the hybrid market mechanisms to satisfy different types of users, the privacy protection for users exposed in the public market, the computational-efficient advanced strategy adaptation designs on both seller and buyer sides, etc. We hope this chapter provides the needed background for spectrum trading and inspire more deep research on this topic.

Acknowledgements This work was partially supported by US National Science Foundation under grants CNS-1343356/CNS-1602172/CNS-1343361, CNS-1409797 and CNS-1423165. The work of M. Pan was also partially supported by US National Science Foundation under grants CNS-1350230 (CAREER) and CPS-1646607. The work of P. Li was also partially supported by US National Science Foundation under grant CNS-1566479 (CAREER). The work of X. Huang was partially supported by the Joint Program of National Science Foundation of China-Guangdong under grants No. U1501255 and No. U1301256. The work of S. Glisic was partially supported by Taseen Käyttö CWC-NS Glisic Menot under 240007101 and ADTEC-2016 Menot under 2410067111.

References

1. Cisco (2016) Cisco visual networking index: global mobile data traffic forecast update, 2015–2020. White paper
2. Jonathan RA, Karen DG (2015) A summary of recent federal government activities to promote spectrum sharing. IDA Science and Technology Policy Institute
3. McHenry MA (2005). NSF spectrum occupancy measurements project summary. Shared Spectrum Company Report
4. President's Council of Advisors on Science and Technology (PCAST), Executive Office of the President (2012) Report to the president: realizing the full potential of government-held spectrum to spur economic growth
5. National Science Foundation (2016) NSF leads federal effort to boost advanced wireless research. https://www.nsf.gov/news/news_summ.jsp?cntn_id=139179
6. Prasad RV, Pawlczak P, Hoffmeyer JA, Berger HS (2008) Cognitive functionality in next generation wireless networks: standardization efforts. IEEE Commun Mag 46(4):72–78
7. Pastircak J, Gazda J, Kocur D (2014) A survey on the spectrum trading in dynamic spectrum access networks. In: Proceedings IEEE ELMAR 2014, pp 1–4
8. Hossain E, Niyato D, Kim DI (2015) Evolution and future trends of research in cognitive radio: a contemporary survey. Wirel Commun Mob Comput 15(11):1530–1564
9. Li XH, Zhao N, Sun Y, Yu FR (2015) Interference alignment based on antenna selection with imperfect channel state information in cognitive radio networks. IEEE Trans Veh Technol 65(7):5497–5511
10. Xu L, Tonjes R, Paila T, Hansmann W, Frank M, Albrecht M (2000) DRiVE-ing to the internet: dynamic radio for IP services in vehicular environments. In: Proceedings of the 25th Annual IEEE Conference on Local Computer Networks, pp 281–289
11. Pan M, Yue H, Fang Y, Li H (2012) The X loss: band-mix selection for opportunistic spectrum accessing with uncertain spectrum supply from primary service providers. IEEE Trans Mob Comput 11(12):2133–2144
12. Huang J (2013) Market mechanisms for cooperative spectrum trading with incomplete network information. IEEE Commun Mag 51(10):201–207
13. Yan Y, Huang J, Wang J (2013) Dynamic bargaining for relay-based cooperative spectrum sharing. IEEE J Sel Areas Commun 31(8):1480–1493
14. Simeone O, Stanojev I, Savazzi S, Bar-Ness Y, Spagnolini U, Pickholtz R (2008) Spectrum leasing to cooperating secondary ad hoc networks. IEEE J Sel Areas Commun 26(1):203–213
15. Zhang Y, Lee C, Niyato D, Wang P (2013) Auction approaches for resource allocation in wireless systems: a survey. IEEE Commun Surv Tutorials 15(3):1020–1041
16. Zhou X, Gandhi S, Suri S, Zheng H (2008) eBay in the sky: strategy-proof wireless spectrum auctions. In: Proceedings of the 14th ACM International Conference on Mobile Computing and Networking, pp 2–13
17. Li Z, Li B, Zhu Y (2015) Designing truthful spectrum auctions for multi-hop secondary networks. IEEE Trans Mob Comput 14(2):316–327
18. Sodagari S, Attar A, Bilen SG (2011) On a truthful mechanism for expiring spectrum sharing in cognitive radio networks. IEEE J Sel Areas Commun 29(4):856–865
19. Feng X, Lin P, Zhang Q (2015) FlexAuc: serving dynamic demands in a spectrum trading market with flexible auction. IEEE Trans Wirel Commun 14(2):821–830
20. Zhou X, Zheng H (2009) Trust: a general framework for truthful double spectrum auctions. In: Proceedings IEEE INFOCOM 2009, pp 999–1007
21. Chen Y, Zhang J, Wu K, Zhang Q (2014) Tames: a truthful double auction for multi-demand heterogeneous spectrums. IEEE Trans Parallel Distrib Syst 25(11):3012–3024
22. Wang S, Xu P, Xu X, Tang S, Li X, Liu X (2010) TODA: truthful online double auction for spectrum allocation in wireless networks. In: Proceedings of the IEEE Symposium on New Frontiers in Dynamic Spectrum, pp 1–10

23. Chen Y, Lin P, Zhang Q (2014) LOTUS: location-aware online truthful double auction for dynamic spectrum access. In: Proceedings of the IEEE International Symposium on Dynamic Spectrum Access Networks (DYSPAN), pp 510–518
24. Zheng Z, Wu F, Tang S, Chen G (2015) AEGIS: an unknown combinatorial auction mechanism framework for heterogeneous spectrum redistribution in noncooperative wireless networks. IEEE/ACM Trans Netw 24(3):1919–1932
25. Dong M, Sun G, Wang X, Zhang Q (2012) Combinatorial auction with time-frequency flexibility in cognitive radio networks. In: Proceedings of IEEE INFOCOM 2012, pp 2282–2290
26. Jiang L, Cai H, Chen Y, Zhang J, Li B (2016) Many-to-many matching for combinatorial spectrum trading. In: Proceedings of the IEEE International Conference on Communications (ICC 2016). https://doi.org/10.1109/ICC.2016.7511434
27. Gopinathan A, Li Z, Wu C (2011) Strategyproof auctions for balancing social welfare and fairness in secondary spectrum markets. In: Proceedings IEEE INFOCOM 2011, pp 3020–3028
28. Wu Y, Wang B, Liu KR, Clancy TC (2009) A scalable collusion-resistant multi-winner cognitive spectrum auction game. IEEE Trans Commun 57(12):3805–3816
29. Pan M, Chen F, Yin X, Fang Y (2009) Fair profit allocation in the spectrum auction using the shapley value. In: Proceedings of the IEEE Global Telecommunications Conference, pp 1–6
30. Li M, Li P, Guo L, Huang X (2015) PPER: privacy-preserving economic-robust spectrum auction in wireless networks. In: Proceedings IEEE INFOCOM 2015, pp 909–917
31. Niyato D, Hossain E (2008) Market-equilibrium, competitive, and cooperative pricing for spectrum sharing in cognitive radio networks: analysis and comparison. IEEE Trans Wirel Commun 7(11):4273–4283
32. Gao L, Wang X, Xu Y, Zhang Q (2011) Spectrum trading in cognitive radio networks: a contract-theoretic modeling approach. IEEE J Sel Areas Commun 29(4):843–855
33. Gao L, Huang J, Chen YJ, Shou B (2013) An integrated contract and auction design for secondary spectrum trading. IEEE J sel Areas Commun 31(3):581–592
34. Yin J, Sun G, Wang X (2013) Spectrum trading in cognitive radio network: a two-stage market based on contract and stackelberg game. In: Proceedings of the IEEE Wireless Communications and Networking Conference (WCNC), pp 1679–1684
35. Jin H, Sun G, Wang X, Zhang Q (2012) Spectrum trading with insurance in cognitive radio networks. In: Proceedings of IEEE INFOCOM 2012, pp 2041–2049
36. Presidential Memorandum (2010) Unleashing the wireless broadband revolution. https://www.whitehouse.gov/the-press-office/presidential-memorandum-unleashing-wireless-broadband-revolution
37. Li M, Li P, Pan M, Sun J (2013) Economic-robust transmission opportunity auction in multi-hop wireless networks. In: Proceedings of IEEE INFOCOM 2013, pp 1842–1850
38. Pan M, Li P, Song Y, Fang Y, Lin P (2012) Spectrum clouds: a session based spectrum trading system for multi-hop cognitive radio networks. In: Proceedings of IEEE INFOCOM 2012, pp 1557–1565
39. Pan M, Li P, Song Y, Fang Y, Lin P, Glisic S (2014) When spectrum meets clouds: optimal session based spectrum trading under spectrum uncertainty. IEEE J Sel Areas Commun 32(3):615–627
40. Li X, Pan M, Song Y, Sun Y, Fang Y (2015) Economic-robust session based spectrum trading in multi-hop cognitive radio networks. In: Proceedings of IEEE Global Communications Conference (GLOBECOM), pp 1–6
41. Huang H, Sun YE, Li XY, Chen S, Xiao M, Huang L (2015) Truthful auction mechanisms with performance guarantee in secondary spectrum markets. IEEE Trans Mob Comput 14(6):1315–1329
42. Fu F, van der Schaar M (2009) Learning to compete for resources in wireless stochastic games. IEEE Trans Veh Technol 58(4):1904–1919

43. Han Z, Zheng R, Poor HV (2011) Repeated auctions with Bayesian nonparametric learning for spectrum access in cognitive radio networks. IEEE Trans Wirel Commun 10(3):890–900
44. Tang W, Jain R (2012) Hierarchical auction mechanisms for network resource allocation. IEEE J Sel Areas Commun 30(11):2117–2125
45. Lin P, Feng X, Zhang Q, Hamdi M (2013) Groupon in the air: a three-stage auction framework for spectrum group-buying. In: Proceedings of IEEE INFOCOM 2013, pp 2013–2021
46. Niyato D, Hossain E, Han Z (2009) Dynamics of multiple-seller and multiple-buyer spectrum trading in cognitive radio networks: a game-theoretic modeling approach. IEEE Trans Mob Comput 8(8):1009–1022
47. Xing Y, Chandramouli R, Cordeiro C (2007) Price dynamics in competitive agile spectrum access markets. IEEE J Sel Areas Commun 25(3):613–621
48. Bajaj I, Lee YH, Gong Y (2015) A spectrum trading scheme for licensed user incentives. IEEE Trans Commun 63(11):4026–4036
49. Xu D, Liu X, Han Z (2013) Decentralized bargain: a two-tier market for efficient and flexible dynamic spectrum access. IEEE Trans Mob Comput 12(9):1697–1711
50. Pan M, Zhang C, Li P, Fang Y (2012) Spectrum harvesting and sharing in multi-hop CRNs under uncertain spectrum supply. IEEE J Sel Areas Commun 30(2):369–378
51. Peng J, Yue H, Xue K, Luo Y, Hong P, Fang Y (2016) Energy-aware scheduling for multi-hop cognitive radio networks. IEEE Trans Cogn Commun Netw 2(4):397–410
52. Wang J, Yue H, Hai L, Fang Y (2016) Spectrum-aware anypath routing in multi-hop cognitive radio networks. IEEE Trans Mob Comput 16(4):1176–1187
53. Pan M, Yue H, Zhang C, Fang Y (2013) Path selection under budget constraints in multi-hop cognitive radio networks. IEEE Trans Mob Comput 12(6):1133–1145
54. Ding H, Fang Y, Huang X, Pan M, Li P, Glisic S (2017, to appear) Cognitive capacity harvesting networks: architectural evolution towards future cognitive radio networks. IEEE Commun Surv Tutorials
55. Li X, Ding H, Pan M, Sun Y, Fang Y (2016) Users first: service-oriented spectrum auction With a two-tier framework support. IEEE J Sel Areas Commun 34(11):2999–3013

Cognitive Radio Networks for Delay-Sensitive Applications: Games and Learning

29

Yuanzhang Xiao and Mihaela van der Schaar

Contents

Y. Xiao (✉)
Department of Electrical Engineering and Computer Science, Northwestern University, Evanston, IL, USA
e-mail: xyz.xiao@gmail.com

M. van der Schaar
Oxford – Man Institute of Quantitative Finance (OMI), Oxford, UK

Department of Engineering Science, University of Oxford, Oxford, UK
e-mail: mihaela.vanderschaar@eng.ox.ac.uk

W. Zhang (ed.), *Handbook of Cognitive Radio*,
https://doi.org/10.1007/978-981-10-1394-2_28

Abstract

We have witnessed an explosion in wireless video traffic in recent years. Video applications are bandwidth intensive and delay sensitive and hence require efficient utilization of spectrum resources. Born to utilize wireless spectrum more efficiently, cognitive radio networks are promising candidates for deployment of wireless video applications. In this chapter, we introduce our recent advances in *foresighted resource allocation mechanisms* that enable multiuser wireless video applications over cognitive radio networks. The introduced resource allocation mechanisms are foresighted, in the sense that they optimize the *long-term* video quality of the wireless users. Due to the temporal coupling of delay-sensitive video applications, such foresighted mechanisms outperform mechanisms that maximize the short-term video quality. Moreover, the introduced resource allocation mechanisms allow wireless users to optimize while learning the unknown dynamics in the environment (e.g., incoming traffic, primary user activities). Finally, we introduce variations of the mechanisms that are suitable for networks with self-interested users. These mechanisms ensure efficient video resource allocation even when the users are self-interested and aim to maximize their individual video quality. The foresighted resource allocation mechanisms introduced in this chapter are built upon our theoretical advances in multiuser Markov decision processes, reinforcement learning, and dynamic mechanism design.

Keywords

Cognitive radio networks · Multimedia communications · Game theory · Reinforcement learning

Introduction

Video applications, such as video streaming, videoconferencing, remote teaching, and surveillance, have become the major applications deployed over wireless networks. Video applications are bandwidth intensive and delay sensitive and hence require efficient allocation of spectrum resources among the users and efficient scheduling of each user's video packets based on its allocated resources.

One promising physical-layer technology to improve the spectrum efficiency is cognitive radio. In cognitive radio, secondary users (SUs) can utilize the idle spectrum when primary users (PUs) are inactive. Due to the potential of high spectrum efficiency, cognitive radio is a promising candidate for the physical-layer technology of video applications. Although cognitive radio is promising, there are several challenges in efficiently deploy video applications over cognitive radio networks.

First, video applications are delay-sensitive, namely, the video packets have to be received before strict deadlines for successful decoding. Therefore, video

applications require not only high spectrum efficiency but also efficient scheduling of video packets.

In addition, there is interdependency across video packets, which makes the issue of delay sensitivity more challenging. Specifically, the successful decoding of some video packets may depend on the successful decoding of others. In other word, even if a video packet is received before its deadline, it may not be decoded if some packets that it depends on were not received by deadlines. This interdependency results in temporal coupling of packet scheduling decisions. Therefore, we need *foresighted* video packet scheduling that aims at maximizing the *long-term* video quality, instead of instantaneous video quality.

Moreover, the delay sensitivity and interdependency mentioned above require not only efficient packet scheduling but also efficient allocation of spectrum resources. More specifically, we need *foresighted* resource allocation among the users in the network, in order to maximize the long-term video quality.

Furthermore, the unknown dynamic environment requires users to make resource allocation and packet scheduling decisions while *learning* the unknown dynamics. Here the unknown dynamics include incoming video traffic, the channel quality, and the PU activities.

Finally, the users in cognitive radio networks are autonomous and may aim to maximize their own video quality (i.e., they are *self-interested*). It is more challenging to design efficient resource allocation mechanism for self-interested users, because they may misreport their information (e.g., their video traffic and channel quality). In this case, the resource allocation mechanism has to be *strategy proof*.

In this chapter, we introduce our solutions to the aforementioned challenges in multiuser wireless video transmission over cognitive radio networks. Specifically, we introduce a framework to design foresighted resource allocation mechanisms and packet scheduling algorithms [1–7]. The introduced resource allocation mechanisms allow wireless users to optimize while learning the unknown dynamics in the environment (e.g., incoming traffic, channel quality, primary user activities). We also describe variations of the mechanisms that are suitable for self-interested users [1–5]. These mechanisms ensure efficient video resource allocation even when the users are self-interested and aim to maximize their individual video quality. The foresighted resource allocation mechanisms introduced in this chapter are built upon our theoretical advances in multiuser Markov decision processes, reinforcement learning, and dynamic mechanism design.

The rest of this chapter is organized as follows. We give a literature review in section "Related Work." We introduce the system model in section "General Model for Video Applications over Cognitive Radio" and then formulate the design problem in section "The Design Problem." We describe the introduced solutions in section "Optimal Foresighted Video Transmission." We also briefly describe the strategy-proof variations of the solutions in section "Strategy-Proof Resource Allocation Mechanisms." Finally, we conclude the chapter in section "Conclusion and Future Directions."

Related Work

Multimedia Applications over Cognitive Radio Networks

A plethora of recent works [1–14] propose distinct solutions to optimize the video quality. Some works [8–16] assume that the users are *myopic*, namely, they only maximize their *instantaneous* video quality over a given time interval without considering the impact of their actions on the *long-term* video quality. They cast the problem in a network utility maximization (NUM) framework to maximize the instantaneous joint video quality of all the users and apply the NUM framework repeatedly when the channel conditions or video traffic characteristics change. However, since the users are optimizing their transmission decisions myopically, their long-term average performance is inferior to the performance achieved when the users are *foresighted* [17]. Some of the works considering the foresighted decision of users focus solely on a *single* foresighted user making sequential transmission decisions (e.g., packet scheduling, retransmissions, etc.) [17]. However, these single-user solutions do not discuss how to allocate resources among multiple users as well as how this allocation is impacted by and impacts the foresighted scheduling decisions of individual users. Static allocations of resources, which are often assumed in the works studying the foresighted decisions of a single user, have been shown to be suboptimal compared to the solutions that dynamically allocate resources among multiple users [6].

In contrast, our introduced solutions, based on [1–7], make *foresighted* resource allocation and packet scheduling decisions over *multiple* video users.

Table 1 summarizes the above discussions. Note that the optimality shown in the last column of Table 1 indicates whether the solution is optimal for the long-term network utility (i.e., the joint long-term video quality of all the users in the network).

Last but not the least, there are a plethora of works that address other important issues in cognitive radio networks with multimedia applications, such as spectrum handoff [18], routing [19], spectrum sensing [20], and applications in smart grid [21]. These works are out of scope of this chapter.

Theoretical Frameworks

Single-user foresighted decision-making in a dynamically changing environment has been studied and formulated as Markov decision process (MDP). Foresighted

Table 1 Related works on video (the first two rows are works introduced in this chapter)

	Users	Foresighted	Learning	Strategy proof	Optimal
[1–5]	Multiple	Yes	Yes	Yes	No
[6, 7]	Multiple	Yes	Yes	No	Yes
[8–16]	Multiple	No	No	Yes/No	No
[17]	Single	Yes	Yes	No	No

Table 2 Related theoretical frameworks (the first row is works introduced in this chapter)

	Decision makers	Foresighted	Learning	Optimal
MU-MDP [6, 7]	Multiple	Yes	Yes	Yes
MDP [17]	Single	Yes	Yes	No
Repeated NUM [16]	Multiple	No	No	No
Lyapunov optimization [22]	Single	Yes	Yes	No

decision-making in a dynamically changing environment can also be solved using the Lyapunov optimization framework [22]. However, the Lyapunov optimization framework is not able to make optimal decisions for video streaming since it disregards specific interdependency and distortion impact of video traffic [23].

Table 2 summarizes the above discussions about existing theoretical frameworks.

General Model for Video Applications over Cognitive Radio

We first present a general model for multiuser wireless video transmission in cognitive radio networks. Then we give an example of a commonly used model as in [6, 14, 17] as an instantiation of our general model.

The General Model

We consider a cognitive radio network with a network manager indexed by 0 and a set $\mathscr{I}$ of I wireless video users, indexed by $i = 1, \ldots, I$. Time is slotted at $t = 0, 1, 2, \ldots$. In the rest of the paper, we will put the user index in the superscript and the time index in the subscript of variables. The multiuser wireless video transmission system is described by the following features.

States

Each user i has a finite state space S^i, from which a state s^i is realized and revealed to user i at the beginning of each time slot. The state s^i may consist of several components, such as the video traffic state and the channel state. An example of a simplified video traffic state can be the types of video frames (I, P, or, B frame) available for transmission and the numbers of packets in each available video frame. Note that the video traffic in our model can come from video sequences that are either encoded in real time, or offline, and stored in the memory before the transmission. An example channel state can be the channel quality reported to the application layer by the lower layers. The network manager has a finite state space S^0 that describes the status of the resource in the network. An example resource state can be the available idle bandwidth.

Actions

At each state s^i, each user i chooses an action $a^i \in A^i(s^i)$. For example, an action can be how many packets within each available video frame should be transmitted. We allow the sets of actions taken under different states to be different, in order to incorporate the minimum video quality requirements that will be discussed.

Payoffs

Each user i has a payoff function $u^i : S^i \times A^i \rightarrow \mathbb{R}$. The payoff function u^i is concave in the action under any state. A typical payoff can be the distortion impact of the transmitted packets minus the cost of energy consumption in transmission.

State Transition

Each user i's state transition is Markovian and can be denoted by $p^i(s^{i\prime}|s^i, a^i) \in \Delta(S^i)$, where $\Delta(S^i)$ is the probability distribution over the set of states.

Resource Constraints

Given the status of the resource (i.e., the network manager's state s^0), we can write the (linear) resource constraint as

$$f(s^0, a^1, \ldots, a^I) \triangleq f^0(s^0) + \sum_{i=1}^{I} f^i(s^0) \cdot a^i \leq 0,$$

where $f^i(s^0)$ is the coefficient under state s^0. When a^i is a vector, $f^i(s^0)$ is a vector of the appropriate length, and $f^i(s^0) \cdot a^i$ is the inner product of the two vectors.

A variety of multiuser wireless video transmission systems can be modeled as special cases of our general model. Next, we present a packet-level video transmission model as an example.

An Example Packet-Level Video Transmission Model

Packet-level video transmission models have been proposed in a variety of related works, including [6–14]. In the following, we briefly describe the model based on [6–14] and refer interested readers to [6–14] for more details.

We first consider a specific video user i and hence drop the superscript before we describe the resource constraints. The video source data is encoded using an H.264 or MPEG video coder under a group of pictures (GOP) structure: the data is encoded into a series of GOPs, indexed by $g = 1, 2, \ldots$, where one GOP consists of N data units (DUs). Each DU $n \in \{1, \ldots, N\}$ in GOP g, denoted DU_n^g, is characterized by its size $l_n^g \in \mathbb{N}_+$ (i.e., the number of packets in it), distortion impact $q_n^g \in \mathbb{R}_+$, delay deadline $d_n^g \in \mathbb{N}_+$, and dependency on the other DUs in the same GOP. The dependency among the DUs in one GOP comes from encoding techniques such as motion estimation/compensation. In general, if DU_n^g depends on DU_m^g, we have $d_n^g \geq d_m^g$ and $q_n^g \leq q_m^g$, namely, DU_m^g should be decoded before DU_n^g and has a higher distortion impact than DU_n^g [17]. Note that in the case of scalable video coding, there is no dependency among the DUs, and the following representation of

the model can be greatly simplified. We will keep the dependency for generality in our exposition.

Among the above characteristics, the distortion impact q_n^g, delay deadline d_n^g, and the dependency are deterministic and fixed for the same DUs across different GOPs (e.g., $q_n^g = q_n^{g+1}$) [6, 17]. As in [6], the sizes of all the DUs are independent random variables and that the sizes of the nth DUs in different GOPs have the same distribution.

States

Each user's state consists of the traffic state T_t and the channel state h_t. We describe the traffic state T_t first. At time slot t, as in [6, 14, 17], we assume that the wireless user will only consider for transmission the DUs with delay deadlines in the range of $[t, t+W)$, where W is referred to as the scheduling time window (STW). Following the model in [6, 17], at time slot t, we introduce *context* to represent the set of DUs that are considered for transmission, i.e., whose delay deadlines are within the range of $[t, t+W)$. We denote the context by $C_t = \left\{DU_j^g | d_j^g \in [t, t+W)\right\}$. Since the GOP structure is fixed, the transition from context C_t to C_{t+1} is deterministic. An illustration of the context is given in Fig. 1.

Given the current context C_t, we let $x_{t,DU}$ denote the number of packets in the buffer associated with a DU in C_t. We denote the buffer state of the DUs in C_t by $x_t = \{x_{t,DU} | DU \in C_t\}$. The traffic state T_t at time slot t is then $T_t = (C_t, x_t)$, where the context C_t represents which DUs are available for transmission, and the buffer state x_t represents how many packets each available DU has left in the buffer.

Next we describe the channel state h_t. At each time slot t, the wireless user experiences a channel condition $h_t \in \mathscr{H}$, where $\mathscr{H}$ is the finite set of possible channel conditions. We assume that the wireless channel is slow fading (i.e., remains the same in one time slot) and that the channel condition h_t can be modeled as a finite-state Markov chain [24].

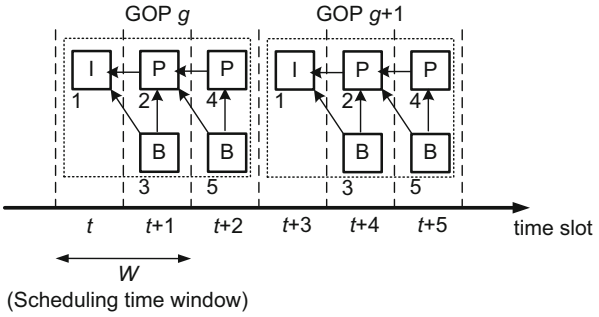

Fig. 1 Illustration of group of pictures (GOP), data unit (DU), and the context. Since the scheduling time window is $W = 2$, the contexts in different time slots are $C_t = \{DU_1^g, DU_2^g, DU_3^g\}$, $C_{t+1} = \{DU_2^g, DU_3^g, DU_4^g, DU_5^g\}$, $C_{t+2} = \{DU_4^g, DU_5^g, DU_1^{g+1}\}$, $C_{t+3} = \{DU_1^{g+1}, DU_2^{g+1}, DU_3^{g+1}\}$, and so on

In summary, the state of a user at each time slot t is $s_t = (C_t, x_t, h_t)$, which includes the current context, buffer state, and channel state.

(Packet Scheduling) Actions
At each time slot t, the user decides how many packets should be transmitted from each DU in the current context. The decision is represented by $a_t(s_t) = \{y_{t,DU} | DU \in C_t, y_{t,DU} \in [0, x_{t,DU}]\}$, where $y_{t,DU}$ is the amount of packets transmitted from the DU.

Payoffs
As in [17], we consider the following *instantaneous payoff* at each time slot t: (The payoff function can be easily extended within our framework to include additional features in the model. For example, when there are packet losses, we can modify the first term to be the expected distortion reduction given the packet loss rate or modify the second term to consider the additional energy consumption associated with packet retransmission.)

$$u(s_t, a_t) = \sum_{DU \in C_t} q_{DU}\, y_{t,DU} - \beta \cdot \rho\left(h_t, \|a_t\|_1\right), \tag{1}$$

where the first term $\sum_{DU \in C_t} q_{DU}\, y_{t,DU}$ is the *instantaneous video quality*, namely, the distortion reduction obtained by transmitting the packets from the DUs in the current context, and the second term $\beta \cdot \rho\left(h_t, \|a_t\|_1\right)$ represents the disutility of the energy consumption by transmitting the packets. Since the packet scheduling action a_t is a vector with nonnegative components, we have $\|a_t\|_1 = \sum_{DU \in C_t} y_{t,DU}$, namely, $\|a_t\|_1$ is the total number of transmitted packets. As in [17], the energy consumption function $\rho(h, \|a\|_1)$ is assumed to be convex in the total number of transmitted packets $\|a\|_1$ given the channel condition h. An example of such a function can be $\rho(h, \|a\|_1) = \sigma^2(e^{2\|a\|_1 b} - 1)/h$, where b is the number of bits in one packet [25]. The payoff function is a trade-off between the distortion reduction and the energy consumption, where the relative importance of energy consumption compared to distortion reduction is characterized by the trade-off parameter $\beta > 0$. In the simulation, we will set different values for β to illustrate the trade-off between the distortion reduction and energy consumption.

The Resource Constraint
Suppose that the users access the channels in a frequency-division multiple access (FDMA) manner. The total bandwidth B is shared by the users. We assume that each user i uses adaptive modulation and coding (AMC) based on its channel condition. In other words, each user i chooses a data rate r_t^i under the channel state h_t^i. Note that the rate selection is done by the physical layer and is not a decision variable in our framework. Then as in [8], we have the following resource constraint:

$$\sum_{i=1}^{I} \frac{\|a_t^i\|_1 b}{r_t^i(h_t^i)} \leq B, \tag{2}$$

where $\frac{\|a_t^i\|_1 \cdot b}{r_t^i(h_t^i)}$ is the bandwidth needed for transmitting the amount $\|a_t^i\|_1 \cdot b$ of bits given the data rate $r_t^i(h_t^i)$.

In this model, the network manager's state s^0 is then the collection of channel states, namely, $s^0 = (h^1, \ldots, h^I)$. The information about the channel states is fed back from the users to the network manager. We can write the constraint compactly as the linear constraint $f(s_t^0, a_t^1, \ldots, a_t^N) \leq 0$ with $f^i(s_t^0) = \frac{b}{r_t^i(h_t^i)}, i = 1, \ldots, I$ and $f^0(s_t^0) = -B$.

The Design Problem

Each user makes decisions based on its state s_t. Hence, each user i's strategy can be defined as a mapping $\pi^i : S^i \to \cup_{s^i} A^i(s^i)$, where $A^i(s^i)$ is the set of actions available under state s^i. We allow the set of available actions to depend on the state, in order to capture the minimum video quality guarantee. For example, at any time, user i has a minimum distortion impact reduction requirement D^i, formulated as

$$A^i(s_t^i) = \left\{ a_t^i : \sum_{DU \in C_t^i} q_{DU} \cdot y_{t,DU}^i \geq D^i \right\}.$$

The users aim to maximize their expected long-term payoff. Given its initial state s_0^i, each user i's strategy π^i induces a probability distribution over the sequences of states $s_1^i, s_2^i, \ldots$, and hence a probability distribution over the sequences of instantaneous payoffs $u_0^i, u_1^i, \ldots$. Taking expectation with respect to the sequences of payoffs, we have user i's *long-term payoff* given the initial state as

$$U^i(\pi^i | s_0^i) = \mathbb{E}\left\{ (1-\delta) \sum_{t=0}^{\infty} \left(\delta^t \cdot u_t^i \right) \right\}, \tag{3}$$

where $\delta \in [0, 1)$ is the discount factor.

The design problem can be formulated as

$$\begin{aligned} \max_{\pi^1, \ldots, \pi^I} \quad & \sum_{s_0^1, \ldots, s_0^I} \sum_{i=1}^{I} U^i(\pi^i | s_0^i) \\ s.t. \quad & \text{minimum video quality guarantee:} \\ & \pi^i(s^i) \in A^i(s^i), \ \forall i, s^i, \\ & \text{resource constraint:} \\ & f(s^0, \pi^1(s^1), \ldots, \pi^I(s^I)) \leq 0, \ \forall s^0. \end{aligned} \tag{4}$$

Note that the design problem (4) is a weakly coupled MU-MDP as defined by [26]. It is a MU-MDP because there are multiple users making foresighted decisions. The MU-MDP is coupled, because the users influence each other through the resource constraints (namely, the choice of one user's action depends on the choices of the other users). However, it is weakly coupled, because the coupling is through the

resource constraints only and because one user's *instantaneous* payoff $u^i(s^i, a^i)$ is not affected by the other users' actions a^j. It is this weak coupling that enables us to decompose the multiuser problem into multiple single-user problems through prices. Such a decomposition of weakly coupled MU-MDPs has been studied in a general setting [26] and in wireless video transmission [6], both adopting a dual decomposition approach based on *uniform* price (i.e., the same Lagrangian multiplier for the resource constraints under all the states).

Note also that we sum up the network utility $\sum_{i=1}^{I} U^i(\pi^i|s_0^i)$ under all the initial states $(s_0^1, \ldots, s_0^I)$. This can be interpreted as the expected network utility when the initial state is uniformly distributed. The optimal stationary strategy profile that maximizes this expected network utility will also maximize the network utility given any initial state.

The design problem (4) is very challenging and has never been solved optimally. To better understand this, let us assume that a central controller would exist which knows the complete information of the system (i.e., the states, the state transitions, the payoff functions) at each time step. Then, this central controller can solve the above problem (4) as a centralized single-user MDP (e.g., using well-known value iteration or policy iteration methods) and obtain the solution to the design problem $\boldsymbol{\pi}^\star$ and the optimal value function $U^\star$. However, the multiuser wireless video system we discussed is inherently informationally decentralized, and there is no entity in the network that possesses the complete information. Moreover, the computational complexity of solving (4) by a single entity is prohibitively high. Hence, our goal is to develop an optimal decentralized algorithm that converges to the optimal solution.

Optimal Foresighted Video Transmission

In this section, we show how to determine the optimal foresighted video transmission policies. We propose an algorithm that allows each entity to make decisions based on its local information and the limited information exchange between the BS and the users. Specifically, in each time slot, the BS sends resource prices to each user, and the users send their total numbers of packets to transmit to the BS. The BS keeps updating the resource prices based on the resource usage by the users and obtains the optimal resource prices based on which the users' optimal individual decisions achieve the optimal network utility.

Decoupling of The Users' Decision Problems

Each user aims to maximize its own long-term payoff $U^i(\pi^i|s_0^i)$ subject to the constraints. Specifically, given the other users' strategies $\boldsymbol{\pi}^{-i} = (\pi^1, \ldots, \pi^{i-1}, \pi^{i+1}, \ldots, \pi^I)$ and states $\boldsymbol{s}^{-i} = (s^1, \ldots, s^{i-1}, s^{i+1}, \ldots, s^I)$, each user i solves the following long-term payoff maximization problem:

$$\pi^i = \arg\max_{\tilde{\pi}^i} U_i(\tilde{\pi}^i|s_0^i) \quad (5)$$
$$s.t. \quad \tilde{\pi}^i(s^i) \in A^i(s^i), \ \forall s^i,$$
$$f(s^0, \tilde{\pi}^i(s^i), \boldsymbol{\pi}^{-i}(\boldsymbol{s}^{-i})) \leq 0.$$

Assuming that the user knows all the information (i.e., the other users' strategies $\boldsymbol{\pi}^{-i}$ and states $\boldsymbol{s}^{-i}$), user i's optimal value function should satisfy the following:

$$V(s^i) = \max_{a^i \in A^i(s^i)} (1-\delta)u^i(s^i, a^i) + \delta \sum_{s^{i\prime}} p^i(s^{i\prime}|s^i, a^i)V(s^{i\prime})$$
$$s.t. \quad f(s^0, a^i, \boldsymbol{\pi}^{-i}(\boldsymbol{s}^{-i})) \leq 0. \quad (6)$$

Note that the above equations would be the Bellman equation, if user i knew the other users' strategies $\boldsymbol{\pi}^{-i}$ and states $\boldsymbol{s}^{-i}$ and the BS' state s^0 (i.e., the channel states of all the users). However, such information is never known to a particular user. Without such information, one user cannot solve the decision problem above because the resource constraint contains unknown variables. Hence, we need to separate the influence of the other users' decisions from each user's decision problem.

One way to decouple the interaction among the users is to remove the resource constraint and add it as a penalty to the objective function. Denote the Lagrangian multiplier (i.e., the "price") associated with the constraint under state s^0 as $\lambda^0(s^0)$. Then the penalty at state s^0 is

$$-\lambda^0(s^0) \cdot f(s^0, a^1, \ldots, a^I) = -\lambda^0(s^0) \cdot \textstyle\sum_{i=1}^I f^i(s^0) \cdot a^i.$$

Since the term $-\lambda^0(s^0) \cdot \sum_{j \neq i} f^j(s^0) \cdot a^j$ is a constant for user i, we only need to add $-\lambda^0(s^0) \cdot f^i(s^0) \cdot a^i$ to each user i's objective function. We define $\lambda^i(s^0) \triangleq \lambda^0(s^0) \cdot f^i(s^0)$. Then we can rewrite user i's decision problem as

$$\tilde{V}^{\lambda^i(s^0)}(s^i) = \max_{a^i \in A^i(s^i)} (1-\delta)\left[u^i(s^i, a^i) - \lambda^i(s^0) \cdot a^i\right]$$
$$+\delta \cdot \textstyle\sum_{s_i'} \left[p^i(s^{i\prime}|s^i, a^i)\tilde{V}^{\lambda^i(s^0)}(s^{i\prime})\right]. \quad (7)$$

By contrasting (7) with (6), we can see that given the price λ^i, each user can make decisions based only on its local information since the resource constraint is eliminated. Note, importantly, that the above decision problem (7) for each user i is different from that in [6] with uniform price. This can be seen from the term $\lambda^i(s^0) \cdot a^i$ in (7), where the price $\lambda^i(s^0)$ is user specific and depends on the state, while the uniform price in [6] is a constant λ. The decision problem (7) is also different from the subproblem resulting from dual decomposition in NUM, because

it is a foresighted optimization problem that aims to maximize the long-term payoff. This requires a different method to calculate the optimal Lagrangian multiplier $\lambda^i(s^0)$ than that in NUM.

Optimal Decentralized Video Transmission Strategy

For the general model described in section "General Model for Video Applications over Cognitive Radio"-A, we propose an algorithm used by the BS to iteratively update the prices and by the users to update their optimal strategies. The algorithm will converge to the optimal prices and the optimal strategy profile that achieves the minimum total system payoff $U^\star$. The algorithm is described in Table 3.

Theorem 1. *The algorithm in Table 3 converges to the optimal strategy profile, namely,*

$$\lim_{t,k\to\infty} \left| \sum_{s_t^1,\ldots,s_t^I} \sum_{i=1}^{I} U_i(\pi^{i,\lambda_k^i}|s_t^i) - U^\star \right| = 0\,.$$

Proof. See the appendix in [7].

We illustrate the BS's and users' updates and their information exchange in one time slot in Fig. 2. At the beginning of each time slot t, the BS and the users exchange information to compute the optimal resource price and the optimal actions to take. Specifically, in each iteration k, the BS updates the resource price λ_k^0. Then based on the user-specific resource price λ_k^i, each user i solves for the optimal individual strategy π^{i,λ_k^i} and sends the BS its resource request $f^i \cdot \pi^{i,\lambda_k^i}(s_t^i)$. Then the BS updates the prices based on the users' resource requests using the stochastic subgradient method, which can be performed easily. The difference from the dual decomposition in NUM is that each user's decision problem in our work is a foresighted optimization problem aiming to maximize the long-term, instead of instantaneous, payoff. Our algorithm is also different from the algorithm in [6] in that we have different prices under different states.

Table 3 Distributed algorithm to compute the optimal strategy at time t

Input: Performance loss tolerance ϵ
Initialization: Set $k = 0$, $\lambda_k^0 = 0$.
Each user i observes s_t^i, the BS observes s_t^0
repeat
Each user i solves the decoupled decision problem (7) to obtain π^{i,λ_k^i}
Each user i submits its resource request $f^i(s_t^0) \cdot \pi^{i,\lambda_k^i}(s_t^i)$
The BS updates the prices (stochastic subgradient update):
$\lambda_{k+1}^i(s_t^0) = \lambda_k^i(s_t^0) + \frac{1}{k+1} f(s_t^0, \pi^{1,\lambda_k^1}(s_t^1), \cdots, \pi^{I,\lambda_k^I}(s_t^I))$
until $\|\lambda_{k+1}^i(s_t^0) - \lambda_k^i(s_t^0)\| \le \epsilon$
Output: optimal price λ_k^0, optimal strategies $\{\pi^{i,\lambda_k^i}\}_{i=1}^I$

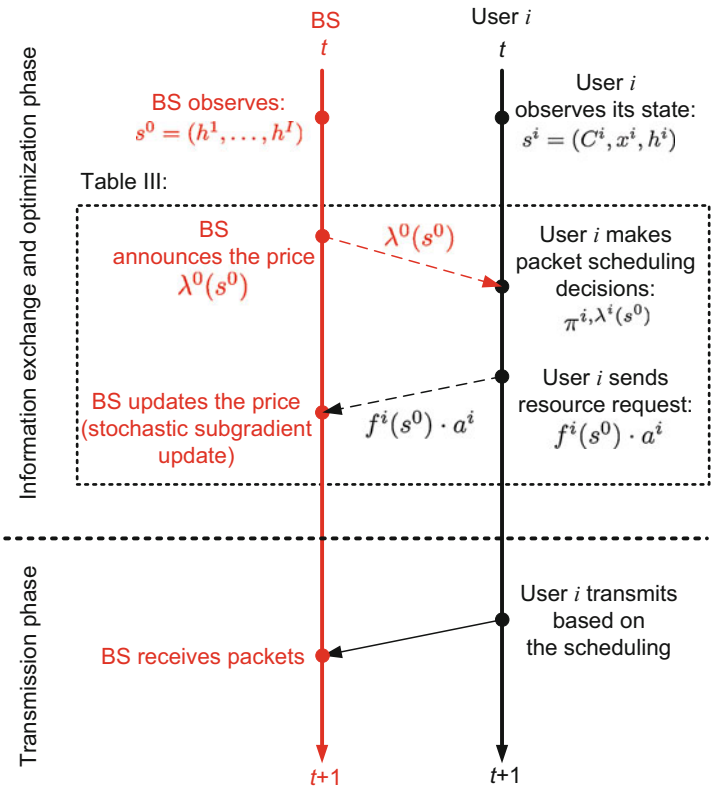

Fig. 2 Illustration of the interaction between the BS and user i (i.e., their decision-making and information exchange) in one period

From Fig. 2, we can clearly see what information (namely, resource prices λ_k^0 and resource requests $f^i \cdot \pi^{i,\lambda_k^i}(s_t^i)$) is exchanged. The amount of information exchange is small ($O(I)$), compared to the amount of information required by each user to solve the decision problem (6) directly ($\prod_{j \neq i} |S_i|$ states plus the strategies $\boldsymbol{\pi}_{-i}$). In other words, the algorithm enables the entities to exchange a small amount ($O(I)$) of information and reach the optimal video transmission strategy that achieves the same performance as when each entity knows the complete information (i.e., the states and the strategies of all the entities) about the system.

Optimal Packet Scheduling

In the previous subsection, we propose an algorithm of optimal foresighted resource allocation and packet scheduling for the general video transmission model described in section "General Model for Video Applications over Cognitive Radio"-A. In

the algorithm, each user's packet scheduling decision is obtained by solving the Bellman equation (7) (see Table 3). The Bellman equation (7) can be solved by a variety of standard techniques such as value iteration. However, the computational complexity of directly applying value iteration may be high, because each user's state contains the information of all DUs, and thus each user's state space can be very large. In the following, we show that for the specific model described in section "General Model for Video Applications over Cognitive Radio"-B, we can greatly simplify the packet scheduling decision problem. The key simplification comes from the decomposition of each user's packet scheduling problem with multiple DUs into multiple packet scheduling problems with single DU. In this way, we can greatly reduce the number of states in each single-DU packet scheduling problem, such that the total complexity of packet scheduling grows linearly, instead of exponentially without decomposition, with the number of DUs.

The decomposition closely follows the decomposition of multiple-DU packet scheduling problems proposed in [17]. The only difference is that the decision problem (7) in our work has an additional term $-\lambda^i(s^0)\cdot a^i$ due to the price, while such a term does not exist in [17] because the *single*-user packet scheduling problem is considered in [17].

Lemma 1 (Structural Result). *Suppose $DU_1 \in C_t$ and $DU_2 \in C_t$. If DU_2 depends on DU_1, we should schedule the packets of DU_1 before scheduling the packets of DU_2.*

Although Lemma 1 is straightforward, it greatly simplifies the scheduling problem because we can now take advantage of the partial ordering of the DUs. However, this still does not solve the scheduling decision for the DUs that are not dependent on each other. Next, we provide the algorithm of optimal packet scheduling in Table 4. The algorithm decomposes the multiple-DU packet scheduling problem into a sequence of single-DU packet scheduling problems and determines how many packets to transmit for each DU sequentially. This greatly reduces the total computational complexity (which is linear in the number of DUs) compared to

Table 4 The optimal packet scheduling algorithm

Input: Directed acyclic graph given the current context: $DAG(C_t)$
Initialization: Set $DAG_1 = DAG(C_t)$.
For $k = 1, \ldots, \lvert C_t \rvert$
$DU_k = \arg \max_{DU \in root(DAG_k)} \max_{0 \le y \le x_{t,DU}} (1-\delta)\left[q_{DU}\cdot y - \lambda_k^i(s^0)\cdot y\right]$
$+ \delta \cdot \sum_{s^{i\prime}} \left[p^i(s^{i\prime} \lvert s^i, a_{f,t}) \tilde{V}^{i,\lambda^{i,(k)}(s^0)}(s^{i\prime}) \right]$
$y^*_{t,DU_k} = \arg \max_{0 \le y \le x_{t,DU_k}} (1-\delta)\left[q_{DU_k}\cdot y - \lambda_k^i(s^0)\cdot y\right]$
$+ \delta \cdot \sum_{s^{i\prime}} \left[p^i(s^{i\prime} \lvert s^i, a_{f,t}) \tilde{V}^{i,\lambda^{i,(k)}(s^0)}(s^{i\prime}) \right]$
$DAG_{k+1} = DAG_k \setminus \{DU_k\}$
End for

solving the multiple-DU packet scheduling problem directly (in which the number of states grows exponentially withe the number of DUs). The algorithm is similar to [17, Algorithm 2]. The only difference is the term $-\lambda^i(s^0)\cdot a^i$.

Learning Unknown Dynamics

In practice, each entity may not know the dynamics of its own states (i.e., its own state transition probabilities) or even the set of its own states. When the state dynamics are not known a priori, each entity cannot solve their decision problems using the distributed algorithm in Table 3. In this case, we can adapt the online learning algorithm based on post-decision state (PDS) in [17], which was originally proposed for single-user wireless video transmission, to the considered deployment scenario.

The main idea of the PDS-based online learning is to learn the post-decision value function, instead of the value function. Each user i's post-decision value function is defined as $\tilde{U}^i(\tilde{x}^i,\tilde{h}^i)$, where $(\tilde{x}^i,\tilde{h}^i)$ is the post-decision state. The difference from the normal state is that the PDS $(\tilde{x}^i,\tilde{h}^i)$ describes the status of the system *after* the scheduling action is made but before the DUs in the next period arrive. Hence, the relationship between the PDS and the normal state is

$$\tilde{x}^i = x^i - a^i,\ \tilde{h}^i = h^i.$$

Then the post-decision value function can be expressed in terms of the value function as follows:

$$\tilde{U}^i(\tilde{x}^i,\tilde{h}^i) = \sum_{x^{i\prime},h^{i\prime}} p^i(x^{i\prime},h^{i\prime}|\tilde{x}^i + a^i,\tilde{h}^i)\cdot \tilde{V}^i(x^{i\prime},\tilde{h}^i).$$

In PDS-based online learning, the normal value function and the post-decision value function are updated in the following way:

$$\begin{aligned} V^i_{k+1}(x^i_k,h^i_k) &= \max_{a^i}\ (1-\delta)\cdot u^i(x^i_k,h^i_k,a^i) \\ &\quad + \delta\cdot U^i_k(x^i_k+(a^i-l^i_k),h^i_k), \\ U^i_{k+1}(x^i_k,h^i_k) &= (1-\frac{1}{k})U^i_k(x^i_k,h^i_k) \\ &\quad + \frac{1}{k}\cdot V^i_k(x^i_k-(a^i-l^i_k),h^i_k). \end{aligned}$$

We can see that the above updates do not require any knowledge about the state dynamics. In particular, we propose the decomposed optimal packet scheduling with PDS-based learning in Table 5. Note that the difference between the learning algorithm in Table 5 with the algorithm assuming statistic knowledge in Table 4

Table 5 The optimal decomposed packet scheduling algorithm with PDS-based learning

Input: Directed acyclic graph given the current context: $DAG(C_t)$
Initialization: Set $DAG_1 = DAG(C_t)$.
For $k = 1, \ldots, \lvert C_t \rvert$
$DU_k = \arg \max_{DU \in root(DAG_k)} \max_{0 \le y \le x_{t,DU}} (1-\delta)\left[q_{DU} \cdot y - \lambda_k^i(s^0) \cdot y\right] + \delta \cdot U_{DU}(C_t, x_{t,DU} - y, h_t)$
$y^*_{t,DU_k} = \arg\max_{0 \le y \le x_{t,DU}} (1-\delta)\left[q_{DU} \cdot y - \lambda_k^i(s^0) \cdot y\right] + \delta \cdot U_{DU}(C_t, x_{t,DU} - y, h_t)$
$DAG_{k+1} = DAG_k \setminus \{DU_k\}$
End for

is that we use the post-decision state value function instead of the normal value function. It is proved in [17] that the PDS-based online learning will converge to the optimal value function. Hence, the distributed packet scheduling and resource allocation solution in Table 3 can be modified by letting each user perform the packet scheduling using the PDS-based learning in Table 5.

Strategy-Proof Resource Allocation Mechanisms

When the users are self-interested, they may not follow the solutions introduced in section "Optimal Foresighted Video Transmission". In particular, they may not be truthful in the message exchange with the network manager. There are several ways of designing strategy-proof resource allocation mechanisms, based on pricing [3] and mechanism design [1–5]. In this section, we describe a representative framework based on auctions [4, 5].

The auction-based resource allocation mechanism is illustrated in Fig. 3. The basic procedure at each time slot is described as follows:

1. The network manager announces the total amount of available resources (e.g., state s^0).
2. The SUs submit bids of how much resources they are willing to get.
3. Based on SUs' bids, the network manager determines the resource allocation and the payments required from SUs.
4. Based on the allocated resources, the SUs schedule their video packets.

As we can see, most elements (e.g., states, rewards) in auction-based mechanisms are the same as in the general model in section "General Model for Video Applications over Cognitive Radio". Here we list some key features of the auction-based mechanism.

- In the auction-based mechanism, the SUs' actions consist of two types of actions, internal actions and external actions. The internal actions, denoted by b_i^t in

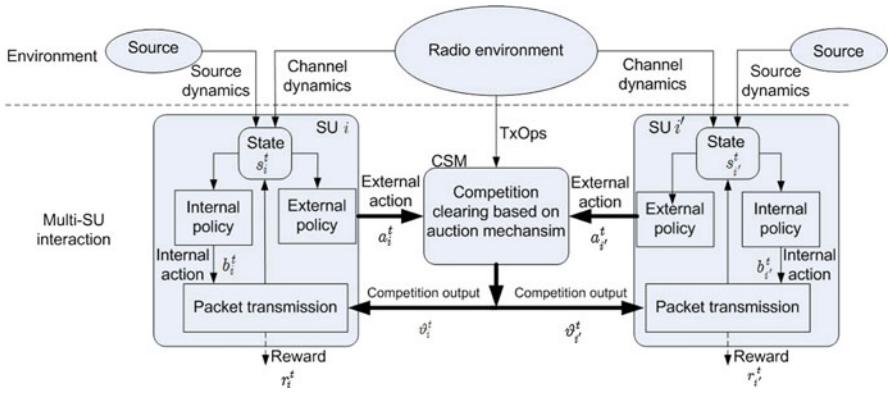

Fig. 3 Illustration of strategy-proof resource allocation mechanism based on auctions

Fig. 3, are the packet scheduling actions described in section "General Model for Video Applications over Cognitive Radio". The external actions are unique in the auction-based mechanism. Specifically, the external action is the amount of resources each SU wants to get (i.e., their bids).

- In the auction-based mechanism, the network manager directly allocates the resources to the SUs and announces the payments required from the SUs. This is different from the mechanism in section "General Model for Video Applications over Cognitive Radio", where the network manager announces the prices and the SUs determine the resource allocation based on the prices.

We refer interested readers to [4, 5] for detailed descriptions and theoretical results of the auction-based mechanisms.

Conclusion and Future Directions

In this chapter, we introduce the optimal foresighted resource allocation and packet scheduling for multiuser wireless video transmission over cognitive radio networks. The introduced solution achieves the optimal long-term video quality subject to each user's minimum video quality guarantee, by dynamically allocating resources among the users and dynamically scheduling the users' packets while taking into account the dynamics of the video traffic and channel states. We develop a low-complexity algorithm that can be implemented by the network manager and the users in an informationally decentralized manner and converges to the optimal solution. We also introduce strategy-proof variations of our solutions for self-interested users.

There are many important future research directions. First, we have focused on the cases where users have orthogonal spectrum access. One interesting direction is to allow non-orthogonal spectrum access through power control. This will further

complicate the coupling among the users. This is because orthogonal spectrum access results in resource allocation constraints as linear inequality, while non-orthogonal spectrum access will destroy the linearity. Theoretically, the resulting problems are *strongly coupled* multiuser MDPs, instead of *weakly coupled* multiuser MDPs in this chapter.

Second, in the scenarios where users are self-interested, theoretical analysis of the efficiency at the equilibrium is yet missing. There are existing works in computer science and economics literature that analyze the Price of Anarchy (PoA) and efficiency of learning in games. However, most of these works focus on one-shot games (i.e., when users are myopic). When the users are foresighted, the problem is more challenging and calls for novel analytical frameworks.

References

1. Fattahi A, Fu F, van der Schaar M, Paganini F (2007) Mechanism-based resource allocation for multimedia transmission over spectrum agile wireless networks. IEEE J Sel Areas Commun 25(3):601–612
2. Fu F, van der Schaar M (2007) Noncollaborative resource management for wireless multimedia applications using mechanism design. IEEE Trans Multimedia 9(4):851–868
3. Fu F, Stoenescu TM, van der Schaar M (2007) A pricing mechanism for resource allocation in wireless multimedia applications. IEEE J Sel Top Sign Process, Spec Issue Netw-Aware Multimedia Process Commun 1(2):264–279
4. Fu F, van der Schaar M (2009) Learning to compete for resources in wireless stochastic games. IEEE Trans Veh Tech 58(4):1904–1919
5. van der Schaar M, Fu F (2009) Spectrum access games and strategic learning in cognitive radio networks for delay-critical applications. Proc IEEE Spec Issue Cogn Radio 97(4):720–740
6. Fu F, van der Schaar M (2010) A systematic framework for dynamically optimizing multi-user video transmission. IEEE J Sel Areas Commun 28(3):308–320
7. Xiao Y, van der Schaar M (2015) Optimal foresighted multi-user wireless video. IEEE J Sel Top Sign Process, Spec Issue Visual Sign Process Wirel Netw 9(1):89–101
8. Yu Y-J, Hsiu P-C, Pang A-C (2012) Energy-efficient video multicast in 4G wireless systems. IEEE Trans Mob Comput 11(10):1508–1522
9. van der Schaar M, Andreopoulos Y, Hu Z (2006) Optimized scalable video streaming over IEEE 802.11 a/e HCCA wireless networks under delay constraints. IEEE Trans Mob Comput 5(6):755–768
10. Su G-M, Han Z, Wu M, Liu KJR (2007) Joint uplink and downlink optimization for real-time multiuser video streaming over WLANs. IEEE J Sel Top Sign Process 1(2):280–294
11. Zhang X, Du Q (2007) Cross-layer modeling for QoS-driven multimedia multicast/broadcast over fading channels in mobile wireless networks. IEEE Commun Mag 45(8):62–70
12. Huang J, Li Z, Chiang M, Katsaggelos AK (2008) Joint source adaptation and resource allocation for multi-user wireless video streaming. IEEE Trans Circuits Syst Video Technol 18(5):582–595
13. Maani E, Pahalawatta P, Berry R, Pappas TN, Katsaggelos AK (2008) Resource allocation for downlink multiuser video transmission over wireless lossy networks. IEEE Trans Image Process 17(9):1663–1671
14. Chou P, Miao Z (2006) Rate-distortion optimized streaming of packetized media. IEEE Trans Multimedia 8(2):390–404
15. Huang J, Wang H, Qian Y (2017) Game user-oriented multimedia transmission over cognitive radio networks. IEEE Trans Circuits Syst Video Tech 27(1):198–208

16. Ji X, Huang J, Chiang M, Lafruit G, Catthoor F (2009) Scheduling and resource allocation for SVC streaming over OFDM downlink systems. IEEE Trans Circuits Syst Video Technol 19(10):1549–1555
17. Fu F, van der Schaar M (2012) Structural solutions for dynamic scheduling in wireless multimedia transmission. IEEE Trans Circuits Syst Video Technol 22(5):727–739
18. Wu Y, Hu F, Kumar S, Zhu Y, Talari A, Rahnavard N, Matyjas J (2014) A learning-based QoE-driven spectrum handoff scheme for multimedia transmissions over cognitive radio networks. IEEE J Sel Areas Comm 32(11):2134–2148
19. Shah G, Alagoz F, Fadel E, Akan O (2014) A spectrum-aware clustering for efficient multimedia routing in cognitive radio sensor networks. IEEE Trans Veh Tech 63(7):3369–3380
20. He Z, Mao S, Kompella S (2016) Quality of experience driven multi-user video streaming in cellular cognitive radio networks with single channel access. IEEE Trans Multimedia 18(7):1401–1413
21. Wang H, Qian Y, Sharif H (2013) Multimedia communications over cognitive radio networks for smart grid applications. IEEE Wirel Commun 20(4):125–132
22. Chen W, Neely MJ, Mitra U (2008) Energy-efficient transmission with individual packet delay constraints. IEEE Trans Inform Theory 54(5):2090–2109
23. Fu F, van der Schaar M (2012) Structure-aware stochasticcontrol for transmission scheduling. IEEE Trans Veh Tech 61(9):3931–3945
24. Zhang Q, Kassam SA (1999) Finite-state Markov model for Rayleigh fading channels. IEEE Trans Commun 47(11):1688–1692
25. Bertsekas D, Gallager R (1987) Data networks. Prentice-Hall, Upper Saddle River
26. Hawkins J (2003) A Lagrangian decomposition approach to weakly coupled dynamic optimization problems and its applications. PhD dissertation, MIT, Cambridge

Further Reading

1. Khan S, Sgroi M, Peng Y, Steinbach E, Kellerer W (2006) Application-driven cross layer optimization for video streaming over wireless networks. IEEE Commun Mag 44(1):122–130
2. De Vleeschouwer C, Frossard P (2007) Dependent packet transmission policies in rate-distortion optimized media scheduling. IEEE Trans Multimedia 9(6):1241–1258
3. Li Z, Zhai F, Katsaggelos A (2008) Joint video summarization and transmission adaptation for energy-efficient wireless video streaming. EURASIP J Adv Sign Process Spec Issue Wirel Video 2008: 1–11
4. Tizon N, Pesquet-Popescu B (2008) Scalable and media aware adaptive video streaming over wireless networks. EURASIP J Adv Sign Process 2008:11, Article ID 218046
5. Wang H, Ortega A (2009) Rate-distortion optimized scheduling for redundant video representations. IEEE Trans Image Process 18(2):225–240
6. IEEE Standard for Local and Metropolitan Area Networks, Part 15.4: Low-Rate Wireless Personal Area Networks (LR-WPANs) Amendment 1: MAC Sublayer. IEEE Computer Society, 16 Apr 2012. Online at: http://standards.ieee.org/getieee802/download/802.15.4e-2012.pdf
7. Kushner H, Yin G (2003) Stochastic approximation and recursive algorithms and applications. Springer, New York

MIMO-Empowered Secondary Networks for Efficient Spectrum Sharing

30

Xu Yuan, Cunhao Gao, Feng Tian, Yi Shi, Y. Thomas Hou, Wenjing Lou, Wade Trappe, Scott F. Midkiff, Jeffrey H. Reed, and Sastry Kompella

Contents

X. Yuan (✉) · C. Gao · Y. T. Hou · W. Lou · S. F. Midkiff · J. H. Reed
Virginia Polytechnic Institute and State University, Blacksburg, VA, USA
e-mail: xuy10@vt.edu; cunhaogao@gmail.com; thou@vt.edu; wjlou@vt.edu; midkiff@vt.edu; reedjh@vt.edu

F. Tian
Nanjing University of Posts and Telecommunications, Nanjing, China
e-mail: tianf@njupt.edu.cn

Y. Shi
Intelligent Automation Inc., Rockville, MD, USA
e-mail: yshi@vt.edu

W. Trappe
Rutgers University, New Brunswick, NJ, USA
e-mail: trappe@winlab.rutgers.edu

S. Kompella
Information Technology Division, Naval Research Laboratory, Washington, DC, USA

U.S. Naval Research Laboratory, Washington, DC, USA
e-mail: sastry.kompella@nrl.navy.mil

W. Zhang (ed.), *Handbook of Cognitive Radio*,
https://doi.org/10.1007/978-981-10-1394-2_29

Abstract

Cognitive radio (CR) and multiple-input multiple-output (MIMO) are two independent physical layer technologies that have made significant impact on wireless networks. In particular, CR operates on the channel level to exploit efficiency across spectrum dimension, while MIMO operates within the same channel to exploit efficiency across spatial dimension. In this chapter, we explore MIMO-empowered CR technique to enhance spectrum access in wireless networks. Specially, we study how to apply MIMO-empowered CR for both interweave and underlay paradigms in multi-hop network environment. With MIMO interference cancelation (IC) capability, we first show how multiple secondary links achieve simultaneous transmission on the same channel under the interweave paradigm. Next, we show how secondary networks achieve simultaneously transmission with the primary network on same channel to achieve transparent coexistence under the underlay paradigm. Through rigorous mathematical modeling, problem formulation, and extensive simulation results, we find that MIMO-empowered CR can offer significant improvement in terms of spectrum access and throughput performance under both interweave and underlay paradigms.

Keywords

Cognitive radio · MIMO · Interference cancelation · Spectrum sharing · Coexistence · Interweave · Underlay · Multi-hop network

Introduction

Since its inception, cognitive radio (CR) has quickly been accepted as the enabling radiotechnology for next-generation wireless communications [8, 22]. A CR promises unprecedented flexibility in radio functionalities via programmability at the lowest layer, which was once done in hardware. Due to its spectrum sensing, learning, and adaptation capabilities, CR has the potential to address the heart of the problem associated with spectrum scarcity (via dynamic spectrum access (DSA)) and interoperability (via channel switching). Already, CR or its predecessor, software-defined radio (SDR), has been implemented for cellular communications [20], the military [10], and public safety communications [13]. It is envisioned that CR will be employed as a general radio platform upon which numerous wireless applications can be implemented.

In parallel to the development of CR, MIMO [2, 19] has already been widely implemented in commercial wireless products to increase capacity. The goal of

MIMO and how it operates are largely independent of and orthogonal to CR. Instead of exploiting idle channels for wireless communications, MIMO attempts to increase capacity within the same channel via space-time processing [6]. In particular, by employing multiple antennas at both the transmit and receive nodes, wireless channel capacity can scale almost linearly with the number of antennas (via spatial multiplexing) [4, 18]. Further, with zero-forcing beamforming (ZFBF) [3, 21], a node may use its degrees of freedom (DoFs) to cancel interference from other nodes or its own interference to other nodes.

In this chapter, we explore MIMO in CR-based secondary networks in both interweave (i.e., interference avoidance or DSA) and underlay paradigms [7] to enhance spectrum efficiency and spatial reuse. In interweave paradigm, to avoid interference to primary network, the secondary networks can only operate on spectrum holes. However, with MIMO IC capability, secondary nodes are allowed to be active simultaneously on the same band in the secondary network. If we assume that each node in a cognitive radio network (CRN) is equipped with A_{MIMO} antennas, then one would expect at least A_{MIMO}-fold capacity increase when compared to a CRN with only a single antenna at each node, due to spatial multiplexing gain from MIMO. Now observing that CR and MIMO handle interference differently (with CR on the channel level and MIMO within a channel), we ask the following fundamental question: *Will joint optimization of CR (via channel assignment) and MIMO (via DoF allocation) offer more than A_{MIMO}-fold in capacity?*

In underlay paradigm, we explore the potential of *simultaneous activation* of a secondary network with the primary network, as long as the interference produced by the secondary nodes can be properly "controlled" (e.g., canceled) by secondary nodes. In other words, secondary nodes are allowed to access the spectrum as long as they can cancel their interference to the primary nodes in such a way that primary nodes do not feel the presence of secondary nodes. In other words, activities by the secondary nodes are made transparent (or "invisible") to the primary nodes. We call this *transparent coexistence*. Although the idea of the transparent coexistence has been explored in the information theory (IT) community, results from the IT and communication (COMM) communities have mainly limited to very simple network settings, e.g., several nodes or link pairs, all for *single-hop* communications [1, 5, 11, 23, 24]. The more interesting problem of how transparent coexistence can be achieved in a *multi-hop* secondary network remains open. As shown in [9, 14], the problem complexity associated with multi-hop CR networks is much higher than single-hop CR networks.

The remainder of this chapter is organized as follows. In sections "MIMO-Based Secondary Network in Interweave Paradigm" and "MIMO-Based Secondary Network in Transparent-Coexistence Paradigm", we explore MIMO-empowered CR for a multi-hop secondary network under the interweave and underlay paradigms, respectively. Through case studies, we demonstrate that MIMO-empowered secondary networks can significantly improve spectrum efficiency and spatial reuse under both interweave and underlay paradigms. Section "Summary and Future Directions" summarizes this chapter.

MIMO-Based Secondary Network in Interweave Paradigm

In this section, we study MIMO-based secondary multi-hop network in interweave paradigm. Our discussion consists of two levels: The first is on channel level, i.e., how does a secondary network exploit available spectrum and handle interference via the use of different channels. The second is within a channel, i.e., how does MIMO mitigate co-channel interference via ZFBF (i.e., using DoF). A thorough understanding of these interference avoidance/cancelation techniques across/within channels is critical to mathematical modeling and ultimately fully exploit the potential of MIMO and CR. Based on this background, we then develop a rigorous mathematical model and study a throughput maximization problem to exploit the potential benefit of MIMO-based secondary network.

Co-channel Interference Cancelation with MIMO DoFs

The total number of antennas at a node is called *degrees of freedom* (or DoFs) [12] at the node. A node can use some or all of its DoFs for either spatial multiplexing (SM) (to achieve multiple concurrent data streams over a link) or co-channel IC (to enable multiple links on the same band), as long as the number of DoFs being used does not exceed the number of antennas at the node.

The allocation of DoFs at a node for SM and IC can be based on an ordering of all nodes in the network [16]. For a given ordered node list, the DoFs at a node can be allocated as follows.

- *DoF Allocation at A Transmit Node.* First, the transmit node needs to allocate DoFs for SM. The number of DoFs to be allocated equals to the number of data streams to be transmitted. Then, for IC, this transmit node must ensure that its transmission does not interfere with those receive nodes that are before this node in the ordered list. To cancel its interference to these receive nodes, this node needs to allocate a number of DoFs that are equal to the received data streams by those nodes. This transmit node does not need to allocate any of its DoFs to null potential interference to those receive nodes that are after itself in the ordered node list.
- *DoF Allocation at A Receive Node.* First, the receive node needs to allocate DoFs for data reception (SM). The number of DoFs to be allocated equals to the number of data streams to be received. Then, for IC, this node must ensure that its reception is not interfered by those transmit nodes that are ordered before this node in the list. To cancel the interference from these transmit nodes, this node needs to allocate a number of DoFs that are equal to the transmitted data streams by those nodes. This receive node does not need to allocate any of its DoFs to null potential interference from those transmit nodes that are after itself in the ordered node list.

An example is given in Fig. 1, where there are four nodes, each equipped with 4 antennas. All nodes operate on the same channel, and there are two mutually

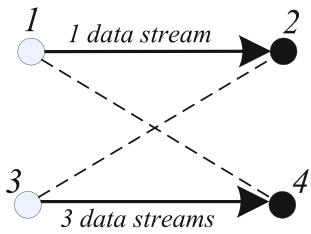

Fig. 1 Simultaneous activation of two secondary links with IC

interfering links in the network: $1 \rightarrow 2$ and $3 \rightarrow 4$. Suppose the ordered node list for DoF allocation is 1, 2, 3, and 4. Further, node 1 is transmitting 1 data stream to node 2 and node 3 is transmitting 3 DoF to node 4 . Now we show how the DoFs at each node are allocated for interference cancelation and spatial multiplexing:

- Starting with node 1, it is the first node in the list and it is a transmit node. Then it allocates 1 DoF for its transmission with 1 data stream. It does not need to allocate any DoF to cancel potential interference to other receive nodes that are after itself in the ordered node list, i.e., node 4.
- The next node in the list is node 2. As a receive node, it allocates 1 DoF for receiving 1 data stream from node 1. It does not need to consider allocating any DoF to cancel interference from other transmit nodes that are after itself in the ordered node list, i.e., node 3.
- The next node in the list is node 3. As a transmit node, it needs to ensure that its transmission does not interfere with any receive node before itself in the list, i.e., node 2. Thus, node 3 uses 1 DoF (equals to the number of received data streams by node 2) to cancel its interference to node 2. Now it has 3 remaining DoFs, which can all be used to transmit data streams (up to 3) to node 4.
- The last node in the list is node 4. As a receive node, node 4 needs to allocate 3 of its DoFs for receiving 3 data streams from node 3. Node 4 also needs to use its remaining 1 DoF (equals to the number of transmitted data streams by node 1) to cancel interference from node 1. This completes the DoF allocation at each node.

Mathematical Modeling

We consider a secondary multi-hop network consisting of a set of $\mathcal{N}$ nodes. At each node $i \in \mathcal{N}$, there is a set of $\mathcal{B}_i$ available frequency bands that can be used for communications. As discussed, $\mathcal{B}_i$ may represent the set of bands that are unused by the primary users and may be different at each node due to geographical difference. Denote the set of commonly available bands between nodes i and j as $\mathcal{B}_{ij} = \mathcal{B}_i \bigcap \mathcal{B}_j$. Also, denote A_i as the number of antennas at node i. Suppose there are multiple sessions in this network. Denote $\mathcal{Q}$ the set of sessions in the network. For a session $q \in \mathcal{Q}$, denote $s(q)$ the source node, $d(q)$ the destination node, and $f(q)$ the flow rate (in b/s). Table 1 lists all notation used in the interweave paradigm.

Table 1 Notation in interweave paradigm

Symbol	Definition
A_i	The number of antennas at node $i \in \mathcal{N}$
A_{MIMO}	The number of antennas at each node
$\mathcal{B}_i$	The set of available bands at node $i \in \mathcal{N}$
$\mathcal{B}_{ij}$	The set of common available bands at nodes $i, j \in \mathcal{N}$
c	The capacity when 1 DoF is used for data transmission on a band over a link
$d(q)$	Destination node of session q
$f(q)$	The rate of session q
g_i^b	A binary indicator. g_i^b is 1 if node i is transmitting or 0 otherwise
h_i^b	A binary indicator. h_i^b is 1 if node i is receiving or 0 otherwise
$\mathcal{I}_i^b$	The set of nodes in the interference range of node i on band b
$\mathcal{L}_{i,b}^{\text{Out}}$	The set of outgoing links on band b at node i
$\mathcal{L}_{i,b}^{\text{In}}$	The set of incoming links on band b at node i
$\mathcal{L}_{\text{Active}}$	The set of links used for routing
$\mathcal{N}$	The set of all nodes in the network
$\mathcal{Q}$	The set of active sessions in the network
$\text{Rx}(l)$	Receiving node of link l
$s(q)$	Source node of session q
$\text{Tx}(l)$	Transmitting node of link l
z_l^b	The number of data streams over link l on band b
θ_{ji}^b	Binary indicator showing the relationship between nodes i and j in the ordered list on band b
λ_{ji}^b	The number of DoFs on band b used by transmitting node i to cancel its interference to node j
μ_{ji}^b	The number of DoFs on band b used by receiving node i to cancel the interference from node j

Half-Duplex Constraint. To model the half-duplex nature of each node in a band, we use two binary variables g_i^b and h_i^b to indicate node i's transmission/reception status on band b, i.e.,

$$g_i^b = \begin{cases} 1 & \text{if node } i \text{ is transmitting on band } b, \\ 0 & \text{otherwise.} \end{cases}$$

$$h_i^b = \begin{cases} 1 & \text{if node } i \text{ is receiving on band } b, \\ 0 & \text{otherwise.} \end{cases}$$

where $i \in \mathcal{N}, b \in \mathcal{B}_i$. Then the half-duplex constraint (i.e., a node cannot transmit and receive at the same time in the same band) can be represented as follows:

$$g_i^b + h_i^b \leq 1, \quad (i \in \mathcal{N}, b \in \mathcal{B}_i). \tag{1}$$

Node Ordering for IC. As discussed in section "Co-channel Interference Cancelation with MIMO DoFs", the DoF allocation (for SM and IC) at each node is determined sequentially based on an ordered node list. This ordering determines DoF allocation behavior in the final solution and should be part of the optimization problem. We point out that such a node ordering approach for DoF allocation is the most efficient approach among all existing DoF models that can guarantee feasibility. As pointed out in [16], an optimal ordering of secondary nodes can be found by inserting a formulation of the ordering relationship into the specific optimization problem.

Denote π^b as an ordered list of the nodes in the secondary network on channel $b \in \mathscr{B}$, and denote π_i^b as the position of node $i \in \mathscr{S}$ in π^b. Therefore, $1 \le \pi_i^b \le S$, where $S = |\mathscr{S}|$. For example, if $\pi_i^b = 3$, then it means that node i is in the third position in the list π^b.

To model the relative ordering between any two secondary nodes i and j in π^b, we define a binary indication variable $\theta_{j,i}^b$ and define it as follows:

$$\theta_{j,i}^b = \begin{cases} 1 \text{ if node } j \text{ is before node } i \text{ in } \pi^b \text{ on channel } b; \\ 0 \text{ otherwise.} \end{cases}$$

It was shown in [16] that the following relationships hold:

$$\pi_i^b - S \cdot \theta_{j,i}^b + 1 \le \pi_j^b \le \pi_i^b - S \cdot \theta_{j,i}^b + S - 1 \,, \quad (i, j \in \mathscr{S}, b \in \mathscr{B}). \tag{2}$$

Transmitter DoF Constraint. Now we consider DoF allocation at a node, which includes DoFs allocated for SM and DoFs allocated for IC.

For transmission and reception, the number of required DoFs is $\sum_{l \in \mathscr{L}_{i,b}^{\text{Out}}} z_l^b$ for a transmit node i and $\sum_{m \in \mathscr{L}_{j,b}^{\text{In}}} z_m^b$ for a receive node j, respectively. As we discussed in section "Co-channel Interference Cancelation with MIMO DoFs", in any given band, the total number of data streams for transmission or reception at a node is limited by its number of antennas. Denote l as a directional link in the network and z_l^b as the number of data streams over link l in band b. Then we have the following two constraints:

$$g_i^b \le \sum_{l \in \mathscr{L}_{i,b}^{\text{Out}}} z_l^b \le g_i^b A_i \qquad (i \in \mathscr{N}, b \in \mathscr{B}_i) \,, \tag{3}$$

$$h_i^b \le \sum_{l \in \mathscr{L}_{i,b}^{\text{In}}} z_l^b \le h_i^b A_i \qquad (i \in \mathscr{N}, b \in \mathscr{B}_i) \,, \tag{4}$$

where $\mathscr{L}_{i,b}^{\text{Out}}$ and $\mathscr{L}_{i,b}^{\text{In}}$ represent the sets of outgoing and incoming links at node i in band b, respectively.

For IC, as discussed in section "Co-channel Interference Cancelation with MIMO DoFs", a transmit node needs to allocate its DoFs to cancel its interference to all receive nodes before itself in the ordered node list. Denote $\mathscr{I}_i^b$ as the set of nodes to which node i can interfere within band b. Then the number of DoFs that node i allocates for IC can be computed as $\sum_{j\in\mathscr{I}_i^b}(\theta_{ji}^b \cdot \sum_{m\in\mathscr{L}_{j,b}^{\text{In}}}^{\text{Tx}(m)\neq i} z_m^b)$, where the inner summation $\sum_{m\in\mathscr{L}_{j,b}^{\text{In}}}^{\text{Tx}(m)\neq i} z_m^b$ gives the number of data streams for a given receive node j, while the outer summation is taken only over those receive nodes that are before node i in the ordered node list. Now considering both the DoFs at a node allocated for SM and IC, we have the following constraint:

$$\sum_{l\in\mathscr{L}_{i,b}^{\text{Out}}} z_l^b + \sum_{j\in\mathscr{I}_i^b}\left(\theta_{ji}^b \cdot \sum_{m\in\mathscr{L}_{j,b}^{\text{In}}}^{\text{Tx}(m)\neq i} z_m^b\right) \leq A_i g_i^b + (1-g_i^b)M, \tag{5}$$

where $i \in \mathscr{N}, b \in \mathscr{B}_i$, and M is a sufficiently large number to ensure the constraint holds when node i is not a transmitnode (e.g., we can set $M = \sum_{j\in\mathscr{I}_i^b} A_j$).

Receiver DoF Constraint. Similarly, if node i is a receive node, we have the following constraint for its DoF allocation:

$$\sum_{l\in\mathscr{L}_{i,b}^{\text{In}}} z_l^b + \sum_{j\in\mathscr{I}_i^b}\left(\theta_{ji}^b \cdot \sum_{m\in\mathscr{L}_{j,b}^{\text{Out}}}^{\text{Rx}(m)\neq i} z_m^b\right) \leq A_i h_i^b + (1-h_i^b)M, \tag{6}$$

where $i \in \mathscr{N}, b \in \mathscr{B}_i$.

For a given route for each session, we can identify the set of links on this route. Denote $\mathscr{L}_{\text{Active}}$ as the set of links that are used by all these routes in the network. Then we have the following capacity constraint on link $l \in \mathscr{L}_{\text{Active}}$.

$$\sum_{q\in\mathscr{Q}}^{l \text{ is traversed by } q} f(q) \leq c \sum_{b\in\mathscr{B}_{\text{Tx}(l),\text{Rx}(l)}} z_l^b \quad (l \in \mathscr{L}_{\text{Active}}), \tag{7}$$

where $f(q)$ is the flow rate of session $q \in \mathscr{Q}$ and c is the capacity when 1 DoF is used for data transmission on a band over link l.

Problem Formulation

Based on the above mathematical model, various problems can be formulated. In this chapter, we study a throughput optimization problem with the objective of maximizing the minimum session rate among all secondary sessions. The optimization problem can be written as follows:

$$
\begin{aligned}
\text{OPT}\ \max\ & f_{\min} \\
\text{s.t}\ & f_{\min} \le f(q) \quad (q \in \mathscr{Q}); \\
& \text{Half-duplex constraints: (1);} \\
& \text{Node ordering constraints: (2);} \\
& \text{Transmitter DoF constraints: (3), (5);} \\
& \text{Receiver DoF constraints: (4), (6);} \\
& \text{Link capacity constraints: (7).}
\end{aligned}
$$

In this formulation, $f_{\min}$, $f(q)$, g_i^b, h_i^b, z_l^b, and θ_{ji}^b are optimization variables and A_i, M, and c are given constants. Due to the nonlinear product term $\sum_{j\in\mathscr{I}_i^b}(\theta_{ji}^b \cdot \sum_{m\in\mathscr{L}_{j,b}^{\text{In}}}^{\text{Tx}(m)\neq i} z_m^b)$ in (5), $\sum_{j\in\mathscr{I}_i^b}(\theta_{ji}^b \cdot \sum_{m\in\mathscr{L}_{j,b}^{\text{Out}}}^{\text{Rx}(m)\neq i} z_m^b)$ in (6), and integer variables, the problem is in the form of mixed-integer nonlinear programming (MINLP).

Mathematical Reformulation

Note that the constraints in (5) and (6) have nonlinear terms (product of variables), which bring in extra complexity in problem formulation. We now show how these nonlinear terms can be removed via linearization. For the nonlinear term in (5), we define a new variable λ_{ji}^b as follows:

$$
\lambda_{ji}^b = \theta_{ji}^b \cdot \sum_{m\in\mathscr{L}_{j,b}^{\text{In}}}^{\text{Tx}(m)\neq i} z_m^b \qquad (i \in \mathscr{N}, b \in \mathscr{B}_i, j \in \mathscr{I}_i^b), \tag{8}
$$

which is the number of DoFs that transmit node i uses to cancel the interference to receive node j. With λ_{ji}^b, (5) can be rewritten as:

$$
\sum_{l\in\mathscr{L}_{i,b}^{\text{Out}}} z_l^b + \sum_{j\in\mathscr{I}_i^b} \lambda_{ji}^b \le A_i g_i^b + (1 - g_i^b)M, \tag{9}
$$

where $i \in \mathscr{N}, b \in \mathscr{B}_i$. Now, we need to add some constraints for λ_{ji}^b. This can be done by examining the definition of λ_{ji}^b in (8). For binary variable θ_{ji}^b, we have the following relaxed constraints: $\theta_{ji}^b \ge 0$, $1 - \theta_{ji}^b \ge 0$. For $\sum_{m\in\mathscr{L}_{j,b}^{\text{In}}}^{\text{Tx}(m)\neq i} z_m^b$, we have $\sum_{m\in\mathscr{L}_{j,b}^{\text{In}}}^{\text{Tx}(m)\neq i} z_m^b \ge 0$, $A_j - \sum_{m\in\mathscr{L}_{j,b}^{\text{In}}}^{\text{Tx}(m)\neq i} z_m^b \ge 0$. Multiplying each constraint involving θ_{ji}^b by one of the two constraints involving $\sum_{m\in\mathscr{L}_{j,b}^{\text{In}}}^{\text{Tx}(m)\neq i} z_m^b$, and replacing the product term $\theta_{ji}^b \cdot \sum_{m\in\mathscr{L}_{j,b}^{\text{In}}}^{\text{Tx}(m)\neq i} z_m^b$ with the new variable λ_{ji}^b, we obtain the following four constraints:

$$
\lambda_{ji}^b \ge 0 \tag{10}
$$

$$
\lambda_{ji}^b \le \sum_{m\in\mathscr{L}_{j,b}^{\text{In}}}^{\text{Tx}(m)\neq i} z_m^b \tag{11}
$$

$$\lambda_{ji}^{b} \leq A_j \cdot \theta_{ji}^{b} \tag{12}$$

$$\lambda_{ji}^{b} \geq A_j \cdot \theta_{ji}^{b} - A_j + \sum_{m \in \mathscr{L}_{j,b}^{\mathrm{In}}}^{\mathrm{Tx}(m) \neq i} z_m^b \tag{13}$$

where $i \in \mathscr{N}, b \in \mathscr{B}_i, j \in \mathscr{I}_i^b$. Note that due to the relaxation of integer variable θ_{ji}^b, $\sum_{m \in \mathscr{L}_{j,b}^{\mathrm{In}}}^{\mathrm{Tx}(m) \neq i} z_m^b$, and product operations, the above four constraints for λ_{ji}^b might be looser than (8). However, for the special case when θ_{ji}^b is a binary variable, it can be easily verified that (8) is equivalent to the four constraints in (10), (11), (12), and (13). Therefore, it is sufficient to have linear constraints (9), (10), (11), (12), and (13) to replace (5).

Similarly, to remove the nonlinear term in (6), we define μ_{ji}^b as the number of DoFs that receive node i uses to cancel the interference from transmit node j. Following the same token, (6) can be replaced by the following linear constraints:

$$\sum_{l \in \mathscr{L}_{i,b}^{\mathrm{In}}} z_l^b + \sum_{j \in \mathscr{I}_i^b} \mu_{ji}^b \leq A_i h_i^b + (1 - h_i^b) M \tag{14}$$

$$\mu_{ji}^b \geq 0 \tag{15}$$

$$\mu_{ji}^b \leq \sum_{m \in \mathscr{L}_{j,b}^{\mathrm{Out}}}^{\mathrm{Rx}(m) \neq i} z_m^b \tag{16}$$

$$\mu_{ji}^b \leq A_j \cdot \theta_{ji}^b \tag{17}$$

$$\mu_{ji}^b \geq A_j \cdot \theta_{ji}^b - A_j + \sum_{m \in \mathscr{L}_{j,b}^{\mathrm{Out}}}^{\mathrm{Rx}(m) \neq i} z_m^b \tag{18}$$

where $i \in \mathscr{N}, b \in \mathscr{B}_i, j \in \mathscr{I}_i^b$.

With the above linearization, we have a revised optimization problem formulation (denoted as OPT-R).

OPT-R max $f_{\min}$
s.t $f_{\min} \leq f(q) \quad (q \in \mathscr{Q})$;
Half-duplex constraints: (1);
Node ordering constraints: (2);
Transmitter DoF constraints: (3), (10), (11), (12), and (13);
Receiver DoF constraints: (4), (14), (15), (16), (17), and (18);
Link capacity constraints: (7).

In this formulation, $f_{\min}$, $f(q)$, g_i^b, h_i^b, z_l^b, θ_{ji}^b, λ_{ji}^b, and μ_{ji}^b are optimization variables and A_i, M, and c are constants. The problem is now in the form of mixed-integer linear programming (MILP), which is NP-hard in general. The computation complexity of MILP is exponential, but fortunately, the branch-and-cut based solution procedure used by a commercial solver such as CPLEX is very efficient. Therefore, we will use CPLEX to solve our MILP problems, which turns out to be very successful for all practical purposes.

Anticipated Results

Before we present numerical results, we offer the following discussion on the possible solution to our problem. Consider a CRN with only a single transmit/receive antenna at each node (i.e., $A_i = 1, i \in \mathcal{N}$). Denote f_{CRN} as the optimal objective value for this CRN with our problem formulation. Now consider a CRN$^{\text{MIMO}}$ with the same topology as the above CRN but now with A_{MIMO} transmit/receive antennas at each node. This CRN$^{\text{MIMO}}$ is a special case of our CRN$^{\text{MIMO}}$ network with all $A_i = A_{\text{MIMO}}, i \in \mathcal{N}$. Denote $f_{\text{CRN}^{\text{MIMO}}}$ as the optimal objective value for this CRN$^{\text{MIMO}}$ under our problem formulation. Comparing $f_{\text{CRN}^{\text{MIMO}}}$ with f_{CRN}, we have the following observation:

$$f_{\text{CRN}^{\text{MIMO}}} \geq A_{\text{MIMO}} \times f_{\text{CRN}} \tag{19}$$

The equality part in (19) can be easily explained by exploiting SM, i.e., constructing the same solution in CRN$^{\text{MIMO}}$ as that in the CRN but with A_{MIMO} data streams on each link.

However, we are more interested in the possible *inequality* part in (19), i.e., with joint channel level (via CR) and co-channel level (via MIMO DoF) optimization within a CRN$^{\text{MIMO}}$, we should anticipate more than A_{MIMO}-fold increase in the optimal solution. The greater the gap is in this inequality, the more potential in the joint CR and MIMO that can be exploited. We shall look into this potential gain via numerical results on various networks in the next section.

A Case Study

In this section, we present some numerical results for various network configurations. We consider randomly generated secondary networks with $|\mathcal{N}| = 30$ nodes in an 100×100 area. For ease of scalability and generality, we normalize all units for distance, bandwidth, and rate with appropriate dimensions. In this case study, we assume there are four sessions in the network with the source node and destination node for each session which are randomly selected. There are $|\mathcal{B}| = 15$ frequency bands available in the network. The set of available bands at each node is being

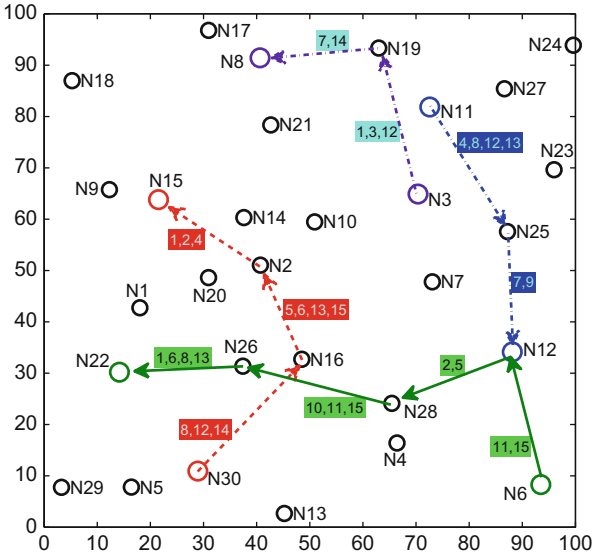

Fig. 2 Assigned bands on each link for the 30-node secondary network

randomly selected from the 15-band pool. The capacity achieved by one band and 1 DoF is normalized to 1. We assume that the transmission range is 30 and the interference range is 60.

Results Before we present results to validate for all 30-node network instance, we select one network instance and explain the details of its optimal solution. This will offer us thorough understanding on what is behind MIMO-based CRN.

The particular network configuration that we will examine is shown in Fig. 2. The location and available bands for each node are listed in Table 2. Table 3 specifies the source and destination nodes for each session. For MIMO, we assume each node in the network is equipped with 4 antennas. We assume minimum-hop routing is used in the network.

Using CPLEX, we can obtain optimal solution to the OPT-R problem. The optimal objective value for this secondary network is 6, which means each session can send at least 6 data streams from its source to its destination.

In addition to the optimal objective value, we show channel level and co-channel level solution to achieve this objective. Figure 2 shows the optimal band assignment to each link for each session. The bands assigned on each link are shown in shaded boxes. This result is also shown in Table 4 (first 3 columns). Also shown in column 4 of Table 4 is the capacity on each band under the optimal solution. In column 5, we show the capacity (in terms of sum of capacity on each band) over each link. Note that this capacity is at least 6, thus guaranteeing each session can transport at least 6 data streams.

Table 2 Each node's location and available frequency bands for the 30-node CRN^{MIMO}

Node	Location	Available bands	Node	Location	Available bands
N1	(18.0, 42.7)	1,2,4,5,6,8,9,10,11,12,13,14	N16	(48.5, 32.7)	2,4,5,6,8,10,11,12,13, 14,15
N2	(40.7, 51.0)	1,2,4,5,6,7,8,9,10,11,13,14,15	N17	(31.0, 96.8)	4,6,7,12,15
N3	(70.4, 64.9)	1,2,3,4,5,7,8,9,12,13,14,15	N18	(5.3, 87.0)	6,7,15
N4	(66.4, 16.4)	2,7,10	N19	(63.0, 93.3)	1,3,4,7,12,14
N5	(16.4, 7.8)	5,6,9,10,12,13,14	N20	(30.9, 48.6)	1,2,4,6,8,9,10,11,12, 13,14
N6	(93.5, 8.3)	11,15	N21	(42.7, 78.4)	1,3,4,7,12,14
N7	(73.1, 47.8)	1,2,3,4,5,7,8,9,13,15	N22	(14.2, 30.2)	1,2,5,6,8,9,10,11,12, 13,14
N8	(40.6, 91.4)	4,6,7,12,14	N23	(99.0, 69.6)	1,2,3,4,7,9,12,13,15
N9	(12.3, 65.8)	1,2,7,14	N24	(99.6, 93.9)	3,9,12
N10	(50.9, 59.5)	1,2,3,4,5,6,7,8,11,14,15	N25	(87.2, 57.6)	1,2,4,5,7,8,9,12,13,15
N11	(72.6, 81.9)	1,2,3,4,5,7,8,9,12,13,14,15	N26	(37.4, 31.4)	1,2,4,5,6,8,9,10,11, 12,13,14,15
N12	(88.1, 34.1)	2,5,7,9,11,15	N27	(86.6, 85.4)	1,2,3,4,7,9,12,13
N13	(45.2, 2.7)	10,12,13,14	N28	(65.5, 24.1)	2,5,7,10,11,15
N14	(37.6, 60.3)	1,2,4,5,6,7,8,10,11,13,14,15	N29	(3.3, 7.8)	5,6,9,13
N15	(21.5, 63.8)	1,2,4,7,8,10,14	N30	(28.9, 10.9)	5,6,8,9,10,11,12,13,14

Table 3 Source and destination nodes of each session in the 30-node CRN^{MIMO}

Session q	Source node $s(q)$	Destination node $d(q)$
1	N30	N15
2	N6	N22
3	N11	N12
4	N3	N8

We now examine co-channel DoF allocation in the optimal solution. Recall that DoF allocation is performed within the same band. Given that we have a total of 15 bands in the network, we shall have DoF allocation within each of the 15 bands. Let's first show DoF allocation in one particular band, say band 1. Note that band 1 is used by links N2 → N15, N3 → N19, N26 → N22 in Fig. 2. The DoF allocation on these 6 nodes are given in Fig. 3 and Table 5. As shown in Fig. 3, there are 2 data streams in each of these 3 links on band 1. The dashed lines in Fig. 3 show the interference relationship among the nodes, i.e., node N2 interferes with N19 and N22, node N3 interferes with N15, and node N26 interferes with N15. These transmission links and interference relationships are also listed in Table 5 (row 1), where "N2 → N15 (N19, N22)" denotes N2 transmits to N15 and interferes with N19, N22, etc. Also shown in the first column of Table 5 is the optimal order for the 6 nodes for DoF allocation in the optimal solution, i.e., N2, N3, N15, N19, N26, and N22. Based on this order, the DoFs at each node are allocated as follows (also see Fig. 3):

Table 4 Details of band assignment, capacity on each band, and capacity on each link in the 30-node CRN^{MIMO}

Session q	Link	Assigned band	Capacity on band	Link capacity
1	N30 → N16	8	1	6
		12	1	
		14	4	
	N16 → N2	5	1	6
		6	3	
		13	1	
		15	1	
	N2 → N15	1	2	6
		2	1	
		4	3	
2	N6 → N12	11	3	6
		15	3	
	N12 → N28	2	3	6
		5	3	
	N28 → N26	10	4	6
		11	1	
		15	1	
	N26 → N22	1	2	7
		6	1	
		8	1	
		13	3	
3	N11 → N25	4	1	6
		8	2	
		12	2	
		13	1	
	N25 → N12	7	2	6
		9	4	
4	N3 → N19	1	2	7
		3	4	
		12	1	
	N19 → N8	7	2	6
		14	4	

- Starting with node N2, it is the first node in the ordered node list and it is a transmit node. Then it allocates 2 DoFs to transmit 2 data streams to node N15. It does not need to allocate any DoF to cancel potential interference to other receive nodes after itself in the node list, i.e., nodes N19 and N22.
- The next node in the list is N3. As a transmit node, it allocates 2 DoFs to transmit 2 data streams to node N19. It does not need to allocate any DoF to cancel potential interference to receive node N15, which is after itself in the ordered node list.

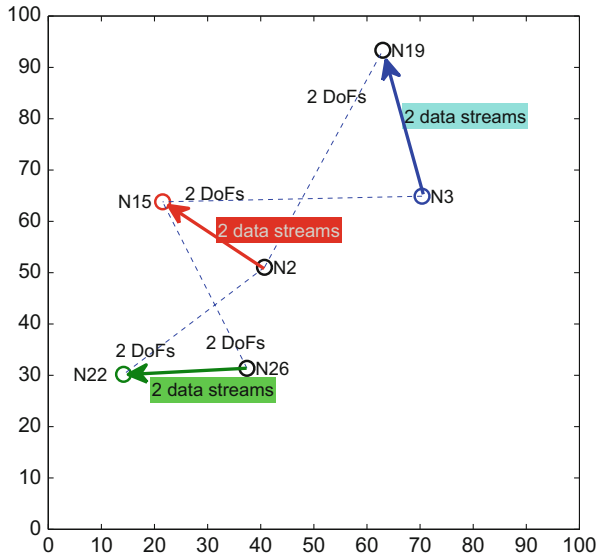

Fig. 3 The DoF allocation in the optimal solution in band 1 for the 30-node CRN^{MIMO} example

Table 5 The DoF allocation in band 1 in the 30-node CRN^{MIMO} example

Transmission and interference	N2 → N15 (N19, N22), N3 → N19 (N15), N26 → N22 (N15)	
Ordered node list	Interference cancelation (# of DoFs, to/from, node)	Spatial multiplexing (# of DoFs, transmit/receive, node)
N2		(2, Transmit, N15)
N3		(2, Transmit, N19)
N15	(2, From, N3)	(2, Receive, N2)
N19	(2, From, N2)	(2, Receive, N3)
N26	(2, To, N15)	(2, Transmit, N22)
N22	(2, To, N2)	(2, Receive, N26)

- The next node in the list is N15. As a receive node, it needs to allocate 2 DoFs to receive 2 data streams from node N2. In addition, it must ensure that its reception is not interfered with by any transmit node before itself in the list, i.e., N3. Thus it allocates the remaining 2 DoFs to cancel the interference from node N3.
- The next node in the list is N19. As a receive node, it allocates 2 DoFs for receiving 2 data streams from node N3. In addition, it allocates the remaining 2 DoFs to cancel interference from transmit node N2 which is before itself in the list.
- The next node in the list is N26. As a transmit node, it needs to ensure that its transmission does not interfere with any receive node before itself in the list, i.e., N15. For this purpose, it allocates 2 DoFs to cancel its interference to node N15. Then it allocates the remaining 2 DoFs to transmit 2 data streams to node N22.

- The last node in the list is N22. As a receive node, it allocates 2 DoFs to receiving 2 data streams from node N22. In addition, it must ensure that its reception is not interfered with by any transmit node before itself in the list, i.e., N2. Thus, it allocates the remaining 2 DoFs to cancel the interference from node N2.

This completes the DoF allocation for each node in the list in band 1. The DoF allocation for the 6 nodes is also listed in Table 5, where we employ the following two abbreviated notations:

- We use the tuple (# of DoFs, From/To, Node) to denote the IC relationship between the nodes. For example, (2, From, N3) denotes current node (in the first column of the same row) allocates 2 DoFs to cancel the interference from N3, whereas (2, To, N15) denotes current node allocates 2 DoFs to cancel its interference to N15.
- We use the tuple (# of DoFs, Transmit/Receive, Node) to denote data transmission relationship between the nodes. For example, (2, Transmit, N15) denotes the current node (in the first column of the same row) allocates 2 DoFs to transmit data streams to N15, whereas (2, Receive, N2) denotes the current node uses 2 DoFs to receive data streams from N2.

Discussions in bands 2 to 15 are similar and are omitted to conserve space.

$$f_{\text{CRN}^{\text{MIMO}}} vs. A_{\text{MIMO}} \times f_{\text{CRN}}$$

The results above show an optimal solution for a 30-node secondary network with $A_{\text{MIMO}} = 4$ antennas at each node. We now validate the result in (19) under different number of antennas at each node. Figure 4 shows the optimal objective values under different number of antennas for the same 30-node network discussed in the last section. Also shown in this figure is a dashed line with a slope of f_{CRN}.

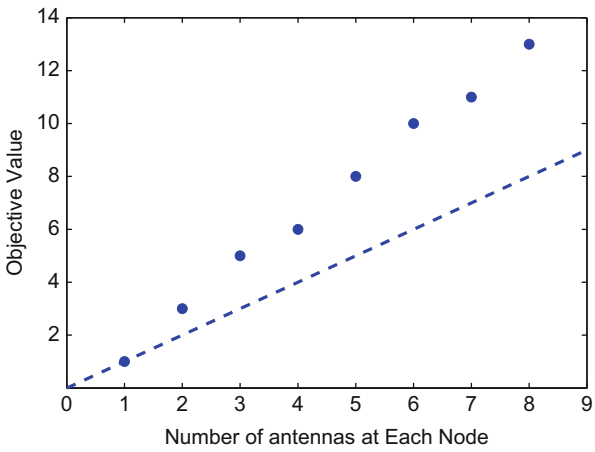

Fig. 4 Objective value under different antennas for the 30-node CRN^{MIMO}

Note that the equality in (19) only coincides for the first point, i.e., single antenna at each node. When the number of antennas at each node is greater than 1, we have an inequality, i.e., $f_{\text{CRN}^{\text{MIMO}}} > A_{\text{MIMO}} \times f_{\text{CRN}}$. That is, with joint channel level (via CR) and co-channel level (via MIMO DoF) optimization within a CRN^{MIMO} network, we have more than A_{MIMO}-fold increase in the optimal solution.

MIMO-Based Secondary Network in Transparent-Coexistence Paradigm

In section "MIMO-Based Secondary Network in Interweave Paradigm", we have studied how multi-hop secondary CR network achieve simultaneous transmission on the same channel among secondary nodes with MIMO-empowered CR under the interweave paradigm. In this section, we study how a multi-hop secondary CR network can coexist with a primary network transparently. A MIMO node's ability to use a subset of its DoFs to cancel interference while using the remaining subset of DoFs for data transmission allows the possibility of simultaneous activation of the secondary nodes with the primary nodes. For a set of channels owned by the primary networks, the primary nodes may use them in whatever manner to suit their needs. On the other hand, the secondary nodes are only allowed to use these channels if they can cancel their interference to the primary nodes. Further, to ensure successful transmission among the secondary nodes, the secondary nodes also need to perform IC to/from the primary nodes as well as potential interference among the secondary nodes. Simply put, all IC burden should rest solely on the secondary nodes and remain invisible to the primary nodes.

It is important to realize that we strive to put all IC burden on the secondary node side. Specifically, the transmitter of a secondary node needs to cancel its interference to all neighboring primary receive nodes who are interfered with by this secondary transmitter; the receiver of a secondary node needs to cancel interference from all neighboring primary transmit nodes who interfere with this secondary receiver. To achieve transparency to primary nodes, it is important for the secondary nodes to have accurate channel state information (CSI). The problem here is: how can a secondary node obtain the CSI between itself and its neighboring primary nodes while remaining transparent to the primary nodes? We propose the following solution to resolve this problem. For each primary node, it typically sends out a pilot sequence (training sequence) to its neighboring primary nodes such that those primary nodes can estimate the CSI for communication. This is the practice for current cellular networks, and we assume such a mechanism is available for a primary network. Then, the secondary nodes can *overhear* the pilot sequence signal from the primary node while staying transparent. Suppose the pilot sequence from the primary nodes is publicly available (as in cellular networks) and is thus known to the secondary nodes. Then the secondary nodes can use this information and the actual received pilot sequence signal from the primary node for channel estimation. Based on the reciprocity property of a wireless channel [17], the

estimated CSI can also be used as CSIT (channel state information at transmitter side). Therefore, a secondary node can obtain complete CSI between itself and a primary node.

Problem Scope

Although the new coexistence paradigm has been explored at the physical layer, its application to a multi-hop network environment is far from trivial. Consider a primary multi-hop ad hoc network $\mathscr{P}$ shown in Fig. 5, which is colocated with a secondary multi-hop network $\mathscr{S}$ in the same geographical region. Suppose that there is a set of channels $\mathscr{B}$ available to the primary network. The primary nodes can use this set of frequency channels freely as if they were the only nodes in the network. The primary nodes do not need to be MIMO-capable. The secondary nodes, however, are allowed to use a channel in $\mathscr{B}$ only if their interference to the primary nodes is canceled properly, with complete transparency to the primary nodes. As discussed, the secondary nodes are assumed to be equipped with MIMO. In this context, we have a number of challenges for the secondary network.

- **Channel Selection** In a secondary network, an intermediate relay node is both a transmitter and a receiver. Due to half-duplex, a node cannot transmit and receive on the same channel at the same time. Therefore, scheduling (either in time slot or channel) is needed. In this chapter, we assume scheduling is performed in the form of channel assignment. Therefore, a secondary relay node needs to select different channels for transmission and reception. Note that scheduling transmission and reception of a secondary node will lead to a different interference relationship among the primary and secondary nodes in the network. This brings in considerable complexity to the mathematical modeling of interference relationship.
- **IC to/from Primary Network** A secondary transmitter needs to cancel its interference to its neighboring primary receivers, while a secondary receiver

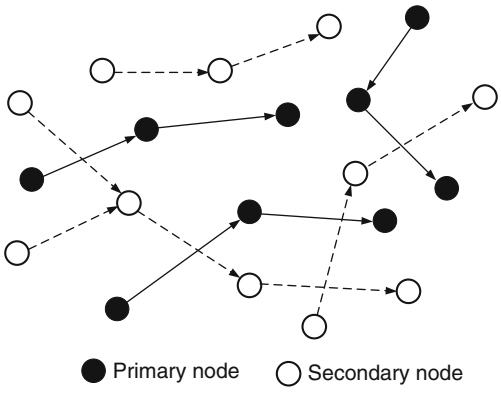

Fig. 5 A multi-hop secondary network colocated with a multi-hop primary network

needs to cancel the interference from its neighboring primary transmitters. Such challenge magnifies when the secondary network is a multi-hop network.

- **IC Within Secondary Network** In addition to interference between the primary and secondary nodes, interference from a secondary node may also interfere another secondary node within their own network. Such interference must also be canceled properly (either by a secondary transmitter or the secondary receiver that is being interfered with) to ensure successful data communications inside the secondary network. Resource allocation to account for such IC is clearly not a trivial problem.

It is important to realize that the above three challenges are not independent, but rather deeply intertwined with each other. In particular, channel selection at a secondary node is directly tied to the interference relationship between primary and secondary nodes as well as interference among the secondary nodes within each channel. Further, the combined channel resource and total DoFs at each node determine a complete resource space in the network: an optimal DoF allocation and channel selection at each secondary node for both IC to/from the primary nodes and within the secondary nodes are critical to achieve the desired network performance objective. A modeling and formulation of transparent-coexistence paradigm would call for a joint consideration of all these components.

Mathematical Modeling

In this section, we develop a mathematical model for the transparent-coexistence paradigm where a multi-hop secondary network shares the same spectrum as a primary network (see Fig. 5).

Referring to Fig. 5, we consider a secondary multi-hop network consisting of a set of nodes $\mathscr{S}$, which is colocated with a primary multi-hop network consisting of a set of nodes $\mathscr{P}$. Suppose that there is a set of channels $\mathscr{B}$ available to the primary network. For the primary network, there is no special node requirement, and we assume that each primary node is a traditional single-antenna node. A primary node may transmit and receive on the same channel but in different time slots or transmit and receive on different channels. We consider the latter in this chapter. Consider a set of multi-hop sessions $\tilde{\mathscr{F}}$ among the primary nodes. For a given routing for each session, denote $\tilde{\mathscr{L}}$ the set of active links in the primary network (shown in solid arrow lines in Fig. 5). Denote $\tilde{z}^b(\tilde{l})$ as the number of data streams over primary link $\tilde{l} \in \tilde{\mathscr{L}}$ on channel b. Then due to single antenna on each primary node, $\tilde{z}^b(\tilde{l}) = 1$ if link $\tilde{l}$ is active on channel b and 0 otherwise.

For the secondary network, we assume MIMO's capability at each node. Denote A_i as the number of antennas on a secondary node $i \in \mathscr{S}$. Suppose there is a set of multi-hop sessions $\mathscr{F}$ in $\mathscr{S}$. For a given routing for each session, denote $\mathscr{L}$ as the set of secondary links (shown in dashed arrow line in Fig. 5). Denote $r(f)$ as the rate of session $f \in \mathscr{F}$. A general goal of throughput maximization is to maximize a function of $r(f)$, $f \in \mathscr{F}$. Table 6 lists all notations used in the underlay paradigm.

Table 6 Notation in underlay paradigm

Primary network	
$\tilde{\mathscr{P}}$	The set of nodes in the primary network
T	The number of time slots in a frame
$\tilde{\mathscr{B}}$	The sets of channels owned by the primary network
B	The number of channels in set $\tilde{\mathscr{B}}$, $B = \lvert\tilde{\mathscr{B}}\rvert$
$\tilde{\mathscr{F}}$	The set of sessions in the primary network
$\tilde{\mathscr{I}}_i$	The set of primary nodes within the interference range of secondary node i
$\tilde{\mathscr{L}}_i^{\text{In}}$	The set of incoming links (from other primary nodes) at node $i \in \tilde{\mathscr{P}}$
$\tilde{\mathscr{L}}_i^{\text{Out}}$	The set of outgoing links (to other primary nodes) at node $i \in \tilde{\mathscr{P}}$
$\tilde{\mathscr{L}}$	The set of links in the primary network
$\tilde{z}_{(\tilde{l})}^b$	The number of data streams over primary link $\tilde{l}$ on channel b
Secondary network	
$\mathscr{S}$	The set of nodes in the secondary network
S	The number of secondary nodes in the network, $S = \lvert\mathscr{S}\rvert$
A_i	The number of antennas at secondary node $i \in \mathscr{S}$
c	The minimum data rate carried by a data stream
$\mathscr{F}$	The set of sessions in the secondary network
$\mathscr{I}_i$	The set of node in $\mathscr{S}$ that are within the interference range of secondary node i
$\mathscr{L}_i^{\text{In}}$	The set of incoming links (from other secondary nodes) at node $i \in \mathscr{S}$
$\mathscr{L}_i^{\text{Out}}$	The set of outgoing links (to other secondary nodes) at node $i \in \mathscr{S}$
$\mathscr{L}$	The set of secondary links
$r(f)$	The data rate of the session $f \in \mathscr{F}$
$r_{\min}$	The minimum data rate among all secondary sessions
$\text{Rx}(l)$	The receiver of link $l \in \mathscr{L}$
$\text{Tx}(l)$	The transmitter of link $l \in \mathscr{L}$
x_i^b	$= 1$ if node $i \in \mathscr{S}$ is a transmitter on channel b and is 0 otherwise
y_i^b	$= 1$ if node $i \in \mathscr{S}$ is a receiver on channel b and is 0 otherwise
$z_{(l)}^b$	The number of data streams over link $l \in \mathscr{L}$ on channel b
$\lambda_{j,i}^b$	The number of DoFs used by transmit node $i \in \mathscr{S}$ to cancel its interference to receive node $j \in \mathscr{S}$ on channel b
$\mu_{j,i}^b$	The number of DoFs used by receive node $i \in \mathscr{S}$ to cancel the interference from transmit node $j \in \mathscr{S}$ on channel b
$\theta_{j,i}^b$	Binary indicator showing the relationship between nodes i and j in ordered list on channel b, $i, j \in \mathscr{S}$
π^b	An ordering for IC among the secondary nodes on channel b
π_i^b	The position of node $i \in \mathscr{S}$ in π^b

Channel Selection. To model channel use behavior at a secondary node for transmission or reception, we denote x_i^b and y_i^b ($i \in \mathscr{S}$ and $b \in \mathscr{B}$) as whether node i selects channel b for transmission or reception, respectively. We have

$$x_i^b = \begin{cases} 1 & \text{if node } i \text{ uses channel } b \text{ for transmission;} \\ 0 & \text{otherwise.} \end{cases}$$

$$y_i^b = \begin{cases} 1 \text{ if node } i \text{ uses channel } b \text{ for reception;} \\ 0 \text{ otherwise.} \end{cases}$$

To consider half-duplex (a node cannot transmit and receive on the same channel at the same time), we have the following constraint on x_i^b and y_i^b:

$$x_i^b + y_i^b \leq 1 \qquad (i \in \mathscr{S}, b \in \mathscr{B}). \tag{20}$$

DoF Allocation at a Secondary Transmitter. Recall that the secondary network is solely responsible for IC to/from the primary network as well as IC within itself. At a secondary transmitter, it needs to expend DoFs for SM, IC to primary receivers, and IC to other secondary receivers:

- For SM, denote $z^b(l)$ and $\mathscr{L}_{i,\text{Out}}^b$ as the number of data streams over link $l \in \mathscr{L}$ and the set of outgoing links from secondary node i on channel b. Then the number of DoFs at secondary node $i \in \mathscr{S}$ for SM on channel b is $\sum_{l \in \mathscr{L}_{i,\text{Out}}^b} z^b(l)$.
- For IC to primary receivers, recall $\tilde{z}^b(\tilde{l})$ is the number of data streams over primary link $\tilde{l}$ on channel b. For a primary node $p \in \tilde{\mathscr{P}}$, denote $\tilde{\mathscr{L}}_{p,\text{In}}^b$ as the set of incoming primary links on channel b. Denote $\tilde{\mathscr{I}}_i$ as the set of neighboring primary nodes that are located within the interference range of secondary transmitter i. Then at node i, the number of DoFs required for IC to primary receivers is $\left(\sum_{p \in \tilde{\mathscr{I}}_i} \sum_{\tilde{l} \in \tilde{\mathscr{L}}_{p,\text{In}}^b} \tilde{z}^b(\tilde{l})\right)$ on channel b.
- For IC to secondary receivers, as discussed earlier, a secondary transmitter i only needs to cancel its interference to those nodes that are before itself in the ordered list. For a secondary node $j \in \mathscr{S}$, denote $\mathscr{L}_{j,\text{In}}^b$ as the set of incoming secondary links. Denote $\mathscr{I}_i$ as the set of neighboring secondary nodes that are located within the interference range of secondary transmitter i. Then at node i, the number of DoFs required for IC to secondary receivers is $\sum_{j \in \mathscr{I}_i} \left(\theta_{j,i}^b \cdot \sum_{k \in \mathscr{L}_{j,\text{In}}^b}^{\text{Tx}(k) \neq i} z^b(k)\right)$ in channel b, and $\text{Tx}(k)$ represents the transmitter of link k.

Putting all three DoF consumptions together at a secondary transmitter i, we have the following constraints:

$$x_i^b \leq \sum_{l \in \mathscr{L}_{i,\text{Out}}^b} z^b(l) + \left[\left(\sum_{p \in \tilde{\mathscr{I}}_i} \sum_{\tilde{l} \in \tilde{\mathscr{L}}_{p,\text{In}}^b} \tilde{z}^b(\tilde{l})\right) + \sum_{j \in \mathscr{I}_i} \left(\theta_{j,i}^b \cdot \sum_{k \in \mathscr{L}_{j,\text{In}}^b}^{\text{Tx}(k) \neq i} z^b(k)\right)\right] \cdot x_i^b \leq x_i^b A_i, \tag{21}$$

which means that if node i is transmitting, its DoF consumptions cannot exceed the total number of DoFs at node i; if node i is not transmitting, there is no

DoF consumption for transmissions, and $\sum_{l\in\mathscr{L}^b_{i,\mathrm{Out}}} z^b(l) = 0$. By introducing a large constant M, which is an upper bound of $\left[\left(\sum_{p\in\tilde{\mathscr{I}}_i}\sum_{\tilde{l}\in\tilde{\mathscr{L}}^b_{p,\mathrm{In}}}\tilde{z}^b(\tilde{l})\right) + \sum_{j\in\mathscr{I}_i}\left(\theta^b_{j,i}\cdot\sum^{\mathrm{Tx}(k)\neq i}_{k\in\mathscr{L}^b_{j,\mathrm{In}}} z^b(k)\right)\right]$ (e.g., $M = \sum_{j\in\mathscr{I}_i} A_j + \sum_{p\in\tilde{I}_i}\sum_{\tilde{l}\in\tilde{\mathscr{L}}^b_{p,\mathrm{In}}}\tilde{z}^b(\tilde{l})$), we can use the following two sets of constraints to replace (21):

$$x^b_i \le \sum_{l\in\mathscr{L}^b_{i,\mathrm{Out}}} z^b(l) + \left(\sum_{p\in\tilde{\mathscr{I}}_i}\sum_{\tilde{l}\in\tilde{\mathscr{L}}^b_{p,\mathrm{In}}}\tilde{z}^b(\tilde{l})\right) + \sum_{j\in\mathscr{I}_i}\left(\theta^b_{j,i}\cdot\sum^{\mathrm{Tx}(k)\neq i}_{k\in\mathscr{L}^b_{j,\mathrm{In}}} z^b(k)\right) \le A_i x^b_i + (1-x^b_i)M, \tag{22}$$

$$\sum_{l\in\mathscr{L}^b_{i,\mathrm{Out}}} z^b(l) \le x^b_i A_i. \tag{23}$$

We can see that when node i is transmitting (i.e., $x^b_i = 1$), (22) becomes (21) and (23) holds trivially; if node i is not transmitting (i.e., $x^b_i = 0$), (23) and (21) are equivalent, which is $\sum_{l\in\mathscr{L}^b_{i,\mathrm{Out}}} z^b(l) = 0$, and (22) holds trivially.

Since (22) has a nonlinear term $\left(\theta^b_{j,i}\cdot\sum^{\mathrm{Tx}(k)\neq i}_{k\in\mathscr{L}^b_{j,\mathrm{In}}} z^b(k)\right)$, we can use *reformulation-linearization technique* (RLT) [15] to reformulate this nonlinear term as several linear terms. We define a new variable $\lambda^b_{j,i}$ as follows:

$$\lambda^b_{j,i} = \theta^b_{j,i}\cdot\sum^{\mathrm{Tx}(k)\neq i}_{k\in\mathscr{L}^b_{j,\mathrm{In}}} z^b(k)\,, \qquad (i\in\mathscr{S}, j\in\mathscr{I}_i, b\in\mathscr{B}).$$

For binary variable $\theta^b_{j,i}$, we have the following related constraints: $\theta^b_{j,i} \ge 0, (1-\theta^b_{j,i}) \ge 0$. For $\sum^{\mathrm{Tx}(k)\neq i}_{k\in\mathscr{L}^b_{j,\mathrm{In}}} z^b(k)$, we have $\sum^{\mathrm{Tx}(k)\neq i}_{k\in\mathscr{L}^b_{j,\mathrm{In}}} z^b(k) \ge 0$ and $A_j - \sum^{\mathrm{Tx}(k)\neq i}_{k\in\mathscr{L}^b_{j,\mathrm{In}}} z^b(k) \ge 0$. We can multiply each constraint involving $\theta^b_{j,i}$ by one of the two constraints involving $\sum^{\mathrm{Tx}(k)\neq i}_{k\in\mathscr{L}^b_{j,\mathrm{In}}} z^b(k)$, replacing the product term $\left(\theta^b_{j,i}\cdot\sum^{\mathrm{Tx}(k)\neq i}_{k\in\mathscr{L}^b_{j,\mathrm{In}}} z^b(k)\right)$ with a new variable $\lambda^b_{j,i}$. Then (22) can be replaced by the following linear constraints:

$$\begin{aligned} x^b_i &\le \sum_{l\in\mathscr{L}^b_{i,\mathrm{Out}}} z^b(l) + \left(\sum_{p\in\tilde{\mathscr{I}}_i}\sum_{\tilde{l}\in\tilde{\mathscr{L}}^b_{p,\mathrm{In}}}\tilde{z}^b(\tilde{l})\right) + \sum_{j\in\mathscr{I}_i}\lambda^b_{j,i} \\ &\le A_i x^b_i + (1-x^b_i)M \quad (i\in\mathscr{S}, b\in\mathscr{B}), \end{aligned} \tag{24}$$

$$\lambda_{j,i}^{b} \geq 0 \qquad (i \in \mathscr{S}, j \in \mathscr{I}_i, b \in \mathscr{B}), \tag{25}$$

$$\lambda_{j,i}^{b} \leq \sum_{k \in \mathscr{L}_{j,\mathrm{In}}^{b}}^{\mathrm{Tx}(k) \neq i} z^{b}(k) \qquad (i \in \mathscr{S}, j \in \mathscr{I}_i, b \in \mathscr{B}), \tag{26}$$

$$\lambda_{j,i}^{b} \leq A_j \cdot \theta_{j,i}^{b} \qquad (i \in \mathscr{S}, j \in \mathscr{I}_i, b \in \mathscr{B}), \tag{27}$$

$$\lambda_{j,i}^{b} \geq A_j \cdot \theta_{j,i}^{b} - A_j + \sum_{k \in \mathscr{L}_{j,\mathrm{In}}^{b}}^{\mathrm{Tx}(k) \neq i} z^{b}(k) \qquad (i \in \mathscr{S}, j \in \mathscr{I}_i, b \in \mathscr{B}). \tag{28}$$

DoF Allocation at a Secondary Receiver. At a secondary receiver, it needs to expend DoFs for SM, for IC from primary transmitters, and for IC from other secondary transmitters. For a primary node $p \in \mathscr{P}$, denote $\tilde{\mathscr{L}}_{p,\mathrm{Out}}^{b}$ as the set of outgoing primary links. Following the same token as our discussion for a secondary transmitter, we can put all DoF consumption at a secondary receiver as follows:

$$y_i^b \leq \sum_{k \in \mathscr{L}_{i,\mathrm{In}}^{b}} z^{b}(k) + \left(\sum_{p \in \tilde{\mathscr{I}}_i} \sum_{\tilde{l} \in \tilde{\mathscr{L}}_{p,\mathrm{Out}}^{b}} \tilde{z}^{b}(\tilde{l}) \right) + \sum_{j \in \mathscr{I}_i} \left(\theta_{j,i}^{b} \cdot \sum_{l \in \mathscr{L}_{j,\mathrm{Out}}^{b}}^{\mathrm{Rx}(l) \neq i} z^{b}(l) \right) \leq A_i y_i^b + (1 - y_i^b) N, \tag{29}$$

$$\sum_{k \in \mathscr{L}_{i,\mathrm{In}}^{b}} z^{b}(k) \leq y_i^b A_i, \tag{30}$$

where $\sum_{k \in \mathscr{L}_{i,\mathrm{In}}^{b}} z^{b}(k)$ represents the number of DoFs used for SM, $\left(\sum_{p \in \tilde{\mathscr{I}}_i} \sum_{\tilde{l} \in \tilde{\mathscr{L}}_{p,\mathrm{Out}}^{b}} \tilde{z}^{b}(\tilde{l}) \right)$ represents the number of DoFs used for suppressing interference from primary transmitters, and $\sum_{j \in \mathscr{I}_i} \left(\theta_{j,i}^{b} \cdot \sum_{l \in \mathscr{L}_{j,\mathrm{Out}}^{b}}^{\mathrm{Rx}(l) \neq i} z^{b}(l) \right)$ represents the number of DoFs consumed for canceling interference from other secondary transmitters, and N represents a large constant, and $\mathrm{Rx}(l)$ represents the receiver of link l.

Again, we can use RLT to linearize the nonlinear term $\left(\theta_{j,i}^{b} \cdot \sum_{l \in \mathscr{L}_{j,\mathrm{Out}}^{b}}^{\mathrm{Rx}(l) \neq i} z^{b}(l) \right)$ in (29). Denote $\mu_{j,i}^{b}$ as $\left(\theta_{j,i}^{b} \cdot \sum_{l \in \mathscr{L}_{j,\mathrm{Out}}^{b}}^{\mathrm{Rx}(l) \neq i} z^{b}(l) \right)$. Then (29) can be replaced by the following linear constraints:

$$y_i^b \leq \sum_{k \in \mathscr{L}_{i,\mathrm{In}}^{b}} z^{b}(k) + \left(\sum_{p \in \tilde{\mathscr{I}}_i} \sum_{\tilde{l} \in \mathscr{L}_{p,\mathrm{Out}}^{b}} \tilde{z}^{b}(\tilde{l}) \right) + \sum_{j \in \mathscr{I}_i} \mu_{j,i}^{b} \leq A_i y_i^b + (1 - y_i^b) N \qquad (i \in \mathscr{S}, b \in \mathscr{B}), \tag{31}$$

$$\mu_{j,i}^{b} \geq 0 \qquad (i \in \mathscr{S}, j \in \mathscr{I}_i, b \in \mathscr{B}), \tag{32}$$

$$\mu_{j,i}^{b} \leq \sum_{l \in \mathscr{L}_{j,\text{Out}}^{b}}^{\text{Rx}(l) \neq i} z^{b}(l) \qquad (i \in \mathscr{S}, j \in \mathscr{I}_i, b \in \mathscr{B}), \tag{33}$$

$$\mu_{j,i}^{b} \leq A_j \cdot \theta_{j,i}^{b} \qquad (i \in \mathscr{S}, j \in \mathscr{I}_i, b \in \mathscr{B}), \tag{34}$$

$$\mu_{j,i}^{b} \geq A_j \cdot \theta_{j,i}^{b} - A_j + \sum_{l \in \mathscr{L}_{j,\text{Out}}^{b}}^{\text{Rx}(l) \neq i} z^{b}(l) \qquad (i \in \mathscr{S}, j \in \mathscr{I}_i, b \in \mathscr{B}). \tag{35}$$

Link Capacity Constraint. For link $l \in \mathscr{L}$, we have the following link capacity constraint:

$$\sum_{f \in \mathscr{F}}^{f \text{ traversing } l} r(f) \leq c \cdot \sum_{b \in \mathscr{B}} z^{b}(l) \qquad (l \in \mathscr{L}), \tag{36}$$

where c is the data rate carried by a data stream.

Formulation

Based on the above mathematical model, various problems can be formulated. In this chapter, we study a throughput optimization problem with the objective of maximizing the minimum session rate among all secondary sessions. The optimization problem can be written as follows:

OPT
max $r_{\min}$
s.t $r_{\min} \leq r(f) \qquad (f \in \mathscr{F})$;
Half-duplex constraints: (20);
Node ordering constraints: (2);
Transmitter DoF constraints: (23), (22), (24), (25), (26), (27), and (28);
Receiver DoF constraints: (30), (31), (32), (33), (34), and (35);
Link capacity constraints: (36).

In this formulation, $r_{\min}, r(f), x_i^b, y_i^b, z^b(l), \pi_i^b, \lambda_{j,i}^b, \mu_{j,i}^b$ and $\theta_{j,i}^b$ are optimization variables, and $A_i, M, N, \tilde{z}^b(\tilde{l})$ and c are given constants. This optimization problem is in the form of a mixed-integer linear program (MILP), which is NP-hard in general. The computation complexity of MILP is exponential but can be solved efficiently by CPLEX solver.

A Case Study

The goal of this section is twofold. First, we want to use numerical results to demonstrate how a secondary network can operate simultaneously with the primary network while being transparent to the primary network. Second, we will show the tremendous benefits in terms of throughput gain under the transparent-coexistent paradigm.

Consider a 20-node primary network and a 30-node secondary network randomly deployed in the same 100×100 area (see Fig. 6). For the ease of scalability and generality, we normalize all units for distance, bandwidth, and throughput with appropriate dimensions. As discussed in section "Mathematical Modeling", the primary nodes are traditional single-antenna device, while the secondary nodes are equipped with MIMO. We assume there are 4 antennas for transmission or reception on each secondary node. Further, we assume all nodes' transmission range and interference range are 30 and 50, respectively, on all channels. There are $|\mathscr{B}| = 10$ channels available in the network. For simplicity, we assume the achievable rate of 1 DoF on a channel is 1 unit. In this case study, we assume there are three active sessions in the primary network and four active sessions in the secondary network and that minimum-hop routing is used for each primary and secondary session. Further, the channel allocation on each hop for a primary session is known a priori (see Fig. 6).

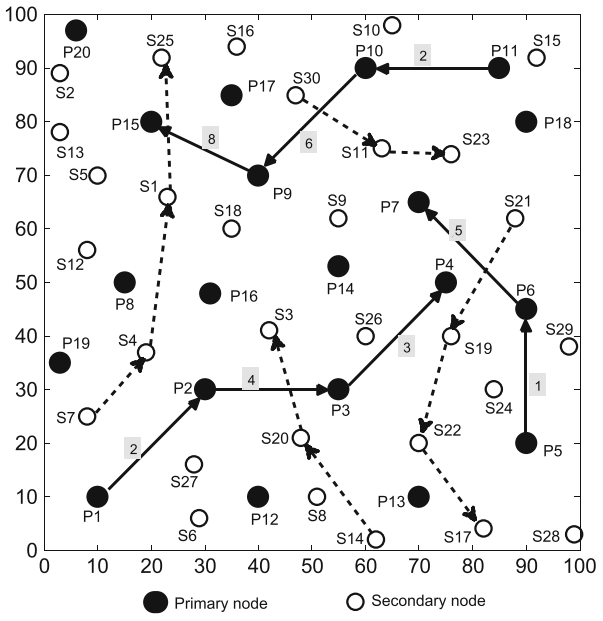

Fig. 6 Active sessons in the primary and secondary networks

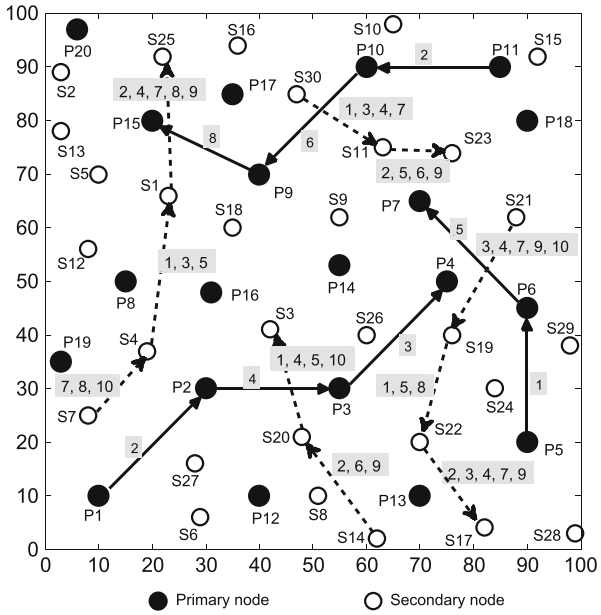

Fig. 7 Channel allocation on each link for the secondary sessions. Channel allocation on each link for the primary sessions is given a priori

For this network setting for the primary and secondary networks, the obtained objective value is 7. The channel allocation on each link for each secondary session is shown in Fig. 7. The details of DoFs used for SM on each channel at each link are shown in Table 7. The achievable rate (i.e., total number of DoFs used for SM) on a link is also shown in this table.

To see how links in the primary and secondary networks can be active in the same channel at the same time, consider channel 2 in Fig. 7. For channel 2, it is active on $P_1 \rightarrow P_2$ and $P_{11} \rightarrow P_{10}$ in the primary network and $S_{14} \rightarrow S_{20}$, $S_{22} \rightarrow S_{17}$, $S_1 \rightarrow S_{25}$ and $S_{11} \rightarrow S_{23}$ in the secondary network. The interference relationships among these 6 links are shown in Fig. 8, where the dotted arrow lines show the interference relationships among them. The 2 primary links $P_1 \rightarrow P_2$ and $P_{11} \rightarrow P_{10}$ do not interfere with each other as the receiver of each link is outside the interference range of the other link's transmitter. But each of these two primary links is within the interference range of its neighboring secondary links. Now consider link $P_1 \rightarrow P_2$:

- To cancel interference from secondary nodes (S_1, S_{14}, and S_{22}) to primary node P_2, secondary transmitters S_1, S_{14}, and S_{22} use 1 DoF to cancel their interference to primary receiver P_2. Consequently, the transmissions on $S_1 \rightarrow S_{25}$, $S_{14} \rightarrow S_{20}$, and $S_{22} \rightarrow S_{17}$ will be transparent to primary node P_2.

Table 7 Channel allocation on each link, DoF allocation on each channel for SM, and achievable data streams on each link for the secondary sessions

Session	Link	Channel allocation	DoF for SM	Achievable data streams
1	$S_7 \longrightarrow S_4$	7	3	7
		8	2	
		10	2	
	$S_4 \longrightarrow S_1$	1	2	7
		3	2	
		5	3	
	$S_1 \longrightarrow S_{25}$	2	1	7
		4	1	
		7	1	
		8	1	
		9	3	
2	$S_{21} \longrightarrow S_{19}$	3	2	7
		4	1	
		7	1	
		9	1	
		10	2	
	$S_{19} \longrightarrow S_{22}$	1	1	7
		5	2	
		8	4	
	$S_{22} \longrightarrow S_{17}$	2	1	7
		3	1	
		4	1	
		7	3	
		9	1	
3	$S_{14} \longrightarrow S_{20}$	2	2	7
		6	4	
		9	1	
	$S_{20} \longrightarrow S_3$	1	2	7
		4	2	
		5	1	
		10	2	
4	$S_{30} \longrightarrow S_{11}$	1	2	7
		3	1	
		4	1	
		7	3	
	$S_{11} \longrightarrow S_{23}$	2	2	7
		5	1	
		6	3	
		9	1	

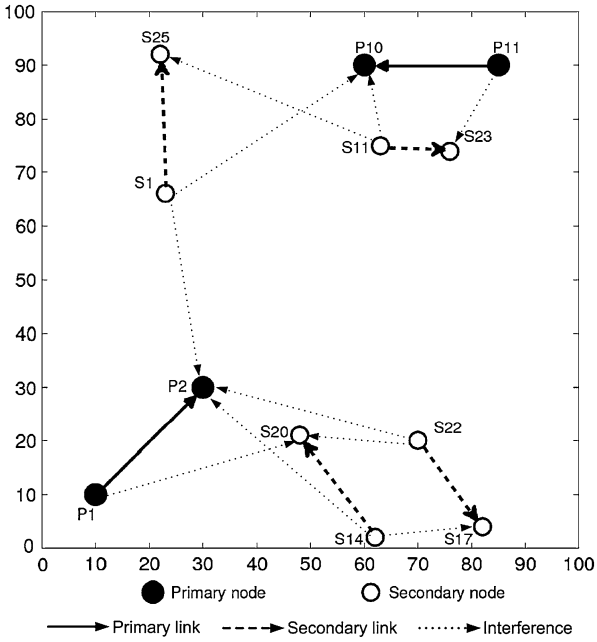

Fig. 8 Illustration of interference relationships among the primary and secondary links on channel 2 in the case study

- To cancel interference from primary node P_1 to secondary receive node S_{20}, S_{20} uses 1 DoF to cancel this interference.
- Among the secondary links, $S_{14} \rightarrow S_{20}$ and $S_{22} \rightarrow S_{17}$ interfere with each other since the receiver of each link falls within the interference range of the transmitter of the other link. To cancel its interference to S_{17}, transmitter S_{14} uses 1 DoF to cancel this interference. On the other hand, to cancel the interference from S_{22}, receiver S_{20} uses 1 DoF to cancel this interference. After IC, nodes S_{14} and S_{20} can use the remaining 2 DoFs for SM (on both transmitter and receiver sides), while nodes S_{22} and S_{17} can only use 1 DoF for SM to meet IC constraints (24) and (31).

The discussion for primary link $P_{11} \rightarrow P_{10}$ is similar and is omitted to conserve space. In addition to channel 2, other channels that exhibit transparent coexistence between the primary and secondary links include channels 1, 3, 4, 5, 6, and 8.

Comparison to Interference-Avoidance Paradigm To see the benefits of transparent-coexistence paradigm, we compare to the interference-avoidance paradigm. Under the interference-avoidance paradigm, a secondary node is not allowed to transmit (receive) on a channel when a nearby primary receiver (transmitter) is using the same channel. Therefore, the set of available channels

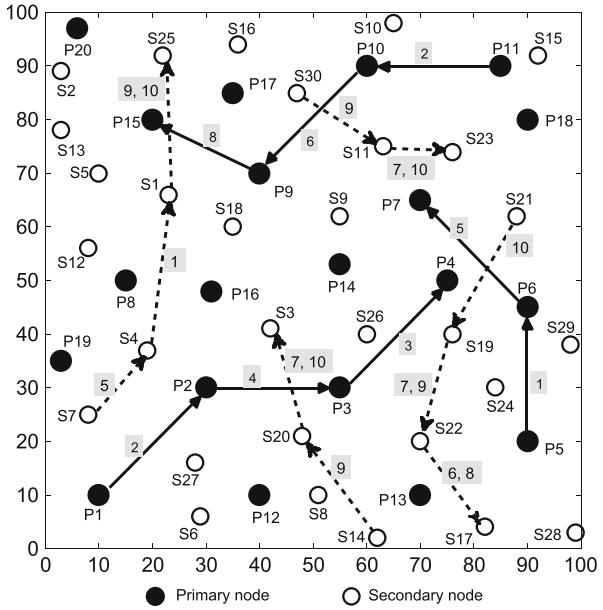

Fig. 9 Channel allocation on each link under the interference-avoidance paradigm

that can be used for secondary nodes is smaller. The problem formulation for this paradigm is simpler (although somewhat similar) than OPT and was presented in section "Mathematical Modeling". In particular, we can remove the second term ($\sum_{p\in\tilde{\mathscr{I}}_i}\sum_{\tilde{l}\in\tilde{\mathscr{L}}^b_{p,\mathrm{In}}}\tilde{z}^b(\tilde{l})$ and $\sum_{p\in\tilde{\mathscr{I}}_i}\sum_{\tilde{l}\in\tilde{\mathscr{L}}^b_{p,\mathrm{Out}}}\tilde{z}^b(\tilde{l})$) in constraints (24) and (31) in OPT that are used for secondary nodes to cancel interference to/from the primary nodes.

Following the same setting as in the case study above, we solve the above optimization problem under the interference-avoidance paradigm. The obtained objective value is 3 (compared to 7 in transparent-coexistence paradigm). The channel allocation on each link for each secondary session is shown in Fig. 9. Comparing Figs. 7 with 9, we find that the set of channels used on each secondary link under interference-avoidance paradigm is smaller than that under transparent-coexistence paradigm.

Summary and Future Directions

In this chapter, we explore MIMO-empowered CR in multi-hop networks for efficient spectrum sharing. Specially, we study joint optimization of CR and MIMO under both interweave and underlay paradigms in multi-hop ad hoc

network environment. In the interweave paradigm, by exploiting CR's behavior at channel level and MIMO's capability within a channel, we showed that we can have much bigger design space to mitigate interference in the network. In the underlay paradigm, by employing the MIMO IC capability, we can achieve simultaneous transmission of primary and secondary networks in the same channel. Under both paradigms, we offer the systematic mathematical modeling, problem formulation, and performance evaluation. The extensive simulation results show that the MIMO-empowered secondary networks offer significant improvement in spectrum efficiency and throughput performance.

Much work remains to be done to transition the ideas in this paper into reality. In particular, the focus of this paper has been on exploring performance gain under idealized network setting (by ignoring many details that may arise from practical operations). We briefly discuss some of the practical issues that must be addressed to apply the MIMO-empowered CR in interweave and underlay paradigms in the real world. First, to perform IC, we assume each secondary node could obtain the accurate CSI based on channel reciprocity. But in reality, the communication channel not only consists of the physical channel but also the antennas, RF mixers, filters, A/D converters, etc., which are not necessarily identical on all the nodes. Therefore, complex calibration among the nodes is needed to achieve channel reciprocity. Such calibration is not a simple task even for a pair of transmitter and receiver and certainly is more complicated among a network of nodes. Second, zero-forcing based IC may not be perfect even if we have perfect CSI. A consequence of non-perfect IC is interference leakage, which is undesirable for both primary and secondary receivers. How to mitigate such interference leakage to a minimal acceptable level should be a key consideration when deploying MIMO-empowered CR technique into secondary network for real applications. Third, the IC and DoF allocation algorithm that we designed for the secondary network is a centralized one. Such a centralized solution serves our purpose of introducing new concepts. It bears similar pros and cons of other centralized algorithm for a wireless network. If a centralized solution is adopted in practice, those issues must be carefully addressed. On the other hand, if a distributed solution is desired, then a different set of issues need to be addressed. These issues include partial network knowledge, limited information sharing, communication overheard, and ensuring IC feasibility at each secondary node, among others. Regardless centralized or distributed solution, flow dynamics (new session initiation, existing session termination) will add additional complexity on information update and algorithm execution. Clearly, there is a large landscape for further research on these practical operation issues. We expect to see more follow-up research in this area in the near future.

Acknowledgements This work was supported in part by the US National Science Foundation (NSF) under Grants 1642873, 1617634, 1443889, 1343222, 1102013, and 1443434 and the Office of Naval Research Grant N00014-15-1-2926. Part of W. Lou's work was completed while she was serving as a Program Director at the NSF. Any opinion, findings, and conclusions or

recommendations expressed in this chapter are those of the authors and do not reflect the views of the NSF. The authors thank Virginia Tech Advanced Research Computing for giving them access to the BlueRidge computer cluster.

References

1. Bakr O, Johnson M, Mudumbai R, Ramchandran K (2009) Multi-antenna interference cancellation techniques for cognitive radio applications. In: Proceedings of the IEEE WCNC, Budapest, pp 1–6
2. Biglieri E, Calderbank R, Constantinides A, Goldsmith A, Paulraj A, Poor HV (2007) MIMO wireless communications. Cambridge University Press, Cambridge
3. Caire G, Shamai S (2003) On the achievable throughput of a multiantenna gaussian broadcast channel. IEEE Trans Inf Theory 49(7):1691–1706
4. Foschini GJ (1996) Layered space-time architecture for wireless communication in a fading envorinment when using multi-element antennas. Bell Labs Tech J 1(2): 41–59
5. Gao F, Zhang R, Liang Y-C, Wang X (2010) Design of learning-based MIMO cognitive radio systems. IEEE Trans Veh Tech 59(4):1707–1720
6. Gesbert D, Shafi M, Shiu DS, Smith PJ, Naguib A (2003) From theory to practice: an overview of MIMO space-time coded wireless systems. IEEE J Sel Areas Commun 21(3): 281–302
7. Goldsmith A, Jafar SA, Maric I, Srinivasa S (2009) Breaking spectrum gridlock with cognitive radios: an information theoretic perspective. Proc IEEE 97(5):894–914
8. Haykin S (2005) Cognitive radio: brain-empowered wireless communications. IEEE J Sel Areas Commun 23(2):201–220
9. Hou YT, Shi Y, Sherali HD (2008) Spectrum sharing for multi-hop networking with cognitive radios. IEEE J Sel Areas Commun 26(1):146–155
10. Joint Tactical Radio System. http://www.globalsecurity.org/military/systems/ground/jtrs.htm/
11. Kim S-J, Giannakis GB (2011) Optimal resource allocation for MIMO ad hoc cognitive radio networks. IEEE Trans Inf Theory 57(5):3117–3131
12. Poon ASY, Brodersen RW, Tse DNC (2005) Degrees of freedom in multiple-antenna channels: a signal space approach. IEEE Trans Inf Theory 51(2):523–536
13. SAFECOM. http://www.safecomprogram.gov/SAFECOM/
14. Sengupta S, Subbalakshmi KP (2013) Open research issues in multi-hop cognitive radio networks. IEEE Commun Mag 52(4):168–176
15. Sherali HD, Adams WP (1999) A reformulation-linearization technique for solving discrete and continuous nonconvex problems, Chapter 8. Kluwer Academic Publishers, Dordrecht
16. Shi Y, Liu J, Jiang C, Gao C, Hou YT (2014) A DoF-based link layer model for multi-hop MIMO networks. IEEE Trans Mob Comput 12(7):1395–1408
17. Smith GS (2004) A direct derivation of a single-antenna reciprocity relation for the time domain. IEEE Trans Antennas Propag 52(6):1568–1577
18. Telatar IE (1999) Capacity of multi-antenna gaussian channels. Eur Trans Telecommun 10(6):585–596
19. Tse D, Viswanath P (2005) Fundamentals of wireless communication. Cambridge University Press, Cambridge
20. Vanu Inc. http://www.vanu.com/
21. Viswanathan H, Venkatesan S, Huang H (2003) Downlink capacity evaluation of cellular networks with known-interference cancellation. IEEE J Sel Areas Commun 21(5): 802–811
22. Wyglinski A, Nekovee M, Hou YT (eds) (2009) Cognitive radio communications and networks: principles and practice. Elsevier. ISBN-13:978-0-12-374715-0

23. Zhang R, Liang Y-C (2008) Exploiting multi-antennas for opportunistic spectrum sharing in cognitive radio networks. IEEE J Sel Top Signal Process 2(1):88–102
24. Zhang YJ, So AM-C (2011) Optimal spectrum sharing in MIMO cognitive radio networks via semidefinite programming. IEEE J Sel Areas Commun 29(2):362–373

Further Reading

1. Shi Y, Hou YT (2007) Optimal power control for multi-hop software defined radio networks. In: Proceedings of the IEEE INFOCOM, Anchorage, pp 1694–1702

Coalition Formation Games for Cooperative Spectrum Sensing in Cognitive Radio Networks

31

Yong Zhou, Zhiyu Dai, Xiaolei Hao, Man Hon Cheung, Zehua Wang, and Vincent W. S. Wong

Contents

Abstract

Cooperative spectrum sensing is an effective technique to enhance the sensing performance and improve the spectrum efficiency in cognitive radio networks

Y. Zhou (✉) · Z. Wang · V. W. S. Wong · X. Hao
Department of Electrical and Computer Engineering, The University of British Columbia, Vancouver, BC, Canada
e-mail: zhou@ece.ubc.ca; zwang@ece.ubc.ca; vincentw@ece.ubc.ca; hao.xiaolei.beijing@gmail.com

Z. Dai
D&B Cloud Innovation Center, Vancouver, BC, Canada
e-mail: zydai2011@gmail.com

M. H. Cheung
Department of Information Engineering, The Chinese University of Hong Kong, Hong Kong, China
e-mail: mhcheung@ie.cuhk.edu.hk

W. Zhang (ed.), *Handbook of Cognitive Radio*,
https://doi.org/10.1007/978-981-10-1394-2_30

(CRNs). This chapter considers a CRN with multiple primary users (PUs) and multiple secondary users (SUs) and presents two cooperative spectrum sensing and access (CSSA) schemes. The first CSSA scheme allows each SU to sense one channel and is formulated as a hedonic coalition formation game, where each coalition is composed of the SUs that sense on the same channel. The value function of each coalition and the utility function take into account both the sensing accuracy and the energy consumption. The algorithms for decision node selection in each coalition and SU decision-making are proposed to obtain a final network partition, which is proved to be both Nash stable and individually stable. This chapter then focuses on a more general scenario, where each SU can simultaneously sense multiple channels based on its traffic demand. The traffic demand-based CSSA scheme is formulated as a nontransferable utility (NTU) overlapping coalitional game, where each SU implements a cooperation strategy based on its expected payoff. Two algorithms, namely overlapping coalition formation (OCF) and sequential coalition formation (SCF), are proposed to obtain a coalition structure. The OCF algorithm guarantees the stability of the coalition structure, while the SCF algorithm reduces the computational complexity and information exchange. Simulation results show that the proposed algorithms significantly enhance the network throughput.

Keywords

Cognitive radio networks · Coalitional game · Cooperative spectrum sensing · Hedonic coalition formation · Overlapping coalitional game · Traffic demand-based cooperation strategy

Introduction

Driven by the rapidly increasing number of connected devices and the popularity of data intensive applications, the global mobile data traffic explosion is expected to continue according to Cisco's forecast [1]. Due to the scarcity of the spectrum resources, the radio spectrum should be efficiently utilized to meet the huge amount of data traffic demand. However, the scarce spectrum is assigned to the licensed users by the Federal Communications Commission (FCC) over a long period of time. Such a static spectrum allocation strategy leads to a large portion of the assigned spectrum being underutilized [2]. This motivates the concept of cognitive radio (CR), which allows the unlicensed users to dynamically and opportunistically access the temporarily unused licensed spectrum that has been allocated to the licensed users.

The FCC defines the CR as follows: "Cognitive radio: A radio or system that senses its operational electromagnetic environment and can dynamically and autonomously adjust its radio operating parameters to modify system operation, such as maximize throughput, mitigate interference, facilitate interoperability, access secondary markets." [3]. Based on this definition, in order to enhance the

spectrum efficiency, a CR user should have the capability to monitor the licensed spectrum and accurately identify the temporarily unoccupied spectrum.

A cognitive radio network (CRN) consists of a primary network and a secondary network. The users of the primary and secondary networks are referred to as the primary users (PUs) and secondary users (SUs), respectively. Generally, the SUs can operate on the licensed spectrum using either spectrum overlay or spectrum underlay. In particular, in an overlay system, the SUs are only allowed to utilize the unoccupied spectrum. On the other hand, spectrum underlay allows the SUs to operate on the occupied spectrum under the condition that the SUs do not cause harmful interference to the PUs.

In order to protect the transmissions of the PUs, local spectrum sensing should be performed by each SU to detect the availability of the spectrum within its operating range before accessing it. However, the local spectrum sensing is susceptible to sensing errors due to shadowing, path loss, or receiver uncertainty [4]. In order to enhance the performance of spectrum sensing, multiple SUs can sense the spectrum cooperatively to exploit the spatial diversity from the observations of spatially located SUs [4–6]. In centralized cooperative spectrum sensing, a central unit is required to collect the sensing results of the cooperative SUs. Based on the received sensing results, the central unit makes the final decision on the availability of the sensed spectrum and sends the final decision to all SUs. After that, the available channels are shared among the SUs that participate in spectrum sensing.

Cooperative spectrum sensing has the potential to enhance the sensing accuracy and network throughput, at the cost of consuming more energy for spectrum sensing. Note that a CRN generally consists of multiple PUs (i.e., multiple licensed channels) and multiple SUs. Hence, it is important to determine the channel for each SU to sense and access while taking into account the sensing accuracy, throughput, and energy efficiency. Many cooperative spectrum sensing strategies have been proposed to achieve high network throughput or improve energy efficiency, as discussed in the following.

- Enhancing network throughput: the SUs are offered the opportunities to access the licensed channel by participating in spectrum sensing. There exists a trade-off between the sensing performance and the network throughput [6]. By optimizing the sensing parameters (e.g., the detection threshold and the sensing duration), the efficient cooperative spectrum sensing scheduling methods can be developed to balance the sensing performance and the network throughput [7, 8]. An adaptive and cooperative spectrum sensing method is proposed in [9], and the impact of cooperative spectrum sensing on the performance of the proposed optimal spectrum sensing scheme is studied. A periodic sensing opportunistic spectrum access scheme is proposed in [10], where the constrained Markov decision processes are utilized to maximize the channel utilization.
- Enhancing energy efficiency: performing spectrum sensing consumes energy, and more SUs participating in spectrum sensing leads to more energy consumption. By allocating spectrum resources to the SUs based on the channel states and the traffic demand, developing efficient scheduling algorithms to assign available

channels to different SUs can improve the energy efficiency [11,12]. The system energy efficiency can also be maximized by optimizing the sensing time, the energy detection threshold, and the number of the SUs [13]. In addition, the constraints of both the transmission power and the sensing performance should be considered to protect the transmission of the PUs [14,15].

Game theory has been widely applied in CRNs to study the cooperative spectrum sensing. The problem of cooperative spectrum sensing in CRNs with multiple channels can be formulated as an evolutionary game, where each SU makes its own decision on whether to sense the spectrum, and an entropy-based coalition formation algorithm is proposed to select the channel for the SUs [16]. To achieve better performance of cooperative sensing and efficiently allocate the spectrum resources among the SUs, coalitional game is also applied in the cooperation strategy design [17], in which Bayesian learning is used to estimate the channel states and Markov chain decision process is applied to make channel access decisions for the SUs. In addition, there exists a trade-off between spectrum sensing and spectrum access [18]. Such a problem can be formulated as a disjoint coalition formation (DCF) game, where each SU joins one coalition to maximize the utility. Note that a collection of coalitions is referred to as a coalition structure. The SUs can serve as cooperative relays of the PUs and obtain channel access in return. It is shown in [19] that the SUs can form the grand coalition structure to maximize the system utility.

Although many studies have been conducted for cooperative spectrum sensing, there are still several issues that should be addressed.

- The traffic demand of the SUs should be taken into account when investigating the cooperative spectrum sensing and channel access in CRNs. Most of the existing works assume that the SUs always have data to transmit, and the channels are always fully utilized if they are assigned to the SUs. However, in practice, the traffic demand of the SUs may change over time, and the amount of data to be transmitted depends on the applications. For instance, an SU that monitors the environment and aims to report the temperature changes does not transmit periodically, while an SU with a video streaming application has higher traffic demand than an SU running a best-effort application. Although the traffic demand of the SUs are considered in [11,20], they focus on spectrum resource allocation rather than spectrum sensing. Besides, they aim to maximize the aggregate system utility instead of developing a cooperation strategy from the perspective of each individual SU.
- Both the energy efficiency and the traffic demand should be taken into account when each SU makes its own decision on whether to participate in the cooperative spectrum sensing. Most of the existing works assume that all SUs in the system participate in cooperative spectrum sensing as in [12,21,22]. However, an energy-constrained SU having no data to transmit within a certain amount of time may prefer to stay in idle to reduce the energy consumption.
- By allowing each SU to join multiple coalitions, each SU can contribute to spectrum sensing for multiple channels at the same time so as to increase the probability of channel access. Most of the existing works assume that each SU

can join only one coalition to perform cooperative spectrum sensing, formulate the problem as a DCF game, and find a nonoverlapping coalition structure. Such an assumption restricts the cooperation opportunities of the SUs. By exploiting the advantage of simultaneously sensing multiple channels, the overlapping coalitional game theory is required. One exception is [23], in which the problem of cooperative spectrum sensing is formulated as an overlapping coalitional game, and a distributed algorithm is proposed to find a stable coalition structure. However, the spectrum resource allocation and additional energy consumption due to joining coalitions are not taken into account.

In the following two sections, two coalitional games for cooperative spectrum sensing and access in CRNs are described to address the aforementioned issues. Section "Hedonic Coalition Game for Cooperative Spectrum Sensing and Channel Access" presents a cooperative spectrum sensing and access (CSSA) scheme for the SUs and formulates the multichannel CSSA problem as a hedonic coalition formation game. The algorithms for decision node selection and SU decision-making are proposed. Section "Overlapping Coalitional Game for Cooperative Spectrum Sensing and Access" proposes a traffic demand-based cooperation strategy for the SUs and formulates it as a nontransferable utility (NTU) overlapping coalitional game. The overlapping coalition formation (OCF) and sequential coalition formation (SCF) algorithms are proposed to solve the problem.

Hedonic Coalition Game for Cooperative Spectrum Sensing and Channel Access

System Model and CSSA Scheme

Consider a CRN consisting of one base station, $|M|$ PUs, and $|N|$ secondary transmitter-receiver (ST-SR) pairs. As the ST performs spectrum sensing and data transmission, the terms SU and ST are used interchangeably. The sets of PUs and STs are denoted as M and N, respectively. Each $PU_i, i \in M$ transmits data to the base station through its own licensed channel with bandwidth B_i. Hence, there are $|M|$ nonoverlapped channels in the system. On the other hand, each ST_j is assumed to always have data to transmit and seeks to exploit possible transmission opportunities over one of the $|M|$ licensed channels.

Consider a frame structure for periodic spectrum sensing, where each time frame has the same frame duration, denoted as T. Each time frame is composed of one sensing subframe and one data transmission subframe. All SUs have the same spectrum sensing duration, denoted as $\delta \in (0, T]$. Hence, the data transmission duration is $T - \delta$. Note that the time duration required for sensing results collection and data fusion is negligible as it is much shorter than the time required for spectrum sensing and data transmission. Each $ST_j, j \in N$ samples the received signal intended for the PU with sampling frequency f_s. Both δ and T are assumed to be a multiple of $1/f_s$.

Each SU senses one channel in each time frame and determines the probabilities of detection and false alarm. The hypotheses that $PU_i, i \in M$ is active and inactive are denoted as $H_{1,i}$ and $H_{0,i}$, respectively. The probability of detection is the probability that the presence of PU_i is correctly detected under hypothesis $H_{1,i}$ (i.e., a busy channel is detected as busy), while the probability of false alarm is the probability of falsely declaring the presence of the primary signal under hypothesis $H_{0,i}$ (i.e., an idle channel is detected as busy).

The noise in the channel of $PU_i, i \in M$ is assumed to be an independent and identically distributed (i.i.d.) random variable with zero mean and variance $\sigma_{n,i}^2 = N_0 B_i$, where N_0 denotes the power spectral density. The signals of the primary users are i.i.d. random variables with zero mean and variance $\sigma_{s,i}^2, i \in M$. Hence, the received signal-to-noise ratio (SNR) of PU_i, $i \in M$ measured at ST_j, $j \in N$ under the hypothesis $H_{1,i}$ is $\gamma_{i,j} = |g_{i,j}|^2 \sigma_{s,i}^2 / \sigma_{n,i}^2$, where $|g_{i,j}|$ denotes the average channel gain of the link between PU_i and ST_j in channel i. Complex phase shift keying (PSK) modulated primary signals and circularly symmetric complex Gaussian (CSCG) noise are considered. By using energy detection [4, 24], the probability of false alarm [6] in channel $i \in M$ by ST_j under hypothesis $H_{0,i}$ is given by

$$\begin{aligned} P_{f,i,j}(\varepsilon, \delta, \sigma_{n,i}^2) &= \Pr(y_{j,i} > \varepsilon \mid H_{0,i}) \\ &= Q\left(\left(\frac{\varepsilon}{\sigma_{n,i}^2} - 1\right)\sqrt{\delta f_s}\right), \end{aligned} \tag{1}$$

where ε denotes the detection threshold for all STs, $y_{j,i}$ denotes the test statistic for the energy detector of ST_j in channel i, and Q denotes the complementary distribution function of the standard Gaussian. If all PUs have the same bandwidth, then $P_{f,i,j}(\varepsilon, \delta, \sigma_{n,i}^2)$ are the same with $\forall\, i \in M$, $\forall\, j \in N$. On the other hand, the probability of detection in channel $i \in M$ by ST_j under hypothesis $H_{1,i}$ is given by

$$\begin{aligned} P_{d,i,j}(\varepsilon, \delta, \sigma_{n,i}^2, \gamma_{i,j}) &= \Pr(y_{j,i} > \varepsilon \mid H_{1,i}) \\ &= Q\left(\left(\frac{\varepsilon}{\sigma_{n,i}^2} - \gamma_{i,j} - 1\right)\sqrt{\frac{\delta f_s}{2\gamma_{i,j} + 1}}\right). \end{aligned} \tag{2}$$

The performance of local spectrum sensing can be degraded by many factors, including the hidden node problem, deep fading, and shadowing [4]. Cooperative spectrum sensing as an effective technique for realizing spatial diversity has been proposed to enhance the detection performance. In particular, each SU senses the channel independently and reports the sensing result to the decision node (DN) when sensing time δ expires. The selection of DN for each channel will be presented in the next subsection. Based on the sensing results from the SUs that sense channel i, DN_i determines the status (i.e., busy or idle) of channel i.

The DN makes the spectrum sensing decision based on the k-out-of-n rule [25]. In particular, a busy channel is determined if k or more SUs individually detect the

presence of primary activity. For $k = 1$, $k = n$, and $k \geq n/2$, k-out-of-n rule becomes the "or" rule, "and" rule, and majority rule, respectively [4]. The local decisions made by the SUs in the same channel are assumed to be independent. Let S_i denote the set of SUs sensing channel i. As each SU can sense only one channel in each time frame, the constraints $S_i \subseteq N$, $\forall\, i \in M$, $\bigcup_{i \in M} S_i = N$, and $S_i \cap S_l = \emptyset$, $\forall\, i, l \in M, i \neq l$ should be satisfied. When $k = 1$, the probability of false alarm under hypothesis $H_{0,i}$ and the probability of detection under hypothesis $H_{1,i}$ in channel $i \in M$ can, respectively, be expressed as

$$P_{f,i} = 1 - \prod_{j \in S_i} \left(1 - P_{f,i,j}\left(\varepsilon,\, \delta,\, \sigma_{n,i}^2\right)\right), \tag{3}$$

$$P_{d,i} = 1 - \prod_{j \in S_i} \left(1 - P_{d,i,j}\left(\varepsilon,\, \delta,\, \sigma_{n,i}^2,\, \gamma_{i,j}\right)\right). \tag{4}$$

For channel $i \in M$, the probabilities that PU_i is active and silent are denoted as $P_{H_{1,i}}$ and $P_{H_{0,i}}$, respectively, and $P_{H_{1,i}} + P_{H_{0,i}} = 1$. If DN_i declares that channel i is busy, then ST_j, $\forall\, j \in S_i$ cannot transmit during the data transmission subframe. On the other hand, if DN_i declares that channel i is idle, then each ST_j, $j \in S_i$ can access channel i with equal probability (i.e., $1/|S_i|$) and only one SU in S_i can be selected to transmit data, where $|S_i|$ denotes the number of the SUs sensing channel i. If channel i is declared to be idle and PU_i is actually silent, then the secondary data transmission in channel i is successful. However, if channel i is declared to be idle but PU_i is actually active (i.e., a missed detection), then the secondary data transmission in channel i interferes with the transmission of PU_i. In this case, if the collision is detected by the base station, then the SUs will be charged $\varphi > 0$ by the base station as a penalty. The value of φ can be selected to map the level of the performance degradation of the PU to the penalty value of the SUs. Hence, it is important to decide which channel each SU should sense and access so as to optimize the performance.

Hedonic Coalition Formation Game

In this subsection, the multichannel energy-efficient cooperative spectrum sensing and access problem is formulated as a hedonic coalition formation game, in which the switch rule is utilized to decide whether the SUs join or leave a coalition. In addition, the formulated hedonic coalition formation game is proved to always converge to the Nash-stable and individually stable partition.

Value Function and Utility Function

To fully exploit the possible transmission opportunities, each SU should carefully decide which channel to sense and access during each time frame. Both the sensing accuracy and the energy consumption should be considered when making the decisions. In particular, the sensing accuracy affects the amount of data transmitted

by the SUs and the penalty charged for interfering with the PUs' transmissions. The energy consumption of the SUs is a critical criterion for spectrum sensing and data transmission in practice.

There are four scenarios in the proposed CSSA scheme, depending on the activity of the PU_i and the decision of DN_i in channel $i \in M$. The payoff of set S_i is defined as the reward (i.e., the amount of data transmitted by the SUs in S_i) minus the penalty (i.e., the payment charged for interfering with PU_i's transmission) during the data transmission subframe. The payoff, the energy consumption, and the probability that each scenario occurs are discussed as follows:

Scenario 1: PU_i is silent, and the decision made by DN_i is not a false alarm. In this scenario, ST_j, $\forall\, j \in S_i$ transmits data within the data transmission subframe. The transmission rate $R_{j,i}$ of ST_j can be expressed as [26]

$$R_{j,i} = B_i \log_2 \left(1 + |h_{j,i}|^2 \frac{P_t}{\sigma_{n,i}^2}\right), \tag{5}$$

where P_t denotes the signal transmission power and $|h_{j,i}|$ denotes the average channel gain of the link between ST-SR pairs j in channel i.

In this scenario, the payoff of set S_i is $v_{0|0,D}(S_i) = \frac{\sum_{j\in S_i} R_{j,i}}{|S_i|}(T-\delta)$, as the transmission of the SUs is successful and the penalty is zero. By denoting the sensing power of ST_j, $\forall\, j \in N$ as P_s, the energy consumption of set S_i is given by $v_{0|0,E}(S_i) = P_s|S_i|\delta + P_t(T-\delta)$, where $P_s|S_i|\delta$ and $P_t(T-\delta)$ represent the energy consumption due to spectrum sensing and data transmission, respectively. The probability that this scenario occurs is $P_{0|0,i} = P_{H_{0,i}}(1 - P_{f,i})$.

Scenario 2: PU_i is silent, and the decision made by DN_i is a false alarm. In this scenario, as no SU transmits during the data transmission subframe and interfere with the PU, the payoff of set S_i is $v_{1|0,D}(S_i) = 0$, and the energy consumption of set S_i is $v_{1|0,E}(S_i) = P_s|S_i|\delta$. The probability that this scenario occurs is $P_{1|0,i} = P_{H_{0,i}} P_{f,i}$.

Scenario 3: PU_i is active, and DN_i detects the presence of PU_i. In this scenario, no SU transmits data during the data transmission subframe. The payoff of set S_i is $v_{1|1,D}(S_i) = 0$, as both the reward and the penalty are zero. In addition, the energy consumption of set S_i is $v_{1|1,E}(S_i) = P_s|S_i|\delta$, and the probability that this scenario occurs is $P_{1|1,i} = P_{H_{1,i}} P_{d,i}$.

Scenario 4: PU_i is active, and DN_i fails to detect the presence of PU_i. In this scenario, both PU_i and $ST_j, j \in S_i$ transmit data during the data transmission subframe. Due to co-channel interference, it is assumed that both transmitted packets are corrupted. The payoff of set S_i is $v_{0|1,D}(S_i) = -\varphi(T-\delta)$, where the reward is zero. The energy consumption of set S_i is $v_{0|1,E}(S_i) = P_s|S_i|\delta + P_t(T-\delta)$. The probability that this scenario occurs is $P_{0|1,i} = P_{H_{1,i}}(1 - P_{d,i})$.

Based on the above discussions, the expected payoff for set S_i over each time frame is given by

$$\begin{aligned} v_D(S_i) &= \sum_{a=0}^{1}\sum_{b=0}^{1} P_{a|b,i}\, v_{a|b,D}(S_i) \\ &= P_{0|0,i}\frac{\sum\limits_{j\in S_i} R_{j,i}}{|S_i|}(T-\delta) - P_{0|1,i}\varphi(T-\delta). \end{aligned} \tag{6}$$

The expected energy consumption for set S_i in each time frame of duration T is

$$\begin{aligned} v_E(S_i) &= \sum_{a=0}^{1}\sum_{b=0}^{1} P_{a|b,i}\, v_{a|b,E}(S_i) \\ &= P_s|S_i|\delta + (P_{0|0,i} + P_{0|1,i})P_t(T-\delta). \end{aligned} \tag{7}$$

The value function of set S_i is defined as the ratio of $v_D(S_i)$ to $v_E(S_i)$, which represents the expected payoff per unit of energy consumed in set S_i:

$$\begin{aligned} v(S_i) &= \frac{v_D(S_i)}{v_E(S_i)} \\ &= \frac{P_{0|0,i}\sum_{j\in S_i} R_{j,i}(T-\delta) - |S_i|P_{0|1,i}\varphi(T-\delta)}{|S_i|\big(P_s|S_i|\delta + (P_{0|0,i} + P_{0|1,i})P_t(T-\delta)\big)}. \end{aligned} \tag{8}$$

The trade-off between the energy efficiency and the protection of the PUs' transmission depends on the value of φ. Specifically, when $\varphi = 0$, $v(S_i)$ equals to the energy efficiency (i.e., the expected amount of data transmitted by the SUs divided by the expected energy consumption) of the CSSA scheme. When φ is large, a higher priority is given to protect the PU from the interference of the SUs. According to (8), the value function takes into account the sensing accuracy by considering the sensing results related to false alarm (i.e., $P_{0|0,i}$ is related to $P_{f,i}$), and detection (i.e., $P_{0|1,i}$ is related to $P_{d,i}$). The value of $v(\emptyset)$ is chosen such that $v(S_i) > v(\emptyset)$, $\forall\, S_i \subseteq N$, and $S_i \neq \emptyset$.

As all SUs that in set S_i perform spectrum sensing have the same probability to access channel i, they receive the same utility. Hence, the utility function of ST_j, $\forall\, j \in S_i$ can be expressed as

$$x_j^{S_i} = \frac{v(S_i)}{|S_i|}. \tag{9}$$

The utility defined in (9) can be used as a performance metric to affect the decision of each SU on which channel to sense and access during each time frame. Note that the utility does not correspond to a physical quantity that can be divided among the SUs in a coalition.

Hedonic Coalition Formation Analysis

In order to formulate the multichannel cooperative spectrum sensing and channel access problem as a coalition formation game with transferable utility (TU) [27], the following basic elements need to be introduced:

- *Players*: the players of the coalition formation game are the $|N|$ SUs (i.e., ST_j, $\forall\ j \in N$).
- *Strategies*: the strategy of each SU is the licensed channel it chooses to sense and access (i.e., ST_j chooses a licensed channel $i \in M$).
- *Utilities*: the utility of each SU depends on which coalition it belongs to, and it is defined in (9) (i.e., the utility of ST_j in coalition S_i is $x_j^{S_i}$).

Based on coalitional game theory, set S_i is referred to as coalition i. Hence, $|M|$ coalitions can be formed in the system, and each SU joins one coalition. By restricting one coalition per channel, different coalitions operate in different nonoverlapping channels. Hence, the SUs of different coalitions do not interfere with each other. The SUs autonomously form coalitions to achieve higher utilities. This game is a hedonic coalition formation game [28], which will be shown later. Before presenting its definition, some basic definitions used in the coalition formation games are introduced as follows.

Definition 1. The set $S = \{S_1, \ldots, S_{|M|}\}$ is a partition (or coalition structure) of N if $S_i \cap S_l = \emptyset$, $\forall\, i, l \in M, i \neq l$ and $\bigcup_{i \in M} S_i = N$.

Definition 2. For any player $j \in N$, a preference relation $\succeq_j$ is defined as a complete, reflexive and transitive binary relation over the set of all coalitions that player j can possibly form [28].

Based on Definition 2, given two coalitions $S_1 \subseteq N$ and $S_2 \subseteq N$, $S_1 \succeq_j S_2$ indicates that player $j \in N$ prefers to be a member of coalition S_1 over to be a member of coalition S_2, or at least, player j prefers both coalitions equally. Similarly, $S_1 \succ_j S_2$ indicates that player j strictly prefers being a member of coalition S_1 over being a member of coalition S_2. The preference function $U_j(S_i)$, $j \in S_i$ is defined as

$$U_j(S_i) = \begin{cases} x_j^{S_i}, & S_i \notin h(j), \\ -\infty, & \text{otherwise}, \end{cases} \tag{10}$$

where $h(j)$ is the history set of ST_j. Note that the preference over different coalitions for ST_j, $\forall\ j \in N$ depends on its utility function defined in (9). The following operation is defined to evaluate the preferences of ST_j, $\forall\ j \in N$:

$$S_1 \succ_j S_2 \Leftrightarrow U_j(S_1) > U_j(S_2), \tag{11}$$

where $S_1 \subseteq N$ and $S_2 \subseteq N$ are any two coalitions containing ST_j.

Based on the above discussions, ST_j, $\forall\ j \in N$ prefers to join a new coalition, which ST_j has never been a member of, if and only if ST_j can obtain a higher utility in this new coalition than ever before. Given the set of players N and a preference relation $\succ_j$ for each player $j \in N$, a hedonic coalition formation game is defined as follows:

Definition 3. A hedonic coalition formation game is a coalitional game that satisfies the following two conditions: (1) The utility of any player depends solely on the members of the coalition to which the player belongs; (2) the coalitions form as a result of the preferences of the players over their possible coalition set. Therefore, a hedonic coalition formation game is defined by the pair $(N, \succ)$, where N is the set of players and $\succ$ is a profile of preferences defined for each player in N.

The formulated game satisfies the conditions of a hedonic coalition formation game. In particular, the utility function of ST_j, $\forall\ j \in S_i$ defined in (9) only depends on the SUs in coalition S_i, $i \in M$, and the preference function of each SU is given in (10). The switch rule for coalition formation is defined as follows.

Definition 4. (Switch rule) Given a partition $S = \{S_1, \ldots, S_{|M|}\}$, ST_j, $j \in S_i$ decides to leave its current coalition S_i and joins another coalition S_l, where $i \neq l$, if and only if $S_l \bigcup \{j\} \succ_j S_i$.

Based on the switch rule, an SU leaves its current coalition and joins another coalition if the new coalition is strictly preferred over the current coalition. Each player makes a selfish decision and moves from the current coalition to a new coalition, regardless the effect of its move on other players. All SUs make decisions to automatically form coalitions based on the switch rule. Hence, the partition of the $(N, \succ)$ hedonic coalition formation game may change in each time frame. The initial partition of the hedonic coalition formation game is denoted as $S^{(0)} = \{S_1^{(0)}, \ldots, S_{|M|}^{(0)}\}$, and the partition at the r-th time frame is denoted as $S^{(r)} = \{S_1^{(r)}, \ldots, S_{|M|}^{(r)}\}$. The history set $h(j)$ of ST_j is defined as follows:

Definition 5. At the r-th time frame, the history set for $ST_j, j \in N$ is given by $h(j) = \{S_{i_0}^{(0)}, \ldots, S_{i_{r-1}}^{(r-1)}\}$, where $i_z \in M$ and $j \in S_{i_z}$ hold at any time frame index $z \in \{0, 1, \ldots, r-1\}$. At the end of the r-th time frame, ST_j will update its history set $h(j)$ by including a new element $S_{i_r}^{(r)}$, where $i_r \in M$ and $j \in S_{i_r}$.

Proposition 1. *If ST_j performs the switch rule in the r-th time frame, in which it leaves its previous coalition S_i (denoted as $S_{i_{r-1}}^{(r-1)}$) and joins another coalition S_l with $i \neq l$, the newly formed coalition $S_l \bigcup \{j\}$ (denoted as $S_{i_r}^{(r)}$) cannot be the same with the previous coalition members in the history set $h(j)$. That is, $S_l \bigcup \{j\} \notin h(j)$ holds before the update of $h(j)$ at the end of the r-th time frame.*

Proof. Please refer to [29].

Before proving that there exists a stable partition in this hedonic coalition formation game, the definitions of Nash-stable and individually stable partitions [30] are presented as follows.

Algorithm 1 Decision node DN_i selection algorithm in channel $i \in M$. The algorithm is executed by ST_j, $\forall\, j \in S_i$

1: **for** iteration $r := 1$ to MAX **do**
2: ST_j broadcasts its measured SNR information $\gamma_{i,j}^{(r)}$ and transmission rate $R_{j,i}$ to other secondary transmitters ST_k, $\forall\, k \in S_i^{(r)} \backslash \{j\}$
3: ST_j receives the measured SNR information $\gamma_{i,k}^{(r)}$ and transmission rate $R_{k,i}$ from other ST_k, $\forall\, k \in S_i^{(r)} \backslash \{j\}$
4: $q := \arg\max_{p \in S_i^{(r)}} \gamma_{i,p}^{(r)}$
5: $DN_i^{(r)} := ST_q$
6: **end for**

Definition 6. A partition $S = \{S_1, \ldots, S_{|M|}\}$ is Nash stable if $\forall\, j \in S_i$ with $\forall\, i \in M$, $S_i \succeq_j S_l \bigcup \{j\}$, $\forall\, l \in M$.

Definition 7. A partition $S = \{S_1, \ldots, S_{|M|}\}$ is individually stable if there does not exist $j \in S_i$ with $i \in M$, and a coalition S_l $(l \neq i)$ such that $S_l \bigcup \{j\} \succ_j S_i$, and $S_l \bigcup \{j\} \succeq_k S_l$ for all $k \in S_l$.

Hence, a coalition partition S is Nash stable if no player has an incentive to move from its current coalition to another coalition (i.e., no player can obtain a higher utility by performing the switch rule). When a partition is Nash stable, it implies that it is individually stable [30] that there does not exist any coalition, where a player strictly prefers to join, while the other players in that coalition do not get hurt by the formation of this new coalition.

Theorem 1. *Starting from any initial partition $S^{(0)}$, all the SUs will always converge to a final partition $S^* = \{S_1^*, \ldots, S_{|M|}^*\}$, which is both Nash stable and individually stable.*

Proof. Please refer to [29].

Note that if the history sets are not used, the partition still converges to stability, but a longer convergence time is required.

Algorithms for Coalition Formation

In this subsection, the implementations of the proposed CSSA scheme and the hedonic coalition formation game are described. Besides, a DN selection algorithm and a coalition formation algorithm based on the switch rule are proposed.

The hedonic coalition formation game has two stages. In stage one, the base station gathers necessary information, including the number of the PUs, the operating frequency, bandwidth B_i of PU_i, $\forall\, i \in M$, the locations of the PUs, the transmit power of the PUs $\sigma_{s,i}^2$, $\forall\, i \in M$, and the channel models. Assuming that the base station does not know exactly when the PUs will be active. The base station sets and broadcasts the initial partition $S^{(0)}$ to all SUs. The initial partition

is set as $S_1^{(0)} = N$ and $S_l^{(0)} = \emptyset$, $\forall\, l \in M \backslash \{1\}$. In stage two, all SUs perform the switch operations until the CRN converges to the final Nash-stable partition S^*. The total number of iterations required to converge is denoted as MAX. Based on Theorem 1, the CRN can always converge to the final Nash-stable partition S^* if the value of MAX is large enough. Note that at each time frame, only one SU can leave its current coalition and move to another coalition to increase its utility. The selection of DN_i, $\forall\, i \in M$ and the switch operations in coalition formation are illustrated in Algorithm 1 and Algorithm 2, respectively. After the final Nash-stable partition S^* is reached, the SUs stay in their current coalitions to sense and access the channels based on the proposed CSSA scheme.

In order to avoid the corruption of the sensing results due to transmission error between ST_j, $j \in S_i$ and DN_i, the SU with the highest detection probability in coalition S_i is selected as DN_i. By selecting the SU with the highest detection probability as the DN, the most reliable sensing result can be directly used in the decision fusion without experiencing any corruption. Hence, the primary data transmission can be protected if PU_i is active. In the r-th iteration of Algorithm 1, ST_j, $\forall\, j \in S_i$ selects $DN_i^{(r)}$ for channel $i \in M$. All SUs in coalition $S_i^{(r)}$ exchange their measured SNR and transmission rate $R_{j,i}$ via a dedicated error-free control channel [31] (lines 2–3). Finally, the SU with the highest measured SNR is selected as $DN_i^{(r)}$ (lines 4–5). As $P_{d,i,j}(\varepsilon, \delta, \sigma_{n,i}^2, \gamma_{i,j})$ is an increasing function of $\gamma_{i,j}$, the following proposition holds.

Proposition 2. *The DN_i selected by Algorithm 1 has the highest detection probability in S_i.*

The r-th iteration of Algorithm 2 consists of two phases: phase one (lines 3–8) and phase two (lines 9–25). In phase one, each SU randomly generates a number (line 4) and broadcasts in the dedicated control channel (lines 6–7). The SU with the largest random number is selected (line 8) to perform the switch operation in phase two. Without the loss of generality, user $ST_j \in S_i^{(r)}$ and channel $\alpha_j \in M$, where $\alpha_j \neq i$ (line 5), are assumed to be selected. In phase two, ST_j is temporarily switched from its current coalition $S_i^{(r)}$ to another coalition $S_{\alpha_j}^{(r)}$ (lines 11–13). Subsequently, ST_j obtains the information of $S_{\alpha_j}^{(r)}$ from $DN_{\alpha_j}^{(r)}$, which include data rates R_{k,α_j} ($\forall\, k \in S_{\alpha_j}^{(r)}$), coalition size $|S_{\alpha_j}^{(r)}|$, and statistics P_{d,α_j}, P_{f,α_j}, and $P_{H_{0,\alpha_j}}$ (line 12). If ST_j has already joined $S_{\alpha_j}^{(r)}$ before (lines 14–17) or its achieved utility is reduced (i.e., $x_j^{S_{\alpha_j}^{(r)}} \leq x_j^{S_i^{(r)}}$) (lines 19–22), then ST_j moves back to its original coalition $S_i^{(r)}$. Otherwise, ST_j remains in coalition $S_{\alpha_j}^{(r)}$. Finally, ST_j updates its history set $h(j)$ (line 25).

The proposed algorithms can adapt to the network changes. Specifically, if new PUs and SUs are deployed, existing PUs and SUs are removed, or the wireless channel conditions are changed, both stages will be performed again to find the new Nash-stable partition. In practice, these two stages can be periodically performed for the CRN to handle occasional changes of network settings. Note that the proposed algorithms can be directly applied to a more general scenario, which is not restricted

Algorithm 2 Coalition formation algorithm based on the switch rule. It is executed by ST_j, $\forall\ j \in N$

Initialization: $S_1^{(0)} := N$; $S_l^{(0)} := \emptyset$, $\forall\ l \in M \backslash \{1\}$
for iteration $r := 1$ to MAX **do**
  $S_i^{(r)} := S_i^{(r-1)}$, where $i \in M$ and $j \in S_i^{(r)}$
  ST_j generates θ_j, which is a Gaussian random variable with mean 0 and variance 1
  ST_j randomly selects another licensed channel α_j such that $\alpha_j \in M$, $\alpha_j \neq i$
  ST_j broadcasts the information of θ_j to other ST_k, $\forall\ k \in N$, $k \neq j$
  ST_j receives the information of θ_k from other ST_k, $\forall\ k \in N$, $k \neq j$
  $m := \arg\max_w \theta_w$, $\forall\ w \in N$
  if $ST_j = ST_m$ **then**
    ST_j computes $x_j^{S_i^{(r)}} := v(S_i^{(r)})/|S_i^{(r)}|$
    $S_i^{(r)} := S_i^{(r)} \backslash \{j\}$
    ST_j requests and obtains the information of $S_{\alpha_j}^{(r)}$ from $DN_{\alpha_j}^{(r)}$
    $S_{\alpha_j}^{(r)} := S_{\alpha_j}^{(r)} \bigcup \{j\}$
    if $S_{\alpha_j}^{(r)} \in h(j)$ **then**
      $S_{\alpha_j}^{(r)} := S_{\alpha_j}^{(r)} \backslash \{j\}$
      $S_i^{(r)} := S_i^{(r)} \bigcup \{j\}$
    else
      ST_j computes $x_j^{S_{\alpha_j}^{(r)}} := v(S_{\alpha_j}^{(r)})/|S_{\alpha_j}^{(r)}|$
      if $x_j^{S_{\alpha_j}^{(r)}} \leq x_j^{S_i^{(r)}}$ **then**
        $S_{\alpha_j}^{(r)} := S_{\alpha_j}^{(r)} \backslash \{j\}$
        $S_i^{(r)} := S_i^{(r)} \bigcup \{j\}$
      end if
    end if
  end if
  ST_j updates $h(j)$ by adding its current coalition at the end of $h(j)$
end for

to using the PSK-modulated signal for transmission and the OR rule for data fusion. In [29], the proposed model is further extended to consider the coalition formation game under the NTU framework.

Performance Evaluation

In this subsection, the performance gain of the proposed CSSA scheme is evaluated and compared with the closest PU (CPU) scheme and the noncooperative spectrum sensing and access (NSSA) scheme. In the CPU scheme, each SU senses the closest PU and joins that coalition to perform cooperative sensing, while the SUs in the NSSA scheme only perform local spectrum sensing. Unless specified otherwise, there are one base station, $|M| = 5$ PUs, and $|N| = 10$ ST-SR pairs. All nodes are randomly placed in a square region of 100×100 m. The average channel gain of the link between PU_i and ST_j is $|g_{i,j}|^2 = 1/d_{i,j}^{\gamma}$, where $d_{i,j}$ denotes the distance

between PU_i and ST_j, and $\gamma = 2$ denotes the path loss exponent. Similarly, the average channel gain of the link between ST_j and SR_j is $|h_{j,i}|^2 = 1/d_{j,i}^{\gamma}$, where $d_{j,i}$ denotes the distance between ST_j and SR_j. The bandwidth of the primary channel B_i is 10 MHz, $\forall\, i \in M$. Other parameters are set as follows: the duration of one time frame T is 100 ms; the sampling frequency f_s is 1 kHz; the transmit power of each ST P_t is 10 mW; the sensing power of each ST P_s is 10 mW; the detection threshold ε is 0.2 mW; the noise power $\sigma_{n,i}^2$ is 0.1 mW for all $i \in M$. The probability that $PU_i, i \in M$ is active is $P_{H_{1,i}} = P_{H_1} = 0.8$, $\forall\, i \in M$. The sensing duration δ and the unit penalty per second φ are to be 5 ms and 100, respectively. The OR rule is used for the data fusion.

Figure 1 shows the average utility of the SUs versus the number of the PUs $|M|$ in the CRN when $|N|$ is equal to 10. It can be observed that the performance of CSSA is better than those of CPU and NSSA. For all schemes, the average utility of the SUs first increases with $|M|$, as more spectrum can be utilized by the SUs. The performance of CPU is worse than that of CSSA, as the SUs in the CPU scheme choose to sense the closest PU, which leads to crowded coalition. When $|M| < 10$ and $|N| > |M|$, CSSA performs better than NSSA due to the cooperative gain of cooperative spectrum sensing. When $|M| \geq 10$, each SU can sense and access a different channel under CSSA and NSSA. Hence, the average utilities of the SUs for both the CSSA scheme and the NSSA scheme are the same. When $|M| \geq 10$, the average utility of the SUs still increases with $|M|$, as each SU may select a better channel when there are more channels available in the CRN. When $|M|$ is large, increasing $|M|$ further will not improve the spectrum utilization, as the number of the SUs is limited and the additional spectrum cannot be utilized by the SUs.

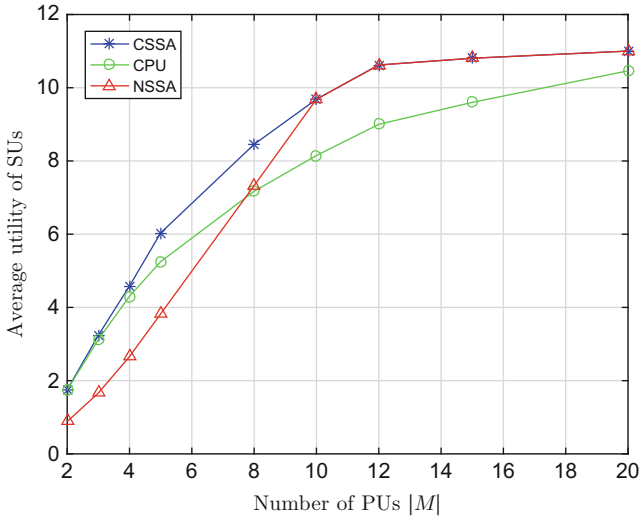

Fig. 1 The average utility of the SUs versus the number of PUs $|M|$ ($|N| = 10$) (Reproduced with permission from the IEEE)

Figure 2 shows the average utility of the SUs versus the probability that the PUs being active P_{H_1}. It can be observed that CSSA outperforms both CPU and NSSA. The performance gap between CSSA and CPU does not change too much with P_{H_1}, but the performance gap between CSSA and NSSA increases with P_{H_1}. When P_{H_1} is small, the improved sensing accuracy due to cooperative spectrum sensing is not

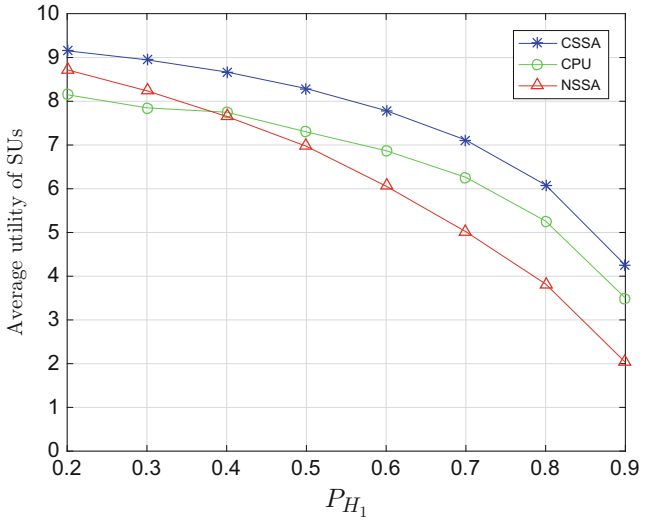

Fig. 2 The average utility of the SUs versus the probability for PUs being active P_{H_1} ($|M| = 5$, $|N| = 10$) (Reproduced with permission from the IEEE)

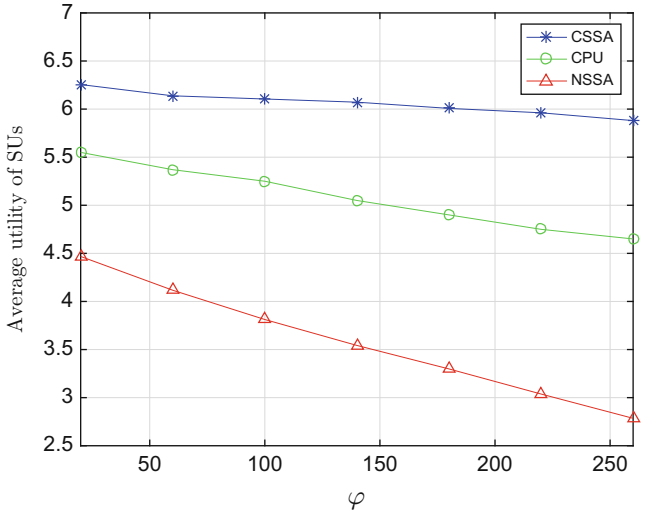

Fig. 3 The average utility of the SUs versus the unit penalty per second φ ($|M| = 5$, $|N| = 10$) (Reproduced with permission from the IEEE)

significant because the channels are vacant for most of the time. With the increase of P_{H_1}, the PUs occupy the channels more frequently. Due to the improved sensing accuracy, the SUs pay less penalty for interfering the PUs' transmissions and makes an effective use of the energy that has been consumed for sensing.

Figure 3 illustrates the average utility of the SUs versus the unit penalty φ. The results show that the performance of CSSA is better than those of CPU and NSSA. The average utility of the SUs decreases with the value of φ. However, the average utility of CSSA decreases much slower. The reason is that when φ is large, each SU is charged a larger penalty if there is a missed detection. Since the probability of detection of CSSA is higher than those of CPU and NSSA, the average utility of the SUs for CSSA does not decrease as significantly as CPU and NSSA when φ is increased.

Overlapping Coalitional Game for Cooperative Spectrum Sensing and Access

In the previous section, the multichannel cooperative spectrum sensing and access problem is formulated as a hedonic coalition formation game, where each SU can only sense one channel at a time and is assumed to always have data to transmit. By relaxing these two assumptions, in this section, a traffic demand-based cooperation strategy is proposed, and this problem is formulated as an NTU overlapping coalitional game. Comparing with the DCF game, the overlapping coalitional game can achieve better performance at the expense of a higher computational complexity.

System Model

As in the previous section, a CRN consisting of one base station, $|M|$ PUs (i.e., $|M|$ licensed channels), and $|N|$ SUs, is considered. Recall that $M = \{1, \ldots, |M|\}$ and $N = \{1, \ldots, |N|\}$ denote the sets of PUs and SUs, respectively, T denotes the frame duration, δ denotes the length of the spectrum sensing period, and S_i denotes the set of SUs choosing to sense and access channel $i \in M$. Assuming that each SU has multiple energy detectors and can sense multiple channels in a sensing period, but each SU can access at most one channel during one time slot [32]. A group refers to all the SUs that sense the same channel, and there are multiple groups in the system. The base station allocates a channel that is detected as idle to a group member. To avoid interference between different SUs, an idle channel can only be allocated to one SU at a time. Different SUs have different amount of data in their buffer waiting to be transmitted. An idle channel can only be assigned to the SU that is participating in sensing. Hence, each SU decides whether or not to participate in cooperative sensing based on the traffic demand and the channel capacity. As the individual sensing result may not be accurate due to path loss and shadowing, the SUs perform cooperative sensing in this work. The base station, which also serves as a fusion center, collects the sensing results from the SUs, and uses the OR rule to

decide the status of each channel. The detection probability of the set of the SUs S_i that sense channel $i \in M$ is given in (4). The false alarm probability of SU $j \in N$ after sensing channel $i \in M$, denoted as $P_{f,i,j}$, is given by

$$P_{f,i,j}\left(P_{d,i,j}, \gamma_{i,j}\right) = Q\left(\sqrt{2\gamma_{i,j}+1}Q^{-1}\left(P_{d,i,j}\right) + \sqrt{N_s}\gamma_{i,j}\right), \tag{12}$$

where N_s denotes the number of sensing samples during the sensing period in a time frame.

To protect the transmission of PU i, the cooperative sensing performance needs to satisfy a target value, denoted as $\bar{P}_{d,i}$ for SUs in set S_i. Hence, the individual target detection probability of SU $j \in S_i$ is given by [33]

$$\bar{P}_{d,i,j} = 1 - (1 - \bar{P}_{d,i})^{\frac{1}{|S_i|}}, \tag{13}$$

where $|S_i|$ denotes the number of SUs sensing channel i.

By substituting (13) into (12), the value of $P_{f,i,j}$ can be obtained. According to the OR rule, the false alarm probability at channel i is given by

$$P_{f,i} = 1 - \prod_{j \in S_i}\left(1 - P_{f,i,j}\right). \tag{14}$$

The transmission rate achieved by SU j over channel i can be expressed as

$$R'_{i,j} = B_i \log_2\left(1 + |g_j|^2 \frac{W_{t,i,j}}{\sigma^2_{n,i}}\right), \tag{15}$$

where $W_{t,i,j}$ denotes the transmit power of SU j when it performs transmission on channel i, and g_j denotes the channel gain of the transmission link of SU j.

The probability that channel i is correctly detected as idle is $P_{I,i}\left(1 - P_{f,i}\right)$, where $P_{I,i}$ denotes the probability that channel i is idle. When a channel is detected as idle, each member in the same coalition has the same probability $\left(\text{i.e., } \frac{1}{|S_i|}\right)$ to access the channel. The base station assigns an idle channel to only one SU that participates in cooperative sensing. Thus, the probability that SU j is allowed to transmit over channel i without interfering the transmission of the PU is given by

$$P^U_{i,j} = P_{I,i}\left(1 - P_{f,i}\right)\frac{1}{|S_i|}. \tag{16}$$

The number of the information bits in the buffer of SU j is denoted by D_j, which is a constant during one time slot. SU j cannot transmit more than the number of the information bits in its buffer. When an idle channel i is assigned to SU j, the

transmission time, denoted as $t_{i,j}$, is given by

$$t_{i,j} = \min\left\{\frac{D_j}{R'_{i,j}}, T-\delta\right\}. \tag{17}$$

Thus, the throughput that SU j can achieve in the time slot is

$$U_{i,j} = \frac{R'_{i,j}t_{i,j}}{T}. \tag{18}$$

An SU can transmit over channel $i \in M$ when the following two cases happen. The first case is that channel i is detected as idle, and it is indeed idle, which occurs with probability $P_{I,i}\left(1-P_{f,i}\right)$. The second case is that channel i is detected as idle but actually it is busy, which occurs with probability $(1-P_{I,i})(1-P_{d,i})$. Based on these two cases, the probability that SU j is assigned channel i and transmits data is

$$P^E_{i,j} = \left((1-P_{I,i})(1-P_{d,i}) + P_{I,i}(1-P_{f,i})\right)\frac{1}{|S_i|}. \tag{19}$$

By participating in multiple coalitions, the SUs can sense multiple channels during the sensing period, and the set of channels that SU j chooses to sense is denoted as A_j. Let K denote a subset of A_j which contains the channels assigned to SU j. The probability that set $K \subseteq A_j$ is obtained on SU j is given by $\prod_{i\in K}\left(P^E_{i,j}\right)\prod_{i\in A_j\setminus K}\left(1-P^E_{i,j}\right)$. Among these $|K|$ channels, SU j selects the channel that can maximize its throughput (i.e., $\max_{i\in K}\{U_{i,j}\}$). Due to mis-detection, the transmission of SU j in channel $\arg\max_{i\in K}\{U_{i,j}\}$ may not always be successful. Hence, the expected throughput of SU j is given by

$$U_j(A_j) = \sum_{K\subseteq A_j}\left(\left(\prod_{i\in K}P^E_{i,j}\prod_{i\in A_j\setminus K}\left(1-P^E_{i,j}\right)\right)\times\frac{P^U_{j,\,\mathrm{argmax}_{i\in K}\{U_{i,j}\}}}{P^E_{j,\,\mathrm{argmax}_{i\in K}\{U_{i,j}\}}}\max_{i\in K}\{U_{i,j}\}\right). \tag{20}$$

where $P^U_{j,\,\mathrm{argmax}_{i\in K}\{U_{i,j}\}}/P^E_{j,\,\mathrm{argmax}_{i\in K}\{U_{i,j}\}}$ denotes the probability that SU j can successfully transmit data over this channel. Note that the expected throughput of SU j increases with the cardinality of set A_j.

An energy-constrained SU should limit the energy spent on sensing and save its energy for data transmission. The power consumption consists of the sensing power consumption and the data transmission power consumption. The energy that SU j spends to sense channel i is $E^s_{i,j} = W_{s,i,j}\delta$, where $W_{s,i,j}$ denotes the sensing power of SU j to channel i. Similarly, the energy spent by SU j on data transmission over channel i is $E^t_{i,j} = W_{t,i,j}t_{i,j}$, where $W_{t,i,j}$ is the transmission power of SU j on

channel i. As a result, the expected power consumption of SU j is a function of the set of channels A_j that it prefers to sense, which is given by

$$E_j\left(A_j\right) = \frac{1}{T}\Bigg(\sum_{K\subseteq A_j}\Bigg(\Big(\prod_{i\in K} P_{i,j}^{E}\prod_{i\in A_j\setminus K}\left(1-P_{i,j}^{E}\right)\Big) \times E^{t}_{j,\,\mathrm{argmax}_{i\in K}\{U_{i,j}\}}\Bigg) + \sum_{i\in A_j} E_{i,j}^{s}\Bigg). \tag{21}$$

Energy efficiency is used as a metric to evaluate an SUs' decision on cooperation. The expected energy efficiency of SU j is defined as [34]

$$\eta_j\left(A_j\right) = \frac{U_j\left(A_j\right)}{E_j\left(A_j\right)}. \tag{22}$$

Each SU aims to maximize its throughput subject to an energy efficiency constraint. When the traffic demand of an energy-constrained SU is low, it may prefer not to participate in the cooperative sensing, as the cost of participating in the cooperation outweighs the payoff. The energy saved can be used to transmit data when there are enough information bits in the buffer. Hence, the problem that how each SU should cooperate with other SUs to sense the channels needs to be addressed.

Overlapping Coalitional Game for Cooperation Strategy

In this subsection, the CSSA problem is formulated as an NTU overlapping coalitional game. Each SU makes its own decision on coalition formation based on the move rules, which take into account both social welfare and individual payoff. An OCF algorithm is proposed to enable SUs to form a stable coalition structure, and a SCF algorithm is proposed to reduce the number of iterations and information exchange among the SUs.

NTU Overlapping Coalitional Game Formation

In this cooperative spectrum sensing and access strategy, the SUs can choose multiple channels and contribute to multiple coalitions, so as to maximize their expected throughput while satisfying the energy efficiency requirements. The SUs that participate in sensing, the same channel forms a coalition. If the channel is detected as idle, the SUs in the coalition share the spectrum resource. Thus, it can be formulated as an overlapping coalitional game where an SU is allowed to join multiple coalitions, and each coalition is formed on one channel that the SU prefers to sense. As the payoff of an SU in one coalition is constrained by its traffic demand,

the utility obtained by an SU in an overlapping coalition game cannot be transferred to other SUs. As a result, this overlapping coalitional game is an NTU game. The NTU overlapping coalitional game [35] is defined as follows:

Definition 8. An NTU overlapping coalitional game $G = (N, v)$ is given by a set of players $N = \{1, \ldots, |N|\}$ and a function $v : S \rightarrow \mathbb{R}^{|S|}$, where $S \subseteq N$ denotes a coalition formed by players and $v(\emptyset) = \mathbf{0}$.

The players of this game are $|N|$ SUs, and they form different coalitions to sense and access different channels. The coalition value is defined as the expected payoff that each SU can obtain in the coalition. Hence, $v(S_i) = (x_j(S_i), \forall j \in S_i)$, where value function v maps each coalition $S \subseteq N$ to an $|S|$-dimensional vector and $x_j(S_i) = P_{i,j}^U U_{i,j}$ is the payoff of SU j in coalition S_i. In a DCF game, a coalition structure is a partition of N [36]. The SUs in an overlapping coalitional game can join multiple coalitions at the same time. The definition of the coalition structure Π in an overlapping coalitional game [37] is given as follows:

Definition 9. An overlapping coalition structure Π over a player set N is defined as a set $\Pi = \{S_1, \ldots, S_{|K|}\}$, where $|K|$ is the number of coalitions. $\forall\ 1 \leq i \leq |K|$, $S_i \subseteq N$ and $\cup_{i=1}^{|K|} S_i = N$. Since coalitions can be overlapped, $\exists\ S_i, S_k \in \Pi, i \neq k$ such that $S_i \cap S_k \neq \emptyset$.

The SUs that choose to sense and access channel $i \in M$ form coalition S_i. On the other hand, the SUs with low-traffic demand may choose to stay in idle to save energy, and they form coalition $S_{|M|+1}$. Hence, the number of the coalitions $|K|$ in the system is equal to $|M| + 1$. Although more than one channel may be available for an SU in a time slot, the SU can only transmit data over one channel. Hence, the total payoff of an SU cannot be calculated by summing up its payoffs from all coalitions that it belongs to. The total payoff of SU j is defined as

$$p_j(\Pi) = \begin{cases} U_j(A_j), & \text{if } \eta_j(A_j) \geq \eta_{\min}, \\ -\infty, & \text{otherwise.} \end{cases} \tag{23}$$

The total payoff of SU j is equal to the expected throughput that it can obtain by choosing channel set A_j to sense, when the expected energy efficiency of SU j is greater than energy efficiency threshold $\eta_{\min}$. Otherwise, it is equal to negative infinity. This payoff definition guarantees that the expected energy efficiency of the SUs during the coalition formation process is not lower than threshold $\eta_{\min}$. The payoff of each SU in set $S_{|M|+1}$ is defined as zero. Each SU that belongs to set $S_{|M|+1}$ does not sense and access any channel and cannot join set $S_i, \forall\ i \in M$. Hence, $S_{|M|+1}$ is an isolated coalition, which does not overlap with any other coalitions.

The proposed preference order of the SUs takes into account both social welfare and individual payoff, which helps SUs compare two coalition structures and select the one that can provide more social welfare and individual payoff at the same time. The social welfare $u(\Pi)$ of a coalition structure Π is the value of coalition structure

Π, which is the sum of the payoff of each individual player. Hence,

$$u(\Pi) = \sum_{j \in N} p_j(\Pi). \tag{24}$$

The social welfare $u(\Pi)$ also represents the expected overall throughput of the SUs when the energy efficiency constraints are met. The preference order of the coalition structures is defined as follows, which takes into account both individual payoff and social welfare.

Definition 10. In an overlapping coalitional game $G = (N, v)$, given two coalition structures Π_p and Π_q over N, Π_p is j-preferred over Π_q, where $j \in N$ is equivalent to $p_j(\Pi_p) > p_j(\Pi_q)$ and $u(\Pi_p) > u(\Pi_q)$. This preference order is represented as

$$\Pi_p \succ_j \Pi_q \Leftrightarrow p_j(\Pi_p) > p_j(\Pi_q) \text{ and } u(\Pi_p) > u(\Pi_q). \tag{25}$$

Based on Definition 10, an SU prefers a coalition structure over another if and only if both the total payoff of the coalition structure and the individual payoff of the SU are increased. Such an preference order not only guarantees the increase of social welfare during the coalition formation but also keeps the spectrum efficiency above a certain level.

Coalition Formation Algorithms

During the process of overlapping coalition formation, each SU makes its own decision to join or leave a coalition based on the proposed preference order. Three move rules for the possible moves of each SU are defined as follows. First, the SU joins a new coalition that it does not belong to. Second, the SU leaves one of its current coalitions. Third, the SU switches from one of its current coalitions to a new coalition. The following three definitions provide the mechanisms for the SUs to form different coalitions by performing these moves.

Definition 11. *Join rule*: consider a coalition structure Π_p over a set of players N, where coalition $S_i \in \Pi_p$ and SU $j \in N \setminus S_i$. A new coalition structure is defined as $\Pi_q = \{\Pi_p \setminus S_i\} \cup \{S_i \cup \{j\}\}$. If $\Pi_q \succ_j \Pi_p$, SU j joins coalition S_i and coalition structure Π_p changes into coalition structure Π_q.

Based on Definitions 10 and 11, SU j in coalition structure Π_p, which does not belong to coalition S_i, joins coalition S_i in new coalition structure Π_q, if coalition structure Π_q is preferred by SU j over coalition structure Π_p. The join rule takes into account both the individual payoff and social welfare. An SU joins a new coalition if and only if both its payoff and the coalition structure value are improved by its move. Hence, SU j does not act selfishly without considering the effects of its move on other SUs.

Definition 12. *Quit rule* [29]: consider a coalition structure Π_p over a set of players N, where coalition $S_i \in \Pi_p$ and SU $j \in N \cap S_i$. A new coalition structure is defined as $\Pi_q = \{\Pi_p \setminus S_i\} \cup \{S_i \setminus \{j\}\}$. If $\Pi_q \succ_j \Pi_p$, then SU j leaves coalition S_i, and coalition structure Π_p changes into coalition structure Π_q.

Based on Definition 12, SU j leaves one of its current coalitions S_i and Π_p changes into Π_q if the newly formed coalition structure is preferred by SU j over the current one. SU j may prefer to leave coalition S_i to avoid a negative payoff in the following two situations. One is that there are too many SUs in coalition S_i to sense channel i, which leads to a low chance of assigning this channel to SU j. The other is that SU j has only several information bits to be transmitted in a time slot.

Definition 13. *Switch rule*: consider a coalition structure Π_p over a set of players N, where coalitions $S_i, S_k \in \Pi_p$ and SU $j \in N$ satisfy $j \in S_i$ and $j \notin S_k$. A new coalition structure is defined as $\Pi_q = \{\Pi_p \setminus \{S_i, S_k\}\} \cup \{S_i \setminus \{j\}\} \cup \{S_k \cup \{j\}\}$. If $\Pi_q \succ_j \Pi_p$, then SU j switches from coalition S_i to coalition S_k, and coalition structure Π_p changes into coalition structure Π_q.

Based on Definition 13, SU j switches from one of its coalitions to a new coalition when the new coalition structure is preferred over the current one. During the coalition structure formation, some channels may be chosen by many SUs, while some other channels are selected by few ones. An SU performs the switch move, when it notices that its payoff can be increased by switching from the coalition chosen by many SUs to another coalition selected by few SUs. As a result, the SUs autonomously distribute their contributions to different coalitions. In this way, the switch rule balances the size of different coalitions and improves the spectrum efficiency. The stability of an overlapping coalition structure is defined as follows:

Definition 14. An overlapping coalition structure Π over a set of players N is stable if any SU $j \in N$ such that $j \in S_i$ and $j \notin S_k$ for coalitions $S_i, S_k \in \Pi$, SU j will not deviate from coalition S_i or join coalition S_k.

Based on Definition 14, each SU $j \in N$ in a stable coalition structure will not leave any of its coalitions or join any new coalition. Therefore, all SUs do not make any change and stay in the current coalitions.

(1) Overlapping Coalition Formation (OCF) Algorithm

Algorithm 3 shows the proposed OCF algorithm, which can reach a stable coalition structure. The proposed algorithm is distributed and executed by each SU $j \in N$.

In Algorithm 3, all SUs are initialized to join quit sensing coalition $S_{|M|+1}$ (line 1). Then SU j exchanges the traffic demand information with other SUs by invoking functions j.broadcast() and j.receive() via a dedicated control channel (lines 2–3). At the beginning of each iteration, SU j randomly selects a coalition that it currently belongs to, denoted as S_k, and a new coalition it does not belong to, denoted as S_i (lines 5–10). SU j calculates its resulted payoff if it leaves coalition S_k and the value of newly formed coalition structure Π_{Quit} according to Eqs. (22), (23) and (24) (lines 6–7). Similarly, SU j calculates its payoffs in potential new coalition structures Π_{Join} and Π_{Switch} due to join move and switch move, and the values of

Algorithm 3 The overlapping coalition formation (OCF) algorithm in CRN for SU $j \in N$

1: **Initialization**: $S_{|M|+1} := N$; $S_i := \emptyset$ for $i \in M$; $\Pi := \{S_1, \ldots, S_{|M|+1}\}$; $\Pi_\ell := \Pi$ for each SU $\ell \in N$.
2: SU j executes j.broadcast(j, D_j).
3: SU ℓ executes ℓ.receive(ℓ, D_ℓ) for each SU $\ell \in N \setminus \{j\}$.
4: **repeat**
5: SU j randomly selects $k \in A_j \cup \{|M|+1\}$ and $i \in M \setminus A_j$.
6: $\Pi_{Quit} := \{\Pi \setminus S_k\} \cup \{S_k \setminus \{j\}\}$.
7: SU j calculates $u(\Pi_{Quit})$ and $p_j(\Pi_{Quit})$.
8: $\Pi_{Join} := \{\Pi \setminus S_i\} \cup \{S_i \cup \{j\}\}$.
9: SU j calculates $u(\Pi_{Join})$ and $p_j(\Pi_{Join})$.
10: $\Pi_{Switch} := \{\Pi \setminus \{S_i,\ S_k\}\} \cup \{S_i \cup \{j\}\} \cup \{S_k \setminus \{j\}\}$.
11: SU j calculates $u(\Pi_{Switch})$ and $p_j(\Pi_{Switch})$.
12: **if** $\Pi_{Quit} \succ_j \Pi$ **then**
13: $\Pi_j := \Pi_{Quit}$; $u(\Pi_j) := u(\Pi_{Quit})$.
14: **else if** $\Pi_{Join} \succ_j \Pi$ **then**
15: $\Pi_j := \Pi_{Join}$; $u(\Pi_j) := u(\Pi_{Join})$.
16: **else if** $\Pi_{Switch} \succ_j \Pi$ **then**
17: $\Pi_j := \Pi_{Switch}$; $u(\Pi_j) := u(\Pi_{Switch})$.
18: **end if**
19: SU j executes j.broadcast$(j, \Pi_j, u(\Pi_j))$.
20: SU ℓ executes ℓ.receive$(\ell, \Pi_\ell, u(\Pi_\ell))$ for each SU $\ell \in N \setminus \{j\}$.
21: $T_{info} := \{\Pi_1, \ldots, \Pi_{|N|}\}$.
22: $\Pi := \arg\max_{\Pi_l \in T_{info}} \{u(\Pi_l)\}$.
23: **until** $\forall\ j \in N$, $\forall\ k \in A_j \cup \{|M|+1\}$ and $i \in M \setminus A_j$, $\Pi_{Quit} \not\succ_j \Pi$, $\Pi_{Join} \not\succ_j \Pi$, and $\Pi_{Switch} \not\succ_j \Pi$.
24: SU j executes j.sense(Π).
25: **if** SU j is assigned channel i **then**
26: SU j calculates $W_{t,i,j}^{opt}$ and transmits data with power $W_{t,i,j}^{opt}$.
27: **end if**

the coalition structures by Eqs. (22), (23) and (24) (lines 9–11), respectively. If the quit move improves the coalition structure, the coalition structure is updated (line 13). Otherwise, SU j considers join move (line 14) and switch move (line 16). After that, SU j updates the coalition structure and its value and exchanges the updated information with other SUs (lines 19–20). All the updated coalition structure information form a set T_{info} (line 21). The coalition structure with the greatest value is selected as the new coalition structure (line 22). The coalition formation process is repeated until all SUs do not deviate from their current coalitions or join other new coalitions (line 23). After the process converges to a stable coalition structure, SU j cooperatively senses the channels with other SUs in corresponding coalitions by invoking function j.sense(Π). During the spectrum access stage, if SU j is allocated a channel, it calculates the optimal transmission power $W_{t,i,j}^{opt}$ to minimize the energy consumption spent on data transmission. Finally, SU j transmits data with the optimal transmission power (line 26). In [38], an adaptive transmission power control scheme is proposed to calculate the optimal transmission power for each SU that has been assigned a channel.

The following theorem guarantees the convergence of the proposed OCF algorithm.

Theorem 2. *The proposed OCF algorithm converges to a stable overlapping coalition structure after a finite number of iterations.*

Proof. Please refer to [38].

According to Algorithm 3, each SUs seeks to increase both its individual utility and the value of the coalition structure in each iteration. Hence, the total payoff for SUs is always increased when the coalition structure Π changes. In addition, the proposed algorithm adapts to network changes (e.g., number of SUs, channel states). Specifically, the SUs adaptively change their cooperation strategies and form a stable coalition structure, when new SUs join in the network, more channels are available, or channel states vary.

(2) Sequential Coalition Formation (SCF) Algorithm

Although Algorithm 3 always converges, the number of iterations required to converge grows exponentially with the number of SUs. As a result, the SCF algorithm is proposed, which reduces the computational complexity and exchanges less information among SUs to form an overlapping coalition structure.

In a sequential game of coalition formation, the coalition structure is formed step by step. In each step, only one player can update the coalition structure according to the rule of order h. Once a player joins a coalition, it remains in the coalition. In the proposed SCF algorithm, the rule of order h depends the traffic demands of SUs. Specifically, the SU that has the highest traffic demand moves first. The active SU makes a decision to join multiple coalitions based on the current coalition structure. The active SU remains in these coalition once it has joined them.

Algorithm 4 shows the proposed SCF algorithm, where the SUs make distributed decisions on coalition formation. However, the behaviors of the SUs are coordinated by a central coordinator. First, each SU reports its traffic demand information to the central coordinator by invoking function j.broadcast() (line 2). The traffic demand information of different SUs forms vector D (line 4). A sorting function $H(X)$ is defined, which maps a vector X to a $|X|$-dimensional vector, and returns a vector with each element representing the sorted index of each X's element in a descending order. The coordinator calculates the rule of order ρ using function $H(D)$ and broadcasts the information of ρ to all SUs (line 5). Then, the coalition formation decision is made by SUs one by one based on ρ. In particular, SU $\rho(1)$ makes the first decision as it has the highest traffic demand and initializes the coalition structure by setting all SUs in quit sensing coalition $S_{|M|+1}$ (line 8). The active SU receives the updated information of Π from previously active SU by invoking function j.receive() (line 10). During the coalition formation process, each active SU checks all channels one by one to find new coalition. For a new channel i, the active SU can join coalition i or switch to coalition i if SU prefers to sense channel i. Assuming an active SU joins coalition S_i (line 13), the SU calculates the payoff and the value of the newly resulted coalition structure based on Eqs. (22), (23) and (24) (line 14). In addition, assuming the active SU switches from a randomly selected

Algorithm 4 The sequential coalition formation (SCF) algorithm in CRN

1: **for** each $j \in N$ **do**
2: SU j executes j.broadcast(j, D_j).
3: **end for**
4: $D := (D_1, D_2, \ldots, D_{|N|})$
5: Coordinator calculates $\rho := H(D)$ and broadcasts ρ to all SUs.
6: **for** $j = 1$ to $|N|$ **do**
7: **if** $j = 1$ **then**
8: SU $\rho(j)$ initializes $S_{|M|+1} := N$; $S_i := \emptyset$, $\forall i \in M$, and $\Pi := \{S_1, S_2, \ldots, S_{|M|+1}\}$.
9: **else**
10: SU j executes j.receive($\rho(j-1), \Pi$).
11: **end if**
12: **for** each $i \in M$ **do**
13: $\Pi_{Join} := \{\Pi \setminus S_i\} \cup \{S_i \cup \{\rho(j)\}\}$.
14: SU $\rho(j)$ calculates $u(\Pi_{Join})$ and $p_{\rho(j)}(\Pi_{Join})$.
15: SU $\rho(j)$ randomly selects $k \in A_{\rho(j)} \cup \{|M|+1\}$.
16: $\Pi_{Switch} := \{\Pi \setminus \{S_i, S_k\}\} \cup \{S_i \cup \{\rho(j)\}\} \cup \{S_k \setminus \{\rho(j)\}\}$.
17: SU $\rho(j)$ calculates $u(\Pi_{Switch})$ and $p_{\rho(j)}(\Pi_{Switch})$.
18: **if** $\Pi_{Join} \succ_{\rho(j)} \Pi$ **then**
19: $\Pi := \Pi_{Join}$.
20: **else if** $\Pi_{Switch} \succ_{\rho(j)} \Pi$ **then**
21: $\Pi := \Pi_{Switch}$.
22: **end if**
23: **end for**
24: **if** $j = |N|$ **then**
25: SU $\rho(j)$ executes $\rho(j)$.broadcast($\rho(j), \Pi$).
26: **else**
27: SU $\rho(j)$ executes $\rho(j)$.send($\rho(j), \rho(j+1), \Pi$).
28: **end if**
29: **end for**
30: **for** each $j \in N \setminus \{\rho(|N|)\}$ **do**
31: SU j executes j.receive($\rho(|N|), \Pi$).
32: **end for**
33: **for** each $j \in N$ **do**
34: SU j executes j.sense(Π).
35: **if** SU j is assigned channel i **then**
36: SU j calculates $W_{t,i,j}^{opt}$ and transmits data with power $W_{t,i,j}^{opt}$.
37: **end if**
38: **end for**

coalition that it belongs (line 15) to coalition S_i (line 16), the SU calculates SU's new payoff and the value of the potential new coalition structure resulting from switch move (line 17). If the resulted coalition structure due to join move Π_{Join} is preferred over the current coalition structure Π, the coalition structure is updated (line 19). On the other hand, if the join move cannot improve the coalition structure, the resulted structure by switch move Π_{Switch} is considered (line 20). After checking all new coalitions, the currently active SU $\rho(j)$ reports the updated information of Π to the next active SU $\rho(j+1)$ by invoking function j.send() (line 27). The last active SU broadcasts the final coalition structure to other SUs (line 25). After the coalition formation process, the SUs perform cooperative sensing in each coalition

according to the final coalition structure. During the transmission stage, the SUs transmit data with the optimal transmission power (lines 34–36).

Although the stability of the final coalition structure is not guaranteed in the SCF algorithm, it can achieve the same aggregate throughput as the OCF algorithm. In addition, the computational complexity of the SCF algorithm is lower than that of the OCF algorithm. As the active SU in the SCF algorithm checks each potential channel only once and makes one move, at most $|M||N|$ iterations are required when running the SCF algorithm. However, in the OCF algorithm, the formation of a coalition structure takes place every time when a new coalition structure is preferred over the current coalition structure. Hence, the number of possible overlapping coalition structures in the OCF algorithm is $2^{|M||N|}$, which is much larger than the number of iterations required in the SCF algorithm. Moreover, as each SU only needs to send the updated coalition structure to the next active SU, less information exchange is required by the SCF algorithm.

Performance Evaluation

In this subsection, the aggregate throughput of the proposed OCF and SCF algorithms is evaluated and compared to the DCF algorithm. In the DCF algorithm, each SU can only join at most one coalition. The base station is placed at the center of a 100 ×100 m square region, in which the SUs are randomly placed. The channel gain of the link between SU j and the base station is modeled as $|g_j|^2 = 1/d_j^n$, where d_j denotes the distance between SU j and the base station, and $n = 2$ is the path loss exponent. The number of packets generated by each SU within one time slot follows the Poisson distribution with rate $\lambda = 0.5$ packet per time slot. The number of sensing samples during the sensing period in one time slot is $N_s = 5000$. The probability of each channel being idle is randomly chosen between $[0.5, 1]$. The bandwidth of channel i, B_i, and noise power, $\sigma_{n,i}^2$, are set to be 100 kHz and 0.01 mW, respectively. A list of simulation parameters is summarized in Table 1.

Table 1 List of Simulation Parameters

Parameter	Value
Number of PUs (licensed channels) $\|M\|$	6
Number of SUs $\|N\|$	10
Target detection probability $\bar{P}_{d,i,j}$	0.99
Received SNR at each SU during the sensing stage $\gamma_{i,j}$	−15 dB
Sensing power of SU j on channel i $W_{s,i,j}$	50 mW
Slot duration T	100 ms
Sensing duration δ	5 ms
Packet size	20 kbit
Buffer size of each SU	200 kbit
Lower bound of the energy efficiency η_{min}	500 kbit/Joule

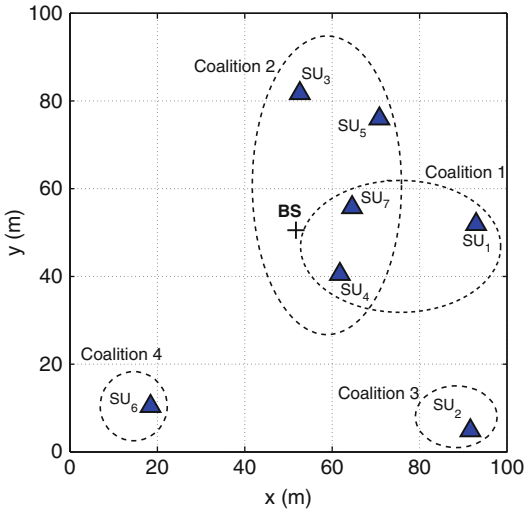

Fig. 4 An example of the stable overlapping coalition structure ($|M| = 3, |N| = 7$) by the OCF algorithm (Reproduced with permission from the IEEE)

Figure 4 shows a snapshot of a stable overlapping coalition structure obtained by using the proposed OCF algorithm, when there are 3 PUs and 7 SUs. The SUs within the same ellipse form a coalition. SUs 1, 4, and 7 form coalition 1 in channel 1. Similarly, SUs 3, 4, 5, and 7 form coalition 2 to sense and access channel 2. SU 2 forms a singleton coalition 3 to sense and access channel 3. SU 6 joins the coalition 4, which is the quit sensing coalition. Hence, the overlapping coalition structure can be expressed as $\Pi = \{\{1, 4, 7\}_1, \{3, 4, 5, 7\}_2, \{2\}_3, \{6\}_4\}$, in which coalitions 1 and 2 overlap with each other, and SUs 4 and 7 belong to both coalitions at the same time. Besides, SU 6 chooses not to cooperate with other SUs and joins the quit sensing coalition due to its low traffic demand.

Figure 5 illustrates the impact of the number of SUs $|N|$ on the aggregate throughput of SUs. Both the OCF and SCF algorithms outperform the DCF algorithm, as the chance of each SU to be assigned a channel is increased by allowing each SU to join multiple coalitions. However, in the DCF algorithm, an SU can only join one coalition and share one channel with other SUs, which limits the chance of being assigned a channel. Moreover, the performance of the SCF algorithm is slightly better than that of the OCF algorithm. This is because the SCF algorithm gives higher priorities to the SUs with greater traffic demands to join coalitions. As a result, these SUs have a higher chance to transmit data than those SUs with lower traffic demands.

Figure 6 shows the impact of the number of PUs $|M|$ (i.e., the number of channels) on the aggregate throughput of the SUs. The SCF algorithm obtains a slightly higher aggregate throughput than the OCF algorithm. The performance gap between the DCF algorithm and the proposed algorithm is small when $|M|$ is small and increases with $|M|$. This is because the SUs in the proposed OCF

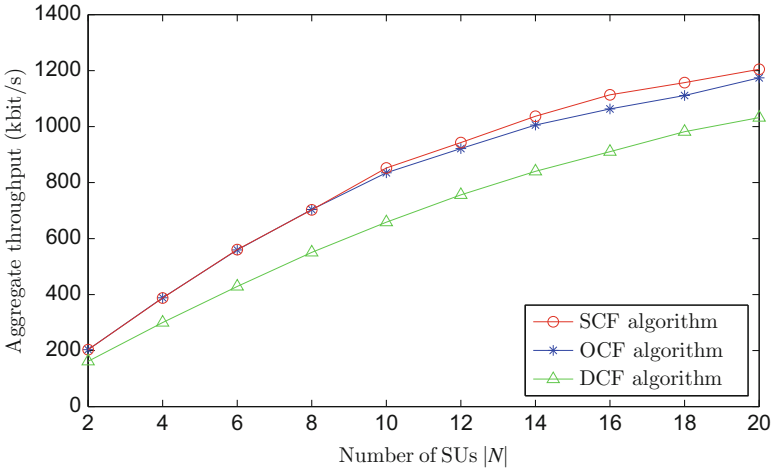

Fig. 5 Aggregate throughput versus the number of SUs in CRN for $|M| = 6$ (Reproduced with permission from the IEEE)

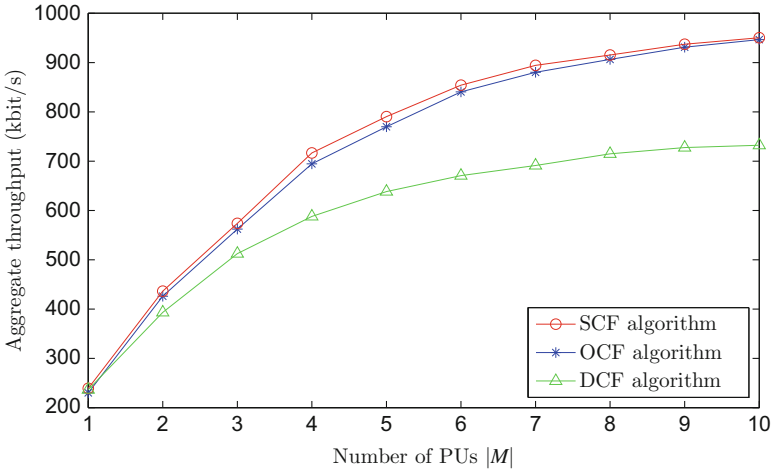

Fig. 6 Aggregate throughput versus the number of PUs in CRN for $|N| = 10$ (Reproduced with permission from the IEEE)

or SCF algorithm can obtain higher throughput when more channels are available by joining multiple coalitions. However, the SUs in the DCF algorithm obtain limited throughput improvement as each SU can sense and access at most one channel.

Conclusion and Future Directions

This chapter has studied cooperative spectrum sensing and access in a CRN with multiple licensed channels. A CSSA scheme has been proposed and formulated as a hedonic coalition formation game, in which the sensing accuracy and energy consumption are taken into account. The algorithm to find Nash-stable partition has been proposed. Simulation results showed that the proposed CSSA scheme outperforms the CPU and NSSA schemes. In addition, this chapter has proposed a traffic demand-based cooperative spectrum sensing and access scheme to achieve high throughput without degrading the energy efficiency. To solve this problem, an overlapping coalition game was formulated, where each SU is allowed to sense multiple channels. An OCF algorithm was proposed to find a stable coalition structure, which takes into account the individual payoff and social welfare. An SCF algorithm was also proposed to reduce the computational complexity and information exchange. Simulation results showed that the proposed OCF and SCF algorithms outperform the DCF algorithm in terms of the aggregate throughput.

In this chapter, all SUs are assumed to have the same sensing duration and sensing power. An extension to a more general setting is interesting but challenging, in which each SU can choose its sensing duration and sensing power as part of its strategy based on the network settings.

References

1. Cisco Systems (2016) Cisco visual networking index: global mobile data traffic forecast update 2015–2020
2. Haykin S (2005) Cognitive radio: brain-empowered wireless communications. IEEE J Sel Areas Commun 23(2):201–220
3. Federal Communications Commission (2005) Notice of proposed rule making and order: facilitating opportunities for flexible, efficient, and reliable spectrum use employing cognitive radio technologies. ET Docket (03–108):1–73
4. Akyildiz IF, Lo BF, Balakrishnan R (2011) Cooperative spectrum sensing in cognitive radio networks: a survey. Phys Commun 4(1):40–62
5. Gandetto M, Regazzoni C (2007) Spectrum sensing: a distributed approach for cognitive terminals. IEEE J Sel Areas Commun 25(3):546–557
6. Liang YC, Zeng Y, Peh EC, Hoang AT (2008) Sensing-throughput tradeoff for cognitive radio networks. IEEE Trans Wireless Commun 7(4):1326–1337
7. Park S, Hong D (2013) Optimal spectrum access for energy harvesting cognitive radio networks. IEEE Trans Wireless Commun 12(12):6166–6179
8. Zhang T, Tsang DH (2011) Cooperative sensing scheduling for energy-aware cognitive radio networks. In: Proceedings of the IEEE ICC, Kyoto
9. Lee WY, Akyildiz IF (2008) Optimal spectrum sensing framework for cognitive radio networks. IEEE Trans Wireless Commun 7(10):3845–3857
10. Zhao Q, Geirhofer S, Tong L, Sadler BM (2008) Opportunistic spectrum access via periodic channel sensing. IEEE Trans Signal Process 56(2):785–796
11. Bayhan S, Alagoz F (2013) Scheduling in centralized cognitive radio networks for energy efficiency. IEEE Trans Veh Technol 62(2):582–595
12. Sun X, Tsang DH (2013) Energy-efficient cooperative sensing scheduling for multi-band cognitive radio networks. IEEE Trans Wireless Commun 12(10):4943–4955

13. Gao Y, Xu W, Yang K, Niu K, Lin J (2013) Energy-efficient transmission with cooperative spectrum sensing in cognitive radio networks. In: Proceedings of the IEEE WCNC, Shanghai
14. Zheng L, Tan CW (2014) Maximizing sum rates in cognitive radio networks: convex relaxation and global optimization algorithms. IEEE J Sel Areas Commun 32(3):667–680
15. Zhai X, Zheng L, Tan CW (2014) Energy-infeasibility tradeoff in cognitive radio networks: price-driven spectrum access algorithms. IEEE J Sel Areas Commun 32(3):528–538
16. Li H, Cheng X, Li K, Xing X, Jing T (2013) Utility-based cooperative spectrum sensing scheduling in cognitive radio networks. In: Proceedings of the IEEE INFOCOM, Turin
17. Jiang C, Chen Y, Yang YH, Wang CY, Liu KR (2013) Dynamic chinese restaurant game in cognitive radio networks. In: Proceedings of the IEEE INFOCOM, Turin
18. Saad W, Han Z, Zheng R, Hjorungnes A, Basar T, Poor HV (2012) Coalitional games in partition form for joint spectrum sensing and access in cognitive radio networks. IEEE J Sel Top Sign Proces 6(2):195–209
19. Li D, Xu Y, Wang X, Guizani M (2011) Coalitional game theoretic approach for secondary spectrum access in cooperative cognitive radio networks. IEEE Trans Wireless Commun 10(3):844–856
20. Gozupek D, Eraslan B, Alagoz F (2012) Throughput satisfaction-based scheduling for cognitive radio networks. IEEE Trans Veh Technol 61(9):4079–4094
21. Cheung MH, Wong VWS, Schober R (2011) SINR-based random access for cognitive radio: distributed algorithm and coalitional game. IEEE Trans Wireless Commun 10(11):3887–3897
22. Jing T, Xing X, Cheng W, Huo Y, Znati T (2013) Cooperative spectrum prediction in multi-PU multi-SU cognitive radio networks. In: Proceedings of the IEEE CROWNCOM, Washington, DC
23. Wang T, Song L, Han Z, Saad W (2013) Overlapping coalitional games for collaborative sensing in cognitive radio networks. In: Proceedings of the IEEE WCNC, Shanghai
24. Zhang W, Letaief KB (2008) Cooperative spectrum sensing with transmit and relay diversity in cognitive radio networks. IEEE Trans Wireless Commun 7(12):4761–4766
25. Atapattu S, Tellambura C, Jiang H (2011) Energy detection based cooperative spectrum sensing in cognitive radio networks. IEEE Trans Wireless Commun 10(4):1232–1241
26. Simeone O, Stanojev I, Savazzi S, Bar-Ness Y, Spagnolini U, Pickholtz R (2008) Spectrum leasing to cooperating secondary ad hoc networks. IEEE J Sel Areas Commun 26(1):203–213
27. Saad W, Han Z, Debbah M, Hjorungnes A, Basar T (2009) Coalitional game theory for communication networks. IEEE Signal Process Mag 26(5):77–97
28. Ray D (2007) A game-theoretic perspective on coalition formation. Oxford University Press, Oxford
29. Hao X, Cheung MH, Wong VWS, Leung VCM (2012) Hedonic coalition formation game for cooperative spectrum sensing and channel access in cognitive radio networks. IEEE Trans Wireless Commun 11(11):3968–3979
30. Bogomolnaia A, Jackson MO (2002) The stability of hedonic coalition structures. Games Econ Behav 38(2):201–230
31. Lo BF, Akyildiz IF, Al-Dhelaan AM (2010) Efficient recovery control channel design in cognitive radio ad hoc networks. IEEE Trans Veh Technol 59(9):4513–4526
32. Zhang X, Su H (2011) CREAM-MAC: cognitive radio-enabled multi-channel MAC protocol over dynamic spectrum access networks. IEEE J Sel Top Sign Proces 5(1):110–123
33. Peh E, Liang YC (2007) Optimization for cooperative sensing in cognitive radio networks. In: Proceedings of the IEEE WCNC, Hong Kong
34. Miao G, Himayat N, Li YG, Swami A (2009) Cross-layer optimization for energy-efficient wireless communications: a survey. Wirel Commun Mob Comput 9(4):529–542
35. Chalkiadakis G, Elkind E, Markakis E, Polukarov M, Jennings NR (2010) Cooperative games with overlapping coalitions. J Artif Intell Res 39(1):179–216
36. Shoham Y, Leyton-Brown K (2008) Multiagent systems: algorithmic, game-theoretic, and logical foundations. Cambridge University Press, Cambridge

37. Zhang Z, Song L, Han Z, Saad W, Lu Z (2013) Overlapping coalition formation games for cooperative interference management in small cell networks. In: Proceedings of the IEEE WCNC, Shanghai
38. Dai Z, Wang Z, Wong VWS (2015) An overlapping coalitional game for cooperative spectrum sensing and access in cognitive radio networks. IEEE Trans Veh Technol 65(10):8400–8413

Contract-Based Secondary Spectrum Trading

32

Lin Gao, Xinbing Wang, Youyun Xu, and Qinyu Zhang

Contents

L. Gao · Q. Zhang (✉)
School of Electronic and Information Engineering, Harbin Institute of Technology, Shenzhen, China
e-mail: gaolin@hitsz.edu.cn; zqy@hit.edu.cn

X. Wang
EE and CS Department in School of Electronic Information and Electrical Engineering, Shanghai Jiao Tong University, Shanghai, China
e-mail: xwang8@sjtu.edu.cn

Y. Xu
National Engineering Research Center for Communications and Networking, Nanjing University of Posts and Telecommunications, Nanjing, China
e-mail: yyxu@njupt.edu.cn

W. Zhang (ed.), *Handbook of Cognitive Radio*,
https://doi.org/10.1007/978-981-10-1394-2_31

Abstract

Secondary spectrum trading is a promising solution to address the economic incentive issue in dynamic spectrum access, by allowing primary users (PUs) to sell the underutilized spectrum to secondary users (SUs) for the temporary access. This chapter studies a *monopoly* secondary spectrum market with a single PU (seller) and multiple heterogeneous SUs (buyers), where SUs have different preferences for spectrum access quality. The key focus is to study the optimal trading mechanism for the PU (that maximizes his profit) under information symmetry or asymmetry, depending on whether the preference of each SU is public information (hence can be observed by the PU) or private information (hence cannot be observed by the PU). The key solution idea to this PU-profit maximization problem is a contract-based spectrum trading mechanism, in which the PU offers a list of quality-price combinations (called a *contract*) for SUs, and each SU chooses the proper quality and price according to his (private or public) preference information. The optimal design for this contract-based trading mechanism consists of two steps: (i) analyze the incentive compatibility (IC) and individual rationality (IR) for feasible contracts, which guarantee the truthful information disclosure of SUs, and (ii) derive the optimal contract that maximizes the PU's profit under each information scenario, based on the IC and IR analysis in the first step. Simulations show that the optimal contract can increase the PU's payoff significantly.

Keywords

Cognitive radio · Dynamic spectrum access · Secondary spectrum sharing · Contract theory · Incentive mechanism

Introduction

Nowadays, wireless spectrum resource is becoming more and more scarce with the explosive growth of wireless services and mobile devices [1]. On the other hand, however, many licensed spectrum bands are often in a low utilization rate (efficiency) due to the temporal and spatial variation of licensed users' behaviors. Taking the VHF/UHF band (licensed for broadcast television services) as an example, it is largely unused during midnight to morning, and the average utilization rate is lower than 40% in many countries [2]. Therefore, it is highly desirable to open the underutilized licensed spectrum for the secondary utilization of unlicensed users who are starving for spectrum. As a consequence, FCC in the USA and Ofcom in UK have approved the license-exempt use of the *unused* or *underutilized* spectrum in the VHF/UHF band (called TV white space [3]) to support new wireless

applications [4, 5]. However, without a proper incentive mechanism, the licensed users may not be willing to open and share their spectrum with others due to the potential interference they may suffer from. This motivates the study of incentive mechanism and secondary spectrum trading in this chapter.

Motivations

Cognitive radio-based dynamic spectrum access (DSA) [6–8] has been recognized as a promising technology for improving the spectrum efficiency and alleviating the spectrum scarcity, by allowing unlicensed secondary users (SUs) access the under-utilized spectrum of licensed primary users (PUs) opportunistically. Obviously, the successful implementation of DSA requires to solve many technical challenges (e.g., how to explore and exploit the idle licensed spectrum efficiently and how to avoid the harmful interference to PUs) as well as economic challenges (e.g., how to incentivize PUs to share their idle spectrum with SUs).

While most of the existing works focused on the technical issues of DSA (e.g., spectrum sensing [9], allocation [10–12], and sharing [13]), this chapter focuses on the economic incentive issue in DSA. In particular, how to incentivize PUs to open their idle licensed spectrum for the secondary access of SUs. Some recent studies have been devoted to the incentive issue in DSA and proposed various incentive mechanisms, including cooperative spectrum sharing [14–18] and secondary spectrum trading [19–29].

In [14–18], authors proposed a *cooperative spectrum sharing* mechanism, in which SUs relay the traffic of PUs in exchange for the opportunities to access the PUs' licensed spectrum. With the cooperative spectrum sharing, PUs can increase their service qualities through the cooperative relay of SUs, and SUs can obtain the opportunities of accessing the PUs' licensed spectrum. Hence, PUs can obtain the necessary incentive to open their spectrum for SUs under a proper mechanism design. However, this mechanism needs to exchange a large amount of control signals between PUs and SUs (e.g., to formulate the cooperative PU-SU pair and to determine their cooperation details) and hence will introduce a large communication overhead. Moreover, it requires strict time synchronization between a pair of cooperative PU and SU. Both limit the use of this mechanism in practice.

In [19–25], authors proposed a *secondary spectrum trading* market, in which PUs directly lease the unused or underutilized licensed spectrum to SUs for the temporary access. Inspired by the classic market theory and numerous maths tools in economics, they proposed various trading mechanisms (e.g., auction, wholesale pricing, and usage-based pricing) for different market scenarios ranging from monopoly market to competitive market. With the secondary spectrum trading, PUs can achieve additional profit directly from the unused or underutilized spectrum, and meanwhile the total spectrum efficiency can be improved. In [26–29], authors further studied the secondary spectrum trading market for TV white space networks. However, the above works considered neither the quality and/or price discrimination in the trading of spectrum nor the information asymmetry between PUs and SUs.

Contributions

This chapter studies a *monopoly* secondary spectrum market with a single PU selling his idle (licensed) spectrum to multiple heterogeneous SUs for the temporary access, where SUs have different efficiencies in accessing spectrum, hence different preferences for spectrum quality. Such a spectrum access efficiency or quality preference is referred to as the *type* of SU. The *quality* of spectrum denotes the constraints (for SUs) of using the spectrum: a higher quality implies a looser constraint. The PU can sell the spectrum to different SUs in different qualities and prices, leading to the *quality and price discrimination spectrum trading*. Our focus is to study the optimal trading mechanisms for the PU (maximizing his profit) under both information symmetry and asymmetry (between the PU and SUs).

Under *information symmetry*, the preference information (i.e., type) of each SU is public information and can be observed by the PU directly. In this case, the PU can derive the best quality and price for each SU (with a particular type) directly, while each SU can only decide whether to accept the quality and price assigned to him. Hence, the optimal trading mechanism that maximizes the PU's profit can be derived by solving the best quality and price for each SU separately.

Under *information asymmetry*, however, the preference information (i.e., type) of each SU is his private information and cannot be observed by the PU. In this case, the PU cannot derive the best quality and price for each SU directly, due to the lack of the SU's preference information. To solve this problem, the *contract theory* [30], a Nobel Prize (in Economics) awarded theory in 2016, is introduced for eliciting the private information of each SU. More specifically, the key solution idea is to propose a contract-based spectrum trading mechanism, in which the PU offers a list of quality-price combinations (called a *contract*) for SUs, each intended for one type of SUs; and each SU chooses the proper quality and price (which can be different from those intended for his type) according to his private preference information. A contract is *incentive compatible* (IC), if each SU can achieve the maximum payoff when choosing the quality and price designed for his type. A contract is *individually rational* (IR), if each SU can achieve a non-negative payoff when choosing the quality and price designed for his type. Obviously, only under a feasible contract that satisfies IC and IR, each SU will choose the quality and price designed for his type. Hence, IC and IR guarantee the acceptance and truthful information disclosure of SUs. This chapter will first design the feasible contracts that satisfy IC and IR and then derive the optimal (and feasible) contract that maximizes the PU's profit.

In summary, the key results and contributions of this chapter are as follows:

- *Model and Solution Novelty:* Study a general monopoly secondary spectrum market, taking the user heterogeneity and information asymmetry into consideration. Contract theory, a Nobel Prize awarded theory, is introduced to solve the PU's profit maximization problem under information asymmetry.

- *Multiple Information Scenarios:* Study the optimal contract design under two typical information scenarios: information symmetry and information asymmetry, depending on whether the PU can observe the type of each SU. Hence, the analysis can be applied to a wide range of situations.
- *Optimal Contract Design:* Design the optimal contract systematically. First, the feasible contracts satisfying IC and IR are designed (to guarantee the truthful information disclosure of SUs). Then, within the feasible contract set, the optimal (and feasible) contract is derived (to maximize the PU's profit).
- *Performance Evaluation:* Simulations show that the optimal contract under information asymmetry can increase the PU's payoff significantly and can achieve 60% $\sim$ 70% of the optimal performance under information symmetry.

The rest of this chapter is organized as follows. Section "System Model and Contract Formulation" provides the system model. Section "Contract Formulation" provides the contract formulation. Sections "Optimal Contract Under Information Symmetry" and "Optimal Contract Under Information Asymmetry" study the optimal contract designs under information symmetry and asymmetry, respectively. Section "Contract Design in Continuous SU-Type Model" extends the discrete SU-type model to the continuous SU-type model. Section "Simulation Results" presents the simulation results, and Section "Conclusion" concludes this work.

System Model and Contract Formulation

Consider a cognitive radio network with a single PU and multiple SUs, where the PU shares the underutilized licensed spectrum with SUs for the temporary access. The PU can be a licensed potable device (e.g., a smartphone), a licensed infrastructure (e.g., a base station) serving multiple subscribers in a small area or even a primary network consisting of multiple infrastructures and serving many subscribers in a wide area. Each SU can be an unlicensed potable device (e.g., a laptop) or infrastructure (e.g., an unlicensed access point) serving multiple unlicensed subscribers. The PU owns some licensed spectrum bands (called *channels*) but not fully utilizes them, while SUs are starving for spectrum but do not have any licensed spectrum channel. Hence, the PU can potentially sell the unused or underutilized channels to SUs for the temporary access, leading to a *monopoly* secondary spectrum market, where the PU is the *monopolist* in the market.

The licensed channels of the PU are *homogeneous*, in the sense that they are in the same frequency band with the same bandwidth and time length. Different channels are orthogonal, and hence the transmissions on different channels do not interfere with each other. Each SU desires for one channel for his service, and multiple SUs can operate on the same channel without mutual interference if they are far enough from each other. Moreover, the PU has sufficient idle channels for SUs such that each SU can get one channel without interference with any other SU.

PU Model

To protect the quality of service (QoS) of the PU, SUs can only access the PU's channels with the specific constraints specified by the PU, such as the maximum transmission power (as required by FCC [4] and Ofcom [5]) and the fast backoff mechanism (to avoid collision with the PU when the PU reoccupies a channel). Obviously, a looser constraint imposed on a channel implies a higher quality of the channel for SUs, as they have more freedom to use the channel. Without loss of generality, in this chapter the *quality* of a channel is defined as the *maximum allowable transmission power of SUs on that channel*. In this sense, a higher-quality channel implies that SUs can transmit with a larger power on that channel. Note that the whole analysis can be applied to a general quality definition.

As the monopolist in the market, the PU can specify the quality $q \geq 0$ and price $\pi \geq 0$ of the channels to be sold to SUs, while SUs decide whether to buy a channel. For the quality q, it further satisfies: $0 \leq q \leq Q_{\max}$, where $Q_{\max}$ is the maximum achievable transmission power of SUs' devices. Moreover, a zero quality $q = 0$ implies that the SU cannot use the channel. Hence, if an SU chooses a zero quality $q = 0$, it is equivalent to say that he decides *not* to buy a channel.

When selling a channel with a quality q to an SU at a price π, the PU's profit (defined as *payoff*) can be computed as follows:

$$R(q, \pi) = \pi - C(q), \tag{1}$$

where π and $C(q)$ are the PU's revenue and cost when selling a channel with quality q to an SU. Here the cost $C(q) \geq 0$ captures the QoS degradation of the PU due to the potential interference and collision of the SU.

It is easy to see that when selling a channel with a higher-quality q to an SU, the PU will incur a higher QoS degradation or cost $C(q)$ potentially. This is because a higher-channel quality implies that the SU can use the channel with less constraint (e.g., larger transmission power), hence imposing a higher interference or collision to the PU potentially. Thus, it is reasonable to assume that:

- $C(q)$ is non-negative and monotonically increases with q.

To facilitate the analysis, we further assume that

- $C(q)$ is a convex function of q.

This implies that $C(q)$ tends to grow faster with the increasing of q. Suppose $C(q)$ is twice differentiable. Let $C'(q) \triangleq \frac{\partial C(q)}{\partial q}$ and $C''(q) \triangleq \frac{\partial^2 C(q)}{\partial q^2}$ denote the first- and second-order derivatives of $C(q)$ with respect to q. Then, the above assumptions can be formally written as: $C'(q) > 0$ and $C''(q) \geq 0$, for all $q \in [0, Q_{\max}]$.

SU Model

When an SU gets a licensed channel from the PU, he can achieve a certain benefit from using that channel. Such a benefit mainly depends on the amount of data that the SU can transmit on that channel, which is highly related to the data rate or channel capacity that the SU can achieve. Moreover, when using a channel with quality q, the maximum channel capacity that an SU can achieve (when transmitting with the maximum allowable transmission power q) is

$$\Phi(\theta, q) = \log(1 + q \cdot \theta) \tag{2}$$

where $\theta \triangleq \frac{1}{|L|} \cdot \frac{1}{|I|+\sigma^2}$ is the SU's signal-to-noise ratio (SNR) under a unit transmission power, called the *efficiency factor*. Here the channel bandwidth is normalized to be one; σ^2 is the average background noise power, which is identical for all SUs on all channels; $|I|$ is the aggregate interference, which may come from the PU, other SUs, or even outside systems operating on the same frequency band; $|L|$ is the average path loss (signal attenuation) of the SU, which depends on both the transmission range and the antenna technology. For example, an SU transmitting a longer distance often has a larger path loss than transmitting a shorter distance; an SU using a directional antenna with an advanced beamforming technology often has a smaller path loss than using an omnidirectional antenna.

Due to the channel homogeneity, each SU has the same pass loss factor L and aggregate interference I on different channels and hence has the same efficiency factor θ on all channels. It is worth noting that different SUs may have different efficiency factors θ, due to the different path loss factors L and/or aggregate interferences I. Such an efficiency factor θ captures not only the SU's efficiency in accessing spectrum but also his *preference* for spectrum access quality. For example, an SU with a higher efficiency θ has a stronger preference for high quality, as he can achieve a higher capacity gain from a quality improvement.

For convenience, the efficiency factor θ of an SU is also referred to as his *type*. SUs are categorized into different classes according to their efficiency factors or types. Namely, the SUs in the same class have the same efficiency factor or type θ, while the SUs in different classes have different efficiency factors or types. Let Θ denote the set of all SU types, and $|\Theta|$ denote the number of types. Let $f_\theta, \forall \theta \in \Theta$, denote the percentage of type-θ SUs among all SUs, where $0 \leq f_\theta \leq 1$ and $\sum_{\theta \in \Theta} f_\theta = 1$. Then, the number of type-θ SUs can be computed by

$$N_\theta = N \cdot f_\theta, \quad \forall \theta \in \Theta,$$

where N is the total number of SUs and $\sum_{\theta \in \Theta} N_\theta = N$. It is easy to see that this is a discrete SU-type model, where each SU's type is chosen from a discrete set Θ. Later section "Contract Design in Continuous SU-Type Model" will extend the above discrete SU-type model to the continuous SU-type model, where the SU-type set Θ is a continuous region.

The *utility* of a type-θ SU from a channel with quality q, denoted by $U(\theta, q)$, is the benefit that he can achieve from using that channel, which can be defined as a strictly increasing function of channel capacity $\Phi(\theta, q)$. Without loss of generality, the utility $U(\theta, q)$ is defined as a linear function of capacity $\Phi(\theta, q)$ as follows:

$$U(\theta, q) = w \cdot \Phi(\theta, q) = w \cdot \log(1 + q \cdot \theta), \tag{3}$$

where $w > 0$ is a constant evaluation factor, indicating the benefit for SUs from one unit of channel capacity. Note that w is a predefined parameter and identical for all SUs. In the rest of this chapter, w will be normalized to be one, i.e., $w = 1$.

The *payoff* of a type-θ SU achieved from purchasing a channel with quality q at price π, denoted by $V(\theta, q, \pi)$, is defined as the difference between the achieved utility and the payment for the channel, i.e.,

$$V(\theta, q, \pi) = U(\theta, q) - \pi = w \cdot \log(1 + q \cdot \theta) - \pi. \tag{4}$$

It is easy to see that the utility $U(\theta, q)$ of SUs increases with the channel quality q, and the increase rate tends to be smaller with the increasing of q. That is,

- $U(\theta, q)$ is a non-negative, concave, and increasing function of q.

Suppose $U(\theta, q)$ is twice differentiable. Let $U'(\theta, q) \triangleq \frac{\partial U(\theta, q)}{\partial q}$ and $U''(\theta, q) \triangleq \frac{\partial^2 U(\theta, q)}{\partial q^2}$ denote the first- and second-order derivatives of $U(\theta, q)$ with respect to q. Then, the above observation can be formally written as $U'(\theta, q) > 0$ and $U''(\theta, q) \leq 0$, for all $q \in [0, Q_{\max}]$.

Social Welfare

The *social welfare* is defined as the aggregate payoff of all involved players, including the PU and all SUs. Specifically, when selling a channel with a quality q to a type-θ SU at a price π, the total generated social welfare is:

$$W(\theta, q) = R(q, \pi) + V(\theta, q, \pi) = U(\theta, q) - C(q), \tag{5}$$

where the price π in both payoff functions cancels each other out.

It is easy to see that $W''(\theta, q) \leq 0, \forall q \in [0, Q_{\max}]$, since $U''(\theta, q) \leq 0$ and $C''(q) \geq 0$, where $W''(\theta, q) \triangleq \frac{\partial^2 W(\theta, q)}{\partial q^2}$ is the second-order derivatives of $W(\theta, q)$ with respect to q. That is, the social welfare $S(\theta, q)$ is a concave function of q. Thus, the socially optimal quality for a type-θ SU, i.e., that maximizes the social welfare $W(\theta, q)$, can be solved by the following first-order condition:

$$U'(\theta, q) - C'(q) = 0.$$

Let $q^\circ(\theta)$ denote the socially optimal quality for a type-θ SU derived by the above first-order condition, and $W^\circ(\theta) = W(\theta, q^\circ(\theta))$ denote the corresponding optimal social welfare generated by a type-θ SU. It is easy to check that both $q^\circ(\theta)$ and $W^\circ(\theta)$ monotonically increase with θ. In other words, from a social perspective, the optimal qualities for SUs with different types are different: a higher type (efficiency) SU will be assigned with a higher-quality channel. This implies that offering different qualities for different types of SUs (i.e., *quality discrimination*) is desired from a social perspective.

Problem Description

As mentioned previously, the PU's decision is to specify the quality and price of the channels to be sold to SUs, and moreover, the quality discrimination is desired from a social perspective. Specifically, with the *quality discrimination* spectrum trading, the PU can offer multiple quality and price choices to SUs, and each SU decides not only whether to buy a channel but also which quality and price he would like to choose (when deciding to buy a channel).

The focus of this chapter is to design the optimal trading mechanism (i.e., the sets of quality and price choices to be offered to SUs) for the PU that maximizes his payoff (profit). The problem is challenging, especially under *information asymmetry*, where the type of each SU is his private information and cannot be observed by the PU. We will study the PU's profit maximization problem under both information symmetry (in section "Optimal Contract Under Information Symmetry") and information asymmetry (in section "Optimal Contract Under Information Asymmetry"), by using the *contract theory* [30]. Contract theory is a widely used theoretic tool in economics and often studies how economic actors can and do construct contractual arrangements, generally in the presence of asymmetric information. Recently, contract theory has also been introduced to solve various wireless communication and networking problems, e.g., cooperative spectrum sharing [14], secondary spectrum trading [23–25], TV white space networking [29], and WiFi community networking [31].

Contract Formulation

As mentioned early, with the *quality discrimination* spectrum trading, the PU can offer multiple quality and price choices to SUs, while each SU decides whether to buy a channel, and if so, which quality and price he would like to choose.

Notice that the SUs in the same class (i.e., those with the same type θ) are homogeneous, in the sense that they have the same preference, decision, utility/payoff functions, and social impact. This implies that it is sufficient for the PU to design one quality and one price for *each class of SUs* (with the same type), instead of for each SU. Let $q(\theta)$ and $\pi(\theta)$ denote the quality and price designed for

the type θ SUs. The set of all quality and price combinations (each for one type of SUs) is called a *contract*, denoted by

$$\Psi \triangleq \{(q(\theta), \pi(\theta)),\ \theta \in \Theta\}, \tag{6}$$

where each quality and price combination $(q(\theta), \pi(\theta))$ is called a *contract item* (for type θ SUs). The aim of the PU (and also the focus of this chapter) is to design the optimal contract that maximizes his profit.

It is important to note that without a proper contract design, a type-θ SU may not be willing to accept a contract item $(q(\theta), \pi(\theta))$ designed for his type θ. For example, if a contract item $(q(\theta), \pi(\theta))$ brings a negative payoff for a type-θ SU, then none of the type-θ SUs are willing to accept it; if a contract item $(q(\theta), \pi(\theta))$ has a higher quality and lower price than another one $(q(\theta'), \pi(\theta'))$, i.e., $q(\theta) > q(\theta')$ and $\pi(\theta) < \pi(\theta')$, then none of the type-$\theta'$ SUs are willing to choose the contract item $(q(\theta'), \pi(\theta'))$. Therefore, a joint design of $q(\theta)$ and $\pi(\theta)$ for all $\theta \in \Theta$ is necessary. This leads to the important concept of *feasible contract*.

Definition 1 (Feasibility). A contract $\Psi = \{(q(\theta), \pi(\theta)), \theta \in \Theta\}$ is feasible, if each SU of type θ is willing to choose the contract item $(q(\theta), \pi(\theta))$ designed for his type θ (hence truthfully reveal his type information).

Note that the feasibility constraint is different under different information scenarios. Specifically, under information symmetry, the PU can observe the type of each SU and hence can assign a specific contract item to each type of SUs. Thus, the feasibility constraint can be satisfied, if each SU of type θ can achieve a non-negative payoff under the contract item $(q(\theta), \pi(\theta))$ assigned to him. This condition is often referred to as the *individual rationality* (IR) [30]. Formally,

Definition 2 (Individual Rationality – IR [30]). A contract $\Psi = \{(q(\theta), \pi(\theta)), \theta \in \Theta\}$ is individually rational, if for all $\theta \in \Theta$,

$$V(\theta, q(\theta), \pi(\theta)) \geq 0. \tag{7}$$

Under information asymmetry, the PU cannot observe the type of each SU and hence cannot assign a specific contract item to each type of SUs. Instead, the PU can only offer all contract items for all SUs, while let SUs choose the best contract items according to their private-type information. Thus, the feasibility constraint can be satisfied, if each SU of type θ can achieve not only the non-negative payoff (IR condition) but also the best payoff among all contract items, under the contract item $(q(\theta), \pi(\theta))$ designed for his type. The latter condition is often referred to as the *incentive compatibility* (IC) [30]. Formally,

Definition 3 (Individual Compatibility – IC [30]). A contract $\Psi = \{(q(\theta), \pi(\theta)), \theta \in \Theta\}$ is incentive compatible, if for all $\theta \in \Theta$,

$$V(\theta, q(\theta), \pi(\theta)) \geq V(\theta, q(\theta'), \pi(\theta')), \quad \forall \theta' \in \Theta, \theta' \neq \theta. \tag{8}$$

Intuitively, under information symmetry, a contract is feasible if it satisfies the IR condition, while under information asymmetry, a contract is feasible only if it satisfies both the IR and IC conditions. Under a feasible contract Ψ, the payoff of the PU can be computed as follows:

$$R(\Psi) = \sum_{\theta \in \Theta} N_\theta \cdot R(q(\theta), \pi(\theta)) = \sum_{\theta \in \Theta} N_\theta \cdot (\pi(\theta) - C(q(\theta))), \tag{9}$$

where N_θ is the number of type-θ SUs. Note that (9) is only available under a feasible contract, where each type-θ SU chooses the contract item $(q(\theta), \pi(\theta))$ designed for his type θ. For an arbitrary contract, however, the PU payoff may not be the form of (9), due to the uncertainty of SUs' choices. This introduces an additional challenge in finding the optimal contract for the PU.

One effective way to resolve this challenge is the *revelation principle* [32], a fundamental principle in mechanism design. Specifically, revelation principle states that for an arbitrary mechanism, the designer can always find a feasible mechanism (where users truthfully report their types) that achieves the same outcome and payoff. By the revelation principle, the PU can restrict his search within the feasible contracts, in which every SU will choose the contract item designed for his type. In other words, the PU can focus on the optimal contract within the feasible contract set, which can achieve the same outcome as a globally optimal contract.

Definition 4 (Optimality). A contract $\Psi = \{(q(\theta), \pi(\theta)), \theta \in \Theta\}$ is optimal, if it is feasible, and meanwhile maximizes the PU payoff given in (9).

Let $\Psi^* = \{(q^*(\theta), \pi^*(\theta)), \theta \in \Theta\}$ denote the optimal contract (within the feasible contract set). Then, it can be formally derived as follows:

$$\begin{aligned} \max_{\Psi} \quad & R(\Psi) = \sum_{\theta \in \Theta} N_\theta \cdot (\pi(\theta) - C(q(\theta))) \\ \text{s.t.} \quad & \Psi \text{ is feasible.} \end{aligned} \tag{10}$$

The feasibility constraint guarantees that each SU is willing to choose the contract item designed for his type; hence the PU payoff can be written as $R(\Psi)$ in (9). As mentioned previously, under information symmetry, it can be satisfied if the IR condition holds, while under information asymmetry, it can be satisfied only if both the IR and IC conditions hold.

Optimal Contract Under Information Symmetry

This section studies the optimal contract design under information symmetry, where the type of each SU is public information and can be observed by the PU. In this case, the PU can assign a specific contract item to each type of SUs, and each SU can only decide whether to accept the quality and price designed for his type. Thus, the

feasibility constraint can be satisfied if each SU can achieved a non-negative payoff under the contract item assigned to him (IR condition); and the optimal contract can be derived by solving the best contract item for each type of SUs separately.

Feasibility of Contract

Under information symmetry, the feasibility of contract can be achieved if the IR condition holds. That is, each SU of type θ can achieve a non-negative payoff under the contract item $(q(\theta), \pi(\theta))$ assigned to him.

Lemma 1. *A contract $\Psi = \{(q(\theta), \pi(\theta)), \theta \in \Theta\}$ is feasible under information symmetry, if and only if the following IR conditions hold:*

$$U(\theta, q(\theta)) - \pi(\theta) \geq 0, \quad \forall \theta \in \Theta.$$

where $U(\theta, q(\theta)) = w \cdot \log(1 + q(\theta) \cdot \theta)$ is the utility of SU defined in (3).

Intuitively, under information symmetry, each SU has only two choices: accept or reject the contract item assigned to him. The latter choice implies that the SU decides not to buy a channel, leading to a zero payoff for the SU. Thus, each SU is willing to accept a contract item if it brings a non-negative payoff for the SU.

Optimality of Contract

The optimal contract can be derived by solving the best quality and price for each type of SUs separately. Formally, for a type-θ SU, the best quality and price, denoted by $q^\dagger(\theta)$ and $\pi^\dagger(\theta)$, can be derived as follows:

$$\begin{aligned} \max_{\{q(\theta), \pi(\theta)\}} \quad & R(q(\theta), \pi(\theta)) = \pi(\theta) - C(q(\theta)) \\ s.t. \quad & U(\theta, q(\theta)) - \pi(\theta) \geq 0; \\ & \pi(\theta) \geq 0, \quad Q_{\max} \geq q(\theta) \geq 0. \end{aligned} \tag{11}$$

Here $U(\theta, q(\theta)) - \pi(\theta) \geq 0$ is the IR condition, which guarantees the feasibility of contract. Let $R^\dagger(\theta) \triangleq R(q^\dagger(\theta), \pi^\dagger(\theta))$ denote the solution of (11), i.e., the maximum payoff that the PU can achieved from a type-θ SU.

To solve (11), it is notable that given any feasible quality $q(\theta)$, the best price strategy for the PU is to charge a price as high as the SU's utility $U(\theta, q(\theta))$, i.e., $\pi^\dagger(\theta) = U(\theta, q(\theta))$. Substitute the above best price into (11), the best quality $q^\dagger(\theta)$ can be solved in the following way:

$$\begin{aligned} \max_{\{q(\theta)\}} \quad & U(\theta, q(\theta)) - C(q(\theta)) \\ s.t. \quad & Q_{\max} \geq q(\theta) \geq 0. \end{aligned} \tag{12}$$

Note that $U(\theta, q(\theta)) - C(q(\theta))$ is exactly the social welfare defined in (5). Thus, the above (12) is exactly the social welfare maximization problem, and the best quality $q^\dagger(\theta)$ is equivalent to the corresponding socially optimal quality $q^\circ(\theta)$. Formally,

Lemma 2. *The optimal contract* $\Psi^\dagger = \{(q^\dagger(\theta), \pi^\dagger(\theta)), \theta \in \Theta\}$ *under information symmetry is given by*

$$q^\dagger(\theta) = q^\circ(\theta) \ \text{ and } \ \pi^\dagger(\theta) = U(\theta, q^\circ(\theta)), \quad \forall \theta \in \Theta.$$

where $q^\circ(\theta)$ *is the socially optimal quality for a type-*θ *SU.*

Intuitively, when the PU can observe the type information of SUs, he can design such an optimal contract, which assigns each SU the corresponding socially optimal quality (hence generates as much social welfare as possible) and charges each SU as high as possible (up to the SU's achieved utility). Thus, the maximum payoff $R^\dagger(\theta)$ that the PU can achieved from a type-θ SU is exactly the maximum social welfare $W^\circ(\theta)$ that can be achieved from a type-θ SU, i.e., $R^\dagger(\theta) = W^\circ(\theta)$.

Optimal Contract Under Information Asymmetry

This section studies the optimal contract design under information asymmetry, where the type of each SU is his private information and cannot be observed by the PU. In this case, the PU cannot assign a specific contract item to each SU; instead, he can only offer all contract items for all SUs, while let SUs choose the best contract items according to their private-type information. Thus, the feasibility constraint can be satisfied if each SU can achieve not only a non-negative payoff (IR condition) but also the best payoff among all contract items (IC condition), under the contract item designed for his type. Accordingly, the optimal contract needs to solve the best contract items for all SU types jointly.

Suppose there is a total of T SU classes (types), with θ_t denoting the type of SUs in the t-th class. Then, the set of SU types can be written as $\Theta = \{\theta_1, \cdots, \theta_T\}$. Assume that $\theta_1 < \theta_2 < \cdots < \theta_T$ without loss of generality. For notational convenience, denote $f_t = f_{\theta_t}$ and $N_t = N_{\theta_t}$ as the percentage and the number of type-θ_t SUs (in the t-th class), respectively, and $q_t = q(\theta_t)$ and $\pi_t = \pi(\theta_t)$ as the quality and price designed for type θ_t SUs, respectively. Then, a contract can be rewritten as

$$\Psi \triangleq \{(q_t, \pi_t),\ t \in \{1, \cdots, T\}\}.$$

Accordingly, the contract optimization problem (10) can be rewritten as

$$\max_{\Psi} \ R(\Psi) = \sum_{t=1}^{T} N_t \cdot (\pi_t - C(q_t)) \qquad (13)$$

$$\text{s.t. IR and IC conditions.}$$

Before discussing the feasibility and optimality of contract, we first introduce the following important property for the utility model: when increasing a quality with a

given value, the utility improvement for a higher-type user is greater than that for a lower-type user. This property is refereed as the *increasing preference* (IP).

Definition 5 (Increasing Preference – IP). Let $u(\theta, q)$ denote the utility of a type-θ user for quality q. Then, the utility model satisfies the property of increasing preference (IP), if for any $\theta > \theta'$ and $q > q'$, the following conditions hold:

$$u(\theta, q) - u(\theta, q') > u(\theta', q) - u(\theta', q'). \tag{14}$$

That is, a higher-type user can achieve a larger utility gain from a given quality improvement than a lower-type user.

It is easy to see that the SU's utility $U(\theta, q)$ defined in (3) satisfied the above IP property. Namely, when increasing the quality with a given value, a higher-type SU (who has a higher efficiency factor) can achieve a larger utility gain than a lower type SU (who has a lower efficiency factor).

In what follows, we will first provide the necessary and sufficient conditions for feasible contracts and then find the optimal contract within the feasible contract set.

Feasibility of Contract

Under information asymmetry, the feasibility of contract can be achieved only if both IR and IC conditions hold. That is, each SU of type θ can achieve not only a non-negative payoff but also the best payoff among all contract items, under the contract item $(q(\theta), \pi(\theta))$ assigned to him.

First, we show the necessary conditions for a contract to be feasible.

Lemma 3. *If a contract* $\Psi = \{(q_t, \pi_t),\ t \in \{1, \cdots, T\}\}$ *is feasible under information asymmetry, then the following necessary conditions hold:*

$$q_i > q_j \quad \textit{if and only if} \quad \pi_i > \pi_j, \quad \forall i, j \in \{1, \cdots, T\},\ i \neq j.$$

Proof. Notice that if a contract is feasible under information asymmetry, it must satisfy the IR and IC conditions defined in (7) and (8).

$\rightarrow$: In this direction, we will show: if $q_i > q_j$, then $\pi_i > \pi_j$. By the IC condition defined in (8), the following condition holds for each type-θ_j SU:

$$U(\theta_j, q_j) - \pi_j \geq U(\theta_j, q_i) - \pi_i,$$

or equivalently,

$$\pi_i - \pi_j \geq U(\theta_j, q_i) - U(\theta_j, q_j) > 0,$$

where the second inequality follows because $U(\theta, q)$ strictly increases with q.

$\leftarrow$: In this direction, we will show: if $\pi_i > \pi_j$, then $q_i > q_j$. By the IC condition defined in (8), the following condition holds for each type-θ_i SU:

$$U(\theta_i, q_i) - \pi_i \geq U(\theta_i, q_j) - \pi_j,$$

or equivalently,

$$U(\theta_i, q_i) - U(\theta_i, q_j) \geq \pi_i - \pi_j > 0,$$

which implies that $q_i > q_j$, as $U(\theta, q)$ strictly increases with q. □

Lemma 3 provides an important property of a feasible contract: *a higher quality must be associated with a higher price*. This lemma also implies that if there exist two qualities (or prices) with the same value, then the associated prices (or qualities) are also the same value. Formally,

Corollary 1. *For any feasible contract* $\Psi = \{(q_t, \pi_t),\ t \in \{1, \cdots, T\}\}$ *under information asymmetry, the following conditions hold:*

$$q_i = q_j \quad \textit{if and only if} \quad \pi_i = \pi_j, \quad \forall i, j \in \{1, \cdots, T\},\ i \neq j.$$

Lemma 4. *If a contract* $\Psi = \{(q_t, \pi_t),\ t \in \{1, \cdots, T\}\}$ *is feasible under information asymmetry, then the following necessary conditions hold:*

$$\textit{if} \quad \theta_i > \theta_j, \quad \textit{then} \quad q_i \geq q_j \quad \forall i, j \in \{1, \cdots, T\},\ i \neq j.$$

Proof. Assume, to the contrary, that there exist $\theta_i > \theta_j$ and $q_i < q_j$. Then, by the IP property defined in (14), the following condition holds:

$$U(\theta_i, q_j) - U(\theta_i, q_i) > U(\theta_j, q_j) - U(\theta_j, q_i)$$

By the IC condition in (8), the following condition holds for each type-θ_i SU,

$$U(\theta_i, q_i) - \pi_i \geq U(\theta_i, q_j) - \pi_j,$$

and for each type-θ_j SU,

$$U(\theta_j, q_j) - \pi_j \geq U(\theta_j, q_i) - \pi_i.$$

Combine the above two IC conditions, we obtain:

$$U(\theta_i, q_j) - U(\theta_i, q_i) \leq U(\theta_j, q_j) - U(\theta_j, q_i),$$

which violates the IP property given above. □

Lemma 4 provides another important property of a feasible contract: *a higher-type SU must be assigned with a higher quality (and also a higher price by Lemma 3)*. Recall that the type of an SU reflects the SU's transmission efficiency, and the quality of a channel reflects the constraint on using the channel. Thus, this lemma implies that the SUs with a higher efficiency can use the channels with a less constraint, which coincides with the social expectation.

Recall that $\theta_1 < \theta_2 < \cdots < \theta_T$. According to Lemmas 3 and 4, a feasible contract $\Psi = \{(q_t, \pi_t),\ t \in \{1, \cdots, T\}\}$ has the following structure:

$$q_1 \leq q_2 \leq \ldots \leq q_T \quad \text{and} \quad \pi_1 \leq \pi_2 \leq \ldots \leq \pi_T, \tag{15}$$

with $q_t = q_{t+1}$ if and only if $\pi_t = \pi_{t+1}$.

Next, we show the sufficient conditions for a contract to be feasible.

Lemma 5. *A contract $\Psi = \{(q_t, \pi_t),\ t \in \{1, \cdots, T\}\}$ is feasible under information asymmetry, if the following sufficient conditions hold:*

$$0 \leq q_1 \leq \cdots \leq q_T \leq Q_{\max} \tag{16}$$

and

$$\begin{cases} 0 \leq \pi_t \leq U(\theta_1, q_1), & t = 1 \\ \pi_{t-1} + A \leq \pi_t \leq \pi_{t-1} + B, & t = 2, \cdots, T \end{cases} \tag{17}$$

where $A \triangleq U(\theta_{t-1}, q_t) - U(\theta_{t-1}, q_{t-1})$ and $B \triangleq U(\theta_t, q_t) - U(\theta_t, q_{t-1})$.

Proof. Prove the lemma by induction. Define a new contract

$$\Psi_{(k)} \triangleq \{(q_t, \pi_t),\ t \in \{1, \ldots, k\}\},$$

which consists of the first k contract items in the original contract Ψ, for the first k types of SUs in the system. Obviously, $\Psi_{(T)} = \Psi$. By induction, the contract Ψ or $\Psi_{(T)}$ is feasible, if the following two conditions hold: (a) $\Psi_{(1)}$ is feasible, and (b) If $\Psi_{(k)}$ is feasible, then $\Psi_{(k+1)}$ is also feasible, for all $k = 1, \cdots, T-1$.

Proof for (a): $\Psi_{(1)}$ is feasible. Since there is only one contract item (q_1, π_1) in $\Psi_{(1)}$ and one SU type θ_1, the sufficient condition for the contract $\Psi_{(1)}$ to be feasible is only the IR condition in (7). By (16) and (17), it is easy to see that: $V(\theta_1, q_1, \pi_1) = U(\theta_1, q_1) - \pi_1 \geq 0$, that is, the IR condition holds, hence $\Psi_{(1)}$ is feasible.

Proof for (b): if $\Psi_{(k)}$ is feasible, then $\Psi_{(k+1)}$ is also feasible, for all $k = 1, \cdots, T-1$. Notice that $\Psi_{(k)}$ consists of the first k contract items in Ψ for the first k types of SUs, while $\Psi_{(k+1)}$ consists of the first $k+1$ contract items in Ψ for the first $k+1$ types of SUs. Thus, to prove that $\Psi_{(k+1)}$ is feasible, we need to show:

- (b.1) For the newly joined SUs with type θ_{k+1}, the IR and IC conditions hold:

$$\begin{aligned} &U(\theta_{k+1}, q_{k+1}) - \pi_{k+1} \geq 0, \\ &U(\theta_{k+1}, q_{k+1}) - \pi_{k+1} \geq U(\theta_{k+1}, q_i) - \pi_i, \quad \forall i = 1, \cdots, k. \end{aligned} \tag{18}$$

- (b.2) For the existing SUs with types $\theta_1, \cdots, \theta_k$, the IC conditions hold:

$$U(\theta_i, q_i) - \pi_i \geq U(\theta_i, q_{k+1}) - \pi_{k+1}, \quad \forall i = 1, \cdots, k. \tag{19}$$

  Note that the IR conditions for the exiting SUs are naturally satisfied by the feasibility of $\Psi_{(k)}$.

Proof for (b.1): the IC and IR conditions for the new SUs with type θ_{k+1}. Since $\Psi_{(k)}$ is feasible, the following IC conditions must hold for the type-θ_k SUs:

$$U(\theta_k, q_k) - \pi_k \geq U(\theta_k, q_i) - \pi_i, \quad \forall i = 1, \cdots, k.$$

According to (17), i.e., $\pi_{k+1} \leq \pi_k + U(\theta_{k+1}, q_{k+1}) - U(\theta_{k+1}, q_k)$, we have:

$$U(\theta_k, q_k) + U(\theta_{k+1}, q_{k+1}) - U(\theta_{k+1}, q_k) \geq U(\theta_k, q_i) - \pi_i + \pi_{k+1}, \ \forall i = 1, \cdots, k.$$

With simple transformation, the above condition can be written as:

$$U(\theta_{k+1}, q_{k+1}) - \pi_{k+1} \geq U(\theta_k, q_i) - U(\theta_k, q_k) + U(\theta_{k+1}, q_k) - \pi_i, \ \forall i = 1, \cdots, k.$$

Notice that $\theta_{k+1} > \theta_k$ and $q_k \geq \cdots \geq q_1$. By the IP property, we have:

$$U(\theta_k, q_i) - U(\theta_k, q_k) + U(\theta_{k+1}, q_k) \geq U(\theta_{k+1}, q_i), \ \forall i = 1, \cdots, k.$$

Based on the above, we can prove the IC conditions for the new type θ_{k+1}:

$$U(\theta_{k+1}, q_{k+1}) - \pi_{k+1} \geq U(\theta_{k+1}, q_i) - \pi_i, \ \forall i = 1, \cdots, k.$$

Notice that $U(\theta_{k+1}, q_i) - \pi_i \geq U(\theta_i, q_i) - \pi_i$ for any $i \leq k$ and $U(\theta_i, q_i) - \pi_i \geq 0$ by the feasibility of $\Psi_{(k)}$. Then, using the above IC conditions, we can prove the IR conditions for the new type θ_{k+1}:

$$U(\theta_{k+1}, q_{k+1}) - \pi_{k+1} \geq 0.$$

Proof for (b.2): the IC conditions for the exiting SUs with types $\theta_1, \cdots, \theta_k$ under the new contract $\Psi_{(k+1)}$. Since $\Psi_{(k)}$ is feasible, the following IC conditions must hold for all the existing SUs with types $\theta_1, \cdots, \theta_k$:

$$U(\theta_i, q_i) - \pi_i \geq U(\theta_i, q_k) - \pi_k, \quad \forall i = 1, \cdots, k.$$

According to (17), i.e., $\pi_k + U(\theta_k, q_{k+1}) - U(\theta_k, q_k) \leq \pi_{k+1}$, we have:

$$U(\theta_i, q_i) - \pi_i \geq U(\theta_i, q_k) + U(\theta_k, q_{k+1}) - U(\theta_k, q_k) - \pi_{k+1}, \quad \forall i = 1, \cdots, k.$$

Notice that $\theta_{k+1} > \theta_k > \cdots > \theta_1$ and $q_{k+1} \geq q_k \geq \cdots \geq q_1$. By IP property, we have:

$$U(\theta_i, q_k) + U(\theta_k, q_{k+1}) - U(\theta_k, q_k) \geq U(\theta_i, q_{k+1}), \quad \forall i = 1, \cdots, k.$$

Based on the above, we can prove the IC conditions for the existing types $\theta_1, \cdots, \theta_k$:

$$U(\theta_i, q_i) - \pi_i \geq U(\theta_i, q_{k+1}) - \pi_{k+1}, \quad \forall i = 1, \cdots, k.$$

Up to now, we have proved that (a) $\Psi_{(1)}$ is feasible, and (b) If $\Psi_{(k)}$ is feasible, then $\Psi_{(k+1)}$ is also feasible. By induction, the contract $\Psi_{(T)}$ or Ψ is feasible. □

It is important to note that the sufficient conditions in Lemma 5 are also necessary for a feasible contract: the necessity of (16) can be proved by Lemma 4, and the necessity of (17) can be proved by the IC and IR conditions directly. Moreover, the conditions in Lemma 5 satisfy the feasible structure in (15). First, $q_k \geq q_{k-1}$ by (16); second, $\pi_k \geq \pi_{k-1}$ as $A \geq 0$; third, if $q_k = q_{k-1}$, then $A = B = 0$ and $\pi_k = \pi_{k-1}$ as $\pi_{k-1} \leq \pi_k \leq \pi_{k-1}$; and forth, if $\pi_k = \pi_{k-1}$, then $A \leq 0 \leq B$, which implies that $q_k \leq q_{k-1}$ and $q_k \geq q_{k-1}$; hence $q_k = q_{k-1}$. In fact, Lemma 5 provides more strict and tight necessary conditions for a feasible contract.

Optimality of Contract

To derive the optimal contract, we first derive the best price set under a given (feasible) quality set and then derive the best quality set. For notational convenience, let $\mathsf{Q} \triangleq \{q_t,\ t \in \{1, \cdots, T\}\}$ and $\mathsf{P} \triangleq \{\pi_t,\ t \in \{1, \cdots, T\}\}$ denote the quality set and the price set of a contract $\Psi = \{(q_t, \pi_t),\ t \in \{1, \cdots, T\}\}$, respectively. Then, a contract can also be written as $\Psi = \{\mathsf{Q},\ \mathsf{P}\}$.

By Lemma 5, a quality set Q is feasible, if and only if $0 \leq q_1 \leq \cdots q_T \leq Q_{\max}$ Let $R^*_{(\mathsf{Q})}$ denote the maximum payoff that the PU can achieve under a given feasible quality set Q, by optimizing the price set P solely. Let $\mathsf{P}^*_{(\mathsf{Q})} \triangleq \{\pi^*_t,\ t \in \{1, \cdots, T\}\}$ denote the best price set given the feasible quality set Q. Formally, the best price set $\mathsf{P}^*_{(\mathsf{Q})}$ and the maximum payoff $R^*_{(\mathsf{Q})}$ can be derived by

$$\begin{aligned} \max_{\mathsf{P}} \ & \sum_{t=1}^{T} N_t \cdot (\pi_t - C(q_t)) \\ \text{s.t.} \ & \text{The Conditions in (17).} \end{aligned} \tag{20}$$

The conditions in (17) are used to guarantee the feasibility of contract.

Lemma 6. *Given a feasible quality set* Q *with* $0 \le q_1 \le \cdots q_T \le Q_{\max}$, *the unique best price set* $\mathsf{P}^* \triangleq \{\pi_t^*,\ t \in \{1, \cdots, T\}\}$ *for problem* (20) *is given by*

$$\begin{cases} \pi_t^* = U(\theta_1, q_1), & t = 1; \\ \pi_t^* = \pi_{t-1}^* + U(\theta_t, q_t) - U(\theta_t, q_{t-1}), & t = 2, \cdots, T. \end{cases} \tag{21}$$

Proof. It is easy to check that the price set in (21) is a feasible price set, and thus the achieved contract (with the given quality set and the derived price set) is feasible. Note that this feasibility is necessary for the optimality.

Next we prove the optimality of the price set in (21). Notice that, given a feasible quality set $\mathsf{Q} = \{q_t,\ t \in \{1, \cdots, T\}\}$, the total cost $\sum_{t=1}^{T} N_t \cdot C(q_t)$ of the PU is a constant. Thus, the PU's profit maximization problem (20) can be transferred into the following revenue maximization problem (22):

$$\max_{\mathsf{P}} \sum_{t=1}^{T} N_t \cdot \pi_t \tag{22}$$
$$\text{s.t. The Conditions in (17).}$$

Assume, to the contrary, that there exists another feasible price set $\mathsf{P}' = \{\pi_t',\ t \in \{1, \cdots, T\}\}$, which is different from P^* in (21) and achieves $\sum_{t=1}^{T} N_t \pi_t' > \sum_{t=1}^{T} N_t \pi_t^*$. Then, there exists at least one price in P' larger than the corresponding price in P^*. Suppose $\pi_k' > \pi_k^*$ without loss of generality. By (17), the following condition must hold for π_k' (in order to guarantee the feasibility of contract):

$$\pi_k' \le \pi_{k-1}' + U(\theta_k, q_k) - U(\theta_k, q_{k-1}).$$

By (21), we have: $\pi_k^* - \pi_{k-1}^* = U(\theta_k, q_k) - U(\theta_k, q_{k-1})$. Thus,

$$\pi_k' \le \pi_{k-1}' + \pi_k^* - \pi_{k-1}^*,$$

or equivalently,

$$\pi_{k-1}' - \pi_{k-1}^* \ge \pi_k' - \pi_k^* > 0.$$

Continue the above process, we can finally reach $\pi_1' - \pi_1^* > 0$, which violates the IR condition for the type-θ_1 SUs. Namely, with a price $\pi_1' > \pi_1^* = U(\theta_1, q_1)$, a type-$\theta_1$ SU will not accept the price contract item (q_1, π_1') assigned to him. Therefore, there does *not* exist another feasible price set $\mathsf{P}' \ne \mathsf{P}^*$ such that $\sum_{t=1}^{T} N_t \pi_t' > \sum_{t=1}^{T} N_t \pi_t^*$, which implies that P^* is the best price set.

Then we prove that P^* in (21) is the unique best price set for (20). Assume, to the contrary, that there exists another feasible price set $\mathsf{P}' = \{\pi_t',\ t \in \{1, \cdots, T\}\}$, which is different from P^* in (21) and achieves the same maximum revenue, i.e., $\sum_{t=1}^{T} N_t \pi_t' = \sum_{t=1}^{T} N_t \pi_t^*$. Since $\mathsf{P}' \ne \mathsf{P}^*$, there exists at least one price in P'

different from the corresponding price in P^*. Suppose $\pi'_k \neq \pi^*_k$ without loss of generality. If $\pi'_k > \pi^*_k$, then we will finally reach $\pi'_1 - \pi^*_1 > 0$, using the similar analysis in the above. If $\pi'_k < \pi^*_k$, then there must exist another price $\pi'_j > \pi^*_j$ since $\sum_{t=1}^{T} N_t \pi'_t = \sum_{t=1}^{T} N_t \pi^*_t$. Similarly, we will finally reach $\pi'_1 - \pi^*_1 > 0$. Therefore, there does *not* exist another feasible price set $\mathsf{P}' \neq \mathsf{P}^*$ such that $\sum_{t=1}^{T} N_t \pi'_t = \sum_{t=1}^{T} N_t \pi^*_t$, which implies that P^* is the unique best price set. □

Lemma 6 states that, given any feasible quality set Q, the best price set P^* is unique and given by (21). By substituting the best price set P^* into (20), the best quality set $\mathsf{Q}^* \triangleq \{q^*_t,\ t \in \{1, \cdots, T\}\}$ can be derived as follows:

$$\max_{\mathsf{Q}} \ R^*_{(\mathsf{Q})} \triangleq \sum_{t=1}^{T} N_t \cdot (\pi^*_t - C(q_t)) \qquad \text{s.t. The Conditions in (16).} \tag{23}$$

The conditions in (16), i.e., $0 \leq q_1 \leq \cdots \leq q_T \leq Q_{\max}$, are used to guarantee the feasibility of contract.

Introduce the notations: $\Delta_1 = 0$ and $\Delta_t = U(\theta_t, q_t) - U(\theta_t, q_{t-1}), \forall t = 2, \ldots, T$. Then, the best price set P^* given in (21) can be rewritten as

$$\pi^*_t = U(\theta_1, q_1) + \sum_{k=1}^{t} \Delta_k, \quad \forall t = 1, \ldots, T. \tag{24}$$

Substitute (24) into (23), the PU's payoff $R^*_{(\mathsf{Q})}$ can be written as follows:

$$R^*_{(\mathsf{Q})} = \sum_{t=1}^{T} N_t \cdot \left(U(\theta_1, q_1) + \sum_{k=1}^{t} \Delta_k - C(q_t) \right), \tag{25}$$

where $\Delta_1 = 0$ and $\Delta_k = U(\theta_k, q_k) - U(\theta_k, q_{k-1}), \forall k = 2, \ldots, T$ as defined above. Rearranging the above equation by putting the terms associated with the same quality together, the PU's payoff $R^*_{(\mathsf{Q})}$ can be rewritten as follows:

$$R^*_{(\mathsf{Q})} = \sum_{t=1}^{T} \left(N_t \cdot U(\theta_t, q_t) - N_t \cdot C(q_t) + \Lambda_t \cdot \sum_{k=t+1}^{T} N_k \right) \tag{26}$$

where $\Lambda_t = U(\theta_t, q_t) - U(\theta_{t+1}, q_t), \forall t = 1, \cdots, T-1$, and $\Lambda_T = 0$. Introduce

$$G_t(q_t) \triangleq N_t \cdot U(\theta_t, q_t) - N_t \cdot C(q_t) + \Lambda_t \cdot \sum_{k=t+1}^{T} N_k.$$

Then, the PU's payoff $R^*_{(\mathsf{Q})}$ can be rewritten as $R^*_{(\mathsf{Q})} = \sum_{t=1}^{T} G_t(q_t)$. Accordingly, the optimization problem (23) can be rewritten as follows:

$$\begin{aligned} \max_{\mathsf{Q}} \quad & \sum_{t=1}^{T} G_t(q_t) \\ \text{s.t.} \quad & \text{The Conditions in (16).} \end{aligned} \tag{27}$$

It is worth noting that $G_t(q_t)$ depends only on the quality q_t, while independent of all other qualities $q_k, \forall k \neq t$. This implies that the optimization problem (27) can be solved by optimizing the quality q_t for each $G_t(q_t)$ separately. Let $\tilde{q}_t^*$, $t = 1, \cdots, T$, denote the quality that maximizes $G_t(q_t)$. That is,

$$\begin{aligned} \tilde{q}_t^* \triangleq \arg\max_{q_t} \quad & G_t(q_t) \\ \text{s.t.} \quad & 0 \leq q_t \leq Q_{\max}. \end{aligned} \tag{28}$$

Note that if the quality set $\widetilde{\mathsf{Q}}^* \triangleq \{\tilde{q}_t^*, \ t = 1, \cdots, T\}$ derived by (28) is a feasible quality set, i.e., satisfying the conditions in (16), then it is exactly the optimal solution of (23). This condition holds for a wide range of SU distributions. For example, with the uniform distribution, i.e., $N_1 = \cdots = N_T$ and $\theta_t - \theta_{t-1} = \delta, \forall t = 2, \cdots, T$, the quality set $\widetilde{\mathsf{Q}}^*$ derived by (28) satisfies the conditions in (16) and hence is the best quality set for the problem (23). Formally,

Theorem 1. *Suppose* $\widetilde{\mathsf{Q}}^* \triangleq \{\tilde{q}_t^*, \ t = 1, \cdots, T\}$ *derived by* (28) *is a feasible quality set satisfying the conditions in* (16)*. Then, the optimal contract* $\Psi^* = \{(q_t^*, \pi_t^*), \ t \in \{1, \cdots, T\}\}$ *under information asymmetry is given by*

$$q_t^* = \tilde{q}_t^* \quad \textit{and} \quad \pi_t^* = U(\theta_1, q_1^*) + \sum_{k=1}^{t} \Delta_k, \quad \forall t = 1, \ldots, T.$$

where $\Delta_1 = 0$ *and* $\Delta_k = U(\theta_k, q_k^*) - U(\theta_k, q_{k-1}^*), \forall k = 2, \ldots, T$.

In a general case, however, the quality set $\widetilde{\mathsf{Q}}^*$ derived by (28) may not satisfy the conditions in (16), hence not feasible. That is, there may exist two qualities $\tilde{q}_t^*$ and $\tilde{q}_{t-1}^*$ such that $\tilde{q}_t^* < \tilde{q}_{t-1}^*$. In this case, similar as in [25], an iterative algorithm can be used to adjust the quality set $\widetilde{\mathsf{Q}}^*$ such that it is feasible. The key idea is to optimize q_t and q_{t-1} together with the constraint $q_t \geq q_{t-1}$. Specifically, any infeasible qualities $\tilde{q}_t^*$ and $\tilde{q}_{t-1}^*$ with $\tilde{q}_t^* < \tilde{q}_{t-1}^*$ will be adjusted in the following way:

$$\begin{aligned} \{\tilde{q}_t^*, \tilde{q}_{t-1}^*\} \triangleq \arg\max_{\{q_t, q_{t-1}\}} \quad & G_t(q_t) + G_{t-1}(q_{t-1}) \\ \text{s.t.} \quad & 0 \leq q_{t-1} \leq q_t \leq Q_{\max}. \end{aligned} \tag{29}$$

Eventually, the feasible quality set $\widetilde{\mathbb{Q}}^*$ can be obtained, by repeating the above process to remove any infeasible quality bundle.

Contract Design in Continuous SU-Type Model

The previous sections study the optimal contract design in the discrete SU-type model with a finite set of SU types $\Theta = \{\theta_1, \cdots, \theta_T\}$. This section will extend such a discrete SU-type model to the continuous one, where the set of SU types Θ is a continuous region $[\theta_{\min}, \theta_{\max}]$. Note that the optimal contract design under information symmetry in the continuous SU-type model is totally same as that in the discrete model (section "Optimal Contract Under Information Symmetry"). Thus, this section will focus on the optimal contract design under information asymmetry in the continuous SU-type model.

Let $f(\theta)$ denote the probability distribution function (pdf) of θ in $\Theta = [\theta_{\min}, \theta_{\max}]$. With the continuous SU types in $\Theta = [\theta_{\min}, \theta_{\max}]$, a contract can be defined as

$$\Psi \triangleq \{(q(\theta), \pi(\theta)),\ \theta \in \Theta\}, \tag{30}$$

where $q(\theta)$ and $\pi(\theta)$ are continuous functions of θ in Θ. Under a feasible contract Ψ, the expected payoff (9) of the PU can be rewritten as

$$\begin{aligned} R(\Psi) &= \int_{\theta\in\Theta} R(q(\theta), \pi(\theta)) \cdot f(\theta) \mathrm{d}\theta \\ &= \int_{\theta\in\Theta} (\pi(\theta) - C(q(\theta))) \cdot f(\theta) \mathrm{d}\theta. \end{aligned} \tag{31}$$

Accordingly, the contract optimization problem (10) can be rewritten as

$$\begin{aligned} \max_{\Psi}\ & R(\Psi) = \int_{\theta\in\Theta} (\pi(\theta) - C(q(\theta))) \cdot f(\theta) \mathrm{d}\theta \\ \text{s.t.}\ & \Psi \text{ is feasible.} \end{aligned} \tag{32}$$

Following the structure of section "Optimal Contract Under Information Asymmetry", in what follows, we will first provide the necessary and sufficient conditions for feasible contracts and then find the optimal contract within the feasible contract set.

Feasibility of Contract

Intuitively, the continuous SU-type model can be achieved from a discrete model with an infinite number of types (i.e., $T \to \infty$) and an infinitesimal gap between any two successive types (i.e., $\theta_{t+1} - \theta_t \to 0$). Thus, the conditions in Lemmas 3, 4,

and 5 for the discrete SU-type model are also applicable to the continuous SU-type model, but with different forms.

Suppose that $q(\theta)$ and $\pi(\theta)$ are continuous and differentiable in Θ. Let $q'(\theta) \triangleq \frac{\partial q(\theta)}{\partial \theta}$ and $\pi'(\theta) \triangleq \frac{\partial \pi(\theta)}{\partial \theta}$ denote the first-order derivatives of $q(\theta)$ and $\pi(\theta)$ with respect to θ, respectively. Then, Lemmas 3, 4, and 5 can be rewritten as follows:

Lemma 7. *If a contract* $\{(q(\theta), \pi(\theta)),\ \theta \in \Theta\}$ *is feasible under information asymmetry, then the following necessary conditions hold:*

$$q'(\theta) > 0 \quad \textit{if and only if} \quad \pi'(\theta) > 0, \quad \forall \theta \in \Theta.$$

Lemma 8. *If a contract* $\{(q(\theta), \pi(\theta)),\ \theta \in \Theta\}$ *is feasible under information asymmetry, then the following necessary conditions hold:*

$$q'(\theta) \geq 0, \quad \forall \theta \in \Theta.$$

By Lemmas 7 and 8, the feasible contract structure in (15) can be rewritten as

$$q'(\theta) \geq 0 \quad \text{and} \quad \pi'(\theta) \geq 0, \quad \forall \theta \in \Theta, \tag{33}$$

with $q'(\theta) = 0$ if and only if $\pi'(\theta) = 0$.

Lemma 9. *A contract* $\{(q(\theta), \pi(\theta)),\ \theta \in \Theta\}$ *is feasible under information asymmetry, if and only if the following conditions hold:*

$$q'(\theta) \geq 0, \quad \forall \theta \in \Theta \tag{34}$$

and

$$\begin{cases} 0 \leq \pi(\theta_{\min}) \leq U(\theta_{\min}, q(\theta_{\min})) \\ \pi'(\theta) = U'(\theta, q(\theta)) \cdot q'(\theta), \quad \forall \theta \in \Theta \end{cases} \tag{35}$$

where $U'(\theta, q(\theta)) = \frac{\partial U(\theta, q)}{\partial q}|_{q=q(\theta)}$ *and* $q'(\theta) \triangleq \frac{\partial q(\theta)}{\partial \theta}$.

Proof. The first two conditions can be easily derived from the corresponding conditions in Lemma 5 for the discrete SU-type model. Therefore, we focus on proving the last condition, i.e., $\pi'(\theta) = U'(\theta, q(\theta)) \cdot q'(\theta),\ \forall \theta \in \Theta$.

As mentioned previously, the continuous SU-type model can be viewed as a discrete model with an infinitesimal gap between any two successive types, i.e., $\theta_t = \theta_{t-1} + \sigma$ where $\sigma \to 0$. Substitute the above θ_t and $\theta_{t-1} = \theta_t - \sigma$ into the third condition in Lemma 5, we can obtain the following condition:

$$\pi(\theta_t - \sigma) + A \leq \pi(\theta_t) \leq \pi(\theta_t - \sigma) + B, \tag{36}$$

where $A \triangleq U(\theta_t - \sigma, q(\theta_t)) - U(\theta_t - \sigma, q(\theta_t - \sigma))$ and $B \triangleq U(\theta_t, q(\theta_t)) - U(\theta_t, q(\theta_t - \sigma))$. From the right inequality of (36), we have:

$$\begin{aligned}\pi'(\theta_t) &= \lim_{\sigma \to 0} \frac{\pi(\theta_t) - \pi(\theta_t - \sigma)}{\sigma} \\ &\leq \lim_{\sigma \to 0} \frac{U(\theta_t, q(\theta_t)) - U(\theta_t, q(\theta_t - \sigma))}{\sigma} \\ &= \lim_{\sigma \to 0} \frac{U(\theta_t, q(\theta_t)) - U(\theta_t, q(\theta_t - \sigma))}{q(\theta_t) - q(\theta_t - \sigma)} \cdot \frac{q(\theta_t) - q(\theta_t - \sigma)}{\sigma} \\ &= U'(\theta_t, q(\theta_t)) \cdot q'(\theta_t).\end{aligned} \tag{37}$$

Similarly, from the left inequality of (36), we have:

$$\pi'(\theta_t) \geq U'(\theta_t - \sigma, q(\theta_t)) \cdot q'(\theta_t) = U'(\theta_t, q(\theta_t)) \cdot q'(\theta_t). \tag{38}$$

Combining the above two inequalities, we have:

$$\pi'(\theta_t) = U'(\theta_t, q(\theta_t)) \cdot q'(\theta_t), \quad \forall \theta_t \in \Theta.$$

Thus, we complete the proof by using the results in the discrete SU-type model. □

Note that Lemma 9 provides the feasible price function $\pi(\theta)$ with the first-order derivative indirectly. The explicit form of the feasible price function can be derived by using the integral calculus. Formally, for any $x \in \Theta$,

$$\begin{aligned}\pi(x) &= \int_{\theta_{\min}}^{x} \pi'(\theta) \mathrm{d}\theta + \pi(\theta_{\min}) \\ &= \int_{\theta_{\min}}^{x} U'(\theta, q(\theta)) \cdot q'(\theta) \mathrm{d}\theta + \pi(\theta_{\min}).\end{aligned} \tag{39}$$

The full derivative of $U(\theta, q(\theta))$ with respect to θ is:

$$\begin{aligned}\frac{\mathrm{d}U(\theta, q(\theta))}{\mathrm{d}\theta} &= \frac{\partial U(\theta, q(\theta))}{\partial \theta} + \frac{\partial U(\theta, q(\theta))}{\partial q(\theta)} \cdot \frac{\partial q(\theta)}{\partial \theta} \\ &= \frac{\partial U(\theta, q(\theta))}{\partial \theta} + U'(\theta, q(\theta)) \cdot q'(\theta).\end{aligned} \tag{40}$$

Substitute the above full derivative into (39), we have: for any $x \in \Theta$,

$$\begin{aligned}\pi(x) &= \int_{\theta_{\min}}^{x} \frac{\mathrm{d}U(\theta, q(\theta))}{\mathrm{d}\theta} - \frac{\partial U(\theta, q(\theta))}{\partial \theta}\mathrm{d}\theta + \pi(\theta_{\min}) \\ &= U(x, q(x)) - U(\theta_{\min}, q(\theta_{\min})) - \int_{\theta_{\min}}^{x} \frac{\partial U(\theta, q(\theta))}{\partial \theta}\mathrm{d}\theta + \pi(\theta_{\min}) \\ &= U(x, q(x)) - U(\theta_{\min}, q(\theta_{\min})) - \int_{\theta_{\min}}^{x} \frac{q(\theta)}{1 + q(\theta)\cdot\theta}\mathrm{d}\theta + \pi(\theta_{\min}),\end{aligned} \tag{41}$$

where the last line follows because $\frac{\partial U(\theta,q)}{\partial \theta} = \frac{\partial \log(1+q\cdot\theta)}{\partial \theta} = \frac{q}{1+q\cdot\theta}$.

Optimality of Contract

Similar as in section "Optimality of Contract", to derive the optimal contract, we first derive the best price function under a given (feasible) quality function and then derive the best quality function. Specifically, given a feasible quality function $q(\theta)$, the best price function $\pi^*(\theta)$ and the maximum payoff $R^*_{q(\theta)}$ can be derived by

$$\begin{aligned}\max_{\pi(\theta)} \quad & \int_{\theta\in\Theta} (\pi(\theta) - C(q(\theta)))\cdot f(\theta)\mathrm{d}\theta \\ \text{s.t.} \quad & \text{The Conditions in (35).}\end{aligned} \tag{42}$$

Similar as Lemma 6, the unique best price function $\pi^*(\theta)$ is given below.

Lemma 10. *Given a feasible quality function $q(\theta)$ with $q'(\theta) \geq 0, \forall\theta \in \Theta$, the unique best price function $\pi^*(\theta)$ for problem (42) is given by*

$$\pi^*(\theta) = U(\theta, q(\theta)) - \int_{\theta_{\min}}^{\theta} \frac{q(x)}{1 + q(x)\cdot x}\mathrm{d}x, \quad \forall\theta \in \Theta. \tag{43}$$

Lemma 10 states that, given any feasible quality function $q(\theta)$, the best price function $\pi^*(\theta)$ is unique and given by (43). By substituting the best price function $\pi^*(\theta)$ into (42), the best quality function $q^*(\theta)$ can be derived as follows:

$$\begin{aligned}\max_{q(\theta)} \quad & R^*_{q(\theta)} \triangleq \int_{\theta\in\Theta} (\pi^*(\theta) - C(q(\theta)))\cdot f(\theta)\mathrm{d}\theta \\ \text{s.t.} \quad & \text{The Conditions in (34).}\end{aligned} \tag{44}$$

Substitute the best price function $\pi^*(\theta)$ in (43) into Lemma (44), the PU's maximum payoff $R^*_{q(\theta)}$ under a given quality function $q(\theta)$ can be written as

$$R^*_{q(\theta)} \triangleq \int_{\theta\in\Theta} \left(U(\theta, q(\theta)) - \int_{\theta_{\min}}^{\theta} \frac{q(x)}{1 + q(x)\cdot x}\mathrm{d}x - C(q(\theta)) \right)\cdot f(\theta)\mathrm{d}\theta \tag{45}$$

Using integration by parts, we have:

$$\begin{aligned}
&\int_{\theta\in\Theta}\left(\int_{\theta_{\min}}^{\theta}\frac{q(x)}{1+q(x)\cdot x}\mathrm{d}x\right)\cdot f(\theta)\mathrm{d}\theta \\
&= F(\theta)\int_{\theta_{\min}}^{\theta}\frac{q(x)}{1+q(x)\cdot x}\mathrm{d}x\Big|_{\theta_{\min}}^{\theta_{\max}} - \int_{\theta\in\Theta}F(\theta)\frac{q(\theta)}{1+\theta q(\theta)}\mathrm{d}\theta \\
&= \int_{\theta\in\Theta}(1-F(\theta))\cdot\frac{q(\theta)}{1+q(\theta)\cdot\theta}\mathrm{d}\theta,
\end{aligned} \tag{46}$$

where $F(\theta)$ is the cumulative distribution function (cdf) of θ. The last line follows because $F(\theta_{\min})=0$ and $F(\theta_{\max})=1$. Thus, we can rewrite (45) as follows:

$$R^*_{q(\theta)} \triangleq \int_{\theta\in\Theta}\left(U(\theta,q(\theta)) - C(q(\theta)) - \frac{1-F(\theta)}{f(\theta)}\cdot\frac{q(\theta)}{1+q(\theta)\cdot\theta}\right)\cdot f(\theta)\mathrm{d}\theta. \tag{47}$$

It is easy to see that (47) has the similar structure as (26) in the discrete SU-type model. Similar as in (26), we introduce:

$$G(\theta,q(\theta)) \triangleq U(\theta,q(\theta)) - C(q(\theta)) - \frac{1-F(\theta)}{f(\theta)}\cdot\frac{q(\theta)}{1+q(\theta)\cdot\theta}.$$

Then, the PU's payoff $R^*_{q(\theta)}$ in (47) can be rewritten as $R^*_{q(\theta)} \triangleq \int_{\theta\in\Theta} G(\theta,q(\theta))\cdot f(\theta)\mathrm{d}\theta$. Accordingly, the optimization problem (44) can be rewritten as follows:

$$\begin{aligned}
&\max_{q(\theta)} \quad R^*_{q(\theta)} \triangleq \int_{\theta\in\Theta} G(\theta,q(\theta))\cdot f(\theta)\mathrm{d}\theta \\
&\text{s.t.} \quad \text{The Conditions in (34).}
\end{aligned} \tag{48}$$

Similar as $G_t(q_t)$ in the discrete SU-type model, here $G(\theta,q(\theta))$ depends only on the quality $q(\theta)$ for type θ while independent of the quality $q(\theta')$ for any other type $\theta' \neq \theta$. This implies that the optimization problem (48) can be solved by optimizing the quality $q(\theta)$ for each $G(\theta,q(\theta))$ separately. Let $\tilde{q}^*(\theta)$ denote the quality that maximizes $G(\theta,q(\theta))$. That is,

$$\begin{aligned}
&\tilde{q}^*(\theta) \triangleq \arg\max_{q} \quad G(\theta,q) \\
&\text{s.t.} \quad 0 \le q \le Q_{\max}.
\end{aligned} \tag{49}$$

If the quality function $\tilde{q}^*(\theta), \forall\theta \in \Theta$, derived by (49) is a feasible quality function, i.e., satisfying the conditions in (34), then it is exactly the optimal solution of (44). In a general case, however, the quality function $\tilde{q}^*(\theta)$ derived by (49)

may not be feasible. A similar iterative algorithm can be used to adjust the quality function $\tilde{q}^*(\theta)$ such that it is feasible. Formally,

Theorem 2. *Suppose* $\tilde{q}^*(\theta), \forall\theta \in \Theta$, *derived by* (49) *is a feasible quality function satisfying the conditions in* (34). *Then, the optimal contract* $\Psi^* = \{(q^*(\theta), \pi^*(\theta)),\ \theta \in \Theta\}$ *under information asymmetry is given by:*

$$q^*(\theta) = \tilde{q}^*(\theta), \quad \forall\theta \in \Theta,$$

and

$$\pi^*(\theta) = U(\theta, q^*(\theta)) - \int_{\theta_{\min}}^{\theta} \frac{q^*(x)}{1 + q^*(x) \cdot x} \mathrm{d}x, \quad \forall\theta \in \Theta.$$

Simulation Results

We evaluate the performance of the proposed optimal contract in a network with $T = 20$ types of SUs. The type of k-th SUs is $\theta_k = k$, and hence the set of all types is $\Theta = \{1, 2, \cdots, 20\}$. The cost function of the PU is defined as $C(q) = c_0 + a \cdot q^b$ where $c_0 = 0.01$, $a = 2$ and $b = 1.2$. The upper-bound of quality is $Q_{\max} = 1$. We study the optimal contracts in three different network scenarios, which differ from each other in the distribution of SU types. In case (a), the percentage of higher-type SUs is larger than that of lower-type SUs; In case (c), the percentage of higher-type SUs is smaller than that of lower-type SUs; and In case (b), the percentage of higher-type SUs is same as that of lower-type SUs. Without loss of generality, we set: (a) $N_k = N \cdot \frac{\theta_k}{\sum_{t=1}^{T} \theta_t}$, (b) $N_k = N \cdot \frac{1}{T}$, and (c) $N_k = N \cdot \frac{\theta_{T-k+1}}{\sum_{t=1}^{T} \theta_t}$.

Figure 1 presents the best quality set and price set under the optimal contracts in three different network scenarios (under information asymmetry). The dark blue bar (SO) denotes the socially optimal quality set (which maximizes the social welfare) and the associated best price set given by Lemma 6. From Fig. 1, we can see that the best qualities in three optimal contracts (under information asymmetry) are smaller than the socially optimal qualities. The quality gap is smaller for a higher type. This implies that in order to elicit the private information of SUs, there will be certain social welfare loss. We can further see that in the network with more higher-type SUs, i.e., case (a), the optimal contract tends to sell channels to less SUs with higher types and charge them higher prices.

Figure 2 presents the PU's payoff achieved by the optimal contracts under information symmetry and information asymmetry. For an illustrative purpose, we also provide the PU's payoff achieved by an non-optimal contract (under information asymmetry) with the socially optimal qualities and the associated prices, i.e., the SO in Fig. 1. Comparing the optimal contracts under information symmetry and asymmetry, we can see that under information asymmetry, the PU can achieve 60% $\sim$ 70% of the maximum payoff under information symmetry.

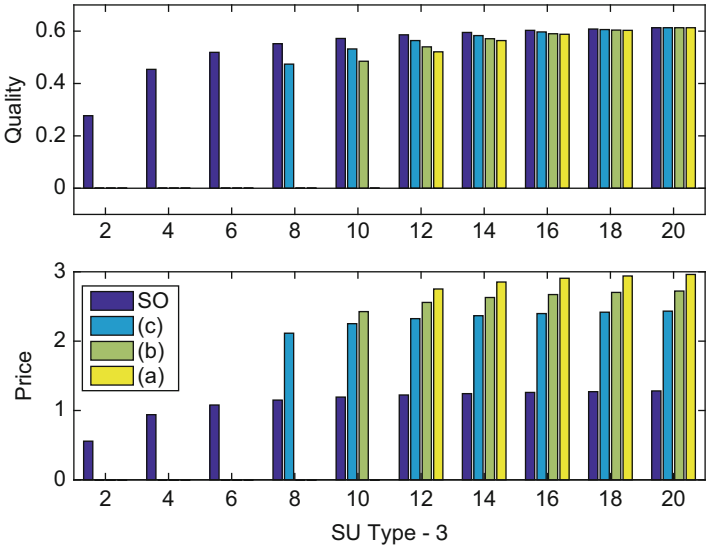

Fig. 1 The best quality assignments and price assignments under the optimal contracts

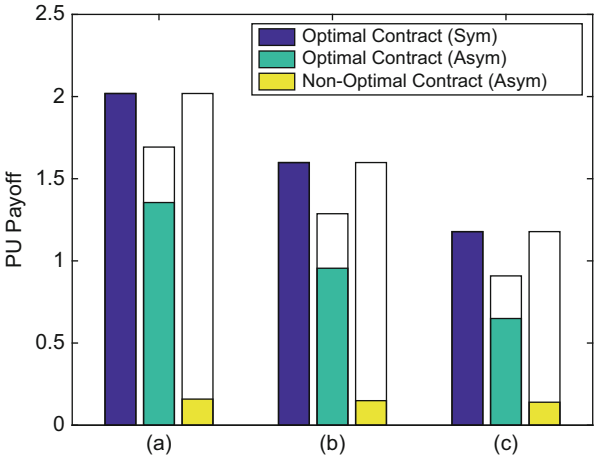

Fig. 2 The social surplus and the revenues of the PO in the optimal contracts

Comparing the optimal and non-optimal contracts under information asymmetry, we can see that by using the optimal contract, the PU can increase his payoff by $400\% \sim 700\%$.

Conclusion

This chapter proposes contract-based spectrum trading mechanism for a monopoly secondary spectrum market with a single PU (seller) and multiple SUs (buyers).

In the proposed mechanism, the PU offers a list of quality-price combinations (contract) for SUs, and each SU chooses the proper quality and price according to his public/private preference information. The necessary and sufficient conditions for feasible contracts (that guarantee the truthful information disclosure of SUs) are proved analytically, and then the optimal (feasible) contract (that maximizes the PU's payoff) is derived under both information symmetry and information asymmetry. This chapter further extends the optimal contract design to the continuous SU-type model. Simulations show that the optimal contract under information asymmetry can increase the PU's payoff significantly and can achieve $60\% \sim 70\%$ of the optimal performance under information symmetry.

In terms of the future extensions, it is important (also challenging) to study the optimal contract design under the more general model with multidimension private information, where each SU's private information consists of multiple dimension parameters (e.g., preferences on both quality and payment). Some recent works (e.g., [31]) have started to consider this issue under some simplified cases, while the complete analysis for the general case is still open. It is also important to study the contract design under the practical constraint of limited price and quality discrimination, where a limited number (often smaller than the number of SU types) of different prices and qualities can be selected in the designed contract. This is important for the implementation of the designed contract in practice. In [33], Li *et al.* have considered this problem and obtained some interesting preliminary results. However, the complete analysis and results are still open.

References

1. Cisco (2016) Cisco visual networking index: global mobile data traffic forecast update 2015–2020. White paper
2. Brown TX, Pietrosemoli E, Zennaro M, Bagula A, Mauwa H, Nleya SM (2014) A survey of TV white space measurements. In: International Conference on e-Infrastructure and e-Services for Developing Countries. Springer International Publishing, pp 164–172
3. Luo Y, Gao L, Huang J (2015) Business modeling for TV white space networks. IEEE Commun Mag 53(5):82–88
4. Federal Communication Commission (2012) Third memorandum opinion and order in the matter of unlicensed operation in the TV broadcast bands. Federal Communication Commission (FCC), Docket, pp 12–36
5. Copsey B (2010) Implementing geolocation. Ofcom, London
6. Akyildiz IF, Lee WY, Vuran MC, Mohanty S (2006) Next generation/dynamic spectrum access/cognitive radio wireless networks: a survey. Comput Netw 50(13):2127–2159
7. Zhao Q, Swami A (2007) A survey of dynamic spectrum access: signal processing and networking perspectives. In: IEEE International Conference on Acoustics, Speech and Signal Processing (ICASSP), vol 4, p 1349–1352
8. Haykin S (2005) Cognitive radio: brain-empowered wireless communications. IEEE J Sel Areas Commun 23(2):201–220
9. Lee WY, Akyildiz IF (2008) Optimal spectrum sensing framework for cognitive radio networks. IEEE Trans Wirel Commun 7(10):3845–3857
10. Nie N, Comaniciu C (2006) Adaptive channel allocation spectrum etiquette for cognitive radio networks. Mob Netw Appl 11(6):779–797
11. Acharya J, Yates RD (2009) Dynamic spectrum allocation for uplink users with heterogeneous utilities. IEEE Trans Wirel Commun 8(3):1405–1413

12. Gao L, Wang X, Xu Y (2009) Multiradio channel allocation in multihop wireless networks. IEEE Trans Mob Comput 8(11):1454–1468
13. Grokop LH, David NC (2010) Spectrum sharing between wireless networks. IEEE/ACM Trans Netw 18(5):1401–1412
14. Duan L, Gao L, Huang J (2014) Cooperative spectrum sharing: a contract-based approach. IEEE Trans Mob Comput 13(1):174–187
15. Gao L, Duan L, Huang J (2016) Two-sided matching based cooperative spectrum sharing. IEEE Trans Mob Comput 16(2):538–551
16. Simeone O, Stanojev I, Savazzi S, Bar-Ness Y, Spagnolini U, Pickholtz R (2008) Spectrum leasing to cooperating secondary ad hoc networks. IEEE J Sel Areas Commun 26(1):203–212
17. Zhang J, Zhang Q (2009) Stackelberg game for utility-based cooperative cognitive radio networks. In: ACM International Symposium on Mobile Ad Hoc Networking and Computing (MobiHoc), pp 23–32
18. Duan L, Gao L, Huang J (2011) Contract-based cooperative spectrum sharing. In: IEEE Symposium on New Frontiers in Dynamic Spectrum Access Networks (DySPAN), pp 399–407
19. Niyato D, Hossain E (2008) Spectrum trading in cognitive radio networks: a market-equilibrium-based approach. IEEE Wirel Commun 15(6):71–80
20. Yu H, Gao L, Li Z, Wang X, Hossain E (2010) Pricing for uplink power control in cognitive radio networks. IEEE Trans Veh Technol 59(4):1769–1778
21. Huang J, Berry RA, Honig ML (2006) Auction-based spectrum sharing. Mob Netw Appl 11(3):405–418
22. Gao L, Xu Y, Wang X (2011) Map: multiauctioneer progressive auction for dynamic spectrum access. IEEE Trans Mob Comput 10(8):1144–1161
23. Gao L, Huang J, Chen YJ, Shou B (2013) An integrated contract and auction design for secondary spectrum trading. IEEE J sel Areas Commun 31(3):581–592
24. Gao L, Shou B, Chen YJ, Huang J (2016) Combining spot and futures markets: a hybrid market approach to dynamic spectrum access. Oper Res 64(4):794–821
25. Gao L, Wang X, Xu Y, Zhang Q (2011) Spectrum trading in cognitive radio networks: a contract-theoretic modeling approach. IEEE J Sel Areas Commun 29(4):843–855
26. Luo Y, Gao L, Huang J (2016) An integrated spectrum and information market for green cognitive communications. IEEE J Sel Areas Commun 34(12):3326–3338
27. Luo Y, Gao L, Huang J (2015) Mine gold to deliver green cognitive communications. IEEE J Sel Areas Commun 33(12):2749–2760
28. Luo Y, Gao L, Huang J (2015) Price and inventory competition in oligopoly TV white space markets. IEEE J Sel Areas Commun 33(5):1002–1013
29. Luo Y, Gao L, Huang J (2013) White space ecosystem: a secondary network operator's perspective. In: IEEE Global Communications Conference (GLOBECOM), pp 925–930
30. Bolton P, Dewatripont M (2005) Contract theory. MIT Press, Cambridge
31. Ma Q, Gao L, Liu YF, Huang J (2016) A contract-based incentive mechanism For crowdsourced wireless community networks. In: International Symposium on Modeling and Optimization in Mobile, Ad Hoc, and Wireless Networks (WiOpt), pp 1–8
32. Dasgupta P, Hammond P, Maskin E (1979) The implementation of social choice rules: some general results on incentive compatibility. Rev Econ Stud 46(2):185–216
33. Li S, Huang J (2014) Price differentiation for communication networks. IEEE Trans Netw 22(3):703–716

Adaptive Learning in Cognitive Radio

33

Husheng Li

Contents

Abstract

Machine learning is a powerful tool for cognitive radio users to learn its sensing and transmission strategy from the experience. This chapter provides a brief

H. Li (✉)
Department of Electrical Engineering and Computer Science, The University of Tennessee, Knoxville, TN, USA
e-mail: hli31@utk.edu

W. Zhang (ed.), *Handbook of Cognitive Radio*,
https://doi.org/10.1007/978-981-10-1394-2_41

introduction to a variety of machine-learning techniques. The basic setup of machine learning, as well as the dichotomy, is explained. Then, the supervised, unsupervised, semi-supervised, and reinforcement learning techniques are briefly discussed. The single-agent learning is then extended to the case of multiagent learning. Then, the machine-learning techniques are applied in various cases of machine learning, such as channel selection and routing.

Keywords
Machine learning · Cognitive radio · Supervised learning · Unsupervised learning · Reinforcement learning

Introduction

Cognitive radio users are equipped with capabilities of sensing (spectrum sensing), thinking (powerful computing devices), and talking (communications). Hence, a cognitive radio can be considered as an intelligent device, which is also endowed the capability of learning. Due to the changing environment (e.g., the dynamically changing frequency spectrum, fast fading channel, and mobile communication network), learning is a necessary requirement for the adaptivity to the environment. Therefore, it is of key importance to study the learning issues in cognitive radio.

This chapter will first provide a brief introduction to the area of machine learning, which consists of supervised, unsupervised, and semi-supervised learning. In particular, it will focus on the reinforcement learning, which is of particular importance in cognitive radio networks, since usually there is no explicit supervision in cognitive radio networks while each learner does receive rewards which can be used to train the decision maker. Comprehensive introductions to machine learning can be found in [15, 22].

Then, this chapter will provide several case studies on the application of machine learning in cognitive radio scenarios. The discussion will focus on the applications of reinforcement learning and multiarmed bandit learning for channel selection and routing. Both the single-user and multiple-user cases will be discussed. The introduction will focus on the general principles, instead of discussing the details and providing a comprehensive survey of works in this area.

Basics of Learning

This section provides a brief introduction to machine learning to make this chapter self-contained and will first introduce the dichotomy of learning and then explain each type of learning techniques. Since reinforcement learning is very useful in cognitive radio, this chapter will use an independent section to introduce its details.

Essence and Dichotomy of Learning

In a machine-learning problem, one is provided a series of samples $\{X_i\}_{i=1,\ldots,N}$ (which is called the training set) with a distribution P_X. Usually the distribution P_X is unknown. The goal of machine learning is to learn a function c, mapping from a given X (which may be beyond the training set) to a Y. Here Y is the outcome of the mapping, which can be considered as a label to the sample X. When Y is discrete, the learning can be considered as a classification problem (namely, assigning a label to a given sample); when Y is continuous, the output means a certain property of the sample X. The procedure is illustrated in Fig. 1. Hence, essentially machine learning is a function approximation problem, where both the true function and the sample distribution are unknown.

There are many possible dichotomies for machine learning. Below are several typical ones, as illustrated in Fig. 2:

- Supervised or not: In the training set, in many cases, the label of each sample is also provided. Hence, the tuples $\{(X_i, Y_i)\}_{i=1,\ldots,N}$ are used in the training. One calls this case the supervised learning. When labels are not available, it is called unsupervised learning. When only a fraction of the labels are available, it is called semi-supervised learning.

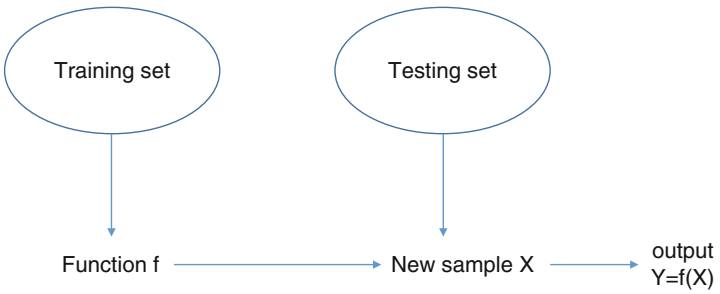

Fig. 1 Illustration of learning problem

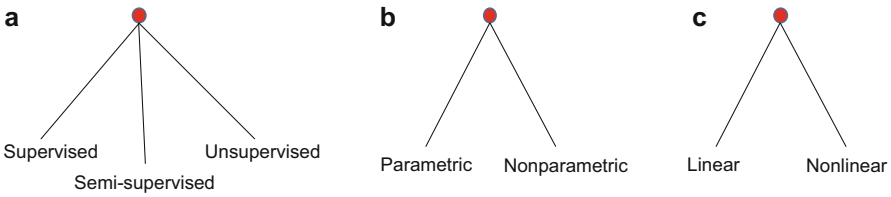

Fig. 2 Dichotomy of machine learning. (**a**) Classification according to the availability of labeled samples. (**b**) Classification the availability of parameterized expressions. (**c**) Classification the application of linear functions

- Parameterized or not: The mapping f could be parameterized or not, thus resulting in parametric and nonparametric ones, respectively.
- Linear or not: The function f, or an intermediate function, could be linear or nonlinear. For example, in classification problems, one may apply a linear function g such that $c(X) = 1(g(X) \geq 0)$, where the characteristic function $1(E)$ equals 1 if the corresponding event E is true and 0 otherwise. Although f itself is not linear (it cannot be linear since the output Y is discrete), the classifier is still called a linear one, since g is linear.

In the following discussion, this chapter follows the dichotomy of supervised/unsupervised/semi-supervised learning.

Supervised Learning

As has been explained, in supervised learning, labeled samples are provided for the training procedure, in which $Y_n = c(X_n)$, $n = 1, \ldots, N$. Since c, usually called concept in the community of machine learning, is actually unknown, the goal is to learn an estimation of c, denoted by h and called hypothesis, such that h can well approximate c and can be well generalized to samples not observed in the training set.

For cognitive radio networks, supervised learning is mainly used in classifications, e.g., how to recognize the modulation and coding schemes of primary users [23]. The learning procedure can be accomplished by training the classifiers using signal with known modulation and coding schemes.

Learning Criterion and Generalization

To find an optimal approximation h to the concept c, one first needs to identify a class of functions for h, which is denoted by $\mathcal{H}$ and is called the hypothesis set. Then, one defines a risk function for each hypothesis h as

$$R(h) = E[r(h(X), c(X))], \tag{1}$$

where the expectation $E[\cdot]$ is over the randomness of sample X and r is the risk of h when the sample is X. Take the binary classification problem for example: the risk r is defined as $1(h(X) \neq c(X))$, namely, whether the classification result is wrong or not. Hence, for this example, one has

$$R_c(h) = E[1(h(X) \neq c(X))] = P(h(X) \neq c(X)), \tag{2}$$

namely the error probability of classification. Then, the optimal selection of hypothesis is given by

$$h_{\text{opt}} = \arg\min_h R(h). \tag{3}$$

Unfortunately, the calculation of h_{opt} in (3) is infeasible, since the expectation in (1) cannot be calculated due to the lack of information on the sample distribution P_X. Hence, a feasible approach is to approximate the expectation using the empirical average, namely

$$R(h) \approx \hat{R}(h) = \frac{1}{N} \sum_{n=1}^{N} r(h(X_n), c(X_n)). \tag{4}$$

Hence, the supervised learning is to minimize the empirical risk, namely

$$h_{\text{emp}} = \arg\min_{h} \sum_{n=1}^{N} r(h(X_n), c(X_n)). \tag{5}$$

When a new sample that is not observed in the training set is given, the gap between the risk for the empirically optimal hypothesis, namely, $r_{\text{rmp}}()$, and the minimum risk can be written as

$$R(h_{\text{rmp}}) - R^* = \underbrace{R(h_{\text{rmp}}) - R(h_{\text{opt}})}_{\text{estimation}} + \underbrace{R(h_{\text{opt}}) - R^*}_{\text{approximation}}, \tag{6}$$

where $R^* = R(c)$ is the minimum risk incurred by the true concept. The two terms in (6) have the following meanings:

- Estimation: The term $R(h_{\text{rmp}}) - R(h_{\text{opt}})$ means that the performance gap between the empirically optimal hypothesis and the optimal hypothesis (both in the hypothesis set $\mathcal{H}$) is due to the limited number of samples. The gap can be reduced by taking more samples such that the empirical average can better approximate the expectation.
- Approximation: The term $R(h_{\text{opt}}) - R^*$ is the performance gap between the optimal hypothesis in $\mathcal{H}$ and the true concept. If $c \in \mathcal{H}$, the gap will be zero. However, since c is unknown, it is impossible to know whether c has been incorporated in $\mathcal{H}$. Therefore, a larger $\mathcal{H}$ can reduce this approximation error. However, a larger (or more complex) $\mathcal{H}$ may increase the estimation error when the number of samples is fixed.

Based on the above two terms of errors, when one designs a learning algorithm, one needs to consider the following two aspects of the hypothesis set $\mathcal{H}$:

- If the cardinality of $\mathcal{H}$ is too small, it cannot well approximate the true concept c even if there are sufficiently many samples (i.e., term of the approximation error will be large).

- If the cardinality of $\mathcal{H}$ is too large, the optimal solution can well approximate the concept c. However, it requires more samples to find a near-optimal hypothesis in $\mathcal{H}$.

Linear Classifier

A simple but effective hypothesis set is the linear functions. Take the classification task for instance. Suppose that the samples are d-dimensional vectors $\mathbf{x}$. A vector $\mathbf{w}$ and an offset b are trained, such that the decision of classification is given by

$$h(\mathbf{x}) = \begin{cases} 1, & \mathbf{w}^T\mathbf{x} + b \geq 0 \\ 0, & \mathbf{w}^T\mathbf{x} + b < 0 \end{cases}. \tag{7}$$

The linear classifier is illustrated in Fig. 3a, where the boundary of the two classes is generated by $\mathbf{w}$ and b. It is possible that the linear classifier cannot achieve perfect performance even in the training set. Hence, it is necessary to introduce nonlinear classifiers, such as support vector machine [15, 22], as illustrated in Fig. 3b. This chapter will introduce a few in the subsequent discussions.

Support Vector Machine

Support vector machine (SVM) is one of the most useful approaches to exploit linear classifiers and nonlinear features. Again, one uses classification task as the example. The discussion begins from the linearly separable case and estimates the weighting coefficient vector $\mathbf{w}$ and offset b. When the two classes of training samples are linearly separable, usually there are many possible choices for $\mathbf{w}$ and b. An example is illustrated in Fig. 4, where both linear boundaries can separate the two classes of samples. However, the boundary in (a) is better since the minimum distance from training samples to the boundary, which is called the margin, is larger. A larger margin means a safer classification, because it can better tolerate a new sample close to the boundary, as illustrated in Fig. 4.

It has been shown that the margin, whose detailed definition is given in [15,22], is equal to $\frac{1}{\|\mathbf{w}\|}$. Hence, the following optimization problem is employed to maximize the margin:

$$\min_{\mathbf{w},b} \frac{1}{2}\|\mathbf{w}\|^2 \tag{8}$$

$$s.t. \quad y_i(\mathbf{w} \cdot \mathbf{x}_i + b) \geq 1, \qquad \forall i = 1, \ldots, m, \tag{9}$$

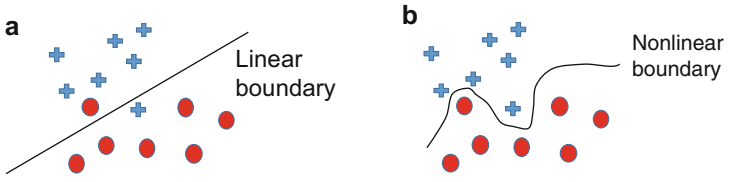

Fig. 3 Illustration of linear and nonlinear classifiers. (**a**) Linear classifier. (**b**) Nonlinear classifier

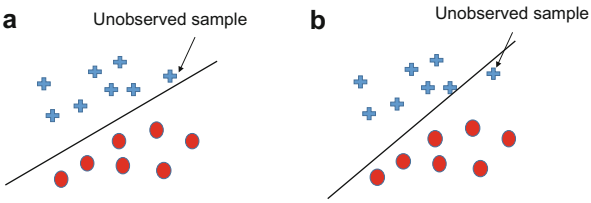

Fig. 4 Illustration of margin in linearly separable case. (**a**) Larger margin. (**b**) Smaller margin

where m is the number of samples. The inequalities in the constraints are used to guarantee the correctness of classification. Using the Lagrange factor method, the above optimization problem can be rewritten as

$$\min_{\mathbf{w},b} \frac{1}{2}\|\mathbf{w}\|^2 - \sum_{i=1}^{m} \alpha_i \left[y_i(\mathbf{w}\cdot\mathbf{x}_i + b) - 1\right], \tag{10}$$

where $\alpha = (\alpha_1, .., \alpha_m)$ is the vector consisting of the Lagrange factors. Using the KKT condition of constrained optimization, one can obtain the following conclusions for the optimization in (10):

$$\begin{cases} \mathbf{w} = \sum_{i=1}^{m} \alpha_i y_i \mathbf{x}_i \\ \alpha_i = 0, \text{ or } y_i(\mathbf{w}^T\mathbf{x}_i + b) = 1 \end{cases}. \tag{11}$$

Hence, one can see that the optimal weighting coefficient vector $\mathbf{w}$ is determined by those samples $\mathbf{x}_i$ with $\alpha_i \neq 0$. These vectors are called the support vectors. Taking the dual form of (10), the optimization problem is converted to

$$\max_{\alpha} \sum_{i=1}^{m} \alpha_i - \frac{1}{2} \sum_{i,j=1}^{m} \alpha_i \alpha_j y_i y_j \mathbf{x}_i^T \mathbf{x}_j \tag{12}$$

$$s.t. \quad 0 \leq \alpha_i \leq C \tag{13}$$

$$\sum_{i=1}^{m} \alpha_i y_i = 0. \tag{14}$$

Although SVM is originally designed for linear models, it can also be extended to nonlinear cases. One can design a nonlinear mapping h, which maps $\mathbf{x}$ to a higher dimension. Then, one can apply the SVM approach to the new vector $h(\mathbf{x})$ and thus result in the following nonlinear function:

$$f(\mathbf{x}) = \mathbf{w}^T h(\mathbf{x}) + b. \tag{15}$$

This discussion will come back to this point later when one discusses the kernel method.

Boosting

An effective nonlinear learning algorithm, called boosting [27], is to train multiple weak learners using simple hypothesis sets and then combine these weak classifiers to obtain a strong classifier. By weak learner, it means hypothesis set $\mathcal{H}$ such that there exist an algorithm of learning and parameters γ and that for any $\delta > 0$, one can always find a sample size m and thus train a hypothesis h satisfying

$$P\left(R(h) \leq \frac{1}{2} - \gamma\right) \geq 1 - \delta. \tag{16}$$

Intuitively speaking, a weak leaner can guarantee a certain performance (an error rate better than random guess) but cannot guarantee to reach one regardless of the training sample size.

A detailed introduction to the procedure of boosting can be found in [27]. The rough procedure of the most typical boosting algorithm, named AdaBoost [27], is given as follows:

- Given m samples, the sampling probability of each sample is set to be identical.
- A weak classifier is learned and the corresponding error probability is evaluated.
- The sampling probability of each sample is reevaluated according to the error rate.
- One repeats the procedure of updating the sampling probability and training new weak classifiers using the new probability.
- After a given number of iterations, a strong classifier is obtained by combining the trained weak learners.

Note that, although the weak learners could be linear, the final resulting classifier of the boosting procedure is nonlinear, thus being more powerful than linear classifiers.

Neural Networks

Another typical nonlinear model for machine learning is neural networks [2, 14], which is motivated by the study on neural systems. In a neural network, there is an input layer which accepts the vector sample $\mathbf{x}$. The output layer outputs $\mathbf{y}$, which could be either vector or scalar. There is also one or multiple hidden layers, linking the input and output layers, as illustrated in Fig. 5. In each layer, there are multiple nodes, accepting the inputs from a lower layer. Consider a node whose output is z_o and input is $\mathbf{z}^i = (z_1^i, \ldots, z_n^i)$. Then, the input-output relationship is given by

$$z_o = g(\mathbf{w}^T \mathbf{z}^i), \tag{17}$$

where $\mathbf{w}$ is the linear coefficients obtained from the training process and g is a nonlinear function such as sigmoid function or max operation. It has been shown that, even when there is only a single hidden layer (called shallow networks), a neural network can approximate functions with arbitrarily small errors, given sufficiently many nodes in the network. The research in recent years has shown that a deep network with many hidden layers can achieve much better performances

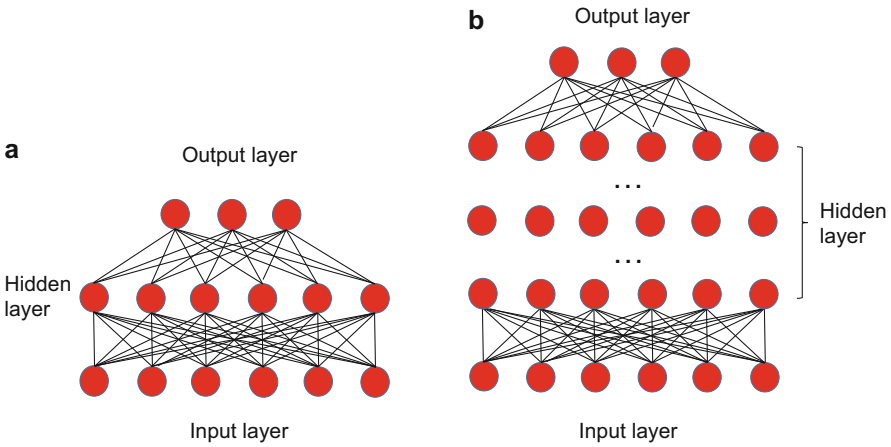

Fig. 5 Illustration of neural networks. (**a**) Shallow networks. (**b**) Deep networks

than the shallow ones and has gained substantial successes in many areas such as artificial intelligence, image processing and speech processing [14]. The training of the neural network can be accomplished by using the famous back propagation (BP) algorithm [14].

Kernel Method

Kernel method is a family of nonlinear models, which has been widely used in machine learning [28]. One calls a two-argument real function $K(x, x')$ a kernel, where $x, x' \in \mathcal{X}$. One wants to define a kernel K such that there exists a mapping $\Phi : \mathcal{X} \to \mathbb{H}$, where $\mathbb{H}$ is a Hilbert space, such that

$$K(x, x') =< \Phi(x), \Phi(x') >, \qquad \forall x, x' \in \mathcal{X}, \tag{18}$$

where $< \cdot, \cdot >$ is the inner product in the Hilbert space $\mathbb{H}$. Here $\mathbb{H}$ is called the feature space. Hence, the mapping Φ maps the original sample $\mathbf{x}$ to a feature of it, which facilitates the further processing. Another typical requirement on the kernel K is to make the matrix $\mathbf{K} = (K(x_i, x_j))_{i,j}$ symmetric and nonnegative definite for any $(x_1, \ldots, x_m) \subset \mathcal{X}$. One calls such kernels positive definite symmetric (PDS) kernels.

To guarantee the existence of Φ, one needs some constraint on the kernel K, which is stated in the following Mercer's condition:

Theorem 1. *Consider a compact set $\mathcal{X} \subset \mathbb{R}^N$ and a continuous and symmetric kernel $K : \mathcal{X} \times \mathcal{X} \to \mathbb{R}$. K can be written as*

$$K(x, x') = \sum_{n=0}^{\infty} a_n \phi_n(x) \phi(x'), \tag{19}$$

if and only if the following Mercer's condition holds:

$$\int\int_{\mathcal{X}\times\mathcal{X}} c(x)c(x')K(x,x')dxdx' \geq 0, \tag{20}$$

for any square-integrable function c.

Obviously, the condition in (20) guarantees the nonnegativity of the inner product. A typical kernel is the Gaussian kernel, which is given by

$$K(\mathbf{x},\mathbf{x}') = \exp\left(-\frac{\|\mathbf{x}-\mathbf{x}'\|^2}{2\sigma^2}\right), \tag{21}$$

for a certain positive σ^2.

The following conclusion is of key importance for the kernel methods.

Theorem 2. *Consider a PDS kernel K. Then there is a Hilbert space* $\mathbb{H}$ *and a mapping* $\Phi : \mathcal{X} \to \mathbb{H}$ *such that*

$$K(x,x') =< \Phi(x), \Phi(x') >, \qquad \forall x, x' \in \mathcal{X}. \tag{22}$$

Moreover, the Hilbert space $\mathbb{H}$ *satisfies the following reproducing property:*

$$h(x) =< h, K(x,\cdot) >, \qquad \forall h \in \mathbb{H}, x \in \mathcal{X}. \tag{23}$$

Here the Hilbert space $\mathcal{H}$ is called the reproducing kernel Hilbert space associated to K.

When a kernel K is fixed, it can be applied to machine learning. For example, for the context of SVM, one can use Φ, associated to the kernel K, to map the sample to a higher-dimensional space, thus resulting in the following SVM optimization:

$$\max_{\alpha} \sum_{i=1}^{m} \alpha_i - \frac{1}{2} \sum_{i,j=1}^{m} \alpha_i \alpha_j y_i y_j \Phi^T(\mathbf{x}_i)\Phi(\mathbf{x}_j) \tag{24}$$

$$s.t.\ \ 0 \leq \alpha_i \leq C \tag{25}$$

$$\sum_{i=1}^{m} \alpha_i y_i = 0. \tag{26}$$

where the maximization can also be written as

$$\max_{\alpha} \sum_{i=1}^{m} \alpha_i - \frac{1}{2} \sum_{i,j=1}^{m} \alpha_i \alpha_j y_i y_j K(\mathbf{x}_i, \mathbf{x}_j). \tag{27}$$

Since K and ϕ are nonlinear, the resulting classifier is also nonlinear. The advantage of changing (24), (25), (26), and (27) is that the computation of $\Phi(\mathbf{x})$ and the subsequent inner product will be very difficult since $\Phi(\mathbf{x})$ is usually of high dimension, while the calculation of the kernel K is straightforward. This is called the kernel trick.

Unsupervised Learning

In unsupervised learning, there is no "teacher"; i.e., the samples are not labeled. What the learner sees is only the samples $\{X_i\}_{i=1,\ldots,N}$, without the Y component. Hence, the learner has to find the inherent pattern of the samples without the direction of the teacher. The following approaches can be used to find the pattern of the samples:

- Density estimation [8]: One can estimate the probability density of X from finitely many samples. It is well known that the density estimation is very challenging, especially when the dimension of X is high.
- Cluster analysis: It is desirable to group the samples into multiple clusters, each of which forms a convex region. Then, the density can be approximated by a mixture of the clusters. Examples of 1-dimensional and 2-dimensional cases are illustrated in Fig. 6.

Below the discussion provides a simple introduction to the clustering. A most popular approach to divide the samples into multiple clusters is the k-means algorithm, which follows the following steps:

1. Set the number of clusters. Randomly initialize the center of each cluster.
2. For each sample, find the closest center and associate it to the corresponding cluster.
3. Calculate the centers by calculating the averages of the samples in the clusters.
4. Go back to step 2 and repeat the procedure until it converges or reaches a maximum number of steps.

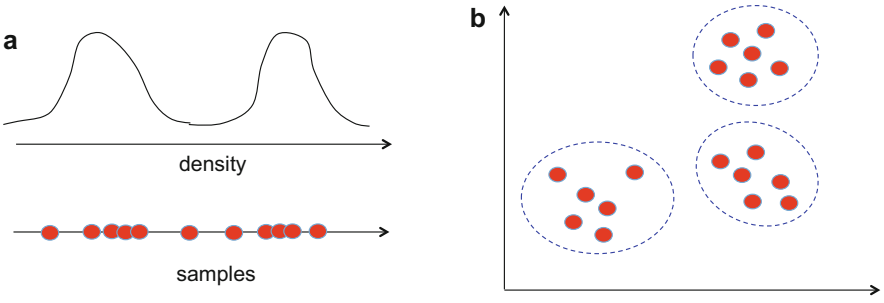

Fig. 6 Examples of 1-dimensional and 2-dimensional cases

Unsupervised learning is not very widely used in cognitive radio. One useful application is to divide the spectrum-sensing outcomes into clusters, each of which is considered as a primary user or an operation mode of primary user [24, 30]. The above k-means clustering algorithm has been used for the cluster analysis.

Semi-supervised Learning

In semi-supervised learning, there are a small set of labeled samples and a large set of unlabeled samples. The challenge is how to incorporate the unlabeled samples into the training procedure. One approach is to regard the missing labels as unobserved data. Then, the standard expectation maximization (EM) algorithm can be applied to handle the unobserved data. More details can be found in [7].

Reinforcement Learning

Introduction

Reinforcement learning [29, 32] has been widely used in cognitive radio. It is different from both supervised and unsupervised learning techniques in the following aspects:

- In unsupervised learning, what the learner sees is only the unlabeled sample; hence, the learning has no standard answer. In reinforcement learning, the learner can receive feedback of reward which may be delayed. Hence, one can say that reinforcement learning does have supervision which is implicit.
- In supervised learning, the learner has labeled samples. Although reinforcement learning does receive feedback through system rewards, the feedback is not labeled; instead it is quantified. It is possible that the feedback could be substantially delayed and be implicit (when you receive a large reward, you may not know which action taken before triggers it).
- In both supervised and unsupervised learning, the training is usually carried out in an offline manner; i.e., the learner first obtains a set of training samples and then apply the learned mapping to testing samples. In reinforcement learning, the training and testing are carried out simultaneously. When a new sample arrives, the reinforcement learning tests its performance and updates its strategy using the feedback of the outcome. Hence, reinforcement learning is in an online manner.

Essentially, supervised and unsupervised learnings are function approximations of input-output mapping, while reinforcement learning is a decision-making problem which determines the action given the current system state and observation. Hence, reinforcement learning is essentially different from the learning tasks introduced in the previous section. However, the strategy, namely, the mapping from system state to the action, can be considered as an input-output relationship; hence,

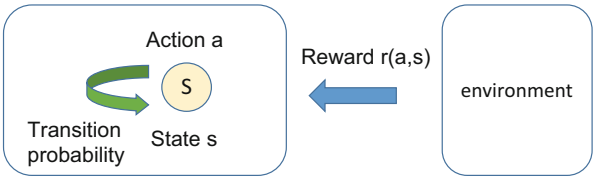

Fig. 7 Illustration of Q-learning

one can also consider reinforcement learning as approximating the optimal strategy. Hence, many techniques in supervised/unsupervised learning can also be applied in the context of reinforcement learning.

There are several types of reinforcement learning. This chapter will introduce them in the subsequent discussion. Note that one considers only the reinforcement learning of a single learner. The learning of multiple learners will be introduced in the next section.

Q-Learning

As a typical reinforcement learning, Q-learning is deeply related to dynamic programming (DP) [5]. A DP problem has the following key elements:

- System state: The learner has N system states, $s_1, \ldots, s_N$, characterizing the current status of the learner.
- Control action: The learner has M possible actions, $a_1, \ldots, a_M$, which is determined by the system state; i.e., there exists a mapping (also called the control strategy) π such that $a = \pi(s)$.
- State transition: The state dynamics of the learner can be considered as a Markov chain. The transition probability is given by $P_a(s_i|s_j)$, which means the probability that the learner transits from state s_j to s_i when the control action is a.
- Reward: When the learner takes an action a when the current system state is s, it receives a reward $r(s, a)$, as a function of s and a.

The goal of DP is to find the optimal strategy π such that the following total reward is maximized:

$$\max_{\pi} E\left[\sum_{t=1}^{T} \alpha^t r(s(t), a(t))\right], \tag{28}$$

where $0 < \alpha < 1$ is a discounting factor and T could be either finite or infinite.

In the context of Q-learning [31], the learner knows the set of system states. However, it does not know the reward function and the transition probability.

The learner has to learn its strategy using its experience. Basically, it needs to achieve a good tradeoff between the exploitation and exploration:

- Exploitation: For each state s, the learner may have found a good action incurring more reward. Hence, it is desirable to take this action more frequently.
- Exploration: It is also important to try actions that have not been considered or have been rarely tried. If the learner uses only the good actions that have been demonstrated, it may miss possibly better actions. Hence, the learner should also explore the actions that have not or have been rarely tested.

To accomplish the tradeoff of exploration and exploitation, Watkins proposed the Q-learning approach, in which the learner keeps a Q-value for each pair of state and action (s, a), which is denoted by $Q(s, a)$. The value of $Q(s, a)$ means the estimated total reward (with discount) in the future after using the action a at state s. These Q-values can be initialized as zeros or random numbers. During the operation, the Q-values are updated using the following rule:

$$\begin{aligned} Q(s(t), a(t)) \leftarrow\ & Q(s(t), a(t)) \\ & + \beta \left(r(t) + \alpha \max_a Q(s(t+1), a) - Q(s(t), a(t)) \right), \end{aligned} \tag{29}$$

where $s(t)$ and $a(t)$ are the state and action of the learner at time t, $r(t)$ is the received reward, and β is a coefficient controlling the learning rate. The term $\alpha \max_a Q(s(t+1), a)$ is an estimation of the future total reward when the state transits to $s(t+1)$. The gap $r(t) + \alpha \max_a Q(s(t+1), a) - Q(s(t), a(t))$, which can be considered as an estimation of the Q-value error, is used to update the new Q-value.

There is still one problem to be solved: how to choose the control action a given the state s, in order to achieve the tradeoff between the exploitation and exploration. One popular approach is to use the Boltzmann distribution; i.e., the probability of taking action a, when the system state is s, is given by

$$P(a|s) = \frac{\exp\left(\frac{Q(s,a)}{T_0}\right)}{\sum_{a'} \exp\left(\frac{Q(s,a')}{T_0}\right)}, \tag{30}$$

where T_0 is called the temperature, which controls the tradeoff between exploitation and exploration: when T_0 is large (hotter), the learner is more inclined to exploration; when T_0 is small (cooler), the learner is more inclined to exploitation. The two extreme cases are:

- When $T_0 \to 0$, the leaner will fix on the action having the highest Q-value.
- When $T_0 \to \infty$, the learner will choose the action in a uniform manner.

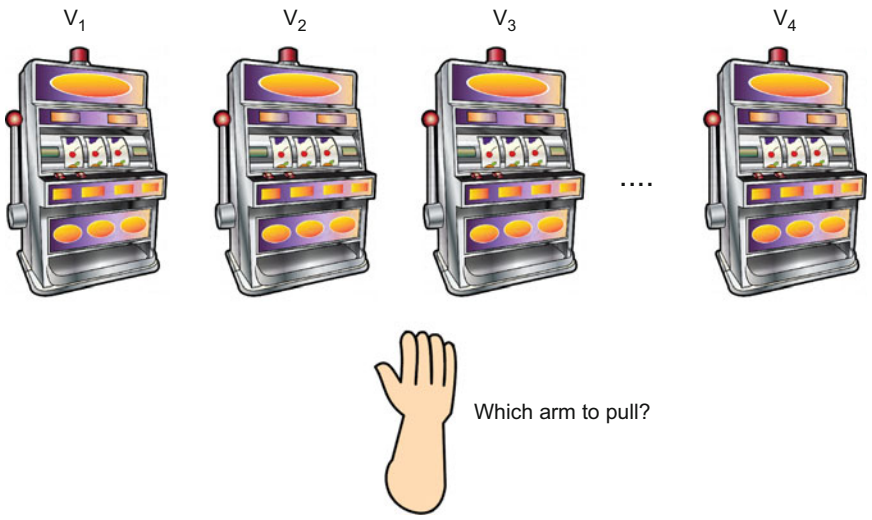

Fig. 8 Illustration of multi-armed bandit problem

It has been shown that the Q-learning can finally converge to the optimal strategy, although the convergence rate is difficult to analyze (Fig. 8).

Multiarmed Bandit

Another setup of reinforcement learning is as follows: at each time, the learner can choose an action a from the set $\{a_1, \ldots, a_n\}$ and receive a random reward r satisfying distribution ν_a. The goal of the learner is to maximize the expected reward. Obviously, when the distribution ν is known, the solution is straightforward: one simply chooses the action having the highest expected reward, namely,

$$a_{\text{opt}} = \arg\max_a E_{\nu_a}[r]. \tag{31}$$

However, the problem is how to make the decision when the distribution $\{\nu_i\}_{i=1,\ldots,n}$ is unknown. This is coined the multiarmed bandit problem [12, 25], which is different from the Q-learning in the following aspect: there is no state at the learner in the multiarmed bandit problem; hence, the learner does not need to consider the explicit impact of the current action on the future rewards, while the Q-learning needs to consider the state transition besides the current reward. The similarity is that both the Q-learning and the multiarmed bandit problem need to address the tradeoff between exploitation and exploration. Hence, the learner should also pull the arms that have not been pulled or have been seldom pulled.

One defines the cost function of the multiarmed bandit problem as the cumulative regret:

$$R_n = n \max_i \{v_i\} - \sum_{t=1}^{n} r(t), \tag{32}$$

where R_n is the regret until time n. Obviously, this is the gap between the optimal reward and the real reward. The learner desires to minimize the regret R_n.

There have been many proposed approaches to handle the multiarmed bandit problem. This chapter will introduce one approach in a subsequent section discussing single-user channel selection.

Multiagent Learning

When multiple agents have coupled dynamics and learn their strategies, the problem is much more complicated than the single-agent learning. It is because, for a certain agent, the behaviors of other agents are part of its environment. However, the behaviors of other agents are changing. Hence, the learning agent is experiencing a changing environment, which is different from the single-agent learning where one assumes that the environment does not change. Hence, it is possible that the dynamics of learning will oscillate and never converge.

Take the channel selection in cognitive radio, for instance. Suppose that many secondary users choose from two channels. Consider the following procedure:

1. All users choose channel 1, and then channel 1 becomes crowded.
2. The users find that channel 1 is congested, and all switch to channel 2.
3. Then channel 2 becomes congested; hence, the users switch to channel 1 again.

The above procedure may repeat and never converge. Hence, it is important to design algorithms that converge for a stable performance. In this section, one introduces two types of multiagent learnings, namely, fictitious play and multiagent reinforcement learning.

Another possibility of multiagent learning is that the rewards of the agents are not coupled. However, the agents can share information with each other, such that they can accelerate the learning process. The discussion will introduce this type of learning by taking the collaborative filtering [1] as the example.

Fictitious Play

For simplicity, one considers the case of two agents. In fictitious play, both agents take simultaneous moves and receive rewards. Suppose that, in each move, the two agents can take actions $a_1 \in \mathcal{A}_1$ and $a_2 \in \mathcal{A}_2$, where $\mathcal{A}_1$ and $\mathcal{A}_2$ are the sets of actions. The rewards are given by $r_1(a_1, a_2)$ and $r_2(a_1, a_2)$, respectively. This is illustrated in Fig. 9

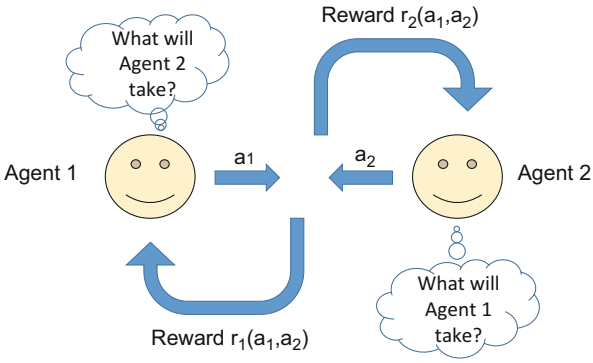

Fig. 9 Illustration of fictitious play

The strategies of both agents are to consider the opponent as having stationary probabilities. Hence, each agent calculates the frequencies of different actions taken by the opponent. Take agent 1, for instance. At round t, it updates the counter for each action, denoted by $\{c_2(a)\}_{a\in\mathcal{A}_2}$, namely,

$$c_2^t(a) = c_2^{t-1}(a) + \begin{cases} 1, \text{ if } a_2(t) = a \\ 0, \text{ if } a_2(t) \neq a \end{cases}. \tag{33}$$

Then, agent 1 updates the frequencies as follows:

$$f_2^t(a) = \frac{c_2^t(a)}{\sum_{a'} c_2^t(a')}. \tag{34}$$

This frequency update can be fit into the Bayesian framework: when more actions of the opponent are observed, the belief of the action distribution is updated. Then, the agent can take actions according to the estimated frequency. For example, it can take the action that maximizes the expected reward if the estimated frequency is true:

$$a_1(t+1) = \arg\max_{a'} f_2^t(a) r(a', a). \tag{35}$$

The analysis of the learning dynamics is complicated. One can consider the counters $\{c_1^t(a)\}_{a\in\mathcal{A}_1}$ and $\{c_2^t(a)\}_{a\in\mathcal{A}_2}$. It is easy to verify that the learning dynamics is nonlinear, which makes the analysis of converge challenging. For such nonlinear dynamics, a most useful approach is the Lyapunov method. For a generic dynamics given by

$$\frac{d\mathbf{x}(t)}{dt} = g(\mathbf{x}(t)), \tag{36}$$

one can try to find a Lyapunov function V, in terms of the system state $\mathbf{x}$, satisfying the following conditions:

- $V : \mathbb{R}^n \to \mathbb{R}$ is continuous.
- V has continuous derivatives and is positive definite.
- The gradient ∇V is nonpositive definite.

One can consider such a Lyapunov function as the energy of the system. Then, if one can prove that,

$$\frac{dV(\mathbf{x}(t))}{dt} < 0, \qquad \forall \mathbf{x} \in \mathbb{R}^n - \{0\}, \tag{37}$$

then, the dynamics is stable and will converge as time evolves. Unfortunately, there is no systematic approach to find such a Lyapunov function.

Multiagent Reinforcement Learning

The fictitious learning does not consider the evolution of system states. When the agents have internal system states, they can employ the reinforcement learning. Since every agent is updating its strategy during the learning procedure, the convergence becomes a major concern. In this chapter, one assumes that every agent employs the Q-learning. A comprehensive survey on multiagent reinforcement learning can be found in [6]. In this chapter, one provides a brief introduction to the basic model, concept, and method.

First, the multiagent reinforcement learning can be formulated as a stochastic game with n agents represented by a tuple $(X, U_1, \ldots, U_n, f, \rho_1, \ldots, \rho_n)$, where the components are illustrated in Fig. 10 and are explained as follows:

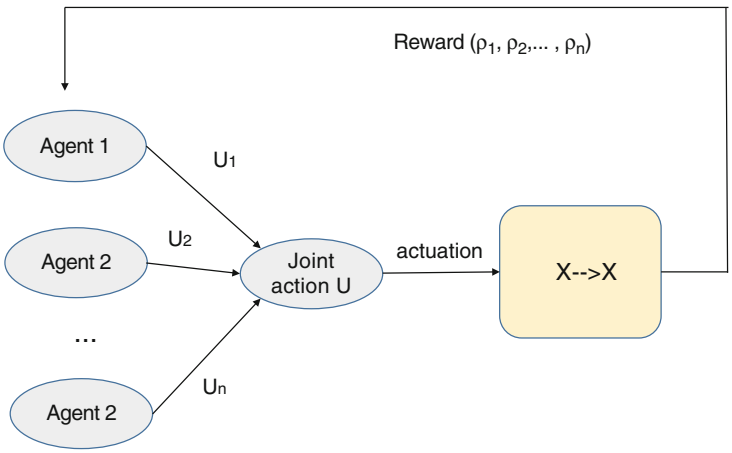

Fig. 10 Illustration of multiagent reinforcement learning

- X is the environment state, which is assumed to be discrete.
- $U_i, i = 1, \ldots, n$ is the action taken by agent n. One defines the joint action as $\mathbf{U} = (U_1, \ldots, U_n)$.
- f is the transition probability of the environment given different joint actions. One can write it as $f_U(X(t+1)|X(t))$.
- $\rho_i, i = 1, \ldots, n$ is the reward of agent i, which can be written as $\rho_i(X(t+1), X(t), U(t))$.

It is assumed that each agent can observe the system state X and choose a random action according to distribution $\pi_i(U|X)$, where π_i is called the policy of agent i. The goal of reinforcement learning is to optimize ρ_i for a larger expectation of reward. Since the reward is dependent on the joint action, the expected reward will also be dependent on the policies of other agents. Therefore, the learning dynamics of the agents are coupled with each other. In the subsequent discussion, several cases of the rewards will be discussed.

Fully Cooperative Tasks

When $\rho_1 = \ldots = \rho_n = \rho$, the agents have the same benefit. Hence, they need to fully cooperate to improve the common reward ρ. Then, each agent can apply the Q-learning by updating the Q-values $Q(X, U_k)$:

$$Q_{t+1}(X_t, \mathbf{U}_t) = Q_t(X_t, \mathbf{U}_{t+1}) + \beta \left[r_{t+1} + \alpha \max_{U'} Q_t(X_{t+1}, \mathbf{U}') - Q_t(X_t, \mathbf{U}_t) \right]. \tag{38}$$

Given the Q-value, the agent needs to choose a good action upon the current system state X. Since the task is fully cooperative, the agent can imagine that all the other agents have similar Q-values and are also trying to maximize the reward. Hence, one can define a Q-value for each local action U_i as follows:

$$Q_i'(X, U_i) = \max_{U_1, \ldots, U_{i-1}, U_{i+1}, \ldots, U_n} Q_i(X, \mathbf{U}), \tag{39}$$

namely, choosing the action that can maximize the reward given the full support of all other agents. Using this Q-value, the agent can choose the corresponding action given the environment state X, e.g., using the Boltzmann distribution.

Fully Competitive Tasks

Suppose that there are two agents, namely, $n = 2$. One assumes that $\rho_1 = -\rho_2$, thus forming a zero-sum game. In this case, if all the information (especially the reward functions) is known, the two agents will form a maxmin equilibrium, according to game theory [10]. Hence, the maxmin principle can also be applied in the learning

procedure. In [20], the maxmin-Q algorithm is proposed, in which each agent learns the rewards of different combinations of actions under different environment states. Hence, the agents will learn the Q-values in the following manner:

$$Q_{t+1}(X(t), U_1(t), U_2(t)) = Q_t(X(t), U_1(t), U_2(t)) + \beta \left[\rho_1(t+1) + \alpha m_1(Q(t), X(t+1)) - Q_{t+1}(X(t), U_1(t), U_2(t))\right], \quad (40)$$

where m_1 is the maxmin reward, which is given by

$$m_1(Q, X) = \max_{\pi_1} \min_{U_2} \sum_{U_1} \pi_1(X, U_1) Q(X, U_1, U_2), \quad (41)$$

namely, the optimal probability of different actions subject to the most detrimental action taken by agent 2. Once the Q-value is updated, the optimal strategy of agent 1 is given by

$$\pi_1(Q, X) = \arg\max_{\pi} \min_{U_2} \sum_{U_1} \pi(X, U_1) Q(X, U_1, U_2). \quad (42)$$

It is complicated to analyze whether the learning procedure can achieve the Nash equilibrium.

Collaborative Filtering

Collaborative filtering has a longer history than cognitive radio systems. It originated from the study of Tapestry system, which helps users to scan a list of documents and select desired ones [13]. Collaborative filtering is proposed to let people collaboratively filter the document list according to their shared interest. Since then, multiple approaches have been proposed. People considered the preferences of all users as a matrix and converted the collaborative filtering into a mathematical problem called matrix completion, i.e., predicting missing entries in a matrix according to some a priori information about the matrix. Quite often, the matrix is singular or near singular due to the similarities among different rows if the preference of each user is considered as a row in the matrix. Then, singular value decomposition (SVD) is applied to reconstruct the matrix by recovering the sparse spectrum of the matrix [3].

Since the beginning of this century, collaborative filtering has been widely applied in e-commercial recommendation systems, which is a popular research topic in computer science. Recommendation systems help users to leverage the experience of other people to achieve a more oriented purchase; i.e., users can purchase goods that have been experienced and recommended by other users, provided that they have similar flavors. Practical systems include eBay's reputation

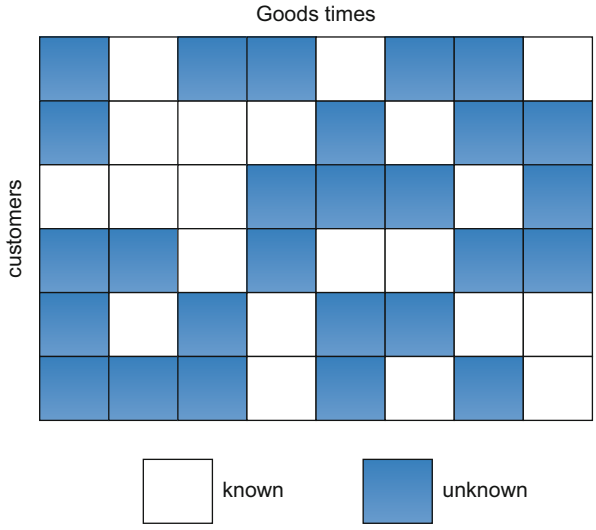

Fig. 11 Illustration of collaborative filtering in terms of matrix completion

system and Amazon's customer review system. Collaborative filtering is a natural and powerful tool to recover the preferences of users (thus completing the matrix) based on the similarities among users. The SVD approach is applied for identifying groups with similar flavors in [9]. In [4], the preference matrix is divided into multiple domains for enhancing the collaborative filtering in websites. When users are distributed, it is difficult to apply the centralized approaches such as SVD or nuclear norm optimization. Therefore, linear predictions are applied to estimate the preferences according to the estimation of Pearson's correlation among different users.

The collaborative filtering can also be considered as a matrix completion. One can consider the customer index as one dimension while the goods item as the second dimension, thus forming a matrix, as illustrated in Fig. 11. Each element corresponding to customer-goods pair is the fondness of the customer to the goods. The simplest case is whether the customer likes or dislikes the goods, thus forming a binary value. However, many elements in the matrix are unknown, because the customer may not know the goods (thus, the fondness is also unknown). However, one believes that the elements in this matrix are not mutually independent because of the similarity of the rows (namely, the similarity of customers) and the similarity of the columns (namely, the similarities of the goods). Hence, the goal of the collaborative filtering is to guess the values of the unknown elements and thus complete the matrix.

A comprehensive introduction to collaborative filtering can be found in [1]. Here an outline of the dichotomy of various collaborative filtering techniques is provided.

Neighborhood-Based Collaborative Filtering

Suppose that there is a set of purchase record for M customers. The set of goods purchased by customer m is denoted by $\mathcal{I}_m$. Obviously, a customer cannot purchase all goods. Hence, it is important to predict the preference of each customer and make recommendations. There are two approaches for the prediction from two different aspects:

- Customer based: One measures the similarity between different customers. Two customers are similar if they purchase similar goods. However, it is tricky to measure the similarity. Many approaches can be found in [1]. Once one detects two customers A and B, one can send recommendations to B about the goods that A has purchased while B has not.
- Goods based: One measures the similarity between two goods. Two goods are similar if they are purchased by similar customers. Again, it is important to devise measures for the similarity between two goods. Once two similar goods A and B have been found, one can send recommendations to the customers that have purchased A but have not purchased B (and vice versa).

Model-Based Collaborative Filtering

The neighborhood-based collaborative filtering can be considered as the method based on raw data, similarly to the k-nearest neighbor classifiers. If structures can be identified from the data, one can first build a model for the data and then use the model to predict unknown elements (Fig. 12).

One possible selection of model is the decision tree, in which multiple attributes are used to judge the path selection in the tree, while each leaf of the tree means a decision. Hence, one can design a decision tree for each goods, while the attributes are the fondness of other goods. When one needs to predict the fondness of one customer for a certain goods, the decision tree can be used to make the decision by using the fondness of the customer for other goods. The missing elements in the matrix incur two challenges for this decision-based approach: (a) how to train

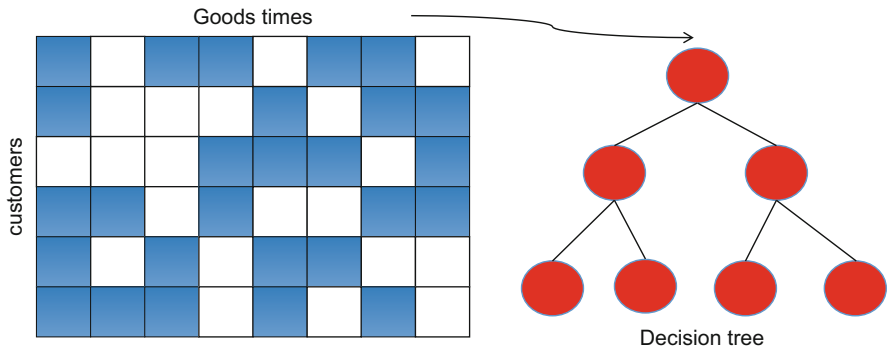

Fig. 12 Illustration of model based collaborative filtering

the decision tree when some of the attributes are missing and (b) given a decision tree, how to make the decision when some attributes are not available. There are systematic approaches to handle them (see Chapter 3 of [1]).

Knowledge-Based Collaborative Filtering

The above approaches do not exploit the domain knowledge of the task; they simply mine the raw data. If there is domain knowledge to be exploited, one can improve the efficiency of the collaborative filtering. The application of knowledge-based collaborative filtering is highly task specific. It is discussed for several scenarios in Chapter 5 of [1]. In the context of cognitive radio, it is intuitive that nearby secondary users are more likely to observe similar spectrum activities. Hence, the distance between two secondary users can also be incorporated into the similarity metric.

Applications in Cognitive Radio

In this section, some illustrative examples will be provided for the applications of learning in cognitive radio networks. One mainly focuses on the reinforcement learning without an explicit supervision and the applications in the channel selection in MAC layer, as well as routing in the network layer.

Channel Selection Using Multiarmed Bandit

In this subsection, one follows the discussion in [17] to introduce the channel selection in the MAC layer.

Channel Model

One considers N communication channels with synchronized timing. At each time slot t, the status of channel i is represented by a Bernoulli random variable $Z_i(t)$, which is equal to 1 (which means that the channel is idle and can be used by secondary user) with probability θ_i and is equal to 0 (which means that the channel is being used by a primary user) with probability $1 - \theta_i$. One assumes that $Z_i(t)$ is independent for different i and different t. This is illustrated in Fig. 13.

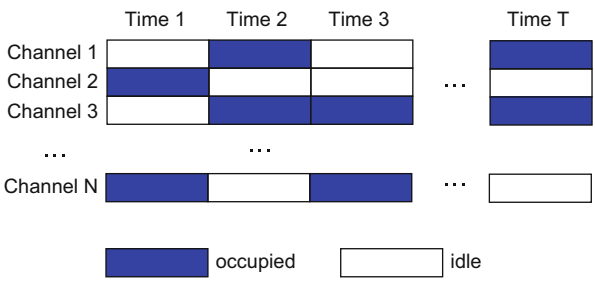

Fig. 13 Channel model for cognitive radio

Problem Formulation

Suppose that the secondary user chooses channel $S(t)$ at time t. Then, the total number of bandwidth it can access in T time slots is given by

$$W = \sum_{t=1}^{T} Z_{S(t)}(t), \tag{43}$$

where one assumes a unit bandwidth for each channel. The goal of the secondary user is to maximize the expected bandwidth given by

$$W = \sum_{t=1}^{T} E[Z_{S(t)}(t)]. \tag{44}$$

If the probabilities $\{\theta_i\}_{i=1,\ldots,N}$ are known, the secondary user can simply choose the channel having the largest probability, namely, $\arg\max_i \theta_i$. However, these probabilities are unknown. Hence, the secondary user needs to determine the selection of channel according to the outcomes of the previous trials.

Multiarmed Bandit Learning

One can consider each communication channel as an arm, thus forming a multi-armed bandit problem. In this chapter, one assumes that the secondary user can sense only one channel, namely, pulling one arm. In [17], the case of simultaneously sensing multiple channels is also discussed.

Multiple approaches can be used to solve the problem:

- Bayesian approach: In this approach, one updates the knowledge about the system parameter $\theta = (\theta_1, \ldots, \theta_N)$. One assumes that θ is a random variable, whose prior probability density function (pdf) is given by $f(\theta)$. When a new decision has been made and the spectrum sensing result is available, the prior pdf f can be updated:

$$f^{t+1}(\theta) = \frac{z_{s(t)}(t)\theta_{s(t)} f^t(\theta) + (1 - z_{s(t)}(t))(1 - \theta_{s(t)}) f^t(\theta)}{z_{s(t)}(t) \int \xi_{s(t)} f^t(\xi) d\xi + (1 - z_{s(t)}(t)) \int (1 - \xi_{s(t)}) f^t(\xi) d\xi} \tag{45}$$

  Based on this Bayesian updating rule for f, the problem can be solved by using DP [5], as illustrated in Fig. 14. One denotes by $V^*(f, T)$ the optimal reward between time 1 and T when the pdf of θ is f. Then, this optimal reward satisfies the following Bellman equation:

$$V^*(f, T) = \max_s E_f\{Z_s + V^*(f_s, T - 1)\}, \tag{46}$$

  where f_s is the possible pdf of θ after the updating step according to the outcome Z_s when the channel selection is s. Then, the optimal channel selection is given by

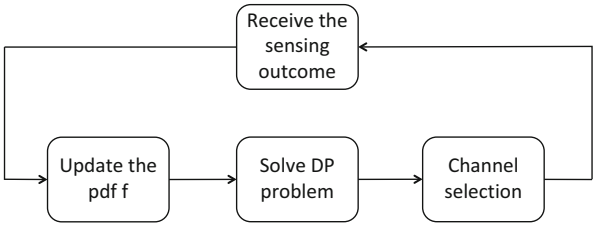

Fig. 14 Bayesian solution to bandit problem

$$s^*(f, T) = \arg\max_s E_f\{Z_s + V^*(f_s, T-1)\}. \tag{47}$$

These equation can be solved in a recurrent manner since, when $T = 1$, one simply chooses the channel with the maximum expected probability $\theta^* = \max_i f(\theta_i)$. However, the challenge is that V^* is a functional in terms of f (since f is a function). Hence, a precise solution to (46) is prohibitively difficult except for some special cases. One possible approach is to discretize the space of f, thus turning V to a vector. Another possible solution is to parameterize the functional V and discretize f.

- Non-Bayesian methods with loss $O(T)$: When the parameter θ is not considered as random variables, there are several approaches for the decision-making of channel selection. One simple approach is simply choose a channel randomly; another simple one is the myopic strategy, namely, choosing the channel having the largest probability estimation (hence, only exploitation; no exploration). In [17], a more intelligent approach is called the strategy of staying with the winner and switching from the loser. The rule is simple. The secondary user begins with a random channel selection. If the channel turns out to be idle, it will sense this channel again in the next time slot. If the channel is busy, then the secondary user will randomly choose one from the remaining channels. It is shown in [17] that the performance loss, which is defined as

$$L(\theta) = \sum_{j=1}^{T} \theta_{i^*} - \sum_{j=1}^{T} \sum_{i=1}^{N} Pr(S(j) = i), \tag{48}$$

where i^* is the index of the optimal channel, is of order $O(T)$. It has been shown in [17] that there exist better algorithms that achieves $O(\log T)$.

- Non-Bayesian methods with loss $O(\log T)$: It has been found in [17] that several approaches can achieve a performance loss defined in (48) of order $O(\log T)$. For example, the order-optimal single-index strategy can achieve the loss $O(\log T)$. In this approach, the secondary user maintains two vector $\mathbf{x}$ and $\mathbf{y}$. Here x_i means the number of times in which the secondary user finds channel i to be idle, while y_i means the times that the secondary user has sensed channel i. The secondary user begins from sensing each channel for one time, such that $\mathbf{y} = (1, 1, 1, \ldots, 1, 1)$. Then, at each time slot, the secondary user updates the probability estimation by

$$\hat{\theta}_i(t) = \frac{x_i(t)}{y_i(t)}, \tag{49}$$

and then assign an index to channel i:

$$\Lambda_i(t) = \hat{\theta}_i(t) - \sqrt{\frac{2\log t}{y_i(t)}}. \tag{50}$$

Then, the secondary user will choose the index having the largest index. As long as y_i increases as fast as $O(\log T)$, the index will converge to the true probability and thus the secondary user will finally keep using the best channel. On the other hand, if a channel has not been sufficiently sensed, the corresponding value of y_i will be small, thus making the index Λ_i large and the secondary user sense this channel. Hence, this mechanism forces the secondary user to sense channels rarely sensed for exploration.

Routing Using *Q*-Learning

Reinforcement learning algorithms usually address problems of a single objective, when scalar rewards are received. Different from the traditional reinforcement learning algorithms, multi-objective reinforcement learning (MORL) introduced by Gabor [11] employs reinforcement learning in problems having multiple objectives, thus forming vector rewards. Note that multiple objectives do exist in wireless communication networks, such as expected delay and packet drop rate, which may conflict with each other. Thus MORL is applicable in the routing of cognitive radio networks to meet the multiple performance goals.

In this chapter, one considers the task of routing with two objectives, whose value functions are represented by $V^{\pi,1}(s)$ and $V^{\pi,2}(s)$, respectively [33]. To handle the two conflicting objectives, one sets a hard constraint on one objective and then optimizes the other one. Then, one has the following optimization problem:

$$\max V^{\pi,1}(s) \tag{51}$$

$$s.t.\ \ V^{\pi,2}(s) \leq R_{\text{constr}}, \tag{52}$$

where R_{constr} is the hard constraint on the second objective. One will use the following assumptions for the cognitive radio under study:

- There exist multiple licensed channels.
- The activities of primary users can be modeled as Markov processes.

- In each time slot, each primary user can be either active or idle. If a primary user is active, it will occupy a fraction of the licensed channels. Before SUs start transmitting packets, they must perform spectrum sensing first.
- One only considers the packet loss due to transmission failures, which is dependent on the link condition.

In this chapter, one focuses on two typical metrics in wireless communication networks, namely, the transmission delay and packet drop rate [33]. When one formulates the algorithm design as an optimization problem, there could be the following two choices:

- One minimizes the transmission delay subject to a constraint of packet drop rate. This is suitable for the scenario of best effort applications.
- One minimizes the packet drop rate subject to a constraint of transmission delay. This is proper for the scenario of real-time applications.

In the MORL-based routing, one will adopt the first one. It is also straightforward to implement the second one within the proposed framework. Meanwhile, in order to simplify the MORL procedure, two Q-value tables will be used in the learning and routing algorithm, one for the transmission delay and the other one for the packet loss rate. Similarly to the standard Q-learning procedure, each Q-value table stores the accumulated reward given the state and corresponding action. Thus the first Q-value table (for transmission delay) uses the negative of one hop transmission delay as the immediate reward, while the second Q-value table uses the negative of the accumulated packet loss rate as the immediate reward. The action is to find the forwarding node for the next hop in order to maximize the Q-values.

An MORL algorithm is proposed for the routing procedure, which is summarized in Procedure 1. Simulations have shown that the proposed learning algorithm can achieve a good performance for the routing task.

Procedure 1 Procedure of MORL routing [33]

```
Initialize all the Q-value tables of all nodes
for Each time slot do
    for Each node forwarding a packet do
        Choose the forwarding node from the local Q-value table. The action should minimize
        the Q-value table for the transmission delay, while maintaining the corresponding value
        of the Q-value table for packet loss rate under a specific constraint.
        Sense the channel. If the channel is occupied by PU, then randomly choose another
        channel.
        if ACK is received then
            Update the Q-value tables.
        end if
    end for
end for
```

Multiple User Learning

In the previous discussion, the discussion focused on the learning procedure of a single secondary user. However, in many cases, multiple secondary users need to compete for limited resources. Hence, it is also important to study the learning procedures of multiple users and examine their interactions. In this subsection, one uses the channel selection for instances.

Multiagent Reinforcement Learning

Here one applies the multiagent reinforcement learning for channel selection [18]. For simplicity, one considers only two secondary users, denoted by A and B, and two channels, denoted by 1 and 2. The reward to secondary user i, $i = A, B$, of channel j, $j = 1, 2$, is R_{ij} if secondary user succeeds in transmitting data over channel j (which is not interrupted by primary user or the other secondary user). Otherwise the reward received by the secondary user is 0. For simplicity, one denotes by j^- the other user (channel) different from user (channel) j.

One has the following assumptions for the system:

- The rewards $\{R_{ij}\}$ are unknown to both secondary users, whereas they are fixed throughout the game.
- Both secondary users can sense both channels simultaneously. However, they can choose only one channel for data transmission.
- One considers only the case that both channels are available. Otherwise the actions that the secondary users can take are obvious (transmit over the only available channel or not transmit if no channel is available).
- There is no direct communication between the two secondary users.

The above channel selection game is a 2×2 one, in which the payoff matrices for player A and B are shown in Fig. 15. The actions, denoted by $a_i(t)$ for user i at time t, in the game are the channel selections. The diagonal elements in the

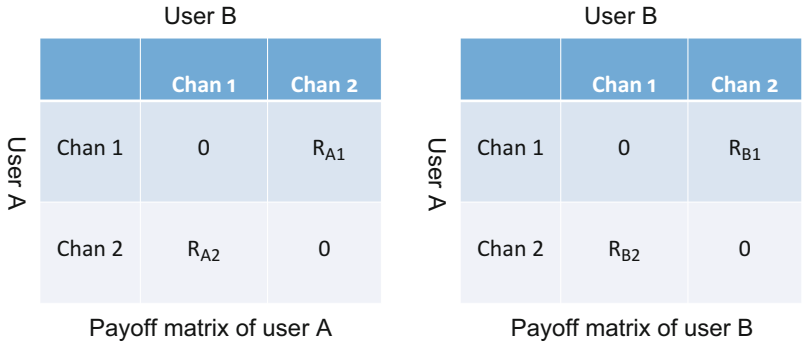

Fig. 15 Payoff matrices in the game of channel selection

payoff matrices are all zero since transmission conflict incurs zero reward. There are two Nash equilibria in the channel selection game, namely, the strategies such that unilaterally changing strategy incurs performance degradation. Both equilibria are pure; i.e. $a_A = 1, a_B = 2$ and $a_A = 2, a_B = 1$ (namely the orthogonal transmission without interference).

Since both channels are available without the interruption of primary users, the system is state-less. Therefore, the Q-value of each player is simply the expected reward of each action; i.e.

$$Q(a) = E[R(a)], \tag{53}$$

where a is the action, R is the reward corresponding to the action while the expectation is over the randomness of the other user's action. Since the action is the channel selection, one denotes by Q_{ij} the value of selecting channel j by secondary user i. The actions in the Q-learning are stochastic for possible exploration. One considers the standard Boltzmann distribution for exploration [29]; i.e.

$$P(\text{user } i \text{ chooses channel } j) = \frac{e^{Q_{ij}/T}}{e^{Q_{ij}/T} + e^{Q_{ij^-}/T}}, \tag{54}$$

where T is the temperature.

When secondary user i selects channel j, the expected reward is given by

$$E[R_i(j)] = \frac{R_{ij} e^{Q_{i^-j^-}/\gamma}}{e^{Q_{i^-j}/\gamma} + e^{Q_{i^-j^-}/\gamma}}, \tag{55}$$

since secondary user i^- chooses channel j with probability $\frac{e^{Q_{i^-j}/\gamma}}{e^{Q_{i^-j}/\gamma}+e^{Q_{i^-j^-}/\gamma}}$ (namely, collision occurs and secondary user i receives no reward) and channel j^- with probability $\frac{e^{Q_{i^-j^-}/\gamma}}{e^{Q_{i^-j}/\gamma}+e^{Q_{i^-j^-}/\gamma}}$ (the transmissions are orthogonal; thus, secondary user i receives reward R_{ij}).

During the operation of the system, the Q-values are updated right after each spectrum access using the following rule:

$$Q_{ij}(t+1) = (1-\alpha_{ij})Q_{ij}(t) + \alpha_{ij}(t) r_i(t) I(a_i(t) = j), \tag{56}$$

where $0 < \alpha_{ij}(t) < 1$ is a step factor (when channel j is not selected by user i, $\alpha_{ij}(t) = 0$) and $r_i(t)$ is the reward that secondary user i receives at time slot t, and I is characteristic function for the event that channel j is selected.

Next, one checks whether the updating rule of Q functions in (56) converges to a point close to the Nash equilibrium if the step factor α satisfies certain conditions. One first provides an intuitive explanation for the convergence using the geometric argument proposed in [21], and illustrated in Fig. 16 (which is called it *Metrick-Polak plot* since it was originally proposed by A. Metrick and B. Polak in [21]). Here the axes represent $\mu_A = \frac{Q_{A1}}{Q_{A2}}$ and $\mu_B = \frac{Q_{B1}}{Q_{B2}}$, respectively. The plane is divided into

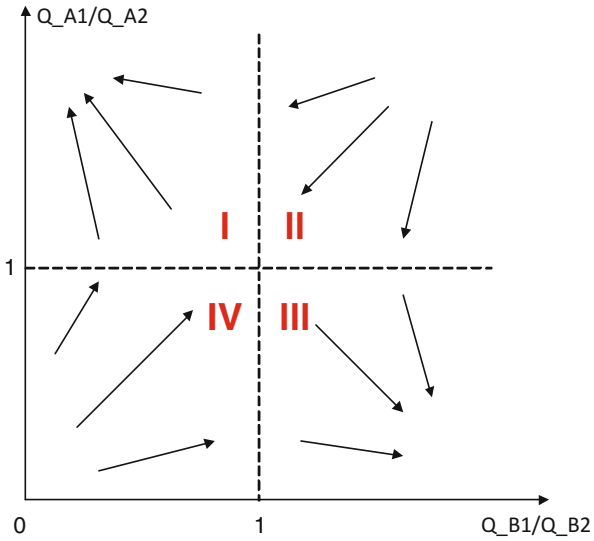

Fig. 16 Illustration of the dynamics in the Q-learning

four regions by two lines $\mu_A = 1$ and $\mu_B = 1$, in which the dynamics of Q-learning follows different patterns. The following four regions are discussed separately:

- Region I: In this region, $Q_{A1} > Q_{A2}$, which means that secondary user A prefers visiting channel 1. Meanwhile, secondary user B prefers to access channel 2 since $Q_{B1} > Q_{B2}$. Then, with a large probability, the strategies of both players will converge to the Nash equilibrium point in which secondary users A and B access channels 1 and 2, respectively.
- Region II: In this region, both secondary users prefer to access channel 1, thus causing collisions. Therefore, both Q_{A1} and Q_{B1} will be reduced until entering either region I or region III.
- Region III: similar to region I.
- Region IV: similar to region II.

The points in regions II and IV are unstable and will move into region I or III with a large probability. In regions I and III, the strategy will move close to the Nash equilibrium points with a large probability. Therefore, regardless of where the initial point is, the updating rule in (56) will yield a stationary equilibrium point with a large probability.

In order to prove the convergence rigorous, one first finds the equivalence between the updating rule in (56) and the celebrated Robbins-Monro iteration [26], which is used to solve equations with unknown expressions. Then, one can apply the conclusion in the theory of stochastic approximation [16] to relate the iteration with an ordinary differential equation (ODE) and thus prove the convergence.

The updating rule of Q-learning is equivalent to the following four equations:

$$Q_{ij} = \frac{R_{ij} e^{Q_{i-j}-/\gamma}}{e^{Q_{i-j}/\gamma} + e^{Q_{i-j}-/\gamma}}, \qquad i = A, B, \ j = 1, 2. \tag{57}$$

Then, one defines $\mathbf{q} = (Q_{A1}, Q_{A2}, Q_{B1}, Q_{B2})^T$, which makes (57) equal to

$$\mathbf{g}(\mathbf{q}) = \mathbf{A}(\mathbf{q})\mathbf{r} - \mathbf{q} = 0, \tag{58}$$

where $\mathbf{r} = (R_{A1}, R_{A2}, R_{B1}, R_{B2})^T$ and the matrix $\mathbf{A}$ is given by

$$\mathbf{A}_{ij} = \begin{cases} \frac{e^{Q_{i-j}-/\gamma}}{e^{Q_{i-j}/\gamma} + e^{Q_{i-j}-/\gamma}}, & \text{if } i = j \\ 0, & \text{if } i \neq j \end{cases}. \tag{59}$$

Then, the iteration in (56) is equivalent to solving the equation in (58). However, the expression of the equation is unknown in advance, since the rewards, as well as the strategy of the other user, are unknown. Hence, one can use the Robbins-Monro algorithm [16], which is given by

$$\mathbf{q}(t+1) = \mathbf{q}(t) + \alpha(t)\mathbf{Y}(t), \tag{60}$$

where $\mathbf{Y}(t)$ is a random and noisy observation on function g; i.e.

$$\begin{aligned} \mathbf{Y}(t) &= \mathbf{r}(t) - \mathbf{q}(t) \\ &= \bar{\mathbf{r}}(t) - \mathbf{q}(t) + \mathbf{r}(t) - \bar{\mathbf{r}}(t) \\ &= \mathbf{g}(\mathbf{q}(t)) + \delta M(t), \end{aligned} \tag{61}$$

where $\mathbf{g}(\mathbf{q}(t)) = \bar{\mathbf{r}}(t) - \mathbf{q}(t)$, $\delta M(t) = \mathbf{r}(t) - \bar{\mathbf{r}}(t)$ is noise for estimating $\bar{\mathbf{r}}(t)$ and $\bar{\mathbf{r}}(t)$ is the expectation of reward, which is given by

$$\bar{\mathbf{r}}(t) = \mathbf{A}(\mathbf{q}(t))\mathbf{r}. \tag{62}$$

As has been shown above, the procedure of using the Robbins-Monro algorithm is the stochastic approximation of the equation solution. It has been shown that the convergence of such a procedure can be determined by an ODE. Since the noise $\delta M(t)$ in (61) is a Martingale difference, it is easy to verify the conditions in Theorem 12.3.5 in [16] and thus obtain the following proposition:

Proposition 1. *With probability 1, the sequence* $\mathbf{q}(t)$ *converges to some limit set of the ODE*

$$\dot{\mathbf{q}} = \mathbf{g}(\mathbf{q}). \tag{63}$$

What remains is to analyze the convergence of the ODE in (63). With a nontrivial proof in [18], the following proposition is obtained for the convergence of the learning procedure:

Proposition 2. *The solution of ODE* (63) *converges to the stationary point determined by* (58).

Multiagent Bandit

The multiarmed bandit algorithm can also be extended to the case of multiple users. Suppose that there are K secondary users in the cognitive radio system [17]. Then, these secondary users need to avoid the interruptions from primary users and interference from other secondary users. The model for the channels can be found in the single user case discussed above.

In this chapter, one assumes that each secondary user can sense and transmit over only one channel. One assumes that the secondary users sharing the same channel use the carrier sense multiple access/collision avoidance (CSMA/CA) protocol to avoid collisions. One denotes by $\mathcal{K}_i(j)$ the set of secondary users sensing channel i at time slot j. Hence, if at time slot j secondary user k finds that channel i is free of primary users, it generates a random number $t_k(j)$ according to a predetermined distribution g. Then, it will wait for a time duration $t_k(j)$, and sense the channel at the end of the waiting period. If the channel is free, the secondary user goes ahead to transmit; otherwise it gives up the transmission. One assumes that the transmission of a packet will span the whole time slot. Hence, only the secondary user having the smallest waiting time will obtain the chance to transmit. Therefore, the throughput of secondary user k within one time slot is given by

$$W_k = \sum_{j=1}^{T} Z_{S_k(j)}(j) I\left\{k = \arg \min_{q \in \mathcal{K}_{S_k(j)}(j)} t_q(j)\right\}, \tag{64}$$

In the setup of multiple secondary users, even if the probabilities θ are known to the secondary users, the strategy for channel selection and accessing is still nontrivial. Different from the single-user case, it is not a good idea to always choose the channel having the least primary user activities, since there will be a congestion among the secondary users if all the secondary users select the idlest channel. Hence, the secondary users should "spread" their selections over more channels in a random manner. It is shown in [17] that the optimal strategy in the multiple user case is given by

$$p_i^* = \begin{cases} \left[1 - \left(\frac{\lambda^*}{K\theta_i}\right)^{\frac{1}{K-1}}\right], & \text{if } \theta_i > 0 \\ 0, & \text{otherwise} \end{cases}, \tag{65}$$

where λ^* is the Lagrange factor to make $\sum_{i=1}^{N} p_i^* = 1$ and $\{x\}^+$ is equal to $\max\{0, x\}$.

When the idle probability θ is unknown, the following rule is adopted in [17]:

1. Initialization: Similarly to the single-user case, each secondary user k maintains two N-vectors: $\mathbf{x}_k$ and $\mathbf{y}_k$, whose meanings are the same as those of the single-user case.
2. At the beginning of each time slot, the secondary user updates the values of $\mathbf{x}_k$ and $\mathbf{y}_k$, according to the sensing result.
3. At the beginning of each time slot j, user k updates the estimation of θ_i using

$$\hat{\theta}_i(j) = \frac{X_{k,i}(j)}{Y_{k,i}(j)}. \tag{66}$$

4. Then, the secondary user will choose channel i using the following probability

$$p_i(j) = \frac{\hat{\theta}_i(j)}{\sum_{i=1}^{N} \hat{\theta}_i(j)}. \tag{67}$$

It is shown that, if K is sufficiently large, the above rule will converge to the Nash equilibrium in probability, as T tends to infinity.

Collaborative Filtering

As has been explained in the previous section, collaborative filtering can be used to find similar users or items such that recommendations can be made for users having not accessed certain items. The recommendation could be positive (namely, this channel is good for you) or negative (namely, this channel is harmful for you). In this discussion, one follows the study in [19] and consider a cognitive radio network having N secondary users. One can use an undirected graph to use to represent the network, where each vertex is a secondary user and each edge means that the corresponding two secondary users can directly communicate with each other. One denotes by $\mathcal{N}_i$ the set of neighbors that can communicate directly to secondary user i. These secondary users are allowed to access M licensed channels, which may be dynamically used by primary users. One considers the following assumptions:

- The system timing is slotted, as illustrated in Fig. 17. In each time slot, each secondary user can choose a channel and sense the spectrum. At the end of each time slot, the secondary user exchanges information for collaborative learning.

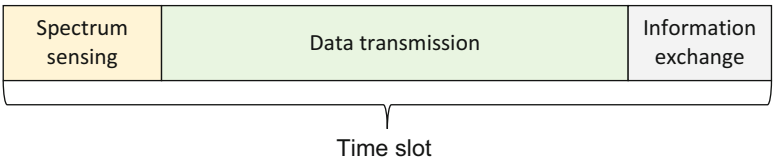

Fig. 17 An illustration of the timing structure

Due to the limited capability of spectrum sensing, each secondary user can sense only one channel in each time slot. It is straightforward to extend the algorithm to the case of sensing multiple channels simultaneously.

- The spectrum sensing result is always correct. This is reasonable when the signal-to-noise ratio (SNR) is good. The study is focused on the competition, instead of low SNR.
- In each time slot, a secondary user can communicate with only one neighbor, due to the limited communication capability. The communication fails with a small probability P_c. The packet containing the information for collaborative learning is protected by parity check bits, such that the receiver can detect possible decoding errors.
- The secondary users have no knowledge about the locations, transmission time and transmit power of primary users. The spectrum activities are independent in different time slots and for different primary users. Different primary users can share the same channel, e.g., using code division multiple access (CDMA).

The activity of each channel can be modeled as a Bernoulli random variable: 0 means that the channel has been occupied by primary users, while 1 means that the channel is usable by secondary users. The Bernoulli assumption is reasonable if each time slot is sufficiently large, such that the time correlation of spectrum occupancy vanishes. One denotes by μ_{ij} the probability that channel j cannot be used by secondary user i. Since μ_{ij} is unknown, it is considered as a random variable in the Bayesian framework. μ_{ij} has a conjugate a priori beta distribution with parameters α and β, which is denoted by beta(α, β). One assumes that α and β are common for all μ_{ij}. The expression of the pdf of $\mu$is thus given by

$$f(\mu; \alpha, \beta) = \frac{\mu^{\alpha-1}(1-\mu)^{\beta-1}}{\int_0^1 q^{\alpha-1}(1-q)^{\beta-1}dq}. \tag{68}$$

Now, the collaborative filtering is discussed. One begins from the simplest case, in which there is only one secondary user. Consider secondary user i. It can use the following unbiased estimation for μ_i:

$$\hat{\mu}_{ii} = \frac{1}{n_i} \sum_{j \in I_{i1}} x_{ij}, \tag{69}$$

where x_{ij} is the observation, 1 or 0, of secondary user i at time slot j.

Then, one considers two neighboring secondary users carrying out the collaborative filtering. One uses the estimation of secondary user 1 to predict the parameter of secondary user 2. Suppose that the estimation of secondary user 1 is given by μ_1. Then, the linear prediction is given by

$$\hat{\mu}_2 = a\mu_1 + b. \tag{70}$$

In the MMSE linear prediction, the optimal coefficients a and b are given by

$$a = \rho_{12}\frac{\sigma_2}{\sigma_1}, \tag{71}$$

and

$$b = E[\mu_2] - aE[\mu_1]. \tag{72}$$

Note that σ_1 and σ_2 are variances of μ_1 and μ_2, respectively. ρ_{12} is the correlation factor of μ_1 and μ_2, which is defined as

$$\rho_{12} = \frac{E[(\mu_1 - E[\mu_1])(\mu_2 - E[\mu_2])]}{\sqrt{\sigma_1}\sqrt{\sigma_2}}. \tag{73}$$

The above estimation can be easily extended to the case of multiple neighbors.

The above calculation assumes that the correlation factor ρ_{12} between secondary users 1 and 2 is known. However, this information is unknown to secondary users in advance. Therefore, each secondary user needs to estimate ρ_{ij} from the history of spectrum sensing in the following procedure:

1. Consider secondary user i, $i = 1, 2$. Each estimates its own expectation and variance using the following equations:

$$\hat{\mu}_{ii} = \frac{1}{T}\sum_{t=1}^{T} x_{it}, \tag{74}$$

and

$$\hat{\mu}_{iim} = \frac{1}{n_{im}}\sum_{t\in I_m}^{T} x_{it}, \forall n_{im} > 0, \tag{75}$$

and

$$\hat{\sigma}_{ii} = \frac{1}{|Z_i|}\sum_{m\in Z_i}(\hat{\mu}_{iim} - \hat{\mu}_{ii})^2. \tag{76}$$

These statistics are obtained from the channels probed by secondary user i before. Secondary user j also carries out the same procedure.

2. The correlation between secondary users i and j is computed using

$$\hat{\rho}_{ij} = \frac{1}{|Z_i \cap Z_j|}\frac{\sum_{m\in Z_i, m\in Z_j}(\hat{\mu}_{iim} - \hat{\mu}_{ii})(\hat{\mu}_{jjm} - \hat{\mu}_{jj})}{\sqrt{\hat{\sigma}_{ii}}\sqrt{\hat{\sigma}_{jj}}}. \tag{77}$$

Once the correlations and expectations have been estimated, the secondary users need to carry out the channel selection. Consider two secondary users 1 and 2. Assume that channel j has been probed by secondary user i for n_{ij} times. When applying the linear prediction proposed in the previous discussion, each secondary user faces the following tradeoff between exploration and exploitation:

- Exploitation: Consider a certain secondary user n. If the availability probability of channel i has been well estimated by another secondary user, say m, secondary user n should exploit the estimation of secondary user m and does not probe channel i, given that the channel availability probabilities of secondary users m and n are similar.
- Exploration: Secondary user n should probe channels that are rarely probed by itself in order to better assess the similarity to other secondary users.

One approach is to borrow the idea of Boltzmann distribution from reinforcement learning. One can adjust the temperature to tune the tradeoff between exploitation and exploration.

One remaining problem is the user selection, namely, how to choose a neighbor to consult about the spectrum situation. Since it is very difficult to derive a theoretically optimal rule, one proposes heuristic algorithms for the information request motivated by the exploration rule used in reinforcement learning. One assumes that, in each time slot, each secondary user can exchange information with at most one neighbor, and it needs to choose a neighbor to request the information of spectrum statistics. It is desirable for a secondary user to exchange information with a neighbor that is more similar to itself. The similarity can be measured by the correlation factor ρ. Therefore, the secondary user can choose a neighbor having the largest correlation factor. However, this approach focuses too much on the exploitation and thus may lose chances of finding better channels. Suppose that one considers the user selection of a generic secondary user i. Then, the considerations of exploration and rejection are discussed as follows:

- Exploration: Since the estimated correlation factors are never precise, it is possible that another secondary user having a smaller estimation of the correlation factor actually has a larger correlation factor. If secondary user i insists on the neighbor currently having the largest correlation factor estimation, it may lose the opportunity to find a neighbor that is actually more similar. Therefore, secondary user i should also explore neighbors other than the one having the largest correlation factor estimation.
- Rejection: Even if a neighbor, say secondary user j, has the largest true correlation, it may not respond to the request of secondary user i. It is possible that user j may have a more similar neighbor, say secondary user k, and thus will communicate to secondary user k, instead of user i. Therefore, secondary user i should try to contact other neighbors if its request is declined by secondary user j for several times.

Based on the above reasons, one approach is to use the Boltzmann distribution to alleviate the tradeoff between exploration and exploitation. Consider secondary user i. The probability that it chooses secondary user j, which is a neighbor of secondary user i, is given by

$$p_i^j = \frac{e^{\frac{\tilde{\rho}_{ij}}{T}}}{\sum_{k \in \mathcal{N}_i} e^{\frac{\tilde{\rho}_{ik}}{T}}}, \tag{78}$$

where T is the temperature, which controls the balance between the exploration and exploitation. To address the problem of possible rejection by the requested secondary user, one can use an exponentially decreasing correlation factor in (78), which is given by

$$\tilde{\rho}_{ij} = \beta^{r_{ij}} \hat{\rho}_{ij}, \tag{79}$$

where $\hat{\rho}_{ij}$ is the estimated correlation obtained from (77), $0 < \beta < 1$ is a decaying factor and r_{ij} is the number of times that the request from secondary user i to secondary user j is rejected, which is reset to 0 once secondary user j grants the request from secondary user i.

Conclusions and Future Directions

Machine learning has widely been applied in the area of cognitive radio networks and will be a promising direction of research. The following techniques in machine learning could be of particular value in cognitive radio networks:

- Deep reinforcement learning: With the substantial success of deep learning, it is prospective to employ deep learning techniques in cognitive radio networks, due to the capability of universal learning of neural networks. Deep reinforcement learning has integrated both deep learning and reinforcement learning, which can be used in the scheduling and routing of cognitive radio networks.
- Distributed learning: The learning procedure in cognitive radio networks is often carried out in a distributed manner. Hence, it is of substantial importance to consider the communication complexity in distributed learning since the efficiency can be improved when the communication overhead can be minimized.

References

1. Aggarwal CC (2016) Recommender systems: the textbook. Springer, New York
2. Anthony M, Bartlett P (1999) Neural network learning: theoretical foundations. Cambridge University Press, Cambridge

3. Azar Y, Fiat A, Karlin A, McSherry F, Saia J (2001) Spectral analysis of data. In: Proceedings of the 33rd ACM symposium on theory of computing (STOC), 6 July 2001, pp 619–626
4. Berkvosky S, Kuflik T, Ricci F (2007) Distributed collaborative filtering with domain specialization. In: Proceedings of ACM conference recommender systems (RecSys), 19 Oct 2007, pp 33–40
5. Bertsekas DP (1987) Dynamic programming: deterministic and stochastic models. Prentice Hall, Englewood Cliffs
6. Busoniu L, Babuska R, Schutter BD (2008) A comprehensive survey of multiagent reinforcement learning. IEEE Trans Syst Man Cybern Part C Appl Rev 38(2):156–172
7. Chapelle O, Scholkopf B, Zien A (2006) Semi-supervised learning. The MIT Press, Cambridge
8. Devroye L, Lugosi G (2001) Combinatorial methods in density estimation. Springer, New York
9. Drineas P, Kerenidis I, Raghavan P (2002) Competitive recommendation systems. In: Proceedings of the 34th ACM symposium on theory of computing (STOC), 19 May 2002, pp 82–90
10. Fudenberg D, Tirole J (1991) Game theory. The MIT Press, Cambridge
11. Gabor Z, Kalmar Z, Szepesvari C (1998) Multi-criteria reinforcement learning. In: Proceedings of the 15th International conference on machine learning (ICML), 24 July 1998, vol 98, pp 197–205
12. Gittins JC (1979) Bandit processes and dynamic allocation indices. J R Stat Soc Ser B (Stat Methodol) 41(2):148–177
13. Goldberg D, Nichols D, Oki BM, Terry D (1992) Using collaborative filtering to weave an information tapestry. Commun ACM 35(12):61–70
14. Goodfellow I, Bengio Y (2016) Deep learning. The MIT Press, Cambridge
15. Hastie T, Tibshirani R, Friedman J (2009) The elements of statistical learning: data mining, inference, and prediction, 2nd edn. Springer, New York
16. Kushner HJ, Yin GG (2003) Stochastic approximation and recursive algorithms and applications. Springer, New York
17. Lai L, Gamal HE, Jiang H, Poor HV (2011) Cognitive medium access: exploration, exploitation, and competition. IEEE Trans Mob Comput 10(2):239–253
18. Li H (2009) Multi-agent Q-learning of channel selection in multi-user cognitive radio systems: a two by two case. In: Proceedings of IEEE International conference on systems, man and cybernetics, 11 Oct 2009, pp 1893–1898
19. Li H (2009) Learning the spectrum via collaborative filtering in cognitive radio networks. In: Proceedings of IEEE symposium on new frontiers in dynamic spectrum (DySPAN), 6 Apr 2010, pp 1–12
20. Littman ML (2001) Value-function reinforcement learning in Markov games. J Cogn Syst Res 2(1):55–66
21. Metrick A, Polak B (1994) Fictitious play in 2×2 games: a geometric proof of convergence. Econ Theory 4(6):923–933
22. Mohri M, Rostamizadeh A, Talwalkar A (2012) Foundations of machine learning. The MIT Press, Cambridge
23. O'Shea TJ, Corgan J, Clancy TC (2016) Convolutional radio modulation recognition networks. In: Proceedings of International conference on engineering applications of neural networks, 2 Sept 2016, pp 213–226
24. O'Shea TJ, Corgan J, Clancy TC (2016) Unsupervised representation learning of structured radio communication signals. In: Proceedings of 1st International workshop on sensing, processing and learning for intelligent machines (SPLINE), 6 July 2016, pp 1–5
25. Robbins H (1952) Some aspects of the sequential design of experiments. Bull Am Math Soc 58(5):527–535
26. Robbins H, Monro S (1951) A stochastic approximation method. Ann Math Stat 2:400–407
27. Schapire RE, Freud Y (2014) Boosting: foundations and algorithms. The MIT Press, Cambridge
28. Schlkopf B, Smola AJ (2001) Learning with kernels: support vector machines, regularization, optimization and beyond. The MIT Press, Cambridge

29. Sutton RS (1998) Reinforcement learning: an introduction. The MIT Press, Cambridge
30. Thilina KM, Choi KW, Saquib N, Hossain E (2013) Machine learning techniques for cooperative spectrum sensing in cognitive radio networks. J Sel Areas Commun 31(11): 2209–2221
31. Watkins CJCH (1989) Learning from delayed rewards. Ph.D. thesis, Cambridge University, Cambridge
32. Wiering M, Otterio M (2012) Reinforcement learning: state-of-the-art. Springer, Berlin/Heidelberg
33. Zheng K, Li H (2011) Multi-objective reinforcement learning based routing in cognitive radio networks: walking in a random maze. In: Proceedings of IEEE International conferences on computing, networking and communications (ICNC), 30 Jan 2011, pp 359–363

Spatial Spectrum Access Game

34

Xu Chen and Jianwei Huang

Contents

Part of the results has appeared in our previous publication in [1].

X. Chen (✉)
School of Data and Computer Science, Sun Yat-Sen University, Guangzhou, China
e-mail: chenxu35@mail.sysu.edu.cn

J. Huang
Department of Information Engineering, The Chinese University of Hong Kong, Shatin, New Territory, Hong Kong, China
e-mail: jwhuang@ie.cuhk.edu.hk

W. Zhang (ed.), *Handbook of Cognitive Radio*,
https://doi.org/10.1007/978-981-10-1394-2_42

Abstract

A key feature of wireless communications is the spatial reuse of wireless resources. However, such a spatial aspect is relatively less understood for the purpose of designing efficient spectrum sharing mechanisms. In this chapter, we propose a framework of spatial spectrum access games, where we model fairly general spatial interference relationships among users as directed interference graphs. We show that a pure Nash equilibrium exists for the two classes of games: (1) any spatial spectrum access games on directed acyclic graphs and (2) any games satisfying the congestion property on directed trees and directed forests. We identify the graphical structures under which the spatial spectrum access games have pure Nash equilibria and further show that under mild conditions, the spatial spectrum access games with random backoff and Aloha channel contention mechanisms on undirected graphs are potential games and have pure Nash equilibria as well. We also quantify the price of anarchy of the general spatial spectrum access game. We then propose a distributed learning algorithm, which only utilizes users' local observations to adaptively adjust the spectrum access strategies. We show that the distributed learning algorithm can converge to an approximate mixed strategy Nash equilibrium for any spatial spectrum access games. We further generalize the spatial spectrum access game framework to accommodate the physical interference model. Numerical results demonstrate that the distributed learning algorithm achieves significant performance improvement over the benchmark algorithms.

Introduction

Cognitive radio is envisioned as a promising technology to alleviate the problem of spectrum underutilization [2]. It enables unlicensed wireless users (secondary users) to opportunistically access the licensed channels owned by legacy spectrum holders (primary users) and, hence, can significantly improve the spectrum efficiency [2].

A key challenge of the cognitive radio technology is how to resolve the resource competition by selfish secondary users in a decentralized fashion. If multiple secondary users transmit over the same channel simultaneously, severe interferences or collisions might occur, and the individual as well as total data rates of all users may get reduced. This highlights the importance of designing efficient spectrum sharing mechanisms for cognitive radio networks.

The competitions among secondary users for common spectrum have often been studied as a noncooperative game (e.g., [3–7] and the references therein). A common assumption of many existing studies is that secondary users are close-by and interfere with each other when they transmit on the same channel simultaneously. However, a unique feature of wireless communication is spatial reuse. If users who transmit simultaneously are located sufficiently far away, then simultaneous transmissions over the same channel may not cause any performance degradation to the users. Such spatial effect on spectrum sharing is less understood than many other aspects in the existing literature [8].

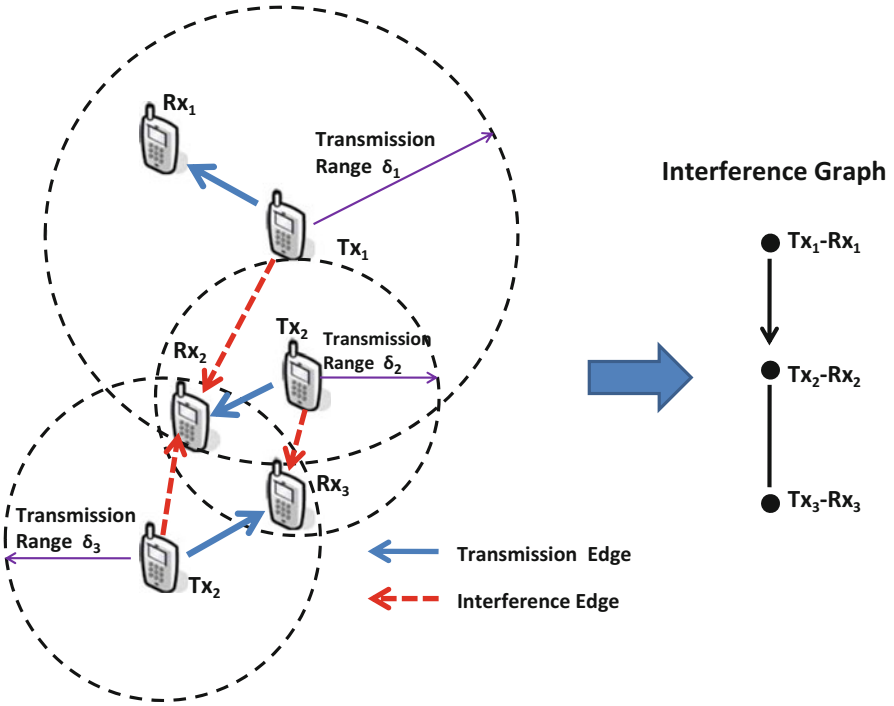

Fig. 1 Illustration of distributed spectrum access with spatial reuse under the protocol interference model. Each user n is represented by a transmitter Tx_n and receiver Rx_n pair. Users 2 and 3 cannot generate interference to user 1, since user 1's receiver Rx_1 is far from user 2 and 3's transmitters. On the other hand, user 1 can generate interference to user 2, since user 2's receiver Rx_2 is within the transmission range of user 1's transmitter Tx_1. Similarly, user 2 and user 3 can generate interferences to each other

Motivated by this, in this chapter, we describe a novel spatial spectrum access game framework to take spatial relationship into account. As illustrated in Fig. 1, the interference relationship among the secondary users can be asymmetric due to the heterogeneous transmission powers and locations of the users. We hence propose a general framework of spatial spectrum access game where secondary users interact over the directed interference graphs, which allows us to model users' heterogeneous resource competition capabilities and asymmetric interference relationship. Moreover, we design a practical distributed algorithm for achieving the equilibria of the spatial spectrum access game. The main results and contributions of this chapter are as follows:

- *General game formulation*: We formulate the distributed spectrum access problem as a spatial spectrum access game on directed interference graphs, with user-specific channel data rates and channel contention capabilities.

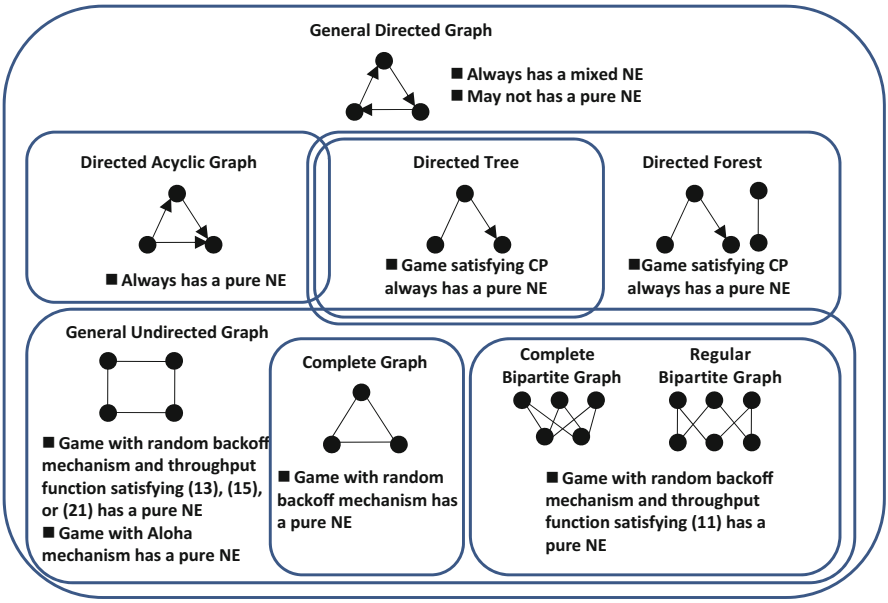

Fig. 2 Summary of the results on the existence of both mixed and pure Nash equilibrium (NE) of spatial spectrum access games. Here CP means congestion property (see section "Existence of Nash Equilibria")

- *Existence of Nash equilibria*: As summarized in Fig. 2, we systematically investigate the existence of Nash equilibrium. Specifically, we show by counter examples that a general spatial spectrum access game may not have a pure Nash equilibrium. We also show that a pure strategy equilibrium exists in the following two classes of games: (1) any spatial spectrum access games on directed acyclic graphs and (2) any games satisfying the congestion property on directed trees and directed forests. We identify the graphical structures under which the spatial spectrum access games have pure Nash equilibria and further show that under mild conditions, the spatial spectrum access games with random backoff and Aloha channel contention mechanisms on undirected graphs are potential games and have pure Nash equilibria as well. We also quantify the price of anarchy of the spatial spectrum access game.
- *Distributed learning for achieving an approximate Nash equilibrium*: We develop a maximum likelihood estimation approach for estimating user expected throughput based on local observations. Based on such local estimations, we then propose a distributed learning algorithm that can converge to an approximate mixed Nash equilibrium for any spatial spectrum access games. Numerical results demonstrate that the distributed learning algorithm achieves significant performance improvement over the random access algorithm.

The rest of the chapter is organized as follows. We first introduce the related work in section "Related Research" and present the system model in section "System

Model". We then present the spatial spectrum access game framework in section "Spatial Spectrum Access Game" and explore the existence of Nash equilibrium in section "Existence of Nash Equilibria". We analyze the price of anarchy and propose the distributed reinforcement learning algorithm in sections "Price of Anarchy and Distributed Learning for Spatial Spectrum Access Game", respectively. We discuss the extension of the spatial spectrum access game in section "Extension to Physical Interference Model", present the numerical results in section "Numerical Results", and finally conclude the chapter in section "Conclusion".

Related Research

A common modeling approach for distributed spectrum access is to consider selfish secondary users and model their interactions as noncooperative games. There is a vast literature along this line, and here we will briefly outline some representative ones. Nie et al. in [9] designed a self-enforcing distributed spectrum access mechanism based on potential games. Niyato and Hossain in [3] proposed a dynamic game approach for analyzing the competition among secondary users for spectrum access. Flegyhzi et al. in [4] proposed a two-tier game framework for cognitive radio medium access control (MAC) mechanism design. Yang et al. in [5] studied a price-based spectrum access mechanism for competitive secondary users. Li et al. in [6] proposed a game theoretic framework to achieve incentive compatible multiband sharing among the secondary users. Law et al. in [7] studied the system performance degradation due to the competition of secondary users in distributed spectrum access game.

When not knowing the spectrum information such as channel availability, secondary users need to learn the network environment and adapt the spectrum access decisions accordingly. Han et al. in [10] and Maskery et al. in [11] used no-regret learning to solve this problem, assuming that the users' channel selections are common information. The learning converges to a correlated equilibrium [12], wherein the common observed history serves as a signal to coordinate all users' channel selections. When users' channel selections are not observable, authors in [13–15] designed a multi-agent multiarmed bandit learning algorithm to minimize the expected performance loss of distributed spectrum access. Li [16] applied reinforcement learning to analyze Aloha-type spectrum access by relying on each individual secondary user's local adaption and experience.

As mentioned above, a commonly adopted assumption of many existing studies is that secondary users are close-by and interfere with each other when they transmit on the same channel simultaneously. Only a few efforts have been made to investigate the spatial reuse feature of distributed spectrum access. In a recent work, Tekin et al. in [17] proposed a novel spatial congestion game framework to take spatial relationship into account. The key idea is to extend the classical congestion game upon an *undirected* graph, by assuming that the interferences among the players are symmetric and a player's throughput depends on the number of players in its neighborhood that choose the same resource. However, as discussed

above the interference relationship among the secondary users can be asymmetric due to the heterogeneous transmission powers and locations of the users. Hence we propose a more general framework of spatial spectrum access game on *directed* interference graphs in this chapter. The congestion game on directed graphs has also been studied in [18], with the assumption that players have linear and homogeneous payoff functions. The game model in this chapter is more general and allows both linear and nonlinear player-specific payoff functions.

System Model

We consider a cognitive radio network with a set $\mathscr{M} = \{1, 2, \ldots, M\}$ of independent and stochastically heterogeneous primary channels. A set $\mathscr{N} = \{1, 2, \ldots, N\}$ of secondary users try to access these channels distributively when the channels are not occupied by primary (licensed) transmissions. Here we assume that each secondary user is a dedicated transmitter-receiver pair.

To take users' spatial relationship into account, we denote $\boldsymbol{d}_n = (d_{Tx_n}, d_{Rx_n})$ as the **location vector** of secondary user n, where d_{Tx_n} and d_{Rx_n} denote the locations of the transmitter and the receiver, respectively. Each secondary user n has a **interference range** ν_n. Then given the location vectors of all secondary users, we can obtain the **interference graph** $G = \{\mathscr{N}, \mathscr{E}\}$ to describe the interference relationship among the users. Here the vertex set $\mathscr{N}$ is the same as the secondary user set. The edge set is defined as $\mathscr{E} = \{(i, j) : ||d_{Tx_i}, d_{Rx_j}|| \leq \nu_i, \forall i, j \neq i \in \mathscr{N}\}$, where $||d_{Tx_i}, d_{Rx_j}||$ is the distance between the transmitter of user i and the receiver of user j. In general, an interference edge can be directed or undirected. If an interference edge is directed from secondary user i to user j, then user j's data transmission will be affected by user i's transmission on the same channel, but user i will not be affected by user j. If the interference edge is undirected (Here the edge is actually bi-directed. We follow the conventions in [17] and ignore the directions on the edge.) between user i and user j, then the two users can affect each other. Note that a generic directed interference graph can consist of a mixture of directed and undirected edges. In the sequel, we call an interference graph undirected, if and only if all the edges of the graph are undirected. We also denote the set of users that can cause interference to user n as $\mathscr{N}_n = \{i : (i, n) \in \mathscr{E}, i \in \mathscr{N}\}$.

Based on the interference model above, we describe the cognitive radio network with a slotted transmission structure as follows:

- *Channel State*: the channel state for a channel m during time slot t is $S_m(t) = 0$ if channel m is occupied by primary transmissions, and $S_m(t) = 1$ otherwise.
- *Channel State Transition*: for a channel m, the channel state $S_m(t)$ is a random variable with a probability density function as ψ_m. In the following, we denote the channel idle probability θ_m as the mean of $S_m(t)$, i.e., $\theta_m = E_{\psi_m}[S_m(t)]$. For example, the state of a channel changes according to a two-state Markovian process. We denote the channel state probability vector of channel m at time t as

$\boldsymbol{q}_m(t) \triangleq (Pr\{S_m(t) = 0\}, Pr\{S_m(t) = 1\})$, which forms a Markov chain as $\boldsymbol{q}_m(t) = \boldsymbol{q}_m(t-1)\Gamma_m, \forall t \geq 1$, with the transition matrix

$$\Gamma_m = \begin{bmatrix} 1-\varepsilon_m & \varepsilon_m \\ \xi_m & 1-\xi_m \end{bmatrix}.$$

Furthermore, the long-run statistical channel availability $\theta_m \in (0, 1)$ of a channel m can be obtained from the stationary distribution of the Markov chain, i.e.,

$$\theta_m = \frac{\varepsilon_m}{\varepsilon_m + \xi_m}. \tag{1}$$

As another example, we can also use the channel idle probability θ_m to indicate the spectrum availability for white-space spectrum access. Due to the fact that the activities of primary users on TV channels typically change very slowly, the most recent FCC ruling requires white-space devices (i.e., secondary users of TV channels) to determine the spectrum availability via a database [19]. In this case, we can set that $\theta_m = 1$ if the TV channel m is vacant for secondary users and $\theta_m = 0$ otherwise.

- *User-Specific Channel Throughput*: for each secondary user n, its realized data rate $b_m^n(t)$ on an idle channel m in each time slot evolves according to a random process with a mean B_m^n, due to users' heterogeneous transmission technologies and the local environmental effects such as fading. For example, we can compute the data rate $b_m^n(t)$ according to the Shannon capacity as

$$b_m^n(t) = W \log_2 \left(1 + \frac{\eta_n z_m^n(t)}{\omega_m^n}\right), \tag{2}$$

where W is the channel bandwidth, η_n is the fixed transmission power adopted by user n according to the requirements such as the primary user protection, ω_m^n denotes the background noise power, and $z_m^n(t)$ is the channel gain. In a Rayleigh fading channel environment, the channel gain $z_m^n(t)$ is a realization of a random variable that follows the exponential distribution.

- *Time Slot Structure*: each secondary user n executes the following stages synchronously during each time slot:
  - *Channel Sensing*: sense one of the channels based on the channel selection decision made at the end of previous time slot.
  - *Channel Contention*: Let a_n be the channel selected by user n and $\boldsymbol{a} = (a_1, \ldots, a_N)$ be the channel selection profile of all users. The probability that user n can grab the chosen idle channel a_n during a time slot is $g_n(\mathcal{N}_n^{a_n}(\boldsymbol{a})) \in (0, 1)$, which depends on the subset of user n's interfering users that choose the same channel $\mathcal{N}_n^{a_n}(\boldsymbol{a}) \triangleq \{i \in \mathcal{N}_n : a_i = a_n\}$. Here are two examples:

1. *Random backoff mechanism*: the contention stage of a time slot is divided into $\lambda_{\max}$ mini-slots (The contention window size $\lambda_{\max}$ plays an important role for optimizing the system performance. If $\lambda_{\max}$ is too small, it would increase the collision probability among users and hence negatively affect the system performance. In general, if $\lambda_{\max}$ is too large, it would reduce the spectrum access time and hence reduce the system throughput. To optimize the system performance, we can adopt the approach in [20] to determine the optimal contention window size.). Each contending user n first counts down according to a randomly and uniformly generated integer backoff time counter (number of mini-slots) λ_n between 1 and $\lambda_{\max}$. If there is no active transmissions till the countdown timer expires, the user monitors the channel and transmits RTS/CTS messages on that channel. If multiple users choose the same backoff counter, a collision will occur, and no users can grab the channel successfully. After a user successfully grabs the channel, he starts to transmit its data packet. In this case, we have

$$\begin{aligned} g_n(\mathcal{N}_n^{a_n}(\boldsymbol{a})) &= Pr\{\lambda_n < \min_{i \in \mathcal{N}_n : a_i = a_n} \{\lambda_i\}\} \\ &= \sum_{\lambda=1}^{\lambda_{\max}} Pr\{\lambda_n = \lambda\} Pr\{\lambda_n < \min_{i \in \mathcal{N}_n : a_i = a_n} \{\lambda_i\} | \lambda_n = \lambda\} \\ &= \sum_{\lambda=1}^{\lambda_{\max}} \frac{1}{\lambda_{\max}} \left(\frac{\lambda_{\max} - \lambda}{\lambda_{\max}} \right)^{K_n^{a_n}(\boldsymbol{a})}, \end{aligned} \tag{3}$$

   where $K_n^{a_n}(\boldsymbol{a}) = |\mathcal{N}_n^{a_n}(\boldsymbol{a})| = \sum_{i \in \mathcal{N}_n} I_{\{a_i = a_n\}}$ denotes the number of user n's interfering users choosing the same channel as user n.
2. *Aloha mechanism*: user n contends for an idle channel with a probability $p_n \in (0, 1)$ in a time slot. If multiple interfering users contend for the same channel, a collision occurs, and no user can grab the channel for data transmission. In this case, we have

$$g_n(\mathcal{N}_n^{a_n}(\boldsymbol{a})) = p_n \prod_{i \in \mathcal{N}_n^{a_n}(\boldsymbol{a})} (1 - p_i). \tag{4}$$

– *Data Transmission*: transmit data packets if the user successfully grabs the channel.
– *Channel Selection*: choose a channel to access during next time slot according to the distributed learning algorithm in section "Distributed Learning for Spatial Spectrum Access Game".

Under a fixed channel selection profile $\boldsymbol{a}$, the long-run average throughput of a secondary user n choosing channel a_n can be computed as

$$U_n(\boldsymbol{a}) = \theta_{a_n} B_{a_n}^n g_n(\mathcal{N}_n^{a_n}(\boldsymbol{a})). \tag{5}$$

Note that in practices, due to hardware constraint, each secondary user typically cannot observe the channel states of all the channels in each time slot. In this case, one possible modeling approach is to formulate the distributed spectrum access problem as a partial-observation dynamic game, such that the game state is defined as the channel states $\{S_m(t)\}_{m=1}^M$ in the current time slot and each secondary user has a partial observation of the game state in each time slot. However, it is well known that such a partial-observation dynamic game is very difficult to analyze and is computationally intractable due to the curse of dimensionality. To enable tractable analysis and achieve an efficient spectrum access, we hence study the distributed spectrum access problem from the long-run average perspective and utilize the statistical channel availability information (i.e., channel idle probability θ_m) to aid secondary users' decision-makings. This is due to the fact that the statistical channel availability information can be learned from the history of a secondary user's local observations, via the maximum likelihood estimation approach described in section "Distributed Learning for Spatial Spectrum Access Game". Moreover, the spatial spectrum access game solution in this chapter can help us solve the complete information dynamic game, where each secondary user is able to globally observe the channel state realization $\{S_m(t)\}_{m=1}^M$ of all the channels in each time slot. Since the secondary users cannot control the transition of channel states, we can easily derive the solution of the complete information dynamic game as follows: for each time slot t, we solve the corresponding stage spatial spectrum access game using the algorithm proposed in this chapter, with the channel idle probabilities $\{\theta_m\}_{m=1}^M$ of the stage game replaced by the channel state realization $\{S_m(t)\}_{m=1}^M$ of time slot t. Since our analysis is from the secondary users' perspective, we will use the terms "secondary user" and "user" interchangeably.

Spatial Spectrum Access Game

We now consider the problem that each user tries to maximize its own throughput by choosing a proper channel in a distributed fashion. Let $a_{-n} = \{a_1, \ldots, a_{n-1}, a_{n+1}, \ldots, a_N\}$ be the channels chosen by all users except user n. Given other users' channel selections a_{-n}, the problem faced by a user n is

$$\max_{a_n \in \mathscr{M}} U(a_n, a_{-n}), \forall n \in \mathscr{N}. \tag{6}$$

We thus formulate the distributed channel selection problem on an interference graph G as a **spatial spectrum access game** $\Gamma = (\mathscr{N}, \mathscr{M}, G, \{U_n\}_{n \in \mathscr{N}})$, where $\mathscr{N}$ is the set of players, $\mathscr{M}$ is the set of strategies, G describes the interference relationship among the players, and U_n is the payoff function of player n.

The distributed nature of the channel selection problem naturally leads to a formulation based on the game theory, such that users can self-organize into a mutually acceptable channel selection, which is defined as follows.

Definition 1 (Pure Nash Equilibrium [21]). A strategy profile $\boldsymbol{a}^* = (a_1^*, a_2^*, \ldots, a_N^*)$ is a pure Nash equilibrium if and only if

$$a_n^* = \arg\max_{a_n \in \mathscr{M}} U(a_n, a_{-n}^*), \forall n \in \mathscr{N}. \tag{7}$$

It is known that not every finite strategic game possesses a pure Nash equilibrium [21]. We then introduce the more general concept of mixed Nash equilibrium. Let $\boldsymbol{\sigma}_n \triangleq (\sigma_1^n, \ldots, \sigma_M^n)$ denote the mixed strategy of user n, where $0 \leq \sigma_m^n \leq 1$ is the probability of user n choosing channel m and $\sum_{m=1}^{M} \sigma_m^n = 1$. For simplicity, we use the same payoff notation $U_n(\boldsymbol{\sigma}_1, \ldots, \boldsymbol{\sigma}_N)$ to denote the expected throughput of user n under the mixed strategy profile $(\boldsymbol{\sigma}_1, \ldots, \boldsymbol{\sigma}_N)$, and it can be computed as

$$U_n(\boldsymbol{\sigma}_1, \ldots, \boldsymbol{\sigma}_N) = \sum_{a_1=1}^{M} \sigma_{a_1}^1 \ldots \sum_{a_N=1}^{M} \sigma_{a_N}^N U_n(a_1, \ldots, a_N). \tag{8}$$

Similarly to the pure Nash equilibrium, the mixed Nash equilibrium is defined as:

Definition 2 (Mixed Nash Equilibrium [21]). The mixed strategy profile $\boldsymbol{\sigma}^* = (\boldsymbol{\sigma}_1^*, \ldots, \boldsymbol{\sigma}_N^*)$ is a mixed Nash equilibrium, if for every user $n \in \mathscr{N}$, we have

$$U_n(\boldsymbol{\sigma}_n^*, \boldsymbol{\sigma}_{-n}^*) \geq U_n(\boldsymbol{\sigma}_n, \boldsymbol{\sigma}_{-n}^*), \forall \boldsymbol{\sigma}_n \neq \boldsymbol{\sigma}_n^*,$$

where $\boldsymbol{\sigma}_{-n}^*$ denotes the mixed strategy choices of all other users except user n.

In the spatial spectrum access game, each secondary user takes both the primary activity levels on different channels and the competition with other secondary users into consideration, in order to improve its long-run average throughput. Nash equilibrium is the natural solution concept for the spatial spectrum access game. At a Nash equilibrium, secondary users are mutually satisfied with their long-run average throughputs, and no user can improve by changing its channel unilaterally. One important property of the mixed Nash equilibrium is that if a user assigns positive probabilities of some actions, then the expected payoff of these actions should be the same at the equilibrium. Otherwise, the user can improve by increasing the probability of the action with a higher expected payoff.

In the following sections, we will study the existence of both mixed and pure Nash equilibria based on the global network information and then discuss how to achieve the Nash equilibria based on the local user observations only.

Existence of Nash Equilibria

In this part, we study the existence of Nash equilibria in a spatial spectrum access game. Since a spatial spectrum access game is a finite strategic game (i.e., with a finite number of players and a finite number of channels), we know that it always admits a mixed Nash equilibrium according to [21].

On the other hand, not every finite strategic game possesses a pure Nash equilibrium [21]. Compared with the mixed Nash equilibrium, a pure Nash equilibrium can achieve the mutually satisfactory spectrum sharing solution without requiring the frequent channel switching and hence helps reduce the system overhead such as energy consumption of frequent channel switching. This motivates us to further investigate the existence of pure Nash equilibria of the spatial spectrum access games.

Existence of Pure Nash Equilibria on Directed Interference Graphs

We first study the existence of pure Nash equilibria on directed interference graphs. First of all, we can construct a game which does not have a pure Nash equilibrium.

Theorem 1. *There exists a spatial spectrum access game on a directed interference graph not admitting any pure Nash equilibrium.*

Figure 3 shows such an example. It is easy to verify that for all eight possible channel selection profiles, there always exists one user (out of these three users) having an incentive to change its channel selection unilaterally to improve its throughput.

We then focus on identifying the conditions under which the game admits a pure Nash equilibrium. To proceed, we first introduce the following lemma (the proof is given in the appendix at the end of the chapter).

Lemma 1. *Assume that any spatial spectrum access game with N users on a given directed interference graph G has a pure Nash equilibrium. Then we can construct a new spatial spectrum access game by adding a new player, who cannot generate interference to any player in the original game and may receive interference from one or multiple players in the original game. The new game with $N + 1$ users also has a pure Nash equilibrium.*

We know that any directed acyclic graph (i.e., a directed graph contains no directed cycles) can be given a topological sort (i.e., an ordering of the nodes), such that if node $i < j$, then there are no edges directed from the node j to node i in the ordering [22]. This is due to that any spatial spectrum access game with $N = 1$

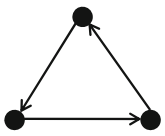

Fig. 3 An example of spatial spectrum access game without a pure Nash equilibrium. There are two channels available and the throughput of a user n is $U_n(\boldsymbol{a}) = p\prod_{i\in\mathcal{N}_n^{a_n}(\boldsymbol{a})}(1-p)$. If all three players (nodes) choose channel 1, then each player has the incentive of unilaterally changing its choice to channel 2 to improve its throughput, assuming that the other two players do not change their channel choices. We can show that such derivation will happen for all eight possible strategy profiles $\boldsymbol{a} = (a_1, a_2, a_3)$, where $a_i \in \{1, 2\}$ for $i \in \{1, 2, 3\}$

user always has a pure Nash equilibrium. By the induction argument, we know from Lemma 1 that

Corollary 1. *Any spatial spectrum access game on a directed acyclic graph has a pure Nash equilibrium.*

To obtain more insightful results, we next impose the following property on the spatial spectrum access games:

Definition 3 (Congestion Property – CP). User n's channel grabbing probability $g_n\left(\mathcal{N}_n^{a_n}(\boldsymbol{a})\right)$ satisfies the congestion property if for any $\tilde{\mathcal{N}}_n^{a_n}(\boldsymbol{a}) \subseteq \mathcal{N}_n^{a_n}(\boldsymbol{a})$, we have

$$g_n(\tilde{\mathcal{N}}_n^{a_n}(\boldsymbol{a})) \geq g_n\left(\mathcal{N}_n^{a_n}(\boldsymbol{a})\right). \tag{9}$$

Furthermore, a spatial spectrum access game satisfies the congestion property if (9) holds for all users $n \in \mathcal{N}$.

The congestion property (CP) means that the more contending users exist, the less chance a user can grab the channel. Such a property is natural for practical wireless systems such as the random backoff and Aloha systems. We can show that the following result (the proof is given in the appendix in the separate supplemental file).

Lemma 2. *Assume that any spatial spectrum access game with N users satisfying the congestion property on a given directed interference graph G has a pure Nash equilibrium. Then we can construct a new spatial spectrum access game by adding a new player, whose channel grabbing probability satisfies the congestion property and who has an interference relationship with at most one player $n \in \mathcal{N}$ in the original game. The new game with $N+1$ users also has a pure Nash equilibrium.*

Definition 4 (Directed Tree [22]). A directed graph is called a directed tree if the corresponding undirected graph obtained by ignoring the edge directions is a tree.

Note that a (undirected) tree is a special case of directed trees. Since any spatial spectrum access game over a single node always has a pure Nash equilibrium, we can then construct the directed tree recursively by introducing a new node and adding an (directed or undirected) edge between this node and one existing node. By using Lemma 2 and the induction argument, we have

Corollary 2. *Any spatial spectrum access game satisfying the congestion property on a directed tree has a pure Nash equilibrium.*

Definition 5 (Directed Forest [22]). A directed graph is called a directed forest if it consists of a disjoint union of directed trees.

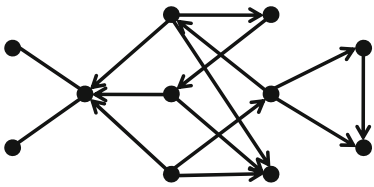

Fig. 4 An interference graph that consists of directed acyclic graphs and directed trees

Similarly, we can obtain from Lemma 2 that

Corollary 3. *Any spatial spectrum access game satisfying the congestion property on a directed forest has a pure Nash equilibrium.*

Note that the directed acyclic graph and directed tree structures are widely observed in many wireless networking systems such as wireless ad hoc and sensor networks [23]. For example, the star topology with sink/hub nodes in wireless sensor networks is a special case of directed tree. Based on Lemmas 1 and 2, we can construct more general directed interference graphs over which a spatial spectrum access game satisfying the congestion property has a pure Nash equilibrium. Figure 4 illustrates such an example.

Existence of Pure Nash Equilibria on Undirected Interference Graphs

We now study the case where the interference graph is undirected. This is a good approximation of reality if the transmitter of each user is close to its receiver and all users' interference ranges are roughly the same. For example, in 802.11 systems, undirected interference graph is widely used to approximate the interference relationships, since the access points are typically close to their associated clients and the carrier sensing ranges are similar.

When an undirected interference graph is a tree, according to Corollary 2, any spatial spectrum access game satisfying the congestion property has a pure Nash equilibrium. However, for those non-tree undirected graphs without a topological sort, the existence of a pure Nash equilibrium cannot be proved following the results in section "Existence of Pure Nash Equilibria on Directed Interference Graphs". This motivates us to further study the existence of pure Nash equilibria on generic undirected interference graphs.

First of all, [24] showed that a 3-players and 3-resources congestion game with user-specific congestion weights may not have a pure Nash equilibrium. Such a congestion game can be considered as a spatial spectrum access game on a complete undirected interference graph (by regarding the resources as channels). When all users have homogeneous channel contention capabilities and all channels have the same mean data rates, [17] showed that the spatial spectrum access game on any undirected interference graphs has a pure Nash equilibrium. Clearly, the applicability of such a channel-homogeneous model is quite limited, since the channel throughputs in practical wireless networks are often heterogeneous. Hence

we will focus on exploring the random backoff and Aloha systems with user-specific data rates, which provide useful insights for the user-homogeneous and user-heterogeneous channel contention mechanisms, respectively.

Our following analysis will rely on the properties of potential game (Note that it is much more difficult to find a proper potential function to take into account users' asymmetric relationships (i.e., directions of edges on graph) when the interference graph is directed. Hence in this study, we only apply the tool of potential game in the undirected case.), defined as follows:

Definition 6 (Potential Game [25]). A game is called a potential game if it admits a potential function $\Phi(\boldsymbol{a})$ such that for every $n \in \mathcal{N}$ and $a_{-n} \in \mathcal{M}^{N-1}$,

$$\operatorname{sgn}\left(\Phi(a_n^{'}, a_{-n}) - \Phi(a_n, a_{-n})\right) = \operatorname{sgn}\left(U_n(a_n^{'}, a_{-n}) - U_n(a_n, a_{-n})\right),$$

where $\operatorname{sgn}(\cdot)$ is the sign function.

Definition 7 (Better Response Update [25]). The event where a player n changes to an action $a_n^{'}$ from the action a_n is a better response update if and only if $U_n(a_n^{'}, a_{-n}) > U_n(a_n, a_{-n})$.

An appealing property of the potential game is that it always admits a pure Nash equilibrium. Furthermore, it enjoys the finite improvement property, which is defined as

Definition 8 (Finite Improvement Property [25]). A game has the finite improvement property if any asynchronous better response update process (i.e., no more than one player updates the strategy at any given time) terminates at a pure Nash equilibrium within a finite number of updates.

Based on the potential game theory, we first study the random backoff mechanism. We show in Theorem 2 that when the undirected interference graph is complete, there exists indeed a pure Nash equilibrium.

Theorem 2. *Any spatial spectrum access game on a complete undirected interference graph with the random backoff mechanism is a potential game with the potential function*

$$\Phi(\boldsymbol{a}) = \prod_{n=1}^{N} \theta_{a_n} B_{a_n}^{n} \prod_{m=1}^{M} \prod_{c=0}^{K_m(\boldsymbol{a})} \sum_{\lambda=1}^{\lambda_{\max}} \frac{1}{\lambda_{\max}} \left(\frac{\lambda_{\max} - \lambda}{\lambda_{\max}}\right)^{c}, \tag{10}$$

where $K_m(\boldsymbol{a})$ is the number of users choosing channel m under the strategy profile $\boldsymbol{a}$ and hence has a pure Nash equilibrium.

The proof is similar to that in [26] and hence is omitted here. We then consider the spatial spectrum access game with the random backoff mechanism on bipartite graphs.

Definition 9 (Bipartite Graph [22]). An undirected graph is called a bipartite graph if the set of its nodes can be decomposed into two disjoint sets, such that no two nodes within the same set are connected by an edge.

Definition 10 (Complete Bipartite Graph [22]). An undirected graph is called a complete bipartite graph if it is a bipartite graph and any two nodes selected from the two disjoint sets, respectively, are connected by an edge.

Definition 11 (Regular Bipartite Graph [22]). An undirected graph is called a regular bipartite graph if it is a bipartite graph and each node is connected by the same number of edges.

Note that a complete bipartite graph that has the same number of vertices in the two disjoint sets is also a regular bipartite graph. Many well-known graphs such as star graphs, circulant graphs, cycle graphs with even number of vertexes, hypercubes, and rectangular lattices are either complete bipartite graphs or regular bipartite graphs. We consider the user-specific throughput as

$$U_n(a_n, a_{-n}) = h_n \theta_{a_n} B_{a_n} g_n(\mathcal{N}_n^{a_n}(\boldsymbol{a})), \tag{11}$$

where h_n represents a user-specific transmission gain. We can show that

Theorem 3. *Any spatial spectrum access game on either a complete bipartite interference graph or a regular bipartite interference graph with user-specific transmission gains and the random backoff mechanism has a pure Nash equilibrium.*

The proof is given in the appendix in the separate supplemental file. We then consider the random backoff mechanism in the asymptotic case that $\lambda_{\max}$ goes to infinity. This can be a good approximation of reality when the number of backoff mini-slots is much greater than the number of interfering users and collision rarely occurs. In this case, we have

$$\begin{aligned} g_n(\mathcal{N}_n^{a_n}(\boldsymbol{a})) &= \lim_{\lambda_{\max}\to\infty} \sum_{\lambda=1}^{\lambda_{\max}} \frac{1}{\lambda_{\max}} \left(\frac{\lambda_{\max}-\lambda}{\lambda_{\max}}\right)^{K_n^{a_n}(\boldsymbol{a})} \\ &= \int_0^1 x^{K_n^{a_n}(\boldsymbol{a})} dx = \frac{1}{1+K_n^{a_n}(\boldsymbol{a})}, \end{aligned} \tag{12}$$

here $K_n^{a_n}(\boldsymbol{a})$ denotes the number of users that choose channel a_n and can interfere with user n. Equation (12) implies that the channel opportunity is equally shared among $1 + K_n^{a_n}(\boldsymbol{a})$ contending users (including user n). This can also apply in TDMA channel access mechanism. We consider the user-specific throughput as

$$U_n(a_n, a_{-n}) = h_n \theta_{a_n} B_{a_n} \frac{1}{1+K_n^{a_n}(\boldsymbol{a})}, \tag{13}$$

We show that

Theorem 4. *Any spatial spectrum access game on any undirected interference graph with user-specific transmission gains and the random backoff mechanism in the asymptotic case is a potential game with the potential function*

$$\Phi(\boldsymbol{a}) = -\sum_{n=1}^{N}\left(\frac{1+\frac{1}{2}K_n^{a_n}(\boldsymbol{a})}{\theta_{a_n}B_{a_n}}\right), \tag{14}$$

and hence has a pure Nash equilibrium.

Theorem 4 is a direct consequence of the more general result Theorem 5. More specifically, we generalize the throughput function in (13) as

$$U_n(a_n, a_{-n}) = h_n\theta_{a_n}B_{a_n}\frac{w_n}{w_n + \sum_{i\in\mathcal{N}_n^{a_n}(\boldsymbol{a})} w_i}, \tag{15}$$

where $w_n > 0$ denotes user-specific channel sharing weight. When $w_n = 1$, the throughput function in (15) degenerates to the equal-sharing case in (13). The physical meaning of (15) is that the channel is shared among the contending users according to their weights. We refer this to the spatial spectrum access game with user-specific sharing weights. Such a proportional channel sharing scheme has been widely used to model the heterogeneous channel access priority assignment for heterogeneous users of different QoS requirements in wireless networks [27]. We show that

Theorem 5. *Any spatial spectrum access game with user-specific sharing weights on any undirected interference graph is a potential game with the potential function as*

$$\Phi(\boldsymbol{a}) = -\sum_{n=1}^{N}\left(\frac{w_n^2 + \frac{1}{2}\sum_{i\in\mathcal{N}_n^{a_n}(\boldsymbol{a})} w_n w_i}{\theta_{a_n}B_{a_n}}\right), \tag{16}$$

and hence has a pure Nash equilibrium.

The proof is given in the appendix in the separate supplemental file. We then consider the random access mechanism under the scenario where all channels are homogeneous to each user (i.e., $\theta_m = \theta$ and $B_m = B$ for all $m \in \mathcal{M}$). This models the case where a licensed spectrum band of a large bandwidth (e.g., TV channel) is divided into equal width logical channels for secondary usage with interleaving technology at the physical layer (e.g., the IEEE 802.16d/e standard), such that all channels exhibit the same primary occupancy and have the same channel gain to the same user (but still different channel gains for different users). In this case, the user throughput function is given as

$$U_n(\boldsymbol{a}) = h_n\theta B g(\mathcal{N}_n^{a_n}(\boldsymbol{a})). \tag{17}$$

We can show that the following result (the proof is given in the appendix in the separate supplemental file).

Theorem 6. *Any spatial spectrum access game on any undirected interference graph with homogeneous channels, user-specific transmission gains, and the random backoff mechanism is a potential game with the potential function*

$$\Phi(\boldsymbol{a}) = \sum_{n=1}^{N} \left(\frac{1 + K_n^{a_n}(\boldsymbol{a})}{\theta B} \right)$$

and hence has a pure Nash equilibrium.

We now consider the Aloha mechanism. According to (4), we have the user throughput function as

$$U_n(\boldsymbol{a}) = \theta_{a_n} B_{a_n}^n p_n \prod_{i \in \mathcal{N}_n^{a_n}(\boldsymbol{a})} (1 - p_i). \tag{18}$$

We can show that the following result (the proof is given in the appendix in the separate supplemental file).

Theorem 7. *Any spatial spectrum access game on any undirected interference graph with the Aloha mechanism is a potential game with the potential function*

$$\Phi(\boldsymbol{a}) = \sum_{i=1}^{N} -\log(1 - p_i) \times \left(\frac{1}{2} \sum_{j \in \mathcal{N}_i^{a_i}(\boldsymbol{a})} \log(1 - p_j) + \log\left(\theta_{a_i} B_{a_i}^i p_i\right) \right)$$

and hence has a pure Nash equilibrium.

As a summary, we depict the results on the existence of pure Nash equilibria of spatial spectrum access games in Fig. 2.

Price of Anarchy

In previous sections, we have considered the existence of Nash equilibrium of spatial spectrum access games. We will further explore the efficiency of the Nash equilibrium.

Following the definition of price of anarchy (PoA) in game theory [28], we will quantify the efficiency ratio of the worst-case Nash equilibrium over the centralized optimal solution. Let $\mathcal{Z}$ be the set of Nash equilibria of a given spatial spectrum access game. Then the PoA is defined as

$$\text{PoA} = \frac{\min_{\boldsymbol{a} \in \mathcal{Z}} \sum_{n \in \mathcal{N}} U_n(\boldsymbol{a})}{\max_{\boldsymbol{a} \in \mathcal{M}^N} \sum_{n \in \mathcal{N}} U_n(\boldsymbol{a})},$$

which is always not greater than 1. A larger PoA implies that the set of Nash equilibrium is more efficient (in the worst-case sense) using the centralized optimum as a benchmark. Let $V_n = \max_{m \in \mathcal{M}} \{\theta_m B_m^n\}$. For a general spatial spectrum access game, we have the following result.

Theorem 8. *The PoA of a spatial spectrum access game* $\Gamma = (\mathcal{N}, \mathcal{M}, G, \{U_n\}_{n \in \mathcal{N}})$ *is at least* $\frac{\min_{n \in \mathcal{N}} \{V_n g_n(\mathcal{N}_n)\}}{\max_{n \in \mathcal{N}} V_n}$.

The proof is given in the appendix in the separate supplemental file. Intuitively, Theorem 8 indicates that we can increase the efficiency of spectrum sharing by better utilizing the gain of spatial reuse (i.e., reducing the interference edges $\mathcal{N}_n$ on the interference graph).

Distributed Learning for Spatial Spectrum Access Game

As mentioned in section "Spatial Spectrum Access Game", both pure and mixed Nash equilibria are important equilibrium concepts for spatial spectrum access games, characterizing system states where secondary users achieve a mutually satisfactory spectrum sharing solution. We hence consider how to achieve the Nash equilibrium for the spatial spectrum access games in this section.

As shown in section "Existence of Nash Equilibria", a generic spatial spectrum access game does not necessarily have a pure Nash equilibrium, and thus it is impossible to design a mechanism that is guaranteed to reach a pure Nash equilibrium in general. However, when the spatial spectrum access game is a potential game, a pure Nash equilibrium exists. In this case, we can apply the Safe Experimentation algorithm in [29] for achieving the pure Nash equilibrium. The key idea is to explore the pure strategy space based on the finite improvement property of the potential game. From the practical application's perspective, we can apply the results obtained in section "Existence of Nash Equilibria" to identify whether the spectrum sharing system satisfies the potential game property. We can then apply the Safe Experimentation algorithm to achieve the pure Nash equilibrium when the system possesses the potential game property.

Since any spatial spectrum access game always admits a mixed Nash equilibrium, we next target on approaching the mixed Nash equilibria. From a practical point of view, if the spectrum sharing system is complex and it is difficult to verify the existence of pure Nash equilibrium, we can consider to achieve a mutually satisfactory spectrum sharing solution by allowing users to choose mixed strategies. Govindan and Wilson in [30] proposed a global Newton method to compute the mixed Nash equilibria for any finite strategic games. This method hence can be applied to find the mixed Nash equilibria for the spatial spectrum access games. However, such an approach is a centralized optimization, which requires each user to have the complete information of other users and compute the solution accordingly. This is often infeasible in a cognitive radio network, since acquiring complete information requires heavy information exchange among the users and setting up

and maintaining a common control channel for message broadcasting demands high system overheads [2]. Moreover, this approach is not incentive compatible since some users may not be willing to share their local information due to the energy consumption of information broadcasting. We thus propose a distributed learning algorithm for any spatial spectrum access games, and the algorithm does not require any information exchange among users. Each user only learns to adjust its channel selection strategy adaptively based on its local throughput observations. We show that the distributed learning algorithm can converge to a mixed Nash equilibrium approximately.

Expected Throughput Estimation

For the distributed learning algorithm, we assume that each user does not have the complete network information and can only estimate its expected throughput locally. Similarly to the approaches in [31] and [32], we can divide the spectrum access time into a sequence of *decision periods* indexed by $T(=1,2,\ldots)$, where each decision period consists of $t_{\max}$ time slots. During a single decision period, a user accesses the *same* channel in all $t_{\max}$ time slots in order to better understand the environment. At the end of each decision period T, a user observes $S_n(T,t)$, $I_n(T,t)$ and $b_n(T,t)$. Here $S_n(T,t)$ denotes the state of the chosen channel (i.e., whether occupied by the primary traffic), $I_n(T,t)$ indicates whether the user has successfully grabbed the channel, i.e.,

$$I_n(T,t) = \begin{cases} 1, & \text{if user } n \text{ successfully grabs the channel,} \\ 0, & \text{otherwise,} \end{cases}$$

and $b_n(T,t)$ is the received data rate on the chosen channel by user n at time slot t. Note that if $S_n(T,t) = 0$ (i.e., the channel is occupied by the primary traffic), we set $I_n(T,t)$ and $b_n(T,t)$ to be 0. At the end of each decision period T, each user n will have a set of local observations $\Omega_n(T) = \{S_n(T,t), I_n(T,t), b_n(T,t)\}_{t=1}^{t_{\max}}$. Based on these observations, each user can then apply the Maximum Likelihood Estimation (MLE) method to estimate its expected throughput U_n. As an example, we next consider the MLE of user expected throughput in the Markovian channel environment introduced in section "System Model".

We first consider the estimation of the channel idle probability θ_m. From the observation set $\Omega_n(T)$ at period T, user n can observe a sequence of channel state transitions as

$$\mathscr{S}_n(T) = \left((S_n(T,1), S_n(T,2)), \ldots, (S_n(T,t_{\max}-1), S_n(T,t_{\max}))\right).$$

Here there are four different transition types between adjacent time slots t and t+1: $(0,0)$, $(0,1)$, $(1,0)$, and $(1,1)$. We denote $C_{00}(T)$, $C_{01}(T)$, $C_{10}(T)$, and $C_{11}(T)$ as the number of occurrences of the four state transitions types in $\mathscr{S}_n(T)$, respectively.

According to the principle of MLE, user n can then compute the likelihood function in terms of channel state transition parameters (ε_m, ξ_m) as

$$\begin{aligned}
&\mathscr{L}[\Omega_n(T)|\varepsilon_m, \xi_m] \\
&\quad = Pr\{\mathscr{S}_n(T)|\varepsilon_m, \xi_m\} \\
&\quad = Pr\{S_n(T,1)|\varepsilon_m, \xi_m\} \times \prod_{t=1}^{t_{\max}-1} Pr\{S_n(T,t+1)|S_n(T,t), \varepsilon_m, \xi_m\} \\
&\quad = Pr\{S_n(T,1)|\varepsilon_m, \xi_m\} \times (1-\varepsilon_m)^{C_{00}(T)} \varepsilon_m^{C_{01}(T)} (1-\xi_m)^{C_{11}(T)} \xi_m^{C_{10}(T)}.
\end{aligned}$$

Then MLE of (ε_m, ξ_m) can be computed by maximizing the log-likelihood function $\ln \mathscr{L}[\Omega_n(T)|\varepsilon_m, \xi_m]$, i.e., $\max_{\varepsilon_m, \xi_m} \ln \mathscr{L}[\Omega_n(T)|\varepsilon_m, \xi_m]$. By the first order condition, we obtain the optimal solution as

$$\begin{aligned}
\tilde{\varepsilon}_m &= \frac{C_{01}(T)}{C_{00}(T) + C_{01}(T)}, \\
\tilde{\xi}_m &= \frac{C_{10}(T)}{C_{11}(T) + C_{10}(T)}.
\end{aligned}$$

According to (1), we can then estimate the channel idle probability θ_m as

$$\tilde{\theta}_m = \frac{\tilde{\varepsilon}_m}{\tilde{\varepsilon}_m + \tilde{\xi}_m}.$$

We then consider the estimation of channel grabbing probability $g_n(T)$. When a channel is idle (i.e., no primary traffic), a user n will contend for the channel and can successfully grab the channel with a probability $g_n(T)$. Since there are a total of $\sum_{t=1}^{t_{\max}} S_n(T,t)$ rounds of channel contentions in the period T and each round is independent, the total number of successful channel captures $\sum_{t=1}^{t_{\max}} I_n(T,t)$ by user n follows the Binomial distribution. User n then computes the likelihood of $g_n(T)$ as

$$\begin{aligned}
\mathscr{L}[\Omega_n(T)|g_n(T)] = &\left(\begin{matrix} \sum_{t=1}^{t_{\max}} S_n(T,t) \\ \sum_{t=1}^{t_{\max}} I_n(T,t) \end{matrix} \right) g_m(T)^{\sum_{t=1}^{t_{\max}} I_n(T,t)} \\
&\times (1-g_m(T))^{\sum_{t=1}^{t_{\max}} S_n(T,t) - \sum_{t=1}^{t_{\max}} I_n(T,t)}.
\end{aligned}$$

Then MLE of $g_n(T)$ can be computed by maximizing the log-likelihood function $\ln \mathscr{L}[\Omega_n(T)|g_n(T)]$, i.e., $\max_{g_n(T)} \ln \mathscr{L}[\Omega_n(T)|g_n(T)]$. By the first-order condition, we obtain the optimal solution as

$$\tilde{g}_n(T) = \frac{\sum_{t=1}^{t_{\max}} I_n(T,t)}{\sum_{t=1}^{t_{\max}} S_n(T,t)}.$$

We finally consider the estimation of mean data rate B_m^n. Since the received data rate $b_n(T,t)$ is also i.i.d. over different time slots, similar to the MLE of the channel grabbing probability $g_n(T)$, we can obtain the MLE of mean data rate B_m^n as

$$\tilde{B}_m^n = \frac{\sum_{t=1}^{t_{\max}} b_n(T,t)}{\sum_{t=1}^{t_{\max}} I_n(T,t)}.$$

By the MLE above, we can then estimate the true expected throughput $U_n(T)$ as $\tilde{U}_n(T) = \tilde{\theta}_m \tilde{B}_m^n \tilde{g}_n(T)$. In the following analysis of distributed learning algorithm, we consider a general setting where the estimated expected throughput $\tilde{U}_n(T)$ of user n can be noisy. More precisely, we assume that $\tilde{U}_n(T) = U_n(T) + w_n$ where $w_n \in (\underline{w}, \overline{w})$ is the random estimation noise with a probability density function $f_n(w_n)$ satisfying $E[w_n] = \int_{\underline{w}}^{\overline{w}} w_n f_n(w_n) dw_n = 0$.

Distributed Learning Algorithm

Based on the expected throughput estimation, we then propose the distributed learning algorithm for spatial spectrum access games. The idea is to extend the principle of single-agent reinforcement learning to a multi-agent setting. Such multi-agent reinforcement learning algorithm has also been applied to the classical congestion games on complete interference graphs [33, 34] by assuming that users are homogeneous (i.e., user's payoff only depends on the number of users choosing the same resource). Here we extend the learning algorithm to the generalized spatial congestion games on any generic interference graphs with heterogeneous users, which lead to significant differences in analysis. For example, we show that the convergence condition for the learning algorithm depends on the structure of spatial reuse, which is different from those results in [33, 34].

More specifically, at the beginning of each period T, a user $n \in \mathcal{N}$ chooses a channel $a_n(T) \in \mathcal{M}$ to access according to its mixed strategy $\boldsymbol{\sigma}_n(T) = (\sigma_m^n(T), \forall m \in \mathcal{M})$, where $\sigma_m^n(T)$ is the probability of choosing channel m. The mixed strategy is generated according to $\boldsymbol{P}_n(T) = (P_m^n(T), \forall m \in \mathcal{M})$, which represents its *perceptions* of the payoff performance of choosing different channels based on local estimations. Perceptions are based on local observations in the past and may not accurately reflect the expected payoff. For example, if a user n has not accessed a channel m for many decision intervals, then perception $P_m^n(T)$ can be out of date. The key challenge for the learning algorithm is to update the perceptions with proper parameters such that perceptions equal to expected payoffs at the equilibrium.

Similarly to the single-agent learning, we choose the Boltzmann distribution as the mapping from perceptions to mixed strategies, i.e.,

$$\sigma_m^n(T) = \frac{e^{\gamma P_m^n(T)}}{\sum_{i=1}^{M} e^{\gamma P_i^n(T)}}, \forall m \in \mathcal{M}, \tag{19}$$

Algorithm 1 Distributed learning algorithm for spatial spectrum access game

1: **initialization:**
2: **set** the temperature γ.
3: **set** the initial perception values $P_m^n(0) = \frac{1}{M}$ for each user $n \in \mathcal{N}$.
4: **end initialization**

5: **loop** for each decision period T and each user $n \in \mathcal{N}$ in parallel:
6: **select** a channel $m \in \mathcal{M}$ according to (19).
7: **estimate** the expected throughput $\tilde{U}_n(\boldsymbol{a}(T))$.
8: **update** the perceptions value $\boldsymbol{P}_n(T)$ according to (20).
9: **end loop**

where γ is the temperature that controls the randomness of channel selections. When $\gamma \to 0$, each user will choose to access channels uniformly at random. When $\gamma \to \infty$, user n always chooses the channel with the largest perception value $P_m^n(T)$ among all channel $m \in \mathcal{M}$. We will show later on that the choice of γ trades off convergence and performance of the learning algorithm.

At the end of a decision period T, a user n estimates its expected throughput as $\tilde{U}_n(\boldsymbol{a}(T))$ and adjusts its perceptions as

$$P_m^n(T+1) = \begin{cases} (1-\mu_T)P_m^n(T) + \mu_T \tilde{U}_n(\boldsymbol{a}(T)), & \text{if } a_n(T) = m, \\ P_m^n(T), & \text{otherwise,} \end{cases} \tag{20}$$

where $(\mu_T \in (0,1), \forall T)$ are the smoothing factors. A user only changes the perception of the channel just accessed in the current decision period and keeps the perceptions of other channels unchanged.

Algorithm 1 summarizes the distributed learning algorithm. We then analyze the complexity of the distributed learning algorithm. In each iteration, Line 6 involves the arithmetic operations over M channels and hence has a complexity of $\mathcal{O}(M)$. The expected throughput estimation in Line 7 typically involves the arithmetic operations based on the observations of the chosen channel in $t_{\max}$ time slots of the decision period and hence has a complexity of $\mathcal{O}(t_{\max})$. In Line 8, the perception value update is only carried out in the chosen channel and hence has a complexity of $\mathcal{O}(1)$. Suppose that it takes K iterations for the algorithm to converge. Then total computational complexity of the algorithm is at most $\mathcal{O}(K(M + t_{\max}))$.

Convergence of Distributed Learning Algorithm

We now study the convergence of the proposed distributed learning algorithm based on the theory of stochastic approximation [35].

First, the perception value update in (20) can be written in the following equivalent form,

$$P_m^n(T+1) - P_m^n(T) = \mu_T[Z_m^n(T) - P_m^n(T)], \forall n \in \mathcal{N}, m \in \mathcal{M}, \tag{21}$$

where $Z_m^n(T)$ is the update value defined as

$$Z_m^n(T) = \begin{cases} \tilde{U}_n(\boldsymbol{a}(T)), & \text{if } a_n(T) = m, \\ P_m^n(T), & \text{otherwise.} \end{cases} \tag{22}$$

For the sake of brevity, we denote the perception values, update values, and mixed strategies of all the users as $\boldsymbol{P}(T) \triangleq \left(P_m^n(T), \forall m \in \mathcal{M}, n \in \mathcal{N}\right)$, $\boldsymbol{Z}(T) \triangleq (Z_m^n(T), \forall m \in \mathcal{M}, n \in \mathcal{N})$, and $\boldsymbol{\sigma}(T) \triangleq (\sigma_m^n(T), \forall m \in \mathcal{M}, n \in \mathcal{N})$, respectively.

Let $Pr\{\mathcal{N}_n^m(\boldsymbol{a}(T))|\boldsymbol{P}(T), a_n(T) = m\}$ denote the conditional probability that, given that the users' perceptions are $\boldsymbol{P}(T)$ and user n chooses channel m, the set of users that choose the same channel m in user n's neighborhood $\mathcal{N}_n$ is $\mathcal{N}_n^m(\boldsymbol{a}(T)) \subseteq \mathcal{N}_n$. Since each user independently chooses a channel according to its mixed strategy $\boldsymbol{\sigma}_n(T)$, then the random set $\mathcal{N}_n^m(\boldsymbol{a}(T))$ follows the Binomial distribution of $|\mathcal{N}_n|$ independent nonhomogeneous Bernoulli trials with the probability mass function as

$$\begin{aligned} &Pr\{\mathcal{N}_n^m(\boldsymbol{a}(T))|\boldsymbol{P}(T), a_n(T) = m\} \\ &\quad = \prod_{i \in \mathcal{N}_n^m(\boldsymbol{a}(T))} (\sigma_m^i(T)) \prod_{i \in \mathcal{N}_n \setminus \mathcal{N}_n^m(\boldsymbol{a}(T))} (1 - \sigma_m^i(T)) \\ &\quad = \prod_{i \in \mathcal{N}_n} (\sigma_m^i(T))^{I_{\{a_i(T)=m\}}} (1 - \sigma_m^i(T))^{1 - I_{\{a_i(T)=m\}}}, \end{aligned} \tag{23}$$

where $I_{\{a_i(T)=m\}} = 1$ if user i chooses channel m and $I_{\{a_i(T)=m\}} = 0$ otherwise.

Since the update value $Z_m^n(T)$ depends on user n's estimated throughput $\tilde{U}_n(\boldsymbol{a}(T))$ (which in turn depends on $\mathcal{N}_n^m(\boldsymbol{a}(T))$), thus $Z_m^n(T)$ is also a random variable. The equations in (21) are hence stochastic difference equations, which are difficult to analyze directly. We thus focus on the analysis of its *mean dynamics* [35]. To proceed, we define the mapping from the perceptions $\boldsymbol{P}(T)$ to the expected throughput of user n choosing channel m as $Q_m^n(\boldsymbol{P}(T)) \triangleq E[U_n(\boldsymbol{a}(T))|\boldsymbol{P}(T), a_n(T) = m]$. Here the expectation $E[\cdot]$ is taken with respective to the mixed strategies $\boldsymbol{\sigma}(T)$ of all users (i.e., the perceptions $\boldsymbol{P}(T)$ of all users due to (19)). We show that

Lemma 3. *For the distributed learning algorithm, the mapping from the perceptions to the expected throughput* $Q(\boldsymbol{P}(T)) \triangleq \left(Q_m^n(\boldsymbol{P}(T)), m \in \mathcal{M}, n \in \mathcal{N}\right)$ *forms a maximum-norm contraction if the temperature satisfies*

$$\gamma < \frac{1}{2 \max_{m \in \mathcal{M}, n \in \mathcal{N}} \{\theta_m B_m^n\} \max_{n \in \mathcal{N}} \{|\mathcal{N}_n|\}}, . \tag{24}$$

The proof is given in the appendix in the separate supplemental file. Lemma 3 implies that when the interference among users becomes more severe (i.e., the maximum degree $\max_{n\in\mathcal{N}}\{|\mathcal{N}_n|\}$ of the interference graph becomes larger), a smaller γ is needed to guarantee the convergence. This is because that interference relationship among users becomes more complicated and users should put more weight to explore the environment. Note that the condition (24) is a sufficient condition to form a contraction mapping, which in turn is a sufficient condition for convergence. Simulation results show that a slightly larger γ may also lead to the convergence of the mapping. Based on the property of contraction mapping, there exists a fixed point $\boldsymbol{P}^*$ such that $Q(\boldsymbol{P}^*) = \boldsymbol{P}^*$. By the theory of stochastic approximations [35], the distributed learning algorithm will also converge to the same limit point $\boldsymbol{P}^*$.

Theorem 9. *For the distributed learning algorithm, if the temperature γ satisfies (24), $\sum_T \mu_T = \infty$ and $\sum_T \mu_T^2 < \infty$, then the sequence $\{\boldsymbol{P}(T), \forall T \geq 0\}$ converges to the unique limit point $\boldsymbol{P}^* \triangleq (P_m^{n*}, \forall m \in \mathcal{M}, n \in \mathcal{N})$ satisfying that*

$$Q_m^n(\boldsymbol{P}^*) = P_m^{n*}, \forall m \in \mathcal{M}, n \in \mathcal{N}. \tag{25}$$

We next explore the property of the equilibrium $\boldsymbol{P}^*$ of the distributed learning algorithm. From Theorem 9, we see that

$$Q_m^n(\boldsymbol{P}^*) = E[U_n(\boldsymbol{a}(T))|\boldsymbol{P}^*, a_n(T) = m] = P_m^{n*}. \tag{26}$$

It means that the perception value P_m^{n*} is an accurate estimation of the expected throughput in the equilibrium. Moreover, we show that the mixed strategy $\boldsymbol{\sigma}^*$ is an approximate Nash equilibrium.

Definition 12 (Approximate Nash Equilibrium [36]). A mixed strategy profile $\bar{\boldsymbol{\sigma}} = (\bar{\boldsymbol{\sigma}}_1, \ldots, \bar{\boldsymbol{\sigma}}_N)$ is a δ-approximate Nash equilibrium if

$$U_n(\bar{\boldsymbol{\sigma}}_n, \bar{\boldsymbol{\sigma}}_{-n}) \geq \max_{\boldsymbol{\sigma}_n} U_n(\boldsymbol{\sigma}_n, \bar{\boldsymbol{\sigma}}_{-n}) - \delta, \forall n \in \mathcal{N},$$

where $U_n(\bar{\boldsymbol{\sigma}}_n, \bar{\boldsymbol{\sigma}}_{-n})$ denotes the expected throughput of player n under mixed strategy $\bar{\boldsymbol{\sigma}}$ and $\bar{\boldsymbol{\sigma}}_{-n}$ denotes the mixed strategy profile of other users except player n. Here $\delta \geq 0$ is the gap from a (precise) mixed Nash equilibrium. For the distributed learning algorithm, we show that

Theorem 10. *For the distributed learning algorithm, the mixed strategy $\boldsymbol{\sigma}^*$ in the equilibrium $\boldsymbol{P}^*$ is a δ-approximate Nash equilibrium, with $\delta = \max_{n\in\mathcal{N}}\{-\frac{1}{\gamma}\sum_{m=1}^{M}\sigma_m^{n*}\ln\sigma_m^{n*}\}$.*

The proof is given in the appendix in the separate supplemental file. The gap δ can be interpreted as the *weighted entropy*, which describes the randomness of

the learning exploration. A larger δ means a worse learning performance. When each user adopts the uniformly random access, the gap δ reaches the maximum value and results in the worst learning performance. In this case, we can obtain the upper-bound of the gap δ as $-\frac{1}{\gamma}\sum_{m=1}^{M}\frac{1}{M}\ln\frac{1}{M} = \frac{1}{\gamma}\ln M$. Theorems 9 and 10 together illustrate the trade-off between the exploration and exploitation through the choice of γ. A small enough γ is required to explore the environment (so that users will not put too many weights on exploitation and get stuck in channels with the *current* best throughputs) and guarantee the convergence of distributed learning to the approximate mixed Nash equilibrium. If γ is too small, however, then the performance gap δ is large due to over-exploration. Numerical results in section "Numerical Results" demonstrate that, by a proper choice of the temperature γ, the performance loss of the approximate mixed Nash equilibrium obtained by distributed learning is at most 10% compared with the exact mixed Nash equilibrium.

Extension to Physical Interference Model

In previous sections, we have focused on studying the spatial spectrum access game under the protocol interference model, which has been widely adopted in wireless network research literature [37, 38]. The protocol interference model uses the interference graph to describe the pair-wide interference relationships among users, i.e., two users can interfere with each other if they are within each other's interference range. This is useful for modeling the data transmission confliction when some random access MAC protocol is adopted. For example, in 802.11 networks, we can construct the interference graph by setting the carrier sensing range as the interference range. Moreover, by carefully constructing the interference edges via the reality check approach in [37] or the measurement-calibrated propagation scheme in [38], the protocol interference model can provide a good approximation to the physical interference model that captures the continuous nature of interference and takes into account the accumulated interference from multiple concurrent transmitters [39, 40].

We next study the spatial spectrum access game under the setting of physical interference model. According to [39], we can compute the data rate of user n under the physical interference model as

$$U_n(\boldsymbol{a}) = \theta_m W \log_2\left(1 + \frac{\eta_n d_n^{-\alpha}}{\omega_0 + \omega_{a_n}^n + \sum_{i\in\mathcal{N}/\{n\}:a_i=a_n}\eta_i d_{in}^{-\alpha}}\right). \tag{27}$$

Here W is the channel bandwidth, η_i is the transmission power of user n, α is the path loss factor, and $d_n^{-\alpha}$ denotes the channel gain between the transmitter and the receiver of user n due to free-space attenuation [39]. Furthermore, ω_0 denotes the background noise, $\omega_{a_n}^n$ denotes the interference from primary users to secondary user n on channel a_n, $\eta_i d_{in}^{-\alpha}$ denotes the interference generated by user i to user n,

and $\sum_{i\in\mathcal{N}\setminus\{n\}:a_i=a_n}\eta_i d_{in}^{-\alpha}$ denotes the accumulated interference from other second users to user n. Similarly to the setting of protocol interference model, we can model the distributed spectrum access problem among users under the physical interference model as a spatial spectrum access game with the payoff function given as in (27). We can show the following result for the case that the channel availability θ_m of all channels are homogeneous, i.e., $\theta_m = \theta$ for any $m \in \mathcal{M}$.

Theorem 11. *When the channel availabilities of all channels are homogeneous, the spatial spectrum access game under the physical interference model is a potential game, with the potential function given as*

$$\Phi(\boldsymbol{a}) = -\sum_i \sum_{j\neq i} \eta_i \eta_j d_{ij}^{-\alpha} I_{\{a_i=a_j\}} - 2\sum_{n=1}^{N} \eta_n \left(\omega_{a_n}^n + \omega_0\right)$$

and hence has a pure Nash equilibrium.

The proof is given in the appendix in the separate supplemental file. Since the spatial spectrum access game is a potential game, we can then apply the Safe Experimentation algorithm in [29] for achieving the pure Nash equilibrium. For the general case that the channel availabilities are heterogeneous, the analysis of spatial spectrum access game is much more challenging and can be an interesting future research direction.

Numerical Results

We now evaluate the proposed distributed learning algorithm by simulations. We consider a Rayleigh fading channel environment. The data rate of user n on an idle channel m is given according to the Shannon capacity, i.e., $b_m^n(t) = W \log_2\left(1 + \frac{\eta_n z_m^n(t)}{\omega_m^n}\right)$. We consider the Rayleigh fading channel environment where channel gain $z_m^n(t)$ is a random variable that follows the exponential distribution with the mean $\bar{z}_m^n$. In the following simulations, we set $W = 10\,\text{MHz}$, $\omega_m^n = -100\,\text{dBm}$, and $\eta_n = 100\,\text{mW}$. By choosing different mean channel gains $\bar{z}_m^n$, we have different mean data rates $B_m^n = E[b_m^n(t)]$ for different channels and users. We set the channel idle probability $\theta_m = 0.5$.

We consider a network of $M = 5$ channels and $N = 9$ users with four different interference graphs (see Fig. 5). Graphs (a) and (b) are undirected, and Graphs (c) and (d) are directed. Let $\boldsymbol{B}_n = \{B_1^n, \ldots, B_M^n\}$ be the mean data rate vector of user n. We set $\boldsymbol{B}_1 = \boldsymbol{B}_2 = \boldsymbol{B}_3 = \{2, 6, 16, 20, 30\}$ Mbps, $\boldsymbol{B}_4 = \boldsymbol{B}_5 = \boldsymbol{B}_6 = \{4, 12, 32, 40, 60\}$ Mbps, and $\boldsymbol{B}_7 = \boldsymbol{B}_8 = \boldsymbol{B}_9 = \{10, 30, 80, 100, 150\}$ Mbps. We implement both the random backoff and Aloha mechanisms for channel contention. For the random backoff mechanism, we set the number of backoff mini-slots in a time slot $\lambda_{\max} = 10$. For the Aloha mechanism, the channel contention probabilities of the users are randomly assigned from the set $\{0.3, 0.5, 0.7\}$. Notice that in this study, we focus on channel choices instead of the adjustment of contention

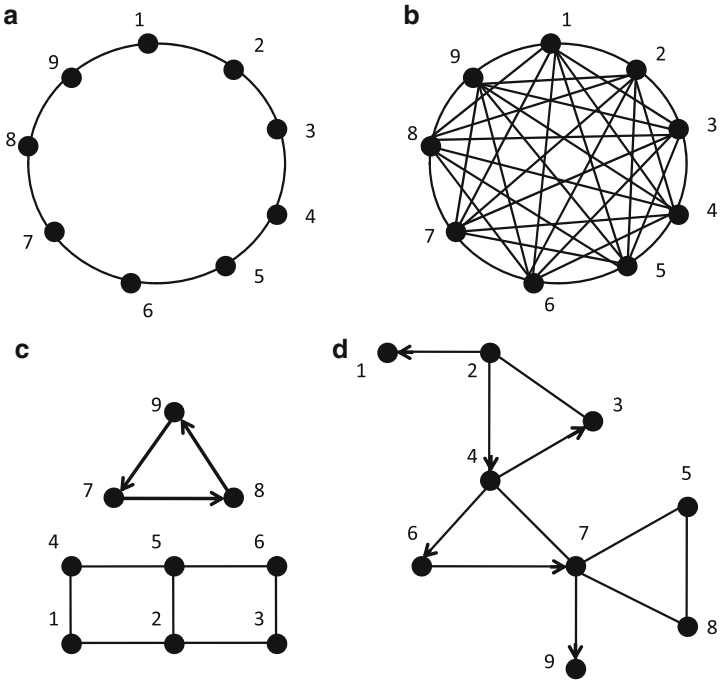

Fig. 5 Interference graphs

probabilities. For the distributed learning algorithm initialization, we set the smooth factor $\mu_T = \frac{1}{T}$, which satisfies the condition $\sum_T \mu_T = \infty$ and $\sum_T \mu_T^2 < \infty$.

We first evaluate the distributed learning algorithm with different choices of temperature γ on the interference graph (d) in Fig. 5. We run the learning algorithm sufficiently long until the time average system throughput does not change. The result in Fig. 6 shows the system performance with different γ and demonstrates that a proper temperature γ can achieve a balance between exploration and exploitation and offer the best performance. When γ is small, the users tend to select the channels randomly (i.e., over-exploration), and the performance gap δ can be large. When γ is very large, the algorithm focuses on exploitation and may get stuck in local optimum, and the performance is again negatively affected. In the following simulations, we set $\gamma = 5.0$ since it achieves good system performance in both random backoff and Aloha mechanisms as in Fig. 6.

We then evaluate the convergence of the distributed learning algorithm. In Fig. 7, we show the number of iterations for the convergence of distributed learning algorithm with random backoff and Aloha mechanisms. We see that as the interference graph becomes more dense (e.g., graph (b)), the convergence time becomes longer. The reason is that when the interference graph becomes more dense and a user can generate interference to more users, the environment becomes more complex, and it hence takes more time overhead to explore. We also observe that the convergence

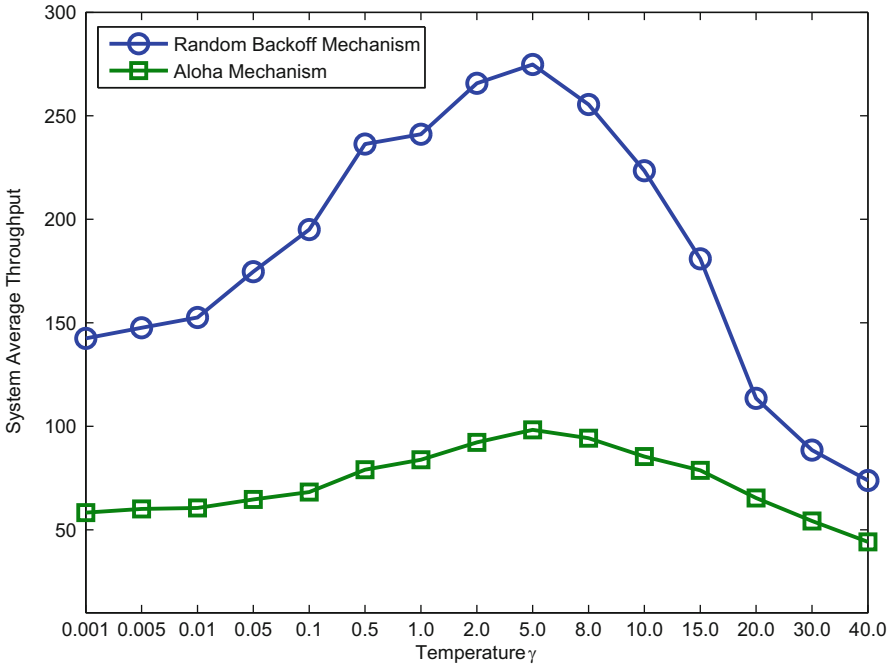

Fig. 6 The system performance of the distributed learning algorithm with different temperature γ

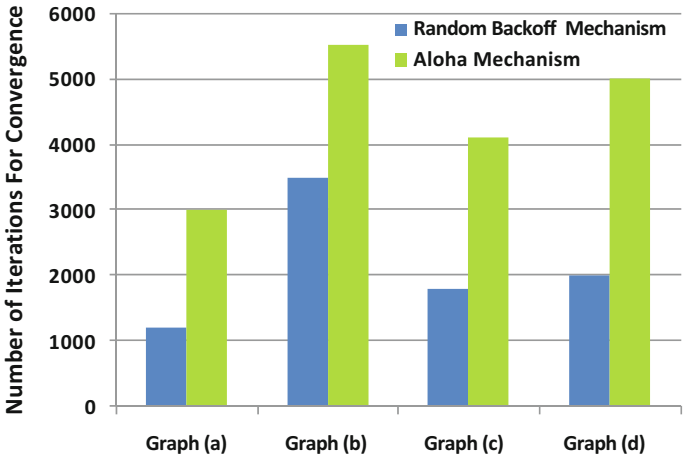

Fig. 7 Convergence time of distributed learning algorithm on different graphs

time of Aloha mechanism is longer than that of random backoff mechanism. This is due to the fact that in Aloha mechanism, users are heterogeneous in terms of channel contention capability; hence the system environment becomes more complicated.

We further compare distributed learning with the solutions obtained by the following benchmark algorithms:

- Random Access: each user chooses a channel to access purely randomly.
- Multiarmed Bandit: we implement the multiarmed bandit solution for distributed spectrum access in [41].
- Mixed NE: we compute the exact mixed Nash equilibrium of the spatial spectrum access game, based on statistical network information using the global Newton method [30].
- Dynamic Game: we compute the solution of the complete information dynamic game for spectrum access, by solving the corresponding stage spatial spectrum access game (using the global Newton method) for each time slot t, with the channel idle probabilities $\{\theta_m\}_{m=1}^{M}$ of the stage game replaced by the channel state realization $\{S_m(t)\}_{m=1}^{M}$ of time slot t.
- Centralized Optimization: the solution obtained by solving the centralized global optimization of $\max_{\boldsymbol{a}} \sum_{n\in\mathcal{N}} U_n(\boldsymbol{a})$.

We implement these algorithms together with the distributed learning algorithm on the four types of interference graphs in Fig. 5. The results are shown in Figs. 8 and 9. We see that the exact mixed Nash equilibrium of spatial spectrum access game based on statistical network information is quite efficient, with an average of less than 8% performance loss compared with the dynamic game solution. This is

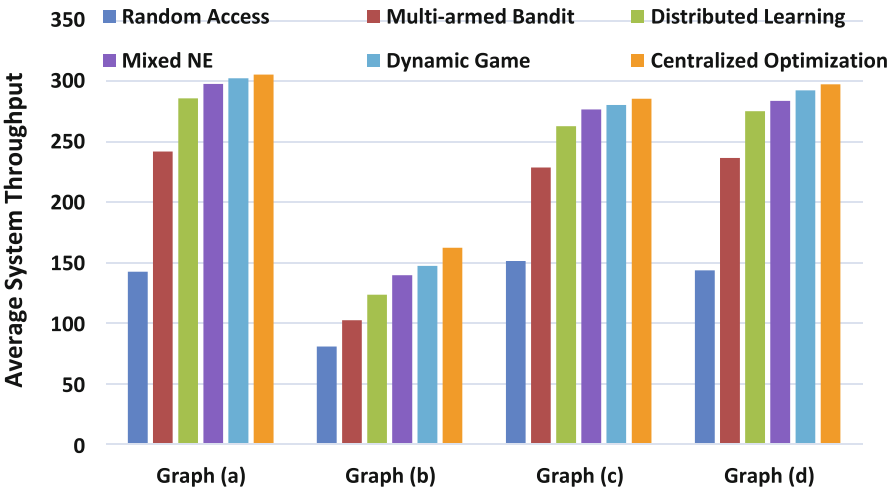

Fig. 8 Comparison of distributed learning, random access, global Newton, and centralized optimization with the random backoff mechanism

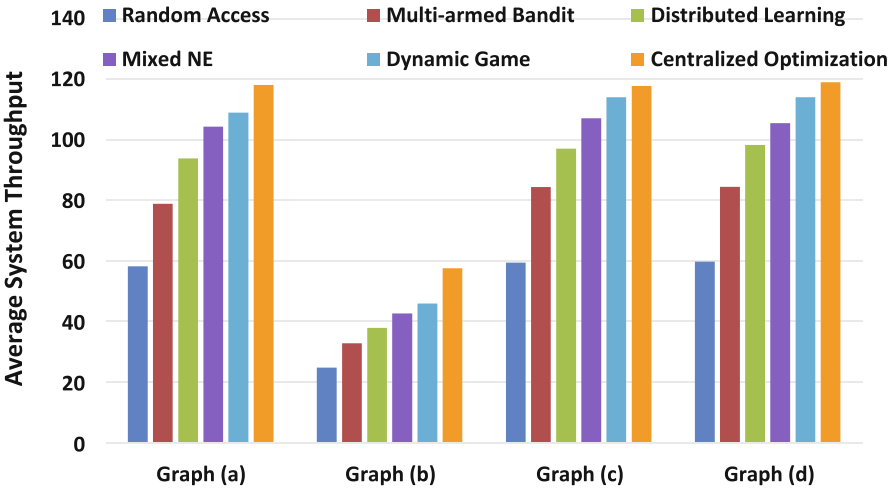

Fig. 9 Comparison of distributed learning, random access, global Newton, and centralized optimization with the Aloha mechanism

due to the fact that in the proposed spatial spectrum access game, each secondary user takes both the primary activity levels on different channels and the competition with other secondary users into consideration. This can help mitigate the congestion within secondary users and exploit the channels of high transmission opportunities. Moreover, the performance gap δ of the approximate mixed Nash equilibrium by distributed learning from the exact mixed Nash equilibrium is small, with a less than 10% performance loss in all cases. For the random backoff (Aloha, respectively) mechanism, we see that the distributed learning algorithm achieves up to 100% (65%, respectively) performance improvement over the random access algorithm. Moreover, we observe that the distributed learning algorithm can achieve a better performance than the multiarmed bandit scheme, with a performance gain of up to 15%. This is because that the design of multiarmed bandit scheme does not take the spatial reuse effect in account. Compared with the centralized optimal solution, the performance loss of the distributed learning in the full-interference graph (b) is 28% (34%, respectively). Such a performance loss is not due to the algorithm design; instead it is due to the selfish nature of the users (i.e., competition in distributed spectrum sharing). In the partial-interference graphs (a), (c), and (d), the performance loss can be further reduced to less than 10% (17%, respectively). This shows that the negative impact of users' selfish behavior is smaller when users can share the spectrum more efficiently through spatial reuse.

Conclusion

In this chapter, we explored the spatial aspect of distributed spectrum sharing and proposed a framework of spatial spectrum access game on directed interference graphs. We investigated the critical issue of the existence of pure Nash equilibria and developed a distributed learning algorithm converging to an approximate mixed Nash equilibrium for any spatial spectrum access games. We further discussed how to extend the framework to the setting of physical interference model. Numerical results showed that the algorithm is efficient and achieves a significant performance gain over a random access algorithm that does not consider the spatial effect.

For the future work, one interesting direction is to design distributed spectrum access mechanisms that can converge to pure Nash equilibria, for those spatial spectrum games which are not potential games but admit pure Nash equilibria. Another important direction is to study the general spatial spectrum access game under the physical interference model. It would be very challenging to show the existence of Nash equilibrium and extend the distributed learning algorithm under such a general physical interference setting.

References

1. Chen X, Huang J (2015) Spatial spectrum access game. IEEE Trans Mob Comput 14(3): 646–659
2. Akyildiz I, Lee W, Vuran M, Mohanty S (2006) Next generation/dynamic spectrum access/cognitive radio wireless networks: a survey. Comput Netw 50(13):2127–2159
3. Niyato D, Hossain E (2008) Competitive spectrum sharing in cognitive radio networks: a dynamic game approach. IEEE Trans Wirel Commun 7(7):2651–2660
4. Felegyhazi M, Cagalj M, Hubaux J-P (2009) Efficient mac in cognitive radio systems: a game-theoretic approach. IEEE Trans Wirel Commun 8(4):1984–1995
5. Yang L, Kim H, Zhang J, Chiang M, Tan CW (2011) Pricing-based spectrum access control in cognitive radio networks with random access. In: 2011 Proceedings of IEEE INFOCOM. IEEE, pp 2228–2236
6. Li D, Xu Y, Liu J, Wang X, Han Z (2010) A market game for dynamic multi-band sharing in cognitive radio networks. In: 2010 IEEE International Conference on Communications (ICC). IEEE, pp 1–5
7. Law LM, Huang J, Liu M, Li S-y et al (2009) Price of anarchy for cognitive mac games. In: IEEE Global Telecommunications Conference (GLOBECOM). IEEE, pp 1–6
8. Weiss M, Al-Tamaimi M, Cui L (2010) Dynamic geospatial spectrum modelling: taxonomy, options and consequences. In: Proceedings of TPRC Conference, Fairfax, Sept 2010
9. Nie N, Comaniciu C (2005) Adaptive channel allocation spectrum etiquette for cognitive radio networks. In: First IEEE International Symposium on New Frontiers in Dynamic Spectrum Access Networks. IEEE, pp 269–278
10. Han Z, Pandana C, Liu KR (2007) Distributive opportunistic spectrum access for cognitive radio using correlated equilibrium and no-regret learning. In: IEEE Wireless Communications and Networking Conference. IEEE, pp 11–15

11. Maskery M, Krishnamurthy V, Zhao Q (2009) Decentralized dynamic spectrum access for cognitive radios: cooperative design of a non-cooperative game. IEEE Trans Commun 57(2):459–469
12. Aumann RJ (1987) Correlated equilibrium as an expression of Bayesian rationality. Econometrica 55:1–18
13. Anandkumar A, Michael N, Tang A (2010) Opportunistic spectrum access with multiple users: learning under competition. In: INFOCOM. IEEE, pp 1–9
14. Lai L, Jiang H, Poor HV (2008) Medium access in cognitive radio networks: a competitive multi-armed bandit framework. In: IEEE 42nd Asilomar Conference on Signals, Systems and Computers. IEEE, pp 98–102
15. Liu K, Zhao Q (2010) Decentralized multi-armed bandit with multiple distributed players. In: IEEE Information Theory and Applications Workshop (ITA). IEEE, pp 1–10
16. Husheng L (2010) Multiagent Q-learning for aloha-like spectrum access in cognitive radio systems. EURASIP J Wirel Commun Netw Article ID 876216, 1:1–15
17. Tekin C, Liu M, Southwell R, Huang J, Ahmad S (2012) Atomic congestion games on graphs and their applications in networking. IEEE/ACM Trans Netw 20(5):1541–1552
18. Bilò V, Fanelli A, Flammini M, Moscardelli L (2008) Graphical congestion games with linear latencies. In: Proceedings of ACM SPAA, Munich, June 2008
19. FCC (2010) Second memorandum opinion and order. 23 Sept 2010. [Online] Available: http://transition.fcc.gov/Daily_Releases/Daily_Business/2010/db0923/FCC-10-174A1.pdf
20. Anouar H, Bonnet C (2007) Optimal constant-window backoff scheme for IEEE 802.11 dcf in single-hop wireless networks under finite load conditions. Wirel Pers Commun 43(4): 1583–1602
21. Nash J (1950) Equilibrium points in n-person games. Proc Natl Acad Sci 36:48–49
22. Biggs N, Lloyd E, Wilson R (1986) Graph theory. Oxford University Press, Oxford
23. Santi P (2005) Topology control in wireless ad hoc and sensor networks. ACM Comput Surv 37(2):164–194
24. Milchtaich I (1996) Congestion games with player-specific payoff functions. Games Econ Behav 13:111–124
25. Monderer D, Shapley LS (1996) Potential games. Games Econ Behav 14:124–143
26. Mavronicolas M, Milchtaich I, Monien B, Tiemann K (2007) Congestion games with player-specific constants. In: Mathematical Foundations of Computer Science 2007, pp 633–644
27. Monisha JH, Uthariaraj VR (2012) User profile based proportional share scheduling and mac protocol for manets. Int J Distrib Parallel Syst (IJDPS) 3(1):269–283
28. Koutsoupias E, Papadimitriou C (1999) Worst-case equilibria. In: STACS 99. Springer, pp 404–413
29. Marden J, Young H, Arslan G, Shamma J (2009) Payoff-based dynamics for multiplayer weakly acyclic games. SIAM J Control Optim 48(1):373–396
30. Govindan S, Wilson R (2003) A global newton method to compute Nash equilibria. J Econ Theory 110:65–86
31. Chen X, Huang J (2012) Imitative spectrum access. In: Proceedings of IEEE WiOpt, Paderborn, May 2012
32. Maskery M, Krishnamurthy V, Zhao Q (2009) Decentralized dynamic spectrum access for cognitive radios: cooperative design of a non-cooperative game. IEEE Trans Commun 57(2):459–469
33. Shah D, Shin J (2010) Dynamics in congestion games. ACM SIGMETRICS Perform Eval Rev 38(1):107–118
34. Cominetti R, Melo E, Sorin S (2010) A payoff-based learning procedure and its application to traffic games. Games Econ Behav 70(1):71–83
35. Kushner H, Yin G (2003) Stochastic approximation and recursive: algorithms and applications. Springer, New York
36. Daskalakisa C, Mehtab A, Papadimitriou C (2009) A note on approximate Nash equilibria. Theor Comput Sci 410(17):1581–1588

37. Shi Y, Hou YT, Liu J, Kompella S (2009) How to correctly use the protocol interference model for multi-hop wireless networks. In: Proceedings of the Tenth ACM International Symposium on Mobile Ad Hoc Networking and Computing. ACM, pp 239–248
38. Zhou X, Zhang Z, Wang G, Yu X, Zhao BY, Zheng H (2013) Practical conflict graphs for dynamic spectrum distribution. In: Proceedings of the ACM SIGMETRICS/International Conference on Measurement and Modeling of Computer Systems. ACM, pp 5–16
39. Gupta P, Kumar PR (2000) The capacity of wireless networks. IEEE Trans Inf Theory 46(2):388–404
40. Yang L, Cao L, Zheng H (2008) Physical interference driven dynamic spectrum management. In: 3rd IEEE Symposium on New Frontiers in Dynamic Spectrum Access Networks. IEEE, pp 1–12
41. Lai L, El Gamal H, Jiang H, Poor HV (2011) Cognitive medium access: exploration, exploitation, and competition. IEEE Trans Mob Comput 10(2):239–253

Part IV
Cognitive Cellular Networks

Coexistence of Heterogeneous Cellular Networks

35

Kaigui Bian and Jung-Min Jerry Park

Contents

K. Bian (✉)
School of EECS, Peking University, Beijing, China
e-mail: bkg@pku.edu.cn

J.-M. J. Park
Department of Electrical and Computer Engineering, Virginia Tech, Blacksburg, VA, USA
e-mail: jungmin@vt.edu

W. Zhang (ed.), *Handbook of Cognitive Radio*,
https://doi.org/10.1007/978-981-10-1394-2_32

Abstract

Many wireless standards for cellular networks (e.g., IEEE 802.11af and IEEE 802.22) have been developed or are currently being developed for enabling opportunistic access to spectrum using cognitive radio (CR) technology. When heterogeneous cellular networks that are based on different wireless standards operate in the same spectrum band, coexistence issues can potentially cause major problems. Enabling coexistence via direct coordination between heterogeneous cellular networks is very challenging due to incompatible MAC/PHY designs of coexisting networks, the conflict of interest issues, as well as customer privacy concerns. This chapter introduces a number of research problems that may arise in the context of coexistence of heterogeneous cellular networks, namely, the hidden terminal problem, the multichannel broadcast problem, the spectrum sharing problem, and the channel contention problem. This chapter also identifies the major challenges for addressing these problems, proposes the guidelines for devising potential solutions, and provides results of performance evaluation on the proposed solutions.

Introduction

Industry and research stakeholders have launched standardization efforts to enable the secondary networks' utilization of unused spectrum by leveraging *cognitive radio* (CR) technology. These efforts include IEEE 802.22 wireless regional area networks (WRAN) [22], IEEE 802.16h Cognitive WiMax, IEEE 802.11af (WiFi over TV white space) [20], ECMA 392 (WPAN over TV white space) [8], etc. All of these standards rely on CR technology to overcome the challenging *vertical* or *incumbent* coexistence problem between primary and secondary networks as well as the *horizontal* coexistence problem between secondary networks.

Heterogeneous vs. homogeneous coexistence: There exists a significant body of work on vertical coexistence [5, 6], and it has been attracting significant interest from academia and industry. In contrast, horizontal coexistence has garnered less attention thus far. Horizontal coexistence can be further categorized into:

- *Heterogeneous* coexistence that refers to the coexistence of networks that employ different wireless technologies (e.g., the coexistence between WiFi and Bluetooth [19, 50], the coexistence of heterogeneous wireless networks over TV white space [21]);

- *Homogeneous* coexistence (aka self-coexistence) that refers to the coexistence of networks that employ the same wireless technology (e.g., neighboring CR networks of the same type [3, 31], or neighboring 802.11 hotspots [30]).

This chapter has a focus on the heterogeneous coexistence between secondary cellular networks that employ different wireless technologies and uses the term "cellular network" to denote a CR-enabled cellular network operating over TV white space.

Existing coexistence schemes: The coexistence schemes for wireless networks can be broadly classified into two categories.

- A *noncollaborative* coexistence scheme is the only feasible approach when there are no means of coordination between the coexisting networks, such as the coexistence of WiFi and ZigBee networks [19, 50].
- A *collaborative* coexistence scheme can be employed when coexisting networks can directly coordinate their operations, such as the self-coexistence schemes for 802.22 networks [3, 31].

Major challenges: Existing coexistence schemes fail to adequately address the heterogeneous coexistence problem in TVWS for a number of technical and policy reasons. Noncollaborative schemes cannot facilitate the coexistence among heterogeneous networks due to their incompatible MAC strategies. Collaborative strategies may require the exchange of potentially sensitive information (e.g., traffic load, bandwidth requirements) across different networks to negotiate the spectrum partitioning [47, 48], which could raise conflict-of-interest issues and customer privacy concerns for competing wireless networks or service providers. Moreover, it is difficult to find a third party that can serve as a global or centralized decision-maker that supervise all heterogeneous networks and allocate spectrum them.

Problems in focus: This chapter studies a few challenging problems that are related to the medium access control (MAC) layer protocol design for coexistence of heterogeneous coexistence of cellular networks.

- *Hidden terminal problem* can be potentially exacerbated by the heterogeneity of the PHY/MAC designs of the coexisting cellular networks, especially when TDM-based cellular networks coexist with CSMA-based networks.
- *Broadcast failure* problem may arise over a single broadcast channel when the broadcast channel is reclaimed by a primary (or licensed) user that has a higher priority of accessing the spectrum, or when secondary users in coexisting cellular networks moves into a region where the co-channel interference is caused.
- *Spectrum sharing* among coexisting heterogeneous cellular networks is very challenging via direct coordination, while a *mediator* system is able to establish an *indirect* coordination mechanism for spectrum sharing between networks.

- *Channel contention* is a distributed inter-network coordination process that enables a CR network in need of more spectrum resources to acquire channels from neighboring networks by exchanging control messages via a local controller.

The following sections discuss each problem and its corresponding solution respectively.

Hidden Terminal Problem

In wireless networks, when more than one transmitter-receiver pairs share a channel, the *hidden terminal problem* can occur. This problem occurs when a transmitter is visible from a receiver node, but hidden from (or out of the sensing range of) another transmitter that is visible from the same receiver. This leads to packet collisions at the receiver when the two transmitters send packets simultaneously. The hidden terminal problem in single-channel environments has been widely studied. In single-channel systems employing CSMA/CA, a handshaking procedure (i.e., using RTS/CTS control packets [29]) has been adopted to address the problem. For handling the hidden terminal problem in *multi*channel wireless networks, some have proposed the use of a fixed control channel to facilitate a handshake procedure between two transceivers [40].

Unfortunately, the aforementioned handshaking procedures do *not* work when the hidden terminal problem is caused by heterogeneous coexistence. This is because the hidden terminal problem in heterogeneous coexistence is different from those mentioned above and is due to the fact that the coexisting networks *cannot understand each others' control messages* because they use different air interfaces (i.e., PHY/MAC stacks). An example is shown in Fig. 1 in which: an 802.22 network is coexisting with an 802.11af network. The 802.22's MAC protocol is TDM (time-division multiplexing) based with PHY resources allocated using OFDMA, while 802.11af relies on a contention-based CSMA protocol. Because the 802.22 base station (BS) and the 802.11af access point (AP) are hidden from each other, packets sent by the BS and the AP may collide at the 802.11af receiver node. Previous works have shown that enabling fair and efficient spectrum sharing is challenging in scenarios where a network with a contention-based MAC protocol (e.g., 802.11af) coexists with a network with a tightly scheduled TDM-based MAC

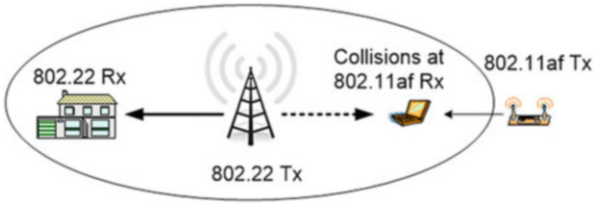

Fig. 1 An example of the hidden terminal problem caused by heterogeneous coexistence

protocol (e.g., 802.22 or 802.16h) [10, 11, 13, 27, 39, 44]. IEEE 802.22 is the first worldwide wireless standard based on CR technology for utilizing TVWS in rural areas. The 802.22 standard prescribes incumbent protection techniques necessary for secondary users to operate in licensed TV bands, while 802.16 does not. It is assumed that the TDM device can distinguish a packet sent by a CSMA device from the background noise. This section focuses on the particular type of heterogeneous coexistence between TDM and CSMA networks.

The hidden terminal problem in this heterogeneous coexistence scenario induces two types of packet collisions:

1. Collisions at the receivers of a TDM MAC network that are caused by hidden transmitters of a CSMA MAC network
2. Collisions at the receivers of a CSMA MAC network that are caused by hidden transmitters of a TDM MAC network

This section presents a coexistence scheme that mitigates the packet collisions caused by the hidden terminal problem in a particular type of heterogeneous coexistence scenario – viz., coexistence of TDM and CSMA MAC networks (e.g., 802.22 and 802.11af networks).

- To mitigate the first type of collisions, a *beacon transmission* mechanism is introduced to enable the receivers in a TDM MAC network to send beacon signals to prevent the hidden CSMA devices from accessing the shared channel, while transmitters of the TDM MAC network occupy the channel.
- To mitigate the second type of collisions, a *dynamic quiet period* mechanism is presented for the TDM MAC networks. This mechanism requires a TDM transmitter to dynamically determine the end point of its current quiet period (QP) in order to reduce the probability of packet collisions. The length of the quiet period is dynamically adjusted in order to maintain long-term weighted fairness in channel access between the coexisting TDM and CSMA networks.

Two Types of Collisions

Type 1: Collisions at the TDM Network Receiver

This type of collisions occur when a TDM receiver is located within the transmission ranges of both the TDM and CSMA transmitters, but the two transmitters are hidden from each other. To reduce this type of collisions, the TDM network has to prevent the CSMA transmitter from transmitting while the TDM transmitter is transmitting.

A straightforward solution to mitigate packet collisions in this scenario is to require the TDM receiver to emit *beacon signals* during a small time fraction at the beginning of every time slot. This time fraction is called the *beaconing fraction* of a time slot. Here, it is assumed that the TDM receiver is within the CSMA transmitter's sensing range – i.e., the CSMA transmitter can sense the

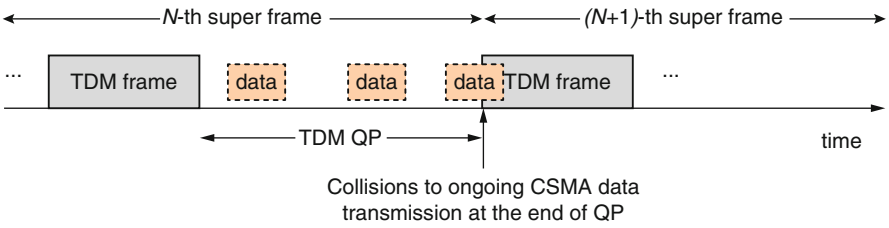

Fig. 2 Collisions at the end of the N-th frame's QP. *Dotted-line rectangles* represent the CSMA data packets

TDM receiver's beacon signals. The beacon signal's presence in the channel will cause the CSMA transmitter to suspend transmissions. It is reasonable to assume that the coexistence enabling system (e.g., 802.19.1 system) mandates the use of beacon signals by the TDM receivers to facilitate coexistence, since the TDM MAC networks are registered.

During the beaconing fraction of a time slot, the TDM transmitter stops transmitting, and the TDM receiver emits beacon signals such that the coexisting CSMA transmitter can detect the beacons and refrain from transmitting in the channel. As a result, the collision-free receptions at the TDM receivers can be guaranteed. Requiring the TDM receiver to transmit beacons can be a costly overhead and thus should be required only when its benefits outweigh the costs.

Type 2: Collisions at the CSMA Network Receiver

This type of collisions occur when the CSMA receiver is located within the transmission ranges of both the TDM and CSMA transmitters, but the two transmitters are hidden from each other. In this scenario, packet collisions occur because the TDM transmitter initiates transmission before the CSMA transmitter has finished transmitting its data packets.

A specific example of this scenario is shown in example in Fig. 2. In the figure, the first TDM frame transmitted by the TDM transmitter in the $(N + 1)$-th superframe collides with the CSMA transmitter's ongoing packet transmissions which started in the QP of the N-th superframe and has continued on past the QP. In this situation, requiring the CSMA receivers to use beacons is not a plausible solution, because they are not under the control of the 802.19.1 system.

During a QP, a TDM transmitter suspends its transmission, and it terminates the QP at the scheduled end time point by transmitting a prescribed number of beacons. After transmitting a prescribed number of beacons, the TDM transmitter terminates the current QP and starts the TDM frame of the next superframe. Note that the TDM transmitter simply terminates the QP at the scheduled time point, and it will not wait until the ongoing transmission for CSMA data and/or ACK packets to be finished.

Beacon Transmission by TDM Receiver

Consider an 802.22 WRAN co-located with an 802.11af WLAN, both sharing the same TV white space channel. To mitigate the first type of collisions, it is recommended to support two modes at the TDM receiver: beaconing and non-beaconing modes. It can switch from one mode to the other depending on the channel conditions, and this procedure of switching contains two steps:

1. First, the network entity performs channel evaluation to determine when to switch from one mode to the other. The TDM receiver measures the received SIR, estimates the channel capacity in the two modes, and makes a decision of which mode to operate in.
2. Then, the TDM receiver will notify the TDM transmitter if it decides to switch to the beaconing mode. In the beaconing mode, the TDM transmitter has to stop transmitting in the beaconing duration.

Beaconing by TDM receivers will incur additional overhead and waste the channel time. That is why a dynamic switch is needed between the two modes to balance the tradeoff between the performance loss due to interference caused by CSMA packets, and the beaconing overhead.

First, calculate the channel capacity in each of the two modes. By estimating the channel access time and packet error rate, the capacity of the shared channel, C, is:

$$C = \left(1 - \frac{u}{t}\right) \cdot (1 - \varepsilon), \tag{1}$$

where t is the length of a time slot, u is the duration of beaconing in a time slot, and ε denotes the packet error rate on the shared channel at the TDM receiver. In (1), $\left(1 - \frac{u}{t}\right)$ represents the ratio of channel access time used for non-beaconing transmission and the length of a time slot and $(1 - \varepsilon)$ shows the rate of successful packet reception given possible packet errors. The packet error can be caused by a few factors, such as noise, interference, fading, etc.

The reduction of channel capacity can be caused by two factors in the considered scenarios of heterogeneous coexistence, namely, the beaconing duration, and the inter-network interference. In the beaconing mode, the beaconing duration, u, is the major cost that may lower the channel capacity, and the inter-network interference can lead to a high packet error rate (i.e., a low channel capacity according to (1)) in the non-beaconing mode. The effect of fading may vary with time, geo-locations, or frequency, and it is independent of whether the beaconing mode is used.

Let γ denote the maximum achievable SIR perceived by the TDM receiver on the shared channel. In [38], Shellhammer describes a way of estimating ε based on γ: the symbol error rate (SER), ρ, can be estimated based on γ; then, ε can be calculated based on the SER. If the modulation is BPSK, the SER $\rho = Q[\sqrt{2\gamma}]$, where the function $Q(\cdot)$ is the integral of the tail of a normalized Gaussian

probability density function [37]. The packet error rate in a packet of m symbols is the probability that at least one symbol is incorrect,

$$\varepsilon = 1 - (1 - \rho)^m.$$

Channel capacity in beaconing mode: To avoid the first type of collisions, the TDM receiver is allowed to block the medium by emitting beacon signals in every time slot. The capacity of the shared channel in this mode can be expressed as

$$C_b = \left(1 - \frac{u}{t}\right) \cdot (1 - \varepsilon).$$

The CSMA transmitter could sense an idle channel during a time period of $(t - u)$ in every TDM time slot. To successfully block the medium, the TDM receiver needs to guarantee that the value of $(t - u)$ is less than the time for channel clear assessment (CCA) in CSMA networks. The time for CCA in WiFi networks is 28 μs [25].

Assume the noise source is additive white Gaussian noise (AWGN) N_0, and the signal-to-noise ratio is represented as E_s/N_0, where E_s denotes the signal energy in a symbol. That is,

$$\gamma = \frac{E_s}{N_0}.$$

Given the modulation, the TDM MAC network is able to estimate C_b using γ.

Channel capacity in non-beaconing mode: If the feature of beacons is disabled, the TDM receiver may experience the first type of collision when there is a nearby CSMA transmitter that is hidden from the TDM transmitter. The channel capacity in the non-beaconing mode can be expressed as

$$C_n = \left(1 - \frac{u}{t}\right) \cdot (1 - \varepsilon) = 1 - \varepsilon.$$

The fundamental principal of this approach in the non-beaconing mode is to equate the interference power at the TDM receiver, after the receive filter, to the equivalent noise power after the receive filter.

Given the AWGN N_0, the signal energy in a symbol of period T is related with the symbol power $P_s = \frac{E_s}{T}$. Let B denote the noise equivalent bandwidth of the receive filter for a symbol period of T, and $B = \frac{1}{T}$. The noise power after the receiver filter is given by $P_n = \frac{N_0}{B}$. The ratio E_S/N_0 can be expressed in terms of the signal power and the noise power after the receiver,

$$\frac{E_s}{N_0} = \frac{P_s T}{P_n T} = \frac{P_s}{P_n},$$

Since the TDM receiver has the same TVWS channel model as the interferer (CSMA transmitter), the noise power after the receive filter is equal to the value of the interference signal, P_I^r, after the receive filter [38], i.e., $P_n = P_I^r$. Therefore,

$$\gamma = \frac{E_s}{N_0} = \frac{P_s}{P_I^r},$$

and C_n can be accordingly estimated.

An approach of switching between two modes: In the proposed approach, the non-beaconing mode over the shared mode is attempted first. If the maximum achievable SIR on the channel is not sufficiently high, it is prescribed that the beaconing mode for TDM networks will block the medium and prevent CSMA devices' access to the channel. One possible approach is introduced here for determining when to enable the beaconing mode.

The network determines which mode for the the TDM receiver to operate in, for a given channel, by comparing γ with the required SIR threshold parameter γ^*. To obtain the value of γ^*, first solve for ε in the equation $C_b = C_n$ and then find the SIR value corresponding to the solved ε, which is used as the value of γ^*.

1. If $\gamma \geq \gamma^*$, the TDM receiver operates in the non-beaconing mode. The benefits of non-beaconing mode (e.g., low control overhead) outweigh the benefits of beaconing (e.g., no collisions).
2. If $\gamma < \gamma^*$, the TDM receiver operates in the beaconing mode. The benefits of beaconing mode outweigh the benefits of non-beaconing mode.

Dynamic Quiet Period at TDM Transmitter

In the proposed approach, the TDM transmitter chooses the appropriate starting time point for TDM transmission in order to avoid overlapped TDM and CSMA transmissions, and it starts occupying the channel immediately after the transmission of a whole CSMA packet and before the transmission of the next CSMA packet.

Quiet Period

In TDM MAC networks, channel access occurs in scheduled blocks of time slots; in CSMA MAC networks, channel access is contention based, and there is no predetermined schedule for channel access. A "universal" superframe structure is representative in TDM MAC networks with coexistence mechanisms (e.g., 802.22 or 802.16 networks). Time is divided into *superframes*, each superframe is divided into *frames*, and each frame contains a number of f time slots.

In 802.16h, a quiet period (QP) that contains an integer number of frames is periodically scheduled [22,36]. During a QP, the BS suspends its data transmissions to provide channel access opportunities for CSMA networks. Similarly, a QP is

scheduled at the end of every superframe, and non-QP frames are considered as *data frames*.

Let q denote the number of frames contained in a QP, and let d denote the number of data frames contained in a superframe. Thus, the number of frames in a superframe is $d + q$, and the number of time slots in a superframe is $(d + q) f$. A TDM network starts transmitting data immediately after the end of a QP (i.e., end of a superframe). The value of q quantifies the number of frames that TDM networks can share with CSMA networks during a superframe. The values of d and q are predetermined collectively by the coexisting TDM MAC networks or determined by the coexistence mediator. During a TDM QP, the CSMA networks sense an idle channel and start to transmit CSMA packets.

The proposed approach is built on top of the superframe structure of TDM MAC networks, and it adopts an innovative way of dynamically determining the length of the quiet period, which reduces the second type of collisions as well as maintains the weighted fairness for the TDM MAC network in channel access. It employs the following algorithms to achieve these objectives.

- *Collision avoidance algorithm*. The TDM transmitter monitors the data traffic during the QP and captures the ACK packets emitted by CSMA networks. To avoid collisions, the TDM transmitter is allowed to terminate the QP immediately after detecting an ACK packet. This will lead to a shortened QP in the current superframe and an advanced frame in the next superframe, which hurts the short-term weighted fairness for the TDM MAC network.
- *Weighted fairness maintenance algorithm*. By counting the number of time slots lost in previous shortened QPs, the TDM transmitter is able to determine whether it needs to increase the length of the next QP such that the long-term fairness can be maintained.

Collision avoidance: In either saturated or unsaturated WLANs, the aggregated traffic pattern (the inter-arrival time between WLAN packets) approximates a Poisson distribution [7, 49]. The experimental results in [19] show that the inter-arrival time of WLAN frame clusters fits a *Pareto* model. It is assumed that the packet arrival of the WLAN follows a Poisson distribution. Let λ denote the WLAN data packets' arrival rate, and thus the mean inter-arrival time is $1/\lambda$.

Definition 1. When the TDM network enters a scheduled QP,

- The *elapsed QP* is the time duration from the start of the QP to the current time point.
- The *residual QP* is the time duration from the current time point to the expected end of the QP.

Figure 3 illustrates the elapsed QP and residual QP.

To avoid collisions to the potential hidden CSMA receiver at the end of the QP (defined as the second type of collisions), the TDM MAC network (or TDM

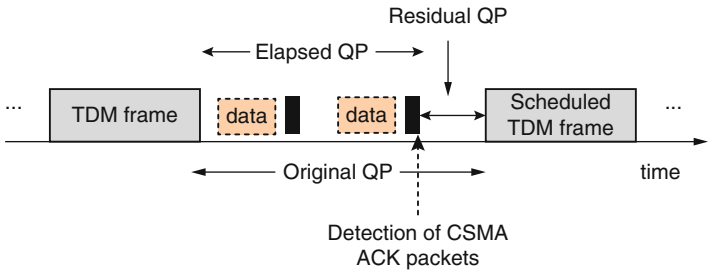

Fig. 3 Illustration of the elapsed QP and residual QP in a superframe of the TDM MAC network

transmitter) has to make a decision upon detecting a CSMA ACK packet: *Is the residual QP long enough for completing another CSMA packet transmission?*

1. If the answer is "yes," the TDM network will keep silent and wait for the next CSMA packet arrival (i.e., the next detected ACK).
2. If the answer is "no," the TDM network should terminate the QP by immediately starting TDM transmissions (or beacon transmissions) such that the CSMA receiver would refrain from operating in the channel.

As a result, it enables the TDM MAC network to autonomously terminate the QP at an "appropriate" time point.

Let e_i denote the duration of the elapsed QP and r_i denote the duration of the residual QP, in the i-th superframe, both of which are on a time slot basis. Let l_d and l_a denote the mean length of WLAN's data packets and the length of ACK packet, respectively. Recall that the number of time slots in a frame is f. Let p denote the probability that the next CSMA packet transmission can be finished in the residual QP, r_i. Upon detection of an ACK packet, the length of the residual QP is r_i, and the TDM network calculates the probability p.

- When $r_i < l_d$, the residual QP is smaller than the mean length of a WLAN data packet, and thus $p = 0$.
- When $r_i \geq l_d$, the residual QP is longer than the mean length of a WLAN data packet, and the next CSMA packet transmission can be finished in the residual QP, only if the packet arrives in next $(r_i - l_d)$ slots.

$$\begin{aligned} p &= \mathbb{P}\{\text{CSMA pkt arrival in next } (r_i - l_d) \text{ slots}\} \\ &= 1 - \mathbb{P}\{\text{no CSMA pkt arrival in next } (r_i - l_d) \text{ slots}\} \\ &= 1 - e^{-\lambda(r_i - l_d)}. \end{aligned} \tag{2}$$

Decision rule of dynamic QP mechanism: Based on the calculated value of p, the TDM network is able to decide whether to terminate the QP upon detection of

CSMA ACK packets, using the following decision rule, in which q_i denotes the *length of QP* (on a frame basis) in the i-th superframe, and the initial value $q_1 = q$. How to dynamically update the value of q_i will be described later.

1. When $e_i < q_i f$, the QP of the current superframe has not finished. Upon the detection of a CSMA ACK packet,
   a. The TDM network predicts that the residual QP is insufficiently long for completing a next CSMA packet transmission if $p < \tau$. Then, it terminates the QP by immediately transmitting beacons;
   b. The TDM network predicts that the residual QP is long enough for completing a next CSMA packet transmission if $p \geq \tau$. Thus, the TDM transmitter waits for the next ACK packet without sending any beacons.

   τ denotes the threshold that represents the *expected probability that the next CSMA packet transmission can be finished in the residual QP*.
2. When $e_i = q_i f$ (i.e., the residual QP $r_i = 0$), it means that the elapsed QP length exceeds the original length of QP in the i-th superframe, and the TDM network has to terminate the QP immediately even without detecting any ACK packet. In unsaturated CSMA networks, the waiting time before a CSMA packet arrival might be very long, which degrades the channel utilization. This step prevents the case that the waiting time is longer than the length of the current QP.

Simulation

This section compares the proposed approach with the fixed QP (FQP) mechanism, and considers a heterogeneous coexistence scenario between TDM networks (e.g., 802.22 networks) and CSMA networks (e.g., 802.11 networks). In each TDM network, there is one BS and multiple user devices, and the BSs of TDM networks are synchronized. Each CSMA network is placed at a location such that the AP is hidden from the BS. All coexisting networks are able to identify available TVWS channels by making queries to the TVWS database or leveraging the spectrum sensing techniques.

A synchronized superframe structure is simulated for all coexisting TDM networks to share the same channel. In each data frame, the TDM receiver is required to adopts the beacon transmission mechanism to prevent the collisions to the TDM packet reception when necessary. In each quiet period, the TDM transmitters suspend their traffic and observe the possible CSMA transmission over the channel to carry out the dynamic QP mechanism. The decision-making threshold $\tau = 0.5$, which implies that in the residual QP, the probability of the next complete CSMA packet transmission is required to be greater than the probability of an incomplete transmission. The length of QP is counted by the number of frames, and each frame contains ten time slots. The CSMA packet duration consists of multiple time slots. The CSMA packet arrival rate quantifies the probability that the CSMA packet arrives in a time slot. In the CS-based spectrum access scheme, $\frac{s}{f} = \frac{1}{5}$, which is the fraction of time a device spends on spectrum sensing in every time slot.

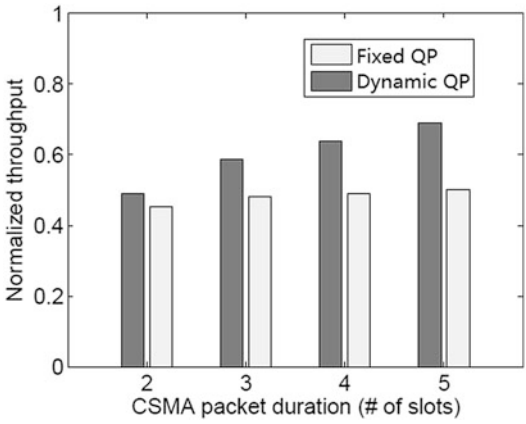

Fig. 4 Normalized throughput under the hidden terminal situation, when varying the basic QP length, $l_d = 2$ and $\lambda = 0.5$

The simulation parameter values were chosen to be consistent with those used by the 802.22 working group [23, 24].

Normalized Throughput in the Quiet Period

In a quiet period-based approach, the packet collision due to the hidden terminals only happens at the end of a QP.

Define the *normalized throughput in the QP* as the ratio between the number of time slots for transmitting CSMA packets without collisions during a QP and the total number of time slots in the QP. In general, Figs. 4 and 5 show that the performance of the dynamic QP approach is better than that of the FQP scheme in all cases.

As shown in Fig. 4, the gap between SHARE and FQP in terms of the normalized throughput narrows as the length of the QP increases. In contrary, the throughput gap between SHARE and FQP becomes wider when the CSMA packet duration l_d increases, as shown in Fig. 5. The reason has been explained above: with an increased CSMA packet duration, the collision probability increases in every QP, which decreases the normalized throughput.

The purpose of this set of simulations is to investigate how much is the performance gain that can be obtained from the proposed protocol.

- In Fig. 4, the performance gain is approximately 20% when the length of the quiet period is as small as the half of a frame length;
- As Fig. 5 shows, the longer the CSMA packet is, the more performance gain can be obtained (approximately 40% when the CSMA packet length is five slots).

Thus, the proposed protocol has a significant performance gain when a CMSA network that has a long packet length coexists with a TDM network that has a small QP length. Meanwhile, it has no significant performance gain given various packet arrival rates.

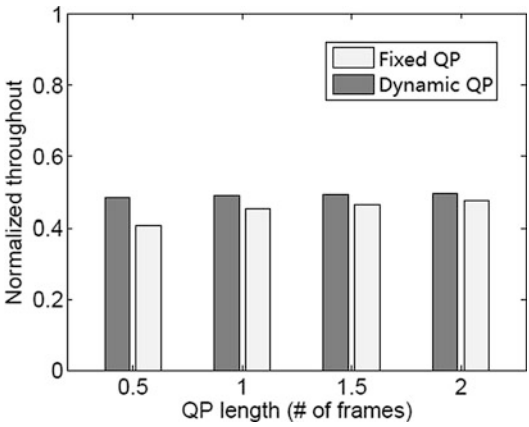

Fig. 5 Normalized throughput when varying the CSMA packet duration, $q = 1$ and $\lambda = 0.5$

Multichannel Broadcast Problem

Broadcast in cellular networks is typically offered as a push-type service for distributing important control information from the base station to a group of users that share radio resources. Moreover, broadcast enables the low-cost delivery of large volumes of popular content (e.g., multimedia content) to users in a cell. There are many existing solutions to broadcast in the market, including mobile TV broadcasting (DVB-H) [32], audio casting, massive software updates, content delivery over WiMax [28], and broadcast (or multicast) service offered by 3GPP in LTE cellular networks [15].

A single channel, referred to as a *broadcast channel*, is usually used by a base station to distribute the same content to a group of users that subscribe to the same service [9]. Meanwhile, a base station may employ multiple broadcast channels for delivering different contents to groups of users that subscribe to different services. A user or a content subscriber is able to successfully receive the broadcasted content when (1) the broadcast channel is available and (2) the user is located within the transmission range of the base station.

In dynamic spectrum access, the *broadcast failure problem* can occur due to the temporal and spatial variations in channel availability. Specifically, the primary users (PU, or licensed users) may reclaim the spectrum band where broadcast channels reside and the unlicensed users have to vacate this channel according to the requirement for protection of licensed users in CR networks. On the other hand, a secondary user is likely to move into a region where the interference is caused by coexisting cellular networks. In either case, the broadcast channel becomes unavailable thereby leading to unsuccessful deliveries of broadcasts.

A vast majority of existing work has focused on tackling this problem in *multi-hop or ad hoc* CR networks. Instead of relying on a single broadcast channel, the control information is transmitted over a preselected set of broadcast channels, which can be derived based on the neighbor graphs [33]. To determine the minimum broadcast schedule length for a CR network, two heuristics are presented and they

can produce schedules that have either optimal or near-optimal lengths [2]. In [26], a mixed broadcast scheduling algorithm is proposed under the unit disk graph (UDG) model, which combines the uni-cast and broadcast collaboratively in order to obtain a small broadcast latency. To broadcast over multiple channels, the channel hopping technique is used by cognitive radios without requiring the knowledge of global network topology or the requirement of time synchronization information [41–43].

This section focuses on the broadcast failure problem in the context of coexisting cellular networks, i.e., *infrastructure-based* CR networks. To guarantee the successful broadcast, a base station has to employ a *multichannel broadcast protocol* – i.e., it delivers contents over multiple broadcast channels using broadcast radios, so as to reduce the chance of colliding with primary users' transmissions or coexisting networks in the spatial or temporal domain.

This section presents a multichannel broadcast protocol, called *Mc-Broadcast*, for delivering contents to secondary users that are located in coexisting cellular networks. Every broadcast radio at a base station selectively transmit over a number of channels via a channel hopping process. The channel hopping sequence is generated using a mathematical construct called *Langford pairing*, such that Mc-Broadcast can only incur a small broadcast latency and guarantee a high successful delivery ratio.

Definition of Langford Pairing (LP)

Given an integer n, Langford pairing is a sequence of length $2n$ that consists of two 1s, two 2s, ..., and two ns and satisfies that there are exactly one number between the two 1's, exactly two numbers between the two 2's, ..., and exactly n numbers between the two n's.

Formally, A *Langford pairing*, $\{l_i\}_{0\le i\le 2n-1}$ of order n, also called a *Langford sequence*, is a permutation of the sequence of $2n$ integers $\{1, 1, 2, 2, 3, 3, \ldots, n, n\}$, and it satisfies the *Langford property*: if $l_i = l_j, 0 \le i < j \le 2n-1$, then $j - i = l_i + 1$.

For example, the sequence $l = \{3, 1, 2, 1, 3, 2\}$ is a Langford pairing of order $n = 3$. There is only one number (that is, 2) between the two 1s, two numbers (they are 1 and 3) between the two 2s and three numbers (they are 1, 2 and 1) between the two 3s. Given $i = 0$ and $j = 4$, then $l_0 = l_4 = 3$, and $j - i = 3 + 1$; given other combinations of i and j, the sequence l also satisfies the Langford property.

Slightly different from LP, an *extended Langford pairing* (ELP) is defined to contain two 0s (note that an LP does not contain any 0s) and that these two 0s be neighboring. Formally, an ELP, $\{l'_i\}_{0\le i\le 2(n+1)-1}$ of order n, which is a permutation of the sequence of $2(n+1)$ integers:

$$\{0, 0, 1, 1, 2, 2, \ldots, n, n\}.$$

The sequence satisfies the Langford property, i.e., if $l_i = l_j, 0 \le i < j \le 2(n+1)-1$, then $j - i = l_i + 1$. For example, the sequence

$$l' = \{0, 0, 3, 1, 2, 1, 3, 2\},$$

is an extended Langford pairing (ELP) of order $n = 3$.

Multichannel Broadcast Process

In a cellular network, the BS and the users in the BS's service area are secondary users, and they are equipped with CRs operating over broadcast channels. Due to PU's activities or interference from coexisting networks, a broadcast channel may become unavailable at any time. Therefore, the BS has to broadcast the content over multiple channels to ensure the successful delivery to users, and such a process is called a *multichannel broadcast* process.

Suppose there are N broadcast channels, labeled as $0, 1, 2, \ldots, N-1$. The BS is equipped with multiple broadcast radios, labeled as $r_1, r_2, \ldots, r_R$, where R is the total number of the BS's broadcast radios. There are U users $s_1, s_2, \ldots, s_U$ in the service area. Every user is equipped with a single radio interface.

Broadcast via Channel Hopping (CH)

To implement the multi-channel broadcast protocol, a BS's broadcast radio or a user's radio can hop across multiple broadcast channels to deliver or to receive the broadcast content. Thus, the channel hopping (CH) sequence is chosen to define the order with which a BS's broadcast radio (or a user's radio) visits the set of broadcast channels.

Consider a time-slotted communication system, where a global system clock exists. The local clock of each node may be synchronized to the global clock or may differ with the global clock by a certain amount of clock drift. A radio is assumed to be capable of hopping between different channels according to a channel hopping sequence and its local clock. A packet can be exchanged between two radios if they hop onto the same channel in the same time slot.

Then, a CH sequence u of period T can be represented as a sequence of channel indices:

$$u = \{u_0, u_1, u_2, \ldots, u_i, \ldots, u_{T-1}\},$$

where $u_i \in [0, N-1]$ represents the channel index of the ith time slot of CH sequence u. If $u_i = u_j, \forall i, j \in [0, T-1]$, the radio using u as its CH sequence stays on the same channel and does not hop.

Given two CH sequences of period T, u and v, if there exists $i \in [0, T-1]$ such that $u_i = v_i = h$, where $h \in [0, N-1]$, we say that a *broadcast delivery* occurs between u and v in the ith time slot on broadcast channel h. The ith time slot is called a *delivery slot* and channel h is called a *delivery channel* between u and v.

Given N channels, let $\mathscr{C}(u, v)$ denote the *set of delivery channels* between two CH sequences u and v. The cardinality of $\mathscr{C}(u, v)$ is called the *number of broadcast delivery channels*, denoted by $|\mathscr{C}(u, v)|$, and $|\mathscr{C}(u, v)| \in [0, N]$. The number of

broadcast delivery channels measures the number of channels in which successful broadcast delivery occurs, i.e., the diversity of broadcast delivery channels.

Let $\mathscr{T}(u, v)$ denote the *set of delivery slots* between two CH sequences u and v, and $|\mathscr{T}(u, v)| \in [0, T]$. The cardinality of $\mathscr{T}(u, v)$ reflects the number of times lots in which successful broadcast delivery occurs within a period.

Broadcast by Multiple Radios

To reduce the broadcast latency, the BS is allowed to use a set of broadcast radios, denoted by $\mathscr{B} = \{r_1, r_2, r_3, \ldots, r_R\}$. Since the BS has multiple radios, the broadcast delivery occurs between the BS and a user s if the broadcast delivery occurs between one of the BS's broadcast radios and the user s's radio – i.e., the broadcast delivery occurs between a radio set $\mathscr{B}$ and a user s if there exists a radio $r_i \in \mathscr{B}$ such that a broadcast delivery occurs between the CH sequences of radios r_i and s. To simplify the notation, it is recommended to use r_i to denote the CH sequence of the BS's broadcast radio $r_i \in \mathscr{B}$ and use s to denote the CH sequence of user s's radio.

The *set of broadcast delivery channels* between the BS with its set of broadcast radios $\mathscr{B}$ and a user s is the union of the sets of broadcast delivery channels between each broadcast radio of the BS and the user s's radio, i.e., let $\mathscr{C}(\mathscr{B}, s) = \bigcup_{r \in \mathscr{B}} \mathscr{C}(r, s)$ denote the set of broadcast delivery channels between the BS with its set of broadcast radios $\mathscr{B}$ and the user s's radio, and the cardinality of $\mathscr{C}(\mathscr{B}, s)$ is called the *number of delivery channels*, denoted by $|\mathscr{C}(\mathscr{B}, s)|$, and $|\mathscr{C}(\mathscr{B}, s)| \in [0, N]$.

Similarly, the *set of delivery slots* between the BS with its set of broadcast radios $\mathscr{B}$ and a user s is the union of the sets of delivery slots between each broadcast radio of the BS and the user s's radio, i.e., let $\mathscr{T}(\mathscr{B}, s) \triangleq \bigcup_{r \in \mathscr{B}} \mathscr{T}(r, s)$ denote the *set of delivery slots* between the BS with its set of broadcast radios $\mathscr{B}$ and the user s's radio, and $|\mathscr{T}(\mathscr{B}, s)| \in [0, T]$.

An Asynchronous Multichannel Broadcast System

Given a CH sequence u, use $rotate(u, k)$ to denote a *cyclic rotation* of CH sequence u by k time slots, i.e.,

$$rotate(u, k) = \{v_0, \ldots, v_j, \ldots v_{T-1}\},$$

where $v_j = u_{(j+k) \bmod T}$, $j \in [0, T-1]$. For example, given $u = \{0, 1, 2\}$ and $T = 3$, $rotate(u, 2) = rotate(u, -1) = \{2, 0, 1\}$.

Define an *asynchronous multichannel broadcast (AMB)* system $\mathscr{M}$ with CH period T as an ordered pair $(\mathscr{B}, \mathscr{U})$:

- $\mathscr{B}$ is the set of CH sequences of period T used by broadcast radios of the BS. Suppose $\mathscr{B} = \{r_1, r_2, r_3, \ldots, r_R\}$, where R is the number of the BS's broadcast radios, and the BS's broadcast radio r_i uses the CH sequence r_i in $\mathscr{B}$.

- $\mathscr{U}$ is the set of CH sequences of period T used by the users. Suppose $\mathscr{U} = \{s_1, s_2, s_3, \ldots, s_U\}$, where U is the number of users, and the user s_j's radio uses the CH sequence s_j in $\mathscr{U}$.

An AMB system must satisfy the *rotation closure property*: $\forall k, l \in [0, T-1]$, $\forall s \in \mathscr{U}$, there exists $r \in \mathscr{B}$ such that $|\mathscr{C}(rotate(s,k), rotate(r,l))| \geq 1$. And thus the design problem of CH sequences of the BS's broadcast radios and users' radios is mapped to the design problem of an AMB system with rotation closure property. And the rotation closure property implies that for all possible clock drifts between the BS and users, every user can have successful broadcast delivery with the BS, i.e., with one of the BS's broadcast radios.

In other words, in an AMB system, the BS, with each broadcast radio using CH sequences in $\mathscr{B}$, can deliver broadcast messages to all users using CH sequences in $\mathscr{U}$ via a channel hopping process for all possible clock drifts.

Performance Metrics

Given an AMB system $\mathscr{M} = (\mathscr{B}, \mathscr{U})$, the following metrics are defined to evaluate its performance.

- **Delivery channel diversity**. The delivery channel diversity for an AMB system measures the lower bound of the number of delivery channels between the BS and an arbitrarily given user for all possible clock drifts. The delivery channel diversity, denoted by $DIV(\mathscr{M})$, is the minimum number of delivery channels $|\mathscr{C}(\mathscr{B}, rotate(s,k))|$ for every $s \in \mathscr{U}$ and every $k \in \mathbb{Z}$, i.e.,

$$\begin{aligned} DIV(\mathscr{M}) &= \min_{s \in \mathscr{U}, k \in \mathbb{Z}} |\mathscr{C}(\mathscr{B}, rotate(s,k))| \\ &= \min_{s \in \mathscr{U}, k \in \mathbb{Z}} |\bigcup_{r \in \mathscr{B}} \mathscr{C}(r, rotate(s,k))|. \end{aligned}$$

- **Broadcast latency**. To quantify the broadcast latency, we define the maximum broadcast latency for a given AMB system as the upper bound of the latency before the first successful broadcast delivery between the BS and an arbitrary user on at least one channel for all possible clock drifts, which can be computed by

$$\max_{s \in \mathscr{U}, k \in \mathbb{Z}} [\min \mathscr{T}(\mathscr{B}, rotate(s,k))].$$

- **Delivery ratio**. To measure the proportion of delivery slots in a period, first it is needed to define the delivery ratio for a CH sequence pair. The delivery ratio for a CH sequence pair r and s, denoted by $\rho(r,s)$, is

$$\min_{k,l \in \mathbb{Z}} (|\mathscr{T}(rotate(r,k), rotate(s,l))|/T).$$

And then introduce the delivery ratio for an AMB system $\mathscr{M} = (\mathscr{B}, \mathscr{U})$, which measures the minimum proportion of delivery slots in all time slots. To be precise, the delivery ratio is

$$\rho(\mathscr{M}) \triangleq \min_{s\in\mathscr{U},k,l\in\mathbb{Z}} \frac{\sum_{r\in\mathscr{B}} |\mathscr{T}(rotate(r,k), rotate(s,l))|}{|\mathscr{B}|T}.$$

Extended Langford Pairing-Based Broadcast Protocols

An AMB system $\mathscr{M} = (\mathscr{B}, \mathscr{U})$ is constructed based on the extended Langford pairing (ELP). To illustrate the design of the ELP-based AMB system, it is better to first investigate a simple scenario in which the BS has a single radio, i.e., $|\mathscr{B}| = 1$, and there is only a single user, i.e., $|\mathscr{U}| = 1$. Then, the problem in a general scenario will be addressed where $|\mathscr{B}|$ and $|\mathscr{U}|$ are generally greater than 1.

CH Sequence Generation

In the ELP-based channel hopping protocol for AMB systems with a single radio pair, $\mathscr{M} = (\{r\}, \{s\})$, where r is the only BS radio and s is the only user.

First look at the simple scenario where $|\mathscr{B}| = |\mathscr{U}| = 1$, i.e., $\mathscr{B} = \{r\}$ and $\mathscr{U} = \{s\}$.

Consider the original Langford pairing (LP). If N is congruent to 0 or 3 modulo 4, there exists an LP $\{l_i\}_{0\le i\le 2N-1}$ of order N. Suppose both r and s use the CH sequence $\{l_i - 1\}_{0\le i\le 2N-1}$ of period $2N$. If s is one time slot ahead, the broadcast delivery cannot occur between r and s. For example, suppose the channel number $N = 3 \equiv 3 \pmod 4$ and $\{3, 1, 2, 1, 3, 2\}$ is an LP of order 3. Both r and s use the CH sequence $\{2, 0, 1, 0, 2, 1\}$ of period 6. If s is one time slot ahead, the broadcast delivery cannot occur between r and s , i.e., $|\mathscr{C}(r, rotate(s, 1))| = 0$.

However, an AMB system can be constructed by using ELP. If the channel number N is congruent to 0 or 1 modulo 4, then $N - 1$ is congruent to 0 or 3, there exists an ELP $\{l'_i\}_{0\le i\le 2N-1}$ of order $N - 1$. For example, when $N = 4$, the ELP-based CH sequence is

$$u = \{0, 0, 3, 1, 2, 1, 3, 2\}.$$

When $N \not\equiv 0, 1 \pmod 4$, easily use the *downsizing scheme* or the *padding scheme* to transform it into an AMB system design problem with the channel number N' congruent to 0 or 1 modulo 4.

Downsizing scheme. Suppose the channel number $N \not\equiv 0, 1 \pmod 4$, let N' be $\max\{N' \le N : N' \equiv 0, 1 \pmod 4\}$. It is easy to see that $|N - N'| \le 2$. The donwsizing scheme will limit the set of broadcast channels to a N'-element subset of the original broadcast channel set, e.g., $\{0, 1, 2, \ldots, N' - 1\}$ is used as the new broadcast channel set.

Padding scheme. Suppose the channel number $N \not\equiv 0, 1 \pmod 4$, let N' be $\min\{N' \geq N : N' \equiv 0, 1 \pmod 4\}$. It is easy to see that $|N - N'| \leq 2$. In contrast with the downsizing scheme, the padding scheme introduces $N' - N$ more channels but maps them to the original broadcast channels in $\{0, 1, 2, \ldots, N-1\}$. For example, suppose $N = 7$ and then $N' = 8$. Now add one more channel, i.e., channel 7, and adjoin channel 7 to the original broadcast channel set $\{0, 1, 2, \ldots, 6\}$, but channel 7 is an alias of channel 0 – i.e., it is mapped to channel 0.

For instance, if $N \equiv 2 \pmod 4$, use the downsizing scheme and $|N - N'| = 1$; if $N \equiv 3 \pmod 4$, use the padding scheme and $|N - N'| = 1$. And this will only lead to a very mild degradation of performance since $|N - N'| = 1$.

With the aid of the downsizing scheme and the padding scheme, the problem in focus becomes the AMB design problem with the channel number N' congruent to 0 or 1 modulo 4.

A Simple Broadcast (S-Broadcast) Scheme for a Single CH Sequence Pair

This section presents a simple broadcast scheme, called *S-Broadcast*, for the simple scenario of the AMB system ($\mathscr{M} = (\{r\}, \{s\})$) design problem.

Motivation. If the broadcast radio r and the user radio s both use the same ELP $u = \{l'_i\}_{0 \leq i \leq 2N'-1}$, the successful broadcast delivery between them is guaranteed; however, the delivery channel diversity is not ensured. If the broadcast radio uses cyclic rotated copies of u and the user radio uses periodically extended u, the delivery channel diversity will be increased.

To be precise, the CH sequences for the broadcast and user radios can be generated as follows:

1. The broadcast radio generates its CH sequence

$$r = \prod_{f=1}^{F} rotate(u, o_f),$$

   where $\{o_f\}_{1 \leq f \leq F}$ is a sequence of integers that are used to deliberately manipulate the clock drift and $\prod_{f=1}^{F} \theta_f$ denotes the concatenation of strings $\theta_1, \theta_2, \theta_3, \ldots, \theta_F$, i.e., $\prod_{f=1}^{F} \theta_f = \theta_1 \parallel \theta_2 \parallel \theta_3 \parallel \cdots \parallel \theta_F$.
2. The user radio generates its CH sequence as $s = \prod_{f=1}^{F} u$, which is the periodic extension of u.

The *delivery channel determination function* is defined as

$$\delta : \mathbb{Z} \to \mathbb{Z}.$$

For $k \in \mathbb{Z}$, $k \equiv g \pmod{2N'}$ where $|g| \leq N'$, then $\delta(k) = |g| - 1$. For example, when $N' = 4$, $\delta(1) = 0$, $\delta(2) = 1$, $\delta(3) = 2$, $\delta(4) = 3$, $\delta(5) = 2$, $\delta(6) = 1$, $\delta(7) = 0$, and in particular $\delta(0) = -1$.

S-Broadcast. The proposed broadcast protocol for the simple scenario of the AMB system ($\mathscr{M} = (\{r\}, \{s\})$) design problem, S-Broadcast, is an asynchronous CH-based channel broadcast protocol that achieves the broadcast latency at most $2N' - 1$, the delivery ratio $\rho = \frac{1}{N'}$ and full diversity. According to the design of S-Broadcast,

- $r = \prod_{f=1}^{2N'} rotate(u, f-1)$.
- $s = \prod_{f=1}^{2N'} u$.

Two examples illustrating the CH sequences of S-Broadcast when $N' = 4$ are shown in Fig. 6.

A Multichannel Broadcast (Mc-Broadcast) Scheme for Multiple CH Sequence Pairs

In the general AMB system design problem, $|\mathscr{B}|$ and $|\mathscr{U}|$ are generally greater than 1, i.e., $\mathscr{B} = \{r_1, r_2, r_3, \ldots, r_R\}$, $\mathscr{U} = \{s_1, s_2, s_3, \ldots, s_U\}$, $R, U \geq 1$. This section presents two ELP-based CH protocols, *A-Broadcast* and *L-Broadcast*, for the case $R \geq 2N'$ and the case $R < 2N'$, respectively.

Then, a multichannel broadcast protocol, called *Mc-Broadcast*, is the hybrid of the two above ELP-based CH protocols – i.e., it adopts A-Broadcast if $R \geq 2N'$ and it adopts L-Broadcast if $R < 2N'$.

Suppose $u = \{l'_i\}_{0 \leq i \leq 2N'-1}$ is an ELP of order $N' - 1$. The roadcast delivery can occur between any two cyclic rotation copies of u, say, between $rotate(u, k)$ and $rotate(u, l)$ – i.e., if $\forall 1 \leq i \leq R$, $r_i = rotate(u, o_i)$, and $\forall 1 \leq j \leq U$, $s_j = u$, $\mathscr{M} = (\mathscr{B}, \mathscr{U})$ is an AMB system. However, full delivery channel diversity ($DIV(\mathscr{M}) = N'$) is not necessarily guaranteed, and it is expected to reduce the broadcast latency. To take the advantage of multiple broadcast radios of the BS, it would be beneficial to select o_i's properly so as to achieve full delivery channel diversity, reduce the broadcast latency down to zero and guarantee successful broadcast delivery in every time slot.

Define the *balance sequences* as

$$\psi_i^{n,k} (0 \leq i < \mathrm{lcm}(n,k)/k),$$

where $\psi_i^{n,k}$ is a sequence of k elements and $\mathrm{lcm}(n,k)$ is the least common multiple of n and k. Denote the j-th element in $\psi_i^{n,k}$ by $\psi_{i,j}^{n,k}$, where $0 \leq j < k$. And let

$$\psi_{i,j}^{n,k} \triangleq (ik + j) \bmod n \in [0, n-1].$$

It is easy to see that $\{ik + j | 0 \leq i < \mathrm{lcm}(n,k)/k, 0 \leq j < k\} = \{0, 1, 2, 3, \ldots \mathrm{lcm}(n,k) - 1\}$. Hence $\forall n_0 \in [0, n-1]$, there exist exactly $\frac{\mathrm{lcm}(n,k)}{n}(i, j)$-pairs such that $\psi_{i,j}^{n,k} = (ik + j) \bmod n = n_0$.

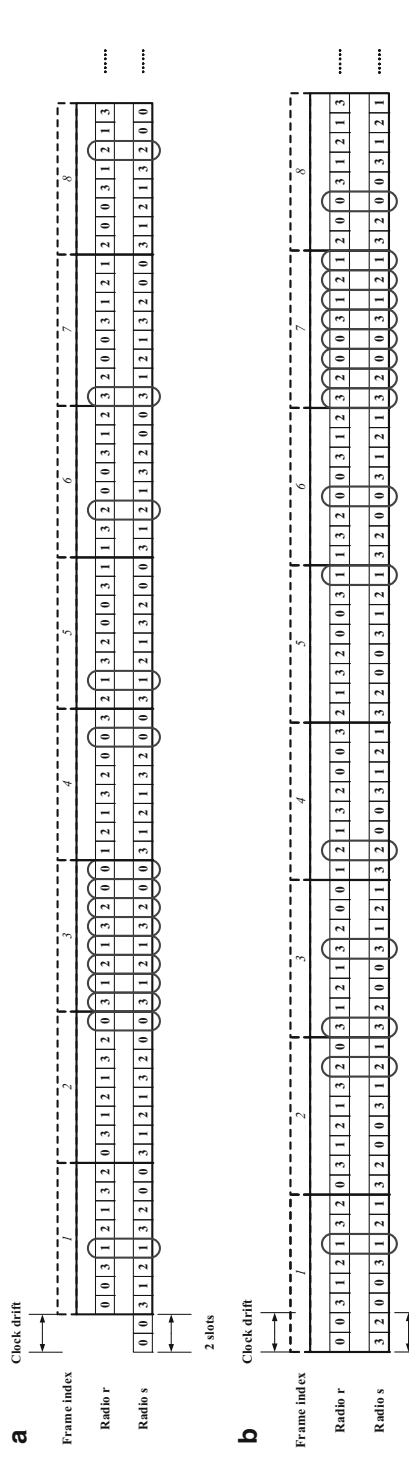

Fig. 6 Example illustrating the CH sequences of S-Broadcast when $N' = 4$. Radio r is the BS's broadcast radio, and there is only one user, i.e., radio s. The CH sequences of the two radios can achieve full diversity within a period of $4N'^2 = 64$ time slots, given a clock drift of two slots either forwards or backwards. The delivery latency in (**a**) and (**b**) is 3 and 5 time slots, respectively, both less than $2N' - 1 = 7$. And the delivery ratios in these two figures are both $\frac{1}{N'} = \frac{1}{4}$

As a result, $\forall n_0 \in [0, n-1]$, there exist exactly $\frac{\text{lcm}(n,k)}{n}$ (i, j)-pairs such that $\psi_{i,j}^{n,k} = (ik + j) \bmod n = n_0$.

A-Broadcast when $R \geq 2N'$: If the BS has a large number of broadcast radios, i.e., $R \geq 2N'$, the AMB system can be designed to have guaranteed successful broadcast delivery in every time slot and full delivery channel diversity. Suppose $R = 2qN' + w$, where $q = \lfloor \frac{R}{2N'} \rfloor \geq 1$ and $0 \leq w < 2N'$. A-Broadcast is designed as follows:

- $\forall 1 \leq i \leq 2qN', r_i = rotate(u, (i-1) \bmod 2N')$.
- $\forall 1 \leq i \leq w$, from time slot $\lfloor \frac{t_B}{2N'} \rfloor$ to time slot $\lfloor \frac{t_B}{2N'} \rfloor + (2N' - 1)$, radio $r_{2qN'+i}$ uses

$$rotate\left(u, \psi^{2N',w}_{\lfloor \frac{t_B}{2N'} \rfloor \bmod \text{lcm}(2N',w)/w, i-1}\right)$$

  as its CH sequence, where t_B is the BS's local clock time (i.e., according to the BS's local clock, it is the t_B-th time slot).
- $\forall 1 \leq j \leq U, s_j = u$.

An example illustrating the CH sequences of A-Broadcast when $N' = 4$ is shown in Fig. 7.

The A-Broadcast protocol has the following properties [4].

- A-Broadcast has zero broadcast latency.
- It achieves full delivery channel diversity. And the interval (i.e., $2N'$) is bounded – within every $2N'$ time slots, it achieves full delivery channel diversity.
- The delivery ratio is $\frac{1}{N'}$.
- In every time slot, every user can receive broadcast delivery from at least $2q$ BS radios, and on average $\frac{R}{N'}$ radios.

L-Broadcast when $R < 2N'$: If the number of BS broadcast radios R is less than $2N'$, we can also use the balance sequence to achieve delivery channel diversity and maximize delivery ratio. L-Broadcast is an ELP-based protocol, which is described as follows:

- $\forall 1 \leq i \leq R$, from time slot $\lfloor \frac{t_B}{2N'} \rfloor$ to time slot $\lfloor \frac{t_B}{2N'} \rfloor + (2N' - 1)$, radio r_i uses

$$rotate\left(u, \psi^{2N',R}_{\lfloor \frac{t_B}{2N'} \rfloor \bmod \text{lcm}(2N',R)/R, i-1}\right)$$

  as its CH sequence, where t_B is the BS's local clock time (i.e., according to the BS's local clock, it is the t_B-th time slot).
- $\forall 1 \leq j \leq U, s_j = u$.

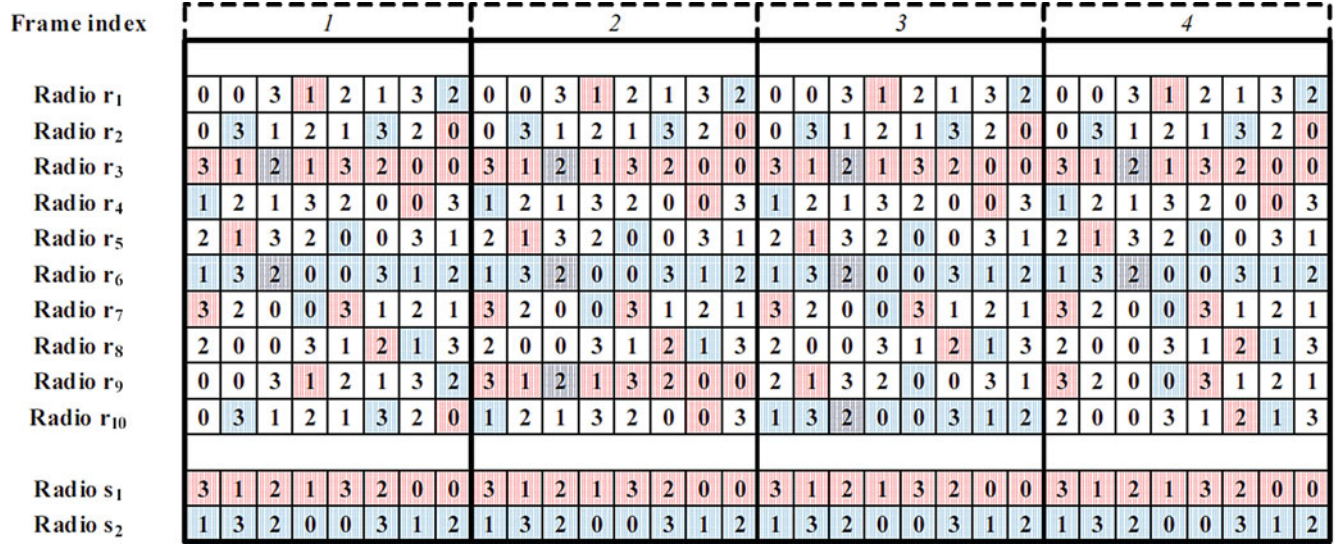

Fig. 7 Example illustrating the CH sequences of A-Broadcast when $N' = 4$. Radios $r_1, r_2, r_3, \ldots, r_{10}$ are the BS's broadcast radios and there are two users – radio s_1 and radio s_2. The clock of radio s_1 is two time slots behind (or six time slots ahead of) that of the BS while the clock of radio s_2 is three times lots ahead of (or five time slots behind) that of the BS. The blocks with *red/blue* fill pattern represents the time slots in which radio s_1/s_2 receives successful broadcast delivery from the BS, respectively, while the blocks with gray fill pattern represents the time slots in which both users (radios s_1 and s_2) receive successful broadcast delivery from the BS simultaneously. Both users can receive broadcast delivery from at least $2q = 2\lfloor \frac{10}{8} \rfloor = 2$ and on average $\frac{R}{N'} = \frac{10}{4} = 2.5$ BS's broadcast radios every time slot and achieve full broadcast channel diversity

An example illustrating the CH sequences of L-Broadcast when $N' = 4$ is shown in Fig. 8.

The L-Broadcast protocol has the following properties [4].

- The broadcast latency of the AMB system that implements L-Broadcast is at most $2N' - 1$.
- It achieves full delivery channel diversity. And the interval (i.e., $2N' \cdot \lceil \frac{2N'}{R} \rceil$) is bounded – it achieves full delivery channel diversity every $2N' \cdot \lceil \frac{2N'}{R} \rceil$ slots.
- In every time slot, every user can receive broadcast delivery from $\frac{R}{N'}$ radios on average.

Simulation

This section compares the performance of the proposed Mc-Broadcast protocol and other existing protocols, including the distributed broadcast protocol (or simply called "distributed") proposed in [43] and the random channel hopping scheme, via simulation results. In each simulated network cell, the BS has R broadcast radios available; a number of U users are connected to the BS, and each user has a single radio interface; each radio can access N broadcast channels (i.e., the number of broadcast channels available to the network is N). The BS or its connected users generate their CH sequences using the agreed broadcast scheme (i.e., either Mc-Broadcast, the distributed protocol, or the random channel hopping protocol) and perform CH in accordance with the sequences. Once two nodes hop onto the same channel that is free of primary user signals, the broadcast delivery between them is successful.

Traffic model. A number of X primary transmitters are simulated, operating on X channels independently, and these channels were randomly chosen in each simulation run. In most existing work, it is assumed that a primary user transmitter follows a "busy/idle" transmission pattern on a licensed channel [12, 18], and the same traffic pattern is assumed here. That is, the busy period has a fixed length of b time slots, and the idle period follows an exponential distribution with a mean of l time slots. A channel is considered "unavailable" when PU signals are present in it. The intensity of primary user traffic can be characterized as $PU = \frac{X}{N} \cdot \frac{b}{l+b}$.

Random clock drift. In a CR network, the BS and the user may lose clock synchronization or even link connectivity at any time when they experience the broadcast failure problem due to primary user affection. Hence, the clock of the BS and those of the users are not necessarily synchronized. In each simulation run, each secondary node (the BS and the users) determines its clock time independently of other nodes. Note that the radios of the BS are synchronized, and there is a random clock drift between the BS and any of its connected users.

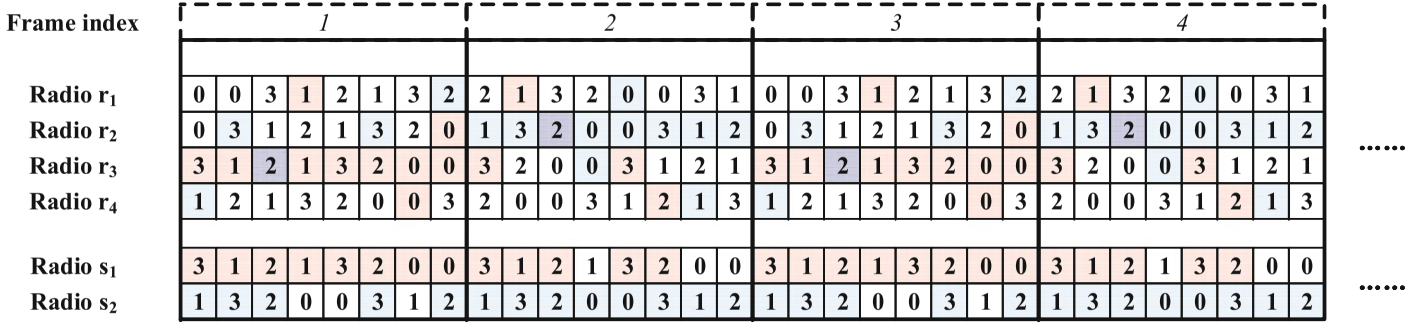

Fig. 8 Example illustrating the CH sequences of L-Broadcast when $N' = 4$. Radios r_1, r_2, r_3, r_4 are the BS's broadcast radios and there are two users – radio s_1 and radio s_2. The clock of radio s_1 is two time slots behind (or six time slots ahead of) that of the BS, while the clock of radio s_2 is three time slots ahead of (or five time slots behind) that of the BS. The blocks with *red/blue* fill pattern represents the time slots in which radio s_1/s_2 receives successful broadcast delivery from the BS, respectively, while the blocks with gray fill pattern represents the time slots in which both users (radios s_1 and s_2) receive successful broadcast delivery from the BS simultaneously. Both users can receive broadcast delivery from $\frac{R}{N'} = \frac{4}{4} = 1$ BS's broadcast radio on average and achieve full delivery channel diversity every $2N' \cdot \lceil \frac{2N'}{R} \rceil = 8 \cdot \frac{8}{4} = 16$ time slots

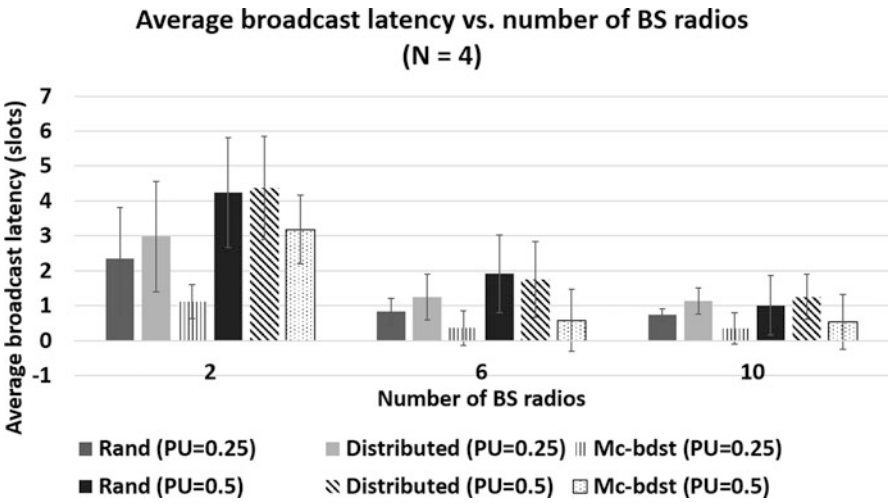

Fig. 9 The average broadcast latency versus the number of broadcast radios at the base station ($N = 4$), with a 95% confidence interval attached to each bar

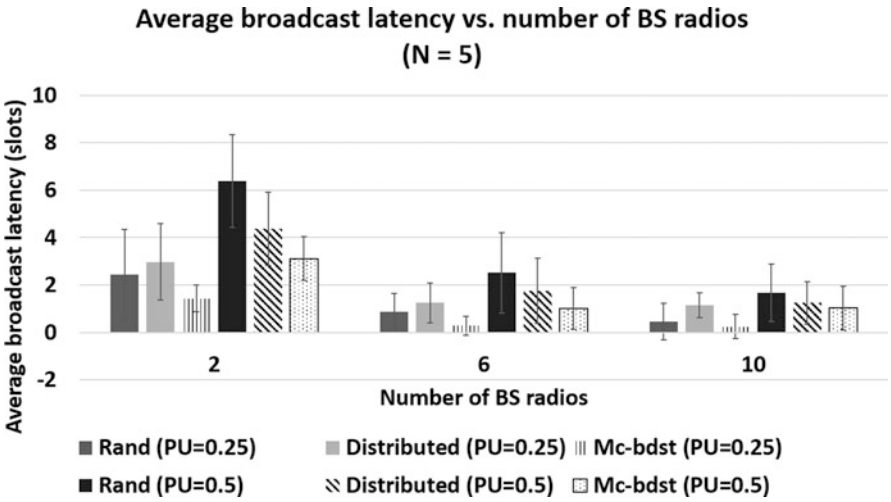

Fig. 10 The average broadcast latency versus the number of broadcast radios at the base station ($N = 5$), with a 95% confidence interval attached to each bar

Average broadcast latency. Figures 9 and 10 show the simulation results with respect to the average broadcast latency under the conditions $N = 4$, 5 and 8, respectively. It is illustrated that as the number of broadcast radios increases, it takes fewer time slots on average before the first successful delivery for both schemes under different PU traffic. This implies that a greater number of broadcast radios is conducive to mitigating the average broadcast latency.

It is noteworthy that for different numbers of available channels and different PU traffic, the average latency of Mc-Broadcast is smaller than those of other existing broadcast protocols.

Spectrum Sharing Problem

This section investigates the spectrum sharing problem among coexisting heterogeneous cellular networks.

To address this problem, it is needed to establish a coexistence framework that employs an *indirect* coordination method for enabling collaborative coexistence among networks. The proposed framework was inspired by the interspecies relations that exist in biological ecosystems. A *symbiotic* relation is a term used in biology to describe the coexistence of different species that form relations via indirect coordination. It exploits a *mediator* system (e.g., the 802.19.1 system) that forwards *sanitized* data to establish the indirect coordination mechanism between coexisting networks. It employs an *ecology inspired spectrum sharing* algorithm inspired by an interspecific resource competition model that enables each CR network to autonomously determine the amount of spectrum that it should appropriate without direct negotiation with competing networks. Results show that this framework guarantees weighted fairness in partitioning spectrum and improves spectrum utilization.

The Mediator System

The recently formed IEEE 802.19.1 task group (TG) was chartered with the task of developing standardized methods, which are radio access technology independent, for enabling coexistence among dissimilar or independently operated wireless networks [21]. This standard is currently being developed, and it has yet to prescribe solid solutions. The IEEE 802.19.1 system is a good candidate to serve as the mediator. The IEEE 802.19.1 system [21] defines a set of logical entities and a set of standardized interfaces for enabling coordination between heterogeneous CR networks. Figure 11 shows the architecture of an 802.19.1 system which includes three entities in the grey box: (1) the coexistence manager (CM) acts as the

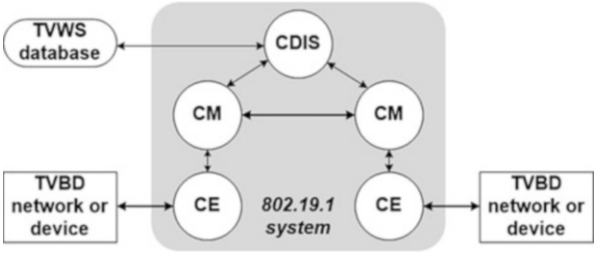

Fig. 11 IEEE 802.19.1 system architecture

local decision-maker of the coexistence process; (2) the coexistence database and information server (CDIS) provides coexistence-related control information to the CMs, and (3) the coexistence enabler (CE) enables communications between the 802.19.1 system and the TV band device (TVBD) network. The TVWS database indicates the list of channels used by primary users and their locations, and it is connected to the 802.19.1 system via backhaul connections.

Interspecific Competition in Ecology

In ecology, interspecific competition is a distributed form of competition in which individuals of different species compete for the same resource in an ecosystem without direct interactions between them [45]. The impact of interspecific competition on populations have been formalized in a mathematical model called the Lotka-Volterra (L-V) competition model [34,46]. In this model, the impact on population dynamics of species i can be calculated separately by a differential equation given below:

$$\frac{dN_i}{dt} = r_i N_i \left(1 - \frac{N_i + \sum_{j \neq i} \alpha_{ij} N_j}{K_i}\right). \tag{3}$$

In this equation, N_i is the population size of species i, K_i is the carrying capacity (which is the maximum population of species i if it is the only species present in the environment), r_i is the intrinsic rate of increase, and α_{ij} is the competition coefficient which represents the impact of species j's population growth on the population dynamics of species i.

Framework Overview

Consider n heterogeneous networks are co-located, and they coexist in the same spectrum band that includes N channels with an identical bandwidth. Let $\mathscr{K}$ denote this set of networks, and all of these networks in $\mathscr{K}$ are registered with the mediator system. Every network is composed of multiple devices and a base station (BS) (or access point). Channels are labeled with indices $0, 1, \ldots, N-1$.

Time-spectrum blocks. Time is divided into periods, each period contains a number of u superframes, and each super-frame contains f frames (such a structure based on frames can be found in IEEE 802.16 and 802.22). A time-spectrum block is the minimum unit for spectrum allocation, which can be defined by a channel index and a frame index. Specifically, a time-spectrum block can be represented using a three-tuple (i, j, k) – i.e., the k-th frame in the j-th superframe over channel i. Over channel i, there are a number of uf blocks that can be allocated during a period. It is assumed that a BS or network with multiple radios is able to scan and access

multiple time-spectrum blocks on different channels simultaneously. Furthermore, define the capacity, C, as the total number of spectrum-time blocks during a period, given N channels.

The bandwidth requirement. Define the *bandwidth requirement* of a network as the number of time-spectrum blocks that it needs to satisfy the QoS requirements of its traffic load. Let R_i denote the bandwidth requirement of network i.

The mediator-based indirect coordination. SHARE establishes a mediator-based *indirect* coordination mechanism between coexisting networks. There is no direct coordination between the coexisting networks, and they have to interact with each other by exchanging control information through a third-party mediator. Specifically, SHARE utilizes a CDIS (which is one of the components of an 802.19.1 system) as a mediator. Note that CDIS is not a global or centralized decision-maker, but rather it is an information directory server with simple data processing capabilities.

Necessity of sanitized information. The mediator helps address conflict-of-interest issues and customer privacy concerns, which may arise when coexisting networks operated by competing service providers are required to exchange sensitive traffic information in order to carry out coexistence mechanisms. The mediator *sanitizes* the sensitive information received from the coexisting networks and then returns the sanitized information back to them. The coexisting networks execute their coordinated coexistence mechanisms using the sanitized data.

Ecology Inspired Spectrum Allocation

As mentioned before, spectrum allocation among the coexisting networks through *direct* coordination may not be possible (due to a lack of infrastructure), may be too costly, or may be shunned by the competing network operators because they do not want to provide their sensitive information. Instead of direct coordination, the SHARE framework adopts an indirect coordination mechanism, which is inspired by an interspecific competition model from theoretical ecology.

Design objective. In a spectrum sharing process, a network has to figure out how much spectrum it can appropriate given its bandwidth requirement. Suppose a time-spectrum block is the minimum unit amount of spectrum allocation. Let S_i denote the *number of time-spectrum blocks* allocated to network $i \in \mathcal{K}$, and S_i refers to as the *spectrum share* of network i.

The objective is that the spectrum sharing process will eventually reach a state of equilibrium, where the number of allocated blocks to each network is proportional to its reported bandwidth requirement.

Inspiration from ecology. In ecology, the population dynamics of a species in the interspecific resource competition process can be captured by the L-V competition

model. In the context of network coexistence, a *weighted* competition model is built to help a network to determine the *dynamics of its allocated spectrum*, given its bandwidth requirement.

Information exchange between the mediator and a network. The mediator exchanges two types of control information with every CR network:

1. *Upload of local report*. Network i reports the current value of S_i to the mediator.
2. *Download of sanitized data*. The mediator replies back to network i with the sanitized data, i.e., sum of numbers of time-spectrum blocks of all other coexisting networks, i.e., $\sum_{j \neq i, j \in \mathscr{K}} S_j$.

Problem Formulation

Suppose that $\mathscr{K}$ denotes a set of n co-located networks that have individual bandwidth requirements $R_1, R_2, \ldots, R_n$, and operate over the same WS. The first objective for coexisting networks is to split the WS into n pieces that are proportional to their individual bandwidth requirements, without sharing individual bandwidth requirements with each other.

Let $\mathbf{S}(\mathscr{K}) = [S_1, S_2, \ldots, S_n]$ denote the *spectrum share vector* for $\mathscr{K}$ over the white space. The *fairness index*, $F(\mathbf{S}(\mathscr{K}))$, for networks in $\mathscr{K}$ is defined as follows:

$$F(\mathbf{S}(\mathscr{K})) = \frac{\left(\sum_{i \in \mathscr{K}} S_i\right)^2}{\sum_{i \in \mathscr{K}} R_i \cdot \sum_{i \in \mathscr{K}} R_i \left(\frac{S_i}{R_i}\right)^2}. \tag{4}$$

The maximum value of $F(\mathbf{S}(\mathscr{K}))$ is one (the best or weighted fair case), where the allocated spectrum share value of a network is proportional to its bandwidth requirement.

Let $\mathscr{I}_i$ denote the *set of shared control information* known by network i, and it is easy to see that $R_i \in \mathscr{I}_i$. However, it is assumed that $R_j \notin \mathscr{I}_i$ – i.e., co-located networks, i and j, do not know each other's bandwidth requirements.

A *weighted fair spectrum sharing allocation* problem is formulated for heterogeneous networks to dynamically determine their spectrum share values.

Problem 1. Given a set of n co-located networks, $\mathscr{K}$, operating over N channels, one has to solve the following problem to find the spectrum share vector for $\mathscr{K}$:

$$\begin{aligned} &\text{Maximize} \quad F(\mathbf{S}(\mathscr{K})) \\ &\text{subject to} \quad \frac{S_i}{S_j} = \frac{R_i}{R_j}, R_j \notin \mathscr{I}_i, \forall i, j \in \mathscr{K}. \end{aligned}$$

The first constraint $\frac{S_i}{S_j} = \frac{R_i}{R_j}$ guarantees the weighted fairness.

Table 1 A mapping between biological and CR network ecosystems

Biological ecosystem	CR network system
A species	A network
Population of a species	Spectrum share of a network
Population dynamics (growth or decline)	Dynamics of spectrum share

An Ecology-Inspired Spectrum Share Allocation Algorithm

The Stable Equilibrium of the L-V Competition Model

The L-V competition model provides a method for defining a state of "stable equilibrium" and finding the sufficient conditions for achieving it. If one considers the interspecific competition process described by equation (3), when $K_i = K_j$ and $\alpha_{ij} = \alpha_{ji}$ for any two species i and j, then the sufficient condition for stable equilibrium is $\alpha_{ij} < 1$.

The Basic Spectrum Competition Model

Table 1 shows a number of analogies between a biological ecosystem and a network system. Based on equation (3) and the analogies, the following *basic* spectrum competition model is obtained:

$$\frac{dS_i}{dt} = rS_i\left(1 - \frac{S_i + \alpha\sum_{j\neq i} S_j}{C}\right), \tag{5}$$

where S_i is the spectrum share for network i, and r is an intrinsic rate of increase. In equation (5), the carrying capacity is equal to the number of time-spectrum blocks in a period given N channels. A competition coefficient $\alpha < 1$ will guarantee a stable equilibrium – i.e., all the competing networks will have the same spectrum share value.

Next section shows how to extend the basic competition model to a weighted fair spectrum competition model that complies with the weighted fairness requirement (i.e., $\frac{S_i}{S_j} = \frac{R_i}{R_j}$ for any two networks i and j) in a state of stable equilibrium.

The Weighted Fair Spectrum Competition Model

The basic spectrum competition model guarantees a stable equilibrium where all the competing networks have the same spectrum share value. However, solutions to Problem 1 must satisfy the requirement of weighted fairness, which implies that the competing networks' spectrum share values are proportional to their bandwidth requirements. For example, if network i has a bandwidth requirement that is twice that of network j, then network i's allocated spectrum share should also be twice the allocated spectrum share of network j.

To support the weighted fairness in spectrum share allocation, a weighted fair spectrum competition model introduces the concept of "subspecies." A network with a higher bandwidth requirement would have a greater number of subspecies than a network with a lower bandwidth requirement. The bandwidth requirement R_i is used as the number of sub-species of network i.

Let $S_{i,k}$ denote the spectrum share allocated to the subspecies k of network i, where $k \in [1, R_i]$. In the *weighted* competition model, every subspecies k of network i calculates the change in its spectrum share according to the following equation:

$$\begin{aligned} \delta_{i,k} &= \frac{dS_{i,k}}{dt} \\ &= rS_{i,k}\left(1 - \frac{S_{i,k} + \alpha \sum_{\kappa \neq k} S_{i,\kappa} + \alpha \sum_{j \neq i} S_j}{C}\right). \end{aligned} \tag{6}$$

Then, network i obtains its spectrum share value by combining the spectrum share values of all its subspecies, i.e., $S_i = \sum_k S_{i,k}$.

Every network i periodically sends its spectrum share value S_i to the mediator, and then the mediator sends back the sanitized data $\beta_i = \sum_{j \neq i} S_j$ to network i. The spectrum share allocation process terminates when $\delta_{i,k} = 0$ for all i and k. Note that the sanitized data β_i is used (instead of actual bandwidth requirement information) to mitigate conflict of interest and privacy issues that may arise between competing networks. The use of sanitized data coincides with the second constraint of Problem 1. The procedure is described as below.

1. A network i starts its spectrum share allocation process by creating a number of R_i sub-species.
2. At the beginning of every frame, every sub-species calculates the change rate of its spectrum share (i.e., $\frac{dS_{i,k}}{dt}$) using the sanitized data β_i obtained from the mediator.
3. If the change rate of the spectrum share is positive (or negative), a subspecies increases (or decreases) its spectrum share by randomly selecting a number of time-spectrum blocks to access (or releasing/freeing a number of occupied time-spectrum blocks).
4. At the end of every iteration, every network i calculates its new spectrum share value by $S_i = \sum_k S_{i,k}$, and sends S_i to the mediator. Meanwhile, the network updates the value of β_i from the mediator.
5. Last three steps are repeated until there is no subspecies with a non-zero change rate of spectrum share; that is $\frac{dS_{i,k}}{dt} = 0$ for every subspecies k of any network i.
6. The allocated spectrum share for network i is $\sum_k S_{i,k}$.

In this framework, the spectrum share allocation algorithm satisfies the requirement of weighted fairness.

Simulation

This section evaluates the performance of the proposed approach by looking into the stable equilibrium achieved by the weighted fair spectrum share allocation scheme.

Consider two CR networks that coexist in a block of spectrum that is divided into 20 channels, and fix the bandwidth requirements of the two networks as $R_1 = 2$ and $R_2 = 3$, which implies that network 1 has two subspecies and network 2 has three in the spectrum share allocation process. In the L-V competition model, the competition coefficient $\alpha < 1$ and the intrinsic rate of increase $r < 2$ [35]. The discussions on how to choose appropriate parameter values to achieve fast convergence to an equilibrium can be found in [35]. In this set of simulations, $\alpha = 0.9$ and $r = 1.95$.

Convergence to an equilibrium. Figure 12 shows the dynamics of the spectrum share value of each network and each subspecies within a network. "Subspecies (i, j)" in the figure legend represents sub-species j within network i. The system converges to an equilibrium state in finite time where all subspecies of every network are allocated the same spectrum share value. The aggregate spectrum share value allocated to a network is proportional to its bandwidth requirement.

Weighted Fairness. In each simulation run, the bandwidth requirement, R_i, of each network i is randomly chosen from the range $[1, 5]$. A "noncollaborative" allocation scheme implies that every coexisting network determines its spectrum share value without coordinating with others. This is equivalent to splitting the available spectrum "randomly" to n pieces and allocates them to n coexisting networks. The fairness values are measured using the fairness index defined in (4). Figure 13 clearly shows that SHARE allocates spectrum in a weighted fair manner, whereas the noncollaborative allocation scheme does not.

Channel Contention Problem

When coexisting networks have a means for direct coordinations, the channel contention protocol is a viable way of addressing the heterogeneous coexistence problem.

A channel contention protocol facilitates the dynamic spectrum allocation among coexisting networks in a *distributed* manner when a network is in need of spectrum to satisfy its *service requirement*. There is no need to start the spectrum sharing process for self-coexistence when the available spectrum is *sufficient* to satisfy all coexisting networks.

When the available spectrum is *insufficient*, every network (or network BS) occupies an amount of spectrum that is no more than it needs (i.e., its service

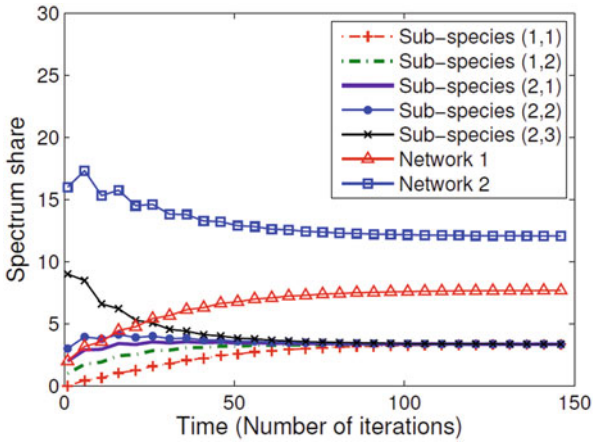

Fig. 12 Convergence to the equilibrium

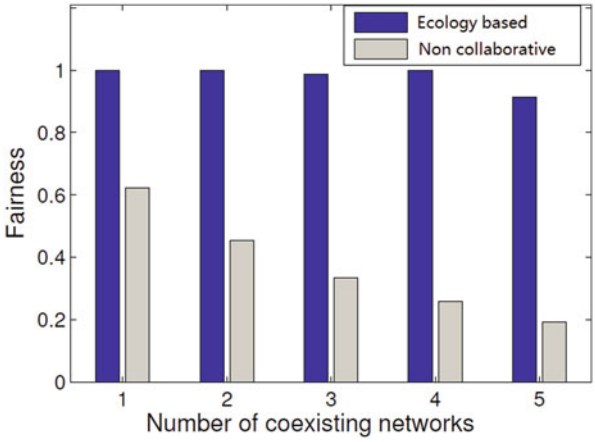

Fig. 13 Measured fairness values

requirement). IEEE 802.22 defines an inter-BS *spectrum contention* protocol for network cells to achieve the goal of self-coexistence.

- A BS that is in need of spectrum (*contention source* BS) is allowed to win channels via pairwise contentions with its neighboring BSs (*contention destination* BSs).
- If the contention source wins the contention, it occupies the contended channels exclusively, while the contention destinations vacate those channels via channel switching.

To ensure the fairness in the contention process, existing proposals adopt a simple *unbiased* contention resolution rule based on random number selection [16, 17], such that either a contention source or a contention destination has an equal probability of winning the pairwise contention.

However, the existing design of a coexistence protocol fails to consider the *successive* events that may be triggered by the spectrum redistribution during a *local* spectrum contention process. For example, the channel redistribution via contentions may satisfy the contention source, but meanwhile the contention destination that loses spectrum may become short of spectrum and successively initiate a *cascading* spectrum contention process to acquire more spectrums.A *cascade* is a series of events, in which the occurrence of an event can trigger the occurrence of successive events. As a result, unrestricted local spectrum contentions may trigger a series of successive contention instances that proliferate over the whole network, which may waste the network resources.

This section systematically studies the *spectrum contention* problem using the percolation theory in the context of coexisting cellular networks. The process of cascading spectrum contentions under existing spectrum contention resolution rules is equivalent to a *site percolation* process that can readily lead to a network-wide cascade. Moreover, a biased spectrum contention protocol is presented to mitigate this problem.

Spectrum Contention

When available spectrum is insufficient to satisfy all coexisting BSs, an 802.22 BS in need of spectrum can initiate an *inter-BS spectrum contention* process so that better channels or more channels can be acquired from neighboring BSs to satisfy the QoS of its workload [22].

1. The BS that initiates the spectrum contention process is the *contention source (SRC)*. A spectrum contention process consists of a number of pairwise contentions, and every pairwise contention is carried out between the SRC and a neighboring BS that is referred to as the *contention destinations (DST)*.
2. The SRC sends a contention request message to contend for a target channel that is currently occupied by a DST. The DST uses a specific *contention resolution rule* to determine the winner of the contention.
3. In the *unbiased* contention resolution rule [16, 17], every BS (either SRC or DST) is required to select a spectrum contention number (SCN) that is uniformly distributed in the range $[0, W-1]$, and exchange the SCN values, where W is a constant representing the contention window size.
4. The BS that has selected the *largest* CN among all participating BSs is the winner of the contention. Other BSs (and their 802.22 networks) that fail to win will vacate the channel.

Site Percolation

A *percolation* process resides in a graph including sites (vertices) or bonds (edges). The most common percolation model takes the graph structure of a regular lattice

(e.g., a square lattice). In the *site percolation process*, every site is either *open* (i.e., open to flow, diffusion, etc.) randomly and independently with probability p, or *closed* (i.e., closed to flow, diffusion, etc.) with probability $1 - p$.

Definition 2. A path is *open* if all its sites are open and it is *close* if all its sites are closed. Sites u and v are said to be *open connected* if there exists an open path that connects u and v. Define v to be open connected to itself.
It follows immediately that open connection is an equivalence relation. Write $u \leftrightarrow v$ if u and v are open connected, and $u \nleftrightarrow v$ if u and v are not open connected.

Definition 3. The *open cluster* $C(v)$ at site v is the set of all sites that are open connected to v, represented as

$$C(v) = \{u \in V | u \leftrightarrow v\}.$$

Intuitively, as p increases, the size of an open cluster also increases. At a critical value of p, the long-range connectivity in the network appears – there is a transition in the topological structure of the network from a macroscopically disconnected to a connected one – and thus this critical value is called the *percolation threshold* or *critical probability* [14]. Let p_c denote the percolation threshold, the following fundamental results can be obtained from percolation theory [14]:

- when $p > p_c$, with probability one, there exists an infinite cluster, and with a positive probability, the origin (or any other fixed point) belongs to an infinite cluster
- when $p < p_c$, all clusters are finite

When the graph structure resides in continuous space (e.g., a random geometric graph), the resulting percolation model is described as *continuum* percolation.

Network Model

Network graph. The placement of BSs of CR networks could transform to an undirected *network graph* $G = (V, E)$, where V is the set of vertices and E is the set of edges. Each vertex $i \in V$ represents a BS of a network cell, and the BS represented by a vertex i is called BS i. If two BSs i and j are neighboring to each other in the network, there is an edge $\{i, j\} \in E$ connecting the two vertices $i, j \in V$ (i.e., an inter-BS communication link connecting the two BSs). In this case, vertex j is said to be a *neighbor* of vertex i. Let $N(i)$ denote the set of all neighbors of vertex i in graph G: $N(i) = \{j \in V | \{i, j\} \in E\}$. The cardinality of $N(i)$ is called the degree of vertex i, written as $d(i) = |N(i)|$.

Base station placement on a lattice. In an 802.22 system, the rural area is divided into regular-shaped cells, which can be hexagonal, square, or some other irregular shapes. They are generalized to the notion of *lattice* [1], and three common types of lattices are triangular, square, and honeycomb lattices.

Service requirement Every BS i requires r_i channels to satisfy the QoS of its admitted workload, and N is the maximum number of available channels. The value of r_i, called the *service requirement of BS* i, depends on the intra-cell traffic demand raised by the secondary users (i.e., CPEs) connected to the BS i. Let A_i denote the set of channels that are occupied by BS i.

Every BS i tries to claim as many unoccupied channels as possible until $|A_i| = r_i$ or there is no unoccupied channels that can be claimed. Thus, $|A_i| \leq r_i$ for any BS i. To avoid co-channel interference, neighboring BSs i and j occupy disjoint sets of channels, i.e., $A_i \cap A_j = \varnothing$.

Network states. Every BS i occupies an amount of spectrum that is no more than its service requirement. It is assumed there are two states for a given CR network – a state wherein the BS is in need of spectrum, and a state wherein the BS does not need additional spectrum. These two states are called "starving" and "satisfied," respectively.

- When $|A_i| < r_i$, BS i is a *starving BS*.
- When $|A_i| = r_i$, BS i is a *satisfied BS*.

Causes for spectrum contention. The root cause for incurring spectrum contention is the existence of a starving BS. There are three factors that make a satisfied BS i become starving: (1) the reclaim of occupied channels in A_i by the primary user, (2) the increase of r_i due to an increased intra-cell workload, and (3) losing channels in A_i due to spectrum contentions.

The probability that a satisfied BS i becomes starving due to all these factors is called the *starving probability* of BS i, denoted by p_i. Meanwhile, call the probability that a satisfied BS i becomes starving due to non-contention (the first two) factors as *spontaneous starving probability*, denoted by $p_{i,0}$.

Problem Formulation

In an inter-BS spectrum contention process, the channel redistribution may satisfy the contention source BS i, but meanwhile a contention destination BS j that loses the target channel may become starving and successively initiate a cascading contention process. Therefore, the event that a BS j becomes starving is caused by a spectrum contention initiated by a starving BS i. That is, a local spectrum contention initiated by a BS may cause a cascade of spectrum

contentions, which will result in futile contention results and waste network resources. Such a phenomenon is referred to as a *cascading spectrum contention*, which is formulated as a site percolation process over the network graph as follows.

Similar to the definitions of open/closed sites (vertices) in the percolation process, define open/closed BSs in the context of CR networks. A vertex i in the network graph G is *open* if BS i is a starving BS, and call it an *open* BS. Otherwise, the vertex i is *closed* if BS i is a satisfied BS, and call it a *closed* BS.

Two BSs i and j are said to be *open connected* if there exists a path in the network graph that connects vertices i and j, and every vertex in this path is open. The *open cluster* at BS i is the set of all BSs that are open connected to BS i.

It is believed that BSs i and j in the same open cluster are related in a certain relationship of spectrum contentions, e.g., there may exist a path starting at BS i and ending at BS j, where a pairwise contention occurs between every pair of BSs along this path, or there exist two contention paths between k and i, k and j, where k is a third BS in the same cluster. The open cluster in the network graph describes the set of BSs that are in the "starving" state that may be caused by cascading spectrum contentions.

The size of an open cluster. Metrics in the percolation theory are used to quantify the magnitude of cascading spectrum contentions. Define the mean open cluster size at BS i as

$$\chi_i(p_i : i \in V) = E_{(p_i:i\in V)}(|C(i)|),$$

where $E_{(p_i:i\in V)}(X)$ denotes the expectation of a random variable X, given that BS i is open independently with probability p_i $(i \in V)$.

Lower bound case with starving probability p. There is a lower bound p of p_i's, i.e., $p \le p_i$, $\forall i \in V$. Thus $\chi_i(p_i : i \in V) \ge \chi_i(p) \triangleq E_p(|C(i)|)$, where $E_p(X)$ denotes the expectation given that every BS is open independently with probability p, i.e. $\chi_i(p)$ is a lower bound of $\chi_i(p_i : i \in V)$.

So far the study of $\chi_i(p_i : i \in V)$ is transformed into the study of $\chi_i(p)$ in a lower bound case where every BS i is open independently with probability p.

Since the placement of BSs of CR networks form a lattice $G = (V, E)$, whose automorphism group acts transitively upon V (also known as *vertex-transitive*) [1], then $\forall i, j \in V$, $C(i) = C(j)$ and $\chi_i(p) = \chi_j(p)$ due to the homogeneity of a lattice. Hence, simply use C and $\chi(p)$ instead of $C(i)$ and $\chi_i(p)$.

Therefore, the cascading spectrum contention process in CR networks is mapped to the lower bound site percolation process over the network graph where every vertex (BS) is open independently with probability p.

Global and Severe Cascades

Since $\chi(p)$ is defined to characterize the magnitude of cascading spectrum contentions, a *global* cascade of spectrum contentions occurs if the mean open cluster size is infinite, i.e., $\chi(p) = \infty$. According to the percolation theory, an infinite open cluster exists ($\chi(p) = \infty$) with probability one, if and only if $p \geq p_c$, where p is the starving probability and p_c is the critical probability.

In the subcritical phase when $p < p_c$, a severe cascade of spectrum contentions is to said to occur if the mean open cluster size $\chi(p) \geq \chi$ (χ is a predefined threshold, e.g., that χ is set to be 50 means that a cascade involving in over 50 BSs is considered to be a severe cascade), which suggests that an average open cluster of BSs is large.

A Biased Spectrum Contention Protocol

Contention Resolution Rule

A biased contention resolution rule is found to be effective to mitigate this problem by reducing the winning probability of a contention source in a pairwise contention. Define a *contention path* between BSs i and j as a path between vertices i and j in the network graph, such that the channel redistribution via a pairwise contention process occurs for every pair of neighboring BSs that belong to the path. The procedure for the biased contention resolution is described below.

1. In the contention request, every contention source BS i includes the target channel number h, its SCN s_i chosen from $[0, W-1]$, and the current length of the contention path l_i measured by BS i. If the BS i does not belong to any contention path, it sets $l_i = 0$, which implies that it is the starting vertex of a new contention path.
2. Every contention destination BS j checks the values of l_i and SCN s_i in the contention request from the contention source BS i. Let $S(j)$ denote the set of contention sources that send contention requests to BS j during a self-coexistence window.
3. If $|S(j)| > 1$, BS j is being reached by more than one contention paths. The contention destination BS j measures its l_j as $\max_{i \in S(j)}\{l_i\} + 1$ and generates its own SCN s_j from a modified contention window $[0, l_j \cdot W - 1]$. The measured value of l_j will be used by BS j in future contention requests if it becomes a contention source.
4. If the contention destination BS j has the greatest SCN value, it wins the contention. Otherwise, the contention source who has the greatest SCN value wins, and the contention destination BS j releases the target channel.

If $p_0 \geq p_c$, a global cascade of spectrum contentions is inevitable. The fact that $p_0 \geq p_c$ strongly suggests the insufficiency of overall spectrum resources. Next section discusses the case when $p_{i,0} < p_c$ for all $i \in V$.

Finite Cluster Size

Decreasing the winning probability of a contention source can prevent the occurrence of infinite contention paths. There is no infinite contention path if the biased contention resolution rule is used for contention resolution in the case of $p_{i,0} < p_c$, $\forall i \in V$.

Simulation

This section compares two contention resolution rules, namely, the unbiased rule and the proposed biased rule, in terms of feasibility of invoking the cascade phenomenon in spectrum contentions under various conditions in CR networks.

Simulation Setup

Topology. Consider simulating three typical lattices: coexisting BSs are placed on a honeycomb lattice ($d = 3$), a square lattice ($d = 4$), and a triangular lattice ($d = 6$), respectively.

Self-coexistence window and inter-BS spectrum contention. In a network cell, the BS provides broadband access to secondary users according to a time schedule consisting of *superframes*. 802.22 provides the inter-BS synchronization mechanism for neighboring BSs to align their superframes. In 802.22, a superframe has 16 frames, and a self-coexistence window (SCW) is periodically scheduled in every frame for spectrum contention.

Service requirement. There are a total number of $N = 30$ channels in the simulations. Every BS requires 10, 20, or 30 channels to satisfy the QoS of its admitted workload. Neighboring BSs occupy disjoint sets of channels, and a BS claims a number of channels which is no more than its service requirement.

Primary user (PU) traffic generation. It is assumed that there is one primary transmitter per cell, and every primary transmitter randomly selects $X \in [0, N_a]$ channels to emit its signals, where N_a is the number of PU's active channels. In most existing work, it is assumed that a primary transmitter follows a "busy/idle" traffic pattern on a licensed channel [12]. Hence, a "busy/idle" pattern is simulated for each primary transmitter: the busy period has a fixed length of b time slots, and the idle period follows an exponential distribution with a mean of l frames. Thereafter, the notation $\lambda_e = \frac{1}{l}$ is the *primary transmission rate*. Every BS is able to detect the signals from the primary transmitter in the same cell. A channel is considered "unavailable" when primary user signals are present in it. All secondary users (BSs) should vacate unavailable channels during the period of primary user transmission.

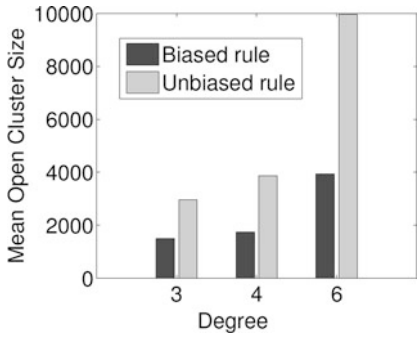

Fig. 14 Mean open cluster size vs. lattice degree

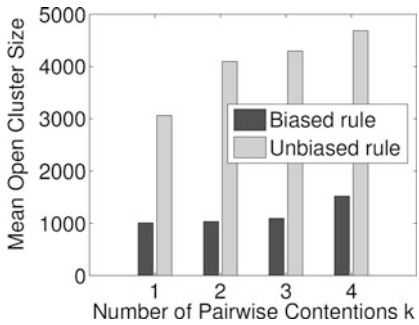

Fig. 15 Mean open cluster size vs. number of pairwise contentions

Phenomenon of Cascading Spectrum Contentions

The mean cluster size, χ, is measured when varying the following parameters: the degree d of the lattice where BSs are placed, the number k of pairwise contentions initiated by a contention source, and the PU traffic pattern (the number N_a of PU's active channels and the primary transmission rate λ_e).

Impact of lattice degree. In this set of simulations, we fix $r = k/d = 1$. In the honeycomb lattice case ($d = 3$), the mean open cluster size is the smallest, while the triangular lattice ($d = 6$) shows the largest mean open cluster size (Fig. 14). These results coincide with the previous conclusion, with $r = k/d$ fixed, there is a positive correlation between χ and d.

Impact of number of pairwise contentions. As is shown in Fig. 15, the more pairwise contentions initiated by a contention source, the larger the mean open cluster size.

Conclusion and Future Directions

This chapter reviews four important research problems for coexistence of heterogeneous cellular networks using cognitive radio technologies. Specifically, the hidden terminal problem can be factored into two types of collision problems, and the

beacon transmission scheme and the dynamic quiet period scheme can address them respectively. Next, it is showed that the channel hopping technique is useful to alleviate the broadcast failure problem in cellular CR networks by leveraging the Langford paring for creating channel hopping sequences. When the inter-network direct coordination is not feasible, a mediator system is able to establish an indirect coordination mechanism for spectrum sharing between networks. On the other hand, when the inter-network direct coordination is not supported, a local controller helps a CR network in need of more spectrum resources to acquire channels from neighboring networks via channel contention without causing the cascading contention problem.

Future work lies in three directions: (1) the evaluation of the coexistence schemes in the real-world scenarios of heterogeneous cellular networks, (2) how to address the violation to the conflict of interests and customer privacy when heterogeneous coexistence of cognitive cellular networks is feasible, and (3) the application of the cutting-edge machine learning techniques to upgrade the existing design principles and frameworks for the coexistence of heterogeneous cellular networks.

References

1. Aizenman M, Newman CM (1984) Tree graph inequalities and critical behavior in percolation models. J Stat Phys 36(1–2):107–143
2. Baykas T, Kasslin M, Cummings M, Kang H, Kwak J, Paine R, Reznik A, Saeed R, Shellhammer SJ (2012) Developing a standard for TV white space coexistence: technical challenges and solution approaches. IEEE Wirel Commun 19(1):10–22
3. Brahma S, Chatterjee M (2009) Mitigating self-interference among IEEE 802.22 networks: a game theoretic perspective. In: IEEE 2009 Global Telecommunications Conference, GLOBECOM 2009, 30 Nov 2009, pp 1–6
4. Chen L, Bian K, Du X, Li X (2015) Multichannel broadcast via channel hopping in cognitive radio networks. IEEE Trans Veh Technol 64(7):3004–3017
5. Chen R, Park JM, Bian K (2008) Robust distributed spectrum sensing in cognitive radio networks. In: The 27th Conference on Computer Communications, INFOCOM 2008, 13 Apr 2008. IEEE
6. Chen R, Park JM, Reed JH (2008) Defense against primary user emulation attacks in cognitive radio networks. IEEE J Sel Areas Commun 26(1):25–37
7. Daneshgaran F, Laddomada M, Mesiti F, Mondin M (2007) On the linear behaviour of the throughput of IEEE 802.11 DCF in non-saturated conditions. IEEE Commun Lett 11(11): 856–858
8. Ecma International (2009) ECMA-392: MAC and PHY for operation in TV white space, 1st edn. Ecma International, Geneva
9. Etemad K, Wang L (2009) Multicast and broadcast multimedia services in mobile WiMAX networks. IEEE Commun Mag 47(10):84–91
10. Fu X, Ma W, Zhang Q (2007) The IEEE 802.16 and 802.11 a coexistence in the license-exempt band. In: 2007 IEEE Wireless Communications and Networking Conference, 11 Mar 2007, pp 1942–1947
11. Gao B, Park JM, Yang Y, Roy S (2012) A taxonomy of coexistence mechanisms for heterogeneous cognitive radio networks operating in TV white spaces. IEEE Wirel Commun 19(4):41–48
12. Geirhofer S, Tong L, Sadler BM (2008) Cognitive medium access: constraining interference based on experimental models. IEEE J Sel Areas Commun 26(1):95–105

13. Ghosh C, Roy S, Cavalcanti D (2011) Coexistence challenges for heterogeneous cognitive wireless networks in TV white spaces. IEEE Wirel Commun 18(4):22–31
14. Grimmett G (1999) Percolation, 2nd edn. Springer, New York
15. Gruber M, Zeller D (2011) Multimedia broadcast multicast service: new transmission schemes and related challenges. IEEE Commun Mag 49(12):176–181
16. Hu W (2009) Frame-based on-demand spectrum contention protocol—the specifications. IEEE docs: IEEE 802.22-07/0024r0
17. Hu W, Gerla M, Vlantis GA, Pottie GJ (2008) Efficient, flexible, and scalable inter-network spectrum sharing and communications in cognitive IEEE 802.22 networks. In: First International Workshop on Cognitive Radio and Advanced Spectrum Management, CogART 2008, 14 Feb 2008, pp 1–5
18. Huang S, Liu X, Ding Z (2009) Optimal transmission strategies for dynamic spectrum access in cognitive radio networks. IEEE Trans Mobile Comput 8(12):1636–1648
19. Huang J, Xing G, Zhou G, Zhou R (2010) Beyond co-existence: exploiting WiFi white space for Zigbee performance assurance. In: 18th IEEE International Conference on Network Protocols (ICNP), 5 Oct 2010, pp 305–314
20. IEEE 802.11 task group af. Wireless LAN in the TV White Space. http://www.ieee802.org/11/
21. IEEE 802.19 Task Group 1. Wireless Coexistence in the TV White Space. http://www.ieee802.org/19/pub/TG1.html
22. IEEE 802.22 Working Group. http://www.ieee802.org/22/
23. IEEE 802.22 Working Group (2005) Reviews of Channel Model. IEEE docs: 22-05-0070-00-0000
24. IEEE 802.22 Working Group (2006) ETRI FT Philips Samsung Proposal. IEEE docs: 22-06-0005-01-0000
25. IEEE standard 802.11 (2007) Wireless LAN medium access control (MAC) and physical layer (PHY) specifications
26. Ji S, Beyah R, Cai Z (2013) Minimum-latency broadcast scheduling for cognitive radio networks. In: 2013 IEEE International Conference on Sensing, Communications and Networking (SECON), 24 Jun 2013, pp 389–397
27. Jing X, Raychaudhuri D (2005) Spectrum co-existence of IEEE 802.11 b and 802.16 a networks using the CSCC etiquette protocol. In: First IEEE International Symposium on New Frontiers in Dynamic Spectrum Access Networks, DySPAN 2005, 8 Nov 2005, pp 243–250
28. Jiang T, Xiang W, Chen HH, Ni Q (2007) Multicast broadcast services support in OFDMA-based WiMAX systems [Advances in mobile multimedia]. IEEE Commun Mag 45(8):78–86
29. Karn P (1990) MACA-a new channel access method for packet radio. In: ARRL/CRRL Amateur radio 9th computer networking conference, vol 140, pp 134–140
30. Khadivi P, Todd TD, Zhao D (2004) Handoff trigger nodes for hybrid IEEE 802.11 WLAN/cellular networks. In: First International Conference on Quality of Service in Heterogeneous Wired/Wireless Networks, QSHINE 2004, 18 Oct 2004, pp 164–170
31. Ko CH, Wei HY (2010) Game theoretical resource allocation for inter-BS coexistence in IEEE 802.22. IEEE Trans Veh Technol 59(4):1729–1744
32. Kornfeld M (2004) DVB-H-the emerging standard for mobile data communication. In: 2004 IEEE International Symposium on Consumer Electronics, 1 Sep 2004, pp 193–198
33. Kondareddy YR, Agrawal P (2008) Selective broadcasting in multi-hop cognitive radio networks. In: 2008 IEEE Sarnoff Symposium, 28 Apr 2008, pp 1–5
34. Lotka A (1925) Elements of physical biology. Williams & Wilkins, Baltimore
35. Murray J (2002) Mathematical biology I: an introduction. Springer, New York
36. Piggin P (2006) An Overview of 802.16h 'Uncoordinated' Coexistence Approach in 3.65–3.7 GHz. S80216h-06_117
37. Proakis J, Salehi M (2001) Communication Systems Engineering, 2nd edn. Prentice Hall, Harlow
38. Shellhammer SJ (2005) Estimation of Packet Error Rate Caused by Interference using Analytic Techniques—A Coexistence Assurance Methodology. IEEE docs: P802.19-05/0028r1

39. Siddique MM, Wenning BL, Gorg C, Muehleisen M (2010) Spectrum sharing between IEEE 802.16 and IEEE 802.11 based wireless networks. In: IEEE International Symposium on a World of Wireless Mobile and Multimedia Networks (WoWMoM), 14 Jun 2010, pp 1–6
40. So J, Vaidya NH (2004) Multi-channel MAC for ad hoc networks: handling multi-channel hidden terminals using a single transceiver. In: Proceedings of the 5th ACM international symposium on Mobile ad hoc networking and computing, 24 May 2004, pp 222–233
41. Song Y, Xie J (2011) A QoS-based broadcast protocol for multi-hop cognitive radio ad hoc networks under blind information. In: IEEE InGlobal Telecommunications Conference (GLOBECOM 2011), 5 Dec 2011. IEEE, pp 1–5
42. Song Y, Xie J, Wang X (2014) A novel unified analytical model for broadcast protocols in multi-hop cognitive radio ad hoc networks. IEEE Trans Mobile Comput 13(8):1653–1667
43. Song Y, Xie J (2012) A distributed broadcast protocol in multi-hop cognitive radio ad hoc networks without a common control channel. In: Proceedings of IEEE INFOCOM, 25 Mar 2012. IEEE, pp 2273–2281
44. Thomas NJ, Willis MJ, Craig KH (2006) Analysis of co-existence between IEEE 802.11 and IEEE 802.16 systems. In: 2006 3rd Annual IEEE Communications Society on Sensor and Ad Hoc Communications and Networks, 28 Sep 2006, vol 2, pp 615–620
45. Tokeshi M (1998) Species coexistence: ecological and evolutionary perspectives. Wiley-Blackwell, Oxford
46. Volterra V (1931) Variations and fluctuations of the number of individuals in animal species living together. In: Chapman RN (ed) Animal ecology. McGraw-Hill, New York
47. Wang T, Song L, Han Z (2013) Coalitional graph games for popular content distribution in cognitive radio VANETs. IEEE Trans Veh Tech 62(8):4010–4019
48. Yu R, Zhang Y, Yi L, Xie S, Song L, Guizani M (2012) Secondary users cooperation in cognitive radio networks: balancing sensing accuracy and efficiency. IEEE Wirel Commun 19(2):30–37
49. Zhang X, Shin KG (2011) Enabling coexistence of heterogeneous wireless systems: case for ZigBee and WiFi. In: Proceedings of the Twelfth ACM International Symposium on Mobile Ad Hoc Networking and Computing, 17 May 2011, p 6
50. Zhou R, Xiong Y, Xing G, Sun L, Ma J (2010) ZiFi: wireless LAN discovery via ZigBee interference signatures. In: Proceedings of the sixteenth annual international conference on Mobile computing and networking, 20 Sep 2010, pp 49–60

Device-to-Device Communications over Unlicensed Spectrum

36

Hongliang Zhang, Yun Liao, and Lingyang Song

Contents

H. Zhang (✉)
School of Electronics Engineering and Computer Science, Peking University, Beijing, China
e-mail: hongliang.zhang@pku.edu.cn

Y. Liao · L. Song
School of Electrical Engineering and Computer Science, Peking University, Beijing, China
e-mail: yun.liao@pku.edu.cn; lingyang.song@pku.edu.cn

W. Zhang (ed.), *Handbook of Cognitive Radio*,
https://doi.org/10.1007/978-981-10-1394-2_33

Abstract

Device-to-device (D2D) communication, which enables direct communication between nearby mobile devices, is an attractive add-on component to improve spectrum efficiency and user experience by reusing licensed cellular spectrum. Nowadays, LTE-unlicensed (LTE-U) emerges to extend the cellular network to the unlicensed spectrum to alleviate the spectrum scarcity issue. In this chapter, we propose to enable D2D communication in unlicensed spectrum (D2D-U) as an underlay of the uplink cellular network to further boom the network capacity. A sensing-based protocol is designed to support the unlicensed channel access for both LTE and D2D users, based on which we investigate the subchannel allocation problem to maximize the sum-rate of LTE and D2D users while taking into account their interference to the existing Wi-Fi systems. Specifically, we formulate the subchannel allocation as a many-to-many matching problem with externalities and develop an iterative user-subchannel swap algorithm. Analytical and simulation results show that the proposed D2D-U scheme can significantly improve the network capacity.

Keywords

Carrier aggregation · Device-to-device unlicensed · Matching theory · Resource allocation

Introduction

With the explosive growth of mobile devices and bandwidth-hungry applications such as video streaming and multimedia file sharing, user demands for mobile broadband are undergoing an unprecedented rise, which pushes the limits of current LTE systems [1]. To improve spectrum efficiency and user experience, device-to-device (D2D) communications underlaying LTE networks have been proposed as a promising approach to facilitate high data rate services in a short range and boost the performance of LTE systems [1–3]. D2D communications underlaying LTE networks enable mobile devices in proximity to establish a direct link without traversing the base station (BS) and reuse the spectrum with the LTE system by the control of the BS [4–8]. With the centralized control at BS and the proximity of communication parties, D2D communications enjoy the benefits of fast access to the radio spectrum in terms of proximity gain, reuse gain, and paring gain [3,4,6].

In addition to excavating more capacity on licensed spectrum, the operators are motivated to expand LTE services to the unlicensed spectrum in order to alleviate congestion. Mobile traffic offloading is a conventional method, in which the data is offloaded to Wi-Fi networks [9–12]. However, the offloading schemes commonly suffer from low efficiency and poor guarantee of quality of service (QoS) due to the inferior performance of Wi-Fi and the lack of coordination between LTE and Wi-Fi systems [13]. In light of these issues, the 3rd Generation Partnership Project (3GPP) has initialed the research on Licensed Assisted Access (LAA) to integrate the unlicensed carriers with the licensed ones for data transmission [14]. Based on

the LAA scheme, the LTE-unlicensed (LTE-U) technology is proposed to extend LTE to the unlicensed spectrum to leverage the existing carrier aggregation (CA) technology [15, 16].

As LTE-U technology shows satisfying performance, a natural idea to further improve spectrum efficiency and system throughput is to extend D2D communications to the unlicensed spectrum, that is, D2D communications work as the underlay of LTE system in not only the licensed spectrum but also the unlicensed one. However, due to the mutual interference among LTE-U users, D2D users, and the opportunistic feature of unlicensed channel access in existing Wi-Fi systems, this extension turns out to be much complicated. In this work, we investigate the extension of the underlaid D2D communications to LTE-U networks, which we refer to as D2D-unlicensed (D2D-U). Different from most previous peer-to-peer communication technologies in the unlicensed spectrum such as Wi-Fi Direct [17–19], which builds the network upon the IEEE 802.11 infrastructure mode and allows users to negotiate with each other in an AP-like method, D2D-U requires assist and control from the central BS. With the involvement of BS, D2D users can work as an underlay of LTE system in both licensed and unlicensed spectra.

As aforementioned, the major challenges of implementing D2D-U are (1) the opportunistic feature of unlicensed channel access due to current 802.11 mechanism adopted by Wi-Fi systems and (2) the interference management issue among the three types of systems, i.e., the access and transmission of D2D-U users cannot cause too much additional interference to the existing Wi-Fi system as well as the LTE-U system. To cope with the first challenge, we design an access protocol in the unlicensed bands for D2D-U and LTE-U users, which is based on the sensing mechanism, to mitigate collision with the ongoing Wi-Fi transmissions. To deal with the second challenge, we first find the cleanest channel for data transmission and elaborate an approximated model to evaluate the interference to Wi-Fi networks. Then, we investigate the subchannel allocation problem to leverage the maximization of the sum-rate of LTE-U and D2D-U users and the protection of Wi-Fi performance. This subchannel allocation problem is originally a mixed integer nonlinear programming (MINLP) problem, which is generally NP-hard. For this reason, we reformulate it as a many-to-many game with externalities [20–24] and solve it with low computational complexity by designing an iterative user-subchannel swap matching algorithm.

The rest of the chapter is organized as follows. In section "Characteristics of LTE-U, D2D, and Wi-Fi Networks", we first introduce the PHY/MAC features of LTE, D2D, and Wi-Fi systems. In section "System Model", we describe the system model for the coexistence among LTE, D2D, and Wi-Fi users and discuss the interference issues. In section "Sensing-Based D2D-U Protocol", a sensing based protocol is elaborated to support LTE-U and D2D-U users in the unlicensed band [25]. Then we formulate the optimization problem for subchannel allocation as a many-to-many matching game with externalities in section "Problem Formulation". In section "Many-to-Many Matching-Based Subchannel Allocation", an iterative algorithm is designed to find a stable matching in the many-to-many matching game. In section "Performance Analysis", the system performance is discussed.

Numerical results in section "Simulation Results" evaluate the proposed algorithm and the performance of the D2D-U. Finally, conclusion remarks are drawn in section "Conclusions".

Characteristics of LTE-U, D2D, and Wi-Fi Networks

In this part, we sequentially elaborate the PHY/MAC characteristics of the coexisting systems, i.e., LTE and D2D users in the licensed/unlicensed bands, and existing Wi-Fi characteristics in the unlicensed band.

LTE-U Network

In PHY layer, LTE-U users can utilize both the licensed and unlicensed spectra, in which the spectrum bandwidth is divided into a series of orthogonal subchannels. We assume that each user is able to occupy multiple subchannels in one subframe. In addition, to guarantee reliable transmission of the control signaling, an active LTE-U user must hold at least one licensed subchannel [16].

For the sake of Wi-Fi protection, the LTE-U system are not allowed to keep occupying the unlicensed channel forever. Instead, there exists reserved transmission period for the Wi-Fi systems, in which the LTE-U users need to evacuate the unlicensed spectrum and allow the Wi-Fi systems enough time for transmission [16]. The reserved duration for Wi-Fi system can be adjusted by the current traffic. In particular, if the channel is sensed clean in the sensing phase, the LTE-U users can occupy the channel for the whole duty cycle.

And as for the MAC layer, the LTE-U system adopts a centralized MAC protocol, which always allocates the subchannels to the user that can maximize the target metric in every subframe.

Underlaid D2D Users

D2D users is allowed to utilize the licensed and unlicensed spectra in the underlay method. That is to say, multiple D2D users are allowed to work in licensed/unlicensed subchannels concurrently occupied by LTE users. Co-channel assignment of the LTE and D2D users will be more efficient and profitable for operators for it can achieve a better overall system performance. Similar to the LTE-U network, a D2D user also needs to occupy one licensed subchannel for control signaling. Besides, due to the low transmit power and short transmission range of D2D communications, the D2D communications are allowed to transmit in the unlicensed spectrum even in the reserved subframes for Wi-Fi system so long as the operating channel is sensed idle by the D2D transmitter.

In the MAC layer, a centralized protocol is also utilized, the BS controls the access of both types of users and decides the subchannel allocation in a centralized

manner to mitigate mutual interference or maximize the system sum-rate after receiving the estimated channel state.

Wi-Fi Systems

The Wi-Fi systems operate only in the unlicensed spectrum. Different from the OFDMA-based channel utilization in LTE systems, the Wi-Fi transmission covers the whole unlicensed channel. Thus, Wi-Fi systems allow only one user to occupy the channel at a time, and concurrent transmission leads to collision. In addition, the OFDM symbol durations in these two systems are different. For LTE the symbol duration is 71.4 ms, while Wi-Fi has a granularity of 4 ms. The PHY layer comparison of these two systems is shown in Fig. 1 [26].

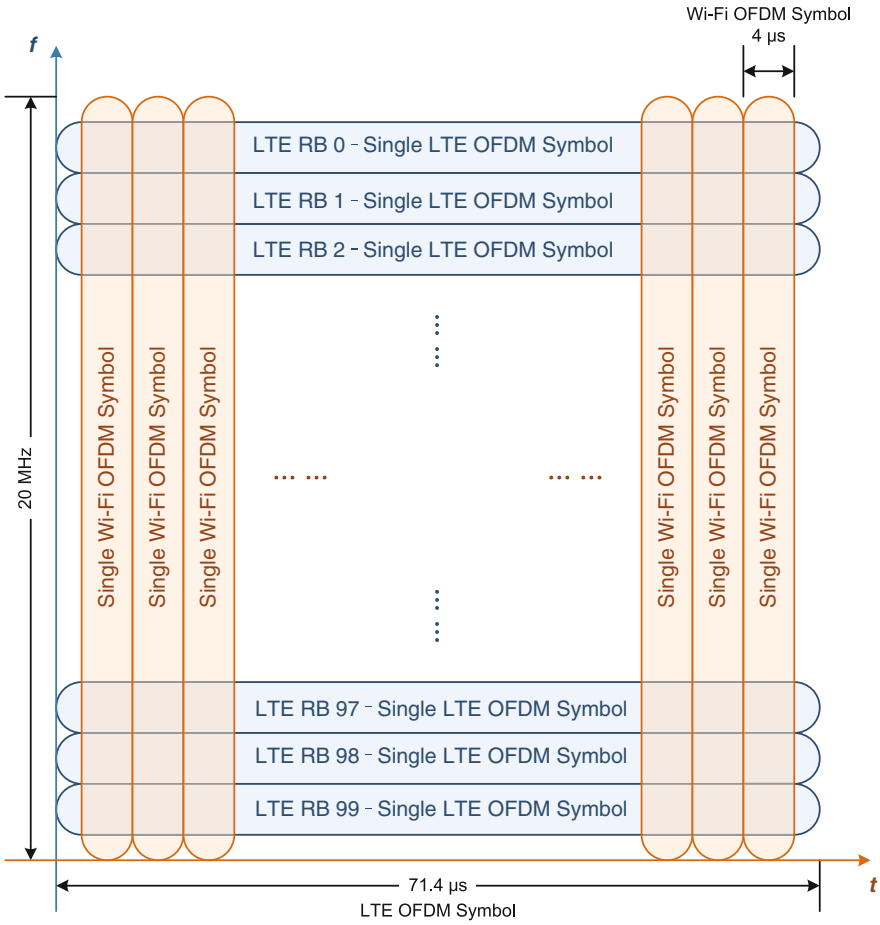

Fig. 1 PHY layer comparisons between LTE and Wi-Fi systems in both time and frequency domains

For the MAC layer, without a central controller, the Wi-Fi systems adopt a sensing and contention-based MAC protocol, i.e., carrier sense multiple access with collision avoidance (CSMA/CA) [27]. Specifically, before transmission, a Wi-Fi user first listens to the intended channel. If the channel is unoccupied, the Wi-Fi user begins backoff process to avoid collision; otherwise, the Wi-Fi user keeps sensing until the channel is judged idle.

System Model

In this section, we present the coexistence scenario of LTE, D2D, and Wi-Fi systems in both licensed and unlicensed spectra. Then, we discuss the interference issues within the coexistence network.

Scenario Description

As shown in Fig. 2, we consider an uplink scenario in an LTE network with one BS and Q Wi-Fi access points (APs), denoted by $q \in \mathcal{Q} = \{1, \ldots, Q\}$. The BS is located at the center, and the APs are randomly located around the BS. There exist N LTE users, denoted by $n \in \mathcal{N} = \{1, \ldots, N\}$, and M D2D users, denoted by $m \in \mathcal{M} = \{1, \ldots, M\}$. The LTE system owns licensed spectrum, and the bandwidth

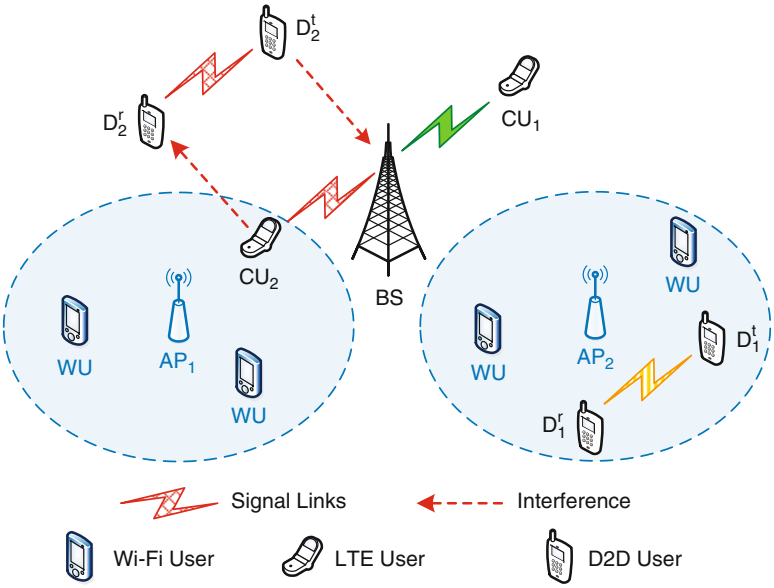

Fig. 2 System model for LTE, D2D, and Wi-Fi coexistence in both licensed and unlicensed spectra

is divided into K subchannels to support orthogonal frequency division multiple access (OFDMA) transmissions. The licensed subchannels are denoted by $\mathscr{K} = \{1, \ldots, K\}$, with uniform bandwidth B_l.

For the Wi-Fi system, we assume that within the coverage of AP q, there exist F_q Wi-Fi users marked by f_q ($f_q = 1, \ldots, F_q$). Besides, we assume that there are L unlicensed channels to support different APs, e.g., there are 23 channels for IEEE 802.11n in the 5 GHz band, and BS will select one of them to support LTE-U/D2D-U users. Since the unlicensed channel is much wider than one licensed subchannel in LTE system, each LTE-U or D2D user only requires a fraction of the unlicensed channel. Thus, to reuse the unlicensed channel more efficiently, the unlicensed channel is divided to K^u unlicensed subchannels with bandwidth B_u [28], marked by $\mathscr{K}^u = \{K + 1, \ldots, K + K^u\}$, so that multiple LTE-U and D2D users can transmit on the unlicensed channel concurrently.

We also assume that all devices transmit with fixed power, specifically, an LTE-U or D2D user transmits on any subchannel with power P^c or P^d, and the transmit power of the APs as well as the Wi-Fi users over the whole unlicensed channel is fixed on P^w. The free-space propagation path loss model with Rayleigh fading is adopted to model the channel gain between any two devices in the network, i.e., for the link from device i to device j, the received power can be expressed as

$$p_{i,j}^r = p_i^t \cdot |h_{i,j}|^2 = p_i^t \cdot G \cdot d_{i,j}^{-\alpha} \cdot |h_0|^2, \tag{1}$$

where p_i^t represents the transmit power of user i, $d_{i,j}$ is the distance between devices i and j, α is the path loss exponent, G is the constant power gains factor introduced by amplifier and antenna, and $h_0 \sim \mathrm{CN}(0, 1)$ is a complex Gaussian variable representing Rayleigh fading. Besides, we assume that the thermal noise at each device satisfies independent Gaussian distribution with zero mean and the same variance σ^2.

Evaluation of Interference to Wi-Fi Systems

When LTE-U and D2D-U users occupy the unlicensed channel, the nearby Wi-Fi users cannot work normally, and the performance of Wi-Fi system would be severely degraded. To quantify the performance degradation brought by LTE-U and D2D users, we introduce the concept of *interference range* on the Wi-Fi network. The interference range is defined as the area in which the Wi-Fi users can detect the reservation signal from the LTE-U/D2D users and suspend their transmission attempts. More specifically, each Wi-Fi user is able to detect the channel unavailable if the received signal power is beyond a certain threshold. With the free-space path loss model, if an LTE-U or D2D user is occupying the unlicensed spectrum, the interference range to the Wi-Fi network is a circle centered at the transmitter, whose radius is positively proportional to the transmit power. Intuitively, the users with large interference range has low probability of being allocated the unlicensed subchannels, because a large number of Wi-Fi users will be interfered by this user.

On contrary, the users with small interference range are more likely to utilize the unlicensed subchannels due to their insignificant interference to the Wi-Fi network.

However, when multiple LTE-U and D2D users transmit on the unlicensed spectrum concurrently, their individual interference circles may overlap, which is hard to derive the closed form expression for the area of the total interference range. In the following of this part, we present an approximated model of the interference range to evaluate the performance degradation in Wi-Fi system. Intuitively speaking, a smaller interference range can be obtained if BS allocates the unlicensed subchannels to those users which are close to each other rather than those whose interference ranges do not overlap. Inspired by this observation, we use the minimum distance between a new LTE-U/D2D users to others to approximate the additional interference introduced by this add-on user. Let L_c and L_d denote the radii of individual interference circles of LTE-U and D2D users, respectively, where $L_d \leq L_c$. Besides, we define $\mathscr{C}^u$ as the user set in which users are allocated to the unlicensed subchannels. With these notations, the weight functions for LTE-U and D2D users are given as below.

LTE-U user

When LTE user n is allocated to the unlicensed subchannel for the first time, and LTE user j, the increased interference range is related to the distance between LTE users n and j, denoted by $L^c_{n,j}$. When the interference ranges of these two LTE users overlaps, i.e., $L^c_{n,j} < 2L_c$, as LTE user 1 and user 2 in Fig. 3, we assume the weight is proportional to the distance $L^c_{n,j}$. And as LTE users 1 and 3 illustrated in Fig. 3, their interference ranges do not overlap, i.e., $L^c_{n,j} \geq 2L_c$, the increased area

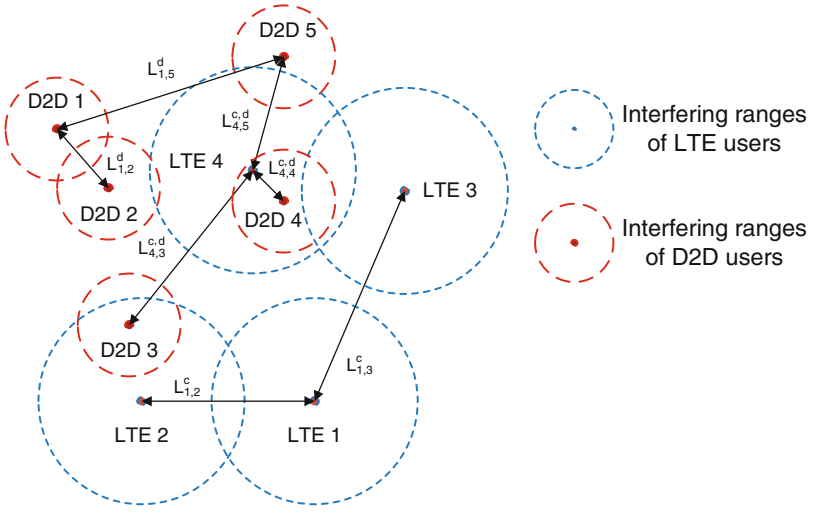

Fig. 3 Illustrations for interference range

will not grow as the distance $L^c_{n,j}$. Therefore, the weight function for the increased area $w^c_{n,j}$ can be expressed as

$$w^c_{n,j} = \begin{cases} L^c_{n,j}, & L^c_{n,j} < 2L_c, \\ 2L_c, & L^c_{n,j} \geq 2L_c. \end{cases} \tag{2}$$

On the other hand, given D2D user m, the increased interference range is also related to the distance between D2D users n and m, $L^{c,d}_{n,m}$. Note that $L_d \leq L_c$, when the interference range of D2D user m is contained by that of LTE user n as LTE user 4 and D2D user 4 in Fig. 3, i.e., $L^{c,d}_{n,m} \leq L_c - L_d$, the increased area is proportional to the increased diameter $2(L_c - L_d)$. When the interference range of LTE user n overlaps with but does not contain that of D2D user m as D2D user 5 and LTE user 4, that is, $L_c - L_d < L^{c,d}_{n,m} < L_c + L_d$, the weight is proportional to the distance $L^{c,d}_{n,m}$ as well. Besides, when the interference ranges of D2D user m and LTE user n do not overlap, such as LTE user 4 and D2D user 3, i.e., $L^{c,d}_{n,m} \geq L_c + L_d$, the increased area is a constant. Therefore, the weight function for the increased area $w^{c,d}_{n,m}$ is written by

$$w^{c,d}_{n,m} = \begin{cases} 2(L_c - L_d), & L^{c,d}_{n,m} \leq L_c - L_d, \\ L^{c,d}_{n,m} + L_c - L_d, & L_c - L_d < L^{c,d}_{n,m} < L_c + L_d, \\ 2L_c, & L^{c,d}_{n,m} \geq L_c + L_d. \end{cases} \tag{3}$$

The weight of an LTE-U user n is the minimum increased interference range between LTE user n and any user allocated to the unlicensed subchannels, that is,

$$w^c_n = \min_{j,m \in \mathscr{C}^u} (w^c_{n,j}, w^{c,d}_{n,m}). \tag{4}$$

D2D user

Similar to the LTE-U users, if D2D users m is allocated to the unlicensed subchannel for the first time, and D2D user j is a D2D user utilizing the unlicensed subchannels, the increased range is related to the distance between the transmitter of D2D user m and the receiver of D2D user j. As illustrated in Fig. 3, the increased range can be calculated under two conditions: (1) the interference ranges of these two D2D users overlap and (2) their interference ranges do not overlap. Thus, the weight function $w^d_{m,j}$ between D2D users m and j is provided by

$$w^d_{m,j} = \begin{cases} L^d_{m,j}, & L^d_{m,j} < 2L_d, \\ 2L_d, & L^d_{m,j} \geq 2L_d. \end{cases} \tag{5}$$

In addition, if there already exists one LTE-U user n, the increased area $f^{c,d}_{n,m}$ is also related to the distance $L^{d,c}_{m,n}$ between LTE user n and D2D user m, which can be given by

$$w_{n,m}^{c,d} = \begin{cases} 0, & L_{m,n}^{d,c} \le L_c - L_d, \\ L_{n,m}^{c,d} + L_d - L_c, & L_c - L_d < L_{m,n}^{d,c} < L_c + L_d, \\ 2L_c, & L_{m,n}^{d,c} \ge L_c + L_d. \end{cases} \tag{6}$$

Therefore, the weight of D2D user m is

$$w_m^d = \min_{j,n \in \mathscr{C}^u} (w_{m,j}^d, w_{m,n}^{d,c}). \tag{7}$$

Interference in the LTE-U/D2D Network

The mutual interference between the LTE-U and D2D users is analyzed in this subsection. We assume that one subchannel can be allocated to a maximum of one LTE user, and a subchannel can be allocated to at most V^s users for the sake of QoS. Besides, we also assume that a user can utilize at most V^u subchannels including licensed and unlicensed ones for the sake of fairness.

First, some notations are listed as follow. The subchannel allocation matrix for LTE and D2D users is denoted by

$$A_{(N+M)\times(K+K^u)} = \begin{pmatrix} \Phi_{N\times(K+K^u)} \\ \Theta_{M\times(K+K^u)} \end{pmatrix}, \tag{8}$$

where $\Phi_{N\times(K+K^u)} = [\phi_{n,k}]$, and $\Theta_{M\times(K+K^u)} = [\theta_{m,k}]$ stand for the subchannel allocation matrices for the LTE-U and D2D users, respectively. The values of $\phi_{n,k}$ and $\theta_{m,k}$ are defined as

$$\phi_{n,k} = \begin{cases} 1, & \text{when subchannel } k \text{ is allocated to LTE user } n, \\ 0, & \text{otherwise,} \end{cases} \tag{9}$$

and

$$\theta_{m,k} = \begin{cases} 1, & \text{when subchannel } k \text{ is allocated to D2D user } m, \\ 0, & \text{otherwise.} \end{cases} \tag{10}$$

Besides, we define the access indicators s_n^c ($n \in \mathscr{N}$) and s_m^d ($m \in \mathscr{M}$) to respectively represent whether the LTE and D2D users can access the unlicensed channel. If the LTE user n can access the unlicensed channel, $s_n^d = 1$, otherwise, $s_n^d = 0$. And it is the same for D2D users. We also define $\mathscr{C}_k$ to represent the set of LTE and D2D users to which subchannel k is allocated.

With this approximated model, the BS only needs to measure the distances between any two users applied for accessing the unlicensed spectrum and evaluates the increased interference range for each pending user compared to the current

subchannel allocation scheme. The increased interference range is regarded as a penalty term in the subsequent subchannel allocation process.

Interference Analysis in the Licensed Spectrum

In the licensed subchannels, under the assumption that a subchannel can be allocated to a maximum of one LTE user, the LTE users can only receive the co-channel interference from the underlaying D2D users, while the interference received by D2D users might be from LTE users and other co-channel D2D users. The SINR at the receiver of BS from LTE user n over licensed subchannel k can be given by

$$\gamma_{n,k}^{c} = \frac{\phi_{n,k} P^{c} |h_{n,B}^{c}|^2}{\sigma^2 + \sum\limits_{m=1}^{M} \theta_{m,k} P^{d} |h_{m,B}^{d}|^2}, \tag{11}$$

where $h_{n,B}^{c}$ and $h_{m,B}^{d}$ represent the channel gains from LTE user n and the transmitter of D2D user m to the BS, respectively. The SINR at the receiver of D2D user m over licensed subchannel k can be expressed as

$$\gamma_{m,k}^{d} = \frac{\theta_{m,k} P^{d} |h_{m,m}^{d}|^2}{\sigma^2 + \sum\limits_{m \neq m', m'=1}^{M} \theta_{m',k} P^{d} |h_{m',m}^{d}|^2 + \sum\limits_{n=1}^{N} \phi_{n,k} P^{c} |h_{n,m}^{c}|^2}, \tag{12}$$

where $h_{m',m}^{d}$ and $h_{n,m}^{c}$ are the channel gains from the transmitter of D2D user m' and LTE user n to the receiver of D2D user m, respectively. The data rates of LTE user n and D2D user m over licensed subchannel k are respectively given by

$$\begin{aligned} R_{n,k}^{c} &= B_l \log_2(1 + \gamma_{n,k}^{c}), \\ R_{m,k}^{d} &= B_l \log_2(1 + \gamma_{m,k}^{d}). \end{aligned} \tag{13}$$

Interference Analysis in the Unlicensed Spectrum

In the unlicensed subchannels, the D2D-U and LTE-U users will not only receive the mutual interference from D2D-U and LTE-U users as in the licensed subchannels but also the interference from the Wi-Fi system. Therefore, the SINR at BS from LTE-U user n over unlicensed subchannel k is

$$\gamma_{n,k}^{c,u} = \frac{\phi_{n,k} P^{c} |h_{n,B}^{c}|^2}{\sigma^2 + \sum\limits_{m=1}^{M} \theta_{m,k} P^{d} |h_{m,B}^{d}|^2 + I_{w}^{c}}, \tag{14}$$

where I_{w}^{c} is the total interference from Wi-Fi system to BS, which can be calculated as $I_{w}^{c} = \sum\limits_{q \in \mathcal{Q}} \frac{P^{w}}{K^{u}} |h_{f,B}^{q}|^2$, where $h_{f,B}^{q}$ is the channel gain from the transmitting Wi-Fi user f associated with AP q to BS. Similarly, the SINR at the receiver of D2D user m over unlicensed subchannel k can be written as

$$\gamma_{m,k}^{d,u} = \frac{\theta_{m,k} P^d |h_{m,m}^d|^2}{\sigma^2 + \sum\limits_{m \neq m', m'=1}^{M} \theta_{m',k} P^d |h_{m',m}^d|^2 + \sum\limits_{n=1}^{N} \phi_{n,k} P^c |h_{n,m}^c|^2 + I_w^d}, \tag{15}$$

where I_w^d is the interference from Wi-Fi system to the receiver of D2D user m, whose value is $I_w^d = \sum\limits_{q \in \mathcal{Q}} \frac{P^w}{K^u} |h_{f,m}^q|^2$, with $h_{f,m}^q$ representing the channel gain from the active Wi-Fi user f to the receiver of D2D user m.

The data rates of LTE user n and D2D user m over unlicensed subchannel k are respectively given by

$$\begin{aligned} R_{n,k}^{c,u} &= B_u \log_2(1 + \gamma_{n,k}^{c,u}), \\ R_{m,k}^{d,u} &= B_u \log_2(1 + \gamma_{m,k}^{d,u}). \end{aligned} \tag{16}$$

Sensing-Based D2D-U Protocol

In this section, we propose a duty cycle-based [29] protocol for LTE-U and D2D-U users to share the unlicensed spectrum with Wi-Fi systems. The basic principle of the protocol is to allow the LTE-U and D2D-U users a chance to access the unlicensed spectrum while protecting the incumbent Wi-Fi performance. Note that the behavior of LTE and D2D-U users on the licensed spectrum still follows the current LTE standard. In this chapter, we only provide the protocol design for accessing the unlicensed spectrum in Fig. 4.

Overview of the Proposed Protocol

As illustrated in Fig. 4, similar to the LTE standard, the timeline is slotted into subframes with length T_{sub} (e.g., 1ms in the LTE standard). There are three types of subframes, namely, sensing subframes (SSs), transmission subframes, and reserved Wi-Fi subframes. The SSs are inserted before the LTE-U, and D2D-U users attempt to initiate a transmission to avoid collision with the ongoing Wi-Fi transmissions. In transmission subframes, the LTE-U and D2D-U users perform transmission as in the conventional LTE standard. Then, to further protect the Wi-Fi performance, we reserve several subframes for Wi-Fi transmission, during which the LTE-U users are not allowed to utilize the unlicensed spectrum, and then the long successive transmission period of LTE-U and D2D-U users follows. The transmission periods for LTE-U and D2D-U systems as well as the Wi-Fi network can be adjusted according to their desired performance; specifically, when the channel is clean, LTE-U and D2D-U users can start transmission at once.

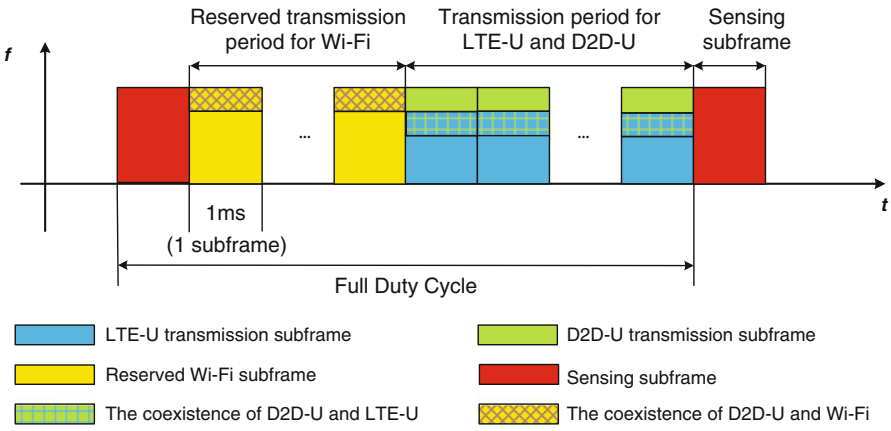

Fig. 4 Sensing-based protocol for LTE and D2D users accessing the unlicensed spectrum

Coexistence Mechanism

In this protocol, two mechanism are used to safeguard that LTE-U/D2D-U users do not bring severe interference to their neighboring users in the unlicensed spectrum. First, channel selection is performed to choose the cleanest channel avoiding the interference between Wi-Fi users and LTE-U/D2D-U users. In the case that no clean channel is found, channel sensing transmission is used to support transmission for D2D-U/LTE-U users, in which LTE-U users are applied with TDM transmission, and D2D-U users are selectively activated, based on the channel sensing result.

Channel Selection

In SS, LTE-U/D2D-U users will scan the unlicensed spectrum and identify a cleanest channel from the L unlicensed channels for uplink data transmission. For a LTE-U/D2D-U users, the transmitter will perform energy detection, and measure the interference level as in CSMA/CA method. If the interference is sensed less than the predefined threshold, the channel will be regarded as clean for this LTE-U/D2D-U user. Then, the LTE-U/D2D-U users will inform the BS whether they are interfered by Wi-Fi users according to the measured result. In the operating channel, if the number of interfered users is larger than a given threshold, and there is another cleaner channel available, i.e., the number of interfered users in this channel is less than that in the operating channel, the transmission will be switched to the new channel.

Some technologies are also used to improve detection sensitivity. For example, Wi-Fi preambles are detected to estimate the number of neighboring Wi-Fi APs in the given channel. In addition, device-assisted enhancements, such as 802.11k, in which users can measure the received signal and recognize the hidden nodes, can be used to address the hidden node effect and thus help to select a better channel.

Channel-Sensing Transmission

For most deployments, the channel selection is usually sufficient to meet the coexistence requirements. While in hyper-dense deployment, there is a possible that no clean channel can be found. For LTE-U users, carrier-sensing adaptive transmission (CSAT) algorithm [29] is used to support the coexistence of LTE-U and Wi-Fi users. In the CSAT scheme, LTE-U and Wi-Fi users coexist in a TDM fashion. In particular, a duty cycle is defined where LTE-U users transmit in a fraction of the cycle and gates off in the remaining time to hand over the unlicensed channel to Wi-Fi users.

However, due to the short transmission range and low transmit power of D2D communications, it is possible to share the unlicensed spectrum with Wi-Fi users during the full duty cycle. After the SS, the unlicensed channel can be still utilized by Wi-Fi users to resume the ongoing data transmission. In these reserved subframes, those D2D-U users which have sensed that the channel idle in SS can utilize the unlicensed subchannels for data transmission, while other D2D and LTE users are only allowed to utilize licensed subchannels. When the reserved subframes for Wi-Fi transmission expires, all the LTE-U/D2D-U users are activated in the unlicensed subchannels. At the beginning of each subframe, the BS allocates licensed and unlicensed subchannels to the LTE-U/D2D-U users; in particular, only active LTE-U/D2D-U users have possibility to utilize unlicensed subchannels, which is elaborated in section "Many-to-Many Matching-Based Subchannel Allocation".

Problem Formulation

In this section, we first formulate subchannel allocation problem considering both the performance of Wi-Fi and the total sum-rate of LTE and D2D users and then reformulate this problem into a many-to-many matching problem in consideration of its computation complexity.

Sum-Rate Maximization Problem Formulation

Our objective is to maximize the total sum-rate of the LTE and D2D users while minimizing the interference range by setting the subchannel allocation variables $\{\phi_{n,k}, \theta_{m,k}\}$ in each subframe.

Since the BS does not hold the information of the interference from LTE-U and D2D users to Wi-Fi systems, we use the approximate model described in the section "Overview of the Proposed Protocol" to evaluate the performance degradation of Wi-Fi system and add it in the objective function as a penalty term. Assumed that the Wi-Fi users are uniformly located in this plane, the number of interfered Wi-Fi users is positively proportional to the interference area, which can be an indicator of the performance degradation of Wi-Fi system. Besides, provided that at least one unlicensed subchannels is allocated to CU_n or D_m, the Wi-Fi users in its interference range cannot perform data transmission; the penalty term is in the

form of sign function. Thus, the penalty items W_n^c and W_m^d for LTE user n and D2D user m are respectively given by

$$\begin{aligned} W_n^c &= w_n^c \operatorname{sgn}\left(\sum_{k\in\mathscr{K}^u} \phi_{n,k}\right), \\ W_m^d &= w_m^c \operatorname{sgn}\left(\sum_{k\in\mathscr{K}^u} \phi_{m,k}\right). \end{aligned} \tag{17}$$

where $\operatorname{sgn}(\cdot)$ is the sign function. Taking the penalty into consideration, the subchannel allocation can be formulated as the following optimization problem:

$$\max_{\{\phi_{n,k},\theta_{m,k}\}} \sum_{k\in\mathscr{K}} \sum_{\mathscr{C}_k} \left(R_{n,k}^c + R_{m,k}^d\right) + \sum_{k\in\mathscr{K}^u} \sum_{\mathscr{C}_k} \left(R_{n,k}^{c,u} + R_{m,k}^{d,u}\right) - \lambda \left(\sum_{n\in\mathscr{N}} W_n^c + \sum_{m\in\mathscr{M}} W_m^d\right), \tag{18a}$$

$$s.t. \sum_{n\in\mathscr{N}} \phi_{n,k} \le 1, \forall k \in \mathscr{K}, \tag{18b}$$

$$\sum_{k\in\mathscr{K}\cup\mathscr{K}^u} \phi_{n,k} \le V^u, \forall n \in \mathscr{N}, \sum_{k\in\mathscr{K}\cup\mathscr{K}^u} \theta_{m,k} \le V^u, \forall m \in \mathscr{M}, \tag{18c}$$

$$\sum_{n\in\mathscr{N}} \phi_{n,k} + \sum_{m\in\mathscr{M}} \theta_{m,k} \le V^s, \forall k \in \mathscr{K} \cup \mathscr{K}^u, \tag{18d}$$

$$\sum_{k\in\mathscr{K}} \phi_{n,k} \ge 1, \forall n \in \mathscr{N}, \sum_{k\in\mathscr{K}} \theta_{m,k} \ge 1, \forall m \in \mathscr{M}, \tag{18e}$$

$$s_n^c \phi_{n,k} = \phi_{n,k}, s_m^d \theta_{m,k} = \theta_{m,k}, \forall k \in \mathscr{K}^u, \tag{18f}$$

where $\lambda \ge 0$ is the sensitivity factor for Wi-Fi systems. Constraint (18b) is given under the assumption that one subchannel can be utilized by at the maximum of one LTE user. Constraints (18c) and (18d) imply that a user utilize at most V^u subchannels, and a subchannel can be utilized by a maximum of V^s users. According to the CA property, each LTE-U or D2D-U user needs to occupy at least one licensed subchannel for control signals, and thus constraint (18e) needs to be satisfied. Constraint (18f) is the sensing constraint, only the LTE-U and D2D-U users which have sensed that the channel is idle can access the unlicensed channel.

Note that the aforementioned problem is an MINLP problem, which is NP-hard [30]. Considering the computational complexity, we reformulate the subchannel allocation as a many-to-many two-sided matching problem, which can be efficiently solved by utilizing the matching games.

Matching Formulation

We consider the set of LTE and D2D users, $\mathscr{U} = \mathscr{M} \cup \mathscr{N}$, and the set of subchannels including licensed and unlicensed, $\mathscr{S} = \mathscr{K} \cup \mathscr{K}^u$, as two disjoint sets of selfish players aiming to maximize their own benefits. Each player can exchange information with one another without extra signaling cost (The BS is assumed to have the full knowledge of the channel side information (CSI), and performs subchannel allocation based on the obtained CSI.), that is, the players have complete information about others. In this many-to-many matching model, if subchannel k is assigned to LTE user n, then LTE user n is said to be matched with subchannel k and form a matching pair, marked by (n, k).

A matching is an assignment of subchannels in $\mathscr{S}$ to users in $\mathscr{U}$, which can be defined as:

Definition 1. Given two disjoint sets, $\mathscr{U} = \mathscr{M} \cup \mathscr{N}$ of the users, and $\mathscr{S} = \mathscr{K} \cup \mathscr{K}^u$ of the subchannels, a many-to-many matching Ψ is a mapping from the set $\mathscr{U} \cup \mathscr{S}$ to the set of all subsets of $\mathscr{U} \cup \mathscr{S}$ such that for every user $n \in \mathscr{N}$ or $m \in \mathscr{M}$, and subchannel $k \in \mathscr{S}$:

1. $\Psi(n) \in \mathscr{S}, \Psi(m) \in \mathscr{S}$;
2. $\Psi(k) \in \mathscr{U}$;
3. $|\Psi(n)| \leq V^u, |\Psi(m)| \leq V^u$;
4. $|\Psi(k)| \leq V^s$;
5. $|\Psi(n) \cap \mathscr{K}| \geq 1, |\Psi(m) \cap \mathscr{K}| \geq 1$;
6. $s_m^d = 0 \Leftrightarrow \Psi(m) \cap \mathscr{K}^u = \emptyset, s_n^c = 0 \Leftrightarrow \Psi(n) \cap \mathscr{K}^u = \emptyset$;
7. $k \in \Psi(n) \Leftrightarrow n \in \Psi(k), k \in \Psi(m) \Leftrightarrow m \in \Psi(k)$.

Conditions 1 and 2 state that each LTE or D2D user is matched with a subset of subchannels, and each subchannel is matched with a subset of users. Conditions 3 and 7 show the utilization constraints for a user and a subchannel. Due to the CA requirement, the users need to occupy to at least one licensed subchannel, as expressed in condition 4. Condition 5 implies that only those users sensed idle unlicensed subchannel can utilize the unlicensed subchannels.

Considering mutual interference items in (12) and (15), any D2D user's sum-rate over its allocated subchannels is related to the set of other LTE users and D2D users sharing this subchannel. Besides, the penalty term in (18a) indicates that the objective of the LTE-U and D2D users is relevant to other users operating in the unlicensed spectrum as well. Thus, each user cares about not only which subchannel it is matched with but also the set of users matching with the same subchannel. For this reason, the aforementioned matching game is a many-to-many matching game with *externalities* [23] or *peer effects* [24].

Affected by the peer effects, the outcome of this matching game greatly depends on the dynamic interactions among the users sharing the subchannels. To better

describe the selection behavior and decision process of each player, we introduce a concept of preference relation $>$ for both users and subchannels. For any two subchannels $k, k' \in \mathscr{S}, k \neq k'$, and any two matchings $\Psi, \Psi', k \in \Psi(m), k' \in \Psi'(m)$:

$$(k, \Psi) >_m (k', \Psi') \Leftrightarrow R^d_{m,k}(\Psi) > R^d_{m,k'}(\Psi'), \tag{19}$$

where $R^d_{m,k}$ is related to the current subchannel allocation results. If D2D user m has not been allocated to unlicensed subchannels, the data rate $R^d_{m,k}$ needs to deduct the penalty item. This implies that the D2D user m prefers k in Ψ to k' in Ψ' if m can have a higher data rate over k than k'. The same process will be done for an LTE user $n \in \mathscr{N}$. LTE-U user n will also prefer the subchannel which can achieve higher data rate.

As for any subchannel $k \in \mathscr{S}$, its preference relation $>_k$ over the set of users can be given in a uniform method. For any two subsets of users $T, T \in \mathscr{U}, T \neq T'$, and any two matchings $\Psi, \Psi', T = \Psi(k), T' = \Psi'(k)$:

$$(T, \Psi) >_k (T', \Psi') \Leftrightarrow R_k(\Psi) > R_{k'}(\Psi'), \tag{20}$$

where R_k also includes the penalty items. This indicates that subchannel k prefers the set of users T to T' only when k can get a higher data rate from T. $(T, \Psi) \geq_k (T', \Psi')$ is also used to indicate that subchannel k likes the set of users T at least as well as T'.

Different from traditional many-to-many matchings in which the players' preferences are substitutable, subchannels' preferences do not satisfy *substitutability*. Specifically, given a subchannel $k \in \mathscr{S}$, let $\mathscr{T}_k \subseteq \mathscr{U}$ represent its most preferred user set that contains two D2D users m and i. Besides, the data rate $R^d_{m,k}$ of D2D user m is higher than $R^d_{i,k}$ of D2D user i when they utilize subchannel k independently. If $m \notin \mathscr{T}_k$, then it is not necessary that $i \in \mathscr{T}_k / \{m\}$. Due to the mutual interference, the data rate may have changed after m is removed from $\mathscr{T}_k$, and thus, k may not prefer i any more.

Due to the externalities, the many-to-many matching model in this work is more complicated than the conventional two-sided matching models. Under traditional definition of stable matching (Traditional stable matching refers to a matching in which there do not exist two players from opposite sets prefer each other to at least one of their current matches such that they form a new matching pair together for the sake of their interests, that is, there are no blocking pairs in a stable matching.) in [23], there is no guarantee that a stable matching exists even in many-to-one matchings. Because of the lack of substitutability, traditional deferred acceptance algorithm [23] cannot be applied to this model anymore. To solve this matching problem, we introduce the swap matching [24] and propose a matching algorithm in section "Many-to-Many Matching-Based Subchannel Allocation".

Many-to-Many Matching-Based Subchannel Allocation

In this section, we propose a matching algorithm to solve the problem formulated in section "Problem Formulation". We first introduce the notations and definitions of *swap matching* and *stability* into our many-to-many matching model and then elaborate on the matching algorithm.

Notations and Definitions

The concepts of *swap matching* and *swap-blocking pair* are defined as below.

Definition 2. Given a matching Ψ, two matching pairs (i, p) and (j, q) with subchannels $p \in \Psi(i)$, $q \in \Psi(j)$, $p \notin \Psi(j)$, and $q \notin \Psi(i)$, *a swap matching* is defined as:

$$\Psi_{i,p}^{j,q} = \{\Psi \backslash \{(i, p), (j, q)\}\} \cup \{(i, q), (j, p)\}. \tag{21}$$

A swap matching is generated via swap operations, which is the two-sided version of the *exchange* operation [31, 32]. In the swap operation, a pair of players exchange their matches while all other matchings remain unchanged. Different from conventional strategy change in one-to-one matching performed by the individual player, the swap operation needs to be approved by both involved players. In the following, we provide the conditions in which the swap operations can be approved by introducing the concepts of *swappable set* and *swap-blocking pair*.

Definition 3. For LTE-U user n or D2D user m, its *swappable set* is defined as a subchannel subset in which the user can swap for subchannel via swap matching. Specifically, if the sensing vector $s_m^d = 1$, the swappable set Ω_m of D2D user m is subchannels set $\mathscr{S}$ including licensed and unlicensed ones; otherwise, its swappable set Ω_m is licensed subchannels set $\mathscr{K}$. And it does the same for LTE user n.

Note that in the reserved subframe for Wi-Fi transmission, only the fraction of D2D users which have sensed the operating channel idle in SS have the unlicensed subchannels in their swappable sets, other users can only swap for licensed subchannels in the swappable sets.

Definition 4. Provided a matching Ψ and a user pair $(i, j), i, j \in \mathscr{U}$, i and j are matched in Ψ, and let Ω_i and Ω_j, respectively, represent the swappable sets of i and j. If there exist subchannels $p \in \Psi(i)$, $p \in \Omega_j$, $q \in \Psi(j)$, and $q \in \Omega_i$ such that:

1. $\forall t \in (i, j, p, q), (\Psi_{i,p}^{j,q}, \Psi_{i,p}^{j,q}(t)) \succeq_t (\Psi, \Psi(t))$,
2. $\exists t \in (i, j, p, q), (\Psi_{i,p}^{j,q}, \Psi_{i,p}^{j,q}(t)) \succ_t (\Psi, \Psi(t))$,
3. $\forall t \in (i, j), |\Psi_{i,p}^{j,q}(t) \cap \mathscr{K}| \geq 1$,

then the swap matching $\Psi_{i,p}^{j,q}$ is *approved*, and the pair (i, j) is called *a swap-blocking pair* in the matching Ψ.

The third condition in Definition 4 is to satisfy the CA requirement in which each user needs to utilize at least one licensed subchannel. The definition implies that once a swap matching is approved, at least one player's data rates will increase, which leads to the increase in the total data rate.

Definition 5. A matching Ψ is *two-sided exchange-stable (2ES)* if and only if there does not exist a swap-blocking pair.

Intuitively speaking, from the perspective of network, a matching Ψ is said to be 2ES implies that there is not any user i or subchannel q, in which i prefers another subchannel p to its match q, or q likes another user j rather than its match i. Such a network-wide stable can be achieved by guaranteeing the involved players are beneficial from the swap operations, given the externalities in current matching Ψ.

Algorithm Description

With the notations of swap matching and the definition of stability, we propose a user-subchannel matching algorithm (Algorithm 1) to obtain a 2ES matching. This algorithm is an extension of the many-to-one matching algorithm proposed in [33] with constraints that $|\Psi(n)| \geq V^u$, $|\Psi(m)| \geq V^u$, and $|\Psi(k)| \geq V^s$.

As a part of Algorithm 1, each LTE or D2D user needs to maintain a preference list. The preference list is established according to the following principles:

1. The subchannels in the preference list need to be contained in the swappable set.
2. The matched subchannel is removed from the preference list for each user.
3. The subchannels which have matched with V^s users is removed from the preference list.
4. If the user is unmatched, i.e., the user has not been allocated to any subchannels, the licensed subchannels have priorities over the unlicensed ones.
5. The preference list is established based on the data rate over each subchannel.

In Algorithm 1, each user will send a proposal to the BS. According to Definition 3, the proposed subchannel needs to be contained by swappable set. For each user, removing the matched subchannel is to avoid multiple proposals for the same subchannel. In addition, under the utilization constraints for a subchannel, the users can only send proposal to the available subchannels. The forth principle is designed in accordance with the CA requirement. This implies that if the user cannot compete for a licensed subchannel, the user needs to be silent. And according to the definition of preference relation in (19), the preference list is maintained based on

Algorithm 1 User-subchannel matching algorithm for LTE and D2D users

Input: Set of users $\mathscr{U}$; set of subchannels $\mathscr{S}$; sensing vectors s_n^c, s_m^d.
Output: A 2ES matching Ψ.
begin
  while $\Psi \neq \Psi'$ **do**
    Let $\Psi' = \Psi$ The preference lists are updated based on the current matching Ψ **if** *i has not been matched with V^u subchannels* **then**
      i sends a proposal to the first subchannel q in the preference list **if** *swap operation $\Psi_{i,0}^{0,q}$ is approved* **then**
        User i matches with subchannel q The current matching Ψ is replaced by swap matching $\Psi_{i,0}^{0,q}$
      else
        User i cannot get access to subchannel q
      end
      The BS searches for swap-blocking pairs **if** *swap operation $\Psi_{i,p}^{j,q}$ is approved* **then**
        User i exchanges its match SC_p with U_j for subchannel q The current matching Ψ is replaced by swap matching $\Psi_{i,p}^{j,q}$
      else
        User i keeps its match subchannel p
      end
    else
      User U_i keeps its matches.
    end
  end
  Terminate with the final matching result Ψ
end

the data rate. Due to the externalities, the preference list is dynamic in the swap matching process. Thus, in each iteration, the preference list will be updated based on the current matching.

The key idea of Algorithm 1 is to consider approving swap matchings among the players so as to obtain a 2ES matching. The algorithm is composed of two phases: initialization phase and swap matching phase. In the initialization phase, the BS will evaluate the channel gains for all users and interference from Wi-Fi system. The swap matching phase contains multiple iterations in which the BS keeps executing the swap matching if there exist swap-blocking pairs and updates the current matching. Note that the higher a user's data rate is, the higher probability it has to be accepted by the subchannel. In each iteration, the user i updates its preference list and sends a proposal to the subchannel q ranked the first in the preference list unless it has been matched with V^u subchannels. The acceptance can be regarded as a swap operation $\Psi_{i,0}^{0,q}$, where the element $\{0\}$ denotes a virtual user or subchannel. If this swap matching is approved, the proposed user i is accepted by the subchannel q, and the matching is updated. Then, the BS will search other swap-blocking pairs and execute the swap matching to renew the current matching. The iterations stop until current matching is the same as the matching in the last iteration, and a final matching is determined.

Performance Analysis

In this section, we first analyze the proposed duty cycle-based protocol regarding the compatibility and signaling issues. Then, we analyze the effectiveness and efficiency of the proposed algorithm and remark some key properties of the LTE-U/D2D network. In the first part, the effectiveness and efficiency of the proposed algorithm is proved. Finally, we discuss how the selection of the sensitivity factor λ impacts the subchannel allocation strategy at the end of this section.

Analysis of the Protocol

Compatibility Analysis

For LTE system, unlike the LBT-based protocol for D2D-U in [34] which requires LBT waveform and transmission modification of current LTE standard, our proposed protocol follows the current LTE PHY/MAC standards, such as frame structures, resource scheduling, and signaling, and thus, it can be directly implemented to current LTE network. And as for Wi-Fi system, D2D/LTE-U users also perform energy detection to avoid the collision with Wi-Fi users. In addition, in a hyper-dense scenario, the protocol support the coexistence of the LTE-U/D2D and Wi-Fi users in a TDM fashion. Therefore, the LTE-U and D2D network can be a good neighbor of Wi-Fi network.

Signaling Analysis

To describe the signaling cost over the control channels for the proposed protocol, we assume that η messages are required to inform the BS, the channel information sensed by a D2D/LTE-U user; μ messages are required for a user to report its location and subchannel estimation results; and ν messages are required for the BS to notify a user the allocated subchannels. In SS, each D2D/LTE-U user $n \in \mathcal{N} \cup \mathcal{M}$ needs to report the sensing result over each channel. Therefore, at most $\eta(M+N)L$ messages are required in the SS. And before each transmission subframe, each LTE-U/D2D user n needs to report their locations and the subchannel estimation results for subchannel allocation, which requires $\mu(M+N)$ messages. Then, the BS will perform resource allocation process with extra information and notify each user by sending $\nu(M+N)$ messages.

Note that in one duty cycle, each LTE-U/D2D user only perform one energy detection over one channel; thus, the signaling cost is under a tolerable level. In addition, the signaling cost of resource allocation is positively proportional to the number of D2D/LTE-U users, which is constrained by the limited subchannel resources. In each subframe, the signaling cost of the resource allocation can be restricted to a tolerable level. Therefore, the signaling cost of the proposed duty cycle-based protocol is acceptable for a practical system.

Stability, Convergence, Complexity, and Optimality

Given the proposed Algorithm 1, we then give remarks on the stability, convergence, complexity, and optimality.

Stability and Convergence

We now provide the stability and convergence of Algorithm 1.

Lemma 1. *Phase II in Algorithm 1 converges after a limited number of swap operations.*

Proof. In each iteration of Algorithm 1, the matching Ψ is updated after a swap operation. Without the loss of generality, we assume that after swap operation l, the matching result is updated by swap matching $\Psi_l = \Psi_{l-1}{}_{i,p}^{j,q}$. According to Definition 4, after swap operation l, the sum-rates of subchannels p and q satisfy $R_p(\Psi_l) \geq R_p(\Psi_{l-1})$ and $R_q(\Psi_l) \geq R_q(\Psi_{l-1})$, and these two equations cannot hold at the same time, while the sum-rates of other subchannels remain unchanged. Therefore, the total sum-rate over all subchannels strictly increases.

Note that the number of potential swap-blocking pairs is finite since the number of users is limited, and the total sum-rate has an upper bound due to limited subchannels. Therefore, there exists a swap operation after which no swap-blocking pairs can be found, and the total sum-rate stops increasing. Then Algorithm 1 converges.

Proposition 1. *Upon the convergence of Phase II, Algorithm 1 reaches a 2ES matching.*

Proof. The proof follows from these two considerations. First, the swap operations only occur when the players' data rate strictly increases. Second, due to the convergency of Phase II, for any user $i \in \mathscr{U}$, it cannot find another user $j \in \mathscr{U}$ to form a swap-blocking pair with their matches when Algorithm 1 terminates. The matches of user M_i must be the best choice for it in current matching. Hence, the terminal matching obtained by Algorithm 1 is 2ES.

Complexity

Having proved the convergence of Algorithm 1, we can then discuss its computational complexity.

Note that in the swap matching phase, a number of iterations are performed to reach the 2ES matching. In every iteration, the BS needs to search for swap-blocking pairs, and all the approved swap operations are executed. Thus, the complexity of the swap matching phase lies in the number of both iterations and potential swap matchings in each iteration.

Proposition 2. *In the t-th iteration of Algorithm 1, at most $(M+N)*[(M+N-1)*(t-1)+1]$, swap matchings need to be considered.*

Proof. In each iteration of Algorithm 1, at most $M + N$, users send proposal to the subchannels which rank first in their preference lists. Therefore, in this step, at most $M + N$, swap matchings need to be considered.

If the proposals from users are accepted by subchannels, they might execute swap matchings with the existing matches. For user U_i, it sends proposal to subchannel p and is accepted. According to Definition 2, this match can only execute swap matchings with matches which do not contain user i and subchannel p. In each iteration, at most 1, match can be added to the current matching for each user. Therefore, for match pair (i, q), there are at most $(M + N - 1) * (t - 1)$ potential swap matchings in the t-th iteration. In the worst case, all the proposal for users are accepted by subchannels, and thus, there are a maximum of $(M + N) * (M + N - 1) * (t - 1)$ potential swap matchings.

Above all, at most $(M+N)*[(M+N-1)*(t-1)+1]$, swap matchings need to be considered in the t-th iteration. In practice, one iteration requires a significantly low number of swap operations, since only a small number of proposals from users can be accepted.

Optimality

We show whether Algorithm 1 can achieve an optimal matching.

Proposition 3. *All local maxima of total sum-rate correspond to a 2ES matching.*

Proof. Suppose the total data rates of matching Ψ is a local maximum value. If Ψ is not a 2ES matching, then there exists at least one swap-blocking pair, and any swap matching strictly increases data rates according to Definition 2. However, this is in contradiction to the assumption that Ψ is a local maximum value. Therefore, Ψ must be 2ES.

However, not all 2ES matchings obtained from Algorithm 1 are local maxima of total data rates. For example, there exists a possibility that a user i does not approve a swap matching $\Psi_{i,p}^{j,q}$, since its data rate will decrease, but the other user j will benefit from this swap matching, and the sum-rates of subchannels p and q increase as well. The total sum-rates will increase at the expense of stability if the swap operation is forced to execute.

To obtain a global optimum matching, we utilize an algorithm (GO Algorithm) proposed in [24] by utilizing a Markov chain Monte Carlo heat bath method. In GO Algorithm, the swap matching does not need to be approved anymore; instead, a swap matching $\Psi_{i,p}^{j,q}$ is executed with a probability P_{swap} which depends on the total sum-rate as shown below:

$$P_{\text{swap}} = \frac{1}{1 + e^{-T[R_{\text{total}}(\Psi_{i,p}^{j,q}) - R_{\text{total}}(\Psi)]}}, \tag{22}$$

where T is a probability parameter. The algorithm keeps track of the optimum matching found so far, even as it moves to worse matchings. After sufficiently large amount of iterations, the matching moves toward the global optimal one [35].

Selection of the Sensitivity Factor λ

Let $R^d_{\max}$ be the maximum rate for a D2D user in an unlicensed subchannel, $R^c_{\max}$ be the maximum rate for an LTE user, and generally $R^d_{\max}/L_d \geq R^c_{\max}/L_c$. How the value of the sensitivity factor λ tunes the performance can be analyzed in the following cases.

- $\lambda \geq R^d_{\max}/(2L_d)$: This case implies that neither a D2D nor LTE user can get access to an unlicensed subchannel; the value of penalty terms is sufficiently large that cannot satisfy all the conditions of swap matching. Therefore, in this case, any D2D or LTE users cannot occupy unlicensed subchannels; the LTE and D2D users can only utilize the licensed spectrum for total sum-rate maximization.
- $R^c_{\max}/(2L_c) \leq \lambda \leq R^d_{\max}/(2L_d)$: This case implies that a D2D user get access to unlicensed subchannels. In this case, any LTE users cannot utilize unlicensed subchannels. As for the D2D users, they can utilize both licensed and unlicensed subchannels. If one D2D user get access to an unlicensed subchannel, those D2D users whose interference ranges overlap with the accessed one will become more easier to get access to the unlicensed subchannels, because the increased interference ranges will be less than that when this D2D user is the first one to get access to the unlicensed subchannels. Thus, in the view of geography, those D2D users over unlicensed subchannels trend to form several clusters.
- $0 < \lambda < R^c_{\max}/(2L_c)$: This case means that both LTE and D2D users can get access to unlicensed subchannels. Similar to case 2, the users accessed to unlicensed subchannels also form several clusters. In addition, the accessed LTE users will decrease with the value of λ grows because of the large interference range; that is, more unlicensed subchannels are allocated to D2D users, and the LTE users are more likely to utilize licensed subchannels.
- $\lambda = 0$: This case is the same as resource allocation problem in licensed scenario. In this case, both licensed and unlicensed subchannels can be regarded as a uniform subchannel; D2D and LTE users will make full use of the whole spectrum to maximize the total sum-rate.

Simulation Results

In this section, we present the simulation results of Algorithm 1, in comparison to the GO Algorithm, a greedy allocation algorithm, and the scenario without D2D, where all the users are LTE users. In the greedy scheme, the users will maintain a static preference list and send proposal to the subchannels according to the preference list. We set the number of iterations as 10^6, $T = 0.5$ in GO Algorithm such that the outcome of GO Algorithm can be regarded as the upper bound of the total sum-rate. Note that the upper bound is unrealistic since the computational complexity is rather high. And the subchannels in the scenario without D2D are also allocated by Algorithm 1. For the simulations, we consider a single-cell layout,

Table 1 Parameters for simulation

LTE-U and D2D-U parameters	Values
Cell radius	500 m
Maximum D2D user distance $D_{\max}$	20 m
LTE's transmit power P^c	13 dBm
D2D's transmit power P^d	3 dBm
Subchannel bandwidth B_l	180 kHz
Number of subchannels	40
Carrier frequency	1.9 GHz
Noise figure	5 dB
Decay factor of the path loss α	3
Power gains factor G	−31.5 dB
Maximum number of subchannels V^s	4
Maximum number of users V^u	4
Wi-Fi parameters	Values
Number of subchannels	40
Subchannel bandwidth B_u	180 kHz
Wi-Fi user's transmit power P^w	23 dBm
Number of APs Q	3
LTE-U interference radius L_c	50 m
D2D-U interference radius L_d	23 m

where the LTE and D2D users are distributed randomly, and the communication distance of D2D users cannot exceed a predefined value. The simulation parameters based on existing LTE/LTE-Advanced specifications [36] are given in Table 1. Note that the transmission power of Wi-Fi user is over the whole unlicensed channel, while the transmission power of LTE or D2D user is over one subchannel.

Figure 5 shows the total sum-rate vs. the number of active D2D users N, with the number of LTE users $M = 20$ and the sensitivity factor $\lambda = 0.1$. We observe that the total sum-rate increases with N. And it can be observed that the sum-rate obtained by proposed Algorithm 1 is 9.23% higher than the greedy algorithm, and 168.5% higher than the scenario without D2D, while it only has 3% gap to the upper bound when $N = 20$. This further implies that the BS can make full use of the unlicensed spectrum resources via D2D communications. The simulation results correspond to optimality analysis in section "Stability, Convergence, Complexity, and Optimality".

Figure 6 shows the total sum-rate vs. the number of active D2D users with the number of LTE users $M = 20$. It can be easily observed that the total sum-rate will decrease as the sensitivity factor λ increases. According to discussions on section "Selection of the Sensitivity Factor λ", $\lambda = 0$ means every D2D and LTE user can use the unlicensed spectrum, the subchannels are sufficient, and the total sum-rate is the maximum. $\lambda = 1$ means that almost they cannot use the unlicensed spectrum; both LTE and D2D users can only utilize the licensed subchannels. Because there are half of subchannels can be utilized, the total sum-rate is close

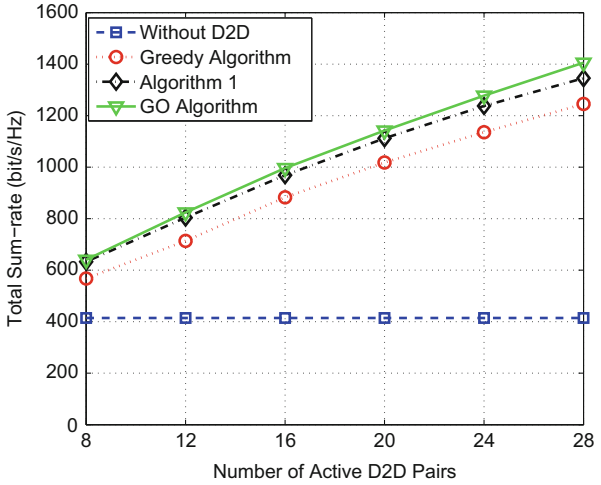

Fig. 5 Total sum-rate vs. number of active D2D users, with the number of LTE users $M = 20$ and $\lambda = 0.1$

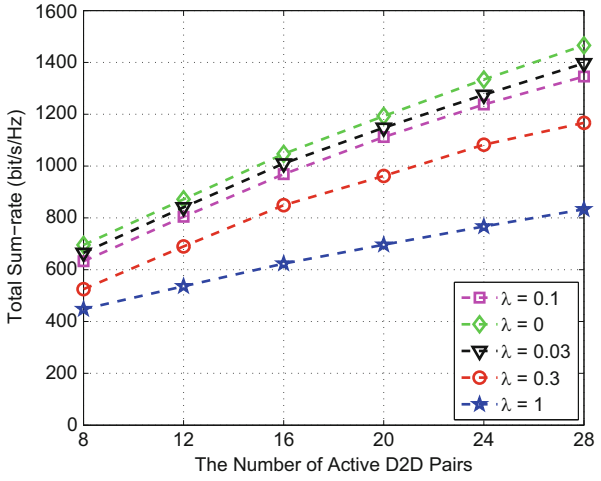

Fig. 6 Total sum-rate vs. number of active D2D users, with the number of LTE users $M = 20$

to the half of sum-rate with $\lambda = 0$. And $\lambda = 0.3$ implies that most LTE users cannot use the unlicensed spectrum; most unlicensed subchannels are used by D2D users. Because of less available subchannels, the total sum-rates decreases.

In Fig. 7, we provide the interference ranges vs. the number of active D2D users N with the number of LTE users $M = 20$. We use a uniform sampling and judge whether this sampling point is in the interference range of any LTE or D2D user using the unlicensed spectrum. The percentage of sampling points in the interference ranges is regarded as the interference ranges. From Fig. 7, it can be observed that the

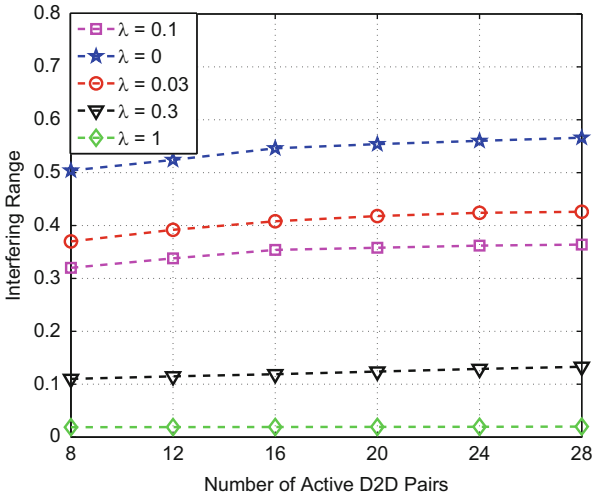

Fig. 7 Interference ranges vs. number of active D2D users, with the number of LTE users $M = 20$

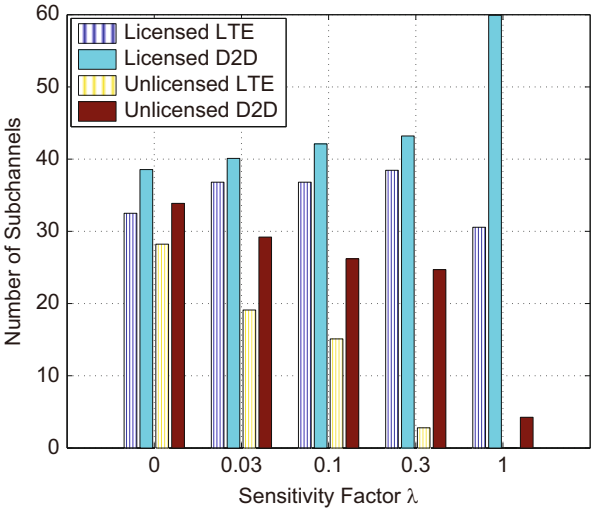

Fig. 8 Number of subchannels vs. sensitivity factor λ, with the number of LTE users $M = 20$ and the number of D2D users $N = 20$

interference ranges will decrease as the value of sensitivity factor λ grows. We can also find out the decrease in interference ranges is at the expense of the total sum-rate from Fig. 7. We can learn that we can use the unlicensed spectrum according to different requirement for the interference by properly setting the value of λ.

Figure 8 provides that the number of subchannels in both licensed and unlicensed spectra vs. the value of sensitivity factor λ with the number of LTE users $M = 20$ and the number of D2D users $N = 20$. Based on the constraint that a user can utilize at most $V^u = 4$ subchannels, the total subchannels of LTE users or D2D

users cannot exceed 80 subchannels. It can be also observed that when the value of λ increases, LTE users can occupy more licensed subchannels, while D2D users will utilize more unlicensed subchannels due to its smaller interference ranges. This is consistent with the discussions in section "Selection of the Sensitivity Factor λ".

Conclusions

In this chapter, we investigate the D2D-U technology, in which the D2D users operate as an underlay to the LTE system in both licensed and unlicensed spectra. A sensing-based D2D-U protocol has been designed for LTE-U and D2D-U users to access the unlicensed spectrum while protecting the existing Wi-Fi systems. Considering the complicated mutual interference between LTE-U, D2D, and Wi-Fi systems, we study the subchannel allocation problem for D2D and LTE-U users sharing both licensed and unlicensed spectra to leverage the performance degradation in Wi-Fi systems and the maximization of the sum-rate in LTE/D2D networks. Specifically, we formulate the allocation problem as a many-to-many matching game with externalities and develop a low-complexity user-subchannel swap matching algorithm. Analytical and simulation results show that enabling D2D communications in LTE-U network can significantly improve the network capacity. Besides, the subchannel allocation strategy for LTE and D2D users is closely related to how the BS adjusts the interference to Wi-Fi systems. In an aggressive strategy where the Wi-Fi performance degradation is not considered seriously, the BS allows more D2D and LTE users to transmit on the unlicensed spectrum. On contrary, in a Wi-Fi-friendly strategy, the BS tends to permit only a small fraction of D2D users to transmit on the unlicensed spectrum, and most of the LTE users are only allocated with licensed subchannels.

References

1. Doppler K, Rinne M, Wijting C, Ribeiro CB, Hugl K (2009) Device-to-device communication as an underlay to LTE-advanced networks. IEEE Commun Mag 47(12):42–49
2. Lei L, Zhong Z, Lin C, Shen X (2012) Operator controlled device-to-device communications in LTE-advanced networks. IEEE Wirel Commun 19(3):96–104
3. Fodor G, Dahlman E, Mildh G, Parkvall S, Reider N, Miklòs G, Turśnyi Z (2012) Design aspects of network assisted device-to-device communications. IEEE Commun Mag 50(3): 170–177
4. Xu C, Song L, Han Z, Zhao Q, Wang X, Cheng X, Jiao B (2013) Efficiency resource allocation for device-to-device underlay communication systems: a reverse iterative combinatorial auction based approach. IEEE J Sel Areas Commun 31(9):348–358
5. Zhang H, Song L, Han Z (2016) Radio resource allocation for device-to-device underlay communication using hypergraph theory. IEEE Trans Wirel Commun 15(7):4852–4861
6. Song L, Niyato D, Han Z, Hossain E (2015) Wireless device-to-device communications and networks. Cambridge University Press, Cambridge
7. Yu CH, Doppler K, Ribeiro CB, Tirkkonen O (2011) Resource sharing optimization for device-to-device communication underlaying cellular networks. IEEE Trans Wirel Commun 10(8):2752–2763

8. Min H, Lee J, Park S, Hong D (2011) Capacity enhancement using an interference limited area for device-to-device uplink underlaying cellular networks. IEEE Trans Wirel Commun 10(12):3995–4000
9. Aijaz A, Aghvami H, Amani M (2013) A survey on mobile data offloading: technical and business perspectives. IEEE Wirel Commun 20(2):104–112
10. Lee K, Lee J, Yi Y, Rhee I, Chong S (2013) Mobile data offloading: how much can WiFi deliver? IEEE/ACM Trans Netw 21(2):536–550
11. Bennis M, Simsek M, Czylwik A, Saad W, Valentin S, Debbah M (2013) When cellular meets WiFi in wireless small cell networks. IEEE Commun Mag 51(6):44–50
12. Dong H, Wang P, Niyato D (2012) A dynamic offloading algorithm for mobile computing. IEEE Trans Wirel Commun 11(6):1991–1995
13. Gu Y, Zhang Y, Cai LX, Pan M, Song L, Han Z (2015) Exploiting student-project allocation matching for spectrum sharing in LTE-unlicensed. In: IEEE Global Communications Conference (GLOBECOM), San Diego
14. 3GPP TR 36.808 (2013) Evolved Universal Terrestrial Radio Access (E-UTRA); Carrier Aggregation; Base Station (BS) radio transmission and reception, Release 10
15. Al-Dulaimi A, Al-Rubaye S, Ni Q, Sousa E (2015) 5G communications race: pursuit of more capacity triggers LTE in unlicensed band. IEEE Veh Technol Mag 10(1): 43–51
16. Zhang R, Wang M, Cai LX, Zeng Z, Shen X, Xie L (2015) LTE-unlicensed: the future of spectrum aggregation for cellular networks. IEEE Wirel Commun 22(3):150–159
17. Chao Y, Zhang H, Song L (2015) Demo: WiFi multihop – implementing device-to-device local area networks by android smartphones. In: ACM International Symposium on Mobile ad hoc Networking and Computing (MobiHoc), Hangzhou
18. Karvounas D, Georgakopoulos A, Tsagkaris K, Stavroulaki V, Demestichas P (2014) Smart management of D2D constructs: an experiment-based approach. IEEE Commun Mag 52(4):82–89
19. WiFi Alliance (2010) Wi-Fi peer-to-peer (P2P) technical specification
20. Di B, Song L, Li Y (2016) Sub-channel assignment, power allocation, and user scheduling for non-orthogonal multiple access networks. IEEE Trans Wirel Commun 15(11):7686–7698
21. Zhou H, Liu B, Liu Y, Zhang N, Gui L, Shen XS, Yu Q (2014) A cooperative matching approach for resource management in dynamic spectrum Access Networks. IEEE Trans Wirel Commun 13(2):1047–1057
22. Semiari O, Saad W, Valentin S, Bennis M, Poor HV (2015) Context-aware small cell networks: how social metrics improve wireless resource allocation. IEEE Trans Wirel Commun 14(11):5927–5940
23. Roth A, Sotomayor M (1992) Two-sided matching: a study in game-theoretic modeling and analysis. Cambridge University Press, Cambridge
24. Baron E, Lee C, Chong A, Hassibi B, Wierman A (2011) Peer effects and stability in matching markets. In: Persiano G (ed) Algorithmic game theory. Lecture notes in computer science, vol 6982. Springer, Berlin/Heidelberg, pp 117–129
25. Zhang H, Liao Y, Song L (2017) D2D-U: Device-to-device communications in unlicensed bands for 5G system. IEEE Trans Wirel Commun 16(6):3507–3519
26. Nihtilä T, Tykhomyrov V, Alanen O, Uusitalo MA, Sorri A, Moisio M, Iraji S, Ratasuk R, Mangalvedhe N (2013) System performance of LTE and IEEE 802.11 coexisting on a shared frequency band. In: IEEE Wireless Communications and Networking Conference (WCNC), Shanghai
27. Malekshan KR, Zhuang W, Lostanlen Y (2014) An energy efficient MAC protocol for fully connected wireless ad hoc networks. IEEE Trans Wirel Commun 13(10):5729–5740
28. Fu J, Zhang X, Cheng L, Shen Z, Chen L, Yang D (2015) Utility-based flexible resource allocation for integrated LTE-U and LTE wireless systems. In: IEEE Vehicular Technology Conference (VTC Spring), Glasgow
29. Qualcomm Research (2014) LTE in Unlicensed Spectrum: Harmonious Coexistence with Wi-Fi

30. Plaisted DA (1976) Some polynomial and integer divisibility problems are NP-HARD. In: 1976 Annual Symposium on Foundations of Computer Science, Houston
31. Cechlarova K, Manlove D (2005) The exchange-stable marriage problem. Discret Appl Math 152(1–3):109–122
32. Irving R (2008) Stable matching problems with exchange restrictions. J Comb Optim 16(4):344–360
33. Pantisano F, Bennis M, Saad W, Valentin S, Debbah M (2013) Matching with externalities for context-aware user-cell association in small cell networks. In: IEEE Global Communications Conference (GLOBECOM), Atlanta
34. Wu Y, Guo W, Yuan H, Li L, Wang S, Chu X, Zhang J (2016) Device-to-device Meets LTE-unlicensed. IEEE Commun Mag 54(5):154–159
35. Haggstrom O (2001) Finite markov chains and algorithmic applications. Cambridge University Press, Cambridge
36. 3GPP TS 36.213 (2014) Evolved Universal Terrestrial Radio Access (E-UTRA) Physical Layer Procedures, Release 12

RF-Based Energy Harvesting Cognitive Cellular Networks

37

Dinh Thai Hoang and Dusit Niyato

Contents

Abstract

Recently, fundamental research has demonstrated great potentials of integrating radio frequency (RF) energy harvesting techniques into cognitive cellular

D. T. Hoang (✉) · D. Niyato
School of Computer Science and Engineering, Nanyang Technological University, Singapore, Singapore
e-mail: thdinh@ntu.edu.sg; dniyato@ntu.edu.sg

W. Zhang (ed.), *Handbook of Cognitive Radio*,
https://doi.org/10.1007/978-981-10-1394-2_34

networks (CCNs). Such an integration can improve spectrum utilization and energy efficiency of wireless communication services. In CCNs with RF energy harvesting capability, when cellular base stations, i.e., primary transmitters, transmit signals to their mobile devices, secondary users (SUs) can harvest energy from the cellular channel, i.e., the primary channel, and store the energy in their batteries. Then, when the cellular channel becomes idle, the SUs can use the harvested energy to transmit data to their receivers. As such, we can utilize not only the available spectrum when the channel is idle but also energy scavenging when the channel is busy. This chapter first presents an overview of RF-based energy harvesting CCNs. Then, limitations are discussed, and some new solutions using ambient backscattering communication techniques are introduced to overcome the limitations. Finally, the chapter concludes with a discussion on the development of such networks and possible research directions.

Keywords
Cellular networks · Cognitive radios · Ambient backscattering · RF energy harvesting · Convex optimization

Introduction

RF Energy Harvesting

Basic Concepts

RF energy transfer is a technique which enables energy transmission from an RF emitter to a distant destination (up to a few kilometers) based on the electromagnetic radiation, i.e., electromagnetic waves propagating through the space. According to Maxwell's theory [1], for electromagnetic waves, changes in the electrical field are always associated with a wave in the magnetic field in one direction and vice versa. This phenomenon happens continuously in the direction of the wave propagation and enables electromagnetic waves to carry information as well as energy to a far distance.

Wireless signal is a typical example of the electromagnetic waves, which is used widely in practice. In order to harvest energy from wireless signals, a mobile device needs to be equipped with a receive antenna, a matching circuit, and an RF-DC conversion circuit, as illustrated in Fig. 1. The mobile signals received at the receive antenna will be transferred to the matching circuit with the aim of maximizing power delivery from the antenna to the remaining circuit and minimizing signal reflections. After that, the RF-DC conversion circuit will convert these signals to DC voltage which can be stored in the mobile device's battery for future use. It was shown in [2] that the efficiency of the RF energy harvesting techniques strongly depends on the sensitivity of the receive antenna, the accuracy of the impedance matching circuit, and the proficiency between the voltage multiplier and the capacitor. The recent prototype implementation [3] demonstrated that RF energy harvesting techniques can achieve the efficiency up to 84% with a 5.8 dBm input power.

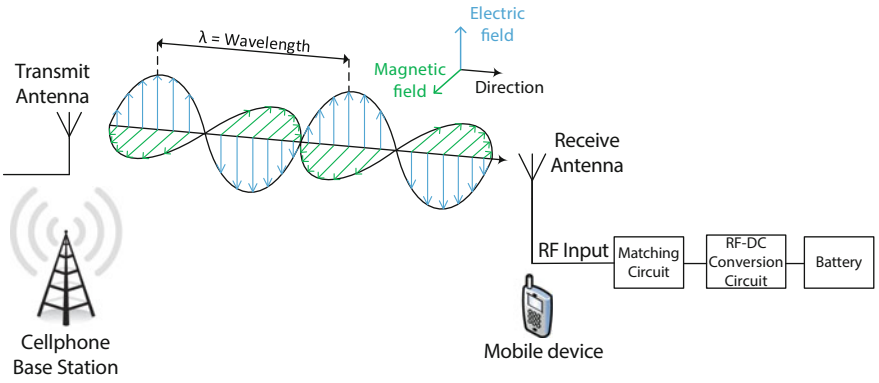

Fig. 1 RF energy harvesting in cellular networks

Energy Propagation Models

There are three RF energy propagation models which are often used to determine the amount of energy harvested at the mobile node.

- *Free space model:* In a free space environment, the energy received at the mobile node can be determined by the Friis equation [4] as follows:

$$P_R = P_T \frac{G_T G_R \lambda^2}{(4\pi d)L}, \tag{1}$$

  where P_R is the received power at the mobile node, P_T is the transmit power of the RF emitter or wireless signal source, e.g., a base station, L is the path loss factor, G_T is the transmit antenna gain, G_R is the receive antenna gain, λ is the mobile wavelength emitted, and d is the distance from the signal source to the mobile device.
- *Two-ray ground model:* In the free space model, there is only one single path from the signal source to the mobile device. However, in practice, signals received at the mobile device are from multiple paths due to the RF scattering and reflection. In this case, the two-ray ground model, which considers the received wireless signals pass through a line-of-sight path and a ground reflected path, can be used. The receive power is calculated from

$$P_R = P_T \frac{G_T G_R h_t^2 h_r^2}{d^4 L}, \tag{2}$$

  where h_t and h_r are the heights of the signal source and mobile device from the ground, respectively.
- *Rayleigh model:* Different from two aforementioned models which characterize RF propagation based on deterministic parameters, Rayleigh model [5] using

probability distribution parameters allows modeling energy propagation process in a more realistic manner. The Rayleigh model is therefore widely used in practice. In the Rayleigh model, the power received at the mobile device is determined as follows:

$$P_R = P_R^d 10^L |r|^2, \tag{3}$$

where P_R^d is the received RF power derived by a deterministic model, $L = -\alpha \log 10(d/d_0)$ is the path loss factor (d_0 is a reference distance), and r is a random number following Gaussian distribution.

Advantages of RF Energy Harvesting to Cognitive Cellular Networks

While there are a few available wireless energy harvesting techniques, e.g., inductive coupling and magnetic resonant coupling, RF energy harvesting is considered as a particularly appropriate solution for cognitive cellular networks because of the following advantages.

- *Pervasive environment:* wireless signals are available almost everywhere now, which provides an abundant energy source for mobile devices.
- *Long distance:* mobile signals can propagate and transfer over long distances, which creates favorable conditions for mobile devices.
- *Multiple directions:* cellular base stations can broadcast signals in all directions, and thus multiple mobile devices can harvest energy from the same source simultaneously.
- *Controllable power:* the amount of transferred energy can be controlled by adjusting the transmit power at the cellular base stations.
- *Stability:* RF energy supply is much more stable than other ambient energy sources such as solar, wind, and vibration.

Challenges and Solutions of Integrating RF Energy Harvesting Techniques into Cognitive Cellular Networks

Although RF energy harvesting is considered as a promising solution to cognitive cellular networks (CCNs), how to efficiently integrate this technique into CCNs is still a challenge. This section reviews related literature.

Channel Access

In [6], a secondary user (SU) harvests energy from primary signals when it is close enough to primary transmitters and stores the energy in a finite energy buffer. In addition, the SU can transmit data to its destination when it is sufficiently far away from primary transmitters. Based on these assumptions, the authors proposed a stochastic geometry model for the CCN where primary users (PUs) and SUs are distributed as independent homogeneous Poisson point processes (HPPPs). In this model, the PUs are protected from interference from the SU by a *guard zone*, and

they transfer a significant amount of RF energy to the SU when they are located in a *harvesting zone*. Based on the stochastic geometry model, the authors used a Markov chain to derive the transmission probability of the SU and then applied a Poisson approximation method to derive the maximum throughput for the SU. An important result found in this paper is that the maximum throughput of the SU is linearly increasing with increasing PUs' density. Furthermore, the PUs' density is inversely proportional to the transmission probability of the SU.

In [6], the authors assumed that all SUs have to be fully charged before they can transmit data. This implies that all SUs transmit data with the same power which may limit the network capacity for the secondary system. Therefore, the authors in [7] proposed the energy-based opportunistic spectrum access (OSA) strategy which allows the SUs to use the variable power mode to transmit data instead of waiting until full charging as in [6]. With the proposed OSA strategy, an SU can transmit data when it is outside of the guard zone, and its harvested energy level is greater than a predefined threshold. As a result, the reliability and stability of the secondary system can be significantly improved.

Park et al. [8] studied an optimal mode selection policy for an SU in a CCN with RF energy harvesting capability. It was assumed that the SU can harvest energy when the PU transmits data or the SU can transmit data when the PU is idle. However, the SU cannot harvest RF energy and access the primary channel simultaneously. Thus, it has to opt between *access mode* and *harvest mode* at the beginning of each time slot. Alternatively, it is assumed that the SU does not have any information about the current state of the channel in advance, but it knows part of channel state (e.g., idle channel probability). Therefore, the partially observable MDP (POMDP) framework was adopted to obtain the optimal mode selection policy for the SU. In order to improve the energy efficiency as well as the spectrum usage efficiency of the proposed model, the authors then introduced appropriate solutions in [9] and [10]. In particular, in [9], the authors developed a method to adjust the energy causality constraint and the collision constraint, which results in increasing the probability of accessing the occupied channel. Likewise, in [10], a theoretical upper bound on the maximum achievable throughput given the aforementioned constraints was derived with the main aim of deeply examining impacts of the temporal correlation of the primary system to the secondary system. Then, in [11], Park et al. designed an optimal spectrum access strategy in order to obtain the theoretical maximum achievable throughput. The numerical results then verified that by taking the temporal correlation of the primary system into account, the proposed strategy can achieve high efficiency in using the harvested energy.

Time Scheduling

In CCNs using energy harvesting techniques, SUs not only find opportunities to access primary channels but also have to harvest energy. The problem is that if the energy harvesting time is too long, the data transmission time will be reduced. By contrast, if the energy harvesting time is insufficient, the harvested energy will not be adequate for the data transmission phase. This leads to the problem of how to

balance between the energy harvesting time and the data transmission time for SUs to maximize their performance.

In [12], the authors proposed an online solution to find the optimal trade-off time between the energy harvesting phase (EHP) and the data transmission phase (DTP) for an underlay CCN. In the first phase, i.e., the EHP, the SU harvests energy from PU's signals and uses this energy to transmit data in the second phase, i.e., the DTP, under interference constraints with the primary system. Then, to find the optimal trade-off time between the EHP and the DTP, the authors adopted the convex optimization technique and derived the optimal value for the time-sharing ratio in a similar way as in [13]. With the proposed solution, the authors showed that the interference constraints with the primary system are under control, and the average achievable rate of the SU is maximized.

The same scenario was also examined in [14], but in [14] the authors also considered a cooperation scenario between the primary system and the secondary system. Specifically, in the second phase, the SU can opt to transmit data to its destination or relay data for the primary system. Consequently, the SU now has to determine not only how much time on the EHP but also how much power for data relay or data transmission to allocate. For both cases, i.e., cooperation and noncooperation, the authors proposed corresponding optimal solutions by using close-form solutions with numerical analysis. Simulation results showed that the proposed solutions can achieve better performance than that of the stochastic cooperation protocol and the optimal underlay transmission protocol.

Li et al. [15] introduced a strategy, called one-step-ahead spectrum sensing, with the aim of balancing the time allocation among three phases, i.e., EHP, SSP, and DTP. For the proposed strategy, based on the information about the current system state, e.g., available channels, the current energy level, and idle channel probabilities, and the estimation about the next state, the SU will make the best decision to maximize its throughput. However, the proposed strategy just can obtain a myopic solution, and thus an optimal saving-sensing-transmitting structure was proposed in [16] to maximize the average throughput for the SU. In particular, the authors first formulated the time allocation optimization problem as a mixed integer nonlinear programming problem and then employed a heuristic algorithm developed from the different evolution algorithms to derive the optimal time structure for three phases. Simulation results verified the efficiency of the proposed solution compared with a stochastic sensing strategy.

Relaying

Relaying for Secondary Systems

Lu et al. [17] studied an application of RF energy harvesting technique in a cognitive amplify-and-forward relaying network. In particular, there is a cognitive radio network with one PU and three SUs, called a source SU (SS), a relay SU (RS), and a destination SU (DS), as illustrated in Fig. 2. The RS forward the information

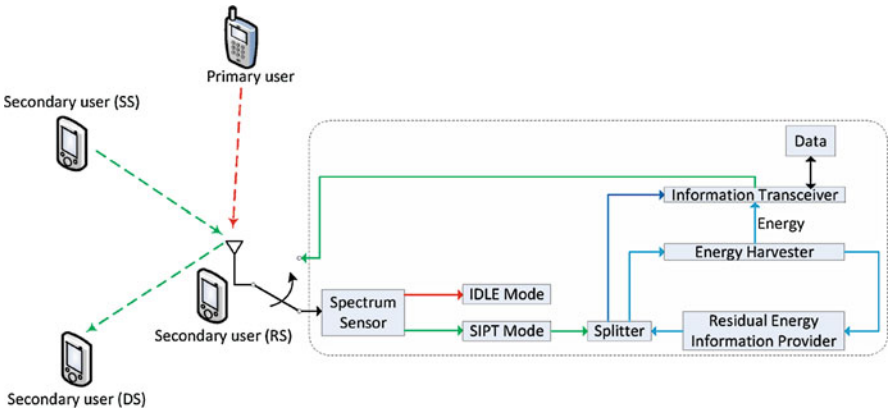

Fig. 2 Relay-assisted cognitive radio networks

received from SS to the DS by using the energy harvested from RF signals of the SS with the aim to maximize the throughput of the secondary system. At the beginning of each time slot, the SUs sense the primary channel. If the primary channel is busy, SUs use the IDLE mode. On the other hand, if the primary channel is idle, SUs can perform the transmit data process which consists of two phases, i.e., from SS to RS and from RS to DS (each phase lasts for $\frac{1}{2}$ time slot). Given the proposed system, the authors formulated the throughput maximization problem and then adopted an approximation method using the upper bound to mitigate the complexity of the optimization problem. In addition, a suboptimal algorithm was developed in order to achieve the near-optimal throughput performance. The results demonstrated that the throughput obtained by the proposed approximation algorithm is close to that of the optimal solution, and it has a significant gain compared with the separate management algorithm. A similar model was investigated in [18], but under the underlay CCN. Moreover, in [18], the authors focused on deriving the outage probability for the secondary system with the aim of improving the energy conversion efficiency for such a secondary system.

In [19], a similar relay cognitive radio model with RF energy harvesting techniques was studied, but different from [17, 18]; in [19] the relay node harvests energy from the primary transmitter's signals instead of the secondary transmitter's signals. In addition, different from [17] which considers an overlay spectrum sharing cognitive radio with the amplify-and-forward relaying technique, in [19], the authors took an underlay spectrum sharing cognitive radio with the decode-and-forward relaying technique into account. The aim of [19] is to demonstrate that the use of relay CCNs with simultaneous wireless information and power transfer (SWIPT) will not cause any loss of diversity gain, although it can reduce the outage performance of the system. Thus, it was concluded that, to improve the network performance, one of the possible ways is adopting the MIMO technique for SWIPT CCNs.

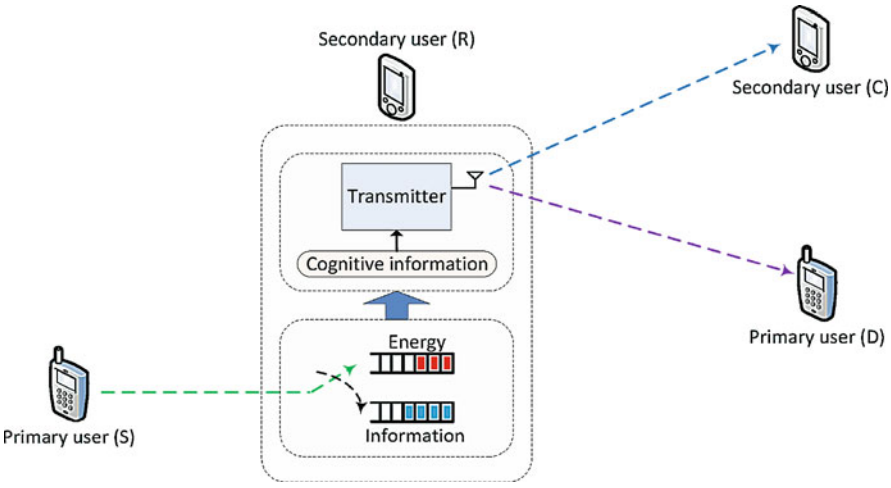

Fig. 3 Two-way cognitive relay network

Relaying for Primary Systems

Wang et al. [20] considered a scenario in which there are two primary users, denoted by S and D, who want to exchange information, but the distance between them is too far and thus they cannot communicate directly with each other. However, there is a secondary user R who volunteers to relay signals for primary users S and D. At the same time, the secondary relay node R also has its own information and wants to transmit to the secondary user C as illustrated in Fig. 3. Consequently, the node R has to transmit the primary relay information and its own information simultaneously. It is assumed that when the relay node R receives signals from the primary node, it is able to extract information and energy from the received RF signals. Then, by using the harvested energy, the relay node can transmit information to primary and secondary nodes. For the proposed aforementioned network, the authors formulated the outage probability expressions for the primary system and derived lower/upper bounds of outage probability for the secondary system. From analysis results, it was demonstrated that the proposed protocol has better outage performance than direct transmission without spectrum sharing. More numerical results can be found in [21].

A similar model was also considered in [22]. However, instead of using the decode-and-forward protocol as in [20], the authors in [22] adopted the amplify-and-forward protocol for the relay process. In addition, in [22], the authors proposed three schemes for the energy and information cooperation problem between PUs and SUs. For each scheme, the authors introduced corresponding optimization solutions, and they also indicated that the scheme based on the power splitting can achieve larger rate region than that of the time splitting scheme if the harvested energy is sufficient. Nevertheless, in [22], the authors did not consider the time constraint in which a secondary relay node needs to forward the whole received PU's signals to the primary receiver. To overcome this issue, the authors in [23] proposed a

time-divided power splitting scheme taking both the influence of time division proportion and the power splitting into account. By using this scheme, it was proved that the relay SU will have enough time to forward all received data from the PU if the energy supply is sufficient.

Power Allocation

Li et al. [24] studied the power allocation problem for a secondary network in which the secondary receiver (SR) is able to harvest RF energy from its secondary transmitter (ST) as well as from a primary transmitter (PT). It was assumed that the secondary system adopts the orthogonal frequency division multiplexing (OFDM) modulation for transmitting data from ST to SR. Thus the main goal of this paper is to find the optimal power allocation policy on each subcarrier and the power splitting ratio (i.e., the power ratio between the energy harvesting process and the information decoding process) at the ST in order to maximize the energy efficiency of the secondary system. The optimization power allocation problem is transformed to an equivalent convex problem that is solved efficiently by using an iterative algorithm. Simulation results showed that the iterative algorithm can achieve a great trade-off between the energy efficiency and high SINR regions.

Differently from [24,25] examined the power allocation problem for the primary system and then analyzed its impacts on both the primary system and the secondary system. First, in the secondary system, the secondary transmitter is allowed to transmit packets to the primary channel iff the channel is not occupied by the PU. In addition, ST can harvest energy from the primary transmitter's signals as well as from the environment. Then, the authors introduced a power allocation scheme for the primary system in which the PT sets the transmission power at time slot t based on the following equation $P_p^*(t) = \frac{N_o W(2^{R_p}-1)}{h_{ppd}(t)}$ where N_o is the additive white Gaussian noise power spectral density, W is the channel bandwidth, R_p is the targeted primary spectral efficiency, and h_{ppd} is the instantaneous channel gain. Under the proposed power allocation policy, the authors analyzed its impacts to both systems and concluded that by using the proposed policy at the primary system and implementing the RF energy harvesting at the secondary system, the throughput for both systems can be enhanced.

Scheduling and Security

In [26], the authors considered a primary system coexisting with an underlay secondary system which consists of one secondary transmitter (ST) and multiple secondary receivers (SU-Rx$_N$). Each SU-Rx$_n$ is able to harvest RF energy from the PU's signals or decode information received from the ST at a time. It means that SU-Rx$_n$ cannot carry out both processes concurrently. To avoid the collision among SU-Rx$_n$' transmissions, there is only one SU-Rx selected to decode information from the ST. Consequently, the SU-Rx with the best channel condition will be scheduled to decode information from the ST, while other SU-Rx will harvest RF energy from the ST's transmission. Then, in order to maximize the network throughput for the secondary system, a threshold condition using the Max-SNR

scheduling [27] was adopted to find the best SU-Rx at each time epoch. Numerical results showed that the proposed scheduling strategy can obtain a desirable QoS for the secondary system.

Similar to [26], the authors in [28] also investigated the scheduling problem for the secondary system by choosing only one secondary receiver at each time slot for data transmission. However, in [28], to guarantee the communication security in the secondary system, the authors employed a resource allocation algorithm which treats both idle secondary receivers and primary receivers as potential eavesdroppers. In addition, different from [26], a non-convex multi-objective optimization problem is formulated with the aim of jointly minimizing the total transmission power of the multi-antenna secondary transmitter and maximizing the efficiency of harvesting energy, while guaranteeing to minimize the interference power leakage-to-transmit power ratio for the primary system. Numerical results then figured out an interesting trade-off between the considered conflicting system design objectives.

Channel Selection

All aforementioned research works just consider only one primary channel at a time. However, in practice, there are multiple channels that the secondary system can utilize at the same time. Different channels have different capacities, e.g., high or low idle channel probabilities. Thus, the secondary transmitter needs to choose the best channel to access at each time slot such that its average throughput is maximized. For example, in the case that the ST wants to transmit data, it will select the channel with a high idle probability. By contrast, if the ST wants to harvest energy, it will prefer the channel with a low idle probability.

To address this problem, the authors in [29] proposed a model which allows secondary users to select the best channel to maximize their throughput. In particular, the authors formulated the channel selection problem for a secondary user by using Markov decision process and used the linear programming technical to find the optimal policy for the secondary user. To deal with the curse-of-model problem in the case when the secondary user has no information about its surrounding environment, the authors proposed a learning algorithm developed from the simulation-based method to find the optimal policy for the secondary user in an online fashion. Through simulation results, the authors showed that the performance of the proposed learning algorithm achieves close to that of the optimal solution, and it can improve the network through for the secondary system significantly.

This work was then extended in [30] with multiple secondary users coexisting in the same environment. Specifically, the authors considered two scenarios in which the secondary users cooperate in centralized and decentralized manner. In the case of centralized cooperation, TDMA method together with the learning algorithm introduced in [29] were adopted to find optimal policies for users. In the case of decentralized cooperation, the authors proposed a decentralized learning algorithm which allows users to determine their optimal policies in an online fashion with a little amount of information exchange. The simulation results clearly showed the

convergence of the learning algorithms as well as their efficiency in terms of network throughput.

Ambient Backscatter Communications: A New Communication Method in Cognitive Cellular Networks

In RF-powered cognitive cellular systems, secondary transmitters are required to harvest energy from radio signals and then use this energy to transmit data to their receivers. However, a new communication method has been introduced, called ambient backscatter communication, which enables secondary users to communication without requiring the energy harvesting process. In ambient backscatter communication, when secondary transmitter (ST) wants to send data to the secondary receiver (SR), the ST first backscatters ambient signals, e.g., mobile signals, to its receiver. The receiver then can decode and obtain the data by using averaging mechanisms.

In the following, the method used by the SR to extract information from the ST in the ambient backscatter communication will be briefly explained. For more details, the readers are referred to [32]. The core idea of ambient backscatter communication is that the ST backscatters information at a lower rate than that of ambient signals, i.e., signals from the PT. Thus, the SR is able to distinguish two signals by using averaging mechanisms. First, the case in which the secondary user is equipped with an analog-to-digital converter (ADC) to perform digital samples and extract information through the signal backscattering process will be considered. Then, based on the concept of signal sampling, the information decoding method using analog circuits which can remarkably reduce the energy consumption for secondary users will be presented.

Extracting Backscatter Information from Ambient Signals Using ADC

Consider a continuous time additive white Gaussian noise (AWGN) channel with bandwidth W Hz, the passband-baseband conversion and the sampling theory [31] (Chapter 5) with the sampling rate at the Nyquist-information rate of the RF signal will be adopted. Then, the received samples at the SR, i.e., $y[n]$, is a combination of the PT signals and the ST's backscattering signals, which can be expressed as:

$$y[n] = x[n] + \eta B[n]x[n] + w[n], \tag{4}$$

where $x[n]$ is the samples of the PT signals received at the SR, $w[n]$ is the noise, η is the complex-valued channel attenuation of the backscattered signals, and $B[n]$ are the bits transmitted by the ST. Here, since the distance between the ST and SR is assumed to be very small (within 1 m), the signal delay between the ST and SR can be ignored, and thus the signal received at the SR by backscattering from the ST is $\eta B[n]x[n]$.

If we assume that the ST transmits information at a fraction of the PT Nyquist rate, e.g., $\frac{1}{N}$, then $B[Ni + j]$ are all equal for $j = 1$ to N. Therefore, if the SR averages the instantaneous power of the N received samples which correspond to a single backscattered bit, it can be derived that

$$\frac{1}{N}\sum_{n=1}^{N}|y[n]|^2 = \frac{1}{N}\sum_{n=1}^{N}\left|x[n] + \eta B x[n] + w[n]\right|^2, \tag{5}$$

where B is either "0" or "1". Since PT signal $x[n]$ is uncorrelated with noise $w[n]$, (5) can be written as

$$\frac{1}{N}\sum_{n=1}^{N}|y[n]|^2 = \frac{|1+\eta B|^2}{N}\sum_{n=1}^{N}x[n]^2 + \frac{1}{N}\sum_{n=1}^{N}w[n]^2. \tag{6}$$

If P is denoted as the average received power at the SR, then $P = \frac{1}{N}\sum_{n=1}^{N}|y[n]|^2$. Ignoring the noise, the received average powers at the SR are $|1+\eta|^2 P$ and P corresponding to $B = 1$ or $B = 0$, respectively. Therefore, even under the change of the PT signals, the SR can still decode information from the ST.

Extracting Backscatter Information from Appropriate Analog Circuit

By using an ADC, the SR can extract information from ambient signals received from the ST. Nevertheless, ADC circuits may consume a significant amount of energy from the wireless nodes. Alternatively, analog circuit can be designed to imitate the operations of ADC circuits, but with less energy consumption.

Figure 4 shows a simple circuit diagram to demodulate the information for the SR. There are two stages, i.e., averaging stage and computing threshold stage. In the first stage, the SR smoothens and averages the natural variations of the PT signals. The output of the averaging stage yields two signal levels, corresponding to the voltage V_0 (bit "0") and the voltage V_1 (bit "1") for $V_1 > V_0$. Then, in the second stage, the SR computes the threshold between these two levels, which is the average of the two signal levels, i.e., $\frac{V_0+V_1}{2}$. If the received signal is higher than

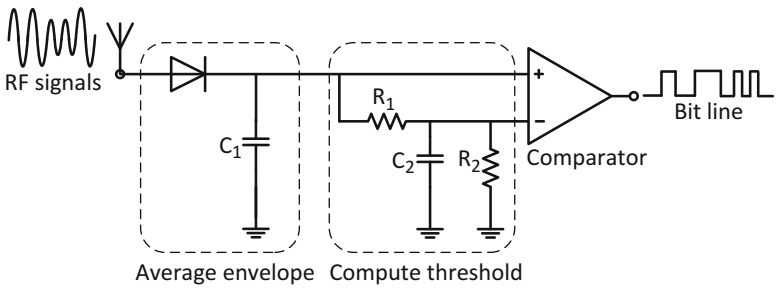

Fig. 4 Circuit diagram for the SR demodulator in the backscatter mode

the threshold, the SR concludes that the received signal is V_1 and V_0 otherwise. Finally, the comparator takes two voltages as inputs and generates a bit "0" or "1" accordingly.

Ambient backscatter communication was first introduced in [32] with the aim of enabling two wireless nodes to communicate without relying on batteries or wires for power. This idea has quickly received great attentions from research communities because it is expected to "*bring us closer to an Internet of Things*" [33]. Recent research work has been focusing on improving the performance for ambient backscatter communication. Specifically, in [34], the authors extended [32] by employing multiple antennas and a novel coding mechanism to improve the backscatter transmission rate as well as the communication range. Through experiments, it was shown in [34] that the backscatter transmission rate and the backscatter communication range can be extended up to 1 Mbps and 20 m, respectively. In [34], Parks et al. developed a coding scheme based on the spread spectrum techniques in which each data bit is represented by one symbol, and each symbol in turn is represented by a predefined chip sequence. Moreover, the authors in [35] proposed a new coding scheme which encodes several bits in a single symbol with the aim of increasing the data rate for ambient backscatter communication. Additionally, there are some other works which considered the security problem [36] and signal detection together with BER analysis [37] for ambient backscatter communication systems.

RF-Powered Cognitive Cellular Networks with Ambient Backscatter Communications: A New Approach

In an RF-powered cognitive cellular network, the secondary transmitter (ST) is able to harvest energy from primary signals and then uses the harvested energy to transmit data to its secondary receiver (SR) through the primary channel without causing harmful interference to primary users. The transmission used in the current RF-powered CCNs is therefore known as the harvest-then-transmit protocol/mode. However, the performance of RF-powered CCNs is dependent largely on the amount of harvested energy and the primary channel activity. For example, when the amount of harvested energy is too small and/or the idle channel period of the overlay CCNs is too short, the total transmitted bits will be remarkably reduced.

Therefore, this chapter introduces an RF-powered backscatter CCN which enables the ST not only to harvest energy from primary signals but also to backscatter these signals to its receiver for data transmission. Nevertheless, as stated in [38], ambient backscatter communication and RF energy harvesting processes cannot be performed concurrently in practice. If the ST backscatters signals, the RF carrier will be modulated by reflection, causing significant reduction in the harvested energy, and mostly it is insufficient to transmit data. Consequently, this leads to a question of how to choose the best mode, i.e., the harvest-then-transmit mode or backscatter mode, given the current radio conditions such that the total transmitted bits received at the SR per time unit is maximized. In the following, two scenarios

will be discussed, i.e., overlay and underlay cognitive cellular networks, and each scenario will present how to find the best trade-off time for the secondary user to maximize its throughput.

RF-Powered Backscatter Overlay Cognitive Cellular Network

Network Model

This section considers an RF-powered backscatter overlay cognitive cellular network (CCN) composed of a primary transmitter (PT) and a secondary transmitter (ST) [39]. In this network, the secondary transmitter (ST) is allowed to transmit signals to a primary channel iff this channel is currently not occupied by primary users. The ST communicates with a secondary receiver (SR). The ST is equipped with an RF energy harvesting module and a backscatter circuit to harvest RF energy and backscatter radio signals, respectively. The ST can also transmit data as normal wireless transmission. When the PT, e.g., a cellular base station (BS), transmits RF signal to its primary receiver (PR), the primary channel is busy. At the same time, the ST can either harvest energy and store it in an energy storage or backscatter the signal for data transmission [32]. The harvested energy is used for direct wireless data transmission to the SR when the primary channel becomes idle. This is referred to as the harvest-then-transmit mode, while the other is referred to as the backscatter mode. It is assumed that the SR perfectly knows the transmit mode of the ST and applies corresponding demodulators to extract useful information.

In the proposed system, when the PT transmits signals, i.e., the primary channel is busy, the ST can transmit data to the SR using backscatter communication (Fig. 5a) or harvest energy (Fig. 5b). Let β denote the normalized channel idle period and $(1-\beta)$ denote the normalized channel busy period as shown in Fig. 5. When the channel is busy, α denotes the time fraction for energy harvesting, and thus $(1-\alpha)$ denotes the time fraction for backscatter communication. The energy harvested

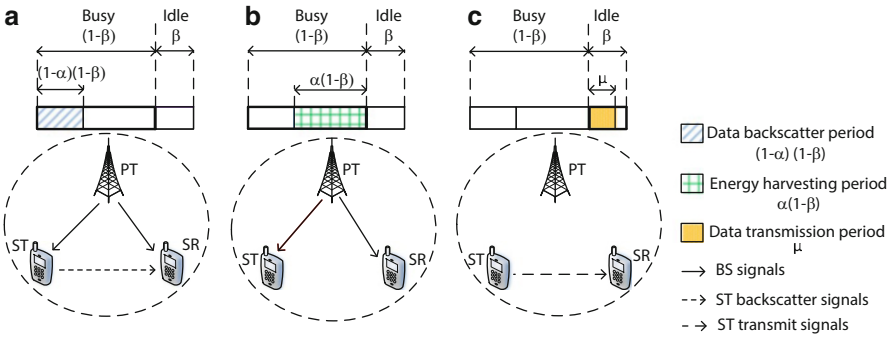

Fig. 5 RF-powered overlay cognitive radio network with ambient backscatter communication. (**a**) Backscattering data. (**b**) Harvesting energy. (**c**) Transmitting data

during the time fraction α will be stored in the ST's energy storage before it is used for direct data transmission during the idle channel period (Fig. 5c). It is observed that there is a trade-off between the time fractions for backscatter communication and energy harvesting. Clearly, the ST can achieve an optimal overall transmission rate through the dual mode of harvest then transmit and backscatter by balancing between backscatter communication and energy harvesting during the busy channel period. Thus, in the following, formulation and solution for the time optimization problem to find an optimal value of α for the ST will be presented.

Problem Formulation

We aim at maximizing the overall transmission rate of the secondary system, which is the number of information bits transmitted by the ST per time unit. We denote R as the overall transmission rate which is obtained as

$$R = R_{\mathrm{b}} + R_{\mathrm{h}}, \tag{7}$$

where R_{b} and R_{h} are the numbers of transmitted bits using the backscatter mode and the harvest-then-transmit mode in a time unit, respectively. Here, note that in the case of the backscatter mode, the interference to the primary receiver does not need to consider because through real experiments in [32], it was demonstrated that the backscattering transmitter does not create any noticeable glitches at the primary receiver unless it is less than 7 in.

Backscatter Mode

Transmission Rate of Backscatter Mode

It was shown in [32] that the transmission rate of the ambient backscatter communication depends on the setting of the RC circuit elements. For example, to transmit data at the transmission rate of 1 and 10 kbps, the values of circuit elements, i.e., R_1, R_2, C_1, and C_2, are set as (150 kΩ, 10 MΩ, 4.7 nF, 10 nF) and (150 kΩ, 10 MΩ, 680 pF, 1 μF), respectively. Therefore, let B_{b} denote the transmission rate of the ambient backscatter communication, i.e., the backscatter transmission rate. The total number of bits transmitted using the backscatter mode per time unit for the RF-powered backscatter CCN is expressed as follows:

$$R_{\mathrm{b}} = (1-\beta)(1-\alpha)B_{\mathrm{b}}. \tag{8}$$

Here, note that based on real implementations in [32], when the ST backscatters signals to the SR, the ST can still harvest energy from RF signals (i.e., when RF signals are absorbed for binary "0"). Although the amount of harvested energy is not enough to transmit data when the channel is idle, it is sufficient to sustain backscatter operations of the ST. Therefore, in (8), there is no need to consider the circuit energy consumption for the backscatter mode.

Harvest-Then-Transmit Mode

The harvest-then-transmit mode includes two phases. First, the ST harvests energy from the PT signals when the channel is busy. Then, the ST uses the harvested energy to transmit data when the primary channel becomes idle.

Harvesting Energy

From the Friis equation [4], the harvested RF power from the PT signals at the ST in a free space can be determined by

$$P_{\mathrm{R}} = \delta P_{\mathrm{T}} \frac{G_{\mathrm{T}} G_{\mathrm{R}} \lambda^2}{(4\pi d)^2}, \tag{9}$$

where P_{R} is the harvested power of the ST, P_{T} is the PT transmit power, $\delta \in [0, 1]$ is the energy harvesting efficiency, G_{T} is the PT antenna gain, G_{R} is the ST antenna gain, λ is the emitted wavelength, and d is the distance between the PT and ST. The total amount of harvested energy over the energy harvesting period $\alpha(1-\beta)$ then can be derived as follows:

$$E_{\mathrm{h}} = \alpha(1-\beta) P_{\mathrm{R}} = \alpha(1-\beta)\delta P_{\mathrm{T}} \frac{G_{\mathrm{T}} G_{\mathrm{R}} \lambda^2}{(4\pi d)^2}. \tag{10}$$

Transmitting Data

After harvesting energy, the ST uses all harvested energy deducted by the circuit energy consumption to transmit data over the data transmission period μ when the channel is idle. Let P^{tr} denote the transmit power of the ST in the data transmission period μ ($\mu \in [0, \beta]$ as shown in Fig. 5c) when the channel is idle. Then, P^{tr} can be obtained from

$$P^{\mathrm{tr}} = \frac{E_{\mathrm{h}} - E_{\mathrm{c}}}{\mu}, \tag{11}$$

where E_{h} is the total harvested energy and E_{c} is the circuit energy consumption. From [40], given the transmit power P^{tr}, the transmit data rate can be determined as follows:

$$r_{\mathrm{h}} = \kappa W \log_2 \left(1 + \frac{P^{\mathrm{tr}}}{P_0}\right), \tag{12}$$

where $\kappa \in [0, 1]$ is the transmission efficiency, W is the bandwidth of the primary channel, and P_0 is the ratio between the noise power N_0 and the channel gain coefficient h, i.e., $P_0 = \frac{N_0}{h}$.

Then, the number of transmitted bits per time unit using the harvest-then-transmit mode is given by

$$R_{\mathrm{h}} = \mu\kappa W \log_2 \left(1 + \frac{P^{\mathrm{tr}}}{P_0}\right) = \mu\kappa W \log_2 \left(1 + \frac{E_{\mathrm{h}} - E_{\mathrm{c}}}{\mu P_0}\right). \tag{13}$$

Here, since R_h in (13) must be non-negative, P^{tr} in (11) must be also non-negative. Therefore, from (11), the following condition is derived

$$E_h = \alpha(1-\beta)P_R \geq E_c, \tag{14}$$

it means

$$\alpha \geq \frac{E_c}{(1-\beta)P_R}. \tag{15}$$

Let's denote $\alpha^\dagger = \frac{E_c}{(1-\beta)P_R}$ as the minimum energy harvesting time to obtain enough energy for supplying the circuit of the ST to use the harvest-then-transmit mode. Then, $\alpha \geq \alpha^\dagger$. Note that since $\alpha \leq 1$, therefore if $\alpha^\dagger \leq 1$, then R_h can be greater than zero. Let's denote $m = \frac{(1-\beta)}{P_0\mu}P_R$ and $n = 1 - \frac{E_c}{P_0\mu}$. Then, from (13), it is derived that

$$R_h = \begin{cases} \mu\kappa W \log_2(n+m\alpha), & \text{if } \alpha^\dagger \leq 1 \text{and } \alpha^\dagger \leq \alpha, \\ 0, & \text{otherwise.} \end{cases} \tag{16}$$

Here, $m > 0$ and $(n + m\alpha) \geq 1$, $\forall \alpha \in [\alpha^\dagger, 1]$.

Then, to maximize the overall transmission rate of the secondary system, an optimization problem can be formulated as

$$\max_{\alpha,\mu} R(\alpha,\mu) = \begin{cases} (1-\beta)(1-\alpha)B_b + \mu\kappa W \log_2(n+m\alpha), & \text{if } \alpha^\dagger \leq 1 \text{ and } \alpha^\dagger \leq \alpha, \\ (1-\beta)(1-\alpha)B_b, & \text{otherwise.} \end{cases} \tag{17}$$

Proposed Solution

First, from (17), when $R(\alpha,\mu) = (1-\beta)(1-\alpha)B_b$, it is easy to show that

$$\max_{\alpha,\mu} R(\alpha,\mu) = R(\alpha=0) = (1-\beta)B_b, \forall \alpha \in [0,1]. \tag{18}$$

This implies that the ST will use only the backscatter mode when the primary channel is busy in this case.

Second, through Theorem 1, it will be proved that when $\alpha^\dagger \leq 1$ and $\alpha^\dagger \leq \alpha$, an optimal overall transmission rate is achieved when the ST transmits data over the entire channel idle period, i.e., $\max_{\alpha,\mu} R(\alpha,\mu) = R(\alpha,\beta)$.

Theorem 1. *When $\alpha^\dagger \leq 1$ and $\alpha^\dagger \leq \alpha$, if R_h from (16) is considered as a function of μ, then R_h reaches the highest value if and only if $\mu = \beta$. In other words,*

$$\max_{\mu} R_h(\mu) = R_h(\beta), \forall \mu \in [0,\beta]. \tag{19}$$

Proof. Since $\alpha^\dagger \leq 1$ and $\alpha^\dagger \leq \alpha$, then from (16), it will be derived that

$$R_{\mathrm{h}} = \mu\kappa W \log_2\left[1 + \frac{1}{P_0\mu}\big(\alpha(1-\beta)P_{\mathrm{R}} - E_{\mathrm{c}}\big)\right]. \tag{20}$$

To prove Theorem 1, let's denote $a = \kappa W$, $b = \frac{1}{P_0}\big(\alpha(1-\beta)P_{\mathrm{R}} - E_{\mathrm{c}}\big)$, where a and b are positive constants since now R_{h} is considered as a function of μ. Then, (16) becomes

$$R_{\mathrm{h}}(\mu) = a\mu \log_2\left(1 + \frac{b}{\mu}\right). \tag{21}$$

Then the first and second derivatives of R_{h} with respect to μ can be derived as follows:

$$R'_h(\mu) = a\log_2\left(1 + \frac{b}{\mu}\right) - \frac{ab}{(\mu+b)\ln 2}, \tag{22}$$

$$R''_h(\mu) = -\frac{ab^2}{\mu(\mu+b)^2\ln 2}. \tag{23}$$

From (23), it is observed that $R''_h < 0$ since a, b, and μ are greater than 0. Hence, $R'_h(\mu)$ is a decreasing function with respect to μ. Moreover, from (22), the following result can be derived

$$\lim_{\mu\to+\infty} R'_h(\mu) = \lim_{\mu\to+\infty} a\log_2\left(1 + \frac{b}{\mu}\right) - \lim_{\mu\to+\infty}\frac{ab}{(\mu+b)\ln 2} = 0. \tag{24}$$

Since when $\mu \to +\infty$, $R'_h(\mu) = 0$, this implies that $R'_h(\mu) > 0, \forall\mu \in [0,\beta]$. As a result, $R_{\mathrm{h}}(\mu)$ is an increasing function over $\mu \in [0,\beta]$, and thus $\max_\mu R_{\mathrm{h}}(\mu) = R_{\mathrm{h}}(\beta), \forall\mu \in [0,\beta]$.

The proof now is completed.

From Theorem 1, the optimization problem in (17) can be rewritten with only one variable α as follows:

$$\max_{\alpha} R(\alpha) = \begin{cases} (1-\beta)(1-\alpha)B_{\mathrm{b}} + \beta\kappa W\log_2(n+m\alpha), & \text{if } \alpha^\dagger \le 1 \text{ and } \alpha^\dagger \le \alpha, \\ (1-\beta)B_{\mathrm{b}}, & \text{otherwise.} \end{cases} \tag{25}$$

Then, the following theorem is hold.

Theorem 2. *When $\alpha \in [\alpha^\dagger, 1]$ and $\alpha^\dagger \le 1$ and the backscatter transmission rate $B_{\mathrm{b}} \in (\frac{\beta\kappa Wm}{(m+n)(1-\beta)\ln 2}, \frac{\beta\kappa Wm}{(m\alpha^\dagger+n)(1-\beta)\ln 2})$, there exists a globally optimal solution of $\alpha^* \in [\alpha^\dagger, 1]$ which maximizes R.*

Proof. For $\alpha \in [\alpha^\dagger, 1]$ and $\alpha^\dagger \le 1$, from (25) the first and second derivatives of $R(\alpha)$ with respect to α can be obtained as follows:

$$R'(\alpha) = -B_{\mathrm{b}}(1-\beta) + \frac{\beta\kappa W m}{(m\alpha+n)\ln 2}, \tag{26}$$

$$R''(\alpha) = -\frac{\beta\kappa W m^2}{(m\alpha+n)^2 \ln 2} < 0, \forall\alpha. \tag{27}$$

From (27), it can be inferred that $R'(\alpha)$ is a decreasing function with respect to α. Furthermore, to guarantee that there exists a value of $\alpha \in [\alpha^\dagger, 1]$ such that $R'(\alpha) = 0$, the following boundary conditions must be satisfied

$$\begin{aligned} R'(\alpha^\dagger) &= -B_{\mathrm{b}}(1-\beta) + \frac{\beta\kappa W m}{(m\alpha^\dagger+n)\ln 2} > 0, \text{ and} \\ R'(1) &= -B_{\mathrm{b}}(1-\beta) + \frac{\beta\kappa W m}{(m+n)\ln 2} < 0. \end{aligned} \tag{28}$$

Then, from (28), the following condition is hold

$$B_{\mathrm{b}} \in \left(\frac{\beta\kappa W m}{(m+n)(1-\beta)\ln 2}, \frac{\beta\kappa W m}{(m\alpha^\dagger+n)(1-\beta)\ln 2} \right). \tag{29}$$

Here, let $\alpha^* \in [\alpha^\dagger, 1]$ correspond to an optimal point of the objective function $R(\alpha)$. From (26), it is derived that

$$\alpha^* = \frac{\beta\kappa W}{B_{\mathrm{b}}(1-\beta)\ln 2} - \frac{n}{m}. \tag{30}$$

Then, it can be concluded that if the condition in (29) is met, an optimal solution $\alpha^* \in [\alpha^\dagger, 1]$ will be always found such that $R'(\alpha^*) = 0$.

From (27), it will be showed that $R(\alpha)$ is a concave function. This implies that the optimal value of α^* is a globally optimal solution and it yields the maximum value of R. Specifically, if $B_{\mathrm{b}} \in \left(\frac{\beta\kappa W m}{(m+n)(1-\beta)\ln 2}, \frac{\beta\kappa W m}{(m\alpha^\dagger+n)(1-\beta)\ln 2}\right)$, then a globally optimal solution can always be found $\alpha^* = \frac{\beta\kappa W}{B_{\mathrm{b}}(1-\lambda)\ln 2} - \frac{n}{m}$ which maximizes the objective function R.

The next theorem shows that if the backscatter transmission rate is high, the ST will backscatter as much as possible. Conversely, if the backscatter transmission rate is low, the ST will harvest energy for data transmission as much as possible.

Theorem 3. *For $\alpha \in [\alpha^\dagger, 1]$ and $\alpha^\dagger \leq 1$, if $B_{\mathrm{b}} \geq \frac{\beta\kappa W m}{(m\alpha^\dagger+n)(1-\beta)\ln 2}$, then $\alpha^* = \alpha^\dagger$. Moreover, when $B_{\mathrm{b}} \leq \frac{\beta\kappa W m}{(m+n)(1-\beta)\ln 2}$, then $\alpha^* = 1$.*

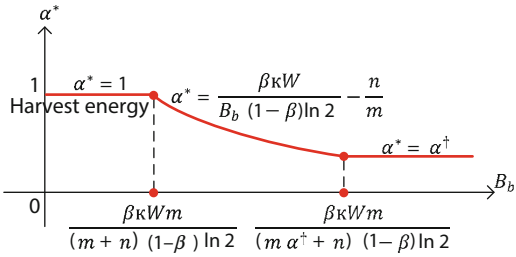

Fig. 6 Optimal value of α under the variation of B_b when $R_\mathrm{h} \geq 0$

Proof. First, it will be proved that if $B_\mathrm{b} \geq \frac{\beta\kappa W m}{(m\alpha^\dagger+n)(1-\beta)\ln 2}$, then $\alpha^* = \alpha^\dagger$. Since $B_\mathrm{b} \geq \frac{\beta\kappa W m}{(m\alpha^\dagger+n)(1-\beta)\ln 2}$, from (26), it will be derived that

$$R'(\alpha) \leq -\frac{\beta\kappa W m}{(m\alpha^\dagger+n)\ln 2} + \frac{\beta\kappa W m}{(n+m\alpha)\ln 2} = \frac{\beta\kappa W m^2(\alpha^\dagger-\alpha)}{(n+m\alpha)(m\alpha^\dagger+n)\ln 2} \leq 0. \tag{31}$$

From (31), there are two cases, i.e., $R'(\alpha) = 0$ or $R'(\alpha) < 0$. If $R'(\alpha) = 0$, i.e., $\alpha = \alpha^\dagger$, then $\alpha^* = \alpha^\dagger$. If $R'(\alpha) < 0$, then $R(\alpha)$ is a decreasing function with respect to α. In other words, $R(\alpha)$ decreases as α increases from $\alpha^\dagger$ to 1. Therefore, $R_{\max}(\alpha) = R(\alpha^\dagger)$. It means that $\alpha^* = \alpha^\dagger$.

Second, it will be proved that for $B_\mathrm{b} \leq \frac{\beta\kappa W m}{(m+n)(1-\beta)\ln 2}$, the ST will always select the harvest-then-transmit mode in order to maximize the objective function R. Since $B_\mathrm{b} \leq \frac{\beta\kappa W m}{(m+n)(1-\beta)\ln 2}$, from (26), it will be derived that

$$R'(\alpha) \geq -\frac{\beta\kappa W m}{(m+n)\ln 2} + \frac{\beta\kappa W m}{(n+m\alpha)\ln 2} = \frac{\beta\kappa W m^2(1-\alpha)}{(m+n)(n+m\alpha)\ln 2}. \tag{32}$$

Since $(n+m\alpha) > 0$ and $m > 0$ (from (16)), then $(n+m) > (n+m\alpha) > 0$, $\forall\alpha \in [\alpha^\dagger, 1]$. Consequently, $R'(\alpha) \geq 0, \forall\alpha \in [\alpha^\dagger, 1]$. Here, there are two cases, i.e., $R'(\alpha) = 0$ or $R'(\alpha) > 0$. If $R'(\alpha) = 0$, i.e., $\alpha = 1$, then $\alpha^* = 1$. If $R'(\alpha) > 0$, then $R(\alpha)$ is an increasing function with respect to α. It means that as α increases from $\alpha^\dagger$ to 1, $R(\alpha)$ will also increase. Therefore, for $\alpha^* = 1$, the ST will always choose the harvest-then-transmit mode to maximize its overall transmission rate when $B_\mathrm{b} \leq \frac{\beta\kappa W m}{(m+n)(1-\beta)\ln 2}$.

The proof is now completed.

From Theorems 2 and 3, it will be showed graphically in the optimal solution $\alpha^* \in [\alpha^\dagger, 1]$ under the variation of B_b in Fig. 6. Note that the convexity of the objective function R is proved in Theorem 2 and demonstrated in Fig. 11a.

Finally, the maximum value of R can be derived by

$$R_{\max} = \begin{cases} \max\left[(1-\beta)B_\mathrm{b}, (1-\beta)(1-\alpha^*)B_\mathrm{b} + \beta\kappa W \log_2(n+m\alpha^*)\right], & \text{if } \alpha \in [\alpha^\dagger, 1], \\ (1-\beta)B_\mathrm{b}, & \text{otherwise.} \end{cases} \tag{33}$$

RF-Powered Backscatter Underlay Cognitive Radio Network

Network Model

Unlike "overlay" CCNs where the secondary transmitter (ST) can harvest RF energy when the primary channel is busy and transmit data when the channel is idle, in the "underlay" CCN, the primary channel is assumed to be always busy. Therefore, the ST has to control the transmit power in order to avoid causing harmful interference to the primary receiver (PR). Therefore, different from the RF-powered backscatter "overlay" CCN studied in section "RF-Powered Backscatter Overlay Cognitive Cellular Network" where we need to find the optimal trade-off between backscattering time and energy harvesting time, in the RF-powered backscatter "underlay" CCN, we need to determine the optimal trade-off among backscattering time, harvesting time, and transmitting time such that the overall transmission rate is maximized. Moreover, the interference to the primary system must be guaranteed under a predefined threshold. Note that the transmit power of the secondary system can be expressed as a function of the transmitting time. This is because the transmit power is equal to the harvested energy from the harvesting time divided by the total transmitting time. Hence, in the following, an optimization problem considering the transmitting time of the ST as a decision variable instead of the transmit power will be presented.

Similar to the case of the overlay CCN, let's denote α as the time fraction for energy harvesting. However, the variable β now stands for the time fraction for data transmission instead of the idle channel period as in section "RF-Powered Backscatter Overlay Cognitive Cellular Network". Consequently, the time fraction for backscattering will be $(1-\alpha-\beta)$ as illustrated in Fig. 7. Then, the following conditions are hold, i.e., $\mathbf{C}_0$, for the values of α and β.

$$\mathbf{C}_0 \quad \text{s.t.} \begin{cases} \alpha, \beta \geq 0, \\ \alpha + \beta \leq 1. \end{cases} \tag{34}$$

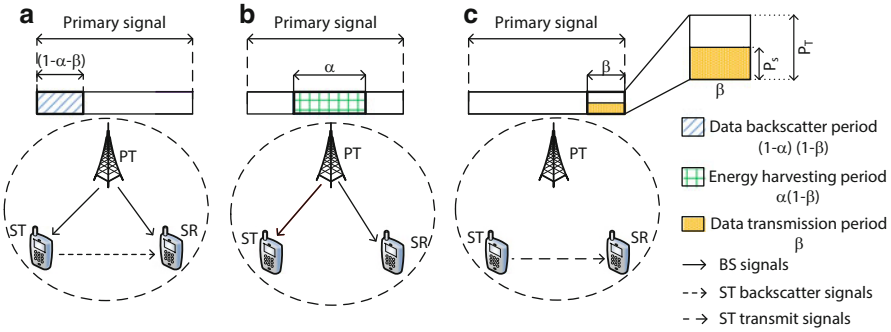

Fig. 7 RF-powered underlay cognitive radio network with ambient backscatter communication. (**a**) Backscattering data. (**b**) Harvesting energy. (**c**) Transmitting data

Problem Formulation

Again, let's denote R, R_b, and R_h as the total number of transmitted bits of the secondary system, the number of transmitted bits of the backscatter mode, and the number of transmitted bits of the harvest-then-transmit mode, respectively. For the case of an underlay CCN, it aims maximizing the overall transmission rate for the secondary system, i.e., R, under the transmit power constraint. First, the optimization problem is formulated, and then the solution to find the optimal trade-off for the ST is proposed by investigating the relation between the values of α and β.

Backscatter Mode

Similar to the previous section, the total number of bits transmitted by using the backscatter mode per time unit is determined as follows:

$$R_b = (1 - \alpha - \beta) B_b, \tag{35}$$

where B_b is the transmission bit rate of the backscatter mode. This rate depends on the hardware configuration of the wireless nodes as shown in [32].

Harvest-Then-Transmit Mode

Harvesting Energy

From the Friis equation [4], the received RF power from the PT at the ST is given in (9). The total amount of harvested energy over the energy harvesting period α in the case of an underlay CCN is obtained as follows:

$$E_h = \alpha P_R = \alpha \delta P_T \frac{G_T G_R \lambda^2}{(4\pi d)^2}. \tag{36}$$

Transmitting Data

After harvesting energy in the first phase, the ST uses all harvested energy deducted by the circuit energy consumption to transmit data over the data transmission period β. Let P_S denote the transmit power of the ST in the data transmission period β. Thus, P_S can be obtained from

$$P_S = \frac{E_h - E_c}{\beta}, \tag{37}$$

where E_h is the total harvested energy and E_c is the circuit energy consumption. If P_c is denoted as the circuit power consumption of the ST, then $E_c = \beta P_c$. Note that this case just considers the circuit energy consumption when the ST transmits data. When the ST harvests energy, the circuit energy consumption can be negligible [9, 13, 14, 22]. For the considered underlay CCN, the transmit power of the ST must be lower than a threshold to guarantee that the interference to the PR is acceptable. Thus, the following constraint is required

$$P_{\mathrm{S}} \leq P^{\ddagger}, \tag{38}$$

where $P^{\ddagger}$ is the maximum transmit power allowed for the ST. From (38), the constraint for α and β can be derived as follows:

$$\begin{aligned} \frac{\alpha P_{\mathrm{R}} - E_{\mathrm{c}}}{\beta} &\leq P^{\ddagger}, \\ \alpha P_{\mathrm{R}} &\leq \beta P_{\mathrm{c}} + \beta P^{\ddagger}, \\ \alpha &\leq \beta \frac{P_{\mathrm{c}} + P^{\ddagger}}{P_{\mathrm{R}}}. \end{aligned} \tag{39}$$

From [40], given the transmit power P_{S}, the transmission rate can be obtained in a similar way as presented in (12) as follows:

$$r_{\mathrm{h}} = \kappa W \log_2 \left(1 + \frac{P_{\mathrm{S}}}{P_0}\right). \tag{40}$$

Then, the number of transmitted bits per time unit using the harvest-then-transmit mode is given by

$$\begin{aligned} R_{\mathrm{h}} &= \beta \kappa W \log_2 \left(1 + \frac{P_{\mathrm{S}}}{P_0}\right) = \beta \kappa W \log_2 \left(1 + \frac{E_{\mathrm{h}} - E_{\mathrm{c}}}{\beta P_0}\right) \\ R_{\mathrm{h}} &= \beta \kappa W \log_2 \left(1 + \frac{\alpha P_{\mathrm{R}} - \beta P_{\mathrm{c}}}{\beta P_0}\right). \end{aligned} \tag{41}$$

Here, since R_{h} in (41) must be no n-negative, P_{S} in (37) must be also non-negative. Consequently, from (36) and (37), the following condition is hold

$$\begin{aligned} E_{\mathrm{h}} = \alpha P_{\mathrm{R}} \geq E_{\mathrm{c}}, \quad &\text{it means} \\ \alpha \geq \frac{E_{\mathrm{c}}}{P_{\mathrm{R}}} &= \frac{\beta P_{\mathrm{c}}}{P_{\mathrm{R}}}, \\ \alpha \geq \beta \frac{P_{\mathrm{c}}}{P_{\mathrm{R}}}&. \end{aligned} \tag{42}$$

The constraint in (42) implies that the length of the harvesting period must be sufficient long to yield energy greater than the circuit energy consumption of the ST to use the harvest-then-transmit mode. Then, from (34), (39), and (42), the constraints for variables α and β can be derived as shown in Fig. 8.

- In Fig. 8, the triangle (OAB) represents the feasible region of α and β which satisfies the constraint $\mathbf{C}_0$.

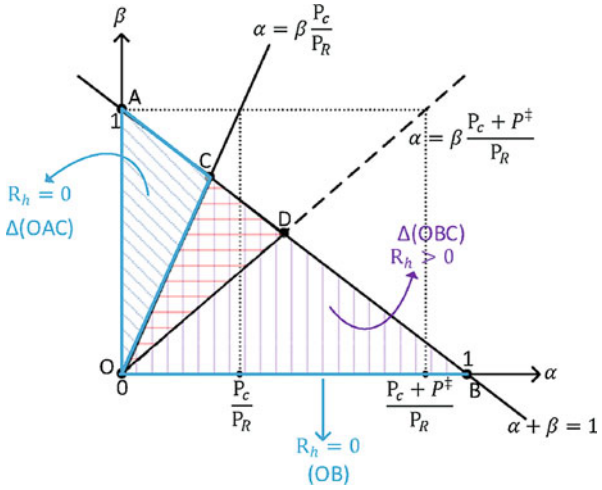

Fig. 8 Variable constraints

- The triangle (OAC) and the segment (OB) correspond to the case when $R_\mathrm{h} = 0$, i.e., when the amount of harvested energy is not enough to transmit data, i.e., $\alpha \leq \beta \frac{P_\mathrm{c}}{P_\mathrm{R}}$, and when the transmission period is zero, i.e., $\beta = 0$, respectively.
- The triangle (OBC) (not including the segments (OC) and (OB)) is the feasible region corresponding to the case when $R_\mathrm{h} > 0$.
- The triangle (ODB) (not including the segments (OB) and (OD)) corresponds to the case when $P_\mathrm{S} > P^{\ddagger}$.
- The triangle (ODC) excluding segment (OC) corresponds to the feasible region in which $R_\mathrm{h} > 0$, and the power constraint of the secondary transmitter, i.e., $\alpha \leq \beta \frac{P_\mathrm{c}+P^{\ddagger}}{P_\mathrm{R}}$, is satisfied.

Note that when $\alpha = 0$, i.e., there is no energy harvesting, β must be zero. Likewise, when $\beta = 0$, i.e., there is no data transmission, then α must be zero because the harvested energy will not be used. Thus, from Fig. 8 and (41), it can be derived that

$$R_\mathrm{h} = \begin{cases} \beta \kappa W \log_2\left(1 + \frac{\alpha P_\mathrm{R} - \beta P_\mathrm{c}}{\beta P_0}\right), & \text{if } \alpha + \beta \leq 1, \alpha > 0, \beta > 0, \text{ and } \alpha > \beta \frac{P_\mathrm{c}}{P_\mathrm{R}}, \\ 0, & \text{if } \alpha + \beta \leq 1, \alpha > 0, \beta > 0, \text{ and } \alpha \leq \beta \frac{P_\mathrm{c}}{P_\mathrm{R}}, \\ & \text{OR if } \alpha\beta = 0, \end{cases}$$

$$\text{s.t. } \alpha \leq \beta \frac{P_\mathrm{c} + P^{\ddagger}}{P_\mathrm{R}}. \tag{43}$$

In (43), the constraint $\alpha \leq \beta \frac{P_\mathrm{c}+P^{\ddagger}}{P_\mathrm{R}}$ is applied when $R_\mathrm{h} > 0$ only. This is because when $R_\mathrm{h} = 0$, there is no interference to the primary system, and thus this constraint is not required. Then, the optimization problem can be formulated as follows:

$$\max_{\alpha,\beta} R(\alpha,\beta) =$$

$$\begin{cases} (1-\alpha-\beta)B_{\mathrm{b}} + \beta\kappa W \log_2\left(1+\frac{\alpha P_{\mathrm{R}}-\beta P_{\mathrm{c}}}{\beta P_0}\right), & \text{if } \alpha+\beta \le 1, \alpha>0, \beta>0, \\ & \text{and } \alpha > \beta\frac{P_{\mathrm{c}}}{P_{\mathrm{R}}}, \\ (1-\alpha-\beta)B_{\mathrm{b}}, & \text{if } \alpha+\beta \le 1, \alpha>0, \beta>0, \\ & \text{and } \alpha \le \beta\frac{P_{\mathrm{c}}}{P_{\mathrm{R}}}, \text{OR if } \alpha\beta = 0 \end{cases}$$

$$\text{s.t. } \alpha \le \beta\frac{P_{\mathrm{c}}+P^{\ddagger}}{P_{\mathrm{R}}}. \tag{44}$$

In (44), it is easy to show that when $R(\alpha,\beta) = (1-\alpha-\beta)B_{\mathrm{b}}$, i.e., only the backscatter mode is used by the ST, the optimization problem is simplified to

$$\max_{\alpha,\beta} R(\alpha,\beta) = R(0,0) = B_{\mathrm{b}}. \tag{45}$$

Accordingly, the optimization problem in (44) can be written as follows:

$$\mathbf{P}_1 \quad \max_{\alpha,\beta} R(\alpha,\beta) =$$

$$\begin{cases} (1-\alpha-\beta)B_{\mathrm{b}} + \beta\kappa W \log_2\left(1+\frac{\alpha P_{\mathrm{R}}-\beta P_{\mathrm{c}}}{\beta P_0}\right), & \text{if } \alpha+\beta \le 1, \alpha>0, \beta>0, \\ & \text{and } \alpha > \beta\frac{P_{\mathrm{c}}}{P_{\mathrm{R}}}, \\ B_{\mathrm{b}}, & \text{if } \alpha+\beta \le 1, \alpha>0, \beta>0, \\ & \text{and } \alpha \le \beta\frac{P_{\mathrm{c}}}{P_{\mathrm{R}}}, \text{ OR if } \alpha\beta = 0, \end{cases}$$

$$\mathbf{C}_1 \quad \text{s.t. } \alpha \le \beta\frac{P_{\mathrm{c}}+P^{\ddagger}}{P_{\mathrm{R}}}. \tag{46}$$

Proposed Solution

It is observed that α and β are not separate variables. For the harvest-then-transmit mode, they are dependent as indicated in [12, 13]. Therefore, the relation between α and β needs to be examined, and then the optimization problem with two variables will be transformed into a new optimization problem with only one variable, which is easier to solve and analyze.

Optimal Time Allocation for Harvest-Then-Transmit Mode

Here, it will be showed that an optimal ratio between the energy harvesting period and the data transmission period can be found. Let γ denote the time fraction for the data transmission and $(1-\gamma)$ denote the time fraction for the energy harvesting as shown in Fig. 9.

Similar to the previous section, the number of transmitted bits per time unit using the harvest-then-transmit mode can be derived by replacing $\alpha = (1-\gamma)$ and $\beta = \gamma$ in (43), i.e.,

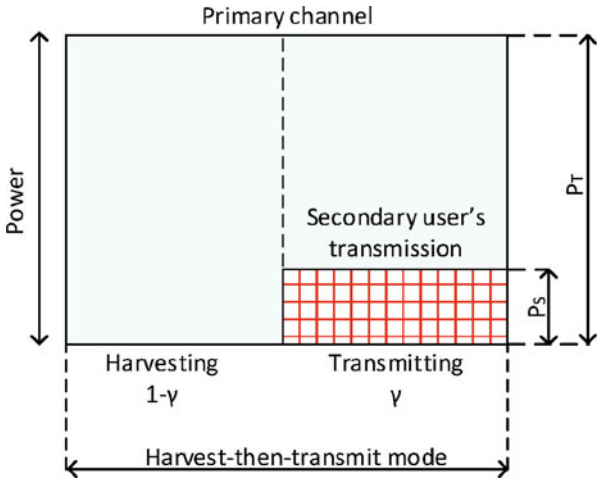

Fig. 9 Optimal time allocation for harvest-then-transmit mode

$$R_{\mathrm{h}} = \begin{cases} \gamma\kappa W \log_2\left(1 + \frac{(1-\gamma)P_{\mathrm{R}} - \gamma P_{\mathrm{c}}}{\gamma P_0}\right), & \text{if } \alpha + \beta \le 1, \alpha > 0, \beta > 0, \text{ and } \alpha > \beta\frac{P_{\mathrm{c}}}{P_{\mathrm{R}}}, \\ 0, & \text{if } \alpha + \beta \le 1, \alpha > 0, \beta > 0, \text{ and } \alpha \le \beta\frac{P_{\mathrm{c}}}{P_{\mathrm{R}}} \\ & \text{OR if } \alpha\beta = 0, \end{cases}$$

$$\text{s.t. } \alpha \le \beta\frac{P_{\mathrm{c}} + P^{\ddagger}}{P_{\mathrm{R}}}. \tag{47}$$

The first condition $\alpha + \beta = (1-\gamma) + \gamma \le 1$ is always satisfied. The second and third conditions

$$\alpha > 0 \text{ and } \beta > 0 \text{ are to ensure that } \gamma < 1 \text{ and } \gamma > 0. \tag{48}$$

For the fourth condition in (47), it will be derived that

$$\alpha > \beta\frac{P_{\mathrm{c}}}{P_{\mathrm{R}}}, \text{so } 1 - \gamma > \gamma\frac{P_{\mathrm{c}}}{P_{\mathrm{R}}}. \text{ Thus } \gamma < \frac{P_{\mathrm{R}}}{P_{\mathrm{c}} + P_{\mathrm{R}}}. \tag{49}$$

For the last condition in (47), it will be derived that

$$\alpha\beta = 0, \text{so } (1-\gamma)\gamma = 0, \text{i.e., } \gamma = 0 \text{ or } \gamma = 1. \tag{50}$$

From the constraint in (47), it will be derived that

$$\begin{aligned} \alpha P_{\mathrm{R}} &\le \beta P_{\mathrm{c}} + \beta P^{\ddagger}, \\ (1-\gamma)P_{\mathrm{R}} &\le \gamma P_{\mathrm{c}} + \gamma P^{\ddagger}, \\ \frac{P_{\mathrm{R}}}{P_{\mathrm{c}} + P^{\ddagger} + P_{\mathrm{R}}} &\le \gamma. \end{aligned} \tag{51}$$

Finally, from (48), (49), (50), and (51), it will be derived that

$$R_{\mathrm{h}} = \begin{cases} \gamma\kappa W \log_2\left(1 + \frac{(1-\gamma)P_{\mathrm{R}} - \gamma P_{\mathrm{c}}}{\gamma P_0}\right), & \text{if } \gamma \in \left(0, \frac{P_{\mathrm{R}}}{P_{\mathrm{c}}+P_{\mathrm{R}}}\right), \\ 0, & \text{if } \gamma \in \left[\frac{P_{\mathrm{R}}}{P_{\mathrm{c}}+P_{\mathrm{R}}}, 1\right) \text{ OR if } (1-\gamma)\gamma = 0, \end{cases}$$

$$\text{s.t. } \gamma \geq \frac{P_{\mathrm{R}}}{P_{\mathrm{c}} + P^{\ddagger} + P_{\mathrm{R}}}. \tag{52}$$

Since $\frac{P_{\mathrm{R}}}{P_{\mathrm{c}}+P^{\ddagger}+P_{\mathrm{R}}} < \frac{P_{\mathrm{R}}}{P_{\mathrm{c}}+P_{\mathrm{R}}}$, for $\gamma \in (0, \frac{P_{\mathrm{R}}}{P_{\mathrm{c}}+P_{\mathrm{R}}})$, the optimization problem for the harvest-then-transmit mode becomes

$$\mathbf{P}_2 \quad \max_{\gamma} R_{\mathrm{h}}(\gamma) = \gamma\kappa W \log_2\left(1 + \frac{(1-\gamma)P_{\mathrm{R}} - \gamma P_{\mathrm{c}}}{\gamma P_0}\right), \tag{53}$$

$$\mathbf{C}_2 \quad \text{s.t.} \begin{cases} \gamma < \frac{P_{\mathrm{R}}}{P_{\mathrm{c}}+P_{\mathrm{R}}}, \\ \gamma \geq \frac{P_{\mathrm{R}}}{P_{\mathrm{c}}+P^{\ddagger}+P_{\mathrm{R}}}. \end{cases}$$

To simplify the presentation, let's denote

$$a = \kappa W, \quad b = 1 - \frac{P_{\mathrm{R}} + P_{\mathrm{c}}}{P_0}, \quad \text{and} \quad c = \frac{P_{\mathrm{R}}}{P_0}. \tag{54}$$

The transmission rate of the harvest-then-transmit mode can be expressed as follows:

$$R_{\mathrm{h}}(\gamma) = a\gamma \log_2\left(b + \frac{c}{\gamma}\right). \tag{55}$$

From (55), the first derivative of R_{h} with respect to γ can be obtained as follows:

$$R'_h = a \log_2\left(b + \frac{c}{\gamma}\right) - \frac{ac}{(b\gamma + c)\ln 2}. \tag{56}$$

In the following, it will be showed that $R'_h = 0$ has a unique solution of γ.

Theorem 4. *If* $1 - \frac{P_{\mathrm{R}}+P_{\mathrm{c}}}{P_0} \geq (1 + \frac{P^{\ddagger}}{P_0})(1 - \ln(1 + \frac{P^{\ddagger}}{P_0}))$, *then a globally optimal solution* γ_1^* *for the optimization problem* $\mathbf{P}_2$ *with the constraint* $\mathbf{C}_2$ *that maximizes* R_{h} *can always be found.*

Proof. Let's define $X = b + \frac{c}{\gamma}$. Then, it will be proved that $X > 1$ and $X \leq 1 + \frac{P^{\ddagger}}{P_0}$ if γ satisfies $\mathbf{C}_2$. From the first constraint in $\mathbf{C}_2$, it will be derived that $\gamma < \frac{P_{\mathrm{R}}}{P_{\mathrm{c}}+P_{\mathrm{R}}}$, so

$$X = b + \frac{c}{\gamma} > b + \frac{c}{\frac{P_R}{P_c+P_R}} > 1 - \frac{P_R + P_c}{P_0} + \frac{\frac{P_R}{P_0}}{\frac{P_R}{P_c+P_R}} > 1. \tag{57}$$

From the second constraint in $\mathbf{C}_2$, it will be derived that $\gamma \geq \frac{P_R}{P_c+P^{\ddagger}+P_R}$, so

$$X = b + \frac{c}{\gamma} \leq b + \frac{c}{\frac{P_R}{P_c+P^{\ddagger}+P_R}} \leq 1 - \frac{P_R + P_c}{P_0} + \frac{\frac{P_R}{P_0}}{\frac{P_R}{P_c+P^{\ddagger}+P_R}} \leq 1 + \frac{P^{\ddagger}}{P_0}. \tag{58}$$

From (56), it will be derived that

$$\begin{aligned} g(X) = R'_h &= a \log_2 \left(b + \frac{c}{\gamma}\right) - \frac{ac}{(b\gamma + c)\ln 2}, \\ &= a \frac{\ln\left(b + \frac{c}{\gamma}\right)}{\ln 2} - \frac{\left(b + \frac{c}{\gamma} - b\right)a}{\left(b + \frac{c}{\gamma}\right)\ln 2}, \\ &= a \frac{\ln\left(b + \frac{c}{\gamma}\right)}{\ln 2} + \frac{ab}{\left(b + \frac{c}{\gamma}\right)\ln 2} - \frac{a}{\ln 2}, \\ &\quad \frac{a}{\ln 2}\left(\ln\left(b + \frac{c}{\gamma}\right) + \frac{b}{b + \frac{c}{\gamma}} - 1\right), \\ &= \frac{a}{\ln 2}\Big(\ln X + \frac{b}{X} - 1\Big), \\ &= \frac{a}{X \ln 2}\Big(X \ln X + b - X\Big). \end{aligned} \tag{59}$$

Then, we need to find the value of $X \in \left(1, 1 + \frac{P^{\ddagger}}{P_0}\right]$ that satisfies $g(X) = R'_h(\gamma) = 0$. It means

$$\frac{a}{X \ln 2}\Big(X \ln X + b - X\Big) = 0,$$

$$X - X \ln X = b \ \ (\text{since } \ a > 0 \ \text{ and} X > 1). \tag{60}$$

Let's denote $G(X) = X - X \ln X$. Then from Fig. 10, it can be concluded that if $b \in [G(1 + \frac{P^{\ddagger}}{P_0}), G(1))$, then a unique solution X^* satisfying the condition in (59) can always be found.

Since $X = b + \frac{c}{\gamma}$, it can be concluded that if $b \in [G(1 + \frac{P^{\ddagger}}{P_0}), G(1))$, then a unique solution $\gamma_1^* = \frac{c}{X^* - b}$ which satisfies $R'_h(\gamma_1^*) = 0$ can always be found. Moreover, since $b = 1 - \frac{P_R + P_c}{P_0}$, $b < G(1) = 1$ is hold. Therefore, if $b = 1 - \frac{P_R + P_c}{P_0} \geq$

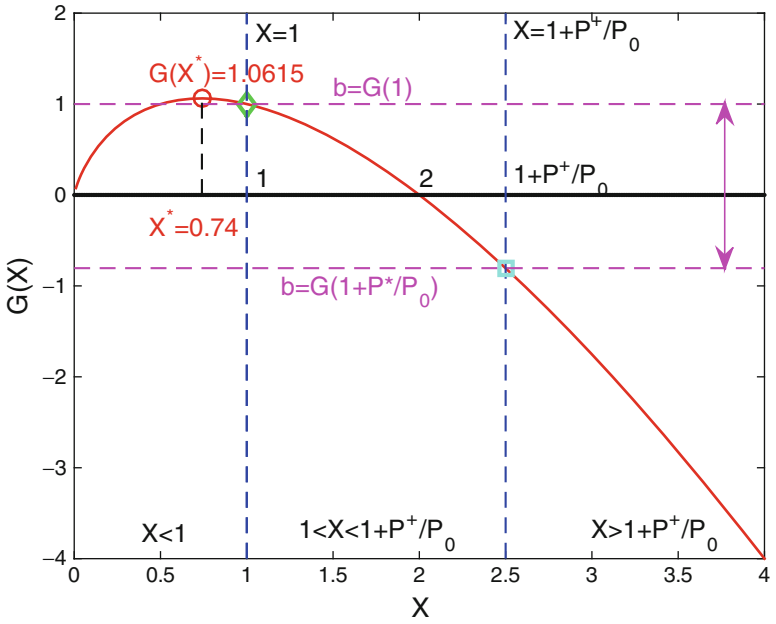

Fig. 10 Function $G(X)$

$G(1+\frac{P_0^\ddagger}{P_0}) = (1+\frac{P_0^\ddagger}{P_0})(1-\ln(1+\frac{P_0^\ddagger}{P_0}))$, then a unique solution γ_1^* such that $R_h'(\gamma_1^*) = 0$ can alawys be found.

Moreover, from (56), the second derivative of R_h can be derived as follows:

$$R_h'' = -\frac{ac^2}{(b\gamma + c)^2 \gamma \ln 2}. \tag{61}$$

Here, since $a = \kappa W > 0$, $\gamma > 0$, and $c > 0$, $R_h'' < 0$. This means that R_h is a concave function. Therefore, if γ_1^* is an optimal solution of $\mathbf{P}_2$, then it is a unique globally optimal solution, and γ_1^* maximizes the objective function R_h.

The proof is now completed.

Theorem 5. *If* $1-\frac{P_\mathrm{R}+P_\mathrm{c}}{P_0} < (1+\frac{P_0^\ddagger}{P_0})(1-\ln(1+\frac{P_0^\ddagger}{P_0}))$, *then a globally optimal solution* γ_2^* *for the optimization problem* $\mathbf{P}_2$ *with constraint* $\mathbf{C}_2$ *which maximizes* R_h *can always be found.*

Proof. From (59), it can be derived that $R_h'(\gamma) = g(X) = \frac{a}{X\ln 2}(b - G(X))$. Since $X \in (1, 1+\frac{P_0^\ddagger}{P_0}]$, from Fig. 10, if $b < G(1+\frac{P_0^\ddagger}{P_\mathrm{R}})$, i.e., $1-\frac{P_\mathrm{R}+P_\mathrm{c}}{P_0} < (1+\frac{P_0^\ddagger}{P_0})(1-\ln(1+\frac{P_0^\ddagger}{P_0}))$, then $R_h'(\gamma) = g(X) < 0$. This implies that R_h is a decreasing function. Thus, there exists a unique value of γ_2^* such that $R_\mathrm{h}(\gamma_2^*)$ is maximized. Additionally, from $\mathbf{C}_2$, it can be derived that $\gamma \in [\frac{P_\mathrm{R}}{P_\mathrm{c}+P^\ddagger+P_\mathrm{R}}, \frac{P_\mathrm{R}}{P_\mathrm{c}+P_\mathrm{R}})$. Thus, $\gamma_2^* = \frac{P_\mathrm{R}}{P_\mathrm{c}+P^\ddagger+P_\mathrm{R}}$.

The proof is now completed.

From Theorems 4 and 5, the optimal value of γ and R_{h} can be derived as follows:

$$(\gamma^*, R_{\mathrm{h}}^*) = \begin{cases} (\gamma_1^*, R_{\mathrm{h}}(\gamma_1^*)), \text{ if } 1 - \frac{P_{\mathrm{R}}+P_{\mathrm{c}}}{P_0} \geq \left(1 + \frac{P^{\ddagger}}{P_0}\right)\left(1 - \ln\left(1 + \frac{P^{\ddagger}}{P_0}\right)\right), \\ (\gamma_2^*, R_{\mathrm{h}}(\gamma_2^*)), \text{ if } 1 - \frac{P_{\mathrm{R}}+P_{\mathrm{c}}}{P_0} < \left(1 + \frac{P^{\ddagger}}{P_0}\right)\left(1 - \ln\left(1 + \frac{P^{\ddagger}}{P_0}\right)\right), \end{cases} \tag{62}$$

where $\gamma_1^* = \frac{c}{X^* - b}$ and $\gamma_2^* = \frac{P_{\mathrm{R}}}{P_{\mathrm{c}} + P^{\ddagger} + P_{\mathrm{R}}}$.

Optimal Time Trade-Off for Backscatter and Harvest-Then-Transmit Modes

Let's denote

$$\gamma^* = \begin{cases} \gamma_1^*, \text{ if } 1 - \frac{P_{\mathrm{R}}+P_{\mathrm{c}}}{P_0} \geq \left(1 + \frac{P^{\ddagger}}{P_0}\right)\left(1 - \ln\left(1 + \frac{P^{\ddagger}}{P_0}\right)\right), \\ \gamma_2^*, \text{ if } 1 - \frac{P_{\mathrm{R}}+P_{\mathrm{c}}}{P_0} < \left(1 + \frac{P^{\ddagger}}{P_0}\right)\left(1 - \ln\left(1 + \frac{P^{\ddagger}}{P_0}\right)\right), \end{cases} \tag{63}$$

where $\gamma^* \in \left[\frac{P_{\mathrm{R}}}{P_{\mathrm{c}}+P^{\ddagger}+P_{\mathrm{R}}}, \frac{P_{\mathrm{R}}}{P_{\mathrm{c}}+P_{\mathrm{R}}}\right)$. Also, let $\tau = \alpha + \beta$, then the following results can be derived $\alpha = (1 - \gamma^*)\tau$ and $\beta = \tau\gamma^*$.

Now the optimization problem has been simplified to find an optimal time ratio, i.e., τ, between the backscatter mode and the harvest-then-transmit mode such that the overall transmission rate of the ST is maximized. Then, for $\tau \in [0, 1]$, the optimization problem $\mathbf{P}_1$ can be rewritten as follows:

$$\mathbf{P}_3 \quad \max_{\tau} R(\tau) = \begin{cases} (1-\tau)B_{\mathrm{b}} + \tau\gamma^*\kappa W \log_2\left(1 + \frac{(1-\gamma^*)P_{\mathrm{R}} - \gamma^* P_{\mathrm{c}}}{\gamma^* P_0}\right), & \text{if } \tau \in (0, 1], \\ B_{\mathrm{b}}, & \text{if } \tau = 0. \end{cases} \tag{64}$$

For $\tau \in (0, 1]$, it is observed that $R(\tau)$ is a linear function with respect to τ and

$$R'(\tau) = -B_{\mathrm{b}} + \gamma^*\kappa W \log_2\left(1 + \frac{(1-\gamma^*)P_{\mathrm{R}} - \gamma^* P_{\mathrm{c}}}{\gamma^* P_0}\right), \tag{65}$$

thus

$$R(\tau) \begin{cases} \text{is a decreasing function, if } R'(\tau) < 0, \\ \text{is an increasing function, if } R'(\tau) > 0. \end{cases} \tag{66}$$

Therefore, the following result is hold

$$\max_{\tau} R(\tau) = \begin{cases} R(\tau = 0) = B_{\mathrm{b}}, & \text{if } R'(\tau) < 0, \\ R(\tau = 1) = \gamma^*\kappa W \log_2\left(1 + \frac{(1-\gamma^*)P_{\mathrm{R}} - \gamma^* P_{\mathrm{c}}}{\gamma^* P_0}\right), & \text{if } R'(\tau) > 0. \end{cases} \tag{67}$$

In other words, the ST will select the backscatter mode if $B_{\mathrm{b}} > \gamma^*\kappa W \log_2\left(1 + \frac{(1-\gamma^*)P_{\mathrm{R}} - \gamma^* P_{\mathrm{c}}}{\gamma^* P_0}\right)$ and the harvest-then-transmit mode otherwise. Here, note that for

$B_{\mathrm{b}} = \gamma^* \kappa W \log_2\left(1 + \frac{(1-\gamma^*)P_{\mathrm{R}} - \gamma^* P_{\mathrm{c}}}{\gamma^* P_0}\right)$, then it will be derived that $R(\tau) = B_{\mathrm{b}} = \gamma^* \kappa W \log_2\left(1 + \frac{(1-\gamma^*)P_{\mathrm{R}} - \gamma^* P_{\mathrm{c}}}{\gamma^* P_0}\right)$. This implies that $R(\tau)$ is a constant. Therefore, the ST can choose either the backscatter mode or the harvest-then-transmit mode since both modes have the same transmission bit rate.

Let $B_{\mathrm{b}}^* = \gamma^* \kappa W \log_2\left(1 + \frac{(1-\gamma^*)P_{\mathrm{R}} - \gamma^* P_{\mathrm{c}}}{\gamma^* P_0}\right)$ denote the threshold of the transmission rate of the backscatter mode, then the optimal transmission policy for the ST in this case can be expressed as a step function as follows:

$$\text{ST's Action} = \begin{cases} \text{Backscatter mode}, & \text{if } B_{\mathrm{b}} \geq B_{\mathrm{b}}^* \\ \text{Harvest-then-transmit mode}, & \text{if } B_{\mathrm{b}} < B_{\mathrm{b}}^*. \end{cases} \tag{68}$$

Numerical Results and Performance Evaluation

To evaluate the performance for the proposed solution, simulation experiments for two scenarios, i.e., RF-powered "overlay" and "underlay" CCNs, will be presented. For each scenario, the overall transmission rate of the proposed solution with the primary signal being FM signal and examine the cases with other PTs, i.e., TV signal, 3G signal, and WiFi signal, will be showed. Then, the transmission policy of the secondary transmitter (ST) under the variation of parameters will be investigated, and the performance of the proposed solution will be compared with other baseline policies, i.e., the harvest-then-transmit protocol [12, 13], and ambient backscatter communication [32].

Experiment Setup

The parameters of the signals are provided in Table 1. Here, note that the transmit power from a macrocell base station is capped at 46 and 24 dBm for a small-cell access point. Therefore, the transmit power of the small-cell and WiFi access points is set at 10 dBm.

The other parameters are set as follows. The PT antenna gain and ST antenna gain are 6 dBi as in [41], and the circuit power consumption is −35 dBm. The energy harvesting efficiency and data transmission efficiency are 0.6. The idle channel ratio, the backscatter transmission rate, the transmit power constraint for the case

Table 1 Referenced parameters

RF source	Transmit power	Frequency	Bandwidth	Distance
FM tower	17 kW	100 MHz	100 KHz	6.7 miles
TV tower	17 kW	915 MHz	6 MHz	2 km
Cellular BS	10 dBm	2.15 GHz	14 MHz	100 m
WiFi AP	10 dBm	2.4 GHz	20 MHz	2 m

of the underlay CCN, and the TV signal frequency will be varied to evaluate the performance as well as the policy of the secondary system.

Overlay Cognitive Radio Networks

Figure 11a shows the overall transmission rate $R(\alpha)$ in (25) as the value of α is varied. Here, the idle channel ratio is set at 0.3 (i.e., the RF source transmits signals 70% of the total time) and the backscatter transmission rate at 33 kbps. In Fig. 11a, it is observed that if the ST uses either the backscatter mode or the harvest-then-transmit mode, then the overall transmission rates of the ST are 23.1 and 22.563 kbps, respectively. However, if the ST spends 41.125% of time (in the busy channel period) for the energy harvesting, i.e., $\alpha = 0.41125$, and 58.875% for backscattering, then the overall transmission rate of the secondary system can be up to 25.2264 kpbs. This can be explained through Fig. 11b. As the value of α increases, R_{b} decreases linearly, while R_{h} increases following the logarithmic function. This is because when α is too small, i.e., the ST spends much time for the backscattering, the ST cannot fully utilize the channel idle period for data transmission because of the small amount of harvested energy. Alternatively, if the value of α is too high, i.e., the ST spends much time for harvesting energy, the overall transmission rate will be low because the backscatter mode is not efficiently utilized during the channel busy period.

Then, the channel idle ratio β is varied, and its impact on the transmission policy as well as performance of the secondary system will be analyzed. As shown in Fig. 12a, when the channel idle ratio is increased from 0.1 to 0.5, the optimal value of α increases quickly from 0.1 to 0.95, and it then remains stable at 1 when β is greater than 0.5. Clearly, for the primary channel with low channel idle ratio, the ST will spend more time for the backscatter mode. By contrast, for the primary channel with a high idle channel ratio, the ST prefers the harvest-then-transmit mode. This is from the fact that the harvest-then-transmit mode can provide higher transmission rate than that of the backscatter mode. Hence, when the channel idle ratio is high, the ST will spend the whole time to harvest energy when the channel is busy.

Figure 12b shows the overall transmission rate obtained by the proposed solution and comparison with two baseline policies, namely, the backscatter only policy (BP) and harvest-then-transmit only policy (HP). With our proposed solution, the overall transmission rate is approximately 2 times greater than that of the HP and 1.3 times greater than that of the BP when the channel idle ratios are 0.1 and 0.6, respectively. Here, for the HP policy, its transmission rate first increases when β increases from 0.1 to 0.3, but if β keeps increasing, its transmission rate will be reduced. The reason is that when the channel idle ratio is low, the ST will have less time to transmit data. On contrary, if the channel idle ratio is high, the ST will have less time for harvesting energy. Therefore, both result in low transmission rate.

Next, the backscatter transmission rate is varied, and the optimal solution together with the performance of the secondary system is evaluated. Here, the idle

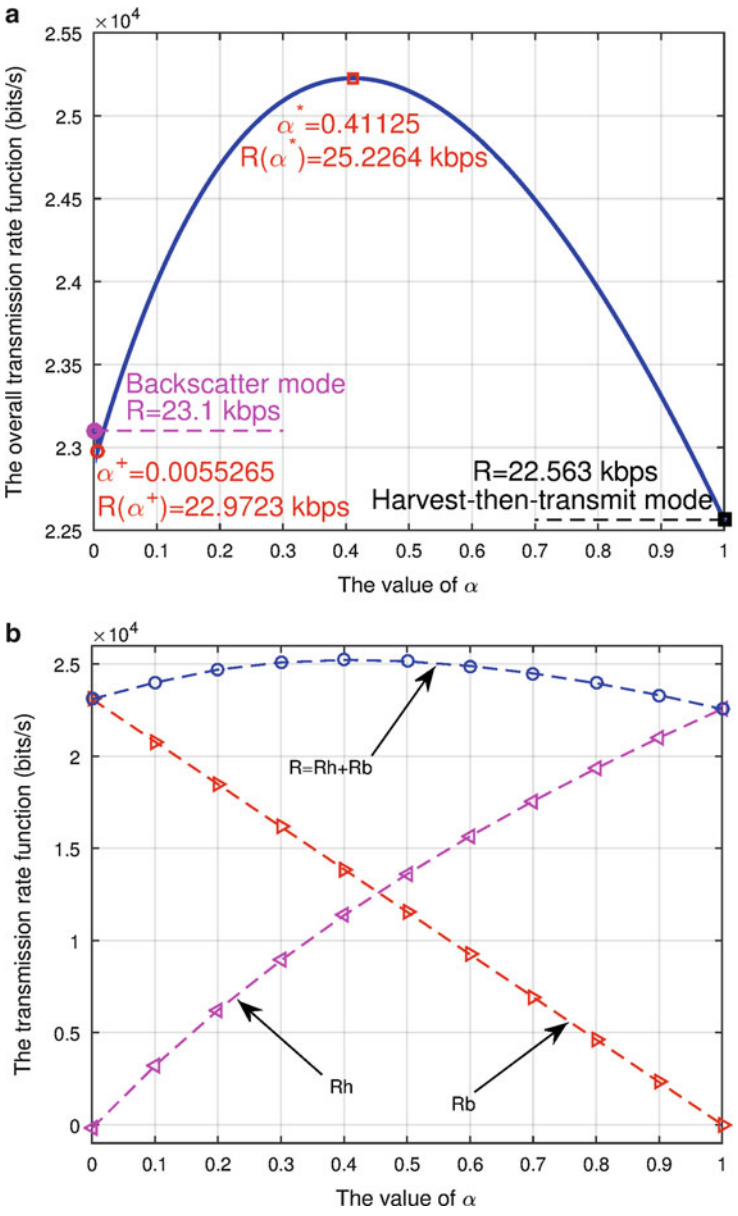

Fig. 11 The overall transmission rate under different values of alpha

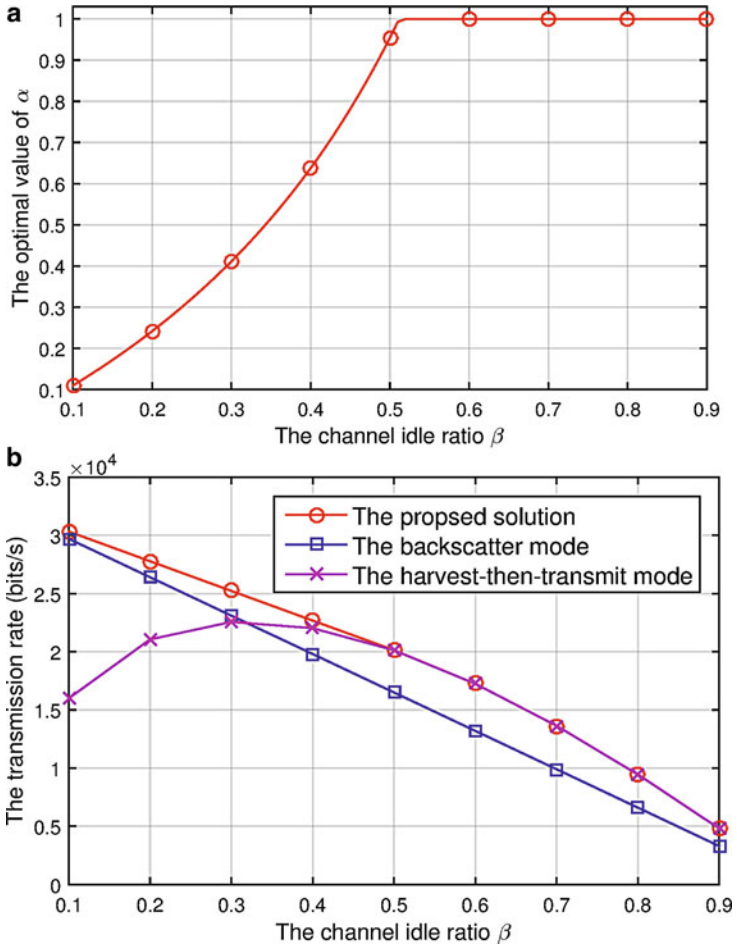

Fig. 12 The performance of the system under the variation of channel idle ratio

channel ratio is set at 0.3. In particular, as shown in Fig. 13a, as the backscatter transmission rate is increased from 1 to 21 kbps, the ST will always choose the harvest-then-transmit mode, i.e., $\alpha = 1$. However, if the backscatter transmission rate keeps increasing, the ST will spend more time for the backscatter mode. When it is greater than 45 kbps, the ST will use the backscatter mode only. Again, here the proposed solution always achieves the best performance compared with those of the BP and the HP as showed in Fig. 13b.

Then, the transmission policy of the ST under different wireless signals from selected practical RF sources is examined. Specifically, Fig. 13c studies three different signals, i.e., FM signals, TV signals, and WiFi signals. As observed in Fig. 13c, the ST will only select the harvest-then-transmit mode when the

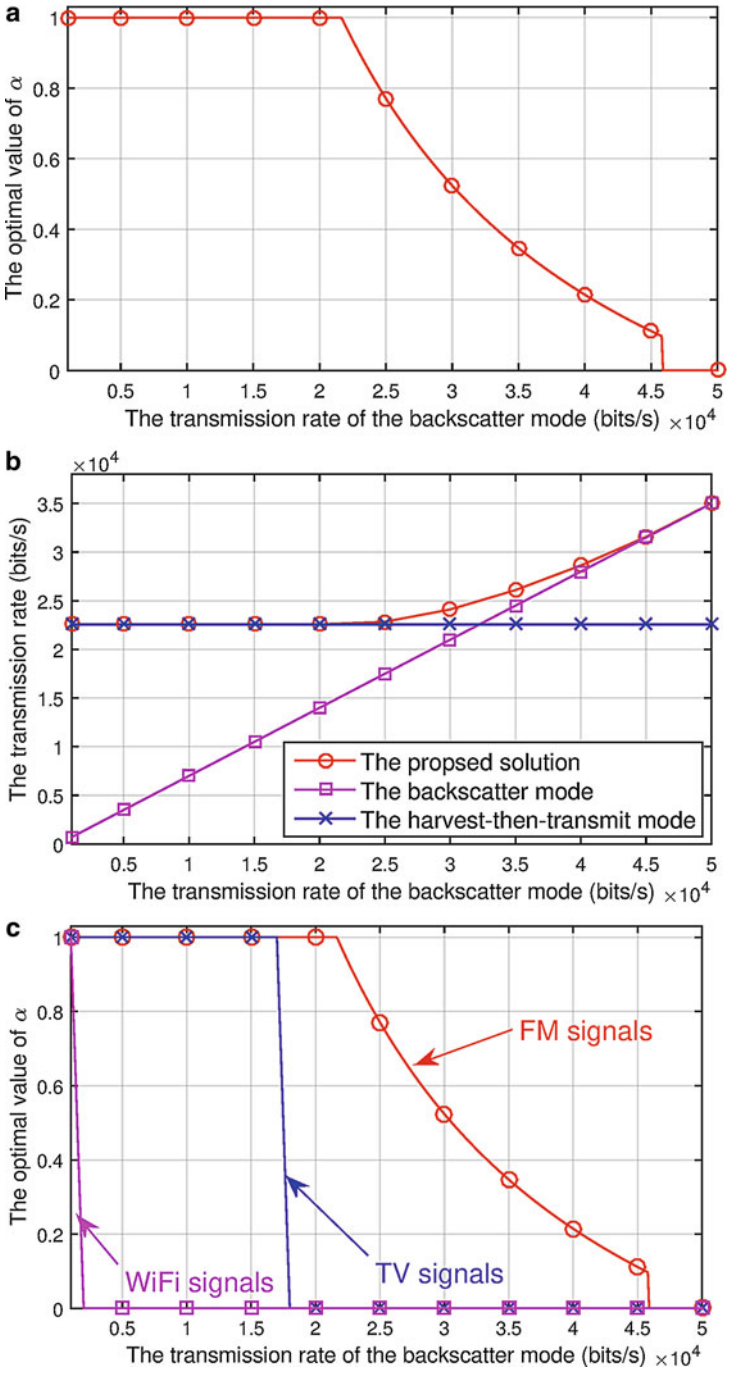

Fig. 13 The performance of the system under the variation of backscatter transmission rate

backscatter transmission rate is lower than 17 and 1 kbps, for TV signals and WiFi signals, respectively. This can be explained through the Friis equation in (9). In particular, for TV signals and WiFi signals, because they are transmitted at high frequencies (i.e., 915 MHz and 2.4 GHz, respectively), the amount of energy harvested at the ST will be reduced significantly, as compared with the FM signal. For WiFi signals, although the secondary system can be placed near the power source, e.g., access point, the source transmit power is relatively small (around 10 dBm as shown in Table 1) and the frequency is very high (few GHz). Therefore, the amount of harvested energy is very small. Consequently, the ST tends to spend more time for the backscatter mode.

Underlay Cognitive Radio Networks

In this section, the objective function of overall transmission rate under the variation of the α and β, i.e., $R(\alpha, \beta)$, is first examined in (46). Figure 14a, b consider two cases, i.e., $B_b = 10$ and 30 kbps, respectively. For $B_b = 10$ kbps, the optimal value of α and β are 0.682 and 0.318, respectively. This corresponds to the case when $\tau = \alpha + \beta = 1$, i.e., the ST will select the harvest-then-transmit mode. Conversely, for $B_b = 30$ kbps (Fig. 14b), the optimal solution is at $\alpha = 0$ and $\beta = 0$ (corresponding to $\tau = 0$). This implies that the ST will use the backscatter mode in this case. This result is also to illustrate the findings in section "RF-Powered Backscatter Underlay Cognitive Radio Network", i.e., the optimal transmission policy of the ST is a step function.

Then, the transmission rate of the backscatter mode is varied, and the policy along with the performance of the secondary system will be evaluated. As observed in Fig. 15a, as the backscatter transmission rate increases, the optimal value of τ will be reduced. Here, note that as stated in section "RF-Powered Backscatter Underlay Cognitive Radio Network", the variation of τ is a step function. In particular, in Fig. 15a, the ST will select the harvest-then-transmit mode if the backscatter transmission rate is lower than 22.6 kpbs and the backscatter mode otherwise. Again, as shown in Fig. 15b, it is confirmed that the proposed solution always achieves the best performance in terms of the overall transmission rate for the secondary system.

Figure 15c, similar to overlay CCNs, also compares the proposed solution of the ST under different types of wireless signals. Four different kinds of signals are examined, i.e., FM signals, TV signals, WiFi signals, and 3G mobile signals, which are generally considered in underlay CCNs. Similar to the overlay CCN, the decision of the ST also depends much on the characteristic of the received signal. For WiFi and 3G signals, although the secondary system can be placed near the power source, e.g., access point and cellular base station, the source transmit power is relatively small (around 10 dBm as shown in Table 1) and the frequency is very high (few GHz). Therefore, the amount of harvested energy is very small, and the ST will prefer using the backscatter mode in the cases of WiFi and 3G signals.

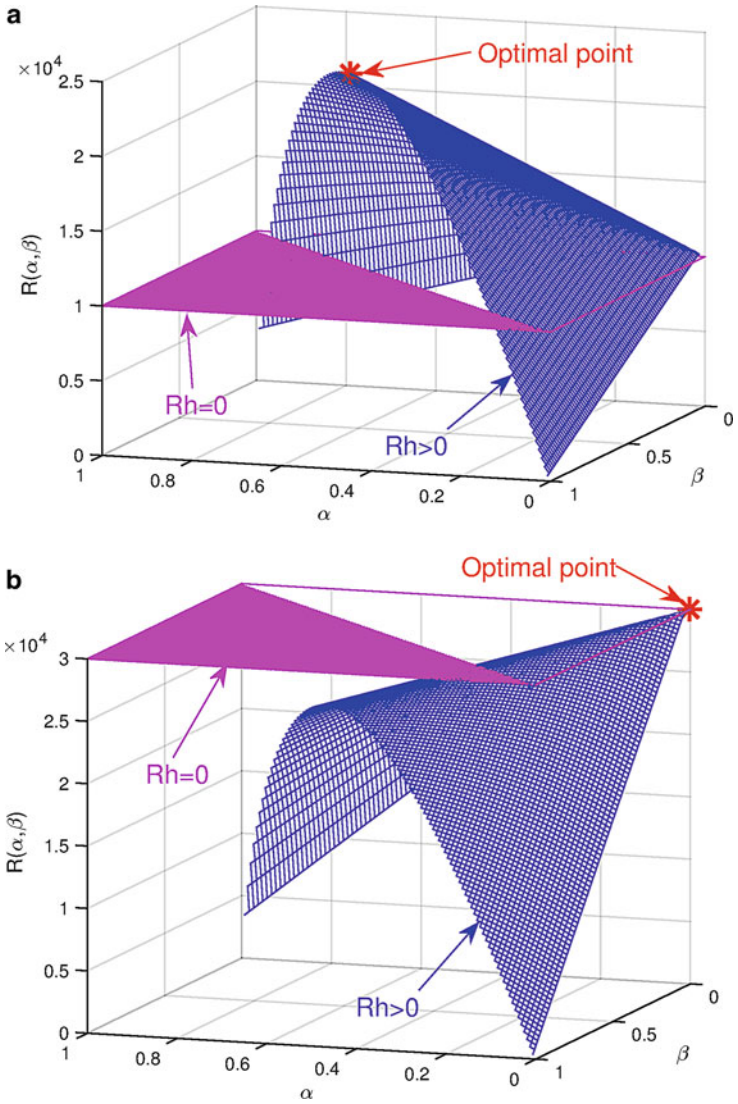

Fig. 14 The overall transmission rate $R(\alpha, \beta)$ under different value of B_b. (**a**) $B_b = 10$ kpbs. (**b**) $B_b = 30$ kpbs

Then, the signal frequency (Fig. 16) and the transmit power constraint (Fig. 17) of the secondary system are varied to investigate their impacts to the optimal policy of the ST. In particular, Fig. 16 shows that as the frequency of the signal increases, the amount of harvested energy will be reduced (Fig. 16a). Consequently, the backscatter mode will be more preferable (Fig. 16b). In Fig. 17, it is observed that when the transmit power constraint of the secondary system is more relaxed

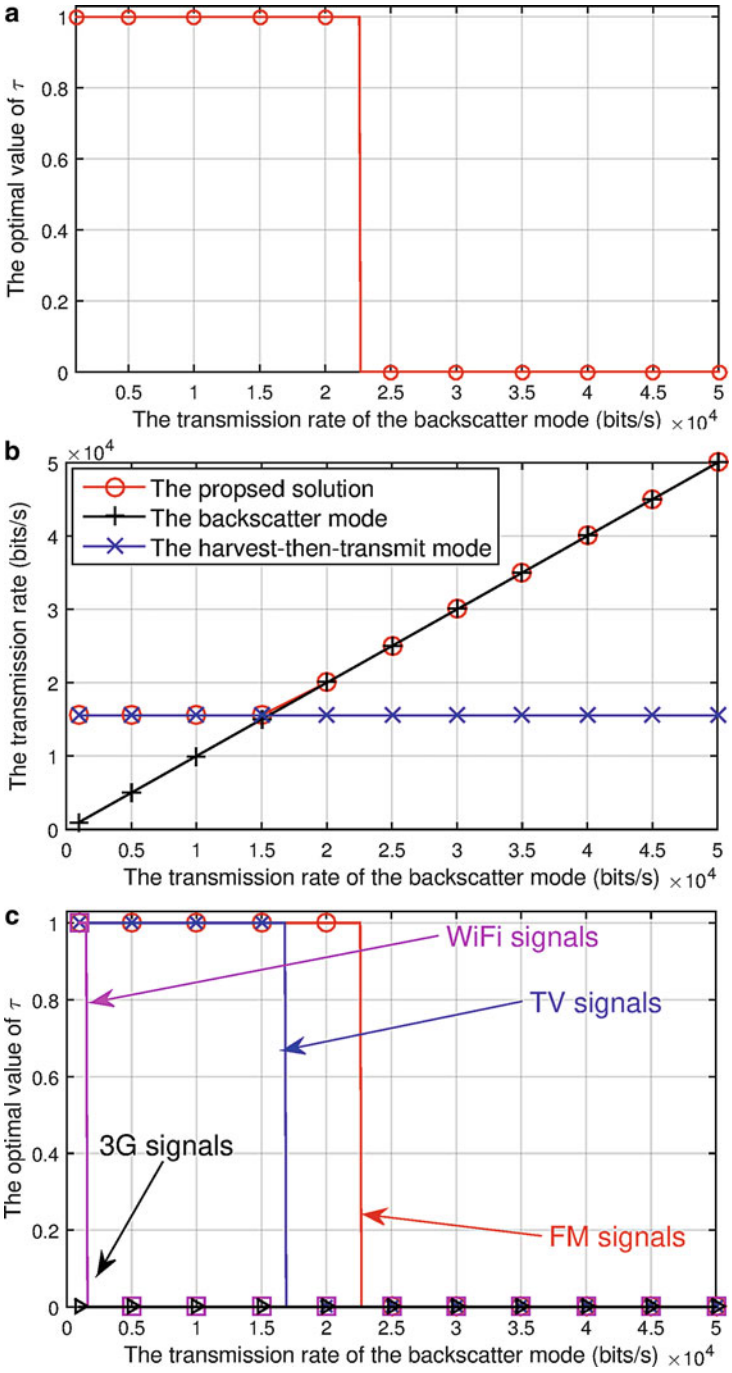

Fig. 15 The performance of the system under the variation of transmission bit rate of the backscatter mode

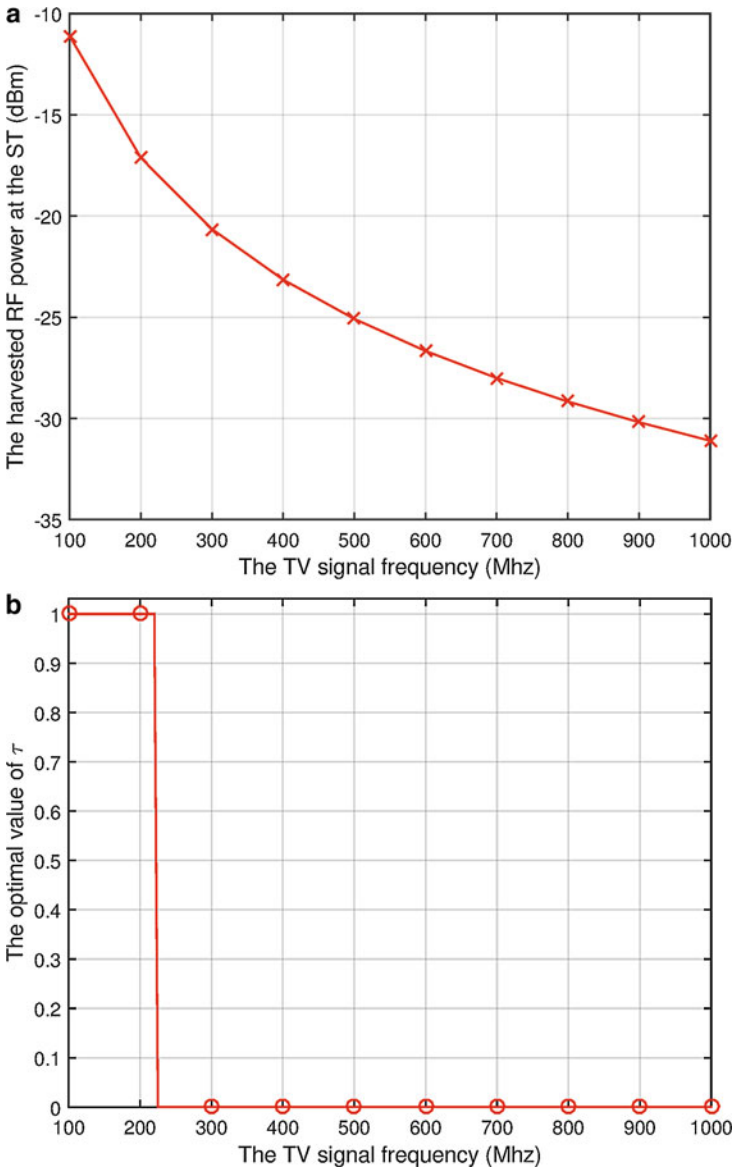

Fig. 16 The harvested RF power and the optimal policy of the ST when the TV signal frequency is varied

(i.e., the power threshold increases), the optimal value of τ also increases. This implies that the ST tends to choose the harvest-then-transmit mode. The reason is that when the transmit power constraint is limited at a low level, the secondary transmitter cannot fully utilize the harvested energy. Consequently, the ST will use the backscatter mode instead.

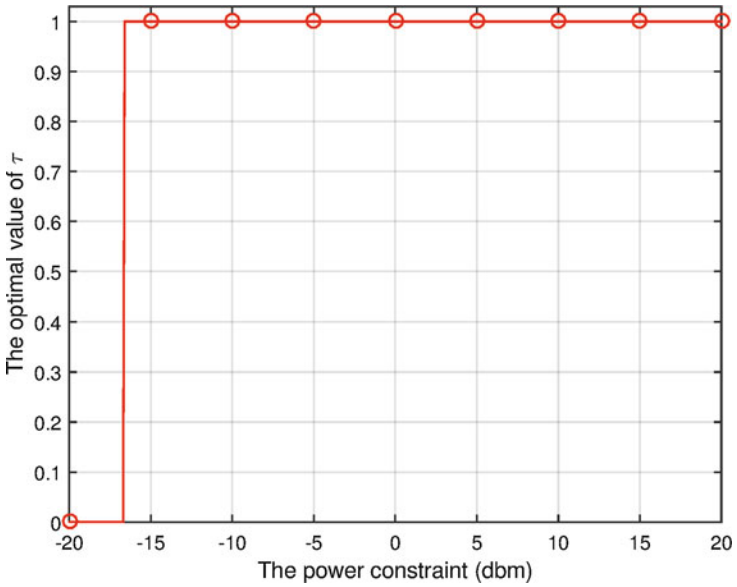

Fig. 17 The optimal policy of the ST under the variation of the power constraint $P^{\ddagger}$

Conclusions and Future Directions

The development of RF energy harvesting techniques together with ambient backscattering communication has opened great opportunities for cognitive cellular systems. In RF-powered cognitive cellular networks with ambient backscattering, secondary users can utilize not only the available spectrum holes when the channel is idle but also energy scavenging when the channel is busy, thereby improving network throughput of secondary systems significantly. This chapter first presents fundamental background on RF energy harvesting techniques and ambient backscattering communications. Then, the challenges of implementing these techniques in cognitive cellular networks are discussed, and the solutions are introduced. After that, two new approaches are presented based on two scenarios in cognitive cellular networks, i.e., overlay and underlay networks. Through numerical results, it is demonstrated that by incorporating the ambient backscatter communication and the conventional harvest-then-transmit protocol in RF-powered cellular cognitive radio networks, the secondary system always achieves the best performance under different setups. Moreover, the numerical results can provide insightful guidance to help a wireless node to choose the best mode.

There are some research directions in this topic.

- *Multiple secondary systems:* This chapter only considers a single secondary system. However, in practice, multiple secondary systems may coexist in the same cognitive cellular network. In this case, the optimal time trade-off problem

is much more complicated because we have to balance the time allocation among multiple secondary transmitters such that the overall network throughput is maximized and QoS requirements of all STs are satisfied. To address this problem, optimization techniques for multiple objectives presented in [13] could be a potential solution.

- *Economic models and game theory:* In the case when the secondary transmitter (ST) and receiver (SR) belong to different entities, the SR may not be interested in decoding information for the ST in the backscattering mode as the SR will lose energy in this process. To encourage an SR to decode information, the ST should incentivize the SR based on its demand on the backscattering time. As a result, economic models, e.g., Stackelberg game, can be adopted in this case. Alternatively, in the case when there are multiple secondary systems coexisting in the same environment, and they do not want to cooperate for the backscattering process as well as harvest-then-transmit process, noncooperative game models can be used to deal with this problem.
- *Extend the communication range:* In particular, because the transmission range of the ambient backscatter technique is relatively limited, i.e., within few meters. Thus, to extend the communication range, the backscatter process can be performed through relay nodes. It means the source node backscatters signals to the relay node, and then the relay node backscatters signals to the destination node. Thus, the transmission range for ambient backscattering systems can be extended greatly.

References

1. Maxwell JC (eds) (1881) A treatise on electricity and magnetism. Oxford, Clarendon
2. Ladan S, Ghassemi N, Ghiotto A, Wu K (2013) Highly efficient compact rectenna for wireless energy harvesting application. IEEE Microw Mag 14(1):117–122
3. Kuhn V, Lahuec C, Seguin F, Person C (2015) A multi-band stacked RF energy harvester with RF-to-DC efficiency up to 84%. IEEE Trans Microw Theory Tech 63(5):1768–1778
4. Balanis CA (eds) (2012) Antenna theory: analysis and design. New York
5. Rappaport TS (eds) (2001) Wireless communications: principles and practice. Upper Saddle River
6. Lee S, Zhang R, Huang K (2013) Opportunistic wireless energy harvesting in cognitive radio networks. IEEE Trans Wirel Commun 12(9):4788–4799
7. Yao Y, Song X, Yin C, Huang S (2015) Opportunistic energy harvesting and energy-based opportunistic spectrum access in cognitive radio networks. In: International Conference on Cognitive Radio Oriented Wireless Networks. Springer International Publishing, pp 187–198
8. Park S, Heo J, Kim B, Chung W (2012) Optimal mode selection for cognitive radio sensor networks with RF energy harvesting. In: IEEE International Symposium on Personal Indoor and Mobile Radio Communications, Sydney, pp 2155–2159
9. Park S, Kim H, Hong D (2013) Cognitive radio networks with energy harvesting. IEEE Trans Wirel Commun 12(3):1386–1397
10. Park S, Hong D (2014) Achievable throughput of energy harvesting cognitive radio networks. IEEE Trans Wirel Commun 13(2):1010–1022
11. Park S, Hong D (2013) Optimal spectrum access for energy harvesting cognitive radio networks. IEEE Trans Wirel Commun 12(12):6166–6179

12. Rakovic V, Denkovski D, Hadzi-Velkov Z, Gavrilovska L (2015) Optimal time sharing in underlay cognitive radio systems with RF energy harvesting. In: IEEE International Conference on Communications, London, pp 7689–7694
13. Ju H, Zhang R (2014) Throughput maximization in wireless powered communication networks. IEEE Trans Wirel Commun 13(1):418–428
14. Yin S, Zhang E, Qu Z, Yin L, Li S (2014) Optimal cooperation strategy in cognitive radio systems with energy harvesting. IEEE Trans Wirel Commun 13(9):4693–4707
15. Li D, Yin S, Li S (2013) One-step-ahead spectrum sensing in cognitive radio systems with wireless energy harvesting. In: IEEE Global High Tech Congress on Electronics, Shenzhen, pp 130–134
16. Yin S, Zhang E, Yin L, Li S (2013) Optimal saving-sensing-transmitting structure in self-powered cognitive radio systems with wireless energy harvesting. In: IEEE International Conference Communications, Budapest, pp 2807–2811
17. Lu X, Xu W, Li S, Lin J, He Z (2014) Simultaneous information and power transfer for relay-assisted cognitive radio networks. In: IEEE International Conference on Communications Workshops, Sydney, pp 331–336
18. Mousavifar SA, Liu Y, Leung C, Elkashlan M, Duong TQ (2014) Wireless energy harvesting and spectrum sharing in cognitive radio. In: IEEE 80th Vehicular Technology Conference, Vancouver, pp 1–5
19. Yang Z, Ding Z, Fan P, Karagiannidis GK (2016) Outage performance of cognitive relay networks with wireless information and power transfer. IEEE Trans Veh Technol 65(5): 3828–3833
20. Wang Z, Chen Z, Yao Y, Xia B, Liu H (2014) Wireless energy harvesting and information transfer in cognitive two-way relay networks. In: IEEE Global Communications Conference, Austin, pp 3465–3470
21. Wang Z, Chen Z, Luo L, Hu Z, Xia B, Liu H (2014) Outage analysis of cognitive relay networks with energy harvesting and information transfer. In: IEEE International Conference on Communications, Sydney, pp 4348–4353
22. Zheng G, Ho Z, Jorswieck EA, Ottersten B (2014) Information and energy cooperation in cognitive radio networks. IEEE Trans Signal Process 62(9):2290–2303
23. Gao Q, Jing T, Xing X, Cheng X, Huo Y, Chen D (2015) Simultaneous energy and information cooperation in MIMO cooperative cognitive radio systems. In: IEEE Wireless Communications and Networking Conference, New Orleans, pp 351–356
24. Li B, Xu W, Gao X (2015) Energy-efficient simultaneous information and power transfer in OFDM-based CRNS. In: IEEE Vehicular Technology Conference, Glasgow, pp 11–14
25. Shafie AE, Ashour M, Khattab T, Mohamed A (2015) On spectrum sharing between energy harvesting cognitive radio users and primary users. In: International Conference on Computing, Networking and Communications, California, pp 214–220
26. Sibomana L, Zepernick H-J, Tran H (2015) Wireless information and power transfer in an underlay cognitive radio network. In: International Conference on Signal Processing and Communication Systems, Cairns, pp 1–7
27. Gesbert D, Alouini MS (2004) How much feedback is multi-user diversity really worth? In: IEEE International Conference on Communications, Paris, pp 234–238
28. Ng DWK, Lo ES, Schober R (2016) Multi-objective resource allocation for secure communication in cognitive radio networks with wireless information and power transfer. IEEE Trans Veh Technol 65(5):3166–3184
29. Hoang DT, Niyato D, Wang P, Kim DI (2014) Opportunistic channel access and RF energy harvesting in cognitive radio networks. IEEE J Sel Areas Commun 32(11):2039–2052
30. Hoang DT, Niyato D, Wang P, Kim DI (2015) Performance optimization for cooperative multiuser cognitive radio networks with RF energy harvesting capability. IEEE Trans Wirel Commun 14(7):3614–3629
31. Tse D, Viswanath P (eds) (2005) Fundamentals of wireless communication. Cambridge University Press, Cambridge

32. Liu V, Parks A, Talla V, Gollakota S, Wetherall D, Smith JR (2013) Ambient backscatter: wireless communication out of thin air. In: Proceedings of the ACM SIGCOMM, Hong Kong, pp 39–50
33. Dunne C (2013) Ambient backscatter: brings us closer to an internet of things. http://www.fastcodesign.com/3017570/ambient-backscatter-brings-us-closer-to-an-internet-of-things
34. Parks AN, Liu A, Gollakota S, Smith JS (2014) Turbocharging ambient backscatter communication. ACM SIGCOMM Comput Commun Rev 44(4):619–630
35. Penichet CP, Varshney A, Hermans F, Rohner C, Voigt T (2016) Do multiple bits per symbol increase the throughput of ambient backscatter communications? In: Proceedings of the International Conference on Embedded Wireless Systems and Networks, TU Graz, pp 355–360
36. You J, Wang G, Zhong Z (2015) Physical layer security-enhancing transmission protocol against eavesdropping for ambient backscatter communication system. In: 6th International Conference on Wireless, Mobile and Multi-Media, Beijing, pp 43–47
37. Lu K, Wang G, Qu F, Zhong Z (2015) Signal detection and BER analysis for RF-powered devices utilizing ambient backscatter. In: International Conference on Wireless Communications & Signal Processing, Nanjing, pp 1–5
38. Zhang P, Ganesan D (2014) Enabling bit-by-bit backscatter communication in severe energy harvesting environments. In: Proceedings of the 11th USENIX Conference on Networked Systems Design and Implementation, pp 345–357
39. Hoang DT, Niyato D, Wang P, Kim DI, Han Z (2016) The tradeoff analysis in RF-powered backscatter cognitive radio networks. In: IEEE GLOBECOM, Washington DC
40. Huang H, Lau VKN (2012) Decentralized delay optimal control for interference networks with limited renewable energy storage. IEEE Trans Sig Process 60(5):2552–2561
41. Kim DY, Kim DI (2010) Reverse-link interrogation range of a UHF MIMO-RFID system in Nakagami-m fading channels. IEEE Trans Ind Electron 57(4):1468–1477

Spectrum Sharing of Drone Networks

38

Chiya Zhang, Zhiqing Wei, Zhiyong Feng, and Wei Zhang

Contents

C. Zhang (✉) · W. Zhang
School of Electrical Engineering and Telecommunications, The University of New South Wales, Sydney, NSW, Australia
e-mail: chiya.zhang@unsw.edu.au; w.zhang@unsw.edu.au

Z. Wei · Z. Feng
Key Laboratory of Universal Wireless Communications, Ministry of Education, Beijing University of Posts and Telecommunications, Beijing, China
e-mail: weizhiqing@bupt.edu.cn; fengzy@bupt.edu.cn

W. Zhang (ed.), *Handbook of Cognitive Radio*,
https://doi.org/10.1007/978-981-10-1394-2_35

Abstract

Drone networks are aerial base stations that can be used to support cellular networks. The underlay spectrum sharing between the three-dimensional (3D) drone small cells (DSCs) downlink network modeled by a 3D Poisson point process and traditional cellular networks modeled by a 2D Poisson point process is introduced. To maximize the DSC network throughput while satisfying the cellular network efficiency constraint, the optimal density of DSC aerial base stations is discussed. The maximum throughput of the DSC user increases almost linearly with the increase of the DSC outage constraint. Effects of directional transmission on DSC networks is further discussed. Besides density control, power and beam control can also be applied in the spectrum sharing between unmanned aerial vehicle (UAV) network and ground network. With the mobility pattern information of UAVs, the delay-tolerant transmissions can be constructed and multiple transmission modes are implemented to carry various types of traffic. Exploiting cognition capability on mobility, UAV network can provide high quality of information services in the highly dynamic environment with limited resources.

Introduction

UAV, commonly known as a drone, refers to an aircraft without a human pilot aboard. We can expect drones developing in many interesting applications, such as policing and surveillance and scientific research. As illustrated in Fig. 1, UAVs aerial base stations can establish communication connection between ground node A and B. UAVs can also act as aerial sensors to collect environment data and transmit data to the control station. UAVs can act as aerial base stations or relays, namely, drone small cells (DSCs), to provide communication services to the areas with natural disasters and traffic congestions. DSCs can be deployed in a high-altitude platform (HAP) which is above 10 km height or in low-altitude platform (LAP) below 10 km [1].

DSC network has several advantages over conventional cellular networks. The fifth generation communication utilizing mmWave signals suffers many propagation-related shortcomings, such as relatively short range and vulnerable to blockage. UAVs can exploit its mobility to avoid the blockage and provide seamless coverage. Further, aerial base stations are robust to environmental changes. Another advantage of UAV networks is the flexibility of reconfiguration. For example, UAVs can be deployed to help offloading cellular networks in wireless congestion events with low cost. In [2], optimal deployment altitude of a drone providing maximum coverage is discussed. The deployment design and performance analysis of DSCs at LAP are further studied in [3], in which the optimal altitude maximizing ground coverage and minimizing required transmit power for a single DSC is derived. Their result shows that the optimal deployment altitude varies according to different environment statistics.

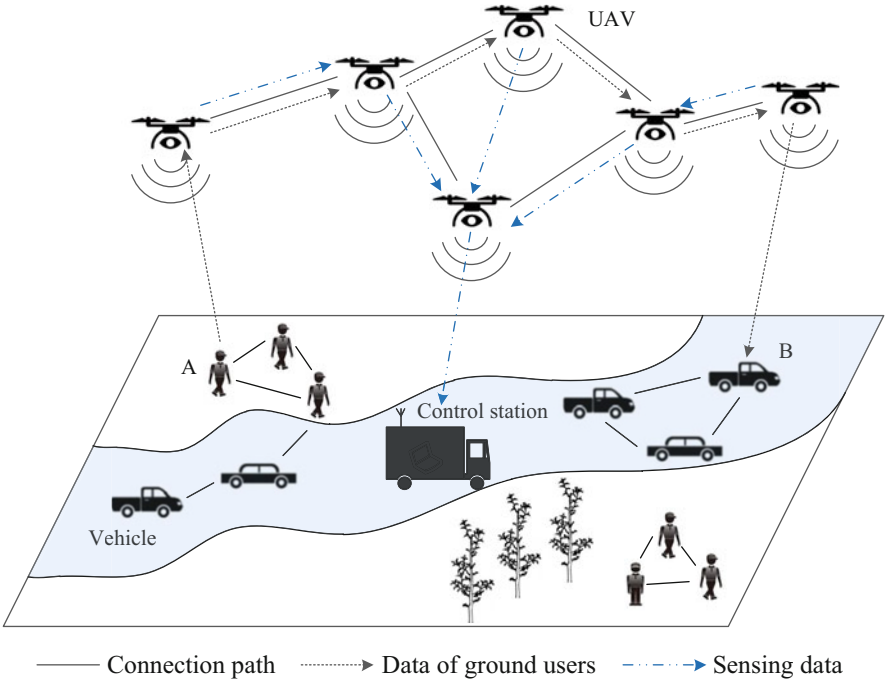

Fig. 1 Application scenario of UAV network

UAVs can be preprogrammed to fly autonomously from the starting point to destination. However, when multiple UAVs acting as cas aerial base stations, the ability of remote control could significantly improve the operation and safety [4]. For instance, if there is a possible collision due to traffic management, it is essential that information is shared to the UAVs promptly. Federal Aviation Administration (FAA) is exploring that each intended UAV use case has certain coverage, latency, and reliability requirements to ensure proper operational control of the UAVs [5]. In a typical multi-UAV network, the ground control station is mainly responsible for dispatching, coordinating, charging, and collecting of UAVs [6].

In the scenario where UAVs have a relatively small transmission range, the traffic is usually generated within the UAVs and transmits to control station via multi-hop transmissions. Repeated data transmissions in multi-hop transmission manner will consume radio resources and decrease network capacity. Thus environment cognition is proposed to improve the capacity of UAV network. Also, broadband UAV network would need to be constructed to support massive data transmission. According to Shannon-Hartley theorem [7], the capacity increases logarithmically with the transmit power. However, the capacity increases linearly with the bandwidth of spectrum. UAVs have limited carrying capacity and energy supply. Thus exploiting more spectrum is a practical way to increase the capacity of UAV network. With multiple sensors such as radar, Global Positioning System (GPS) ,

and camera implemented in UAVs, the environment cognition besides traditional spectrum sensing can be realized to further improve the capacity and adaptability of UAV network.

One of the most important problems on the coexistence between DSC and cellular network is the interference management. Underlay spectrum sharing between a 3D DSC network and a 2D cellular network is proposed for interference management [8, 9]. Underlay spectrum sharing refers to the simultaneous transmissions from DSC network and cellular network as long as the interference level at the cellular user side remains acceptable. The cellular signal would degrade dramatically if DSC network exceeds the predefined tolerable interference threshold. It has been demonstrated in traditional cellular network that spectrum sharing technologies can provide complementary benefits to dedicated spectrum. Effort was made toward spectrum sharing technologies of DSCs [10].

The spectrum sharing of 2D cellular wireless networks has been well studied in recent years [11, 12]. Different interference management strategies in 2D Poisson cognitive radio networks have been developed, for example, inter-cell interference coordination and intra-cell diversity [13]. It is also revealed from [13] that the general stochastic results for PPP base station deployments are independent to the shadow fading distribution as long as the shadowing is independent and identically distributed. The primary exclusive regions (PERs) centered at every primary receiver are designed in [14]. PER is a fixed region centered at each primary receiver in which no secondary transmitter is allowed to transmit signals. Applying PERs provides extra level of control to the network performance. It is often used to further guarantee the primary performance, e.g., when the primary users require a very small outage. The relationship between shadowing with path loss exponent and PERs is further analyzed in [15]. As the idea of PER effectively guarantees the primary service under limited spectrum resources, research efforts have been made to implement PERs into the optimization of different spectrum sharing schemes [16, 17]. Assuming all transmitters are 2D Poisson distributed nodes with limited feedback of channel quality information from their local receiver, two limited feedback-based underlay spectrum sharing schemes are proposed in [16], with and without PERs, respectively.

Further, it is discovered that there exist temporal spectrum opportunities in PER. The architecture of three regions including black, gray, and white regions is proposed in [18]. Black region is surrounded by gray region and gray region is surrounded by white region [18]. In black region, SUs are not allowed to transmit. In gray region, SUs can exploit temporal spectrum opportunities. Namely, SUs can use the spectrum that is not used by primary users (PUs). In white region, because SUs are far away from PUs, SUs can transmit all the time with maximum power. When primary receivers are densely deployed, the union of PERs of all primary receivers forms a layer. When a UAV is located below the layer, it is not allowed to transmit. Moreover, the architecture of three regions can be applied in UAV network. As illustrated in Fig. 2, layer 1 and layer 2 divide the 3D space into three regions. In region 1, since UAVs are close to the ground users, UAVs are not allowed to transmit. In region 2, UAVs are farther to ground users. Thus UAVs can exploit the temporal spectrum opportunities. In region 3, since UAVs are sufficiently high

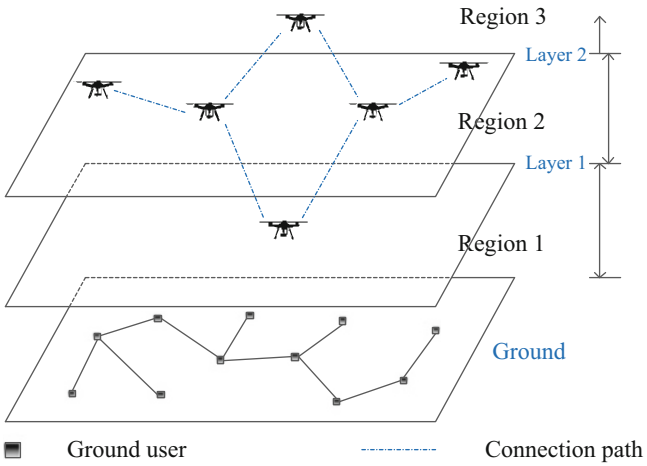

Fig. 2 PER layers of UAV network

above the ground, UAVs can transmit all the time. Regions 1, 2, and 3 are similar to the black, gray, and white regions, respectively in [19]. It is verified in [19] that the capacity of secondary network with three regions is larger than that with PER. Hence the architecture of three regions can also be applied in cognitive UAV network.

Stochastic geometry theory provides effective tools to study the average behavior over spatial realizations of a large wireless network [20]. For 2D networks, there are several empirical and theoretical results indicating that a Poisson point process (PPP) is an appropriate point process to model base station deployments with tractability. PPP is widely used to model different types of networks, for instance, cognitive radio networks [16], cellular networks [21], and wireless sensor networks [22]. It is shown in [23] that under certain appropriate conditions, the stochastic results obtained by modeling wireless networks as spatial PPPs are still valid, even if in reality the positioning of transmitting nodes does not appear Poisson.

One of the future trends of cellular networks is to have smaller cells to deserve the growing number of communications [24]. The standard concept of planar cellular networks is extended into 3D space in [25]. Different cell shapes in 3D cellular networks achieving full coverage are investigated in [26]. It is demonstrated that truncated octahedral cell results in the best strategy. Applying stochastic tools to 3D ultradense cellular networks, different coverage probability and throughput scaling behaviors in terms of the path loss components using a dual path loss model are discussed in [21].

In this chapter, the study of DSC network underlay spectrum sharing with cellular network is presented. Taking advantage of the tractability of Poisson point process, explicit expressions for the DSC coverage probability and achievable throughput are derived by stochastic geometry. To maximize the DSC network throughput while satisfying the cellular network efficiency constraint, the optimal density of DSC aerial base stations is discussed. The maximum throughput of the DSC user increases almost linearly with the increase of the DSC outage constraint. Effects of PERs and directional transmission on DSC networks are further discussed.

Besides density control, power and beam control can also be applied in the spectrum sharing between UAV network and ground network. The traditional cognitive radio technology focuses on spectrum sensing, spectrum decision and spectrum sharing, etc. However, since UAVs are robotic system, the mobility of UAVs can be controlled to improve network capacity. The concept of mobility cognitive UAV network is then proposed. Mobility pattern cognition aims to discover returning UAVs to construct the delay-tolerant transmission scheme, which carries the delay-insensitive traffic with Store-Carry-and-Forward (SCF) mode to avoid multi-hop transmissions consuming radio resources. The delay-sensitive traffic is still carried by multi-hop transmission manner.

Spectrum Sharing of UAV Network

Optimal DSC Density

As shown in Fig. 3, DSC networks distribute in 3D space. Assume that DSC aerial base stations follow a 3D-PPP $\{X_i \in \Phi_d\}$ with density λ_d in an infinite 3D space $\mathbb{V}$, but the height is limited to L, that is, $\mathbb{V} = \{(x, y, z) : x, y \in \mathbb{R}, z \in [0, L]\}$. The channel between any pair of DSC aerial base station and the user here is assumed to undergo path loss and the small-scale fading. The path loss is proportional to $x^{-\alpha}$, where x is the distance between the transmitting aerial base station and the typical user and α is the mean path loss exponent. The power gain of small-scale fading channel h_i is exponentially distributed with unit mean, and the noise N_0 is additive white Gaussian noise following the distribution $N_0 \sim N(0, N)$. DSCs only transmit while they are static [10,27], e.g., moving DSCs will perform transmission on certain "stop points."

Assume that all aerial base stations transmit at the same power level P_d. For a typical link, the received signal power is hence $P_d h_0 D^{-\alpha}$, where D is the distance between a typical user and a typical aerial base station. The transmission is successful if the received SINR at a receiver is larger than a certain threshold. Set the SINR thresholds of DSC users to θ. A typical DSC user at the origin O will receive interference from other transmitting DSC base stations while receiving the desired signal. The received SINR of a typical user at the origin O is:

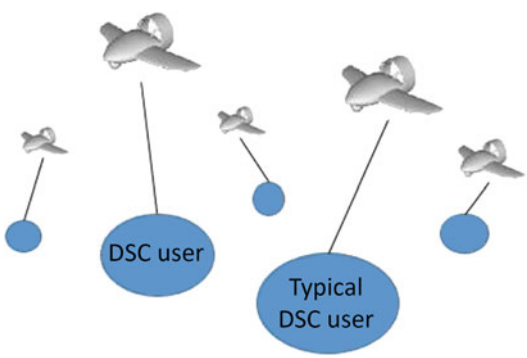

Fig. 3 DSC networks

$$SINR_d = \frac{P_d h_0 D^{-\alpha}}{N + \sum_{x_i \in \Phi_d \setminus \{0\}} P_d h_i x_i^{-\alpha}}. \tag{1}$$

The transmission rate of a network is defined as [11]:

$$T_d = \lambda_d P(SINR_d > \theta) \log(1 + \theta). \tag{2}$$

Assuming that the DSC network has an outage probability constraint $\varepsilon_d \ll 1$, the optimal DSC base station density can be obtained by solving the following optimization problem:

$$\begin{aligned} &\underset{\lambda_d}{\text{maximize}} \quad T_d && (G1) \\ &\text{subject to} \quad P(SINR_d > \theta) > 1 - \varepsilon_d. \end{aligned}$$

Next, the optimal DSC base station density for a single-tier DSC downlink network in 3D space can be derived. Let $I = \sum_{x_i \in \Phi_d \setminus \{0\}} h_i x_i^{-\alpha}$. From (1) we have the coverage probability as

$$\begin{aligned} P(SINR_d > \theta) &= P\left(\frac{h_0 D^{-\alpha}}{\frac{N}{P_d} + I} > \theta\right) && (3) \\ &= \mathbb{E}_I\left[P\left(h_0 > \theta D^{\alpha}\left(\frac{N}{P_d} + I\right)\right) | I\right] \\ &= \mathbb{E}_I\left[\exp\left(-\theta D^{\alpha}\frac{N}{P_d}\right)\exp(-\theta D^{\alpha} I)\right] \\ &= \exp\left(-\theta D^{\alpha}\frac{N}{P_d}\right)\mathscr{L}_I(\theta D^{\alpha}). && (4) \end{aligned}$$

where $\mathscr{L}_I(\theta D^{\alpha})$ is the Laplace transform of the interference $I = \sum_{x_i \in \Phi_d \setminus \{0\}} h_i x_i^{-\alpha}$, which can be further derived as:

$$\begin{aligned} \mathscr{L}_I(\theta D^{\alpha}) &= \mathbb{E}_I[\exp(-\theta D^{\alpha} I)] && (5) \\ &= \mathbb{E}_{\Phi_d, h_i}\left[\prod_{x_i \in \Phi_d \setminus \{0\}} \exp(-\theta D^{\alpha} h_i x_i^{-\alpha})\right] && (6) \\ &= \mathbb{E}_{\Phi_d}\left[\prod_{x_i \in \Phi_d \setminus \{0\}} \mathbb{E}_{h_i}[\exp(-\theta D^{\alpha} h_i x_i^{-\alpha})]\right] && (7) \\ &= \mathbb{E}_{\Phi_d}\left[\prod_{x_i \in \Phi_d \setminus \{0\}} \frac{1}{1 + \theta D^{\alpha} x_i^{-\alpha}}\right]. && (8) \end{aligned}$$

where (7) follows because of the i.i.d. distribution of h_i and its further independence from the point process Φ_d. Equation (8) follows because h_i is exponential distributed with unit mean. The probability generating functional of a set $\mathbb{V}$ is given by [28]:

$$\mathbb{E}\left(\prod_{x_i \in \Phi} f(x)\right) = \exp\left(-\lambda_d \int_{\mathbb{V}} [1 - f(x)] dx\right). \tag{9}$$

Applying (9) into (8), we have

$$\mathscr{L}_I(\theta D^\alpha) = \exp\left(-\lambda_d \int_{\mathbb{V}} \left(1 - \frac{1}{1 + \theta D^\alpha x^{-\alpha}}\right) dx\right) \tag{10}$$

$$= \exp\left(-\lambda_d \int_0^L \int_0^{2\pi} \int_0^\infty \left(1 - \frac{1}{1 + \theta D^\alpha (\sqrt{r^2 + z^2})^{-\alpha}}\right) r dr d\phi dz\right) \tag{11}$$

$$= \exp\left(-2\pi\lambda_d \int_0^L \int_0^\infty \frac{\theta D^\alpha r (\sqrt{r^2 + z^2})^{-\alpha}}{1 + \theta D^\alpha (\sqrt{r^2 + z^2})^{-\alpha}} dr dz\right)$$

$$= \exp(-\lambda_d H(L, \theta, D, \alpha)) \tag{12}$$

where

$$H(L, \theta, D, \alpha) = \int_0^L \int_0^\infty \frac{2\pi\theta D^\alpha r (\sqrt{r^2 + z^2})^{-\alpha}}{1 + \theta D^\alpha (\sqrt{r^2 + z^2})^{-\alpha}} dr dz. \tag{13}$$

With (4), (5), (6), (7), (8), (9), (10), (11), and (12), we are now able to solve the optimization problem $(G1)$.

$$\begin{aligned} &\underset{\lambda_d}{\text{maximize}} \quad T_d \qquad\qquad (G1) \\ &\text{subject to} \quad P(SINR_d > \theta) > 1 - \varepsilon_d. \end{aligned}$$

Since T_d in (2) is unimodal in terms of λ_d and $P(SINR_d > \theta)$ is a decreasing function of λ_d, Karush-Kuhn-Tucker (KKT) conditions [16] are applicable. The Lagrange function of the above optimization problem is given by:

$$\mathscr{L}(\lambda_d) = T_d + \mu(P(SINR_d > \theta) - 1 + \varepsilon_d). \tag{14}$$

where μ is the Lagrange multiplier. Then, the KKT conditions are given as:

$$\frac{d\mathscr{L}(\lambda_d)}{d\lambda_d} = \frac{dT_d}{d\lambda_d} + \mu \frac{dP(SINR_d > \theta)}{d\lambda_d}. \tag{15}$$

$$\mu(P(SINR_d > \theta) - 1 + \varepsilon_d) = 0. \tag{16}$$

$$P(SINR_d > \theta) - 1 + \varepsilon_d \geq 0. \tag{17}$$

$$\mu \geq 0 \quad \text{and} \quad \lambda_d \geq 0. \tag{18}$$

Solving Eqs. (15) to (18) yields the optimal of DSC aerial base stations, as follows:

$$\lambda_d^* = \frac{[-\ln(\frac{1-\varepsilon_d}{\exp(-\theta D^\alpha \frac{N}{P_d})})]^+}{H(L, \theta, D, \alpha)}. \tag{19}$$

where $[.]^+$ denotes $\max(., 0)$. The maximum DSC network throughput is given by

$$T_d^* = \frac{\left[-\ln\left(\frac{1-\varepsilon_d}{\exp(-\theta D^\alpha \frac{N}{P_d})}\right)\right]^+}{H(L, \theta, D, \alpha)}(1 - \varepsilon_d)\log(1 + \theta). \tag{20}$$

It can be seen from (19) that the optimal primary density is obtained when the success probability just meets the outage constraint. Since $\varepsilon_d \ll 1$, we have $\ln(1 - \varepsilon_d) \approx -\varepsilon_d$. Therefore, for small ε_d, both optimal DSC density and potential throughput are linear with the DSC network outage constraint ε_d.

Effect of Different Path Loss Models

In this section, effect of a more specific air-to-ground path loss model is discussed. Different air to ground channel path loss models have been proposed and measured to suit in different environments [29]. Simplified mean path loss model for the spectrum sharing analysis in this chapter is given by:

$$l(x) = x^{-\alpha}. \tag{21}$$

Another air-to-ground path loss model $l(x, \gamma)$ for an air vehicle locating at distance x and elevation angle γ from the origin is given by [1]:

$$l(x, \gamma) = P_{LOS} x^{-\alpha_1} + P_{NLOS} k x^{-\alpha_1}. \tag{22}$$

in which α_1 and k are the path loss exponent and parameter corresponding to different type of links. $P_{NLOS} = 1 - P_{LOS}$. P_{LOS} is the line of sight probability. It is further given by:

$$P_{LOS} = \frac{1}{1 + a\exp(-b[\gamma - a])}. \tag{23}$$

where a and b are parameters determined by environment.

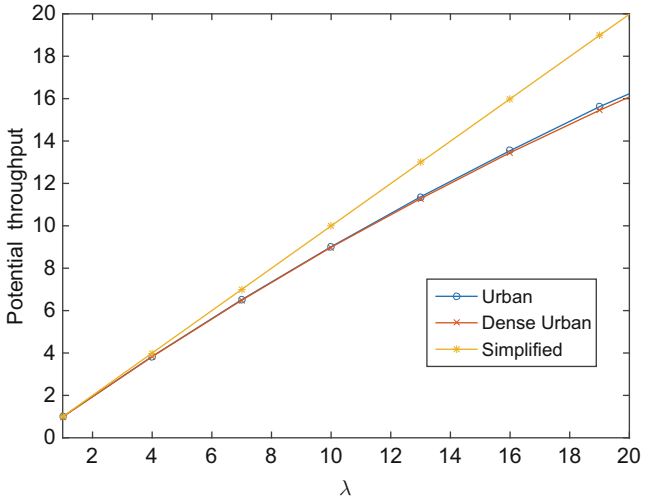

Fig. 4 Potential throughput of different path loss models $L = 0.1$, $D = 0.05$

Table 1 Radio-frequency propagation parameters

Environment	(a,b)	$\alpha(\alpha_1)$	k
Simplified		4	
Urban	(9.61,0.16)	2	20dB
Dense Urban	(12.08,0.11)	2	23dB

Radio frequency 2,000 MHz [1]

Figure 4 plots the scaling behavior of network throughput in terms of the drone density λ by simulations. The numerical values of the parameters of the air-to-ground channels for different environments are presented in Table 1. It can be observed that the potential throughput of drone network monotonically increases with node density for all different path loss models. As the research on modeling the air-to-ground channel is ongoing, the insight of underlay spectrum sharing results in this chapter is applicable for more precise path loss models in the future.

Spectrum Sharing Between DSC Network and Cellular Network

Optimal DSC Density

As shown in Fig. 5, cellular base stations are distributed on the ground as a 2D PPP with density λ_c. The distance between a typical cellular base station and its associated user is d. Similar to that of DSC network, we assume that all cellular base stations transmit with power P_c. The channel between any base station and the user undergoes path loss and the small-scale fading. The power gain of the small-scale

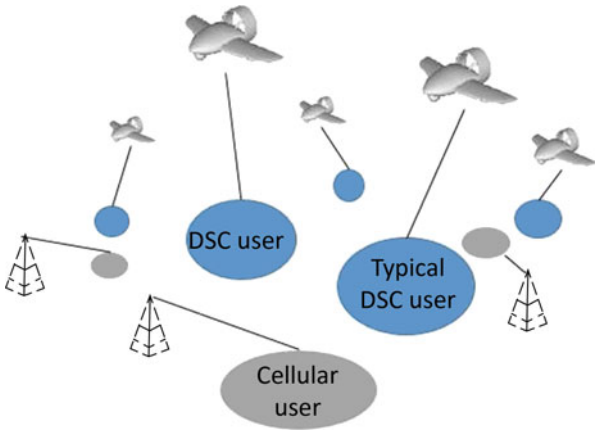

Fig. 5 Spectrum sharing between drone small cells (DSCs) networks and cellular networks

fading channel h_j is exponentially distributed with the unit mean, and the noise is $N_0 \sim N(0, N)$. Each cellular transmitter decides to transmit if the received SINR is larger than a certain threshold θ_c with a 1-bit feedback from the cellular receiver [16]. The active cellular base stations follow a thinned 2D PPP $\{Y_j \in \Phi_c\}$. Considering a typical DSC user at the origin O, it will receive interference not only from transmitting DSC base stations but also from transmitting cellular base stations. The SINR of the typical DSC user is given by

$$SINR_{dc} = \frac{P_d h_0 D^{-\alpha}}{N + P_d \sum_{i \in \Phi_d \setminus \{0\}} h_i x_i^{-\alpha} + P_c \sum_{j \in \Phi_c} h_j y_j^{-\alpha}}. \tag{24}$$

The SINR expressions of a typical cellular user with and without the DSC network are given by, respectively, as follows:

$$SINR_c = \frac{P_c h_0 d^{-\alpha}}{N + P_d \sum_{i \in \Phi_d} h_i x_i^{-\alpha} + P_c \sum_{j \in \Phi_c \setminus \{0\}} h_j y_j^{-\alpha}}. \tag{25}$$

$$SINR'_c = \frac{P_c h_0 d^{-\alpha}}{N + P_c \sum_{j \in \Phi_c \setminus \{0\}} h_j y_j^{-\alpha}}. \tag{26}$$

The throughputs of DSC and cellular networks are:

$$T_{dc} = \lambda_{dc} P(SINR_{dc} > \theta) \log(1 + \theta). \tag{27}$$

$$T_c = \lambda_c P(SINR_c > \theta_c) \log(1 + \theta_c). \tag{28}$$

$$T'_c = \lambda_c P(SINR'_c > \theta_c) \log(1 + \theta_c). \tag{29}$$

where T_c and T_c' are the cellular network throughput with and without DSC network, respectively. Define δ as the cellular efficiency loss ratio $\delta = \frac{T_c - T_c'}{T_c}$ and r_{th} as the cellular efficiency loss constraint [16]. The optimal DSC base station density coexisting with a cellular network λ_{dc} can be obtained by solving the following optimization problem:

$$\begin{aligned} \underset{\lambda_{dc}}{\text{maximize}} \quad & T_{dc} \qquad (G2) \\ \text{subject to} \quad & P(SINR_{dc} > \theta) > 1 - \varepsilon_{dc} \\ & \delta \le r_{th}. \end{aligned}$$

Next, we derive the optimal DSC base station density when coexisting with cellular networks.

Consider the DSC network coexists with a 2D cellular network. Denote $I_c = \sum_{j \in \Phi_c} h_j y_j^{-\alpha}$. The success probability of the typical DSC user is given by

$$P(SINR_{dc} > \theta) = P\left(\frac{h_0 D^{-\alpha}}{\frac{N}{P_d} + I + \frac{P_c}{P_d} I_c} > \theta\right) \tag{30}$$

$$= \exp\left(-\theta D^{\alpha} \frac{N}{P_d}\right) \mathbb{E}_I[\exp(-\theta D^{\alpha} I)] \mathbb{E}_{I_c}\left[\exp\left(-\theta D^{\alpha} \frac{P_c}{P_d} I_c\right)\right]. \tag{31}$$

where I was given in (3). The second term in (31) has been evaluated by (4), (5), (6), (7), (8), (9), (10), (11), and (12). The third term in (31) is the interference from other active cellular base stations following a 2D-PPP and can be derived as [16]:

$$\mathbb{E}_{I_c}\left[\exp\left(-\theta D^{\alpha} \frac{P_c}{P_d} I_c\right)\right] = \exp\left(-\lambda_c C D^2 \left(\frac{P_c}{P_d}\theta\right)^{\frac{2}{\alpha}} \exp\left(-d^{\alpha} \frac{N}{P_c}\theta_c\right)\right). \tag{32}$$

where $C = \frac{2\pi^2}{\alpha \sin\left(\frac{2\pi}{\alpha}\right)}$.

The success probability of a typical DSC user is

$$P(SINR_{dc} > \theta) = A_1 \exp(-A_2 \lambda_d) \exp(-A_3 \lambda_c) \tag{33}$$

where

$$A_1 = \exp\left(-\theta D^{\alpha} \frac{N}{P_d}\right).$$

$$A_2 = H(L, \theta, D, \alpha).$$

$$A_3 = CD^2 \left(\frac{P_c}{P_d}\theta\right)^{\frac{2}{\alpha}} \exp\left(-d^\alpha \frac{N}{P_c}\theta_c\right). \tag{34}$$

With the success probability expressions, we are able to solve the optimization problem (G2):

$$\begin{aligned} \underset{\lambda_{dc}}{\text{maximize}} \quad & T_{dc} \qquad (G2) \\ \text{subject to} \quad & P(SINR_{dc} > \theta) > 1 - \varepsilon_{dc} \\ & \delta \le r_{th}. \end{aligned}$$

Likewise, to derive the success probability of a typical cellular user, along with (28) and (29), the cellular efficiency loss ratio is first calculated:

$$\begin{aligned} \delta &= \frac{T_c - T_c'}{T_c} \\ &= 1 - \exp\left(-H\left(L, \theta_c \frac{P_d}{P_c}, d, \alpha\right)\lambda_{dc}\right). \end{aligned} \tag{35}$$

The Lagrange function of the optimization problem $(G2)$ is hence given by

$$\mathscr{L}(\lambda_{dc}) = T_{dc} + \mu_1(P(SINR_{dc} > \theta)) - \mu_2(\delta - r_{th}). \tag{36}$$

The KKT conditions are listed as follows:

$$\frac{d\mathscr{L}(\lambda_{dc})}{d\lambda_{dc}} = \frac{dT_{dc}}{d\lambda_{dc}} + \mu_1 \frac{d(P(SINR_{dc} > \theta)}{d\lambda_{dc}} - \mu_2 \frac{d\delta}{d\lambda_{dc}}.$$

$$\mu_1(P(SINR_{dc} > \theta) - 1 + \varepsilon_{dc}) = 0. \tag{37}$$

$$\mu_2(\delta - r_{th}) = 0. \tag{38}$$

$$(-1 + \varepsilon_{dc}) \le P(SINR_{dc} > \theta). \tag{39}$$

$$\delta \le r_{th}. \tag{40}$$

$$\mu_1 \ge 0, \mu_2 \ge 0 \quad \text{and} \quad \lambda_{dc} \ge 0. \tag{41}$$

Solving the above equations yields:

$$\begin{aligned} &\text{If} \quad \varepsilon_{dc} < \eta, \\ &\lambda_{dc}^* = \frac{\left[-\ln(1-\varepsilon_{dc}) - D^\alpha \frac{N}{P_d}\theta - A_3\lambda_c\right]^+}{A_2} \\ &\text{If} \quad \varepsilon_{dc} \ge \eta, \end{aligned} \tag{42}$$

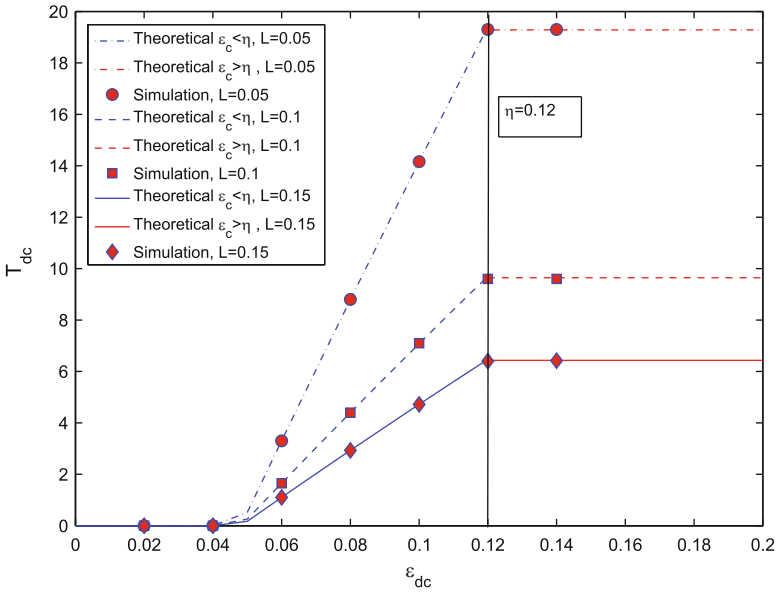

Fig. 6 Maximum throughput of a 3D-PPP with limited height coexisting with a cellular network, $\alpha = 4$, $\theta = 1$, $\theta_c = 5$, $\lambda_c = 1$, $P_d = 1$, $P_c = 1$

$$\lambda_{dc}^{*} = \frac{-\ln(1-r_{th})}{H(L, \theta_c \frac{P_d}{P_c}, d, \alpha)}. \tag{43}$$

where $\eta = 1-\exp(-A_3\lambda_c)A_1(1-r_{th})^{\frac{A_2}{H(L,\theta_c\frac{P_d}{P_c},d,\alpha)}}$. We have the maximized potential throughput:

$$T_{dc}^{*} = \lambda_{dc}^{*} P(SINR_{dc*} > \theta)\log(1+\theta). \tag{44}$$

where $P(SINR_{dc*} > \theta)$ can be evaluated by substituting λ_{dc}^{*} into (33). For $\varepsilon_{dc} < \eta$, since $1-\varepsilon_{dc} \approx 1$, $\ln(1-\varepsilon_{dc}) \approx -\varepsilon_{dc}$. The approximated optimal DSC density and potential throughput are both linear with the DSC network outage constraint ε_{dc}. For $\varepsilon_{dc} > \eta$, both optimal DSC density and potential throughput are constants which are independent of ε_{dc}.

Numerical Examples

In this section, some numerical examples are given to validate the theoretical results and discuss the effects of several parameters on the coverage and rate of DSCs and cellular networks.

In Fig. 6, the simulation results of the maximal throughput of a 3D DSC network with the coexistence of a cellular network are compared with the analytical results derived from (44). The simulation of optimal node density is done by two steps. The optimal DSC base station density and the maximal throughput are plotted as functions depending on the DSC outage constraint. The values of λ_d and T_d are zero at the small ε region since the outage probability cannot satisfy its outage constraint. In the region where the outage probability is able to satisfy its outage constraint, both λ_{dc} and T_{dc} increase almost linearly with the increase of ε_{dc}, until they flatten out and coincide with (43). The flattening is because cellular network constraints are restricting the DSC node density, even more DSC outage could be tolerated by the DSC network. Moreover, it is noticed that η is independent of the limited height of the 3D network, as it represents when the cellular network interference constraints become dominant. The scaling behaviors of DSC outage constraints provide us the following insight: as we relax the restrictions for DSC network, the dependence of optimal DSC base station deployment moves from the constraints of DSC network to constraints of cellular network.

Spectrum Sharing of UAV Networks with Directional Antennas

UAVs are above the ground with a certain altitude, which creates opportunities for UAV network to share the spectrum of ground network. In this section, we present the study of UAV network spectrum sharing exploring the benefits of beam and power control in 3D and 2D deployment scenarios, respectively.

3D Deployment

Density and Power Control

When UAVs are deployed in 3D space and share the spectrum of ground networks, the density and transmit power of UAVs need to be controlled to mitigate the interference to ground network. In section "Spectrum Sharing Between DSC Network and Cellular Network", UAV network shares spectrum with a ground cellular network, where the density of UAV network is optimized to maximize the network capacity with the constraints of the outage probability of UAV network and the capacity loss of cellular network. Besides density control, power control can also be applied in the spectrum sharing between UAV network and ground network. UAVs with low altitude should transmit with small transmit power to mitigate the interference to ground users. Meanwhile, UAVs with high altitude can transmit with a relatively large transmit power because they are distant from the ground users. With power control, the deployment density and capacity of UAVs can be improved.

Beam and Power Control

In previous sections, UAVs are implemented with omnidirectional antennas. When UAVs are implemented with directional antenna, more efficient spectrum sharing

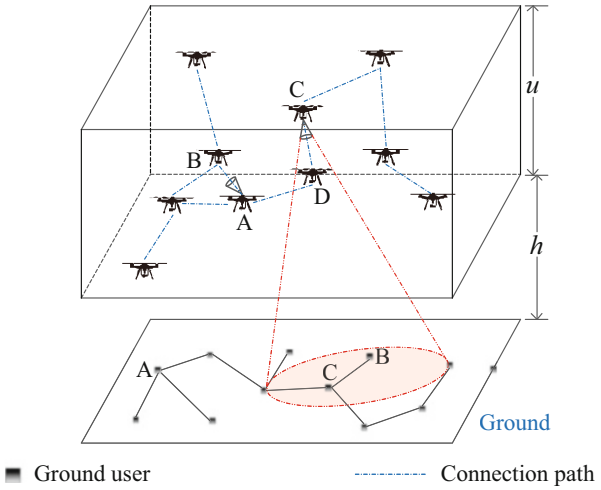

Fig. 7 Directional transmission scenario of UAV network

schemes can be explored. As illustrated in Fig. 7, UAVs are distributed in 3D space and transmit directionally. The 3D space is modeled by a cuboid with height u and the height of the bottom of this cuboid from the ground is h. Notice that the UAVs with low altitude have small probability to transmit downward because their destinations have large probability to be located above them. However, when a UAV transmits downward, it may cause interference to ground nodes, such as UAV C in Fig. 7. If the signal radiation of a UAV is modeled as a spherical cone, the projection of the signal on ground is an ellipse. If the beam of signal is sufficiently narrow, the probability that the signal of UAV causes interference to ground nodes is small. Besides, power control can also be applied to control the interference from UAVs to ground users.

However, the control of beam and power is not necessary for each direction. There is a beam control angle for each UAV. When transmission direction is not in the beam control angle, the beam and power control are not necessary. In Fig. 8, the beam control angles of UAVs A, B, and C are α_1, α_2, and α_3, respectively, where $\alpha_3 = 0$. With the increase of the altitude of UAV, the beam control angle is decreasing. The beam control angle can be derived as follows. Take UAV A as an example; the distance between UAV A and a ground user A$'$ is X_1. When X_1 is increasing, γ_1 is decreasing and the probability of non-line-of-sight (NLoS) transmission between UAV A and ground node A$'$ is increasing. With the increase of X_1 and NLOS probability, the interference from UAV A to ground node A$'$ is decreasing. When the distance X_1 is increased to X_1^* such that the expectation of the interference from UAV A to ground node A$'$ is smaller than a threshold, the beam control angle α_1 is determined. When a UAV is high above the ground such that the interference to the ground node is small, the beam control angle for this UAV does not exist.

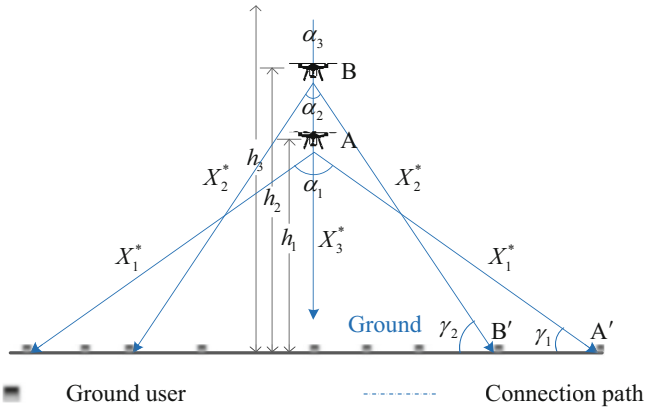

Fig. 8 Directional transmission in UAV network with different angles

In Fig. 8, the beam control angles of three UAVs are illustrated. Notice that if we do not consider the NLOS transmissions, the value of X_1^* equals X_2^*. However, because the UAV with high altitude has a larger angle of elevation compared with the UAV with low altitude, the length of X_1^* is smaller than X_2^*. UAV can freely transmit in the non-beam control angle. However, if a UAV transmits in the beam control angle, more sophisticated transmission schemes need to be implemented. The following schemes may be applicable:

1. Spectrum sensing If a UAV transmits in the beam control angle, it performs spectrum sensing and transmits when ground users are absent.
2. Narrow beam If a UAV transmits in the beam control angle with narrow beam, the interference probability to ground users will decrease. However, this requires sophisticated beamforming algorithm.
3. Power control When a UAV transmits in the beam control angle, if the power of UAV can be controlled to mitigate the interference to ground users, the transmission opportunities can also be exploited.

With these schemes, UAVs can share the spectrum of ground users in every direction and altitude, which will increase the number of wireless channel and improve the capacity of UAV network.

2D Deployment

In previous section, we explore the spectrum sharing between 3D UAV network and 2D ground network. However, when UAVs are used to monitor or search specific targets on ground, they may be distributed in an aerial 2D plane, which is illustrated

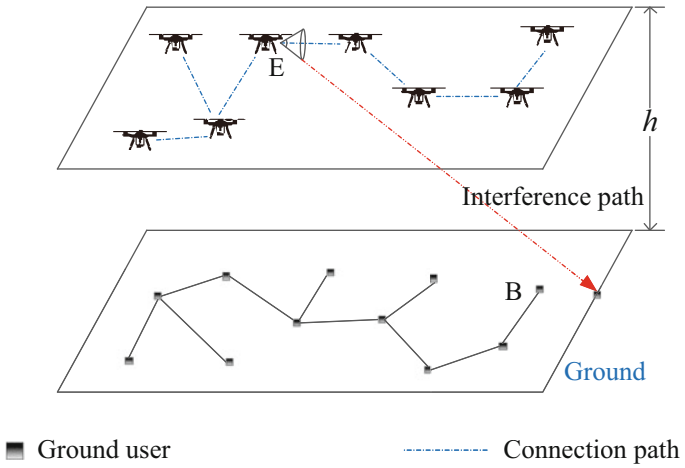

Fig. 9 2D UAV networks with 2D ground networks

in Fig. 9. In this section, we discuss the spectrum sharing between 2D UAV network and 2D ground network.

Altitude, Density, and Power Control

When UAVs are deployed in an aerial 2D plane, the altitude, density, and transmit power can be coordinated to mitigate the interference to ground users. In [30], assuming UAV network has air-to-ground transmissions, we derived the optimal altitude of UAVs with fixed transmit power and density. When the altitude of UAVs is fixed, the density and transmit power of UAVs can be optimized to maximize the capacity of UAV network with the constraint of capacity loss of ground network. Furthermore, the altitude, density, and power of UAVs can be jointly optimized.

Beam Control

Similar with section "Beam and Power Control", when UAVs are implemented with directional antennas, efficient spectrum sharing schemes can be designed. As illustrated in Fig. 9, when UAV E transmits directionally, it will not cause interference to ground node B. Assuming that the beam width of UAV is β, when β is decreasing, the interference from UAV network to ground users is correspondingly decreasing. Thus beam control can realize interference coordination between UAV network and ground network. Intuitively, the directional transmission in UAV network is equivalent to increasing the altitude of UAVs. Thus with beam control of UAV network, the spectrum sharing between UAV network and ground network is feasible.

Numerical Results

The spectrum sharing between an aerial 2D UAV network and a ground ad hoc network is investigated in [30]. The scenario of Fig. 9 is simulated. Namely, UAV network shares spectrum with a ground ad hoc network and UAVs are implemented with directional antennas. Assume that the signal to interference and noise ratio (SINR) threshold for signal reception is 1. In a 1000×1000 m area, 100 ground users are uniformly deployed and 25 UAVs are uniformly deployed above the ground users. The path loss exponent of ground-to-ground channel is 3, and the path loss exponent of air-to-ground channel is 2. The air-to-ground channel model is borrowed from [10], where the probability of line-of-sight (LOS) is an increasing function of the angle of elevation.[1] The transmit power of UAV is 5 W and the transmit power of ground node is 1 W. With these parameters configuration, the coverage probability of ground ad hoc network is provided in Fig. 10. The interference from UAV network to ground network has an impact on the coverage probability of ground network. With the increase of the altitude of UAVs, the length of propagation path from UAV to ground user is increasing. Meanwhile, the angle of elevation from ground user to UAV is increasing. The increase of propagation path will decrease the interference from UAV to ground user. However, the increase of the angle of elevation will enlarge the probability of LOS and increase the interference from UAV to ground user. In Fig. 10, for UAV networks with omnidirectional antennas, when the altitude of UAVs is smaller than h^*, the angle of elevation is dominated. Thus with the increase of the altitude, the interference from UAV network to ground user is increasing and the coverage probability of ground network is decreasing. However, when the altitude of UAVs is larger than h^*, the length of the propagation path is dominated. The interference from UAV network to ground users is decreasing with the increase of the altitude in this situation. Thus the coverage probability is increasing with the increase of altitude.

When the beam width of UAV, namely, β is decreasing, the interference from UAVs to ground network is reduced and the coverage probability of ground network is improved. As illustrated in Fig. 10, when $\beta = 2\pi/3$, the improvement of coverage probability is not significant. However, when $\beta = \pi/6$, the coverage probability will rapidly increase to the maximum value with the increase of altitude. Thus directional transmission in UAV network creates spectrum sharing opportunities between UAVs and ground network.

Mobility Pattern Cognition of UAV Networks

UAVs have specific mobility pattern and the mobility of UAVs can be exploited to improve network capacity. With the mobility pattern information of UAVs, the delay tolerant transmissions can be constructed and multiple transmission modes

[1] Reader could refer to (8) and (9) in [10] for the details of air-to-ground channel model.

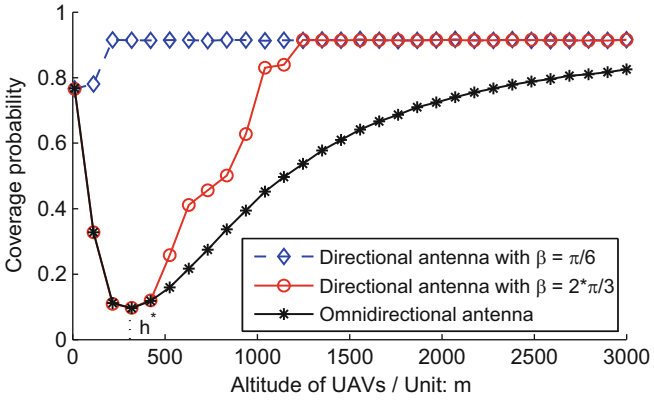

Fig. 10 The coverage probability of ground ad hoc network

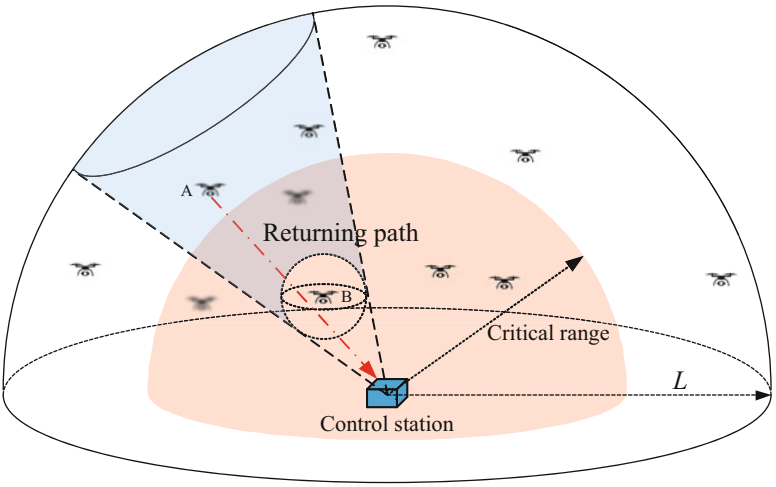

Fig. 11 UAV network with mobility pattern cognition. UAV sensors are deployed in 3D space

are implemented to carry various types of traffic. Figure 11 illustrates the scenario that UAVs act as aerial sensors and transmit sensing data to control station.

In Fig. 11, when UAV A returns, it will encounter UAV B. The returning UAV A can store and carry the data of UAV B to control station. Thus in addition to multi-hop transmission mode, the delay-tolerant transmission mode is constructed to improve the capacity of UAV networks. UAV network with multi-hop and SCF transmission modes can adapt the demands of diverse traffic. The delay-insensitive and delay-sensitive traffic can be forwarded through SCF transmission mode and multi-hop transmission mode, respectively. In the following sections, we discuss the SCF transmission modes.

Mobility Pattern Cognition

The process of the discovery of a returning UAV and the establishment of communication link between the returning UAV and a UAV along the returning path is illustrated in Fig. 12. Assume that UAV A will return to the control station and UAV B is located in the returning path of UAV A. Each UAV has a state bit. When a UAV is returning, the state bit is set as 0. Otherwise, the state bit is set as 1. The neighbor discovery function of UAV B will detect nearby UAVs. Once UAV B detects a UAV, it sends synchronize (SYN) signal. Meanwhile, the returning UAV A is also detecting the UAVs along its returning path. Once UAV A discovers a UAV and this UAV is sending SYN signal, UAV A feedbacks the state bit indicating that it is returning and synchronize/acknowledge (SYN/ACK) signal containing channel information for communication link establishment. Then UAV B sends ACK signal and establishes communication connection. When the data transmission is finished, the communication session is released and UAV A continues returning.

With mobility pattern information, the SCF transmission modes for 3D and 2D UAV network are introduced in the following sections.

3D UAV Deployment

As illustrated in Fig. 11, when UAV A returns, it can store and carry the data of UAV B to the control station. Assume that UAVs return in straight line path. In Fig. 11, when the UAVs in the shaded region return, they will assist UAV B to deliver data to control station. With the increase of the distance between the control station and UAV B, the volume of shaded region is decreasing and the number of returning UAVs assisting the data transmission of UAV B is also decreasing.

In [6], a critical range is discovered, which is illustrated in Fig. 11. Within critical range, the number of returning UAVs is sufficiently large, such that the capacity of UAVs within critical range contributed by SCF mode is higher than that outside of critical range. Thus the mobility of the returning UAVs outside of critical range needs to be controlled to improve the capacity. Mobility control schemes are as follows:

1. Returning path control: The returning path outside of critical range should be fold line such as zigzag curve to increase the length of returning path, such that more data can be delivered with SCF mode.
2. Pause time control: The returning UAVs outside of critical range pause for a time to gather the data of neighbor UAVs, such that the capacity of SCF mode can be improved.

However, all the mobility control scheme aiming to improve the capacity of SCF mode will increase the energy consumption of UAVs because the returning time will be longer than that without mobility control. Hence there is a trade-off between energy consumption and capacity improvement.

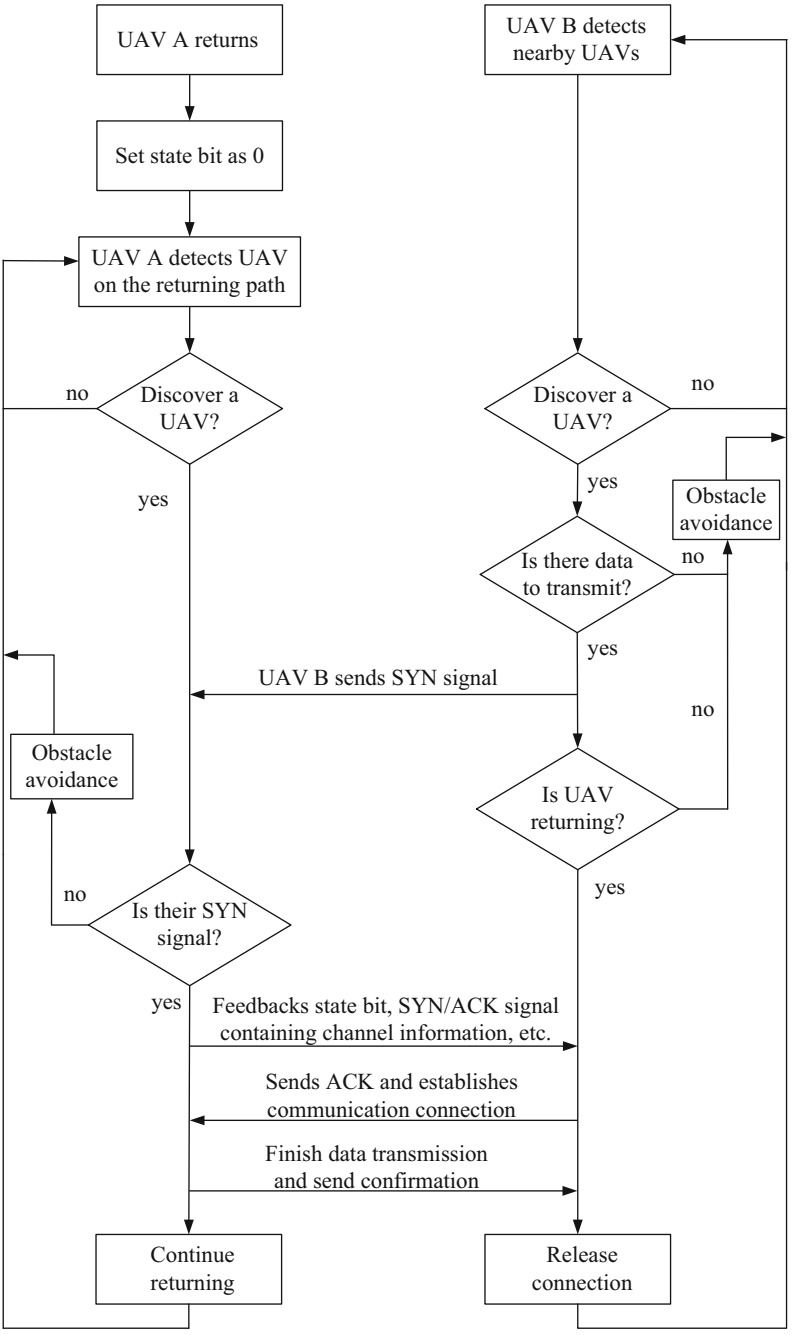

Fig. 12 The establishment of SCF transmission link

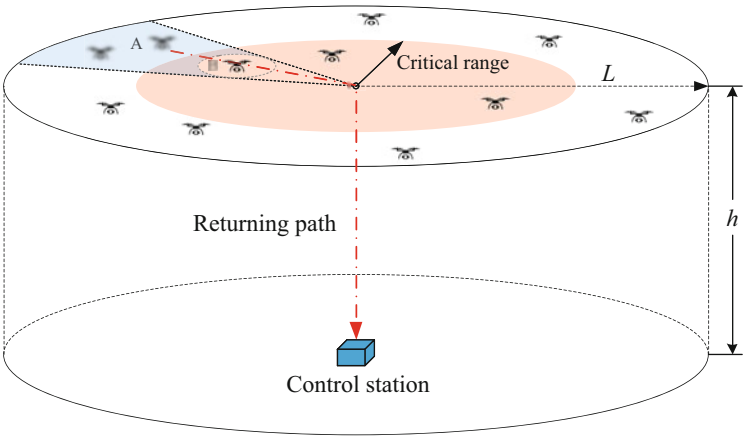

Fig. 13 UAV network with mobility pattern cognition. UAV sensors are deployed in an aerial 2D plane

2D UAV Deployment

When UAVs are deployed in an aerial 2D plane, the returning path of UAV is redesigned. As illustrated in Fig. 13, the UAVs are deployed in a circle above the ground. When UAV A returns, it will firstly flies to the center of the circle. Then UAV A flies downward to control station. With this returning path, the returning UAV A can deliver the data of UAV B to control station with SCF mode. In 2D deployment of UAVs, the critical range also exists and the mobility of the returning UAVs outside of critical range should be controlled to improve the capacity of SCF mode.

The previous discussions consider the scenario that UAVs act as aerial sensors. In the scenario that UAVs act as aerial base stations, the mobility pattern information can also be applied to construct SCF transmission mode. As illustrated in Fig. 14, UAVs are deployed in the sky to provide communication connections for ground nodes. For example, when ground node C transmits data to ground node D, it will firstly transmit to UAV A, then UAV A will transmit the data with multi-hop manner to UAV B. Finally, the data is forwarded from UAV B to ground node D. However, with SCF mode, if UAV A is a returning UAV passing ground node C, ground node C will forward data to UAV A. Then the data is brought to control station via UAV A. When UAV B is departing from control station and passing ground node D, UAV B will bring the data of ground node C and forward the data to ground node D. In this way, the multi-hop transmission can be avoided, such that the wireless channels will not be consumed by repeated data transmission in multi-hop transmission.

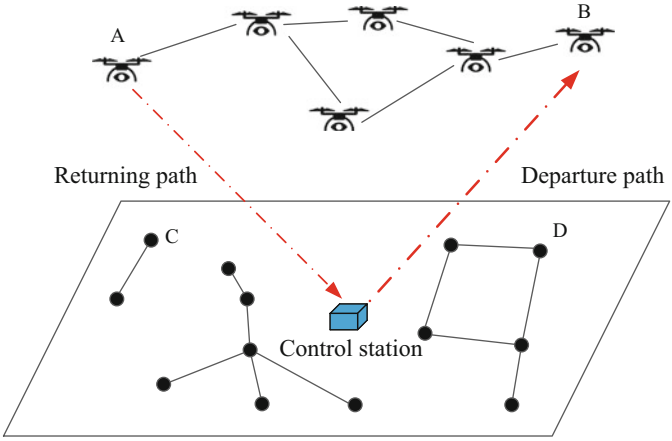

Fig. 14 UAV network with mobility pattern cognition. UAVs act as base stations

Summary and Future Work

This chapter presents the spectrum sharing between the drone network and traditional ground cellular network under different scenarios. It has provided explicit solutions of the optimal density of DSCs modeled by a 3D Poisson point process with limited height. It was demonstrated that larger deployment height limit results larger optimal DSC density. For DSC network underlay spectrum sharing with cellular network, as we relax the restrictions for DSC network, the dependence of optimal DSC base station deployment moves from the constraints of DSC network to constraints of cellular network. Effects of directional transmission on DSC networks are further discussed. Exploiting cognition capability on mobility, UAV network can provide high quality of information services in the highly dynamic environment with limited resources.

The spectrum sharing of drone networks is an emerging field with numerous interesting applications. We conclude by discussing some fruitful avenues for future research:

- *UAV Channel Modeling* As mentioned in the chapter, the characteristics of UAV wireless channels are very different from those of terrestrial wireless channels. More empirical measurements can be expected for developing more accurate channel models.
- *Multi-UAV Scheduling* Based on the analytical framework for drone spectrum sharing presented, it would be interesting to further design the scheduling scheme for multiple UAVs. The cooperation between UAVs can further improve the network performance.
- *UAV to Infrastructure/Vehicle Spectrum Sharing* We have focused on the spectrum sharing between UAVs and conventional cellular networks. There are

also ongoing thrusts on the coexisting between UAV and infrastructure/vehicle networks. Since UAVs can provide extra coverage, how to integrate the aerial base stations and relays with the existing ground networks deserves further study.

References

1. Al-Hourani A, Kandeepan S, Jamalipour A (2014) Modeling air-to-ground path loss for low altitude platforms in urban environments. In: IEEE global communication conference (GLOBECOM), Austin, pp 2898–2904. https://doi.org/10.1109/GLOCOM.2014.7037248
2. Al-Hourani A, Kandeepan S, Lardner S (2014) Optimal LAP altitude for maximum coverage. IEEE Wirel Commun Lett 3(6):569–572. https://doi.org/10.1109/LWC.2014.2342736
3. Mozaffari M, Saad W, Bennis M, Debbah M (2015) Drone small cells in the clouds: design, deployment and performance analysis. In: IEEE global communication conference (GLOBECOM), San Diego, pp 1–6. https://doi.org/10.1109/GLOCOM.2015.7417609
4. Lin X et al (2018) The sky is not the limit: LTE for unmanned aerial vehicles. IEEE Commun Mag 56(4):204–210. https://doi.org/10.1109/MCOM.2018.1700643
5. Federal Aviation Administration (FAA) (2017) UAS traffic management research transition tea plan. Technical report. https://www.faa.gov/uas/research/utm/media/FAA_NASA_UAS_Traffic_Management_Research_Plan.pdf
6. Wei Z, Wu H, Huang S, Feng Z (2017) Scaling laws of unmanned aerial vehicle network with mobility pattern information. IEEE Commun Lett 21(6):1389–1392. https://doi.org/10.1109/LCOMM.2017.2671861
7. Cover T, Thomas J (2012) Elements of information theory. Wiley, New York
8. Zhang C, Zhang W (2017) Spectrum sharing for drone networks. IEEE J Sel Areas Commun 35(1):136–144. https://doi.org/10.1109/JSAC.2016.2633040
9. Zhang C, Zhang W (2016) Spectrum sharing in drone small cells. In: Proceedings of IEEE global communication conference (GLOBECOM), Washington. https://doi.org/10.1109/GLOCOM.2016.7842290
10. Mozaffari M, Saad W, Bennis M, Debbah M (2016) Unmanned aerial vehicle with underlaid device-to-device communications: performance and tradeoffs. IEEE Trans Wirel Commun 15(6):3949–3963. https://doi.org/10.1109/TWC.2016.2531652
11. Andrews JG, Baccelli F, Ganti RK (2011) A tractable approach to coverage and rate in cellular networks. IEEE Trans Commun 59(11):3122–3134. https://doi.org/10.1109/TCOMM.2011.100411.100541
12. Bai T, Heath RW Jr (2015) Coverage and rate analysis for millimeter wave cellular networks. IEEE Trans Wirel Commun 14(2):1100–1114. https://doi.org/10.1109/TWC.2014.2364267
13. Zhang X, Haenggi M (2014) A stochastic geometry analysis of inter-cell interference coordination and intra-cell diversity. IEEE Trans Wirel Commun 13(12):6655–6669. https://doi.org/10.1109/TWC.2014.2339273
14. Vu M, Devroye N, Tarokh V (2009) On the primary exclusive region of cognitive networks. IEEE Trans Wirel Commun 8:3380–3385. https://doi.org/10.1109/TWC.2009.080454
15. Bagayoko A, Tortelier P, Fijalkow I (2010) Impact of shadowing on the primary exclusive region in cognitive networks. In: European wireless conference (EW), Lucca, pp 105–110. https://doi.org/10.1109/EW.2010.5483402
16. Wang Z, Zhang W (2014) Opportunistic spectrum sharing with limited feedback in Poisson cognitive radio networks. IEEE Trans Wirel Commun 13(12):7098–7109. https://doi.org/10.1109/TWC.2014.2363676
17. Dahama R, Sowerby KW, Rowe GB (2013) Estimating protection distances in spectrum sharing systems. IEEE Trans Signal Process 61(17):4284–4295. https://doi.org/10.1109/TSP.2013.2269901

18. Wei Z, Feng Z, Zhang Q, Li W (2015) Three regions for space-time spectrum sensing and access in cognitive radio networks. IEEE Trans Veh Technol 64(6):2448–2462. https://doi.org/10.1109/GLOCOM.2012.6503290
19. Wei Z, Feng Z, Zhang Q, Li W (2015) Three regions for space-time spectrum sensing and access in cognitive radio networks. IEEE Trans Veh Technol 64(6):2448–2462. https://doi.org/10.1109/TVT.2014.2342612
20. Guo A, Haenggi M (2015) Asymptotic deployment gain: a simple approach to characterize the SINR distribution in general cellular networks. IEEE Trans Commun 63(3):962–976. https://doi.org/10.1109/TCOMM.2014.2387170
21. Gupta AK, Zhang X, Andrews JG (2015) SINR and throughput scaling in ultradense urban cellular networks. IEEE Wirel Commun Lett 4(6):605–608. https://doi.org/10.1109/LWC.2015.2472404
22. Lee S, Zhang R, Huang K (2013) Opportunistic wireless energy harvesting in cognitive radio networks. IEEE Trans Wirel Commun 12(9):4788–4799. https://doi.org/10.1109/TWC.2013.072613.130323
23. Keeler HP, Ross N, Xia A (2015) When do wireless network signals appear Poisson. Available via DIALOG. https://arxiv.org/abs/1411.3757
24. Andrews JG, Buzzi S, Choi W, Hanly SV, Lozano A, Soong ACK, Zhang JC (2014) What will 5G be? IEEE J Sel Areas Commun 32(6):1065–1082. https://doi.org/10.1109/JSAC.2014.2328098
25. Carle J, Myoupo JF, Seme D (2001) A basis for 3-D cellular networks. In: Proceedings of the 15th international conference on information networking, Beppu City, pp 631–636. https://doi.org/10.1109/ICOIN.2001.905525
26. Alam SM, Haas ZJ (2006) Coverage and connectivity in three-dimensional networks. In: Proceedings of the 12th annual international conference on mobile computing and networking, Los Angeles, pp 346–357. https://doi.org/10.1145/1161089.1161128
27. Zeng Y, Zhang R, Lim TJ (2016) Wireless communications with unmanned aerial vehicles: opportunities and challenges. IEEE Commun Mag 54(5):36–42. https://doi.org/10.1109/MCOM.2016.7470933
28. Streit RL (2010) Probability generating functional. In: Poisson point processes: imaging, tracking, and sensing. Springer Science & Business Media, Berlin, p 27
29. Zhou L, Yang Z, Zhou S, Zhang W (2018) Coverage probability analysis of UAV cellular networks in Urban environments. In: Proceeding IEEE international conference on communication (ICC), Kansas City
30. Guo Z, Wei Z, Feng Z, Fan N (2017) Coverage probability of multiple UAVs supported ground network. Electron Lett 53(13):885–887. https://doi.org/10.1049/el.2017.0800

User-Cognizant Scalable Video Transmission over Heterogeneous Cellular Networks

39

Liang Wu and Wenyi Zhang

Contents

L. Wu (✉)
Department of Electronic Engineering and Information Science, University of Science and Technology of China, Hefei, China

Huawei Technologies, shanghai, China
e-mail: tuohai@mail.ustc.edu.cn

W. Zhang
Key Laboratory of Wireless-Optical Communications, Chinese Academy of Sciences, Hefei, China

Department of Electronic Engineering and Information Science, University of Science and Technology of China, Hefei, China
e-mail: wenyizha@ustc.edu.cn

W. Zhang (ed.), *Handbook of Cognitive Radio*,
https://doi.org/10.1007/978-981-10-1394-2_36

Abstract

With the increase of mobile video applications in people's daily life as well as industrial manufacture, such as video streaming, surveillance, and so on, video has been the main service in cellular networks. Operators and service providers are struggling to enhance the mobile video service, while user requirements for abundant, high-definition, and low-delay video have nearly drained the transmission capacity of current networks. Moreover, the large population of user equipments (UEs) exhibit differentiated video demands and various network transmission environments. Traditional networking, which is static and base station (BS) concentric, can hardly deal with these challenges. Thus, adaptive video transmission schemes are needed by jointly considering the interplay among user demand, video source characteristics, and networking. This work focuses on user-cognizant scalable video transmission over heterogeneous cellular networks. The video source is encoded using scalable video coding, which enables dynamic adaption of source information to the requirements of UEs and is suitable for cellular networks in which the transmission link quality varies substantially over space and time. Three novel transmission schemes are proposed, layered digital transmission, layered hybrid digital-analog transmission, and cooperative digital transmission. Leveraging tools from stochastic geometry, a comprehensive analysis is conducted focusing on three key performance metrics: outage probability, high-definition probability, and average distortion. The associated spectrum allocation and video transmission are chosen based on the user-cognizant information, such as the requirements for video service, wireless channel status, and the connections with the BSs. The results show that the proposed user-cognizant transmission schemes can provide a scalable video experience for UEs.

Keywords

Coordinated multipoint · Heterogeneous cellular networks · Hybrid digital-analog · Scalable video coding · Stochastic geometry · User cognizant

Introduction

Emerging wireless communication technologies as well as powerful and versatile mobile terminal devices have changed people's daily life, and the data traffic grows explosively, among which a substantial portion is attributed to multimedia such as mobile video. According to the Cisco Visual Networking Index, mobile video is expected to grow at an average growth rate of 62% until 2020, and within the 30.6 exabytes of data per month crossing mobile networks by 2020, 23.0 exabytes will be video related, such as video on demand, real-time streaming video, video

conferencing, and so on. The ever-increasing demand for abundant, high-definition, and low-latency mobile video brings great challenges to the mobile network with time-varying wireless channel. Moreover, with the release of different types of UEs, the requirements on data rate of video transmission vary in a wide range.

Compared to the IP transmission network and cellular core network, the bottleneck of the end-to-end transmission degrading the Quality of Experience (QoE) of video lies in the radio access network due to user traffic congestion and packet loss. Current LTE/LTE-A networks are not inheritably built for QoE-aware video delivery. The application-specific information exists at Packet Data Network Gateway (P-GW), while the wireless channel quality and connection status are restrictively known by eNodeB.

State-of-art design of cellular networks is base station (BS) concentric, which means that the resource allocation and transmission schedule are completed at the BSs and are not on-demand for UEs. The information bits are treated equally and the transmission strategy is not UE specific. As for the video transmission of a typical UE, the UE would require the video content with different video qualities based on its terminal capacity. Meanwhile, the UE can choose different service mechanisms provided by the cellular network based on the connection status.

Taking into account of time-varying wireless channel conditions and congestion, video streams are adapted to reduce the transmission bitrates. Traditionally, rate adaptation of video streams is realized by packet/frame dropping or transcoding with some serious drawbacks, since packet/frame dropping significantly degrades the video quality and transcoding is computationally complex. Advanced source coding techniques provide a new dimension of dynamically provisioning wireless resources for the varying requirements and the varying link conditions of UEs, thus creating the possibility of extracting video scaled in multiple dimensions, e.g., spatial, temporal, and quality. Scalable Video Coding (SVC) is an extension of the H.264/MPEG-4 AVC video compression standard [1] and has been evolved to Scalable High-Efficiency Video Coding (SHVC) [2], in which the bitstream is encoded into multiple layers, namely, a base layer (BL) and at least one enhancement layer (EL). The quality of reconstructed video depends on the number of layers decoded and stays the same until a higher enhancement layer is successfully decoded. The number of layers and their code rates may be determined by the requirement and the link condition of the subscribing UE.

On the other hand, cellular networks are evolving from a homogenous architecture to a composition of heterogeneous networks, comprised of various types of base stations (BSs) [3, 4]. Each type of BSs has its characteristic transmit power and deployment intensity: for example, macro BSs (MBSs) have larger transmit power, aiming at providing global coverage; femto access points (FAPs) are small BSs targeted for home or small business usages. As the distance between a UE and its serving FAP is small, the UE enjoys a high-quality link and achieves power savings. Meanwhile, the reduced transmission range also enhances spatial reuse and alleviates multiuser interference. In addition, different types of BSs can transmit cooperatively the same video content to the UE to enhance the quality of experience. The user-cell association approach for heterogenous networks should be addressed

to exploit context information as well as channel-related information extracted from UEs. Generally speaking, there are two different service modes, separate mode and cooperative mode. In separate mode, the macro cells and the small cells (e.g., femto cells) transmit different video streams to the UEs in a manner of dual connectivity. In cooperative mode, both the macro cells and small cells transmit the same video content to the UE in a manner of coordinated multipoint transmission. In this paper, we study the problem of scalable transmission over heterogeneous networks and demonstrate the performances of several user-cognizant transmission schemes to exploit the combination of multi-layer video transmission and multitier cellular networks.

Related Work

The prior works that consider video transmission over wireless networks mainly focus on scalable coding of video source or adaptive networking techniques separately. Furthermore, UE is regarded as a dummy terminal, and thus their differentiated demand and status are neglected. The analysis usually focuses on homogeneous networks, and the common feature of the layered structure of SVC and HCNs is not exploited. In [5], an overview of SVC and its relationship to mobile content delivery are discussed focusing on the challenges due to the time-varying characteristics of wireless channels. In [6], a per-subcarrier transmit antenna selection scheme is employed to support multiple scalable video sequences over a downlink cognitive network, and the outage probability is reduced because of video scalability. In [7], real-time use cases of mobile video streaming are presented, for which a variety of parameters like throughput, packet loss ratio, and delay are compared with H.264 single-layer video under different degrees of scalability. In [8], the proposed scheme employs WiFi: the BL is always transmitted over a reliable network such as cellular, whereas the EL is opportunistically transmitted through WiFi. Technical issues associated with the simultaneous use of multiple networks are discussed. In [9], HCNs with storage-capable small-cell BSs are studied: versions and layers of video have different impacts on the delay-servicing cost tradeoff, depending on the user demand diversity and the network load.

Some works related to QoE-aware or adaptive strategies have also been studied previously. Chen et al. [10] proposed an admission control strategy that was designed to maximize the number of video users satisfying the QoE constraints on their second-order statistics. Although the admission control strategy damages the QoE of the blocked users, the overall percentage of users satisfying the QoE constraints among both admitted and blocked users can be significantly improved. Thakolsri et al. [11] proposed a content-aware scheduling and resource allocation, taking into account the content characteristics of the video streams, and performs video rate adaptation at the BS. Fu et al. [12] proposed a QoE-aware video delivery by considering the hierarchical architecture of LTE/LTE-A network. Different video flows are marked at the core network to transform the video content information into QoE-aware priority classes. A packet dropping strategy addressing the transmission

capacity at the eNodeB is also proposed. But the priority marking process at the core network is unaware of channel status.

Considering the wireless video transmission techniques, there are several approaches to enhance the QoE of video users. The above literature is based on digital transmission, consisting of digital source coding (e.g., quantization and entropy coding), digital modulation (e.g., QPSK, 64QAM), and digital channel coding (e.g., turbo or LDPC). Unfortunately, digital transmission results in cliff effect. The cliff effect refers to the drastic degradation in video quality when the signal strength fades below the decoding threshold (as opposed to a graceful degradation). There exist certain SINR thresholds at which the video quality changes drastically; in between these thresholds, the quality stays approximately constant. The recently revitalized analog transmission has shown promising potential in handling channel variations and user heterogeneities for wireless video communication. The analog scheme consists of analog source coding and analog modulation that directly maps a source signal into a linearly transformed channel signal without channel coding. SoftCast [13] is an analog video broadcast scheme that transmits a linear transform of the video signal without quantization, entropy coding, or channel coding. It is claimed to realize continuous quality scalability. However, information-theoretic studies (such as [14,15]) show that analog schemes with linear mapping (from source signals to channel signals) are relatively inefficient for video transmission, while hybrid digital-analog transmission is asymptotically optimal under matched channel conditions for optimally chosen power allocations between the analog and digital parts. The hybrid digital-analog scheme combines digital with analog schemes, transmitting digital and analog signals simultaneously using TDMA, FDMA, or superposition transmission. The authors in [16] propose a hybrid digital-analog scheme for broadcasting, showing a substantial performance gain. However, these works did not consider the impacts of HCNs and the spatial distribution of wireless networks, let alone the design of scalable transmission algorithms utilizing the structure of HCNs.

Moreover, coordinated multipoint (CoMP) transmission is intensively studied to enhance the system performance of LTE-A. By coordinating multiple BSs, the interference at the UE can be alleviated, or multiple received signals can be merged. The studies in [17, 18] evaluate the potential system gain of CoMP and discuss the appropriate deployment scenarios. The authors also review the necessary techniques of signal processing, backhaul link design, and supported protocols. There exist two types of cooperative transmissions, namely, coherent and noncoherent joint transmission. Many previous studies considered noncoherent joint transmission because it requires less channel status information. The authors in [19,20] analyze the performance of noncoherent joint transmission in heterogeneous cellular networks and give the distribution of SINR for a user in a random position and cell edge, respectively. In addition, the impact of channel status information is also studied. Most previous works neglect the spectrum sub-band allocation, but the same sub-band is required when two BSs transmit cooperatively. Bang et al. [21] combines frequency fraction reuse and CoMP, and proposes an allocation to minimize the system power. Zhang et al. [22] and Kosmanos et al. [23] propose a

joint sub-band allocation and power optimization scheme to improve the spectrum efficiency for LTE-A when BS and relay transmit cooperatively.

In order to give a theoretic analysis of the system performance, stochastic geometry has been utilized as an effective tool for modeling and analyzing cellular networks; see, e.g., [24–26] and references therein. Generally, the spatial distribution of BSs is modeled as a spatial point process, such as the homogeneous Poisson point process (PPP) for single-tier networks, for which the coverage probability is derived in [27]. For HCNs, the spatial distribution of heterogeneous BSs is often modeled as multiple independent tiers of PPPs, and several key statistics are analyzed in [20, 28]. A comprehensive treatment of the application of stochastic geometry in wireless communication and content can be found in [29, 30].

A User-Cognizant Solution

Most existing works on heterogenous networks have focused on admission control, resource allocation, and transmission coordination. The serving BS associated to a particular UE is assigned based on indicators of the wireless link quality at the UEs, such as the received signal strength indicators (RSSIs) or the SINRs. The same priority is allocated to each information bit for different video data flows in the scheduling stage. All these networking designs again verify that the current network is inefficient for video transmission. To enhance the QoE, one promising approach for efficient networking is by making the network better informed of its environment and user requirements.

Thus, considering scalable video transmission over HCNs, we have previously proposed two user-cognizant transmission schemes. In [31], the common layer structures of both video source data and network topology are employed to enhance the video transmission, based on the user's video requirement and association status. In [32], analog transmission of enhancement layer of video stream is proposed in order to make the video reception quality changing continuously with channel quality, thus degrading the staircase effect of digital transmission. Here the cooperative transmission is taken into consideration, where the macro BS and small BS work in a manner of coordinated multipoint transmission.

In all, three user-cognizant transmission schemes are proposed, which are layered digital transmission, layered hybrid digital-analog transmission, and cooperative digital transmission, respectively. The user is cognizant of its video service requirement, mobility, and connection status.

An analytical performance assessment of user-cognizant SVC transmission over two-tier HCNs utilizing tools from stochastic geometry is studied. The contributions of the are:

1. Three user-cognizant transmission schemes are proposed to enhance the QoE of video users exploiting the interplay among user demand, video source characteristic, and networking.

2. An analytical framework is proposed for scalable video transmission exploiting the common feature of a layered structure of SVC and HCNs. A digital and a hybrid digital-analog transmission scheme are proposed and studied. The impact of UE load, i.e., the number of UEs served in a cell, is also considered.
3. The power allocation between the digital BL signal and the analog EL signal is also analyzed to minimize the average distortion. The hybrid digital-analog scheme can further improve the system performance by avoiding the cliff effect and realizing continuous quality scalability when the proportion of frequency resource allocated to the femto tier exceeds a certain threshold.
4. A noncoherent joint transmission cooperative scheme is proposed, and moreover, the impact of sub-band allocation is also studied.

The remaining part of this paper is as follows: section "System Model" describes the system model, including the transmission schemes and spectrum allocation methods. Section "UE Load and Sub-band Occupancy" derives the distributions of the number of UEs per cell and sub-band occupancy probabilities. Section "SINR Distribution and Data Rate" derives the SINR and data rate distributions. Section "System Performances" evaluates the performance metrics, namely, outage probability, HD probability, and average distortion. Section "Simulation and Discussion" presents simulation results and related discussions. Section "Conclusion and Future Directions" concludes this paper.

System Model

The downlink performance of SVC over a two-tier HCN is considered; see Fig. 1. When a video user needs to request for a particular video, it would first collect the information about video quality requirement due to possessing ability of the UE and connection status due to its mobility and the network topology. The user sends the user-cognizant information to the serving BS (or BSs), and the BS or BSs choose an appropriate transmission strategy. The video data stream is traversing through the video server, IP transmission network, cellular core network, radio access network, and finally reaching at the user.

Layered Video Model

The SVC video content is split into two layers, BL and EL. The BL is always modulated into a digital signal, and the data rate is R_{B}, while the EL is modulated into a digital signal or an analog signal in these transmission schemes accordingly. If the EL is modulated into a digital signal, then the data rate is R_{E}. Here we focus on the streaming video service; the video can be decoded successfully when the data rate requirements of the BL and the EL are met.

Actually, the proposed analytical framework can be extended to video signals that are encoded to J layers using a fine granularity, and the BS chooses the first

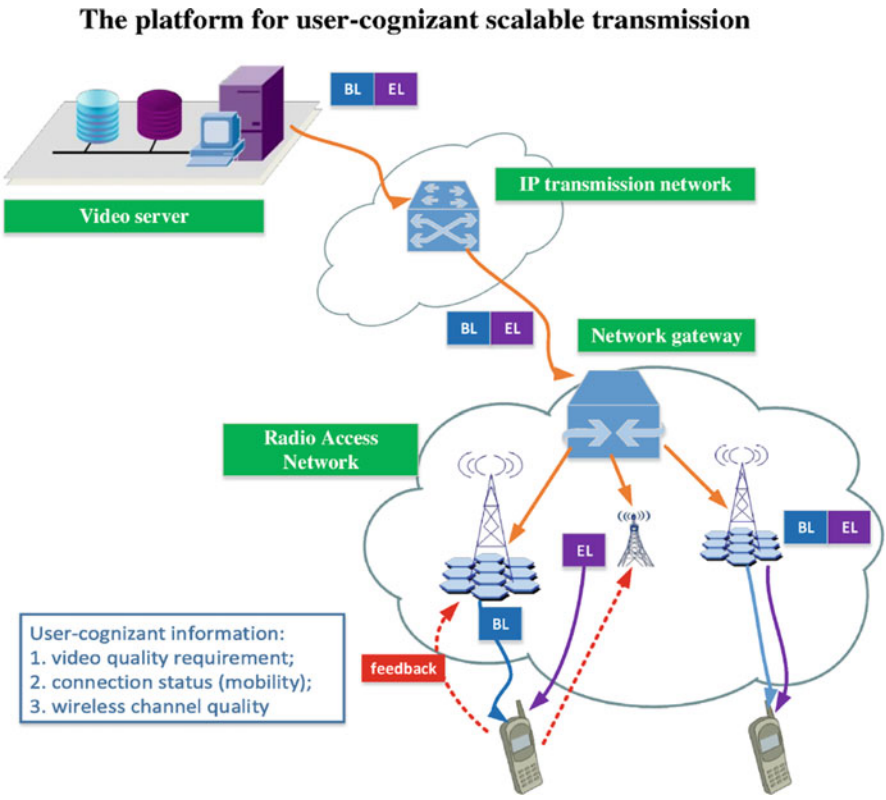

Fig. 1 Illustration of the platform for user-cognizant scalable transmission

J_1 layers for the BL and the following J_2 layers for the EL based on the channel quality for each UE, where $J_1 + J_2 \leq J$.

It should be aware that SVC allows three types of scalable encoding (spatial, temporal, SNR quality) to be combined and create a single layer [1,5]. The proposed layered video model is generic and is not restricted by the specifications of the layered encoding and the optimal selection of scalability combinations. Each layer is generated by some combinations of video scalabilities, and the required data rates are the main parameters from the view of networking.

Network Model

The two-tier HCN consists of two types of BSs, namely, MBSs and FAPs. These two types of BSs are modeled by two independent tiers of homogeneous PPPs, Φ_{mb} and Φ_{fb}, whose intensities are λ_{mb} and λ_{fb}, respectively. FAPs aim at providing network access to UEs in their vicinity within a coverage radius R_{f}. Suppose that there exist

N sub-bands each of bandwidth W. The transmit powers of an MBS and an FAP over each sub-band are set as P_{m} and P_{f}, respectively. The path loss model is $r^{-\alpha}$, and here for simplicity, it is assumed that the path loss exponent is the same for MBS and FAP, and the effect of shadowing is ignored. The small-scale fading distribution is exponential with mean unity in squared magnitude, i.e., Rayleigh fading. The fading is assumed to be frequency flat within each sub-band and independent among different sub-bands. The noise variance at each UE is denoted by σ^2.

There are two types of UEs, macro UEs and femto UEs. The locations of macro UEs form a homogeneous PPP Φ_{mu} with intensity λ_{mu}, and each macro UE connects to the nearest MBS. The locations of the femto UEs form a Matern cluster process Φ_{fu} [30] with parent process Φ_{fb} (the FAPs), i.e., the UEs in each cluster form a finite PPP of intensity λ_{fu} on the disk of radius R_{f} centered at each FAP, implying that the mean number of users per cluster is $\bar{U}_{\mathrm{f}} = \lambda_{\mathrm{fu}} \pi R_{\mathrm{f}}^2$. Each femto UE connects to the FAP located at the parent point of the corresponding cluster, called the parent FAP. The access mechanism is as follows: a femto UE always connects to its parent FAP when accessing a femto BS and connects to the MBS closest to its parent FAP when accessing a macro BS; a macro UE can only connect to the nearest MBS, even if it is situated within the coverage of an FAP. This corresponds to a closed-access femto network, in which only subscribers are allowed to be served by an FAP.

Transmission Schemes

Considering the connection status of UEs and their differentiated demand, three transmission schemes are proposed, i.e., layered digital (LD) [31], layered hybrid digital-analog (LHDA) [32], and cooperative digital (CD). For the macro UEs, they only connect to the MBS. Since the MBS aims at providing the coverage service, macro UEs attempt to obtain their BL contents from their serving MBSs and forego the EL. For the femto UEs, since they are covered by the MBS and the FAP, they have two choices: one is that they attempt to obtain their EL contents from their serving FAPs, and they attempt to obtain their BL contents either from their serving MBSs with probability p or from their serving FAPs with probability $1 - p$. The other one is that they receive the video contents which are transmitted cooperatively by the MBS and the FAP in the manner of CoMP.

1. *LD transmission*: See Fig. 2. Both the BL and the EL are modulated into digital signals. For a macro UE, the data stream of encoded BL signals is transmitted from the serving MBS. For a femto UE, the data stream of encoded BL signals for small SINR or jointly encoded signals of both the BL and the EL for large SINR is transmitted from the serving FAP when $p = 0$; the digital BL data stream is transmitted from its serving MBS, while the digital EL data stream is transmitted from its serving FAP when $p = 1$; a mixed transmission is adopted when $0 < p < 1$.
2. *LHDA transmission*: See Fig. 2. The BL is modulated into a digital signal, while the EL is modulated into an analog signal. For a macro UE, the data stream of

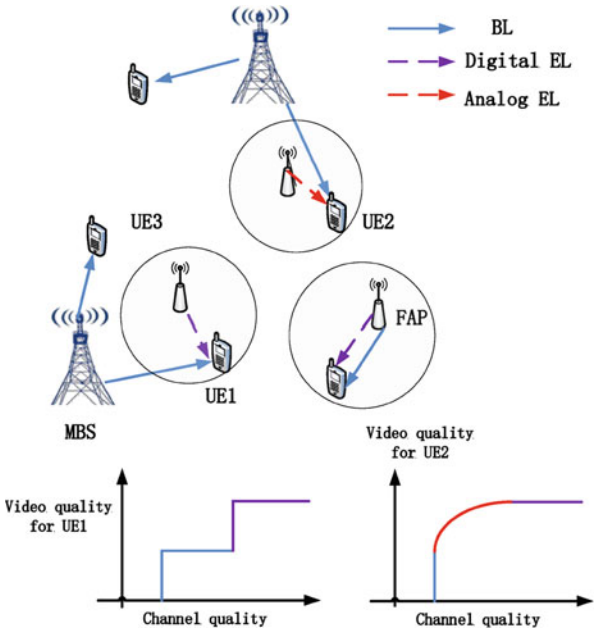

Fig. 2 Qualitative illustration of the performances of LD and LHDA transmissions. LD transmission shows a staircase effect, while LHDA transmission shows continuous quality reception with respect to the channel quality

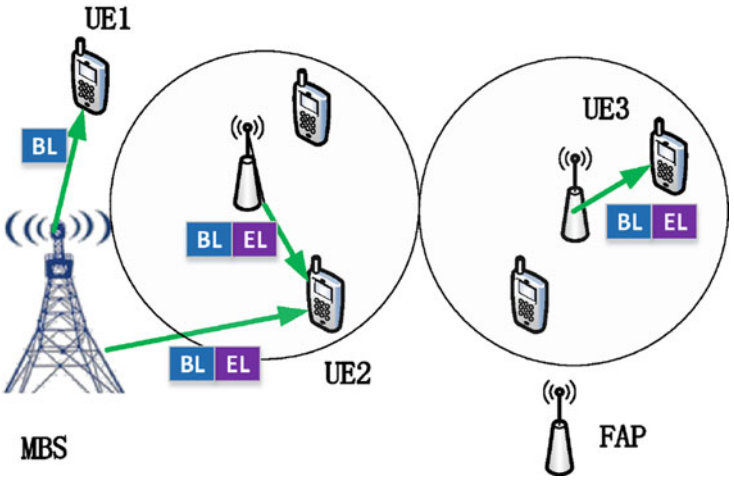

Fig. 3 Illustration of the CD transmission model

encoded BL signals is transmitted from the serving MBS. For a femto UE, the superposition of the digital BL signal and the analog EL signal is transmitted from the serving FAP when $p = 0$; the digital BL data stream is transmitted from its serving MBS, while the analog EL data stream is transmitted from its serving FAP when $p = 1$; a mixed transmission is adopted when $0 < p < 1$.

3. *CD transmission*: See Fig. 3. Both the BL and the EL are modulated into digital signals. For a macro UE, the data stream of encoded BL signals is transmitted from the serving MBS. For a femto UE, if it can claim the same sub-band from both the MBS and the FAP, then the data stream of jointly encoded signals of both the BL and the EL is transmitted from the serving MBS and FAP cooperatively in the manner of noncoherent joint transmission, otherwise, the data stream of jointly encoded signals of both the BL and the EL is transmitted from the serving FAP.

Since the video source is encoded into multiple layers, different layers are transmitted to the UE based on the channel quality, thus providing scalable video quality. Specifically, for those UEs in less favorable conditions, only the BL with relatively low data rate is received in order to ensure basic video experience. When the channel quality improves, the EL is also received for enhanced video experience. Thus, the LD and CD transmissions can provide two-level scalable video for the UEs, and LHDA can provide a continuous quality scalability.

UE Load and Sub-band Occupancy

UE Load

Since the distribution of femto UEs in an FAP coverage disk is a PPP with intensity λ_{fu}, the number of femto UEs connected to an FAP is a Poisson random variable (r.v.) with mean $\bar{U}_{\mathrm{f}}$,

$$\mathbb{P}\{U_{\mathrm{f}} = i\} = \frac{(\bar{U}_{\mathrm{f}})^i}{i!} e^{-\bar{U}_{\mathrm{f}}}, \quad i = 0, 1, \cdots. \tag{1}$$

For LD and LHDA transmissions, an MBS not only serves the macro UEs situated in its Voronoi cell but also the femto UEs that belong to the FAPs in this Voronoi cell and connect to the MBS to receive the BL contents. We denote the number of macro UEs in the Voronoi cell as U_{MBS} and the total number of femto UEs served by the MBS as U_{FAP}, which is given by $U_{\mathrm{FAP}} = \sum_{i=1}^{N_{\mathrm{c}}} N_{\mathrm{f},i}$, where N_{c} denotes the number of the FAPs in the Voronoi cell and $N_{\mathrm{f},i}$ denotes the number of femto UEs which belong to the ith FAP but connect to the MBS to receive the BL contents. The total number of UEs served by an MBS is thus

$$U_{\mathrm{m}} = U_{\mathrm{MBS}} + U_{\mathrm{FAP}}. \tag{2}$$

U_{MBS} is conditionally independent of U_{FAP} given the area of the Voronoi cell. Denote the area of a Voronoi cell by S; the probability generating function (pgf) of U_{m} conditioned on S, denoted by $G_{\mathrm{m}}(z \mid S)$, is

$$G_{\mathrm{m}}(z \mid S) = G_{\mathrm{MBS}}(z \mid S) G_{\mathrm{FAP}}(z \mid S), \tag{3}$$

where $G_{\mathrm{MBS}}(z \mid S)$ and $G_{\mathrm{FAP}}(z \mid S)$ are the pgfs of U_{MBS} and U_{FAP} conditioned on S, respectively.

U_{MBS} is a Poisson r.v. with mean $\lambda_{\mathrm{mu}} S$, and the conditional pgf of U_{MBS} is

$$G_{\mathrm{MBS}}(z \mid S) = e^{\lambda_{\mathrm{mu}} S(z-1)}. \tag{4}$$

Since a femto UE attempts to connect to its serving MBS with probability p in LD and LHDA transmissions, a thinning occurs, i.e., $N_{\mathrm{f},i}$ is a Poisson random variable with mean $p\bar{U}_{\mathrm{f}}$. Meanwhile, N_{c} is also a Poisson r.v. with mean $\lambda_{\mathrm{fb}} S$ because of the PPP distribution of the FAP locations. U_{FAP} is a compound Poisson r.v. with conditional pgf

$$G_{\mathrm{FAP}}(z \mid S) = e^{\lambda_{\mathrm{fb}} S(e^{p\bar{U}_{\mathrm{f}}(z-1)}-1)}. \tag{5}$$

There is no known closed form expression of the probability density function (pdf) of the area S of the typical Poisson Voronoi cell, but the following approximation [33]

$$f_S(x) \approx \frac{(\lambda_{\mathrm{mb}} c)^c}{\Gamma(c)} x^{c-1} e^{-c\lambda_{\mathrm{mb}} x}, \tag{6}$$

where $c = \frac{7}{2}$ and $\Gamma(c) = \int_0^\infty t^{c-1} e^{-t} \mathrm{d}t$, has been known to be handy and sufficiently accurate (see, e.g., [34]). Aided by this approximation, with some manipulations, the pgf of U_{m} is

$$G_{\mathrm{m}}(z) = c^c \left(c - \frac{\lambda_{\mathrm{mu}}}{\lambda_{\mathrm{mb}}}(z-1) + \frac{\lambda_{\mathrm{fb}}}{\lambda_{\mathrm{mb}}} \left(1 - e^{p\bar{U}_{\mathrm{f}}(z-1)} \right) \right)^{-c}, \tag{7}$$

and the distribution of U_{m} follows as

$$\mathbb{P}\{U_{\mathrm{m}} = i\} = \frac{G_{\mathrm{m}}^{(i)}(0)}{i!}, \quad i = 0, 1, \cdots, \tag{8}$$

where $G_{\mathrm{m}}^{(i)}(0)$ is the i-th derivative of $G_m(z)$ evaluated at $z = 0$.

For CD transmission, all the femto UEs attempt to connect to the MBS to obtain cooperative gain; thus distribution of U_{m} is similar to that in LD and LHDA transmissions with $p = 1$.

Sub-band Occupancy

Since the number of served UEs for each BS is random, the sub-band frequency resource will be underutilized in some BSs and overutilized in some other BSs. As

the UE loads in the MBS and the FAP are different under different transmission schemes, the sub-band occupancy is calculated accordingly.

Spectrum Allocation for LD and LHDA

Of the N sub-bands, let N_{m} sub-bands be allocated to the macro tier and N_{f} sub-bands to the femto tier. Each UE requires one sub-band for each transmission. We consider the following two spectrum allocation methods [35]:

1. *Orthogonal spectrum allocation:* The N sub-bands are split as $N = N_{\mathrm{m}} + N_{\mathrm{f}}$, where the N_{m} sub-bands used by all the MBSs of the macro tier are orthogonal to those N_{f} sub-bands used by all the FAPs of the femto tier. So there is no inter-tier interference.

   It is assumed that the available sub-bands are uniformly and independently allocated to the UEs by the BS. There are N_{m} available sub-bands for the MBS, and each sub-band is equally likely to be chosen. If the number of UEs is smaller than that of sub-bands, the MBS randomly chooses U_{m} out of the total N_{m} sub-bands. Otherwise, all the sub-bands are chosen. The probability that a sub-band is used by an MBS is

$$P_{\mathrm{busy}}^{\mathrm{m},\perp} = \frac{1}{N_{\mathrm{m}}} \sum_{i=0}^{\infty} \min\{i, N_{\mathrm{m}}\} \mathbb{P}\{U_{\mathrm{m}} = i\}, \tag{9}$$

   and similarly the probability that a sub-band is used by an FAP is

$$P_{\mathrm{busy}}^{\mathrm{f},\perp} = \frac{1}{N_{\mathrm{f}}} \sum_{i=0}^{\infty} \min\{i, N_{\mathrm{f}}\} \mathbb{P}\{U_{\mathrm{f}} = i\}. \tag{10}$$

2. *Non-orthogonal spectrum allocation:* Compared with the orthogonal case, here the two sets of sub-bands may overlap: each MBS (resp. FAP) independently randomly selects N_{m} (resp. N_{f}) sub-bands from the N sub-bands. The values of both N_{m} and N_{f} can be chosen from 1 to N flexibly and need not add to N. So there is inter-tier interference, while the available spectrum will be abundant as N_{m} and N_{f} grow large.

   For the non-orthogonal case, both the MBS and the FAP choose a sub-band randomly from N sub-bands, so the probability that a sub-band is used by an MBS is

$$P_{\mathrm{busy}}^{\mathrm{m},\not\perp} = \frac{1}{N} \sum_{i=0}^{\infty} \min\{i, N_{\mathrm{m}}\} \mathbb{P}\{U_{\mathrm{m}} = i\}, \tag{11}$$

   and similarly the probability that a sub-band is used by an FAP is

$$P_{\mathrm{busy}}^{\mathrm{f},\not\perp} = \frac{1}{N} \sum_{i=0}^{\infty} \min\{i, N_{\mathrm{f}}\} \mathbb{P}\{U_{\mathrm{f}} = i\}. \tag{12}$$

The spatial point process of BSs that use a given sub-band is an approximately independent thinning of the original point process Φ_{mb} (resp. Φ_{fb}) by the probability $P_{\text{busy}}^{\text{m,s}}$ (resp. $P_{\text{busy}}^{\text{f,s}}$), denoted by $\tilde{\Phi}_{\text{mb}}$ (resp. $\tilde{\Phi}_{\text{fb}}$) with the intensity $\tilde{\lambda}_{\text{mb}} = \lambda_{\text{mb}} P_{\text{busy}}^{\text{m,s}}$ (resp. $\tilde{\lambda}_{\text{fb}} = \lambda_{\text{mb}} P_{\text{busy}}^{\text{m,s}}$) [34], where the superscript $\text{s} \in \{\perp, \not\perp\}$ indicates whether the orthogonal or the non-orthogonal spectrum allocation method is used.

Spectrum Allocation for CD

Since both the macro UEs and femto UEs connect to the MBS, if the number of UEs connected to MBS $U_{\text{m}} \leq N$, each UE is allocated one sub-band, otherwise, if $U_{\text{m}} \geq N$, all the UEs share the sub-bands in a round-robin mechanism. Then the FAPs allocate sub-bands to femto UEs in a similar way by comparing U_{f} and N. For a femto UE, if it is chosen by both the MBS and the FAP, the MBS and the FAP allocate the same sub-band to the UE, thus making it working in a cooperative mode. Otherwise it is only served by the FAP and works in a noncooperative mode.

Since both the macro and femto tiers employ the total N sub-bands, similar to that of the LD case, the probability that a sub-band is used by an MBS is

$$P_{\text{busy}}^{\text{m,CoMP}} = \frac{1}{N} \sum_{i=0}^{\infty} \min\{i, N_{\text{m}}\} \mathbb{P}\{U_{\text{m}} = i\}, \tag{13}$$

and similarly the probability that a sub-band is used by an FAP is

$$P_{\text{busy}}^{\text{f,CoMP}} = \frac{1}{N} \sum_{i=0}^{\infty} \min\{i, N_{\text{f}}\} \mathbb{P}\{U_{\text{f}} = i\}. \tag{14}$$

SINR Distribution and Data Rate

SINR Distribution

The complementary cumulative distribution function (ccdf) of the SINR is defined as $\mathcal{P}(\theta) = \mathbb{P}\{\text{SINR} > \theta\}$, where θ is the SINR threshold. The SINR distributions of a UE connected to the MBS and the FAP are derived under three transmission schemes.

LD Transmission

For analytical tractability, we assume that both the BL and the EL are modulated into digital signals according to a Gaussian codebook.

For the typical UE which is assumed to be located at the origin and connected to its MBS, the received signal denoted by Y can be written as

$$Y = P_{\mathrm{m}}^{1/2}\|x_0\|^{-\alpha/2}h_{x_0}X_{x_0} + \sum_{x\in\tilde{\Phi}_{\mathrm{mb}}\setminus\{x_0\}} P_{\mathrm{m}}^{1/2}\|x\|^{-\alpha/2}h_x X_x + \kappa \sum_{y\in\tilde{\Phi}_{\mathrm{fb}}} P_{\mathrm{f}}^{1/2}\|y\|^{-\alpha/2}h_y X_y + Z, \tag{15}$$

where the first item of right side of the equation denotes the received signal symbol, the second and the third items denote the interference symbols from the macro and the femto tier, respectively, and Z denotes the Gaussian noise with zero mean and variance σ^2. We use x_0 to denote the location of the serving MBS. X_{x_0} is the signal symbol, while X_x is the interference symbol transmitted by the interfering MBS x. $X_{x_0}, X_x \sim \mathbb{CN}(0,1)$. X_y is the interference symbol transmitted by the interfering FAP y, and $X_y \sim \mathbb{CN}(0,1)$. The indicator $\kappa \in \{0,1\}$ indicates the orthogonal and non-orthogonal spectrum allocation methods, respectively.

Thus, the received SINR is

$$\gamma_{\mathrm{LD}}^{\mathrm{m}} = \frac{P_{\mathrm{m}}\|x_0\|^{-\alpha}|h_{x_0}|^2}{I_{\mathrm{m}} + \kappa I_{\mathrm{f}} + \sigma^2}, \tag{16}$$

where $I_{\mathrm{m}} = \sum_{x\in\tilde{\Phi}_{\mathrm{mb}}\setminus\{x_0\}} P_{\mathrm{m}}\|x\|^{-\alpha}|h_x|^2$ is the interference from the macro tier, and $I_{\mathrm{f}} = \sum_{y\in\tilde{\Phi}_{\mathrm{fb}}} P_{\mathrm{f}}\|y\|^{-\alpha}|h_y|^2$ is the interference from the femto tier.

For the typical femto UE which is assumed to be located at the origin and connected to its FAP, the received signal can be written as

$$Y = P_{\mathrm{f}}^{1/2}\|y_0\|^{-\alpha/2}h_{y_0}X_{y_0} + \sum_{y\in\tilde{\Phi}_{\mathrm{fb}}\setminus\{y_0\}} P_{\mathrm{f}}^{1/2}\|y\|^{-\alpha/2}h_y X_y + \kappa \sum_{x\in\tilde{\Phi}_{\mathrm{mb}}} P_{\mathrm{m}}^{1/2}\|x\|^{-\alpha/2}h_x X_x + Z, \tag{17}$$

where y_0 denotes the location of the serving FAP. Note that the FAP transmits the encoded EL signals only or the jointly encoded signals of both the BL and the EL to the typical UE based on user request. X_{y_0} is the signal symbol transmitted by the serving FAP, and X_y is the interference symbol transmitted by the interfering FAP y.

Thus, the received SINR is

$$\gamma_{\mathrm{LD}}^{\mathrm{f}} = \frac{P_{\mathrm{f}}\|y_0\|^{-\alpha}|h_{y_0}|^2}{I_{\mathrm{f}} + \kappa I_{\mathrm{m}} + \sigma^2}, \tag{18}$$

where $I_{\mathrm{f}} = \sum_{y\in\tilde{\Phi}_{\mathrm{fb}}\setminus\{y_0\}} P_{\mathrm{f}}\|y\|^{-\alpha}|h_y|^2$ denotes the interference from the femto tier and $I_{\mathrm{m}} = \sum_{x\in\tilde{\Phi}_{\mathrm{mb}}} P_{\mathrm{m}}\|x\|^{-\alpha}|h_x|^2$ denotes the interference from the macro tier.

The following theorem gives the ccdf of the SINR for the typical UE,

Theorem 1. *For LD transmission, the ccdf of the SINR for the typical UE connected to its serving MBS is*

$$\mathcal{P}_{\mathrm{LD}}^{\mathrm{m}}(\theta) = \mathbb{P}\{\gamma_{\mathrm{LD}}^{\mathrm{m}} > \theta\}$$
$$= \int_0^{\infty} \pi\lambda_{\mathrm{mb}} \exp\Bigg(- \pi v(\lambda_{\mathrm{mb}} + \tilde{\lambda}_{\mathrm{mb}}\rho(\theta,\alpha))$$
$$- \frac{\theta v^{1/\delta}\sigma^2}{P_{\mathrm{m}}} - \kappa\left(\frac{P_{\mathrm{f}}\theta}{P_{\mathrm{m}}}\right)^{\delta} v\tilde{\lambda}_{\mathrm{fb}}\delta\pi^2\csc(\delta\pi)\Bigg)\mathrm{d}v, \tag{19}$$

and the ccdf of the SINR for the typical femto UE connected to its serving FAP is

$$\mathcal{P}_{\mathrm{LD}}^{\mathrm{f}}(\theta) = \mathbb{P}\{\gamma_{\mathrm{LD}}^{\mathrm{f}} > \theta\}$$
$$= \int_0^{R_{\mathrm{f}}^2} \frac{1}{R_{\mathrm{f}}^2} \exp\left(- \frac{\theta v^{1/\delta}\sigma^2}{P_{\mathrm{f}}} - \delta\pi^2\csc(\delta\pi)\theta^{\delta} v\left(\tilde{\lambda}_{\mathrm{fb}} + \kappa\left(\frac{P_{\mathrm{m}}}{P_{\mathrm{f}}}\right)^{\delta}\right)\tilde{\lambda}_{\mathrm{mb}}\right)\mathrm{d}v, \tag{20}$$

where $\delta = 2/\alpha$, $\tilde{\lambda}_{\mathrm{mb}} = \lambda_{\mathrm{mb}} P_{\mathrm{busy}}^{\mathrm{m,s}}$, $\tilde{\lambda}_{\mathrm{fb}} = \lambda_{\mathrm{fb}} P_{\mathrm{busy}}^{\mathrm{f,s}}$, *and* $\rho(\theta,\alpha) = \theta^{\delta}\int_{\theta^{-\delta}}^{\infty} \frac{1}{1+x^{1/\delta}}\mathrm{d}x$. *In orthogonal spectrum allocation,* $\kappa = 0$, *while in non-orthogonal spectrum allocation,* $\kappa = 1$.

Proof. Let $\|x_0\|$ be the distance from the typical UE to its serving MBS, which is the nearest MBS, so the pdf of $\|x_0\|$ is $f_{\|x_0\|}(r) = e^{-\lambda_{\mathrm{mb}}\pi r^2} 2\pi\lambda_{\mathrm{mb}} r$.

The SINR experienced by the typical UE connected to its serving MBS is given by $\gamma_{\mathrm{LD}}^{\mathrm{m}} = \frac{P_{\mathrm{m}}\|x_0\|^{-\alpha}|h_{x_0}|^2}{I_{\mathrm{m}}+\kappa I_{\mathrm{f}}+\sigma^2}$, where $I_{\mathrm{m}} = \sum_{x\in\tilde{\Phi}_{\mathrm{mb}}\setminus\{x_0\}} P_{\mathrm{m}}\|x\|^{-\alpha}|h_{x_0}|^2$ is the interference from the macro tier, and $I_{\mathrm{f}} = \sum_{y\in\tilde{\Phi}_{\mathrm{fb}}} P_{\mathrm{f}}\|y\|^{-\alpha}|h_y|^2$ is the interference from the femto tier. $\kappa \in \{0,1\}$ is the indicator that whether the orthogonal or the non-orthogonal spectrum allocation is used. Due to the independent thinning approximation, the set of interfering MBSs is a PPP $\tilde{\Phi}_{\mathrm{mb}}$ with intensity $\tilde{\lambda}_{\mathrm{mb}}$, and the set of interfering FAPs is a PPP $\tilde{\Phi}_{\mathrm{fb}}$ with intensity $\tilde{\lambda}_{\mathrm{fb}}$.

The ccdf of the SINR experienced by the typical UE connected to its serving MBS

$$\mathcal{P}_{\mathrm{LD}}^{\mathrm{m}}(\theta) = \mathbb{P}\{\gamma_{\mathrm{LD}}^{\mathrm{m}} > \theta\}$$
$$= \int_0^{\infty} 2\pi\lambda_{\mathrm{mb}} r e^{-\pi\lambda_{\mathrm{mb}}r^2}\mathbb{P}\left\{\frac{P_{\mathrm{m}}|h_{x_0}|^2 r^{-\alpha}}{I_{\mathrm{m}}+\kappa I_{\mathrm{f}}+\sigma^2} > \theta\right\}\mathrm{d}r$$
$$\overset{(a)}{=} \int_0^{\infty} 2\pi\lambda_{\mathrm{mb}} r e^{-\pi\lambda_{\mathrm{mb}}r^2 - \frac{\theta r^{\alpha}\sigma^2}{P_{\mathrm{m}}}}\mathcal{L}_{I_{\mathrm{m}}+\kappa I_{\mathrm{f}}}\left(\frac{\theta r^{\alpha}}{P_{\mathrm{m}}}\right)\mathrm{d}r. \tag{21}$$

where (a) follows from $|h_{x_0}|^2 \sim \mathrm{Exp}(1)$.

After excluding the serving BS x_0, $\tilde{\Phi}_{\mathrm{mb}} \setminus \{x_0\}$ is still a PPP, so we apply the pgfl of PPP to obtain the Laplace transform of I_{m}

$$\mathcal{L}_{I_{\mathrm{m}}}(s) = \exp\left(-2\pi\tilde{\lambda}_{\mathrm{mb}}\int_r^{\infty}\left(1-\frac{1}{1+sP_{\mathrm{m}}x^{-\alpha}}\right)x\mathrm{d}x\right)$$
$$= e^{-\pi\tilde{\lambda}_{\mathrm{mb}}r^2\rho\left(\frac{sP_{\mathrm{m}}}{r^{\alpha}},\alpha\right)}. \tag{22}$$

Since $\tilde{\Phi}_{\mathrm{fb}}$ is a PPP, the Laplace transform of I_{f} is

$$\mathcal{L}_{I_{\mathrm{f}}}(s) = \exp\left(-2\pi\tilde{\lambda}_{\mathrm{fb}}\int_0^{\infty}\left(1-\frac{1}{1+sP_{\mathrm{f}}x^{-\alpha}}\right)x\mathrm{d}x\right)$$
$$= e^{-\delta\pi^2\csc(\delta\pi)\tilde{\lambda}_{\mathrm{fb}}(sP_{\mathrm{f}})^{\delta}}. \tag{23}$$

Substituting (22) and (23) into $\mathcal{P}_{\mathrm{LD}}^{\mathrm{m}}(\theta)$, we can obtain (19).

Let y_0 be the distance between the typical femto UE and its serving FAP. Since femto UEs are uniformly distributed in the circular coverage area of radius R_{f} of each FAP, the pdf of y_0 is given by $f_{y_0}(r) = \frac{2r}{R_{\mathrm{f}}^2}$.

The received SINR for the typical femto UE connected to its serving FAP follows as $\gamma_{\mathrm{LD}}^{\mathrm{f}} = \frac{P_{\mathrm{f}}\|y_0\|^{-\alpha}|h_{y_0}|^2}{I_{\mathrm{f}}+\kappa I_{\mathrm{m}}+\sigma^2}$, where $I_{\mathrm{f}} = \sum_{y\in\tilde{\Phi}_{\mathrm{fb}}} P_{\mathrm{f}}\|y\|^{-\alpha}|h_y|^2$ is the interference from the femto tier, and $I_{\mathrm{m}} = \sum_{x\in\tilde{\Phi}_{\mathrm{mb}}} P_{\mathrm{m}}\|x\|^{-\alpha}|h_{x_0}|^2$ is the interference from the macro tier.

The ccdf of the SINR experienced by the typical femto UE connected to its serving FAP is

$$\mathcal{P}_{\mathrm{LD}}^{\mathrm{f}}(\theta) = \mathbb{P}\{\gamma_{\mathrm{LD}}^{\mathrm{f}} > \theta\}$$
$$= \int_0^{R_{\mathrm{f}}} \frac{2r}{R_{\mathrm{f}}^2}\mathbb{P}\left\{\frac{P_{\mathrm{f}}|h_{y_0}|^2 r^{-\alpha}}{I_{\mathrm{f}}+\kappa I_{\mathrm{m}}+\sigma^2} > \theta\right\}\mathrm{d}r$$
$$= \int_0^{R_{\mathrm{f}}} \frac{2r}{R_{\mathrm{f}}^2} e^{\frac{-\theta r^{\alpha}\delta^2}{P_{\mathrm{f}}}}\mathcal{L}_{I_{\mathrm{f}}+\kappa I_{\mathrm{m}}}\left(\frac{\theta r^{\alpha}}{P_{\mathrm{f}}}\right)\mathrm{d}r, \tag{24}$$

which, after expanding the Laplace transform of I_{m}, I_{f}, and further manipulations, leads to (20).

LHDA Transmission

The BL is modulated to a digital signal, while the EL is modulated to an analog signal. The digital modulation is based on a Gaussian codebook, and the EL signal after analog modulation is also modeled as a Gaussian source with zero mean and unit variance [36, 37]. For analog modulation, it is assumed that the source bandwidth is equal to the channel bandwidth [14, 16].

For the typical UE which is assumed to be located at the origin and connected to its serving MBS, the received signal can be written as

$$Y = P_{\mathrm{m}}^{1/2}\|x_0\|^{-\alpha/2}h_{x_0}X_{x_0} + \sum_{x\in\tilde{\Phi}_{\mathrm{mb}}\setminus\{x_0\}} P_{\mathrm{m}}^{1/2}\|x\|^{-\alpha/2}h_x X_x + \kappa \sum_{y\in\tilde{\Phi}_{\mathrm{fb}}} P_{\mathrm{f}}^{1/2}\|y\|^{-\alpha/2}h_y X_y + Z, \tag{25}$$

which is nearly the same as (15) in LD transmission, the difference lies in that X_y is the analog EL interference symbol or the superposition of digital BL and analog EL interference symbol transmitted by the interfering FAP y based on the transmission scheme of y, and $X_y \sim \mathbb{CN}(0,1)$.

Thus the received SINR is

$$\gamma_{\mathrm{LHDA}}^{\mathrm{m}} = \frac{P_{\mathrm{m}}\|x_0\|^{-\alpha}|h_{x_0}|^2}{I_{\mathrm{m}} + \kappa I_{\mathrm{f}} + \sigma^2}, \tag{26}$$

where $I_{\mathrm{m}} = \sum_{x\in\tilde{\Phi}_{\mathrm{mb}}\setminus\{x_0\}} P_{\mathrm{m}}\|x\|^{-\alpha}|h_x|^2$ is the interference from the macro tier and $I_{\mathrm{f}} = \sum_{y\in\tilde{\Phi}_{\mathrm{fb}}} P_{\mathrm{f}}\|y\|^{-\alpha}|h_y|^2$ is the interference from the femto tier.

For the typical femto UE which is assumed to be located at the origin and connected to its FAP, according to the transmission scheme, it receives only the EL, or it receives the superposition of the digital BL signal and the analog EL signal.

- *Case 1:* The typical femto UE connected to its FAP receives only the EL. The received signal for the typical femto UE is

$$Y = P_{\mathrm{f}}^{1/2}\|y_0\|^{-\frac{\alpha}{2}}h_{y_0}X_{y_0}^{\mathrm{E}} + \sum_{y\in\tilde{\Phi}_{\mathrm{fb}}\setminus\{y_0\}} P_{\mathrm{f}}^{1/2}\|y\|^{-\frac{\alpha}{2}}h_y X_y + \kappa \sum_{x\in\tilde{\Phi}_{\mathrm{mb}}} P_{\mathrm{m}}^{1/2}\|x\|^{-\frac{\alpha}{2}}h_x X_x + Z, \tag{27}$$

  where $X_{y_0}^{\mathrm{E}}$ is the EL signal symbol transmitted by the serving FAP and X_y is the interference symbol transmitted by the interfering FAP y.

  Thus, the received SINR for the femto UE connected to its FAP to receive the EL is

$$\gamma_{\mathrm{LHDA}}^{\mathrm{f}} = \frac{P_{\mathrm{f}}\|y_0\|^{-\alpha}|h_{y_0}|^2}{I_{\mathrm{f}} + \kappa I_{\mathrm{m}} + \sigma^2}, \tag{28}$$

  where $I_{\mathrm{f}} = \sum_{y\in\tilde{\Phi}_{\mathrm{fb}}\setminus\{y_0\}} P_{\mathrm{f}}\|y\|^{-\alpha}|h_y|^2$ is the interference from the femto tier and $I_{\mathrm{m}} = \sum_{x\in\tilde{\Phi}_{\mathrm{mb}}} P_{\mathrm{m}}\|x\|^{-\alpha}|h_x|^2$ is the interference from the macro tier.
- *Case 2:* The typical femto UE connected to its FAP receives the superposition of the digital BL signal and the analog EL signal. The received signal for the typical femto UE is

$$Y = \|y_0\|^{-\alpha/2} h_{y_0} \left(\sqrt{P_{\mathrm{f}}^{\mathrm{B}}} X_{y_0}^{\mathrm{B}} + \sqrt{P_{\mathrm{f}}^{\mathrm{E}}} X_{y_0}^{\mathrm{E}} \right) + \sum_{y \in \tilde{\Phi}_{\mathrm{fb}} \setminus \{y_0\}} P_{\mathrm{f}}^{1/2} \|y\|^{-\alpha/2} h_y X_y + \kappa \sum_{x \in \tilde{\Phi}_{\mathrm{mb}}} P_{\mathrm{m}}^{1/2} \|x\|^{-\alpha/2} h_x X_x + Z, \tag{29}$$

where $X_{y_0}^{\mathrm{B}}$ is the BL signal symbol transmitted by the serving FAP, and $X_{y_0}^{\mathrm{E}}$ is the EL signal symbol transmitted by the serving FAP.

Thus, the received SINR for the typical femto UE connected to its FAP to receive the BL, denoted by $\gamma_{\mathrm{LHDA}}^{\mathrm{f,B}}$, is

$$\gamma_{\mathrm{LHDA}}^{\mathrm{f,B}} = \frac{P_{\mathrm{f}}^{\mathrm{B}} \|y_0\|^{-\alpha} |h_{y_0}|^2}{P_{\mathrm{f}}^{\mathrm{E}} \|y_0\|^{-\alpha} |h_{y_0}|^2 + I_{\mathrm{f}} + \kappa I_{\mathrm{m}} + \sigma^2}. \tag{30}$$

Successive interference cancellation (SIC) [38] is adopted to demodulate the EL signal. Conditioned on the successful reception of the BL, the received SINR for the typical femto UE connected to the FAP to receive the EL signal, denoted by $\gamma_{\mathrm{LHDA}}^{\mathrm{f,E}}$, is

$$\gamma_{\mathrm{LHDA}}^{\mathrm{f,E}} = \frac{P_{\mathrm{f}}^{\mathrm{E}} \|y_0\|^{-\alpha} |h_{y_0}|^2}{I_{\mathrm{f}} + \kappa I_{\mathrm{m}} + \sigma^2}. \tag{31}$$

The following theorem gives the ccdf of the SINR for the typical UE:

Theorem 2. *For LHDA transmission, the ccdf of the SINR for the typical UE connected to its serving MBS is*

$$\mathcal{P}_{\mathrm{LHDA}}^{\mathrm{m}}(\theta_{\mathrm{B}}) = \mathbb{P}\{\gamma_{\mathrm{LHDA}}^{\mathrm{m}} > \theta_{\mathrm{B}}\} = \mathcal{P}_{\mathrm{LD}}^{\mathrm{m}}(\theta_{\mathrm{B}}); \tag{32}$$

the ccdf of the SINR for the typical femto UE connected to its serving FAP to receive the EL is given by:

$$\mathcal{P}_{\mathrm{LHDA}}^{\mathrm{f}}(\theta_{\mathrm{E}}) = \mathbb{P}\{\gamma_{\mathrm{LHDA}}^{\mathrm{f}} > \theta_{\mathrm{E}}\} = \mathcal{P}_{\mathrm{LD}}^{\mathrm{f}}(\theta_{\mathrm{E}}), \tag{33}$$

and the joint ccdf of the SINR for the typical femto UE connected to its serving FAP to receive the superposition of the digital BL and the analog EL is given by (40).

Proof. Similar to the derivation of $\mathcal{P}_{\mathrm{LD}}^{\mathrm{m}}(\theta)$, the ccdf of $\gamma_{\mathrm{LHDA}}^{\mathrm{m}}$ follows as:

$$\mathcal{P}_{\mathrm{LHDA}}^{\mathrm{m}}(\theta) = \mathbb{P}\{\gamma_{\mathrm{LHDA}}^{\mathrm{m}} > \theta\} = \mathcal{P}_{\mathrm{LD}}^{\mathrm{m}}(\theta). \tag{34}$$

According to the transmission scheme, the FAP transmits the analog EL signal with probability p or the superposition of the digital BL signal and the analog EL signal with probability $1 - p$.

Case 1: The received SINR for the typical femto UE connected to the FAP receives the EL follows as $\gamma^{\mathrm{f}}_{\mathrm{LHDA}} = \frac{P_{\mathrm{f}}\|y_0\|^{-\alpha}|h_{y_0}|^2}{I_{\mathrm{f}}+\kappa I_{\mathrm{m}}+\sigma^2}$. Similar to the derivation of $\mathcal{P}^{\mathrm{f}}_{\mathrm{LD}}(\theta)$, the ccdf of $\gamma^{\mathrm{f}}_{\mathrm{LHDA}}$ follows as

$$\mathcal{P}^{\mathrm{f}}_{\mathrm{LHDA}}(\theta) = \mathbb{P}\{\gamma^{\mathrm{f}}_{\mathrm{LHDA}} > \theta\} = \mathcal{P}^{\mathrm{f}}_{\mathrm{LD}}(\theta). \tag{35}$$

Case 2: The received SINR for the typical femto UE connected to the FAP receives the superposition of the digital BL signal and the analog EL signal is

$$\gamma^{\mathrm{f,B}}_{\mathrm{LHDA}} = \frac{P^{\mathrm{B}}_{\mathrm{f}}\|y_0\|^{-\alpha}|h_{y_0}|^2}{P^{\mathrm{E}}_{\mathrm{f}}\|y_0\|^{-\alpha}|h_{y_0}|^2 + I_{\mathrm{f}} + \kappa I_{\mathrm{m}} + \sigma^2}, \tag{36}$$

where $P^{\mathrm{E}}_{\mathrm{f}}\|y_0\|^{-\alpha}|h_{y_0}|^2$ is the interference of the superposed EL.

$$\begin{aligned}\mathbb{P}\{\gamma^{\mathrm{f,B}}_{\mathrm{LHDA}} > \theta\} &= \int_0^{\infty} \frac{2r}{R_{\mathrm{f}}^2} e^{-\frac{\theta r^{\alpha}\sigma^2}{P^{\mathrm{B}}_{\mathrm{f}}-\theta P^{\mathrm{E}}_{\mathrm{f}}}} \mathcal{L}_{I_{\mathrm{f}}+\kappa I_{\mathrm{m}}}\left(\frac{\theta r^{\alpha}}{P^{\mathrm{B}}_{\mathrm{f}}-\theta P^{\mathrm{E}}_{\mathrm{f}}}\right) \mathrm{d}r \\ &= \int_0^{R_{\mathrm{f}}^2} \frac{1}{R_{\mathrm{f}}^2} \exp\Bigg(-\frac{\theta v^{1/\delta}\sigma^2}{P^{\mathrm{B}}_{\mathrm{f}}-\theta P^{\mathrm{E}}_{\mathrm{f}}} - \delta\pi^2 \csc(\delta\pi)\theta^{\delta} v \\ &\quad \times \left(\tilde{\lambda}_{\mathrm{fb}}\left(\frac{P_{\mathrm{f}}}{P^{\mathrm{B}}_{\mathrm{f}}-\theta P^{\mathrm{E}}_{\mathrm{f}}}\right)^{\delta} + \kappa\tilde{\lambda}_{\mathrm{mb}}\left(\frac{P_{\mathrm{m}}}{P^{\mathrm{B}}_{\mathrm{f}}-\theta P^{\mathrm{E}}_{\mathrm{f}}}\right)^{\delta}\right)\Bigg)\mathrm{d}v.\end{aligned} \tag{37}$$

SIC is adopted to decode the EL signal. After successful reception of the BL, the received SINR for the EL signal is $\gamma^{\mathrm{f,E}}_{\mathrm{LHDA}} = \frac{P^{\mathrm{E}}_{\mathrm{f}}\|y_0\|^{-\alpha}|h_{y_0}|^2}{I_{\mathrm{f}}+\kappa I_{\mathrm{m}}+\sigma^2}$.

The ccdf of $\gamma^{\mathrm{f,E}}_{\mathrm{LHDA}}$ follows as:

$$\begin{aligned}\mathbb{P}\{\gamma^{\mathrm{f,E}}_{\mathrm{LHDA}} > \theta\} &= \int_0^{\infty} \frac{2r}{R_{\mathrm{f}}^2} e^{-\frac{\theta r^{\alpha}\sigma^2}{P^{\mathrm{E}}_{\mathrm{f}}}} \mathcal{L}_{I_{\mathrm{f}}+\kappa I_{\mathrm{m}}}\left(\frac{\theta r^{\alpha}}{P^{\mathrm{E}}_{\mathrm{f}}}\right) \mathrm{d}r \\ &= \int_0^{R_{\mathrm{f}}^2} \frac{1}{R_{\mathrm{f}}^2} e^{-\frac{\theta v^{1/\delta}\sigma^2}{P^{\mathrm{E}}_{\mathrm{f}}} - \delta\pi^2\csc(\delta\pi)\theta^{\delta} v\left(\tilde{\lambda}_{\mathrm{fb}}\left(\frac{P_{\mathrm{f}}}{P^{\mathrm{E}}_{\mathrm{f}}}\right)^{\delta} + \kappa\tilde{\lambda}_{\mathrm{mb}}\left(\frac{P_{\mathrm{m}}}{P^{\mathrm{E}}_{\mathrm{f}}}\right)^{\delta}\right)} \mathrm{d}v.\end{aligned} \tag{38}$$

The joint ccdf of $\gamma^{\mathrm{f,B}}_{\mathrm{LHDA}}$ and $\gamma^{\mathrm{f,E}}_{\mathrm{LHDA}}$ is

$$\begin{aligned}\mathcal{P}_{\mathrm{LHDA}}(\theta_{\mathrm{B}}, \theta_{\mathrm{E}}) &= \mathbb{P}\{\gamma^{\mathrm{f,B}}_{\mathrm{LHDA}} > \theta_{\mathrm{B}}, \gamma^{\mathrm{f,E}}_{\mathrm{LHDA}} > \theta_{\mathrm{E}}\} \\ &= \mathbf{1}\left(\theta_{\mathrm{B}} > \frac{\theta_{\mathrm{E}} P^{\mathrm{B}}_{\mathrm{f}}}{(1+\theta_{\mathrm{E}})P^{\mathrm{E}}_{\mathrm{f}}}\right)\int_0^{R_{\mathrm{f}}^2}\end{aligned}$$

$$\frac{1}{R_{\mathrm{f}}^2} e^{-\frac{\theta_{\mathrm{B}} v^{1/\delta} \sigma^2}{P_{\mathrm{f}}^{\mathrm{B}} - \theta_{\mathrm{B}} P_{\mathrm{f}}^{\mathrm{E}}} - \delta\pi^2 \csc(\delta\pi) \theta_{\mathrm{B}}^{\delta} v \left(\frac{\tilde{\lambda}_{\mathrm{fb}} P_{\mathrm{f}}^{\delta} + \kappa \tilde{\lambda}_{\mathrm{mb}} P_{\mathrm{m}}^{\delta}}{\left(P_{\mathrm{f}}^{\mathrm{B}} - \theta_{\mathrm{B}} P_{\mathrm{f}}^{\mathrm{E}}\right)^{\delta}} \right)} \mathrm{d}v$$

$$+ \mathbf{1}\left(\theta_{\mathrm{B}} \leq \frac{\theta_{\mathrm{E}} P_{\mathrm{f}}^{\mathrm{B}}}{(1+\theta_{\mathrm{E}}) P_{\mathrm{f}}^{\mathrm{E}}}\right) \int_0^{R_{\mathrm{f}}^2}$$

$$\frac{1}{R_{\mathrm{f}}^2} e^{-\frac{\theta_{\mathrm{E}} v^{1/\delta} \sigma^2}{P_{\mathrm{f}}^{\mathrm{E}}} - \delta\pi^2 \csc(\delta\pi) \theta_{\mathrm{E}}^{\delta} v \left(\tilde{\lambda}_{\mathrm{fb}} \left(\frac{P_{\mathrm{f}}}{P_{\mathrm{f}}^{\mathrm{E}}} \right)^{\delta} + \kappa \tilde{\lambda}_{\mathrm{mb}} \left(\frac{P_{\mathrm{m}}}{P_{\mathrm{f}}^{\mathrm{E}}} \right)^{\delta} \right)} \mathrm{d}v. \tag{39}$$

$$\begin{aligned}
\mathcal{P}_{\mathrm{LHDA}}(\theta_{\mathrm{B}}, \theta_{\mathrm{E}}) &= \mathbb{P}\{\gamma_{\mathrm{LHDA}}^{\mathrm{f,B}} > \theta_{\mathrm{B}}, \gamma_{\mathrm{LHDA}}^{\mathrm{f,E}} > \theta_{\mathrm{E}}\} \\
&= \mathbb{P}\left\{ |h_{x0}|^2 > \frac{\theta_{\mathrm{B}} I_{\mathrm{total}}}{(P_{\mathrm{B}} - \theta_{\mathrm{B}} P_{\mathrm{E}}) \|x_0\|^{-\alpha}}, |h_{x0}|^2 > \frac{\theta_{\mathrm{E}} I_{\mathrm{total}}}{P_{\mathrm{E}} \|x\|^{-\alpha}} \right\} \\
&= \mathbb{P}\left\{ |h_{x0}|^2 > \max\left(\frac{\theta_{\mathrm{B}} I_{\mathrm{total}}}{(P_{\mathrm{B}} - \theta_{\mathrm{B}} P_{\mathrm{E}}) \|x_0\|^{-\alpha}}, \frac{\theta_{\mathrm{E}} I_{\mathrm{total}}}{P_{\mathrm{E}} \|x\|^{-\alpha}} \right) \right\} \\
&= \mathbb{P}\{\gamma_{\mathrm{LHDA}}^{\mathrm{f,B}} > \theta_{\mathrm{B}}\} \mathbf{1}\left(\theta_{\mathrm{B}} > \frac{\theta_{\mathrm{E}} P_{\mathrm{f}}^{\mathrm{B}}}{(1+\theta_{\mathrm{E}}) P_{\mathrm{f}}^{\mathrm{E}}} \right) \\
&\quad + \mathbb{P}\{\gamma_{\mathrm{LHDA}}^{\mathrm{f,E}} > \theta_{\mathrm{E}}\} \mathbf{1}\left(\theta_{\mathrm{B}} \leq \frac{\theta_{\mathrm{E}} P_{\mathrm{f}}^{\mathrm{B}}}{(1+\theta_{\mathrm{E}}) P_{\mathrm{f}}^{\mathrm{E}}} \right),
\end{aligned} \tag{40}$$

where $I_{\mathrm{total}} = I_{\mathrm{f}} + \kappa I_{\mathrm{m}} + \sigma^2$.

CD Transmission

For the macro UE, the video transmission from the serving MBS is the same as that of LD; thus the ccdf of the SINR denoted by $\mathcal{P}_{\mathrm{CD}}^{\mathrm{m}}(\theta)$ is equal to $\mathcal{P}_{\mathrm{LD}}^{\mathrm{m}}(\theta)$ with $p = 1$ and $\kappa = 1$.

For the femto UE, based on the sub-band allocation from the MBS and the FAP, it can work in a cooperative or noncooperative modes.

- In the noncooperative case, since the femto UE can only connect to the FAP, the received signal can be written as

$$\begin{aligned}
Y &= P_{\mathrm{f}}^{1/2} \|y_0\|^{-\frac{\alpha}{2}} h_{y_0} X_{y_0} + \sum_{y \in \tilde{\Phi}_{\mathrm{fb}} \setminus \{y_0\}} P_{\mathrm{f}}^{1/2} \|y\|^{-\frac{\alpha}{2}} h_y X_y \\
&\quad + \sum_{x \in \tilde{\Phi}_{\mathrm{mb}}} P_{\mathrm{m}}^{1/2} \|x\|^{-\frac{\alpha}{2}} h_x X_x + Z,
\end{aligned} \tag{41}$$

Thus, the received SINR is

$$\gamma_{\mathrm{CD}}^{\mathrm{f,non}} = \frac{P_{\mathrm{f}}\|y_0\|^{-\alpha}|h_{y_0}|^2}{I_{\mathrm{f}} + I_{\mathrm{m}} + \sigma^2}. \tag{42}$$

The ccdf of the $\gamma_{\mathrm{CD}}^{\mathrm{f,non}}$, denoted as $\mathcal{P}_{\mathrm{CD}}^{\mathrm{f,non}}(\theta)$, is equal to $\mathcal{P}_{\mathrm{LD}}^{\mathrm{f}}(\theta)$ with $p = 1$ and $\kappa = 1$.

- In the cooperative case, since the femto UE is served jointly by the MBS and the FAP, the received signal can be written as

$$Y = P_{\mathrm{m}}^{1/2}\|x_0\|^{-\alpha/2}h_{x_0}X_0 + P_{\mathrm{f}}^{1/2}\|y_0\|^{-\alpha/2}h_{y_0}X_0 + \sum_{x\in\tilde{\Phi}_{\mathrm{mb}}\setminus\{x_0\}} P_{\mathrm{m}}^{1/2}\|x\|^{-\alpha/2}h_x X_x + \sum_{y\in\tilde{\Phi}_{\mathrm{fb}}\setminus\{y_0\}} P_{\mathrm{f}}^{1/2}\|y\|^{-\alpha/2}h_y X_y + Z, \tag{43}$$

where the fist and second items of right side of the equation denote the received signal symbols from the serving MBS and FAP, respectively, and the following two items denote the interference symbols from the macro and femto tiers, respectively

The noncoherent joint transmission is adopted, and the SINR of the received signal is

$$\gamma_{\mathrm{CD}}^{\mathrm{f,CoMP}} = \frac{\left|P_{\mathrm{m}}^{1/2}\|x_0\|^{-\alpha/2}h_{x_0} + P_{\mathrm{f}}^{1/2}\|y_0\|^{-\alpha/2}h_{y_0}\right|^2}{I_{\mathrm{m}} + I_{\mathrm{f}} + \sigma^2}, \tag{44}$$

where the interference from the macro tier is $I_{\mathrm{m}} = \sum_{x\in\tilde{\Phi}_{\mathrm{mb}}\setminus x_0} P_{\mathrm{m}}\|x\|^{-\alpha}h_x$, and the interference from the femto tier is $I_{\mathrm{f}} = \sum_{y\in\tilde{\Phi}_{\mathrm{fb}}\setminus y_0} P_{\mathrm{f}}\|y\|^{-\alpha}h_y$.

Theorem 3. *For CD transmission, when the femto UE works in a cooperative mode, the ccdf of the SINR is*

$$\mathcal{P}_{\mathrm{CD}}^{\mathrm{f,CoMP}}(\theta) = \int_0^\infty \int_0^{R_{\mathrm{f}}} e^{-\frac{\mu\theta\sigma^2}{P_{\mathrm{m}}r_{\mathrm{m}}^{-\alpha}+P_{\mathrm{f}}r_{\mathrm{f}}^{-\alpha}} - \pi\tilde{\lambda}_{\mathrm{mb}}r_{\mathrm{m}}^2\rho\left(\frac{\theta}{1+\frac{P_{\mathrm{f}}r_{\mathrm{f}}^{-\alpha}}{P_{\mathrm{m}}r_{\mathrm{m}}^{-\alpha}}},\alpha\right) - \pi\tilde{\lambda}_{\mathrm{fb}}r_{\mathrm{f}}^2\rho\left(\frac{\theta}{1+\frac{P_{\mathrm{m}}r_{\mathrm{m}}^{-\alpha}}{P_{\mathrm{f}}r_{\mathrm{f}}^{-\alpha}}},\alpha\right) - \lambda_{\mathrm{mb}}\pi r_{\mathrm{m}}^2} \times 2\pi\lambda_{\mathrm{mb}}r_{\mathrm{m}}\frac{2r_{\mathrm{f}}}{R_{\mathrm{f}}^2}\mathrm{d}r_{\mathrm{m}}\mathrm{d}r_{\mathrm{f}}. \tag{45}$$

Proof. Let $\|x_0\|$ be the distance from the typical femto UE to its serving MBS, and the pdf of $\|x_0\|$ is $f_{\|x_0\|}(r_{\mathrm{m}}) = e^{-\lambda_{\mathrm{mb}}\pi r_{\mathrm{m}}^2}2\pi\lambda_{\mathrm{mb}}r_{\mathrm{m}}$.

Let $\|y_0\|$ be the distance from the typical femto UE to its serving FAP, and the pdf of r_f is $f_{\|y_0\|}(r_\mathrm{f}) = \frac{2r_\mathrm{f}}{R_\mathrm{f}^2}$.

The ccdf of SINR $\gamma_{\mathrm{CD}}^{\mathrm{f,CoMP}}$ is

$$\begin{aligned}
\mathcal{P}_\mathrm{f}^{\mathrm{CoMP}}(\theta) &= \mathbb{P}\{\gamma_\mathrm{f}^{\mathrm{CoMP}} > \theta\} \\
&= \mathbb{P}\left\{\left|P_\mathrm{m}^{\frac{1}{2}} r_\mathrm{m}^{-\frac{\alpha}{2}} h_\mathrm{m} + P_\mathrm{f}^{\frac{1}{2}} r_\mathrm{f}^{-\frac{\alpha}{2}} h_\mathrm{f}\right|^2 > \theta(I_\mathrm{m} + I_\mathrm{f} + \sigma^2)\right\} \\
&\overset{(a)}{=} \mathbb{E}_{I_\mathrm{m}, I_\mathrm{f}, r_\mathrm{m}, r_\mathrm{f}}\left\{e^{-\frac{\mu\theta(I_\mathrm{m}+I_\mathrm{f}+\sigma^2)}{P_\mathrm{m} r_\mathrm{m}^{-\alpha} + P_\mathrm{f} r_\mathrm{f}^{-\alpha}}}\right\} \\
&= \mathbb{E}_{r_\mathrm{m}, r_\mathrm{f}}\left\{e^{-\frac{\mu\theta\sigma^2}{P_\mathrm{m} r_\mathrm{m}^{-\alpha} + P_\mathrm{f} r_\mathrm{f}^{-\alpha}}} \mathcal{L}_{I_\mathrm{m}}\left(-\frac{\mu\theta}{P_\mathrm{m} r_\mathrm{m}^{-\alpha} + P_\mathrm{f} r_\mathrm{f}^{-\alpha}}\right)\right. \\
&\quad \left.\mathcal{L}_{I_\mathrm{f}}\left(-\frac{\mu\theta}{P_\mathrm{m} r_\mathrm{m}^{-\alpha} + P_\mathrm{f} r_\mathrm{f}^{-\alpha}}\right)\right\}, \qquad (46)
\end{aligned}$$

where (a) follows that h_m and h_f are independent Gaussian variable $\mathcal{N}(0, 1)$.

The Laplace transform of I_m is

$$\begin{aligned}
\mathcal{L}_{I_\mathrm{m}}(s) &= \exp\left(-2\pi\tilde{\lambda}_\mathrm{mb} \int_{r_\mathrm{m}}^{\infty} (1 - \mathcal{L}_h(sP_\mathrm{m} x^{-\alpha}))x\mathrm{d}x\right) \\
&= e^{-\pi\lambda'_m r_\mathrm{m}^2 \rho(\frac{sP_\mathrm{m}}{\mu r_\mathrm{m}^{\alpha}}, \alpha)}. \qquad (47)
\end{aligned}$$

The Laplace transform of I_f is

$$\begin{aligned}
\mathcal{L}_{I_\mathrm{f}}(s) &= \exp\left(-2\pi\tilde{\lambda}_\mathrm{fb} \int_{r_\mathrm{f}}^{\infty} (1 - \mathcal{L}_h(sP_\mathrm{f} x^{-\alpha}))x\mathrm{d}x\right) \\
&= e^{-\pi\lambda'_f r_\mathrm{f}^2 \rho(\frac{sP_\mathrm{f}}{\mu r_\mathrm{f}^{\alpha}}, \alpha)}. \qquad (48)
\end{aligned}$$

Data Rate

The instantaneous data rate that a sub-band channel of bandwidth W can accommodate is $R = W \log_2(1 + \mathrm{SINR})$. For LD transmission, since both the MBS and the FAP transmit digital signals; the channel from the typical UE to its serving MBS can accommodate the data rate $R_\mathrm{m} = W \log_2(1 + \gamma_{\mathrm{LD}}^{\mathrm{m}})$, and the channel from the typical UE to its serving FAP can accommodate the data rate $R_\mathrm{f} = W \log_2(1+\gamma_{\mathrm{LD}}^{\mathrm{f}})$. For LHDA transmission, only the BL is modulated to a digital signal, so the data rate is defined only for the BL, the channel from the typical UE to its serving MBS

can accommodate the data rate $R_{\mathrm{m}} = W \log_2(1 + \gamma_{\mathrm{LHDA}}^{\mathrm{m}})$, and the channel from the typical UE to its serving FAP can accommodate data rate $R_{\mathrm{f}} = W \log_2(1 + \gamma_{\mathrm{LHDA}}^{\mathrm{f,B}})$.

The actually achieved UE data rates, after taking into consideration the UE load and sub-band occupancy, are given below. Without loss of generality, we take an MBS as an example. When the number of UEs in a macro cell does not exceed the total number of sub-bands (i.e., $U_{\mathrm{m}} \leq N_{\mathrm{m}}$), each UE can exclusively occupy a sub-band, and its achieved data rate is R_{m}; when $U_{\mathrm{m}} > N_{\mathrm{m}}$, the U_{m} UEs share the N_{m} sub-bands, and the data rate is thus discounted into $\frac{N_{\mathrm{m}}}{U_{\mathrm{m}}} R_{\mathrm{m}}$, assuming a round-robin sharing mechanism. So the average achieved data rate of a UE served by an MBS is given by:

$$R_{\mathrm{mu}} = \xi_{\mathrm{m}} R_{\mathrm{m}}, \tag{49}$$

where ξ_{m} is the scheduling index denoting the probability that a UE is scheduled by the MBS,

$$\xi_{\mathrm{m}} = \frac{\sum_{i=1}^{N_{\mathrm{m}}} \mathbb{P}\{U_{\mathrm{m}} = i\} + \sum_{i=N_{\mathrm{m}}+1}^{\infty} \mathbb{P}\{U_{\mathrm{m}} = i\} \frac{N_{\mathrm{m}}}{i}}{1 - \mathbb{P}\{U_{\mathrm{m}} = 0\}}. \tag{50}$$

Similarly, the average achieved data rate of a UE served by an FAP is given by

$$R_{\mathrm{fu}} = \xi_{\mathrm{f}} R_{\mathrm{f}}, \tag{51}$$

where ξ_{f} is the scheduling index denoting the probability that a UE is scheduled by the FAP,

$$\xi_{\mathrm{f}} = \frac{\sum_{i=1}^{N_{\mathrm{f}}} \mathbb{P}\{U_{\mathrm{f}} = i\} + \sum_{i=N_{\mathrm{f}}+1}^{\infty} \mathbb{P}\{U_{\mathrm{f}} = i\} \frac{N_{\mathrm{f}}}{i}}{1 - \mathbb{P}\{U_{\mathrm{f}} = 0\}}. \tag{52}$$

System Performances

In this section we evaluate several important performance metrics, namely, the outage probability, the HD probability, and the average distortion. The outage probability is the probability that a UE cannot receive the BL, namely, the UE data rate is less than R_{B}. The HD probability is the probability that a UE can receive high-definition content, i.e., both the BL and the EL, namely, the UE data rate is greater than $R_{\mathrm{B}} + R_{\mathrm{E}}$. The average distortion evaluates the difference between the received video and source video, which is measured using the distortion-rate function. Note that, for LHDA transmission, the HD probability for the femto UE is not defined since the EL is transmitted as an analog signal and the data rate for an analog signal is undefined.

LD Transmission

For a macro UE, only the BL is transmitted from its serving MBS, so the outage probability, denoted by $P_{\text{out}}^{\text{LD,m}}$, is

$$\begin{aligned} P_{\text{out}}^{\text{LD,m}} &= \mathbb{P}\{R_{\text{mu}} < R_{\text{B}}\} \\ &= \mathbb{P}\left\{\gamma_{\text{LD}}^{\text{m}} < 2^{\frac{R_{\text{B}}/\xi_{\text{m}}}{W}} - 1\right\} \\ &= 1 - \mathcal{P}_{\text{LD}}^{\text{m}}\left(2^{\frac{R_{\text{B}}/\xi_{\text{m}}}{W}} - 1\right). \end{aligned} \tag{53}$$

For a femto UE, it either connects to its serving MBS with probability p or its serving FAP with probability $1-p$ to receive the BL, so the outage probability, denoted by $P_{\text{out}}^{\text{LD,f}}$, is

$$\begin{aligned} P_{\text{out}}^{\text{LD,f}} &= p\mathbb{P}\{R_{\text{mu}} < R_{\text{B}}\} + (1-p)\mathbb{P}\{R_{\text{fu}} < R_{\text{B}}\} \\ &= p\mathbb{P}\left\{\gamma_{\text{LD}}^{\text{m}} < 2^{\frac{R_{\text{B}}/\xi_{\text{m}}}{W}} - 1\right\} + (1-p)\mathbb{P}\left\{\gamma_{\text{LD}}^{\text{f}} < 2^{\frac{R_{\text{B}}/\xi_{\text{f}}}{W}} - 1\right\} \qquad (54) \\ &= p\left(1 - \mathcal{P}_{\text{LD}}^{\text{m}}\left(2^{\frac{R_{\text{B}}/\xi_{\text{m}}}{W}} - 1\right)\right) + (1-p)\left(1 - \mathcal{P}_{\text{LD}}^{\text{f}}\left(2^{\frac{R_{\text{B}}/\xi_{\text{f}}}{W}} - 1\right)\right). \qquad (55) \end{aligned}$$

To receive the high-definition video content, a femto UE receives the BL from the MBS and receives the EL from the FAP with probability p, or it receives both the BL and the EL from the FAP with probability $1-p$. Thus, the HD probability for a femto UE, denoted by P_{HD}^{f}, is

$$\begin{aligned} P_{\text{HD}}^{\text{f}} &= p\mathbb{P}\{R_{\text{mu}} > R_{\text{B}}, R_{\text{fu}} > R_{\text{E}}\} + (1-p)\mathbb{P}\{R_{\text{fu}} > R_{\text{B}} + R_{\text{E}}\} \\ (a) &= p\mathbb{P}\{R_{\text{mu}} > R_{\text{B}}\}\mathbb{P}\{R_{\text{fu}} > R_{\text{E}}\}(1-p)\mathbb{P}\{R_{\text{fu}} > R_{\text{B}} + R_{\text{E}}\} \\ &= p\mathbb{P}\left\{\gamma_{\text{LD}}^{\text{m}} > 2^{\frac{R_{\text{B}}/\xi_{\text{m}}}{W}} - 1\right\}\mathbb{P}\left\{\gamma_{\text{LD}}^{\text{f}} > 2^{\frac{R_{\text{E}}/\xi_{\text{f}}}{W}} - 1\right\} \\ &\quad + (1-p)\mathbb{P}\left\{R_{\text{fu}} > 2^{\frac{(R_{\text{B}}+R_{\text{E}})/\xi_{\text{f}}}{W}} - 1\right\} \\ &= p\mathcal{P}_{\text{LD}}^{\text{m}}\left(2^{\frac{R_{\text{B}}/\xi_{\text{m}}}{W}} - 1\right)\mathcal{P}_{\text{LD}}^{\text{f}}\left(2^{\frac{R_{\text{E}}/\xi_{\text{f}}}{W}} - 1\right) + (1-p)\mathcal{P}_{\text{LD}}^{\text{f}}\left(2^{\frac{(R_{\text{B}}+R_{\text{E}})/\xi_{\text{f}}}{W}} - 1\right), \end{aligned} \tag{56}$$

where (a) follows from the tier independence approximation.

The distortion-rate function $D(R)$ [14, 39] is used to measure the distortion per source sample when the source rate is R bits/sample. As the bandwidth of a sub-band is W and the data rate of the BL (resp. the EL) is R_{B} (resp. R_{E}), the source rate is $\frac{R_{\text{B}}}{W}$ (resp. $\frac{R_{\text{E}}}{W}$). Since the source signal is modeled as a Gaussian signal with zero mean and unit variance, the distortion of the received video signal can be divided into three cases based on the reception. If the BL is not decoded correctly,

the distortion is $D_0 = 1$; if the BL is decoded correctly while the EL is not, then the distortion is $D_{\mathrm{B}} = 2^{-2\frac{R_{\mathrm{B}}}{W}}$; if both the BL and the EL are decoded correctly, the distortion is $D_{\mathrm{HD}} = 2^{-2\frac{R_{\mathrm{B}}+R_{\mathrm{E}}}{W}}$.

The average distortion for femto UEs, denoted by D_{LD}, is given by

$$D_{\mathrm{LD}} = P_{\mathrm{out}}^{\mathrm{LD,f}} D_0 + (1 - P_{\mathrm{out}}^{\mathrm{LD,f}} - P_{\mathrm{HD}}^{\mathrm{f}}) D_{\mathrm{B}} + P_{\mathrm{HD}}^{\mathrm{f}} D_{\mathrm{HD}}. \tag{57}$$

LHDA Transmission

For a macro UE, only the BL is digitally transmitted from its serving MBS; just the same as that in LD transmission, the outage probability $P_{\mathrm{out}}^{\mathrm{LHDA,m}}$ is

$$P_{\mathrm{out}}^{\mathrm{LHDA,m}} = \mathbb{P}\{R_{\mathrm{mu}} < R_{\mathrm{B}}\} = P_{\mathrm{out}}^{\mathrm{LD,m}}. \tag{58}$$

For a femto UE, since it receives the BL from the MBS with probability p or receives the BL from the FAP with probability $1-p$, the outage probability, denoted by $P_{\mathrm{out}}^{\mathrm{LHDA,f}}$, is

$$\begin{aligned} P_{\mathrm{out}}^{\mathrm{LHDA,f}} &= p\mathbb{P}\{R_{\mathrm{mu}} < R_{\mathrm{B}}\} + (1-p)\mathbb{P}\{R_{\mathrm{fu}} < R_{\mathrm{B}}\} \\ &= p\mathbb{P}\left\{\gamma_{\mathrm{LHDA}}^{\mathrm{m}} < 2^{\frac{R_{\mathrm{B}}/\xi_{\mathrm{m}}}{W}} - 1\right\} + (1-p)\mathbb{P}\left\{\gamma_{\mathrm{LHDA}}^{\mathrm{f,B}} < 2^{\frac{R_{\mathrm{B}}/\xi_{\mathrm{f}}}{W}} - 1\right\} \\ &= p\left(1 - \mathcal{P}_{\mathrm{LHDA}}^{\mathrm{m}}\left(2^{\frac{R_{\mathrm{B}}/\xi_{\mathrm{m}}}{W}} - 1\right)\right) + (1-p)\left(1 - \mathcal{P}_{\mathrm{LHDA}}\left(2^{\frac{R_{\mathrm{B}}/\xi_{\mathrm{f}}}{W}} - 1, 0\right)\right). \end{aligned} \tag{59}$$

The femto UE has two choices to receive the video content, and the average distortion is calculated accordingly.

1. *Case 1:* The femto UE receives the BL from MBS and receives the EL from FAP. Since the EL signal is analog, an MMSE estimator is employed for the estimation of the EL, and thus we have MMSE $= \frac{1}{1+\gamma_{\mathrm{LHDA}}^{\mathrm{f}}}$, where $\gamma_{\mathrm{LHDA}}^{\mathrm{f}}$ is the received SINR. Since there are multiple femto UEs in a FAP, a round-robin mechanism is used to schedule time slots for each femto UE to transmit the EL. If a UE is scheduled, its distortion for the EL is MMSE; otherwise, its distortion is unity. So the distortion is $e_{\mathrm{LHDA}} = \xi_{\mathrm{f}} \cdot \frac{1}{1+\gamma_{\mathrm{LHDA}}^{\mathrm{f}}} + (1-\xi_{\mathrm{f}}) \cdot 1$. Since the EL is estimated only if the BL is decoded successfully, the cdf of e_{LHDA} conditioned on the successful reception of the BL is given by

$$\begin{aligned} \mathbb{P}\{e_{\mathrm{LHDA}} < T \mid R_{\mathrm{mu}} \geq R_{\mathrm{B}}\}(a) &= \mathbb{P}\{e_{\mathrm{LHDA}} < T\} \\ &= \mathbb{P}\left\{\xi_{\mathrm{f}} \frac{1}{1+\gamma_{\mathrm{LHDA}}^{\mathrm{f}}} + (1-\xi_{\mathrm{f}})1 < T\right\} \end{aligned}$$

$$= \mathbb{P}\left\{\gamma^{\mathrm{f}}_{\mathrm{LHDA}} > \frac{1-T}{T-1+\xi_{\mathrm{f}}}\right\}$$
$$= \mathcal{P}^{\mathrm{f}}_{\mathrm{LHDA}}\left(\frac{1-T}{T-1+\xi}\right), \tag{60}$$

where (a) follows from the tier independence approximation.

Since for a positive random variable X, $\mathbb{E}\{X\} = \int_{t>0} \mathbb{P}\{X > t\}\mathrm{d}t$, the mean distortion for the EL, denoted by D_{E}, is

$$D_{\mathrm{E}} = \mathbb{E}\{e_{\mathrm{LHDA}} \mid R_{\mathrm{mu}} \geq R_{\mathrm{B}}\}$$
$$= 1 - \xi_{\mathrm{f}} + \int_{1-\xi_{\mathrm{f}}}^{1}\left(1 - \mathcal{P}^{\mathrm{f}}_{\mathrm{LHDA}}\left(\frac{1-T}{T-1+\xi_{\mathrm{f}}}\right)\right)\mathrm{d}T. \tag{61}$$

Since the EL corresponds to the residual between the BL and the source signal, the distortion when both the BL and the EL are received, denoted by D_{HD}, is given by $D_{\mathrm{HD}} = D_{\mathrm{B}} D_{\mathrm{E}}$.

So the average distortion for the femto UE in *Case 1*, denoted by $D^{(1)}_{\mathrm{LHDA}}$, is

$$D^{(1)}_{\mathrm{LHDA}} = \mathbb{P}\{R_{\mathrm{mu}} < R_{\mathrm{B}}\}D_0 + \mathbb{P}\{R_{\mathrm{mu}} \geq R_{\mathrm{B}}\}D_{\mathrm{HD}}$$
$$= 1 - \mathcal{P}^{\mathrm{m}}_{\mathrm{LHDA}}\left(2^{\frac{R_{\mathrm{B}}}{\xi_{\mathrm{m}}W}} - 1\right) + \mathcal{P}^{\mathrm{m}}_{\mathrm{LHDA}}\left(2^{\frac{R_{\mathrm{B}}}{\xi_{\mathrm{m}}W}} - 1\right)2^{-2R_{\mathrm{B}}}$$
$$\times\left(1 - \xi_{\mathrm{f}} + \int_{1-\xi_{\mathrm{f}}}^{1}\left(1 - \mathcal{P}^{\mathrm{f}}_{\mathrm{LHDA}}\left(\frac{1-T}{T-1+\xi_{\mathrm{f}}}\right)\right)\mathrm{d}T\right). \tag{62}$$

2. *Case 2:* The femto UE receives both the BL and the EL from the FAP. Since the EL signal is analog and superposed with the digital BL signal, an MMSE estimator is employed for the estimation of the EL conditioned on the correct reception of the BL; thus we have MMSE $= \frac{1}{1+\gamma^{\mathrm{f,E}}_{\mathrm{LHDA}}}$, where $\gamma^{\mathrm{f,E}}_{\mathrm{LHDA}}$ is the received SINR after the cancellation of the BL. The distortion for the EL is $e_{\mathrm{LHDA}} = \xi_{\mathrm{f}}\frac{1}{1+\gamma^{\mathrm{E}}_{\mathrm{LHDA}}} + (1-\xi_{\mathrm{f}})1$. The cdf of e_{LHDA} conditioned on the successful reception of the BL is given by

$$\mathbb{P}\{e_{\mathrm{LHDA}} < T \mid R_{\mathrm{fu}} \geq R_{\mathrm{B}}\} = \mathbb{P}\left\{\xi_{\mathrm{f}}\frac{1}{1+\gamma^{\mathrm{E}}_{\mathrm{hc}}} + (1-\xi_{\mathrm{f}})1 < T \;\middle|\; R_{\mathrm{fu}} \geq R_{\mathrm{B}}\right\}$$
$$= \mathbb{P}\left\{\gamma^{\mathrm{f,E}}_{\mathrm{LHDA}} > \frac{1-T}{T-1+\xi_{\mathrm{f}}} \;\middle|\; \gamma^{\mathrm{f,B}}_{\mathrm{LHDA}} > 2^{\frac{R_{\mathrm{B}}/\xi_{\mathrm{f}}}{W}} - 1\right\}$$
$$= \frac{\mathcal{P}_{\mathrm{LHDA}}\left(2^{\frac{R_{\mathrm{B}}/\xi_{\mathrm{f}}}{W}} - 1, \frac{1-T}{T-1+\xi_{\mathrm{f}}}\right)}{\mathcal{P}_{\mathrm{LHDA}}\left(2^{\frac{R_{\mathrm{B}}/\xi}{W}} - 1, 0\right)}. \tag{63}$$

Then, we can obtain the distortion of the EL as

$$\begin{aligned} D_{\mathrm{E}} &= \mathbb{E}\{e_{\mathrm{LHDA}} < T \mid R_{\mathrm{fu}} \geq R_{\mathrm{B}}\} \\ &= 1 - \xi_{\mathrm{f}} + \int_{1-\xi_{\mathrm{f}}}^{1} \left(1 - \frac{\mathcal{P}_{\mathrm{LHDA}}\left(2^{\frac{R_{\mathrm{B}}}{W\xi_{\mathrm{f}}}} - 1, \frac{1-T}{T-1+\xi_{\mathrm{f}}}\right)}{\mathcal{P}_{\mathrm{LHDA}}(2^{\frac{R_{\mathrm{B}}}{W\xi_{\mathrm{f}}}} - 1, 0)} \right) \mathrm{d}T. \end{aligned} \tag{64}$$

So the average distortion for the femto UE in *Case 2*, denoted by $D_{\mathrm{LHDA}}^{(2)}$, is

$$\begin{aligned} D_{\mathrm{LHDA}}^{(2)} &= \mathbb{P}\{R_{\mathrm{fu}} < R_{\mathrm{B}}\} D_0 + \mathbb{P}\{R_{\mathrm{fu}} \geq R_{\mathrm{B}}\} D_{\mathrm{HD}} \\ &= 1 - \mathcal{P}_{\mathrm{LHDA}}\left(2^{\frac{R_{\mathrm{B}}/\xi_{\mathrm{f}}}{W}} - 1, 0\right) + \mathcal{P}_{\mathrm{LHDA}}\left(2^{\frac{R_{\mathrm{B}}/\xi_{\mathrm{f}}}{W}} - 1, 0\right) 2^{-2R_{\mathrm{B}}} \Bigg(1 - \xi_{\mathrm{f}} \\ &\quad + \int_{1-\xi_{\mathrm{f}}}^{1} \left(1 - \frac{\mathcal{P}_{\mathrm{LHDA}}\left(2^{\frac{R_{\mathrm{B}}/\xi_{\mathrm{f}}}{W}} - 1, \frac{1-T}{T-1+\xi_{\mathrm{f}}}\right)}{\mathcal{P}_{\mathrm{LHDA}}(2^{\frac{R_{\mathrm{B}}/\xi_{\mathrm{f}}}{W}} - 1, 0)} \right) \mathrm{d}T \Bigg). \end{aligned} \tag{65}$$

Since a femto UE follows *Case 1* with probability p and follows *Case 2* with probability $1 - p$, the average distortion for a femto UE, denoted by D_{LHDA}, is

$$D_{\mathrm{LHDA}} = pD_{\mathrm{LHDA}}^{(1)} + (1-p)D_{\mathrm{LHDA}}^{(2)}. \tag{66}$$

CD Transmission

For a macro UE, only the BL is transmitted from MBS, so the outage probability, denoted by $P_{\mathrm{out}}^{\mathrm{CD,m}}$, is

$$\begin{aligned} P_{\mathrm{out}}^{\mathrm{CD,m}} &= \mathbb{P}\{R_{\mathrm{mu}} < R_{\mathrm{B}}\} \\ &= 1 - \mathcal{P}_{\mathrm{CD}}^{\mathrm{m}}\left(2^{\frac{R_{\mathrm{B}}/\xi_{\mathrm{m}}}{W}} - 1\right). \end{aligned} \tag{67}$$

For a femto UE, if it is chosen by the MBS and the FAP, it works in a cooperative mode with the probability $\eta = \xi_{\mathrm{m}}/\xi_{\mathrm{f}}$. Thus, the outage probability, denoted by $P_{\mathrm{out}}^{\mathrm{CD,f}}$ is

$$\begin{aligned} P_{\mathrm{out}}^{\mathrm{CD,f}} &= \mathbb{P}\{R_{\mathrm{fu}} < R_{\mathrm{B}}\} \\ &= \eta\left(1 - \mathcal{P}_{\mathrm{CD}}^{\mathrm{f,CoMP}}\left(2^{\frac{R_{\mathrm{B}}/\xi_{\mathrm{f}}}{W}} - 1\right)\right) + (1-\eta)\left(1 - \mathcal{P}_{\mathrm{CD}}^{\mathrm{f,non}}\left(2^{\frac{R_{\mathrm{B}}/\xi_{\mathrm{f}}}{W}} - 1\right)\right). \end{aligned} \tag{68}$$

For a femto UE, the HD probability, denoted as $P_{\mathrm{HD}}^{\mathrm{CD,f}}$, is

$$P_{\mathrm{HD}}^{\mathrm{CD,f}} = \mathbb{P}\{R_{\mathrm{fu}} > R_{\mathrm{B}} + R_{\mathrm{E}}\} = \eta \mathcal{P}_{\mathrm{CD}}^{\mathrm{f,CoMP}} \left(2^{\frac{(R_{\mathrm{B}}+R_{\mathrm{E}})/\xi_{\mathrm{f}}}{W}} - 1\right) + (1-\eta)\, \mathcal{P}_{\mathrm{CD}}^{\mathrm{f,non}} \left(2^{\frac{(R_{\mathrm{B}}+R_{\mathrm{E}})/\xi_{\mathrm{f}}}{W}} - 1\right). \quad (69)$$

Simulation and Discussion

In this section, the outage probabilities, the HD probabilities, and the average distortions are evaluated for the three transmission schemes. Meanwhile, the optimal power allocation for the digital BL and the analog EL for LHDA transmission is assessed. Unless otherwise specified, the system parameters are listed in Table 1.

Figure 4a displays the performance of LD transmission in the orthogonal case. In that case, N_{m} sub-bands for the macro tier and N_{f} sub-bands for the femto tier that are orthogonal with $N_{\mathrm{m}}+N_{\mathrm{f}} = N$. As N_{m} increases, more resources are allocated to the macro tier, and the outage probabilities decrease for both macro UEs and femto UEs, except that the femto UE outage probabilities slightly increase for very large values of N_{m}. The HD probability of the femto UE with $p = 0$ decreases with N_{m} because the EL transmission via FAPs deteriorates as the resources for the femto tier are reduced. The HD probabilities of the femto UE for $p = 0.5$ and $p = 1$ increase for small N_{m} and then decrease as N_{m} grows large, reflecting the tension between the resources for the BL transmission and the EL transmission.

Figure 4b displays the performance of LD transmission in the non-orthogonal case. For comparison with Fig. 4a, we still let $N_{\mathrm{m}} + N_{\mathrm{f}} = N$ but let the sub-bands be selected by each BS independently. The general trend is similar to that in the orthogonal case, but the difference lies in that the curves show less variability with

Table 1 System parameters

Symbol	Description	Typical value
N	Number of sub-bands	20
W	Bandwidth of a sub-band (MHz)	5
P_{m}	MBS transmit power per sub-band (dBm)	39
P_{f}	FAP transmit power per sub-band (dBm)	13
σ^2	Noise power (dBm)	−104
λ_{mb}	MBS intensity (m^{-2})	1E-5
λ_{fb}	FAP intensity (m^{-2})	5E-5
λ_{mu}	Macro UE intensity (m^{-2})	2E-4
λ_{fu}	Femto UE intensity in coverage (m^{-2})	8E-3
R_{f}	Coverage radius of FAP (m)	20
α	Path loss exponent	4
R_{B}	Rate for the BL transmission (Mbps)	0.5
R_{E}	Rate for the EL transmission (Mbps)	4.5

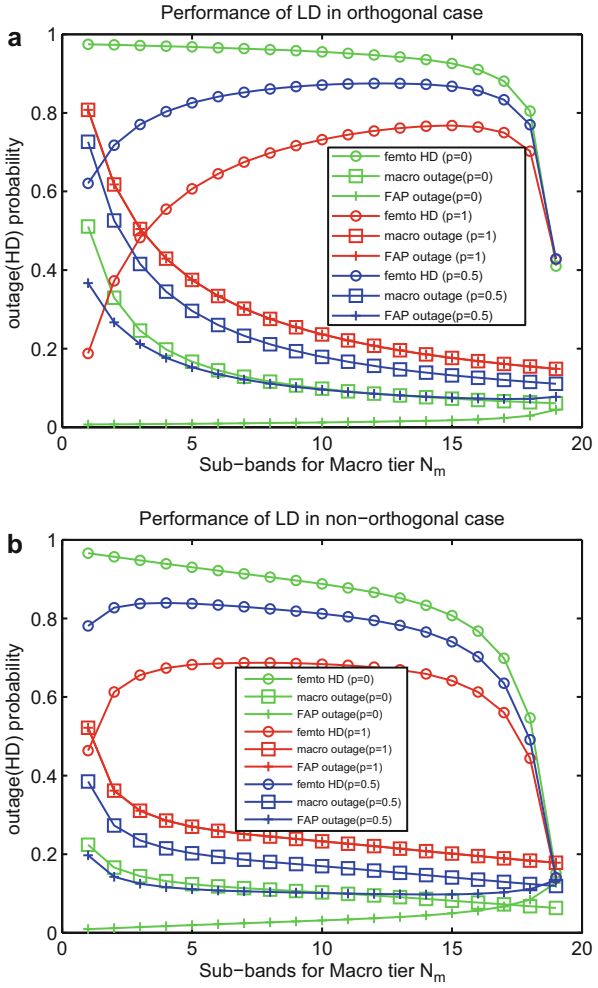

Fig. 4 Performances of LD in both orthogonal and non-orthogonal cases

N_{m} (except for those values near to N). The reason for such a practically desirable insensitivity is due to the lessened tension between the resources for macro tiers and femto tiers from randomized sub-band selection.

Note that if p is large, the femto UE tends to connect to an MBS to receive the BL; the outage probability increases, and the HD probability decreases, i.e., the performance deteriorates. However, since an MBS can provide continuous coverage while an FAP cannot, if a femto UE is moving, then it may prefer to connect to an MBS to receive the BL, which prevents frequent handover between femto cells and enables uninterrupted reception of the BL video.

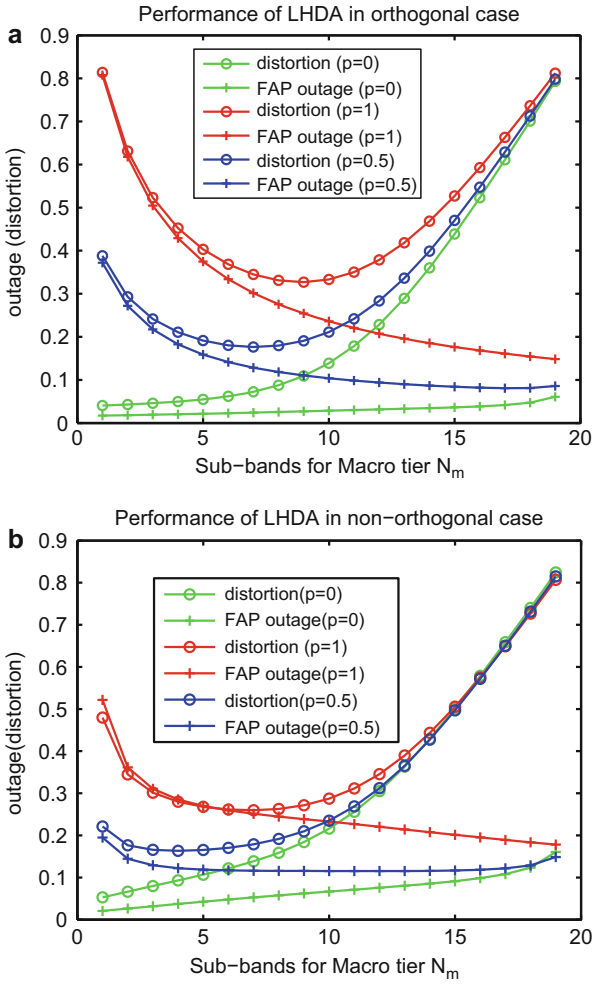

Fig. 5 Performances of LHDA in both orthogonal and non-orthogonal cases

Figure 5a displays the performance of LHDA transmission in the orthogonal case. The outage probability for macro UE is the same as that in LD transmission, so we just neglect it in LHDA transmission. Since the frequency resource allocated to the macro tier increases, the resource for the femto tier decreases. The outage probability for the femto UE connected to the FAP (corresponding to $p = 0$) to receive the BL increases, while the outage probability for the femto UE connected to the MBS (corresponding to $p = 1$) to receive the BL decreases. The case where $p = 0.5$ shows a tradeoff of these two extreme cases: the outage probability for femto UE first decreases and then slightly increases when the allocated resource for the FAP is small. When N_{m} is small, the performance of the macro tier is poor, and

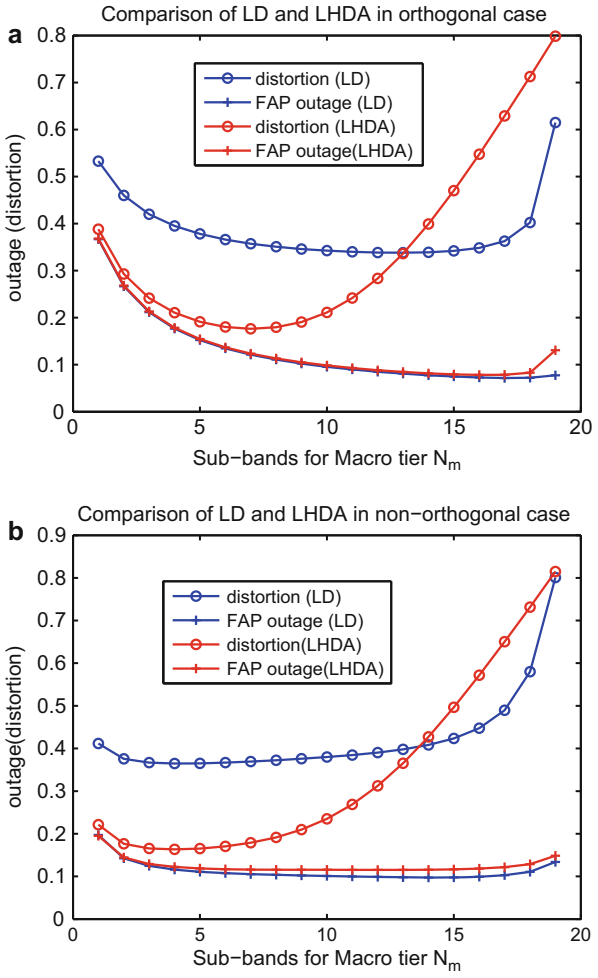

Fig. 6 Comparisons between LD and LHDA in both orthogonal and non-orthogonal cases

thus the distortion for the UE connected to the MBS to receive the BL is large. When increasing N_{m}, the performance of the macro tier becomes good, while that of the femto tier is poor.

Figure 5b displays the performance of LHDA transmission in the non-orthogonal case. The general trends of the curves of the outage and the average distortion are almost the same as that of Fig. 5a. The difference lies in that the outage probability is lower in the non-orthogonal case than that in the orthogonal case when N_{m} is small.

Figure 6 displays the comparison between LD transmission and LHDA transmission. Since the comparisons for different p are more or less the same, we set $p = 0.5$

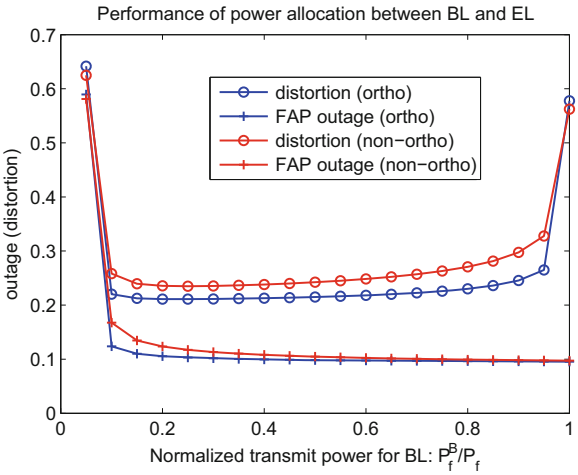

Fig. 7 Power allocation between the BL and the EL in FAPs for LHDA transmission

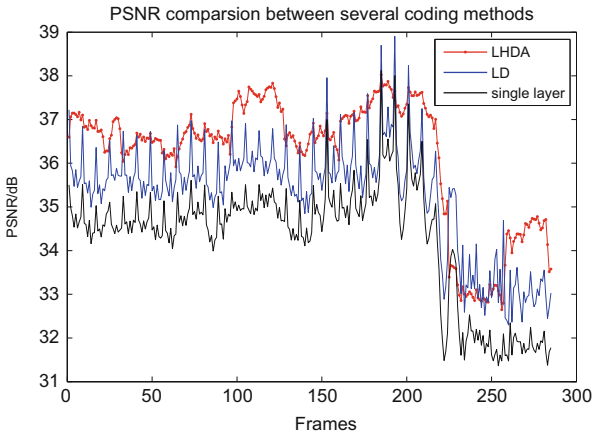

Fig. 8 Comparisons of LHDA and LD and single-layer coding video transmission

as an example. In both orthogonal and non-orthogonal cases, LHDA outperforms LD when the proportion of frequency resource allocated to the femto tier exceeds a certain threshold, for example, 35% (i.e., $N_f \geq 7$) in the current deployment, as the outage probability is slightly increasing while the average distortion is obviously decreasing when N_m is small. The reason is that analog transmission avoids the cliff effect and offers the continuous quality scalability.

Figure 7 displays the power allocation between the digital BL and the analog EL for LHDA transmission. If the power allocated to the BL is increasing, the outage probability decreases monotonously and then approaches stable as the network is interference limited. With P_f^B increasing, the distortion for the BL is sharply decreasing, while the distortion for the EL is increasing. Thus, the total distortion firstly decreases owing to superior transmission of the BL and then increases owing to inferior transmission of the EL. Because of the tradeoff between the transmissions

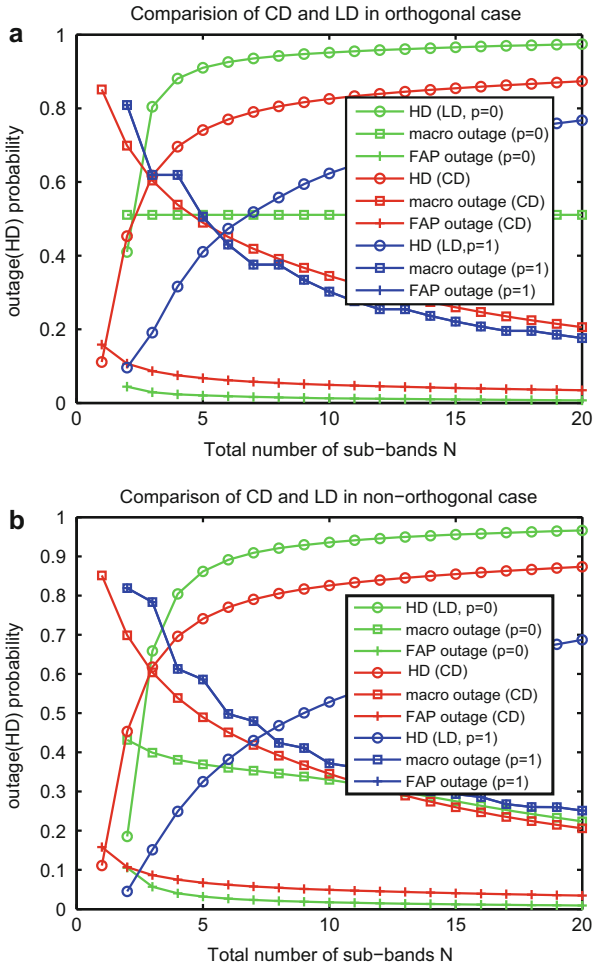

Fig. 9 Comparisons of CD and LD in both orthogonal and non-orthogonal cases

of the BL and the EL, the average distortion varies little when the power allocation ratio $P_{\mathrm{f}}^{\mathrm{B}} / P_{\mathrm{f}}$ lies in a wide range; thus the power allocation is robust.

QoE reflects the user experience and satisfaction, and its evaluation can be performed via subjective tests with the help of a panel of users. The mean opinion score (MOS) which reflects the quality perceived by the observers is dependent on human observation as well as time demanding and costly, while objective video metrics are mathematical-based metrics which are easy and fair to evaluate. The peak signal-to-noise ratio (PSNR) is usually chosen as the objective video metric.

Figure 8 displays the comparisons of performance of LHDA and LD and single-layer coding video transmission in a practical scenario. A standard video called Foreman.yuv is chosen, then it is encoded through H.264/AVC to a single layer or is

encoded through H.264/AVC to two layers to exploit the spatial scalability. LHDA and LD are employed to transmit the layered video contents. The performance peak signal-to-noise ratio (PSNR) of all the 288 frames is compared for the three transmission schemes. The performance of LHDA is the best, since it achieves the highest PSNR, and the variation of PSNR with respect to different frame is stable. The performance of LD is better than single-layer coding video transmission.

Figure 9 displays the comparison between CD transmission and LD transmission with $p = 0$ and $p = 1$ under orthogonal and non-orthogonal spectrum allocation methods. Since different N_{m} result in different performance, here the optimal N_{m} is chosen to achieve the minimal outage probability given the total number of sub-bands is N. It can be found that the HD probability of CD is between that of LD with $p = 0$ and $p = 1$. Meanwhile the outage probabilities of macro UE and femto UE are nearly minimal.

Conclusion and Future Directions

In order to overcome the challenges of the mobile networks induced by the rapidly growing video traffic, efficient networking strategy as well as providing optimal QoE is an urgent task for mobile operators. In this work, we proposed an analytical framework for user-cognizant scalable video transmission, which exploits the interplay among user demand, video source characteristic, and networking.

Specifically, three scalable transmission schemes are presented, i.e., LD, LHDA, and CD, which are shown to be an effective means for providing differentiated services for users. Through the analysis and comparison of system performance metrics, i.e., outage probability, HD probability, and average distortion, under different spectrum allocation methods, it is observe that:

(1) Compared to the traditional non-scalable video transmission, our schemes can adaptively provide basic or high-definition video.
(2) The frequency resource should be elaborately allocated between tiers to achieve good performance, and the choice of orthogonal and non-orthogonal spectrum allocation methods for LD and LHDA depend on the system configuration.
(3) The hybrid digital-analog transmission can further improve the system performance by reducing video distortion and providing continuous quality scalability of high-definition video, and the performance is quite insensitive to the power allocation between the digital BL and the analog EL.
(4) Cooperative video transmission can achieve relatively high HD probability with a little increase of outage probability.

To further enhance the networking performance and user QoE, the work can be extended to incorporate wireless caching and rateless codes. The heterogeneity of video quality and video popularity can be exploited to optimize the caching and transmission schemes [40]. Since the UE may simultaneously connect to the MBS and the FAP, rateless codes such as fountain codes [41, 42] can be employed

to reduce the complexity of synchronization of these two links. Moreover, rate adaption and shaping strategies can also be studied with some background traffic, such as file downloading and over-the-top (OTT) services.

References

1. Schwarz H, Marpe D, Wiegand T (2007) Overview of the scalable video coding extension of the H. 264/AVC standard. IEEE Trans Circuits Syst Video Technol 17(9):1103–1120
2. Sullivan GJ, Boyce JM, Chen Y, Ohm JR (2013) Standardized extensions of high efficiency video coding (HEVC). IEEE J Sel Top Signal Process 7(6):1001–1016
3. Chandrasekhar V, Andrews JG, Gatherer A (2008) Femtocell networks: a survey. IEEE Commun Mag 46(9):59–67
4. Ko C-H, Wei H-Y (2011) On-demand resource-sharing mechanism design in two-tier OFDMA femtocell networks. IEEE Trans Veh Technol 60(3):1059–1071
5. Schierl T, Stockhammer T, Wiegand T (2007) Mobile video transmission using scalable video coding. IEEE Trans Circuits Syst Video Technol 17(9):1204–1217
6. Bocus MZ, Coon JP, Canagarajah CN, Armour S, Doufexi A, McGeehan JP (2012) Per-subcarrier antenna selection for H. 264 MGS/CGS video transmission over cognitive radio networks. IEEE Trans Veh Technol 61(3):1060–1073
7. Radhakrishnan R, Nayak A (2012) Cross layer design for efficient video streaming over LTE using scalable video coding. In: Proceedings of IEEE International Conference on Communications, pp 6509–6513
8. Gupta V, Somayazulu S, Himayat N, Verma H, Bisht M, Nandwani V (2012) Design challenges in transmitting scalable video over multi-radio networks. In: Proceedings of IEEE Globecom Workshops, pp 46–51
9. Poularakis K, Iosifidis G, Argyriou A, Tassiulas L (2014) Video delivery over heterogeneous cellular networks: optimizing cost and performance. In: Proceedings of IEEE INFOCOM, pp 1078–1086
10. Chen C, Zhu X, De Veciana G, Bovik AC, Heath RW (2013) Rate adaptation and admission control for video transmission with subjective quality constraints. IEEE J Sel Top Signal Process 9(1):22–36
11. Thakolsri S, Khan S, Steinbach E, Kellerer W (2009) QoE-driven cross-layer optimization for high speed downlink packet access. J Commun 4(9):669–680
12. Fu B, Staehle D, Kunzmann G, Steinbach E, Kellerer W (2015) QoE-based SVC layer dropping in LTE networks using content-aware layer priorities. ACM Trans Multimedia Comput Commun Appl 12(1):1–23
13. Jakubczak S, Katabi D (2011) A cross-layer design for scalable mobile video. In: Proceedings of ACM Proceedings of Annual International Conference on Mobile Computing and Networking, pp 289–300
14. Gao Y, Tuncel E (2010) New hybrid digital/analog schemes for transmission of a Gaussian source over a Gaussian channel. IEEE Trans Inf Theory 56(12):6014–6019
15. Minero P, Lim SH, Kim Y-H (2015) A unified approach to hybrid coding. IEEE Trans Inf Theory 61(4):1509–1523
16. Yu L, Li H, Li W (2014) Wireless scalable video coding using a hybrid digital-analog scheme. IEEE Trans Circuits Syst Video Technol 24(2):331–345
17. Altieri A, Vega LR, Galarza CG, Piantanida P (2011) Cooperative strategies for interference-limited wireless networks. In: IEEE International Symposium on Information Theory Proceedings (ISIT), pp 1623–1627
18. Lee J, Kim Y, Lee H, Ng BL, Mazzarese D, Liu J, Xiao W, Zhou Y (2012) Coordinated multipoint transmission and reception in lte-advanced systems. IEEE Commun Mag 50(11):44–50

19. Nigam G, Minero P, Haenggi M (2013) Coordinated multipoint in heterogeneous networks: a stochastic geometry approach. In: IEEE Globecom Workshops, pp 145–150
20. Nigam G, Minero P, Haenggi M (2014) Coordinated multipoint joint transmission in heterogeneous networks. IEEE Trans Commun 62(11):4134–4146
21. Bang I, Kim SH, Kim SM, Sung DK (2012) Energy-efficient subchannel allocation scheme based on adaptive base station cooperation in downlink cellular networks. In: Wireless Communications and Networking Conference (WCNC), pp 2434–2439
22. Zhang X, Shen XS, Xie L-L (2014) Joint subcarrier and power allocation for cooperative communications in LTE-advanced networks. IEEE Trans Wirel Commun 13(2):658–668
23. Kosmanos D, Argyriou A, Liu Y, Tassiulas L, Ci S (2015) A cooperative protocol for video streaming in dense small cell wireless relay networks. Signal Process Image Commun 31: 151–160
24. Chan CC, Hanly SV (2001) Calculating the outage probability in a CDMA network with spatial Poisson traffic. IEEE Trans Veh Technol 50(1):183–204
25. Haenggi M, Andrews JG, Baccelli F, Dousse O, Franceschetti M (2009) Stochastic geometry and random graphs for the analysis and design of wireless networks. IEEE J Sel Areas Commun 27(7):1029–1046
26. ElSawy H, Hossain E, Haenggi M (2013) Stochastic geometry for modeling, analysis, and design of multi-tier and cognitive cellular wireless networks: a survey. IEEE Commun Surv Tutorials 15(3):996–1019
27. Andrews JG, Baccelli F, Ganti RK (2011) A tractable approach to coverage and rate in cellular networks. IEEE Trans Commun 59(11):3122–3134
28. Dhillon HS, Ganti RK, Baccelli F, Andrews JG (2012) Modeling and analysis of K-tier downlink heterogeneous cellular networks. IEEE J Sel Areas Commun 30(3):550–560
29. Baccelli F, Blaszczyszyn B (2009) Stochastic geometry and wireless networks: volume 1 – theory, vol 1. Now Publishers Inc, Boston
30. Haenggi M (2012) Stochastic geometry for wireless networks. Cambridge University Press, Cambridge
31. Wu L, Zhong Y, Zhang W, Haenggi M (2015) Scalable transmission over heterogenous networks. In: Proceedings of International Symposium on Modeling and Optimization in Mobile, Ad Hoc, and Wireless Networks (WiOpt), pp 459–466
32. Wu L, Zhong Y, Zhang W, Haenggi M (2016) Scalable transmission over heterogeneous network: a stochastic geometry analysis. IEEE Trans Veh Technol 66(2):1845–1859
33. Ferenc J-S, Néda Z (2007) On the size distribution of Poisson Voronoi cells. Phys A Stat Mech Appl 385(2):518–526
34. Zhong Y, Zhang W (2013) Multi-channel hybrid access femtocells: a stochastic geometric analysis. IEEE Trans Commun 61(7):3016–3026
35. Cheung WC, Quek TQ, Kountouris M (2012) Throughput optimization, spectrum allocation, and access control in two-tier femtocell networks. IEEE J Sel Areas Commun 30(3):561–574
36. Prabhakaran VM, Puri R, Ramchandran K (2011) Hybrid digital-analog codes for source-channel broadcast of Gaussian sources over Gaussian channels. IEEE Trans Inf Theory 57(7):4573–4588
37. Kochman Y, Zamir R (2011) Analog matching of colored sources to colored channels. IEEE Trans Inf Theory 57(6):3180–3195
38. Wildemeersch M, Quek TQ, Kountouris M, Rabbachin A, Slump CH (2014) Successive interference cancellation in heterogeneous networks. IEEE Trans Commun 62(12):4440–4453
39. Xu X, Gunduz D, Erkip E, Wang Y (2005) Layered cooperative source and channel coding. In: Proceedings of IEEE International Conference on Communications, pp 1200–1204
40. Wu L, Zhang W (2016) Caching-based scalable video transmission over cellular networks. IEEE Commun Lett 20(6):1156–1159
41. Luby M (2002) LT codes. In: Symposium on Foundations of Computer Science, pp 271–280
42. Shokrollahi A (2006) Raptor codes. IEEE/ACM Trans Netw 14(SI):2551–2567

Precoding and Power Allocation for Two-Tier Heterogeneous Networks

40

Shengjie Guo and Xiangwei Zhou

Contents

Abstract

In two-tier heterogeneous networks, the cross-tier interference and co-tier interference significantly affect the network performance. In this chapter, cascaded precoders in orthogonal frequency-division multiplexing systems are investigated to protect *macro-cell user equipments* (MUEs) from the cross-tier interference caused by co-located small cells and at the same time to satisfy the *quality-of-service* (QoS) requirements of *small-cell user equipments* (SUEs). An outer precoder ensures that the signals intended for the SUEs are orthogonal to the MUEs thus avoids the cross-tier interference from the second tier. Moreover, optimal power allocation through an inner precoder at each *small base station* (SBS) yields better performance of the SUEs and guarantees their

S. Guo (✉) · X. Zhou
Louisiana State University, Baton Rouge, LA, USA
e-mail: sguo12@lsu.edu; xwzhou@lsu.edu

W. Zhang (ed.), *Handbook of Cognitive Radio*,
https://doi.org/10.1007/978-981-10-1394-2_37

QoS requirements. With consideration of the dense deployment of SBSs, an SBS selection algorithm is studied to further reduce the computational complexity. Simulation results demonstrate that the cascaded precoders are effective in mitigating the interference and enhancing the capacity of small cells.

Introduction

Recently, the deployment of *small base stations* (SBSs) such as femtocells has emerged as a promising technology to extend service coverage, increase network throughput, and improve energy efficiency [1–3]. Because of their low-power and low-cost features, SBSs are mostly installed in offices or at homes for better indoor performance [4]. Since SBSs are usually deployed to overlay with *macro base stations* (MBSs), cross-tier interference is introduced, which limits the performance of two-tier networks. Moreover, since both cross-tier interference and co-tier interference need to be considered, the complexity in designing algorithms increases. To address these issues, an effective scheme with cascaded precoders will be disscussed in this chapter.

Coexistence Problem in Two-Tier Networks

In two-tier heterogeneous networks, both small cells and macro cells face the cross-tier interference and co-tier interference from the network elements belonging to different and the same tiers, respectively. When SBSs are randomly deployed with high density, the cross-tier interference and co-tier interference dramatically limit the performance of the heterogeneous network [5].

Current Techniques

To address the above issues, many researches have been devoted to frequency partitioning, power allocation, and precoding.

Frequency Partitioning

To avoid cross-tier interference, frequency partitioning is a direct and effective method [6–9]. By dividing frequencies into multiple nonoverlapping blocks, the network assigns different tiers to different blocks that can totally avoid cross-tier interference.

According to locations [6,7], traffic volumes [8], and user types [9], different frequency partitioning schemes for two-tiered heterogeneous networks serve different purposes.

Power Allocation

Power allocation is widely adopted in two-tiered heterogeneous networks to mitigate both cross-tier and co-tier interference, especially when the frequency is shared within two tiers. The main idea of power allocation is limiting the transmit power to alleviate the interference to the other parties in the shared frequency [10–13].

The power allocation method has been exploited from various aspects, i.e., game theory [10, 11], sleep mode [12], and distributed manner [13]. Power allocation renders a trade-off between interference mitigation and spectrum efficiency.

Precoding

Precoding scheme exploits the diversity and *degree of freedom* (DoF) of the transmission. Recently, several state-of-art precoding schemes have been presented in [14–18] to deal with the cross-tier interference and co-tier interference in two-tier heterogeneous networks. The precoding schemes utilize the spatial DoF [14] and frequency DoF [15–18] in multi-cell multiple-input-multiple-output networks and cognitive two-tier networks, respectively.

For better spectrum efficiency, frequency partitioning method is not discussed in this chapter and the focus of this chapter is to study precoding and power allocation in two-tier heterogenous networks. With consideration of combining power allocation and precoding, cascaded precoders dealing with both the cross-tier interference and co-tier interference in heterogeneous networks are discussed. First, an outer precoder is designed at each SBS to eliminate the cross-tier interference to the existing *macro-cell user equipments* (MUEs). Then to mitigate the co-tier interference in the second tier, an inner precoder for power allocation is studied.

The rest of this chapter is organized as follows. A two-tier heterogeneous system model is presented in section "System Model". In section "Cascaded Precoders", the cascaded precoders for two-tier networks are studied. An SBS selection algorithm to reduce the complexity of the cascaded precoders and the system performance under channel estimation are discussed in section "Discussion". Simulation results are given in section "Simulation Results". Finally, conclusions and future directions are provided in section "Conclusion and Future Directions".

System Model

As shown in Fig. 1, the coexistence of one MBS and K SBSs in a downlink system is considered. The MBS serves M single-antenna MUEs and each SBS serves one single-antenna SUE. The MBS adopts *orthogonal frequency-division multiple* (OFDM) based transmission with N subcarriers and a *cyclic prefix* (CP) of length L to avoid inter-symbol interference. Since the MBS usually covers a large area, the first tier is regarded as a primary user and oblivious of the existence of the second tier. The cross-tier interference mitigation strategy is only implemented in the second tier. No cooperation is considered between different tiers or among different SBSs in the same tier. Therefore, the precoders are designed in a distributed manner. All transmissions are assumed to be synchronized and no radio frequency

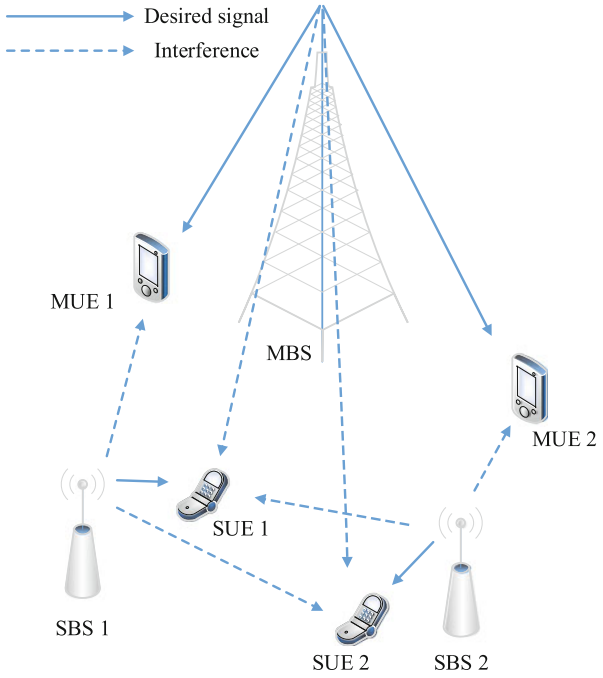

Fig. 1 System model

impairments at the receiver are considered. The knowledge of perfect *channel state information* (CSI) for all links is assumed. The influence of imperfect CSI will be discussed in section "Discussion".

Subscript s denotes the SBSs and m denotes the MBS. $\mathbf{x}_s^{(i)} \in \mathbb{C}^{(N+L)\times 1}$ denotes the precoded signal vector in time domain at the i-th SBS. Then

$$\mathbf{x}_s = [\mathbf{x}_s^{(1)T}, \mathbf{x}_s^{(2)T}, \ldots, \mathbf{x}_s^{(K)T}]^T \in \mathbb{C}^{K(N+L)\times 1} \tag{1}$$

is the equivalent aggregate signal vector of the SBSs. $\mathbf{H}_{sm}^{(i,j)}$ denotes the channel matrix from the i-th SBS to the j-th MUE. Then

$$\mathbf{H}_{sm}^{(j)} = [\mathbf{H}_{sm}^{(1,j)}, \mathbf{H}_{sm}^{(2,j)}, \ldots, \mathbf{H}_{sm}^{(K,j)}] \in \mathbb{C}^{N\times K(N+L)} \tag{2}$$

is the aggregate channel matrix from the SBSs to the j-th MUE and expressed as

$$\mathbf{H}_{sm}^{(i,j)} = \begin{bmatrix} h_{sm}^{(i,j)}(L) & \cdots & h_{sm}^{(i,j)}(0) & 0 & \cdots & 0 \\ 0 & \ddots & & \ddots & \ddots & \vdots \\ \vdots & \ddots & \ddots & & \ddots & 0 \\ 0 & \cdots & 0 & h_{sm}^{(i,j)}(L) & \cdots & h_{sm}^{(i,j)}(0) \end{bmatrix}, \tag{3}$$

where $h_{sm}^{(i,j)}(L)$, $h_{sm}^{(i,j)}(L-1)$, …, and $h_{sm}^{(i,j)}(0)$ represent the channel taps from the i-th SBS to the j-th MUE.

The received signal vectors of length N in frequency domain at the j-th MUE and i-th SUE are expressed as

$$\mathbf{y}_m^{(j)} = \mathbf{F}(\mathbf{H}_{mm}^{(j)}\mathbf{A}\mathbf{F}^{-1}\mathbf{s}_m^{(j)} + \mathbf{H}_{sm}^{(j)}\mathbf{x}_s + \mathbf{n}_m^{(j)}) \tag{4}$$

and

$$\mathbf{y}_s^{(i)} = \mathbf{F}(\mathbf{H}_{ss}^{(i,i)}\mathbf{x}_s^{(i)} + \sum_{\substack{u=1 \\ u\neq i}}^{K} \mathbf{H}_{ss}^{(u,i)}\mathbf{x}_s^{(u)} + \mathbf{H}_{ms}^{(1,i)}\mathbf{A}\mathbf{F}^{-1}\mathbf{s}_m^{(j)} + \mathbf{n}_s^{(i)}), \tag{5}$$

respectively, where $\mathbf{s}_m^{(j)} \in \mathbb{C}^{(N+L)\times 1}$ is the input signal vector in time domain at the MBS for the j-th MUE, $\mathbf{n}_m^{(j)}$ and $\mathbf{n}_s^{(i)}$ are the corresponding equivalent noise vectors for the MUEs and SUEs, respectively, $\mathbf{F}$ is an $N \times N$ unitary discrete Fourier transform matrix with the entry in the $(k+1)$-th row and $(l+1)$-th column $[\mathbf{F}]_{(k+1),(l+1)} = \frac{1}{\sqrt{N}} e^{-i2\pi\frac{kl}{N}}$ for $k, l = \{0, \ldots, N-1\}$, $\mathbf{A}$ is an $(N+L) \times N$ cyclic prefix insertion matrix given by

$$\mathbf{A} = \begin{bmatrix} \mathbf{0_{L,N-L}}, \mathbf{I_L} \\ \mathbf{I_N} \end{bmatrix}, \tag{6}$$

where $\mathbf{0_{N,L}}$ and $\mathbf{I_N}$ denote an $N \times L$ zero matrix and an $N \times N$ identity matrix, respectively, $\mathbf{H}_{mm}^{(j)} \in \mathbb{C}^{N\times(N+L)}$ is the channel matrix from the MBS to the j-th MUE, which is

$$\mathbf{H}_{mm}^{(1,j)} = \begin{bmatrix} h_{mm}^{(1,j)}(L) & \cdots & h_{mm}^{(1,j)}(0) & 0 & \cdots & 0 \\ 0 & \ddots & & \ddots & \ddots & \vdots \\ \vdots & \ddots & \ddots & & \ddots & 0 \\ 0 & \cdots & 0 & h_{mm}^{(1,j)}(L) & \cdots & h_{mm}^{(1,j)}(0) \end{bmatrix}, \tag{7}$$

where $h_{mm}^{(1,j)}(L)$, $h_{mm}^{(1,j)}(L-1)$, …, and $h_{mm}^{(1,j)}(0)$ are the channel taps between the MBS and the j-th MUE, $\mathbf{H}_{ss}^{(u,i)}$ and $\mathbf{H}_{ms}^{(1,i)}$ are the channel matrices from the u-th SBS and the MBS to the i-th SUE, respectively, and constructed as

$$\mathbf{H}_{ss}^{(u,i)} = \begin{bmatrix} h_{ss}^{(u,i)}(L) & \cdots & h_{ss}^{(u,i)}(0) & 0 & \cdots & 0 \\ 0 & \ddots & & \ddots & \ddots & \vdots \\ \vdots & \ddots & \ddots & & \ddots & 0 \\ 0 & \cdots & 0 & h_{ss}^{(u,i)}(L) & \cdots & h_{ss}^{(u,i)}(0) \end{bmatrix}, \tag{8}$$

and

$$\mathbf{H}_{ms}^{(1,i)} = \begin{bmatrix} h_{ms}^{(1,i)}(L) & \cdots & h_{ms}^{(1,i)}(0) & 0 & \cdots & 0 \\ 0 & \ddots & & \ddots & \ddots & \vdots \\ \vdots & \ddots & \ddots & & \ddots & 0 \\ 0 & \cdots & 0 & h_{ms}^{(1,i)}(L) & \cdots & h_{ms}^{(1,i)}(0) \end{bmatrix}, \tag{9}$$

where $h_{ms}^{(1,i)}(L)$, $h_{ms}^{(1,i)}(L-1)$, …, $h_{ms}^{(1,i)}(0)$ and $h_{ss}^{(u,i)}(L)$, $h_{ss}^{(u,i)}(L-1)$, …, and $h_{ss}^{(u,i)}(0)$ represent the L channel paths from the MBS to the i-th SUE and from the u-th SBS to the i-th SUE, respectively.

Cascaded Precoders

In this section, cascaded precoders are studied. Specifically, the outer precoder and inner precoder are designed and analyzed.

The structure of cascaded precoders is illustrated in Fig. 2. The precoded signal vector is obtained from the direct input symbol vector. Specifically,

$$\mathbf{x}_s^{(i)} = \mathbf{W}^{(i)}\mathbf{s}^{(i)}, \tag{10}$$

where $\mathbf{s}^{(i)} \in \mathbb{C}^{L\times 1}$ is an *independent identical distributed* (i.i.d.) zero-mean unit-variance direct input symbol vector from the i-th SBS and $\mathbf{W}^{(i)}$ is the overall precoding matrix for the i-th SBS, which is constructed from two cascaded precoders,

$$\mathbf{W}^{(i)} = \mathbf{E}^{(i)}\mathbf{G}^{(i)}, \tag{11}$$

where $\mathbf{E}^{(i)}$ is the outer precoder to cancel the cross-tier interference from the i-th SBS to the MUEs and $\mathbf{G}^{(i)}$ is the inner precoder to mitigate the co-tier interference from the i-th SBS through power allocation in the second tier.

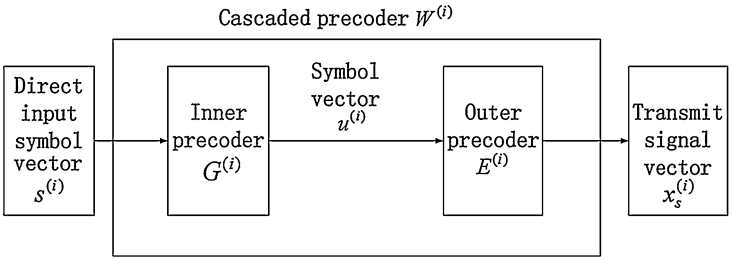

Fig. 2 Proposed cascaded precoder structure

Out Precoder Design

The outer precoder is designed to prevent the first tier from the cross-tier interference. To protect the j-th existing MUE, it is preferred to eliminate the cross-tier interference from the second tier, i.e.,

$$\mathbf{H}_{sm}^{(j)}\mathbf{x}_s = \mathbf{0}, \quad \forall\, j \in 1, 2, \ldots, M. \tag{12}$$

The transmitted signal $\mathbf{x}_s^{(i)}$ from the i-th SBS is designed as

$$\mathbf{x}_s^{(i)} = \mathbf{E}^{(i)}\mathbf{u}^{(i)}, \tag{13}$$

where $\mathbf{u}^{(i)} \in \mathbb{C}^{L\times 1}$ is the symbol vector at the i-th SBS and $\mathbf{E}^{(i)} \in \mathbb{C}^{(N+L)\times L}$ is a linear precoder for the i-th SBS to render

$$\mathbf{H}_{sm}^{(i,j)}\mathbf{E}^{(i)} = \mathbf{0}. \tag{14}$$

Since $\mathbf{H}_{sm}^{(i,j)}$ is an $(N + L)$ by N matrix with independent elements, the rank of $\mathbf{H}_{sm}^{(i,j)}$ is N and thus the dimension of the null space of $\mathbf{H}_{sm}^{(i,j)}$ is $(N + L) - N = L$. Therefore, the LQ decomposition method [17] can be used to construct an $(N + L) \times L$ precoder $\mathbf{E}^{(i)}$ to transmit L symbols aligned with the null space of $\mathbf{H}_{sm}^{(i,j)}$. The equivalent channel matrix $\mathbf{H}_{sm}^{(i,j)}$, representing the interfering link between the i-th SBS and the j-th MUE, is decomposed as

$$\mathbf{H}_{sm}^{(i,j)} = \mathbf{L}_{sm}^{(i,j)}\mathbf{Q}_{sm}^{(i,j)}, \tag{15}$$

where $\mathbf{L}_{sm}^{(i,j)} \in \mathbb{C}^{N\times(N+L)}$ is a lower triangular matrix and $\mathbf{Q}_{sm}^{(i,j)} \in \mathbb{C}^{(N+L)\times(N+L)}$ is a unitary matrix given by

$$\mathbf{Q}_{sm}^{(i,j)} \triangleq [\mathbf{q}_1, \mathbf{q}_2, \cdots, \mathbf{q}_{N+L}]. \tag{16}$$

Then the outer precoder $\mathbf{E}^{(i)}$ is constructed as

$$\mathbf{E}^{(i)} \triangleq [\mathbf{q}_{N+1}, \mathbf{q}_{N+2}, \cdots, \mathbf{q}_{N+L}] \tag{17}$$

and therefore the equivalent signal model in the first tier is rewritten as

$$\mathbf{y}_m^{(j)} = \mathbf{F}(\mathbf{H}_{mm}^{(j)}\mathbf{A}\mathbf{F}^{-1}\mathbf{s}_m^{(j)} + \mathbf{n}_m^{(j)}), \tag{18}$$

which is free of the cross-tier interference from the second tier.

Inner Precoder Design

To reduce the influence of the co-tier interference and achieve higher throughput, an inner precoder is designed to render optimal power allocation.

The Inner Precoder Structure

The inner precoding matrix $\mathbf{G}^{(i)} \in \mathbb{C}^{L\times L}$ is used to generate the symbol vector of the i-th SBS, i.e.,

$$\mathbf{u}^{(i)} = \mathbf{G}^{(i)}\mathbf{s}^{(i)}. \tag{19}$$

The received signal vector at the i-th SUE is

$$\mathbf{y}_s^{(i)} = \mathbf{F}(\mathbf{H}_{ss}^{(i,i)}\mathbf{E}^{(i)}\mathbf{G}^{(i)}\mathbf{s}^{(i)} + \sum_{\substack{u=1\\u\neq i}}^{K}\mathbf{H}_{ss}^{(u,i)}\mathbf{E}^{(u)}\mathbf{G}^{(u)}\mathbf{s}^{(u)} + \mathbf{v}_s^{(i)}), \tag{20}$$

where $\mathbf{v}_s^{(i)} = \mathbf{H}_{ms}^{(1,i)}\mathbf{A}\mathbf{F}^{-1}\mathbf{s}_m^{(j)} + \mathbf{n}_s^{(i)}$.

Define matrix $\widetilde{\mathbf{F}}$ such that

$$\widetilde{\mathbf{F}} = \mathbf{F}\widetilde{\mathbf{A}}, \tag{21}$$

where $\widetilde{\mathbf{A}}$ denotes the cyclic prefix removal matrix, which is

$$\widetilde{\mathbf{A}} = \left[\mathbf{0}_{\mathbf{N},\mathbf{L}}, \mathbf{I}_{\mathbf{N}}\right]. \tag{22}$$

Then the precoded symbol of the i-th SBS in frequency domain, $\mathbf{X}_s^{(i)}$, can be expressed as

$$\mathbf{X}_s^{(i)} = \widetilde{\mathbf{F}}\mathbf{E}^{(i)}\mathbf{G}^{(i)}\mathbf{s}^{(i)}. \tag{23}$$

The average transmit power of the i-th SBS over the j-th subcarrier, $P^{(i,j)}$, is given by

$$P^{(i,j)} = \mathbb{E}\{[\mathbf{X}_s^{(i)}]_{(j,1)}^2\}, \tag{24}$$

where $\mathbb{E}\{\cdot\}$ denotes the expectation operation. Because $\mathbf{s}^{(i)}$ is i.i.d. with zero-mean and unit-variance,

$$P^{(i,j)} = [\widetilde{\mathbf{F}}\mathbf{E}^{(i)}\mathbf{G}^{(i)}\mathbf{G}^{(i)T}\mathbf{E}^{(i)T}\widetilde{\mathbf{F}}^{T}]_{(j,j)}. \tag{25}$$

Let $\mathbf{B}^{(i)} = \widetilde{\mathbf{F}}\mathbf{E}^{(i)}\mathbf{G}^{(i)}$ and the entry in the m-th row and n-th column be $b_{(m,n)}^{(i)}$. The following N equations are obtained

$$\begin{aligned} b_{(1,1)}^{(i)2} + b_{(1,2)}^{(i)2} + \cdots + b_{(1,L)}^{(i)2} &= P^{(i,1)}, \\ b_{(2,1)}^{(i)2} + b_{(2,2)}^{(i)2} + \cdots + b_{(2,L)}^{(i)2} &= P^{(i,2)}, \\ &\vdots \\ b_{(N,1)}^{(i)2} + b_{(N,2)}^{(i)2} + \cdots + b_{(N,L)}^{(i)2} &= P^{(i,N)}. \end{aligned} \tag{26}$$

Define matrix $\mathbf{C}_n$ as

$$\mathbf{C}_n = \begin{bmatrix} \sqrt{P^{*(1,nL+1)}} & \cdots & 0 \\ \vdots & \ddots & \vdots \\ 0 & \cdots & \sqrt{P^{*(1,nL+L)}} \end{bmatrix}. \tag{27}$$

To achieve the desired power $P^{*(i,j)}$ for $j = 1, 2, \cdots, N$, $\mathbf{B}^{(i)}$ should be designed as

$$\mathbf{B}^{(i)} = \begin{bmatrix} \mathbf{C}_1 \\ \mathbf{C}_2 \\ \vdots \\ \mathbf{C}_z \\ \mathbf{C}'_{z+1} \end{bmatrix}, \tag{28}$$

where z is the largest integer that is smaller than $\frac{N}{L}$ and $\mathbf{C}'_{z+1}$ is constructed with the first $(N - zL)$ rows of $\mathbf{C}_{z+1}$. Then the full rank inner precoding matrix $\mathbf{G}^{(i)}$ can be obtained through

$$\mathbf{G}^{(i)} = ((\widetilde{\mathbf{F}}\mathbf{E}^{(i)})^H \widetilde{\mathbf{F}}\mathbf{E}^{(i)})^{-1} (\widetilde{\mathbf{F}}\mathbf{E}^{(i)})^H \mathbf{B}^{(i)}, \tag{29}$$

where superscript H denotes the Hermitian transpose operation.

The Optimal Power Allocation

Power allocation at each SBS is optimized through the designed inner precoder. Since the power allocation of the MBS is not affected by the second tier, the interference from the first tier is always fixed during the power allocation of the SBSs. Therefore, the interference from the MBS is treated as noise with fixed power during the SBS power optimization and absorbed in the noise expression, $\sigma_{(i,j)}^2$, for simplicity.

Through the precoding matrix $\mathbf{G}^{(i)}$, the transmit power $P^{(i,j)}$ is allocated to maximize the achievable rate $R^{(i)}$ of the i-th SUE. Thus the following optimization problem is formulated

Algorithm 1 QoS guarantee algorithm

Initialize: The total transmit power of the i-th SBS $P^{(i)} = P^{(i)}_{\max}$, $P^{(i,j)} = 0$, i = 1,2,. . .,K, j = 1,2,. . .,N.
loop
  loop
    Solve (30) for all $i = 1, 2, \ldots, K$ and $j = 1, 2, \ldots, N$. Set $P^{(i,j)}$ and transmit power $P^{(i)}$.
    Set $R^{(i)}$ according to (30).
  end loop
  for i = 1 to K,
    if $R^{(i)} > R_{re} + \varepsilon$, set $P^{(i)} = P^{(i)} - \xi$.
    if $R^{(i)} < R_{re}$, set $P^{(i)} = P^{(i)} + \xi$.
    if $P^{(i,j)} > P^{(i)}_{\max}$, $P^{(i,j)} = P^{(i)}_{\max}$.
  end for
  until $R^{(i)} > R_{re}$ for all $i = 1, 2, \ldots, K$. Then set $P^{(i,j)} = P^{*(i,j)}$.
end loop

$$\max R^{(i)} = \sum_{j=1}^{N} \log_2 \left(1 + \frac{|g^{(j)}_{i,i}| P^{(i,j)}}{\sum_{u \in \mathscr{S}^{[i]}} |g^{(j)}_{u,i}| P^{(u,j)} + \sigma^2_{(i,j)}} \right),$$

$$\text{subject to} \sum_{j=1}^{N} P^{(i,j)} \leq P^{(i)}_{\max}, \tag{30}$$

where $P^{(i)}_{\max}$ is the maximum transmit power of the i-th SBS, $\mathscr{S}^{[i]}$ denotes the set of SBSs excluding the i-th SBS, $\sigma^2_{(i,j)}$ is the noise power for the i-th SUE over the j-th subcarrier, and $|g^{(j)}_{u,i}|$ denotes the channel gain from the u-th SBS to the i-th SUE over the j-th subcarrier, which can be obtained from $\mathbf{H}^{(u,i)}_{ss}$ as

$$|g^{(j)}_{u,i}| = |[\mathbf{F}\mathbf{H}^{(u,i)}_{ss}\mathbf{F}'^{H}(\widetilde{\mathbf{F}}\widetilde{\mathbf{F}}^{H})^{-1}]_{(j,j)}|^2. \tag{31}$$

The Lagrangian function for (30) is

$$\begin{aligned} &\mathscr{L}(P^{(i,j)}, \alpha_i) \\ &= -\sum_{j=1}^{N} \log_2 \left(1 + \frac{|g^{(j)}_{i,i}| P^{(i,j)}}{\sum_{u \in \mathscr{S}^{[i]}} |g^{(j)}_{u,i}| P^{(u,j)} + \sigma^2_{(i,j)}} \right) \\ &+ \alpha_i \left(\sum_{j=1}^{N} P^{(i,j)} - P^{(i)}_{\max} \right), \end{aligned} \tag{32}$$

where α_i is a Lagrangian multiplier.

By setting the differentiation of (32) with respect to $P^{(i,j)}$ to be 0, the power allocated over the j-th subcarrier of the i-th SBS is

$$P^{(i,j)} = \left[\frac{1}{\alpha_i \ln 2} - \frac{1}{\beta}\right]^+, \tag{33}$$

where $\frac{1}{\alpha_i \ln 2}$ is a constant that ensures the power constraint (30) to be satisfied and $\beta = \frac{|g_{i,i}^{(j)}|}{\sum_{u \in \mathscr{S}^{[i]}} |g_{u,i}^{(j)}| P^{(u,j)} + \sigma_{(i,j)}^2}$. Here, $[x]^+ = \max(x, 0)$. Equation (33) is a standard form of water-filling power allocation. Given the coupled power allocation in (30) for different i's, the iterative water-filling in [19] is effective to optimize the power allocation $P^{(i,j)}$.

To guarantee the QoS of SUEs, Algorithm 1 is adopted to ensure that the achievable rate satisfies the rate requirement R_{re} for each SUE by adjusting the power allocation. Here the parameters ε and ξ are used to reach the desired accuracy. With the optimal power $P^{*(i,j)}$ for the i-th SBS over the j-th subcarrier, the precoding matrix $\mathbf{G}^{(i)}$ can be designed according to (27), (28), and (29).

Discussion

Algorithm to Reduce Computational Complexity

Given channel fading and path loss, an SBS may not introduce interference to the other SUEs even with the maximum transmit power. Thus Algorithm 2 is considered to exclude the SBSs from set $\mathscr{S}^{[i]}$ that do not interfere with the i-th SBS, which reduces the computational complexity of the algorithm.

Algorithm 2 SBS selection algorithm

1: **Initialize**: Set $P_{\text{cons}}^{(u)}$ for $u = 1, 2, \ldots, K$. Set $\mathscr{S}^{[i]} = \emptyset$, for $i = 1, 2, \ldots, K$.
2: **for** $i = 1$ to K,
3: **for** $u = 1$ to K, $u \neq i$,
4: Calculate $P_{arrive}^{(u,i)}$ according to (34).
5: **if** $P_{arrive}^{(u,i)} \geq \varepsilon_p$, set $\mathscr{S}^{[i]} = \mathscr{S}^{[i]} + \{u\}$.
6: **if** $P_{arrive}^{(u,i)} < \varepsilon_p$, set $\mathscr{S}^{[i]} = \mathscr{S}^{[i]}$.
7: **end for**
8: **end for**

Let $P_I^{(u,i)}$ be the interference power from the u-th SBS at the i-th SUE. If $P_I^{(u,i)}$ does not exceed the threshold ε_p when the u-th SBS uses the maximum power allowed, $P_{\max}^{(u)}$, the u-th SBS will not be considered as an interferer to the i-th SUE.

Given channel fading and path loss, $P_I^{(u,i)}$ can be expressed as

$$P_{I(dBm)}^{(u,i)} = \gamma_{u,i\,(dB)} + P_{\max(dBm)}^{(u)} - P_{L(dB)}^{(u,i)}, \tag{34}$$

where $\gamma_{u,i}$ is the channel fading coefficient from the u-th SBS to the i-th SUE and $P_L^{(u,i)}$ denotes the path loss from the u-th SBS to the i-th SUE.

For a system with K SBSs and N subcarriers, the complexity of the power allocation optimization and inner precoding matrix design increases with the number of SBSs, K. Through the SBS selection algorithm, the number of SBSs involved in the computation decreases and thus the complexity of optimization reduces.

Imperfect Channel Estimation

In section "Cascaded Precoders", perfect CSI is assumed to obtain the proposed precoder. However, in practice, it is difficult to obtain perfect CSI. Therefore, the performance of the proposed cascaded precoding scheme under channel estimation is analyzed in this subsection. There has been some discussion regarding the cross-tier interference elimination outer precoder under estimated channel in [15]. As in [20], the estimated channel matrix from the i-th SBS to the j-th SUE $\widehat{\mathbf{H}}_{ss}^{(i,j)}$ can be written as

$$\widehat{\mathbf{H}}_{ss}^{(i,j)} = \mathbf{H}_{ss}^{(i,j)} - \widehat{\mathbf{Er}}_{\mathbf{ss}}, \tag{35}$$

where $\widehat{\mathbf{Er}}_{\mathbf{ss}}$ denotes the channel estimation error that is a zero-mean circularly symmetric complex Gaussian matrix, i.e., $\widehat{\mathbf{Er}}_{\mathbf{ss}} \sim (0, \sigma^2_{\widehat{Er}_{ss}}\,\mathbf{I})$, with variance $\sigma^2_{\widehat{Er}_{ss}} = \mathbb{E}(|\mathbf{H}_{ss}^{(i,j)}|^2) - \mathbb{E}(|\widehat{\mathbf{H}}_{ss}^{(i,j)}|^2)$. With the estimated channel matrix, the received signal at the i-th SUE is given by

$$\begin{aligned}
\mathbf{y}_s^{(i)} =& \mathbf{F}(\widehat{\mathbf{H}}_{ss}^{(i,i)}\mathbf{E}^{(i)}\widehat{\mathbf{G}}^{(i)}\mathbf{s}^{(i)} + \sum_{u\in\mathscr{S}^{[i]}} \widehat{\mathbf{H}}_{ss}^{(u,i)}\mathbf{E}^{(u)}\widehat{\mathbf{G}}^{(u)}\mathbf{s}^{(u)} + \mathbf{v}_s^{(i)}) \\
=& \mathbf{F}(\mathbf{H}_{ss}^{(i,i)}\mathbf{E}^{(i)}\widehat{\mathbf{G}}^{(i)}\mathbf{s}^{(i)} + \sum_{u\in\mathscr{S}^{[i]}} \mathbf{H}_{ss}^{(u,i)}\mathbf{E}^{(u)}\widehat{\mathbf{G}}^{(u)}\mathbf{s}^{(u)} + \mathbf{v}_s^{(i)} \\
& \underbrace{- \widehat{\mathbf{Er}}_{ss}^{(i,i)}\mathbf{E}^{(i)}\widehat{\mathbf{G}}^{(i)}\mathbf{s}^{(i)} - \sum_{u\in\mathscr{S}^{[i]}} \widehat{\mathbf{Er}}_{ss}^{(u,i)}\mathbf{E}^{(u)}\widehat{\mathbf{G}}^{(u)}\mathbf{s}^{(u)}}_{\text{channel estimation error part}}),
\end{aligned} \tag{36}$$

where $\widehat{\mathbf{G}}^{(i)}$ is the inner precoding matrix of the i-th SBS considering channel estimation error. To design the elements of $\widehat{\mathbf{G}}^{(i)}$, the power allocation under channel

estimation, $\widehat{P}^{(i,j)}$, is obtained by replacing channel power gain $g_{u,i}^{(j)}$ with $\widehat{g}_{u,i}^{(j)}$ in the optimization problem (30).

The data rates with perfect and imperfect CSI, respectively, have a gap introduced by the channel estimation error part, which will be discussed with simulation results.

Simulation Results

In this section, simulation results are presented to illustrate the performance with the cascaded precoders. In the simulation, $K = 12$ SBSs are randomly deployed in a circle with radius $R = 50$ m and each SBS serves one SUE. The maximum transmit power is 100 mW for each SBS and 10 W for the MBS. The number of subcarriers and the length of CP are $N = 64$ and $L = 16$, respectively. According to [21], a path loss model $37 + 32\log_{10}(d)$ in decibels for all links is adopted, where d is the distance between a base station and a user.

In Fig. 3, the evolution of SUE data rates is illustrated with the iterations in Algorithm 1. The data rate requirement is $R_{re} = 5$ bps/Hz and the data rates of 3 selected SUEs are shown in Fig. 3. The data rate requirement is satisfied for all the SUEs. And the data rates of the SUEs converge fast in a few iterations while the QoS requirements of all the SUEs are met.

The average data rates of all the SUEs with perfect CSI and imperfect CSI under channel estimation are compared in Fig. 4. As shown in the figure, there is a gap

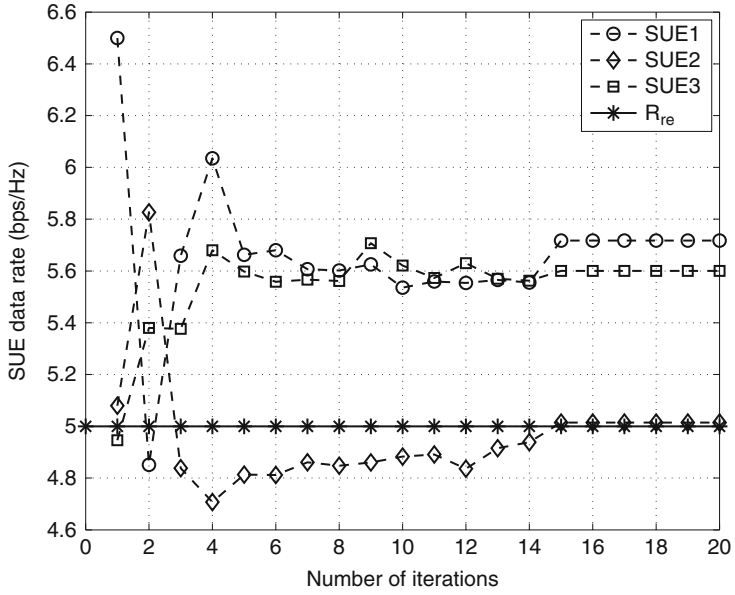

Fig. 3 SUE data rate versus number of iterations

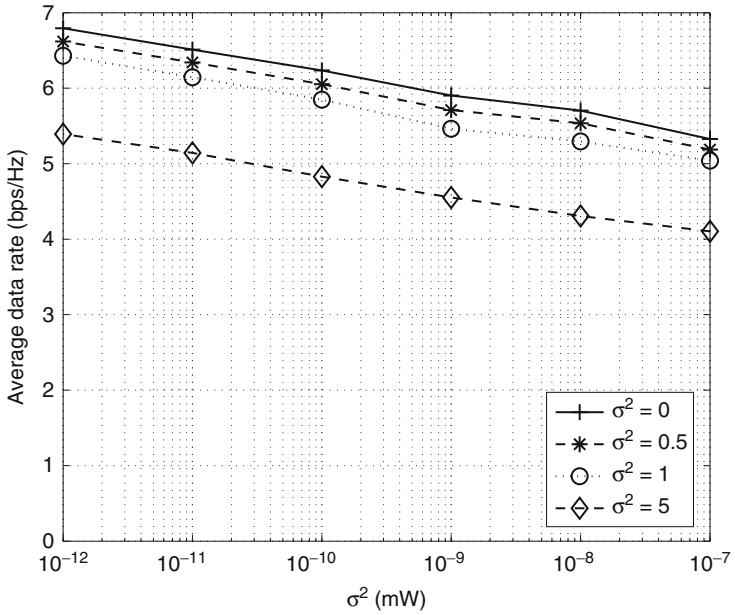

Fig. 4 Average data rate versus noise power under channel estimation

between the network performance with perfect CSI and imperfect CSI. It is obvious that the performance is becoming worse when the error variance increases. However, the average data rate under channel estimation is comparable with the perfect case when the error variance is 1, which is large enough in channel estimation according to [20]. Therefore, the cascaded precoders achieve acceptable performance with imperfect CSI.

In Fig. 5, the performance of the second tier with and without SBS selection algorithm is illustrated. Because of the random deployment and varying channel conditions, some SBSs do not cause co-tier interference to others even in dense deployment with the maximum power. With the SBS selection algorithm, the SBSs not affecting the i-th SBS will be eliminated from set $\mathscr{S}^{[i]}$. Then each SBS could serve its SUE with a higher power to achieve a better data rate and reduce the computational complexity with a smaller number of SBSs included in the optimization.

The performance of equal power allocation without inner precoder and with cascaded precoders is shown in Fig. 6. The cascaded precoders that suppress the co-tier interference render obviously higher data rate than the equal power allocation. Since the fixed co-tier interference in (30) dominates in the equal power allocation scheme, the performance gap increases when the noise power decreases.

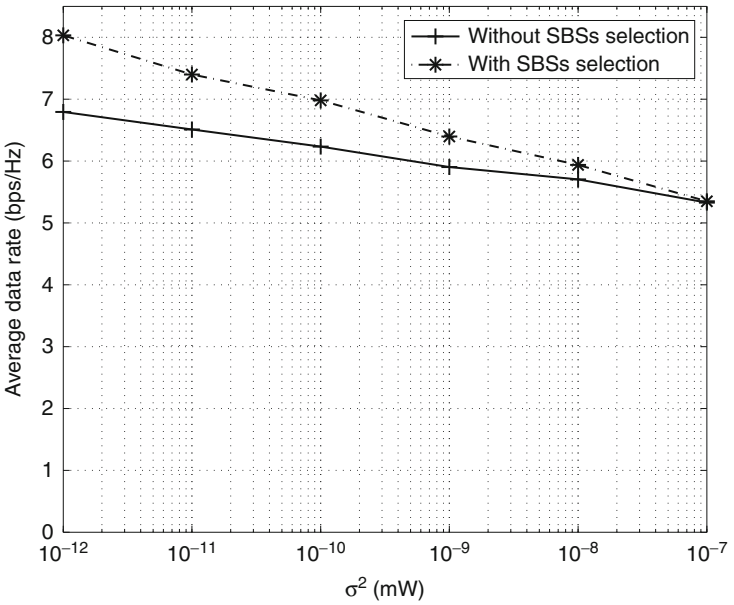

Fig. 5 Average data rate versus noise power with and without SBS selection algorithm

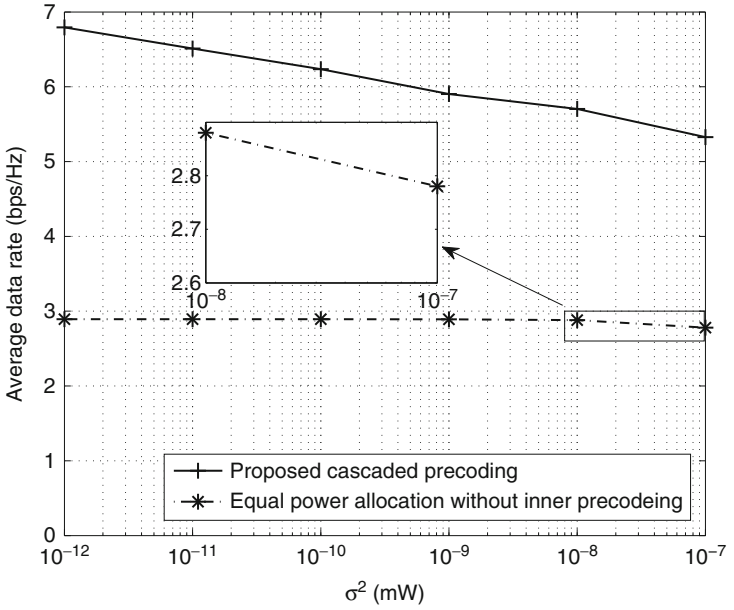

Fig. 6 Average data rate versus noise power in different schemes

Conclusion and Future Directions

In this chapter, cascaded precoders combining precoding and power allocation are discussed to enhance the throughput of the two-tier heterogeneous networks. With the designed outer precoder, the cross-tier interference from SBSs to MUEs is eliminated. Meanwhile, an inner precoder is derived to improve the performance of the second tier, which allocates the powers of SBSs optimally. Moreover, an SBS selection algorithm is presented to reduce the computational complexity of the proposed scheme. The system performance under channel estimation is also discussed. Simulation results illustrate the effectiveness of the cascaded precoders.

For further directions, the interference from the first tier to the second tier can be considered to design more advanced precoders. The precoding and power allocation in cooperative two-tier heterogeneous networks and MIMO networks are expected to be exploited.

References

1. Chandrasekhar V, Andrews J, Gatherer A (2008) Femtocell networks: a survey. IEEE Commun Mag 46:59–67
2. Li Q, Hu RQ, Xu Y, Qian Y (2013) Optimal fractional frequency reuse and power control in the heterogeneous wireless networks. IEEE Trans Wirel Commun 12:2658–2668
3. Navaratnarajah S, Saeed A, Dianati M, Imran MA (2013) Energy efficiency in heterogeneous wireless access networks. IEEE Wirel Commun 20:37–43
4. Ha VN, Le LB (2014) Fair resource allocation for OFDMA femtocell networks with macrocell protection. IEEE Trans Veh Technol 63:1388–1401
5. Damnjanovic A, Montojo J, Wei Y, Ji T, Luo T, Vajapeyam M, Yoo T, Song O, Malladi D (2011) A survey on 3GPP heterogeneous networks. IEEE Wirel Commun 18:10–21
6. Chandrasekhar V, Andrews JG (2009) Spectrum allocation in tiered cellular networks. IEEE Trans Commun 57:3059–3068
7. Chen D, Jiang T, Zhang Z (2015) Frequency partitioning methods to mitigate cross-tier interference in two-tier femtocell networks. IEEE Trans Veh Technol 64:1793–1805
8. Singh S, Andrews JG (2014) Joint resource partitioning and offloading in heterogeneous cellular networks. IEEE Trans Wirel Commun 13:888–901
9. Bao W, Liang B (2015) Uplink interference analysis for two-tier cellular networks with diverse users under random spatial patterns. IEEE Trans Wirel Commun 14:1252–1265
10. Kang X, Zhang R, Motani M (2012) Price-based resource allocation for spectrum-sharing femtocell networks: a Stackelberg game approach. IEEE J Sel Areas Commun 30:538–549
11. Shen S, Lok TM (2013) Dynamic power allocation for downlink interference management in a two-tier OFDMA network. IEEE Trans Veh Technol 62:4120–4125
12. Kim DI, Shin EH, Jin MS (2015) Hierarchical power control with interference allowance for uplink transmission in two-tier heterogeneous networks. IEEE Wirel Commun 14:616–627
13. Wang H, Wang J, Ding Z (2015) Distributed power control in a two-tier heterogeneous network. IEEE Trans Wirel Commun 14:6509–6523
14. Chen J, Lau VKN (2014) Two-tier precoding for FDD multi-cell massive MIMO time-varing interference networks. IEEE J Sel Areas Commun 32:1230–1238
15. Cardoso LS, Kobayashi M, Cavalcanti FRP, Debbah M (2013) Vandermonde-subspace frequency division multiplexing for two-tiered cognitive radio networks. IEEE Trans Commun 61:2212–2220

16. Maso M, Debbah M, Vangelista L (2013) A distributed approach to interference alignment in OFDM-based two-tiered networks. IEEE Trans Veh Technol 62:1935–1949
17. Maso M, Cardoso LS, Debbah M, Vangelista L (2013) Cognitive orthogonal precoder for two-tiered networks deployment. IEEE J Sel Areas Commun 31:2338–2348
18. Yao R, Liu Y, Lu L, Li GY, Maaref A (2016) Cooperative precoding for cognitive transmission in two-tier networks. IEEE Trans Commun 64:1423–1436
19. Yu W, Ginis G, Cioffi JM (2002) Distributed multiuser power control for digital subscriber lines. IEEE J Sel Areas Commun 20:1105–1115
20. Yoo T, Goldsmith A (2006) Capacity an power allocation for fading MIMO channels with channel estimation error. IEEE Trans Inf Theory 52:2203–2214
21. Son K, Lee S, Yi Y, Chong S (2011) REFIM: a practical interference management in heterogeneous wireless access networks. IEEE J Sel Areas Commun 29:1260–1272

Distributed Resource Allocation for Network Virtualization

41

Huaqing Zhang and Zhu Han

Contents

Abstract

The explosive development of mobile data service makes our lives convenient and efficient. However, due to the limitation of resources and high flexibility of users' requirements, the resource management and allocation remain challenging. In this chapter, we first overview the development of mobile network. Based on the increasingly complicated mobile network, we analyze the current trends for service architecture, and show the features of distributive control and network

H. Zhang (✉) · Z. Han
Electrical and Computer Engineering Department, University of Houston, Houston, TX, USA
e-mail: markasjunior@gmail.com; hanzhu22@gmail.com

W. Zhang (ed.), *Handbook of Cognitive Radio*,
https://doi.org/10.1007/978-981-10-1394-2_39

virtualization in the future data services. According to the service architecture, game theory is adopted to discuss the distributed behaviors of each service provider and user. We model the resource allocation problem as a hierarchical game, where the strategies for each service provider and each mobile user is proposed to achieve optimal and stable utilities. Finally, we conclude the chapter and put forwards future directions for distributed resource allocation problem in the virtualized data service network.

Development of Mobile Network

Ever since the digital revolution, the past half century has witnessed the information explosion in every perspective of the world. Nowadays, with the increasing popularity of smart mobile devices, a large variety of wireless data services and applications have effectively improved the efficiency and convenience of business and our daily lives. According to Cisco [1], at the end of 2016, global mobile data traffic has reached 7.2 EB (EB is equivalent to one billion GB) per month, which is 63% more compared with the global mobile data traffic of 4.4 EB at the end of 2016, and 18-fold over the past 5 years, compared with the global mobile data traffic of 400 PB (PB is equivalent to one million GB) per month at the end of 2011. Moreover, most emerging data services and applications, such as augmented reality, vehicle-to-vehicle communication, and live video feed, not only require large volume of transmitted data but also low service delay and delay jitter, which plays significant role on the quality of service (QoS) for mobile users [2].

In order to perform wireless data transmission from service providers to mobile users, the traditional cellular network is able to provide the coverage for data services. As shown in Fig. 1a, within a large communication cell, the base station processes and transmits data for mobiles users and forwards the data to the core network via backhaul. However, due to the limited amount of wireless resources, when there are mobile users requesting large volume of data transmission within the same communication cell, the base station cannot allocate sufficient wireless resources for all mobile users, and the QoS of mobile users at the cell edge is severely affected. Accordingly, in order to meet the requirements for the increasing data transmission trends, in these years, many solutions have been proposed for the communication network and can be generally summarized in the following three directions.

The Heterogeneous Architecture Within the Cellular Network

In urban areas, considering the high density of mobile users in specific areas and poor indoor coverage with the traditional cellular network, it is significant and beneficial to add different sizes of the communication cells, such as microcell, picocell, and femtocell, on the traditional macrocell network and form a heterogeneous wireless service architecture. As shown in Fig. 1b, in the areas with high volume of data transmission, the implementation of small cells reduce the data transmission

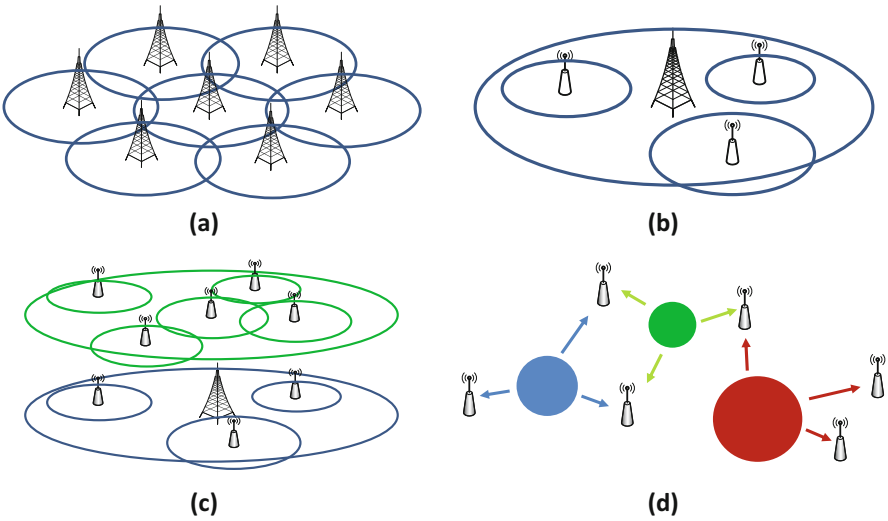

Fig. 1 Development of mobile network

distance between transmitters and receivers, resulting in high capacity for mobile users and high spectrum reuse factors for service providers. Meanwhile, in other areas with limited nomadic users, the macrocells are required and sufficient to guarantee the data transmission coverage. Accordingly, based on the distribution of data requirements, the heterogeneous network is able to efficiently improve the QoS of all mobile users.

Service Cooperation with Other Networks

The heterogeneous architecture of communication network is able to significantly improve the efficiency of wireless resources. However, when the total amount of wireless resource is limited but the volume of data transmission requirements keeps increasing, the QoS for mobile users eventually decreases. Therefore, it is fundamental to increase the total amount of feasible spectrum for wireless communication. As currently the majority of radio spectrum is licensed to other users or networks, while the application within the radio spectrum is spare sometimes, it is promising to explore the cooperations with other users or networks and obtain a large amount of available radio spectrum for data transmission, as shown in Fig. 1c. Such cooperations have been widely applied in cellular network with several examples shown as follows.

- In 1998, the concept of cognitive radio was initially put forward by Joseph Mitola in a seminar at KTH Royal Institute of Technology in Stockholm, and the article [3] was published with Gerald Q. Maguire in the following year. In the cognitive

radio network, the primary users are allocated with a large amount of spectrum resources, while the secondary users, without sufficient spectrum, try to reuse the licensed spectrum from primary users without causing interference. Accordingly, the secondary users are required to quickly sense the radio environment and effectively capture the vacant channels from primary users [4]. In IEEE 802.22 standard, the white spaces in the television frequency spectrum are allowed to be accessed for wireless regional area network with cognitive radio technology [5].

- With fast development in wireless local area network (WLAN), in 2008, the 802.11ac and 802.11ad standards have already been able to achieve the data rate of 6.9 and 6.7 Gbps, respectively. Accordingly, it is beneficial for the wireless cellular network to off-load its data services to WLAN to achieve high performance. By 2009, AT&T Inc. has deployed over 20,000 Wi-Fi hotspots to assist data transmission in the USA [6], and nearly 27 million AT&T customers receive access to the domestic Wi-Fi services. Moreover, as shown in Cisco, in 2016, 60% of total mobile data traffic has off-loaded onto Wi-Fi or femtocell [1].

Content-Centric Analysis for Resource Allocation

With the increasing popularity of smart mobile devices, the wireless services are experiencing a fundamental transition from the traditional connection-centric communications, such as phone calls and emails, to the content-centric communication, such as various mobile applications and video streaming [7]. Accordingly, the resource allocation protocol is no longer focused on the network links, but on the features and influences of content or data itself, as shown in Fig. 1d. Due to the content diversity [8] or content reuse [9], the same content may be requested by multiple mobile users. Therefore, the multi-casting and caching are able to be adopted to improve the QoS of mobile users.

Moreover, in cloud computing, the data storage and computation are normally applied by massive data centers, which are located far away from mobile users, causing high transmission cost and transmission delay. In order to fulfill the requirement of real-time applications, it is necessary to pull the cloud closer to mobile users. In the Internet of things (IoT), fog computing is put forward by Cisco as a promising solution, where multiple low-power computing or storage devices, known as the fog nodes, are allocated close to the users and can provide disaster resilient, fast response and location-awareness services. Similarly, in wireless radio access network, the concept of mobile edge computing is put forward by ETSI (European Telecommunications Standards Institute), where the network edge are able to perform data computation and storage in an isolated environment, so as to reduce network congestion and improve QoS. Therefore, considering the purpose of transmitted data and the deployment of multiple fog nodes or small computing devices, the allocated resources for both networking and computation are supposed to be considered simultaneously to further improve the QoS.

Service Architecture

According to the development of mobile network, the structure is becoming increasingly complicated. It is trending that the resource allocation in data transmission, computation and storage should be jointly considered, and various cooperations and competitions among multiple autonomous characters in the data services are included during the data services. In order to clearly show the complex service architecture for further analysis, we summarize the key framework in the mobile data services and itemize them as follows:

- **Service layer**: In service layer, a large variety of mobile data applications are provided by service operators. Based on different demands of the data services and applications, the service authorization, billing, network routing, and mobility managements are considered and adopted in the layer.
- **Infrastructure layer**: The infrastructure layer consists of various physical facilities which are able to perform data computation, data storage or caching, and data transmission for provided mobile data services. The facilities not only contain massive data centers or macrocell base stations which are established and maintained by professional corporations but also include enterprise data centers or personal mobile devices which are owned by small groups or individuals.
- **Resource layer**: The resource layer includes all kinds of resources required for data computation, storage, and transmission in mobile data services. Some resources may be offered and charged by resource providers such as computation resources from personal mobile devices in the neighborhood, while some may be public and free for data services such as unlicensed spectrum for wireless communication.
- **User layer**: The user layer contains all kinds of mobile users requesting various mobile data services from service providers.

According to the framework, in the following subsections, we analyze the current trends of resource allocation in mobile data services and further depict the future network architecture with network virtualization.

Traditional Service Architecture

In the traditional data service network, in order to provide mobile service to users, each service provider is required to purchase and maintain its own facilities and resources. As shown in Fig. 2, we observe that the facilities and resources for the mobile data services are combined with unique service providers vertically in the architecture. Accordingly, in peak hours, there are many mobile users subscribing the data services from one service provider, in order to meet the requirements of all mobile users, the service provider is required to purchase large amount of facilities and resources. However, most of the time, few data services are requested by mobile

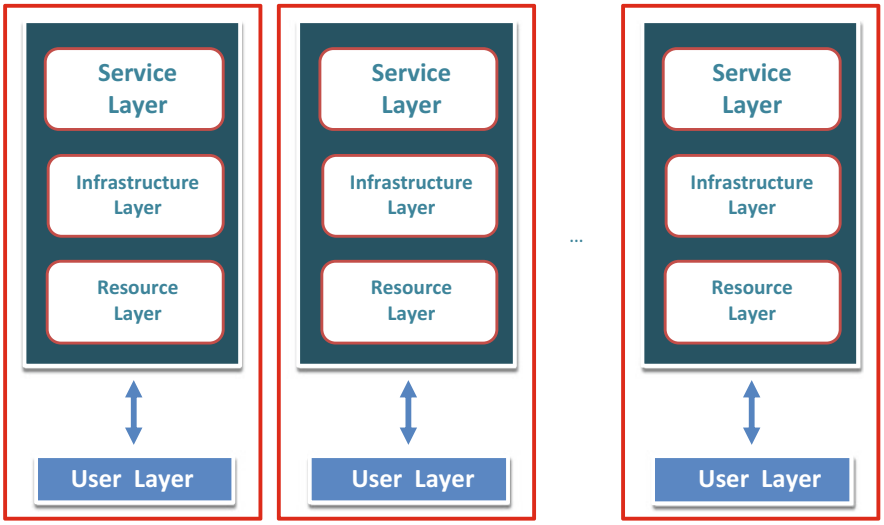

Fig. 2 Traditional service architecture

users, which brings big waste and low efficiency for the usage of facilities and resources. Moreover, due to the high cost on the purchasing and maintenance of facilities and resources, the mobile users may suffer high service price from the service provider.

The Development of Service Architecture

In order to improve the efficiency and capacity of mobile data services, based on the development of mobile network, in these years, the service architecture changes correspondingly. Based on the proposed service framework, we take the following two examples in mobile network to further analyze the development of data service architecture.

The Mobile Data Service in Heterogeneous Network

In the heterogeneous network, as some small cell base stations are purchased and maintained by private enterprises, families, or individuals, the closed access mode is adopted and a private wireless network is established in the indoor environment. However, due to the high cost and low efficiency when allocating unique licensed spectrum for small cell services, the small cell base stations are required to share the spectrum resources with traditional cellular network. Therefore, strong interference may occur between the macrocells and small cells and aggravate the performance of mobile data services. Accordingly, as shown in the Fig. 3, the small cell service network is required to cognitively sense the usage of resource layer of traditional

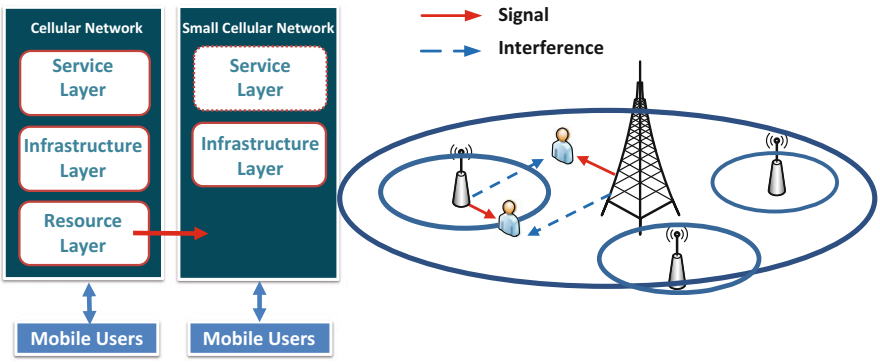

Fig. 3 The mobile data service in heterogeneous network

cellular network and smartly allocate some licensed spectrum with proper transmit power to guarantee the performance of mobile users in traditional cellular network.

Based on the service architecture, further spectrum allocation between the macrocell and small cells have been studied in literature. In [10], in order to obtain sufficient spectrum resources, wireless cooperations are established where the small cell base stations help macrocell base stations to off-load some data services and gain licensed spectrum as rewards. In [11], the optimal power strategies have been analyzed considering the possible cheating behaviors of small cells during the wireless cooperation between small cells and macrocells.

The Mobile Data Service with Visible Light Communication

Visible light communication (VLC) utilizes the illuminating LED for mobile data transmission, which can provide large amount of spectrum resources for wireless data transmission. However, because of the natural property of the visible light, transmission signals are easy to be blocked or severely interfered by other lighting sources. Thus, the coverage region for VLC is limited. Considering the ubiquitous distribution of mobile devices, it is promising to combine the VLC with device-to-device communication (D2D) to help serve mobile users [12]. As shown in Fig. 4, during the service, the VLC network is required to rent the mobile devices from other networks and allocate licensed spectrum for the D2D communication from cellular networks. The whole data service process cannot be finished with the facilities and resources of the VLC networks alone.

Future Service Architecture

According to above analysis, compared with the traditional service architecture, the infrastructure layer and resource layer tends to be separated from its service layer and flexibly allocated to other service providers. Moreover, as the service provider is able to rent the facilities and resources from other networks, it may reduce the total

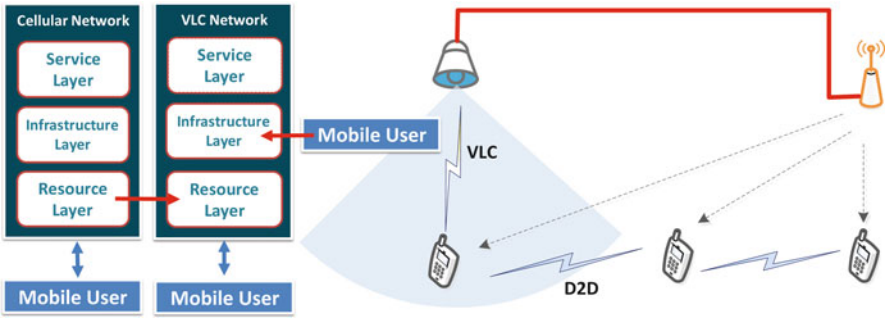

Fig. 4 The mobile data service with VLC

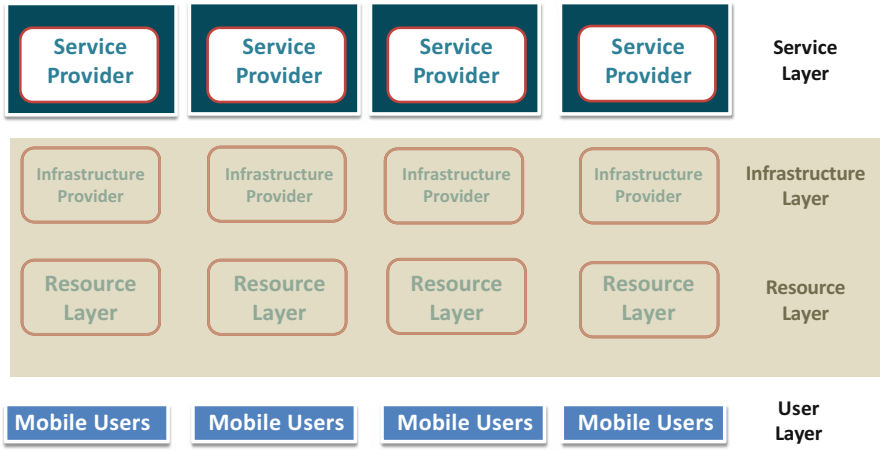

Fig. 5 Future service architecture

amount of purchasing facilities and resources for data services. Thus, there exist new infrastructure providers or resource providers which purchase and maintain the facilities or resources only and provide them to the service providers.

Based on the above, we depict the future service architecture as shown in Fig. 5, where there exist multiple service providers, infrastructure providers, and resource providers in the service layer, infrastructure layer, and resource layer, respectively. The service providers, infrastructure providers, and resource providers are autonomous companies or individuals, which are able to make smart decisions independently for high revenues. Notably, based on different purposes and requirements, some companies or individuals may act as some service providers, infrastructure providers, and resource providers at the same time.

During the data service, due to the security and complexity of the network, the infrastructure layer and resource layer are unknown to mobile users. Thus, the mobile users are only required to determine its service providers for its data services.

As the service provider actually doesn't provide any physical connections and services for the mobile users, we denote the interactions between the service providers and mobile users as a virtualized network, where the virtualized data services are able to be offered by the service providers based on all kinds of requirements of subscribed mobile users. In order to map the physical data connections and services to the virtualized network, the service provider is required to motivate infrastructure provider and resource provider to offer suitable facilities and resources for the data services the mobile users. Accordingly, based on the motivation and selection of service providers, some infrastructure provider and resource provider are able to provide suitable physical facilities and resources for the data services of mobile users. Thus, the facilities and resources in the mobile network can be flexibly and efficiently adopted, and all service providers, infrastructure providers, resource providers, and mobile users are able to achieve high revenues from the data services.

Hierarchical Game Analysis for Resource Allocation

Considering the future service architecture, all service providers, infrastructure providers, resource providers, and users are assumed to be autonomous and selfish, which are required to make decisions distributively to achieve high revenues for themselves. Game theory, which has been shown as an effective and powerful tool, can be applied for the distributed resource allocation problem in the modeled service architecture [13]. In this chapter, based on the relations among all service providers, infrastructure providers, resource providers, and mobile users, a hierarchical game approach is proposed, which consists of three sub-games corresponding to the interactions between service providers and mobile users, between service providers and infrastructure and resource providers, and between infrastructure and resource providers and mobile users. As shown in Fig. 6, following the sequential manner, we summarize the hierarchical game structure as follows:

- We first consider the virtualized data service between the service providers and mobile users as Stackelberg game, where the service providers, acting as leaders, charge mobile users for their virtualized data services, and the mobile users, i.e., the followers, determine the total amount of virtualized resources to purchase to achieve high utilities. The utility of the mobile users is defined as the total revenues received from the mobile data service minus service delay penalty as well as the payment for service providers. The utility of the service provider consist of the total income from the mobile users' payment minus the rewards for motivating the infrastructure & resource providers.
- Based on the prediction of subscribed virtualized data services from the mobile users, the service providers motivates the infrastructure providers and resource providers to offer physical facilities and resources for the data services with moral hazard, considering the utility of each infrastructure & resource provider, which is defined as the total rewards minus the cost for serving different mobile users.

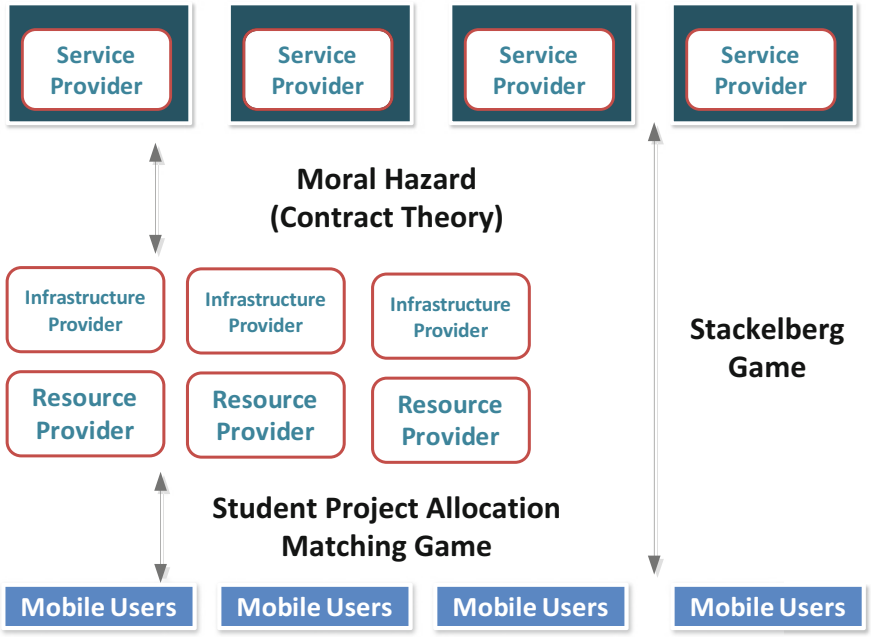

Fig. 6 Hierarchical game model

- According to the total amount of offered resources in physical facilities from infrastructure & resource providers and the total amount of virtual resource requested by the mobile users, a student-project allocation matching game is employed between resources and mobile users, where the mobile users prefers to be served with high QoS, while the infrastructure & resource providers selects its preferred mobile users based on the ratio of collected rewards over the service delay.

In the following sections, with backward induction, we sequentially analyze the interactions between the players within two different layers, which are the interactions between infrastructure and resource providers and mobile users, between service providers and infrastructure and resource providers, and between service providers and mobile users, so as to determine the optimal strategies for all service providers, infrastructure providers, resource providers, and mobile users.

Interactions Between Infrastructure and Resource Providers and Mobile Users

In this section, we suppose the offered facilities and the amount of resources from the infrastructure and resource providers and the requested amount of resources from each mobile user are known. The resource is defined as the combination of both

computation and storage resources within the offered facilities and radio resources from the offered facilities to the mobile users, which is regarded as a resource pair and mapped to requested mobile users. The mapping between the resource pairs and mobile users can be suitably modeled as a student project allocation problem [14], which belongs to a many-to-many stable matching problem. The original problem is described as follows. During the studies in universities, students are instructed to select a number of projects in classes by lecturers. With different judgements, students have different preferences on the projects. Aiming to train students for their expertise, the lecturers may also have different preferences over different (student, project) pairs. In order to guarantee the quality of the class, the maximum number of joining students for each project is constrained, called the capacity of the project. Accordingly, based on the preferences of both students and lecturers, it is expected to achieve a stable matching result where no students in the matched (student, project) pairs are able to find other available projects with higher preferences.

When mapping the student project allocation problem to the resource allocation problem in mobile data service network, the service providers, resource pairs, and mobile users act as lecturers, projects, and students, respectively [15]. The preference list of each mobile user is established according to the total profits obtained from the mobile data service minus delay penalty as well as the payment to the service provider. Moreover, in the perspective of the service provider, the payment from the mobile users is able to increase its revenues, while the service delay with a certain resource pair reduces its profits. Thus, the service providers set high priorities to the mobile users which are willing to pay high prices. The preference list of each service provider over a certain resource pair is based on the ratio of price collected from a mobile user over its delay. In order to achieve a stable matching between service providers and mobile users, the SPA-(S,P) algorithm can be adopted based on the set-up preference lists of both sides [15, 16]. In the algorithm, according to the preference list, each mobile user firstly proposes to its currently most preferred resource pair. For each resource pair, if the total amount of proposals from mobile users exceeds its capacity, then the service provider ranks the combination of resource pairs and mobile users based on its preference list, selects the worst one and rejects its corresponding mobile user. Receiving the rejected notification, the mobile user deletes the resource pair from its preference list and continues to propose to the next favorite one in its list. The proposals of all mobile users iterates until all mobile users are either matched with a resource pair or have an empty preference list. By the iterated proposing and rejecting actions of mobile users and service providers, the algorithm is guaranteed to converge eventually, with a stable matching result.

In Fig. 7, we evaluate the relations between mobile users and service delay with the proposed SPA-(S,P) algorithm. When the number of mobile increases, due to the limited amount of resource pairs, generally, the ratio of mobile users which are qualified for the delay requirement decreases. Compared with the random matching result, the ratio of mobile users with low delays in the proposed SPA-(S,P) algorithm is able to keep in higher values.

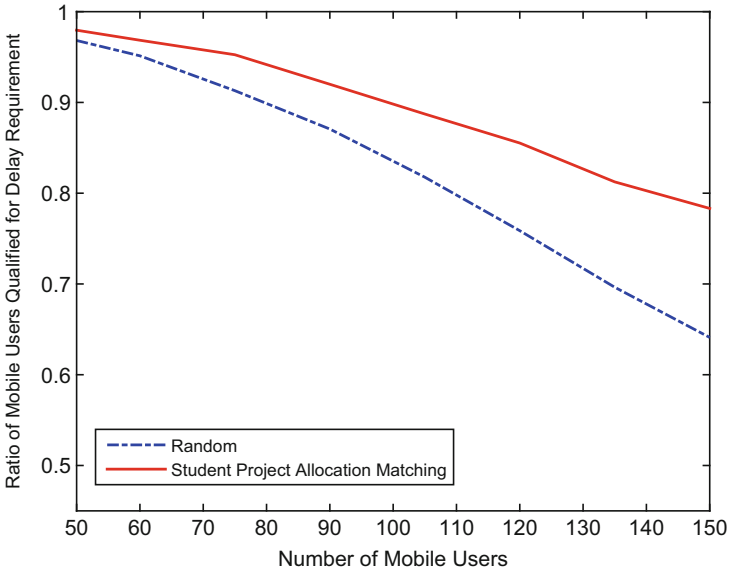

Fig. 7 The performance evaluation of SPA-(S,P)

Interactions Between Service Providers and Infrastructure and Resource Providers

Considering the possible matching results between the infrastructure and resource providers and mobile users, given the amount of subscribed virtual resource from mobile users, each service provider is required to consider the motivation strategies for infrastructure and resource providers to supply the suitable facilities and resources with high QoS for mobile users.

The motivation problem from mobile users to infrastructure and resource providers can be considered as a moral hazard in contract theory. The problem of moral hazard refers to the situations that the employees' actions are hidden form the employers [17]. As the service provider, acting as employers, do not know the resource usage information within each infrastructure and resource provider, if one service provider off-loads its mobile data services to infrastructure and resource providers with limited resource or facilities far from mobile users, the mobile users will suffer poor QoS and switch to other service providers. Accordingly, such a kind of asymmetric information between service providers and infrastructure and resource providers severely reduces the revenues of both service providers and mobile users.

In order to overcome the problem, a resource payment bundle (a, r) in the contract is proposed between service providers and infrastructure and resource providers. a refers to the physical facilities and resources offered by infrastructure and resource providers, and r denotes rewards from service providers to

infrastructure and resource providers. Therefore, in order to motivate the infrastructure and resource providers to offer more physical facilities and resources, the rewards r should be increased correspondingly. Notably, considering different data requirements, usage and transmission distance between infrastructure and resource providers and mobile users, the relations between a and r is also different.

In order to motivate infrastructure and resource providers to offer sufficient resource and suitable facilities, when one infrastructure and resource provider agrees to provide resources or facilities for mobile users, the service provider pays fixed payment to the infrastructure and resource providers. Furthermore, if the infrastructure and resource provider can offer more resource to improve the QoS of mobile users, the service operator will supplement an extra bonus. Thus, the rewards from each service operator to infrastructure and resource providers can be denoted as the addition of both the fixed payment plus extra bonus. The utility of each infrastructure and resource provider is defined as the total rewards from service providers minus the costs of operations. The utility of each service provider is denoted as the revenues from mobile users minus the total rewards for infrastructure and resource providers. In order to maximize the utility of each service provider with the selfish behaviors of infrastructure and resource providers, the optimal value of fixed payment and extra bonus is determined for each infrastructure and resource provider in a contract.

In simulation results, the proposed payment method is compared with four other motivation strategies. In the single bonus plan, we assume each infrastructure and resource provider can offer limited amount of resource to each service provider. In the stochastic independent plan, we assume the measurement error from the service operator to all infrastructure and resource providers equals zero. For the technologically independent plan, the cost for adopting resource within each infrastructure and resource provider is assumed to be independent from each other. The independent plan combines both stochastic independent and technologically independent plans. As shown in Fig. 8, when the cost coefficients of resource increase, as the service operator should pay more to motivate infrastructure and resource providers, the utility of the service provider generally decreases. Furthermore, when the amount of asymmetric information between service providers and infrastructure and resource providers increases, the utility of service provider decreases. Accordingly, the utility of the service provider in the independent payment plan is the highest, followed by the utilities in the stochastic independent plan, technologically independent plan, and our proposed plan. The single bonus plan has the lowest utility, due to the limited amount of offered resource.

Interactions Between Service Providers and Mobile Users

Considering the motivation strategies for infrastructure and resource providers and the matching results between the offered physical resources and the requested virtualized resource, each service provider determines its service price to the mobile users for high utility. In the virtualized data service network, all service providers

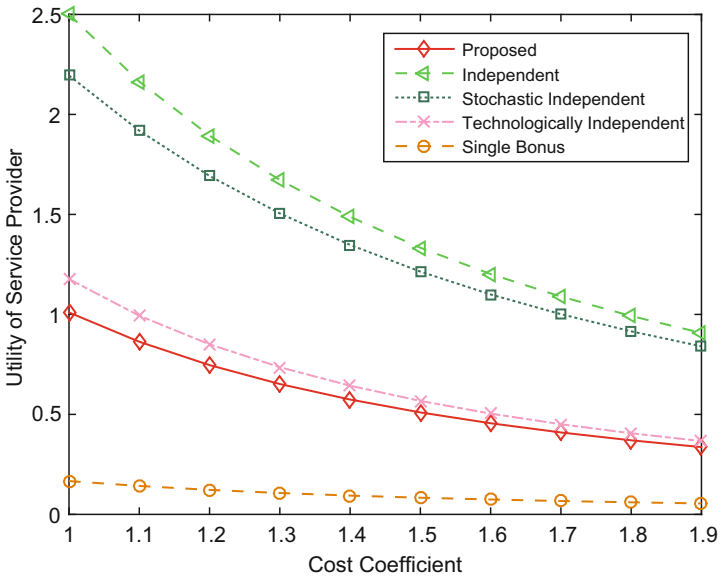

Fig. 8 The performance in moral hazard between service providers and infrastructure & resource providers

first broadcast the prices of their virtualized services. Based on different prices, each mobile user selects its preferred service provider and purchase optimal amount of virtual resources. The relations between service providers and mobile users can be modeled as Stackelberg game, where the service providers play as the leaders and the mobile users play as the followers. Due to the first-mover advantage, each service provider is able to predict the reactions of its serving mobile users and set its optimal service price for the highest utility. As neither service providers nor mobile users are able to change its behaviors for higher utility, the Stackelberg equilibrium exists between service providers and mobile users [18, 19].

Furthermore, the service providers also compete with each other to serve mobile users. If one service provider sets prices much higher than other service providers, the mobile users may switch to other service providers for low payment. Therefore, in the relations among multiple service providers, there is also a noncooperative game. Accordingly, in order to attract more mobile users and maintain high utility at the same time, each service provider can follow the sub-gradient algorithms in [18, 19], where each service provider initially sets its service price in high values and no mobile users are willing to choose its data services. Based on the utility it can achieve, the service provider then adjusts its service price with a small value. If the adjustment is able to improve the utility, the service provider set the adjusted prices in the next round. If the adjustment reduce the utility, the DSO keeps the service price unchanged in the next round. The iteration continues with reduced size of adjustment values until no service operators can change its prices for higher utility.

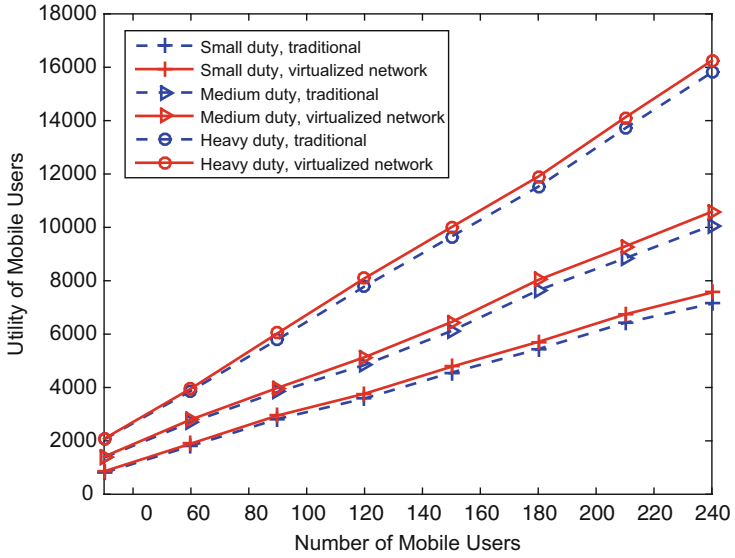

Fig. 9 The utility of all mobile users versus the number of mobile users

Based on the strategies of service operators and mobile users in the Stackelberg game, we evaluate the performances of mobile users in mobile data service network. As shown in Fig. 9 [19], when the number of mobile users increases, whatever the data size for services, the total utility of mobile users generally increases. In addition, when the service price of the service providers and data size for services are fixed, due to the flexible resource allocation with low transmission delay, the utility of the mobile users in the virtualized network performs better than the utility in traditional network. Nevertheless, as the service providers can announce high prices in the virtualized network to gain high revenues, the improvement gap of the mobile users utility from virtualized network to the traditional network is limited.

Conclusion Remarks and Future Works

With all kinds of distributions and demands from mobile data services and applications, the mobile network is becoming increasingly complicated. In order to meet the requirements of all mobile users, the network virtualization is the current trends for resource allocation and management. In this chapter, we first put forward the mobile data service framework, which is constitute of service layer, infrastructure layer, resource layer, and user layer. Based on the distributed and autonomous behaviors of service providers, infrastructure providers, resource providers, and users, the hierarchical game approach is proposed based on the general data service architecture, which provides distributed strategies for each service provider, infrastructure provider, resource provider, and user to gain high and stable revenues.

Based on the three-layer hierarchical game architecture, there are still potentials to analyze the optimal strategies of service operators, infrastructure and resource providers, and mobile users suitable to different scenarios. In this section, we list several future research directions that can be explored in mobile data service network.

Considerations of Both Competitive and Coordinated Behaviors for Service Providers

In the network, not only the competitive strategy but also some coordinated behaviors may exist among the service providers. The coordination among service providers are able to improve the total utility, but the fairness cannot be guaranteed. In order to further improve the total utilities of coordinated service providers, some potential coordinated algorithms can be considered. Following the ideas in [20], the Kalai-Smorodinsky bargaining game can be designed among service providers when setting prices to mobile users. The Kalai-Smorodinsky bargaining game is able to maintain the ratios of maximal gains when all coordinated service providers set prices, so the fairness among service providers can be guaranteed.

Coalition Game Among Infrastructure and Resource Providers

During the resource allocation between physical resource provided by the infrastructure and resource providers and the virtualized resource requested by the mobile users, if there exist cooperations before the matching, the utility of both infrastructure and resource providers and mobile users can be further improved. In [21], a combination of coalitional game and matching game is proposed. As the coalitions of infrastructure and resource providers are able to improve quality of matching results, the total utility is proved to have significant improvement. Therefore, in the student project matching game between infrastructure and resource providers and mobile users, if the infrastructure and resource providers are able to cooperate and form coalitions, the mobile users may be able to further receive higher QoS with low costs.

Switches Between Infrastructure and Resource Providers and Mobile Users

As the mobile users and infrastructure and resource providers may switch to each other, the mobile users and infrastructure and resource providers may be regarded as the same type of players. Considering the possible data transmission between any pair, a graphical game is a promising analytical tool [12], where players are regarded as nodes and the transactions between players are denoted as edges. Accordingly, a general graph is formed where each node considers its optimal

strategies. As the graphical game design considers the flexible switches between infrastructure and resource providers and mobile users, the total utility for each mobile user or infrastructure and resource provider within a long-time interval may be significantly improved.

References

1. Cisco (2017) Cisco visual networking index: global mobile data traffic forecast update, 2016–2021. Cisco White paper, ID:1454457600805266. Available via DIALOG http://www.cisco.com/c/en/us/solutions/collateral/service-provider/visual-networking-index-vni/mobile-white-paper-c11-520862.html
2. Yi S, Li C, Li Q (2015) A survey of fog computing: concepts, applications and issues. In: Proceedings of the 2015 Workshop on Mobile Big Data, Hangzhou, pp 37–42
3. Mitola J, Maguire GQ (1999) Cognitive radio: making software radios more personal. IEEE Pers Commun 6(4):13–18
4. Liang YC, Chen KC, Li GY, Mahonen P (2011) Cognitive radio networking and communications: an overview. IEEE Trans Veh Technol 60(7):3386–3407
5. Stevenson CR, Chouinard G, Lei Z, Hu W, Shellhammer SJ, Caldwell W (2009) IEEE 802.22: the first cognitive radio wireless regional area network standard. IEEE Commun Mag 47(1):130–138
6. AT&T (2009) AT&T Wi-Fi: at a glance. Available via DIALOG https://www.att.com/Common/about_us/files/pdf/wifi/Wi-Fi_at_a_Glance.pdf
7. Tao M, Chen E, Zhou H, Yu W (2016) Content-centric sparse multicast beamforming for cache-enabled cloud RAN. IEEE Trans Wirel Commun 15(9):6118–6131
8. Liu H, Chen Z, Tian X, Wang X, Tao M (2014) On content-centric wireless delivery networks. IEEE Wirel Commun 21(6):118–125
9. Golrezaei N, Molisch AF, Dimakis AG, Caire G (2013) Femtocaching and device-to-device collaboration: a new architecture for wireless video distribution. IEEE Commun Mag 51(4):142–149
10. Zhang L, Jiang T, Luo K (2016) Dynamic spectrum allocation for the downlink of OFDMA-based hybrid-access cognitive femtocell networks. IEEE Trans Veh Technol 65(3):1772–1781
11. Zhang H, Niyato D, Song L, Jiang T, Han Z (2016) Zero-determinant strategy for resource sharing in wireless cooperations. IEEE Trans Wirel Commun 15(3): 2179–2192
12. Zhang H, Ding W, Song J, Han Z (2016) A hierarchical game approach for visible light communication and multi-hop D2D heterogeneous network. In: 2016 IEEE Global Communications Conference (GLOBECOM), Washington, DC
13. Han Z, Niyato D, Saad W, Basar T, Hjorungnes A (2011) Game theory in wireless and communication networks: theory, models and applications. Cambridge University Press, Cambridge/New York
14. El-Atta AHA, Moussa MI (2009) Student project allocation with preference lists over (student, project) Pairs. In: Second International Conference on Computer and Electrical Engineering, Dubai
15. Gu Y, Chang Z, Pan M, Song L, Han Z (2017, preprint) Joint radio and computational resource allocation in IoT fog computing: a student project allocation matching. arXiv:1777723
16. Abraham DJ, Irving RW, Manlove DF (2003) The student-project allocation problem. In: 14th International Symposium, ISAAC, Kyoto, pp 474–484
17. Zhang Y, Han Z (2017) "Multi-dimensional Payment Plan in Fog Computing with Moral Hazard", book chapter of Contract Theory for Wireless Networks. Springer International Publishing, pp. 73–88.

18. Zhang H, Xiao Y, Bu S, Niyato D, Yu R, Han Z (2016) Fog computing in multi-tier data center networks: a hierarchical game approach. In: IEEE International Conference on Communications(ICC), Kuala Lumpur
19. Zhang H, Xiao Y, Bu S, Niyato D, Yu R, Han Z (2017) Computing Resource Allocation in Three-Tier IoT Fog Networks: a Joint Optimization Approach Combining Stackelberg Game and Matching. In: IEEE Internet of Things Journal PP(99):1–1.
20. Zhang H, Xiao Y, Cai LX, Niyato D, Song L, Han Z (2015) Hieratical competition for LTE unlicensed using stackelberg game and bargaining. In: IEEE Global Communications Conference, San Diego
21. Saad W, Han Z, Zheng R, Debbah M, Poor HV (2014) A college admissions game for uplink user association in wireless small cell networks. In: IEEE Conference on Computer Communications, Toronto, pp 1096–1104

Many-to-Many Matching for Distributed Spectrum Trading

42

Jin Zhang, Linshan Jiang, Haofan Cai, and Yanjiao Chen

Contents

Abstract

In cognitive radio networks, service providers with spare channels can sell the spectrum to those in need of them. The redistribution of the spectrum among service providers reduces the waste of spare spectrum, therefore enhances the spectrum utilization. It also provides the service provider more revenue from the sail of spectrum. Traditional method of spectrum trading mainly based on double auction, which requires an auctioneer, is a trustworthy third-party authority, to centrally enforce a certain spectrum allocation policy. In this chapter, we take a

J. Zhang (✉) · L. Jiang · H. Cai
Southern University of Science and Technology, Shenzhen, China
e-mail: zhang.j4@sustc.edu.cn; jiangls@mail.sustc.edu.cn; caihf@mail.sustc.edu.cn

Y. Chen
Wuhan University, Wuhan, China
e-mail: chenyj.thu@gmail.com

W. Zhang (ed.), *Handbook of Cognitive Radio*,
https://doi.org/10.1007/978-981-10-1394-2_40

different and new perspective, proposing to use matching as an alternative tool to realize spectrum trading in a distributed way for a free market, which consists of only buyers and sellers, without a trustworthy third-party authority. In this chapter, we will first give a brief introduction of the whole chapter in the first section and then present the fundamentals of the matching theory in the second section. In the third section, matching theory is leveraged in spectrum trading among service providers to decide the spectrum allocation and trading price, the distinctive challenge of spectrum matching compared with conventional matching is analyzed, and a two-stage distributed algorithm is proposed to solve the spectrum matching problem. In the fourth section, we considered a more general case, where multiple channels can be bought by the same service provider, and the spectrum matching algorithm for combinatorial spectrum trading is proposed to enable the spectrum allocation. For both algorithms, the proposed algorithm can achieve a Nash-stable matching, and the simulation shows that the proposed algorithms achieve good performance compared with centralized schemes.

Keywords

Spectrum trading · Multi-item matching · Combinatorial auction · Mechanism design · Cognitive radio

Introduction

To support the ever-increasing volume of wireless traffic with limited spectrum availability, dynamic spectrum access has been proposed to better leverage the underused channels [1, 2]. A wireless service provider can sell spare spectrum to others when her traffic demand is light and buy additional spectrum from others when her demand becomes heavy. Conventionally, such spectrum exchange is assumed to be achieved via double auctions, where a third-party auctioneer determines the spectrum allocation in a centralized manner, based on auction participants' bids and certain optimization objectives.

A truthful spectrum double auction was first proposed in [3]. In [4], a multi-auctioneer progressive auction mechanism was designed, with all sellers assuming the role of auctioneers. In [5], local availability of the spectrum license and its influence on spectrum auctions were studied. In [6, 7], heterogeneous interference graphs for different channels were built for spectrum reuse. Apart from single-round auction mechanisms, dynamic spectrum auction mechanisms were proposed in [8, 9]. The major drawback of double auctions is the need for a third-party authority to enforce the spectrum allocation in a centralized way, which is not applicable for the free spectrum markets with only buyers and sellers but no third-party rule-enforcing authorities.

Taking a completely different viewpoint, we propose to leverage *matching* as an alternative framework for spectrum redistribution. The seminal work of Gale and Shapley [10] pioneers the research on matching items in two different sets

with stability. The concept of stable matching, compared with optimal matching (i.e., the social welfare of buyers and sellers is the highest), matters more in free spectrum markets for two reasons. Firstly, stable matching ensures that no buyer or seller is willing to deviate from the current matching result. Optimal matching, if unstable, will not be obeyed by buyers and sellers, unless it is enforced by a third-party authority. Secondly, stable matching can be realized through *deferred acceptance*, an algorithm that is both efficient and fully distributed. Stable matching has been widely applied to computer science, such as resource management in the cloud [11], user association in small cells [12], as well as resource sharing in device-to-device communication [13]. We will introduce the fundamentals of matching theory in section "Fundamentals on Matching Theory".

Finding a stable matching in free spectrum markets is quite challenging. In this chapter, we refer this challenge problem as the *spectrum matching* problem. This spectrum matching problem is quite different from traditional matching problems, such as the well-known college admission problem [10]. In the college admission problem, each student can attend only one college, and each college can admit multiple students but subject to a fixed quota. In spectrum matching, the fundamental constraint is no longer fixed quotas but *interference:* non-interfering buyers can freely reuse the same channel, while interfering buyers have to operate on separate channels. In other words, the "quota" of a channel is infinite for non-interfering buyers but reduced to one for interfering buyers. The unique feature of spectrum reusability has been widely discussed in spectrum auctions yet has never been considered within a stable matching framework.

In section "System Model", we propose to use the spectrum matching framework as a new economic model for distributed spectrum exchange in free spectrum markets. Sellers who own multiple channels and buyers who demand multiple channels are represented by corresponding numbers of dummies. In this way, spectrum exchange can be formulated as a many-to-one matching problem, where a buyer can be matched to no more than one seller and a seller can be matched to multiple non-interfering buyers (spectrum reuse). To address spectrum heterogeneity, different interference graphs are constructed for different channels to determine spectrum reuse.

In this context, we propose a two-stage distributed algorithm to achieve the objective of stable spectrum matching (section "Spectrum Matching"). The final matching result is proved to be individual rational and Nash-stable. Through extensive simulations, we demonstrate that our proposed distributed algorithm can achieve more than 90% of the maximum social welfare obtained by centralized optimal (but unstable) matching.

In section "Spectrum Matching", a more general case is considered, where multiple channels can be bought by the same service provider, and the value of multiple spectrum combination is different from the sum of each spectrum, which is a unique characteristic of spectrum compared with other commodity. Under this scenario, the spectrum matching algorithm for combinatorial spectrum trading is proposed to enable the spectrum allocation. Buyers can freely express their preferences for different combinations of channels, and the same channel can

be reused by multiple non-interfering buyers. To address spectrum heterogeneity, different interference graphs are constructed for different channels to determine spectrum reuse [7]. We prove that the matching result is individual rational, strong pairwise stable, and is a subgame-perfect Nash equilibrium of the corresponding spectrum bargaining game. Extensive simulations are conducted to evaluate the performance of the proposed many-to-many spectrum matching framework. It is shown that it takes only a few iterations for the proposed algorithm to reach a stable matching result.

Fundamentals on Matching Theory

Gale and Shapley first studied the problems of stable matching in [10] and proposed the deferred-acceptance algorithm to achieve a stable matching in a distributed way.

The stable marriage problem has been stated as follows: Given n men and n women, where each person has ranked all members of the opposite sex in order of preference, marry the men and women together such that there are no two people of opposite sex who would both rather have each other than their current partners. When there are no such pairs of people, the set of marriages is deemed stable.

David Gale and Lloyd Shapley [10] proved that, for any equal number of men and women, it is always possible to solve the SMP and make all marriages stable. They presented an algorithm to do so.

The Gale-Shapley algorithm involves a number of "rounds" (or "iterations"). In the first round, first (a) each unengaged man proposes to the woman he prefers most, and then (b) each woman replies "maybe" to her suitor she most prefers and "no" to all other suitors. She is then provisionally "engaged" to the suitor she most prefers so far, and that suitor is likewise provisionally engaged to her. In each subsequent round, first (a) each unengaged man proposes to the most preferred woman to whom he has not yet proposed (regardless of whether the woman is already engaged), and then (b) each woman replies "maybe" if she is currently not engaged or if she prefers this guy over her current provisional partner (in this case, she rejects her current provisional partner who becomes unengaged). The provisional nature of engagements preserves the right of an already-engaged woman to "trade up" (and, in the process, to "jilt" her until-then partner). This process is repeated until everyone is engaged. The algorithm is also called defer and acceptance algorithm.

This algorithm guarantees that:

- *Everyone gets married*: At the end, there cannot be a man and a woman both unengaged, as he must have proposed to her at some point (since a man will eventually propose to everyone, if necessary) and, being proposed to, she would necessarily be engaged (to someone) thereafter.
- *The marriages are stable*: Let Alice and Bob both be engaged, but not to each other. Upon completion of the algorithm, it is not possible for both Alice and Bob to prefer each other over their current partners. If Bob prefers Alice to his current partner, he must have proposed to Alice before he proposed to his current

partner. If Alice accepted his proposal, yet is not married to him at the end, she must have dumped him for someone she likes more and therefore does not like Bob more than her current partner. If Alice rejected his proposal, she was already with someone she liked more than Bob.

Afterwards, the research in economics explores all kinds of variants of matching problems [14, 15]. Matching has been widely used for resource allocation in computer science. In [11], online and offline algorithms were proposed to match virtual machines to heterogeneous sized jobs in the cloud. In [12], matching was used to associate users to small cells. In [13], device-to-device users were matched to cellular users for resource sharing. In [16], secondary users were matched to primary users for data relay. In [17, 18], a friendly jammer was matched to a transmission pair to help protect them from eavesdropping.

Non-combinatorial Many-to-Many Spectrum Matching

According to section "Fundamentals on Matching Theory", stable matching compared with optimal matching (i.e., the social welfare of buyers and sellers is the highest) matters more in free spectrum markets for two reasons. Firstly, stable matching ensures that no buyer or seller is willing to deviate from the current matching result. Optimal matching, if unstable, will not be obeyed by buyers and sellers, unless it is enforced by a third-party authority. Secondly, stable matching can be realized through *deferred acceptance*, an algorithm that is both efficient and fully distributed. Stable matching has been widely applied to computer science, such as resource management in the cloud [11], user association in small cells [12], as well as resource sharing in device-to-device communication [13]. Stable matching can also be used in spectrum trading problem.

Unfortunately, the *spectrum matching* problem is quite different from traditional matching problems, such as the well-known college admission problem [10]. In the college admission problem, each student can attend only one college, and each college can admit multiple students, but subject to a fixed quota. In spectrum matching, the fundamental constraint is no longer fixed quotas but *interference:* non-interfering buyers can freely reuse the same channel, while interfering buyers have to operate on separate channels. In other words, the "quota" of a channel is infinite for non-interfering buyers but reduced to one for interfering buyers. The unique feature of spectrum reusability has been widely discussed in spectrum auctions yet has never been considered within a stable matching framework.

In this section, we introduce the spectrum matching framework as a new economic model for distributed spectrum exchange in free spectrum markets (section "System Model"). Sellers who own multiple channels and buyers who demand multiple channels are represented by corresponding numbers of dummies. In this way, spectrum exchange can be formulated as a many-to-one matching problem, where a buyer can be matched to no more than one seller and a seller can be

matched to multiple non-interfering buyers (spectrum reuse). To address spectrum heterogeneity, different interference graphs are constructed for different channels to determine spectrum reuse.

In this context, we propose a two-stage distributed algorithm to achieve the objective of stable spectrum matching (section "Spectrum Matching"). Stage I is inspired by the deferred-acceptance (Gale-Shapley) algorithm, which we adapt to enable spectrum reuse and avoid interference among buyers. Stage I converges to an interference-free but unstable matching, due to the complicated interference relationship among buyers. Therefore, we introduce Stage II, which allows buyers to transfer to more preferred channels and sellers to invite previously rejected buyers, if the interference condition permits. The final matching result is proved to be individual rational and Nash-stable.

To address the synchronization problems in the real implementation of the proposed two-stage algorithm, i.e., buyers and sellers are not coordinated to end Stage I and enter Stage II simultaneously, we design rules for individual buyers and sellers to independently decide the timing of their stage transition (section "Implementation of Spectrum Matching").

Through extensive simulations (section "Simulation"), we demonstrate that our proposed distributed algorithm can achieve more than 90% of the maximum social welfare obtained by centralized optimal (but unstable) matching. We also show the influence of different parameters on the final matching results. One interesting finding is that, if buyers have diverse utilities in using different channels, the overall social welfare will be higher, because more buyers will be matched to their desired channels.

System Model

Spectrum Market

In a free spectrum market, service providers with spectrum supply or demand serve as sellers or buyers, respectively. Spectrum reuse must conform to interference constraints.

Market participants. Assume that there are I sellers and J buyers in the spectrum market. Seller i owns m_i channels, and buyer j requests n_j channels. Let $\sum_{i=1}^{I} m_i = M$ and $\sum_{j=1}^{J} n_j = N$ denote the total numbers of supplied and demanded channels, respectively. Inspired by the idea in [7], we create m_i and n_j dummies for seller i and buyer j, respectively. Hence, there are M virtual sellers and N virtual buyers, and each virtual buyer or seller can trade only one channel. In the remainder of this chapter, we omit the term "virtual" without confusion (For simplicity, we assume that channels are independent from each other. Therefore, the value of a combination of channels is exactly the sum of values of each individual channel. We will consider that channels may be complementary or substitute goods (e.g., in a combinatorial auction) in the future. We also use the index of a seller for her channel, e.g., seller i's channel is referred to as channel i.

Utility of buyers and sellers. A service provider obtains different utilities when operating on different channels. We assume that buyer j has a utility vector $B_j = (b_{1,j}, b_{2,j}, \ldots, b_{M,j})$, in which $b_{i,j}$ is the utility for her to use channel i. The higher $b_{i,j}$ is, the more valuable channel i is to buyer j, and buyer j is willing to pay more for channel i. We assume that $b_{i,j}$ is also the price that buyer j offers to seller i. A seller's utility equals the total offered price of all buyers matched to her.

Interference relationship. The key feature of the spectrum resource is interference-restricted reuse. To characterize interference heterogeneity of different channels [7], we construct a series of interference graphs $\{G^i = (V, E^i)\}_{i=1}^{M}$, in which each node $v \in V$ represents a buyer and each edge $e^i \in E^i$ connects a pair of interfering buyers on channel i. If two virtual buyers originate from the same buyer, they are viewed as interfering buyers, since they should not be matched to the same channel. Let $e^i_{j,j'} \in \{0, 1\}$ denote the interference status between buyers j and j' regarding channel i.

Optimal Matching

We introduce the optimal matching as a benchmark to be compared later with our proposed stable matching. The optimal matching maximizes social welfare while complying with the interference constraint. Following the norm of spectrum auctions, we define social welfare as the sum of buyers' utility from acquiring the channels through spectrum matching. Let $\{x_{i,j}\}_{i=1,j=1}^{i=M,j=N}$ denote the matching result. $x_{i,j} = 1$ if and only if buyer j is matched to seller i. The optimal matching is the solution to the following centralized maximization problem:

$$\max_{x_{i,j}} \sum_{i=1}^{M} \sum_{j=1}^{N} b_{i,j} x_{i,j}, \tag{1}$$

$$\text{subject to} \sum_{i=1}^{M} x_{i,j} \leq 1, \forall j, \tag{2}$$

$$x_{i,j} \cdot x_{i,j'} = 0, \text{if } e^i_{j,j'} = 1, j \neq j', \forall i, j, j', \tag{3}$$

$$x_{i,j} \in \{0, 1\}, \forall i, j. \tag{4}$$

The first constraint indicates that each (virtual) buyer can only get one channel. The second constraint restricts that no interfering buyers can be matched to the same channel. The optimal matching, if unstable, can only be implemented by a third-party authority, who solves the above nonlinear integer programming problem, which is NP-hard. In comparison, our proposed distributed matching algorithm can reach an interference-free stable matching in linear time, and our simulation results show that it can achieve 90% of maximum social welfare yielded by the optimal matching.

Spectrum Matching

Preliminaries

We formally define spectrum matching as follows.

Definition 1 (Spectrum matching). Given the set of sellers $\mathscr{M}$ and the set of buyers $\mathscr{N}$, a spectrum matching is a function μ from $\mathscr{M} \cup \mathscr{N}$ to subsets of $\mathscr{M} \cup \mathscr{N}$, such that

- For every buyer $j \in \mathscr{N}$, $\mu(j) = \{i\}$ if buyer j is matched to seller i, and $\mu(j) = \{j\}$ if buyer j is unmatched;
- For every seller $i \in \mathscr{M}$, $\mu(i) \subseteq \mathscr{N}$;
- For every seller i and buyer j, $\mu(j) = \{i\}$ if and only if $j \in \mu(i)$.

In the traditional college admission problem, a preference profile is built for each student, indicating her willingness of attending different colleges; a preference profile is also built for each college, indicating its willingness of accepting different students. In spectrum matching, however, a buyer's willingness to be matched to a channel depends not only on her utility of using the channel but also on whether her interfering neighbors are matched to the same channel. In comparison, in the college admission problem, a student's willingness of attending a college will not be affected by other students at the same college. We assume that if a buyer is matched to a channel without her interfering neighbors, she obtains full utility; otherwise, she gets zero utility because of interference. To deal with such peer effects in spectrum matching, we construct preference profiles on spectrum coalition, rather than individual buyers or sellers. A spectrum coalition consists of a seller and the buyer's matched to this seller or includes a single unmatched seller or buyer.

For buyer j, we can construct a complete, reflexive, and transitive preference relation $\triangleright$ over all spectrum coalitions, based on her utility in the coalition. Assume that buyer j is a member of two coalitions C^{i_1} and C^{i_2}, containing seller i_1 and seller i_2, respectively. Buyer j prefers C^{i_1} to C^{i_2} in two cases: (1) buyer j prefers channel i_1 to channel i_2, and buyer j does not have any interfering neighbor in C^{i_1}; (2) buyer j has some interfering neighbors in C^{i_2}. We implicitly assume that a buyer is indifferent toward two coalitions both involving her interfering neighbors, and she is indifferent towards a coalition of herself (unmatched) and a coalition with her interfering neighbors.

$$C^{i_1} \triangleright_j C^{i_2} \Longleftrightarrow \begin{cases} \forall j' \in C^{i_1}, e^{i_1}_{j,j'} = 0, b_{i_1,j} > b_{i_2,j}, \text{or} \\ \exists j' \in C^{i_2}, e^{i_2}_{j,j'} = 1. \end{cases} \tag{5}$$

For seller i, we can also build a preference relation over all coalitions, based on her utility in the coalition. Assume that seller i is a member of two coalitions C^i and C'^i, containing different groups of buyers. Seller i prefers C^i to C'^i in two cases: (1) the total offered price of buyers in C^i is higher than that of buyers in C'^i, and buyers

in C^i are all noninterfering; (2) there are interfering buyers in C'^i. We also assume that a seller is indifferent toward two coalitions both involving interfering buyers, and she is indifferent toward a coalition of herself (unmatched) and a coalition with interfering buyers.

$$C^i \rhd_i C'^i \iff \begin{cases} \forall j, j' \in C^i, e^i_{j,j'} = 0, \sum\limits_{j \in C^i} b_{i,j} > \sum\limits_{j \in C'^i} b_{i,j}, \text{or} \\ \exists j, j' \in C'^i, e^i_{j,j'} = 1. \end{cases} \tag{6}$$

Distributed Matching Algorithm

Stage I: Adapted Deferred Acceptance

Algorithm 1 Stage I: adapted deferred acceptance

Initialization
$\forall i \in \mathcal{M}$, the waiting list $\mathcal{L}_i = \Phi$, the current proposer list $\mathcal{P}_i = \Phi$.
$\forall j \in \mathcal{N}$, the unproposed seller list $\mathcal{A}_j = \mathcal{M}$.
while ∃ unmatched buyer with nonempty unproposed seller list **do**
  for all Unmatched buyer j with nonempty unproposed seller list **do**
    i = the most preferred seller in $\mathcal{A}_j$.
    Buyer j proposes to seller i.
    Add buyer j to seller i's current proposer list, $\mathcal{P}_i = \mathcal{P}_i \cup \{j\}$.
    Remove seller i from the unproposed seller list, $\mathcal{A}_j = \mathcal{A}_j \setminus \{i\}$.
  end for
  for all Seller i with nonempty current proposer list **do**
    Form the most preferred coalition $C^i \subseteq \mathcal{L}_i \cup \mathcal{P}_i, \forall C'^i \subseteq \mathcal{L}_i \cup \mathcal{P}_i, C^i \rhd_i C'^i$.
    Set the waiting list as $\mathcal{L}_i = C^i$.
  end for
end while
for all $i \in \mathcal{M}$ **do**
  $\mu(i) = \mathcal{L}_i$.
end for
for all $j \in \mathcal{N}$ **do**
  if $\exists i, j \in \mathcal{L}_i$ **then**
    $\mu(j) = \{i\}$.
  else
    $\mu(j) = \{j\}$.
  end if
end for

The traditional deferred-acceptance algorithm, designed to solve the college admission problem, runs as follows [10]. There is a set of students to be admitted to a set of colleges, each with a fixed quota. In the first round, each student applies to her favorite college. Among all applicants, a college with a quota q temporarily puts the top q students in the waiting list, or all students if the number of applicants is smaller than q, and rejects others. In the following rounds, each rejected student applies to her most preferred college which has never rejected her before. Each

college updates its waiting list by selecting the top q students among the current applicants and those in the previous waiting list. This process is repeated until all students have exhausted their applications.

We adapt the original deferred-acceptance algorithm for spectrum matching in Algorithm 1. Unlike the college admission problem, we are not able to determine the "quota" of each seller, since the "quota" depends on the interference relationship among buyers. Instead, at each round, we let a seller to form her most preferred spectrum coalition, i.e., to select a group of buyers who do not interfere with each other according to the interference graph, and whose total offered price is the highest. To find a group of non-interfering buyers with maximum offered price is equivalent to finding a maximum weighted independent set on the interference graph, which is NP-hard. Greedy algorithms have been proposed to solve the maximum weighted independent set (MWIS) problem in linear time [19], which we will adopt in our algorithm.

Proposition 1. *Algorithm 1 is guaranteed to converge, and the running time is* $O(MN)$.

Proof. Each time an unmatched buyer makes a proposal, she will remove one seller from her unproposed seller list. Therefore, each buyer will eventually become matched or exhaust her unproposed seller list; thus, Algorithm 1 comes to an end.

The worst case is that the interference graph on every channel is a complete graph. Then, the spectrum matching problem is reduced to a one-to-one matching problem, and Algorithm 1 is equivalent to the original deferred-acceptance algorithm, whose running time is $O(MN)$.

Toy example. As shown in Fig. 1, there are five buyers $\{1, 2, 3, 4, 5\}$ and three sellers $\{a, b, c\}$. The interference graph on each channel is shown in Fig. 1a; the buyers' utility vectors are shown in Fig. 1b. We make the simplified assumption that $f(b_{i,j}) = b_{i,j}$. Figure 2 shows the process of the adapted deferred-acceptance algorithm. In the first round, buyer 1 and buyer 2 propose to seller a; buyer 3

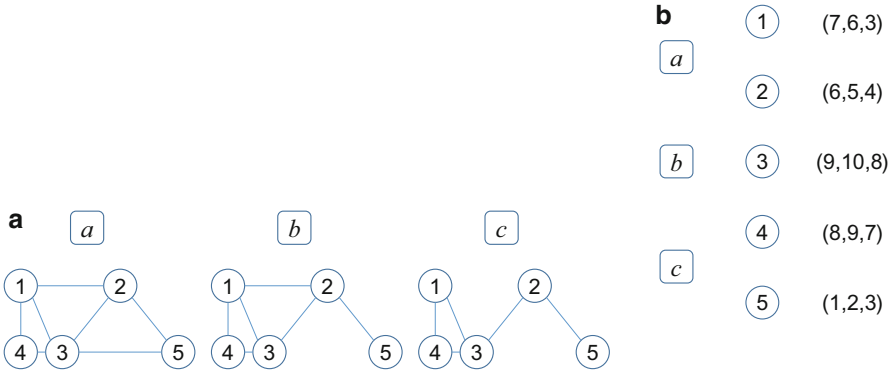

Fig. 1 Toy example. (**a**) Interference graph. (**b**) Preference relations

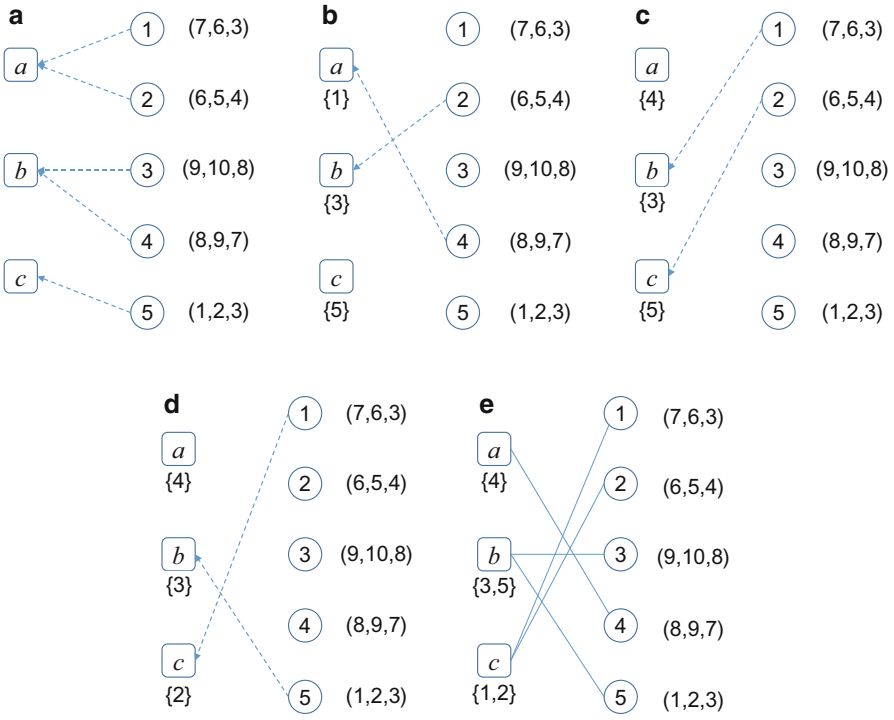

Fig. 2 Stage I: adapted deferred acceptance. (**a**) First round proposal. (**b**) Second round proposal. (**c**) Third round proposal. (**d**) Fourth round proposal. (**e**) Matching result

and buyer 4 propose to seller b; and buyer 5 proposes to seller c, as shown in Fig. 2a. After the first round, all sellers' waiting lists are shown in Fig. 2b. Then, the unmatched buyer 2 and buyer 4 propose to seller b and seller a, respectively. Seller a evicts buyer 1 to form a better coalition with buyer 4 in the waiting list. Figure 2c, d shows the following rounds, and the final matching result is shown in Fig. 2e, with a social welfare of 27.

Stage II: Transfer and Invitation

The deferred-acceptance algorithm produces a stable matching result for college admission problem [20], i.e., there is no pair of student and college who both prefer each other to their current choices. However, the matching result of the adapted deferred-acceptance algorithm is not stable for spectrum matching. For instance, in Fig. 2e, buyer 2 can be matched to seller a without interfering with buyer 4, and both buyer 2 and seller a are better off. This instability is a result of the peer effect of spectrum matching, caused by complicated interference relationship among buyers. Buyer 2 has a better chance of being chosen by seller a in the presence of her non-interfering buyer 4, but a worse chance in the presence of her interfering neighbor 1 (e.g., in the first round).

To improve the matching result and achieve a stable matching, we propose a transfer and invitation algorithm as a second stage, as shown in Algorithm 2. At Stage II Phase 1, buyers send transfer applications to sellers who are more preferred than their currently matched sellers. This means that buyers send transfer applications to sellers whom they have proposed to in Stage I. But unlike Stage I, sellers cannot evict any currently matched buyers in Stage II. Hence, a buyer's transfer application to a seller can only be accepted if she does not interfere with any buyers matched to the seller. In Stage I, we do not allow buyers to re-propose to sellers who have rejected them, because this may lead to ping-pong effect, where buyers continuously make proposals and the algorithm never converges. In Stage II, such ping-pong effect would not happen because each buyer can only send transfer application *once* to each seller who is more preferred than her currently matched seller, and the number of such sellers is *limited*.

At Stage II Phase 2, as a seller's previously matched buyers may have transferred to other sellers, she can invite some of the buyers whom she has rejected in Phase 1. In simulations, we find that the invitation opportunities are scarce, but Stage II Phase 2 has to be included to guarantee the stability of the final matching result.

Toy example. Figure 3 shows the process of our transfer and invitation algorithm. Given the matching result in Fig. 2e, buyer 1 and buyer 2 send transfer applications

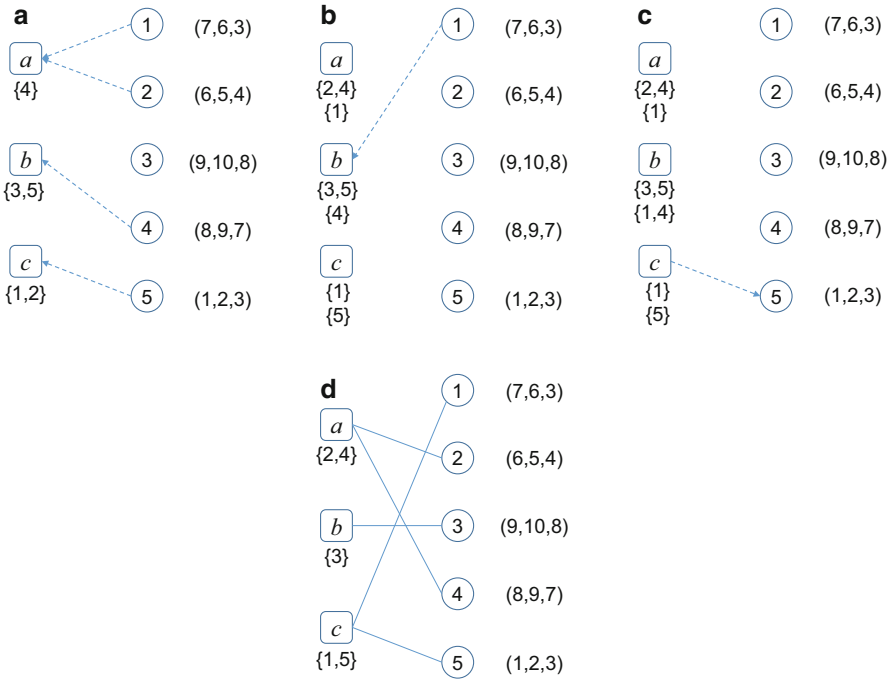

Fig. 3 Stage II: transfer and invitation. (**a**) First round transfer. (**b**) Second round transfer. (**c**) First round invitation. (**d**) Final matching result

to seller a; buyer 4 sends transfer application to seller b; and buyer 5 sends transfer application to seller c. Buyer 2's application is granted, while other buyers are rejected and added to the sellers' rejecting lists, shown under the matching lists. After Phase 1, seller c sends invitation to buyer 5, and the final matching result is shown in Fig. 3d, with a social welfare of 30.

Algorithm 2 Stage II: transfer and invitation

Initialization
$\forall i \in \mathscr{M}$, the current applicant list $\mathscr{D}_i = \Phi$, the invitation list $\mathscr{R}_i = \Phi$.
$\forall j \in \mathscr{N}$, the unapplied seller list $\mathscr{T}_j = \{i | b_{i,j} > b_{\mu(j),j}\}$.
Phase 1: Transfer
while $\exists$ buyers with nonempty unapplied seller list **do**
  for all Buyer j with nonempty unapplied seller list **do**
    i = the most preferred seller in $\mathscr{T}_j$.
    Buyer j sends a transfer application to seller i.
    Add buyer j to seller i's current applicant list $\mathscr{D}_i = \mathscr{D}_i \cup \{j\}$.
    Remove seller i from the unapplied seller list $\mathscr{T}_j = \mathscr{T}_j \setminus \{i\}$.
  end for
  for all Seller i with nonempty current applicant list **do**
    Select the most preferred coalition $C^i = \mu(i) \cup \mathscr{S}, \mathscr{S} \subseteq \mathscr{D}_i, \forall C'^i = \mu(i) \cup \mathscr{S}', \mathscr{S}' \subseteq \mathscr{D}_i, C^i \triangleright_i C'^i$.
    Update the matching, $\mu(i) = C^i, \forall j \in C^i, \mu(j) = i$.
    Set the invitation list as $\mathscr{R}_i = \mathscr{R}_i \cup \mathscr{D}_i \setminus \mathscr{S}$.
  end for
end while
Phase 2: Invitation
for all $i \in \mathscr{M}$ **do**
  Screen non-interfering buyers in the invitation list $\mathscr{R}_i = \{j | j \in \mathscr{R}_i, \forall j' \in \mu(i), e^i_{j,j'} = 0\}$.
end for
while $\exists$ seller with nonempty invitation list **do**
  for all Seller i with nonempty invitation list **do**
    j = buyer with the highest offered price.
    Seller i send invitation to buyer j.
    if Seller i is more preferred than $\mu(j)$ **then**
      Buyer j accepts invitation.
      Update the matching, $\mu(i) = \mu(i) \cup \{j\}, \mu(j) = i$.
      Remove buyer j's interfering neighbors in the invitation list $\mathscr{R}_i = \mathscr{R}_i \setminus \{j | j' \in \mathscr{R}_i, e^i_{j,j'} = 1\}$.
    end if
    Remove buyer j from the invitation list $\mathscr{R}_i = \mathscr{R}_i \setminus \{j\}$.
  end for
end while

Proposition 2. *Algorithm 2 is guaranteed to converge, and the running time of Phase 1 is $O(M)$, of Phase 2 is $O(N)$.*

Proof. Each buyer sends transfer application once to each more preferred seller, so Phase 1 will terminate in a limited number of rounds. In Phase 2, each seller has a

finite invitation list and only sends invitation at most once to each buyer in the list; thus, Phase 2 will also end in a limited number of rounds.

In Phase 1, each buyer has at most M more preferred sellers, so the running time is $O(M)$. Unlike Stage I, no buyer will be evicted in Stage II; therefore, the running time is $O(M)$ rather than $O(MN)$. In Phase 2, each seller has at most N buyers in the invitation list, so the running time is $O(N)$.

Properties

In this section, we prove that the matching result of the proposed distributed algorithm is individual rational and Nash-stable.

Definition 2 (Individual rational).

A matching result is blocked by seller i if she prefers not to be matched to some of her currently matched buyers. In other words, $\exists \mathscr{S} \subseteq \mu(i), \mathscr{S} \neq \Phi, C^i = \{i\} \cup \mu(i), C'^i = \{i\} \cup \big(\mu(i) \setminus \mathscr{S}\big), C'^i \rhd_i C^i$.

A matching result is blocked by buyer j if she prefers being unmatched to being matched to the current seller. In other words, $\{j\} \rhd_j \big(\mu(j) \cup \mu(\mu(j))\big)$.

A matching result is individual rational if it is not blocked by any buyer or seller.

Proposition 3. *The matching result of the proposed distributed algorithm is individual rational.*

Proof. For seller i, the matching result $\mu(i)$ of the proposed algorithm is interference-free. In this case, removing any buyers in $\mu(i)$ will reduce the total offered price and result in a less preferred matching result.

For a matched buyer j, she does not have interference neighbors in $\mu(\mu(j))$. Therefore, her utility is positive, higher than the utility of being unmatched, which is zero.

Deferred-acceptance algorithm can achieve pairwise stability for the college admission problem, i.e., no pair of detached student and college would both be better off if they are matched together. Due to peer effects in spectrum matching, pairwise stability cannot be preserved, whereas we can guarantee a weaker form of stability.

Definition 3 (Nash-stable). A matching result is Nash-stable if no buyer prefers to be a member of another spectrum coalition rather than stay in the current spectrum coalition, i.e., $\forall j \in \mathscr{N}, i = \mu(j), i' \neq i, \big(i \cup \mu(i)\big) \rhd_j \big(i' \cup \mu(i') \cup j\big)$.

Proposition 4. *The matching result of the proposed distributed algorithm is Nash-stable.*

Proof. We prove this by contradiction. Assume that the final matching result is not Nash-stable. There exists at least one buyer j who prefers to join another spectrum coalition with seller $i \neq \mu(j)$. This implies that in Stage II Phase 1, buyer j must have sent a transfer application to seller i because buyer j prefers i to $\mu(j)$. Seller

i must have rejected j and put j in her rejecting list. In Stage II Phase 2, seller i cannot have sent an invitation to buyer j; otherwise, j will accept the invitation and be matched to seller i. This implies that buyer j must interfere with some buyers in $\mu(i)$. Therefore, buyer j would not like to join seller i's spectrum coalition because her utility will become zero, which contradicts the assumption. Hence, the matching result of the proposed algorithm is Nash-stable.

Discussions

In this section, we discuss the limitations of the proposed matching algorithm. The deferred acceptance can achieve a matching result that is pairwise stable and student-optimal for the traditional college admission problem. (Note that the definition of the optimal matching here is different from that in section "System Model".) Unfortunately, our two-stage algorithm based on adapted deferred acceptance cannot achieve these two ideal properties, which may inspire future research in this direction.

Definition 4 (Pairwise stability). A matching is blocked by a pair of seller i and buyer $j \notin \mu(i)$, if there exists $\mathscr{S} \subseteq \mu(i)$ such that:

- Non-interfering condition: $\forall j' \in \mathscr{S}, e^i_{j,j'} = 0$.
- Seller improvement: $\big(\{i\} \cup \{j\} \cup \mathscr{S}\big) \rhd_i \big(\{i\} \cup \mu(i)\big)$.
- Buyer improvement: $\big(\{i\} \cup \{j\} \cup \mathscr{S}\big) \rhd_j \big(\mu(j) \cup \mu(\mu(j))\big)$.

A matching is pairwise stable if it is not blocked by any seller-buyer pair.

Unfortunately, the proposed spectrum matching algorithm cannot ensure pairwise stability. A counterexample is given in Figs. 5 and 4. We ignore Stage II since the matching result will not change in this example. Given the final matching result in Fig. 4e, seller b and buyer 2 form an unstable pair. According to Definition 4, we know that $\mathscr{S} = \{3, 7\}$; seller b prefers the spectrum coalition $\{b, 2, 3, 7\}$ to the current spectrum coalition $\{b, 3, 4, 7\}$; and buyer 2 prefers seller b to the currently matched seller c. Seller b and buyer 2 have incentives to be matched together at the sacrifice of buyer 4, which is, however, not allowed by the proposed matching algorithm.

Another nice property of the deferred-acceptance algorithm is that its matching result realizes an optimal assignment of students among all pairwise stable matching result, that is, no student can get admitted by a better college in another pairwise stable matching result. (When the students initiate the proposal, the matching result is optimal for students but is not guaranteed to be optimal for colleges.) As the spectrum matching can only achieve Nash-stability, we give the following definition for optimality regarding Nash-stable matching.

Definition 5 (Optimality). A Nash-stable matching result μ is buyer-optimal, if there does not exist another Nash-stable matching result μ', in which no buyer

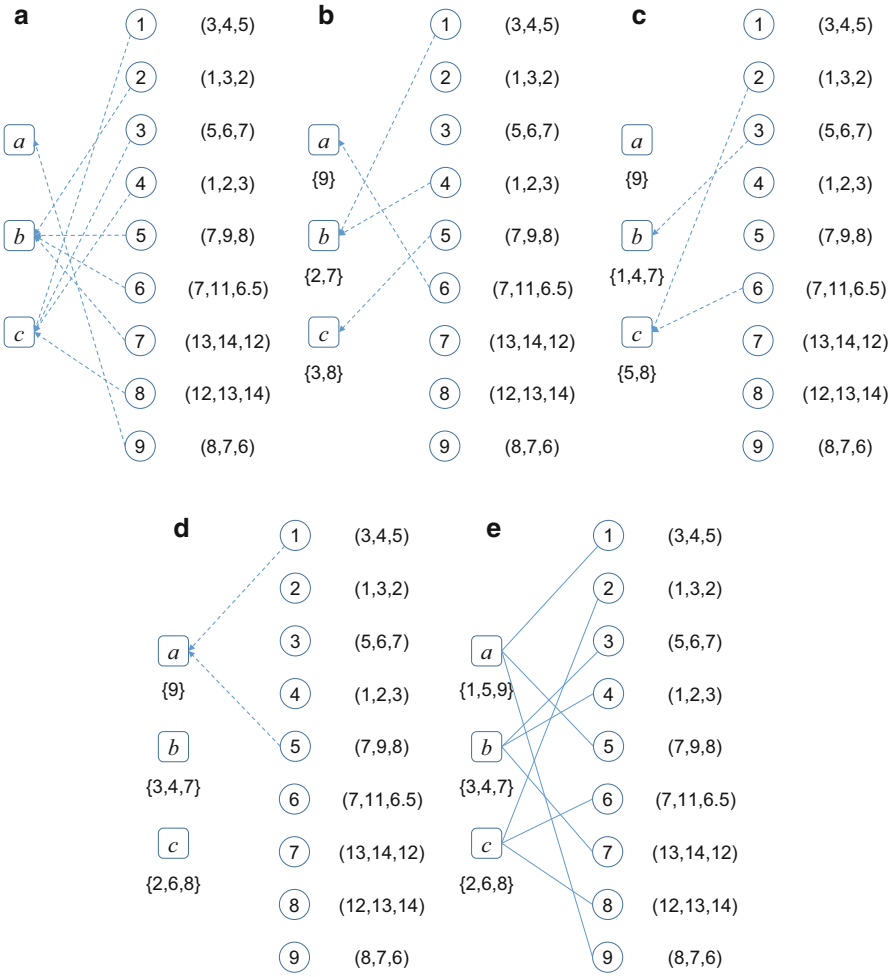

Fig. 4 Counterexample, proposed spectrum matching algorithm. (**a**) First round proposal. (**b**) Second round proposal. (**c**) Third round proposal. (**d**) Fourth round proposal. (**e**) Final matching result

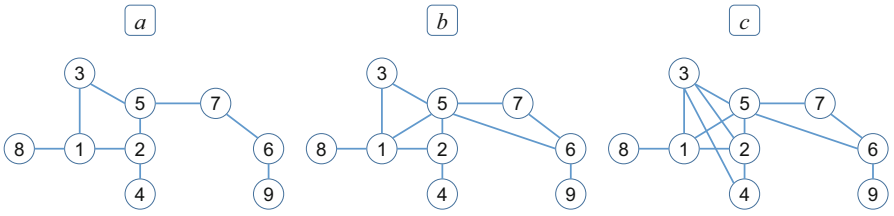

Fig. 5 Counter example, interference graph

is worse off and some buyers are better off. In other words, $\forall j \in \mathcal{N}, \left(\mu(j) \cup \mu(\mu(j))\right) \rhd_j \left(\mu'(j) \cup \mu'(\mu'(j))\right), \forall \mu'$ that is Nash-stable.

Using the same counterexample in Figs. 5 and 4, we show that the matching result of the proposed algorithm is not optimal. Swap buyer 2 and buyer 4 to seller b and seller c, respectively. It can be easily checked that the new matching result is Nash-stable. The new matching result is strictly better than the one produced by the proposed algorithm, in that not only buyer 2 and buyer 4 but also seller b and seller c are better off, and other buyers and sellers are unaffected. In Stage II Phase 1, such a swap cannot be accomplished because seller b is not aware that buyer 4 can transfer to seller c, as long as she accepts the transfer application from buyer 2, who is matched to seller c and interferes with buyer 4. How to enable such a swap, which requires a coordination among different sellers and buyers, is an interesting topic for future works.

Implementation of Spectrum Matching

The proposed two-stage matching algorithm runs in a distributed fashion within each stage and each phase. Nevertheless, asynchronization problem arises during stage or phase transition. More specifically, Stage II commences when all buyers exhaust their proposals and start the transfer application. Unfortunately, it is impossible for a buyer to know whether all other buyers have stopped making proposals. Similar problem exists during phase transition in Stage II. Therefore, in this section, we specify practical rules for stage or phase transition, facilitating the implementation of the proposed two-stage matching algorithm in perfectly distributed manner.

Assume that each round in the proposed algorithm takes one time slot. Propositions 1 and 2 give the running time of Algorithms 1 and 2, respectively, based on which we have the following default transition rule.

Default transition rule. From the very beginning, all buyers and sellers wait for MN time slots to transit to Stage II, then M time slots to transit to Stage II Phase 2, and finally N time slots to end the matching process.

The default transition rule can be extremely inefficient. For instance, given the toy example in Fig. 9, according to the default transition rule, the whole matching process takes 23 time slots, but in fact, 7 time slots are enough to reach the final matching result as shown in Figs. 2 and 3. To tackle this problem, we design the following transition rules.

Stage Transition Rules on Buyers' Side

For a buyer, the risk of a premature entrance into Stage II is being evicted after she starts to send transfer applications but no more proposals. A transfer application has a lower chance of being accepted than a proposal, as the seller will not evict any currently matched buyers upon a transfer application. Therefore, a buyer should transit to Stage II only when her risk of being evicted by the currently matched seller

is low. One observation is that a buyer only faces the threat from her interfering neighbors, so we have the following transition rule.

Stage Transition Rule I for Buyers
A buyer can transit to Stage II if all her interfering neighbors have proposed to her currently matched seller. Stage transition rule I for buyers guarantees that a buyer's matching result in Stage I will not change anymore, but the condition may be hard to meet. For example, in Fig. 2, buyer 4 will never detect buyer 3's proposal to seller a because buyer 3 never proposes to seller a.

To design a more operable rule, we estimate the probability of a buyer being evicted after she performs the stage transition. The smaller this probability is, the less risky for the buyer to enter Stage II. Assume that all buyers' prices follow identically independent distribution (i.i.d.) with a cumulative distributed function $F(\cdot)$.

Consider buyer j who is matched to seller i till the $(k-1)$th round, and n of her interfering neighbors have not proposed to seller i yet. Let p_x^k denote the probability that, at the kth round, x of buyer j's interfering neighbors proposes to seller i, and at least one of their offered prices is higher than buyer j's.

$$p_x^k = \binom{n}{x}\left(\frac{1}{M}\right)^x\left(1-\frac{1}{M}\right)^{n-x}\left(1-F^x(b_{i,j})\right). \tag{7}$$

The probability of buyer j being evicted in the kth round can be estimated as $p^k = \sum_{x=1}^{n} p_x^k$. The probability of buyer j being evicted in the $(k+1)$th round but not in the kth round is $(1-p^k)p^k$. Following the same logic, the probability of buyer j being evicted through the kth round till the MNth round is

$$\begin{aligned} P^k &= p^k + (1-p^k)p^k + \cdots + (1-p^k)^{MN-k}p^k \\ &= 1-(1-p^k)^{MN-k+1} \end{aligned} \tag{8}$$

P^k decreases with k, so it is more secure for a buyer to commence Stage II at a later round.

Stage Transition Rule II for Buyers
A buyer can transit to Stage II at the kth round if P^k is less than a threshold.

We have one more transition rule for buyers that are incurred by sellers. When a seller determines to carry out stage transition, she will inform all her currently matched buyers, which ensures that the seller will no longer evict these buyers.

Stage Transition Rule III for Buyers
A buyer can transit to Stage III if she receives the transition notification from her currently matched seller.

Stage Transition Rule on Sellers' Side

A seller has to make the stage transition decision if she receives no proposal but some transfer applications in the current time slot. After stage transition, a seller cannot grant proposals anymore. In other words, none of her currently matched buyers can be expelled to make room for new buyers. We estimate the probability of a seller getting better proposals after she makes the stage transition. If the probability is low, a seller may begin to process the transfer applications, thus completing the stage transition.

Consider seller i who is, at the $(k-1)$th round, matched to a group of buyers, among which buyer j has the lowest offered price of $b_{i,j}$. There are n buyers who haven't proposed to seller i yet. Let θ denote the probability that an unproposed buyer does not interfere with anyone in $\mu(i)$ except buyer j. θ is an empirical value, which can be estimated by analyzing the interference relationship between buyers in and out of $\mu(i)$. Let q_y^k denote the probability that, at the kth round, y buyers propose to seller i, and at least one of them offers a price higher than $b_{i,j}$, and this buyer do not interfere with anyone in $\mu(i)$ other than buyer j.

$$q_y^k = \binom{n}{y}\left(\frac{1}{M}\right)^y\left(\frac{M-1}{M}\right)^{n-y} \left[1-\Big(F(b_{i,j})+(1-\theta)(1-F(b_{i,j}))\Big)^y\right]. \tag{9}$$

Similar to (8), the probability of seller i receiving better proposals through the kth round till the MNth round is $Q^k = 1-(1-q^k)^{MN-k+1}$, in which $q^k = \sum_{y=1}^{n} q_y^k$. Q^k also decreases with k, thus it is less likely for a seller to obtain more favorable proposals at a later round.

Stage Transition Rule for Sellers

A seller can transit to Stage II at the kth round if Q^k is less than a threshold.

Upon stage transition, a seller will notify all her currently matched buyers, and these buyers will transit to Stage II as well, as specified by stage transition rule III for buyers.

Phase Transition Rule and Matching Termination

We will use the default transition rule for phase transition in Stage II, as the simulation results show that Stage II Phase 1 lasts for approximately M rounds. Buyers and sellers have to decide when to terminate the matching process so that spectrum exchange can be finalized. The simulation results show that Stage II Phase 2 only runs a few rounds, as the opportunities for sellers to send invitations to buyers are rare. Nonetheless, the invitation phase is indispensable to guarantee the stability of the final matching result. We set the rule that each seller will put an end to the matching process when she has no invitation to make and let the user to access her channel.

Simulation

Simulation Settings

We assume that buyers are randomly located in a 10×10 area. The transmission range of each channel is randomly chosen in the range $(0, 5]$. The interference graph of each channel is established based on users' locations and the transmission range of the channel. Users' utility vectors are independently and identically distributed (i.i.d.), following a uniform distribution in $[0, 1]$. The numbers of buyers and sellers are specified in each simulation scenario. The similarity across buyers' utility vectors are quantified by the Spearman's rank correlation coefficient (SRCC) [21], which assesses whether the relationship between two variables can well be described as monotonic. We compute the SRCC for every pair of buyer's utility vectors and obtain the average value. If the result is close to 1, buyers' utility vectors are perfectly similar to one another. If the result is close to 0, buyers' utility vectors are perfectly random and independent from one another. To study the utility similarity and its influence on the matching result, we maneuver buyers' utility vectors as follows. First, we sort all buyers' utilities in the ascending (or descending) order. In this way, the average SRCC is 1. Then, for each buyer, we randomly select m out of M items from her utility vector and perform an $m-$permutation. As m increases, the average SRCC will decrease, indicating that the buyers' utility vectors become more dissimilar to one another. When $m = M$, the SRCC is approximately 0.

Performance of the Proposed Matching Algorithm

We compare the social welfare of the matching result generated by the proposed algorithm and that of the optimal matching result derived by (1) (the optimal matching result is derived by the brute-force approach. As the running time exponentially increases with the numbers of buyers and sellers, we can only simulate small-scale spectrum markets), as shown in Fig. 6. Our proposed distributed matching algorithm can obtain more than 90% of the social welfare from the optimal matching result. Moreover, the running time of the proposed algorithm is only $O(MN)$, while the optimal matching problem in (1) is NP-hard. The social welfare grows with the number of buyers or sellers. If the buyers' utility vectors are similar to each other, multiple buyers will compete for the same channel, and it is hard to satisfy every buyer's requirement; on the contrary, if buyers' utility vectors are more diverse, they will pursue different channels, and the final matching result can satisfy more buyers.

Two-Stage Distributed Algorithm

In Figs. 7 and 8, we demonstrate the social welfare and running time of different stages and phases in our proposed two-stage matching algorithm. Note that the social welfare is accumulated with each stage and phase, while the running time is separately counted for each stage and phase. Most of the social welfare improvement in Stage II comes from Phase 1, while Phase 2 makes a minor contribution. Nevertheless, Phase 2 is indispensable to guarantee the stability of the final matching result.

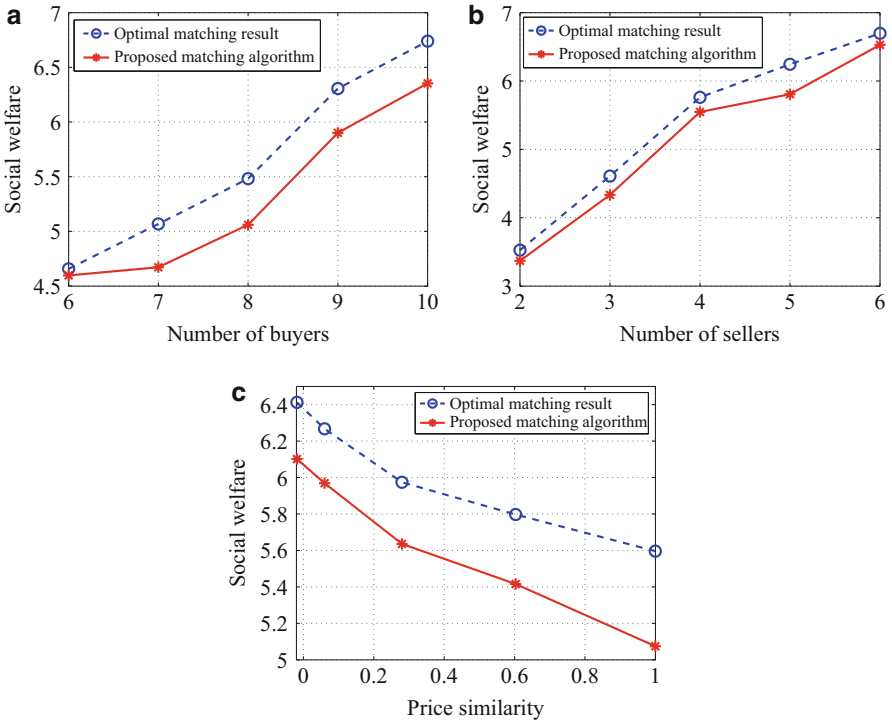

Fig. 6 Optimal matching result versus the proposed distributed spectrum matching algorithm. (**a**) $M = 4$; (**b**) $N = 8$; (**c**) $M = 5, N = 8$

When the number of buyers is far greater than the number of sellers, the running time of Stage I is mostly influenced by the number of sellers. The running time of Stage II Phase 1 is theoretically $O(M)$: it linearly increases with the number of sellers, irrespective of the number of buyers and their offered prices, as shown in Fig. 8. Stage II Phase 2 only runs for a few rounds, as opportunities for sellers to send invitations to buyers are rare.

Combinatorial Many-to-Many Spectrum Matching

In section "Non-combinatorial Many-to-Many Spectrum Matching", we simply assume that channels are independent from each other, i.e., the value of a combination of channels is exactly the sum of values of each individual channel. However, this assumption is not true in real case. The service providers usually value more on two continuous channels than the sum of the individuals, because the effective bandwidth is increased to save the guard band. This is significantly different from conventional commodity where the value is usually in linear proportional with the quantity of the commodity. To take this characteristic into consideration,

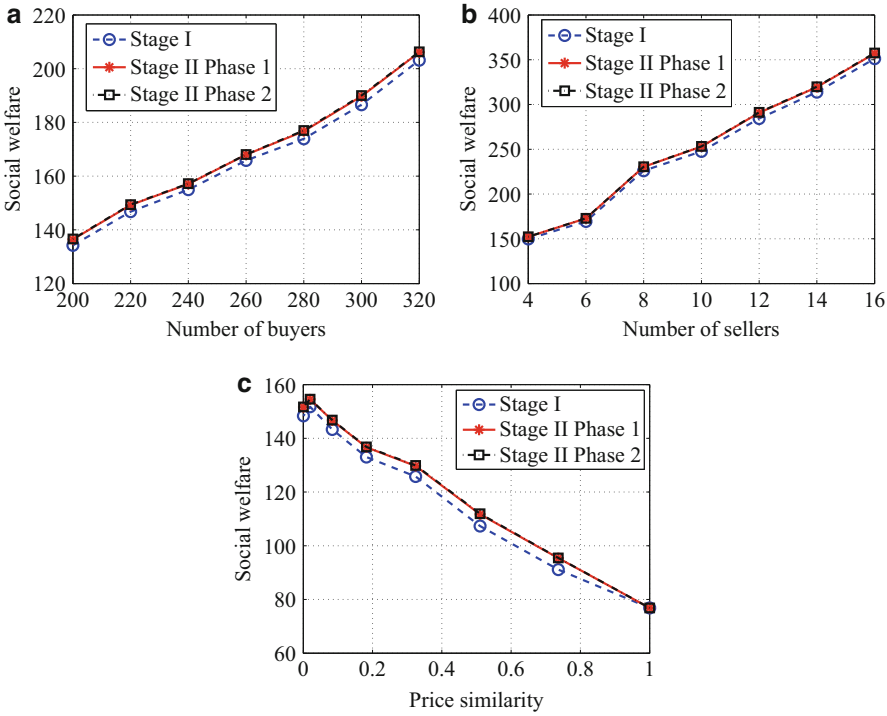

Fig. 7 The social welfare of the two-stage distributed spectrum matching algorithm. (**a**) $M = 10$; (**b**) $N = 500$; (**c**) $M = 8, N = 300$

the spectrum trading becomes a combinatorial spectrum trading, where for each combination of spectrum, the value needs to be redefined. There are many previous works on combinatorial auction. Due to the intractability of combinatorial auctions, a number of greedy algorithms have been proposed with bounded approximation ratio [22–24]. Combinatorial spectrum auction is studied in [25,26]. However, the combinatorial auction has the disadvantage of intractability and collusion problem, which can be addressed by the spectrum matching framework.

In the rest of the section, we leverage matching as an alternative framework for dynamic spectrum access. More specifically, to realize a combinatorial auction alike spectrum market, we propose to use many-to-many matching, where a buyer can purchase multiple channels, and a seller's channel can be assigned to multiple non-interfering buyers. Instead of maximizing social welfare, the aim of matching is to achieve a stable status. The stability concept is attractive because it keeps an equilibrium status for both sellers and buyers. Besides, the matching process can be free from a third-party auctioneer, avoiding potential collusion between the auctioneer and the buyers or sellers. In fact, stable matching has been widely applied to computer science, such as resource management in the cloud [11].

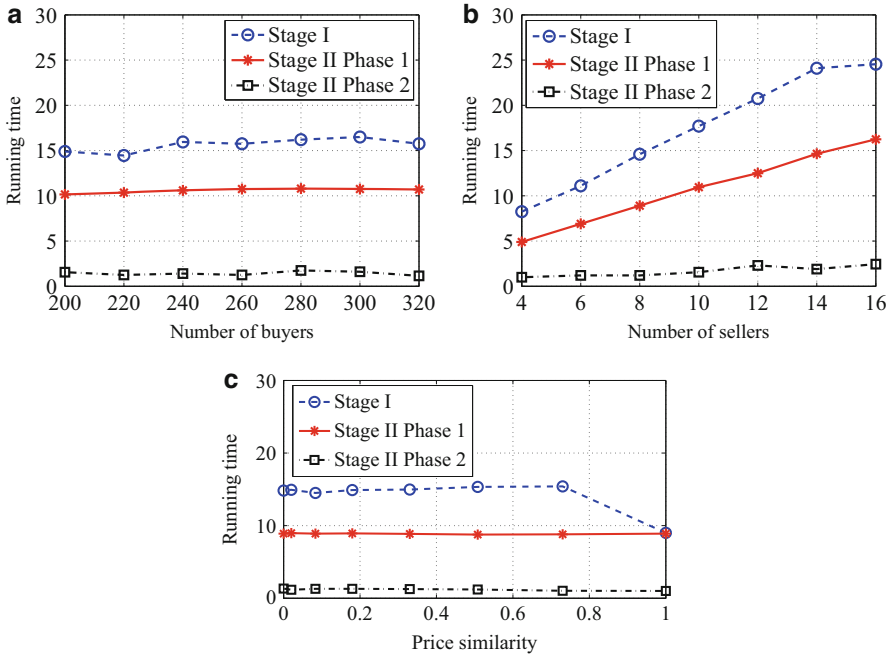

Fig. 8 The running time of the two-stage distributed spectrum matching algorithm. (**a**) $M = 10$; (**b**) $N = 500$; (**c**) $M = 8, N = 300$

Matching has been widely studied in the economics and mathematics communities. In the pioneer work of David Gale and Lloyd Shapley [10], *deferred-acceptance* algorithms are proposed to reach a stable matching for the marriage problem (one-to-one matching) and the college admission problem (many-to-one matching). Compared with one-to-one matching and many-to-one matching, many-to-many matching is much more complicated, and it is more difficult to reach a stable matching result. Based on the deferred-acceptance algorithm, in [27], the authors proposed a competitive adjustment process for labor markets with perfect information. In [28], an iterative T-algorithm is proposed, which can realize many nice properties, such as pairwise stability, setwise stability, and core stability.

In this section, we propose a novel many-to-many spectrum matching framework for combinatorial spectrum trading. Buyers can freely express their preferences for different combinations of channels, and the same channel can be reused by multiple non-interfering buyers. To address spectrum heterogeneity, different interference graphs are constructed for different channels to determine spectrum reuse [7]. We propose an algorithm, which can reach a stable matching result and also improve spectrum utilization through spectrum reuse. We make the following key contributions:

- We propose a many-to-many spectrum matching framework to realize combinatorial spectrum trading for dynamic spectrum access.
- We propose a matching algorithm which addresses spectrum heterogeneity and spectrum reuse. We prove that the matching result is individual rational, is strong pairwise stable, and is a subgame-perfect Nash equilibrium of the corresponding spectrum bargaining game.
- We conduct extensive simulations to evaluate the performance of the proposed many-to-many spectrum matching framework. It is shown that it takes only a few iterations for the proposed algorithm to reach a stable matching result.

The rest of the section is organized as follows. We describe the system model in details in section "System Model". In section "Spectrum Matching", we present the many-to-many spectrum matching framework and matching algorithm. Simulation results are shown in sections "Simulation".

System Model

Assume there is a set of sellers $\mathscr{M} = \{1, 2, \ldots, m\}$ and a set of buyers $\mathscr{N} = \{1, 2, \ldots, n\}$ in the market. Each seller owns one channel, which can be matched to multiple non-interfering buyers. Buyer j has a basic price offer for all channels $B_j = (b_{1,j}, b_{2,j}, \ldots, b_{m,j})$, in which $b_{i,j}$ is buyer j's valuation for a single channel i. For a bundle of channels $\mathscr{A}$, buyer j may be willing to pay more than the sum $\sum_{i \in \mathscr{A}} b_{i,j}$, for example, two continuous channels may bring more benefit to a buyer. We will express such complementariness of channels in buyers' preference profiles.

The key feature of spectrum allocation is interference-restricted spatial reuse. To characterize interference heterogeneity of different channels, we construct a series of interference graphs $\{G^i = (V, E^i)\}_{i=1}^m$, in which each node $v \in V$ represents a buyer and each edge $e^i \in E^i$ connects a pair of interfering buyers on channel i. Let $e^i_{j,j'} \in \{0, 1\}$ represent the interference status between buyers j and j' regarding channel i.

The preference profile $\succ_i$ of seller i is a complete, reflexive, and transitive binary relation on all sets of buyers $2^{\mathscr{N}}$. Due to interference constraint, a seller prefers the empty set $\emptyset$ to any buyer set that contains interfering buyers. For two buyer sets that are both interference-free (not any two buyers in the set interfere with each other), the seller prefers the one with a higher aggregate basic offer price. Let $\mathscr{S}, \mathscr{S}' \in 2^{\mathscr{N}}$ denote buyer sets, we have:

- If $\mathscr{S}$ is interference-free, $\mathscr{S} \succ_i \emptyset$; if $\mathscr{S}$ is not interference free, $\emptyset \succ_i \mathscr{S}$.
- If $\mathscr{S}$ is interference-free, but $\mathscr{S}'$ is not, $\mathscr{S} \succ_i \mathscr{S}'$, vice versa.
- If both of $\mathscr{S}$ and $\mathscr{S}'$ are interference-free, $\mathscr{S} \succ_i \mathscr{S}' \iff \sum_{j \in S} b_{i,j} > \sum_{j' \in S'} b_{i,j'}$.
- If neither of $\mathscr{S}$ and $\mathscr{S}'$ is interference-free, the seller randomly decides the preference relation between $\mathscr{S}$ and $\mathscr{S}'$.

The preference profile $\succ_j$ of buyer j is a complete, reflexive, and transitive binary relation on all sets of channels (sellers) $2^{\mathscr{M}}$. The preference profile on all sets of channels instead of individual channels is quite expressive to cater to buyers' requirements. First, buyers are able to express their preference for certain bundles of channels. For example, buyer j may have $\{s_1, s_2\} \succ_j \{s_1, s_3\}$, which means that she prefers the continuous channels $\{s_1, s_2\}$ to non-continuous channels $\{s_1, s_3\}$. Second, buyers can easily comply with their budget constraints by preferring empty set to large (therefore expensive) channel bundles. For example, buyer j may have $\emptyset \succ_j \{s_1, s_2, s_3\}$ since the aggregate basic offer price of $\{s_1, s_2, s_3\}$ exceeds her budget. Our proposed many-to-many spectrum matching algorithm works with general preference profiles without any restrictions.

Spectrum Matching

Preliminaries

We formally define many-to-many spectrum matching as follows.

Definition 6 (Many-to-Many Spectrum Matching). Given the set of sellers $\mathscr{M}$ and the set of buyers $\mathscr{N}$, a many-to-many spectrum matching is a mapping μ from the set $\mathscr{M} \bigcup \mathscr{N}$ into the set of all subsets of $\mathscr{M} \bigcup \mathscr{N}$ (i.e., $2^{\mathscr{M} \cup \mathscr{N}}$), such that

- For every seller $i \in \mathscr{M}$, $\mu(i) \subseteq 2^{\mathscr{N}}$;
- For every buyer $j \in \mathscr{N}$, $\mu(j) \subseteq 2^{\mathscr{M}}$;
- For every seller i and buyer j, $j \subseteq \mu(i)$ if and only if $i \subseteq \mu(j)$.

We also define the pre-matching, which will be the intermediate result in our proposed matching algorithm.

Definition 7 (Pre-matching). A pre-matching is a pair $\nu = (\nu_m, \nu_n)$, in which ν_m is a mapping from the seller set $\mathscr{M}$ into all subsets of buyers $2^{\mathscr{N}}$ and ν_n is a mapping from the buyer set $\mathscr{N}$ into all subsets of seller $2^{\mathscr{M}}$, that is,

- For every seller $i \in \mathscr{M}$, $\nu_m(i) \in 2^{\mathscr{N}}$;
- For every buyer $j \in \mathscr{N}$, $\nu_n(j) \in 2^{\mathscr{M}}$.

Note that a pre-matching is a matching if ν is such that $\nu_m(i) = j$ if and only if $\nu_n(j) = i$ for all $i \in \mathscr{M}$, $j \in \mathscr{N}$.

Given a buyer j and a set of sellers $\mathscr{S}$, let $Ch(\mathscr{S}, \succ_j)$ denote buyer j's most preferred subset of $\mathscr{S}$ according to j's preference relation $\succ_j$. More specifically, $Ch(\mathscr{S}, \succ_j)$ is the unique subset $\mathscr{S}'$ of $\mathscr{S}$ such that $\mathscr{S}' \succ_j \mathscr{S}''$ for all $\mathscr{S}'' \subseteq \mathscr{S}, \mathscr{S}'' \neq \mathscr{S}'$. Similarly, given seller i and a set of buyers $\mathscr{S}$, $Ch(S, \succ_i)$ is seller i's most preferred subset of $\mathscr{S}$ according to i's preference relation $\succ_i$.

Matching Algorithm

We propose a many-to-many matching algorithm to realize a stable and interference-free spectrum matching, as shown in Algorithm 3. The key component in the matching algorithm is the $T(\cdot)$ operation on the pre-matching ν. We iteratively perform the $T(\cdot)$ operation until we reached the fixed point ($T(\nu) = \nu$) or the number iterations reached the threshold. To define the $T(\cdot)$, we first introduce two sets. Given a pre-matching $\nu = (\nu_m, \nu_n)$, we have:

$$\begin{aligned} U(i,\nu) &= \{j \in \mathscr{N} : i \in Ch(\nu_n(j) \cup \{i\}, \succ_j)\} \\ V(j,\nu) &= \{i \in \mathscr{M} : j \in Ch(\nu_m(i) \cup \{j\}, \succ_i)\} \end{aligned} \tag{10}$$

The set $U(i,\nu)$ is the set of buyers who are willing to obtain seller i's channel, given their currently matched channels. Similarly, the set $V(j,\nu)$ is the set of sellers who are willing to sell their channels to buyer j, given their currently matched buyers (and their interference relationships).

Now, we can define the $T(\cdot)$ operation as:

$$T(\nu) = \begin{cases} Ch(U(i,\nu), \succ_i), \forall i \in \mathscr{M} \\ Ch(V(j,\nu), \succ_j), \forall j \in \mathscr{N} \end{cases} \tag{11}$$

The purpose of the $T(\cdot)$ operation on seller i is to find the optimal set of buyers among those who are willing to purchase seller i's channel. Likewise, the purpose the $T(\cdot)$ operation on buyer j is to find the optimal set of sellers (channels) among those who are willing to sell their channels to buyer j.

Though similar to the definition in [28], the $T(\cdot)$ operation is quite different for spectrum matching. The main reason is that spectrum matching exhibits buyer externality: the matching result of a buyer will affect those of other buyers. More specifically, if a buyer is matched to a seller, her interfering neighbors will be unwilling to be matched to the same seller, even if they have a high preference for that seller's channel. For the same reason, when choosing the optimal set of buyers, a seller not only considers their basic offer price but also their interference relationship.

In (11), the operation $Ch(U(i,\nu), \succ_i)$ requires seller i to find the optimal set of buyers with the highest total basic offer price, given the set $U(i,\nu)$. This is equivalent to finding the maximum weighted independent set (MWIS) on the interference graph G^i regarding buyers in $U(i,\nu)$. However, it has been proved that the MWIS problem is NP-hard. A naive brute-force solution is to exhaustively search all possible subsets of $U(i,\nu)$, resulting in exponential running time. To address this problem, we adopt the greedy algorithm in [19]. The key idea of the greedy algorithm is to select the buyer with the maximum price/degree ratio, remove her and all her neighbors, and repeat this process until the graph becomes empty. The selected buyers at all iterations are the output independent set.

It is proved in [28] that the fixed point $\nu = T(\nu)$ is a matching, that is, $\nu_m(i) = j$ if and only if $\nu_n(j) = i$ for all $i \in \mathscr{M}$ and $j \in \mathscr{N}$. However, due to the complexity

of spectrum matching, it is analytically difficult to prove that this property can still be preserved. Our simulation results in section "Simulation" numerically show that the output of Algorithm 3 is indeed a matching, the properties of which we will analyze in section "Properties". We will work on theoretically proving this in our future work.

In Algorithm 3, the input pre-matching ν is not specified. The simplest way is to initiate the pre-matching as $\nu_m(i) = \emptyset, \nu_n(j) = \emptyset, \forall i \in \mathscr{M}, j \in \mathscr{N}$. An alternative way is to randomly assign one buyer to one channel at the start (assuming there are more buyers than sellers), i.e., $\nu_m(i) = j, \forall i \in \mathscr{M}; \nu_n(j) = i$, if $\exists i, \nu_m(i) = j$, otherwise, $\nu_n(j) = \emptyset$. Now we give a toy example to show how the proposed algorithm works.

Algorithm 3 Many-to-many spectrum matching

Require: Preference relation $\succ$; interference graphs $\{G^i\}_{i=1}^M$; interference-free pre-matching ν_0; iteration threshold Num.
Ensure: An interference-free (pre-)matching ν
1: $iteration = 0$.
2: $\nu = T(\nu_0)$.
3: **while** $\nu \neq \nu_0$ or $iteration \leq Num$ **do**
4: $\quad \nu_0 = \nu$.
5: $\quad \nu = T(\nu_0)$.
6: $\quad iteration = iteration + 1$.
7: **end while**

Toy example. Suppose the set of sellers is $\mathscr{M} = \{i_1, i_2, i_3\}$ and the set of buyers is $\mathscr{N} = \{j_1, j_2, j_3, j_4\}$. The basic offer of buyer j_1 is $(1, 3, 5)$, of buyer j_2 is $(5, 1, 3)$, of buyer j_3 is $(1, 5, 3)$, and of buyer j_4 is $(3, 5, 1)$. Therefore, we can construct the buyers' preference profiles as:

$$\begin{aligned}
&\succ_{j_1}: \{i_2, i_3\} \succ_{j_1} \{i_1, i_3\} \succ_{j_1} \{i_1, i_2\} \succ_{j_1} i_3 \succ_{j_1} i_2 \succ_{j_1} i_1 \\
&\succ_{j_2}: \{i_1, i_3\} \succ_{j_2} \{i_1, i_2\} \succ_{j_2} \{i_2, i_3\} \succ_{j_2} i_1 \succ_{j_2} i_3 \succ_{j_2} i_2 \\
&\succ_{j_3}: \{i_2, i_3\} \succ_{j_3} \{i_1, i_2\} \succ_{j_3} \{i_1, i_3\} \succ_{j_3} i_2 \succ_{j_3} i_3 \succ_{j_3} i_1 \\
&\succ_{j_4}: \{i_1, i_2\} \succ_{j_4} \{i_2, i_3\} \succ_{j_4} \{i_1, i_3\} \succ_{j_4} i_2 \succ_{j_4} i_1 \succ_{j_4} i_3
\end{aligned} \tag{12}$$

We assume that no buyer can afford the set $\{i_1, i_2, i_3\}$, so we omit this set, which is less preferred than the empty set due to budget constraint. The buyers' interference graph is shown in Fig. 9, so we can construct the sellers' preference profiles which are:

$$\begin{aligned}
&\succ_{i_1}: \{j_2, j_4\} \succ_{i_1} j_2 \succ_{i_1} j_4 \succ_{i_1} \{j_1, j_3\} \succ_{i_1} j_1 \succ_{i_1} j_3 \\
&\succ_{i_2}: \{j_1, j_3\} \succ_{i_2} \{j_2, j_4\} \succ_{i_2} j_3 \succ_{i_2} j_4 \succ_{i_2} j_1 \succ_{i_2} j_2 \\
&\succ_{i_3}: \{j_1, j_3\} \succ_{i_3} j_1 \succ_{i_3} \{j_2, j_4\} \succ_{i_3} j_2 \succ_{i_3} j_3 \succ_{i_3} j_4
\end{aligned} \tag{13}$$

Fig. 9 A Toy example

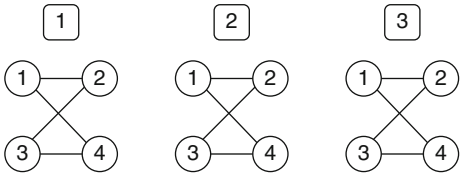

The interference graph.

Table 1 A Toy example

	$\nu_m(i_1)$	$\nu_m(i_2)$	$\nu_m(i_3)$	$\nu_n(j_1)$	$\nu_n(j_2)$	$\nu_n(j_3)$	$\nu_n(j_4)$
0	$\emptyset$	$\emptyset$	$\emptyset$	$\emptyset$	$\emptyset$	$\emptyset$	$\emptyset$
1	$\{j_2, j_4\}$	$\{j_1, j_3\}$	$\{j_1, j_3\}$	$\{i_2, i_3\}$	$\{i_1, i_3\}$	$\{i_2, i_3\}$	$\{i_1, i_2\}$
2	$\{j_2, j_4\}$	$\{j_1, j_3\}$	$\{j_1, j_3\}$	$\{i_2, i_3\}$	i_1	$\{i_2, i_3\}$	i_1
3	$\{j_2, j_4\}$	$\{j_1, j_3\}$	$\{j_1, j_3\}$	$\{i_2, i_3\}$	i_1	$\{i_2, i_3\}$	i_1

We assume that the pre-matching is $\nu_m(i) = \nu_n(j) = \emptyset, \forall i, j$. In the first iteration, for seller i_1, $U(i_1, \nu) = \mathscr{N}$, and it can be easily found that the optimal buyer set is $\nu_m(i_1) = \{j_2, j_4\}$; for buyer j_1, $V(j_1, \nu) = \mathscr{M}$, so that after the $T(\cdot)$ operation, we have $\nu_n(j_1) = \{i_2, i_3\}$. The results after the first iteration is shown in the third row of Table 1. Similarly, we can proceed through the second iteration, whose result can be checked as a fixed point and a matching.

Properties

In this section, we first prove that the matching result of the proposed Algorithm 3 is individual rational in general cases. Then, we show that with specific preference profiles, the matching result is strong pairwise stable and is a subgame-perfect Nash equilibrium of the corresponding spectrum bargaining game.

Definition 8 (Individual rational).

A matching result is blocked by seller i if she prefers not to be matched to some of her currently matched buyers. In other words, $\exists S \subseteq \mu(i), \left(\mu(i) \setminus S\right) \succ_i \mu(i)$.

A matching result is blocked by buyer j if she prefers not to be matched to some of her currently matched sellers. In other words, $\exists S \subseteq \mu(j), \left(\mu(j) \setminus S\right) \succ_j \mu(j)$.

A matching result is individual rational if it is not blocked by any buyer or seller.

Proposition 5. *The matching result of the proposed Algorithm 3 is individual rational.*

Proof. Let μ be the matching result. μ is a fixed point of the $T(\cdot)$ operation. So for any buyers $j \in \mathscr{N}$:

$$\begin{aligned} Ch(\mu_n(j), \succ_j) &= Ch(U(Ch(U(j, \mu), \succ_j)), \succ_j) \\ &= Ch(U(j, \mu), \succ_j) = \mu_n(j) \end{aligned} \tag{14}$$

$Ch(\mu_n(j), \succ_j) = \mu_n(j)$ indicates that there is no *block* for buyers. The proof for sellers is similar. Therefore, the matching result of the proposed Algorithm 3 is individual rational.

Now, we consider a special constraint, *substitutability*, on buyers' preference profiles. First introduced in [27], substitutability is widely studied in the matching literature.

Definition 9 (Substitutability). A buyer j's preference profile $\succ_j$ satisfies substitutability, if for any seller set S and $S' \subseteq S, i \in Ch(S \cup i, \succ_j) \Rightarrow i \in Ch(S' \cup i, \succ_j)$.

An interpretation of substitutability is that, if buyer j wants to have channel i among an available channel set $S \cup i$, then she still wants channel i among a smaller channel set $S' \cup i$. Substitutable preference profile can be easily satisfied, as shown by the following example. There are three sellers/channels $\{i_1, i_2, i_3\}$, buyer j's basic offer is $(b_{i_i,j}, b_{i_2,j}, b_{i_3,j}) = (1, 2, 3)$. For any two-channel bundles of i and i', buyer j is willing to pay $1.1 * (b_{i,j} + b_{i',j})$. The three-channel bundle exceeds buyer j's budget constraint. Following this logic, buyer j's preference profile is:

$$\begin{aligned} \{i_2, i_3\} \succ_j \{i_1, i_3\} \succ_j \{i_1, i_2\} \succ_j i_3 \\ \succ_j i_2 \succ_j i_1 \succ_j \emptyset \succ_j \{i_1, i_2, i_3\} \end{aligned} \tag{15}$$

It can be easily checked that this preference profile is substitutable. When all buyers' preference profiles satisfy substitutability, the matching results of the proposed Algorithm 3 are strong pairwise stable and are a subgame-perfect Nash equilibrium of the corresponding spectrum bargaining game.

Definition 10 (Strong pairwise stability). A matching result is blocked by a pair $(S, j) \in 2^{\mathscr{M}} \times \mathscr{N}$ in which $S \neq \emptyset$, if $S \cap \mu(j) = \emptyset$, $S \subseteq Ch(\mu(j) \cup S, \succ_j)$, and $j \in Ch(\mu(i) \cup j, \succ_i)$ for all $i \in S$.

A matching result is strong pairwise stable if it is not blocked by any pair of buyer and seller and individual rational.

Proposition 6. *The matching result of the proposed Algorithm 3 is strong pairwise stable.*

Proof. Assume there is a block pair (S, j) and $S \neq \emptyset$. Since $j \in Ch(\mu(i) \cup j, \succ_i)$, $\forall i \in S$, by definition of $V(j, \mu)$, we have $S \subseteq V(j, \mu)$. Thus, for any subset $A \subseteq \mu(j)$, as $\mu(j) \subseteq V(j, \mu)$, we have $A \cup S \subseteq V(j, \mu)$. Due to individual rationality, $\mu(j) = Ch(V(j, \mu), \succ_j)$. So $\mu(j) \succeq_j Ch(A \cup S, \succ_j) \succeq_j A \cup S$, in which $\succeq_j$ means that the two sets may be the same. This contradicts the fact that $S \cap \mu(j) = \emptyset$ and $S \subseteq Ch(\mu(j) \cup S, \succ_j)$. Therefore, there cannot be any blocks in the matching result μ.

Now we regard the spectrum matching as a noncooperative bargaining game. To begin with, every buyer j proposes a set of channels $\eta_j \subseteq \mathscr{M}$. After observing the proposals, every seller i proposes a set of buyers $\xi_i \subseteq \mathscr{N}$. All buyers or sellers make the proposals simultaneously. A buyer and a seller will be matched if seller i

proposes to buyer j and buyer j proposes to seller i. The strategy space for buyer j is $\eta_j \subseteq \mathscr{M}$ and for seller i is $\xi_i(\eta) \subseteq \mathscr{N}$. Now we define *subgame-perfect Nash equilibrium* (SPNE) for such a bargaining game.

Definition 11 (Subgame-perfect Nash equilibrium). Given the preference profiles $\succ$ of buyers and sellers, a strategy profile (η^*, ξ^*) is called a subgame-perfect Nash equilibrium (SPNE), if $\forall i \in \mathscr{M}, j \in \mathscr{N}$,

$$\begin{aligned} &\eta_j^* \cap \{i : j \in \xi_i^*(\eta^*)\} \succeq_i P \cap \{i : j \in \xi_i^*(P, \eta_{-j}^*)\}, \forall P \subseteq \mathscr{M} \\ &\xi_i^*(\eta) \cap \{j : i \in \eta_j^*\} \succeq_j S, \forall S \subseteq \{j : i \in \eta_j^*\} \end{aligned} \tag{16}$$

In other words, (η^*, ξ^*) is SPNE if η_j^* is optimal given other buyers' proposal η_{-j}^*, and $\xi_i^*(\eta^*)$ is an optimal proposal given all buyers' proposal η^*.

Proposition 7. *The matching result of the proposed Algorithm 3 is an SPNE of the spectrum bargaining game.*

Proof. Let μ be the matching result of the proposed Algorithm 3. Define (η^*, ξ^*) as $\eta_j^* = \mu(j)$ and $\xi_i^*(\eta^*) = Ch(\{j : i \in \eta_j^*\}, \succ_i)$. Let μ' be the outcome of the strategy (η^*, ξ^*). Now we show that (η^*, ξ^*) is an SPNE and $\mu' = \mu$.

For any i and j, $\{j : i \in \eta_j^*\} \cup j = \mu(i) \cup j$, therefore,

$$\begin{aligned} &\{i : j \in Ch(\{j : i \in \eta_j^*\} \cup j, \succ_i)\} \\ &= \{i : j \in Ch(\mu(i) \cup j), \succ_i\} = U(i, \mu). \end{aligned} \tag{17}$$

So we have $\eta_j^* = \mu(j) = Ch(U(j, \mu), \succ_j)$, which means that η_j^* is optimal given η_{-j}^*. By definitions we know that $\xi_i^*(\eta')$ is optimal, given η^*. Thus (η^*, ξ^*) is an SPNE.

Since μ is a matching, we have $j \in \mu(i)$ if and only if $i \in \mu(j) = \eta_j^*$, so that $\{j : i \in \eta_j^*\} = \mu(i)$. According to individual rationality, we have $\xi_i^*(\eta^*) = Ch(\{j : i \in \eta_j^*\}, \succ_i) = Ch(\mu(i), \succ_i) = \mu(i)$. Therefore, $i \in \mu'(j)$ if and only if $i \in \eta_j^* = \mu(j)$, and $j \in \mu'(i)$ if and only if $j \in \xi_i^* = \mu(i)$. This proves that $\mu' = \mu$.

Simulation

Simulation Settings

We assume that buyers are located in a 10×10 square. The transmission range of a channel is randomly chosen in the range $(0, 5]$. Based on buyers' locations and the transmission range of a channel, we can construct the interference graph of each channel. Preference profiles are generated as follows. We first assume that buyers' basic offer prices for individual channels are uniformly distributed in $(0, 10]$, based on which we can construct sellers' preference profiles according to section "System

Model". Then, we assume that for a combination of channels S, buyer j is willing to pay $\alpha \sum_{i \in S} b_{i,j}$, in which $\alpha > 1$ is a gain factor. If the number of channels in the combination is higher, α is higher. But there is a threshold on the size of a combination, beyond which we assume that the buyer is not willing to purchase the combination due to budget constraint. Buyers' preference profile is based on their willingness to pay for a combination of channels.

Performance of the Proposed Matching Algorithm

The influence of the number of buyers, the number of sellers, and the budget constraint (the threshold on the size of channel combinations) on social welfare of the matching result is shown in Fig. 10. When the number of buyers increases, social welfare grows quickly at first and then slows down because more buyers compete for limited channels, and the chance of obtaining channels becomes smaller. Social welfare also goes up with the number of sellers because more channels are available for the buyers to acquire. As buyers have higher budget, social welfare improves, because buyers can attain more channels with higher budget. We have checked that all fixed points of the simulation results are matching (instead of pre-matching), and the iteration times of the proposed many-to-many matching algorithm is shown

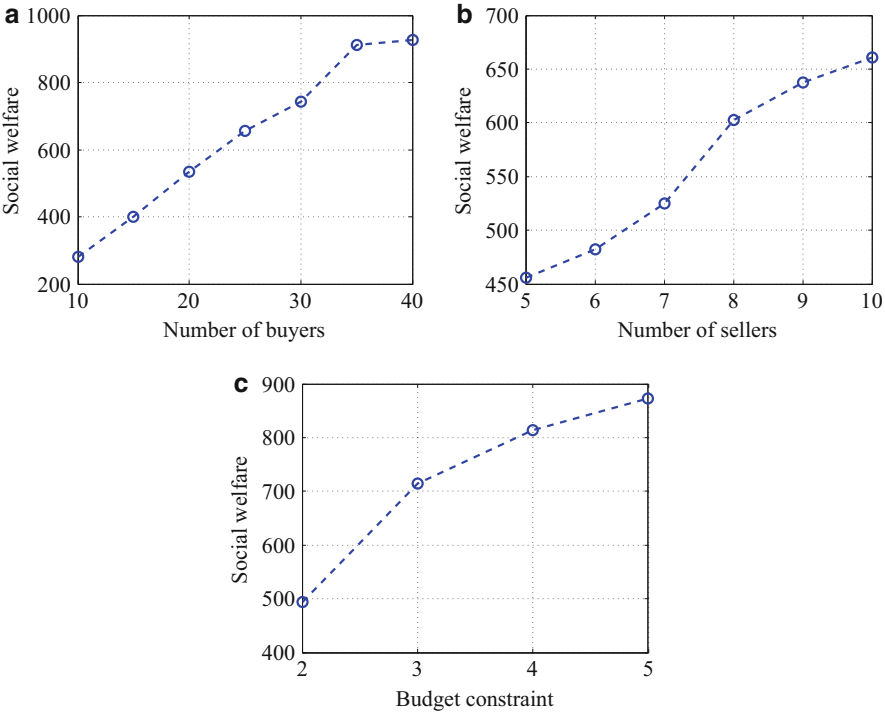

Fig. 10 Social welfare of the proposed many-to-many matching algorithm. (**a**) $M = 10$; (**b**) $N = 25$; (**c**) $M = 8, N = 30$

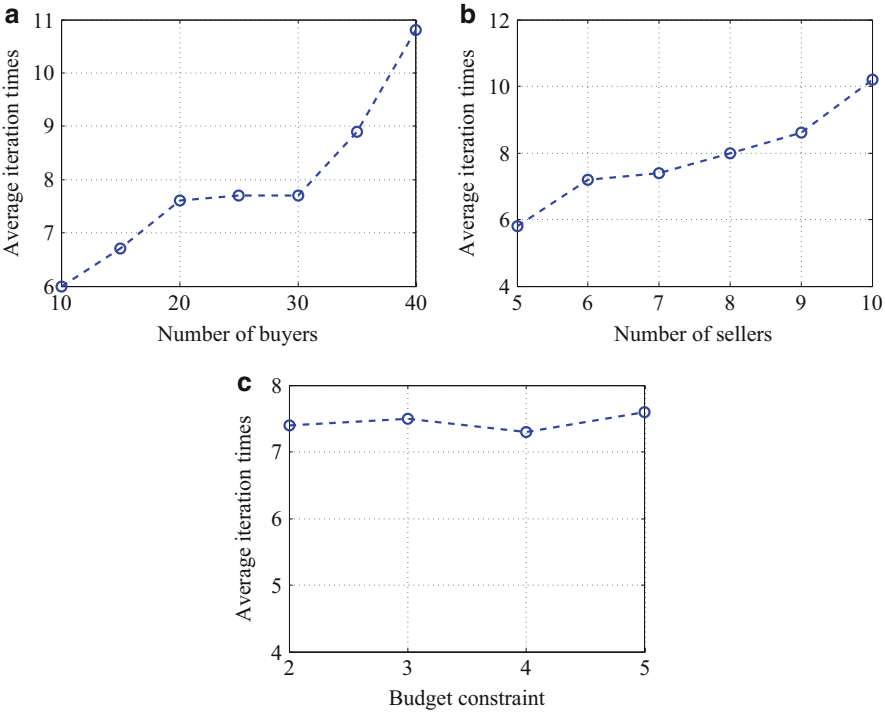

Fig. 11 Iteration times of the proposed many-to-many matching algorithm. (**a**) $M = 10$; (**b**) $N = 25$; (**c**) $M = 8, N = 30$

in Fig. 11. We can see that the proposed algorithm can converge to the fixed point within a few iterations. The iteration times are mainly affected by the number of buyers and the number of sellers. The change of budget constraint does not have a significant impact on iteration times as the number of buyers and sellers stay the same.

Conclusion and Future Directions

In this chapter, we first present the matching framework for distributed spectrum exchange in a free spectrum market and then propose the many-to-many matching framework for combinatorial spectrum trading. In stark contrast to prior double auction mechanisms, spectrum matching in section "Non-combinatorial Many-to-Many Spectrum Matching" does not require the centralized management of a third-party authority. We have designed a two-stage distributed algorithm, with consideration of the interference constraint in spectrum matching. We have theoretically proved the convergence of our algorithm, as well as the stability of the matching result. Simulations have demonstrated the efficiency of the proposed distributed algorithm,

as the final matching results can attain 90% of the maximum social welfare from optimal matching that needs centralized enforcement.

Compared with combinatorial auction which is usually NP-hard, spectrum matching in section "Combinatorial Many-to-Many Spectrum Matching" is easier to implement and is immune to collusion between the auctioneer and buyers or sellers. We theoretically prove that the matching result is individual rational, is strong pairwise stable, and is a subgame-perfect Nash equilibrium of the corresponding spectrum bargaining game. We conducted extensive simulations to evaluate the performance of the proposed many-to-many matching framework. It is shown that social welfare increases with the number of buyers or sellers, as well as buyers' budget constraint. The iteration times only depend on the number of buyers or sellers.

Matching is very promising in spectrum trading market and can be carried out easily since it requires only buyers and sellers but no third-party rule-enforcing authorities. Future work will be dedicated to investigating more research challenges. In particular, online spectrum trading where buyers and sellers join or leave the market dynamically should be taken into consideration. And the computation complexity of the algorithm also needs further discussion when testing on practical market.

References

1. Feng X, Zhang J, Zhang Q (2011) Database-assisted multi-ap network on tv white spaces: architecture, spectrum allocation and AP discovery. In: IEEE symposium on new frontiers in dynamic spectrum access networks (DySPAN), Aachen
2. Chen X, Huang J (2013) Database-assisted distributed spectrum sharing. IEEE J Sel Areas Commun (JSAC) 31(11):2349–2361
3. Zhou X, Zheng H (2009) TRUST: a general framework for truthful double spectrum auctions. In: IEEE international conference on computer communications (INFOCOM), Rio de Janeiro
4. Gao L, Xu Y, Wang X (2010) MAP: multi-auctioneer progressive auction for dynamic spectrum access. IEEE Trans Mob Comput (TMC) 10(8):1144–1161
5. Wang W, Li B, Liang B (2011) District: embracing local markets in truthful spectrum double auctions. In: IEEE international conference on sensing, communication, and networking (SECON), Salt Lake City
6. Feng X, Chen Y, Zhang J, Zhang Q, Li B (2012) TAHES: a truthful double auction mechanism for heterogeneous spectrums. IEEE Trans Wirel Commun (TWC) 11(11):4038–4047
7. Chen Y, Zhang J, Wu K, Zhang Q (2014) TAMES: a truthful double auction for multi-demand heterogeneous spectrums. IEEE Trans Parallel Distrib Syst (TPDS) 25(11):3012–3024
8. Wang SG, Xu P, Xu XH, Tang SJ, Li XY, Liu X (2010) TODA: truthful online double auction for spectrum allocation in wireless networks. In: IEEE international symposium on dynamic spectrum access networks (DySPAN), Baltimore
9. Chen Y, Lin P, Zhang Q (2014) LOTUS: location-aware online truthful double auction for dynamic spectrum access. In: IEEE international symposium on dynamic spectrum access networks (DySPAN), McLean
10. Gale D, Shapley LS (1962) College admissions and the stability of marriage. Am Math Mon 69(1):9–15
11. Xu H, Li B (2013) Anchor: a versatile and efficient framework for resource management in the cloud. IEEE Trans Parallel Distrib Syst (TPDS) 24(6):1066–1076

12. Saad W, Han Z, Zheng R, Debbah M, Poor HV (2014) A college admissions game for uplink user association in wireless small cell networks. In: IEEE international conference on computer communications (INFOCOM)
13. Gu Y, Zhang Y, Pan M, Han Z (2014) Cheating in matching of device to device pairs in cellular networks. In: IEEE global communications conference (GLOBECOM)
14. Pycia M (2005) Many-to-one matching without substitutability. MIT industrial performance center working paper vol 8, p 2005
15. Bodine-Baron E, Lee C, Chong A, Hassibi B, Wierman A (2011) Peer effects and stability in matching markets. In: Algorithmic game theory, pp 117–129
16. Bayat S, Louie RHY, Li Y, Vucetic B (2011) Cognitive radio relay networks with multiple primary and secondary users: distributed stable matching algorithms for spectrum access. In: IEEE international conference on communications (ICC)
17. Bayat S, Louie RHY, Han Z, Vucetic B, Li Y (2013) Physical-layer security in distributed wireless networks using matching theory. IEEE Trans Inf Forensics Secur 8(5):717–732
18. Bayat S, Louie RHY, Han Z, Li Y, Vucetic B (2012) Distributed stable matching algorithm for physical layer security with multiple source-destination pairs and jammer nodes. In: IEEE wireless communications and networking conference (WCNC)
19. Sakai S, Togasaki M, Yamazaki K (2003) A note on greedy algorithms for the maximum weighted independent set problem. Discret Appl Math 126(2):313–322
20. Gusfield D, Irving RW (1989) The stable marriage problem: structure and algorithms. MIT press, Cambridge
21. McDonald JH (2009) Handbook of biological statistics, vol 2. Sparky House Publishing, Baltimore
22. Zurel E, Nisan N (2001) An efficient approximate allocation algorithm for combinatorial auctions. In: Electronic commerce. ACM, New York
23. Mu'Alem A, Nisan N (2008) Truthful approximation mechanisms for restricted combinatorial auctions. Games Econ Behav 64(2):612–631
24. Vöcking B (2013) A universally-truthful approximation scheme for multi-unit auctions. Games Econ Behav. Available online http://www.sciencedirect.com/science/article/pii/S0899825613001735
25. Zheng Z, Wu F, Chen G (2014) A strategy-proof combinatorial heterogeneous channel auction framework in noncooperative wireless networks. IEEE Trans Mob Comput 14(6):1123–1137
26. Yi C, Cai J (2014) Two-stage spectrum sharing with combinatorial auction and Stackelberg game in recall-based cognitive radio networks. IEEE Trans Commun 62(11):3740–3752
27. Kelso AS Jr, Crawford VP (1982) Job matching, coalition formation, and gross substitutes. Econometrica: J Econ Soc 50(6):1483–1504
28. Oviedo J, Echenique F (2005) A theory of stability in many-to-many matching markets. In: 2005 meeting papers, number 233. Society for Economic Dynamics

Cooperation in Cognitive Cellular Heterogeneous Networks

43

Ahmed R. Elsherif, Hesham M. Elmaghraby, and Zhi Ding

Contents

Abstract

A recent drive by mobile network operators to mitigate the network capacity crunch and to improve indoor coverage involves the development of cellular heterogeneous networks. Cellular heterogeneous networks consist of the existing macrocells plus shorter range cells referred to as small cells. Coexistence of macrocells and small cells sharing the same spectrum represents a special case of cognitive networking, where small cells and their users can be viewed as secondary users, whereas the macrocell and its users act as the primary legacy users. Unlike the traditional listen-before-talk concept in cognitive radio spectrum sensing, this chapter presents techniques for utilizing inherent Radio Link Control (RLC) messages and feedback information in existing cellular systems. It develops a more-advanced cognitive approach that takes into account actual

A. R. Elsherif (✉) · H. M. Elmaghraby · Z. Ding
University of California, Davis, CA, USA
e-mail: arelsherif@ucdavis.edu; hmelmaghraby@ucdavis.edu; zding@ucdavis.edu

W. Zhang (ed.), *Handbook of Cognitive Radio*,
https://doi.org/10.1007/978-981-10-1394-2_43

primary user's interference tolerance and facilitates more efficient spectrum sharing. The chapter first introduces the idea of implicit cooperation through the use of inherent feedback information in cellular heterogeneous networks. Explicit cooperation is then discussed in the chapter before introducing the concept of cooperation in hybrid-access cellular heterogeneous networks as well as in dense enterprise femtocell deployments. The chapter concludes by summarizing the most recent trend of integrated access between both cellular and wireless local area network (WLAN) interfaces at small cells for traffic offloading and for improving network capacity.

Introduction

Mobile network operators (MNOs) have been facing a difficult challenge to meet the increasing demand of expansive high-data services given their limited spectrum resources. Acquisition of more spectrum is not only costly but also requires actions from the typically slow regulatory entities. Thus, MNOs have been searching in other dimensions to increase their system capacity while preparing for fifth-generation (5G) cellular systems. The concept of cell densification has been envisioned for 5G systems by deploying smaller range and lower power cells such as picocells and femtocells that are collectively referred to as small cells, in addition to the existing macrocells [1]. Throughout this chapter, femtocell is exchangeably referred to as femto base station (FBS) or home eNode B (HeNB). Similarly, femtocell user equipment (FUE) is exchangeably referred to as home user equipment (HUE).

The coexistence of macrocells, picocells, and femtocells has given rise to the concept of cellular heterogeneous networks. Macrocells and small cells can, in principle, occupy different spectra, which is not generally favored by MNOs due to the scarcity of spectrum resources. Alternatively, the common configuration of cellular heterogeneous networks is for macrocells and small cells to share the spectrum, thereby giving rise to a cognitive overlay scenario. Coexistence in cellular heterogeneous networks can happen through explicit coordination between the legacy macrocells and the newly deployed picocells/femtocells or through cognitive deployment of picocells/femtocells in the coverage of macrocells. This chapter focuses on techniques for cognitive coexistence in cellular heterogeneous networks while providing insight into cooperative operation in cellular heterogeneous networks in general.

Spectrum sharing in cellular heterogeneous networks is a direct application of the cognitive radio concept, in which small cells (e.g., picocells or femtocells) act as the secondary transmitter during downlink to serve their associated user equipments (UEs) acting as the secondary receivers. Currently, the spectrum is occupied only by the existing macrocell and its subscribers acting as the primary transmitter and receivers, respectively. We first describe various schemes for applying implicit

cooperation in cognitive networks by exploiting the concept of overhearing in cellular heterogeneous networks for resource allocation and interference management. The scope is then expanded to scenarios with limited explicit cooperation between primary users (or PUs) in the macrocells and secondary users (or SUs) in the femtocells.

Traditional cognitive radios have often focused on the idea of sensing-before-transmitting or listen-before-talk (LBT) [2], where a secondary user searches for unoccupied channel vacancies (bands) to avoid collision with the primary user transmissions. However, we note that cellular networks have inherent Radio Link Control (RLC) signaling and feedback information that may be utilized by secondary users in more efficient ways beyond the LBT paradigm. Such RLC information is already available in practical cellular systems such as LTE, including Channel Quality Indicator (CQI), power control information, and receiver ACK/NACK. Thus, they require no additional cost. Exploiting such information by secondary users (SUs) makes it possible to achieve better spectrum efficiency while satisfying the Quality of Service (QoS) requirements of primary users (PUs). Moreover, such information reflects primary receiver's actual service experience (e.g., level of interference from different sources) more accurately than spectrum sensing which focuses on transmitter activities. The basic principle of implicit cooperation in cognitive cellular networks is illustrated in Fig. 1.

In this model, secondary users transmitters (SU-Tx) and receivers (SU-Rx) can listen to primary user transmitter (PU-Tx) and can overhear link layer signal feedback reports from the primary user receiver (PU-Rx). Utilizing such feedback information represents a more mature and sophisticated level of secondary user

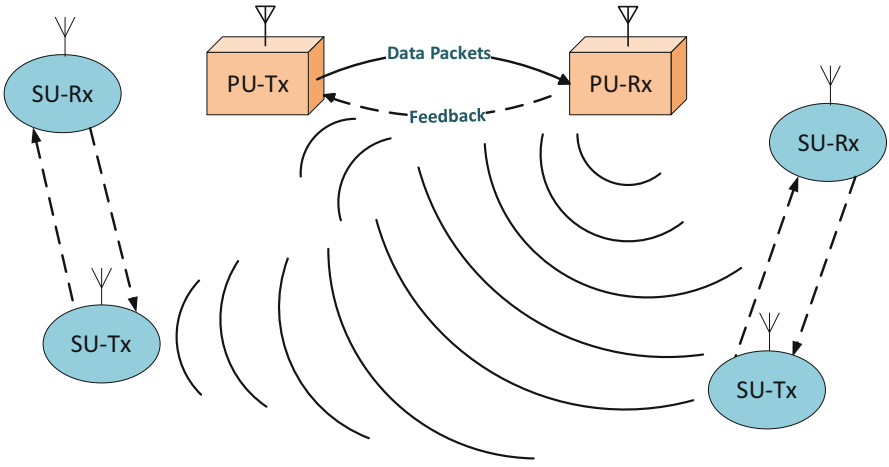

Fig. 1 Feedback overhearing concept in cellular heterogeneous networks

cognitive capability. This "overhearing concept" where secondary users can overhear the feedback information of primary transmission is at the core of various techniques to be presented in this chapter.

Implicit Cooperation in Cellular Heterogeneous Networks

This section presents a survey of various works under the implicit cooperation framework addressing different aspects of coexistence in cellular cognitive networks. In these schemes, there is no explicit cooperation between the PUs and SUs.

Dynamic Spectrum Access with Network-Layer Performance Assurance

A general requirement in cognitive radio deployments is to guarantee the performance of the PU. A PU would not be satisfied if its performance is seriously degraded by the presence of an SU overlaying on the PU spectrum. Various works have focused on PU protection from Physical (PHY) layer perspective such as limiting interference power from SU [3] or link layer perspective such as imposing collision probability constraints [4].

In [5], PU network-layer performance is characterized in terms of PU queue stability. A network access optimization for cognitive radio nodes is developed with the objective of throughput maximization for the SU under the constraint of PU queue stability. This work depends on opportunistic access by allowing the SU to overhear and utilize the ACK/NACK feedback signal, as well as PU activity/inactivity, where PU inactivity is an indication of empty PU queue. This work develops a Lagrangian formulation for SU rate maximization and links the resulting Lagrange multiplier to the PU's queue length to achieve PU rate assurance. The proposed forward equilibrium loading algorithm (FELA) for distributive SU transmission control achieves near optimal SU throughput with PU queue stability in both single SU link and multiple SU link applications.

Dual Sensing for Primary User Detection

Traditional cognitive radios employ spectrum sensing as the main approach for assessing the presence and/or activity of a PU on a specific channel [6]. The main drawback of this traditional approach is that the SU yields to the PU transmissions irrespective of the SU's transmission impact on the PU receivers. In [7, 8], a dual sensing approach is presented for PU detection. In this approach, the SU detects both the spectrum occupancy of the user band that it attempts to access and also decodes the PU Rx feedback signals that it overhears which can reflect the quality

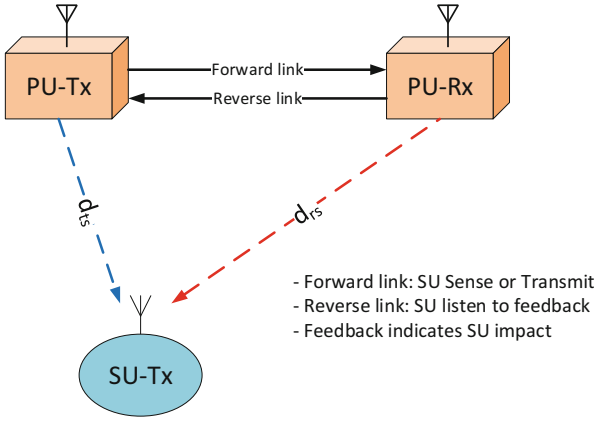

Fig. 2 Dual sensing for primary user detection

of the PU channel as well as the impact of the SU transmissions on the PU Rx, as shown in Fig. 2. This information allows a better control of the SU channel access.

The major advantage of this dual sensing approach is that noticeable change in SU-Tx channel access parameters will be reflected in feedback information of the PU-Rx. This work focuses on monitoring the ACK/NACK signal of the PU link as the main feedback information reflecting the impact of SU transmission. To devise an admission control policy for secondary users, this work uses a partially observable Markov decision process (POMDP) given a general primary busy/idle distribution. The true state (quality) of the forward link at time t, s_t, is defined as a binary state taking the value 0 when the primary channel is busy or 1 when it is idle. The state s_t is partially observable by the SU through both spectrum sensing of PU transmission and overhearing PU Rx feedback information. This approach uses past and current observations to estimate the traffic transition of the primary user through a maximum a posteriori (MAP) estimator. The use of this MAP estimator achieves high-network throughput for the secondary users while guaranteeing robust protection of the primary users.

Resource Allocation in Heterogeneous Networks Using Shadow Chasing

We have studied in [9] femtocell opportunistic resource allocation in shared spectrum heterogeneous networks. Our work presents a resource allocation scheme at FBS that maximizes the throughput of FUEs and mitigates downlink interference to nearby macrocell user equipments (MUEs). In this work, we propose a resource allocation framework called Shadow Chasing for femtocell resource allocation to achieve interference mitigation in heterogeneous networks serving both MUEs and

FUEs. A Shadow Chasing FBS uses downlink control information (DCI) together with overheard MUE ACK/NACK feedbacks and CQI reports to assign its own downlink resources to mitigate downlink interference to MUEs. Since the FBS receives outdated DCI due to backhaul delay, a likelihood metric for each resource unit being either empty or assigned to a (low-interference) outdoor MUE based on a finite-state Markov chain (MC) model for each resource unit is derived. By dynamically separating MUE and FUE assignments, the Shadow Chasing scheme can better control the downlink interference to MUEs for QoS assurance. It effectively reduces the probability of resource collision and MUE interference compared to schemes not considering backhaul delay effect or user feedbacks.

The principle of Shadow Chasing is illustrated in Fig. 3. The DCI messages are received and decoded at the FBS after a delay D that accounts for the delay of the backhaul connection plus the decoding delay. In the figure, T_m is the MBS scheduling period in Transmission Time Interval (TTI) units and we assume that $T_m \geq D$. The larger the MUE scheduling period T_m is relative to the backhaul delay D, the more confident the FBS is in the outdated DCI information it receives. On the other hand, if T_m is comparable to D, the actual MUE resource chunk assignment may be completely different from the received outdated DCI which leads more likely to incorrect FBS assignment decisions.

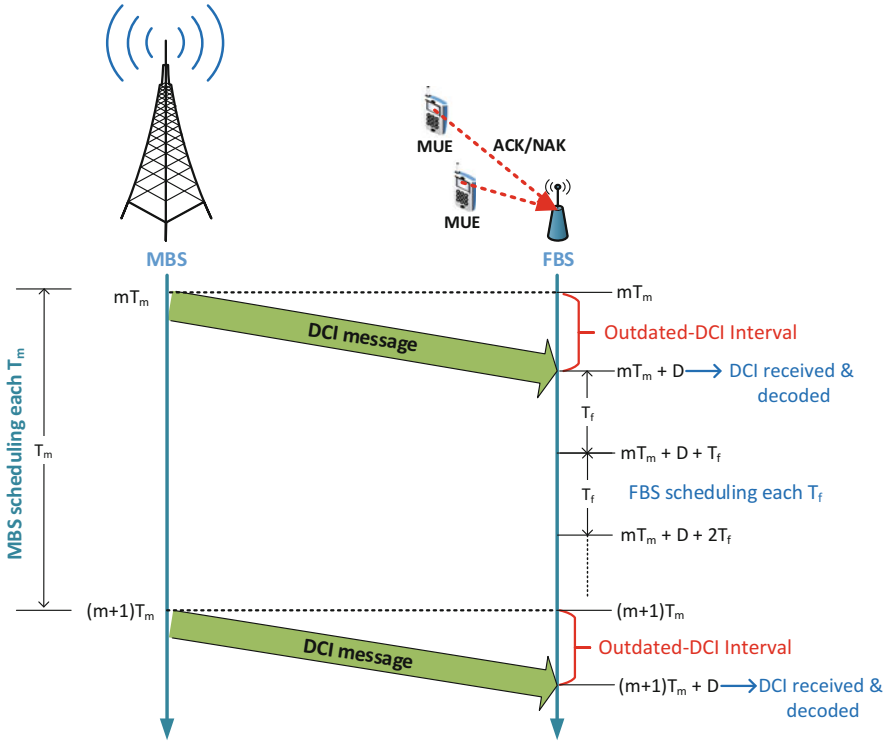

Fig. 3 Shadow chasing principle

The FBS classifies MUEs as outdoor/indoor using the DCI together with the overheard ACK/NACK in MUEs uplink feedback. From the DCI, the FBS knows Physical Resource Block (PRB) assignment pattern of different UEs. If the DCI shows that some PRBs are assigned to a certain MUE but neither ACKs nor NACKs are heard from that MUE, this means that monitored MUE is far enough such that we can fairly assume the MUE to be outdoor and unaffected. On the other hand, if either ACKs or NACKs are received from an MUE, then it is likely to be close as the FBS is already able to hear its feedback signals. Moreover, the FBS can learn from the DCI if some PRBs are not assigned to any UE.

Based on UE classification, each resource follows an MC model with three states: empty, indoor, and outdoor. The three states are defined as follows:

- State 0 : PRB/resource chunk is empty (unoccupied).
- State 1 : PRB/resource chunk is assigned to the outdoor MUE (M_o).
- State 2 : PRB/resource chunk is assigned to the indoor MUE (M_i).

The trellis diagram for this MC model is shown in Fig. 4.

The FBS assumes a certain MUE resource allocation policy that can be shared between the MBS and FBS statically or semi-statically through backhaul. An example of such MUE resource allocation policy is that an MUE assigned a PRB/resource chunk k at time $n-1$ will be assigned the same PRB/resource chunk at time n if one of the following is true:

- The MUE has good channel quality on PRB/resource chunk k at time n.
- The MUE does not have good channel quality on PRB/resource chunk k but there are no sufficient empty and good PRBs/resource chunks at time n for the MUE.

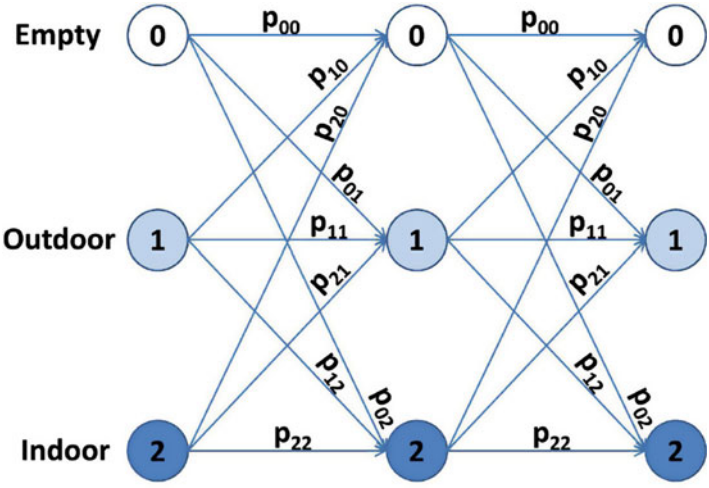

Fig. 4 Markov chain trellis diagram for shadow chasing

The probability of an MUE having a good channel quality can be defined as the probability that the CQI value reported by the MUE is greater than or equal to a channel quality threshold γ. Therefore, the probability that an outdoor MUE M_o has good channel quality on PRB/resource chunk k at time n is given by

$$p_{g_1}(k,n) = Pr(\mathrm{CQI}_1(k,n) \geq \gamma). \tag{1}$$

Based on the probabilities that a PRB/resource chunk assigned to an outdoor MUE, $p_{g_1}(k,n)$, or indoor MUE, $p_{g_2}(k,n)$, the FBS calculates the transition probabilities in Fig. 4 and forms a transition probability matrix $\mathscr{P}_k$. Moreover, at each DCI update time instance, $mT_m + D$, the FBS updates the initial state of the MC model based on the received DCI as follows:

$$p_k^{(0)} = \begin{cases} [1\ 0\ 0] & \text{resource chunk } k \text{ is empty} \\ [0\ 1\ 0] & \text{resource chunk } k \text{ is assigned to } M_o \\ [0\ 0\ 1] & \text{resource chunk } k \text{ is assigned to } M_i, \end{cases} \tag{2}$$

where $p_k^{(0)}$ denotes the initial state of the MC of PRB/resource chunk k. Referring to Fig. 3, after receiving and decoding a new DCI message at time $mT_m + D$, the FBS does not need to update the MC state till $(m+1)T_m + D$. Next in the Outdated-DCI interval $[(m+1)T_m, (m+1)T_m + D)$, the FBS updates the MC state since the MBS scheduling in this interval is uncertain to the FBS. Thus, an MC state update time index n' is defined as follows:

$$n' = \begin{cases} n - \left\lfloor \frac{n}{T_m} \right\rfloor T_m, & n \in [mT_m, mT_m + D) \\ 0 & n \in [mT_m + D, (m+1)T_m), \end{cases} \tag{3}$$

where $\lfloor x \rfloor$ is the largest integer less than or equal to x. Assuming a homogeneous MC, the state probabilities at time n can thus be given as

$$p_k^{(n)} = p_k^{(0)} \mathscr{P}_k^{n'}. \tag{4}$$

The probability of a PRB/resource chunk k being empty, outdoor, or indoor at time n is, consequently, given by $p_e(k,n) = p_k^{(n)}(0)$, $p_o(k,n) = p_k^{(n)}(1)$, or $p_i(k,n) = p_k^{(n)}(2)$, respectively. The FBS develops a likelihood metric for each resource being empty, outdoor, or indoor as follows:

$$L(k,n) = \begin{bmatrix} p_e(k,n) & p_i(k,n) & p_o(k,n) \end{bmatrix}. \tag{5}$$

Based on this likelihood metric, the order of preference for FBS resource scheduling to the FUE will be empty PRBs (if any), outdoor PRBs (since this results in very little interference), then indoor PRBs (if needed).

Figure 5 compares the sum MUE rate for three schemes, namely, "Random Assignment," "DCI-Following" (where the FBS uses the DCI information about MBS scheduling but without accounting for backhaul delay), and the proposed

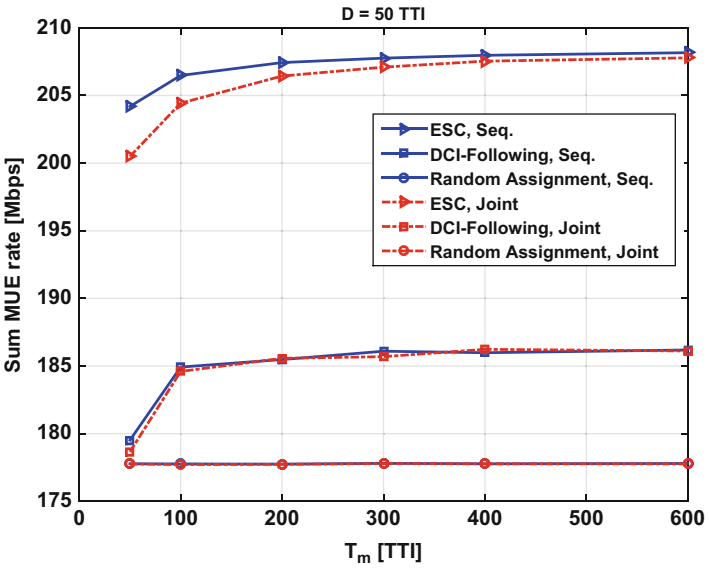

Fig. 5 Shadow chasing performance

Enhanced Shadow Chasing (ESC) scheme. As the MBS scheduling period, T_m, increases relative to the backhaul delay, D, the probability of FBS interference to the indoor MUE drops and, hence, the effect of D becomes less significant. Consequently, in the following figure, the sum MUE rate improves. The figure also shows that sequential scheduling at the MBS gives higher sum MUE rate compared to joint scheduling when associated with Shadow Chasing at the FBS. The reason for this difference is that sequential scheduling is a two-step approach that inherently allows swapping between resource chunks assigned to indoor and outdoor MUEs whereas joint scheduling is done in one step with no swapping between resource chunks assigned to indoor and outdoor MUEs. Thus, sequential scheduling can provide more good resource chunks for both MUEs versus joint scheduling that is limited by the availability of empty resource chunks with good CQI qualities.

Resource Allocation in Cellular Heterogeneous Networks Using CQI Feedback

Another work [10,11] that exploits the "overhearing concept" addresses the resource allocation problem in femtocells using MUE CQI feedback to the MBS to estimate the channel gain distribution. This work provides a decentralized technique for FBS resource scheduling using the overheard CQI report and a priori statistical channel information. In order to achieve this objective, each FBS has to use certain cognitive capabilities that allow it to sense the CQI of neighboring MUEs. Unlike

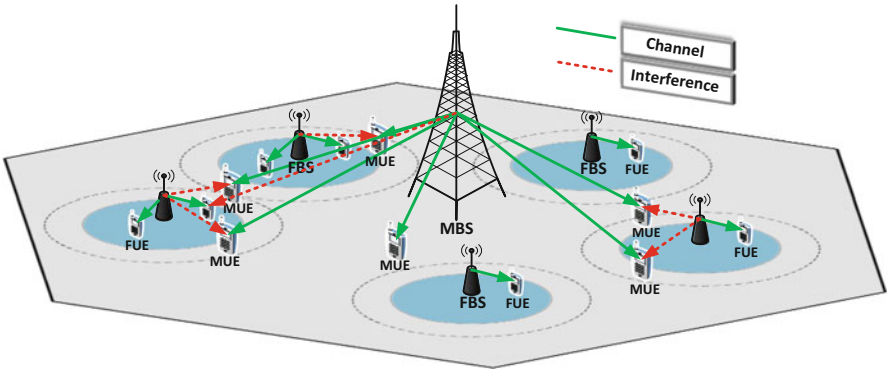

Fig. 6 Network model for closed access FBSs

most of existing works [12–14], this work does not assume channel gain information exchange between FBS and MBS, hence considered implicit cooperation. Specifically, the work studies femtocell downlink scheduling and power assignment based on listening to CQI reports from nearby and impacted MUEs to the MBS. The objective is to maximize the FBS total mean capacity while maintaining minimum QoS for the MUEs that share the same downlink spectrum.

This work considers femtocells in closed access mode where the cellular network adopts the standard LTE-A time division duplex (TDD) frame structure. Figure 6 depicts a two-tier macro-femto network, consisting of a central MBS, owned and operated by a cellular service operator, and a number of FBSs deployed by the femto clients with cellular subscription. Each FBS shares its assigned bandwidth with the MBS while avoiding the intra-tier interference with other FBSs. Due to the orthogonal resource assignments for adjacent femtocells, the intra-tier interference effect is avoided [15, 16]. Each FBS will be provided with cognitive capabilities in order to assist in the scheduling and power assignment process. Additional details on how these cognitive capabilities can assist the FBS to acquire the needed information are discussed in [10].

Also this work assumes that each FBS has a signal footprint (shown by the dashed circle in Fig. 6) such that the MUEs within this footprint and assigned the same FBS bandwidth will experience noticeable FBS interference (represented by red dashed lines in Fig. 6) due to spectrum sharing. Such co-channel interference outside the footprint is neglected. The presented formulation focuses on one MBS and one FBS in isolation by allocating orthogonal channels to adjacent FBSs, justified by the possibility for each FBS in the network to use the proposed scheme independently.

According to [11], the network channel gains are classified into known and unknown channels. Any channel gain that the FBS can estimate directly or can be estimated by the user and reported to the FBS through a control channel (indirectly) is considered known, while unknown channels cannot be estimated by the FBS directly or indirectly. Channel estimation error is included in the known channel

model for robustness considerations, while for the unknown channels, channel modeling relied on the overheard MUE CQI information.

To provide a decentralized technique, the problem formulation captures the scheduling of all FBSs in the heterogeneous network. The main objective is to maximize the mean total rate for all the FUEs served by the FBS subject to resource assignment, QoS, and power constraints while optimizing the users' assigned power levels (**P**) as well as the assignment indicator (**A**). The problem formulation is given as

$$\max_{\mathbf{P},\mathbf{A}} \left(\sum_{i=1}^{N_f} \sum_{j=1}^{N_c} a_{i,j} \mathbf{E}[R_{i,j}] \right) \tag{6a}$$

$$s.t. \quad \sum_{i=1}^{N_f} a_{i,c} \leq 1 \qquad \sum_{j=1}^{N_c} a_{u,j} = 1, \tag{6b}$$

$$\mathbf{Pr}\left(\sum_{j=1}^{N_c} a_{u,j} \gamma_{u,j} \geq \gamma_r \right) \geq \alpha, \quad u = 1 \ldots N_f, \tag{6c}$$

$$\mathbf{Pr}\left(\sum_{j=1}^{N_c} \xi_{v,j} \gamma_{v,j} \geq \gamma_r \right) \geq \beta, \quad v = 1 \ldots N_M, \tag{6d}$$

$$P_b \leq P_{u,c} \leq P_t, \quad u = 1 \ldots N_f, \quad c = 1 \ldots N_c, \tag{6e}$$

where $a_{i,j}$, $\xi_{i,j} = \{0, 1\}$ are indicator variables for FUEs and MUEs to indicate whether or not user i occupies channel j. $R_{i,j}$ and $\gamma_{i,j}$ are the rate and signal to interference-plus-noise ratio (SINR) of UE i when using channel j, respectively. The parameters N_f, N_c, and N_M are the number of FUEs, number of available channels, and number of neighboring MUEs, respectively. **P** is $(N_f \text{x} N_c)$ matrix representing FUE power assignments and is expressed as $\mathbf{P} = [P_{i,j}]$ where $P_{i,j}$ is the power assigned for FUE i on channel j. **A** is the matrix of indicator coefficients of FUEs and is expressed as $\mathbf{A} = [a_{i,j}]$ $\forall i \in \{1, 2 \ldots N_f\}, j \in \{1, 2 \ldots N_c\}$. Based on its cognitive capabilities, the authors assume that FBS can overhear the scheduling information $(\xi_{i,j}(t))$ of the neighboring MUEs [10]. To ensure QoS for all UEs, FUE QoS constraint is considered in (6c), meanwhile (6d) guarantees an acceptable interference level at neighboring MUE sharing the same spectrum.

The presented optimization problem is considered to be a mixed integer nonlinear (MINL) optimization problem which is non-convex and NP hard in general [17]. To overcome the high complexity of conventional solutions, problem reduction can help develop a solution.

The main idea is to transform the underlying problem from a general form (MINL) to a known form for which there exists a known optimal and efficient algorithm. One common use of problem reduction is to show that a specific problem belongs to a certain class of complexity like P, NP, or NP-complete [18]. The

reduction method is based on the users SINR distribution analysis made for two different channel models.

In the problem formulation, we added FUE and MUE QoS coverage probability constraints. These constraints can be transformed into power constraints using the cumulative distribution function (CDF) of the UE SINR. Moreover, our algorithm transforms the given problem into maximum weighted bipartite matching problem that can be solved optimally using the (Kuhn-Munkres) Hungarian algorithm in polynomial time or even suboptimally by applying greedy algorithm in linear time [19,20].

The work in [10] illustrates the importance of considering estimation error through comparing the maximum total mean capacity of the served FUEs with and without considering estimation error in the channel model. It also compares the Hungarian and greedy algorithm performance. Figure 7 shows the total mean capacity of the served FUEs versus the coverage probability β, from which we can observe the performance difference for considering and ignoring estimation error. Furthermore, this result verifies the achievable gain when applying the Hungarian algorithm versus the greedy algorithm.

Another work in [11] focuses on presenting the performance when using the available feedback information (CQI) instead of explicitly transmitting the channel gain information. Two cases are considered: in the first case (Case I), the FBS receives the channel gain information for all MBS-MUE channels at $t-1$ ($G_{M,v}(t-1)$), whereas in the second case (Case II), the FBS overhears the CQI of neighboring MUEs to estimate the distribution of their channel gains based

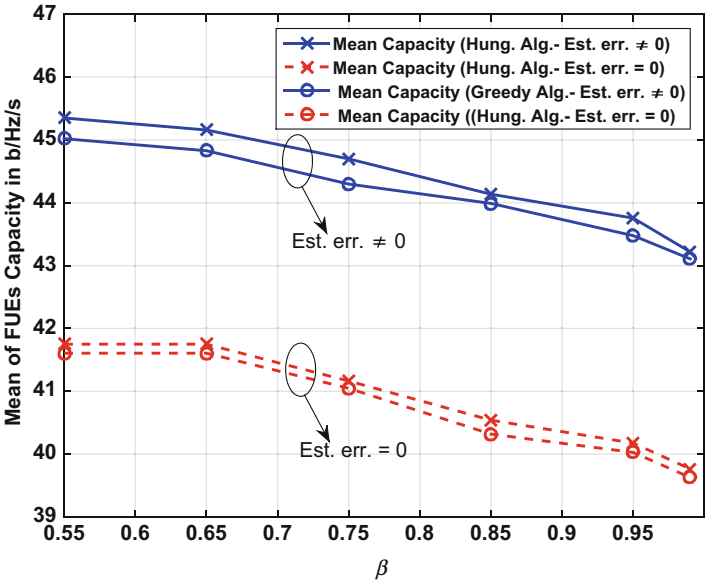

Fig. 7 Solutions results according to error assumptions for different β

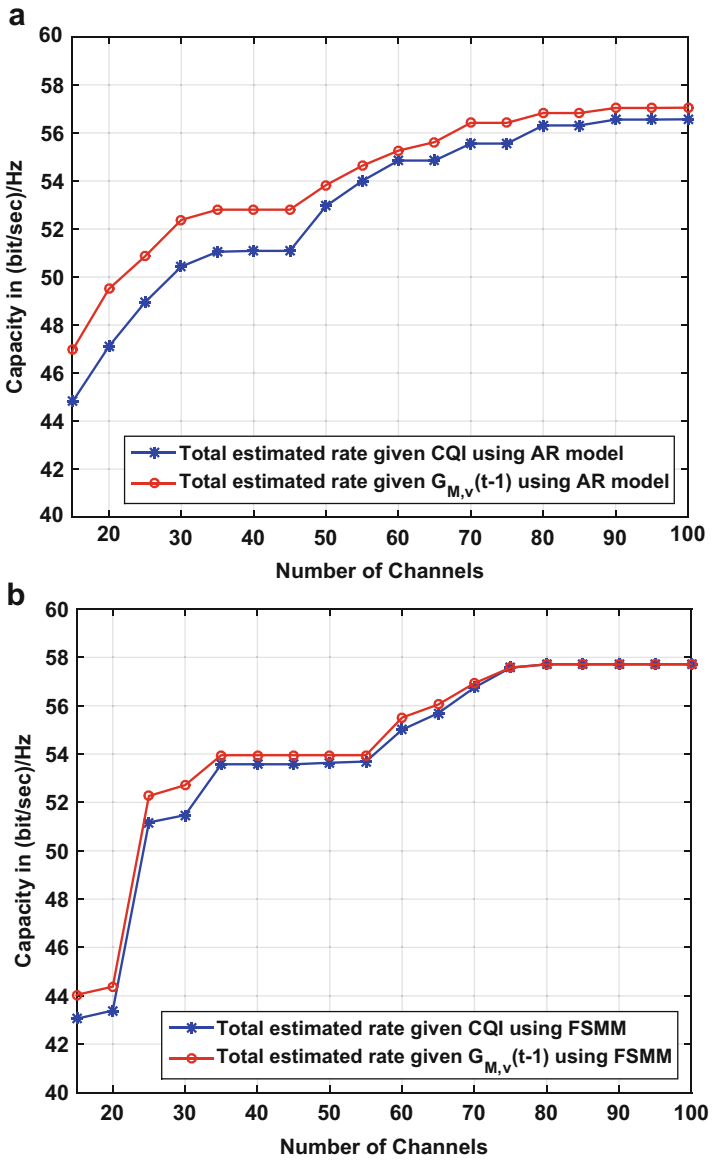

Fig. 8 (**a**) Total mean capacity versus the available number of channels using AR model; (**b**) Total mean capacity versus the available number of channels using FSM model

on the CQI report. Figure 8 depicts the total mean capacity as the number of channels grow using two different channel models, the 1st order autoregressive (AR) channel model and the finite state Markov model (FSMM). Clearly, as the number of available channels for scheduling increases, the gap between the two cases becomes increasingly insignificant.

Explicit Cooperation in Cellular Heterogeneous Networks

This section describes schemes where macrocells and femtocells cooperate for resource allocation and/or interference management. Interference coordination in cellular heterogeneous networks has been discussed actively in 3GPP standards under the Enhanced Inter-Cell Interference Coordination (eICIC) framework [21, 22]. Such techniques entail explicit coordination of messages between the macrocell and femtocells for interference mitigation [23]. Examples of these eICIC techniques include time domain techniques such as the use of almost blank subframes (ABSFs) as well as frequency domain techniques such as orthogonalizing control and reference signals of macrocells and small cells [24]. In ABSFs, a femtocell only sends reference signals such as pilots, i.e., it does not send any data or control information in order to reduce the interference to nearby MUEs. Frequency-domain eICIC techniques include transmitting control and reference signals on non-overlapping frequencies. Such orthogonalization can be done statically or dynamically through coordination between the macrocell and small cells. For examples, when there are some victim MUEs in the vicinity of a small cell and the macrocell detects this through the MUE feedback reports, the macrocell can send this information to the interfering small cell to send its control and reference signals on a different frequency channel.

Another example of explicit cooperation in cellular heterogeneous networks is based on MIMO precoding in the framework of using MUE feedback signals overheard by the femtocell as in the rest of the techniques in this chapter or delivered to the femtocell by the macrocell through backhaul. Both approaches are feasible in cellular heterogeneous networks where the different tiers of the heterogeneous networks are generally operated by the same cellular carrier. The work in [25] investigates interference mitigation in cellular heterogeneous networks consisting of traditional macrocells and overlaid femtocells through dynamic MIMO precoding by designing distributed low-complexity beamforming mechanisms that are compliant with current cellular technology standards. In this work, we also provide an analysis of the mean throughput under the proposed precoding schemes in the format of a simple closed form that provides insight on how the mean throughput depends on basic transmitter, channel, and receiver parameters.

The paper takes advantage of a special LTE standard feature known as MIMO precoder restriction for interference control between HeNB and MUE. Based on MUE feedback signals overheard at the HeNB, the HeNB can choose a precoder for downlink transmission to HUEs that can effectively reduce interference to MUE which share the same frequency spectrum. The paper presents three beamforming schemes for interference mitigation that take into account the QoS requirement of both femtocell and macrocell clients. These MIMO precoding strategies improve flexibility in resource provisioning and signaling requirement while responding to different QoS needs. For example in the MUE Restricted Subset (MRS) scheme, a connection is established between the MUE and the interfering HeNB. This connection is used to exchange information between the HeNB and the MUE. First, MUE estimates the cross-channel response based on HeNB downlink reference

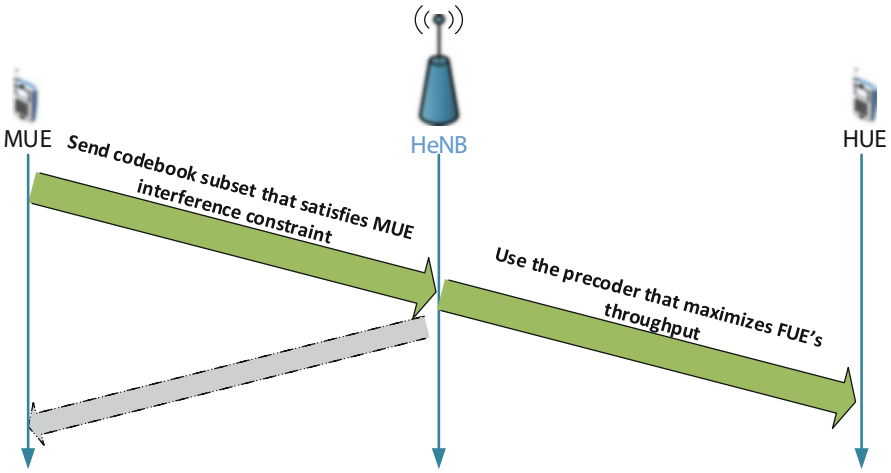

Fig. 9 MRS MIMO precoding scheme in cellular heterogeneous networks

signals (pilots). The MUE sends to the HeNB a subset of indices in the codebook that meet its QoS requirement. The QoS requirement of the MUE is expressed as a maximum tolerable HeNB interference level. After receiving the set of indices satisfying MUE requirement, the HeNB chooses the one that maximizes the SINR to its HUEs. This procedure is summarized in Fig. 9.

The proposed algorithms achieve HeNB precoder selection in two steps: precoder subset restriction at the MUE or HeNB and final precoder selection out of the restricted subset at the HeNB or MUE, respectively. For example, in the MRS scheme, the MUE first selects a subset of precoders that meet its maximum tolerable interference requirement as follows:

$$\mathscr{W}_1 = \left\{ \mathbf{w}_i : \; P_f G_{10} \left\| \mathbf{H}_{10} \mathbf{w}_i \right\|^2 \leq \varepsilon \right\}. \tag{7}$$

where ε is the maximum tolerable interference power at the MUE, $\mathscr{W}_1$ is the set of restricted precoders for the MRS scheme, P_f is the HeNB transmission power, and $\mathbf{H}_{10}$ and G_{10} are the channel and power gain between the HeNB and the MUE, respectively. This subset is sent to the HeNB, which, accordingly, selects the optimum precoder $\mathbf{w}_{i*}$ out of this subset that maximizes its HUEs SINR as

$$w_{i*} = \max_{\mathbf{w}_i \in \mathscr{W}_1} \frac{P_f G_{11} \left\| \mathbf{H}_{11} \mathbf{w}_i \right\|^2}{P_m G_{01} \left\| \mathbf{H}_{01} \mathbf{w}_{m*} \right\|^2 + N_0 B_f}, \tag{8}$$

where P_m is the macrocell transmission power, $\mathbf{w}_{m*}$ is the precoder used by the macrocell, $\mathbf{H}_{11}$ and G_{11} are the channel and power gain between the femtocell and the HUE, respectively, $\mathbf{H}_{01}$ and G_{01} are the channel and power gain between the macrocell and the HUE, respectively, N_0 is the noise power, and B_f is the HUE bandwidth.

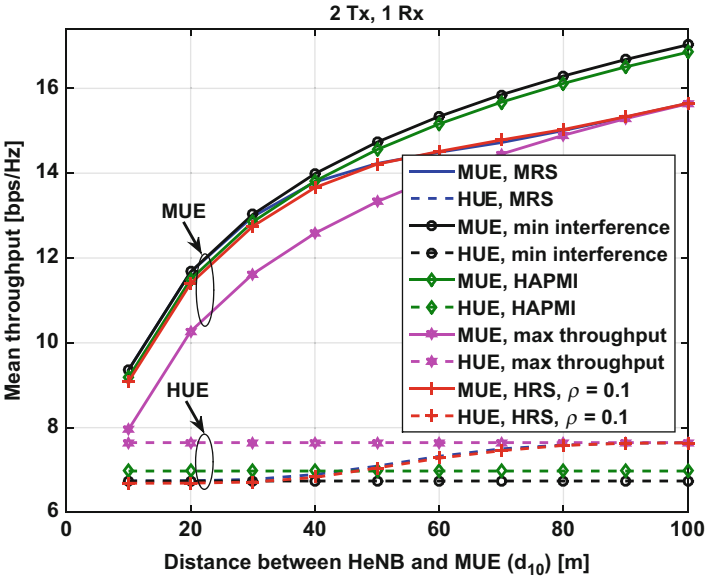

Fig. 10 Performance comparison for MIMO precoding schemes in cellular heterogeneous networks

Figure 10 shows the 5% outage capacity of both MUE and HUE versus HeNB-to-MUE distance, d_{10} for the different proposed schemes. As shown in the figure, the system has the flexibility to assign priority to MUE interference mitigation in heavily loaded networks (by using the MRS scheme) or to HUE throughput maximization in lightly loaded networks (by using the HUE Augmented PMI (HAPMI) scheme). For the MRS scheme, we notice that as d_{10} increases, HUEs throughput grows because the interference power at the MUE drops and, therefore, it becomes easier to satisfy the maximum interference conditions. Consequently, the size of precoder subset becomes larger which gives more flexibility for HUEs throughout maximization. The HRS (HeNB Restricted Subset) scheme in Fig. 10 is a modification of the MRS scheme, where the HeNB estimates the channel between itself and the MUE based on channel reciprocity with a reciprocity error variance of ρ. This scheme does not need any explicit coordination between the HeNB and the macrocell. Therefore, the HRS scheme can be considered an example of implicit cooperation in cellular heterogeneous networks.

Cooperation in Hybrid Access Cellular Heterogeneous Networks

In explicit cooperation scenarios, there exists a better chance to get more cooperation between MBS and FBSs. This kind of cooperation can be used to increase the network throughput. One example for such cooperation is shown in [26], where it

is used to motivate FBS to adopt hybrid access mode instead of the closed access mode. Basically, user access to femtocells can be one of three types: open access, closed access, and hybrid access [27–29].

In open access, all network users (MUEs or FUEs) can access the FBSs. In closed access, only subscriber FUEs are granted FBS access but not MUEs. In general, open access is advantageous from the MUE's perspective [27, 30]. For limited FBS resources, FUE performance in open access may be negatively affected by too many MUEs [28]. On one hand, closed access is easy to implement and gives FUEs better rate and privacy. On the other hand, certain MUEs may receive weak signal from MBS but suffer from strong interference signal by the FBS. Furthermore, spectrum utilization of closed access networks is lower due to the lack of flexibility to serve MUEs even if spare resource is available.

Hybrid access mode offers a trade-off between the first two modes, allowing MUEs to access the FBS so long as the QoS of target FUEs are guaranteed. This means that MUEs can access the FBS without causing serious harm to FUEs. In [31] and [32], the authors have shown that hybrid access outperforms either closed access or open access by significantly reducing cross-tier interference while guaranteeing the performance of FUEs. The practical challenge in hybrid access femtocell is basically how to incentivize FBS to share their spare resources with the MUEs when it can afford to [33, 34]. In [26], we assume that FBS and MBS do not possess prior knowledge of all interference channel state information (CSI), unlike existing work. Practically, such prior knowledge on CSI would require well-coordinated measurement control and signaling. Furthermore, substantial network bandwidth or backhaul must be used to exchange the measured link and interference CSI. Thus, the problem is motivated by the network need for interference management while, at the same time, reducing the excessive burden for interference CSI measurement and transfer.

We develop a refunding framework to stimulate the FBS to serve MUEs with poor channel conditions referred to as hybrid MUEs (hMUEs). This framework will require cooperation between MBS and underlying FBSs and accordingly will reward FBSs when serving MUEs while guaranteeing minimum QoS for the served users (FUEs and MUEs). We formulate this optimization problem as follows:

$$\max_{\mathbf{A},\mathbf{b},\mathbf{P},\mathbf{P}^F} \mathscr{H}(g_F) - \nu F_r \tag{9a}$$

$$s.t. \quad \sum_{i=1}^{N_f} a_{i,c} \leq 1 \qquad \sum_{j=1}^{N_c} a_{u,j} = 1, \tag{9b}$$

$$\mathbf{Pr}\left(\sum_{j=1}^{N_c} a_{u,j}\gamma_{u,j} \geq \bar{\gamma}\right) \geq \alpha, \quad u = 1, 2 \ldots N_f, \tag{9c}$$

$$\mathbf{Pr}\left(\sum_{j=1}^{N_c} \xi_{v,j}\gamma_{v,j} \geq \bar{\gamma}\right) \geq \beta, \quad v = 1, 2 \ldots N_m, \tag{9d}$$

$$\mathbf{Pr}\big(\eta_w \geq \bar{\eta}\big) \geq \varepsilon, \qquad w = 1, 2 \ldots N_h, \tag{9e}$$

$$F_r + \sum_{i=1}^{N_h} b_i \mathbf{E}[R_i^F] \leq R_T, \tag{9f}$$

$$P_b \leq P_i^F \leq P_t, \quad i = 1, 2 \ldots N_f + N_h, \tag{9g}$$

where N_f, N_h, N_m, and N_c are the number of FUEs, hMUEs, MUEs, and channels, respectively, g_F is the FBS gain function, F_r is the expected sum rate of the FUEs in the femtocells, and $\mathscr{H}(.)$ is a 1-to-1 monotone function that converts power to rate, in order to unify the units of g_F and F_r (g_F is summation of power). $\mathbf{P}$ is $(N_f \mathrm{x} N_c)$ matrix representing FUE power assignments and is expressed as $\mathbf{P} = [P_{i,j}]$, while $\mathbf{A}$ is the matrix of indicator coefficients of FUEs and is expressed as $\mathbf{A} = [a_{i,j}]\ \forall i \in \{1, 2 \ldots N_f\}, j \in \{1, 2 \ldots N_c\}$. Also $\mathbf{P}^F$ and $\mathbf{b}$ represent $(1 \times N_h)$ vectors containing power assignments and indicator coefficients of the hMUEs, respectively, such that entries of $\mathbf{P}^F = [P_i^F]$ and $\mathbf{b} = [b_i]\ \forall i \in \{1, 2 \ldots N_h\}$. P_b, P_t are the minimum and maximum power levels allowed for each user respectively, while $P_{i,j}$, P_i^F are the power assigned for user i on channel j and the power assigned for user i from the FBS respectively. $a_{i,j}$, $\xi_{i,j} = \{0, 1\}$ are respectively indicator variables for FUEs and MUEs to indicate whether or not user i occupies channel j, while $b_i = \{0, 1\}$ is indicator variable for hybrid MUEs to indicate whether or not user i will be served by the FBS. $\gamma_{u,j}, \gamma_{v,j}$ are the SINR of the FUE u, MUE v on channel j respectively, η_w is the SNR of hMUE w, while $\bar{\gamma}$ and $\bar{\eta}$ are respectively the required SINR and SNR that guarantee reliable communication for the requested service. $\alpha, \beta, \varepsilon$ are the coverage probability values (outage probability additive inverse). R_T is the upper bound on the average backhaul rate for the FBS and $\mathbf{E}[R_i^F]$ represents is the expected rate of the hMUE i.

We refer to the constraints shown in (9b) as the assignment constraints which guarantee that each user will be assigned no more than one channel, while (9c), (9d) and (9e) are noted as the QoS constraints. These constraints are meant to keep the QoS of the users above certain threshold. Using (9f), the FBS will limit overall FBS backhaul rate such that the total expected rate of all users served by the FBS (FUEs and hMUEs) should not exceed the backhaul rate limit R_T.

The constant $\nu \in \{0, 1\}$ determines the FBS objective dependency. On one hand, when $\nu = 0$, the FBS objective will fully depend on the gain from serving hMUEs as long as the FUEs QoS and power constraints are satisfied. On the other hand, when $\nu = 1$, the FBS will try to minimize the mean sum rate of the FUEs while maximizing the FBS gain. Basically, by varying the value of ν, the problem remains unchanged. To be more specific, in terms of the optimum solution sets for each case, the solution set of the problem when $\nu = 1$ is included in the solution set when $\nu = 0$. Therefore, by setting $\nu = 1$, we only tighten our optimum solution set.

A two-step solution approach was proposed in [26]. Step (1) starts by decomposing the given optimization problem into two decoupled problems. The first problem handles the FUE scheduling such that each user maintains the required QoS, while the second problem deals with the hMUE power assignments. Moreover, the FBS backhaul rate limitation is considered, which will directly affect the FBS capacity to serve hMUEs. Additionally, Step (2) reduces the decomposed problems into well-known forms as in [10,11]. The provided reduction is based on the SINR distribution analysis results.

The optimality of the proposed solution was tested through comparing it with the exhaustive search solution as shown in Fig. 11. Moreover, the paper provides a comparison between the proposed mechanism and the fractional frequency reuse (FFR) presented in [35]. FFR is based on dividing the entire spectrum into sub-bands and assigning each base station different sub-bands. Allocating non-overlapped spectrum will mitigate the induced intra-tier interference between FBSs as well as the cross-tier interference between each FBS and the MBS. The results in Fig. 12 illustrate that the proposed algorithm in [26] provides a negligible difference in the mean sum rate compared to FFR at different levels of spectrum/bandwidth saving. This bandwidth saving benefit is made possible by trading more power for better spectral efficiency, as shown in Fig. 12b. The results in Fig. 12b show that the proposed scheme requires higher FBS power consumption as the percentage of bandwidth saving increases. It is clear that because of the higher spectral efficiency of the proposed technique in [26], the power needed to deliver the same service is higher.

Cooperation in Dense Enterprise Femtocell Networks

This section discusses cooperation in dense enterprise deployments consisting of multiple neighboring femtocells such as in corporate premises, shopping malls, stadiums, or conference venues. Unlike home deployments of femtocells, enterprise deployments are generally dense resulting in large co-channel interference among femtocells if they reuse the same frequency. On the other hand, orthogonal frequency allocation can result in lower area spectral efficiency. Due to the large amount of cooperation needed for resource allocation and interference management in enterprise deployments, a central controller is generally needed as in [36–38].

Our work in [38] addresses the problem of interference management and coarse resource allocation using a central controller through an adaptive graph coloring approach (AGC). The block diagram of the solution presented in [38] is shown in Fig. 13. Each femtocell estimates the total number of resources needed to meet the requirements of its associated FUEs based on their traffic type, in a step referred to as Load Estimation. To minimize interference to adjacent femtocells, each femtocell n solves an optimization problem with the objective of minimizing the number of resources (PRBs) needed to meet minimum rate requirements of the associated FUEs as follows:

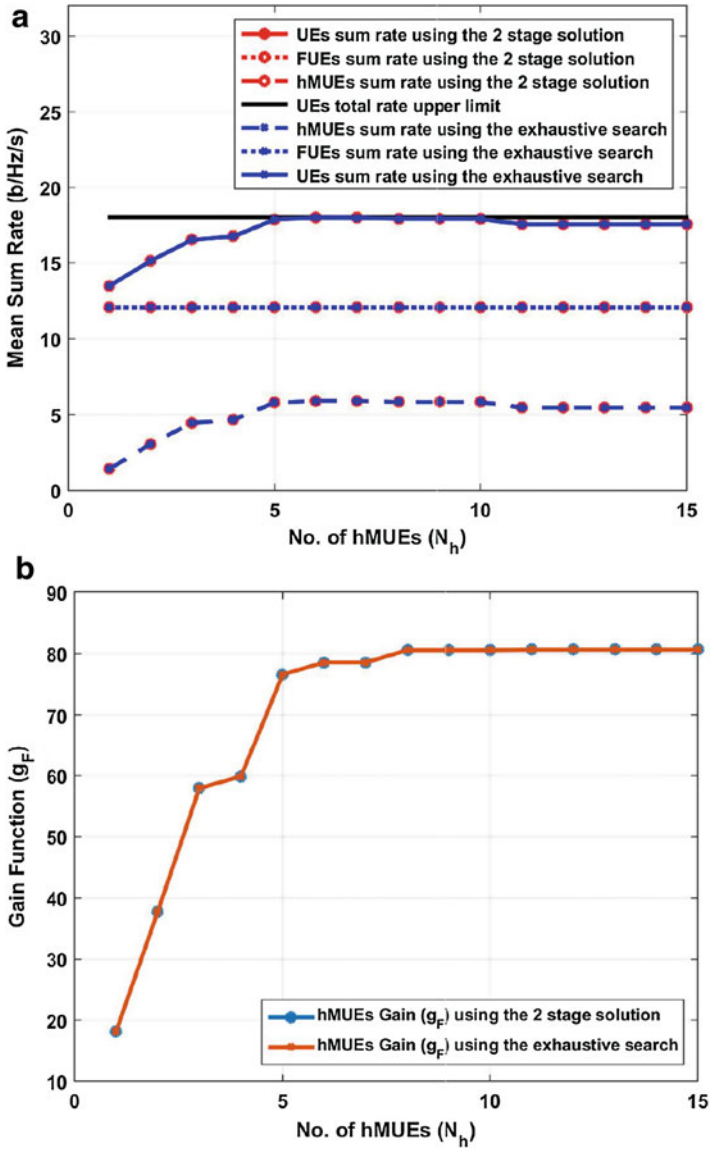

Fig. 11 (**a**) The UEs (FUEs, hMUEs) mean sum rate at $\nu = 1$; (**b**) FBS gain function (g_F) at $\nu = 1$

$$\min_{\{w_i^{(n)}, P_i^{(n)}\}} \sum_{i \in \Omega_n} w_i^{(n)} \tag{10a}$$

$$s.t.\ w_i^{(n)} \frac{B}{K} \log_2 \left(1 + \frac{P_i^{(n)} H_i^{(n)}}{w_i^{(n)} \sigma^2}\right) \geq \bar{r}_i^{(n)}, \quad \forall i \in \Omega_n, \tag{10b}$$

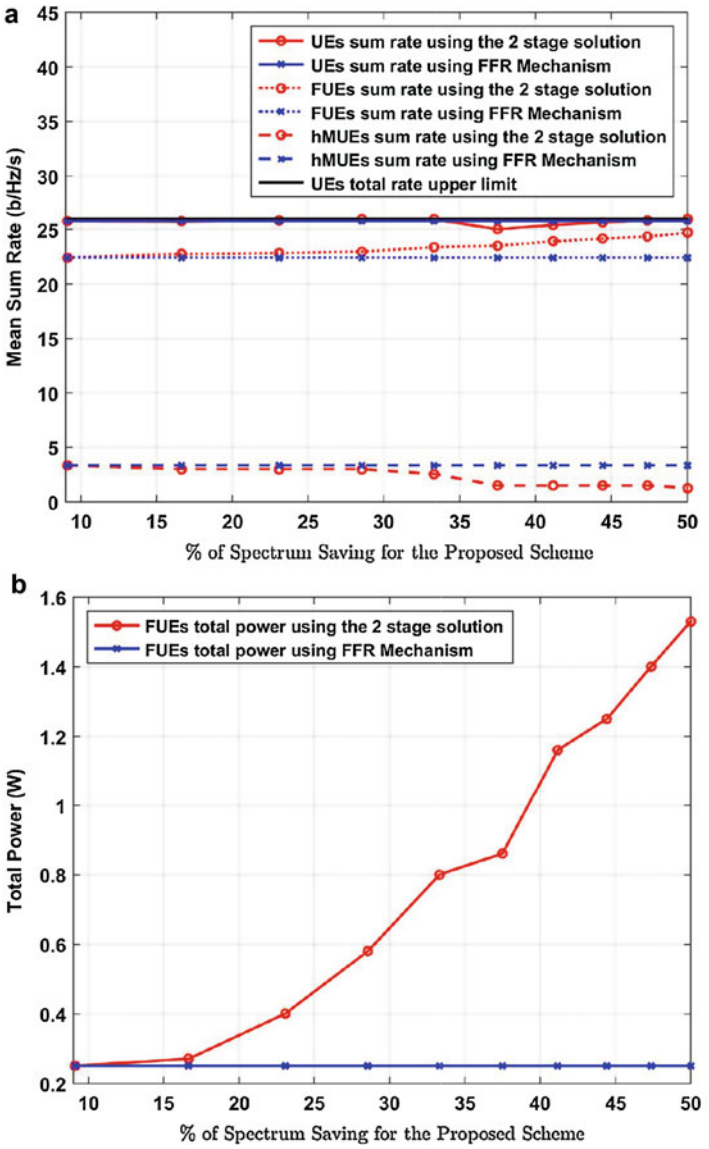

Fig. 12 (**a**) The UEs (FUEs, hMUEs) mean sum rate variation with the percentage of spectrum saving; (**b**) FBS total power consumption variation with the percentage of spectrum saving

$$\sum_{i \in \Omega_n} P_i^{(n)} \leq P_{\max}^{(n)} \tag{10c}$$

$$\sum_{i \in \Omega_n} w_{i,c}^{(n)} \leq K \tag{10d}$$

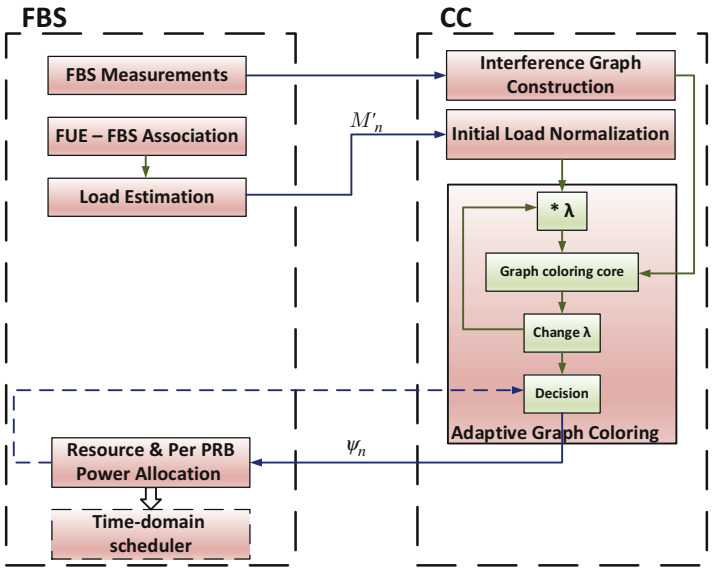

Fig. 13 Adaptive graph coloring block diagram

$$P_i^{(n)} \geq 0, \ \forall i \in \Omega_n \tag{10e}$$

$$w_{i,c}^{(n)} \geq 0, \ \forall i \in \Omega_n, \ \forall c \in C_i^{(n)} \tag{10f}$$

In (10), $w_i^{(n)}$ and $\bar{r}_i^{(n)}$ are the estimated number of required PRBs and the minimum rate requirement for FUE i associated with femtocell n, respectively, $P_i^{(n)}$ is the average per-PRB power allocated to FUE i, $P_{\max}^{(n)}$ is the maximum transmission power of femtocell n, Ω_n is the set of FUEs associated with femtocell n, B is the total system bandwidth, K is the total number of PRBs, and $H_i^{(n)}$ is the average channel power between femtocell n and FUE i. The formulation in (10) is a convex optimization problem in the variables $w_i^{(n)}$ and $P_i^{(n)}$. The outcome of this load estimation step at each femtocell n is the sum of the number of PRBs required for the FUEs associated with femtocell n, denoted as $M'_n = \sum_{i \in \Omega_n} w_i^{(n)}$. This estimated load represents a coarse estimate of the actual number of resources needed by the FUE since interference from neighboring femtocells is not considered in this step yet.

Based on the estimated load from each femtocell, the central controller then performs resource allocation among the femtocells using a graph coloring approach. The graph coloring approach allocates resources among femtocells in an iterative greedy fashion allowing frequency reuse and minimizing inter-cell interference among femtocells. The outcome of the graph coloring step is a set of resources, Ψ_n, for each femtocell n that can then be used by the femtocell locally to distribute

among its associated FUEs. The central controller also calculates the amount of interference among femtocells based on graph coloring results and sends this information to each femtocell.

After the graph coloring step, each femtocell locally performs resource and per-PRB power allocation to its associated FUEs. Different objective functions for resource allocation at each femtocell can be max-min fairness or sum rate maximization. For example, the max-min fairness optimization problem is formulated as follows:

$$\max_{\{p_{i,k}^{(n)}, s_{i,k}^{(n)}\}} \min_{i} \quad \frac{B}{K} \sum_{k \in \Psi_n} s_{i,k}^{(n)} \log_2 \left(1 + \frac{p_{i,k}^{(n)} h_{i,k}^{(n)}}{s_{i,k}^{(n)} (\sigma^2 + \sum_{m \in \mathscr{I}_k} P_k^{(m)} G_{mni})} \right) \tag{11a}$$

$$s.t. \quad R_i^{(n)} \geq \bar{r}_i^{(n)} \tag{11b}$$

$$\sum_{k \in \Psi_n} \sum_{i \in \Omega_n} p_{i,k}^{(n)} \leq P_{\max}^{(n)} \tag{11c}$$

$$\sum_{i \in \Omega_n} s_{i,k}^{(n)} = 1, \ \forall k \in \Psi_n \tag{11d}$$

$$p_{i,k}^{(n)} \geq 0, \ \forall i \in \Omega_n, \forall k \in \Psi_n \tag{11e}$$

$$s_{i,k}^{(n)} \geq 0, \ \forall k \in \Psi_n, \tag{11f}$$

where B is the total system bandwidth, K is the total number of PRBs, $s_{i,k}^{(n)}$ is the time sharing coefficient of PRB k for FUE i connected to FBS n, $p_{i,k}^{(n)}$ and $h_{i,k}^{(n)}$ are the transmission power and channel gain from FBS n to FUE i on PRB k, respectively, σ^2 is the noise power, $\mathscr{I}_k$ is the set of interfering FBSs on each PRB k, $P_k^{(m)}$ is the average transmission power of every interfering FBS m in the set $\mathscr{I}_k$ on PRB k, and G_{mni} is the path loss from FBS m to FUE i associated with FBS n. The problem in (11) is a convex optimization in the variables $p_{i,k}^{(n)}$ and $s_{i,k}^{(n)}$.

On top of the described baseline graph coloring approach, paper [38] presents an adaptive graph coloring scheme that finds the best trade-off between frequency reuse and orthogonal allocation among femtocells. In low-interference regimes, a higher frequency reuse allows better spectral efficiency, whereas in high-interference regimes, orthogonal allocation would be preferred. To reach a good compromise between both extremes, the central controller searches for the best scale parameter λ for the number of resources assigned to femtocells to achieve a certain objective function. Two methods are proposed for adapting the scale parameter λ, namely, estimation-based adaptive graph coloring (EB-AGC) and feedback-based adaptive graph coloring (FB-AGC). In EB-AGC, the central controller estimates the rate of each femtocell based on candidate graph coloring results and in FB-AGC, each femtocell reports to the central controller its attained rate to aid in choosing the best graph coloring result for the whole network.

Besides the EB-AGC and FB-AGC schemes, the following resource allocation schemes are considered for performance comparison:

- **Uniform Zero Frequency Reuse (Uniform ZFR)**
  Orthogonal resource allocation with each femtocell allocated an equal number of PRBs given by $M_n = \left\lfloor \frac{K}{N} \right\rceil \quad \forall n$ regardless of the actual FBS load.
- **Proportional Zero Frequency Reuse (Proportional ZFR)**
  Orthogonal resource allocation among femtocells with proportional allocation to the initial estimated load by each femtocell as in (10).
- **Full Frequency Reuse (FuFR)**
  Reusing all available resources for all femtocells, i.e., each femtocell is allocated all K available PRBs ($M_n = K \quad \forall n$).

Figure 14 shows the average minimum FUE achieved rate using max-min fairness criteria at each femtocell versus the normalized noise power level in dBm/Hz. The normalized noise power level represents the sum of all noise sources including cellular or noncellular interference. In this figure, a sparse femtocell deployment with nine femtocells in a $180 \times 180\,\mathrm{m}^2$ square area with FUE density of $0.001/\mathrm{m}^2$ is considered. The minimum required rate for each FUE, $\bar{r}_i^{(n)}$, is set as 1 Mbps. As shown in Fig. 14, for interference-limited region where noise power level is low, Proportional ZFR gives higher average minimum FUE rate than FuFR. On the other

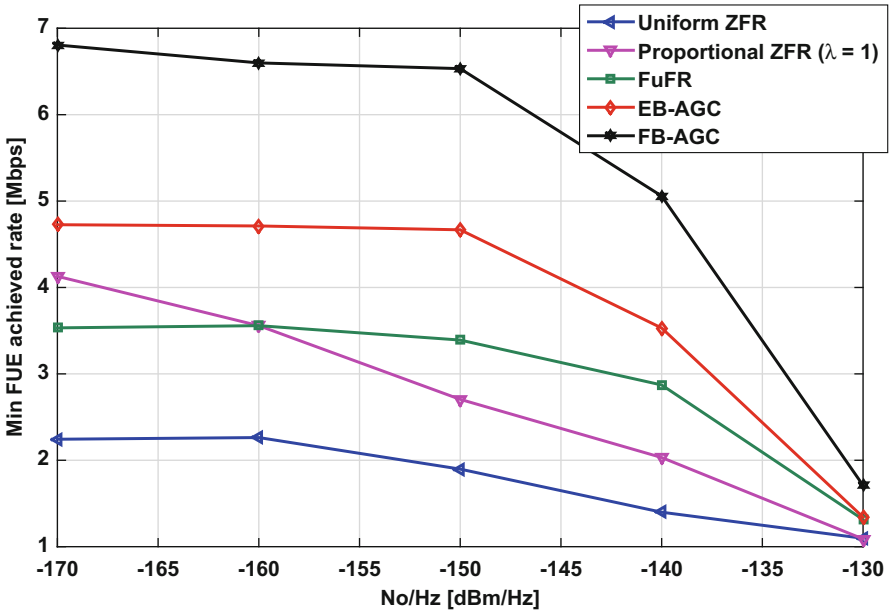

Fig. 14 Minimum FUE rate vs. noise power level

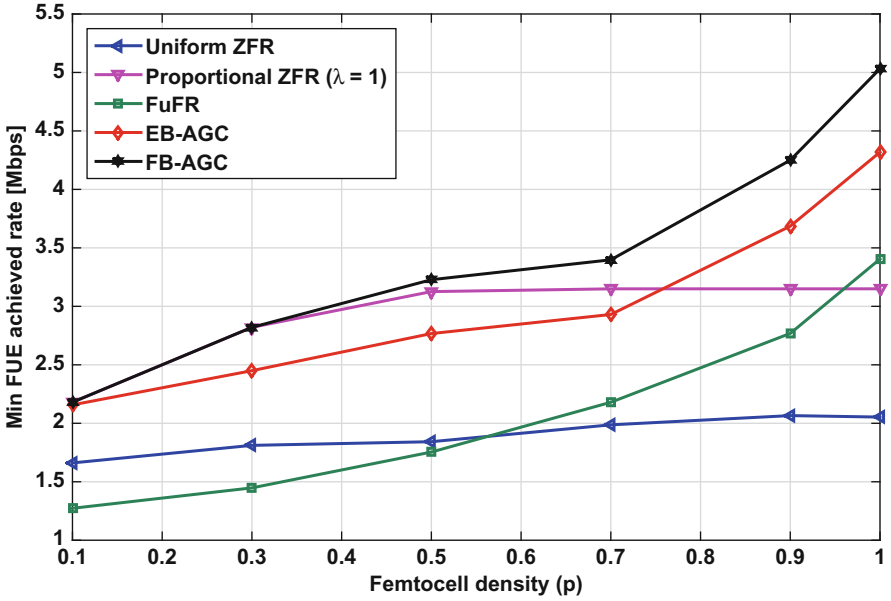

Fig. 15 Minimum FUE rate vs. femtocell density p

hand, in bandwidth-limited region with high noise power level, FuFR achieves better spectral efficiency and higher minimum FUE throughput than orthogonal allocation. Both AGC schemes can achieve better minimum FUE throughput for different levels of normalized noise power. The gain for AGC schemes arise from selecting a better fractional frequency reuse compromise between orthogonal resource allocation and full frequency reuse.

Figure 15 studies the performance of the aforementioned algorithms in dense enterprise deployments. A 5×5 grid model is considered in a $50 \times 50\,\mathrm{m}^2$ square area representing a single-floor building with 25 blocks of $10 \times 10\,\mathrm{m}^2$ each [39]. Along with the higher femtocell density compared to Fig. 14, a higher FUE density of $0.03/\mathrm{m}^2$ is also considered. For each block, a femtocell is randomly dropped with a probability p. As p increases, the femtocell density increases. Moreover, unlike the results in Fig. 14, the random femtocell deployment here can result in an irregular deployment.

As shown in Fig. 15, the FB-AGC algorithm gives higher minimum FUE rate compared to other schemes for different femtocell densities p. As p increases, the number of femtocells covering the whole area increases, and, thus, the number of FUEs per femtocell increases leading to a higher minimum achieved FUE rate. This shows that the FB-AGC can achieve a better solution than both orthogonal allocation and full frequency reuse for femtocell densities ranging from a sparse deployment with $p = 0.1$ to a very dense deployment with $p = 1$, i.e., 25 femtocells in a $50 \times 50\,\mathrm{m}^2$ square area.

Cooperation in Integrated WLAN-Cellular Heterogeneous Networks

A recent trend in the deployment of cellular heterogeneous networks is the integration of both WLAN (e.g., WiFi) and cellular (e.g., 3G and LTE) technologies at small cells. The large number of WiFi hotspots and the adoption of WiFi interfaces in almost all smart phones and portable devices make it increasingly attractive to MNOs to offload traffic from congested cellular networks to WiFi hotspots.

In [40, 41], we present a resource allocation and inter-cell interference management scheme for small cells with integrated licensed and unlicensed band interfaces. We propose a joint and adaptive allocation of resources over both bands with fairness constraints among small cell user equipments (SUEs), implemented as minimum SUE rate constraints, and QoS guarantees to neighboring MUEs, implemented as maximum tolerable interference constraints. The QoS requirements of different types of traffic for the SUEs are considered by controlling the distribution of resources over both licensed and unlicensed bands. For example, QoS cannot be guaranteed over WiFi networks for delay-sensitive applications such as voice conversations and real-time gaming.

The system model considered in [40] is shown in Fig. 16, where the MBS has M associated MUEs and the Small eNode B (SeNB) has S SUEs with both cellular (licensed) and WLAN air (unlicensed) interfaces as well as W wireless nodes (WNs) with WLAN air interface only. The rate of an SUE i in the licensed band is denoted $R_\ell^{(i)}$ and is given by

$$R_\ell^{(i)} = \alpha^{(i)} \psi_\ell^{(i)} B = \alpha^{(i)} \eta_b \eta_c \left[\beta \log_2 \left(1 + \frac{P_s |G_i|^2}{(N_o + P_m |J_i|^2) \eta_s} \right) + (1 - \beta) \log_2 \left(1 + \frac{P_s |G_i|^2}{N_o \eta_s} \right) \right] B, \tag{12}$$

where $\alpha^{(i)}$ is the probability that a PRB is assigned to SUE i associated to the SeNB, $\psi_\ell^{(i)}$ is the average effective spectral efficiency attained by SUE i, and B is the total SeNB bandwidth. The parameter $\alpha^{(i)}$ can also be thought of as the percentage of the total bandwidth assigned to SUE i. Similarly, β is the access probability of the MBS for a given PRB, i.e., the probability that a PRB is assigned by the MBS to any of its associated MUEs. P_s is the transmit power of the SeNB, G_i and J_i are respectively the channel gain between the SeNB and SUE i and the MBS and SUE i, N_0 is the noise power per PRB, and the parameters η_b, η_c, and η_s are modeling the throughput of a typical practical cellular system as a function of bandwidth and SINR implementation efficiency. With probability β, a PRB will be used by the MBS and therefore suffers interference from the MBS to SUE i as in the first term in the square bracket in (12), and with probability $1 - \beta$ the PRB will not suffer interference as in the second term.

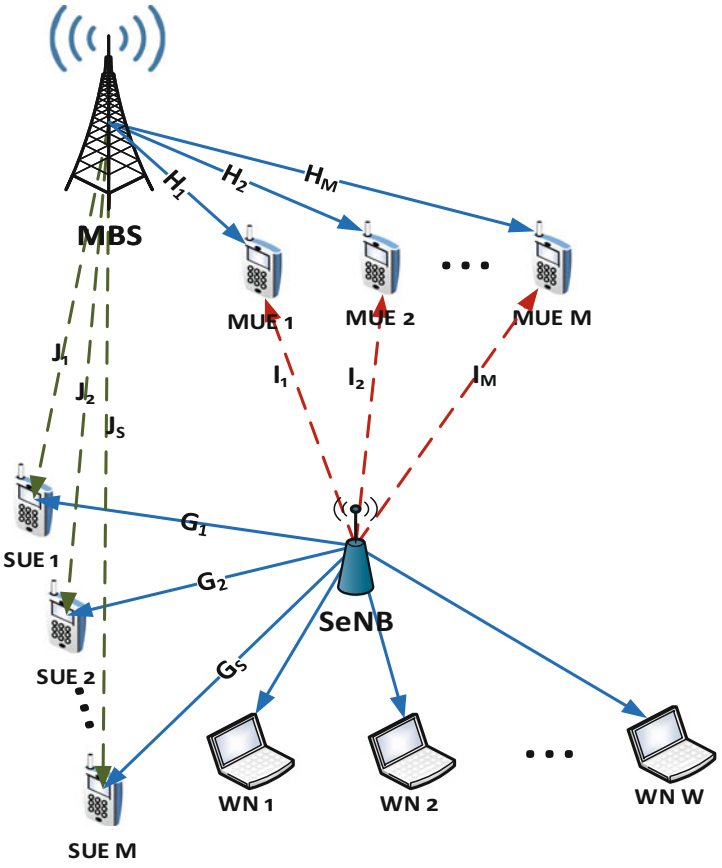

Fig. 16 Integrated WLAN-cellular heterogeneous networks system model

The QoS of MUEs is maintained by limiting the interference caused by the SeNB at MUE j below a predetermined threshold ε_j. This is formulated as $Pr[\alpha_s \beta^{(j)} P_s |I_j|^2 \leq \varepsilon_j] \geq \zeta,\ j = 1, \ldots, M,$, where I_j is the channel gain between the SeNB and MUE j and ζ is the QoS guarantee probability, e.g., 95%. The interference channel I_j can be decomposed into large scale fading component I_j^{ℓ} representing path gain and small scale fading random component I_j^s. Assuming I_j^s to be a complex Gaussian scalar random variable with zero mean and unity variance, the random variable $|I_j^s|^2$ becomes exponentially distributed with rate parameter of 1. The maximum interference constraint can thus be rewritten as:

$$1 - \exp\left(\frac{-\varepsilon_j}{\alpha_s \beta^{(j)} P_s |I_j^{\ell}|^2}\right) \geq \zeta,$$

or alternatively,

$$\alpha_s \leq \frac{\varepsilon_j}{\beta^{(j)} P_s |I_j^{\ell}|^2 \ln(\frac{1}{1-\zeta})}.$$

The joint resource allocation on both licensed and unlicensed bands can be formulated as an optimization problem with the objective of maximizing sum SUE rate while maintaining both minimum SUE rate and maximum MUE interference requirements as follows:

$$\max_{\{\boldsymbol{\alpha}, \boldsymbol{R_u}\}} \quad \sum_{i=1}^{S} \left[\alpha^{(i)} \psi_{\ell}^{(i)} B + R_u^{(i)}\right], \tag{13a}$$

$$s.t. \quad \sum_{i=1}^{S} R_u^{(i)} \leq R_{AP} - \sum_{k=1}^{W} r_w^{(k)}, \tag{13b}$$

$$\alpha^{(i)} \psi_{\ell}^{(i)} B + R_u^{(i)} \geq r^{(i)}, \; i = 1, \ldots, S, \tag{13c}$$

$$Pr[\alpha_s \beta^{(j)} P_s |I_j|^2 \leq \varepsilon_j] \geq \zeta, \; j = 1, \ldots, M, \tag{13d}$$

$$\sum_{i=1}^{S} \alpha^{(i)} \leq \rho - \beta = \bar{\alpha}_s, \tag{13e}$$

$$0 \leq \alpha^{(i)} \leq 1, \; i = 1, \ldots, S, \tag{13f}$$

$$0 \leq R_u^{(i)} \leq R_{u,\max}^{(i)}, \; i = 1, \ldots, S, \tag{13g}$$

where $R_u^{(i)}$ is the throughput of SUE i in the unlicensed band, R_{AP} is the SeNB throughput on the unlicensed band, $r_w^{(k)}$ and $r^{(i)}$ are the minimum rate requirement for WN k and SU i, respectively, and ρ controls the percentage of probabilistic bandwidth sharing between the MBS and the SeNB. The parameter $R_{u,\max}^{(i)}$ sets an upper bound on the unlicensed band rate for SUE i which is chosen as a function of the traffic type for each SUE. The optimization problem in (13), can be reformulated as a linear program in the variables $\boldsymbol{\alpha} = [\alpha^{(1)} \; \cdots \; \alpha^{(S)}]$ and $\boldsymbol{R_u} = [R_u^{(1)} \; \cdots \; R_u^{(S)}]$ representing resource allocation on both licensed and unlicensed bands, respectively.

Figure 17 shows the sum rate of MUEs, SUEs (with both LTE and WiFi interfaces), and WNs (with WiFi interface only) for different resource allocation schemes. The figure compares the proposed joint optimization approach (Proposed) against two existing solutions, namely, WiFi offloading and Conventional femto, and two other baseline schemes with LTE and WiFi integration, namely, Fixed and Sequential allocation schemes. The results show that the proposed solution

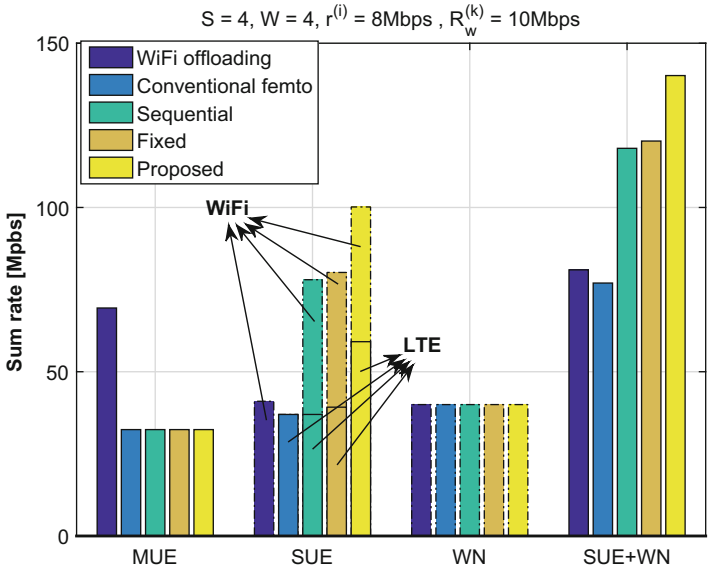

Fig. 17 Sum rate comparison for different algorithms for dual-access small cells

achieves better (or at least the same) performance compared to other schemes while maintaining fairness among SUEs and controlling the amount of inter-cell interference to neighboring MUEs. In this simulation, conventional femto, sequential, fixed, and proposed schemes generate the same amount of interference to MUEs, resulting in the same sum MUE rate, whereas the WiFi offloading scheme causes no interference to MUEs and, therefore, gives the largest sum MUE rate. Although both conventional femto and the proposed schemes use the same resource allocation method in the licensed band, the throughput obtained by SUEs on the licensed band in the proposed scheme is larger than that obtained by conventional femto. The reason for this is that the proposed scheme has more flexibility in satisfying the minimum SUE rate requirements compared to conventional femto as the proposed scheme can satisfy each individual constraint using the licensed and/or unlicensed bands rather than the licensed band only for the conventional femto case. Additionally, compared to the sequential and fixed schemes that also use both the licensed and unlicensed band, the proposed scheme gives higher sum SUE rate. The reason for this is that the proposed scheme solves the resource allocation problem over both bands jointly, in contrast with the sequential scheme, and adaptively (i.e., the distribution of traffic over both bands is adapted to the channel condition, availability of LTE resources and WiFi capacity, and rate requirement of each SUE), in contrast with fixed partitioning of traffic over both bands in the fixed scheme. This joint and adaptive allocation of resources over the licensed and unlicensed bands allows the proposed scheme to achieve higher sum throughput for the SUEs compared to other solutions.

Conclusion and Future Directions

This chapter introduced several techniques for cooperative spectrum sharing in heterogeneous networks by exploiting the inherently available feedback information in most communication systems such as CQI and ACK/NACK feedback. Taking advantage of such information within different types of cooperation by different network players can achieve better overall QoS and network throughput.

Several research thrusts have demonstrated efficient utilization of implicit and explicit cooperation between the MBS and overlaying small cells in order to reduce the direct information transfer among BSs. One major challenge that this chapter addresses is the spectrum sharing of macrocell and small cells while guaranteeing MUE's QoS. From the interference perspective, such implicit feedback information can help secondary transmitters to partially observe the unknown interference channel state and learn severity of its interference to the primary receiving users (e.g., MUEs). The chapter also presented works on resource allocation and interference management in dense deployment scenarios through a central controller to coordinate spectrum allocation among neighboring femtocells. Moreover, cooperation in heterogeneous networks can be extended to more general cooperative networks integrating both cellular and noncellular access.

One potentially interesting extension for the present direction is to reformulate a number of interference management problems by taking advantage of the inherent signal feedback in most two-way communication systems. A number of existing works on interference management in wireless networks often rely on assumptions of available information that are often either impractical or costly. Revisiting some of these important design challenges by utilizing inherent feedback signals to relax their originals assumptions can lead to highly exciting solutions to important practical problems.

References

1. Bhushan N, Li J, Malladi D, Gilmore R, Brenner D, Damnjanovic A, Sukhavasi RT, Patel C, Geirhofer S (2014) Network densification: the dominant theme for wireless evolution into 5G. IEEE Commun Mag 52(2):82–89
2. Sadek AK, Zhang W, Shellhammer SJ (2008) Listen-before-talk versus treating interference as noise for spectrum sharing. In: 3rd IEEE Symposium on New Frontiers in Dynamic Spectrum Access Networks (DySPAN 2008), pp 1–6
3. Gao L, Wu P, Cui S (2007) Power and rate control with dynamic programming for cognitive radios. In: IEEE GLOBECOM 2007-IEEE Global Telecommunications Conference, pp 1699–1703
4. Xiao Q, Li Y, Zhao M, Zhou S, Wang J (2009) Opportunistic channel selection approach under collision probability constraint in cognitive radio systems. Comput Commun 32(18): 1914–1922
5. Lapiccirella FE, Liu X, Ding Z (2013) Distributed control of multiple cognitive radio overlay for primary queue stability. IEEE Trans Wirel Commun 12(1):112–122
6. Yücek T, Arslan H (2009) A survey of spectrum sensing algorithms for cognitive radio applications. IEEE commun Surv Tutorials 11(1):116–130

7. Lapiccirella FE, Ding Z, Liu X (2012) Improved spectrum access control of cognitive radios based on primary ARQ signals. IET commun 6(8):900–908
8. Lapiccirella FE, Ding Z, Liu X (2010) Cognitive spectrum access control based on intrinsic primary ARQ information. In: IEEE International Conference on Communications (ICC)
9. Elsherif AR, Ding Z, Liu X, Hamalainen J (2013) Resource allocation in two-tier heterogeneous networks through enhanced shadow chasing. IEEE Trans Wirel Commun 12(12): 6439–6453
10. Elmaghraby HM, Qin D, Ding Z (2015) Downlink scheduling and power allocation in cognitive femtocell networks. In: Cognitive radio oriented wireless networks. Springer, pp 92–105
11. Elmaghraby HM, Ding Z (2015) Cognitive femtocell scheduling and power allocation based on channel quality report. In: 2015 IEEE Global Communications Conference (GLOBECOM), pp 1–6
12. Sun D, Zhu X, Zeng Z, Wan S (2011) Downlink power control in cognitive femtocell networks. In: 2011 International Conference on Wireless Communications and Signal Processing (WCSP), pp 1–5. https://doi.org/10.1109/WCSP.2011.6096947
13. Zhang L, Yang L, Yang T (2010) Cognitive interference management for LTE-A femtocells with distributed carrier selection. In: 2010 IEEE 72nd Vehicular Technology Conference Fall (VTC 2010-Fall), pp 1–5. https://doi.org/10.1109/VETECF.2010.5594585
14. Xie R, Yu F, Ji H (2012) Spectrum sharing and resource allocation for energy-efficient heterogeneous cognitive radio networks with femtocells. In: 2012 IEEE International Conference on Communications (ICC), pp 1661–1665. https://doi.org/10.1109/ICC.2012.6364100
15. Peng M, Liu Y, Wei D, Wang W, Chen HH (2011) Hierarchical cooperative relay based heterogeneous networks. IEEE Wirel Commun 18(3):48–56
16. Mukherjee S (2012) Distribution of downlink SINR in heterogeneous cellular networks. IEEE J Sel Areas Commun 30(3):575–585
17. Burer S, Letchford AN (2012) Non-convex mixed-integer nonlinear programming: a survey. Surv Oper Res Manage Sci 17(2):97–106
18. Karp RM (1972) Reducibility among combinatorial problems, Springer, Boston, pp 85–103
19. Kuhn HW (1955) The hungarian method for the assignment problem. Nav Res Logist Q 2(1–2):83–97
20. Munkres J (1957) Algorithms for the assignment and transportation problems. J Soc Ind Appl Math 5(1):32–38
21. 3GPP (2012) Evolved universal terrestrial radio access (E-UTRA) and evolved universal terrestrial radio access network (E-UTRAN); overall description; stage 2. 3GPP Tech Spec TS 36300, Ver 1080
22. R1-104968 (2010) Summary of the description of candidate eICIC solutions. 3GPP Std
23. R1-101369 (2010) Considerations on interference coordination in heterogeneous networks. 3GPP Std
24. Lopez-Perez D, Guvenc I, De la Roche G, Kountouris M, Quek TQ, Zhang J (2011) Enhanced intercell interference coordination challenges in heterogeneous networks. IEEE Wirel Commun 18(3):22–30
25. Elsherif AR, Ding Z, Liu X (2014) Dynamic MIMO precoding for femtocell interference mitigation. IEEE Trans Commun 62(2):648–666
26. Elmaghraby HM, Ding Z (2017) Scheduling and power allocation for hybrid access cognitive femtocells. IEEE Trans Wirel Commun 16(4):2520–2533. https://doi.org/10.1109/TWC.2017.2665618
27. Andrews J, Claussen H, Dohler M, Rangan S, Reed M (2012) Femtocells: past, present, and future. IEEE J Sel Areas Commun 30(3):497–508. https://doi.org/10.1109/JSAC.2012.120401
28. De La Roche G, Valcarce A, López-Pérez D, Zhang J (2010) Access control mechanisms for femtocells. IEEE Commun Mag 48(1):33–39
29. Golaup A, Mustapha M, Patanapongpibul LB (2009) Femtocell access control strategy in UMTS and LTE. IEEE Commun Mag 47(9):117–123

30. Xia P, Chandrasekhar V, Andrews J (2010) Open vs. closed access femtocells in the uplink. IEEE Trans Wirel Commun 9(12):3798–3809. https://doi.org/10.1109/TWC.2010.101310.100231
31. Choi D, Monajemi P, Kang S, Villasenor J (2008) Dealing with loud neighbors: the benefits and tradeoffs of adaptive femtocell access. In: Global Telecommunications Conference (GLOBECOM 2008). IEEE, pp 1–5
32. Valcarce A, López-Pérez D, De La Roche G, Zhang J (2009) Limited access to OFDMA femtocells. In: 2009 IEEE 20th International Symposium on Personal, Indoor and Mobile Radio Communications, pp 1–5
33. Zhang L, Jiang T, Luo K (2015) Dynamic spectrum allocation for the downlink of OFDMA-Based hybrid access in cognitive femtocell networks. IEEE Trans Veh Technol (99):1–1. https://doi.org/10.1109/TVT.2015.2414424
34. Chen Y, Zhang J, Zhang Q (2012) Utility-aware refunding framework for hybrid access femtocell network. IEEE Trans Wirel Commun 11(5):1688–1697
35. Saquib N, Hossain E, Le LB, Kim DI (2012) Interference management in OFDMA femtocell networks: issues and approaches. IEEE Wirel Commun 19(3):86–95
36. 3GPP standard (2012) Technical specification group services and system aspects; evolved universal terrestrial radio access (E-UTRA); FDD Home eNode B (HeNB) radio frequency (RF) requirements analysis (release 11). 3rd Generation Partnership Project (3GPP), Sophia Antipolis Cedex, France, 3GPP TR 36921 11.0.0. https://jwcn-eurasipjournals.springeropen.com/articles/10.1186/1687-1499-2012-54
37. Sadr S, Adve R (2012) Hierarchical resource allocation in femtocell networks using graph algorithms. In: 2012 IEEE International Conference on Communications (ICC), pp 4416–4420
38. Elsherif AR, Chen WP, Ito A, Ding Z (2015) Adaptive resource allocation for interference management in small cell networks. IEEE Trans Commun 63(6):2107–2125
39. 3GPP standard (2010) Evolved universal terrestrial radio access (E-UTRA); further advancements for E-UTRA physical layer aspects (release 9). 3rd Generation Partnership Project (3GPP), Sophia Antipolis Cedex, 3GPP TS 36814 9.0.0. https://jwcn-eurasipjournals.springeropen.com/articles/10.1186/1687-1499-2012-54
40. Elsherif AR, Chen WP, Ito A, Ding Z (2015) Resource allocation and inter-cell interference management for dual-access small cells. IEEE J Sel Areas Commun 33(6):1082–1096
41. Elsherif AR, Chen WP, Ito A, Ding Z (2013) Adaptive small cell access of licensed and unlicensed bands. In: IEEE International Conference on Communications (ICC)

Cognitive Multihoming System for Enhanced Cellular Experience

44

Satyam Agarwal and Swades De

Contents

Abstract

Cellular network service providers are facing acute spectrum shortage due to surging mobile data traffic demand. On the contrary, spectrum measurement studies reveal that large part of the licensed spectrum is being underutilized.

S. Agarwal (✉)
Indian Institute of Technology Guwahati, Guwahati, India
e-mail: satyama@iitg.ernet.in; satyam6099@gmail.com

S. De
Indian Institute of Technology Delhi, New Delhi, India
e-mail: swadesd@iitd.ac.in; swadesd@ee.iitd.ac.in

W. Zhang (ed.), *Handbook of Cognitive Radio*,
https://doi.org/10.1007/978-981-10-1394-2_55

In this chapter, a cognitive multihoming (CM) framework is presented for the cellular network service providers to meet the escalating data demands and provide enhanced quality of service (QoS) to the users. In CM, the conventional cellular base stations (BS) are enabled with cognitive radio (CR) access functionality. Thus, these CR-enabled BS transmit simultaneously to the users over the licensed cellular bands as well as over the CR bands. Communication over CR incurs lower transmission cost at the expense of higher energy consumption due to frequent channel sensing. On the other hand, communication over licensed cellular bands is expensive due to its licensing premium. Performance of CM is analyzed in two scenarios. Multiple real-time (RT) and non-RT users requesting for unicast downlink content are considered in the first scenario, while the second scenario considers multiple users requesting for scalable video content from the network. For the two scenarios, optimal resource allocation and call admission control algorithm are presented. Through the performance results presented in this chapter, it is inferred that the CM strategy can enable the cellular network providers to serve a higher number of users as well as improve the user's QoS in terms of reduced service cost.

Introduction

There has been a manifold growth in Internet traffic demand in recent times. Recent research report by Cisco indicates that the mobile data traffic is expected to grow 10 times by 2022 [1]. Due to these increased demands, it is expected that the present cellular network infrastructure will fall short of providing adequate and high-quality service to the users in the upcoming years [2]. Main reason for this accounts for the lack of adequate licensed spectrum availability. On the other hand, various spectrum measurement studies have indicated that only a small fraction of the licensed spectrum is being used [3]. Cognitive radio (CR) techniques can be employed to combat spectrum resource scarcity in the conventional cellular bands for mobile broadband quality of service (QoS) support.

On the receiver technology front, emergence of multihomed devices (multi-radio clients) [4] has enabled simultaneous access to multiple radio access technology (RAT) in a heterogeneous network. Conventionally, multihoming capability of user devices is used for concurrent multipath transfer (CMT) [5] of data from remotely located source via multiple networks. This approach invites challenges due to network dynamics, leading to selective packet loss over multiple paths and hence the user's difficulty in data decodability. In order to alleviate the spectrum scarcity problem in licensed cellular networks (LCNs) and quality degradation in conventional CMT via wireless networks, a novel paradigm, called cognitive multihoming (CM), was proposed in [6, 7].

Cognitive Multihoming

As depicted in Fig. 1, in CM system the cellular network BS is also equipped with the CR functionality. The BS controller buffers the data packets from the remote data server across the Internet and divides the data stream suitably as per the available LCN and CR network (CRN) resources, and the BS transmits them to the user via LCN and CRN, simultaneously. Multihoming capable users are considered which are equipped with the functionality to operate on both the networks simultaneously. It is considered that the network operates over at least one licensed cellular band and one CR band. LCN can include one of the cellular networks, for example, LTE, WCDMA standards, etc. On the other hand, CRNs can operate over the TVWS bands, ISM bands, etc., utilizing one of the existing IEEE standards such as IEEE 802.22, IEEE 802.11af, etc. Thus, the band over which the LCN and CRN operate are different.

Let us consider downlink communication from BS to the users. In general, the downlink communication is the main bottleneck in providing broadband access to the users. While providing service, the content to be transmitted to the users is pre-buffered at the BS from the external server. Consider that the BSs are enabled with high bandwidth backhaul network such that the content requested by the users can be made available at the BS at a lower delay. Once the user content is buffered, the BS splits the data optimally across the two networks and transmits simultaneously to the users across both the networks.

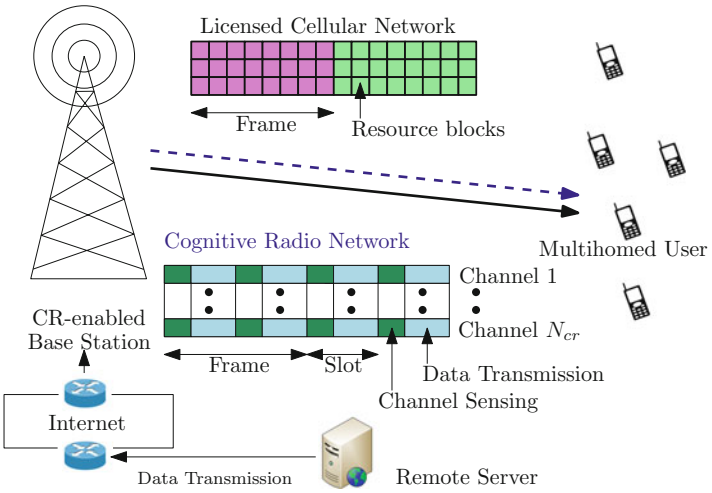

Fig. 1 Illustration of cognitive multihoming

One of the advantage of CM is that the data is split at the BS (last hop to the user) and the external server from which the data is being fetched is not involved in this split. Thus, any additional overhead between BS and data server is saved which is usually not the case in concurrent multipath transmissions. Further, in CMT, packets may arrive out of order due to variable delays along multiple paths leading to congestion-related delays. Thus, this congestion-related delays present in conventional multihoming are not present in CM.

To meet dynamic demands of the real-time users, the service provider (SP) would want to keep its licensed band as idle as possible by making most use of CRN resource. To encourage usage of more CRN resources, data transmission over the CRN is offered at a discounted rate. This is in consonance with the fact that the cellular bands are costly, as the SP pays a huge premium for licensing. Operations over CRNs do not levy high cost to the users due to the opportunistic (secondary) usage of the PU bands.

Transmission cost could be reduced if most of the content is transmitted via CRN. However, due to intermittent PU arrivals and imperfect channel sensing, there could be low throughput over CRN. Moreover, the channel needs to be sensed at regular intervals which further reduces the throughput and energy efficiency. Hence, reception over CRN can be characterized by low cost, low QoS, and low energy efficiency. On the other hand, transmissions over LCN are marked by high cost and high QoS. So, there is an apparent cost-quality-energy tradeoff. The possible degradation in energy efficiency and QoS in CRN can be controlled in CM by optimally allocating resources from LCN and CRN as a function of a user's demand.

LCN and CRN system specific models and assumptions are presented below.

Transmission over LCN

For LCN, let us consider a framework similar to the LTE networks. The LCN resources are divided into time-frequency resource blocks (RBs). Denote B_{rb} and T_{rb}, respectively, as the bandwidth and time duration of an RB. Transmitter rate over an RB depends on the channel conditions. Consider block fading across an RB such that the channel gain remains constant over an RB duration T_{rb}. Let $P_{(lc,tx)}$ denote the BS transmit power. The received signal power $P_{(lc,rx)}$ at a location r distance away from the BS is given by the Friis formula:

$$P_{(lc,rx)} = P_{(lc,tx)} \mathsf{G}_T \mathsf{G}_R \left(\frac{\Lambda}{4\pi r} \right)^{\varepsilon}.$$

Here, G_T and G_R are, respectively, the transmitter and receiver antenna gains, ε is the path loss coefficient, and Λ is the transmitted signal wavelength. Consider Rayleigh fading with zero mean and unit variance between the BS and user. The rate offered to the user by the BS over an RB is given by Shannon's capacity formula $I = B_{rb} \log_2 \left(1 + \frac{h_{lc} P_{(lc,rx)}}{\sigma^2_{(lc,n)}} \right)$, where h_{lc} is the channel fading power gain and

$\sigma^2_{(lc,n)}$ is the noise variance. Outage probability at the user while the BS transmits at rate R bps is given as:

$$P_{out,lc}(R) = Pr(I \leq R) = 1 - exp\left(-\frac{\sigma^2_{(lc,n)}(2^{R/B_{rb}} - 1)}{P_{(lc,rx)}}\right). \tag{1}$$

Transmission over CRN

CRNs make opportunistic use of the licensed PU channels. Consider that there are N_{ch} number of PU channels available at the BS with each PU channel having bandwidth B_{cr}. Time is slotted with each slot duration of T_{cr} units. ON-OFF model [8] for PU transmission is considered over the cognitive radio bands. In this ON-OFF model, PU transmits over a slot in a particular channel with a certain fixed probability. The probability of kth PU channel being idle in a slot is denoted as $p_{cr,k}$. Transmission over CR bands requires sensing the channel for certain duration and transmitting only when the channel is sensed idle. The CR-enabled BS senses the channel for a duration ζ over a slot. If the channel is sensed idle, it transmits over the channel for the remaining time $T_{cr} - \zeta$. The users and the BS are considered colocated in a small geographical area relative to the PU coverage area. Thus, channel conditions at the BS and the users are similar. Probabilities of false alarm $p_{fa}(\zeta)$ and misdetection $p_{md}(\zeta)$ as a function of sensing duration ζ are, respectively, given as [9]:

$$p_{fa}(\zeta) = \text{erfc}\left(\left(\frac{\varepsilon}{\sigma^2_{(cr,u)}} - 1\right)\sqrt{\zeta f_s}\right) \tag{2}$$

$$p_{md}(\zeta) = \text{erfc}\left(\left(\frac{\varepsilon}{\sigma^2_{(cr,u)}} - \gamma - 1\right)\sqrt{\frac{\zeta f_s}{2\gamma + 1}}\right) \tag{3}$$

where $\sigma^2_{(cr,u)}$ is the noise power variance, ε is the sensing threshold, f_s is the channel sampling frequency, and γ is the PU signal SNR at the CR node. The BS transmits to the user over the remaining part of the slot at the rate of R bps if the channel is sensed idle. Packet transmission probability over CRN in a slot is given as:

$$J(\zeta) = (1 - p_{cr})p_{md}(\zeta) + p_{cr}(1 - p_{fa}(\zeta)). \tag{4}$$

Similar to (1), outage probability over the PU channel in CRN due to channel fading is:

$$P_{out,cr}(R) = 1 - exp\left(-\frac{\sigma^2_{(cr,n)}(2^{R/B_{cr}} - 1)}{P_{(cr,rx)}}\right) \tag{5}$$

where $\sigma^2_{(cr,n)}$ is the channel noise variance and $P_{(cr,rx)}$ is the received power over the CRN.

Consider that there are N_u users in the network. Each user requests for a unicast content over the downlink. BS allocates resources over a frame duration. Frame duration $\mathscr{T}$ could be taken as the time over which the packets in a delay-sensitive application are correlated (e.g., duration of group of pictures (GOP) in a video). Denote $\mathscr{N}_{rb}$ as the maximum number of RBs available to the users in a GOP. Channel is sensed by the BS in each slot, and it transmits over the remaining slot if the channel is sensed idle. It is assumed that the BSs efficiently manage the PU bands over which each of them would operate such that there is no interference caused to the users due to transmissions from different BSs operating over CRN.

To understand the performance of CM, two example scenarios are considered. In the general scenario, multiple heterogeneous users request different type of traffic (real-time (RT) or non-RT (NRT)), with each user having different rate requirements and cost constraints. The resources from the two networks can be split according to the cost constraints of the different users to ensure their satisfaction while maintaining some degree of fairness. Due to a minimum rate requirement for the RT users, all RT-QoS requests may not be admitted. To this end, call admission control along with the optimal multihomed resource allocation algorithm is presented to maximize the network utility.

In the application-specific scenario, the multihomed users request unicast scalable video encoded content from the CM network. For battery-operated devices, user satisfaction depends on the received video quality, device battery level, and the cost it paid for the content reception. To this end, in addition to transmission rate adaptation over single network [10], in the presented CM approach, two novel techniques of video packet priority-dependent sensing duration adaptation and network selection for packet retransmission are included to enhance user experience (QoS, energy saving, cost) without causing PU performance degradation.

Performance Evaluation of CM-Based Access

Performance of CM is evaluated against two test scenarios. In the first scenario, multiple multihomed users request either real-time (RT) or non-RT traffic. In the second scenario, users request for unicast scalable video from the network.

General Performance Measures

In this scenario, multiple multihomed users are considered requesting heterogeneous content from the network. Users request heterogeneous content which can be broadly classified under two types: RT and NRT. An RT application, like video streaming and voice over IP, typically requires a minimum data rate d_{min} for its operation, while its requested rate is d_{req} to ensure a high QoS. For NRT (delay-tolerant) applications, such as file transfers and web browsing, the typical demanded

rate per user is d_{req}, while $d_{min} = 0$. For the analytical exposition, all users' rates d_{min} and d_{req} are denoted as per-frame rates.

Consider that the BS transmits to the users at a fixed rate of R_{lc} bps over LCN and $R_{cr,k}$ bps over the kth PU channel. The probability of successful packet transmission over an RB is given as $s_{lc} = 1 - P_{out,lc}(R_{lc})$. Data transmitted per RB is $d_{rb} = R_{lc}T_{rb}$. Over the CRN, consider that the BS senses the PU channel for a fixed duration of ζ. The successful packet transmission probability over the kth PU channel is given as $s_{cr,k} = (1 - p_{cr,k})(1 - p_{fa}(\zeta))(1 - P_{out,cr}(R_{cr,k}))$. The amount of data transmitted over the kth PU channel is $d_{cr,k} = R_{cr,k}(T_{cr} - \zeta)$ bits per slot.

User satisfaction can be expressed in terms of QoS offered and cost charged. QoS of a user is defined as the quality of content received, which is modeled as a utility function. Users are charged based on the amount of data they receive via CM. A cost constraint metric $\chi \in [0, 1]$ is maintained by each user. This metric indicates *the maximum fraction of cost (compared to the cost required for service through LCN) the user is willing to pay for its service*. A higher χ indicates that the user is willing to pay a higher premium for its service.

The SP's goal is to maximize the network utility, which is the sum of all users utility. This is achieved by optimally allocating the resources across different networks to the different users in CM. User's utility and cost are introduced next.

User Utility and Cost

User QoS is modeled in terms of a utility function, which is expressed as a function of the amount of resources allocated to the user by the network [11]. User's utility $\mathscr{U}$ depends on whether the user requests for an RT or an NRT traffic. The successful transmission rate of a user per frame is denoted as d_{suc}. $\mathscr{U}$ is given as [12]:

$$\mathscr{U} = \begin{cases} 1 - e^{(-c_1 d_{suc}/d_{req})}, & \text{NRT application} \\ \frac{1}{1+c_2 e^{(-c_3 d_{suc}/d_{req})}}, & \text{RT application} \end{cases}. \tag{6}$$

c_1, c_2, and c_3 are positive constants determined by the minimum and maximum utility obtained by the users corresponding to their successful transmission rates $d_{suc} = \{0, d_{req}\}$. Figure 2a plots the utility for NRT users which shows a steeply increasing nature with the increase in d_{suc}. On the other hand, Fig. 2b presents the utility for the RT users which follows the sigmoid function.

Denote a_{lc} as the total number of RBs allocated to the user from LCN and denote $a_{cr,k}$ as the number of slots allocated over the kth channel of CRN per frame. These are determined by the resource allocation algorithm presented in section "Resource Allocation Optimization Problem". Successful data transmission $d_{suc} = b_{lc}d_{lc} + \sum_{k=1}^{N_{ch}} b_{cr,k}d_{cr,k}$, where b_{lc} is the number of RBs out of a_{lc} with successful packet transmission and $b_{cr,k}$ is the number of successful transmission slots in $a_{cr,k}$ allocated slots.

Next, let us arrive at a relation between b_{lc} (or $b_{cr,k}$) and a_{lc} (or $a_{cr,k}$). The user utility depends on the successful transmissions per frame. Probability that $b_{lc} = j$ out of a_{lc} RBs in LCN is successful is expressed as:

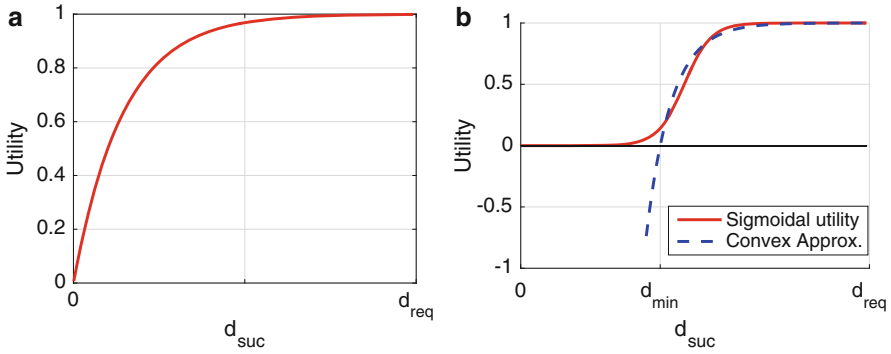

Fig. 2 User utility plot for RT and NRT traffic. (**a**) Non real-time. (**b**) Real-time

$$Pr(b_{lc} = j) = \binom{a_{lc}}{j} (s_{lc})^j (1 - s_{lc})^{(a_{lc} - j)} \tag{7}$$

which follows a binomial distribution. Similarly the probability of $b_{cr,k} = j$ successful slots out of $a_{cr,k}$ over CRN is:

$$Pr(b_{cr,k} = j) = \binom{a_{cr,k}}{j} (s_{cr,k})^j (1 - s_{cr,k})^{(a_{cr,k} - j)}. \tag{8}$$

The total number of successful slots for a user is given as:

$$d_{suc} = b_{lc} d_{lc} + \sum_{k=1}^{N_{ch}} b_{cr,k} d_{cr,k}. \tag{9}$$

d_{suc} is the sum of $N_{ch} + 1$ binomial random variables. Probability mass function (pmf) of d_{suc} is obtained by the convolution of (7) and (8) $\forall\ k = 1, 2, \cdots, N_{ch}$ PU channels. Closed form expression for pmf of d_{suc} is not possible. Hence, numerical techniques must be used as suggested in [13].

As computation of d_{suc} is analytically intractable (the closed form for d_{suc} cannot be obtained) and computationally intensive (obtaining d_{suc} using numerical methods scales up exponentially with N_{ch}), the mean value of d_{suc}, i.e., $d_{suc} = a_{lc} d_{lc} s_{lc} + \sum_{k=1}^{N_{ch}} a_{cr,k} d_{cr,k} s_{cr,k}$ is considered for the utility computation in further analysis.

The cost $\mathscr{C}$ to a user is the price charged by the SP in successfully transmitting the data via CM. This is given as:

$$\mathscr{C} = b_{lc} d_{rb} \mathscr{C}_{lc} + \sum_{k=1}^{N_{ch}} b_{cr,k} d_{cr,k} \mathscr{C}_{cr} \tag{10}$$

where $\mathscr{C}_{lc}$ is the price charged per successful bit transmission over LCN by the SP, while $\mathscr{C}_{cr}$ is the price charged by the SP per successful bit transmission over the CRN. A user maintains a cost constraint χ, which specifies the maximum amount it is willing to pay for its request. Accounting χ, user's cost is bounded by

$$\mathscr{C} \leq c_{max} = \chi d_{req} \mathscr{C}_{lc}. \tag{11}$$

Resource Allocation Optimization Problem

There are a total of N_u users in the system requesting for unicast downlink content from the BS. Each RT user specifies its d_{min}, d_{req}, and the cost constraint χ. Similarly, each NRT user specifies its d_{req} and χ. To indicate the individual requirements, for the ith user, the superscript i is used over the variable.

The controller objective is to maximize the overall network utility, which is a sum of all users' utility. The optimization problem can be formulated as:

$$\begin{aligned}
\underset{a^i_{lc}, a^i_{cr,k}}{\text{maximize}} \quad & \sum_{i=1}^{N_u} \mathscr{U}^i \\
\text{s.t.} \quad & \mathscr{C}^i \leq c^i_{max}, \ \forall i = 1, 2, \cdots, N_u, \\
& \frac{\left(\sum_{i=1}^{N_u} \sum_{k=1}^{N_{ch}} a^i_{cr,k} d_{cr,k}\right)^2}{N_u \sum_{i=1}^{N_u} \left(\sum_{k=1}^{N_{ch}} a^i_{cr,k} d_{cr,k}\right)^2} \geq \beta, \\
& \sum_{i=1}^{N_u} a^i_{lc} \leq \mathscr{N}_{rb}, \\
& \sum_{i=1}^{N_u} a^i_{cr,k} \leq \frac{\mathscr{T}}{T_{cr}}, \ k = 1, \ldots, N_{ch}.
\end{aligned} \tag{12}$$

In the above optimization problem, the first constraint limits the cost incurred by the users to their maximum desired cost. The second constraint limits a fair usage of CRN resources among different users. The left-hand side of the second constraint is based on Jain's fairness index [14] on resources allocated to the users via CRN. For the ith user, $\sum_{k=1}^{N_{ch}} a^i_{cr,k} d_{cr,k}$ is the resource allocated via CRN. The fairness index is lower bounded to a constraint β to ensure that the low-cost CRN resources are fairly allocated among the users. This ensures that the greedy users are not unduly benefited by choosing a low χ. The third and the forth constraints are the maximum resource availability constraints.

The utility function of RT users is a sigmoid function which is nonconvex. The first, third, and forth constraints in this problem are linear, while the second constraint is convex. To obtain an equivalent convex problem for this optimization problem, the convex approximation of the sigmoid function is presented next followed by the solution to this problem.

Solution to the Optimization Problem and Call Admission Control Algorithm

The utility function for an RT application is a sigmoid function (cf. (6)) which is nonconvex. Consider $\mathscr{U}_c$ as the convex approximation to this function, which is given as:

$$\mathscr{U}_c = 1 - e^{-c_4(d_{suc} - d_{min})/d_{req}} \tag{13}$$

where c_4 is a constant. Here, it is noted that the utility function of the RT users for $d_{suc} < d_{min}$ is close to 0 as shown in Fig. 2b. This is indicative of the fact that RT applications require a minimum resource d_{min} to work. With $\mathscr{U}_c$, the convex approximation function closely matches with the sigmoid function in the range $d_{suc} \geq d_{min}$. However, for $d_{suc} < d_{min}$, the value of the convex approximation is negative which serves as a penalty, indicating that for an RT application, rate lower than d_{min} is inadmissible. If, for a particular RT user, its $\mathscr{U}_c$ turns out to be negative after optimization, it is better to drop the user because in this case the network is unable to provide the user its minimum data rate requirement. This would be seen later in this section.

A new convex optimization problem is formulated with the utility function of RT users replaced by its convex approximation as seen in (13). Typically the network operates in the saturation region where all the network resources are allocated to the users. Hence $\sum_{i=1}^{N_u} \sum_{k=1}^{N_{ch}} a_{cr,k}^i d_{cr,k}$ can be taken equal to $\sum_{k=1}^{N_{ch}} d_{cr,k} \mathscr{T}/T_{cr}$. The optimal allocation of resources (a_{lc}^i and $a_{cr,j}^i$) to the ith user can be obtained by solving the formed convex optimization problem using the dual decomposition and subgradient method [15].

After optimization of the formulated convex optimization problem, for some RT users, their obtained utility from the approximated convex function could be negative. This is because the network is unable to provide a minimum data rate d_{min} to these users. Hence, the network chooses to block these users resulting in nonadmission into the network. In the resource allocation optimization process, the RT user with most negative $\mathscr{U}_c$ is blocked/dropped, a new optimization problem with the remaining users is solved using similar method, and the process is repeated. The process is repeated until all the users obtain positive $\mathscr{U}_c$. At this point, the solution obtained is considered the optimal solution to the optimization problem. Figure 3 presents a flowchart for the admittance of users in the network and computation of the optimal resource allocation.

Algorithm Performance

Two example scenarios are considered to demonstrate the performance of the presented convex approximation algorithm. In the first scenario, a network consisting of 50 RT users is considered, while, in the second scenario, network with 40 RT users is considered. All RT users request for data rate uniformly distributed in the range of 0.5 to 1 Mbps. For the two scenarios, the actual network utility and the network utility corresponding to the convex approximation function (cf. (13)) are plotted

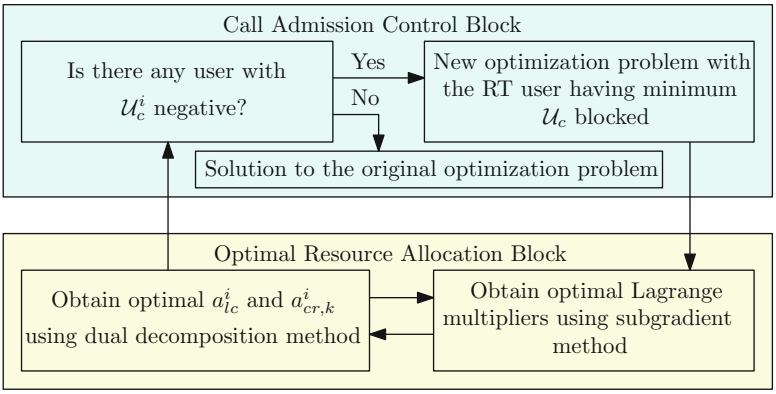

Fig. 3 Algorithm for optimal resource allocation

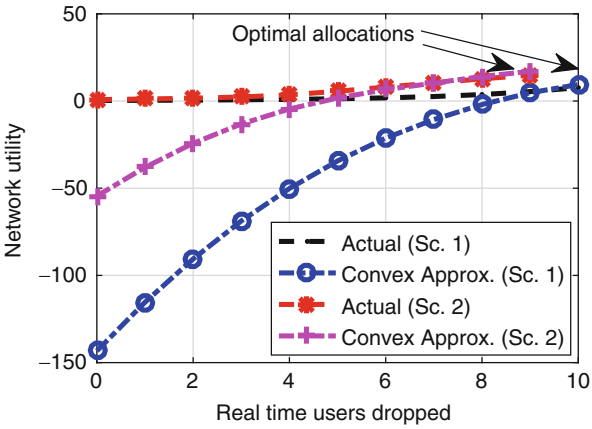

Fig. 4 Convergence of the presented convex approximation algorithm. $\beta = 0.7$. (Sc.: Scenario)

in Fig. 4. A user is blocked at each iteration whenever its utility corresponding to the convex approximation function $\mathscr{U}_c$ is negative at the optimal resource allocation. After each iteration, the optimization problem is solved with the remaining users and the resources are again allocated among those users. It is observed that the network utility via convex approximation converges toward the actual network utility at each iteration. At the optimal point, it is concluded that the actual utility and the utility via convex approximation closely match. Additionally, the number of iterations is upper bounded by the number of RT users present in the system.

CM performance in the video-specific application scenario is presented below.

Application-Specific Considerations

In this scenario, multiple multihoming capable users request unicast scalable video encoded content from the network. The user devices are battery operated. For these

devices, user satisfaction depends on the video quality received, device battery level, and the cost the user paid for the content reception. Toward this goal, in the considered CM approach, video packet priority-dependent sensing duration and transmission rate adaptation and network selection for packet retransmission are included to enhance user experience (QoS, energy saving, cost) without causing PU performance degradation.

The video traffic model, user device capabilities, and video transmission mechanism to a CM user are briefly introduced below.

Video Traffic Model

Multihomed users request for scalable video coding (SVC) encoded video content from the network. SVC video encoder allows graceful degradation of video quality caused by wireless channel fading. It consists of a base layer (denoted as layer 1) and several enhancement layers (denoted as layers $2, 3, \cdots, L$). Layer l_1 has a higher priority over layer l_2 if $l_1 < l_2$. Base layer provides the basic quality level of the video, and it is decoded independently of the higher layers. Enhancement layer l_1 can only be decoded once all the layers $l < l_1$ are decoded. Each layer is independently encoded at a specific rate.

Similar to the approaches in [4, 16], distortion of H.264/SVC encoded video can be quantified in terms of video encoding-induced distortion and distortion due to packet loss in video transmission. It can be quantified as $\mathscr{D} = \mathscr{D}_{enc} + \mathscr{D}_{loss}$. $\mathscr{D}_{enc}$ is the average encoding distortion, given as $\mathscr{D}_{enc} = D_0 + \frac{\theta_0}{X - \mathscr{R}_0}$. Here, X is the average bit rate, and parameters D_0, θ_0, and $\mathscr{R}_0$ are constants that depend on the encoder and video characteristics. Packet-loss-induced distortion $\mathscr{D}_{loss}$ is independent of $\mathscr{D}_{enc}$. Denoting φ_l as the probability of lth layer content loss, $\mathscr{D}_{loss}$ can be expressed as:

$$\mathscr{D}_{loss} = \sum_{l=1}^{L} \varphi_l \Omega_l, \quad \text{where } \Omega_l = \left(\frac{\theta_0}{X_{l-1} - \mathscr{R}_0} - \frac{\theta_0}{X_l - \mathscr{R}_0} \right). \tag{14}$$

Ω_l is the weight associated with the lth layer and X_l is the rate of the video content up to l layers.

Video quality metric $\mathscr{Q}$ is defined as the distortion impact of the packets received correctly to the total available packets [17]. It is given as:

$$\mathscr{Q} = \frac{\sum_{l=1}^{L} \Omega_l (1 - \varphi_l)}{\sum_{l=1}^{L} \Omega_l} \cdot 100\%. \tag{15}$$

Video stream is divided into group of pictures (GOP) with each GOP duration of $\mathscr{T}$ units.

User Device Capability

The users are equipped with multihoming capable devices. All user devices are considered battery operated, and therefore their respective reception processes are sensitive to the remaining battery energy. Part of this energy consumption is due to

reception of the video content over the two networks. Consequently, the remaining battery level determines the upper bound on energy consumption for video reception and the quality of video (number of layers) requested by the user.

As noted in the experimental studies in [18, 19], energy consumption in mobile devices due to network interface is mainly on three fronts, namely, ramp, tail, and data transfer energy. Ramp energy is consumed when the radio transits from *idle* state to *transmit* state. Data transfer energy is proportional to the duration of time the radio is transmitting/receiving. Tail energy refers to the lingering of the radio at high-energy states during the inactivity period after the transmission is over, which is on the order of tens of seconds [18]. The network transmits to the device for a fraction of time in a GOP. Thus, reception energy is consumed for the time device is actually receiving, and the tail energy is consumed when the device is idle in a GOP. The device does not incur ramp energy consumption, as the radio mostly remains in the high-energy state during the reception.

Along with meeting the energy consumption constraints, the network should ensure high-quality video reception to the user end at a low cost. The communication cost (cost charged to the user) is proportional to the amount of resources allocated via the two networks. A user is more satisfied when it receives the video content at a lower cost while satisfying its energy consumption constraint.

Video Transmission to CM User

The BS transmits video stream to a user optimally across the two networks such that the user's cost is minimized subject to the user's energy consumption and video quality constraints. Note that the user cost minimization by SP does not affect its revenue maximization objective, as the profit to SP may be completely different over the two networks. Video content for a GOP is considered available at the BS before the GOP starts. Consider that the BS is capable of performing layer-based video transmission. It can form packets of desired length and transmits them to a user. A lost packet is retransmitted by the BS (based on acknowledgement (ACK) notification via independent LCN RBs) to the user up to a layer-dependent predefined number (n_l) of retransmission attempts. The undelivered packets within a GOP duration are dropped, resulting in distortion. For enhanced user experience, transmission rate adaptation over the LCN, sensing duration and transmission rate adaptation over the CRN, and number of retransmission attempts and network selection for retransmission are optimized for each layer of video transmission. These three mechanisms are detailed as follows.

Transmission rate adaptation over LCN/CRN: According to (1) and (5), a higher transmission rate has a lower probability of success. However, higher transmission rate introduces lower cost as well as energy consumption to the user. Hence, while the lower layers (high distortion impact) are transmitted at a lower rate so that their correct reception probability is higher, the higher layers are transmitted at a higher rate.

Sensing duration adaption over CRN: Sensing duration ζ over a slot plays a key role in determining the reception performance. With a small ζ, probabilities of misdetection and false alarm are large, but the available transmission duration is also longer. Therefore, for balanced cost and quality, the different priority of video packets ζ can be accordingly chosen.

Cross network retransmissions: Video packets transmitted can be lost due to path loss, channel fading, or channel sensing misdetections. Such packets are retransmitted within the allowable GOP time window to reduce distortion at the receiver. Network selection for retransmission is also critical. Retransmission over CRN could reduce cost, however, at a higher energy consumption. If the retransmission request for the lth layer content initially transmitted over LCN is received by the BS, it can either retransmit the content over LCN or CRN.

Analysis of CM-Based Resource Allocation

The multiuser scenario is considered, where a fixed pool of total channel resource is traded with multiple user demands of video content delivery. First, the multiuser resource allocation optimization problem is presented. Subsequently, to achieve solution of the multiuser optimization, for an individual user, single-user cost minimization problem is solved.

Problem Formulation

Due to limited resource availability at the BS, out of N_u users requesting scalable video content, some of the user requests may not be fulfilled, leading to their nonadmission to the network. Resource allocation by the BS is such that the user cost is minimized while the number of users served is maximized. In this example scenario, only a single PU channel is considered available at the BS to serve the users.

For a user requesting L layers of video content, let d_l amount of data (in bits) be transmitted for the lth layer content over a GOP. The BS transmits data of layer l at a rate $R_{lc,l}$ over LCN and at a rate $R_{cr,l}$ over CRN. Denote the sensing duration for layer l packet as ζ_l. Also, denote that the lth layer content can be retransmitted at most $\lceil n_l \rceil$ times, where n_l can take a fractional value in general. It is upper bounded by n_{max}, which is the maximum number of retransmissions allowed for any individual packet within a GOP. Let $p_{lc,l}^{rtx}$ (respectively, $p_{cr,l}^{rtx}$) be the probability that the retransmission of lth layer content transmitted initially over LCN (respectively, CRN) is carried out over LCN (respectively, CRN) itself.

As the data stream d_l is split across the two networks, let u_l amount be initially transmitted over CRN. The remaining data volume $(d_l - u_l)$ is initially transmitted over LCN. To compute the total traffic over LCN for the lth layer content, it is noted that, due to wireless channel uncertainties, part of the failed

data is retransmitted over LCN (with probability $p_{lc,l}^{rtx}$). The remaining volume of retransmission is over CRN, with probability $(1 - p_{lc,l}^{rtx})$. Given the maximum number of retransmissions n_l for the lth layer, $\sum_{i=0}^{n_l} P_{out,lc}(R_{lc,l})^i = \frac{1-P_{out,lc}(R_{lc,l})^{n_l+1}}{1-P_{out,lc}(R_{lc,l})}$ is the expected number of transmission attempts carried out including the initial transmission for the part of data retransmitted over LCN. Hence, for transmitting $(d_l - u_l)$ data over LCN, the expected data transmission over LCN is $(d_l - u_l)\left(p_{lc,l}^{rtx}\left(\frac{1-P_{out,lc}(R_{lc,l})^{n_l+1}}{1-P_{out,lc}(R_{lc,l})}\right) + 1 - p_{lc,l}^{rtx}\right)$. The data transmitted over CRN could also be lost due to misdetection in channel sensing, path loss, and channel fading. The probability of packet transmission failure $P_{e,cr}(\zeta_l, R_{cr,l})$ over CRN is given as:

$$P_{e,cr}(\zeta_l, R_{cr,l}) = (1 - p_{cr})p_{md}(\zeta_l) + p_{cr}(1 - p_{fa}(\zeta_l))P_{out,cr}(R_{cr,l}). \tag{16}$$

Part of the lost data is retransmitted over LCN. Out of the original share of transmitted data u_l over CRN, the amount of data retransmitted over LCN is $u_l(1 - p_{cr,l}^{rtx})P_{e,cr}(\zeta_l, R_{cr,l})$. The expected number of retransmissions over LCN is $\sum_{i=0}^{n_l-1} P_{out,lc}(R_{lc,l})^i = \frac{1-P_{out,lc}(R_{lc,l})^{n_l}}{1-P_{out,lc}(R_{lc,l})}$ for the data retransmitted over LCN. Overall, the total amount of data transmitted over LCN for the lth layer in a GOP is:

$$\begin{aligned} w_{lc,l} =& (d_l - u_l)\left(p_{lc,l}^{rtx}\left(\frac{1 - P_{out,lc}(R_{lc,l})^{n_l+1}}{1 - P_{out,lc}(R_{lc,l})}\right) + 1 - p_{lc,l}^{rtx}\right) \\ &+ u_l(1 - p_{cr,l}^{rtx})P_{e,cr}(\zeta_l, R_{cr,l})\frac{1 - P_{out,lc}(R_{lc,l})^{n_l}}{1 - P_{out,lc}(R_{lc,l})}. \end{aligned} \tag{17}$$

Similarly, total lth layer data transmission over CRN in a GOP is obtained as:

$$\begin{aligned} w_{cr,l} =& u_l\left(p_{cr,l}^{rtx}\left(\frac{1 - P_{e,cr}(\zeta_l, R_{cr,l})^{n_l+1}}{1 - P_{e,cr}(\zeta_l, R_{cr,l})}\right) + 1 - p_{cr,l}^{rtx}\right) \\ &+ (d_l - u_l)(1 - p_{lc,l}^{rtx})P_{out,lc}(R_{lc,l})\frac{1 - P_{e,cr}(\zeta_l, R_{cr,l})^{n_l}}{1 - P_{e,cr}(\zeta_l, R_{cr,l})}. \end{aligned} \tag{18}$$

Probability of packet transmission failure for the data transmitted (including retransmission) via LCN is $P_{out,lc}(R_{lc,l})^{n_l+1}$, while that for the data transmitted over LCN and retransmitted over CRN is $P_{out,lc}(R_{lc,l})P_{e,cr}(\zeta_l, R_{cr,l})^{n_l}$. Hence, for $(1 - u_l/d_l)$ fraction of lth layer content initially transmitted over LCN, probability of failure after retransmissions is $(p_{lc,l}^{rtx}P_{out,lc}(R_{lc,l})^{n_l+1} + (1 - p_{lc,l}^{rtx})P_{out,lc}(R_{lc,l})P_{e,cr}(\zeta_l, R_{cr,l})^{n_l})$. Similarly for u_l/d_l fraction of the lth layer content, the probability of transmission failure is $\left(p_{cr,l}^{rtx}P_{e,cr}(\zeta_l, R_{cr,l})^{n_l+1} + (1 - p_{cr,l}^{rtx})P_{e,cr}(\zeta_l, R_{cr,l})P_{out,lc}(R_{lc,l})^{n_l}\right)$. Consolidating, probability of lth layer content loss is given as:

$$\varphi_l = \left(1 - \frac{u_l}{d_l}\right)\left(p_{lc,l}^{rtx} P_{out,lc}(R_{lc,l})^{n_l+1} + (1 - p_{lc,l}^{rtx}) P_{out,lc}(R_{lc,l}) P_{e,cr}(\zeta_l, R_{cr,l})^{n_l}\right) + \frac{u_l}{d_l}\left(p_{cr,l}^{rtx} P_{e,cr}(\zeta_l, R_{cr,l})^{n_l+1} + (1 - p_{cr,l}^{rtx}) P_{e,cr}(\zeta_l, R_{cr,l}) P_{out,lc}(R_{lc,l})^{n_l}\right). \tag{19}$$

The overall received video quality is quantified using (15).

A packet is transmitted per RB/slot with a header overhead of H_l bits. From (17), the amount of LCN RBs required by the user is given as:

$$N_{rb} = \sum_{l=1}^{L} \frac{w_{lc,l}}{(R_{lc,l} T_{rb} - H_l)} \tag{20}$$

while the spectrum leasing duration over CRN using (18) is:

$$T = T_{cr} \sum_{l=1}^{L} \frac{w_{cr,l}}{J(\zeta_l)(R_{cr,l}(T_{cr} - \zeta_l) - H_l)}. \tag{21}$$

Over LCN, cost of communication charged to the user is proportional to the number of RBs allocated to the user. Denoting cost charged per unit time as $\mathbb{C}_{lc}$, cost to the user over LCN is:

$$\mathscr{C}_{lc} = \mathbb{C}_{lc} T_{rb} \sum_{l=1}^{L} \frac{w_{lc,l}}{(R_{lc,l} T_{rb} - H_l)}. \tag{22}$$

Over the CRN, cost to the user is considered proportional to the time duration the spectrum is leased for its service. Let $\mathbb{C}_{cr}$ be the cost to the user per unit time. So, the user cost over CRN is:

$$\mathscr{C}_{cr} = \mathbb{C}_{cr} T_{cr} \sum_{l=1}^{L} \frac{w_{cr,l}}{J(\zeta_l)(R_{cr,l}(T_{cr} - \zeta_l) - H_l)}. \tag{23}$$

Energy consumption on account of reception over LCN is:

$$\Phi_{lc} = (\xi_{lc,rx} - \xi_{lc,ta}) T_{rb} \sum_{l=1}^{L} \frac{w_{lc,l}}{(R_{lc,l} T_{rb} - H_l)} + \xi_{lc,ta} \mathscr{T} \tag{24}$$

where reception and tail power consumption over LCN are, respectively, $\xi_{lc,rx}$ and $\xi_{lc,ta}$. Over CRN, the device remains in receive mode in the entire slot duration. Denoting receive and tail power consumption over CRN, respectively, as $\xi_{cr,rx}$ and $\xi_{cr,ta}$, total energy consumption in reception over CRN is:

$$\Phi_{cr} = (\xi_{cr,rx} - \xi_{cr,ta}) T_{cr} \sum_{l=1}^{L} \frac{w_{cr,l}}{J(\zeta_l)(R_{cr,l}(T_{cr} - \zeta_l) - H_l)} + \xi_{cr,ta} \mathscr{T}. \tag{25}$$

For the multiuser resource allocation optimization formulation, superscript k is used over a variable to denote it for the kth user. Depending on the remaining battery level, the kth user requests $L^{(k)}$ layers of the video content at a minimum quality threshold $\mathscr{Q}_{th}^{(k)}$ and a maximum energy consumption constraint $E_{th}^{(k)}$. Let $\psi^{(k)} = 1$ (respectively, 0) denote the user k served (respectively, not served). A reward Θ is associated with each user admitted. The resource allocation optimization problem is presented in (26).

$$\mathscr{C}_{net}^{*} = \text{minimize} \sum_{k=1}^{N_u} \left(\mathscr{C}_{lc}^{(k)} + \mathscr{C}_{cr}^{(k)} - \Theta \right) \psi^{(k)} \tag{26}$$

$$\text{s.t.} \quad C1: \frac{\sum_{l=1}^{L^{(k)}} \Omega_l^{(k)} \left(1 - \varphi_l^{(k)}\right)}{\sum_{l=1}^{L} \Omega_l^{(k)}} \cdot 100\% \geq \mathscr{Q}_{th}^{(k)}, \; k \in 1, 2, \cdots, N_u,$$

$$C2: \Phi_{lc}^{(k)} + \Phi_{cr}^{(k)} \leq E_{th}^{(k)}, \; k \in 1, 2, \cdots, N_u,$$

$$C3: p_{md}^{(k)}(\zeta_l) \leq p_{md}^{th}, \; \forall \; l \in 1, 2, \cdots, L^{(k)}, \; k \in 1, 2, \cdots, N_u,$$

$$C4: n_l^{(k)} \leq n_{max}, \; \forall \; l \in 1, 2, \cdots, L^{(k)}, \; k \in 1, 2, \cdots, N_u,$$

$$C5: u_l^{(k)} \leq d_l^{(k)}, \; \forall \; l \in 1, 2, \cdots, L^{(k)} \; k \in 1, 2, \cdots, N_u,$$

$$C6: \sum_{k=1}^{N_u} N_{rb}^{(k)} \psi^{(k)} \leq \mathscr{N}_{rb},$$

$$C7: \sum_{k=1}^{N_u} T^{(k)} \psi^{(k)} \leq \mathscr{T},$$

$$C8: \psi^{(k)} \in \{0, 1\}, \; \forall \; k \in 1, 2, \cdots, N_u.$$

The optimization problem (26) jointly maximizes the number of users served and minimizes the cost of video transmission to the users while ensuring their demanded quality (cf. C1) and energy consumption (cf. C2) constraints. To protect the PUs from interference due to CR activity, the sensing duration is chosen such that the probability of misdetection is upper bounded by p_{md}^{th} (cf. C3). C4 bounds the number of packet retransmissions to n_{max}, while C5 upper bounds u_l to the lth layer content d_l. Constraints C6 and C7 are the resource availability constraints, respectively, over LCN and CRN.

Due to the integer variable $\psi^{(k)}$, the above problem is an integer optimization problem which is NP hard. The solution to this problem is presented below.

Algorithm 1: Resource allocation in multiuser scenario

1. Obtain optimal resource requirements for each user k. Optimal cost to the user, number of LCN RBs, and PU channel leasing duration are $\mathscr{C}^{(k)*}$, $N_{rb}^{(k)*}$, and $T^{(k)*}$, respectively;
2. Arrange the users in the increasing order of their optimal cost $\mathscr{C}^{(k)*}$;
3. Set the available resources: $N_{rb}^{a} \leftarrow \mathscr{N}_{rb}$ and $T^{a} \leftarrow \mathscr{T}$ and $j = 1$;

while $j \leq N_u$ **do**
  if $N_{rb}^{(j)*} \leq N_{rb}^{a}$ *and* $T^{(j)*} \leq T^{a}$ **then**
    4. Allocate resources to the jth user;
    5. Update the available resources $N_{rb}^{a} \leftarrow N_{rb}^{a} - N_{rb}^{(j)*}$ and $T^{a} \leftarrow T^{a} - T^{(j)*}$;
    6. $j \leftarrow j + 1$;
  else
    if $N_{rb}^{(j)*} > N_{rb}^{a}$ **then**
      7. Drop the user ;
      8. $j \leftarrow j + 1$;
    else
      9. Recompute optimal resource requirements with available CRN resource constraint $T^{(j)} \leq T^{a}$;
      10. Sort the remaining users (including the jth user) again in the increasing order of their optimal cost $C^{(j)*}$;
    end
  end
end

Solution to the Optimization Problem

A higher number of users can be served if the users are allocated resources in the increasing order of their demands. From (22) and (23), it is noted that the cost to a user is directly proportional to the resource allocated. For each user, the optimal resource requirement and corresponding optimal cost to the user are independently computed (as would be seen later in this section). A user with lower cost is served first, subject to resource availability. As noted later in section "Multiuser Operation", the users with stronger energy consumption constraint are allocated resources via LCN as they cannot be supported by CRNs. Thus, if for a user the available LCN RBs are less than the required RBs, the user would not be admitted in to the network. On the other hand, if the available CRN resource is less than the required CRN resource for a user, then optimal resource requirement for the user is recomputed after updating the CRN resource constraint. The remaining users are again sorted in the increasing order of their optimal cost and the allocation process continues. The algorithm is presented in Algorithm 1, which provides an optimal solution as it simultaneously achieves low cost to the users while maximizing the number of users served.

Resource allocation optimization to single user: In steps 1 and 9 of Algorithm 1, the optimal resource and cost to the individual users are required. To obtain this, a cost minimization problem is solved for a single user. The optimization problem

is formulated in (27), where superscript k (to indicate the kth user) is omitted for brevity.

$$\mathscr{C}^* \triangleq \mathscr{C}^*_{lc} + \mathscr{C}^*_{cr} = \underset{\substack{R_{lc,l},\zeta_l,R_{cr,l},u_l,\\ n_l,p^{rtx}_{lc,l},p^{rtx}_{cr,l}}}{\text{minimize}} \sum_{l=1}^{L} \left(\mathbb{C}_{lc} T_{rb} \frac{w_{lc,l}}{(R_{lc,l} T_{rb} - H_l)} + \mathbb{C}_{cr} T_{cr} \frac{w_{cr,l}}{J(\zeta_l)(R_{cr,l}(T_{cr} - \zeta_l) - H_l)} \right) \tag{27}$$

s.t. $C1 - C5$ from (26) (superscript k removed for brevity),

$$C6a : \sum_{l=1}^{L} \frac{w_{lc,l}}{(R_{lc,l} T_{rb} - H_l)} \leq N^a_{rb},$$

$$C7a : \sum_{l=1}^{L} \frac{w_{cr,l}}{J(\zeta_l)(R_{cr,l}(T_{cr} - \zeta_l) - H_l)} \leq \frac{T^a}{T_{cr}},$$

$$C9 : (d_l - u_l) \left(p^{rtx}_{lc,l} \left(\frac{1 - P_{out,lc}(R_{lc,l})^{n_l+1}}{1 - P_{out,lc}(R_{lc,l})} \right) + 1 - p^{rtx}_{lc,l} \right) + u_l (1 - p^{rtx}_{cr,l}) \cdot P_{e,cr}(\zeta_l, R_{cr,l}) \frac{1 - P_{out,lc}(R_{lc,l})^{n_l}}{1 - P_{out,lc}(R_{lc,l})} = w_{lc,l} \ \forall\ l \in 1, 2, \cdots, L,$$

$$C10 : u_l \left(p^{rtx}_{cr,l} \left(\frac{1 - P_{e,cr}(\zeta_l, R_{cr,l})^{n_l+1}}{1 - P_{e,cr}(\zeta_l, R_{cr,l})} \right) + 1 - p^{rtx}_{cr,l} \right) + (d_l - u_l)(1 - p^{rtx}_{lc,l}) \cdot P_{out,lc}(R_{lc,l}) \frac{1 - P_{e,cr}(\zeta_l, R_{cr,l})^{n_l}}{1 - P_{e,cr}(\zeta_l, R_{cr,l})} = w_{cr,l} \ \forall\ l \in 1, 2, \cdots, L.$$

N^a_{rb} in C6a and T^a in C7a are the available resources over LCN and CRN, respectively. C9 and C10 are the constraints corresponding to the amount of lth layer content transmitted over LCN ($w_{lc,l}$) and CRN ($w_{cr,l}$), respectively.

The factor $J(\zeta_l)$ appearing in the energy (cf. (25)), cost (cf. (23)), and in the CRN resource constraint C7a is nonconvex in ζ_l. The terms $P_{out,lc}(R_{lc,l})$ and $P_{e,cr}(\zeta_l, R_{cr,l})$ in constraints C1, C9, and C10 are also nonconvex. Hence, the overall optimization problem is nonconvex with nonconvex constraints. Therefore, solution to (27) is NP hard. In the following, the problem is transformed to a difference of convex (DC) optimization problem and solved using the convex-concave procedure (CCP). Before proceeding further, the DC optimization problem is briefly discussed along with some useful lemmas.

DC optimization problem: A DC optimization problem can be written in the following form:

$$\begin{aligned} \underset{\mathbf{x}}{\text{minimize}} \quad & f_0(\mathbf{x}) - g_0(\mathbf{x}) \\ \text{s.t.} \quad & f_i(\mathbf{x}) - g_i(\mathbf{x}) \leq 0, \forall\, i \in 1, 2, \cdots M \end{aligned} \tag{28}$$

where f_i and g_i are convex functions of vector $\mathbf{x}$. The following two lemmas are used to transform (27) to a DC optimization problem.

Lemma 1. *A function of product of two convex functions $f(x) \cdot g(x)$, $x \in \mathbb{R}$ is convex if $f(x)$ and $g(x)$ are positive and both the functions are either increasing or decreasing.*

Proof. Let us express $h(x) = f(x) \cdot g(x)$. Hessian h''_{xx} of $h(x)$ is:

$$h''_{xx} = f''_{xx} g(x) + f(x) g''_{xx} + 2 f'_x g'_x.$$

Hessian of a convex function is positive. Thus, f''_{xx} and g''_{xx} are > 0. As $f(x)$ and $g(x)$ are positive, the first two terms in h''_{xx} expression are positive. Given that both the functions are either increasing or decreasing, their derivatives are of same sign (either positive or negative). Thus, the last term is also positive. Consequently, h''_{xx} is positive, and hence $h(x)$ is convex.

Lemma 2. *A function of product of two convex functions $f(x) \cdot g(y)$, $(x, y) \in \{\mathbb{R}^2 | f(x) + g(y) \geq 0\}$ can be written as a difference of two convex functions as:*

$$f(x) \cdot g(y) = \frac{(f(x) + g(y))^2}{2} - \left(\frac{f(x)^2}{2} + \frac{g(y)^2}{2} \right). \tag{29}$$

Proof. Using binomial expansion of $(f(x)+g(y))^2$, the above expression for $f(x) \cdot g(y)$ is obtained. From Lemma 1, square of a convex function is convex. Thus, $f(x)^2/2$ and $g(y)^2/2$ are convex. Consider $h(x, y) = (f(x) + g(y))^2$. Hessian $\mathbf{h}''$ of $h(x, y)$ is given as:

$$\begin{bmatrix} 2f''_{xx}(f(x) + g(y)) + 2(f'_x)^2 & 2f'_x g'_y \\ 2f'_x g'_y & 2g''_{yy}(f(x) + g(y)) + 2(g'_y)^2 \end{bmatrix}$$

Given that $f(x)$ and $g(y)$ are convex, diagonal terms in $\mathbf{h}''$ are positive. Determinant of $\mathbf{h}''$ is $4f''_{xx}g''_{yy}(f(x) + g(y)) + 4f''_{xx}(f(x) + g(y))(g'_y)^2 + 4g''_{yy}(f(x) + g(y))(f'_x)^2$. As $(x, y) \in \{\mathbb{R}^2 | f(x) + g(y) \geq 0\}$, determinant of $\mathbf{h}'' > 0$. Hence, $(f(x) + g(y))^2$ is also convex.

These two lemmas are used to reformulate (27) to a DC optimization problem as described below.

Optimization problem reformulation into DC: The number of RBs over LCN and number of slots over CRN used for the lth layer video transmission obtained from (22) and (23), respectively, are nonconvex. Using epigraphs, these expressions are transformed into constraints as follows:

$$\frac{w_{lc,l}}{(R_{lc,l}T_{rb} - H_l)} \leq \omega_l \tag{30}$$

$$\frac{w_{cr,l}}{J(\zeta_l)(R_{cr,l}(T_{cr} - \zeta_l) - H_l)} \leq \upsilon_l. \tag{31}$$

By replacing the above expressions in (27) with ω_l and υ_l, (27), C2, C6a, and C7a are transformed to linear functions of ω_l and υ_l. These newly introduced constraints are converted to DC constraints as follows: Rewriting (30) as $w_{lc,l} - \omega_l R_{lc,l} T_{rb} + \omega_l H_l \leq 0$. The term $\omega_l R_{lc,l} T_{rb}$ is nonconvex, which is converted to DC by using Lemma 2. Similarly, (31) is rewritten using (4) as $w_{cr,l} - \upsilon_l(p_{cr} p_{md}(\zeta_l) + (1 - p_{cr})(1 - p_{fa}(\zeta_l)))(R_{cr,l}(T_{cr} - \zeta_l) - H_l) \leq 0$. The terms $(1 - p_{cr})(1 - p_{fa}(\zeta_l))R_{cr,l}\zeta_l$ and $\upsilon_l p_{cr} p_{md}(\zeta_l)$ in the above expression are nonconvex and are converted to DC by Lemma 2.

The probability of transmission failure $P_{out,lc}(R)$ over a LCN RB and the probability of transmission failure $P_{out,cr}(R)$ due to channel fading and path loss over a slot in CRN from (1) and (5), respectively, are nonconvex. Similarly, the expressions $\frac{1-P_{out,lc}(R_{lc,l})^{n_l+1}}{1-P_{out,lc}(R_{lc,l})}$, $\frac{1-P_{out,lc}(R_{lc,l})^{n_l}}{1-P_{out,lc}(R_{lc,l})}$, $\frac{1-P_{e,cr}(\zeta_l,R_{cr,l})^{n_l}}{1-P_{e,cr}(\zeta_l,R_{cr,l})}$, $\frac{1-P_{e,cr}(\zeta_l,R_{cr,l})^{n_l+1}}{1-P_{e,cr}(\zeta_l,R_{cr,l})}$, $P_{out,lc}(R_{lc,l})^{n_l}$, and $P_{e,cr}(\zeta_l, R_{cr,l})^{n_l}$ appearing in the constraints C1a, C9, and C10 are also nonconvex. These are linear approximated using the first order Taylor series. For a function $f(x)$, its linear approximation is $f(x_\kappa) + \bigtriangledown f_x(x_\kappa)'(x - x_\kappa)$ around a point x_κ. Once these are approximated, the original constraints are expressed in DC using Lemmas 1 and 2.

Thus, the modified optimization problem constitutes a convex objective with DC constraints. Below, the convex-concave procedure (CCP) [20] is used to solve the DC optimization problem.

Solution to the DC optimization problem: In CCP, the DC functions $f_i(\mathbf{x}) - g_i(\mathbf{x})$ are approximated to convex functions. Linear approximation of the negative convex part, i.e., $g_i(\mathbf{x})$, is used to convert the DC to convex function. First order Taylor series is used to obtain the linear approximation. At a point $\mathbf{x}_k$, the linear approximation of the DC function is given as $f_i(\mathbf{x}) - g_i(\mathbf{x}) \approx f_i(\mathbf{x}) - g_i(\mathbf{x}_\kappa) - \bigtriangledown g_i(\mathbf{x}_\kappa)'(\mathbf{x} - \mathbf{x}_\kappa)$. Once the DC functions are convex approximated, convex optimization is applied to obtain the solution. At each iteration, once the optimal values are obtained, the approximation to the DC functions is improved to obtain a better solution. Convergence of this algorithm has been provided in [21].

A feasible initial point is required as input to this algorithm, which may be challenging given the number of variables involved. In [22], it was shown that the need for an initial feasible point could be overcome by making use of slack variables in the constraints and penalizing the violations. Naming this modified algorithm as

Algorithm 2: Penalty convex-concave procedure

Initial point $\mathbf{x}_0$, $\tau_0 > 0$, τ_{max}, $\varkappa$, and ε. $\kappa = 0$
while $|F_\kappa - F_{\kappa-1}| < \varepsilon$ **do**
1. Form $\hat{g}_j(\mathbf{x}; \mathbf{x}_\kappa) \triangleq g_j(\mathbf{x}_\kappa) + \nabla g_j(\mathbf{x}_\kappa)'(\mathbf{x} - \mathbf{x}_\kappa)$ for $j = 0, 1, \cdots, M$.
2. Set the value of $\mathbf{x}_{\kappa+1}$ to the solution of

$$
\begin{aligned}
F_\kappa = \underset{\mathbf{x}}{\text{minimize}} \quad & f_0(\mathbf{x}) - \hat{g}_0(\mathbf{x}, \mathbf{x}_\kappa) + \tau_\kappa \sum_{j=1}^{M} v_j \\
\text{subject to} \quad & f_j(\mathbf{x}) - \hat{g}_j(\mathbf{x}; \mathbf{x}_\kappa) \leq v_j, \forall\ j \in 1, 2, \cdots M, \\
& v_j \geq 0, j = 1, 2, \cdots, M.
\end{aligned}
$$

3. Update τ: $\tau_{\kappa+1} = min(\varkappa \tau_\kappa, \tau_{max})$.
end

penalty CCP, Algorithm 2 describes the steps involved. In step 1, the DC constraints are linear approximated around point $\mathbf{x}_\kappa$. Slack variable v_j is considered for each constraint, τ is the penalty factor added to the objective, and $\varkappa$ is the multiplying factor which increments the penalty factor in each iteration. τ_{max} is the upper limit of τ. In each iteration, an approximate convex optimization problem is solved in step 2. The algorithm stops when the change in the objective function value is less than a small constant ε.

Complexity analysis and convex problem decomposition: In step 2 of the Algorithm 2, a convex optimization problem is solved. For solving (27), a number of variables are $(20L + 4)$, where $7L$ are the required parameters ($R_{lc,l}$, ζ_l, $R_{cr,l}$, u_l, n_l, $p_{lc,l}^{rtx}$, and $p_{cr,l}^{rtx}$), $4L$ are the additional introduced variables ($w_{lc,l}$, $w_{cr,l}$, ω_l, and υ_l), and $9L+4$ are slack variables (v_i) corresponding to each constraint. Solving this convex problem involves high complexity. Therefore, the decomposition method is employed to solve this convex problem.

Due to the specific structure of the problem, it is decomposed with each layer forming a separate subproblem. The Lagrange function of the approximated convex problem is decomposed into L subproblems corresponding to each layer and $9L + 4$ subproblems corresponding to the slack variables. The subproblems corresponding to each layer are nonlinear, while the subproblems corresponding to the slack variables are linear. The problem is iteratively solved, where the subproblems are fed with the Lagrange multipliers to obtain the optimal parameters. Using these optimal values from each subproblem, the main problem computes the optimal Lagrange multipliers using the subgradient method [23].

This decomposition results in a total of $10L + 4$ subproblems with 15 variables for the L subproblems corresponding to each layer and 1 variable for the $9L + 4$ subproblems corresponding to each slack variable. Complexity for solving subproblems corresponding to L layers is $\mathcal{O}(15^3)$, and they can be solved in parallel. Closed form expressions are obtained for solving the $9L + 4$ subproblems corresponding to

each slack variable. Their computation complexity is negligible. The computation of optimal Lagrange multipliers requires only a few arithmetic operations. Thus, the decomposition method reduces the complexity significantly.

For CM-basic, the parameters in (27) are made layer independent. Thus, decomposition method is not required in CM-basic. The solution to (27) for CM-basic is obtained using the penalty CCP method as presented in Algorithm 2. There are 22 variables, where 7 are the desired parameters, 4 are the additional variables introduced, and 13 are the slack variables corresponding to the constraints. Complexity of solving this problem is $\mathcal{O}(22^3)$. Though its complexity is lower than CM-optimal, as will be noted in section "Video Application-Specific Performance", the performance of CM-basic is inferior to CM-optimal.

Discussion: The optimization problem (27) provides optimal parameters for the transmission of L-layer video content via the two networks. The user-provided parameters (viz., $E_{th}^{(k)}$, $\mathcal{Q}_{th}^{(k)}$, and $L^{(k)}$) change with the remaining battery level of the device, which is on the order of minutes. While these computations are done on the BS, which have high processing capabilities, the optimization problem computation can be easily parallelized to meet the deadlines.

Results

Performance of the CM system is captured in two scenarios. The performance of the CM network is compared against single network access (SNA) scheme, where the users associate themselves to a single network either LCN (SNA-LCN) or CRN (SNA-CRN).

General Performance

In this section, numerical results are presented to demonstrate the performance of CM in the general scenario with heterogeneous user traffic demands. Frame duration $\mathcal{T}$ is taken as 260 ms considering the case of video transmission of 30 fps with GOP duration of 8 pictures. LTE network is considered as LCN with 5 MHz bandwidth available. Slot duration in LTE is 0.5 ms with 50 RBs per slot. Data transmission over each RB is 0.5 Kb. Over the CRN, 2 channels of bandwidth 7 MHz each are considered with the data rate over each channel is 26.7 Mbps (as in IEEE 802.11af). Slot duration is taken as 0.5 ms. SU channel sensing duration is taken such that the probability of misdetection is bounded within 0.1. PU channel activity parameter is taken as $p_{cr} = \{0.3, 0.4\}$ [24]. For demonstration purpose, consider cost per bit transmission in LCN ($\mathscr{C}_{lc}$) and CRN ($\mathscr{C}_{cr}$) as 0.1 and 0.05, respectively. Fairness constraint β is taken to be 0.7, unless otherwise stated.

As stated earlier, for comparison purpose, SNA scheme is considered where the users are allocated resources via a single network. Users associate themselves to

a specific network based on their cost constraint χ. Low χ users (say, $\chi < \chi_{th}$) are low-paying users and hence they choose CRN, while the high χ users choose LCN. Depending upon the users in each network, the controller in each network allocates resources such that their individual network utility is maximized. The overall network utility is taken as the sum of the individual network utility of the two networks. It is of interest to obtain the optimal threshold χ^*_{th} that maximizes the network utility.

Comparative Performance of CM

A network of 60 users is considered where the percentage of RT users varied as $\{10, 30, 50, 70, 90\}\%$ of the total users. Users are randomly deployed across the cell. Each user uniformly chooses its $d_{req} \in [0.2, 1]$ Mbps and cost constraint $\chi \in (0.2, 1)$. d_{min} for RT users is considered 40% of d_{req}. Constants c_1, c_2, c_3, and c_4 are taken as 10, 1000, 25, and 15, respectively.

Figure 5 plots the user utility in CM and SNA along with their cost constraint χ for the network with 50% RT users. In SNA, via simulations maximum network utility (sum of the network utility of the two networks) is obtained. Corresponding to the maximum network utility is the optimal $\chi^*_{th}(SNA)$. The users with $\chi < \chi^*_{th}(SNA)$ associate themselves to the CRN, while the others associate

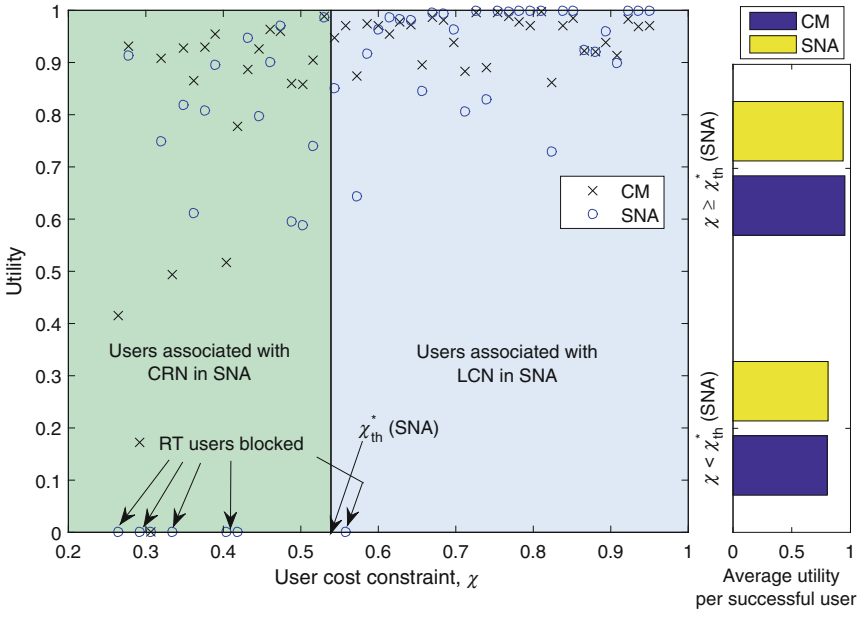

Fig. 5 Users' utility along with their cost constraint (χ) and average utility observed by successful users in different χ regimes for the network with 50% RT users. $\beta = 0.7$

themselves with the LCN in SNA. Bar plot shows the average utility obtained by the successful users (those users which have been provided service) in the two χ regimes, i.e., $\chi < \chi^*_{th}(SNA)$ and $\chi \geq \chi^*_{th}(SNA)$.

From the plot, it is observed that the utility for high χ users is higher in CM as compared to SNA. Users operating over SNA in this regime obtain their resources via LCN only which is an expensive resource. In SNA, the users with moderate χ suffer as they can only be allocated a fraction of their required resource via LCN due to their cost constraint. CM does better in QoS because of flexible shared resource allocation.

In the low χ regime ($\chi < \chi^*_{th}(SNA)$), all users are associated with CRN in SNA. Because of intermittent PU activity in CRN, SNA in this regime offers a much lower user utility compared to that in CM. Average utility per successful user is comparable in both the cases. This is because, a higher number of users are blocked in SNA. Similar conclusion can be drawn for network with different proportion of RT users. Thus, CM offers a high QoS to the users at low cost (low to moderate χ users) along with high-paying users, while SNA can provide high QoS only to high-paying LCN users.

Figure 6a shows the percentage of users blocked in CM and SNA for various network instances. As the proportion of RT users increases in the network, a higher number of users are blocked because it becomes difficult for the network to meet the minimum rate requirements of all these RT users. The blocked users are mostly

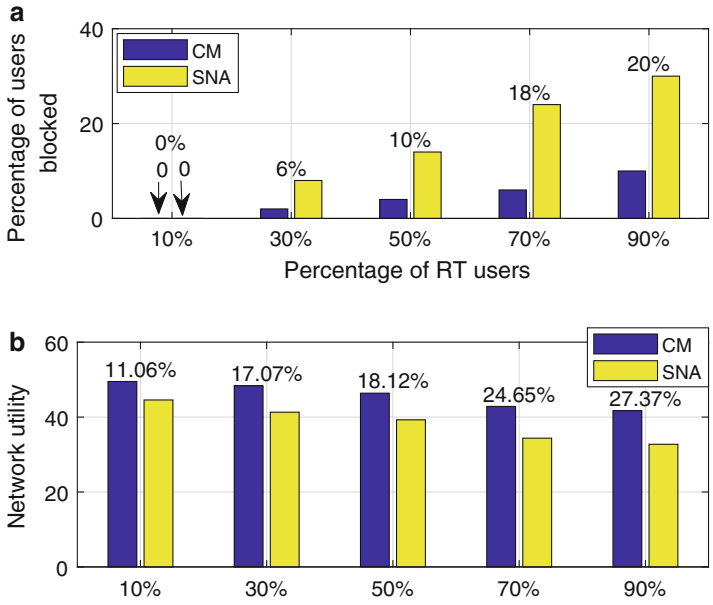

Fig. 6 (**a**) Number of users blocked and (**b**) network utility obtained. $\beta = 0.7$. Values above the bar shows the percentage gain in CM

low-χ users (see Fig. 5), because these users seek most resource from CRN, which is a scarce resource (due to high demand of CRN resources by other users and also due to intermittent PU activity). In the CM system, a lower number of users get blocked as compared to the SNA due to optimal allocation of resources to the users via the two networks. It is noted that, in the chosen RT versus NRT user scenarios, on average 10.8% less users are blocked in CM.

Network utility in CM and SNA scheme is shown in Fig. 6b. As expected, CM performs better than the SNA in all cases as the resources are optimally and fairly allocated to the users according to their cost constraints and required resources. It is also observed that the gain increases with the proportion of RT users in the network as high number of users get blocked in SNA for higher RT users proportion in the network. Gain in network utility is seen to vary from 11% to 27%, with an average gain of 19.6%.

Effect of Fairness Constraint

Finally, to observe the effect of fairness constraint β, the network utility versus β is plotted in Fig. 7. Fairness constraint limits the controller to allocate the CRN resources unevenly among users. A stringent fairness threshold pushes the controller to allocate the CRN resources more evenly among users. This adversely affects the low χ users leading to low network utility, though at the cost of maintaining high degree of fairness. Thus, the inclusion of fairness constraint in the optimization problem ensures that the greedy users are not unduly benefited from the CRN by having low-cost constraint.

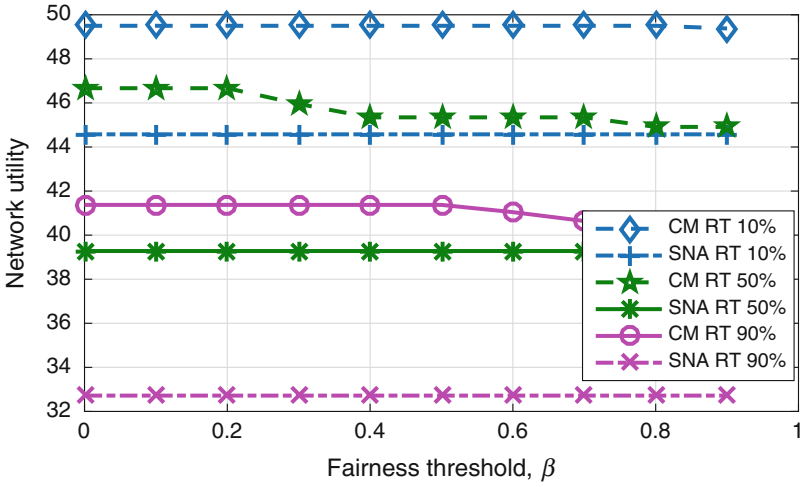

Fig. 7 Network utility as a function of fairness constraint, β

Video Application-Specific Performance

The user cost in video reception via CM is evaluated in this subsection. A single cell scenario is considered with 1 Km cell radius. The CR-enabled BS is located at the cell center. LCN RBs are of duration 0.5 ms with bandwidth of 5 MHz (LTE in 900 MHz band is considered). CRN operation is considered over UHF band (500 MHz) with PU channel bandwidth of 6 MHz. Slot duration is 10 ms (as in IEEE 802.22). Channel idling probability is 0.7 [24]. Misdetection probability threshold is set to 0.05 [8]. Transmission power over LCN and CRN is 24 and 20 dBm, respectively, while noise variance is 10^{-4} [25]. Path loss exponent is 3.76 [26].

$\mathbb{C}_{CR}/\mathbb{C}_{LC} \triangleq \rho$ is the ratio of cost charged by CRN and LCN per unit time. In this study, it is considered that the user is charged monetary cost 100 units per unit time for operation over LCN, and $\rho = 0.5$ (50 units per unit time for PU spectrum leasing). Device power consumption for reception is 1737 mW, while its tail power consumption is 1325 mW [18]. Device energy consumption is a function of the number of layers it intends to receive. In 3GPP, channel state feedback is provided within 6 ms [27]. Hence, for each packet reception error, the receiver can inform the BS almost within the next CRN slot. For this study, maximum retry limit n_{max} is considered to be 5.

City and *Mobile* QCIF video sequences are encoded into SNR scalable bitstreams with a base layer and 3 enhancement layers, with 30 frames per second (fps) and with GOP of duration 16 frames having structure "IPPPPPPPPPPPPPPP." For the *City* sequence, base layer data rate is 71 Kbps, while the enhancement layers 2, 3, and 4 are encoded at rates 34, 110, and 236 Kbps, respectively. For the *Mobile* sequence, base layer data rate is 162 Kbps, while the enhancement layers 2, 3, and 4 are encoded at rates 203, 535, and 1497 Kbps, respectively. The encoding is done using JSVM [28]. This data is suitably divided into packets with per-packet overhead of 24 Bytes, as in IEEE 802.11.

The performance of the CM is compared with CM-basic, SNA-LCN, and SNA-CRN. If the user is associated only with LCN (i.e., SNA-LCN), transmission rate is optimized for its optimal performance. In SNA-CRN, where the user is only associated with CRN, sensing duration and transmission rate adaptation are performed to guarantee optimal performance. To explicitly demonstrate the benefit of layer-dependent parameter adaptation in the CM (call it as optimized CM, or CM-optimal), the comparative scheme, namely, basic CM (CM-basic), is considered. In CM-basic, transmission rate adaptation over the LCN and CRN, sensing time adaptation, and number of retransmission and network selection for retransmission are optimally chosen for all video packets without distinguishing their respective priority levels, to obtain low-cost transmission to the users.

Video Transmission to a Single CM User

A user located at a distance of 0.5 Km from the BS requests for *City* video sequence with 4 layers. The minimum desirable video quality is 95%. In the following, the single-user performance is presented in terms of device and network constraints and user preference.

Effects of User Preference

Figure 8a, b present, respectively, the user cost and energy consumed versus energy consumption threshold. Compared to SNA-LCN, SNA-CRN offers service at a lower cost due to its opportunistic spectrum access. However, operation over CRN requires a higher minimum energy E_{th}^{*} as opposed to $E_{th}^{\#}$ in SNA-LCN (i.e., $E_{th}^{*} \geq E_{th}^{\#}$, as noted in Fig. 8b), because of the additional activity of the device due to intermittent sensing and channel imperfections. CM-basic provides service in all regimes as it exploits both CRN and LCN. For $E_{th} > E_{th}^{*}$, cost is same as in SNA-CRN, because all content is transmitted via CRN. As the device energy consumption constraint becomes more stringent ($E_{th} < E_{th}^{\#}$), the SNA-LCN and CM-basic go into outage because energy consumption in SNA-LCN exceeds the threshold. In contrast, less resource requirement in CM-optimal allows to serve a user with even more stringent energy constraints. Though the energy consumption in CM-optimal is higher than that in SNA-LCN, CM-optimal serves the user at a lower cost due to concurrent transmissions via LCN and CRN. Overall, CM-optimal outperforms CM-basic (hence SNA-LCN and SNA-CRN) by reducing the cost on average by up to 44.1%.

Figure 9 presents the impact of video quality threshold $\mathcal{Q}_{th}$ on user cost. $\mathcal{Q}_{th}$ is varied from 90% to 99%, with $E_{th} = 680$ mJ. A higher $\mathcal{Q}_{th}$ requires higher resources, thereby increasing energy consumption and cost. With the considered E_{th}, SNA-CRN can guarantee service only up to $\mathcal{Q}_{th} \leq \mathcal{Q}_{th}^{*}$. In contrast, SNA-LCN meets the user demand at a lower energy consumption, though at a higher cost. CM performs better by using CRN at lower $\mathcal{Q}_{th}$ for reduced cost and optimally dividing the stream over LCN and CRN to meet higher $\mathcal{Q}_{th}$ at a reduced cost. Compared to SNA, CM-optimal provides on an average 42% cost reduction along with providing service to the users with more stringent E_{th} and $\mathcal{Q}_{th}$ requirements.

Effects of Network Parameters

Figure 10a shows the cost to the user in various schemes with the change in CRN versus LCN cost ratio ρ. Observe that cost to the user increases with the increase in ρ (ϕ_{cr}). User cost in SNA-CRN surpasses SNA-LCN at $\rho = \rho^{*}$. To achieve a low-cost transmission, the CM-optimal delivers all the data via CRN for $\rho < \rho^{*}$, while the data is transmitted via LCN for $\rho > \rho^{*}$.

The effect of PU activity parameter on user cost is plotted in Fig. 10b. PU channel idling probability p_{cr} is varied from 0.25 to 1. Lower idling probability induces the use of higher number of CRN slots to transmit a video content, thus increasing energy consumption and cost. For $p_{cr} < p_{cr}^{*}$, the energy consumption constraint is violated in SNA-CRN resulting in service outage. CM-optimal chooses the radio access optimally to maintain low cost to the user at all times.

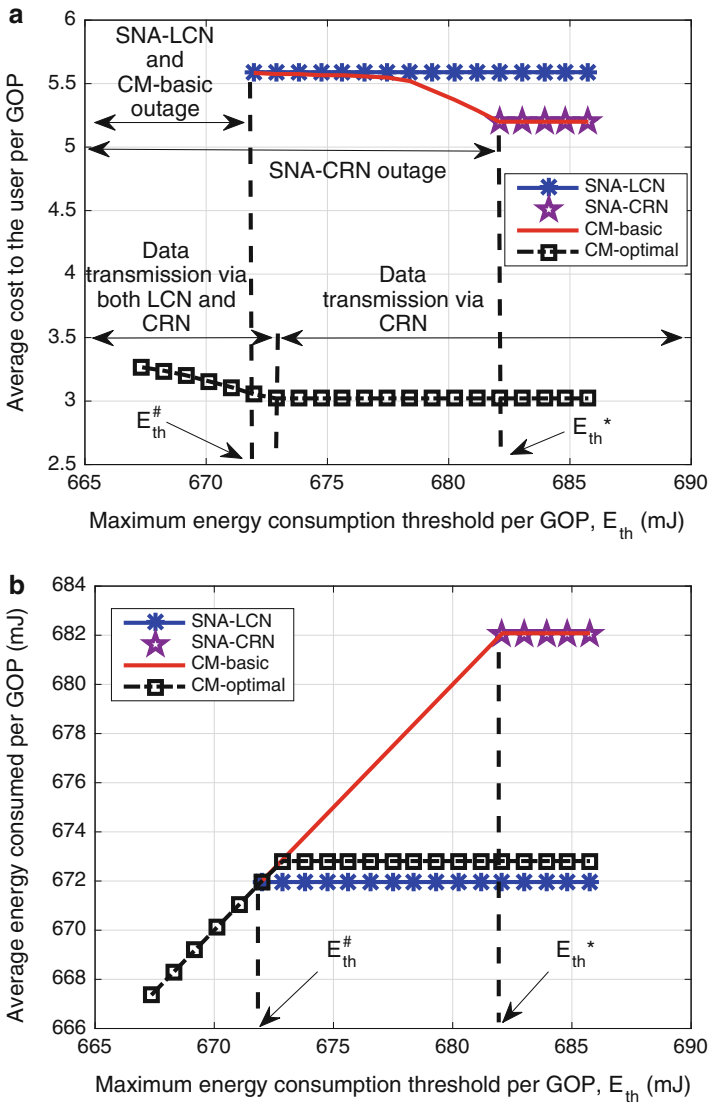

Fig. 8 Variation in (**a**) user cost and (**b**) energy consumed, versus energy consumption threshold. $\mathscr{Q}_{th} = 95\%$. $\rho = 0.5$, $p_{cr} = 0.7$, $L = 4$

Effects of User Device Battery Energy Constraint

As discussed in section "User Device Capability", to aid continued reception, user's requested video quality and maximum energy consumption constraint has been considered to be a function of its remaining battery level. For demonstration, let us consider a mobile device with maximum energy consumption threshold and requested number of video layers L, as shown in Fig. 11.

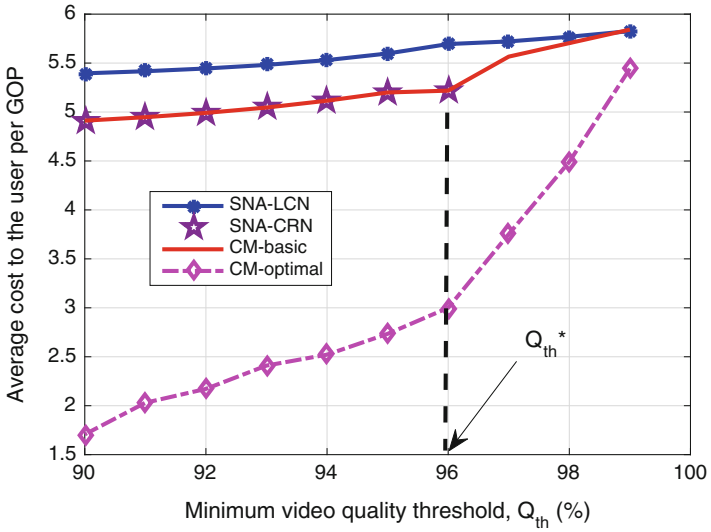

Fig. 9 Variation in user cost versus video quality constraint. $E_{th} = 680$ mJ, $\rho = 0.5$, $p_{cr} = 0.7$, $L = 4$

A lower remaining battery level induces lower video quality and E_{th}. $\mathscr{Q}_{th}$ is maintained at 95%. Figure 12a presents the user cost in video transmission in the various schemes. SNA-CRN goes into outage for some E_{th} regimes, though providing service at a lower cost. The gain in CM-optimal as compared to SNA as well as CM-basic scheme is higher when L is higher. This is because the advantage with layer-dependent parameter adaptation diminishes for lower number of requested layers. Figure 12b presents the mean received video PSNR for different battery levels of the user device. The PSNR increases with the increased number of layers requested. As $\mathscr{Q}_{th}$ is maintained at 95%, the PSNR remains constant for a fixed number of layers requested. Thus, CM-optimal intelligently distributes data via the two networks depending on the individual network cost and availability, to ensure low cost to the user without affecting the video reception quality.

Multiuser Operation

Let us consider a single cell scenario with 80 CM users uniformly randomly distributed across the cell. Three network scenarios are considered. In the first, all users request *"City"* video sequence, while in the second all users request *'Mobile'* video sequence. In the third scenario, the users request one of the two video sequences: *"City"* or *"Mobile"*, with equal probability. Remaining battery level of user device is distributed uniformly between [0 100]%. Depending on the remaining battery level, the user's maximum energy consumption constraint and number of

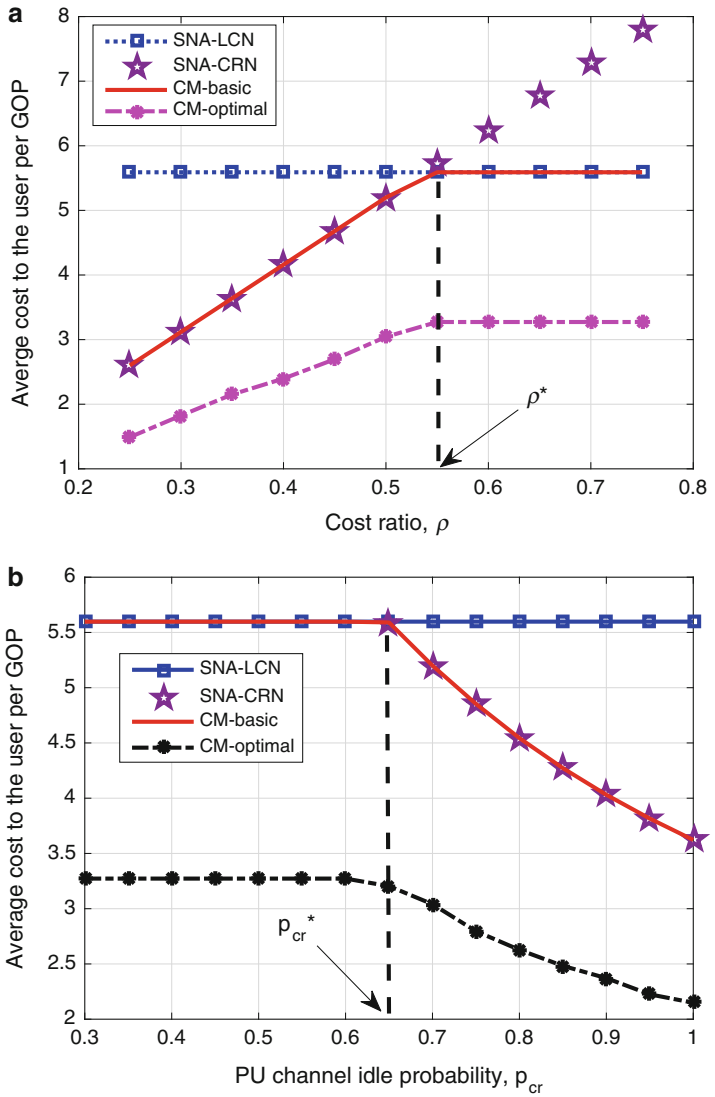

Fig. 10 User cost versus change in (**a**) cost ratio ρ, with $p_{cr} = 0.7$; (**b**) PU channel idling probability p_{cr}, with $\rho = 0.5$. $\mathcal{Q}_{th} = 95\%$, $E_{th} = 680$ mJ, and $L = 4$

layers requested are obtained from the characteristics in Fig. 11. The minimum video quality constraint is fixed to 95% for all users. Three random instances of the network in each of the three scenarios are studied, and the average performance is evaluated.

Figure 13 presents an example of resources requested/allocated via the two networks for a random network instance in the third scenario. Optimal resources

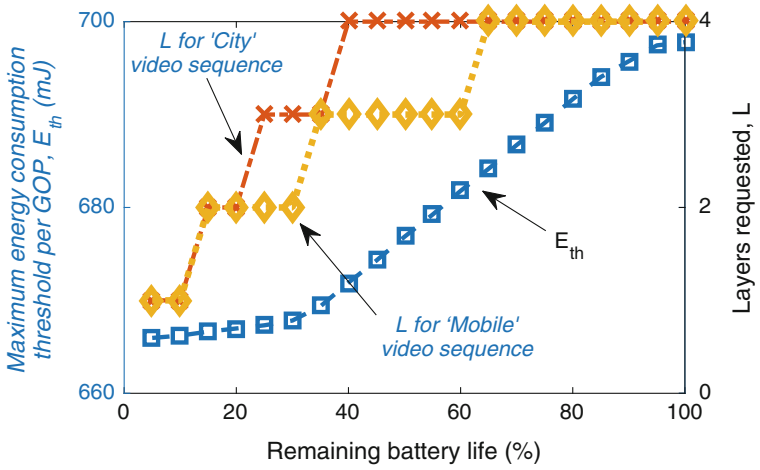

Fig. 11 User's demanded video quality and energy constraint with the remaining battery level

requested by the individual users are computed using (27). Following Algorithm 1, the users are served in an increasing order of their cost or equivalently the number of layers requested. The users meeting the resource availability criteria are served (marked *allocated* in Fig. 13). If the CRN resources are insufficient, (27) is recomputed to obtain the revised resource allocation. If a user's revised resource allocation is acceptable, the user is served (marked by arrow in Fig. 13). A user is dropped if its resource requirement is not met. Overall, the users requesting lower resources are served, while the users with higher demands are more likely to be dropped.

Figure 14a, b present, respectively, the total network cost $\mathscr{C}^*_{net}$ (cf. (26)) and the average number of users served in the three scenarios. The number of users served is higher in scenario 1 as the data rate of the *City* video sequence is lower compared to the *Mobile* video sequence. Total network cost in SNA schemes is seen to be higher than (inferior to) the CM system because the users are optimally allocated resources from the two networks simultaneously in CM. Further, the number of users served in CM is higher compared to the other schemes. Figure 14c shows the average PSNR of the users served. It is observed that the average PSNR in CM-optimal is better than that in all the other schemes as higher number of users are served in CM-optimal. Due to layer-dependent parameter optimization, CM-optimal outperforms SNA-LCN schemes by serving on average 48.2% more users with about 3% higher PSNR on average.

To gain further insights, Fig. 15a, b present the average cost per user and fraction of users served versus number of layers requested in the first scenario. From Fig. 15a, it is observed that the average cost per user served is the lowest in CM-optimal, which is due to its layer-dependent parameter optimization. Cost reduction in CM-optimal is higher for higher number of requested layers. As the

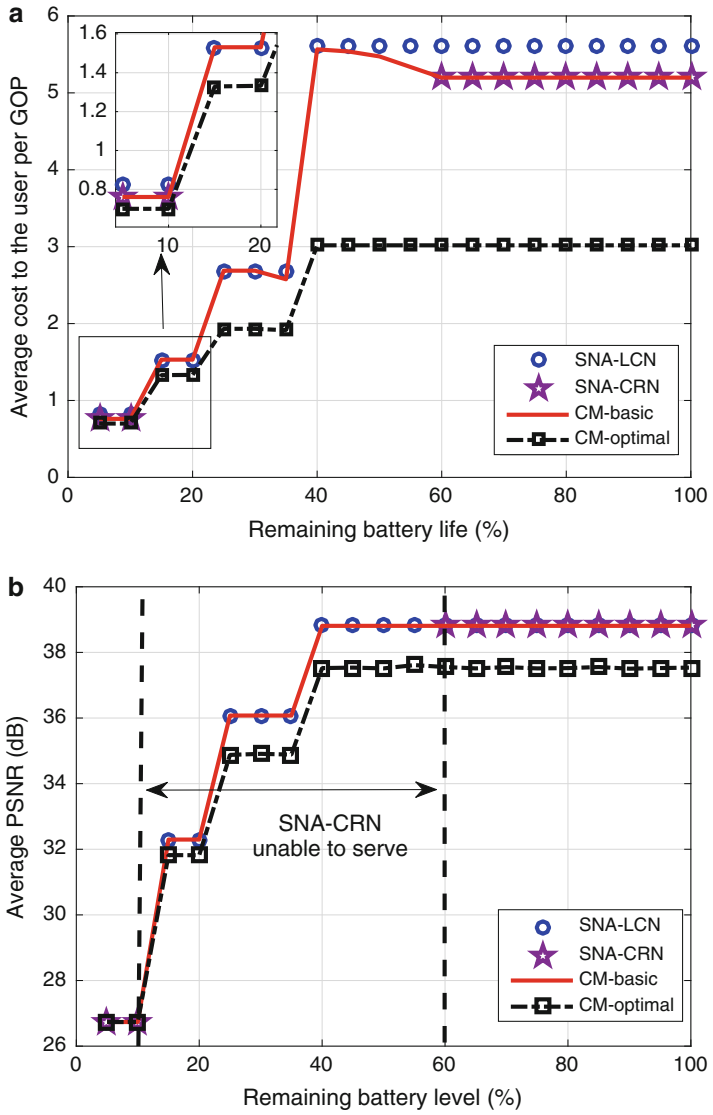

Fig. 12 User (**a**) cost and (**b**) received video quality (PSNR) with the remaining battery level for the *"City"* video request. $\mathscr{Q}_{th} = 95\%$, $\rho = 0.5$, and $p_{cr} = 0.7$

users are served in an increasing order of the number of layers requested, the users requiring higher number of layers are more likely to be dropped (see Fig. 15b). However, in CM system, where the data is optimally transmitted via the two networks, the fraction of users served is higher. Similar trends are observed in the other scenarios as well. Compared to SNA, CM system serves a higher number of users with a higher average video reception quality and at a lower cost.

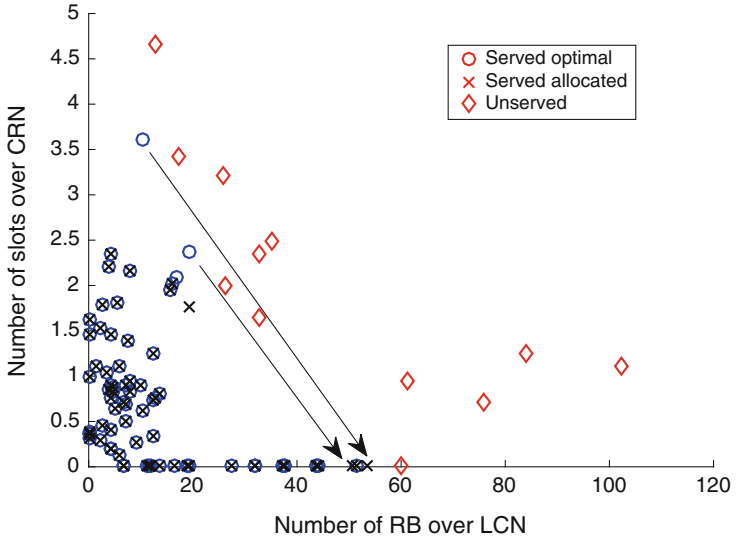

Fig. 13 Requested and allocated resources to the users via the two networks for a network instance in Scenario 3. $N_u = 80$, $\mathcal{Q}_{th} = 95\%$, $\rho = 0.5$, and $p_{cr} = 0.7$

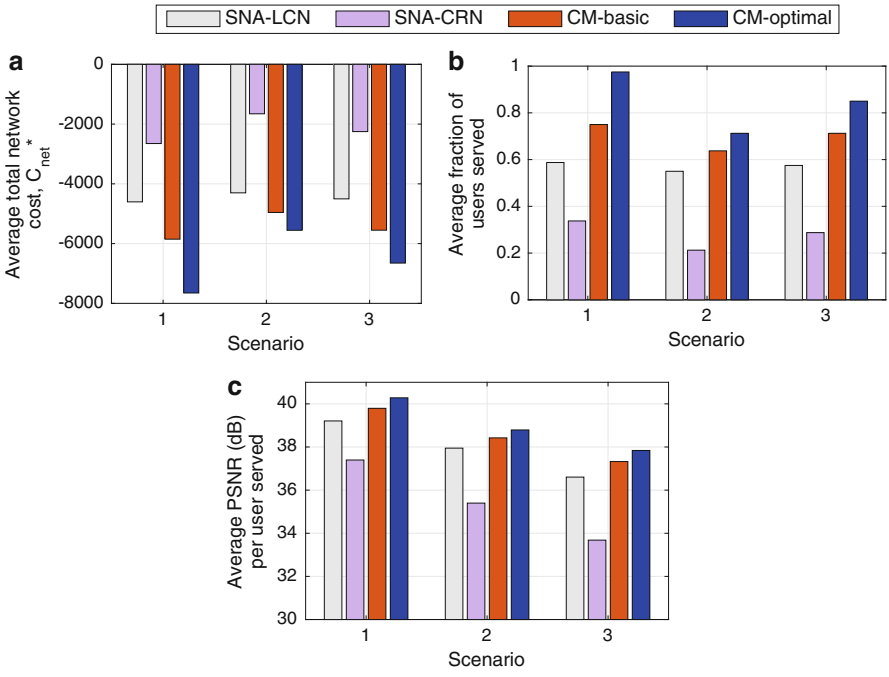

Fig. 14 Average (**a**) total network cost, (**b**) fraction of users served, and (**c**) PSNR per user served in the three scenarios. $N_u = 80$, $\mathcal{Q}_{th} = 95\%$, $\rho = 0.5$, $p_{cr} = 0.7$, and $\Theta = 100$

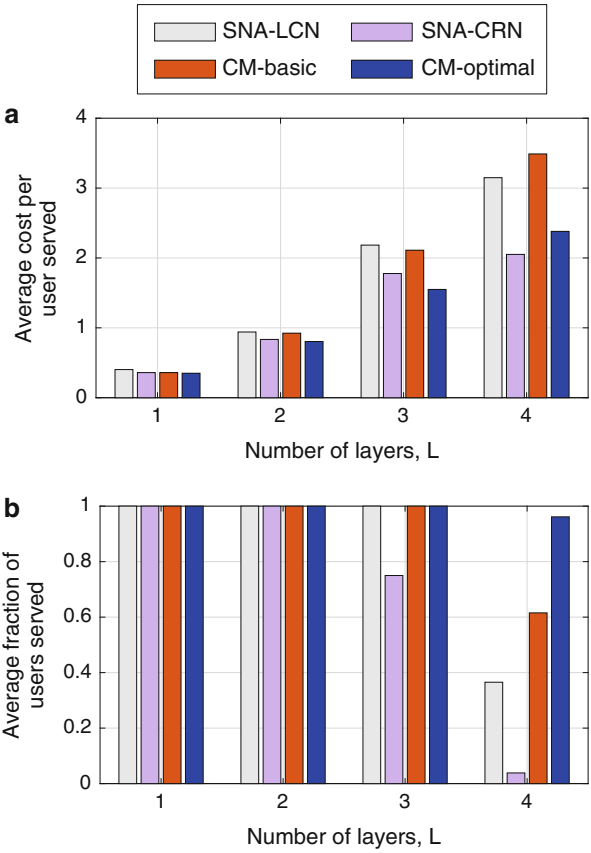

Fig. 15 (**a**) Average cost per user served and (**d**) average fraction of users served for users requesting different number of layers in Scenario 1. $N_u = 80$, $\mathscr{Q}_{th} = 95\%$, $\rho = 0.5$, $p_{cr} = 0.7$, and $\Theta = 100$

Concluding Remarks

Summary and Discussion

In this chapter, a cognitive multihoming system concept has been introduced to enhance the cellular network experience. Here, the user data is optimally split across LCN and CRN before transmission to the multihomed users. The CM approach aids in mitigating the spectrum scarcity problem of LCN, which CRN alone cannot solve. Two test scenarios were considered. In the general scenario, compared to the SNA approach, CM offers about 19% increase in average network utility and about 11% increase in average number of users served. In the application-specific scenario, where the users request for scalable video content, the optimized CM has been shown to outperform the SNA schemes by reducing the cost up to 51% and serving almost 55% more number of users.

Challenges and Future Directions

CM involves aggregating LCN and CRN to provide high-quality service to the users. CM can be easily realized in practice by utilizing the LTE-WiFi aggregation (LWA) technique standardized by the 3GPP in Release-13. LWA offers seamless usage of both LTE and WiFi networks to increase network performance. LWA can be used for CM deployment by replacing the WiFi network component with the CRN.

However, regulations are required to carry out opportunistic transmissions over unused licensed bands. A few countries, for example, the USA and some countries in Europe have introduced regulations for exploiting unused TV spaces. Yet, no regulation has been introduced for dynamic spectrum access in other licensed bands, which is required from the government agencies before CRN techniques could be commercially realized.

Furthermore, the BSs need additional capability of streaming the data stream from the remote data server and splitting the stream optimally across LCN and CRN for each user. This requires servers with high computation power at the BS which can carry out the optimization in real time. One aspect for future works is to study and develop novel real-time algorithms which can be implemented on low-end off-the-shelf hardware platforms and require minimal changes in the existing BS ecosystem.

The discussion in this chapter considers only the downlink communication via CM. Analysis of CM system for uplink transmissions can be studied likewise. There could be multiple cellular networks in a specific geographical region accessing the same CR channels. Coexistence studies among multiple such networks are useful from the point of performance and resource allocation via CM.

Acknowledgements This work was supported in parts by ITRA Media Lab Asia Project under Grant ITRA/15(63)/Mobile/MBSSCRN/01 and the Department of Science and Technology under Grant SB/S3/EECE/0248/2014

References

1. Cisco Systems C, Jose S (2017) Cisco visual networking index: global mobile data traffic forecast update, 2017–2022, white paper
2. Xu C, Liu T, Guan J, Zhang H, Muntean G-M (2013) CMT-QA: quality-aware adaptive concurrent multipath data transfer in heterogeneous wireless networks. IEEE Trans Mobile Comput 12(11):2193–2205
3. Lopez-Benitez M, Casadevall F (2013) Time-dimension models of spectrum usage for the analysis, design, and simulation of cognitive radio networks. IEEE Trans Veh Technol 62(5):2091–2104
4. Freris N, Hsu C-H, Singh J, Zhu X (2013) Distortion-aware scalable video streaming to multinetwork clients. IEEE/ACM Trans Netw 21(2):469–481
5. Wu J, Cheng B, Yuen C, Shang Y, Chen J (2015) Distortion-aware concurrent multipath transfer for mobile video streaming in heterogeneous wireless networks. IEEE Trans Mobile Comput 14(4):688–701

6. Agarwal S, De S, Seo J-B (2015) Cognitive multihoming: maximizing network utility over CR-assisted cellular network. In: Proceedings of IEEE SDRANCAN GLOBECOM workshop, San Diego
7. Agarwal S, De S (2016) Cognitive multihoming system for energy and cost aware video transmission. IEEE Trans Cogn Commun Netw 2(3):316–329
8. Pei Y, Liang Y-C, Teh K, Li HK (2011) Energy-efficient design of sequential channel sensing in cognitive radio networks: optimal sensing strategy, power allocation, and sensing order. IEEE J Sel Areas Commun 29(8):1648–1659
9. Liang Y-C, Zeng Y, Peh E, Hoang AT (2008) Sensing-throughput tradeoff for cognitive radio networks. IEEE Trans Wirel Commun 7(4):1326–1337
10. Chuah S-P, Chen Z, Tan Y-P (2013) Energy minimization for wireless video transmissions with deadline and reliability constraints. IEEE Trans Circuits Syst Video Technol 23(3):467–481
11. DaSilva LA (2000) Pricing for QoS-enabled networks: a survey. IEEE Commun Surv Tuts 3(2):2–8. Second Quater
12. Shenker S (1995) Fundamental design issues for the future internet. IEEE J Sel Areas Commun 13(7):1176–1188
13. Butler K, Stephens M (1993) The distribution of a sum of binomial random variables. Technical report, no. 467
14. Jain R, Chiu D-M, Hawe W (1984) A quantitative measure of fairness and discrimination for resource allocation in shared computer systems. Eastern Research Laboratory, Digital Equipment Corporation, Technical report
15. Boyd S, Vandenberghe L (2004) Convex optimization. Cambridge University Press, New York
16. Fallah Y, Mansour H, Khan S, Nasiopoulos P, Alnuweiri H (2008) A link adaptation scheme for efficient transmission of H.264 scalable video over multirate WLANs. IEEE Trans Circuits Syst Video Technol 18(7):875–887
17. Ismail M, Zhuang W (2014) Mobile terminal energy management for sustainable multi-homing video transmission. IEEE Trans Wirel Commun 13(8):4616–4627
18. Deng S, Balakrishnan H (2012) Traffic-aware techniques to reduce 3G/LTE wireless energy consumption. In: Proceedings of international conference on emerging networking experiments and technology, Nice, pp 181–192
19. Balasubramanian N, Balasubramanian A, Venkataramani A (2009) Energy consumption in mobile phones: a measurement study and implications for network applications. In: Proceedings of ACM SIGCOMM conference on Internet measurement, Chicago, pp 280–293
20. Yuille AL, Rangarajan A (2003) The concave-convex procedure. Neural Comput 15(4): 915–936
21. Lanckriet GR, Sriperumbudur BK (2009) On the convergence of the concave-convex procedure. Adv Neural Inf Process Syst 22:1759–1767
22. Lipp T, Boyd S (2014) Variations and extensions of the convex-concave procedure. http://stanford.edu/~boyd/papers/pdf/cvx_ccv.pdf
23. Geirhofer S, Tong L, Sadler B (2007) Cognitive radios for dynamic spectrum access – dynamic spectrum access in the time domain: modeling and exploiting white space. IEEE Commun Mag 45(5):66–72
24. Wang S, Wang Y, Coon J, Doufexi A (2012) Energy-efficient spectrum sensing and access for cognitive radio networks. IEEE Trans Veh Technol 61(2):906–912
25. Zhao F, Wei L, Chen H (2016) Optimal time allocation for wireless information and power transfer in wireless powered communication systems. IEEE Trans Veh Technol 65(3): 1830–1835
26. Long Y, Li H, Yue H, Pan M, Fang Y (2014) SUM: spectrum utilization maximization in energy-constrained cooperative cognitive radio networks. IEEE J Sel Areas Commun 32(11):2105–2116
27. 3GPP (2010) Further advancements for E-UTRA physical layer aspects. 3rd generation partnership project, TR 36.814
28. Reichel J, Schwarz H, Wien M (2007) Joint scalable video model JSVM-12. In: Joint video team (JVT) of ISO/IEC MPEG and ITU-T VCEG Doc. JVT-Y202

Part V
Spectrum Policy and Cognitive Radio Standards

Spectrum Policy and Cognitive Radio Standards

45

Oliver Holland

Contents

Abstract

Standards, fundamental in many areas of technology, are particularly vital in communications as they provide the foundations upon which radio devices, network elements, and other essential parts and functionalities in the communication chain can talk to each other. Moreover, standards are of even further accentuated importance in CR and spectrum sharing scenarios, as such scenarios imply direct or indirect interaction involving a wider range of stakeholders,

O. Holland (✉)
Centre for Telecommunications Research, King's College London, London, UK
e-mail: oliver.holland@kcl.ac.uk

W. Zhang (ed.), *Handbook of Cognitive Radio*,
https://doi.org/10.1007/978-981-10-1394-2_46

including regulators – implying different forms of standards (e.g., regulatory conformance standards). Given such observations, this chapter addresses standardization in the context of CR and spectrum sharing, particularly aiming to provide an opening and front matter to the more detailed coverage of some particular standards that are addressed in later chapters of this section of the book. In addition to providing this introductory material, this chapter addresses the broader scope of a number of relevant standards that are not detailed in the dedicated chapters. These include the TVWS regulatory conformance standard ETSI EN 301 598, the IEEE DySPAN-SC and IEEE 1900 series standards on various aspects of spectrum sharing and dynamic spectrum access, the IEEE 802.15.4m wireless personal area networks in TVWS standard, and the ECMA 392 TVWS MAC/PHY standard.

Introduction

Standards serve a number of purposes. On the one hand, they enable elements of communication systems to be developed and operated by a number of different manufacturers and operators, those elements still being able to communicate with each other with given expectations on performance, capabilities, technical characteristics, and overall outcome more generally. This has paved the way for the creation of systems such as GSM, UMTS, and LTE, with end-users and operators not being constrained to the use of mobile phones and network equipment created by a single manufacturer, for example. Such attributes are fundamentally essential to achieve sufficient economies of scale and market diversity to make mobile communications economically viable and also to make mobile communications acceptable from a policy perspective, e.g., not leading to a monopoly or dominance by a single manufacturer.

On the other hand, standards allow for coexistence among different elements or entities using spectrum or another common resource. In this context, there might often be a requirement from an overarching policy entity such as a regulator or regional/international regulatory coordinator (e.g., the CEPT, ITU) that certain standards are adhered to for coexistence and other purposes. This is in order to guarantee compatibility and performance in achieving coexistence, noting that the correctness of coexistence among (and implemented by) the participating entities becomes something of a legal requirement in such contexts.

Particularly in the context of spectrum sharing technologies, coexistence etiquette and associated functional requirements are basic impositions on the range of systems sharing the spectrum, or on the "secondary" users if such sharing is in a primary/secondary context. Standards are often required for key reasons such as to ensure that (i) the decisions or actions on spectrum sharing are either made or implemented correctly; (ii) the correct protocols for communication with a spectrum sharing decision making entity are implemented; (iii) the correct parameters and/or capabilities of spectrum sharing supporting functionalities and other capabilities are implemented; (iv) compatible decisions on spectrum sharing, e.g., from an

interference perspective, are made and implemented; and (v) the correct fail-safe and/or hardware intervention functions are implemented, among many others.

A good example here is the requirement of the UK regulator Ofcom [1] that white space devices imparted the status of "license exempt" for operation in TV White Space (TVWS) in the UK correctly implement the ETSI EN 301 598 standard [2]. Such a requirement equally applies to all European Union (EU) countries that decide to implement TVWS technology, by virtue of ETSI EN 301 598 being a "Harmonized European Standard." This standard specifies aspects such as the white space devices' emission requirements, their communications with geolocation databases and listings of geolocation databases, and their actions based on responses from the geolocation databases, among many other aspects. The adherence to such a standard is ensured at the certification stage of the creation of equipment, noting that no other input to the devices can be required in the operational stage given their status as "license exempt," i.e., the devices must operate without any specific input from the user or other entity, aside from communicating with a geolocation database.

In the following sections, we delve into detail on some of the specific standards and standards coordinating entities in the context of spectrum sharing and white spaces, cognitive radio (CR), and related areas of interest to this book. It is noted again that there are dual intentions here: (i) to provide front matter to the detailed coverage that is given on particular standards in later chapters, and (ii) to address some interesting and related standards that are not covered in the later chapters.

ETSI EN 301 598 Harmonized European Standard

The ETSI EN 301 598 Harmonized European Standard [2] is absolutely central to TVWS in the EU, as it defines the conformance requirements of white space devices in order for them to be allowed to operate in the EU. In essence, it also captures key aspects of the EU framework for TVWS, through the descriptions of the required actions and characteristics of white space devices. In line with this, ETSI EN 301 598 specifies detailed conformance tests that white space devices must pass, each test matching a characteristic or requirement as defined in a mirroring section of the standard.

The aspects of white space devices' characteristics and requirements defined in this standard, hence associated conformance tests, include:

- Definitions of types white space devices and associated requirements: Type A (fixed operation) and Type B (non-fixed operation), and their antenna types, noting that Type A has the additional flexibility in terms of an external antenna being allowed as opposed to only integral or dedicated antennas as for Type B.
- Transmission channel definitions and the need to specify transmission "nominal" channel bandwidths (as per bonding, i.e., a multiple of 8 MHz) and the total "nominal" bandwidth should the white space device use multiple such collections of channels.
- RF power (EIRP) and PSD (EIRP) definitions and limit requirements.

Table 1 ETSI white space device spectrum mask classes ("dB's down" per 100 kHz compared with power in intended 8 MHz channel) [2]

Adjacent channel distance from intended channel n	Adjacent frequency leakage ratio (AFLR)				
	Class 1	Class 2	Class 3	Class 4	Class 5
$n \pm 1$	74	74	64	54	43
$n \pm 2$	79	74	74	64	53
$n \pm 3$ or more	84	74	84	74	64

- Unwanted emission requirements of the white space devices, including:
  - Unwanted emissions outside of the TV band, specified as overall emitted power per 100 kHz in various frequency ranges below 1 GHz, and per 1 MHz above 1 GHz.
  - Unwanted emissions inside the TV band, specified in terms of "dB's down" per 100 kHz compared with the intended 8 MHz channel, for the adjacent channel, the next adjacent channel after that, and the next one again after that for which all further out channels have the same limit. It is noted that ETSI EN 301 598 specifies five different such mask classes, ranging from extremely tough to extremely lenient. Table 1 details these classes.
- White space device reverse intermodulation requirements.
- Identification requirements of white space devices.
- Requirements regarding communication with a regulatory-provided listing of valid geolocation databases.
- Communication of master white space devices characteristics, locations, heights, identities, etc., with the geolocation databases.
  - The correct implementation of the responses from the geolocation database (i.e., allowed EIRPs/channels).
  - Requirements on notification of the database of the chosen channel(s)/EIRP(s) and the reception of an acknowledgement before being allowed to transmit.
- Similar requirements for the slave white space devices, via a master white space device and association with the master white space device; definition of "generic" and "specific" parameters, and associated procedures, supporting this process of initial slave parameter exchange.
- Receiver spurious emission requirements.
- Geolocation capability requirements.
- Software, firmware, and related security requirements.

IEEE 802.22 Wireless Regional-Area Networks in TVWS

IEEE 802.22 is first completed IEEE standard specifically dedicated to the use of white space access. The standard builds on IEEE developments for other contexts of deployment, adapting them to the specific case of TVWS – a particular starting point being the work on IEEE 802.16 (WiMAX) [3]. Through this, IEEE 802.22

has aimed to provide a radio interface serving wireless regional area networks (WRANs), covering (at least in terms of MAC capabilities) ranges of potentially up to 100 km, compared with a few 10's of km which the next-best coverage IEEE specification set, WiMAX wireless metropolitan area networks (WMANs), might achieve. In line with its intended coverage and characteristics through the use of TVWS, and in comparison with the monkers "WiFi" and "WiMAX" of some other prominent IEEE systems, 802.22 has been given the tag "WiFar" – most often represented as "Wi-Far."

The baseline IEEE 802.22 standard was approved for publication in 2011 and is therefore denoted as IEEE Std 802.22™-2011 [4]. IEEE 802.22 has further worked on other standards within its scope, namely, 802.22.1 on "Enhanced Interference Protection of the Licensed Devices" (approved for publication in 2010, denoted as IEEE Std 802.22.1™-2010 [5]), effectively specifying a beaconing network to protect low-power licensed devices, and 802.22.2 "Recommended Practice for Installation and Deployment of IEEE 802.22 Systems" (approved for publication in 2012, denoted as IEEE Std 802.22.2™-2012 [6]), which simply gives recommendations on deployment of IEEE 802.22 networks, noting that such an IEEE Recommended Practice standard is a form of informative content and not binding by definition. IEEE 802.22 has also recently started working on standard 802.22.3, "Standard for Spectrum Characterization and Occupancy Sensing," aiming to define a spectrum sensing system to add value to current 802.22 white space systems through more advanced spectrum sensing capabilities. Among other benefits, this facilitates a better choice of which channel should be used by an 802.22 system based on the channels' characteristics, such as background interference.

IEEE 802.22 has also worked on two amendments to IEEE Std 802.22™-2011, 802.22a "Management and Control Plane Interfaces and Procedures and enhancement to the Management Information Base (MIB)," and 802.22b "Enhancement for Broadband Services and Monitoring Applications." IEEE 802.22a was approved for publication in 2014 (therefore denoted as IEEE Std 802.22a™-2014 [7]), and 802.22b was very recently approved for publication at the end of 2015 (denoted as IEEE Std 802.22b™-2015). At the time of writing, in addition to IEEE 802.22.3, IEEE 802.22 is further working on a revision of the baseline IEEE Std 802.22™-2011, aiming to bring it to other spectrum sharing bands and applications, as well as a revision of IEEE Std 802.22.1™-2010.

IEEE 802.22 Physical Layer

The PHY of 802.22 is heavily based on a variation of the WiMAX amendment standard IEEE 802.16e. The 802.22 PHY use 2,048 OFDM subcarriers irrespective of the utilized channel bandwidth, noting that 802.22 supports bandwidths of 6, 7 and 8 MHz, respectively, with transmission bandwidths of 5.625, 6.561, and 7.499 MHz. Out of these, 368 subcarriers are guard subcarriers, with the utilized

subcarriers comprising 1,440 data subcarriers and 240 pilot subcarriers. The basic unit of resource allocation is known as a sub-channel, defined as 24 data subcarriers plus 4 pilot subcarriers.

IEEE 802.22 supports BPSK, QPSK, 16-QAM, and 64-QAM modulation. Pertaining to various extraordinary modes of operation and preambles, 802.22 uses BPSK in uncoded mode only for CDMA opportunistic mode on the uplink, which is applicable in the USA, as well as QPSK with 1/2-rate coding and repetitions 2, 3, and 4. Repetition 4 is for superframe control header (SCH) transmission and also the superframe preamble, as well as the coexistence beacon protocol (CBP) packet preamble, repetition 3 is for the CBP transmission, and repetition 2 is for frame control header (FCH) transmission as well as the frame preamble. For data communication, more generally, 802.22 supports QPSK, 16-QAM, and 64-QAM modulation, each with convolutional coding rates of 1/2, 2/3, 3/4, or 5/6. The highest rate modulation and coding scheme, 64-QAM modulation with 5/6 coding, can achieve a peak data rate of 22.69 Mbps for a spectral efficiency of 3.78 bps/Hz in a 6 MHz channel assuming the entirety of that channel is used in the denominator of the calculation (i.e., not just the transmission bandwidth). 802.22 also supports three different optional advanced coding methods: duo-binary convolutional turbo codes, shortened block turbo codes, and low-density parity check codes.

Interleaving is achieved using a turbo interleaver, applied to coded bits and to carriers, the latter with different parameters.

Far more information on the 802.22 PHY can be obtained, e.g., from [8].

IEEE 802.22 MAC Layer

The 802.22 MAC is again very similar in form to that of IEEE 802.16 (WiMAX), with additional functionality incorporated to cope with the protection requirements of incumbent services in TVWS. This additional functionality includes geolocation capability and interaction with geolocation databases; synchronicity in the superframe structure achieved by a common clock such as GPS, to allow for spectrum sensing among other benefits; and spectrum sensing itself, among others. The MAC is connection oriented and centralized in terms of resource allocation and QoS control.

The 802.22 frame structure consists of superframes and frames. A superframe is 160 ms long and contains 16 frames of 10 ms duration each. The first frame in a superframe starts with the superframe preamble, the frame preamble, the SCH, and then the FCH. Frames otherwise start with a frame preamble then FCH. The SCH is a broadcast by base stations that can be seen as a type of beacon and carries information that effectively "boots" consumer premises equipment (end users) on to the cell/access, configuring them accordingly based on the characteristics of that cell/access. It is sent with a very robust modulation and coding, as described above, for this reason. The FCH includes information on the downlink and uplink structuring in the frame. As well as the aforementioned preamble, upfront information, and downlink and uplink traffic, the frame structure

of 802.22 includes a third part dedicated to coexistence: termed the self-coexistence window (SCW). This enables intercell communication, utilized for self-coexistence and incumbent protection in CR systems, and is scheduled by the BS at the end of some frames. The SCW extends over five symbols.

As would be expected for a centralized protocol serving CR principles, there are a number of highly sophisticated aspects of its MAC layer design. These capabilities include, among others:

- System-level coordination among cell resource usages.
- Time-sharing of resource usages among cells in the case of over overlapping cells, if desired.
- An urgent messaging procedure to stop transmissions incorporated into the MAC structure for coexistence emergencies (e.g., unexpected emergence/detection of an incumbent spectrum user).
- Fully specified sensing support (not only coordinated quiet periods but also messaging for sensing measurements, fully specified information sets, etc.).
- A highly configurable frame structure, e.g., based on downlink/uplink traffic requirements.

Far more information on the 802.22 MAC can be obtained, e.g., from [8].

IEEE 802.22 Spectrum Manager

In line with the centralized nature of the IEEE 802.22 design, and noting the complexity of spectrum coordination in such cases, 802.22 also includes a centralized "Spectrum Manager" entity. As well as efficient spectrum coordination in the context of spectrum usage within the 802.22 deployment, the entity deals with aspects of incumbent protection and adherence to regulatory policies. More specifically, it is responsible for:

- Maintenance of spectrum availability information.
- Channel classification and selection.
- Association control.
- Regulatory policy enforcement.
- Channel management.
- Self-coexistence with other 802.22 systems.

The maintenance of spectrum availability information is achieved through combining a range of information sets on incumbents, namely, from spectrum sensing and geolocation databases. The channel classification and selection assigns operational statuses of channels to MAC/PHY elements in the 802.22 network. A number of classes are given to channels in these assignments, including operating channels, backup channels, and candidates for backup channels, among others [8]. Association control manages association between CPEs and BSs, granting

association rights accordingly. The regulatory policy enforcement is achieved by interfacing with a regulatory policy entity and instructing all necessary elements in accordance with the response from that. For instance, such information might include the required frequency of checking availability with a geolocation database. Channel management is responsible for the assignment of the actual operational channels to 802.22 network elements, including associated actions such as switching to backup channels, e.g., if an incumbent is detected, perhaps even terminating a cell if there are no appropriate channels, among other aspects. Self-coexistence with other 802.22 networks combines the information from all CPEs of other 802.22 networks in the area and selects channels accordingly or switches to "self-coexistence mode." Self-coexistence mode is the special mode for time-sharing of resources among cells/networks, anticipated to be rarely needed.

Again, far more information on the 802.22 Spectrum Manager, as well as the detail of 802.22 in general, can be obtained, e.g., ▸ Chap. 49, "ETSI-RRS Reconfigurable Radio Systems Standards".

IEEE 802.11af Wireless Local Area Networks in TVWS

IEEE 802.11af (approved for publication in 2013, therefore denoted as IEEE Std 802.11af™-2013 [9]) is the amendment of the IEEE's 802.11 wireless local area networking (WLAN) specification to extend it to operability in TVWS.

IEEE 802.11af Physical Layer

The IEEE 802.11af PHY is heavily based on IEEE 802.11ac, simply downclocking the OFDM-based "very high throughput" 40 MHz PHY mode of 802.11ac. 802.11af supports modulation and coding schemes BPSK 1/2, QPSK 1/2 and 3/4, 16-QAM 1/2 and 3/4, 64-QAM 2/3, 3/4, and 5/6, and 256-QAM 3/4 and 5/6. The theoretical maximum throughput in 6 and 8 MHz channels, respectively, for a short guard interval implementation are 26.7 and 35.6 Mbps. Among other PHY aspects, 802.11af supports convolutional coding and optional LDPC coding, channel aggregation is optionally supported bonding up four channels in one or two contiguous blocks, and up two four spatial multiplexing streams are optionally supported. If all these characteristics are implemented together, the theoretical maximum throughput of 802.11af increases to 426.7 Mbps in 6 MHz channelization, and 568.8 Mbps in 8 MHz channelization. Regarding OFDM structure, 802.11af implements 108 data subcarriers, 6 pilot subcarriers, and 3 null subcarriers per channel.

IEEE 802.11af MAC Layer

Being an amendment to the IEEE 802.11 standard, much of the MAC characteristics and functionalities therein are maintained, as expected. However, there are, by necessity or in order to improve optimality, some key differences and

added functionalities of 802.11af compared with the baseline 802.11 and its other amendments.

Some differences relate to self-coexistence. The 802.11af MAC layer defines the optional concept of the registered location secure server (RLSS). If 802.11af access points (APs) are placed in close proximity, the associated RLSS manages the channel allocation among them. This represents a novel self-coexistence function in order to better coordinate the channel usage in TVWS. However, the conventional IEEE 802.11 self-coexistence mechanism of CSMA is also maintained.

An AP in 802.11af is a master device as per TVWS terminology, and a Station (STA – i.e., the end user device, e.g., a WiFi-capable laptop) is a slave device. However, despite the infrastructure-based hierarchy, 802.11af does not support cellular operation in the sense that 802.22 does. This is in line with the conventional 802.11 wireless local area networks structure as a "nomadic" wireless network. In contrast, 802.11af maintains its support for ad hoc modes of operation as in 802.11, which are not supported by 802.22.

Clearly, in order to be compliant with TVWS rules, 802.11af must implement communications with geolocation databases as well as all other such requirements as specified by regulators. This is implemented by the 802.11af MAC. However, 802.11af does not specify the intricate solutions for sensing-based access, as are specified in 802.22 (see section "IEEE 802.22 Wireless Regional-Area Networks in TVWS"). Our assessment is that this in because 802.22 undertook a lot of its early work at a time when the pending rules for TVWS in the USA were very different from what they are now, being significantly based on sensing until late 2010. The rules then changed almost in totality to being based on geolocation database-enabled access, with sensing-based access only being allowed in the US case and only for an extremely low transmission power of 50 mW in the 6 MHz channel, or −0.4 dBm per 100 kHz PSD, neither of which can be violated. 802.11af was developed entirely within the duration that the new rules applied. However, it is noted that TVWS rules might still vary further internationally; hence, the flexibility that 802.22 has in terms of aspects such as sensing support might have benefits, depending on the implementation scenario.

More information on 802.11af, linked specifically to implementation and trialing of it, can be found in ▸ Chap. 49, "ETSI-RRS Reconfigurable Radio Systems Standards".

IEEE 802.15.4m Wireless Personal Area Networks in TVWS

IEEE 802.15.4m (approved for publication in 2014, therefore denoted as IEEE Std 802.15.4m™-2014 [11]) is the amendment to IEEE 802.15.4 for operation in TVWS. IEEE 802.15 is the standards working group for wireless personal area networks (WPANs), and IEEE 802.15.4 the standard for low-rate such WPANs (LR-WPANs) under that scope. Examples of deployment purposes for such capabilities include smart utility networking, wireless sensor networking, active radio-frequency identification, and low-energy critical infrastructure monitoring, among others.

Like IEEE 802.11af, IEEE 802.15.4m doesn't assume sensing capability up front and therefore doesn't explicitly define it or support capabilities to the extent that IEEE 802.22 does (see section "IEEE 802.22 Wireless Regional-Area Networks in TVWS"); however, 802.15.4m doesn't rule out access being based on sensing either. It is perfectly conceivable for a separate sensing capability to be deployed that will allow such a system to operate in TVWS, e.g., with the much lower channel power limit of 50 dBm as is permitted in such cases in US deployments. 802.15.4m does specify all the geolocation database communications that are necessary in order to allow white space access as the dominant method internationally.

IEEE 802.15.4 specifies two levels of device functionality: full-function devices (FFDs) and reduced-function devices (RFDs). FFDs may serve as coordinators or as simple nodes in the WPANs and can undertake functionalities such as relaying messages in the coordinator role. RFDs are very basic devices, e.g., with very constrained batteries and limited communication capability, and cannot act as coordinators. There is also a higher-level concept of a PAN coordinator that communicates directly with the geolocation database and deals with synchronization of the network. Based on such capabilities, 802.15.4m supports cluster-tree topologies (i.e., interconnections of trees), and star topologies, and can also support mesh-based topologies.

Regarding the PHY of 802.15.4m, keeping in mind that it is an amendment, 802.15.4 and its other amendments define a total of 12 different PHY alternatives. Far more information on these can be obtained from [11, 12]. However, 802.15.4m defines three new PHYs/variants for operation specifically in TVWS: a frequency-shift keying based PHY, a wideband OFDM-based PHY, and a narrow-band OFDM-based PHY. Regarding the MAC of 802.15.4m, interesting capabilities such as "dynamic band switching" are defined, allowing 802.15.4 (as amended by 802.15.4m, and other amendments) to switch back to other bands/modes where TVWS is not available or perhaps not yet permitted under regulations. Power-saving functionality is also defined, involving the scheduling of listening periods and sleep modes in between.

More information on 802.15.4m can be found in [11, 12].

IEEE DySPAN-SC and IEEE 1900 Standards Working Groups

The IEEE Dynamic Spectrum Access Networks Standards Committee (DySPAN-SC) [13] and associated IEEE 1900 working groups (see [14–20]) are concerned with the standardization of aspects of DySPAN and related technologies such as Dynamic Spectrum Access (DSA), CR, and TVWS, among others. DySPAN-SC is responsible for the oversight and sponsoring the development of standards in the IEEE 1900 working groups. Many of the standards that are worked on and developed by IEEE 1900 working groups take an overarching viewpoint. They often intend to be either broadly applicable to generic concepts among a range of types of systems (e.g., the terms and definitions harmonization work of IEEE 1900.1 [26], or the heterogeneous networks management scope of IEEE

1900.4 [29], among other examples), or ultimately applicable to a wide range of use cases (e.g., the white spaces radio interface standard of IEEE 1900.7, among other examples; although it is noted that 1900.7 is still in the process of defining amendment standards that will likely broaden the use cases it covers).

Such a direction has strong links to DySPAN-SC's definition as based on a particular class of technologies (DySPAN/DSA) and therefore standardizing the different and broadly applicable aspects of those technologies. This is in contrast to the IEEE 802 standards committee [21] and its working groups (IEEE 802.11 [22], IEEE 802.15 [23], IEEE 802.16 [24], IEEE 802.22 [25], etc.), which for the most part concentrate on very specific use cases and scenarios for computer communications, such as local area networking, personal area networking, and metropolitan area networking, among others, and therefore define their standards based on those use cases. Further, in defining the scope of IEEE DySPAN-SC and its standards, it is recognized that flexibility is needed in order to serve the capabilities and characteristics of a range of different systems. The broad, often technology-agnostic nature of IEEE DySPAN-SC and some of its IEEE 1900 standards underlines the operational flexibility within which they aim to flourish.

IEEE 1900 Working Groups

The IEEE 1900 working groups and their titles/topics are listed as follows:

- IEEE 1900.1: Definitions and Concepts for Dynamic Spectrum Access: Terminology Relating to Emerging Wireless Networks, System Functionality, and Spectrum Management [14].
- IEEE 1900.2: Recommended Practice for the Analysis of In-Band and Adjacent Band Interference and Coexistence Between Radio Systems [15].
- IEEE 1900.3: Recommended Practice for Conformance Evaluation of Software-Defined Radio (SDR) Software Modules (disbanded) [16].
- IEEE 1900.4: Architectural Building Blocks Enabling Network Device Distributed Decision Making for Optimized Radio Resource Usage in Heterogeneous Wireless Access Networks [17].
- IEEE 1900.5: Policy Language and Policy Architectures for Managing Cognitive Radio for Dynamic Spectrum Access Applications [18].
- IEEE 1900.6: Spectrum Sensing Interfaces and Data Structures for Dynamic Spectrum Access and other Advanced Radio Communication Systems [19].
- IEEE 1900.7: Radio Interface for White Space Dynamic Spectrum Access Radio Systems Supporting Fixed and Mobile Operation [20].

Figure 1 depicts the relationships among the IEEE 1900 working groups, as well as their statuses. In the following sections, we go into a bit more detail on these groups, including their topics, purposes, and current or emerging standards.

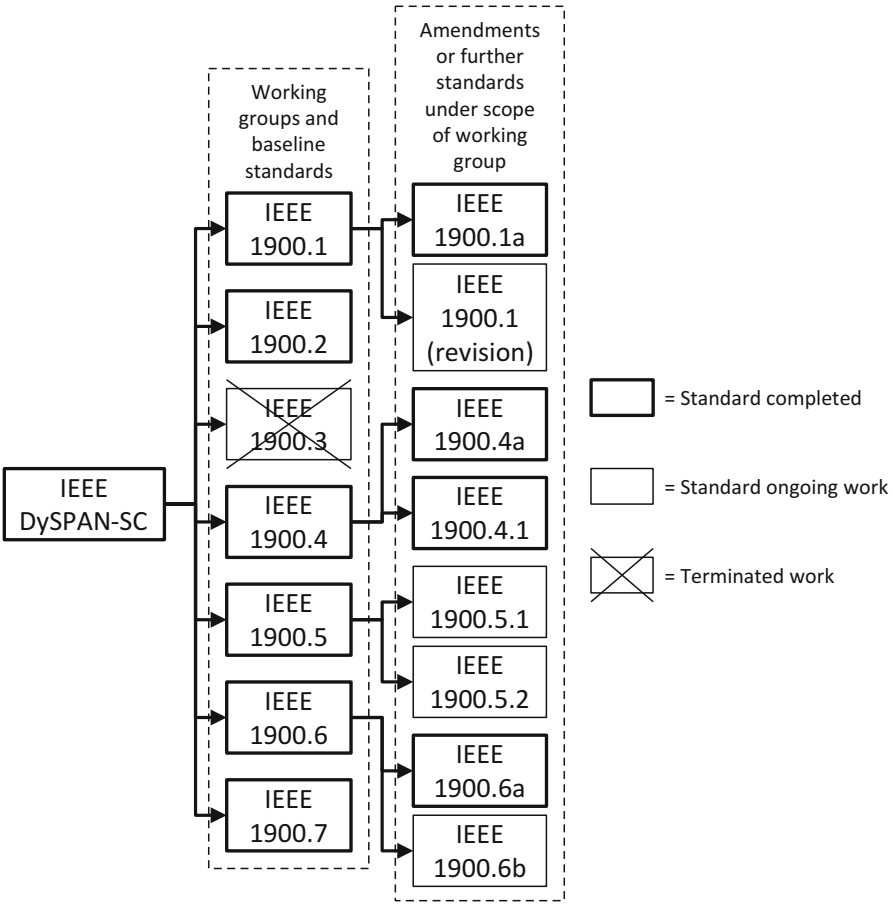

Fig. 1 IEEE DySPAN-SC and IEEE 1900 working groups and standards

IEEE 1900.1

IEEE 1900.1 aims to facilitate the development of DySPAN-related technologies (including DSA, white spaces, CR, etc.) by clarifying the terminology and aspects of how these technologies relate to each other, noting that many of the terms used in the fields of DSA and the wide range of related technologies do not have precise definitions or have multiple/unclear definitions. The baseline 1900.1 standard was approved and published in 2008 (therefore denoted as IEEE Std 1900.1™-2008 [26]), and an amendment covering new terms and definitions that have emerged since the publication of the baseline standard in the scope of other IEEE 1900 working groups was approved in late 2012 and published in January 2013 (therefore denoted as IEEE Std 1900.1a™-2012 [27]). IEEE 1900.1 has since worked on a revision of its published 2008 standard, also incorporating the text of the IEEE

1900.1a-2012 amendment as is usual procedure. This work should complete the end of 2017 at the latest.

The baseline IEEE 1900.1-2008 standard presents terms and definitions in the following categories:

- Definitions of advanced radio system concepts.
- Definitions of radio system functional capabilities.
- Definitions of network technologies that support advanced radio system technologies.
- Spectrum management definitions.
- Glossary of ancillary terminology.

Further, the IEEE 1900.1a-2012 amendment has added the category of definitions of decision making and control concepts that support advanced radio system technologies.

The annexes of the baseline standard, all of which are "informative" in nature, cover additional aspects such as the consideration of the implications of DySPAN and related technologies (e.g., for regulation), some detailed consideration of the relationships between the technologies hence their hierarchical inheritance, and observations on the purposes of the technologies and aspects of their architectures. One example of the latter is a detailed study on the different forms of flexible radio. There is also discussion on roadmapping for such technologies, among other aspects.

The 1900.1 revision is reviewing the terms with regard to and changes in their use in the community, new terms/definitions that are required or the deletion of terms, structuring of the terms, and other aspects. It will also further consider upcoming concepts and related terminology such as those stemming from the commercial dynamic use of shared spectrum.

IEEE 1900.2

IEEE 1900.2 provides guidance, which is primarily technical in nature, on the analysis of the potential for coexistence or interference between radio systems operating in the same frequency band and between different frequency bands. In essence, IEEE 1900.2 facilitates the realization – in a viable way – of a range of spectrum coexistence technologies.

Regarding content of the IEEE 1900.2-2008 baseline standard, published in 2008 (denoted as IEEE Std 1900.2™-2008 [28]), it includes a range of normative content, such as the specification a key concepts such as "harmful interference" and "measurement events," among others, and the definition of scenarios for interference assessment, interference assessment criteria and important variables, and commentary on the analysis and modelling of interference.

IEEE 1900.2 has been dormant since 2008 with no additional work items currently envisaged. IEEE 1900.2 will, however, be required to undergo the usual IEEE process of periodic revisions or affirmations of IEEE standards. Revision or affirmation of published IEEE standards is required to occur every 10 years at most.

IEEE 1900.3

The IEEE 1900.3 standards work was initiated in May 2005, but the working group was disbanded in late 2008 [16]. The intended purpose of the standard was to provide guidance on how to ensure the conformance with relevant specifications (e.g., security in particular) of software intended for deployment in a SDR terminal.

IEEE 1900.4

IEEE 1900.4, until relatively recent years, has been one of the most active of the working groups under IEEE DySPAN-SC. It is currently, however, in hibernation having completed its standards work, awaiting further revisions of those standards if and when necessary and any further upcoming topics.

The baseline IEEE 1900.4 standard (denoted as IEEE Std 1900.4™-2009 [29]) was published in February 2009. The purpose of this standard, and IEEE 1900.4 in general, is to define management capabilities to improve overall composite capacity and quality of service of wireless systems in multiple radio access technology environments, through instantiation of an appropriate system architecture and protocols to facilitate the optimization of radio resource usage. 1900.4 works on the assumption of a three-level resource management hierarchy: The network or inter-network level, then the radio access network (RAN) level under that, and finally the terminal level. It is noted that IEEE 1900.4 facilitates a range of spectrum sharing (and management thereof) technologies of interest to the community, although particularly emphasizes those that are network driven as might be managed by a mobile communications operator, for example, owning a range of spectrum bands and with various radio access technologies available that can adapt to operate in the different bands.

The two key entities of 1900.4 are the Network Reconfiguration Manager (NRM) and Terminal Reconfiguration Manager (TRM). Other entities such as the operator spectrum management (OSM) entity are assumed, although some are not defined in detail – in the OSM example this is because it is taken to be proprietary within the scope of the given network operator. The NRM resides at the top of the management hierarchy, managing resources at the network or inter-network level and producing instructions/constraints (directives, policies) for the TRM accordingly, and also instructing RANs based on its decisions. The TRM implements the instructions/constraints from the NRM and also manages resources at the terminal level but sticking within the constraints conveyed by the NRM. There are also processes of feedback from the TRM to the NRM, with associated functionalities defined, and from RANs to the NRM.

IEEE 1900.4 has also published an amendment to the 1900.4-2009 standard, in the form of 1900.4a (denoted as IEEE Std 1900.4a™-2011 [30]), Architecture and Interfaces for Dynamic Spectrum Access Networks in White Space Frequency Bands, and has published an additional standard within the scope of 1900.4's work, 1900.4.1 (denoted as IEEE Std 1900.4.1™-2013 [31]), IEEE Standard for Interfaces and Protocols Enabling Distributed Decision Making for Optimized Radio Resource Usage in Heterogeneous Wireless Networks. The IEEE 1900.4a-2011 amendment standard considers extensions to the spectrum management cases in 1900.4 to cover

access to TVWS, with minimal constraints on the used radio interface (physical and media access control layers), by defining additional components of the IEEE 1900.4 system. A key addition in 1900.4a is the White Space Manager (WSM) entity, which provides regulatory context information to the networks or composite systems that might be using TVWS. On the network-side, the Cognitive Base Station Reconfiguration Manager (CBSRM) entity is also introduced, in order to enable the control of the base stations white space access according to the regulatory rules and flexibility that is allowed given context information, and a mirroring entity to control the terminal side in white space is also introduced.

The IEEE 1900.4.1-2013 standard provides a description of the interfaces and service access points defined in the baseline 1900.4-2009, enabling distributed decision making in heterogeneous wireless networks and obtaining context information for this decision making. This standard delves into more detail on the information exchanges between the 1900.4 elements and the associated state transitions of those elements based on the information exchanges. It considers precise signaling interactions for the purpose of implementing 1900.4 decisions, among other aspects. Noting that the information model in 1900.4-2009 was abstract in the sense of specifying only the high-level ASN.1 characteristics and requirements, 1900.4.1-2013 delves down to the level of precise bit-level header structures.

IEEE 1900.5

IEEE 1900.5 defines a policy language (or a set of policy languages or dialects) to specify interoperable, vendor-independent control of CR functionality and behavior for DSA resources and services. The definition of such policies is an essential step toward the facilitation of autonomous spectrum coexistence of devices and systems, in primary-secondary access and in other contexts. The distinction is made between policy reasoning and policy generation and validation, in that policy reasoning is accomplished within a defined policy-based radio node and that policy generation and validation is accomplished through a policy generation system prior to provision of the policy to the policy-based radio node.

The baseline standard of IEEE 1900.5 (denoted as IEEE Std 1900.5™-2011 [32]) was published in 2012, and at the time of writing, IEEE 1900.5 is working toward the publication of two further standards within its scope: IEEE 1900.5.1 Draft Standard Policy Language for Dynamic Spectrum Access Systems and IEEE 1900.5.2 Standard Method for Modeling Spectrum Consumption. The latter is in the final stages of approval and publication by the IEEE, whereas the former is still at a relatively early stage in its work. 1900.5.2 specifies a generalized method to model spectrum consumption of any use of spectrum and the associated computations for arbitrating the compatibility among models. The methods of modeling are chosen to support the development of tractable algorithms for determining the compatibility between models and for performing various spectrum management tasks that operate on a plurality of models. This work concentrates on the application of the vision presented in [33, 34] where the Spectrum Consumption Modeling Markup Language (SCMML) is used.

IEEE 1900.5.1 work is toward defining a vendor-independent policy language for managing the functionality and behavior of DySPAN based on the language requirements defined in the IEEE 1900.5 standard. Reflecting the current status and thinking at the time of writing, the standard will take into consideration both the policy language requirements of IEEE 1900.5 and the results of the Modeling Language for Mobility Work Group (MLM-WG) within the Wireless Innovation Forum (SDRF v2) Committee on Advanced Wireless Networking and Infrastructure [35].

IEEE 1900.6

IEEE 1900.6 defines the interfaces and data structures for communication between spectrum sensors and their clients in dynamic spectrum access and other advanced radio communication systems. This might be applicable for cooperative and/or collaborative distributed sensing scenarios, as well as other scenarios where the intelligence that makes spectrum access and other decisions, and spectrum sensors, are at different physical locations – although it is noted that IEEE 1900.6 can also serve cases where subsets of the various entities involved can reside at the same physical location. The logical interfaces and supporting data structures in 1900.6 are defined abstractly, without constraining the sensing technology, client design, or data link between sensors and their clients. Of course, the facilitation of sensing technologies through standards such as IEEE 1900.6 assists many spectral sharing techniques that utilize locally-obtained spectrum information.

The baseline standard of IEEE 1900.6 (denoted as IEEE Std 1900.6™-2011 [36]), addressing its key purposes as mentioned above, was published in April 2011. This standard defines three basic elements: Spectrum sensors, the cognitive engine, and the data archive. These, and the interfaces between them that IEEE 1900.6 addresses, are illustrated in Fig. 2. Among these elements, the relatively simple spectrum sensors are assumed to merely obtain spectrum usage information

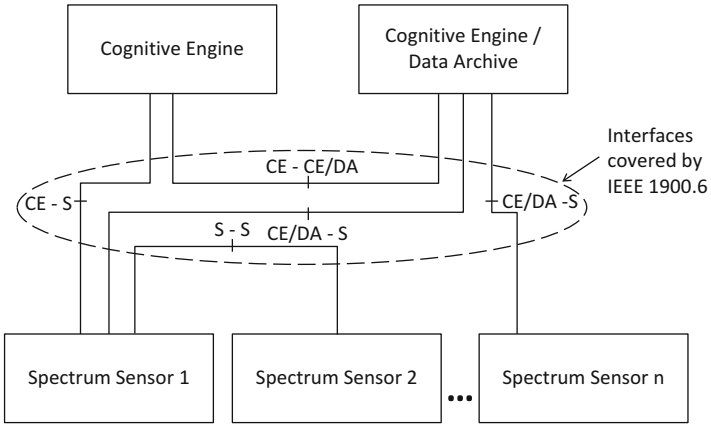

Fig. 2 IEEE 1900.6 entities and considered interfaces

such as the energy in a particular band at a given location, however, there is scope given collaborative spectrum sensing scenarios for example, for some sensors to act as cluster heads for other sensors and undertake limited processing of the sensed information from those other sensors before forwarding the result (e.g., performing a logical OR on sensed decisions to assess if there are any positive results among the sensors). The cognitive engine is the intelligent element that uses the spectrum sensing information, e.g., to make decisions on viable opportunities for spectrum access. The data archive is a store of sensed information that might be utilized to assist decisions, e.g., for learning capabilities based on past experience.

IEEE 1900.6 has also published an amendment (IEEE Std 1900.6a™-2014 [37]), on Procedures, Protocols, and Data Archive Enhanced Interfaces. This covers a number of aspects of the precise nature of the procedure and protocols, including the interaction with non-compliant systems, consideration of professional installations in which sensors may not have location information (e.g., GPS) but may instead have their location professionally verified, data-archive assisted sensing decisions such as related to propagation maps that the data archive has access, support for wideband sparse sensing implementation, and support for use of the 1900.6 subsystem for connectivity awareness, among many other additions.

At the time of writing, IEEE 1900.6 is working on a new amendment, IEEE 1900.6b, covering the application and extension of the standard to the case of spectrum sensing systems being used to augment or otherwise assist spectrum databases – geolocation databases in the context of TVWS being one example thereof. Initial work on this amendment has aimed to satisfy use cases including the application of spectrum sensing to spectrum databases in TVWS, the application to Spectrum Access System and Environmental Sensing Capability capabilities such as employed for the 3.5 GHz Citizens Broadband Radio Service in the USA, and the use of such sensing information by self-organizing networks.

A further work item, at the time of writing recently completed, approved, and published as a corrigendum, is a minor revision of the terms and definitions covered in 1900.6 to harmonize with IEEE 1900.1 terms and definitions and the terms and definitions in IEEE 1900/DySPAN-SC in general.

IEEE 1900.7

IEEE 1900.7 work is concerned with the definition a new radio interface (PHY/MAC, and related aspects) for white space access. The aim is for this radio interface to be generic, applicable to a range of use cases and spectrum bands. However, in practice, 1900.7 has thus far considered TVWS as the most appealing and key focus area, as TV bands are the only bands currently allowed from a regulatory perspective for white space access.

The baseline standard of IEEE 1900.7 (denoted as IEEE Std 1900.7™-2015) has recently been completed and published at the time of writing. It has aimed to address a wide range of use cases, from wireless sensor networking, to in-building provisioning (e.g., wireless local area networking), to backhaul provisioning, and to maritime coverage enhancement through white spaces, among many others. The defined PHY, currently, is based on filter bank multicarrier (FBMC) technology,

Table 2 IEEE 1900.7 modulation and coding schemes, and associated peak throughputs

Modulation	Coding	Peak throughput in 2 MHz/ Mbps	Peak throughput in 8 MHz/ Mbps
BPSK	1/2	0.93	3.78
QPSK	1/2	1.86	7.56
QPSK	1/4	2.79	11.34
16-QAM	1/2	3.72	15.12
16-QAM	3/4	5.58	22.68
64-QAM	2/3	7.44	30.24
64-QAM	3/4	8.37	34.02
64-QAM	5/6	9.30	37.80

and the MAC is based on a variation on the 802.11 CSMA MAC, incorporating an adaptive algorithm in the collision back-off mechanism to enhance fairness and performance. The current published 1900.7 standard also assumes a master-slave mode of operation, noting that such a mode is compatible with regulations for white space as are out there currently.

The 1900.7 PHY assumes multiples of 2 MHz operation, in theory being able to aggregate across channels (even with non-contiguous aggregation) through transmission in subsets of 2 MHz as specified by a mask applied to the set of 2 MHz sub-channels. This fits well with regulatory approaches allowing aggregation (see, e.g., [1, 2]), as well as potential future advancements such as being able to filter out 2 MHz chunks, e.g., to avoid interference with wireless microphones. Regarding modulation and coding, those schemes in Table 2 are defined. The peak rates supported by these modulation and coding schemes are also given in Table 2.

At the time of writing, 1900.7 is considering the initiation of additional possible amendments to its baseline standard, which will likely achieve the objective of satisfying some of the use cases that it is more challenging for FBMC and CSMA to realize: an example being wireless sensor networking. It therefore seems likely that further options for the PHY/MAC will be formulated as part of such work, should it progress, as well as other aspects such as the mode of operation which could conceivably also be expanded. Of course, this would be done compatibly with regulatory requirements.

ETSI Reconfigurable Radio Systems (RRS) Standards

The European Telecommunications Standards Institute (ETSI) has produced and is producing a number of CR- and TVWS-related standards, as well as standards on spectrum sharing technologies in general. ETSI standards on these topics are most commonly developed under the ETSI Reconfigurable Radio Systems (ETSI-RRS) technical committee [38], with the ETSI 301 598 standard, as covered earlier in

section "ETSI EN 301 598 Harmonized European Standard," being a clear exception to this. At the time of writing, ETSI-RRS is divided into four working groups:

- RRS Working Group 1: "System Aspects"
- RRS Working Group 2: "Radio Equipment Architecture"
- RRS Working Group 3: "Functional Architecture and Cognitive Pilot Channel"
- RRS Working Group 4: "Public Safety"

Again at the time of writing, ETSI-RRS has thus far developed 20 standards and technical reports, as follows. ETSI-RRS is currently very active in producing additional standards.

- TR 102 967: Reconfigurable Radio Systems (RRS); Use cases for dynamic equipment reconfiguration
- EN 303 387: Reconfigurable Radio Systems (RRS); Signalling Protocols and information exchange for Coordinated use of TV White Spaces; Interface between Cognitive Radio System (CRS) and Spectrum Coordinator (SC)
- EN 303 146-1: Reconfigurable Radio Systems (RRS); Mobile Device Information Models and Protocols; Part 1: Multiradio Interface (MURI)
- EN 303 143: Reconfigurable Radio Systems (RRS); System architecture for information exchange between different Geo-location Databases (GLDBs) enabling the operation of White Space Devices (WSDs)
- EN 303 144: Reconfigurable Radio Systems (RRS); Enabling the operation of Cognitive Radio System (CRS) dependent for their use of radio spectrum on information obtained from Geo-location Databases (GLDBs); Parameters and procedures for information exchange between different GLDBs
- EN 303 145: Reconfigurable Radio Systems (RRS); System Architecture and High Level Procedures for Coordinated and Uncoordinated Use of TV White Spaces
- TS 103 235: Reconfigurable Radio Systems (RRS); System architecture and high level procedures for operation of Licensed Shared Access (LSA) in the 2300–2400 MHz band
- EN 303 095: Reconfigurable Radio Systems (RRS); Radio Reconfiguration related Architecture for Mobile Devices
- TS 103 146-2: Reconfigurable Radio Systems (RRS); Mobile Device Information Models and Protocols; Part 2: Reconfigurable Radio Frequency Interface (RRFI)
- TS 103 145: Reconfigurable Radio Systems (RRS); System Architecture and High Level Procedures for Coordinated and Uncoordinated Use of TV White Spaces
- TS 103 143: Reconfigurable Radio Systems (RRS); System architecture for information exchange between different Geo-location Databases (GLDBs) enabling the operation of White Space Devices (WSDs)
- EN 302 969: Reconfigurable Radio Systems (RRS); Radio Reconfiguration related Requirements for Mobile Devices

- TS 103 154: Reconfigurable Radio Systems (RRS); System requirements for operation of Mobile Broadband Systems in the 2300–2400 MHz band under Licensed Shared Access (LSA)
- TS 102 946: Reconfigurable Radio Systems (RRS); System requirements for Operation in UHF TV Band White Spaces
- TS 103 146-1: Reconfigurable Radio Systems (RRS); Mobile Device Information Models and Protocols; Part 1:Multiradio Interface (MURI)
- TR 102 947: Reconfigurable Radio Systems (RRS); Use Cases for building and exploitation of Radio Environment Maps (REMs) for intra-operator scenarios
- TR 102 945: Reconfigurable Radio Systems (RRS); Definitions and abbreviations
- TR 103 067: Reconfigurable Radio Systems (RRS); Feasibility study on Radio Frequency (RF) performance for Cognitive Radio Systems operating in UHF TV band White Spaces
- TS 103 095: Reconfigurable Radio Systems (RRS); Radio Reconfiguration related Architecture for Mobile Devices
- TR 102 970: Reconfigurable Radio Systems (RRS); Use Cases for spectrum and network usage among Public Safety, Commercial and Military domains

A dedicated ▸ Chap. 49, "ETSI-RRS Reconfigurable Radio Systems Standards", provides far more detail and background reasoning on this range of standards and technical reports, so we don't address them directly here.

ECMA-392

This standard originates from perhaps a lesser-known group: ECMA. This was the European Computer Manufacturers Association (ECMA) until 1994, since then has been internationalized and just maintained ECMA as a trademark. The ECMA-392 MAC and PHY for Operation in TV White Space standard was the first TVWS standard to actually be completed, having been published in December 2009.

ECMA-392 specifies a MAC sub-layer and a PHY for personal/portable cognitive wireless networks operating in TV bands. It also specifies a MUX sub-layer for higher-layer protocols. It supports master-slave, peer-to-peer, or mesh configurations and three types of devices: master devices, slave devices, and peer devices. The master (or peer) coordinates dynamic frequency selection, transmit power control, and channel measurements.

ECMA-392 names various incumbent protection mechanisms which may be used to meet regulatory requirements; the mechanisms themselves are outside of the scope of ECMA-392, and the geolocation database interaction is seen as a higher-layer function and therefore not specified. However, the network structures defined in ECMA-392 (e.g., the definition of master and slave devices) support current regulatory approaches well, and the information structures defined (e.g., channel availabilities) also assist.

The primary application of ECMA-392 is intended to be in-home multimedia distribution. To this end, the PHY is OFDM-based, comprising 128 subcarriers, out of which 26 are guard subcarriers, 98 are data subcarriers, and 4 are pilot subcarriers. These values stay the same whether the standard is transmitting in the supported 6, 7, or 8 MHz channel widths, with the spacing between sub-channels changing. Modulation schemes QPSK, 16-QAM, and 64-QAM are supported and a range of convolutional coding rates dependent on the modulation, varying from 1/2-rate to 5/6. The highest-rate modulation and coding option (64-QAM, 5/6 coding) can achieve a throughput of 23.74 Mbps, and with 2×2 spatial multiplexing implemented (which is also supported), this can increase to 47.48 Mbps.

The MAC of ECMA-392 consists of superframes and 256 medium access slots (MASs) within each superframe. The MASs are assigned to either a beacon period, a data transfer period, or a contention signaling window. A reservation-based signaling window can also be used, as can quiet periods similarly to the case of IEEE 802.22 in section "IEEE 802.22 Wireless Regional-Area Networks in TVWS." Beacon periods are used to transmit beacons, e.g., on used channels – the master and peer devices are therefore beaconing devices with associated beacon slots in the beacon period. The defined signaling windows are likewise used to convey important network management information, noting that the reservation-based signaling window is not needed for peer-to-peer network deployments.

The ECMA-392 standard is available freely online, at the time of writing, at [39].

Conclusion and Future Directions

In the context of communications, standards can be looked on as defining the spoken language of how systems communicate with each other. In spectrum sharing scenarios, they become even more essential, also defining the protocol for how the spectrum is shared, in a way that is agreeable to those sharing the spectrum, or, in the case of secondary spectrum access (e.g., TVWS), agreeable to the incumbent user of the spectrum. In this context, such standards are not only implemented by stakeholders such as manufacturers and operators, but may also be enforced (and depending on the case in question, implemented) by a higher-level responsible entity such as the regulator.

This section has provided some detail on a range of standards that have been created for CR- and TVWS-related scenarios, mostly in the context of the realization of CR and TVWS communication between devices, but also in one case providing an example of a vital regulatory standard for TVWS operation in Europe, namely, the ETSI EN 301 598 Harmonized European Standard. For fundamental reasons, standards will continue to be absolutely essential to the achievement of CR and white space communications networks, and spectrum sharing in general.

References

1. Ofcom statement (2015) Implementing TV white spaces. Accessible at: http://stakeholders.ofcom.org.uk/consultations/white-space-coexistence/statement. Accessed Jan 2016
2. ETSI EN 301 598 (2014) White space devices (WSD); wireless access systems operating in the 470 MHz to 790 MHz frequency band; Harmonized EN covering the essential requirements of article 3.2 of the R&TTE Directive, v1.1.1. Accessible at: https://www.etsi.org/deliver/etsi_en/301500_301599/301598/01.01.01_60/en_301598v010101p.pdf. Accessed Jan 2016
3. IEEE Std 802.16™-2012 (2012) IEEE standard for air interface for broadband wireless access systems. Accessible at: https://standards.ieee.org/about/get/802/802.16.html. Accessed Jan 2016
4. IEEE Std 802.22™-2011 (2011) Standard for local and metropolitan area networks – specific requirements – Part 22: cognitive wireless RAN medium access control (MAC) and physical layer (PHY) specifications: policies and procedures for operation in the TV Bands. Accessible at: https://standards.ieee.org/about/get/802/802.22.html. Accessed Jan 2016
5. IEEE Std 802.22.1™-2010 (2010) IEEE standard for local and metropolitan area networks – specific requirements Part 22.1: standard to enhance harmful interference protection for low-power licensed devices operating in TV broadcast bands. Accessible at: https://standards.ieee.org/about/get/802/802.22.html. Accessed Jan 2016
6. IEEE Std 802.22.2™-2012 (2010) IEEE recommended practice for information technology – telecommunications and information exchange between systems wireless regional area networks (WRAN) – specific requirements – Part 22.2: installation and deployment of IEEE 802.22 systems. Accessible at: https://standards.ieee.org/about/get/802/802.22.html. Accessed Jan 2016
7. IEEE Std 802.22a™-2014 (2014) IEEE standard for information technology – telecommunications and information exchange between systems wireless regional area networks (WRAN)– Specific requirements – Part 22: cognitive wireless RAN medium access control (MAC) and physical layer (PHY) specifications: policies and procedures for operation in the TV bands amendment 1: management and control plane interfaces and procedures and enhancement to the management information base (MIB). Accessible at: https://standards.ieee.org/about/get/802/802.22.html. Accessed Jan 2016
8. Mody A, Chouinard G, Shellhammer SJ, Ghosh M, Cavalcanti D (2015) Cognitive wireless regional area network standard. In: Holland O, Bogucka H, Medeisis A (eds) Opportunistic spectrum sharing and white space access: the practical reality. Wiley, Hoboken. ISBN:978-1-118-89374-6
9. IEEE Std 802.11af™-2013 (2014) IEEE standard for information technology – telecommunications and information exchange between systems – local and metropolitan area networks – specific requirements – Part 11: wireless LAN medium access control (MAC) and physical layer (PHY) specifications amendment 5: television white spaces (TVWS) operation. Accessible at: https://standards.ieee.org/findstds/standard/802.11af-2013.html. Accessed Jan 2016
10. Ishizu K et al (2015) Cognitive wireless regional area network standard. In: Holland O, Bogucka H, Medeisis A (eds) Opportunistic spectrum sharing and white space access: the practical reality. Wiley, Hoboken. ISBN:978-1-118-89374-6
11. IEEE Std 802.15.4m™-2014 (2014) IEEE standard for local and metropolitan area networks – Part 15.4: low-rate wireless personal area networks (LR-WPANs) – amendment 6: TV white space between 54 MHz and 862 MHz physical layer. Accessible at: https://standards.ieee.org/about/get/802/802.15.html. Accessed Jan 2016
12. Sum C-S, Lu L, Ming-Tuo Z, Kojima F, Harada H (2013) Design considerations of IEEE 802.15.4m low-rate WPAN in TV white space. IEEE commun 51(4):74–82
13. IEEE DySPAN Standards Committee (DySPAN-SC), http://www.dyspan-sc.org. Accessed Jan 2016
14. IEEE 1900.1 Working Group, http://grouper.ieee.org/groups/dyspan/1/index.htm. Accessed Jan 2016

15. IEEE 1900.2 Working Group, http://grouper.ieee.org/groups/dyspan/2/index.htm. Accessed Jan 2016
16. IEEE 1900.3 Working Group, http://grouper.ieee.org/groups/dyspan/3/index.htm. Accessed Jan 2016
17. IEEE 1900.4 Working Group, http://grouper.ieee.org/groups/dyspan/4/index.htm. Accessed Jan 2016
18. IEEE 1900.5 Working Group, http://grouper.ieee.org/groups/dyspan/5/index.htm. Accessed Jan 2016
19. IEEE 1900.6 Working Group, http://grouper.ieee.org/groups/dyspan/6/index.htm. Accessed Jan 2016
20. IEEE 1900.7 Working Group, http://grouper.ieee.org/groups/dyspan/7/index.htm. Accessed Jan 2016
21. IEEE 802 LAN/MAN Standards Committee, http://www.ieee802.org. Accessed Jan 2016
22. IEEE 802.11 Wireless Local-Area Networks Working Group, http://www.ieee802.org/11. Accessed Jan 2016
23. IEEE 802.11 Wireless Personal-Area Networks Working Group, http://www.ieee802.org/15. Accessed Jan 2016
24. IEEE 802.11 Wireless Metropolitan-Area Networks Working Group, http://www.ieee802.org/16. Accessed Jan 2016
25. IEEE 802.22 Wireless Regional-Area Networks Working Group, http://www.ieee802.org/22. Accessed Jan 2016
26. IEEE Std 1900.1™-2008 (2008) IEEE standard definitions and concepts for dynamic spectrum access: terminology relating to emerging wireless networks, system functionality, and spectrum management. Accessible at http://ieeexplore.ieee.org/xpl/articleDetails.jsp?tp=&arnumber=4633734. Accessed Jan 2016
27. IEEE Std 1900.1a™-2012 (2013) IEEE standard definitions and concepts for dynamic spectrum access: terminology relating to emerging wireless networks, system functionality, and spectrum management. Amendment 1: addition of new terms and associated definitions. Accessible at http://ieeexplore.ieee.org/xpl/articleDetails.jsp?tp=&arnumber=6422300. Accessed Jan 2016
28. IEEE Std 1900.2™-2008 (2008) IEEE recommended practice for the analysis of in-band and adjacent band interference and coexistence between radio systems. Accessible at: http://ieeexplore.ieee.org/xpl/articleDetails.jsp?tp=&arnumber=4584236. Accessed Jan 2016
29. IEEE Std 1900.4™-2009 (2009) IEEE standard for architectural building blocks enabling network-device distributed decision making for optimized radio resource usage in heterogeneous wireless access networks. Accessible at: http://ieeexplore.ieee.org/xpl/articleDetails.jsp?tp=&arnumber=4798288. Accessed Jan 2016
30. IEEE Std 1900.4a™-2011 (2011) IEEE standard for architectural building blocks enabling network-device distributed decision making for optimized radio resource usage in heterogeneous wireless access networks. Amendment 1: architecture and interfaces for dynamic spectrum access networks in white space frequency bands. Accessible at: http://ieeexplore.ieee.org/xpl/articleDetails.jsp?tp=&arnumber=6022707. Accessed Jan 2016
31. IEEE Std 1900.4.1™-2013 (2013) IEEE standard for interfaces and protocols enabling distributed decision making for optimized radio resource usage in heterogeneous wireless networks. Accessible at: http://ieeexplore.ieee.org/xpl/articleDetails.jsp?tp=&arnumber=6544530. Accessed Jan 2016
32. IEEE Std 1900.5™-2011 (2012) IEEE standard for policy language requirements and system architectures for dynamic spectrum access systems. Accessible at: http://ieeexplore.ieee.org/xpl/articleDetails.jsp?tp=&arnumber=6132379. Accessed Jan 2016
33. Stine J, Schmitz S (2014) Model-based spectrum management, Part 1: modeling and computation manual version 2.0, MITRE technical report. Accessible at: http://www.mitre.org/sites/default/files/publications/13-4541-MBSM_Modeling_Manual_v2%200.pdf. Accessed Jan 2016

34. Bastidas C, Stine J (2013) Spectrum markets and sharing via spectrum consumption models, MITRE technical report. Accessible at: https://www.mitre.org/sites/default/files/publications/13-2941.pdf. Accessed Jan 2016
35. The Wireless Innovation Forum, http://www.wirelessinnovation.org. Accessed Jan 2016
36. IEEE Std 1900.6™-2011 (2011) IEEE standard for spectrum sensing interfaces and data structures for dynamic spectrum access and other advanced radio communication systems. Accessible at: http://ieeexplore.ieee.org/xpl/articleDetails.jsp?tp=&arnumber=5756728. Accessed Jan 2016
37. IEEE Std 1900.6a™-2014 (2013) IEEE draft standard for spectrum sensing interfaces and data structures for dynamic spectrum access and other advanced radio communication systems. Amendment: procedures, protocols and data archive enhanced interfaces. Accessible at: http://ieeexplore.ieee.org/xpl/articleDetails.jsp?tp=&arnumber=6619393. Accessed Jan 2016
38. ETSI Technical Committee on Reconfigurable Radio Systems (ETSI-RRS), http://www.etsi.org/technologies-clusters/technologies/radio/reconfigurable-radio. Accessed Jan 2016
39. ECMA-392 (2012) MAC and PHY for operation in TV white space, 2nd edn. Accessible at: http://www.ecma-international.org/publications/standards/Ecma-392.htm. Accessed Jan 2016

Further Reading

1. ETSI EN 303 387 (2015) Reconfigurable radio systems (RRS); signalling protocols and information exchange for coordinated use of TV white spaces; interface between cognitive radio system (CRS) and spectrum coordinator (SC). Accessible at: http://www.etsi.org/deliver/etsi_en/303300_303399/303387/01.01.01_60/en_303387v010101p.pdf. Accessed Jan 2016
2. ETSI EN 303 143 (2015) Reconfigurable radio systems (RRS); system architecture for information exchange between different geo-location databases (GLDBs) enabling the operation of white space devices (WSDs). Accessible at: http://www.etsi.org/deliver/etsi_en/303100_303199/303143/01.02.01_60/en_303143v010201p.pdf. Accessed Jan 2016
3. ETSI EN 303 144 (2015) Reconfigurable radio systems (RRS); enabling the operation of cognitive radio system (CRS) dependent for their use of radio spectrum on information obtained from geo-location databases (GLDBs); parameters and procedures for information exchange between different GLDBs. Accessible at: http://www.etsi.org/deliver/etsi_en/303100_303199/303144/01.01.01_60/en_303144v010101p.pdf. Accessed Jan 2016
4. ETSI EN 303 145 (2015) Reconfigurable radio systems (RRS); system architecture and high level procedures for coordinated and uncoordinated use of TV white spaces. Accessible at: http://www.etsi.org/deliver/etsi_en/303100_303199/303145/01.02.01_60/en_303145v010201p.pdf. Accessed Jan 2016
5. ETSI TS 103 235 (2015) Reconfigurable radio systems (RRS); system architecture and high level procedures for operation of licensed shared access (LSA) in the 2300 MHz–2400 MHz band. Accessible at: http://www.etsi.org/deliver/etsi_ts/103200_103299/103235/01.01.01_60/ts_103235v010101p.pdf. Accessed Jan 2016
6. ETSI TS 103 154 (2014) Reconfigurable radio systems (RRS); system requirements for operation of mobile broadband systems in the 2300 MHz–2400 MHz band under licensed shared access (LSA). Accessible at: http://www.etsi.org/deliver/etsi_ts/103100_103199/103154/01.01.01_60/ts_103154v010101p.pdf. Accessed Jan 2016
7. ETSI TS 102 946 (2014) Reconfigurable radio systems (RRS); system requirements for operation in UHF TV band white spaces. Accessible at: http://www.etsi.org/deliver/etsi_ts/102900_102999/102946/01.01.01_60/ts_102946v010101p.pdf. Accessed Jan 2016
8. ETSI TR 103 067 (2013) Reconfigurable radio systems (RRS); feasibility study on radio frequency (RF) performance for cognitive radio systems operating in UHF TV band white spaces. Accessible at: http://www.etsi.org/deliver/etsi_tr/103000_103099/103067/01.01.01_60/tr_103067v010101p.pdf. Accessed Jan 2016

IEEE 802.11af Wi-Fi in TV White Space

46

Kentaro Ishizu, Keiichi Mizutani, Takeshi Matsumura, Zhou Lan, and Hiroshi Harada

Contents

Abstract

TV White Space is expected to make the radio resource utilization more flexible by adopting spectrum sharing concept to TV band. IEEE 802.11af is the world-first standard of PHY and MAC for operation of wireless LAN in the TV band. As

K. Ishizu (✉)
National Institute of Information and Communications Technology, Yokosuka, Japan
e-mail: ishidu@nict.go.jp

K. Mizutani · T. Matsumura · H. Harada
Department of Communications and Computer Engineering, Kyoto University, Kyoto, Japan
e-mail: mizutani@i.kyoto-u.ac.jp; takeshi.matsumura@i.kyoto-u.ac.jp; matsumura@nict.go.jp; hiroshi.harada@i.kyoto-u.ac.jp

Z. Lan
Broadcom Ltd., Irvine, CA, USA
e-mail: zhou.lan@broadcom.com

W. Zhang (ed.), *Handbook of Cognitive Radio*,
https://doi.org/10.1007/978-981-10-1394-2_53

radio regulations, such as spectrum mask and maximum transmission power, are different depending on countries, it is not so simple to implement the standard. Therefore, it is necessary for the standard to conduct investigation on implementation of the standard by prototyping according to the specific regulations, measurements of performances in various use scenarios, and discussion on its feasibility. This chapter covers from the IEEE 802.11af standard to its prototypes and field experiments. It is believed that the chapter helps to understand not only the specific standard but also the concept and practical experiences of TV White Space operations. The prototyping was based on radio regulations of US FCC and UK Ofcom. The field experiments introduced in the chapter were conducted under the TV White Space Pilot organized by UK Ofcom. Measurements were taken through the experiments in indoor and outdoor environments and analyzed to show feasibility and features of the standard and potentials of TV White Space utilization for IP communications. Note that this chapter includes several world-first achievements on IEEE 802.11af related R&D.

Keywords
IEEE 802.11af · TV White Space · Interference · TV band · Wireless LAN · PHY · MAC · Prototype · Radio propagation · Field trials

Introduction

IEEE 802.11af is an amendment standard that defines modifications to both the 802.11 physical layers (PHY) and the 802.11 medium access control (MAC) layer, to meet the legal requirements for channel access and coexistence in the TV White Space (TVWS). The standard enables Wi-Fi to operate TVWS. Traditional Wi-Fi is operated in 2.4 and 5 GHz, and its transmission range is very limited, normally within several tens meters. However, the expected range of the standard is larger than several km because the operation band is mainly UHF band and the maximum transmission power is 1 W.

The IEEE 802.11af is a combination standard by IEEE 802.11 families as shown in Fig. 1 and the PHY has compatibility with IEEE 802.11ac on the basis of OFDM. Table 1 shows main parameters of IEEE 802.11af. The IEEE802.11ac is based on 40 MHz operation with 128 FFT. But the bandwidth of TV is 6 or 7 or 8 MHz per channel. The downclocking therefore is required. In the case of usage in TV channel with 6 MHz channel spacing, the occupied bandwidth is $6\,\text{MHz} \times 128/144 = 5.33\,\text{MHz}$.

Figure 2 shows the fundamental network architecture based on IEEE 802.11af. All stations (STAs) need to communicate with each other via access points (APs). The APs need to have two new functions. The first is to protect primary users such as TV broadcasting companies because the IEEE 802.11af-based APs and STAs are secondary operation in the TVWS and should not interfere with the primary users. The second is to protect other secondary users that use same communication systems based on IEEE 802.11af.

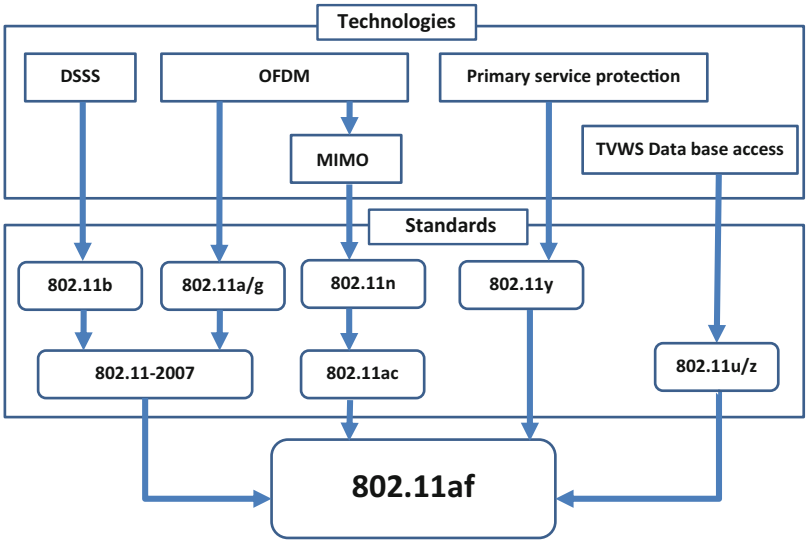

Fig. 1 Configuration of IEEE 802.11af standards

Table 1 Basic parameters of IEEE 802.11af

Parameters	Specification
Frequency range	54–862 MHz
Multiple access	CSMA
Payload modulation	QPSK-OFDM, 16QAM-OFDM, 64QAM-OFDM, 256QAM-OFDM (Option)
FEC coding rate	1/2, 2/3, 3/4, 5/6
Number of FFT-points	128
Number of effective subcarriers	114
Based 802.11ac operational bandwidth	40 MHz
Nominal bandwidth	5.33 MHz (6/7 MHz), 7.11 MHz (8 MHz)
Downclocking factor from 802.11ac 40 MHz bandwidth	7.5 (6/7 MHz), 5.625 (8 MHz)
Maximum number of spatial stream (NSS)	4
Cyclic Prefix (CP) Modes	3.0/ 6 us (6/7 MHz), 2.25/ 4.5 us (8 MHz)
Maximum net throughput	Mandatory 20.0 Mbps (6/7 MHz, 64 QAM, R = 5/6, NSS = 1,CP = 3.0 us), Optional 426.7 Mbps (24/28 MHz, Base 256 QAM, NSS = 4, R = 5/6, CP = 3.0 us)

To protect the primary users, the APs must access to white space database (WSDB) to get available spectrums in the TVWS. Moreover, the control to STAs from AP is also operated to meet the regulatory requirement. There are two ways to configure the system [1].

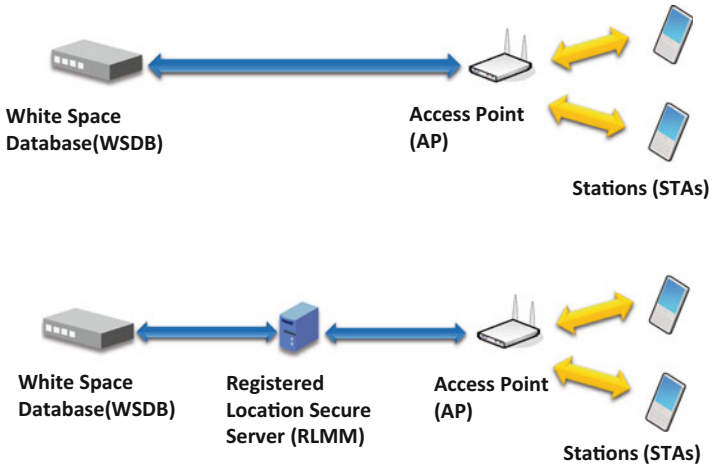

Fig. 2 Basic parameters of IEEE 802.11af

The first is that APs directly talk to the database through the Internet connection that they have. All the APs independently operate according to the available spectrum information obtained from the WSDB. Therefore, this scenario lacks of flexibility of utilizing the neighborhood information of the APs. Assuming APs are located closely, the available spectrum information might be identical. However, the spectrum is not efficiently utilized when the APs blindly choose the same channel to operate.

The second is to deploy a registered location secure server (RLSS) in between APs and WSDB in order to reduce the interference between secondary users' use of IEEE 802.11af. There are several benefits to use such a server. Firstly, the server collects neighborhood information of APs and helps them to choose channels with less collision with both primary and secondary users. Secondly, the APs may request the WSDB through the RLSS to tune their transmission power based on the out-band emissions of the APs.

This chapter is organized as follows. In section "Physical Layer", the PHY layer specification of IEEE 802.11af is introduced. Section "MAC Layer" describes the specification of IEEE 802.11af MAC layer. The IEEE 802.11af prototype has been developed and the detailed information is described in section "Prototypes," and finally the field trial results based on the developed prototype are introduced in section "Field Trials."

Physical Layer

This subsection introduces the overview of the physical layer (PHY) specification of the IEEE 802.11af [2]. The PHY of the IEEE 802.11af is developed for the WLAN operating on TVWS band. Table 2 shows the PHY layer parameters of the

Table 2 IEEE 802.11af PHY layer parameters

Air interface	OFDM
Channel bandwidth	6.0, 7.0, 8.0 (MHz) (Depend on regulation of each country)
Modulation	BPSK, QPSK, 16QAM, 64QAM, 64QAM, 256QAM[a]
Channel coding	Block convolutional coding (BCC), LDPC coding[a]
FFT size	128
Number of data subcarriers	108 (From −58 to −2 and from +2 to +58)
Number of pilot subcarriers	6(−53, −25, 11, +11, +25, +53)
Sampling frequency	6.0 (MHz) × 128/144 = 5.33 (MHz) (For 6.0 MHz channel bandwidth) 7.0 (MHz) × 128/168 = 5.33 (MHz) (For 7.0 MHz channel bandwidth) 8.0 (MHz) × 128/144 = 7.11 (MHz) (For 8.0 MHz channel bandwidth)
Guard interval	Long-GI: 1/4, Short-GI[a]: 1/8
Channel aggregation[a]	1, 2, 4 channels (Contiguous and Non-contiguous)
Spatial multiplexing[a]	Up to 4 steams (users)

[a]indicates option.

IEEE 802.11af. The size of FFT to generate OFDM signal is 128. The PHY layer configuration of the IEEE 802.11af is based on the downclocking PHY of the VHT (Very High Throughput) 40 MHz mode of the IEEE 802.11ac [3]. To operate under the law regulation of each country, several types of channel bandwidth (6.0, 7.0, and 8.0 MHz) are supported. Sampling frequencies are 6.0 MHz × 128/144 = 5.33 MHz, 7.0 MHz × 128/168 = 5.33 MHz, and 8.0 MHz × 128/144 = 7.11 MHz and in cases of the channel bandwidth are 6, 7, and 8 MHz, respectively. Two type guard interval (GI) modes are supported, i.e., Long-GI (mandatory mode) and Short-GI (option mode). The GI length of the Long-GI mode and the Short-GI mode is 1/4 and 1/8 of the IFFT output, respectively. As an option, the IEEE 802.11af supports channel aggregation mode up to four channels, and spatial multiplexing mode up to four streams.

Table 3 shows the modulation and coding scheme (MCS) levels of the IEEE 802.11af. The values of the data rate in this table are with the case of 6.0 MHz channel bandwidth mode using single-input single-output (SISO) transmission mode. As the mandatory mode, BPSK, QPSK, 16QAM, and 64QAM are supported. 256QAM modulation scheme is an option mode. Block convolutional coding (BCC) is adopted to the channel coding scheme as mandatory mode. LDPC coding is also supported as an optional mode.

Figure 3 shows subcarrier allocation of the payload in case of the 6.0 MHz channel bandwidth mode. The payload consists of 108 data subcarriers (subcarrier index, from 58 to 2 and from +2 to +58), 6 pilot subcarriers (subcarrier index, 53, 25, 11, +11, +25, and +53), and 3 null subcarriers (subcarrier index, 1, 0, and +1). The transmit spectrum of the IEEE 802.11af has 583 kHz effective guard band on both side in the 6.0 MHz channel bandwidth case.

Table 3 Modulation and coding schemes (MCS)

MCS index	Modulation scheme	Coding rate	Data rate (Long-GI)	Data rate (Long-GI)
0	BPSK	1/2	1.8 Mbps	2.0 Mbps
1	QPSK	1/2	3.6 Mbps	4.0 Mbps
2	QPSK	3/4	5.4 Mbps	6.0 Mbps
3	16QAM	1/2	7.2 Mbps	8.0 Mbps
4	16QAM	3/4	10.8 Mbps	12.0 Mbps
5	64QAM	2/3	14.4 Mbps	16.0 Mbps
6	64QAM	3/4	16.2 Mbps	18.0 Mbps
7	64QAM	5/6	18.0 Mbps	20.0 Mbps
8[a]	256QAM	3/4	21.6 Mbps	24.0 Mbps
9[a]	256QAM	5/6	24.0 Mbps	26.7 Mbps

[a]indicates option.

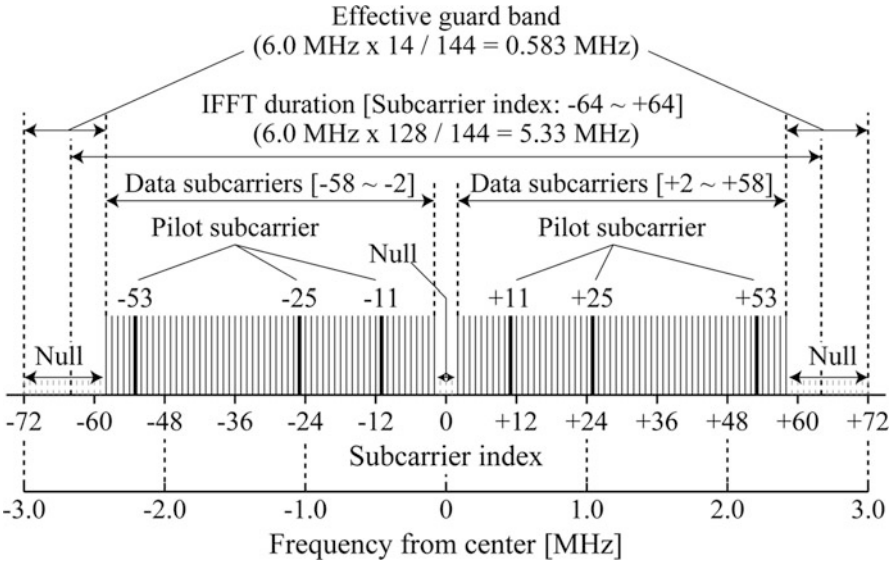

Fig. 3 OFDM subcarrier allocation of IEEE 802.11af TVHT_MODE_1 (Case of 6 MHz mode)

Figure 4 shows the frame configuration of the IEEE 802.11af consists of the Legacy field, the TV High Throughput (TVHT) field, and the payload. The Legacy field includes Legacy Short Training Field (L-STF), Legacy Long Training Field (L-LTF), and Legacy Signal Field (L-SIG). By using the Legacy field, coarse and fine synchronization and automatic gain control (AGC) are operated. The TVHT field includes TVHT-SIGNAL-A (TVHT-SIG-A), TVHT-STF, TVHT-LTF, and TVHT-SIGNAL-B (TVHT-SIG-B). In the TVHT-SIG-A, the required information for demodulation such as the number of channel aggregation, the number of spatial multiplexing, the type of guard interval (GI), and the type of channel coding scheme are included. The number of subcarriers of the TVHT field and the payload is larger than one of the Legacy fields except for TVHT-SIG-A. Therefore, the AGC

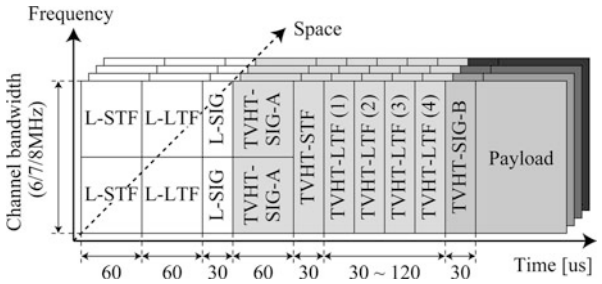

Fig. 4 IEEE 802.11af PHY frame format

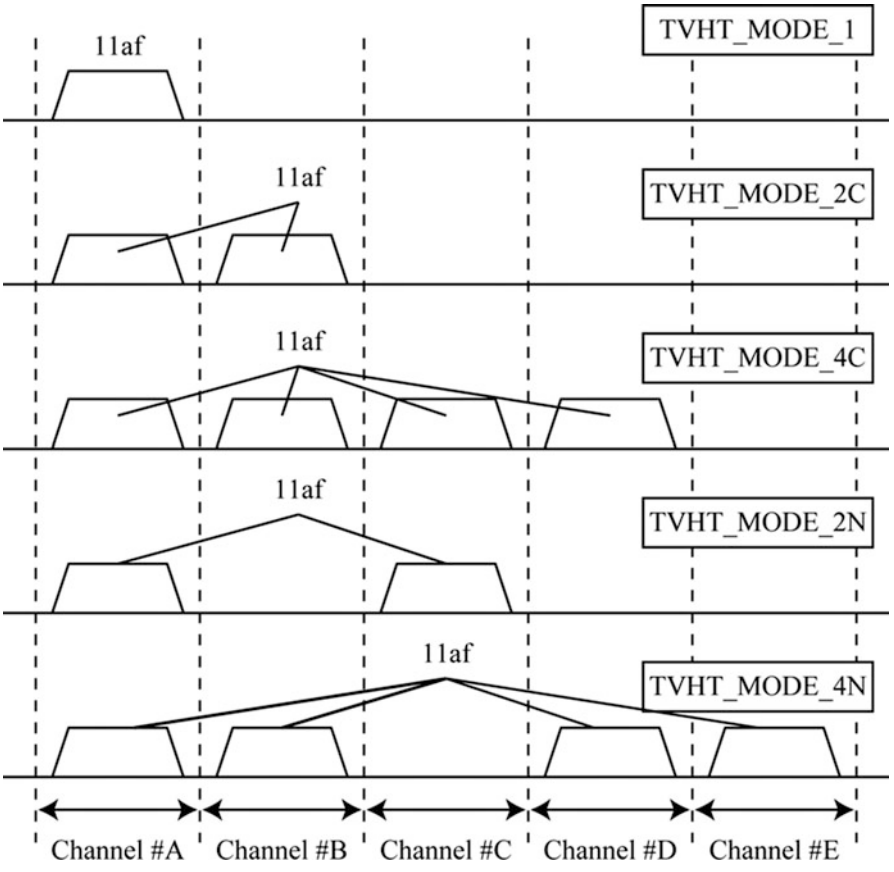

Fig. 5 Channel aggregation pattern

is reoperated by using TVHT-STF. TVHT-LTF is used for the channel estimation to demodulate the payload. Finally, the modulation and coding scheme (MCS) level and the length of the payload for each spatial stream are included in the TVHT-SIG-B.

Furthermore, a multichannel mode is supported as an option. The operating channel can be aggregated up to four channels to increase transmission data rate as shown in Fig. 5.

MAC Layer

The FCC rules of unlicensed operation in TVWS took about 10 years. It started in 2002 with FCC releasing the TV Broadcast Notice of Inquiry. In 2008 and 2010, the base rules were specified and updated based on the comments received from both industry and regulation parties. The final rule was released in 2012. The FCC rules of the secondary users in TVWS rely on geo-location database approach. Protection of the primary users by sensing technologies remains in the final rules and, however, changed from mandatory to optional. Ofcom is the independent telecommunication regulator and competition authority for the communication industries in the UK. In July 2009, Ofcom published its statement report on TVWS usage. According to the report, accessing TV band database with geo-location is the most important mechanism to protect primary users in short and medium terms. The Ofcom final rules were published in 2012. Other countries are also conducting feasibility study on TVWS. The European Conference of Postal and Telecommunications Administrations (CEPT) created a working group to define technical and operational requirements for the operation of cognitive radio systems in the TVWS. In Singapore, the Info-communications Development Authority (IDA) is very active for the promotion of the TVWS. The Ministry of Internal Affairs and Communications (MIC) of Japan has established a discussion group to carry out examination of the new frequency usage such as TVWS.

The challenges of enabling Wi-Fi systems in TVWS mainly come from regulatory requirements. In order to operate in TVWS, there are regulatory rules for the protection of existing primary services. The operation of the Wi-Fi systems must not jeopardize the operation of these existing primary services. Because traditional Wi-Fi systems of 2.4 or 5 GHz bands are unlicensed based, the existing mechanisms are not sufficient for primary user protections. In addition, the propagation characteristics of VHF and UHF bands are quite different from that of 2.4 and 5 GHz bands. The physical layer design of the existing Wi-Fi systems in 2.4 or 5 GHz cannot be directly used in these new bands.

Regulators only permit certain types of device that fulfill the device requirements to operate. Both FCC and Ofcom permit fixed type of device and portable type of device. Fixed devices don't have geo-location capability. Their antenna is permanently mounted on a nonmoving platform by a professional installer or responsible communication provider. On the other hand, portable device is those that don't have a permanently mounted antenna and may change their location upon configurations. Both FCC and Ofcom have the concept of master and slave device in their rules. FCC calls their master device as mode II portable device and slave device as mode I device. Master device has geo-location capability and can talk to the regulatory database for operation parameters, while slave device has to be under control of a master device for operation. The major difference between FCC and Ofcom regarding the device type is that Ofcom allows a fixed device as master or slave device. FCC specified fixed device as a particular device group and doesn't put any master or slave role to fixed device. A Wi-Fi access point can be categorized into a fixed or mode II portable device according to FCC rules and master fixed

or portable device according to Ofcom rules. FCC and Ofcom also support sensing type of devices.

The maximum allowable transmission power is also different. FCC specified fixed maximum transmission power, while Ofcom allows flexibility of tunable maximum transmission power according to the interference level. According to the FCC rules, a fixed device can transmit up to 4 W Effective Isotropic Radiated Power (EIRP) out of the protection contour of primary users. A portable device can transmit up to 100 mW outside of the protection contour of the primary users on co-channel and adjacent channel and reduces EIRP to 40 mW on adjacent channel if being wanted to operate inside the protection contour. Ofcom allows device to report their transmission parameters such as the spectrum mask to the database; database feeds back the maximum allowable transmission power accordingly. There are also strict rules specified for out-of-band emissions to protect primary users on adjacent channels. For fixed device of FCC, the out-of-band emission on the adjacent channel must be lower than −42.8 dBm on every 100 KHz and −52.8 dBm for personal/portable device. Ofcom supports four classes of device with different out-of-band emission requirement. The most relaxed requirement is on class 4 with −54 dBr on the adjacent channel from the 8 MHz TV channel.

Figure 4 presents the network architecture of an 802.11af system. Due to the requirement of database access, the function of a Wi-Fi access point (AP) is extended. More than providing Internet accesses to stations associated, AP is enhanced as a control entity that queries database for available spectrum. There are two typical usage scenarios. The first is that APs directly talk to the database through the Internet. This type of operation meets the FCC ruling that requires mode II portable device to directly talk to the database without a proxy. Assuming APs are located closely, the available spectrum information might be identical. Therefore, when APs blindly choose the same channel to operate, the spectrum is not efficiently utilized. The second is to deploy a registered location secure server (RLSS) between APs and database. RLSS is a proxy for the APs to talk to the database. The proxy approach is supported by Ofcom. There are several benefits of using such server. RLSS collects neighborhood information and helps APs to choose channels with less collision. APs may also request the database through the RLSS to provide tunable transmission power based on the out-of-band emission level.

Figure 5 presents the basic sequence to initiate communications of Wi-Fi devices in TVWS. Before starting operation, APs ask database for the available spectrum information. Both the identification and geo-location information is needed for the database to provide available spectrum information. The identification information indicates what and who the AP is, i.e., AP tells the database what type of device the AP is and what the FCC ID and serial number are. The geo-location information needs to be within the accuracy of 50 m. Once receiving the information, database calculates the available spectrum for the AP to operate based on the interference criteria of licensed operation and feeds back the available spectrum information to the AP. The protocol for the above communication procedure is out of scope of IEEE 802.11af. However, the format to convey the device identification and geo-location information is defined, so that the APs from different manufactures can

talk to the database using the same interface. There are standard groups working on the protocols for database access, such as IETF PAWS.

According the FCC rules, every 60 s, a mode II device needs to confirm its geo-location. If the mode II device finds its position has been changed 100 m (50 m in Ofcom rules) from the place where the last database access took place, the mode II device needs to contact the database again to obtain a new available spectrum. A mobile AP is also a mode II device. The message exchange with the database would be intensive if the mobile AP moves fast. FCC has enhanced the rules to provide better supports on mobile operations. As shown in Fig. 6, mode II devices are allowed to submit several locations before starting operation. The database may respond with the spectrum that is available on the bounded area defined by the locations queried, or the database may respond with the spectrum available on each location and let the device to figure out the common part of available spectrum to use. 802.11af defines interface to support the above two options. The AP submits its current geo-location together with several anchor locations to the database. There is a bounded area defined by the anchor locations and current location. If there is no common spectrum in the bounded area, only the spectrum available on the current location is responded. There is another option supported. Instead of sending multiple locations, the AP may send only two locations, the current location and a second location with an uncertainty value to define the bounded area. For example, an AP may submit a location with uncertainty of 500 m in longitude and 400 m in latitude. Eventually the bounded area will be a $400 \times 500\,m^2$ where the AP can move around without contacting the database. The current location submitted together is for the database to verify that the AP is capable of determining its geo-location within 50 m as required by the rules (Fig. 7).

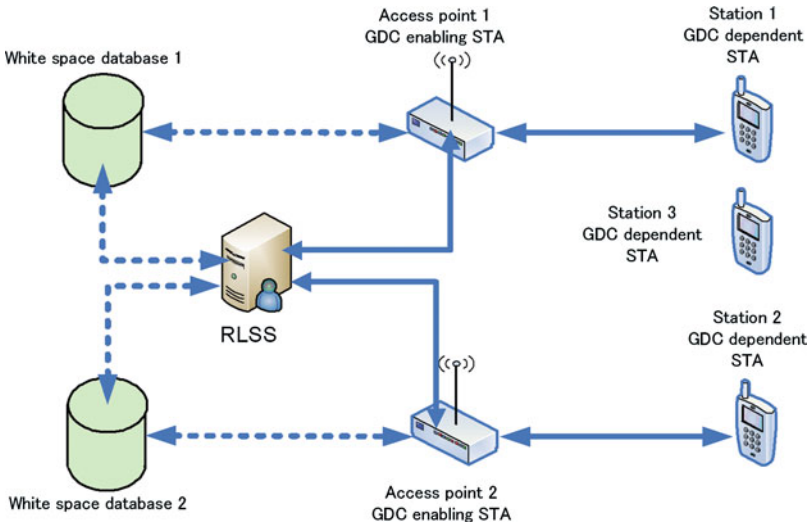

Fig. 6 Network architecture of 802.11af

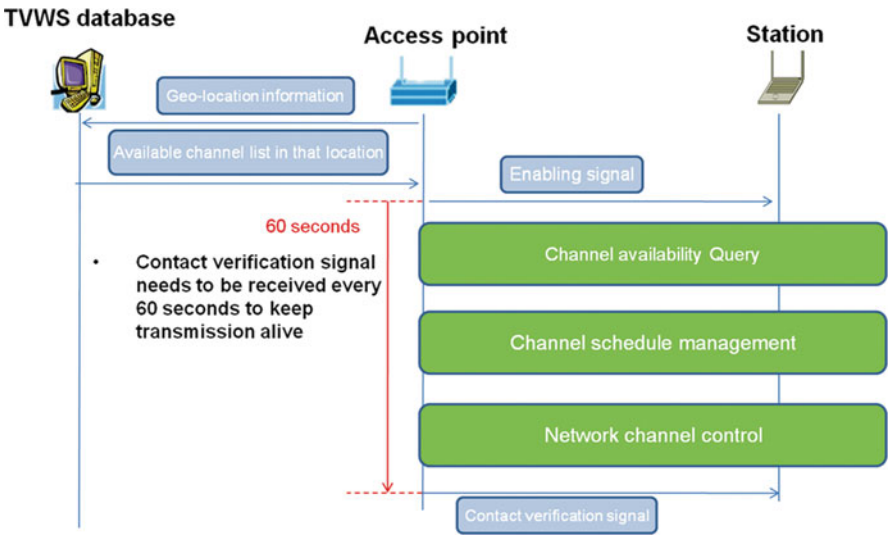

Fig. 7 Major MAC mechanisms specified in 802.11af

FCC rules state that a mode I device has to operate under the control of a mode II device. It can utilize the same spectrum that is available on the mode II device that is controlling it. There are three mechanisms defined in 802.11af to guarantee the control relation between the AP and stations, enabling signal, channel availability query (CAQ), and contact verification signal (CVS).

Enabling Signal

A mode I device is not allowed to release signal on the air unless receiving an enabling signal from a mode II device. 802.11af implements this enabling signal with the beacon frame. AP as a mode II device announces the existence with the beacon. The beacon has to be sent in the TVWS bands. The stations intent to operate in TVWS scan the channels in TVWS. Once a beacon operating as an enabling signal is received, the station is allowed to release signal on TVWS band for initial contact with the AP.

CAQ

A mode I device needs the available spectrum to operate. We have described the procedure for an AP to obtain available spectrum from database. Before a station performs CAQ procedure with an AP, we can assume the AP already obtained the available spectrum from database. The CAQ procedure between a station and an AP is for the station to submit its own identification to the AP; AP verifies this identification with the database whether the station is an authorized mode I device or not. Once the station is verified, AP responses to the station with the available spectrum information. In order to meet the security requirements, the CAQ procedure can only be performed, after secured association and authentication have already been completed.

CVS

In order to make sure the slave device is under control of a master device, FCC specified a rule that a mode I device needs to receive a CVS every 60 s from the mode II device that is controlling it. Beacon is not an option for CVS, because beacon is non-securely broadcasted. Therefore, the CVS of 802.11af is defined as a unicast frame that is sent to all the stations one at a time. The frame is protected by the keys generated during the negotiation of secured association procedure. The frame needs to activate its acknowledgment option to allow station to indicate the receipt of the CVS.

There is another folder of requirement that also needs to be considered. Wi-Fi systems are designed to operate in unlicensed band. Stations content for resource before transmitting frames. This nature makes the successful story of Wi-Fi systems. However, TVWS is different from other unlicensed bands. There is licensed user coexisting in the same bands. The spectrum is not always available there to use. Coordination and interference mitigation mechanisms are the key to efficiently utilize the spectrum. Two important mechanisms that are developed for this purpose in the 802.11af are channel schedule management (CSM) and network channel control (NCC). Both mechanisms are related with the RLSS which serves the role of a proxy to the database and also a local coordinator for spectrum allocation.

CSM

Licensed services such as DTV or wireless microphone have timely characteristics, i.e., the service is not always occupying the channel. For example, a big sport event may require hundreds of wireless microphones for only 1 h. Many DTV channels stop at 2:00 am and restart 6:00 am in the morning. There are 4 h available in between for the unlicensed operation to utilize. FCC has specified that a mode II device obtains the channel schedule information up to 48 h and stores the schedule information to operate in case database access lost. The implication of this rule is to allow the available spectrum to be shared in time domain. The RLSS may further divide the spectrum obtained from database and allocate the spectrum to different Wi-Fi devices to improve spectrum efficiency. 802.11af developed the protocol between AP and RLSS for secured information exchange. And the mechanism, namely, CSM, is developed based on the protocol for the AP to negotiate with RLSS for the available spectrum in time domain. An AP who is requesting the CSM is called a CSM requesting station; the requesting station constructs a CSM query to a CSM responding station asking for schedule information on the interested channels. The responding station normally is the RLSS; it responds to the requesting station with the time periods of available spectrum to operate. Because APs in the neighborhood access the database through RLSS, RLSS understands the interested channel that the APs want to operate. It can smartly allocate spectrum orthogonal in time to different users to avoid interference. RLSS may also reject the request from certain APs when spectrum availability is less in order to reduce the interference to licensed operation. The responding station of a CSM can also be another AP. One AP may obtain the available spectrum and schedule information via another AP.

NCC

NCC is another mechanism developed to improve spectrum efficiency. Different from CSM that handles spectrum in time domain, NCC handles the spectrum in frequency domain. NCC follows the same architecture of requesting and responding stations. Requesting station queries the responding station about the interested channels to operate. When a mode II device obtained available spectrum information from database, all the information is delivered in a form of TV channel across the whole VHF and UHF bands, 6, 7, or 8 MHz depending on the regulatory domain. However, with respect to a Wi-Fi device, it operates in a WLAN channel plan. RLSS as the responding station once receiving the query from a requesting station needs to map the WLAN channel into TV channel and check whether the interested WLAN channels are available for operation. The other important feature of NCC is to deliver the spectrum mask information. Spectrum mask is defined for a device to reduce the out-of-band emissions so that the licensed operation on the adjacent channel is not interfered. FCC and Ofcom have different approaches of suppressing out-of-band emissions. FCC specified a very stringent rule as described in previous section. The rule guarantees protections of licensed operation on the adjacent channel with a price of increased cost of portable Wi-Fi devices. In order to implement a filter to achieve such power suppression, both the size and cost of Wi-Fi chip have to increase. As a consequence, this rule hampers portable Wi-Fi from having a broad market. On the other hand, Ofcom is more flexible in dealing with out-of-band emission. Rather than specifying a very stringent spectrum mask, the rule allows device to provide its own spectrum mask to the database. Database gives less transmission power to the AP, if the spectrum mask is not sharp. This approach encourages AP that is capable of reducing out-of-band emission to transmit more power and consequently obtain more opportunities for the spectrum.

Prototypes

Introduction

IEEE 802.11af-based system has attracted attentions for its superior propagation characteristics in the UHF band enabling 100 m or longer-range communication. On the other hand, leading regulators impose a rigorous spectrum mask limitation on the TVWS (TV White Space) devices to avoid the interference with primary users such as TV broadcasters and wireless microphones. In addition, TVWS (TV White Space) communication systems are necessary to implement some specific functions for acquiring and updating the TVWS availability. Accordingly, IEEE 802.11af-based systems and devices should be developed or prototyped by taking into account these regulations and requirements. In this section, regulations and requirements imposed on the IEEE 802.11af-based systems and devices are briefly summarized first. Then, IEEE 802.11af-based working systems prototyped by NICT (National Institute of Communications Technology, Japan) are introduced.

Requirements

Power and Emission Limits

For the TVWS utilization, each regulator has stated a similar but different policy by reflecting each national circumstance. In the FCC regulations, TVWS devices are classified into four types according to the operation mode as shown in Table 4 [4]. The power limit and the adjacent channel emission limit are individually defined for each category and every limit is specified by an absolute power. Table 5 shows the adjacent channel leakage power (ACLP) limits defined by the ETSI [5] that were applied for the Ofcom TVWS pilot program in 2014. The ETSI basically accepts the same power level as the FCC for the TVWS devices, while the TVWS devices are categorized into five types according to the ACLP performance. Conversely, each category has individual ACLP limit and every limit is specified by a relative value to the transmission power, i.e., the adjacent channel leakage power ratio (ACLR). Here, P_{OOB} which means leakage power in a 100 kHz bandwidth outside the using channel can be calculated by

$$P_{\mathrm{OOB}}\ (\mathrm{dBm}/(100\,\mathrm{kHz})) \leq \max\{P_{\mathrm{IB}}\ (\mathrm{dBm}/(8\,\mathrm{MHz})) - ACLR\ (\mathrm{dB}), -84\ (\mathrm{dBm}/(100\,\mathrm{kHz}))\},$$

where P_{IB} is output power in an 8 MHz bandwidth of the using channel and *ACLR* is defined in Table 5. The IDA in Singapore also defines the original regulations by following the FCC and the ETSI regulations with regard to the power limit and the adjacent channel emission limit [6]. IEEE 802.11af-based TVWS devices must conform to these requirements in actual operations.

Table 4 Power and emission limit regulated by FCC [6]

Type of TV bands device	Power limit (6 MHz)	Power spectrum density limit (100 kHz)	Adjacent channel emission limit (100 kHz)
Fixed	30 dBm (1 W)	12.6 dBm	−42.8 dBm
Sensing only	16 dBm (40 mW)	−1.4 dBm	−56.8 dBm
Personal/portable (adjacent channel)	17 dBm (50 mW)	−0.4 dBm	−55.8 dBm
All other personal/portable	20 dBm (100 mW)	2.6 dBm	−52.8 dBm

Table 5 ACLR for different device emission classes [7]

Where P_{OOB} falls within nth adjacent DTT channel	ACLR (dB)				
	Class 1	Class 2	Class 3	Class 4	Class 5
$n = \pm 1$	74	74	64	54	43
$n = \pm 2$	79	74	74	64	53
$n \geq +3, n \leq -3$	84	74	84	74	64

WSDB Access

Before starting the communication in the TVWS, TVWS devices need to know whether they can transmit the power without any interference to/from primary users and/or other TVWS devices. But, how can they know it? Regulators simply offer two solutions. One is the sensing function recognizing whether the target TV bands are empty or not by the TVWS device itself. The other one is the WSDB access approach for acquiring the availability of the target TV bands. The former requires an implementation of a highly sensing capability to sense a very weak signal level of, for instance, −114 dBm/6 MHz and −107 dBm/100 kHz as defined by the FCC [4]. However, high-performance sensing units are generally costly and not small for implementation in practical consumer devices. The latter is a common function defined by many regulators including the FCC and the Ofcom, because this function only requires constant accessibility to the WSDB via the Internet, while high-performance and expensive units are not necessary. As above, the IEEE 802.11af-based communication system was standardized on a more rational WSDB approach basis.

Implementation

This section is a summary of IEEE 802.11af-based system and device prototypes developed by NICT. Here, three types of prototype devices are described. The first one is a low-power type prototype with superior spectrum emission characteristics. The second one is a high-power type prototype enabling long-haul communication with a maximum output power of +30 dBm. These two prototypes are costly and consuming a lot of power due to the FPGA-based baseband (BB) circuits. The last one is the compact card-type prototype incorporating the world's first IEEE 802.11af-based BB IC. This prototype achieves dramatic downsizing, power saving, and even cost saving and paves the way to the practical use of the IEEE 802.11af-based communication system. This section describes a brief summary of each device. For more detailed information, refer to each reference (Fig. 8).

System Architecture

The IEEE 802.11af-based prototype system shown in Fig. 9 consists of an access point (AP), a station (STA), a WSDB, and a registered location secure server (RLSS). In this system, the AP is operating as a master device and has to access the WSDB via the Internet before starting the communication with the STA. In general, the AP first informs the WSDB of some essential information such as geo-location, antenna height, and device parameters, which are defined by the regulators, and then the WSDB calculates and provides an available channel list with some additional information to the AP. After the AP selects optimal channel(s) to use and starts beacon transmission to its slave devices, i.e., STAs. The beacon also includes some essential information such as permitted maximum output power, and thus, STAs can set the optimal radio parameters. Eventually, STAs answer the AP, and then the TVWS communication starts. The RLSS is an optional component in this system.

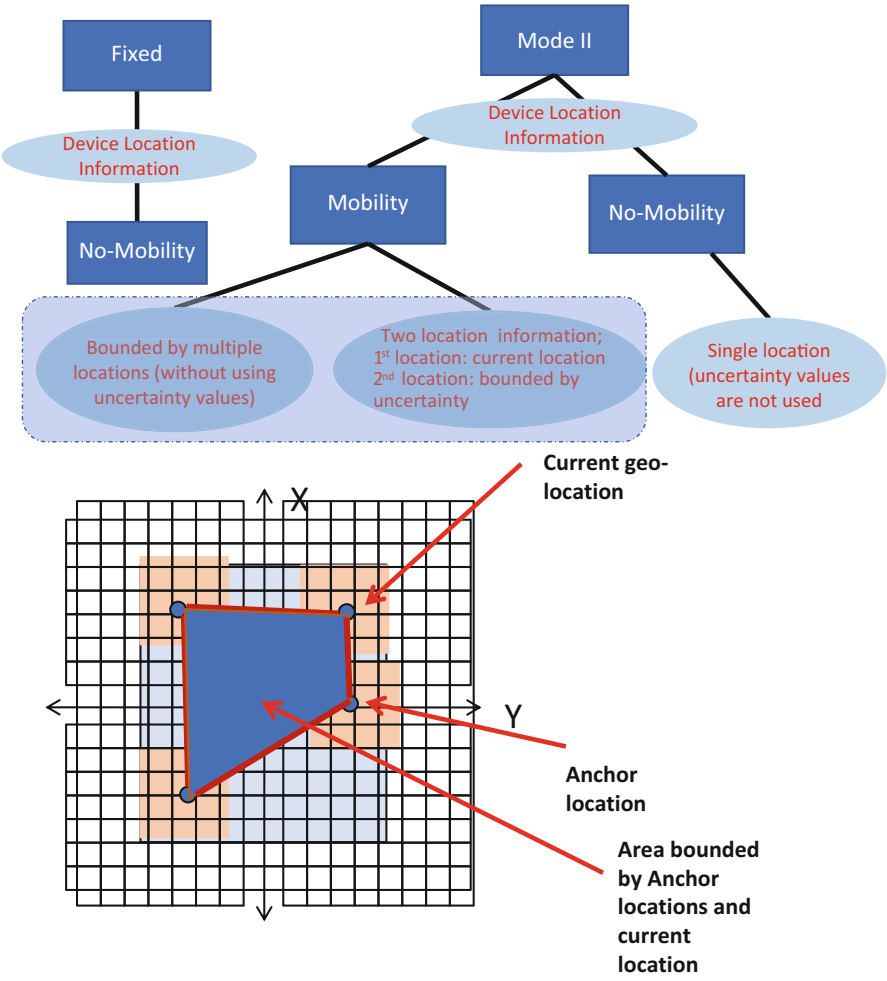

Fig. 8 Multi-location operation of 802.11af

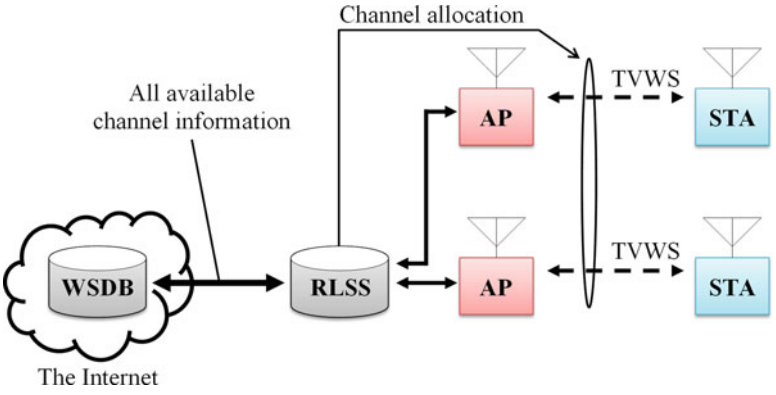

Fig. 9 IEEE 802.11af-based prototype system

If some APs operate in the same area and frequency, they will interfere with each other. To avoid the interference between secondary users, the RLSS allocates an appropriate channel to each AP according to the information from the WSDB and the geo-location information of the AP.

Low-Power Type Prototype Conforming to Both FCC and ETSI Regulations

Figure 10 shows the low-power type prototype [4]. This prototype consists of a CPU board, a BB board, a DAC/ADC board, an RF board, and an antenna. Table 6 shows specifications of the prototype. To conform to the rigorous requirements of the FCC and the ETSI, a three-stage heterodyne architecture is applied in the transmitter for sharply suppressing the adjacent channel emissions, as shown in Fig. 11. The spectrum emission of the prototype complies with the regulations defined by the FCC and the ETSI with an output power of +3.5 dBm, as shown in Fig. 12.

Fig. 10 Low-power type prototype

Table 6 Specification of the low-power type prototype

Item	Description
Supporting frequency range	470–710 MHz
Bandwidth	6 MHz
Maximum output power	+10 dBm
Receiver dynamic range	−88 to −35 dBm
Size	300 mm(W) × 210 mm(L) × 100 mm(H)
Weight	5 kg
Power supply	AC 100–240 V
Current consumption	<70 W

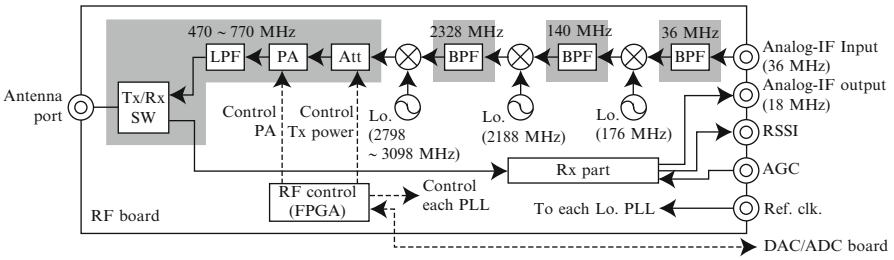

Fig. 11 Transmitter block diagram of the low-power type prototype

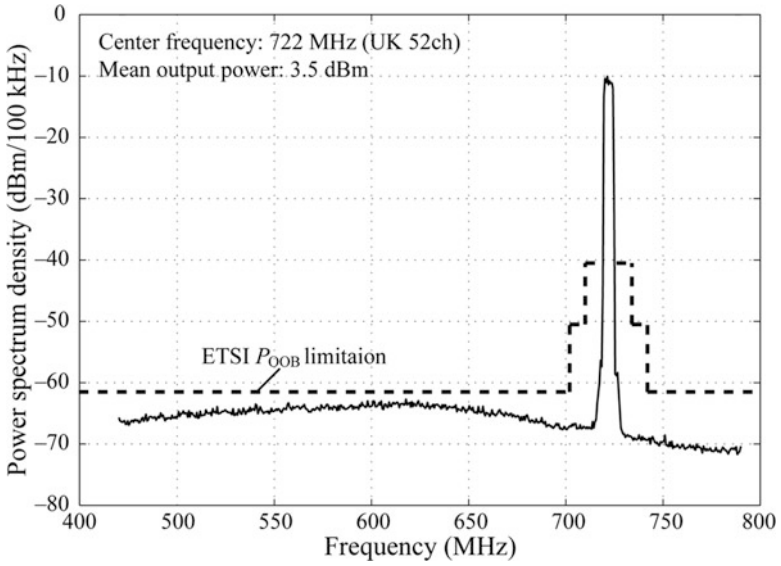

Fig. 12 Spectrum emission characteristics of the low-power type prototype

High-Power Type Prototype Conforming to the ETSI Regulation

Figure 13 shows the high-power type prototype [5]. This prototype is based on the abovementioned low-power type prototype, but direct conversion architecture is applied in the RF circuits as shown in Fig. 14. Table 7 shows the RF specification of the prototype. This prototype is capable of an output power of +30 dBm in conformity to the ETSI regulations, while the supporting frequency range is limited to 500–710 MHz due to the difficulty in a design of a wideband amplifier enabling a high output power of more than +30 dBm in the entire TV band. Figure 15 shows a typical spectrum emission with an output power of +27 dBm. The out-of-band emissions are under the P_{OOB} limitation defined by the ETSI in the entire TV band. By adjusting the output power to less than +20 dBm, spectrum emission conforms to the FCC regulations.

Fig. 13 High-power type IEEE 802.11af-based prototype

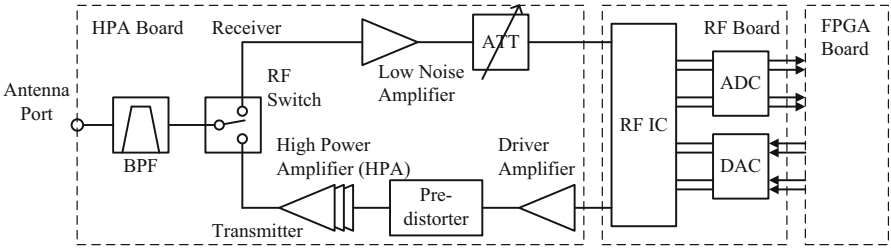

Fig. 14 RF block diagram of high-power type IEEE 802.11af-based prototype

Table 7 Specification of the high-power type prototype

Item	Description
Supporting frequency range	500–710 MHz
Bandwidth	6 MHz
Frequency accuracy	±2ppm
Output power	+30 dBm
Tuning range of output power	>40 dB
Receiver dynamic range	−88 to −20 dBm

Compact Card-Type Prototype Incorporating Baseband IC

For practical use of the IEEE 802.11af-based technologies, there are still some major difficulties in downsizing, power saving, low cost, easy installation, etc. In the low-power and high-power prototype devices, the BB signal processing circuits were designed and implemented by using an FPGA, and thus, practical size and power consumption were difficult to achieve [7, 8]. To solve this problem,

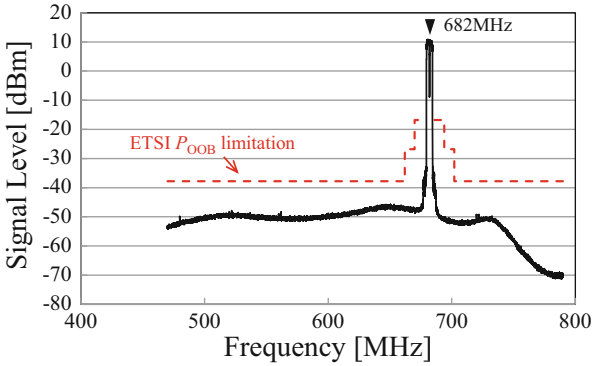

Fig. 15 Spectrum mask with 682 MHz transmission signal

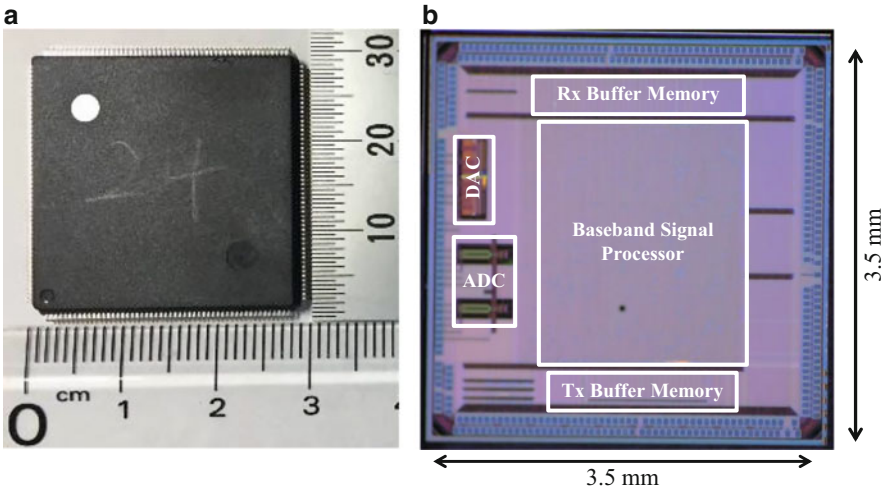

Fig. 16 World's first IEEE 802.11af-based baseband IC

more sophisticated technologies driving downsizing, power saving, and even cost saving are strongly required as well as conventional communication systems such as Wi-Fi and mobile communication systems. An integration of the BB signal processing circuits is one of the promising technologies that wipe out these concerns.

NICT has developed the world's first IEEE 802.11af-based BB IC with a 65-nm mixed CMOS process, as shown in Fig. 16 [9, 10]. The BB circuits are based on the previously developed prototype of the low-power device. By implementing this prototype BB IC, NICT has also developed a compact card-type prototype in all-in-one package including an antenna, as shown in Fig. 17, and has demonstrated

Fig. 17 Card-type IEEE 802.11af-based prototype

Table 8 Specification of the card-type prototype

Item	Description
Supporting frequency range	470–710 MHz
Bandwidth	6 MHz
Maximum output power	+20 dBm
Receiver dynamic range	−86 to −35 dBm
Size	50 mm(W) × 170 mm(L) × 18.8 mm(T)
Weight	170 g
Power supply	DC 5 V
Current consumption	<5 W

the practicality of the prototype BB IC. The card-type prototype is equipped with the USB interface enabling an easy connection to a host PC and a simple control for operation. Table 8 shows specifications of the card-type prototype. By comparing with the low-power type prototype, the card-type prototype achieves 1/40 downsizing, 1/30 weight saving, and 1/15 power saving with a maximum output power of +20 dBm. With regard to the spectrum emissions, the output power is capable of +20 dBm and +16 dBm for the rules regulated by the ETSI and the FCC, respectively. Power consumption of the card-type prototype is about 5 W, and thus, this prototype operates with a power supply from USB3.0 interface.

Registered Location Secure Server (RLSS)

RLSS is an IEEE 802.11af specific functional entity to avoid interference between WSDs conforming to this standard. As IEEE 802.11af defines PHY and MAC; an interface of RLSS is not the scope of the standard.

The specific mechanisms of RLSS is as follows:

— Query channel availability to geographical database(s) (GDB) for an area or a geo-location
— Enable APs to form a network and maintain the network under the control of GDB
— Retrieve the available white space channels and transmit power restrictions
— Schedule channel utilization such as start and end time of each WSD for each available white space channel

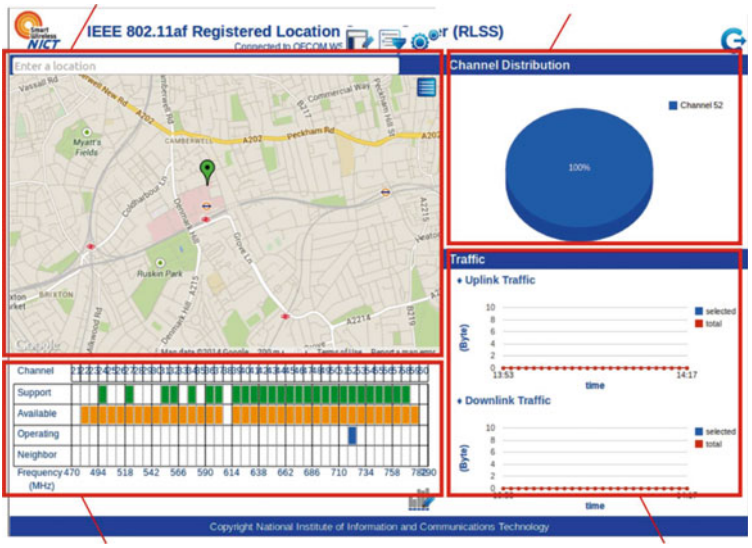

Fig. 18 Screenshot of RLSS management software

The use of RLSS in a particular regulatory domain depends on the specific regulatory requirements. Each of the mechanisms is required, informative, or not applicable according to regulatory requirements. Also, time requirement of each mechanism may be daily, hourly, or minute responsiveness. Implementers of RLSS need to carefully refer to the regulatory sources to be satisfied.

A screenshot of management GUI of a prototype RLSS under operation is shown in Fig. 18, as an example of implementation. Locations of WSDs are shown on a map, so that operators easily grasp overall TVWS operation around a specific area. A list of supported channels, available channels, operating channels, and neighboring channels is shown regarding a WSD specified on the map. The supported channels are channels where the WSD is capable of operation. TV band is quite wide for RF hardware implementation, and therefore the channels for transmission and receiving may be limited on some WSDs. Available channels are channels that a GDB informs to RLSS. Operating channels are channels on which WSDs are operating at this point of time. Operating channels are single or multiple as the PHY and MAC support the multiple TV channel utilization. Neighboring channels indicate channels that are operated by other WSDs nearby within a certain distance enough to be interfered. The neighboring channel is considered in channel

assignment not to overlap with a channel(s) to be operated by other WSDs. Uplink and downlink traffic can be monitored per WSD selected on the map.

Field Trials

To investigate IEEE 802.11af in terms of real field performances and environment-specific issues; the National Institute of Information and Communications Technology (NICT) of Japan conducted experiments in indoor and outdoor environments under TV White Spaces Pilot organized by Ofcom of the UK.

The pilot required a license issued by Ofcom to operate TV White Space devices (WSD), which are AP and STA in case of IEEE 802.11af system. The WSD needs to access one of TVWS databases (WSDB) qualified by Ofcom for the pilot. NICT obtained the licenses for WSD operation and qualification of WSDB operation.

This section explains environments and results in indoor and outdoor use cases. The experiments were conducted jointly with King's College of London (KCL) in July 2014 [7, 8, 11–13].

Indoor Experiment

The indoor experiment was conducted in the second floor of the institute of psychiatry building in the Denmark Hill Campus of KCL [7, 13]. The floor is mainly composed of two corridors (X and Y) and two computer education rooms (A and B) as shown in Fig. 19. Detailed information of the environment is listed in Table 9. Four routes (A to D) are defined for separated measurements. The Routes A and B are along Corridor X; Routes C and D are along Corridor Y. An AP is fixed in between Routes A and B. STA moves along the routes measuring RSSI and throughput. The throughput is measured using the "iperf" tool in UDP mode. The MCS of AP and STA are set to 3. AP, and STA had omnidirectional whip antennas with 2.2 dBi gain at 1.3 m height above the ground using RF cables with 1.0 dB loss. Transmission power was set to 3.5 dBm; therefore, output ERIP was 4.7 dBm as listed in Table 10.

Measured RSSI and throughput on each route are separately shown in the graphs in Fig. 19. The deflection effect is observed near P5 on route C where RSSI is still high regardless of non-line-of-sight (NLoS) from the AP, and therefore throughput is kept as high as in P5 which is line-of-sight (LoS). This is estimated to be due to the TV band which is lower than ordinary wireless LAN bands. Focusing on route B, the throughput is partly deteriorated although RSSI is still high and the STA is LoS from the AP. This is thought to be due to multipath fading. The reason why the RSSI is high on route D is because the penetration loss inside the Room A is not high because of less metal materials metal for walls or bookshelf. The measurements in the indoor environment show that IEEE802.11af AP can cover wider area, that is, not only LoS but also NLoS.

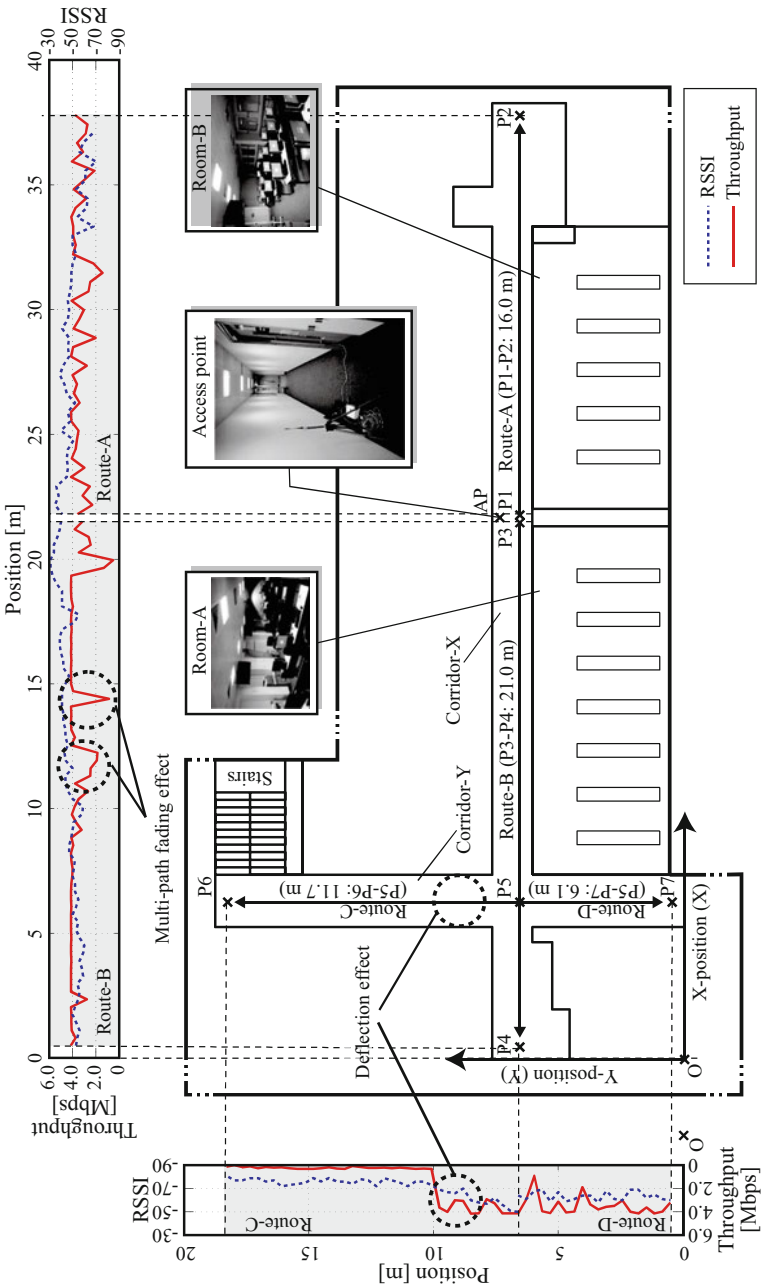

Fig. 19 Indoor experiment environment and measurement results

Table 9 Details of indoor experiment environment

Corridor X	Length: 38.3 m, Width: 1.6 m
Corridor Y	Length: 18.8 m, Width: 2.1 m
Room A	Length: 14.2 m, Width: 5.5 m
Room B	Length: 10.9 m, Width: 5.5 m
Ceiling	Height: 2.4 m
Antenna	Height: 1.3 m

Table 10 Device setup for indoor experiment

Operation mode	IEEE802.11af TVHT_MODE_I
MCS	3 (16QAM, 1/2 coding rate)
Transmission power	3.5 dBm (average)
Antenna gain	2.2 dBi (Omni directional)
RF cable loss	1.0 dB
Transmission ERIP	4.7 dBm

Outdoor Experiment

The outdoor experiment was conducted in the center of London, UK [8]. The purpose of this experiment was to study feasibility of establishment of long-distance link using IEEE 802.11af as a backhaul network. Two fixed sites were selected in London, from campuses of King's College London, Guy's Campus, and Denmark Hill Campus. Distance of the two sites is 3.7 km. A STA and an AP were installed at Guy's and Denmark Hill campuses, respectively. Heights of antenna were 65 and 37 m, respectively, in the same order. Three-element ring Yagi antennas with 7.6 dBi gain were used at the two locations. Directions of the antenna were carefully tuned so to maximize the RSSI at each side. Transmission EIRP at both sides was 36 dBm. As shown in Fig. 20, the antenna was set up inside a glass window at the Guy's Campus, whereas it was open air at the Denmark Hill Campus. Throughput of the link was measured using "iperf" again in UDP mode.

The measured throughput was 2.2 Mbps with MCS 0 where the RSSI was −60 dBm. It was observed that higher throughput could not be obtained with higher MCS than 0. The reason is considered that TV broadcasting signals transmitted from Crystal Palace to London area is quite strong and Crystal Palace is approximately on the same direction as from Guy's Campus to Denmark Hill Campus. This resulted in strong TV signal input to the RF circuit of the STA at the Guy's Campus. For this experiment, the STA and AP had just a broadband front-end filter covering whole the TV band where such extremely strong TV signals were beyond assumption. It is assumed that the signal input caused saturation of RF circuit of the STA. Also, according to other measurements and analysis, penetration loss of the window in front of the antenna at the Guy's Campus is more than 10 dB, which further deteriorated the performance. However, establishment of a long-distance wireless link over 3.7 km was anyway demonstrated based on IEEE 802.11af and feasibility of its functions and protocols was verified. The issue related to the strong signal input needs to be addressed in product development phase.

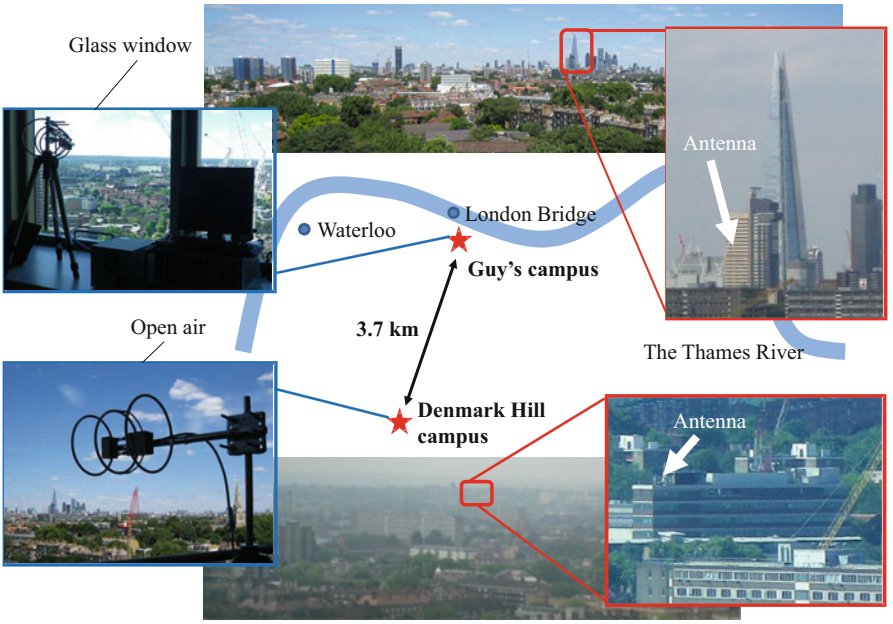

Fig. 20 Overview of outdoor experiment

Conclusion

Utilization of TV White Space is realized based on advanced spectrum sharing concept. Its requirements are hard to protect; TV broadcastings and radio regulations are various according to policies. IEEE 802.11af is one of the standards to enable the TV White Space operation. Especially, since IEEE 802.11af is based on the wireless LAN concept, prices of its products are expected to be reasonable and deployment of its system would be less complicated compared with other TV White Space systems. So far, various use scenarios are proposed to apply TV White Space, backhaul link between islands, mountain area mobile communications, robots for disaster recovery, and so on, taking advantage of good radio propagations in TV band. This chapter is expected to contribute to the development of TV White Space applications.

References

1. Lan Z, Sun C, Alemseged Y, Villardi G, Tran H, Harada H (2012) WiFi in TVWS – an overview of IEEE 802.11af. Technical report of IEICE, SR 2011-114, pp 73–78
2. IEEE Std 802.11af™ -2013 (2014)
3. IEEE Std 802.11ac™ -2013 (2014)

4. FCC (2010) Unlicensed Operation in the TV Broadcast Bands, Second Memorandum Opinion and Order. FCC. 10-174
5. ETSI (2014) White space devices (WSD); wireless access systems operating in the 470 MHz to 790 MHz TV broadcast band; Harmonized EN covering the essential requirements of article 3.2 of the R&TTE directive. Final draft ETSI EN 201 598 V1.0.9
6. IDA (2014) Regulatory Framework for TVWS Operation in the VHF/UHF Band
7. Mizutani K, Ishizu K, Matsumura T, Tran H, Sawada H, Murakami H, Kojima F Harada H (2015) IEEE 802.11af indoor experiment in UK Ofcom TVWS trial pirot program. IEEE VTC Spring 2015, pp 1–5
8. Matsumura T, Ishizu K, Mizutani K, Tran H, Murakami H, Kojima F, Harada H (2015) Long-haul communication trial in London TV white-space with IEEE 802.11af-based high power prototype. WPMC2015
9. NICT (2015) NICT develops world's first IEEE802.11af-compatible baseband IC for TV white-space wireless LAN systems. https://www.nict.go.jp/en/press/2015/12/16-1.html. Accessed 20 Feb 2017
10. Matsumura T, Ibuka K, Ishizu K, Murakami H, Kojima F, Harada H (2017) IEEE 802.11af-based baseband IC prototype enabling compact and low power consumption TV white-spaces devices. IEEE DySPAN2017
11. Holland O et al (2015) Some initial results and observations from a series of trials within the Ofcom TV White Spaces pilot. IEEE VTC Spring 2015
12. Tran H et al (2015) Development and evaluation of a TVWS database for the UK Ofcom TVWS trial. IEICE Tech Rep 114(165):21–26
13. Sawada H et al (2015) Path loss and throughput estimation models for an IEEE 802.11af prototype. IEEE VTC Spring 2015

Further Reading

1. Mizutani K et al (2013) Prototype hardware of IEEE 802.11af/D.5.0 for wireless LAN systems operating on TV White Spaces. IEICE Tech Rep 113(266):69–76

Cognitive Radio: The Need to Align Regulations with Technology

47

Peter Anker

Contents

Abstract

Cognitive radio holds an interesting promise for improved utilization of the radio spectrum. However, there is a considerable degree of uncertainty regarding the potential application of cognitive radio. One of the reasons for this uncertainty is the need for changes in the regulatory regime to allow for more dynamic forms of spectrum access. In addressing the necessary changes in regulations, the regulator should be well aware of the perspective of the entrepreneur. Eventually it is the entrepreneur who invests in CR technology and thereby realizes the goal of improved utilization of the radio spectrum.

P. Anker (✉)
Ministry of Economic Affairs, Delft University of Technology, Haarlem, The Netherlands
e-mail: p.d.c.anker@minez.nl

W. Zhang (ed.), *Handbook of Cognitive Radio*,
https://doi.org/10.1007/978-981-10-1394-2_45

This chapter addresses the relationship between the regulations and the CR technology. Both the regulations and the CR technology will pose limitations on the possible business cases. It further proposes a way forward to come to a successful exploitation of CR technology in which the objectives of both the entrepreneur and the regulator can be realized.

Keywords
Dynamic spectrum access · Regulations · Licensed shared access · Geolocation database · White space · Spectrum pooling

Introduction

Cognitive radio (CR) is a promising innovative technology that can be used to improve spectrum utilization. Especially the ability of cognitive radiotechnology to provide access to spectrum that is already assigned to other user(s) or usage but partly unused when considered on a time or geographical basis holds an interesting promise. The concept of CR was proposed already more than 15 years ago by Mitola. Trials with the commercial use of cognitive radio are ongoing since the historic decision of the FCC in 2008 to allow CR technology in the TV broadcasting bands. However, commercial use of cognitive radio is still very limited. The question is what went wrong and how to proceed?

One of the main reasons for the limited practical and commercial use of CR technology is uncertainty. An important aspect of this uncertainty is the regulatory model. Although there are possibilities to use cognitive radio under the current radio spectrum management regime, the current regulatory model is not conducive for dynamic access of spectrum made possible by cognitive technology. Regulatory provisions are needed to align the regulations with the new capabilities of CR technology of flexible and more efficient utilization of the radio spectrum [1].

In drafting regulatory provisions, governments are facing a dilemma. The liberalization prevailing policy that suggests a technology-neutral assignment of radio spectrum, while enabling the deployment of a specific technology, i.e., cognitive radiotechnology, is of public interest to achieve more efficient utilization of the radio spectrum. It appears that in this light, regulation to allow the deployment of a specific type of CR technology in parts of the radio spectrum that would otherwise be underutilized or not used at all is justified [11].

As CR encompasses a very versatile set of technologies, the subsequent challenge governments are facing is the choice among some of the more fundamental features of CR technology, such as the technology used to make a CR aware of its radio environment and the band in which the CR is allowed to operate. Their choices will need to be well informed as their choices play a pivotal role in the business models of the entrepreneurs. The way governments allocate the use of radio spectrum to particular radio communication services on the (inter)national level and assign the rights to use the radio spectrum on the national level is determining the viability of the business case for particular radio communication products and services.

In this respect there is the issue of "the chicken and the egg": certain types of radio spectrum rights assignment facilitate certain types of usage, while certain types of perceived usage will require a particular type of assignment. In other words, entrepreneurs are reluctant to invest in new products and/or services based on CR technology because of the degree of regulatory uncertainty, and regulators cannot provide this certainty because it is uncertain if their choices will support a viable business case.

This chapter proposes a way forward to deal with this dilemma by explaining the relationship between the regulations and the CR technology. Choices on both regulations and CR technology will greatly influence possible business cases for the introduction of new products and/or services based on CR technology. It is proposed to use an actor-centric approach to deal with this issue of alignment between the technology and the regulatory provisions. After all, cognitive radio is a technology to share spectrum among various users. The various users of the spectrum, the industry that has to develop the equipment and the government that has to provide the necessary regulations, will have to coordinate to make the right decisions in order to come to a successful exploitation of CR. The actors involved in this coordination will all have their own objectives and incentives.

This chapter is structured as follows. It starts with an explanation of the regulatory provisions and its influence on possible business cases for CR. This is followed by an explanation of the relationship between CR technology and possible business cases. This exploration is used to introduce a framework to assess the alignment between the regulations and the technology. This approach is illustrated by an analysis of the so far best known intended use of CR technology: white space access in the TV bands. Based on the results of this analysis, it is proposed to explore use cases within a community of practice as the way forward for realizing the necessary coordination between the actors involved to facilitate the successful deployment of cognitive radio and to realize – at the same time – the goal of improved utilization of the radio frequency spectrum. This proposal is also based on experiences gained at the national level, in the Netherlands, with a community of practice related to cognitive radio.

Spectrum Regulations of Dynamic Spectrum Access

In the current spectrum management model, radio spectrum is divided into fixed and non-overlapping blocks, separated by so-called guard bands. These blocks are assigned to different services and wireless technologies, while a lot of spectrum usage is only local and limited in time. In an economic sense, there appears to be a paradox whereby the rights to the radio spectrum are fully assigned, but a lot of radio spectrum remains unused in practice when considered on a time or geographical basis.

Cognitive radio, as a technology, is an enabling tool to realize increased flexibility in access to the radio spectrum. The key feature of a cognitive radio is its ability to recognize unused parts of radio spectrum that are assigned to conventional

users and adapt its communication strategy to use these parts while minimizing the interference that it causes to the conventional users. An important consequence is that cognitive radio can be an enabling technology to facilitate a paradigm shift for spectrum management from a regime based on static spectrum assignments to a regime based on more dynamic forms of spectrum access [1, 13].

Scenarios for Dynamic Spectrum Access

There are different possibilities to exploit dynamic spectrum access. It can be used to pool spectrum between a number of users or user groups or it can be used to dynamically access white spaces. Spectrum pooling is the situation in which a common "pool of spectrum" is shared among multiple users [10]. Access to the pool may be restricted to specific users through the use of licenses or the pool may be open to all under certain use restrictions. All users have the same rights to access the spectrum. Therefore, this kind of sharing is also referred to as horizontal sharing.

This is in contrast to the other case in which white space users are only allowed access to the radio spectrum as long as the primary users are not needing access. The white space users are on a secondary level of usage of the spectrum. Therefore, this type of sharing is also referred to as vertical sharing. This secondary usage may also be restricted to specific (licensed) users or open to all.

This leads to four different scenarios for the implementation of dynamic spectrum access. The different scenarios are summarized in the following Table 1.

The way in which the regulatory regime allows access to spectrum will greatly influence the business opportunities. This section gives an overview of the impact of the regulatory regime on the business opportunities.

White Space Access

CR technology is proposed to improve radio spectrum utilization by using white spaces within spectrum that is allocated but actually not used at a given time and location. The question is whether there is enough capacity in these unused white spaces that can be made available to support the underlying business case for CR technology and if the business case is solid enough to recoup the necessary investments in this new technology.

The ease of making unused spectrum available for cognitive use depends on the characteristics of the incumbent user. It is easier to find a white space if conventional user(s) and usage is relatively static than when conventional users are mobile and/or their usage fluctuates.

Table 1 Four different regulatory scenarios for dynamic spectrum access

	Horizontal sharing (spectrum pooling)	Vertical sharing (white space access)
Licensed access	Spectrum owners dynamically share spectrum	Owners of the spectrum grant specific cognitive radio's access to their white spaces
Unlicensed access	All CR devices dynamically share spectrum on an equal footing	cognitive radio's dynamically access white spaces from incumbent users

Moreover, the fact that large parts of the radio spectrum are not utilized does not imply that an attractive business case for the remaining unused parts exists. A simple example can clarify this. A mobile operator will have more radio spectrum is use than in rural areas. The fact that in rural areas mobile spectrum is underutilized does not necessarily mean that there is a viable business case for these unused mobile frequency channels, at least not for mobile communications. The business case for the exploitation of these white spaces will have to be distinctively different from the business case of the conventional user.

In the white space access regimes, the CR devices will always have to respect the needs of the primary user. White space access is only possible as long as there is no need for the spectrum by the primary user and no interference is created to the primary user. This sets limitations to the business case for unlicensed white space access with an unrestricted number of devices. There will never be a guarantee that a CR device can have access to a white space and there is always the possibility that a CR device has to cease its operation because a primary user wants access to the spectrum. This makes this regulatory regime less suitable for time critical CR applications.

White space access can be used to share bands between licensed users and unlicensed short-range devices in bands that were difficult in the classic scenario. A good example of this is the use of the 5 GHz band. In this case, RLANs uses CR technology to sense its radio environment, i.e., to detect and avoid incumbent radar systems.

Licensed owners of spectrum can also grant access to parts of their radio spectrum that they do not need in a certain geographic area and/or for a certain period of time to secondary devices on a non-exclusive (unlicensed) basis. These devices can get access to this spectrum after an explicit request for permission to the owner of the spectrum. The owner will need a mechanism to facilitate requests from secondary devices for permission to use spectrum. Cellular operators can use their existing infrastructure to handle these requests. For example, a mobile operator can set aside a mobile channel for this purpose.

An incentive for licensees to open "its" white spaces might be to introduce easements in spectrum licenses. In other words, if a spectrum owner is in possession of radio spectrum that (s)he actually does not use, everybody is entitled to use this spectrum in an opportunistic way as long as the transmissions of the rightful owner are not subject to interference from this opportunistic spectrum access. This is an incentive which might prevent market players from hoarding spectrum [2].

Licensing of white space devices provides the possibility to restrict access to the white spaces to a specific user group. Since the secondary users are now known, this provides the possibility for active coordination between the incumbent user and the secondary (cognitive) user about the likelihood of interference and on guarantees about access to spectrum. Restricted access may also increase the level of trust for the incumbent user and may make them more willing to share their white spaces with a known and trusted CR user.

This licensed form of white space access has become known as Licensed Shared Access (LSA). LSA is a regulatory approach that focuses on facilitating a more

efficient use of spectrum in frequency bands assigned to one or more incumbent users by introducing additional licensed users on a shared basis allowing predictable quality of service for all rights holders [17].

An example of a service that needs guaranteed access to spectrum but only in a very local area and for a short period of time is public safety. Public safety organizations have their own network for day-to-day operations. However, during an emergency situation, they have a huge demand for communications on the spot [15]. A public safety organization might make an agreement to alleviate their urgent local needs with other frequency users. In the agreement sharing arrangements are covered but the actual spectrum usage can be based on the local conditions and the local use of the primary user.

A good opportunity to start this form of sharing is in bands of the military. The military already have a long-standing practice of cooperation with public safety organizations. This may raise the level of trust to a level that is high enough to start an experiment.

Spectrum Pooling

In case spectrum is pooled between a number of users or user groups, CR technology is used to dynamically share the spectrum resources. In a licensed regime, dynamic access to spectrum is obtained through buying, leasing, or renting access rights from the owners of the spectrum. This regime provides the possibility for active coordination between the incumbent user and the cognitive user about the likelihood of interference and on guarantees about access to spectrum. If the barriers to instant trading are removed, the opportunity to buy and sell rights to access spectrum can be based on the actual demand for spectrum. This creates the opportunity to use dynamic spectrum access for higher valued service offerings, such as mobile telephony, and for a spot market to be introduced. A spot market is a perfect means to acquire or sell rights to spectrum access based on the actual demand at any given moment in time.

A spot market can be used among operators to pool the spectrum in such a way that the rights to spectrum access are based on the actual demand for spectrum by their respective users. One of the suggested implementation scenarios is that mobile operators use a part of their spectrum to provide the basic services to their respective customers and pool the rest of their spectrum to facilitate temporarily high demands for spectrum. However, cooperation between mobile operators that are in direct competition to each other is not likely to happen [4].

This kind of sharing spectrum might be a more viable option for implementation in border areas to ease the problem of border coordination. Nowadays the use of spectrum in border areas is based on an equal split of the use of spectrum between neighboring countries through the definition of preferential rights. However, there is no relationship with the actual demand for spectrum at either side of the border. A prerequisite is that the spectrum market is introduced at both sides of the border or in a region, e.g., the European Union.

Pooling spectrum between different services that are not in direct competition to each other might be a more promising approach. This can help to make licensed

spectrum that is not fully used available to others users. In this case access to spectrum is based on an negotiable acceptable level of interference, instead of the worst case scenarios based on harmful interference that are used by regulators to introduce a new service in an already used band. This may open bands for alternative use which might otherwise be kept closed. The incumbent licensee may now have an incentive to open its spectrum for other, secondary, users. The incumbent licensee is in full control because it can earn money with unused spectrum, while the access to its spectrum of the secondary user is on the incumbents own conditions.

A spectrum market can only function if information about the actual ownership of the spectrum property rights is readily available to facilitate trading. The regulator is ideally positioned to perform the task to keep a record of the ownership of these rights. Inclusion of monitoring information about actual usage of spectrum can further facilitate trading by giving more insights in the possibilities for secondary usage.

A special case of licensed spectrum pooling is pooling whereby a single operator who is the exclusive owner of the spectrum uses cognitive radiotechnology to perform a flexible redistribution of resources among different radio access technologies within its own licensed frequency bands to maximize the overall traffic by an optimum use of spatial and temporal variations of the demand. This could be used by mobile operators to realize a flexible spectrum allocation to the various radio access technologies in use or to have an optimal distribution of spectrum between the different hierarchical layers of the network, for example, to realize an optimal allocation of spectrum to femto cells that takes account of the actual user demand without affecting the macro network. A prime requisite for such a scenario is that the license from the operator is flexible enough and technology neutral.

CR technology can also be used to pool spectrum between unlicensed applications. Knowledge of the radio environment is in this case used to realize a fair distribution of access to spectrum between an undefined number of devices.

A very promising application for a true commons whereby unlicensed devices dynamically pool their spectrum is in-house networking. An in-house network is an ad hoc network by its very nature. No two in-house networks are exactly alike and devices are turned on and off during the day, new devices are brought in, devices leave the house, and the neighboring houses have the same ad hoc way of working. The number of wireless devices in a household is rising while the users want to have new equipment that is "plug and play." A new device that is put into service should be able to find its own possibilities to communicate within the in-house network.

A second example of ad hoc networking is the radio network between vehicles as part of intelligent transportation systems (ITS). Restricting access to the pool for certain applications with a polite cognitive protocol may alleviate the tragedy of the commons. In that case, the number of devices outnumbers the available spectrum in such amount that the spectrum is of no use to all. However, even if a polite cognitive protocol is used and the band is restricted to a certain type of applications, the amount of spectrum that is made available must be enough to cater for the intended business case.

Table 2 Impact of the regulatory regime for spectrum access on the business case for CR applications

	Horizontal sharing (Spectrum pooling)	Vertical sharing (white space access)
Unlicensed acces (spectrum commons)	• Sharing between an undefined number of devices	
	Fair distribution of spectrum access between the devices	No guarantees for spectrum access, i.e., less suitable for time critical applications
Licensed access	• Restricted group of users • Increased level of trust • More certainty about access to spectrum • Better suited for infrastructure based service offerings	
	CR user groups not in direct competition with each other	Possibility for active coordination. More guarantees for spectrum access

Impact Assessment of Spectrum Access on the Business Case

The regulatory regime has a huge impact on the business case for cognitive radio. Each regulatory regime will facilitate a different kind of CR applications and/or service offerings. A mixture of these regimes will be necessary to unlock the full potential of CR technology in increased spectrum efficiency. The impact on the business case of the regulatory regime under which the CR application will operate is summarized in Table 2.

Especially the use of CR technology for a restricted group of users can help to bring this technology further for two reasons. First, restricting access to a controlled group may increase the level of trust between the users who share the spectrum. Second, restricted access can provide certainty about access to spectrum over a longer period of time needed to recover the investments to be made in CR technology.

The Impact of Cognitive Radio Capabilities on the Business Case

The fundamental difference between a cognitive radio and a conventional radio is that a cognitive radio uses information of the radio environment to select and deploy the most appropriate communications profile, such as frequency band, access technique, and modulation method. There are various techniques possible to obtain information about the radio environment. Each of them will have different implications for potential CR applications and the magnitude of the required investments.

Sensing

In its basic form a cognitive radio senses the radio environment to acquire information on the local usage. The CR device relies thereby on its own judgment of the local use of the spectrum to transmit over sections of the spectrum that are considered free. No matter how good the sensing technology is, a system that only relies on its own judgment to obtain information about spectrum usage might come in a situation where it inadvertently is not able to detect usage of a radio channel. This means that with a cognitive radio based on sensing alone, there is always the possibility of interference to the conventional users of the band. To limit this risk, restrictions on the output power of the CR devices will have to be set. As a consequence, the CR can only be used for applications which use low power in relation to the incumbent usage.

Sensing can be used without the need for coordination with the "outside world." Sensing can be used by stand-alone applications, whereby there is no need for investments in the rollout of associated infrastructure. However, there is always the possibility that the device is not able to detect a white space. Hence, dynamic spectrum access based on sensing is expected to be restricted to low-end applications involving low power devices.

Sensing is also of interest to military users. Since the radio only relies on its own judgement, it makes it possible to communicate without making the whereabouts and communication needs of the military radios known to others. This will make their communications less vulnerable.

The probability of finding a white space that can be utilized depends on the activities of the incumbent user(s), the range of frequencies which is sensed, and the number of active white space devices. Sensing will have to take place over a sufficiently large frequency range to support the capacity needed by the CR application. Sensing becomes more challenging, and more expensive, when a wider range of frequencies and/or a wider range of conventional user applications are to be taken into account. At the current state of technology and field experience on sensing, a case-by-case approach will be required which takes into consideration the existing spectrum usage. Hence, for new CR regulations to be meaningfully applied, i.e., before making available a band for white space devices, an assessment should be made of the amount of white spaces that can be made available against the capacity needed for the introduction of the application that uses these white spaces.

A possibility to ease the problem of the (un)reliability of sensing is to focus sensing in a band that is not too wide in a completely unlicensed environment to create a true commons for short-range devices. The regulator should pinpoint a band for dynamic spectrum access in cooperation with industry. To reach economies of scale, this band could be designated on a regional level, for example, on a European level.

An obvious example is the earlier mentioned in-house network. Sensing can be used to realize that devices pool the spectrum available for in-house network in a "plug and play" manner. A new device senses its environment and coordinates its use within the local in-house network. A possible band to start is, e.g., the 60 GHz band.

Sensing can be made more reliable by cooperation between the sensing devices [12]. Cooperation can improve the probability of detection and reduces the detection time and thus increase the overall agility of the system. Drawbacks are the need for a common signaling channel between the devices and the additional overhead needed to exchange sensing information over this channel.

Especially the need for a signaling channel makes this coordinated approach complex. The cognitive devices become part of a network. This makes this coordinated approach especially feasible in applications where the CR device is already part of a (local) network, e.g., in-house networks. Coordination is a less attractive option for stand-alone CR applications.

Another possibility is to use sensing in a more controlled environment between licensed users. This will give more control over the environment, because the users are known. This type of sharing could be used to broaden the amount of accessible spectrum for temporarily users who need a guaranteed quality of service. This makes this type of sharing a perfect fit for, e.g., electronic news gathering and other programme making and special events services. Electronic news gathering only requires spectrum for short periods of time and for a restricted local area, but it requires guaranteed access during the operation.

Geolocation Database

Since sensing is in its present form is not reliable enough, regulators around the world have turned their focus from sensing toward a geolocation database. This will require investments in a database and related infrastructure that need to be recouped. Entrepreneurs will only invest in this infrastructure if there is long-term assurance for access to spectrum and willingness to pay from customers. This shifts the orientation from a device centric approach to a service centric approach. Such a business case is better supported by a regulatory regime based on licensed access.

The database should contain the relevant information on the frequencies that can be used at a certain location as well as the applicable restrictions. The database will have to be kept up to date, which makes this option especially suitable in cases where spectrum usage of the conventional user(s) does not change frequently, e.g., in a broadcasting band or a band for fixed satellite communications.

The restrictions for the CR application imposed by the use of a geolocation database are twofold. First of all, the CR device needs to be (made) aware of its geographical location. This information can be programmed in the device during the installation of the CR device for fixed applications. Mobile CR devices will need a means to acquire that information, for instance, by incorporating radio navigation in the terminal. However, the use of radio navigation will be difficult for indoor applications.

Secondly, the CR device will need to have access to this database on a regular basis. Access to the database is easier to arrange if the CR device is already part of a network than for stand-alone CR applications. The rate at which the CR devices have to obtain updated information on the local radio environment depends on the

rate at which the information on the incumbent user may change and on the degree of mobility of the CR device.

The use of a geolocation database is proposed to enable mobile broadband communications in the 2300–2400 MHz band. Licensed Shared Access based on a geolocation database is the recognized approach in Europe for the introduction of mobile communications in the band while maintaining the current incumbent use. Among the incumbent users to protect are programme making and special events (PMSE) applications (wireless video camera's). Although the concept of LSA with a geolocation database was originally developed for the introduction of mobile communications in the band, it could also be used to enhance efficient use of the band by the wireless camera's themselves. In the latter case, the database is used to electronically assign a license to a wireless camera, but only for the time duration and the location it is actually needed.

Cognitive Pilot Channel

Coordination between CR devices can be realized through a so-called cognitive pilot channel (CPC). A CPC is a dedicated carrier providing information about the availability of spectrum and possibly usage restrictions to the CR devices in a certain area. The CPC can be used to (1) give general –local– information on the availability of white spaces in relation to the service to be protected or (2) to coordinate the use of the spectrum resources by the CR devices competing for spectrum access or (3) a combination of both [4, 5].

The first option requires that the CPC broadcasts information on channels that are available and possibly the associated use restrictions, unless these restrictions are already known beforehand by the CR device. The second option is more complex because there is also a need for the network to know which channels are actually used by the CR devices, and therefore there is a need for a feedback channel.

Implementation of a CPC will require a radio-infrastructure to support the CPC. The CPC can be provided by a dedicated, autonomous network, but this will require substantial investments. The necessary investments can be lowered if the CPC uses a logical channel within an existing network, e.g., within a mobile network.

Because a CPC can provide real-time information, a CPC is highly suitable in cases where spectrum usage of the user(s) with which the band has to be shared is more dynamic. In this case, the network will need to have up-to-date information of the spectrum usage of all user(s) at all times.

Impact Assessment of CR Technology on the Business Case

The means a CR uses to acquire information on the radio environment has a significant impact on the business case for CR applications. An outline of the main conclusions of the impact of the CR technology on the CR application, and thereby on restrictions for a viable business case, is given in Table 3.

Table 3 The impact of the CR technology on the CR application

	Implication to potential CR applications	Remarks
Sensing	Low power in relation to the primary user Sensing over a relatively small band sets limits to the data transfer capacity available. Wide band sensing increases the capacity available, but is more complex and expensive. Can be used for stand-alone applications	There remains a potential for interference to the conventional user.
Geolocation database	Can be used for applications which need a higher power. The location of the CR device needs to be known. Application needs a connection to the database on a regular basis	Only useful in bands with relatively static conventional users Costs of database service will have to be recovered
Cognitive pilot channel	Can be used for applications which need a higher power. Need for a radio-infrastructure to support the CPC. Large-scale deployment more expensive than a database	Can also be used in case conventional use varies

An apparent difference between sensing on the one hand and a geolocation database or Cognitive Pilot Channel on the other hand is that the latter two will require investments in infrastructure. This means that sensing can be used for stand-alone applications, while the other options are better suited for the delivery of services with an associated infrastructure rollout, i.e., sensing can be used in a business case based on the sales of equipment, whereas the database and CPC are better suited for a service provider-driven business case based on the sales of a service. In that case, there will be a direct relationship between the service provider and the customer. This relationship is necessary to recoup the investments in infrastructure.

Of course, it is always possible to use a combination of techniques. Especially a combination of database access and sensing seems promising. The database can be used to protect existing services with which the band is shared, and sensing can be used to assess whether the opportunity is really available or already in use by another CR device.

Another possibility is the use of a local CPC (or so-called beacon) to reduce some of the drawbacks of sensing, especially the complexity and associated costs of sensing devices. A relatively complex master device can be used to process the sensing results of a range of locally connected devices. The master device decides

based on this information on what channel the connected devices may operate and sends this information to these devices over a local beacon. This solution can only be used if these devices form a local network. The relatively expensive master device acts as an intelligent central node for the relatively cheap connected devices. A good example is a local area network, whereby the router can serve as a master to provide information to the wireless devices that are active in the network. This configuration provides possibilities to open bands for additional use that were closed otherwise, such as the earlier mentioned 5 GHz band.

Two Levels of Alignment

While alignment between new technologies, such as CR, and the associated regulations is an important prerequisite, it is not enough to assure a successful introduction of this new technology. There are numerous examples on the introduction of new technologies where the necessary alignment between the technology and the regulations was in place but the market for the provisioning of products and services based on this new technology did not mature.

Our analysis of the underlying causes is that firms will only decide to invest in new products and/or services if they can expect a future return. These investment decisions are driven by three major considerations: (1) the prospective demand and willingness to pay for new products and/or services, (2) the magnitude of the investments required, and (3) the degree of risk or uncertainty involved.

The profile of the business case, in terms of depth of investment and the recovery period required, will influence the ability to obtain the necessary (external) funding. As such the business case is especially challenging for service provisioning that requires a huge, up-front investment, e.g., an infrastructure rollout to provide mobile telephony. In these cases, the right to exploit the radio spectrum or any other infrastructure over a significant period of time and on an exclusive basis will contribute to the willingness of firms to invest as it reduces the uncertainty, which may make the business case more viable [11].

Although the regulator can't do much about technological and market uncertainties as such, the regulator plays a crucial role. The regulator should create a regulatory environment in which these uncertainties are lowered to an acceptable level for commercial applications to emerge. This environment should, among other things, give clear directions on the expectations of CR technology [1].

However, in setting up institutional arrangements, governments will steer technology and possible business cases in a certain direction. Ostrom [14] showed that the specificities of the entry and authority rules will favor certain types of usage over other types of use. This is also true the other way around; certain types of perceived usage will require particular entries and authority rules. Although Ostrom made this observation in the investigation of common pool resources, the problems associated to the provisioning of telecommunication services are quite similar as shown by Künneke and Finger [9]. They argue that infrastructures (including energy,

communication, transport, and postal services) can be perceived as common pool resources providing essential services to society.

Hence, decisions made by governments on the market design and associated regulations will have an influence on the viability of possible business cases. For example, decisions made in spectrum policy on the amount of spectrum allocated, whether the spectrum is made available on a license exempt basis or not, the number of licenses issued, the rollout and other obligations attached to the licenses, and the award mechanism for the licenses (e.g., an auction or a beauty contest), will all influence the required investments and the possibilities to exploit a certain business case. This is quite well demonstrated by mobile communications (GSM) which could flourish under a strict licensing regime and Wi-Fi that could develop under a license exempt regime.

Governments will need to be very well informed to make the right decision in order to let the intended business case flourish. Lessons learned from the past seem to suggest that a too "pushy" approach from governments may be counterproductive and retard or stall technological development [8]. Governments will need to take decisions that are not only in line with their own goal(s) but also make it possible for entrepreneurs to realize their goals. After all, it is through the actions of the firms, individually and collectively, that the governmental goals will be realized. This is illustrated in Fig. 1 [3].

The government and the entrepreneurial firm have different objectives, in a somewhat simplistic view of the world, since the liberalization governments have, above all, an objective of economic efficient use of spectrum. This is accompanied

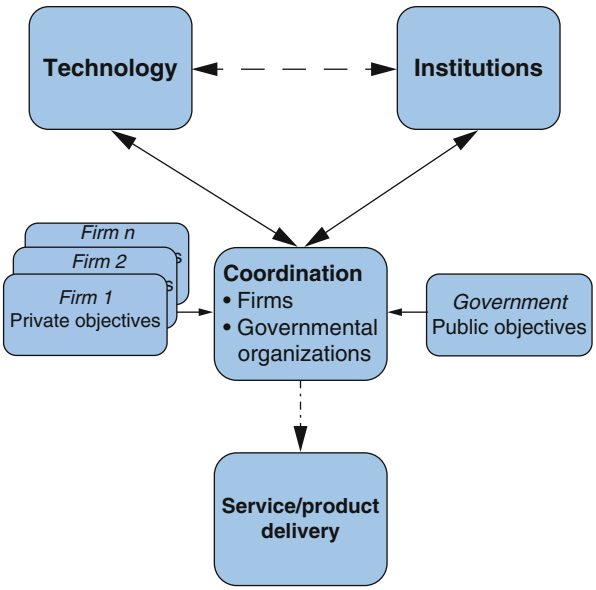

Fig. 1 Two levels of alignment

by societal objectives, such as universal service delivery, and in some cases also by industry policy. Governments rely on a market design and associated regulations to serve this mixture of economic and societal objectives. In the case of mobile communications, radio spectrum policy is used to create a market for mobile telephony. Specific auction rules may be used to allow new entrants and to influence the number of players on the market. Specific obligations are attached to the licenses to serve societal objectives, e.g., a coverage obligation.

Firms, on the other hand, have a completely different objective. They want to invest in (new) technology to develop products and services with the aim to maximize profit. The government and the firm are highly interdependent in the realization of their objectives. The institutional arrangements that are set up will have to provide certainty to entrepreneurial firms to invest in new technology and the exploitation thereof. If, as a result of profit maximization considerations, firms decide not to use the system as intended, the government fails in realizing its governance objectives.

Use of the new technology in such a way that both the government and the entrepreneurs can realize their objectives is what we call a "sweet spot." A sweet spot is only possible if the use of certain technology and the associated institutional arrangements are aligned in such a way that both the intended business opportunity and the public objectives can be realized [3].

Analyzing the Case of White Space Access in the Television Broadcasting Band

Having established this actor-centric perspective, we will now apply this perspective to a case of which its resolution lies in the future. It concerns one of the first applications for CR that was put forward: the introduction of cognitive radiotechnology in the so-called white spaces in TV bands. The US Federal Communication Commission (FCC) made these white spaces available for unlicensed broadband Internet. Its intended use is, above all, to provide more affordable broadband deployment in rural areas [6, 7].

In this case CR technology is intended to share the TV band with the legitimate primary users, the TV broadcasting stations, and low power auxiliary service stations (notably wireless microphones). Given the latter, it is understandable that the FCC removed sensing from the original requirements and took alternative measures to guarantee access to spectrum for wireless microphones and to prevent wireless microphones from being subjected to interference from CR devices. First of all, at the current state of technology, sensing is not sufficiently reliable. More importantly, to prevent interference to the primary user, the output power of the CR device should be low relative to the primary users (see section "Sensing"). These primary users are not only TV broadcasting stations but also these low power wireless microphones. Restriction of the output power of CR devices to a level that is low compared to the wireless microphones would have been detrimental for the business case of rural broadband access.

In taking the perspective of the private actor, the first question to be asked is as follows: Why is there no service provided at the moment? There certainly is no scarcity of radio spectrum; the 2G/3G bands are underutilized in these rural areas. The main reason appears to be that the costs to provide the service are too high in relation to the willingness to pay for the provided service.

The second question to be asked is as follows: How will the business case for CR improve the situation? For the business case to become viable, either the willingness to pay for the CR enabled services has to become higher or the cost reduction needs to be greater than the additional costs associated with the new (more capable and sophisticated) cognitive technology. Combined they need to bridge the gap between the provision of services based on the current technology and the current willingness to pay.

Under the FCC white space ruling, rural broadband access is made more feasible due to the fact that a lower frequency range is made available, which extends the coverage area of a base station, compared to the existing alternatives to provide the service. However, existing mobile networks operate at frequencies that are just above the television band. This means that the gains of using a lower frequency are very limited. (As the use of white spaces is considered to be free of charge, this represents a benefit compared to the business case for existing 2G/3G deployments, which may be subject to the recovery of a hefty auction fee. However, in serving the rural areas, economists will consider the auction fee as sunk costs and will calculate the business case on marginal costs.) Therefore, the business case for deployment of a wide area network in rural areas based on white space access remains highly questionable. It is much more likely that white space access will be used to provide localized access to the Internet at specific backbone nodes. This is a business case that is comparable to Wi-Fi hot space access, although over larger distances.

The next question is whether the capacity that can be supported by white space access is high enough to support the demand from users. In areas where the required demand for capacity is bigger, the coverage area of the base station may have to be made smaller. This conflicts with the reasoning to make these lower frequencies available. This means that the business case will be restricted to areas with a population density below a certain limit. This limit will be lower if the demand per customer is higher. It remains to be seen whether the assigned band will have enough white space capacity available for the intended application – broadband Internet access – to support a successful business case. Moreover, the already limited capacity that is available for white space access is under pressure, because the FCC decided in 2012 to auction off part of the TV band (the so-called 600 MHz band) for use by public mobile operators, based on a preceding incentive auction for TV licensees to give up their licenses. This limits the available white space capacity even further.

The final question is if there are private actors that are willing to provide the intended business case. When the FCC proposed to make use of a geolocation database instead of relying on sensing, a shift was made from a device-oriented business case toward a business case where there is a need to invest in infrastructure to build the database and to provide access to this database. However, the FCC

retained the institutional setting of unlicensed access to white spaces. Given the fact that there is limited capacity available and there are no guarantees to spectrum access in an unlicensed access regime will reduce incentives for private actors to invest in the infrastructure. This would explain why the intended service providers are relatively absent in the standardization activities and other discussions around white space access in the UHF TV band and why the number of TV white space devices deployed is still limited although the FCC has allowed access to TV white space since February 2009 and a commercial service offering was made possible after the FCC permitted white space database administration to provide the necessary database services. In the Third Memorandum Opinion and Order of 2012, the FCC made some changes to the rules mainly to lower the cost for WISPs to provide broadband access in rural areas. However, the white spaces do not seem to attract WISPs to provide their service in rural areas. Moreover, in this institutional setting ,it is also not very clear what the business model for commercial operation of the database should be.

To conclude, the white space access regulations appear to be a technological fit instead of a business case fit, driven by the regulator to realize a societal objective. The FCC took a very careful step by step approach to implement regulations that are aligned with the current state of technology. However, whether there is alignment between the public objective of the FCC to provide broadband access in rural areas with the objectives of the private actors remains to be seen. It is highly questionable whether the intended social objective will materialize in a viable business opportunity to provide wireless broadband access in rural areas and for the exploitation of the associated database.. It would explain why the intended service providers are relatively absent in the standardization activities and other discussions around white space access in the TV band. Moreover, it may explain why there is, as yet, no viable business model for the commercial operation of a database in support of sharing the spectrum with wireless microphones.

Next Steps: Finding a Sweet Spot for Cognitive Radio

Although there are possibilities to use cognitive radio under the current radio spectrum management regime, there is still no compelling business case. To assure development and deployment of CR technologies, it is worthwhile to review potential product-market combinations where CR functionality provides a “value add” and determine whether these cases are attractive enough to be taken up by the industry as first applications of CR, as first steps on the road toward broader deployment of CR technologies.

The government can facilitate this process through the initiation of a platform in which the equipment industry, the service providers, and the government itself closely cooperate with the aim to find a sweet spot. This sweet spot serves as a catalyst to both the private sector and the government, for the private sector to develop products and services based on cognitive technology and for the government to realize the ultimate goal of more efficient use of spectrum.

The RSPG (Radio Spectrum Policy Group) has already recommended creating a platform to allow researchers, academia, manufacturers, operators, service providers, and regulators to coordinate research activities. According to the RSPG, this platform could build upon already existing platforms with comparable purposes, notably COST-TERRA [16]. This notion of the RSPG on COST-TERRA is quite relevant. The discussions within COST-TERRA were very fruitful, but were rather academic in nature.

As the discussion within COST-TERRA were too academic, discussions will benefit from a new extended platform that serves as a community of practice that involves all stakeholders. In order to do so, participation should be widened in two directions. Firstly, participation should be extended to service providers and users of spectrum. This may strengthen the discussions on the incentives for primary users and possible business cases for the primary and secondary users. Secondly, participation should be widened to industry players to incorporate the ideas and solutions in the development of new technology and technology standards.

In this platform, all participants should work together with the national spectrum regulators to find and enable a sweet spot. A sweet spot needs a fit between a specific CR technology, an initial business opportunity and an associated regulatory regime. The regulators can enable this sweet spot on a European level by specifying the necessary and specific regulatory regime in a European decision and/or European recommendation.

This requires participation at the working level. Intended participation is largely the same as those of the workshops that were organized by ERO, the national spectrum regulators as organized within the ECC, in association with COST-TERRA, and the industry actors as organized within ETSI.

There is already some experience with a community of practice related to CR in the Netherlands (CRplatform.NL). This community of practice aims to identify the uncertainties surrounding potential deployment areas of CR and through discussion among stakeholders to find ways and means of addressing and reducing these uncertainties, thereby facilitating the successful deployment of CR-based products and services. This initiative evolved from the regular interaction between representatives of the Ministry of Economic Affairs, responsible for radio spectrum policy and the industry.

The platform organizes meetings and workshops and has a repository on the Internet with information considered useful for the participants. The main focus of the workshops is to explore potential application areas of cognitive radio, so-called use cases. Some of the workshops are dedicated to the state of the art of the technology and to the theoretical framing of sharing spectrum through cognitive radiotechnology. Each workshop brought together potential users, industry, service providers, policy makers, and regulators, as well as academic researchers.

The workshops on the use cases take the perspective of the user itself. The use case is introduced by the case owner. A presentation is given of the use case centered around the communication needs. The discussion that follows is centered around solutions to these communication needs and the question whether the use of cognitive radio has added value. The following application areas have been among

the topics of a use case workshop during the first two years: container terminals in the Rotterdam harbor; special events captured by broadcasting organizations; public safety communications by the police force; high-intensity communications at airports; and domotica. Moreover, manufacturers of cognitive radio and related shared access products and technology have had an opportunity to present their solutions, such as hybrid radio, professional wireless audio equipment, and high-density Wi-Fi solutions.

In these explorations, one of the first questions to be asked is what are the gains from the use of this new technology, and are these gains high enough to cover the increased cost of the use of this technology compared to the alternatives? The use cases as discussed suggest that cognitive radio functionality adds most value in situations that are typically niche applications or are a small segment of the overall market for wireless technologies. One of the reasons is the fact that cognitive radiotechnology is basically a technology to (more efficiently) share the radio spectrum. As cognitive radio provides additional functionality compared to current radiotechnology, this will come at increased costs, at least initially. Situations of high-intensity demand are expected to provide the highest willingness to pay by the end users.

Each use case discussed so far addressed a specific market segment, or even a market niche. Hence, potential market volumes are (relatively) low to moderate, which impacts the viability of the cognitive radio business case. Nonetheless, the use cases also show similarities, in particular if cognitive radio-based solutions are considered as variants of a more generic cognitive radio-platform solution. Especially the combined business case of the communication needs of the public safety services in case of an emergency and the registration of this emergency and other news gathering seems to be logical and promising. This became apparent during the Use Case Workshop on Special Events, as during (ad hoc) events, the needs of public safety and broadcasting converge at the same place and time. The type of communication needs to show a strong parallel. Hence, pursuing solutions for one group of actors (broadcasters) should best be done cognizant of the needs of the other group of actors (public safety).

This example shows that finding a sweet spot for cognitive radio might be easier if the solutions for one group are similar to the solutions for the other group, at least on the platform level. This increases the addressable market and hence the viability of the business case. The unresolved issue is the capacity issue. How much capacity is available for cognitive radio use and is there enough capacity available to support the (combined) business case?

The use cases further show that a viable business case for cognitive radio will require economies of scale. This extends the need for coordination to the European Union level, if not at the global level. Such coordination may still be left to be organized by the industry actors. However, the use case experience suggests that lacking a very compelling business case, the likelihood that industry actors will take the lead is expected to be low. This ties in with the fact that discussions within the community of practice confirmed the role of the regulator to facilitate this search for a sweet spot [3].

Conclusions and Recommendations

For successful introduction of cognitive radio, it is necessary but not enough to align the specific CR technology with the regulatory environment that is chosen. Next to it, the business opportunities that are enabled by specific choices should serve the objectives of both the entrepreneur and the government. In other words, the regulations and the technology should be carefully chosen such that both the private objectives of the entrepreneur and the public objectives can be realized.

Exploring use cases can be a good instrument to bring all interested parties together and to find and enable a "sweet spot" for the use of new technology in an explorative modus. A sweet spot is enabled if the institutional arrangements and the characteristics of the new technology are aligned in such a way that both the intended business opportunity and the public objectives can be realized.

This exploration can take place in a community of practice. An initial exploration of possible business cases revealed that the type of CR technology to be used and the appropriate regulatory regime to support it depend on the specifics of the intended business case and the specifics of the users with which the bands will be shared. When a viable combination is found, the spectrum regulator should set up the specific regulations to facilitate the CR deployment and thereby make an important step toward a more efficient utilization of the radio spectrum.

It is recommended to introduce this community of practice for cognitive radio on a European level. Such a community could make use of, and build upon, the experiences of COST-TERRA. In order to encompass all interested stakeholders, this platform should be broader than the COST-TERRA participation. It should include representatives of service providers, user communities, industry players, academia, and national regulators.

References

1. Anker P (2010) Does cognitive radio need policy innovation? Compet Regul Netw Ind 11(1): 2–26
2. Anker P (2010) Cognitive radio, the market and the regulator. In: 2010 IEEE Symposium on New Frontiers in Dynamic Spectrum Access Networks (DySPAN 2010)
3. Anker P, Lemstra W (2013) Cognitive radio: how to Proceed? An actor-centric approach. Commun Strateg 90(2nd Quarter 2013):77–95
4. Bourse D, Agusti R et al (2007) The E2R II Flexible Spectrum Management (FSM) Framework and Cognitive Pilot Channel (CPC) concept – technical and business analysis and recommendations. E2R II white paper
5. ETSI (2009) ETSI TR 102 683 V1.1.1: Reconfigurable Radio Systems (RRS); Cognitive Pilot Channel (CPC). ETSI
6. FCC (2004) FCC 04–113. Notice of proposed rulemaking, in the matter of unlicensed operation in the TV broadcast bands (ET Docket no. 04-186) and additional spectrum for unlicensed devices below 900 MHz and in the 3 GHz band (ET Docket no. 02–380). Federal Communications Commission, Washington, DC
7. FCC (2010) FCC 10–174 second memorandum opinion and order in the matter of unlicensed operation in the TV broadcast bands (ET Docket No. 04-186) and additional spectrum for unlicensed devices below 900 MHz and in the 3 GHz Band (ET Docket no. 02–380). Federal Communications Commission, Washington

8. Haug T (2002) A commentary on standardization practices: lessons from the NMT and GSM mobile telephone standards histories. Telecommun Policy 26(3–4):101–107
9. Künneke R, Finger M (2009) The governance of infrastructures as common pool resources. In: Fourth Workshop on the Workshop (WOW4). Indiana University, Bloomington
10. Lehr W, Jesuale N (2008) Spectrum pooling for next generation public safety radio systems. In: 3rd IEEE Symposium on New Frontiers in Dynamic Spectrum Access Networks (DySPAN 2008)
11. Lemstra W, Anker P et al (2011) Cognitive radio: enabling technology in need of coordination. Compet Regul Netw Ind 12(3):210–235
12. Mishra S, Sahai A et al (2006) Cooperative sensing among cognitive radios. In: IEEE International Conference on Communications 2006 (ICC'06)
13. Olafsson S, Glover B et al (2007) Future management of spectrum. BT Technol J 25(2):52–63
14. Ostrom E (1990) Governing the commons: the evolution of institutions for collective action. University Press, Cambridge
15. Pawelczak P, Prasad RV et al (2005) Cognitive radio emergency networks–requirements and design. In: First IEEE International Symposium on New Frontiers in Dynamic Spectrum Access Networks (DySPAN 2005)
16. RSPG (2011) RSPG10-348 final RSPG opinion on cognitive technologies, Brussels
17. RSPG (2013) RSPG13-538 RSPG opinion on licensed shared access, Brussels

Spectrum Sharing Policy at Global Level

48

Marja Matinmikko and Miia Mustonen

Contents

Abstract

Spectrum sharing developments exploiting cognitive radio technology will change the traditional spectrum management models, which calls for discussions and decisions in the policy making domain. Efficient governance of natural resources such as the radio spectrum requires actions in different policy making levels ranging from national level all the way to the international level. This chapter will introduce spectrum sharing related policy making activities in the

M. Matinmikko (✉)
Centre for Wireless Communications (CWC), University of Oulu, Oulu, Finland
e-mail: marja.matinmikko@oulu.fi

M. Mustonen
VTT Technical Research Centre of Finland Ltd., Oulu, Finland
e-mail: miia.mustonen@vtt.fi

W. Zhang (ed.), *Handbook of Cognitive Radio*,
https://doi.org/10.1007/978-981-10-1394-2_47

global level presenting the actions taken at the International Telecommunication Union Radiocommunication (ITU-R) sector. We will introduce the groups within ITU-R and their related activities and introduce cognitive radio and spectrum sharing related terminology developed at the ITU-R. Special emphasis is put to the ITU-R studies on cognitive radio systems (CRS) with a set of capabilities for obtaining knowledge, decision-making and adjustment, and learning, to enhance the efficiency of spectrum use. We will introduce the CRS capabilities and present scenarios and applications where vertical and horizontal spectrum sharing using CRS capabilities could take place. Other sharing related activities at the ITU-R are also presented including spectrum management, spectrum monitoring and spectrum occupancy measurement studies, as well as more general ongoing work on regulatory tools to enable spectrum sharing and CRS from the point view of spectrum management. Finally, a future outlook is given for spectrum sharing policy developments toward the fifth generation (5G) networks.

Introduction

Research community has made extensive studies on cognitive radio techniques for spectrum sharing to enable several radio systems to operate in the same frequency band on a shared basis. In the early cognitive radio research studies, the focus was on technical approaches to detect users with higher priority of spectrum access rights by using spectrum sensing techniques [1] and to select operational channels according to some optimization criteria such as interference minimization and throughput maximization [2]. While the early studies on cognitive radio work were about new spectrum management techniques, the link between the cognitive radio techniques developed in the research domain and the actual spectrum management principles adopted in the spectrum regulatory domain remained loose. Thus, the criteria for the development of cognitive radio techniques in the research domain did not thoroughly address the real requirements set for spectrum policy by the regulators and the concerns of involved stakeholders in terms of, e.g., interference issues.

As the term "cognitive radio" very rapidly became commonly used in the research domain in the beginning of the century with various definitions and interpretations, there was a need for a global spectrum policy making body to give guidance on the definition itself and the evolution of the entire cognitive radio topic. While spectrum management and development of spectrum sharing methods and models are a national matter, decided by the local regulatory authorities in the regulatory domain, there is a strong need for coordination between neighboring countries and for harmonization to achieve economies of scale. Therefore, regional and international levels need to develop and promote feasible solutions with potential for widespread adoption. The United Nations based International Telecommunication Union Radiocommunication (ITU-R) sector [3–5] plays the key role in spectrum policy making as the truly global body where relevant stakeholders are represented to take decisions on spectrum matters. ITU-R conducts studies on technical and

spectrum management aspects and provides a global forum for discussions and disseminating best practices [3–5].

Since the cognitive radio topics studied and developed in the research domain introduced a novel way of spectrum sharing and coexistence using technical advances to detect other spectrum users and to coordinate interference between different wireless systems in a more dynamic way, there was a need to investigate at the ITU-R whether changes are required in the traditional spectrum management and allocation principles due to the introduction of the cognitive radio concept. This process resulted in a number of studies conducted at the ITU-R and outputs published in several ITU-R documents.

This chapter will discuss cognitive radio and the related spectrum sharing policy activities at the global level by introducing the relevant activities at the ITU-R and their link to the research domain. By starting with the basic requirements for efficient governance models for natural resources, spectrum sharing related governance principles are first discussed in a high level. Then, the different groups at the ITU-R with activities on cognitive radio and spectrum sharing topics are then summarized including their activities around spectrum sharing and especially cognitive radio systems (CRS) as called by the ITU-R. Finally, a future outlook for the spectrum sharing policy developments are given depicting directions for 5G.

Spectrum Sharing in Governance Framework

Management of the radio spectrum belongs to the broader framework of governance of natural resources that have been extensively studied in many fields [6]. The development of effective governance mechanisms is at the heart of managing the precious resources. Efficient management of natural resources requires governance models at different levels ranging from the local level all the way to the global level [6]. Management of the radio spectrum is about defining bundles of property rights over the radio spectrum, and spectrum sharing introduces new bundles of rights that vary with the sharing model [7]. More specifically, the radio spectrum can be seen as a common pool resource (CPR) that is characterized by difficulty to exclude and high subtractability of use [7]. Difficulty to exclude refers to how complicated it is to prevent others from using the same resource. Subtractability of use indicates whether one person's use of the resources diminishes someone else's ability to use the same resources which takes place in the case of the radio spectrum. The guidelines from the management of CPR can provide useful insight into the development of spectrum management and particularly spectrum sharing models.

General principles for robust governance of environmental resources introduce several requirements including providing information, dealing with conflict, inducing rule compliance, providing infrastructure, and being prepared for change [6]. Promising strategies to meet these requirements include dialogue among interested parties; layered institutions including a mix of institutional types; and designs that facilitate experimentation, learning, and change and rules that evolve [6]. Best governance systems in fact are polycentric indicating that there are several points

of decision-making control that may partially overlap in scope and hierarchy and interact with each other in complex ways that evolve over time [7].

In terms of management of the radio spectrum and particularly introducing dynamic spectrum sharing, *efficient governance highlights the different levels of governance* for providing information, dealing with conflict, inducing rule compliance, and providing infrastructure and readiness for change. Different radio systems that want to use spectrum such as broadcasting, mobile communications, satellite, and fixed and the specific systems within these services need to be coordinated by mechanisms at various levels to manage the complicated interference scenarios. Thus, spectrum policy discussion and spectrum sharing related activities take place at several levels in the policy making. While the actual awarding of spectrum access rights is done at the national level, spectrum sharing related developments exploiting cognitive radio technologies need international-level activities. In the following, we will focus on the global level for spectrum sharing by presenting spectrum sharing developments within the spectrum governance framework at the international level.

Role of ITU-R

For spectrum sharing policy making at the global level, the ITU-R plays the key role in the governance framework regarding the global harmonization on spectrum matters. The role of ITU-R is "to ensure the rational, equitable, efficient and economical use of the radio-frequency spectrum by all radiocommunication services, including those using satellite orbits, and to carry out studies and approve Recommendations on radiocommunication matters" [5]. The activities taken at the ITU-R aim at providing an environment that enables the sustainable development of radio communications. In practice, this means ensuring interference-free operation of the different radio applications to guarantee quality and reliability of services, harmonization of frequency usage, promotion of new technologies while protecting existing users, and ensuring efficient spectrum utilization. One particularly important part of the ITU-R work is to create conditions for harmonized development and efficient operation of existing and new systems while taking into account the different stakeholders' often conflicting concerns. This becomes a highly complicated task as the ITU-R brings together approximately 40 different radio services that compete for the spectrum allocations. This results in a complex environment for coordinating the various interference scenarios between different services with different technical and operational characteristics.

As being the global body in spectrum policy making, the specific role of the ITU-R is to maintain and extend international cooperation between different countries for the improvement and rational use of telecommunications [3–5]. With this respect, the detailed roles taken by the ITU-R as described in [3–5] are to:

- effect allocation of bands of the radio frequency spectrum, the allotment of radio frequencies, and the registration of radio frequency assignments and of associated

orbital positions in the geostationary satellite orbit in order to avoid harmful interference between radio stations of different countries;
- coordinate efforts to eliminate harmful interference between radio stations of different countries and to improve the use made of radio frequencies and of the geostationary-satellite orbit for radiocommunication services.
- create the regulatory and technical basis for the development and effective operation of satellite and terrestrial climate monitoring and data systems.

Avoidance of harmful interference is a key principle in the above roles of the ITU-R, and there are several mechanisms to attain that goal. The global use and management of the radio spectrum requires a high level of international cooperation, and an important task of the ITU-R is thus to facilitate the intergovernmental negotiations to develop legally binding agreements between different countries. To ensure interference-free operations of the different radio systems, the key tool of the ITU-R is the Radio Regulations (RR) that is the international treaty governing the use of the radio frequency spectrum and satellite orbits. The RR is reviewed and revised regularly through the World Radiocommunication Conferences (WRC) arranged by the ITU-R [8] as shown in Fig. 1. The RR defines the recommended allocations of frequency bands to the different radio services and their related technical parameters and procedures for coordination. In preparation for WRCs, the ITU-R conducts detailed studies in order to improve the international spectrum

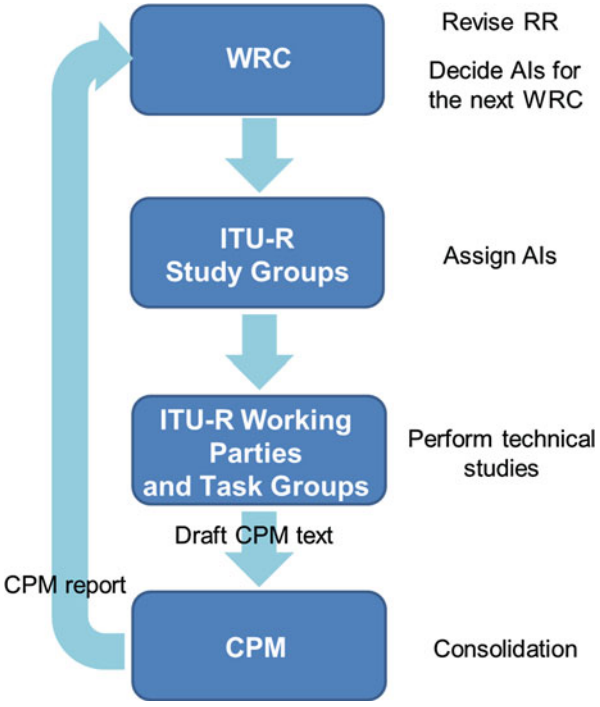

Fig. 1 The ITU-R process for revision of RR

regulatory framework with respect to the evolution of existing, emerging, and future applications, systems, and technologies. The WRC is organized to deal with topics covered by different agenda items (AI), and the previous WRC specifies the AIs for the next WRC. These AIs are assigned to different working parties (WP) or task groups (TG) by study groups (SG) where the actual preparatory work is carried out. WPs and TGs are responsible for technical studies for the AIs, such as sharing and coexistence studies between different radiocommunication services when preparing for new spectrum allocations. Detailed sharing considerations related to the specific implementation of the bands are left to the regional and national regulatory bodies. The results of the WRC preparatory studies from the various WPs and TGs are provided to the Conference Preparatory Meeting (CPM) prior to the WRC in the form of draft CPM text. The CPM then prepares a consolidated report on the ITU-R preparatory studies and possible solutions to the WRC AIs.

In addition to maintaining and revising process of RR through the WRCs, ITU-R promotes the development of radio systems and their new technologies to ensure the efficient use of the radio spectrum by studying technical and spectrum management related aspects in various SGs. The results of these studies are published in reports, handbooks, and recommendations. Best practices of spectrum usage are collected and disseminated in workshops, seminars, and publications. The current study groups of the ITU-R are [4]:

- SG1: Spectrum management,
- SG3: Radiowave propagation,
- SG4: Satellite services,
- SG5: Terrestrial services,
- SG6: Broadcasting service,
- SG7: Science services.

The study groups are presented in more detail in [4]. The key tool for the organization of these studies at the ITU-R is the Radiocommunication Assembly (RA) that is responsible for the structure, program, and approval of radiocommunication studies. RAs are normally convened held every four years and often associated in time and place with WRCs. The RAs determine the questions to be studied in detail in the different study groups of the ITU-R, assign WRC conference preparatory work and other questions to the study groups, and respond to other requests. RAs also acts as the forum to approve and issue ITU-R recommendations and questions developed by the study groups, to set the program for study groups, and to reshape the study group structure.

The ITU-R has developed its terminology for the global governance of the radio spectrum to fulfill policy making goals which can differ from the terminology defined and used in the research domain. For example, the ITU-R terminology on spectrum allocations in terms primary and secondary differs from those that were commonly used in the wireless communications research literature on cognitive radios. According to the ITU-R terminology used in the RR [8], “stations of

secondary service shall not cause harmful interference to stations of primary services to which frequencies are already assigned or to which frequencies may be assigned at a later date." In addition, they "cannot claim protection from harmful interference from stations of a primary service to which frequencies are already assigned or may be assigned at a later stage". However, "stations of a secondary service can claim protection from harmful interference from stations of the same or other secondary service(s) to which frequencies may be assigned at a later date" [8].

Interference is defined in RR [8] as "the effect of unwanted energy due to one or a combination of emissions, radiations, or inductions upon reception in a radiocommunication system, manifested by any performance degradation, misinterpretation, or loss of information which could be extracted in the absence of such unwanted energy". Harmful interference is interference "which endangers the functioning of a radionavigation service or of other safety services or seriously degrades, obstructs, or repeatedly interrupts a radiocommunication service operating in accordance with Radio Regulations" [8].

The dynamic spectrum sharing work in the form of cognitive radio technology development originally initiated in the research domain has been vetted into the ITU-R process of going through studies to become part of the global spectrum regulatory framework. In fact several of the study groups within the ITU-R and the key events (WRC and RA) have been involved in this process. In particular, spectrum sharing using cognitive radio system (CRS) technologies has been studied at the ITU-R in several groups from different perspectives. In the following, we present these groups and their activities describing their activities around CRS and dynamic spectrum sharing.

Overview of Dynamic Spectrum Sharing Related Studies at ITU-R

Cognitive radio research has considered new innovative ways of accessing the radio spectrum to improve the spectrum utilization efficiency. In the early cognitive radio studies, the system models assumed that the wireless devices themselves could decide on starting to transmit in a frequency channel based on observing the status of the outside world [9]. More specifically, the devices could dynamically share the spectrum by opportunistically accessing channels with the aid of spectrum sensing techniques to protect incumbent primary users by avoiding occupied channels. These approaches made the inherent assumption on the use of spectrum sensing techniques as the mechanism for the protection of incumbent systems from harmful interference. However, the link between what harmful interference meant in the technical studies in the research domain and in the regulatory domain was vague. Thus, early on for promoting real-life deployment of the cognitive radio technology, there was the need to introduce the cognitive radio principles developed in the research domain into the spectrum regulatory process in the global level.

As a concrete step, the ITU-R decided at its WRC in 2007 (WRC-07) to address the topic of cognitive radio at the following WRC in 2012 (WRC-12). The agenda item 1.19 of WRC-12 was *to consider regulatory measures and their relevance, in order to enable the introduction of software-defined radio and cognitive radio systems, based on the results of ITU R studies, in accordance with Resolution 956 (WRC 07)*. WRC-07 adopted Resolution 956 [10] that invited the ITU-R to study the need for regulatory measures for cognitive radio system (CRS) and software-defined radio (SDR). The responsibility on the spectrum management related aspects of CRS was assigned to SG1 and specifically its working party 1B (ITU-R WP1B), while the technical studies on its use particularly in the land mobile service were to be conducted in SG5 by its working party 5A (ITU-R WP5A).

Prior to WRC-07, the RA in 2007 (RA-07) issued Question ITU-R 241 [11] on studies of cognitive radio systems in the mobile service. This question seek to obtain answers to ITU definition of cognitive radio systems; closely related radio technologies and their functionalities; key technical characteristics, requirements, performance, and benefits; and potential applications of cognitive radio systems and their impact on spectrum management, operational implications, and cognitive capabilities that could facilitate coexistence. As the ITU-R Question 241 [11] was specifically focused on the use of cognitive radio systems within the mobile service, it was the topic of SG5 and particularly its working party ITU-R WP5A and ITU-R WP5D regarding the land mobile service and IMT systems, respectively.

As a starting point for the preparations for WRC-12, the ITU-R WP1B defined cognitive radio system (CRS) in 2009 in [12] as "A radio system employing technology that allows the system to obtain knowledge of its operational and geographical environment, established policies and its internal state; to dynamically and autonomously adjust its operational parameters and protocols according to its obtained knowledge in order to achieve predefined objectives; and to learn from the results obtained." [12] Technical studies used as a basis for the AI on CRS were conducted in ITU-R WP5A and WP5D, and the results of these studies were contained in reports [13] and [14], respectively. These reports included deployment scenarios, capabilities, as well as potential challenges and benefits arising from the cognitive technologies. These three ITU-R reports formed the basis for CPM text for the AI on cognitive radio for WRC-12.

As a result, the WRC-12 concluded that the introduction of CRSs does not require any changes to the RR and developed a WRC recommendation on the deployment and use of CRSs [15]. In fact, it was clarified that a CRS is not a radiocommunication service, but rather a system that employs technology that in the future may be implemented in a wide range of applications in the land mobile service. The WRC-12 concluded that any radio system implementing CRS technology needs to operate in accordance with the RR and that the obligations on the protection of stations of other administrations operating in accordance with the RR still hold.

However, it was determined that further studies would be required to explore the potential of cognitive radios. As a result, RA-12 developed Resolution

ITU-R 58 [16] regarding further studies on the implementation and use of cognitive radio systems which instructed the ITU-R to continue with the CRS studies. It urged the ITU-R to study operational and technical requirements, characteristics, performance, and possible benefits associated with the implementation and use of CRS in relevant radiocommunication services and related frequency bands and to give particular attention to enhancing coexistence and sharing among radiocommunication services [16]. The need for the further studies on CRS presented in ITU-R Resolution 58 [16] was further confirmed at the WRC in the development of WRC recommendation [15] that recommended administrations to actively participate in the studies. In fact, the resolution triggered a number of studies that are described in more detail in this chapter. The resolution was further updated in 2015.

To conclude, the studies on CRS at the ITU-R were based on responding to the topics raised in ITU-Resolution 58 [16] and ITU-R Question 241 [11]. In the course of work, ITU-R Resolution 58 [16] was updated in 2015 after its initial launch in 2012, and ITU-R Question 241 [11] was updated in 2012 and 2015 after its launch in 2007. The spectrum management related work is conducted in SG1 and particularly ITU-R WP1B. While the scope of ITU-R Resolution 58 [16] was more generic on the implementation and use of CRS in different radiocommunication services, the focus of Question ITU-R 241 [11] was specific to the mobile service. In fact the technical CRS related work within the ITU-R was mainly focused on the land mobile service while applications to other radiocommunication services are also possible. Thus, the technical work was mainly done in SG5. In particular, the ITU-R WP5A developed two reports on CRS in the land mobile service [13, 17], and ITU-R WP5D one report on CRS specific to IMT systems [14]. Moreover, other ITU-R study groups started to address the topic of CRS from the perspective of being impacted by CRS. For example, ITU-R WP5C studied the impact of CRS on the fixed service and started to prepare a report on it. In SG6, ITU-R WP6A started to study potential interference into broadcasting from CRS devices in the 470–790 MHz band and prepare a report on it but later ended the work.

The cognitive radio studies in the research domain were often motivated by measurements on the spectrum occupancy in different frequency bands in different countries [18]. The spectrum measurement and monitoring related activities within the ITU-R are dealt within ITU-R WP1C. In fact there were ITU-R studies that are directly related to the measurements conducted by the researchers providing guidelines responding to two ITU-R questions [19, 20]. ITU-R Question 233 [19] was originally assigned in 2007 and updated in 2011 and extended in 2015 on the measurement of spectrum occupancy. ITU-R Question ITU-R 235 [20] from 2011 and extended in 2015 dealt with spectrum monitoring evolution. It specifically addresses monitoring from the administrations' perspective regarding new considerations for monitoring of radiocommunication systems based on new technologies.

In the following sections, we will describe the studies related to CRSs in the mobile service and other related spectrum management studies in more detail.

CRS in Land Mobile Service

The technical studies on CRS at the ITU-R have focused on the use of CRS technology within the mobile service in response to ITU-R Question 241 [11]. This section reviews the work done at the ITU-R WP5A that resulted in two published reports on CRS in the land mobile service [13, 17]. The first report ITU-R Report M.2225 [13] was published in 2011, and it addressed a subset of the questions of the first version of ITU-R Question 241 [11] and provided technical features and capabilities, potential benefits, technical challenges, and deployment scenarios for CRS. The second report ITU-R Report M.2330 [17] addressed the updated questions in Question ITU-R 241 [11] from 2012 that asked the ITU-R to study closely related radio technologies and their functionalities; key technical characteristics, requirements, performance improvements, and/or other benefits; potential applications of CRS and their impact on spectrum management; how CRS promote efficient use of spectrum; operational implications (including privacy and authentication); CRS cognitive capabilities and CRS technologies that could facilitate sharing and coexistence between the mobile service and other services; and factors to be considered for the introduction of CRS technologies in the land mobile service.

As the starting point for the studies, ITU-R WP5A used the ITU-R definition for CRS [12] that identified three key CRS capabilities: (1) obtaining knowledge, (2) decision-making and adjustment, and (3) learning. These general capabilities could be applied to different systems in different bands on a case-by-case basis, and within these capabilities, there are several individual techniques. For example, knowledge of spectrum availability for sharing could be obtained via control channels, databases, or spectrum sensing techniques. Decision-making can take centralized or distributed forms, and the parameter to be decided can include frequency channels or power levels for operations among others.

The initial benefits of CRS to operators and end users were depicted in Report ITU-R M.2225 [13]. They include improvements in the efficiency of spectrum use; increased flexibility, self-correction, and fault tolerance; resilience in disaster or emergency situation; improved power efficiency; and potential for new mobile communication applications. The report [13] further identified four CRS deployment scenarios:

1. Use of CRS technology to guide reconfiguration of connections between terminals and multiple radio systems,
2. Use of CRS technology by an operator of a radiocommunication system to improve the management of its assigned spectrum resource,
3. Use of CRS technology as an enabler of cooperative spectrum access,
4. Use of CRS technology as an enabler for opportunistic spectrum access in bands shared with other systems and services.

The first two scenarios address an intra-system situation where an operator can use CRS technology to obtain more efficient use of resources within its networks.

The latter two are intersystem scenarios that involve spectrum sharing between different operators and systems. In the third scenario, wireless systems collaborate and exchange information about their spectrum use in order to avoid mutual interference. In the fourth scenario, CRSs may access unused spectrum band on a shared basis without causing harmful interference to other systems which resembles the traditional cognitive radio use cases extensively considered in the research domain. Scenarios are also discussed in [21, 22].

ITU-R WP5A continued the work in ITU-R Report M.2330 [17] that was published in 2014 providing answers to the remaining topics of the updated ITU-R Question 241 [11]. The report [17] introduced applications of CRS, details of CRS capabilities and enabling technologies, high-level characteristics, high-level technical and operational requirements, aspects related to CRS performance, potential benefits, factors related to introduction of CRS, and migration issues.

CRS Applications

ITU-R Report M.2330 [17] specifically addressed spectrum sharing where two or more radio systems operate in the same frequency band as well as coexistence where two or more radio systems operate in adjacent frequency bands. Noting that CRSs could share spectrum with other radio systems that are not necessarily CRSs, as well as with other CRSs, the report introduced two general level spectrum sharing cases:

- *Vertical spectrum sharing*: The case where one or more radio systems with CRS capabilities share the band of another radio system that does not necessarily have CRS capabilities. The radio systems with CRS capabilities are only allowed to utilize frequencies within the band as long as the other radio system is not affected by harmful interference from the CRSs;
- *Horizontal spectrum sharing*: The case where multiple radio systems with CRS capabilities are accessing the same shared spectrum band.

Figure 2 illustrates vertical and horizontal spectrum sharing cases where horizontal spectrum sharing refers to systems operating with the same level of access rights, while vertical spectrum sharing introduces sharing between systems with different levels of spectrum access rights. Horizontal and vertical spectrum sharing are not mutually existing, and both of them can be simultaneously present in various forms in practical applications. Report ITU-R M.2330 [17] identified the following benefits related to vertical and horizontal spectrum sharing:

- Interference minimization: The CRS capability of obtaining knowledge, for example, using databases can give information on the current protection requirements thus allowing the radio systems to adapt their operations in accordance within the given rules and policies.
- Efficient spectrum use: Additional spectrum can be made available by allowing radio systems to share spectrum with other radio systems leading to increase

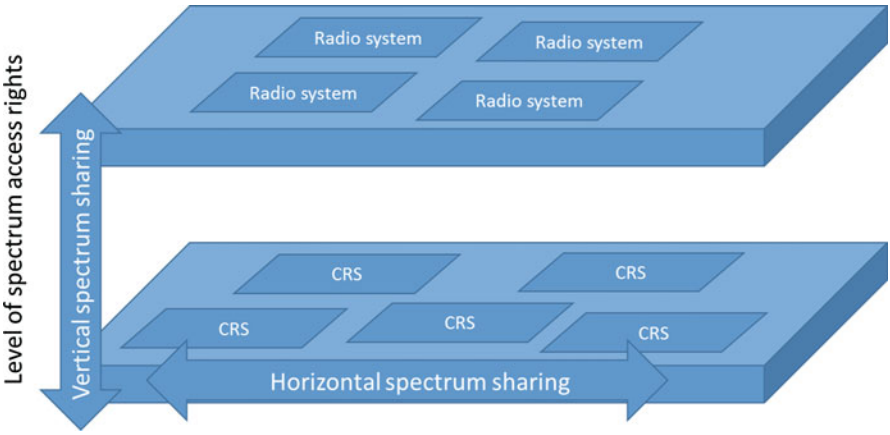

Fig. 2 Horizontal and vertical spectrum sharing in the context of CRSs

efficiency of spectrum use which can lead to capacity enhancements for the systems employing CRS technologies.

– Flexible operations: In sharing and coexistence situation, CRS system is flexible and could operate over various system configurations, and information shared between the involved CRS nodes would ensure that the relevant nodes have the most accurate information of available spectrum in a timely manner.

The Report ITU-R M.2330 [17] introduced a collection of CRS applications including existing, emerging, and potential applications. An existing application is the radio local area network (RLAN) system operating in the 5250–5350 MHz and 5470–5725 MHz bands on a co-primary basis with radiolocation systems and radar utilizing dynamic frequency selection (DFS) protocol to avoid harmful interference. The RLAN is required to use DFS to ensure by sensing/detection techniques that radiolocation systems are not operating in the same channels and vacate the channels when they appear as described in [23].

An emerging application is the use of TV white space which according to [13] refers to "A portion of spectrum in a band allocated to the broadcasting service and used for television broadcasting that is identified by an administration as available for wireless communication at a given time in a given geographical area on a non-interfering and non-protected basis with regard to other services with a higher priority on a national basis." Some administrations are allowing license-exempt devices to operate on a non-interfering basis in these TV white spaces with the help of CRS capability of geolocation with database access.

Examples of potential CRS applications identified in [17] include cognitive networks exploiting reconfigurable nodes, cognitive mesh networks, heterogeneous system operation using CRS capabilities, intra-system inter-RAT handover, inter-system handover, coordinated spectrum access in heterogeneous radio environment, and vertical and horizontal spectrum sharing enabled by CRS technologies. Several

examples of the last application are under study by several administrations to allow additional users to access spectrum with existing incumbent usage with the help of CRS to provide appropriate protection of other radio systems. These examples include Licensed Shared Access (LSA) in Europe and Citizens Broadband Service (CBRS) in the USA.

CRS Capabilities

Report ITU-R M.2330 [17] also elaborated the CRS capabilities identified in [12,13] and provided detailed descriptions of the three key capabilities and their enabling technologies which are depicted in Fig. 3. For obtaining knowledge of its operational and geographical environment, established policies, and its internal state, the CRS can listen to wireless control channels, use spectrum sensing techniques, and/or access databases. Examples of wireless control channels include cognitive control channel (CCC) and cognitive pilot channel (CPC). CCC aims at enhancing coordination between the CRS devices by providing real-time communication channel between distributed CRS nodes within a specific geographic area. CPC is a pilot channel that broadcasts radio environment information to CRS devices. Challenges of using wireless control channels for obtaining knowledge of the operational environment include power consumption, synchronization between nodes, contention resolution mechanisms, reliability of information, and strict requirements for timeliness of the data.

Spectrum sensing is another enabling technique identified in [17] for obtaining knowledge and has been widely studied in the cognitive radio research [1, 2, 9]. Spectrum sensing is the capability to detect other signals around the CRS node. There are different sensing techniques with varying sensing capabilities, requirements for a priori information, and degrees of complexity. Moreover, the use of sensing techniques can be with single or multiple devices and by CRS nodes themselves or by dedicated listening devices or community sensor networks. There are several challenges related to the use of spectrum sensing for obtaining knowledge or the operational environment including hidden node problem, reliability of sensing, implementation of particularly wideband sensing, power and processing consumption, signaling cost, performance in realistic settings, and detection of receive-only nodes. The report discussed that the implementation of opportunistic spectrum access could not rely solely on spectrum sensing techniques but would additionally require alternative methods.

The third technique for obtaining knowledge in [17] is the use of databases often combined with geolocation capability where the CRS node knows its location. CRS nodes can access a database that provides information about the locally usable frequencies ensuring that incumbent services remain protected from harmful interference. Databases can provide information of vacant frequency channels as well as the rules related to the use of the channels in certain locations. Many of the CRS applications introduced previously such as TV white space, LSA, and CBRS have taken the database approach. The implementation can take various forms such

as single open database, multiple open databases, proprietary close databases, or clearinghouse that aggregates and host raw data from multiple providers. Definition of open interfaces and protocols is important for allowing different types of CRS nodes to access different databases. Challenges for the database approach with geolocation include, e.g., timely update of data, availability of information about the stations to be protected, and security and privacy aspects.

The CRS capability of decision-making and adjustment of operational parameters and protocols (see Fig. 3) discussed in Report ITU-R M.2330 [17] involves the CRSs to take actions in link level and network level that take into account underlying policies in the dynamic operational environment. The report identifies centralized and distributed decision-making techniques and provides examples of channel selection and cognitive network management for CRS in the land mobile service. Centralized decision-making assumes a centralized entity for decision-making that informs the CRS nodes about adaptations of operational parameters such as spectrum resources. Distributed decision-making is based on localized decisions of distributed CRS nodes which can involve coordination between nodes. In the case of spectrum sharing, decision-making can involve the selection of channels for operation. Moreover, for dynamic adjustment of reconfigurable nodes in a network, cognitive network management functions are needed.

Finally, learning as a CRS capability can enable performance improvement by allowing the CRS to use stored information of its own actions and other's actions and the results of the actions to help in the decision-making process. Learning can make the operations of the CRS more efficient by, e.g., improving fault tolerance,

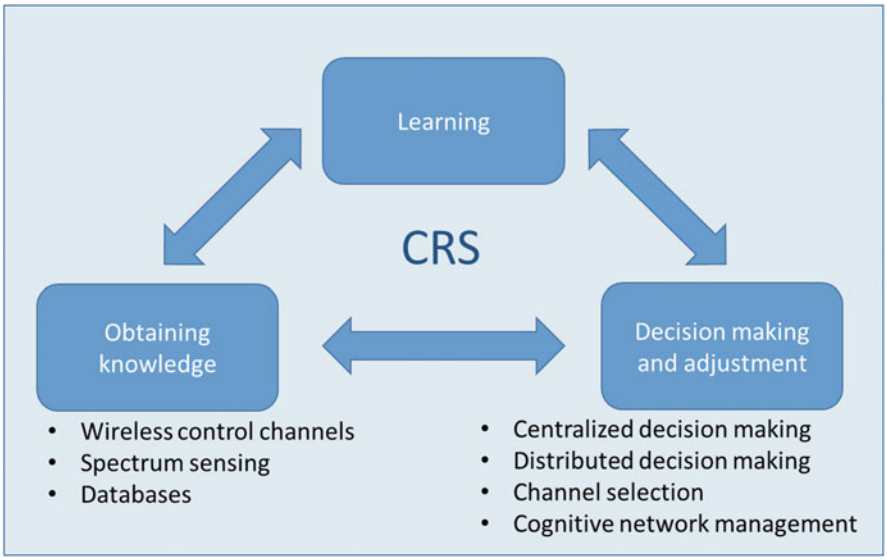

Fig. 3 CRS capabilities and enabling technologies

learning traffic patterns in different frequency channels for channel selection, and enhancing network management to adjust to different requirements.

CRS Characteristics, Requirements, and Performance Aspects

CRS introduces new high-level characteristics over conventional radio systems including aspects related to flexible spectrum management in temporal, frequency, and geographical domains to improve spectrum efficiency and dynamic coordination among radio systems to facilitate spectrum sharing and coexistence [17]. More accurate knowledge of the characteristics and operations of other systems combined with dynamic interference management could help the CRSs to avoid causing harmful interference and share the spectrum more efficiently in horizontal and vertical spectrum sharing cases.

New requirements for CRSs over traditional radio systems arise from CRS internal operations as well as from interactions with other systems operating in the same channel or adjacent channel in spectrum sharing and coexistence cases, respectively. Horizontal and vertical spectrum sharing and coexistence with other systems set requirements on the CRSs requesting them to support specific technical features and functionalities to avoid harmful interference to other radio systems with same level or higher level of spectrum usage rights in dynamic conditions where the spectrum use of the channels changes.

CRSs that introduce radio operations with dynamic availability of spectrum call for new metrics to characterize the system internal performance, interference considerations in spectrum sharing and coexistence between radio systems, and overall spectrum usage efficiency. Initial benefits from [13] are expanded in [17] specifically to vertical and horizontal spectrum sharing cases which were discussed above. In addition, CRS can provide benefits for operators by introducing dynamic spectrum reconfiguration, radio resource optimization, and dynamic device context provision. Finally, introduction of CRS capabilities into the land mobile service introduces migration aspects which were also discussed in [17] including inclusion of information exchange between different systems to facilitate spectrum sharing.

CRS for IMT Systems

The International Mobile Telecommunications (IMT) systems, the ITU-R terminology encompassing the mobile communication networks from 3G to upcoming 5G, are addressed in ITU-R WP5D. While majority of the studies on cognitive radio techniques at the ITU-R was focused on mobile communication systems in response to ITU-R Question 241 [11] encompassing both IMT and non-IMT systems, the IMT specific work on spectrum sharing and CRS remained limited. In fact in the research domain, a lot of effort was put on developing cognitive radio techniques for cellular systems where spectrum sharing was assumed between operators or between cellular systems and other systems. However, the work at the ITU-R on

CRS specific for IMT systems resulted in only one report ITU-R M.2242 developed by the ITU-R WP5D in 2011 [14]. The report studied the impact of adding CRS capabilities to existing IMT systems, and analyzed the benefits, challenges and impacts of CRSs in IMT, particularly regarding the impact on the use of IMT spectrum. The report emphasized that an IMT system employing CRS technology should still meet the minimum requirements for IMT systems and that the existing IMT systems should not suffer from harmful interference and quality-of-service (QoS) degradation from the introduction of CRS technology.

The report [14] took a very cautious view on what CRS could mean for IMT systems and only focused on single-operator scenarios where an operator would use CRS technology to enhance its own performance as the exclusive owner of the spectrum. The report preferred the operator centric intra-operator approach as the scenario for IMT to benefit from some CRS capabilities. It is restricted to improvement in the spectrum usage efficiency by accessing spectrum resources from one IMT system for other IMT systems inside the domain of a single operator. The report [14] identified the following scenarios for CRS in IMT systems:

1. Update of a network for optimized radio resource usage,
2. Upgrade of an existing radio interface or a network with a new radio interface,
3. In-band coverage/capacity improvement by relays,
4. Self-configuration and self-optimization of femtocells,
5. Multimode coexistence and simultaneous transmission.

The intra-operator scenarios involved cases where an operator who is the exclusive owner of the spectrum may use cognitive radio features to better manage its heterogeneous radio access networks. CRS scenarios for IMT are also discussed in [24].

The report identified benefits from CRS in IMT in the intra-operator case and in terms of overall spectrum efficiency and capacity improvement, radio resources utilization flexibility, and interference mitigation. The report concluded that the introduction of CRS in IMT systems in intra-operator case is the preferred scenario which did not include vertical or horizontal spectrum sharing. Even in that case, a concern is to ensure that existing radio systems do not suffer from harmful interference or QoS degradation from CRS technology, which shows the caution of the operators about the topic.

There has been a lot of work at the ITU-R on sharing and compatibility studies between IMT systems and other radiocommunication systems for the potential use of IMT systems in the bands currently used by other services. These studies take into account the characteristics of the IMT systems and the other systems to identify the potential interferences between the systems. They typically identify for protection criteria in terms of, e.g., separation distance, transmission power limit, interference mitigation techniques, and feasibility of sharing. These studies typically characterize the static situations without the use of CRS capabilities and dynamic spectrum sharing as such. To some extent, they have taken into account the use of interference mitigation techniques which has seen to reduce the protection

distances. In fact the CRS capabilities could help in the sharing studies to relax the conditions and improve opportunities for sharing and coexistence between different radio systems.

The most recent IMT developments are now focusing on the fifth generation (5G) of mobile communication systems denoted as IMT-2020 at the ITU-R. The IMT the work at the ITU-R is specifically addressing the preparations for WRC-19 AI 1.13 about the possible new spectrum allocations for IMT systems in the frequency range between 24 and 86 GHz.

Spectrum Management Related Studies at ITU-R

While the technical studies on CRS were conducted in SG5 of the ITU-R, spectrum management related aspects of CRS belong to SG1. The CRS related spectrum measurement studies and new spectrum management principles studied at SG1 are reviewed next.

Spectrum Measurements and Occupancy Studies

Many of the cognitive radio studies in the research domain were motivated by spectrum measurement studies conducted by research people where the spectrum occupancies of different frequency bands were analyzed as summarized in [18]. In fact a number of spectrum measurement campaigns were conducted around the world to quantify the percentage of time that the received signal levels exceed some threshold giving an indication of the channel occupancies. The main findings from the research studies indicated very low levels of spectrum occupancy in many bands which gave motivation for the studies to introduce dynamic spectrum sharing in bands with low occupancy levels. While these measurements were mainly done by the research community, spectrum measurement and monitoring had been a standard tool in the spectrum regulatory domain for a long time. However, the basic guidelines developed in the regulatory domain were not applied to a large extent in the research domain.

At the same time, as the CRS studies were conducted at the ITU-R, there were studies about the measurement of spectrum occupancy and spectrum monitoring that took place in SG1. In fact, studies addressed two ITU-R questions, ITU-R Question 233 [19] about measurement of spectrum occupancy and ITU-R Question ITU-R 235 [20] on spectrum monitoring evolution. ITU-R Question 233 [19] originated from RA-07 and was updated in 2011 and expanded in 2015. It called for identifying techniques to perform frequency channel and frequency band occupancy measurements including processing and presentation methods. It also seek to define the term "occupancy" for frequency channel and frequency band measurements and define and apply threshold levels in practical situations. Question ITU-R 235 [20] initiated in 2011 was extended in 2015 and focused on spectrum monitoring evolution with the advent of new technologies. It looked for

new considerations for monitoring of radiocommunication systems including new approaches in terms of organization, procedures, and equipment to monitor systems based on future radiocommunication technologies. It is particularly concerned with the administrations' positions and seeks for the needs for administrations in order to implement the new approaches to monitor systems based on future radiocommunication technologies.

The studies have resulted in several reports and recommendations published by the ITU-R [25–28]. Recommendation ITU-R SM.2039 [25] on spectrum monitoring evolution published in 2013 provides answers to Question ITU-R 235 [20] and recommends new technologies to be used in spectrum monitoring evolution to extend monitoring coverage including detection of weak signals, co-frequency signal separation, and multimode location based on a combination of techniques. Report ITU-R SM.2355 [26] published in 2015 highlights the role of spectrum monitoring as an important tool in the management of radio spectrum by providing monitoring data, including spectrum occupancy and characteristic of signal, such as field strength, bandwidth, modulation type, location of emitter, etc. The report addresses the challenges of future spectrum monitoring systems that should have the capability for monitoring new radiocommunication technologies and systems including those with CRS capabilities, such as detection of weak signal, co-frequency signal separation, and multimode location based on digital signal processing and network. The report also provides examples of advanced monitoring techniques.

Recommendation ITU-R SM.1880 [27] on spectrum occupancy measurement and evaluation originally published in 2011 and revised in 2015 specifies the measurement procedures and techniques in response to Question ITU-R 233 [19]. It recommends the use of Report ITU-R SM.2256 [28] and ITU-R Handbook on spectrum monitoring [29] to be used as guidance and equipment that should fulfill the requirements set in those documents. Report ITU-R SM.2256 [28] on spectrum occupancy measurement and evaluation was published in 2012 and further updated in 2016. The report provides a comprehensive description of spectrum occupancy measurement terminology and methodology and acts as the guideline for conducting spectrum occupancy measurements. The report includes relevant terminology, measurement parameters, measurement procedure, calculation of occupancy, presentation of results, as well as interpretation and use of results. Finally, the ITU-R Handbook on spectrum monitoring [29] whose latest edition is from 2011 contains ITU-R guidelines for monitoring.

New Spectrum Management Principles

In ITU-R, the nontechnical spectrum management related issues are handled in the WP 1B "Spectrum management methodologies and economic strategies" of SG1. The WP1B considers, for example, spectrum management fundamentals, methodologies, as well as both national and international regulatory frameworks. The studies performed in this WP are done in a technology and service neutral

manner. After completing of the preparatory work for WRC-12 on CRS, the WP1B is currently working on two reports regarding more dynamic spectrum use. Similarly to prior studies on the CRS, the first report is being developed in response to ITU-R Resolution 58 [16]. This current working document toward a preliminary draft new (PDN) report on spectrum management challenges [30] is addressing spectrum management principles and spectrum engineering techniques for the dynamic access to spectrum by radio system employing CRS capabilities. Whereas the previous CRS reports were service specific and concentrated on the technical aspects of CRS developed in ITU-R WP5A and ITU-R WP5D, the focus of this report is to study general framework and highlight some challenges related to CRS techniques including the means to ensure the protection of incumbent services sharing the same band or operating in the adjacent bands.

The second working document toward a PDN report on innovative regulatory tools [31] is being developed within the framework of an ITU-R Question 208-1/1 [32] "Alternative methods of national spectrum management." This report aims to provide a collection of regulatory mechanisms which may be implemented on a national basis that have been experimented and are recognized as best practices in terms of spectrum management solutions by administrations. Currently, the draft report includes the European LSA approach and an approach to share spectrum between multiple mobile operators.

Conclusions and Future Outlook

At the international level, the ITU-R has developed general guidelines for dynamic spectrum sharing using the CRS technology. These guidelines form the ground for spectrum sharing in the global scale. The main conclusions of the CRS work for WRC-12 was that the introduction of CRS does not require any changes to the RR and that a system employing CRS technology needs to operate in accordance with the RR.

As defined by the ITU-R, the CRS is a set of capabilities for obtaining knowledge, decision-making and adjustment, and learning, which can be applied to different radiocommunication services. The CRS work within the ITU-R mainly focused on the land mobile service while applications to other radiocommunication services are also seen possible. The ITU-R introduced vertical and horizontal spectrum sharing applications where the distinction comes from the different levels of spectrum usage rights between the wireless systems operating in the same spectrum band.

In fact the ITU-R guidelines for CRS have been there for a few years now. ITU-R studies on CRS capabilities expanded the considerations from pure spectrum sensing techniques to wireless control channels and databases. In the research domain, the interest in pure cognitive radio technology has shifted to the development of specific spectrum sharing models that exploit CRS capabilities. At the same time, these sharing models have been introduced at the ITU-R level to exchange information about new spectrum management approaches. The role of the ITU-R

continues to be the global forum for gathering and disseminating best practices, providing place for discussions by all stakeholders, and conducting studies of technical and spectrum management aspects.

The development of fifth generation (5G) networks is a major ongoing effort in research, industry, and regulatory domains regarding future mobile communication systems. While the prior work carried out in the scope of CRS specific to the IMT systems at the ITU-R remained limited and focused only on intra-operator scenarios, spectrum sharing will have a more prominent role in 5G. In the future, spectrum sharing will find new application areas in the development and deployment of 5G networks. 5G networks are envisaged to be deployed in a wide variety of frequency bands ranging from the existing bands with mobile allocation toward higher frequency range between 24 and 86 GHz studied for WRC-19. In the context of 5G, spectrum sharing in vertical and horizontal dimensions will play an increasingly important role to allow efficient utilization of the spectrum for the different stakeholders. Operations in these higher frequencies will call for new models and techniques for both horizontal and vertical spectrum sharing to allow local deployments and to protect possible incumbents, respectively.

References

1. Yücek T, Arslan H (2009) A survey of spectrum sensing algorithms for cognitive radio applications. IEEE Commun Surv Tutorials 11(1):116–130
2. Akyildiz IF, Lee WY, Vuran MC, Mohanty S (2008) A survey on spectrum management in cognitive radio networks. IEEE Commun Mag 46:40–48
3. ITU-R (2014) ITU-R Radiocommunication. Committed to connecting the world. International Telecommunications Union Radiocommunication sector. Available at http://www.itu.int/dms_pub/itu-r/opb/gen/R-GEN-OVW-2014-PDF-E.pdf
4. ITU-R (2013) ITU-R study group booklet. International Telecommunications Union Radiocommunication sector. Available at http://www.itu.int/dms_pub/itu-r/opb/gen/R-GEN-SGB-2013-PDF-E.pdf
5. ITU-R (2017) Welcome to the ITU-R. International Telecommunications Union Radiocommunication sector. Available at http://www.itu.int/en/ITU-R/information/Pages/default.aspx
6. Dietz T, Ostrom E, Stern PC (2003) The struggle to govern the commons. Science 302: 1907–1912
7. Weiss MBH, Lehr WH, Acker A, Gomez MM (2015) Socio-technical considerations for Spectrum Access System (SAS) design. In: IEEE International Symposium on Dynamic Spectrum Access Networks (DySPAN), Stockholm, pp 35–46
8. ITU (2016) The Radio Regulations. International Telecommunications Union Radiocommunication sector, Geneva
9. Haykin S (2005) Cognitive radio: brain-empowered wireless communications. IEEE J Sel Areas Commun 23:201–220
10. ITU-R (2007) Regulatory measures and their relevance to enable the introduction software-defined radio and cognitive radio systems. Resolution 956 (WRC-07). International Telecommunication Union Radiocommunication sector
11. ITU-R (2015) Cognitive radio systems in the mobile service. ITU-R Question 241-3/5. International Telecommunication Union Radiocommunication sector
12. ITU-R (2009) Definitions of software-defined radio (SDR) and cognitive radio system (CRS). Report ITU-R SM.2152. International Telecommunications Union Radiocommunication sector

13. ITU-R (2011) Introduction to cognitive radio systems in the land mobile service. Report ITU-R M.2225. International Telecommunications Union Radiocommunication sector
14. ITU-R (2011) Cognitive radio systems specific for International Mobile Telecommunications systems. Report ITU-R M.2242. International Telecommunications Union Radiocommunication sector
15. ITU-R (2012) Deployment and use of cognitive radio systems. Recommendation 76 (WRC-12). International Telecommunications Union Radiocommunication sector
16. ITU-R (2012) Studies on the implementation and use of cognitive radio systems. ITU-R Resolution 58. International Telecommunications Union Radiocommunication sector
17. ITU-R (2014) Cognitive radio systems in the land mobile service. Report ITU-R M.2330. International Telecommunications Union Radiocommunication sector, Geneva
18. Höyhtyä M, Mämmelä A, Eskola M, Matinmikko M, Kalliovaara J, Ojaniemi J, Suutala J, Ekman R, Bacchus R, Roberson D (2016) Spectrum occupancy measurements: A survey and use of interference maps. IEEE Commun Surv Tutorials 18:2386–2414
19. ITU-R (2011) Question ITU-R 233-1/1. International Telecommunications Union Radiocommunication sector
20. ITU-R (2011) Spectrum monitoring evolution. Question ITU-R 235/1. International Telecommunications Union Radiocommunication sector
21. Mustonen M, Matinmikko M (2014) Scenarios for CRS from ITU-R. In: Medeisis A, Holland O (eds) Cognitive radio policy and regulation: techno-economic studies to facilitate dynamic spectrum access. Springer, Cham
22. Filin S, Murakami H, Harada H, Yoshino H, Kashiki K, Shibata T (2011) ITU-R standardization activities on cognitive radio systems. In: 6th International ICST Conference on Cognitive Radio Oriented Wireless Networks and Communications (CROWNCOM), Osaka, pp 116–120
23. ITU-R (2011) Dynamic frequency selection in wireless access systems including radio local area networks for the purpose of protecting the radiodetermination service in the 5 GHz band. Recommendation ITU-R M. 1652-1. International Telecommunications Union Radiocommunication sector
24. Sayrac B, Uryga H, Bocquet W, Cordier P, Grimoud S (2013) Cognitive radio systems specific for IMT systems: operator's view and perspectives. Telecommun Policy 37:154–166
25. ITU-R (2013) Spectrum monitoring evolution. Recommendation ITU-R SM.2039. International Telecommunications Union Radiocommunication sector
26. ITU-R (2015) Spectrum monitoring evolution. Report ITU-R SM.2355. International Telecommunications Union Radiocommunication sector
27. ITU-R (2015) Spectrum occupancy measurement and evaluation. Recommendation ITU-R SM.1880-1. International Telecommunications Union Radiocommunication sector
28. ITU-R (2016) Spectrum occupancy measurements and evaluation. Report ITU-R SM.2256-1. International Telecommunications Union Radiocommunication sector
29. ITU-R (2011) Handbook on spectrum monitoring. International Telecommunications Union Radiocommunication sector
30. ITU-R (2016) Working Document toward PDNR SM. [CRS Spectrum Management Challenges]. International Telecommunication Union Radiocommunication sector
31. ITU-R (2016) Working Document toward PDNR SM. [Regulatory_Tools]. International Telecommunication Union Radiocommunication sector
32. ITU-R (2015) Alternative methods of national spectrum management. ITU-R Question 208-1/1. International Telecommunications Union Radiocommunication sector

ETSI-RRS Reconfigurable Radio Systems Standards

49

Markus Mueck

Contents

Abstract

The evolution of classical, static Radio Systems toward Reconfigurable Radio Systems is a clear trend in the industry for several reasons – first, the lack of spectral resources forces manufacturer to exploit novel technological trends in order to meet 5G-related promises in terms of quality of service, latency,

M. Mueck (✉)
Next Generation and Standards, INTEL Deutschland GmbH, Neubiberg, Germany
e-mail: Markus.Dominik.Mueck@intel.com

W. Zhang (ed.), *Handbook of Cognitive Radio*,
https://doi.org/10.1007/978-981-10-1394-2_48

reliability, etc. Second, the fast evolution and heterogeneous nature of the radio environment combined with an ever-increasing computation power in mobile devices call for new ways of ensuring that the diverse environment is exploited in the best possible way; software reconfigurability is the key to dynamically adapt any target device to the specific needs of its owner through installation of tailored and targeted software components. All this flexibility, however, is useless without access to real-time, reliable context information which feeds decision-making entities in the network and in the mobile device or implemented in a distributed way such that the network and mobile devices participate in the decision-making process. The European Commission has recognized this trend in an early stage and acted correspondingly. ETSI received EC Mandate M/512 "Standardisation Mandate to CEN, CENELEC and ETSI for Reconfigurable Radio Systems" which has led to the development of the Licensed Shared Access Spectrum Sharing solution in ETSI's Technical Committee Reconfigurable Radio Systems (TC RRS). Furthermore, the new Radio Equipment Directive creates a clear framework for Software Reconfigurable Radio Equipment in Europe. This section details the respective technical solutions and trends as they are currently being developed in ETSI standards.

Keywords
Cognitive radio systems · ETSI · Reconfigurable radio systems · Software reconfiguration · Spectrum sharing

Introduction

Within the European Telecommunications Standards Institute (ETSI), the Reconfigurable Radio Systems (RRS) Technical Committee (TC) is focusing on standardization activities in all relevant areas of Reconfigurable Radio Systems encompassing system solutions related to software-defined radio (SDR) and cognitive radio (CR). TC RRS is therefore the center of competence within ETSI for cognitive radio and Reconfigurable Radio Systems standards development. Still, TC RRS sees its activities to be horizontal across ETSI and thus interacts with other TCs as required in order to ensure the proliferation of RRS and CR technology.

This section summarizes available standards and ETSI activities in the space of RRS and CR technology. The key focus is in particular on:

- Reconfigurable Radio Systems and cognitive radio on a political, regulation, and standards level;
- Spectrum sharing, in particular Licensed Shared Access (LSA) and TV White Space (TVWS) access, as an enabler for future 5G capacity;
- Software reconfigurability of radio equipment, including mobile terminals as well as network equipment, in order to enable a dynamic adaptation to an ever-changing heterogeneous system environment.

Reconfigurable Radio Systems and Cognitive Radio on a Political, Regulation, and Standards Level

On a political and regulation level, a number of steps have been undertaken in order to accelerate the adoption of RRS and related technology in the European market. In the sequel, the following specific steps will be further outlined and commented:

- Through the publication of a novel *Radio Equipment Directive* [6], the European Commission has created an official framework for RRS and related technology. The conditions for granting access to the single European market are clearly defined and outlined.
- In *EC M/512 Standardisation Mandate To CEN, CENELEC and ETSI For Reconfigurable Radio Systems* [41], the European Commission has furthermore addressed all European Standards Organizations (ESOs), i.e., CEN, CENELEC, and ETSI, to develop Reconfigurable Radio Systems-related standards. In particular ETSI has answered to this request and has developed a series of standards in the field.
- The European Conference of Postal and Telecommunications Administrations (CEPT) has furthermore developed a regulation framework where required – this was in particular the case for Licensed Shared Access (LSA) and TV White Space (TVWS)-based spectrum sharing technology for which a number of *recommendations* and *decisions* were developed.
- The UK regulator, OFCOM UK, has taken the initiative within Europe to drive the adoption of TVWS technology [39, 48].
- The US Federal Communications Commission (FCC) has furthermore issued a series of rulings related to the usage of so-called TV White Space (TVWS) bands and related requirements, including the usage of TVWS databases [42].

As stated above, the European Commission has revised the *Radio and Telecommunication Terminal Equipment (R&TTE) Directive* [5] for the first time since 1999. It was replaced by the novel Radio Equipment Directive [6] which specifically includes provisions to enable the introduction of RRS technology onto the single European market. Note in particular articles (3)(3)(i) and 4 which address requirements related to software reconfiguration:

> *Article 3:* **Essential requirements**
>
> . . .
>
> *3. Radio equipment within certain categories or classes shall be so constructed that it complies with the following essential requirements:*
>
> . . .
>
> *(i) radio equipment supports certain features in order to ensure that* ***software can only be loaded*** *into the radio equipment where the* ***compliance of the combination of the radio equipment and software has been demonstrated***

Article 4: **Provision of information on the compliance of combinations of radio equipment and software**

1. Manufacturers of radio equipment and of software allowing radio equipment to be used as intended shall provide the Member States and the Commission with information on the ***compliance of intended combinations of radio equipment and software*** *with the essential requirements set out in Article 3. Such information shall result from a conformity assessment carried out in accordance with Article 17, and shall be given in the form of a statement of compliance which includes the elements set out in Annex VI. Depending on the specific combinations of radio equipment and software, the information shall precisely identify the radio equipment and the software which have been assessed, and it shall be continuously updated.*

. . .

The upper text gives legal clarity on the requirements to be met in order to introduce corresponding equipment into the single European market. To have it finally implemented, however, so-called delegated act and implementing act need to be triggered. The European Commission is currently working on these requirements which will finally *activate* the corresponding articles. As it will be outlined in the sequel, ETSI has developed a number of *European norms* which provide a technical, security, and regulation solution for software reconfiguration [11,15–18]. ETSI furthermore analyzed key software reconfiguration use cases from a feasibility and regulation perspective in ETSI TR 102 967 [22]. The latter document in particular outlines how the requirements of the Radio Equipment Directive [6] may translate into technical solutions. Finally, ETSI has considered security channels and introduces a corresponding security framework in [21,22,33].

Concerning EC Mandate M/512 [41], ETSI and CEPT interacted closely in order to develop/ensure consistency between the available regulation framework and ETSI standards in the field of TWS and LSA technology in particular. CEPT has developed a number of recommendations and decisions [4,7,38] enabling the usage of LSA in the 2300–2400 MHz band in Europe. ETSI, on the other hand, has developed in its Technical Committee (TC) Reconfigurable Radio Systems (RRS) the required standards [30–32] based on an initial System Reference document (SRdoc) related to LSA [26], which is the official way for ETSI to inform CEPT about the intended definition and deployment of new radio technologies. Note that ETSI is in close contact with 3GPP – a split of responsibilities has been agreed with 3GPP defining the technology required within the 3GPP network; a corresponding has started in 3GPP [1].

In terms of TVWS technology, CEPT has issued a number of reports [3,37,47]. ETSI has considered the problem from various angles. In order to enable an immediate deployment of related systems, typically under the applicable UK framework [39, 48], a so-called harmonised standard [9] was issued which comprises all technical requirements to be met in order to introduce corresponding products to the single European market. Further, ETSI considered a possible evolution, in particular

in terms of spectrum access coordination among secondary devices themselves (in order to increase quality-of-service (QoS) levels for secondary devices by reducing mutual interference) and by introducing advanced solutions for database management and inter-database coordination [12–14, 19, 21, 23, 28].

Spectrum Sharing

Spectrum sharing technology will be one of the key ingredients for future 5G systems. It is indeed expected that 5G systems will require between 1000× and 10,000× the capacity of legacy 4G systems. As illustrated in Fig. 1, major analysts expect a growth by a factor of 6×–10× by 2019 – and the full-fledged 5G rollout will only begin in 2020! Over the lifetime of the 5G system, massive capacity requirements are thus obvious and lead to expected factors up to 10,000× as mentioned above.

In this context, it is fair to ask the question which main enabler will be available to achieve the capacity objectives. In the opinion of the author of this section, there are four key vectors which are mutually exclusive (at least to some extend) as illustrated in Fig. 2: spectrum sharing, higher frequencies, spectrum efficiency, and densification. Very roughly speaking, it will be required to achieve a 10× capacity for each of those vectors in order to achieve the 10,000× target.

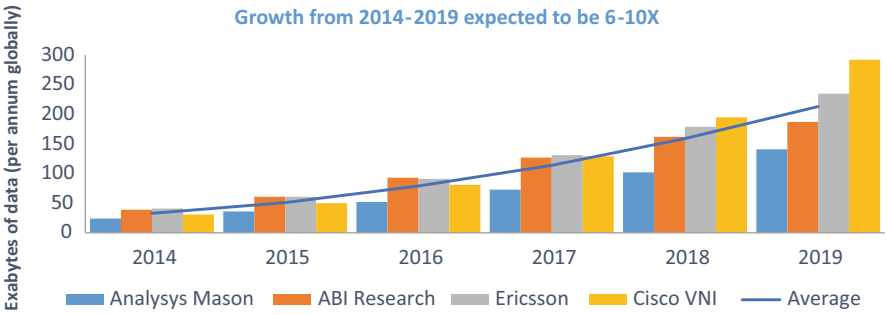

Fig. 1 Wireless traffic growth predictions until 2019

Fig. 2 Key enablers for 5G capacity growth

Note that the FCC has already acted and made approx. 11 GHz of spectrum available in the mmWave bands [36]. Previously, approx. 1.2 GHz were available for licensed and unlicensed commercial services taken together, so this corresponds to the 10× expectations for the corresponding "higher frequencies" vector in Fig. 2. Similar decisions are expected for Europe.

The "densification" vector is addressed in the current trend to move toward small cells in frequency ranges such as 3.5–6 GHz. The "spectrum efficiency" vector should not be understood as a required capacity increase in terms of Shannon capacity of a single link but rather as a requirement to work toward a better integration of heterogeneous radio systems, reduce signaling overhead, etc.

The "spectrum sharing" vector is orthogonal to the "higher frequencies" vector in some sense, since spectrum sharing can be applied independently to classical frequency bands below 6 GHz as well as to higher mmWave bands. The importance of spectrum sharing will furthermore depend on the availability of robust and reliable solutions of mmWave communication in commercial user equipment. It is currently unclear whether such solutions will be available in a reasonable time frame and at a reasonable cost for all user scenarios. In particular, medium to high mobility scenarios are an obvious challenge. If this "source of capacity" will not be available in some scenarios, the importance of spectrum sharing technology will grow even beyond the current level of critical need for it.

Currently, the following spectrum sharing technologies are considered to be candidates for future 5G systems:

- TV White Space usage
  - The technology has been extensively investigated, and a database-based usage approach was defined in the USA [42] and Europe [9]. OFCOM UK has implemented the corresponding regulation framework, while other European countries are currently hesitant. The commercial success of TVWS technology for wireless broadband applications is still limited. In the opinion of the author of this section, the main reasons lie in (i) the unclear business model (there is no interaction between spectrum owners and secondary users), (ii) the lack of QoS guarantees for secondary users, and (iii) the lack of certainty that TVWS spectrum will be available in the future for a given geographic area. The adoption rate may increase with the proliferation of 5G where a strong need for additional spectral resources may arise. The corresponding ETSI solutions are detailed in the sequel.
- Licensed Shared Access (LSA) and Spectrum Access System (SAS)
  - Following the experience from TVWS-based spectrum sharing technology, regulation administrations have further evolved the concept with the objective to address the shortcomings addressed above. This has finally led to the creation of the Licensed Shared Access (LSA) technologies in Europe and Spectrum Access System (SAS) in the USA. In the sequel, both technologies are briefly introduced, and then a more detailed description is given on ETSI's work focusing on LSA. SAS-related activities are mainly done in the Wireless Innovation Forum [49].

– Licensed Shared Access (LSA)
  The main use case for LSA technology relates to the extension of cellular capacity below 6 GHz in Europe. LSA specifically enables a 3GPP LTE network to be operated on licensed shared basis in the 2.3–2.4 GHz frequency band, which corresponds to 3GPP LTE band 40. It is expected that LTE mobile network operators (MNOs) will engage in a multiyear sharing contract with incumbents such as military stakeholders, professional video camera services, and others. Sharing contracts are typically 10 years or more in length. This long-term certainty is a key requirement for justifying large-scale investments into cellular network infrastructure. Still, the incumbent (tier-1) user is prioritized over the licensee (tier-2), i.e., the concerned MNO (or other LSA licensee) is required to vacate the LSA band for the given geographic area, the given frequency range, and the given period of time for which the incumbent is requiring access to the resource.
  Typically, the LSA band is combined with LTE operation in dedicated licensed spectrum through suitable carrier aggregation mechanisms. Because legacy LTE systems in Europe are mainly employing frequency division duplex (FDD) technology, the 3GPP Release-12 FDD/TDD carrier aggregation feature is required for a suitable combination of existing deployments with LTE LSA modes. The basic principle is illustrated in Fig. 3.
– Spectrum Access System (SAS)
  The main use case for SAS technology is similar to the LSA case above but currently defined for usage in the US market – as illustrated by Fig. 4.

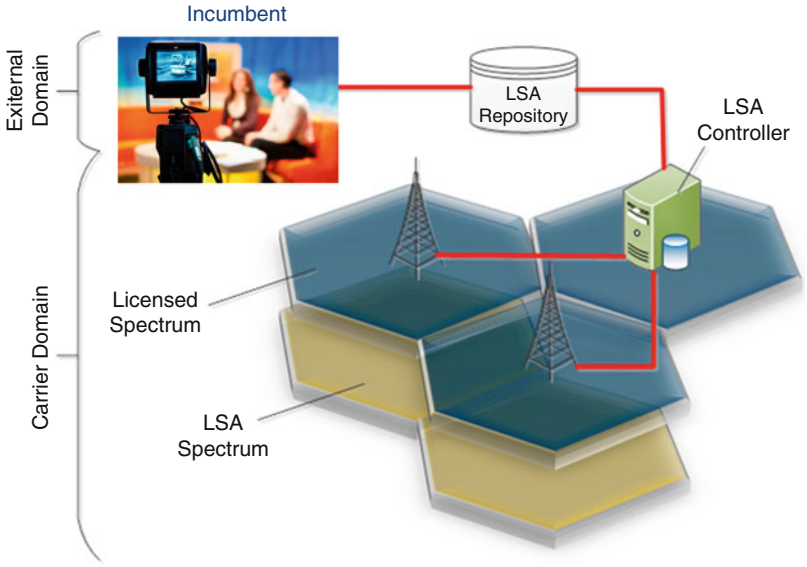

Fig. 3 The Licensed Shared Access (LSA) system approach

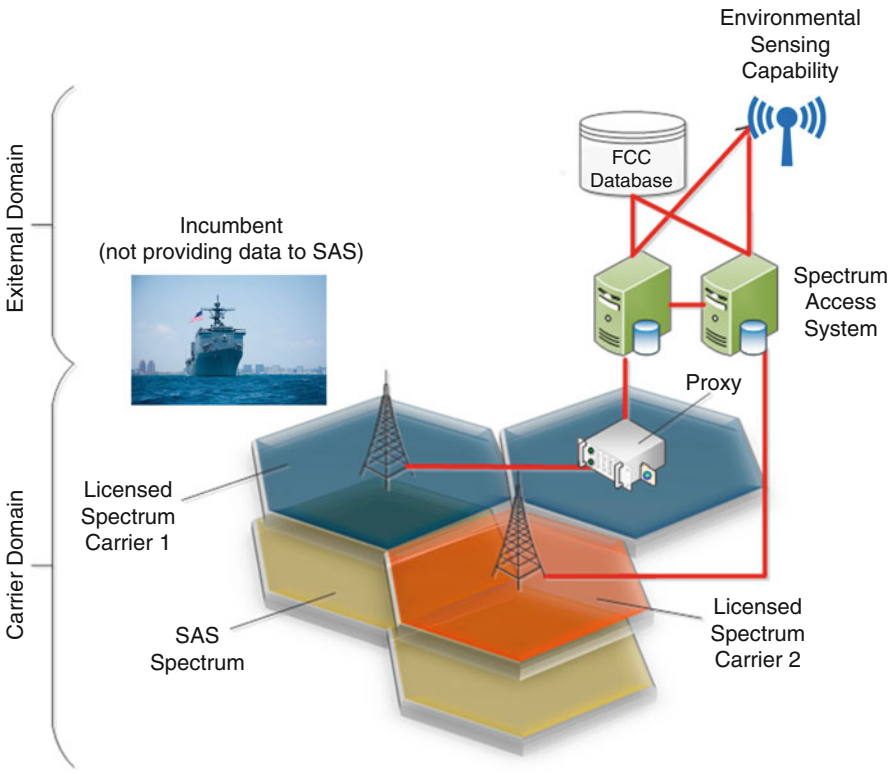

Fig. 4 The Spectrum Access System (SAS) approach

A so-called Citizens Broadband Radio Service (CBRS) network, such as a 3GPP LTE network, is operated on licensed shared basis in the 3.55–3.7 GHz frequency band, i.e., 3GPP LTE TDD bands 42 and 43. A major difference to LSA consists in the fact that licensed shared spectrum slots are only available in parts of the entire SAS band (up to 70 MHz) for so-called Priority Access License (PAL) tier-2 users. The remaining part of the spectrum and unused portions of the PAL spectrum ("use-it-or-share-it" rule) are available to a new user class called General Authorized Access (GAA) tier-3 users. This tier-3 class does not exist in the LSA system definition. GAA users may typically operate systems which have originally been defined for industrial, scientific, and medical (ISM) radio bands, such as LTE License-Assisted Access (LAA)-type systems or similar, including modifications in order to be adapted to the SAS requirements imposed by the FCC [43] (employing a "license-by-rule" framework).

– Comparison of Licensed Shared Access (LSA) vs Spectrum Access System (SAS)
  It should be noted that both systems – LSA and SAS – are currently defined for usage in a specific frequency band. The basic operational principles of

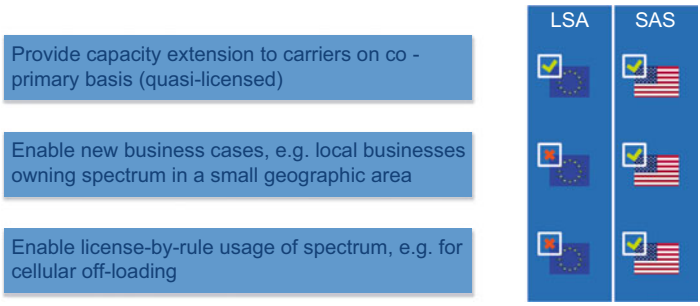

Fig. 5 Comparison of the Licensed Shared Access and Spectrum Access System (SAS) approaches

those systems, however, are frequency agnostic and can be applied to other bands. NRAs will be able to utilize the technologies as a new tool in the frequency management toolbox in order to allocate suitable bandwidth to wireless broadband systems.

A high-level overview on the difference is given in Fig. 5.

The LSA system is based on two tiers: incumbents and LSA licensees which each gets exclusive access right to the spectrum while they are using it. Furthermore, the incumbent populates a database indicating when the LSA licensee can access the spectrum in a given geographic area, a given frequency band, and a given period of time. The 3.5 GHz spectrum has three tiers with a tier-3 component to it (requiring communication capabilities with the SAS entities for interference mitigation, etc.) which closely relates to unlicensed operation and does not exist in the LSA system. However the most notable difference is the fact that the federal SAS incumbents (in particular the DoD) will not populate any databases giving usage information and it has to be entirely determined by sensing. It puts accurate and reliable sensing technologies in the forefront unlike LSA, where sensing could be used to improve network performance but is not essential for accessing the band.

The interference mitigation problem is also enhanced in the 3.5 GHz system for two reasons. First, the size of a census tract (i.e., the minimum geographic area which can be auctioned/used independently for each 10 MHz band) is based on population and not area. As a result, in densely populated urban areas, these census tracts could be as small as a few blocks and greatly increases the coordination needed for interference mitigation along each of these boundaries. Second, the GAA users need to be actively managed to prevent interference to the PAL users, something that is not needed in LSA. Finally, SAS expects to make the system attractive to new stakeholder and user groups who can acquire spectrum over a single census tract only, e.g., for providing access to a local business or similar. LSA, on the other hand, is rather designed for providing additional spectral resources to major MNOs over a large geographic area, such as an entire country.

Fig. 6 Mid-/long-range wireless access, no mobility

TV White Space

TV White Space Use Cases

A cognitive radio vision has been published by ETSI in ETSI TR 102 802 [20], and a number of active working items are currently dealing with (TV) White Space-related standardization. In this chapter, selected key use cases and scenarios are presented as they have been derived by ETSI TR 102 907 [21] – the below presented selection among available use cases was done with a focus on opportunistic sharing applications.

Use Case: Mid-/Long-Range Wireless Access over (TV) White Space Frequency Bands

A base station is providing Internet access to the end users by utilizing (TV) White Space frequency bands over ranges comparable to today's cellular systems, e.g., in the range of 0–10 km.

This use case is considered in further detail in the following scenarios:

- **Mid-/long range, no mobility**

In this scenario, a base station is providing wireless access toward fixed devices, e.g., a nonmobile home base station/access point. The geo-location of both the base station and from the fixed device is well known (Fig. 6).

- **Mid-/long range, low mobility**

In this scenario, a base station is providing wireless access toward mobile devices where the users have low mobility, e.g., they are staying at their location or are moving at walking speed. In that respect, the mobility of the user does not lead to invalid sensing results for primary users retrieved for the current location. The geo-location of the base station is well known. The geo-location of the mobile device must be determined during operation, e.g., via GPS, GLONASS, Galileo or BeiDou system, or cellular positioning systems.

- **Mid-/long range, high mobility**

In this scenario, a base station is providing wireless access toward mobile devices, and the concerned mobile devices may move at high speed, e.g., because a user is in a car or a train. In that respect, sensing results for primary users retrieved for the current location may get invalid quickly due to the mobility of the user. Thus, this use case leads to challenging constraints for the detection of primary users, and it needs to be evaluated if high mobility can be suitably supported in (TV) White Spaces at all.

Use Case: Short-Range Wireless Access Over (TV) White Space Frequency Bands

An access point or a base station is providing Internet access to the end users via short-range wireless communication (e.g., in the range of 0–50 m) by utilizing (TV) White Space frequency bands.

This use case is considered in further detail in the following scenarios:

- **Networks without coexistence management**

In this scenario one or more independent networks access (TV) White Space frequency bands. The access points require knowledge on the incumbent users of the spectrum (e.g., via (TV) White Space incumbent geo-location databases, sensing, etc.). However, in this first scenario, the different networks are uncoordinated, and thus they have no knowledge on other secondary networks and other users operating in the (TV) White Space bands.

- **Networks with distributed coexistence management**

In this scenario multiple networks access (TV) White Space frequency bands. The different networks are independent, and different network operators provide the backbone connectivity. Such a scenario can be envisaged, e.g., in an apartment building, where residents independently acquire their own local area access points operating in (TV) White Space frequency bands. Typically, the concerned access points can be operated and maintained by the residents themselves or the Internet service providers.

In order to work properly, effective coexistence mechanisms are required for (TV) White Space frequency access (Fig. 7).

- **Networks with centralized coexistence management**

In this case a (TV) White Space operator operates the (TV) White Space networks in the proximity in coordinated manner. Examples of this kind of usage can be small-scale corporate networks, networks for academic institutions, etc. (Fig. 8).

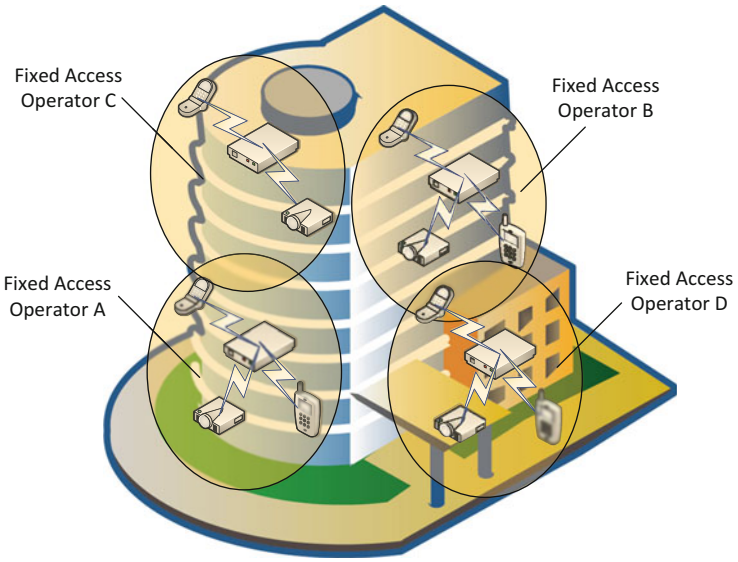

Fig. 7 Use case scenario of internet access by networks with distributed coexistence management on (TV) White Space frequency bands

Fig. 8 Short-range wireless access, coordinated networks

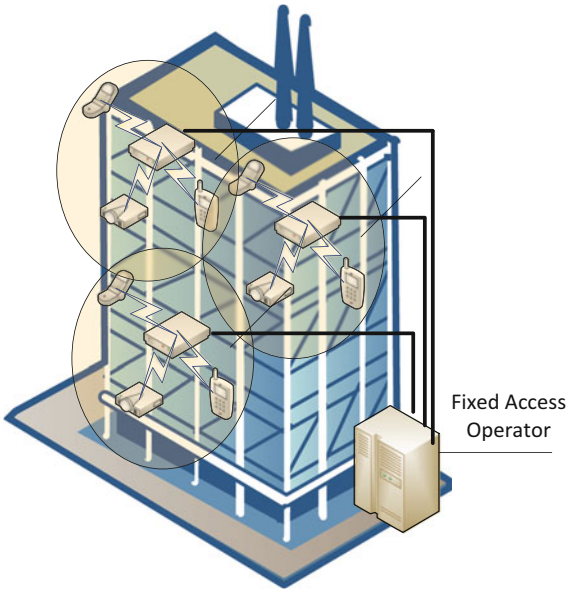

- **Hybrid of networks with distributed and centralized coexistence management**

This scenario combines the above two scenarios, i.e., in the same geographic area, there are centralized coexistence management and distributed coexistence management applied. Such setup typically occurs in combinations of public and private places, like campus areas and shopping malls, where, e.g., the "official" local area networks, operating under centralized coexistence management, are complemented by independent access points set up independently by some individuals.

The overall coexistence management in this scenario is distributed, due to the existence of the independent networks (Fig. 9).

Use Case: Sporadic Use of (TV) White Space Frequency Bands

In this use case, (TV) White Space resources are only available sporadically for secondary users, such as multimode user terminals being able to operate, among

Fig. 9 Use case scenario of internet access by hybrid of networks with distributed and centralized coexistence managements on (TV) White Space frequency bands

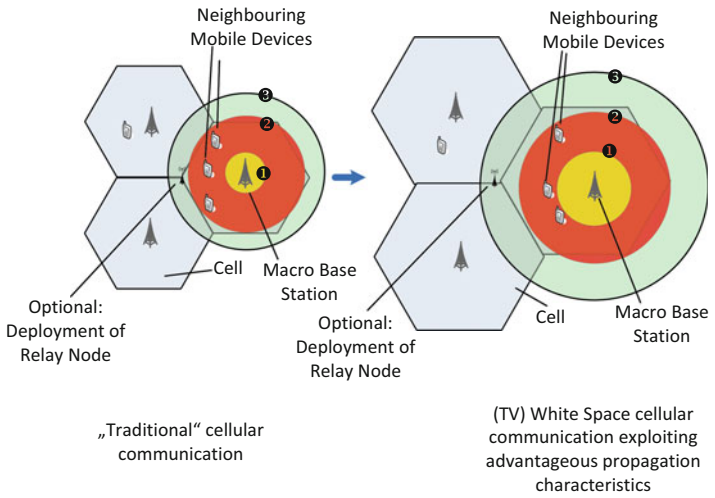

Fig. 10 Reduced propagation loss in (TV) White Spaces and thus improved coverage (the symbols ❶, ❷, ❸ indicate decreasing throughput levels, QoS, etc.)

other systems, cellular systems in licensed and unlicensed spectrum. The supported unlicensed spectrum is assumed to include (TV) White Spaces, i.e., the 470–790 MHz range in Europe/Region 1 (Fig. 10).

TVWS Medium Access Control Standards: A Coordinated and an Uncoordinated Approach

First-generation TVWS systems will focus on the protection of incumbent system, since this is a key regulation requirement. For an efficient usage of the technology, however, it is important to consider the resource sharing among multiple TVWS systems themselves. Otherwise, a chaotic and uncontrolled access to the resource will make the system hard to handle – in particular in dense environments. For this purpose, [29] introduce a system architecture and corresponding procedures for coordinated and uncoordinated use of TVWS.

The proposed approach builds on three entities as introduced in [29]: the cognitive radio system (CRS), the spectrum coordinator (SC), and the geo-location database (GLDB)) as shown in Fig. 11. The use of SC is specific to coordinated approach (Fig. 11).

The cognitive radio system (CRS) consists of a TVWS device (WSD) or network of WSDs (i.e., a master WSD and some slave WSDs). The CRS uses available TVWS resources which are identified with the help of geo-location database (GLDB), and/or the CRS uses available TVWS resources by exploiting the GLDB and with additional knowledge of spectrum usage by its neighbor CRSs by the spectrum coordinator (SC).

The operation of a GLDB is mandated or authorized by a regulatory authority and that provides a WSD in a CRS with location-specific information on the

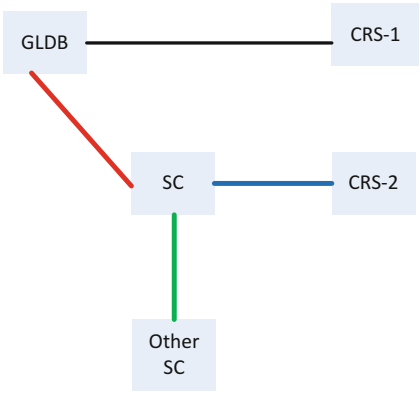

Fig. 11 Overview of TVWS system

available frequencies and associated maximum EIRP values. The concerned WSD is permitted to use the service which allows for protection of the incumbent service.

The SC is coordinating spectrum usage of CRSs. For this purpose, information is requested from GLDB and is communicated to CRSs, as well as supplemental spectrum usage data from different CRSs using its service. Different SCs are capable of communicating with each other.

Coordinated Usage of TVWS

In this section, it is outlined how several (distinct) CRSs can be coordinated among themselves in order to ensure access to required amount of spectrum and protection from harmful interference for secondary systems.

Spectrum Coordination

A SC uses spectrum coordination to serve CRSs such that they can operate in available spectrum resources of TVWS without causing harmful interference to each other and having a predictable access to the spectrum resources. The SC coordinates the management of radio resources among a set of CRSs that are potentially interfering with each other (coexistence) and allows for channel assignment requested by a CRS that requests guaranteed access to full capacity of a channel and with priority over other CRSs (priority-based channel assignment). The priority-based channel assignment is managed by the SC based on some minimum protection requirements requested by the CRS, which includes minimum bandwidth, minimum SINR (or maximum allowable interference), and some guaranteed minimum availability time. There are two basic approaches on how to implement priority access: (i) In the first approach, the SC translates these requirements into protection criteria, which are used by the GLDB to ensure that the priority-based channel assignment is maintained in the presence of other WSDs not using the SC; (ii) In the second approach, the SC stores the spectrum usage of the priority access, and the GLDB checks with the SC before providing available channels to other CRSs not using SC. From the perspective of the CRSs, coexistence and priority-based channel

assignments are provided as a set of two available SC services: the information service (for coexistence only) and the management service (for both coexistence and priority-based channel assignment). Each SC provides at least an information service or a management service for CRSs or provides both services.

Information Service

CRSs can be subscribed to an information service. In this case, a SC provides information about selected operational parameters (e.g., the operational parameters of other CRS in the available spectrum resources). In the information service, a SC does not make decision on the operational parameters to be used by those CRSs, but rather, all decisions are made by the CRS itself. However, the SC may process information about the current usage of spectrum to provide it to the CRS in order to support the CRS decision-making processes (such as ranking the potential operational parameters according to the resulting expected performance).

Management Service

For CRSs that are subscribed to the management service, a SC provides the operational parameters to be used by a CRS based on its requests and, if requested, certain QoS and usage time requirements. A CRS will not make any decision for its operational parameters (e.g., channel and transmit power) that are determined by the SC.

High-Level Operation Sequence

An overview of coordinated usage of TVWS is shown in Fig. 12. A CRS consists of a master WSD and one or more slave WSDs. The master WSD sends device parameters to a GLDB via the SC. The SC typically acts as relay and can also store the device parameters of the master WSD. The SC, during the process, maintains additional data about spectrum usage of the different CRSs using its service. This additional data contains information on the current state of spectrum usage, including spectrum measurement data from WSDs, and usage maps or areas of occupancy of the different CRSs. It also contains information related to the Radio Access Technology of each CRS that facilitates coexistence. A GLDB receives

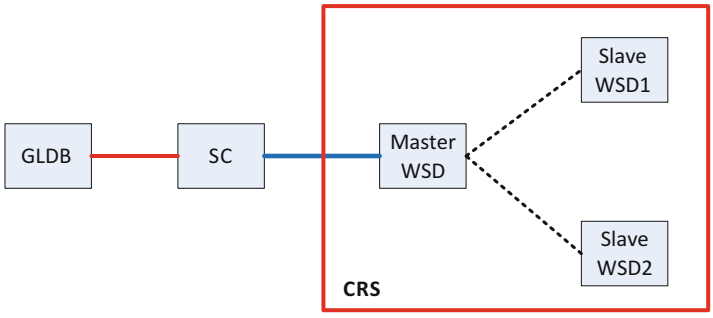

Fig. 12 Overview of coordinated usage of TVWS system

information from the master WSD about the characteristics of that WSD in order to generate operational parameters for that WSD. The GLDB provides operational parameters to the master WSD via the SC. During this process, the SC determines the operational parameters using the information obtained from the GLDB as well as the additional data about spectrum usage provided by the different CRSs and sends these operational parameters to the master WSD in response to the request for TVWS access. The operational parameters determined by the SC will not violate the protection criteria of the incumbent and are therefore compliant with the information obtained from the GLDB. The master WSD then sends the selected channel usage parameter to the GLDB via the SC. The SC will also update its additional spectrum usage data based on information sent by the WSD. At any time in the process of assigning channels to the CRSs, the SC could reconfigure the channel usage of the CRSs to ensure an efficient use of spectrum, such as reducing fragmentation in the available spectrum. The GLDB can either access SC or use channel usage parameters sent by the SC to ensure that WSDs can operate in the presence of other WSDs not using the SC (Fig. 12).

Uncoordinated Usage of TVWS

While the upper approach introduces coordination among CRSs, the uncoordinated usage of TVWS spectrum ensures a protection of the incumbents without providing specific protection for interference between the secondary users themselves (Fig. 13).

An overview of uncoordinated usage of TVWS is shown in Fig. 13. A CRS consists of a master WSD and one or more slave WSDs. The master WSD communicates with a GLDB to obtain its operational parameters in TVWS. A GLDB receives information from a WSD about the characteristics of that WSD in order to generate operational parameter for that WSD. A GLDB maintains a record of the actual usage of the TVWS. This information could be used to enable offending WSDs to be readily identified if interference to incumbent users were to occur and to allow the GLDB to know the extent to which available TVWS are being used.

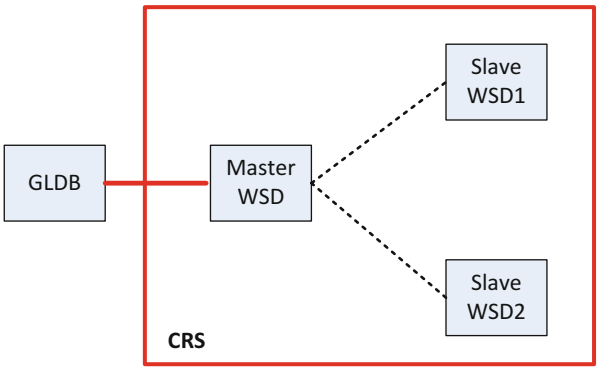

Fig. 13 Overview of uncoordinated usage of TVWS system

Licensed Shared Access (LSA)

In the sequel, a detailed overview on ETSI's solution for LSA is given.

System Design

The LSA system will address the needs of the following stakeholders:

- Incumbent user(s), i.e., primary users who may sublicense spectrum to LSA licensees under certain conditions;
- LSA licensee(s) operating a wireless system under a sharing agreement, typically a MNO providing 3GPP LTE services;
- NRA(s), which will monitor spectrum sharing activities.

Note that the upper guidelines imply a substantial change over legacy spectrum sharing technology, overcoming in particular the insufficiencies of the TVWS communication system approach. The LSA scheme provides a clear business case in which a long-term rental relationship between incumbents and LSA licensees leads to a defined money flow with LSA licensees obtaining guaranteed quality-of-service (QoS) conditions in a given geographic area, frequency band, and time period. TVWS neither offer such a clear business model for all stakeholders nor a guaranteed level of QoS, which may at least partly explain the technology's lack of commercial success. Further, the LSA approach is supported by major stakeholders, which is a key advantage for LSA in gaining marketplace acceptance.

In Europe, the 2.3–2.4 GHz band has been identified for an initial deployment of LSA [26]. This band corresponds to LTE TDD band 40 and is used in other regions as dedicated licensed LTE spectrum. ETSI's Reconfigurable Radio Systems (RRS) Technical Committee has developed corresponding system requirements [30] and system architecture [31] documents, defining the key building blocks and interfaces related to the upper framework.

The LSA repository (LR) is an entity providing database and other functionalities as it will be detailed below. In the European LSA context, the LSA repository plays a key role because relevant information related to spectrum occupancy is provided by the incumbent(s) to the database. The US model follows a different strategy for users entering (coastal) protection zones: all such information needs to be derived by an ESC and must comply with strict confidentiality requirements, as detailed further on in this in paper. The LSA controller features processing and decision-making capabilities building on the data elements provided by the LSA srepository. The LSA controller will interact with an MNO's (or other LSA licensee's) operations, administration, and management (OA&M) framework in order to indicate spectrum availability and request short-term vacating of the spectrum and other functions as illustrated in Fig. 14.

In accordance to the definitions in [31], the LSA repository and LSA controller components are illustrated by Fig. 15:

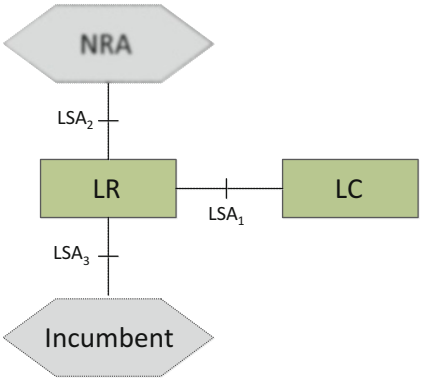

Fig. 14 LSA architecture reference model

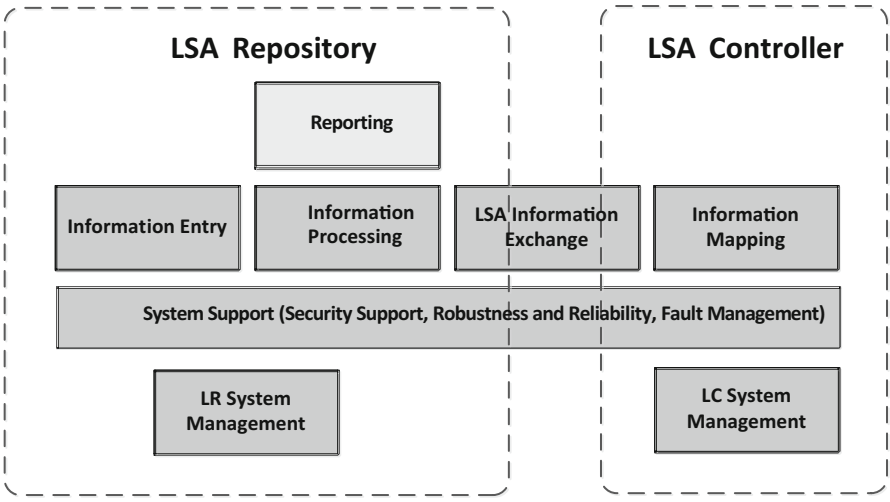

Fig. 15 Mapping of high-level functions and function groups to logical elements

The high-level functions introduced in Fig. 15 are derived from the ETSI requirement document [30], and they are further detailed below:

- The information entry function enables the entry and storage of information which is required for the operation of the LSA system and is comprised of the following:

  (i) Information on the sharing of framework between incumbent(s) and LSA licensee(s) indicating mutually agreed sharing conditions for the concerned band(s);
  (ii) LSA licensee information such as its identity;
  (iii) Information on the incumbents' LSA spectrum resource usage and protection requirements.

- The information processing function supports the derivation of LSA spectrum resource availability information for each licensee, to be provided to the information exchange function for forwarding to the respective Information Mapping function of the LSA licensee. This function uses data provided through the information entry function. It also includes support for multiple incumbents and multiple LSA licensees, scheduled and on-demand modes of operation, and logging of processing information.
- The information mapping function receives LSA spectrum resource availability information, confirms reception, and initiates respective operations in the MFCN. Furthermore, it provides acknowledgments to the information exchange function (for forwarding to the information processing function) when changes in the MFCN are processed.
- The reporting function is responsible for creating and providing reports regarding the LSA system operation to administration/NRA, incumbent(s), and/or LSA licensee(s) on an on-demand or scheduled basis.
- The LSA information exchange function supports communication mechanisms, internal to the LSA system, to exchange LSA spectrum resource availability information, and related acknowledgment information.
- The system support function group is comprised of the following elements:

  (i) Security support function for support of authentication and authorization as well as services to support integrity and confidentiality of data;
  (ii) Robustness and reliability function for support of mechanisms to maintain robustness and reliability against failures and malicious attacks;
  (iii) Fault management function for support of failure detection in the LSA system, subsequent generation and delivery of respective failure notification(s) to LSA licensee(s) and incumbent(s), and initiation of respective operations in the LSA system.

- The system management function group includes:

  (i) Operation, administration, and maintenance tasks in the LSA system,
  (ii) Identity management (comprising user identity and authentication management and user authorization profiles)
  (iii) System management is separate for LR and LC since these logical entities belong to different operation domains.

It is expected that the upper system approach is able to satisfy the needs of all stakeholders, including incumbents, LSA licensees, NRAs, and others such that:

(i) The incumbent(s) will be able to monetize spectrum which is underused in a given geographic area, a given frequency band, and a given time;
(ii) The LSA licensee will be able to access additional spectrum enjoying guaranteed QoS conditions and
(iii) The NRAs ensure the best possible usage of already allocated spectrum.

Standards and Regulation Framework

LSA and SAS-related standard (system definitions) activities are currently ongoing in the ETSI Reconfigurable Radio Systems (RRS) Technical Committee with a focus on LSA, in the Wireless Innovation Forum (WInnForum) with a focus on SAS, and in 3GPP targeting a global solution.

Thus far, the ETSI work has mainly produced documents [26, 30], and [31] and currently finalizes stage-3 interface definitions in [32] which are outside of the 3GPP system, such as the definition of the LSA1 Interface as illustrated in Fig. 14.

3GPP is discussing the integration and linkage of the LSA and SAS components into the 3GPP architecture. Document [40] proposes one possible option on how to include both sides under a common umbrella as it is illustrated in Fig. 16. As defined in [2], the corresponding entities provide the following functionalities:

- A network manager (NM) provides a package of end-user functions with the responsibility for the management of a network, mainly as supported by the EM(s), but it may also involve direct access to the network elements. All communication with the network is based on open and well-standardized interfaces supporting management of multi-vendor and multi-technology network elements;
- A domain manager (DM) provides element management functions and domain management functions for a subnetwork. Interworking domain managers provide multi-vendor and multi-technology network management functions;
- An element manager (EM) provides a package of end-user functions for management of a set of closely related types of network elements. These functions

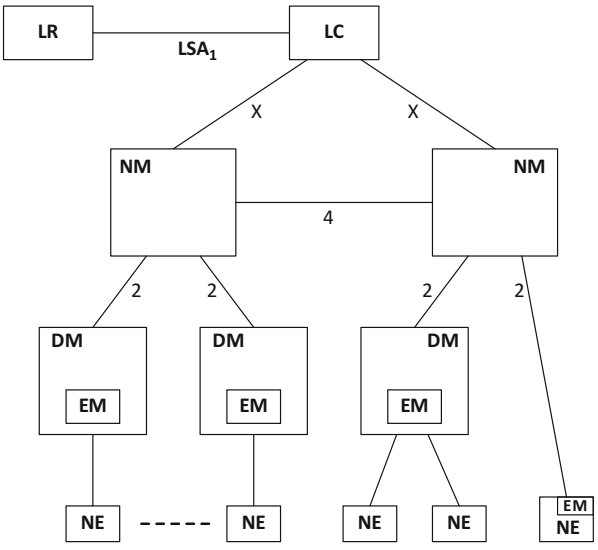

Fig. 16 Integration and linkage of LSA components to 3GPP SA5 architecture

can be divided into two main categories: element management functions and subnetwork management functions;
- A network element (NE) corresponds to a discrete telecommunications entity, which can be managed over a specific interface, e.g., the RNC.

The WInnForum leverages its long-term relationship with the US Department of Defense (DoD) in order to define a SAS system approach compatible with the needs of the US incumbents, which include in particular naval shipborne radar and satellite services. Protection of satellite services is a key aspect of the FCC's second further notice of proposed rulemaking [43].

From a regulatory perspective, the European CEPT organization has acted following investigations and a corresponding mandate by the European Commission [35, 44, 45]. CEPT has produced a number of reports, recommendations, and decisions [4, 7, 38] and has finally closed the corresponding working groups. From a CEPT perspective, the work is complete, and the actual usage of the LSA band in Europe now depends on NRAs to enable the usage of spectrum sharing in the national territories.

Protection of Incumbents and Neighboring Licensees

The current usage of the 2.3–2.4 GHz LSA band varies over the European Countries. While professional video camera services represent the main incumbents for some countries, others have allocated the spectrum also to (military) aircraft telemetry services, amateur radio, police wireless communication, and others. Detailed information for each country is available in the ECO Frequency Information System [8]. Based on information where corresponding incumbent systems are operated and which level of protection they require, the maximum LSA output power levels can be derived as shown in Fig. 17, which illustrates France as an example. Note that in this example, major parts of the country are available without major restrictions, including the capital of France: Paris.

Traditionally, incumbent systems are protected by so-called exclusion zones which prohibit the usage of interfering equipment within a given zone. In order to ensure a sufficient level of protection, corresponding zones are typically defined for a geographic area of substantial size, since the interfering system can operate without restrictions starting from the boundaries of the exclusion zone. In order to maximize the geographic area in which the operation of LSA is possible, the standards committee ETSI RRS has identified further zone types to reduce the constraints on the LSA system [30]:

- **LSA exclusion zone**: geographical area within which LSA licensees are not allowed to have active radio transmitters. Note: An exclusion zone is normally applicable for a defined frequency range and time period.
- **LSA restriction zone**: geographical area within which LSA licensees are allowed to operate radio transmitters, under certain restrictive conditions (e.g., maximum EIRP limits and/or constraints on antenna parameters). Note: A

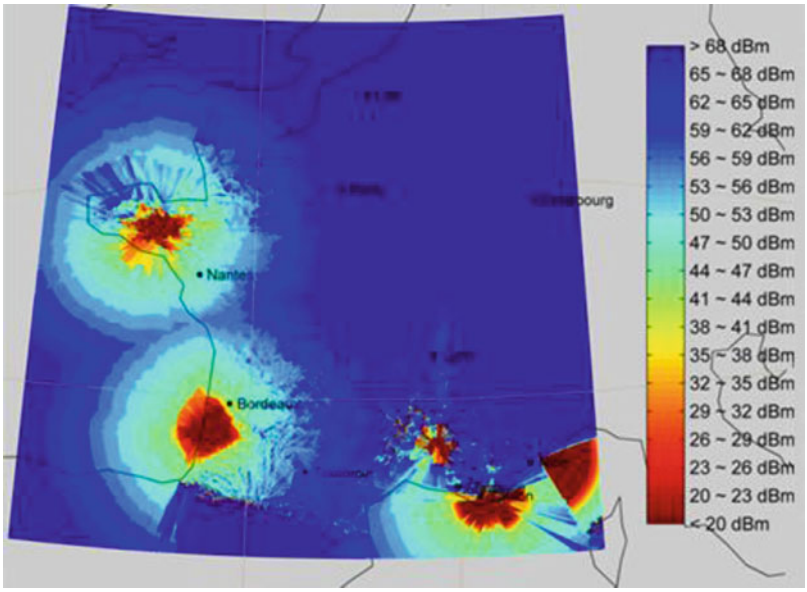

Fig. 17 LSA spectrum availability in France [46]

restriction zone is normally applicable for a defined frequency range and time period.

- **LSA protection zone**: geographical area within which incumbent receivers will not be subject to harmful interference caused by LSA licensees' transmissions. Note: A protection zone is defined using specific measurement quantities and thresholds (e.g., a mean field strength that does not exceed a defined value in dBμV/m/MHz at a defined receiver antenna height above ground level). A protection zone is normally applicable for a defined frequency range and time period.

Concerning requirements on protection of neighboring (LSA) systems operated by distinct MNOs (or other LSA licensees), mainly cross-border issues need to be considered for an efficient operation close to national country borders. Note that complex interference mitigation between distinct licensees is not required for LSA across small geographic areas – it is assumed that an LSA license is allocated to an MNO (or other LSA licensee) across an entire country or at least for a large geographic area (with the inherent limitations for exclusion, restriction, and protection zones). This is in contrast to the FCC SAS concept, where interference mitigation is required between neighboring Census Tracts which may be of small geographic size in particular in densely populated areas. Intra-MNO (or other intra-licensee) interference mitigation, on the other hand, may be employed as it is detailed in the next section.

Intra-MNO-System Interference Mitigation Through LSA

Future 5G network deployments will provide increased energy efficiency and spatial utilization of the licensed spectrum, but such a diverse and heterogeneous cell deployment will create some important technical challenges that need to be overcome first. One of the critical aspects in such high dense heterogeneous networks is a rich and uncoordinated inter-cell interference within the system of a given MNO (or other LSA licensee). LSA is expected to provide a new tool in order to address at least some of the interference cases.

While LSA spectrum can straightforwardly be used as additional spectrum for voice and data communication, the available LSA spectrum can be also exploited for inter-cell interference coordination. As LSA provides additional spectral resources over a given geographic area, for a given time interval, and a given frequency band, depending on interference levels and the need for interference mitigation, a trade-off can be made between LSA resources assigned for voice and data and LSA resources assigned for inter-cell interference coordination. Introducing collaborative spectrum sensing and more flexibility in spectrum sharing, the licensed users can dynamically access and share spectrum without causing interference to primary users. By intelligently allocating LSA spectrum to center and cell-edge cells in a network, interference can be reduced significantly, and implementation of complex and high-cost interference mitigation techniques in the user equipment receiver chain can be avoided.

Challenges and Next Steps

The regulatory circumstances related to LSA have been developed by CEPT, and the corresponding work is complete. The standards work is in an advanced stage in ETSI's RRS Technical Committee, while 3GPP's activities have only recently been initiated for Release 13. The technology is likely to further evolve in 3GPP Release 14 and beyond. A commercial availability, however, can be envisaged before the standards work is finally achieved. Thus, the main challenge relates to the possibility for the NRAs to finally enable the usage of the target 2.3–2.4 GHz band and possibly other bands in the future. Corresponding trials are ongoing in France and Italy, and additional countries are expected to follow. Once LSA has been proven to operate efficiently, it is expected that NRAs will open the 2.3–2.4 GHz band for licensed shared cellular usage under the LSA framework and to start identifying additional target bands. It is expected that LSA will become a key tool in the regulation toolbox in order to provide spectrum resources for 5G systems and beyond in order to meet the target 1000× to 10,000× capacity requirements.

Software Reconfigurability

ETSI TC RRS has developed a set of six European norms detailing a software reconfiguration framework for mobile device reconfigurability [10, 11, 15–18]:

- [10] Introduces the related system requirements;
- [11] Defines the system architecture;

- [15] Details the Multiradio Interface (MURI) which introduces in particular functions to (un)install radio applications packages (RAPs), to select suitable operational modes (e.g., simultaneous operation of multiple RATs), to access to the data pipes of the active RATs, and to access to radio parameter measurements.
- [16] Introduces Reconfigurable Radio Frequency Interface (RRFI), which complements existing Radio Interfaces, such as DigRF and others. It enables RAPs to access radio parameters and introduces the concept of Radio Protection Classes. These protection classes allow a (third party) software developer to choose a trade-off between the level of the mobile device "openness" to developers (e.g., access to Application Programming Interfaces (APIs)) and the required recertification complexity (and thus cost) of the platform.
- [17] Finally defines the Radio Programming Interface (RPI). The key novel concept consists of the Radio Virtual Machine (RVM) which is an abstract machine capable of executing Configcodes independent of the available hardware on the target platform. Its particularity is that it does not require a middleware for execution and thus lead to a far more efficient device reconfigurability compared to state-of-the-art approaches.

This set of European norms is complemented by a study on use cases for dynamic equipment reconfiguration [22]. This study introduces the following five basic use cases:

(1) OEM establishing initial conformity of reconfigurable equipment platform.
(2) DoC/StoC (Declaration of Conformity/Statement of Conformity) verification of reconfigurable equipment
(3) OEM upgrade of reconfigurable equipment (individual or en masse).
(4) Third-party upgrade of reconfigurable equipment (individual or en masse).
(5) Configuration enforcement of reconfigurable equipment.

Finally, security solutions are outlined in [24, 25, 27, 34].

Reconfiguration Capabilities: Mobile Device Reconfiguration Classes

As it is expected that the reconfiguration capabilities of a mobile device will evolve over time, mobile device reconfiguration classes (MDRC) are introduced. As shown in Fig. 18, seven different classes of reconfigurable MD are introduced (MDRC-0 corresponds to a non-reconfigurable device).

A reconfigurable MD belongs to a defined class according to the reconfiguration capabilities, which are determined by the type of resource requirements and the form of the Radio Application Package. Reconfigurable MD classes are defined as follows (see also Fig. 2):

- **MDRC-0:** No MD reconfiguration is possible; MDRC-0 represents legacy radio implementations and does not allow for MD reconfiguration (except for bug fixing and release updates through firmware updates) or exploitation of cognitive

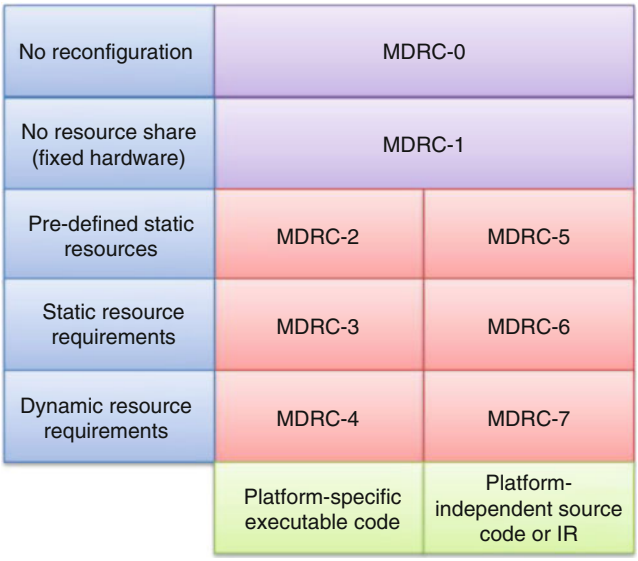

Fig. 18 Definition of MDRCs according to reconfiguration capabilities [10]

radio (CR) features. MDRC-0 represents legacy radio implementations and does not allow for MD reconfiguration.

- **MDRC-1:** Radio applications use different fixed resources; in this scenario, at least some of the radios are implemented with non-software-defined radio (SDR) technology, e.g., with dedicated Application-Specific Integrated Circuits (ASICs), and are resource-wise independent of each other. Simple CR functionality may be supported through radio parameter management to the extent which the radio implementations allow.
  MDRC-1 implements multiple radio applications with fixed resources allocation and no resource sharing.
- **MDRC-2:** Radio applications use predefined static resources; MDRC-2 implements multiple radio applications, but no dynamic resource management is available. The radio applications for MDRC-2 come from a single Radio Application Package which is normally provided by a reconfigurable MD vendor or SDR chipset manufacturer. In this scenario, we assume that software radio components in the Radio Application Package are provided in platform-specific executable code.
- **MDRC-3:** Radio applications have static resource requirements; for MDRC-3, a resource budget is defined for each radio application. This budget contains a static resource measure that represents the worst-case resource usage of the application, generated at radio application compile time. If an application is being started, the resource manager installed in a reconfigurable MD of MDRC-3 checks its resource budget and the sum of all resource budgets of already running

applications and admits the new application only if the resources can still be guaranteed for all running applications. In this scenario, we assume that software radio components in the Radio Application Package are provided in platform-specific executable code.

- **MDRC-4:** Radio applications have dynamic resource requirements; this scenario assumes a similar resource manager in a reconfigurable MD as for MDRC-3, but in addition, radio applications have now varying resource demands based on their current type of activity. Applications have separate operational states for different types of activity, and a resource budget is assigned to each operational state. In this scenario, we assume that software radio components in the Radio Application Package are provided in platform-specific executable code.
- **MDRC-5:** Radio applications use predefined static resources, on-device compilation of software radio components. This class corresponds to MDRC-2 with the difference that all or part of the software radio components are provided in the Radio Application Package as platform-independent source code or platform-independent intermediate representation (IR), which is compiled on the reconfigurable MD itself. It particularly means that the reconfigurable MD should include a proper compiler in order to convert the source code or IR of the software radio components into an executable code that runs on a given modem chip of a reconfigurable MD. It is assumed that the methods of radio programming and the tools to support this category have become sufficiently standardized so that third-party vendors may create radio applications and activate them to different platforms with relative ease. The formal description of the resource management is the same as for MDRC-2.
- **MDRC-6:** Radio applications have static resource requirements, on-device compilation of software radio components. This class corresponds to MDRC-3 with the difference that all or part of the software radio components are provided in the Radio Application Package as platform-independent source code or platform-independent IR, which is compiled on the reconfigurable MD itself. As in the case of MDRC-5, it particularly means that the reconfigurable MD should include a proper compiler in order to convert the source code or IR of the software radio components into an executable code that runs on a given modem chip of a reconfigurable MD. As in the case of MDRC-5, it is assumed that the methods of radio programming and the tools to support this category have become sufficiently standardized so that third-party vendors may create radio applications and activate them to different platforms with relative ease. The formal description of the resource management is the same as for MDRC-3.
- **MDRC-7:** Radio applications have dynamic resource requirements, on-device compilation of software radio components. This class corresponds to MDRC-4 with the difference that all or part of the software radio components are provided in the Radio Application Package as platform-independent source code or platform-independent IR, which is compiled on the reconfigurable MD itself. As in the case of MDRC-5 or MDRC-6, it particularly means that the reconfigurable MD should include a proper compiler in order to convert the source code or IR of the software radio components into an executable code that

Table 1 Summary of MDRCs

	Multi-radio system	Resource share (among Radio applications)	Resource manager	Multitasking	Resource measurement	Resource allocation
MDRC-0	No	No	No	no	Design time	Design time
MDRC-1	Yes	No	No	no	Design time	Design time
MDRC-2 MDRC-5	Yes	No[a]	Yes[b]	Yes[c]	Design time	Design time
					Design time/install time	Design time/install time
MDRC-3 MDRC-6	Yes	yes	Yes	yes	Design time	Run time
					Design time/install time	
MDRC-4 MDRC-7	Yes	yes	Yes	yes	Design-time	Run time
					Design time/install time	

[a]Resource share can exist among Radio Access Technologies (RATs) in a given Radio Application.
[b]This is for a fixed resource allocation only. Resource management and resource allocation among RATs (in a single RA) are predetermined in a static manner by Radio Application provider.
[c]Multitasking in this case is for multiple RATs within a single radio application.

runs on a given modem chip of a reconfigurable MD. As in the case of MDRC-5 or MDRC-6, it is assumed that the methods of radio programming and the tools to support this category have become sufficiently standardized so that third-party vendors may create radio applications and activate them to different platforms with relative ease. The formal description of the resource management is the same as for MDRC-4.

The definition of MDRCs described above can be summarized as shown in Table 1.

Note that radio conformance tests are mandatory for MDRC-1 to MDRC-7 in order to ensure that the joint operation of (dynamically) reconfigured base bands and RF front ends is in compliance with the relevant conformance requirements before the device is introduced into the market.

The Basic Technical Approach for Software Reconfiguration

The ETSI RRS approach for software reconfiguration introduces a complex tool set enabling an end-to-end ecosystem for software reconfiguration taking technical, security, and certification solutions into account. This section explains how a subset of the entire framework can be used to introduce a simple software reconfiguration framework offering the basic functionalities independent of the underlying target hardware platform (Fig. 19).

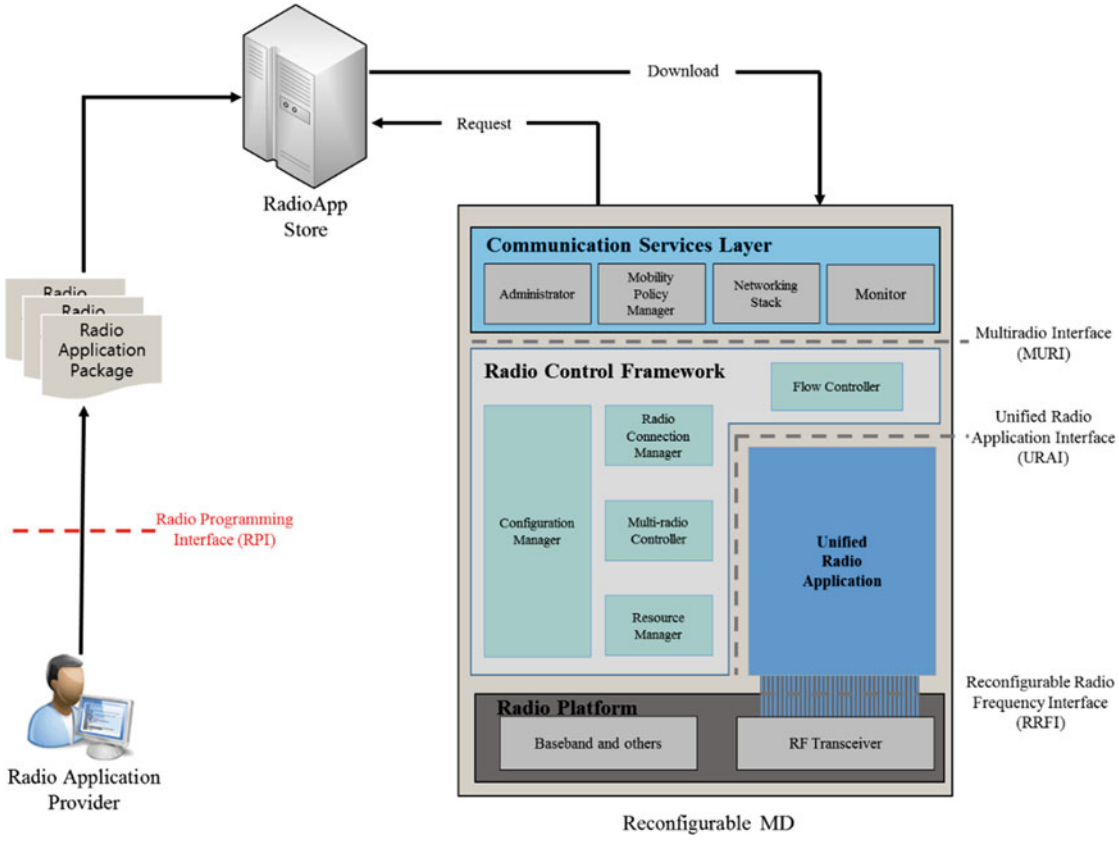

Fig. 19 The reconfigurable mobile device architecture and four sets of interfaces for reconfigurable MD introduced in [11]

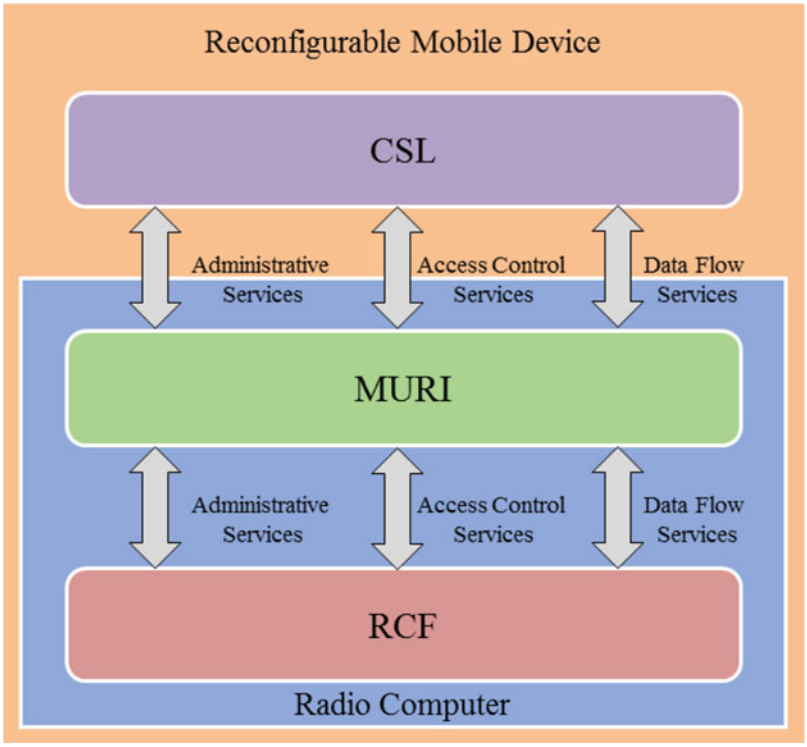

Fig. 20 Interconnection between CSL and RCF using MURI for reconfigurable MD [15]

A basic implementation of the framework may comprise the communication services layer (CSL) and the Multiradio Interface (MURI) to be complemented by the minimum set of required functions in the Radio Control Framework.

As shown in Fig. 20, MURI supports three kinds of services:

- **Administrative Services:** These services are used by some device configuration application, i.e., administrator which is included in the CSL, to (un)install a new unified radio application (URA) into the reconfigurable MD and create/delete an instance of the URA. Installation and loading may take place both at device start-up time to set up the network connection and during run time, whenever reconfiguration of available URAs is needed. MURI does not make any assumption on how and when the mobile device will detect the need of the reconfiguration.
- **Access Control Services:** These services are used by the MPM to maintain the user policies and preferences related to the usage of different RATs and to make a selection between them. Modeling of such preferences and selection algorithms is not in the scope of the present document; however, the MURI specification covers the information exchange of RAT selection decisions between CSL and

RCF. The preferences themselves may originate either locally from applications or end-user settings as well as in a distributed manner from network operator or from a cognitive radio management framework.

- **Data Flow Services:** These services are used by the networking stack of the reconfigurable MD, such as the TCP/IP stack. Therefore data flow services represent the set of (logical) link layer services, which are provided in a uniform manner regardless of which URAs are active.

With these basic features, it is possible to:

- Enable the installation and activation of a unified radio application;
- Parameterize the configuration, e.g., select a number of RATs to be operated simultaneously;
- Access to data flow services
- Perform the deactivation and uninstallation of a Unified Radio Application

Regulation Considerations

With the development of a unified radio application, the radio behavior of the target devices typically changes, and the conformity to the application regulation must be (re)validated. In Europe, annex VII of the Radio Equipment Directive [6] introduce a useful tool in order to update the applicable Declaration of Conformity of a radio equipment. In this context, Radio Virtual Machine (protection) classes are introduced in order to find a trade-off between (re)certification effort and base-band code development flexibility [10].

At one extreme of RVM class, a high-level RVM class corresponds to full reconfigurability of the low-level parameters of an RVM and accordingly necessitates a relatively more extensive certification testing process after the RVM has been reconfigured. At the other extreme of RVM class, a low-level RVM class corresponds to a limited reconfigurability of the low-level parameters of an RVM. As the reconfigurability of the low-level parameters of this particular class of RVM is limited, a relatively less extensive certification testing process is necessitated after the RVM has been reconfigured. Moreover, an RVM can have different RVM classes associated with different components of the RVM that relates to the reconfigurability of the low-level parameters of the respective components of the RVM.

Reconfiguration of an RVM of the highest-level RVM class may necessitate that the overall certification testing process focuses on the certification of each reconfigured software components of the RVM. In such a situation, each respective reconfigured software component may need to be separately certified before one or more sets of reconfigured software components are certified together. For example, a reconfigured RVM software component “A” (e.g., Wi-Fi) may need to be separately certified from a reconfigured and certified RVM software component “B” (e.g., LTE). The certification process may then be such that the joint operation of separately certified reconfigured RVM software components “A” and “B” may then take place jointly.

At the other extreme of RVM classes, the lowest-level RVM class corresponds to a restricted reconfigurability of the low-level parameters of an RVM. For such a restricted level of reconfigurability, a developer of radio applications would only have limited access to the low-level parameters of an RVM. For example, the lowest-level RVM class would permit a radio application developer to have access to only the low-level parameters of the receive chain of an RVM. Accordingly, the lowest-level of RVM class would not need to utilize a corresponding detailed and thorough certification testing process because, for example, a radio platform operating a malfunctioning reconfigured RVM would not interfere with other radio platforms. Thus, level of certification testing for the lowest RVM class would be less extensive certification testing process than that used for the highest RVM class.

One or more medium- or intermediate-level RVM classes may also be established between the two extreme RVM classes that correspond to intermediate levels of reconfigurability of the low-level parameters of an RVM. An intermediate-level RVM class, for example, would allow more flexibility for reconfiguring low-level parameters of an RVM than the lowest-level RVM class but would not permit the degree of reconfigurability that would be associated with the highest-level RVM class. Depending on the level of reconfigurability to the low-level parameters of an RVM, an intermediate-level RVM class may necessitate a certification testing process for a compiled reconfigured RVM and underlying hardware that is more extensive than that corresponding to the lowest-level RVM class but less extensive than that corresponding to the highest-level RVM class. For example, a certification based on the intermediate-level RVM software component might be obtained by contacting an authorized notified body and providing only a serial number for the RVM software component and an identification of the target device type on which the compiled reconfigured RVM would operate. In another example, there could be no requirement for a joint certification based on an RVM software component for a simultaneous operation with other RVM software components. That is, a certificate based on an RVM software component "A" (e.g., Wi-Fi) and a separate certificate based on another RVM software component "B" (e.g., LTE) would allow for a simultaneous operation of reconfigured components "A" (e.g., Wi-Fi) and "B" (e.g., LTE).

Another exemplary situation that may necessitate a relatively less extensive certification testing process would be a Radio Application developer that only reconfigures non-transmission-related low-level parameters, for example, low-level parameters relating to a data interleaver and/or a channel coder in the transmit/receive (TX/RX) chain of an RVM that otherwise has been defined to be of the highest-level RVM class. As nothing related to the spectral shaping of a transmitted signal is reconfigured by the reconfiguration of the data interleaver and/or channel coder, a relatively less extensive certification testing process could be used. Another exemplary situation that may necessitate a less extensive certification testing process would be a reconfiguration that involves changes targeting predefined frequency bands and/or bandwidths. In still other exemplary situations, there may be reconfigurations for which a certification testing process may not be necessary.

The Radio Virtual Machine

The Radio Virtual Machine usage is defined in [18]. It introduces highly efficient software reconfigurability without requiring the usage of a (inefficient) middleware while still enabling code portability.

It is typically up to the manufacture to decide which components of a target platform may be made available to a (third party) software developer. In the past, it has proven difficult to fully open up a highly complex hardware environment, so at least in a first time it may be preferable to enable such third parties to replace one or multiple of selected components by novel software components. Figure 21 illustrates the replacement of an abstract component B through a novel implementation by (third party) software developers.

The Radio Virtual Machine (RVM) is an abstract machine which is capable of executing Configcodes, and it is independent of the hardware. The implementation of a RVM is target radio computer specific, and it has access to the back-end compiler (on the platform itself or externally) for just-in-time (JIT) or ahead-of-time (AOT) compilation of Configcodes.

The RVM executes a particular algorithm presented as a data flowchart. In other words, the RVM is the result of replacing all operators and tokens in the particular data flowchart with abstract processing elements (APEs) and data objects (DOs), respectively. Each APE executes computations marked by the replaced operator identifier. These computations are taken from the Radio Library.

Figure 21 illustrates a conceptual view of RVM processing. This process requires APE, DO, and Radio Library, of which the definitions are as follows:

- APE abstracts a computational resource corresponding to the operation in a particular data flow chart;

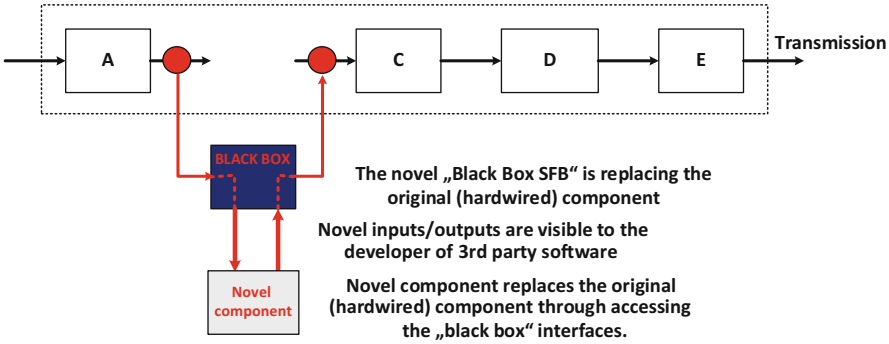

Fig. 21 Example replacement of a component through interfacing with novel SFB provided by a (third party) software provider [18]

- DO abstracts a memory resource. In other words, DO is an abstracted memory for storing data used during the procedure of radio processing;
- Reference/Native Radio Library includes normative definitions/native implementation of all Standard Functional Blocks (SFBs) for front-end/back-end compilation. Note that the computations included in the Radio Library are represented in terms of normative definitions or native implementations of SFBs depending upon whether the Radio Library is used for front-end or back-end compilation, respectively.

Note: User-defined function blocks (UDFBs) will be created through combination of SFBs and represented as a data flowchart to be executed in the RVM. Alternatively, a UDFB is implemented as a stand-alone module/function which can be mapped (i) into one APE (i.e., this UDFB can be considered atomic) or (ii) into an eRVM/RVM (i.e., not atomic). UDFBs are not in general included into the Radio Library, but they are part of the Radio Application Package.

The RVM begins to work immediately after some DO initialization. All APEs execute computations asynchronously and concurrently. An individual APE executes the allocated operator if all the corresponding input DOs are full. APEs access DOs with operations "read," "read-erase," or "write." After reading input data from DOs, the APE executes the allocated operator, and, if output DOs are empty, then the APE writes processed data. Any full output DO blocks the corresponding writing operation. The RVM executes computations until reaching the state when all APEs become inactive. In this state, there are not enough full DOs, which can activate the

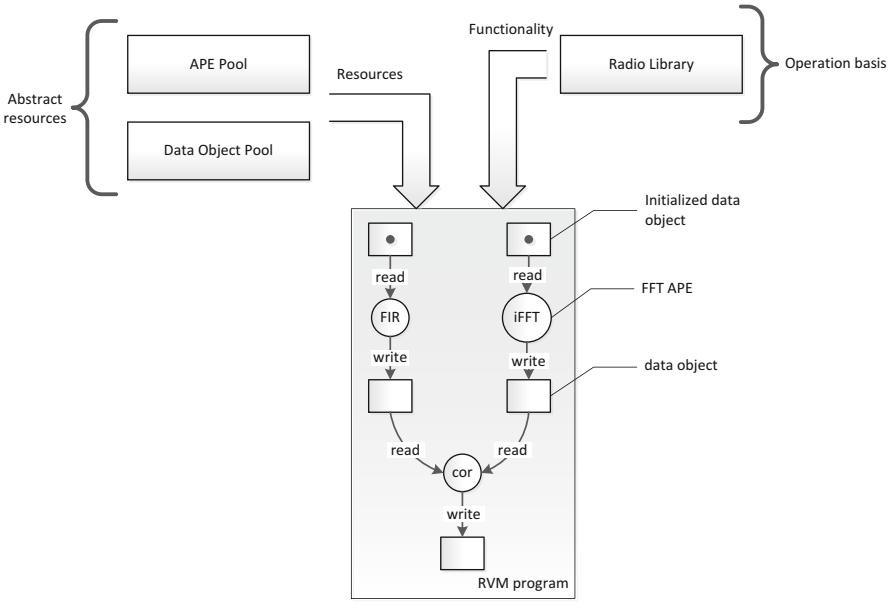

Fig. 22 Conceptual diagram of radio virtual machine processing [18]

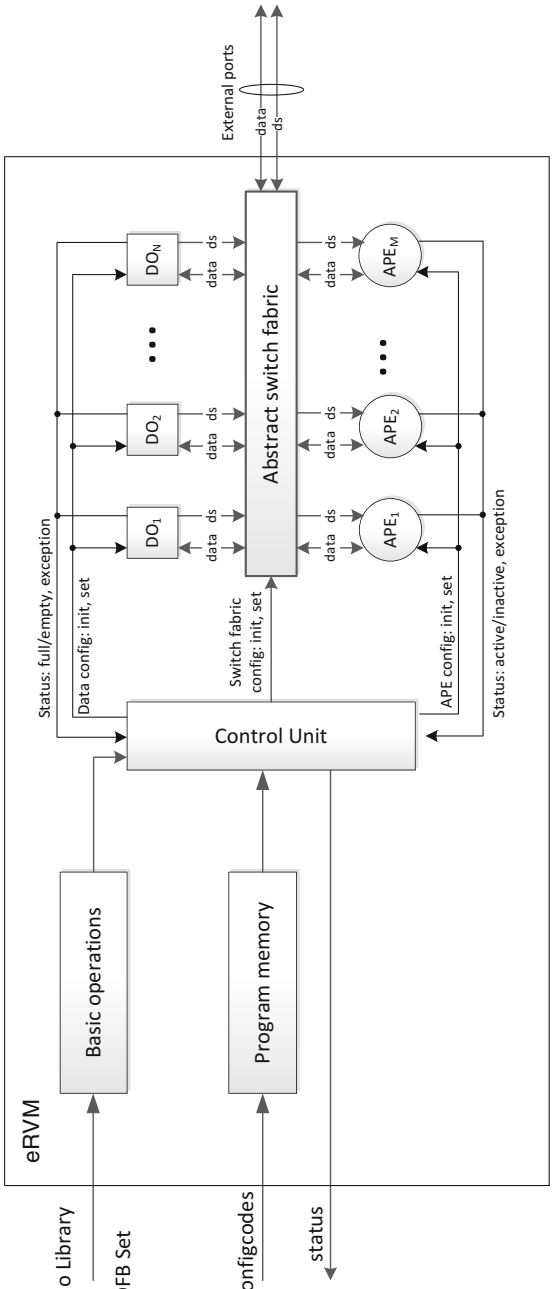

Fig. 23 Elementary RVM [18]

inactive operators. The result of computations is full DOs, which cannot activate the inactive operators.

Note: An output DO can become an input DO for a subsequent operator. Then, this input DO can activate the subsequent operator. Furthermore, the state or operation of a given APE is independent on the state of other APEs, i.e., each APE is atomic (Fig. 22).

In the sequel, the elementary RVM (eRVM) approach is described. An eRVM consists of components of basic operations, program memory, control unit (CU), abstract switch fabric (ASF), as well as APEs and DOs, of which the definitions are as follows. eRVM does not contain another eRVM or RVM.

Basic operations include operators either provided (i) from Radio Library as SFBs and/or (ii) from UDFB set as UDFBs, each of which is mapped onto one single APE.

Note: Since UDFBs might be implemented as a stand-alone module/function which can be mapped into one APE, in this case, basic operations include operators provided by UDFB set as well as by Radio Library as SFBs. Note that those UDFBs are atomic.

Note: For a RVM, the SFB or UDFB can be mapped onto an APE or RVM or eRVM. In the eRVM case, the mapping to RVM or eRVM is not possible since it is the lowest level of hierarchy. Furthermore, from an execution perspective, there is no difference between SFBs and UDFBs.

The program memory is provided with Configcodes which determine the eRVM configuration.

The CU generates initialization and setup instructions for APEs, DOs, and ASF based on decoding Configcodes stored in the program memory.

The ASF connects APEs and DOs in accordance with CU signals. One DO can be connected with multiple APEs. One APE can be connected with multiple DOs. DO from other eRVMs can be connected with ASF through external data ports.

Figure 21 illustrates a block diagram of eRVM. Basic Operations in eRVM consist of operations provided by the Radio Library and/or UDFB set.

Note: A target platform may or may not provide accelerators for some/all SFBs and/or UDFBs. Furthermore, three cases can be considered: (i) RAP includes only SFBs, (ii) RAP includes only UDFBs, and (iii) RAP includes SFBs and UDFBs. Finally, and independent of the upper note, basic operations may include (i) SFBs only, (ii) UDFBs only, or (iii) SFBs and UDFBs (Fig. 23).

Conclusion

In future 5G communication systems, the usage of hardware and spectrum resources will be dramatically different from previous generations. ETSI RRS deliverables will help to provide an efficient spectrum sharing framework based on Licensed Shared Access technology, which will lead to an overall higher spectrum usage efficiency and thus better QoS for the single end user. Software Reconfigurability solutions will allow chipset manufacturers to develop generic solutions which

can then be tailored to a multitude of vertical applications, including medical, automotive, industrial, mass market commercial, etc. ETSI RRS has developed an entire reconfiguration ecosystem which provides solutions for technical, security, and conformity needs. The underlying solution is different from existing state-of-the-art software reconfiguration approaches in the sense that (i) the manufacturer can choose any appropriate level of "openness" of the underlying platform (allowing for the replacement of an entire RAT or only specific components) and (ii) the Radio Virtual Machine approach ensures a highly efficient approach that allows code portability without requiring the usage of an (inefficient) middleware.

References

1. 3GPP TR 32.855, Technical Report 3rd Generation Partnership Project; Technical Specification Group Services and System Aspects; Telecommunication management; Study on OAM support for Licensed Shared Access (LSA); (Release 13)
2. 3GPP TS 32.101 (V11.2.0), Technical Specification 3rd Generation Partnership Project; Technical Specification Group Services and System Aspects; Telecommunication management; Principles and high level requirements (Release 11)
3. Complementary Report to ECC Report 159. Further definition of technical and operational requirements for the operation of white space devices in the band 470–790 MHz, ECC Report 185, 2013
4. Cross-border coordination for mobile/fixed communications networks (MFCN) and between MFCN and other systems in the frequency band 2300–2400 MHz, ECC Recommendation (14)04
5. Directive 1999/5/EC of the European Parliament and of the Council of 9 March 1999 on radio equipment and telecommunications terminal equipment and the mutual recognition of their conformity. http://eur-lex.europa.eu/legal-content/EN/TXT/?uri=CELEX:31999L0005
6. Directive 2014/53/EU of the European Parliament and of the Council of 16 April 2014 on the harmonisation of the laws of the Member States relating to the making available on the market of radio equipment and repealing Directive 1999/5/EC. http://eur-lex.europa.eu/legal-content/EN/TXT/?uri=celex:32014L0053
7. ECC Decision of 27 June 2014 on Harmonised technical and regulatory conditions for the use of the band 2300–2400 MHz for Mobile/Fixed Communications Networks (MFCN)
8. ECO Frequency Information System. http://www.efis.dk/
9. ETSI EN 301 598 V1.1.1 (2014-04) White Space Devices (WSD); Wireless Access Systems operating in the 470 MHz to 790 MHz TV broadcast band; Harmonized EN covering the essential requirements of article 3.2 of the R&TTE Directive
10. ETSI EN 302 969 V1.2.1 (2014-11) Reconfigurable Radio Systems (RRS); Radio Reconfiguration related Requirements for Mobile Devices
11. ETSI EN 303 095 V1.2.1 (2015-06) Reconfigurable Radio Systems (RRS); Radio Reconfiguration related Architecture for Mobile Devices
12. ETSI EN 303 143 (2015) Reconfigurable Radio Systems (RRS); System architecture for information exchange between different Geo-location Databases (GLDBs) enabling the operation of White Space Devices (WSDs)
13. ETSI EN 303 144 (2015) Reconfigurable Radio Systems (RRS); Enabling the operation of Cognitive Radio System (CRS) dependent for their use of radio spectrum on information obtained from Geo-location Databases (GLDBs); Parameters and procedures for information exchange between different GLDBs
14. ETSI EN 303 145 (2015) Reconfigurable Radio Systems (RRS); System Architecture and High Level Procedures for Coordinated and Uncoordinated Use of TV White Spaces

15. ETSI EN 303 146-1 V1.2.1 (2015-11) Reconfigurable Radio Systems (RRS); Mobile Device Information Models and Protocols; Part 1: Multiradio Interface (MURI)
16. ETSI EN 303 146-2 V1.2.1 (2016-06) Reconfigurable Radio Systems (RRS); Mobile Device (MD) information models and protocols; Part 2: Reconfigurable Radio Frequency Interface (RRFI)
17. ETSI EN 303 146-3 V1.2.1 (2016-08) Reconfigurable Radio Systems (RRS); Mobile Device (MD) information models and protocols; Part 3: Unified Radio Application Interface (URAI)
18. ETSI EN 303 146-4 V1.1.2 (2017-04) Reconfigurable Radio Systems (RRS); Mobile Device (MD) information models and protocols; Part 4: Radio Programming Interface (RPI)
19. ETSI EN 303 387 (2015) Reconfigurable Radio Systems (RRS); Signalling Protocols and information exchange for Coordinated use of TV White Spaces; Interface between Cognitive Radio System (CRS) and Spectrum Coordinator (SC)
20. ETSI TR 102 802. Reconfigurable Radio Systems (RRS); Cognitive Radio System Concept. Available at http://www.etsi.org
21. ETSI TR 102 907 (2012) Reconfigurable Radio Systems (RRS); Use Cases for Operation in White Space Frequency Bands, V1.2.1
22. ETSI TR 102 967 (2015) Reconfigurable Radio Systems (RRS); Use cases for dynamic equipment reconfiguration, V1.2.1
23. ETSI TR 103 067 (2013) Reconfigurable Radio Systems (RRS); Feasibility study on Radio Frequency (RF) performance for Cognitive Radio Systems operating in UHF TV band White Spaces
24. ETSI TR 103 087 (2016) Reconfigurable Radio Systems (RRS);Security related use cases and threats in Reconfigurable Radio Systems
25. ETSI TR 103 087 V1.1.1 (2016-06) Reconfigurable Radio Systems (RRS); Security related use cases and threats in Reconfigurable Radio Systems
26. ETSI TR 103 113 (2013) Electromagnetic compatibility and Radio spectrum Matters (ERM); System Reference document (SRdoc); Mobile broadband services in the 2300 MHz–2400 MHz frequency band under Licensed Shared Access regime
27. ETSI TR, under development, Reconfigurable Radio Systems (RRS); Applicability of RRS with existing Radio Access Technologies and core networks Security aspects
28. ETSI TS 102 946 (2014) Reconfigurable Radio Systems (RRS); System requirements for Operation in UHF TV Band White Spaces
29. ETSI TS 103 145 V1.1.1 (2015-01) Reconfigurable Radio Systems (RRS); System Architecture and High Level Procedures for Coordinated and Uncoordinated Use of TV White Spaces
30. ETSI TS 103 154 (2016) Reconfigurable Radio Systems (RRS); System requirements for operation of Mobile Broadband Systems in the 2300 MHz–2400 MHz band under Licensed Shared Access (LSA)
31. ETSI TS 103 235 (2016) Reconfigurable Radio Systems (RRS); System architecture and high level procedures for operation of Licensed Shared Access (LSA) in the 2300 MHz–2400 MHz band
32. ETSI TS 103 379 (2016) Reconfigurable Radio Systems (RRS); Information elements and protocols for the interface between LSA Controller (LC) and LSA Repository (LR) for operation of Licensed Shared Access (LSA) in the 2300 MHz–2400 MHz band
33. ETSI TS 103 436 (2016) Reconfigurable Radio Systems (RRS); Security requirements for reconfigurable radios
34. ETSI TS 103 436 V1.1.1 (2016-08) Reconfigurable Radio Systems (RRS); Security requirements for reconfigurable radios
35. European Commission (EC) mandate to CEPT for the 2300–2400 MHz frequency band in the EU issued in March 2014
36. FCC Report and Order, FCC 16-89, Issued On: 14 Jul 2016. Available at https://www.fcc.gov/document/spectrum-frontiers-ro-and-fnprm
37. Guidance for national implementation of a regulatory framework for TV WSD using geolocation databases, ECC Report 236, 2015

38. Guidance for the implementation of a sharing framework between MFCN and PMSE within 2300–2400 MHz, ECC Recommendation (15)04
39. Holland O, Ping S, Aijaz A, Chareau J-M, Chawdhry P, Gao Y, Qin Z, Kokkinen H (2015) To white space or not to white space: that is the trial within the Ofcom TV white spaces pilot. In: 2015 IEEE International Symposium on Dynamic Spectrum Access Networks (DySPAN 2015)
40. LSA management architecture, INTEL contribution, 3GPP TSG SA WG5 (Telecom Management) Meeting #102, 24–28 Aug 2015, Beijing
41. M/512, Standardisation Mandate to CEN, CENELEC and ETSI for Reconfigurable Radio Systems, Nov 2012. http://www.etsi.org/images/files/ECMandates/m512.pdf
42. Overview of FCC's New Rules for TV White Space Devices and database updates, FCC, Allen Yang, 2014. http://www.itu.int/en/ITU-R/study-groups/workshops/RWP1B-SMWSCRS-14/Presentations/USA%20-%20Overview%20of%20FCC%e2%80%99s%20New%20Rules%20for%20TV%20White%20Space%20Devices%20and%20database%20updates.pdf
43. Report and Order and Second Further Notice of Proposed Rulemaking, FCC 15–47, Adopted: 17 Apr 2015 Released: 21 Apr 2015
44. Report on CUS and other spectrum sharing approaches, RSPG (Radio Spectrum Policy Group), RSPG11-392, 2011b
45. RSPG Opinion on Licensed Shared Access, RSPG (Radio Spectrum Policy Group), RSPG13-538, 2013
46. Spectrum Availability Simulation Environment, RED Technologies, 2015
47. Technical and operational requirements for the possible operation of cognitive radio systems in the 'white spaces' of the frequency band 470–790 MHz, ECC Report 159, 2011
48. TV white spaces – approach to coexistence. Technical report, OFCOM, OFCOM UK, Sept 2013
49. Wireless Innovation Forum. http://www.wirelessinnovation.org/

Spectrum Sharing Policy in Europe

50

Miia Mustonen, Marja Matinmikko, and Jarkko Paavola

Contents

Abstract

While the importance of harmonization on spectrum matters in the global scale is well known and the national regulatory authorities possess the power to govern the spectrum use within their territory, the regional level regulatory

M. Mustonen (✉)
VTT Technical Research Centre of Finland Ltd., Oulu, Finland
e-mail: miia.mustonen@vtt.fi

M. Matinmikko
Centre for Wireless Communications (CWC), University of Oulu, Oulu, Finland
e-mail: marja.matinmikko@oulu.fi

J. Paavola
Turku University of Applied Sciences, Turku, Finland
e-mail: jarkko.paavola@tuas.fi

W. Zhang (ed.), *Handbook of Cognitive Radio*,
https://doi.org/10.1007/978-981-10-1394-2_49

activities are important to bridge the gap between these two levels. This chapter introduces the spectrum management framework and spectrum sharing initiatives in the regional level in Europe. The roles of major European regulation and standardization authorities are outlined as well as the cooperation framework between these entities. Additionally, the activities promoting spectrum sharing in Europe is discussed. These European spectrum sharing policy developments have addressed the introduction of additional users in a spectrum band considering both individual usage rights and general authorization by developing specifically licensed shared access and TV white space sharing concepts. These sharing concept are introduced on general level as well as on the basis of introducing the underlying regional regulatory and standardization activities that have led to harmonized overall framework, leaving national administrations the freedom to decide on details of the implementation of the concept.

Introduction

The current spectrum regulatory framework consists of three levels: the international, regional, and national level. The role of the ITU-R at international level has been discussed in ▸ Chap. 48, "Spectrum Sharing Policy at Global Level" as the global forum for spectrum harmonization. The purpose of regional regulation is to harmonize ITU-R spectrum allocations at the regional level. This is especially critical in Europe with small countries with multiple borders and limited national markets. Harmonization in the regional level brings industry confidence on the continuity of spectrum availability, QoS guarantees, and scale of the solutions developed for spectrum management and spectrum sharing to guarantee return of investment and helps the regulators in coordination of spectrum between different radiocommunication services.

The use of mobile data has increased rapidly in the last few years as the increased amount of smartphones, tablets, and other devices has changed the usage patterns of users [1]. Meanwhile, regulatory authorities are struggling to find solutions to guarantee spectrum resources required to support this trend, as the regulatory process for traditional spectrum allocation is becoming too time-consuming and complex. In addition, finding harmonized spectrum for exclusive mobile use is getting increasingly difficult due to existing usage. This has motivated regulatory authorities to consider new concepts and tools to allow more flexibility in spectrum management and enable spectrum sharing.

There are several forums influencing spectrum management and particularly the spectrum sharing policy in Europe including the European Commission (EC), the Electronic Communications Committee (ECC) of European Conference of Postal and Telecommunications Administrations (CEPT), and the European Telecommunications Standards Institute (ETSI). These bodies have established close collaboration framework to promote new technology and services in order to guarantee compatibility of solutions leading to maximal benefit for the society. The European spectrum management framework and spectrum sharing-related activities have also been discussed previously in [2, 3] and [4].

The rest of this chapter is organized as follows. First, the European spectrum regulatory framework is introduced including the introduction of the relevant forums and description of the cooperation framework between them. Second, European activities to promote shared use of spectrum are introduced. Third, activities to develop the licensed shared access (LSA) concept are reviewed followed by sharing initiatives in the ultrahigh frequency (UHF) band. The chapter considers only sharing concepts that are based on individual licensing, leaving out the activities based on general authorization. Finally, conclusions are drawn.

European Regulatory Framework for Spectrum Management

European regional regulatory authorities regarding spectrum issues are the European Commission (EC) and the Electronic Communications Committee (ECC) of European Conference of Postal and Telecommunications Administrations (CEPT). The European Telecommunications Standards Institute (ETSI) is the European standardization organization. In the following sections, the roles of each of these entities as well as the means of cooperation between them are discussed.

The European Commission

The member states (MSs) of the European Union (EU) manage the radio spectrum at the national level in line with the EU level legislation. The MSs need to implement the EU level decisions and supply information on the status of national implementations such as on frequency allocations when requested by the EC. Thus, the EU level decisions on spectrum matters shape the spectrum sharing policy in the MSs. The EC is divided into directorate-generals (DGs). The DGs dealing with spectrum related issues are Communications Networks, Content and Technology (CNECT) and Mobility and Transport (MOVE). DG CNECT is the main DG dealing with mobile communications. It considers aspects such as digitization, regulatory environment for electronic communications, future internet, cyber security, digital privacy, and digital trust policy [5]. The aim of the DG MOVE is to promote efficient, safe, secure, and environmentally friendly mobility and to create the conditions for a competitive industry. Regarding mobile communications, for example, intelligent transport systems and plain and train-related communication issues fall under jurisdiction of DG MOVE.

The Radio Spectrum Policy Group (RSPG) is a high-level advisory group consisting of senior representatives of the MSs and the official representative of the EC. These include representatives from both the regulatory authorities and the ministries having responsibility for radio spectrum-related matters in each MS. The RSPG assists the EC in the development of radio spectrum policy by giving advice on radio spectrum policy issues, coordination of policy approaches, and harmonized conditions, where appropriate, with regard to the availability and efficient use of radio spectrum necessary for the establishment and functioning of the internal market [6]. This is illustrated in Fig. 1. The RSPG can also be requested by the

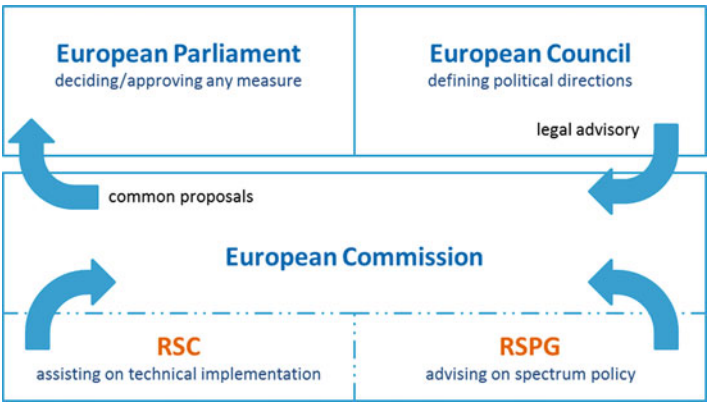

Fig. 1 Roles of different groups of the European Commission and cooperation

European Parliament and/or the Council to issue an opinion or produce a report on specific radio spectrum policy issues relating to electronic communications [7]. The RSPG consults all relevant stakeholders on a variety of technological, market, and regulatory developments relating to the use of radio spectrum. These include both commercial and noncommercial radio spectrum users as well as any other interested party. The Radio Spectrum Committee (RSC) assists EC on the development of technical implementing decisions to ensure harmonized conditions across Europe for the use of radio spectrum. The RSC is composed of MS representatives and is chaired by the EC [8]. EC discusses its proposals with national administrations before implementation in order to ensure that any measure is optimized to the various national situations.

Body of European Regulators for Electronic Communications (BEREC) was established by the European Parliament in 2009 to promote competition, contribute to the development of the internal market, and promote the interests of EU citizens. BEREC has recognized the radio spectrum to be essential to the development of the market and of innovative products and services and supports the study of innovative sharing mechanisms as means to optimize spectral efficiency.

ECC of CEPT

The CEPT is a recognized regional organization representing 48 European national regulatory administrations in the field of posts and telecommunications. Thus, it spans over a wider area than the EC. The goal of Electronic Communications Committee (ECC) of CEPT is to develop common policies and nonbinding regulations in electronic communications and related applications in order to harmonize the use of the radio spectrum across Europe [9]. European proposals developed in ECC represent European interests in the ITU and other international organizations.

The ECC undertakes compatibility studies and establishes conditions and parameters for sharing between different spectrum users. Results of ECC studies are reported to public in the form of ECC Decisions, ECC Recommendations, ECC Reports, and CEPT Reports. ECC Decisions are measures to harmonize the use of spectrum and numbering across the CEPT membership. ECC Recommendations describe measures that national administrations are encouraged to apply. ECC Reports support ECC Recommendations and ECC Decisions by describing results of studies conducted by the ECC. CEPT Reports describe technical studies carried out by in response to mandates from the EC. Results of ECC studies are based on consensus between the member countries.

ETSI

ETSI is officially recognized European Standards Organization which produces standards for information and communication technologies (ICT), including fixed, mobile, radio, converged, broadcast, and internet technologies [10]. ETSI is an independent, nonprofit association; members include national administrations, companies, and international organizations. ETSI produces and maintains technical standards and other deliverables. In accordance to the EC standardization mandate M/536 [11], ETSI develops their part of harmonized standards for radio equipment under the Radio Equipment Directive (RED) [12]. This Directive covers products, including unlicensed devices, which use spectrum. Applying harmonized standards enable manufacturers and service providers to sell, deploy, and put into service the radio equipment within the whole EU. Additionally, ETSI develops technical reports, so-called system reference documents, SRdocs, which provide technical, legal, and economic background on new radio systems under standardization.

Cooperation Framework

The relationship between the EC, ECC, and ETSI is illustrated in Fig. 2 [13]. Partnership between these three aims to facilitate the delivery of technologies and services for the benefit of society. EC may issue study mandates to ECC of CEPT

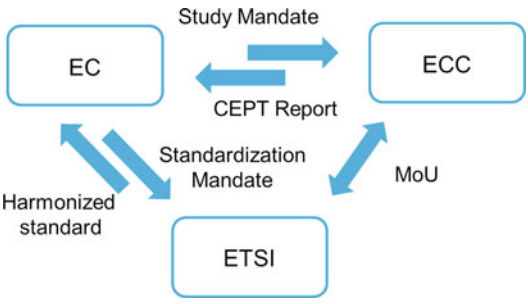

Fig. 2 Cooperation between European regulatory and standardization entities

for the development of technical implementing measures to ensure harmonized conditions for the use of radio spectrum. These mandates specify the task to be undertaken and the timeframe in which they should be achieved. ECC of CEPT communicates technical implementation measures to the EC in the form of CEPT Reports.

The EC submits standardization mandates to ETSI, which responses to these mandates via harmonized standards. Those CEPT Reports that are adopted as EC Decisions by the EC become mandatory for all MSs of the EU [13]. The cooperation agreement between ECC of CEPT and ETSI, so-called memorandum of understanding (MoU), ensures, for example, that deliverables from these parties do not contradict each other and the results from sharing studies are mutually acceptable and implemented consistently by both parties. A MoU has been established also between the CEPT and the EC to support activities on harmonization of radio spectrum.

Promoting Shared Use of Spectrum in Europe

Meeting the growing demand for wireless connectivity with traditional spectrum regulation based on exclusive usage or license-exempt usage is becoming increasingly difficult in the absence of vacant spectrum. In addition, making existing bands available for new type of usage is often expensive, involves delays, and runs the occasional risk of having to "switch off" existing users. Advances in technologies, for example, cognitive radio technology, make it possible for different types of wireless systems with different technologies to operate in the same frequency band. To make shared use of spectrum reality, there is a need to promote such new technologies and make shared use of spectrum easier in the regional level in Europe. Common European framework is needed to achieve economies of scale.

As the early steps to promote shared use of spectrum in 2008, the ECC published a CEPT report that identified white space as a part of the spectrum, which is available for a radiocommunication application (service, system) at a given time in a given geographical area on a non-interfering/non-protected basis with regard to primary services and other services with a higher priority on a national basis [14]. The report discussed cognitive techniques for white space applications in ultrahigh frequency (UHF) band including spectrum sensing, geolocation, and local beacons.

Further to promote shared use of spectrum, the EC has published a report on cognitive radio technologies in 2010 [15]. The purpose of the report was to clarify the concepts and the terminology used as well as to provide an overview of various enabling technologies for cognitive radio, for example, sensing, databases, cognitive pilot channels, and learning. It also provided an overview on various experiences with precognitive technologies and considered regulatory frameworks. Based on their study, the RSPG concluded that more efforts are needed to study the subject to provide adequate confidence on all stakeholders [15]. In 2011 RSPG together with Body of European Regulators for Electronic Communications (BEREC) published a report on infrastructure and spectrum sharing in mobile networks. The report

defined spectrum sharing as the simultaneous usage of a specific radio frequency band in a specific geographical area by a number of independent entities, leveraged through mechanisms other than traditional multiple- and random-access techniques. The report specifically denoted spectrum sharing to consist of common exploitation of frequencies among several operators [16].

As a continuation the EC published a communication to promote shared use of spectrum and highlighted the importance of identifying beneficial sharing opportunities in both licensed and license-exempt frequency bands [12]. These approaches could be based on national administrations granting shared spectrum access rights. The main drivers and enablers identified by the EC for spectrum sharing in Europe were (1) wireless broadband, (2) wireless-connected society, and (3) research and innovative technologies. The main benefits identified by the EC were cost savings for mobile network operators, affordable Internet connectivity, and infrastructure sharing possibilities as well as increased innovation potential arising from lowered spectrum access barrier. The greatest challenges were considered to arise from interference management, incentivizing and safeguarding all stakeholders and capacity of license-exempt bands.

In relation to the mission of the EC to set up annual and multiannual work programs for the European Union in the various economic fields, regarding spectrum management, the EC proposed in 2012 the Radio Spectrum Policy Program (RSPP) [17]. Core mission of the RSPP is to facilitate a strategy toward a digital agenda for Europe leading to a common digital market, part of which should be the efficient use of the spectrum by introducing more reliable approaches to share the resources. In this regard, the RSPP highlights considerations, for example, on the following topics:

- Innovative types of authorization
- CRS as a means to facilitate spectrum sharing based on geolocation
- A spectrum inventory to benefit spectrum sharing opportunities
- Harmonized standards for efficient use of spectrum and spectrum sharing

These considerations lead to decisions related to:

- The identification and sharing of best practices on authorization conditions and procedures
- Establishing a spectrum inventory, which could help to identify the bands suitable for reallocation and spectrum sharing
- The exploration of new ways of spectrum sharing

Regarding the spectrum inventory, the RSPG proposed a three-phased spectrum review process [18]. In the first phase, the demand for spectrum is assessed by collecting and analyzing information on the current and future demands for spectrum using, for example, trends in technology development, surveys, and forecasts of demand in relevant markets. In the second phase, the supply of spectrum is quantified based on the information about the actual use of the frequency bands.

In the third phase, the demand and supply of spectrum is analyzed to determine whether current allocations are adequate to meet the future demand and, if not, identify technically suitable bands to meet the increased demand.

Regarding the spectrum sharing, the EC has identified two dynamic sharing approaches that relate spectrum availability into time and geographical area:

- Collective use of spectrum (CUS): "*Collective Use of Spectrum allows an unlimited number of independent users and/or devices to access spectrum in the same range of designated CUS frequencies at the same time and in a particular geographic area under a well-defined set of conditions*" [19].
- Licensed shared access (LSA): "*A regulatory approach aiming to facilitate the introduction of radio communication systems operated by a limited number of licensees under an individual licensing regime in a frequency band already assigned or expected to be assigned to one or more incumbent users. Under the LSA framework, the additional users are allowed to use the spectrum (or part of the spectrum) in accordance with sharing rules included in their rights of use of spectrum, thereby allowing all the authorized users, including incumbents, to provide a certain QoS*" [20].

CUS concept is based on general authorization without any control on the number of users sharing the band [19]. A device is allowed to use spectrum that it finds unused through its capabilities. This type of usage is generally considered irreversible, and it may make the band unusable for other applications due the potential interference. Interference may be mitigated with power limits, duty cycle limits, or coordination between users. Alternatively, introduction on the higher-frequency ranges could be considered. Without any control mechanism, QoS offered for users depends on the amount of other traffic.

In the LSA concept, an incumbent user is able to share the spectrum assigned to it with one or several new users (so-called LSA licensees) in accordance with a set of conditions negotiated between the primary user and the LSA licensee and implemented under the direction of the NRA [19]. Since the incumbent user continues the use of spectrum while enabling the use of the same spectrum by other users, the efficiency of spectrum use is improved. The LSA concept allows the LSA licensee a faster access to a spectrum band in comparison to a lengthy repurposing process. Both the incumbent user and the LSA licensee are guaranteed protection from harmful interference and predictable QoS. A reliable sharing agreement and a database (or another system for updating the conditions of spectrum access) were considered as critical items for success of LSA by the RSPG. In its opinion on June 2013, the RSPG stated that [21] "To meet the growing demand for spectrum the industry and administrations are under pressure to introduce new technologies and regulatory mechanisms to optimise the use of the limited frequency resources. In this context, the promotion of the shared use of radio spectrum resources is a valuable means to offer additional spectrum access to broadband communications, for licence exempt but also licensed usage, which is a new paradigm referred to as Licensed Shared Access."

The development on the LSA concept has been continued by CEPT and ETSI as well as by Administrations in terms of live experimentation as will be discussed in the following section. It could be concluded that the EC values and supports the development of new concepts, related technologies, and authorization conditions for sharing the scarce spectrum resources in future. In the Digital Single Market (DSM) initiative of the EC [22], one of the key actions as announced by the EC is to *present an ambitious overhaul of EU telecoms rules. This includes more effective spectrum coordination and common EU-wide criteria for spectrum assignment at national level, creating incentives for investment in high-speed broadband; ensuring a level playing field for all market players, traditional and new; and creating an effective institutional framework* [23].

There are new activities in the development of next-generation mobile communication networks known as 5G. These efforts are specifically addressing new spectrum for the mobile service in preparation for WRC-19 in the frequency range between 24 and 86 GHz. In these discussions, spectrum sharing will play an increasingly important role. The 5G Action plan for Europe published by the EC in 2016 states that the potential for spectrum sharing, including under license-exempt use, should be maximized as it generally supports innovation and market entry [24]. RSPG published an early opinion on spectrum aspects for 5G in 2016 providing a strategic roadmap toward 5G for Europe [25]. As a specific point, the RSPG was requested to identify and analyze spectrum-related challenges, such as spectrum sharing, usage, and license conditions, which will be addressed in a subsequent detailed opinion. A communication from the EC in 2016 toward a gigabit society promotes shared use of spectrum, either on the basis of general authorization or individual rights of use, as it can enable more efficient and intensive exploitation of spectrum especially in the new millimeter spectrum bands foreseen for 5G communications [26]. CEPT roadmap for 5G published in 2016 urges to investigate new sharing opportunities and challenges that new technologies (e.g., MIMO) can bring [27].

Licensed Shared Access

The development of the LSA concept was initiated by industry with their concept of providing mobile industry means to access spectrum that was occupied by other services. Based on this initiative, the LSA at its current form was introduced by the EC as a general concept to facilitate controlled sharing between any two systems in such way that predictable QoS is provided [19]. Thus, the entrant user, so-called LSA licensee, may present any industry field. The incumbent user will maintain higher spectrum usage rights and is allowed to reclaim spectrum when needed. This will increase the efficiency of spectrum use considerably, especially when considering sporadic or spatially restricted incumbent usage.

In LSA, access to the shared band is based on licensing regime and a sharing framework. Depending on the national approach and incumbent usage, the LSA license may be limited in time or geographical area. The sharing framework defines

the set of conditions for shared access, and it is negotiated between the incumbent user, the LSA licensee, and the NRA. The conditions should be defined in reasonable accuracy to provide enough predictability toward the future access to spectrum for the LSA licensee, to invest in equipment and network.

The first use case of LSA considered in the standardization and regulation in Europe has been the application to the 2.3–2.4 GHz band to enable mobile operations on the band [28–31], and [32]. This band has been allocated to mobile service and identified for international mobile telecommunications (IMT) by the WRC-2007 of the ITU-R on a globally harmonized manner. However, due to the incumbent usage on the band, it is not available for mobile use on an exclusive basis globally or even in all European countries. The incumbent use on the band includes Programme Making and Special Events (PMSE), wireless cameras, telemetry, fixed service, unmanned aircraft systems, and amateur service depending on the country [28]. The amateur service, however, is on the secondary basis and therefore has no protection from LSA usage. Tools for LSA need to be flexible enough to function regardless of the difference characteristics of the incumbent usage. Task of the European regulatory and standardization activities is to develop harmonized solutions for LSA in order to create a European internal market. The activities of ECC of CEPT and ETSI on LSA are explained below and summarized in Fig. 3.

The first report from ECC of CEPT on LSA was aimed at providing a description of the general LSA framework that could be applied to enable sharing between any two services in accordance to the definition of RSPG [33]. Studies were made on the compatibility of the LSA framework with the current regulatory framework on the use of spectrum, current spectrum management, and management of frequency authorizations. Additionally, some general guidelines were given on the applicability criteria of LSA when applied to the mobile communications. Regarding the application of the LSA concept to the 2.3–2.4 GHz band, the work was initiated by the EC by sending a study mandate to CEPT on harmonized conditions for mobile use on the band [34]. As a response, ECC of CEPT developed guidelines for the application of LSA into this band and communicated them to EC in the form of two CEPT Reports. In the first report, technological and regulatory options for sharing between mobile broadband and the relevant incumbent services were identified [28]. The report included an overview of different incumbent services on the band in the European countries as well as options for sharing for these services. In the second report, focus was on the technical sharing solutions between the mobile broadband and PMSE, which is the most common incumbent usage on the band [29]. The report included a step-by-step approach for the implementation of an LSA sharing framework. The following steps were identified: determining the extent and type of incumbent use, calculating the protection criteria for the incumbent, and identifying operational conditions for sharing, such as implications on the mobile network.

The use case considered for LSA in ETSI RRS is bandwidth expansion to an existing MNO [30]. In practice this means additional bandwidth to an MNO that is already operating LTE in a licensed band in that given area. This can be used either for macro- or small cell deployment. The first system reference document from ETSI provided an overview of the LSA concept, including aspects such

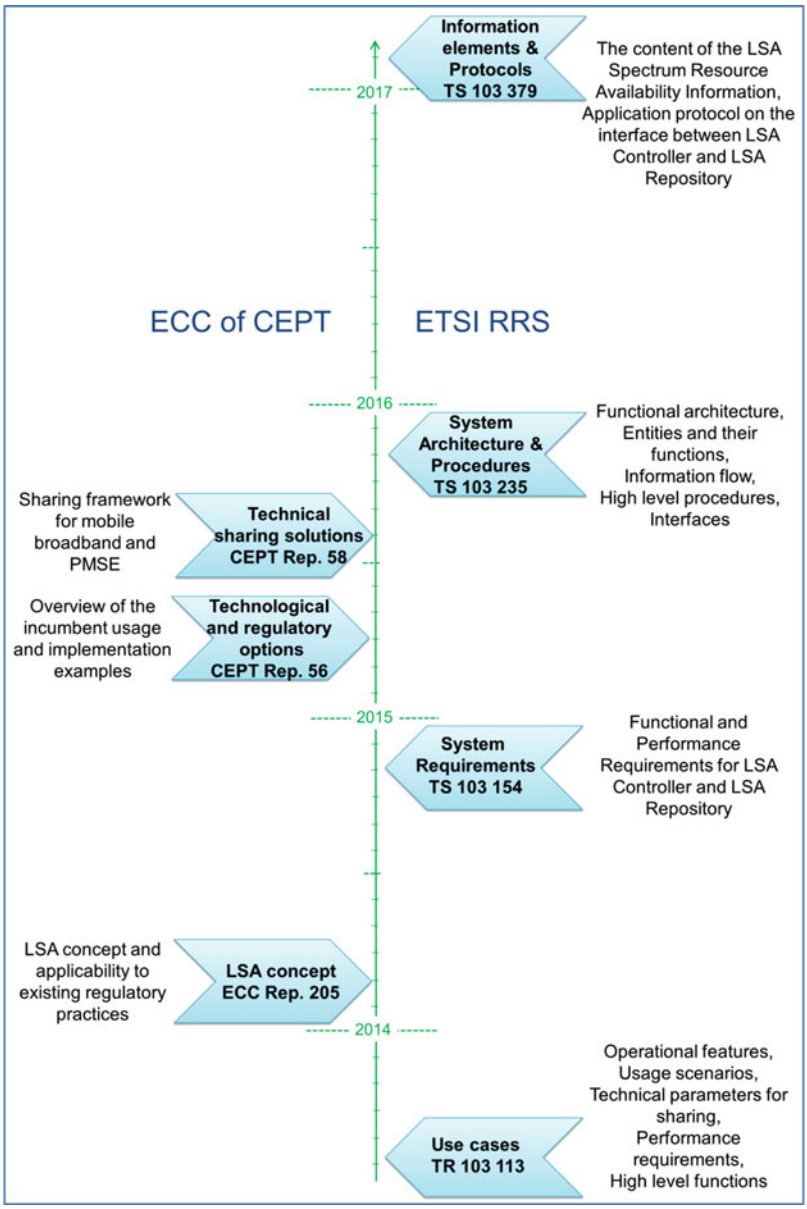

Fig. 3 Activities on LSA in ECC of CEPT and ETSI RRS

as operational features, performance requirements, and high-level functions [30]. At this point, it was outlined that the LSA architecture would be based on two functional units on top of the existing cellular network: LSA controller (LC) and LSA repository (LR). This is illustrated in Fig. 4 [30]. In this initial report, the

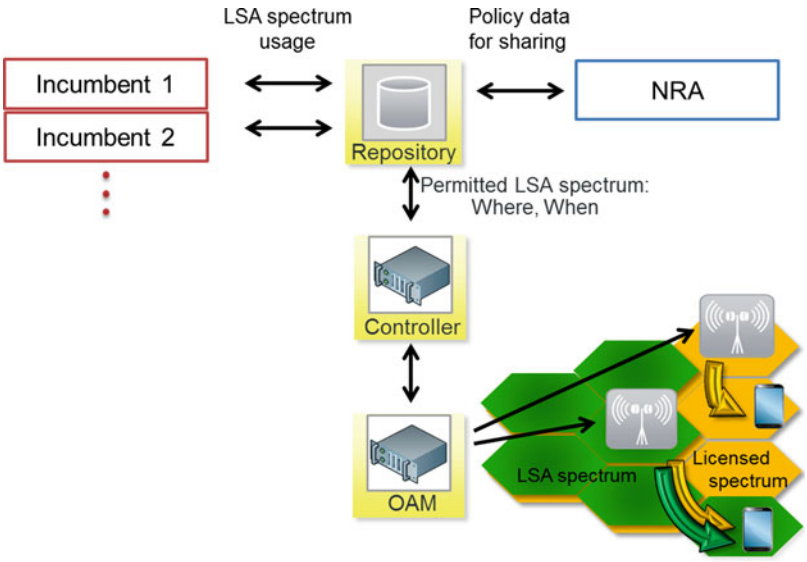

Fig. 4 An example architecture for LSA according to ETSI RRS

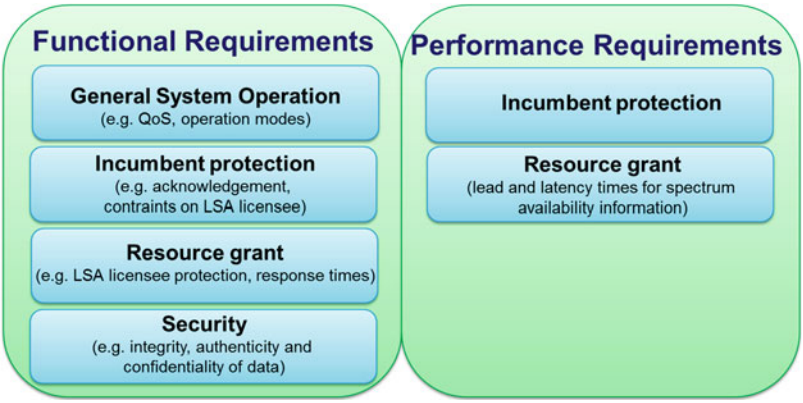

Fig. 5 Requirements for the LSA system defined by ETSI RRS

LR was defined as a database that contains information on the incumbent spectrum usage and LC as a control unit that uses this information together with additional information on, e.g., access rules to compute the spectrum availability information. This initial definition was then complemented in the second report which provided a full list of functional and performance requirements for the LSA system, consisting of LC and LR, that would enable mobile broadband access to the band [31]. These requirements were categorized as shown in Fig. 5. Functional requirements relate to the general system operations, to the protection of the incumbent user, to the

process of granting the rights of use of LSA spectrum resource to the LSA licensee, and to security. Performance requirements relate to the timescales required by the LSA system for delivering spectrum usage information. Third report defined high-level functions and mapped them into the two logical elements, LC and LR [32]. It also defined high-level procedures, messaging, and information exchange between these elements. The last report defined the application protocol LC and LR, and the content of the LSA spectrum resource availability information (LSRAI) conveyed by this protocol [35].

One of the major benefits of the LSA is that it requires no changes to internal procedures or air interfaces of the mobile network or to the user equipment. Therefore, there is no need to change the mobile network internal procedures or protocols defined by the 3rd Generation Partnership Project (3GPP) standardization. This reduces the time required for implementation considerably. The fact that LSA can be implemented using additional logical units on top of the cellular architecture also means that the MNO can continue using the existing equipment regardless of whether it needs to implement LSA or not. However, on an architecture level, 3GPP is working on defining a harmonized LSA solution supported by the 3GPP network management architecture and internal interfaces [36].

Sharing Concepts Targeted for the UHF Band

For several decades the ultrahigh frequency (UHF) band has been used for broadcasting linear over-the-air TV services in Europe, but the broadcasting sector received pressure particularly from the mobile communication sector to give up parts of its traditional UHF broadcasting spectrum to be used by the mobile service. As a consequence, almost half of the original UHF broadcasting band (470–862 MHz) has been or is being cleared from broadcasting service and repurposed for mobile use in Europe (694–862 MHz). In addition, there are spectrum sharing initiatives specifically addressing the UHF band which are discussed next.

TV WS

The CEPT defines a white space (WS) as a part of the spectrum, which is available for a radiocommunication application (service, system) at a given time in a given geographical area on a non-interfering/non-protected basis with regard to primary services and other services with a higher priority on a national basis [14]. The European regulatory activities on TV WSs were initiated in ECC of CEPT within Working Group (WG) Spectrum Engineering (SE) in May 2009. A dedicated Project Team (PT) SE43 "*White Spaces-cognitive radio systems*" began its work by defining technical and operational requirements for the possible operation of cognitive radio systems in the white space of the frequency band 470–790 MHz. Terms of reference to SE43 was to (1) define technical and operational requirements for the operation of cognitive radio systems in the white spaces of the UHF broadcasting band

(470–790 MHz) to ensure the protection of incumbent radio services/systems and investigate the consequential amount of spectrum potentially available as white space; (2) provide, if required, technical assistance on further issues related to white spaces and cognitive radio systems that ECC may identify in the future; and (3) liaise directly with relevant groups within ECC and ETSI as necessary [37].

The first report from SE43 addressed technical and operational requirements for the possible operation of cognitive radio systems in the white spaces needed to ensure the protection of the incumbent radio services [38]. The report identified a range of possible deployment scenarios as well as set up some key working assumptions and protection criteria to be used in sharing studies for different incumbent services existing on the band. In the second report, additional technical investigations to facilitate development of the regulation for white space devices (WSDs) were performed [39]. The report described the protection of incumbents, digital terrestrial television (DTT) broadcasting and PMSE wireless microphones, protection of services on the bands adjacent to UHF TV band, and the classification and technical characteristics of WSDs. It also included measurement campaigns which detailed DTT and PMSE protection ratios tests with example WSD technologies. The third report described the use of information in a centralized manner from a geolocation database to guarantee the protection of the incumbent services [40]. The report provided detailed framework proposal based on new modeling techniques and a range of measurement campaigns as well assessed the appropriateness of the geolocation technique for protecting incumbent services coexisting and adjacent bands. The report also provided more detailed guidance on general principles and basic requirements for WSDs operating under the geolocation database.

The work of SE43 was later on complemented by the work of ECC WG Frequency Management (FM) PT 53 group [41]. In this group, a report was developed for describing overall framework for TV WSD using geolocation databases and for providing guidance for national implementation [42]. Additionally, the report described options for database policy and provision. Annex 2 of the report contained a high-level description of an example of national implementation of TVWS framework and calculation of operational parameters from Ofcom UK.

The standardization for TVWS has been performed in ETSI RRS. ETSI has carried out extensive standardization efforts for operation in TV white spaces by defining and publishing technical specifications for use cases [43], system architecture and high-level procedures [44], and system architecture for information exchange between different geolocation databases [45]. The European standard for TV white space devices was published in [46]. Harmonized standard covering the essential requirements of article 3.2 of the Radio and Telecommunication Terminal Equipment (R&TTE) Directive [47], which includes WSD radio frequency (RF) requirements to prevent harmful interference to DTT incumbents by setting specific limits for the radiated power in the assigned and adjacent channels of the WSD. In addition, ETSI has published an European standard on parameters and procedures for information exchange between different geolocation databases (GLDBs) in [48] and signaling protocols and information exchange for coordinated use of TV White Spaces in [49].

Flexible Use of UHF Band

The flexible use of UHF band has been under active discussion in the last few years as the media convergence has inspired a lot of investigations on the broadcast broadband converge and its impact on spectrum and network [50]. In Europe, the high-level group (HLG), comprised of nineteen executive-level representatives from the mobile and broadcasting sectors, was convened by the EC in 2013 to deliver strategic advice to the EC for developing a European strategy on the future use of the UHF band. The results of the 6-month long debate in the group were reported by one of the group members [51]. In parallel, the regulatory group ECC of CEPT TG6 "long-term vision UHF" prepared a report, long-term vision for the UHF broadcasting band, identifying and analyzing possible scenarios for the development of the UHF band in the long term [52].

RSPG of the EC issued a draft opinion on the future use of the UHF band 470–790 MHz supporting the provisioning of wireless broadband services in the 700 MHz band [53]. In the opinion, RSPG recommended that the frequency band 470–694 MHz will remain available for broadcasting in the future. However, it also encouraged flexibility for countries to use the band for wireless broadband in downlink. In line with the RSPG view, the EC published a draft decision to allow mobile downlink use on the band [54]. This would allow member states of the EU to introduce mobile use on the band on a national basis in accordance to the current regulatory boundary conditions, without causing interference or claiming protection from broadcasting in the neighboring countries. In practice the availability of the spectrum would vary within country. The shared use with broadcasting and variable availability of the spectrum may motivate the implementation and further development of spectrum sharing concepts such as LSA.

Conclusion and Future Directions

The regional-level regulatory activities on spectrum matters aim to bridge the gap between the international harmonization and governance of spectrum by national administrations. Regional harmonization plays a critical role especially in Europe with small national markets for countries. The purpose of the harmonization at the regional level is to provide industry confidence and visibility to the future opportunities as well as to guarantee economies of scale for the sharing solutions to guarantee return of investment. It also aids European administrations to manage spectrum in their country in an efficient manner as well as to coordinate between the neighboring countries.

In the last few years, extensive efforts have been taken at the European level to develop new spectrum sharing concepts that introduce additional users in a frequency band on a shared basis while protecting the incumbent users. This has led to considerations on concepts targeted for specific bands (e.g., UHF band) as well as development of more general sharing frameworks such as LSA. In addition

to currently considered use case of mobile broadband, LSA has potential not only for mobile as currently considered but also to enable sharing between any two radio systems.

Importance of spectrum sharing will significantly grow in the development of 5G systems that will operate in a wide range of frequency bands. In particular, the operation in higher-frequency bands will require sharing with incumbents as well as between 5G networks where the development of European level harmonization will be important. Spectrum sharing becomes more relevant to all future use cases for 5G, and it is therefore essential to understand how to develop the frameworks within which different technologies and services can coexist in the same frequency band.

References

1. Cisco (2016) Cisco Visual Networking Index: Global Mobile Data Traffic Forecast Update, 2015–2020, 39p
2. Anker P (2014) International regulations and DSA. In: Medeisis A, Holland O (eds) Cognitive radio policy and regulation. Springer, Switzerland, pp 2–14
3. Medeisis A (2014) European regulatory developments related to CR. In: Medeisis A, Holland O (eds) Cognitive radio policy and regulation. Springer, Switzerland, pp 14–19
4. Anker P (2015) International regulatory framework for spectrum and spectrum sharing. In: Holland O, Bogucka H, Medeisis A (eds) Opportunistic spectrum sharing and white space access. John Wiley & Sons, Inc., New Jersey, pp 259–275
5. EC (2016) DG Connect, Who we are. Available: https://ec.europa.eu/digital-single-market/en/who-we-are-dg-connect. Accessed 18 Jan 2017
6. EC (2002) Commission Decision of 26 July 2002 establishing a Radio SpectrumPolicy Group. European Commission. 2002/622/EC
7. EC (2009) Commission Decision of 16 December 2009 amending Decision 2002/622/EC establishing a Radio Spectrum Policy Group. 2009/978/EU
8. EC (2002) Decision No 676/2002/EC of the European Parliament and of the Council of 7 March 2002 on a regulatory framework for radio spectrum policy in the European Community (Radio Spectrum Decision). European Commission. 676/2002/EC
9. ECC (2016) ECC All about our organization, v. 2. Available: http://cept.org//files/1051/ECC/Who%20are%20we/ECC%20Leaflet%20pdf/ECC_Leaflet_v2-Nyropsgade.pdf. Accessed 18 Jan 2017
10. EU (2012) Regulation (EU) No 1025/2012 of the European Parliament and of the Council of 25 October 2012 on European standardization. Official Journal of the European Union
11. EC (2015) Commission implementing decision of 4.8.2015 on a standardisation request to the European Committee for Electrotechnical Standardisation and to the European Telecommunications Standards Institute as regards radio equipment in support of Directive 2014/53/EU of the European Parliament and of the Council. M/536
12. Directive 2014/53/EU of the European Parliament and of the Council of 16 April 2014 on the harmonisation of the laws of the Member States relating to the making available on the market of radio equipment and repealing Directive 1999/5/EC. 2014/53/EU
13. ECC & ETSI (2016) The European regulatory environment for radio equipment and spectrum. An introduction, v. 2.1. Available: http://www.etsi.org/e-brochure/radio/ETSI_ECC%20Brochure_2016_Web.pdf. Accessed 18 Jan 2017
14. ECC (2008) A preliminary assessment of the feasibility of fitting new/future applications/services into non-harmonised spectrum of the digital dividend (namely the so-called “white spaces” between allotments). Report C from CEPT to the European Commission in

response to the Mandate on: "Technical considerations regarding harmonisation options for the Digital Dividend". CEPT Report 24
15. RSPG (2011) Final RSPG Report on Cognitive Technologies. European Commission, Radio Spectrum Policy Group. RSPG10-348
16. BEREC & RSPG (2011) BEREC-RSPG report on infrastructure and spectrum sharing in mobile/wireless networks. Body of European Regulators for Electronic Communications and Radio Spectrum Policy Group. BoR (11)16, RSPG11-374
17. EU (2012) Decision No 243/2012/EU of the European Parliament and of the Council of 14 March 2012 establishing a multiannual radio spectrum policy programme. Off J Eur Union 55:7–17
18. RSPG (2012) Final RSPG Opinion on Review of Spectrum Use. European Commission, Radio Spectrum Policy Group. RSPG12-408
19. RSPG (2011) Report on Collective Use of Spectrum (CUS) and other spectrum sharing approaches. European Commission, Radio Spectrum Policy Group. RSPG11-392
20. RSPG (2013) RSPG Opinion on Licensed Shared Access. European Commission, Radio Spectrum Policy Group. RSPG13-538
21. RSPG (2013) RSPG Opinion on strategic challenges facing Europe in addressing the growing spectrum demand for wireless broadband. European Commission, Radio Spectrum Policy Group. RSPG13-521 rev1
22. EC (2015) A Digital single market strategy for Europe. Communication from the Commission to the European Parliament, the Council, the European Economic and Social Committee and the Committee of the Regions, European Commission. COM(2015) 192 final
23. EC (2015) A Digital Single Market for Europe: Commission sets out 16 initiatives to make it happen. Press release. Available: http://europa.eu/rapid/press-release_IP-15-4919_en.htm. Accessed 18 Jan 2017
24. EC (2016) 5G action plan from EC. Communication from the Commission to the European Parliament, the Council, the European Economic and Social Committee and the Committee of the Regions. European Commission. COM(2016) 588 final
25. RSPG (2016) Strategic roadmap towards 5G for Europe. Radio Spectrum Policy Group. European Commission. RSPG16-032 final
26. EC (2016) Communication from the Commission to the Parliament, the Council, the European Economic and Social Committee and the Committee of the Regions. Connectivity for a Competitive Digital Single Market – Towards a European Gigabit Society. European Commission, COM (2016) 587 final
27. ECC (2016) CEPT Roadmap for 5G. Electronic Communications Committee of European Conference of Postal and Telecommunications Administrations, ECC(16)110 Annex 17. Available: http://cept.org/Documents/ecc/33486/ecc-16-110-annex-17_cept-roadmap-for-5g. Accessed 18 Jan 2017
28. ECC (2015) Technological and regulatory options facilitating sharing between Wireless broadband applications (WBB) and the relevant incumbent services/applications in the 2.3 GHz band. CEPT Report 56
29. ECC (2015) Technical sharing solutions for the shared use of the 2300–2400 MHz band for WBB and PMSE. CEPT Report 58
30. ETSI (2013) Mobile Broadband services in the 2300–2400 MHz frequency band under Licensed Shared Access regime. ETSI TR 103.113 v.1.1.1
31. ETSI (2014) System requirements for operation of Mobile Broadband Systems in the 2300 MHz–2400 MHz band under Licensed Shared Access (LSA). ETSI TS 103 154 v.1.1.1
32. ETSI (2015) System Architecture and High Level Procedures for operation of Licensed Shared Access (LSA) in the 2300 MHz–2400 MHz band. ETSI TS 103 235 v.1.1.1
33. ECC (2014) Licensed Shared Access (LSA). ECC Report 205
34. EC (2014) Mandate to CEPT to develop harmonised technical conditions for the 2300–2400 MHz ('2.3GHz') frequency band in the EU for the provision of wireless broadband electronic communication services. European Commission, DG CONNECT/B4

35. ETSI (2016) Information elements and protocols for the interface between LSA Controller (LC) and LSA Repository (LR) for operation of Licensed Shared Access (LSA) in the 2300 MHz–2400 MHz band. ETSI TS 103 379 v0.0.14
36. 3GPP (2016) Study on OAM support for Licensed Shared Access (LSA). 3rd Generation Partnership Project. TR 32.855 v14.0.0
37. ECC (2017) SE43 working group. Available: http://www.cept.org/ecc/groups/ecc/closed-groups/se-43. Accessed 18 Jan 2017
38. ECC (2011) Technical and operational requirements for the possible operation of cognitive radio systems in the white spaces of the frequency band 470–790 MHz. ECC Report 159
39. ECC (2013) Complementary Report to ECC Report 159. Further definition of technical and operational requirements for the operation of white space devices in the band 470–790 MHz. ECC Report 185
40. ECC (2013) Technical and operational requirements for the operation of white space devices under geo-location approach. ECC Report 186
41. ECC (2017) FM53 working group. Available: http://www.cept.org/ecc/groups/ecc/closed-groups/fm-53/. Accessed 18 Jan 2017
42. ECC (2015) Guidance for national implementation of a regulatory framework for TV WSD using geo-location databases. ECC Report 236
43. ETSI (2010) Use Cases for Operation in White Space Frequency Bands, ETSI TR 102 907 v.1.1.1
44. ETSI (2014) System Architecture and High Level Procedures for Coordinated and Uncoordinated Use of TV White Spaces. ETSI TS 103 145 v.1.1.1
45. ETSI (2014) System architecture for information Exchange between different Geo-Location databases (GLDB's) enabling the operation of White Space Devices (WSDs). ETSI TS 103 143 v.1.1.1
46. ETSI (2014) White Space Devices (WSD); Wireless Access Systems operating in the 470 MHz to 790 MHz frequency band; Harmonized EN covering the essential requirements of article 3.2 of the R&TTE Directive. ETSI EN 301 598 v1.1.1
47. ETSI (2014) System requirements for Operation in UHF TV Band White Spaces. ETSI TS 102 946 v.1.1.1
48. ETSI (2015) Parameters and procedures for information exchange between different GLDBs. ETSI EN 303 144 v.1.1.1
49. ETSI (2015) Signalling Protocols and information Exchange for Coordinated use of TV White Spaces; part 1: interface between Cognitive Radio System (CRS11) and Spectrum Coordinator (SC). ETSI EN 303 387 v.1.1.1
50. Lewins D et al (2014) Challenges and opportunities of broadcast – broadband con-vergence and its impact on spectrum and network use. Plum and Farncombe Consulting
51. Lamy P (2014) Results of the work of the high level group on the future use of the UHF band (470–790 MHz). Technical Report. Available: http://ec.europa.eu/newsroom/dae/document.cfm?doc_id=6721. Accessed 18 Jan 2017
52. ECC (2014) Long Term Vision for the UHF broadcasting band. ECC Report 224
53. RSPG (2014) Draft RSPG Opinion on a long-term strategy on the future use of the UHF band (470–790 MHz) in the European Union. RSPG14-585rev1
54. EC (2016) Proposal for a Decision of the European Parliament and of the Council on the use of the 470–790 MHz frequency band in the Union. European Commission. COM/2016/043

Further Reading

1. EC (2012) Promoting the shared use of radio spectrum resources in the internal market. In: European Commission (COM 2012), p 478

Novel Regulatory Solutions for Cognitive Radio and Spectrum Sharing in the United States

51

Lee Pucker

Contents

L. Pucker (✉)
The Wireless Innovation Forum, Reston, VA, USA
e-mail: Lee.Pucker@wirelessinnovation.org

W. Zhang (ed.), *Handbook of Cognitive Radio*,
https://doi.org/10.1007/978-981-10-1394-2_50

Abstract

The regulation of spectrum in the United States is managed by two independent agencies: the National Telecommunications and Information Administration, who is responsible for spectrum used by US government agencies such as the Department of Defense and the National Weather Service, and the Federal Communications Commission, who is responsible for all nonfederal spectrum. Both agencies are mandated by law to maximize the efficient use of spectrum, and toward that end, both agencies are working to share underutilized spectrum to the greatest extent possible. This chapter will explore various initiatives by these two agencies to achieve this objective, both independently and in cooperation.

Introduction

Regulation of spectrum sharing in the United States is oftentimes more complex than in other countries because spectrum is managed by multiple regulatory agencies (see Fig. 1) [1]. Through the Communication Act of 1934, the US Congress established the Federal Communications Commission (the FCC or "Commission") as an independent body with broad powers to regulate both wireline and wireless communications for nonfederal use including commercial, private, and state and local government use. Through the same act, Congress reserved for the President of the United States the authority to assign operating frequencies for federal government use. In 1978, the President issued an executive order effectively delegating these powers to the newly established National Telecommunications and Information Administration (NTIA) operating within the Department of Commerce and led by the Assistant Secretary of Commerce for Communications and Information. Congress later codified the functions defined in this order in the National Telecommunications and Information Administration Organization Act, making the delegation permanent.

The regulation of spectrum is managed differently by the FCC and NTIA. Regulations from the FCC are largely created through a rulemaking process [2]. For each new rule, a docket is opened to act as an electronic file for all the rulemaking documents issued. Once a docket is opened, a notice of public rulemaking (NPRM) can be released, defining the need for and the text of the proposed rule to allow for public comment. Comments and reply comments (comments about the comments) are reviewed, and the Commission can then choose to leave the docket open, issue a further notice of proposed rulemaking with an amended proposal, or issue a final rule, or Order. The Commission may also release a notice of inquiry or other public notice in support of the rulemaking process. The FCC's rules and regulations are in Title 47 of the Code of Federal Regulations (CFR), which are published and maintained by the Government Printing Office. Parties disagreeing with the final rules may issue a petition for reconsideration or seek court review of the decision. The FCC is supported in this rulemaking process through a Technological Advisory Council (TAC), which is comprised of leading experts and is chartered to

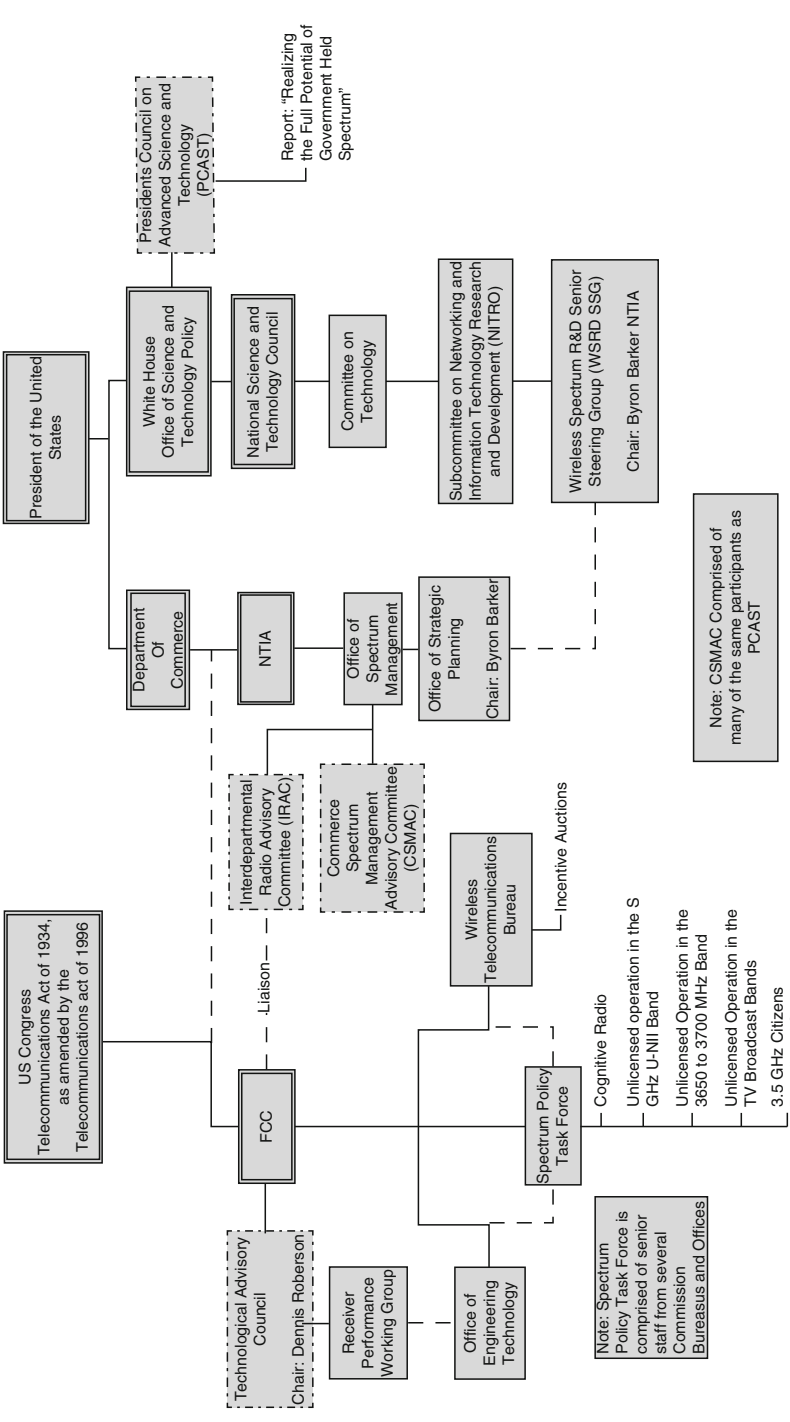

Fig. 1 Relationships between organizations regulating and managing spectrum in the United States

help the Commission keep abreast of current innovations and understand relevant technologies [3].

Spectrum management at NTIA follows a different model. Policies and procedures for assigning federal spectrum within the United States are established by NTIA's Office of Spectrum Management (OSM) [4]. To help facilitate this task, OSM chairs the Interdepartmental Radio Advisory Committee (IRAC) consisting of representatives from 19 federal government agencies who advise the NTIA on policies and regulations for the use of federal spectrum [5]. OSM coordinates with the IRAC to set policy for the assignment of spectrum, the results of which are published in the NTIA "Manual of Regulations and Procedures for Federal Radio Frequency Management," also known as the "Red Book" [6]. In addition to the IRAC, OSM receives support in this area from the Commerce Spectrum Management Advisory Committee (CSMAC), comprised of government and industry experts chartered to advise NTIA on spectrum management policy [7].

The Communications Act of 1934 does not allocate exclusive use of specific bands for federal and nonfederal use, so all allocations stem from coordination and agreement between the FCC and NTIA. To help in this process, the FCC appoints a representative to act as a liaison between the IRAC and the Commission. Through this coordination, 54.2% of spectrum below 3.1 GHz in the United States is already shared, with 31.7% and 14.1% allocated, respectively, to the private sector and government on an exclusive basis [8]. Until recently, most sharing has been through static allocations; however, this is changing, and new regulations are being looked at for federal and nonfederal use to utilize more dynamic sharing to improve efficiency to free spectrum for new applications. The remainder of this chapter will explore existing and emerging regulations related to these new dynamic spectrum sharing regulations, with a focus on the technical details of the defined policies and rules.

Managing Spectrum Sharing Among Federal Users

Frequency sharing is assumed for federal users, and the Red Book specifically states:

> Sharing of frequencies is necessary for the fullest utilization of the radio spectrum. This may entail the acceptance of some interference but does not contemplate requiring the acceptance of harmful interference.

With that in mind, Chapter 8 of the Redbook defines the specific procedures followed for the coordination and assignment of frequencies [9]. In summary:

- Each federal agency evaluates telecommunications needs on a mission-by-mission basis. As a part of this evaluation, agencies perform technical studies, select potential frequencies for each mission, and coordinate with other agencies as necessary, with a requirement to neither cause harmful interference to nor receive harmful interference from other authorized users, as outlined in Red Book Chapter 10 [10].

- Once this evaluation is complete, the agency files an application with the NTIA Office of Spectrum Management for consideration of the Frequency Assignment Subcommittee (FAS) of the IRAC. Preparation of these applications is outlined in Chapter 9 of the Redbook [11] and includes requirements for technical data on transmit and receive equipment, geolocation information, application descriptions, and other usage information. Applications can request a regular or permanent assignment, a temporary assignment, a trial assignment, or a group assignment.
- The FAS considers applications and takes action within the established policy guidelines. Principles followed by the FAS in frequency assignment include frequency sharing, planned frequency utilization, and the justification for frequency assignments.

Frequency assignments are made with a specific geographic location, a specific service area, and performance requirements levied against stations in a close geographic proximity. If multiple assignments are made in the same area, Priority Access is generally given to the assignment made first. Other frequency assignment regulations defined in the Red Book take into account the type of service and band of operation. Under these rules, OSM processes between 8000 and 10,000 assignment actions each month while maintaining a database of over 400,000 assignment entries [12]. On 11 April 2014, the NTIA published a new online resource detailing these assignments and use [13].

One important item to note: the sharing of spectrum between federal and nonfederal users discussed later in this chapter is facilitated through this same process. The FCC, through their IRAC liaison, files frequency assignment applications for nonfederal use of shared bands and in cases where operation in nonfederal bands may impact federal spectrum use. Processing of the application then follows the standard course.

Early Regulations Supporting Nonfederal Spectrum Sharing

A key element of the Act of 1934, as amended, directs the Commission to "generally encourage the larger and more effective use of radio in the public interest" and to seek to promote "efficient and intensive use of the radio spectrum" [14]. In 2000, the FCC began looking at new models to achieve these objectives with a move toward higher levels of spectrum sharing for nonfederal users through two early rulemakings: one on software-defined radio and the other on secondary markets. In 2002, the Commission took these actions a step further in forming the Spectrum Policy Task Force. This task force was made up of senior staff and chartered to "provide specific recommendations to the Commission for ways in which to evolve the current "command and control" approach to spectrum policy into a more integrated, market-oriented approach that provides greater regulatory certainty, while minimizing regulatory intervention" and "assist the Commission in addressing ubiquitous spectrum issues, including, interference protection, spectral

efficiency, effective public safety communications, and implications of international spectrum policies" [15]. Through this task force, a host of other proceedings advanced spectrum sharing, including an early proceeding on smart radio systems. This section will explore these early regulations.

FCC Rulemaking on Software-Defined Radio (Docket 00-47)

In March of 2000, the FCC issued a notice of inquiry seeking comment on a variety of issues related to software-defined radios (SDR) [16]. A key element of this notice was an exploration of several spectrum sharing scenarios that could be enabled by SDR, allowing a lessee to reconfigure a radio to meet with the requirements of a specific band manager at a specific moment in time. Twenty-four parties filed comment on this NOI, and in December of 2000, the FCC followed with a Notice of Proposed Rulemaking. The NPRM proposed a regulatory definition of SDR and rules for SDR equipment authorization. Through the NPRM, the Commission recognized the potential for SDR to increase spectrum efficiency, but concluded that no additional rules were required at that time with respect to this capability. The Commission later went on to issue a Report and Order, building on the 14 comments and 8 reply comments to modify the proposed SDR definition and to finalize voluntary authorization requirements (Table 1).

Table 1 Timeline for early regulations

	2000	2001	2002	2003	2004	2005
Early regulations Report and Order on SDR	Notice of inquiry on SDR			NPRM on employing cognitive radio technologies		Report and Order on cognitive radio technologies
	NPRM on eliminating barriers to the development of secondary markets			Report and Order and further NPRM on eliminating barriers to the development of secondary markets	Second Report and Order and further NPRM on eliminating barriers to the development of secondary markets	
			Spectrum policy task force formed			

Elimination of Barriers to the Development of Secondary Markets (Docket 00-230)

In November of 2000, the FCC issued a Notice of Proposed Rulemaking on "Promoting the Efficient Use of Spectrum through Elimination of Barriers to the Development of Secondary Markets" [17]. Through this NPRM, the Commission recognized that spectrum may be being used inefficiently, especially in rural areas, and, given the increased demand for spectrum, sought ways to encourage license holders to lease underutilized spectrum on a temporary basis. Concurrent with this NPRM, the Commission also issued a policy statement outlining its long-term principles for encouraging the development of such secondary markets.

A key issue that the NPRM tried to address was clearly defining who was responsible should harmful interference occur under the defined scenarios. In addressing this issue, the NPRM introduced the concept of a "band manager," which is a class of licensee specifically authorized to lease unused spectrum. The NPRM also proposed a database approach for band managers to utilize in managing secondary users, concluding that "the private sector is better suited both to determine what types of information parties might demand, and to develop and maintain information on the licensed spectrum that might be available for use by third parties."

Thirty seven parties commented on this NPRM and 21 filed reply comments. Based on these comments, in 2003 the FCC issued a Report and Order and Further Notice of Proposed Rulemaking. The Order established two options for use in secondary markets:

- A spectrum license holder may enter into an agreement with an entity wishing to lease spectrum without Commission interaction. In doing so, the licensee must maintain legal responsibility for the leased spectrum. The licensee acts as the "spectrum manager" in this option and may lease any or all of their licensed spectrum in any geographic area for any length of time they wish. Technical and interference-related rules associated with the license still apply, and the licensee is liable for any violations.
- A streamlined process for a licensee to transfer control to an entity wishing to lease the spectrum. Referred to as de facto transfer leasing, the lease can apply to any amount of spectrum in any geographic area and for any period of time. All the original service rules and policies apply; however for the period of the lease, the leasing entity is the responsible party and is liable for any violation.

In addition, the Commission issued a second NPRM seeking comment on issues fundamental to the development of secondary markets. Questions contained in this NPRM included what additional steps the Commission needed to take, whether there would need to be a clearing house mechanism to provide real-time information for "opportunistic" devices, and what role the Commissions should take, if any, in regulating such a clearing house.

The Commission received five petitions for reconsideration on the order, along with 21 comments and 10 reply comments on the NPRM. In July of 2004, the Commission responded with a Second Report and Order, Order on Reconsideration, and Second Further Notice of Proposed Rulemaking (NPRM). In summary, the order:

- Adopted immediate approval procedures for certain categories of de facto transfer leasing agreements and streamlined the procedures for establishing a short term de facto lease
- Clarified policies related to "smart" or "opportunistic" use technologies, including reinforcing that the rules allow for dynamic forms of spectrum leasing and that licensees and those entities that are leasing their spectrum may share use of the same spectrum on a nonexclusive basis for the term of the lease
- Established a new type of secondary market that facilitates the development of a private commons in licensed spectrum, allowing groups of licensees or lessee to make spectrum available to a group of users that do not use the licenses or lessees network infrastructure

The second further NPRM sought comment on ways in which new technologies could make opportunistic use of licensed spectrum, including types of uses of opportunistic spectrum and examples of private commons and ways to improve the private commons model. Only three comments were received, and so in April 2007, the Commission issued a third Report and Order that reaffirmed the existing Report and Order without change.

FCC Rulemaking on "Smart Radio" Systems (Docket 03-108)

In May of 2003, the FCC Office of Engineering and Technology (OET) hosted a workshop exploring the use of cognitive radiotechnologies to enable more efficient use of spectrum [18]. In December 2003, the FCC followed up on this workshop by launching a Notice of Public Rulemaking on "Facilitating Opportunities for Flexible, Efficient, and Reliable Spectrum Use Employing Cognitive Radio Technologies." Through this NPRM, the Commission sought comment on all issues related to cognitive radio technology, with a specific focus on:

(1) Allowing unlicensed devices to operate in higher power levels in rural areas
(2) Allowing unlicensed devices to operate at higher power levels in bands with limited spectrum use
(3) Enabling spectrum leasing, including:
    a. The ability of cognitive radio to support/enable for interruptible spectrum leasing, allowing a lessor to take back spectrum from a lessee,
    b. Applicability of interruptible spectrum leasing models to allow secondary commercial use of public safety spectrum
(4) Dynamically coordinating spectrum sharing, allowing ad hoc sharing of licensed spectrum

(5) Facilitating interoperability between communications systems, especially first responder public safety communications systems
(6) Forming ad hoc or mesh networks with the ability to self-heal

The NPRM also sought comment on proposed rule changes allowing automated frequency selection for unlicensed devices, allowing manufacturers to build devices that can operate worldwide when unlicensed frequency bands are not harmonized.

Through the associated Order, Docket 00-47 was closed, with the further evolution of the regulation of SDR now falling under a combined SDR/CR docket. The NPRM also revisited equipment authorization for SDRs, noting that in the 2 years since the rules were passed, no manufacturers had filed applications to certify an SDR, even though many of the devices certified by the FCC met the Commission's broad definition of SDR. With this in mind, the NPRM sought comment on whether it should become mandatory for manufacturers to declare certain types of equipment as SDR, rules on the types of security features that SDR must incorporate, and the approval process for SDR contained within modular transmitters.

The Commission received 56 comments and 14 reply comments to this NPRM and based on this issued a Report and Order in March 2005. The report covered a wide range of cognitive radio topics, recognizing that both software-defined radio and cognitive radio will continue to evolve over time. The report also described the technical requirements for interruptible spectrum leasing as follows:

(1) The licensee must have positive control as to when the lessee can access the spectrum.
(2) The licensee must have positive control to terminate the use of the spectrum by the lessee so it can revert back to the licensee's use.
(3) Reversion must occur immediately upon action by the licensee unless that licensee has made specific provisions for a slower reversion time.
(4) The equipment used by the licensee and the lessee must perform access and reversion functions with an extremely high degree of reliability.
(5) The equipment used by the licensee and the lessee must incorporate security features to prevent inadvertent misuse of, and to thwart malicious misuse of, the licensee's spectrum

The Commission did not adopt any particular technical model in this area, stating that this was best left to the licensee to be satisfied that the technical mechanism implemented meets with their requirements for reclaiming leased spectrum.

Through the associated Order, the Commission broadened the definition of software-defined radio to include changes in software that could make a transmitter noncompliant with Commission emission rules. They also changed the equipment authorization rules to require that equipment in which the software controlling the radio-frequency operating parameters is expected to be modified by a party other than the manufacturer must be certified as an SDR. Certification as an SDR remains optional for equipment that is not expected to be modified by a third

party. In addition, the Order allowed certification of unlicensed transmitters that are capable of operating outside of US unlicensed frequency bands, provided that they incorporate automatic frequency selection mechanisms to ensure they operate only on allowed frequencies inside the United States.

Results from Early Regulations for Nonfederal Spectrum Sharing

The market success of these early proceedings, in and of themselves, has been limited. A search of the FCC's license database shows that there are only 92 active leases [19]. Although the exact reason for this low number is unknown, if one believes the published studies showing that commercial spectrum is largely underutilized (e.g., [20,21]), it must be assumed that the business case for spectrum leasing does not surpass the business case for not leasing. One can speculate that this is because holding unused spectrum versus leasing creates a barrier to entry for potentially competing services. Likewise, while a review of the licensing database showed that there was significant early activity in licensing software-defined radios, that activity declined following the publication of the revised rules. Industry continued to advance SDR technology, however, and the Wireless Innovation Forum now estimates that roughly 95% of defense, public safety, and cellular infrastructure radios are now software defined [22]. All this said, even though these proceedings, taken individually, have not been considered business successes, the proceedings provided significant data to the Commission and provided an important basis for future proceedings.

Early Regulation to Facilitate Spectrum Sharing Between Federal and Nonfederal Users

Building on these earlier rulings, the FCC began initiating proceedings in 2004 to enable spectrum sharing between federal and nonfederal users. Two rulings are of significant interest: the 5 GHz U-NII ruling and the 3650 to 3700 MHz band ruling. Regulations from these proceedings are addressed below (Table 2).

FCC 5 GHz U-NII Rulemaking (Docket 03-122)

Prior to 2002, Unlicensed National Information Infrastructure (U-NII) devices were permitted to operate in the United States over a total of 300 megahertz of spectrum spread across the 5 GHz band [23]. The majority of U-NII devices operating in this band supported the IEEE 802.11a standard, and in January of 2002, the Wireless Ethernet Compatibility Alliance (WECA, now the Wi-Fi Alliance) petitioned for rulemaking to provide an additional 255 MHz of spectrum for use by these types of devices in the 5470 to 5725 MHz band. In response to this petition, 17 comments

Table 2 Timeline for initial regulations for sharing between federal and nonfederal users

	2002	2003	2004	2005	2006	2007	. . .	2013	2014
Federal and nonfederal spectrum sharing		NPRM on 5 GHz U-NII Report and Order on 5 GHz U-NII			Memorandum Opinion and Order on 5 GHz U-NII			NPRM Extending 5 GHz U-NII band	Report and Order Extending 5 GHz U-NII band
	Unlicensed Spectrum Notice of Inquiry		NPRM on Unlicensed Spectrum in the 3650 Band	Report and Order on 3650 band		Memorandum Opinion and Order on 3650 band			

and 10 reply comments were filed, and upon reviewing these comments, the FCC issued a Notice of Public Rulemaking in May of 2003.

In the NPRM, the FCC agreed with WECA that current allocation was insufficient for growth. However, the 5350 to 5650 band was currently allocated to radiolocation and used by the US Department of Defense (DoD) for a number of radar systems, including systems used for national security. The DoD was concerned that U-NII devices would cause interference to its radar systems and therefore asked that if this petition were granted, its radiolocation services be upgraded from secondary to primary status in this band.

In addition, NTIA working with the FCC, NASA, and the DoD reached the following agreement on International Telecommunications Union World Radiocommunications Conference 2003 (WRC-03) Agenda Item 15 to establish an international recommendation that:

(1) Radiolocation service in the 5350 to 5650 MHz band be upgraded to primary status
(2) An allocation be added in the 5305 to 5460 MHz band for Space Research Services (SRS) and in the 5460 to 5560 for SRS and the Earth Exploration Satellite Service (EESS)
(3) A mobile allocation be added to the 5150 to 5350 MHz and 5470 to 5725 MHz bands
(4) U-NII or HiperLAN users in the 5250 to 5350 MHz and 5470 to 5725 MHz bands be required to employ dynamic frequency selection (DFS) using a listen-before-transmit mechanism with the following detection thresholds: −64 dBm for devices that operate with an Effective Isotropic Radiated Power (EIRP) of between 200 mW and 1 W and −62 dBm for devices that operate with an EIRP of less than 200 mW.

Based on this agreement, through the NPRM the Commission sought comment on proposals to upgrade affected federal government radiolocation service to primary status; to upgrade the affected nonfederal government radiolocation services, primarily used for weather radar, to co-primary status; to add primary federal Government and secondary nonfederal government allocations for SRS and EESS; and to allow U-NII devices to operate as per the WECA petition on a noninterference basis.

Technical requirements for unlicensed operation proposed in the NPRM were as follows:

- 1 watt EIRP peak
- Devices operating in the 5250 to 5350 MHz and 5470 to 5725 MHz bands employ DFS to monitor spectrum and determine if radar signals are present (listen before talk) with detection thresholds as per the WRC-03 agreement. In addition, the Commission sought comment on:
  - A proposed correction factor for devices with under 1 MHz BW
  - The minimum number of radar pulses and observation time for reliable detection

- A proposal that devices operating under control of a central controller or master not be required to have DFS, proposing that only the master be required to have DFS capability
- As U-NII devices in the 5250 to 5350 MHz band currently operate without DFS capability, the Commission proposed establishing a transition period

The Commission also sought comment on a proposal to require devices operating in the 5470 to 5725 MHz band employ Transmit Power Control (TPC) to further protect EESS and SRS operations. The Commission's proposal was that the power level be reduced by 6 dB when triggered and requested comment on a suitable trigger. The Commission also requested comment on whether TPC should be required for devices that operate at less than 500 mW EIRP. Finally, the Commission requested comments on test procedures necessary to ensure compliance with the DFS and TPC requirements.

Twenty-nine comments and 12 reply comments were filed in response to this NPRM, and the Commission quickly followed up to issue a Report and Order in November of 2003. Through this Order, the Commission established rules to make the 255 MHz requested by the WECA available in the 5470 to 5725 MHz band for Unlicensed National Information Infrastructure (U-NII) devices. As a part of this ruling, the FCC upgraded federal and nonfederal radiolocation services to primary status as proposed and added primary federal and secondary nonfederal government allocations for SRS and EESS. The Commission declined to adopt a specific mobile allocation and instead chose to treat devices equally as unlicensed intentional radiators, allowing to operate on a noninterfering basis.

On the technical side, the Report and Order adopted the power requirements and DFS requirements as proposed. The order exempted remote devices under control of a central controller from the DFS requirement, but did not exempt controller or master devices. The Order required Transmit Power Control for devices operating at power levels of greater than 500 mW. In doing so, the Commission declined to provide a triggering mechanism but rather asked that applicants seeking equipment authorization for U-NII devices provide a statement in the certification application explaining how they comply. Finally, the Order provided an interim test procedure to allow immediate certification.

This Order was followed in June of 2006 with a Memorandum Opinion and Order clarifying the rules for TPC and providing a revised test procedure for determining DFS compliance. Then, in 2013, the Commission issued a new NPRM (Docket 13-49) proposing an additional 100 MHz bandwidth in the 5 GHz band for U-NII devices [24]. This was followed by an Order in April of 2014 allocating this new bandwidth as a part of the regulations.

FCC 3650 MHz Rulemaking (Docket 04-151)

The Omnibus Budget Reconciliation Act passed by the US Congress in 1993 required the US Secretary of Commerce to identify at least 200 MHz of spectrum allocated for use by the federal government agencies to be transferred to the private

sector [25]. NTIA released a final report on reallocation in 1995, identifying the 3650 MHz band for transfer on the condition that government radiolocation stations in two locations continue to operate in that band and that spectrum in the adjacent 3600 to 3650 MHz band continue to be used for high-power radar. In 1998, the Commission issued an NPRM (Docket 98-237) proposing to allocate the 3650 band for nongovernment fixed service on a primary basis. In 2000, the FCC issued an associated Report and Order that allocated the 3650 MHz band to fixed and mobile terrestrial services on a co-primary basis but to protect grandfathered fixed satellite service (FSS) earth stations and radiolocation operations operating on a primary basis. This order limited mobile service allocation to base station use only and established that new FSS earth stations were only allowed to operate in the band on a secondary basis. The Commission received four petitions for reconsideration, requesting that FSS be returned to full allocation and deleting the fixed service and mobile service allocations. Concurrent with the issue of 3650 MHz allocation Report and Order, the Commission issued a 3650 Service Rules Second NPRM. In response to this NPRM, the FCC received 17 comments and 7 reply comments. Comments submitted on behalf of telecommunications providers serving rural areas and Internet service providers who provide wireless internet to their customers were interested in licensed terrestrial services. FSS providers submitted comments that licensed fixed and mobile services would cause interference.

Later, in December 2002, the Commission issued an Unlicensed Spectrum Notice of Inquiry (Docket 02-380). This inquiry sought to assess the feasibility of releasing additional spectrum for unlicensed use below 900 MHz (TV bands) and in the 3 GHz band. The inquiry specifically sought comment on whether unlicensed devices could operate in these bands at higher power levels than was previously allowed and asked whether licensed and unlicensed devices should be allowed to operate in unused portions of the spectrum on a noninterfering basis.

A number of commenters supported the ideas proposed by the Commission; however, numerous comments were also received from those incumbent licensed users in these bands with mixed opinions on whether such operation would cause interference, especially when operating in band adjacent to those supporting licensed operation (adjacent band interference).

With this as background, in April of 2004, the FCC issued a Notice of Public Rulemaking. Through this NPRM, the Commission deferred comment on petitions for reconsideration defined above and instead sought comment on whether new FSS stations could operate in band on a co-primary basis using smart/cognitive radio technologies. The Commission also sought comment on a proposal to delete fixed service and mobile service allocations in favor of unlicensed operation and sought comment on proposed fixed and non-fixed unlicensed operation as follows:

- Fixed operation
  - Primary use will be to provide wireless broadband connectivity by wireless Internet service providers (WISPs) in rural areas
  - A certified professional installer would be required to ensure fixed unlicensed devices operate in a manner that will avoid causing interference with FSS earth stations

  - Maximum allowed EIRP of 25 watts, with comment sought on the proposed use of sectorized or scanning spot beam antennas
  - Fixed devices would be prohibited from operating within protection zones defined as 180 km within +/−15 degrees of the FSS antenna main-beam azimuth and 25 km otherwise
- Non-fixed operation
  - Maximum allowed EIRP of 1 W
  - DFS like listen before talk function required, with power to be adjusted based on detected FSS receiver signal strength.
  - Device prohibited from transmitting if detects an uplink signal greater than −76 dBm in a 1 MHz bandwidth.
  - Device must lower EIRP to 500 mW if FSS signal strength of between −79 and −82 dBm is detected
  - Device must lower EIRP to 250 mW if FSS signal strength of −76 and −79 dBm is detected

The NPRM also proposed to prohibit operation by unlicensed devices within 8 km of the US/Mexico border and proposed to require all unlicensed devices to broadcast identification information at regular intervals. Through the NPRM, the Commission also sought comment on the use of geolocation or a dedicated FSS beacon signal to protect incumbents and sought comment on options for licensed use or combinations of licensed and unlicensed use.

The Commission received responses to this NPRM from over 100 parties. In March of 2005, they followed up with a Report and Order and Memorandum Opinion and Order. Through this Order, the FCC maintained the existing FSS and fixed service allocations established in the 2000 Order and removed the base station-only restriction on the mobile service allocations. The Order established that the fixed service and mobile service access would be through nonexclusive nationwide licensing in lieu of the unlicensed scheme discussed in the NPRM. The Order also allowed new FSS earth stations but limited them to secondary status.

The Order required that licensees cooperate to avoid generating harmful interference and to facilitate this required that they register their fixed and base stations in a common database. The Order further required a contention-based protocol to manage interference in the shared spectrum, but did not specify the protocol, and left this to industry standards bodies. Fixed station power was limited to 25 W EIRP in any 25 MHz band, and mobile station power was limited to 1 W EIRP over the same bandwidth.

In response to this Order, the Commission received eight petitions for reconsideration, with 160 oppositions, replies, or comments to those petitions. After consideration, in June of 2007, the FCC issued another Memorandum Opinion and Order reaffirming the nonexclusive licensing and retaining the requirement for contention-based protocols but clarified that the rules allow for the certification of a variety of different protocols and contention avoidance mechanisms [26]. This included unrestricted protocols such as listen before talk or restricted protocols which can only prevent interference from other devices utilizing the same protocol. To avoid contention between these types of devices, the Order limited devices using

restricted protocols to the lower 25 MHz of the band. No other reconsideration of power levels or other petition items occurred.

Results from Early Regulations to Facilitate Spectrum Sharing Between Federal and Nonfederal Users

Through these proceedings, the Commission made over 400 MHz of spectrum available for shared use, and from a business perspective, the proceedings can be considered a success. The U-NII band is broadly used to support the millions of wireless local area network and broadband access devices. There are currently 78 protected sites in the 3650 rulemaking, and a search of the FCC license database shows that there are 2608 active licenses operating in that band [27]. The success of these can be attributed to the amount of available spectrum and the ease in meeting the license requirements.

Unlicensed Operation in the TV Broadcast Bands (Docket 04-186)

As part of the Docket 02-380 Notice of Inquiry, the FCC also asked questions concerning the unlicensed use of unused spectrum below 900 MHz [28]. Comments received from wireless technology suppliers and wireless Internet service providers generally support the concept; however, television broadcasters expressed concerns that the technology to determine if a television station is active in a specific location and the ability to quickly change frequency is unproven. Based on these comments, in May of 2004, the FCC issued a Notice of Public Rulemaking with a stated goal to enable wireless Internet service providers to offer expanded services by allowing unlicensed operation in the broadcast television spectrum at locations where that spectrum is not being used. The hope was that such operation would also provide synergy between WISPs and traditional broadcast operations to offer broadcasters the opportunity to provide additional services.

Initial Regulations for TV Band Operations

The approach taken by the FCC through the NPRM was to ensure no harmful interference to authorized users of spectrum by requiring that "smart radio" technology be used to identify unused TV channels in a specific geographic area. Two types of operation were proposed by the FCC:

(1) *Personal/portable devices.* Personal/portable devices were envisioned by the FCC to be used as Wi-Fi-like cards in home computers and for in-home local area networks. For these types of devices, the Commission proposed that interference could be prevented through the use of a control signal sent by TV transmitters in the vertical blanking interval of a standard TV signal.

Transmission of this control signal was voluntary, and parties could receive compensation for transmitting. The control signal would be current on a 24 h cycle.

For personal/portable devices, a TV channel would only be considered vacant if no portion of the service area of an authorized station assigned to use that channel was within the service area of the station transmitting the control signal.

(2) *Fixed access devices.* Fixed access devices were envisioned by the FCC to be used for commercial service. The Commission proposed that for these devices, interference would be prevented through the use of geolocation information. The location of the device would be set with 10 m accuracy using a GPS or certified professional installer to establish and set the location. Once the location was set, the device would access a database, provide its location, and retrieve information to calculate what channels are available in its area. Once a frequency of operation was selected by a device, the Commission proposed that the device register with a separate database indicating its operating frequency and location.

The Commission received numerous comments and reply comments to this NPRM. WISPs, manufacturers of unlicensed TV band devices (TVBDs), and potential users of TVBDs all expressed support for the proposals. Broadcasters and other licensed incumbents expressed strong concerns as to whether unlicensed devices could in fact operate without causing interference. Several comments were also received from several parties who felt that the operations of TVBDs should be licensed.

Upon reviewing these comments, the Commission issued a First Report and Order and Further Notice of Proposed Rulemaking in October of 2006. Through this Order, the Commission concluded that allowing low-power devices to operate in the TV band in frequencies that are not used could have significant benefits for the public by enabling the development of new wireless devices, systems, and services. The Commission also reiterated its belief that properly regulated devices could operate in the TV bands without causing interference; however based on comments received, the Commission concluded that it needed more data to set those regulations, including in the area of spectrum sensing.

Sensing Versus Geolocation Databases

The original NPRM made no specific proposals on spectrum sensing to detect active TV signals, but sought comment on spectrum sensing technologies, including levels that must be detected and ways of dealing with the hidden node problem that occurs when the TV signal is blocked from the sensing device but not from a TV receiver in range of the unlicensed wireless transmitter. The Commission noted that in the comments to this NPRM, no party provided sufficient technical information on the use of spectrum sensing for rules to be established. As such, in the further NPRM, the Commission reiterated that technical rules are necessary if sensing devices are

to be used to ensure that such devices adequately sense incumbents and sought comment on the following proposal for sensing TV band signals, modified from the radar signal sensing rules adopted for the 5 GHz U-NII band:

- Detection threshold of −116 dBm (based on work of 802.22) as well as factors that may affect this threshold such as number of false positives and antenna height, addressing the hidden node problem through technologies such as distributed sensing or sensing in combination with geolocation information.
- Devices will sense before occupying a channel and then periodically recheck the channel, with a proposed recheck period of every 10 s, with sensing only required in the adjacent channels during recheck

The Commission also raised a number of questions on which it sought comment such as whether the sensing bandwidth should be regulated and whether antenna gain should be limited to 0 dBi as proposed by 802.22

In response to requirement for data to set regulations established in the Report and Order, FCC Office of Engineering and Technology invited submittal of prototype devices for initial testing in December of 2006. Two prototype devices were provided for testing, which focused on "detect and avoid" or "listen before talk" strategies using spectrum sensing. The test results from this initial testing were released in July of 2007, concluding that:

> . . . sample prototype White Space Devices submitted to the Commission for initial evaluation do not consistently sense or detect TV broadcast or wireless microphone signals. Our tests also found that the transmitter in the prototype device is capable of causing interference to TV broadcasting and wireless microphones.

In August of 2007, OET held a meeting with interested parties to review the test results and define a way forward. Based on the outcome of this meeting, the Commission announced a second phase of testing beginning in January of 2008 following a revised test procedure. In July of 2008, the Commission also initiated filed trials of TV White Space devices. Results of the Phase II Testing were published in October 2008, with conclusions summarized as follows:

(1) All devices were able to reliably detect a clean DTV signal on a single channel; however, results varied in a noisy real-world environment.
(2) Signals in adjacent channels degraded detection capability in channel
(3) All devices were able to detect wireless microphones when no other signals were present. TV signals in adjacent channels degraded performance in detecting wireless microphones to the point that it was no longer reliable.
(4) In most cases, devices correctly reported occupied channels in field tests, but there were some errors and high false alarm rates
(5) The use of a geolocation database in combination with sensing was 100% reliable in detecting DTV
(6) Wireless microphone field tests failed in that false alarms eliminated all bands or when sensitivity was adjusted indicating channels were available when in fact they were not.
(7) Under certain conditions, direct pickup was possible

Based on these results, in November of 2008, the Commission issued a Second Report and Order and Memorandum Opinion and Order. Through this Order, the Commission continued to allow for both fixed and personal/portable devices; however, they modified the original proposed rules to require that devices, except personal/portable devices operating in client mode, access a geolocation database over the Internet. The rules also required that all devices employ spectrum sensing as a further means of minimizing potential interference, but the database will be the controlling mechanism as test results showed that more developmental work was needed before spectrum sensing can be the principal means of identifying unoccupied channels. The rules also established that fixed devices were prohibited from operating in adjacent channels; fixed devices must register with the database to provide FCC ID, location, and responsible party info and that wireless microphones could be registered in the database for protection. Through this order, the Commission eliminated the control signal option for determining available channels but agreed to revisit if economics or other circumstances make it more favorable. No regulation was established for coexistence of TVBDs.

The Commission received 17 petitions for reconsideration in response to this First Memorandum and Order and following review and analysis issued a Second Memorandum Opinion and Order in September of 2010. Among changes to the rules made by the Commission in addressing the petitions was the elimination of the requirement that TVBDs support sensing and allowed database-only solutions. In doing so, the Commission stated that they continue to believe that sensing will evolve, that sensing has promise, and left open the possibility of sensing-only devices. The Commission also allowed sensing to be used on a voluntary basis (Table 3).

Table 3 Timeline for TV White Space regulations

	2004	2005	2006	2007	2008	2009	2010	2011	2012
TV White Space	NPRM on unlicensed operation in TV bands		First Report and Order and further NPRM on unlicensed operation in TV bands Initial prototype devices invited for testing	Phase I test results released	Phase II testing Phase II test results released Second Report and Order and First Memorandum Opinion and Order on unlicensed operation in TV bands		Second Memorandum Opinion and Order on unlicensed operation in TV bands		Third Memorandum Opinion and Order on unlicensed operation in TV bands Incentive auctions ordered by Congress

Other Technical Rules and Other Requirements

The rules established by the FCC through these proceedings allowed for operation of TVBDs in all channels except:

- Channels 4
- Channel 37, which was being used for radio astronomy
- Channels 52 to 69, which were being reallocated in the digital TV transition

Operation was allowed in channels 14 to 20 but must avoid interference with PLMRS/CMRS and offshore radio telephone service. For all devices, out-of-band emissions in the first adjacent channel are limited to a level of 55 dB below the power in the channel they occupy and measured in a 100 kHz bandwidth.

Technical criteria for determining when a TV channel would be considered vacant were established through the use of protected contours defining service areas based on service types (digital TV, low-power TV, etc.) with defined propagation curves. The rules established desired to undesired signal protection ratios based again on service type, channel separation (co-channel or adjacent channel), and propagation curves. The rules required that calculations would be made to determine if operation within a specific location would create an undesired signal strength from the unlicensed device within the service area that is too high.

Other technical requirements established for fixed and personal portable devices are summarized as follows:

- Fixed devices
  - Maximum transmit power of 1 W, with 4 W maximum EIRP. For antennas with gains above 6 dBi, the transmit power must be reduced so that EIRP does not exceed 4 W
  - Power spectral density limits on conducted output power of 16.7 mW (12.2 dBm) when measured in a 100 kHz bandwidth
  - Should use Transmit Power Control to limit maximum power where possible
  - Allowed to communicate with other fixed devices and personal portable devices
  - Must incorporate geolocation capability or have location set by professional installer
  - Must transmit identifying information, following a standard to be established by the industry
  - Restricted fixed devices from operating in locations where the ground HAAT is greater than 250 m. The Commission established that HAAT would be calculated by the database provider.
- Personal portable devices
  - 100 mW maximum EIRP, except when operating adjacent to a TV station or licensed station within the protected coverage area, in which case limited to 40 mW. Power should typically be adjusted to less than the maximum permitted power when possible

- Power spectral density limits on conducted output power of 1.67 mW (2.2 dBm) for personal/portable devices and 0.7 mW (−1.8 dBm) for personal portable in adjacent channels when measured in a 100 kHz bandwidth
- Two modes
  - Mode I – client that is controlled by a fixed device or a personal portable device operating in mode II
  - Mode II – determines available channels from internal geolocation/database access. Can act as a master to a mode I device in a master client link
- Both modes must establish location each time they are activated and must reverify their location each time they detect they have moved. Mode II devices must not transmit if location is unknown

The order also established a fixed adjacent channel emission limit of 72.8 dB below the maximum power limit for each type of device.

The Order established that all fixed devices and mode II personal portable devices are allowed to operate in master mode. Each network would have at least one master, and a master is allowed to transmit without receiving an enabling signal from any other device. A personal portable device communicating with a fixed master is required to use channels and frequencies as directed by the fixed device. If a fixed device does not have direct connection to the Internet, and has not initialized and registered with the database system, then it can communicate to another TVBD that does have a connection and is registered over a channel that device is using. That link must then be used to register with the database and receive a list of channels for use. Mode I devices must either receive a current list of available channels from a mode II or fixed device once per minute or must contact the mode II or fixed device once per minute to reverify/reestablish channel availability. Finally, a mode I personal portable device that does not have geolocation capability can listen for and then communicate with a mode II or fixed device over a channel that device has already used. The mode II device must then immediately obtain a list of channels.

The Order also established that the database system for fixed stations and mode II personal portable devices would be managed by database administrators selected by OET. The database requirements established are summarized as follows:

- Databases will be privately owned and operated service, with database service providers allowed to charge fees for registration of fixed devices and to provide available channels to all devices
- More than one entity may be authorized to operate as a TV band database provider, with final decision based on expressions of interest
- Database providers must share registration information with each other and with the Commission
- Fixed and mode II TVBDs must re-sync with the database at least once per day and, after a 1-day grace period, must stop transmitting
- Database administrators are not required to resolve claims of interference by TVBDs

- Services must be made available by database providers to all TVBDs on a nondiscriminatory basis
- TVBDs shall only be capable of contacting databases operated by administrators designated by the Commission, the database must not provide channel information to uncertified TVBDs, and communication between TVBDs and database be secure. The Commission did not require specific technologies to meet these requirements.
- All database information required by the Commission be publicly available. In doing so, the Commission stated that public disclosure was not required and that data not required by the Commission does not have to be disclosed by a database administrator
- Information on TV stations in Canada and Mexico border areas be included in the database

The rules also established that two channels between 14 and 51 would be reserved in all markets nationwide for wireless microphones and disallowed unlicensed wireless microphone and other low-power auxiliary devices operating without a license to be registered in the database, stating that these devices will not be afforded protection from interference from TV band devices on channels were TV band devices are allowed to operate. Established that operators of licensed low-power auxiliary stations including wireless microphone may register their site directly with one of the designated database administrators. Established that entities operating or otherwise responsible for the audio systems of major events where large numbers of wireless microphones will be used may request a registration of the event.

Finally, rules established that the FCC would be the certifying authority for TVBDs and databases and establish a proof of performance standard to allow certification of sensing-only devices that demonstrate the capability to detect protected services with a high level of accuracy.

In compliance with these orders, the FCC OET began accepting applications for White Space database administrators. To date, ten organizations have been designated as database administrators, and four have databases that have been approved for operation:

Organization	Status
Google	Designated Database Administrator, Database Approved
Keybridge Global	Designated Database Administrator, Database Approved
Spectrum Bridge	Designated Database Administrator, Database Approved
iconectiv	Designated Database Administrator, Database Approved
Comsearch	Designated Database Administrator, Database Approval Pending
LS Telecom	Designated Database Administrator, Database Approval Pending
Microsoft	Designated Database Administrator, Database Approval Pending
Airity	Designated Database Administrator
Frequency Finder	Designated Database Administrator
Neustar	Designated Database Administrator

The Commission has also published a compliance guide for TV band devices and a guide for database administrators.

Standards for Unlicensed Operation in TV Bands

Standard development in support of TV band device regulations has been somewhat scattered. Pre-standard development for database to device communications began in the Wireless Innovation Forum. At the same time, the White Space database administrators formed a closed group to do pre-standard development of a database-to-database interoperability specification. Both of these efforts fed into the Protocol to Access White Space Database (PAWS) Effort of the Internet Engineering Task Force (IETF) [29].

Results from Unlicensed Operation in TV Bands

The potential success of this proceeding is still unknown. While there have been some initial trials and early deployments across the United States, there has not been a large commercial investment in this band to date. The reason for this is likely tied to the regulatory uncertainty surrounding the TV band spectrum. In February 2012, Congress directed the FCC to hold a reverse auction, or incentive auction, which freed up broadcast spectrum for use by cellular operators "by encouraging <broadcasters> to voluntarily relinquish spectrum usage rights in exchange for a share of the proceeds from an auction of new licenses to use the repurposed spectrum" [30]. If successful, these incentive auctions, which are currently scheduled for 2015, will necessarily reduce the amount of White Space that is available in the TV broadcast bands. The uncertainty in the amount of White Space spectrum that will be available following these auctions has effectively frozen the market by delaying investment.

The impact of these regulations outside of the United States, however, has been more positive. In 2014, Ofcom, the UK regulator, launched a White Space pilot program that eventually led to the TVWS regulations in the United Kingdom. These regulations specifically referenced the European Telecommunications Standards Institute (ETSI) harmonized requirement standard, which mirrors the technical requirements outlined in the US regulatory proceeding in many areas, including defining multiple device types and master-slave operation. Canada, Singapore, and a host of other countries also followed suit implementing TVWS test beds and field trials, which often have resulted in follow-up regulatory actions. As a result of this activity, Markets and Markets anticipates that:

> The global TV white space spectrum market . . . is expected to reach USD 53.1 Million (approximately) by 2022, at a CAGR of 74.30% during the forecast period. [31]

Without the United States leading the way in the development of TV White Space regulations, it is reasonable to conclude that many of these efforts would have been, at the very least, delayed.

Citizens Broadband Radio Service (Docket 12-354)

In June of 2010, the President of the United States issued an executive memorandum on "Unleashing the Wireless Broadband Revolution" [32, 33]. This memorandum recognized that "America's future competitiveness and global technology leadership depend, in part, upon the availability of additional spectrum" and that "We can also unlock the value of otherwise underutilized spectrum and open new avenues for spectrum users to derive value through the development of advanced, situation-aware spectrum sharing technologies." Through this memorandum, the President directed the Secretary of Commerce, working through the NTIA, to collaborate with the FCC and other federal agencies to make 500 MHz of federal spectrum available for nonfederal use within a 10 year time frame. In support of this initiative, NTIA undertook a fast-track review of the 1675 to 1710 MHz band, 1755 to 1780 MHz band, 3500 to 3650 MHz band, 4200 to 4220 MHz band, and 4380 to 4400 MHz band to determine the near-term viability of nonfederal broadband access within the 10 year time frame [34]. Through this study, NTIA identified the 1675 to 1710 MHz bands and the 3550 to 3650 MHz bands as early candidates for commercial use. They also identified several additional bands that may be viable but required further study. In response to this report, in March of 2011, the FCC issued a Notice of Inquiry under Docket 10-123 seeking comment on the proposed bands, noting that the 3550 to 3650 MHz band was already shared for WiMAX as federal operations were geographically limited [35]. In November of 2010, the FCC also issued a Notice of Inquiry on Dynamic Spectrum Access Technologies (Docket 10-237), as a means of building a record on current state of dynamic spectrum sharing technologies [36].

In the meantime, the President's Council of Advisors on Science and Technology (PCAST) was preparing a report on "Realizing the Full Potential of Government-Held Spectrum to Spur Economic Growth" [37]. This report, published in 2012, had a number of key findings related to the 500 MHz Initiative, the first of which was that "clearing and reallocating Federal spectrum is not a sustainable basis for spectrum policy." The report cited as an example the March 2012 report by NTIA entitled "An Assessment of the Viability of Accommodating Wireless Broadband in the 1755 to 1850 MHz Band" [38]. The report indicates that this band is currently used for fixed point-to-point microwave systems, military tactical radio relay, air combat training systems, precision-guided munitions, tracking and telemetry, video surveillance, and UAVs. Moving these systems to other spectrum to allow dedicated use by nonfederal users is estimated to cost approximately $18 billion over 10 years. The PCAST reports that the last successful auction of 90 MHz in 2006 yielded only 13.7 billion in revenue, bringing into question the business case for clearing the 1755 MHz band.

The PCAST report offered an alternative view instead, recommending a federal spectrum architecture where "the norm for spectrum use should be sharing, not exclusivity." The report urged the President to issue a new memorandum directing the Secretary of Commerce to find 1000 MHz for sharing, building on a number of elements including the following:

(1) Spectrum should not be fragmented for use, but allocated in as large of frequency bands as possible. These bands should not be allocated for the use of specific technologies, but rather be technology neutral allowing the greatest possible flexibility in use.
(2) Spectrum should be managed via a Spectrum Access System (SAS), similar to the White Space database but with additional features and capabilities
(3) Access to shared spectrum should take a three-tier approach:
    a. Protected nonexclusive use by primary users.
    b. Protected, nonexclusive access for certain priority secondary users so long as they do not interfere with primary users.
    c. General authorized access for all other devices. Such access is not protected and must not interfere with primary users or priority secondary users.
(4) Spectrum management should include not only transmission characteristics but also receiver characteristics, recognizing that receiver performance will increasingly impact the ability of spectrum to be shared as poor receiver design will increase the likelihood that the receiver will receive harmful interference from adjacent channel or co-channel transmitters.

Building on this report and in support of the President's initiative, the FCC opened a new docket (12-354) and issued a Notice of Proposed Rulemaking in January 2013 proposing the creation of a Citizens Broadband Radio Service (CBRS) in the 3550 to 3650 MHz band. The Commission positioned this spectrum as an innovation band, allowing the exploration of new spectrum sharing paradigms and providing low barriers to entry to emerging small cell technologies.

Evolution of the CBRS Regulations

In the initial Notice of Proposed Rulemaking, the Commission proposed a three-tier access model as per the PCAST report, with the Priority Access tier limited to critical users under the defined model. Through the Notice, the Commission sought comment as follows:

- *Design of the Spectrum Access System*. Building from the TV White Space proceedings, the Commission sought comment on whether the government, a commercial entity, or a public private partnership should manage the SAS and, if a commercial entity was used, whether the Commission should select a single database administrator or allow multiple administrators. The Commission also sought comment on the requirements for registration with the database and on a number of security issues including the management of classified and unclassified data, cross-domain access, and techniques to manage sensitive but unclassified federal information. Finally, the Commission sought comment on whether data within the database be available for public inspection.
- *CBRS devices.* The Commission sought comment on the proposal that all CBRS devices include geolocation technology, on power levels for Priority Access

and GAA devices for fixed base station and mobile station operation, and whether lower power should be allowed near or within an exclusion zone versus outside of an exclusion zone. The Commission also sought comment on HAAT and minimum/maximum emission bandwidth and allowances for out-of-band emissions.

- *Geographic area exclusion.* The Commission sought comment on the geographic exclusion area defined in the NTIA fast-track report based on high-power WiMAX models.
- *Other related items.* The Commission also sought comment on a whole host of other items, including equipment authorization, receiver protection, spectrum sensing, and indoor use-only models. The Commission also sought comment on whether the proposal should be extended to the 3.65 to 3.70 GHz band and alternative two-tier schemes based on the European Authorized Shared Access/Licensed Shared Access models. Public notice seeking comment on licensing models and technical requirements.

In a follow-up to this NPRM, the FCC Wireless Telecommunications Bureau and Office of Engineering Technology hosted a workshop on the proposed SAS in January of 2014. In parallel with this activity and based on a review of the record from the NPRM, the Commission issued a Public Notice soliciting further comment on alternative licensing proposals inspired by suggestions made by the commenters to the original NPRM. Through this Public Notice, the Commission sought to explore whether Priority Access should be made open to a broader class of users, including commercial users, allowing some level of assured access beyond the critical access users defined in the NPRM. Expanding on this, the Commission sought comment on licensing Priority Access by auction, to include proposed licensing term as well as the geographic, temporal, and frequency dimensions associated with such licenses. The Notice also sought comment on a defined floor proposed for GAA spectrum availability, allowing GAA access to unused Priority Access bandwidth, managed by the SAS, to maximize dynamic use of unutilized spectrum, and a proposal to allocate a portion of the Priority Access bandwidth for the critical users defined in original NPRM. Through the Notice, the Commission sought comment on technical implementation issues, including limiting the maximum power to 24 dBm with maximum antenna gain of 6 dBi for a composite 30 dBm EIRP, and how to facilitate coexistence. Finally, the Commission sought comment on whether the formation of one or more stakeholder groups, as defined under Docket 13-101, should be encouraged to study receiver standards.

The Commission received extensive comments on both the NPRM and the Public Notice and, based on an analysis of these comments and the outputs from the workshops held, issued a Further Notice of Proposed Rulemaking in April of 2014. Through this new NPRM, the Commission proposed to increase the band for consideration to include the 3650 to 3700 MHz band, and confirmed the three-tier licensing model across, but established open eligibility for Priority Access as per the Public Notice.

Since Priority Access will no longer be limited to critical users under the defined model, the Commission proposed accommodating these users by setting aside 20 MHz of GAA spectrum with protection similar to Priority Access users inside the confines of their facility, such as a hospital. This effectively created a fourth tier referred to as Contained Access Users.

The Notice proposed to allow users at the PA or GAA tiers to select whether to provide access under common carrier or non-common carrier basis and sought comment on whether a SAS could effectively coordinate to allow GAA users to provide common carrier services. The Notice also proposed that there would be no fixed channel assignments. Instead, the SAS will manage assignments within each geographic area and can reassign channels from time to time as required, indicating that SAS providers are free to agree upon a convention for reassignment, but such convention will not be in the rules. The NPRM also proposed that GAA devices can use PAL spectrum that is not used at a given location and time, again with the SAS to coordinate.

In April of 2015, the FCC issued a Report and Order amending the Commission's rules with regard to the 3550 to 3650 MHz band (Docket 12-354). The Report and Order is established in Part 96 of the regulations and largely aligned with the rules outlined in the related Notice of Proposed Rulemaking and Further Notice of Proposed Rulemaking. In conjunction with the Report and Order, the Commission also released a Second Further Notice of Proposed Rulemaking, the Commission. In the FNPRM, the Commission explored three questions:

(1) Defining the use of PAL frequencies. The Report and Order allowed GAA use of PAL spectrum when not in active use by a Priority Access licensee. The FCC proposed an engineering, economic, and hybrid definition of what constitutes "not in active use" and proposed and sought comment on the proposed definitions.
(2) Implementing Secondary Markets in Priority Access Licenses. The Commission sought comment on changes required in the rules to facilitate the establishment of a secondary market for PALs, including allowing partitioning and disaggregation of PALs in terms of frequency and location.
(3) Optimizing protections for FSS. The Commission sought comment on proposals for both in-band and out-of-band protection of FSS. For in-band protection, five topics were presented:
    a. Calculation methodology
    b. Propagation modeling
    c. Interference protection criteria (IPC)
    d. Avoiding policy concerns related to aggregate IPC
    e. End user devices

    In terms of out-of-band protections for C-Band FSS Earth Stations, the Commission sought comment on whether the proposed in-band IPC was sufficient to address out-of-band protection or if other criteria should be applied.

In October 2015, the FCC released a Public Notice seeking comment on a proposed two-prong approach for determining a grandfathered wireless protection zone:

(1) Protection is provided for unregistered customer premise equipment (CPE) by establishing a protection radius of 4.4 km around each base station.
(2) Protection is provided for registered CPEs by establishing a protection sector determined by the azimuth and beamwidth of the registered base station antenna and a radius determined by the location of the furthest CPE (normally not more than 18 km).

In May 2016, the Commission released an Order on Reconsideration and Second Report and Order addressing the eight petitions for reconsideration received for the First Report and Order and the second Further Notice of Proposed Rulemaking. Through this Order, the Commission addressed the eight petitions for reconsideration received on the First Report and Order covering areas that included PAL License Terms and Renewability, PAL Auctions, SAS and CBSD Response Time, CBSD Power Limits, Out-of-Band Emission and Adjacent Channel Emission Limits, Emission Power Measurements and Testing Methodology, Device Geolocation, PAL Protection Criteria, and FSS Protection. In addition the Second Report and Order addressed the three issues raised in the second Further Notice of Proposed Rule Making. In August of 2016, the Commission extended these rules further in defining the methodology for determining the Grandfathered Wireless Protection Zones in the 3650 to 3700 MHz band based on the inputs received from the October 2015 Public Notice (Table 4).

Table 4 Timeline for CBRS regulations

	2013	2014	2015	2016
CBRS	Notice of Public Rulemaking	Further Notice of Proposed Rulemaking	Report and Order and Second Further Notice of Proposed Rulemaking	Order on Reconsideration and Second Report and Order
	3.5 GHz Workshop		Public Notice on Protection of Grandfathered 3650 to 3700 MHz Licensees	Methodology Adopted on Protection of Grandfathered 3650 to 3700 MHz Band Licensees
	Public Notice on 3.5 GHz Licensing Framework		First Wave Applications for SAS Administrators and ESC Operators	Conditional Approval of SAS Administrators

Technical Rules and Other Requirements

The rules in Part 97 define a three-tier structure as follows:

- Tier 1: Incumbents. This tier includes:
  - Military shipborne radars on 17 ships with current-generation radar, about 75% of which are homeported in Norfolk, VA; San Diego, CA; and Seattle, WA
  - Military ground-based radars with occasional in-band operations in 3650–3700 MHz at three sites: St. Inigoes, MD; Pensacola, FL; and Pascagoula, MS, and below 3500 MHz radar operations at isolated military bases spread around the United States.
  - Receive-only fixed satellite service (FSS) earth stations operating in band in 35 sites around the United States (mostly coastal sites, limited to inter-continental international satellites) and in the adjacent band 3700 to 4200 (thousands of sites around the United States).
  - Wireless broadband services (Part 90 services) operating in the 3650 to 3700 MHz band. In extending the regulations to include the 3650 to 3700 band, the Commission "grandfathered" existing license holders in this band for 5 years.
- Tier 2: Priority Access License (PAL). PALs are licensed by auction for a 3 year term, with license areas defined by the approximately 74,000 census tracts in the United States, each supporting a population of approximately 4000 people. Each PAL license will define a single 10 MHz channel in a single census tract, and each census tract will have from zero to seven PALs. PALs will be limited to the lower 3550 to 3650 MHz portion of the band. Anticipated use cases for PALs include:
  - Capacity/offload networks for established wireless service providers
  - QoS-managed enterprise networks
  - Utility networks
  - Backhaul
  - Wireless broadband service (after 5-year sunset on Part 90 3650–3700 MHz operations)
- Tier 3: General authorized access (GAA). GAA licenses allow the use of ANY frequency in any location in the 3550 to 3700 MHz band not being used at a given time by a higher tier licensee. The definition of unused is yet to be defined beyond the explicit statement that must not interfere with incumbents and PALs. GAA licensees are afforded no interference protection. GAA is licensed by rule, with no a priori bandwidth limit or license area. The regulations require that a minimum of 80 MHz and a maximum of 150 MHz be reserved for GAA in each census tract, subject to incumbent activity. Anticipated use cases for GAA include (Fig. 2):
  - Personal & small business hot spots
  - Campus hot spots

- PAL offload during periods of incumbent activity interrupting PAL spectrum
- Unprotected capacity/offload for established wireless providers
- Wireless broadband services
- Backhaul

Access to spectrum in Tiers 2 and 3 is facilitated through the use of Citizens Broadband Radio Service Devices (CBSDs) acting as fixed base station/access points for end user devices (EUDs). CBSDs can only operate under the authority and management of a centralized Spectrum Access System (SAS), which manages interference to incumbents by Tiers 2 and 3, interference among Tier 2 devices, and interference from Tier 3 into Tier 2 (see Fig. 3). To support this function, each CBSD wishing a spectrum grant must register with a SAS and provide its location

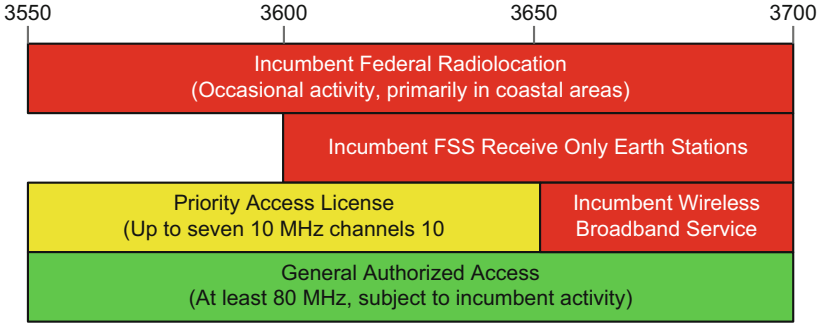

Fig. 2 3.5 GHz Band Overview

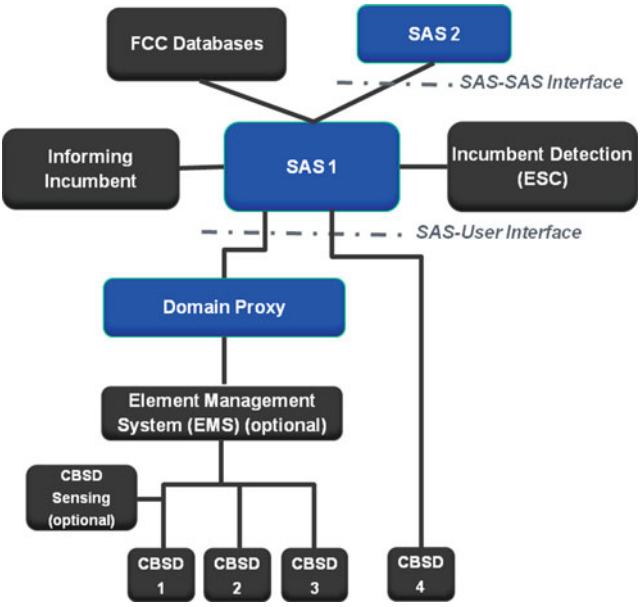

Fig. 3 SAS functional architecture [39]

and other information [40]. The SAS then determines and provides to the CBSD the permissible channels or frequencies and the maximum permissible transmission power level available at its location. Aggregate interference to protected users from all CBSDs is calculated by each SAS, and SAS share information as required to resolve conflicting uses of the band while maintaining, as much as possible, a stable radio-frequency environment.

Within Part 96, CBSDs are broken into two categories: Category A and Category B. Category A devices are envisioned primarily for indoor use as access points, femtocells, etc. Category A devices are limited to 30 dBm Effective Isotropic Radiated Power (EIRP), and if used outdoors, Category A devices are limited to 6 m height above average terrain (HAAT). Conversely, Category B devices are only allowed to operate outdoors with a 47 dBm maximum EIRP. Category B devices must be professionally installed and allow for both point-to-point and point-to-multipoint operation. The location of both Category A and Category B devices is required by the regulations to be accurate to $+/-50$ m horizontal and $+/-3$ m vertical, and CBSDs are required to report to the SAS within 60 s if their location changes.

End user devices in the CBRS system communicate exclusively with CBSDs: peer-to-peer communication is prohibited. The EIRP for end user devices is limited to 23 dBm.

Incumbent Protection

Protection for incumbent radar under Part 96 is initially provided through exclusion zones which effectively define keep out areas for CBSDs. The regulations also allow, however, the use of an environmental sensing capability (ESC) in lieu of exclusion zones to monitor for incumbent radar activity in coastal areas and near inland military bases. When incumbent activity is detected, and ESC communicates that information to a SAS, and the SAS or SASs will reconfigure local devices within 300 s to avoid interfering with incumbent radars, current incumbent radar will impact at most two channels in one area, and while the specific area of impact is to be determined, these radars operate infrequently, and so the use of a ESC will significantly improve access to spectrum over the defined exclusion zones.

Protection for PAL holders under Part 96 is established through the use of PAL Protection Areas (PPAs). The PPA defines a protection contour surrounding the CBSDs associated with a PAL holder that are in use in a specific location. A PPA may cross census track boundaries and therefore may be associated with multiple Priority Access licenses. PPAs are determined by a default protection contour based on a signal strength of -96 dBm/10 MHz around each CBSD or alternatively are self-reported by the PAL holder so long as they do not exceed the default contour. Areas outside the PPA are available for GAA use so long as the aggregate interference generated by CBSDs does not exceed -80 dBm/10 MHz within or at the PPA boundary.

Protection of legacy fixed satellite service providers was defined separately in the Report and Order for in-band and out-of-band services. For fixed satellite services operating in the 3550 to 3700 MHz band, the SAS shall ensure that the aggregate passband power spectral density at the location of the FSS earth station operating

in the 3600 to 3700 produced by emissions of co-channel CBSDs within 150 km operating in the Citizens Band Radio Service do not exceed a median RMS value of −129 dBm/MHz. In addition, the aggregate RF power at the location of the FSS earth station operating in the 3600 to 3700 produced by emissions of ALL CBSDs within 40 km operating in the Citizens Band Radio Service do not exceed a median RMS value of −60 dBm. Similarly, the SAS shall ensure that the aggregate passband power spectral density at the location of the FSS earth station operating in the adjacent 3700 to 4200 MHz band by emissions of CBSDs within 40 km operating in the Citizens Band Radio Service do not exceed a median RMS value of −129 dBm/MHz. The aggregate RF power at the location of the FSS earth station operating in the 3700 to 4100 MHz band produced by emissions of ALL CBSDs within 40 km operating in the Citizens Band Radio Service does not exceed a median RMS value of −60 dBm.

This level of protection is only afforded to those FSS earth stations that are registered annually, and such registration must provide detailed information on technical and operational characteristics, including antenna characteristics. If any information changes, the FSS operator has an obligation to update the SAS with the new information. CBSDs may operate within areas that may cause interference to FSS earth stations, in excess of the levels described so long as the licensee of the FSS earth station and the authorized user of the CBSD mutually agree on such operation and the terms of any such agreement are provided to an SAS Administrator that agrees to enforce them. In addition, the SAS must be capable of receiving and responding to complaints of interference from FSS operators.

In terms of protection for grandfathered broadband wireless service providers, protection is provided through use of a protection zone established in one of two ways:

- For sectors encompassing unregistered customer premises equipment (CPE), a 5.3 km radius sector from each registered base station based on the azimuth and beamwidth registered for that base station;
- For sectors encompassing registered CPE, a sector centered on each base station with the registered azimuth and beamwidth covering all registered subscriber stations within that sector.

The Commission established that aggregate power of co-channel CBSDs must be no greater than −80 dBm/10 MHz at any point inside these protection zones.

Standard Development

In its Report and Order establishing rules for the Citizens Broadband Radio Service ("CBRS") in the 3550 MHz band, the Commission observed that "a multi-stakeholder group focused on the complex technical issues raised by this proceeding could provide us with a wealth of valuable insights and useful information." In response to this need, in January of 2015, the Wireless Innovation Forum stood up a Spectrum Sharing Committee (SSC) to serve as a common industry

and government standard body to support the development and advancement of spectrum sharing technologies based on the three-tier architecture proposed for the 3.55 GHz rulemaking activities [41]. This Committee is intended to facilitate the interpretation and implementation of FCC rulemaking to a level that allows industry and government parties to collaborate on implementation of a common, efficient, well-functioning ecosystem around this technology.

The participants of this Committee include:

- Developers and operators of SAS, wireless equipment and devices, and sensor systems
- Operators and service providers interested in deploying in the spectrum
- Suppliers of systems and components operating on this spectrum
- Representatives of incumbent users including DoD/DISA, satellite operators, and utilities
- General users of spectrum outside of main providers
- Policy makers, academics, and researchers
- Representatives from other standard groups where interfaces or joint work is desired or necessary

These participants are organized into five work groups that work collaboratively to develop the reports, recommendations, and standards necessary to establish a commercial CBRS ecosystem (Fig. 4).

In the Report and Order, the Commission proposed a number of areas where a multistakeholder group would take action in supporting the band. The SSC Steering Group has reviewed these "callouts" and assigned them to the committee work groups as follows (Table 5):

Thus far, the Wireless Innovation Forum Spectrum Sharing Committee balloted, approved, and released three technical reports in support of this mandate:

- Technical reports
  - WINNF-15-P-0051-V1.0.0 Interim SAS to SAS Protocol Technical Report-A
  - WINNF-15-P-0023-V1.0.0 Interim SAS to CBSD Protocol Technical Report-A
  - WINNF-15-P-0060-V1.0.0 SSC WG4 Certification Process
  - WINNF-15-P-0047-V1.0.0 SAS Functional Architecture
  - WINNF-15-P-0062-V1.0.0 Interim SAS to CBSD Protocol Technical Report B
  - WINNF-16-P-0063-V1.0.0 Interim SAS to SAS Protocol Technical Report B
  - WINNF-16-P-0089-V1.0.0 CBRS Threat Model
- Recommendations
  - WINNF-15-R-0200-V1.0.0 WInnForum Comments on 3650 Protection Contours
  - WINNF-15-R-0092-V1.0.0 Emission Measurement Ex Parte
  - WINNF-15-R-0058/0059-V1.0.0 Reply Comments on the Second FNPRM
  - WINNF-15-R-0045-V1.0.0 WInnForum Comments on the Report and Order

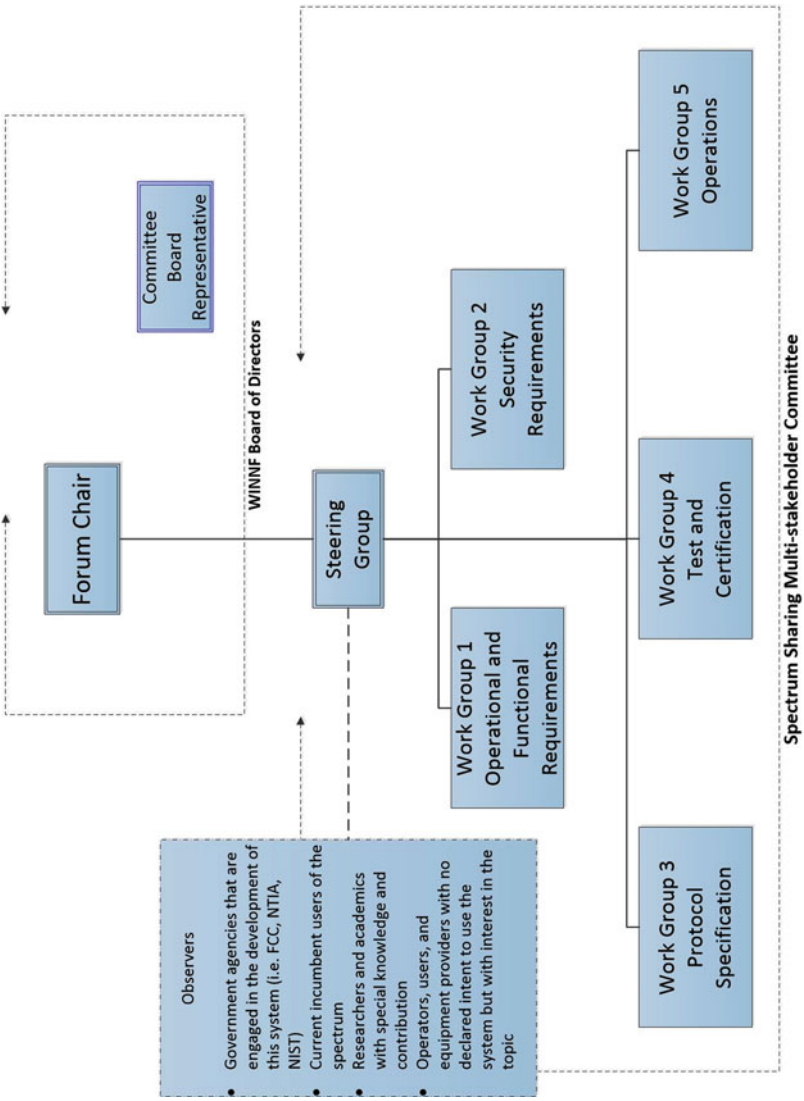

Fig. 4 WInnForum Spectrum Sharing Committee Structure

- Specifications and standards
  - WINNF-15-S-0112-V1.0.0 CBRS Operational and Functional Requirements
  - WINNF-15-S-0065 CBRS Communications Security Technical Specification
  - WINNF-15-S-0071-V1.0.0 CBRS Operational Security
  - WINNF-16-S-0016-V1.0.0 SAS to CBSD Technical Specification
  - WINNF-16-S-0096-V1.0.0 SAS to SAS Technical Specification

Table 5 SSC work group assignments for Report and Order multistakeholder group callouts

Paragraph	Callout	Work Group
59	We acknowledge that SAS Administrators, potential licensees, and other industry stakeholders will need to develop various implementation details to facilitate development of the Citizens Broadband Radio Service. As described elsewhere in this *Report and Order*, we believe that many of these issues can be addressed during the SAS Approval Process and through the efforts of a multistakeholder group	WG1
195	We recognize that ensuring compliance with this limit at the boundary is likely challenging on a real-time basis and there are legitimate questions relative to how to develop appropriate predictive models. We also recognize that the use of an aggregate metric could be challenging in a multi-user environment. We encourage any multistakeholder group formed to address technical issues raised by this proceeding to consider how this limit should be applied	WG1
214	For example, it might be possible that instead of the bright-line urban/rural distinction implemented in these initial rules, industry stakeholders (perhaps working through a multistakeholder forum) could agree on a "congestion metric" and associated methodology for SASs to reduce CBSD power levels in high-demand areas. We intend to continue an informal dialog with stakeholders on this topic and welcome the submission of additional technical analysis or reports of technological developments that can inform us going forward	WG1
222	Given the importance of accurate reporting by professional installers, we strongly encourage the SAS and user community, through multistakeholder fora or industry associations, to develop programs for accrediting professional installers who receive training in the relevant Part 96 rules and associated technical best practices	WG4 in partnership with another organization TBD
234	We encourage multistakeholder groups to consider the issues raised by the registration rules described in this section, including acceptable contact intervals between CBSDs and SASs, and to suggest appropriate operational parameters.	WG1
237	We encourage industry to develop detailed metrics regarding issues like received signal strength, packet error rate, and technology specific parameters of signal and interference metrics. These metrics could be developed by an industry multistakeholder group. Such guidance could be incorporated in the SAS Approval process described in section IIIH)(3)(b) or incorporated independently by authorized SAS Administrators, subject to Commission review	WG3

(*continued*)

Table 5 (continued)

Paragraph	Callout	Work Group
240	We encourage the industry to develop best practices for end-to-end security that can be validated in the equipment and SAS certification processes	WG2
268	We also require SAS Administrators to implement protocols to respond to directions from the President of the United States or another designated federal entity to manually discontinue operations of its associated CBSDs in a given area pursuant to 47 U.S.C. §606. SAS Administrators must also implement protocols to manually discontinue operations of their associated CBSDs in response to enforcement actions taken by the Commission	WG3
289	We agree with Federated Wireless, Google, Motorola Solutions, SIA, the Wireless Innovation Forum, and others, that a multistakeholder process could provide insight into the technical factors and interference limits between coexisting services in the 3.5 GHz Band	WG1
319	We continue to believe that a "light touch" regulatory approach is appropriate for this band and that the rules should include only the high-level requirements necessary to ensure the effective development and operation of fully functional SASs. We agree with commenters that support collaborative, industry-wide efforts to create standards and best practices governing SAS operations. The Commission will assist these efforts through the SAS Administrator approval process, as set forth in III(H)(3)(b). We also believe that an active multistakeholder group could help develop industry consensus around the best methods of meeting the SAS requirements	All
346	We require potential SAS Administrators to develop and demonstrate that their systems include robust communications and information security features during the SAS Approval process.745 CBSDs shall demonstrate compliant security features during the equipment authorization process. These security protocols will be subject to the Commission's review and approval, with input from NTIA and DoD. We anticipate that given the immense value of industry-wide interoperability, groups – such as the types of multistakeholder groups discussed in section III(K) – will develop security models that SAS Administrators may consider, subject to Commission review	WG2
438	We seek comment on what propagation model(s) are best suited for SAS-based protections of FSS. We solicit measurement results that validate model parameters for combined short range and long range propagation scenarios, involving indoor and outdoor propagation channels. What model(s) are the most accurate in accounting for urban clutter and other environmental factors such as rain attenuation, ducting, etc., and most suitable for modeling statistical variations to support analysis – including possible Monte-Carlo analysis – of many potential interfering sources? In order to generate the same exclusion distances between CBSDs and any individual FSS earth stations in 3650–3700 MHz, we expect each SAS to enforce the same minimum separation distance and we tentatively conclude that each SAS must use the same propagation model. We seek comment and objective analysis from anyone who believes otherwise	WG1

(*continued*)

Table 5 (continued)

Paragraph	Callout	Work Group
440	We also invite comment as to whether we can establish a default earth station protection area based on an assumed minimum earth station receiving system gain-to-temperature ratio (G/T) and minimum antenna elevation angle, and what the assumed values of the G/T and elevation angle should be. CBSD operation outside of such a default protection area would be assumed not to cause interference to earth stations receiving in the 3700–4200 MHz band. Such a default protection area would be adjusted by the SAS to accommodate the actual operating characteristics of earth stations that are registered in order to achieve additional protection	WG1

SAS Administrators and ESC Operators (Docket 15-319)

In December of 2015, the FCC opened a new docket allowing "First Wave" applications for SAS administrators and ESC operators [42]. Seven organizations applied to be SAS administrators and six applied to be ESC operators:

SAS administrator applicants	ESC operator applicants
Amdoc	
Comsearch	Comsearch
CTIA	CTIA
Federated Wireless	Federated Wireless
Google	Google
Keybridge Global	iPosi
Sony	Keybridge Global

In December of 2016, the Commission conditionally approved all seven SAS administrator applicants, based upon a review of the proposals submitted and subsequent amendments.

Current Status and Future Plans

The next step in the evolution of the CBRS band is the certification of SAS for commercial use, followed by certification of ESC and CBSD products. Such testing is expected to occur in the first half of 2017, with commercial deployments expected later that same year. In anticipation of this, the CBRS ecosystem has undertaken a number of activities:

- 3GPP has approved "Band 48" for LTE operation in the CBRS
- Google and Federated Wireless have both announced trials involving multiple operators and equipment manufacturers in the United States [43].

- Google and Federated Wireless have validated the SAS to SAS interface protocol standard through an interoperability demonstration [44].

While not conclusive, this level of activity indicates significant interest by the industry in the success of this new band.

Many of the SAS administrators are also seeking to extend elements of the CBRS framework to other bands. Google, for example, has publicly announced support for Part 96 rules in 5G [45], and the University of Oulu has led an effort to field trial CBRS as a part of the Finnish Spectrum Sharing Trial [46]. Keybridge Global has signed a contract with more immediate impact. In November of 2013, the US DoD and the Broadcasting Industry agreed to relocate DoD operations in the 1755 to 1780 MHz spectrum to the 2025 to 2110 MHz band, currently used by broadcasters for remote news gathering operations [47]. Doing so allows the 1755 to 1780 MHz band to be paired with the 2155 to 2180 MHz band as a part of the AWS-3 auction. DoD use of the 2025 to 2110 spectrum would be on a co-primary shared basis with nonfederal users. Nonfederal operation will have priority over DoD operations in this band, with the fixed and mobile military stations operating in the band incorporating frequency agile technology to ensure they shall not cause harmful interference to nonfederal users. In October 2016, Keybridge Global signed a contract to become the SAS administrator for the 2025 to 2110 MHz band [48].

Conclusion

Through the regulatory activities highlighted in this chapter, the FCC working in cooperation with NTIA have made hundreds of megahertz of spectrum available for sharing at various different levels. The results of these activities to date have been mixed. Spectrum sharing regulations appear to be successful when the amount of available spectrum is relatively well known, and the mechanism for obtaining a license is relatively straightforward. Where the regulations are less successful from a business perspective, the hurdles to success are generally not technical. Instead, regulatory uncertainty has limited investment, or a failure to overcome business disincentives to share has limited the actual availability of spectrum. Open proceedings in the 500 MHz initiative and in other initiatives ongoing in this area indicate that the FCC and NTIA are learning from these proceedings in their efforts to better facilitate the effective use of spectrum in serving the public interest.

Acknowledgements Portions of the entry were extracted from the Wireless Innovation Forum's "Spectrum Sharing Annual Report" (Document WINNF-14-P-0001-V1.0.0) [49], funded by the Wireless Innovation Forum.

References

1. http://www.ntia.doc.gov/book-page/who-regulates-spectrum
2. http://www.fcc.gov/encyclopedia/rulemaking-process-fcc
3. http://www.fcc.gov/encyclopedia/technological-advisory-council
4. http://www.ntia.doc.gov/office/OSM
5. http://www.ntia.doc.gov/page/irac-functions-and-responsibilities
6. http://www.ntia.doc.gov/page/2011/manual-regulations-and-procedures-federal-radio-frequency-management-redbook
7. http://www.ntia.doc.gov/files/ntia/publications/csmac_2013_charter.pdf
8. http://www.ntia.doc.gov/book-page/how-spectrum-shared
9. http://www.ntia.doc.gov/files/ntia/publications/redbook/2013/8_13.pdf
10. http://www.ntia.doc.gov/files/ntia/publications/redbook/2013/10_13.pdf
11. http://www.ntia.doc.gov/files/ntia/publications/redbook/2013/9_13.pdf
12. http://www.ntia.doc.gov/book-page/national-telecommunications-and-information-administration
13. http://www.ntia.doc.gov/other-publication/2014/federal-government-spectrum-compendium
14. http://transition.fcc.gov/Reports/1934new.pdf
15. http://transition.fcc.gov/sptf/
16. https://www.fcc.gov/ecfs/search/filings?proceedings_name=00-47&sort=date_disseminated,DESC
17. https://www.fcc.gov/ecfs/search/filings?proceedings_name=00-230&sort=date_disseminated,DESC
18. https://www.fcc.gov/ecfs/search/filings?proceedings_name=03-108&sort=date_disseminated,DESC
19. http://wireless.fcc.gov/uls/index.htm?job=home
20. Roberson et al (2011) Long-term Spectral Occupancy Findings in Chicago. In: Proceedings of DySpan 2011
21. McHenry M, Roberson R. Spectrum Occupancy Measurements: Chicago. http://www.sharedspectrum.com/wp-content/uploads/NSF_Chicago_2005-11_measurements_v12.pdf
22. Wireless Innovation Forum (2011) SDR Market Size Study
23. https://www.fcc.gov/ecfs/search/filings?proceedings_name=03-122&sort=date_disseminated,DESC
24. https://www.fcc.gov/ecfs/search/filings?proceedings_name=13-49&sort=date_disseminated,DESC
25. https://www.fcc.gov/ecfs/search/filings?proceedings_name=04-151&sort=date_disseminated,DESC
26. http://hraunfoss.fcc.gov/edocs_public/attachmatch/FCC-07-99A1.pdf
27. http://wireless.fcc.gov/services/index.htm?job=service_home&id=3650_3700
28. https://www.fcc.gov/ecfs/search/filings?proceedings_name=04-186&sort=date_disseminated,DESC
29. Pucker L (2012) Standards for DSA system implementation: a harmonized requirements approach. In: Proceedings of the Wireless Communications and Networking Conference Workshops (WCNCW)
30. http://www.fcc.gov/topic/incentive-auctions
31. http://www.marketsandmarkets.com/Market-Reports/tv-white-space-spectrum-market-71081100.html
32. https://www.fcc.gov/ecfs/search/filings?proceedings_name=12-354&sort=date_disseminated,DESC
33. http://www.whitehouse.gov/the-press-office/presidential-memorandum-unleashing-wireless-broadband-revolution

34. http://www.ntia.doc.gov/report/2010/assessment-near-term-viability-accommodating-wireless-broadband-systems-1675-1710-mhz-17
35. https://www.fcc.gov/ecfs/search/filings?proceedings_name=10-123&sort=date_disseminated,DESC
36. https://www.fcc.gov/ecfs/search/filings?proceedings_name=10-237&sort=date_disseminated,DESC
37. http://www.whitehouse.gov/sites/default/files/microsites/ostp/pcast_spectrum_report_final_july_20_2012.pdf
38. http://www.ntia.doc.gov/files/ntia/publications/ntia_1755_1850_mhz_report_march2012.pdf
39. Wireless Innovation Forum. SAS Functional Architecture. http://www.wirelessinnovation.org/assets/work_products/Reports/winnf-15-p-0047-v1%200%200%20sas%20functional%20architecture.pdf
40. Wireless Innovation Forum. Requirements for Commercial Operation in the U.S. 3550 to 3700 MHz Citizens Broadband Radio Service Band. http://www.wirelessinnovation.org/assets/work_products/Specifications/winnf-15-s-0112-v1.0.0%20cbrs%20operational%20and%20functional%20requirements.pdf
41. The Wireless Innovation Forum. Spectrum Sharing Committee Scope and Operations. https://winnf.memberclicks.net/assets/SSC/spectrum%20sharing%20committee%20scope%20and%20operations%20-%20v1.0.0.pdf
42. https://www.fcc.gov/ecfs/search/filings?proceedings_name=15-319&sort=date_disseminated,DESC
43. Hamblin M (2016) multiple US Trials Underway for Shared 3.5 GHz Wireless Spectrum. ComputerWorld. http://www.computerworld.com/article/3075748/mobile-wireless/multiple-u-s-trials-underway-for-shared-3-5ghz-wireless-spectrum.html
44. BusinessWire. Federated Wireless and Alphabet's Access Team Demonstrate Operational Viability of Shared Spectrum Solution for CBRS Band. http://www.businesswire.com/news/home/20161214006343/en/Federated-Wireless-Alphabet's-Access-Team-Demonstrated-Operational
45. Dano M (2016) Google Engineer: Wireless Industry Needs to Break the Model of Exclusive Spectrum. FierceWireless. http://www.fiercewireless.com/tech/google-engineer-wireless-industry-needs-to-break-model-exclusive-spectrum
46. Wireless Innovation Forum. WInnComm Europe 2016 Innovation Showcase. http://www.europe.wirelessinnovation.org/2016-showcase-demos
47. http://www.ntia.doc.gov/files/ntia/publications/ntia_aws-3_ltr_11252013_.pdf
48. Keybridge Global (2016) Keybridge Signs Spectrum Sharing Contract ofr Defense Information Systems Agency. https://keybridgeglobal.com/company/news/story.xhtml?uri=tag%3Ablogger.com%2C1999%3Ablog-6667646702756364360.post-7754372270063786695
49. Wireless Innovation Forum. Dynamic Spectrum Sharing Annual Report 2014. http://www.wirelessinnovation.org/assets/work_products/Reports/winnf-14-p-0001-v1.0%20dynamic%20spectrum%20sharing%20annual%20report%202014.pdf

Novel Regulatory Solutions for Cognitive Radio and Spectrum Sharing in the UK

52

Toby Youell

Contents

T. Youell (✉)
Spectrum Group, Ofcom (writing in a personal capacity), London, UK
e-mail: Toby.Youell@ofcom.org.uk; toby.youell@googlemail.com

W. Zhang (ed.), *Handbook of Cognitive Radio*,
https://doi.org/10.1007/978-981-10-1394-2_51

Abstract

More than half (58%) of the spectrum in the UK is shared between different classes of users. Typically, this has been enabled by authorizing individual applications to use specific frequencies at specific locations on a first-come-first-served basis.

But technological developments, the focus of this book, have presented Ofcom with promising opportunities to share spectrum more effectively. Ofcom has taken advantage of these technologies within the UHF band (470–790 MHz) in the context of the digitization of terrestrial television. More recently, Ofcom has focused on establishing a systematic way of enabling spectrum sharing in general and has taken preliminary steps in exploring how to share the 3.8–4.2 GHz band.

Keywords

TV White Space · Spectrum sharing · Cognitive radio · Ofcom · 470–790 MHz · 3.8–4.2 GHz · Tiered spectrum access

Introduction

Spectrum Regulation in the UK

Ofcom was established in late 2003 in anticipation of convergence in communications. It has a mandate to regulate (among other things) telecommunications, broadcasting, and radio spectrum in the UK.

Its work regarding radio spectrum is driven by two pieces of legislation, the Communications Act 2003 [1] and the Wireless Telegraphy Act 2006 [2]. Broadly speaking, the former sets out the high-level objectives that Ofcom must work to, and the latter provides Ofcom with the authority to authorize access to radio spectrum in the service of those objectives, as well as further guidance. European law is embedded in both Acts. In particular, through its regulation of spectrum, Ofcom must always apply objective, transparent, nondiscriminatory, and proportionate regulatory principles.

Section 3 of the Communications Act provides that Ofcom's principal duty is to further the interests of citizens in relation to communication matters and to further the interests of consumers in relevant markets, where appropriate, by promoting competition.

In carrying out these functions, section 3(2) provides that Ofcom is required, among other things, to secure the optimal use for wireless telegraphy of the electromagnetic spectrum and the availability throughout the UK of a wide range of electronic communication services.

It follows that when considering spectrum policy in the UK, Ofcom always keeps in mind its requirement to "secure the optimal use for wireless telegraphy of the electromagnetic spectrum." This provokes Ofcom to consider cognitive radio and/or spectrum sharing if it is thought that it would make the use of the spectrum more "optimal."

The Wireless Telegraphy Act 2006 confers on Ofcom the authority to fulfill its statutory duties by authorizing access to spectrum. It also imposes a number of further obligations regarding how it carries out these duties. Specifically, section 3(2) requires Ofcom to have regard to (among other things) the desirability of promoting the efficient management and use of the spectrum, the economic and other benefits that may arise from the use of wireless telegraphy, and the development of innovative services and competition in the provision of electronic communications services. When taking into account the desirability of those things, Ofcom must have regard to the extent to which the spectrum is available for use and to the demand, both current and future, for use of the spectrum.

Clearly, making a judgment on what use of spectrum would comprise a given frequency's "optimal" use for wireless telegraphy (any form of wireless communication) is a difficult task. This is only partially mitigated against by the guidance articulated through additional duties set out in the Wireless Telegraphy Act, especially when there could be a tension between these objectives.

For example, taking into account the desirability of the development of innovative services means that for a given part of the spectrum, Ofcom should look to encourage technical innovation, including cognitive radio and spectrum sharing. At the same time, a given policy that would enable spectrum sharing might not be thought by some to deliver, for example, the greatest economic benefits from the use of (a hypothetical) part of the spectrum.

Altogether, the duty to secure the optimal use of radio spectrum, and to also have regard to the desirability of developing innovative technologies when authorizing access to spectrum, means that the preconditions are in place to allow Ofcom to enable cognitive radio and spectrum sharing.

Sharing Within the UK Legal Framework

The Wireless Telegraphy Act empowers Ofcom to authorize transmissions under two circumstances:

- A licensee has obtained a Wireless Telegraphy Act license and transmits according to the conditions specified in the license. These conditions will typically be (where possible) technology neutral and could be focused on avoiding undue interference into adjacent channels. For example, a mobile network operator (MNO) may have a WT Act license that gives it permission to transmit within a certain assignment within a given band. The MNO may have obtained the license through an auction mechanism, and transmissions will have to follow certain parameters referred to in the license, alternatively.
- A stakeholder is exempted from requiring a license in order to transmit under certain circumstances and in certain spectrum bands that have been defined by Ofcom. Section 8(5) of the WT Act sets down a series of conditions that have to be met for Ofcom to establish such rules, including that license-exempt use may not cause undue interference to wireless telegraphy (as additionally set down in WT Act Section 55).

The use of spectrum to receive signals is exempted from licensing under the Wireless Telegraphy Apparatus (Receivers) (Exemption) Regulations 1989 [3]. Ofcom does not "protect" receivers from undue interference. Nonetheless, some of its policies have a similar effect in that they allow a stakeholder to benefit from "benchmark spectrum quality," which may be defined as a particular interference level at a given site. When doing so, Ofcom sometimes makes grants of Recognised Spectrum Access available to stakeholders. These grants allow Ofcom to take a certain usage into account when regulating spectrum access, even though Ofcom does not directly license its transmission. For example, the transmitter may be a "Crown" user (the UK Government) or could be a naturally occurring phenomenon in outer space that radio astronomers wish to be able to receive in the UK.

This framework enables spectrum sharing because license-exemption and WT Act licenses only authorize transmissions and in principle do not comprise "exclusive" use of a given spectrum band. This means that there is no legal barrier preventing another stakeholder from using spectrum (for transmitting and/or receiving) that is already assigned to another stakeholder through a WT Act license.

One way of achieving spectrum access could be for the new entrant to enter into a commercial arrangement with the licensee (e.g., leasing), if permitted under the terms of the relevant license. Alternatively, the new entrant could obtain a WT Act license where it would be up to Ofcom to decide whether or not to allow such spectrum sharing by issuing such a new license.

In an international context, in particular in the Radio Regulations [4], spectrum managers typically discuss a hierarchy of spectrum rights based on the concept of primary and secondary users of spectrum. According to this understanding, the primary user can transmit and receive without undue interference. This means that the secondary user must not cause undue interference to primary services and cannot claim protection from undue interference from the primary service, even if a specific deployment of a primary service was established after the secondary service. In some frequency bands, particularly those designated for industrial, scientific, and medical applications (ISM bands), all spectrum users are secondary and cannot claim protection against each other regarding undue interference.

In this context, cognitive radio and spectrum sharing could depend on secondary spectrum access, where a secondary user can "borrow" spectrum already assigned to another (often primary) user.

In the UK context, however, because of the legal framework described above, Ofcom is not able to issue licenses that provide explicitly "primary" or "secondary" spectrum access rights; rather, any distinction between primary and secondary users may only exist when they are embedded in the conditions set down within authorizations or the processes that Ofcom itself undertakes when authorizing spectrum access.

In some bands, Ofcom authorizes spectrum access on a site-by-site or area-defined basis where a hierarchy is established on the basis of when an authorization has been issued. In these bands, sometimes referred to as "Ofcom Managed Bands," Ofcom issues WT Act licenses, or grants of Recognised Spectrum Access on a first-come-first-served basis subject to Ofcom coordination and Ofcom technical

frequency assignment criteria. The conditions in each new WT Act license will be designed to avoid interference to already-existing users. For example, a fixed link license might be issued with quite detailed technical specifications that Ofcom has found to be necessary to protect nearby satellite Earth stations with a grant of Recognised Spectrum Access for a given band. Altogether, these bands comprise around half of the radio spectrum in the UK [5].

Seeing as spectrum sharing is already so widespread in the UK, it is more appropriate to discuss innovative forms of spectrum sharing, potentially enabled by cognitive radio, as "enhanced spectrum sharing."

In sum, in pursuing its general duties, Ofcom has sought to enable the development of cognitive radio and spectrum sharing, working with the authorization tools at its disposal. Secondary spectrum access, which might enable cognitive radio and spectrum sharing, can only exist in the UK when embedded in the conditions of access authorizations or through Ofcom's internal processes. Ofcom can enable new entrants to access spectrum even though there may already be a licensee because Ofcom does not in principle issue "exclusive" licenses.

The rest of this chapter considers two examples of this, one where spectrum sharing is now authorized on a license-exempt basis (or in some cases WT Act licenses) and one where Ofcom's policy is still in development.

TV White Space

Introduction

Terrestrial broadcasting has traditionally been a cornerstone of economic and cultural activity in the UK, and it has long been a policy objective to ensure near-universal access to the service. The 470–790 MHz band has been used to achieve this because it is considered to comprise the "sweet spot" where high-capacity signals can be transmitted over a very wide area.

Partly because the infrastructure predates the concept of "spectrum scarcity" (and market-based spectrum fees), the network is based on high-power high-tower transmitters that require relatively few sites to provide universal coverage. The disadvantage of this is that interference can only be prevented by using different frequencies in different areas for the same multiplexes.

This legacy requirement for geographical separation of broadcasting transmitters (as shown in an early illustration made by Ofcom given in Fig. 1) [6] means that in most places, most of this spectrum is theoretically available for alternative use. The presence of unused UHF spectrum at a given location is referred to as interleaved spectrum or TV White Space.

Programme Making and Special Events (PMSE) applications already use TV White Spaces (TVWS), where Ofcom issues licenses to PMSE users that provide a degree of protection against undue interference from a third party, such as another PMSE user. PMSE licenses are only issued to frequencies that are not issued to DTT at a particular location or where its use will not cause undue interference to DTT

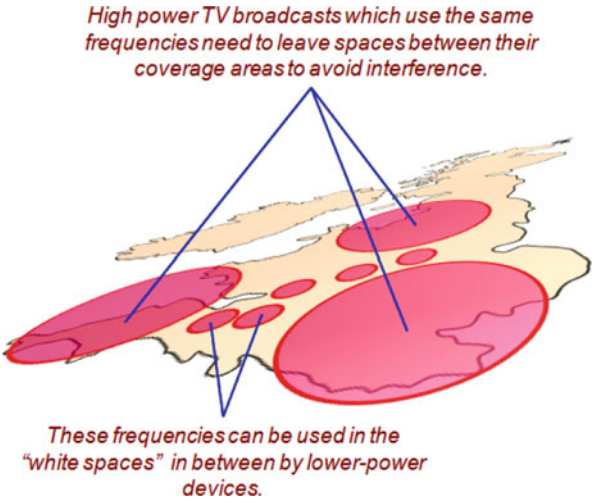

Fig. 1 Geographical separation of broadcasting transmitters (Source: Ofcom (2012) TV White Space: a consultation on white space device requirements. Available online at https://www.ofcom.org.uk/__data/assets/pdf_file/0022/40477/condoc.pdf)

(such as in an indoor environment). These licenses can be conceived of as operating on a second tier to DTT as practically speaking a license would not be issued to PMSE where undue interference would be caused to the primary tier (DTT).

Ofcom has now established a framework whereby a new class of radios, known as white space devices (WSDs), can also access these TV White Spaces on a license-exempt basis or on an interim basis through a WT Act license. Effectively this establishes a third tier for where use is permitted as long as it does not cause undue interference to any licensed user.

It should be noted that the concept of a first, second, and third tier does not correspond to primary and secondary spectrum access, which as described in the introduction does not exist in Ofcom's authorizations.

The Scale of the Opportunity

Digital terrestrial television (DTT) is based upon six national multiplexes, each of which carries eight to 13 channels. Three of these (used for public service broadcasting) provide coverage to around 98.5% of the UK population, while the other three provide coverage to 90% of the population. There are also local multiplexes in some areas. Additionally, there are interim multiplexes that can operate until 2020, or beyond albeit with diminished rights, and are intended to promote the adoption of more advanced digital terrestrial television technology (DVB-T2).

Each multiplex uses a single 8 MHz block of spectrum, meaning that only a fraction of the 320 MHz allocated to the broadcasting service is required in any particular location in the UK for the reception of DTT.

It is worth noting that this conception of TV White Space is different than the one used in the USA. In the UK, the "white spaces" refer to the channels that are not in

use at a particular place taking into account any nearby viewer antenna locations and the relevant transmitters, whereas in the USA white space refers to the geographical areas between TV coverage areas that are not used in a particular channel. The difference in conception is a function of the fact that the DTT offering in the UK is almost universal, whereas in the USA there are some areas with relatively little DTT usage, as well Ofcom's policy to only protect DTT antennas that are actually in use.

Notwithstanding the more limited conception of TVWS in the UK, spectrum is still abundantly available.

In preparation for the TVWS Framework Statement [7], Ofcom calculated the availability of spectrum for different types of devices operating at different power levels at different locations.

It found that if one assumes a geographically fixed WSD transmitting at 23 dBm within a strict emissions class at a height of 10 m (e.g., as part of a municipal Wi-Fi network), then there would be 14 channels (112 MHz) available at 85% of locations in London. The graph below demonstrates how the availability of spectrum would differ according to power limit and number of locations (Fig. 2).

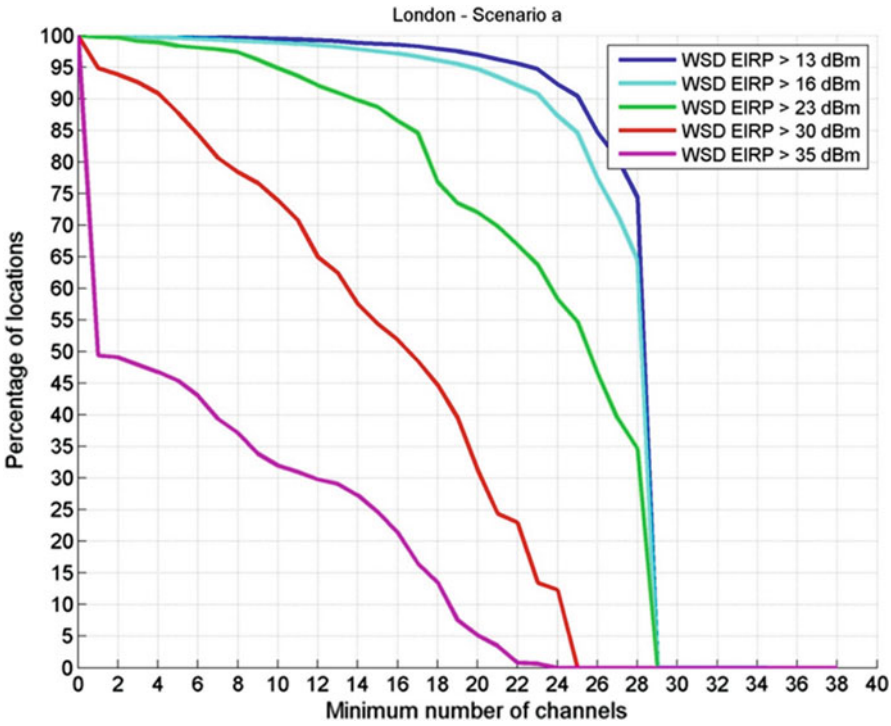

Fig. 2 Availability of TV White Space in central London (Source: Ofcom (2015) Implementing TV White Spaces. Available online at https://www.ofcom.org.uk/__data/assets/pdf_file/0034/68668/tvws-statement.pdf)

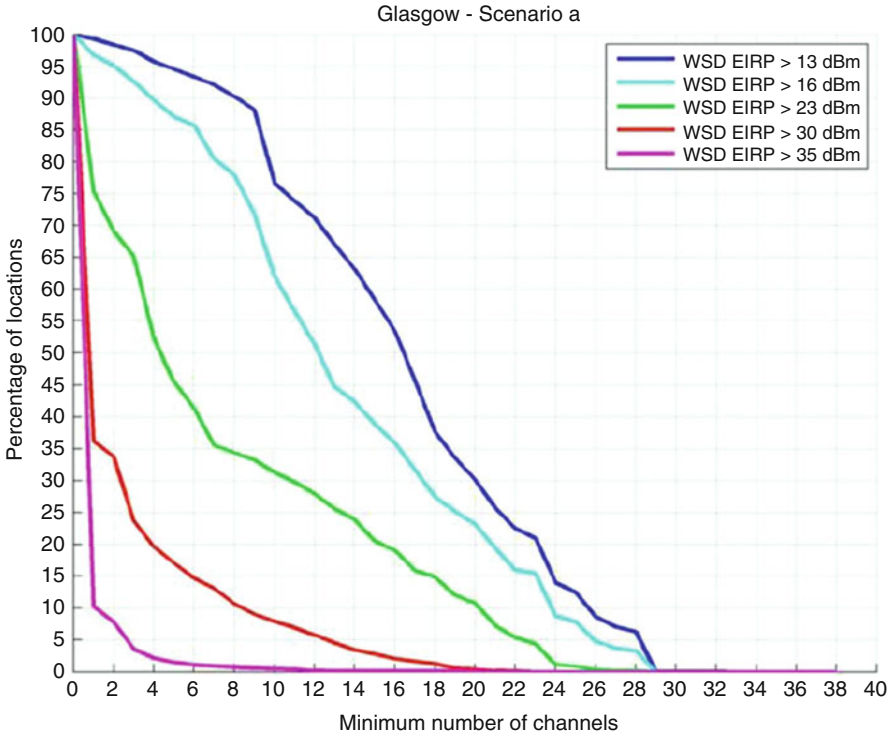

Fig. 3 Availability of TV White Space in Glasgow (Source: Ofcom (2015) Implementing TV White Spaces. Available online at https://www.ofcom.org.uk/__data/assets/pdf_file/0034/68668/tvws-statement.pdf)

However, the London case is favorable for TVWS availability because it is dominated by a single high-tower high-power transmitter (Crystal Palace). In other areas, there is a significant overlap between the different transmitters, resulting in less TVWS available. For example, in Glasgow there would be no channels available under the circumstances described above. Instead, power would have to be reduced to 13 dBm, and even then only 9 channels (72 MHz) would be available, as shown below (Fig. 3).

In general, the opportunity to use this spectrum more intensively has long been perceived and exploited by services auxiliary to broadcasting, now known as Programme Making and Special Events (PMSE) applications. These devices, such as wireless microphones and in ear monitors, typically use 200 kHz channels at low power. Additionally, other applications such as audio links and video links use different bandwidths and are planned on the basis of an 8 MHz channel, although the user can often plan many devices in one channel. PMSE users currently obtain time- and location-specific licenses to access TV White Spaces from Ofcom or can alternatively obtain from Ofcom a license for Channel 38 (606–614 MHz), which is uncoordinated and typically used for news-gathering.

PMSE equipment is typically used in venues such as theaters, studios, or churches on a regular basis. Peak demand comes from special events such Formula One or music festivals.

Permitting Cognitive Radio in Principle

Terrestrial broadcasting's digitization in the last decades both enhanced the capabilities of the platform and allowed Ofcom to reuse parts of the spectrum for mobile, eventually comprising the 800 MHz mobile band. It also prompted Ofcom to review its policy toward the band as part of its Digital Dividend Review [8].

As discussed in the introduction, Ofcom's principal duty is to secure the optimal use of spectrum. A prevalent interpretation of this is that it should seek to ensure that the radio spectrum is being used as intensively as possible. Ofcom's additional duty to consider future requirements also requires Ofcom to monitor the opportunities presented by new technologies.

These duties indicated to Ofcom when it was undertaking its Digital Dividend Review that it should consider allowing cognitive radios to use this band.

One could argue that the most effective way to promote innovation would have been to set spectrum aside for cognitive radios operating on a license-exempt basis, thus creating a "sandpit" for innovation. In the absence of spectrum licenses, this would have required devices to find their own technical solutions to undue interference arising from the use of radios by third parties. This approach has been praised for fostering technologies such as Wi-Fi and Bluetooth in the 2.4 GHz band. However, there are plenty of other sandpits across the radio spectrum, and Ofcom felt that the loss of benefits (the opportunity cost) arising from not allowing licensed services (in this case DTT, PMSE, or Mobile) to use these bands were seen to be greater than the potential benefits of allowing only licence-exempt users access to a portion of the band.

Bearing in mind the large amount of spectrum available within TV White Spaces, as explained above, there remained ample opportunities for cognitive radio to access spectrum without reserving spectrum. Doing so would allow the spectrum to be used more "optimally," as it would otherwise probably be unused.

It therefore decided in 2008 to allow the interleaved parts of the band to be used by cognitive devices on a license-exempt basis, providing Ofcom was satisfied that licensed users of the band (DTT and PMSE) would be protected from undue interference.

Authorizing Access to Spectrum

Typically under license exemption, the regulator shifts the responsibility to protect a user from undue interference from the regulator to the user itself. To do this, a device needs to know whether or not its transmissions will be able to be received by the

intended receiver using information about the interference environment. This could be done through the use of beacons, sensing technology, or geolocation databases.

Beacons could theoretically use the same sites used for DTT multiplexes to transmit information about available spectrum within the reception area of a given transmitter. If a WSD could not receive signals from a beacon, then the WSD would not be permitted to transmit within TV White Spaces at all. A principle advantage of this approach is that it would be effective in preventing the emergence of scenarios where a WSD would cause undue interference to another spectrum user.

However, the infrastructure necessary for this was deemed to be expensive to construct and maintain, and it was not clear who would be responsible for creating standards for this technology and who would maintain it. Additionally, it was also anticipated at the time that this approach would be inherently too conservative as the beacons would need to transmit at a lower power than that of the multiplexes so that the beacon signal could not be received outside of the geographic area where DTT transmission was intended to be received. The consequence of this is that WSDs would not be able to receive the signal from the beacon, even though it may be safe to transmit. This would not result in the optimal use of spectrum.

Sensing, where a device itself would detect whether or not spectrum was available to use would be much less conservative. An added advantage would be that no infrastructure would need to be constructed. However, sensing also generated challenges. For example, a White Space Device (WSD) might not be able to detect a weak signal in a given channel from a distant transmitter and may begin transmissions that would cause interference to a nearby DTT receiver.

Additionally, a reliance on sensing would create the hidden node problem, whereby the transmitter path remains blocked but the interference path remains open. The image below, created by Ofcom as part of a policy statement it made on the subject [9], demonstrates how this might occur in the context of WSDs. Here, it is imagined that a cognitive WSD may not be able to detect a DTT transmission because of an obstacle so would start to use a given frequency. However, these transmissions would cause undue interference to a DTT receiver that is reliant on the frequency for its DTT reception (Fig. 4).

Seeing as Ofcom had sought to be satisfied that there was a low probability of undue interference *to* the licensed users of the band *from* the license-exempt device, this was not seen as a viable solution for the time being.

Alternatively, a WSD may be able to obtain information about the spectrum environment at its particular geolocation from a database that can compute this information based on its knowledge of DTT transmitters, PMSE licenses, and (in some cases) other WSD deployments. The use of geolocation was judged to be able to provide a good balance between optimizing the use of spectrum (allowing as much WSD use of the spectrum as possible), while satisfying Ofcom that undue interference to licensed users would be unlikely [10]. An additional advantage of this approach is that it allows Ofcom to retain control on WSDs' access to spectrum. For example, if interference were to be found to be occurring at a particular location due to changes in the performance of a DTT transmitter, then the databases could be updated to take account of this.

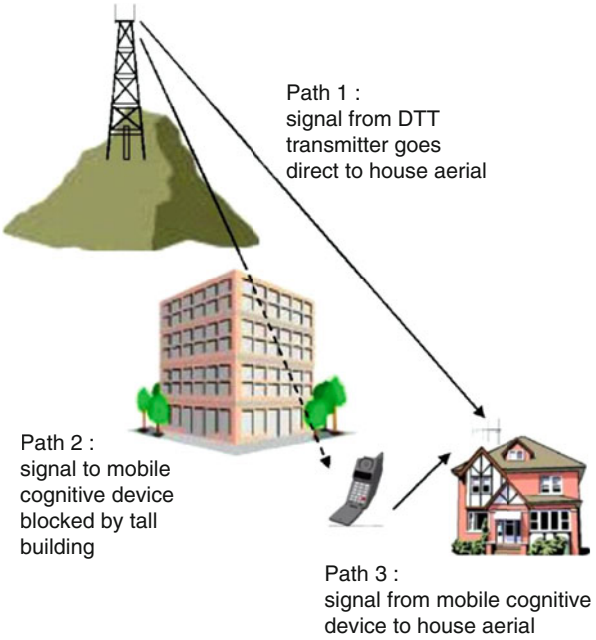

Fig. 4 The hidden-terminal issue (Source: Ofcom (2009) Digital dividend: cognitive access. Available online at https://www.ofcom.org.uk/__data/assets/pdf_file/0023/40838/statement.pdf)

Seeing as WSDs in the UK depend on geolocation databases, it is not strictly accurate to describe the devices as cognitive radios. As explained later, the cognition required for an effective deployment of dynamic spectrum access is undertaken by the geolocation database.

Geolocation databases could theoretically have been provided by Ofcom itself, or by a third party on its behalf. However, in order to keep costs to a minimum, and to allow the development of white space services to develop without regulatory constraints, it was felt that geolocation databases should be provided by third parties according to their own business models. In this scenario, white space service providers negotiate with geolocation database providers on a commercial basis for use of the database.

A disadvantage of allowing third parties to operate geolocation databases is that Ofcom needed to create an overall framework that would ensure that databases would work correctly (as it would not have direct control).

An additional problem is that the UK's legal framework concerning spectrum does not currently allow for such geolocation databases to be registered through Ofcom. To overcome this problem, Ofcom has entered into contractual arrangements with geolocation providers. In the interests of simplicity and clarity, it is proposed as part of the Digital Economy Bill 2016/17 that geolocation databases may be registered by Ofcom. At the time of writing, this bill is being considered in the UK Parliament and may become an Act in the future.

The Database Approach

An overview of the database approach to TV White Space in the UK is given in the diagram below. This was created by Ofcom as part of its *Implementing TV White Spaces* statement in 2015 [11] (Fig. 5).

The database approach establishes two types of WSDs:

- **Master WSDs**. These devices are able to communicate with a White Space Database (WSDB) without using TV White Space spectrum. They provide information about their own characteristics and the characteristics of their slave WSDs to the database. These characteristics are known as device parameters.
- **Slave WSDs**. These devices must be under the control of a master WSD and are not allowed to communicate with a WSDB directly.

Before communicating with a WSDB, the master WSD must regularly interrogate a machine-readable page on Ofcom's website to find out which WSDBs are registered with Ofcom. Once it has obtained a list of WSDBs, the master WSD sends information about its device parameters to its chosen WSDB, including device parameters concerning slave WSDs.

The WSDB then performs calculations using the device parameters and provides the master WSD with information on which frequencies can be used by the master WSD and slave WSD and at what power level. These are referred to as operational parameters.

The master WSD chooses which frequencies to use at what power and informs the WSDB of its channel usage parameters (the lower- and upper-frequency

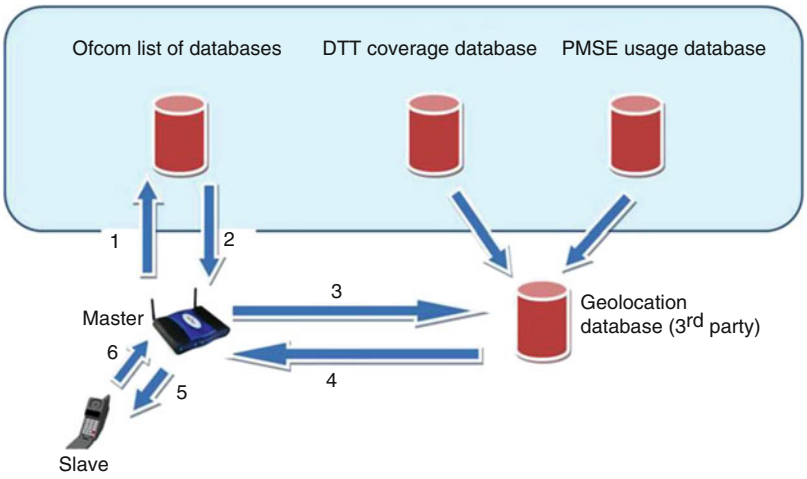

Fig. 5 Overview of TV White Spaces framework (Source: Ofcom (2015) Implementing TV White Spaces. Available online at https://www.ofcom.org.uk/__data/assets/pdf_file/0034/68668/tvws-statement.pdf)

boundaries within which the WSD will transmit and the maximum in-block EIRP spectral density).

Ofcom has chosen to adopt a more complex form of TV White Space access than other countries (notably the USA) so as to allow for the optimal use of spectrum. For example:

- The operating parameters generated by WSDBs will vary the power levels permitted by WSDs based on the specific location of WSDs. Conversely, in the USA a WSD may either operate at full power or not at all, depending on whether or not transmission in a certain frequency and place risks causing undue interference to a licensed user. The UK approach means it is possible for a WSD to transmit at a greater proximity to licensed receivers, as long as the power levels are appropriately moderated. This is designed to take into account the fact that the UK's DTT network is near-universal, resulting in a different conception of TV White Space, as explained above;
- *Specific operating parameters* are generated by databases in order to allow high-performing WSDs to transmit at a higher power in some cases (although never higher than 36 dBm/8 MHz). More information about specific operating parameters in provided below.

Specific Operating Parameters

Once a connection is established between the master and slave WSDs, the master WSD may update the WSDB with device parameters concerning a specific slave WSD.

These parameters include:

– Device category (master or slave)
– Device type (fixed or non-fixed)
– Geolocation and geolocation uncertainty
– A unique identifier
– Device emission class (nonmandatory)
– Technology identifier (nonmandatory)
– Spectral mask improvement and reverse intermodulation attenuation improvement (nonmandatory)

This will allow the WSDB to generate specific operational parameters for the slave WSD. These are likely to be much less restrictive for the WSD. For example, the WSDB will initially assume that the slave could be in any 100×100 m pixel within a given radius of the master WSD and will generate generic operational parameters that take into account the powers in the most restrictive pixel within that area for each channel. Once a more specific location is known, then fewer pixels will be taken into account, and it is likely that higher powers will be permissible.

Additionally, generic operational parameters assume that the performance of WSDs is the minimum permitted under the ETSI standard (EN 301 598) [12], which is known as Class 5. WSDs conforming to higher classes have lower out of block emissions, meaning that its transmissions have a lower impact on adjacent channels. The effect of this is that when the WSDB calculates the permitted power levels across the available channels, there is likely to be greater availability and, at higher power, for better performing WSDs. These can only be taken advantage of if specific operational parameters have been obtained.

The master WSD will always need to inform the WSDB of the channel usage parameters of each WSD under its control, regardless of whether it is using generic operating parameters or specific operating parameters.

Data Used by the Geolocation Databases

In line with equipment used for TVWS access in the USA, the maximum power level of any WSD is 36 dBm. In many cases, the permissible power level will be lower than this, depending on the result of calculations undertaken by the database.

The algorithms have been defined by Ofcom, and database operators have had to demonstrate that they are able to carry these out before they are qualified by Ofcom.

When calculating the operating parameters that master WSDs (Master OPs) must use when communicating with their slave WSDs, the databases use four datasets provided by Ofcom. This is shown in the diagram below, which was created by Ofcom as part of its *Implementing TV White Spaces* statement:

(1) **PMSE data**. Ofcom provides information on licensed PMSE use, which must be used by WSDBs according to algorithms designed to ensure adequate separation in frequency between WSDs and PMSE devices for a given location.
(2) **Location agnostic data**. Ofcom provides general power limits applicable to WSDs operating in channels 34–41 in order to protect PMSE use of Channel 38 from undue interference & users in adjacent bands & international users. WSDs cannot operate in channel 38.
(3) **DTT coexistence data**. Ofcom provides for WSDBs information about the permissible power level for a WSD in each 100 × 100 m pixel in the UK taking into account the need to ensure a low probability of undue interference.
These calculations are based on the DTT planning model (UKPM), which has information on the predicted wanted signal level, taking into account receiver characteristics and interference from other DTT transmitters, at each 100 × 100 m pixel in the UK for each channel. Ofcom then adds statistics about the potential additional interference caused by a WSD, taking into account factors such as how far away the WSD would be from the nearest DTT receiver in terms of geography and frequency.

These calculations take into account both in-band emissions and out-of-band emissions from the WSD.
This calculation is repeated for each channel and for each pixel in the relevant area.
These calculations are complex and many (although not all) of the assumptions adopted are designed to be conservative.
These calculations are based on the assumption that households receive only intended DTT transmissions (i.e., that the aerial is pointing the right way).
In line with Ofcom's general policy, indoor aerials are not protected from interference from WSDs. Nevertheless, Ofcom believes that if the risk of interference to an outdoor aerial is low, then the risk to the indoor aerial is likely to be low too, as long as the WSD is located outside the building because the path loss generated by the building is likely to have a similar effect on both DTT and WSD signals.
The DTT coexistence data also takes into account the UK's international obligations concerning protecting DTT reception in neighboring countries.

(4) **Unscheduled adjustments data**. These are revised power limits that may need to be introduced into a particular geographic area on an ad hoc basis (Fig. 6).

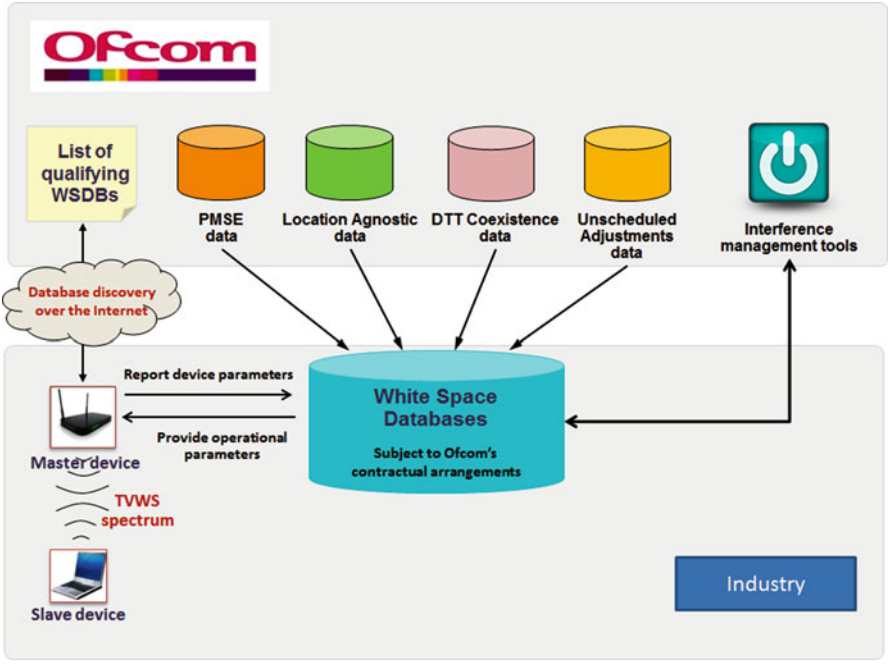

Fig. 6 Framework for authorising the use of TVWS including the interactions between WSDs and white space databases (WSDBs) (Source: Ofcom (2015) Implementing TV White Spaces. Available online at https://www.ofcom.org.uk/__data/assets/pdf_file/0034/68668/tvws-statement.pdf)

Interference Management Tools

Ofcom has also established several safeguards against undue interference:

- **White Space Information Platform**. This is a single interface where Ofcom can request information about active WSDs from all WSDBs simultaneously through a single API. During the pilot, Ofcom had relied on a White Space Devices Information System based on multiple WSDB interfaces, but this was demonstrated to be impracticable in the event of an interference case.
- **Requirements to cease transmissions**. WSDs must re-query a database for their operational parameters at least every 15 min. Should a device be suspected of causing interference Ofcom are able to instruct a database to cease providing selected master devices with operational parameters. This instruction must be relayed to the selected master devices at the next re-query following the instruction. Ofcom recognize that such a "cease transmission" instruction is a fairly blunt instrument insofar as it has the potential to impact an entire network of master and its slave nodes (which are dependent on the master for their operational parameters). Partly for this reason Ofcom has developed other interference management options that they are able to apply using the WSIP.
- **Adjustments to the maximum power at which WSDs can operate**. Contrary to its original intentions, Ofcom retains control over the calculations concerning DTT reception. This gives Ofcom the ability to revise the results it gives taking into account new evidence it may receive where, for example, the UKPM may be found to be inaccurate regarding the signal levels delivered to particular 100 $\times$ 100 m pixels.
- **Requirements to cease providing WSDB services**. WSDBs are subject to a process of qualification, which includes testing whether or not a database is capable of implementing Ofcom's coexistence framework. Ofcom retains the ability to instruct WSDBs to stop providing certain services, potentially for a specific timeframe. Ultimately, Ofcom may remove a WSDB from the list of qualifying WSDBs on its website if there are found to be repeated breaches.

The License-Exempt Approach

Most mass market devices using radio spectrum do so on a license-exempt basis as this approach minimizes the costs related to intrusive regulation. However, Ofcom has been careful in implementing its TVWS framework to only allow devices to be available on a license-exempt basis if they can demonstrate automatic geolocation.

It was found during Ofcom's pilot of TV White Space spectrum access that none of the WSDs being trialed were able to demonstrate an automatic geolocation capability. To get around this problem, researchers typically manually configured the devices so that they could report their geolocation to a WSDB.

Manual configuration was permitted during the pilot as the researchers were operating under nonoperational licenses (previously known as test and development Licenses). However, allowing this approach to continue indefinitely would introduce conditions where undue interference could theoretically be caused.

For example, it is possible to imagine a scenario where a master WSD inaccurately reports that its slave WSD is at a suburban location and receives permission to transmit on several channels that are to be used in theaters at that time. If the slave WSD were in front of a theater and started to transmit, then there would be a high risk of undue interference to PMSE devices used in that production. Clearly this would not comprise the optimal use of this spectrum.

To address this problem, equipment adhering to the relevant ETSI standard (EN 301 598) specifies that the device must be able to geolocate automatically (i.e., it cannot be manually configured).

Under EU law, radio transmissions can only be performed by devices adhering to the Radio Equipment Directive [13]. The simplest way for manufacturers to achieve this is to self-declare that their device complies with the specifications cited in a European Telecommunications Standards Institute (ETSI) standard. It is also possible to obtain type approval from a notified body.

Under the TVWS framework, which has been operational since the end of 2015, license exemption is only permitted for devices that comply with the ETSI standard.

However, recognizing that it may be some years before devices adhering to the ETSI specifications become mass produced, Ofcom has set up a transitional arrangement whereby manually configurable WSDs may operate under a standard Ofcom license (under the terms of the Wireless Telegraphy Act) [14]. These licenses cover an unlimited number of manually configured WSDs, but the licensees must keep comprehensive and accurate installation records and make them available to Ofcom through a web tool.

Ofcom hopes this can allow benefits to be generated to UK citizens and consumers through the use of WSDs in the interim period before devices adhering to the ETSI standard are easily available.

Ofcom issued a statutory instrument [15] in December 2015 authorizing license-exempt use of TVWS by cognitive radios, providing they comply with the ETSI standard.

The Spectrum Sharing Framework and the 3.8–4.2 GHz Band

The Spectrum Sharing Framework

Ofcom's *Spectrum Management Strategy* [16] published in 2013 observed that the demand for spectrum was continuing to grow rapidly. In the past, Ofcom would typically address this by creating conditions where the spectrum can be used by the entity that values it the most. This could include clearing users out of a given spectrum band, meaning that often alternative solutions would need to be identified for those users, and then auctioning the spectrum to the highest bidder. This complex

process typically takes years and is often delayed further due to litigation regarding one or more of the many difficult policy decisions required in this process.

Bearing in mind improvements in the efficient use of spectrum over the last decades, the Strategy acknowledged that fewer and fewer spectrum bands are left where current users can be "cleared" so that new entities can start using the spectrum. Notwithstanding the fact that the same document found that 58% of the spectrum was shared (Ofcom Managed and license-exempt bands), Ofcom found that there should be more spectrum sharing in order to address growing demands.

This insight demanded Ofcom allow for new thinking to flow through its decision-making process. To enable this, Ofcom published a series of documents culminating in a *framework for spectrum sharing* [17].

A Framework for Spectrum Sharing

The *framework for spectrum sharing* establishes a systematic approach that Ofcom takes when it appears that an opportunity for spectrum sharing could arise or when it appears that spectrum sharing could be a solution for future spectrum demand.

This could take place, for example, when stakeholders' demand for spectrum cannot be met through existing authorization products. Alternatively, Ofcom may become aware of new developments, for example, advances in technology, that could comprise a tool or enabler for spectrum sharing. These circumstances are illustrated in Fig. 7, which was provided as part of Ofcom's statement on its *framework for spectrum sharing*

Under these circumstances, Ofcom would arrive at potential sharing proposals by considering the relevant *high-level characteristics of use*, *barriers*, *tools and enablers*. These concepts are defined below.

High-level characteristics of use allow Ofcom to make sure it is asking the right questions when it is analyzing potential, or current, users of spectrum. Ofcom has identified eight of these and has set out the thinking that would be employed when defining a given application's characteristics of use:

- **Time and duration**. What are the temporal requirements of the service – is it always-on, a set time, or unpredictable? Does the service require spectrum for long-term use or temporarily? What are the temporal requirements of the individual transmissions? What duty cycle do these use?
- **Geography and coverage**. Will the service cover the whole UK or be restricted to certain areas? Will it be ground based; will it be used outdoors or indoors? Is the location predictable – is the service in a fixed location or mobile? If it has control over end users, does the user know where its end users are?
- **Quality of service**. What type of reliability does the service require – guaranteed availability vs. best effort? What level of interference is acceptable? Is the service critical, e.g., used for critical national infrastructure?

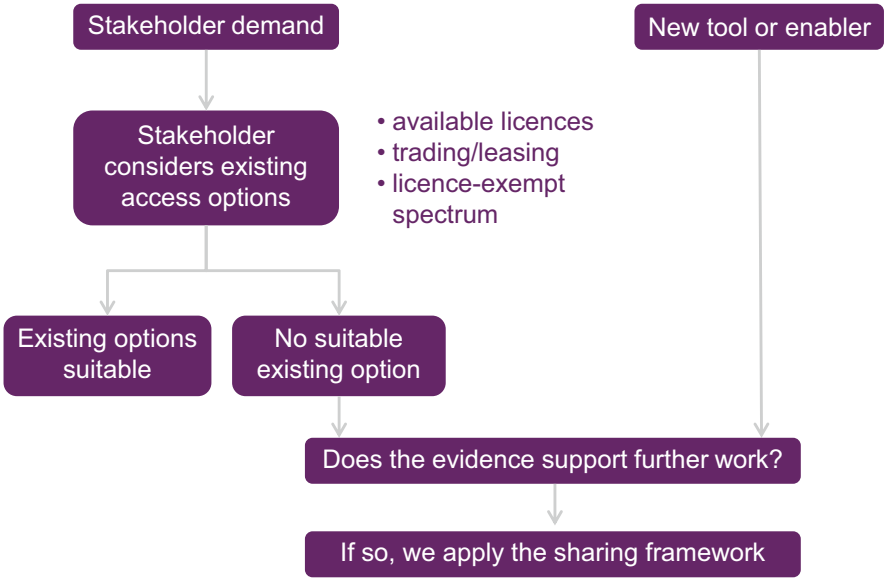

Fig. 7 Use of the spectrum sharing framework (Source: Ofcom (2016) A framework for spectrum sharing. Available online at https://www.ofcom.org.uk/__data/assets/pdf_file/0028/68239/statement.pdf)

- **High-level technical characteristics**. EIRP (power), typical transmitter height and location (i.e., urban, rural, on hills, etc.) and antenna characteristics (beam widths directionality), typical receiver sensitivity (minimum receivable signal), and receiver locations and antenna characteristics.
- **Capacity requirement**. How much capacity is needed for each device and for the whole service? Is this a core capacity requirement or for additional capacity, e.g., for occasional overflow?
- **Density of use**. What is the approximate number of devices in use, i.e., whether a mass market consumer use or a limited number of terminals?
- **Evolution of characteristics over the life of an authorization**. How will each of these characteristics evolve over the term of the authorizations involved? What is the best way of approaching the uncertainty over longer timeframes? What is the payback period on the investment?
- **Harmonization required [for potential new applications]**. How essential are the benefits from international harmonization? What extent of economies of scale is necessary (e.g., one or several world regions or just UK specific)? What is essential to securing sufficient harmonization?

Having established the relevant characteristics of use, Ofcom then identifies the *barriers* and *tools and enablers* that flow from this analysis. According to the framework, *tools and enablers* are introduced to address the *barriers*. These aspects relate to information, the market, technology, and authorization conditions.

How these concepts relate to each other is shown in the following table:

	Barrier	Tool/Enabler
Information	Lack of information prevents identification of opportunities	Provision of information about spectrum assignment and use
Market	Transaction costs, concerns about impact on spectrum value, uncertainty about constraints on future use	Spectrum trading and leasing, spectrum pricing, auctions and awards (such as the DECT guard band concurrent license awards)
Authorization conditions	Terms of authorization can limit flexible use; Ofcom's commitment to sharing and regulatory timescales	Information requirements, tiered authorization approach;
Technology	Coexistence adds complexity and cost	Protocols for accessing shared spectrum (such as CSMA used in Wi-Fi), geolocation database technologies, sensing, automatic reporting of interference, frequency and band agile equipment

These *barriers* and *tools and enablers* are anticipated to change over time. For example, as Ofcom found during its work in TVWS, it is not clear that sensing can currently be considered to be an effective tool for sharing, but this may change as technologies evolve with time. After analyzing the appropriate tools and enablers, Ofcom may be in a position to make proposals related to spectrum sharing

Ofcom decided to use the proposed sharing approach identified in the framework for the first time on the 3.8–4.2 GHz band. These insights fed in to a Call for Input (CFI), which was published in April 2016 [18]

Opportunities for Innovation at 3.8–4.2 GHz

Ofcom's policy development regarding TVWS was in part driven by the insight that the UHF band comprises a "sweet spot" where large amounts of data can be transmitted over relatively large distances. Technological advances, and more investment in infrastructure, have arguably extended this "sweet spot" into higher frequencies.

The 3.8–4.2 GHz band is one of the "Ofcom Managed Bands" that comprise around half of radio frequencies in the UK.

The entire band is currently shared by the fixed and fixed-satellite services, while an 84 MHz block (3925–4009 MHz) of it is also used by UK Broadband. Ofcom authorizes point-to-point fixed links on a first-come-first-services basis, subject to Ofcom coordination and Ofcom technical frequency assignment criteria. These links are coordinated by Ofcom so that there is no undue interference caused to the assignments to the fixed-satellite service that are taken into account on Ofcom's

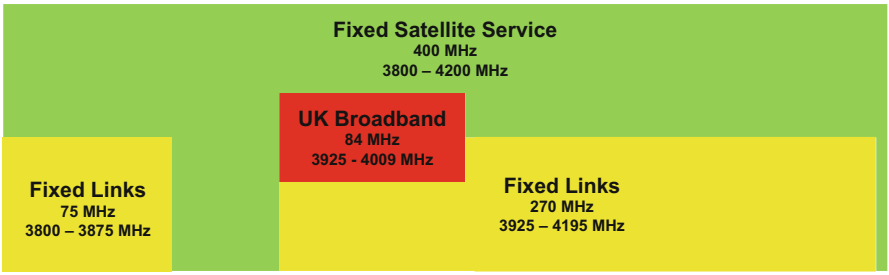

Fig. 8 The 3.8–4.2 GHz band (Source: Ofcom (2016) 3.8–4.2 GHz band: opportunities for innovation. Available online at https://www.ofcom.org.uk/__data/assets/pdf_file/0031/79564/3.8-GHz-to-4.2-GHz-band-Opportunities-for-Innovation.pdf)

planning tool. A stakeholder is taken into account when it has a permanent Earth station license or grant of Recognised Spectrum Access that includes reception of space-to-Earth transmissions in the 3.8–4.2 GHz band at a particular satellite Earth station. UK Broadband has a nationwide spectrum access license, but its deployments also have to be coordinated through Ofcom so as to avoid interference with the other services. The frequency allocations of this band are shown in Fig. 8, which Ofcom created as part of its Call for Input to demonstrate how the band is used.

Much like the UHF bands, there appears to be scope to enhance the current sharing of the band. For the UHF bands, this is because at most locations there are many unused frequencies. This is also the case for the 3.8–4.2 GHz band, but additionally for much of the band, the spectrum is only being used in a few dozen locations at most.

For example, while the band is available for space-to-Earth transmissions anywhere in the UK, in reality its use is confined to 28 sites with satellite Earth stations (not including links operated by foreign governments). Further, these satellite Earth stations tend to be clustered in relatively small portions of the UK. Aside from a handful of important facilities such as Goonhilly in Cornwall and the Meteorological Office at Exeter, the use of the band is focused on Aberdeen and the home counties. Fixed links also tend to be concentrated geographically. All of the locations of these applications are shown in Fig. 9 (not taking into account UK Broadband's use of the 3925–4009 MHz range), which was created by Ofcom as part of its April 2016 Call for Input.

Further, each satellite Earth station will have several assignments authorized to it by Ofcom related to discrete blocks of spectrum and orbital positions. This means that not all of the spectrum will be used at each satellite Earth station. Similarly, each fixed link uses a 2×30 MHz block of spectrum, meaning that of the 65 fixed links in this band, only a few of these would be used in any particular part of the spectrum.

The way that their duplex channel plan is arranged (2×270 MHz within the 3.6–4.2 GHz band) additionally allows for a 50 MHz gap (3875–3925 MHz) where use is confined to the satellite Earth stations.

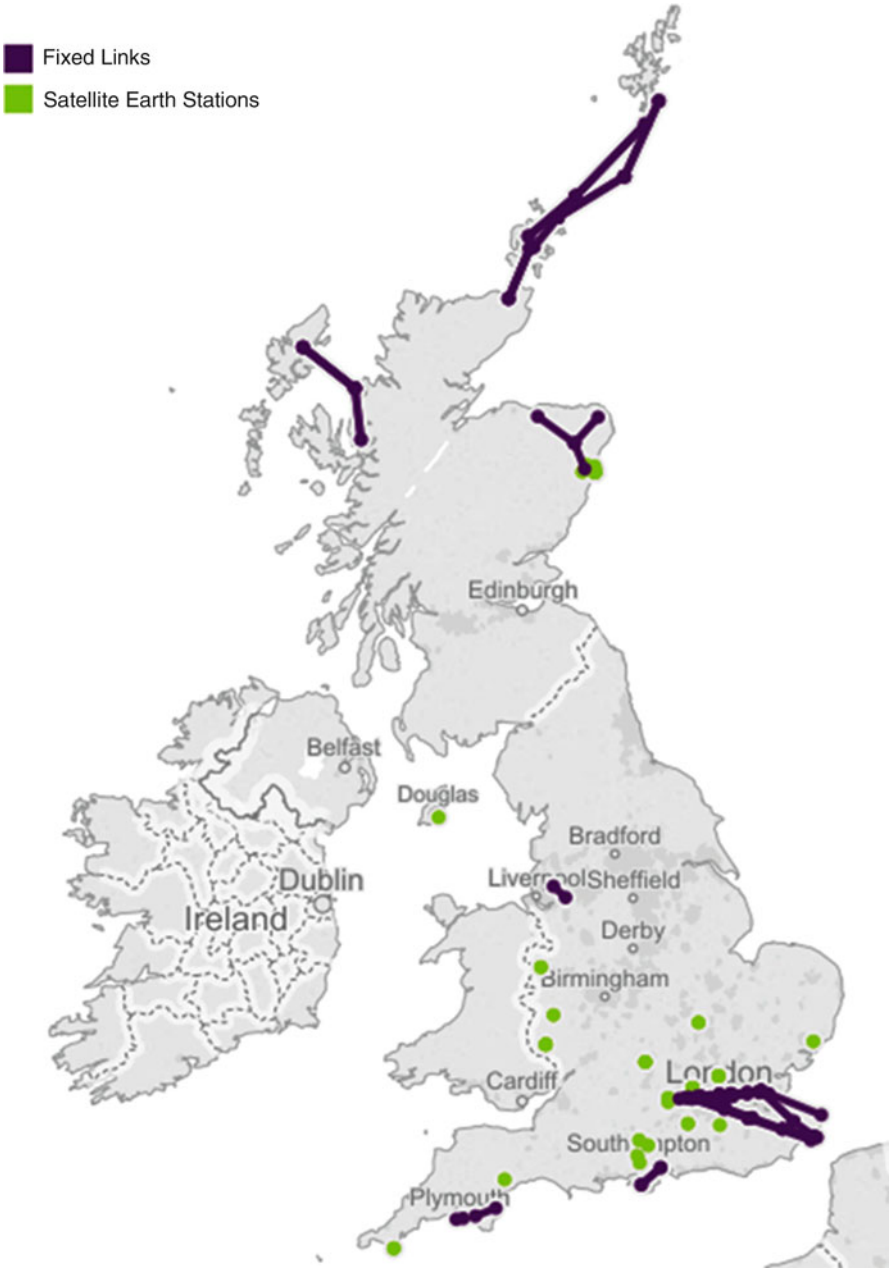

Fig. 9 Current users of the 3.8–4.2 GHz band (Source: Ofcom (2016) 3.8–4.2 GHz band: opportunities for innovation. Available online at https://www.ofcom.org.uk/__data/assets/pdf_file/0031/79564/3.8-GHz-to-4.2-GHz-band-Opportunities-for-Innovation.pdf)

Characteristics of Use

To take the language of the Framework, the scale of the opportunity for sharing in this band derives from the current users' characteristics of use. The following table compares these high-level characteristics of use for major users in the UHF and 3.8–4.2 GHz band. WSDs are not included in this table as their use cases are varied.

	470–790 MHz		3.8–4.2 GHz	
	Digital terrestrial television	Audio Programme Making and Special Events	Fixed links	Satellite Earth stations
Time	Continuous	Variable	Continuous	
Geography/Coverage	Near-universal coverage required	Concentrated around a few locations at any given time, apart from channel 38, which could be needed anywhere	Concentrated around specific locations	Concentrated in certain regions
Quality of service	High levels of availability		High levels of availability	
Capacity requirement	High	Low for individual devices, but many devices may be required	Variable	
Density of use	Millions of TV receivers at UK premises	Many hundreds of thousands	Several dozen in the UK	Dozens in the UK
Evolution of these criteria	Stable for the medium to long term	Stable for the medium to long term. Growth in demand could be partly mitigated against by new band availability	Some change possible in medium term for some channels due to mobile data strategy at 3.6–3.8 GHz [20]	Stable, although some change possible in medium term due to mobile data strategy at 3.6–3.8 GHz band

One can observe that a major difference between these bands is that the use of the UHF band is much more "dynamic," because PMSE assignments change on a regular basis whereas current users of the 3.8–4.2 GHz band operate on indefinite licenses and have usage requirements that do not change substantially year by year. This makes sharing by time difficult, but also means that sharing may not be dependent on complex technologies, as is required for the Citizen Broadband Radio Service [19] in the USA at 3550–3700 MHz. It should be noted that, as explained earlier, even in geographic areas containing current users there are

typically frequencies that are not being used due to the channeling arrangements in this band.

It is also clear that there are fewer current users of the 3.8–4.2 GHz band than in the UHF band and that the usage tends to be concentrated in fewer areas than in those bands. As set out in the section above, this indicates that a more optimal use of this spectrum could involve finding a way of allowing spectrum access for additional applications in more areas of the UK, seeing as in many areas of the UK there is no current use of the spectrum.

As explained in the section above, it is the geography and coverage, density of use, and (relatively little) evolution of these characteristics of use that make the 3.8–4.2 GHz band a good opportunity for innovation in terms of securing a more optimal use of the spectrum.

Barriers and Enablers

Bearing in mind the high-level characteristics of use defined above, one could identify the following as potential barriers/enablers:

- **Information**. An absence of accurate information concerning current use of the band would prevent stakeholders from sharing this band as they would not understand its users' characteristics of use. However, in this case, Ofcom makes available high-level information on all fixed link deployments and the majority of satellite Earth stations (excluding those operated by foreign governments) on the Wireless Telegraphy Register.
- **Market**. In principle, some stakeholders have an incentive to prevent sharing, for example, from uncertainty about constraints on future use. In this case, regarding fixed links and satellite Earth stations, it is not clear that any market mechanism could enable sharing, seeing as the authorizations refer to specific applications at specific locations (i.e., they are not technology neutral), and are assumed to be required at all times. Spectrum assigned to UK Broadband (3925–4009 MHz) could in principle be shared through spectrum leasing (which is permitted under its licence for this band), and it is possible that fees could produce incentives for this outcome.
- **Technology**. Ofcom manages authorizations in this band because the coexistence challenges arising from the wide diversity of relevant equipment (i.e., highly sensitive receivers used in satellite Earth stations and high-power fixed link transmitters) are significant. Any technological innovation that can ensure that Ofcom does not need to directly coordinate spectrum authorizations in this band would need to be sophisticated enough to take into account the fact that satellite Earth stations operate on a receive-only basis in this band. For this reason, sensing or the use of protocols for accessing shared spectrum is not likely to be appropriate.
- **Authorisation**. Arguably, a significant barrier to enhanced sharing of the 3.8–4.2 GHz band is the absence of appropriate regulatory tools. For example, a

new user wishing to deploy a local fixed wireless access service could not use this band as a fixed link license would only allow transmissions under certain circumstances, and licenses for satellite Earth stations would not authorize any sort of transmissions within this band. The exception to this is UK Broadband (in the 3925–4009 MHz band only), which is able to use this band but only if Ofcom is satisfied that other users of the band will not suffer undue interference from a particular deployment.

A Potential Tool: The Tiered Approach

One could argue that one of the barriers to enhanced sharing in this band is the lack of an authorization mechanism for additional users.

A potential enabler to overcome this could be to introduce new licensing products that would support an overall tiered access model for spectrum access.

Ofcom imagined one scenario how this might be enabled in the future. A map generated by Ofcom to demonstrate this scenario is shown in Fig. 10, which shows how a given range of spectrum might be authorized across the UK.

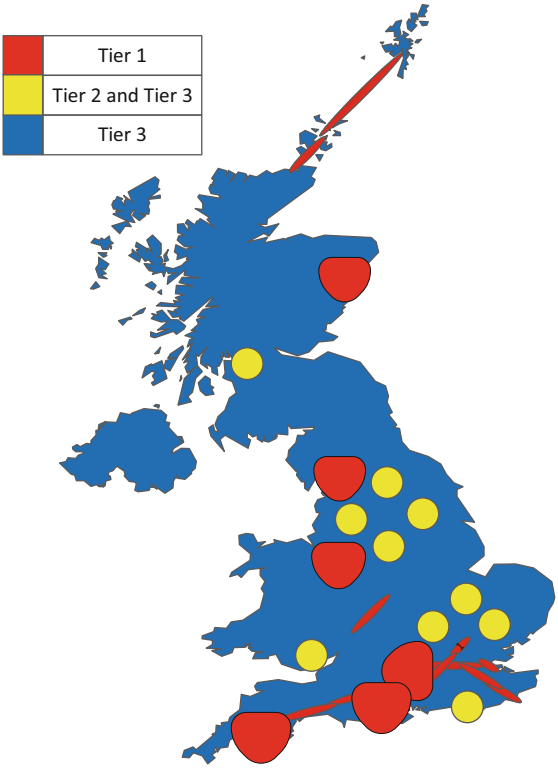

Fig. 10 A potential tiered approach to the 3.8–4.2 GHz band (Source: Ofcom (2016) 3.8–4.2 GHz band: opportunities for innovation. Available online at https://www.ofcom.org.uk/__data/assets/pdf_file/0031/79564/3.8-GHz-to-4.2-GHz-band-Opportunities-for-Innovation.pdf)

The scenario speculated on how much of the spectrum (the 316 MHz not assigned to UK Broadband) could be used more effectively.

In the imagined scenario, "Tier 1" would comprise the current point-to-point terrestrial links licenses, permanent Earth station licenses, and grants of Recognised Spectrum Access that are made available by Ofcom on a first-come-first-served basis. The majority of stakeholders responding to the Call for Input expressed the view that any changes in this band should allow for the continued further availability of these products.

Additionally, Ofcom could issue regional licenses for spectrum access as part of a "Tier 2." As an example, these could comprise a 10 MHz block for a local mobile service provided in areas where mobile network operators have not built a network. These licenses could be issued for areas at a large distance away from Tier 1 deployments, in order to minimize the risk of interference.

Ofcom did not consider the authorization mechanism for such a tier; nor did it consider how geographic areas would be defined (e.g., by Ofcom dividing up the country or by specific requests from stakeholders).

The third tier could comprise "opportunistic" spectrum access, which would be akin to a "secondary" service. While holders of Tier 2 license products could be granted some form of certainty of spectrum access (arising from the way Ofcom could issue authorizations), users in this layer would have no such guarantees. As with TVWS, the successful operation of this layer might require some mechanism by which users in other tiers could be sure that they would not suffer undue interference from Tier 3 users. As a preliminary suggestion, Ofcom raised the possibility of using databases as a means of giving such assurances. Databases have the advantage of being a proven and demonstrated concept during the TVWS pilot.

In the UHF band, the only incumbent user of the spectrum whose deployments frequently change is PMSE. In the 3.8–4.2 GHz band, current use (Tier 1) is assumed to be static seeing as current authorization products in this band are indefinite. Some potential future use of the band (Tier 2) is assumed to be relatively static, although the Call for Input did not include any discussion of whether or not Tier 2 licenses would be time limited.

Opportunistic spectrum users, however, are often assumed to have dynamic characteristics of use, so the deployment of databases could also ensure that there is minimal undue interference caused between these users, notwithstanding the fact that they would all operate on a "secondary" basis. An additional potential advantage of databases is that they could also in principle allow opportunistic spectrum users to access spectrum assigned to a Tier 2 users, if information about Tier 2 use was also included in the database. As discussed at the beginning of this chapter, the WT Act licenses granted by Ofcom allow Ofcom to authorize additional use in the band. However, the extent to which a database might control users has not been discussed in the Call for Input.

Responses to the Call for Input were in general supportive of Ofcom's analysis and overall intentions. Many respondents advocated two-tier sharing where, for example, current licensees would share with mobile, which may correspond to the

form of Licensed Shared Access envisaged in some European countries for the 3.6–3.8 GHz band.

In August 2016 Ofcom published an update. In general, Ofcom confirmed its interest in enhanced sharing for (nonspecific) authorizations that, according to Ofcom's preliminary analysis, should be geographically defined. Geographically defined means that authorizations could be, for example, based on regional licenses and/or for a specific geographic point plus an area around it based on a given radius, defined as pixels, as is authorized under TV White Space spectrum access.

Conclusions and Future Directions

This chapter explained how the legal framework in the UK has provoked Ofcom to exploring novel regulatory solutions for spectrum sharing.

Its Spectrum Management Strategy and subsequent Framework for Spectrum Sharing have underlined that it considers spectrum sharing to be a priority going forward.

A test-bed for this new approach has been the 3.8–4.2 GHz band, where it has demonstrated an interest in finding novel regulatory solutions for spectrum sharing in service of Ofcom's principal duty, to secure the optimal use of the radio spectrum in the UK.

In the short term, it seems possible that industry focus on spectrum sharing is likely to be on TV White Space. The last words of this chapter reflect on the future directions for this form of spectrum access.

As previously noted, terrestrial broadcasting plays a very important role in public life in the UK. Bearing this in mind, Ofcom has in general taken a conservative approach in ensuring that there will be an adequately low probability of interference to these users.

It is possible that the combined effect of these conservative assumptions has resulted in an overall over-restrictive approach to TV White Space, and Ofcom may in the future review these assumptions. Equally, it may consider that these assumptions are not conservative enough. For example, it does not currently consider the effect of an aggregation of WSDs being authorized to transmit on the same frequency from different databases. While the probability of this is deemed low in the initial stages, this may require attention in the future. This could, for example, be resolved through the sharing of information between WSDBs, seeing as WSDBs are not aware of the channel usage parameters being reported to other WSDBs.

Future change to Ofcom's framework for TV White Space is likely to be dependent on market developments, not least the proliferation and performance of WSDs using this spectrum. It is true that the adoption of cognitive radio in TVWS has been slower than predicted by some, although the pilot saw interesting use cases that had not originally been anticipated, such as digital signage and webcam backhaul. In turn manufacturers are likely to closely monitor changes to the use of the band by the broadcasting service internationally.

At the World Radiocommunication Conference in 2012 (WRC-12), the countries in ITU Region 1 (Africa, the Middle East, Europe, and the former Soviet Union) agreed to allocate the 700 MHz band (694–790 MHz) for mobile services from 2015, bringing its spectrum allocations more in line with the rest of the world. This agreement was confirmed at WRC-15. The introduction of mobile into the 700 MHz band could in some cases reduce the amount of TV White Spaces available for cognitive radio. In the UK, this change of use could begin from 2020 [21], which is when the spectrum is expected to be auctioned for mobile services.

This will partly be enabled by reducing use of the interim multiplexes, which may somewhat mitigate against the loss of spectrum available for cognitive radios.

Another mitigation is that Ofcom has made the 960–1164 MHz band available for low-power audio PMSE applications on a shared basis with [21] aeronautical radionavigation services.

In the very long run, the future of the DTT platform itself will have to be considered. The issue will be considered again in the run-up to WRC-2023 (23), although the consensus within EU member states is to retain the platform until at least 2030, revisiting the issue again from 2025.

Therefore, the future availability of the UHF band for cognitive radio might in the long run be to some extent dependent on society's idea of what broadcasting services should be made available universally and what platform can best deliver that. These considerations might take into account the proliferation (or nonproliferation) of alternative broadcasting platforms (including IPTV) among the population at large, including the most vulnerable members of society.

Additionally, although by definition license-exempt applications are not in general directly protected from undue interference by regulators, it is possible that the benefits that cognitive radio may deliver to citizens and consumers could also be taken into account in such discussions.

References

1. Communications Act 2003. Available at http://www.legislation.gov.uk/ukpga/2003/21/contents
2. Wireless Telegraphy Act 2006. Available at http://www.legislation.gov.uk/ukpga/2006/36/contents
3. Wireless Telegraphy Apparatus (Receivers) (Exemption) Regulations 1989. Available at http://www.legislation.gov.uk/uksi/1989/123/contents/made
4. International Telecommunications Union (2016) Radio regulations. Available at https://www.itu.int/itu_mt_main/catalog/home.jsf?wec-appid=EBOOKSHOP_B2B&wec-locale=en_US&area=R-REG-RR-2016&filter=ZITU_LANGUAGE%3dEnglish%26ZITU_MEDIATYPE%3dElectronic
5. Ofcom (2013) Spectrum attribution metrics. Available at https://www.ofcom.org.uk/__data/assets/pdf_file/0028/81658/spectrum_attribution_metrics.pdf
6. Ofcom (2012) TV White Spaces A consultation on white space device requirements. Available at https://www.ofcom.org.uk/__data/assets/pdf_file/0022/40477/condoc.pdf?lang=en
7. Ofcom (2015) Implementing TV White Spaces. Available at https://www.ofcom.org.uk/__data/assets/pdf_file/0034/68668/tvws-statement.pdf

8. Ofcom (2007) Digital dividend review. Available at https://www.ofcom.org.uk/consultations-and-statements/category-1/ddr/statement
9. Ofcom (2009) Digital dividend: cognitive access. Available at https://www.ofcom.org.uk/__data/assets/pdf_file/0023/40838/statement.pdf
10. Ofcom (2011) Implementing geolocation. Available at https://www.ofcom.org.uk/__data/assets/pdf_file/0035/46889/statement.pdf
11. Ofcom (2015) Implementing TV White Spaces. Available at https://www.ofcom.org.uk/__data/assets/pdf_file/0034/68668/tvws-statement.pdf
12. European Telecommunications Standards Institute (2014) ETSI EN 301 598 V1.1.1. Available at http://www.etsi.org/deliver/etsi_en/301500_301599/301598/01.01.01_60/en_301598v010101p.pdf
13. Directive of the European Parliament and the Council (2014) On the harmonisation of the laws of the Member States relating to the making available on the market of radio equipment and repealing Directive 1999/5/EC. Available at http://eur-lex.europa.eu/legal-content/EN/TXT/PDF/?uri=CELEX:32014L0053&qid=1480523814812&from=en
14. Ofcom (2015) Licensing manually configurable white space devices. Available at https://www.ofcom.org.uk/__data/assets/pdf_file/0023/84209/licensing_manually_configurable_white_space_devices.pdf
15. The Wireless Telegraphy (White Space Devices) (Exemption) Regulations 2015 Spectrum Management Strategy. Available at http://www.legislation.gov.uk/uksi/2015/2066/contents/made
16. Ofcom (2016) A framework for spectrum sharing. Available at https://www.ofcom.org.uk/__data/assets/pdf_file/0028/68239/statement.pdf
17. Ofcom (2016) 3.8–4.2 GHz band: opportunities for innovation. Available at https://www.ofcom.org.uk/__data/assets/pdf_file/0031/79564/3.8-GHz-to-4.2-GHz-band-Opportunities-for-Innovation.pdf
18. Ofcom (2016) Improving consumer access to mobile services at 3.6 to 3.8 GHz. Available at https://www.ofcom.org.uk/__data/assets/pdf_file/0035/91997/3-6-3-8ghz-consultation.pdf
19. Ofcom (2016) Maximising the benefits of 700 MHz clearance. Available at https://www.ofcom.org.uk/__data/assets/pdf_file/0031/92659/Maxi mising-the-benefits-of-700-MHz-clearance-Statement.pdf
20. Federal Communications Commission Report and Order and Second Further Notice of Proposed Rulemarking (2015) In the matter of amendment of the commission's rules with regard to commercial operations in the 3550–3650 MHz band. Available at https://apps.fcc.gov/edocs_public/attachmatch/FCC-15-47A1.pdf
21. Ofcom (2016) New spectrum for audio PMSE. Available at https://www.ofcom.org.uk/__data/assets/pdf_file/0021/62481/New-Spectrum-for-Audio-PMSE-statement.pdf

Further Reading

1. International Telecommunications Union (2015) Provisional Final Acts: World Radio Communication Conference (WRC-15). Available at https://www.itu.int/dms_pub/itu-r/opb/act/R-ACT-WRC.11-2015-PDF-E.pdf

Spectrum Sharing Policy in the Asia-Pacific Region

53

Zhiyong Feng and Zhiqing Wei

Contents

Abstract

In this chapter, we investigate the spectrum measurement results in Asia-Pacific region. Then the spectrum sharing policy in Asia-Pacific region is reviewed in details, where the national projects and strategies on spectrum sharing in China, Japan, Singapore, India, Korea, and Australia are Investigated. Then, we

Z. Feng (✉) · Z. Wei
Key Laboratory of Universal Wireless Communications, Ministry of Education, Beijing University of Posts and Telecommunications, Beijing, China
e-mail: fengzy@bupt.edu.cn; weizhiqing@bupt.edu.cn

W. Zhang (ed.), *Handbook of Cognitive Radio*,
https://doi.org/10.1007/978-981-10-1394-2_52

introduce the spectrum sharing test-bed developed in China, which is a cognitive radio-enabled TD-LTE test-bed utilizing TV white space (TVWS). This chapter provides a brief introduction to the spectrum sharing mechanism and policy in Asia-Pacific region.

Radio spectrum resources play a fundamental role in wireless communication systems. The fast-growing demand for wireless communication services and the inefficient spectrum allocation methods result in the scarcity of spectrum resources, greatly hindering the development of future wireless communication systems [6,27].

For example, in China, the state radio regulatory commission of China (SRRC) divides the entire available spectrum resources into multiple frequency bands and assigns them to different license services such as broadcast TVs and cellular networks for exclusive use. Such fixed spectrum allocation approach ensures that wireless applications and devices dont cause harmful interference with each other. However, it will result in inefficient use of current radio spectrum. Some bands are heavily occupied by busy radio services, while other bands are rarely used. There exist great difficulties to find unassigned spectrum for new broadband wireless communication systems such as time division long-term evolution (TD-LTE).

One of the most promising solutions to overcome this problem is cognitive radio (CR). A CR device has the ability to identify and access an unoccupied spectrum band for temporary usage. Therefore, CR is viewed as a technology to overcome the current inefficient use of radio spectrum resources [32,55].

Due to its importance, a lot of research funds have been invested in developing cognitive radio technology. National research programs have already been founded to support CR technology in China such as the Major State Basic Research Development Program (973 Program), the National High Technology Research, the Development Program of China (863 Program), and the National Natural Science Foundation of China. Government policy regulators such as SRRC are now considering modifying the current spectrum allocation policies in order to enable dynamic spectrum access technologies. However, if they fail to fully understand the current spectrum occupancy patterns, the investments and efforts may not produce expected accomplishments.

In the rest of this chapter, we first introduce the spectrum measurement in Asia-Pacific region and then describe the spectrum sharing policies. In addition, the main spectrum sharing technologies such as spectrum sensing and geo-location database-based spectrum sharing schemes are introduced. Finally, we give a brief introduction to the spectrum sharing test-bed in China.

Spectrum Measurement in Asia-Pacific Region

Spectrum occupancy survey is essential for spectrum management and provides policy makers with necessary information on the frequency usage pattern of different services in different frequency bands. Until now, several measurement

campaigns have already been conducted in the United States, Singapore, Vietnam, and Germany [2, 20, 31, 52]. All these studies show a common discovery that a large portion of assigned spectrum resources are seldom used, while some particular spectrum bands are overcrowded. In this chapter, we make a brief survey on the spectrum occupancies in Asia-Pacific region.

China

The spectrum occupancies in Beijing are measured by our team [4, 51]. We have measured the spectrum band from 440 to 2700 MHz for 2 weeks in Beijing. This measurement not only fills the gap of the current lack of knowledge on the radio spectrum usage pattern in Beijing but also finds out the frequency bands suitable for future dynamic spectrum access products like CR devices. Our measurement consists of two parts, the fixed measurement and the mobile measurement, which are introduced in the following sections.

Spectrum measurement

Fixed measurement

The fixed measurement was adopted to measure the spectrum band from 440 to 2700 MHz. Our fixed measurement was taken on the roof top of a 30-story building near the central business district (CBD) in Beijing. Without any higher buildings surrounding the measurement site, it ensures us to measure the radio activities accurately. The equipment includes omnidirectional broadband antenna BOGER DA753G that has a frequency range of 75 MHz∼3 GHz, Agilent high-performance spectrum analyzer N9030A with a dynamic range from −154 to 30 dBm, and a computer. As illustrated in Fig. 1 (left), the antenna was installed on the roof top and connected to the spectrum analyzer by a low-loss cable. The spectrum analyzer was controlled by a computer which was used for parameters setting and data saving. Both the spectrum analyzer and the computer were kept in an indoor metal box as shown in Fig. 1 (right). The resolution bandwidth (RBW) of the spectrum analyzer was set to be 200 kHz. The measurement started in June 2012 and lasted for seven consecutive days. In total, around 100 billion data samples were collected.

Mobile Measurement

As illustrated in Fig. 2 (left), the instruments utilized in the mobile measurement and their connections are mostly the same as the fixed measurement. It is worthwhile to mention that a GPS is connected to the computer in order to record the geographical coordinates of data samples. The GPS we used is Garmin 72HGPS with a location precision of 5 m. To ensure that the mobile measurement captures the actual spectrum occupancies in Beijing, a proper route is crucial. Therefore, the following three principles are adopted for the selection of measurement route.

Fig. 1 Equipment and measurement environment of fixed measurement

Fig. 2 Equipment and route of mobile measurement

(1) The route should be a helix circling the TV transmitters. The distance from the TV transmitter changes gradually, such that the relationship between signal strength and distance can be captured.
(2) To avoid the distortion caused by Doppler effect, the speed of the vehicle must be kept low. In addition, the performance of the instruments may be affected by the turbulence at high speed. So we maintained a speed around 20 Km/h in the measurement.
(3) To make the measurement convincing, the route should cover all typical places including business district, residents living quarters, open outdoor areas, etc.

The selected measurement route is plotted in Fig. 2 (right). Here different colors denote different kinds of places. In this map, yellow stands for residential areas, purple for business districts, and white marks the open areas with sparse buildings. The measurement was conducted from 9 a.m. to 5 p.m. each weekday.

The Measurement Results

Spectrum Measurement of 440–2700 –MHz

The spectrum band from 450 to 470 MHz is authorized for radio navigation, radio localization, and land mobile services such as interphone. The average spectrum occupancy is observed as 18%. A temporary usage pattern can be observed for part of frequency channels in this band, which mainly are interphone services resulting in relatively low spectrum occupancy. The spectrum measurement results in Beijing are shown in Fig. 3.

The spectrum band from 470 to 806 MHz is allocated for the broadcasting services, which are Chinese analog TV service PAL-DK and Chinese digital TV service "Digital Television Terrestrial Multimedia Broadcasting (DTMB)." The average spectrum occupancy of spectrum band from 470 to 806 MHz is about 42%. However, not all TV stations work for 24 h each day. Some TV channels are closed between 00:10 a.m. and 5:50 a.m.

The spectrum band from 880 to 960 MHz is assigned to the mobile cellular services (GSM900). The average spectrum occupancy of this spectrum band is 45.52%. Note that the spectrum occupancy patterns of uplink and downlink of GSM900 are quite different. Similar signal occupancy pattern is observed in the GSM1800 and 3G services. This may result from that the transmit power of uplink of the cellular systems is relatively lower than the transmit power of downlink. And the uplinks are silent when there are no active communication sessions. The

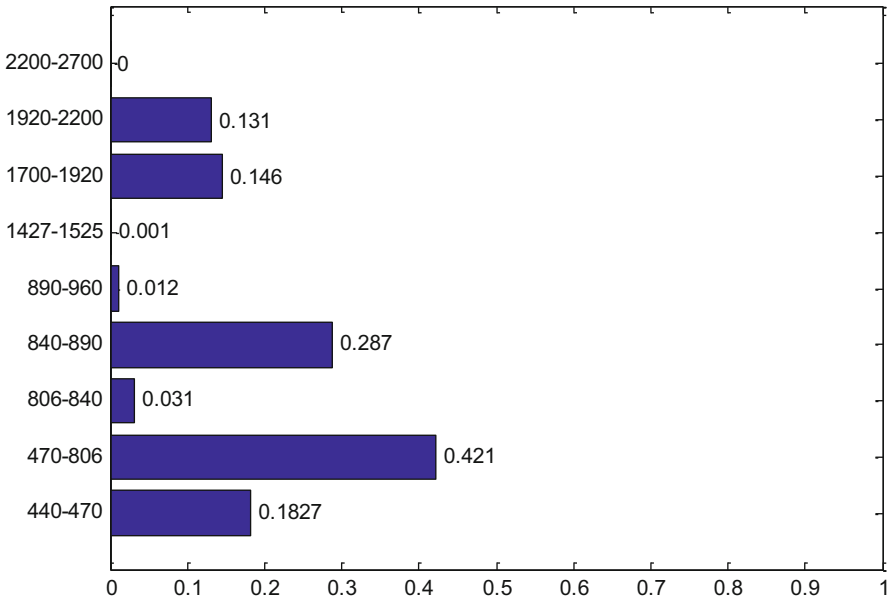

Fig. 3 Spectrum occupancy in Beijing

TD-SCDMA band A (1880∼1900 MHz) was not detected in our experiment, and its service only existed in band B (2010∼2025 MHz). CDMA2000 signals were not detected during the 2-week period. The average spectrum occupancy of 1700-1920 MHz is about 14.6%, and the average spectrum occupancy of 1920-2200 MHz is about 13.1%.

The spectrum occupancy of the industrial, scientific, and medical band (ISM band), ranging from 2400 to 2500 MHz, appears to be completely unused during 2-week observation. High-likelihood signal occupancy pattern is found in the radar spectrum band from 2500 to 2700 MHz, TD-SCDMA candidate band C 2300∼2400 MHz, and 1427∼1525 MHz band for pointing to multipoint microwave communication system, which is currently utilized by military services. The occupancy estimations of ISM and radar bands may not be the real situation of the systems such as WLAN and Bluetooth. Since the measurement site is on the roof top of a 30-story (115-m-high) building, the ISM signals may not reach the measurement point. Besides, ISM signals may not penetrate through walls. Radar signals may need special detection methods and equipment, since its pulse is too short to be detected and may result in a very low probability to be captured.

The summary of average spectrum occupancy in Beijing city is presented in Fig. 3. The results indicate the sparse usage characteristics both in time and frequency domains. The spectrum occupancy rate in average is 13.5% in Beijing for 450∼2700-MHz frequency band. Therefore, nearly 86.5% of allocated spectrum is unused.

Spectrum Measurement of TV Band

We conducted fixed and mobile measurement of the 470∼806 MHz spectrum band in Beijing. The frequency, time, and space domain [18] and the specific TV standards are all considered in our analysis. Similar to previous measurements, the fixed measurement and mobile measurement are both conducted.

In China, the spectrum band originally allocated for terrestrial TV broadcasting service is between 470 and 806 MHz. Due to historical reasons, 566∼606 MHz band is reallocated to trunking communication service, which is omitted in our analysis. Thus the TV band takes up to 296 MHz bandwidth. Currently, both analog television (ATV) and digital television (DTV) are utilized in Beijing. The channel bandwidth is 8 MHz for both DTV and ATV. Therefore, TV band contains 37 channels. Their transmit power is very high, which means that these channels are occupied almost all the time, like 750∼758 MHz. In the second case, both the maximum and the average transmit powers are high. However, a certain difference exists between them, which suggests that these frequency bands are only partially used, like 478∼486 MHz. In the last case, the maximum power is high, while the average power is close to the noise floor, like 700∼730 MHz. Since TV broadcasting system usually works stably over a long period of time, these channels may be utilized by wireless microphones or interphones.

The water fall map of the spectrum band is depicted in the lower subfigure of Fig. 4. It can be observed that some spectrum bands are not utilized during the time interval 00:00∼06:00. To show whether the spectrum utilization has periodicity over

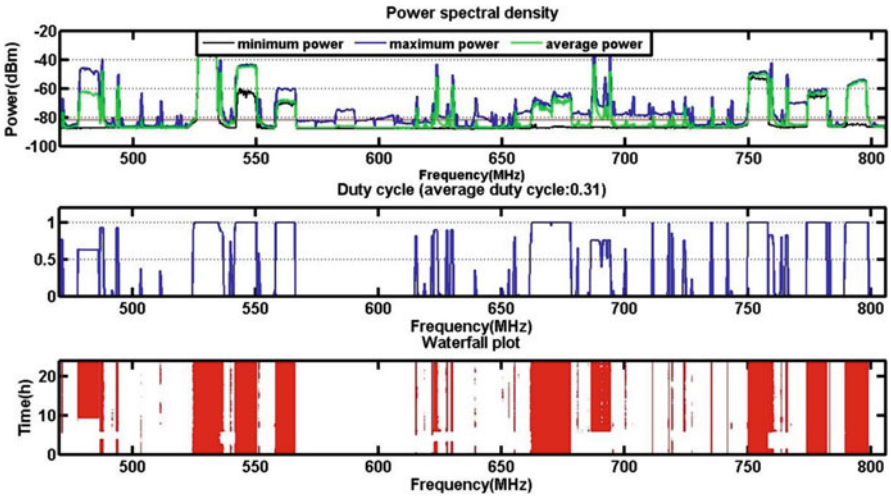

Fig. 4 The utilization of TV band

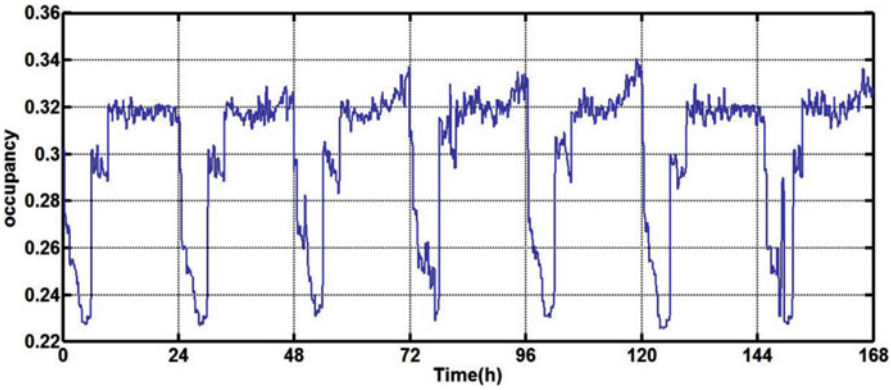

Fig. 5 Spectrum occupancy versus time in the 7-day measurement

time, the spectrum occupancy versus time in the 7-day measurement is plotted in Fig. 5.

It is obvious that the entire spectrum band occupancy shows strong periodicity with 1-day period. As illustrated in Fig. 5, the lowest occupancy appears in 00:00∼06:00, which can be explained by the fact that some TV transmitters are shut down at midnight due to the small number of audiences. The occupancy is almost identical for each day during a week, which depicts the static feature of the TV channels. Ripples in the occupancy curve can be explained by measurement errors and illegal usage. Notice that the high utilization period of TV band coincides with the busy period of the public communication systems such as CDMA and WLAN.

An interesting paradox is that even though spectrum opportunity in the time domain is sufficient in 00:00∼06:00, the spectrum demand may not exist in this period.

Suggestions on Spectrum Innovation in TV Band of China

Based on the analysis of both fixed and mobile measurement above, we would like to provide our suggestions on spectrum innovation for the TV band of China.

Our first suggestion is that China should accelerate the transition from ATV to DTV. The advantages of DTV are obvious. Firstly, the DTMB standard developed by China can provide a data rate as high as 30 Mbps via OFDM, which is sufficient for HDTV. So the experience of the audiences will be greatly enhanced. Secondly, the receiver design and out-of-band performance of DTMB are better than PAL-DK and make DTMB robust to adjacent channel interference. The replacement of ATV with DTV will eliminate the hidden occupancy problem, resulting in fewer requirements on the device using this band. Thirdly, Chinese DTV standard has its unique single-frequency network (SFN) technology. To cover a huge area, the same TV program is traditionally broadcasted using different channels to avoid the interference among transmitters. However, in SFN, a TV program can be synchronously broadcasted across the entire area via only one channel. Thus spectrum efficiency can be improved, and more channels can be relieved for reallocation. Finally, multiple TV programs can be carried by a DTV channel, and the channels needed for TV broadcasting can be further reduced. The transition to DTV is an international trend which has been accomplished in many countries. China began the transition from 2008 and is more likely to accomplish in 2020.

We believe spectrum reallocation should be the main spectrum innovation strategy in the TV band of China. As the measurement indicates, the overall occupancy of TV band is merely 38%, which is very low. Thus, the vacant band can be reallocated to other services. However, the spectrum allocation for TV band varies in the different areas of the country. To leave a universal band for other services, national-wide adjustment of TV spectrum band may be required. Moreover, the spectrum occupancies show that there exist the time domain spectrum opportunity in the midnight and space domain spectrum opportunity in the suburb of city. However, there are difficulties to use these spectrum opportunities. Besides, indoor spectrum opportunities exist for short-distance communication technologies like femtocell. However, a further measurement is needed to justify the possibility to implement femtocell in TV white space.

Other Countries and Regions

Contreras et al. in [5] carried out the spectrum occupancy measurements in three locations of Kanto area in Japan. The spectrum band from 90 MHz to 3 GHz is measured. It has been found that only 6.9% of the spectrum between 90 MHz and 3 GHz is used for more than 10% of time, which indicates the great potential for deploying spectrum sharing systems in Japan.

Table 1 Spectrum occupancies in Japan [5]

Subband	Bandwidth	Occupancy	Services
90∼108 MHz	18 MHz	23.58%	TV broadcast (until 07/11)
108∼170 MHz	62 MHz	12.91%	Miscellaneous communications
170∼222 MHz	52 MHz	17.46%	TV broadcast (until 07/11)
222∼470 MHz	248 MHz	0.63%	Miscellaneous communications
470∼810 MHz	340 MHz	13.9%	TV (until 07/12), radio microphones
810∼958 MHz	148 MHz	28.55%	Cellular networks, disaster prevention, RFID
958∼1710 MHz	752 MHz	0.09%	Miscellaneous services
1710∼2300 MHz	590 MHz	5.9%	IMT 2K, spatial applications
2300∼3000 MHz	700 MHz	0.018%	Radar, IMT 2K, ISM, public communications

Table 2 Spectrum occupancies in Malaysia [21]

Service	Frequency range (MHz)	Bandwidth (MHz)	Average duty cycle (%)
GSM 900	880∼960	80	35.31
GSM 1800	1710∼1880	170	9.59
3G (IMT-2000)	1885∼2200	315	26.08
VHF TV	174∼230	56	10.92
UHF TV	470∼798	328	13.36

The spectrum occupancies of different sub-bands are provided by [5], which is presented in Table 1. It is noted that the highest spectrum occupancy is 810∼958 MHz, which is occupied by cellular networks. On the other hand, the spectrum bands which are occupied by radar, TV broadcasting system, etc. are relatively idle. Overall, the spectrum measurement in Japan has demonstrated the great potential for deploying spectrum sharing systems in Japan all along the evaluated spectrum from 90 MHz to 3 GHz [5].

Jayavalan et al. in [21] investigated the spectrum occupancy of cellular and TV broadcasting spectrum bands in Malaysia, as shown in Table 2. Malaysia is closely located with Singapore, Thailand, and Indonesia, so some of the TV spectrum bands are not utilized in this country due to cross-border spectrum coordination. Specifically, TV broadcasting in VHF and UHF bands has the average duty cycles of 11% and 13%, respectively [21]. Besides, Jayavalan et al. found that the utilization of most allocated TV spectrum bands is below 15%. Thus their work provides the motivation for spectrum sharing in Malaysia and can bring economic and social welfare to this country.

Spectrum Sharing Policy in the Asia-Pacific Region

China

According to the prediction of ITU, the spectrum demand of international mobile telecommunications (IMT) in 2020 will be 1340∼1960 MHz. SRRC estimates that

spectrum demand in 2020 will be 1490∼1810 MHz. However, there is still around 1000 MHz shortage of spectrum for China [53].

In this situation, the spectrum refarming, spectrum sharing, etc. are proposed to improve the spectrum utilization. In China, government policy regulators such as the ministry of industry and information technology (MIIT), SRRC, etc. are considering modifying current spectrum allocation policies in order to enable dynamic spectrum access technologies. The Chinese government has already released the regulations that allow the spectrum sharing among the radio access technologies (RATs) within an operator. In 2016, MIIT of China firstly carried out spectrum audit, which aims to evaluate the spectrum usage to enhance the radio spectrum resource regulation. Through this work, Chinese government obtains the actual use of key spectrum bands of 7 public mobile communication systems consisting of 25 spectrum bands. Thus Chinese government has enhanced the monitoring level of the spectrum, which paves the road for spectrum refarming and spectrum sharing.

Moreover, in order to satisfy the requirements of future mobile broadband systems in 5G, such as ultrahigh traffic and ultrahigh data rates, more spectrum and wider bandwidth are needed to improve the performance. Therefore, the innovative spectrum utilization methods should be further investigated to discover the available spectrum of IMT under horizontal or vertical spectrum sharing systems. Spectrum sharing is a dynamic and optimized allocation of multi-RAT spectrum resources, which involves some key factors such as deployment scenario, network load, and user experience. Spectrum efficiency improvement and interference control are benefited from the optimized dynamic spectrum allocation and management among different networks or systems. Besides, self-adaption functions of autonomous access networks and handover between networks can be realized. Furthermore, air interface efficiency and coverage are enhanced for the efficient, dynamic, and flexible spectrum utilization. Therefore, the utilization efficiency of spectrum can rise.

Spectrum sharing technologies can be classified by the application scenarios, including intra-operator inter-RAT spectrum sharing, inter-operator spectrum sharing, spectrum sharing in the unlicensed band, and spectrum sharing in secondary access. There are various implementation choices for spectrum sharing such as independent control node, database-based control, etc. The specific functionalities of spectrum sharing contain multiple priority spectrum allocation, interference coordination, and so on. In the following sections, we will introduce the development of spectrum sharing technologies in China.

Spectrum Refarming

In the United States, Finland, etc., the spectrum bands of 2G mobile communication systems are reallocated to the 4G mobile communication systems. In China, there are also some cases of spectrum refarming. In 1998, the personal handy-phone system (PHS) entered into China market. Until October 2006, the number of the users of PHS system in China is 93 million. However, in October 2008, MIIT of China announced that the spectrum band of PHS (1900∼1920 MHz) was planned to be reallocated to time division-synchronous code division multiple access

(TD-SCDMA) system, a third-generation mobile communication system proposed by China. In January 2011, PHS system began to be officially withdrawn from the market of China. In October 2014, the base stations of PHS were completely closed in China.

TD-SCDMA has inherited the spectrum band of PHS system in China. However, when the TD-SCDMA began its commercial operation, the 4G mobile communication system has been already on the way. Besides, the time division long-term evolution (TD-LTE) and TD-SCDMA are both operated by China Mobile Communications Corporation (China Mobile). Hence TD-SCDMA fell in an awkward situation. In 2013, China Mobile determined that the voice service of 4G will fall back to GSM system rather than TD-SCDMA system. In 2014, China Mobile announced that the investment to TD-SCDMA had been stopped. And the users of TD-SCDMA will be moved to TD-LTE, which means that TD-SCDMA network will be naturally withdrawn in the future. Actually, China Mobile has already started some trials to refarm the spectrum of TD-SCDMA. In 2015, China Mobile allocated the spectrum band A (1880∼1920 MHz) of TD-SCDMA to TD-LTE, such that the data rate of TD-LTE can be improved to 79.8 Mbps. Besides, China Telecom and China Unicom started to refarm the spectrum of CDMA 800 MHz and GSM 900 MHz [53].

Spectrum Sharing

In China, the mobile Internet plays an important role in economic development and everyone's life. Driven by the devices such as smartphones and tablet PCs and the services, such as social networking, streaming media, and online game, the amount of mobile traffic dramatically increases, which gives birth to the fifth-generation (5G) mobile networks. One of the quality of service (QoS) requirements of 5G is the 1000× capacity improvement compared to 4G. With such large capacity demand in the future mobile communication system, the spectrum refarming cannot totally solve the shortage of spectrum. Hence the spectrum sharing is regarded as the long-term solution in the 5G era.

Recently, with the emergence of sharing economy or collaborative consumption, the spectrum sharing becomes more and more popular. Similar as the business model of Uber and Didi, the government believes that spectrum sharing can stimulate the economy. In 2013, the Broadband China Strategy was proposed by China government, where optimized spectrum planning was initialized as one of the strategies.

In the spectrum planning of Broadband China Strategy, the government of China regarded the dynamic spectrum allocation as a promising approach to improve the utilization of spectrum resources. To achieve this goal, the interference mitigation technology and equipment are required to be addressed to enable the spectrum sharing among various wireless services. Meanwhile, the spectrum regulation for multiple wireless devices operating on the public spectrum is essential, which aims to maintain the order of spectrum utilization among the spectrum sharing wireless networks and devices.

The TV white spaces (TVWSs), 2.3 and 3.5 GHz, etc. are widely regarded as the promising spectrum bands that can be shared with other wireless systems. In the Broadband China Strategy, the spectrum band of 2300∼2400 MHz, which was originally allocated to the radar system, was planned to be shared with wireless communication systems. The spectrum bands that are utilized locally, such as spectrum bands of TV and radar, are commonly regarded as the ideal candidate spectrum sharing bands. However, the TV white spaces in China are difficult to be shared because of the policy issues, although the sharing of TV white spaces has been already deeply studied in China's academia.

National projects of Cognitive Radio

The government of China has supported a lot of national projects to study the cognitive radio and spectrum sharing, etc. In 2005, the National High-Tech R&D Program (863 Program) began to support the research on cognitive radio. In 2008, the National Natural Science Foundation of China established a group of the projects on cognitive radio. The Beijing University of Posts and Telecommunications (BUPT), Tsinghua University, PLA University of Science and Technology, etc. were all supported by this group.

Specifically, in 2008, BUPT was supported by the Major State Basic Research Development Program of China (973 Program) to study the architecture of cognitive radio networks, multi-domain cognition theory and method, autonomous resource management and control schemes of cognitive radio networks, etc. The proposed architecture of cognitive radio network was illustrated in Fig. 6, which consists of four modules.

(1) End-to-end goal management: This module consists of two aspects: the end-to-end goals and cognitive specification language. The cognitive information collection and autonomous resource management module are guided by the end-to-end goals. The cognitive specification language maintains the connection among different modules.
(2) Cognition coordinator: Cognition coordinator is mainly used to set the filter to obtain cognitive information from multi-domain environment. Then cognition coordinator establishes the precise mapping between multi-domain environment and cognitive information. Finally, cognition coordinator extracts the relevant cognitive information.
(3) Self-organization coordinator: With the goals of end-to-end utility, the autonomous resource management module generates the optimization strategy based on the collected cognitive information.
(4) Reconfiguration management: Based on the optimization decision, the related reconfiguration model is established to execute the reconfiguration command and reconstruct the network parameters.

In the architecture of cognitive network, the entire architecture is driven by end-to-end performance. And the learning function is realized through the interaction between the theoretical model and the modules. As illustrated in Fig. 7, the

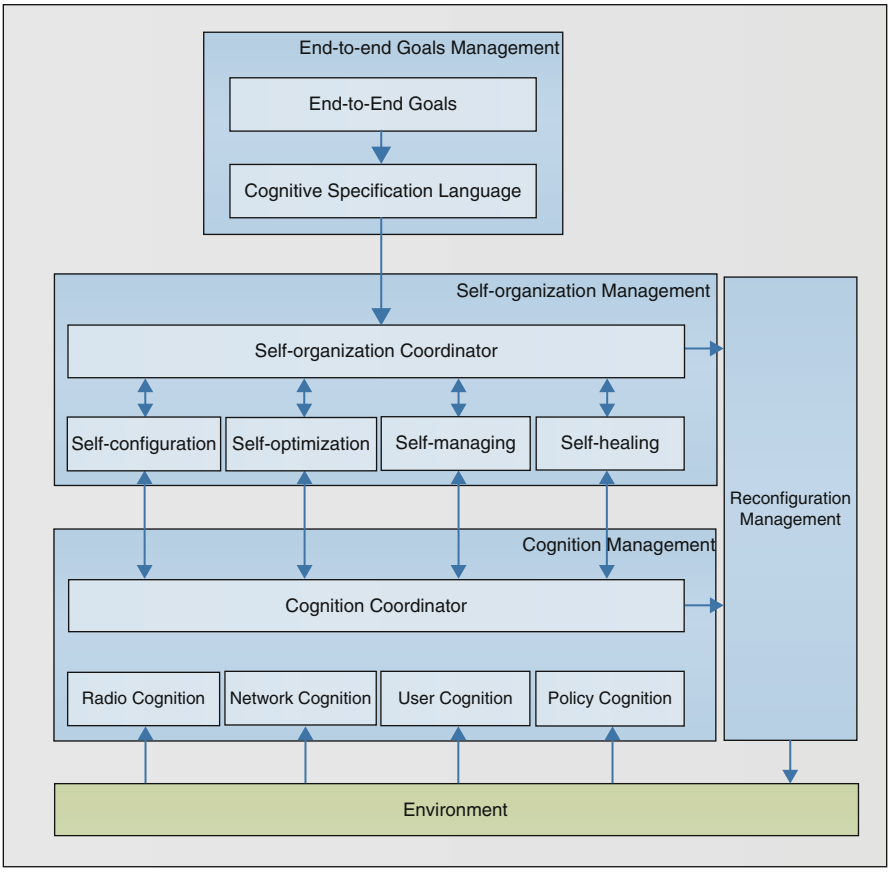

Fig. 6 The architecture of cognitive radio proposed by China

cognitive information flows from the cognitive management module to the end-to-end module, the self-organization module, and the reconfiguration module.

Apart from BUPT, the University of Electronic Science and Technology of China (UESTC) was also supported by the 863 Program. UESTC designed the architecture of cognitive radio networks and developed the test-bed of cognitive radio networks with the support of 863 program.

Cognitive Radio Networks in China

It is noted that in China, the cognitive TD-LTE system was proposed by BUPT, which can be regarded as one of the precursors of LTE-U. In LTE-U, LTE system shares the unlicensed band. The cellular network is the pillar of telecommunication industry. Thus utilizing cognitive technology to solve spectrum usage in cellular network is of great importance. To improve the spectrum efficiency of cellular system, the following requirements must be satisfied.

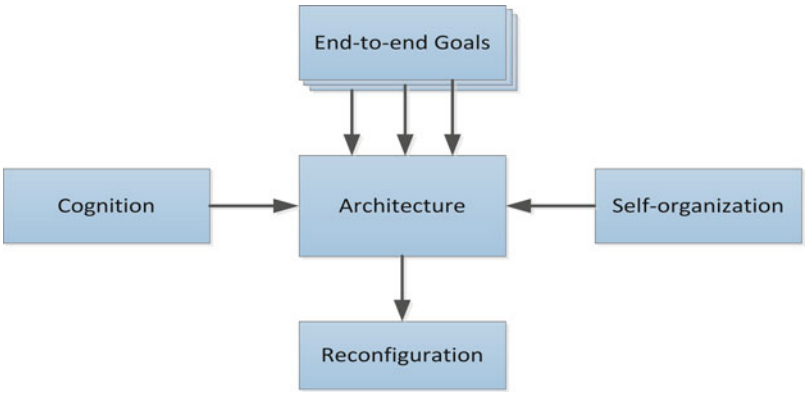

Fig. 7 The main modules in the architecture of cognitive radio

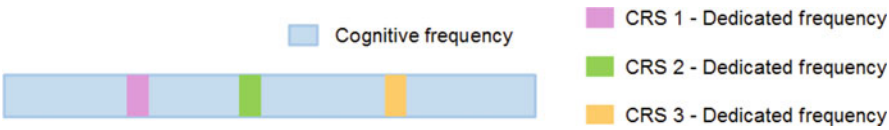

Fig. 8 The spectrum allocation in cognitive radio

(1) Accurate and efficient vacant spectrum awareness.
(2) Dynamic spectrum management.
(3) Flexible and adaptive transmission and dynamic spectrum utilization.

Notice that time division duplex (TDD) mode can be operated in unpaired spectrums, whereas frequency division duplex (FDD) requires paired spectrums. Thus TDD offers more flexibility in spectrum allocation. The capacity of TD-LTE system can be improved with the assistance of cognitive radio.

The cognitive TD-LTE system coexisting with TV broadcast services enables high efficiency of spectrum utilization. Based on the field test of the spectrum band allocated to broadcast TV services, the band 698∼806 MHz is selected for the cognitive TD-LTE system. However, the dedicated spectrum is also necessary to guarantee the control signaling and basic data transmission. The dedicated spectrum is allocated to a certain cognitive cellular system to guarantee cognitive information transmission and basic data transmission. Different dedicated spectrum bands are allocated to multiple cognitive cellular systems to work together without any interference to each other, as shown in Fig. 8. Hence it is challenging to design the dynamic spectrum management for the cognitive cellular system with statically utilized dedicated frequency and dynamically utilized cognitive frequency.

Besides, as illustrated in Fig. 9, two-level spectrum management architecture is proposed to enable the spectrum regulation among TD-LTE and TV broadcast services, consisting of global layer and local layer [7, 8].

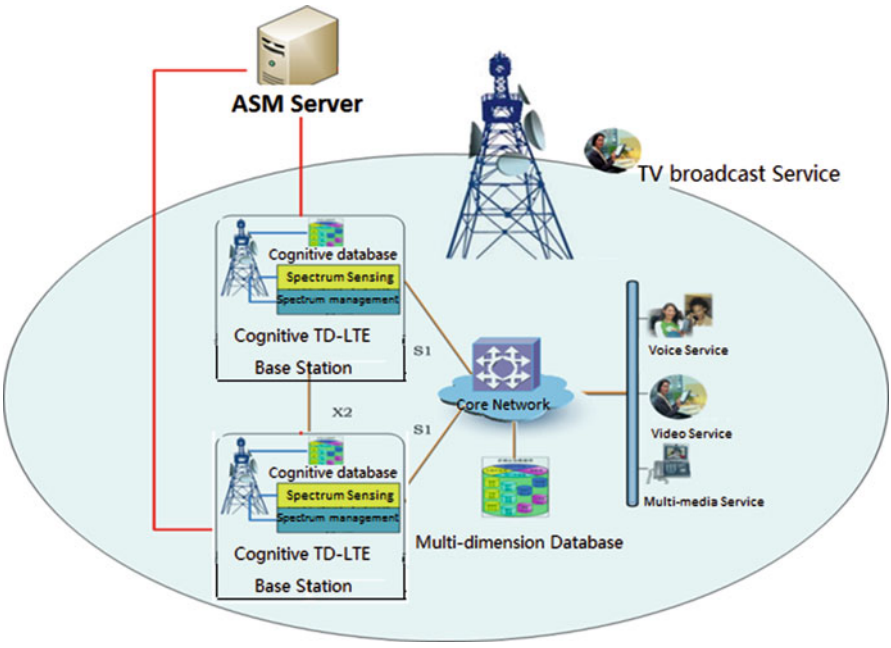

Fig. 9 The two-level spectrum management architecture

(1) Global layer: The advanced spectrum management (ASM) server is operated in the global layer and is responsible for the inter-cell spectrum management, which is a large time granularity spectrum planning.
(2) Local layer: In practice, the spectrum occupancies vary in the space and time dimensions. Hence the local layer spectrum management is also necessary. In the local layer spectrum management, the combination of cognitive database and spectrum sensing is essential to capture the spatial and temporal spectrum fluctuations and coordinate the possible interference between TD-LTE and TV broadcasting networks.

Policy and Regulation Challenges of Spectrum Sharing in China

The major difference between the spectrum policy of China and that of western countries is that spectrum bands are not allocated by auction. Thus the operators in China, like China Mobile, China Unicom, and China Telecom, do not need to pay for the dedicated spectrum. In the United States, Britain, Germany, etc., the spectrum is always billion dollar asset. Hence in these countries, the spectrum sharing is highly motivated to improve the spectrum efficiency. When Qualcomm proposed the LTE-U and LAA technologies, the motivation was due to the expensive spectrum. When the operators try to improve the network capacity, the unlicensed spectrum is one of reasonable choices. Hence in China, from the operators' point of view, the motivation of spectrum sharing is not strong enough compared to other countries.

Meanwhile, the sharing of TV white spaces is not well developed owing to the policy issues.

However, on the other hand, Chinese government has strong incentive to push spectrum sharing forward because the spectrum sharing can stimulate the industry innovation and boost the economic development. The spectrum regulation entities like MIIT and SRRC have launched a large number of regulations and projects to study the possibility to share the spectrum bands of TV and radar. The sharing of infrastructures and spectrum can save public resources and avoid the waste of resources, such as reputably building the base stations and low spectrum utilization. Hence Chinese government has promoted to establish the China Tower company, which aims to share the base stations among the operators. From the vision of development, the spectrum sharing in China is challenging while on the way.

Japan

The spectrum policy of Japan is administrated by the Radio Regulatory Commission, which is an independent agency under Japan government [47]. The Ministry of Internal Communications (MIC) of Japan established a committee in 2004 to formulate the policies on spectrum regulation. The telecommunications policy functions of the Ministry of Posts and Telecommunications (MPT) moved to the Ministry of Internal Communications (MIC) in 2001 [30]. MIC releases the radio legislation, the spectrum rules and the spectrum allocation table [30].

In Japan, with the innovation of wireless technologies such as small cells, code division multiple access (CDMA), and high-speed packet access/evolution-data only (HSPA/EVDO) [41], the spectrum utilization is significantly improved compared to traditional spectrum usage. However, the spectrum in Japan has been nearly exhausted. Hence the emerging wireless technologies have great difficulties in finding new spectrum bands, similarly in China. With the severe spectrum usage, the development of mobile Internet faces great challenges. However, the economy is boosted by the information and communication technology (ICT), where the mobile communication plays an important role. With the upgrade of the different generations of wireless communication systems, the ideal frequency bands are allocated to the prior wireless communication system, which makes the spectrum resources to be scarce. In addition, the mobile communication operators need to provide new services to attract consumers. Therefore the spectrum resource is also in shortage supply. Hence the mobile communication operators need to find an approach to efficiently use spectrum. In this situation, spectrum sharing is one of the promising technologies to efficiently improve the spectrum efficiently [41].

Cognitive Radio Architecture Proposed by Japan

Spectrum sharing aims to use the vacant spectrum bands. In spectrum sharing, the vacant spectrum bands and vacant time slots of primary users can be exploited by secondary users. By sensing and accessing the vacant spectrum in spatial and temporal dimensions, secondary users can use adequate spectrum bands to improve

the capacity of cognitive radio networks. In the implementation of spectrum sharing in cognitive radios, the cooperation among heterogeneous wireless networks is essential to coexist among them and improve the spectrum utilization.

In Japan, the cognitive wireless cloud (CWC), a kind of architecture of cognitive radio network was proposed by NICT [15]. The cognitive radio systems cooperated with primary networks are called dynamic spectrum access network or cognitive wireless clouds [15]. In CWC, a network reconfiguration manager (NRM) installed in secondary networks collects the sensing data of secondary users. The sensing data includes data rate, delay, throughput and signal strength, and so on. The NRM analyzes the collected sensing data and feedbacks the controlling information to secondary users, such that secondary users can access to the most appropriate wireless networks.

White Space Sharing in Japan

It is worth noting that Japan is a small island country with population of 126.81 million and is close to Busan, one of South Korea's major cities. Therefore the geographic features of Japan are different compared to many other countries that have multiple land borders with neighboring countries. Large population and small area make Japan's spectrum resources particularly scarce. The government of Japan attaches great importance to the efficient use of spectrum.

To solve the shortage of spectrum resources, MIC released a series of the related policies to improve spectrum utilization. The exploitation of white space is an important part. MIC announced the action plan for spectrum reuse in 2004, with the latest revision accomplished in October 2015 [11]. For the implementation of the plan, the government of Japan conducts annual audits for spectrum. Through the investigation and evaluation of specific spectrum bands, they developed spectrum recovery programs and use the frequency compensation mechanism to promote spectrum migration.

In July 2011, Japan finished the transition from ATV to DTV. Spectrum band of 710∼722 MHz was released on July 24, 2006. Spectrum band 722∼770 MHz was released in July 24, 2012, which was no longer used for the broadcasting service [43]. The spectrum band 90 $\sim$ 108 MHz and 170 $\sim$ 222 MHz cannot be used for TV broadcasting after July 25, 2011 [43]. As illustrated in Fig. 10, TV white space (TVWS) devices must be separated from the protected area of TV channel within a distance based on their transmission power and antenna height. Typically, the protected area of TV channel is the area where the corresponding transmitter provides the required signal strength for acceptable TV service. According to [34], there were more than 20 available TVWS channels in central Tokyo in 2012. There are many wireless systems aiming to be operated in TVWS, such as sensor networks, wireless microphones, and public safety communication systems. The possibility of adopting geo-location database in spectrum sharing is under the investigation by the TVWS working group established by MIC, which has so far investigated the feasibility of allowing small-area broadcasting systems, wireless microphones, sensor networks, and public safety communication systems to access TVWSs [34].

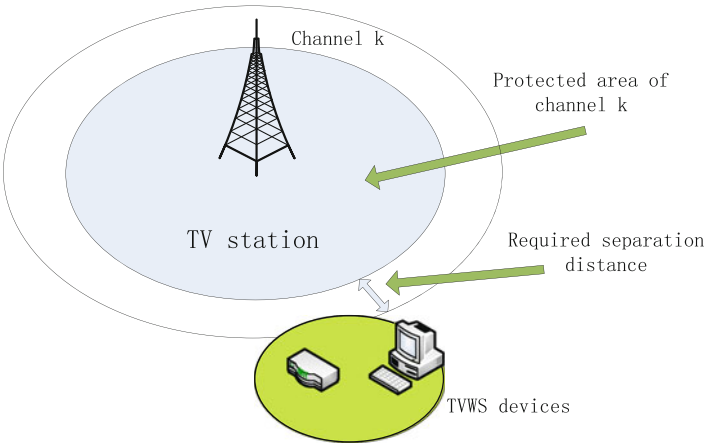

Fig. 10 Basic concept of TVWS device regulations [34]

In Japan, the spectrum has already been allocated to a variety of services. Spectrum sharing also faces the political barrier, which is not purely a technical problem. Hence, the realization of spectrum sharing will still have a long way to go.

Singapore

White Space Sharing in Singapore

Due to its restricted area and large population similarly as Japan, the government of Singapore is highly concerned about the efficient use of spectrum. There are also many trial experiences to investigate the possibility to use spectrum efficiently. ATV to DTV transition produces a large number of idle spectrum bands, and the new spectrum utilization method, namely, spectrum sharing, is proposed to improve the spectrum efficiency [45].

TVWS is a good choice to be utilized to enrich the available spectrum. The VHF spectrum (174 and 230 MHz) and the UHF spectrum (470 and 806 MHz) for TVWS operations were not fully utilized [38]. Such spectrum bands could potentially be redeployed for other wireless services. Info-communications Development Authority in Singapore (IDA) has the authority to plan the spectrum bands. The white space equipment operates without permission as long as it complies with IDA's technical specifications. The license-free approach allows the users to explore a range of business models, which reduces user's costs and stimulate innovative services.

As early as 2006, the Singapore Institute of Information and Communications (I2R) participated in the standardization of TVWS in IEEE [17]. In 2008, I2R proposed an experimental prototype exploiting TVWS to the Federal Communications Commission (FCC), which is the original development of the spectrum sharing in

Singapore. In 2009, IDA completed Singapore's regulatory framework for TVWS deployment [36]. In 2011, IDA carried out the spectrum planning in white spaces and development of relevant regulatory framework. In 2012, Singapore set up a TVWS test working group. More than 40 locations were tested within 2 years, and it is found that the use of TVWS has many obvious advantages.

The use of TVWS has been found to have many obvious advantages. It is estimated that Singapore has TVWS of up to 180 MHz [39]. Once the TVWS is open to use, the capacity of wireless networks can be boosted. IDA has developed a regulatory framework in November 2014 to allocate the 180 MHz TVWS to unlicensed users. In 2015, TVWS regulatory framework was further pushed forward. It allows other wireless networks to use TVWS to increase capacity and create broadband wireless networks. Singapore is the second country in the world after the United States who agrees to access TVWS for unlicensed users [39]. The concept of dynamic spectrum access can optimize and enable the access to underutilized spectrum, which can be used in many areas such as smart grid, wireless broadband, and machine-to-machine communication. Moreover, the geo-location database approach will be a practical method for white space devices to access TVWS. Allowing unlicensed users accessing TVWS will motivate potential new technologies and business models, which will bring opportunities for small- and medium-sized enterprises. Although the companies wish to use TVWS without license, they need to comply with the technical regulations proposed by IDA. Manufacturers and suppliers of TVWS equipment must register their devices in IDA, similarly for the manufacturers and suppliers of mobile phones and communication equipment [40].

Furthermore, the Minister of Communications and Public Information in Singapore announced the latest development blueprint, namely, Master Plan 2025, to tackle the shortage of the spectrum facing the great spectrum demand of mobile Internet [42].

National Projects of Cognitive Radio in Singapore

Singapore has developed a white space test-bed cognitive radio venue (CRAVE) to evaluate the promising technologies to improve spectrum utilization. The test locations of CRAVE are Malaysian coast, Indonesia coast, near broadcast tower, dense urban environment, and in-building environment [28]. The performance of WSD devices is evaluated by this program.

Policy and Regulation Challenges of Spectrum Sharing in Singapore

Singapore is a country with small area and limited natural resources. Facing the grow of elderly population and the process of urbanization, the high-tech products such as sensors, robots, and wireless networks are widely deployed to build a smart nation that improves people's life quality. It is also the common aspiration of Singapore government and the people. Spectrum-related policies are important for the construction of smart country.

The realization of spectrum sharing faces many open and critical challenges, for example, is low-power transmission of secondary user able to meet the transmission requirements, what transmit power level should be adopted and how to control it, how to effectively estimate the users interference [29], etc. All these questions need to be addressed in the policy design.

India

White Space Sharing in India

Unlike the developed countries, India has a lot of licensed but unutilized TV spectrum band [33], namely, TVWS. Since the UHF television band has ideal radio propagation characteristics, Indian authorities plan to use this spectrum band and fiber-based point of presence (POP) connections to cover the 250,000 rural offices. Since most of the Indian citizens live in rural areas, the communications engineers of India addressed the possibility to use TVWSs as the broadband access in rural areas [35]. Some researchers in India proposed to create a geo-location database that can broadcast TVWS information on rate constrained channels, such that multi-hop mesh network can operate in TV UHF band [14]. With this solution, the TV UHF band is used to provide seamless connectivity between the gram panchayat and village users [26]. The network can coexist with TV broadcasts through a licensed shared access mechanism.

National Projects of Cognitive Radio in India

India government has launched some projects on cognitive radio. Among them, an emergency network based on cognitive radio was proposed in Adaptive Ad hoc Free (AAF) Band Project [54]. Besides, the authorities of India approved the spectrum sharing, which allows the operators to share the spectrum of a particular band to improve spectrum utilization.

Policy and Regulation Challenges of Spectrum Sharing in India

The authorities in India are determined to change the situation that many citizens cannot access to broadband Internet. Spectrum sharing is a promising answer to solve this problem. Therefore, the government of India approved the operators to share a specific spectrum band within the service area to improve spectrum utilization, which is regarded as a big step toward spectrum sharing.

Korea

White Space Sharing in Korea

The South Korea government has recently proposed a TVWS field demonstration system that meets the requirements of the Federal Communications Commission (FCC). The measurements of TV band device (TVBD) networks have been

conducted in Jeju, South Korea. The measurement results show that the service's coverage of mobile network can be extended to more than 2 km when TVBD operates on the available TV spectrum bands [24]. The primary service in TV band is the digital television (DTV) [23]. With the DTV service, both the co-channel and adjacent channel deployment scenarios of TVBD network are investigated in Korea.

Policy and Regulation Challenges of Spectrum Sharing in Korea

The government of Korea has launched some projects on cognitive radio. The service coverage measurements on TVBD networks were implemented in Jeju, Korea [24]. Besides, the Korea Communications Commission (KCC) has proposed a new spectrum strategy based on dynamic spectrum access technologies, such as LBT universal spectrum for RFID, UWB-DAA, and flexible access (FACS) [25]. The KCC also considers spectrum sharing for TVWS after the transition from ATV to DTV and pays much attention to the improvement of spectrum efficiency [25].

Australia

Australia is a large continental country with population of 23.8 million. However, the distribution of populations in Australia is highly inhomogeneous. Australia is highly urbanized, and nearly half of the populations live in the two largest cities: Sydney and Melbourne. Most people in Australia live in the big cities near the coastline. About 70% of Australia's land is arid or semiarid, and most of the central area is not suitable for human habitation. Hence in the central area or rural area of Australia, the distribution of the people is very sparse.

According to Prof. Y. Jay Guo's report, the Federal Government of Australia has started a 43 billion dollar project to build a national broadband network (NBN) [22]. NBN will deliver 100 Mbps broadband services to 90% of the population. The rest of the populations, which mainly live in rural area, will be served by wireless and satellite communications networks [22]. In this situation, the TVWSs are proposed as the suitable spectrum bands to provide coverage for rural area.

In Australia, with the process of switching off ATV beginning in 2010 and completing at the end of 2013, the UHF spectrum allocated to broadcasting in Australia shrinks from 300 (520∼820 MHz) to 174 MHz (520∼694 MHz) [10]. Thus there are considerable TVWSs emerging in Australia. To provide wireless services to rural area of Australia, CSIRO has developed cognitive radio technologies to dynamically access the TVWSs. These technologies include reconfigurable antennas, reconfigurable active devices, out-of-band interference suppression techniques, and adaptive and reconfigurable multiple input and multiple output (MIMO) systems [22]. Hence, due to the special geographical feature and population distribution, Australia has great motivation to perform spectrum sharing and has already obtained some achievements in spectrum sharing.

Spectrum Sharing Test-Bed in China

The explosive growth of mobile Internet has led to a surge of data traffic. Hence, the next-generation cellular network is facing both opportunity and challenge. Under this background, the new unlicensed spectrum widely known as TVWS offers new opportunities to improve spectrum efficiency [49]. The 4G cellular networks adopt long-term evolution (LTE) technology based on all-IP network architecture and significantly improve area spectrum efficiency [1]. LTE can support both frequency division duplex (FDD) and time division duplex (TDD) operations over a variety of allocated frequency bands. In Asia, typically 1800, 1900, 2100, 2300, and 2500 MHz are often utilized [19]. To meet the requirement of high data rate services, TDD LTE (TD-LTE) with flexible downlink and uplink time slot ratio without stringent requirements for paired uplink and downlink frequencies can better utilize fragmented TVWS.

However, the available licensed spectrum bands for 4G cellular networks using LTE technology in Asia are around 2 GHz and above, which may increase the network cost for large area coverage. According to spectrum occupancy measurements in Beijing, significant white space opportunities exist in TV broadcasting bands around 700 MHz [55]. Hence, the 4G cellular networks can be operated in TVWS. Such opportunistic operation will require dynamic spectrum access (DSA), which is based on effective cognitive radio principles. Compared to the strict requirements of the paired downlink and uplink spectrum bands with appropriate spectrum separation in FDD LTE, the TD-LTE system with multiplexed downlink and uplink in the same spectrum band can fully utilize the fragmented TVWS. In addition, to meet the service demands in hot spots, multi-tier heterogeneous radio access networks are deployed with overlapped coverage areas, which will bring much challenge for spectrum allocation and interference coordination among multi-tier heterogeneous networks. Therefore DSA and efficient spectrum management technologies should be applied in heterogeneous radio access networks.

Standardization activities on TVWS utilization include IEEE 802.22 [16] for wireless regional area networks (WRAN), European computer manufacturers association (ECMA) 392 [48] for wireless personal area network (WPAN), and IEEE 802.11af task group [13] for wireless local area network (WLAN). Generally speaking, the above standards consist of the mechanisms for coexistence between the secondary and primary networks, where a variety of use cases are addressed such as long-range outdoor services for 802.22 and short-range indoor services for ECMA-392 and 802.11. With respect to spectrum sensing, these standards mostly advocate a quiet period for spectrum sensing by interrupting an existing communication session. This is not appropriate for TD-LTE system which has strict QoS requirements for latency in the voice service and precludes interrupting a communication session [3]. Therefore, some new and simple modifications to the existing TD-LTE protocol stack are needed to exploit TVWS.

In this section, a cognitive radio-enabled TD-LTE test-bed that operates in TVWS is proposed [9]. It supports multi-tier heterogeneous radio access networks. Specifically, an efficient feature detection-based spectrum sensing method is proposed for TD-LTE which can achieve 99.9% detection probability and 1% false alarm probability. The proposed cognitive radio-enabled TD-LTE frame structure utilizes the guard period and adjacent vacant uplink subframe for spectrum sensing by the cognitive eNodeB (CeNB), which requires the minimum protocol stack modifications. In particular, cognitive control channel (CogCCH) is proposed in medium access control (MAC) layer to transmit CR-related radio resource control (RRC) information. Physical cognitive channel (PCogCH) is also proposed in physical (PHY) layer to broadcast the spectrum decision information to CR user. To mitigate the potential adjacent channel interference between the TD-LTE system and the TV broadcasting system, appropriate guard bands between these two systems are needed. The width of guard bands is determined through the simulations and field experiments. To the best of our knowledge, our proposed test-bed is the first CR-enabled TD-LTE system operating in TVWS.

CR-Enabled TD-LTE Test-Bed Utilizing TVWS

The TD-LTE-based spectrum sharing test-bed is developed by the Beijing University of Posts and Telecommunications (BUPT) [9, 56]. To solve the challenges of deploying CR-enabled TD-LTE system operating in TVWS, both solutions and analysis are proposed, including an efficient spectrum sensing method for TV signal detection, interference analysis, and the CR-enabled TD-LTE protocol stack to support the efficient utilization of TVWS, which will be introduced in the following sections.

Spectrum Sensing in TVWS

The cognitive eNodeB (CeNB)-based spectrum sensing method is proposed for spectrum sensing in TVWS with two advantages. Firstly, the spectrum occupied and signaling overhead for information exchange between CR users and CeNBs can be minimized. Secondly, the energy consumption for spectrum sensing by CR users can be saved.

Unlike the United States where TVWS exists among digital TV signals, analog TV signals will be the dominant primary users in China for years. Therefore, we propose a feature detection-based spectrum sensing method exploring the specific characteristic of the analog TV signals. According to the spectral characteristics of analog TV signals (PAL-D) in China [2], the energy of the baseband TV signals is mostly concentrated on 1.25 MHz, chroma vice carrier on 5.68 MHz and audio FM carrier on 7.75 MHz as illustrated in Fig. 11. The procedure of the proposed feature detection method for analog TV signals is shown in Fig. 12. The TV RF signal is digitized directly via fast ADC, which is then down-converted to a baseband signal.

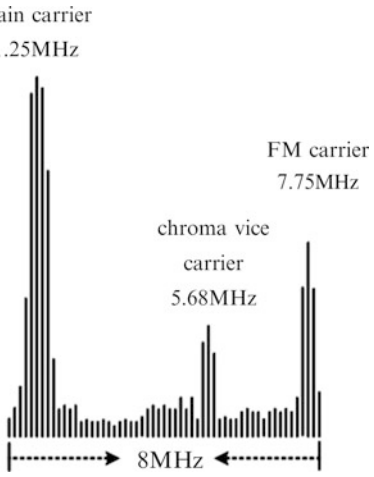

Fig. 11 Spectrum characteristics of analog TV signals

If there are narrow band signals existing on 1.25, 5.68, and 7.75 MHz, and the signal waveform is similar to the analog TV signals, the analog TV signal is then detected. Otherwise, the spectrum is assumed to be unoccupied by the TV signal. Because the detection bandwidth is only 200 kHz compared to 8 MHz for each TV channel, it can increase the spectrum sensing speed for each TV channel with an improvement of 16 dB. The proposed feature detection method can also reduce the noise and the sampling time, which has a good performance under the low signal-to-noise ratio (SNR) condition.

The field experiments are implemented to test the performance of the proposed feature detection method, which is programmed into a baseband signal process board of the spectrum sensing modules. The Agilent N5182A MXG signal generator is used to generate analog TV signals. Spectrum sensing module receives analog TV signals through a cable and reports the detection results to the computer. The detection probability and false alarm probability can be determined by the experiment in Fig. 13, which shows that the detection probability can be 99.9% with at most 1% false alarm probability. Besides, the proposed feature detection method improves the weak signal detection capability significantly with the TV signal power level of −120 dBm.

Furthermore, in order to utilize the vacant spectrum in time-frequency-space multi-domains in TVWS, an efficient spectrum utilization scheme called three regions is proposed in [50], which applies the joint geo-location database and spectrum sensing scheme in order to reduce the complexity and cost of traditional spectrum sensing. Firstly, CeNBs of the TD-LTE system access to the geo-location database to find their locations and decide their specific regions, i.e., the black region, gray region, and white region. Geo-location database is a database system that maintains the records of all authorized services in TV frequency bands and is capable of determining vacant channels at a specific location based on the

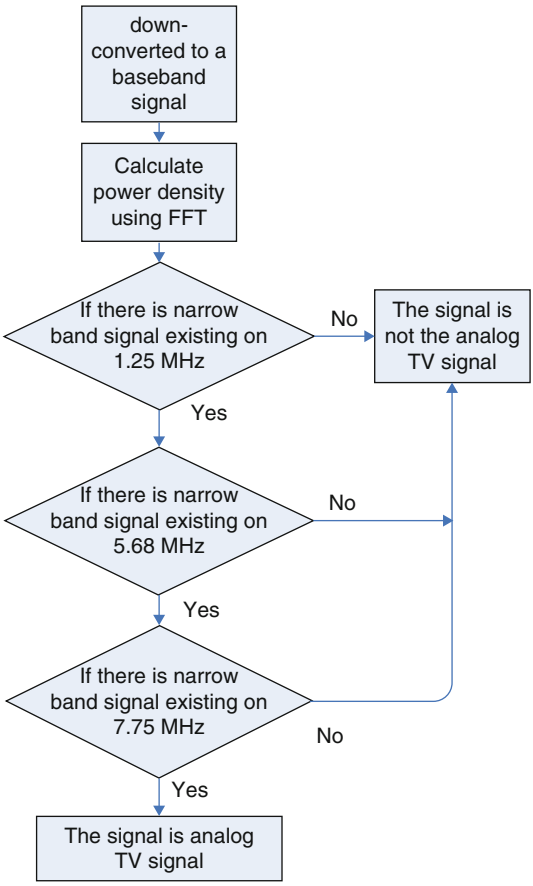

Fig. 12 Procedure of the feature detection method for analog TV signals

interference protection requirements. Black region is defined as the region where the CeNB within it cannot reuse the spectrum of TV broadcasting system. Gray region is a region where the CeNB should apply the spectrum sensing to utilize TVWS. White region is defined as a region where the CeNB can reuse the spectrum of the TV broadcasting system freely without implementing the spectrum sensing procedure. Therefore, by checking the position information in the geo-location database, the CeNB can decide its specific region and make an appropriate decision on whether to apply the spectrum sensing. The scheme of three regions can improve the efficiency and reduce the cost of spectrum utilization.

Interference Analysis

One approach to the reduction of the adjacent channel interference (ACI) between the TD-LTE system and TV broadcasting system is reconfiguring the central frequency of the TD-LTE system and setting the appropriate guard bands between two systems, which will reduce available spectrum resources. Another approach is

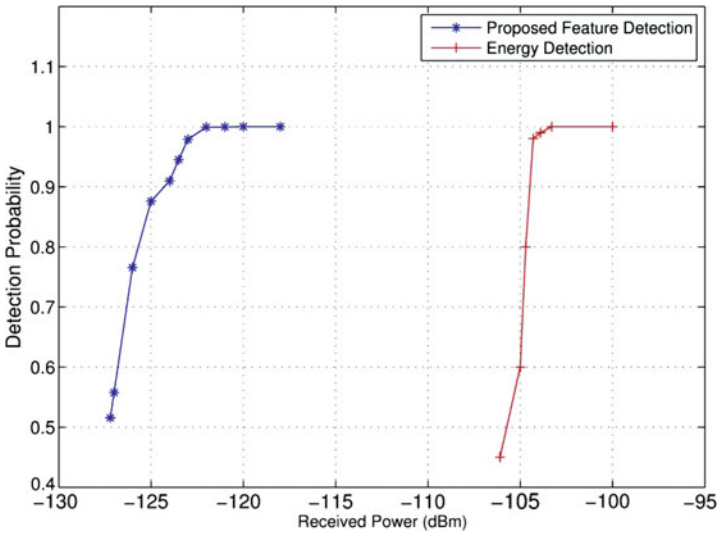

Fig. 13 Detection probability against the received power level of TV signals

to use power control scheme to transmit with a lower power on adjacent channels close to the active TV channels. Based on the geo-database approach, if the TD-LTE system is close to TV receivers, it can use the spectrum bands far from the active TV channels to reduce the interference.

Firstly, we conduct simulation experiments to analyze the interference between two systems. We establish the TV circle-shaped system and TD-LTE honeycomb-shaped network topology (19 CeNBs and 57 sectors) and then assign TV receivers and TD-LTE users, configure transmitter/receiver and channel models, and upload resource scheduling and user mobility schemes to simulate the real system operation states. Moreover, TV receivers and TD-LTE users are assumed to be uniformly distributed. During the simulations, system configurations are the category B in [44]. The left part of Fig. 14 shows the interference probability of the TV broadcasting system versus ACIR, where interference probability is defined as the percentage of TV users that cannot receive signals normally due to the interference. It denotes that the interference decreases as ACIR becomes larger. It also depicts that the interference from CeNB is bigger than that from CR users, which is caused by a much higher CeNB transmit power compared to CR users. The right part of Fig. 14 depicts the interference from the TV broadcasting system to the TD-LTE system. Similarly, we define the percentage of interference-caused capacity decline as the capacity loss, and the larger ACIR leads to a less capacity loss of the TD-LTE system, and the uplink capacity is prone to be decreased compared to the downlink capacity. In general, from the engineering point of view, 5% system performance loss is acceptable for the TD-LTE system. Thus 75/30 dB ACIR (TV interfered by TD-LTE downlink/uplink) and 27/78 dB ACIR (TD-LTE downlink/uplink interfered

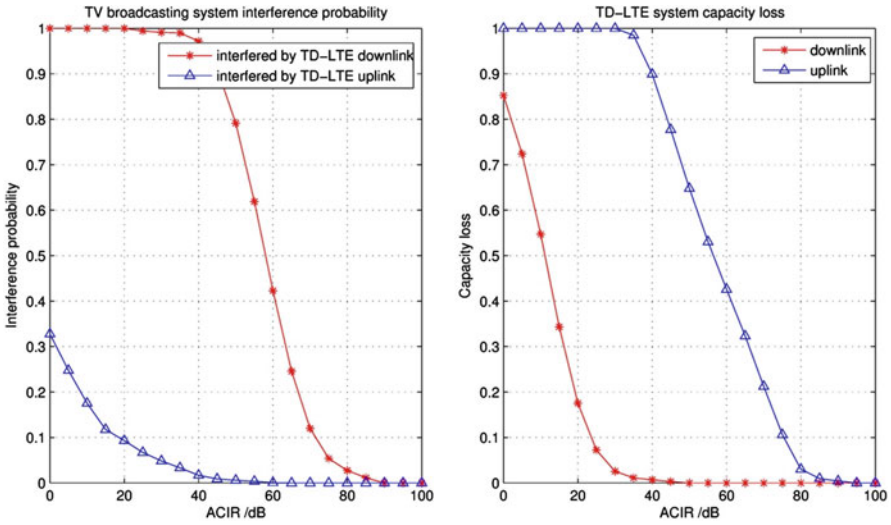

Fig. 14 Performance of the TV broadcasting system and the TD-LTE system against ACIR

by TV) are acceptable for the TV broadcasting system and the TD-LTE system, respectively. Based on the mapping relationship between ACIR and the width of guard bands [44], the frequency separation bandwidth of 7 MHz is appropriate to enable the coexistence of two systems.

Secondly, further field experiments are performed to find the width of the guard bands. The Agilent E4438C signal generator and Agilent N5182A MXG signal generator are applied to generate downlink TD-LTE and TV broadcasting signals, respectively, which go through the signal emulator (EB propsim F8) to emulate different indoor and outdoor channel environments. Then an R&S ETL TV broadcasting signal analyzer acts as a TV receiver to measure the quality of received TV signals with the interference from TD-LTE signals. The central frequency of both TD-LTE and the TV signals is set to be 700 MHz at first, and then the central frequency of the TD-LTE system increases until the TV signal analyzer indicates that the received TV signal quality reaches the normal standard [12]. Then, the separation bandwidth between two signals is the width of the guard bands. The results show that a frequency separation of 6 MHz between TD-LTE and TV signals is an appropriate value, which will not cause harmful interference between them. Therefore, 7 MHz guard band can be used for the coexistence between two systems.

The CR-enabled TD-LTE protocol stack

The protocol stack of the TD-LTE system should be designed with the minimum modifications in order to support CR functions. In addition, the spectrum sensing results and network information exchange among the CeNBs should be supported.

As illustrated in Fig. 15, the modifications to the TD-LTE protocol stack for both the CeNBs and the CR users are designed to support CR functions.

In the RRC layer, the spectrum decision management module in CeNB is introduced to make spectrum decision according to the spectrum sensing information received from the spectrum sensing module. Two main spectrum management functions are proposed for RRC. The first is called the long-term spectrum management among the different CeNBs for the efficient allocation and utilization of TVWS. The second is called the short-term spectrum management within CeNB.

The MAC layer provides different types of data transmission on different types of logic channels such that the types of logical channels are determined by data types. To accomplish the interaction of the CR-related information, a new logic channel called CogCCH is proposed both in CeNBs and CR users to transmit CR-related RRC messages.

In the PHY layer, a physical channel named PCogCH is proposed both in CeNB and CR users to carry the spectrum decision information on the transport channel called cognitive channel (CogCH) and broadcast the spectrum decision information to CR users through the special subframes. The CR users execute the spectrum decision after receiving the broadcast information. To reduce the power consumption and signaling overhead for the CR users, the spectrum sensing module is only added in CeNB to perform the spectrum sensing and report the spectrum sensing results to RRC layer. Meanwhile, through the X2 interface among CeNBs, cooperative spectrum sensing can be performed accordingly and will be used between the adjacent CeNBs for spectrum sensing, information exchange, and long-term spectrum management.

Furthermore, the TD-LTE frame structure is modified to enable CR functions, as demonstrated in the lower part of Fig. 15. Within 10 ms TD-LTE frame, the guard period (GP) in the special subframe #1 is used for spectrum sensing, which will not disrupt the communication between CeNBs and CR users. Moreover, the adjacent vacant uplink subframe #2 is also used for spectrum sensing when the candidate TVWS is too wide. Thus, the TD-LTE system performs the spectrum sensing within 2 ms within each 10 ms frame period. In the meantime, the spectrum sensing module will perform spectrum sensing and deliver the results to the RRC layer. The DwPTS in the special subframe is chosen to transfer both spectrum sensing and spectrum decision information of the previous frame.

Test-Bed and results

Considering the industrial trend of future telecommunication networks in China, a CR-enabled TD-LTE test-bed has been designed and developed in the Beijing University of Posts and Telecommunications (BUPT) with two CeNBs and eight CR users. Both CeNBs and CR users are implemented with a unified hardware platform [46], where the baseband signal processing functions are implemented on TI C6487 DSP. For the three-core DSP, one core is used for downlink signal processing, another is used for uplink signal processing, and a third is for scheduling. AD/DA operation is implemented in Xilinx FPGA, with the AURORA interface to DSP. In

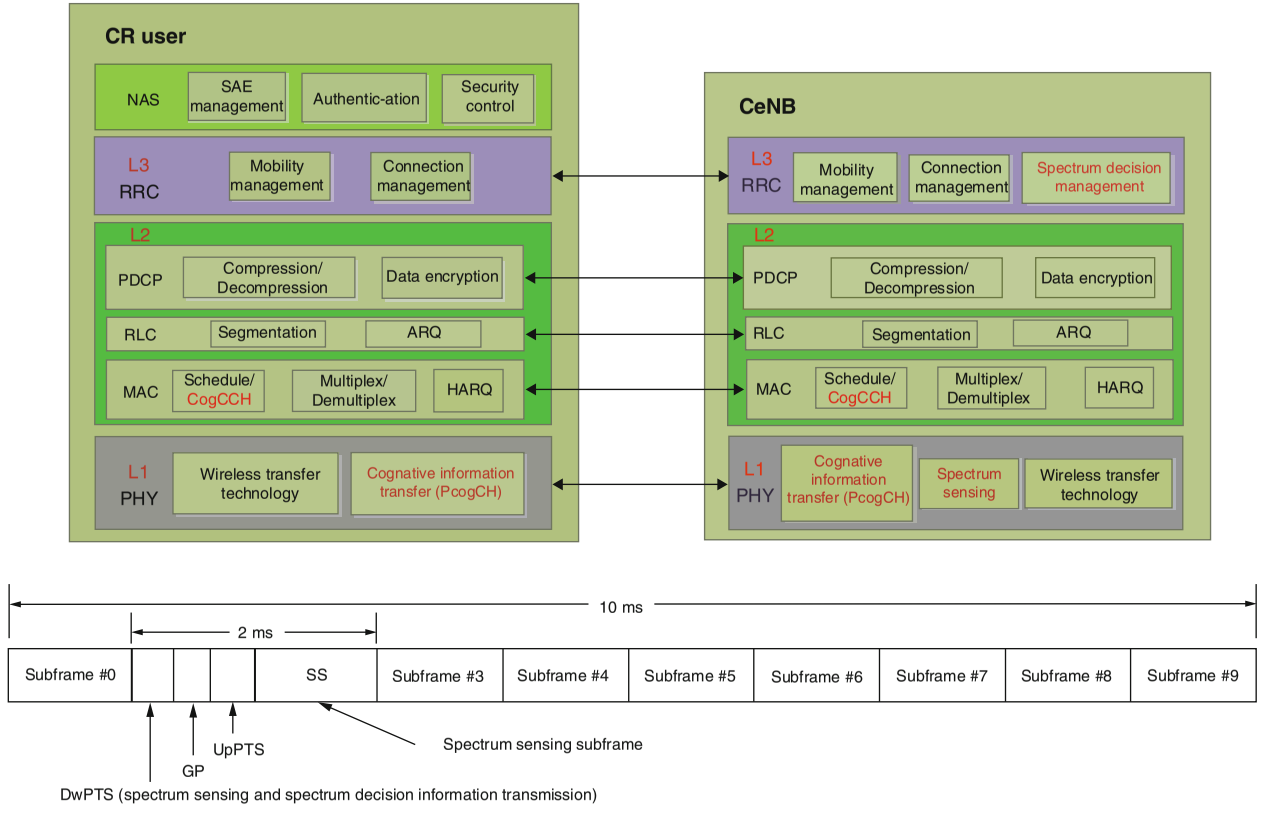

Fig. 15 Proposed CR-enabled TD-LTE protocol stack and frame structure

addition, the platform can also download different protocols from DSP dynamically and be capable of reconfiguring its work mode and parameters intelligently to utilize TVWSs efficiently.

Each TV channel occupies a frequency of 8 MHz in China; thus the TD-LTE system can be implemented with 20 MHz system bandwidth when three continuous TV channels (24 MHz) are all vacant. After the CeNB detects the TV signal, it will execute spectrum handover and switch to another vacant spectrum band accordingly. Furthermore, the spectrum sensing results will also be sent to the TVWS database for vacant spectrum information update, which is used for vacant spectrum information coordination and synchronization among CeNBs. In addition, considering the scenario that continuous TV channels are less than three, the test-bed can apply the dynamic system bandwidth adjustment technology, which means that 15 MHz bandwidth is used when two continuous TV channels are both vacant, while 5 MHz bandwidth is used if only one TV channel is available. Therefore, the test-bed can dynamically change its system bandwidth to adapt the different vacant spectrum conditions in practical scenarios.

The proposed CR-enabled TD-LTE test-bed has both the outdoor and indoor scenarios. In the outdoor scenario, CeNB is deployed on the roof of a building with two mobile CR users. In the indoor scenario, the trial of the test-bed is illustrated in Fig. 16 with three analog TV signal transmitters deployed as the primary TV broadcasting system. The CeNB and CR users are placed inside a room with a light-of-sight (LOS) propagation. The antennas for both CeNB and CR users are 6 dBi rod-antenna. The transmit power of the CeNB is 20 dBm. In addition, the CeNBs are connected to the TVWS database and advanced spectrum management (ASM) subsystem. The TVWS database will collect and update the crude data of spectrum sensing results from different CeNBs, the database of the mobile network, TV broadcasting operators, and the database of state spectrum regulators, in order to draw the global spectrum occupancy graph. Moreover, based on the global spectrum occupancy graph from the TVWS database, the ASM subsystem is responsible for an efficient spectrum management and coordination among different CeNBs by making decisions on the efficient vacant spectrum allocation.

Fig. 16 CR-enabled TD-LTE test-bed

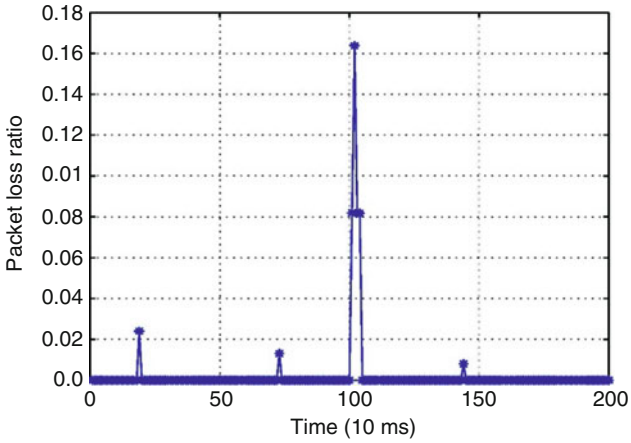

Fig. 17 Packet loss ratio during spectrum handover

In Fig. 17, the packet loss ratio of the CR-enabled TD-LTE system is plotted during a period of 2 s by 200 samples with 10 ms for each sample. During the experiment, the TV transmitter is turned on at 1 s, and the packet loss ratio of the CR-enabled TD-LTE system is fairly steady before 1 s and increases significantly after 1 s as depicted by the surge at the point of 100 samples. This indicates that the interference from TV signals is fairly strong and results in a tremendous packet loss. However, due to the accurate and timely TV signal detection and spectrum handover, the packet loss ratio of the CR-based TD-LTE system can be quickly restored within a short time of 50 ms, as shown in Fig. 5. In contrast to the silence period applied by IEEE 802.22 standard in [6], the proposed CR-enabled TD-LTE test-bed can achieve the spectrum handover within 50 ms on average without severe performance deterioration or service dropout, which significantly outperforms the avoiding time of 2 s in [6].

References

1. Astely D, Dahlman E, Furuskar A, Jading Y, Lindstrom M, Parkvall S (2009) LTE: the evolution of mobile broadband. IEEE Commun Mag 47(4):44–51
2. Bao VNQ, Thuan TD, Quy NT, Trung LM et al (2011) Vietnam spectrum occupancy measurements and analysis for cognitive radio applications. In: IEEE international conference on advanced technologies for communications (ATC), pp 135–143
3. Chen S, Wang Y, Ma W, Chen J (2012) Technical innovations promoting standard evolution: from TD- SCDMA to TD-LTE and beyond. IEEE Wirel Commun 19(1):60–66
4. Chen K, Min J, Han X, Yan X, Duan Y, Zhang L, Feng Z (2014) Spectrum survey for TV band in Beijing. In: IEEE international conference on telecommunications (ICT), pp 267–271
5. Contreras S, Villardi G, Funada R, Harada H (2011) An investigation into the spectrum occupancy in Japan in the context of TV white space systems. In: IEEE cognitive radio oriented wireless networks and communications (CROWNCOM), pp 341–345

6. FCC (2008) Second report and order and memorandum opinion and order (FCC 08-260). Federal Communications Commission, vol 4, no 04-186
7. Feng Z, Li W, Li Q, Le V, Gulliver TA (2011) Dynamic spectrum management for WCDMA/DVB heterogeneous systems. IEEE Trans Wirel Commun 10(5):1582–1593
8. Feng Z, Li Q, Li W, Gulliver TA, Zhang P (2015) Priority-based dynamic spectrum management in a smart grid network environment. IEEE J Sel Areas Commun 33(5):933–945
9. Feng Z, Zhang Q, Wei Z (2015) A cognitive TD-LTE system operating in TV white space: test-bed design. IEEE COMSOC TCCN Commun 1(1):34–37
10. Freyens BP, Loney M (2011) Opportunities for white space usage in Australia. In: International conference on wireless communication, vehicular technology, information theory and aerospace & electronics systems technology (Wireless VITAE), pp 1–5
11. Frequency Assignment Plan. http://www.tele.soumu.go.jp/e/adm/freq/search/share/plan.htm
12. GB 3174-1995 (1996) Characteristics of PAL-D television broadcasting system. China Telecommunications
13. Ghosh C, Roy S, Cavalcanti D (2011) Coexistence challenges for heterogeneous cognitive wireless networks in TV white spaces. IEEE Wirel Commun 18(4):22–31
14. Ghosh S, Naik G, Kumar A, Karandikar A (2015) OpenPAWS: an open source PAWS and UHF TV white space database implementation for India. In: IEEE national conference on communications(NCC), pp 1–6
15. Harada H, Murakami H, Ishizu K, Filin S et al (2007) A software defined cognitive radio system: cognitive wireless cloud. In: IEEE global telecommunications conference (GLOBECOM), pp 294–299
16. IEEE Std. 802.22 (2011) Information Technology-Telecommunications and Information Exchange between Systems-Wireless Regional Area Networks (WRAN) Specific Requirements-Part 22: Cognitive Wireless RAN Medium Access Control (MAC) and Physical Layer (PHY) Specifications: Policies and Procedures for Operation in the TV Bands http://www.ieee802.org/22/
17. Li J, Lin J, Zhong X (2014) Case study of Microsoft TVWS development. http://www.mic.iii.org.tw/aisp/reports/reportdetail_register.asp?docid=3020&rtype=freereport
18. Li Q, Feng Z, Li W, Gulliver TA, Zhang P (2014) Joint spatial and temporal spectrum sharing for demand response management in cognitive radio enabled smart grid. IEEE Trans Smart Grid 5(4):1993–2001
19. LTE and LTE advanced frequency bands and spectrum allocations. http://www.3glteinfo.com/lte-and-lte-advanced-frequency-bands-and-spectrum-aloactions-20120224/
20. Islam MH, Koh CL, Oh SW, Qing X, Lai YY et al (2008) Spectrum survey in Singapore: occupancy measurements and analyses. In: IEEE cognitive radio oriented wireless networks and communications (CrownCom), pp 1–7
21. Jayavalan S, Mohamad H, Aripin NM, Ismail A et al (2014) Measurements and analysis of spectrum occupancy in the cellular and TV bands. Lect Notes Softw Eng 2(2):133
22. Jay Guo Y (2010) Keynote speech 4: cognitive radio and Australia's national broadband network. In: 10th international symposium on communications and information technologies, pp 1–2
23. Kang K-M, Park JC, Cho S-I, Jeong BJ, Kim Y-J et al (2012) Deployment and coverage of cognitive radio networks in TV white space. IEEE Commun. Mag. 50(12):88–94
24. Kang K-M, Jeong BJ (2014) TV band device for TV white space field trial. In: IEEE international conference on consumer electronics (ICCE), pp 450–451
25. Kim C-J, Kim S-W, Kim J, Pyo C (2010) Dynamic spectrum access/cognitive radio activities in Korea. In: IEEE new frontiers in dynamic spectrum access networks (DySPAN), pp 1–5
26. Kumar A, Kumar R, Rathod P, Karandikar A (2015) How much TV UHF band spectrum is sufficient for rural broadband coverage? In: IEEE international symposium on modeling and optimization in Mobile, Ad Hoc, and Wireless Networks (WiOpt), pp 419–426
27. Kolodzy P, Avoidance I (2002) Spectrum policy task force. Federal Communications Commission, no 02-135

28. Leng TG (2010) Spectrum-sharing research and policy formulation in Asia-Pacific. Infocomm Dev Authority Singapore. https://www.its.bldrdoc.gov/media/33655/TanISART-Spectrum%20Sharing%20in%20Asia%20Pacific%20210710.pdf
29. Liang Y-C Cognitive radio: opportunities and challenges. http://slideplayer.com/slide/718743/
30. Marcus MJ (2015) Spectrum policy in Japan [Spectrum policy and regulatory issues]. IEEE Wirel Commun 22(3):6–7
31. McHenry MA, Tenhula PA, McCloskey D, Roberson DA, Hood CS (2006) Chicago spectrum occupancy measurements & analysis and a long-term studies proposal. In: ACM technology and policy for accessing spectrum (TAPAS)
32. Mitola J, Maguire GQ (1999) Cognitive radio: making software radios more personal. IEEE Pers Commun Mag 6(4):13–18
33. Naik G, Singhal S, Kumar A, Karandikar A (2014) Quantitative assessment of TV white space in India. In: IEEE national conference on communications (NCC), pp 1–6
34. Oyama T, Shimomura T, Seki H (2012) TV white space availability in Japan estimated using D/U-based and I/N-based protection rules. In: IEEE global communications conference (GLOBECOM), pp 1302–1307
35. Patil K, Skouby KE, Prasad R (2013) Cognitive access to TVWS in India: TV spectrum occupancy and wireless broadband for rural areas. In: IEEE wireless personal multimedia communications (WPMC), pp 1–5
36. Policies, collaboration crucial to support Singapore innovation. https://www.tech.gov.sg/en/TechNews/DigitalGov/2014/06/Policies-collaboration-crucial-to-support-Singapor
37. Schwartzman D (1993) The Japanese television cartel: a study based on Matsushita v. Zenith. University of Michigan Press, Ann Arbor
38. Singapore to introduce new regulations for use of TV white space spectrum. http://www.enterpriseinnovation.net/article/singapore-introduce-new-regulations-use-spectrum-tv-white-space-1904105599
39. Singapore will open TV white spaces. http://intl.ce.cn/specials/zxgjzh/201406/18/t20140618_2995873.shtml
40. Singapore releases TV white space regulatory framework. http://www.zdnet.com/article/singapore-releases-tv-white-space-regulatory-framework/
41. Spectrum management policy in Japan. TEL41/LSG/RR/007 session 2. May 2010
42. Speech by Dr Yaacob Ibrahim, minister for communications and information at the launch of Infocomm Media 2025. https://www.tech.gov.sg/en/Media-Room/Speeches/2015/08/Speech-by-Dr-Yaacob-Ibrahim-Minister-for-Communications-and-Information
43. Toward a new era of digital terrestrial television broadcasting. https://www.nhk.or.jp/strl/publica/bt/en/tn0008-2.html
44. TR 36.942 (2011) LTE: evolved universal terrestrial radio access (E-UTRA): radio frequency (RF) system scenarios. 3GPP Technical Report v.10.2.0
45. TV white spaces: smart city development trends and opportunities. http://sdf.hkeic.org.hk/upload/files/1/file/57f35861694c2.pdf
46. Universal software defined radio platform SP2010. http://www.starpointcomm.com/products.php
47. Uozumi S (1995) The short life of Japanese FCC: social and legal origins of the radio regulatory commission. Master's thesis, University of Hawaii
48. Wang J, Song MS, Santhiveeran S, Lim K, Ko G, Kim K et al (2010) First cognitive radio networking standard for personal/portable devices in TV white spaces. In: IEEE new frontiers in dynamic spectrum access networks (DySPAN), pp 1–12
49. Wang B, Liu KR (2011) Advances in cognitive radio networks: a survey. IEEE J Sel Top Sign Proces 5(1):5–23
50. Wei Z, Feng Z, Zhang Q, Li W (2015) Three regions for space-time spectrum sensing and access in cognitive radio networks. IEEE Trans Veh Technol 64(6):2448–2462
51. Xue J, Feng Z, Chen K (2013) Beijing spectrum survey for cognitive radio applications. In: IEEE vehicular technology conference (VTC), pp 1–5

52. Yin S, Chen D, Zhang Q, Liu M, Li S (2012) Mining spectrum usage data: a large-scale spectrum measurement study. IEEE Trans Mob Comput 11(6):1033–1046
53. Zhang H, MIIT released spectrum sharing signal. News of C114 China Communication Network. Available at URL: http://www.srrc.org.cn/wap/content.aspx?id=15683
54. Zhang Q, Kokkeler AB, Smit GJ (2006) A reconfigurable radio architecture for cognitive radio in emergency networks. In: IEEE european conference on wireless technology (EuWiT), pp 35–38
55. Zhang P, Liu Y, Feng Z, Zhang Q, Li Q, Xu D (2012) Intelligent and efficient development of wireless networks: a review of cognitive radio networks. Chin Sci Bull 57(28):3662–3676
56. Zhang P, Li J. Feng Z, Zhang Q (2014) Research on basic theory and key technology of cognitive radio network. Telecommun Sci 2:1–13

IEEE 802.22/802.22.3 Cognitive Radio Standards: Theory to Implementation

54

Apurva Mody, Anindya Saha, Ivan Reede, Gianfranco Miele, and Gianni Cerro

Contents

A. Mody (✉)
WhiteSpace Alliance®, Chelmsford, MA, USA
e-mail: apurva.mody@WhiteSpaceAlliance.org

A. Saha
Saankhya Labs Pvt Ltd, Bangalore, India
e-mail: anindya@saankhyalabs.com; asaha20@gmail.com

I. Reede
AmeriSys, Oviedo, FL, USA

G. Miele · G. Cerro
Department of Electrical and Information Engineering, University of Cassino and Southern Lazio, Cassino, Italy
e-mail: g.miele@unicas.it; g.cerro@unicas.it

W. Zhang (ed.), *Handbook of Cognitive Radio*,
https://doi.org/10.1007/978-981-10-1394-2_54

Abstract

In an earlier book chapter published in the Book titled Opportunistic Spectrum Sharing and White Space Access: The Practical Reality, First Edition (Holland et al., 1st edn. Wiley, 2015), we provided an in-depth overview of the IEEE 802.22 standard for cognitive wireless regional area networks. The discussion featured the motivation and the need for that standard, white space regulations around the world, in-depth analysis of the IEEE 802.22-2011 standard along with a brief overview of the new features present in the amendment to the IEEE 802.22 standard.

IEEE 802.22 standard for wireless regional area networks (WRANs), also known as Wi-FAR® (IEEE Std 802.22-2011) proposes to use the unused television band channels (the so called white spaces) in the VHF and the UHF bands to provide fixed and nomadic, high-throughput, long-range communications. Applications of this standard include remote and rural broadband Internet access, Frugal 5G for e-Education, e-Health, e-Banking, e-Payments, ship to shore communications, homeland security, border protection and surveillance, environment monitoring, smart grid applications such as supervisory control and data acquisition (SCADA), as well as low latency applications such as protective relaying at a future date. The IEEE Std. 802.22-2011 has been approved by ISO, and its interoperability testing is being carried out by the WhiteSpace Alliance under the commercial brand name of Wi-FAR®.

In this book chapter, we focus on an early implementation of the IEEE 802.22 standard. We also focus on the emerging IEEE 802.22.3 Standard on Spectrum Characterization and Occupancy Sensing and the implementation challenges based on software defined radio platforms. It would be nice if the readers have some basic understanding of the IEEE 802.22 standard, but as such, this book

chapter is self-contained for the new readers. The readers wanting to go deeper into the IEEE 802.22 spec may get the IEEE 802.22-2011standard at no cost using the following URL: http://standards.ieee.org/about/get/802/802.22.html

Introduction

While the wireless technologies have moved to 3G/4G and now even 5G, the connectivity to rural parts of the world, as well as developing countries has severely lagged behind. There are many technologies that can bring broadband internet connectivity. While developed economies can afford the price of bringing cable or optical fibre to the curb, Satellite Communications (SATCOM) or advanced cellular services, these are not viable options in rural areas and developing economies due to their hight cost. In case of 3G/4G cellular services, the higher cost comes from spectrum that needs to be licensed through auctions process, and deployment of many cellular towers or satellites. This is a costly process, where the cost that is incurred, is passed down to the consumers. Hence, the traditional wireless carriers have focused on urban areas with high population density which typically results in faster Return on Investment (RoI). Another problem for rural areas and developing countries are the distances. Distances between homes could span anywhere from few meters to a few kilometers (km). Traditional technologies have been unable to provide large area wireless coverage under Non-Line-of-Sight (NLoS) conditions present in rural area to build successful and viable business models. This has resulted in a digital divide and this situation tends to be worse in developing and under-developed countries.

Figure below shows a recent statistics on the percentage of households that have broadband Internet connectivity in developed, developing, and least developed countries. The statistics are truly alarming (Fig. 1).

The table below further shows the distribution of the affordable monthly communications expenditure as we traverse through the seven billion people around the world. In his analysis, Richard Thanki [13] shows why tackling the global connectivity problem is a challenging one (Table 1).

One of the core issues facing the digital divide that exists today is a lack of cost-effective middle-mile solution. Middle-mile solution refers to the gap between some optical fiber, wired or wireless backhaul connection at the edge of the regional area, and the last-mile solution which may use technologies such as Wi-Fi® or LTE. The middle-mile range requirement map spans between a few kilometers (km) to tens of km. In many areas of the world, such middle-mile gaps have uneven terrains, requiring NLoS solutions, and in many cases there is an absence of electric power which means that the wireless connectivity needs to be powered using solar cells. Hence, every joule of energy must be consumed in a "Frugal" manner, technology should be able to overcome foliage and terrain issues, and spectrum should be such, so that a little transmit power can go very far.

The use of Television (TV) Band WhiteSpaces can alleviate the digital divide that exists today. This has been enabled by analog to digital TV transition where

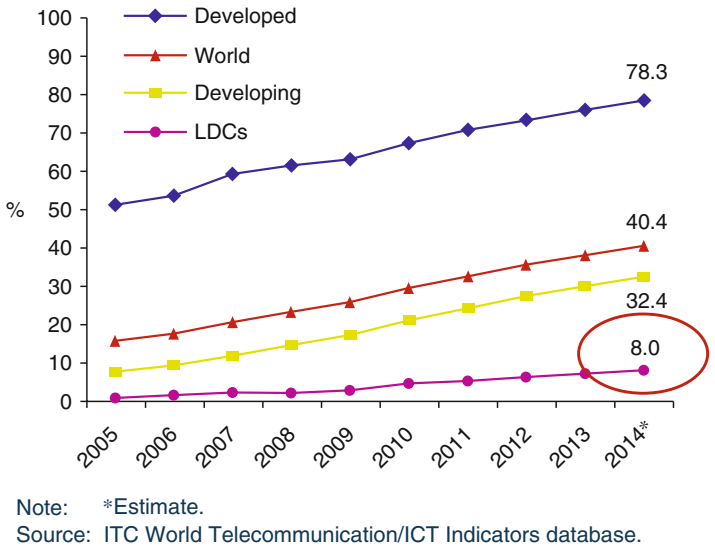

Fig. 1 International telecommunications union broadband Internet penetration statistics

Table 1 Reality of Internet Affordability: Providing Internet Connectivity to the Remaining Three Billion People is Going to Require Low-Cost Long Range Communications Solutions

Billions of people on the Earth	Average annual income per annum	Affordable monthly communications spend
1st Billion	$29,206	$205
2nd Billion	$12,722	$53
3rd Billion	$5,540	$23
4th Billion	$2,987	$12
5th Billion	$1,771	$7
6th Billion	$1,065	$4.4
7th Billion	$540	$2.25

one digital TV station can potentially transmit 5 standard definition signals on the same channel. As such, in many countries around the world, not all the TV channels are being used by the broadcasters. In urban areas, more TV transmitters operate as compared to the rural areas. So you can envision the spectrum occupancy in every country by the region to be like swiss cheese, where large swathes of channel by the region are un-occupied or un-used. These channels are termed as White Spaces TV Channels in very high frequency - ultra high frequency (VHF/UHF) bands and have highly favorable propagation characteristics for long-distance reach.

In addition, many administrations are moving towards establishing regulations that allow opportunistic license-exempt usage of the spectrum on a non-interfering basis with the TV receivers using cognitive radio techniques.

Fig. 2 WRAN coverage

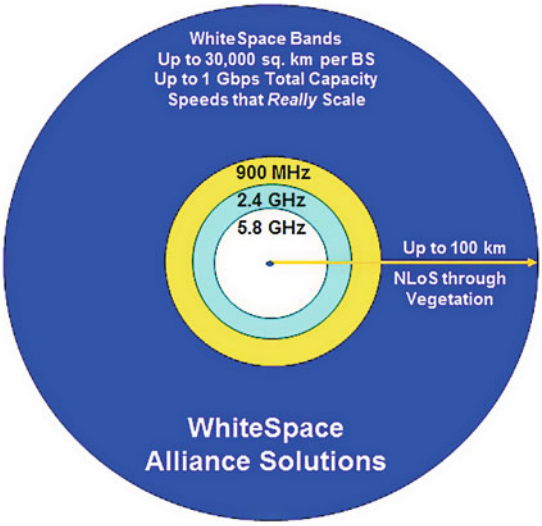

Favorable propagation characteristic of TV channels combined with opportunistic license-exempt use of spectrum creates a synergy that is perfect to provide middle-mile broadband connectivity to rural areas and developing countries in a cost-effective manner. When this is combined with favorable technologies, it can result in communications ranges of nearly 30 km as shown in Fig. 2. Hence it has a great promise to bridge the digital divide that exists today.

After the 2004 Federal Communications Commission (FCC)' s Notice of Inquiry (NoI) to open up TV WhiteSpaces for communications, the Institute of Electrical and Electronics Engineers (IEEE) Local Area Networks Metropolitan Area Networks (LAN/MAN) Standards Committee initiated the IEEE 802.22 Project on Cognitive Radio (CR) enabled Wireless Regional Area Networks (WRANs). The work resulted in a standard that was approved in 2011 for wireless access in the TV white space spectrum using cognitive radio techniques. The resulting type of wireless networks are referred to as wireless regional area networks (WRAN) which was later given a trade name of Wi-FAR® by the industry alliance called the WhiteSpace Alliance® [16]. In this book chapter, the terms WRAN, Wi-FAR™ or IEEE Std. 802.22™-2011 or IEEE 802.22 will be inter-changeably used.

Other similar activities of the IEEE 802 Standards Committee include the IEEE Std. 802.11af™-2013 amendment that specifies wireless local area networks (WLAN) operation, the IEEE Std. 802.15.4m™-2013 amendment that specifies the wireless personal area networks (WPAN), and the IEEE Std. 802.19.1™-2014 that specifies co-existence between various systems in the TV Band white spaces respectively. Similarly the internet engineering task force (IETF) has completed its protocol to access white spaces (PAWS) specification for the geolocation database access.

Since 2011, the IEEE 802.22-2011 standard has had two amendments. The 802.22a-2014 Amendment on Management Information Base (MIB)s and the

IEEE 802.22b-2015 Amendment on Enhancements for Broadband Servies and Monitoring Applications. Currently IEEE 802.22 Group is working on revising this standard, which will fold in these amendments, provide support for new frequency bands where spectrum sharing is allowed, and also new technologies such as Full Duplex Communications, also known as Simultaneous Transmit and Receive (STAR).

The IEEE 802.22 Spec uses orthogonal frequency division multiple access (OFDMA) physical layer. This OFDMA implementation supports long range operation by accommodating long signal turn-around times by providing sufficient cyclic prefixes to absorb long excess delay multipath. The medium access control (MAC) layer includes the traditional MAC layer features as well as support for various cognitive radio capabilities. These include management messages for the Base Stations (BS) to control spectrum sensing carried out at the Customer Premises Equipment (CPEs) and to query for various results, and for the CPEs to signal Urgent Coexistence Situation (UCS) to the BS. The MAC layer implementation is described in section "MAC Layer Architecture".

IEEE Std 802.22 allows geolocation of the devices by providing an interface to the Global Positioning System (GPS) receiver interface. Geolocation may also be enabled using on-line database of licensed services that compiles the location and radio frequency characteristics of these licensed services, whether they are permanent or temporary services, and when they are in operation. This geo-location and database access capability is fundamental in determining which TV channels are vacant of licensed services (e.g., TV white space) and hence are available for use by a WRAN. A description of these two capabilities is provided in section "Geolocation and Database".

The WRAN Base Station (BS) determines which channel to be utilized. The entity that makes the final decision on which channel the WRAN should use is called the *Spectrum Manager*. This entity can utilize the geo-location information of the base station and of each associated Customer Premises Equipment (CPE), the database of licensed services and optionally the Spectrum Sensing reports from the base station and the CPEs to decide which channel is to be used by the WRAN.

The TV WhiteSpaces regulatory rules are more elaborate than the rules for most other unlicensed devices, like the rules for operation in the 2.4 GHz industrial scientific and medical (ISM) band. A summary and analysis of the FCC rules for operation in the TV white space spectrum is given in section "Summary of FCC Rules on Operation in the TV White Space".

IEEE Std 802.22 also includes spectrum sensing which enables the devices to make observations of the radio frequency spectrum and deduces from those observations whether a channel is occupied by a licensed transmitter or if the channel is vacant and hence can be used by a WRAN. Spectrum sensing is performed at both the base station and the CPEs. The IEEE 802.22 has provided primitives that allow the spectrum sensing to be performed at the CPEs and transmitted to the BS, or the sensing to be performed at the BS itself.

In 2014, the IEEE 802.22 working group formed the IEEE 802.22.3 task group on Spectrum Characterization and Occupancy Sensing (SCOS) to create standards

and protocols to enable distributed spectrum monitoring. More information on this standard may be found in section "Distributed Spectrum Monitoring: IEEE 802.22.3 Standard on Spectrum Characterization and Occupancy Sensing".

WRAN System Overview

The Wi-FAR network consists of a base station and a set of fixed and portable client devices, called CPE. CPEs are typically installed with directional antennas. CPE may be connected to a Wi-Fi router for last mile connectivity. IEEE 802.22 supports 6, 7 and 8 MHz bandwidth operation which corresponds to the channel width in various countries. These channels are in both the very high frequency (VHF) and ultra high frequency (UHF) bands. In the United States, for example, the VHF band consists of channels 2–13 while the UHF band consists of channels 14–51.

The Wi-FAR technology specifically focuses on regional and rural broadband access. Also it is the first standard that embeds many cognitive radio features to avoid interference to the primary users. FCC and other regulations require that wireless networks support several cognitive radio features such as geo-location and access to a regulatory approved database and optionally spectrum sensing. In order to operate properly, these WRANs may also include additional features such as adaptation to regulatory dependent policies, channel set management, spectrum etiquette and self coexistence mechanisms.

Summary of FCC Rules on Operation in the TV White Space

Many administrations, such as Canada, United Kingdom, Colombia, India, European Union, Japan, Singapore, Botswana, South Africa, Malawi etc. have issued or are expected to issue rules for operation in TVWS. United States has been the first administration to initiate development of the regulatory rules for TVWS. Organizations such as the WhiteSpace Alliance urged FCC to use the spectrum in the most efficient way possible. Based on the recommendations of WhiteSpace Alliance, FCC has started doctrines such as use it or share it. The FCC has issued more recent additions to the rules on TVWS that allow for more efficient use of spectrum. For example, previous rules did not allow that adjacent channels to TV stations within the protected contour to be used by the whitespace devices (WSDs). This meant that three channels had to be available for one in the middle to be used. This was relaxed by the FCC, where they allowed WSD operation even when two consecutive channels were available, by letting the WSDs be operating in the middle of the two available channels. This section provides an overview of the FCC R&O [12], the second MO&O [11], and the third MO&O [14] on operation in the TV white space. The FCC refers to the devices that use the TV white space as TV band devices (TVBDs).

Classes of TV Band Devices

TV band devices are divided into two categories: fixed devices and personal/portable devices. Personal/portable devices can operate in one of two modes: Mode I and Mode II. Mode I devices can only operate in TV channels identified as an *available channel* by either a fixed or a personal/portable Mode II device to which they are usually associated. Mode I operation does not require geo-location capability nor access to the *TV band database* since it is assumed that such Mode I devices will be in the vicinity of the Mode II or fixed devices. Geo-location and TV bands databases are described below. Mode II personal/portable operation does require both geo-location capability and access to the TV bands database.

IEEE 802.22 devices can be fixed devices or Mode II devices: usually organized as a fixed BS and a set of fixed and/or Mode II CPEs. A fixed WSD transmits from a fixed location while a personal/portable device transmits either from an unknown location or while in motion (e,g., nomadic).

Permissible TV Channels

The FCC specifies a set of permissible channels, not occupied by licensed services, in which fixed and personal/portable devices may be permitted to transmit. There are a few channels that are excluded from use by TV band devices (i.e., channels 3, 4 and 37). Channels 36 and 38 are also excluded since they would require excessive adjacent channel emission rejection, being adjacent to Channel 37 that is reserved for use for medical telemetry. These two channels are reserved for wireless microphone operation. If channels 36 and/or 37 are used by local TV stations, the reserve channels would then become 35 and 38. Some channels may only be used by fixed devices (i.e., channels 2–20), whereas other channels may be used by both fixed and personal/portable devices (i.e., 21–51).

In thirteen metropolitan areas, some channels out of Channels 14–20 are used for public land mobile radio systems (LMRS). In those metropolitan areas, fixed TVBD may not operate co-channel or adjacent channel to the channels used by any PLMRS. Which channels are used for PLMRS in each of those metropolitan areas is specified by the FCC.

A summary of permissible channels for fixed and personal/portable, along with the frequencies of operation, are provided in Table 2.

Transmission Power Limits

Fixed devices have a maximum transmit power of 30 dBm (1 watt) with up to 6 dBi antenna gain, resulting in a maximum effective isotropic radiated power (EIRP) of 36 dBm. It is allowed to transmit lower power and have higher antenna gain as long as the maximum EIRP does not exceed 36 dBm. IEEE 802.22 standard uses this

Table 2 Permissibility of TV Channels usage by TV band devices

TV channel	Frequency (MHz)	Fixed permitted	Personal/Portable permitted
2	54–60	Yes	No
3–4	60–72	No	No
5–6	76–88	Yes	No
7–13	174–216	Yes	No
14–20	470–512	Yes	No
21–35	512–602	Yes	Yes
36	602–608	No	Yes
37	608–614	No	No
38	614–620	No	Yes
39–51	620–698	Yes	Yes

option to increase the antenna gain for the CPEs for the fixed devices. Antenna gain increase is normally less easily applicable in the case of the BS since its coverage needs to be broader to reach all CPEs.

Personal/portable devices have a maximum transmit power of 20 dBm (100 mW) with a 0 dBi antenna gain resulting in a maximum EIRP of 20 dBm. It is allowed to lower the transmit power and increase the antenna gain as long as the maximum EIRP does not exceed 20 dBm. Personal/portable devices operating on an adjacent channel to a TV broadcast within the protected contour are allowed a maximum EIRP of 16 dBm (40 mW).

TV band devices must incorporate transmit power control (TPC) to limit their transmit power to the minimum necessary for successful communication.

Antenna Requirements

For fixed TV band devices, the transmit antenna is allowed to be no more than 30 meters above ground. The receive antenna used for sensing has to be mounted outdoors at least 10 meters above ground and should be capable of receiving equally in all directions and on all polarization orientations. The IEEE 802.22 CPE transmit receive (TX/RX) antenna is used for communication between the BS and a fixed CPE is directional and points towards the BS. When RF sensing is performed, there is a need for a separate omnidirectional sensing antenna mounted at least 10 m above ground and not lower than the CPE transmit antenna. Antennas on personal/portable TV band devices have to be permanently attached.

Out of Band Emissions

There are three out-of-band emission (OOBE) requirements specified by the FCC for TV band devices. The first requirement specifies the power density in an adjacent

Table 3 PSD and Adjacent Channel Emission Limits

Type of TV bands device	Power limit (6 MHz)	PSD limit (100 kHz)	Adjacent channel limit (100 kHz)
Fixed	30 dBm (1 W)	12.6 dBm	−42.8 dBm
Personal/portable (adj. channel)	16 dBm (40 mW)	−1.4 dBm	−56.8 dBm
Sensing only	17 dBm (50 mW)	−0.4 dBm	−55.8 dBm
Other personal/portable	20 dBm (100 mW)	2.6 dBm	−52.8 dBm

TV channel relative to the total power in the band of operation. The second is the requirement to meet FCC Section 15.209(a) requirement beyond the two adjacent channels. And the third requirement is the emissions in Channel 37, and its two adjacent channels (Channels 36 and 38).

In each of the two TV channels adjacent to the channel being used by the TV band device, the maximum in-channel power spectrum density and adjacent channel emission limits in a measurement bandwidth of 100 kHz shall be as indicated in Table 3.

Outside the channel of operation and the two TV channels adjacent to the channel of operation, the out-of-band emissions shall meet FCC Section 15.209(a) requirement. That is, in the band 216–960 MHz, the electromagnetic field strength measured at 3 meters from the radiating source must not exceed 200 microvolts/meter, when measured in a 120 kHz bandwidth. In order to appreciate this requirement we must understand the relationship between transmit power and electromagnetic field strength measured at a specified distance from the transmitter.

This corresponds to a differential of 55.4 dB between the maximum PSD level within the channel for the maximum rated transmission power in each category to the maximum allowable PSD in the first adjacent channels for all four cases indicated in Table 3. This is much more demanding than in the case of other similar wireless systems such as Wi-Fi (20–28 dB) and WiMax (25–32 dB).

For all four cases indicated in Table 3, this corresponds to a differential of 55.4 dB between the maximum PSD level within the channel for the maximum rated transmission power in each category to the maximum allowable PSD in the first adjacent channels. This is much more demanding than in the case of other similar wireless systems such as Wi-Fi (20–28 dB) and WiMax (25–32 dB).

From [9] we have that for free space propagation,

$$\frac{PG}{4\pi d^2} = \frac{E^2}{R_{FS}} \tag{1}$$

where P is the transmit power, G is the transmit antenna gain, d is the distance in meters, E is the electric field strength, and R_{RS} is impedance of free space and is given by $R_{FS} = 120\pi$. Solving for the field strength, we get

$$E^2 = \frac{30PG}{d^2} \tag{2}$$

Taking logarithms and multiplying by 10, we have

$$20\log(|E|) = 10\log(P) + 10\log(G) + 10\log(30) - 20\log(d) \tag{3}$$

We would like to represent the field strength in dBu (microvolts/meter) and the transmit power in dBm. To make these conversions, we let

$$FS_{dBu} = 20\log(|E|) + 120 \tag{4}$$

$$P_{dBm} = 10\log(P) + 30 \tag{5}$$

This gives the following formula for the electromagnetic field strength in dBu for free space propagation,

$$FS_{dBu} = P_{dBm} + 10\log(G) + 10\log(30) + 90 - 20\log(d) \tag{6}$$

After simplification we get

$$FS_{dBu} = P_{dBm} + 10\log(G) + 104.77 - 20\log(d) \tag{7}$$

Now this formula gives us the field strength for free space propagation. We would like to convert back from field strength to transmit power. To be more specific, since in the IEEE 802.22 standard it is expected that the in-band transmissions will be more accurately specified by the EIRP, we can combine the transmit power and antenna gain into the EIRP though the following formula, $EIRP_{dBm} = P_{dBm} + 10\log(G)$. Utilizing this in the formula for the field strength and solving for EIRP in terms of the resulting field strength, we get

$$EIRP_{dBm} = FS_{dBu} - 104.77 + 20\log(d) \tag{8}$$

We can then determine the permitted out-of-band emission EIRP beyond the second adjacent channel, when measured in 120 kHz bandwidth. As we recall, the field strength must be below 200 μv/m. When converted to dBu, this is 23.01 dBu. Since this is measured at 3 m, we have $d = 3$. Therefore, the maximum EIRP measured in 120 kHz beyond the second adjacent channel is

$$EIRP_{dBm} = 46.02 - 104.77 + 9.54 = -49.21\,\text{dBm} \tag{9}$$

In order to relate this to our in-band emission, we must calculate the corresponding EIRP in 100 kHz bandwidth as used to define the rejection in the first adjacent channel,

$$EIRP_{dBm} = -49.21 + 10\log\left(\frac{100}{120}\right) = -50.02\,\text{dBm} \tag{10}$$

The maximum allowed EIRP in 100 kHz in the second channel and beyond, relative to the total 36 dBm transmitted in-channel EIRP from fixed devices, is therefore

$$\Delta EIRP_{dBm} = 36 - (-50.02) = 86.02\,\text{dB} \tag{11}$$

This corresponds to a differential in power spectrum density between in band and out of band in the second adjacent channel and beyond, for the IEEE 802.22 standard with an occupied bandwidth of 5.625 MHz of

$$\text{Relative OOBE} = 36 - 10\log\left(\frac{5.625}{0.1}\right) - (-50.02) = 68.52\,\text{dB} \tag{12}$$

The same calculations can be done for the personal/portable devices with their maximum EIRP of 20 dBm, and this will result in

$$\Delta EIRP_{dBm} = 20 - 50.02 = 70.02\,\text{dB} \tag{13}$$

$$\text{Relative OOBE} = 20 - 10\log\left(\frac{5.625}{0.1}\right) - (-50.02) = 52.52\,\text{dB} \tag{14}$$

If the EIRP of the fixed and/or personal/portable devices is not at the stated maximum but less by some dBs, the OOBE requirement becomes less stringent by this amount of dBs.

Interference Avoidance Mechanisms

Protection of licensed systems shall be provided by a combination of geolocation with database access and spectrum sensing.

Geolocation and Database Access

Fixed TV band devices shall have a known location to within ±50 m, through either an integrated geolocation capability (e.g., GPS) or through a professional installation, as defined in the IEEE standard and later by the FCC. A Mode II portable device shall incorporate a geolocation capability with an accuracy of ±50 m. A Mode II device is required to reestablish its location after power cycling.

Fixed devices must access a TV band database prior to initial transmission and may only operate on TV channels indicated as available at that location. Fixed devices must subsequently access the database at least once a day.

Mode II portable devices must access the TV band database prior to initial transmission. Mode II devices must also access the database after every power cycle. It must also access the database at least every 60 s.

Mode I portable devices shall obtain a list of available channels from a master device. A master device can transmit without receiving an enabling signal. Fixed and Mode II portable devices can both be master devices for Mode I devices.

Spectrum Sensing

If protection of TV band incumbents is to be achieved through RF sensing, all TV band devices, both fixed and portable, must be capable of detecting ATSC (Advanced Television Systems Committee) and NTSC (National Television System Committee) signals down to −114 dBm and wireless microphone signals down to −107 dBm. These detection levels are referenced to a 0 dBi sensing antenna with no coupling or cable loss. If the minimum antenna gain is less than 0 dBi and/or there is coupling or cable loss present, then the detection level shall be reduced by the difference between a 0 dBi antenna gain and the minimum antenna gain and the eventual amount of coupling or cable loss.

A TV band device must determine that the TV channel is unoccupied by either a TV signal or a wireless microphone signal above the detection threshold for 30 s before it can utilize the TV channel. If a TV signal is detected above the detection threshold on a channel indicated as available by the TV database, the TV band device will notify the base station so that it may optionally remove the channel from the local list of available channels. The base station may also indicate the presence of such signal to the database service.

A TV band device must check the availability of the channel in use at least every 60 s.

If a wireless microphone is detected on the operating channel, the TV band device must cease transmissions within 2 s.

The IEEE 802.22 working group carried out a thorough evaluation of the spectrum sensing techniques by providing over-the-air-collected ATSC and NTSC signal samples to various participants. As a result of this evaluation, many sensing techniques were accepted to be incorporated into an informative annex of the standard. These techniques range from simple energy detector, to time and/or frequency domain matched filters, to covariance, higher-order statistics (HOS), or cyclostationary processing approaches. Typically, more complex techniques such as the ones based on cyclostationary processing provide better sensitivity at an increased cost in complexity.

Since the FCC Second and Third MO&O encourages the use of spectrum sensing, but does not require it, the IEEE 802.22 working group decided to provide a regulatory domain-dependent switch which can be turned off if spectrum sensing operation is not required or not desired.

Additional Requirements

A TV band device must display available channels and its operating channel. In IEEE 802.22 systems, this will correspond to the operating channels and the list of backup channels provided by the base station.

A fixed TV band device must transmit identifying information that conforms to a standard format recognized by an industry standards setting organization. For IEEE 802.22 systems, a set of primitives has been included in the standard that can be used by the base station to communicate with the database. A standard protocol is being defined by the Internet Engineering Task Force IETF-PAWS Working Group [6]. The IEEE 802.22 working group members have also been in touch with several database service providers to make sure that adequate interfaces are defined.

A fixed TV band device without database access can transmit on channels indicated from another fixed TV band device to register its location and receive a list of channels that are available for it to use. This slave fixed device corresponds to a CPE in IEEE 802.22 systems, whereas the master fixed device corresponds to the base station.

A Mode I portable device may only transmit on channels indicated as being available by a fixed or Mode II portable device.

Protection Contours

The FCC rules provide a table of protection contours for analog and digital TV in the lower VHF, upper VHF, and UHF bands. While Fixed devices are permitted in both VHF and UHF bands, portable devices are only permitted in the UHF band. In the UHF band, the protection contour is defined at 41 dBu reception signal level for ATSC and 64 dBu for NTSC.

The devices must be outside these contours by a specified distance depending on their antenna height as indicated in the following Table 4.

Table 4 Required minimum separation distance from TV broadcast contours as a function of the TVBD antenna height

Antenna height above average terrain of unlicensed device	Required separation (km) from digital or analog TV (full service or low power) protected contour	
	Co-Channel (km)	Adjacent channel (km)
$h < 3$ m	4.0	0.4
$3 \leq h < 10$ m	7.3	0.7
$10 \leq h < 30$ m	11.1	1.2
$30 \leq h < 50$ m	14.3	1.8
$50 \leq h < 75$ m	18.0	2.0
$75 \leq h < 100$ m	21.1	2.1
$100 \leq h < 150$ m	25.3	2.2
$150 \leq h < 200$ m	28.5	2.3
$200 \leq h \leq 250$ m	31.2	2.4

The rules also provide detailed requirements regarding operation near the cable head-ends, fixed broadcast auxiliary services, and portable land mobile radio systems (PLMRS). See [12] for all the details.

Fixed TV band devices are not permitted to operate within 1 km of registered wireless microphones, and this distance is reduced to 400 m for portable TV band devices.

Implementation of the IEEE 802.22 Standard Using a Software-Defined Radio Chip

In this section, we provide some insights into the implementation of the IEEE 802.22 standard based on a Software-defined radio (SDR) architecture. The implementation as described in this section is based on one SDR architecture based on customized system on a chip (SoC) digital signal processing (DSP) from one of the vendors [10]. Later in this section, we also provide some insights on another implementation.

The predominant difference between a white space band receiver and a regular Wi-Fi receiver is the dynamic range (DR) of signals that the white space receivers may experience. For example, the receiver operator may want to receive a distant and weak white space signal from a 4 watt base station while being in an environment where one or many high-power TV transmitter is present in the same band. Such a situation imposes stringent requirements on the receiver design and can only be solved by careful and experienced analog front design.

A second difference is that Wi-Fi devices are designed to communicate over short distances. The 802.11 standard compliant devices typically communicate of distances of a few meters up to a maximum of 100 m. They operate in radio bands where the wavelength is in the order of few centimeters. This is very useful for indoor and portable devices, as small antennas can be used in these bands. However, it has a drawback when longer range communications may require the signal to go through vegetation. When such a signal encounters the leave of a tree, the signal bounces off the leaf in an arbitrary direction. It may then bounce of yet another leaf and finally reach the receiver. However, because of the jagged path it has followed, it has traveled a longer distance than a signal that would not have encountered leaves. This causes the received signal to disperse as it crossed vegetated areas, which can muddle up the signal to the point it becomes unintelligible.

The Wi-FAR spec has been designed to circumvent this problem by really stretching out the signal and coding it in such a fashion that it is more intelligible, even in the presence of such dispersion. The industry refers to this a NLoS transmission. Radio signals do not go through rock but do go through vegetation. Signals coded following the Wi-FAR coding are up to 100 times more intelligible after dispersion, in comparison to Wi-Fi signals. Moreover, due to their much longer wavelengths, they are less affected by leaves. To be an efficient reflector, the size of a leaf has to be at least 10% of the size of the wavelength. In the VHF and UHF television bands, wavelengths begin in the order of meters instead of a few centimeters, and hence, the dispersion is reduced. Hardened coding in

conjunction with reduced dispersion yields a signal that is far more tolerant of vegetation impairments. This can be observed by the fact that ADSL TV signals, which were designed with the same impairments in mind, quite easily penetrate through vegetation and provide an excellent user experience.

An additional difficulty in designing a white space device is in the fact that the signal of such a transmitter must not interfere with adjacent TV transmissions. As the white space networks have to coexist with regular TV broadcasts, the signal purity needed is very high. TV broadcasters can achieve such signal purity by placing expensive cavity filters designed to pass their specific frequency and sharply reject splatter in adjacent bands.

Contrary to a TV broadcaster which operates on a specific frequency, the TV band white space regulations call for frequency agile transmitter, able to operate on any given channel and quickly hop to another channel upon demand. This renders impossible the use of the fixed frequency filters typically used by TV broadcasters. Regular Wi-Fi devices are allowed to splatter many MHz away from their frequency of operation with as little as 30 dB suppression, allowing for a lowest possible cost design. On the other hand, white space transmitters must drop their out-of-band emission by 55 dB and do so within 200 kHz of their intended transmission channel.

The IEEE 802.22 WRAN system is a cognitive radio-based network but has similarities to modern-day cellular networks. A typical Wi-FAR system uses the time division duplex (TDD) mode of operation. TDD provides larger range compared to FDD for the same transmitter power, due to lack of self-interference. For the same reason, TDD also reduces the system complexity, especially for the RF front end. A frequency division duplex FDD) system needs duplexers which could become expensive especially if the band separation is not high and higher rejections become necessary. For the Wi-FAR operation, CPEs are likely to be stationary, and issues related to mobility like handoff do not exist. In a typical deployment, the average distance supported between the base station and the CPE is determined by a link budget analysis. The link budget analysis considers aspects of transmitter and receiver like frequency of operation, transmit power, receiver sensitivity, the respective antenna gains, heights of antenna above sea level, and Fresnel zone clearance. Depending on the desirable robustness, appropriate fading margin also needs to be considered.

The BS is the central controller within a WRAN cell responsible for managing the traffic flow to the different CPE endpoints. The base station is connected to a backhaul network of relatively higher throughput. Typically this backhaul network may terminate in an Internet service provider (ISP) gateway. The different base stations are expected to communicate among each other via the backhaul network.

A base station can service a cell using either an omnidirectional antenna or several sectored antennas depending on the relative CPE distribution around it. The CPE is a device which resides with the user or group of users who are receiving the network service. The CPE can be connected to a wired network interface like Ethernet or a wireless access point which enables a group of users to share the service.

Architecture of the Signal Chain for Downlink and Uplink Paths

The BS performs the functions of downlink (DL) transmit to various CPEs and uplink (UL) receive from various CPEs in the WRAN cell. A typical signal chain for the operations performed in the physical layer or Layer 1 (L1) including the base station transmit and CPE receive operation is shown in Fig. 3.

On the downlink transmit side, the data packets received from the medium access control (MAC) Layer 2 (L2) are randomized using the scrambler and encoded using convolutional code as per the desired code rates and undergo bit interleaving using the desired turbo interleaver parameters. The interleaved data passes through the mapper, and frequency interleaving operations, the required pilots, and frame preambles are added and converted to time domain using the IFFT operation. The time domain signal is passed through a spectral mask filter to ensure that the output signal adheres to the desired transmit spectral mask. The time domain analog signal finally obtained is up-converted in the desired frequency band of operation and transmitted.

On the DL receive side, the signal passes through the RF tuner. The receiver synchronizes to the DL frame and subsequently demodulates the OFDM symbols. The soft decision bits from the demapper undergo bit deinterleaving and subsequently decoded using tail-biting Viterbi decoder. The decoded bits are descrambled and passed on to the MAC/L2 for further processing.

The various CPEs perform the functions of UL transmit to the BS and DL receive from the BS in the WRAN cell. Once the CPE powers up and achieves DL synchronization, it registers to the BS using the process of initial ranging. Ranging is the process of estimating and adjusting the delays, transmitting power and frequency offsets of various CPEs with respect to the references fixed at the BS. Once initial ranging is successful, the CPEs are time aligned to BS. From this point on, the UL transmit and DL receive process is similar to equivalent processes described earlier.

The BS typically consists of three significant components – RF unit, baseband unit, and protocol stack unit as shown in Fig. 4.Typically one RF unit serves as sector and connects to a sector antenna. Based on the processing capability, there could be one or multiple baseband units which interface to one of the RF units serving a single sector. Each baseband unit consists of multiple cards of baseband

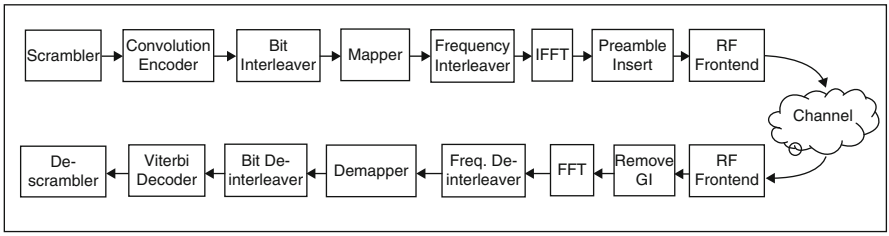

Fig. 3 Downlink signal flow from base station to CPE

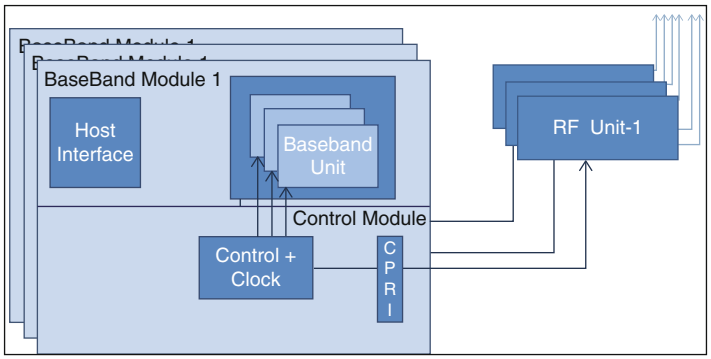

Fig. 4 Base station unit architecture

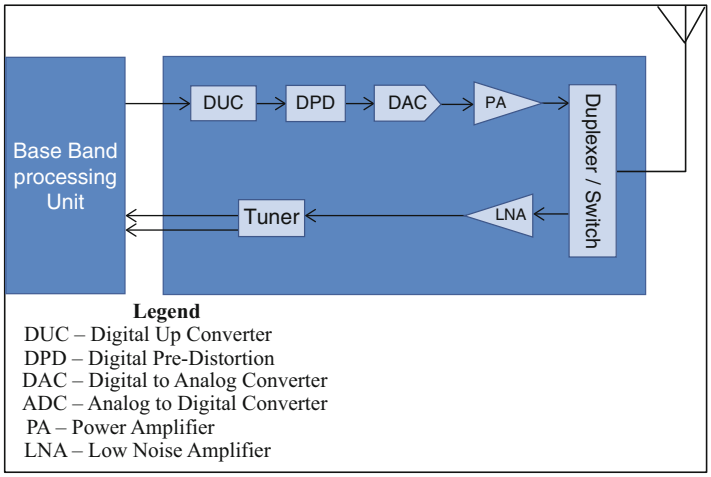

Fig. 5 Baseband and RF unit architecture

unit serving a set of users. Typically a single host processor interfaces to all the baseband units. The block diagram of the combined baseband and RF unit is shown in Figs. 4 and 5. The protocol stack unit is responsible for performing the L2 (MAC) and L3 functions.

Baseband and RF Module Architecture

The baseband module is based on software-defined radio (SDR) platform architecture which performs OFDMA processing for both uplink receive and downlink transmit processing. The baseband SoC is a SDR capable of supporting multiple radio technologies including custom waveforms. This is described in detail in the section on SDR platform. The RF unit interfaces to the sectored antenna via a TDD

RF switch. The input path from the TDD switch goes to a high gain LNA and a tuner having the ability to receive VHF-UHF bands of interest. The tuner typically generates a differential low-IF or zero-IF signal which connects to the receive SDR SoC for performing uplink receive functions. It is important to note that base station receives a signal which is a sum total of all the uplink waveforms transmitted by the CPEs. Hence the input DR of BS receiver needs to be carefully chosen and gain control loops appropriately handled.

MAC Layer Architecture

The protocol stack will have an abstraction layer that will make the PHY design compatible to that of 802.22 WRAN stack model. The abstraction layer will map all MAC messages to the PHY layer. The MAC provides mechanisms for flexible and efficient data transmission. In the downstream direction, data are scheduled over consecutive MAC slots, while in the upstream direction, the channel capacity is shared by the CPE units based on a demand-assigned multiple access (DAMA) scheduling scheme. The concept of a connection plays a key role in the MAC. The mapping of all services to connections, as performed in the convergence sub-layer, facilitates bandwidth allocation, quality of service (QoS) and traffic parameter association, and data delivery between the corresponding convergence sub-layer. The MAC employs a superframe structure in order to efficiently manage data communication and facilitate WRAN synchronization. Each MAC frame, with a 10 ms frame size, comprises a DL subframe and an UL subframe with an adaptive boundary in between as shown in Fig. 6. While the DL subframe only contains a single PHY protocol data unit (PDU), the UL subframe may have a number of PHY PDUs scheduled from different CPE units, as well as contention intervals for initialization and bandwidth request. Because the DL traffic for CPE located far from the BS can be scheduled early in the DL subframe, such a data layout allows the MAC to absorb the round-trip delay for large distances. In addition to these functions, the MAC also controls the network entry and initialization procedures which are accomplished using several processes such as synchronization, ranging, capacity negotiation, authorization, registration, and connection setup. In a typical base station, the protocol stack and MAC functions are handled using a high-performance reduced instruction set computing (RISC) processor (like dual-core ARM-9-based SoC).

Customer Premise Equipment (CPE)

The customer premise equipment housed at the user end consists of a similar subsystem as present on the base station side with much lower processing capabilities as shown in Fig. 7. The CPE unit typically consists of three significant components – RF unit, baseband unit, and protocol stack unit (similar to base station). The RF unit connects to a directional antenna with its main lobe pointing

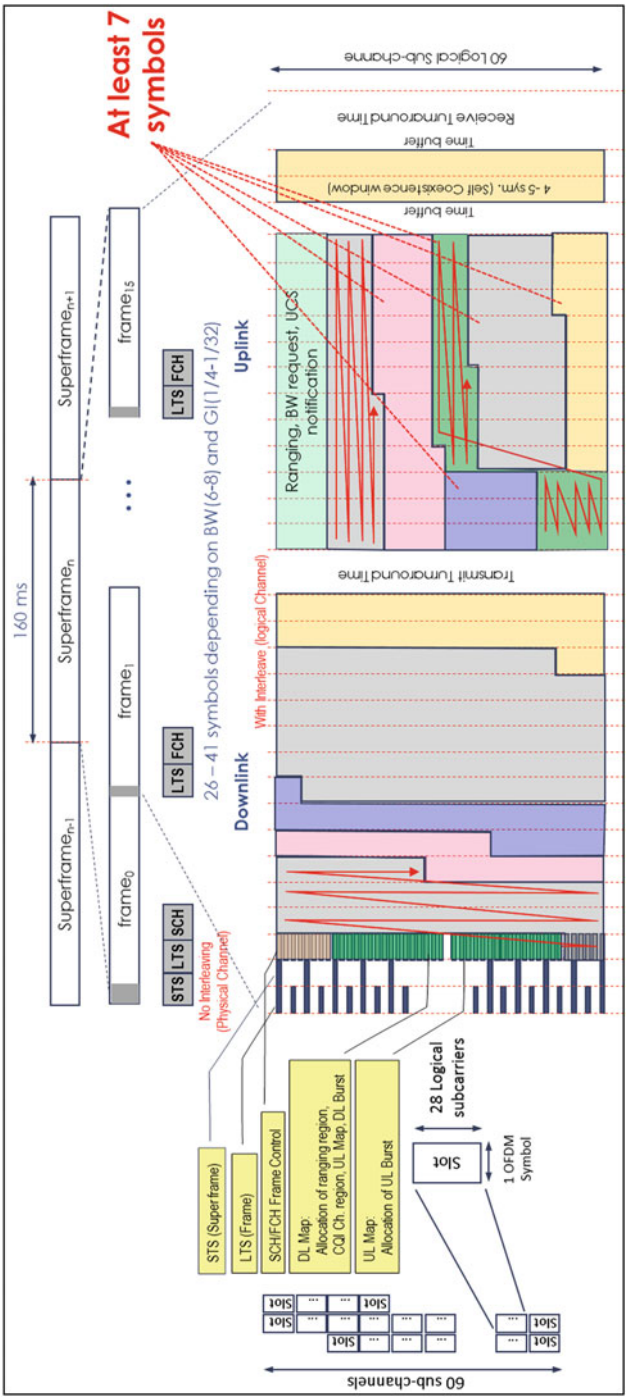

Fig. 6 IEEE 802.22 Frame Structure

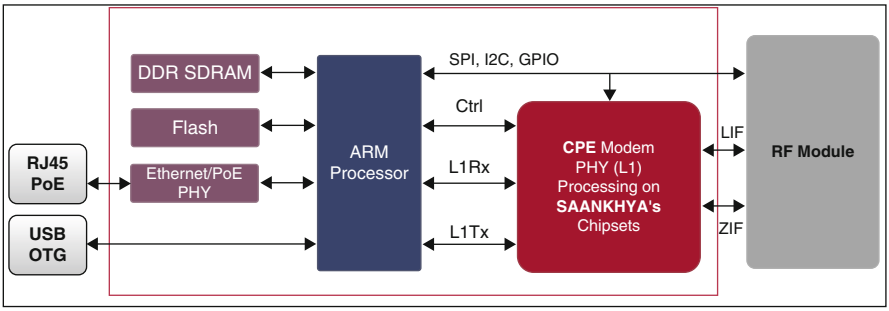

Fig. 7 Customer premise equipment unit

toward the base station. A single or dual baseband unit based on the SDR architecture performs the uplink transmit and downlink receive functions. In addition to this, the protocol stack unit typically consisting of an ARM-based SoC is responsible for performing the L2 (MAC) and L3 functions (Fig. 7).

The RF front end consists of both transmit and receive paths. The front end contains the following functionality low noise amplifier (LNA), receive/transmit (Rx/Tx) mixers, RX/TX filters, synthesizers, Rx gain control and required Rx variable gain amplifier (VGA), Tx power control, power amplifier (PA) driver, and the PA. The RF front end is expected to cover the UHF-VHF frequency range as intended. The functional block diagram of the RF unit is shown in Fig. 8.

On the transmit side, the RF front end interfaces to a differential real and imaginary (IQ) digital-to-analog converter (DAC) outputs from the baseband device. The DAC outputs are filtered using on-board DAC image rejection filters. The output of the filters passes through a stage of VGA and then is fed to an IQ up-converter mixer. The IQ-mixer and up-converter output is fed to a PA driver. The PA driver is finally connected to an external power amplifier which drives an output. The power amplifier is designed to meet the adjacent channel leakage ratio (ACLR) requirements of 55dBr for N+/− 1 channel. Additional power amplifiers can be connected to increase the final transmit power based on requirements.

On the receive side, the RF front end interfaces to a zero-intermediate frequency (IF) or low-IF analog to digital converter (ADC) interface with differential inputs. The received input from the antenna is fed to a combination of LNA, complex mixer and gain stages, and a baseband filter. Alternately this signal chain can be replaced with a tuner which operates in the desirable RF band.

SDR Platform

Platform Description

The architecture of the software-defined radio (SDR) subsystem for communication processing is shown in Fig. 9.

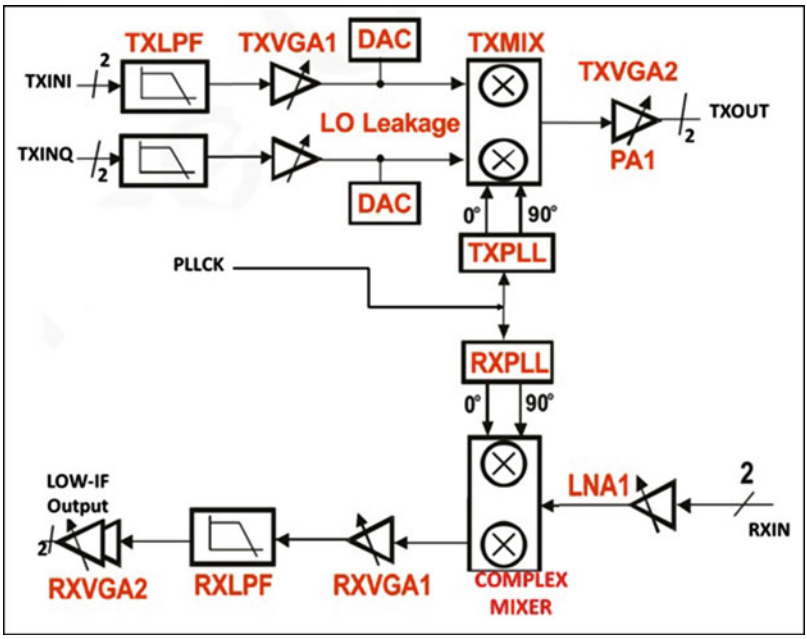

Fig. 8 Functional blocks of the radio frequency unit

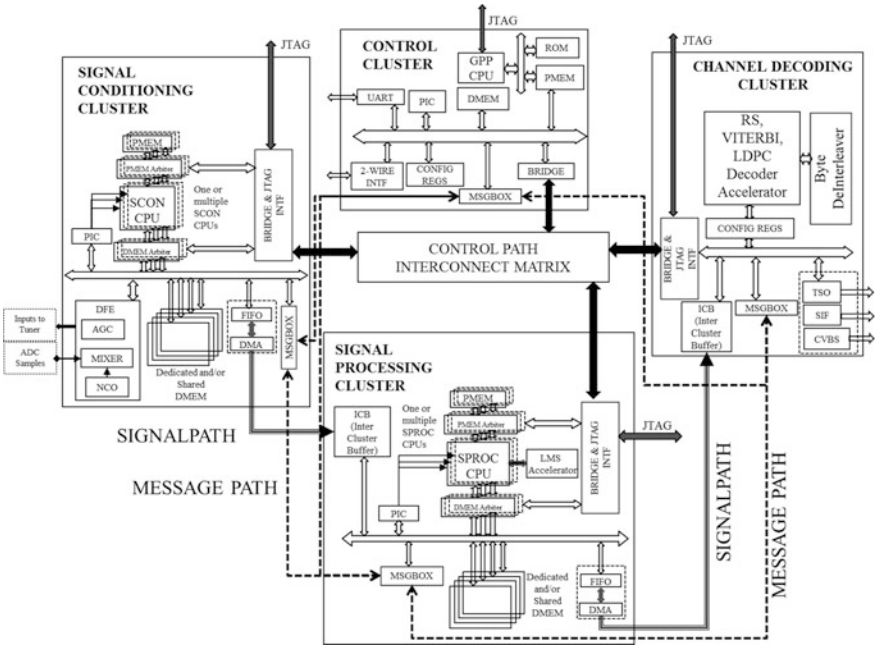

Fig. 9 Architecture of SDR Platform for demodulation

The architecture consists of signal conditioning cluster, signal processing cluster, and channel decoding cluster. The channel decoding cluster performs the tasks of Viterbi, Reed-Solomon, LDPC decoding along with bit/byte deinterleaver. The decoded data is packetized and exported out through a FIFO-like interface or to an on-chip/off-chip DAC. The overall scheduling and control of the entire SDR subsystem is performed by a control cluster which consists of a RISC processor with some general purpose peripherals. The control cluster accesses all individual clusters via the bridge. The signal conditioning cluster (SCC) consists of the following key components:

- One or multiple signal conditioning (SCON) CPUs.
- Digital front end (DFE),
- SCC-FIFO and SCC-DMA blocks.

The SCC cluster is responsible for digital down-conversion from intermediate frequency (IF) rate samples to symbol-rate samples. The associated peripheral block, namely, message box (MSG), is used to interact with other CPU clusters, while programmable interrupt controller (PIC) is used to interface to interrupts generated on chip from same or different clusters. The SCC cluster interfaces to control cluster via the bridge and to the intercluster buffer (ICB) memory of SPC cluster via DMA.

The digital front end (DFE) receives samples obtained by digitizing the incoming intermediate frequency (IF) signal from ADC. The DFE has a numerically controlled oscillator (NCO) operating at sample-rate frequency and a mixer. The mixer obtains a digitally synthesized waveform and is responsible for down-conversion of signal from IF to base band. In addition an AGC circuitry is also present which helps in ensuring that the full-scale range of ADC is used effectively. In addition to this the DFE has an internal FIFO using which incoming samples converted to baseband are stored. These samples are transferred in blocks of samples to SCON CPU. The DFE interfaces with the SCON CPU as a memory-mapped device on the DMEM data bus.

Signal Conditioning (SCON) CPU

The SCON CPU is a VLIW vector CPU with Wide multiply-accumulate units as shown in Fig. 10. This can interface to high-speed streaming input samples and implement finite impulse response (FIR), infinite impulse response (IIR), and sample-rate conversion filters. In addition it also performs carrier synchronization by implementing PLL's in software. In cases when input samples are obtained from IQ ADC, this CPU also performs the task of IQ imbalance correction. The CPU has four execution slots, namely, vector MAC slot, load-store broadcast slot, arithmetic slot, and logical slot. The SCON CPU has a dedicated program memory which interfaces via the program memory interface. SCON CPU interfaces to its dedicated data memory (SCC Data Memory), DFE, FIFO, and DMA using the DMEM interface. The salient features of the different execution units are as follows:

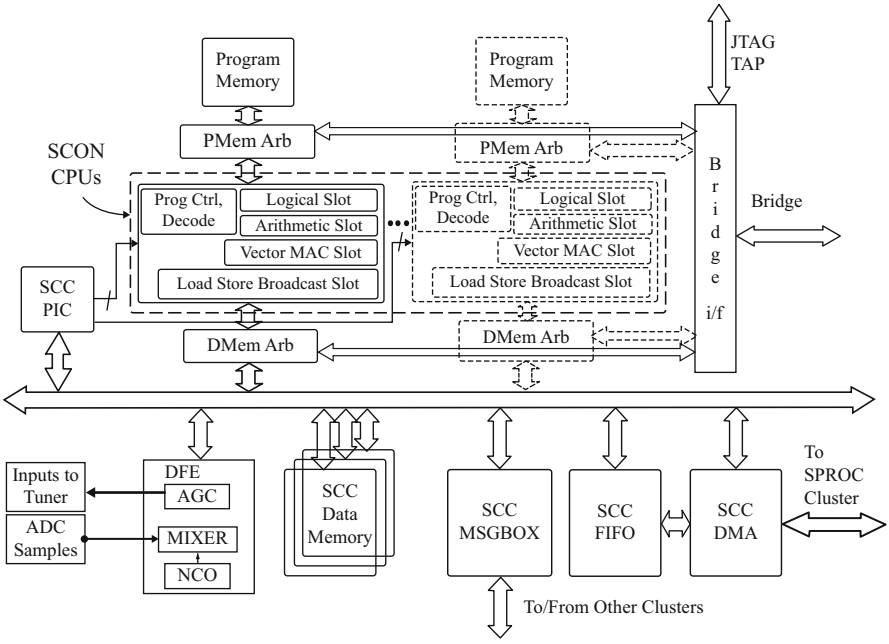

Fig. 10 Details of signal conditioning cluster

- Vector Slot with Real Multiply and Real MAC Capability with Wide MACs: This is capable of doing high sample-rate FIR and IIR filtering, decimation, interpolation, down-sampling, and up-sampling.
- Load-Store Broadcast Slot: This unit is capable of quad-word-sized load-store operations. The broadcast load capability is used to replicate a wide bit-width sample to the vector slot in single cycle.
- Arithmetic Slot: This unit is capable of basic arithmetic functions like add, subtract, absolute finding, exponent calculation, and swapping of IQ pair of complex signals. In addition this unit also does processing of accumulator values by doing summation with post-scaling.
- Logical Slot: This unit is capable of supporting basic logical operations like Boolean operations and compare operations.

The bridge interface is used for transferring control information from the control CPU (in control cluster) to the SCON cluster. The SCON data memory bus is a wide bit-width bus internal to the SCON cluster through which the SCON CPU and bridge can access slaves on data memory bus. The SCON program memory bus is of wide bit-width. The bridge is used at boot-up time to download each CPU code into its program memory. After completion of processing by the SCON CPU, the data is written by the SCON CPU over DMEM bus to the SCC FIFO. The SCC FIFO serves either as store and forward or cut-through buffer. The attached DMA

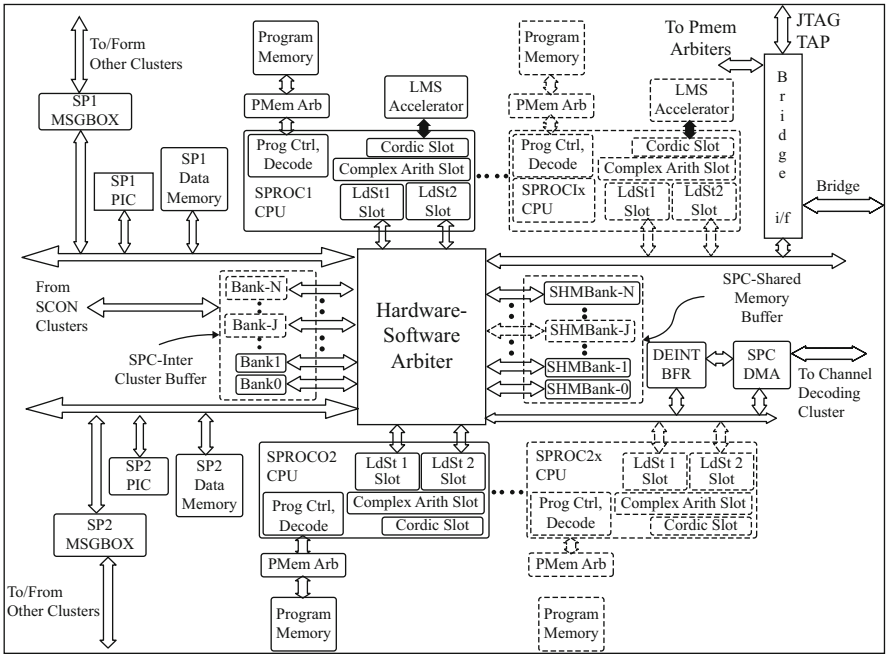

Fig. 11 Details of signal processing cluster

engine (SCC-DMA) moves the data from the FIFO through a dedicated interface independent of data memory bus, once the programmed threshold is reached. The SCC-DMA moves the data from FIFO and transfers it out of the SCC cluster to the intercluster buffer (ICB) of SPROC cluster. Associated with SCON CPU is a message box (SCC MSGBOX) which allows the CPU to exchange messages with each of the other CPU's in different clusters. It receives messages in its inbox from all other CPU's and sends messages to other CPU's via outbox. SCON cluster has a programmable interrupt controller (SCC PIC) which aggregates multiple source events into two levels of interrupts (INT1, INT2) and an exception (EXCP) for SCON CPU.

The signal processing cluster (SPC) as shown in Fig. 11 consists of the following key components:

- One or multiple SPROC CPUs (SP1, SP2,... SPx...),
- Least mean squares (LMS) coprocessor,
- Intercluster buffer (SPC-ICB),
- Shared memory buffer (SPC-SHMB),
- Packing buffer (DEINT BFR) and SPC-DMA blocks.

The signal processing cluster (SPC) performs the bulk of tasks comprising of symbol synchronization, channel estimation, channel correction, and demapping to

bits. It contains one or more SPROC CPUs (e.g., in case of a need of 2 CPUs, we name them SPROC1 and SPROC2) which does most of these tasks. An LMS coprocessor is tightly coupled to one SPROC CPU and designed to handle high sample-rate adaptive filtering required for time domain equalization. The SPC intercluster buffer (SPC-ICB) is used to receive inputs for processing from the previous signal conditioning cluster. The SPC shared memory buffer (SHMBank) is organized to effectively be used across the multiple CPUs in this cluster. A packing buffer (DEINT BFR) and a DMA are present to send processed data to the channel decoding cluster in the signal chain. Each SPROC CPU comes with its associated blocks, namely, message box (SPx-MSGBOX where x = 1, 2) and a programmable interrupt controller (SPx-PIC where x = 1, 2).

Signal Processing (SPROC) CPUs

This cluster contains one of multiple identical SPROC CPUs. The SPROC CPU is a VLIW core optimized for signal processing of complex signals. It is capable of handling complex arithmetic computations like complex MACs and complex multiply and is also capable of handling large (8192-, 4096-, or 2048-point) FFTs including non-power of 2, prime factor DFT computation. In OFDM-like standards, these CPUs are used for symbol synchronization, channel impulse response interpolation, and symbol deinterleaving and demapping. It has four execution slots, which consist of a complex arithmetic slot, a cordic slot (capable of twiddle factor generation and Arc-tan computation), and two wide bit-width slots. Special instructions for dividing complex signal by a real signal and single depth trace-back for Viterbi decoding are provided for channel estimation.

The salient features of the signal processing execution slots are as follows:

- 2× wide bit-width Load-Store Slots: This unit is capable of load and store operations. It supports linear, circular, and bit-reverse addressing. Some registers are marked in the register file as address pointers. In addition to load-store operations, this unit is also capable of performing Boolean, compare, and extract operations.
- Complex Arithmetic Slot: This unit is capable of performing operations on complex signals. It supports complex multiply and division, complex MAC, real multiply, and real MAC operations. It also supports efficient FFT butterfly operations which enable low cycle count FFT operations.
- Cordic Slot: This unit is capable of generating twiddle factors (sine and cosine operations) as well as non-normalized magnitude and phases of complex signals. This unit has a tight coupling with the LMS coprocessor which enables fast equalizer operations.

Each SPROC CPU has a dedicated program memory to which it interfaces via the PMEM interface. Each SPROC CPU interfaces to its dedicated data memory over the exclusive DMEM interface. The message box and PIC peripherals also interface using this data memory interface.

SPC Cluster Access Paths

The SPC cluster access paths are as follows. The access to SPC intercluster banks is arbitrated between different SPROC CPUs (SPROC1, SPROC2,..,SPROC1x, SPROC2x). This could be either priority based or round-robin based. Since the access paths to bridge are also required, they could also have similar types of access schemes.

There are specific registers for programming SPC-DMA and DEINT BFR to select between different SPROC CPUs, to ensure that only one CPU has exclusive access. The access to shared memory banks (SHM) and CPU-exclusive slaves (PIC, MSGBOX) is arbitrated between the SPROC CPU and bridge either using priority based or round-robin algorithm.

SPC Intercluster Buffer (SPC ICB)

SPC intercluster buffer is a bank-based memory with wide data width meant for continuous transfer of processed signal from SCON cluster to be consumed by SPROC cluster. The SPC ICB can be written by SCC DMA (one bank at a time) and can be read (multiple banks at a time) by one of the SPROC CPUs. Banks are contiguous in address space and are used in a circular mode by SCC DMA because it is provided for transferring continuous signal data.

SPC Shared Memory Buffer (SHMBank)

SPC Shared Memory (SPC SHM) is a bank-based buffer with wide datapath meant for storage and exchange of computed results between SPROC CPUs (this could be between SPROC1, SPROC2, SPROC1x, and SPROC2x CPUs). Each bank can be accessed by either of the two load-store ports of SPROC1, SPROC2, and so on. Bridge access is shared with any of the above ports. Either CPU is guaranteed fixed-latency access if it is the owner of a given bank. If nonowner accesses a bank, it will be allowed only on cycles where owner is not accessing that bank.

SPx-Data Memory and SPx-Program Memory

There is a dedicated data memory for each CPU, and it can be accessed by both load-store units of that CPU provided they are not in the same cycle. Both memories can also be accessed by bridge. In addition each SPROC CPU also has its dedicated program memory. The control cluster writes into program memory during boot-up time to download each CPU code.

Packing Buffer (DEINT BFR) and SPC-DMA Operation

The Packing buffer (SPC DEINT BFR) assists in data packing operation to be performed on data written by SPx CPU before it is transferred by SPC-DMA to channel decoding cluster. The packing buffer accepts data of a certain programmed data width from SPx CPU in nonsequential order. The SPC-DMA waits for an indication that data block is ready along with the block size from DEINT BFR after which it transfers data to intercluster buffer of channel decoding cluster.

Channel Decoding Operation and Generation of Payload Data

The SPC-DMA pushes the data into ICB of the channel decoding cluster. Here the channel decoding cluster consists of accelerators performing the tasks of Viterbi and TCM decoder, Reed-Solomon decoder, and LDPC decoder. In addition the byte deinterleaver is also present in this cluster. These processes act on the data in various phases as inner decoder and outer decoder. Additional processes like inner deinterleaver, outer deinterleaver and derandomizer, etc. are also taken care in the channel decoding cluster. The decoded data is finally collected via a ping-pong buffer that accepts packets and sends them out in 8-bit parallel or serial mode outputs. In certain cases the processed data from the SPROC cluster is bypassed through the channel decoding cluster and routed to the IQ-DAC.

Suitability of the Platform for 802.22 Implementation

SDR Partitioning for Demodulation

Figure 12 shows how the various OFDM demodulation processes are partitioned across the different clusters. The numerically controlled oscillator (NCO) and mixer followed by IF to baseband converter, down-sampler, adjacent channel filtering, and sample-rate convertor are performed on the SCON cluster. The time domain synchronization, fast Fourier transform (FFT), frequency domain synchronization, pilot processing, fine symbol synchronization, frame sync detection, channel estimation and correction, symbol demapping, and bit interleaving are performed on the SPROC cluster using one or multiple CPUs. The LMS equalizer is optionally used for long echo channel shortening. The remaining processes constituting Viterbi decoding, outer deinterleaver, Reed-Solomon decoder, and derandomizer are expected to be done in the channel decoding cluster. This final output from channel decoding cluster is the transport stream packet.

The proposed SDR subsystem consisting of signal processing clusters and signal conditioning cluster can be used along with an additional channel encoding cluster to implement a transmit path function as shown in Fig. 13. In such a case, the channel encoding cluster performs the tasks of RS encode, convolution encode, LDPC encoding, and interleaving functions by collecting the required payload data. The data from the channel decoding cluster is passed to the signal processing cluster and from signal processing cluster to signal conditioning cluster. This is done by interchanging the components of FIFO, DMA, and intercluster buffer as compared to the previous configurations across the clusters. Once this configuration change is done, the signal path traverses from channel encoding to signal processing and finally to signal conditioning.

The signal processing cluster does the function of mapping the bits to waveform and performing IFFT for the case of OFDM-based standards or performing the required modulation as per the communication standard of choice. Once the signal is modulated, it is transferred to the signal conditioning cluster for spectrum shaping and filtering. The spectrum-shaped signal is transmitted out either by optionally

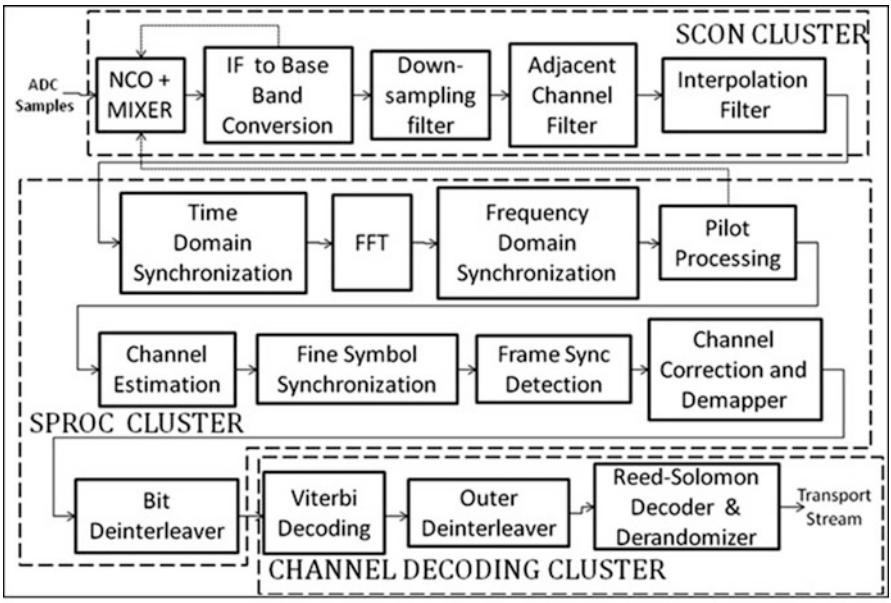

Fig. 12 OFDM demodulation on the SDR chip

up-converting using a mixer and NCO combination or could be send out as is at baseband from the DFE sub-module of signal conditioning cluster. In case a baseband signal is send out, the up-conversion can be performed externally before transmitting it. This data is passed through a digital-to-analog converter (DAC) to transmit a baseband signal or an IF signal. In a similar manner, the transmitter path of other digital communication standards can also be mapped and implemented using the SDR subsystem.

The proposed SDR subsystem consisting of signal processing (SPROC) clusters and signal conditioning (SCON) cluster can be used along with an additional channel encoding cluster and channel decoding clusters to implement universal modulator and demodulator (MODEM) functionality. A scheme to implement this is shown in Fig. 14.

In this scheme we have shown the transmit path (TX-SDR) and receive path (RX-SDR). The transmit path consists of outgoing data being processed via channel encoding cluster (as explained earlier), followed by signal processing (SPROC) cluster and finally to be send out after being processed by the signal conditioning (SCON) cluster. This outgoing signal is fed to a digital-to-analog converter which is up-converted and sent via the transmit antenna. The receive path consists of incoming signals from the receive antenna which pass through the tuner to get intermediate frequency or zero IF signals. These signals are digitized using an analog to digital (ADC) converter to generate real or complex samples. As explained in the previous sections, the real or complex signals are processed by signal

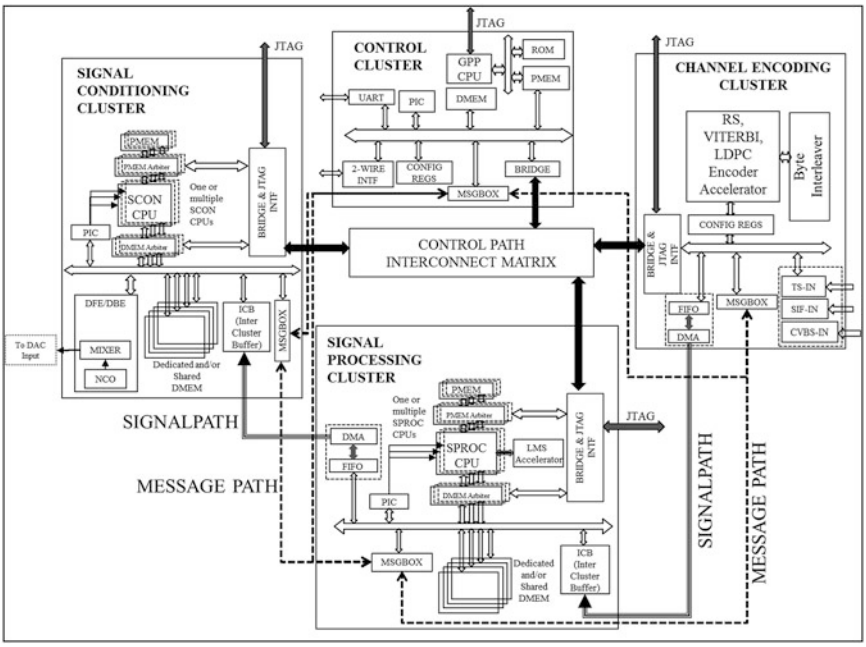

Fig. 13 SDR Platform for Modulator function

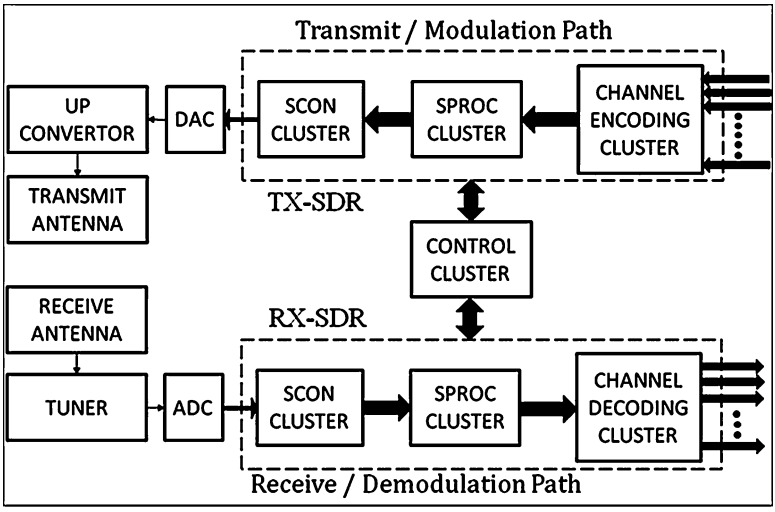

Fig. 14 Usage of SDR systems for implementing modem functionality

conditioning (SCON) cluster for sample processing followed by signal processing (SPROC) cluster for symbol processing and finally demapped to generate bits. The generated bits are passed through the channel decoder to remove errors and get a final data bits. Figure 14 also shows a control cluster which will interact with the transmit and receive SDR paths for performing control and supervisory functions. Thus the proposed SDR subsystem is versatile and can be reused as a basic building block for implementing a universal modem.

802.22 WRAN PHY Implementation on SDR Platform

This section describes how the 802.22 WRAN physical layer is implemented on the SDR platform described in the previous section for the base station as well as the CPE. Base Station (BS). The base station performs the functions of downlink transmit and uplink receive to and from all the CPEs.

Downlink Transmit Processing

The downlink transmit processing chain is shown in Fig. 15. The data obtained from the MAC layer is packetized, randomized using the scrambling sequence in the channel encoding cluster. The payload contains bits which needs to be transmitted to different users. The scrambled packet is convolutional encoded and punctured appropriately, following which it undergoes bit interleaving using the turbo interleaver. The interleaved bits intended for multiple users are combined and sent to the SPROC cluster where it undergoes the process of mapping to different OFDM carriers. The pilots transmitted in the frame are also boosted here. These carriers are interleaved in frequency domain, and pilots are added as desired for the different frames. Superframe preamble and preamble generations happen in this cluster based on the type of frame to be transmitted. The mapped carriers are converted to time domain via process of IFFT and sent to the SCON cluster. The SCON cluster performs the tasks of up-sampling and adherence to spectral mask using filtering operations. The up-sampled and filtered signal is eventually converted to baseband analog waveform using IQ-DACs.

Uplink Receive Processing

The uplink receive processing chain is shown in Fig. 16. The base station RF front end receives signals from different CPEs which are sampled by the ADC. The ADC samples are filtered to remove the effects of adjacent channel interference, in the SCON cluster. The filtered samples are transferred to SPROC cluster where they are aligned on proper boundary and FFT is performed to get frequency domain samples. The frequency domain samples are subsequently deinterleaved, and further processes of channel estimation, equalization, and demapping are performed after removing the CDMA pilot carriers. The demapped soft bits are segregated on a user-specific basis and then undergo the processes of bit deinterleaving, Viterbi decoding, and descrambling. The user-specific payloads are passed to the MAC layer.

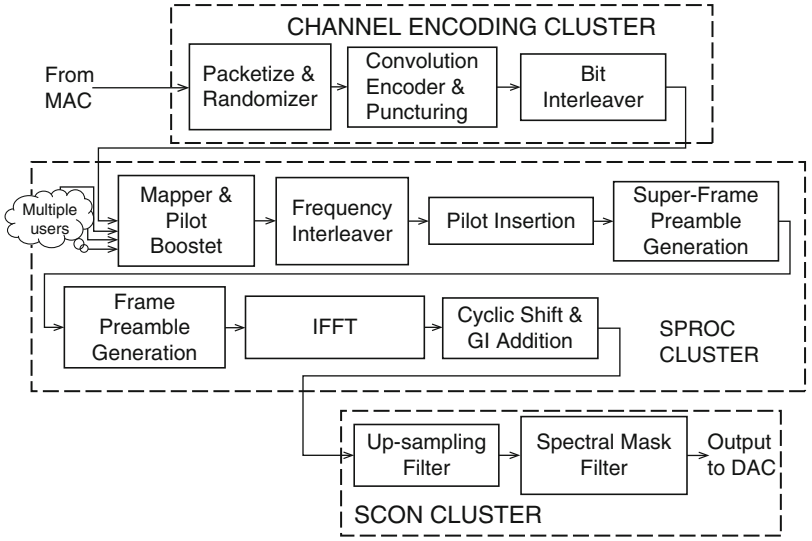

Fig. 15 Downlink transmit task partitioning on the SDR platform

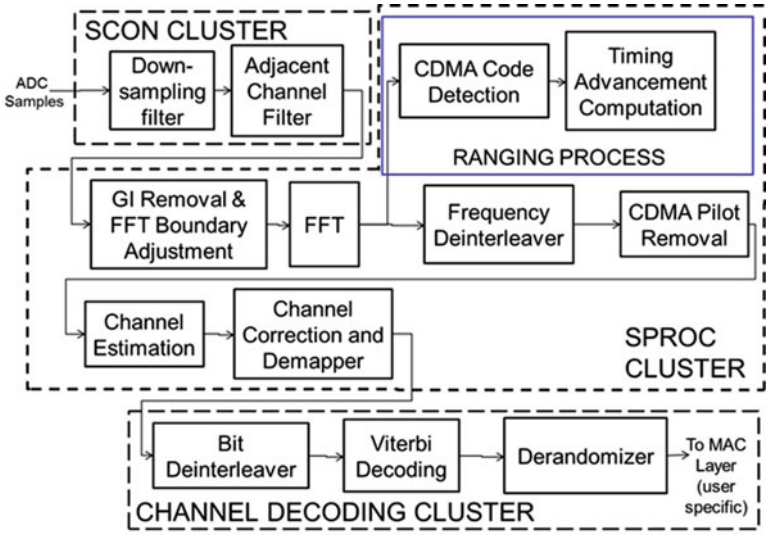

Fig. 16 Uplink receive task partitioning on the SDR platform

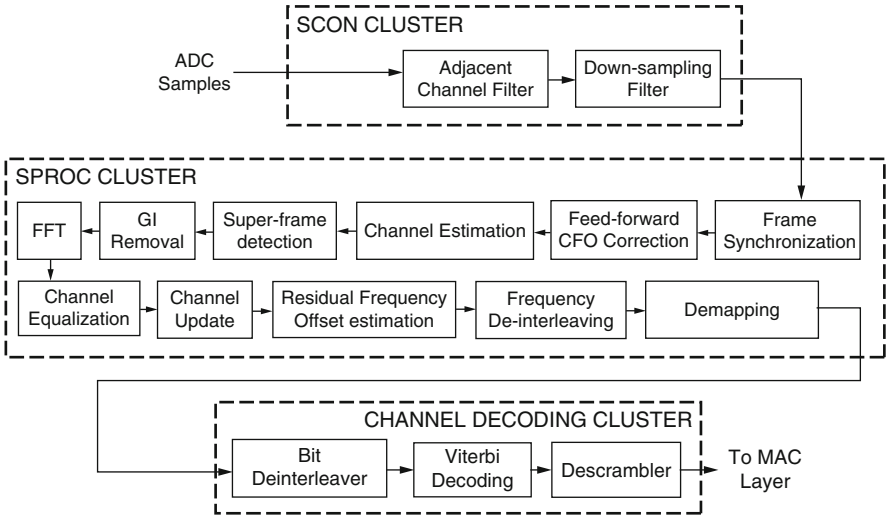

Fig. 17 Downlink receive task partitioning on the SDR platform

Customer Premise Equipment (CPE)

The customer premise equipment performs the functions of downlink receive and uplink transmit from and to the base stations.

The downlink receive processing chain is shown in Fig. 17. The signals received by the RF front end are sampled by the ADC and then filtered to remove the effects of adjacent channel interference in the SCON cluster.

The filtered samples are subsequently processed in the SPROC cluster for frame synchronization and carrier-frequency offset correction. Subsequently the tasks of channel estimation, superframe detection, and frequency domain conversion via FFT are performed. This is followed by channel equalization, channel update, residual frequency offset estimation, frequency deinterleaving, and demapping in the SPROC cluster. The soft-bits are deinterleaved and undergo Viterbi decoding and descrambling in the channel decoding cluster. The final bits obtained are packetized as payload and passed to the MAC layer.

The uplink transmit processing chain is shown in Fig. 18. The channel encoding cluster receives the payload bits from MAC layer, scrambles, and packetizes it. The scrambled payload undergoes convolutional encoding and bit interleaving and is transferred to SPROC cluster. The SPROC cluster further performs the tasks of mapping data to the OFDM carriers and symbol-wise frequency interleaving (characteristic of 802.22 uplink frames) before insertion of CDMA carriers required for ranging. The frequency domain data is converted to time domain via IFFT, and any frequency offset introduced in the CPE is compensated. An additional task of timing advance correction is performed on the uplink side from all CPEs to ensure that all waveforms from different CPEs arrive at the same time at the base station. The time domain data subjected to timing advance correction is subjected to spectral

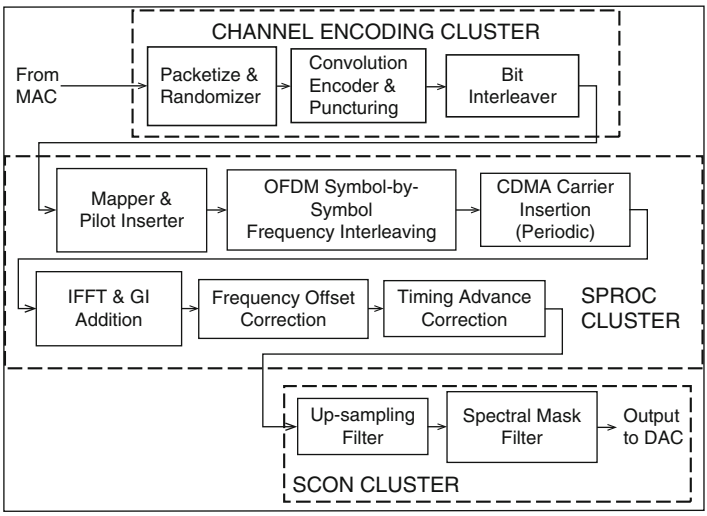

Fig. 18 Uplink transmit task partitioning on the SDR platform

mask filtering in the SCON cluster to be exported to the DAC which generated the baseband analog waveform.

MAC Layer Implementation

The 802.22 MAC primarily consists of the convergence sublayer and common part sublayer on both the CPE and base station side. The different components of the MAC are detailed in Fig. 19.

Each module is expected to be implemented such that it can execute as a thread, task, and function or even be located in a different processor.

Test Methodology for the IEEE 802.22 and Results

The setup shown in Fig. 20 is used to inject different kinds of impairments between the transmit and receive chains for validating the correctness of IEEE 802.22 WRAN system.

This setup enables testing and performance benchmarking of the TVWS (IEEE 802.22) modem implementation for different impairments, viz., additive white Gaussian noise (AWGN), multipath, phase noise, carrier-frequency offset, sampling frequency offset, etc. The unique frame structure specific to 802.22 consisting of superframes and frames is verified using correlation techniques.

The correlation plots shown in the following Fig. 21 help us identify the superframe and frame boundary detection.

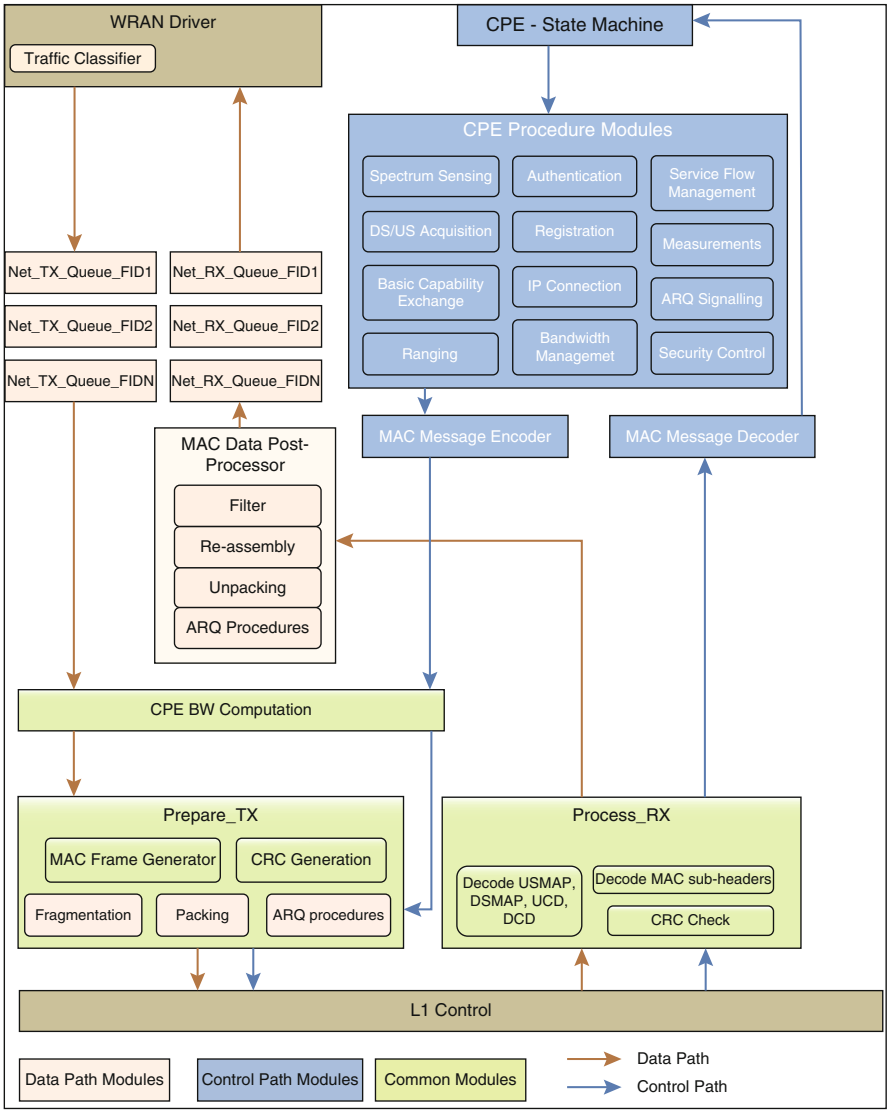

Fig. 19 MAC functional architecture

Figure 22 shows the channel path delay profiles used for verification of the IEEE 802.22 implementation. Red components indicate that the channel profile falls outside 1/32 guard interval (GI) window.

These channel models have been defined based on extensive work carried out over many years by the IEEE 802.22 working group. Some of these models have been derived directly from over the air measurements that have been carried out by the broadcasters as shown in Table 5.

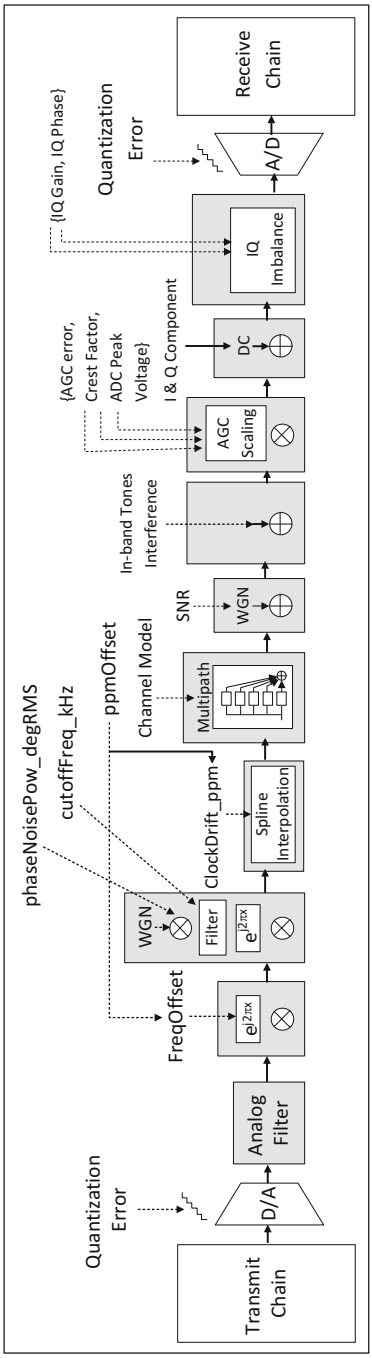

Fig. 20 Simulation setup for 802.22 modem

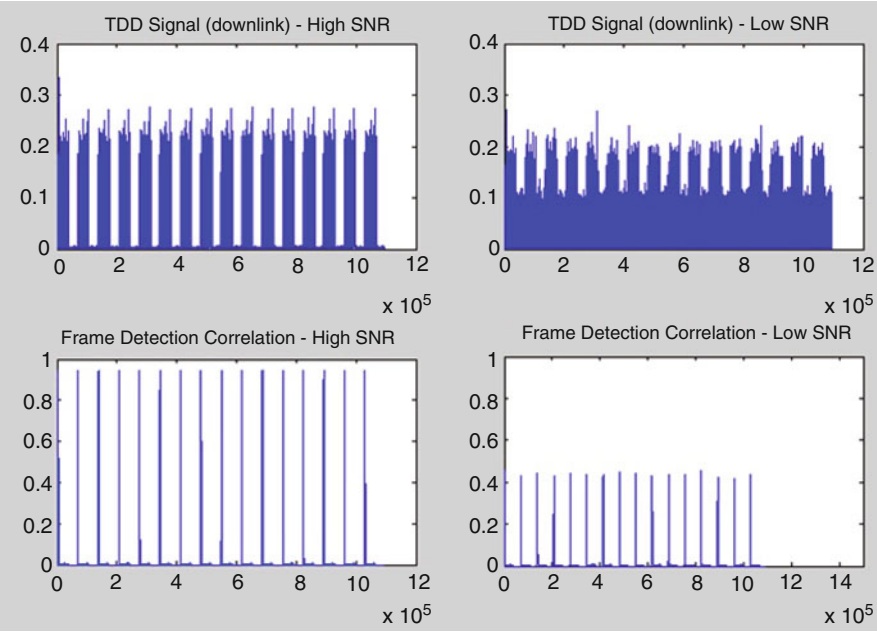

Fig. 21 Correlation plots of packet detection and initial symbol timing

Spectrum Mask

Fig. 23 shows the typical output spectrum obtained at the power amplifier output at base station/CPE side. As can be seen, the spectrum mask complies with the FCC regulations. This is one of the most challenging aspects of the white space device implementation, and based on the techniques described earlier, one can comply with the regulations.

Effect of Carrier-Frequency Offset and Sampling Frequency Offset

Figure 24 describes the constellation in the presence of residual frequency offset and sampling frequency offset. As can be seen, all these offsets need to be taken care of and equalized in order to recover the bits contained in the signal.

Over-the-Air Tests of the IEEE 802.22 Device

This section describes over-the-air tests performed in India for the 802.22 WRAN systems. These tests were done as a technology demonstrator and proof of

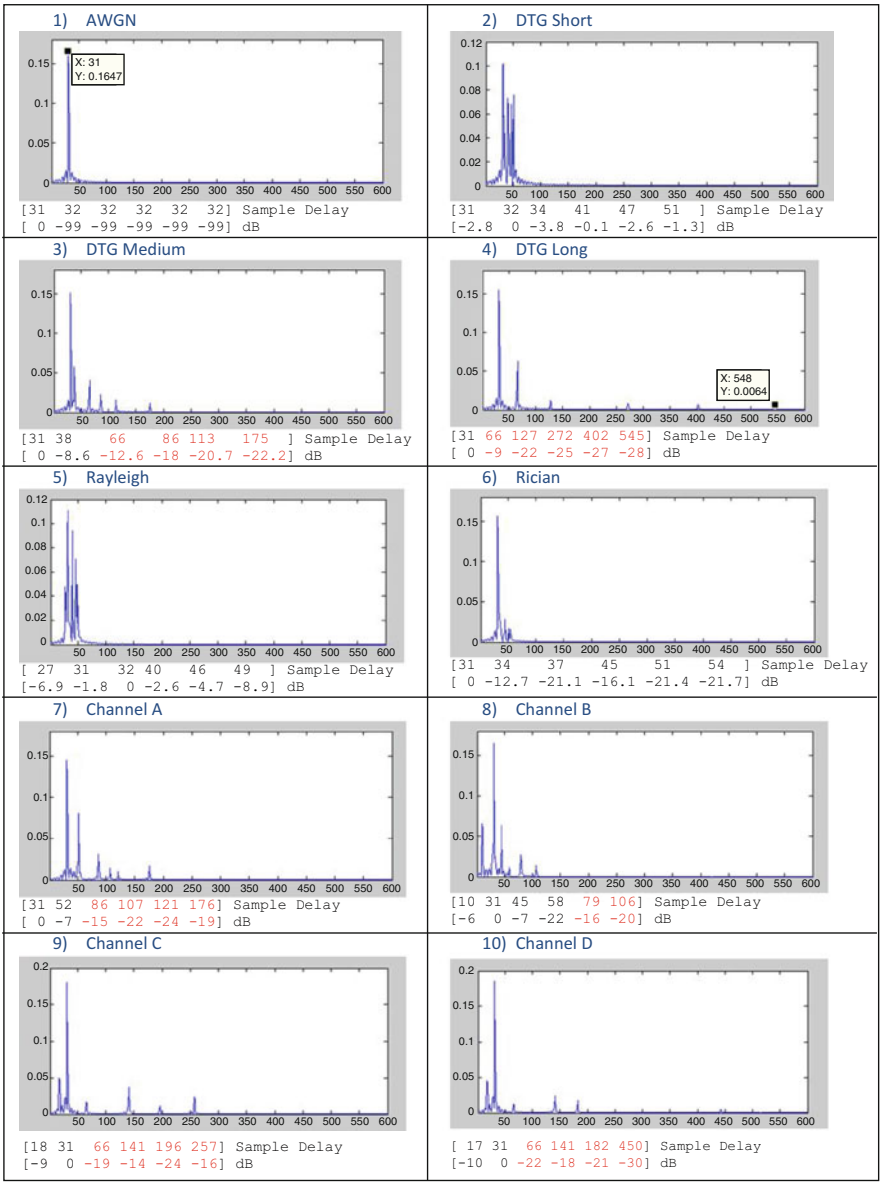

Fig. 22 Channel type for performance verification (Red components indicate, they fall outside 1/32 GI window)

Table 5 Channel types used to conduct the IEEE 802.22 performance evaluation

Channel type	Sample delay and power delay profile
AWGN	[31 32 32 32 32 32] [0 −99 −99 −99 −99 −99] dB
DTG short	[31 32 34 41 47 51] [−2.8 0 −3.8 −0.1 −2.6 −1.3] dB
DTG medium	[31 38 66 86 113 175] [0 −8.6 −12.6 −18 −20.7 −22.2] dB
DTG long	[31 66 127 272 402 545] [0 −9 −22 −25 −27 −28] dB
Rayleigh	[27 31 32 40 46 49] [−6.9 −1.8 0 −2.6 −4.7 −8.9] dB
Rician	[31 34 37 45 51 54] [0 −12.7 −21.1 −16.1 −21.4 −21.7] dB
Channel A	[31 52 86 107 121 176] [0 −7 −15 −22 −24 −19] dB
Channel B	[10 31 45 58 79 106] [−6 0 −7 −22 −16 −20] dB
Channel C	[18 31 66 141 196 257] [−9 0 −19 −14 −24 −16] dB
Channel D	[17 31 66 141 182 450] [−10 0 −22 −18 −21 −30] dB

concept in collaboration with Education and Research Network (ERNET) in India.

ERNET India is the National Research and Education Network dedicated to support the needs of the research and education community within the country. It was established in 1998 as an autonomous scientific society under the Ministry of Electronics and Information Technology (MeitY), Government of India. It operates ERNET network – a pan-Indian terrestrial and satellite network with 15 points of presence at premier research and academic institutions [1].

The main objectives were as follows:

- Test point-to-point and point-to-multipoint link scenarios.
- Test for long-, mid-, and short-distance ranges
- Measure data rates with iperf benchmarks.
- Video conference using Internet backhaul

Srikakulam district of Andhra Pradesh was chosen for one of the trials. This is a typical rural scenario where the base station was installed at Voppangi (on an existing BSNL tower) and connectivity was demonstrated with 2 schools located at Ponnada (located 6.5 km from Voppangi) and Dharmavaram (located 10.6 km from Voppangi).

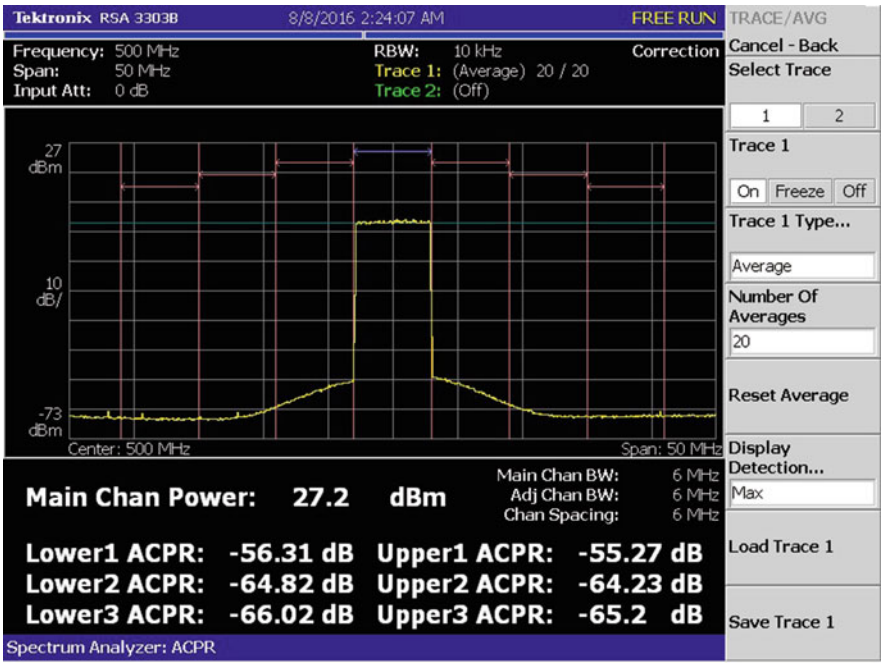

Fig. 23 802.22 implementation spectrum mask

Base station characteristics (Voppangi)

- Configuration:
  Mode: FDD
  Band width: 6 Mhz
  Frequency Band: Down link: 647 MHz, Up Link: 695 MHz
- Antenna
  Gain: 9 dBi
  Height above ground level: 58 ft
- EIRP
  32 dBm
- Back haul (Courtesy: BSNL broadband)
  Downlink: 9.45 Mbps
  Uplink:5.6 Mbps

The directional antennas at the CPE locations were oriented toward the base station for getting the best signal strength.

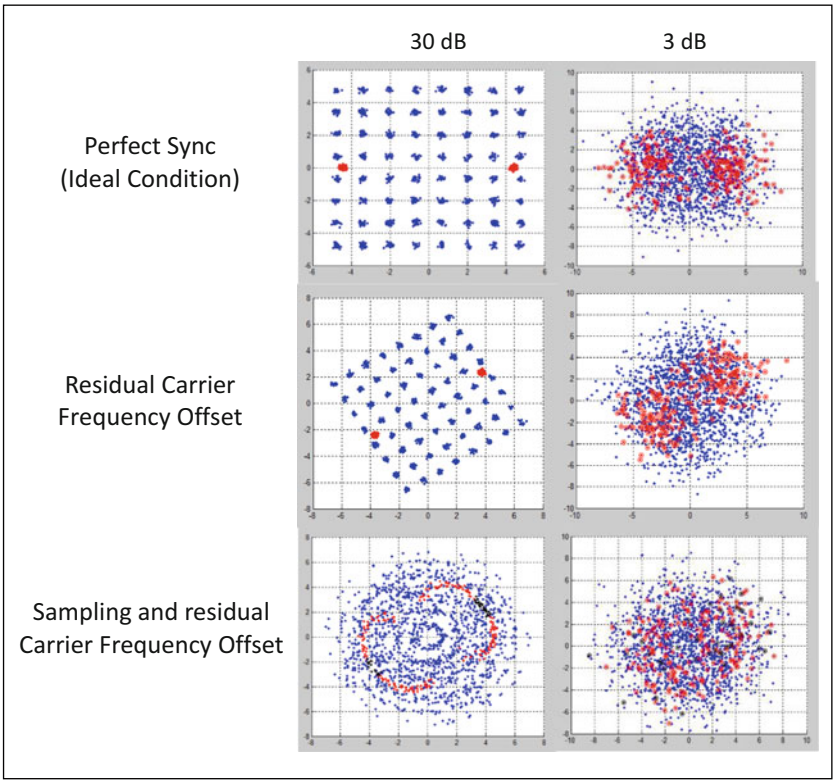

Fig. 24 Constellation in presence of residual frequency offset and sampling frequency offset

CPE location 1 (Z.P.H School, Ponnada)

- Configuration:
  Distance from Voppangi:6.5 KMS
  Frequency band: Downlink: 647 MHz, Up Link: 695 MHz
- Antenna:
  Gain: 9 dBi
  Height: 40 ft
- EIRP
  32 dBm
- Results:
  Point-to-point configuration
  Iperf
  Downlink: 6.95 Mbps (16-QAM, 2/3 code rate).
  Uplink: 4.56 Mbps (QPSK, 3/4 code rate).

Point-to-multipoint(2 Cpe) configuration
Iperf
Downlink: 3.4 Mbps (16-QAM, 2/3 code rate).
Uplink: 1.4 Mbps (QPSK, 1/2 code rate).

CPE location 2 (Z.P.H School, Dharmavaram)

- Configuration
  Distance from Voppangi: 10.6 KMS
  Frequency band: Downlink: 647 MHz, Up Link: 695 MHz
- Antenna:
  Gain: 9 dBi
  Height: 30 ft
- EIRP
  32 dBm
- Results: Point-to-point configuration
  Downlink: 3.89 Mbps (QPSK, 3/4 code rate).
  Uplink: 2.94 Mbps (QPSK, 1/2 code rate)
- Point-to-multipoint (2 Cpe) configuration
  Downlink: 1.76 Mbps (QPSK, 3/4 code rate).
  Uplink: 0.84 Mbps (QPSK, 1/2 code rate)

Another case study for over-the-air trials was the trials done in conjunction with IIT-Hyderabad. In these trials the base station was mounted on top of academic building, and several CPEs were mounted at the following locations:

- CPE1 at Main Gate, IIT Hyderabad: The aerial distance from base station: 1.3 Kms
- CPE2 at Utharpalle School: The aerial distance from base station: 7.5 Kms
- CPE3 at Mallepalle School: The aerial distance from base station: 8.5 Kms
- CPE4 at Terpole School: The aerial distance from base station: 11.8 Kms

The goal of this project was to provide Internet connectivity to students in villages in and around IIT-Hyderabad Campus. The typical configurations used for the base station and CPE equipment are as follows:

- Base station configuration
  Band width: 6 MHz
  FDD: Downlink frequency: 502–508 MHz, Uplink Frequency: 514–520 MHz
  BS antenna type/gain: Sectoral/7 dBi
  BS antenna height(m):20
- Total EIRP @ BS: 31 dBm(1.25 W)
- CPE configuration
  Band width: 6 MHz
  FDD: Downlink frequency: 502–508 MHz, uplink frequency: 514–520 MHz

Table 6 Results of some of the initial field tests for the IEEE 802.22 Wi-FAR Technology

CPE	Distance from the Base station (km)	CPE antenna Height (m)	Downlink (Mbps)	Uplink (Mbps)	Total throughput (Mbps)
CPE1: IIT Main Gate	0.3	1.8	10	12	22
CPE2: Uttarpally	7.5	6	10	12	22
CPE3: Mallepalle	8.5	6	4.74	1	5.74
CPE4: Terpole	11.8	0.6	0.9	1.5	1.4

CPE antenna type/gain: Directional/6 dBi
Total EIRP @ CPE: 30 dBm(1 W)

The summary of the results obtained from point-to-point links is summarized in the following Table 6.

Implementation Challenges of the IEEE 802.22 Standard

Several challenges exist in the design of customer premise equipment and Base Station compliant to the 802.22 standard using SDR approach.

AGC Response Time

The receiver RF chain used in 802.22 mostly makes use of existing TV tuners, since they operate in the band of interest. However, the drawback posed due to the usage of TV tuners is that they have long AGC response times. However, if we consider the frame durations of 802.22 system, they are much lesser in comparison to these response times. This poses a challenge in terms of AGC loops not being able to completely settle. Consequently, the task of gain control cannot be left to RF tuner completely under such circumstances. The SDR architecture as explained earlier also participates in signal normalization and gain control to some extent.

Turbo-Like Interleaver Implementation on SDR

Turbo-like interleavers (TLI) used for frequency interleaving and bit interleaving pose a significant challenge in SDR platforms because of their pattern computation incorporating a modulo operation. If we consider the scenario when extremely high data rates need to be supported, the rate of bit interleaving computation required also becomes significant. Such type of complexities forced two different types of TLI implementation, one for frequency interleaving where the compute requirements are significantly lower and the other (bit interleaving) which needs

much higher compute capability. Hence these types of disparate requirements force the programmer to give up on a modular approach to programming.

Compliance to 802.22 Spectrum Mask

The 802.22 emission mask is very stringent because it is a secondary mode of transmission. The requirement is to have a rejection of 55dBr in N+1 and N-1 channels and 69dBr in N+2 and N−2 channels. These stringent mask requirements become difficult to meet especially because the noise floor in the transmit RF chain also gets amplified by the gain stages when we want to transmit at a certain required power level. To ensure that the spectrum mask is adhered to it is important to pay attention to the noise floor starting from the DAC which converts the digital baseband signal to analog. The designer can choose the DAC with the appropriate noise floor or somehow ensure that in the stages following the DAC (i.e., the post-DAC filters), the noise floor is appropriately shaped and suppressed so that at the power amplifier output, the mask is met. In addition to noise floor shaping, it is also observed that the power amplifier needs to operate mostly in Class A or linear region so that the contribution of nonlinear components is kept to a minimum. It is for reasons of compliance to the tight spectrum mask are why we find the power amplifier having poor efficiency. There are certain implementations which have overcome this deficiency and adopted power amplifier linearizers in the transmit chain to meet the spectrum mask as well as have better power amplifier efficiency.

Alternate Implementation of the IEEE 802.22 Spec

Another manufacturer of the IEEE 802.22 equipment uses advanced, state-of-the-art digital filters coupled with high-resolution digital-to-analog converters, essentially synthesizing on the fly a signal that meets all these requirements. This is then followed by analog antialiasing filters before the complex signal is modulated, amplified, and finally transmitted. Such digitally controlled transmissions have been found to truly mimic simulation predictions in compliance with all of the above requirements.

The received design begins with a gallium arsenide front end, providing an exceptionally low noise figure and a large dynamic range. The signal is then demodulated and passed through a first analog filter. This filter ensures the signal can then be sampled with minimal aliasing, further filtered by a state-of-the-art digital filter, decimated, and further filtered before it is digitally processed to extract every ounce of intelligibility it may contain. The net result is an exquisite sensitivity and an excellent performance in the presence of dispersion, out of band TV transmitter signals, instabilities caused by vegetation shimmering in the wind, etc.

With a useful range of 100 km, the IEEE 802.22 line of radios can provide up to 22 Mbps of robust transmission to areas where other technologies such as LTE, 4G, WiFi, and WiMax fall short. As such, it is not positioned as a replacement for these

technologies but rather as a complement, expanding the service area beyond what more traditional or legacy technologies can provide.

The manufacturer also uses an open-source Linux operating system. Proprietary drivers interface the open-source code to the radio board, the latter ensuring that FCC compliance is achieved despite changes the operator may do at the operating system level. Since the radio uses well-known Linux distributions, there are plenty of experienced personnel available and a plethora of documentation for any operator who would like to use the radio in a customized fashion, all the while knowing that the transmitter/receiver continues to operate in compliance with standards and country-specific regulations.

Rather than relying on global positioning system (GPS) receivers, radios provide exquisite location capabilities, as they implement standardized terrestrial fine ranging, as described in the 802.22 standard. Therefore, this implementation of the radios can operate under adverse conditions where GPS signaling may fail. They are therefore less susceptible to weather and are immune to GPS jamming. With the proper software, these radios can actually map an entire area, acting as a superb swarm of highly precise OFDMA 3D radars. After a natural disaster, all these attributes may be of vital importance in an emergency deployment of these devices to reconstruct a basic telecommunications infrastructure.

Geolocation and Database

Protection of licensed incumbent systems in the TV bands can be provided by either geolocation and access to an incumbent database over the Internet, or spectrum sensing or a combination thereof. This section deals with the first means, whereas spectrum sensing is dealt with in section "Distributed Spectrum Monitoring: IEEE 802.22.3 Standard on Spectrum Characterization and Occupancy Sensing".

Two modes of geolocation can be used with the IEEE 802.22 WRAN technology and satellite-based and terrestrially based geolocation. The satellite-based mode relies on global navigation systems such as GPS, Glonass, and Galileo. The WRAN BS will use its satellite-based geolocation capability to determine the latitude and longitude of its transmitting antenna as well as its altitude above mean sea level from a geolocation receiver installed on the antenna. Each CPE also needs a geolocation receiver to acquire its geolocation and transmit it to the BS using a standard NMEA string at the time of association. The BS can also query the CPE for its geolocation at any time to verify that it is always at the same place.

The terrestrially based geolocation mode relies on the inherent transmission capabilities of the IEEE 802.22 WRAN system. Terrestrial geolocation is based on the time of arrival (ToA) ranging technique which relies on the propagation time on the round trip between the BS and its CPE obtained by the normal ranging process of the wireless system but with an augmented accuracy resulting from the consideration of the relative phase of the frame preamble carriers as received at the CPE on the downstream and the relative phase of dedicated CDMA ranging carriers as received at the BS on the upstream. This information is extracted through the

normal OFDM signal processing of the WRAN system and can be made available to the BS. It is also based on the range between CPEs obtained by the propagation time of the CBP bursts from one CPE to another. Again, the accuracy is augmented by the consideration of the relative phase of the carriers contained in the CBP burst preamble as it is received by the second CPE which, meanwhile, keeps its synchronization with the BS.

A geolocator is used at the BS to initiate the ranging requests on which the BS will act by querying the CPE for the differential carrier phase information and requesting a CDMA ranging burst to be transmitted by the selected CPE to carry out the precise BS-CPE-BS ranging and by requesting specific CPEs to send their CBP bursts and other CPEs to capture these bursts and send the resulting differential carrier phase information to the BS. The geolocator will then compute the distance between the BS and each of its CPEs as well as the distance between the selected CPEs and establish their geolocation by triangulation based on a number of reference WRAN devices for which the precise geolocation is known. Upon completion of the triangulation calculations, the geolocator will return a NMEA longitude-latitude string to the BS for each CPE that it has successfully triangulated.

Once the BS has acquired the geolocation of its CPEs, it can register these geolocations with the incumbent database using standardized primitives through the higher layers of the backhaul transmission so that the database sends back the list of TV channels available at the specific CPE location or the maximum EIRP that the CPE can use at that specific location on each available channel to avoid interference to incumbents.

Both options on the type of information to be provided by the database have been considered and included in the IEEE 802.22 standard since these are the two main ways by which the various databases in the different countries may specify the constraints on TVBD operation, i.e., list of available channels or maximum EIRP that can be used by the TVBD at its location on each channel of interest. The second option includes the first since the indication of the protected channels can be signaled by a much-reduced EIRP level that would not allow WRAN operation on a specific channel. However, this second option would allow operation with reduced EIRP in some instances where a communication link between the BS and the CPE can still be established, resulting in a tapering-off of the EIRP when the BSs and CPEs get close to a protected contour rather than an abrupt transition from full EIRP operation to disallowed operation. Since the BS fully controls the EIRP of its CPEs through the transmit power control (TPC), interference control is centralized at the base station.

However, means had to be developed at the CPE to make sure that the BS actually controls the maximum EIRP and not only the conducted power going to the antenna. The IEEE 802.22 standard includes the requirement that unless an integrated CPE/antenna is used where conformance testing can be done on the entire unit, the antenna will have to indicate its on-axis gain on all the TV channels on which it can operate once it is connected to the CPE (e.g., a PROM in the antenna readable from the CPE). A special signaling interface has been included in the IEEE 802.22 standard for this antenna-to-CPE data communication so that

the BS can securely control the EIRP of the CPE even if the attached antenna can be changed.

A standardized set of primitives to support the interface between the BS and the database has been developed and included in the IEEE 802.22-2011 [5]. This set of primitives should constitute the basis of a communication protocol between the database and the various TV white space unlicensed devices. This set of primitives was presented to the IETF-PAWS which has taken the task of developing such protocol.

IEEE 802.22 Future Enhancements and Other Activities

Many enhancements to the IEEE 802.22 standard are under way in form of amendments or revisions. The IEEE 802.22 working group is working on the IEEE 802.22b amendment on enhancements for broadband services and monitoring applications [8]. The IEEE 802.22b has currently recommended ten new usage cases [15]. The usage cases can be categorized as smart grid and monitoring, broadband service extension, and combined services. The smart grid and monitoring applications include regional area smart grid/metering, agriculture/farm house monitoring, critical infrastructure/hazard monitoring, environment monitoring, homeland security/monitoring, and smart traffic management and communications, which have properties of low capacity/complexity CPEs, very large number of monitoring CPEs, real-time monitoring, low duty cycle, high reliability and security, etc. The broadband service extension applications, on the other hand, including temporary broadband infrastructure such as emergency broadband infrastructure, remote medical service, and archipelago/marine broadband service, have properties of relatively high capacity CPEs; high QoS, reliability, and security; high data rate; and easy network setup.

Based on the above use cases and the functional requirements [2], the IEEE 802.22b amendment and the proposed revision to the IEEE 802.22 standard will provide the following additional features:

- Operation of the IEEE 802.22 beyond TV band white spaces, including new bands of operation. These bands include 1300 to 1750 MHz, 2700 to 3700 MHz and the VHF/UHF TV broadcast bands between 54 and 862 MHz.
- Aggregated throughput of 802.22b to be at least two times the maximum throughput supported by the IEEE Std. 802.22-2011 and in some cases four times the maximum throughput as a result of channel aggregation, channel bonding, and multiple input multiple output (MIMO) operation.
- Support for two new classes of CPEs for different service applications of broadband services and monitoring applications and shall support at least 2048 CPEs to cover a regional area network for monitoring applications.
- The amendment may provide mechanisms to meet the regulatory requirements on spectrum mask,
- Support for multi-hop connections,

- Support for QoS mechanisms for real-time monitoring applications.
- This amendment will provide enhancement to existing or alternate security mechanisms, provide a means for alternative channelization, and provide methods for cost-effective compliance with regulatory spectral mask.

The 802.22 WRAN standard uses the features of cognitive radio primarily for spectrum sensing. In future we envision that most of the CPE and base stations will be based on SDRs. This has the potential of converting modern-day cellular networks into a cognitive RAN (CRAN) network. A CRAN network will learn constantly and update itself in real time. It does so by sensing the current environment and learning from past data. This will lead to hyper-personalization for all devices that operate in the network. Some of the salient characteristics of such devices will be the following:

- All devices will operate at their optimal performance level for all users in the network.
- The modulation (and demodulation) schemes will be designed based on real-time inputs – almost on the fly.
- Devices and the infrastructure elements will apply deep learning to figure out the optimal use of compute resources.
- In such a network, each end point of the network will be a virtual machine, thus leading to virtualization of the interface between different RAN components.

Such a network will marry the concepts of big data, cognitive radio, and machine learning to generate a self-organizing network which updates itself based on environment, device capabilities, and past data. [7]

Distributed Spectrum Monitoring: IEEE 802.22.3 Standard on Spectrum Characterization and Occupancy Sensing

In 2014, the IEEE 802.22 working group formed a task group to commence activities on the IEEE P802.22.3 standard on spectrum characterization and occupancy sensing.

The IEEE 802.22.3 standard will help solve the urgent need for issues such as on-demand spectrum survey and reporting; collaborative spectrum measurement and calibration; labeling of systems using the spectrum; spectrum planning; spectrum mapping; coverage analysis for wireless deployment; terrain and topology – shadowing and fading analysis; quantification of the available spectrum through spectrum observatories; complementing the database access for spectrum sharing by adding in situ awareness and faster decision-making; space-time-frequency spectrum hole identification and prediction where non-time-sensitive tasks can be performed at certain times and at certain locations, when the spectrum use is sparse or nonexistent; as well as identification and geolocation of interference

sources. We will devote some time to this new upcoming standard and some SDR implementations of the distributed spectrum monitoring systems, as well as interference mitigation in cellular networks.

The large amount of wireless services and the consequent growth in terms of request for new allocation in terms of spectrum bands are leading toward a fast saturation of spectrum resources. On the other hand, several studies [4] on the actual occupation status of the allocated bands show how spectrum channels are idle most of the time, and the percentage of average usage in under 30%, on a daily basis. A CR system is an intelligent wireless communication system that is aware of its surrounding environment and uses the methodology of understanding by building to learn from the environment and adapt its internal states to statistical variations in the incoming RF stimuli by making corresponding changes in certain operating parameters (transmit-power, carrier-frequency, and modulation strategy) in real time [13]. Such a definition implies two needed capabilities: the first one is the awareness of the surrounding environment in terms of spectrum occupancy status. This piece of knowledge is the input for the intelligent access to the wireless medium. The second capability is the intelligence, i.e., the radio cannot work in a standard way, but needs to have some processing capabilities and choose the best parameters for each environmental condition. To achieve these goals, the spectrum sensing task is a crucial phase of the cognitive communication. In particular, a cognitive device has two opportunities to be aware of the surrounding electromagnetic environment: the first is to perform spectrum sensing locally and thrust on the output of the sensing method to access idle channels and the second is to query a geolocation database, where sensing outputs are stored by other distributed systems.

Sensing Engines: Spectrum Analyzer, Low-Cost Solutions, and SDR

A sensing engine [3] can be defined as a device, or a part of it, which is able to perform sensing task, composed of two subtasks: sampling phase and processing phase. In particular, a good sensing engine should have some peculiarities, such as efficiency, flexibility, reliability, and capability of continuous recording. The first one, efficiency, is defined as the ratio between the sampling time and the total time (sampling + processing) needed to perform sensing. It approaches 100% if the processing time is negligible with respect to the sampling time. It is very important that the processing time is minimized, since during this period the sensing cannot acquire, in normal single radio operations, new samples and so it becomes blind to the changes of the spectrum occupancy status.

Several sensing devices are available today on the market. They can be coarsely divided into three categories: spectrum analyzers, low-cost USB devices, and SDR. Devices belonging to the first category are able to scan very wide frequency ranges, but they are extremely costly and they are usually not customized to perform channel assessment. They can acquire spectrum records just for a few seconds, due to

the high-frequency resolution they need to apply for good visualization. Further processing is still needed to run more complex outcomes.

We will provide further insights on the IEEE 802.22.3 standard during future revisions of this book chapter.

Conclusions

In this chapter we provided insights on the implementation of the IEEE 802.22 (Wi-FAR) standard for wireless regional area networks. The IEEE 802.22 standard is the first standard that specifically focuses on regional and rural broadband access. Also it is the first standard that embeds many cognitive radio features to avoid interference to the primary users as a result of license-exempt operation. The regional and rural broadband wireless access is enabled as a result of using empty or vacant channels in the TV band frequencies which have exceptional propagation characteristics. Although the population density may be limited in rural areas, this allows deployment of such large regional area networks that can typically cover 300 sq. km with a single BS, or 30,000 sq. kms when exceptional propagation conditions are available. This allows adequate customer base per cell, thus making the rural area network business model viable. The PHY layer is based on orthogonal frequency division multiple access, to counter potentially harsh multipath environments. The MAC layer incorporates a number of features to support the cognitive radio capabilities. Geolocation, incumbent database, and spectrum sensing are utilized to provide protection for the incumbent services in the TV bands. The spectrum manager combines the geolocation, spectrum sensing information, regulatory-dependent policies, and channel set management to decide on the choice of TV channel to be utilized.

In this chapter we also discussed trials, certification, and interoperability testing of the IEEE 802.22-based Wi-FAR^{TM} systems.

References

1. Education and Research Network. http://www.ernet.in/l
2. Functional Requirements for IEEE 802.22b amendment. https://mentor.ieee.org/802.22/dcn/12/22-12-0012-03-000b-functional-requirements-for-ieee-802-22b-amendment.doc
3. Get IEEE 802.22 Standard. http://standards.ieee.org/about/get/802/802.22.html
4. Holland O, Bogucka H, Medeisis A (2015) Opportunistic spectrum sharing and white space access: the practical reality, 1st edn. Wiley
5. IEEE Std 802.22-2011 (2011) Standard for wireless regional area networks part 22: cognitive wireless RAN medium access control (MAC) and physical layer (PHY) specifications: policies and procedures for operation in the TV Bands
6. Internet Engineering Task Force (IETF), Protocol to Access White-Space (PAWS) Working Group. Protocol to Access White-Space (PAWS) Databases, draft-IETF-paws-protocol-12. https://datatracker.ietf.org/wg/paws/documents/
7. Mody A et al (2007) Machine learning based cognitive communications in both the white and the gray space. In: Proceedings of the IEEE MILCOM

8. PAR for Enhanced Broadband and Monitoring Amendment. https://mentor.ieee.org/802.22/dcn/11/22-11-0118-04-rasg-par-for-enhanced-broadband-and-monitoring-amendment.doc
9. Rappaport T (1996) Wireless communications: principals and practice. Prentice Hall
10. Saankhya Labs IEEE 802.22 Standard Implementation. http://www.saankhyalabs.com/products/white-space-base-station/
11. Second memorandum opinion and order in the matter of unlicensed operation in the TV broadcast bands, additional spectrum for unlicensed devices below 900 MHz and in the 3 GHz band. Federal Communication Commission, Docket Number 10–174, 23 Sept 2010
12. Second report and order and memorandum opinion and order in the matter of unlicensed operation in the TV broadcast bands, additional spectrum for unlicensed devices below 900 MHz and in the 3 GHz band. Federal Communication Commission, Document 08–260, 14 Nov 2008
13. Thanki R. Measuring the Local Impact of the TV WhiteSpace Broadband. http://dynamicspectrumalliance.org/assets/DSA_Presentations/5-1_DSA_2015_GlobalSummit_Day2_Richard_Thanki.pdf
14. Third memorandum opinion and order in the matter of unlicensed operation in the TV broadcast bands, additional spectrum for unlicensed devices below 900 MHz and in the 3 GHz band. Federal Communication Commission, Docket Number 12–36, 5 Apr 2012
15. Usage Cases in 802.22 Smart Grid and Critical Infrastructure Monitoring. https://mentor.ieee.org/802.22/dcn/11/22-11-0073-02-0000-usage-cases-in-802-22-smart-grid-and-critical-infrastructure-monitoring.ppt
16. WhiteSpace Alliance™. http://www.whitespacealliance.org

Further Reading

1. Anderson N (2009) First white space broadband deployment in small Virginia town, ARS TECHNICA. www.arstechnica.com/tech-policy/news/2009/10/first-white-space-broadband-deployment-in-small-virginia-town.ars
2. ATSC digital television standard (A/53) revision E, with amendments No. 1 and 2. Advanced Television Systems Committee, Sept 2006
3. Caldwell W (2008) Policy engine, IEEE 22-0973r1
4. Cavalcanti D, Ghosh M (2008, Invited) Cognitive radio networks: enabling new wireless broadband opportunities. In the Proceedings of the Third International Conference on Cognitive Radio Oriented Wireless Networks and Communications (IEEE CrownCom 2008), Singapore
5. Chounard G (2009) Sensing performance from 802.22.1 wireless microphone beacon, IEEE 802.22-09/68r1
6. Chouinard G (2010) RF sensing in the TV white space. In: 8th Conference on Communications Networks and Services Research (CNSR2010), Montreal
7. Clanton C, Kenkel M, Tang Y (2007) Wireless microphone signal simulation model, IEEE 802.22
8. Cordeiro C, Challapali K, Birru D, Shankar S (2005) IEEE 802.22: the first worldwide wireless standard based on cognitive radios. In: IEEE DySPAN
9. Cordeiro C, Ghosh M, Cavalcanti D, Challapali K (2007, Invited) Spectrum sensing for dynamic spectrum access of TV bands. In: Proceedings of the IEEE CROWNCOM 2007
10. Document US/6A-1 U.S. Annex to the Working Document Towards a Preliminary Draft New Report ITU-R BT CRS BS Bands, Feb 2014
11. Dolan B (2010) Google eyes white space for wireless health, MOBI Health News. www.mobihealthnews.com/8913/google-eyes-white-space-for-wireless-health/
12. Hamblen M. Big Tech Firms Back Wi-FAR for Remote, Rural Broadband. http://www.computerworld.in/news/big-tech-firms-back-wi-far-for-remote,-rural-broadband
13. http://www.airu.net/about/

14. http://giglibraries.net/Default.aspx?pageId=1628969; see also e.g., http://www.skokienet.org/whitespace
15. http://www.saankhyalabs.com/
16. http://www.tvtechnology.com/article/west-virginia-university-launches-first-super-wifi-campus-white-space-network/220307
17. IEEE 802.16 Working Group on Broadband Wireless Standards. http://www.wirelessman.org/, IEEE Standards Association, Piscataway, NJ
18. IEEE P802.22.1/D4 (2008) Part 22.1: standard to enhanced harmful interference protection for low-power licensed devices operating in the TV broadcast bands
19. Kay S, Marple SL Jr (1981) Spectral analysis: a modern perspective. In: Proceedings of the IEEE, pp 1380–1419
20. Mendel JM (1991) Tutorial on higher order statistics (Spectra) in signal processing and systems theory: theoretical results and some applications. In: Proceedings of the IEEE, pp 278–305
21. Mody A et al (2008) Protocol reference model enhancements in 802.22, document number 22-08-0121-06
22. Nation's First Smart Grid White Spaces Network Trial, The Smart Grid Observer, 25 June 2010. www.smartgridobserver.com/n6-25-10-2.htm
23. NICT and Hitachi Kokusai, IEEE 802.22 and IEEE 802.11af Field Trials. http://www.nict.go.jp/en/press/2014/01/23-1.html
24. OET Nationwide TVWS Roll-Out Notice
25. Other WhiteSpace Pilot Programs. http://www.dynamicspectrumalliance.org/pilots.html
26. Part 74 – Experimental Radio, Auxiliary, Special Broadcast and Other Program Distributional Services
27. Shellhammer SJ (2008) Spectrum sensing in IEEE 802.22. In: Cognitive Information Processing Workshop
28. Shellhammer SJ, Nandagopalan S, Tandra R, Tomcik J (2006) Performance of power detector sensors of DTV signals in IEEE 802.22 WRANs. In: TAPAS Workshop
29. Taher T et al (2014) Global spectrum observatory network setup and initial findings. In: 2014 9th International Conference on Cognitive Radio Oriented Wireless Networks and Communications (CROWNCOM), Oulu, pp 79–88. https://doi.org/10.4108/icst.crowncom.2014.255402
30. Tandra R (Spring 2005) Fundamental limits of detection in low SNR. Masters thesis, University of California Berkeley
31. The IEEE 802.22.1 Revision PAR. http://www.ieee802.org/22/
32. Tutorial on Spectrum Characterization and Occupancy Sensing. https://mentor.ieee.org/802.22/dcn/14/22-14-0089-00-0000-spectrum-occupancy-sensing-tutorial-presentation.pdf
33. Urkowitz H (1967) Energy detection of unknown deterministic signals. In: Proceedings of the IEEE, pp 523–531
34. Vos E (2010) Wilmington, NC uses white spaces for smart city, eco-friendly wireless applications, MUNI Wireless. http://www.muniwireless.com/2010/02/24/wilmington-uses-white-spaces-for-smart-city-ecofriendly-wireless-applications/
35. WhiteSpace Alliance Pilot and Trials. http://www.whitespacealliance.org/Pilots.html

Part VI
Cognitive Radio Applications and Practices

Spectrum Database and Smart Spectrum

55

Takeo Fujii, Kei Inage, and Koya Sato

Contents

T. Fujii (✉)
Advanced Wireless and Communication Research Center, The University of Electro-Communications, Tokyo, Japan
e-mail: fujii@awcc.uec.ac.jp

K. Inage
Electrical and Electronics Engineering Course, Tokyo Metropolitan College of Industrial Technology, Tokyo, Japan
e-mail: inage@metro-cit.ac.jp

K. Sato
Department of Electrical Engineering, Tokyo University of Science, Tokyo, Japan
e-mail: ksato@ieee.org

W. Zhang (ed.), *Handbook of Cognitive Radio*,
https://doi.org/10.1007/978-981-10-1394-2_56

Abstract

In this chapter, spectrum management technologies based on a spectrum database are introduced. Statistical spectrum maps and spectrum databases are important components for understanding a spectrum environment that has locality due to geolocation, surrounding structures, frequency, and so on. The typical spectrum database provides spectrum information according to a radio propagation model for estimating the unused spectrum for spectrum sharing. However, the original geolocation spectrum database does not consider the site-specific environment because a statistical radio propagation model is used. Here, in order to improve the accuracy of the spectrum database, the measurement-based spectrum database is considered. The highly accurate spectrum database can improve spectrum-sharing performance and spectrum efficiency. Finally, a future spectrum management concept, called a smart spectrum, is introduced to open up the possibility for a new wireless world.

Introduction

In order to share the spectrum in cognitive radio, the detection of a primary user (PU) and protection from interference from the secondary users (SUs) to the PU are important. Spectrum sensing and geolocation databases are considered for comprehension of the existence of the PU. Although spectrum sensing can check the current status of the PU by detecting the PU signal, misdetection generates interference toward the PU, and a false alarm may eliminate the opportunity to transmit the signal from SUs. These errors degrade the reliability of spectrum sharing. On the other hand, the geolocation database stores the available frequency for SUs without creating interference toward the PUs. Therefore, the SU can know the available frequency of a certain location by checking the data stored in the database. However, the real-time PU status cannot be understood from the database because the available frequency is usually calculated by conservative radio propagation model for avoiding the interference toward the PU.

Because spectrum sensing cannot guarantee the protection of PUs, the current practical discussion on spectrum sharing for TV white space is based on geolocation databases, like the Federal Communications Commission (FCC)-defined spectrum database and Office of Communications (Ofcom)-defined spectrum database [1, 2]. The geolocation database stores and provides geographical radio information and is expected to achieve interference avoidance influenced by the probabilistic behavior of wireless channels. The database stores radio environment information, such as the transmitter position and the received signal power from each transmitter to any location in each channel. The main information consists of the propagation loss and the transmitter and receiver locations. This empirical propagation model is derived from the enormous amount of propagation data collected from urban, suburban, and rural environments.

However, the propagation model-based geolocation database cannot support the locality of radio propagation, like shadowing, and a conservative spectrum-sharing design is required for protecting PUs. In order to improve the accuracy of the database considering the locality of propagation, spectrum databases generated by measurement results, called measurement-based spectrum databases, are considered [3, 4]. The measurement-based spectrum database gathers the measurement results from mobile terminals with their location information, and the spatial spectrum map is generated by statistically processing the gathered datasets. The typical registered information is the average received power with a mesh-divided area, which can be used to estimate the propagation of the PU and SU signals. In order to make a highly accurate and wide-coverage measurement-based spectrum database, spatial interpolation is an important technique that does not require high-density measurement data. In this chapter, we introduce the statistical interpolation techniques for measurement-based spectrum databases, and the effectiveness of such techniques on spectrum sharing is discussed.

Finally, we consider a future wireless world with dynamic spectrum use based on spectrum measurement, modeling, database, and management, which are collectively referred to as the smart spectrum [5]. The current spectrum allocation policy is based on exclusive spectrum use by a primary system determined by the regulator in each county. However, exclusive spectrum use reduces the efficiency of the spectrum, because flexible spectrum use according to user demand is difficult and a large spatial margin is required to avoid interference. In order to improve spectrum efficiency, a smart spectrum has been proposed for future wireless networks. In this chapter, we introduce the smart spectrum, and future spectrum policy is discussed with a hierarchical spectrum database and spectrum manager.

Throughout this chapter, we would like to open a future wireless world with flexible spectrum use based on user demand.

Geolocation Database

At the beginning of spectrum sharing, harmful interference toward license services is to be avoided using spectrum sensing with a white-space device. In this case, the white-space device can only transmit its own signal on the license band if the result of spectrum sensing is idle; collision avoidance between the licensed system and white-space device can subsequently be achieved in the temporal, spatial, and/or spectral domains. This concept is device-driven with respect to interference avoidance; therefore, it is important to detect the idle channel with high accuracy for the protection of licensed services. However, the radio regulations defined by organizations such as the FCC and Ofcom set a spectrum-sharing policy independent of spectrum sensing, caused by poor performance of spectrum sensing in low-SNR regions. In other words, it is difficult to protect the licensed service with satisfactory accuracy using spectrum sensing. The FCC and Ofcom offer an outline for a possible alternative, interference management by geolocation database [1, 2]. The geolocation database stores and relays geographical radio information and is

expected to achieve interference avoidance influenced by probabilistic behavior of the wireless channel. Database-driven spectrum sharing has attracted attention as an alternative solution with satisfactory accuracy.

In spectrum sharing assisted by geolocation database, a white-space device queries the database with its own parameters and current location to determine the availability of communication over the licensed band. The geolocation database responds with the allowable transmission parameters, such as the available channel list in the FCC rule or the maximum transmit power in the Ofcom rule. This response is derived from the database information and the specified parameter of the white-space device based on the utilization rule. The white-space device begins transmitting signals over the licensed band according to the database response. In other words, the interference toward licensed system is managed by the database response. The rules for management of harmful interference is divided into two categories: channel allocation and power allocation. The FCC rule is a channel-allocation type, in which white-space devices coexist with Digital TV systems and other white-space devices by utilizing the channel provided by database response. On the other hand, the Ofcom rule is a power-allocation type. Critical interference can be avoided by suppression of the maximum transmit power. The major difference between the FCC and Ofcom rules is the design of the database response as a policy for interference avoidance.

This section summarizes the concept of the geolocation database required by FCC and Ofcom rules, for clarity of the measurement-based spectrum database.

Radio Propagation Prediction from Empirical Model

A common feature of geolocation and measurement-based spectrum databases is the storage of radio environment information such as the transmitter position and received signal power from each transmitter to any location within each channel. The main information consists of the propagation loss and the transmitter and receiver locations. In other words, the performance of the geolocation database is dependent on the accuracy of the propagation loss prediction. In traditional wireless communications, channel prediction is a major topic for system design in terms of transmitter geometry, coverage size, and system capacity under performance constraints. Various empirical propagation models have been proposed, for example, the Okumura model [6], Hata model [7], and COST Hata model [8]. These empirical models are derived from enormous propagation data collected from urban, suburban, and rural areas.

The main purpose of deriving empirical models is to construct a versatile model with low error from the actual values in a real environment. In order to achieve a versatile model, measurement data is obtained from a wide area, and the impact of a site's specific character is suppressed by mean reversion. However, measurement data from an oversized area leads to an increase in the error between the predicted and actual values. The radio environment, as typified by propagation loss, is referenced from surrounding environments, such as geography and aboveground

structures. The empirical model predicts the relationship among the received signal power and the typical feature quantities in urban, suburban, and rural areas. The predicted value from the above empirical model is different from the actual value averaged over a short term. This residual error is called the shadowing factor and also indicates a unique characteristic at the specific location. With regard to accuracy, it is better to confine the measurement area to model the propagation loss, although collection and utilization of small measurements or specific area data cause a lack of versatility of the propagation model. Therefore, the empirical propagation model creates a dilemma for versatile prediction with high accuracy.

The geolocation database utilizes one of the above types of empirical propagation model for signal prediction. However, this does not mean that the geolocation database provides the licensed signal power at every location. Generally, the edge of service coverage for each transmitter is calculated in the geolocation database, as illustrated in Fig. 1. Nevertheless, it is not always possible to predict every location with high accuracy using the geolocation database. In order to avoid harmful interference due to prediction error, a protective margin is added to the calculated service coverage.

Protection of the licensed system often requires maintaining a signal-to-interference ratio (SIR) of the licensed receiver above the threshold demanded by the licensed system. In spectrum sharing, there could be two causes of situations in which there is harmful interference toward the licensed system. The first is the overestimation of the licensed signal power at the coverage edge. The other is the underestimation of the interference from the white-space device. To mitigate the former risk, licensed signal prediction must avoid overestimation by setting a protective margin. In particular, service coverage is extended from the estimated edge by the margin distance. This is expected to prevent regional overestimation of the weak signal area due to the shadowing effect and to attenuate harmful interference received within the true service coverage. However, the prediction error of the regional area in the geolocation database leads to the degradation of spectral efficiency in the spatial domain.

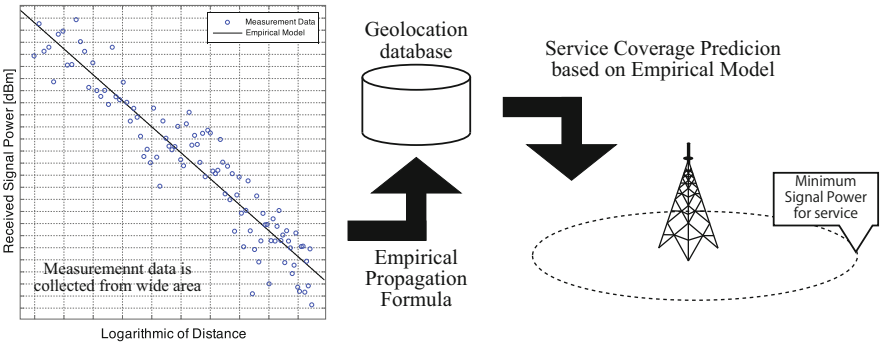

Fig. 1 Signal prediction from empirical propagation formula

Available White Space

As mentioned in section "Radio Propagation Prediction from Empirical Model", the licensed signal is predicted based on the empirical model. Similarly, the transmitted signal from the white-space device, or the harmful interference, is predicted through the empirical model. In fact, different empirical propagation models of the licensed system are often used for white-space devices because of the different system parameters. In the geolocation database, the boundaries of two kinds of wireless signal are obtained through prediction of the signal. The response of the geolocation database is also obtained from these prediction results.

In order to find the available white space, the transmit parameters that satisfy the relative position of the two boundaries are calculated. The relationship between the two boundaries is divided into two cases: overlapping and non-overlapping. As shown Fig. 2a, two boundaries are crossed, and the white-space device interferes with the receiver of the licensed system. If the SIR at the edge of licensed coverage exceeds the lower limit of the SIR requirement, then the white-space device cannot transmit its own signal. In other words, there is no available white space for spectrum sharing in Fig. 2a. The geolocation database derives the transmit parameters of the white-space device from these geographical results.

Because Ofcom's database is power-allocation type, the maximum transmit power of the white-space device is decreased from Fig. 2a. With decreasing transmit power, the interference area decreases to eliminate overlap with the service coverage of the licensed system, as shown in Fig. 2b. On the other hand, the FCC uses a channel-allocation database. This database searches the channels that satisfy the non-overlap condition between the licensed coverage and interference area by changing the channel, as shown in Fig. 2c. After that, the database responds with the solution parameters under the geographical constraint, which is the non-overlapping case with the white-space device. The FCC database responds with the available channel list, and the Ofcom database responds with the maximum transmit power of the white-space device.

Measurement-Based Spectrum Database

The spectrum database facilitates users to acquire global knowledge of surrounding radio environment. However, many databases that are under consideration for practical use including FCC-defined spectrum database are constructed based on a path loss model. Such a path loss model cannot take into account the effect of shadowing sufficiently, often a large estimation error occurs in the path loss-based spectrum database. Therefore, SUs is required to set a large interference margin. In addition, although there are complex models that consider a larger number of variables (i.e., terrain models), these models do not necessarily make better predictions [9].

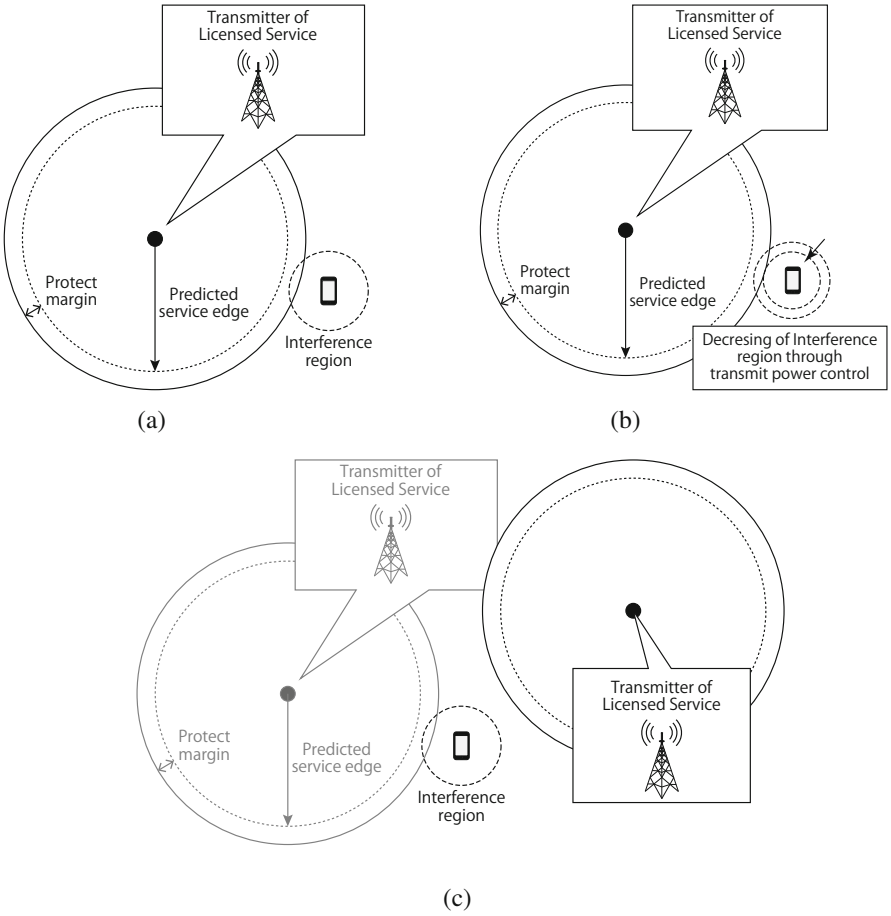

Fig. 2 Relationship between licensed system and white-space device. (**a**) Interfering case. (**b**) Availability case by controlling transmit power. (**c**) Availability case by changing channel

On the other hand, the accuracy of the spectrum database can be improved via actually measured information of the radio environment. Figure 3 shows a concept of measurement-based spectrum database. The database is a hybrid system, combining spectrum sensing and a spectrum database. The spectrum database consists of radio environment information that is measured by SUs (e.g., highly accurate spectrum analyzer, smartphones, and vehicles). The collected dataset is related to the measurement location and is reported to the database. After enough data are gathered, the database estimates the radio environment characteristics of the PUs by statistical processing with the large created dataset. Because the data include actual propagation losses and shadowing effects, accurate channel statuses can be determined.

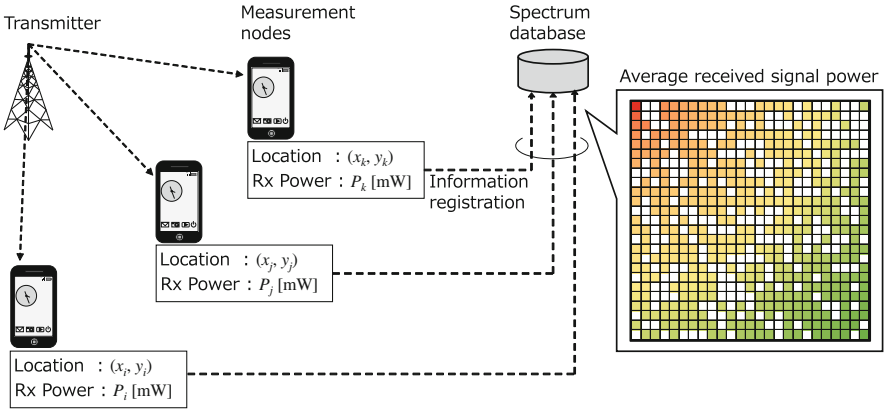

Fig. 3 Measurement-based spectrum database

In this section, we summarize basics of statistical analysis of radio environment based on the actual observation. We especially focus on the map of average received signal power, often called *Radio Environment Map* (REM), for a fixed transmitter such as TV broadcaster and cellular base station.

Geostatistics for Radio Environment Analysis

Overview of Spatial Interpolation in Wireless Communications

In the frequency reuse over the spatial domain, such as in cellular systems and spectrum sharing over TVWS, the average received signal power and communication coverage are important factors for appropriate interference management between transmitters. The measurement-based spectrum database can accurately estimate the information via the map of the average received signal power, often called REM. In this section, we introduce the fundamentals of map cartography.

In wireless communications, the instantaneous received signal power from a transmitter is often modeled as

$$\begin{aligned} P_{\mathrm{Rx}}(\boldsymbol{x}) &= P_{\mathrm{Tx}} - 10\eta \log_{10} ||\boldsymbol{x}_{\mathrm{Tx}} - \boldsymbol{x}|| + W(\boldsymbol{x}) + F \quad [\mathrm{dBm}] \\ &= \overline{P}_{\mathrm{Rx}}(\boldsymbol{x}) + F, \end{aligned} \tag{1}$$

where $\boldsymbol{x}$ is the receiver location, $\boldsymbol{x}_{\mathrm{Tx}}$ is the transmitter location, P_{Tx} [dBm] is the transmission power, η is the path loss index, W [dB] is the log-normal shadowing with zero mean and standard deviation σ [dB], and F [dB] is the effect of multipath fading. Because the communication coverage depends on $\overline{P}_{\mathrm{Rx}}(\boldsymbol{x})$ and the value is uniquely determined by the receiver location, the main task of the map is to provide $\overline{P}_{\mathrm{Rx}}(\boldsymbol{x})$ accurately.

When the database collects radio environment information measured by mobile terminals, as shown in Fig. 3, the database consists of instantaneous received signal power, including the multipath fading factor F. In order to obtain $\overline{P}_{\mathrm{Rx}}$, the measurement area is divided into a square grid with a side length of a few meters, and the instantaneous information is averaged in each grid. Here, by only averaging such datasets, the tooth missing map can be obtained, as shown on the right side of Fig. 3. Therefore, after averaging, we need to consider the interpolation of the tooth missing information.

The spatial interpolation can be implemented by considering the spatial correlation of shadowing. It is empirically known that shadowing has a spatial correlation that follows the function [10]

$$\begin{aligned}\rho_{i,j} &= \frac{\mathrm{E}\left[W(\boldsymbol{x}_i)W(\boldsymbol{x}_j)\right]}{\sigma_i \sigma_j} \\ &\approx \exp\left(-\frac{||\boldsymbol{x}_i - \boldsymbol{x}_j||}{d_{\mathrm{cor}}}\ln 2\right),\end{aligned} \tag{2}$$

where d_{cor} [m] is the correlation distance. Therefore, by taking the weighted average shown in the following equation and assigning suitable weight factors, we can implement a highly accurate spatial interpolation:

$$\hat{Z}(\boldsymbol{x}_0) = \sum_{i=1}^{N} \omega_i Z(\boldsymbol{x}_i), \tag{3}$$

where Z is a random variable, N is the number of datasets, $\boldsymbol{x}_0$ is the interpolated location, $\boldsymbol{x}_i$ is the measured location, and ω_i is the weight factor multiplied to $Z(\boldsymbol{x}_i)$. Intuitively, by assigning a high weight factor for nearby datasets and a small weight factor for distant datasets, an accurate interpolation will be performed. Estimation problems for such spatially random variables have been established in the field of geostatistics (see [11, 12]), and recent works show the effects in the field of wireless communications [3].

Inverse distance weighting (IDW) is the simplest technique for spatial interpolation. This method designs ω_i according to the inverse of the distance from the interpolation point to the pth power, and ω_i is calculated by the following equation:

$$\omega_i = \frac{1}{\sum_{j=1}^{N} ||\boldsymbol{x}_0 - \boldsymbol{x}_j||^p} \cdot \frac{1}{||\boldsymbol{x}_0 - \boldsymbol{x}_i||^p}. \tag{4}$$

Generally, a value of about 1–2 is set for p. However, because IDW produces a constant weight factor for a certain distance regardless of the spatial correlation characteristics of the random variable, its guideline leaves room for consideration.

On the other hand, *Kriging* determines the optimum weights that minimize the variance of the estimation error.

$$\sigma_k^2 = \mathrm{Var}\left[\hat{Z}(\boldsymbol{x}_0) - Z(\boldsymbol{x}_0)\right] \tag{5}$$

In the following section, we describe the procedure of the Kriging interpolation. After semivariogram modeling and ordinary Kriging are explained for a general random variable Z, we show the procedure for map cartography in wireless systems.

Semivariogram

Kriging methods are subdivided on the basis of the decision rule of ω_i and assumptions about Z, but all the methods must preliminarily estimate the spatial-covariance structure of the random process from the datasets.

In the field of geostatistics, the semivariogram is used for the analysis of the spatial-covariance structure, which is the semivariance of the difference of all pairs of points $Z(\boldsymbol{x}_i)$ and $Z(\boldsymbol{x}_j)$ at distance $\boldsymbol{h} \triangleq ||\boldsymbol{x}_i - \boldsymbol{x}_j||$,

$$\gamma(\boldsymbol{h}) = \frac{1}{2}\mathrm{Var}[Z(\boldsymbol{x}_i) - Z(\boldsymbol{x}_j)]. \tag{6}$$

The semivariogram allows the influence of a spatially varying mean to be filtered for sufficient small distances and does not depend on the mean of the field when the mean is constant:

$$\mathrm{Var}\left[Z(\boldsymbol{x}_i) - Z(\boldsymbol{x}_j)\right] = \mathrm{E}\left[\left(Z(\boldsymbol{x}_i) - Z(\boldsymbol{x}_j)\right)^2\right]. \tag{7}$$

To obtain the semivariogram in the measurement area, it is necessary to estimate the empirical semivariogram from the available data. Under the assumption of a constant mean, a natural estimator based on the method of moments can be written as

$$\hat{\gamma}(\boldsymbol{h}) = \frac{1}{2|N(\boldsymbol{h})|}\sum_{N(\boldsymbol{h})}\left\{Z(\boldsymbol{x}_i) - Z(\boldsymbol{x}_j)\right\}^2, \tag{8}$$

where $N(\boldsymbol{h})$ denotes the set of nodes that are separated by a distance $\boldsymbol{h}$. Note that this averaging procedure is called *binning*. Once $\hat{\gamma}(\cdot)$ has been estimated, it must be fitted into a theoretical semivariogram model. Table 1 summarizes the major theoretical semivariogram models. Here, τ^2, $\tau^2+\sigma^2$, σ^2, and $1/\phi$ are called *nugget*, *sill*, *partial-sill*, and *range*, respectively. Examples of the theoretical semivariogram models are shown in Fig. 4. In wireless communications, because the shadowing correlation follows the exponential function shown in Eq. (2), the exponential model is often chosen as the theoretical model.

Figure 5 draws an example of semivariogram modeling. All of $\{Z(\boldsymbol{x}_i) - Z(\boldsymbol{x}_j)\}^2/2$, called *variogram cloud*, are plotted in Fig. 5a. As shown in Fig. 5b, after the semivariograms are averaged over a given interval, the theoretical semivariogram can be fitted. Here, because $N(\boldsymbol{h})$ becomes smaller as $||\boldsymbol{h}||$ becomes larger, there is a problem in which the averaged semivariogram is used for curve fitting. This is generally determined by trial and error, and Cressie introduces a practical

Table 1 Examples of theoretical semivariogram models

Model	Equation
Linear	$\gamma(\boldsymbol{h}) = \begin{cases} \tau^2 + \sigma^2 \|\|\boldsymbol{h}\|\| & \text{if } \|\|\boldsymbol{h}\|\| > 0 \\ 0 & \text{otherwise} \end{cases}$
Spherical	$\gamma(\boldsymbol{h}) = \begin{cases} \tau^2 + \sigma^2 & \text{if } \|\|\boldsymbol{h}\|\| > 1/\phi \\ \tau^2 + \sigma^2 \left\{ \frac{3}{2}\phi \|\|\boldsymbol{h}\|\| - \frac{1}{2} (\phi \|\|\boldsymbol{h}\|\|)^3 \right\} & \text{if } 0 < \|\|\boldsymbol{h}\|\| < 1/\phi \\ 0 & \text{otherwise} \end{cases}$
Exponential	$\gamma(\boldsymbol{h}) = \begin{cases} \tau^2 + \sigma^2 \{1 - \exp(-\phi \|\|\boldsymbol{h}\|\|)\} & \text{if } \|\|\boldsymbol{h}\|\| > 0 \\ 0 & \text{otherwise} \end{cases}$
Gaussian	$\gamma(\boldsymbol{h}) = \begin{cases} \tau^2 + \sigma^2 \{1 - \exp(-\phi^2 \|\|\boldsymbol{h}^2\|\|)\} & \text{if } \|\|\boldsymbol{h}\|\| > 0 \\ 0 & \text{otherwise} \end{cases}$

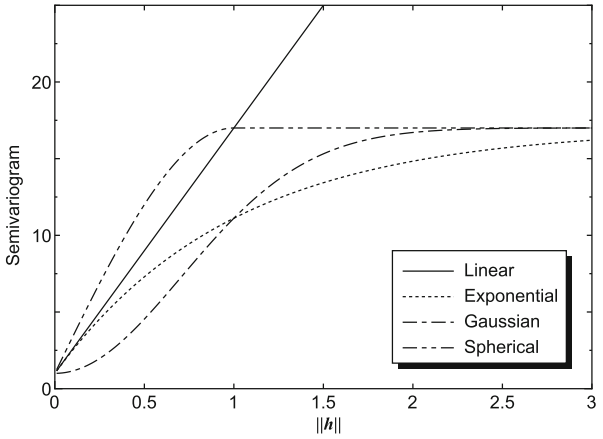

Fig. 4 Examples of theoretical semivariogram where $\tau = 1.0$, $\sigma = 4.0$ and $\phi = 1.0$

rule: the averaged semivariogram, in which $N(\boldsymbol{h}) > 30$ and $||\boldsymbol{h}||$ are smaller than the maximum $||\boldsymbol{h}||$, is used for curve fitting, as a guideline [13].

Ordinary Kriging

Ordinary Kriging is assumed to be constrained in the local neighborhood of each estimation point, i.e., $\mathrm{E}[Z(\boldsymbol{x})] = const.$ for each nearby data value. In order to achieve the best linear unbiased estimator (BLUE), this method determines the weights that minimize the variance of the estimation error $\sigma_k^2 = \mathrm{E}[\{\hat{Z}(\boldsymbol{x}_0) - Z(\boldsymbol{x}_0)\}^2]$ under the condition

$$\sum_{i=1}^{N} \omega_i = 1. \tag{9}$$

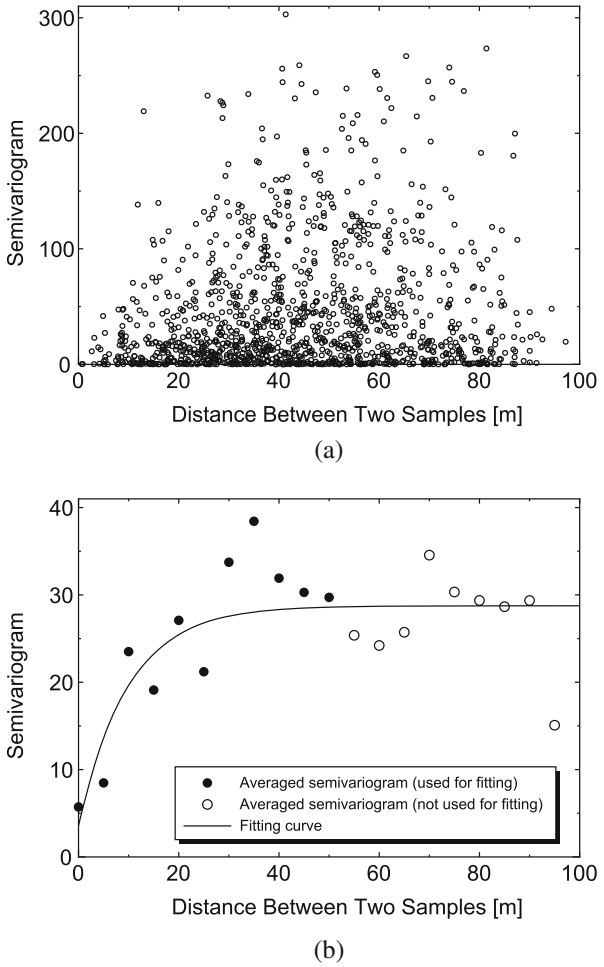

Fig. 5 Example of semivariogram modeling. (**a**) Variogram cloud. (**b**) Averaged variogram and estimated curve

This constraint can be derived from the condition of unbiased estimation,

$$\mathrm{E}\left[\hat{Z}(\boldsymbol{x}_0) - Z(\boldsymbol{x}_0)\right] = 0. \tag{10}$$

Using the Lagrange multiplier method, the objective function $\phi(\omega_i, \mu)$ can be written as

$$\phi(\omega_i, \mu) = \sigma_k^2 - 2\mu\left(\sum_{i=1}^{N}\omega_i - 1\right), \tag{11}$$

where μ is the Lagrange multiplier. Here, σ_k^2 can be written as the following equation:

$$\sigma_k^2 = -\gamma(d_{0,0}) - \sum_{i=1}^{N}\sum_{j=1}^{N}\omega_i\omega_j\gamma(d_{i,j}) + 2\sum_{i=1}^{N}\omega_i\gamma(d_{i,0}), \tag{12}$$

where $d_{i,j} \triangleq ||\boldsymbol{x}_i - \boldsymbol{x}_j||$.

From the partial derivatives in Eq. (12), we can obtain $N + 1$ simultaneous equations

$$\begin{pmatrix} \gamma(d_{1,1}) & \cdots & \gamma(d_{1,N}) & 1 \\ \gamma(d_{2,1}) & \cdots & \gamma(d_{2,N}) & 1 \\ \vdots & \vdots & \vdots & \vdots \\ \gamma(d_{N,1}) & \cdots & \gamma(d_{N,N}) & 1 \\ 1 & \cdots & 1 & 0 \end{pmatrix} \begin{pmatrix} \omega_1 \\ \omega_2 \\ \vdots \\ \omega_N \\ \mu \end{pmatrix} = \begin{pmatrix} \gamma(d_{1,0}) \\ \gamma(d_{2,0}) \\ \vdots \\ \gamma(d_{N,0}) \\ 1 \end{pmatrix}. \tag{13}$$

From the above simultaneous equations, the weights that minimize σ_k^2 can be derived. Here, the minimized σ_k^2 is called the *Kriging variance*, and σ_k is called the *Kriging standard deviation*.

Procedure for Received Signal Power Estimation

Both semivariogram modeling and ordinary Kriging shown above assume $\mathrm{E}[Z(\boldsymbol{x})] = const.$ for each nearby data value. On the other hand, $\mathrm{E}[P_{\mathrm{Rx}}(\boldsymbol{x})]$ is not constant because of the effect of path loss $10\eta\log_{10}||\boldsymbol{x}_{\mathrm{Tx}} - \boldsymbol{x}||$: such a location dependence is called a *trend* in the geostatistics. A way to consider the dependence is the use of *universal Kriging* (see [11]). If we apply ordinary Kriging for the map cartography, in a precise sense, the path loss modeling and the shadowing estimation should be separated as follows.

1. Path loss factor η and transmission power P_{Tx} are estimated from the dataset with a traditional method for path loss modeling such as the least squares (LS) method. Then, each shadowing factor is extracted via

$$\hat{W}(\boldsymbol{x}_i) = P_{\mathrm{Rx}}(\boldsymbol{x}_i) - \hat{P}_{\mathrm{Tx}} - 10\hat{\eta}\log_{10}||\boldsymbol{x}_{\mathrm{Tx}} - \boldsymbol{x}_i||, \tag{14}$$

   where $\hat{\eta}$ is the estimated path loss factor and $\hat{P}_{\mathrm{Tx}}$ is the estimated transmission power.
2. The variogram cloud between $\hat{W}(\boldsymbol{x}_i)$ is generated.
3. The theoretical semivariogram is fitted to the variogram cloud.

4. The weight factor ω_i is calculated via ordinary Kriging.
5. $P_{\mathrm{Rx}}(\boldsymbol{x}_0)$ is interpolated by

$$\hat{P}_{\mathrm{Rx}}(\boldsymbol{x}_0) = \hat{P}_{\mathrm{Tx}} - 10\hat{\eta}\log_{10}||\boldsymbol{x}_{\mathrm{Tx}} - \boldsymbol{x}_0|| + \sum_{i=1}^{N} \omega_i \hat{W}(\boldsymbol{x}_i). \tag{15}$$

Note that some works show that we can perform an accurate interpolation even when the semivariogram analysis and ordinary Kriging are applied directly to $P_{\mathrm{Rx}}(\boldsymbol{x}_i)$ [3, 14]. This is because the fluctuation of the path loss is gradual in the area away from the transmitter.

Here, Kriging has a powerful property: the statistical performance of the estimation error $\{\hat{Z}(\boldsymbol{x}_0) - Z(\boldsymbol{x}_0)\}$ can be roughly estimated via the Kriging standard deviation σ_k. If the random variable Z spatially fluctuates with a Gaussian process, the estimation error follows a Gaussian distribution. This behavior can be applied to typical radio propagation because the shadowing follows a logarithmic Gaussian process. Because this interpolation procedure achieves unbiased estimation, we can estimate that the error $\hat{P}_{\mathrm{Rx}}(\boldsymbol{x}_0) - P_{\mathrm{Rx}}(\boldsymbol{x}_0)$ nearly follows a log-normal distribution with mean 0 [dB] and standard deviation σ_k [dB] (Kriging standard deviation means the standard deviation of the estimation error under the perfect semivariogram modeling. Because the semivariogram is modeled from datasets, the true estimation error exceeds σ_k. Therefore, the upper bound of $\mathrm{E}[\sigma_k]$ is equal to the standard deviation of the estimation error [11]).

Effect of Measurement-Based Spectrum Database on Spectrum Sharing

Let us discuss the effect of the knowledge of radio propagation information on spectrum sharing from a theoretical perspective. Now, we consider a typical spectrum-sharing environment in which a secondary transmitter shares a spectrum with a primary link, as shown in Fig. 6. To evaluate the spectrum-sharing efficiency, we calculate the allowable transmission power at the secondary transmitter under given channel information. Note that the following discussion does not consider the knowledge of instantaneous multipath fading gain: the SU only knows the path loss gain and shadowing gain. This is because the acquisition of the instantaneous factor requires some feedback from the primary receiver. On the other hand, in spectrum sharing with legacy wireless systems, such feedback is *not* a realistic

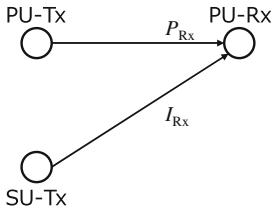

Fig. 6 Spectrum-sharing model

assumption. Aiming for the improvement of spectrum-sharing efficiency in the legacy systems, this section considers the case with no instantaneous feedback from the PUs.

Spectrum-Sharing Model

First, P_{Rx} [dBm] is defined as the received signal power at the primary receiver PU-Rx from the primary transmitter PU-Tx. We assume the value fluctuates according to the path loss and the log-normal shadowing, as follows:

$$P_{\mathrm{Rx}} = P_{\mathrm{P,\,Tx}} - L_{\mathrm{P}} + W_{\mathrm{P}} \quad [\mathrm{dBm}] \tag{16}$$

$$\triangleq \overline{P}_{\mathrm{Rx}} + W_{\mathrm{P}}, \tag{17}$$

where $P_{\mathrm{P,\,Tx}}$ [dBm] is the transmission power at PU-Tx, L_{P} [dB] is the path loss in the primary link, and W_{P} [dBm] is the shadowing gain following an i.i.d. log-normal distribution with zero mean and standard deviation σ_{P} [dB].

Next, we assume that SU-Tx interferes with PU-Rx with the following power:

$$I_{\mathrm{Rx}} = P_{\mathrm{S,\,Tx}} - L_{\mathrm{S}} + W_{\mathrm{S}} \quad [\mathrm{dBm}] \tag{18}$$

$$\triangleq \overline{I}_{\mathrm{Rx}} + W_{\mathrm{S}}, \tag{19}$$

where $P_{\mathrm{S,\,Tx}}$ is the transmission power at SU-Tx, L_{S} is the path loss in the interference link, and W_{S} is the shadowing gain. W_{S} follows an i.i.d. normal distribution with zero mean and standard deviation σ_{S} [dB] and is statistically independent from W_{P}. Under the above conditions, we utilize the SIR as the protection criterion for primary communication according to a typical rule of spectrum sharing. Here, the SIR at PU-Rx can be written as

$$\Gamma = P_{\mathrm{Rx}} - I_{\mathrm{Rx}} \quad [\mathrm{dB}]. \tag{20}$$

If the PU determines the desired SIR as Γ_{d} [dB], the outage event can be formulated as $\Gamma_{\mathrm{d}} > \Gamma$. Thus, considering the desired protection probability $1 - p_{\mathrm{out}}$, the SU must satisfy the protection probability at PU-Rx, given by the following equation:

$$\Pr[\Gamma \geq \Gamma_{\mathrm{d}}] \geq 1 - p_{\mathrm{out}}. \tag{21}$$

Using the channel information in both the primary link and the interference link, SU-Tx estimates the maximum transmission power

$$\max P_{\mathrm{S,\,Tx}} \triangleq P_{\mathrm{S,\,max}} \quad [\mathrm{dBm}], \tag{22}$$

which is subject to Eq. (21). We analyze the performance of the maximum transmission power under two conditions: P_{Rx} can be estimated via the measurement-based

spectrum database, and only $\overline{P}_{\mathrm{Rx}}$ and σ_{P} can be estimated. For simplicity, we assume that both of the conditions only include information on L_{S} and σ_{S} for the interference link.

Error Characteristics of Geostatistics-Assisted Radio Propagation Estimation

Before discussing the performance of the database-assisted spectrum sharing, we model the error characteristics of the geostatistical radio propagation estimation. Let us define $\hat{P}_{\mathrm{Rx}}$ [dBm] as the estimated values for P_{Rx}. By introducing the error factor ε_{P} [dB], the relationship between the estimated and true values can be written as

$$\begin{aligned}\hat{P}_{\mathrm{Rx}} &= P_{\mathrm{Rx}} - \varepsilon_{\mathrm{P}} \\ &= \left(\overline{P}_{\mathrm{Rx}} + W_{\mathrm{P}}\right) - \varepsilon_{\mathrm{P}}.\end{aligned} \tag{23}$$

We assume that $\hat{P}_{\mathrm{Rx}}$ is estimated by the Kriging-based database construction. As mentioned in section "Procedure for Received Signal Power Estimation", if the received signal power follows a log-normal distribution, the estimation error follows a log-normal distribution with median zero [dB]. Because the estimated and true values are highly correlated in the log domain, P_{Rx} and $\hat{P}_{\mathrm{Rx}}$ follow a bivariate normal distribution with median $\overline{P}_{\mathrm{Rx}}$ and covariance matrix

$$\begin{pmatrix} \sigma_{\mathrm{P}}^2 & \rho_{\mathrm{P}}\sigma_{\mathrm{P}}\sigma_{\hat{P}_{\mathrm{Rx}}} \\ \rho_{\mathrm{P}}\sigma_{\hat{P}_{\mathrm{Rx}}}\sigma_{\mathrm{P}} & \sigma_{\hat{P}_{\mathrm{Rx}}}^2 \end{pmatrix}, \tag{24}$$

where σ_{P} [dB] is the standard deviation of W_{P}, $\sigma_{\hat{P}_{\mathrm{Rx}}}$ is the standard deviation of $\hat{P}_{\mathrm{Rx}}$, and ρ_{P} is the correlation coefficient between P_{Rx} and $\hat{P}_{\mathrm{Rx}}$. The PDF of $\varepsilon_{\mathrm{P}} = P_{\mathrm{Rx}} - \hat{P}_{\mathrm{Rx}}$ can be derived from the bivariate normal distribution. Because ε_{P} consists of the difference between two variables following a bivariate normal distribution and Kriging can perform unbiased estimation, ε_{P} also follows a log-normal distribution with median zero. In addition, its variance can be calculated by

$$\sigma_{\varepsilon_{\mathrm{P}}}^2 = \sigma_{\mathrm{P}}^2 + \sigma_{\hat{P}_{\mathrm{Rx}}}^2 - 2\rho_{\mathrm{P}}\sigma_{\mathrm{P}}\sigma_{\hat{P}_{\mathrm{Rx}}}. \tag{25}$$

For simplicity, we approximate $\sigma_{\hat{P}_{\mathrm{Rx}}}$ by σ_{P}. From this relationship, $\sigma_{\varepsilon_{\mathrm{P}}}^2$ can be derived as

$$\sigma_{\varepsilon_{\mathrm{P}}}^2 \approx 2\sigma_{\mathrm{P}}^2\left(1 - \rho_{\mathrm{P}}\right). \tag{26}$$

Using these characteristics, we can easily emulate the Kriging-based radio propagation estimation by σ_{P} and ρ_{P}. Note that ρ_{P} strongly depends on the estimation conditions, such as the number of datasets and the correlation distance of the shadowing. In addition, $\sigma_{\varepsilon_{\mathrm{P}}}^2$ can be directly estimated from the Kriging variance σ_k^2.

Performance of Spectrum-Sharing Capability

According to the error characteristics mentioned above, we derive the allowable transmission power of SU-Tx $P_{\mathrm{S,max}}$ that satisfies the interference constraint defined in Eq. (21).

First, for the comparison, we derive the allowed transmission power when the SU-Tx only knows $\overline{P}_{\mathrm{Rx}}$ and σ_{P}. In this situation, the SIR follows a log-normal distribution with a median $\overline{P}_{\mathrm{Rx}}-\overline{I}_{\mathrm{Rx}}$ and a standard deviation $\sqrt{\sigma_{\mathrm{P}}^2+\sigma_{\mathrm{S}}^2}$. Therefore, its cumulative distribution function (CDF) can be formulated as

$$F_{\Gamma}(\Gamma_{\mathrm{d}}|\overline{P}_{\mathrm{Rx}},L_{\mathrm{S}}) = \frac{1}{2}\left\{1+\mathrm{erf}\left(\frac{\Gamma_{\mathrm{d}}-\left(\overline{P}_{\mathrm{Rx}}-\overline{I}_{\mathrm{max}}\right)}{\sqrt{2\left(\sigma_{\mathrm{P}}^2+\sigma_{\mathrm{S}}^2\right)}}\right)\right\} \tag{27}$$

$$= p_{\mathrm{out}}, \tag{28}$$

where $\mathrm{erf}(\cdot)$ is the error function and $\overline{I}_{\mathrm{max}} \triangleq P_{\mathrm{S,\,max}} - L_{\mathrm{S}}$ is the median of the allowed interference power. Therefore, the allowed transmission power can be determined by

$$\begin{aligned} P_{\mathrm{S,\,max}} &= L_{\mathrm{S}} + \overline{I}_{\mathrm{max}} \\ &= L_{\mathrm{S}} + \overline{P}_{\mathrm{Rx}} - \Gamma_{\mathrm{d}} - \sqrt{2(\sigma_{\mathrm{P}}^2+\sigma_{\mathrm{S}}^2)}\mathrm{erf}^{-1}(1-2p_{\mathrm{out}}), \end{aligned} \tag{29}$$

where $\mathrm{erf}^{-1}(\cdot)$ is the inverse error function.

Next, we evaluate the performance in which the SU-Tx can estimate the signal power P_{Rx} via the measurement-based spectrum database. Because the SU-Tx knows $\hat{P}_{\mathrm{Rx}}$ and $\overline{I}_{\mathrm{Rx}}$, the SIR $\Gamma = (\hat{P}_{\mathrm{Rx}}+\varepsilon_{\mathrm{P}})-I_{\mathrm{Rx}}$ follows a log-normal distribution with median $\hat{P}_{\mathrm{Rx}} - \overline{I}_{\mathrm{Rx}}$ and standard deviation $\sqrt{\sigma_{\varepsilon_{\mathrm{P}}}^2+\sigma_{\mathrm{S}}^2}$. Thus, based on the condition of $P_{\mathrm{S,\,max}}$, we can formulate the CDF of the SIR as

$$F_{\Gamma}(\Gamma_{\mathrm{d}}|\hat{P}_{\mathrm{Rx}},L_{\mathrm{S}}) = \frac{1}{2}\left\{1+\mathrm{erf}\left(\frac{\Gamma_{\mathrm{d}}-\left(\hat{P}_{\mathrm{Rx}}-\overline{I}_{\mathrm{max}}\right)}{\sqrt{2\left(\sigma_{\varepsilon_{\mathrm{P}}}^2+\sigma_{\mathrm{S}}^2\right)}}\right)\right\} \tag{30}$$

$$= p_{\mathrm{out}}. \tag{31}$$

Therefore, $\overline{I}_{\mathrm{max}}$ can be formulated as

$$P_{\mathrm{S,\,max}} = L_{\mathrm{S}} + \hat{P}_{\mathrm{Rx}} - \Gamma_{\mathrm{d}} - \sqrt{2\left(\sigma_{\varepsilon_{\mathrm{P}}}^2+\sigma_{\mathrm{S}}^2\right)}\mathrm{erf}^{-1}(1-2p_{\mathrm{out}}). \tag{32}$$

A numerical example is shown in Fig. 7. If the SU-Tx only knows $\overline{P}_{\mathrm{Rx}}$ and σ_{P}, the spectrum-sharing opportunity decreases in proportion to the intensity of the shadowing variation. The measurement-based spectrum database can improve performance, although $\hat{P}_{\mathrm{Rx}}$ has an estimation error.

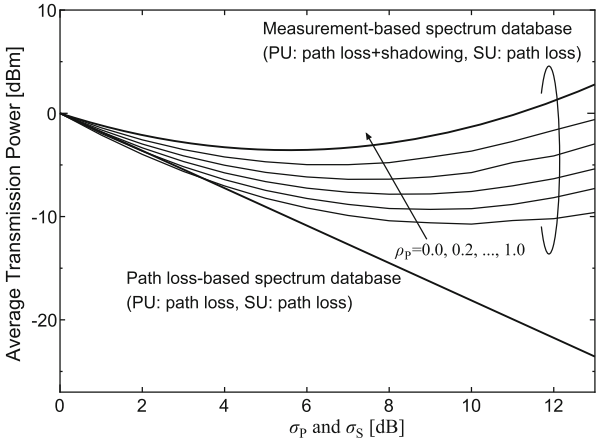

Fig. 7 Effects of channel state information on average transmission power where $p_{\text{out}} = 0.10$, $\Gamma_{\text{d}} = 10$ [dB], $L_{\text{S}} = 100.0$ [dB], and $\overline{P}_{\text{Rx}} = -90.0$ [dBm]

Future Smart Spectrum World

Spectrum Allocation Policy and Smart Spectrum

In the current spectrum allocation policy, International Telecommunication Union Radiocommunication Sector (ITU-R) decides the global spectrum allocation policy, and the detailed spectrum utilization is allocated in each country by a spectrum regulator, such as the FCC in the USA, Ofcom in the UK, and the Ministry of Internal Affairs and Communications (MIC) in Japan. Roughly speaking, spectrum allocation policies can be categorized into two types. One is "Command and Control," and the other is "Spectrum Commons." "Command and Control" is the spectrum management policy in which the regulator centrally allocates the spectrum to systems with the usage of the spectrum. Therefore, the spectrum is allocated to systems without duplication. On the other hand, "Spectrum Commons" is the spectrum-sharing method in which the users access the spectrum in a distributed manner. The Industry, Science, and Medical radio (ISM) band is a spectrum managed by a "Spectrum Commons" policy. "Command and Control" can exclusively allocate the spectrum to a certain system to avoid intersystem interference. Currently, almost all licensed spectra are exclusively allocated to the system. However, exclusive allocation may reduce the spectrum efficiency because it is required to give a spatial margin for sharing multiple systems in the same spectrum. Moreover, even if the system does not continuously transmit radio waves due to the various traffic, such as in a public safety system, the spectrum is occupied by the primary licensed systems. Therefore, spectrum redundancy over the spatial and time domains becomes a serious problem. On the other hand, "Spectrum Commons" can utilize the spectrum based on user demand.

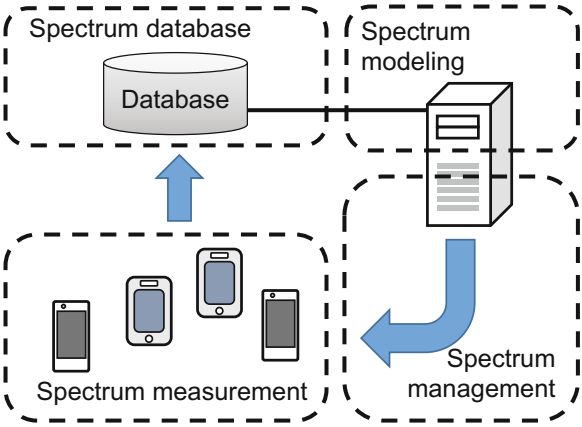

Fig. 8 Concept of smart spectrum

Currently, the listen-before-talk technique based on carrier sense function is used for wireless LANs and wireless sensor networks. However, because of its distributed control based on carrier sensing, the reliability of communication is not high. The hidden node problem and dense installed access points in the crowded area deteriorate the quality and throughput of distributed networks. In order to improve the spectrum utilization in future wireless networks, a smart-spectrum concept has been proposed [5]. The smart spectrum is a dynamic spectrum-utilization scheme based on measurement and modeling, in which on-demand spectrum allocation is applied for spectrum management. The basic issues of smart spectrum comprise four categories: spectrum measurement, modeling, database, and management, as shown in Fig. 8. The spectrum database is a key component of the smart spectrum, and the physical radio spectrum environment is projected into the spectrum database. In order to generate the spectrum database, the spectrum is modeled by gathering the results of the spectrum measurement at mobile terminals and/or measurement equipment. The spectrum allocation is managed by the spectrum manager in cooperation with the spectrum database. Therefore, the smart spectrum can utilize the spectrum according to the demand of the users by considering the exact radio environment based on spectrum efficiency and user demand.

Hierarchical Spectrum Database

The spectrum database can be used for managing the spectrum utilization of wireless systems. In a spectrum database defined by the FCC for TV white space, a simple database storing the spectrum availability according to location is installed in a large area. However, if we consider the measurement-based spectrum database, a large amount of spectrum data with locality must be registered in the database. In order to support the spectrum data with different granularities and supporting areas, the spectrum database with a hierarchical structure is considered, as shown

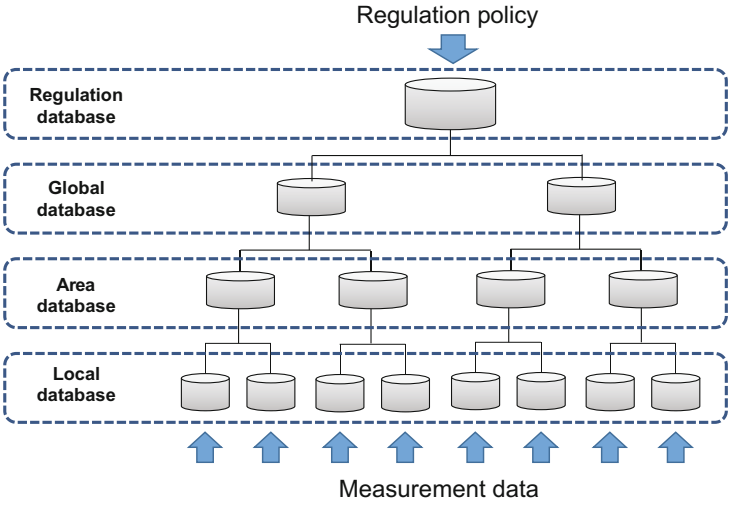

Fig. 9 Example hierarchical spectrum database

in Fig. 9 [5]. The upper layer of the hierarchical spectrum database can be used to define the spectrum regulation policy. For example, the data in this database can be registered and updated by the radio regulators of each country, like the FCC, Ofcom, and MIC. A small number of databases are prepared in each country. However, the lower layer of the hierarchical spectrum database supports a small area, and the measurement data generated by local mobile terminals can be registered. The spectrum environment of each location is managed in a distributed manner. The measurement results are statistically processed, and a self-organizing spectrum allocation according to user demand can be supported. The middle-layer databases can be used for coordinating (1) the upper layer spectrum policy and the lower-layer measurement-based spectrum environment and (2) the adjacent databases belonging to the lower layer for smooth spectrum allocation beyond the supporting area of each local database. The lowest-layer spectrum database may be located in each mobile terminal, and the spectrum database in the second-lowest layer may be located in the access point of wireless LAN systems or the base station of cellular networks.

The spectrum database can manage the spectrum of its supporting area in conjunction with spectrum servers. An example of spectrum management using the spectrum server and the spectrum database is shown in Fig. 10. The users request the spectrum by a demand of communication, such as data rate, error rate, throughput, stability, and reliability, and the available spectrum is allocated to the users with consideration for the spectrum efficiency by the spectrum manager with the spectrum database. The spectrum efficiency can be improved compared with the current fixed-allocated spectrum because on-demand spectrum allocation can be realized. In particular, the real-time spectrum status can be recognized by the measurement results, on-demand spectrum assignment with efficient spectrum-

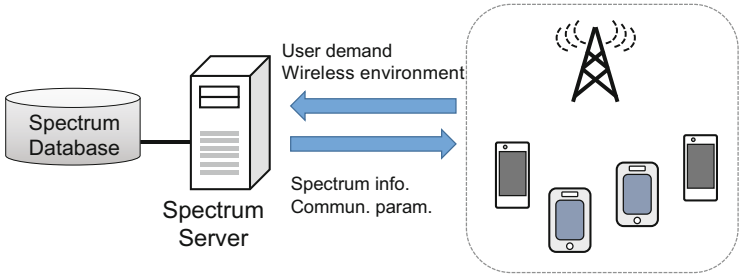

Fig. 10 Spectrum management server

sharing performance, and guaranteeing the user demand. Therefore, it can be considered that the hierarchical spectrum database with measurement results can change the current fixed-spectrum allocation policy.

In order to obtain the measurement results of the spectrum, wireless measurement equipment, like a spectrum analyzer, can be used. However, measurement equipment to gather the measurement results in every location is expensive. In order to solve the cost of measurement, crowd-sensing techniques using mobile terminals, such as smart phones, can be used. Today, the computational availability of mobile terminals increases, and multiple frequencies and systems are supported. Therefore, these terminals can be used for spectrum environment in a large area with low cost. Crowd sensing is a low-cost measurement technique and is already used for estimating the cellular performance by telecom operators [15].

Components of Smart Spectrum

Smart spectrum is a concept of dynamic spectrum management based on the measurement results from multiple terminals and statistical modeling for a future wireless world. The smart spectrum is realized by a cycle of components, which are spectrum measurement, modeling, database, and management, as shown in Fig. 8.

"Spectrum measurement" is the first step for obtaining the surrounding wireless environment. The typical measurement data is the received power of radio signals corresponding to the radio frequency. The basic technique is similar to spectrum sensing, and the following soft information is the basic measurement information for the smart spectrum.

$$P_r = \frac{1}{N} \sum_{n=1}^{N-1} |h[n]s[n] + w[n]|^2, \tag{33}$$

where $h[n]$ is the channel coefficient, $s[n]$ is the signal component, and $w[n]$ is the noise. N is the number of samples and n is the sample index. These sensed data are measured at each terminal and gathered in the spectrum database. The measurement

data can be expanded to other physical data, like angle of arrival, Doppler shift, delay spread, as well as network information, such as the number of active mobile terminals, throughput, and the location of mobile terminals.

"Spectrum modeling" is the statistical model of the measurement results for easy utilization of spectrum-sharing and reliable wireless communications. The typical statistical models are the averaged received power and the channel occupancy ratio. The averaged received power can be used for creating a spectrum map of the primary system. The channel occupancy ratio is useful for providing ON/OFF characteristics of wireless systems, like wireless LAN and other unlicensed systems. As these systems share the spectrum of the time domain, the channel occupancy ratio can be used for the basis of channel congestion for time-division spectrum sharing. In addition, the channel transition rate and the channel occupancy duration can be used for similar statistical information.

"Spectrum database" is used for storing the spectrum measurement data and modeling data for on-demand spectrum utilization. The hierarchical structure supports regulatory issues and local radio environments observed by the measurement results. The detailed structure is explained in the previous subsection.

Finally, "smart-spectrum management" is a dynamic spectrum management system according to the spectrum environment data stored in the spectrum database. On-demand spectrum allocation considering the user demand and current spectrum environment, considering spectrum efficiency, is the ultimate spectrum utilization for future wireless systems.

Case and Future Spectrum Policy Based on Smart Spectrum

Here, cases of a measurement-based spectrum database and its applications are introduced. Several reports of spectrum databases for TV white space (TVWS) have been published for estimating the area of TV broadcasting based on the measurement results [3,4]. The reference paper [3] discussed the linear interpolation technique for estimating the area of TV broadcasting by using the results of the measurement campaign in the UK. The reference paper [4] discussed the comparison with the current propagation model-based spectrum database and the measurement-based spectrum database by using the results of the measurement campaign in Japan. The accurate received power estimation performance by using the measurement-based spectrum database is confirmed. The similar idea has been considered in cellular networks for minimizing the drive test to check the communication quality in the support area using user equipment measurement logging in the 3GPP standard [15]. These cases assume that the transmitter is fixed like a TV broadcasting station and cellular base station. The measurement-based spectrum database for the distributed system has been reported for vehicle-to-vehicle (V2V) communication [16]. This database can be used for predicting the communication reliability of the intersection with many buildings in advance, and the usual broadcast-based V2V packets like IEEE 802.11p can be used as the dataset storing in the database, as shown in Fig. 11. The issue with this database is that

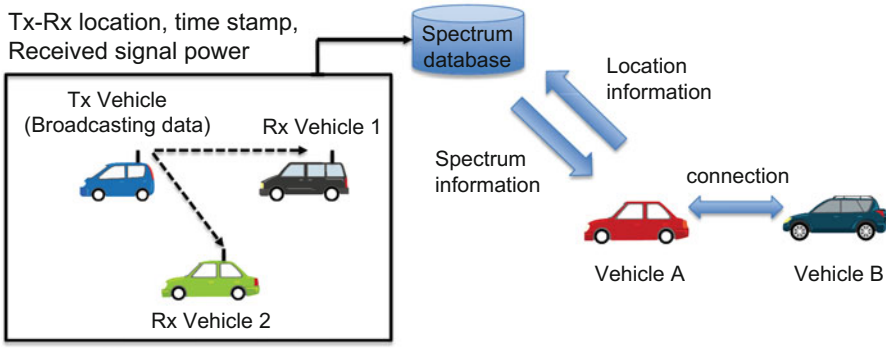

Fig. 11 Sepctrum database for V2V communication

the registered data becomes large because the database must be prepared for each transmit position. The appropriate mesh size and the database support area are important practical databases. It can be used for automated and connected vehicles with highly reliable wireless communications according to the demand.

As seen in this section, the smart spectrum can be used for smart dynamic spectrum utilization considering the local wireless environments and user demand as well as the radio regulation policy. The smart spectrum can be used not only to improve spectrum-sharing performance but also to guarantee reliable communication because the exact spectrum environment can be known at communication terminals. As a result, the current spectrum allocation policy can be changed by using smart spectrum, and a new wireless world with highly efficient spectrum use can be realized in the future.

Conclusion and Future Directions

More than 100 years, spectrum allocation regulation policy has been based on exclusive spectrum use by a primary system determined by the regulator in each country. However, exclusive spectrum use degrades the spectrum utilization efficiency due to inflexible spectrum use without considering demands of users. Cognitive radio and software defined radio technologies have possibility to change this regulation policy to more flexible spectrum use according to the demand of users. The most important issue for launching the new dynamic spectrum allocation is to recognize the exact wireless environment. Recognizing the accurate wireless environment can avoid intersystem interference with minimum spatial separation. In this chapter, we have introduced spectrum databases for providing wireless environment information to users. We have shown that the measurement-based spectrum database can improve the accuracy of the wireless environment recognition. We have also introduced the concept of smart spectrum which is a future spectrum management based on spectrum measurement, spectrum modeling,

spectrum database and smart spectrum management. By using the smart spectrum, the current exclusive spectrum allocation can be changed to on-demand spectrum allocation with highly efficient spectrum use in the future.

References

1. FCC (2008) In the matter of unlicensed operation in the TV broadcast bands, additional spectrum for unlicensed devices below 900 MHz and in the 3 GHz band. FCC adopted rules for unlicensed use of television white spaces documents
2. Ofcom (2014) TV white spaces: pilot database provider contract
3. Achtzehn A, Riihijärvi J, Mähönen P (2014) Improving accuracy for TVWS geolocation databases: results from measurement-driven estimation approaches. In: Proceeding of IEEE DySPAN April 2014, McLearn, VA, pp 392–403
4. Sato K, Kitamura M, Inage K, Fujii T (2015) Measurement-based spectrum database for flexible spectrum management. IEICE Trans Commun E98-B(10):2004–2013
5. Fujii T, Umebayashi K (2017) Smart spectrum for future wireless world. IEICE Trans Commun E100-B(9):1661–1673
6. Okumura T, Ohmori E, Fukuda K (1968) Field strength and its variability in VHF and UHF land mobile service. Rev Elec Commun Lab 16:825–873
7. Hata M (1980) Empirical formula for propagation loss in land mobile radio services. IEEE Trans Veh Tech 29:317–325
8. European Cooperative in the Field of Science and Technical Research EURO-COST 231 (1991) Urban transmission loss models for mobile radio in the 900 and 1800 MHz bands. rev.2
9. Phillips C, Sicker D, Grunwald D (2011) Bounding the error of path loss models. In: Proceeding of IEEE DySPAN May 2011, Aachen, pp 71–82
10. Gudmundson M (1991) Correlation model for shadow fading in mobile radio systems. Electron Lett 27(23):2145–2146
11. Cressie N (1993) Statistics for spatial data. Wiley, New York
12. Gelfand A, Diggle P, Guttorp P, Fuentes M (2010) Handbook of spatial statistics. CRC Press, Boca Raton
13. Cressie N (1985) Fitting variogram models by weighted least squares. Math Geol 12(2): 115–125
14. Sato K, Fujii T (2017) Kriging-based interference power constraint: integrated design of the radio environment map and transmission power. IEEE Trans Cog Commun Netw 3(1):13–25
15. Study on minimization of drive-tests in next generation networks;(release 9), 3GPP TR 36.805, Technical report
16. Katagiri K, Sato K, Fujii T (2017) Crowdsourcing-assisted radio environment maps for V2V communication systems. In: Proceeding of IEEE VTC 2017-Fall, Toronto, pp 1–5

Dynamic Spectrum Access for Machine to Machine Communications: Opportunities, Standards, and Open Issues

56

Luca Bedogni, Marco Di Felice, and Luciano Bononi

Contents

Abstract

Cognitive radio can be applied to a multitude of domains, one of which is M2M communication. Specifically, M2M communication refers to communication between devices without human intervention. Hence, devices should be able to organize themselves and run the communication protocol autonomously. If cognitive radio is used, tasks such as dynamic spectrum access (DSA), spectrum sensing, and alike present additional challenges compared to traditional network, as all the decision framework should be implemented and automatized in the

L. Bedogni · M. Di Felice (✉) · L. Bononi
Department of Computer Science and Engineering, University of Bologna, Bologna, Italy
e-mail: luca.bedogni4@unibo.it; marco.difelice3@unibo.its; luciano.bononi@unibo.it

W. Zhang (ed.), *Handbook of Cognitive Radio*,
https://doi.org/10.1007/978-981-10-1394-2_57

devices. In this chapter, we focus on DSA techniques for M2M. The main difference from other kinds of communication is relative both to the energy efficiency and to the low protocol overhead, as devices should run for long periods of time and run without human intervention. At first we present related work from literature, categorizing the different tasks devices which want to leverage DSA on M2M have to perform. At the end of the chapter, we present a proof of concept of a general framework, which can be applied to different scenario concerning M2M, encompassing all the spectrum management and measurement tasks M2M devices should generally perform. Finally, we derive open challenges and future research directions concerning this scenario.

Introduction

Machine to machine (M2M) communication refers to interactions which occur between devices with no human intervention. M2M has gained attention mostly thanks to the Internet of things (IoT) paradigm, where a multitude of devices communicate together with little to no human intervention. M2M communication inherently has such unique characteristics which differ from standard communication and is typically used on resource limited devices, hence posing additional constraints on the communication.

Over the years, many proposals, technologies, and standards have been proposed and are used to realize the M2M paradigm. However, such a plethora of different technologies also raises challenges on the interoperability and ability to communicate. The risk is to create the so-called intranet of things, or islands of things, meaning that devices are able to communicate only within the same ecosystems.

This heterogeneous scenario, in which different manufacturers and consortiums develop different technologies, is due to the extreme diverse scenario in which M2M communication can take place. These can span from healthcare scenarios, in which M2M technologies should provide reliability in the first place, to video surveillance installation, in which also the data rate is an important aspect. Productive scenario, such as predictive maintenance, often requires long operational times; hence, energy efficiency is key. All of the above has contributed in creating a vast ecosystem, in which different technologies share some characteristics and differ in other.

Besides the aforementioned scenarios, also cognitive M2M technologies can play an important role. Basically, cognitive networks sense the environment and reconfigure their communication parameters in order to better adapt to the scenario and possibly communicate. Among all the facets of cognitive networks, one of the most studied and investigated is certainly dynamic spectrum access (DSA), through which cognitive networks can transmit in the so-called spectrum holes, that is, part of the spectrum which are currently free and not occupied by others. Clearly, DSA requires extra computation on the device side, hence requiring more performing hardware and possibly reducing the energy efficiency.

In this chapter we present the different technologies, standards, and applications of M2M technologies. We also derive potential challenges and future research work on the topic.

Use Cases

In this section we review the applications that would benefit from cognitive M2M communication. In general, cognitive M2M communication helps deploying services in specific scenarios. For instance, M2M communication deployed in TVWS is beneficial for applications requiring an extended range compared to classical wireless solutions and for applications requiring good propagation through obstacles like building walls. This is especially interesting for indoor/outdoor networks, in which nodes are placed inside homes and need to communicate between each other as well as with other buildings. For instance, the new smart grid network is certainly a good representative of this category, as nodes should gather the consumptions of the home and balance the load of the network by aggregating the data coming from different sources.

Smart Grid Communication

One of the most prominent and most investigated topics regarding M2M communication in general, and specifically with TVWS, is certainly smart grid communication. Nowadays, and with a foreseen increase in presence over the next years, utility meters will be deployed in homes to report consumptions and balance the load. The scenario is that of multiple sensor devices deployed in homes, which monitor and report loads either to an in-home aggregator or to the utility operator. The former is for automatic balance of the consumptions locally; the latter is to enable the operator to balance the network.

As said, TVWS have been widely studied specifically for this scenario, due to their characteristics which make them appealing for such a deployment. The possibility to cover large distances, even if the meters are located in the basement [4], and the reduced energy consumptions to send data locally [3] are just two of the characteristics of TVWS that are interesting for this specific scenario.

Specifically in [59] it has been firstly seen in the term cognitive M2M (CM2M), to enhance the flexibility and the reliability of M2M communication.

There is a natural bind between devices needed in a smart utility network (SUN) like the smart grid and the TVWS device classes. In [49] it is highlighted this, which candidates TVWS as one of the most prominent technologies to realize these kind of networks. They identify four classes of devices needed in SUNs, namely: – Utility provider base station – Data collector – Utility meter – Mobile data collector They bind to the different classes of TVWS devices foreseen by regulations. The base station is clearly the static device, which is able to transmit at high power (up to 4 W) and thus covers larger distances. The data collector and

the utility meter are, respectively, Mode II and Mode I devices. They do not need sensing capabilities, which are instead required by the mobile data collector, carried by operators to gather data from meters. TVWS would be beneficial for SUNs thanks to the larger coverage range, which make them attractive particularly in rural areas.

This is also the path taken by [10], which present a test-bed deployed in Scotland specifically focused on smart grid communication. The motivation leading to the use of TVWS is mainly economical: more expensive systems such as fiber optic or DSL are not economically viable in rural areas, where few people live. Instead, TVWS are more economic and explored for this deployment, following results in [46]. The underlying protocol for this network test-bed is 802.11, which runs in the UHF bands instead of ISM bands over channel 57 (758–766 MHz). Another interesting feature, going toward the energy efficiency required by M2M communication, is that of a wind turbine for power supply mounted on top of the base station, making it autonomous from an energy supply. Wind power is an attractive option for Scotland, and clearly other options should be explored in other countries and environments, where wind may not be the most efficient method of energy production. The work presented in [10] is one of the first aimed at deploying an M2M network directly on the field.

Another work which studies the deployment of smart grid communication in TVWS is [4], which presents both a measurement study to deploy smart grid networks in TVWS and TV gray space and field results on the indoor propagation of narrowband signals in the TVWS. What emerges from the study is that the superior propagation characteristics of UHF bands are able to deliver the signal much farther compared to classical ISM bands. Moreover, it is interesting to note that if deployed indoors and at a low floor such as in the basements, the DVB-T receiver can easily compensate possible interference coming from the smart meters, thanks to the high directionality of its antenna.

The battery savings are presented in [3], where the authors foresee clusters of smart meters that communicate together through TVWS and one of them eventually reports the load measurements to the remote utility aggregator. Here the main advantage of TVWS networks relies in its duality: it can be used as a local communication technology, using low power but still penetrating obstacles better than technologies in higher-frequency bands. When needed, for instance, when the meter has to report the data to the aggregator, it can increase its transmitting power to cover a larger range.

Sensor Networks

Apart from the specific case of smart grid communication, as we already mentioned, M2M networks can also be built with the focus on energy efficiency. This allows building sensor networks in general with battery-powered devices, for a range of possible applications:

- Environmental monitoring: through TVWS networks it is easier to build large-scale networks for battery-powered devices, which by transmitting in narrowband channels can reduce their power consumption keeping a satisfactory transmission range.
- Industrial monitoring: wireless sensor networks have been deployed in several machines and automated tools, mainly for machinery condition-based maintenance. The use of M2M in this domain would help reduce the problems when machines are placed in hard-to-reach places, and thus shadowing effects could reduce the signal to undetectable levels.
- eHealth: in eHealth, devices could be either implanted in patients or deployed as wearable computing devices. They report the patient health with important parameters such as the heart rate or the blood oxygen level. Doctors can then monitor the patient remotely and be alarmed whenever health parameters fall below or rise above a predefined threshold.

ITS

Another interesting application of M2M communication is related to intelligent transportation systems (ITS). Here, cars report their state and gather information about the road situation, to possibly inform the driver of alternate paths in presence of road works or accidents. An important aspect is that vehicular communication happens at the ground level, and thus possible interference to the primary receiver is naturally mitigated.

Messages in safety VANETS are typically of two kinds: Emergency safety messages (ESM) and periodic beacon messages (PBM) [37]. The aim of the work is to show how to deliver ESM messages faster than classical dedicated short-range communication (DSRC), thanks to better propagation and penetration into other cars and buildings. Examples of ESM messages are stopped cars on blind turns, cars driving in the opposite way, or cars approaching too fast. Given their nature, it is straightforward to understand how reliable and fast the communication has to be. The classical approach for DSRC communication would be multihop, with vehicles relaying the message to eventually reach farther drivers. Although it is possible to enhance the IEEE 802.11p to meet stringent delivery requirements [17], it would still be challenging to guarantee the reception of the message to all the interested cars with such a congested network. Moreover, multihop communication raises the well-known problem of the broadcast storm, in which too many relays could interfere with each other and reduce the communication performance. Thus, the benefits for V2V are mainly in the longer transmission range, which make them ideal to deliver safety messages. At the same time, the challenges reside in the spectrum availability. ESM messages cannot depend solely on opportunistic communication, since in areas with scarcity of spectrum, or when the licensee is using its spectrum band, the ESM messages should still be delivered. So the main idea is to use opportunistic communication when available, but switch back to classical DSRC when this is not possible. Another issue to consider is about the

time needed to get the available channels on which the message should be delivered. For classic DSA protocols, the key challenge is to achieve this information rapidly, as the ESM message cannot be delayed. For the case of TVWS, the car should get the list of available channels from the remote spectrum database in advance, since this cannot be done when the emergency occur, so that the client already have to send the message; otherwise, it would incur in too much delay. So clients should ask in advance to the database or other clients what are the channels available on the road they are traveling [16]. This would reduce the time needed to send the ESM, as the car already has the channel list in which it can transmit when needed.

Studies in literature have also demonstrated the feasibility of the aforementioned approaches, like [2] and [29]. In [2] the test-bed is built in Massachusetts, while [29] is deployed in Japan. Both are realized thanks to the GNU radio platform and show in practice how it is possible to build VANETs using TVWS.

When we consider M2M communication for cars, it is also important to commonly agree on the protocol to be used. For vehicular communication, the IEEE standardized the well-known IEEE 802.11p protocol, in which are foreseen two periods of time: one is used to transmit safety messages over a common control channel (CCC) and the other one to offer services such as infotainment. One of the issues with 802.11p, analyzed in [17], is about the timely delivery of messages, particularly those containing safety information. A possible solution is to rely on licensed communication for mission critical messages and rely on DSA for all the other messages, such as control information. This also goes in the direction foreseen by [37], which proposes to use TVWS to transmit safety messages which could then reach farther cars and possibly use DSRC communication for critical information. Another possible protocol proposed for V2V communication is 802.11af, studied in this particular scenario in [60]. 802.11af for V2V is certainly feasible and an interesting option, which could also be used together as 802.11p, by using DSRC and 802.11af together, as we already stated before.

Industry 4.0 and IoT

An area which is not much explored but that can certainly represent one peculiar application scenario for M2M in TVWS is certainly the upcoming Industry 4.0. In this environment, machines and devices are able to talk without human intervention, to offer new and enhanced services, ranging from predictive analytics to enhanced services for the end users.

Industry 4.0 refers to the plethora of tools, technologies, and methodologies needed to revolutionize normal industries with enhanced technologies, such as wireless sensor network and big data, which will open up services which would had never been possible. For instance, wireless technologies should be adapted to this changing environment, which will likely have multiple devices running different standards, which need not to prevent others from working [53]. Here, multiple gateways, able to speak different wireless protocols, are envisioned, so that they can bring messages from one network to the other [15]. For instance, access to

users can be provided either through Ethernet or WiFi; however, this is not feasible for battery-powered devices, which might also be located in hard-to-reach places [42].

Another scenario which hugely benefits from M2M communication is predictive analytics [34], defined as the ability for a system to monitor its assets and forecast the remaining life of each one, hence optimizing maintenance and reducing downtimes. This is done by monitoring components and through big data analysis and machine learning techniques recognizes unusual behaviors, such as never seen before vibrations, exceeding threshold values, and so on. Then, maintenance may be performed to multiple components at once, reducing the costs and arguably maintaining machines in better health. In fact, the cost of replacing a component before its end of life is generally much lower than having the machine to stop for a period of time, waiting for that component to be replaced.

To realize the IoT vision, it needs a technology that glues together different networks together, like the TVWS, as IoT networks can be locally sparse. For example, smart crossing lights can broadcast their status to nearby cars, which in turn could dynamically update the travel time, to proactively activate smart objects at homes. What typically happen is that these communication links can be realized through different technologies. In the previous example, the crossing light might transmit locally using WiFi, the car could use the cellular connection, and the messages are delivered in the smart home through a DSL connection or fiber optic. In this heterogeneous scenario, TVWS is one of the candidate technologies to possibly offer a bridge to all these devices, since they could propagate the messages farther than other technologies and can thus deliver the messages to more devices. Crossing lights would then be able to talk between each other and disseminate locally not only their status but also on the crossroads, so cars can infer more information.

Even if this is only an example, it exemplifies the potential of M2M communication in TVWS. Longer range means potentially more devices to be connected and from which obtain and give data.

eHealth

Another interesting domain for TVWS M2M is that of eHealth services, in which patients are monitored through wireless devices, and enhanced medical services can be provided also in hard-to-reach areas. TVWS network can provide useful services such as patient monitoring and locate them in the premises of a hospital. In addition, TVWS networks can also realize the remote patient monitoring, so that people can still be monitored at home, by constantly communicating with the doctor, without the need for human intervention, which can be warned only when needed, by setting for instance appropriate triggers. Moreover, many medical devices rely on the wireless medical telemetry system (WMTS), which operates in similar bands of TVWS. Therefore, they would need little intervention to be adapted to also use a larger spectrum band. However, there are several interference issues that need to be

carefully studied, since medical devices would compete also with other, consumer-like devices in the same bands.

It is worth noting the ongoing development of an eHealth test-bed in the Philippines [27], aimed at connecting 100 sites in rural areas of Philippines. The goal/plan initially is to use TVWS as a public service allowing for connectivity for education, eHealth, eGovernment services, environmental sensor networks such as those used by PAGASA and DOSTs Project NOAH, as well as Internet access in public places such as halls and town plazas. The trial is ongoing, proceeding slowly, mostly due to a precise policy missing.

A similar trial is ongoing also in Africa [29], where Microsoft is partnering with the Botswana-University of Pennsylvania, to provide medical services in poorly connected regions. They selected TVWS since it represents a less costly, faster, and farther-reaching Internet connection that is a promising option for connecting the previously unconnected populations of remote and underserved areas." Thus, TVWS are again selected as a candidate technology to practically realize services where the communication range is an issue and also because they represent a cheaper technology, compared to other well-known wireless standards. In addition, it is worth to note that once TVWS will roll out, the economy of scale might decrease even more the price of the devices, as more TVWS chips will be produced. Also in Bhutan TVWS are currently investigated to provide last mile connectivity, particularly for eHealth services, as patients incur in high costs to reach healthcare centers.

Apart from human medicine, TVWS networks are also currently investigated for animal treatment and monitoring. In particular, recently the London Zoo partnered with Google [38] to monitor endangered species through the use of a TVWS network. Moreover, animals can also be viewed online through video streaming by people through the Internet. TVWS have been selected as the ideal technology as animals can be hidden behind trees or in caves, and therefore the carrier wireless technology in use should be resilient to environmental obstacles. In areas such as rainforests and deserts, where animals can travel long distances and where therefore it is difficult to monitor animals for long period of times, TVWS can definitely fill the technology gap by meeting these needs. The test-bed has been rolled out in the London ZOO, and it is planned to extend it also to wider areas. Apart from wild animals, there is also an interest in TVWS for livestock monitoring [51] through the use of smart geofences, which can monitor animals inside a huge area, thanks to the propagation characteristics of TV bands.

M2M Operational Characteristics

In this section we present the details of M2M characteristics and how these are tackled by cognitive networks.

Generally speaking, M2M communications are typically referred to small and battery-powered devices, although this is not always true. For instance, video surveillance cameras where it is also performed image recognition, either on the

edge or on the cloud, can be still seen as M2M, as no human intervention is performed in the middle of the communication. However, it is also true to say that most of the M2M deployed scenario envision small, battery-powered devices which report different kind of data to a central entity, in charge of analyzing them and inform the users. Clearly, the number of intermediate levels can change, as intermediate computation may be performed to achieve network optimization.

Focusing only on the communication slice of the picture, we define the following operational characteristics of M2M communication:

- **Self-instantiated**: no human intervention should be envisioned, like checking connectivity or acknowledging any sort of data in order to establish a new M2M connection.
- **Self-healing**: in case of network disruption, such as nodes that depart the network either voluntarily or because they have run out of batteries, the network should be able to heal itself.
- **Battery efficient**: although we mentioned that M2M communication can be in main powered devices, M2M communication should be designed to be energy efficient. Hence, M2M devices are typically sleeping and wake up only upon certain events. Hence, it should not be assumed that they can receive a message, and optional device configuration should be performed by the device station in reply to events on which M2M devices wake up.
- **Lightweight**: M2M protocol should also be designed to carry the minimum amount of protocol overhead possible, as this would require additional time and computation to be achieved, such as CRC an alike.
- **Multiple transmissions**: unlike human communication, M2M may perform many, simultaneous connections. Coupled with the battery efficiency requirement, this involves developing novel techniques to access the channel by M2M devices. Imagine the Industry 4.0 scenario, in which thousands of tiny devices installed report sensed data to a central entity. Clearly, these devices should access the channel fast, and the high number of them poses technical challenges on how this should be performed.
- **Heterogeneous kind of traffic**: M2M traffic can be characterized in two different shapes: `bursty` or `sporadic`. `Bursty` traffic refers to devices which typically sleep and when they wake up send a large amount of information. This may be surveillance cameras which perform image recognition locally and, only when something which requires additional analysis has to performed, send that information to a central entity. `Sporadic` refers to anything which is not bursty and comprises periodic beaconing of information to a central station.
- **Security**: although not a specific requirement of M2M communication, security can take a dual meaning in M2M communication. At first, there is the communication security, which may mean encryption. However, this should also be tailored to battery-powered devices; hence, it should not require excessive computation power. There is also the security of the device itself, since they can be stolen, and hence they should be able to sense unusual behaviors and events and report those to the central entity.

- **Latency**: depending on the scenario, latency may be or not a constraint. For critical scenario, such as eHealth, clearly latency becomes a more severe constraint. However, it is also worth to mention the latency when data has to be synchronized through different M2M devices, for instance, for predictive analytics, when considering Industry 4.0 scenarios or of building structure monitoring. There, latency becomes of paramount importance, to determine the sequence of events reported by different devices.

It is also worth to say that cognitive networks should be carefully tailored to meet M2M communication. For instance, tasks such as spectrum sensing and spectrum decision, which are normally battery consuming, have to be reengineered to meet the constraints this scenario poses. For this reason, among others, dynamic spectrum access and cognitive networks have a narrow area of application for M2M. In fact, the overhead needed by cognitive networks is not particularly suitable for battery-powered devices, which may waste considerable amount of energy to perform network maintenance and access tasks. In fact, in the M2M domain, typically network operations are performed vastly on a remote central unit, and less consuming tasks are left to the edge of the network, formed by the end nodes.

A fundamental difference which has to be made between different M2M scenarios is about the operational range. M2M scenarios can be built either for short-range or long-range communication, and several technologies and protocols have been proposed for both. In the following, we outline some of the major differences between the two and protocols and standards which have been proposed.

M2M Range

Short-Range M2M

Short-range M2M technologies are historically used to build wireless sensor networks (WSN), due to their ability to form networks of devices in close to each other. Certainly, one of the most adopted technologies in this field is IEEE 802.15.4, although more recently also IEEE 802.15.1 (Bluetooth Low Energy) has gained interest.

Among the IEEE 802.15.4 family, it is interesting to discuss the IEEE 802.15.4m amendment, which is the use of IEEE 802.15.4 on the TV white space (TVWS) bands.

TVWS are frequency bands which are progressively becoming available for secondary user operations, thanks to the digital TV switchover. Basically, thanks to the transition from analog to digital TV, several channels are not used anymore and can possibly be exploited for other use cases. TVWS have already shown interesting performance in scenario such as communication in rural areas, thanks to the low-frequency band used which helps in achieving a large communication range. Many standards have been proposed to work in TVWS, like IEEE 802.22 for regional networks, IEEE 802.11af for indoor, WiFi like deployments, and IEEE 802.15.4m for M2M communication and more oriented to IoT and WSN.

At the moment of writing, not all the countries in the world have regulations to transmit in TVWS. It is worth mentioning the US case, in which the FCC already published the rules to access TVWS, and the UK case, where Ofcom followed a similar path. Although they differ in details, they share the fundamental building block of the TVWS architecture, which is the remote spectrum database. Basically, it contains the positions of the TV transmitter, and through path loss models, it determines in which areas a given channel is free or occupied. Devices which need to access the TVWS should firstly query the remote spectrum database and ask for free channels, by providing their position. The remote spectrum database will eventually reply with a list of available channels on which the device can transmit, since they are free at that moment.

IEEE 802.15.4m has been proposed in 2014 [7, 28], and the major differences over the standard IEEE 802.15.4 standard are devoted to the physical layer, with the IEEE 802.15.4m defining three novel PHY layers, an FSK PHY, an OFDM PHY, and a narrowband OFDM PHY (NB-OFDM). They are designed to operate on TVWS frequency bands, up to 862 MHz.

The OFDM layer, which is the one which offers the highest data rate among the available ones, offers six different modulation and coding schemes (MCS), ranging from around 390 kb/s with a BPSK modulation to a maximum of 1562.5 kb/s, when using a 16-QAM. Note that these values can be increased up to four times when using channel bonding. The study in [7] summarizes the practical use of IEEE 802.15.4m, finding that in practical scenarios free of noise, the highest throughput can reach around 30 m, with a transmitting power of 20 dBm. Clearly, this can be increased if higher transmission powers are allowed or when using stronger MCS which require lower link budget.

Concerning dynamic spectrum access, IEEE 802.15.4m should ask to the remote spectrum database the available channels. However, [32] finds that when using bursty transmissions, which are typical of M2M scenarios, TV receivers better compensate for interference. Hence, [7] shows that it is possible to transmit small packets even on occupied channels, without causing interference to the primary user of the channel.

Long-Range M2M

While short-range M2M achieves a maximum transmission range of tenths of meters, long-range M2M foresees to connect devices which are located several kilometers away. This is generally done either by increasing the transmitting power or by reducing the communicating band. Recently, a lot of standards have been proposed and are now used in different scenarios. These include LoRa, LTE-M, and Weightless.

LoRa is a technology developed by the LoRa alliance and is rapidly becoming one of the most used standards in the M2M and IoT world. Its network topology is a star of stars, which means that each device is directly connected to a LoRa gateway, which can communicate to the central entity, called the LoRa NetServer, which also handles the authentication and association of the devices. Basically, the LoRa gateway is simple, acting mostly as a relay, since the complexity is

moved to the LoRa NetServer. Hence, features such as mobility and information redundancy elimination are inherently supported, as the NetServer manages them all. Concerning the data rate, LoRa devices can reach a peak of 50 kbps, transmitting at a maximum power of 24 dBm.

LTE-M is an LTE version which enables machine type communication, particularly for constrained devices. This technology has the clear advantage of relying on a vastly deployed technology such as LTE, and transmitting in smaller bands enables longer range and battery savings when reducing the transmission power. This would also enable hybrid devices, which might leverage on the full LTE stack when needing bandwidth hungry data transfer and switch to the more efficient LTE-M for smaller communication. The 3GPP studied LTE-M in the area of Washington [1], achieving a maximum of more than 10 km. NB-LTE-M further improves the capabilities of LTE-M, by reducing the bandwidth to 200 kHz and allowing a maximum transmitting power of 23 dBm instead of 20 dBm like in LTE-M.

Finally, Weightless is a set of technologies originally proposed by Neul and now developed by the Weightless Special Interest Group (SIG). It is composed basically of three different technologies, namely, Weightless-N, which uses a narrowband transmission scheme, achieving a maximum range of 5 km. For bi-directional communication there is Weightless-P, although this reduces the maximum transmission range from 5 to 2 km. Finally, Weightless-W is based on TVWS, which tops the other two in terms of communication range, achieving a maximum of 10 km.

Dynamic Spectrum Access for M2M

The need for dynamic spectrum access (DSA) comes from the scarcity of the spectrum resources, which is also the basis for the birth of cognitive networks in general. Basically, we are living in a world where almost all the spectrum are statically allocated to different services. In [21] the FCC shows the current allocation of frequency spectrum up to 3000 GHz, and it is possible to note how little space is left for new services. Apart from the ISM bands such as the 868/915 MHz, 2.4 GHz, and 5.8 GHz where different services take place, it is challenging to license new bands for other purposes. However, a lot of studies have shown how little licensed space is used. We mention [39, 44, 55] for the European-related measurement studies, [14,41,50] for the USA, [30,56,57], for Asia, and [40] for Africa. Clearly, measurement bands differ, and also the purpose of the study varies. However, there is a global consensus that some licensed bands are heavily underutilized. As new services are deployed, which build upon new technologies, spectrum is a scarce hence valuable resource. With these premises, cognitive networks are born, and more specifically the building block which takes into account the so-called spectrum holes is named DSA [36].

DSA can be mainly implemented through two different architectures: centralized DSA or distributed DSA. In the centralized DSA architecture, it is foreseen as a server which allocates the radio resources to clients, while in distributed DSA the

devices compete or cooperate together to access the spectrum. Contention can occur, for instance, through a control channel, where devices declare their willingness to transmit and reach agreement together.

Certainly, one of the major challenges to tackle is the fairness between clients. While such achievement might be easy to obtain in centralized DSA, as the remote server has a global view of all the clients and the air time allocated to them, achieving fairness in distributed DSA is more challenging. One possible solution would be to gain access to the spectrum proportionally to the sensing time [35]. If a client senses the spectrum more, hence gives to the neighboring devices more information about the spectrum state, it should be given more opportunities to communicate. However, in the domain of M2M communication, where devices are typically on batteries and with low duty cycle, this technique is clearly inefficient. This can be mitigated using solutions like the one presented in [26], where forced vacation periods for devices must take place; hence, sooner or later a device will have the opportunity to transmit. However, for M2M communication distributed DSA solution requires energy hungry operations such as sensing and requires to wait some time to understand the state of neighboring devices, hence which are not suitable for battery operated devices.

Cognitive networks are realized through different modules, in charge of performing tasks related to recognize, access, and efficiently use the spectrum. For the purpose of M2M, we will look at spectrum sensing, spectrum sharing, and spectrum management. Spectrum sensing is the ability for a device to sense the spectrum and identify potential spectrum holes, which are portion of the spectrum band at a given time and frequency which are not utilized by anyone. Spectrum sharing is performed across multiple devices, which share the resources to gain access to it. Finally, Spectrum management relates to all the operations needed to grant access to the spectrum and manage the resource between the clients. In other words, it is the overarching architecture composed of other submodules, in charge of executing different tasks.

Spectrum Sensing

As we already introduced, spectrum sensing is the ability for a device to sense the environment and acquire information about the spectrum occupancy, on a given frequency band. This is generally done by listening to the channel and analyzes the signals received. The spectrum detection, which is the task of determining whether a channel is occupied or not, can be done with different degrees of complexity, which clearly lead to different results.

In general, we can divide spectrum sensing in two broad categories, namely, energy detection spectrum sensing and cyclostationary spectrum sensing. Energy detection has the advantage of being simpler; hence, they require less resources to be run. Moreover, they do not need any information on the nature of the signal they are sensing. However, they are generally less accurate than other techniques, and they cannot distinguish between primary signals and secondary signals. More

accurate techniques, such as the cyclostationary one, analyze the signal to determine whether a primary user is present or not. Generally speaking, they are more accurate, at the cost of a higher computation power required, and knowing the nature of the primary signal. At the same time, they may also distinguish between primary signal and secondary signal, opposite to the energy detection systems which only sense an occupied channel.

In [45] the authors proposed a compressive spectrum sensing algorithm, designed specifically for M2M communication. Specifically, the design is for UHF TV, thanks to TVWS technology. TVWS have been targeted as highly interesting for M2M [58], as they have favorable characteristics that bind well with M2M. The main idea behind the proposed solution is to sense only a part of the spectrum, instead of a wider band. Instead of sampling the whole band with fast update rates, the spectrum is sampled at sub-Nyquist rates, and only specific portions of the spectrum are further evaluated, thus reducing the overall complexity of the algorithm. Clearly, knowing which part of the spectrum needs further analysis has multiple benefits:

- If information is shared among M2M devices, it could reduce the complexity also for other devices, at the cost of adding further overhead both on the management part and on the battery consumed to transmit the information.
- If the device can make a decision without involving complex techniques, it saves battery. Clearly, this cannot come at the cost of potentially interfering with the primary user.
- Through cooperative sensing, devices may share the computation costs, so that the energy required for each one is lower.

Energy detection, although fascinating for M2M communication, thanks to its simplicity, presents other drawbacks that need to be tackled [12]. For instance, it is difficult to set an appropriate threshold for the sensing, as setting a too low threshold may lead to missed communication opportunities due to environmental, and a high threshold may result in being too conservative. In fact, carefully setting the threshold is certainly the most challenging part in designing an efficient spectrum sensing algorithm, and this has been the main focus of several works which can be found in literature [19, 52]. While [52] provides general considerations and boundaries for energy detectors, [19] proposes a novel spectrum sensing algorithm, which involves cooperation between the nodes. In particular, they communicate to reach a consensus on the optimal energy threshold to be used. Even though this comes at the cost of involving additional communication, [19] shows that the gains are in favor of their solution.

Cooperative spectrum sensing uses shared knowledge among the nodes to reach a decision about the spectrum occupancy. A major challenge which arises with other techniques is related to the well-known hidden node problem, that is, nodes which might be sensed by some devices and not by others. In cooperative spectrum sensing, the hidden node problem is tackled by sharing the channel occupancy by nodes placed in different positions, hence reducing the probability that the hidden node is not sensed by anyone.

In cooperative spectrum sensing, we may have three different architectures:

- **Centralized Cooperative Sensing**, in which nodes report spectrum measurements to a central entity, usually main powered, which analyzes the results and reports either hard or soft decisions to the clients.
- **Distributed Cooperative Sensing**, in which there is not a central entity, but spectrum measurements are shared among nodes in a distributed way. Clearly, synchronization challenges have to be tackled.
- **Relay Cooperative Sensing**, in which nodes send their measurements to other devices, which relay them to a central entity. The closer to the central entity, the higher the energy consumption, since a higher number of measurements should be reported.

Regardless of the specific architecture used, cooperative spectrum sensing also carries the problem of user selection, which is the subset of devices chosen for the next round of sensing. These devices should be representatives (i.e., cover the area of interests) and possibly be independent (i.e., in different positions, to limit the hidden node problem) [47].

Spectrum Sharing

Spectrum sharing refers to the techniques needed in order to share the spectrum resource between devices. Techniques vary, but the underlying idea is that devices could either compete for the spectrum, such as through auctions [20,54], or through cooperative schemes [11, 23, 25, 59]. In particular, [25] is focused specifically on M2M communication, and by exploiting some of the M2M constraints, such as a small packet length, it shows how it is possible to transmit leveraging WiFi whitetimes, which is the inter-time between subsequent WiFi transmissions. In other words, in [25] vision M2M communication, thanks to its bursty nature and small packet lengths, can coexist with other transmissions by using period of non-transmissions in normally occupied channels.

Moreover, we can also distinguish between two different architectures of spectrum sharing:

- **Centralized Spectrum Sharing**, in which the access to the spectrum is managed by a central entity, which is often named as **Spectrum Coordinator**. It can lease the spectrum in a competitive way, sending the same information to all the devices which eventually compete to access to it, or controlled, in which it decides which portion of spectrum should be leased to a given device.
- **Distributed Spectrum Sharing**, in which devices take decision locally, based on the information they have, which could also be obtained through cooperation with other nodes. Again, cooperation improves the overall performances of the spectrum sharing, at the cost of an increased overhead and energy consumption.

Much work has been done on spectrum sharing architectures. Many works explore the possibilities offered by game theory, modeling games in which the objective of the client is accessing the spectrum [24,31,43].

Southwell et al. [48] focuses on quality of service games for spectrum sharing. Their solutions are totally distributed, and they also show the overarching benefits of a distributed solution over a centralized one.

A novel paradigm of spectrum sharing also exploits the height of the devices, as a countermeasure to reduce interference between devices accessing the spectrum, named 3D spectrum sharing, proposed in [5,8]. The idea is that generally spectrum is considered free or occupied at a certain location, without considering the height of the buildings which may have been constructed there. For specific M2M use cases such as smart metering [4], this may significantly help in finding spectrum opportunities, as spectrum sharing is considered on a per-floor basis.

More formally, we can define the spectrum occupancy at a given location $\mathscr{L}$ as

$$S_{\mathscr{L}} = \mathscr{O} \tag{1}$$

where $S_{\mathscr{L}}$ is the spectrum information regarding location $\mathscr{L}$ and $\mathscr{O}$ is the result obtained through a given technique of spectrum sharing. Since $\mathscr{L}$ is a location, it is generally defined as

$$\mathscr{L} =< Lat, Lng >$$

where Lat and Lng represent the latitude and the longitude, respectively. Most notably, this is the definition used by the TVWS spectrum database [9], which has been shown to offer less communication opportunities than those which may be used without interfering with the primary users. 3D spectrum sharing modifies the definition of $\mathscr{L}$, changing it into

$$\mathscr{L}_{3D} =< Lat, Lng, \mathscr{H} >$$

where $\mathscr{H}$ is defined as the height from ground floor. In tall buildings, or in the case of specific networks such as TVWS, 3D spectrum sharing has shown good results in finding additional spectrum sharing opportunities, compared to other techniques. Of course, this comes at an additional cost and with additional constraints. At first, devices should know which are their $\mathscr{H}$. This can be either manually defined when the device is installed, or it can be determined by the device during its operations. If manual configuration is used, the spectrum occupancy estimation may become inaccurate, due to the fact that devices may be moved or substituted. In case of the device determining its $\mathscr{H}$, additional costs for building it should be accounted for, due to the need of a barometric sensor. Moreover, pressure value changes during the day, due to natural events such as thunderstorms or clouds, which should be again detected and properly managed [6].

An additional aspect crucial to M2M communication is related to the energy consumption. Switching from a 2D to a 3D space may involve additional

computation costs, as more complex spectrum propagation and detection techniques should be used. However, this may be solved by using a spectrum manager which is in charge of handling all the spectrum information of a building. Again, this is not straightforward to implement, due to devices which may not be in the range of the spectrum manager and should then use relays to reach it in order to report measurements or to obtain information about the free channels.

Spectrum Management

Spectrum management comprises different tasks to be achieved, to efficiently utilize the available spectrum. This does not involve only spectrum sensing or spectrum sharing, as they may be relative to a specific frequency band. In fact, in spectrum management it is also foreseen that clients may have access to multiple bands, which may be exploited for specific needs. This may include multiband devices, able to utilize both WiFi channels and others, depending on the scenario and on the instant needs, like [22], where the authors design a system which leverages both cellular technologies such as LTE-A, to other opportunistic technologies like TVWS. The underlying idea is to utilize LTE-A to perform spectrum management tasks and also to query the remote spectrum database for TVWS availability.

Other solutions leverage TVWS to overcome other technology limitations in specific scenarios, such as video streaming [7]. Here, the scenario of interest is different from M2M, but the general architecture presents many similarities, like the use of a technology to query the database like WiFi and occasionally TVWS if WiFi performance is not enough to support the video streaming.

We can characterize multiband solutions, based on the spectrum availability and on the technologies characteristics overlapping, into the following categories:

- Two technologies, both always available, similar characteristics: this is the case, for instance, of technologies such as WiFi and Bluetooth, which do not have to rely on other entities to assess the spectrum availability, as they use the ISM bands. They share similar characteristics; hence, their use together is limited.
- Two technologies, both always available, different characteristics: this is the case, for instance, of WiFi and LTE, assuming coverage. In this scenario, typically technologies complement each other: for instance, modern smartphones have the possibility to switch to LTE should the WiFi connection presents low performance.
- Two technologies, one always available: this is the case of TVWS, in which another technology such as LTE or WiFi is used to gain access to the TVWS network, by asking to the remote spectrum database the list of channels available at a given location.

Concerning M2M communication, most notably here is the work presented in [13], which compares LTE-Direct and WiFi-Direct over classical LTE communication, in the specific scenario of M2M. Cellular communication has been extensively

looked at as one of the most prominent candidates for M2M, as they have a large coverage and present characteristics favorable for this kind of communication, like a longer range of communication over other technologies. However, they should be optimized to fully unleash the potential of M2M, like optimizing them for bursty transmissions or a better energy efficiency for battery-powered devices.

In [13] the authors show that both LTE-Direct and WiFi-Direct outperform classical LTE, mostly thanks to a specific design targeted at M2M communication. However, no clear winner arises, as LTE offers the best energy efficiency, particularly with a high number of devices, while WiFi has an advantage when considering small packets.

Other proposals do not focus on different access technologies but rather use M2M to enhance the main network basically by providing enhanced coverage, by using M2M devices which act as relay [33]. Even though this kind of communication has to be considered M2M, as no human intervention is foreseen in between, it is hard to think at those devices as battery powered and only communication to other devices. In fact, they can be devices which offer different services, one of which is M2M communication to extend the transmission range.

Spectrum management can thus be considered both a solution which enhances and optimizes the performance of M2M device. At the same time, it requires additional computation resources which eventually lead to increased battery consumption and reduced device life. Hence, there is a trade-off between using specific technologies, which may not be well suited for a specific scenario, even though they are simple to be managed, and to a more complex spectrum management which involves different bands and requires algorithms to successfully exploit additional technologies. Needless to say, also the cost of the device increases, and possibly the size of it, as different technologies may require different antennas and transceivers to operate.

Case Study: Cooperative M2M for Smart Metering

In this section we describe in detail a specific use case for M2M, related to smart metering applications. The scenario we model is depicted in Fig. 1, where multiple devices need to report their data to a central aggregator. Devices can have different capabilities and different residual energy; hence, algorithms which make them cooperate can significantly extend their battery life.

System Model

We model a generic network scenario S, composed by $\mathcal{N}$ secondary devices (SUs), operating in the same area. In other words, we assume they are able to sense the same signals. Each SU operates a DSA-enabled device, able to sense signals over

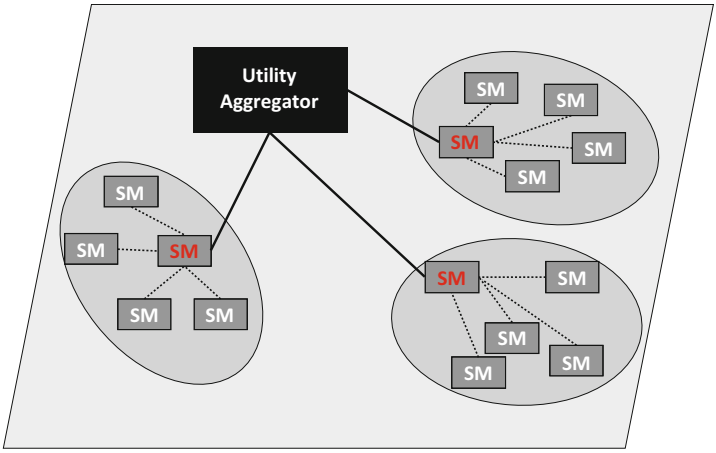

Fig. 1 Scenario for M2M smart metering communication. Multiple heterogeneous devices need all to report their data to a central aggregator, which is in charge of merging them. Devices can either report the measurements alone, hence consuming a considerable amount of battery, or they can form clusters, in which only one of them sends the measurements to the aggregator, and information about the other measurements is shared within the cluster. In this picture, we picture in red smart meters which report information of all the smart meters in the cluster, and in white those smart meters which only transmit intra-cluster. Clearly, the device which reports the data to the utility aggregator may change in time

all the frequencies of interest. We study the use case for the specific frequency band of TV white space (TVWS), although it can be easily extended to other frequency bands as well.

In TVWS, devices should query the remote spectrum database to obtain access to the list of channels available on a given area. This can be done by a device to obtain the list for its own purposes or to share the list to other devices which may not have access to the remote spectrum database. Hence, we also assume that devices also have an interface such as WiFi, through which they can access the remote spectrum database.

As the devices are close to each other, we can also assume that they are at most at one hop from the device which executes the query to the remote spectrum database. Hence, we call the querying device `master device` (MD) and all the other $\mathcal{N}-1$ as `slave devices` (SDs). Energy smart meters may be main powered, but for other kind of smart meters, such as those measuring gas, it is not possible to assume main power, but battery power is viable, and eventually energy efficiency has to be accounted for.

The set of activities $\mathcal{S}$ MD i has to perform through the day can be summarized as:

- **Sense**: based on the measure and on regulations, the device has to acquire the measure of interest and store it locally.

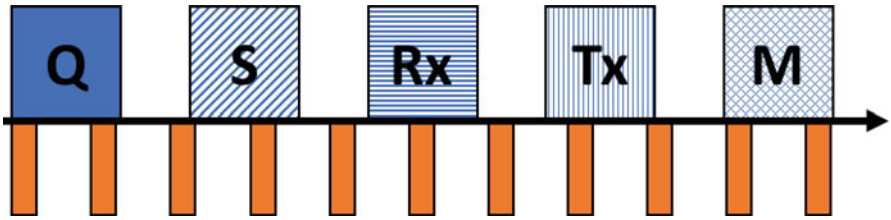

Fig. 2 The daily schedule of an MD. Below the lines there are the `Sense` operations, while on the upper line, we show the communication operation, starting from **Q**, which is relative to the `Query` operation. After getting the channel information, the MD can `Share` it through the **S** operation. Then the MD is ready to receive data from the SDs through the **Rx** operation and transmit it to the utility aggregator in the **Tx** phase. Finally, `Maintenance` operation can be performed through the **M** phase

- **Query**: this task has to be done to acquire access to the spectrum. Depending on the network, it can vary.
- **Share**: in this task, the MD and SD share information about the available channels.
- **Rx**: the MD, which should reports all the measurements of the SDs, receives measurement updates by them, which transmit their data to it.
- **Tx**: the MD eventually sends its measurements and those received by the SDs to the utility aggregator.
- **Maintenance**: based on its residual energy, the MD decides whether to drop its role to another device, which in this case should be informed.

Clearly, an SD performs a subset $\int \in \mathscr{S}$ of activities, where

$$\int =< Sense, Share, Rx, Maintenance >$$

We depict the typical day routine of smart meters in Fig. 2.
To model the energy consumption of the MD, we define the following Equation:

$$E_{MD} = E_{\text{sense}} + E_q + E^{MD}_{\text{share}} + E^{MD}_{rx} + E_{tx} + E^{MD}_{m}, \tag{2}$$

where E_{sense} is the energy consumed by the sensing operation, common to both the MD and SDs, E_q is the energy needed to query the remote spectrum database, E^{MD}_{share} is the energy consumed by sharing the measurements from the MD perspective, E^{MD}_{rx} accounts for the energy spent receiving measurements from SDs, E_{tx} is relative to the energy needed to transmit the measurements to the utility aggregator, and E^{MD}_{m} accounts for the maintenance costs, in terms of energy, from the MD perspective.

Table 1 Symbols table

Symbol	Description
E_r	Energy per reading
$\mathscr{F}$	Number of readings per day
γ	Energy needed to transmit locally
ϵ	Sleep energy
α	Energy while in Rx
t_α^{MD}	Time in which the MD listens for SD data
t_β^{SD}	Time in which the SD listens for MD data
$\mathscr{N}$	Number of nodes
E_i^{start}	Starting energy

Clearly, each SD has a similar behavior, more precisely as follows:

$$E_{SD} = E_{\text{sense}} + E_{\text{share}}^{SD} + E_{rx}^{SD} + E_m^{SD},$$

where $E_{\text{share}}^{S} D$ accounts for the energy spent to acquire the list of channels available, E_{rx}^{SD} is relative to SDs sending their measurements to the MD, and finally E_m^{SD} is relative to management operations.

The general model we just presented can be tailored to meet specific needs, depending on the scenario and on the target objective. For instance, if all the devices have to query the spectrum database, then E_q has to be counted also for SD. Another case would be the use of a fixed MD: this case can be modeled by putting $E_m^{MD} = E_m^{SD} = 0$.

To compute each term, we refer to Table 1, where we report all the symbols used to model the scenario.

In detail, we obtain

$$E_{\text{sense}} = E_r \cdot \mathscr{F} \tag{3}$$

$$E_{\text{share}}^{MD} = \gamma \cdot (\mathscr{N} - 1) \tag{4}$$

$$E_{rx}^{MD} = \alpha \cdot t_\alpha^{MD} \tag{5}$$

$$E_m^{MD} = \mathscr{H} \cdot \gamma \cdot (N - 1) \tag{6}$$

where $\mathscr{H}$ is a 0−1 variable indicating whether management has to be performed or not, depending on the policy used.

Concerning the SDs, the following equations are then defined:

$$E_{\text{share}}^{SD} = \gamma + t_\beta^{SD} \cdot \alpha \tag{7}$$

$$E_{rx}^{SD} = \gamma \tag{8}$$

$$E_m^{SD} = t_\beta^{SD} \cdot \alpha \tag{9}$$

Based on the above model, and having all the data about the devices, it is then possible to compute the devices lifetime. Moreover, it is also possible to design specific algorithms which manage the cluster, such as the one defined in [3], where the authors also define the cluster goal, which is the minimum lifetime the cluster should be able to achieve. Since devices are heterogeneous, achieving a higher goal requires that some devices never become an MD, in order to save battery, while others will have a higher probability of being the MD.

Here we present three different algorithms, derived from [3], which are summarized as follows:

- **Greedy**: a device remains as MD as much as it can, before reaching a point where it must save battery to reach the final lifetime goal.
- **Highest**: at the end of each day, the MD drops its role to the device having the highest residual energy. This can be realized with different techniques, and here we leverage on the dynamic backoff. Basically, when the MD advertises, it wants to change its role to SD; each SD computes a backoff to reply to the election proportional to its residual energy. The higher the residual energy, the shorter the backoff time. If a device hears a reply from another SD, it cancels its transmission, since a new MD has been found. This solution has also been used in other scenarios, such as vehicular communication [18].
- **Cost Aware**: since devices can be heterogeneous, this algorithm updates periodically the actual costs of being an SD or an MD, and during the `Maintenance` slot, it selects the client which has done less for the cluster. In other words, the device which has been less days an MD compared to others will be elected.

In this domain, several metrics of interest exist. Within the scope of this analysis, we consider the following:

- **Lifetime**: defined as the time from the start till the first device runs out of battery.
- **Elections**: this is the number of times an MD changes its role. It gives an idea of the overhead involved in each protocol, hence the additional energy used to perform the `Maintenance`.
- **Fairness**: the fairness of the system $\in [0, 1]$. A higher value means that clients shared the workload based on their capabilities, while a low value indicates that there is a considerable variation in the workload between them. More precisely, the fairness is computed as

$$F = 1 - \left(\max_{i \in [0,n[} \left(\frac{D_i}{MD_i} \right) - \min_{i \in [0,n[} \left(\frac{D_i}{MD_i} \right) \right), \tag{10}$$

  where D_i is the amount of time device i has been MD, and MD_i is the maximum time device i can be an MD to keep its lifetime goal.

Figure 3 shows the overhead needed by the three protocols. In Fig. 3a we show the number of elections per day, when considering a cluster of 500 nodes. Setting

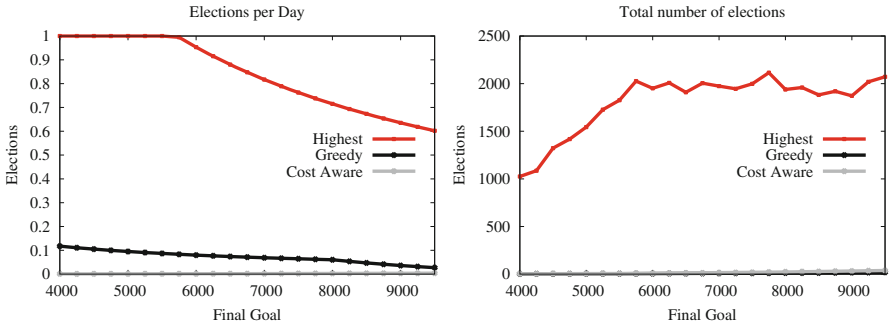

Fig. 3 Analysis on the elections, which translates to the algorithm overhead. A higher number of elections translate into a higher consumption by the devices, which need to send several messages to reach a consensus on the MD. (**a**) Elections per day. (**b**) Total number of elections

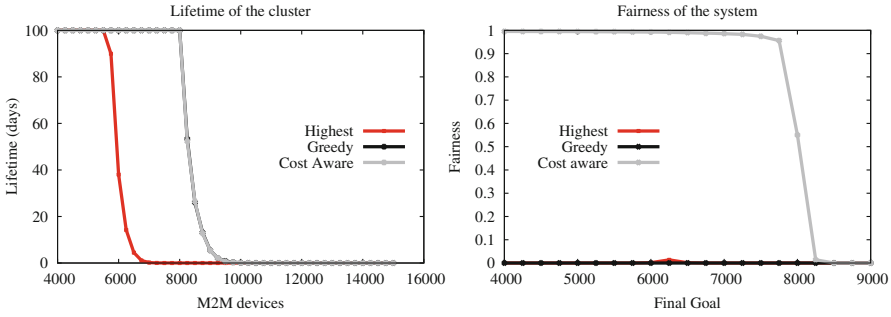

Fig. 4 Lifetime and fairness of the cluster. Setting a higher minimum goal may result in an unfeasible scenario, as the client cannot reach the goal, hence a lower average cluster lifetime. The fairness of the system is achieved only when using the **Cost Aware** protocol, as the other two do not share the load among the devices but only select those which better suit the MD role at the moment. (**a**) Lifetime of the cluster. (**b**) Fairness of the cluster

a higher minimum goal to reach for the devices increases the performance of the system, and the number of elections per day decreases, as devices tend to keep the MD role for a longer time and save battery. This is also confirmed by Fig. 3b, where it is straightforward to note that the total number of elections remains stable after a certain point, which is clearly dependent on the initial configuration of the nodes.

Figure 4 shows the cluster lifetime, along with the fairness. A higher minimum goal for the cluster pushes the capabilities of the devices, and some may not be able to support such high demands. Hence, on the average the cluster lifetime may be reduced. Figure 4a shows the percentage of cluster which are able to reach the goal, which obviously decreases as the minimum goal is increased. These results should only be regarded as qualitative, as precise quantitative results can be obtained only by setting appropriate parameters on the framework, depending on the specific scenario and on the characteristics of the devices.

The fairness of the system is an important parameter, as it shows the workload share. This is of paramount importance when performing maintenance operations, as having only one device which runs out of battery, while all the others still have energy remaining, raises the maintenance costs for such device. On the other hand, achieving a discharge which goes at the same pace for each one, depending on the different capabilities, can end up in having all the cluster to have similar energy remaining, hence perform maintenance operations on all the devices at once, thus decreasing the maintenance cost per single device.

Conclusion and Future Directions

In this chapter we presented the benefits and the challenges of DSA for M2M communication. M2M communication should be performed by devices without or with little human intervention. Thus, they should encompass self-healing and self-configuring capabilities. Cognitive network, hence DSA, is a technology that could help to overcome some of the challenges that M2M networks face, such as the energy constraints and the possible long range of the communication. Several experiments, both theoretic as well as simulative and with test-beds, have demonstrated both the benefits and the limits of M2M communication when considering DSA. In particular, energy efficiency should be taken into account when deploying M2M networks, and it becomes even more constrained when using spectrum agile techniques such as spectrum sensing and DSA.

Clearly, there is a plethora of topics which can be explored and further analyzed, which we have identified and commented in this chapter, and which we summarize here:

- **Energy efficiency**: even though we stated that M2M device may not be battery powered, it is also straightforward to understand that in a vast set of scenarios, they will be. Energy efficiency can be optimized in several parts of the device, either on the computation, on the transmission, or on the architecture level, where improvements are obtained through device collaboration.
- **Spectrum sensing**: it can be expensive both in terms of computation cost and also simply on the energy needed to listen to the channels, even more depending if a large spectrum is considered. Different techniques can be applied, such as cooperative spectrum sensing, in which devices organize and divide the tasks so that the energy consumption per single device is reduced. Other solutions involve identifying smaller portions of spectrum so that the task of sensing becomes more feasible. Regardless of the technique used, spectrum sensing is vital for DSA, and it is also an operation which needs to be repeated multiple times, as spectrum utilization may change suddenly.
- **Test-beds**: most of the presented results have been studied through simulations or with devices which implement only some of the tasks a cognitive M2M device should utilize. Hence, it is challenging to find wider analysis, which take

into account M2M communication and DSA accounting for realistic scenarios. In particular, primary user activity on the spectrum may be challenging to understand in real scenarios, rather than simulations where it can be controlled.

References

1. 3GPP. Study on provision of low-cost machine-type communications (MTC) user equipments (UEs) based on LTE. TSG GERAN R1
2. Altintas O et al (2011) Demonstration of vehicle to vehicle communications over TV white space. In: 2011 IEEE vehicular technology conference (VTC Fall), San Francisco, pp 1–3
3. Bedogni L, Trotta A, Di Felice M, Bononi L (2013) Machine-to-Machine communication over TV white spaces for smart metering applications. In: 2013 22nd international conference on computer communications and networks (ICCCN), Nassau, pp 1–7
4. Bedogni L, Achtzehn A, Petrova M, Mähönen P (2014) Smart meters with TV gray spaces connectivity: a feasibility study for two reference network topologies. In: 2014 eleventh annual IEEE international conference on sensing, communication, and networking (SECON), Singapore, pp 537–545
5. Bedogni L, Trotta A, Di Felice M (2015) On 3-dimensional spectrum sharing for TV white and gray space networks. In: 2015 IEEE 16th international symposium on a world of wireless, mobile and multimedia networks (WoWMoM), Boston, pp 1–8
6. Bedogni L, Franzoso F, Bononi L (2016) A self-adapting algorithm based on atmospheric pressure to localize indoor devices. In: 2016 IEEE global communications conference (GLOBECOM), Washington, DC, pp 1–6
7. Bedogni L, Trotta A, Di Felice M, Gao Y, Zhang X, Zhang Q, Malabocchia F, Bononi L (2017) Dynamic adaptive video streaming on heterogeneous TVWS and Wi-Fi networks. IEEE/ACM Trans Netw (IEEE TON) 25:3253–3266
8. Bedogni L, Achtzehn A, Petrova M, Mähönen P, Bononi L (2017) Performance Assessment and Feasibility Analysis of IEEE 802.15.4m Wireless Sensor Networks in TV Grayspaces. *ACM Trans Sensor Netw* 13(1), Article 8 (January 2017), 27 pages
9. Bedogni L, Malabocchia F, Di Felice M, Bononi L (2017) Indoor use of gray and white spaces: another look at wireless indoor communication. IEEE Veh Technol Mag 12(1):63–71
10. Brew M, Darbari F, Crockett LH, Waddell MB, Fitch M, Weiss S, Stewart RW (2011) UHF white space network for rural smart grid communications. In: 2011 IEEE international conference on smart grid communications (SmartGridComm), Brussels, pp 138–142
11. Chang HB, Chen KC (2011) Cooperative spectrum sharing economy for heterogeneous wireless networks. In: 2011 IEEE GLOBECOM workshops (GC Wkshps), Houston, pp 458–463
12. Chatziantoniou E, Allen B, Velisavljevic V (2015) Threshold optimization for energy detection-based spectrum sensing over Hyper-Rayleigh fading channels. IEEE Commun Lett 19(6):1077–1080
13. Condoluci M, Militano L, Orsino A, Alonso-Zarate J, Araniti G (2015) LTE-direct vs. WiFi-direct for machine-type communications over LTE-A systems. In: 2015 IEEE 26th annual international symposium on personal, indoor, and mobile radio communications (PIMRC), Hong Kong, pp 2298–2302
14. Cui P, Liu H, Rajan D, Camp J (2014) A measurement study of white spaces across diverse population densities. In: 2014 12th international symposium on modeling and optimization in mobile, ad hoc, and wireless networks (WiOpt), number WiNMeE, May 2014. IEEE, pp 30–36
15. Datta SK, Bonnet C (2014) Smart M2M gateway based architecture for M2M device and endpoint management. In: 2014 IEEE international conference on internet of things (iThings), and IEEE green computing and communications (GreenCom) and IEEE cyber, physical and social computing (CPSCom), Taipei, pp 61–68

16. Di Felice M, Chowdhury KR, Bononi L (2010) Analyzing the potential of cooperative cognitive radio technology on inter-vehicle communication. In: Wireless days (WD), 2010 IFIP, Venice, pp 1–6
17. Di Felice M, Bedogni L, Bononi L (2012) DySCO: a dynamic spectrum and contention controlframework for enhanced broadcast communication invehicular networks. In: Proceedings of the 10th ACM international symposium on mobility management and wireless access (MobiWac'12)
18. Di Felice M, Bedogni L, Bononi L (2013) Group communication on highways: an evaluation study of Geocast protocols and applications. Elsevier's Ad Hoc Netw J 11: 818–832
19. Ebrahimzadeh A, Najimi M, Andargoli SMH, Fallahi A (2015) Sensor selection and optimal energy detection threshold for efficient cooperative spectrum sensing. IEEE Trans Veh Technol 64(4):1565–1577
20. Fang YX, Xue G (2012) HERA: an optimal relay assignment scheme for cooperative networks, selected areas in communications. IEEE J 30(2):245–253
21. Federal Communications Commission. FCC online table of frequency allocations. Available online: https://transition.fcc.gov/oet/spectrum/table/fcctable.pdf
22. Gao Y, Qin Z, Feng Z, Zhang Q, Holland O, Dohler M (2016) Scalable and reliable IoT enabled by dynamic spectrum management for M2M in LTE-A. IEEE Internet Things J 3(6): 1135–1145
23. Gao L, Duan L, Huang J (2017) Two-sided matching based cooperative spectrum sharing. IEEE Trans Mob Comput 16(2):538–551
24. Gu Y, Saad W, Bennis M, Debbah M, Han Z (2015) Matching theory for future wireless networks: fundamentals and applications. IEEE Commun Mag 53(5):52–59
25. Harris J, Beach M, Nix A, Thomas P (2016) Spectrum sharing for M2M applications through Whitetime exploitation in WiFi networks. In: 2016 IEEE wireless communications and networking conference, Doha, pp 1–6
26. Hsu LK, Chou CT (2013) A dynamic spectrum access (DSA)-based multichannel protocol for large scale machine-to-machine (M2M) networks. In: 2013 9th international wireless communications and mobile computing conference (IWCMC), Sardinia, pp 1217–1222. https://doi.org/10.1109/IWCMC.2013.6583730
27. ICT-DOST. TV white space deployment in Philippines. http://icto.dost.gov.ph/tv-white-space-deployment-in-ph-the-largest-in-asia/
28. IEEE 802.15.4m standard. Available online: https://standards.ieee.org/findstds/standard/802.15.4m-2014.html
29. Ihara Y et al (2013) Distributed autonomous multi-hop vehicle-to-vehicle communications over TV white space. In: 2013 IEEE consumer communications and networking conference (CCNC), Las Vegas, pp 336–344
30. Islam MH, Koh CL, Oh SW, Qing X, Lai YY, Wang C, Liang YC, Toh BE, Chin F, Tan L, Toh W (2008) Spectrum survey in Singapore: occupancy measurements and analyses. In: Proceedings of the 3rd international conference on cognitive radio oriented wireless networks and communications (CrownCom), May 2008. IEEE
31. Ji Z, Liu KJR (2007) Cognitive radios for dynamic spectrum access – dynamic spectrum sharing: a game theoretical overview. IEEE Commun Mag 45(5):88–94
32. Kerttula J, Jäntti R (2011) DVB-T receiver performance measurements under secondary system interference. In: Proceedings of COCORA 2011
33. Laya A, Wang K, Widaa AA, Alonso-Zarate J, Markendahl J, Alonso L (2014) Device-to-device communications and small cells: enabling spectrum reuse for dense networks. IEEE Wirel Commun 21(4):98–105
34. Lee J, Bagheri B, Kao H-A (2015) A cyber-physical systems architecture for industry 4.0-based manufacturing systems. Manuf Lett 3:18–23. ISSN:2213–8463
35. Li TL, Chou CT, Hsu LK (2015) Proportional sharing in distributed dynamic spectrum access-based networks. IEEE Trans Mob Comput 14(1):155–168

36. Liang YC, Chen KC, Li GY, Mahonen P (2011) Cognitive radio networking and communications: an overview. IEEE Trans Veh Technol 60(7):3386–3407. https://doi.org/10.1109/TVT.2011.2158673
37. Lim JH, Kim W, Naito K, Yun JH, Cabric D, Gerla M (2014) Interplay between TVWS and DSRC: optimal strategy for safety message dissemination in VANET. IEEE J Sel Areas Commun 32(11):2117–2133
38. London ZOO TVWS animal monitoring. http://www.dailymail.co.uk/sciencetech/article-2788044/using-tv-whitespaces-save-endangered-animals-gaps-digital-frequencies-monitor-creatures-remote-areas.html
39. Marcu I, Marghescu I (2010) Evaluation of spectrum occupancy in an urban environment in a cognitive radio context. Adv Telecommun 3(3):172–181
40. Masonta MMT, Johnson DL, Mzyece M (2011) The white space opportunity in Southern Africa: measurements with Meraka cognitive radio platform. In: Proceedings of AFRICOMM. Lecture notes of the institute for computer sciences, social informatics and telecommunications engineering, vol 92. Springer, pp 64–73
41. McHenry MA, Tenhula PA, McCloskey D, Roberson DA, Hood CS (2006) Chicago spectrum occupancy measurements & analysis and a long-term studies proposal. In: Proceedings of the first international workshop on technology and policy for accessing spectrum (TAPAS)
42. Montori F, Contigiani R, Bedogni L (2017) Is WiFi suitable for energy efficient IoT deployments? In: A performance studyİon proceedings of the 3rd IEEE internal forum on research and technologies for society and industry, technologies for smarter societies (IEEE RTSI), 11–13 Sept, Modena
43. Niyato D, Hossain E (2008) Competitive spectrum sharing in cognitive radio networks: a dynamic game approach. IEEE Trans Wirel Commun 7(7):2651–2660
44. Pérez-Romero J, Noguet D, López-Benítez M, Casadevall F (2011) Towards more-efficient spectrum usage: spectrum-sensing and cognitive-radio techniques. in *URSI Radio Science Bulletin*, 2011(336):59–74, March 2011
45. Qin Z, Gao Y, Plumbley MD, Parini CG, Cuthbert LG (2014) Efficient compressive spectrum sensing algorithm for M2M devices. In: 2014 IEEE global conference on signal and information processing (GlobalSIP), Atlanta, pp 1170–1174
46. Reed JH (2010) Enabling rural Virginia's smart grid through white space communications, Virginia Tech, Technical report
47. Selen Y, Tullberg H, Kronander J (2008) Sensor Selection for Cooperative Spectrum Sensing. *2008 3rd IEEE Symposium on New Frontiers in Dynamic Spectrum Access Networks*, Chicago, pp. 1–11
48. Southwell R, Chen X, Huang J (2014) Quality of service games for spectrum sharing. IEEE J Sel Areas Commun 32(3):589–600
49. Sum CS, Harada H, Kojima F, Lan Z, Funada R (2011) Smart utility networks in tv white space. IEEE Commun Mag 49(7):132–139
50. Taher TM, Bacchus RB, Zdunek KJ, Roberson DA (2011) Long-term spectral occupancy findings in Chicago. In: Proceedings of IEEE international symposium on dynamic spectrum access networks (DySPAN), pp 100–107, May 2011
51. Tracking and monitoring of animals with combined wireless technology and geofencing, US Patent Application US20130340305
52. Umar R, Sheikh AUH, Deriche M (2014) Unveiling the hidden assumptions of energy detector based spectrum sensing for cognitive radios. IEEE Commun Surv Tutor 16(2):713–728. Second Quarter 2014
53. Varghese A, Tandur D (2014) Wireless requirements and challenges in industry 4.0. In: 2014 international conference on contemporary computing and informatics (IC3I), Mysore, pp 634–638
54. Wang J, Liu A, Yan T et al. (2018) Peer-to-Peer Netw Appl. 11:(679)
55. Wellens M, Wu J, Mähönen P (2007) Evaluation of spectrum occupancy in indoor and outdoor scenario in the context of cognitive radio. In: 2007 2nd international conference on cognitive

radio oriented wireless networks and communications (CROWNCOM), Aug 2007. IEEE, pp 420–427
56. Yin S, Chen D, Zhang Q, Liu M, Li S (2012) Mining spectrum usage data: a large-scale spectrum measurement study. IEEE Trans Mob Comput 11(6):1033–1046
57. Ying X, Zhang J, Yan L, Zhang G, Chen M, Chandra R (2013) Exploring indoor white spaces in metropolises. In: Proceedings of the 19th annual international conference on Mobile computing & networking – MobiCom'13, New York. ACM Press, p 255
58. Yuan Ma, Gao Y, Parini CG (2015) Sub-Nyquist rate wideband spectrum sensing over TV white space for M2M communications. In: 2015 IEEE 16th international symposium on a world of wireless, mobile and multimedia networks (WoWMoM), Boston, pp 1–6
59. Zhang Y, Yu R, Nekovee M, Liu Y, Xie S, Gjessing S (2012) Cognitive machine-to-machine communications: visions and potentials for the smart grid. IEEE Netw 26(3):6–13
60. Zhou H et al (2015) Enabling efficient and wide-coverage vehicular content distribution over TV white spaces. In: 2015 international conference on wireless communications & signal processing (WCSP), Nanjing, pp 1–6

Reinforcement Learning-Based Spectrum Management for Cognitive Radio Networks: A Literature Review and Case Study

57

Marco Di Felice, Luca Bedogni, and Luciano Bononi

Contents

Abstract

In cognitive radio (CR) networks, the cognition cycle, i.e., the ability of wireless transceivers to learn the optimal configuration meeting environmen-

M. Di Felice (✉) · L. Bedogni · L. Bononi
Department of Computer Science and Engineering, University of Bologna, Bologna, Italy
e-mail: marco.difelice3@unibo.it; luca.bedogni4@unibo.it; luciano.bononi@unibo.it

W. Zhang (ed.), *Handbook of Cognitive Radio*,
https://doi.org/10.1007/978-981-10-1394-2_58

tal and application requirements, is considered as important as the hardware components which enable the dynamic spectrum access (DSA) capabilities. To this purpose, several machine learning (ML) techniques have been applied on CR spectrum and network management issues, including spectrum sensing, spectrum selection, and routing. In this paper, we focus on reinforcement learning (RL), an online ML paradigm where an agent discovers the optimal sequence of actions required to perform a task via trial-end-error interactions with the environment. Our study provides both a survey and a proof of concept of RL applications in CR networking. As a survey, we discuss pros and cons of the RL framework compared to other ML techniques, and we provide an exhaustive review of the RL-CR literature, by considering a twofold perspective, i.e., an application-driven taxonomy and a learning methodology-driven taxonomy. As a proof of concept, we investigate the application of RL techniques on joint spectrum sensing and decision problems, by comparing different algorithms and learning strategies and by further analyzing the impact of information sharing techniques in purely cooperative or mixed cooperative/competitive tasks.

Introduction

A cognitive radio (CR) can be defined as a wireless device that is able to autonomously control its configuration based on the environmental conditions and on the quality of service (QoS) requirements of the applications [1]. Since its original proposal in 1999 [2], the node architecture has been considered the core novelty of a CR device, being the fusion of advanced dynamic spectrum access (DSA) functionalities at the radio level and of intelligent decision-making provided by a cognition module (CM) at the software level. Through the DSA, a CR is able to observe the network environment and to dynamically adjust transmission parameters like the operative frequency, the modulation and coding scheme, or the power level. To this purpose, the dynamic reuse of vacant portion of the licensed spectrum, in overlay or underlay mode, has emerged as the prominent use-case of the CR technology: CR devices, also known as secondary users (SUs), aim to maximally exploit all the available spectrum frequencies, including both licensed and unlicensed ones, without affecting the performance of the frequency owners, also known as primary users (PUs) [1]. The research literature on channel sensing techniques, required to detect PU-free transmission opportunities on the frequency and time domains, is vast [3, 4], as well as the number of proposed network architecture and standards regulating the operations of the SUs [5, 6]. On top of the DSA module, the CM leverages the perceptions and measurements gathered during the sensing phase for the decision-making process, i.e., to properly adjust the radio configuration and plan the network operations, by means of advanced learning and reasoning functionalities [7]. For this reason, a significant portion of the literature on CR networking is investigating the utilization of machine learning (ML) techniques [8] for the device and network configuration, optimization, and planning; the ML approaches adopted so far are extremely heterogeneous and include supervised

learning techniques (e.g., neural networks and Bayesian classifiers), unsupervised learning techniques, and dynamic games [9–11].

In this paper, we focus on reinforcement learning (RL) [12, 13], a well-known ML paradigm where the agent learns the optimal sequence of actions in order to fulfill a specific task via trial-and-error interactions with a dynamic environment; at each action performed, the agent observes its current state and receives a numeric reward, which quantifies the effectiveness of the action. The agent behavior, also known as the *policy*, should choose actions that tend to increase the long-term sum of rewards [13]. The literature on RL dates back to the 1960s [12] and comprises several different techniques and variants [14–17]. The online nature of the learning process fits well the architecture of a CR device: the DSA module provides context-awareness via explicit feedbacks and channel measurements, and based on such rewards, the RL-CM is able to learn the optimal state-action mapping. Differently from supervised learning [8], RL algorithms might work without assuming any previous knowledge of the environment and of the reward function [11]. At the same time, a RL agent continuously adjusts its current policy based on the interactions with the environment: hence, policy adaptiveness is implicitly addressed also in dynamic and nonstationary environments.

This property is particularly interesting in CR networking scenarios, which are dynamic by nature due to the mobility of the SU devices, the PU activity patterns, and the likely varying propagation and traffic load conditions, and constitutes another significant advantage compared to traditional optimization approaches. Thanks to these benefits, several recent works have demonstrated that RL techniques can be applied on spectrum management issues [18–20], including channel sensing, channel selection, or power control problems, as well as on many CR network management issues, including routing, cooperation control, and security [21, 22]. At the same time, the application of RL techniques in CR scenarios hides a number of technical challenges, like the impact of exploration phase on the system performance Ozekin et al. [23, 24] and the convergence in distributed environments characterized by the presence of SUs that compete for shared resources (e.g., channel frequency) while cooperating on keeping the aggregated interference below a predefined QoS threshold [25, 26].

This paper investigates the application of RL techniques on CR networking by providing two kinds of scientific contributions, i.e., (i) a survey of the RL-CR-related literature, which can serve also as a tutorial for readers approaching the topic for the first time, and (ii) a proof of concepts of RL techniques on novel CR use-cases. Regarding the survey/tutorial, after a brief presentation of the RL theory and of the main algorithms, we discuss advantages and drawbacks of the RL framework for CR networking, and we compare it against other ML approaches. We then provide an up-to-date and exhaustive review of the RL-CR-related literature through a twofold taxonomy. The first taxonomy is based on the CR application domains, focusing on spectrum management and network configuration issues (i.e., spectrum sensing, decision, power allocation, and routing); on each category, we further classify the studies according to the proposed goal being addressed. The second taxonomy is learning methodology-driven, i.e., we review

the literature according to specific RL modeling features which are orthogonal to the application domain, like the modeling of the environment and of the reward function. Regarding the proof of concepts, we describe a novel application of RL techniques on joint channel sensing and decision problems (hence, combining two research issues which are treated separately in the survey): more specifically, we show how the SUs can autonomously learn the optimal channel allocation, as well as the optimal balance of sensing/transmitting actions on each channel, so that the secondary network performance are maximized, while the harmful interference to PU receivers are kept below a QoS threshold. We formulate the problem as an instance of a Markov decision process (MDP) [12, 13], and we tested different algorithms (Q-Learning and Sarsa) and learning models, on two different task goals: independent learning and collaborative agents on a fully cooperative task (e.g., PU-SU interference minimization) and distributed coordinating agents on a mixed cooperative/competitive task (e.g., SU-SU and PU-SU interference minimization). The experimental results show that RL-based solutions can greatly enhance the performance in dynamic CR environments compared to non-learning-based solutions; at the same time, they unveil the impact of RL parameter tuning, knowledge sharing techniques, and algorithm selection, hence paving the way to further researches on the topic.

The rest of the paper is structured as follows. Section "Related Works" reviews the existing surveys addressing ML and RL applications in CR networks and points out the novelties of this paper. Section "Overview of Reinforcement Learning" provides an overview of the RL theory, by introducing a taxonomy of the existing techniques and by also summarizing the operations of the most popular RL algorithms. Advantages and drawbacks of RL-CR approaches are discussed in section "Reinforcement Learning in Cognitive Radio Scenarios: Pros and Cons". Section "Reinforcement Learning in Cognitive Radio Scenarios: Applications-Driven Taxonomy" reviews the existing RL-CR studies according to an application-driven taxonomy. The existing works are further classified by means of a learning methodology-driven taxonomy in section "Reinforcement Learning in Cognitive Radio Scenarios: Learning Methodology-Driven Taxonomy". The case study is presented in section "Case Study: RL-Based Joint Spectrum Sensing/Selection Scheme for CR Networks", together with the RL formulation, proposed algorithms and performance evaluation results. Conclusions are drawn in section "Conclusions and Open Issues".

Related Works

The most comprehensive surveys investigating the applications of ML techniques on CR networking are probably [9, 10], and [11]. More specifically, [10] describes the existing applications of ML techniques on CR networking, considering both supervised and unsupervised learning techniques and including also the RL-based approaches. Moreover, the authors investigate the learning challenges in non-Markovian environments and discuss policy-gradient algorithms. An impressive

review of model-free learning-based solutions in CR networks is presented in [11], where the existing works are grouped in three main categories, i.e.: (i) strategy-learning schemes based on single-agent systems, (ii) strategy-learning schemes based on loosely coupled multi-agent systems, and (iii) strategy-learning schemes in the context of games. In [9], the authors survey the ML-CR literature by considering an interesting distinction between learning aspects of cognition – which include RL and dynamic games – and reasoning aspects. These latter are in charge of applying inference on the acquired and the learned knowledge, hence enriching the current knowledge base; applications of policy-based reasoning to predict spectrum handover operations or to enhance spectrum opportunity detections are evaluated in a test-bed [9]. The strict relationship occurring between learning and reasoning in CR networks is also investigated in [7]. By focusing on the RL-CR literature, the authors of [20] demonstrate how the RL framework, and in particular the Q-routing algorithm, can be utilized as modeling tool in four different problems, regarding dynamic channel selection (DCS), DCS and route selection, DCS and congestion control, and packet scheduling in QoS environments. Similarly, the authors of [18] show how three different CR problems (routing, channel sensing, and decision) can be modeled via the Markov decision process (MDP) introduced by the RL framework. Applications, implementations, and open issues of RL techniques in CR networks are extensively discussed in [19], which is the work most similar to our paper. Our paper provides two additional contributions compared to [19]: (i) it provides an up-to-date review of the RL-CR literature from two different perspective, i.e., a CR networking perspective and a learning perspective, and (ii) it evaluates gains and drawbacks of the RL framework on a realistic CR use-case, addressing joint spectrum sensing, and selection.

Overview of Reinforcement Learning

Reinforcement learning (RL) constitutes an area of machine learning (ML) [8] addressing the problem of an agent that must determine the optimal sequence of actions to perform over time, so that a predefined goal is achieved [12, 13]. Differently from supervised techniques, the learning process is based on trial-error interactions with the environment, i.e., at each action, the agent receives a numeric reward which is a proxy for its optimality (see Fig. 1). The optimal sequence is the

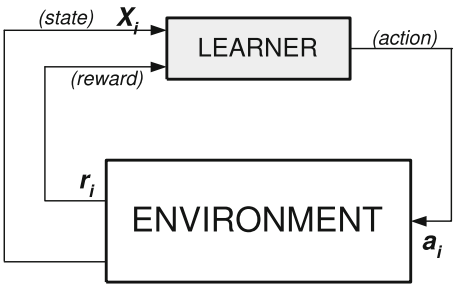

Fig. 1 The reinforcement learning (RL) model

one maximizing the summation of the expected rewards received by the agent over time.

More formally, the RL problem can be modeled by using a discrete Markov decision process (MDP), represented by the tuple $< S, A, R, ST >$, where:

- S is the (discrete) set of *available States*; let s_t denote the current state of the agent at time t.
- A is the (discrete) set of *Actions*; let $A(s_t)$ denote the set of actions available in state s_t.
- $R : S \times A \rightarrow \Re$ is the *Reward* function indicating the numeric reward received at each state/action; more specifically, let r_t indicate the reward received by the agent while being in state s_t and executing action $a_t \in A(s_t)$.
- $ST : S \times A \rightarrow S$ is the *State Transition* function, which indicates the next state s'_{t+1} after executing action $a_t \in A(s_t)$ from state s_t; in case of nondeterministic environments, the ST function is a probabilistic distribution over the set of actions and states, i.e., $ST : S \times A \times S \rightarrow [0 : 1]$.

Another component of the RL framework is the policy function $\pi : S \rightarrow A$, which indicates, for each state s_t, the proper action a_t to execute. Similarly to the state transition function, also the policy function can be modeled as a probabilistic distribution over the set of actions and states, i.e., $\pi : S \times A \rightarrow [0 : 1]$. The goal of the agent is to discover the optimal policy π^* which maximizes a specific function of the received rewards over time. In the infinite-horizon discount model [13], the policy aims to maximize the long-run expected reward; however, it discounts the rewards received in the future, i.e.:

$$goal \rightarrow maximize\ E\left(\sum_{t=0}^{\infty} \gamma^t \cdot r_t\right) \tag{1}$$

where $0 \leq \gamma \leq 1$ is a factor discounting the future rewards. If $\gamma = 0$, the agent aims to maximize the immediate rewards.

In order to compute the optimal policy, several RL algorithms employ two additional data structures: the state-value function (V^π) and the state-action function (Q^π) [12, 13]. For each state $s \in S$, the state-value function $V^\pi(s_t)$ represents the expected reward when following policy π from state s_t. The $V^\pi(s_t)$ value can be computed as follows:

$$V^\pi(s_t) = \sum_{a_t \in A(s_t)} \pi(s_t, a_t) \cdot \sum_{s' \in S} ST(s_t, a_t, s') \cdot \left(R(s_t, a_t) + \gamma \cdot V^\pi(s')\right) \tag{2}$$

Analogously, the state-action function $Q^\pi(s_t, a_t)$ represents the expected reward when the agent is in state s_t, executes action a_t, and then follows the policy π. More formally:

$$Q^\pi(s_t, a_t) = \sum_{s' \in S} ST(s_t, a_t, s') \cdot \left(R(s_t, a_t) + \gamma \cdot V^\pi(s')\right) \tag{3}$$

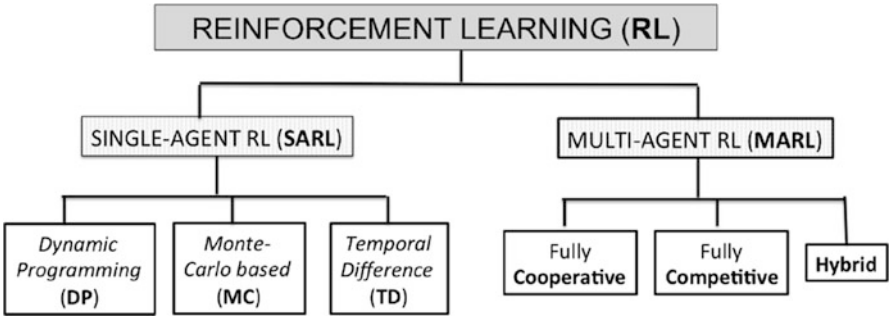

Fig. 2 Taxonomy of reinforcement learning (RL) algorithms

RL techniques can be classified into single-agent RL (SARL) and multi-agents RL (MARL) (see Fig. 2); the main characteristics of each approach are illustrated in the following section.

SARL Algorithms

In a SARL framework, each agent acts independently and aims to maximize its long-run expected reward (Eq. 1). Different techniques have been proposed in order to determine the optimal policy π^*, including dynamic programming (DP), Monte Carlo-based, and temporal-difference (TD) learning algorithms. DP techniques assume a perfect knowledge of the environment, i.e., of the reward (R) and of the state transition (ST) functions; hence, the exact value of $V^{\pi}(\cdot)$ can be computed by solving Eq. 2. The DP algorithms alternate between a policy-evaluation phase, during which the value of the current policy $V^{\pi}(s)$ is determined for each state $s \in S$, and a policy improvement phase, where the current policy π is modified into π' so that $\pi'(s) = \text{argmax}_{a \in A} Q^{\pi}(s, a)$ [12]. Monte Carlo methods do not assume the knowledge of the environment, but they are mainly used on episodic tasks [12]. Vice versa, TD methods implement an online, step-by-step learning process without assuming a model of the environmental dynamics. Among the several existing TD-based solutions, we cite the popular Sarsa and Q-learning algorithms [16, 17]: they both update the Q-table after each received reward, till converging to the optimal Q^* values. More specifically, each time the agent chooses action a_t from state s_t (receiving reward r_t), and action a_{t+1} from next state s_{t+1}, the Sarsa algorithm [17] updates the $Q(s_t, a_t)$ entry as follows:

$$Q(s_t, a_t) = Q(s_t, a_t) + \alpha \cdot [r_t + \gamma \cdot Q(s_{t+1}, a_{t+1}) - Q(s_t, a_t)] \tag{4}$$

where α is a learning rate factor. The Q-learning algorithm [16] employs a slightly different update rule, since it is independent from the policy being followed (offline policy learning), i.e.:

$$Q(s_t, a_t) = Q(s_t, a_t) + \alpha \cdot \left[r_t + \gamma \cdot \max_{a_{t+1} \in A(s_{t+1})} Q(s_{t+1}, a_{t+1}) - Q(s_t, a_t) \right] \tag{5}$$

Both Sarsa and Q-learning algorithms are guaranteed to converge to the optimal Q^* values, under the assumption that all state-action pairs are visited an infinite number of times, and proper tuning of the α factor [16, 17]. This poses a challenging trade-off between exploration and exploitation actions, i.e.: (i) insufficient exploration might affect the convergence to the optimal Q^* values, while (ii) excessive exploration might determine performance fluctuations caused by the selection of random actions. A well-known approach to balance exploration and exploitation actions is via the Boltzmann Equation [12], which assigns a probability to each action and state as a graded function of the estimated $Q(s, a)$ value:

$$p(s, a) = \frac{e^{Q(s,a)/TE}}{\sum_{a' \in A(s)} e^{Q(s,a')/TE}} \tag{6}$$

where $TE > 0$ is the temperature parameter and controls the exploration/exploitation phases. Indeed, high temperature values cause the actions to be all equiprobable, while, if $TE \to 0$, the greedy action a^* associated to the highest $Q(s, a^*)$ value is always selected, for each state $s \in S$.

MARL Algorithms

The MARL framework generalizes the MDP to the case of a multi-agent environment. Let N be the number of learning agents and S^i and A^i be the state and action sets for agent i. The state of the MARL at time t, $\widehat{s_t}$, is then defined as the combination of the individual states of the agents, i.e., $\widehat{s_t} = \{s_t^1, s_t^2, \ldots s_t^N\}$. Similarly, the system action $\widehat{a_t}$ is defined as the combination of the individual actions performed by the agents, i.e., $\widehat{a_t} = \{a_t^1, a_t^2, \ldots a_t^N\}$; based on $\widehat{a_t}$ and $\widehat{s_t}$, a vector of rewards is produced, i.e., $\widehat{r_t} = \{r_t^1, r_t^2, \ldots r_t^N\}$. According to the way such rewards are computed, and to the interactions among the agents, [14, 15] further classify MARL techniques as *fully cooperative*, *fully competitive*, or *hybrid*. In the first case, all the agents receive the same reward, i.e., $r_t^1 = \ldots = r_t^N$, and the goal is to determine the optimal joint policy maximizing a common discounted return; although such policy could be also determined via SARL techniques assuming that all the agents keep the full Q-table of $\widehat{s}$ and $\widehat{a}$ values, most of the MARL algorithms work by decomposing the Q-table and introducing indirect coordination mechanisms [27]. In fully competitive MARL frameworks, a min-max principle can be applied, for instance, when $N = 2$, $r_t^1 = +\zeta$ and $r_t^1 = -\zeta$ [14]. Finally, hybrid MARL techniques apply on not fully cooperative nor fully competitive problems, where the reward function might assume a complex shape depending on the joint action being implemented by the agents; this is the case, for instance, of agents competing for a shared resource, like SUs determining the optimal channels

where to transmit and taking into account the interference caused by other players (we further investigate such use-case in section "Case Study: RL-Based Joint Spectrum Sensing/Selection Scheme for CR Networks"). Hybrid MARL frameworks usually employ distributed coordination techniques derived from the game theory. We do not further elaborate on MARL techniques; interested readers can refer to [14] and [15] for a detailed illustration.

Reinforcement Learning in Cognitive Radio Scenarios: Pros and Cons

In CR networking, the cognition cycle, i.e., the ability of wireless transceivers to learn the optimal configuration meeting the characteristics of the environment and the QoS requirements of the applications, is considered as important as the hardware components which enable the spectrum reconfiguration capabilities. To this purpose, several ML techniques have been applied on CR-related use-cases [10], like spectrum sensing, spectrum selection, or routing; beside the RL techniques, which are the main topic of the paper, we cite approaches based on the game theory (GT), neural networks (NN), or Bayesian classifier (BC). On the SCOPUS database, we counted around 400 scientific papers addressing ML-based approaches in CR networks[1]: 23% of them are based on RL schemes, more than the supervised learning schemes but still less than GT-based approaches. In any case, Fig. 3 shows that there is no ML solution fitting all the solutions. This is because RL techniques provide clear advantages but also formidable drawbacks when applied on CR-related use-cases. About the advantages, RL techniques can considered highly suitable for CR applications because of these characteristics:

1. *Experience-based Learning*. In supervised learning, a cognitive agent must be instructed on how to perform a classification task by means of a knowledge base containing both positive and negative instances. In CR-related applications, building the knowledge base from real experiments can pose practical issues in terms of scalability and costs. Another issue pertains to the generalization of the learning process, i.e., to the problem of classifying novel instances which are considerably different from those occurring in the knowledge base. This aspect is particularly critic in CR environments, since the network performance is affected by a high number of parameters and by environmental conditions (like the PU activity model, the SU traffic load, the channel error rate, etc.); as a result, a transmitting policy learnt by a CR agent via supervised techniques might not be effective on a different network scenarios or even on the same scenario in presence of dynamic changes of environmental conditions. Vice versa, RL techniques do not require the creation of a knowledge base, rather they leverage on trial-and-error interactions with the environments. In addition, some

[1]The classification rule is based on the occurrence of specific keywords in the paper title.

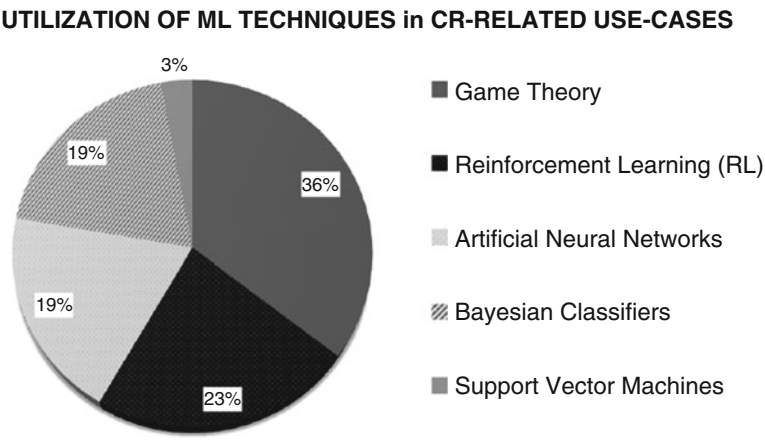

Fig. 3 Machine learning (ML) techniques utilized in the RL literature

model-free algorithms like Sarsa and Q-learning [11, 16, 17] do not assume an a priori knowledge of the environmental dynamics (i.e., of the reward and state transition functions); as a result, the same learning algorithm deployed on different network scenarios can automatically discover differentiated transmitting policies, without any need of adaptation or tuning of the RL algorithm.

2. *Context adaptiveness*. Through the concepts of rewards and Q-values, the RL framework provides effective building blocks in order to implement adaptive, spectrum-aware solutions. Indeed, since any RL agent continuously evaluates its current policy and improves it, any change in the received reward might cause a policy switch, or it might trigger new exploration actions, hence leading to the discovery of better actions to perform in some states. Moreover, the presence of aggregated rewards can indirectly boost the context-awareness in another way. As already said, performance of CR networks can be affected by multiple factors, whose interactions might be difficult to model analytically. Instead of addressing a single factor at a time, a RL agent can observe all the factors as a state, receive an aggregate feedback (e.g., the cost of each transmission), and optimize a general goal as a whole, e.g. throughput [28].
3. *Reduced complexity*. In most cases, RL techniques provide a simple yet effective modeling approach [12]. Model-free RL algorithms like Q-learning or Sarsa require only the storing of the Q-table. The number of state-action values can be further reduced via function approximation techniques; an example related to CR spectrum management can be found in [29]. In addition, it is worth remarking that the update rule of Q-learning or Sarsa algorithms can be implemented in few lines of codes. This feature makes RL techniques suitable also in resource-constrained environments, like CR-based sensor networks [30], where the wireless devices must face severe energy issues.

These advantages are counterbalanced by formidable drawbacks, which should be taken into account when working on CR networks, i.e.:

1. *Continuous Discovery.* Properly balancing the exploitation/exploration phase is a unique challenge of the RL framework [23]. On the one side, RL agents are required to perform random actions in order to explore the state-action space and then compute the optimal policy. In dynamic environments, the exploration phase cannot be ended after the boot phase; rather it must be continuously performed over time. This is the case, for instance, of SUs aimed to learn the available spectrum opportunities in a multiband scenario; while transmitting on a PU-free channel, the SU should also keep track of the opportunities on other channels, so that a spectrum handoff can be quickly performed in case of PU appearance [31]. On the other hand, a random selection might translate into suboptimal actions being executed, e.g., into the selection of low-quality or PU-busy channels, and hence lead to temporary performance degradation. Permanent performance degradation can occur when the exploration phase has been too short, or too long; hence, the optimal trade-off between exploration and exploitation can be complex to achieve, as investigated in section "Case Study: RL-Based Joint Spectrum Sensing/Selection Scheme for CR Networks".
2. *Convergence Speed.* Many RL techniques (specially time discounted methods [12]) guarantee convergence to the optimal policy only if each action is executed in each state an infinite number of times. This is clearly not realistic for most of CR applications; moreover, the fact that environmental conditions can quickly change over time can pose additional requirements on the speed of convergence. The issue is further exacerbated in MARL scenarios, where the optimal joint action must be determined, e.g., in spectrum selection or power adaptation problems [32, 33] where the SUs should maximize their own performance while collectively mitigating the interference to PUs. For these reasons, MARL-based algorithms are often enhanced with GT mechanisms which guarantee the emergence of a Nash equilibrium under specific assumptions [25, 26].

Reinforcement Learning in Cognitive Radio Scenarios: Applications-Driven Taxonomy

In this section, we describe the applications of RL techniques in four different CR use-cases, e.g., spectrum sensing, power allocation, spectrum decision, and routing. For each use-case, we provide a taxonomy of the existing works, and we briefly discuss their technical contributions, by mainly focusing on the problem formulation through the MDP. Figure 4 depicts the classification adopted throughout this section.

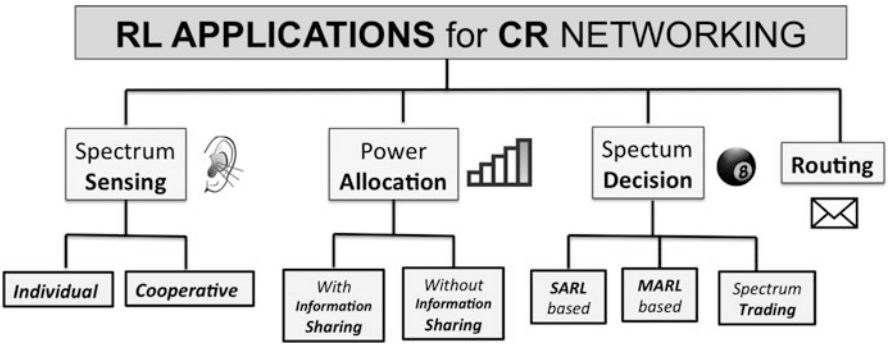

Fig. 4 Applications-driven taxonomy of the RL-CR literature

Spectrum Sensing

In CR, spectrum sensing techniques play the crucial role to identify the available spectrum resources for the SUs [1]. As a result, most of research is focused on advanced signal processing schemes aimed to achieve robust PU detection under different signal-to-noise ratio (SNR) conditions [3]. Beside this, the scheduling of sensing actions is also a crucial task affecting the performance of the SUs [34], mainly due to the fact that half-duplex radios cannot transmit on a channel while listening to it. The optimal sensing schedule can be determined via experiments and analytical models [4] or dynamically learnt via trial-and-error interactions with the environment [35]. About this latter, existing RL-based sensing schemes can be further classified into *individual* or *cooperative* approaches. We discuss them separately in the following.

Individual Sensing Scheduling

Frequency and duration of the sensing phase constitute a challenging trade-off between PU detection accuracy and throughput of the secondary network: too long sensing intervals might cause buffer overflow and/or TCP time-outs, while too short sensing intervals might lead to poor throughput due to SU-PU collisions [34]. Moreover, SUs should periodically explore all the available channels in order to detect spectrum opportunities over time. For these reasons, recent studies like [36, 37] and [38] investigate the problem on how to optimally balance sensing, transmission, and exploration actions, so that the performance of SU networks are maximized, while the PU detection accuracy is always kept higher than a safety threshold. More specifically, the authors of [36] formulate the problem via a MDP defined as follows: the set of states $S = \{s_1, s_2, ..s_{|S|}\}$ represents the available (licensed) resources. On each channel s, a SU can perform three actions:

- a_1: sense channel s and transmit in case the channel is found idle (*exploitation*).
- a_2: sense channel $s' \neq s$ (*exploration*).
- a_3: switch to channel $s' \neq s$ (*exploitation*).

For actions a_1 and a_2, the reward is expressed by the number of PU-free subcarriers detected on the sensed channel; vice versa, for action a_3 the reward is always equal to zero. The study in [37] extends such formulation, by taking into account the channel switching delay in the reward of action a_3 and by decoupling the transmit action from the sensing action; for sensing actions, the reward is equal to 1 in case of PU detection, 0 otherwise. Vice versa, the reward of transmit actions is computed as the average number of MAC retransmissions for each successful data transmission. The simulation results in [37] show that the proposed RL-based scheme is able to dynamically adjust the sensing frequency according to the perceived PU activity on each channel. Similarly, in [38], the authors aim to balance transmission and sensing actions on each channel; a cost function $C_s(\tau)$ is decreased each time a sensing action is performed on channel s, and this latter is found idle. When $C_s(\tau)$ is lower than a threshold Γ, then the SU can perform a transmission attempt; vice versa, if $C_s(\tau) > \Gamma$, then SU defers its attempt and keeps sensing the channel. When the channel is found occupied by a PU, the cost function $C_s(\tau)$ is reset to a maximum value. In [39], the problem of determining the optimal sequence of channels sensed by each SU is formulated through the RL framework; here, a state is defined as an ordered couple $< o_k, f_j >$, where o_k is the current position at the sensing order and f_j is the k-th channel sensed in the current slot. At each state $< o_k, f_j >$, the list of available actions will include all the channels (not visited yet) which could be sensed at the next position of the sensing order (o_{k+1}). The reward function for a specific sensing order action takes into account the time spent sensing the channels and the transmission rate experienced by the SU on the selected channels [39].

Cooperative Sensing Scheduling

Sensing techniques can be prone to errors in presence of shadowing or multipath fading conditions on the current licensed channel. For this reason, cooperative sensing techniques [3] aim to enhance the PU detection by aggregating channel measurements from multiple SUs and by averaging the gathered results. However, the network overhead might limit the cooperative gain: for instance, the transmission delay might be higher in presence of cooperative sensing, since each SU should gather the measurements from other peers before taking a decision about the spectrum availability. For this reason, studies like [40,41] and [42] employ the RL framework in order to determine the optimal set of cooperating neighbors for each SU; the goal is to maximize the PU detection accuracy while avoiding unnecessary measurements sharing among correlated SUs. In [40], the set of states S for SU i coincides with the list of neighbors, plus one start and one end state. There is an action which allows to move from any couple of states; the sequence of actions correspond to the list of cooperative sensing neighbors, i.e., neighbors to query in order to get channel measurements. The reward function combines the amount of correlation among the gathered sensing samples plus the total reporting delay. In [42], the authors investigate how to coordinate the sensing actions of a secondary network, in order to meet the optimal trade-off between two goals: (i) the maximum number of spectrum opportunities is detected, and (ii) the probability of missed detection on each channel is kept below a safety threshold. Such probability is

estimated based on the number of SUs currently sensing the channel. Since the SUs cannot directly observe the PU state on each channel, the sensing problem is formulated via a partially observable MDP (POMDP).

Power Allocation

In both underlay and overlay CR spectrum paradigms, the SUs should properly tune their transmitting power levels so that the probability of generating harmful interference to any active PU is minimized. Differently from spectrum sensing, which can be considered an individual or, in presence of knowledge sharing, a fully cooperative task, power allocation is a natively hybrid competitive/collaborative task, since the reward function, i.e., the aggregated interference perceived by PU receivers, depends on the joint action performed by the SUs, i.e., on the selected transmitting power level of each SU. For this reason, power allocation can be easily modeled via a MARL framework (see section "Overview of Reinforcement Learning"). A straightforward approach in order to determine the optimal power allocation consists in storing the complete MARL Q-table for each state/action/learning agent and by computing the optimal $\widehat{a}_t$ through Eq. 4. This methodology is employed in [43], assuming a centralized CR network with a single learning agent, i.e., the cognitive base station, which is charge of determining the optimal power level of each SU, based on the cumulative interference caused to the PUs. In distributed deployments, storing and updating the complete MARL Q-table at each SU might not be practical especially when the number of learning agents (i.e., the SUs) increases. For this reason, most of recent works employ decentralized MARL with two different approaches. In the first case (described in section "RL-Based Power Allocation Based on Information Sharing"), the SUs share rewards or rows of their Q-table after each local action, so that the interference caused by the joint action $\widehat{a}_t$ can be computed. In the other case (described in section "RL-Based Power Allocation Without Information Sharing"), each SU acts according to the local information only, but the secondary network still aims to achieve a global coordination, often expressed by the notion of Nash equilibrium (NE).

RL-Based Power Allocation Based on Information Sharing

In decentralized MARL frameworks, information sharing can be used for two different objectives: (i) speedup the learning process of the individual agents, by reducing the amount of exploration needed; or (ii) favor the identification of joint optimal actions at each learning agent. The docitive paradigm discussed in [44,45] is an example of the first use-case; here, the learning agents are secondary base stations (femtocells) which must determine the optimal transmitting profile so that the aggregated interference at the primary receivers is kept below a specific threshold ($SINR_{Th}$). The problem is modeled through the MDP defined as follows:

- The state set is defined as the set of couples $\{I_t^i, d_t^i\}$, where $I_t^i \in \{0; 1\}$ is a binary indicator specifying whether the CR base station i is generating an aggregated

interference above or below the $SINR_{Th}$ threshold, and d_t^i is the approximated distance between i and the protection contour region of the primary system.
- The action set coincides with the discrete set of power levels which can be assigned to each CR base station.
- The reward function $R(i) = (SINR_t^i - SINR_{Th})^2$ expresses the difference between the SINR value measured by SU i and the expected threshold.

In addition, docitive SUs can teach the discovered policies to other peers, by sharing parts of the local Q-table. In [44] , three different information-sharing techniques are evaluated, namely, start-up docition, adaptive docition, and iterative docition. This latter (involving continuous sharing of the Q-table entries) maximizes the system performance, although introducing the highest network overhead. In [45], the docitive scheme is extended for the case of partially observable environments, i.e., when the SUs lack of complete information about aggregated interference at the protection contour regions. A similar learning-from-experts MARL approach is followed in [46] and [47] but also introducing expertness measures which estimate the amount of knowledge which can be transferred between each couple of SUs. More specifically, the authors of [47] address a generic power-spectrum selection problem; at each step, an agent can decide whether to stay idle, to switch to a different channel, or to increase/decrease the current transmitting power. The current state reflects the buffer occupancy of each SU, while the reward function is related to the energy efficiency of each action. Periodically, all the SUs update their Q-entries by considering a weighted combination of location information and received Q-values, i.e., $Q_i^{\text{new}} = \sum_j W_{i,j} \cdot Q_j^{\text{old}}$, where $W_{i,j}$ is a measure on how much SU i relies on knowledge produced by SU j. The scheme in [47] employs information sharing in order to speed up the individual learning process; however, there is no guarantee that the optimal joint action will be determined. In order to fulfill this second requirement, the authors of [48] propose a cooperative RL-based power allocation scheme aimed to control the aggregated interference generated by SU femtocells. The MDP model is similar to [44, 45]; however , each SU shares only a row of its Q-table. At each time-slot, a SU chooses action a_i maximizing the summation of the Q-values considering the current states of all the N neighbors, i.e.:

$$a_i = \text{argmax}_a \left(\sum_{i \le j \le N} Q_j(s_j, a) \right) \tag{7}$$

RL-Based Power Allocation Without Information Sharing

Differently from the previous works, studies like [32] and [33] address the power selection problem without assuming information sharing among the SUs; each SU tunes its transmitting power based on local (possibly inaccurate) interference measurements, but at the same time, it observes or makes conjectures about the behavior of other SUs. Based on such estimations, each SU adjusts its transmitting

power so that a global NE is achieved, i.e., no SU can experience better rewards by following a different policy. The MDP is formulated as follows:

- The state set is defined as the set of couples $\{I_i, p_i(a_i)\}$, where $I_i \in \{0; 1\}$ is a binary indicator specifying whether the SINR of SU i is higher or lower than a predefined safety threshold and $p_i(a_i)$ denotes the current power level.
- The action set coincides with the discrete set of power levels which can be assigned to each SU.
- The reward function R is a proxy for the energy efficiency of the transmission attempt, i.e., of the average number per bits received per unit of energy consumption; if I_i=1, the reward is set to zero.

Differently from [44, 45], each SU keeps internal conjunctures about how the other SUs will react to their current action. More specifically, at each action performed in state s_t, SU i updates its Q-table as follows:

$$Q^{t+1}(s_i, a_i) = (1-\alpha) \cdot Q^t(s_i, a_i) + \alpha \cdot \left(\sum_{a_{-i}} \overrightarrow{c}^t(s_i, a_{-i}) \cdot r_t + \beta \max_{b_i} Q(s_i', b_i) \right) \tag{8}$$

where $\overrightarrow{c}^t(s_i, a_{-i})$ denotes the conjecture of SU i regarding the behavior of the other players and is updated as follows:

$$\overrightarrow{c}^{t+1}(s_i, a_{-i}) = \overrightarrow{c}^t(s_i, a_{-i}) - \omega_i^{s_i, a_{-i}} \cdot \left[\pi_i^{t+1}(s_i, a_i) - \pi_i^t(s_i, a_i) \right] \tag{9}$$

Spectrum Selection

Dynamic channel selection (DCS) constitutes the most investigated RL application in the field of wireless networking [20, 49–53]. In overlay RL networks, each SU must select the proper channel where to transmit in order to fulfill two main requirements: (i) minimize the interference caused to PU receivers tuned on the same or adjacent spectrum bands (G_0) and (ii) maximize its own performance, by taking into account the channel contention and the MAC collisions caused by other SUs operating on the same band (G_1). Moreover, the SUs should continuously execute channel selection in order to adapt to dynamic changes of the PU activities, to the traffic loads generated by the SUs, and to varying propagation and channel state conditions. It is easy to notice that the RL framework fits well the requirements of adaptive protocol design. G_0 is usually addressed via the SARL techniques presented in section "SARL-Based DCS". Vice versa, meeting both G_0 and G_1 requires some form of coordination among the SUs: for this reason, the DCS problem is modeled via MARL techniques enhanced with game theory concepts, so that a stable channel allocation is achieved (details are provided in section "MARL-Based DCS"). Another way of classifying the existing RL-DCS schemes proposed in the literature is by focusing on the learning

agent, i.e., on where the RL framework is implemented. The solutions presented in sections "SARL-Based DCS" and "MARL-Based DCS" refer to a scenario where channel selection is performed by each SU, and the PU is unaware about the presence of opportunistic users. Vice versa, in spectrum trading models, the PUs borrow portions of its spectrum to the SUs, receiving in return a monetary revenue; the problem formulation through the RL framework allows determining the optimal portion of spectrum band which can be leased to the SUs without compromising the QoS requirements of the primary network. Details about RL-based spectrum trading schemes are provided in section "RL-Based Spectrum Trading".

SARL-Based DCS

This subcategory includes all the works where a SU learns in isolation the optimal sequence of channels where to transmit, without receiving any explicit feedback from other SUs and without keeping any implicit model of the opponents behaviors. At the same time, the reward function is often modeled in order to reflect some network performance (e.g., throughput or delay metrics) which are also affected by the joint strategy, i.e., by the channel selection performed by the other SUs. While this approach greatly simplifies the problem formulation, it might introduce some oscillating behaviors when also goal G_1 is taken into account: a SU might keep adjusting its operating channel as a consequence of channel selection performed by the other SUs. SARL-based DCS schemes can be further classified as *state-full* or *stateless* approaches. In the first case, the RL framework contains both actions and states, hence following the traditional structure discussed so far. Examples of state-full SARL-based DCS schemes are presented in [20] and [49]. More specifically, in [49] the authors propose an opportunistic spectrum model, in which each SU is associated to a home band (where it has the right to transmit), but it may also seek for spectrum opportunities in the licensed bands (at condition of minimizing the interference caused to the licensed users). The DCS problem is modeled through the following MDP:

- The state set $S = \{s_0^i, s_1^i, \ldots, s_M^i\}$ coincides with the list of available channels; s_0^i corresponds to the home channel of the SU, while $s_1^i, \ldots, s_M^i$ are the licensed channels.
- The action set $A = a_0, a_1, \ldots a_P$ indicates the output of the channel selection process; a_0 is the action of transmitting on the home channel, while action $a_i, i > 0$ perform explorations, i.e., the SU will transmit on the M licensed frequency by following a specific channel sequence.
- The reward R is a function of the quality communication level, which can be determined via link-metrics (e.g., SNR or packet success rate).

The simulation results in [49] show that the RL-based DCS scheme can greatly enhance the performance compared to random access schemes, also in presence of PU load variability. In [20], the authors propose a joint RL-based DCS and congestion control scheme, which performs channel selection by taking into account the traffic load produced by each SU and the amount of PU activity on each band.

This is achieved by enriching the definition of states of the RL framework; each state is a combination of four variables, which models, respectively , the amount of required bandwidth, the current data packet dropping probability, the amount of good white space in the current channel, and the amount of good white space across the various channels.
Stateless SARL-based DCS schemes simplify the RL framework, by eliding the states, and considering only the action set A which often coincides with the list of available channels; executing action a_i corresponds to switching to frequency f_i, sensing it, and transmitting in case no PU activity is detected. In [51], the Q-learning update rule of Eq. 4 is simplified to:

$$Q^i_{t+1}(a) = (1-\alpha) \cdot Q^i_t(a) + \alpha \cdot r^i_t \tag{10}$$

Here, the reward r^i_t is the throughput experienced by SU i at time-slot t. In order to avoid oscillations in the learning process, sequential exploration is employed, i.e., a single SU can undergo exploration within a neighborhood. In [30], the authors propose three different RL-based DCS schemes, all based on the update rule of Eq. 10 but adopting three different formulation of the reward function, i.e.: the transmission successful rate in each epoch (named Q-learning+ scheme), the SINR metric (named Q-Noise scheme), and the SINR plus the historical behavior of the SUs (named Q-Noise+). A similar approach is also followed in [54], where the SUs aim to learn the optimal channel selection probability and the amount of PU activity on each channel. It is also worth noting that stateless RL frameworks can be considered instances of the multiarmed bandit (MAB) problem [55]. Several MAB-based DCS algorithms have been proposed in the literature. We cite, among others, the study in [56], where the authors compare two popular MAB schemes, named the UCB and the WD techniques, to the DCS problem in RL scenarios, assuming error-free sensing and that the temporal occupation of each channel follows a Bernoulli distribution. The output of the learning process is hence to learn the PU channel occupation probability of each channel, limiting the summation of regret[2] over time. The MAB framework of [56] is extended in [57] by considering cooperation techniques, aimed to improve the sensing accuracy, and coordination techniques, aimed to mitigate the impact of secondary interference.

MARL-Based DCS

In [52] and [53], the authors formulate the DCS problem through a MARL framework, by extending the previous SARL formulation [51]; the goal of the SUs is to discover the optimal joint action addressing both G_0 and G_1 requirements. This is performed via a payoff propagation mechanism, i.e., each SU i maintains – in addition to the Q table – a μ-table with size $|\Gamma(i) \times A|$ where $\Gamma(i)$ denotes its set of neighbors and A is the set of actions, which coincides with the channel list. Each

[2] In MAB theory [55], the regret is defined as the expected difference between the reward sum associated with an optimal strategy and the sum of the collected rewards of the actual strategy.

time SU plays action a_k (i.e., switches to channel a_k), it transmits a payoff message including its $Q^i_{t+1}(a_k)$ value, while all the other SUs $j \in \Gamma(i)$ will store such value in their μ-table. When selecting the next channel $\widehat{a}_{t+1}$, SU i will take into account both the local Q-table as well as the payoff table, i.e.:

$$\widehat{a}_{t+1} = \text{argmax}_{a \in A} | Q^i_t(a) + \sum_{j \in \Gamma(i)} \mu_{ji}(a) | \tag{11}$$

The simulation results show that the MARL-based and SARL-based DCS schemes provide similar level of throughput, although the MARL-based scheme greatly reduces the number of channel switching operations. The converge of MARL-based DCS schemes to a Nash equilibrium (NE) is investigated in [25] and [58]. More specifically, in [58] the authors consider a simplified SU interference model where maximum one SU can operate on each channel and demonstrate that a Q-learning-based DCS scheme without any SU cooperation and regardless of the initial allocation can converge to a stationary channel allocation. The result holds only under the assumption that all the SUs have perfect knowledge of the complete system state, i.e., of the PU occupancy of all the available channels. In [25], the authors remove such assumption and propose a probabilistic DCS scheme which is demonstrated to converge to a NE. To this purpose, each SU updates the selection probability $p_{t+1}(k)$ at each transmission attempt on channel k according to a linear reward-inaction model, i.e.:

$$p_{t+1}(k) = p_t(i) + r_t \cdot (e_k - p_t(k)) \tag{12}$$

where r_t is a function of the SINR metric perceived by the SU receiver, and e_k is the unit vector [25].

RL-Based Spectrum Trading

Spectrum trading can be considered as a variant of DCS problems where spectrum operations involve both the PU, who is in charge of deciding the amount of frequencies to borrow to the SUs, and SUs, who can request specific portions of the spectrum. In [59], the authors propose a RL-based scheme which helps a PU in deciding which requests to accept and which to reject, assuming that SUs belong to different classes, mapped on different QoS requirements. The MDP formulation is as follows:

- the state set S coincides with the number of SU traffic classes; the value of s_i is the number of SU requests accepted belonging to class i.
- the action set $A = \{0, 1\}$ includes only two choices, corresponding to the option of accepting a new incoming request or to refuse it.
- the reward function $R = P - C$ combines the expected monetary profit (P) that should be paid by the SU with the cost C, which is proportional to the number of already leased channels.

In addition, the authors of [59] show how to dynamically adjust the spectrum price and the size of the spectrum leased over time, based on the dynamic SU traffic load conditions. In [60], the RL-based spectrum leasing problem is inverted, i.e., the SUs learn to improve the bidding policy in the spectrum auction game, by using the transmission capability of each channel as immediate reward.

Spectrum-Aware Routing

In multi-hop wireless networks, routing protocols are in charge of discovering a feasible path between any source and a destination nodes; the path creation is performed through a distributed node selection process guided by end-to-end/global (e.g., delay) or link-by-link/local (e.g., SNR) metrics. In CR networks, routing protocols must address additional challenges caused by the dynamic variation of spectrum opportunities, like (i) the need of selecting forwarding nodes, so that the interference caused to PU receivers is minimized; (ii) the need of fast rerouting mechanisms, so that alternative, back-up paths can be used when the main path is invalidated due to the appearance of a PU [61]. For this reason, several existing routing schemes for CR networks address joint node and frequency selection [61, 62]. The routing problem can be easily modeled in the RL framework: each CR node must learn the optimal next-hop toward the destination via trial-and-error interaction. At each data transmission, the SU receives a reward which is a proxy for the forwarding cost, like the mean-access delay or the amount of energy consumed. Changes in the environment, like the appearance of a PU or the SUs mobility, are reflected in changes of the received feedbacks, which in turn translate into the selection of an alternative path. The MDP process for a generic RL-enabled routing protocol can be described as follows:

- The state set S coincides with the set of SU nodes N_{SU} in the network.
- The action set A_i is defined for each node $i \in N_{SU}$; more specifically, $a_j^{(s,d)} \in A_i$ denotes the action of forwarding data toward next-hop j, where s and d are, respectively, the source and destination communication end-points.
- The reward $R(i, a_j^{(s,d)})$ is a network metric reflecting the effectiveness for node i of using j as next-hop node toward the destination d.

The above model has been implemented by Q-routing [63], which is a popular routing protocol for dynamically changing networks, also applied over generic multi-hop wireless ad hoc networks [64]. In Q-routing, each node i maintains a *table* of Q-entries for each destination d; the entry $Q_i(j, d)$ is the *expected delivery time* toward destination d when using next-hop node j. After forwarding a packet via node j toward destination d, node i updates its Q-Table as follows [63]:

$$Q_i(j, d) = q_i + \delta + min_z Q_d(y, z) \tag{13}$$

where q_i is the time spent by the packet in the queue of node i, δ is the transmission delay on the $i-j$ link, and $\min_z Q_j(z,d)$ is the best delivery time at node j and for destination d. The same learning framework than Q-routing has also been adopted by several CR routing protocols, like [21, 65] and [66] although properly adapting the reward function to the CR scenario. In [65], the reward $R(i, a_j^{(s,d)})$ is the per-link delay, which also takes into account the retransmissions caused by SU-PU collisions. In [21], the reward function is an estimation of the average channel available time, i.e., average OFF period of PUs interfering over the bottleneck link along the route from j to d. In addition, the authors of [21] investigate the performance of the proposed RL routing protocol on a real test-bed environment using USRP platforms; the experimental result demonstrates that the RL scheme provides better result than a greedy approach in terms of end-to-end metrics (i.e., throughput and packet delivery ratio). A multi-objective Q-routing scheme for CR networks is discussed in [66]; more specifically, the proposed algorithm aims to minimize the packet loss rate under desired constraint of transmission delay. The multi-objective is implemented by employing two rewards for each successful transmission (e.g., loss rate and delay) and by storing two separate Q-values at each node. The authors of [28] propose two RL-based spectrum-aware routing protocols for CR networks. Here, the $Q_i(j,d)$ value denotes the number of available PU-free channels on the route from SU i to SU d via SU j; the SU j providing the highest Q-value is the preferred next-hop candidate. The Q-values are updated after each successful transmission, using a dual RL algorithm. In [67], the RL framework is used in order to properly tune the transmitting parameters of the popular AODV routing protocol. A different RL formulation for CR routing is proposed in [68], considering both the delay minimization requirement of each SU-SU flow and the interference minimization requirement of each SU-PU link and assuming no cooperation occurs among the SUs. The MDP is defined as follows:

- The state set of SU i is defined as the tuple: $< \eta_i(t), \lambda_1(t), \lambda_2(t), \ldots, \lambda_{|PU|}(t) >$, where $\eta_i(t)$ is the packet arrival rate of SU i and $\lambda_x(t)$ is the packet transmission rate of PU x at time t.
- The action set of SU $iA = \{a_0, NH_i^1, NH_i^2, .., NH_i^k, \}$ includes the no-forwarding action a_0 and the transmission toward next-hop node NH_i^j.
- The reward function is equal to the delay experienced by packets flowing from SU i to the destination node, in case the interference caused to PUs is kept below a safety threshold; it is set to a large value in case the no-forwarding action is selected or in case the interference caused to the PUs is higher than the threshold.

Since no information sharing is assumed, each SU forms conjectures on the other SUs routing strategies by using local observations of the environment; the convergence to proposed routing protocol is also investigated in [68] through an analytical framework and network simulations.

Reinforcement Learning in Cognitive Radio Scenarios: Learning Methodology-Driven Taxonomy

While the aim of the previous section was to analyze the existing literature from a networking perspective, in this section we provide an alternative review from the learning perspective, i.e., on the way different components of the RL framework are modeled for CR-related issues and on the overall evaluation method adopted. To this purpose, we decompose the learning process into six steps, which are depicted in Fig. 5 and discussed separately in the following:

- *State representation*. The state of SUs is often modeled through a single discrete variable or a combination of discrete variables. However, the reviewed RL-CR studies differentiate on whether the state variables are *fully observable* by the SU or are only *partially observable*. In the first case, the state variable is expressed by parameters which are internal to the SU or by network conditions which can be measured by the DSA without perception errors. This is the case, for instance, of the MDP model proposed in [44], where each state takes into account both internal (i.e., the current distance from the PU) and network metrics (i.e., the aggregated interference caused by the secondary network). Vice versa, a minority of the cited studies takes into account the impact of perception errors on the network observation: we cite, for instance, the MDP proposed in [41] and [42] where the SU state is the belief that a given frequency is vacant, hence subject to the accuracy of the sensing scheme.
- *Model representation*. Almost the totality of the proposed RL-CR solutions employs *model-free* strategies with very few exceptions [68, 69], i.e., the agent does not keep any representation/estimation of the state transition and of the reward functions (the T and R functions in section "Overview of Reinforcement Learning"); rather, it updates the Q-table after each immediate reward through the popular Q-learning or Sarsa algorithms. This choice can be justified since, on several use-cases like DSA problems, the reward values are associated to network metrics (e.g., the actual throughput or the SNR) which are stochastically by nature and whose trends are hard to predict without having full knowledge of the network and channel conditions; moreover, both the state transition and the reward functions can dynamically vary in nonstationary environments

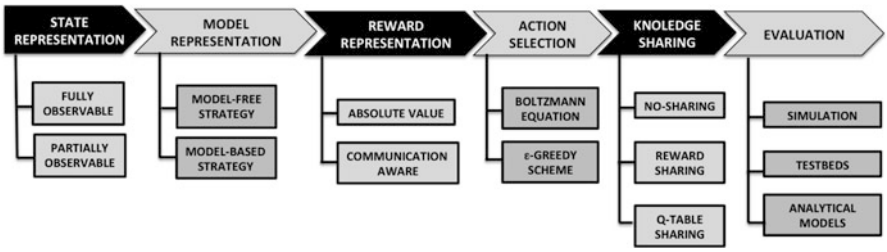

Fig. 5 Application-driven taxonomy of the existing RL-CR literature

due, e.g., to SU or PU mobility. For this reason, most of the works prefer to adjust the policy as a blind consequence of the received reward, instead of attempting to unveil the rules behind it. Some foundational results on this topic are provided in [70], where the authors investigate the relationship between the learning capabilities of the SUs in RL-DCS applications and the complexity of the PU pattern activity, measured through the Ziv-Lempel complexity metric. The experimental results demonstrate that, for specific levels of Ziv-Lempel complexity, the PU spectrum occupancy pattern can be learnt in an effective way by the SUs, hence justifying the utilization of model-based solutions.

- *Reward representation*. The modeling of the reward function clearly depends on the specific CR use-case. However, we can distinguish between two main approaches: *absolute* representation and *communication-aware* representation. In the first case, the reward is a scalar value, which can assume positive or negative values in order to encourage good actions or to penalize bad actions, but it is not related to any network metric. This is the case, for instance, of the RL-DCS scheme proposed in [29], where different rewards are introduced according to the outcome of each SU-SU transmission (i.e., successful, failed due to CRPU interference, failed due to CR-CR interference, failed due to channel errors). Vice versa, in communication-aware scheme, the reward takes into account node-related (e.g., the energy efficiency in [47]), link-related (e.g. the SNR in [43]) or network-related (e.g., the throughput in [20]) metrics. The clear advantage of this second approach is that the Q-table will converge over time to the actual system performance for the selected metric; at the same time, this might introduce additional protocol complexity, especially in presence of aggregated or cumulative metrics (e.g., the end-to-end path delay in Q-routing [63]).
- *Action Selection*. Strategies for action selection play a crucial role since they are in charge of balancing the exploration/exploitation phases, which in turn affect the performance of the RL-based solutions. Two main strategies have been employed in the RL-CR literature reviewed so far: the *Boltzmann rule*, which is based on Eq. 6 and relies on the temperature parameter TE in order to balance the exploration/exploitation phases, or the ε-*greedy rule*, which selects the optimal action with ε probability, while it performs random actions with $1-\varepsilon$ probability. Both such strategies might guarantee adaptiveness to nonstationary environments; however, the way the TE and ε parameters are set and discounted over time is barely addressed, except for [23, 24]. More in details, [24] proposes an interesting self-evaluation mechanism which is added to a basic RL-DSA framework: each time the SU receives a predecided number of negative rewards in exploitation mode, it assumes that there has been a change in the environment and reacts by forcing an aggressive channel exploration phase.
- *Knowledge Sharing*. In several CR use-cases modeled through a MARL, the SUs can share learnt information in order to speed up the exploration phase or to implement distributed coordination mechanisms. From the analysis presented in section "Reinforcement Learning in Cognitive Radio Scenarios: Applications-Driven Taxonomy", we can further classify the existing MARL-

CR works in three major families: (i) *no-sharing*, (ii) *reward-based*, or (iii) *Q-table-based*. The first category includes all works where the SUs update their Q-table independently and without receiving any feedback from the other peers, although the instantaneous reward might depend from the joint action executed by the secondary network (e.g., the throughput in [30]). We include in this group also centralized approaches, where the global Q-table is managed by a network coordinator (e.g., the cognitive base station in [43]), or solutions where each SU keeps conjectures about the future behavior of the other SUs [32,68]. The second category includes approaches like the docitive [44, 45] or payoff propagation paradigms [52, 52] where the SUs share the immediate rewards or rows of the Q-table. The received data are then merged with the local data, by using expertness measures controlling the knowledge transfer [46, 47] or action selection methods for achieving distributed coordination [48]. The impact of knowledge sharing on MARL-DCS problems is further investigated in section "Case Study: RL-Based Joint Spectrum Sensing/Selection Scheme for CR Networks".

- *Evaluation method*. Performance of RL-based solutions can be investigated through *simulation* studies, *testbeds*, or *analytical* models. The first two methods allow understanding the network performance gain introduced by RL techniques compared to non-learning approaches: at the best of our knowledge, [21, 71] and [72] are the only experimental studies in the literature. More specifically, [21] investigates the ability of a RL-enhanced routing protocol to select PU-free routes on a network environment consisting of ten USRP SU nodes, while [71] and [72] implement a RL-based DCS algorithm, respectively, over GNU-radio and USRP N210 platforms, and evaluate the way CR devices are able to learn the PU spectrum occupancy patterns. Both [21] and [71] confirm the effectiveness of RL-based solutions compared to state-of-the-art (non-ML-based) approaches. Analytical studies like [58] investigate the convergence of proposed RL algorithms to the optimal solution. Such theoretical results can be considered highly relevant from a pure scientific perspective but less practical in real-world network deployments, since the convergence property is assumed asymptotic and without accounting for the impact of exploration phase on the short-term system performance.

Case Study: RL-Based Joint Spectrum Sensing/Selection Scheme for CR Networks

In this section, we describe an application of RL techniques to CR networks, in order to highlight gains and drawbacks of different RL algorithms and also to investigate the impact of learning parameters on the system performance. By referring to the taxonomy presented in section "Reinforcement Learning in Cognitive Radio Scenarios:
Applications-Driven Taxonomy", we consider here a joint spectrum sensing/selection (JSS) problem, in which a SU must learn the optimal channel where

to transmit among the available frequencies and also the optimal balance between sensing and transmit actions on each channel. In section "System Model", we introduce the system model and the problem goals. The problem is formulated by using the RL framework in section "RL-Based Problem Formulation". Then, we evaluate the performance of RL-based solutions by neglecting the impact of secondary interference (section "Analysis I: SU-PU Interference Only"). Such assumption is removed in section "Analysis II: SU-PU and SU-SU Interference".

System Model

We model a generic network scenario composed by N couples of SUs operating within the same sensing domain. Each SU is equipped with a DSA transceiver, able to switch over K frequencies of the licensed band, and over a common control channel (CCC) implemented in the unlicensed band. Each couple i is formed of one SU transmitter (SU_i^{tx}) and one SU receiver (SU_i^{rx}). Data packets are transmitted over a licensed channel, while the signaling traffic is transmitted over the CCC. On each frequency f_j, there is an active PU which transmits according to an exponential ON/OFF distribution with parameters $< \alpha_j, \beta_j >$. Hence, frequency j is vacant with a posteriori probability equal to $\frac{\alpha_j}{\alpha_j+\beta_j}$, while it is occupied by the PU with probability equal to $\frac{\beta_j}{\alpha_j+\beta_j}$. In addition, we model the packet error rate (PER) on each channel; let φ_j be the PER of channel f_j. Each SU_i^{tx} can implement three different time-slots:

- *Sensing* slot, i.e., SU_i^{tx} senses the frequency to which it is currently tuned, in order to determine the PU presence. The sensing length is equal to t_{slot}. We assume a default energy-detection sensing scheme [3]: let p_D indicate the probability of correct detection and $1 - p_D$ the probability of sensing errors (including both false-positive and true negative instances).
- *Transmit* slot, i.e., SU_i^{tx} attempts transmitting exactly one packet to SU_i^{rx} by using a CSMA MAC scheme. In case the MAC ACK frame is not received, SU_i^{tx} retransmits the packet till a maximum number of attempts equal to $MAX\_ATTEMPTS$. Otherwise, the packet is discarded.
- *Switch* slot, i.e., SU_i^{tx} switches to a different licensed frequency and communicates the new channel to the SU_i^{rx} on the CCC. Let t_{switch} represent the time overhead required for the handover.

Figure 6 shows an example of the time-slot sequences for three different SU transmitters. We indicate with τ_i^k the type of k-th time-slot implemented by SU i, where $\tau_i^k = \{\texttt{SENSE}, \texttt{TRANSMIT}, \texttt{SWITCH}\}$ and with $T_i = \{\tau_i^0, \tau_i^1, \ldots\}$ the slot schedule of SU i. Each SU i can decide its own schedule T_i, but subject to these constraints: (i) if τ_i^k=SENSE, and the channel is found busy, then τ_i^{k+1}=SENSE or τ_i^{k+1}=SWITCH, i.e., the SU can keep sensing or switching to a different channel, but it cannot perform a transmission and (ii) if τ_i^k=SWITCH, then τ_i^{k+1}=SENSE,

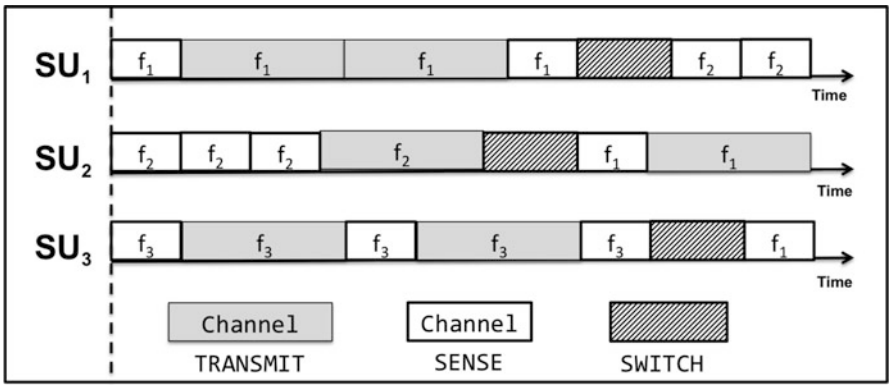

Fig. 6 Example of time-slot sequences for three different SU transmitters

i.e., the SU must sense the new channel in order to discover its availability.
Similarly, let NTX_i be the total number of transmissions performed by SU i (including the retransmissions). We denote with $STX_i(l)$ the outcome of the $l-$th transmission (with $0 \leq l < NTX_i$) performed by SU i. Based on the channel conditions, and on the SUs and PUs activities, the $STX_i(l)$ variable can assume one of these four values: (i) $STX_i(l)$=`OK` if the transmission has been acknowledged by SU_i^{rx}, (ii) $STX_i(l)$=`FAIL-PU-COLLISION` if the transmission has failed due to collision with an active PU (i.e., PU is ON during the SU transmission); (iii) $STX_i(l)$=`FAIL-SU-COLLISION` if the transmission has failed due to collision with other SU transmissions on the same channel; and (iv) $STX_i(l)$=`FAIL-CHERROR` if the transmission has failed due to channel errors.
The JSS problem can be formulated as the problem of determining the optimal schedule T_i of each SU i, $0 \leq i < N$, so that the total number of successful transmissions is maximized, while the probability to interfere with the PUs is kept below a predefined threshold (ψ). More formally:

(**JSS Problem**) Determine the optimal schedule T_i $\forall i, 0 \leq i < N$, so that:

- $\sum_{0 \leq i < N, 0 \leq l < NTX(i)} I(STX_i(l) =$`OK`$)$ is maximized;
- $\frac{\sum_{0 \leq i < N, 0 \leq l < NTX(i)} I(STX_i(l)=\texttt{FAIL-PU-COLLISION})}{\sum_{0 \leq i < N} NTX(i)} > \psi$, where $I(\cdot)$ is the identity function.

RL-Based Problem Formulation

We model the JSS Problem via a SARL model; each SU_i^{tx} is a learning agent. Figure 7 depicts the corresponding MDP for the case of K=2. More in details:

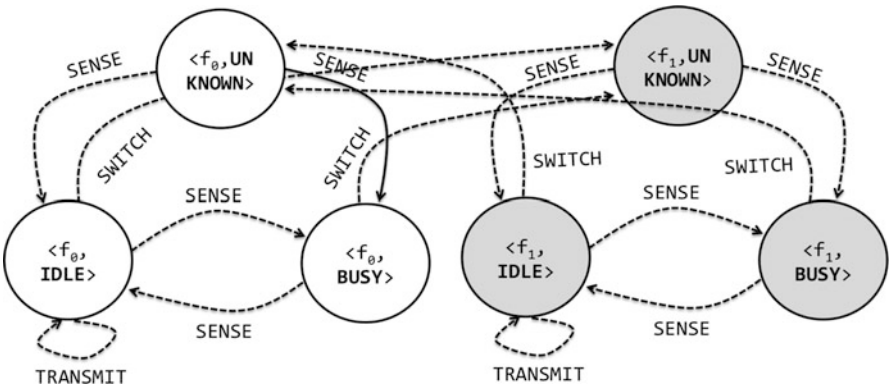

Fig. 7 The Markov decision process (MDP) for the JSS problem

- The set of states S is the set of couples $< f_j, \{\texttt{IDLE, BUSY, UNKNOWN}\} >$ where the first field is the frequency $f_j \in K$ and the second field is the estimated availability of frequency f_j, based on the output of the sensing action.
- The set of actions $A = \{\texttt{SENSE}, \texttt{TRANSMIT}, \texttt{SWITCH}\}$ coincides with the slot types previously introduced.
- The reward function $R : S \times A \rightarrow [0 : 1]$ is defined in different ways according to the action implemented by SU_i^{tx}. More specifically, $R(< f_j, \cdot >, \texttt{SENSE})$ is set to 1 whether channel f_j is found BUSY, 0 otherwise. In case of transmit action, $R(< f_j, \texttt{IDLE} >, \texttt{TRANSMIT})$ is set as follows:

$$R(< f_j, \texttt{IDLE} >, \texttt{TRANSMIT}) = 1 - \frac{\#Retransmissions}{\texttt{MAX\_ATTEMPTS}} \tag{14}$$

  where $\#Retransmissions$ denotes the number of retransmissions performed. Hence, the reward is set to 1 whether the packet is acknowledged without any retransmission. Vice versa, it is set to 0 whether the packet is discarded since the maximum number of retransmission attempts has been reached. Finally, in case of channel switch, the reward $R(< f_j, \texttt{UNKNOWN} >, \texttt{SWITCH})$ is set to zero.
- The transition function $T : S \times A \times S \rightarrow [0 : 1]$ is defined as follows, i.e.:

$$T(< f_j, \cdot >, \texttt{SENSE}, < f_j, \texttt{IDLE} >) = \frac{\beta_j}{\alpha_j + \beta_j}$$

$$T(< f_j, \cdot >, \texttt{SENSE}, < f_j, \texttt{BUSY} >) = \frac{\alpha_j}{\alpha_j + \beta_j}$$

$$T(< f_j, \texttt{IDLE} >, \texttt{TRANSMIT}, < f_j, \texttt{TRANSMIT} >) = 1$$

$$T(< f_j, \cdot >, \texttt{SWITCH}, < f_k, \texttt{UNKNOWN} >) = 1$$

$$T(< f_j, \texttt{UNKNOWN} >, \texttt{SENSE}, < f_j, \texttt{IDLE} >) = \frac{\beta_j}{\alpha_j + \beta_j}$$

$$T(< f_j, \texttt{UNKNOWN} >, \texttt{SENSE}, < f_j, \texttt{BUSY} >) = \frac{\alpha_j}{\alpha_j + \beta_j}$$

For all the other input values, the transition function assumes output value equal to 0. In the equations above, we neglect the impact of channel sensing errors, and we assume that the next channel f_k has already been determined. In any case, the T matrix is interesting only from the theoretical side, since in practice we assume that the SUs do not know its values.

We consider three RL-based learning algorithms addressing the JSS problem, i.e.:

- **Q-Learning based**: each SU_i^{tx} stores a Q-table for each state/action and updates it after each `TRANSMIT` or `SENSE` action through Eq. 4. Moreover, at the end of slot k, SU_i^{tx} decides the next action through a probabilistic scheme. The probability of `TRANSMIT` or `SENSE` actions is set through Eq. 6, while the probability of a `SWITCH` action is computed as follows:

$$p(< f_j, \cdot >, \texttt{SWITCH}) = \max\{\max_{0 \leq v < K, v \neq j} Q(< f_v, \texttt{IDLE} >, \texttt{TRANSMIT}) - Q(< f_j, \texttt{IDLE} >, \texttt{TRANSMIT}), \theta\} \quad (15)$$

  Here, the first term of the max operator denotes the maximum gain achievable when switching to a channel different from the current one (f_j), while the $0 \leq \theta \leq 1$ parameter indicates the probability of spectrum exploration. In case a `SWITCH` action is implemented, another probabilistic step is executed in order to select the channel: with probability θ, a random value is selected in range $\{0 \ldots K\}$; otherwise, the best channel is selected (the one equal to $\text{argmax}_{0 \leq v < K, v \neq j} Q(< f_v, \texttt{IDLE} >, \texttt{TRANSMIT}) - Q(< f_j, \texttt{IDLE} >, \texttt{TRANSMIT})$. The values of the temperature TE (see Eq. 6) and of γ are set to a large initial value, and then progressively discounted at each slot in order to ensure convergence, but they cannot decrease below predefined minimum $TE_{\min}$ and $\theta_{\min}$ values. We investigate the impact of the initial temperature value TE in section "Analysis I: SU-PU Interference Only".
- **Sarsa based**: the scheme works similarly to the Q-learning except for the update rule of the `TRANSMIT` and `SENSE` actions, which is based on Eq. 5.
- **Information Dissemination Q-Learning based** (IDQ-Learning): the scheme works similarly to the Q-learning. In addition, each SU_i^{tx} shares the information about its state, action, and received reward, at each slot. All the SU_j^{tx}, $j \neq i$ update their Q-values consequently as if the action was performed locally.

Analysis I: SU-PU Interference Only

We modeled the CR network scenario and the RL-based algorithms through the NS2-CRAHN simulator described in [34]. Unless stated otherwise, we considered a scenario composed of 20 SU couples (i.e., N=20) and K= 6 licensed channels. The other parameters are p_D=10%, $MAX\_ATTEMPTS$=7, TE_{ini}=50, $TE_{\min}$=5,

$\theta_{\text{ini}} = 80\%$, and $\theta_{\text{min}} = 10\%$. Each of the six channels exhibits different PU activity levels (PUL) and PER values, as reported in the table below.

We consider a constant bit rate (CBR) application; each SU_i^{tx} generates a new packet destined to SU_i^{rx} every 0.005 seconds. The packet length is 1000 bytes.

In this analysis, we assume that each SU does not interfere with other SUs tuned to the same channel. Hence, the goal of the learning algorithm is to identify vacant spectrum opportunities over the K channels. We compare the performance of the three RL-based schemes described in section "RL-Based Problem Formulation" with those of a non-learning scheme, named *Sequential* in the following. The protocol operations of the sequential scheme are straightforward: each SU senses the channel before any transmission attempt; in case the current channel f_j is detected as busy, the SU switches to channel $f_{(j+1)\%K}$; otherwise, it transmits one packet and then senses the channel again.

Figure 8a shows the system throughput when varying the number of transmitting SUs (N) on the x-axis. It is easy to notice that all the RL-based algorithms greatly outperform the sequential scheme. No significant differences can be appreciated between Q-learning and Sarsa. Vice versa, IDQ-learning provides the highest throughput, and the gain produced by the cooperation becomes more evident when increasing the number of involved SUs. This result can be justified as follows: (i) the RL-based schemes estimate the quality of each channel and then concentrate most of the SU transmissions on channels 5, 2, and 4 characterized by favorable PUL and PER values and (ii) on these channels, the RL-based schemes reduce the amount of sensing actions while still guaranteeing satisfactory PU detection (see next results). In addition, compared to Q-learning and Sarsa, IDQ-learning guarantees better exploration and quicker convergence of all the SUs to the optimal state-action policy (which is equal for all the SUs). This is made evident in Fig. 8b, which shows the throughout over time, for a network scenario with N=20. Till second 100, both Q-learning and Sarsa perform poorly because they are performing exploration, caused by the high values of the TE and θ parameters. After second 100, the throughput of both schemes sharply increases because they exploit more aggressively the learnt policy. In IDQ-learning, the impact of random actions is greatly mitigated since the exploration phase is shorter: at each round, each SU can receive N different rewards and hence discounts more quickly the TE and θ parameters. At the same time, the exploration phase is more effective since all the SUs converge to the same policy guaranteeing the highest throughput. Figure 8c confirms the same trend of Fig. 8a, by showing the packet delivery ratio (PDR) of the four schemes for different values of N. The PDR of the sequential, Q-learning and Sarsa schemes are not affected by N since – in this analysis – we are neglecting the impact of SU channel contention. The PDR of the IDQ-learning increases with N, again due to the positive impact of the SU cooperation.

Figure 9a reveals that the PDR and throughput enhancements do not come at the expense of increased interference caused to the PUs. On the y axis, we show the PU interference probability, defined as the rate of SU transmissions ending in state `FAIL-PU-COLLISION` over the total number of transmissions performed by the SUs. The Q-learning and Sarsa schemes guarantee a value which is comparable

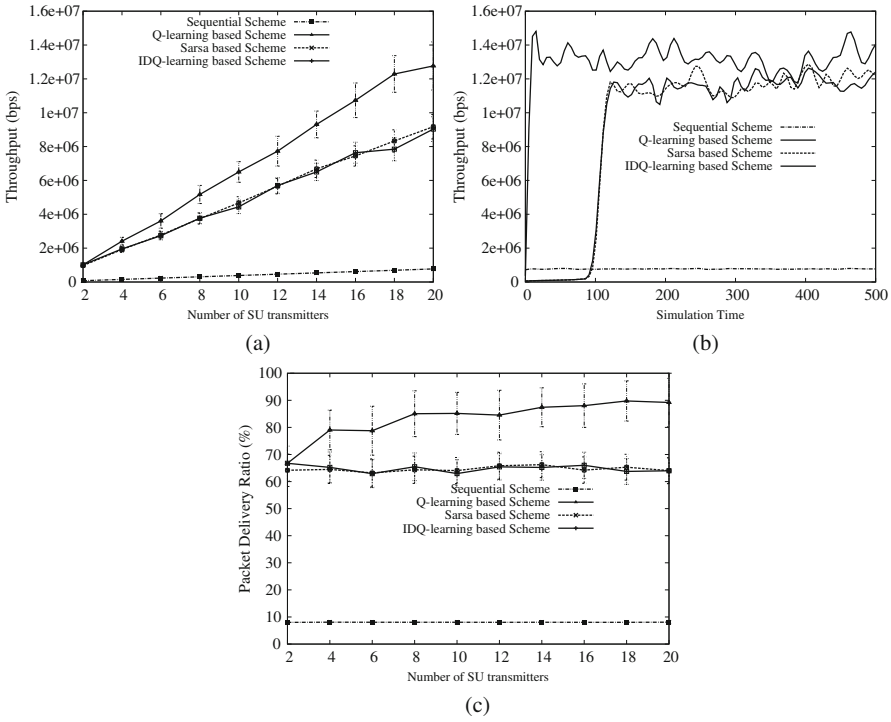

Fig. 8 The throughput and packet delivery ratio (PDR) of the sequential and of the RL-based schemes are shown in (**a**) and (**c**), respectively. The throughput over simulation time for N=20 is shown in (**b**)

with the performance of the sequential scheme and in any case lower than 2%. The IDQ-learning exhibits a counterintuitive behavior: the risk of interference with PUs even reduces when increasing the number of potential interferers (i.e., the SUs), again thanks to the reward dissemination mechanisms, through which all the SUs converge to the optimal channel sequence and to the optimal balance between `SENSE` and `TRANSMIT` actions on each channel. To this purpose, Fig. 9b shows the average frequency rate of each action (different color bars) and on each channel (on the x axis), experienced by the IDQ-learning (N=20). It is easy to notice that our learning scheme (i) concentrates most of transmissions on channels 5 and 2 (which are the one most favorable toward the PUs in terms of PUL and PER values) and (ii) significantly reduces the frequency of sensing actions on channel 5, while it maximizes sensing on channels 0 and 3 (characterized by high PU activity). Hence, the graph confirms the ability of the IDQ-learning scheme to learn the optimal sequence of spectrum opportunities, and the amount of sensing on each channel, without knowing in advance the PER and PUL values. Finally, in Fig. 9c we investigate the impact of the initial temperature value (TE_{ini}) on the throughput (on the $y1$ axis) and on the number of channel switches (on the $y2$ axis). Again,

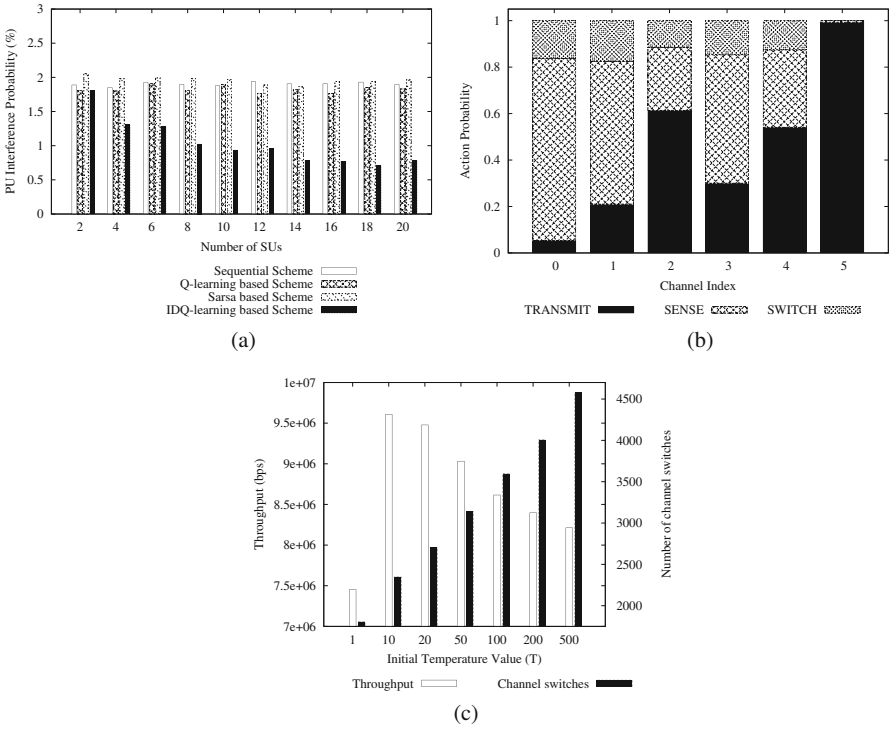

Fig. 9 The PU interference probability over N is shown in (**a**). The selection rate of the three actions (`TRANSMIT`, `SENSE`, and `SWITCH`) on each of the K channels and for the IDQ-learning scheme is depicted in (**b**). The impact of the initial temperature value (TE_{ini}) on the throughput and on the number of channel switches is shown in (**c**)

we evaluate the IDQ-learning scheme with $N = 20$. We can notice that there is an optimal TE_{ini} value (equal to 10 in our case) maximizing the throughput: when $TE_{\text{ini}} < 10$, the exploration phase is too short and hence the optimal policy cannot be discovered, vice versa when $TE_{\text{ini}} \gg 10$, the impact of suboptimal actions during exploration becomes significant. On the other side, the number of channel switches increases proportionally with TE_{ini}.

Analysis II: SU-PU and SU-SU Interference

In this section, we complete the analysis by considering also the impact of SU-SU interference on the system performance. In addition to the channel model presented so far, a SU transmission might result in state `FAIL-SU-COLLISION`, i.e., it can fail due to collisions with other SU transmissions operating on the same channel. Such collisions can occur despite the utilization of a MAC protocol providing distributed channel contention orchestration mechanisms (we assume all the SUs

follow a CSMA/CA protocol). As a result, SUs cannot merely implement all the same policy; besides determining the optimal balance of sensing actions, SUs must also learn the optimal coordinated action, which leads to the optimal allocation of the SUs to the available frequency. The goal is a hybrid collaborative/competitive MARL problem; no solutions could be found in the literature for this specific JSS problem instance, although close problems have been modeled via game theory-based approaches and distributed collaboration techniques (e.g., the payoff propagation mechanism described in [52, 53]). Far from determining the optimal solution, we introduce here an addition RL-based scheme, named distributed Q-learning, which is based on the frequency maximum Q-value (FMQ) heuristic [27]. This latter attempts to achieve SU coordination without any explicit policy exchange and also with minimal extra-storage requirements compared to the basic SARL techniques. We present the protocol operations in brief:

- **Distributed Q-Learning** (DistQ-Learning): the protocol works similarly to the Q-learning scheme described in section "RL-Based Problem Formulation", with two significant differences. First, each time SU_i^{tx} performs a `TRANSMIT` action on a given channel; it computes a local reward $r_i^L = 1 - \frac{\#Retransmissions}{\texttt{MAX\_ATTEMPTS}}$ and shares it with all the other SUs. By averaging the received r_j^L values, $j \neq i$, each SU_i^{tx} computes the average network reward $r^G = \frac{\sum_{0 \leq i < N} r_i^L}{N}$, which is a proxy for the network throughput. Second, once computing the r^G value, each SU_i^{tx} updates the Q-table for the `TRANSMIT` action on channel f_j by following the FMQ rule [27], i.e.:

$$Q(< f_j, \texttt{IDLE} >, \texttt{TRANSMIT}) = Q(< f_j, \texttt{IDLE} >, \texttt{TRANSMIT}) + \frac{C^i_{\max}(r^G_{\max}, f_j)}{C^i(f_j)} \cdot r^G_{\max}(f_j) \tag{16}$$

  where $r^G_{\max}(f_j)$ is the maximum global reward observed when SU_i^{tx} is tuned to channel f_j, $C^i_{\max}(r^G_{\max}, f_j)$ is the number of times such values has been observed, and $C^i(f_j)$ is the total number of transmission attempts on frequency f_j. As a result, each SUs pushes its policy toward channels where an optimal network reward r^G is achieved, although no SU keeps track on the global MARL Q-table nor it makes conjectures about the opponents' behaviors; the r^G value reflects indirectly the optimality of the joint action performed by the other SUs, and based on it each SU adjusts its own policy.

In Fig. 10a, b, and c, we compare the performance of the DistQ-learning scheme against the sequential and the IDQ-learning algorithms previously introduced in section "Analysis I: SU-PU Interference Only". We consider the same network environment of the previous analysis, except for the number of licensed frequencies (K= 9 instead of $K = 6$); the channels 7-8-9 have the same PUL-PER profiles of channels 3-4-5 (see Table 1). Figure 10a shows the network throughput when

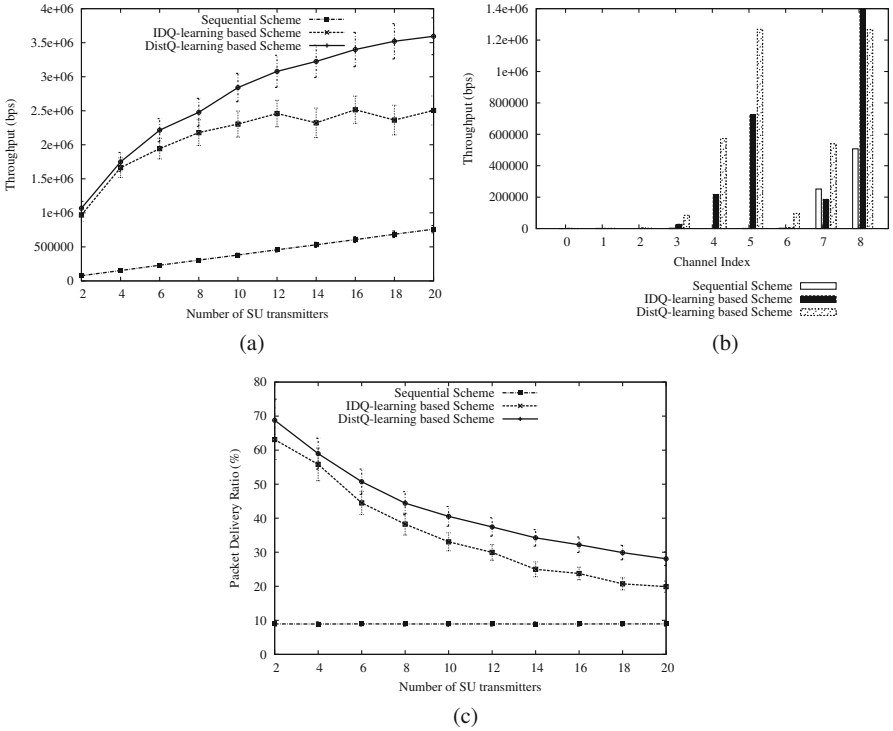

Fig. 10 The throughput and packet delivery ratio (PDR) of the sequential and of the RL-based schemes are shown in (**a**) and (**c**), respectively. The throughput on each of the $K = 9$ channel, for N=20, is shown in (**b**)

Table 1 PUL/PER profiles of the $K = 5$ licensed channels

Channel index	PUL	PER	PUL profile: $< \alpha, \beta >$	PER
0	High	Medium	<10,2>	50%
1	Medium	Medium	<5,5>	50%
2	Low	Medium	<2,10>	50%
3	High	Low	<10,2>	10%
4	Medium	Low	<5,5>	10%
5	Low	Low	<2,10>	10%

varying the number of transmitting SUs (N). The throughput values are lower than Fig. 8a and also decrease with N as a consequence of the SU contention on each channel. We can notice that the DistQ-learning scheme provides significantly better performance than the sequential scheme but also than the IDQ-learning scheme. Using this latter, all the SUs attempt to discover the same policy, i.e., they transmit on the same channels and balance `TRANSMIT` and `SENSE` actions in the same way. Vice versa, the DistQ-learning aim at achieving implicit coordination among

SUs through Eq. 16; the SUs learn differentiated policies – at least regarding the Q-value of the TRANSMIT action on each channel – so that the maximum, network-wide reward can be achieved. This is also visible in Fig. 10b which shows the network throughput on each of the K channels, for the three different algorithms and $N = 20$. The IDQ-learning scheme concentrates most of the SU transmissions on channel 8 and 4 (which are the most favorable to SUs for PUL/PER profiles) but clearly increasing the contention level on those frequencies and hence the risk of packet losses due to SU-SU collisions. Vice versa, the DistQ-learning scheme achieves better distribution of the SUs over the available spectrum opportunities, which also translates into enhancements in terms of PDR, as depicted in Fig. 10c.

Conclusions and Open Issues

In this paper, we have addressed the utilization of reinforcement learning (RL) techniques in cognitive radio (CR) networks. A twofold taxonomy of the existing RL-CR studies has been proposed, from a networking perspective and a learning perspective. The review of the literature has confirmed that RL techniques are quite popular in RL networking and that they have been applied on several different use-cases and on dynamic network scenarios, often enhancing the performance of non-learning-based solutions. At the same time, despite the number of published papers, we believe there is great room for improvement, since some RL-CR issues have been only superficially addressed by the academic research. We focus here on three main research issues:

- *Accurate performance evaluation in real-world CR network scenarios*. Despite few experimental works [68, 71, 72], the evaluation of RL-based solutions have been mainly conducted through simulation studies, in which the spectrum occupancy pattern is modeled by using well-known probability distribution (like the exponential [4] or the Bernoulli [56] distributions). However, spectrum bands might exhibit different complexity of the PU occupancy pattern, based the signal waveform and regulations of licensed users transmitting on those frequency [70]. Hence, differentiated RL learning algorithms (e.g., by considering model-free or model-based approaches, MDP or POMDP frameworks) can be tested and deployed on different frequencies, also based on the predictability of the spectrum availability. Additional works based on real-world spectrum traces are required in order to address this issue.
- *Analysis of RL techniques for CR applications with strict QoS network requirements*. Several multimedia applications pose strict QoS requirements (e.g., the maximum packet drop rate or jitter for video-streaming services) that must be continuously met by the network, in order not to affect negatively the users' experience. In RL-CR solutions, the SUs must continuously balance the exploitation and exploration phases during the system lifetime: when the SU selects random, possibly suboptimal actions, the QoS requirements of the CR multimedia applications are not guaranteed. Proper techniques that provide effec-

tive state-action exploration without causing detectable performance degradation for CR applications with strict QoS network requirements have not designed so far.

- *Enhancement of the learning framework*. Most of the reviewed works in the RL-CR literature provide an accurate modeling of the CR network scenario, including the operations of the main actors (PUs and SUs); the same level of complexity cannot be found on the learning part, since in most cases, the RL framework consists in a straightforward application of model-free algorithms (Q-learning or Sarsa algorithms overall). However, the RL theory is vast and is not limited to such results [12]; moreover, it is continuously extended by novel contributions coming from an active research community [73]. CR networking can benefit from the novel RL architectures introduced so far: we cite, among others, the utilization of deep RL techniques (i.e., RL framework enhanced with artificial neural networks for state-action representation) for better coordination in distributed scenarios [74] or for more efficient exploration [75].

About the second contribution of this paper, i.e., the application of RL techniques on joint spectrum sensing and selection problems, the evaluation results have revealed that the information-sharing schemes can considerably enhance the performance of RL-based schemes in fully cooperative tasks, like SUs seeking for PU-vacant channels. Vice versa, in mixed cooperative/competitive tasks, like SUs seeking for PU-vacant channels and also minimizing their mutual interference, information-sharing schemes can be counterproductive unless enhanced with distributed coordination strategies. Current and future research activities on the case study include the convergence analysis in multi-agent scenarios, the implementation of proposed RL schemes on a small-case test-bed, and the extension of the proposed modeling approach for the case of partially observable environments.

References

1. Akyildiz IF, Lee WY, Vuran MC, Mohanty S (2006) NeXt generation/dynamic spectrum access/cognitive radio wireless networks: a survey. Comput Netw J 50(1):2127–2159
2. Mitola J (2000) Cognitive radio an integrated agent architecture for software defined radio. PhD Dissertation, KTH Stockholm
3. Yucek T, Arslan H (2009) A survey of spectrum sensing algorithms for cognitive radio applications. J IEEE Commun Surv Tutor 11(1):116–130
4. Lee WY, Akyildiz I (2008) Optimal spectrum sensing framework for cognitive radio networks. IEEE Trans Wirel Commun 7(10):3845–3857
5. Sherman M, Mody AN, Martinez R, Rodriguez C, Reddy R (2008) IEEE standards supporting cognitive radio and networks, dynamic spectrum access, and coexistence. IEEE Commun Mag 46(7):72–79
6. Flores AB, Guerra RE, Knightly EW (2013) IEEE 802.11af: a standard for TV white space spectrum sharing. IEEE Commun Mag 51(10):92–100
7. Clancy C, Hecker J, Stuntbeck E, OShea T (2007) Applications of machine learning to cognitive radio networks. IEEE Wirel Commun 14(4):47–52
8. Mitchell T (1997) Machine learning. McGraw Hill, New York

9. Gavrilovska L, Atanasovksi V, Macaluso I, DaSilva L (2013) Learning and reasoning in cognitive radio networks. IEEE Commun Surv Tutor 15(4):1761–1777
10. Bkassiny M, Li Y, Jayaweera SK (2013) A survey on machine-learning techniques in cognitive radios. IEEE Commun Surv Tutor 15(3):1136–1159
11. Wang W, Kwasinksi A, Niyato D, Han Z (2016) A survey on applications of model-free strategy learning in cognitive wireless networks. IEEE Commun Surv Tutor 18(3):1717–1757
12. Barto AG, Sutton R (1998) Reinforcement learning: an introduction. MIT Press, Cambridge
13. Kaelbling LP, Littman ML, Moore AW (1996) Reinforcement learning: a survey. J Artif Intell Res 4(1):237–285
14. Busoniu L, Babuska R, De Schutter B (2008) A comprehensive survey of multiagent reinforcement learning. IEEE Trans Syst Man Cybern 38(2):156–171
15. Busoniu L, Babuska R, De Schutter B (2006) Multi-agent reinforcement learning: a survey. In: Proceedings of IEEE ICARCV, Singapore
16. Watkins CJ, Dayan P (1992) Technical note: Q-learning. Mach Learn 8(1):279–292
17. Rummery GA, Niranjan M (1994) Online Q-learning using connectionist systems. Technical Report
18. Di Felice MK, Wu C, Bononi L, Meleis W (2010) Learning-based spectrum selection in cognitive radio ad hoc networks. In: Proceedings of IEEE/IFIP WWIC, Lulea
19. Yau KLA, Komisarczuk P, Teal PD (2012) Reinforcement learning for context awareness and intelligence in wireless networks: review, new features and open issues. J Netw Comput Appl 35(1):235–267
20. Yau KLA, Komisarczuk P, Teal PD (2010) Applications of reinforcement learning to cognitive radio networks. In: Proceedings of IEEE ICC, Capetown
21. Raza Syed A, Alvin Yau KL, Qadir J, Mohamad H, Ramli N, Loong Keoh S (2016) Route selection for multi-hop cognitive radio networks using reinforcement learning: an experimental study. In: Proceedings of IEEE access 4(1):6304–6324
22. Vucevic N, Akyildiz IF, Romero JP (2010) Cooperation reliability based on reinforcement learning for cognitive radio networks. In: Proceedings of IEEE SDR, Boston
23. Jiang T, Grace D, Mitchell PD (2011) Efficient exploration in reinforcement learning-based cognitive radio spectrum sharing. IET Commun 5(10):1309–1317
24. Ozekin E, Demirci FC, Alagoz F (2013) Self-evaluating reinforcement learning based spectrum management for cognitive ad hoc networks. In: Proceedings of IEEE ICOIN, Bangkok
25. Macaluso I, DaSilva L, Doyle L (2012) Learning Nash equilibria in distributed channel selection for frequency-agile radios. In: Proceedings of IEEE ECAI, Montpellier
26. Lall S, Sadhu AK, Konar A, Mallik KK, Ghosh S (2016) Multi-agent reinforcement learning for stochastic power management in cognitive radio network. In: Proceedings of IEEE Microcom, Durgapur
27. Kapetanakis S, Kudenko D (2002) Reinforcement learning of coordination to cooperative multi-agent systems. In: Proceedings of AAAI, Menlo Park
28. Wahab B, Yang Y, Fan Z, Sooriyabandara M (2009) Reinforcement learning based spectrum-aware routing in multi-hop cognitive radio networks. In: Proceedings of IEEE CROWNCOM, Hannover
29. Chowdhury K, Wu C, Di Felice M, Meleis W (2010) Spectrum management of cognitive radio using multi-agent reinforcement learning. In: Proceedings of IEEE AAMAS, Toronto
30. Faganello LR, Kunst R, Both CB (2013) Improving reinforcement learning algorithms for dynamic spectrum allocation in cognitive sensor networks. In: Proceedings of IEEE WCNC, Shanghai
31. Wu Y, Hu F, Kumar S, Zhu Y, Talari A, Rahnavard N, Matyjas JD (2014) A learning-based QoE-driven spectrum handoff scheme for multimedia transmissions over cognitive radio networks. IEEE J Sel Areas Commun 32(11):2134–2148
32. Chen X, Zhao Z, Zhang H (2013) Stochastic power adaptation with multiagent reinforcement learning for cognitive wireless mesh networks. IEEE Trans Mob Comput 12(11):2155–2166
33. Zhou P, Chang Y, Copeland JA (2010) Learning through reinforcement for repeated power control game in cognitive radio networks. In: Proceedings of IEEE Globecom, Miami

34. Di Felice M, Chowdhury K, Kim W, Kassler A, Bononi L (2011) End-to-end protocols for cognitive radio ad hoc networks: an evaluation study. Perform Eval (Elsevier) 68(9): 859–875
35. Reddy YB (2008) Detecting primary signals for efficient utilization of spectrum using Q-learning. In: Proceedings of IEEE ITNG, Las Vegas
36. Berhold U, Fu F, Van Der Schaar M, Jondral FK (2008) Detection of spectral resources in cognitive radios using reinforcement learning. In: Proceedings of IEEE Dyspan, pp 1–5
37. Di Felice M, Chowdhury KR, Kassler A, Bononi L (2011) Adaptive sensing scheduling and spectrum selection in cognitive wireless mesh networks. In: Proceedings of IEEE Flex-BWAN, Maui
38. Arunthavanathan S, Kandeepan S, Evans RJ (2013) Reinforcement learning based secondary user transmissions in cognitive radio networks. In: Proceedings of IEEE Globecom, Atlanta
39. Mendes AC, Augusto CHP, da Silva MWR, Guedes RM, de Rezende JF (2011) Channel sensing order for cognitive radio networks using reinforcement learning. In: Proceedings of IEEE LCN, Bonn
40. Lo BF, Akyldiz IF (2010) Reinforcement learning-based cooperative sensing in cognitive radio ad hoc networks. In: Proceedings of IEEE PIMRC, Istanbul
41. Lunden J, Kulkarni SR, Koivunen V, Poor HV (2011) Exploiting spatial diversity in multiagent reinforcement learning based spectrum sensing. In: Proceedings of IEEE CAMSAP, San Juan
42. Lunden J, Kulkarni SR, Koivunen V, Poor HV (2013) Multiagent reinforcement learning based spectrum sensing policies for cognitive radio networks. IEEE J Sel Top Signal Process 7(5):858–868
43. Jao Y, Feng Z (2010) Centralized channel and power allocation for cognitive radio network: a Q-learning solution. In: Proceedings of IEEE FNMS, Florence
44. Galindo-Serrano A, Giupponi L, Blasco P, Dohler M (2010) Learning from experts in cognitive radio networks: the docitive paradigm. In: Proceedings of IEEE CROWNCOM, Cannes
45. Galindo-Serrano A, Giupponi L (2010) Distributed Q-learning for aggregated interference control in cognitive radio networks. IEEE Trans Veh Tech 59(4):1823–1834
46. Chowdhury KR, Di Felice M, Doost-Mohammady R, Meleis W, Bononi L (2011) Cooperation and communication in cognitive radio networks based on TV spectrum experiments. In: Proceedings of IEEE WoWMoM, Lucca
47. Emre M, Gur G, Bayhan S, Alagoz F (2015) CooperativeQ: energy-efficient channel access based on cooperative reinforcement learning. In: Proceedings of IEEE ICCW, London
48. Saad H, Mohamed A, ElBatt T (2012) Distributed cooperative Q-learning for power allocation in cognitive femtocell networks. In: Proceedings of IEEE VTC-Fall, Quebec City
49. Venkatraman P, Hamdaoui B, Guizani M (2010) Opportunistic bandwidth sharing thorough reinforcement learning. IEEE Trans Veh Tech 59(6):3148–3153
50. Bernardo F, Augusti R, Perez-Romero J, Sallent O (2010) Distributed spectrum management based on reinforcement learning. In: Proceeding of IEEE CROWNCOM, Hannover
51. Yau KLA, Komisarczuk P, Teal PD (2010) Context-awareness and intelligence in distributed cognitive radio networks: a reinforcement learning approach. In: Proceedings of IEEE AusCTW, Canberra
52. Yau KLA, Komisarczuk P, Teal PD (2010) Enhancing network performance in distributed cognitive radio networks using single-agent and multi-agent reinforcement learning. In: Proceedings of IEEE LCN, Denver
53. Yau KLA, Komisarczuk P, Teal PD (2010) Achieving context awareness and intelligence in distributed cognitive radio networks: a payoff propagation approach. In: Proceedings of IEEE WAINA, Singapore
54. Kakalou I, Papadimitriou GI, Nicopoliditis P, Sarigiannidis PG, Obaidat MS (2015) A reinforcement learning-based cognitive MAC protocol. In: Proceedings of IEEE ICC, London
55. Agrawal R (1995) Sample mean based index policies with o(log(n)) regret for the multi-armed bandit problem. Adv Appl Prob 27(1):1054–1078
56. Robert C, Moy C, Wang CX (2014) Reinforcement learning approaches and evaluation criteria for opportunistic spectrum access. In: Proceeding of IEEE ICC, Sydney

57. Jouini W, Di Felice M, Bononi L, Moy C (2012) Coordination and collaboration in secondary networks: a multi-armed bandit based framework. In: Technical Report. Available at: https://arxiv.org/abs/1204.3005
58. Li H (2010) Multi-agent Q-learning for competitive spectrum access in cognitive radio systems. In: Proceedings of IEEE SDR, Boston
59. Alsarhan A, Agarwal A (2010) Resource adaptations for revenue optimization in cognitive mesh network using reinforcement learning. In: Proceedings of IEEE GLOBECOM, Miami
60. Teng Y, Zhang Y, Niu F, Dai C, Song M (2010) Reinforcement learning based auction algorithm for dynamic spectrum access in cognitive radio networks. In: Proceedings of IEEE VTC Fall, Ottawa
61. Cesana M, Cuomo F, Ekici E (2011) Routing in cognitive radio networks: challenges and solutions. Ad Hoc Netw (Elsevier) 9(3):228–248
62. Chowdhury KM, Di Felice (2009) SEARCH: a routing protocol for mobile cognitive radio ad-hoc networks. Comput Commun (Elsevier) 32(18):1983–1997
63. Litman M, Boyan J (1994) Packet routing in dynamically changing networks: a reinforcement learning approach. Adv Neural Inform Process Syst 7(1):671–678
64. Chetret D, Tham C, Wong L (2004) Reinforcement learning and CMAC-based adaptive routing for MANETs. In: Proceedings of IEEE ICON, Singapore
65. Al-Rawi AHA, Alvin Yau KL, Mohamad H, Ramli N, Hashim W (2014) A reinforcement learning-based routing scheme for cognitive radio ad hoc networks. In: Proceedings of IEEE WMNC, Vilamoura
66. Zheng K, Li H, Qiu RC, Gong S (2012) Multi-objective reinforcement learning based routing in cognitive radio networks: walking in a random maze. In: Proceedings of IEEE ICNC, Maui
67. Safdar T, Hasbulah HB, Rehan M (2015) Effect of reinforcement learning on routing of cognitive radio ad hoc networks. In: Proceedings of IEEE ISMSC, Ipon
68. Pourpeighhambar B, Dehghan M, Sabaei M (2017) Non-cooperative reinforcement learning based routing in cognitive radio networks. Comput Commun (Elsevier) 106(1):11–23
69. Dowling J, Curran E, Cunningham R, Cahill V (2005) Using feedback in collaborative reinforcement learning to adaptively optimize MANET routing. IEEE Trans Syst Man Cybern 35(3):360–372
70. Macaluso I, Finn D, Ozgul BAL, DaSilva (2013) Complexity of spectrum activity and benefits of reinforcement learning for dynamic channel selection. IEEE J Sel Areas Commun 31(11):2237–2246
71. Ren Y, Dmochowski P, Komisarczuk P (2010) Analysis and implementation of reinforcement learning on a GNU radio cognitive radio platform. In: Proceedings of IEEE CROWNCOM, Cannes
72. Moy C, Nafkha A, Naoues M (2015) Reiforcement learning demonstrator for opportunistic spectrum access on real radio signals. In: Proceedings of IEEE DySPAN, Stockholm
73. Dayan P, Niv Y (2008) Reinforcement learning: the good, the bad and the ugly. Curr Opin Neurobiol 18(1):1–12
74. Naparstek O, Cohen K (2017) Deep multi-user reinforcement learning for distributed dynamic spectrum access. In: CoRR abs/1704.02613
75. Ferreira VP, Paffenroth R, Wyglinski RMA, Hackett MT, Bilen GS, Reinhart CR, Mortense JD (2017) Multi-objective reinforcement learning-based deep neural networks for cognitive space communications. In: Proceedings of IEEE CCAA, Cleveland

Overview of Recent Applications of Cognitive Radio in Wireless Communication Systems

58

Miguel López-Benítez

Contents

Abstract

Cognitive radio (CR) is one of the most intensively researched paradigms in recent wireless communication systems. The great deal of attention that CR has attracted can be ascribed to its demonstrated capability to increase spectrum efficiency and overall network capacity through interference-free spectrum sharing among several wireless communication systems. CR provides intelligence to wireless networks, enabling users to access multiple air interfaces and select the most appropriate alternative under varying communication needs and operation conditions. The potential benefits of CR have not gone unnoticed to many wireless communication systems, which nowadays have effectively benefited

M. López-Benítez (✉)
Department of Electrical Engineering and Electronics, University of Liverpool, Liverpool, UK
e-mail: M.Lopez-Benitez@liverpool.ac.uk

W. Zhang (ed.), *Handbook of Cognitive Radio*,
https://doi.org/10.1007/978-981-10-1394-2_59

from the adoption of CR techniques and operating principles. This chapter provides an overview on the introduction of CR principles into two prominent wireless communication systems, namely, mobile and satellite communication networks. A detailed discussion is provided on the background and motivation for the adoption of the CR technology and how CR techniques have been introduced in these two systems. A brief discussion is also provided on the adoption of the CR technology in other wireless communication systems, including military communications, public safety and emergency networks, aeronautical communications, and wireless-based Internet of Things. This chapter is aimed at illustrating the practical implementation of the theoretical CR principles widely discussed in the literature.

Keywords
Cognitive radio · Dynamic spectrum access · Mobile communications · Satellite communications

Introduction

While the concept of cognitive radio (CR) [39] in its broadest sense can find a wide range of applications in wireless communications, dynamic spectrum access (DSA) [3] is certainly the most popular one (as a matter of fact, the term CR is often used to refer to DSA). The main motivation for the development of DSA/CR is to overcome the conflicts between spectrum demand growth and spectrum underutilization arising from legacy static spectrum allocation policies. This spectrum access paradigm allows several wireless communication systems to coexist in the same region of the spectrum, thus enabling a more efficient exploitation of the available spectrum resources. The potential benefits that the CR technology can bring into a broad variety of wireless communication systems have not gone unnoticed by academia, industry, and regulatory bodies, which over the last years have constantly explored new ways to introduce the principles of CR and DSA into existing wireless communication networks. This chapter provides an overview of how CR principles and techniques have been adopted in wireless communication systems. Two prominent examples have been selected to this end, namely, mobile communication networks (section "Mobile Communication Networks") and satellite communication networks (section "Satellite Communication Networks"). This chapter discusses the background and motivation for the introduction of CR in these systems and how CR techniques have been adopted by different standardized technologies, which illustrates the practical implementation in real deployments of the theoretical CR principles widely discussed in the literature [34]. The adoption of the CR technology in other wireless communication systems is briefly discussed as well (section "Cognitive Radio in Other Wireless Communication Systems").

Mobile Communication Networks

Mobile communication systems have always experienced an ever-increasing capacity demand since the early days [30]. The replacement of the first generation (1G) of analogic devices with digital handsets based on the second-generation (2G) global system for mobile communication (GSM) standard [15] unleashed a worldwide expansion of mobile communications to the general public and the creation of a mass market for mobile communications. The decade following the deployment of GSM networks witnessed an astonishing increase in the number of subscribers to the mobile service that has never decreased. The third-generation (3G) universal mobile telecommunications service (UMTS) standard [16] introduced true data services in mobile networks for the first time and represented the beginning of a race to increase the network capacity in response to the sustained increase in the number of subscribers as well as the introduction of more demanding data-hungry services. This trend can be clearly appreciated by comparing the requirements set for the fourth-generation (4G) long-term evolution (LTE) standard [17] and the fifth-generation (5G) systems: while 4G radio requirements [10] were set at peak data rates of 100 Mbit/s in downlink and 50 Mbit/s in uplink in a 20 MHz bandwidth (which required a spectral efficiency of up to 5 bit/s/Hz, i.e., 2–4 times greater than that of UMTS Release 6), the 5G radio requirements [13] have been set at peak data rates of 1 Gbit/s in downlink and 500 Mbit/s in uplink (for indoor hot spots) and 50 Mbit/s in downlink and 25 Mbit/s in uplink (for outdoor macro-environments), with prospective field (i.e., not theoretical maximum) peak data rates of up to 10 Gbit/s being widely accepted in the industry community. This continuous increase in traffic demand has strained mobile operators, which have been forced to find new ways to increase the network capacity.

The capacity of a wireless communication system can be increased by achieving higher spectrum efficiency, denser network deployments, and obtaining more spectrum resources. All three approaches have been exploited in different ways by mobile network operators, some of which are summarized below.

- *More spectrum efficiency.* This approach is aimed at increasing the number of bits transmitted per time and spectrum unit (i.e., bit/s/Hz) by means of innovative physical layer solutions. This includes new modulation and coding schemes such as orthogonal frequency-division multiplexing (OFDM) or filter bank multicarrier (FBMC) which can reduce the space between modulated subcarriers [9, 38], multiple antenna techniques such as massive MIMO (multiple-input multiple-output) [22], full-duplex radios [32,41] which can transmit and receive simultaneously in the same time and frequency thus potentially enabling (in theory) an increase in the spectrum efficiency by a factor of 2, non-orthogonal multiple access techniques [7] which use the power domain to separate signals from each other (high-power signals can be isolated to be detected and then cancelled out to leave the low-power signals), or orthogonal polarizations used to transmit different data streams (however, the radio propagation environment can

modify the polarization of the signal components and cause mutual interference). Research in this area has been intensive, and the current state of the art has closely approached the well-known Shannon limit [43], which represents an upper bound on the maximum attainable spectrum efficiency. This suggests that this approach has almost hit the performance wall and the room for further improvements appears to be limited [8].

- *More dense network deployments.* This approach is aimed at increasing the spatial reutilization of spectrum resources by means of network densification. A basic method to increase the capacity of a cellular network is to reduce the radius of coverage (size) of each cell [30], since a more dense reuse of the available frequencies over shorter distances enables a higher density of subscribers. While the 2G GSM system was designed for macro-cell radii of up to 35 km, subsequent generations have targeted progressively smaller coverage areas such as microcells (few kilometers), picocells (few hundreds of meters), and femtocells (few tens of meters) [35]. This trend has led to heterogeneous scenarios with overlaying cells of different sizes, which has made necessary the development of more complex inter-cell interference coordination (ICIC) mechanisms [25], in particular with the introduction of more aggressive frequency reuse patterns (e.g., fractional frequency reuse and single-frequency networks). The extent to which a network can be densified is theoretically upper bounded [14]; however, such limitation can be overcome with the introduction of beamforming techniques, which can reconfigure the antenna radiation pattern in order to target specific user locations and minimize interference in other directions.
- *More spectrum resources.* This approach provides more network capacity by making new spectrum available. The amount of additional spectrum that can be gained at higher frequencies is virtually unlimited and only constrained by the ability of the available technology to efficiently transmit and receive signals at such high frequencies. One option to realize this approach is the exploitation of new high-frequency bands in the region of millimeter waves (typically 10 GHz and above) [33]. These bands can provide unprecedented large amounts of spectrum and therefore offer the potential to achieve extremely high network capacity. However, several important challenges need to be overcome. Propagation characteristics at such high frequencies not only limit the application of these bands to short-range communications but also pose new challenges for the design of network protocols and radio resource management methods to cope with unreliable links that can drop frequently and unexpectedly. Moreover, the equipment for use at these high frequencies is typically more expensive. As a result, in parallel with this alternative, the idea of opportunistically exploiting unused spectrum at lower frequencies with better radio propagation conditions (below 6 GHz) has recently gained interest from both industry and academia. The principle of DSA based on the CR paradigm in the context of mobile communication systems has led to several initiatives, which are presented in the following sections.

Spectrum Coexistence in Licensed Bands

The main initiatives for spectrum coexistence of mobile communication systems in licensed bands are the licensed shared access (LSA), which is focused on the sharing of the 2.3 GHz band in Europe, and the spectrum access system (SAS), which is focused on the sharing of the 3.5 GHz band in the USA [40]. These initiatives allow licensed spectrum to be used by more than one entity and provide the means for mobile networks to increase their capacity through additional spectrum in bands originally licensed to other systems. Mobile network operators can combine the new spectrum obtained from these bands with their own licensed spectrum by means of carrier aggregation techniques [57].

LSA was envisaged as a means to provide access to licensed spectrum bands that otherwise would not be possible in some European countries [29]. LSA defines a framework to enable (rather than enforce) spectrum sharing between a license holder or incumbent (tier 1) and an LSA licensee (tier 2) whereby the license holder agrees to grant exclusive use of part of its licensed spectrum at a given time and location (likely on a long-term basis, typically 10 years or more). The key features of LSA are that it is voluntary (this framework enables but does not enforce spectrum sharing), licensed (spectrum sharing takes places under an agreed license), and exclusive (the licensee is guaranteed exclusive access to the new spectrum). The LSA framework also guarantees the protection of the incumbent system and its use of the spectrum. A particular case of LSA is authorized shared access (ASA), which refers to spectrum sharing between an incumbent system (other than a mobile communication system) and a mobile communication system. As a matter of fact, the main use case for the LSA technology is the extension of the capacity of cellular mobile communication systems in the sub-6 GHz band in Europe. LSA allows 3GPP LTE mobile networks to be operated on a licensed shared basis in the 2300–2400 MHz band (3GPP LTE band 40) along with incumbents such as military stakeholders or professional video camera services, among others [40].

The SAS technology relies on the same principle as LSA but refers to the use case in the US market, where the so-called citizens broadband radio service (CBRS) network, such as an LTE network, is operated on a licensed shared basis in the 3550–3700 MHz band (3GPP LTE bands 42–43). The main difference with respect to LSA relies on the available spectrum slots based on a three-tier hierarchy (as opposed to the two-tier hierarchy of LSA). Licensed 10 MHz spectrum slots (up to 70 MHz) are only available in parts of the entire band (3550–3650 MHz) for the second tier priority access license (PAL) users, while the third tier general authorized access (GAA) users are guaranteed at least 80 MHz of spectrum throughout the 3550–3700 MHz band. The third tier (GAA), which does not exist in LSA, is intended for "Wi-Fi-type systems" and therefore not protected from interference; the second tier (PAL) is protected from GAA, and the first tier (incumbents) is protected from all users.

While LSA and SAS share some common features, there are differences as well. LSA relies on a central database that is populated by incumbents with accurate

Table 1 Comparison between LSA and SAS

	LSA	SAS
Geographic domain	Europe	United States
Frequency band	2.3 GHz (2300–2400 MHz) 3GPP LTE band 40	3.5 GHz (3550–3700 MHz) 3GPP LTE bands 42–43
Spectrum awareness	Central database populated by incumbents	Spectrum sensing plus exclusion/ protection zones
Tiers	Tier 1: Incumbent Tier 2: LSA licensee	Tier 1: Incumbent Tier 2: PAL Tier 3: GAA
Incumbents	Country-dependent (e.g., military stakeholders, professional video cameras)	Military services (e.g., radars) around coastal areas

information on spectrum usage over space and time. This database is used to either grant access to an LTE network or request to vacate specific bands through an LSA controller. On the other hand, SAS relies on spectrum occupancy information obtained from spectrum sensing combined with the definition of exclusion and protection zones around coastal areas, where SAS incumbents (mostly military services) are operated. It is worth noting that both systems (LSA and SAS) are defined for specific frequency bands but can be applied to other bands as well. Table 1 summarizes the main features of both systems.

Spectrum Coexistence in Unlicensed Bands

The most popular initiatives for spectrum coexistence of mobile communication systems in unlicensed bands are LTE unlicensed (LTE-U), licensed assisted access (LAA), and MuLTEfire [26, 27, 49, 59]. These initiatives are designed to operate in the unlicensed 5 GHz band (5150–5925 MHz), which is also known as the unlicensed national information infrastructure (U-NII) band (3GPP LTE bands 46–47) and is mostly utilized by radar systems and wireless local area networks (WLAN) based on IEEE 802.11a/g/n/ac (*WiFi* networks). Both LTE-U and LAA operators will typically employ the dedicated licensed spectrum as the primary carrier for signalling traffic (i.e., control channels) and provide data services with high QoS requirements, while a secondary set of carriers in the unlicensed spectrum will be added by means of carrier aggregation techniques to provide data services with less demanding QoS requirements.

LTE-U (standardised in 3GPP LTE Releases 10/11/12) was designed for quick launch and deployment in countries that do not require the implementation of the listen-before-talk (LBT) technique (e.g., USA, South Korea, India, and China). This allowed existing LTE systems to operate in unlicensed spectrum with no changes to the air interface protocol by simply exploiting mechanisms provided by the standard. LAA (standardised in 3GPP LTE Release 13) was introduced to allow

spectrum coexistence in unlicensed bands in countries where the implementation of the LBT protocol is required (e.g., Europe and Japan). The third variant of LTE in unlicensed bands, MuLTEfire, was designed as a stand-alone version of LTE for small cells relying exclusively on unlicensed spectrum as the primary and only carrier.

LTE-U was developed by the LTE Forum (established in 2014) with the aim to exploit the latest 3GPP LTE features to enable operation in unlicensed frequency bands. The approach of LTE-U was not to introduce changes to the standard, which would have required a long development time, but instead adapt the existing features provided by the standard so that operation in unlicensed bands could be enabled within a short time frame. Three main simple mechanisms are exploited by LTE-U to operate in unlicensed bands (see Fig. 1):

- On-off switching: In order to minimize interference to other users within the unlicensed band, transmissions in the unlicensed spectrum are performed only when needed. If the LTE traffic load exceeds a certain threshold and there exist active users within the unlicensed spectrum band, then the carrier in the unlicensed band is turned on to offload LTE traffic. On the other hand, when the main (licensed) carrier of the LTE network operator is sufficient to manage the traffic demand (or when there is no active user within the unlicensed band), then the carrier in the unlicensed band is turned off. This mechanism is referred to as

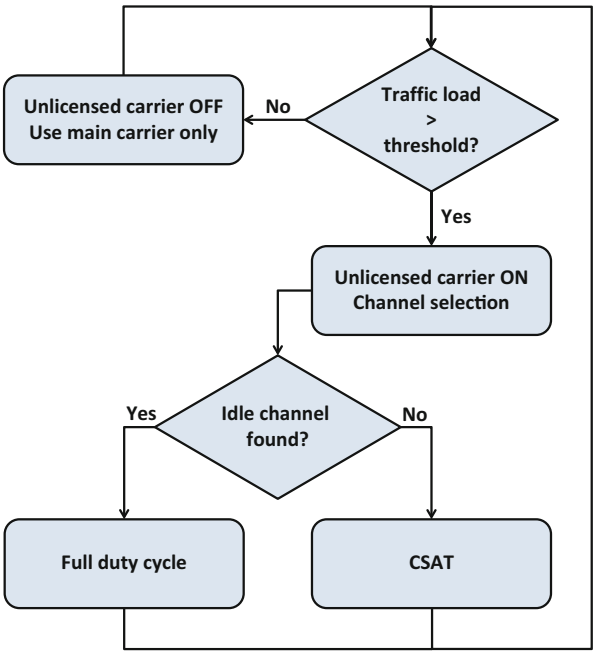

Fig. 1 LTE-U operation

opportunistic supplementary downlink (SDL) since LTE-U only uses unlicensed spectrum for additional downlink capacity.

- Carrier selection: The LTE base station scans the unlicensed spectrum and monitors the power level in each available channel. An unused channel will eventually lead to a low measured power and therefore to a low prospective interference if the LTE network operates in that channel. Based on this premise, the channel with the lowest detected signal power is selected. Since the sources and types of interference in an open unlicensed band are unknown, the power level is measured based on energy detection. Power measurements are usually performed both at the beginning power-up stage and later on periodically during active transmission (typically every 10 s). If interference is detected, LTE-U will attempt to switch to other channels with lower interference levels.
- Carrier-sensing adaptive transmission (CSAT): When no unused channel is found within the unlicensed spectrum, an active channel is selected. The CSAT mechanism allows LTE systems to share an active channel with other users on a time-division multiplex (TDM) basis as illustrated in Fig. 2. The LTE base station senses periodically the channel (for a relatively long period that can be anywhere between 0.5 and 200 ms) to determine if a signal is present (typically using an energy detection principle with a decision threshold of −62 dBm). Based on the detection result, CSAT will adjust the transmission duty cycle by deciding for how many frames the LTE system will transmit or remain quiet. If low channel activity is detected during LTE off periods, the duty cycle will be increased and vice versa (within some constraints of minimum and maximum durations for LTE on/off periods). During the LTE transmission periods, LTE accesses the channel without performing sensing; however, it regularly leaves some short transmission gaps to allow for latency-sensitive Wi-Fi services.

The distributed coordination function (DCF) used by Wi-Fi devices to access the channel includes a clear channel assessment (CCA) mechanism which dictates that the channel can only be accessed if it has been idle for a certain period. Moreover, Wi-Fi devices will vacate the channel if a collision is detected during the transmission, after which they will enter a back-off mode where they will wait for a random time before a new transmission is attempted. As a result of this channel

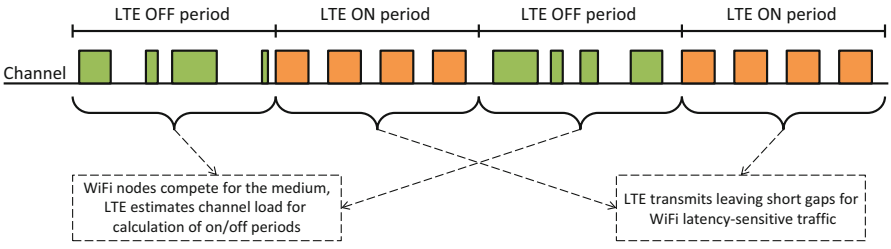

Fig. 2 Example of coexistence between LTE-U and WiFi [36]

access protocol, the performance of Wi-Fi users can be severely degraded by the presence of LTE-U users monopolizing the unlicensed spectrum.

LAA was developed and standardized by 3GPP in Release 13 with the aim to enable a fair coexistence between LTE and Wi-Fi. Fairness is defined as the capability of LTE "to not impact WiFi services more than an additional WiFi network on the same carrier, with respect to throughput and latency" [11]. An LBT mechanism with random back-off and a variable contention window size, similar to that of Wi-Fi, was introduced as the main means to enable such fair coexistence. The main idea to prevent LTE users from monopolizing the spectrum is to first sense the channel (based on energy detection) and transmit only if the medium is sensed to be idle for a minimum period of time. This process is referred to as clear channel assessment (CCA), and the LBT mechanism includes both initial and extended CCA (see Fig. 3). The back-off mechanism is designed to avoid collisions when two or more nodes sense the channel as idle and transmit at the same time. The back-off counter N is randomly drawn from a uniform distribution within a dynamic contention window (CW), which is increased exponentially (up to a predefined maximum value) when a collision is detected (typically when at least 80% of the HARQ reports indicate erroneous transmission) and reset (to a predefined minimum value) when the transmission is successfully completed. The required N idle slots do not need to be contiguous; however, when a busy slot is detected, the back-off process is suspended until the channel has been idle for at least a predefined extended defer period, after which the counter can be decreased again with each idle slot. As a result of this channel access protocol, LTE behaves similarly to Wi-Fi as illustrated in Fig. 4, which leads to a *fair coexistence* as defined in [11].

In 3GPP LTE Release 13, where the use of unlicensed spectrum is supported for downlink only, the eNodeB follows the procedure shown in Fig. 3 for transmission in the physical downlink shared channel (PDSCH). An enhanced-LAA (eLAA) version that supports transmission in the uplink, via the physical uplink shared channel (PUSCH), was introduced in 3GPP LTE Release 14, which enables the user equipment to access the unlicensed spectrum following a largely similar procedure.

There exist specific regulations in many countries that prevent from continuous transmission. As a result, LTE operators cannot transmit in unlicensed spectrum for unlimited periods of time. When a transmission opportunity arises, LTE can transmit for a predefined amount of time, after which the channel has to be vacated even if there are more data to transmit. This resembles the behavior of Wi-Fi nodes, which utilize the channel for a limited time to allow for medium access competition. 3GPP introduced four different priority classes for LAA (the smaller the priority class number, the higher the priority). The maximum channel occupancy time for the commonly used category 4 LBT is typically 10 ms. Certain countries may have additional requirements (e.g., for LAA operation in Japan, the eNodeB should sense the channel to be idle after every 4 ms of transmission). To allow for a more flexible access to the unlicensed spectrum, LAA has a slightly different frame structure (Type 3). This frame is also based on ten 1 ms subframes; however, transmissions do not necessarily start or end at the boundary of a subframe [12].

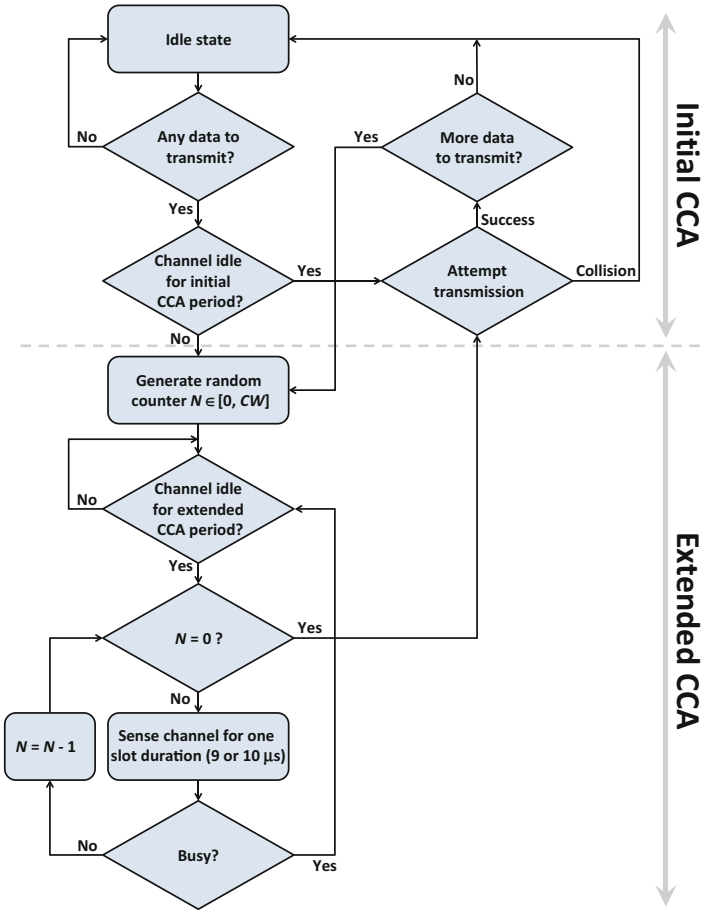

Fig. 3 LAA operation [11]

Table 2 summarizes the main features of LTE-U and LAA. A related technology is LTE-WLAN aggregation (LWA), introduced in 3GPP LTE Release 13 to enable mobile terminals equipped with LTE and Wi-Fi employ both links simultaneously through the LTE dual connectivity architecture introduced in Release 12 (but using a Wi-Fi access point instead of an LTE secondary base station) and aggregate the data traffic of both links at the radio access network level (instead of aggregating the traffic at the core network level through the interfaces introduced in Release 8). Unlike LTE-U and LAA, in LWA, there is no spectrum coexistence between LTE (operating in licensed spectrum) and Wi-Fi (operating in unlicensed spectrum), and CR techniques are therefore not applicable in this case. In general, LWA provides a performance comparable to that of LAA (which outperforms LTE-U as a result of the fair coexistence with Wi-Fi networks enabled by the LBT mechanism).

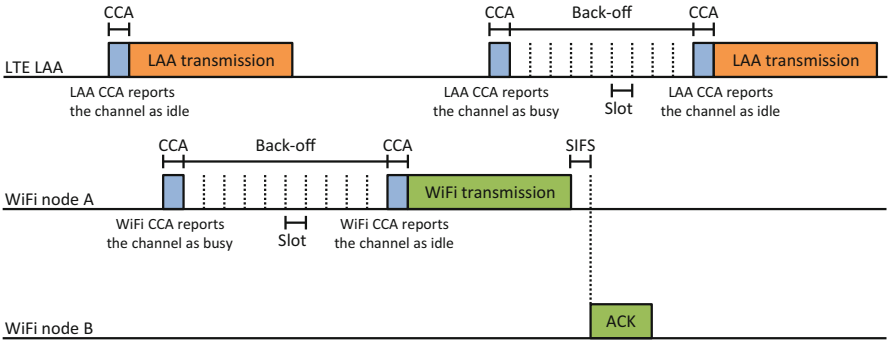

Fig. 4 Example of coexistence between LAA and WiFi [36]

Table 2 Comparison between LTE-U and LAA

	LTE-U	LAA
Geographic domain	Countries that do not require LBT (US, South Korea, India, China)	Countries that do require LBT (Europe, Japan)
Frequency band	5 GHz (5150–5925 MHz) 3GPP LTE bands 46–47	5 GHz (5150–5925 MHz) 3GPP LTE bands 46–47
Spectrum awareness	Sensing (energy detection)	Sensing (energy detection)
Incumbents	IEEE 802.11 WiFi networks	IEEE 802.11 WiFi networks
Release (operation mode)[a]	Rel. 10–12 (downlink only)	Rel. 13 (downlink only) Rel. 14 (downlink and uplink)
Coexistence mechanisms	On-off switching Carrier selection CSAT	Carrier selection LBT (WiFi-like)

[a]Both use the licensed spectrum as the primary carrier and are backward-compatible with Rel. 9

Other Applications in Mobile Communication Networks

The increase of the mobile network capacity by exploiting unused spectrum in other (licensed and unlicensed) bands is not the only application of CR techniques in the context of mobile communications. CR principles can be exploited in other contexts and scenarios as well. CR has the potential to provide simple solutions to overcome some of the challenges faced by mobile communication networks and improve the effectiveness and efficiency of already existing solutions [20].

The trend of network densification (i.e., the deployment of cells with smaller coverage areas as a means to increase network capacity) has resulted in heterogeneous network scenarios where macro-, micro-, pico-, and/or femtocells coexist in the same area and typically in the same spectrum as well. The application of CR principles in the context of femtocells has led to the concept of *cognitive femtocells*, which has received significant attention. Femtocells are consumer-deployed access points designed to provide low-power short-range broadband

coverage at homes, offices, public hotspots (e.g., airports, malls), and other indoor scenarios. Femtocell access points (FAPs) are connected to the operator's network through broadband wired connections or wireless backhaul links and can therefore be seen as gateways for indoor terminals. The deployment of FAPs is carried out by the customer and is therefore uncoordinated (i.e., without network planning), which usually leads to potential cross-layer interference with the macrocell as well as co-layer interference with other femtocells. Traditional solutions include the use of coordinated resource allocation schemes (which is in general challenging due to the lack of a direct communication interface defined between the femtocell and macrocell access points) and static or dynamic frequency reuse schemes (where different portions of spectrum are allocated to macro-/femtocells, which usually results in sub-optimum exploitation of the spectrum resources). The limitations of both approaches can be overcome with the adoption of CR techniques in the FAPs, thus leading to a dynamic spectrum coexistence scenario where the femtocell plays the role of a cognitive (secondary) system accessing opportunistically the spectrum of the incumbent (primary) macrocell without generating harmful interference. This approach results in a more efficient exploitation of the spectrum than frequency partitioning methods, without the need of direct coordination mechanisms between femtocells and macrocells or other femtocells. The femtocell can sense the spectrum to detect free channels not used by the macrocell or another femtocell (which can be performed by the FAP to remove the need of additional infrastructure as well as battery life issues in mobile terminals), select the carrier frequency that best suits the requirements of the femtocell users, and exploit the free carrier using either interweave or underlay techniques, depending on the detected spectrum activity, tolerable interference levels, and user traffic requirements [54]. Cognitive femtocells can observe the surrounding radio environment and adapt dynamically to exploit spectrum opportunities and avoid co-layer and cross-layer interference in a manner that is transparent to the macrocell. This approach enables an uncoordinated deployment of femtocells while allowing an efficient exploitation of the spectrum allocated to the mobile communication network, without having to resort to additional spectrum bands. Alternatively, under high traffic demands, femtocells can exploit the cognitive capabilities to access other spectrum bands (e.g., Wi-Fi bands using LTE-U/LAA techniques).

Another area of application of CR in mobile communications is in device-to-device (D2D) communications. D2D was introduced in 3GPP LTE Release 12 to enable nearby mobile terminals establish a direct communication link, bypassing their corresponding cellular base station. By enabling a low-power direct D2D link instead of a higher-power dual-hop link through the base station (uplink/downlink), the D2D concept can reduce congestion and improve radio resource utilization and spectral efficiency at the base station, reduce interference at the macrocell, and improve latency and power consumption at mobile terminals. While the network may be aware (even take control) of D2D links, it is in network-unaware D2D links where CR can unleash its full potential by allowing mobile terminals detect the proximity of the other terminals, sense the spectrum to find suitable frequencies for the establishment of D2D links, and reconfigure the operation parameters to allow

opportunistic use of the spectrum [42]. Cognitive D2D communications can enable efficient radio resource utilization and interference management among coexisting cellular and D2D users with limited or no intervention from the cellular base station.

With the advent of the Internet of Things (IoT), mobile communication networks have emerged as one of the main connectivity technologies. In this context, the narrowband IoT (NB-IoT) was standardized by 3GPP in Release 13 to enable a wide range of IoT devices to be connected using LTE networks. The NB-IoT technology has been designed to coexist with standard LTE users in the spectrum allocated to LTE (using the same radio resource block bandwidth of 180 kHz) where LTE used to operate exclusively. This can lead to interference problems between LTE and NB-IoT carriers when only some base stations are NB-IoT-capable. While the adjacent channel interference may be negligible [53], low-power NB-IoT devices may be affected by strong co-channel interference from base stations that are LTE-capable only. CR techniques can also be exploited in this context to mitigate this harmful interference (e.g., by means of selective LTE resource blanking [37]).

Satellite Communication Networks

Satellite communication networks are nowadays fundamental to meet the challenging objectives of future fast broadband access for everyone. Their inherently large coverage footprint makes them the ideal candidate to reach areas where the deployment of wired and wireless networks is not economically feasible. While satellite communications may be better known to the general public for direct-to-home (DTH) interactive video broadcasting services, they have certainly found a broader range of applications in market niches such as land mobile, aeronautical, maritime, transports, military, and rescue and disaster relief.

Similar to the evolution of mobile communication networks, satellite communications have also suffered a substantial increase in traffic and capacity demands over recent years. This has historically been addressed with the gradual optimization of the single-user satellite link by means of more spectrum-efficient technologies, for instance, the different families of the digital video broadcasting (DVB) standard (DVB-S, DVB-SH and DVB-RCS). This process is well documented in the existing literature. Given that the current state of the art has closely approached the well-known Shannon limit [43] and further improvements usually provide incremental performance enhancements, satellite communication research has recently shifted toward multiuser communication techniques, many of which have already demonstrated great potentials for performance improvements in the context of terrestrial communications. In line with this trend, the introduction of CR techniques is currently inspiring the next generation of satellite communication systems.

While the application of CR principles to terrestrial communication networks has been investigated for over a decade, it has not been until more recently that the potential benefits that CR techniques may bring into satellite communications have started to be explored. Flexible spectrum utilization is a cornerstone for the efficient exploitation of the scarce spectrum resources, and CR techniques have broadly

demonstrated their potential benefits in the context of terrestrial communication networks (e.g., more efficient exploitation of the scarce spectrum resources, rollout of new and optimized services at lower costs for the end user, or new revenue streams for operators from secondary services). Future satellite communication systems may also benefit from the capability to access spectrum opportunities in frequency bands other than the dedicated licensed spectrum. CR techniques can be implemented in satellite communications to enable spectrum sharing and provide its associated benefits by effectively managing interference.

Long-term persistent interference from terrestrial or other satellite systems pose a major challenge to satellite operators as interference has a significant impact on the obtained revenues. In this context, CR techniques can help relieve interference. Certain types of interference may be difficult to mitigate by the introduction of CR techniques. This is the case of cross-polarization interference, which is typically caused by misaligned antennas, incompatible modulation types in opposite polarizations, or sometimes inappropriate training of the operators. Given its inherent nature, CR techniques can provide limited benefits in the relief of cross-polarization interference, which is solved by addressing the source of interference (usually a time-consuming and labor-intensive task). However, CR techniques can help relieve interference in scenarios of spectrum coexistence. This interference can occur from or to terrestrial fixed or mobile services and other satellites or satellite constellations in both geostationary and non-geostationary orbits (GSO/NGSO). Adjacent satellite interference is usually accidental and caused by inadequate coordination between systems. While this type of interference can be solved between satellite operators, CR techniques can be introduced as a countermeasure to mitigate its consequences. Interference between terrestrial and satellite services can be more severe and depends on the considered frequency band, geographic region, and enforced regulatory framework. For example, interference is in general lower in DTH markets in developed countries than in very small aperture terminal (VSAT)-oriented markets, while it is currently low (but increasing) in the Ka band and higher in the Ku and C bands. An interesting and useful application of CR solutions in this context is the use of dynamic adaptation methods for interference-free dynamic spectrum sharing in order to exploit unused or underused frequency bands assigned to other (satellite or terrestrial) services on an incumbent/primary or secondary basis.

Satellite Bands of Interest for Cognitive Radio

Satellite communication systems operate over a wide range of spectrum bands. Several beneficial applications of CR principles have been identified in the Ka (27–40 GHz), Ku (12–18 GHz), C (4–8 GHz), and S (2–4 GHz) bands [4, ch. 10]. Some characteristics as well as the motivation for introducing CR techniques for spectrum sharing in these bands are reviewed in this section. The exploration of the potential applications and benefits of CR techniques at higher frequencies such as the Q (35–50 GHz), V (40–75 GHz), and W (75–110 GHz) bands has

Table 3 Satellite bands of interest for cognitive radio

IEEE designation[a]	Frequency range	Motivation for the introduction of CR
Ka band	27–40 GHz	Capacity extension through secondary cognitive access to adjacent spectrum
Ku band	12–18 GHz	Capacity extension and exploitation of fragmented spectrum
C band	4–8 GHz	Capacity extension and mitigation of interference from LTE/WiMAX
S band	2–4 GHz	Capacity improvement through mitigation of intra-system (satellite/ground segments) and inter-system (UMTS) interferences

[a]IEEE Standard Letter Designations for Radar-Frequency Bands (IEEE Std 521-2002)

been suggested as well; however, most of the interest has mainly focused on lower frequencies, and these are therefore the bands considered in this section (see Table 3).

As a result of the long-standing demand of broadband via satellite from users out of reach to high-speed terrestrial networks, a general trend in the evolution of satellite communications has been the migration of systems and services to higher-frequency bands, where larger portions of contiguous spectrum can be found, in order to deploy the so-called high-throughput satellite (HTS) systems (communication satellites that can provide at least twice the total throughput of a classic FSS satellite for the same allocated spectrum, although in practice, this is typically exceeded by a factor of 20 or more). One advantage of the Ka band over lower-frequency bands (Ku, C, S) is the possibility to exploit higher-frequency bands with smaller spot beam cell sizes and higher degrees of frequency reuse (i.e., reuse of the allocated frequency band several times over the coverage area, similar to cellular networks in the terrestrial domain), which enables a more efficient exploitation of the available frequency resources and therefore an increase of the overall system capacity and a reduction of the cost per bit per second per Hertz. Consequently, the use of the Ka band has been targeted by the majority of satellite operators as a technical pathway to deliver high capacity services at economically affordable and sustainable rates. The Ka band is nowadays populated by HTS able to deliver maximum throughput rates typically between 70 and 100 Gbit/s over contiguous coverage areas ranging from small to regional and even continental scales. The increasing attention received by the Ka band and the perspective of broadband satellite applications motivate the additional use of some adjacent spectrum in the Ka band as a means to extend the overall satellite capacity in this band and further drive down the cost per bit per second per Hertz. This adjacent spectrum may be accessed on a cognitive/opportunistic basis through the adoption of CR techniques.

The Ku band is used extensively for DTH applications (in particular the downlink), and the current trend is an increase in the capacity demand (by a factor of around 1000 transponder equivalents over a 10-year period) mainly driven by DTH and VSAT services, followed by mobility and video distribution services.

Within the heavily exploited Ku spectrum, an additional issue is the fragmented use due to interference or other reasons. CR techniques are well suited to exploit and share non-contiguous regions of the spectrum and therefore become a natural (and promising) candidate to cater for the increasing capacity demand in Ku band.

The C band is significantly less affected by rain and humidity than the Ka and Ku bands, which results in better radio propagation conditions. The atmospheric fading conditions are excellent for highly reliable, weather-independent links over very large coverage areas (at continental and intercontinental scales) with very high availability rates. This band has traditionally been used by satellite communication systems extensively and is still appreciated for satellite service deployments, which include mainly point-to-point and point-to-multipoint links for IP backbone connections. The bandwidth required for backhaul, trunking and professional services, and the continuously increasing bit rates of digital video distribution services provided in the C band are expected to push the required capacity in this band. This challenge has traditionally been addressed by means of new combinations of wide beams, spot beams, and frequency reuse patterns along with enhanced connectivity options between beams and new improvements of antenna technologies. In this context, the adoption of CR principles can provide a new dimension for further capacity enhancements. However, it is in the management of interference in the C band where the introduction of CR techniques can unleash its full potential and provide the most significant improvements. Despite the robustness under all atmospheric conditions, the current deployments found in the C band are very sensitive to interference and, as a result, are facing numerous challenges to provide reliable and efficient services to the standard required by the customers. Given the high imbalance of power levels between satellite and terrestrial signals, any terrestrial interference toward satellite systems has a strong negative impact on the satellite signal quality and the resulting end-user QoS. The relatively recent deployment of LTE cellular services and broadband wireless access (BWA) systems such as WiMAX in the so-called *extended* C band (3.4–3.6 GHz) has led to severe interference problems on C band satellite systems. The extended C band was globally allocated to IMT-2000 cellular services on an incumbent basis with no real system impact considerations (or insufficient analysis) and without protection to satellite communications, which has led to numerous interference concerns for satellite operators as well as reported coexistence problems with LTE, in particular for transmissions into low elevation angles for GSO satellite links. Moreover, the presence of WiMAX signals, which typically operate at power levels approximately 40 dB higher than satellite signals, has resulted in problems of obliterating in-band interference, harmful interference from out-of-band emissions, and blocking of signals resulting from saturation of the low-noise amplifiers used by satellite receivers. Typical countermeasures employed to date in order to mitigate the negative impact of terrestrial interference include the increase of separation distances, use of larger dishes (antennas) at the receivers, and deployment of new expensive filters or other hardware upgrades of the end-user equipment. Unfortunately, the technology available today may not be able, in some cases, to mitigate completely the interference, in particular when it comes to high data rate services requiring very high signal-to-noise ratios. In exceptional cases,

this has required spectrum refarming from regulators and price reductions from operators given the inability to provide suitable levels of service to the customers. Such interference problems (mainly in the reception of digital TV) led some Asian countries (Philippines, Indonesia, Malaysia, Vietnam) to refuse or withdraw WiMAX licenses in the extended C band, while European regulatory regimes have started to review more strictly licenses in the lower part of the C band. However, with LTE and WiMAX services already deployed in the extended C band, the damage has already been caused, which claims for novel technological solutions to mitigate the existing interference problems. In this context, CR emerges as a promising solution given its demonstrated ability to manage and control interference through several techniques, mechanisms, and protocols. The introduction of CR techniques is expected to significantly relieve interference problems in the C band and relax the demanding requirements currently imposed on other interference-mitigating techniques. An adequate interference mitigation in C band is relevant not only for the coexistence of satellite systems in this band with LTE/WiMAX terrestrial systems but also for many other satellites that today operate in other higher-frequency bands but carry out telemetry, tracking, and control (TTC) operations in C band.

The S band is typically populated by hybrid networks composed of a satellite segment and a complementary ground segment, both of which may be integrated and coordinated by the same operator to provide holistic service coverage and delivery over urban, suburban, and rural areas but may utilize potentially different broadcast and interactive technologies in the space and terrestrial segments. The frequency planning of these networks is quite complex and requires a careful consideration not only of the potential intra-system interference between satellite and ground segments (a problem usually worsen by the presence of mobile user terminals in the ground segment) but also the potential inter-system interference arising from 3G UMTS cellular deployments in adjacent spectrum allocations, which are heavily used in Europe and other regions. CR techniques can find several useful applications in this context as a tool to mitigate both intra- and inter-system interferences and increase the overall system throughput. Either the satellite or complementary ground segment can be the primary/incumbent part of the integrated network, while the other segment plays the role of a secondary/cognitive network, or the fixed part of the network acts as primary/incumbent, while the mobile terminals dynamically adapt the forward and return links to the changing interference scenario on a secondary/cognitive basis.

Spectrum Coexistence Scenarios

Several scenarios in satellite communications offer the potential for flexible spectrum sharing and interference mitigation through the adoption of CR techniques. Some possible application areas include the secondary use of satellite spectrum by terrestrial systems, satellite systems as cognitive secondary users of the terrestrial spectrum, extension of terrestrial networks using satellite networks, and wider

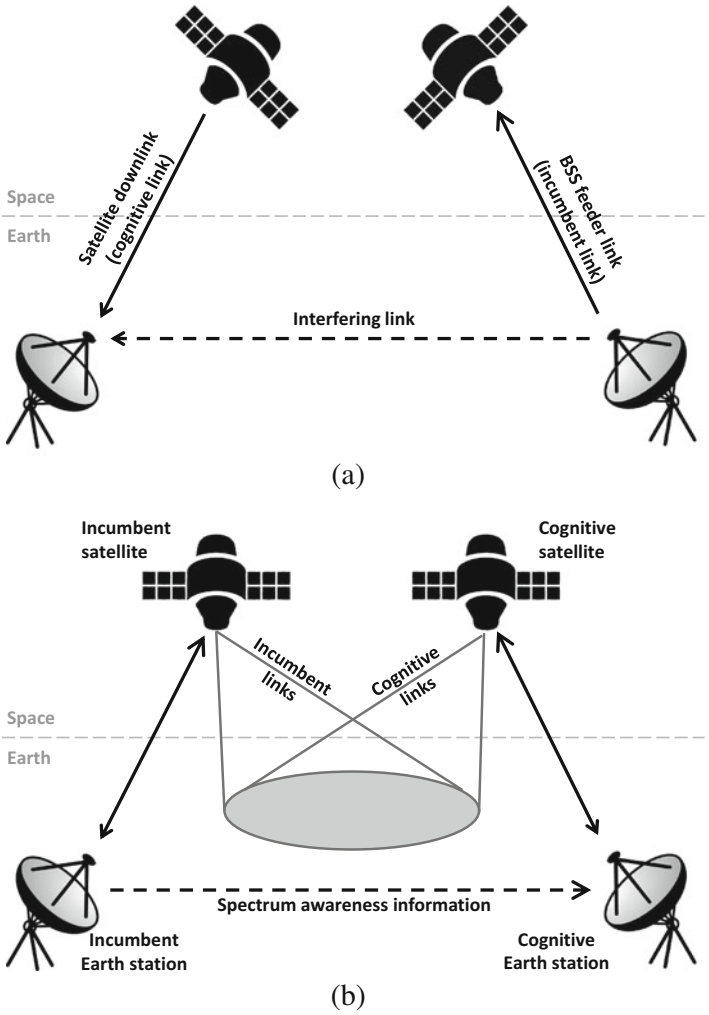

Fig. 5 Spectrum sharing scenarios in satellite communications (satellite-satellite) [4, ch. 10]

cognition for more efficient use of resources in the satellite network (with or without involvement of a terrestrial network) [19]. Figures 5 and 6 illustrate some representative scenarios of satellite-satellite and satellite-terrestrial spectrum coexistence, respectively. Each scenario is defined by the frequency band of operation, the provided services, and the enforced regulatory framework, which are discussed in more detail in the following.

The scenario shown in Fig. 5a is applicable to the downlink of GSO satellites in Ka band (17.3–17.7 GHz). The 17.3–17.7 GHz band is mainly allocated to satellite systems (with the exception of some particular countries where this band may

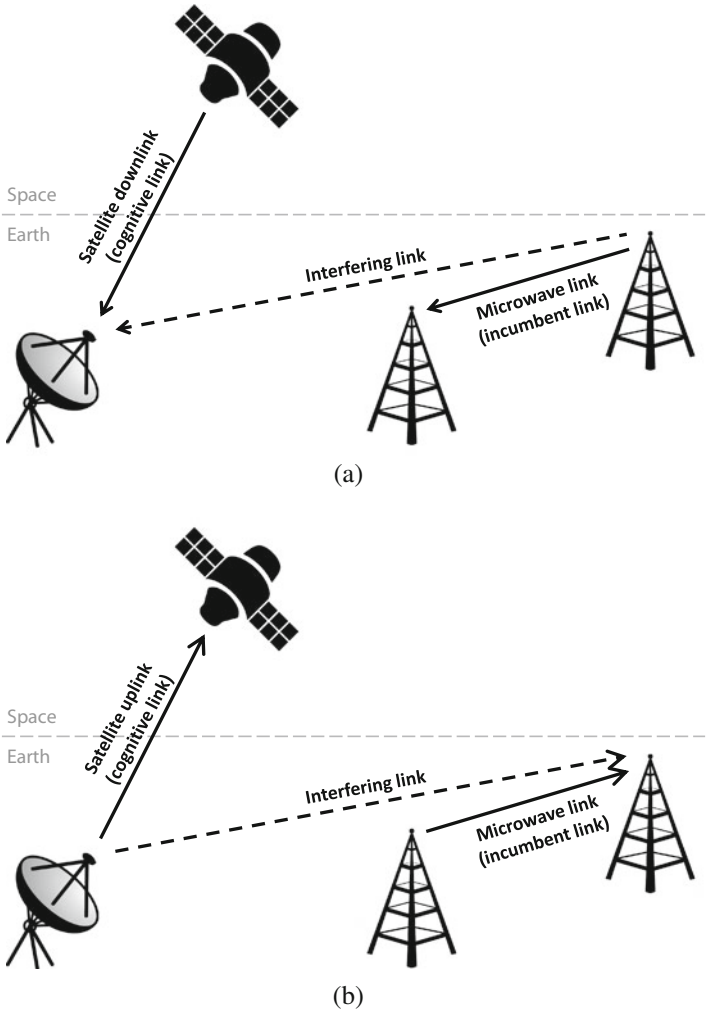

Fig. 6 Spectrum sharing scenarios in satellite communications (satellite-terrestrial) [4, ch. 10]

also be allocated to some terrestrial services on an incumbent basis). This band is typically allocated to high-density applications in the fixed satellite service (HDFSS), without prejudice to its use by GSO broadcasting satellite service (BSS) feeder uplinks. Spectrum regulations also allow the deployment in this band of uncoordinated fixed satellite service (FSS) Earth stations and contemplate the harmonized use of Earth stations on mobile platforms (ESOMP). The deployment of uncoordinated FSS Earth stations may eventually take place in locations subject to long-term interference from BSS feeder uplinks as well as temporary, short-term interference from satellite terminals on mobile platforms. In this context, the

adoption of CR techniques can provide the means required for an interference-free coexistence among the involved parties and an increased frequency exploitation by means of flexible spectrum usage.

The scenario shown in Fig. 5b is applicable to the uplink and downlink of GSO satellites in Ku band (10.7–12.75, 12.75–13.25 and 13.75–14.5 GHz). These bands are allocated to GSO satellite systems, which use these regions of the spectrum on a primary/incumbent basis. However, an additional (secondary/cognitive) GSO satellite system may be overlaid, thus leading to a dual GSO satellite system. In this scenario, the cognitive GSO satellite system can adopt the use of CR techniques in both uplink (12.75–13.25 GHz and 13.75–14.5) and downlink (10.7–12.75 GHz) to dynamically adapt to the interference environment of the incumbent GSO satellite system and exploit the available spectrum opportunities in order to achieve a more efficient exploitation of these bands. A detailed discussion of this scenario can be found in [4, ch. 12].

The scenario shown in Fig. 6a is applicable to the downlink of GSO satellites in Ka band (17.7–17.9 GHz) and C band (3.4–3.8 GHz). The 17.7–17.9 GHz band can be used by FSS and terrestrial fixed services (FS) such as microwave links. In this band, FSS Earth stations can be deployed anywhere, however without the right of protection from interference from the FS transmitters. CR techniques can be adopted to provide such protection and enable the FSS to reuse the spectrum in this band in the vicinity of terrestrial FS transmitters. Satellite operators can exploit this to gain significant user capacity by extending the 19.7–20.2 GHz band (exclusive for wideband downlink FSS) with additional contiguous spectrum in the 17.7–19.7 GHz band. The presence of ESOMP in this band needs to be taken into account as well. In the 3.4–3.8 GHz band, which is also shared between terrestrial FS and satellite services, the incumbent system can be either the satellite or terrestrial service. In this context, CR techniques can be exploited to enable a more intense use of the spectrum by allowing satellite systems adapt their frequency usage in the downlink according to the interference environment generated by the incumbent satellite and terrestrial FS. Information on the FS frequency assignment would enable the local selection of suitable frequencies that would enable satellite operation while avoiding interference from microwave links.

The scenario shown in Fig. 6b is applicable to the uplink of GSO satellites in Ka band (27.5–29.5 GHz). The 27.5–29.5 GHz band is segmented between FS and uncoordinated FSS Earth stations. The FS segment is typically subject to a low level of utilization (in particular through Europe), which motivates the flexible reuse of the FS segment by FSS stations through the adoption (in the satellite uplink) of CR techniques able to dynamically control the potential interference to FS stations.

The scenarios in Fig. 6a, b are also applicable to the downlink and uplink, respectively, of NGSO satellites in Ka band (17.7–19.7, 27.8285–28.4445 and 28.9485–29.4525 GHz), where similar coexistence and interference issues can be found and similar solutions through the adoption of CR techniques can be applied.

It is worth noting that in some scenarios, in particular those shown in Figs. 5a and 6a, the relevant interference is from the incumbent system to the cognitive

system. This is a distinguishing feature of satellite communications with respect to terrestrial scenarios where this type of interference is irrelevant and the focus typically is on avoiding interference in the reverse direction (i.e., from the cognitive system to the incumbent system). On the other hand, in the scenarios shown in Figs. 5b and 6b, the relevant interference is from the cognitive system to the incumbent system, which resembles the traditional scenarios typically found in terrestrial CR networks. There exist some additional interference relations besides those shown in Figs. 5 and 6; however, these typically correspond to *weak interference* and can be considered negligible in practice. This is usually the case of interference links between Earth and space stations, where the long distances along with the use of directional antennas lead to very low (negligible) levels of interference, or between Earth-Earth and space-space stations where interference occurs through side or back lobes of the antennas and is negligible in practice as well. The interference links shown in Figs. 5 and 6 correspond to *strong interference* that determines the performance limits of spectrum coexistence between services.

Cognitive Radio in Satellite Communications

Spectrum exploitation in satellite communications has traditionally relied on static approaches such as separation of frequency bands on the basis of geographical service areas, service types, or angle of the satellite signals. While these traditional static approaches have provided effective mechanisms for interference-free operation of satellite communication systems, they do not allow for dynamic adaptation to the evolving conditions of traffic demand, geographical mobility, or temporal and spatial interference. They introduce significant inefficiencies that leave a substantial margin for improvement in the exploitation of the allocated spectrum and are currently regarded as suboptimal. Most (if not all) existing CR techniques have been inspired by terrestrial scenarios, and their applicability to satellite communication systems is not always straightforward, thus requiring an exhaustive revision and potential redesign of the existing CR technology taking into account the specific features of satellite communication systems (e.g., much lower received signal levels, much larger coverage areas, much longer delays, or very limited ability to update in-orbit infrastructures).

This section presents an overview of some of the main CR techniques of interest for application in satellite communications, with discussions on specific particularities of satellite scenarios and differences with respect to their terrestrial counterparts. These techniques can be classified into *spectrum awareness* solutions used to obtain relevant information and knowledge of the surrounding radio environment (spectrum sensing and geolocation databases) and solutions for *spectrum utilization* aimed at enabling interference-free coexistence between incumbent and cognitive systems (cognitive zone, power control, carrier allocation, beamforming).

Spectrum sensing is one of the simplest forms of spectrum awareness in CR-based systems and, with some special considerations, may be applicable to satellite communications. Spectrum sensing aims at detecting the presence of

incumbent user signals by scanning some selected frequency bands and processing the captured samples with advanced signal processing methods. The signal to be detected may be fully known, partially known, or unknown, and this determines the range of spectrum sensing methods that can be applied as well as their performance [58]. One of the main limitations of spectrum sensing as a spectrum awareness technique is its detection reliability. The unavoidable presence of errors in the idle/busy decisions of spectrum sensing methods leads to interference and efficiency problems. This problem is accentuated in satellite communications, where received signal levels are significantly lower than in terrestrial scenarios as a result of the limited transmission power of satellite stations along with substantial signal attenuation due to cloud, rain, and other atmospheric effects, which can deteriorate significantly the quality of incumbent signals received at cognitive sensors. Devices based on energy detection methods may need to employ highly directed antennas toward the satellite, which may require the deployment of separate stations with parabolic antennas for the task of spectrum sensing [18]. Other detection methods such as matched filter or feature detection can provide better detection performance by exploiting signal inherent features such as cyclo-stationarity, specific autocorrelation, pilot symbols (e.g., in DVB-S2 signals typically used in satellite communications), or signal polarization [44,46]; however, these techniques require a priori information on the signal to be detected and its properties. Cooperation among spectrum sensors is a well-known approach to improve the overall detection performance while reducing the sensitivity requirements imposed on individual sensors. The existence of multiple users that belong to the same network (and can therefore communicate among them) exploiting the same band can be exploited to use cooperative spectrum sensing techniques. However, this approach faces additional problems in satellite communications: firstly, finding another sensor with better channel conditions for cooperation may sometimes mean finding a sensor hundreds of kilometers away given the large coverage areas of satellite communications; secondly, the design of an efficient means for intercommunication among cooperative users spread over large geographical areas is an additional issue to be addressed; and thirdly, the heterogeneity of satellite communications scenarios (satellite/terrestrial stations, uplink/downlink, incumbent/cognitive roles) requires a case-by-case analysis and design of cooperative spectrum sensing. In addition to the challenge of providing a reliable incumbent signal detection, satellite communications also face the problem of having to deal with channel bandwidths significantly larger than those usually found in terrestrial communications, which require the use of more powerful analog-to-digital converters (ADC). The use of sub-Nyquist sampling techniques such as sparse power spectrum estimation or compressive wideband spectrum sensing may help relieve the problem [2,50,56]; however, this still remains an important challenge, in particular in certain cases such as low Earth orbit (LEO) constellations, which are affected by mobility and frequency issues [31].

A popular alternative to spectrum sensing is the use of geolocation databases, which has also been considered in the context of satellite communications [18,23] [4, ch. 14]. Secondary nodes are required to implement the means to know their

own location (e.g., GPS receiver), which is sent to a centralized database in order to produce a report with the relevant spectrum awareness information for that location. A database for CR applications in satellite communications will typically contain information on geographic characteristics (coverage, service, and capture areas of space and terrestrial stations), incumbent and cognitive devices present in the area of interest and their characteristics (location, elevation and azimuth angles, coverage footprint, device type, height and altitude, antenna type, and directivity), and the surrounding radio environment (incumbent available frequencies, power levels and polarizations, spectrum masks). This rich set of data can be exploited to produce spectrum awareness information that would be difficult to acquire by individual spectrum sensors. This, along with the reliability problems associated with spectrum sensing, makes databases the most favored approach for spectrum awareness.

Spectrum sensing and databases have their specific advantages and limitations and provide different tradeoffs among performance, accuracy, complexity/cost of terminals and infrastructure, reliability, and legacy compatibility (see [34] for a detailed discussion). These approaches provide complimentary characteristics in terms of spectrum dynamism. In general, geolocation databases are not well suited for operation in spectrum bands with highly dynamic spectrum occupancy patterns. The procedure for determining the location of a cognitive node, sending a request to a database, and producing a report on the available spectrum and exploitation constraints is a time-consuming process. In highly dynamic bands, this may result in a cognitive node retrieving outdated information that does not reflect the current spectrum use scenario by the time it is received. On the other hand, spectrum sensing is well suited to obtain instantaneous spectrum awareness information even in highly dynamic, fast-changing bands. In general, geolocation databases are suitable for static scenarios where the transmitter characteristics (location, frequency, power, etc.) are stable or change very infrequently, such as geostationary Earth orbit (GEO) satellites (where the coverage and visibility of the satellite are almost fixed) or FS terrestrial stations (which are deployed at geographically fixed locations and with fixed frequency plans, similar to TV bands where databases are a popular approach as well). Databases may also be suitable for scenarios where spectrum occupancy patterns vary over relatively long time scales, such as medium Earth orbit (MEO) satellites (with altitudes of 10,000–20,000 km and pass times of 130–300 min) and even low Earth orbit (LEO) satellites (with altitudes of 200–1400 km and pass times of 7–2 min) [4, ch. 14]. On the other hand, the use of spectrum sensing may be necessary in bands where mobile terminals are present (e.g., ESOMPs) or a database is not available at all. Ideally, spectrum awareness information would be obtained by the joint use of a centralized database and the local spectrum usage detection of cognitive sensors; spectrum sensing can be used to support the database-based access; however, it should not be used as a stand-alone method in satellite bands.

Once the cognitive system has obtained adequate spectrum awareness information about the incumbent system, it can exploit that information to access spectrum opportunities by means of appropriate spectrum utilization techniques that can guarantee interference-free operation. One simple technique for interference

protection is the definition of a *cognitive zone*, which is a geographical region around a potentially interfered receiver where prospective interferers are not allowed to transmit unless they implement appropriate CR techniques that can mitigate interference to acceptable levels, which will be discussed later on. Interference outside this region is considered to be below the acceptable interference threshold, and transmission is allowed in a non-cognitive manner (i.e., without CR techniques). In terrestrial scenarios, where interference occurs from cognitive to incumbent users, the cognitive zone is typically defined around incumbent receivers. However, in satellite scenarios, where interference may occur in both directions (i.e., from cognitive to incumbent users and vice versa), the cognitive zone may need to be defined around either incumbent or cognitive users. For example, in Figs. 5a and 6a, the cognitive zones would be calculated around the satellite cognitive receiver, while in Fig. 6b, it would be calculated around the terrestrial incumbent receiver. Sometimes the cognitive zone may need to be defined around both, and the most restrictive one needs to be applied in order to guarantee that both systems can coexist simultaneously in the same region of the spectrum (e.g,, if bidirectional communication is assumed in the scenarios of Fig. 6). The cognitive zone can be defined around one or more individual stations or sometimes may need to be defined around a whole satellite spot beam or coverage area (e.g., in Fig. 5b). Cognitive zones are typically computed based on information from satellite and terrestrial databases along with interference modelling techniques that take into account the interferer's transmission power, the amount of aggregated interference tolerated by the interfered receiver, and the propagation channel between both including a range of propagation mechanisms such as line of sight, diffraction, tropospheric scattering, surface ducting, and anomalous propagation (ducting and layer reflection/refraction) as well as environmental factors such as frequency of operation, climate, distance, and path topography. If an accurate and complete database is not available, cognitive zones may then be designed based on spectrum sensing measurements, but worst-case designs should be adopted, which may result in loose zones. In any case, the use of cognitive zones has been proven to be effective for interference protection in satellite communications [45].

Within the cognitive zone, several spectrum utilization techniques can be employed. The most popular CR techniques proposed for satellite communications are based on underlay and interweave spectrum access approaches, while overlay-based solutions are less popular due to their inherent complexities and practical issues [45]. A typical underlay CR technique is the traditional location-aware power control [52], while a widely explored interweave CR technique is carrier allocation (other dynamic radio resource methods such as channel selection, admission control, and user scheduling have also been explored in the context of satellite communications [4, ch. 10] [5]). Carrier allocation techniques proposed for satellite communications are typically aimed at maximizing either the total overall throughput or the fairness (i.e., availability of carriers to as many users as possible according to their data rate requirements) [28] and can be combined with carrier aggregation techniques, which are popular in the context of LTE mobile communication networks and very appealing for the exploitation of the fragmented

spectrum in Ku band. Carrier allocation techniques have been proposed for the dynamic allocation of both incumbent and cognitive carrier frequencies to the users, not only in specific time and/or geographical locations but also exploiting additional degrees of freedom available in satellite communications such as polarization and angular direction (since satellites are seen at high elevation angles, depending on the latitude, an adequate design of antenna radiation diagrams can help reduce mutual interference and enable cognitive frequency reuse [23]).

Specific antenna radiation diagrams can be achieved by means of beamforming, a multiple-antenna signal processing technique that operates separately the individual elements of an antenna array in such a way that the combined radiations form a desired overall radiation (beam) pattern. Beamforming enables transmission/reception along certain spatial directions of interest while cancelling or mitigating signal components along non-desired directions. The spatial discrimination and filtering provided by beamforming can be exploited to enable spectral coexistence of two systems in the angular domain [47] and can be combined with resource allocation methods for a more efficient use of the spectrum [48]. Beamforming can be applied both in reception (e.g., in the cognitive satellite receiver of Figs. 5a and 6a) and transmission (e.g., in the cognitive satellite transmitter of Figs. 5b and 6b) as a passive/active interference mitigation technique, respectively. The introduction of beamforming techniques may very likely require significant upgrades in current satellite communication systems, both in the terminal and satellite sides, such as the introduction of multiple radiation elements (e.g., multi-LNB receivers) in order to create the desired beam patterns (which can be challenging in scenarios with high density of desired and/or interfering links) as well as modifications to enable full frequency reuse and perform the advanced signal processing required by beamforming. Moreover, in addition to the channel state information at the transmitter, which is crucial to design suitable beamforming techniques, location information of the terminals is required as well. If databases of both interfering and interfered systems are available and the interference links are fixed (e.g., fixed FSS or FS links), the direction of interference links can be calculated from the available database information; otherwise, spectrum sensing can be combined with beamforming to detect the direction of arrival (DoA) of interfering signal components. In practice, the DoA of the desired and interfering signals are not perfectly known, and the use of some DoA estimation algorithm is required, which not only provides more accurate estimations of the DoA but also has the advantage of compensating for antenna array imperfections and multipath signals. A more detailed discussion on cognitive beamforming for satellite communications can be found in [4, ch. 13].

Given the large variety of scenarios, services, users, potential interferences, and alternatives for the adoption of primary/secondary roles, a detailed discussion of the possibilities for the application of CR techniques in satellite communications is beyond the scope of the overview provided in this section; however, the interested reader can refer to the literature where a rich set of solutions specifically designed for dual satellite scenarios, hybrid satellite-terrestrial scenarios, or both can be found (see [4, ch. 10] [5] and references therein).

Cognitive Radio in Other Wireless Communication Systems

The two wireless communication systems reviewed in this chapter are some examples of prominent use cases of the CR technology in established systems but are certainly not the only possible application scenarios. The principles of the CR paradigm are helpful not only to increase spectrum usage efficiency and enhance network capacity but also to improve many aspects of wireless communications, providing intelligence to wireless communication networks and enabling users to access multiple air interfaces under varying communication needs and conditions. A detailed discussion is beyond the scope of this chapter, but the application of CR in some other scenarios is briefly mentioned in this section.

One of the early developments of the CR technology was in the context of military communications, where CR can be used to automatically find spectrum opportunities in regions with different frequency allocations or when communications are jammed by an enemy. Public safety and emergency networks can also benefit from the adoption of CR to provide reliable and flexible communications in disaster scenarios where the network infrastructure is partially damaged or completely destroyed [51]. CR-enabled devices can spontaneously configure new communication links among surviving nodes and communicate on an ad hoc basis. The infrastructureless, distributed, self-configuring multi-hop features of ad hoc networks are well suited for the implementation of the CR principles. Cognitive ad hoc networks involve challenging practical problems that have attracted significant research efforts for generic ad hoc networks [1] as well as particular types thereof, such as vehicular ad hoc networks [6]. The potential applications of CR techniques in the context of aeronautical communication systems have been considered as well [21]. The growth of the aviation industry and steady rise in air traffic have led to the depletion of aeronautical radio channels, which has worsen in recent years with the widespread deployment of unmanned aerial systems needing a vast amount of spectrum for remote real-time operation. CR techniques can be introduced to provide a more efficient exploitation of the aeronautical spectrum and mitigate interference in the broad range of systems and technologies involved in aeronautical communications, which includes air-ground systems, air-air systems, satellite-based communications, in-flight information and entertainment (infotainment) systems, and LTE air-ground (LTE A/G) links, among others (see [21] for a detailed discussion).

Table 4 shows some wireless communication systems where CR principles have been adopted. The adoption of CR in wireless communication systems has not only led to the definition of new standards but also the extension of existing ones to incorporate CR-based techniques:

- IEEE: In addition to the creation of new specific CR standards such as the IEEE 802.22 standard for WRANs in TVWS and the IEEE 1900 series of standards for dynamic spectrum access networks, IEEE has also extended some of its existing standards for WLANs (e.g., 802.11af for operation in TVWS, 802.11 h for dynamic frequency sharing and transmit power control extensions in the 5 GHz

Table 4 Adoption of the CR technology in some wireless communication systems

Body/group	Standard/document	Description
IEEE	802.11 [af/h/y]	Wireless local area networks (WLANs)
	802.15 [.2]	Wireless personal area networks (WPANs)
	802.16 [a/h/m]	Wireless metropolitan area networks (WMANs)
	802.19	Coexistence between unlicensed wireless standards
	802.22 [a/b/.1/.2/.3]	Wireless regional area networks (WRANs)
	SCC41/1900 [.1-7]	Dynamic spectrum access networks
3GPP	23.402, 24.302	Non-3GPP network access
	24.312	Access network discovery and selection function (ANDSF)
ECMA	ECMA-392	In-home HD video streaming, interactive TV broadcasting
ITU-R	M.2225	CR systems in the land mobile service
	M.2242	CR systems in the IMT service
ETSI	Technical reports	Feasibility studies and standardisation needs/opportunities
WINNF	Technical reports	Definitions, benefits, use cases in public safety

band in Europe, and 802.11y for operation in the 3650–3700 MHz band in the USA), WPANs (e.g., 802.15.2 for coexistence with other devices in unlicensed bands), and WMANs (e.g., 802.16a for operation in the 2–11 GHz band, 802.16 h for improved license-exempt coexistence, and 802.16 m for coexistence of fixed and mobile broadband wireless systems) and existing IEEE 802.19 standards for the coexistence among wireless standards for unlicensed devices.

- 3GPP: Besides the accommodation of features required for operation of mobile communication networks in licensed and unlicensed bands, 3GPP standards also include CR-like capabilities to enable integration for inter-system mobility between 3GPP and non-3GPP networks (e.g., WLAN or WiMAX) by means of modifications in the network architecture (3GPP TS 23.402) and the definition of access approaches (3GPP TS 24.302) as well as an access network discovery and selection function (3GPP TS 24.312).
- ECMA: The European Computer Manufacturers Association (ECMA) released ECMA-392, the first standard for personal/portable devices operating in TVWS [55], designed for applications such as in-home high-definition video streaming and interactive TV broadcasting services. The standard defines the PHY and MAC layers of a CR system with flexible network formation, mechanisms for protection of primary users, adaptation to different regulatory requirements, and support for real-time multimedia traffic.

Other important organizations have published technical reports and other documents addressing specific aspects of CR-enabled systems, including, for example:

- ITU-R: The International Telecommunication Union (ITU) has published reports addressing aspects of CR systems specific to the land mobile

(ITU-R M.2225) and international mobile telecommunication (ITU-R M.2242) services (LMS/IMT) such as technical features and capabilities, potential benefits, and deployment scenarios.

- ETSI: The European Telecommunications Standards Institute (ETSI) Technical Committee for Reconfigurable Radio Systems (RRS) has published a series of technical reports (TR 102 838) summarizing various feasibility studies on topics such as control channels for CR systems (TR 102 684), performance of CR systems operating in UHF TVWS (TR 103 067), and coexistence between CR systems operating in TVWS and existing radio frequency cable networks (TR 101 571). Other reports examine standardization needs and opportunities, including functional (TR 102 682) and coexistence (TR 102 908) architectures, system requirements for operation in TVWS (TR 102 946), network-aided spectrum awareness methods such as the cognitive pilot concept (TR 102 683), and use cases (TR 102 907).
- WINNF: The Wireless Innovation Forum (WINNF) has published a number of reports on CR deployments in TVWS, including potential benefits (WINNF-09-P-0012) and use cases for CR application in public safety networks (WINNF-09-P-0015) and LTE in white spaces (WINNF-12-P-0003), among others.

As new radio technologies and wireless communication paradigms appear, CR consistently continues to be an important candidate taken into account. The recent popularity of the IoT paradigm has opened new research directions in CR. The IoT concept involves a rich variety of interconnected smart devices that enable remote collection and exchange of data (with little or no human intervention) across existing network infrastructure, creating unlimited opportunities for the integration of the physical world into communication networks. While the Internet has historically been a wired network, wireless technologies are gaining popularity for the delivery of IoT services due to their flexibility and ability to provide connectivity anytime, anywhere, with anyone and anything. Traffic forecasts predict tens of billions of IoT devices in the foreseeable future, a significant part of which will be connected to the IoT through wireless links. This poses unprecedented challenges to network operators and claims not only for the utmost efficient exploitation of the already allocated spectrum but also the urgent need to gain additional capacity at much faster pace than spectrum regulations and allocations typically evolve. Relying on the already demonstrated benefits brought into legacy and modern wireless communication systems, CR emerges in this context as a promising concept to also increase the spectrum efficiency and network capacity of future IoT systems [24].

Conclusion and Future Directions

The CR paradigm has deeply impacted the way spectrum is accessed, shared, and exploited in modern (and will be in the future) wireless communication systems. CR provides wireless communication systems with an effective and elegant way

to overcome the challenge of increasing traffic demands, by opportunistically accessing and sharing spectrum bands that are not efficiently exploited. An increasing number of spectrum bands are being targeted by multiple wireless technologies to gain additional network capacity. However, besides the common vision of CR as a DSA method to increase the amount of spectrum available to a wireless network, CR can actually enhance many aspects of wireless communications through a more efficient exploitation of the allocated radio resources and mitigation of interference. This chapter has provided an overview on how CR techniques have been adopted by some prominent wireless communication systems (taking into account system-specific aspects and features) in order to gain additional network capacity, efficiently manage radio resources, mitigate interferences, or a combination thereof. CR has demonstrated its potentials in legacy and modern wireless communications and will, with no doubt, contribute to the evolution of the future radio technologies to come.

Cross-References

- Cognitive Management Strategies for Dynamic Spectrum Access
- Coexistence of Heterogeneous Cellular Networks
- Device-to-Device Communications over Unlicensed Spectrum
- IEEE 802.11af Wi-Fi in TV White Space
- Modeling and Performance Analysis of Cognitive Radio Systems from a Deployment Perspective
- Opportunities and Enabling Technologies for 5G and Beyond-5G Spectrum Sharing
- Spectrum Sensing, Database, and Its Hybrid
- Spectrum Database and Smart Spectrum

References

1. Akyildiz IF, Lee WY, Chowdhury KR (2009) CRAHNs: cognitive radio ad hoc networks. Ad Hoc Netw 7(5):810–836
2. Arianandа DD, Leus G (2012) Compressive wideband power spectrum estimation. IEEE Trans Signal Process 60(9):4775–4789
3. Buddhikot MM (2007) Understanding dynamic spectrum access: taxonomy, models and challenges. In: Proceedings of the 2nd IEEE international symposium new frontiers in dynamic spectrum access networks (DySPAN 2007), pp 649–663
4. Chatzinotas S, Ottersten B, de Gaudenzi R (eds) (2015) Cooperative and cognitive satellite systems. Academic, Amsterdam
5. Chatzinotas S, Evans B, Guidotti A, Icolari V, Lagunas E, Maleki S, Sharma SK, Tarchi D, Thompson P, Vanelli-Coralli A (2017) Cognitive approaches to enhance spectrum availability for satellite systems. Int J Satell Commun Netw 35(5):407–442
6. Cheng N, Zhang N, Lu N, Shen X, Mark JW, Liu F (2014) Opportunistic spectrum access for CR-VANETs: a game-theoretic approach. IEEE Trans Vehic Tech 63(1):237–251
7. Ding Z, Liu Y, Choi J, Sun Q, Elkashlan M, Chih-Lin I, Poor HV (2017) Application of non-orthogonal multiple access in LTE and 5G networks. IEEE Commun Mag 55(2):185–191

8. Dohler M, Heath RW, Lozano A, Papadias CB, Valenzuela RA (2011) Is the PHY layer dead? IEEE Commun Mag 49(4):159–165
9. Farhang-Boroujney B (2011) OFDM versus filter bank multicarrier. IEEE Signal Process Mag 28(3):92–112
10. 3rd Generation Partnership Project Technical Specification Group Radio Access Network (2009) Requirements for Evolved UTRA (E-UTRA) and Evolved UTRAN (E-UTRAN), Release 9. 3GPP TR 25.913, v9.0.0
11. 3rd Generation Partnership Project Technical Specification Group Radio Access Network (2015) Study on licensed-assisted access to unlicensed spectrum, Release 13. 3GPP TR 36.889, v13.0.0
12. 3rd Generation Partnership Project Technical Specification Group Radio Access Network (2017) Physical channels and modulation, Release 15. 3GPP TS 36.211, v15.0.0
13. 3rd Generation Partnership Project Technical Specification Group Services and System Aspects (2018) Service requirements for the 5G system, Stage 1, Release 15. 3GPP TR 22.261, v15.3.0
14. Gupta P, Kumar PR (2000) The capacity of wireless networks. IEEE Trans Inf Theory 46(2):388–404
15. Halonen T, Romero J, Melero J (2003) GSM, GPRS and EDGE performance: evolution towards 3G/UMTS. Wiley, Chichester
16. Holma H, Toskala A (2010) WCDMA for UMTS – HSPA evolution and LTE. Wiley, Chichester
17. Holma H, Toskala A (2011) LTE for UMTS – evolution to LTE-advanced. Wiley, Chichester
18. Höyhtyä M (2013) Secondary terrestrial use of broadcasting satellite services below 3 GHz. Int J Wirel Mob Netw 5(1):1–14
19. Höyhtyä M, Kyröläinen J, Hulkkonen A, Ylitalo J, Roivainen A (2012) Application of cognitive radio techniques to satellite communication. In: Proceedings IEEE international symposium dynamic spectrum access networks (DySPAN 2012), pp 540–551
20. Hu F, Chen B, Zhu K (2018, in press) Full spectrum sharing in cognitive radio networks toward 5G: a survey. IEEE Access 6:15754–15776
21. Jacob P, Sirigina RP, Madhukumar AS, Prasad VA (2016) Cognitive radio for aeronautical communications: a survey. IEEE Access 4:3417–3443
22. Ji H, Kim Y, Lee J, Onggosanusi E, Nam Y, Zhang J, Lee B, Shim B (2017) Overview of full-dimension MIMO in LTE-Advanced Pro. IEEE Commun Mag 55(2):176–184
23. Kandeepan S, Nardis LD, Benedetto MGD, Guidotti A, Corazza GE (2010) Cognitive satellite terrestrial radios. In: Proceedings of the IEEE global communications conference (Globecom 2010), pp 1–6
24. Khan AA, Rehmani MH, Rachedi A (2017) Cognitive-radio-based internet of things: applications, architectures, spectrum related functionalities, and future research directions. IEEE Wirel Commun 24(3):17–25
25. Kosta C, Hunt B, Quddus AU, Tafazolli R (2013) On interference avoidance through inter-cell interference coordination (ICIC) based on OFDMA mobile systems. IEEE Commun Surv Tutorials 15(3):973–995
26. Kwon HJ, Jeon J, Bhorkar A, Ye Q, Harada H, Jiang Y, Liu L, Nagata S, Ng BL, Novlan T, Oh J, Yi W (2017) Licensed-assisted access to unlicensed spectrum in LTE release 13. IEEE Commun Mag 55(2):201–207
27. Labib M, Marojevic V, Reed JH, Zaghloul AI (2017) Extending LTE into the unlicensed spectrum: technical analysis of the proposed variants. IEEE Commun Stand Mag 1(4):31–39
28. Lagunas E, Sharma S, Maleki S, Chatzinotas S, Grotz J, Krause J, Ottersten B (2015) Resource allocation for cognitive satellite uplink and fixed-service terrestrial coexistence in Ka-band. In: Proceedings of the international ICST conference cognitive radio oriented wireless networks and communications (CROWNCOM 2015), pp 487–498
29. Lavender T, Hogg T (2015) Licensed shared access. UK Spectrum Policy Forum
30. Lee WCY (1989) Mobile cellular telecommunications systems. McGraw-Hill, New York

31. Li F, Li G, Li Z, Wang Y, Lu C (2017) Wideband spectrum compressive sensing for frequency availability in LEO-based mobile satellite systems. Int J Satell Commun Netw 35(5):481–502
32. Li R, Chen Y, Li GY, Liu G (2017) Full-duplex cellular networks. IEEE Commun Mag 55(4):184–191
33. Li Y, Pateromichelakis E, Vucic N, Luo J, Xu W, Caire G (2017) Radio resource management considerations for 5G millimeter wave backhaul and access networks. IEEE Commun Mag 55(6):86–92
34. López-Benítez M (2013) Cognitive radio. In: Chu X, López-Pérez D, Yang Y, Gunnarsson F (eds) Heterogeneous cellular networks: theory, simulation and deployment, chap 13. Cambridge University Press, Cambridge, pp 383–425
35. Lopez-Perez D, Valcarce A, Roche GDL, Zhang J (2009) OFDMA femtocells: a roadmap on interference avoidance. IEEE Commun Mag 47(9):41–48
36. Maglogiannis V, Naudts D, Shahid A, Giannoulis S, Laermans E, Moerman I (2017) Cooperation techniques between LTE in unlicensed spectrum and Wi-Fi towards fair spectral efficiency. Sensors 17(9):1–26
37. Mangalvedhe N, Ratasuk R, Ghosh A (2016) NB-IoT deployment study for low power wide area cellular IoT. In: Proceedings of the IEEE 27th international symposium personal, indoor and mobile radio communications (PIMRC 2016), pp 1–6
38. Medjahdi Y, le Ruyet D, Bader F, Martinod L (2014) Integrating LTE broadband system in PMR band: OFDM vs. FBMC coexistence capabilities and performances. In: Proceedings of the 11th international symposium wireless communications systems (ISWCS 2014)
39. Mitola J (2006) Cognitive radio architecture. Wiley-Interscience, New York
40. Mueck MD, Srikanteswara S, Badic B (2015) Spectrum sharing: licensed shared access (LSA) and spectrum access systems (SAS). Intel White Paper
41. Noh G, Wang H, Shin C, Kim S, Jeon Y, Shin H, Kim J, Kim I (2017) Enabling technologies toward fully LTE-compatible full-duplex radio. IEEE Commun Mag 55(3):188–195
42. Sakr AH, Tabassum H, Hossain E, Kim DI (2015) Cognitive spectrum access in device-to-device-enabled cellular networks. IEEE Commun Mag 53(7):126–133
43. Shannon CE (1948) A mathematical theory of communication. Bell Syst Tech J 27(3):379–423
44. Sharma SK, Chatzinotas S, Ottersten B (2012) Exploiting polarization for spectrum sensing in cognitive SatComs. In: Proceedings international ICST conference cognitive radio oriented wireless networks and communications (CROWNCOM 2012), pp 36–41
45. Sharma SK, Chatzinotas S, Ottersten B (2012) Satellite cognitive communications: interference modeling and techniques selection. In: Proceedings 6th advanced satellite multimedia systems conference and 12th signal processing for space communications workshop (ASMS/SPSC 2012), pp 111–118
46. Sharma SK, Chatzinotas S, Ottersten B (2012) Spectrum sensing in dual polarized fading channels for cognitive SatComs. In: Proceedings of the IEEE global communications conference (Globecom 2012), pp 3419–3424
47. Sharma SK, Chatzinotas S, Ottersten B (2013) Transmit beamforming for spectral coexistence of satellite and terrestrial networks. In: Proceedings international ICST conference cognitive radio oriented wireless networks and communications (CROWNCOM 2013), pp 275–281
48. Sharma SK, Maleki S, Chatzinotas S, Grotz J, Krause J, Ottersten B (2015) Joint carrier allocation and beamforming for cognitive SatComs in Ka-band (17.3-18.1 GHz). In: Proceedings international conference communications (ICC 2015), pp 2476–2481
49. Thalanany S, Irizarry M, Saxena N (2017) License-assisted access considerations. IEEE Commun Standards Mag 1(2):106–112
50. Tian Z, Tafesse Y, Sadler BM (2012) Cyclic feature detection with sub-Nyquist sampling for wideband spectrum sensing. IEEE J Sel Top Sign Process 6(1):58–69
51. Uchida N, Sato G, Takahata K, Shibata Y (2011) Optimal route selection method with satellite system for cognitive wireless network in disaster information network. In: Proceedings 25th IEEE international conference on advanced information networking and applications (AINA 2011), pp 23–29

52. Vassaki S, Poulakis MI, Panagopoulos AD, Constantinou P (2017) Power allocation in cognitive satellite terrestrial networks with QoS constraints. IEEE Commun Lett 17(7): 1344–1347
53. Wang Y, Wu Z (2016) A coexistence analysis method to apply ACLR and ACS between NB-IoT and LTE for stand-alone case. In: Proceedings of the 6th international conference on instrumentation and measurement, computer, communication and control (IMCCC 2016) pp 375-379
54. Wang W, Yu G, Huang A (2013) Cognitive radio enhanced interference coordination for femtocell networks. IEEE Commun Mag 51(6):37–43
55. Wang J, Song MS, Santhiveeran S, Lim K, Ko G, Kim K, Hwang SH, Ghosh M, Gaddam V, Challapali K (2010) First cognitive radio networking standard for personal/portable devices in TV white spaces. In: Proceedings of the IEEE international symposium dynamic spectrum access networks (DySPAN 2010), pp 1–12
56. Yen CP, Tsai Y, Wang X (2013) Wideband spectrum sensing based on sub-Nyquist sampling. IEEE Trans Signal Process 61(12):3028–3040
57. Yuan G, Zhang X, Wang W, Yang Y (2010) Carrier aggregation for LTE-advanced mobile communication systems. IEEE Commun Mag 48(2):88–93
58. Yucek T, Arslan H (2009) A survey of spectrum sensing algorithms for cognitive radio applications. IEEE Commun Surv Tutorials 11(1):116–130
59. Zhang J, Wang M, Hua M, Xia T, Yang W, You X (2018) LTE on license-exempt spectrum. IEEE Commun Surv Tutorials 20(1):647–673

TVWS: From Trial to Commercial Operation in the UK

59

Andrew Stirling and Jim Beveridge

Contents

A. Stirling (✉)
Larkhill Consultancy Limited, Surrey, UK
e-mail: andrew@larkhillconsult.co.uk

J. Beveridge
Faileas Limited, Buckinghamshire, UK
e-mail: Jimbeveridge@hotmail.com

W. Zhang (ed.), *Handbook of Cognitive Radio*,
https://doi.org/10.1007/978-981-10-1394-2_61

Abstract

The UK has long held a reputation for innovation in the TV bands. This chapter explains how the UK regulator's (Ofcom) openness to innovation, together with long established TV industry collaboration, enabled a robust regulatory framework for TV white spaces to be put in place. This chapter considers how the UK broadcasting heritage led up to this point and shapes the TV white spaces capacity availability. It also considers how industry cooperation in substantive trials produced results that encouraged the regulator to finalise its framework development and enact the required regulation, by the start of 2016.

Summary

The UK has embraced the principle of opening access to the TV white spaces (TVWS) and is applying the dynamic spectrum access mechanisms to enable more efficient sharing of other parts of spectrum, in the future.

Due to the established place of terrestrial broadcasting in UK domestic life, Ofcom, the UK's communications regulator, took considerable care in evaluating the effectiveness of cognitive sharing techniques. As in the USA, the regulator favored license-exempt access to the TV white spaces and found that the use of geolocation databases was the only practical approach which provided sufficient security for the licensed spectrum users – broadcasters and PMSE applications.

Development and evaluation of the regulatory approach to TV white spaces involved considerable cooperation between the regulator and industry – and between existing spectrum users and those who advocated dynamic spectrum access.

Ofcom needed to see strong industry interest, in order to justify the considerable effort needed to develop the regulations in full. This interest was demonstrated in two substantive TVWS trials – one in Cambridge and the other on the Isle of Bute. The trials demonstrated that the technology worked to deliver new applications and did not disrupt existing spectrum users.

When the regulatory framework had been worked up in detail, Ofcom invited participants from across the UK to participate in a pilot of the new framework. This attracted a diverse range of applications and enabled Ofcom to confirm and finalize its approach – albeit with more cautious parameters than it had initially proposed. Finally, the new UK regulation entered into force at the start of 2016.

Although the UK invested in laying the foundations for Europe-wide TV white space access, it still remains the only European country to have enacted the enabling regulations. Others have considered license-shared access to higher frequency bands, but the UHF bands used for broadcasting have proved more politically

complex to share. This has been compounded by the recent clearances of the 800 and 700 MHz bands, for reallocation to mobile broadband.

In implementing TV white spaces regulation, the UK has shown itself to be open to innovation. This openness, together with the cooperative approach taken by incumbents and newcomers, has enabled more efficient use of spectrum, without compromising existing services.

Introduction/Background

Political interest in improving Internet connectivity is as strong in the UK as anywhere else in the world. Policy makers have been considering a range of spectrum options to enhance Internet access performance – particularly in rural areas, where sub-megabit speeds have been a common frustration.

The UK Government has attempted to find mechanisms to encourage major operators to fill in the rural gaps, but with mixed success to date, as the commercial justification is weak.

An alternative approach for regulators is to make spectrum available in such a way that local operators or individuals can access it – either free or at low cost. License-exempt access is the main way to achieve this – since there are no fees for spectrum and the technical conditions on spectrum use are met by the equipment, without requiring any special skills or knowledge of the end user.

Wireless technology has the potential to improve rural connectivity rapidly, flexibly, and cost-effectively, but the lack of available spectrum for new networks has hindered its application.

Regulators have made cleared spectrum available for new wireless applications but mostly through national auctions. The inevitable winners are the mobile network operators (MNOs), which are prepared to spend large sums of money on securing exclusive access to spectrum and as well on network rollout. Given their commercial nature, the MNOs have tended to favor more densely populated areas. Many rural areas have been left with significant holes in network coverage.

Wireless Access Technology Is a Good Fit with Improving Rural Broadband Connectivity

In the early 2000s, the rapid growth in Internet use had started to reveal a stark rural/urban difference. In urban areas, residents and business generally had a way to get a reasonable (broadband) Internet connection. However, because its means of delivery was predominantly wired (either via a telephone wire or a cable TV system coaxial cable), homes in rural areas were at a real disadvantage.

This problem had already been seen in the USA, where typical telephone line lengths are much longer than in Europe, reflecting lower housing densities in urban areas.

- Wired cable TV systems are not widely deployed in rural areas
- The typically longer length of telephone wire connections in rural areas does not work well with the default broadband-over-telephone distribution technology (DSL)

License-Exempt Access Is a Key Tool in Community Service Provision

The license-exempt model has proved highly successful with Wi-Fi, Bluetooth, and other wireless communication technologies, but given the relatively high frequency of the available bands and the low transmission power limits, the range that could be achieved was quite limited.

The Attraction of Spare Frequencies in the TV Band

Wireless technology, on the other hand, was eminently suitable for filling coverage gaps – especially when using cost-effective Wi-Fi hardware. The problem was that the only frequencies available with sufficient bandwidth, on a license-exempt basis, were too high to achieve wide area coverage needed for serving rural communities (with the transmission power restrictions imposed by a regulation). The answer was to look for lower frequencies, under 1 GHz, but there was little or no spare spectrum available. Or at least the frequencies had already been assigned.

On closer inspection, however, it is clear that not all of the allocated frequencies are in use all the time in all places. This creates opportunities for sharing. In particular, the terrestrial TV bands (UHF IV and V) tend to have many, quite stable, white spaces. The beauty of spare capacity in the TV bands is that terrestrial television broadcasting uses UHF spectrum in all countries around the world, so there is great scope for harmonizing technology to harness capacity in this band – with the result that equipment cost can be much lower than it would if different hardware was needed for each market.

However, although there are overlaps in the frequency bands assigned for broadcasting, regulatory approaches for allowing access to the white spaces have differed, with the UK adopting a more cautious and complex framework than was used in the USA, where the first TVWS rules emerged, back in 2008.

Part of the reason for the additional caution, on the part of the UK, is the popularity and political importance of terrestrial TV broadcasting.

A Brief History of UK TVWS

UK TVWS interest can be traced back to the desire of the US IT players, Microsoft, Intel, and Compaq to inject IT technology into consumer electronics and realization that Internet connectivity was key. The industry's interest was articulated in 1997 at the NAB conference in Las Vegas where Craig Mundie, from Microsoft, presented

his vision for the future of television [1]. It came soon after the company's acquisition of WebTV, whose business was based on a merger of the Internet and television.

This vision of the TV, the Internet, and the PC coming together was shared by Intel and Compaq, among others.

Concerns Over Poor Connectivity Drove Interest in the TV White Spaces

Recognition of the need for Internet connectivity led the IT majors to look at how to extend the reach of Wi-Fi, beyond the home, office, and coffee shop.

In the UK, the planned switchover from analogue to digital TV provided a major opportunity to secure more efficient use of the spectrum that was to be retained for broadcasting.

Nature of TV White Spaces in the UK

Essentially white spaces are unused spectrum, but their exact capacity and location are, at least partly, a matter of definition. The national regulator has ultimate control of this, determining the areas where services do not need to be protected (even if they happen to be receivable – e.g., with high-gain antennas).

Development of the UK TVWS Rules

Ofcom has generally welcomed innovation and has sought to enable spectrum access to facilitate it. This was one of the key motivations for digital TV switchover, which started in 2005. The main objective at the time was to clear 112 MHz of UHF spectrum which could then be offered for new applications (mobile broadband being the most likely, especially given the bidding resources of the major UK mobile operators).

Television Broadcasting in the UK

Television (TV) broadcasting started back in the late 1920s, building on the early success of radio broadcasting. The British Broadcasting Corporation (BBC) was set up by the radio manufacturers to stimulate demand for new receivers, by providing suitably attractive content. Early experiments with TV began in 1928 using a system devised by John Logie Baird, transmitted in the VHF band. This rudimentary service progressed to a 405-line (vertical dimension) monochrome picture service, in 1936. At this stage, there was a single BBC TV channel to be broadcast, with relatively few transmitter stations, operating in a high-power, high-tower, transmitter network.

Over the following decades, TV's popularity grew, as receivers became more affordable. There were also steady improvements in the production and distribution technology. In the 1960s broadcasters wanted to increase the picture resolution and introduce a color service. The VHF bands lacked capacity, so some UHF bands (IV and V) were cleared of defense applications and made available for terrestrial TV broadcasting. The allocated frequency range was 470–860 MHz, providing 48 possible broadcast channels (each 8 MHz wide) – each could carry a single analogue TV signal – comprising picture and sound components. However, at that stage only three channels were needed at any given transmitter site – for BBC1, BBC2, and ITV.

National/Regional Coverage Approach Has Created more Openings for TVWS

Due to the national and regional nature of public service broadcasting in the UK and other parts of Europe and the limited scope of UHF transmissions, it was necessary to construct networks with multiple transmitters (in rural and suburban locations) – to ensure contiguous coverage. This contrasts with the pattern in the USA and other countries where private broadcasters drive the show and city-based broadcasting is the norm.

- National/regional coverage in the UK is provided by a network of main transmitter stations and linked (lower-power) relay stations. In the UK, there are 50 main stations and around 1100 relay (lower-power) stations. The top 80 stations (50 main + 30 relays) cover around 95% of the population (around half of the land area), and the remaining 1070 or so, added over a number of decades, provide coverage for an additional 3% to 4% of the population
- Currently each transmitter can (in the latest digital television configuration) carry up to nine multiplexes (groups of TV channels) – each multiplex requiring its own frequency. Frequencies used by adjacent transmitters need to be avoided, so that terrestrial networks resemble a "patchwork quilt" of frequencies where frequencies can only be reused at a certain transmitter spacing. The large capacity available in the broadcast band is traded off against nation- or region-wide coverage
- Television white spaces (TVWS) are the unused frequencies in each coverage area. In remote rural areas, they can approach 100% of the frequencies in the broadcast band range.

Future DTT Planning Evolution Squeezes White Spaces

Across the world, regulators continue their search for harmonizable spectrum bands which can be released to enhance mobile broadband capacity (and coverage in some

cases). This has included significant rollback of spectrum allocated for broadcasting in the UHF bands.

More efficient modulation schemes together with the increasing use of single-frequency network configurations will allow broadcasters to pack more TV channels in and/or move more services to higher definition. In principle, this means that white spaces capacity would reduce, over time. However, broadcasting regulations and business models will ultimately determine how much of the effective capacity is actually taken up by broadcast services.

Single-Frequency Networks

UK broadcast network planners achieved wide national regional/coverage through the reuse of frequencies in a "patchwork quilt" (multifrequency) pattern – so that adjacent transmitters do not disrupt each other's coverage. However, the digital terrestrial technology can be configured to allow adjacent transmitters on the same frequency – provided that key parameters (such as the distance between them) stay within certain ranges. This mode of operation is referred to as "single-frequency" network, since only one frequency is used for a given TV station, across an entire region. This works well when the content to be delivered across the region is the same, but it doesn't support local inserts, e.g., for advertising. Content boundaries therefore define the limits to single-frequency network size and the spectrum usage efficiency that can be gained.

White Space Pioneers: Program Making and Special Events

Broadcasting was not the only user of the broadcast bands. With many channels remaining unused in any given location, broadcasters and event/performance producers found that this spectrum provided a convenient way to accommodate short-distance wireless links – especially from microphones. Each microphone channel can take around 200 kHz, and with many tens of microphones in use during performances at some of the major shows in London, for example, this use can be quite intensive – albeit within a limited geographic scope.

A Cooperative Approach Toward Establishing TVWS Regulations

The UK terrestrial TV market has been largely cooperative – necessitated by the separation between (often publicly funded) broadcasters and private-sector receiver manufacturers. The BBC was originally founded by radio manufacturers, who were trying to create a market for the new devices. The separation between content providers and receiver manufacturers has enabled choice and value for consumers, in receiving systems. However, it has been necessary for the two sides to cooperate so that technology advances can be introduced smoothly. This contrasts with the

UK Pay TV industry – which was confined to cable and satellite platforms until 1998, when digital terrestrial TV was launched. In the Pay TV market, proprietary delivery solutions have favored integrated service provider and device provision.

The spirit of cooperation in the UK TV industry remains strong and is needed more than ever as distribution technology keeps advancing rapidly and choice offered to viewers multiplies. The growth of mobile broadband has led to more intensive sharing of spectrum, which has also required coordination between regulators, broadcasters, and TV device manufacturers, to ensure that disruption to television services is minimized.

Ofcom Working Group

To support a decision announced at the end of 2007, Ofcom formed a working group to look at the regulatory options for enabling access to the TV white spaces. The group was chaired by the then Head of Technology Research at Ofcom – Professor William Webb. It comprised members of industry as well as the regulator. Existing UHF users, including the broadcasters and PMSE industry, were well represented – together with a representative from Microsoft and occasionally from others advocating license-exempt access to the TV white spaces.

The working group's output fed into Ofcom consultations and statements.

After looking at the spectrum sensing and beacon models for facilitating spectrum access, it became clear that the combination of device geolocation and spectrum databases (dubbed geolocation database for short) was the only option which was both sufficient to meet the concerns of incumbents and practical to implement.

Ofcom consulted on this conclusion in November 2010 and then developed more detailed proposals, which were published in September 2011 [6].

TV White Spaces Advantages for Applications

TVWS technology was seen as a powerful tool for filling rural broadband gaps, due to the improved coverage that lower frequencies bring. The relatively broad channels into which UHF (and therefore TVWS) is partitioned (8 MHz wide in ITU Region 1) are well suited to broadband applications – including high-quality video and audio streaming, as well as aggregating narrowband network traffic. The flexibility afforded by dynamic spectrum access also seemed to lend itself to the as yet little known requirements of the emerging "Internet of Things."

First UK TV White Spaces Trials: Cambridge and Isle of Bute

UK industry interest in applying TV white spaces grew with development of the enabling regulations. This, together with the availability of prototype TVWS

equipment, led to trials of the new technology. The trials, in turn, encouraged Ofcom to invest in detailing and finalizing its TVWS regulations.
Two sites emerged for the earliest TV white spaces trials in the UK:

- On the Isle of Bute, in Scotland,
- In and around the City of Cambridge
- Both venues offered the chance to illustrate the coverage potential of TV white spaces, though the Scottish Island was the more representative of the remote rural coverage challenges and a closer approximation to a consumer broadband service.

Wireless connectivity can support a very wide range of applications, with diverse spectrum access needs. Some applications, such as video streaming, require wide-band continuous access. Others are more modest in their capacity requirements and may function quite effectively with even intermittent access to spectrum.

The Isle of Bute Trial

The Isle of Bute is located in the Firth of Clyde, in South West Scotland. It provided more evident terrain challenges than Cambridge – with hills and adjacent marine areas.

It also had a severe connectivity deficit, with many residents having had little or no broadband access.

The newly formed Centre for White Space Communications, at the University of Strathclyde, pulled together a consortium of key industry players (including the BBC and BT), supported by the UK Government's Technology Strategy Board to trial the application of TV white space technology, to the delivery of broadband to a number of residential properties in the south end of Bute.

The details of the deployment, operation, and results of the trial are reported in [2].

The Cambridge Trial

Cambridge is a well-established technology innovation hub, with the research centers of many leading technology companies located there, next to the renowned university. Microsoft's Research Centre, was the focus hub for the organization of the trial. Cambridge proved to be an excellent location to hold a TV white spaces trial, given the skills and resources available to deploy and maintain the emerging technology.

At the time the trial was staged, it was the largest TV white spaces trial, and its results [3] were influential beyond its target UK and European markets. By the time the trial concluded, the following organizations were involved: Adaptrum, Alcatel Lucent, Arqiva, BAE Systems, BBC, BT, Cambridge Consultants, Cambridge

Silicon Radio, CRFS, Digital Television Group, Jaguar Land Rover, Microsoft, Neul, Nokia, Samsung, Sky, Spectrum Bridge, TTP, and Virgin Media.

Preparations

A consortium was created to assist Ofcom in its regulatory work on TVWS and enable industry members to better understand TVWS' potential impact on their businesses. The members included a broadcaster, a broadcaster network operator, and technology vendors (including manufacturers of operator equipment and mobile devices).

A number of sites around the city were evaluated; for ease of installation and potential network coverage, Ofcom provided a test license to cover all of the likely sites for TV white spaces access points. To ensure compliance with the test license, Arqiva, the UK broadcast network operator, conducted a thorough survey – pre- and post-commissioning of each site. This was to check, for example, the proximity of DTT reception antennas and thus avoid the risk of disrupting neighbors' TV reception.

Hardware for deployment was sourced from a locally based start-up, called Neul, which had identified the TV white spaces as a key enabler for the emerging Internet of Things. Neul had designed its own radios from scratch, and it provided the radios for installation at sites around Cambridge as well as technical support to the trial operations. Silicon valley-based TVWS pioneer Adaptrum made available its prototype radio hardware to assist with the demonstration and measurements of TVWS coverage and link performance.

Cambridge Trial Applications

A prime application was rural broadband – given the poor broadband availability/performance experienced by many living and working in areas outside the main conurbations.

Other applications could be grouped under:

- Local area communications and content distribution
- Internet of Things applications – where devices, sensors, etc. can use wireless connections to form intelligent systems

Rural Broadband

As discussed earlier, lack of connectivity is a significant problem for many rural and some urban residents and businesses. This applied to villages around Cambridge as well as remote rural communities in Scotland.

TV white spaces technology, at the time of the trials (2011), offered connections with around 10 megabits/second (Mbps), using a single UHF channel (8 MHz wide). This was considered a reasonable broadband performance at the time and a great step-up from what many rural dwellers could access – even today (2018). The use of UHF spectrum enabled longer link lengths (for a given transmission power and receiver sensitivity) and less impairment due to intervening trees and hills than is experienced with fixed wireless access technology – using higher frequency

bands (2.4 and 5 GHz). The white spaces link provided backhaul to a Wi-Fi access point in single residential property. Conventional Wi-Fi then enabled end users to benefit from the broadband connection using existing devices – laptops, tablets, and smartphones.

Local Content Distribution

The combination of range and potentially high capacity offered by TV white spaces enables a convenient mechanism for local content distribution. A single access point could be used to drive display boards across a community. For example, such a board it might be used to provide news, information, and entertainment content.

Location-Based Content

The propagation range of TVWS can be used effectively to deliver content to individual users within a local area (such as a campus or retail center).

TV white spaces technology was coupled with a mobile device and exhibits at the Duxford Air Museum (part of the Imperial War Museum). As the mobile device user approached an "active" exhibit, interesting content relating to that exhibit could be presented to the user. For example, text summaries, photographs, and video clips are all helpful for understanding of the importance of a particular exhibit and give the visitor a sense of what it might have been like in operation.

Pop-Up Wi-Fi Hotspots

Cambridge offers a number of green open spaces amid its historic and more recent buildings. The open spaces are valued for leisure in general and also host major public events – such as summer festivals.

Users would benefit from connectivity, but the limited range of traditional Wi-Fi hotspots means that open spaces are largely out of reach.

Links from TVWS base stations around the city could be used to create temporary Wi-Fi hotspots – using a portable equipment set (e.g., carried in a backpack), consisting of a battery power supply and TVWS client connected to a Wi-Fi access point. At an event, this configuration could be hosted in a refreshments tent, ice cream stall, etc.

Internet of Things: Waste Management

With an increasing use of cloud-based services to manage a widening array of aspects of modern life, it is important to enable wireless cloud access from devices of all kinds.

Local authorities face a range of challenges to delivery high-quality public services with increasingly constrained budgets.

One such service is waste collection – which involves trucks circulating around the city streets through the week, to empty household and business bins. This provides a consistent service, but not all bins need emptying when the truck calls.

With a small amount of embedded hardware, it is possible to determine how full a bin is. The challenge was to read the level remotely, to determine which bins really need to be emptied and how the truck route could therefore be optimized.

In the trial, a link from an intelligent bin to the cloud via white spaces was demonstrated, allowing immediate indication of its current loading. The use of TV white spaces would enable relatively few access points to provide sufficient coverage across the city. Given the low data rate needed by this application – the 8 MHz TV white spaces channel could be used with a robust modulation to allow even greater coverage to be achieved from a base station.

Trial Measurements: Proving the Rules

Trials/pilots played a key role in building industry confidence in the application of the TV white spaces and shaping the regulatory approach to managing coexistence with licensed services sharing the band. The Cambridge white spaces trial was the largest of its time 2011/2012 and was a watershed moment in UK TVWS developments – with influence far beyond the UK.

Measurements made during the trial included:

- The data link capacity of wireless links into rural village locations
- Coverage and capacity achieved around TV white spaces access points – external and within buildings
- Spectrum usage around the city

The results of the measurements are summarized in the Cambridge TVWS Trial Technical Findings report [4]. They were fed into the Ofcom working group on the TV white space regulations and into the European regional spectrum regulatory working group CEPT SE43, where they helped in establishing recommendations for coexistence between TVWS applications and existing spectrum users.

Ofcom's UK TVWS Pilot

Following the Cambridge and Bute trials, Ofcom decided to complete the required regulations to enable access to the TV white spaces. It made use of an open working group – with participants from companies across the world – to help it develop the required approach to coexistence with established services.

Ofcom piloted the draft regulations before finalizing the details. This evaluation ran over the period 2013 to 2014.

Applications were invited from across the UK, and a number of groups applied for a TVWS pilot license. Among these were:

- a cooperation between Google and London Zoo to create a video link from animal cages, to allow remote viewing
- a project to extend Internet connectivity to the ferries that travel between the islands in Orkney.
- a flood monitoring network, around Oxford

The Centre for White Space Communications (CWSC), at the University of Strathclyde, ran a pilot in Glasgow, with support from the Scottish Government, Microsoft, Sky, 6Harmonics, and MediaTek. The project was aimed at assisting Ofcom in its efforts to progress toward finalizing the regulations and assisting the industry to evaluate potential benefits and opportunities associated with enabling access to the TV white spaces (UHF spectrum).

UK TVWS Pilot: Glasgow Tri-band Wi-Fi

The application chosen by CWSC was wireless home networking, in which "standard" Wi-Fi in the 2.4 GHz ISM band and the 5 GHz UNII bands was augmented with the use of spectrum in the UHF band (suing TVWS technology). Earlier results from Ofcom research had indicated that UHF frequencies would provide coverage benefits within buildings, complementing what the established Wi-Fi bands could deliver [5].

The IEEE had recently ratified the IEEE 802.11af standard, which added TVWS features to the IEEE 802.11 family of specifications, opening the possibility of mass market adoption. This was significant for Internet service providers (ISP), which could potentially benefit from the improved range and bandwidth that might be expected from using TVWS. With ISP requirements in mind, CWSC investigated the performance of IEEE 802.11af in a number of homes around Glasgow and carried out a comparison of IEEE 802.11af (TVWS), with Wi-Fi at 2.4 GHz and Wi-Fi at 5 GHz. CWSC worked with MediaTek and 6Harmonics, who agreed to provide access to their prototype IEEE 802.11af radios, along with engineering support. It also worked with broadcaster and communications service provider, Sky, which offered practical assistance with test locations.

The test results indicated that the IEEE 802.11af radios had the potential to significantly increase Wi-Fi coverage over that of IEEE 802.11n systems (using the 2.4 and 5 GHz bands). Quantifying the amount by which coverage might be improved was difficult, but it was particularly noticeable from the results of tests described in *the final report* [5] that IEEE 802.11af was able to provide coverage throughout the older homes of sandstone and brick construction (and outside), while an IEEE 802.11n network operating at 5 GHz struggled to penetrate beyond the room in which the access point was located.

Finalizing the Regulation

The pilot projects yielded a considerable wealth of data, enabling Ofcom to adjust the draft regulations. In general, its adjustments were toward greater caution – protecting existing users more and hence reducing the TV white space capacity available.

The regulatory framework was divided into two parts:

- The statutory instrument – which license-exempted TV white space access devices meeting suitable technical requirements. The requirements are laid down in ETSI 301 598
- Geolocation databases – validated by Ofcom, holding information on which channels are available in each possible location. Around eight companies applied for validation and there are now two providers in operation: Nominet and FairSpectrum.

The statutory instrument was in place by the start of 2016, and the first databases had already been validated by that point.

Into Commercial Service

With the TVWS regulations in place, it became possible to start commercial network deployments. A UK company called Broadway Partners recognized the opportunity to use the new technology to fill gaps in rural broadband provision, around a new model in community service provision. Broadway identified an initial opportunity to apply the technology on the Isle of Arran, in Scotland, and worked with the local community to define the requirements. It enlisted the help of a database partner and Microsoft to deploy the UK's commercial service using TV white space technology. Arran's rugged and rolling topography provides a representative challenge to network provision and much has been learned about how best to use TVWS to illuminate the least reachable locations.

Arran Broadband continues its rollout around the island, reaching out to the unconnected (or under-connected). Meanwhile Broadway has gone on to tackle broadband challenges facing other remote communities in Scotland and Wales.
Other companies applying TV white space technology, that we know of, are:

- *Cloudnet* in Orkney, which has been providing Internet connectivity on the inter-island ferries and support adjacent rural applications
- New entrant *Whitespace UK*, which has been rolling out rural broadband networks in Dumfries and Galloway, as well as the beautiful, but remote highland village called Balquhidder.

Cross-References

▸ IEEE 802.11af Wi-Fi in TV White Space
▸ Spectrum Sharing Policy in Europe

References

1. Remarks by Craig Mundie, Group Vice President, Platforms and Applications, Microsoft Corporation. National Association of Broadcasters Conference, 6 Apr 1997
2. Centre for Whitespace Communications, University of Strathclyde, Report on the Bute TV white spaces trial. http://www.wirelesswhitespace.org/projects/white-space-trial-on-the-isle-of-bute/
3. Cambridge TV white spaces Consortium, Recommendations for Implementing the Use of White Spaces: Conclusions from the Cambridge TV White Spaces Trial, Apr 2012. https://www.microsoft.com/en-us/research/wp-content/uploads/2016/02/spectrum-cambridge-tv-white-spaces-trial-recomms.pdf
4. Cambridge TV white spaces Consortium – A summary of the technical findings, Apr 2012. https://www.microsoft.com/en-us/research/wp-content/uploads/2016/02/spectrum-cambridge-tv-white-spaces-trial-findings.pdf
5. Ofcom, Research Report: In Home Propagation, 4 Nov 2011. https://www.ofcom.org.uk/__data/assets/pdf_file/0034/55879/ihp_final_report.pdf
6. Ofcom, September 2011, Implementing Geolocation. https://www.ofcom.org.uk/__data/assets/pdf_file/0035/46889/statement.pdf
7. Centre for White Space Communications, In-Home TVWS Measurements Using IEEE 802.11af, May 2015. https://www.wirelesswhitespace.org/wp-content/uploads/2016/06/cwsc_report_for_sky_v01_01.pdf?1ac0be&1ac0be

Cognitive Radio and TV White Space (TVWS) Applications

60

J. H. Martin, L. S. Dooley, and K. C. P. Wong

Contents

J. H. Martin (✉)
IP/Optical Networks (ION), Nokia, Bristol, UK

School of Computing and Communications, The Open University, Milton Keynes, UK
e-mail: john.h.martin@nokia.com

L. S. Dooley · K. C. P. Wong
School of Computing and Communications, The Open University, Milton Keynes, UK
e-mail: laurence.dooley@open.ac.uk; patrick.wong@open.ac.uk

W. Zhang (ed.), *Handbook of Cognitive Radio*,
https://doi.org/10.1007/978-981-10-1394-2_62

Abstract

As more user applications emerge for wireless devices, the corresponding amount of traffic is rapidly expanding, with the corollary that ever-greater spectrum capacity is required. Service providers are experiencing deployment blockages due to insufficient bandwidth being available to accommodate such devices. *TV White Space* (TVWS) represents an opportunity to supplement existing licensed spectrum by exploiting unlicensed resources. TVWS spectrum has materialized from the unused TV channels in the switchover from analogue to digital platforms. The main obstacles to TVWS adoption are reliable detection of *primary users* (PU) i.e., TV operators and consumers, allied with specifically, the *hidden node* problem. This chapter presents a new *generalized enhanced detection algorithm* (GEDA) that exploits the unique way *digital terrestrial TV* (DTT) channels are deployed in different geographical areas. GEDA effectively transforms an energy detector into a feature sensor to achieve significant improvements in detection probability of a DTT PU. Furthermore, by framing a novel margin strategy utilizing a *keep-out contour*, the hidden node issue is resolved and a viable secondary user sensing solution formulated. Experimental results for a cognitive radio TVWS model have formalized both the bandwidth and throughput gains secured by TVWS users with this new paradigm.

Introduction

Mobile communications have become integral to our daily lives with the mobile phone now having developed into a smart device that is able to interact with its user. Commensurately, mobile data traffic has grown exponentially due to a vast array of services and applications for smartphones including interactive gaming, video and music streaming, web browsing, and e-mail [1,2].

In many countries, terrestrial TV broadcast networks are changing from analogue to digital delivery platforms, a process already completed in North America, the UK, and Europe [3,4]. This switchover process has continued apace because during migration, maintenance updates were necessary to channel allocations, with the most recent, respectively, being in 2016 and 2015 for the UK [5] and USA [6]. The switchover released valuable spectrum in the UHF band which was subsequently split into two categories. The first, known as the *digital dividend*, denoted spectrum no longer used by terrestrial TV broadcast networks. This was auctioned for mobile operators to develop application technologies like *Long-Term Evolution* (LTE) [3,4]. The second, known as *TV White Space* (TVWS) or interleaved spectrum, relates to unused spectrum within given geographical locations that avoids adjacent and co-channel interference with *digital terrestrial TV* (DTT) transmitters. Since the *digital*

dividend spectrum has already been sold off, TVWS has come to be the primary spectrum for *cognitive radio network* (CRN) services and applications.

With 5G mobile technology evolving, there are two nascent views for how it will be successfully realized: (i) a focus on greater coverage [7–9] and (ii) increasing throughput and lower latency [7–9]. The emergence of CRN technology [2, 10, 11] and TVWS provides new access opportunities for unlicensed *secondary users* (SU), and since TVWS exists in the low UHF band, it offers greater coverage and increased throughput so satisfying a major 5G requirement. This chapter presents a framework for how TVWS can effectively fulfill the aforementioned 5G criteria allowing services to not only exploit the increased spectrum released by TVWS but also ensure long-term SU access benefits, especially as bandwidth scarcity is still a major 5G issue [5, 6].

Sensing Strategies

CRN offers an efficient and autonomous TVWS solution to facilitate SU access by sensing the RF environment within licensed *primary user* (PU) spectrum [12, 13]. Since TVWS is static spectrum, channels do not change in a particular location, so relaxing the need for efficient PU updates as channels varies only on a spatial and not temporal basis [12, 14]. To access unused TVWS, *spectral holes* [10, 11] must be identified using *dynamic spectrum access* (DSA) techniques [10, 14) which enable the CRN to learn about its neighboring RF environment and make access decisions accordingly. DSA techniques for TVWS are generally classified into three categories: beacons, sensing, and static databases [12, 13].

Beacons are dedicated in-band signals that advertise for SU access in the licensed spectrum, though since the PU must administer this process, it is not practical for DTT broadcasters due to the prohibitive overheads incurred.

Sensing techniques in contrast automatically update a PU static database to reduce operational costs, though the ubiquitous *hidden node* problem [4] must be overcome for them to be viable.

Static databases require manual upkeep, but as interference margins for PU protection are theoretically calculated rather than based on actual measurements, system accuracy can be compromised. This approach offers greater flexibility in embracing scenarios where sensing is not feasible, such as *program making and special event* (PMSE) radio microphones.

The principal requirement for TVWS access is reliable PU detection to avoid interference to local DTT users. Both Ofcom and FCC favor the geo-location database approach [12], though this entails expense to implement and maintain the database infrastructure. It is for these reasons that alternative sensing mechanisms are considered in this chapter. Another key sensing issue to resolve is the *hidden node* problem [11, 15, 16], where a SU sensing receiver is obstructed from a

PU transmitter, so a spectral hole is falsely detected, potentially causing major PU disruption. This is especially critical at the cell edge where signal strength is generally low.

While assorted cooperative sensing solutions exist [17] to overcome hidden nodes, the novel GEDA solution presented in this chapter does not rely on either cooperative mechanisms or compromises SU bandwidth availability. It exploits the unique deployment pattern of DTT frequencies to determine if a PU channel is occupied, applying an energy detector for local real-time measurements in the decision-making, so effectively turning it into a feature detector. We will now investigate in greater depth the rich opportunity TVWS spectrum affords for providing extra bandwidth for SU access.

TV White Space (TVWS)

The DTT switchover from analogue TV reduced the number of TV channels, with some being released for auction, while the remainder were allocated as DTT channels. Unused DTT channels in a particular geographic area are TVWS (interleaved spectrum) and in the most recent standards [5, 6] are assigned to CRN applications. The UK 8 MHz DTT channels are shown in Fig. 1, with TVWS channels being the unused (interleaved) spectrum in any location. The purple channels are DTT, green channels have been auctioned, and the pink channel is for PMSE applications.

In [3], it was noted that in the UK, 50% of locations can release 150 MHz of spectrum and from 90% of locations, 100 MHz of TVWS. The key issue distilled from this analysis is that for a CRN to utilize TVWS, it must be able to allocate non-contiguous channels to all its SU. Figure 2 shows the non-contiguous nature

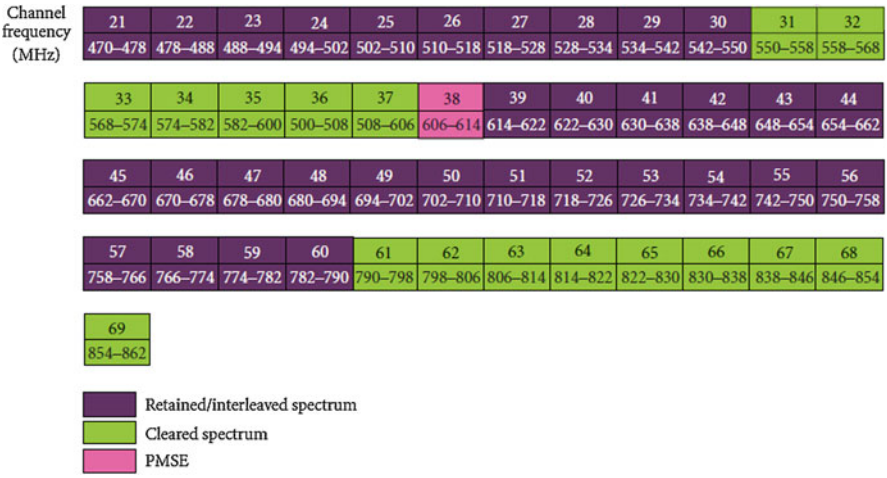

Fig. 1 Channel allocation after DTT conversion in the UK [5]

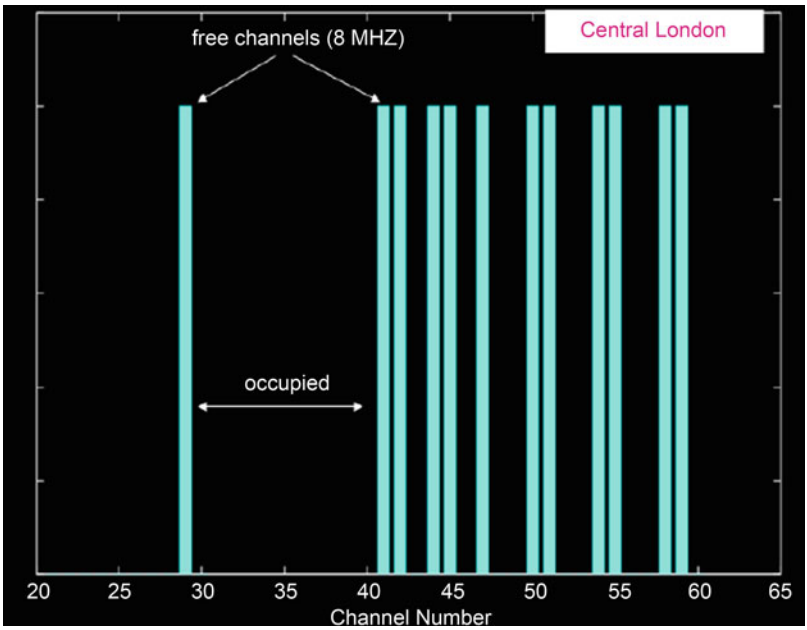

Fig. 2 Contiguous TVWS Channels in Central London [3]

of channels allocated in London, where each cyan bar represents a free 8 MHz channel. It is evident the maximum contiguous channel capacity is 16 MHz, i.e., two adjacent cyan bars, so to achieve greater capacity, non-contiguous techniques such as assembly and disassembly of non-contiguous OFDM channels must be employed.

Figure 3 provides some examples of contiguous channel capacities for other UK locations.

As evidenced in [18], the minimum number of TVWS channels available in the UK for a SU using a 10 m antenna and transmitting at 15 dBm yielded an extra 80 MHz of bandwidth for 90% of households and 184 MHz for 50% of households, so confirming there are significant gains to be leveraged on available SU bandwidth within the TVWS band. The next section briefly reviews the regulatory steps to enable this unlicensed bandwidth to be exploited. It is interesting to note both Ofcom and FCC [18, 19] have opened a TVWS band for industry proposals, while recently the use of TVWS for autonomous vehicles has been proposed [20].

Regulatory Standards

The adopted Ofcom and FCC standards permit CRN broadband devices to operate in TVWS [12,13,21,22]; with the main TVWS engagement parameters specified by both regulators alongside the corresponding IEEE 802.22 standard [13, 15], values

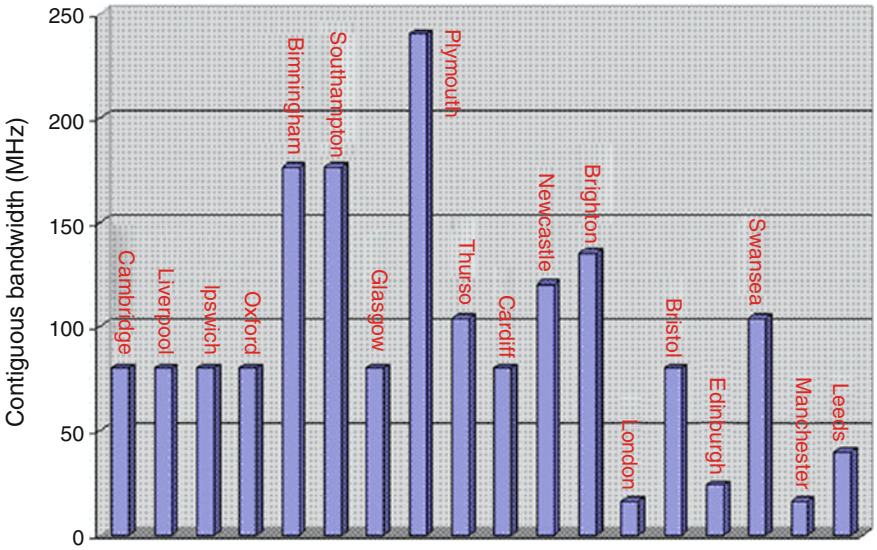

Fig. 3 Maximum Contiguous capacity values for UK [3]

Table 1 Regulatory TVWS engagement parameters [13, 15]

Rule	Parameter	OFCOM	FCC	IEEE802.22
1	DTT sensing threshold	−120 dBm	−114 dBm	−114 dBm
2	Wireless microphone threshold	−126 dBm	−114 dBm	−114 dBm
3	SU transmit power fixed network node 1st adjacent Ch - $P_{BS(N+1)}$	4 dBm	16 dBm	–
4	SU transmit power fixed network node 2nd adjacent Ch - $P_{BS(N+2)}$	17 dBm	30 dBm	36 dBm
5	SU transmit power mobile network node 1st adjacent Ch - $P_{M(N+1)}$	4 dBm	16 dBm	–
6	SU transmit power mobile network node 2nd adjacent Ch - $P_{M(N+2)}$	17 dBm	20 dBm	–
7	Out-of-Band powers	<−46 dBm	−55 dBc	–
8	DTT bandwidth	8 MHz	6 MHz	6 MHz
9	Probability of detection P_d	1	1	0.9
10	Probability of false detection P_f	–	–	0.1

are defined in Table 1. These include the respective probabilities of PU detection (P_d) and false detection (P_f), the DTT sensing noise floor, SU transmit RF power for a *base station* (BS) node in the presence of PU adjacent channels, and SU transmit RF power for a mobile node in the presence of PU adjacent channel.

The Ofcom and FCC settings in Table 1 are committed to PU protection in their respective countries. Conversely, IEEE802.22 is a SU-focused standard, with the

specified parameters being the maximum allowable transmit-power requirements, while corresponding PU protection is the responsibility of the respective country regulators. While sensing has been considered by the regulators, Ofcom currently has only proposed a geo-location database solution for industry consultation, while FCC is focusing on the database solution, with any sensing proposal having to undergo stringent certification with reduced radiating power [23].

The IEEE802.11af wireless networking standard [23], which is also known as White Space Wi-Fi (White-Fi) and Super Wi-Fi, permits WLAN operation in TVWS in both the VHF and UHF bands between 54 and 790 MHz. CRN technology can transmit on unused DTT channels, with crucially this particular standard stipulating PU interference bounds.

Enabling Technologies for Spectral Sensing

Historically the *Open Systems Interconnection* (OSI) communication stack has been used to communicate information between layers; however, for CRN applications this is limited by both parameter availability and acquisition time scales. Once the parameters have been acquired, some analysis is required to interpret an unpredictable RF environment. In the regulatory parameter settings in Table 1, the RF transmit power can vary between a fixed SU BS and a mobile SU user. Furthermore, the mobile SU uses minimum RF power in order to minimize the local noise temperature outside the coverage area of the SU BS which can occur if the mobile SU is at the edge of the BS coverage area. To achieve the coverage area of a fixed SU BS, the mobile SU uplink must employ ad hoc routing [24, 25]. The following sections detail some of the supporting technologies for CRN access of TVWS.

Cross-Layer Processing

Cross-layer processing (CLP) design strategies attempt to optimize key parameters by using information from other OSI layers, allied with information not readily available within the OSI communication stack. Unlike normal OSI stack information exchange, CLP is not constrained to information that is of necessity, contained within adjacent layers. This enables faster information retrieval because the information does not have to be transferred through several layers before reaching the requisite layer. Furthermore, not all information required within a layer to perform its function is passed to other layers, so CLP permits information to be utilized by any OSI layer.

The benefits of CLP are that it reduces the overhead within the protocol stack, lowering the time to acquire information and configure parameters. In [10], it was shown that if CR routing in the network layer uses information from the spectrum management block, then enhanced routing performance can be achieved.

There are two drawbacks of CLP. Firstly, proprietary information models must be implemented across the cross-layer block which will vary between implementations. Standards can be formulated between all stakeholders to frame a rigid information model for interoperability; however, this requires considerable time overhead to establish such a standard. The second limitation is that a higher computational cost is incurred in implementing a CLP block with an associated increase in power resources.

To date, this has not been an issue in CRN research [10,11], because the focus has largely been on the physical layer. Now, however, the emphasis has shifted toward optimizing resources to improve the *quality-of-service* (QoS) provision for the SU, so the CRN needs to simultaneously influence parameters in the significant OSI layers. Examples include optimizing the RF power for routing to spectrum access decisions which are tailored to the application layer (Layer 7) requirements, which directly relate to the QoS user experience.

This chapter also introduces a novel cross-layer mechanism called the *cross-layer cognitive engine* (CLCE) which shares information between the *medium access control* (MAC) and physical layers, so sensing measurements can readily influence spectrum access decisions. Some of the challenges in successfully implementing the CLCE [2, 15, 26] include:

- **Modularity** – The OSI layers are designed to be modular so they operate independently of each other. CLP design can compromise this property, so avoiding technology-specific parameters being passed to the CLCE by abstraction alleviates the need for a bespoke solution in different cross-layer blocks.
  - **Information interpretability** – Choosing a knowledge representation base which is able to accommodate different implementations of the layer modules is vital.
  - **Imprecision and uncertainty –** Since parameters to be exported can contain measurement inaccuracies, cross-layer blocks must be able to manage imprecision which makes incorporating a fuzzy capability an attractive option**.**
  - **Complexity and scalability –** CRN must operate with different wireless configurations to be able to be scalable, so to optimize the wireless link to user requirements, the cross-layer block can become complex because of the number of possible parameters to be exported.

A number of cross-layer block implementations currently exist, with the most prominent being considered below [26–29]:

- **Radio Knowledge Representation Language** [28, 29] – Each micro-world represents a specific wireless technology which implies the CLCE needs explicit knowledge about these technologies. This is contrary to the aforementioned modularity and scalability features.

- **Artificial intelligence (AI)** [2, 27, 30] – Solutions such as neural networks and genetic algorithms are well suited to handling large datasets, but they concomitantly require long training periods to be effective which is not practical in most wireless applications.
- **Fuzzy logic controllers** [2, 26, 27] – These are modular, so technology-specific information is retained in the layers with more generic information used in the cross-layer block. Improved information interpretability is achieved using linguistic attributes for each defined membership function. Precision and accuracy issues are avoided by using an imprecise knowledge representation base. The complexity of the cross-layer block is also lower than other proposals.

Ad Hoc Routing

Section "Regulatory Standards" stressed that regulatory requirements mean the RF transmit power of both fixed and mobile SU nodes can vary up to the maximum values in Table 1, and because of the fixed node antenna height being higher than the mobile node, greater coverage is achieved. To compensate for this asymmetrical coverage in the down and uplink directions, ad hoc routing can be innovatively applied in the uplink direction (mobile to fixed node) to achieve the same coverage in both directions.

To enable frequency reuse and thus increase spectral efficiency, low RF power needs to be used, though a corollary of this is that ad hoc routing must be employed to ensure CR messages reach their destination via other CR nodes. To minimize latency in time-sensitive applications, consideration must be paid to how the message is routed through the CRN to their destination [2, 15].

Routing protocols for *mobile ad hoc networks* (MANET) [2, 15, 24, 25] are well established, though CRN introduce some new challenges which need to be solved. These include:

i. Link availability – In the example in Fig. 4, there is a short spectral hole for the CRN to exploit; however, unlike in a MANET, the availability window is measured in milliseconds rather than seconds, except in the case of TVWS.
ii. Unidirectional links – Typical wireless networks use bi-directional links though this is questionable for CRN for the above reason. Also, in TVWS scenarios, due to the regulatory SU unidirectional power allocation, pragmatically there is only the prospect of unidirectional links which imposes a specific design constraint on the network layer.
iii. Heterogeneous wireless networks – Normal wireless networks are structured, while CRN have a more ad hoc, heterogeneous node structure. This means CRN require inter-system handover but with very short duration links routing relying on cooperative relaying. Such heterogeneous networks pose a security risk because the link duration is so small; there is insufficient time to authenticate any security certificate.

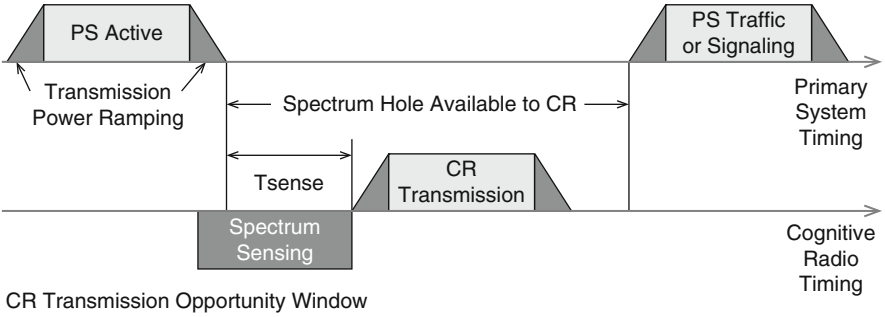

Fig. 4 CRN transmission opportunity window [15]

Reactive protocols devised for typical wireless networks can be adopted for CRN to overcome some of the above issues. The two most common routing protocols are *Dynamic Source Routing* (DSR) [24] and *Ad Hoc On Demand Distance Vector* (AODV) [25].

The DSR protocol is based on source routing whereby all the routing information is maintained by the mobile nodes. It is a simple and efficient routing protocol designed specifically for use in multi-hop links for mobile nodes. DSR allows the network to be completely self-organizing, without the need for any existing network administration. The protocol is composed of two main phases, namely, "Route Discovery" and "Route Maintenance," which work together to allow nodes to discover and maintain routes to destinations in the ad hoc network. All aspects of the protocol operate entirely on demand, allowing the routing packet overhead of DSR to scale automatically, since only after a route to the destination node has been identified does packet transmission occur.

In contrast, the AODV routing protocol is intended solely for use by mobile nodes in ad hoc networks. It offers quick adaptation to dynamic link conditions, low processing and memory overheads, and low network utilization and determines unicast routes to destinations within the network. AODV route table entries are dynamically set up at each intermediate node as the packet is transmitted toward the destination, reducing the traffic overhead.

Existing Sensing Techniques

The regulatory framework in Table 1 has formed the basis for a variety of spectrum sensing proposals including noncooperative feature sensing and cooperative sensing using a non-Gaussian noise covariance Rao test. This section critically analyses these sensing solutions within a regulatory context.

Noncooperative Feature Sensing

In [21, 22], an autocorrelation algorithm for spectrum sensing was developed based upon the correlation of the frame headers and synchronization blocks which are a form of matched filter feature detection. Spectrum sensing is explored in the context of the three main TV standards deployed in China, namely, Digital Terrestrial Multimedia Broadcast (DTMB), China Multimedia Mobile Broadcasting (CMMB), and Phase Alternating Line – D/K (PAL-D/PAL-K). For comparative purposes, only DTMB is considered in this discussion because it is the standard that most closely resembles the UK DVB-T standard in term of frame structure and transmission bandwidth. In [21], a simulation platform was constructed along with a prototype model with the detection results being displayed in Fig. 5.

Figure 5 shows both the simulation and laboratory prototypes at *false detection rates*, $P_f = 0.1$ and $P_f = 0.001$. The *detection rate* (P_d) for the prototype is generally 3–4 dB lower compared to the simulation results which is explained by the simulation not including analogue RF stage impairments like frequency offsets and amplifier nonlinearity. Interestingly, by comparing the detection and false detection probabilities for the IEEE 802.22 standard, $P_d = 0.9$, $P_f = 0.1$ at a signal strength of -114 dBm (Table 1), while the corresponding simulation results for $P_f = 0.1$ in Fig. 5 reveal only a $P_d = 0.7$ at -114 dBm, so this sensing solution fails to comply with the IEEE 802.22, Ofcom or FCC requirements defined in Table 1.

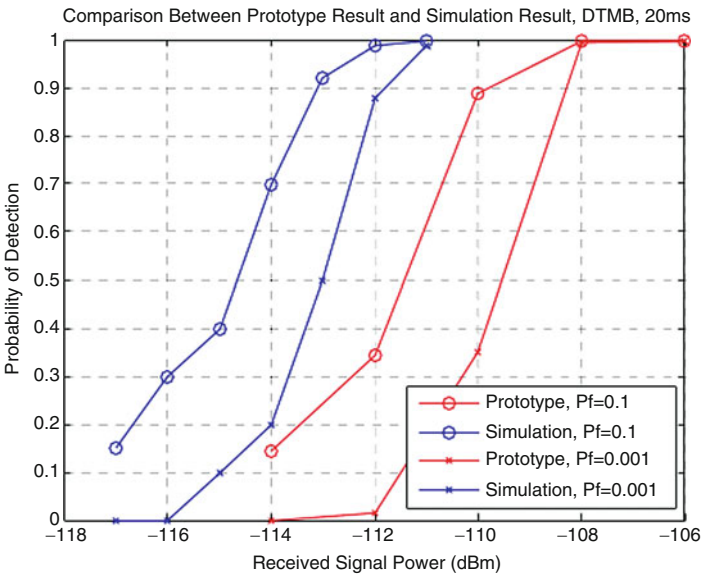

Fig. 5 Simulation and laboratory results for DTMB detection [21]

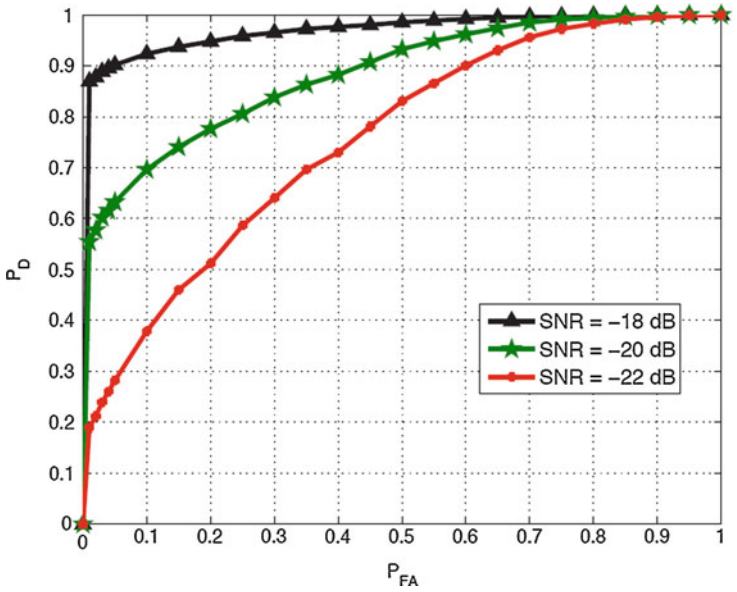

Fig. 6 Probability curves for ATSC DTT Signals at different levels of SNR [22]

The North American approach [22] examined the development of spectrum sensing algorithms for *Advanced Television Systems Committee* (ATSC), *National Television System Committee* (NTSC), and radio microphones. Sensing for both ATSC and NTSC involves a unified signature-based, spectrum sensing algorithm, which, in the case of the US DTT standard ATSC, is the autocorrelation of the SYNC segment of the frame.

ATSC results are plotted in Fig. 6, which shows detection probability (P_d) against the probability of false detection P_f at different SNR values.

If a noise floor of -100 dBm is assumed within a 6 MHz bandwidth, which is the TVWS bandwidth in the USA, then a SNR $= -18$dB is represented by a signal of -118 dBm which is below the sensing threshold of -114 dBm for both IEEE 802.22 and FCC (Table 1). From Fig. 6, at SNR $= -18$ dB, $P_d = 0.9$ and $P_f = 0.05$ which is the only SNR value which upholds IEEE 802.22, though it still does not comply with the FCC detection probability requirement in Table 1. The other SNR values (-20 and -22 dB) do not comply with IEEE 802.22 and FCC sensing thresholds.

Cooperative Sensing Using a Non-Gaussian Noise Covariance Test Rao [31]

Spectrum sensing for CRN in the presence of non-Gaussian noise is challenging due the CR having to have knowledge of both the PU and SU. To overcome

this limitation, the *generalized likelihood ratio test* (GLRT) can be applied which combines unknown parameter estimation with a likelihood ratio test. While GLRT is an optimal detector, it must compute a maximum likelihood estimation (MLE) for the received signal power of the desired signal, the noise variance, and the unwanted signal and so consequently incurs a large computational burden. The Rao test is an approximate form of the GLRT which only estimates system model parameters for unwanted signal conditions. This simplifies the Rao structure and [31] examined its use in the cooperative mode, which is a commonly used technique in spectrum sensing since it overcomes the harmful effects of fading and shadowing by taking advantage of spatial diversity. It thus offers a solution to PU sensing for non-Gaussian noise conditions. Cooperative spectrum sensing is a viable solution for a CR sub-network comprising one SU BS and multiple SU mobiles, which collectively detect the presence/absence of a PU within a given frequency band. Each SU employs a Rao detector to independently sense the PU signal in the presence of non-Gaussian noise, with local SU decisions then forwarded to the BS which makes a final access decision.

The cooperative spectrum sensing system in [31] is an IEEE 802.22-based solution that uses the Rao test to measure the non-Gaussian noise level to improve the energy detection performance and includes a multiuser extension where β defines the noise model used. Figure 7 shows the results for four SU sensors at differing β settings which represent various noise profiles ranging from Gaussian ($\beta = 2$) to Laplacian ($\beta = 1$). Also, the results evaluate four strategies for

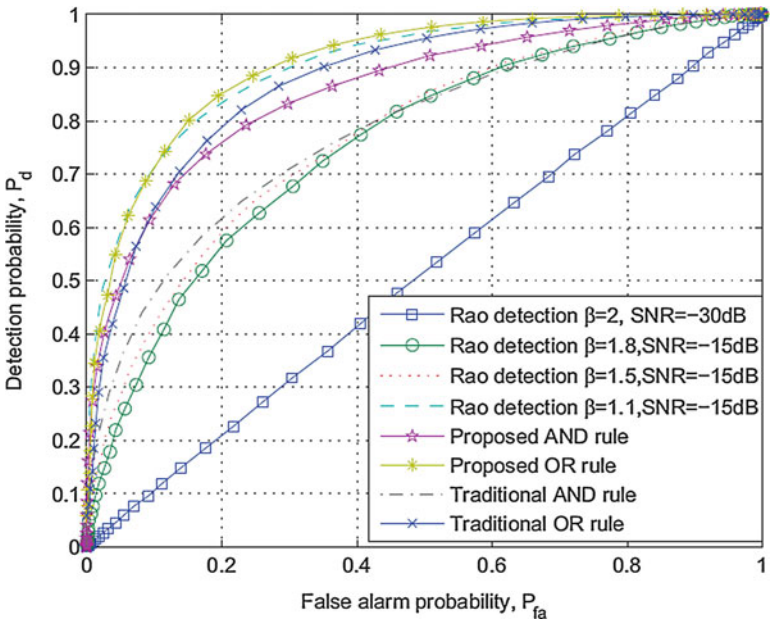

Fig. 7 Family of ROC curves of cooperative for different values of β [31]

cooperative sensing. The first is the traditional cooperative sensing technologies (OR, AND) where the proposed solution uses the cooperative technologies coupled with the Rao test measure.

In summary, the results for both noncooperative sensing in [21, 22] and cooperative sensing [31] corroborate that the requisite detection and false detection rates specified in Table 1 are not upheld. This provided the motivation to investigate new sensing strategies which are able to fulfil the strict sensing regulatory requirements of OFCOM and FCC, with one innovative solution being detailed in the following sections.

Enhanced Detection Algorithm (EDA)

This PU detection technique [17, 32, 33] was introduced to specifically facilitate access to TVWS channels by employing the *cross-layer cognitive engine* mechanism introduced in section "Cross-Layer Processing". This shares information between the MAC and physical layers, so energy sensing measurements can dynamically influence the DSA decisions [10, 17]. EDA exploits inherent patterns in the DTT frequency deployment to determine whether a PU occupies a particular DTT channel using a fuzzy logic model to make channel occupancy decisions. By scanning adjacent frequencies on either side of the channel under investigation, this effectively turns the energy detector into a feature detector, with a *scan range* parameter B determining the number of channels to be sequentially scanned. Hence, if *Ch_A* is the DTT channel under review, EDA symmetrically scans *Ch_A*$\pm$ 1, *Ch_A*$\pm$ 2...up to *Ch_A*$\pm$ B. Symmetrical scanning is used due to the equiprobability of a neighboring DTT channel being either below or above the channel of interest.

EDA affords a unique sensing option for DTT transmitters because regional DTT frequencies are deployed in clusters of 6 channels in the UK, and due to DTT domestic receiver antennae groupings [34], these 6 channels can only lie within a possible bandwidth of 16 DTT channels. The corollary is that by scanning B channels either side of the channel of interest, the majority of occupied DTT channels in a region are detected, with crucially, low false detection probabilities being achieved by maintaining a low B value. Selecting the best choice of B will be discussed shortly. EDA uses the sensed energy values in the scanned channels to resolve whether the DTT channel is occupied. This approach allied together with a geo-location database means EDA generates an accurate map of PU channel usage. The advantage of EDA, when coupled with a geo-location database, is that an accurate mapping of PU channel usage is obtained. PMSE devices can also be included in the database so reducing PU interference and increasing the available bandwidth for SU.

The next section introduces the design principles underpinning EDA.

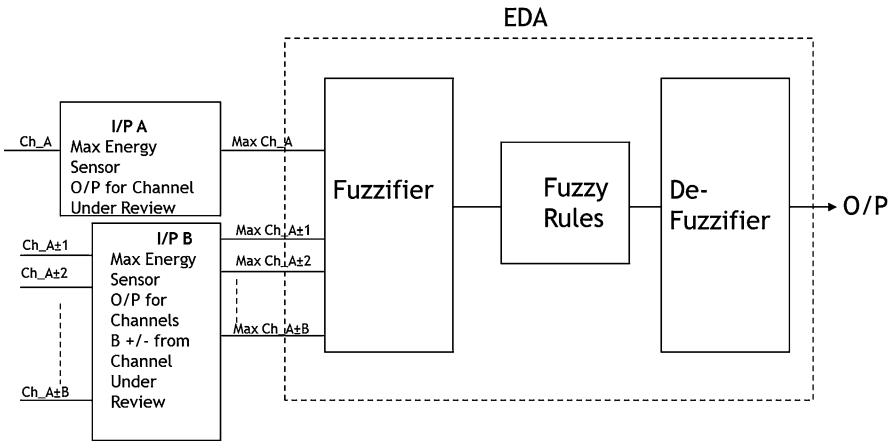

Fig. 8 EDA block diagram [17, 32, 34]

EDA Design

Figure 8 shows a block diagram of the EDA [17, 32, 33], with fuzzy logic inference model employing a classical fuzzy logic framework [26], so I/P (input) A is the sensor output for the channel under investigation, while I/P B is the maximum sensor output for 1 to B channels either up or down from the channel under investigation.

The role of the fuzzifier is to translate the input into a fuzzy set which is allocated a membership function. This follows a normal (Gaussian) probability function used for RF detection. The fuzzy rule block defines how EDA behaves under practical conditions, while the de-fuzzifier produces a final crisp output using the *centre of area* method [26].

B Parameter Selection

The choice of B is critical to EDA detection performance as it scans channels up and down from the channel under investigation to B, where B is the integer number of channels to be scanned. Three membership functions *Lo*, *Med*, and *Hi* are used to assess the occupancy status of a specific channel. If a particular channel lies within the *Med* probability range and another channel which is either within B up or down and also lies within either the *Med* or *Hi* probability detection ranges, then the outcome is weighted according to a set of fuzzy rules [34] which is defined above and a crisp occupied or unoccupied result is returned. This reflects the phenomena that DTT channels in a local area are generally deployed in a cluster configuration due to DTT antenna groupings [34] in which another DTT channel either B channels up or down can be located. EDA detection/false detection response against B for

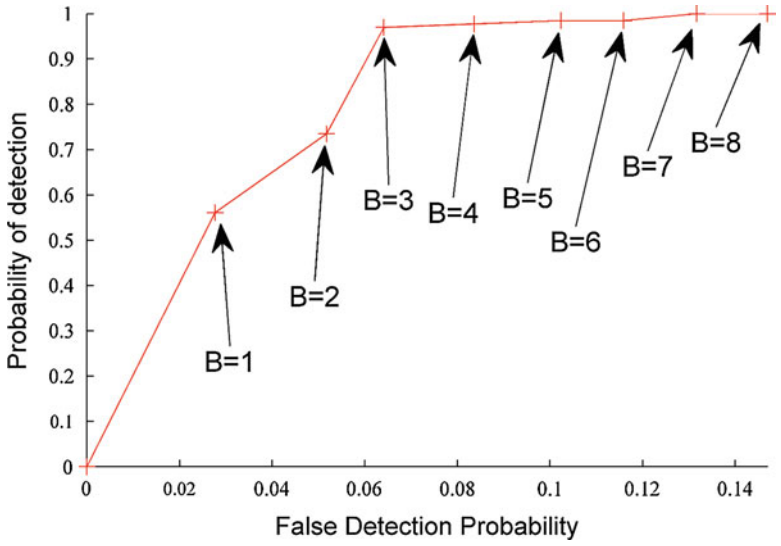

Fig. 9 B Response for the UK

signal strength of −120 dBm and averaged over 22 major DTT transmitter sites in the UK is shown in Fig. 9, with B dynamically determined. Note, B will always be bespoke to the country of the DTT channel deployment.

The corollary from Fig. 9 is that by scanning B channels either side of a channel of interest, the majority of occupied DTT channels in a region are detected with crucially, low false detection probabilities P_f achieved by maintaining a low B value. EDA then uses the sensed energy values in the scanned channels to determine whether the DTT channel is occupied.

EDA Performance

The detection performance of EDA is shown in Fig. 10 in comparison with [21]. This reveals EDA consistently out performs existing PU detection algorithm by up to 9 dB when applying the IEEE 802.22 standard detection thresholds of $P_d = 0.9$ and $P_f = 0.1$, though importantly both techniques fail the stringent Ofcom requirement of $P_d = 1.0$ at a signal strength of −120 dBm.

Despite its performance limitations, EDA demonstrated that a sensing strategy for TVWS applications was feasible, and consequently it became an integral constituent block in a novel adaptive-based sensing framework known as *Generalized EDA* (GEDA) [17], which achieves 100% PU detection under for all regulatory scenarios. GEDA will now be reviewed.

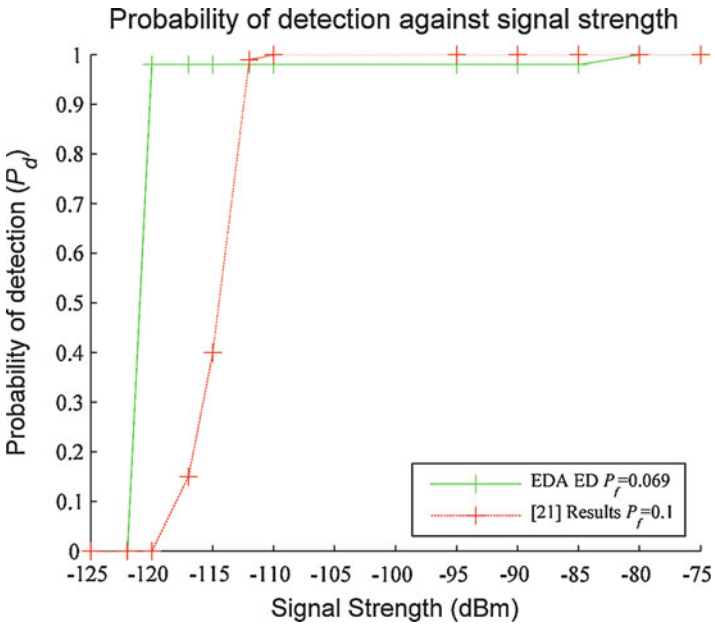

Fig. 10 Detection probabilities versus signal strength

Generalized EDA (GEDA)

Introduction

As highlighted in section "Enhanced Detection Algorithm (EDA)", while EDA upholds the $P_f = 0.1$ requirement of IEEE 802.22 [22], it failed to achieve $P_d = 1.0$ for the DTT sensing threshold in Table 1. This provided the motivation for the development of the GEDA paradigm, which reuses key EDA components, while crucially integrating a new adaptive mechanism for selecting the B parameter to secure significant performance improvements.

GEDA Design

Figure 11 shows the block diagram of the GEDA model which reveals the key role EDA plays. In comparison with EDA, GEDA introduces three new system parameters, namely, B_{Pri}, B_{Sec} and a *scaling factor* (*SF*). B_{Pri} is the initial scan range value of B used to evaluate channel occupancy in accordance with the IEEE 802.22 standard, i.e., $P_d = 0.9$ and $P_f = 0.1$, while B_{Sec} is a higher B value, if required, which ensures an overall $P_d = 1$ once the first frequency scan using B_{Pri} has been completed. It is important to stress that B_{Sec} cannot be directly used at

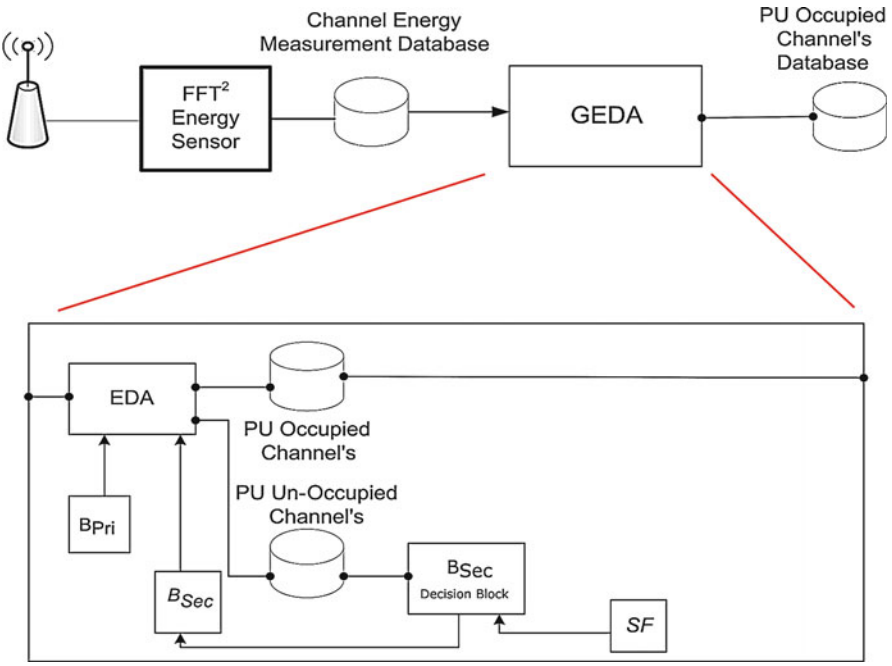

Fig. 11 GEDA block diagram

the outset of sensing by GEDA because its higher value increases the likelihood of false detections which compromises detection performance. It is, thus, only used on occupied DTT channels that B_{Pri} cannot detect. Both B_{Pri} and B_{Sec} are country-specific and are determined applying EDA using the corresponding B value that yields the respective P_d and P_f values.

GEDA detection can thus use either B_{Pri} or B_{Sec} for its DTT scanning range. The former is the initial scan range B value, and, in many cases, this is the only value required. In a few cases, however, B_{Sec} has to be used to achieve $P_d = 1$. Whether B_{Sec} is used is governed by the *SF*, which is the ratio of the highest to the lowest DTT frequency energy values, both of which are stipulated by the relevant regulatory authority [13, 34]. The role of *SF* will now be further investigated.

Scaling Factor (SF)

Using this highest frequency (lowest RF energy) to the lowest frequency (highest RF energy) ratio enables a window of energy measurements to be defined within which it is feasible that a PU DTT channel may trigger using B_{Sec}, provided the channel is in the unoccupied channel database. Thus, by scaling the lowest-frequency energy measurement in the DTT channel occupied database obtained using B_{Pri}, a threshold for using B_{Sec} on an unoccupied DTT channel is established. SF is formally expressed as:

$$SF = \frac{\left|\mathcal{F}\left(RSS_{Hi\_DTTFreq}\right)\right|^2}{\left|\mathcal{F}\left(RSS_{Lo\_DTTFreq}\right)\right|^2} \quad (1)$$

where $RSS_{Hi\_DTTFreq}$ and $RSS_{Lo\_DTTFreq}$ are the respective *received signal strength* (RSS) measurements for the highest and lowest DTT frequencies for a preset distance between the DTT transmitter and receiver.

GEDA Mechanism

Using B_{Pri}, the initial PU sensing results are determined using EDA, from which a PU unoccupied list is compiled. If the criteria in Eq. (2) is upheld, EDA is reapplied, but this time the DTT channel scanning is performed using B_{Sec} to assemble the final PU DTT channel occupied list [17] with y being the energy measurement of the lowest occupied DTT channel.

$$IF\ unoccupied\ DTT\ channel\ energy \geq y \cdot SF \quad THEN\ B = B_{Sec} \quad (2)$$

Numerical Evaluation of the GEDA Mechanism

To demonstrate how GEDA resolves undetected PU channels which are outside the B_{Pri} capture range, we shall examine the Yorkshire-Belmont UK scenario. To illustrate how GEDA is easily transferrable to other countries, the Washington DC FCC (6) scenario is also examined.

Yorkshire-Belmont: UK Channel Deployment GEDA Analysis

The first part of the analysis is where the B_{Pri} value is calculated for the UK DTT channel deployment plan using the algorithm in section "GEDA Design". From this analysis, $B_{Pri} = 4$ which gives a P_d of 0.98 and P_f of 0.0692.

From this DTT channel deployment, the B_{Sec} parameter will be invoked for two transmitter sites, namely, Yorkshire Belmont and Central-Waltham. For the latter case, only one channel is not detected by B_{Pri}; however, using B_{Sec} in the same transmitter region resolves this channel. Yorkshire-Belmont is chosen as the most challenging case study due to having two PU channels not detected, while Scunthorpe is the location for the SU BS, since it is at the edge of the DTT transmission area. The two channels which are not resolved to be occupied are DTT channels 53 and 60, and the way GEDA effectively resolves these channels for the Yorkshire-Belmont DTT transmitter is detailed in [5] and is summarized here.

Firstly, the *SF* for the UK is calculated from (1). The lowest DTT frequency in the UK is 474 MHz and the highest is 786 MHz, and the energy references were 60 km away from a 100 KW DTT transmitter. The DTT propagation model is used to obtain the two energy values below from the sensor with stated parameters:

$$SF = 3.4482118 \times 10^4 / 1.4930635 \times 10^5 = 0.23$$

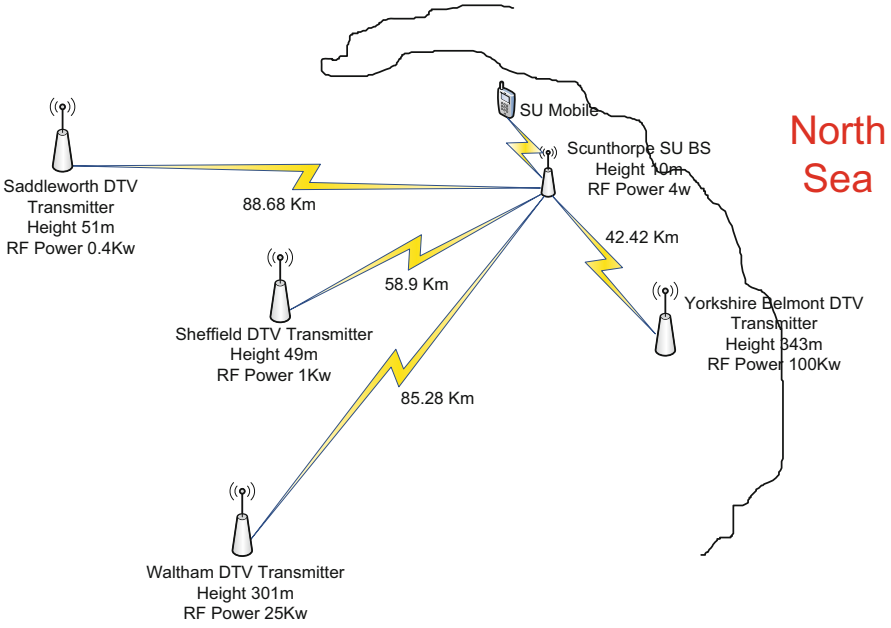

Fig. 12 Yorkshire-Belmont Analysis

Table 2 Energy responses for the Yorkshire-Belmont transmitter area to a Scunthorpe SU BS

Transmitter site and channel	Sensor measurement at SU BS in Scunthorpe
Saddleworth Ch 39	6.0904529×10^{1}
Sheffield Ch 21	6.2628017×10^{1}
Waltham Ch 29	6.3129225×10^{1}
Yorkshire Belmont Ch 53	2.5336327×10^{5}
Yorkshire Belmont Ch 60	2.0449943×10^{5}
Yorkshire Belmont Ch 22 lowest channel detected by GEDA using B_{Pri}	8.4410224×10^{5}

The next step is to map the Yorkshire-Belmont scenario which is shown in Fig. 12, where Yorkshire-Belmont is the primary DTT transmitter and Saddleworth, Sheffield, and Waltham are, respectively, the adjacent region transmitters.

The energy responses for each DTT transmitter is calculated to a SU BS in Scunthorpe by the DTT distance model using the SU BS antenna height (10 m). The corresponding sensor results are shown in Table 2.

The next step is to calculate the trigger for expediting a scan for a channel using B_{Sec}. This is calculated from taking the lowest-frequency channel sensor measurement which is detected by the GEDA using B_{Pri} which in this case is channel 22 and multiplying by SF (0.23) to obtain the trigger point. From Table 2, this will be $8.4410224 \times 10^5 \times 0.23 = 1.94143 \times 10^5$.

Now applying GEDA, the unoccupied channel scan using $B_{Sec} = 7$ is conducted, and if the channel sensor output is $\geq 1.94143 \times 10^5$, which means from Table 2, the Yorkshire-Belmont DTT channels 53 and 60, then the B_{Sec} parameter is triggered. This means when applying $B_{Sec} = 7$, both these DTT channels are detected.

The GEDA mechanism has been fully validated for all UK scenarios though not all countries follow the same channel deployment rules. Hence in order to demonstrate the agility of this novel sensing algorithm, an alternative North American scenario is now presented to exhibit this flexibility.

Washington DC: North American Channel Deployment GEDA Numerical Analysis

The major differences between the North American and UK scenarios are:

1. The DTT channel bandwidth utilized in North America is 6 MHz as opposed to 8 MHz in the UK.
2. The modulation scheme utilized in North America is 8 *Vestigial Sideband* (VSB) modulation where in the UK both 64 and 256 *Quadrature Amplitude Modulation* (QAM) are used.
3. The way the DTT channels are distributed is quite different and mainly driven by geography. In the North American case, distributed transmitter sites [6] are used to service a region because real estate is not a driving factor, with the number of channels varying between 3 and 21 depending on terrain and size of region.

For this analysis, data is required upon channel and RF parameters for the DTT deployment which is generally available from the relevant regulator (6). Using the channel deployment in [6], P_d was calculated using $B_{Pri} = 4$ giving a $P_d = 0.9016$ and $P_f = 0.053$, which conforms to the IEEE 802.22 P_d and P_f criteria. The channel deployment matrix is converted into a detection matrix by using the previously mentioned *detection probability* algorithm.

From the detection matrix, it was noted that channel 15 for Washington DC was not detected when using $B_{Pri} = 4$. Figure 13 shows the Washington DC DTT transmitter model along with a SU BS in the center of Washington in which this forms the basis of the analysis, with ten DTT channels allocated to the Washington DC region, supported by six transmitter sites. Each transmitter is identified by a four-letter call sign, with the particular transmitter of interest being WFDC, which is the channel which cannot be detected. WNVC is the transmitter whose channel is the lowest frequency detected using B_{Pri}, while WMPB is in the adjacent region to Washington DC.

Channel 15 cannot be detected using B_{Pri}, and the lowest frequency which can be detected using B_{Pri} is channel 24. Figure 14 shows the model for these two transmitters WNVC (Channel 24) and WFDC (Channel 15). WMPB (Channel 29), which is a channel servicing Baltimore which is an adjacent region to Washington DC, is also included to demonstrate that false triggering of B_{Sec} will not be caused

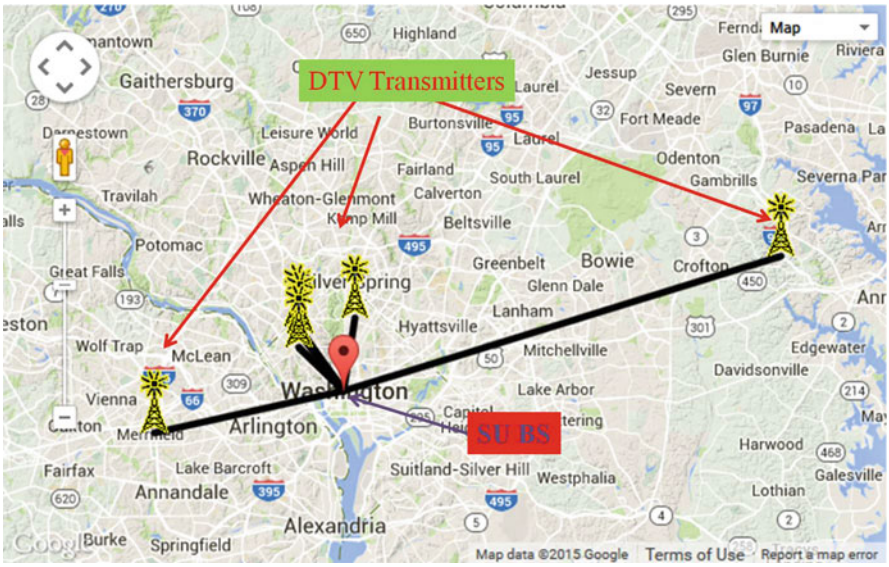

Fig. 13 Washington DC DTT Model [6]

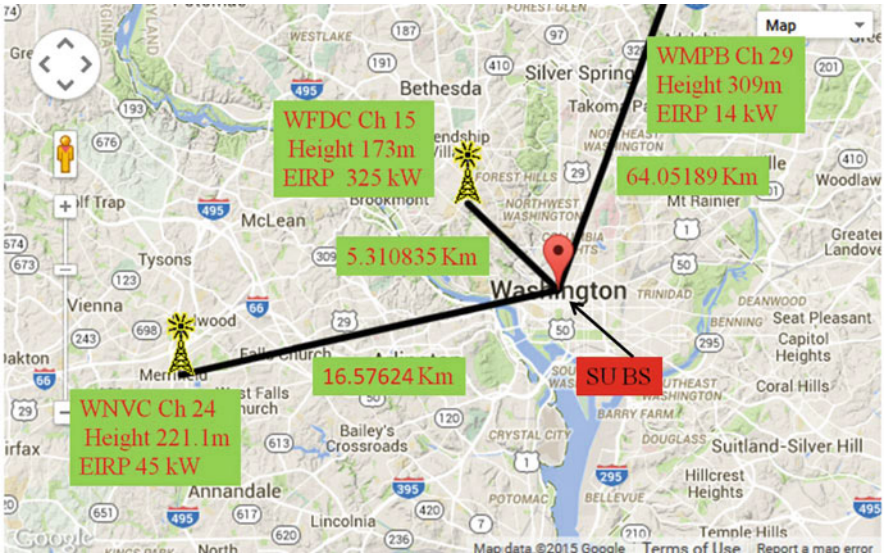

Fig. 14 Washington DC – WNVC, WFDC, and WMPB DTT Model [6]

by any adjacent region, as this would have the effect of increasing the probability P_f , thereby unnecessarily triggering B_{Sec}.

WFDC (channel 15) is not detected using B_{Pri} and WNVC, which is the lowest frequency detected in the Washington DC region thus defines the value at which

Table 3 Washington Model sensor measurements

Transmitter site and channel	Sensor measurement at SU BS in Washington
WFDC Ch 15	1.1846454×10^{10}
WMPB Ch 29 adjacent region	4.9109495×10^{4}
WNVC Ch 24 lowest channel detected by GEDA using B_{Pri}	2.0910753×10^{7}

B_{Sec} is to be used in conjunction with *SF*. Again using (1), the *SF* is calculated using the lowest and highest DTT frequencies in the USA, which are 473 and 887 MHz, respectively.

$$SF = 1360281/7907096.5 = 0.172033$$

This value is now used to calculate the sensor outputs for the three transmitters in Fig. 14 to the SU BS in Table 3.

As with the UK scenario, the next step is to determine the trigger for advancing the scan for a channel using B_{Sec}. This is calculated by taking the lowest-frequency sensor measurement detected by GEDA using B_{Pri}, which in this case is channel 24 and multiplying it by *SF* (0.172033) to give the trigger point. Using Table 3, this is $2.0910753 \times 10^7 \times 0.172033 = 3.597339 \times 10^6$. Now applying GEDA, the unoccupied channel scan using B_{Sec} is conducted, and if the channel sensor measurement is $\geq 3.597339 \times 10^6$, then this means for WFDC (channel 15) B_{Sec} is triggered. Thus, by using $B_{Sec} = 9$ in both the detection and false detection algorithms, this channel is successfully detected.

GEDA Results

The sensing performance of GEDA has been critically compared with two disparate DTT datasets. The first is DTMB which is the DTT standard in China (21), while the other is a North American study [22]. Both results were generated from a DTT deployment matrix of 22 sites. Given the Chinese scenario closely follows the UK in terms of DTT bandwidth and modulation schemes, this was compared to GEDA in a UK scenario using the same channel bandwidths and modulation schemes.

UK GEDA Results Compared to DTMB Standard [21]

DTMB channels have a bandwidth of 8 MHz and employ five modulation constellations, namely, 4-QAM NR, 4-QAM, 16-QAM, 32-QAM, and 64-QAM. The UK DTT standard DVB-T also has eight MHz channels but only two modulation constellations, which are 64-QAM and 256-QAM. To ensure the worst-case UK scenario is evaluated for GEDA, the latter is used because 64 QAM will display a greater energy level than 256 QAM, i.e., higher signal bit energy per noise energy

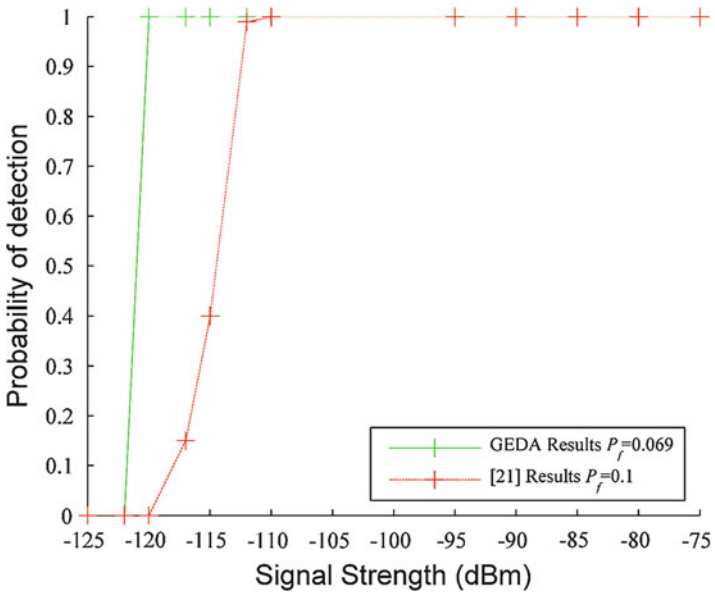

Fig. 15 Comparative detection results for GEDA and DTMB standard

(E_b/N_o) is required to decode 256 QAM signals for the same throughput as per Shannon's law [35].

The B_{Pri} and B_{Sec} values are calculated using the detection and false detection probability algorithms for compliance to $P_d = 1$ and found to be $B_{Pri} = 4$ and $B_{Sec} = 7$ for the UK scenario. The GEDA results are displayed in Fig. 15 along with the corresponding Chinese detection rates [21] at a $P_f = 0.1$. The results confirm that unlike DTMB, GEDA achieves $P_d = 1$ at a signal strength of -120 dBm in accordance with Ofcom requirements (Table 1) and overall produces a 9 dB improvement over [21]. It also achieves a lower comparative $P_{fd} = 0.069$ compared to 0.1 in [24].

US GEDA Results

The next set of results in Fig. 16 show how GEDA performs against the associated North American scenario in [22]. For FCC channel deployment, $B_{Pri} = 4$ and $B_{Sec} = 9$, however, to have an equitable comparison, both B_{Pri} and B_{Sec} values were varied between 1 and 9, so a wide range of P_f values were analyzed.

The results clearly demonstrate GEDA superior robustness across the range of SNR values. The reason for this is that the comparators in [21] and [22] depend on the detection of frame headers, which requires a certain SNR to exist. In contrast, GEDA energy measurements are combined with DTT channel deployment patterns, which effectively becomes a feature detector that is not dependent on demodulating the frame and is thus autonomous of the prevailing noise environment.

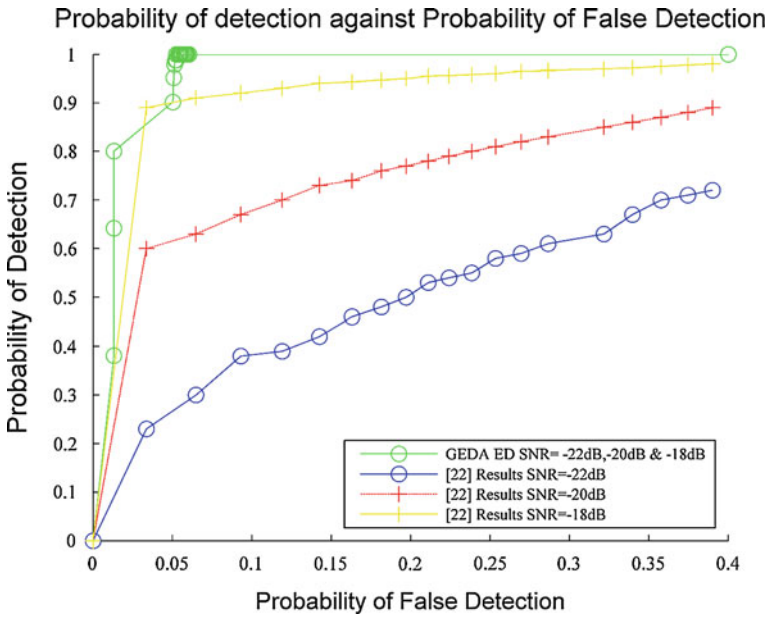

Fig. 16 FCC SNR GEDA results

Comparison of GEDA Results for UK and US

In Figs. 15 and 16, GEDA has been evaluated against other sensing solutions deployed in the UK and USA; however, GEDA was not compared using the same criteria. This section analyzes GEDA performance for both countries using SNR, and the detection and false detection metrics, with Fig. 17 displaying their comparative performance.

The graphs show the US sensing results attain a $P_d = 1$ before GEDA, though both sets of results secure a $P_d = 1$ and $P_f = 0.1$ to uphold both regulatory and IEEE 802.22 requirements. The difference is attributable to the diverse DTT channel deployment patterns between the UK and USA (demonstrated by different the B values used) for the same sensing threshold $= -120$ dBm.

Bandwidth Available for TVWS Devices

This section critically evaluates the potential of TVWS to make available extra bandwidth for SU cognitive devices. Two key concepts are firstly introduced.

(i) The *Protection contour* [34], which is a function of the DTT receiver being able to decode a DTT picture signal, even at the edge of a reception area, without incurring co-channel interference

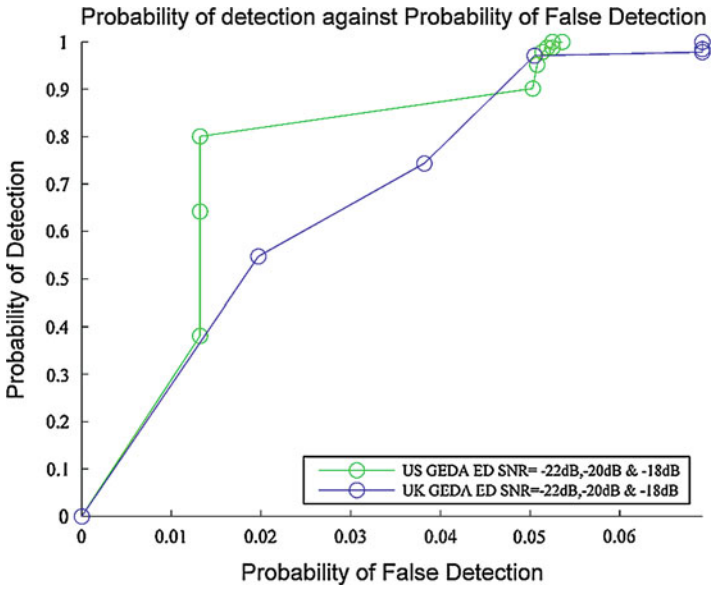

Fig. 17 Comparison between GEDA UK and US results

(ii) The *keep-out contour* which combines the protection contour and hidden node issue to establish a dedicated sterilization zone for each specific DTT channel

To consider how real DTT systems operate in the UK, both the average coverage distance from the transmitter for the Mendip area [17, 34] and the matching Egli terrain factor were calculated. Using the Mendip DTT area as the case study [34], without loss of generality, the Egli terrain value was empirically found to be 97%. It will now be shown how the concepts of a *protection contour* and *keep-out contour* can be innovatively coupled to define how much bandwidth is available for SU TVWS cognitive devices to access. Each will be now individually considered.

Protection Contour and Interference Management

This contour [34] crucially depends upon the RSS at the edge of the Mendip DTT area, which is the worst-case scenario for a PU where no co-channel interference occurs. The related protection contour geometry is shown in Fig. 18.

The *protection contour distance* ($Dist_{PC}$) [34] at the edge of the receivable DTT signal (BER $= 2 \times 10^{-6}$) for the Mendip area is 54.023 km for Channel 54. This $Dist_{PC}$ value does not, however, take account of two different sources of interference:

(i) *Co-channel* – interferers on the same channel
(ii) *Adjacent channel* – interferers on channels adjacent to the PU

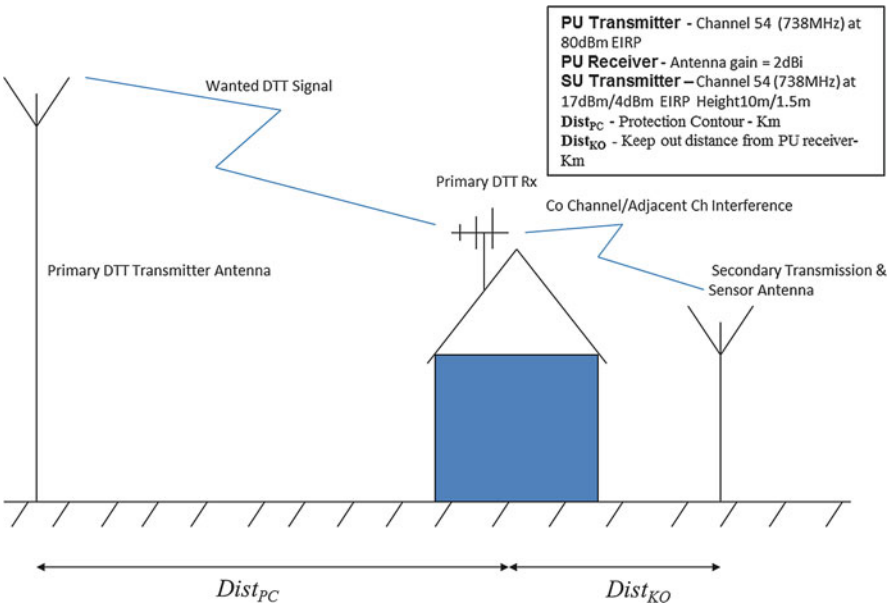

Fig. 18 Protection contour geometry for the Mendip DTT area

For (i), the DTT receiver is located on the protection contour, which for the Mendip area means $RSS_{PC} = -86.2429$ dBm. The co-channel interference signal is now increased until the BER exceeds the 2×10^{-6} threshold, which occurs at $RSS = -131.9$ dBm. Using this value, a model was developed to determine the distance from the protection contour that would generate an interference of -131.9 dBm at the DTT receiver. It was assumed SU BS transmit *effective isotropic radiated powers* (EIRP) of 17 and 4 dBm [12] are used along with the TVWS parameters defined in Table 1, 16 QAM at 32Mbps raw data (user application data together with IP and MAC overheads), and an 8 MHz DTT bandwidth. This equates to a minimum keep-out distance ($Dist_{KO}$) of 3.75 km from the DTT receiver on the protection contour for the 17 dBm SU while $Dist_{KO} = 1.77$ km for the 4 dBm SU. Both $Dist_{KO}$ distances crucially assume no margin for a hidden node.

For adjacent channel interference, the adjacent channel interference signal (N+1) was increased on the DTT receiver at the protection contour until the BER exceeded the 2×10^{-6} limit, which occurred when $RSS = -47.77$ dBm. This is the maximum allowable SU signal strength in this adjacent channel. Undertaking the same analysis for the $(N + 2)$ adjacent channel gave a maximum $RSS = 196.4$ dBm for a SU.

To critically evaluate whether the OFCOM SU maximum transmit EIRP of 4 dBm for $(N + 1)$ and 17 dBm for the $(N + 2)$ adjacent channel interference provides sufficient DTT PU defense against interference, the SU BS and mobile scenarios where the interfering RSS is calculated for both 4 and 17 dBm SU transmit EIRP on $(N + 1)$, 14 m away from a DTT receiver which is assumed to be the

minimum separation of a SU BS from a PU receive antenna. The respective $(N+1)$ BS results were -47.78 and -34.78 dBm, which endorse the Ofcom decision to limit the $(N+1)$ transmit EIRP to only 4 dBm, as this is lower than -47.77 dBm, so it will not generate interference from 14 m unlike the 17 dBm SU BS. The SU mobile scenario for $(N+1)$ using 4 dBm SU transmit EIRP gives protection to the PU receiver up to 5.4 m away from the PU receiver. In contrast, for the $(N+2)$ channel case, the -13 dBm RSS caused by a 17 dBm SU BS at 4 m from the PU receiver is much lower than 196.4 dBm, so no interference is generated. In the 17 dBm SU mobile case, a $RSS = -5.4$ dBm is generated when 1 m away from the PU receiver which again is much lower than 196.4 dBm, so no interference is produced to any PU.

While these co-channel results demonstrate the minimum distance away from the protection contour a SU can reliably transmit on the same channel, the *hidden node* issue [17, 34] is not reflected. It is clear from the above discussion that no interference is generated provided the Ofcom settings (Table 1) on the $(N+1)$ and $(N+2)$ SU power restrictions are upheld.

So far, the *hidden node* effect has been only considered in sensing a PU very close to an obstacle, i.e., 10 and 20 m away. The graph in Fig. 19 shows the sensor output at distances more than 55 km away from a DTT transmitter, for differing obstacle heights in the range 15-90 m [32–34]. The graph reveals that while the distance to the *keep-out contour* distance varies between points (2), which are the minimum, and points (3), the maximum, depending on the obstacle height, the keep-out margin X_{KO} remains constant.

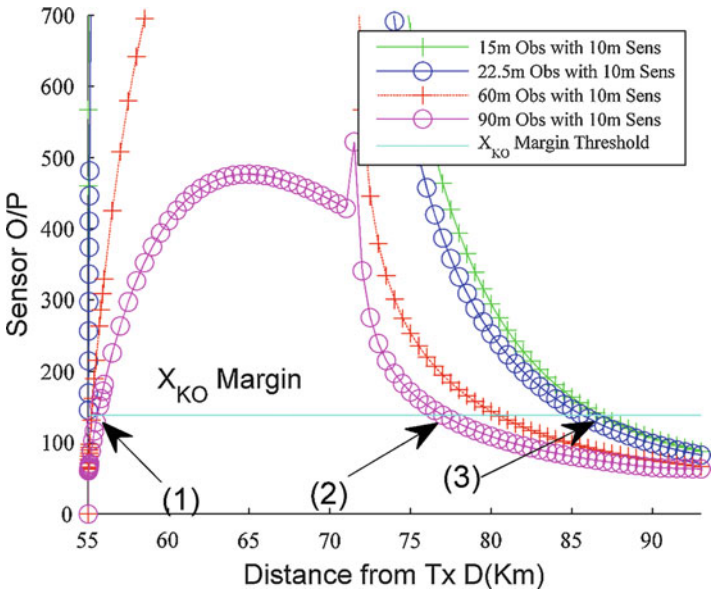

Fig. 19 Mendip keep-out contour at 738 MHz

At point (2), the minimum distance at 76.89 is 22.87 km from the nearest DTT receiver ($Dist_{KO}$) on the protection contour. This means from Table 1 where the maximum allowed Ofcom transmit power is 17 dBm, a minimum distance of 3.75 km is required to avoid co-channel interference. It can then be assumed that by using the *keep-out margin* X_{KO}, no interference is caused by a SU transmitter with an obstacle height of 90 m. For a typical residential scenario and a 15 m obstruction, the maximum *keep-out contour* distance is 86.69 km at point (3), which is the value used in channel reuse calculations. Note, the distance from the obstruction to point (1) is just 0.58 km which represents a special case where PU detection is only achievable using either a cooperative sensing strategy or special sensor heights as discussed in [33] and needs to be within 1 km of the obstruction.

Keep-Out Contour

This contour defines the exclusion zone around the DTT transmitter which protects the PU receiver by applying the *protection contour* even when there is a hidden node present. It also provides sufficient bandwidth to TVWS devices to ensure their users receive the best *QoS*. The difference between the protection and keep-out contours is that the latter includes a margin loss alongside the protection contour to permit prescribed interference RSS in the presence of hidden nodes as illustrated in Fig. 20.

In the *keep-out contour* geometry of Fig. 20, the main parameters are:

$Dist_{PC}$ = *Protection contour* for the lowest modulation scheme in the DTT deployment
$Dist_{KO}$ = Distance from the *protection contour* to *keep-out contour*

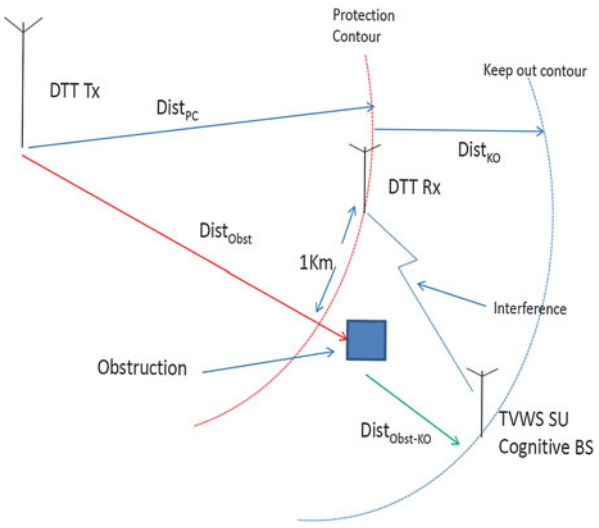

Fig. 20 Keep-out contour geometry

Table 4 Power control parameters

X_{KO}	Keep-out contour energy (section "Ad Hoc Routing")
$P_{BS(N+1)}$	Regulatory definition for base station EIRP for adjacent channel (Table 1)
$P_{BS(N+2)}$	Regulatory definition for base station EIRP (Table 1)
$P_{M(N+1)}$	Regulatory definition for mobile EIRP for adjacent channel (Table 1)
$P_{M(N+2)}$	Regulatory definition for mobile EIRP (Table 1)
DB_{PU}	GEDA identified PU channel database
DB_{DTT}	DTT channel database containing channel numbers and energy measurements
$DB_{DTT}^{(Ch)}$	DTT channel database channel number
$DB_{PU}^{(Ch)}$	GEDA identified PU Channel database channel number
$DB_{DTT}^{(E)}$	DTT channel database energy measurement

$Dist_{Obst}$ = Distance between an obstruction and DTT transmitter
$Dist_{Obst-KO}$ = Distance from an obstruction to the *keep-out contour*

To define the *keep-out contour*, the distance from the *protection contour* in the worst-case scenario must be determined, namely, a 36 dBm SU BS (maximum RF power in Table 1) producing an interference signal strength of −120.8 dBm plus a margin for the hidden node. This margin is derived from the mid-variation point of the 90 m obstacle diffraction loss at distances up to 400 m away from an obstacle, where the most significant changes occur at 41.33 dB. Using the interference models, the corresponding distance $Dist_{KO}$ for this margin in the Mendip DTT region is 47 km. Distance $Dist_{KO} + Dist_{PC}$ now determines the minimum sensor threshold X_{KO} for the *keep-out contour*. For the Mendip DTT area, this is 138.73, which means any sensor output value lower than 138.73 will trigger the *keep-out contour* to enable the SU to access that particular channel as shown in Fig. 19.

Figure 19 reveals that while the distance to the *keep-out contour* varies between the highlighted points (2) and (3), depending on the obstacle height, X_{KO} remains constant. For the most typical residential scenario and a 15 m obstruction, it can be assumed the maximum *keep-out contour* distance is 86.69 km, which is the value used in channel reuse calculations. Note, the distance from the obstruction to point (1) is just 0.58 km which represents a special case where PU detection is only achievable using either a cooperative sensing strategy or special sensor heights [33, 34].

The GEDA model employs the *keep-out contour* to both determine active PU channels and to govern whether these channels can be accessed by a SU. The complete adjacent and co-channel interference management process is presented in pseudo-code form in [17], with Table 4 defining the key parameters.

The interference management algorithm [17] checks every DTT channel in the PU database, which is created during the GEDA process, against the current channel under review. If the sensor output of the DTT under review is greater than (X_{KO}) and the channel number is specified in the PU database, i.e., it is a co-channel, then a SU cannot access this particular channel. However, if the channel under review does

not reside in the PU database or the sensor output is less than X_{KO}, then a SU may access the channel using RF powers of $P_{M(N+2)}$ and $P_{M(N+2)}$, respectively. Finally, if the channel under review lies in an adjacent channel $N + 1$ or $N + 2$, then the SU may use RF powers; $P_{M(N+1)}$, $P_{M(N+2)}$, $P_{BS(N+1)}$, or $P_{BS(N+2)}$, respectively, without crucially impacting upon the PU.

In [14] and [36], the available TVWS bandwidth calculation at any location was determined from physical RF surveys, which incurred extensive resources, so instead GEDA adopted the innovative strategy to assess the amount of SU bandwidth available using the *keep-out contour* and *sterilization index* (SI) [33].

The UK DTT network consists of major regions, with each having minor transmitters operating within their boundaries to overcome local propagation issues so ensuring populated areas have service coverage. The USA DTT deployment in contrast has distributed major transmitter sites covering a region, though notably the *SI* concept is still applicable.

Let the *keep-out contour* area of adjacent main DTT transmitters transmitting intersecting a major DTT area be F km^2 per DTT channel per transmitter. If Y km^2 is the area covered by the furthest *keep-out contour* of a major transmitter serving a UK DTT region, then for a distributed deployment like the US, this will represent the area covered by the radius of the furthest- away transmitter *keep-out contour*, added to the distance from the transmitter to the center of the region under analysis. *SI* is thus formally expressed as:

$$SI = \frac{F}{Y} \tag{3}$$

where the *SI* is calculated on per channel (n), per transmitter (m) basis, with each individual si_{mn} value used to construct a primary area SI' matrix.

$$SI' = \begin{pmatrix} si_{11} & \cdots & si_{1n} \\ \vdots & \ddots & \vdots \\ si_{m1} & \cdots & si_{mn} \end{pmatrix} \tag{4}$$

where the number of DTT channels $n = 32$ in the UK and m the number of transmitters radiating into area Y. If two different transmitters use the same channel, with one *keep-out contour* area nested within another, then the lower si_{mn} value is set to zero.

The final step is to sum all columns and resulting rows in Eq. (4) to form a final *SI* value.

$$SI = \sum_{i=1}^{n} \sum_{j=1}^{m} SI'_{ij} \tag{5}$$

The *SI* determines the available bandwidth in the DTT area under investigation by (*N*-*SI*) x *BW* MHz, where N DTT channels of bandwidth of *BW* MHz area assumed

in the country of interest. The next section investigates how the *SI* can be applied to determine the number of TVWS channels available in the specific case study area of the Mendip region.

UK Case Study for TVWS in the Mendip DTT Transmitter Area

All the major, adjacent, and minor transmitters of either 50 W or more (5) in the Mendip DTT transmitter area, together with their corresponding *SI* values, are given in Table 5.

Using the individual *SI* values in Table 5, the overall *SI* in (5) is 15.1194 which equates to an available bandwidth of 135 MHz for TVWS SU devices, when considering all transmitters of either 50 W or greater. However, there are 60 minor DTT transmitters operating below 50 W that must also be taken into account. To do this efficiently, the average antennae heights and EIRP values are used to determine the *SI*. The *SI* for each channel was found to be 0.0133, and since three channels are allocated to each minor transmitter, $SI = 2.4$. This is now added to (5) giving a total $SI = 17.5194$, so the average available bandwidth for TVWS over the entire Mendip area is 115.85 MHz. While this represents the average available bandwidth for the Mendip DTT region, this value will vary according to locality. In heavily populated areas, it will reduce while in rural areas it will increase. This corroborates the findings in [13], which, based on measured availability and geo-location database access, showed that in the largest city (Bristol) in the Mendip DTT region, 104 MHz of bandwidth was available for TVWS devices.

Other Ofcom studies [13] suggest that over 90% of the population can access at least 100 MHz, aggregated across the interleaved spectrum. They also estimated that $\approx$50% of the population could have access to 150 MHz or greater and some rural communities could enjoy more over 200 MHz of this spare capacity [17]. These findings underscore the importance the *keep-out contour* threshold and *SI* play in

Table 5 Corresponding SI values for the DTT major, adjacent, and minor transmitters of 50 W or over

Transmitter site	SI
Mendip	6
Wenvoe	3.495
Pontypool	0
Bristol Kings	0.36
Cirencester	0.12
Stroud	0.162
Bath	0.132
Hannington	0.942
Cerne Abbas	0.1584
Stocklands Hill	3.15
Salisbury	0.6
Bristol IC	0

releasing valuable bandwidth for SU TVWS exploitation while upholding the *QoS* provision for PU DTT users. As an illustration, the SU gains secured for the Mendip region using the *SI* is approximately 6×20 MHz LTE RF bearers per location. This translates to an increase in the number of active data users in a LTE cell location from 800 to 4600, if a TVWS access node is used in conjunction with an LTE eNodeB, i.e., an improvement of more than a factor of 5.

Future Research Challenges in TVWS and 5G

Emerging 5G technologies [7–9] recognize that coverage, throughput, and latency are the overarching objectives in both framing and advancing any new wireless standard. This chapter has presented a flexible framework for how TVWS can effectively fulfill some of these aims by enabling 5G services to not only utilize the increased spectrum released by TVWS but also safeguard long-term access benefits for unlicensed SU.

Central to this novel TVWS access framework is the GEDA model which uniquely depends on the DTT channel deployment patterns. It is thus motivated by the narrowband nature of DTT UHF receiver antenna, which means only a narrowband of channels are allocated to a specific region. To exploit the SU access benefits of GEDA in other spectrum opportunities such has the millimeter spectrum, it will need to be modified to be able to detect other patterns, such as timing of the PU signals, or when new spectrum is allocated to a PU by administrators, such patterns are factored into the allocation.

Another key challenge is to improve the SU transport QoS metrics of *packet error rate* (PER) and latency when accessing TVWS. Existing TVWS regulatory requirements [13] mean SU BS transmits at far higher RF power compared to SU mobile units, so to achieve adequate SU coverage, the uplink signal from the mobile device to BS needs to employ newly developed innovative routing models to achieve the additional coverage through multi-hop network arrangements.

Furthermore, heterogeneous network environments have been introduced to access different technologies to meet user requirements. An underlying assumption of this development is that TVWS spectrum would be shared between multiple mobile operators, with each setting up a separate WLAN. An interesting alternative strategy would be to critically investigate open WLAN arrangements, involving some commercial agreements between operators for resource sharing [37]. Multi-operator heterogeneous networks have the advantage that any mobile operator can route packets so increasing the number of mobiles in a routing area because it is not restricted to one operator. This will increase the mobile routing population in an area so reducing the PER. A major research question for such an environment, however, would be how best to create a cross-operator heterogeneous implementation framework on existing platforms, including the cognitive TVWS access framework presented in this chapter.

Conclusion

This chapter has investigated how *cognitive radio* (CR) technologies can address the scarcity of spectrum for the increasing demands made by today's wireless applications. It, in particular, explores how *TV White Space* (TVWS) offers a unique, low-risk option to enhance existing licensed spectrum by exploiting unlicensed resources due to the static temporal characteristics of the *primary user* (PU) spectrum. The key hurdles to TVWS adoption are reliable PU detection allied with resolving the *hidden node* issue. A review of existing TVWS regulatory standards has been presented with the PU-centric country-related requirements detailed together with the SU-centric requirements. A key conclusion is that any proposed sensing solution needs to robustly demonstrate resilience to the omnipresent *hidden node* problem.

Supporting technologies which facilitated the introduction of CRN including cross-layer processing and ad hoc routing were also reviewed to address the challenges of both supporting SU access to TVWS and overcoming latency issues of ensuring the correct information is delivered to the required OSI layers in a timely fashion. Ad hoc routing has been highlighted as the favored solution for ensuring the unidirectional transmission caused by the SU RF power differentials, which do not negatively impact on user QoS.

Finally, PU interference management has been analyzed with a novel *generalized enhanced detection algorithm* (GEDA) detailed which exploits the unique way *digital terrestrial TV* (DTT) channels are deployed in different geographical areas. GEDA transforms an energy detector into a feature sensor to achieve significant sensing improvements compared to existing detection solutions. By applying a *keep-out contour* together with a novel *sterilization index*, the *hidden node* problem is resolved and a practical SU sensing solution is formulated. GEDA and the *keep-out contour* interference management paradigm leverages extra bandwidth for SU in TVWS to achieve notably enhanced QoS provision as demonstrated in a UK DTT transmitter case study. The advantages of GEDA has also been shown to be equally effective in DTT deployments in other countries.

References

1. Cisco (2016) Cisco Visual Networking Index: Global Mobile Data Traffic Forecast Update, 2015–2020 [Online], Available at http://www.cisco.com/c/dam/m/en_in/innovation/enterprise/assets/mobile-white-paper-c11-520862.pdf. Accessed Feb 2016
2. Hossain E, Niyato D, Han Z (2009) Dynamic spectrum access and management in cognitive radio networks. Cambridge University Press, Cambridge
3. Nekovee M (2010) Cognitive radio access to TV white spaces: spectrum opportunities, commercial applications and remaining technology challenges. In: IEEE DySPAN, Singapore, 6–9 Apr 2010. IEEE, pp 1–10
4. Fitch M, Nekovee M, Kawade S, Briggs K, MacKenzie R (2011) Wireless service provision in TV white space with cognitive radio technology: a telecom operator's perspective and experience. IEEE Commun Mag 49(3);64–73

5. OFCOM (2016) Digital Switchover Transmitter Details [Online]. Available at https://www.ofcom.org.uk/spectrum/information/transmitter-frequency. Accessed 14 Mar 2017
6. FCC (2015) Engineering DTV Maps [Online], Available at https://www.fcc.gov/media/engineering/dtvmaps. Accessed Jan 2015
7. GSMA (2014) Understanding 5G: perspectives on future technological advancements in mobile [Online]. Available at https://www.gsmaintelligence.com/research/?file=141208-5g.pdf&download. Accessed Feb 2016
8. NGMN (2015) NGMN 5G White Paper. Frankfurt Germany, NGMN, Version 1.0
9. EPRS (2016) 5G network technology- putting Europe at the leading edge, Brussels, European Parliament, PE 573.892
10. Akyildiz IF, Lee W-Y, Chowdhury KR (2009) CRAHNs: cognitive radio ad hoc networks. Netw IEEE 23(4):6–12
11. Haykin S (2005) Cognitive radio: brain empowered wireless communication. IEEE JSAC 23(2):201–220
12. Nekovee M (2011) Current trends in regulation of secondary access to TV white spaces using cognitive radio. In: IEEE globecom 2011, Kathmandu, 5–9 Dec 2011. IEEE, pp 1–6
13. Nekovee M (2012) TV white space services in the UK: current status and future. In: *Directions*, BT, HSN 2012 conference presentation, 12/1/2012 Jeju Island
14. Cambridge White Spaces Consortium (2012) Cambridge TV white spaces trial, a summary of the technical findings [online]. Available at http://www.cambridgewireless.co.uk/docs/Cambridge. Accessed 20th Apr 2013
15. Chen K-C, Prasad R (2009) Cognitive radio networks. Wiley, Chichester
16. Akyildiz IF, Lee W-Y, Vuran MC, Mohanty S (2006) Next generation/dynamic spectrum access/cognitive radio wireless networks: a survey. Comput Netw 50:2127–2159
17. Martin JH, Dooley LS, Wong KCP (2016) A new dynamic spectrum access algorithm for TV white space cognitive radio networks. IET Commun J 10(18):2591–2597
18. OFCOM (2015) Implementing TV white spaces. London, OFCOM, 12 Feb 2015
19. Ramjee R, Roy S, Chintalapudi K (2016) A critique of FCC's TV white space regulations. GetMobile 20(1):20–25
20. Nominet (2018) Autonomous vehicles [Online]. Available at https://www.nominet.uk/emerging-technology/autonomous-vehicles-driven/. Accessed Feb 2018
21. Lei Qiu Jing C, Viessmann A, Kocks C, Bruck GH, Jung P, Qingyang Hu R (2011) A spectrum sensing prototype for TV white space in China. In: GLOBECOM 2011, Kathmandu, 5–9 Dec 2011. IEEE, pp 1–6
22. Chen H-S, Gao W (2011) Spectrum sensing for TV white space in North America. IEEE J Sel Areas Commun 29(2):1–11
23. IEEE (2013) 802.11af™-2013: IEEE standards- amendment 5: television white spaces (TVWS) operation. IEEE Computer Society
24. Sheng L, Shao J, Ding J (2010) A novel energy-efficient approach to DSR based routing protocol for ad hoc network. In: ICECE 2010, Wuhan, 25–27 June 2010. IEEE, pp 2618–2620
25. Yuanzhou L, Weihua H (2010) Optimization strategy for mobile ad hoc network based on AODV routing protocol. In: WiCOM 2010, Chengdu, 23–25 Sept 2010. IEEE, pp 1–4
26. Baldo N, Zorzi M (2008) Fuzzy logic for cross-layer optimization in cognitive radio networks. IEEE Commun Mag 46(4):64–71
27. Mitola J, Maguire GQ (1999) Cognitive radio: making software radios more personal. IEEE Pers Commun 6(4):13–18
28. Ghosh C, Agrawal DP (2007) ROPAS: cross-layer cognitive architecture for wireless mobile adhoc networks. In: IEEE international conference on mobile adhoc and sensor systems, Pisa, pp 1–7
29. Kokar MM, Lechowicz L (2009) Language issues for cognitive radio. Proc IEEE 97(4):689–707
30. He A, Bae KK, Newman TR, Gaeddert J, Kim K, Menon R, Morales-Tirado L, Neel J, Zhao Y, Reed JH, Tranter WH (2010) A survey of artificial intelligence for cognitive radios. IEEE Trans Veh Technol 59(4):1578–1592

31. Zhu X, Champagne B, Zhu W-P (2013) Cooperative spectrum sensing based on the rao test in non-Gaussian noise environments. In: WCSP 2013, Hangzhou, 24–26 Oct 2013. IEEE, pp 1–6
32. Martin JH, Dooley LS, Wong KCP (2011) A new cross-layer design strategy for TV white space cognitive radio applications. In: IEEE IWCLD, pp 1–5
33. Martin JH, Dooley LS, Wong KCP (2013) A new cross-layer dynamic spectrum access architecture for TV white space cognitive radio applications. In: IET ISP, pp 1—5
34. COGEU (2009) Cognitive radio systems for efficient sharing of TV white spaces in European context [Online]. Available at http://www.ict-cogeu.eu/pdf/COGEU_D2_1%20(ICT_248560).pdf. Accessed 20 Apr 2015
35. Taub H, Schilling DL (1986) Principles of communication systems. McGraw-Hill, New York
36. Kang K-M, Park JC, Cho S-I, Jeong BJ (2012) Deployment and coverage of cognitive radio networks in TV white space. IEEE Commun Mag 50:88–95
37. Alcatel-Lucent and BT (2013) WI-FI roaming – building on ANDSF AND HOTSPOT2.0 [Online]. Available at http://www.tmcnet.com/tmc/whitepapers/documents/whitepapers/2013/6686-wi-fi-roaming-building-andsfand-hotspot20.pdf. Accessed July 2015

Opportunities and Enabling Technologies for 5G and Beyond-5G Spectrum Sharing

61

Maziar Nekovee

Contents

Abstract

In this paper an overview is given of the current status of 5G industry standards, spectrum allocation, and use cases, followed by initial investigations of new opportunities for spectrum sharing in 5G and the underlying technologies to enable efficient sharing, considering both licensed and unlicensed scenarios and spectrum both below 6 GHz and in the millimeter-wave frequency range.

Keywords

5G NR · Millimeter wave · Spectrum · 3GPP · ITU · Cognitive radio · LLA · LSA · CBBS

M. Nekovee (✉)
Department of Engineering and Design, School of Engineering and Informatics, University of Sussex, Brighton, UK
e-mail: m.nekovee@sussex.ac.uk

W. Zhang (ed.), *Handbook of Cognitive Radio*,
https://doi.org/10.1007/978-981-10-1394-2_63

What Is 5G?

5G is the next generation of mobile communications technology and is being designed to provide (in comparison with 4G) greater capacity and faster data speeds and offer very low latency and very high reliability, enabling innovative new services across different industry sectors. The first wave of 5G commercial products is expected to be available in 2020 although some "pre-5G" deployments are already expected in 2018. 5G technology standards are currently under development and will include both an evolution of existing (4G) and new radio technologies (5G NR).

5G Use Cases

According to the International Telecommunication Union ITU [4] who has defined the vision and requirements of IMT2020 [1], potential 5G services and applications can be grouped into three different classes:

- Enhanced Mobile Broadband. Together with an evolution of the services already provided by 4G, 5G is expected to provide much faster and more reliable mobile broadband, offering a richer experience to consumers for application such a virtual reality (VR) and augmented reality (AR) as well as cloud-based services. The specific requirements are a minimum of 100 Mbps user-experience data rates and 20 Gbps peak data rate.
- Massive Machine-Type Communications. The Internet of Things (IoT) – where sensors, actuators, consumer electronics appliances, street lighting, etc. wirelessly connect to the Internet and each other. This is already happening on existing 4G networks, and the technology is being used in everything from smart homes to wearables. 5G should help the evolution of IoT services and applications and improve the interaction between different platforms as well as enable the vision of 50 billion devices becoming connected by 2030. Possible future applications could include real-time health monitoring of patients, optimization of street lighting to suit the weather or traffic, and environmental monitoring and smart agriculture. Data security and privacy issues will need to be considered given huge amounts of data could be transferred over a public network. We note that many IoT services are already being offered or will be offered in the next few years over existing and evolved 4G networks, e.g., using narrowband IoT (NB-IOT), LTE-M, or NB-LTE-M technologies. 5G, in this area, is likely to kick in by about 20205 where we expect to see through the explosion of new IoT services for which the evolution of LTE is unable to address the required scalability requirements.
- Ultrareliable and low-latency communications. This class is likely to rely on the new radio developments and includes services requiring a very high

Fig. 1 Exemplar use cases of 5G and their requirements

reliability and/or a very low latency. Possible applications include connected and autonomous cars and aerial vehicles, remote control of robots in extreme conditions and hazardous situations and for industry automation (Industry 4.0), remote surgery, and the so-called tactile Internet as well as some of the applications in the context of smart grids.

These different services have different requirements in terms of speed, coverage, latency, and reliability, which will demand different network solutions (the evolution of existing network and potentially new networks) and different deployment models (including many small cells), an appropriate network infrastructure (which will include both fiber and wireless connectivity to the core network), and access to different spectrum bands. Therefore, the concept of network slicing is being put forward, where different slices of the overall 5G network infrastructure (including spectrum) may be allocated to different types of services to end users (Fig. 1).

We note that in addition to the above three categories of 5G use cases, perhaps surprising a new use case for 5G, the so-called fixed wireless access (FWA) or fiber-like wireless, has recently emerged [2,3]. FWA refers to the provision of high-data-rate (>100 Mbps) broadband wireless access to residential customers and enterprise premises using pre-5G/5G access technologies, including full-dimensional MIMO (FD-MIMO), massive MIMO, and millimeter-wave radio access technologies. The FWA concept has been around for quite a long time (being known also as wireless local loop), but only with 5G the techno-economic case for this use case has become a compelling alternative to wired solutions, such as next-generation cable, copper-based G-fast, and Fiber-to-the-Premises (FTTP) (Fig. 2).

Fig. 2 5G fixed wireless access architecture

Radio Access Technologies for 5G

Different from previous generations, where a new radio access technology replaced the old one, 5G will integrate different radio technologies. Some of these will be the evolution of already existing radio access technologies; some will be new. Different service classes could rely on different radio interfaces. Evolutions of the latest version of the 4G radio interface (LTE-Advanced Pro) are likely to be used to provide a coverage layer via macro cells. A new cellular radio interface (being developed in 3GPP under the name "New Radio" or "NR") operating in frequencies up to 50 GHZ will be used to provide very high data rates and ultralow latencies and to serve a very large number of devices via a large number of small cells. Low-cost, low-battery consumption IoT services are likely to be delivered initially using evolved 4G technologies, as described in the Introduction, with a gradual transition/phaseout to 5G by 2025. Wi-Fi evolutions will also play an important role for consumers, in particular to provide 5G services within homes or offices. In addition it is also expected that satellite technologies also play a role in 5G, in particular for wide area coverage in IoT application space (e.g., tracking of goods and vehicles) and also as a mechanism to off-load broadcast and multicast linear TV traffic from 5G cellular networks.

5G Standards Timelines

Figure 3 shows the latest (as of 25/06/2017) timeline of 3GPP (Third Generation Partnership Project), which is responsible for developing a global industry standard for 5G mobile communication technologies. As can be seen from this figure, 5G phase 1 standards, which are mainly focusing on enhanced mobile broadband (eMBB) with some element of ultralow latency included, are expected to be ready mid-2018, with an initial "non-stand-alone" version of the standard to be released already by the end of 2017. The second phase of 5G technology, which encompasses massive machine-type communications and ULL, is expected to be ready by the end

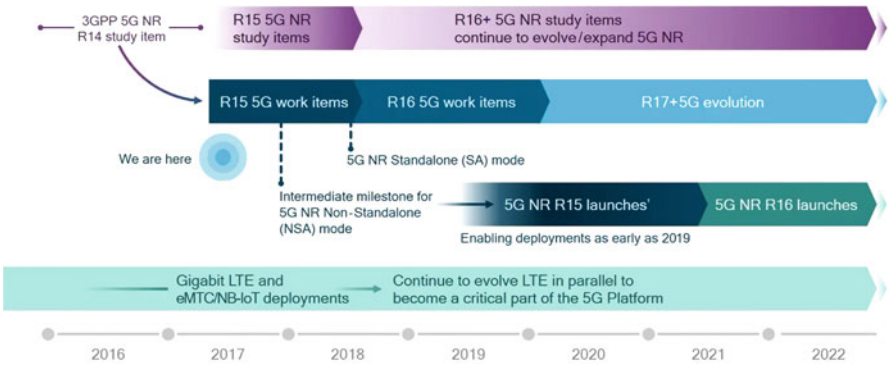

Fig. 3 5G standardization timeline according to 3GPP

of 2019, in time for the standard to be proposed to ITU as a candidate technology which fulfils the IMT 2020 requirements.

Spectrum for 5G

Spectrum is a critical component of wireless networks. It makes up the "airwaves" that underpin the communication services we use every day, such as mobile, Wi-Fi, and TV. The diverse set of 5G services and applications, described above, will require a diverse set of spectrum bands, with different characteristics, addressing different requirements and combining both low and high frequencies:

- Spectrum at lower frequencies, and in particular below 1 GHz, to enable 5G coverage to wide areas;
- Spectrum at higher frequencies with relatively large bandwidths below 6 GHz, to provide the necessary capacity to support a very high number of connected devices and to enable higher speeds to concurrently connected devices; and
- Spectrum at very high frequencies above 24 GHz (e.g., millimeter wave) with very large bandwidths, providing ultrahigh capacity and very low latency. Cells at these frequencies will have smaller coverage (between 50 and 200 m), and it is likely that build-out of 5G networks in millimeter wave bands will initially be focused on areas of high traffic demand or to specific locations or premises requiring services with very high capacity and/or peak data rates (Gbps) (Fig. 4).

5G Spectrum Allocation

The 2015 World Radio Congress (WRC-15) agreed on a WRC-19 agenda item (1.13) to consider the identification of frequency bands for the future development of International Mobile Telecommunications (IMT), including possible additional

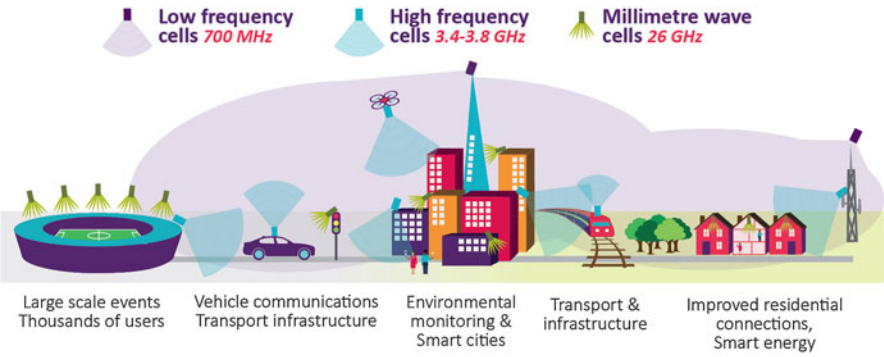

Fig. 4 Radio spectrum for 5G and its uses [Ofcom]

allocations to the mobile service on a primary basis, in accordance with Resolution 238 (WRC-15). This involves conducting and completing the appropriate sharing and compatibility studies for a number of bands between 24 and 86 GHz in time for WRC-19. The compatibility and sharing studies for these bands are being carried out in ITU-R Task Group 5/1 until 2018. This follows work in ITU-R on spectrum needs, deployment scenarios, sharing parameters, and propagation models which were completed in March 2017.

Candidate bands identified for further study in WRC-15 are shown in Fig. 5. It can be seen that there are regional differences, and in particular in the 20–30 GHz range, it can be expected that the 27.5–29.5 band will be only available in Americas, while other regions, including Europe, are likely to converge around the 24.25–27.5 range.

In parallel on the European level, Radio Spectrum Policy Group (RSPG) has developed in 2016 a strategic road map for 5G in Europe. In particular, the road map identified the following building blocks for 5G:

- Low-bandwidth spectrum at **700 MHz**; Medium-bandwidth spectrum at **3.4–3.8 GHz** as a "primary" band, which will provide capacity for new 5G services; and
- High-bandwidth spectrum at **24.25–27.5 GHz** as the "pioneer" millimeter wave band to give ultra-high capacity for innovative new services, enabling new business models and sectors of the economy to benefit from 5G. In addition, a European Commission Mandate to CEPT was approved by member states with regard to the development of harmonized technical conditions in two "pioneer" bands: 3.4–3.8 GHz and the 26 GHz band.

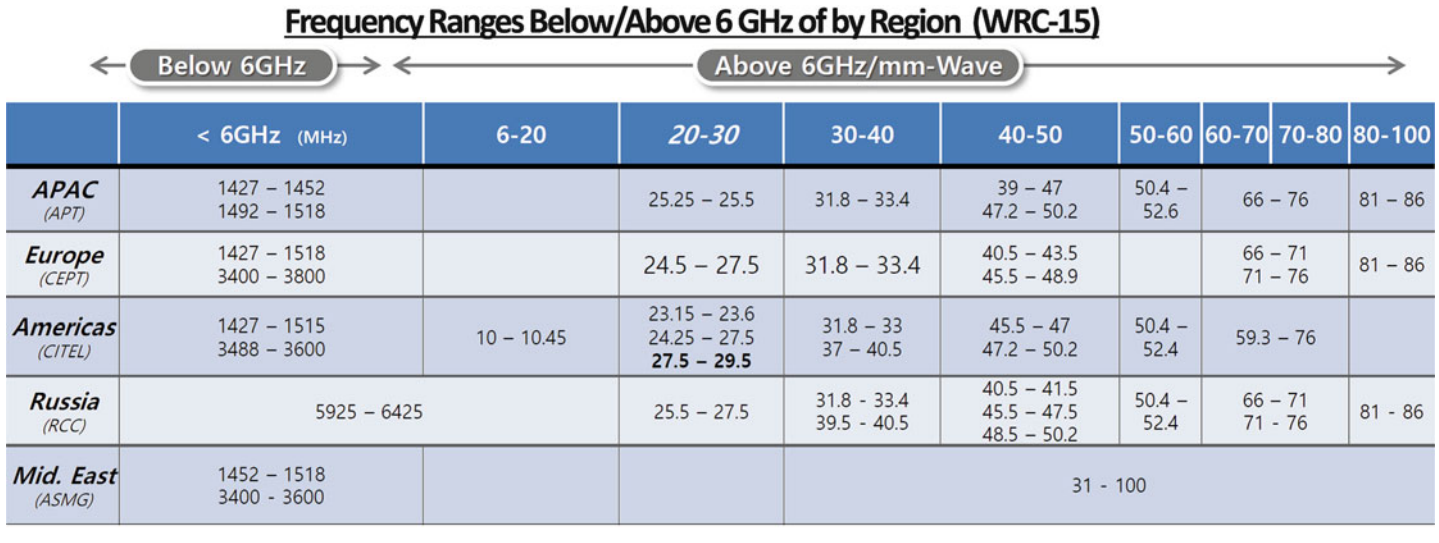

	< 6GHz (MHz)	6-20	20-30	30-40	40-50	50-60	60-70	70-80	80-100
APAC (APT)	1427 – 1452 1492 – 1518		25.25 – 25.5	31.8 – 33.4	39 – 47 47.2 – 50.2	50.4 – 52.6	66 – 76		81 – 86
Europe (CEPT)	1427 – 1518 3400 – 3800		24.5 – 27.5	31.8 – 33.4	40.5 – 43.5 45.5 – 48.9		66 – 71 71 – 76		81 – 86
Americas (CITEL)	1427 – 1515 3488 – 3600	10 – 10.45	23.15 – 23.6 24.25 – 27.5 **27.5 – 29.5**	31.8 – 33 37 – 40.5	45.5 – 47 47.2 – 50.2	50.4 – 52.4	59.3 – 76		
Russia (RCC)	5925 – 6425		25.5 – 27.5	31.8 - 33.4 39.5 - 40.5	40.5 – 41.5 45.5 – 47.5 48.5 – 50.2	50.4 – 52.4	66 – 71 71 - 76		81 - 86
Mid. East (ASMG)	1452 – 1518 3400 - 3600			31 - 100					

※ APT : Asia-Pacific Telecommunity (APT)
CITEL : Inter-American Telecommunication Commission
ASMG : Arab Spectrum Management Group

CEPT : European Conference of Postal and Telecommunications Administrations
RCC : Regional Commonwealth in the Field of Communications (Russia etc.)

Fig. 5 Candidate frequency bands for 5G as identified in WRC15

5G Spectrum Sharing

Sharing Below 6 GHz Spectrum

While above 6 GHz large chunks of spectrum are expected to become available for 5G systems, the amount of spectrum the sub-GHz and below 6 GHz range is far more limited. The sub-6GHz band is expected to support important applications of 5G, such a machine-type communications due to excellent propagation and indoor penetration characteristics, while the first wave of 5G mobile communication systems are expected to be deployed in 3.6 GHz frequency range, where in conjunction with the use of massive MIMO and full-dimensional MIMO (FD-MIMO) technologies 100Mbps+ data rates could be supported while also keeping cell sizes sufficiently large for viable deployment. It is, therefore, of great importance to explore options for the sharing of these very precious portions of 5G spectrum.

Due to quality of service requirement of 5G use cases that are expected to be supported, a very important option for the sharing of these bands is the evolution of Licensed Shared Access (LSA) [5]. In this approach licensed users, called LSA licensees, can access underutilized licensed spectrum on an exclusive basis, thus enjoying predictable QoS, when it is not being used by the incumbent, hence protecting it from harmful interference.

In 2017, the Federal Communications Commission (FCC) opened up 150 MHz of spectrum in the USA around 3.5 GHz that it named *Citizens Broadband Radio Service (CBRS)* [12]. Similar to the LSA approach, CBRS enables others to use the spectrum while it is still being used by existing incumbents, such as the military or satellite communication (see Fig. 6). However, in addition to sharing with incumbents – CBRS adds a "third tier" of general usage. In this third tier, anyone can use the spectrum when it is not used by the higher tiers (the incumbents or users that paid for a license) (see Fig. 2). Of course, if there are multiple third-tier users in the same area, then they will share the available spectrum with each other in a fair manner. The complexity of managing three tiers will require some additional control. To this effect, the FCC has defined a Spectrum Access System (SAS) – a type of database, in effect – and the *Wireless Innovation Forum* is helping to specify the details to ensure that it all works in accordance with the FCC rules.

CBBS can be used by existing mobile operators to offer Gigabit LTE in more places by making more spectrum available. One can also use this spectrum for small-cell deployments to extend coverage and add capacity indoors. Another foreseen

Fig. 6 CBBS spectrum sharing scenario in 3.5 GHZ between an incumbent system (in this case Navy radar) and secondary users

use is the so-called neutral host, which is a LTE deployment that can be used by subscribers irrespective of their service provider.

Sharing mm-Wave Spectrum

Millimeter-wave (mm-wave) communications have emerged as a key disruptive technology for both cellular networks (5G and beyond) [6] and wireless local area networks (802.11ad and beyond). While spectrum availability is limited in traditional bands below 6 GHz, mm-wave frequencies offer order of magnitude greater bandwidths. In addition, mm-wave communication is typically characterized by transmissions with very narrow beams, enabling further gains from directional isolation between mobiles. This combination of massive bandwidth and spatial degrees of freedom may make it possible for mm wave to meet some of the boldest 5G requirements, including higher peak per user data rate, high traffic density, and very low latency. The use of mm-wave bands for 5G presents a number unique features not present at lower frequencies:

- **Beamforming as a mandatory requirement**: A common characteristic of all systems operating in mm-wave frequencies is that beamforming is mandatory to compensate for the significantly higher path loss in these frequencies. For example, the IEEE 802.11ad standard supports up to 4 transmitter antennas, 4 receiver antennas, and 128 sectors. Beamforming is mandatory in802.11ad, and both transmitter-side and receiver-side beamforming are supported. Furthermore specification of beamforming for 5G is expected to be finalized by 3GPP, as part of 5G New Radio (NR) work item. Consequently, beams provide a common new dimension for the sharing of spectrum among multiple access technologies.
- **Potential for "infinite" spatial reuse:** Wireless communications systems already rely on spatial sharing of spectrum in two dimensions, and the entire concept of cellular communications relies on spatial reuse of radio spectrum. In mm-wave systems with the use of transmit-side and receive-side beamforming, spatial spectrum reuse can be pushed even further down close to one dimension, which the footprint of interference from each transmission link becoming very close to the line, rather than an area, in two dimensions. In the idealized case of ultra-narrow beams, this would allow infinite spatial reuse of spectrum.

Sharing with Satellite Services

FSS (Fixed Satellite Service) is the official classification for geostationary communications satellites that provide, for instance, broadcast feeds to television stations, radio stations, and broadcast networks. The FSS uplink (from FSS to satellite) is allocated in the band from 27.5 to 30 GHz, which is adjacent to the 24.25–27.5 GHz band identified for 5G. Therefore, there could be potential issues with the

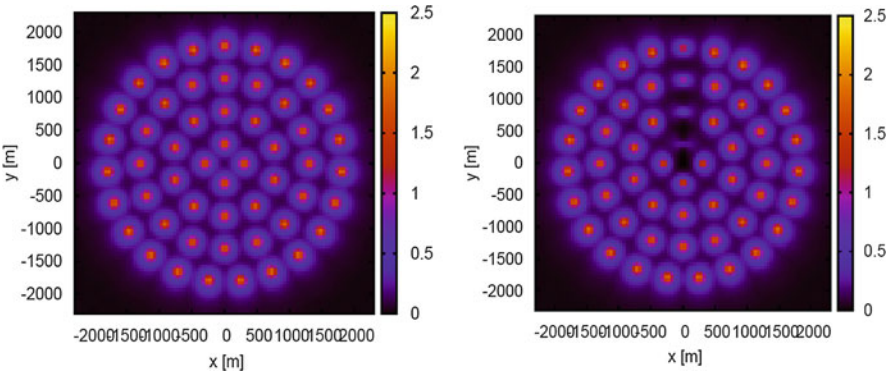

Fig. 7 Impact of FSS uplink transmission on the coverage of a mm-wave 5G network in the worse-case co-channel sharing of 28 GHz spectrum. Coverage maps are shown in the absence (left panel) and presence (right panel) of a FSS's highly directional transmitter positioned at the center of the area

sharing between 5G and FSS due to adjacent channel interference. Several cognitive techniques can be applied to mitigate and improve the 5G-FSS coexistence.

The coexistence between FSSs and mobile cellular BSs in the mm-wave bands has been the subject of only few, and mainly theoretical, studies. Important new parameters that need to be considered are how the interference levels could be reduced by exploiting multiple antenna configurations by 5G mm-wave systems as well as investigating the aggregate interference resulting from massive deployment of 5G systems on uplink FSS. The studies in [7, 8], performed in the worse-case scenario of co-channel sharing, have indicated that due to the use of a beamforming technology, combined with the relatively short range of communications in mm-wave frequencies, spatial sharing is much more feasible than in the case of IMT-advanced systems. In particular, even in this worse-case scenario, the required protection distance around FSS is much smaller (~1 km as opposed to hundreds of km) than those recommended previously. Furthermore, by using coordination among multiple 5G BS, further gains in spectrum sharing can be achieved. These studies also indicate that the presence of highly directional FSS transmission can cause outage in the coverage of 5G mm-wave network. However, due to the highly directional FSS transmission, the outage region is well-confined, and its impact could be mitigated using a combination of null forming at 5G UEs and cooperation by multiple BS to boast signal strengths at the victim UE (Fig. 7).

Sharing Between Access and Backhaul (Fixed) Links

The 26 GHz frequency range is used in many countries for 4G backhaul links, also known as fixed links (FL). Therefore it is of prominent importance to investigate the compatibility of using the 24.25–27.5 GHz for 5G access. A recent study of coexistence between FL and 5G access links has been performed by Ofcom [ofcom]. The study considered the deployment of 5G mm-wave base stations (BS) in London

overlaid on the existing FS deployment. It was assumed that, to avoid harmful interference to FS links, 5G BS can only operate if they are outside the denial area of FS links. Denial areas where assumed to be circular and were derived from interference analysis of a single 5G BS on a single FS link (Fig. 8).

The analysis shows that, in the non-LoS case, 5G BS would not be able to be rolled out within 0.5 km of a typical FL without a 20% probability of causing unacceptable levels of interference in all directions. This probability significantly increases in the pointing direction of the FL, while the distance at which a 20% probability of causing unacceptable levels of interference increases to 1.2 km. Therefore, to ensure that unacceptable interference was not caused to this incumbent FL, this area would have to be denied to IMT-2020 BSs. In fact, dependent on the requirements of the incumbent FL and what probability of interference they were willing to accept, this denial area may need to be significantly larger.

Figure 9 shows what impact this denial area would have on a mobile operator wanting to deploy 5G BSs in an urban conurbation, provided they were willing to ensure that their 5G BS did not have LoS to any FL. In this figure a denial area of 1.2 km is placed over all FLs in London which overlap with the block of 400 MHz of spectrum from 24.5 to 24.9 GHz (shown in red).

Sharing Unlicensed mm-Wave Spectrum

A recent trend in cellular communication is to utilize both the licensed and unlicensed spectrum simultaneously for extending available system bandwidth. In this context, LTE in unlicensed spectrum, referred to as LTE-U, is proposed to enable mobile operators to off-load data traffic onto unlicensed frequencies more efficiently and effectively and provides high performance and seamless user experience. Integration of unlicensed bands is also considered as one of the key enablers for 5G cellular systems. However, unlike the typical operation in licensed bands, where operating base stations (BS) have exclusive access to spectrum and therefore are able to coordinate by exchanging of signalling to mitigate mutual interference, such a multi-standard and multi-operator spectrum-sharing scenario (as shown in Fig. 4), this imposes significant challenges on coexistence in terms of interference mitigation. Licensed Assisted Access (LAA) with listen-before-talk (LBT) protocol has been proposed for the current coexistence mechanism of LTE-U. In case of mm-wave unlicensed sharing, a major issue is that the use of highly directional antennas as one of the key enablers for 5G networks becomes problematic for the current coexistence mechanisms where omnidirectional antennas were mostly assumed. For example, as shown in Fig. 10, transmission by a different nearby 5G BS or WiGig access point (AP) may not be detected due to the narrow beam that has been used, resulting in "beam collision" which can cause even more excessive interference than in conventional systems (Fig. 10).

We note that such beam-collision interference scenarios can also occur in exclusively used mm-wave spectrum as well. However in such scenarios, centralized resource allocation algorithms from 4G can be extended to include beam scheduling among multiple base stations to avoid such excessive interference scenarios. In the case of unlicensed sharing of mm-wave spectrum, centralized coordination is

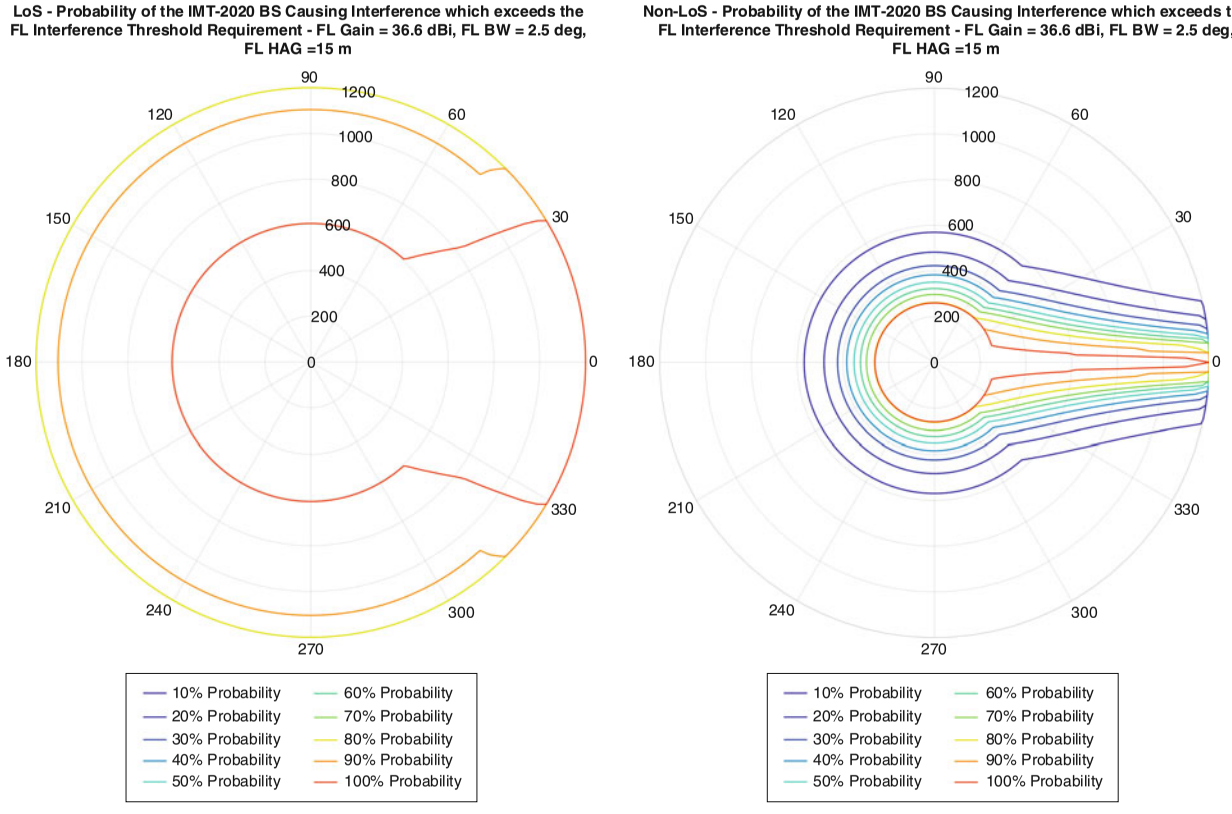

Fig. 8 Contour plots showing the probability of a 5G base station causing harmful interference to a fixed link operating in 26 GHz assuming line-of-sight (left panel) and non-line-of-sight (right panel) results [11]

Fig. 9 Denial area within 1.2 km of all backhaul links in London operating in the 24.9 GHz [11]

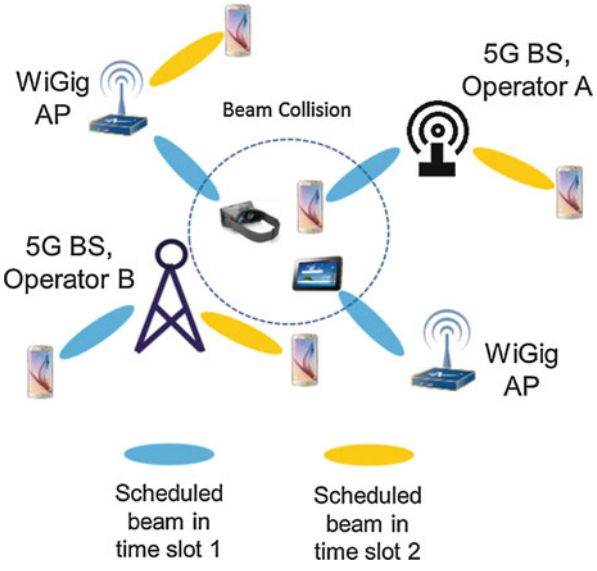

Fig. 10 Multi-standard and multi-operator sharing of unlicensed mm-wave bands in future 5G systems, showing also a beam-collision interference scenario [9]

not possible, and novel mechanisms need to be developed. Work in this direction has only recently being started as part of a new study item in 3GPP 5G-NR which is expected to be completed in 2018 [10]. Various mechanisms for sharing are being proposed, including distributed and self-organized mechanism for beam coordination [9], and approaches based on spectrum pooling [13].

Conclusion

With industry standards for 5G cellular systems rapidly progressing and firming up, issues and challenges related to future sharing and coexistence of spectrum are starting to take a center stage. Furthermore, there is a strong desire from governments and regulators for efficient allocation and use of 5G spectrum. Therefore, given the maturity of technologies such as LSA, LLA, cognitive radio, and mm-wave communications, we can expect that spectrum sharing will be a very prominent area for innovation, standardization, and spectrum regulation in the next few years. Finally beyond 5G mm-wave frequencies, the World Radio Congress in 2019 is expected to consider new spectrum beyond 300 GHz [14], where new opportunities for spectrum sharing can be expected.

Cross-References

- ▸ Cognitive Radio: The Need to Align Regulations with Technology
- ▸ Coexistence of Heterogeneous Cellular Networks
- ▸ Novel Regulatory Solutions for Cognitive Radio and Spectrum Sharing in the UK
- ▸ Spectrum Sharing Policy at Global Level
- ▸ Spectrum Sharing Policy in Europe
- ▸ Spectrum Sharing Policy in the Asia-Pacific Region

References

1. Recommendation ITU-R M.2083-0, IMT Vision – framework and overall objectives of the future development of IMT for 2020 and beyond, Sept 2015
2. Ovum (Sponsored by Samsung), 5G fixed-wireless access, providing fiber speeds over the air while also helping pave the way for 5G full mobility, 2016
3. Laraqui K, Tombaz S, Furuskär A, Skubic B, Nazari A, Trojer E (2016) Fixed wireless access on massive scale for 5G, Ericsson Technology Review, Dec 2016
4. ITU-R Working Party 5D, Minimum requirements related to technical performance for IMT-2020 radio interface(s), Feb 2017
5. Matinmikko M et al (2014) Spectrum sharing using licensed shared access: the concept and its workflow for LTE-advanced networks. IEEE Wirel Commun Mag 21:72–79
6. Roh W, Seol J-Y, Park J, Lee B, Lee J, Kim Y, Cho J, Cheun K, Aryanfar F (2014) Millimeter-wave beamforming as an enabling technology for 5G cellular communications: theoretical feasibility and prototype results. IEEE Commun Mag 52(2):106–113
7. Guidolin F, Nekovee M (2015) Investigating spectrum sharing between 5G millimeter wave networks and fixed satellite systems. In: IEEE GLOBECOM Workshops 2015, San Diego, pp 1–7
8. Guidolin F, Nekovee, Badia L., Zorzi M. (2015) A study on the coexistence of fixed satellite service and cellular networks in a mmWave scenario. In: IEEE ICC 2015, London, pp 2444–2449
9. Nekovee M, Qi Y, Wang Y (2017) Self-organized beam scheduling as enabler for coexistence in 5G unlicensed bands. IEIC Trans vE100.B:1181–1189

10. 3G PPP TSG RAN Meeting # 75, RP-170828, Study on NR-based Access to Unlicensed Spectrum, Mar 2017
11. UK Contribution, to ECC PT1 Meeting #56, 4–8 Sept 2017, CG on 26 GHz Fixed Link Studies – IMT -2020 Base Station and Microwave Fixed Links co-existence Study, Ofcom
12. https://www.fcc.gov/document/fcc-puts-final-rules-place-new-citizens-broadband-radio-service
13. Rebato M, Boccardi F, Mezavilla M, Zorzi M (2017) Hybrid spectrum sharing in mmWave cellular networks. IEE Trans Cog Commun Netw 3(2):155–168
14. The World Radio Congress 2015, Resolution 767, Studies towards an identification for use by administration for land-mobile and fixed service operating in the frequency range 275–450 GHz

Learning Dynamic Jamming Models in Cognitive Radios

62

Andrea Toma, Carlo Regazzoni, Lucio Marcenaro, and Yue Gao

Contents

A. Toma (✉)
Department of Electrical, Electronic, Telecommunications Engineering and Naval Architecture (DITEN), University of Genoa, Genoa, Italy

School of Electronic Engineering and Computer Science (EECS), Queen Mary University of London, London, UK
e-mail: andrea.toma@ginevra.dibe.unige.it; a.toma@qmul.ac.uk

C. Regazzoni · L. Marcenaro
Department of Electrical, Electronic, Telecommunications Engineering and Naval Architecture (DITEN), University of Genoa, Genoa, Italy
e-mail: carlo.regazzoni@unige.it; lucio.marcenaro@unige.it

Y. Gao
School of Electronic Engineering and Computer Science (EECS), Queen Mary University of London, London, UK
e-mail: yue.gao@qmul.ac.uk

W. Zhang (ed.), *Handbook of Cognitive Radio*,
https://doi.org/10.1007/978-981-10-1394-2_64

Abstract

Cognitive radio (CR) integrates results from software-defined radio (SDR), machine learning (ML), and neuroscience for smart radio transmission devices. SDR enables devices to be digitally and dynamically configured in online applications; methodologies and techniques developed to introduce self-awareness in existing systems can be based on ML. Specifically, CR can adaptively regulate its internal parameters in response to the changes in the surrounding environment. New physical layer security issues are also emerging, for example, smart jamming attacks aim to reduce the quality of service or to disrupt legitimate communications. In this context, the electromagnetic spectrum represents the environment, while signals inside it are the individual entities. A CR-to-spectrum interaction consists of a dynamic process that can be driven by a CR device. Learning dynamic and measurement models from spectrum data is the main objective in CR applications.

To learn a model, statistical signal processing techniques can be used. Such models can be considered as parametric Bayesian filters that allow a CR to estimate current state of observed entities (including CR itself) and to predict their actions in the near future. Adaptive hierarchical Bayesian filters able to cover nonstationary entity behaviors can be described through probabilistic graphical models (PGM). *Interacting entities* can be modelled by coupling multiple PGMs related to different entities.

In this chapter, state-of-the-art on representation and learning of dynamic models for physical layer security is introduced along with some future directions. An experimental framework is then presented with two currently investigated applications: *Spectrum Intelligence* and *TV White Spaces (TVWS)*.

Keywords

Dynamic jamming models · Cognitive radio · Learning models · PHY-layer security · TVWS · Interactive and Cognitive Environment · Dynamic spectrum access · Time-frequency analysis · Self-awareness · Learning interactions

Introduction

An *Interactive and Cognitive Environment (ICE)* [17] can be defined as a physical environment with artificially extended capabilities obtained through digital artificial cognition based on information and communication technologies (ICT). An ICE

requires the capability to understand and to actively modulate human-machine interactions by learning from experiences.

A CR device can be seen as an actor of an ICE. In particular, the physical nature of the appropriate environment for a CR is the electromagnetic (EM) spectrum. Considering that, since a CR is equipped with antennas to send signals on the spectrum as well as to sense the frequency content in the same spectrum, it can perform a cognitive cycle and, consequently, becomes progressively smarter provided that it can learn models from experiences that associate the signal that the CR can sense to signals it can send. In other words, the CR becomes smarter if it can learn models that are able to adapt the cognitive cycles applied to maintain a dynamic equilibrium with the external environment. Recent advances in both SDR and ML can make this possible. SDR is a paradigm which enables a full software implementation of radio devices making them general purpose and dynamically reconfigurable devices (even in online applications). This means that internal parameters can be regulated and controlled by software according to some internal and/or external state. Implementation of real-time adaptive systems is then feasible. By employing ML, a paradigm is available consisting of methodologies and techniques developed to translate big amounts of sensed data into classification and generative models that can be used to detect and predict situations. Self-awareness can be introduced in existing systems (such as radar, robots, and wireless equipments) that can enable radios to become more adaptive, cognitive, and interactive. The success encountered in this field has resulted in innovative techniques in radio communications like *dynamic spectrum access* (DSA) which enables opportunistic transmission on shared spectrum and *defense against jamming attacks* to address the physical layer (PHY-layer) security problem. *Spectrum Intelligence (SI)* and *TVWS* are two current applications of Interactive and Cognitive devices as described in this chapter.

Since the environment is assumed to be dynamic, *time information* is a decisive factor when analyzing and processing signals. To this end, *time-frequency analysis* is the tool which retains both frequency and time information of signals, namely, not only where signals are inside the spectrum of interest but also when they are in specific bands that represent the contextual spectrum environment. Specifically, dynamic features can be extracted from the two-dimensional representations (such as bandwidth, central frequency, transmitting power, and shape) of each signal. These features constitute a way to indirectly observe the state (hidden or non-observable) in the dynamical model for each entity. The spectrum of interest is the dynamic environment, while signals inside it represent the observations by which the hidden state of the entities can be measured. Once the problem is described, signal representation is the framework which enables entities and interactions modelling. There are several techniques to perform signal representation, namely, modelling entities in the specific environment. Basically, dynamic systems are used in which the state is observed through noisy measurements. They consist of both a *dynamic model* of the state and a *measurement model*. Transition probabilities of the state refer to the probabilities of changing from an initial state to a new state. In an

ICE scenario, single entities are described by stand-alone models, while interacting (multiple) entities are described by linked coupled models.

In this chapter, different features and signal representations are presented along with probabilistic models. This is necessary to go through the learning process in order to estimate and predict state and transitions for each single entity as well as interactions for multiple interacting entities.

The remainder of the chapter is organized as follows: firstly, PHY-layer security is introduced in section "PHY-Layer Security" with particular emphasis to jamming attacks and intelligent jammers. Afterwards, in section "Dynamic Signal Representation" different representations for dynamic signals are described from conventional features, including time-frequency representation, to probabilistic graphical models to represent single entity state and interacting entities situation assessment. Learning dynamic Bayesian representations is then presented in detail in section "Learning Dynamic Bayesian Representations" including techniques in the state-of-the-art employed to learn dynamic models for both single and interacting entities. To this end, several current techniques and algorithms, with some probable future work, are discussed in this context. Subsequently, *Spectrum Intelligence* and *TV White Spaces*, two currently investigated applications, are included in the experimental framework in section "Experimental Framework and Results", and some preliminary results are shown. A discussion about cognitive dynamic jamming can be found in section "A Discussion of Application Directions of ML Techniques to Cognitive Dynamic Jamming". Finally, some future directions are introduced in the conclusion of the chapter.

PHY-Layer Security

Signals can be transmitted in the shared spectrum with different objectives which means that legitimate users occupy the spectrum in a licit way complying with the security requirements and avoiding interference to other users, while malicious signals are transmitted to produce interference or disrupt legitimate communications. Indeed, radio communications in wireless environments introduce security issues due to external attacks from malicious devices. In particular, the PHY-layer is extremely vulnerable to *jamming attacks*. A malicious node in wireless networks can readily generate intentional interference for disrupting the data communications between legitimate users, which is referred to as a jamming attack (also known as denial of service – DoS – attack) [48]. In addition, the jammer may prevent authorized users from accessing wireless network resources by, for example, continuously transmitting a signal over a shared wireless channel so that legitimate nodes always find the channel busy and keep deferring their data transmissions. This impairs the network availability for the legitimate users.

Due to the recent developments in SDR and ML, both legitimate users and smart (or intelligent) jammers can quickly learn the transmission parameters of the other users in the spectrum of interest and adaptively adjust its transmission parameters to maximize the utility function and the damaging effect, respectively [47].

Recently, in addition to *SI* and *TVWS* discussed in the experimental framework of this chapter, substantial efforts have also been devoted to the research and development of the fifth-generation (5G) mobile systems. Indeed, strict security requirement is desired for the 5G systems, since more and more sensitive information will be transmitted wirelessly. To this end, physical layer security will be a beneficial complement to conventional security mechanisms [48].

In this context, *spectrum sensing (SS)* is the fundamental method which provides radio devices with information about the wireless spectrum in the surrounding environment in which signals with different characteristics, such as different modulation schemes, different communication standards, or different objectives, are transmitted taking into account spectrum sharing techniques. In literature, various SS techniques have been proposed for CRs, such as energy detection [9], matched filtering detection [46], cyclostationary feature detection (CFD) [34], and wavelet transform [42].

Dynamic Signal Representation

The first step toward learning dynamic models is signal representation through feature-based, graphical, and probabilistic methods. This is a decisive step because the performance of the learning process is strongly influenced by the chosen signal representation. Consequently, features representing the signal of interest, the corresponding model, and the necessary parameters should be selected carefully since a sensible choice of them may produce better learning accuracy.

Features are extracted from the signal and represented in the corresponding feature space. Some of the extracted features can provide information about the state variable of the entity whose state needs to be dynamically estimated. They could be, e.g., central frequency, bandwidth, transmitting power, shape, and other more complex entity state descriptors (of analog and digital modulated signals) as presented in this section.

Consequently, probabilistic representation of random variables related to the signal as random process can be obtained by using the extracted features. Specifically, dynamic models (which include the state variable and its noisy observations) are described by PGMs such as DBNs from Bayesian theory.

In this section, after discussing conventional features and algorithms to extract them, time-frequency analysis is introduced, and then, probabilistic models corresponding to both single and interacting entities are discussed.

Conventional Features and Detectors

In the CR framework, there are many SS schemes such as energy detector, matched filter detector, cyclostationary feature detector, and wavelet-based SS.

– *Energy detector (ED)*: this process formally corresponds to solving the decision problem between the following two hypotheses [12]:

$$Z(n) = \begin{cases} \eta(n), & H_0 \\ S(n) + \eta(n), & H_1 \end{cases}; \quad n = 1, ..., N_S \tag{1}$$

where $Z(n)$, $S(n)$, and $\eta(n)$ are the received signal, the transmitted signal, and the noise samples, respectively. H_0 is the *null hypothesis* corresponding to the absence of the signal (in this case, received signal consists of only noise), and H_1 is the *alternative hypothesis* corresponding to the presence of the signal, while N_S is the number of samples acquired during the sampling process.

Finding the appropriate threshold is the principal challenge of any energy detection scheme. The most common approaches are the constant detection rate (CDR) and constant false alarm rate (CFAR) detectors. Energy detection is easy to implement and does not require prior signal parameters, but its performances are highly dependent on noise levels and interference.

– *Matched filter detector (MFD)*: the received signal is convolved with a conjugated time-reverse version of the transmitted signal and then compared with a particular threshold level to recover the transmitted signal without any error. MFD is the optimal linear filter for maximizing the signal-to-noise ratio (SNR) in the presence of additive stochastic noise. Although in general this requires a non-flat frequency response, the associated distortion is not significant in situations such as radar and digital communications, where the original waveform is known and the objective is to detect the presence of this signal against the background noise.

The main advantage of the matched filter detector is that it achieves both high processing gain due to coherency and good robustness to noise uncertainty with moderate computational complexity. On the other hand, it requires a priori knowledge of the primary user signal such as the modulation type and order, the pulse shape, and the packet format. If this information is not accurate, the matched filter performs poorly [28]. In addition, matched filtering detector requires a dedicated receiver structure which may not be possible in a practical CR terminal.

– *Cyclostationary feature detector (CFD)*: it exploits the cyclostationarity of modulated signals by detecting spectral peaks in spectral correlation function (SCF) [34]. Major advantage of CFD-based detector lies on its abilities to perform better than energy detector at low signal-to-noise ratio (SNR) values and to distinguish different modulated signals. Furthermore, the cyclic spectral analysis has been used as a robust tool for signal classification when the carrier frequency and bandwidth information is unavailable. This performance is achieved at the cost of increased implementation complexity.

A process $x(t)$ is said to be wide-sense cyclostationary with period T_0 if its mean $E[x(t)] = \mu_x(t)$ and autocorrelation $E[x(t)x^*(t+\tau)] = R_x(t,\tau)$ are both periodic with period T_0; in such case, they can be defined, respectively, as $\mu_x(t+T_0) = \mu_x(t)$ and $R_x(t+T_0,\tau) = R_x(t,\tau)$. The major benefit of spectral correlation is its insensitivity to background noise. Furthermore, different types of modulated signals (BPSK, AM, FSK, MSK, QAM, PAM) with overlapping power spectral densities have highly distinct SCFs.

– *Wavelet-based detector*: wavelet transform (WT) is employed to characterize singularities and edges exhibited in the local singular structure of the PSD of a wideband signal $r(t)$, denoted by $S_r(f)$ in frequency. Edges in the spectrum correspond to the locations of frequency discontinuities $\{f_i\}_{i=1}^{N-1}$ to be identified.

WT provides good precision to detect the occupied spectrum and to identify and locate spectrum holes in the signal spectrum even for faded signals [42].

Formally, $\Psi(f)$ is a wavelet smoothing function with a compact support, m vanishing moments, and m times continuously differentiable. Widely used examples for $\Psi(f)$ include the Gaussian function and the perfect reconstruction filter bank (PRFB). The dilation of $\Psi(f)$ by a scale factor s is given by

$$\Psi_s(f) = \frac{1}{s}\Psi\left(\frac{f}{s}\right) \tag{2}$$

where s takes values from powers of 2, i.e., $s = 2^j$, $j = 1, 2, \cdots, J$. Letting $*$ denote convolution, the continuous wavelet transform (CWT) of $S_r(f)$ is given by $\mathscr{W}_s S_r(f) = S_r * \Psi_s(f)$. It has been shown that the local extrema of the first derivative and the zero-crossings of the second derivative characterize the signal irregularities.

The first-order and second-order derivatives of $S_r(f)$ smoothed by the scaled wavelet $\Psi_s(f)$ are derived in [42].

Time-Frequency Analysis and Features

The capability of describing the frequency content of a signal is a critical objective in diverse fields of science. Although the conventional Fourier transform (FT) is an extremely important signal and image analysis tool, it assumes that a signal is stationary, i.e., that the frequency content is constant at all times in a signal or at all locations in an image. However, in real applications like speech processing, geology, astronomy, or medicine, signals are nonstationary and frequency changes over time or space [5]. Consequently a series of techniques have been developed which analyze dynamic signals and extract time information about their spectral content by representing a signal as a function of both time and frequency. These methodologies are the foundation of time-frequency analysis, and the corresponding signal representations are commonly referred to as time-frequency distributions (TFDs). Cohen showed that these distributions are related to each other and provided a generalized equation for (TFDs) in [10].

Since TF operates in two-dimensional space, both time and frequency resolutions have to be considered, and such resolutions depend on the window choice. Time and frequency resolutions cannot be improved simultaneously: when the frequency resolution increases, the time resolution decreases, as a consequence of the time-frequency uncertainty principle [33]. Several TF approaches are here described.

– *Short-time Fourier transform (STFT)*: it is the most basic form of linear time-frequency transform [1] and defined as follows:

$$STFT\,(t,\omega) = \int x\,(\tau)\,h\,(\tau - t)\,e^{-j\omega\tau}d\,\tau \tag{3}$$

where $x\,(t)$ is the signal to be analyzed and $h\,(t)$ is the window function which is a symmetric function and is utilized to select a certain time interval of the signal. Changes in frequency over time are captured by sliding the window function to provide time localization. Due to the aforementioned time-frequency uncertainty principle, high frequency resolution is obtained with the window function as long as possible, which contradicts the time domain resolution. The commonly used window functions include rectangular window, triangular window, Hanning window, Hamming window, and Gauss window (in Gabor transform).

The discrete version of the STFT distribution can be found in [26]:

$$X\,(n,k) = \sum_{m=-\infty}^{+\infty} x\,[m]\,w\,[n-m]\exp^{-j2\pi km/N}\,R_N\,[k] \tag{4}$$

where $R_N\,[k] = u\,(k) - u\,(k - N + 1)$.

– *Wigner-Ville Transform (WVT)*: another fundamental distribution in the TF analysis is the Wigner-Ville distribution [3]. It is defined as the Fourier transform of the bilinear product (indeed, unlike linear time-frequency transform, the signal appears twice in bilinear time-frequency transform):

$$WVT\,(t,\omega) = \int x\left(t + \frac{\tau}{2}\right)x^*\left(t - \frac{\tau}{2}\right)e^{-j\omega\tau}d\,\tau \tag{5}$$

where $x^*\,(t)$ is the conjugate of the signal $x\,(t)$.

Even though this distribution provides improved resolution over a single-window spectrogram, it suffers from cross-terms due to its bilinear nature which can clutter the corresponding TF signature [27]. Indeed, for multicomponent signals, cross-terms are introduced, and the SNR is reduced. The more the multicomponents are, the more the cross-terms are generated. To reduce the cross-terms, the Cohen distribution introduced a kernel function $g\,(\theta,\tau)$ to perform as a two-dimensional low-pass filter. There are many kernel functions, including Born-Jordan, Choi-Williams, etc.

The discrete WVD of the time series $x\,(n)$ is given by:

$$DWVT\,(n,k) = \sum_{m=0}^{N-1} x\,(n+m)\,x^*\,(n-m)\,e^{-j2\pi mk/N} \tag{6}$$

where n and m are time indexes, while k denotes the frequency index, and N is the number of samples in the discrete time series.

– *Wavelet transform (WT)*: it improves on the STFT by introducing the concept of progressive resolution [14]. Transforms that incorporate progressive resolution are known to provide better, more consistent time-frequency representations across

the entire spectrum. The WT provides the equivalent of finer time resolution at high frequencies and finer frequency resolution at low frequencies. However, the WT does not measure frequency but only an analogue, called scale. Additionally, the WT provides either no phase information or phase measurements which are all relative to different local references. This is in contrast to the conventional concept of phase, as provided by the FT, where all phase measurements are relative to a global reference.

Wavelet is a waveform function $\Psi(t)$ with limited support in time and zero average which indicates that it is an oscillating function. Wavelets are not periodic and may have discontinuous derivatives; signals with rapid changes are analyzed better with the nonperiodic wavelets. The WT is defined as the projection of the time signal $f(t)$ onto a set of functions $\Psi_{s,d}(t)$ (daughter wavelets) obtained by translating and scaling the original wavelet $\Psi(t)$ (mother wavelet). They determined as:

$$\Psi_{s,d}(t) = \frac{1}{\sqrt{s}}\Psi\left(\frac{t-d}{s}\right) \tag{7}$$

where s is the positive adimensional scale parameter and d is the delay. The scale parameter stretches or compresses the mother wavelet and is connected to the frequency (low scale gives compressed wavelet and thus it can better analyze rapidly changing features which means high frequency components of a signal and vice versa). The delay parameter shifts the wavelet along the time axis and is connected to the time. Both parameters vary continuously. The WT of the signal is then:

$$W^f(s,d) = \int_{-\infty}^{+\infty} f(t)\,\Psi^*_{s,d}(t)\,dt = \int_{-\infty}^{+\infty} f(t)\,\frac{1}{\sqrt{s}}\Psi^*_{s,d}\left(\frac{t-d}{s}\right)dt \tag{8}$$

where wavelet coefficients $W^f(s,d)$ are functions of scale and delay. The basis of WT is not unique and should be chosen according to the characteristics of the signal. Time and frequency resolutions depend on the wavelet choice. There are a number of mother wavelets that can be used for analysis such as Gabor mother wavelet which has the best time-frequency resolution.

The discrete version of the wavelet transform can be found in [18].

– *Stockwell transform (ST)*: developed by Stockwell et al. [40] and based on a sliding Gaussian window distribution. It exhibits globally referenced phase and frequency measurements similar to those of the STFT, as well as the progressive resolution of the WT. This combination of desirable features makes ST particularly suitable in several fields, such as biomedical signal and image analysis applications, and has shown promise in one of the most recent applications which has been employing the ST extensively, namely, the automatic modulation recognition (AMR) [39], although the computational demands of the ST, due to redundant representation of time-frequency, in some cases limit its utility and prevent more widespread usage.

The ST of a nonstationary time signal is defined as

$$S(\tau, v) = \int_{-\infty}^{+\infty} g(t) \frac{|v|}{\sqrt{2\pi}} e^{-\frac{(\tau-t)^2 v^2}{2}} e^{-i2\pi vt} dt \tag{9}$$

where τ and v are the transform time and frequency coordinates. This equation has the same form as that of the FT but adds a normalized-area Gaussian window for time localization. The center of the window is τ, and the variance of the window is $1/v^2$; consequently the width of the window decreases with increasing frequency. This automatically adjusts the ST window to provide progressive resolution.

The ST of a discrete time series $r[p]$ is given by [2]:

$$S_T[m,n] = \sum_{p=0}^{P-1} r[p] \frac{|n|}{\sqrt{2\pi} kN} e^{-\left(n^2(m-p)^2/2k^2N^2 + j2\pi pn/N\right)} \tag{10}$$

when $m = 0, \cdots, M-1$; $n = 1, \cdots, N-1$; and by

$$S_T[m,0] = \frac{1}{P} \sum_{p=0}^{P-1} r[p] \tag{11}$$

when $n = 0$; m is the time delay of the sliding window, n denotes the index of frequency range, p denotes the time index, and k is a scaling factor that controls the time-frequency resolution. When k increases, the frequency resolution increases, with a corresponding loss of time resolution.

– *Hilbert-Huang transform (HHT)*: a multicomponent nonstationary signal is decomposed by using the empirical mode decomposition (EMD) technique [25], and then, the Hilbert transform (HT) is applied to the obtained components known as intrinsic mode functions (IMFs). Although the decomposition is adaptive and therefore highly efficient, IMFs suffer from mode mixing issue that result in an improper time-frequency representation.

From time-frequency analysis described in this section, features for each signal such as the central frequency, bandwidth, and transmitting power can be extracted and used as input dataset for the learning step to estimate model parameters for each signal, transition probability, and interaction as discussed in section "A Discussion of Application Directions of ML Techniques to Cognitive Dynamic Jamming".

Single Entity State

To represent the state of each entity, *probabilistic graphical models (PGMs)* provide a graph-based representation as in [30]. The main idea is to encode complex distributions over high-dimensional spaces where causality links are defined among model components. In the basic graphical representation depicted in Fig. 1a, random variables of the system model such as state and observables are represented by

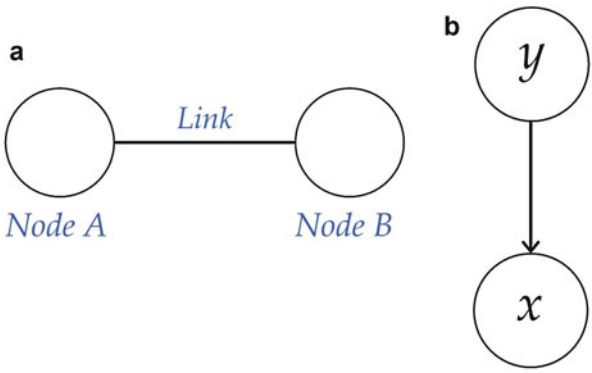

Fig. 1 (**a**) Basic probabilistic graphical model structure consisting of two nodes connected through a link, (**b**) graphical representation of the conditional probability $f_{\mathbf{X}|\mathbf{Y}}(\mathbf{x}|\mathbf{y})$

nodes, while edges (or links) express direct probabilistic relationships between them. Temporal dependencies among nodes can also be represented (often by horizontal edges) as can be seen later in this section. Furthermore, graphical models also introduce a compact representation for independencies among variables in the distribution described by corresponding graph. Considering that, probability distribution functions (PDFs) are often in the form of some parametric functions; the probabilistic relationship described by $p(\mathbf{x}|\mathbf{y}) = f(\mathbf{x}, \mathbf{y}, \theta)$ is represented as in Fig. 1b where $\mathbf{x}$ could be the state (hidden variable) of a dynamic system, $\mathbf{y}$ the corresponding observable, and θ the unknown parameter.

PGMs provide a statistical framework to model interactions and cause-effect relationships like in interaction analysis and enable formalizing and handling the uncertainties. The basic idea is to provide a graphical tool to decompose a multivariate probability distribution into a factored form by providing an intuitive and manageable visual description.

– *Dynamic Bayesian Networks (DBNs)* are based on Bayesian network (BN) approach which is a graph model describing the statistical relationships among a group of n random variables $\mathbf{X} = \{X_i\}_{i=1,2,\ldots,n}$. A BN is determined by its graph structure G and distribution parameter Θ. A variable X_i is independent of its non-descendants given all its parents $Pa(X_i)$ in G. Therefore, the joint probability distribution over $\mathbf{X}$ can be decomposed by:

$$Pr(\mathbf{X}) = \prod_{i=1}^{n} Pr(X_i | Pa(X_i)). \tag{12}$$

The parameter set $\Theta = \{\theta_i\}_{i=1,2,\cdots,n}$ specifies the parameters of each conditional distribution in (12). A Dynamic Bayesian Network (DBN) is the extension of a BN to model temporal processes. In DBN, a set of random processes is represented by the $\mathbf{X}(k) = \{X_i(k)\}_{i=1,2,\cdots,n}$, and $X_i(k)$ is the random variable of process at discrete time k. The network structure G now defines the dependency among variables over a period of time as well as those within the same time epoch. Assuming Markovian and causal processes, a node in graph G is only linked from the other nodes in the same or previous epoch [31]. Thus

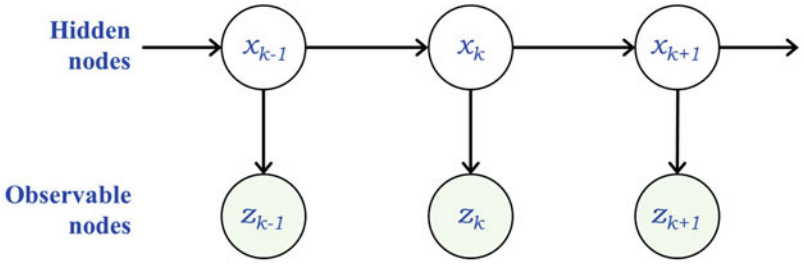

Fig. 2 Hidden Markov Model representation: **x**'s is latent variables, and **z**'s is the observable variables, while the horizontal arrows describe temporal dependencies

$$Pr\left(\mathbf{X}\left(k+1\right)|\mathbf{X}\left(0:k\right)\right) = Pr\left(\mathbf{X}\left(k+1\right)|\mathbf{X}\left(k\right)\right), \quad k = 0, 1, 2, ... \tag{13}$$

Several basic dynamic models which can be represented by DBNs are now introduced.

– a *Hidden Markov Model (HMM)* is a tool for representing probability distributions over sequences of observations and is in fact a special case of the more general DBNs [22]. In Markov models, the state is directly visible to the observer, and therefore, the state transition probabilities are the only parameters to be considered, whereas, in a HMM, the state is not directly visible, but only outputs, dependent on the state, are visible.

The HMM assumes that the observation at time k was generated by some process whose state $\mathbf{x}_k$ is hidden from the observer. It also assumes that the state of this hidden process satisfies the Markov property, which is, given the value of $\mathbf{x}_{k-1}$, the current state $\mathbf{x}_k$ is independent of all the states prior to $k-1$. Graphically we can explain it as shown in Fig. 2. The graph shows the dependencies between the variable of the model. $\mathbf{X} = \{\mathbf{x}_1, \mathbf{x}_2, \mathbf{x}_3, \cdots, \mathbf{x}_k\}$ is a sequence of unobservable states and $\mathbf{Z} = \{\mathbf{z}_1, \mathbf{z}_2, \mathbf{z}_3, \cdots, \mathbf{z}_k\}$ is a sequence of observable emissions. Considering that the probability of being in a particular state at step i is known once the state at step $i-1$ is known and that the probability of seeing a particular emission at step i is known once the state step i is known, the joint distribution of a sequence of states and observations can be factored in the following way:

$$P\left(\mathbf{x}_{1:k}, \mathbf{z}_{1:k}\right) = P\left(\mathbf{x}_1\right) P\left(\mathbf{z}_1|\mathbf{x}_1\right) \prod_{i=2}^{k} P\left(\mathbf{x}_i|\mathbf{x}_{i-1}\right) P\left(\mathbf{z}_i|\mathbf{x}_i\right) \tag{14}$$

– a *Switching linear dynamical system (SLDS)* is defined in [20] by:

$$\begin{cases} \mathbf{x}_k = \mathbf{A}^{(a_k)}\mathbf{x}_{k-1} + \mathbf{v}_k^{(a_k)} \\ \mathbf{z}_k = \mathbf{C}\mathbf{x}_k + \mathbf{w}_k \end{cases} \tag{15}$$

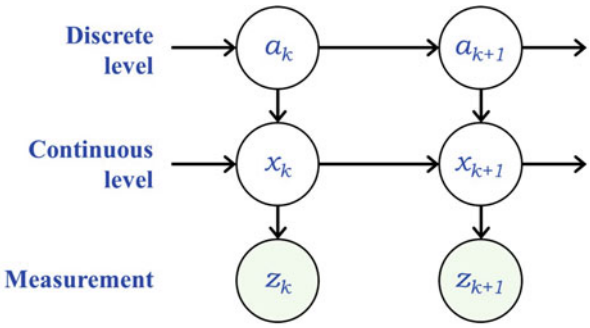

Fig. 3 A SLDS representation in which ¸'s are the categorical variables

with $a_k|a_{k-1} \sim \pi_{a_{k-1}}$. a_k belongs to a set $S \triangleq \{1, 2, \cdots, s\}$ consisting of a finite number of modes (i.e., categorical variable). When a discrete first-order Markov chain a_k with transition probabilities $\{\pi_{ij}\}$, $i, j \in S$, indexes the mode-specific linear dynamic system at time index k driven by Gaussian noise $\mathbf{v}_k^{(a_k)} \sim \mathcal{N}\left(0, \Sigma^{(a_k)}\right)$, it is called Jump Markov Linear System (JMLS). A JMLS can be seen as an extension of the (HMM), which has the same mode evolution, but conditionally independent observations. The corresponding probabilistic graphical representation is shown in Fig. 3. *Rao-Blackwellized particle filter* is an example of a commonly used filter associated with a switching model.

In general, the filtering process is performed to filter (estimate) and predict variables belonging to the dynamic models including nodes and links. Common filters also include:

– *Kalman filter* provides optimal finite-dimensional algorithm for recursive Bayesian state estimation in linear-Gaussian cases. A linear dynamic system is described by the following state-space equations:

$$\mathbf{x}_k = \mathbf{F}_{k-1}\mathbf{x}_{k-1} + \mathbf{n}_{k-1} \tag{16}$$

$$\mathbf{z}_k = \mathbf{H}_k\mathbf{x}_k + \mathbf{w}_k \tag{17}$$

Equation (16) represents the *process model*, while Eq. (17) represents the *measurement model*. Kalman filter assumes that the posterior pdf $p(\mathbf{x}_k|\mathbf{z}_k)$ at every step is Gaussian and then it can be completely characterized by the mean and the covariance. These assumptions hold if $\mathbf{n}_{k-1}$ and $\mathbf{w}_k$ are drawn from Gaussian density, and the dynamic system is linear.

The matrices $\mathbf{F}_k$ and $\mathbf{H}_k$ define the linear functions in the dynamic system. Random sequences $\mathbf{n}_k$ and $\mathbf{w}_k$ are mutually independent zero-mean white Gaussian with covariance $\mathbf{Q}_k$ and $\mathbf{R}_k$, respectively. Mean and covariance predictions are given by:

$$\hat{\mathbf{x}}_{k|k-1} = \mathbf{F}_{k-1}\hat{\mathbf{x}}_{k-1|k-1} \tag{18}$$

$$\mathbf{P}_{k|k-1} = \mathbf{Q}_{k-1} + \mathbf{F}_{k-1}\mathbf{P}_{k-1|k-1}\mathbf{F}_{k-1}^T \tag{19}$$

respectively. In the update process, the prediction is compared to the observation which results in the estimated mean and covariance are as follows:

$$\hat{\mathbf{x}}_{k|k} = \hat{\mathbf{x}}_{k|k-1} + \mathbf{K}_k \left(\mathbf{z}_k - \mathbf{H}_k \hat{\mathbf{x}}_{k|k-1}\right) \tag{20}$$

$$\mathbf{P}_{k|k} = \mathbf{P}_{k|k-1} - \mathbf{K}_k \mathbf{S}_k \mathbf{K}_k^T = \left[\mathbf{I} - \mathbf{K}_k \mathbf{H}_k\right] \mathbf{P}_{k|k-1} \tag{21}$$

where $\mathbf{z}_k - \mathbf{H}_k \hat{\mathbf{x}}_{k|k-1}$ is called innovation and denoted as $\mathbf{v}_k$, $\mathbf{S}_k$ is its covariance, and $\mathbf{K}_k$ is the Kalman gain. In presence of high Kalman gain, i.e., when the $\mathbf{P}_{k|k-1}$ is large or the $\mathbf{S}_k$ is small, the innovation is considered as reliable. A large Kalman gain value occurs when the prediction is not consistent and/or the innovation is trustworthy, and it implies that the estimate $\mathbf{x}_{k|k}$ relies more on the innovation than on prediction.

– the *Extended Kalman filter (EKF)* is a suboptimal solution of the Bayesian filtering problem for nonlinear systems with additive noise

$$\mathbf{x}_k = \mathbf{f}_{k-1}\left(\mathbf{x}_{k-1}\right) + \mathbf{n}_{k-1} \tag{22}$$

$$\mathbf{z}_k = \mathbf{h}_k\left(\mathbf{x}_k\right) + \mathbf{w}_k \tag{23}$$

The basic idea is to linearize the nonlinear functions by the first term in the Taylor series expansion. Prediction and innovation are computed using, respectively, nonlinear functions $\mathbf{f}_{k-1}$ and $\mathbf{h}_k$.

By substituting $\mathbf{f}_{k-1}$ and $\mathbf{h}_k$ with their local linearization (first-order Taylor approximation):

$$\hat{\mathbf{F}}_k = \left[\nabla_{\mathbf{x}_{k-1}} \mathbf{f}_k^T\left(\mathbf{x}_{k-1}\right)\right]^T \Big|_{\mathbf{x}_{k-1}=\hat{\mathbf{x}}_{k-1|k-1}} \tag{24}$$

$$\hat{\mathbf{H}}_k = \left[\nabla_{\mathbf{x}_k} \mathbf{h}_k^T\left(\mathbf{x}_k\right)\right]^T \Big|_{\mathbf{x}_k=\hat{\mathbf{x}}_{k|k-1}} \tag{25}$$

where

$$\nabla_{\mathbf{x}_k} = \left[\frac{d}{d\mathbf{x}_k\left[1\right]} \cdots \frac{d}{d\mathbf{x}_k\left[n_x\right]}\right]^T \tag{26}$$

and $\mathbf{x}_k\left[i\right]$ is the i-th component of the state vector, a linearized Kalman filter is obtained as in Eqs. (16), (17), (18), (19), (20), (21).

Unscented Kalman filter (UKF), cubature Kalman filter (CKF), and Gauss-Hermite Kalman filter (GHKF) are also variations of KF which handle the nonlinear Gaussian problem. Furthermore, nonlinear filtering also includes *particle filter and its variants*.

Interacting Entities Situation Assessment

The previous section investigated single entity representation through PGMs which well-capture dependencies of variables. More specifically, *temporal dependencies* (dynamics of the system) and *entity-to-entity dependencies* (interactions among objects) can be represented in graphical models.

To introduce entity-to-entity dependencies, interaction-oriented DBN structures can be employed with linked nodes belonging to different entities (interacting entities). Specifically, the DBN structure corresponding to a system consisting of two interacting objects described through a SLDS model (introduced in the previous section) is shown in Fig. 4.

Such kind of links defines the probability that a random variable of an entity influences (or is influenced by) one or more random variables of a different entity. Interactions may also happen among three or more objects; each of them can be represented through PGMs.

From neuroscience, cognition and interaction are two interrelated functionalities of biological systems. A *bio-inspired* approach is the main idea toward the concept of cognitive dynamic systems (CDSs) and the development of interactive

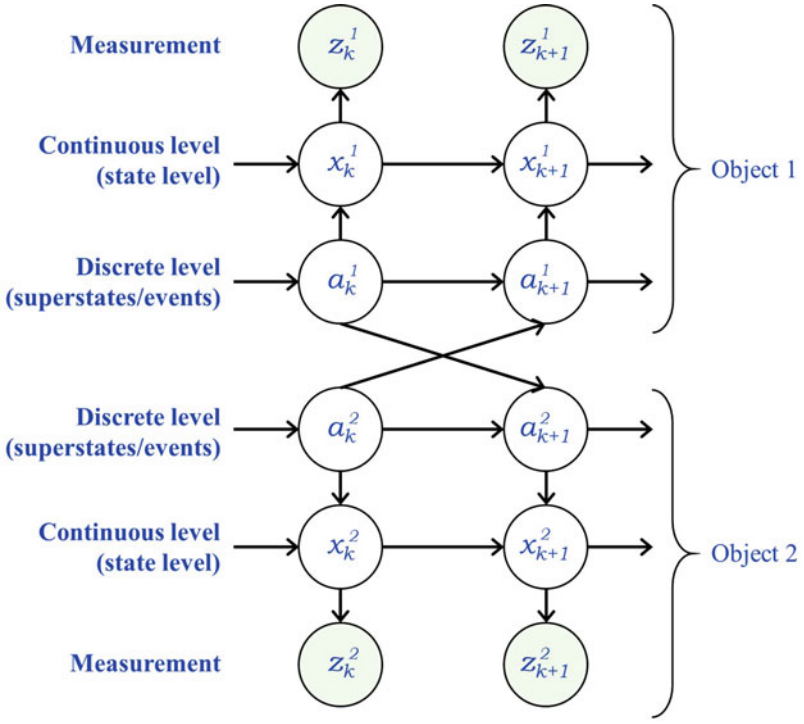

Fig. 4 Interaction-oriented SLDS structure with linked nodes belonging to two interacting objects

systems [17]. Dynamic systems take into account embodied and situated cognition by adaptively changing their state. The goal of dynamic systems is to maintain stability of the equilibrium between the object and the environment (i.e., maintenance of the proper level of security and/or safety). CDSs build up rules of behavior over time through learning from continuous experiential interactions with the environment and thereby deal with environmental uncertainties.

Specifically, a CDS can be described as a system whose design closely mimics the human brain and is motivated by human cognition. Cognitive reasoning is based on dynamical dispositional representations of the interactions between an object in contextual scenario and the changed organism state it causes [13]. Such dispositional representation of external objects with respect to a self-object is the key aspect of the knowledge embedded on bio-inspired CDSs. The capability of *learning from experience* and the idea of *autobiographical memory (AM)* are drawn from the bio-inspired approach of the interactions occurring between the system and the user. Indeed, this concept is based on neurophysiological observations of human brain structure for modelling and learning interactions between the user and the system and provides engineering implications in the development of context-aware learning and predicting strategies.

Self-awareness plays a key role in the development of *self-adaptation* techniques. In particular, self-adaptation based on self-awareness at the individual level means that one single entity receives inputs both from itself or some of its components and from the external environment and uses the input to adjust to the current conditions [32]. *Multiple entity adaptation* is then obtained by introducing the interaction of different self-adaptation techniques at the level of the single individual.

Learning Dynamic Bayesian Representations

Learning *dynamic models* can be considered a main objective in CR applications where the spectrum of interest hosts several signals whose parameters (such as central frequency, transmit power, modulation scheme, and so forth) may change across the measurement time. To this end, *learning from available data* (current and past data) should in perspective become a major approach used in this framework. Basically, in order to learn a model which describes a *single entity*, parameters are estimated and predicted by using statistical signal processing techniques and Bayesian filters. The cycle observation-update-prediction performs learning of parameters and dynamic models at successive time instants. In other words, when the system collects a new observation of the state, both the predicted transition probability of the state and the predicted measurements (obtained at the previous step) are updated with the new data, and their predictions for the subsequent time instant are also computed, as introduced in the KF description, for example. Again, when a new observation is collected, a new cycle observation-update-prediction is performed.

In this section, after introducing the basic concepts of learning, several techniques employed to learn causal conditioned probabilities, dynamic models, and

interactions are described along with some current work and probable future directions in the field of learning dynamic models.

Learning Vocabulary, State, and State Changes

A learning approach in a Bayesian framework starts with some a priori knowledge about both probabilistic distributions of the model structure (namely, edges in the graphical model) and the model parameters. A prior probability distributions over model structures and model parameters represent this initial knowledge which is then updated using the data to obtain the corresponding posterior probability distribution over models and parameters [21]. Denoting the prior distribution over model structures with $P(\mathbf{M})$, the priori distribution over parameters for each model structure with $P(\theta|\mathbf{M})$, and the dataset as $\mathbf{Y} = \{\mathbf{y}_1, \mathbf{y}_2, \cdots, \mathbf{y}_t\}$, the posterior distribution over models can be obtained through Bayes rule as follows:

$$P(\mathbf{M}|\mathbf{Y}) = \frac{\int P(\mathbf{Y}|\theta, \mathbf{M})\, P(\theta|\mathbf{M})\, d\theta\, P(\mathbf{M})}{P(\mathbf{Y})} \tag{27}$$

which takes into account the uncertainty in the parameters. The posterior distribution over the parameters, for a given model structure, can be obtained through:

$$P(\theta|\mathbf{M}, \mathbf{Y}) = \frac{P(\mathbf{Y}|\theta, \mathbf{M})\, P(\theta|\mathbf{M})}{P(\mathbf{Y}|\mathbf{M})} \tag{28}$$

Now, based on available data and models, the next observation $\mathbf{y}_{t+1}$ can be computed by Bayesian prediction as:

$$P(\mathbf{y}_{t+1}|\mathbf{Y}) = \int P(\mathbf{y}_{t+1}|\theta, \mathbf{M}, \mathbf{Y})\, P(\theta|\mathbf{M}, \mathbf{Y})\, P(\mathbf{M}|\mathbf{Y})\, d\theta d\mathbf{M} \tag{29}$$

based on averages over both the uncertainty in the model structure and in the parameters. This is known as *predictive distribution* for each model.

Typically, the state-space model (SSM) of a *dynamic system* consists of three random processes, namely, *state model*, *process model* of the state of a signal (or entity) which describes the transition of the state, and *measurement model* which describes observations of the state:

$$\begin{aligned} \mathbf{x}_0 &\sim p_0(\mathbf{x}_0) \\ \mathbf{x}_t|\mathbf{x}_{t-1} &\sim p_f(\mathbf{x}_t|\mathbf{x}_{t-1}) \\ \mathbf{z}_t|\mathbf{x}_t &\sim p_g(\mathbf{z}_t|\mathbf{x}_t) \end{aligned} \tag{30}$$

where $\mathbf{x}_t$ and $\mathbf{z}_t$ are the state and measurement vectors at time t, p_0 is the initial state probability distribution function (PDF), p_f is a conditional probability

density function (CPDF) representing the dynamics of the state, and p_g is a CPDF representing the measurement process. Interaction-oriented models include linked dynamic systems, as described in the previous section, to represent *interacting entities* in an ICE scenario.

Changes in the state of a dynamic system, described by the corresponding transition probability, are referred to as *trajectories*. Each entity adopts a strategy inside the spectrum of interest, which defines its behavior. *Normal behavior* means that it is predictable because already observed, and consequently the implemented model is capable of obtaining accurate estimates (and predictions) of the parameters and model by using learned information gathered from past experience. When the hypothesized model does not produce the estimates (and predictions) accurately, the behavior is said to be *abnormal*. This happens when the strategy has not been observed in past experiences or from a security point of view, that behavior is different (or not allowed) from legitimate behavior.

Learning Causal Conditioned Distributions

Learning techniques can be classified in *supervised learning* based on labelled data, but it is always an expensive training algorithm and difficult to obtain, and *unsupervised learning* which does not need the labelled data making it a better training algorithm. On the other hand, *semi-supervised learning* is a class of ML techniques which is receiving increasing interest in the last decade. These techniques combine both labelled and unlabelled data items in their training process. Therefore, they are usually applied in datasets in which only a small subset of data items may be effectively labelled, due to the high costs and time required in the labelling process [4]. In this section, some methods used in the literature to learn model parameters are introduced.

– *HMMs* are one of the most important techniques to model and classify sequential data with several applications in sequence modelling problems like speech recognition, human activity recognition (HAR), or time series analysis [35]. The Expectation-Maximization (EM) algorithm is the classical method used to learn the parameters of HMMs. However, it exhibits two main problems: (1) the likelihood is multimodal so the EM is guaranteed to converge only to local maxima, and (2) the multiple initializations required for minimizing the effects of the local convergence and the more than quadratic growth with the number of hidden states make EM computationally heavy with large training dataset. Bayesian inference methods including Gibbs sampling, variational optimization, or Bayesian non-parametric methods are even computationally heavier, and global convergence is still not guaranteed. A spectral algorithm for learning HMMs with discrete observations is proposed in [24]. This method adjusts the model by moment matching instead of maximizing the likelihood, and it relies on the use of the observable operators view of the HMM [35].

Learning of SLDSs is introduced in the practical example of section "A Discussion of Application Directions of ML Techniques to Cognitive Dynamic

Jamming". Now, two supervised learning methods are briefly described, while some unsupervised techniques are discussed in section "Some Current Learning Techniques and Probable Future Directions".

– *Support vector machines (SVMs)* are supervised learning models with associated learning algorithms that analyze data used for classification and regression analysis. In this chapter, SVD for regression is presented. The support vector method for regression is formulated in solving a convex optimization problem, more specifically a quadratic programming (QP) problem [15].

In SVM for nonlinear function regression, the main idea is to approximate the dataset

$$D = \{(\mathbf{x}_1, y_1), \cdots, (\mathbf{x}_k, y_k), \cdots, (\mathbf{x}_N, y_N)\}, \quad \mathbf{x}_k \in R^n, \quad y_k \in R \tag{31}$$

with a nonlinear function

$$f(\mathbf{x}) = < \boldsymbol{\omega}, \phi(\mathbf{x}) > + b \tag{32}$$

where $< \cdot, \cdot >$ denotes the dot product, $\boldsymbol{\omega} \in R^{n_h}$ is the weight vector in primal weight space, $\phi(\cdot) : R^n \rightarrow R^{n_h}$ is the nonlinear function that maps the input space to a high dimensional feature space where linear regression is performed, and b is the bias term. The optimization problem is given by:

$$\min \frac{1}{2}\|\boldsymbol{\omega}\|^2 + C\sum_{k=1}^{N}\left(\xi_k + \xi_k^*\right) \quad s.t. \quad \begin{cases} y_k - < \boldsymbol{\omega}, \phi(\mathbf{x}) > -b \leq \varepsilon + \xi_k \\ < \boldsymbol{\omega}, \phi(\mathbf{x}) > + b - y_k \leq \varepsilon + \xi_k^* \\ \xi_k, \xi_k^* \geq 0 \end{cases} \tag{33}$$

where ε is the approximation accuracy that can be violated by means of the slack variables ξ, ξ^* for the non-feasible case. The constant $C > 0$ determines a trade-off between flatness of f and the amount up to which deviations larger than ε are tolerated. A smaller value of C tolerated a larger deviation. From the constrained optimization problem in Eq. 33, the Lagrange function can be written as in [44] with multipliers α and α^*. Consequently, the resulting SVM takes the form:

$$f(\mathbf{x}) = \sum_{k-1}^{N}\left(\alpha_k - \alpha_k^*\right) < \phi(\mathbf{x}), \phi(\mathbf{x})_k > + b \tag{34}$$

where the inner product $< \phi(\mathbf{x}), \phi(\mathbf{x})_k >$ can be defined through a kernel $K(\mathbf{x}, \mathbf{x}_k)$.

However, the major drawback of SVM is its higher computational burden because of the required constrained optimization programming. Major breakthrough has been obtained at this point with a least squares version of SVM, called LS-SVM.

– *Gaussian processes (GPs) for regression* are a powerful supervised learning algorithm well-suited to high dimensional data analysis and nonlinear estimation problems [6]. Basically, given the covariance function, it provides an analytical

solution to any regression estimation problem. It does not only provide point estimates but it also gives confidence intervals for them. In GPs for regression, the optimization step to set the hyperparameters of the covariance function is performed by maximum likelihood. GPs method assumes a zero-mean GP prior over the space of possible functions and a Gaussian likelihood model. The posterior can be analytically computed; it is a Gaussian density function as well as the predictions given by the model.

Given a labelled training dataset ($D = \{\mathbf{x}_i, y_i\}_{i=l}^{n}$, where the input $\mathbf{x}_i \in \mathscr{R}^{d\times 1}$ and the output $y_i \in \mathscr{R}$) and a new input location $\mathbf{x}^*$, the probability distribution for its output y^*, i.e., $p(y^*|\mathbf{x}^*, D)$, can be predicted. Assuming a Gaussian linear prediction model for $y_i : p(y_i|\mathbf{x}_i, \mathbf{w}) = \mathscr{N}\left(y_i; \mathbf{w}^T\phi(\mathbf{x}_i), \sigma_v^2\right)$, where $\phi(\cdot)$ defines a transformation of the input space and a zero-mean Gaussian prior over $\mathbf{w}$, $p(\mathbf{w}) = \mathscr{N}\left(\mathbf{w}; \mathbf{0}, \sigma_{\mathbf{w}}^2\mathbf{I}\right)$, the posterior for the weight vector w using Bayes theorem is given by:

$$p(\mathbf{w}|D) = \frac{p(y_i|\mathbf{X}, \mathbf{w})\, p(\mathbf{w})}{p(y_i|\mathbf{X})} = \mathscr{N}(\mathbf{w}; \mu_{\mathbf{w}}, \Sigma_{\mathbf{w}}) \tag{35}$$

where $\mu_{\mathbf{w}} = \Phi^T\Phi/\sigma_v^2 + \mathbf{I}/\sigma_{\mathbf{w}}^2$, $\mathbf{y} = [y_1, \cdots, y_n]^T$, $\Phi = [\phi(\mathbf{x}_1), \cdots, \phi(\mathbf{x}_n)]^T$, and $\mathbf{X} = [\mathbf{x}_1, \cdots, \mathbf{x}_n]^T$. The prediction for y^* is obtained integrating out the posterior over $\mathbf{w}$ times its likelihood:

$$p\left(y^*|\mathbf{x}^*, D\right) = \int p\left(y^*|\mathbf{x}^*, \mathbf{w}\right) p(\mathbf{w}, D)\, d\mathbf{w} = \mathscr{N}\left(y; \mu_{y^*}, \sigma_{y^*}\right) \tag{36}$$

where

$$\mu_{y^*} = \phi^T\left(\mathbf{x}^*\right)\mu_{\mathbf{w}} = \mathbf{k}^T\mathbf{C}^{-1}\mathbf{y} \tag{37}$$

$$\sigma_{y^*}^2 = \phi^T\left(\mathbf{x}^*\right)\Sigma\mathbf{w}\phi\left(\mathbf{x}^*\right) = k\left(\mathbf{x}^*, \mathbf{x}^*\right) + \mathbf{k}^T\mathbf{C}^{-1}\mathbf{k} \tag{38}$$

being $k\left(\mathbf{x}_i, \mathbf{x}_j\right) = \phi^T(\mathbf{x}_i)\phi^T\left(\mathbf{x}_j\right)$, $(\mathbf{C})_{ij} = k\left(\mathbf{x}_i, \mathbf{x}_j\right) + \frac{\sigma_\mu^2}{\sigma_w^2}\delta_{ij}$, and $\mathbf{k} = [k(\mathbf{x}^*, \mathbf{x}_1), \cdots, k(\mathbf{x}^*, \mathbf{x}_n)]$. To obtain the estimation given by a GP model for regression, it is necessary only to specify its covariance function $k(\cdot, \cdot)$.

Learning Interactions

A decision support-based system should be capable of inferring on occurring behaviors and interactions of each entity in the corresponding environment. Behaviors are the specific activities defined as actions of each individual object without any external influence, while interactions are the actions inducted by pairwise exchanges of influences between the objects [7].

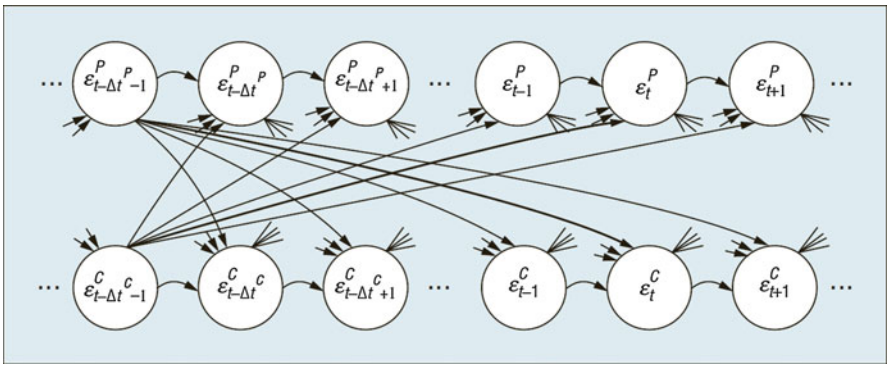

Fig. 5 Dynamic Bayesian Network (DBN) model representing bio-inspired interactions in [16] with linked proto- and core-self nodes

Basically, coupled DBNs are introduced as appropriate models to represent interactions between the entities [8]. Indeed, probabilistic processes and graphical models are characterized by their capability of working in the presence of uncertainty and noise in the environment of interest as well as with a large number of interrelated variables. In addition to these intrinsic capabilities of DBNs, the computational load is kept to a manageable level even with coexistence of many entities and models.

A probabilistic model based on a specific type of event takes inspiration from a bio-inspired approach and the concept of AM as described in section "Interacting Entities Situation Assessment". Damasio describes the cognitive entities as complex systems with incremental learning capabilities based on experience of the interactions between themselves and the external world [13]. Two specific brain processes can be defined to formalize the above concept called proto-self and core-self.

The DBN model proposed in [16] (Fig. 5) takes into account the conditioned probability densities (CPDs) given by $p\left(x_t^P | x_{t-1}^P\right)$ and $p\left(x_t^C | x_{t-1}^C\right)$ relative to the state of each individual object in the environment, denoted through the random variables x_t^P and x_t^C, regardless of the presence of other objects, while the interactions between two objects are defined in terms of casual events ε^P and ε^C through the CPDs:

$$p\left(x_t^P | x_{t-t^C}^C\right) \quad \text{and} \quad p\left(x_t^C | x_{t-t^P}^P\right) \tag{39}$$

In particular, the two conditioned probabilities in Eq. (39) describe the probability that the event ε^C, which occurred at time t^C, provokes the event ε^P in the proto node and the probability that the event ε^P, which occurred at time t^P, provokes the event ε^C in the core node, respectively. Causal relationships between the two entities are then described by the following two CPDs:

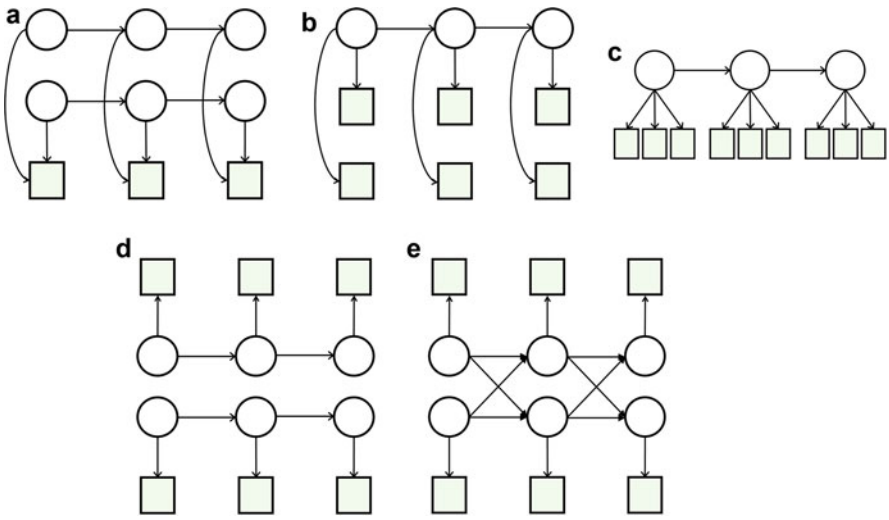

Fig. 6 Graphical representation of five different dynamic models [41]: (**a**) Factorial HMMs (FHMMs), (**b**) Observation Decomposed HMMs (ODHMMs), (**c**) Multiple Observation HMMs (MOHMMs), (**d**) Parallel HMMs (PaHMMs), and (**e**) Coupled HMMs (CHMMs)

$$p\left(x_t^P | x_{t-t^C}^C, x_{t-t^P}^P\right) \quad \text{and} \quad p\left(x_t^C | x_{t-t^P}^P, x_{t-t^C}^C\right) \tag{40}$$

which consider both the interactions in Eq. (39) and the initial situation given by $x_{t-t^P}^P$ and $x_{t-t^C}^C$. In other words, the entity's initial state, an external stimulus (the cause) and its consequence on the behavior of the entity (the effect) can learn an entity's most frequent reaction to the action of another element in the scene.

Several widely used dynamic probabilistic methods in the literature are shown in Fig. 6.

Some Current Learning Techniques and Probable Future Directions

– *Deep learning* has dramatically improved the state-of-the-art in many different ML topics like object detection, speech recognition, and machine translation. Following the initial development of neural networks, the recent success of deep learning is due to its deep architecture based on the idea of a system that simulates human brain [45]; this allows deep learning to solve many more complicated tasks.

The main objective is now to maintain the strength of neural networks while reducing the number of computation units (or neurons). Indeed, it has been shown that the representation of a $(k-1)$-layer neural network with exponentially many neurons is equivalent to a k-layer structure with polynomial many neurons.

In the framework of deep generative models, two examples that have been proposed recently are generative adversarial networks (GANs) and variational autoencoders (VAEs), discussed later in this section. Typically, learning the underly-

ing data distribution of unlabelled signals or images can be highly challenging, and inference on such distributions is highly computationally expensive or intractable. GANs and VAEs provide efficient approximations, making it possible to learn tractable generative models of unlabelled data [43]. Recent works have also extended the VAE and the GAN from unsupervised to semi-supervised settings.

– *Variational autoencoders* consider a dataset $\mathbf{X} = \{\mathbf{x}^{(i)}\}_{i=1}^{N}$ consisting of N i.i.d. samples of observed variables $\mathbf{x}$ [29]. The data are assumed to be generated from some random process that involves latent variables $\mathbf{z}$ as follows: (1) a value $\mathbf{z}^{(i)}$ is drawn from a prior distribution $p_\theta(\mathbf{z})$, and (2) a value $\mathbf{x}^{(i)}$ is drawn from a conditional distribution $p_\theta(\mathbf{x}|\mathbf{z})$ where θ is the true parameter. Both $p_\theta(z)$ and $p_\theta(\mathbf{x}|\mathbf{z})$ are assumed to come from some distribution family parametrized by θ. To learn this generative process with the presence of only observed data, it is often required to estimate the posterior distribution $p_\theta(\mathbf{x}|\mathbf{z})$; however, with moderately complex conditional distributions $p_\theta(\mathbf{x}|\mathbf{z})$, true posterior distributions are generally intractable. A variational autoencoder addresses this issue by introducing an encoder and a decoder. The probabilistic decoder maps the latent variable $\mathbf{z}$ to the conditional distribution $p_\theta(\mathbf{x}|\mathbf{z})$, while the probabilistic encoder maps the observed variable $\mathbf{x}$ to the approximated posterior distribution $q_\phi(\mathbf{x}|\mathbf{z})$, also called recognition model, an approximation of the true posterior $p_\theta(\mathbf{x}|\mathbf{z})$.

– *Generative adversarial networks* have been proposed in [23] to sidestep difficulties in deep generative models of approximating many intractable probabilistic computations and of leveraging the benefits of piecewise linear units in the generative context.

In the adversarial nets framework, the generative model is pitted against an adversary: a discriminative model that learns to determine whether a sample is from the model distribution or the data distribution. The generative model can be thought of as analogous to a team of counterfeiters, trying to produce fake currency and use it without detection, while the discriminative model is analogous to the police, trying to detect the counterfeit currency. Competition in this game drives both teams to improve their methods until the counterfeits are indistinguishable from the genuine articles. This framework can yield specific training algorithms for many kinds of model and optimization algorithm. In [23], the generative model generates samples by passing random noise through a multilayer perceptron, and the discriminative model is also a multilayer perceptron. To learn the generators distribution p_g over data $\mathbf{x}$, a prior on input noise variables $p_{\mathbf{z}}(\mathbf{z})$ is defined, and then, a mapping to data space as $G\left(\mathbf{z}; \theta_g\right)$ is represented, where G is a differentiable function represented by a multilayer perceptron with parameters θ_g, while a second multilayer perceptron $D(\mathbf{x}; \theta_d)$ outputs a single scalar. $D(\mathbf{x})$ represents the probability that $\mathbf{x}$ came from the data rather than p_g. D is trained to maximize the probability of assigning the correct label to both training examples and samples from G, while G is trained to minimize $\log(1 - D(G(\mathbf{z})))$. D and G play the following two-player minimax game with value function $V(G, D)$:

$$\min_G \max_D V(D, G) = \mathscr{E}_{\mathbf{x}\sim p_{\text{data}}(\mathbf{x})}[\log D(\mathbf{x})] + \mathscr{E}_{\mathbf{z}\sim p_z(\mathbf{z})}[\log(1 - D(G(\mathbf{z})))]. \tag{41}$$

Other learning techniques could be considered from the *Game theory* framework such as *Pursuit evasion game* and *Multi-armed bandit*.

Experimental Framework and Results

Research in CR and PHY-layer security has been carried on in different fields for both civil and military purposes. In this section, two current applications are introduced: the *SHIELD project* along with *SPD-Driven Smart Transmission layer* which implement Spectrum Intelligence for security against jamming attacks and *TVWS* to mitigate the shortage of wireless bands. Recent research in TVWS also addresses the problem of jamming attacks in the digital TV band. Some results are then described for future developments in learning dynamic jamming models.

The SHIELD Project and Smart SPD-Driven Transmission Layer

Nowadays, cyber-physical systems (CPSs) and Internet of Things (IoT) are rapidly expanding [19], and new business opportunities are being developed thanks to the dynamic interaction between the entities involved in the business. Indeed, dynamic interactions between entities represent the recent evolution of collaborations between entities for Internet-based services. In this context, autonomous decisions are enabled by dynamic modelling, but the lack of a measurable security makes information exchanges one of the big challenges. Current research on security in CPSs is far less intensive than research on security in computing and networking leaving many devices vulnerable to attacks.

The need for measurable security in the context of interoperating services, applications, systems, and devices in a CPS framework requires the development of an appropriate paradigm. A step forward in that direction is made by *SHIELD* which consists of methodologies for building secure embedded systems. Specifically, the basic approach specifies security through the terms security (S), privacy (P), and dependability (D).

The test-bed, shown in Fig. 7, is a SDR platform which consists of two SWAVE HHs (Secure Wideband Multi-role–Single-Channel Handheld Radios) connected through a dual directional coupler with 20dB nominal coupling (Agilent 778D 100 MHz–2 GHz) [12]. Because of the high output power of the radios, one programmable attenuator is included in the communication path and programmed to their maximum attenuation value – 30dB. The SWAVE HH radio terminal is capable of generating the digital SelfNET Soldier Broadband Waveform (SBW) waveform with bandwidth up to 5 MHz and provides operability in both very high frequency band, VHF (30–88 MHz), and ultrahigh frequency band, UHF (225–512 MHz). Every 3 s, a burst of 8192 consecutive complex samples of the spectrum of interest is outputted over the RS-485 serial port. The bandwidth of the spectrum is 120 MHz. Additional equipment can be connected to the dual directional coupler

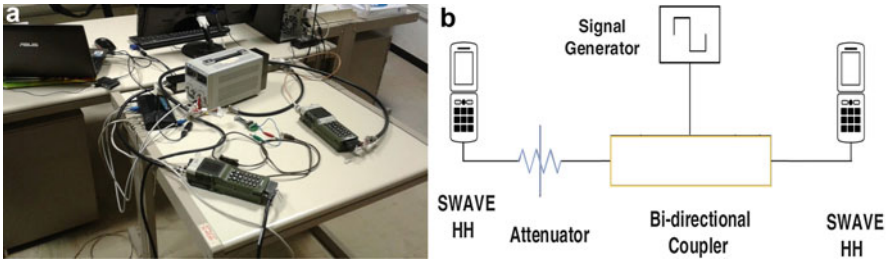

Fig. 7 SDR test-bed in the SHIELD project utilized to generate dynamic signals in the 0–120 MHz spectrum including the SBW signal: (**a**) hardware platform, (**b**) diagram of the main components of the test-bed and their connections

such as a signal generator to inject further modulated signals into the spectrum of interest. Full details on the test-bed architecture may be found in [11].

In order to comply with the minimum requirements for smart and secure data transmission in shared spectrum, SDR-capable devices are based on a set of services implemented at the network level to form a *smart SPD-driven transmission layer* [19]. This is made possible thanks to both the SDR technology with its reconfigurability properties and the CR technology with its learning and self-adaptive capabilities. Cognitive functionalities include self-awareness, spectrum awareness, spectrum intelligence, jamming detection and counteraction, and self-protection.

SPD-driven smart transmission layer addresses the problem of jamming attacks to PHY-layer by providing safe and reliable communication in wireless environments. Anti-jamming methodologies include retroactive frequency hopping (namely, channel surfing), transmission power changing, modifying the modulation of the transmitted waveform, as well as spread spectrum techniques. In particular, when channel surfing is applied, the operating frequency of the radio is changed whenever a strong interfering signal is detected. The probability of detection and reconstruction of a signal may be enhanced by increasing the transmission power and/or gain. Modulation altering may also be decisive in alleviating RF jamming interference, provided that the radios are equipped with automatic modulation recognition capabilities, allowing them to detect and classify the modulation-related features of jamming waveforms.

Research in TVWS

In recent years, the rapid development of wireless devices and wireless services resulted in an ever-growing demand and shortage of the wireless spectrum [36]. For this reason, CR was proposed to efficiently utilize spectrum resources by allowing unlicensed usage of vacant spectrum. Indeed, as reported by the Federal Commu-

nications Commission (FCC) and the UK Office of Communications (Ofcom), a large percentage of spectrum resources is underutilized. This has encouraged the governments to take critical steps toward releasing multiple bands for dynamic spectrum sharing. Consequently, spectrum holes in the licensed spectrum can now be used by secondary users (SUs) without causing any interference to primary users (PUs). In particular, TV White Spaces (TVWS) is one of the most promising paradigms for dynamic spectrum sharing in the digital TV band.

The experimental test-bed in [37] employed for TVWS research consists of a RFeye node, an antenna in the digital TV band [470–790 MHz], and a processing unit (Fig. 8a). The corresponding RF spectrum is shown in Fig. 8b in which there are I = 40 channels over TVWS spectrum (each of them with bandwidth of 8 MHz) ranging from 470 to 790 MHz. Among these TVWS channels, channel 27 is generally vacant, whose frequency ranges from 518 to 526 MHz. During the measurement, channel 27 was randomly corrupted by Digital Video Broadcasting-Terrestrial (DVB-T) signals in order to mimic a malicious user.

To this end, SS is a promising solution to identify potential spectral holes and is one of the most challenging tasks in CR networks [37]. Cooperative SS (CSS) is an effective approach to offer significant performance gain in detecting spectrum holes, by exploiting the spatial diversity of collaborative secondary users (SUs). However, due to the openness of low-layer protocol stacks, CSS networks are vulnerable to attacks from SS data falsification (SSDF). The main goals of malicious attacks come from two aspects: decreasing detection probability for disturbing the normal operation of PUs and increasing false alarm probability to deprive access opportunities for honest SUs. In decentralized CSS networks, sensing results are exchanged between neighboring SUs to improve the network reliability to link failure. However, this characteristic makes decentralized CSS more vulnerable to malicious attacks, as the observations at honest SUs are also available to malicious users during the information exchanging and convergence process. Furthermore, corrupted data can be integrated into the decisions of honest neighbor SUs, which eventually brings significant performance degradation to the whole CSS network.

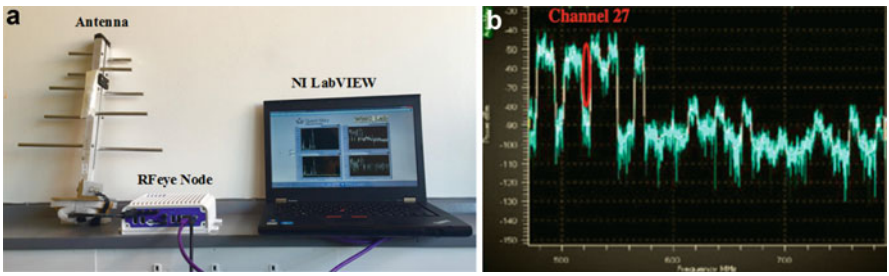

Fig. 8 (**a**) Measurement set-up for collecting real-world data (Queen Mary University of London); (**b**) real-world signals over TVWS collected by a portable RFeye node with the corrupted channel 27

Dual Resolution ST Approach

As mentioned in the previous section, SS is a challenging task in CR devices. In an ICE context, dynamic signal should be processed through time-frequency techniques such as the ST whose complexity often limits its applicability to wideband (i.e., high sampling rate) signals. In the Stockwell transform framework, the dual resolution (DR) technique is conceived to exploit learning mechanisms to adaptively learn the ST parameters for a better trade-off between time resolution and computational time in future work. The DR greatly reduces the computational time of the conventional ST by increasing time delay of the sliding window. Specifically, the signal vector is divided up into sub-blocks in which the wideband signal is assumed to be locally stationary and the sliding window is moved on the first sample of each sub-block. This technique has been validated in a dynamic scenario consisting of real data collected through a SDR test-bed.

Specifically, let $r[p]$, $p = 0, 1, \cdots, P-1$ denote the discrete time series corresponding to a continuous signal $r(t)$ with a time sampling interval T. The corresponding discrete ST is given in Eqs. (10), (11). Considering that the time index m in the discrete ST is the time delay of the sliding window over the signal $r[p]$ and assuming that the signal is locally stationary within the time corresponding to several time delays m, a different approach is proposed in this paper which reduces the computational load of the discrete ST.

From Fig. 9, the P samples of the locally stationary signal are divided into s sub-blocks consisting of P/s samples. This approach computes the ST on s equally spaced values for m belonging to the set $\{0, \cdots, P-1\}$, while $n = 0, \cdots, P-1$ remains as before. Indeed, since in this way the time delay of the sliding window is increased, all the values of m in each sub-block (unless the first one) are not directly included in the computation of the ST (it is sufficient to increase the sliding window length, by increasing k, to also cover the discarded samples). This is based on the consideration that the signal is locally stationary over P/s m's or (P/s)-stationary, namely, variations of the parameters happen no faster than the time

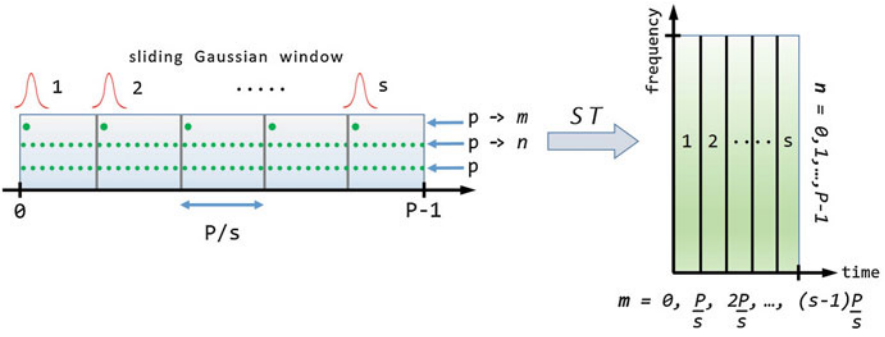

Fig. 9 The dual resolution ST technique for high sampling rate signals

corresponding to P/s samples and not necessarily at the boundary between two consecutive sub-windows. For quicker changes, the length of the sub-blocks can be reduced by increasing s accordingly. This introduces a new capability of the ST, namely, a trade-off between time resolution and computational time that can be adaptively controlled through s, P, and k. The frequency resolution can be changed by regulating P or k (or both).

The (m, n) element in the transformation matrix $\mathbf{T}$ can be written in a vectorial form as follows:

$$S_T[m, n] = \mathbf{T}_{mn}\mathbf{r} \tag{42}$$

where the $P \times 1$ vector $\mathbf{r} = [\, r[0], r[1], \cdots, r[P-1] \,]^T$ is the discrete series, while the following $1 \times P$ vector

$$\mathbf{T}_{mn} = \left[\, T_{mn,0}, T_{mn,1}, \cdots, T_{mn,(P-1)} \,\right]$$

consists of elements given by [2]:

$$T_{mn,p} = \frac{|n|}{\sqrt{2\pi}kN} e^{-\left(n^2(m-p)^2/2k^2N^2 + j2\pi pn/N\right)} \tag{43}$$

$p = 0, \cdots, P-1$. By using the $sN \times P$ transform matrix

$$\mathbf{T} = \left[\, \mathbf{T}_{00}^T, \cdots, \mathbf{T}_{0(N-1)}^T, \mathbf{T}_{\frac{P}{s}0}^T, \cdots, \mathbf{T}_{\frac{P}{s}(N-1)}^T, \cdots, \mathbf{T}_{\frac{P(s-1)}{s}0}^T, \cdots, \mathbf{T}_{\frac{P(s-1)}{s}(N-1)}^T \,\right]^T \tag{44}$$

the discrete ST can be modelled as a linear vectorial equation:

$$\mathbf{s} = \mathbf{T}\mathbf{r} \tag{45}$$

in which the $sN \times 1$ vector $\mathbf{s}$ consists of elements s_{mn} corresponding to $S_T[m, n]$. The dimensionality of Eq. (45) is drastically reduced because $m = m_s P/s$ where $m_s = 0, \cdots, s-1$ is the delay index, instead of $m = 0, 1, 2, \cdots, P-1$.

To validate the proposed dual resolution approach, the discrete ST has been applied to real data in the 0–120 MHz band which includes the VHF band, as described in section "The SHIELD Project and Smart SPD-Driven Transmission Layer". Specifically, at four different time instants, the carrier frequency of the transmitted SBW signal assumes sequentially the values 41 - 51 - 61 - 71 [MHz], while the transmit power is 7dBm. The other waveforms extracted from the spectrum of interest include four sub-signals close to one other (spacing about 0.5–1 MHz) at low frequencies, two interference signals at 20 and 80 MHz, respectively, and three sub-signals in the FM band (spacing about 2.5 and 7 MHz). The carrier frequency of each of these waveforms is fixed over the measurement time.

According to Table 1, the analyzed parameters are P (number of samples in the signal to be S-transformed), s (number of sub-blocks), and the scaling factor k

Table 1 Parameters used to validate the dual resolution ST

P				s			k		
256	512	640	1024	16	32	64	5	17.5	25

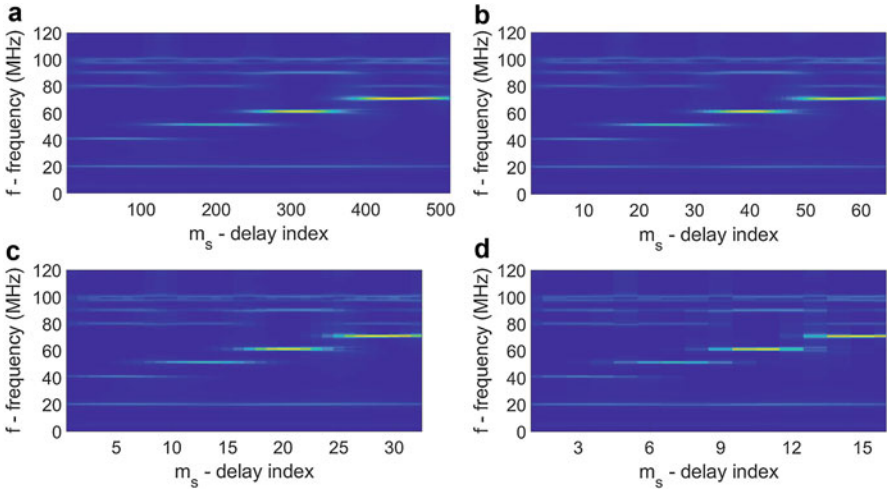

Fig. 10 ST representation of the wideband signal with $P = 512$ and $k = 17.5$: (**a**) without DR; and with dual resolution where (**b**) $s = 64$, (**c**) $s = 32$, and (**d**) $s = 16$. The SBW jumps among 41-51-61-71 MHz at different time instants

described in section "Time-Frequency Analysis and Features". The SBW signal is at least (P/s)-stationary in each configuration.

Figure 10a is the conventional ST, obtained with $k = 17.5$ and without DR, of a signal which consists of $P = 512$ samples. m_s is the delay index, namely, the time variable after ST. The waveforms in the spectrum can be clearly distinguished. In particular, the SWB signal in the middle of the figure jumps sequentially to the four different frequencies at four consecutive time instants. In the bottom, there are the BB peaks (they are very close to each other; the progressive resolution of ST produces fine frequency resolution at low frequencies [5]). Just above them, there is the interference at 20 MHz. Beyond the SBW signal, the interference at 80 MHz and the three FM sub-signals can be seen (the progressive resolution of ST produces low frequency resolution at high frequencies [5]). In this case, the amount of frequency-time samples is $P \cdot P$. The dual resolution algorithm produces the ST in Fig. 10b–d in which s is 64, 32, and 16, respectively. Although the time resolution gets worse by reducing the number of sub-blocks, the signals in the spectrum remain clear. In particular, the dynamic hopping of the SWB signal can be still observed. The main advantage is that the amount of frequency-time samples is reduced to $P \cdot s$, with $s \ll P$.

To show the effective benefits obtained with the proposed algorithm, Fig. 11 illustrates three different indicators: the time to create the $\mathbf{T}$ matrix, the time to compute the ST through Eq. (45), and the $L2$-norm error which illustrates the

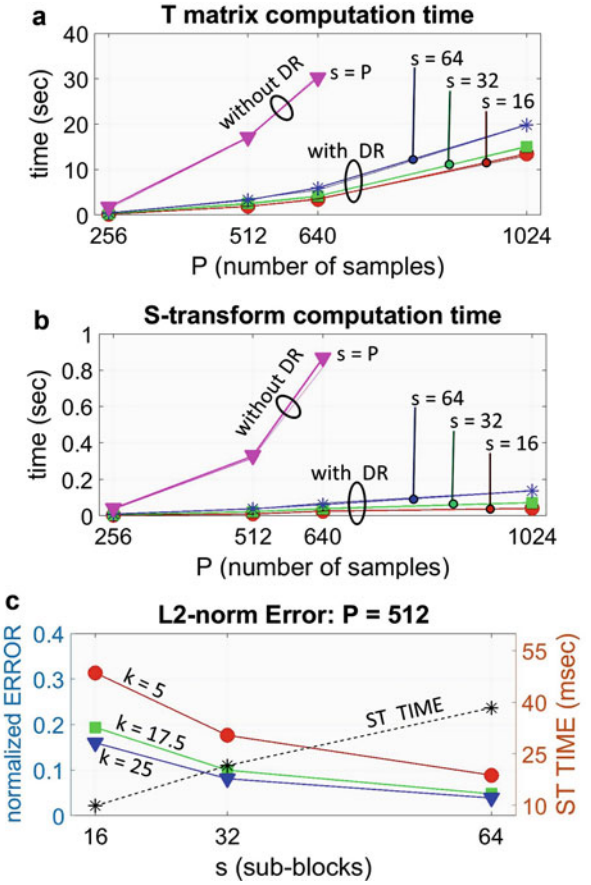

Fig. 11 Performance indicators: (**a**) time to generate **T**, (**b**) ST computation time, (**c**) normalized $L2$-norm error

difference between the 2D TF representation without DR and the corresponding representation with DR ($s = 64, 32, 16$). Specifically, let ε_n be the normalized $L2$-norm error defined as $\frac{\|\mathbf{X}_s - \mathbf{X}_P\|_2}{\|\mathbf{X}_P\|_2}$, where the matrix $\mathbf{X}_s$ is the expanded ST representation with DR, obtained through P/s replicas of each column, the matrix $\mathbf{X}_P$ is the ST representation without DR, and $\|\cdot\|_2$ is the $L2$-norm function.

Figure 11a, b show that in the conventional ST without DR the computational time to both generate the **T** matrix and perform the ST increases sharply when P is increased from 256 to 640. With $P = 1024$, Matlab is no longer capable of generating **T** because of its large dimensions ($P \cdot P$ rows and P columns), while the dual resolution approach reduces dramatically the computational time, and $P = 1024$ is also feasible. This means that the frequency resolution can be improved. Basically, k does not influence the computational time which is through increased by s.

Figure 11c, where $P = 512$, shows that both s and k influence ε_n. As expected, the error (mostly related to the time resolution) increases when at least one between

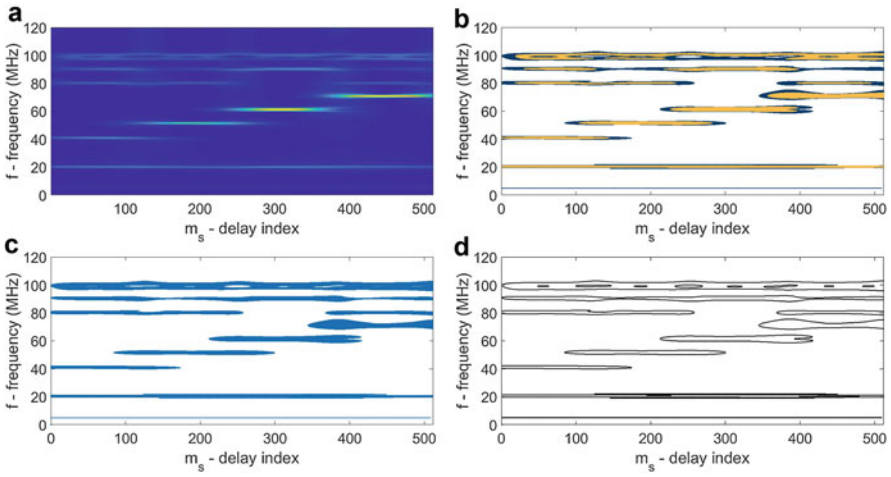

Fig. 12 (**a**) ST representation of the observed 0–120 MHz spectrum with $P = 512$ and $k = 17.5$ and without DR ($s = P$), (**b**) energy locations with threshold = $2\mu_{ST}$ (external dark-blue areas) and with threshold = $4\mu_{ST}$ (internal light-orange areas), (**c**) energy locations with threshold = $2\mu_{ST}$, (**d**) contours of the energy locations with threshold = $2\mu_{ST}$

s and k decreases, and it can be reduced by increasing k when s is small. In Fig. 11c, the corresponding ST computation time is also included which is inversely proportional to the error. The same results hold when a different value for P is considered.

As shown in Fig. 12, contours for each signal in the observation spectrum can be extracted from the time-frequency representations of the wideband signal:

(i) ST representation of the observed 0–120 MHz spectrum is in Fig. 12a;
(ii) energy locations obtained with threshold = $2\mu_{ST}$ and with threshold = $4\mu_{ST}$ are in Fig. 12b–c; μ_{ST} is the mean value of the ST representation;
(iii) contours of the occupied regions detected with threshold = $2\mu_{ST}$ are in Fig. 12d.

Dynamic features can be extracted from the two-dimensional contours of each signal such as bandwidth, central frequency, transmitting power, and shape.

A Discussion of Application Directions of ML Techniques to Cognitive Dynamic Jamming

A possible shared radio environment, as basis for future ICE, is depicted in Fig. 13 in which there are several interacting agents such as a jammer, which aims to "catch" legitimate signals and a user whose objective is to avoid the jammer. In addition, a network manager (NM) is an external observer of the spectrum, e.g., a primary

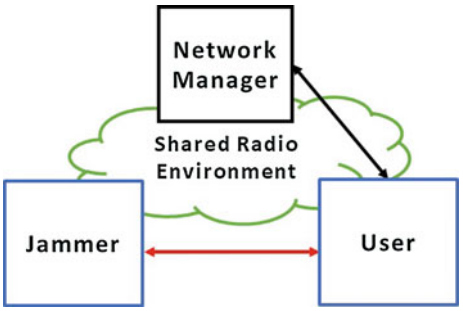

Fig. 13 A practical example in a shared radio environment consisting of two interacting agents, a jammer and a user, with opposite objectives and a network manager. The NM interacts with the user

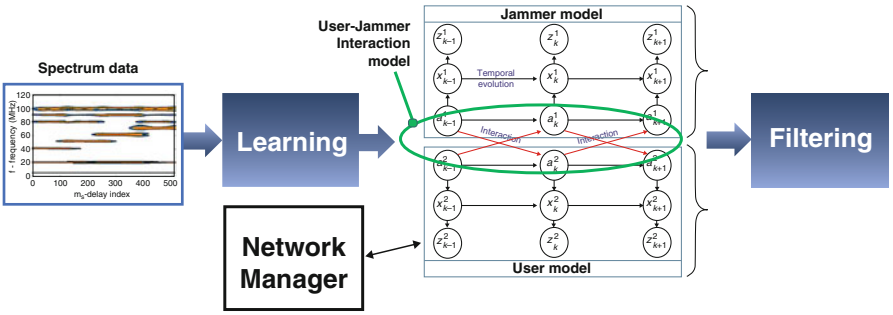

Fig. 14 The proposed example in which jammer, user, and their interactions are modelled through JMSs. The NM observes the spectrum and interacts with the user. Learning and filtering blocks are also shown in the picture

base station, that monitors dynamical spectrum joint situations generated by actions of both the jammer and the user. Such a station can interact with the user and could be either a human operator or an ICE system. The NM can be useful, for example, in case the spectrum sensing computational resources are too intensive to be implemented directly in the user device and the spectrum monitoring facility is shared among many users of the network. Furthermore, in case the NM is the only CDS, it can be in charge to continuously check the normality of an observed situation, namely, to predict if the user behavior is in line with avoiding the jammer.

In general, each of the three radios representing the user, the jammer, or the NM can be a cognitive radio that can be modelled as a CDS. In this example, the NM is assumed to be a CDS that use two JMSs to model the observed interaction between user and jammer as in Fig. 14. The goal is to provide a discussion on how this model can be learned from observed spectrum behaviors where the user successfully avoids the jammer. Such data series correspond to normality patterns that can be used as examples from which to train NM's CDS. First of all, features coming from spectrum monitoring methods are extracted, e.g., by using the time-frequency representation of the spectrum of interest as described at the end of section "Dual Resolution ST Approach". Such spectrum data can be used by the *learning* algorithm to estimate parameters of the switching models. In other words,

normality models are learned corresponding to models where rules that allow the user to avoid the jammer are estimated from the data series examples where this is known to have happened successfully. Such rules describe a dynamic equilibrium condition that should be verified according to previous experiences recorded in such data series if a normal situation occurs. Normal training samples are much easier to collect than abnormality samples whose dataset could be insufficient or unavailable [38]. After having trained the switching models using only normal data in order to learn a representation of the normal spectrum activities, the *filtering* phase produces predictions of the corresponding hidden variables and observation at each time instant. Filtering can be also thought as a generative block for abnormality detection; indeed, since the JMSs are not able to generate abnormal events at testing time because trained with normal data only, a normality condition is said to be probabilistically verified if updates and related predictions are consistent, while excess of deviations of updated observations from predictions corresponds to abnormalities where the jammer's behavior is different from the patterns observed during the training and the user is no longer capable of avoiding it.

From Eq. (15), the state vector $\mathbf{x}_k^i$ for the i-th entity can be augmented into $\tilde{\mathbf{x}}_k^{i\,T} = \left[\mathbf{x}_k^{i\,T}, \mathbf{a}_k^{i\,T}\right]$, where $i = \{1, 2\}$; then the corresponding nonlinear state-space model (NLSSM) is given by:

$$\begin{cases} \tilde{\mathbf{x}}_k^i = f\left(\tilde{\mathbf{x}}_{k-1}^i, \mathbf{v}_k^i\right) \\ \mathbf{z}_k^i = h\left(\tilde{\mathbf{x}}_k^i, \mathbf{w}_k^i\right) \end{cases} \tag{46}$$

The NLSSM for interactive entities evolves according to

$$\Pi\left(\mathbf{a}_k^i|\mathbf{a}_{k-1}^i\right), \quad p\left(\mathbf{x}_k^i|\mathbf{x}_{k-1}^i, \mathbf{a}_k^i, \mathbf{a}_{k-1}^j\right), \quad p\left(\mathbf{z}_k^i|\mathbf{x}_k^i, \mathbf{a}_k^i, \mathbf{a}_{k-1}^j\right); \quad i, j = \{1, 2\}, \; i \neq j \tag{47}$$

and [16]

$$\Pi\left(\mathbf{a}_k^1|\mathbf{a}_{k-1}^2\right), \quad \Pi\left(\mathbf{a}_k^2|\mathbf{a}_{k-1}^1\right) \tag{48}$$

Specifically, in this example *learning* aims to estimate (from available data) model parameters, continuous- and discrete-valued states, and transition and interaction probability distributions in nonlinear state-space models with Markovian switching structure. Discrete switching variables (a's), probabilistic distributions described by links between the discrete nodes (namely, Π matrices) including entity-to-entity interactions, and probabilistic distributions described by links between discrete variables and continuous state variables (x's) can be learnt through unsupervised clustering techniques such as *Dirichlet process mixture (DPM)* model, while continuous state variables, transition models between the state at time k and its value at time $k-1$, and likelihood models between observations (z's) and state variables can be learnt through techniques like *Gaussian process (GP) regression* or *GaNs*.

The *filtering* block estimates and predicts sequentially the latent states $\{\mathbf{x}_k^i, \mathbf{a}_k^i\}$ given the densities for the initial state $\{\mathbf{x}_0^i, \mathbf{a}_0^i\}$ and the measurements up to time k ($\mathbf{z}_{1:k}^i$). For this purpose, *particle filtering*-based methods can be used such as *Markov Jump Particle Filter* (MJPF) or *Rao-Blackwellized Particle Filter* (RBPF).

Conclusion and Future Directions

This chapter addresses the application of learning techniques to dynamic models for wireless communications. Indeed, PHY-layer security is gathering ever-growing interest in the research world due to the high vulnerability of wireless communications to external attacks such as jamming attacks. This is the main objective for which a detailed discussion of selected techniques and scientific results in the current state-of-the-art is provided throughout the above sections. Some probable and interesting future directions in this framework are also introduced in order to show the evolution of CR, which has been conceived to overcome the shortage of available bands in the wireless spectrum, toward a wider paradigm designed for interactive and cognitive environments. Considering that, *dynamic* is a decisive concept to enable cognition and interactions which are on the basis of self-aware and self-adaptive devices. To this end, time information seems to be a key component in processing dynamic signals. For this reason, time-frequency analysis is included in this chapter as a first step to detect signals in the spectrum of interest and to extract both time and frequency information. Afterward, several statistical models are described; most of them are based on a Bayesian approach and represented through probabilistic graphical models which highlight both temporal dependencies, namely, dynamic of the system, and entity-to-entity dependencies, namely, interactions. In this framework, the concepts of *learning*, *cognition*, and *interactions* come from recent results obtained in computational neuroscience. Specifically, autobiographical memory results from a bio-inspired approach which enables cognition and interactions with external entities. To this end, several techniques from ML and data mining are described which are employed to learn parameters, models, and interactions.

A more practical point of view is described in the experimental framework section which includes two applications in dynamic environments: TVWS to overcome the shortage of spectrum availability, which can be vulnerable to jamming attacks, and the SHIELD project which aims to implement measurable security, privacy, and dependability (SPD) in cyber-physical systems. A time-frequency analysis is also introduced which extracts both time and frequency information from real dynamic signals with controllable resolution in both the domains. The corresponding contours are then extracted for future work. In addition, a practical example about application directions of ML techniques for cognitive dynamic jamming lays the foundations toward complex CDSs to make ICEs become a reality.

In particular, probable future directions include employing techniques and algorithms used for data analysis, image and video processing, robotics, and so

forth, in wireless communications. Indeed, general concepts such as entity, state, and trajectory can be specified to CR as signal, central frequency and bandwidth, and time-frequency information, respectively. Specifically, representation of wireless signals (including jammers) through, for example, multilayer perceptron, variational autoencoders, or HMMs are not found in the current state-of-the-art, and, consequently, learning techniques to learn such kind of dynamic models in a jamming context are not either.

In addition, a bio-inspired approach, as described in this chapter, could enhance the learning process by combining cognition with self-awareness and self-adaptation in CR devices for future PHY-layer security.

Cross-References

- Adaptive Learning in Cognitive Radio
- Cognitive Radio Network Security
- Dynamic Spectrum Sharing in Secure Cognitive Radio Networks
- Spectrum Sensing, Measurement, and Modeling
- Spectrum Sensing Methods and Their Performance
- Spectrum Sensing Using Markovian Models

References

1. Allen JB, Rabiner LR (1977) A unified approach to short-time fourier analysis and synthesis. Proc IEEE 65(11):1558–1564
2. Baiqiang Y, Yigang H (2015) A fast matrix inverse s-transform algorithm for MCG denoise. In: IEEE international conference on electronic measurement and instruments (ICEMI), Qingdao, pp 315–319
3. Bouachache B, Flandrin P (1982) Wigner-ville analysis of time-varying signals. In: IEEE international conference on acoustics, speech, and signal processing (ICASSP), Paris, pp 1329–1332
4. Breve FA, Pedronette DCG (2016) Combined unsupervised and semi-supervised learning for data classification. In: 2016 IEEE 26th international workshop on machine learning for signal processing (MLSP), Salerno, pp 1–6
5. Brown RA, Lauzon ML, Frayne R (2010) A general description of linear time-frequency transforms and formulation of a fast, invertible transform that samples the continuous s-transform spectrum nonredundantly. IEEE Trans Sig Process 58(1):281–290
6. Caro S, Perez-Cruz F, Murillo-Fuentes JJ (2006) Gaussian processes for regression in channel equalization. In: 14th European signal processing conference (EUSIPCO 2006), Florence
7. Castaldo F, Palmieri FAN, Regazzoni CS (2016) Bayesian analysis of behaviors and interactions for situation awareness in transportation systems. IEEE Trans Intell Trans Syst 17(2):313–322
8. Chiappino S, Marcenaro L, Morerio P, Regazzoni C (2013) Run length encoded dynamic Bayesian networks for probabilistic interaction modeling. In: 21st European signal processing conference (EUSIPCO 2013), Marrakech, pp 1–5
9. Chin W, Li J, Chen H (2015) Low-complexity energy detection for spectrum sensing with random arrivals of primary users. IEEE Trans Veh Technol 65(2):947–952
10. Cohen L (1989) Time-frequency distributions-a review. Proc IEEE 77(7):941–981

11. Dabčević K, Marcenaro L, Regazzoni CS (2014) SPD-driven smart transmission layer based on a software defined radio test bed architecture. In: 4th international conference on pervasive and embedded computing and communication systems (PECCS), Lisbon
12. Dabčević K, Mughal M, Marcenaro L, Regazzoni CS (2014) Spectrum intelligence for interference mitigation for cognitive radio terminals. In: Wireless innovation forum European conference on communications technologies and software defined radio (WInnComm-Europe), Rome
13. Damasio A (2000) The feeling of what happens: body and emotion in the making of consciousness. Recorded Books, Prince Frederick
14. Daubechies I (1990) The wavelet transform, time-frequency localization and signal analysis. IEEE Trans Inf Theory 36(5):961–1005
15. Dhar S, Cherkassky V (2017) Universum learning for SVM regression. In: 2017 international joint conference on neural networks (IJCNN), Anchorage, pp 3641–3648
16. Dore A, Regazzoni C (2010) Interaction analysis with a Bayesian trajectory model. IEEE Intell Syst 25(3):32–40
17. Dore A, Cattoni AF, Regazzoni CS (2010) Interaction modeling and prediction in smart spaces: a bio-inspired approach based on autobiographical memory. IEEE Trans Syst Man Cybern Part A Syst Humans 40(6):1191–1205
18. Dzakmic S, Namas T, Dzafic I (2017) Fault classification using multi-resolution analysis and discrete wavelet transforms. In: 2017 XXVI international conference on information, communication and automation technologies (ICAT), Sarajevo, pp 1–6
19. Fiaschetti A, Noll J, Azzoni P, Uribeetxeberria R (2017) Measurable and composable security, privacy, and dependability for cyberphysical systems: the SHIELD methodology. CRC Press, Boca Raton
20. Fox E, Sudderth EB, Jordan MI, Willsky AS (2011) Bayesian nonparametric inference of switching dynamic linear models. IEEE Trans Signal Process 59(4):1569–1585
21. Ghahramani Z (2001) An introduction to hidden Markov models and Bayesian networks. Int J Pattern Recognit Artif Intell 15(01):9–42
22. Gomes SR, Saroar SG, Mosfaiul M, Telot A, Khan BN, Chakrabarty A, Mostakim M (2017) A comparative approach to email classification using naive Bayes classifier and hidden Markov model. In: 2017 4th international conference on advances in electrical engineering (ICAEE), Dhaka, pp 482–487
23. Goodfellow I, Pouget-Abadie J, Mirza M, Xu B, Warde-Farley D, Ozair S, Courville A, Bengio Y (2014) Generative adversarial networks. ArXiv e-prints 1406.2661
24. Hsu D, Sham MK, Zhang T (2012) A spectral algorithm for learning hidden Markov models. J Comput Syst Sci 78(5):1460–1480. JCSS Special Issue: Cloud Computing 2011
25. Huang N et al (1998) The empirical mode decomposition and Hilbert spectrum for nonlinear and nonstationary time series analysis. Proc R Soc London Ser A Math Phys Eng Sci 454(1971):903–995
26. Jesus MAD, Teixeira M, Vicente L, Rodriguez Y (2006) Nonuniform discrete short-time fourier transform a goertzel filter bank versus a fir filtering approach, vol 2. In: 2006 49th IEEE international midwest symposium on circuits and systems, Island of Kos, pp 188–192
27. Jokanovic B, Amin MG, Ahmad F (2016) Effect of data representations on deep learning in fall detection. In: 2016 IEEE sensor array and multichannel signal processing workshop (SAM), Rio de Janerio, pp 1–5
28. Kapoor S, Rao S, Singh G (2011) Opportunistic spectrum sensing by employing matched filter in cognitive radio network. In: 2011 international conference on communication systems and network technologies (CSNT 2011), Proceedings of a meeting held 3–5 June 2011, Katra, Jammu, pp 580–583
29. Kingma D, Welling M (2013) Auto-encoding variational Bayes. ArXiv e-prints 1312.6114
30. Koller D, Friedman N (2009) Probabilistic graphical models: principles and techniques – adaptive computation and machine learning. The MIT Press, Cambridge

31. Liu Y, Cai B (2015) A reliability analysis framework based on time-varying dynamic Bayesian network. In: 2015 IEEE international conference on industrial engineering and engineering management (IEEM), Singapore, pp 21–25
32. Maggio M, Abdelzaher T, Esterle L, Giese H, Kephart J, Mengshoel O, Papadopoulos A, Robertsson A, Wolter K (2017) Self-adaptation for individual self-aware computing systems. Springer International Publishing, Cham, pp 375–399
33. Malegori G, Ferrini G (2010) Tip-sample interactions on graphite studied using the wavelet transform. Beilstein J Nanotechnol 1:172–181
34. Nawaz T, Mughal M, Marcenaro L, Regazzoni C (2015) Exploiting cyclic features for jammer detection in wide-band cognitive radios. In: WInnComm-Europe'15, Erlangen
35. Nazábal A, Artés-Rodríguez A (2015) Discriminative spectral learning of hidden Markov models for human activity recognition. In: 2015 IEEE international conference on acoustics, speech and signal processing (ICASSP), South Brisbane, pp 1966–1970
36. Qin Z, Gao Y, Plumbley M, Parini C (2016) Wideband spectrum sensing on real-time signals at sub-nyquist sampling rates in single and cooperative multiple nodes. IEEE Trans Signal Process 64(12):3106–3117
37. Qin Z, Gao Y, Plumbley MD (2018) Malicious user detection based on low-rank matrix completion in wideband spectrum sensing. IEEE Trans Signal Process 66(1):5–17
38. Ravanbakhsh M, Nabi M, Sangineto E, Marcenaro L, Regazzoni CS, Sebe N (2017) Abnormal event detection in videos using generative adversarial nets. In: 2017 IEEE international conference on image processing (ICIP), Beijing, pp 1577–1581
39. Satija U, Mohanty M, Ramkumar B (2015) Automatic modulation classification using s-transform based features. In: 2nd international conference on signal processing and integrated networks (ICSPIN), South Brisbane, pp 708–712
40. Stockwell RG, Mansinha L, Lowe RP (1996) Localization of the complex spectrum: the S transform. IEEE Trans Signal Process 44(4):998–1001
41. Suk HI, Sin BK, Lee SW (2009) Analyzing human interactions with a network of dynamic probabilistic models. In: 2009 workshop on applications of computer vision (WACV), Snowbird, pp 1–6
42. Tian Z, Giannakis G (2006) A wavelet approach to wideband spectrum sensing for cognitive radios. In: IEEE 1st international conference on cognitive radio oriented wireless networks and communications, Crowncom, pp 1–5
43. Wan C, Probst T, Gool LV, Yao A (2017) Crossing nets: combining GANs and VAEs with a shared latent space for hand pose estimation. In: 2017 IEEE conference on computer vision and pattern recognition (CVPR), Honolulu, pp 1196–1205
44. Wang H, Hu D (2005) Comparison of SVM and LS-SVM for regression. In: 2005 international conference on neural networks and brain, Beijing, vol 1, pp 279–283
45. Wang H, Raj B (2017) On the origin of deep learning. ArXiv e-prints 1702.07800
46. Xinzhi Z, Feifei G, Rong C, Tao J (2015) Matched filter based spectrum sensing when primary user has multiple power levels. China Commun 12(2):21–31
47. Yang D, Xue G, Zhang J, Richa A, Fang X (2013) Coping with a smart jammer in wireless networks: a stackelberg game approach. IEEE Trans Wirel Commun 12(8):4038–4047
48. Zou Y, Zhu J, Wang X, Hanzo L (2016) A survey on wireless security: technical challenges, recent advances, and future trends. Proc IEEE 104(9):1727–1765

Index

W. Zhang (ed.), *Handbook of Cognitive Radio*,
https://doi.org/10.1007/978-981-10-1394-2

O